EAC-2012
Granada
European Aerosol Conference
2-7 Sept 2012

EAC2012 GRANADA

European Aerosol Conference Handbook

C·E·A·M·A

Universidad de Granada

Fundación *El legado andalusí*

EAA – European Aerosol Assembly
AECTA – Spanish Science and Technology Aerosol Association

Organised by: Atmospheric Physics Research Group, Andalusian Center for Environmental Studies (CEAMA), University of Granada

European Aerosol Conference 2012,

Granada, Spain, September 2 to 7, 2012

Conference chairs: Lucas Alados Arboledas and Francisco José Olmo Reyes
Hosting Aerosol Association: Asosiación Española de Ciencia y Tecnología de Aerosoles (AECyTA)

Contents:

Abstracts:

Wednesday, September 5, 2012

Thursday, September 6, 2012

Friday, September 7, 2012

GRIMM Aerosol Technik
continuous research

IAQ

Your all-in-one solution provider for the measurement of airborne particles

Sizes from 0.8 nm to > 30 µm
Indoor & Outdoor
Counts, size distributions
mass, surface area, PM 10 / 2.5 / 1
Inhalable, thoracic, alveolic
Filter & ventilation testing
Particle generators

Nano

Satisfied customers for over 30 years.
Just contact us
or meet us face-to-face at the EAC!

Phone: +49 (0)8654 . 578-0
contact@grimm-aerosol.com

Enviro

GRIMM

www.GRIMM-aerosol.com

Preface

The European Aerosol Conference is the meeting place in Europe for the international research community working in the field of aerosol science and technology. These conferences are organized under de auspices of the European Aerosol Assembly (EAA) and in 2012 the conference takes place from 2nd to 7th September in Granada, Spain. It is organized by the Spanish Science and Technology Aerosol Association and hosted by the University of Granada, gathering world-class scientists in all fields of aerosol science from fundamentals to applications.

The conference follows the format of previous editions, with oral sessions preceded by a daily plenary lecture in one of the key areas of active aerosol research. Sessions are organized according to the 11 thematic areas of the EAA Working Groups with additional 5 special sessions. The program ensures key sessions dealing with cutting edge activities encouraging the interaction of the community, especially young scientists. Poster sessions are accommodated in the afternoons on Monday, Tuesday and Thursday; with also room for societies and boards meetings requested.

The organizers of the EAC2012 gratefully acknowledge the effort of the EAA Working Groups and the support of the Scientific Committee in the review process, the identification of plenary speakers and setting up of the special sessions. Last but not least, a grateful thank-you to all sponsors and exhibitors for their financial support.

Lucas Alados Arboledas and Francisco José Olmo Reyes
Co-chairs of EAC2012

Front cover: Alhambra Palace, Granada

NOTES:

Table of Contents

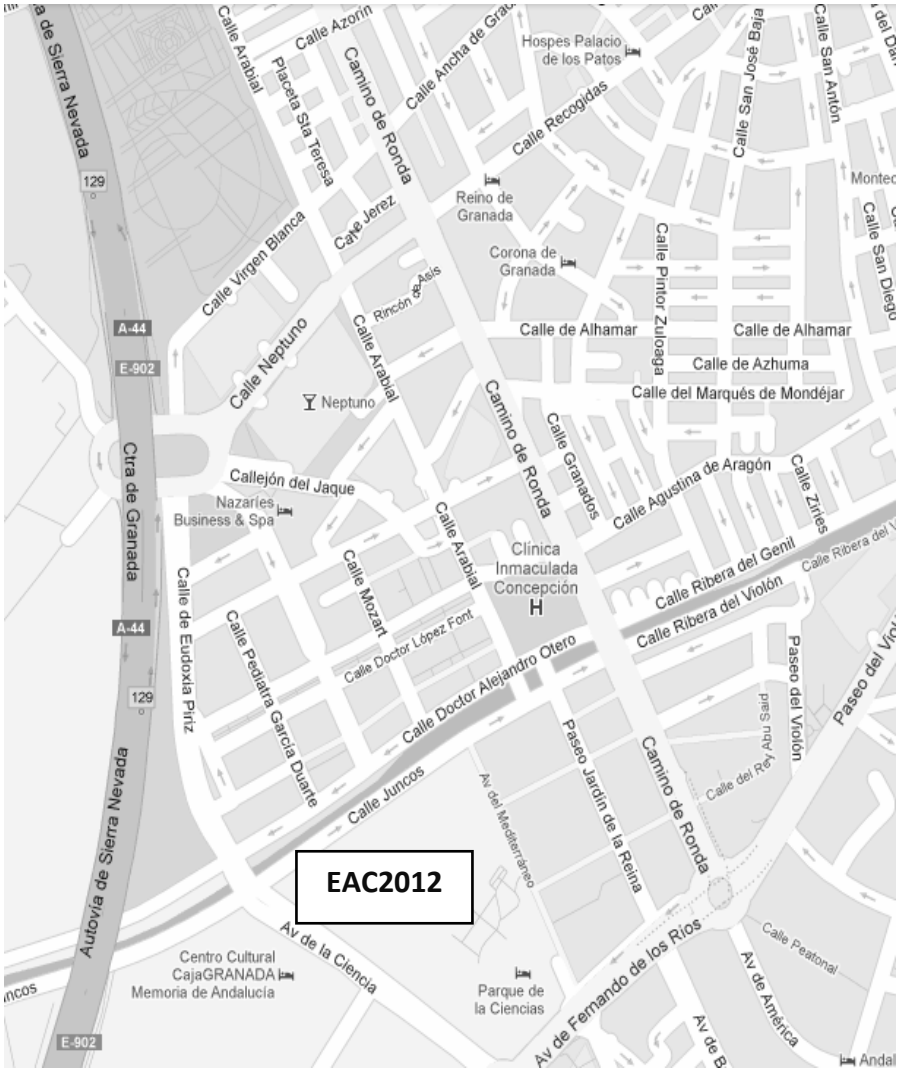

Walk route from Hotels

http://www.eac2012.com/index.php/accommodation

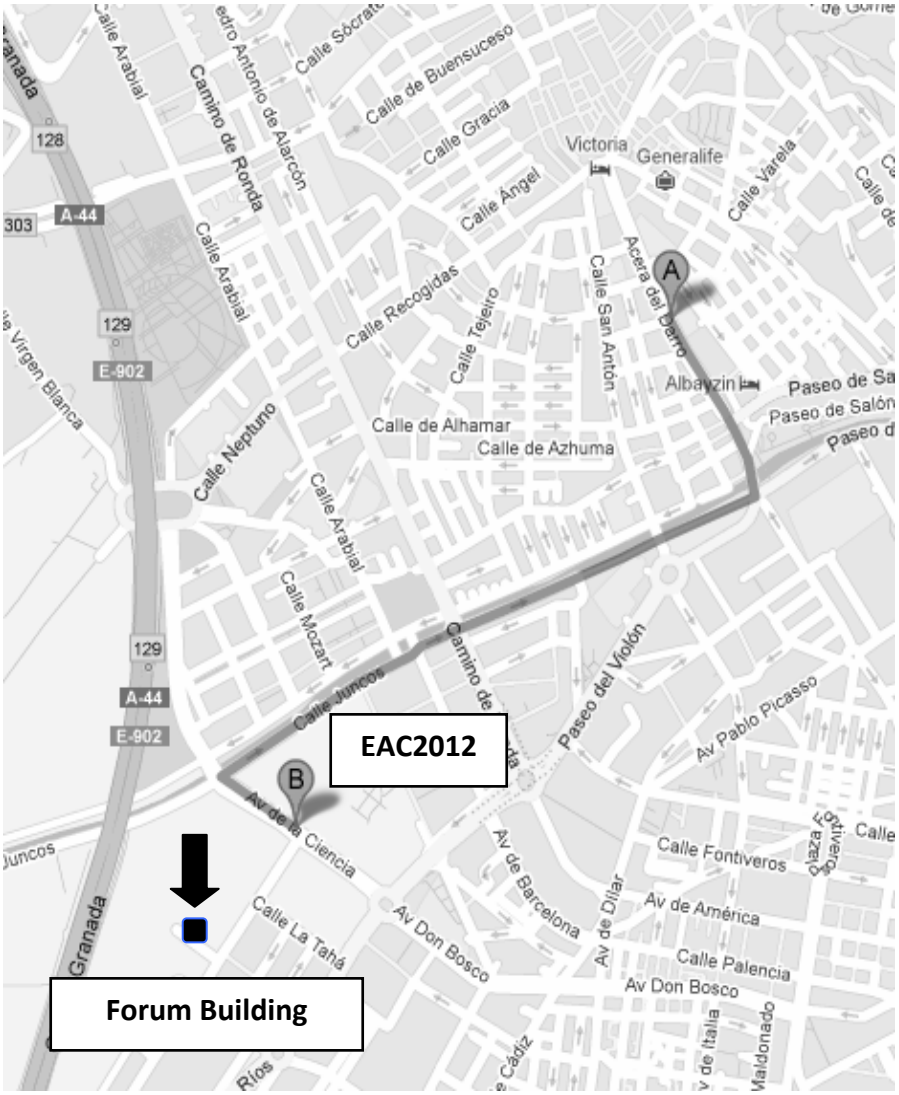

Walk route from the city center

PARQUE DE LAS CIENCIAS

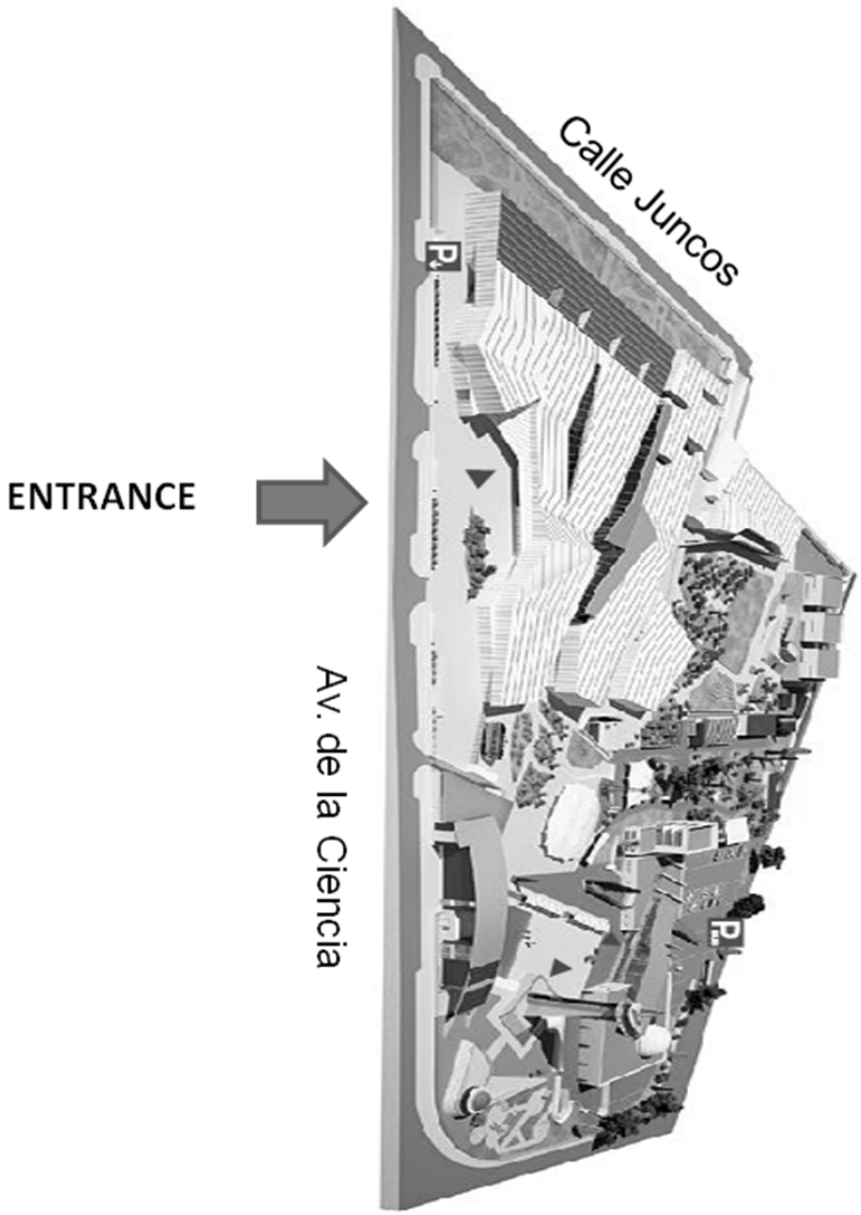

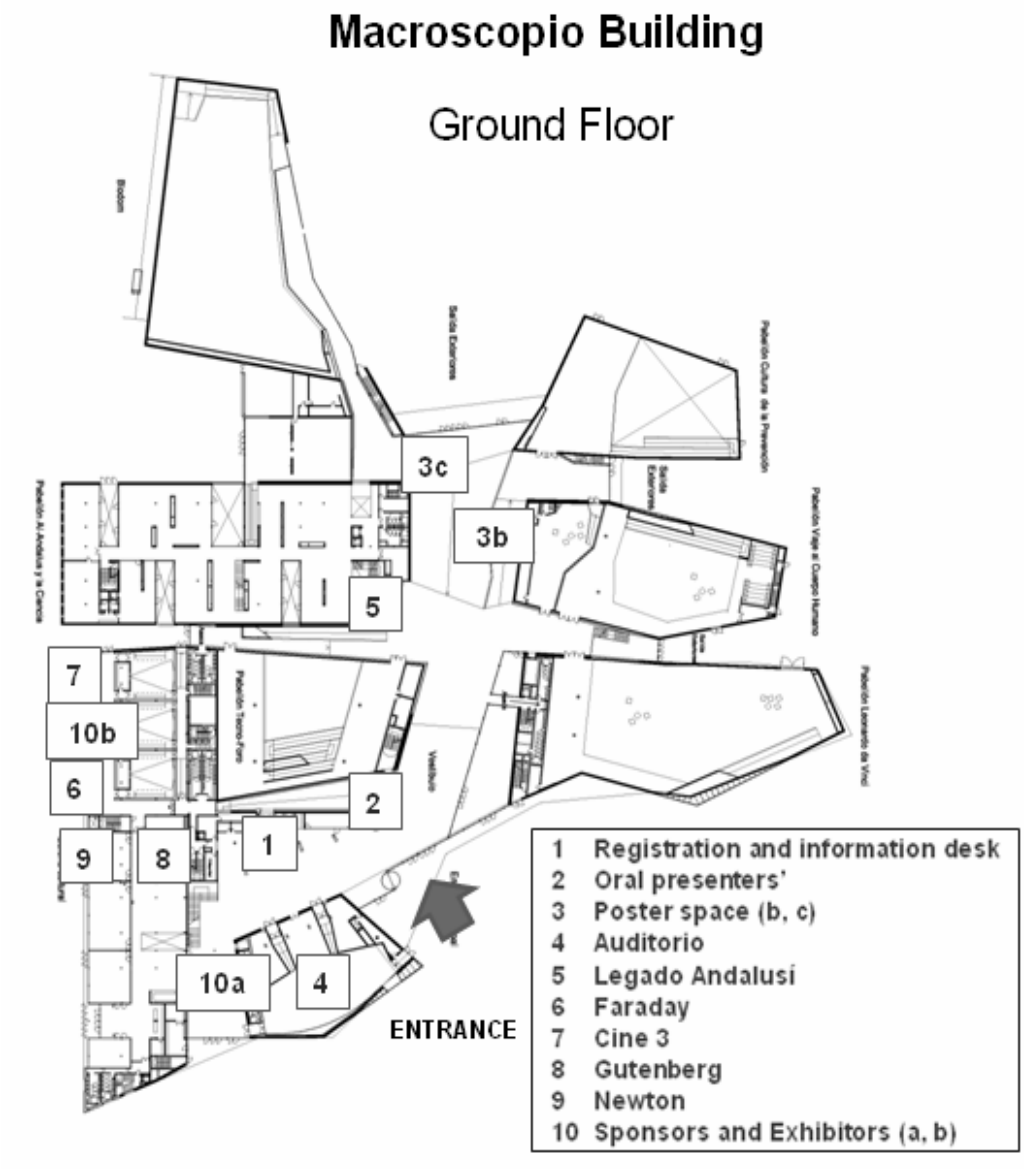
Macroscopio Building
Ground Floor
3c
3b
5
7
10b
6
2
1
9
8
10a
4
ENTRANCE
1 Registration and information desk
2 Oral presenters'
3 Poster space (b, c)
4 Auditorio
5 Legado Andalusí
6 Faraday
7 Cine 3
8 Gutenberg
9 Newton
10 Sponsors and Exhibitors (a, b)

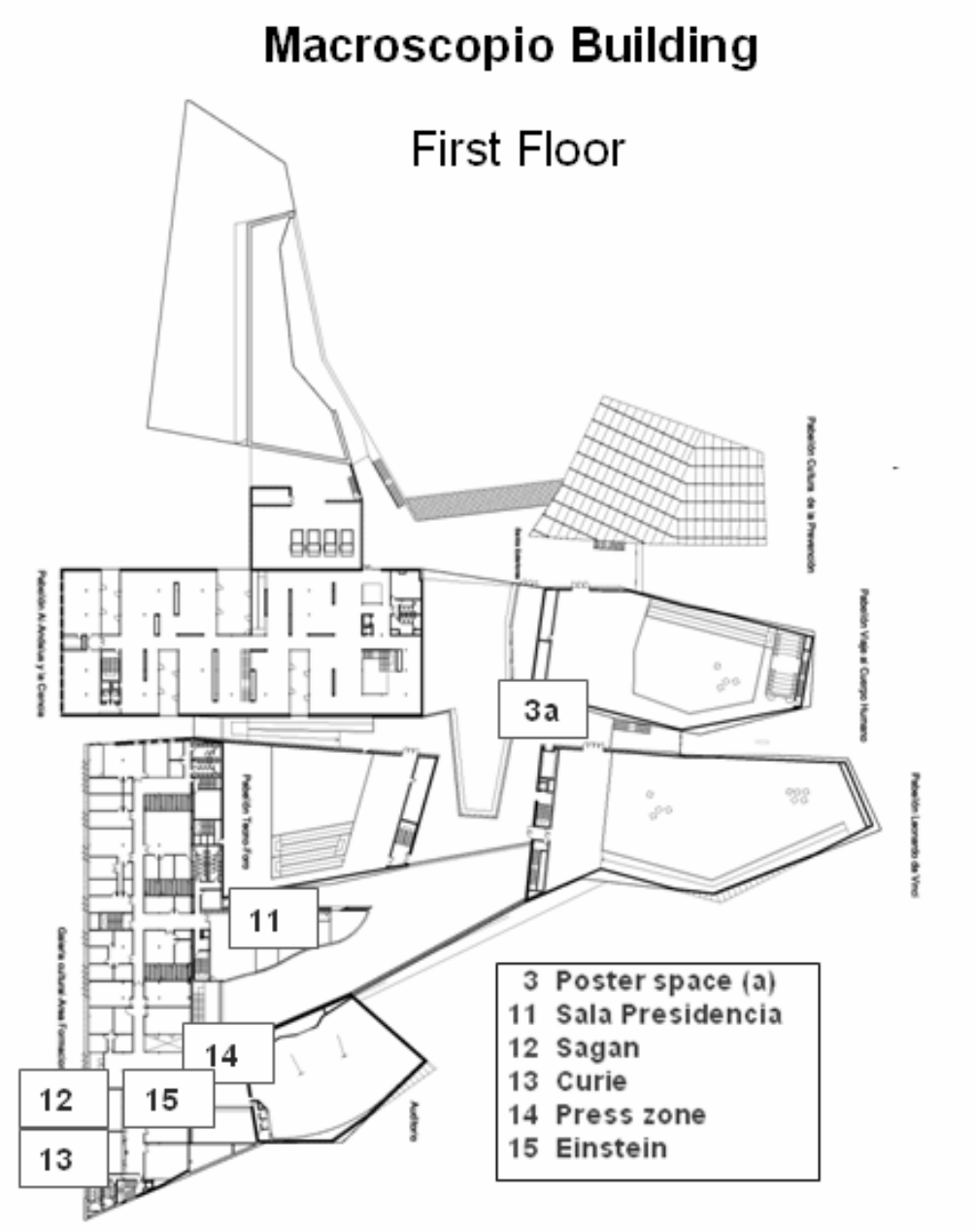
Macroscopio Building
First Floor
3a
11
14
12
15
13
3 Poster space (a)
11 Sala Presidencia
12 Sagan
13 Curie
14 Press zone
15 Einstein

Poster space 3a (First Floor)

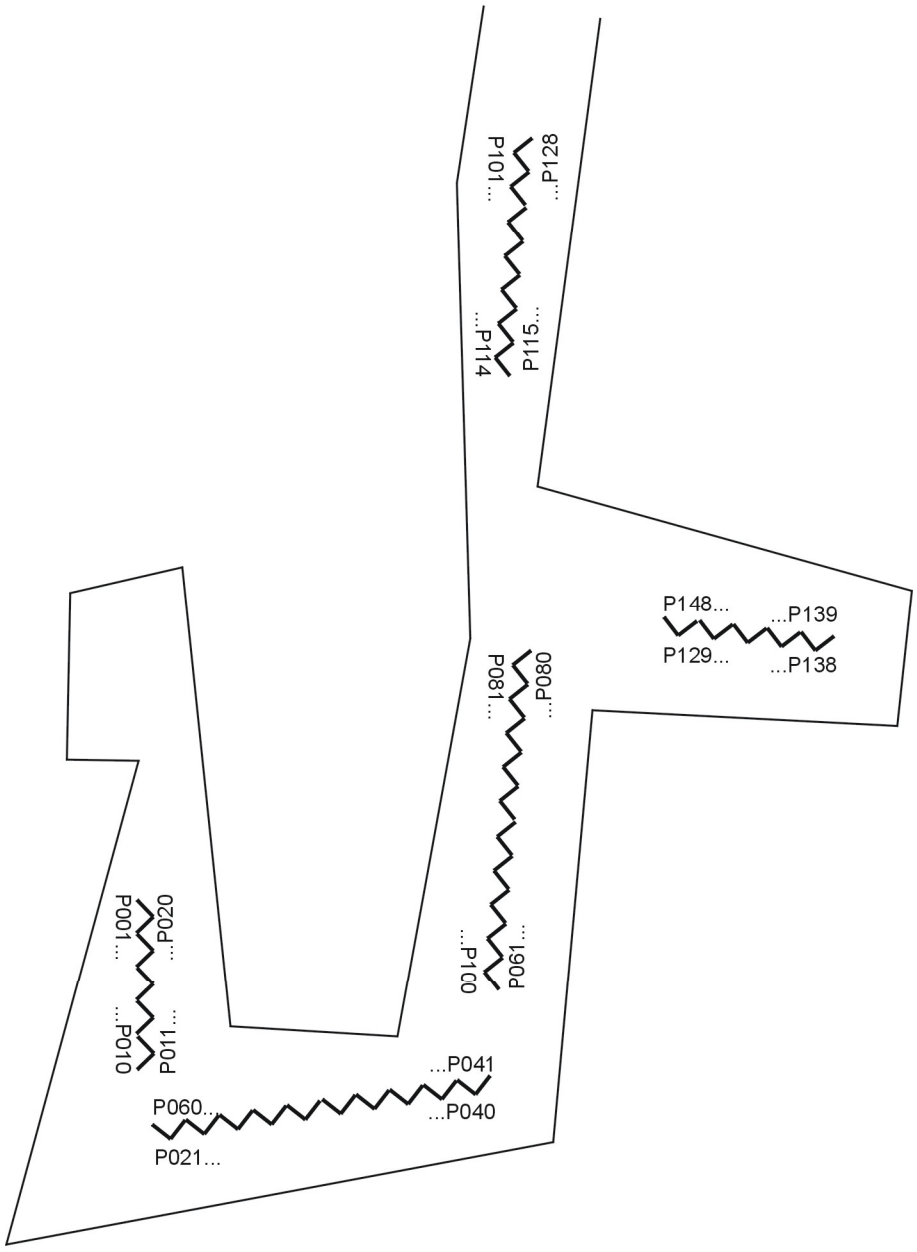

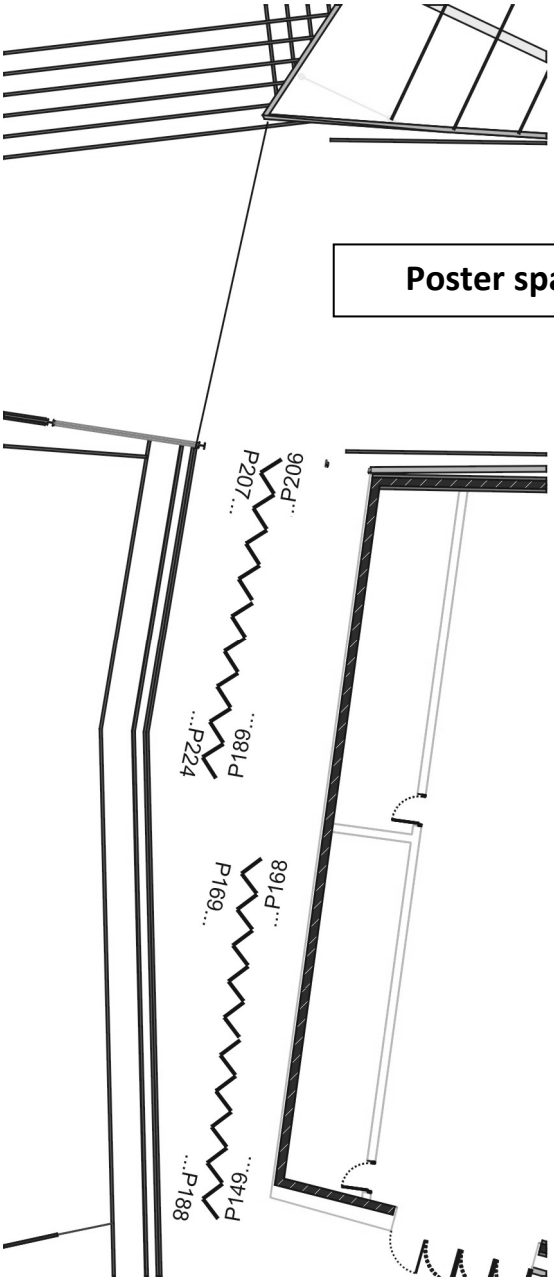
Poster space 3b (Ground Floor)
P207...
...P206
...P224
P189...
P169...
...P168
...P188
P149...

Poster space 3c (Ground Floor)

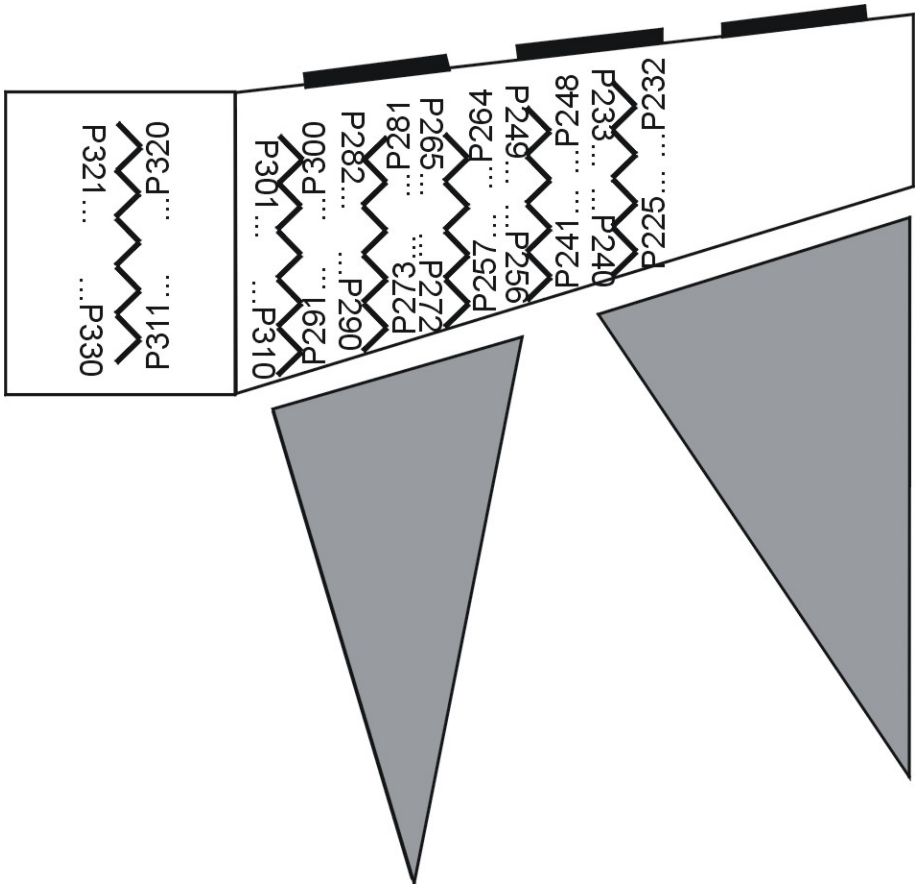

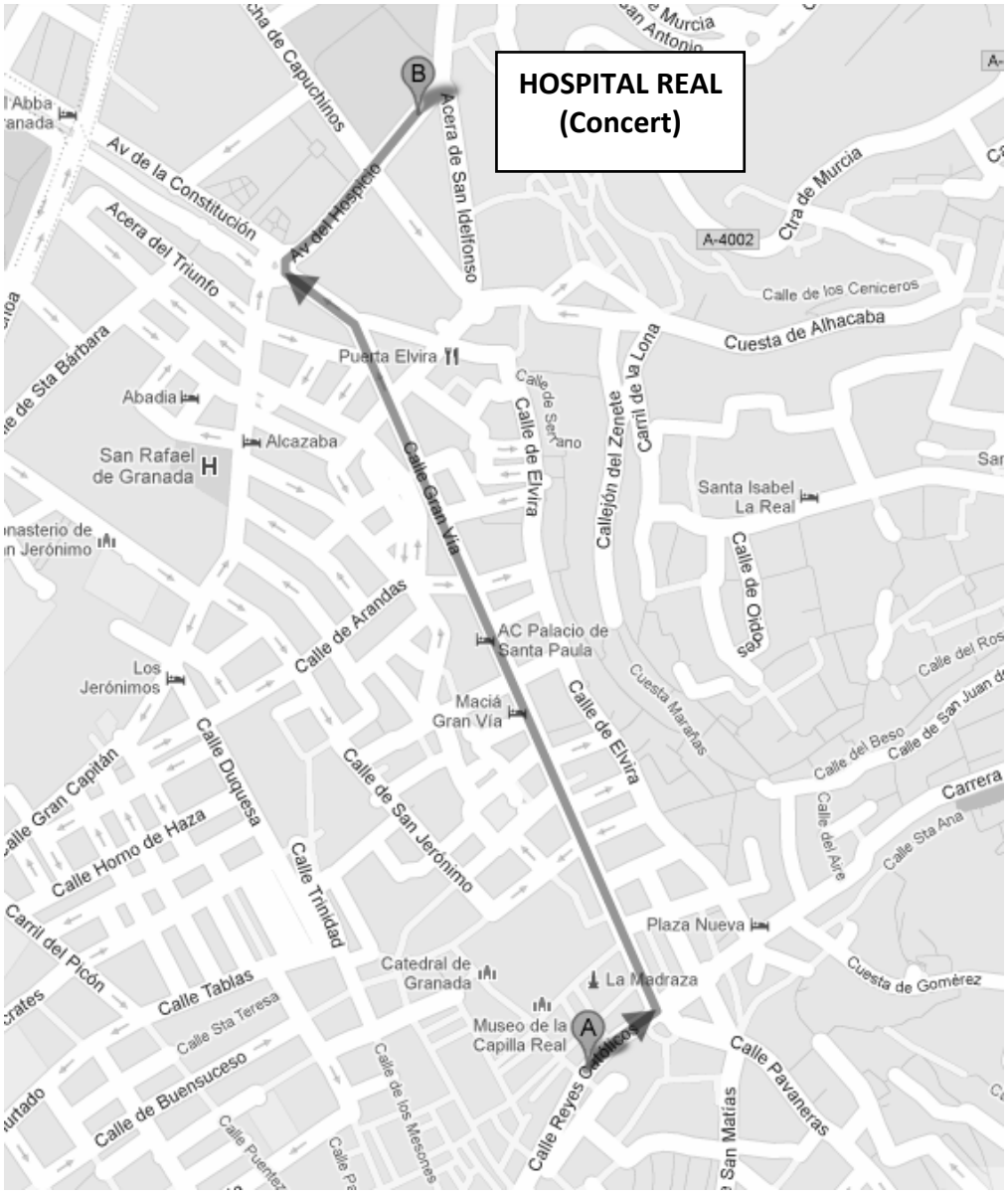

Walk route from the city center (~15 minutes)

Closest BUS STOP: Constitución 1

From Parque de las Ciencias: Lines 1, 5

Other Bus Lines: 3, 4, 6, 7, 9, 11, 21, 24, 33, C

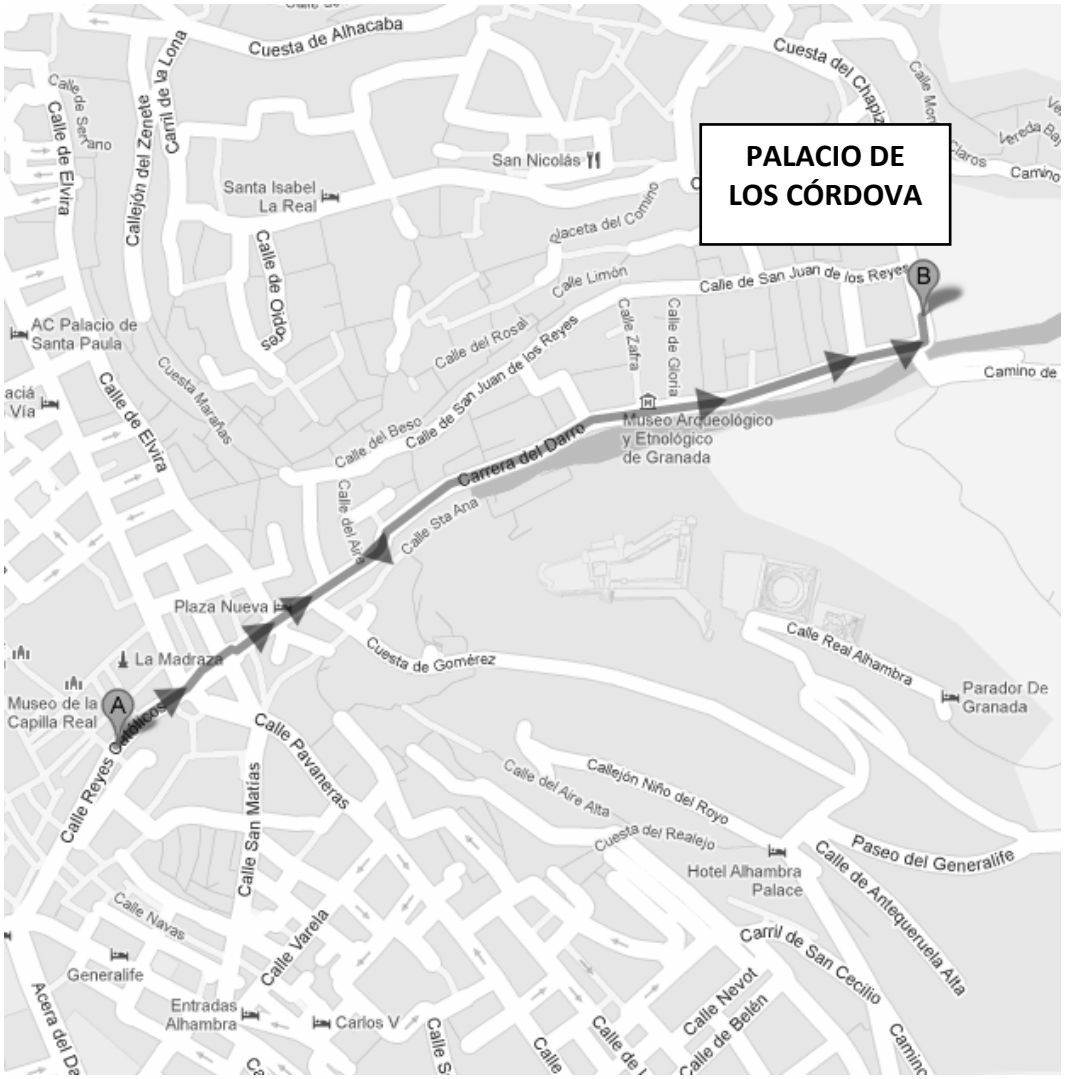

Walk route from the city center (~15 minutes)

Committees

Conference Chairman: Lucas Alados-Arboledas
Conference Co-Chairman: Francisco José Olmo Reyes

Organising Committee:

- Inmaculada Foyo Moreno
- Jesús Fernández Gálvez
- Hassan Lyamani
- Francisco Navas Guzmán
- Juan Antonio Bravo Aranda
- Antonio Valenzuela Gutiérrez
- María José Granados Muñoz
- Gloria Titos Vela
- Arturo Quirantes Sierra
- Mª Ángeles Rivas Romera

Technical Program Committee (also responsible for abstracts reviewing):

- Lucas Alados-Arboledas
- Juan Luis Guerrero Rascado
- Rami Alfarra
- Christoph Asbach
- Ari Asmi
- Darrel Baumgardner
- George Biskos
- Andrei Bologa
- David Broday
- Jeroen Buters
- José L. Castillo
- Charles Clement
- Aladar Czitrovszky
- Yannis Drossinos
- Luca Ferrero
- Ian Ford
- Gary Fuller
- Pedro L. García-Ybarra
- Martin Gysel
- Andreas Held
- Regina Hitzenberger
- Helmuth Horvath
- Otto Klemm
- Thomas Kuhlbusch
- Yoshi Iinuma
- Martina Krämer
- François-Xavier Ouf
- Hanns-Rudolf Paur
- Andreas Petzold
- Johannes Schneider
- Manabu Shiraiwa
- Olli Sippula
- Roberta Vecchi
- Elisabetta Vignati
- Birgit Wehner
- Wendelin Stark
- Sabine Wurzler
- Caner Yurteri

The European Aerosol Assembly

The European Aerosol Assembly (EAA) consists of 12 national or regional societies across Europe, though membership of these societies is not limited to European nationals. The major activity of the EAA and its working groups takes place at the European Aerosol Conference, held in three out of every four years.

The Spanish Science and Technology Aerosol Association

The Spanish Science and Technology Aerosol Association (AECTA, Asociación Española de Ciencia y Tecnología de Aerosoles) was born in 2006 during the 7th International Aerosol Conference held in Minnesota (USA) and had its first official meeting in Madrid in 2007. It is a forum of aerosol scientists and technologists in Spain coordinating activities on aerosols sciences as well as holding annual meetings and summer schools within the field of aerosols.

General Information

Venue
The European Aerosol Conference 2012 is held at the Parque de las Ciencias (Sciences Park, www.parqueciencias.com), Av. de la Ciencia s/n. 18006 Granada. The plenary, oral and poster sessions as well as exhibitions take place in the Macroscopio Building, the brand new area of the largest science park in Andalusia. The Parque de las Ciencias is an interactive museum, of more than 70,000 m^2, placed a few minutes of the historical center of Granada with one of the most varied offers of Europe's cultural and scientific leisure.

Transport to the Conference Centre
By taxi
Tele-Radio-Taxi 958 280 654
Radio-Taxi-Genil 958 132 323
Taxis-Granada 958 35 71 36
A typical taxi fare from the Conference Centre to the city centre is 4-6 €.

By bus
Tourist and city bus: 1, 5 directly to the Science Park (Stop: Parque de las Ciencias), 4, 10, 11 y 21 (Stop: Plaza de las Américas), 22 (Stop: Jardín de la Reina).

Train Station: bus 11, 21.

Bus Station: bus 10.

More bus details: http://www.transportesrober.com/transporte/lineas.htm#

By train
National Railways of Spain (RENFE):
http://www.renfe.com/EN/viajeros/index.html

By plane
Granada Airport,
http://www.aena-aeropuertos.es/csee/Satellite/Aeropuerto-Federico-Garcia-Lorca-Granada-Jaen/en/Page/1047397546288/
Málaga Airport,
http://www.aena-aeropuertos.es/csee/Satellite/Aeropuerto-Malaga/en /

On foot
It is about 15 min from the city centre.

Name badges
Upon registration you will receive a delegate badge which should be worn at all conference events including social activities. The double sided badge is designed for maximum visibility.
Please ensure you wear your delegate badge as this will be your entry identification and it will allow you to freely move around the garden of the Parque de las Ciencias.

Lunch, coffee/tea and snacks
Coffee/tea points
Refreshments will be available at coffee/tea points in the Macroscopio Building during the designated morning and afternoon breaks. There is also a restaurant and a cafeteria inside the Science Park.

Lunch boxes
Sandwich lunches will be provided in boxes during the designated lunch breaks. A vegetarian option will be available upon request. This is inclusive in the registration fee.

Cafeterias/Restaurants outside the Science Park
There are a large number of cafeterias and restaurants around the Conference Venue with opening hours from 8am to 11pm. Lunch is normally served from 1:30pm to 3:30pm and dinner from 7:30pm.

Internet
A Wi-Fi internet connection is available throughout the conference buildings.

The conference website www.eac2012.com will have uptaded information about the conference.

The emergency number is 112
Ambulance
Police
Fire department

Banks
Opening hours Monday to Friday from 9:00 to 14:00.

Credit cards
Credit cards are widely accepted. They can be used in stores, restaurants and hotels.

Tipping
In restaurants and taxis, service is included in the price. Tipping is not necessary but customers may leave a tip if they wish.

Smoking
Smoking is prohibited indoors in public places.

Drinking water
Granada tap water is of good quality and can be consumed safely throughout the city. Bottled mineral and spring water is available in shops and restaurants.

Sponsors and Exhibitors

The organisers wish to acknowledge the support of the many exhibitors present at EAC2012. Please visit their stands on the Macrospocio Building and consult their entries at the back of this handbook. The exhibitors are listed below:

Air Monitors Ltd	GRAW Radiosondes	Sunset Laboratory Inc
Alava Ingenieros	Grimm Aerosol Tech.	Tellus-B
Cambustion Ltd	Ingenieros Asesores	Topas GmbH
Certio	IONER - RAMEM S.A.	TSI
Copley Scientific Ltd	Magee Scientific	URG Corporation
Dekati Ltd	Matter Aerosol	
Droplet Measurement	Metrohm AppliKon	
Ecotech Pty Ltd	Palas GmbH	

Conference Information

Technical Secretariat EAC2012
Mrs. Ángela Luzón
Viajes El Corte Inglés - División de Congresos, Convenciones e Incentivos
Centro de Negocios Camara Comercio Granada
C/ Luis Amador nº 26 18014 Granada
Tel. +34 958 536 820
Fax. + 34 958 254 892
e-mail: eac2012granada@viajeseci.es

General information
Organizing Committee info@eac2012.com
Technical Programme Committee techprog@eac2012.com

Main presentation sessions
The conference will open at 8:45 on Monday 3rd September and close at 13:30 on Friday 7th September according to the schedule shown later in this handbook.

Exhibition
Exhibitors are located next to the main conference rooms in the Macroscopio Building and will be available during the conference hours from Monday to Friday.

Registration and information desk
The registration and information desk will be open at the entrance of the Macroscopio Building in the Science Park as follows:

Sunday, Sept 2: 18:00 –20:00
Monday, Sept 3: 08:00 –18:00
Tuesday, Sept 4: 08:30 –18:00
Wednesday, Sept 5: 08:30 –13:30
Thursday, Sept 6: 08:30 –18:00
Friday, Sept 7: 08:30 - 13.30

Certificate of attendance
Certificates will be available upon request at the registration and information desk.

Social Programme

Sunday 2nd September
Welcome Reception
Forum Building (5 min walk from the Conference Venue)
Time: 20:00 - 21:00

There will be a free welcome party on Sunday 2th September in the Forum Building, 5 min walk from Parque de las Ciencias. This will be an opportunity to meet colleagues.

Monday 3rd September
Concert
Hospital Real, Cuesta del Hospicio
Time: 20:30 - 21:30

The concert will be held in the Royal Hospital, nowadays the headquarters of the University of Granada for the vice-chancellorship and other university services. It was built during the Catholic Kings´ reign as a place to assist injured persons that were fighting in the war against the Arabs. It is one of the few civil monuments in this capital city. The building is a mixture of different styles: Mudejar, Gothic and Renaissance. We suggest being on time due to the limited capacity of the Hall.

The choir “El Orfeón de Granada” will delight us with its more recent production “De lo divino y de lo humano” that will take us back to the Twentieth Century in a sonorous trip representing a tribute to the popular

and classical music, through songs that have become masterpieces of the contemporary music.

Tuesday 4th September
Granada Mayor's Reception
Palacio de Los Córdova, Cuesta del Chapiz
Time: 20:30 - 21:30

The Palace of Los Córdova holds nowadays the City Historical Archive. It was originally built around 1530 at Placeta de las Descalzas more than 1 km away from its actual location at Cuesta del Chapiz when it was reconstructed in 1960. With the enjoyable view of the Alhambra from its gardens, the Mayor of Granada will welcome EAC2012 participants with a cocktail reception offered by the Conference. Afterwards you will have the opportunity to explore the heart of the Albaycín (UNESCO World Heritage Site) with its rich repository of Moorish vernacular architecture.

Thursday 6th September
Conference Dinner
Rte La Mamunia
Time: Drinks from 20:30, Dinner at 21:00

The conference dinner will be held on Thursday 6th September in La Mamunia Restaurant, Granada. This will be a nice opportunity to meet colleagues in a relaxing and charming atmosphere. There will be a separate fee to attend the dinner. Please book your place on the registration page. There will be bus service available from Parque de las Ciencias (departure at 20:00 from the main entrance).

If you have any special dietary requirements, please ensure you email at eac2012granada@viajeseci.es

Dress Code is smart casual, this means smart trousers and a shirt for men (there is no need for a tie or jacket) and the comparable for women.

Awards

Smoluchowski Prize
The award will be given by GAeF to a young researcher (as a rule under 40 years of age) who has achieved and published significant new results in aerosol science in the preceding 3 years.

Best Poster Prizes

To recognize excellence in poster presentation, the EAA will award a number of Best Poster Prizes at the conference. The criteria for selection will be effective design, clarity of communication and scientific quality.

The Prize Committee will be chaired by Dr. Nonne Prisle.

All presentations accepted for poster presentation are eligible for award, but to be included for consideration, participants must send a pdf-copy of the poster to Dr. Prisle at Nonne.prisle@helsinki.fi by 26th August 2012 at the latest. By sending in a pdf-copy of the poster, you can either nominate yourself or alternatively you can nominate the student/colleague presenting the poster.

Board meetings

- GAeF Board Meeting. Monday 3rd September, 12:50-14:00. Room: Sala Presidencia.
- Elsevier Board Meeting. Monday 3rd September 17:00-19:30. Room: Faraday.
- EAC2015 Organizing Meeting. Monday 3rd September 18:30-19:30. Room: Cine 3.
- Journal of Aerosol Science Board Meeting. Monday 3rd September 17:00-19:30. Room: Gutenberg.
- Ioner Meeting. Wednesday 5th September 14:00-17:00. Room: Cine 3.
- EMEP Meeting. Wednesday 5th September 14:00-16:00. Room: Gutenberg.

Assemblies

- Spanish Aerosol Society Assembly. Monday 3rd September 18:30-19:30. Room: Auditorio.
- GAeF General Assembly. Tuesday 4th September 18:30-19:30. Room: Auditorio.

EAA Working Group meetings

The purpose of these meetings is to discuss general matters within the various topic areas and to help plan future events, particularly the next EAC. All delegates are welcome.

Tuesday 4th September 16:00-17:00. The following groups meet at:

WG 1:	Atmospheric Aerosols: Aerosol Processes and Properties	Auditorio
WG 2:	Atmospheric Aerosols: Specific Aerosols Types	Auditorio
WG 3:	Aerosol Chemistry	Faraday
WG 4:	Combustion Aerosols	Gutenberg
WG 5:	PMx	Cine 3
WG 6:	Particle Lung Interactions	Legado Andalusí
WG 7:	Aerosol-based Nanotechnology	Einstein
WG 8:	Instrumentation	Sagan
WG 9:	Aerosol Modelling	Curie
WG 10:	Fundamentals	Newton
WG 11:	Electrical Effects	Sala Presidencia

Presentation Information

Abstracts
All accepted abstracts are published in the EAC2012 Electronic Abstract Book, included in a USB memory together with your conference bag.

Instructions for oral presentations
Please report to the Oral Presenters' Office in advance to upload your presentation electronically. Morning sessions' presenters must upload their presentations during the previous afternoon and afternoon sessions' presenters must upload their presentations during the current morning.

Due to logistical reasons, personal laptops cannot be used for presentations. Electronic formats allowed are Microsoft PowerPoint, OpenOffice Impress and PDF. A copy of your presentation will be available on the PC installed in the appropriate conference room. Oral presenters are requested to be at least 10 minutes prior to beginning of the session and identify themselves to the corresponding chairs.

The time available for oral presentations is 20 minutes (15 minutes for the talk and 5 minutes for discussion).

Instructions for oral reserve presentations

Oral reserve presentations are poster presentations that will also be offered a slot for oral presentation should a vacancy become available. Presenters should check the status with chairs at the beginning of the corresponding session.

Instructions for poster presentations

Posters are displayed on the Poster Space on the first floor (3a) and ground floor (3b, 3c) of the "Parque de las Ciencias". The poster designation A-code, B-code or C-code indicates session A (Monday), session B (Tuesday) or session C (Thursday). The number of board is listed in the next pages and the location of board is indicated on the poster hall plans in this handbook.

– Poster session A, Monday 3rd September, 16:00 – 18:30.

Posters for this session must be mounted from Monday morning and left on display until Tuesday morning before the Plenary Session.

– Poster Session B, Tuesday 4th September, 17:00 – 18:30.

Posters for this session must be mounted from Tuesday morning coffee break and left on display until Thursday morning before the Plenary Session.

– Poster Session C, Thursday 6th September, 16:00 – 18:30.

Posters for this session must be mounted from Thursday morning coffee break and left on display until Friday morning coffee break.

Presenting authors are kindly asked to be available to present their posters during the poster sessions. Posters should be A0, in portrait orientation (841mm wide x 1189mm high). There will be material for fixing your poster, please do not use your own fixing material.

Late posters

Late posters will be displayed on the Poster Space (3c) on the ground floor of the Science Park, during poster session B on Tuesday 4th September.

Internet

A Wi-Fi internet connection is available throughout the Conference Building. Please select Wi-Fi connection "EAC2012" with Password "Angstroem2012".

Next Aerosol Meetings

Bilbao Talks on Aerosol Science
September 10-11, 2012. Bilbao

http://www.ehu.es/bilbaotalks2012/
E-mail: congreso.bilbaotalks@ehu.es

The 10th International Conference on Industrial Ventilation
Ventilation 2012.
September 17-19, 2012. Paris

http://www.inrs-ventilation2012.fr/en/
ventil2012@inrs.fr

Aerosol and Atmospheric Optics, Visibility & Air Pollution
September 24-28, 2012. Whitefish, MT

http://visibility.awma.org/

PARTEC-2013. International Congress on Particle Technology
April 23-25, 2013. Nuremberg

http://www.partec.info/

European Aerosol Conference. EAC-2013
September 1-6, 2013. Prague

http://www.eac2013.cz/
E-mail: eac2013@cbttravel.cz

Scientific Programme

Sunday 2nd September	18:00-20:00	Registration (Parque de las Ciencias)
	20:00-21:00	Welcome party (Forum building, 5 min walk from the Conference Venue)

		Auditorio	Legado Andalusí	Faraday	Cine 3	Gutenberg
Monday 3rd September	08:45-09:00	Opening Ceremony (Auditorio)				
	09:00-10:00	Plenary 1. Vincent Castranova (Auditorio)				
	10:00-10:30	Coffee Break				
	10:30-12:50	WG01S1O	WG02S1O	WG03S1O	WG06S1O	WG08S1O
	12:50-14:00	Lunch (meal box) & GAeF Board Meeting (Sala Presidencia, 1st floor)				
	14:00-16:00	WG01S2O	WG02S2O	WG03S2O	WG06S2O	WG08S2O
	16:00-17:00	Coffee & Poster Session A				
	17:00-18:30			Elsevier Board Meeting		Journal of Aerosol Science Board Meeting
	18:30-19:30	Spanish Aerosol Society Assembly			EAC2015 Organizing Meeting	
	20:30-21:30	Concert (Hospital Real)				

		Auditorio	Legado Andalusí	Faraday	Cine 3	Gutenberg
Tuesday 4th September	08:45-09:45	Plenary 2. Gelsomina Pappalardo (Auditorio)				
	09:45-10:30	Coffee Break				
	10:30-12:50	SS01S1O	WG02S3O	WG03S3O	WG07S1O	WG08S3O
	12:50-14:00	Lunch (meal box), EAA board meeting (Sala Presidencia, 1st floor) & IARA meeting (Sagan, 1st floor)				
	14:00-16:00	WG01S3O	WG02S4O	WG03S4O	WG07S2O	WG05S1O
	16:00-17:00	Working Group Meetings (see Appendix 1)				
	17:00-18:30	Coffee & Poster Session B				
	18:30-19:30	GAeF General Assembly				
	20:30-21:30	Granada Mayor's Reception (Palacio de los Córdova)				

		Auditorio	Legado Andalusí	Faraday	Cine 3	Gutenberg
Wednesday 5th September	08:45-09:45	Plenary 3. Ulrike Lohmann (Auditorio)				
	09:45-10:00	Smoluchowski Award (Auditorio)				
	10:00-10:30	Coffee Break				
	10:30-12:50	WG01S4O	WG02S5O	SS02S1O	WG07S3O	WG09S1O
	12:50-14:00					
	14:00-16:00				Ioner meeting	EMEP meeting
	16:00-17:00			FREE		
	17:00-18:30					
	18:30-19:30					

		Auditorio	Legado Andalusí	Faraday	Cine 3	Gutenberg
Thursday 6th September	08:45-09:45	Plenary 4. Barbara Turpin (Auditorio)				
	09:45-10:30	Coffee Break				
	10:30-12:50	WG01S5O	WG05S2O	WG04S1O	WG10S1O	WG09S2O
	12:50-14:00	Lunch (meal box) & EAA Working Group Chairs' Meeting (Sala Presidencia, 1st floor)				
	14:00-16:00	WG01S6O	WG05S3O	WG04S2O	WG10S2O	WG09S3O
	16:00-17:00	Coffee & Poster Session C				
	17:00-18:30					
	20:00	Conference dinner: departure from Parque de las Ciencias				

		Auditorio	Legado Andalusí	Faraday	Cine 3	Gutenberg
Friday 7th September	08:45-09:45	Plenary 5. Helmuth Horvath (Auditorio)				
	09:45-10:00	Best Poster Awards (Auditorio)				
	10:00-10:30	Coffee Break				
	10:30-12:50	WG01S7O	SS03S1O	SS04S1O	WG11S1O	SS05S1O
	12:50-13:30	Closing Ceremony (Auditorio)				

Working Groups

WG 1: Atmospheric Aerosols: Aerosol Processes and Properties
WG 2: Atmospheric Aerosols: Specific Aerosols Types
WG 3: Aerosol Chemistry
WG 4: Combustion Aerosols
WG 5: PMx
WG 6: Particle Lung Interactions
WG 7: Aerosol-based Nanotechnology
WG 8: Instrumentation
WG 9: Aerosol Modelling
WG 10: Fundamentals
WG 11: Electrical Effects
Special Sessions

Sessions

WG 1

WG01S1O. Optical Properties
WG01S2O. New Particle Formation
WG01S3O. Remote Sensing of Aerosol Properties
WG01S4O. Physical and chemical properties + Transport 1
WG01S5O. Physical and chemical properties + Transport 2
WG01S6O. Climate effects of aerosols
WG01S7O. Aerosol Cloud Interaction

WG 2

WG02S1O. Biomass Burning and Bioaerosol
WG02S2O. Mineral Dust
WG02S3O. Urban Aerosol in Large Cities (1)
WG02S4O. Marine and Carbonaceous Aerosol
WG02S5O. Urban Aerosol Chemical and Physical Properties (2)

WG 3

WG03S1O. Chemistry of Organic Aerosol: Laboratory Study 1
WG03S2O. Chemistry of Organic Aerosol: Laboratory Study 2
WG03S3O. Characterisation Techniques for Organic Aerosol
WG03S4O. Chemistry of Organic Aerosol: Field Study

WG 4

WG04S1O. Combustion and industrial aerosols
WG04S2O. Engines related emissions

WG 5

WG05S1O. Physical and chemical analysis of PMx
WG05S2O. Carbonaceous aerosol and wood burning contribution to PMx
WG05S3O. PMx source apportionment

WG 6

WG06S1O. Particle toxicity
WG06S2O. Particle lung deposition

WG 7

WG07S1O. Application of engineered nanoparticles
WG07S2O. Fundamentals and measurement of nanoparticles
WG07S3O. Gas phase synthesis of nanoparticles

WG 8

WG08S1O. New Instrumentation I
WG08S2O. New Instrumentation II
WG08S3O. Measurement Methods

WG 9

WG09S1O. Aerosol Modelling: Atmospheric Applications
WG09S2O. Aerosol Modelling: Emission inventories, transport and transformation
WG09S3O. Aerosol Modelling: New particle formation and further topics

WG 10

WG10S1O. Aerosol Nucleation, Condensation and Coagulation
WG10S2O. Aerosol Dynamics

WG 11

WG11S1O. Electrical effects

Special Session

SS01S1O. ACTRIS
SS02S1O. A ground-based integrated study of chemical aerosol-cloud interaction (HCCT2010)
SS03S1O. Source apportionment
SS04S1O. Chemical characterization of combustion aerosols
SS05S1O. Field observations and modeling of special events (Fukushima accident and Eyjafjallajökull ash plume)

Appendix 1: location of Working Group Meetings

Working Group	Place
WG 1: Atmospheric Aerosols: Aerosol Processes and Properties	Auditorio
WG 2: Atmospheric Aerosols: Specific Aerosols Types	
WG 3: Aerosol Chemistry	Faraday
WG 4: Combustion Aerosols	Gutenberg
WG 5: PMx	Cine 3
WG 6: Particle Lung Interactions	Legado Andalusí
WG 7: Aerosol-based Nanotechnology	Einstein
WG 8: Instrumentation	Sagan
WG 9: Aerosol Modelling	Curie
WG 10: Fundamentals	Newton
WG 11: Electrical Effects	Sala Presidencia

Monday 3rd September

08:45-09:00	Opening Ceremony (Auditorio)
09:00-10:00	Plenary 1. **Vincent Castranova** *Characterization of Responses to Carbon Nanotubes and Carbon Nanofibers* Room: Auditorio Chair: J.L. Castillo
10:00-10:30	Coffee-break
10:30-12:50	**Session WG01S1O. Optical Properties** Room: Auditorio Chairs: H. Horvath / J. Andrey

10:30	WG01S1O01	**Profiling of the aerosol hygroscopicity in the planetary boundary layer** B. Rosati, E. Weingartner, P. Zieger, G. Wehrle, U. Baltensperger
10:50	WG01S1O02	**The effect of hygroscopicity on the aerosol extinction** V. Gácser, A. Molnár
11:10	WG01S1O03	**Nephelometric study of fine aerosol fraction in Beijing** M.A. Sviridenkov, A.S. Emilenko, V.M. Kopeikin and Wang Gengchen
11:30	WG01S1O04	**Observed darkening of the aerosol** J.P. Putaud, F. Cavalli, A. Dell'Acqua, C. Gruening, and S. Martuins Dos Santos
11:50	WG01S1O05	**Spectral dependence of aerosol light absorption obtained from several field experiments** S. Mogo, V.E. Cachorro1, A. de Frutos, B. Torres, J.F. López, C. Toledano, A. Berjón and B. Barja
12:10	WG01S1O06	**Measuring the optical properties of single particles and aerosol ensembles using cavity ring down spectroscopy** B.J Mason, R.E.H. Miles, S.-J. King, K. Manfred, J.S.

		Walker, A.E. Carruthers, A.J. Orr-Ewing and J.P. Reid
12:30	WG01S1O07	**Modelling radiative properties of light-absorbing carbon aggregates encapsulated in a sulphate shell** M. Kahnert, T. Nousiainen, H. Lindqvist, and M. Ebert
Reserve paper	WG01S1B00	**Optical properties of SiO2 particles: inversion data from laboratory IR absorption spectra** D. Petitprez, H. Herbin

10:30-12:50 **Session WG02S1O. Biomass Burning and Bioaerosol**
Room: Legado Andalusí
Chairs: J. Schneider / C. Ruzene

10:30	WG02S1O01	**Impact of prescribed burning on urban air quality: a case study** C. He, B. Miljevic, L. Crilley, L. Morawska, F. Salimi, G. A. Ayoko, J. Bartsch, E. Uhde
10:50	WG02S1O02	**Physical and chemical properties of aerosol particles from wild fires in South Africa** V. Vakkari, P. Tiitta, H. Laakso, A. Venter, K. Jaars, M. Josipovic, C. Walsh, P. Dagsson Waldhauserova, G. Mafusire, T. Korhola, M. Paramonov, M. Vana, M. Kulmala, J.P. Beukes, P.G. van Zyl, J.J. Pienaar and L. Laakso
11:10	WG02S1O03	**Impact of wood combustion on the ambient aerosol in Augsburg, Germany: A joint measurement campaign using innovative on-line and off-line mass spectrometric systems for chemical profiling** R.Zimmermann, M.Oster, M. Elsasser, J. Schnelle-Kreis, J. Orasche, G. Abbaszade, M. Crippa, A.S.H. Prévôt, T. Gustafson, J.B.C.Pettersson
11:30	WG02S1O04	**Airborne measurements of biomass burning layers over Central Europe: A case study** F. Dahlkötter, B. Weinzierl, D. Sauer, A. Minikin, M. Gysel, C. Voigt, and A. Ansmann
11:50	WG02S1O05	**Comparison of methods for generating bioaerosols** J. Löndahl, O. Nerbrink, N. Burman, A. Thedeby, A. Massling, T. Santl Temkiv, M. Bohgard
12:10	WG02S1O06	**Seasonal and spatial characteristics of fungal**

		spore tracers in Taiwan G. Engling, S.H. Chen and B.J. Tsuang
12:30	WG02S1O07	**Numerical modelling of pollen concentrations: a comparison to measured concentrations** K. Zink, A. Pauling, B. Clot and M.W. Rotach
Reserve paper	WG02S1B00	**Real-time measurement of continuous thermal-inactivated bioaerosols by aerosol fluorescence sensor with dual UV- and Vis-channels** Jae Hee Jung, Gwi Byoung Hwang, Bo Mi Kwon, Jung Eun Lee, and Gwi Nam Bae

10:30-12:50 **Session WG03S1O. Chemistry of Organic Aerosol: Laboratory Study 1**
Room: Faraday
Chairs: R. Alfarra / Y. Iinuma

10:30	WG03S1O01	**Do Organic Aerosols Shrink?** N.M. Donahue, E. S. Robinson, A. Ahern, E. Trump, and R. Saleh
10:50	WG03S1O02	**Gas phase formation of extremely oxidized α-pinene reaction products and their role in aerosol particle formation** M. Ehn, E. Kleist, H. Junninen, T. Petäjä, G. Lönn, S. Schobesberger, M. Sipilä, M. Dal Maso, R. Tillmann, A. Trimborn, M. Kulmala, D. R. Worsnop, A. Wahner, J. Wildt, Th. F. Mentel
11:10	WG03S1O03	**α-Pinene and β-pinene ozonolysis - Effect of CO on SOA formation and product distribution-** A. Kahnt, Y. Iinuma, A. Mutzel, O. Böge and H. Herrmann
11:30	WG03S1O04	**Is the chemical composition of α-pinene secondary organic aerosol dependent on particulate water content?** L. Pfaffenberger, P. Barmet, R. Wolf, J. G. Slowik, J. Dommen, A. S. H. Prévôt and U. Baltensperger
11:50	WG03S1O05	**Kinetic multi-layer model of gas-particle interactions in aerosols and clouds (KM-GAP): linking condensation, evaporation and reactions of organics, oxidants and water** M. Shiraiwa, C. Pfrang, T. Koop and U. Pöschl
12:10	WG03S1O06	**The effect of humidity on the ozonolysis of**

		unsaturated compounds in aerosol particles and on particle phase M. Kalberer, F.D. Pope, P.J. Gallimore, P. Achakulwisut J. Lee, J. F. Davies, V. Garrascon, S. Fuller, A. Björkegren and D. R. Spring
12:30	WG03S1O07	**Composition, Reactivity, and Energetics of Sulphuric Acid Clusters Containing Ammonia and Amines** B. R. Bzdek, J. W. DePalma, J. Laskin, D. P. Ridge and M. V. Johnston
Reserve paper	WG03S1B00	**Simultaneous study of gas and particulate products formed from isoprene oxidation: laboratory and field measurements** C. Rio, S. Rossignol, S. Fable, L. Chiappini

10:30-12:50 **Session WG06S1O. Particle toxicity**
Room: Cine3
Chairs: W. Hofmann / O. Schmid

10:30	WG06S1O01	**Characterization of an Air-Liquid Interface Cell Exposure system for Cigarette Smoke (ALICE_CS) using fluorescence imaging and a quartz crystal microbalance** M. Shoaib, A. G. Lenz, F. Prade, B. Lentner, M. Schmidmeir, T. Stoeger, O. Eickelberg, O. Schmid
10:50	WG06S1O02	**Analysis of the Dosimetric Properties of a Novel Thermal Precipitator for Cell Exposure to Nanoparticles at Air-Liquid Interface** D. Broßell, S. Plitzko, G. Linsel, N. Azong-Wara, C. Asbach, H. Fissan, A. Schmidt-Ott
11:10	WG06S1O03	**Estimation of biodurability of smectite particles in (synthetic) lung fluids** M.E. Ramos, C. Cappelli, M. Rozalén, S. Fiore and F.J. Huertas
11:30	WG06S1O04	**Toxicity testing of domestic wood combustion aerosols** S. Mülhopt, S. Gauggel, D.R. Dietrich, T. Schröder, B. van der Burg, H.-R. Paur
11:50	WG06S1O05	**An experimental comparison of dust resuspension due to human walking** Yilin Tian, Kyung Sul, Jing Qian and Andrea Ferro
12:10	WG06S1O06	**Identification of plant DNA in air: DNA analysis**

		and relevance for human health I. Müller-Germann, J. Fröhlich-Nowoisky, U. Pöschl,and V. R. Després
12:30	WG06S1O07	**Effective density of particles in an urban environment – measured with a DMA-APM system for lung dose estimations** J. Rissler, P.T. Nilsson, J. Pagels, A. Eriksson, E. Nordin, E. Swietlicki, B. Svenningsson, M. Frosch, E. Ahlberg, C. Wittbom, J. Löndahl, A. Wierzbicka, J.G. Hemmingsen, S. Loft, S. Sjögren
Reserve paper	WG06S1B00	**Effects of different combustion conditions on the toxicological properties of PM1 in adjustable biomass combustion reactor** O. Uski, J. Leskinen, P. Jalava, A. Virén, H. Lamberg, T. Kaivosoja,T. Kettunen, I. Nuutinen, M. Happo, T. Torvela, J. Tissari, O. Sippula, J. Jokiniemi, M.-R. Hirvonen

10:30-12:50 **Session WG08S1O. New Instrumentation I**
Room: Gutenberg
Chairs: O. Bischof / C. Asbach

10:30	WG08S1O01	**LOAC: a new small balloon-borne aerosol counter/sizer with some particle characterization** J.-B. Renard, G. Berthet, F. Dulac, J. Sciare, J. Nicolas, M. Mallet, P. Durand, C. Thaury, S. Salles,J.-L. Mineau, T. Tonnelier and N. Verdier
10:50	WG08S1O02	**Aerosol detection with induced currents** M. Fierz, D.Meier, P.Steigmeier and H. Burtscher
11:10	WG08S1O03	**Remote sensing of atmospheric aerosols with the spectropolarimeter SPEX** J. de Boer, G. van Harten, F. Snik, O. P. Hasekamp, H. Volten, A. Apituley, C. U. Keller, J. H. H. Rietjens, J. M. Smit, D. M. Stam, and P. Stammes
11:30	WG08S1O04	**Evaluation of the Cavity Attenuated Phase Shift (CAPS) Extinction Monitor** A.Petzold, T. Onasch, P. Kebabian, A. Freedman
11:50	WG08S1O05	**Improvement of the nanoparticle charging efficiency by using sheath air flow in a single-wire corona unipolar charger** C.L. Chien, C.J. Tsai, V. Wattanmekhinkul
12:10	WG08S1O06	**An optical set-up for the multi-wavelength**

		characterization of carbonaceous particulate matter D. Massabò, M.C. Bove, E. Cuccia, P. Prati, V. Bernardoni, G. Valli, R. Vecchi
12:30	WG08S1O07	**A new expansion chamber CPC applicable to atmospheric measurements** T. Pinterich, P.M. Winkler, P.E. Wagner and A. Vrtala
Reserve paper	WG08S1B00	**A new device for fast measurements of nanoparticle size distributions** Hans Grimm, Lothar Keck, Markus Pesch, Matthias Richter, Hans-Joachim Schulz

14:00-16:00 **Session WG01S2O. New Particle Formation**
Room: Auditorio
Chairs: T. Petäjä / E. Coz

14:00	WG01S2O01	**The role of marine microcolloids in new particle formation over the Arctic Ocean** M. Karl, E. Coz and C. Leck
14:20	WG01S2O02	**Response of Cloud Condensation Nuclei (> 50 nm) to changes in ion-nucleation** M. B. Enghoff, H. Svensmark, and J. O. P. Pedersen
14:40	WG01S2O03	**Estimating the effect of gas-phase kinetics and nanoparticle dynamics on observed particle formation rate dependencies** M. Dal Maso, H. Korhonen, K. Lehtinen, H. Vehkamäki
15:00	WG01S2O04	**The role of amines in atmospheric nucleation** Almeida-Simões, João, Curtius, Joachim, Kirkby, Jasper
15:20	WG01S2O05	**Atmospheric amine measurements with CI-APi-TOF** T. Jokinen, M. Sipilä, H. Junninen, M. Ehn, G. Lönn, J. Hakala, T. Petäjä, R. L. Mauldin III, M. Kulmala and D.R. Worsnop
15:40	WG01S2O06	**Lewis bases as the unifying concept for ion-induced and neutral H2SO4 nucleation** Theo Kurtén, Ismael K. Ortega, Oona Kupiainen, Tinja Olenius, Ville Loukonen and Hanna Vehkamäki
Reserve paper	WG01S2B00	**Differences between Classes of Nucleation Events during the Summer Period in Thessaloniki, Greece: Kerbside versus urban background measurements** D. Siakavaras, C. Samara, M. Petrakakis, G. Biskos

14:00-16:00 **Session WG02S2O. Mineral Dust**
Room: Legado Andalusí
Chairs: L. Ferrero / J. A. García Orza

14:00	WG02S2O01	**The importance of Nocturnal Low-level Jets for simulating mineral dust emission** S. Fiedler, K. Schepanski, B. Heinold, P. Knippertz and I. Tegen
14:20	WG02S2O02	**Resuspension and wind erosion in semi-arid SE Spain: overview and key results from field campaigns in 2005 – 2012** J.A.G. Orza, M. Cabello, M.A. Barrero, L. Cantón, A. Berasaluce, A. Romero-Díaz, F. Belmonte-Serrato, V. Lidón and J. Martínez
14:40	WG02S2O03	**Long-term observations of mineral dust deposition to the Northeast Atlantic Ocean and hygroscopic properties at the Cape Verde Islands** N. Niedermeier, T. Müller, A. Held, K. Kandler, and A. Wiedensohler
15:00	WG02S2O04	**Elemental Composition of Air Particulate Matter in Cape Verde** M. Almeida-Silva, S. M. Almeida, C.A. Pio, T. Nunes, J. Cardoso
15:20	WG02S2O05	**Optical behaviour of mineralogical composition. A laboratory study** T. Ajtai, Á. Filep, N. Utry, M. Pintér, Z. Bozóki, G. Szabó
15:40	WG02S2O06	**The Amsterdam-Granada Light Scattering Database** O. Muñoz, F. Moreno, D. Guirado, D.D. Dabrowska, H. Volten, J.W. Hovenier
Reserve paper	WG02S2B00	**CLIMARENO 2011 campaign: a multi-instrumental characterization of a Saharan dust intrusion over the Iberian Peninsula by airborne and ground-based instrumentation** J. Andrey, J. Fernández-Gálvez, J.L. Guerrero-Rascado, M. Sorribas-Panero, G. Titos-Vela, A. Corrales-Sierra, M. Gil-Ojeda, V. Cachorro, B. de la Morena F.J. Olmo and L. Alados-Arboledas

14:00-16:00 **Session WG03S2O. Chemistry of Organic Aerosol: Laboratory Study 2**
Room: Faraday
Chairs: M. Kalberer / M. Shiraiwa

14:00	WG03S2O01	**A source of oxygenated organic aerosol and oligomers from primary emitted gases** John Liggio, Shao-Meng Li and Alexander Vlasenko
14:20	WG03S2O02	**Uptake of glyoxal by organic and inorganic seed aerosols: Optical, physical and chemical properties of the product aerosols** M. Trainic, A. A. Riziq, A. Lavi, J. M. Flores and Y. Rudich
14:40	WG03S2O03	**Secondary organic aerosol formation from glyoxal** J.G. Slowik, E.M. Waxman, C.J. Kampf, J. Timkovsky, B. Nozière, A.P. Praplan, L.Pfaffenberger, T. Hoffmann, T. Kuipers, R. Holzinger, J. Dommen, A.S.H. Prévôt, U. Baltensperger, and R. Volkamer
15:00	WG03S2O04	**Evolution of SOA chemical composition during ageing: impact of irradiation, cloud processing and presence of pre-existing seeds** N. Maurin, E.Perraudin, J. F. Doussin, P. Pardon, H. Budzinski
15:20	WG03S2O05	**Size dependence of growth rates: results of experiments in the CLOUD chamber** A. Franchin, S. Schobesberger, T. Nieminen K. Lehtipalo, H.E. Manninen
15:40	WG03S2O06	**Modelling study on the effect of salt formation on the atmospheric nanoparticle growth** T. Yli-Juuti, K. Barsanti, L. Hildebrandt Ruiz, A.-J. Kieloaho, T. Kurtén, U. Makkonen, T. Petäjä, M. Äijälä, M. Kulmala and I. Riipinen
Reserve paper	WG03S2B00	**Primary and Secondary Organic Aerosol from Road Vehicles** S. Platt, I. El Haddad, A.A. Zardini, M. Clairotte, C. Astorga, R. Wolf, J. G. Slowik, B. Temime-roussel,N. Marchand, I. Jezek, L. Drinovec, G. Mocnik, O. Möhler, U. Baltensperger and A.S.H. Prévôt

14:00-16:00 **Session WG06S2O. Particle lung deposition**
Room: Cine 3
Chairs: D. Broday / W. Hofmann

14:00	WG06S2O01	**Determining the regional deposition of tobacco smoke in the human respiratory system** C.J. Dickens, C.M. McGrath, J. Perkins, P. Biggs, R.A. Cabot, J.J. McAughey
14:20	WG06S2O02	**Phase transition of inhaled particles within the human respiratory system** L. Pichelstorfer and W. Hofmann
14:40	WG06S2O03	**Particle deposition under transient high frequency ventilation air flow in a physiologically realistic bifurcation** E. Makris, M. Pilou ,P. Neofytou,S. Tsangaris and C.Housiadas
15:00	WG06S2O04	**Dynamics of exhaled aerosol with mixed composition** D. Katoshevski, D. Parienta, L. Morawska, G.R. Johnson, Z.D. Ristovski, M. Hargreaves, K. Mengersen, S. Corbett, C.Y.H. Chao, Y. Li
15:20	WG06S2O05	**In vivo regional deposition of submicron-sized airborne particles in the baboon respiratory model** J. Pourchez, I. Albuquerque-Silva, M. Durand, J. Avet, D. LePennec, M. De Monte, J. Montharu, M. Cottier, F. Dubois, L. Vecellio
15:40	WG06S2O06	**Not only Asbestos exposure, but also inherited susceptibility, is responsible for the occurrence of mesothelioma in humans** F. Cetta, P. Paladini, C. Ghiribelli, M. Monti, F. Granato, R. Borrelli, V. Guercio, D. Stergiou and G. Gotti
Reserve paper	WG06S2B00	**Personal daily exposure of children to ultrafine particles and black carbon** C. Vargas Trassierra, S. Marini, L. Stabile, A. Russi, F. Fuoco, G. Buonanno

14:00-16:00 **Session WG08S2O. New Instrumentation II**
Room: Gutenberg
Chairs: I. Agranovski / R. Caldow

14:00	WG08S2O01	**Characterization of the Airmodus A20 Condensation Particle Counte** K. Lehtipalo, J. Vanhanen, T. Toivola, J. Mikkilä, T. Petäjä and M. Kulmala

14:20	WG08S2O02	**Broadband Aerosol Extinction Spectrometer, a new instrument for measuring the spectral dependence of aerosols** R.A. Washenfelder, J.M. Flores, C.A. Brock, S.S. Brown and Y. Rudich
14:40	WG08S2O03	**Comprehensive Laboratory Characterization of a New Nano Water-based CPC and Performance Comparison to an Ultrafine CPC** A. Kupc, O.F. Bischof, M. Beeston, T. Tritscher, T. Krinke and P.E. Wagner
15:00	WG08S2O04	**Calibration and performance of a novel particle sensor for automotive application** L. Ntziachristos, S. Amanatidis, A. Rostedt, J. Keskinen, K. Janka, J. Tikkanen
15:20	WG08S2O05	**A novel portable instrument for exposure analysis in nanotechnology workplaces** C. Asbach, H. Kaminski, H. Fissan, T.A.J. Kuhlbusch, N. Azong-Wara, D. Broßell, R. Caldow, J. Scheckman, H.-G. Horn
15:40	WG08S2O06	**Device for Measuring Electrical Mobility Size and Concentration of Nanoparticles** S. Elzey, R. Caldow, J.P. Johnson, M. Grose, S. Morell, D. Jensen
Reserve paper	WG08S2B00	**Effect of particle diffusivity on DMAs with multiple monodisperse-particle outlets: theory validation and design optimization** M.Giamarelou, M. Stolzenburg, D.-R. Chen and G. Biskos

POSTER SESSION A

001	A-WG01S1P01	**Aerosol optical properties over East Asia: An integrating CMAQ-simulated and satellite-retrieved aerosol data using a data assimilation technique** C.H. Song, R.S. Park, K.M. Han and M.E. Park
002	A-WG01S1P02	**Temporal variations of the single scattering albedo in the southwestern Iberian Peninsula (Portugal)** S.N. Pereira, F. Wagner and A.M. Silva
003	A-WG01S1P03	**Retrieval of Single Scattering Albedo values from Brewer spectrophotometer irradiance measurements at Uccle, Belgium** V. De Bock and H. De Backer
004	A-WG01S1P04	**Constraining optical properties and refractive index**

		of soot through combined experimental and modelling studies J. Kim, H. Bauer, T. Dobovicnik, R. Hitzenberger, D. Lottin, D. Ferry and A. Petzold
005	A-WG01S1P05	**Modelling light scattering by mineral particles with small-scale surface roughness** M. Kahnert, T. Nousiainen, M. A. Thomas, and J. Tyynelä
006	A-WG01S1P06	**Physical and optical properties of atmospheric aerosol in Eastern Antarctica** A. Mangold, H. De Backer, V. De Bock, C. Hermans, I. Gorodetskaya and W. Maenhaut
007	A-WG01S1P07	**Aerosol Scattering and Absorption Angström Exponents during desert dust events over Granada** A.Valenzuela, F.J. Olmo, H. Lyamani, M. Antón, A.Quirantes, and L. Alados-Arboledas
008	A-WG01S1P08	**DIAPASON: A better assessment of the impact of Saharan dust on PM measurements** G.P. Gobbi, H. Wille, R. Sozzi, S. Frey, A. Bolignano, F. Costabile, F. Angelini, and F. Barnaba
009	A-WG01S1P09	**Spatial variation of aerosol optical properties around the high-alpine site Jungfraujoch** P. Zieger, E. Kienast, M. Starace, von Bismarck, N. Bukowiecki, U. Baltensperger, F.G. Wienhold, T. Peter, T. Ruhtz, M. Collaud Coen, L. Vuilleumier, O. Maier, E. Emili, C. Popp, and E. Weingartner
010	A-WG01S1P10	**Light scattering by ice-covered carbonaceous aerosol particles** S.S. Vlasenko,E.F. Mikhailov
011	A-WG01S1P11	**First ambient aerosol measurements with a polar nephelometer** M. Paixão, T. Müller and A. Wiedensohler
012	A-WG01S1P12	**Spectral dependence of in-situ aerosol optical properties** F. Costabile, F. Angelini, F. Barnaba and G.P. Gobbi
013	A-WG01S1P13	**Aerosol Characteristics and Radiative Forcing during summer and winter seasons over Pakistan** Khan Alam, Thomas Trautmann, Thomas Blaschke
014	A-WG01S1P14	**Seasonal distinctions and temporal trends in frequency of different types of hygrograms in West Siberia** S.A. Terpugova, T.A. Dokukina, E.P. Yausheva and M.V. Panchenko
015	A-WG01S1P15	**Trends in aerosol optical properties using AERONET surface observations** Aswathy V Nair and S. K. Satheesh

016	A-WG01S1P16	**Optical properties of SiO2 particles : inversion data from laboratory IR absorption spectra** Denis Petitprez, Hervé Herbin
017	A-WG01S1P17	**Climatology of aerosol optical properties with a synergy of remote sensing/altitude in situ measurements.** M.Hervo, K. Sellegri, J-C. Roger
018	A-WG01S1P18	**Combined observations with multi-wavelength Raman lidars and sun photometers on the southern Iberian Peninsula** J. Preißler, J.A. Bravo-Aranda, F. Wagner, M.J. Granados-Muñoz, F. Navas-Guzmán, J.L.Guerrero-Rascado, H. Lyamani, and L. Alados-Arboledas
019	A-WG01S1P19	**Seasonal and regional variation of the vertical optical properties of aerosol from CALIPSO validated with aircraft in situ measurements** A. Cazorla, P.S. Praveen, K.A. Prather and V. Ramanathan
020	A-WG01S1P20	**Optical Characterization of Aerosols at a Rural Site in Southeast England During the Winter ClearfLo IOP** P. Massoli, A. Aiken, K. Gorkowski, S. Herndon, E. Fortner, J. Jayne, J. Franklin, W. Brooks, P. Chhabra, T. Onasch, L. Williams, M. Dubey, D. Worsnop and A. Freedman
021	A-WG01S1P21	**Long term measurements of aerosol optical depth in the UV range in central Poland** J. Jarosławski
022	A-WG01S1P22	**Retrieving aerosol properties over the Mediterranean basin with a climate model** N. Hatzianastassiou, P. Ginoux, V. Ramaswamy
023	A-WG01S1P23	**Day and night columnar aerosol properties at Granada (Spain) using sun and star photometry measurements** D. Perez-Ramirez, H. Lyamani, F.J. Olmo, D.N. Whiteman and L. Alados-Arboledas
024	A-WG01S1P24	**Absorption closure – filter-based absorption instruments compared to extinction-scattering measurements** E. Andrews, P. Massoli, A.G. Hallar, A. Sedlacek, A. Freedman, J. A. Ogren and P. Sheridan
025	A-WG01S1P25	**Continuous measurements of aerosol size distribution at two Siberian stations: new particle formation bursts** M.Yu. Arshinov, B.D. Belan, A.V. Kozlov , P.N. Antokhin, D.K. Davydov and V.G. Arshinova

026	A-WG01S1P26	**Insights into the nucleation by organic compounds involving oxidation products of pinanediol and sulphuric acid** F. Bianchi, S. Schobesberger, S. Ehrhart, H. Junninen, N. M. Donahue, J. Dommen, M. Kajos, S. Schallhart, T. Ruuskanen, M. Kulmala, D. R. Worsnop U. Baltensperger and the CLOUD collaboration
027	A-WG01S1P27	**Differences between Classes of Nucleation Events during the Summer Period in Thessaloniki, Greece: Kerbside versus urban background measurements** D. Siakavaras, C. Samara, M. Petrakakis, G. Biskos
028	A-WG01S1P28	**Source apportionment of ultrafine and fine particles in Huelva industrial city** R. Fernández-Camacho, S. Rodríguez, J. de la Rosa, A.M. Sánchez de la Campa, Y. González-Castanedo
029	A-WG01S1P29	**Basic Statistics of New Particles Formation Events at Kosetice Station** N. Zikova and V. Zdimal
030	A-WG01S1P30	**Investigation of consecutive particle formation events in mixed residential and mining area in South Africa** A. Hirsikko, V.Vakkari, P. Tiitta, V.-M. Kerminen, J. Hatakka, J.P. Beukes, H.E. Manninen, M. Kulmala, D. Mabaso, and L. Laakso
031	A-WG01S1P31	**New particle formation events in Hungarian background air at K-puszta, 2008-2011** Zs. Bécsi, Á. Molnár, K. Imre, T. Nieminen, J. Hakala, T. Petäjä and M. Kulmala
032	A-WG01S1P32	**Continental source for secondary biogenic aerosols in Antarctica** E.-M. Kyrö, A. Virkkula, V.-M. Kerminen, M. Dal Maso, J. Parshintsev, J. Ruiz-Jimenez L. Forsström
033	A-WG01S1P33	**NanoShip: Mapping of new particle formation events over the North Sea** N. Kelbus, A. Massling, M. Fiebig, B. Henzing, M. Glasius, M. Bilde, M. Moerman, G. de Leeuw, M. Dal Maso, and A. Kristensson
034	A-WG01S1P34	**Direct observations of atmospheric sub-2 nm neutral and charged clusters** J. Kontkanen, M. Kulmala, K. Lehtipalo, H.E. Manninen, T. Petäjä, M. Sipilä, H. Junninen, S. Schobesberger, P. Rantala, A. Franchin, T. Jokinen, E. Järvinen, M. Äijälä, J. Kangasluoma, T. Nieminen, J. Hakala, P.P. Aalto, P. Paasonen, J. Mikkilä, J. Vanhanen, J. Aalto, T. Ruuskanen, R.L. Mauldin III, J. Dublissy, J. Bäck, I. Riipinen, M.

		Johnston, J.N. Smith, V.-M. Kerminen and D.R. Worsnop
035	A-WG01S1P35	**Cloud Condensation Nucleus Production from Nucleation Events at a Semi-Rural Environment: Puijo station, Eastern Finland** A. Hamed, M. Komppula, H. Portin, A. Leskinen, S. Romakkaniemi, K.E.J. Lehtinen, J. Smith1, J. Joutsensaari and A. Laaksonen
036	A-WG01S1P36	**Formation of halogen-induced secondary organic aerosol (XOA)** K. Kamilli, J. Ofner, C. Zetzsch, A. Held
037	A-WG01S1P37	**Spectra of positive air ions up to 40 nm as a function of selected trace gases** T.-E. Parts, M. Noppel, A. Luts, K. Komsaare, and U. Hõrrak
038	A-WG01S1P38	**NanoMap: Methodology for geographical mapping of new particle formation events** M. Johansson, A. Kristensson, E. Swietlicki, M. Dal Maso, N. Kivekäs, T. Hussein, T. Nieminen, H. Junninen, H. Lihavainen, P. Tunved, and M. Kulmala
039	A-WG01S1P39	**Trends in atmospheric new particle formation - 16 years of observations in boreal forest** T. Nieminen, M. Dal Maso, T.Petäjä, P. P. Aalto, V.-M. Kerminen, P. Hari and M. Kulmala
040	A-WG01S1P40	**Characterization of new particles formation events at Izaña Mountain Observatory (Tenerife, Canary Islands): formation, growth rates and influencing atmospheric parameters** M.I. García, S. Rodríguez, R.D García and Y. González
041	A-WG01S1P41	**Influence of meteorological parameters and air mass history on new particle formation events at K-puszta, Hungary** A. Molnár and Zs. Bécsi
042	A-WG01S1P42	**Micrometeorological measurement of dry deposition of aerosols pollutants (PAH, PCB, metals) on a wetland (Seine river estuary)** O. Connan, M. Millet, D. Hébert, J.J Schwartz, F.Guéguen, P. Roupsard, R. Goujon, D.Maro, B. Letellier
043	A-WG01S1P43	**Experimental study of the submicron aerosol dry deposition in the urban canopy: original methodology and first results** P. Roupsard, D. Maro, A. Coppalle, V. Ruban, S. Percot, O. Connan, P. Laguionie, L. Solier, M. Rozet, D. Hébert and M. Talbaut
044	A-WG01S1P44	**First in situ measurements of atmospheric particle dry deposition velocity by eddy-correlation method**

		using the the new 0.1 s time-response Pegasor Particle Sensor P. Laguionie, D. Maro, D. Hébert and F. Sanson
045	A-WG01S1P45	**Turbulent aerosol fluxes in a forest clearing measured with a fast mixing-type CPC** F. Kittler, F. Ditas, B. Wehner and A. Held
046	A-WG01S1P46	**Highly size resolved particle fluxes: Results from biannual measurements using OPCs in an urban environment.** M.J. Deventer, O. Klemm and F.Grießbaum
047	A-WG01S1P47	**Direct numerical simulation of aerosol growth processes in a turbulent mixing layer** Antonio Attili, Kun Zhou and Fabrizio Bisetti
048	A-WG01S1P48	**Emission Factors for ultrafine particles obtained in Stockholm and Helsinki** Matthias Vogt, E Douglas Nilsson, Christer Johansson, Lena Järvi, Ivan Mammarella, Annika Nordbo, Timo Vesala
049	A-WG01S1P49	**Analytical solution on the minimum scavenging efficiency particle size for below-cloud scavenging process using the harmonic mean method** S.Y. Bae, C.H. Jung, Y.P. Kim and R.J. Park
050	A-WG01S1P50	**The results of the coastal area of bitter-salty lakes in the Altai Territory in the summer of 2011 water and air samples study** A.S. Safatov, G.A. Buryak, S.E. Olkin, I.K. Reznikova, Yu.V. Marchenko, B.M. Desyatkov, N.A. Lapteva, I.S. Andreeva, A.S. Kozlov, S.B. Malyshkin, I.A. Sutorihin, V.I. Bukatyi, S.A. Litvinenko, B.S. Smolyakov, and M.P. Shinkorenko
051	A-WG01S1P51	**Spatial and Temporal Concentration of Ultrafine Particles in Rural and Urban Sites in the Po Valley (Bologna)** M. Rossi, L. Pasti, E. Sarti, E. Nava
052	A-WG01S1P52	**Attenuation of shock wave from a point blast in a dusty air** A.G. Girin
053	A-WG01S1P53	**The Variation of Aerosol Number Concentrations in Relation with 3D wind components in the Ieodo Ocean Research Station** Sung-Hwa Park, Sang-Min Jang, Dong-In Lee, Woon-Seon Jung and Jong-Hoon Jeong
054	A-WG01S1P54	**Time lag between the tropopause height and 7Be activity concentrations on surface air** A. Ioannidou, A. Vasileiadis and D. Melas
055	A-WG01S1P55	**Aerosol Measurements Evaluating the Effects of the**

		Red Mud Disaster in Hungary A. Nagy, A. Czitrovszky, D. Oszetzky and A. Kerekes
056	A-WG01S1P56	**Correlation between measurement results for three-type portable air purifiers: filter, ionizer and wet ones** Bangwoo Han, Hak-Joon Kim and Yong-Jin Kim
061	A-WG02S1P01	**Drug-resistance and heavy metal tolerance of airborne microbes** O. Nikiforou, A. Kikna, M. Lazaridis, and E. Katsivela
062	A-WG02S1P02	**Investigation of bioaerosols distribution in greenhouse for orchid growth** C.Y. Chuang, S. Yang, M.Y. Chang, C.H. Luo, Y.C. Huang, P.C. Huang and W. Fan.
063	A-WG02S1P03	**Autofluorescence of atmospheric bioaerosols – fluorescent biomolecules, biological standard particles and potential interferences** C. Pöhlker, J. A. Huffman , U. Pöschl
064	A-WG02S1P04	**Fluorescent Biological Aerosol Particle (FBAP) Number Concentrations & Size Distributions Measured by the Waveband Integrated Bioaerosol Sensor (WIBS-4) at Environmental Research Station Schneefernerhaus (UFS)** Emre Toprak and Martin Schnaiter
065	A-WG02S1P05	**Ice Activity of Atmospheric Fungi** Janine Froehlich, Thomas C. J. Hill, Gary D. Franc and Ulrich Poeschl
066	A-WG02S1P06	**Characterization and validation of an easy-to-assemble kit of visible LED lights employed for inactivation of environmental bioaerosols** C.H. Luo and H.K. Chang
067	A-WG02S1P07	**Molecular genetic analysis of biological aerosol particles from African dust storms** Cristina Ruzene-Nespoli, Janine Fröhlich-Nowoisky, T. Nunes, J. Cardoso, S. M. Almeida & Ulrich Pöschl
068	A-WG02S1P08	**Survival of airborne influenza on surfaces** Cordonnier, Florian, Ha,Thi-Lan, Robine, Enric and Gehin, Evelyne
069	A-WG02S1P09	**Internally controlled multiplex bioaerosol detection procedure** E.V. Usachev and I.E. Agranovski
070	A-WG02S1P10	**Could BFFB mode breath aerosol play a role in H5N1 transmission?** L. Morawska, G.R. Johnson and S.C. Bell

071	A-WG02S1P11	**Recent advances in bioaerosol control methods** Byung Uk Lee
072	A-WG02S1P12	**Study on the ventilation and air dispersion in a hospital Intensive Care Unit (ICU) using simulation techniques** J.H. Song, J.Y. Jang, M.Y. Cho, D.S. Park and S.-B. Kwon
073	A-WG02S1P13	**Real-time measurement of continuous thermal-inactivated bioaerosols by aerosol fluorescence sensor with dual UV- and Vis-channels** Jae Hee Jung, Gwi Byoung Hwang, Bo Mi Kwon, Jung Eun Lee, and Gwi Nam Bae
074	A-WG02S1P14	**The numerical pollen dispersion model COSMO-ART: model design and operational use at MeteoSwiss** A.Pauling, K. Zink, H. Vogel and B. Vogel
075	A-WG02S1P15	**Rapid Inactivation of Biological Species in the Air using Atmospheric Pressure Non-thermal Plasma** Yongdong Liang, Yan Wu, Ke Sun, Qi Chen, Fangxia Shen, Jue Zhang, and Maosheng Yao, Tong Zhu, Jing Fang
076	A-WG02S1P16	**Single-particle fluorescence spectroscopy of atmospheric relevant fungal spores and bacteria and potential interferences** S. Saari, M. Putkiranta and J. Keskinen
077	A-WG02S1P17	**Microbial and fungal bioaerosol concentrations in Lithuanian schools** I. Radziuniene, D. Martuzevicius, D. Ciuzas, E. Krugly, and T. Prasauskas
078	A-WG02S1P18	**Airborne bacterial deposition in Sierra Nevada National Park** G. D´Orta, N. Mladenov and I. Reche
079	A-WG02S1P19	**Neutralization of Viable Aerosolized Microorganisms due to Exposure to Combustion of Reactive Materials** S.A. Grinshpun, A. Adhikari, M. Yermakov, T. Reponen, E. Dreizin, M. Schoenitz, and V. Hoffmann
080	A-WG02S1P20	**Carbonaceous compounds emitted from domestic biomass burning** M.A.C. Duarte, A.I. Calvo, L.A.C. Tarelho, T. Nunes, M. Evtyugina, C.A. Alves
081	A-WG02S1P21	**Inventory of emissions from residential wood combustion in Portugal** C. Gonçalves, C. Alves and C. Pio
082	A-WG02S1P22	**Aerosol aging during transport from Thailand to Taiwan**

		C.-T. Lee, M.-T. Chuang, N.-H. Lin, K. Sopajareepom, S.-Y. Chang, Y.-J. Chang
083	A-WG02S1P23	**Summer 2010 forest fires in central Portugal: characterisation of trace gases and aerosol emissions** A.M. Vicente, C.A. Alves, A.I. Calvo, A.P. Fernandes, T. Nunes, A.C. Monteiro, M. Evtyugina, L.A.Tarelho and C.A. Pio
084	A-WG02S1P24	**Contribution to PM2.5 from domestic wood burning in a small community in Sweden** P. Molnár and G. Sallsten
085	A-WG02S1P25	**Characterisation of regional ambient biomass burning organic aerosol mixing ratios** M. D. Jolleys, H. Coe, G. McFiggans, G. Capes, J. D. Allan, J. Crosier, P. I. Williams, G. Allen and J. L. Jimenez
086	A-WG02S1P26	**Large use of wood combustion for domestic heating in France: impacts on the air quality in rural environments** C. Piot, J. Cozic, J.-L. Besombes and J.-L. Jaffrezo
087	A-WG02S1P27	**Burning of Olive Tree Branches: A Major Organic Aerosol Emission Source in the Mediterranean** E. Kostenidou, C. Kaltsonoudis, E. Louvaris, M. Tsiflikiotou, and S.N. Pandis
088	A-WG02S1P28	**Airborne measurements in the lower atmosphere in Finland during Russian wildfires in the summer 2010** K. Leino, R. Väänänen , T. Pohja , P.P. Aalto , T. Petäjä A. Virkkula and M. Kulmala
089	A-WG02S1P29	**Measurement of fluorescence from ambient aerosol particles using WIBS-4 instrument** F. Taketani, Y. Kanaya, W. R. Stanley and P.H. Kaye
090	A-WG02S1P30	**Carbonaceous species and anhydrosugars measurements in coarse and fine aerosols size fractions at an urban area in the Po Valley, Italy** T.M.G. La Torretta, L.A. Stante, A. Malaguti, R. Nuzzi, M. Berico
091	A-WG02S1P31	**Mobile measurements for the detection of wood combustion: a case study in a rural environment** M. Van Poppel, N. Bleux, J. Peters, J. Van den Bossche P. Berghmans
092	A-WG02S1P32	**An exceptional air pollution event in the southwest of Europe** J.A. Adame, M. Sorribas, M.A. Hernández-Ceballos,

		J.P. Bolivar and B.A. De la Morena
093	A-WG02S1P33	**Identification of African dust influence to PM10 concentrations at the Athens air quality monitoring network during 2010** V. Aleksandropoulou and M. Lazaridis
094	A-WG02S1P34	**Identifying desert aerosols episodes in Cáceres (Spain)** M.A. Obregón, A. Serrano and M.L. Cancillo
095	A-WG02S1P35	**Mineralogical composition and origin of airborne particles during dust events in the Eastern Mediterranean** Kopanakis Ilias, Thodoros Glytsos, Despoina Pentari, and Mihalis Lazaridis
096	A-WG02S1P36	**Aerosol deposition in the main African dust transport region: establishing a long-term time series at Sao Vicente, Cape Verde** K. Kandler, L. Mendes Neves, N. Niedermeier, and T. Müller
097	A-WG02S1P37	**Influence of Saharan dust in deposition fluxes of nutrients in Spain** S. Castillo, X. Querol, A. Alastuey, A. Ávila, E. Cuevas, and J. de la Rosa
098	A-WG02S1P38	**Laboratory investigations of contact and immersion freezing of mineral dust using two techniques: vertical wind tunnel and acoustic levitator** K. Diehl, H. Schmithüsen, M. Debertshäuser, S.K. Mitra, and S. Borrmann
099	A-WG02S1P39	**Long-term Chemical Characterization of Aerosol at the CVAO** K. Müller, K. W. Fomba, E. Brüggemann, T. Gnauk, G. Spindler, H. Herrmann
100	A-WG02S1P40	**Effects of desert dust aerosols on surface UV radiation from OMI satellite instrument at Granada (Spain)** M. Antón, A. Valenzuela, R. Román, H. Lyamani, N. Krotkov, A. Arola, F.J. Olmo, L. Alados-Arboledas
101	A-WG02S1P41	**Aerosol sampling and coarse mode aerosol measurement of African mineral dust during Fennec 2011 field campaign** J.K.Brooke, M.Bart, J. Trembath, J.B. McQuaid, B.J.Brooks, P. Rosenberg, T. Malkin and S.Osborne
102	A-WG02S1P42	**Optical properties and radiative impact of intense dust outflows in the Mediterranean basin, based on a synergistic use of satellite,**

		ground-based measurements and modelling A. Gkikas, N. Hatzianastassiou, S. Kazadzis, V. Amiridis, S. Basart, E. Marinou, M. Taylor, J.M. Baldasano
103	A-WG02S1P43	**Combination of AERONET and CALIPSO data for the study of Saharan dust outbreaks over Valencia (Spain)** C.R. Marcos, R. Pedrós, J.L. Gómez-Amo, J.A. Martínez-Lozano, M.P. Utrillas
104	A-WG02S1P44	**Experimental study of hygroscopic properties of mineral dust particles** T.I. Ryshkevich, E.F. Mikhailov and S.S. Vlasenko
105	A-WG02S1P45	**Optical properties of a desert dust cloud after long-range transport using scattering matrix formalism and a polarization Lidar** G. David, B. Thomas, A. Miffre and P. Rairoux
106	A-WG02S1P46	**Desert-dust episodes over a background European environment: relationship between optical and physical properties by in-situ and columnar-integrated techniques** M. Sorribas, J.A. Ogren, F.J. Olmo, R. Fraile, B.A. de la Morena and L. Alados- Arboledas
107	A-WG02S1P47	**Estimation of dust emission amount for spring in East Asia using WRF/Chem** Jung-Yoon Kang and Soon-Chang Yoon
108	A-WG02S1P48	**Carbonaceous and inorganic water soluble species in PM in Cape Verde atmosphere** Teresa Nunes, João Cardoso, Danilo Custódio, Mário Cerqueira, Suzana Marta Almeida, M. Almeida-Silva and Casimiro Pio
109	A-WG02S1P49	**Ground-based measurements of suspended and re-suspended volcanic ash in Iceland after the Grímsvötn eruption in 2011** S. von Löwis, C. Fischer, A. Vogel, K. Weber, R. Reichardt and T. Jóhannsson
110	A-WG02S1P50	**Development of a certified reference material for Asian mineral dust (Gobi Kosa)** M. Nishikawa, I. Matsui, T. Sano, M. Ukachi, K. Nagano, K. Onishi, D.Batdorj, N. Enkhmaa and I.Mori
111	A-WG02S1P51	**Planetary Boundary Layer and Saharan Air Layer top height determination using Ceilometer and Micro Pulse Lidar. Intercomparison for two case studies** Y. Hernández, S. Alonso-Pérez, E. Cuevas, C. Camino, J. de Bustos, A.J. Gomez-Pelaez, R. Ramos,C. Córdoba-Jabonero

		and M. Gil
112	A-WG02S1P52	**An empirical relationship to estimate mineral dust concentration from visibility observations** C. Camino, S. Alonso-Pérez, E. Terradellas, S. Rodríguez, A.J. Gomez-Pelaez, P.M. Romero-Campos, Y.Hernández, S. Basart, J.M.Baldasano, E. Cuevas
113	A-WG02S1P53	**Particulate Matter Deposition Monitoring: Neglected Importance of Titanium?** G. Jereb, G. Dražič and B. Poljšak
114	A-WG02S1P54	**Diurnal variation of particulate concentration by size and micrometeorology in semi-arid rural environments** M. Cabello, J.A.G. Orza, M.A. Barrero, L. Cantón, A.Berasaluce, V. Lidón and J. Martínez
115	A-WG02S1P55	**Mineralogy of Atmospheric Dust in Santiago island, Republic of Cape Verde: preliminary results** F. Rocha, A. Quintela, D. Terroso, C. Costa, J. Cardoso; T. Nunes; C.A. Pio, S. M. Almeida and M.C. Freitas
116	A-WG02S1P56	**Modelling of long-range transport of mineral dust in Cape Verde** O. Tchepel, J. Ferreira, A.P. Fernandes, C. Gama, JM Baldasano, C. Borrego, J. Cardoso, S.M. Almeida, C. Pio
117	A-WG02S1P57	**CLIMARENO 2011 campaign: a multi-instrumental characterization of a Saharan dust intrusion over the Iberian Peninsula by airborne and ground-based instrumentation** J. Andrey, J. Fernández-Gálvez, J.L. Guerrero-Rascado, M. Sorribas-Panero, G. Titos-Vela,A. Corrales-Sierra, M. Gil-Ojeda, V. Cachorro, B. de la Morena F.J. Olmo and L. Alados-Arboledas
118	A-WG02S1P58	**The influence of the Atlas Mountains and the meteorological situation on the impact of African dust outbreaks on the Iberian Peninsula** J.A.G. Orza, M. Cabello
149	A-WG03S1P01	**Computational investigation of vinylhydroperoxide dissociation: there is a barrier** Theo Kurtén, Neil M. Donahue
150	A-WG03S1P02	**Reaction of airborne allergenic protein with different nitrating agents** K. Selzle, C. Ackaert, S. Kofler, G.J. Oostingh and U. Pöschl
151	A-WG03S1P03	**Temperature dependence of water activity in aqueous solutions of alcohols and organic acids** Gouri Ganbavale, Claudia Marcolli, U. K. Krieger, Greta Stratmann, Andreas Zuend, Thomas Peter

152	A-WG03S1P04	**Heterogeneous Uptake of HO2 Radicals onto Submicron Atmospheric Aerosols** P. S. J. Matthews, I. J. George, B. Brooks, A. Goddard, L. K. Whalley, M. T. Baeza-Romero and D. E. Heard
153	A-WG03S1P05	**How do night-time oxidants affect the fate of an organic coated aerosol droplet?** F. Sebastiani, R.A. Campbell, I. Hoare and C. Pfrang
154	A-WG03S1P06	**From free electrons to H2SO4 - assessing the efficiency of ion catalysed SO2 oxidation** N. Bork and H. Vehkamäki
155	A-WG03S1P07	**Simultaneous study of gas and particulate products formed from isoprene oxidation: laboratory and field measurements.** C. Rio, S. Rossignol, S. Fable, L. Chiappini
156	A-WG03S1P08	**Aerosol yields from ozonolysis of α- and β-pinene in simulation chamber experiments with low precursor concentrations** H. Saathoff, K.-H. Naumann, and O. Möhler
157	A-WG03S1P09	**Phase-changes during oxidation of atmospheric aerosols: ozonolysis of levitated droplets containing oleic acid** C. Pfrang, A. M. Squires, M. Rittman, M. Ghosh, K. Rastogi, and A. D. Ward
158	A-WG03S1P10	**Characteristics of polymer blend particles produced by evaporation of binary solution droplets of incompatible polymers** V. Rajagopalan, E. A. Grulke and A. K. Ray
159	A-WG03S1P11	**An Inversion Method for Aerosol Particle Concentrations in the CERN CLOUD Experiment** C. Williamson, D Wimmer, K.Lehtipalo, J. Curtius and the CLOUD collaboration
160	A-WG03S1P12	**Development of an aqueous-phase mechanism for secondary organic aerosol formation** F. Couvidat, K. Sartelet and C. Seigneur
161	A-WG03S1P13	**Capturing of low-level CO2 using AC particles** Y. H. Lim, Y. M. Jo
162	A-WG03S1P14	**SOA Formation from Acid Catalysed Rearrangement Reactions** Y. Iinuma, A. Kahnt, O. Böge and H. Herrmann
163	A-WG03S1P15	**Surface tension and aggregate formation in nanoaerosols containing model HULIS compounds** T. Hede
164	A-WG03S1P16	**Formation and aging of secondary organic aerosol through evaporation of aqueous phase processed**

		isoprene reaction products F. Siekmann, P. Renard, B. Temime-Roussel and A. Monod
165	A-WG03S1P17	**Influence of reaction conditions on the formation of dimers and peroxides originating from the ozonolysis of a-pinene and the OH reaction of nopinone** A.Mutzel, Y. Iinuma, O. Böge, A. Kahnt and H. Herrmann
166	A-WG03S1P18	**Comparison of sesquiterpene oxidation products in secondary organic aerosol from different vegetation zones** A. van Eijck, C. Kampf, T. Hoffmann
167	A-WG03S1P19	**Ozonolysis of ultra fine particles of oleic acid: a detailed study mixing on line gas and condensed phase analyses** Maxence Mendez, Vincent Crenn, Véronique Riffault, Sylvie Gosselin, Nicolas Visez, Denis Petitprez
168	A-WG03S1P20	**Effect of ions on the measurement of sulphuric acid at CLOUD** Rondo, Linda, Kürten, Andreas Ehrhart, Sebastian, Curtius, Joachim and the CLOUD collaboration
169	A-WG03S1P21	**Characterisation of thin films on optically trapped single aerosols using broadband white light Mie spectroscopy** S.H. Jones, M.D King and A.D. Ward
170	A-WG03S1P22	**Study on the effect of CO2 partial pressure on mechanism of sulfation of calcium carbonate sorbent particle** Seongha Jeong, Kang Soo Lee, Sang In Keel, Jin Han Yun, and Sang Soo Kim
171	A-WG03S1P23	**Pressure dependence of sulfuric acid induced SOA formation** P. T. M Carlsson, J. E. Dege, C. Keunecke, B. C. Krüger, J. L. Wolf and T. Zeuch
172	A-WG03S1P24	**Changes in hygroscopicity and cloud-activation of diesel exhaust aerosols upon ageing** C.Wittbom, B. Svenningsson, J.Rissler, A. Eriksson, E. Swietlicki, E. Nordin, P. Nilsson and J. Pagels
173	A-WG03S1P25	**Hygroscopicity and optical properties of secondary organic aerosol formed in CESAM simulation chamber** C. Denjean, P. Formenti, B. Picquet-Varrault, Y. Katrib, E. Pangui, P. Zapf and J.F. Doussin
174	A-WG03S1P26	**Secondary Organic Aerosol formation from isoprene photooxidation**

		L. Brégonzio, J.F. Doussin, E. Pangui, A. Monod, F. Siekmann, B. Temime, M. Camredon, B. Aumont
175	A-WG03S1P27	**AMISOC 2012: Multi-instrument campaign for assessment of trace gas-aerosol interactions** O. Puentedura, M. Gil, J.A. Adame, J. Andrey, C. Córdoba-Jabonero, L. Gómez, T. Hay, M. Navarro, C. Prados-Román, A. Saiz-López, M. Sorribas, D. Toledo and B. de la Morena
176	A-WG03S1P28	**Direct Surface Analysis of Size- and Time- Resolved Organic Aerosol** S.J Fuller, M. Kalberer, Y. Zhao, A.S Wexler
177	A-WG03S1P29	**The Manchester Photochemical Aerosol Chamber: Formation, Transformation and Properties of Secondary Organic Aerosols** M.R Alfarra, A. Buchholz, W. Hesson, J.F. Hamilton, K.P. Wyche, I. White, P. Monks, A. Lewis, and G.B. McFiggans
178	A-WG03S1P30	**Compound specific condensation to secondary organic aerosols providing size dependent information** D. Mogensen, D. Lowe, G. Capes, D. O. Topping, G. B. McFiggans, S. Smolander, M. Kulmala and M. Boy
179	A-WG03S1P31	**Direct observations of surface/bulk partitioning and acid/base speciation in aqueous solutions of the atmospheric surfactant sodium decanoate using synchrotron X-ray photoelectron spectroscopy** N.L. Prisle, N. Ottosson, G. Öhrwall, J. Söderström, M. Dal Maso, and O. Björneholm
180	A-WG03S1P32	**13-Carbon Isotopic Fractionation in Secondary Organic Aerosol Formation** C. Meusinger, U. Dusek, S.M. King, R. Holzinger, M. Bilde, T. Röckmann and M.S. Johnson
181	A-WG03S1P33	**Sizing, Infrared Spectra and Phase Transitions of Neutral Water Clusters** C.C. Pradzynski, R.M. Forck, U. Buck and T. Zeuch
182	A-WG03S1P34	**Growing clusters involving pinanediol oxidation products during nucleation experiments in the CLOUD chamber, observed by APi-TOF ion mass spectrometers** Schobesberger, Siegfried; Franchin, Alessandro; Junninen, Heikki; Bianchi, Federico; Dommen, Josef; Donahue, Neil; Ehrhart, Seba
183	A-WG03S1P36	**Aerosol mass spectrometer study of secondary organic aerosol formed during isoprene and methacrolein reaction chamber experiments -**

		Composition and effect of humidity F. Siekmann, L. Bregonzio, B. Temime-Roussel, S. Ravier, J.F. Doussin andA. Monod
184	A-WG03S1P37	**Pathways from aromatic aldehydes to aerosol in urban atmosphere: a competition between oxidation and photopolymerization** T.A. Maksimova, G.G. Dultseva and S.N. Dubtsov
185	A-WG03S1P38	**Atmospheric Degradation of Oxygenated Volatile Organic Compounds on Mineral Aerosol Surfaces** Cristina Iuga, C. Ignacio Sainz-Díaz, and Annik Vivier-Bunge
186	A-WG03S1P39	**Primary and Secondary Organic Aerosol from Road Vehicles** S. Platt, I. El Haddad, A.A. Zardini, M. Clairotte, C. Astorga, R. Wolf, J. G. Slowik, B. Temime-roussel, N. Marchand, I. Jezek, L. Drinovec, G. Mocnik, O. Möhler, U. Baltensperger and A.S.H. Prévôt
187	A-WG03S1P40	**Optimization of a GC/MS method to analyse products from photo-oxidation of biogenic and anthropogenic mixtures of VOCs** O. Pindado Jimenez, R.Mª Pérez-Pastor, M. García Vivanco, M. Santiago Aladro.
188	A-WG03S1P41	**Development of a new tool to study atmospheric aerosol particles origin** L. Bourcier and B. Geypens
189	A-WG03S1P42	**Aerosol chemical characterization by PMF analysis of single particle ATOFMS spectra** C. Giorio, A. Tapparo, M. Dall'Osto, R.M. Harrison, D.C.S. Beddows and E. Nemitz
190	A-WG03S1P43	**Analysis of surgical aerosols by on-line single particle and high resolution mass spectrometry** K.-P. Hinz, A. Fendt, K.-C. Schäfer, Z. Takats and B. Spengler
191	A-WG03S1P44	**Artefacts Associated with ChemVol® Impactor Sampling of Semivolatile Organic Compounds (SVOCs)** E. Galarneau, M. Patel, G. Poole, J.-P. Charland, and J. Brook
192	A-WG03S1P45	**In-situ methylation thermal extraction GC-MS method for the determination of anhydro-sugars in atmospheric aerosol samples** G. Matuschek, A. Wüst
193	A-WG03S1P46	**Studying Atmospheric Aerosols by Acoustic Levitation: Linking Head Space Solid-Phase Micro-Extraction (HS-SPME) with Gas Chromatography-Mass Spectrometry (GC-MS)**

		S. Almabrok, G. Marston and C. Pfrang
194	A-WG03S1P47	**Calibration of CPCs at low temperatures using the CLOUD chamber** D. Wimmer, F.Kreissl, A. Kürten, J. Curtius, F. Riccobono, A. Kupc, K. Lehtipalo and the CLOUD collaboration
195	A-WG03S1P48	**A method for assigning AMS measured nitrates and sulphates into molecular subgroups.** Äijälä, Mikko, Junninen, Heikki, Ehn, Mikael, Häkkinen, Silja, Hong, Juan, Petäjä, Tuukka, Kulmala, Markku and Worsnop, Douglas
196	A-WG03S1P49	**Simplifying the complex nature of water-soluble organic matter from atmospheric aerosols: new insights from comprehensive two-dimensional liquid chromatography** R.M.B.O Duarte, A.C. Barros and A.C. Duarte
197	A-WG03S1P50	**Characterization of a thermal desorption mass spectrometer for freshly nucleated secondary aerosol particles** S. G. Gonser and A. Held
198	A-WG03S1P51	**Comparison of two Laser Ablation Time-Of-Flight Aerosol Mass Spectrometers** S. R. Zorn, K.-P. Hinz, P. Croteau, B. Spengler, D. R. Worsnop, J. T. Jayne and A. M. Trimborn
199	A-WG03S1P52	**Complexation of transition metal ions by organic and inorganic ligands in size-segregated atmospheric aerosol particles in Melpitz, Germany** S. Scheinhardt, K. Müller, D. van Pinxteren, K. Fomba, A. Grüner, G. Spindler, H. Herrmann
200	A-WG03S1P53	**The organic carbon and total protein concentrations in atmospheric aerosol of Southwestern Siberia boundary atmospheric layer** A.S. Safatov, G.A. Buryak, S.E. Olkin, I.K. Reznikova, V.I. Makarov and S.A. Popova
201	A-WG03S1P54	**PM2.5 and PM10 composition in São Paulo city Atmosphere – Summer and Winter campaigns** P.C. Vasconcellos, B. Oraggio, P.V. Veiga, A. Soreira, E. G. Alves, J.B De Andrade
202	A-WG03S1P55	**Aliphatic and aromatic amines in atmospheric aerosol particles** J. Ruiz-Jimenez, J. Parshintsev, T. Laitinen, K. Hartonen, T. Petäjä, M. Kulmala, M.–L. Riekkola
203	A-WG03S1P56	**Organic composition of fog: transformation between liquid and interstitial phase** S. Schüttauf, J. Matschullat, D. van Pinxteren, Y. Iinuma, H.

		Herrmann
204	A-WG03S1P57	**Secondary particulate matter formation during foggy days** A.Piazzalunga, M.Anzano, V.Bernardoni, P.Fermo, M.Urbani, G.Valli and R.Vecchi
205	A-WG03S1P58	**Fingerprint of shipping emissions on PM10 at Barcelona** J. Pey, N. Pérez, A. Alastuey, X. Querol, J. Cortés
206	A-WG03S1P59	**Characteristics of surface ozone over Qinghai Lake area in Northeast Tibetan Plateau, China** Zhenxing Shen, Xin Wang, Junji Cao, Zhuzi Zhao
207	A-WG03S1P60	**Seasonal and diurnal variations of mono- and di-carbonyls in Xi'an, China** W.T. Dai, S.S.H. Ho, K.F. Ho, W.D. Liu, J.J. Cao, S.C. Lee
208	A-WG03S1P61	**Gas conversion to sulfate and nitrate in fine particulate matter at southern Taiwan** J.H. Tsai, J.H. Lin and L.P. Chang
209	A-WG03S1P62	**Regional contributions of arsenic species in Southwestern Spain** González-Castanedo Y, Sánchez-Rodas D., Sánchez de la Campa A.M., Fernández-Camacho R., de la Rosa J. D
210	A-WG03S1P63	**Water soluble compounds in Arctic aerosols (Ny Alesund, Svalbard)** R. Zangrando, C. Turetta, E. Barbaro, P. Zennaro, N. M. Kehrwald, J. Gabrieli, A. Gambaro, C. Barbante
211	A-WG03S1P64	**Aerosol-fog chemical interactions: a case study in the Po Valley (Northern Italy)** L.Giulianelli, S. Gilardoni, M. Rinaldi, S. Decesari, M. Paglione, C. Carbone, S. Fuzzi and M.C. Facchini
212	A-WG03S1P65	**Sulfur containing Polycyclic Aromatic Hydrocarbons (PASHs): new perspectives of tracers for source apportionment of aerosols** B. Golly, C. Piot, J.L. Jaffrezo, D. Chapuis, J.L. Besombes
213	A-WG03S1P66	**Physical-chemical characterization and origin of atmospheric particulate material in Cordoba City – Spain** E. García-Lorenzo, J.D. de la Rosa, A.M. Sánchez de la Campa, Y. González-Castanedo and R. Fernández-Camacho.
214	A-WG03S1P67	**Chemical composition and microphysical parameters of fog samples in a 27 year long study in the Po Valley (Italy)** Giulianelli, Lara; Rinaldi, Matteo; Carbone, Claudio; Decesari, Stefano; Facchini, Maria Cristina; Fuzzi, Sandro

215	A-WG03S1P68	**Determination of Molecular Composition in Boreal Forest Aerosols (PM1.0), Hyytiala, Finland using Ultra-High Resolution Mass Spectrometry** I. Kourtchev, S. Fuller, J. Aalto, T. Ruuskanen, W. Maenhaut, M. Kulmala, and M. Kalberer
216	A-WG03S1P69	**Nucleation and Aitken mode atmospheric particles in relation to O_3 and NO_X at semirural background in Denmark** Q.T. Nguyen, J.K. Nøjgaard, M. Glasius and L.L. Sørensen
217	A-WG03S1P70	**Preliminary results on the characterisation of organic aerosols in urban schools by Aerosol Mass Spectrometry** L. Crilley, G. A. Ayoko, E.R. Jayaratne, L. Morawska
218	A-WG03S1P71	**Pb isotope of atmospheric aerosols in the Iberian Pyrite Belt, SW Spain** J. de la Rosa, A.M. Sánchez de la Campa, Y. González-Castanedo, J.C. Fernández Caliani, A. Romero, I. González-Díez
219	A-WG03S1P72	**Metals and trace element characterization of weather condition - air quality relationships due to event based measurements of particulate matter** Silvia Leise, Frank Zimmermann, Jörg Matschullat
220	A-WG03S1P73	**Characterization of humic-like substances (HULIS) in size segregated atmospheric aerosol** G. Kiss, N. Törő, A. Hoffer, J. Dautovic, S. Frka, Z. Kozarac, M. Harir, P. Schmitt-Kopplin
221	A-WG03S1P74	**A multi-tracer approach to better understand Secondary Organic Aerosol sources and (trans)formation processes in the Mediterranean region** J. B. Nicolas, J. Sciare, R. Sarda-Estève, N. Mihalopoulos, G. Kouvarakis and F. Dulac
222	A-WG03S1P75	**Size-resolved measurement of the mixing state of soot in the megacity Beijing, China: diurnal cycle, aging and parameterization** Y. F. Cheng, H. Su, D. Rose, S. S. Gunthe, M. Berghof, B. Wehner, P. Achtert, A. Nowak, N. Takegawa, Y. Kondo, M. Shiraiwa, Y. G. Gong, M. Shao, M. Hu, T. Zhu, Y. H. Zhang, A. Wiedensohler, M. O. Andreae, and U. Pöschl
223	A-WG03S1P76	**Impact of urban atmospheric aerosols on cultural heritage objects of Granada, Southern Spain** C. Cardell, M. Urosevic, B. Horemans, V. Kontozova-Deutsch, S. Potgieter-Vermaak, E. Sebastián-Pardo and R. Van-Grieken
225	A-WG06S1P01	**Characterisation of nasal spray drug delivery**

		K.Inthavong, M.C.Fung, W.Yang and J.Y. Tu
226	A-WG06S1P02	**Evolution of droplet size distribution during nebulization of liposomes** T.R. Sosnowski
227	A-WG06S1P03	**Bipolar Charge Analyzer for inhaler particles** J. Kannosto, V. Niemelä, H. Isherwood, J. Yli-Ojanperä, J. Keskinen, R. Hillamo, A. Frey and A. Ukkonen
228	A-WG06S1P04	**Characterizing the Time-Dependant Hygroscopic Response of Aerosols Generated From Commercially Available Nebuliser Formulations** A.E. Haddrell, J.F. Davies, L.A. Dailey, D. Murnane and J.P. Reid
229	A-WG06S1P05	**Using the carbon-nanotube plasma for removal of indoor bioaerosols** S. Yang, C.H. Luo, Y.C. Huang, C.Y. Chuang, H.Z. Chen, P.C. Hung
230	A-WG06S1P07	**Periodical interruption of chronic exposure to PM in metropolitan areas could be of benefits to prevent chronic alterations of respiratory function in humans** G. Schiraldi, F. Cetta, P. Paladini, J. Martellucci, F. Granato, B. Lorenzi, R. Zangari, V. Guercio, E. Bolzacchini, M. Monti, G. Gotti and L.Allegra
231	A-WG06S1P08	**A 4-years follow-up study of traffic related respiratory changes in school children in Milan, Italy** M. Sala, F. Cetta, S. Argirò, P. Ballista, R. Zangari, V. Guercio, E. Bolzacchini, M. Monti and M. Mandelli
232	A-WG06S1P09	**Spirometric and laboratory assessment of the respiratory function as an effect of PM exposure in asymptomatic subjects living in a metropolitan area (Milan, Italy) and in a remote alpine site (Aprica)** L.Allegra, F. Cetta, G. Schiraldi, R. Zangari, V. Guercio, D. Stergiou, C. Ghiribelli, P. Paladini, L. Luzzi, E. Bolzacchini, M. Monti and G. Gotti
233	A-WG06S1P10	**Cryo-imaging as a quantitative pre-clinical method to determine the amount and spatial distribution of drugs in lung tissue: A feasibility study for fluorescent substances** Friedrich Prade, Nikolaos C. Deliolanis, Katie Dextraze, Nirav Barapatre, Vasilis Ntziachristos, Oliver Eickelberg, Otmar Schmid
234	A-WG06S1P11	**Stochastic rat lung dosimetry for radon progeny: A surrogate for the human lung**

		M.Hussain , R. Winker-Heil, and W. Hofmann
235	A-WG06S1P12	**Aerosol infection of chickens by avian influenza virus A/H5N1** Ar.A. Sergeev, O.K. Demina, O.V. Pyankov, O.G. Pyankova, A.P. Agafonov, S.A. Kiselev, I.E. Agranovski, Al.A. Sergeev, A.N. Shikov, L.N. Shishkina, A.S. Safatov and A.N. Sergeev
236	A-WG06S1P13	**A better knowledge of causative pathophysiological mechanisms, in addition to proper markers of effects, as key tools for a deeper insight into health effects of air pollution** F. Cisternino, V. Guercio, M. Monti, F. Granato, B. Lorenzi, J. Martellucci, R. Zangari and F. Cetta
237	A-WG06S1P14	**Aerosolization system for experimental inhalation study of metal oxides nanoparticules** Presumé, M, Attoui, M., Lanone, S.
238	A-WG06S1P15	**Comparison of methods for measurement of surface area for six different nanomaterials** M. Levin, I. K. Koponen, S. Bau, O. Witschger, E. Jankowska, C. Guiot, O. Spalla, K. A. Jensen
239	A-WG06S1P16	**Medical effect from nanoparticlate hypotensive drugs inhaled by male rats** A. A. Onischuk, T. G. Tolstikova, M. V. Khvostov, I. V. Sorokina, A.M. Baklanov, O. V. Borovkova, V. V. Boldyrev, V. M. Fomin
240	A-WG06S1P17	**Aerosol Particles in Different Types of Museum Environment** L. Maškova, J. Smolik, and M. Ohlidalova
241	A-WG06S1P18	**Transport of particulate matter in the indoor environment of the National Library in Prague** J. Smolik[1], L. Maškova
242	A-WG06S1P19	**Temporal evolution of pyrethroid aerosol concentrations after insecticide spray treatment in indoor atmosphere using a High Resolution Aerosol Time-of-Flight Mass Spectrometer (HR-ToF-AMS)** Aude Vesin, Nicolas Marchand, Etienne Quivet, Brice Temime-Roussel, Henri Wortham
243	A-WG06S1P20	**Particulate matter in school classrooms and outdoor air** C. Alves, T. Nunes, J. Silva, M. Duarte, C. Borrego
244	A-WG06S1P21	**Indoor and outdoor ultrafine particle characterisation in primary schools in Barcelona** M. Viana, I. Rivas, J. Sunyer, L. Bouso, M. Álvarez, Sioutas C, A. Alastuey and X. Querol
245	A-WG06S1P22	**Variations of PM concentrations in Lithuanian**

		multifamily buildings: Preliminary results from INSULAtE study Tadas Prasauskas, Dainius Martuzevicius, Edvinas Krugly, Darius Ciuzas, Ulla Haverinen-Shaughnessy, Mari Turunen, Virpi Leivo, Anu Aaltonen and the INSULAtE Project Group
246	A-WG06S1P23	**Personal daily exposure of children to ultrafine particles and black carbon** C. Vargas Trassierra, S. Marini, L. Stabile, A. Russi, F. Fuoco, G. Buonanno
247	A-WG06S1P24	**Assessing workers inhalation exposure and dose during production TiO2 particles** A.J. Koivisto, J. Lyyranen, J. Jokiniemi, T. Tuomi and K. Hämeri
248	A-WG06S1P25	**Semi-volatile partitioning effect on indoor PM: inorganic ions and PAHs.** G. Sangiorgi, M.G. Perrone, L. Ferrero, C. Lo Porto, B. Ferrini, S. Petraccone
249	A-WG06S1P26	**Variation of Wintertime PM2.5 and PM10 in Primary Schools of Kaunas, Lithuania** E. Krugly, T. Prasauskas, L. Kliucininkas, D. Ciuzas, D. Martuzevicius
250	A-WG06S1P27	**Biomass burning source: Indoor - Outdoor comparison** Andriani E., Dambruoso P., de Gennaro G., Demarinis Loiotile A, Di Gilio A., Marzocca A., Mazzone A. , Palmisani J. and Tutino M.
251	A-WG06S1P28	**Comparison of nasal deposition efficiency between Taiwanese and Caucasian adults** Y.M. Sun, C.W. Lee and D.J. Hsu
252	A-WG06S1P29	**Lung deposition of charged aerosol particles – particle characterisation and experimental setup for a human volunteer study** M.D. Wright, M.F. Biddiscombe, J.C. Matthews, S.R. Underwood, D.L. Henshaw, O.S. Usmani and D.E. Shallcross
253	A-WG06S1P30	**Theoretical and experimental investigation of aerosol deposition in realistic human airway model** A. Kerekes, A. Nagy, A. Czitrovszky
254	A-WG06S1P31	**Computational study of aerosol flow in a physiologically realistic bifurcation under the influence of an external magnetic field** M. Pilou, E. Makris, P. Neofytou, S. Tsangaris and C. Housiadas
255	A-WG06S1P32	**Cytotoxicity of organic extracts of particles emitted from a soy-biodiesel fuelled generator**

		J.H. Tsai, S.J. Chen, K.L. Huang, C.C. Lin1 and W.Y. Lin
256	A-WG06S1P33	**Toxicological effects of indoor PM10 in primary schools under different street traffic intensities** T. Moreno, A. Langford, K. BéruBé, T. Jones, W. Gibbons and BREATHE participants
257	A-WG06S1P34	**Layered silicate nanofillers and their influence on the pulmonary surfactant** D. Kondej and T.R. Sosnowski
258	A-WG06S1P35	**The increasing importance of "perinatal susceptibility window" to PM exposure in the pathogenesis of cardiovascular and respiratory diseases occurring later in life** F. Granato, M. Sala, E. Riva, V. Guercio, R. Zangari, B. Lorenzi, J. Martellucci M. Monti, O. Caratozzolo, E. Bolzacchini and F. Cetta
259	A-WG06S1P36	**Cytotoxicity and genotoxicity of emission particles from heavy EURO4 engine operated with conventional and biobased diesel fuels and compressed natural gas.** P.I. Jalava, M.S. Happo, T. Murtonen, P. Yli-Pirilä, P. Hakulinen, P. Aakko-Saksa, J. Mäki-Paakkanen, J. Jokiniemi and M-R. Hirvonen
260	A-WG06S1P37	**Experimental study of aerosol transport in semi-realistic human airway model** J. Jedelsky, F. Lizal, J. Elcner and M. Jicha
261	A-WG06S1P38	**Hygroscopic particle deposition in the human lung – a model comparison** W. Hofmann, R. Winkler-Heil, G.A. Ferron and B. Asgharian
262	A-WG06S1P39	**Effects of different combustion conditions on the toxicological properties of PM1 in adjustable biomass combustion reactor** O. Uski, J. Leskinen, P. Jalava, A. Virén, H. Lamberg, T. Kaivosoja,T. Kettunen, I. Nuutinen, M. Happo, T. Torvela, J. Tissari, O. Sippula, J. Jokiniemi, M.-R. Hirvonen
263	A-WG08S1P01	**Aircraft Engine Soot Emissions and Smoke Number Uncertainties** M.E.J. Stettler and A.M. Boies
264	A-WG08S1P02	**Estimation of uncertainty of elemental concentration in PM 1** G. Valotto, E. Pecorari, G. Rampazzo, F. Visin and D. Zannoni
265	A-WG08S1P03	**Collection efficiency and interstage nanoparticle loss in MOUDI** A. Awasthi, C. N. Liu, B. Gumgamsetty and C.J. Tsai

266	A-WG08S1P04	**On the calibration of the Single Particle Soot Photometer (SP2)** M. Gysel, M. Laborde, P. Mertes, P. Zieger, J. Dommen, and U. Baltensperger
267	A-WG08S1P05	**Using a CPMA-Electrometer System as a Suspended Mass Standard** T.J. Johnson , J.P.R. Symonds, K.St.J Reavell, J.S. Olfert
268	A-WG08S1P06	**First field application of a thermal desorption resonance-enhanced multiphoton-ionisation single particle time-of-flight mass spectrometer for on-line measurements of particle bound polycyclic aromatic hydrocarbons and source identification** M. Oster , G. Dragan, M. Elsasser, J. Schnelle-Kreis and R. Zimmermann
269	A-WG08S1P07	**A Study of the Shape and Fluorescence of SOA using ASPECT combined with AFS** M.V.Ghosh, I. Hoare, S. Almabrok, L. Chen, J.M. Clark, G.Cartwright, G. Marston and C. Pfrang
270	A-WG08S1P08	**Rupture event scanning: a novel procedure based on QCM to measure particle size within the nanometer range** F.N. Dultsev , S.N. Dubtsov
271	A-WG08S1P09	**Counting efficiency of Nano-LDA equipment in 100nm polystyrene particles experiments** P. Jani, L. Vámos, A. Nagy, P. Schlosser
272	A-WG08S1P10	**Field measurements with the dual wavelength optical particle analyzer** A. Nagy A. Czitrovszky, A. Kerekes, W.W. Szymanski, Z. Bozóki, T. Ajtai, Á. Filep
273	A-WG08S1P11	**Atmospheric Aerosol Sampling using All-in-one Balloon System** Kang Ho Ahn, Hong Ku Lee, Eun Hee Ram, Gun Ho Lee
274	A-WG08S1P12	**A new device for fast measurements of nanoparticle size distributions** Hans Grimm, Lothar Keck, Markus Pesch, Matthias Richter, Hans-Joachim Schulz
275	A-WG08S1P13	**Sampling test of particle concentration for single-nozzle impactor with collection trap** C-H Huang , S-W Shen , C-J Wu , C-Y Tai and M. Alonso
276	A-WG08S1P14	**Environmental monitoring of ultrafine particles in NW Europe (Joaquin project)** J. Staelens, G.P.A. Kos, E.P. Weijers, D. de Jonge, E. Frijns, P. Berghmans, C. Matheeussen and E.oekens

277	A-WG08S1P15	**A seven Aethalometer correction algorithm intercomparison** J. Backman, A. Virkkula, A. Hyvärinen, A. Dell'acqua
278	A-WG08S1P16	**Water Soluble Organic Carbon (WSOC) Measurement: A Theoretical Analysis** M. Psichoudaki, S.N. Pandis
279	A-WG08S1P17	**Insights on BC determination on quartz-fibre and PTFE filters: results of two field experiments in Milan (Italy)** R. Vecchi, G. Valli, V. Bernardoni, C. Paganelli, and A. Piazzalunga
280	A-WG08S1P18	**Comparison of methods for measuring black carbon in medium speed diesel engine exhaust** S. Saarikoski, S. Carbone, M. Happonen, A. Rostedt, T. Rönkkö, J. Ristimäki, J. Keskinen and R. Hillamo
281	A-WG08S1P19	**Efficiency of portable counters in measuring particle number and lung deposited surface area concentrations** C. Vargas Trassierra, G. Buonanno, P. De Felice, L. Stabile, F. Cardellini, A. Russi
282	A-WG08S1P20	**Comparison between offline and semi-continuous analyzers for aerosol organic and elemental carbon detection** G. Belz, A. Cinieri, P.R. Dambruoso, B.E. Daresta, G. de Gennaro, A. Giove, G. Miglietta, R.M. Nacci, C. Tortorella
283	A-WG08S1P22	**Investigating aerosol functionalization using HRMS: inputs, advantages, validation in controlled environment and comparison with AMS.** G. Salque-Moreton, D. Voisin, N. Marchand, F. Siekmann, A. Monod, B. Nozières, B. D'Anna, J.-L. Jaffrezo, J.-L. Besombes and R. Thissen
284	A-WG08S1P23	**Determination of site specific correction parameters for Aethalometer using multi-wavelength photoacoustic data.** Á. Filep, T. Ajtai, N. Utry, Z. Bozóki, G. Szabó
285	A-WG08S1P24	**Comparison of new UFP monitor with SMPS system in urban sites, in Athens, Greece** E. Diapouli, S. Vratolis, V. Vasilatou, M. Gini, G. Habilomatis, S. Cheristanidis, A. Chaloulakou, S. Pothos and K. Eleftheriadis
286	A-WG08S1P25	**A dry high altitude astronomical observatory in continental Europe** A. Gardini, E. Pérez and J.A. Quesada
287	A-WG08S1P26	**Batch-to-Batch-Variability of Stöber synthesized**

		SiO2 nanoparticles– Comparison of DLS and SMPS data within Q-NANO S. Mülhopt, M. Hauser, E. Mahon, Reinhard Schneider, H.-R. Paur
288	A-WG08S1P27	**Field experiment with ozone scrubber for monitoring of PAHs** L. Hejkrlík, I. Nikolova, H. Plachá
289	A-WG08S1P28	**Retrieval of sky radiance at three wavelengths using a sky camera** R. Román, M. Antón, A. Cazorla, A. de Miguel, F.J. Olmo, J. Bilbao and L. Alados-Arboledas
290	A-WG08S1P29	**Correlating the extinction-based dustiness to the morphology of particles** S. Bach, E. Schmidt
291	A-WG08S1P30	**Indoor aerosols sampling and analysis using personal aerosol sampler and filters** A. Akachat, H. Rebbah
292	A-WG08S1P31	**Chemical composition of commonly used CPC calibration ions in the sub 2nm range** J. Kangasluoma, J. Mikkilä, K. Lehtipalo, J. Vanhanen, H. Junninen, M. Sipilä, M. Kulmala, T. Petäjä
293	A-WG08S1P32	**Methodology for mapping air pollution in an urban environment: the background issue** M. Van Poppel, J. Peters, N. Bleux
294	A-WG08S1P33	**On the use of Direct Analysis in Real Time/Quad-Time of Flight (DART/Q-TOF) for the analysis of Organic Aerosol** A. Sylvestre, S. Ravier and N. Marchand
295	A-WG08S1P34	**Using a Single Particle Soot Photometer to detect and distinguish different absorbing aerosol types** K. Heimerl, B. Weinzierl, M. Gysel, D. Baumgardner, G. Kok, C. Linke, M. Schnaiter, J. Schwarz, P. Sheridan, R. Subramanian and J. Walker
296	A-WG08S1P35	**Detection efficiency of a TSI Environmental Particle Counter 3783 particle counter: experimental and simulated results** J. Hakala, H.E. Manninen, T. Petäjä and M. Sipilä
297	A-WG08S1P36	**Evaluation of collection efficiency for the Aerodyne Aerosol Chemical Speciation Monitor using long-term ambient air data** M. Maasikmets, F. Canonaco, J.G. Slowik, A.S.H. Prévôt, U. Baltensperger
298	A-WG08S1P37	**An innovative and efficient method for the analysis of levoglucosan in ambient air particulate matter by**

		thermal desorption coupled with GS/MS. E. Grandesso, P. Perez Ballesta, K. Valler, K. Kowalewski, C. A. Belis
299	A-WG08S1P38	**The use of quartz filters as reference material for analysis of PAHs in particulate matter ambient air samples** P. Pérez Ballesta, E. Grandesso, K. Kowalewski, C. A. Belis
300	A-WG08S1P39	**Deposition chamber for in vitro toxicity tests of nanoparticles** N. Jeannet, D. Egli, P. Steigmeier, M. Geiser, M. Fierz, Zs. Juranyi, M. Kalberer, and H. Burtscher
301	A-WG08S1P40	**A new Nano ion-DMPS for measuring the charging state of the sub-3 nm aerosol particles** E. Järvinen, H. E. Manninen, P. P. Aalto, M. Sipilä, K. Lehtipalo, T. Petäjä, V.-M. Kerminen and M. Kulmala
302	A-WG08S1P41	**Developments towards an NO2 denuder for elevated temperatures** J. C. Wolf and R. Niessner
303	A-WG08S1P42	**Development of a portable instrument to determine the fractal dimension from angular light scattering meaurements** Zs. Jurányi, A. Keller and H. Burtscher
304	A-WG08S1P43	**iSPEX: Measure aerosols with your smartphone!** H. Volten representing the iSPEX team
305	A-WG08S1P44	**Near-ground hyperspectral imaging for urban scale remote sensing of aerosols, during nighttime – laboratory and upscaling study** Y. Etzion, D.M. Broday
306	A-WG08S1P45	**New instrument to investigate size-resolved chemical composition of nano-particles** A. Kürten, J. Hoker, C. Fuchs and J. Curtius
307	A-WG08S1P46	**Development of New Particle Size Magnifier Using Cooling Nucleation Tube** T. Yamamoto and M. Adachi
308	A-WG08S1P47	**High Temperature Condensation Particle Counter** K. Rongchai and N. Collings
309	A-WG08S1P48	**Effect of particle diffusivity on DMAs with multiple monodisperse-particle outlets: theory validation and design optimization** M.Giamarelou, M. Stolzenburg, D.-R. Chen and G. Biskos
310	A-WG08S1P49	**Influence of Turbulent Diffusion in an Electrical Mobility Spectrometer** J. Salm, P. Intra, A. Yawootti, N. Tippayawongand, U. Hõrrak

311	A-WG08S1P50	**A Micro-Orifice Volatilization Impactor (MOVI) coupled to an ion trap mass spectrometer with a soft ionization source (APCI-IT/MS) for the analysis of secondary organic aerosols** M. Brueggemann, A. Vogel and T. Hoffmann
312	A-WG08S1P51	**A Novel Compact Aerosol Mass Spectrometer - the ToF-ACSM: Instrument Performance and First Field Deployment** R. Fröhlich, M. J. Cubison, J. G. Slowik, A. S. H. Prévôt, U. Baltensperger, U. Rohner, M. Gonin J. R. Kimmel, D. R. Worsnop and J. T. Jayne
313	A-WG08S1P52	**Novel Polar Nephelometer for the Measurement of the Particle Asymmetry Parameter** Paul L. Kebabian, Timothy B. Onasch, Joda C. Wormhoudt and Andrew Freedman
314	A-WG08S1P53	**Scattering Coefficients and Asymmetry Parameters derived from the Polar Nephelometer Aurora4000** T. Müller, M. Paixão and A. Wiedensohler
315	A-WG08S1P54	**Feasibility study of a Differential Aerodynamic Diameter Analyzer** D. Kiesler and F.E. Kruis
316	A-WG08S1P55	**Experimental comparison of two Very Long DMAs** J. Uin, E. Tamm
317	A-WG08S1P56	**Applying Particle Size Magnifier to nano-particle measurements** J. Mikkilä, K. Lehtipalo, J. Kangasluoma, J. Vanhanen, T. Petäjä and M. Kulmala
318	A-WG08S1P57	**Novel continuous ambient air quality monitoring system that simultaneously reports multiple PM-fractions, number concentration and size distribution** M. Weiss, J. Spielvogel
319	A-WG08S1P58	**Direct probing of aerosol surfaces by synchrotron-radiation-based XPS** J. Werner, Y. Cai, N. L. Prisle, G. Öhrwall, J. Söderström, M. Dal Maso and O. Björneholm
320	A-WG08S1P59	**Liquid sample nanoparticle sizing system** J.E. Farnsworth, K. Erickson, B.L. Osmondson, and R. Caldow
321	A-WG08S1P60	**Approximate relationship between mobility and voltage for Brownian particles in a cylindrical DMA** M. Alonso, F.J. Alguacil and C.H. Huang
322	A-WG08S1P61	**Evaluation of Size Selective PM10 Sampling Inlets in Aerosol Wind Tunnel**

		Sangil Lee, Miae Yu, Hyun Ho Kim
323	A-WG08S1P62	**Enhanced multiple charge inversion algorithm for mobility size spectrometers** S. Pfeifer, T. Müller and A. Wiedensohler
324	A-WG08S1P63	**Thermodynamic characterization of the atmosphere during a Saharan dust intrusion over South Spain with onboard and remote sensing instrumentation: CLIMARENO** N. Seoane-Vieira, J. Andrey-Andrés, M.J. Granados-Muñoz, J. Fernández-Gálvez, R. González-Armengod, J.A. Adame, J. Tabrizi Sirvani, F. Lahoz-Pequerul,O. Serrano, M. Marco-Saurín
325	A-WG08S1P64	**Integrated instrument data and control for CLOUD chamber** J. Almeida, A. Amorim, A. David, P. Pereira, A. Tomé and Cloud Collaboration
326	A-WG08S1P65	**Reducing measurement error of Cloud Droplet Probe with a statistical smoother** S.Mikkonen, H. Portin, M. Komppula, A. Laaksonen and S. Romakkaniemi
327	A-WG08S1P66	**Off-line organic aerosol analyses of filter samples using aerosol mass spectrometry** I. El Haddad, J. Slowik, U. Baltensperger, A.S.H. Prévôt

Tuesday 4th September

08:45-09:45 Plenary 2. **Gelsomina Pappalardo**. *ACTRIS Research Infrastructure for coordinated long-term observation of aerosols, cloud-aerosol Interactions, and trace gases in Europe*
Room: Auditorio
Chair: Urs Baltensperger

09:45-10:30 Coffee-break

10:30-12:50 **Session SS01S1O. ACTRIS**
Room: Auditorio
Chairs: G. Pappalardo / P. Laj

10:30	SS01S1O01	**Long-term trends of aerosol number concentrations at GAW stations** A. Asmi, M. Collaud Coen, E. Andrews, M. Fiebig, A. M. Fjaeraa, P. Laj, J.A. Ogren, P. Sheridan, A. Virkkula, U. Baltensperger and E. Weingartner
10:50	SS01S1O02	**Long-term trend analysis of aerosol optical variables at GAW stations** M. Collaud Coen, E. Andrews, A. Asmi, M. Fiebig, A. M. Fjaeraa, P. Laj, C. Lund Myhre, J. A. Ogren, J.-P. Putaud, P. J. Sheridan, A. Virkkula, A. Wiedensohler, U. Baltensperger, and E. Weingartner
11:10	SS01S1O03	**Soot absorption over Europe combining observations and models** E. Vignati, M. Schulz, F. Cavalli, T. Mueller, A. Virkkula, C. Lund Myhre, A. Wiedesohler and P. Laj
11:30	SS01S1O04	**Merging air ion spectrometer and particle mobility size spectrometer measurements** H.E. Manninen, T. Petäjä, P. Aalto, W. Birmili, M. Kulmala and A. Wiedensohler
11:50	SS01S1O05	**Retrieval of aerosol microphysical properties profiles by combination of Lidar and sun photometer measurements. Application to mineral dust and volcanic aerosols** M.J. Granados-Muñoz, J.A. Bravo-Aranda, F. Navas-Guzmán, J.L. Guerrero-Rascado, H. Lyamani, A. Chaikovsky, J. Wagner, U. Wandinger, F.J.Olmo and L. Alados-Arboledas

12:10	SS01S1O06	**Optical and microphysical characterization of volcanic sulphate particles in the lower troposphere by Raman lidar** F. Navas-Guzmán, D. Müller,J. A. Bravo-Aranda, D. Pérez-Ramírez, F.J. Olmo, J.L. Guerrero-Rascado, U. Wandinger and L. Alados-Arboledas
12:30	SS01S1O07	**ACTRIS Data Centre: An atmospheric data portal** Cathrine Lund Myhre, Aasmund Fahre Vik, Robert Logna, Kjetil Tørseth, Holger Linné, Ewan O'Connor

10:30-12:50 **Session WG02S3O. Urban Aerosol in Large Cities (1)**
Room: Legado Andalusí
Chairs: T. Kuhlbusch / G. Fuller

10:30	WG02S3O01	**SAPUSS Solving Aerosol Problems by using synergistic strategies in Barcelona, Spain** M. Dall'Osto, A. Alastuey, M. A. Pedemonte, B. L. van Drooge, M. Pandolfi, M. C. Minguillon, F. Amato, T. Moreno, J. Pey, C. Reche, M. Cusak, M. Viana, A. Roca, J. Gietl, D. Beddows, Roy M. Harrison, J. Wenger, E. Mc Gillcuddy, J. Sudou, R. Healy, D. Ceburnis, G. Martucci, C. O'Dowd, F. Lucarelli, S. Nava, J. L. Jimenez, F. Gomez Moreno, B. Artinono, A. S. H. Prevot, L. Pfaffenberger, S. Frey, F. Wilsenack, S. Ng, D. Worsnop, D. Casabona Fina, P. Jiménez Guerrero and X. Querol
10:50	WG02S3O02	**Simultaneous Single Particle Mass Spectrometry Measurements at Two Different Urban Sites and Comparison with Quantitative Techniques** Eoin McGillicuddy, Manuel Dall'Osto, Franco Lucarelli, Silvia Nava, Xavier Querol, Roy M. Harrison, Johanna K. Gietl, David C. S. Beddows, Deborah Gross, Robert Healy, John Wenger , John Sodeau
11:10	WG02S3O03	**Hourly elemental concentrations at two different urban locations in Barcelona, Spain** F. Lucarelli, S. Nava, G. Calzolai, M. Chiari, M. Dall'Osto, X. Querol
11:30	WG02S3O04	**Seasonal comparison of comprehensive aerosol measurements in London during ClearfLo** D.E. Young, J.D. Allan, P.I. Williams, M.J. Flynn, D. Liu, J.D. Whitehead, N.H. Robinson, A.S.H. Prevot, S. Visser, M. Furger, M.W. Gallagher, and H.Coe

11:50	WG02S3O05	**A mobile measurement network for ultrafine particulate matter in the city of Zurich** A. Richard, P. Steigmeier, H. Burtscher and M. Fierz
12:10	WG02S3O06	**High-resolution mobile monitoring of traffic emissions in an urban area in Finland** L. Pirjola, T. Lähde, A. Malinen, J.V. Niemi, A. Kousa, T. Rönkkö,P. Karjalainen, J. Keskinen, A. Frey, and R. Hillamo
12:30	WG02S3O07	**Spatial and Seasonal Variations of Black Carbon and NO2 Concentrations in an Urban Environment and correlation with UFP concentrations at selected locations** M. Van Poppel, C. Matheeussen, P. Berghmans
Reserve paper	WG02S3B00	**Spatial distribution of particle number concentrations measured with the AERO-TRAM** B. Vogel, R. Hagemann, R. Rinke, A. Wieser, U. Corsmeier, Ch. Kottmeier

10:30-12:50 **Session WG03S3O. Characterisation Techniques for Organic Aerosol**
Room: Faraday
Chairs: A. Held / J. Schneider

10:30	WG03S3O01	**Single particle mass spectrometry of bacteria – lab measurements as reference for the identification of ambient bioaerosols** B. Sierau, F. Freutel, A. Roth, J. Schneider, C. Oehm, O. Möhler, and A. A. Mensah
10:50	WG03S3O02	**On-line analysis of organic aerosols with an ion-trap aerosol mass spectrometer** S.J. Gallavardin, J. Fachinger, F. Helleis, F. Drewnick, and S. Borrmann
11:10	WG03S3O03	**Organic particle and gas phase measurements with a new MOVI-CI-TOF-MS** C. Mohr, F. Lopez-Hilfiker, J. D. Wargo, R. L. N. Yatavelli, and J. A. Thornton
11:30	WG03S3O04	**Urban organic aerosols composition measured by ultra-high resolution mass spectrometry** A.G. Rincón, A.I. Calvo, M. Dietzel, M. Kalberer
11:50	WG03S3O05	**Unravelling the molecular organic signature of the EC/OC fractions of PM: Coupling of an EC/OC-carbon analyzer to photo-ionization mass**

		spectrometry J.Grabowski, T.Streibel, M.Sklorz, J.Chow, J.Watson and R.Zimmermann
12:10	WG03S3O06	**A long pathlength absorbance photometer for the determination of peroxide content and brown carbon in primary and secondary organic aerosol** J. Dommen, P. Mertes, S.M. Platt, I. El Haddad, L. Pfaffenberger, A.S.H. Prévôt, M. Kalberer, and U. Baltensperger
12:30	WG03S3O07	**Investigation of Free Radicals Formed in the Oxidation of Acoustically Levitated Alpha-Pinene Droplets by Electron Spin Resonance** M.V.Ghosh, P.Ionita, S. Almabrok, G. Marston, and C. Pfrang
Reserve paper	WG03S3B00	**Studying Atmospheric Aerosols by Acoustic Levitation: Linking Head Space Solid-Phase Micro-Extraction (HS-SPME) with Gas Chromatography-Mass Spectrometry (GC-MS)** S. Almabrok, G. Marston and C. Pfrang

10:30-12:50 **Session WG07S1O. Application of engineered nanoparticles**
Room: Cine3
Chairs: S. Pratsinis / A. Nasibulin

10:30	WG07S1O01	**Plasmonic biosensors with composite nanosilver structures** G.A. Sotiriou, C. O. Blattmann and S. E. Pratsinis
10:50	WG07S1O02	**Tailoring Single-walled Carbon Nanotube Diameters in Aerosol Synthesis Method** A. G. Nasibulin Y. Tian, M. Timmermans, A. O. Kaskela, K. Mustonen, T. Susi, I. V. Anoshkin, E. I. Kauppinen
11:10	WG07S1O03	**Aerosol-derived antimony doped-tin oxide nanoparticles and studies on the influence of organic and inorganic shells in nanoparticle assemblies on the overall conductance** S.B. Bubenhofera, C.M. Schumachera, G.A. Sotirioub, R.N. Grassa and W.J. Stark
11:30	WG07S1O04	**Synthesis of well-structured Pt catalysts on spherical SiO2 support by a CVS/CVD process using novel metal-organic precursors** M. Faust, K. Gao, M. Enders, S. Bräse, W. Gerlinger and

		M. Seipenbusch
11:50	WG07S1O05	**Different hybrid and single-phase nanoparticles by aerosol-photopolymerization** E. Akgün, W. Gerlinger, M. Wörner, B. Sachweh, J. Hubbuch
12:10	WG07S1O06	**Continuous, electrostatic controlled synthesis of organic-inorganic composite particles** S. Sigmund, E. Akgün, J. Meyer, M. Wörner, W. Gerlinger and G. Kasper
12:30	WG07S1O07	**Room temperature ultraviolet nanophosphor of geometrical MgO nanoparticles** P.V. Pikhitsa, C.H. Kim, S. Chae, S. Shin, S. Jung and M. Choi
Reserve paper	WG07S1B00	**Electrospray deposition of graphene nanosheets** L. B. Modesto-Lopez, O. V. Bilousov, J. J. Carvajal, F. Díaz and J. Rosell-Llompart

10:30-12:50 **Session WG08S3O. Measurement Methods**
Room: Gutenberg
Chairs: R. Niessner / V. Szymanski

10:30	WG08S3O01	**The use of Nuclear Reaction Analysis technique for the determination of Nitrogen in aerosol samples collected on Teflon filters** I. García Orellana, S. Becagli, G. Calzolai, M. Chiari, J. García López, S. Nava, F. Lucarelli, M. Respaldiza, R. Vecchi
10:50	WG08S3O02	**Laser Vaporizer-AMS for exposure assessment and detection of airborne engineered metal nanoparticles** P.T. Nilsson, A. C. Eriksson, M. E. Messing, C. Isaxon, M. Hedmer, H. Tinnerberg, B. O. Meuller, C. R. Svensson, K. Deppert, M. Bohgard and J. Pagels
11:10	WG08S3O03	**Size and surface area characterization of Carbon nanoparticle aggregates by means of a cascade epiphaniometer** M.I. Gini, K. Eleftheriadis, S. Vratolis, C. Helmis, K. Giannakopoulos, D. Papanastasiou, G.Orfanopoulos E. Raptakis
11:30	WG08S3O04	**TwinPAS – a photoacoustic instrument for the parallel, time-resolved analysis of soot and NO2 in exhaust gas** C. Haisch and R. Niessner

11:50	WG08S3O05	**Investigation of Fast Scanning SMPS Measurements: 16s and Below** K. Erickson, F. Quant, J. Farnsworth and R. Caldow
12:10	WG08S3O06	**New portable device for high time resolved measurements of particle size distributions** H. Grimm, D. Huhn, M. Pesch, M. Richter and F. Schneider
12:30	WG08S3O07	**Experimental aerosols characterization for the evaluation of source term from RDE's (Radiological Dispersion Events)** F.G. Di Lemma, J.Y. Colle, H. Thiele and R.J.M. Konings
Reserve paper	WG08S1B00	**Batch-to-Batch-Variability of Stöber synthesized SiO2 nanoparticles– Comparison of DLS and SMPS data within Q-NANO** S. Mülhopt, M. Hauser, E. Mahon, R. Schneider, H.-R. Paur

14:00-16:00 **Session WG01S3O. Remote Sensing of Aerosol Properties**
Room: Auditorio
Chairs: L. Alados-Arboledas / P. Sheridan

14:00	WG01S3O01	**In situ aerosol measurements for the validation and improvement of CALIPSO lidar extinction retrievals** P. Sheridan, J.A. Ogren, E. Andrews, J.L. Tackett, and D.M. Winker
14:20	WG01S3O02	**CLIMARENO-GRA 2011 campaign: Aerosol optical properties characterization from ground-based instrumentation** J.A.Bravo-Aranda, F. Navas-Guzmán, J. Andrey, M.J. Granados-Muñoz, J.L. Guerrerro-Rascado, M. Gil, H. Lyamani, A. Valenzuela, G. Titos, J. Fernández-Gálvez, F.J. Olmo and L. Alados-Arboledas
14:40	WG01S3O03	**Tropospheric aerosols remote sensing with a sensitive and accurate UV-VIS polarization Lidar** G. David, B. Thomas, A. Miffre and P. Rairoux
15:00	WG01S3O04	**Study on the influence of different error sources on sky radiance measurementsand inversion-derived aerosol products in the frame of AERONET** B. Torres, C. Toledano, A.J. Berjón, O. Dubovik, V. E.

		Cachorro, Y. Bennouna, D. Fuertes,R. González, P. Goloub, T. Podvin, L. Barel, A. M. de Frutos
15:20	WG01S3O05	**Evaluation of aerosol OC / BC estimations derived from AERONET data, using in-situ ground measurements** D. Paraskevopoulou, S. Kazadzis, N. Mihalopoulos, A. Arola, K. Eleftheriadis, C. Theodosi, A. Bougiatioti, E. Diapouli and E. Gerasopoulos
15:40	WG01S3O06	**Retrieving MODIS Aerosol Optical Depth in real time at 500 m resolution: urban-scale evaluation over Hong Kong** M. Bilal, J. E. Nichol, M. P. Bleiweiss, D. Dubois
Reserve paper	WG01S3B00	**Aerosol vertical distribution and its variability over Sweden during nighttime: A view from the CALIOP-CALIPSO and AIRS instruments** M.A. Thomas, A. Devasthale and M. Kahnert

14:00-16:00 **Session WG02S4O. Marine and Carbonaceous Aerosol**
Room: Legado Andalusí
Chairs: D. Baumgardner / A. I. Calvo Gordaliza

14:00	WG02S4O01	**Radiocarbon analysis on organic and elemental carbon in aerosol samples and source apportionment at an urban site in Northern Italy** V. Bernardoni, G. Calzolai, M. Chiari, M. Fedi, F. Lucarelli, S. Nava, A. Piazzalunga, F. Riccobono, F. Taccetti, G. Valli, R. Vecchi
14:20	WG02S4O02	**Results of monitoring campaign from a cruise ship in the Western Mediterranean** M.C. Bove, G. Calzolai, F. Cavalli, M. Chiari, E. Cuccia, J. Hjorth, D. Massabò, A. Piazzalunga, P. Prati, C. Schembari
14:40	WG02S4O03	**Organic Carbon detection in crude oil plant emissions in South Italy** M. Calvello, F. Esposito, G. Pavese, M. Lovallo, L. Mangiamele
15:00	WG02S4O04	**The Seasonal Cycle of Sea Spray Emissions: Long term Eddy Covariance Aerosol Flux measurements from Östergarnsholm, Baltic Sea (57°27`N ,18°59` E)** E. Douglas Nilsson and Monica E. Mårtensson

15:20	WG02S4O05	**Diurnal cycle of fossil and non-fossil carbon using 14C analyses during CalNex** P. Zotter, A.S.H. Prévôt, I. El-Haddad, Y. Zhang, S. Szidat, L. Wacker, X. Zhang, R. Bahreini, P. Hayes, J.B. Gilman, J.A. de Gouw, J.L. Jimenez, R. Weber, U. Baltensperger
15:40	WG02S4O06	**A new sea-salt module implemented within the NMMB/BSC Chemical Transport Model** M. Spada, O. Jorba, C. Pérez, Z.I. Janjic and J.M. Baldasano
Reserve paper	WG02S4B00	**New Findings on Submicron Sea Salt Source Flux** J. Ovadnevaite, D. Ceburnis, H. Berresheim and C. O'Dowd

14:00-16:00 **Session WG03S4O. Chemistry of Organic Aerosol: Field Study**
Room: Faraday
Chairs: J. Dommen / I. Kourtchev

14:00	WG03S4O01	**Observations of monoterpene organosulfates in wintertime aerosols** A.M.K. Hansen, K. Kristensen, F. Cozzi, A. Zare, M.F. Lauridsen and M. Glasius
14:20	WG03S4O02	**Simultaneous study of gas and particulate products formed from limonene oxidation: smog chamber and citrus fruit field measurements** L. Chiappini, S. Rossignol, C. Rio, S. Fable, G. Grignion, J.L. Savelli
14:40	WG03S4O03	**Quantification of nitrocatechols and related aromatic compounds in atmospheric aerosols** Z. Kitanovski, I. Grgić, M. Claeys, R. Vermeylen and W. Maenhaut
15:00	WG03S4O04	**Contribution of Cooking Emissions to Primary and Secondary Organic Aerosol in Urban Atmospheres** I. El Haddad, S.M. Platt, J. Slowik1, C. Mohr, M. Crippa, B. Temime-roussel, A. Detournay, N. Marchand, U. Baltensperger, A. S. H. Prévôt
15:20	WG03S4O05	**Interpretation of Sources and Formation Processes of Sub-micron Aerosols near Denver, Colorado from Tower Measurements during NACHTT 2011** Öztürk, F., Bahreini, R., Wagner, N., Dubé, W., Young, C., Brown, S.S., Brock, C., Ulbrich, I.M, Jimenez, J and Middlebrook, A.M.

15:40	WG03S4O06	**Composition and formation of organic aerosol particles in the Amazon** C. Pöhlker, K. T. Wiedemann, B. Sinha, M. Shiraiwa, S. S. Gunthe, M. Smith, H. Su, P. Artaxo, W. Elbert, M. K. Gilles, A. L. D. Kilcoyne, R. C. Moffet, M. Weigand, S. T. Martin, U. Pöschl, M. O. Andreae
Reserve paper	WG03S4B00	**Characterization of humic-like substances (HULIS) in size segregated atmospheric aerosol** G. Kiss, N. Törő, A. Hoffer, J. Dautovic, S. Frka, Z. Kozarac, M. Harir, P. Schmitt-Kopplin

14:00-16:00 **Session WG05S1O. Physical and chemical analysis of PMx**
Room: Gutenberg
Chairs: W. Maenhaut / A. Alastuey

14:00	WG05S1O01	**Inhalable aerosol chemistry of transboundary particulate intrusions into western Japan** T. Moreno, T. Kojima, X. Querol, A. Alastuey, F. Amato, F. Lucarelli, J. de la Rosa and W. Gibbons
14:20	WG05S1O02	**Size-segregated Characterization of PM10 in German low lands (EMEP site Melpitz) using a five-stage Impactor: A six year study** G. Spindler, A. Grüner, Y. Iinuma, K. Müller, S. Scheinhardt, H. Herrmann
14:40	WG05S1O03	**Ultrafine particles and PM1 measurements in a hot-spot pollution area: size distribution, mass closure and source apportionment** R. Vecchi, V. Bernardoni, A. Bigi, M. Elser Fritsche, P. Fermo, G. Ghermandi, A. Piazzalunga, R. Gonzales Turrion, M. Urbani, G. Valli
15:00	WG05S1O04	**Factors influencing levels and composition of PM in the Barcelona's city subway system** Querol X., Moreno T., Karanasiou A., Reche C., Alastuey A., Viana M., Font O., Gil J., de Miguel E., Capdevila M
15:20	WG05S1O05	**Chemical characterization and source apportionment of oxidized organic aerosol components by advanced spectroscopic techniques in the Po Valley, Italy** M. Paglione, S. Decesari, M. Dall'Osto, R. Hillamo, S. Carbone, S. Saarikoski, R. Harrison, C. O'Dowd, and M.C. Facchini

15:40	WG05S1O06	**Towards an identification of sources of HUmic LIke Substances (HULIS) by statistical analysis** J. Guilhermet, C. Piot, J. Vessaire, C. Baduel, J.-L. Jaffrezo and D. Voisin
Reserve paper	WG05S1B00	**Personal monitoring of ambient particulate matter – online monitoring and offline filter sample analysis** J. Schnelle-Kreis G. Abbaszade, J. Cyrys, J. Gu, M. Pitz, A. Peters, R. Zimmermann

14:00-16:00 **Session WG07S2O. Fundamentals and measurement of nanoparticles**
Room: Cine 3
Chairs: A. Schmidt-Ott / G. Kasper

14:00	WG07S2O01	**Physical defect formation in few layer graphene-like carbon on aerosol-made metal nanoparticles** C.M. Schumacher, R.N. Grass, M. Rossier, E.K. Athanassiou and W.J. Stark
14:20	WG07S2O02	**Measurement of the velocity of nanoparticles in a molecular beam of a particle mass spectrometer** W. Baumann, H. Mätzing, J. Seibold, M. Hauser, H.-R. Paur and H. Seifert
14:40	WG07S2O03	**Scaling-up the production of monodisperse nanoparticles by means of a high-flow rate parallel plate DMA** M. Rouenhoff, E. Hontañón, A. Azabal, E. Ramiro and F. E. Kruis
15:00	WG07S2O04	**Direct Transfer and Stabilization of Aerosol Particles into Liquid Suspensions by Meansof a Wet Electrostatic Precipitator** C. Anderlohr, K. Schaber, W. Gerlinger
15:20	WG07S2O05	**An Aerosol Process for Fabrication of a Carbon NanoTube Membrane with Tuneable Pore Size** M. Valenti, A.C. Zonnevylle, V. Vons, C.W. Hagen, R. van Ommen and A. Schmidt-Ott
15:40	WG07S2O06	**Structural determination of charged nanoparticles in a Polarizable Gas** C. Larriba and C. Hogan
Reserve paper	WG07S2B00	**A MEMS sensor based personal sampler for ultrafine particles** S. Merzsch, H.S. Wasisto, E. Peiner, I. Kirsch and E. Uhde

POSTER SESSION B

001	B-WG01S2P01	**Estimation of the aerosol optical depth in the UV region at Caceres (Spain) by the Angstrom formula** M.A. Obregón, A. Serrano and M.L. Cancillo
002	B-WG01S2P02	**Calculation of aerosol microphysical properties by neural network inversion of ground-based AERONET data** M. Taylor , S. Kazantzis, A. Tsekeri, A. Gkikas and V. Amiridis
003	B-WG01S2P03	**Aerosol fine fraction characterization by integrated in-situ and columnar measurements** M. Calvello, F. Esposito and G. Pavese
004	B-WG01S2P04	**SPEX: Multi-Angle Spectropolarimetry for aerosol and cloud characterization from the ISS** O.P. Hasekamp, M. Smit, J. Rietjens, F. Snik, G. van Harten & the SPEX team
005	B-WG01S2P05	**Intercomparison of lidar aerosol backscatter and in-situ size distribution measurements** A. Held, T. Seith, I.M. Brooks, S.J. Norris and S.D. Mayor
006	B-WG01S2P06	**SEVIRI based aerosol optical depth and type retrieval** S. Nevens, N. Clerbaux, A. Velazquez Blazquez, E. Baudrez, I. Decoster, S. Dewitte, A. Ipe
007	B-WG01S2P07	**Lidar observations of stratospheric aerosol over the Northern Hemisphere from Nabro volcano: MPLNET, EARLINET, CALIPSO, NDACC synergy** P. Sawamura, J.P.Vernier, J. E.Barnes, T.A. Berkoff, E.J. Welton, L.Alados-Arboledas, F. Navas-Guzmán, L.Mona, D. Lange, M.Sicard, S. Godin-Beekmann, G. Payen, Z. Wang and R.M. Hoff
008	B-WG01S2P08	**Detection of the stratospheric volcanic aerosol plume from the Nabro eruption in summer 2011 in the framework of SPALINET** J.L. Guerrero-Rascado, J.A. Bravo-Aranda, F. Wagner, C. Córdoba-Jabonero, F. Molero, D. Lange, M. Granados-Muñoz, J. Preißler, D. Toledo, A.J. Fernández, M. Sicard, F. Navas-Guzmán, Y. Hernández, A.M. Silva, M. Pujadas, A. Comerón, S. Pereira, F. Rocadenbosch, and L. Alados-Arboledas
009	B-WG01S2P09	**CLIMARENO-GRA 2011 campaign: retrieval of vertically-resolved aerosol microphysical properties by lidar at daytime** J.L. Guerrero-Rascado, M. J. Granados-Muñoz, F. Navas-Guzmán, J. A. Bravo-Aranda, F. J. Olmo, J. Andrey, M. Gil,

		A. Chaikovsky, U. Wandinger and L. Alados-Arboledas
010	B-WG01S2P10	**First profiling of aerosol microphysical properties from combination of multiwavelength lidar (EARLINET) and sun-photometric (AERONET) data at Évora (Portugal)** J.L. Guerrero-Rascado, A. M. Silva, M. J. Costa, J. Preißler, S. Pereira, A. Chaikovsky and F. Wagner
011	B-WG01S2P11	**A case study of a strong aerosol load over Heraclion Crete (Greece), detected with ground-based lidar and in situ airborne measurements** P. Kokkalis, G. Tzeremes, A. Papayannis, V. Amiridis, E. Armandillo
012	B-WG01S2P12	**PBL determination from ground based lidar over Herakleion-Crete Greece** P. Kokkalis, G. Tzeremes, A. Papayannis, and E. Armandillo
013	B-WG01S2P13	**Saharan Air Layer (SAL) over Tenerife: Summertime statistic analysis from lidar measurements** C. Córdoba-Jabonero, D. Toledo, J.A. Adame, Y. Hernández, E. Cuevas and M. Gil
014	B-WG01S2P14	**Polar Stratospheric Clouds observations in coastal Antarctica based on Micro Pulse Lidar measurements. I. Depolarization ratio comparison with CALIOP** C. Córdoba-Jabonero, J.L. Guerrero-Rascado, D. Toledo, M. Parrondo, M. Yela, M. Gil and H. Ochoa
015	B-WG01S2P15	**Polar Stratospheric Clouds observations in coastal Antarctica based on Micro Pulse Lidar measurements. II. PSC-type discrimination assessment** D. Toledo, C. Córdoba-Jabonero, J.L. Guerrero-Rascado, M. Parrondo, M. Yela, M. Gil and H. Ochoa
016	B-WG01S2P16	**Multiwavelength Raman lidar observations of aerosols at Gual Pahari, India** E. Giannakaki, T. Mielonen, K. Korhonen, H. Lihavainen, A.-P. Hyvärinen, D. Mülle, H. Baars, R. Engelmann, D. Althausen, T.S. Panwar, R.K. Hooda, V.P. Sharma, K.E.J. Lehtinen, Y. Viisanen and M. Komppula
017	B-WG01S2P17	**Preliminary results from the new portable backscatter aerosol lidar in Turkey** K. R. Allakhverdiev, A. Secgin, M. F. Huseyinoglu and Z. Salaeva
018	B-WG01S2P18	**Aerosol vertical distribution and its variability over Sweden during nighttime: A view from the CALIOP-CALIPSO and AIRS instruments** M.A. Thomas, A. Devasthale and M. Kahnert

019	B-WG01S2P19	**Aerosol variability over Lemesos, Cyprus: Use of ground based data, satellite observations and model simulations.** RE Mamouri, S. Kleanthous, S. Basart, V. Amiridis, Nisantzi, A., D.G Hadjimitsis, A. Agapiou and J.M.Baldasano
020	B-WG01S2P20	**Nine years of aerosol optical depth measurements over north-central Spain from ground (AERONET-RIMA) and their comparison with satellite (MODIS) observations** Y.S. Bennouna, V.E. Cachorro, B. Torres, R. Rodrigo, C. Toledano, A. Berjón and A.M. de Frutos
021	B-WG01S2P21	**A first approach to study the aerosol indirect effect over Madrid by means of multiwavelength Raman lidar** A.J. Fernández, F. Molero and M. Pujadas
022	B-WG01S2P22	**Single scattering albedo and fine mode faction retrieved with AATSR satellite instrument** E. Rodríguez, P. Kolmonen, A-M Sundström, L. Sogacheva, T. Virtanen, G. de Leeuw
023	B-WG01S2P23	**Optical and Microphysical properties from Raman lidar and depolarization data** F. Navas-Guzman, L. Osterloh, C. Böckmann, M.J. Granados-Muñoz, and L. Alados Arboledas
024	B-WG01S2P24	**Towards a remote sensing tool for aerosol hygroscopicity studies combining lidar and passive microwave radiometry** F. Navas-Guzmán, J. Bravo-Aranda, M.J. Granados-Muñoz, J.L. Guerrero-Rascado, J. Fernández-Gálvez, A.J. Fernández and L. Alados-Arboledas
025	B-WG01S2P25	**A first estimation of aerosol radiative forcing at Málaga (Spain) through the direct method** I. Foyo-Moreno, Alados, I. H. Lyamani, Olmo, F.J. and L. Alados-Arboledas
026	B-WG01S2P26	**Cloud screening and quality control algorithms for star photometry.** D. Pérez-Ramírez, H. Lyamani, F.J. Olmo, D.N. Whiteman, F. Navas-Guzmán and L. Alados-Arboledas
027	B-WG01S2P27	**Mixing height from passive remote sensing at high temporal resolution** J.Fernández-Gálvez, M.J. Granados-Muñoz, F.J. Olmo and L. Alados-Arboledas
028	B-WG01S2P28	**EARLINET and the international ChArMEx and PEGASOS measurement campaigns in summer 2012** L. Mona, M. Sicard, A. Amodeo, A. Apituley, L.Alados-

		Arboledas, D. Balis, C. Böckmann, A. Chaikovsky, A. Comeron, G. D'Amico, F. De Tomasi, V. Freudenthaler, A. Giunta, I. Grigorov, M. Haeffelin, M. Iarlori, H. Linnè, M. McAuliffe, F. Molero, V. Mitev, D. Nicolae, N.Papagiannopoulos, A. Papayannis, M.R. Perrone, A. Pietruczuk, M. Pujadas, J.-P. Putaud, V. Rizi, F. Rocadenbosch, V. Simeonov, N. Spinelli, K. Stebel, T. Trickl, U. Wandinger, X. Wang, F. Wagner, M. Wiegner and G. Pappalardo
029	B-WG01S2P29	**Climatology of aerosol optical properties over a tropical –urban location in western India** G. R. Aher and G. V. Pawar
030	B-WG01S2P30	**Calibration and intercomparison results in the Spanish network on environmental DMAs** F. J. Gómez-Moreno, B. Artíñano, V. Juncal Bello, M. Piñeiro Iglesias, P. López Mahía, N. Pérez, J. Pey, A. Alastuey, B. A. de la Morena, M. I. García, S. Rodríguez, M. Sorribas, G. Titos, H. Lyamani and L. Alados-Arboledas
031	B-WG01S2P31	**Influence of the thermophoresis on aerosol deposition on warm urban surfaces** P. Roupsard, D. Maro, A. Coppalle, H. Branger, O. Connan, D. Hébert and B. Letellier
032	B-WG01S2P32	**Long Term Trends in Arctic Aerosol Composition at Kevo, Finland** P.K. Hopke, J.R. Laing, L. Hussain, V.A. Dutkiewicz, J. Paatero, and Y. Viisinen
033	B-WG01S2P33	**Hygroscopicity of organic/inorganic internally mixed particles by infrared spectroscopy** Lorena Miñambres, Estíbaliz Méndez, María N. Sánchez, Fernando Castaño and Francisco J. Basterretxea
034	B-WG01S2P34	**General assessment of the main factors governing the particle concentrations in urban and regional background environments** J.F. Nicolás, J. Crespo, E. Yubero, N. Galindo, J. Moltó and E. Mantilla.
035	B-WG01S2P35	**Non-volatile aerosol in the Arctic Winter Stratosphere and its role for PSC formation.** R. Weigel, M. Ebert, K. Kandler, S. Molleker, W. Frey, M. Klingebiel, C. M. Volk, G. Günther, H. Schlager, F. Cairo, S. Kaykin, S. Borrmann
036	B-WG01S2P36	**Chemical Characterization of Impactor Samples from seven Sites in Germany** K. Müller, G. Spindler, T. Gnauk, Y. Iinuma, H. Herrmann
037	B-WG01S2P37	**Physicochemical Properties of Ultrafine Aerosol**

		Particles in the North Aegean during the AEGEAN_GAME Field Campaign E. Triantafyllou, M.Giamarelou, S. Bezantakos, K. Barmpounis, E. Bossioli, Ch. Theodosi, M. Tombrou, N. Mihalopoulos, K. Eleftheriadis, G. Biskos
038	B-WG01S2P38	**Physico-chemical characterization of HULIS from different environments** T.B. Kristensen, L. Du, Q.T. Nguyen, H.G. Kjærgaard, C.B. Koch, J.K. Nøjgaard, A.G. Hallar, D.H. Lowenthal, B. Nekat, D. van Pinxteren, M. Glasius and M. Bilde
039	B-WG01S2P39	**Photophoresis of soot aerosols in the atmospheric radiation field** L.B. Kochneva and S.A. Beresnev
040	B-WG01S2P40	**Chemistry of Size Separated Aerosols over the Indian Arctic Station, Himadri** M.P. Raju, S. M. Sonbawne, P.D. Safai, P.S.P. Rao and P.C.S. Devara
041	B-WG01S2P41	**Two years of measurements of atmospheric aerosols at a remote mountain site in NE Spain** A. Ripoll, M.C. Minguillón, J. Pey, X. Querol, A. Alastuey
042	B-WG01S2P42	**Investigating physicochemical properties of marine aerosol over the Atlantic Ocean** S. Huang, L. Poulain , Z. Wu, F. Höpner, H. Herrmann, A. Wiedensohler
043	B-WG01S2P43	**Evaluation of aerosols properties using ground based instruments in Magurele, Romania** J. Vasilescu, L. Marmureanu, A. Nemuc and L. Belegante
044	B-WG01S2P44	**Size-segregated inorganic aerosol compounds during different meteorological scenarios** M. A. Revuelta, F. J. Gómez-Moreno, L. Núñez, M. Pujadas, B. Artíñano
045	B-WG01S2P45	**Ionization of the atmosphere induced by cosmic rays: Full model and practical applications** I.G. Usoskin
046	B-WG01S2P46	**Long term observations of aerosol light absorption and particle volatility properties in the lower tropical free troposphere** T. Hamburger, R. Krejci, M. Matisans, J. Ström, P. Tunved, G. Hoschild, J. Gross, S. Calderon and P. Hoffmann
047	B-WG01S2P47	**Aerosol long-term volatility measurements in a boreal forest environment** S.A.K. Häkkinen, M. Äijälä, K. Lehtipalo, H. Junninen, J. Backman, A. Virkkula, T. Nieminen, M. Vestenius, H. Hakola, M. Ehn, D. R., Worsnop, M. Kulmala, T. Petäjä and I. Riipinen

048	B-WG01S2P48	**Aerosol water soluble organic matter: Characterization of surface active substances by electrochemical method** Z. Kozarac, B. Ćosović, S. Frka, J. Dautović, G. Kiss, A. Hoffer
049	B-WG01S2P49	**Hygroscopic Properties of Ultrafine Aerosol Particles over the Aegean Sea** S. Bezantakos, K. Barmpounis, E. Bossioli, M. Tombrou, N. Mihalopoulos, K. Eleftheriadis, J. D. Allan, H. Coe A. Bacak, G. Biskos
050	B-WG01S2P50	**Hygroscopic Properties of Fine and Ultrafine Aerosol Particles over an Urban Background Site in Athens, Greece** S. Bezantakos, S. Vratolis, L. Diapouli, K. Eleftheriadis, G. Biskos
051	B-WG01S2P51	**Determination of the parameters of the critical nucleus that is formed on the seed particles during heterogeneous nucleation** S.V. Valiulin, V.V. Karasev, S.V. Vosel, A.A. Onischuk, A.M. Baklanov, S. di Stasio
052	B-WG01S2P52	**A Tandem DMA study on selected sugars and sugar alcohols** N.Zannoni, J.Hong, A.A. Zardini, K.Lieke, M. Bilde
053	B-WG01S2P53	**Vertical Profiles of Aerosol Properties and Black Carbon in the Arctic during spring and summer 2011: relationship with nucleation events and ship plumes** L. Ferrero, D. Cappelletti, B. Moroni, V. Vitale, R. Udisti, G. Sangiorgi, M.G. Perrone, M. Busetto, C. Lanconelli, M. Mazzola, A. Lupi, S. Becagli, R. Traversi, D. Frosini, M. Maturilli, R. Neuber, C. Ritter, J. Graeser, M. Fierz, G. Mocnik and E. Bolzacchini
054	B-WG01S2P54	**Influence of adsorbed organic films on ice particle growth under conditions relevant to the upper troposphere** X. Kong, E.S. Thomson, P. Papagiannakopoulos, N. Markovic and J.B.C. Pettersson
055	B-WG01S2P55	**Continuous multiple-year atmospheric nitrate record from East Antarctic plateau** R. Traversi, S. Becagli, D. Frosini, M. Severi, M. Mazzola, C. Lanconelli, V. Vitale and R. Udisti
056	B-WG01S2P56	**Volume-based k-interaction model, hygroscopicity parameters and solute interaction coefficients** E. Mikhailov, S. Vlasenko, D. Rose and U.Pöschl
057	B-WG01S2P57	**Aerosol optical properties at Santiago Island, Cape**

		Verde M. Cerqueira, C. Pio, P. Fialho, J. Cardoso, T. Nunes and S. M. Almeida
058	B-WG01S2P58	**Mass scattering efficiency and chemical composition of different aerosol types at a coastal area of the Gulf of Cadiz (SW Spain)** J.F. López, V.E Cachorro, Y. González-Castanedo, J.D. de la Rosa and A.M. de Frutos
059	B-WG01S2P59	**Long-term atmospheric aerosol deposition in Southern Portugal: first results on chemical and morphological characterization of particles by VP-SEM+EDS** F. Wagner, N. Schiavon, K. Kandler, L. Tobias and J.Mirão
060	B-WG01S2P60	**Arctic aerosol sampled at Ny Ålesund: results from size-segregated samples** G. Calzolai, S. Becagli, C. Ghedini, F. Rugi, D. Frosini, S. Nava, M. Chiari, F. Lucarelli, R. Traversi and R. Udisti
061	B-WG01S2P61	**Carbonaceous aerosol characterization in Piacenza (Italy)** M. Calvello, F. Esposito, G. Pavese, G, Lonati, S. Ozgen and G. Ripamonti
062	B-WG01S2P63	**Saharan vs. local influence on atmospheric aerosol deposition in the southern Iberian Peninsula: significance for N and P inputs** R. Morales-Baquero, C. Pérez-Martínez
063	B-WG01S2P64	**Observations of aerosol of different origin by Siberian - Far Eastern lidar network and photophoresis** A.A. Cheremisin, V.N. Marichev, V.V. Bychkov, B.M. Shevtsov, P.V. Novikov, I.S. Shnipov
064	B-WG01S2P65	**Direct observations and model simulations of long-range transported aerosols over Northeast Asia inferred from ground, airborne and satellite measurements** M.G. Cayetano, Y.J. Kim, J.S. Jung, K.Y. Lee, K.C. Kim, R. S. Park, C.H. Song, M. Koike and Y. Kondo
065	B-WG01S2P66	**Analysis of particle size distribution on urban and rural sites with connection to meteorological conditions** B. Kotlík, J. Keder, L. Černikovský
066	B-WG01S2P67	**Temperature influence on the natural aerosol budget over boreal forests** L. Liao, H. Junninen, M. Kulmala and M. D. Maso
067	B-WG01S2P68	**Large particle climatology in Finland – Estimating**

		the effect of aerosols in extinction of infrared radiation N. Kivekäs, T. Mielonen, H. Portin, T. Kaurila, I. Rajakallio, K.E.J. Lehtinen and H. Lihavainen
068	B-WG01S2P69	**Comparison of new particle formation events and an analysis of aerosol dynamics between three sites in northern Scandinavia** R. Väänänen, T. Nieminen, M. Dal Maso, A. Virkkula, B. Svenningsson, N. Kivekäs, T. Holst, A. Arneth, V-M. Kerminen, M. Kulmala
069	B-WG01S2P70	**The Impact of Meteorological Conditions on PM air pollution in Tartu, Estonia** E.-S. Kerner, M. Eller
070	B-WG01S2P71	**Aerosol investigations with light aircraft during the Grímsvötn eruption and during Etna volcanic activities in the year 2011** Weber, K., Reichardt, R., Elíasson, J., Vogel, A., Fischer, C., Moser, H.M. , Palsson, A., Palsson, T, Sturm, K
071	B-WG02S2P01	**Indoor and Outdoor Particle Concentrations and Elemental and Organic Carbon at 17 Primary Schools** L. Morawska, M. Mazaheri, F. Salimi, R. Laiman, L. Crilley, G. Ayoko
072	B-WG02S2P02	**Carbonaceous aerosols in Barcelona during the SAPUSS campaign** A. Karanasiou, M. Dall'Osto, M. Viana, A. Alastuey, X. Querol
073	B-WG02S2P03	**Carbonaceous content of PM_{10} and $PM_{2.5}$ in urban-traffic and urban background sites within the Thessaloniki Major Area (TMA), northern Greece** C. Samara, D. Voutsa, A. Kouras, Th. Maggos
074	B-WG02S2P04	**Characteristics of fine carbonaceous aerosol at a coastal rural site in the Central Mediterranean as given by OCEC online measurements** Antonella Malaguti, Mihaela Mircea, Teresa M.G. La Torretta, Chiara Telloli, Massimo Berico
075	B-WG02S2P05	**Black carbon optical properties measured in Pasadena, Los Angeles during CalNex** J.W. Taylor, J.D. Allan, M.J. Flynn, D. Liu, P. L. Hayes, J.L. Jimenez, B. Lefer and H. Coe
076	B-WG02S2P06	**FTIR-ATR spectroscopy of water-soluble organic matter from atmospheric aerosols** S.M.S. Freire, R.M.B.O Duarte and A.C. Duarte
077	B-WG02S2P07	**Seasonal and diurnal observations of black carbon**

		and trace gases in the north suburb of Nanjing influenced by industiral areas L.L Tang, X.Z Zhang, D.T. Liu, J. Allan, Hugh Coe
078	B-WG02S2P08	**Organic, elemental and water-soluble organic carbon in size segregated aerosols in the Eastern Mediterranean** A. Bougiatioti, P. Zarmpas, E. Koulouri, M. Antoniou, C. Theodosi, G. Kouvarakis, S. Saarikoski, T. Mäkelä, R. Hillamo and N. Mihalopoulos
079	B-WG02S2P09	**A yearly cycle of radiocarbon in organic and elemental carbon at a rural site in the Netherlands** U. Dusek, M. Monaco, S. Szidat, H. A. J. Meijer, J. van der Plicht, T. Röckmann
080	B-WG02S2P10	**Characterisation of trace metals in airborne carbonaceous aerosols by single-particle EDX - Scanning Electron Microscopy** A. Pietrodangelo, S. Pareti and C. Perrino
081	B-WG02S2P11	**δ13C values of TC, EC+CC and OC in size segregated aerosol particles** A. Garbaras, R. Bariseviciute, K. Kvietkus, R. Skipityte, I. Garbariene, A. Masalaite and V. Remeikis
082	B-WG02S2P12	**Comparison of PM1 Organic and Elemental carbon between an urban and a regional background station** E. Yubero, J.F. Nicolás, Crespo J, M. Chiari, S. Nava, G. Calzolai, F. Lucarelli
083	B-WG02S2P13	**Organic matter and non-refractory aerosol over the remote Pacific: oceanic and combustion sources** L. M. Shank, S. Howell, A. D. Clarke, S. Freitag, V. Brekhovskikh, V. Kapustin, C. McNaughton, T. Campos, R. Wood
084	B-WG02S2P14	**Organic export from the ocean to the atmosphere - first investigations** M. V. Pinxteren, C. Müller, Y. Iinuma, C. Stolle and H. Herrmann
085	B-WG02S2P15	**Investigating primary marine aerosol properties: CCN activity of sea salt and mixed inorganic-organic particles** S.M. King, A.C. Butcher, T. Rosenoern, E. Coz, K. I. Lieke, G. de Leeuw, E. D. Nilsson, M. Bilde
086	B-WG02S2P16	**Aerosol particle distribution in the Baltic Sea marine boundary layer with the enlarged continental outflows and ship exhaust emissions** K. Plauškaitė, N. Špirkauskaitė, S. Kecorius, T. Petelski, T. Zielinski, and V. Ulevicius

087	B-WG02S2P17	**Sub-Antarctic marine aerosol: Significant contributions from biogenic sources** J. Schmale, J. Schneider, E. Nemitz, S.Y. Tang, U. Dragosits, T.D. Blackall, P.N. Trathan, G. Phillips and C.F. Braban
088	B-WG02S2P18	**Amino acids in Arctic aerosols** A. Gambaro, E. Scalabrin, R. Zangrando, E. Barbaro and C. Barbante
089	B-WG02S2P19	**Oceanic energy dissipation and the relationship to laboratory generated SSA** A.C. Butcher, S.M. King, E.D. Nilsson, and M. Bilde
090	B-WG02S2P20	**Shipboard characterization of a wet scrubber system: Influence on particle number concentration, particle size distribution and chemical composition** A.G. Hemmersam, M.K. Lykkegaard, K. Fuglsang, T. Rosenoern, J.B. Markussen, J.P. Hansen, K.I. Lieke and M. Bilde
091	B-WG02S2P21	**New Findings on Submicron Sea Salt Source Flux** J. Ovadnevaite, D. Ceburnis, H. Berresheim and C. O'Dowd
092	B-WG02S2P22	**The composition of Sea Spray Aerosol (SSA) produced from coastal Baltic seawaters** K. Plauskaite, V. Ulevicius, J. Ovadnevaite, M. Rinaldi, M.C. Facchini, C. O'Dowd and D. Ceburnis
093	B-WG02S2P23	**Laboratory based studies of primary sea-spray generation in plankton-enriched sea-water** D. Ceburnis, J. Ovadnevaite, M. Zacharias, J. Bialek, S. Connan, M. Rinaldi, C. Monahan, M.C. Facchini, H. Berresheim, D.B. Stengel and C. O'Dowd
094	B-WG02S2P24	**Characterization of PM1 sampled in the "Marco Polo" airport area (Tessera-Venice)** G. Valotto, D. Bassano, E. Pecorari, E. Rampado, G. Rampazzo, S. Sollecito, F. Visin and D. Zannoni
095	B-WG02S2P25	**Monitoring of ultrafine particles at an urban environment in southern Europe** G. Titos, H. Lyamani, M. Sorribas, I. Foyo-Moreno and L. Alados-Arboledas.
096	B-WG02S2P26	**Short term control efficiencies of dust suppressants to reduce fugitive dust** Sehyun Han, Yoonho Seo and Yongwon Jung
097	B-WG02S2P27	**Source apportionment of PM-bound PAHs, *n*-alkanes and inorganic ions in an urban environment in southeastern Spain** J. Gil-Moltó, N. Galindo, M. Varea and C. Chofre
098	B-WG02S2P28	**An original device for the measure of aerosol**

		deposition. Results of a one year survey period on the Pin Sec catchment in Nantes, France Stéphane Percot, Véronique Ruban, Pierre Roupsard, Denis Maro and Maurice Millet
099	B-WG02S2P29	**Evidence of regional-scale biomass burning contributions to urban aerosols in the Western Mediterranean** M. Viana, C- Reche, F. Amato, A. Alastuey, T. Moreno, F. Lucarelli, S. Nava, M. Rico, J. Gracia and X. Querol
100	B-WG02S2P30	**The effect of size, location, occupancy and microclimatic factors on air quality of university lecture rooms** M. Braniš and K. Stupková
101	B-WG02S2P31	**Impact of port activities on urban air quality at a Mediterranean coastal city** N. Pérez, J. Pey, C. Reche, X. Querol, A. Alastuey and J. Cortés
102	B-WG02S2P32	**Comparative study of ultrafine aerosol within a city** I. Salma, T. Borsós, Z. Németh, P. Aalto and M. Kulmala
103	B-WG02S2P33	**Black carbon mixing state in Paris megacity** M. Laborde, M. Gysel, T. Tritscher, M. Crippa, Zs. Jurányi, P.F. DeCarlo, A. Prévot, U. Baltensperger
104	B-WG02S2P34	**Seasonal variations of saccharides in PM2.5 aerosols in urban area** K. Křůmal, N. Kubátková, P. Mikuška and Z. Večeřa
105	B-WG02S2P35	**Source apportionment of the organic aerosol fraction by comparing positive matrix factorization, EC-tracer-method and 14C-analysis** Wagener, Sandra, Langner, Marcel, Perron, Nolwenn, Hansen, Ute, Moriske, Heinz-J, and Endlicher, Wilfried
106	B-WG02S2P36	**Chemical and optical characterization of aged fossil fuel aerosol** L. Marmureanu, J. Vasilescu, A. Nemuc, D. Nicolae and L. Belegante
107	B-WG02S2P37	**Influence of Meteorological Variables on Particle Number Concentration in Madrid** E. Alonso-Blanco, A. Hidalgo, F.J. Gómez-Moreno, and B. Artiñano
108	B-WG02S2P38	**Characterization of Particulate-phase High Molecular Weight Mono-carbonyls and Dicarbonyls in Urban Atmosphere of Xi'an, China** Kin-Fai Ho, Wen-Ting Dai, Steven Sai Hang Ho, Jun-Ji Cao
109	B-WG02S2P39	**Spatial patterns of high-resolution AOD and PM over Israel**

		Sorek-Hamer M., Broday D.M, and Levy R.C
110	B-WG02S2P40	**Real time characterization of ambient aerosol at Prague suburban site during wintertime** P. Vodička, O. Makeš, J. Ondráček and J. Schwarz
111	B-WG02S2P41	**Levels and chemical composition in airborne particulate matter (PM10) of eastern Andalusia (SE Spain)** A.M. Sánchez de la Campa, R. Fernández-Camacho, Y. González-Castanedo and J.D. de la Rosa
112	B-WG02S2P42	**PM level in Seoul metropolitan subway cabin indoor during the rush hour** S.-B. Kwon, J.B. Kim, J.H. Song, Y. Cho, D.S. Park, W. Jeong and C.H. Shin
113	B-WG02S2P43	**School Children's Personal Exposure to Ultrafine Particles in Urban Environments** M. Mazaheri, M. Mokhtar, R. Jayaratne and L. Morawska
114	B-WG02S2P44	**Distribution characteristics and trends of PM2.5 and PM1 -bound polycyclic aromatic hydrocarbons (PAHs) over an urban Mediterranean area** St. Pateraki, D.N. Asimakopoulos, Th. Maggos, and Ch.Vasilakos
115	B-WG02S2P45	**Particle number size distribution characteristics in the urban background in Helsinki** B. Mølgaard, H. Hannuniemi, G. Ripamonti, T. Wegner, S. Weber, L. Järvi, T. Vesala, K. Hämeri, T. Hussein
116	B-WG02S2P46	**Ionic composition of PM_{10} and $PM_{2.5}$ in urban-traffic and urban background sites within the Thessaloniki Major Area (TMA), northern Greece** E. Gounari, D. Lazarou, E. Manoli, D. Voutsa, C. Samara
117	B-WG02S2P47	**Particle size distribution of *n*-Alkanes and PAHs in urban and industrial areas of Algiers, Algeria** R. Ladji, S. Khedidji, A. Lemou, L. Rabhi and N. Yassaa
118	B-WG02S2P48	**The air pollutants emitted from biomass burning in North Korea to the air quality in Seoul, South Korea** In Sun Kim, Yong Pyo Kim, Ji Yi Lee, Lan Jin
119	B-WG02S2P49	**Analysis of PM10 concentrations in the urban area of Volos, Greece** G.T. Proias, S. Katartzis, P.T. Nastos, A.G. Paliatsos
120	B-WG02S2P50	**Preliminary results of first intensive observation program campaign of "Supersite" Project in Emilia-Romagna region (Italy)** S. Ferrari, I. Ricciardelli, C. Maccone, A. Trentini, F. Scotto, C. Sartini, D. Bacco, S. Gilardoni, M.C. Facchini and V. Poluzzi

121	B-WG02S2P51	**Bias caused by adsorbed water in standard gravimetric PM10 measurements** K. Imre, A. Gelencsér, A. Molnár and V. Dézsi
122	B-WG02S2P52	**Chemical characterization of fine particulate matter collected in Budapest** T. Szigeti, V.G. Mihucz, M. Óvári and Gy. Záray
123	B-WG02S2P53	**Spatial distribution of particle number concentrations measured with the AERO-TRAM** B. Vogel, R. Hagemann, R. Rinke, A. Wieser, U. Corsmeier, Ch. Kottmeier
124	B-WG02S2P54	**Short-term variation in near-highway air pollutant gradients** P. Berghmans, E. Frijns, M. Van Poppel
125	B-WG02S2P55	**Effect of the shutdown of a coal-fired power plant on urban mercury species** Yungang Wang, Philip K. Hopke, Jiaoyan Huang and Thomas M. Holsen
126	B-WG02S2P56	**^{7}Be and ^{210}Pb in both bulk deposition and atmospheric aerosols from Southwest Spain** R.L. Lozano, E.G. San Miguel and J.P. Bolívar
127	B-WG02S2P57	**The effect of winter salting on PM10 concentrations in the Rhine-Ruhr area** D. Gladtke, A. Olschewski, Th. Retny and P. Risthaus
128	B-WG02S2P58	**Composition and Source Identification of Ambient Single Particles on Haulbowline Island, Cork Harbour** J. Arndt, R.M. Healy, D. Healy, L. Hacker, J.R. Sodeau and J.C. Wenger
129	B-WG02S2P59	**Characterization of aerosols released from agricultural operations in the Po Valley** Antonella Malaguti, Chiara Telloli, Massimo Berico, Carmela Vaccaro, Mihaela Mircea
130	B-WG02S2P60	**Atmospheric fluxes of radionuclides at Málaga (Spain)** C. Dueñas, M.C. Fernández, S. Cañete, E. Gordo and M. Pérez
131	B-WG02S2P61	**The importance of forest fires and dust on aerosol over Portugal's background** J.V. Monjardino, A.C. Carvalho, L. Mendes and F. Ferreira
132	B-WG02S2P62	**Primary and secondary marine aerosol at Station Concordia (East Antarctica). Seasonal pattern and implications for atmospheric transport from a multi-year continuous data-set** R. Udisti, S. Becagli, M. Busetto, M. Chiari, U. Dayan, D.

		Frosini, C. Lanconelli, F. Lucarelli, S. Nava, C. Scarchilli, M. Severi, R. Traversi, V. Vitale
133	B-WG02S2P63	**Aerosol and gas concentrations at the Finnish Antarctic station Aboa in Queen Maud Land and comparisons with the Norwegian station Troll** A.Virkkula, S.Begagli, X.Chi, W.Maenhaut, M.Fiebig, H.Hellén, H.Hakola, E.Asmi, S. Häkkinen, J.Backman, T.Vihma, T.Valkonen, S.Kirkwood and M.Kulmala
134	B-WG02S2P64	***In situ* aerosol measurements at Dome C, Antarctica, in 2007 - 2011** A.Virkkula, E. Järvinen, T.Nieminen, R.Väänänen, H. Manninen, P.P. Aalto, E. Asmi, J.Backman, M. Busetto, C. Lanconelli, R. Schioppo, A. Lupi, V. Vitale, R. Hillamo and M.Kulmala
149	B-WG07S1P01	**Advanced gas-phase synthesis of LTO nanocomposites for Li-ion battery applications** T. Karhunen, A. Lähde, J. Leskinen, T. Torvela, E. Pohjalainen, M. Karppinen, O. Waser, R. Büchel, U. Tapper, J. Jokiniemi
150	B-WG07S1P02	**Flame-spray pyrolysis of copper-based p-type semiconducting oxide nanoparticles and their application in printable electronics** D. Kilian, B. Meyer, M.P.M. Jank, M. Voigt, S. Polster, L. Frey and W. Peukert
151	B-WG07S1P03	**Aerosol-derived antimony doped-tin oxide nanoparticles and studies on the influence of organic and inorganic shells in nanoparticle assemblies on the overall conductance** S.B. Bubenhofer, C.M. Schumacher, G.A. Sotiriou, R.N. Grass and W.J. Stark
152	B-WG07S1P04	**Size controlled flame synthesis of CuO nanoparticles for Li-ion batteries** O. Waser, A. Güntner, M. Heß, P. Novák and S.E. Pratsinis
153	B-WG07S1P05	**IrRuO particles for hydrogen generation** J. Forsman, U. Tapper, A. Auvinen, A. Pasanen, M. Johansson, T. Karhunen, J. Jokiniemi, P. Kauranen
154	B-WG07S1P06	**Multimineral supplementation with nano-CaO as carrier matrix** J.T.N. Knijnenburg, F.M. Hilty, M.B. Zimmermann and S.E. Pratsinis
155	B-WG07S1P07	**Flexible superparamagnetic-plasmonic nanocomposite films with flame-made fillers** Georgios A. Sotiriou, Christoph Blattmann and Sotiris E. Pratsinis
156	B-WG07S1P08	**Electrospray deposition of graphene nanosheets**

		L. B. Modesto-Lopez, O. V. Bilousov, J. J. Carvajal, F. Díaz and J. Rosell-Llompart
157	B-WG07S1P09	**A MEMS sensor based personal sampler for ultrafine particles** S. Merzsch, H.S. Wasisto, E. Peiner, I. Kirsch and E. Uhde
158	B-WG07S1P10	**Detecting the Morphology of SiO2 Aerosols using the Universal NanoParticle Analyzer (UNPA)** R. Wernet, A. Gutsche, B. Sachweh, G. Kasper, M. Seipenbusch
159	B-WG07S1P11	**Mass-Mobility Characterization of Flame-made ZrO2 Aerosols: the Primary Particle Diameter** M.L. Eggersdorfer, A.J. Gröhn, C.M. Sorensen, P.H. McMurry and S.E. Pratsinis
160	B-WG07S1P12	**Determination of soot size distributions from spectra extinction measurements: a feasibility study** C. Caumont-Prim, J. Yon, A. Coppalle and K.F. Ren
161	B-WG07S1P13	**Conductivity for Soot Sensing: Possibilities and Limitations** B. Grob, J. Schmid, N. P. Ivleva and R. Niessner
162	B-WG07S1P14	**Concentrations of particles emitted during spraying of product with silver nanoparticles** Jankowska E. and Łukaszewska J.
163	B-WG07S1P15	**Continuous tandem DMA determination of the mass and charge distribution ofelectrosprayed nanometer polystyrene particles** M. Attoui, J. Fernandez-García, J. Cuevas, G. Vidal and J. Fernandez de la Mora
164	B-WG07S1P16	**A carbon nanotubes suspension study by vortex shaker : Sampling and mass analysis** A. Ustache, D. Bernard, O. Le Bihan, E. Peyret, O. Aguerre-Chariol
165	B-WG07S1P17	**Influences on nanoparticle size distributions generated by the spark principle** J. Spielvogel, R. Joachim, M. Schmidt
166	B-WG07S1P18	**Nanoparticle emission measurement during polymer extrusion experiments** Yu-Ying Kuo, Jelena Buha, Haijun Zhang, Andreas Gerecke, Giuseppino Fortunato and Jing Wang
167	B-WG07S1P19	**Dissociation rates of Fe2+, Fe2-, and Fe2** M. Noppel
168	B-WG07S1P20	**Surface concentration of particles emitted during burning of foams with nano-objects** Jankowska E., Sobiech P., Łukaszewska J. and Zatorski W.

169	B-WG07S1P21	**Real-time measurement of airborne nanoparticles released to a windtunnel and filtration test** I.M. Kammenou, J. Wang
170	B-WG07S1P22	**Structure deformation of Ag nanoparticle clusters induced by deposition onto carbon nanotubes** T. Shinohara, N. Nishida, H. Tanaka
171	B-WG07S1P23	**Reactant depletion in chemical reactions inside nanoscale particles** V.V. Levdansky, J. Smolik, V. Zdimal and P. Moravec
172	B-WG07S1P24	**Monitoring a CVD process for the synthesis of nanostructured particles by means of low-pressure impaction** F.Weis, M. Seipenbusch and G. Kasper
173	B-WG07S1P25	**Electro-hydrodynamic atomization of solutions with strongly electrolytic behaviour – governing parameters and applications** A. Maißer, M.B. Attoui, A.M. Ganan-Calvo and W.W. Szymanski
174	B-WG07S1P26	**The effect of charge on ultrafine particle deposition: an experimental pilot study** L.L. Guo, L.Morawska, G.Johnson, R. Jayaratne and W.Hofmann
175	B-WG07S1P27	**A new method for characterizing bounce and charge transfer properties of nanoparticles** H. Kuuluvainen, A. Arffman, E. Saukko, A. Virtanen and J. Keskinen
176	B-WG07S1P28	**Influence of flow conditions and process parameters on the production rate and characteristics of nanoparticles produced by spark discharging** M. Wagner, M. Wild, F. Weis and M. Seipenbusch
177	B-WG07S1P29	**Variability of nanoparticles number concentration during summer in a humid region** V. Juncal-Bello, S. Iglesias-Samitier, M. Piñeiro-Iglesias, P. López-Mahía, S. Muniategui and D. Prada
178	B-WG07S1P30	**Characterization of different CNT using a thermo-optical elemental carbon / organic carbon analyzer in view of workplace aerosol measurements** A.C. John, M. Renker and T.A.J. Kuhlbusch
179	B-WG07S1P31	**(Quasi) Real-time detection of catalytically active nanoparticles in presence of a background aerosol** N. Neubauer, M. Seipenbusch and G. Kasper
180	B-WG07S1P32	**Release of carbon nanotubes from an epoxy-based nanocomposite during an abrasion process**

		L. Schlagenhauf, B.T.T. Chu, J. Buha, F. Nüesch and J. Wang
181	B-WG07S1P33	**Enabled Aerosol-based Methods for Assessing the Toxicity of Engineered Nanoparticles** A. Kourmouli, P. Kavarnoy, K. Barmpounis, O.I. Kalantzi, G. Biskos
182	B-WG07S1P34	**Nanoparticle Balancing from Release to Dose** H. Fissan, B. Stahlmecke, C. Asbach, T.A.J. Kuhlbusch
183	B-WG07S1P35	**Cytotoxicity of nanosilver with different sizes: Effect of Ag+ ion release** A.Pratsinis, P. Hervella, S. E. Pratsinis, J-C. Leroux and G. A. Sotiriou
184	B-WG07S1P36	**Investigations on nanoparticle release from artificially weathered coatings and composites that experience different treatment processes** D. Göhler, A. Nogowski, P. Fiala and M. Stintz
185	B-WG07S1P37	**Assessment of exposure to airborne nanomaterials using a pragmatic, tiered approach** C. Asbach, D. Dahmann, M. Voetz, B. Stahlmecke, H. Kaminski, Thomas A.J. Kuhlbusch, U. Götz, S. Engel, S. Plitzko
186	B-WG07S1P38	**Aerosol particle emissions from sanding coated plates: effect of the sanding paper and filtering method to the human exposure** I.K. koponen, M. Levin and K.A. Jensen
187	B-WG07S1P39	**Expossure and Risk Assessment during Production of Nanoparticles by Plasma Synthesis** Jelena Buha, Drew Thompson, Marc Leparoux, Christian Jäggi, David Y.H. Pui and Jing Wang
188	B-WG07S1P40	**Analysis of aerosol solid nanoparticles produced during soldering using metal alloys** Virginia Gómez, Silvia Irusta, Francisco Balas and Jesús Santamaría
189	B-WG07S1P41	**Particle characterisation from reducing Cl-process producing Cu and Cu-CNT like nanoparticles - safety issues to consider for scale-up** J. Lyyränen, J. Hokkinen, U. Backman, A. Auvinen, J. Jokiniemi
190	B-WG07S1P42	**Particle characterisation during melting of nanoparticle containing coated and uncoated window glass** J. Lyyränen, J. Hokkinen, U. Backman, A. Auvinen, J. Jokiniemi and A. Kurz
191	B-WG07S1P43	**Atmospheric new particle formation in the Central European boundary layer: A long-term study using**

		Neutral Cluster Air Ion Spectrometer (NAIS) data J. Größ, W. Birmili, A. Hamed, A. Sonntag, A. Wiedensohler, G. Spindler, . E. Maninnen, M. ulmala, U. Hõrrak, C. Plass-Dülmer
192	B-WG07S1P44	**Nanostructured catalytic layers for fuel cell electrodes prepared by electrospray** S. Martin, B. Martinez-Vazquez, P.L. Garcia-Ybarra and J.L. Castillo
193	B-WG07S1P45	**Control of phase composition of LiFePO4 prepared with spray pyrolysis** A. Lähde, T. Karhunen, T. Torvela and J. Jokiniemi
194	B-WG07S1P46	**Two-component aerosol nanoparticle coating for paperboard on roll-to-roll process** J. Haapanen, M. Aromaa, H. Teisala, M. Tuominen, M. Stepien, J.J. Saarinen, Toivakka, J. Kuusipalo and J.M. Mäkelä
195	B-WG07S1P47	**Plasmonic properties of size-selected spherical silver nanoparticles** J. Harra, J. Mäkitalo, R. Siikanen, M. Virkki, G. Genty, T. Kobayashi, M. Kauranen and J.M. Mäkelä
196	B-WG07S1P48	**Synthesis of germanium nanoparticles in an aerosol reactor** C. Mehringer, R. Körmer, B. Butz, E. Spiecker and W. Peukert
197	B-WG07S1P49	**Gas-Phase Synthesis of Metal-Decorated Titanium Dioxide Nanoparticles** N. Alam and A.M. Boies
198	B-WG07S1P50	**Spark Generated Intermetallic Mg-Ti Nanoparticles for Hydrogen Storage** R. J. Canales-Perez, T. V.Pfeiffer, A. Anastasopol, J. Middelkoop, S.W.H. Eijt, and A. Schmidt-Ott
199	B-WG07S1P51	**Generation of sub 10 nm self charged particles with a spark generator in positive andnegative mode** Michel ATTOUI
200	B-WG07S1P53	**Morphology dependency of electrospray-generated polymer particles and coatings on ambient humidity** E. Bodnár, P. Kiselev, J. Grifoll and J. Rosell-Llompart
201	B-WG07S1P54	**Formation of rutile nanoparticles from the condensed disperse phase at a surface of high-temperature particles of the titanium** N.Kh. Kopyt, K.I. Semenov, N..N. Kopyt and A.K. Semenov
202	B-WG07S1P55	**Obtaining of nanoparticles near moving heated metal particle** K.I. Semenov, N.Kh. Kopyt, A.K. Semenov and N..N. Kopyt

203	B-WG07S1P56	**Investigation of the particle formation mechanism in flame spray pyrolysis of silica nanoparticles based on optical techniques** D. Kilian, M.Voigt, S. Engel, Y.Gao, A. F. Kögler, T.Seeger, A. Leipertz and W. Peukert
204	B-WG07S1P57	**Formation of advanced SiC and carbon structures with controlled annealing ofpreceramic silicon-carbon nanoparticles** A. Lähde, M. Miettinen, J. Hokkinen ,T. Karhunen, T. Torvela, U. Tapper and J. Jokiniemi
205	B-WG07S1P58	**In situ observation of sintering behavior of Pt particles supported on silica nanoparticles** Kun Gao, Philipp Müller, Matthias Faust, Reinhard Schneider and Martin Seipenbusch
206	B-WG07S1P59	**Synthesis of copper nanoparticles formed on carbon nanotubes by photochemical process** N. Nishida, A. Miyashita, and H. Tanaka
207	B-WG07S1P60	**Aerosol synthesis of building blocks for layered catalyst structures for Fischer–Tropsch reaction** Lintao Zeng and Alfred P. Weber
208	B-WG07S1P61	**The Spark Generator as a Simple Source of sub-Nanometer Atomic Clusters** M.D. Barankin, K.Barmpounis, G. Biskos, T. Bosboom, A. Maisser, T.V. Pfeiffer, A. Schmidt-Ott
225	B-SS01S1P01	**The analysis of size-segregated cloud condensation nuclei counter (CCNC) data from SMEAR II and its implications for aerosol-cloud relations** M. Paramonov, T. Petäjä, P.P. Aalto, M. Dal Maso, N. Prisle, V.-M. Kerminen and M. Kulmala
226	B-SS01S1P02	**Results of elemental and organic carbon (EC-OC) regular measurements within EUSAAR and ACTRIS projects 2009-2011 at the Košetice Observatory** M.Vana, J. Čech, A.Holubová Šmejkalová, E. Chalupníčková and J.Schwarz
227	B-SS01S1P03	**Particle formation and growth in the boundary layer over boreal forest** L. Zhou, M. Boy, H. Vuollekoski, C. Watcharapaskorn, D. Mogensen, S. Smolander, A. Sogachev and Markku Kulmala
228	B-SS01S1P04	**Aerosol particle number concentration studies based on Fourier and wavelet analysis** S. Byčenkienė, S. Kecorius, K. Plauškaitė, J. Andriejauskienė and V. Ulevicius
229	B-SS01S1P05	**A Mediterranean Atmospheric Network for in-situ**

		aerosol measurements: Motivation and Objectives J. Sciare, A. di Sarra, R. Ellul, E. Gerasopoulos, H.C. Hansson, S. Kleanthous, N. Mihalopoulos, J. Pey, A. Alastuey and N. Yassaa
230	B-SS01S1P06	**OVOC – precursors for SOA: measurements within ACTRIS-WP4** J. Englert, C. Plass-Dülmer, E. Tensing, K. Michl and A. Werner
231	B-SS01S1P07	**The "Dual-Spot" Aethalometer: Improved measurement of Aerosol Black Carbon with real-time loading compensation** L. Drinovec, G. Močnik, P. Zotter, A.S.H. Prévôt, C. Ruckstuhl, A.D.A. Hansen
232	B-SS01S1P08	**New particle formation in the western Mediterranean regional background** M. Cusack, A. Alastuey, X. Querol, N. Pérez, A. Wiedensohler
233	B-SS01S1P09	**A Finnish remote-sensing network for monitoring aerosol, clouds, and the boundary layer** A. Hirsikko, E.J. O´Connor, M. Komppula, M. Bauer-Pfundstein, A. Poikonen, M. Kurri, E. Giannakaki, T. Karppinen, H. Lihavainen, A. Laaksonen, Kari E.J. Lehtinen and Y. Viisanen
234	B-SS01S1P10	**Long-term observation of time-resolved submicron aerosol chemical composition in the region of Paris (France)** J-E. Petit, R. Sarda-Estève, J. Sciare, O. Favez
235	B-SS01S1P11	**Characterize aerosol properties observed over Lemesos, Cyprus using passive and active remote sensing instruments** A. Nisantzi, RE Mamouri, P. Kokkalis and D. G. Hatzimitsis
236	B-SS01S1P12	**The AERONET-Europe calibration facility: access within the ACTRIS project** P. Goloub, V.E. Cachorro, E. Cuevas, L. Blarel, A. Berjón, C. Toledano, T. Podvin, A. Lapionak, C. Guirado, R. Ramos, R. González, D. Fuertes
237	B-SS01S1P13	**Data interoperability solutions for the Finnish SMEAR station network** M. Dal Maso, P. Kolari, H. Junninen, P.P. Aalto, P. Keronen, P. Järveläinen, S. Sorvari and M. Kulmala
238	B-SS02S1P01	**Using sulfur isotope analyses to understand in-cloud sulfate formation during HCCT 2010** E. Harris, B. Sinha, P. Hoppe, J. Schneider, D. van Pinxteren, W. Fomba, T. Gnauk, B. Fahlbusch, S. Mertes, T. Lee, S. Foley, S. Borrmann and H. Herrmann

239	B-SS02S1P02	**Inorganic cloud chemistry and its relation to the valley sites particle chemistry during HCCT** K. Müller, G. Spindler, D. T. Lee, J. Collett Jr., van Pinxteren, H. Herrmann
240	B-SS02S1P03	**Evaluation of PM10 and trace gas measurements with the MARGA during the HCCT 2010 campaign** B. Fahlbusch, G. Spindler, L. Poulain, A. Grüner, M. Wallasch and H. Herrmann
241	B-SS02S1P04	**HOx measurements at the upwind site during HCCT** D. Amedro, C. Schoemaecker, C. Fittschen and Jean-François Pauwels
242	B-SS02S1P05	**Characterisation of biological and biomass burning monosaccharides during Hill Cap Cloud Thuringia 2010 (HCCT 2010) campaign** Y. Iinuma and H. Herrmann
243	B-SS02S1P06	**Trace metal characterization during HCCT2010** K. Wadinga Fomba, K. Müller, T. Lee, J. Collett Jr., H. Herrmann
244	B-SS02S1P07	**Cloud influence on local aerosol chemical composition during the Hill Cap Cloud Thuringia 2010** L. Poulain, Z.J. Wu, A. Tilgner, D. van Pinxteren, B. D' Anna, C. George, J. Schneider, A. Wiedensohler and H. Herrmann
245	B-SS02S1P08	**Particle hygroscopicity during atmospheric new particle formation events: Implications for the chemical species contributing to particle growth** Z.J. Wu, W. Birmili, L. Poulain, M. Merkel, B. Fahlbusch, D. van Pinxteren, H. Herrmann, A. Wiedensohler
246	B-SS02S1P09	**The effect of cloud processing on the chemical composition and mixing state of accumulation mode aerosol: A combined SEM-NanoSIMS study during HCCT 2010** B. Sinha, E. Harris, P. Hoppe, S. Mertes, T. Gnauk, J. Schneider, D. van Pinxteren and H. Herrmann
247	B-SS02S1P10	**Physico-chemical analysis of cloud drop residues and interstitial particles sampled inside clouds within the Hill Cap Cloud Thuringia (HCCT) Experiment 2010** S. Mertes, J. Schneider, R. Otto, K. Diekmann, W. Birmili, D. van Pinxteren, A. Roth, Frank Stratmann, and H. Herrmann
248	B-SS02S1P11	**Meteorological characterisation of the HCCT-2010 hill cap cloud experiments: Synoptic and local meteorological conditions, tracer experiments and**

		flow connectivity A. Tilgner, L. Schöne, P. Bräuer, D. van Pinxteren, H. Deneke, W. Birmili, R. Otto, M. Merkel, K. Weinhold, A. Wiedensohler, G. Spindler, and H. Herrmann
249	B-SS02S1P12	**Cloud chemistry during HCCT-2010: Mono- and dicarboxylic acids** Dominik van Pinxteren, Monique Teich, Stephan Mertes, Taehyoung Lee, Jeff Collett, Hartmut Herrmann
250	B-SS02S1P13	**Cloud chemistry during HCCT-2010: Water soluble organic carbon** Dominik van Pinxteren, Stephan Mertes, Johannes Schneider, Stephan Borrmann, Taehyoung Lee, Jeff Collett, Hartmut Herrmann
251	B-SS03S1P01	**Concentrations of organic and trace element PM species and derivation of freeway-based emission rates in Los Angeles** J. Liacos, W. Kam, R.J. Delfino, J.J. Schauer and C. Sioutas
252	B-SS03S1P02	**The impact of harbour activities on the air quality of the city of Genoa: source apportionment and simulation by dispersion models** P. Brotto, M.C. Bove, F. Cassola, E. Cuccia, D. Massabò, A. Mazzino, A. Piazzalunga and P. Prati
253	B-SS03S1P03	**Assessment of vehicular profiles vis-à-vis real-world traffic emissions** Pallavi Pant and Roy M. Harrison
254	B-SS03S1P04	**PMF vs CMB for source apportionment of PM: advantages, limitations, complementarity of the two models explored by applications at different types of environments** C. Piot, M.F.D. Gianini, J. Cozic, L. Polo, J.-L. Besombes, J.-L. Jaffrezo and C. Hueglin
255	B-SS03S1P05	**Concentrations and source contributions of particulate organic matter before and after implementation of a low emission zone** R.M. Qadir, G. Abbaszade, J. Schnelle-Kreis and R. Zimmermann
256	B-SS03S1P06	**Source apportionment of fine aerosol in Athens by positive matrix factorization and Unmix analysis** A. Karanasiou, M. Scoullos, K. Eleftheriadis
257	B-SS03S1P07	**Wintertime aerosol source apportionment in the metropolitan area of Paris by Chemical Mass Balance** E. Abidi, A. Monod, J. Cozic, J.L. Jaffrezo, M. Crippa, J. Slowik, U. Baltensperger, A.S.H. Prévôt and N. Marchand

258	B-SS03S1P08	**Source Apportionment of Particles in London Paddington Station** U. Chong, J.J. Swanson and A.M. Boies
259	B-SS03S1P09	**Chemical mass balance modelling for the source estimation of high PM2.5 concentrations in Milan, Northern Italy** Perrone M.G., Larsen B.R., Ferrero L., Sangiorgi G., De Gennaro G., Udisti R., Zangrando R., Gambaro A. and Bolzacchini E.
260	B-SS03S1P10	**Impacts of industrial and harbor activities on fine particles over Marseille** D. Salameh, A. Detournay, H. Wortham, J.L. Jaffrezo, J. Cozic, A. Armengaud, D. Piga, J. Dron, P. Chamaret, M. Parra, M. Deveze and N. Marchand
261	B-SS03S1P11	**Absorption Ångström exponent, and its correlation with other aerosol variables such as number size distribution, gas phase- and trace elements of the atmosphere. A field study** T. Ajtai, Á. Filep, N. Utry, M. Pintér, Z. Bozóki, G. Szabó
262	B-SS03S1P12	**Source apportionment of indoor and outdoor PM2.5 in an apartment situated in central Athens, Greece** D.E. Saraga, M. Seleventi, C.G. Helmis, Ch. Vasilakos and Th. Maggos
263	B-SS03S1P13	**Source apportionment of PM during 2008-2010 at Station Nord, North East Greenland** J.K. Nøjgaard, H. Skov, L.L. Sørensen, B.J. Jensen, A.G. Grube, A. Massling, M. Glasius and Q.T. Nguyen
264	B-SS03S1P14	**Structural properties of mineral dust from vehicle resuspension** E. Coz, C. Barrios, C. Martín, A. Domínguez and B. Artíñano
265	B-SS04S1P01	**Thermo-chemical properties of fleet ship emitted aerosols: relation to composition and structure** H. Bladt, J. Schmid, E. Kireeva, O. B. Popovicheva, J. Moldanová, N. P. Ivleva and R. Niessner
266	B-SS04S1P02	**Detailed chemical characterization of ultrafine particles from vehicle exhaust** F. Donaz, L. Polo, C. Piot, J. Cozic, B. Golly, N. Marchand, J.L. Besombes and J.L. Jaffrezo
267	B-SS05S1P01	**The field experiments on the HTO washout from the atmosphere** A.V. Golubev, S.V. Mavrin, V.N. Golubeva, A.V. Stengach, Yu.S. Balashov, V.P. Kovalenko, I.I. Solomatin
268	B-SS05S1P02	**Long-range transport of radionuclides released**

		from Fukushima accident into the Iberian Peninsula M.A. Hernández-Ceballos, R.L.Lozano, E.G. San Miguel and J.P. Bolívar
269	B-SS05S1P03	**Atmospheric radioactivity in the High Arctic following the Fukushima nuclear accident** J. Paatero, J. Vira, J. Hatakka, K. Holmén, A.-P. Hyvärinen and Y. Viisanen
270	B-SS05S1P04	**Airborne fission products from the Fukushima accident in the air over Milano, Italy** A. Ioannidou, E. Giannakaki, S.Manenti, L.Gini and F. Groppi
271	B-SS05S1P05	**Modification of cloud properties by the Eyjafjallajökull eruption** H Vogel, M. Bangert, B. Vogel, A. Wintzen, D. Barahona, A. Nenes, and J. Förstner
272	B-LP01S1P01	**Comparison of three particle number concentration standards for CPC calibration in the particle size range from 10 nm up to 10 µm** Jaakko Yli-Ojanperä, Hiromu Sakurai, Kenjiro Iida, Jyrki M. Mäkelä, Kensei Ehara and Jorma Keskinen
273	B-LP01S1P02	**Large-scale modelling of polycyclic aromatic hydrocarbons and polychlorinated dibenzodioxins in open fire aerosols: On the contribution of biomass burning to POPs in air in Africa** G. Lammel, A. Heil and I. Stemmler
274	B-LP01S1P03	**Gas-particle partitioning and air-sea exchange of polycyclic aromatic hydrocarbons and polychlorinated biphenyls in the central and eastern Mediterranean** Marie D. Mulder, Jana Klánová, Petr Kukučka, Jan Kuta, Gerhard Lammel, Roman Prokeš
275	B-LP01S1P04	**Biothreat and distant detection of bioaerosol** P.Grzybowski and T.Ciach
276	B-LP01S1P05	**Mechanistic insights into the formation of 2-methyltetrols from the photooxidation of isoprene under low-NO x conditions** W. Wang, Y. Iinuma, A. Kahnt, O. Ryabtsova, A. Mutzel, R. Vermeylen, P. Van der Veken, W. Maenhaut, H. Herrmann and M. Claeys
277	B-LP01S1P06	**A non-invasive method to sample exhaled endogenous particles from the respiratory tract** Susanna Lohman, Ann-Charlotte Almstrand, Anna Bredberg, Per Larsson, Ekaterina Mirogrodskaya, Evert Ljungström and Anna-Carin Olin

278	B-LP01S1P07	**Field-Performance of a new time-resolved sampler for the collection of dry aerosol particles** A. Eiguren-Fernandez, G.S. Lewis, S.R. Spielman and S.V. Hering
279	B-LP01S1P08	**High Resolution Ion Mobility Spectrometer (HRIMS): a new instrument for aerosol nucleation studies** E. Montoya, S. López-Vidal, P. Dohányosová, E. Ramiro
280	B-LP01S1P09	**Pre-industrial atmospheric elemental carbon concentrations** Tanveer Ahmed, Akhtar Shareef, Abdul Bari, Liaquat Husain
281	B-LP01S1P10	**Nanoparticle synthesis from manganese(II) acetylacetonate** P. Moravec, J. Smolík, S. Bakardjieva and V.V. Levdansky
282	B-LP01S1P11	**Formation of secondary organic aerosol: OH initiated oxidation of dodecane in the presence of NOx** A. Gratien, M. Camredon, Y. Mohamed Yassin, B. Aumont, and J.F. Doussin
283	B-LP01S1P12	**Some considerations about Langley method on the retrieval of spectral irradiance at the TOA and of the total atmospheric optical depth** M. Melgão, M.J. Costa and A.M. Silva
284	B-LP01S1P13	**Reduction of combustion alkali aerosols by addition of kaolin to pelletized biomass fuels** C. Boman, J. Fagerström, G. Gårdbro, E. Steinvall and D. Boström
285	B-LP01S1P14	**Morphology-Controllable of Porous Hyaluronic Acid Prepared using A Spray-drying Method** Asep Bayu Dani Nandiyanto, Takashi Ogi, and Kikuo Okuyama
286	B-LP01S1P15	**Prague Aerosol Supersite, Suchdol (PASS, urban background)** V. Ždímal, J. Ondráček, N. Zíková, P. Vodička, O. Makeš, D. Řimnáčová, L. Štefancová, J. Šilhavý, J. Smolík and J. Schwarz
287	B-LP01S1P16	**Synthesis and Characterization of Pt/WO 3 Nanoparticles Photocatalyst Prepared by Flame Spray Pyrolysis** Takashi Ogi, Asep Bayu Dani Nandiyanto, Agus Purwanto, Kikuo Okuyama
288	B-LP01S1P17	**TiO 2 Thin Film Morphologies Controlled by Aerosol Flame Deposition Process**

		Jinrui Ding and Kyo-Seon Kim
289	B-LP01S1P18	**Chemical Composition and Hygroscopic Properties of Ultrafine Aerosol Particles in the Atmosphere over an Urban Background Site in Patras, Greece** S. Bezantakos, E. Konstenidou, A. Bougiatioti, K. Eleftheriadis, N. Mihalopoulos, A. Nenes, S. Pandis, G. Biskos
290	B-LP01S1P19	**Size resolved penetration of commercial filter materials** J. Ondráček, N. Zíková and V. Ždímal
291	B-LP01S1P20	**Comparison of Chemical Characteristics of Diesel Particulates from a Euro 0, Japanese and US Engines** T.H. Gan, P. Hield, P.J. Hanhela, M. Leist, W. Mazurek and R. Gillett
292	B-LP01S1P21	**Droplet formation via a 1.7 MHz ultrasonic droplet generator** K. Zhong, G. Peabody, A. Marshall, H. Glicksman, and S. Ehrman
293	B-LP01S1P22	**Spatial distribution of the air quality in Portugal (rural, urban, and archipelagos)** A.M.J. Cruz, S.M. Sarmento, A.V. Silva, T. Verburg, S. Almeida, C. Alves, M.C. Freitas, H. Th. Wolterbeek
294	B-LP01S1P23	**Liquid Filter Evaluation using the New TSI Nanoparticle Nebulizer** T.Y. Ling, A. Zerrath and D.Y.H. Pui
295	B-LP01S1P24	**An update on ChArMEx (the Chemistry-Aerosol Mediterranean Experiment) activities and plans for aerosol studies in the Mediterranean region** F. Dulac and an international ChArMEx Team
296	B-LP01S1P25	**TiO 2 thin film structures prepared by controlling the particle formation and deposition in PCVD system** Hoang Hai Nguyen and Kyo-Seon Kim
297	B-LP01S1P26	**Polarized Imaging Nephelometer for Field and Aircraft Measurements of Aerosol Phase Function** G. Dolgos, J.V. Martins
298	B-LP01S1P27	**Water diffusion in glassy aerosol investigated using a new Raman isotope tracer method** H.C. Price, B.J. Murray, J. Mattsson and L.G. Benning
299	B-LP01S1P28	**Exploring the use of satellite-derived whitecap data to improve sea-spray emission estimatesM.F.M.A.** Albert, M.D. Anguelova, G. de Leeuw, A.M.M. Manders, and M. Schaap

Wednesday 5th September

08:45-09:45 Plenary 3. **Ulrike Lohmann**
Aerosols, clouds and climate
Room: Auditorio
Chair: Sabine Wurzler

09:45-10:00 Smoluchowski Award

10:00-10:30 Coffee-break

10:30-12:50 **Session WG01S4O. Physical and chemical properties + Transport 1**
Room: Auditorio
Chairs: A. Petzold / D. Topping

10:30	WG01S4O01	**Fluorescence lifetime imaging of aerosol viscosity and phase** F.D. Pope, N.A. Hosny, C. Fitzgerald, M.Kalberer, and M.K. Kuimova
10:50	WG01S4O02	**Phase state and humidity-induced phase transition studies of SOA particles from biogenic and anthropogenic precursors** E. Saukko,A.T. Lambe, , P. Massoli, T. Koop, J.P. Wright, D.R. Croasdale, D.A. Pedernera, T.B. Onasch, A. Laaksonen,P. Davidovits, D.R. Worsnop and A. Virtanen
11:10	WG01S4O03	**Overview of ClearfLo Detling Site: Study of Aerosol Sources and Processing at a Rural Site Southeast of London** L. R. Williams, S. Herndon, J. Jayne, A. Freedman, B. Brooks, J. Franklin, P. Massoli, E. Fortner, P. Chhabra, M. Zahniser, H. Stark, T. Onasch, D. R. Worsnop, F. Lopez-Hilfiker, C. Mohr, J. Thornton, N. L. Ng, L. Xu, M. Kollman, W. B. Knighton, M. Dubey, A. Aiken, K. Gorkowski, T. Martin and R. Coulter
11:30	WG01S4O04	**Aircraft measurements of gases and particles during CAREBeijing-2008 in surrounded Beijing areas** W.J. Zhang, Z.P Bai, T. Zhu, W. Yang, B.H. Yin
11:50	WG01S4O05	**Single particle characterization using a high resolution time-of-flight aerosol mass spectrometer: Atmospheric observation in Nagoya, Japan**

		T. Mihara and M. Mochida
12:10	WG01S4O06	**Long term measurements of chemical composition of ambient ions** H. Junninen, M. Ehn, S. Schobesberger, G. Lönn, T. Petäjä, D. R Worsnop and M. Kulmala
12:30	WG01S4O07	**Using a new unified model to revisit the relationship between aerosol size and composition** D. Topping, A. Buchholz and M. McFiggans
Reserve paper	WG01S4B00	**Non-volatile aerosol in the Arctic Winter Stratosphere and its role for PSC formation** R. Weigel, M. Ebert, K. Kandler, S. Molleker, W. Frey, M. Klingebiel, C. M. Volk, G. Günther, H. Schlager, F. Cairo, S. Kaykin, S. Borrmann

10:30-12:50 **Session WG02S5O. Urban Aerosol Chemical and Physical Properties (2)**
Room: Legado Andalusí
Chairs: T. Kuhlbusch / G. Fuller

10:30	WG02S5O01	**Summer ammonia measurements in a densely populated Mediterranean city** M. Pandolfi , F. Amato, C. Reche, A. Alastuey, R. P. Otjes, M.J. Blom and X. Querol
10:50	WG02S5O02	**Seasonal variations of black carbon and number size distribution in Paris (France)** J. Sciare,T. Petäjä, J. Hakala, K. Lehtipalo, E. Herrmann, R. Sarda-Estève, J.B. Nicolas, N. Bonnaire and P.P. Aalto
11:10	WG02S5O03	**Effects of the Low Emission Zone on Black Carbon and Ultrafine Particles in Leipzig** A. Wiedensohler, W. Birmili, F. Rasch, K. Weinhold, M. Merkel, A. Sonntag, G. Löschau, A. Hausmann
11:30	WG02S5O04	**Wintertime urban background measurements of PM1, particle lung-deposited surface area, black carbon and particle number concentrations** U. Quass, H. Kaminski, T. A .J. Kuhlbusch B. Bergmans, D. Muck, F. Lenartz
11:50	WG02S5O05	**Soot externally mixed with Asian dust particles in the submicron rangein the marine atmosphere** K.I. Lieke, D. Zhang, K. Kandler, S. Weinbruch, and M. Bilde
12:10	WG02S5O06	**Sources and processes affecting coarse aerosols**

		at street canyon and urban locations in London, UK D. C Green and, G. W Fuller
12:30	WG02S5O07	**Highly time and size-resolved trace elemental composition of aerosols during CalNex-LA 2010** S. Visser, M. Furger, U. Flechsig, K. Appel, A. S. H. Prevot, U. Baltensperger
Reserve paper	WG02S5B00	**Comparative study of ultrafine aerosol within a city** I. Salma, T. Borsós, Z. Németh, P. Aalto and M. Kulmala

10:30-12:50 **Session SS02S1O. A ground-based integrated study of chemical aerosol-cloud interaction (HCCT2010)**
Room: Faraday
Chairs: Y. Inuma / D. Heard

10:30	SS02S1O01	**Hill Cap Cloud Thuringia 2010 (HCCT-2010): Overview and highlight results** D. van Pinxteren, W. Birmili, B. Fahlbusch, W. Fomba, T. Gnauk, Y. Iinuma, S. Mertes, K. Dieckmann, M. Merkel, C. Müller, K. Müller, L. Poulain, G. Spindler, M. Schäfer, F. Stratmann, A. Tilgner, L. Schöne, P. Bräuer, K. Weinhold, A. Wiedensohler, W. Zhijun, S. Borrmann, E. Harris, A. Roth, J. Schneider, B. Sinha, I. George, D. Heard, L. Whalley, B. D'Anna, C. George, M. Müller, W. Haunold, A. Engel, A. Wéber, D. Amedro, C. Fittschen, C. Schoemaecker, J. Collett, T. Lee, and H. Herrmann
10:50	SS02S1O02	**Influence of Cloud Processing on CCN Activation Behavior in the Thuringian Forest, Germany** K. Dieckmann, M. Schäfer, P. Zedler, H. Wex, S. Henning, H. Herrmann, D. van Pinxteren, W. Birmili, M. Merkel, Z. Wu, A. Wiedensohler, Th. Mentel, and S. Stratmann
11:10	SS02S1O03	**Relating particle hygroscopicity to chemical composition during HCCT-2010 field campaign** Z.J. Wu, L. Poulain, W. Birmili, M. Merkel, K. Dieckmann, M. Schäfer, D. van Pinxteren, S. Stratmann, H. Herrmann, A. Wiedensholer
11:30	SS02S1O04	**Cloud residual analysis using two types of aerosol mass spectrometers within the Hill Cap Cloud Thuringia (HCCT) Experiment 2010** J. Schneider, A. Roth, S. Mertes, D. van Pinxteren, H. Herrmann, and S. Borrmann

11:50	SS02S1O05	**Composition analysis of cloud residual and aerosol particles by single particle massspectrometry during the Hill Cap Cloud Thuringia Experiment 2010** A. Roth, S. Mertes, D. van Pinxteren, T. Klimach, J. Schneider and S. Borrmann
12:10	SS02S1O06	**The impact of clouds on radical concentrations: Observations of OH and HO2 during HCCT-2010** L.K. Whalley, I.J. George, D. Stone and D.E. Heard
12:30	SS02S1O07	**SPACCIM model studies on the multiphase chemistry occurring in orographic hill cap clouds during the HCCT-2010 field campaign** A. Tilgner, P. Bräuer, R. Wolke and H. Herrmann
Reserve paper	SS02S1B00	**Cloud influence on local aerosol chemical composition during the Hill Cap Cloud Thuringia 2010** L. Poulain , Z.J. Wu , A. Tilgner , D. van Pinxteren , B. D' Anna , C. George , J. Schneider , A. Wiedensohler and H. Herrmann

10:30-12:50 **Session WG07S3O. Gas phase synthesis of nanoparticles**
Room: Cine 3
Chairs: E. Kruis / J. Jokiniemi

10:30	WG07S3O01	**Aerosol synthesis of ZnO tetrapods for flexible and transparent UV sensors** Albert G. Nasibulin, Simas Rackauskas, Kimmo Mustonen, Terhi Järvinen, Marco Mattila, Olga Klimova, Hua Jiang, Oleg Tolochko, Harri Lipsanen, Esko I. Kauppinen
10:50	WG07S3O02	**Synthesis of germanium-silicon hybrid particles in an aerosol reactor** C. Mehringer, R. Körmer, B. Butz, E. Spiecker and W. Peukert
11:10	WG07S3O03	**Thermostability of flame synthesized core-shell TiO2/SiO2 nanoparticles and its photocatalytic activity** Qi, Fei, Moiseev, Anna, Deubener, Joachim, Weber, Alfred P
11:30	WG07S3O04	**Synthesis of aluminium nanoparticles with the aid of a customized atmospheric plasma**

		E. Daskalos, H. Mandilas, G. Karagiannakis and A. G. Konstandopoulos
11:50	WG07S3O05	**Synthesis of Magnesium Hydride by Spark Discharge in Argon/Hydrogen Mixtures** T.V. Pfeiffer, A. Anastasopol, S.W.H. Eijt, and A. Schmidt-Ott
12:10	WG07S3O06	**WO3-based thin films produced by Electrostatic Spray Deposition** J. Gaury, E. M. Kelder, G. Biskos
12:30	WG07S3O07	**Core-shell nanomagnets** Forsman, Johann, A. Ari, Tapper, Unto, Koskela, Pirjo, van Dijken Sebastiaan, J. Jorma
Reserve paper	WG07S3B00	**Nanostructured catalytic layers for fuel cell electrodes prepared by electrospray** S. Martin, B. Martinez-Vazquez, P.L. Garcia-Ybarra and J.L. Castillo

10:30-12:50 **Session WG09S1O. Aerosol Modelling: Atmospheric Applications**
Room: Gutenberg
Chairs: A. Asmi / B. Vogel

10:30	WG09S1O01	**Regional modelling of the tropospheric multiphase system using COSMO-MUSCAT: 2D-sensitivity-studies** R. Schrödner, A. Tilgner and R. Wolke
10:50	WG09S1O02	**Simulating the impact of controlled sea salt emissions on cloud optical properties in the Southeast Pacific** K. Lundgren, T. Schad, M. Bangert, B. Vogel, A. Ferrone, and H. Vogel
11:10	WG09S1O03	**Atmospheric boundary layer height estimation by different methods: Application to lidar measurements** D. Toledo, C. Córdoba-Jabonero, E. Cuevas and M. Gil
11:30	WG09S1O04	**The impact of the NAO on aerosol concentration levels in Europe** P. Jiménez-Guerrero, S. Jerez, J.P. Montávez and R.M. Trigo
11:50	WG09S1O05	**CCN formation from biogenic VOCs studied with the global climate model ECHAM5-HAM** R. Makkonen, A. Asmi, V.-M. Kerminen, M. Boy, A. Arneth, A. Guenther and M. Kulmala

12:10	WG09S1O06	**Solar radiation management with high speed civil aircrafts and sulfur-enhanced fuel** A. Laakso, H. Kokkola, A-I. Partanen, A. Laaksonen, K.E.J. Lehtinen and H. Korhonen
12:30	WG09S1O07	**Modelling of particle number size distribution over Europe with chemistry transport model LOTOS-EUROS** A. Manders, A. Visschedijk, H. D. van der Gon, B. Henzing, M. Schaap
Reserve paper	WG09S1B00	**Secondary organic aerosol formation during summer 2010 over Central Europe** B. Langmann, K. Sellegri and E. Freney

Thursday 6th September

08:45-09:45 Plenary 4. **Barbara Turpin**
Secondary organic aerosol formation through aqueous chemistry: atmospheric evidence, chemistry, partitionning and prediction
Room: Auditorio
Chair: Cristina Gutiérrez-Cañas

09:45-10:30 Coffee-break

10:30-12:50 **Session Physical and chemical properties + Transport 2**
Room: Auditorio
Chairs: A. Held / P. Zieger

10:30	WG01S5O01	**Summer Campaign on Aerosol Optics, Microphysics, Chemistry and Mineralogy in Portugal – Overview** F. Wagner, K. Kandler, N. Schiavon, L. Tobias, S. Pereira, J. Preißler, A. Candeias and J. Mirão
10:50	WG01S5O02	**Climatology of aerosol optical properties in Amazonia** P. Artaxo, L.V. Rizzo, E. Swietlicki, A. Arana, E. T. Sena, A. Wiedensohler
11:10	WG01S5O03	**Influence of water uptake on the aerosol light scattering at the regional continental site Melpitz, Germany** P. Zieger, R. Fierz-Schmidhauser, L. Poulain, W. Birmili, T. Müller, M. Nan, A. Wiedensohler, E. Weingartner, and U. Baltensperger
11:30	WG01S5O04	**Black carbon hygroscopic properties influenced by coating content and chemical compositions** D. Liu, J. Allan, B. Bandy, H. Coe, Zoe Fleming, Michael Flynn, G. McFiggans, J. Whitehead and D. Young
11:50	WG01S5O05	**Hygroscopicities, ethanol affinities and composition of nanoparticles in CLOUD** H. Keskinen, G. Tsagkogeorgas, J. Duplissy, F. Bianchi, J. Joutsensaari, P. Miettinen, J. Slowik, M. K. Kajos, S.

		Schobesberger, S. Schallhart, T.Ruuskanen, H. Wex, F. Stratmann, D. Worsnop, M. Kulmala, A. Virtanen , and A. Laaksonen
12:10	WG01S5O06	**Hygroscopicity and cloud forming properties of Arctic aerosol during one year** S. Silvergren, U. Wideqvist , J. Ström, and B. Svenningsson
12:30	WG01S5O07	**Particles measured in a low speed ship engine: Cloud condensation nuclei and mixing state on the nano scale** K. I. Lieke, T. Rosenørn, A. C. Butcher, S. M. King, T. G. Frederiksen, K. Fuglsang, J. B. Pedersen, D. Larsson and M. Bilde
Reserve paper	WG01S5B00	**Long Term Trends in Arctic Aerosol Composition at Kevo, Finland** P.K. Hopke, J.R. Laing, L. Hussain, V.A. Dutkiewicz, J. Paatero, and Y. Viisinen

10:30-12:50 **Session WG05S2O. Carbonaceous aerosol and wood burning contribution to PMx**
Room: Legado Andalusí
Chairs: C. Pio / T. Moreno

10:30	WG05S2O01	**Levels of carbonaceous aerosols in remote, rural, urban and industrial sites of Spain** Querol X., Alastuey A., Viana M., Moreno T., Reche C., Minguillón M.C., Ripoll A., Pandolfi M., Amato F., Pérez N., Pey J., Cusack M., Vázquez R., de la Rosa J., Sánchez de la Campa A., Rodriguez S, Pío C., Alados-Arboledas L., Titos G., Atíñano B., Salvador P., García Dos Santos S., Fernández Patier R
10:50	WG05S2O02	**Long term monitoring of black carbon at eight measurement sites in Switzerland** H. Herich, C. Hueglin, A. Fischer and B. Buchmann
11:10	WG05S2O03	**Cartography and long term trends (1998-2011) of polycyclic aromatic hydrocarbons in France** A. Albinet, M. Beauchamp, G. Harel, L. Malherbe and E. Leoz
11:30	WG05S2O04	**On the contribution from wood burning to the PM10 aerosol in Flanders, Belgium** W. Maenhaut, R. Vermeylen, M. Claeys, J. Vercauteren, C. Matheeussen and E. Roekens
11:50	WG05S2O05	**Contribution of wood burning to the exceedance**

		of PM10 limit values in residential areas of the Rhine-Ruhr conurbation (Germany) U. Pfeffer, L. Breuer and D. Gladtke
12:10	WG05S2O06	**A UK-wide assessment of black carbon and PM from wood burning** Gary W. Fuller, David C Green and David Butterfield
12:30	WG05S2O07	**Insight into the primary and secondary organic fraction of the organic aerosols in and around Barcelona** B.L. van Drooge, M. Alier, R. Tauler, J.O. Grimalt

10:30-12:50 **Session WG04S1O. Combustion and industrial aerosols**
Room: Faraday
Chairs: A. Keller / C. Gutiérrez-Cañas

10:30	WG04S1O01	**Effects of Zn on the physicochemical and toxicological properties of PM1 in pellet combustion** T. Kaivosoja, O. Uski, H. Lamberg, J. Leskinen, A. Virén, T. Torvela, J. Tissari, O. Sippula, S. Paukkunen, M.-R. Hirvonen, J. Jokiniemi
10:50	WG04S1O02	**Comparison of particle concentrations measured direct from hot flue gas and diluted sample gas from wood combustion** J. Tissani, H. Lamberg, O. Sippula, J. Jokiniemi
11:10	WG04S1O03	**Continuous flow reactor for a defined measurement of the SOA formation potential of wood burning emissions** A. Keller, H. Burtscher
11:30	WG04S1O04	**A two component optical absorption model for interpretation of different combustion conditions** T. Dobovicnik, H. Bauer, H. Puxbaum, A. Petzold, A. Ibrahim, R. Hitzenberger, G. Mocnik
11:50	WG04S1O05	**Heavy metals contained in the Particulate Matter emitted from Foundries** J.J. Rodríguez-Maroto, J.L. Dorronsoro-Arenal, D. Sanz-Rivera, E. Rojas-García, M. Fernández-Díaz, P. Galán-Valera and E. Conde Vilda
12:10	WG04S1O06	**Coagulation of Combustion-Formed Nanoparticles in Medium Temperature Regime** M. Sirignano, and A. D'Anna

12:30	WG04S1O07	**Nucleation and growth of welding fumes on the vicinity of the welder: Implications on health effects assessment and protection strategy** Marroquin ML, C. Gutierrez-Canas, Egizabal, Aragon G., Mugica I., Casas N., Flor B. and Larrion M.
Reserve paper	WG04S1B00	**Results and experience of long-term study of reduction of fine particle emissions from wood combustion boiler by a compact electrostatic precipitator** A. Bologa, H.-R. Paur and K. Woletz

10:30-12:50 **Session WG10S1O. Aerosol Nucleation, Condensation and Coagulation**
Room: Cine 3
Chairs: J.L. Castillo / A.G. Konstandopoulos

10:30	WG10S1O01	**Novel Features of (Re-) Crystallization and Particle Population Dynamics In Compressed Gas-Expanded Liquid** D. E. Rosner
10:50	WG10S1O02	**New insight into organic driven particle formation and growth during the CLOUD experiment** F. Riccobono, E. Weingartner, U. Baltensperger and the CLOUD collaboration
11:10	WG10S1O03	**Saturation fluctuations and rain initiation** Charles Clement
11:30	WG10S1O04	**Thermophoretic coating with molybdenum oxide nanoparticles** L, Boskovic and I. E. Agranovski
11:50	WG10S1O05	**Studies on thermal diffusion and Dufour effect in condensation of a trace gas and a near-pure vapor: water droplets on Earth and CO2 ice crystals on Mars** C. Listowski, A. Määttänen, I. Riipinen, F. Montmessin, F. Lefèvre
12:10	WG10S1O06	**Design of well-mixed aerosol chambers for stable aerosol generation** J.T.N. Knijnenburg, M.L. Eggersdorfer and S.E. Pratsinis
12:30	WG10S1O07	**Nucleation and droplet growth measured by a pulse-expansion wave tube** M.A.L.J Fransen, J. Hrubý and D.M.J. Smeulders
Reserve	WG10S1B00	**3D study of fractal combustion aerosols using**

paper		**Electron Tomography** D. Lottin, D. Ferry, D. Delhaye, F.-X. Ouf and J. Yon

10:30-12:50 **Session WG09S2O. Aerosol Modelling: Emission inventories, transport and transformation**
Room: Gutenberg
Chairs: S. Wurzler / P. Makar

10:30	WG09S2O01	**A 40-year retrospective high-resolution European radon flux inventory including climatological variability** I. López-Coto, J.L. Mas and J.P. Bolivar
10:50	WG09S2O02	**Modelling Contribution of Biogenic VOCs to New Particle Formation in the Julich Plant Atmosphere Chamber** L. Liao, M. Boy, D. Mogensen, T. F. Mentel, E. Kleist, A. K.-Scharr, R. Tillman, H. Vuollekoski, M. Kulmala and M. D. Maso
11:10	WG09S2O03	**Development of emission inventories of recreational boats** V. Agranovski
11:30	WG09S2O04	**The Role of Compensating Errors in Reaction-Transport Models of Atmospheric Aerosol** P.A. Makar, R. Nissen, A. Teakles, J. Zhang, Q. Zheng, M.D. Moran, H.Yau
11:50	WG09S2O05	**Application of Process Analysis in the CAMx model for evaluating physical and chemical processes affecting PM in Switzerland** G. Ciarelli, S. Aksoyoglu, J. Keller, D.C. Oderbolz, A.S.H. Prévôt
12:10	WG09S2O06	**Modeling aerosol chemical properties: impact on cloud and precipitation formation** C. Barbet, L. Deguillaume and N. Chaumerliac
12:30	WG09S2O07	**Effect of precursor emissions on PM2.5 concentrations over Europe** E. Tagaris, R.E.P. Sotiropoulou, N. Gounaris and S. Andronopoulos

14:00-16:00 **Session WG01S6O. Climate effects of aerosols**
Room: Auditorio
Chairs: M. Krämer / J.P. Díaz

14:00	WG01S6O01	**Model results of cirrus cloud modifications in a climate engineering framework** H. Muri, J.E. Kristjánsson, T. Storelvmo, D. L. Mitchell and M.A. Pfeffer
14:20	WG01S6O02	**The influence of aerosols on the European heat-wave of 2003: a study with the regional model system COSMO-ART** A. Ferrone, H. Vogel, and C. Kottmeier, B. Vogel
14:40	WG01S6O03	**Are indirect forcing estimates sensitive to cloud formation parameterizations, emission scenarios and meteorological fields?** R.E.P. Sotiropoulou, E. Tagaris,N. Meskhidze, J. Kouatchou, L. Oreopoulos, J.M. Rodriguez and A. Nenes
15:00	WG01S6O04	**Airborne measurements of elevated aerosol layers over Central Europe** B. Weinzierl, F. Dahlkötter, D. Sauer, K. Heimerl, A. Minikin, A. Petzold, C. Voigt, H. Flentje, F. Schnell, V. Freudenthaler, M. Wiegner, and A. Ansmann
15:20	WG01S6O05	**The importance of wood burning as a source of absorbing aerosols in the European Arctic** K.E. Yttri, C. Lund Myhre, A. Stohl, C. Dye, D. Hirdman, J. Ström
15:40	WG01S6O06	**Horizontal Meter Scale Variability of Elemental Carbon in Surface Snow** J. Svensson, J. Ström, M. Hansson and H. Lihavainen

14:00-16:00 **Session WG05S3O. PMx source apportionment**
Room: Legado Andalusí
Chairs: R. Vecchi / F. Amato

14:00	WG05S3O01	**Tracer-based source-apportionment from the EUCAARI project and comparison with the EMEP model** D. Simpson, C. Alves, R. Bergström, S. Decesari, J. Genberg, S. Gilardoni, G. Kiss, E. Swietlicki and E. Vignati
14:20	WG05S3O02	**Intercomparison of source apportionment approaches within the EU-MED APICE project** A. Detournay, D. Salameh, J.L. Jaffrezo, J. Cozic, J.Pey, N.

		Perez, X. Querol, P. Prati, M.C. Bove, E. Cuccia, D. Massabo, J. Bartzis, D. Saraga, E. Tolis, K. Filiou, A. Latella, F. Liguori, S. Patti, A. Armengaud, D. Piga and N. Marchand
14:40	WG05S3O03	**European Intercomparison for Receptor Models: Preliminary Results** F. Karagulian, C.A. Belis, F. Amato, D.C.S. Beddows, V. Bernardoni, S. Carbone, D. Cesari, E. Cuccia, D. Contini, O. Favez, I. El Haddad, R.M. Harrison, T. Kammermeier, M.Karl, F. Lucarelli, S.Nava, J. K. Nøjgaard, M. Pandolfi, M.G. Perrone, J.E. Petit, A. Pietrodangelo, P. Prati, A.S.H. Prevot, U. Quass, X. Querol, D. Saraga, J. Sciare, A. Sfetsos, G. Valli, R. Vecchi, M. Vestenius, J.J. Schauer, J.R. Turner, P. Paatero, P.K. Hopke
15:00	WG05S3O04	**Identification of continental and marine aerosol sources in Paris using high resolution aerosol mass spectrometry** M. Crippa, D. Peter F., S. Jay G., El Haddad Imad, M. Claudia, H. Maarten F., C. Roberto, M. Nicolas, B. Urs, P. Andre. S. H.
15:20	WG05S3O05	**PMF source apportionment of PM10 and PM2.5 daily and hourly aerosol data in Tuscany (Italy)** Lucarelli, F., Becagli, S., Calzolai, G., Chiari, M., Giannoni, M., Martellini, T., Rugi, F., Nava, S., Traversi, R. & Udisti, R.
15:40	WG05S3O06	**Source apportionment of indoor, outdoor and personal PM2.5 exposure of pregnant women** M.C. Minguillón, M. Triguero-Mas, A. Schembari, A. de Nazelle, P. Dadvand, F. Figueras, J.A. Salvado, J.O. Grimalt, M. Nieuwenhuijsen, X. Querol
Reserve paper	WG05S3B00	**Comparison of receptor models using synthetic organic aerosol mass spectra** H. Hagino, and T. Morikawa

14:00-16:00 **Session WG04S2O. Engines related emissions**
Room: Faraday
Chairs: A. Petzold / M. Vojtisek-Lom

14:00	WG04S2O01	**Particulate matter emissions from a winter operation of a modern on-road diesel engine powered by heated rapeseed oil.** M. Vojtisek-Lom, M. Pechout, M. Mazač

14:20	WG04S2O02	**Role of exhaust after-treatment devices in diesel exhaust nanoparticle formation processes** T. Rönkkö, J. Heikkilä, T. Lähde, L. Pirjola, F. Arnold, H. Schlager, D. Rothe and J. Keskinen
14:40	WG04S2O03	**The influence of oxygenated organic aerosols (OOA) and its volatile organic content on the oxidative potential of diesel particulate mater** S. Stevanovic, B. Miljevic, N.C. Surawski, P.Vaattovaara, R. J. Brown, Z.D. Ristovski
15:00	WG04S2O04	**Size-resolved particle emission factors for individual ships** Å.M. Jonsson, J. Westerlund and M. Hallquist
15:20	WG04S2O05	**Towards an identification of aircraft soot among urban background: focus on nanoparticles emitted by CFM56 turbofan engines** D. Lottin, D. Ferry, J.-M. Gay and D. Delhaye
15:40	WG04S2O06	**Evolution of Jet Engine Exhaust Aerosol in an Aging Plume** D.E. Hagen, P. Lobo, J. Keehn, M. Trueblood, and P.D. Whitefield
Reserve paper	WG04S2B00	**Exhaust emissions and particle hygroscopicity with a diesel engine run with HVO fuel-oxygenate blend** M. Happonen, J. Heikkilä, P. Aakko-Saksa, T. Murtonen, K. Lehto, A. Rostedt, T. Sarjovaara, M. Larmi, J. Keskinen, A. Virtanen

14:00-16:00 **Session WG10S2O. Aerosol Dynamics**
Room: Cine 3
Chairs: P.L. García-Ybarra / C. Clement

14:00	WG10S2O01	**The mobility radius of small fractal aggregates in the slip-flow regime** A.D. Melas, A.G. Konstandopoulos and Y. Drossinos
14:20	WG10S2O02	**Study of thermophoretic velocity of soot particles with a new device: the radial flow thermophoretic analyser** E. Brugière, F. Gensdarmes, F.-X. Ouf , J. Yon and A. Coppalle
14:40	WG10S2O03	**Forces on a porous particle in an oscillating flow** P. Vainshtein and M. Shapiro

15:00	WG10S2O04	**Stick and rebound of single nanoparticles and nanoparticle agglomerates** S. Rennecke and A.P. Weber
15:20	WG10S2O05	**The Friction Factor and Collision Kernel for Aggregates in the Mass and Momentum Transition Regimes** C. J. Hogan Jr, C. Zhang, T. Thajudeen, R. Gopalakrishnan, C. Larriba, T. Schwartzentruber
15:40	WG10S2O06	**Separation of gas-borne nanoparticles in bubble columns** D. Koch, A.P. Weber
Reserve paper	WG10S2B00	**Modeling of the behavior of droplets deposited on the smooth and rough fiber surfaces** J.M. Gac and L. Gradoń

14:00-16:00 **Session WG09S3O. Aerosol Modelling: New particle formation and further topics**
Room: Gutenberg
Chairs: S. Wurzler / A. Asmi

14:00	WG09S3O01	**Nucleation rate parametrization in the CLOUD experiment over all tropospheric conditions** Almeida-Simões, J., C. Joachim, K. Jasper, C., Ken, D. Eimear, and the CLOUD collaboration
14:20	WG09S3O02	**Modelling of ion-induced binary nucleation in the CERN CLOUD experiment** S. Ehrhart, L. Ickes, J. Kazil, K. D. Froyd, E. R. Lovejoy, J. Curtius and the CLOUD collaboration
14:40	WG09S3O03	**Atmospheric new particle formation mystery unveiled?** I.K. Ortega, O. Kupiainen, T. Olenius, M. McGrath.T. Kurtén, P. Pasonen, M. Kulmala and H. Vehkamäki
15:00	WG09S3O04	**Simulating the contribution of primary emissions and secondary formation to aerosol number concentrations in Europe** C. Fountoukis, I. Riipinen, D. Patoulias, H. D. van der Gon, P.E. Charalampidis, C. Pilinis, and S.N. Pandis
15:20	WG09S3O05	**Modeling Reactive Aerosols in Oxidizing Atmospheres: Severe Accidents in Sodium Fast Reactors** M. García, L.E. Herranz

15:40	WG09S3O06	**The global distribution of aerosol model uncertainty** L.A. Lee, K.S. Carslaw, K.J. Pringle
Reserve paper	WG09S3B00	**Determining the particle diameter growth rate from the fraction of charged particles** J. Leppä, S. Gagné, L. Laakso, K. E. J. Lehtinen, M. Kulmala and V.-M. Kerminen

POSTER SESSION C

001	C-WG01S3P01	**Biomass burning event in Spain: aerosol size distribution, aerosol optical properties and associated radiative forcing** E. Alonso-Blanco, V. Pont, A. Castro, A.I. Calvo, M. Mallet, R. Fraile
002	C-WG01S3P02	**Estimate of direct radiative forcing by aerosols over East Asia with the assimilated aerosol optical properties** C.H. Song, R.S. Park, C.E. Chung, J.H. Lee, and J. Kim
003	C-WG01S3P03	**9-year analysis of the aerosol radiative forcing over a Mediterranean urban coastal site** A.R. Esteve, V. Estellés, M.P. Utrillas and J.A. Martínez-Lozano
004	C-WG01S3P04	**6 years of continuous aerosol size distribution measurements from the foothills of Central Himalayas** A.-P. Hyvärinen, R.K. Hooda, M. Komppula, K. Neitola, E. Asmi, V.P. Sharma, T.S. Panwar, and H. Lihavainen
005	C-WG01S3P05	**Description of the Soot on Snow experiment (SoS 2012) at Jokioinen, Finland** N. Kivekäs, D. Brus, A. Hyvärinen, O. Järvinen, J. Svensson, A. Aarva, O. Meinander, A. Heikkilä and A. Virkkula
006	C-WG01S3P06	**Influence of kappa-Köhler theory based water uptake scheme on a global climate/aerosol model** D. O'Donnell
007	C-WG01S3P07	**Aerosol and cloud SW radiative forcing in the south of Portugal** V. Salgueiro, M.J. Costa, A.M. Silva and D. Bortoli
008	C-WG01S3P08	**Investigating aerosol – radiation feedbacks in high-emission areas using WRF/Chem model** A.Balzarini, G.Pirovano, G.M. Riva

009	C-WG01S3P09	**The Soot on Snow experiment 1 (SoS 2011): Soot from burning organics** A. Virkkula, O. Järvinen, H. Lihavainen, A. Hyvärinen, J. Svensson, T. Mäkelä, N.Kivekäs, R. Väänänen, J. Backman, A. Heikkilä, A. Aarva, E.-M. Kyrö, and G. Leeuw
010	C-WG01S3P10	**A4: Arctic Absorbing Aerosols and Albedo of Snow (2012-2015)** O. Meinander, A. Aarva, L. Backman, A. Heikkilä, P. Kolmonen, A. Kontu, E. Kyrö, H. Lihavainen, N. Kivekäs, J. Pulliainen, P. Räisänen, M. Sofiev, A. Virkkula and G. de Leeuw
011	C-WG01S3P11	**Experimental study of the surface shortwave aerosol forcing efficiency** J.L. Anastasio, I. Foyo-Moreno , A. Valenzuela, M. Antón, F.J. Olmo and L. Alados-Arboledas
012	C-WG01S3P12	**Aircraft Measurements of Aerosol, Cloud Droplet and CCN Distribution Characteristic over Northern China** Duan Ying, Yin Yu, Duan Jing
013	C-WG01S3P13	**A note of caution concerning particle evaporation during measurements of their Cloud Condensation Nucleus potential** H. Wex, P. Herenz, J. Voigtländer and F. Stratmann
014	C-WG01S3P14	**Indirect aerosol effects from Chemistry Transport model coupled to a Regional Climate model** M.A. Thomas, M. Kahnert, H. Kokkola, C. Andersson, R. Bergström, C. Bennet, L. Robertson, U. Hansson, C. Jones and U. Willen
015	C-WG01S3P15	**Mass spectrometric analysis of cloud residuals in tropical trade wind cumuli at Pico Este, Puerto Rico, during PRADACS 2011** J. Schneider, A. Roth, J. Schmale, S. Mertes, L. Schenk, O. L. Mayol-Bracero, C. J. Valle, F. Zurcher, and S. Borrmann
016	C-WG01S3P16	**New cloud chamber experiments on the crystallization and heterogeneous ice nucleation ability of sodium chloride dihydrate particles** R. Wagner, O. Möhler, H. Saathoff and M. Schnaiter
017	C-WG01S3P17	**Experimental and modelled characterization of diffuse spectral UV irradiance under cloudy conditions: impact of aerosol properties** D. Mateos, A. di Sarra, J. Bilbao, M. Cacciani, G. Casasanta, D. Meloni, G. Pace, and A. de Miguel
018	C-WG01S3P18	**Overview of Puijo Cloud Experiments (PuCE 2010 & 2011)** Portin, Harri, Leskinen, Ari, Brus, David, Neitola, Kimmo,

		Hyvärinen, Antti-Pekka, Kortelainen, Aki, Hao, Liqing, Miettinen, Pasi, Jaatinen, Antti, Lihavainen, Heikki, Romakkaniemi, Sami, Laaksonen, Ari, Lehtinen, Kari E.J. and Komppula, Mika
019	C-WG01S3P19	**Experimental study in situ conditions of below-cloud scavenging of aerosol particles** G. Depuydt, O. Masson, J.L. Brenguier, P. Boissery
020	C-WG01S3P20	**Identifying cloud processed aerosol particles with light depolarization** D. Baumgardner, R. Newton, O.L. Mayol-Bracero, C.J. Valle-Diaz, F. Zurcher, S. Mertes
021	C-WG01S3P21	**Inhibition of Heterogeneous Ice Nucleation of Mineral Dust Particles Exposed to Ozone** Z.A. Kanji, A. Welti, C. Chou and O. Stetzer
022	C-WG01S3P22	**Aerosol activation behaviour in liquid-phase clouds at the Jungfraujoch: A comparison of in-situ measurements and box modelling data** E. Hammer, N. Bukowiecki, M. Gysel, C. R. Hoyle, Z. Jurányi, M. Leuenberger, U. Baltensperger and E. Weingartner
023	C-WG01S3P23	**Cloud condensation nuclei (CCN) properties of mixed organic-sulphate particles** Å.K. Watne, R. K. Pathak, A. Eriksson, C. Wittbom, Th. F. Mentel, J. Pagels, B. Sveningsson, E. Swietlicki and M. Hallquist
024	C-WG01S3P24	**Mixed-phase clouds observations at Pallas subarctic background site** D. Brus, K. Neitola, J. Svensson and H. Lihavainen
025	C-WG01S3P25	**First measurements of marine stratocumulus microphysical parameters at a subtropical Atlantic station (Friolera Peak Lab, FPL, 28.6ºN, 16.2ºW)** J.P. Díaz, F.J. Expósito, J.C. Pérez and A. González
026	C-WG01S3P26	**Combustion Particles as Ice Nuclei in an Urban Environment: Evidence From Single-Particle Mass Spectrometry** J.C. Corbin, P. J. G. Rehbein, G. J. Evans and J.P.D. Abbatt
027	C-WG01S3P27	**A Case Study of Cloud Events by High Resolution Aerosol Mass Spectrometer in a Semi-urban Aerosol-cloud Interaction Observation Station** L.Q. Hao, A. Kortelainen, A. Jaatinen, P. Miettinen, S. Romakkaniemi, H. Portin, M. Komppula, A. Leskinen, A. Virtanen, J.N. Smith, D.R. Worsnop and A. Laaksonen
028	C-WG01S3P28	**A new ice selective inlet for the characterization of the atmospheric ice phase** P. Kupiszewski, P. Vochezer, M. Schnaiter, E. Weingartner

029	C-WG01S3P29	**Cloud resolving model simulations of geoengineering of marine stratocumulus cloud by sea salt injections** Z. Maalick, H. Korhonen, H. Kokkola, A. Laaksonen and S. Romakkaniemi
030	C-WG01S3P30	**Size distribution and chemical composition of ice nuclei at a rural site in Germany** M. Ebert, T. Hermann, H. Bingemer, H. Klein, J. Curtius, and S. Weinbruch
031	C-WG01S3P31	**The regime dependency of the susceptibility of convective mixed-phase clouds and precipitation** Di Chang, Hang Su, Philipp Reutter, Jörg Trentmann, Meinrat O. Andreae, and Ulrich Pöschl
032	C-WG01S3P32	**Measuring tropical maritime cumulus cloud particle residual composition and ice nuclei concentration during the ICE-T field campaign** A. Cazorla, K.J. Suski, G.R McMeeking, P.J. DeMott, S.G. Lasher-Trapp, C.H. Twohy and K.A. Prather
033	C-WG01S3P33	**Hygroscopic and CCN properties of submicron atmospheric aerosol in a boreal forest environment during the summer of 2010** J. Hong, M. Paramonov and T. Petäjä
034	C-WG01S3P34	**Ultra-fine aerosol particles above Amazon rainforest** M. Matisans, L. Rizzo, R. Krejci, P. Artaxo, P. Tunved, I. Riipinen, T. Hamburger, E. Swietlicki
035	C-WG01S3P35	**Impacts of Emission Controls and Perturbations on an Intense Convective Precipitation Event during the 2008 Beijing Olympic Games** Y. F. Cheng, C. Wei, P. Marrupu, P. Saide, S. Kulkarni, M. Lin, Q. Zhang, D. G. Streets, H. Su, A. Wiedensohler, G. R. Carmichael
036	C-WG01S3P36	**Relationships between aerosols, cloud condensation nuclei and cloud droplets on a background subarctic site** T. Anttila, D. Brus, A.-H. Hyvärinen, A. Jaatinen, N. Kivekäs, S. Romakkaniemi, H. Lihavainen
037	C-WG04S1P01	**Fate of volatile and non-volatile elements from biomass burned in stoves and boilers** Torben Seidel & Hans Ruppert
038	C-WG04S1P02	**Control of trace pollutants in fuidised bed biomass-residues co-combustion fly-ash.** D. Sanz, J. J. Rodríguez, J. L. Dorronsoro, E. Rojas, R. Ramos, R. Escalada, M. E. Borjabad, M. A. Martínez, M. P. Sanz, A. De La Torre, P. Galán , A. Bahillo, C. Gutierrez-Cañas, G. Aragón and S. Astarloa

039	C-WG04S1P03	**Aerosol mass spectrometer measurements on wood combustion experiments** A. Kortelainen, J. Joutsensaari, A. Jaatinen, P. Miettinen, L. Hao, D. R. Worsnop, J. Jokiniemi and A. Laaksonen
040	C-WG04S1P04	**Effect of improved combustion technology on emissions in hybrid masonry heater from combustion of pellets and wood logs** A. Virén, H. Lamberg, T. Kaivosoja, O. Sippula, J. Tissari, J. Jokiniemi
041	C-WG04S1P05	**Effective density of particles emitted from different biomass combustion conditions** J. Leskinen, A. Virén, H. Lamberg, T. Kaivosoja, T. Kettunen, I. Nuutinen, T. Torvela, O. Sippula, J. Tissari, J. Jokiniemi
042	C-WG04S1P06	**Zinc enrichment in ultrafine particles formed in biomass combustion** T. Torvela, T. Kaivosoja, O. Sippula, A. Virén, J. Leskinen, T. Kettunen, I. Nuutinen, H. Lamberg, J. Tissari, J. Jokiniemi
043	C-WG04S1P07	**Particle formation during combustion of solid recovered fuels in a grate system** W. Baumann, H. Mätzing, H.-J. Gehrmann, M. Hauser, P. Nowak, H.-R. Paur and H. Seifert
044	C-WG04S1P08	**Particulate emissions from the co-combustion of forest biomass waste and sewage sludge in a bubbling fluidised bed** A.I. Calvo, L.A.C. Tarelho, E.R. Teixeira, T. Nunes, C. Alves, M. Duarte, E. Coz, A. Castro, B. Artiñano, R. Fraile
045	C-WG04S1P09	**Ignition and combustion of coal dusts with different fuel mass concentrations** S.G. Orlovskaya, V.V. Kalinchak and O.N. Zuy
046	C-WG04S1P10	**Reduction of particulate matters emitted from a diesel-generator fuelled by waste-edible-oil biodiesel with acetone and isopropyl alcohol addition** J.H. Tsai, S.J. Chen, K.L. Huang, C.C. Lin and W.Y. Lin
047	C-WG04S1P11	**Study of paraffin droplets evaporation and burning** S.G. Orlovskaya, M.S. Shkoropado, F.F. Karimova
048	C-WG04S1P12	**Testing performance of fume hood in chemical laboratory** T. Jankowski
049	C-WG04S1P13	**Anthropogenic influence in bulk deposition fluxes in an urban-industrial area in the southwest of Spain** S. Castillo, J. de la Rosa, Y. González-Castanedo, A. Sánchez de la Campa, R. Fernández and X. Querol

050	C-WG04S1P14	**Number size distribution of welding fumes** M. Manigrasso, C. Fanizza, P. Carrai, and P. Avino
051	C-WG04S1P15	**Clogging of industrial High Efficiency Particulate Air (HEPA) filters in case of fire: extension of an empirical model to realistic fire conditions** F.-X. Ouf, V.-M. Mocho, S. Pontreau and Z. Wang
052	C-WG04S1P16	**Elemental and morphological characterization of combustion by-products released from coal-fired thermal power plants in India** Rakesh Kumar and Sudesh Yadav
053	C-WG04S1P17	**Characterisation of particle number, nitrogen oxides and ozone concentrations in an urban background area located near a municipal waste incinerator** A.Donateo, D.Contini, F.Belosi, F. Prodi, F.M. Grasso
054	C-WG04S1P18	**Analysis of Soot deposit for post fire investigation: comparison between full scale experiment and theoretical approach** A. Bellivier, M. Vigreux, F.X. Ouf and H. Bazin
055	C-WG04S1P19	**Electrical Properties of Carbonaceous Particles Collected from Laminar Premixed Flames** G. De Falco, M. Commodo, V. Pagliarulo, G.P. Pepe P. Minutolo, A. D'Anna
056	C-WG04S1P20	**Towards a discrimination between particle emission from wood/biomass combustion and road traffic by Raman microspectroscopy** N.P. Ivleva, C. W. Müller, I. Kögel-Knabner and R. Niessner
057	C-WG04S1P21	**Field scale evaluation of ultrafine particles emissions from stationary combustion and industrial sources** S.Cernuschi, G. Lonati, M. Giugliano, S. Ozgen, G. Ripamonti
058	C-WG04S1P22	**Characterization of aerosols produced by a commercial combustion aerosol generator MiniCAST^{TM} 5201: EC/TC, size distribution, morphology and optical properties** F.-X. Ouf, E. Brugière, D. Ferry, S. Pontreau and J. Yon
059	C-WG04S1P23	**Selective catalytic NH_3 using rare-earth oxides of gasified biomasses fuels. Part 1. Materials structural characterization** Chang-Mao Hung, Shui-Jen Chen, Wei-Bang Lin and Wen-Liang Lai
060	C-WG04S1P24	**Selective catalytic NH_3 using rare-earth oxides of gasified biomasses fuels. Part 2. Catalytic activity and mechanism study** C.-M. Hung, S.-J. Chen, W.-B. Lin and W.-L. Lai

061	C-WG04S1P25	**Selective catalytic NH_3 using rare-earth oxides of gasified biomasses fuels. Part 3. Reaction kinetic behavior study** Chang-Mao Hung, Shui-Jen Chen, Wei-Bang Lin and Wen-Liang Lai
062	C-WG04S1P26	**Results and experience of long-term study of reduction of fine particle emissions from wood combustion boiler by a compact electrostatic precipitator** A. Bologa, H.-R. Paur and K. Woletz
063	C-WG04S1P27	**Comparison of Methods for On-Line Measurement of Diesel Particulate Matter** Z. Liu, J. Swanson, D.B. Kittelson and D.Y.H. Pui
064	C-WG04S1P28	**Laboratory investigation of PAH transformation during NO2-based DPF regeneration** J. C. Wolf and R. Niessner
065	C-WG04S1P29	**Comparison of genotoxicity of exhaust from a diesel, biodiesel and rapeseed oil powered engine – pilot study** J. Topinka, A. Milcova, J. Schmuczerova, M. Mazac, M. Pechout, M. Vojtisek-Lom
066	C-WG04S1P30	**Experimental Investigations of Sensitivity of Lichens to Diesel Exhaust under Lab Conditions** U. Langmann, P. Madl, W. Hofmann, G. Brunauer, R. Türk
067	C-WG04S1P31	**Nanoparticle emissions from ships calling the port of Gothenburg** J. Westerlund, M. Hallquist and Å.M. Jonsson
068	C-WG04S1P32	**Detailed chemical characterization of PM and COV, and source apportionment near a French highway** L. Polo, C. Piot, A. Charron, J. Cozic, B. Temime-Roussel, N. Marchand, J.L. Besombes and J.L. Jaffrezo
069	C-WG04S1P33	**Time-resolved NO_2 analysis in the presence of soot** J. C. Wolf, K. Thaler, R. Niessner, and C. Haisch
070	C-WG04S1P34	**Particle size and number distribution of particles emitted by a modern diesel engine using mineral diesel and Biodiesel from Soybean** C. C. Barrios S, A. Domínguez-Sáez, C. Martín Jiménez
071	C-WG04S1P35	**Measuring black carbon emission factors of cars in real driving conditions** I. Ježek, G. Močnik
072	C-WG04S1P36	**2D study of the size and morphological properties of soot emitted by an aircraft advanced combustion chamber** D. Delhaye, D. Lottin, D. Ferry, J.-M. Gay and X. Vancassel

073	C-WG04S1P37	**Exhaust emissions and particle hygroscopicity with a diesel engine run with HVO fuel-oxygenate blend** M. Happonen, J. Heikkilä, P. Aakko-Saksa, T. Murtonen, K. Lehto, A. Rostedt, T. Sarjovaara, M. Larmi, J. Keskinen, A. Virtanen
074	C-WG04S1P38	**Effective Density and Fractal–like Dimension of Diesel Soot Aggregates as a Function of Mobility Diameter** P. Baltzopoulou, E. Papaioannou, M. Kostoglou, A.G. Konstandopoulos
075	C-WG05S1P01	**PM10 is responsible for a greater IL-6 secretion after "in vitro" incubation with synoviocytes from patients with Rheumatoid Arthritis than in those with osteoarthrosis** V. Guercio, F. Cetta, F. Laghi Pasini, E. Selvi, E. Balistreri I. Santi, M. Monti , L. Cantarini, E. Bolzacchini and M. Galeazzi
076	C-WG05S1P02	**Damage to newborns, in terms of risks for diseases occurring even decades after exposure to PM, as a crucial item in the global effects of air pollution to a given population** B. Lorenzi, F. Cetta, V. Guercio, P. Paladini, F. Granato, R. Zangari, M. Monti , M. Giovannini, E. D'Auria, M. Mandelli and M. Sala
077	C-WG05S1P03	**A plea for greater caution before extending "in vitro" assessment of PM to risk assessment in humans** J. Martellucci, F Cetta ,V. Guercio, D. Stergiou, B. Lorenzi , M. Monti and E. Bolzacchini
078	C-WG05S1P04	**Source-specific mutagenicity and carcinogenicity of PM2.5-bound polycyclic aromatic hydrocarbons in a large city of North-eastern Italy** M. Masiol, S. Squizzato, A. Hofer, F. Benetello, G. Rampazzo, B. Pavoni
079	C-WG05S1P05	**Quantitative and qualitative relationship between AOD obtained by AERONET and PM2.5 from in situ measurements in Brazilian Amazonia over several years** M. Paixão, D. Mourao, A. Correia, S. Hacon, P. Artaxo
080	C-WG05S1P06	**Statistics of PM10 concentrations in Mazovia, central Poland (2007 – 2011)** A. Pietruczuk, J. Jarosławski and I. Pawlak
081	C-WG05S1P07	**Anions, Cations, Total Carbon and Water Soluble Organic Carbon in PM2.5 and PM1 samples**

		monitored near a waste incinerator plant in the Po Valley (Bologna) M. Rossi, L. Pasti, L. Tositti, S. Zappoli, E. Brattich, S. Parmeggiani, M. Stracquadanio
082	C-WG05S1P08	**Water-soluble fraction Metals in PM2.5 and PM1 samples collected near a waste incinerator plant in the Po Valley (Bologna)** M. Rossi, L. Pasti, M. Remelli, A. Pagnoni and E. Sarti
083	C-WG05S1P09	**Polycyclic Aromatic Hydrocarbons and Nitro-Derivatives PAHs in PM2.5 and PM1 samples collected near a waste incinerator plant in the Po Valley (Bologna)** M. Rossi, L. Pasti, I. Scaroni and P. Casali
084	C-WG05S1P10	**PM2.5 and PM1 aerosol monitoring near a waste incineration plant located next to Bologna, in the Po Valley: the MONITER Project Campaign** M. Rossi, G. Bonafè, F. Scotto, A. Trentini, L. Pasti
085	C-WG05S1P11	**Concentrations of PMx, NO2 and NH3 in the metropolitan area of Barcelona: APICE long monitoring campaign** J. Pey, N. Pérez, A. Alastuey, X. Querol, J. Cortés
086	C-WG05S1P12	**Searching the relationship between PM10 and MODIS aerosol optical depth at Granada (Spain): urban location and background EMEP station** A.I. Calvo, J.L. Guerrero-Rascado, L. Alados-Arboledas, F.J. Olmo
087	C-WG05S1P13	**Origin of PM2.5 and Secondary Inorganic Aerosol (SIA) and relationship with gaseous pollutants in the Venice area** S. Squizzato, M. Masiol, E. Innocente, E. Pecorari, G. Rampazzo, B. Pavoni
088	C-WG05S1P14	**Analysis of the episodes of high PM10 concentrations from January to April and October to November 2011 in Central and Western Europe with focus on North-Rhine Westphalia** S. Wurzler, H. Hebbinghaus, P. Bruckmann, A. Baltruschat, U. Romberg, J. Friesel, U. Pfeffer, W. Straub, J.Geiger
089	C-WG05S1P15	**Health relevant organic compounds on particulate matter (PM2.5) at two urban sites in Munich: Critical data evaluation** J. Lintelmann, K. Fischer, R. Zimmermann
090	C-WG05S1P16	**Variations of PM-10 and its relationship with BE-7 measurements using a high-volume air sampler at Málaga**

		C. Dueñas, M.C. Fernández, E. Gordo, S. Cañete and M. Pérez
091	C-WG05S1P17	**EDXRF analysis of elemental composition of PM2.5 particles sampled in Taif, Saudi Arabia** A. A. Shaltout, D. R. Almallway, Z. F. Shehadeh, J. Boman
092	C-WG05S1P18	**Time-resolved Measurements of Atmospheric Particulate Matter** M. Amodio, E. Andriani, P. R. Dambruoso, G. de Gennaro, A. Di Gilio
093	C-WG05S1P19	**The changes in chemical composition of fine PM between 1994 and 2010 at rural background site Košetice, Czech Republic** J. Schwarz, V. Havránek, R.Krejčí, P. Tunved, E. Swietlicki, and. V. Ždímal
094	C-WG05S1P20	**Temporal and spatial variability of the total particle number concentration in the Venice area** Pigozzo, A., De Bortoli, A., Patti, S., Manodori, L.
095	C-WG05S1P21	**Takeoff – but what was left behind? In an African perspective** M. J. Gatari, J. Boman, V. Kivaya, D. Maina and A. Wagner
096	C-WG05S1P22	**Air Quality Monitoring Strategies for Urban Areas – A Data Base on New Monitoring Technologies, New Metrics and Proxies** T.A.J. Kuhlbusch, M. Viana, A. Borowiak, E.P. Weijers, K. Torseth, X, Querol, P. Quincey, R. Gehrig, C. Hüglin, K. Katsouyanni and U. Quass
097	C-WG05S1P23	**Magnetic properties of PM10x collected at rural site during heating and non-heating seasons** E. Petrovsky, B. Kotlik, A. Kapicka, R. Zboril and M. Roxer
098	C-WG05S1P24	**Comparison of different operational parameters for thermal-optical EC/OC measurements of filter samples from Flanders, Belgium** W. Maenhaut, M. Claeys, J. Vercauteren and E. Roekens
099	C-WG05S1P25	**Road traffic impact on size-segregated atmospheric aerosols loading at Madrid** F. Mirante, C. Alves, C. Pio, M. Fernandez, M.A. Revuelta and B. Artiñano
100	C-WG05S1P26	**Preliminary research on the ammonium content of particulate matter from indoor air of pig housing systems** T. Ulens, N. Van Ransbeeck, H. Van Langenhove and P. Demeyer
101	C-WG05S1P27	**Seasonal variations of ions and metals in urban PM1 aerosol**

		P. Mikuška, K. Křůmal, M. Vojtěšek, N. Kubátková and Z. Večeřa
102	C-WG05S1P28	**Comparison of online measurements with an Aethalometer and an HR-ToF-AMS and offline chemical analysis data for the characterization of PM2.5 aerosols** V. Crenn, V. Riffault, I. Fronval and D. Petitprez
103	C-WG05S1P29	**Spatial and seasonal distribution of dicarboxylic acids and sugars in the surroundings of a municipal waste incinerator near Bologna, Italy** M.C. Pietrogrande, D. Bacco, M. Rossi
104	C-WG05S1P30	**GC-MS method for the simultaneous analysis of water-soluble organic compounds in PM: response surface methodology for optimizing solvent extraction.** M.C. Pietrogrande, D. Bacco, S. Chiereghin
105	C-WG05S1P31	**Total and water-soluble fraction trace element analysis of PM2.5 samples from the city of Patras, Greece** M. Manousakas, H. Papaefthymiou, K. Eleftheriadis
106	C-WG05S1P32	**Recent changes in PM10 levels and associated ions in an industrial environment in Spain** E. Yubero, N. Galindo, J.F. Nicolás, D. Martínez, M. Santacatalina, and A. Carratalá
107	C-WG05S1P33	**Particle source characterisation of a cement plant with automated scanning electron microscopy** M.F. Meier, T. Zünd and B. Grobety
108	C-WG05S1P34	**Indoor Air Quality in Gymnasiums** C.A. Ramos, S. M. Almeida, S. Cabo Verde, S. Viegas, C. Viegas
109	C-WG05S1P35	**Observations of elevated aerosol particle number and mass concentration events in Vilnius city** S. Kecorius, K. Plauškaitė, S. Byčenkienė and V. Ulevicius
110	C-WG05S1P36	**Mobile platform measurements of PM mass and number concentrations and black carbon in the Greater Athens Area** E. Diapouli, S. Vratolis, V. Vasilatou, M. Gini, A. Tsakis, L. Chasapidis, F. Akritidis, A. Konstantopoulos, G. Mocnik, S. Pothos and K. Eleftheriadis
111	C-WG05S1P37	**PM concentration and chemical speciation measurements at two sites in Athens, Greece** S. Vratolis, E. Diapouli, V. Vasilatou, M. Gini, Th. Maggos, D. Saraga, Th. Ntoka and K. Eleftheriadis
112	C-WG05S1P38	**Determination of refinery emission pollutants**

		impact on an urban atmosphere M.A. Barrero, M. Goikoetxea and L. Cantón
113	C-WG05S1P39	**Determination of water content in atmospheric particulate matter** C. Farao, C. Perrino, S. Canepari, E. Marconi, M.L. Astolfi
114	C-WG05S1P40	**Long-range transport influence on PM2.5 measurements performed in Southern Italy** S. Trippetta, R. Caggiano, S. Fiore, A. Lettino, M. Macchiato and S. Sabia
115	C-WG05S1P41	**Particulate air pollution exposure during commuting in three European cities** P. Taimisto, A. Pennanen, E. Vouitsis, Z. Samaras, M.P. Keuken and T. Lanki
116	C-WG05S1P42	**Two years of measurements at a regional background site in the Balearics: first results** J. Pey, C. Bujosa, S. Caballero, X. Querol, A. Alastuey, M Sicard, B. Artíñano
117	C-WG05S1P43	**Effect of flooring, cleaning and foot traffic on indoor air particulates** N. Mansouri, I. Colbeck
118	C-WG05S1P44	**Personal monitoring of ambient particulate matter – online monitoring and offline filter sample analysis** J. Schnelle-Kreis G. Abbaszade, J. Cyrys, J. Gu, M. Pitz, A. Peters, R. Zimmermann
119	C-WG05S1P45	**Evolution of PM10, PM2.5 and PM1 in a semi-arid industrial environment** M. Santacatalina and A. Carratalá
120	C-WG05S1P46	**Emission measurement of PM size distribution from road wear** M. Maasikmets, E. Teinemaa, T. Arumäe
121	C-WG05S1P47	**PM10 sampling inlets comparison: EPA vs EU** P. Panteliadis, H.J.P.Helmink, P.C.Koopman, M.Hoonhout, D.de Jonge and J.H.Visser
122	C-WG05S1P48	**Source apportionment and sector analysis of organic aerosol in southern Sweden** J. Genberg, M. Sporre and E. Swietlicki
123	C-WG05S1P49	**PM2.5 PCA-APCS Source Apportionment of a site monitored near a waste incinerator plant located in Bologna Area** M. Rossi, L. Pasti
124	C-WG05S1P50	**Source apportionment of PM1 aerosols sampled with an HR-ToF-AMS at an urban background site and an industrialized coastal site using PMF** V. Crenn, V. Riffault, S. Sauvage and D. Petitprez

125	C-WG05S1P51	**The effect of local heating on indoor and outdoor air quality in a rural settlement** M. Braniš and J. Kozáková
126	C-WG05S1P52	**Origin of low-molecular-weight mono and dicarboxylic acids in urban, industrial and suburban environments** G.A. Blanco, M.I. Turnes-Carou, P. López-Mahía, S Muniategui-Lorenzo and D. Prada-Rodríguez
127	C-WG05S1P53	**Modelling of particulate matter concentration at regional and local scale** P. Brotto, F. Cassola, A. Mazzino, T. Giannaros, K. Markakis, A. Poupkou, D. Melas and P. Prati
128	C-WG05S1P54	**Comparison of receptor models using synthetic organic aerosol mass spectra** H. Hagino, and T. Morikawa
129	C-WG05S1P56	**Indoor PM2.5 Source Apportionment from Primary School in Rural Area, Portugal** N. Canha, S.M. Almeida, M.C. Freitas, H.T. Wolterbeek, J. Cardoso, C.A. Pio, A. Caseiro
130	C-WG05S1P57	**Characteristics of heavy metals in PM2.5 at Fukuoka, Japan, based on daily analysis of year-round samples** N. Kaneyasu, A. Takami, K. Sato, S. Ymamamoto, Y-P. Kim and I-S. Kim
131	C-WG05S1P58	**An application of positive matrix factorization and cluster analysis to discriminate the sources of PM10 in a coastal site near Venice (Italy)** M. Masiol, S. Squizzato, D. Ceccato, G. Rampazzo, B. Pavoni
132	C-WG05S1P59	**Source Apportionment of PM2.5 at Burnaby South and Abbotsford, British Columbia, using Positive Matrix Factorization** R. So, R. Vingarzan, S. Meyn, E. Dabek-Zlotorzynska, D. Mathieu, L. Ding, T. Dann, V. Celo, D. Wang
133	C-WG05S1P60	**Application of Positive Matrix Factorization to particle size distribution data from a suburban site in South East Queensland, Australia** Mark Hallas, Adrian J. Friend, Godwin A. Ayoko
134	C-WG05S1P61	**Impact of the Traffic on the Air Particulate Matter from the Urban Area of Setúbal, Portugal** S.M. Almeida, Alexandra V. Silva, A.I. Pedro, A. Ferreira
135	C-WG05S1P62	**Contribution of Residential Wood Combustion to Ambient PM2.5 in a Suburb in Eastern Finland** T. Yli-Tuomi, T. Siponen, R.P. Taimisto, M. Aurela, K. Teinilä, A. Frey, R. Hillamo, J. Pekkanen, R.O. Salonen, T.

		Lanki
136	C-WG05S1P63	**Aerosol chemical characterization and source quantification in a semi-urban area of Indo-Gangetic plains** Hooda, Rakesh K, A.-P. Hyvärinen, S. Gilardoni , a, V.P. Sharma, E. Vignati, T.S. Panwar, b, Viisanen, Y. and H. Lihavainen
137	C-WG05S1P64	**Determination of the elemental composition and the source profiles of particulate matters in Bolu** E. Özlü and S. Yenisoy-Karakaş
138	C-WG05S1P65	**Characterization of PM2.5 in a residential area of Beijing, China** R.R. Shen, K. Schäfer, P. Suppan, N. Schleicher, U. Kramar, S. Norra, J. Schnelle-Kreis, L.Y. Shao, J. Wang, J. Y. Wang, K. Cen, Y.S. Wang, S. Schrader
139	C-WG05S1P66	**Anthropic and natural sources of PM10 in central Mediterranean Sea by bulk and size-segregated samples** S. Becagli, R. Traversi, M. Marconi, C. Ghedini, S. Nava, M. Chiari, F. Lucarelli, G. Calzolai, A. di Sarra, G. Pace, D. Meloni, C. Bommarito, D. M. Sferlazzo , R. Udisti
140	C-WG05S1P67	**The contribution of Rome-Ciampino airport to the surrounding air quality** A. Di Menno di Bucchianico, G. Cattani, A. Gaeta, A. Caricchia, F. Troiano, R. Sozzi, A. Bolignano, F. Sacco, S. Damizia, S. Barberini, R. Caleprico, T. Fabozzi, C. Ancona, L. Ancona, G. Cesaroni, F. Forastiere, G.P. Gobbi, F. Costabile, F. Angelini, F. Barnaba, M. Inglessis, F. Tancredi, L. Palumbo, L. Fontana, A. Bergamaschi, I. Iavicoli
141	C-WG05S1P68	**PM2.5 source apportionment in Milan by UNMIX receptor model** G. Lonati, C. Colombi and S. Cernuschi
142	C-WG05S1P69	**Source apportionment of ambient PM10-1 and PM1 in Granada** G. Titos, H. Lyamani, A.Alastuey, M. Pandolfi, J.A. Bravo-Aranda and L. Alados-Arboledas
143	C-WG05S1P70	**The effect of local wood combustion on fine particles in suburban small house areas in Helsinki Metropolitan Area, Finland** A. Kousa, J. Niemi, A. Svens, K. Teinilä, R. Hillamo and T. Koskentalo
144	C-WG05S1P71	**Overview of the impact of wood burning emissions on carbonaceous aerosols and PM in the Alpine region** H. Herich, M.F.D. Gianini, Ch. Piot, J. Cozic, J.L. Jaffrezo , J.L.

		Besombes, A.S.H. Prevot, and Ch. Hueglin
145	C-WG05S1P72	**Indoor-outdoor relationships of airborne particles and nitrogen dioxide inside Parisian buses** R. Molle, E. Géhin, S. Mazoué and A. Ionescu
146	C-WG05S1P73	**Fungal Bio-Aerosols Quantification - Comparison between q-PCR and Ergosterol Analysis** Naama Lang-Yona, Karen Dannemiller, Naomichi Yamamoto, Noa Burshtein, Jordan Peccia, Oded Yarden, Yinon Rudich
147	C-WG05S1P74	**Comprehensive evaluation of dust cleaning in a subway indoor** W. R. Kim, H. W. Park, Y. M. Jo
148	C-WG05S1P75	**Results from the second Netherlands Research Program on Particulate Matter (BOP II)** E. van der Swaluw, M. Keuken, E. Weijers, M. Schaap, G. Kos, J. Matthijsen, H. Denier van der Gon and R. Hoogerbrugge
149	C-WG09S1P01	**Single molecule water catalysis of atmospheric OH oxidation reactions** Theo Kurtén, Ditte Linde Thomsen, Solvejg Jørgensen, Signe Baggesen, Cecilie Aalling, Henrik Kjærgaard
150	C-WG09S1P02	**Intercomparison of dust prediction models in the framework of the WMO SDS-WAS programme** E. Terradellas, S. Basart, M. Schulz, J. M. Baldasano, J.-J.Morcrette, G. Pejanovic, L. Menut, A. Benedetti, O. Jorba, S. Nickovic and F. Benincasa
151	C-WG09S1P03	**Secondary organic aerosol formation during summer 2010 over Central Europe** B. Langmann, K. Sellegri and E. Freney
152	C-WG09S1P04	**Simulation and evaluation of ozone and its precursor gases over Indian region using the high resolution CHIMERE chemical transport model** Chinmay Jena, Sachin D. Ghude, G. Beig and D.M. Chate
153	C-WG09S1P05	**Climate change impacts on atmospheric gas and particulate mercury levels and deposition rates** A. G. Megaritis, B. N. Murphy, and S. N. Pandis
154	C-WG09S1P06	**Air Quality in Paris - A modeling study** A. G. Megaritis, K. Skyllakou, C. Fountoukis, and S. N. Pandis
155	C-WG09S1P07	**Development of a microphysical model for the H2SO4 - H2O clouds on Venus** A. Määttänen, S. Bekki, F. Montmessin, S. Lebonnois
156	C-WG09S1P08	**Evaluation of the Marco Polo Venice and the Treviso airports impact in two hot spots areas** E. Pecorari, G. Valotto, G. Rampazzo, S. Sollecito, D.

		Bassano, F. Bertoldo and E. Rampado
157	C-WG09S1P09	**Nucleation studies with regional aerosol-climate model REMO-HAM** J.-P. Pietikäinen, S. Mikkonen and A. Laaksonen
158	C-WG09S1P10	**Research Needs Identified In a First-Generation Regional Air Quality Model for Polycyclic Aromatic Hydrocarbons** E. Galarneau, P.A. Makar, Q. Zheng, J. Zhang, and M.D. Moran
159	C-WG09S1P11	**Modelling dust aerosol impacts on heating rate profiles over the Iberian Peninsula and Atlantic Ocean** D. Santos, M. J. Costa, R. Salgado and A. M. Silva
160	C-WG09S1P12	**Modelling PM2.5 chemical composition with CAMx in southwest Spain** C. Milford, N. Castell, C. Marrero, A. Sánchez de la Campa, R. Fernández-Camacho, S. Rodríguez, J. D. de la Rosa and A. F. Stein
161	C-WG09S1P13	**Simulation of mineral dust particle contribution to urban aerosol loading in Greater Beijing with the model system COSMO-ART** S. Schrader, B. Vogel, H. Vogel, K. Schäfer, R. R. Shen, P. Suppan, S. Norra
162	C-WG09S1P14	**Effects of modal representation of aerosol distribution on aerosol activation and optical properties** Korhola, T., Kokkola, H., Korhonen, H., Partanen, A.-I., Laaksonen, A. , Romakkaniemi, S.
163	C-WG09S1P15	**Aerosol observations and predictions in the southeastern Europe during the extreme summer 2007** E. Athanasopoulou, E. Gerasopoulos, H. Vogel, S. Kazadzis, E. Liakakou, M. Gratsea, and B. Vogel
164	C-WG09S1P16	**Application of a SOA parameterization for a-pinene and limonene photooxidation to different conditions** Manuel Santiago, Marta G. Vivanco and Ariel F. Stein
165	C-WG09S1P17	**PM modelling: old challenges and new possibilities** S. Tsyro, D. Simpson, H. Fagerli, W. Aas and M. Schulz
166	C-WG09S1P18	**Modelling the microphysics of Martian CO2 ice clouds** C. Listowski, A. Määttänen, F. Montmessin, F. Lefèvre
167	C-WG09S1P19	**Aerosol generation in atmosphere – data development and modelling**

		V.A. Zagaynov, D.V.Vodyanik, S.F. Timashev, A.A. Lushnikov, Yu.G. Biryukov, I.E. Agranovski, V.V. Maksimenko
168	C-WG09S1P20	**Evaluation of the hydrophobic SOA species estimated by the CHIMERE model considering experiments in a chamber** Marta G. Vivanco and Manuel Santiago
169	C-WG09S1P21	**Influence of Schmidt Number on dispersion modelling using CFD tools: Assessment of urban breathability for urban design and management** M. Tomé, C.A. Alves, R. Santos
170	C-WG09S1P22	**The influence of ion-induced nucleation on atmospheric aerosols based on data from the CERN CLOUD experiment** E.M. Dunne, K.S. Carslaw, J. Almeida,, and the CLOUD collaboration
171	C-WG09S1P23	**Numerical study of the effect of dilution process on the measurement of particle number emissions** Yan Wang, Bo Yang, Eric M. Lipsky, Allen L. Robinson, Topi Ronkko, Jorma Keskinen, K. Max Zhang
172	C-WG09S1P24	**Water bus emission factor model in Venice area** E. Pecorari, G. Rampazzo, A. Ferrari, G. Cuzzolin
173	C-WG09S1P25	**Verification of the NOx emission inventories over South Korea** Na Kyung Kim, Yong Pyo Kim, Yu Morino, Junichi Kurokawa, and Toshimasa Ohara
174	C-WG09S1P26	**Modelling the chemically speciated PM2.5 over the French Northern region using the WRF-Chem system coupled to EMEP and regional emission inventories.** Maxence Mendez, Vincent Crenn, Valérie Fèvre-Nollet, Patrick Lebègue, Denis Petitprez, Véronique Riffault, Nicolas Visez, Rafael Borge
175	C-WG09S1P27	**New method for estimating cigarette smoke emissions** Victoria Agranovski
176	C-WG09S1P28	**The contribution from natural sources to primary and secondary PM emissions over the metropolitan areas of Athens and Thessaloniki** V. Aleksandropoulou, Kjetil Torseth and M. Lazaridis
177	C-WG09S1P29	**Effect of the Lagrangian integral time scale estimation on particle deposition** G. Lecrivain, T. Barth and U. Hampel
178	C-WG09S1P30	**Sulphuric Acid Aerosols in Industrial Processes – Simulation, Estimation of Coagulation and CPC**

		measurement L. Brachert, S. Sinanis and K. Schaber
179	C-WG09S1P31	**Microscopic observation of aerosol particle deposition in turbulent channel flows** T. Barth, G. Lécrivain, J. Preuß and A. Lehmann
180	C-WG09S1P32	**Experimental and Numerical Investigation of Hygroscopic Aerosols Transport, Kinetics and Deposition in an Enclosure** M.A. Zatevakhin, A.A. Ignatiev, Y.N.Vashlyaev, A.A. Zaitsev, A.A. Lukyanov, A.S.Mikheev, D.V.Sumin, O.V.Supotnitskaya
181	C-WG09S1P33	**Mathematical study of inhalable fraction in low velocity conditions** A.K. Gilfanov, I.T. Mukhametzanov, S.K. Zaripov
182	C-WG09S1P34	**Transnational assessment of emerging health relevant air quality parameters (Joaquin)** S. Adriaenssens, F.Fierens, E.Trimpeneers, D.Celis, E. Van der Swaluw, R. Hoogerbrugge and K.V. Wyche
183	C-WG09S1P35	**Development of a workflow for integration of fresh slaughterhouse porcine lungs into an active lung simulation** K. Stiglbrunner, M. Forjan, Z. Bureš and A. Drauschke
184	C-WG09S1P36	**Ion-induced vs. base-induced sulfuric acid nucleation** O. Kupiainen, T. Olenius, I.K. Ortega, T. Kurtén, and H. Vehkamäki
185	C-WG09S1P37	**Parameterization for two-component H2SO4 - H2O nucleation applicable for very low relative humidities and correct at the one-component limit** A. Määttänen, J. Julin, I. K. Ortega and H. Vehkamäki
186	C-WG09S1P38	**First modelling study on new particle formation and growth in Southern African savannah environment** R. Gierens, L. Laakso, V. Vakkari, D. Mogensen, and M. Boy
187	C-WG09S1P39	**Comparing simulated and experimental molecular cluster distributions** T. Olenius, I.K. Ortega, O. Kupiainen, T. Kurtén, S. Schobesberger and H. Vehkamäki
188	C-WG09S1P40	**Simulation of Aerosol Nucleation Bursts: A Case St**udy J. Salm, A. Luts, U. Hõrrak, M. Vana and H. Tammet
189	C-WG09S1P41	**Efficient second-order time-integration for simulation of single-species aerosol dynamics** C. Winkelmann, M. Nordlund, A. Kuczaj, S. Stolz and B.J. Geurts
190	C-WG09S1P42	**To the theory of drop shattering in high-speed flows**

		A. G. Girin
191	C-WG09S1P43	**Particulate Fugitive Emissions in Harbours: characterization and emission factors estimation** A.V.Silva, S.M.Almeida, A.I. Miranda, F. Martín
192	C-WG09S1P44	**Simulation of aerosol growth in chamber conditions** M. Vesterinen, H. Kokkola, H. Korhonen, H. Keskinen and K.E.J. Lehtinen
193	C-WG09S1P45	**Oxidation of SO2 by O2−(H2O)n molecular clusters – a density functional theory study** N.T. Tsona, N. Bork and H. Vehkamaki
194	C-WG09S1P46	**Determining the particle diameter growth rate from the fraction of charged particles** J. Leppä, S. Gagné, L. Laakso, K. E. J. Lehtinen, M. Kulmala and V.-M. Kerminen
195	C-WG09S1P48	**Determining the proton affinity of atmospheric molecular ions** K. Ruusuvuori, T. Kurtén, I. K. Ortega and H. Vehkamäki
196	C-WG09S1P49	**Particle generation in electric arc: experiment and modelling** V.A. Zagaynov, E.V. Zhukova, A.A. Lushnikov, Yu.G. Biryukov, I.E. Agranovsky, V.V. Maksimenko
197	C-WG09S1P50	**Impact of horizontal grid resolution on predicting fine PM with a regional 3-D Chemical Transport Model** C. Fountoukis, A.G. Megaritis, D.S. Koraj, H.A.C. Denier van der Gon, P.E. Charalampidis, C. Pilinis, and S.N. Pandis
198	C-WG09S1P51	**Development of an observation-based box model to investigate secondary inorganic particle behaviors in the urban atmosphere** J. Xue, Z.B. Yuan, J.Z. Yu, A.K.H. Lau and T. Yao
199	C-WG09S1P52	**Simulation of Droplet Nucleation and Growth in a Laminar Counterflow via the Quadrature Method of Moments** A.O. Alshaarawi, K. Zhou and F. Bisetti
200	C-WG09S1P53	**Vertical wind as the dominating factor for spatial-temporal distribution of stratospheric aerosol** V.I. Gryazin and S.A. Beresnev
201	C-WG09S1P54	**Presents to the nearest neighbours: contribution of transboundary transport to the PM10 and PM2.5 concentrations in Central Europe with focus on NRW** H. Hebbinghaus, S. Wurzler, M. Memmesheimer, G. Piekorz, E. Friese, H. J. Jakobs, C. Kessler, A. Ebel
202	C-WG09S1P55	**Validation of ECHAM5-SALSA aerosol climate model against EARLINET lidar network**

		H. Niskanen, E.,Giannakaki, H. Korhonen, K. E. J. Lehtinen, T. Mielonen, A. Lindfors, M. Komppula, L. Alados-Alboledas, U. Wandinger, D. Balis, G. Pappalardo and H. Kokkola
203	C-WG09S1P57	**Numerical simulations of mixing conditions and aerosol dynamicsin the Cern CLOUD chamber** J. Voigtländer, J. Duplissy, L. Rondo, A. Kürten, F. Stratmann, and the CLOUD collaboration
204	C-WG09S1P58	**Experimental Studies on Tin Oxide Dry Aerosol Deposition in Piping assembly under Flow and High Thermal Gradient conditions: Comparison with SOPHAEROS code** Rajni Modi, Arshad Khan, Sunil Ganju, Manish Joshi, Pallavi Khandare, B. K. Sapra and Y. S. Mayya
205	C-WG09S1P59	**Evaluation of black carbon estimations by the regional aerosol-climate model REMO-HAM** A.I. Hienola, J.-P. Pietikäinen, A.-P. Hyvärinen, H. Lihavainen and A. Laaksonen
206	C-WG09S1P60	**Effects of vapor properties on modelled particle growth in the model UHMA** A. Rusanen1 and M. Boy
207	C-WG09S1P61	**Scanning Mobility Particle Sizer: Fast data Inversion and uncertainty analysis** L. Coquelin, N. Fischer, T. Mace, C. Motzkus, F. Gensdarmes, G. Fleury, L. Lebrusquet
208	C-WG09S1P62	**Novel informatics software for automated individual aerosol component property predictions and complex ensemble predictions – an online community facility** D. Topping, M. Bane, M. Barley, D. Lowe, R. Pinning and M. McFiggans
209	C-WG09S1P63	**Contributions of Traffic Emissions to the Ambient Aerosol in an Industrial Area** Sílvia M. Garcia, Gonçalo Domingues, Clara Santos, Carla Gomes, Alexandra V. Silva, S. Marta Almeida
210	C-WG09S1P64	**Evaluating the impact of flooring types on exposure to fine (PM2.5) and coarse (PM2.5 – 10) particles within the residential micro-environment** Lisa Bramwell, Jing Qian, Sumona Mondal, Andrea R. Ferro
225	C-WG10S1P01	**Dynamics of Spray Flames in Oscillating Flow with Droplet Grouping** D. Katoshevski and J. B. Greenberg
226	C-WG10S1P02	**Nonlinear oscillations and deposition of aerosol in tubes** D.A. Gubaidullin, R.G. Zaripov, A.L. Tukmakov and L.A.

		Tkachenko
227	C-WG10S1P03	**Dispersion and dissipation of weak waves in aerosols** Gubaidullin Damir, Nikiforov Anatoly, Teregulova Eugenia and Fedorov Yury
228	C-WG10S1P04	**Gravito-photophoresis of aerosols: the insufficiency of "accommodation" forces action** M.S. Vasiljeva and S.A. Beresnev
229	C-WG10S1P05	**The Polydispersity of Primary Particles in Aggregates undergoing Sintering** M.L. Eggersdorfer and S.E. Pratsinis
230	C-WG10S1P06	**Temperature and particle vertical profiles: suitability of the ML concept under weak cyclonic conditions** J. Giménez, J.F. Nicolás, C.Pastor, R.Castañer, E. Yubero, M.J. Cuesta-Bolao, J. Crespo and S. Caballero
231	C-WG10S1P07	**Two-phase polydisperse spray in a wake of shattering drop** A. G. Girin
232	C-WG10S1P08	**Ab initio molecular dynamics study of sulfuric acid clusters with ammonia/dimethylamine** V. Loukonen, I-F. W. Kuo, M. J. McGrath and H. Vehkamäki
233	C-WG10S1P09	**A turbulent model for the study of dust mobilisation in closed enclosures** J.R. García-Cascales, F.J. Sánchez-Velasco, R. Otón-Martínez and F. Vera-García, A. Bentaib, N. Maynet
234	C-WG10S1P10	**Microgravity experiments on particle motion in the region of negative thermophoresis** A.A. Vedernikov, S.A. Beresnev and A.V. Markovich
235	C-WG10S1P11	**High order operator splitting adaptive time marching Monte Carlo for aerosol dynamics** Kun Zhou and Fabrizio Bisetti
236	C-WG10S1P12	**Modeling of the behavior of droplets deposited on the smooth and rough fiber surfaces** J.M. Gac and L. Gradoń
237	C-WG10S1P13	**Parameters affecting deposition on fibrous filters** Sarah J. Dunnett, Charles F. Clement
238	C-WG10S1P14	**Application of filter utility factor in the filtration of dust and liquid aerosol** T. Jankowski
239	C-WG10S1P15	**Simultaneous removal characteristics of particulate and nitrogen oxides by the SCR catalyst packed high temperature pleated filter bags** Y.O. Park, N.Hasolli
240	C-WG10S1P16	**Dust Cake Cleaning Characteristics of PPS Pleated**

		Bags with Double Venturi and Standard Venturi Y.O. Park, N. Hasolli
241	C-WG10S1P17	**Filtration of airborne carbon nanotubes with nanofiber filters** Y.K. Bahk and J. Wang
242	C-WG10S1P18	**Cellulose nanofibrils filters for environmental applications** L. Alexandrescu, K. Syverud, F.Belosi, G.Santachiara, F. Prodi, A. Donateo
243	C-WG10S1P19	**Aerosol retention in the secondary side of a tube bundle: Insights into a key scenario for nuclear safety** R.D. Tardáguila, C. Lopez, L.E. Herranz, M. García
244	C-WG10S1P20	**Deposition efficiency of charged aerosol particles in cylinder array** T.S. Zaripov, A.G. Egorov
245	C-WG10S1P21	**Inertial deposition of aerosol particles on a porous cylinder** O.V. Grigorieva, S.K. Zaripov
246	C-WG10S1P22	**Soot Nanoparticle Aggregate Filtration in Layer-Coated Diesel Particulate Filters** N. D. Vlachos, A.G. Konstandopoulos
247	C-WG10S1P23	**Experimental study on small cyclones for combustion engine gas cleaning** B. Sagot and J. Giardi
248	C-WG10S1P24	**The calculating method of resuspension based on the combination deterministic and statistical approaches** D.V.Tsaplin and V.N. Piskunov
249	C-WG10S1P25	**Analysis of asymptotic behavior of disperse systems with particle coagulation and breakage** V.N.Piskunov
250	C-WG10S1P26	**Analytical tests for simultaneous coagulation and condensation of composite particles** V.N.Piskunov
251	C-WG10S1P27	**Collapsing self-similarity in systems with coagulation and fragmentation of particles** V.N.Piskunov, I.V.Piskunova
252	C-WG10S1P28	**Thermophoretically Modified Brownian Coagulation** M. Arias-Zugasti and D. E. Rosner
253	C-WG10S1P29	**Calculation of the mobility radius of fractals in the continuum regime from their geometry**

		A.D. Melas, A.G. Konstandopoulos, L. Isella and Y. Drossinos
254	C-WG10S1P30	**Virtual generation of realistic soot particles: Impact to their morphological and optical properties.** A.Bescond, J.Yon, C. Rozé, F. X. Ouf
255	C-WG10S1P31	**3D study of fractal combustion aerosols using Electron Tomography** D. Lottin, D. Ferry, D. Delhaye, F.-X. Ouf and J. Yon
256	C-WG10S1P32	**Impaction dynamics of TiO2 agglomerates with different properties** M. Ihalainen, T. Lind, T. Torvela, K.E.J. Lehtinen and J. Jokiniemi
257	C-WG10S1P33	**Study of fluorescent imaging quantitative evaluation in protective equipment validation** S. Yang, C.H. Luo, M.Y. Syu, C.Y. Wen, K.H. Lin, S.H. Chiu and C.P. Chang
258	C-WG10S1P34	**Vibrational Spectroscopy of the Atmospherically Relevant Ions $A^-(H2SO4)m(HNO3)n(H2O)o$ with A^- = $HSO4^-$, $NO3^-$** N. Heine, T.I. Yacovitch, C. Hock, D.M. Neumark, C. Brieger, T. Wende, G. Meijer and K.R. Asmis
259	C-WG10S1P35	**Microhydration of Conjugate Base Anions Probed by Gas Phase Vibrational Spectroscopy** K.R. Asmis, N. Heine, T. Wende, L. Jiang, G. Meijer, T.I. Yacovitch, D.M. Neumark
260	C-WG10S1P36	**Heat effects at self-similar regime of droplet diffusion growth and the vapor-gas outflow** A.E. Kuchma and A.K. Shchekin
261	C-WG10S1P37	**High temperature oxidation of tungsten particles with account of Stefan flow** S.G. Orlovskaya, M.S. Shkoropado and F.F. Karimova
262	C-WG10S1P38	**Heat and mass transfer and thermal decomposition of firm aerosols when laser radiation action** L.I. Ryabchuk and S.K.Protas
263	C-WG10S1P39	**Flow and Heat Transfer in a Particle Laden Differentially Heated Cavity** J. Kalilainen, P. Rantanen, T. Lind, A. Auvinen, A. Dehbi, S. Güntay and J. Jokiniemi
264	C-WG10S1P40	**Modelling of spray drying of multicomponent aerosols** J.M. Gac and L. Gradoń
265	C-WG10S1P41	**The effect of droplet size on the evaporation and mass accommodation processes of water: a**

		molecular dynamics study Jan Julin and Ilona Riipinen
266	C-WG10S1P42	**Design of a simulation facility for workplace relevant aerosols of semi-volatile organic hydrocarbons: Set-up and first results** G.C. Dragan, E. Karg, H. Nordsieck, J. Schnelle-Kreis and R. Zimmermann
267	C-WG10S1P43	**Measurement of neutral sulphuric acid dimer concentration during CLOUD** A. Kürten, L. Rondo, S. Ehrhart, J. Curtius and the CLOUD collaboration
268	C-WG10S1P44	**Nucleation and condensation on presence of aerosols in boundary-layer flows** L.L. Bonilla and M.D. Camejo
269	C-WG10S1P45	**Particle nucleation in urban subtropical atmosphere** F. Salimi, L. Morawska, Z. Ristovski and M. Mazaheri
270	C-WG10S1P46	**Growth of sulfuric acid nano-particles at dry and wet conditions** L. Škrabalová, D. Brus, V. Ždímal and H. Lihavainen
271	C-WG10S1P47	**Using A09 Particle Size Magnifier for resolving formation and growth rates below 2 nm** K. Lehtipalo, A. Franchin, T. Nieminen, S. Schobesberger, J. Kangasluoma, J. Mikkilä, J. Vanhanen, T. Petäjä, and M. Kulmala
272	C-WG10S1P48	**Two amine campaigns; H2SO4 detection with different methods** K. Neitola, D Brus, U. Makkonen and H. Lihavainen
273	C-WG10S1P49	**Investigation of proton behaviour in water-sulphuric acid clusters using Path Integral Molecular Dynamics** J.L. Stinson, I.J. Ford, S.M. Kathmann and A. Michaelides
274	C-WG10S1P50	**Absorbing aerosols at high relative humidity: closure between hygroscopic growth and optical properties** J. Michel Flores, R. Z. Bar-Or, N. Bluvshtein, A. Abo-Riziq, A. Kostinski, S. Borrmann, I. Koren, and Y. Rudich
275	C-WG10S1P51	**Detecting correlations between the morphological parameters of multi-fractal samples of fractal-like aggregates** M. Woźniak, F.R.A. Onofri, S. Barbosa, J. Yon, C. Caumont, J. Mroczka
276	C-WG11S1P01	**Electrostatic and diffusion loss of charged nanoparticles in cylindrical tube connections with electric potential difference** D.K. Song, W.S. Hong and W.H. Shin
277	C-WG11S1P02	**Charge control of particles in air using centrifugal**

		force acting under applied electric field S. Matsusaka and K. Satoh
278	C-WG11S1P03	**Data inversion and calibration of a particle number concentration monitor** L. Hillemann, A. Zschoppe
279	C-WG11S1P04	**Structured chain-like aggregates by coagulation of charged particles** L. Knobel and H.-J. Schmid
280	C-WG11S1P05	**Influence on the bipolar stationary charge distribution** L. Knobel, A. Jain and H.-J. Schmid
281	C-WG11S1P06	**Break-up of charged ionic salt solution droplets at super-Rayleigh limits** Asit Ray and Kuo-Yen Li
282	C-WG11S1P07	**Performance of 85Kr, Soft X-ray and AC Corona Charging Sources for Particles <20 nm** J.J. Swanson, A.M. Boies, A. Collins
283	C-WG11S1P08	**Characterization of charging effects on different particles and discharge electrodes** Wen-Yinn Lin, Yuan-Yi Chang, Jin-Yuan Syu, Shao-Hao Lu, Chih-Chieh Chen
284	C-WG11S1P09	**Selective electrostatic deposition of airborne engineered nanoparticles on a patterned substrate of silicon cantilever sensor** H. S. Wasisto, S. Merzsch , A. Waag, E. Uhde, I. Kirsch and E. Peiner
285	C-WG11S1P10	**Post-corona diffusion charging versus radial ion profile in axisymmetric arrangement** Jidenko Nicolas, Alonso Manuel and Borra Jean-Pascal
286	C-WG11S1P11	**Sub-second diffusion charging** N. Jidenko, D. Maro, F. Gensdarmes, D. Boulaud and J.-P. Borra
287	C-WG11S1P12	**Atmospheric small-ion mobility downwind and upwind of AC high-voltage power lines** M.D. Wright, A.J. Buckley, J.C. Matthews and D.L. Henshaw
288	C-WG11S1P13	**Charging and collection of fine mists from a wet scrubber using activated oxidation catalysts** Bangwoo Han, Hak-Joon Kim and Yong-Jin Kim
289	C-WG11S1P14	**Removal performance of an electrostatic precipitator with edge to plate geometry for particulates in combustion gases for marines** H.J. Kim, B. Han, G.B. Cho and Y.J. Kim
290	C-WG11S1P15	**Enhancement of the filtration performance of metallic foam filter for diesel particulates by**

		electrostatic charging and collection H.J. Kim, B. Han, G.B. Cho and Y.J. Kim
291	C-WG11S1P16	**Numerical simulations of electrosprays including induced gas flow** A.K. Arumugham, J. Grifoll and J. Rosell-Llompart
292	C-WG10S1P52	**Hybrid QMOM-Orthogonal-Collocation Method: Application to Aerosol Dynamics under Coagulation** M. Arias-Zugasti

Friday 7th September

08:45-09:45 Plenary 5. **Helmuth Horvath**
Photophoresis – the forgotten force
Room: Auditorio
Chair: F.J. Olmo

09:45-10:00 Best Poster Awards

10:00-10:30 Coffee-break

10:30-12:50 **Session WG01S7O. Aerosol Cloud Interaction**
Room: Auditorio
Chairs: M. Gysel / Z. Kanji

10:30	WG01S7O01	**Combustion Aerosol over Marine Stratus: Long Range Transport, Subsidence and Aerosol-Cloud Interactions over the SE Pacific** A. D Clarke, J. Kazil, G. Feingold, S. Freitag, C. McNaughton, J. Snider, T. Lynn Campos, V. Breckhovskikh
10:50	WG01S7O02	**Aerosol cloud interactions of trade wind cumuli - A single cloud contact analysis** F. Ditas, B. Wehner, H. Siebert, R.A. Shaw, H. Wex, T. Schmeißner, G. Roberts, A. Wiedensohler
11:10	WG01S7O03	**Aerosol optical properties before, during, and after cloud events at Puijo** A. Leskinen, A. Arola, H. Portin, S. Romakkaniemi, A.-P. Hyvärinen, A. Laaksonen, K.E.J. Lehtinen and M. Komppula
11:30	WG01S7O04	**Mixing state resolved hygroscopicity closure between sub- and supersaturation in Paris** Zs. Jurányi, M. Gysel, T. Tritscher, E. Weingartner, M. Laborde and U. Baltensperger
11:50	WG01S7O05	**Immersion freezing of biological particles** S. Hartmann, T. Š. Temkiv, B. G. Pummer, S. Augustin, T. Clauss, D. Niedermeier, H. Wex, J. Voigtländer, U. G. Karlson, H. Grothe and F. Stratmann
12:10	WG01S7O06	**Ice formation via deposition mode nucleation on hydrophobic and hydrophilic surfaces** J.B.C. Pettersson, X. Kong, E.S. Thomson, and N. Markovic´

12:30	WG01S7O07	**Cloud particle detection at the AIDA chamber & over the UK and Northern Canada** M. Krämer, J. Meyer, A. Afchine M. Schnaiter O. Möhler S. Benz A. Abdelmonem, M. Gallagher, J. Dorsey, P. Brown, A. Wooley, C. Schmitt, R. Newton and D. Baumgardner
Reserve paper	WG01S7B00	**Inhibition of Heterogeneous Ice Nucleation of Mineral Dust Particles Exposed to Ozone** Z.A. Kanji, A. Welti, C. Chou, and O. Stetzer

10:30-12:50 **Session SS03S1O. Source apportionment**
Room: Legado Andalusí
Chairs: A. Prevot / X. Querol

10:30	SS03S1O01	**Towards a European Common Protocol for Receptor Modelling** C.A. Belis, F. Karagulian, B. R. Larsen, F. Amato, O. Favez, I. El Haddad, R.M. Harrison, A. Prevot, U. Quass, R. Vecchi, M. Viana, P. Paatero, P.K. Hopke
10:50	SS03S1O02	**Application of PMF to the Source Apportionment of Polycyclic Aromatic Hydrocarbons** Roy M. Harrison, Eunhwa Jang and Mohamed S. Alam
11:10	SS03S1O03	**Comparing source apportionment results by a chemistry transport model against PMF analyses for north western Europe** M. Schaap, C. Hendriks, R. Kranenburg, T.A.J. Kuhlbusch, U. Quass and J. Vercauteren
11:30	SS03S1O04	**Multilinear engine 2 applied to long-term on-line data of non-refractory submicron aerosol in the city of Zurich** F. Canonaco, J. Slowik, U. Baltensperger, A.S.H. Prévôt
11:50	SS03S1O05	**Aging fingerprints on the carbon functional groups in 2-stroke scooter exhaust particles with STXM/NEXAFS** E. Coz, S. Platt, I. El Haddad, J. G. Slowik, A. S. H. Prévôt, S. Steimer, G. Grzinic, M. Lampimäki, B. Artíñano and M. Ammann
12:10	SS03S1O06	**Considering the different thermal behaviour of wood-burning and diesel emissions for 14C-based source apportionment of elemental carbon** S. Szidat, Y.L. Zhang, G. Ciobanu, P. Zotter, N. Perron, M.C. Minguillón, L. Wacker, U. Baltensperger, and A.S.H. Prévôt

12:30	SS03S1O07	**Safe PMF: Minimizing the Impact of Erroneous Data in Source Apportionment** P. Paatero and P.K. Hopke
Reserve paper	SS03S1B00	**PMF vs CMB for source apportionment of PM: advantages, limitations, complementarity of the two models explored by applications at different types of environments** C. Piot, M.F.D. Gianini, J. Cozic, L. Polo, J.-L. Besombes, J.-L. Jaffrezo and C. Hueglin

10:30-12:50 **Session SS04S1O. Chemical characterization of combustion aerosols**
Room: Faraday
Chairs: R. Niessner / F. Ouf

10:30	SS04S1O01	**Soot Aerosol – Hard nuts to crack for an analyst** R. Niessner
11:10	SS04S1O02	**Organic emissions from modern small scale wood combustion appliances – Chemical characterization and toxic potential of fine particular matter** J. Orasche, J. Schnelle-Kreis, G. Abbaszade, H. Hartmann,H. Ruppert, R. Zimmermann
11:30	SS04S1O03	**On-line characterization of aerosols from transient biomass combustion** E. Z. Nordin, A. C. Eriksson, R. Nyström, E. Pettersson, J. Rissler, E. Swietlicki, M. Bohgard, C. Boman and J. Pagels
11:50	SS04S1O04	**Impact of iron content on structure and thermo-chemical characteristics of multicomponet soot aerosol** H. Bladt, J. Schmid, E. Kireeva, O. B. Popovicheva, N. P. Ivleva and R. Niessner
12:10	SS04S1O05	**Black carbon sources characterized using the soot-particle aerosol mass spectrometer (SP-AMS)** J.C. Corbin, A. A. Mensah, M. Gysel, M. Laborde, A. Keller, J. Kim, A. Petzold, and B. Sierau
12:30	SS04S1O06	**Chemical and physical characterization of combustion aerosols** J. Jokiniemi

Reserve paper	SS04S1B00	**Detailed chemical characterization of ultrafine particles from vehicle exhaust** F. Donaz, L. Polo, C. Piot, J. Cozic, B. Golly, N. Marchand, J.L. Besombes and J.L. Jaffrezo

10:30-12:50 **Session WG11S1O. Electrical effects**
Room: Cine 3
Chairs: A. Bologa / C. Yurteri

10:30	WG11S1O01	**Indirect Photoelectric Diffusion Charging of Aerosols** B. Grob and R. Niessner
10:50	WG11S1O02	**High resolution mobility and mass spectra of corona-generated ions** H.E. Manninen, A. Franchin, E. Järvinen, J. Kangasluoma, S. Schobesberger, T. Petäjä and M. Kulmala
11:10	WG11S1O03	**Study of the corona discharge in the syngas at various gas temperatures and pressure** A. Bologa, H.-R. Paur, H. Seifert and K. Woletz
11:30	WG11S1O04	**Stability of the cone-jet mode in electrohydrodynamic spraying** J.L. Castillo, S. Martin, A. Perea and P.L. Garcia-Ybarra
11:50	WG11S1O05	**Electrospray deposition of nanoparticles onto airborn microparticles** C.U. Yurteri, N. Ellis, J.R. van Ommen
12:10	WG11S1O06	**Determination of the Transition Regime Collision Rate in the Presence of Potential Interactions from Mean First Passage Time Calculations** C. J. Hogan Jr., R. Gopalakrishnan, H. Ouyang
12:30	WG11S1O07	**Charge Distribution of Primary Nanoparticles Generated by Spark Discharge** K.Barmpounis, T.V. Pfeiffer,G. Biskos, A. Schmidt-Ott
Reserve paper	WG11S1B00	**Selective electrostatic deposition of airborne engineered nanoparticles on a patterned substrate of silicon cantilever sensor** H. S. Wasisto, S. Merzsch , A. Waag, E. Uhde, I. Kirsch and E. Peiner

10:30-12:50 **Session SS05S1O. Field observations and modeling of special events**
Room: Gutenberg
Chairs: M. Krämer / S. Wurzler

10:30	SS05S1O01	**Physico-chemical properties of airborne radiocesium released from the Fukushima nuclear accident** N. Kaneyasu, H. Ohashi, F. Suzuki, and T. Okuda
10:50	SS05S1O02	**Environmental Impact of Fukushima Fallout in Southeast Spain** F. Piñero-García, J. Drożdżak and M.A. Ferro-García
11:10	SS05S1O03	**Atmospheric dispersion and ground deposition induced by the Fukushima Nuclear Power Plant accident at local scale: simulation and sensitivity study** I. Korsakissok, A. Mathieu and D. Didier
11:30	SS05S1O04	**Observations in Germany, France, and Great Britain during eruptions of the Eyjafjallajökull volcano in 2010** S. Wurzler, P. Bruckmann, J. Friesel, J. Geiger, H. Hebbinghaus, W. Straub, D. Gladtke, Pfeffer, T. Kuhlbusch, R. Lumpp, S. Heupel Santos, M. Memmesheimer, H. Jakobs, E. Friese, L. Nieradzik, H. Elbern, D. Klugmann, S. Gilge, O. Favez, A. Colette, L. Chiappini
11:50	SS05S1O05	**Volcanic ashes, desert dust and flying ashes from forest fires: all radiactive clouds!** O. Masson, J.C. Sabroux, D. Piga, R. Gurriaran, J. Loyen
12:10	SS05S1O06	**Eyjafjallajokull volcanic dust characteristics from LIDAR data and in-situ aerosol size distributions** M. Del Guasta, P. Cristofanelli, A. Marinoni, P. Bonasoni
12:30	SS05S1O07	**Eyjafjallajökull volcanic ash number concentration retrieval at Lyon (France) with a UV-polarization Lidar** G. David, B. Thomas, A. Miffre and P. Rairoux
Reserve paper	SS05S1B00	**Modification of cloud properties by the Eyjafjallajökull eruption** H. Vogel, M. Bangert, B. Vogel, A. Wintzen, D. Barahona, A. Nenes, and J. Förstner

12:50-13:30 Closing Ceremony. Room: Auditorio

Sponsors and Exhibitors

Airmodus Ltd

Gustaf Hällströmin katu 2 A
00560 Helsinki
Finland

Tel: +358 44 3038 378
E-mail: info@airmodus.com
HYPERLINK "http://www.airmodus.com" www.airmodus.com

Airmodus is a group of aerosol physicists specialized in aerosol particle measurement technology, having long experience both in laboratory and field experiments. The company is based in Helsinki and as a spin-off company from the University of Helsinki it has straight contact to the leading research in the field of aerosol physics. We specialize in providing tools for measuring the smallest sub - 2 nm aerosol particles.

Airmodus offers Particle Size Magnifiers that allow you to detect particles as small as 1 nm in diameter; easy to use Condensation Particle Counters with a cut-off size fit for your measurement needs; and special mass spectrometer inlets for detection of challenging gaseous compounds (e.g. sulfuric acid, ammonia, amines).

Alava Ingenieros Group has been providing high technology solutions in the Testing, Measurement, Communications Security, Defence and Preventive Maintenance fields since it was first founded in 1973. The group offers consultancy, engineering, distribution, training and technical services, providing turn-key projects for several sectors including Research Centres, Universities Aerospace, Automotive, Security, Defence, Communications and Finance, as well as Testing, Public Services and Industry in general.

Alava Ingenieros Group, as technological partner of TSI in Spain and Portugal, bring you the possibility to know the new solutions launched by TSI, which are described in the previous lines. Besides, Alava Ingenieros Group launches new solutions from other technological partners, such as Unitec and Sigma Space, for the following applications:

- Long term measurements of vertical aerosol distribution
- Tracking of volcano ash and aerosols
- Observation of multiple cloud layers
- Air quality monitoring

We look forward to seeing you at our booth No 11-13

Contact:

Alava Ingenieros, S.A.
C/ Albasanz, 16 - Edificio Antalia
28037 Madrid
Spain
Telephone: +34 91 567 97 00
Fax: +34 91 567 97 11
E-mail: alava@alava-ing.es
Web: www.alavaingenieros.com

Cambustion Ltd

J6 The Paddocks
347 Cherry Hinton Road
Cambridge CB1 8DH
United Kingdom

Tel: +44 1223 210250
Email: cambustion@cambustion.com
www.cambustion.com

Cambustion instrumentation is already used in over 25 countries for both academic research and commercial R&D, with local representation in China, France, India, Japan and North America.

The new Centrifugal Particle Mass Analyzer (CPMA) allows classification of ultrafine aerosol according to mass: charge ratio. With a touch screen interface plus analog and digital connectivity to other aerosol instruments (e.g. CPCs) the CPMA facilitates a wide range of aerosol studies.

Our DMS series instruments offer the fastest (from 200 ms $T_{10\text{-}90\%}$ at 10 Hz) real-time electrical mobility size/number spectra available from 5nm – 2.5µm, with unrivalled sensitivity. Applications include ambient monitoring, combustion aerosol, workplace exposure and engineered nanoparticle research.

With fully integrated sampling and dilution options, DMS series instruments can be used for both ambient applications and straightforward direct sampling of high concentration aerosol sources through software selection of appropriate dilution.

Meet us at the Cambustion exhibit – booth No. 3

CERTIO MEDIO AMBIENTE,S.L.

c/ Fragua 4A – 28760 Tres Cantos (Madrid)
Tel. +34 918 036 433 - Fax. +34 918 036 433

Razón Social: c/ Baza, parcela 6 I
Polígono Juncaril - Albolote (Granada)
Tel. +34 958 490 045 - Fax. +34 958 49 00 46

E-mail: aperez@certio.com
www.certio.com

Certio Environmental is the result of the implementation of a process of concentration of environmental sector companies working under internatio-nally recognized quality systems

Improving Sustainable Development

Certio Environmental was created with the aim of providing improved services in sustainable development through the provision of inspection, testing, inspection and maintenance of systems that ensure the environmental quality

Specialization

The main objective is to bring specialized services in four business lines: Air, Water, Soil and Noise.
In Air business line our specialization is:

- ✓ Environmental control networks for measuring the air quality in emission and inmission levels: remote stations, data transmission systems, processing data centers and presentation of the information for the intended audience
- ✓ Maintenance of Control Air Quality Networks
- ✓ Supply, start up, reparation and maintenance of Air quality analyzers (O3, CO, SO2, NOx, BTX, PM10, PM2,5….)
- ✓ ENAC Accreditation Calibration Lab. according UNE-EN ISO/IEC 17025
- ✓ ENAC Accreditation Inspection Activities in Environmental Area, according UNE-EN ISO/IEC 17020
- ✓ CEMs
- ✓ Meteorological measurement systems

Customer proximity

Deep knowledge of the needs of our clients allows us to detect, analyze and evaluate problems, offer solutions and streamline processes. Solutions based on new technologies to add value in Environmental Control Systems and Industrial Automation Systems. Marketing teams of environmental pollution control and automatic measure, from leading international manufacturers

Copley Scientific Limited

Colwick Quays Business Park
Private Road No. 2
Colwick
Nottingham NG4 2JY
United Kingdom

Tel: +44 (0)115 961 6229
E-mail: sales@copleyscientific.co.uk
www.copleyscientific.com

Copley Scientific is a major supplier of air sampling and aerosol characterisation equipment for academic research and industrial applications. In the pharmaceutical industry, the company is also recognised as the world's leading manufacturer and supplier of inhaler test equipment and is a major provider of testing systems for other pharmaceutical dosage forms.

Having offices in the UK and Switzerland, Copley Scientific works in partnership with US based aerosol particle science experts MSP Corporation, whose air sampling and aerosol characterisation products the company distributes throughout Europe. Such products include the market leading range of MOUDI cascade impactors, the real-time fibre monitor model 7400AD, the Water-based Condensation Particle Counter (CPC) and the wide-range particle spectrometer (WPS) with electrical ionizer, covering the particle size range: 5 nm to 10 microns.

Dekati Ltd.
Osuusmyllynkatu 13
33700 Tampere
Finland

Tel: +358 3357 8100
E-mail: sales@dekati.fi
www.dekati.com

Dekati Ltd. develops, manufactures and markets instrumentation needed in fine particle measurement and sampling. In 1995, Dekati introduced the world's first real-time fine particle concentration and size distribution measurement instrument. Since then, our R&D department has continually increased the range of products. Through the extensive global sales network, we are able to serve our customers around the world.

Dekati develops new products in close co-operation with the world's leading universities and companies. Our mission is to provide our customers with innovative fine particle measurement solutions that guarantee accurate results.

Dekati instruments are used for example in the following application areas:

- Combustion Processes (Diesel, Gasoline, Oil, Coal, Bio-fuels etc.)
- Environmental Ambient Aerosol Research and Monitoring
- Pharmaceutical Drug Screening and Inhalator R&D
- Nanotechnology
- Material Processing

Visit www.dekati.com for more details on our company and our products, or contact us at sales@dekati.fi for further information.

Droplet Measurement Technologies

2545 Central Avenue
Boulder
Colorado, 80301
United States

Tel: +1 303-440-5576
E-mail: info@dropletmeasurement.com
www.dropletmeasurement.com

Droplet Measurement Technologies offers accurate and sensitive instruments for real-time measurement of aerosol particle physical, optical, chemical and biogenic properties. The Ultra-High Sensitivity Aerosol Spectrometer (UHSAS) measures particle size from 60 nm to 1000 nm, the new Photoacoustic Extinctiometer (PAX) and Photoacoustic Soot Spectrometer (PASS) measure particulate light absorption and scattering at different wavelengths, producing BC mass and climate-relevant properties like single scattering albedo (SSA) from a single instrument. The Single Particle Soot Photometer (SP2) measures incandescence from BC-containing particles providing BC mass (independent of mixing state), number concentration and size distribution. Both techniques measure particles in-situ, eliminating filter artifacts. The CCN-100 and Single Particle Ice Nucleus (SPIN) spectrometer measure the concentrations of CCN and IN and the Waveband. Integrated Bioaerosol Sensor WIBS-4 measures the size spectra of primary biological aerosol particles (PBAP).

DMT's extensive line of electro-optical particle analyzers are used by scientists worldwide for airborne and ground-based measurement applications in atmospheric and climate research, air quality monitoring, meteorology, aircraft certification, spray characterization, weather modification and cloud seeding,. In addition to black carbon, DMT instruments characterize aerosols, dust, volcano ash, sprays, cloud droplets, ice crystals, fog and precipitation, and cloud condensation nuclei.

For more information, please visit us in the exhibition hall, call +1 303-440-5576, visit our website www.dropletmeasurement.com, or email info@dropletmeasurement.

Ecotech Pty Ltd

1492 Ferntree Gully Road
Knoxfield
Victoria 3180
Australia

Tel: +61 3 9730 7800
E-mail: info@ecotech.com
www.ecotech.com

With our expanding range of scientific research instrumentation and sophisticated data collection, validation and reporting software, Ecotech provides solutions that ensure air quality and climate data are accessible to everyone without compromising on quality and reliability.

Our Aurora integrating nephelometers range from single to multiple wavelength versions and incorporate both polar and particle correlating options. Using an innovative LED light source, the Aurora 3000 nephelometer simultaneously measures at 525nm (green), 450nm (blue) and 635nm (red) to enable wide and in-depth analysis of particulate matter.

Complimenting this range and also working with other manufacturer's aerosol instruments, is our sample conditioning system. Allowing the simultaneous measure of two parallel aerosol instruments in real time, this system gives scientists the ability to analyse the difference in humidity on the same sample.

With more than 35 years designing and supplying air quality instrumentation Ecotech is regarded as one of the world's leading suppliers in air monitoring. Our commitment to R&D ensures that we stay at the forefront of innovation.

GRAW Radiosondes GmbH & Co. KG

Muggenhofer Str. 95
90429 Nuremberg
Germany
Tel.: +49 911 3201 100
Fax: +49 911 3201 150
E-mail: info@graw.de
Website: www.graw.de

GRAW is a well-established company developing and manufacturing Upper Air Sounding Systems since 1938. GRAW's customers are academic research and meteorological institutions worldwide.

Our product portfolio includes:

- Radiosondes
- Ground stations
- Visualization and evaluation software for meteorological data
- Antenna systems
- Accessories for balloon ascents
- Complete Upper Air Sounding Systems

As a 100% daughter of the family-owned NORIS Group, GRAW has access to more than 200 professionals worldwide but still benefits from the flexibility and fast decisions of a family owned business.

Have we piqued your interest? Please visit our website to see our complete range of products or call us.

GRIMM Aerosol Technik GmbH & Co. KG
Achim Edfelder
Dorfstrasse 9
83404 Ainring
Germany

Tel: +49 (0) 8654 578-33
E-mail: ae@Grimm-Aerosol.com

www.grimm-aerosol.com

GRIMM Aerosol Technik GmbH & Co.KG was founded over 25 years ago by Dr.-Ing. Hans-Jurgen Grimm in Bavaria/Germany. Today, GRIMM Aerosol Technik is one of the worldwide leading companies in the field of high-tech aerosol measurement instrumentation due to its innovations and quality manufacturing.

GRIMM Aerosol Technik offers a wide range of complete solutions for the continuous measurement of fine and ultrafine aerosols.

Instruments such as Environmental Dust Monitors, Aerosol Spectrometers, Particle Counters and Sizers, Filter Testers, and Aerosol Generators consistently meet the requirements of a world-wide increasing number of customers in research and industry. Specialists in-house will advise about the correct instruments for particular applications, e.g. for ambient air, emission, occupational health, filter efficiency and / or exhaust gas measurements, for quality control and for pharmaceutical, atmospheric or epidemiological studies.

Recently expanded production facilities are located in Pouch/Saxony-Anhalt/Germany. World-wide first-class customer service is offered through our U.S. subsidiary and our offices in Canada, UK, Middle East and Asia, and supplemented by a close network of international representatives.

INGENIEROS ASESORES, S.A.

Parque Tecnológico, 39
33428 Llanera (Asturias)
Tfno.: 985.98.00.50
Fax: 985.98.55.51
comun@ingenierosasesores-sa.es
www.ingenierosasesores.com

Ingenieros Asesores, S.A. was established in 1985 and its only mission is satisfying companies' demand of environmental services, encompassing all type of solutions, from the design of environmental strategies, to the measurements of pollutant parameters.
Our strategy has focused on offering these solutions on a technological base. The services that we offer differ from others due to our exclusive specialization in environment and our advanced technological proposals.

Automatic Systems Department for Environmental Control:

The environmental legislation increasingly requires automatic control of pollutant parameters, both air and water.
Ingenieros Asesores S.A., specializes in all aspects of environmental control, having developed a set of action items that allow you to meet any demand in this field, from the simplest sensor to the comprehensive control system more sophisticated, addressing the following activities:

- Air pollution monitoring networks
- Emissions measurement systems
- Mobile laboratories
- Communication Systems
- Public Information
- Calibration and audit

Our company is certified under ISO 9001 for supply, installation, maintenance and calibration of instruments and systems for continuous monitoring of air pollution and water.

IONER®, a trademark of RAMEM S.A.

AEROSOL & VOLATILE ANALYZING TECHNOLOGY
www.ioner.eu www.ramem.com
Tel: (+34) 91 404 45 75
Fax:(+34) 91 403 45 96
Email: sales@ioner.eu

RAMEM-IONER® is a Spanish company dedicated to the development of innovative aerosol instruments. RAMEM-IONER will be introducing at EAC 2012 in Granada its HRIMS (High Resolution Ion Mobility Spectrometer), an instrument based in a planar, high resolution DMA for the study of the early stages of nucleation.

Visit us at booth number 4.

Magee Scientific is the originator of the Aethalometer®, the most-widely-used instrument for the real-time measurement of Black Carbon aerosol particles in the atmosphere. These particles reduce visibility; adversely impact human health; and contribute to regional and global climate change. Aethalometers are installed on all continents: from cities in China to the South Pole, from the Sahara Desert to the Amazon basin.

Research into methods for the real-time measurement of light absorbing aerosols began in Berkeley in approximately 1978. The first-ever Aethalometer® was deployed in a field study in the summer of 1980: the first aircraft measurements were made in 1982, and in 1986 an Aethalometer started making measurements of aerosol Black Carbon at the most remote location on the planet, the South Pole Observatory. Magee Scientific Company was established that same year to develop the Aethalometer further and make it available to the aerosol research and monitoring community. From 1999 to 2001, the instruments were also distributed by Andersen Instruments Inc. and subsequently Thermo Environmental Instruments as identical hardware, but with the chassis painted in 'Andersen' or 'Thermo' colors and name. Distribution by Andersen/Thermo has now been discontinued.

Aethalometers have been used in increasing numbers over the years: a large number of reports have been published in the open scientific literature. A compendium of these reports is found at the literature link.

Contact us:

Magee Scientific Corporation
1916A M. L. King Jr. Way
Berkeley CA 94704
USA
tel: +1 510.845.2801
fax: +1 510.845.7137

Aerosol d.o.o.
Kamniška 41
SI-1000 Ljubljana
Slovenia
tel: +386 59 191 220
fax: +386 59 191 221

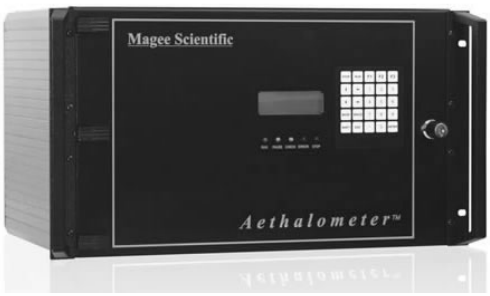

Matter Aerosol

Andreas Knecht
Bremgarterstrasse 62
5610 Wohlen
Switzerland

Tel: +41 56 6186630
Fax: +41 56 6186639
E-mail: infot@matter-aerosol.ch
www.matter-aerosol.ch

Matter Aerosol (formally Matter engineering) specialises in the measurement and characterisation of nanoparticles from combustion processes and nanoparticles in ambient air. Matter Aerosol combines over 50 years of experience in instrument design and development with latest research results about nanoparticles, for application in laboratories to real-world problems.

Key Competencies:

- Equipment - design, development and production of equipment to sample, dilute, measure and characterise nanoparticles from combustion and ambient air.

- Services - nanoparticle emission measuring and testing programs for combustion engines, boilers, particle traps, fuels and additives at our partners' test benches or at the customer's site.

- Transfer - conferences and seminars on nanoparticle measurement.

Metrohm Applikon, headquartered in Schiedam, the Netherlands has more than 35 years' experience in delivering solutions for laboratory, at-line and on-line wet chemical analysis.

Part of the worldwide Metrohm AG group, Metrohm Applikon has access to Metrohm's know-how and expertise in ion analysis.

MARGA (**M**onitor for **A**e**R**osols and **G**ases in ambient **A**ir) is an on-line ion chromatograph that measures the concentration of soluble inorganic species in aerosols and their related gas phase components in ambient air. Hourly simultaneous results for gases and aerosols can be accessed from a remote workstation, with result quality being maintained by an internal standard and detailed system diagnostics.

Jointly developed with ECN, The Netherlands**, MARGA** is distributed world-wide through Metrohm Applikon's distributor network; most members of which belong to the Metrohm group of companies.

Contact information:

Metrohm Applikon B.V.
P.O. Box 149
3100 AC Schiedam
The Netherlands
T: +31 (0)10 29 83 555
F: +31 (0)10 437 96 48
E: ELe@metrohm-applikon.com
W: www.metrohm-applikon.com

Palas® GmbH
Greschbachstr. 3b
76229 Karlsruhe
Germany

Tel: +49 (0)721 96213-0
Fax: +49 (0)721 96213-33
E-mail: mail@palas.de
www.palas.de

With more than 60 submitted patents, the Palas® GmbH has effectively set standards in aerosol technology since 1983. Today, Palas® offers a complete product range for the continuous aerosol generation and measurement from 5 nm to 100 µm.

Our innovations result in superior quality and durability of the products that lead to unique technical and economic advantages for our customers.
Our core competencies are:

- Particle generation
- Particle measurement systems (for high pressures, temperatures, processes, environment and workplace, inhalation)
- Nanoparticle measurement systems
- Filter test systems
- Continuous fine dust monitoring systems
- Dilution systems
- Cleanroom particle technology
- Calibration systems

Well-known industrial enterprises and research institutions worldwide have decided in favour of Palas® products and have thus established Palas® as a worldwide market leader.

Sunset Laboratory Inc

Main Office and Sales
10180 SW Nimbus Avenue
Suite J/5
Tigard, OR 97223-4338
Tel: 503 624 1100
E-mail: ben@sunlab.com
http://www.sunlab.com

Sunset Laboratory Inc. has specialized in the analysis of air pollution for carbon aerosols since 1984. As well as performing the OCEC analysis, Sunset Laboratory also provides instrumentation for carbon aerosol analysis. Our equipment is suitable for the laboratory or in the field, and ready for use with the NIOSH method 5040, IMPROVE, and EUSAAR 2 protocols. Clients include researchers working for government regulatory agencies, private companies, commercial laboratories, and universities.

Topas GmbH

Tel: +49 (351) 21 66 43 - 0
Fax: +49 (351) 21 66 43 55
E-Mail: office@topas-gmbh.de
www.topas-gmbh.de

Topas GmbH Dresden is a specialist company in the field of particle technology and filter testing systems. Our standard product range comprises:

- aerosol generators (mono - and polydisperse, solid and liquid particles)
- particle size measuring instruments for aerosols and liquids
- aerosol dilution systems
- electrostatic aerosol neutralizers
- process aerosol monitors
- filter testing technology and instruments
- clean room measuring equipment
- pore size measuring instruments

Topas also provides solutions for special applications like the dispersion of complex powders, test stands for particle filters and for adsorptive filters, filter media testing, blow-by measuring etc. Our corporate philosophy allows us to meet of a variety of customer needs. Many years of experience, our know-how as well as close cooperation with universities, research centres and industrial partners is the ideal basis for the development of new and innovative solutions. Our reliable measuring and testing equipment has proven successful worldwide.

TSI

For more than 50 years TSI Particle Instruments have been trusted by researchers to provide reliable, repeatable results. During EAC in Granada TSI's engineers will give you an overview of new products in the field of nanotechnology including the new NanoScan 3910 and the Optical Particle Sizer (OPS) Model 3330. Stop by and learn about:

- Sizing of Nanoparticles in the Gas and Liquid phase
- Workplace safety
- Experience and Solutions for Nanoparticle Characterization for scientific research, Industrial R&D, and process and quality control.

We look forward to seeing you at our booth No 11-13

Contact:

TSI GmbH
Neuköllner Strasse 4
52068 Aachen
Germany
Telephone: +49 241-52303-0
Fax: +49 241-52303-49
E-mail: answersEU@tsi.com
Web: www.tsi.com/Nanotechnology

URG Corporation

116 South Merritt Mill Rd.
Chapel Hill, North Carolina 27516 USA

Tel: 919-942-2753
E-mail: info@urgcorp.com
www.urgcorp.com

URG Corporation manufactures the **Ambient Ion Monitor (AIM) System** for the *continuous direct* measurement of particulate nitrate, sulfate, ammonium in PM2.5 plus gas measurements of nitric acid, SO_2 and ammonia. The **AIM System** analyzes particles, gases and organics. The **AIM System** incorporates a **Dionex Reagent-Free Ion Chromatograph**. The **AIM System** has detection limits of 0.1μg/m^3 for each of the required analytes and 0.081μg/m^3 for ammonia. The multi-pollutant data is instantly available on an hourly basis.

URG provides a wide variety of instruments for indoor and outdoor air sampling. Our **Annular Denuder System (ADS)** collects both acidic and basic gases and is designed to meet USEPA's Compendium Method IO-4.2. URG's complete collection of **aluminium cyclone inlets** are Teflon© coated, a patented process that minimizes the losses of reactive gases such as HNO_3 and NH_3 to the internal surfaces of the cyclone. URG provides **stainless steel cyclones** and **filter holders** for diesel emissions.

URG air sampling instrumentation is used in Europe, Asia, North America, Australia, Antarctica, Africa and South America.

Our latest innovations...

Ecotech's quality and expertise in manufacturing integrating nephelometers is well known, so this year visit us to find out what else we can do for you.

- Wet/dry sample conditioning system to compliment any aerosol instrument
- Airodis data evaluation & reporting software
- WinAQMS data acquisition systems
- Aurora 4000 polar nephelometer
- Aurora series of 1 & 3 wavelength nephelometers

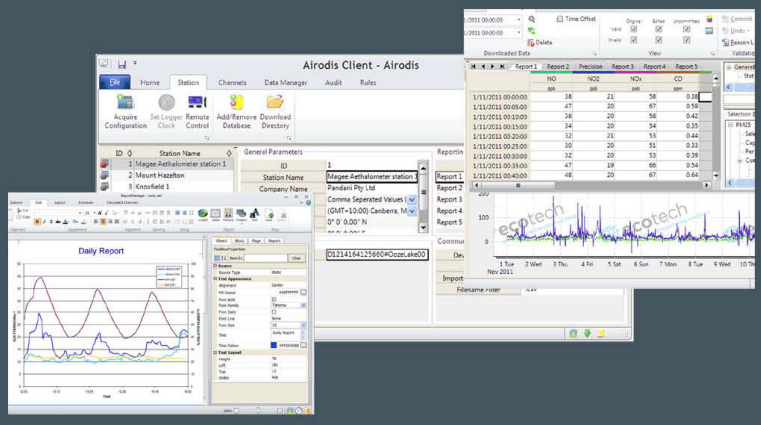

Visit booth 6 to discuss our innovative solutions for conditioning, measuring and reporting

www.ecotech.com

ecotech
environmental monitoring solutions

info@ecotech.com

Monday, September 3, 2012

Plenary 1

Characterization of Responses to Carbon Nanotubes and Carbon Nanofibers

V. Castranova

National Institute for Occupational Safety and Health, Morgantown, West Virginia, USA
Keywords: nanoparticles, carbonaceous particles, lung/particle interaction, occupational health
Presenting author email: vic1@cdc.gov

Methods have been perfected to arrange carbon atoms in a crystalline graphene lattice with a tubular morphology. A single-walled carbon nanotube (SWCNT) is composed of a single cylindrical sheet of graphene and has a diameter of 0.5-2 nm. Multi-walled carbon nanotubes (MWCNT) consist of multiple tubes within a tube and have diameters of 10-80 µm, depending on the number of concentric tubes forming the structure. CNT can range in length from 0.5-30 µm. Carbon nanofibers are composed of graphene layers arranged at an angle to the fiber axis. CNF range from 70-200 nm in diameter and 10-100 µm in length.

CNT exhibit high tensile strength, possess unique electrical properties, are resistant to acid or high temperature, and can be easily functionalized. Therefore, application as structural materials, in electronics, as heating elements, in batteries, in production of conductive and stain resistant fabric, for bone grafting and dental implants, as well as in targeted drug delivery are being developed. CNF are strong, flexible fibers which are currently being used to produce strong but light weight composite materials.

CNT and CNF can be aerosolized readily upon agitation with peak airborne particulate concentrations being associated with workplace activities such as: weighing, transferring, mixing, blending, or sonication. Most airborne CNT or CNF found in workplaces are loose agglomerates of micrometer (µm) diameter. However, due to their low density, they remain in workplace air for a considerable time and a large fraction of these structures are respirable. Since inhalation of CNT or CNF by workers is possible, it is critical to evaluate the possible adverse effects of such exposure.

In rat and mouse models, pulmonary exposure to SWCNT, MWCNT or CNF has been reported to cause the following dose-dependent pulmonary reactions: 1) acute pulmonary inflammation and injury, 2) rapid and persistent formation of granulomatous lesions at deposition sites of large CNT agglomerates, and 3) rapid and progressive alveolar interstitial fibrosis at deposition sites of more dispersed CNT or CNF structures. On an equal mass lung burden basis, SWCNT are more fibrogenic than MWCNT or CNF. In addition, functionalization of MWCNT with carboxylic groups has been shown to decrease their inflammatory and fibrotic potency.

Pulmonary exposure to CNT has also been associated with various systemic effects. Pulmonary exposure to SWCNT has been shown to induce oxidant stress in aortic tissue and increase plaque formation in an atherosclerotic mouse model. Pulmonary exposure to MWCNT depresses the ability of coronary arterioles to respond to dilators. These cardiovascular effects may be due to neurogenic signals from sensory irritant receptors in the lung. The involvement of such a neuro-mediated mechanism is supported by the fact that pulmonary exposure to MWCNT induces upregulation of mRNA for inflammatory mediators in selected brain regions, and pulmonary exposure to SWCNT upregulates the baroreceptor reflex. There is also evidence that pulmonary exposure to MWCNT can induce levels of inflammatory mediators in the blood, which may affect the cardiovascular system.

Since CNT and CNF have been shown to be biologically active in animal models and workplace aerosolization has been measured, it appears prudent to develop strategies to minimize workplace exposure. Evidence indicates that engineering controls and personal protective equipment are effective in significantly decreasing inhalation of CNT and CNF by workers. In addition, administrative controls, worker training, and implementation of good handling practices have been recommended by NIOSH.

Monday, September 3, 2012

Session WG01S1O. Optical Properties

Optical properties of SiO_2 particles : inversion data from laboratory IR absorption spectra.

Denis PETITPREZ[1], Hervé HERBIN[2],

[1]Laboratoire de Physico-Chimie des Processus de Combustion et de l'Atmosphère (PC2A), UMR CNRS 8522, Université Lille 1, Cité Scientifique - Bâtiment C11, 59655 Villeneuve d'Ascq, France

[2]Laboratoire d'Optique Atmosphérique (LOA), UMR CNRS 8518, Université Lille 1, Cité Scientifique - Bâtiment P5, 59655 Villeneuve d'Ascq, France

Keywords: optical properties, SiO_2, refractive index
Presenting author email: Denis.Petitprez@univ-lille1.fr

Due to their ability to absorb and to scatter radiations, airborne particles play an important role in the energy budget of the earth-atmosphere system. It is assumed that aerosols are one of the atmospheric constituents participating to the cooling effect, but estimates are highly uncertain owing to the large spatial and temporal variability of aerosol concentration and physical properties.

The measurements from space-borne instruments are the only means for observing aerosol distributions from local to global scale. In particular, thermal infrared imagers such as MODIS or SEVIRI are routinely used to detect aerosols. Nevertheless, these broadband sensors are not suitable to distinguish the aerosol composition. Recent high spectral resolution sounders such IASI or Tanso-FTS are able to overcome these limitation. However, to fully exploit the hyperspectral instruments capabilities it is essential to have reference optical properties of various particles and mainly refractive indices.

Indeed, the knowledge of refractive indices is essential because it describe the proportioning of scattering and absorption of light by such particle matter. Moreover, the refractive index is strongly depending on the aerosol composition, size and shape.

The aim of this work is to measure high resolution transmittance spectra of model airborne SiO_2 particles in the infrared region and to use a Mie inverse algorithm to retrieve complex refractive indices. Refractive index measurements are generally performed by measuring absorbance or transmittance with bulk material of interest or particles diluted in solid pellets. In this study, we have recorded transmittance spectra of calibrated airborne particles by IRTF spectroscopy.

Aqueous solutions of calibrated SiO_2 microspheres (Bangs Laboratories, Inc.) were generated using an atomizer (TSI 3076). After drying, the continuous flow of aerosol particles was directed into a 10 m absorption length multipass cell within an IRTF spectrometer (Antaris Thermo Scientifique). The size distribution of the particles was measured at the exit of the multipass cell using an aerodynamic particle sizer spectrometer (TSI APS 3321). Concentration between 500 and 6000 particles per cubic centimetre were used for each 3 particle diameter: 0.5, 1 and 2 µm. 300 IRTF records were collected and averaged at a spectral resolution of 2 cm^{-1}. The IRTF spectra for SiO_2 microspheres (Ø = 2 μm) is displayed Fig1 showing an intense band around 1100 cm^{-1} .

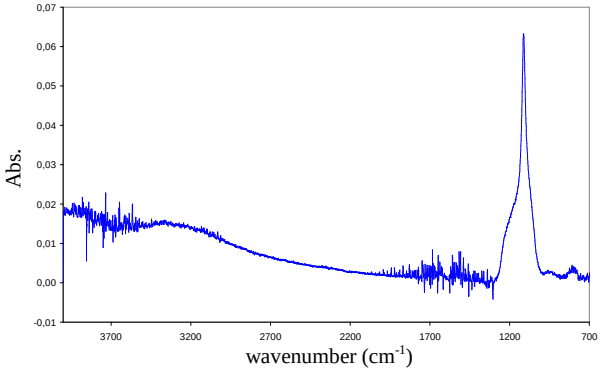

Fig. 1: Absorption spectra of calibrated SiO_2 particles Ø = 2 μm, $[SiO_2]$ = 1430 particle.cm^{-3}.

The complex refractive indices of particles are obtained at each wavenumber by combining the Mie theory, the Kramers-Kronig relations, and a Levenberg-Marquardt algorithm. This inverse model allows avoiding some errors introduce by the extrapolated formulas of Kramers-Kronig relations. This methodology has the advantage to can be applied for any spherical particles.

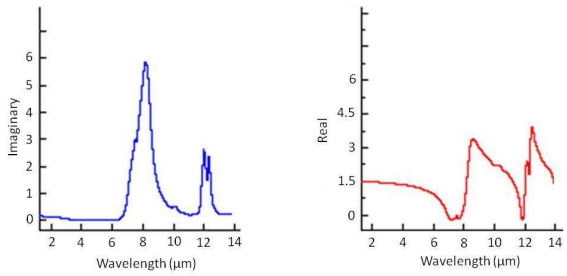

Fig. 2: Retrieved imaginary and real refractive indices of SiO_2 particles.

Experiments with particles (Ø = 0.5 μm and Ø = 1 μm) are currently in progress highlighting size dependence.

Profiling of the aerosol hygroscopicity in the planetary boundary layer

B. Rosati[1], E. Weingartner[1] , P. Zieger[1], G. Wehrle[1], U. Baltensperger[1] and the PEGASOS collaboration

[1]Laboratory of Atmospheric Chemistry, Paul Scherrer Institut, CH-5232 Villigen PSI, Switzerland
Keywords: hygroscopicity, growth factor, OPS, refractive index.
Presenting author email: bernadette.rosati@psi.ch

The aerosol direct effect relates to the interactions that aerosols have with the incoming solar radiation. Depending on the composition of the particles they can either scatter or absorb the light. Laboratory studies are typically performed at dry conditions but the ambient relative humidity (RH) is usually much higher therefore leading to hygroscopic growth which strongly influences the particle size and refractive index and hence the optical properties (Zieger et al., 2011). The knowledge of these aerosol properties is crucial for climate forcing calculations and for the validation of remote sensing measurements with in-situ ones. This is of particular importance if the chemical composition and thus the hygroscopicity changes with altitude (Morgan et al., 2010). Therefore, measurements of vertical profiles are essential to enable more accurate model calculations and improve remote sensing retrievals.

Within the **P**an-**E**uropean **G**as-**A**ero**so**ls-climate interaction **S**tudy (PEGASOS) a Zeppelin is used to explore the planetary boundary layer. The WHOPS (white-light humidified optical particle spectrometer) is a newly developed instrument to investigate the particles' hygroscopic and optical properties on this platform. The idea is to first dry the ambient aerosol and then select a specific mobility diameter with a differential mobility analyzer (DMA). The monodisperse particles are then exposed to a well defined RH (typically 95%) and again measured with a white-light optical particle spectrometer (OPS-Welas) to finally retrieve information on the hygroscopic growth factor and mixing state. Intermittently, the humidifier can be bypassed allowing the comparison of dry mobility and dry optical diameters to deduce information on the particles' optical properties (e.g. refractive index) (Flores et al., 2009). The WHOPS is highly suitable for airborne measurements since it records data at a high sampling rate of 1 Hz and detects diameters up to 10 µm for the humidified particles. First measurements will be conducted in Spring/Summer 2012 at Cabauw (Netherlands) and in the Po Valley (Italy). In the latter case, flights are also planned over the Adriatic Sea to investigate marine aerosols. In addition, atmospheric aging processes will be explored by drifting in a freshly emitted plume. We will present laboratory studies which include tests and calibration measurements with known inorganic salts, as well as first airborne measurements using the WHOPS.

Figure 1 shows an example measurement of ammonium sulfate (AS) for two different dry mobility diameters (300 nm and 500 nm). The red and blue lines are the dry and the humidified (RH=95±3%) optical measurements, respectively. In the top graph the influence of doubly charged particles and their growing behavior is nicely seen. The diameter set by the DMA and measured by the OPS compare quite well: The maximum dry (singly charged) optical diameters are 328 nm and 487 nm, respectively. The differences to the respective mobility diameters can be explained by two reasons: first, the OPS was calibrated with latex spheres with a different refractive index (1.59) compared to AS (1.52–1.55) and secondly the calculated scattering cross sections of latex spheres are only weakly diameter dependent at 300 nm which introduces higher uncertainties to retrieve an unambiguous diameter for a certain scattering intensity.

The apparent hygroscopic growth factors at RH=95% are lower than predicted by Köhler theory. This can be related to the high refractive index used for the calculations. In an improved retrieval the refractive index of water (1.33) will be considered for the wet particles using volume weighted mixing rules.

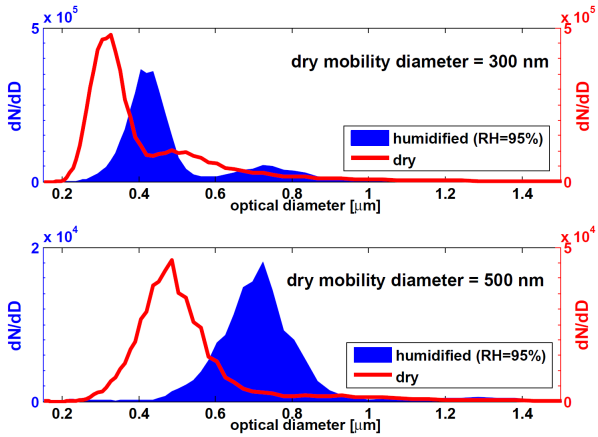

Figure 1: Laboratory experiments with AS; red: dry size distributions; blue: humidified size distributions; for two dry mobility diameters selected by a DMA.

This work is supported by the EU-funded project PEGASOS.

J.M. Flores *et al.*, Effective broadband refractive index retrieval by a white light optical particle counter, *Phys. Chem. Chem. Phys.* **11**(2009), 7943-7950.

W.T. Morgan *et al.*, Enhancement of the aerosol direct radiative effect by semi-volatile aerosol components: Airborne measurements in North-Western Europe, *Atmos. Chem. Phys.* **10**(2010), 8151-8171.

P. Zieger *et al.*, Comparison of ambient aerosol extinction coefficients obtained from in-situ, MAX-DOAS and LIDAR measurements at Cabauw, *Atmos. Chem. Phys.* **11**(2011), 2603-2624.

The effect of hygroscopicity on the aerosol extinction

V. Gácser, A. Molnár

Department of Earth and Environmental Sciences, University of Pannonia, Veszprém 8200, Hungary
Keywords: Visibility, Aerosol extinction, Relative humidity, Hygroscopic growth.
Presenting author email: vera.gacser@chello.hu

It is well known that visibility, which is an important factor in our everyday life, is the function of the shortwave light extinction, first of all the extinction of the aerosol particles. The light extinction of the particles is determined by Mie scattering of the fine particles. Since aerosol particles in the optically active size range (0.1-1.0 μm) are mainly composed of hygroscopic (sulfate, nitrate and organic) compounds, these particles can take up significant quantity of water from the atmosphere. With increasing ambient relative humidity the size of the particles increases; and consequently their optical properties change considerably (Malm and Kreidenweis, 1997; Liu et al. 2008) having an important influence on the control of the visibility.

In a previous study the relationship between the extinction coefficient and the relative humidity were studied in two sampling campaigns in Budapest in 2009. The data of these campaigns revealed that hygroscopic growth is substantially different in winter and in summer. In winter the growth rates (at 80 and 90% RH) were two times higher than in summer.

The aim of this present work is to study how the seasonal variation of the hygroscopic growth rate can be considered as a general phenomenon. In this work the hygroscopic behavior of aerosol extinction coefficient under different environments is presented. The extinction coefficients are derived from visibility data measured regularly at urban as well as non-urban locations for a longer period (1995-2002) in Hungary (Integrated Surface Hourly Observations, NOAA National Data Center).

The extinction coefficients were calculated from visual range observations using the Koschmieder formula, and dry extinction coefficients were estimated by the gamma-approach (Zhou et al., 2001):

$$\sigma_{ext} = 10^{c} \times (1 - \frac{RH(\%)}{100})^{-\gamma}$$

According to our results this seasonality can be observed at all monitoring sites (in large and small cities and other places); the smallest and the highest rates are found in summer and winter, respectively. On the other hand, the seasonal change in the hygroscopic growth rates is rather variable; it can be very different even at locations not far from each other. E.g. the growth rates of the extinction coefficient at two sites in Budapest (Budapest-Lőrinc and Liszt Ferenc Airport) are shown in Fig.1. At Budapest-Lőrinc site, at 80% relative humidity the mean growth rates are ~1.7 and ~3.2 in summer and winter, respectively, while at Liszt Ferenc Airport the corresponding values are ~1.1 in summer and ~1.7 in winter.

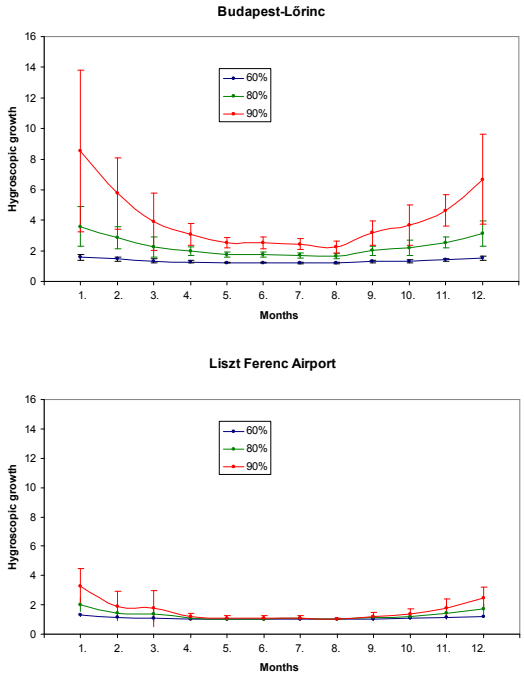

Fig. 1: Seasonal variation of the hygroscopic growth rate of the extinction coefficient at Budapest-Lőrinc and at Liszt Ferenc Airport at 60%, 80% and 90% RH.

The seasonal difference in hygroscopic behavior of extinction coefficient is probably due to the change in the chemical composition of the aerosol particles. We suppose that volatile and semi volatile compounds can play an important role in this variability. On the other hand, the spatial variation of the growth rates can be effected significantly by the local aerosol sources.

This work was supported by the TÁMOP 4.2./B-10/1-2010-0025 project.

http://ols.nndc.noaa.gov

Liu, X., Cheng, Y., Zhang, Y., Jung, J., Sugimoto, N., Chang, S., Kim, Y., Fan, S. and Zeng, L. (2008): Influences of relative humidity and particle chemical composition on aerosol scattering properties during the 2006 PRD campaign. *Atmospheric Enviroment*, 42, 1525-1536.

Malm, W.C., Kreidenweis, S.M, (1997): The effects of models of aerosol hygroscopicity on the apportionment of extinction. *Atmospheric Enviroment*, 31, 1965-1976.

Zhou, J., Swietlicki, E., Berg, O.H., Aalto, P.P., Hämeri, K.,Nilsson, E.D., Leck, C. (2001): Hygroscopic properties of aerosol particles over Arctic Ocean during summer. *J. Geophysical Research*, 106, 32111-32123.

Nephelometric study of fine aerosol fraction in Beijing

M.A. Sviridenkov[1], A.S. Emilenko[1], V.M. Kopeikin[1] and Wang Gengchen[2]

[1]A.M. Obukhov Institute of Atmospheric Physics, Russian Academy of Sciences, Moscow, 119017, Russia
[2]Institute of Atmospheric Physics, Chinese Academy of Sciences, Beijing, 100029, China
Keywords: atmospheric aerosols, optical properties, microstructure, urban pollution
Presenting author email: misv@mail.ru

Beijing, one of the biggest megacities, is characterized by high mean level of the aerosol pollution and its significant variability. IAP RAS in collaboration with IAP CAS has started study of the pollution of Beijing air basin in 1990s. Optical properties of the fine aerosol fraction were investigated using a nephelometer-polarimeter PhAN. Some results of 2003 - 2004 were presented at EAC-2005 (Sviridenkov *et al*., 2005). In the present paper, the results of measurements in the period from 2003 to 2010 (except for 2008) are summarized.

Measurements were usually carried out in fall season (in 2005 - in August). The nephelometer was installed in the building of the IAP CAS, located in the northern part of Beijing. Observations were conducted in two modes – continuous automatic recording of the single characteristic - aerosol scattering at the angle of 45° and wavelength of 510 nm, and periodic measuring of 7 parameters (angular scattering coefficients D at the scattering angle of 45° and wavelengths of 410, 510 and 630 nm and their polarized constituents at the scattering angle of 90° and wavelengths of 450 and 520 nm). The set of parameters, measured by PhAN, allows to solve the inverse problem and to retrieve both size spectra of the fine fraction and the values of the particle refractive index. Inversion results are most reliable in the size range 0.05 – 0.6 μm (Panchenko *et al.* 2008). Measured in routine regime D(45°, 510 nm) is closely correlated with volume scattering coefficient and volume concentration of fine aerosol fraction. In parallel with optical measurements, aerosol probes were sampled to fibre filters for further determination of BC content. In 2003, 2004, 2005 and 2007, observations were also taken at Mountain Observatory Xinglong located at 150 km to the north-east from Beijing at the height of 1 km.

Aerosol concentration in Beijing is characterized by both significant mean level and strong variability. Typical example of a temporal behaviour of D(45°, 510 nm) is shown in Figire 1. It can be seen in Figure 1 that periods of gradual growth of the aerosol pollution with duration of several days are interrupted by the air mass change accompanied usually by rains. In the final stage of smog formation, the visual range decreases sometimes up to values of hundred meters. Analysis of transformation of the aerosol microstructure and BC content during smog formation revealed the tendency of decreasing the particle refractive index and BC fraction and increasing the effective radius with growth of the aerosol loading.

Mean aerosol size distributions of fine aerosol fraction for Beijing and Xinglong are shown in Figure 2. They all are unimodal with modal radius in the interval of 0.1 - 0.2 μm (except for August 2005 in Beijing). Although the average aerosol concentration at Xinglong is much less than in Beijing, it is several times greater than in rural areas and even in such cities as Moscow.

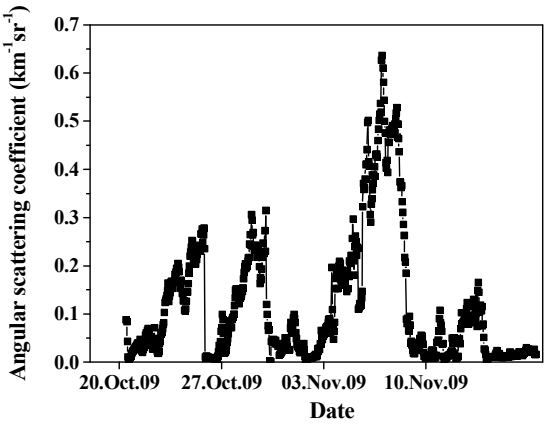

Figure 1. Temporal variations of D(45°, 510 nm) in Beijing in October and November 2009.

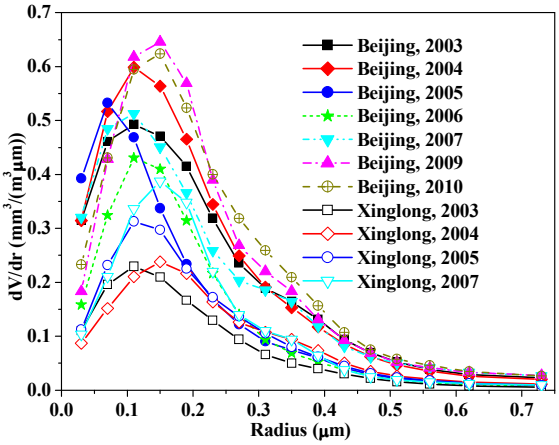

Figure 2. Mean volume size distributions in Beijing and Xinglong.

This work was partially supported by Russian Foundation for Basic Research under Project 10-05-01019.

Sviridenkov, M.A., Emilenko, A.S., Isakov, A.A. and Kopeikin, V.M. (2005) *Proc. EAC-2005, Ghent, Belgium*. 708.

Panchenko, M.V., Sviridenkov, M.A., Terpugova, S.A. and Kozlov, V.S (2008) *Int. J. Rem. Sens*. **29,** 2567-2583.

Observed darkening of the aerosol

J.P. Putaud, F. Cavalli, A. Dell'Acqua, C. Gruening, and S. Martuins Dos Santos

European Commission, Joint Research Centre, Ispra, VA, 21027, Italy
Keywords: aerosol, absorption, scattering, single scattering albedo.
Presenting author email: jean.putaud@jrc.ec.europa.eu

The Po Valley in Northern Italy can be identified from space as one of the most polluted areas in Europe (e.g. Koelemeijer et al., 2006). It is therefore a region where the effects of European policies and international protocols for abating air pollution should be most visible.

Aerosol remote sensing and in-situ measurements at the ground have been performed at the station for atmospheric research located in Ispra (45°49'N, 8°38'E), Italy, for more than 18 and 8 years, respectively. Instruments were run according to the quality assurance programs developed by within the networks AERONET (AErosol RObotic NETwork), EUSAAR (EUropean Supersites for Atmospheric Aerosol Research), and ACTRIS (Aerosols, Clouds, and Trace gases Research InfraStructure network). The station was favorably audited in 2010 by the World Calibration Centre for Aerosol Physics (WCCAP).

Measurements show that while the aerosol extinction coefficient and optical thickness (AOT) decreased over the last decade, the aerosol absorption coefficient and optical thickness (AAOT) did not decrease that much. This means that not only the aerosol cooling power has been vanishing, but also that the aerosol single scattering albedo decreased (Fig. 1). A simple climate forcing simulation shows that the aerosol is consequently getting closer to shift from a cooling to a heating climate forcer in this region.

The changes in aerosol optical properties we observed can be related to changes in the particulate matter ($PM_{2.5}$) chemical composition, with increasing percentages of carbonaceous compared to inorganic species.

These data show that to avoid fast climate change over the next decade, policies should now address more specifically short-lived climate warming agents, among which elemental carbon (EC). EC is also perhaps one of the targets to be aimed at for reducing adverse health effects of air pollution.

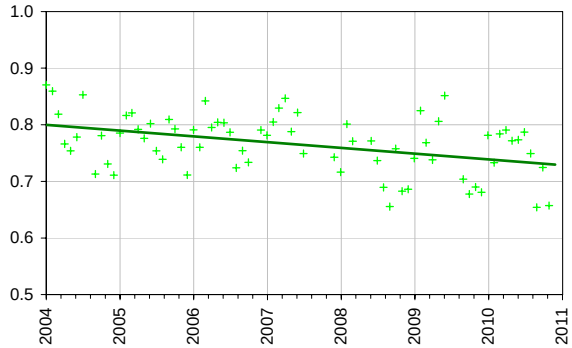

Figure 1. Monthly mean aerosol single scattering albedo at 550 nm observed in Ispra (IT) at ground level in dry conditions. The straight line represents the least square linear fitting curve.

This work was supported by the EC projects EUSAAR (contract RII3-CT-2006-026140) and ACTRIS (contract INFRA-2010-1.1.16).

Koelemeijer, R.B.A., Homan, C.D., and Matthijsen, J. (2006) Comparison of spatial and temporal variations of aerosol optical thickness and particulate matter over Europe, Atmos. Environ. 40, 5304-5315

Spectral dependence of aerosol light absorption obtained from several field experiments

S. Mogo[1,2,3], V.E. Cachorro[1], A. de Frutos[1], B. Torres[1], J.F. López[1], C. Toledano[1], A. Berjón[1,4] and B. Barja[5]
[1]Grupo de Óptica Atmosférica, Univ. de Valladolid, Valladolid, Spain
[2]Dpto. de Física, Univ. da Beira Interior, Covilhã, Portugal
[3]Instituto Dom Luis, Portugal
[4]Centro de Investigación Atmosférica de Izaña, Tenerife, Spain
[5]Grupo de Óptica Atmosférica de Camagüey, Centro Meteorológico de Camagüey, Camagüey, Cuba
Keywords: aerosol optics, absorption coefficient, alpha Ångström coefficient, optical properties.
Presenting author email: chiqui@goa.uva.es

The dependency of the aerosol absorption coefficient on wavelength is usually described by the absorption Ångström exponent, α_a. Depending on the particle's characteristics, the spectral dependence of the aerosol absorption coefficient is given by the empirical expression (Ångström, 1964; Bond, 2001; Moosmüller and Chakrabarty, 2011):

$$\frac{\sigma_a(\lambda)}{\sigma_a(\lambda_0)} = \left(\frac{\lambda}{\lambda_0}\right)^{-\alpha_a}, \quad (1)$$

where $\sigma_a(\lambda)$ is the absorption coefficient, λ is the wavelength, λ_0 is an arbitrary reference wavelength (usually taken as 1 μm in extinction studies) and α_a is the absorption alpha exponent or absorption Ångström exponent, which represents the aerosol complex refractive index influence on the wavelength. This power law expression characterizes the steepness of the slope of the curve σ_a *versus* λ.

For measurements of the absorption coefficient $\sigma_a(\lambda_1)$ and $\sigma_a(\lambda_2)$ taken at any two different wavelengths λ_1 and λ_2 respectively, the absorption Ångström exponent is given by:

$$\alpha_a = -\frac{\ln \frac{\sigma_a(\lambda_1)}{\sigma_a(\lambda_2)}}{\ln \frac{\lambda_1}{\lambda_2}}. \quad (2)$$

In this way, if the absorption coefficient at one wavelength and the absorption Ångström exponent are known, the absorption coefficient can be computed at any other wavelengths within the range of validity of this formula. In practice, measurements of the aerosol absorption coefficients are made at two or more wavelengths, and the absorption Ångström exponent is estimated from these measurements using Eq. 2.

Over recent years, absorption Ångström exponents of aerosol particles have been observed by the Atmospheric Optics Group from the University of Valladolid (GOA-UVa) at a number of sites around the world. Measurements have been performed over different time periods, in short campaigns or in continuous measurements. Several instrumentation have been used (integrating plate, integrating sphere, PSAP) and each study reports the data in particular conditions and different wavelength ranges. We have collected our existing data representing 13 individual campaigns and compare the results for different places and conditions. All the alpha values have been calculated for the pair of wavelengths 400-650 nm for easier comparison.

Campaign	Mean	Median	Min	Max	Std
UVa 2004	1.04	1.07	0.08	2.52	0.53
INTA May 2004	0.14	0.10	-0.38	0.78	0.45
INTA Summer 2004	0.66	0.55	0.23	1.84	0.32
Granada 2007	1.12	1.19	0.78	1.25	0.18
ALOMAR 2007	0.88	0.89	0.18	1.53	0.24
ALOMAR 2008	0.82	0.89	-1.09	1.81	0.34
Cuba 2008	0.27	0.20	-0.02	0.97	0.24
Covilhã PF 2008	0.43	0.42	0.31	0.61	0.09
Covilhã 2007	1.23	1.23	1.17	1.30	0.09
Covilhã 2008	1.19	1.18	1.07	1.35	0.06
Covilhã 2009	1.15	1.15	1.02	1.49	0.08
Covilhã 2010	1.20	1.19	0.86	1.44	0.10

Table 1: Statistics on the α_a value for several campaigns, calculated for the pair of wavelengths 400-650 nm.

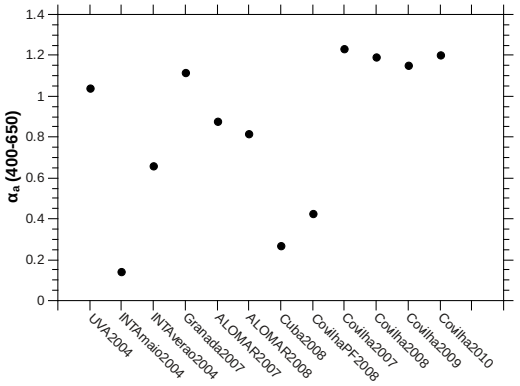

Figure 1: α_a experimental data.

Financial support from the Spanish MICINN (projects of ref. CGL2008-05939-CO3-01/CLI and CGL2009-09740 and "Acción Complementaria" CGL2011-13085-E) are gratefully acknowledged.

Ångström, A. (1964). *Tellus*, **16**, 64–75.

Bond, T. (2001). *Geophys. Res. Lett.*, **28**(21), 4075–4078.

Moosmüller, H. and Chakrabarty, R. (2011). *Atmos. Chem. Phys.*, **11**, 10677–10680.

Measuring the optical properties of single particles and aerosol ensembles using cavity ring down spectroscopy

B.J Mason, R.E.H. Miles, S.-J. King, K. Manfred, J.S. Walker, A.E. Carruthers, A.J. Orr-Ewing and J.P. Reid

Department of Chemistry, University of Bristol, Bristol, BS8 1TS, United Kingdom
Keywords: Cavity ring down spectroscopy, optical properties, refractive index, single particle analysis
Presenting author email: bm6225@bristol.ac.uk

Aerosols, both natural and anthropogenic, influence climate change by directly scattering and absorbing light from the sun and indirectly by acting as cloud condensation nuclei. Both these effects, however, have a large uncertainty associated with them as presented in the 2007 IPCC report of climate change (Forster, Ramaswamy et al. 2007). The refractive index (RI) of a particle can be used directly to describe its absorbing and scattering properties and can thus be directly related to its climate radiative forcing. Laboratory measurements of the RI of a range of anthropogenic and naturally occurring aerosols allow us to better estimate their total effect on radiative forcing.

In recent years ensemble aerosol cavity ringdown spectroscopy (A-CRDS) has been used to retrieve the RI of various atmospherically relevant aerosols such as single, mixed component and coated systems (Rudich, Riziq et al. 2007). Atmospheric relative humidity (RH) varies significantly with altitude, latitude and urbanisation meaning that it is important to know how the RI of an aerosol varies with water fraction. Sodium nitrate ($NaNO_3$) can be introduced directly into the atmosphere from fertiliser and indirectly from reactions with sea salt aerosol. As yet, using A-CRDS for absolute measurements of the RH dependent refractive index of an aerosol at multiple relative humidities has not been attempted. In this work we present A-CRDS determination of the refractive index of $NaNO_3$ at 30, 40 and 50 % RH (figure 1). The accuracy to which we can retrieve the RI as a function of RH and the inherent uncertainties involved have been previously analysed by members of our group (Miles, Rudic et al. 2011).

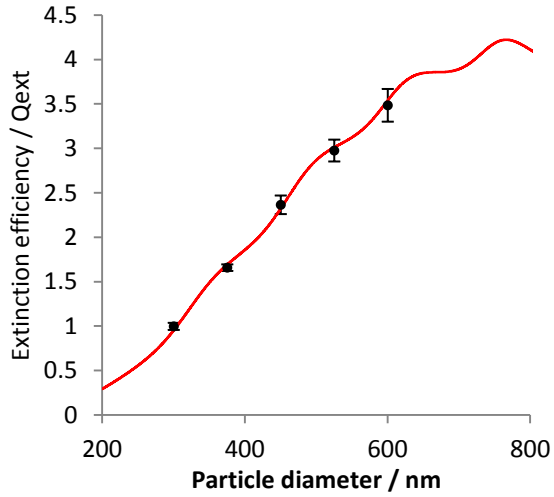

Figure 1. Typical experimental data set of $NaNO_3$. Particles of different sizes at 30 % RH are selected by the DMA and optically probed using the CRDS. The red line shows the fit of the experimental data to Mie theory (RI = 1.441 ± 0.02).

A significant source of error for ensemble A-CRDS arises from the assumption that the aerosol fraction selected by the DMA is monodisperse. This is incorrect for two reasons: firstly the DMA intrinsically selects doubly charged particles (DCPs) in addition to singly charged particles and secondly because the size distribution passed by the DMA, due to its transfer function, can have a significant effect on the optical measurement. Quantification of such effects is important as even a small (~1%) fraction of DCPs can have a significant effect on the observed RI.

Our aim is to take advantage of the sensitivity of A-CRDS and to couple it with accurate measurements of the change in optical properties with environmental conditions whilst avoiding many of the inherent uncertainties in ensemble measurements. To achieve this we are benchmarking an innovative new single particle A-CRDS instrument able to determine the optical properties of individual aerosol particles in the accumulation mode. In such experiments a particle is levitated by a vertically propagating Bessel beam optical trap which bisects a horizontal optical cavity. By changing the power of the Bessel beam a trapped particle can be moved in and out of the optical cavity to perform the ring down measurement. The change in optical properties with environmental conditions can be directly monitored on the same particle by controlling the relative humidity of the surrounding gas phase. This allows the effect on the aerosol optical properties of hygroscopic changes in particle size to be measured. The size of the particle can be measured independently from elastic light scattering.

A key advantage over the ensemble technique is the ability to precisely measure the time-dependence in optical properties of aerosol during transformation on a single particle basis (eg. hygroscopic growth, heterogeneous aging). We believe this new technique represents a significant advance in the accuracy with which measurements of aerosol optical properties and studies of aerosol processing can be made.

This work is funded by the EPSRC and the NERC.

Forster, P., V. Ramaswamy, et al. (2007). Cambridge, United Kingdom and New York, NY, USA, Cambridge University Press.

Miles, R. E. H., S. Rudic, et al. (2011). Aerosol Science and Technology **45**(11): 1360-1375.

Rudich, Y., A. A. Riziq, et al. (2007). Atmospheric Chemistry and Physics **7**(6): 1523-1536

Modelling radiative properties of light-absorbing carbon aggregates encapsulated in a sulphate shell

M. Kahnert[1,2], T. Nousiainen[3], H. Lindqvist[3], and M. Ebert[4]
[1]Swedish Meteorological and Hydrological Institute, Research Department, SE-601 76 Norrköping, Sweden
[2]Chalmers University of Technology, Department of Earth and Space Science, SE-412 96 Gothenburg, Sweden
[3]Department of Physics, P. O. Box 48, FI-00014 University of Helsinki, Finland
[4]Technical University of Darmstadt, Institute for Applied Geosciences, DE-64287 Darmstadt, Germany
Keywords: Light absorbing carbon, aerosol optics, radiative forcing.
Presenting author email: michael.kahnert@smhi.se

Light absorbing carbon is one of the most important classes of short-lived climate forcing agents. Owing to the high absorption cross section, LAC aerosols cause a positive radiative forcing at the tropopause, and a negative forcing at the surface. To quantify the radiative impact of LAC requires reliable information on the extinction cross section, single scattering albedo, and asymmetry parameter.

Because of the high morphological complexity of LAC aerosols, solving the light-scattering problem is a challenging task. Freshly emitted LAC particles can be described as aggregates consisting of small spherules. As the aerosols age in the atmosphere, the fractal dimension increases, and the LAC aggregates become internally mixed with soluble compounds, such as sulphate and organic matter (OM). The objective of this study is to test the suitability of simplified model particles by comparing their radiative properties to those obtained from reference computations performed for realistic encapsulated aggregate models.

We perform detailed light scattering computations for model particles consisting of LAC aggregates encapsulated in a sulphate shell. Figure 1 shows an example for one of the model particles considered. The reference computations brace the range of relevant sizes, wavelengths, and volume fractions. In parallel, we perform computations for external mixtures of homogeneous, spherical LAC and sulphate particles, internal encapsulated geometries described by a homogeneous LAC sphere coated by a concentric spherical sulphate shell, and homogeneous internal mixtures of LAC and sulphate. For the latter, we test different effective medium theories (EMT) for computing the effective refractive index of the LAC-sulphate mixture. Remarkably enough, the core-shell model does not provide the most accurate description of the optical properties of encapsulated LAC aggregates. This model usually underpredicts the absorption cross section C_{abs}, and it often overpredicts the scattering cross section C_{sca}. Thus, the single-scattering albedo ω is significantly overestimated. The Maxwell-Garnett EMT reproduces the reference computations somewhat better than the core shell model. However, it tends to over-estimate C_{abs} and underestimate C_{sca}. The Bruggemann EMT and the inverse

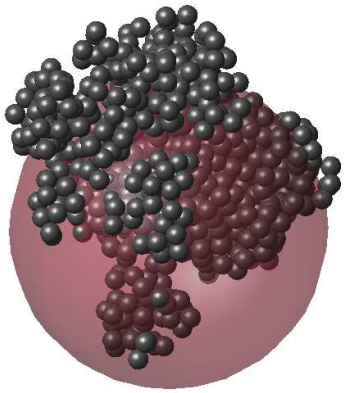

Figure 1: Example of model particle used in this study.

Maxwell-Garnett rule perform, in general, slightly worse than the Maxwell-Garnett EMT, although not as poorly as the core-shell model. As expected, the external mixture model performs worst.

Physically, the problems observed for the core-shell model are caused by the fact that a massive LAC sphere absorbs much less electromagnetic energy than an LAC aggregate, since the electromagnetic field does not penetrate deeply into a compact sphere of highly absorbing material. On the other hand, the homogeneous mixture model distributes the LAC mass too evenly within the sulphate host particle, thus allowing too much LAC mass to interact with the external field. We propose an improved model for encapsulated LAC aggregates based on a concentric core-shell-shell geometry. The model particles have a spherical sulphate core, a concentric LAC inner shell, and a concentric sulphate outer shell. The absorbing material is distributed such that more LAC mass can interact with the external field as compared to the core-shell model, yet not as much mass as in the homogeneous mixture model. The core-shell-shell particles reproduce the radiative properties computed for the encapsulated LAC aggregates reasonably well for all sizes, wavelengths, and volume fractions considered. The improvements over the other model particles are particularly pronounced at visible wavelengths near the maximum of the solar spectral radiance.

Monday, September 3, 2012

Session WG02S1O. Biomass Burning and Bioaerosol

Real-time measurement of continuous thermal-inactivated bioaerosols by aerosol fluorescence sensor with dual UV- and Vis-channels

Jae Hee Jung[1], Gwi Byoung Hwang[1], Bo Mi Kwon[1], Jung Eun Lee[2], and Gwi Nam Bae[1]

[1]Center for Environment, Health and Welfare Research, Korea Institute of Science and Technology (KIST), Hawolgok-dong, Seongbuk-gu, Seoul 136-791, Republic of Korea
[2]Institute of Health and Environment, Graduate School of Public Health, Seoul National University, Gwanak-ro, Gwanak-gu, Seoul 151-742, Republic of Korea
Keywords: Bioaerosol, Real-time detection, Fluorescence, Measurement (Characterization).
Presenting author email: jaehee@kist.re.kr

Airborne particles, primarily bacteria, virus, and fungi, are a primary means of disease transmission in humans and other animals. Due to renewed concerns over biological airborne contaminants such as new strains of flu or anthrax, many researchers have investigated the real-time technique that can be continuously monitored for potentially harmful biological aerosols.

Recently, the focus on fluorescence-based optical sensors has been to improve characterization by individual fluorescence spectral analysis. The fluorescence spectrum varies from material to material, and the evidence obtained from laboratory measurements indicates that effective differentiation from likely interferents should be possible with broadband spectral differentiation (Pan *et al*., 2011; Kaye et al., 2005). There has also been a focus on developing simpler, more robust, and lower-cost real-time sensors for intelligent network deployments.

The aerosol fluorescence sensor (AFS; Biral, Bristol, UK) is a promising monitoring device for the continuous real-time detection of airborne microorganisms, which is based upon the principle of Ultra-violet light induced fluorescence (UV-LIF) targeting the intrinsic fluorescence response from common amino acids found in living matter. The sensor uses an UV optical excitation source of 280 (+20/-40) nm to illuminate an airstream flowing drawn continuously through the sensor detection volume. Fluorescence from all particles instantaneously present within a sensing volume is measured using two photomultiplier detectors optically filtered to detect radiation in the bands 305-385 nm (UV) and 415-550 nm (Vis), enabling a generic discrimination between different aerosol populations.

This study describes the continuous real-time fluorescence characteristics of bacterial bioaerosols (*E. coli, B. subtilis and S. epiderdmids*) with various cell viabilities using the AFS. To control cell viability, the test bacterial bioaerosols were continuously exposed at various surrounding temperature with very short-time in the thermal electric tube furnace and passed into the AFS (Jung *et al*., .2009).

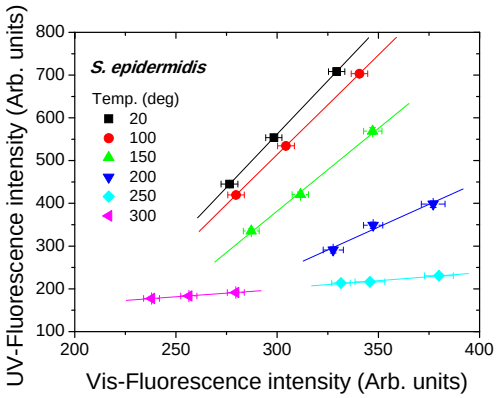

Figure 1. Variation of fluorescence characteristics of *S. epidermidis* bioaerosols under various thermal conditions.

Laboratory data show that these UV- and Vis-fluorescence intensities from the bacterial bioaerosols were decreased with increasing surrounding temperature following the decrease of bacteria viability.

In particular, this slope reduction value has statistically significant relationship ($p<0.05$) with the bacterial cell viability reduction. These experimental results provide basic information about the feasibility of AFS for real-time cell viability assessment of bacterial bioaerosols and may contribute in various applications such as indoor air quality, public health, and military defense against bioterrorism.

This research was supported by the Converging Research Center funded by the Ministry of Education, Science and Technology (2011K000750).

Pan, Y., Hill, S. C., Pinnick, R. G., House, J. M., Flagan, R. C., and Chang, R. K. (2011) *Atmos. Environ*. 45, 1555-1563.
Kaye, P. H., Baxter, K. L,. and Hirst, E. (2005) Opt. Express 13, 3583-3593.
Jung, J. H., Lee, J. E., and Kim, S. S. (2009) Sci. Total Environ. 407, 4723-4730.

Impact of Prescribed Burning on Urban Air Quality: A Case Study

C. He[1], B. Miljevic[1], L. Crilley[1], L. Morawska[1], F. Salimi[1], G. A. Ayoko[1], J. Bartsch[2], E. Uhde[2]

[1]International Laboratory for Air Quality and Health, |Institute of Health and Biomedical Innovation, Queensland University of Technology (QUT), Brisbane, 4001, Australia
[2]Material Analysis & Indoor Chemistry, Fraunhofer Wilhelm-Klauditz-Institute (WKI), Braunschweig, 38108, Germany
Keywords: biomass burning, aerosol chemistry, particle concentration, AMS, VOCs, PM_{10}
Presenting author email: c.he@qut.edu.au

For fuel management and/or ecological reasons prescribed burnings are conducted each year across Australia. Smoke from prescribed burnings could be the major source of air pollution in urban environment during the period of intensive prescribed burning. To investigate the impact of prescribed burning on air quality and the characteristics of prescribed burning particles, field measurements were conducted during the end period of a prescribed burning event in September 2011, Brisbane, Australia.

In this project, time series of ambient particle number concentration, submicrometer particle size distributions (0.009-0.414 µm) and supermicrometer particle size distributions (0.523-19µm) were measured by a TSI condensation particle counter (WCPC 3787), a TSI scanning mobility particle sizer (SMPS) and a TSI UVAPS, respectively. An Aerodyne time of flight aerosol mass spectrometer (AMS) was used to characterize the composition of the submicrometer, non-refractory aerosol. Particle elemental carbon (EC), organic carbon (OC), Levoglucosan (a biomass burning marker) and volatile organic compounds (VOCs) were also measured. Brisbane air quality data for September 2011 was collected from the Department of Environment and Resources Management.

The prescribed burning event started on 14 Sep 2011 and stopped on 21 Sep 2011. The measured and collected data are grouped according to the burning event (14-21 September) and the non-burning event (1-13 and 22-30 September). 24-hour average PM_{10} and $PM_{2.5}$ concentrations in September 2011 are presented in Figure 1. It can be seen from Figure 1 that both 24-hour average PM_{10} and $PM_{2.5}$ concentrations significantly increased during the prescribed burning event. The 24-hour average PM_{10} concentrations in 18 and 19 Sep were higher than the Australian ambient air quality standard (50 µg m^{-3}). The 24-hour average $PM_{2.5}$ concentrations during 17 - 19 Sep were higher than the Australian advisory ambient air quality standard (25 µg m^{-3}) and there were two days that $PM_{2.5}$ concentrations were more than twice as the advisory standard.

A summary of the statistical analysis of average submicrometer PN concentrations ($\times 10^3$ p cm^{-3}), supermicrometer PN concentrations (p cm^{-3}), PM_{10}, (µg m^{-3}) $PM_{2.5}$ (µg m^{-3}) concentrations, as well as maximum 8-hour CO (ppm), maximum 4-hour O_3(ppm), maximum 1-hour NO_2 (ppm), 24-hour SO_2 (ppm), 24-hour Benzene (ppb), 24-hour Toluene (ppb), 24-hour Total Xylenes (ppb) and 24-hour Formaldehyde (ppb) concentrations is given in Tables 1. From Table 1, it can be seen that, except Total Xylenes all pollutant levels during the burning period are higher those during the non-burning period, especially for submicrometer particle number concentration.

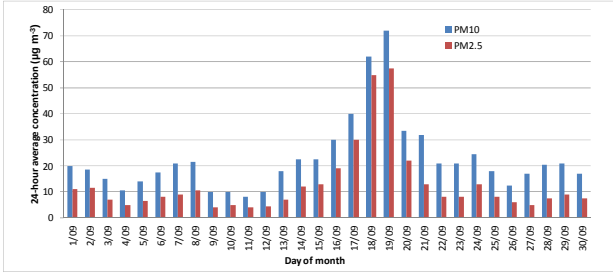

Figure 1. The 24-hour average PM_{10} and $PM_{2.5}$ concentrations of Brisbane city in September 2011.

Table 1. Summary of the statistical analysis of average concentration of the pollutants (units: as above)

	Burning		Non-burning		Ratio*
	Average	S.D	Average	S.D	
Sup PN	4.1	2.6	2.3	0.5	1.78
Sub PN	376	270	7.81	6.36	48.1
PM_{10}	39.3	18.2	16.7	4.7	2.36
$PM_{2.5}$	27.7	18.6	7.5	2.5	3.69
CO	0.9	0.2	0.5	0.1	1.62
O_3	0.057	0.032	0.032	0.004	1.79
NO_2	0.035	0.008	0.026	0.004	1.33
SO_2	0.003	0.001	0.001	0.000	2.31
Ben.	1.4	0.3	1.0	0.1	1.38
Tol.	2.5	1.3	1.1	0.4	2.16
TXy.	2.4	1.5	3.6	0.6	0.65
Form.	6.0	1.7	4.7	1.0	1.26

Note: *****: Ratio of Average concentrations during the burning event and during the non-burning event, Sup: supermicrometer, Sub: submicrometer, Ben.: Benzene, Tol.: Toluene, TXy.: Total Xylenes, Form.: Formaldehyde

AMS results indicated that the mass loadings were more than 20µg m^{-3}, which is not typical for Brisbane measurement site. Particles (PM_1) contained a substantial amount of organics (75% +/- 10% of the total AMS mass). High f44 (tracer for oxygenated organic compounds) value 0.16 (0.12-0.2) indicates that organic component was highly oxygenated, suggests that the particles at the measurement site were aged.

Physical and chemical properties of aerosol particles from wild fires in South Africa

V. Vakkari[1], P. Tiitta[2], H. Laakso[1], A. Venter[3], K. Jaars[3], M. Josipovic[3], C. Walsh[4], P. Dagsson Waldhauserova[5,6], G. Mafusire[7], T. Korhola[8], M. Paramonov[1], M. Vana[1], M. Kulmala[1], J.P. Beukes[3], P.G. van Zyl[3], J.J. Pienaar[3] and L. Laakso[3,9]

[1]Department of Physics, University of Helsinki, P.O. BOX 64, 00014 University of Helsinki, Finland
[2]Department of Environmental Science, University of Eastern Finland, Kuopio, Finland
[3]School of Physical and Chemical Sciences, North-West University, Potchefstroom, South Africa
[4]Lund University, Lund, Sweden
[5]University of Iceland, Reykjavik, Iceland
[6]Agricultural University of Iceland, Hvanneyri, Iceland
[7]University of Johannesburg, Johannesburg, South Africa
[8]Department of Physics and Mathematics, University of Eastern Finland, Kuopio, Finland
[9]Finnish Meteorological Institute, Research and Development, Finland

Keywords: wild fires, biomass burning, South Africa
Presenting author email: ville.vakkari@helsinki.fi

Submicron aerosol particles are well known to affect our lives via direct and indirect climate effects as well as adverse health effects (Seinfeld and Pandis, 2006). In Southern Africa wild fires form a large source of aerosol particles especially during the dry season, from June to September (Swap et al., 2003).

The main source of information on aerosol particles from wild fires in southern Africa are the SAFARI 1992 and 2000 campaigns (Swap et al., 2003), which, while intensive, had instrumentation limitations. In the SAFARI 2000 campaign the lower detection limit of the aerosol size distribution measurements was 100 nm and the chemical analysis of the aerosol particles were determined from filter samples.

In this study, we utilise long-time measurements of aerosol size distributions from 12 to 840 nm in two measurement locations in South Africa, i.e. in Botsalano game reserve close to the Botswana border from July 2006 to February 2008 (Laakso et al., 2008) and in Welgegund (www.welgegund.org), 100 km south-west of Johannesburg, from May 2010 to September 2011. At the Welgegund measurement site we also had an Aerodyne ACSM online aerosol mass spectrometer (Ng et al., 2011) for chemical composition measurements of the sub-micron aerosol and a Thermo model 5012 MAAP running on a PM1 inlet, which was used to estimate the black carbon content in the aerosol.

The ground-based measurements were related to wild fires by combining 96-hour HYSPLIT back-trajectories and MODIS Burned Area product. Only cases when fire-generated aerosol could be clearly separated from the pre-existing aerosol were used. 82 plumes were identified, of which 20 also had online chemical composition data available.

The median chemical composition of the fire-generated aerosol (Figure 1) was dominated by organic compounds. However, in the night time plumes the fraction of organic compounds was 13 percentage points lower than in day time plumes, suggesting photo-oxidation of volatile organic compounds to contribute significantly to the total mass.

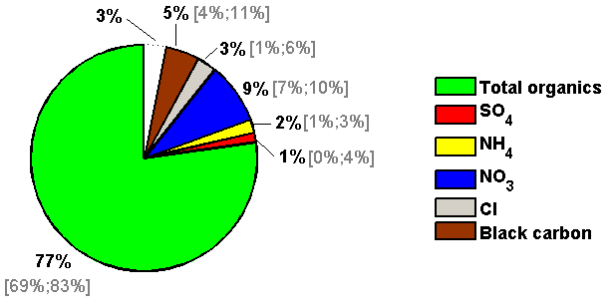

Figure 1. Median chemical composition of fire-generated aerosol from ACSM and MAAP. The median fractions of different compounds do not add up to 100%, hence the unaccounted 3% in the graph. The 25th and 75th percentiles are given in gray.

This work was supported by the Academy of Finland, the Saastamoinen säätiö and the North-West University.

Laakso, L., Laakso, H., Aalto, P.P., Keronen, P., Petäjä, T., Nieminen, T., Pohja, T., Siivola, E., Kulmala, M., Kgabi, N., Molefe, M., Mabaso, D., Phalatse, D., Pienaar, K. and Kerminen, V.-M. (2008). *Atmos. Chem. Phys.*, **8**, 4823-4839.

Ng, N., Herndon, S., Trimborn, A., Canagaratna, M., Croteau, P., Onasch, T., Sueper, D., Worsnop, D., Zhang, Q., Sun, Y., Jayne, J. (2011). *Aerosol Sci. Tech.*, **45**, 780-794.

Seinfeld, J. H. and Pandis, S. N. (2006) *Atmospheric Chemistry and Physics: From Air Pollution to Climate Change*, Wiley, New York.

Swap, R., Annegarn, H.J., Suttles, J.T., King, M.D., Platnick, S., Privette, J.L., Scholes, R.J. (2003). *J. Geophys. Res.*, **108**, 8465-8480.

Impact of wood combustion on the ambient aerosol in Augsburg, Germany: A joint measurement campaign using innovative on-line and off-line mass spectrometric systems for chemical profiling

R.Zimmermann[1], M.Oster[1], M. Elsasser[1], J. Schnelle-Kreis[1], J. Orasche[1], G. Abbaszade[1], M. Crippa[2], A.S.H. Prévôt[2], T. Gustafson[3], J.B.C.Pettersson[3]

[1] Joint Mass Spectrometry Centre / Chair of Analytical Chemistry, University of Rostock, 18051 Rostock, Germany, Helmholtz Zentrum München, 85764 Neuherberg, Germany
[2] Laboratory of Atmospheric Chemistry, Paul Scherrer Institute, Villigen, 5232, Switzerland
[3]Department of Chemistry, University of Gothenburg, 412 96 Gothenburg, Sweden

Keywords: wood combustion, stationary and mobile measurements, urban aerosol, aerosol mass spectrometric methods, organic and inorganic source apportionment tracer.
Corresponding author email: ralf.zimmermann@helmholtz-muenchen.de

In Augsburg, a city of 260.000 inhabitants, close to Munich in the south of Germany, the Helmholtz Zentrum München is operating since 2002 an urban background aerosol monitoring site. A long term source apportionment study based on daily measured organic PM constituents suggests a rather strong impact of wood combustion on the ambient aerosol in Augsburg (Schnelle-Kreis et al. 2007). This holds true for the PM10 values as well as for the concentrations of the health relevant polycyclic aromatic hydrocarbons (PAH). Motivated by these findings, an intense measurement campaign was conducted in Augsburg in order to address the impact of wood combustion (WC) on the ambient aerosol in the winter season 2010. On the one hand different on-line and off-line mass spectrometry based methods were applied at a central stationary measurement site. This includes a High Resolution Time of Flight Aerosol Mass Spectrometer (HR-ToF-AMS, Aerodyne Research Inc.) based on a thermal desorption-electron ionisation process, a home-built thermal ionisation mass spectrometer for detection of alkali ions from particles (Alkali AMS, University of Gothenburg, Svane *et al.* 2004) and a home-built thermal desorption-REMPI laser ionisation mass spectrometer for single particle resolved detection of polycyclic aromatic hydrocarbons (TD-REMPI-ATOFMS, Joint Mass Spectrometry Centre, Helmholtz Zentrum München, Oster, *et al.* 2011). Figure 1 shows Augsburg ambient aerosol mass spectra recorded by the three different aerosol mass spectrometers during the campaign.

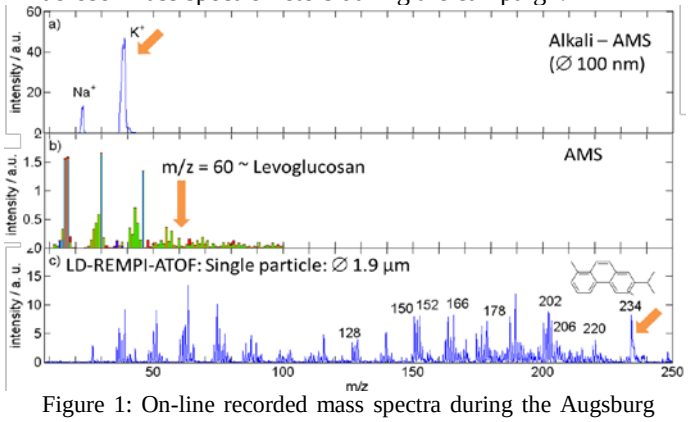

Figure 1: On-line recorded mass spectra during the Augsburg winter 2010 measurement campaign

The high potassium content of the particles recorded by the Alkali-MS reflect the wood combustion contribution (Fig. 1, upper trace). The AMS spectrum is dominated by organic fragments (due to the 70 eV electron ionization). However, the enhanced peak at m/z=60 can be explained partially due to a levoglucosan fragment (Fig. 1, middle trace). The single particle mass spectrum of a 1.9 µm particle recorded by TD-REMPI-ATOFMS depicts a rich pattern of PAH masses (128, 166, 178, 202 m/z). Furthermore the peak at 234 m/z is due to the molecule retene, which is a well-known marker for coniferous wood combustion. In addition to on-line aerosol mass spectrometry PM 2.5 was continuously sampled on filters with a daily resolution while PM1 was collected for several days even with hourly time resolution. The filter samples were analysed with a newly developed in-situ-derivatization thermal desorption gas chromatography time-of-flight mass spectrometry method which allows detecting non polar (e.g. polycyclic aromatic hydrocarbons) as well as polar (levoglucosan) compounds simultaneously (IDTD-GC-TOFMS, Orasche, 2011). The comparison between on-line (e.g. AMS) and off-line analyses (IDTD-GC-TOFMS) show good accordance. To complete the stationary measurements also mobile measurements were carried out in the city of Augsburg, using a further High Resolution Time-of-Flight Aerosol MS which was set up in a mobile atmospheric pollution laboratory (Paul Scherrer Institute, Mohr, *et al.* 2011).

In the contribution the whole measurement campaign (on-line, off-line and mobile measurements) are summarized and concluded.

The health effects of organics in wood combustion aerosols are currently further investigated in the framework of the Helmholtz Virtual Institute of Complex Molecular Systems in Environmental Health, HICE (www.hice-vi.eu).

Schnelle-Kreis, J., Sklorz, M., Orasche, J., Stölzel, M., Peters, A., Zimmermann, R. (2007) Environ. Sci. Technol. 41, 3821 – 3828

Mohr, C., Richter, R., DeCarlo, P. F., Prévôt, A. S. H., and Baltensperger, U. (2011) *Atmos. Chem. Phys.*, 11, 7465-7482.

Svane, M., Hagström, M., and Pettersson, J.B.C., (2004). *Aerosol Sci. Technol.*, 38, 655-663.

Oster, M, Elsasser, M., Schnelle-Kreis, J. and Zimmermann, R. (2011) *Anal.Bioanal.Chem.* **401**, 8991-9004.

Orasche, J., Schnelle-Kreis, J., Abbaszade, G., and Zimmermann, R., *Atmos. Chem. Phys* 11, 8977-8993, 2011.

Airborne measurements of biomass burning layers over Central Europe: A case study

F. Dahlkötter[1], B. Weinzierl[1,2], D. Sauer[2,1], A. Minikin[1], M. Gysel[3], C. Voigt[1,4], and A. Ansmann[5]

[1]Deutsches Zentrum für Luft- und Raumfahrt, Institut für Physik der Atmosphäre, Oberpfaffenhofen, Germany
[2] Ludwig-Maximilians-Universität München, Meteorologisches Institut, München, Germany
[3] Paul Scherrer Institut, Laboratory of Atmospheric Chemistry, Villigen, Switzerland
[4] Johannes Gutenberg-Universität Mainz, Institut für Physik der Atmosphäre, Mainz, Germany
[5] Leibniz-Institut für Troposphärenforschung, Leipzig, Germany

Keywords: biomass burning, airborne particles, black carbon, optical properties, aerosol dynamics.
Presenting author email: Florian.Dahlkoetter@dlr.de

Biomass burning aerosol exerts a significant direct radiative forcing by scattering and absorption of solar radiation (IPCC, 2007) and causes a large uncertainty on the estimates of aerosol radiative forcing driven climate change. Biomass burning aerosol layers are highly variable in time and space and can occur throughout the entire troposphere and lower stratosphere. To determine the impact of particle layers containing absorbing materials like black carbon (BC), on the Earth's radiation budget, it is necessary to learn more about their particle size distributions and mixing state, the aerosol aging, and optical properties. These layers can be characterized directly using airborne in-situ measurements.

During the CONCERT 2011 (Contrail and Cirrus Experiment) campaign in September 2011 eleven research flights were conducted over Central Europe with the DLR research aircraft Falcon. CONCERT 2011 focussed on microphysical, chemical and radiative properties of contrails and natural cirrus clouds, but also several elevated aerosol layers from different origins were detected with extended aerosol in-situ instrumentation.

On 16 September 2011 an elevated biomass burning aerosol layer was measured at altitudes between 10000 m and 11500 m above sea level over north-eastern Germany. Backward trajectories show that this layer originated from boreal forest fires in Northern America around 3 - 5 days before measurement. The biomass burning layer was not only detected by the Falcon, but also by several ground-based LIDAR stations, e.g. at IfT in Leipzig. The combination of airborne and ground-based data provides information on the vertical and horizontal extent of this layer which is necessary to quantify the layer's radiative effects. In our presentation we show data from a Single Particle Soot Photometer (SP2) which demonstrate that a distinct fraction of the particles (6 – 13 %) contains a BC core core (> 70 nm BC mass equivalent diameter) surrounded by a volatile coating. Such coatings can enhance the absorption of BC particles (e.g. Schwarz et al., 2008). The calculated coating thickness of the BC particles in the biomass burning layer is unusually high and distinctly larger than the coating thickness of freshly emitted boundary layer aerosol particles (Fig. 1). BC mass concentrations of the layer reach up to 0.13 µg m^{-3} in the BC (core) mass equivalent diameter range of roughly 70 nm up to 440 nm with the mode of distribution in-between 140 and 220 nm.

We performed additional calculations of optical properties for the biomass burning layer. The imaginary part of refractive index is lower than that of tropical biomass burning layers observed during the SAMUM campaign (Weinzierl et al., 2011). The Ångström exponents of absorption are larger than expected for pure black carbon but agree well with brown carbon (BrC), which can be produced during biomass burning events.

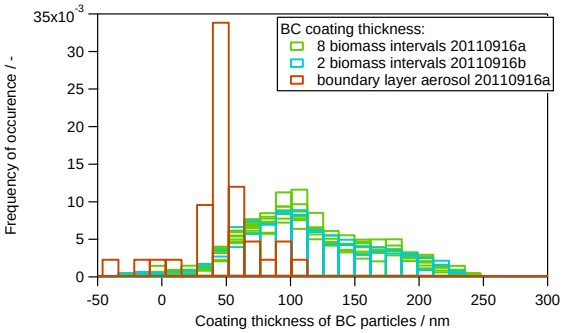

Fig. 1: Coating thickness of BC particles from observed layer (green and blue) in comparison to boundary layer BC particles (red).

This work was funded by the Helmholtz Association (HGF) under grant number VH-NG-606 (Helmholtz Young Investigators Group AerCARE). The field experiment was organized and in part funded by the HGF grant VH-NG-309 (Helmholtz Young Investigators Group AEROTROP) and the DLR project CATS.

Weinzierl, B. et al. (2011). *Microphysical and optical properties of dust and tropical biomass burning aerosol layers in the Cape Verde region - An overview of the airborne in situ and lidar measurements during SAMUM-2.* Tellus, 63B, 589–618.

IPCC, 2007. *Climate change 2007. The physical science basis.* In: Contribution of Working Group 1 to the Fourth Assessment Report of the Intergovernmental Panel on Climate Change (IPCC) (eds. Solomon, A. and co-editors). Cambridge University Press, Cambridge, United Kingdom and New York, NY, USA.

Schwarz, J. P. et al. (2008) *Coatings and Their Enhancement of Black Carbon Light Absorption in the Tropical Atmosphere*. J. Geophys. Res.—Atmospheres 113(D3):D03203.

Comparison of methods for generating bioaerosols

J. Löndahl[1], O. Nerbrink[2], N. Burman[1], A. Thedeby[1], A. Massling[3], T. Santl Temkiv[3], M. Bohgard[1], U. Gosewinkel Karlson[3]

[1]Department of Design Sciences, Lund University, Lund, SE-22100, Sweden
[2]FOI, Umeå, Swedish Defence Research Agency, Umeå, SE-901 82, Sweden
[3]Department of Environmental Science, Aarhus University, Roskilde, DK-2000, Denmark
Keywords: bioaerosols, generation of aerosols, atmospheric aerosols, bacterial activity
Presenting author email: jakob.londahl@design.lth.se

Bioaerosols include viable bacteria, viruses, dead bacterial cells, pollen, fungi and cell fragments, as well as numerous organic compounds derived from biomolecules as, for example, sugars, amino acids and methyl-derivatives. It has been shown that airborne bacteria may be viable also in the harsh conditions at high altitudes in the atmosphere and transmit diseases as well as act as cloud condensation nuclei (CCN) and ice nuclei (IN). Furthermore, they are able to influence cloud chemistry (Santl Temkiv, 2012).

In order to study the properties of bioaerosols in a laboratory setting it is necessary to use a generation methodology that preserves bacterial viability and minimize coating with redundant solvent impurities as this will increase particle size and distort chemical analysis. Few studies describe generation of bioaerosols, especially with respect to aerosol coating, background concentration and viability. The objective of this work is to compare various aerosol generators for bacteria, spores and vesicles.

Seven aerosol generators are investigated: atomizer (TSI Inc., Model 3075), Collison nebulizer (BGI Inc., 3-jet), vibrating orifice aerosol generator (VOAG, TSI model 3450), electrospray (TSI Inc., Model model 3480) and a bubble flask, a medical nebulizer (Dolema, Aeroneb ProX) and a custom-built liquid bubbler.

At this point, exclusively *Rhodoccocus sp.* (a common soil bacterium) is studied. Particle number size distributions were measured with a scanning mobility particle sizer (SMPS, design: Lund University) and an aerodynamic particle sizer (APS, TSI Inc., Model 3321) in a 1 m^3 stainless steel chamber ("Bio-cube") with controlled ventilation, temperature and relative humidity. Bacterial viability is analysed by counting colony forming units (CFU) on gelatin membrane filters and – in future studies – possibly also by fluorescence.

Figure 1 shows the particle number size distribution of the particles produces with the TSI atomizer. There is a peak of bacteria at 0.75 µm. The number concentration of bacteria were around 4 cm^{-3}, while the background salt particles in the range 10 to 200 nm (GMD 40 nm) had a concentration around 3000 cm^{-3}. The bubble flask generated lower bacterial concentrations, but also lower background. The VOAG produced uniform, but comparably large droplets (typically 20-40 µm). When dried, the background particles therefore had a size around 500 nm, while the bacteria had a peak at about 1.7 µm which indicates a significant coating. The electrospray could not be used for bacteria, since they are too large, but may be appropriate for bacterial outer membrane vesicles and spores.

The full matrix of generation methodologies is not yet available, but the preliminary results clearly show that many of the methods commonly used for generation of bioaerosols are unsuitable for examination of key properties of the particles such as CCN or IN ability. A surface coating of bioaerosols may significantly alter these abilities especially when soluble substances are involved. Any background in the measurements may also make a systematic evaluation difficult.

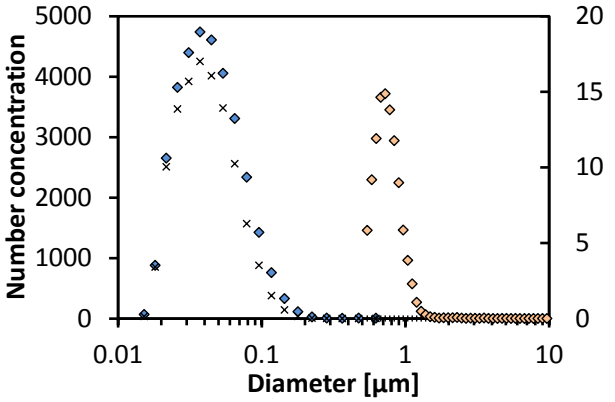

Figure 1. Particle number size distribution for bacterial solution (filled makers) and distilled water (x) produced with nebulizer.

It is often difficult to provide bioaerosols from distilled water of high purity since the organism typically need some surrounding additives (salts etc.) for survival.

It seems that the electrospray method is suitable for particles up to 200 nm. This instrument leaves a minor surface coating due to a small initial droplet size. For larger particles it may be crucial to estimate the amount of surface material in order to draw conclusions about particle properties while they are airborne.

Acknowledgements: This work was supported by the Swedish research council under grant 621-2011-3560.

References

Santl Temkiv, T., 2012, "Bacteria in clouds", PhD dissertation, Aarhus University, Denmark

Seasonal and spatial characteristics of fungal spore tracers in Taiwan

G. Engling[1], S.H. Chen[1] and B.J. Tsuang[2]

[1]Department of Biomedical Engineering & Environmental Sciences, National Tsing Hua University, Hsinchu 300, Taiwan
[2]Department of Environmental Engineering, National Chung-Hsing University, Taichung, Taiwan
Keywords: bioaerosol, ambient PM, molecular tracer, arabitol
Presenting author email: guenter@mx.nthu.edu.tw

Biological aerosol particles are found in ambient air in form of pollen, fungi, bacteria, viruses, algae, and plant fragments. Recent estimates have shown that such bioaerosols may constitute a substantial component of atmospheric particulate matter (PM) on global scale, and specifically in coarse aerosol particles (Jaenicke *et al* 2007, Heald and Spracklen 2009). Fungal spores in particular are an important type of bioaerosol (Elbert *et al* 2007).

A new approach for estimating fungal spore contributions to ambient PM was proposed by Bauer *et al* (2008a), utilizing molecular source tracers, i.e., the sugar alcohols arabitol and mannitol. Recent measurements by our group, applying the method introduced by Bauer *et al* (2008a,b), revealed that fungal spore contributions to coarse PM can be rather high in tropical regions (up to 26% of organic carbon (OC) and up to 18% of PM_{10} (Zhang *et al* 2010).

Ambient conditions, such as temperature and relative humidity, will influence biological activity, including fungal spore release rates. Furthermore, fungal species in different locations likely have varying polyol contents. It is, therefore, important to determine the abundance of these tracers in ambient PM as a function of environmental conditions and location.

For this study, size-resolved PM samples were collected at several locations across Taiwan, including urban, rural, coastal, and mountain sites, using Hi-vol samplers. The polyols arabitol and mannitol, as well as other carbonaceous species, were quantified in the PM samples by high-performance anion exchange chromatography with pulsed amperometric detection (HPAEC-PAD).

While only fine particles ($PM_{2.5}$) were collected at an urban site in northern Taiwan (Taipei) and at a remote forest site in the southern part of the island (Liouguei, Kaohsiung County), both fine and coarse PM ($PM_{2.5-10}$) samples were obtained from a remote high-altitude site in central Taiwan (Bei Tung-Yen Shan, 2080 m asl) and at a coastal site at the northern tip of Taiwan (Fuguei Jiao).

The preliminary results from this study showed distinct temporal patterns in the ambient concentrations of the fungal spore tracers, as well as a particle-size dependence. Surprisingly high arabitol concentrations of up to 50 ng/m^3 were observed during summer in $PM_{2.5}$ at the urban site. Utilizing the conversion factors from Bauer *et al* (2008a,b), these ambient levels correspond to contributions to organic carbon (OC) of roughly 10%. In contrast, during winter and spring the ambient tracer concentrations decreased drastically to values below 1 ng/m^3, indicating minimal fungal activity during the cold season (Figure 1).

At the mountain site, the absolute tracer levels were comparatively smaller throughout the year, likely due to the lower ambient temperatures in the alpine environment. Nevertheless, the tracer concentrations showed again a clear seasonal pattern with lowest values in autumn and winter, and relatively high levels during spring. No diurnal patterns were observed in the tracer levels at any of the sites and during any season. Ambient concentrations of arabitol and mannitol were well correlated, especially in coarse PM, indicating common sources, i.e., fungal spores.

In summary, characteristics of molecular fungal spore tracers in size-resolved PM were observed in various subtropical environments, showing clear spatial and temporal patterns in the ambient tracer concentrations. Additional work is needed, and is in progress in our lab, in order to investigate fungal spore characteristics as a function of different fungal species and other environmental conditions.

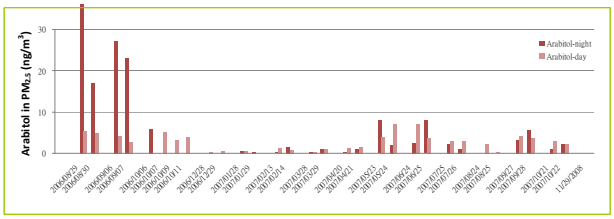

Figure 1. Ambient concentrations of arabitol in $PM_{2.5}$ at the urban site (Taipei).

Bauer, H., Claeys, M., Vermeylen, R., Schueller, E., Weinke, G., Berger, A. and Puxbaum, H. (2008a) *Atmos. Env.* **42**, 588-593.

Bauer, H., Schueller, E., Weinke, G., Berger, A., Hitzenberger, R., Marr, I.L. and Puxbaum, H. (2008b) *Atmos. Env.* **42**, 5542-5549.

Elbert, W., Taylor, P.E., Andreae, M.O. and Poeschl, U. (2007) *Atmos. Chem. Phys.* **7**, 4569-4588.

Heald, C.L. and Spracklen, D.V. (2009) *Geophys. Res. Lett.* **36**, L09806.

Jaenicke, R., Matthias-Maser, S., and Gruber, S. (2007) *Env. Chem.* **4**, 217-220.

Zhang, T., Engling, G., Chan, C.Y., Zhang, Y.N., Zhang, Z.S., Lin, M., Sang, X.F., Li, Y.D. and Li, Y.S. (2010) *Env. Res. Let.* **5**.

Numerical modelling of pollen concentrations: a comparison to measured concentrations

K. Zink[1], A. Pauling[1], B. Clot[1] and M.W. Rotach[2]

[1]Federal Office of Meteorology and Climatology MeteoSwiss, Bio-Environmental Applications, Zurich, Switzerland
[2] Institute for Meteorology and Geophysics, University of Innsbruck, Innsbruck, Austria
Keywords: Aerosol emissions, Air pollution modelling, Bioaerosols, Modelling (regional), Statistical analysis.
Presenting author email: katrin.zink@meteoswiss.ch

Pollen allergies are a very common disease in modern society. Pollen forecasts are frequently used to help doctors and patients in their diagnosis and treatment of the allergenic symptoms. Traditionally, these forecasts are based on pollen monitoring, climatological information about the typical pollen seasons and the current weather forecasts. The main drawbacks of this approach are its limitations regarding spatial and temporal resolution. A new approach that has just been set into operation is the use of numerical weather prediction systems to calculate the dispersion of pollen grains in the atmosphere.

The model system COSMO-ART

The numerical modelling of pollen concentrations requires several input variables and parameterizations within the model. The full life cycle of pollen grains has to be accounted for, starting with the growing of the plant, the ripening and release of the pollen grains, their transport within the atmosphere and ending with their removal from the atmosphere by sedimentation and deposition. The transport and removal processes can be calculated using the equations that were developed for other aerosol types, such as mineral dust or sea salt. At MeteoSwiss, we are using the NWP system COSMO-ART, an extension of the COSMO model developed at the Karlsruhe Institute of Technology (Vogel *et al*, 2009). It is designed for the distinct calculation of **A**erosols and **R**eactive **T**race gases, but also includes modules for soot, mineral dust, sea salt, and pollen. The calculation of the emission flux of pollen grains requires knowledge about the sources (i.e. plant distribution maps), the current state of the pollen season and a parameterization of the biological and meteorological processes leading to pollen emission.

Parameterizing pollen emission

Helbig *et al* (2004) have developed an emission parameterization that has been used for tree pollen emission. It has been implemented into COSMO-ART and used for simulations of birch (Vogel *et al*, 2008) and ragweed pollen (Zink *et al*, 2011). However, this parameterization shows some drawbacks, especially when applied to smaller plants, such as ragweed or grasses. To overcome some of these drawbacks and to strengthen the biological processes, we have developed a new parameterization. It focuses on the description of the individual steps that lead to the ripening of the pollen grains, the rupture of the anthers, the removal of the grains from the flowers, and their entrainment into the atmosphere.

Case study: simulating an entire pollen season

We have implemented the new emission parameterization into COSMO-ART. A first test, taking the birch pollen season of 2010 as an example, has shown that the simulations using the new emission parameterization score similarly compared to the ones using the Helbig *et al* (2004) parameterization (see Figure 1). In both cases, statistical analyses have been used to compare the numerical values to measurements of pollen concentrations.

It should be noted that in the first test phase of 2010, the new parameterization has not been tuned yet. On the contrary, we are using the data of 2010 to adapt the parameters used in the formulations. The pollen season of 2011 will then be used as a case study to compare the performance of the two model variations.

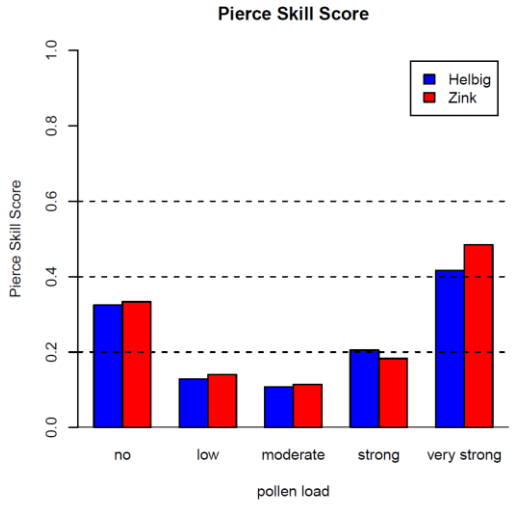

Figure 1. Pierce Skill Score (for formulas and explanations see Wilks, 2006) for different pollen classes using the new (Zink) and old (Helbig) emission parameterizations.

Helbig, N., Vogel, B., Vogel, H., Fiedler, F. (2004) *Aerobiologia* **3**, 3–19.

Vogel, H., Pauling, A., Vogel, B. (2008) *Int. J. Biometeorol.* **52**, 805–814.

Vogel, B., Vogel, H., Bäumer, D., Bangert, M., Lundgren, K., Rinke, R., Stanelle, T. (2009) *Atmos. Chem. Phys.* **9**, 8661–8680.

Wilks, D.S. (2006) *Statistical Methods in the Atmospheric Sciences*, Academic, Amsterdam.

Zink, K., Vogel, H., Vogel, B., Magyar, D., Kottmeier, C. (2011) *Int. J. Biometeorol.* doi:10.1007/s00484-011-0468-8.

Monday, September 3, 2012

Session WG03S1O. Chemistry of Organic Aerosol: Laboratory Study 1

Simultaneous study of gas and particulate products formed from isoprene oxidation: laboratory and field measurements

C. Rio[1], S. Rossignol[1], S. Fable[1], L. Chiappini[1]

[1]Institut National de l'Environnement Industriel et des Risques (INERIS), 60 550 Verneuil-en-Halatte, France
Keywords: Isoprene, SOA, Gas-particle distribution, Smog chamber.
Presenting author email: caroline.rio@ineris.fr

Isoprene is one of the most abundant non-methane hydrocarbons emitted by vegetation into the troposphere. For a long time, it has been generally accepted that isoprene oxidation did not contribute to global SOA burden because of the volatility of its main oxidation products (methacrolein, methyl vinyl ketone…) (Pandis, 1991). It is only recently that isoprene oxidation contribution to SOA formation has been proven (Edney, 2005; Kroll, 2006).

There are still remaining uncertainties on the importance of isoprene contribution to atmospheric SOA and further studies combining ambient measurements of tracers, identified in laboratory experiments, coupled with atmospheric modeling are needed to better parameterize SOA yields and quantitatively model SOA production from isoprene oxidation (Carlton, 2009).

Therefore, the first part of this work focuses on laboratory experiments to study isoprene oxidation under realistic conditions in the EUropean PHOtoREactor (EUPHORE) in Valencia during the period 13–22 September 2010 (Figure 1(a)): seed aerosols (10 µg/m^3) were present in the chamber before isoprene and H_2O_2 introduction (70 ppb and 4 ppm respectively) under sunlight irradiation and a relative humidity close to 30 %. Moreover this study of the (isoprene + OH) reaction was performed under free-NOx condition.

A method recently developed in our laboratory (Rossignol, 2012) was used to investigate the chemical composition of both gas and particulate phases of SOAs formed.

This method consists in using stainless steel Tenax-TA adsorbent tubes previously coated with PFBHA (to specifically study carbonyl compounds) or MTBSTFA (to specifically study hydroxyl compounds) to collect the gas phase. Particulate sample are collected onto filters (quartz and Teflon-Quartz) subsequently exposed to PFBHA or MTBSTFA before analysis. These tubes and filters are subsequently analyzed by thermal-desorption coupled with gas chromatography and mass spectrometry (TD-GC-MS) analysis.

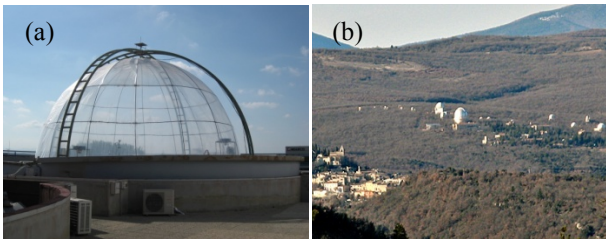

Figure1: (a) EUPHORE smog chamber, (b) St.Michel l'Observatoire with OHP in the background

About thirty compounds have been positively or tentatively identified in gas and/or particle phases. Some of these are monofunctionalized such as methacrylic acid or methacrolein, others are polyfunctionalized such as malic acid. These compounds have been quantified and for those identified in both gas and particulate phases, an experimental partitioning coefficient was calculated.

In a second time, these results will be compared to real atmosphere samples during a field campaign which will take place in June 2012 at the Observatoire de Haute provence (OHP; situated in southeast France) (Figure 1(b)) as a part of the CANOPEE field campaign. This work falls within the framework of a research program about the study of combined model-measurement of intra canopy chemistry. Not only gas and particles samplings will be realized but particles formation and isoprene emission will be observed at the same time.

Results obtained in both smog chamber and field campaign during isoprene oxidation will be presented and discussed.

Carlton A. G., Wiedinmyer C., and Kroll J. H. (2009) *Atmos. Chem. Phys.*, **9**, 4987–5005.

Edney, E. O., Kleindienst, T. E., Jaoui, M., Lewandowski, M., Offenberg, J. H.,Wang,W., and Claeys, M. (2005*) Atmos. Environ.*, **39**, 5281–5289.

Kroll, J. H., Ng, N. L., Murphy, S. M., Flagan, R. C., and Seinfeld,J. H. (2006) *Environ. Sci. Technol.*, **40**, 1869–1877.

Pandis, S. N., Paulson, S. E., Seinfeld, J. H., and Flagan, R.C. (1991) *Atmos. Environ.* ; **25**, 997–1008.

Rossignol, S., Chiappini, L., Perraudin, E., Rio, C., Fable, S., Valorso, R., and Doussin, J. F (2012) *Atmos. Meas. Tech. Discuss.;* **5**, 1153-1231.

Do Organic Aerosols Shrink?

N.M. Donahue[1], E. S. Robinson[1], A. Ahern[1], E. Trump, and R. Saleh[1]
[1]Center for Atmospheric Particle Studies, Carnegie Mellon University, Pittsburgh, Pennsylvania, 15213, USA
Keywords: dilution, organic aerosol, aerosol dynamics.
Presenting author email: nmd@andrew.cmu.edu

There is considerable current controversy about whether atmospherically relevant organic aerosols show significant semi-volatile behavior or whether they are less volatile than they were once thought to be. Furthermore, "less volatile" could mean that the organic aerosol is comprised of constituents that simply have a lower saturation vapor pressure than thought, or it could mean that relatively volatile organic compounds have some strange affinity for the condensed phase and thus remain in a disequilibrium state with an excess in the particle phase.

We have addressed this question experimentally and theoretically via a number of avenues. Using single particle measurements of prepared external mixtures, often with isotopic labeling, we observe the mixing behavior of organic particles via gas-phase vapor exchange (which necessarily requires evaporation of constituents from their original particles). Using the common model α-pinene SOA system, we have injected aliquots of fresh α-pinene SOA into a clean receptor chamber at dilution ratios of 100-1000 and observed the evaporation behavior of the aerosol. We have performed these experiments over a range of relative humidities, testing the hypothesis that absorbed water might plasticized the potentially glassy but demonstrably water soluble SOA. Finally, we have added water to an initially stable α-pinene SOA system, generated at low RH, to explore the sensitivity of the SOA mass and composition to absorbed water.

For test external mixtures we can indeed observe rapid mixing, though some systems with relatively low saturation concentrations remain externally mixed over the timescale of our experiments. We can thus observe systems that do and do not mix with each other.

The α-pinene SOA does contain some organic matter that evaporates more slowly than simple models based on SOA growth experiments predict: roughly 1/3 of the SOA evaporates very quickly, while the remaining 2/3 evaporates slowly over the course of many hours, never appearing to reach a stable equilibrium value. However, the general behavior is not a function of relative humidity and thus does not appear to have anything to do with the makeup of the condensed phase. We thus conclude that it is most likely that the SOA includes a portion of quite low volatility compound, which either simply evaporate slowly or which decompose on a several hour timescale into volatile fragments.

Finally, the slow humidification experiments allow us to follow the influence of water on the phase partitioning of organics over a wide range of RH and total organic aerosol loading.

We have developed a dynamical model of these mixtures, and will present comparisons of the modeled evaporation / equilibration of the organic systems studied with the observed behavior.

Gas phase formation of extremely oxidized α-pinene reaction products and their role in aerosol particle formation

M. Ehn[1], E. Kleist[2], H. Junninen[3], T. Petäjä[3], G. Lönn[3], S. Schobesberger[3], M. Sipilä[3], M. Dal Maso[3], R. Tillmann[1], A. Trimborn[1,4], M. Kulmala[3], D. R. Worsnop[3,5], A. Wahner[1], J. Wildt[2], Th. F. Mentel[1]

[1] Institute for Energy and Climate Research (IEK-8), Forschungszentrum Jülich, 52425 Jülich, Germany
[2] Institute of Bio- and Geosciences (IBG-2), Forschungszentrum Jülich, 52425 Jülich, Germany
[3] Department of Physics, P.O.Box 64, 00014 University of Helsinki, Finland
[4] Aeromegt GmbH, Verbindungsstraße 27, 40723 Hilden, Germany
[5] Aerodyne Research, Inc., 45 Manning Road, Billerica, MA 01821, USA
Keywords: Aerosol formation, mass spectrometry, alpha-pinene oxidation, secondary organic aerosol (SOA)
Presenting author email: m.ehn@fz-juelich.de

High-sensitivity, high-resolution time-of-flight mass spectrometers (TOFs) have become increasingly more common in atmospheric science during the last years. In this work, we have taken advantage of the newest instrumentation, using a novel combination of TOFs for α-pinene oxidation studies, with a focus on the ability of the gas-phase products to form aerosol particles.

The TOF instruments used were:

1) Atmospheric pressure interface TOF (APi-TOF; Junninen et al., 2010)
2) Proton transfer reaction TOF (PTR-TOF; Jordan et al., 2009)
3) Acetate chemical ionization APi-TOF (Ac-CIMS; Bertram et al., 2011)
4) Nitrate chemical ionization APi-TOF (NO3-CIMS; Jokinen et al., 2011)

The APi-TOF measures naturally charged ions formed by cosmic rays and radon decay. This method is extremely sensitive, but selective, to very stable negative or positive ions. The PTR-TOF is the most widespread and well-characterized MS of the four, capable of measuring volatile organic compounds (VOCs) with proton affinities higher than water. The Ac-CIMS detects acids stronger than acetic acid, and is thus sensitive to most gas-phase acids. The NO3-CIMS detects ions that are either charged by clustering with, or by transferring a proton to, NO_3^-. In practice this means that it is mainly selective to very strong acids.

Initially, only the APi-TOF was used to detect and identify a new group of highly oxidized multi-functional organics (HOMs) from α-pinene ($C_{10}H_{16}$) ozonolysis at the Jülich plant atmosphere chamber (JPAC). The HOMs typically contained all the original ten C atoms, while reaching O:C ratios of 0.7-1.3. The spectra resembled APi-TOF spectra acquired in a boreal forest to stunning detail (Ehn et al., 2012). The HOMs are expected to have extremely low vapor pressures, and thus can play an important role in new aerosol particle formation. Motivated by these results, a novel measurement setup was deployed at JPAC to study the oxidation process of α-pinene, and relate the products to aerosol particle formation. The setup included a PTR-TOF, Ac-CIMS, and an NO3-CIMS. A particle size magnifier (PSM) was deployed to count the newly nucleated particles in the size range where they are formed (1-2 nm). In addition to these instruments, the standard JPAC setup includes basic particle (CPC, SMPS) and gas-phase (O_3, RH, OH (by tracer), etc.) measurements.

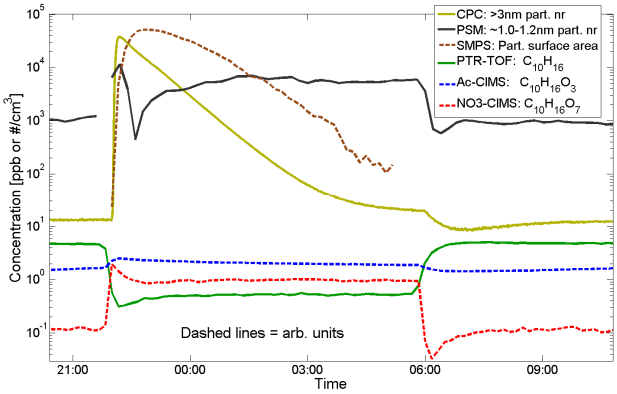

Fig. 1. Selected traces from 6 different instruments during one OH-initiated nucleation event from α-pinene. UV lights were on 22:00-06:00. Dashed traces in a.u.

As an example of the strength of the measurement setup, traces from 6 different instruments are presented in Fig. 1. The bottom three traces depict example gas-phase molecules, with α-pinene in green, and two oxidation products in blue and red (currently only in a.u.). The red trace is an example of the newly discovered HOMs. The upper traces are particle signals, which show sharp increases in both PSM (1.0-1.2 nm) and CPC (>3 nm) number at 22:00 when the UV lamps are turned on, coinciding with a large increase of $C_{10}H_{16}O_7$ (and many other HOMs).

The main findings from similar studies, under varying conditions to probe several different atmospheric conditions, will be presented.

This work was supported by the Emil Aaltonen foundation.

Bertram, T. et al., *Atmos. Meas. Tech.*, 4, 1471-1479, 2011.
Ehn, M. et al., *Atmos. Chem. Phys. Discuss.,* 12, 4589-4625, 2012.
Jokinen, T. et al., *Atmos. Chem. Phys. Discuss.*, 11, 31983-32002, 2011.
Jordan, A. et al., *Int. J. Mass Spectrom.*, 286 (2-3), pp. 122-128, 2009.
Junninen, H. et al., *Atmos. Meas. Tech.*, 3, 1039–1053, 2010.

α-Pinene and β-pinene ozonolysis
- Effect of CO on SOA formation and product distribution -

A. Kahnt*, Y. Iinuma, A. Mutzel, O. Böge and H. Herrmann

Leibniz Institute for tropospheric research (IfT), Department of Chemistry, Leipzig, D-04177, Germany
* Present address: Department of Pharmaceutical Sciences, University of Antwerp, Antwerp, B-2610, Belgium
Keywords: SOA, Smog chamber, Aerosol characterisation.
Ariane.Kahnt@ua.ac.be

The past studies have shown that an HO_2/RO_2 ratio influences the SOA formation chemistry in alkene ozonolysis. Depending on the structures of alkenes, the production of SOA increases or decreases as the HO_2/RO_2 ratio increases. While the influence of high HO_2/RO_2 ratio on SOA yields is established, its impact on the product distribution is rarely studied. In the present study, we examine SOA formation from monoterpene ozonolysis in the presence of CO as an OH radical scavenger and different seed particle acidities. The addition of CO results in the formation of HO_2 radicals from the reaction of the scavenger with OH radicals, leading to a high HO_2/RO_2 ratio in the system. CO is an attractive OH radical scavenger for aerosol chamber experiments because it achieves an HO_2/RO_2 ratio similar to that of ambient atmosphere under low NO_x conditions (< 100 ppt), which is typically between 0.25 – 1.33 (e.g., Stevens et al., 1997; Hanke et al., 2002; Mihelcic et al., 2003; Fuchs et al., 2008). Based on simulations using the COPASI 4.8 model, the HO_2/RO_2 ratio under the conditions applied in the present study is simulated to be 1 that is close to ambient conditions.

In the presence of CO, an increase in SOA formation was observed for the endocyclic α-pinene whereas an opposite was the case for exocyclic β-pinene. As shown in Figure 1 for the α-pinene ozonolysis, the presence of CO and acidic seed particles resulted in the highest organic mass increase at a given hydrocarbon conversion. Furthermore, an increase in SOA formation was observed for all the experiments using acidic seed particles for α-pinene.

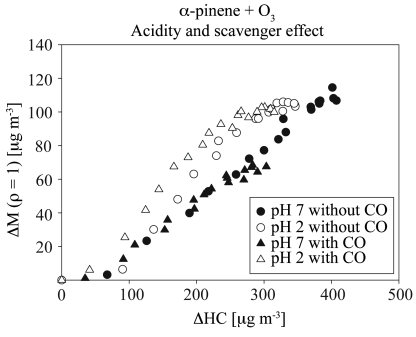

Figure 1. SOA growth curves from α-pinene ozonolysis with (triangle) and without (circle) CO as an OH radical scavenger. The different seed particle acidities are shown with filled symbols for pH 7 and open symbols for pH 2.

In contrast the ozonolysis of β-pinene resulted only in a marginal increase in organic mass in the presence of CO and acidic seed particles (see Figure 2).

As shown in Figure 2 the experiments performed without CO showed no acidity dependency in organic mass formation.

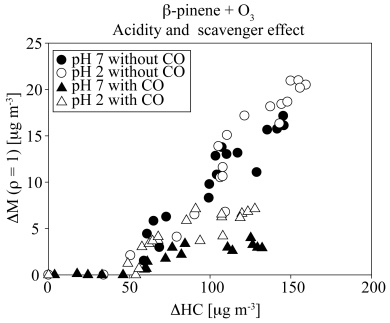

Figure 2. SOA growth curves from β-pinene ozonolysis with (triangle) and without (circle) CO as an OH radical scavenger and different seed particle acidities.

The results obtained in the present study support the differences in the products of α- and β-pinene ozonolysis as proposed by Docherty et al. (2005). While the ozonolysis of α-pinene at elevated HO_2 levels likely resulted in a C10 hydroperoxide, β-pinene oxidation led to a more volatile C9 ketone hydroperoxide. The enhanced SOA growth observed in α-pinene ozonolysis when the CO and acidic seed particles co-existed may be explained by an acid-catalysed reaction of the organic peroxides that led to the formation of higher molecular weight compounds.

The aerosol analysis supports this suggestion as only marginal differences in the relative contribution of carboxylic acid and carbonyl compounds to the detected total organic mass were observed regardless of the experimental conditions.

Docherty, K.S., Wu, W., Lim, Y.B., Ziemann, P.J. (2005) *Environ. Sci. Technol.* **39**, 4049-4059.

Fuchs, H., Holland, F., Hofzumahaus, A. (2008) *Rev. Sci. Instrum.* **79**.

Hanke, M., Uecker, J., Reiner, T., Arnold, F. (2002) *Int. J. Mass. Spectrom.* **213**, 91-99.

Mihelcic, D., Holland, F., Hofzumahaus, A., Hoppe, L., Konrad, S., Müsgen, P., Pätz, H.W., Schäfer, H.J., Schmitz, T., Volz-Thomas, A., Bächmann, K., Schlomski, S., Platt, U., Geyer, A., Alicke, B., Moortgat, G.K. (2003) *J. Geophys. Res.-Atmos.* **108**. -.

Stevens, P.S., Mather, J.H., Brune, W.H., Eisele, F., Tanner, D., Jefferson, A., Cantrell, C., Shetter, R., Sewall, S., Fried, A., Henry, B., Williams, E., Baumann, K., Goldan, P., Kuster, W. (1997) *J. Geophys. Res.-Atmos.* **102**, 6379-6391.

Is the chemical composition of α-pinene secondary organic aerosol dependent on particulate water content?

L. Pfaffenberger, P. Barmet, R. Wolf, J. G. Slowik, J. Dommen, A. S. H. Prévôt and U. Baltensperger

Laboratory of Atmospheric Chemistry, Paul Scherrer Institut PSI, Villigen, 5232, Switzerland

Keywords: AMS, Photochemical processes, SOA (Secondary Organic Aerosols), Water soluble organic compounds

Organic aerosols (OA) represent with 20-90% a major fraction of the submicron aerosol (Jimenez et al., 2009). Potential sources and processes which lead to the formation of secondary organic aerosol (SOA) are still rather poorly understood, although SOA contributes to a large amount to the OA burden. To determine properties relevant for aerosol yield, in particular volatility and degree of oxygenation, the formation and aging of particles have to be investigated more intensively.

Several laboratory studies showed the importance of aqueous phase SOA formation that is thought to be almost as important as SOA compounds that form in the gas phase and then partition to the aerosol phase (Ervens et al., 2011).

The uptake of water-soluble organic compounds depends on the water content of the particles and is higher for larger particle diameters. In this study, the aerosol chemical composition as a function of the vacuum aerodynamic diameter (d_{va}) is investigated using an Aerodyne aerosol mass spectrometer (AMS) equipped with a PM 2.5 lens.

In the PSI smog chamber, the aerosol precursor α-pinene was exposed to UV and xenon lights in the presence of a seed, various relative humidities and NO_x concentrations. NH_4HSO_4 was used as a hygroscopic seed to provide a large water volume capable of taking up soluble oxidation products like glyoxal and methylglyoxal. A wide diameter range, ~50 to 2500 nm, was covered by the particle phase instruments. The aging time in the chamber is related to the atmospheric oxidation time using the OH exposure derived from the decay of an OH tracer added into the bag (Barmet et al. 2011).

Fig. 1 shows the normalised mass spectra for two different diameter bins (100nm-500nm and 500nm-2500nm) averaged over the whole experiment duration in the lower panel and the difference in those spectra in % (upper panel). The presented experiment was conducted at 72 ± 1 % relative humidity and 1.0 ± 0.2 ppb NO_x.

Significant changes are seen in several masses referring to a change in chemical composition. *m/z* 44, a surrogate for the degree of oxygenation, is enhanced in the larger particles compared to the smaller ones.

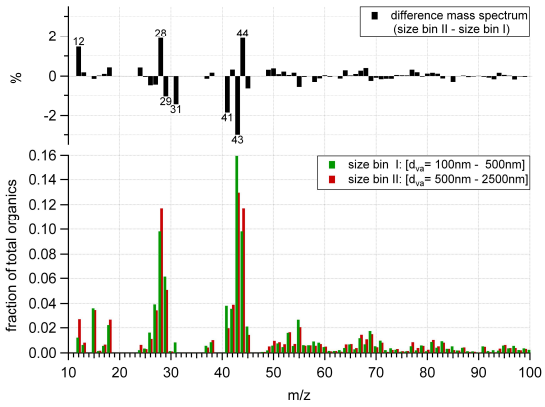

Figure 1: Normalized average mass spectra of two different diameter ranges (lower panel) and the difference [size bin II-size bin I] (upper panel).

This could be due to the larger available water contents which would favour aqueous phase processes and lead to more highly oxygenated products like acids. However, composition-dependent differences in particle vaporization time could also contribute to such differences. The relative importance of these effects will be assessed by analysis of single particle mass spectra acquired using a light scattering module integrated with the AMS.

Further investigations on the evolution of the chemical composition during the experiments and the dependency on the prevailing relative humidity will be part of this study.

This work was supported by EUROCHAMP-2, a research project within the EC 7th Framework Programme, as well as the Swiss National Science Foundation.

Jimenez, J. L. et al. (2009) *Science*, **326**(5959): 1525-1529.

Ervens, B. et al. (2011) *Atmos. Chem. Phys.*, **11**, 11069–11102.

Barmet, P. et al. (2011) *Atmos. Meas. Tech. Discuss.*, **4**, 7471-7498.

Kinetic multi-layer model of gas-particle interactions in aerosols and clouds (KM-GAP): linking condensation, evaporation and reactions of organics, oxidants and water

M. Shiraiwa[1], C. Pfrang[2], T. Koop[3] and U. Pöschl[1]

[1] Max Planck Institute for Chemistry, Biogeochemistry Department, Mainz, Germany
[2] University of Reading, Department of Chemistry, Reading, UK
[3] Bielefeld University, Faculty of Chemistry, Bielefeld, Germany

Keywords: gas-particle partitioning, semi-volatile species, oxidative aging, secondary organic aerosol.
Presenting author email: m.shiraiwa@mpic.de

We present a novel kinetic multi-layer model for gas-particle interactions in aerosols and clouds (KM-GAP) that treats explicitly all steps of mass transport and chemical reaction of semi-volatile species partitioning between gas phase, particle surface and particle bulk (Shiraiwa et al., 2011). KM-GAP is based on the PRA model framework (Pöschl et al., 2007), and it includes gas phase diffusion, reversible adsorption, surface reactions, bulk diffusion and reaction, as well as condensation, evaporation and heat transfer. The size change of atmospheric particles and the temporal evolution and spatial profile of the concentration of individual chemical species can be modeled along with gas uptake and accommodation coefficients. Depending on the complexity of the investigated system, unlimited numbers of semi-volatile species, chemical reactions, and physical processes can be treated, and the model shall help to bridge gaps in the understanding and quantification of multiphase chemistry and microphysics in atmospheric aerosols and clouds.

In this study we demonstrate how KM-GAP can be used to analyze, interpret and design experimental investigations of changes in particle size and chemical composition in response to condensation, evaporation, and chemical reaction. For the condensational growth of water droplets, our kinetic model results provide a direct link between laboratory observations and molecular dynamic simulations, confirming that the accommodation coefficient of water at ~270 K is close to unity (Fig. 1). Literature data on the evaporation of dioctyl phthalate as a function of particle size and time can be reproduced (Fig. 2), and the model results suggest that changes in the experimental conditions like aerosol particle concentration and chamber geometry may influence the evaporation kinetics and can be optimized for efficient probing of specific physical effects and parameters. With regard to oxidative aging of organic aerosol particles, we illustrate how the formation and evaporation of volatile reaction products like nonanal can cause a decrease in the size of oleic acid particles exposed to ozone.

So far the formation and aging of secondary organic aerosol (SOA) has generally been described by thermodynamic models assuming quasi-instantaneous gas-particle partitioning. If, however, the phase state of SOA is not liquid but (semi-)solid (Virtanen et al., 2010), this assumption may break down and the SOA partitioning may be kinetically limited (Shiraiwa et al., 2011). We suggest and intend to use KM-GAP for the investigation of such effects.

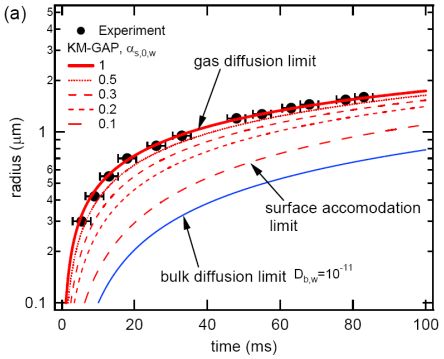

Figure 1. Water droplet growth curve simulated by KM-GAP with different surface accommodation coefficient of H_2O in comparison with data by Winkler et al. (2006).

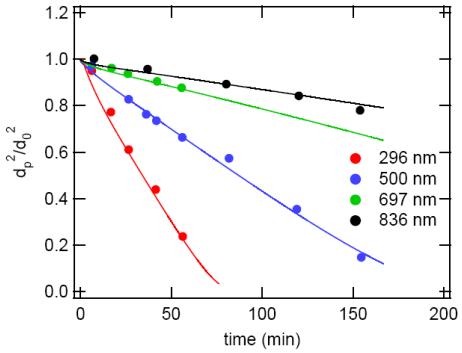

Figure 2. Evaporation of dioctyl phthalate simulated by KM-GAP as a function of time with different particle diameters. The data points are from Vaden et al. (2011).

This work was funded by the Max Planck Society (MPG) and the European Commission under the projects EUCAARI (grant no. 036833-2) and PEGASOS (grant no. 265148).

Pöschl, U., Rudich, Y. and Ammann, M. *Atmos. Chem. Phys.*, 7, 5989-6023, 2007.
Shiraiwa, M., et al., *PNAS*, 108(27) 11003, 2011.
Shiraiwa, M., Pfrang, C., Koop, T., and Pöschl, U.: *Atmos. Chem. Phys. Discuss.*, 11, 33689, 2011.
Vaden, T. D. et al., *PNAS*, 108, 2190-2195, 2011.
Virtanen, A., et al., *Nature*, 467: 824-827, 2010.
Winkler, P. M. et al.: *J. Geophys. Res.*, D19202, 2006.

The effect of humidity on the ozonolysis of unsaturated compounds in aerosol particles and on particle phase

M. Kalberer, F.D. Pope, P.J. Gallimore, P. Achakulwisut J. Lee, J. F. Davies, V. Garrascon, S. Fuller, A. Björkegren and D. R. Spring

[1]Department of Chemistry, University of Cambridge, Cambridge, CB2 1EW, UK
Keywords: Aerosol Chemistry, Hygroscopic Growth, Particle Phase.
Presenting author email: markus.kalberer@atm.ch.cam.ac.uk

Atmospheric aerosol particles are important in many atmospheric processes such as light scattering, light absorption, and cloud formation. Oxidation reactions continuously change the chemical composition of aerosol particles, especially organic components, which are often a dominant fraction. These ageing processes are poorly understood but are known to affect the cloud formation potential of aerosol particles.

In this study we investigate the effect of humidity and ozone on the chemical composition and phase of three model organic aerosol systems: oleic, maleic and arachidonic acid. Two experimental techniques are combined in this investigation. An electrodynamic balance (EDB) is used to levitate single particles and assess changes in particle size and mass (due to water uptake and/or loss of volatile ozonolysis products) and phase (liquid or solid) during and after chemical processing with ozone (Pope et al., 2010). An aerosol flow tube was used to investigate the chemical composition of the processed aerosol particles with off-line ultra high-resolution mass spectrometry (Gallimore et al., 2011).

The role of relative humidity (RH) in the oxidation scheme of the three carboxylic acids is very compound specific (Lee et al., 2012). RH was observed to have a major influence on the oxidation scheme of maleic acid and arachidonic acid, whereas no dependence was observed for the oxidation of oleic acid. In addition, the particle phase has a strong effect on the particle processing and the effect of water on the oxidation processes. Oleic acid is liquid under all conditions at room temperature (dry or elevated humidity, pure or oxidized particle). Thus ozone can easily diffuse into the bulk of the particle irrespective of the oxidation and RH conditions.

This is very different for maleic and arachidonic acid, which change their phase from liquid to solid upon oxidation or upon changes in humidity. In a solid particle the reactions of ozone and water with the organic particle are restricted to the particle surface. Only an exposure to high humidity, i.e. the formation of liquid particles allows for a diffusion of ozone into the particle bulk and an oxidative processing of the entire particle. Oxidation products of maleic acid and arachidonic acid are much more hygroscopic and therefore water is present in the liquid, oxidized particles in much higher mole fractions at elevated RH than in oleic acid particles.

The differences in the oxidation schemes of the three carboxylic acids are mainly explained by the very different reactivity (i.e. electron deficiency) of the Criegee intermediate (CI), one of the first reaction products in the oxidation scheme of all three systems (Figure 1). Reactions of the CI of oleic acid with other primary oxidation products leads to the formation of oligomers. In contrast, the maleic acid oxidation products are mostly monomeric and only dimers (but no higher oligomers) were formed in esterification reactions from stable oxidation products.

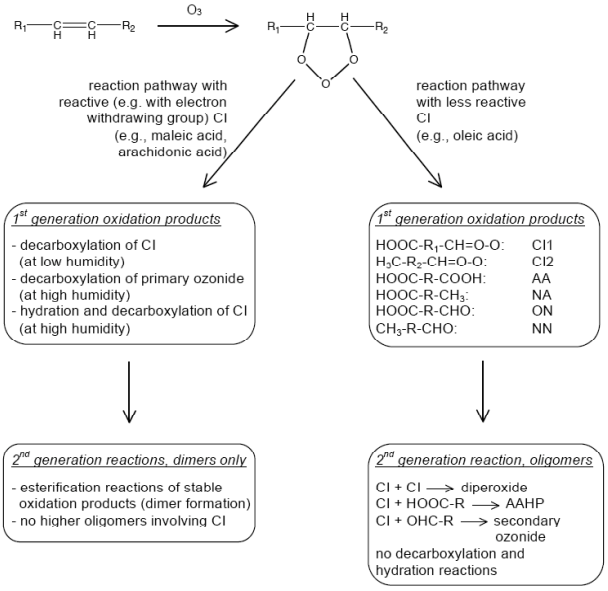

Figure 1. Schematic oxidation scheme of unsaturated compounds with ozone emphasizing the different reaction pathways due to the different reactivity of the Criegee intermediate.

In more complex and atmospherically relevant laboratory model systems such as secondary organic aerosol formed from terpenes ester formation are likely explaining a major fraction of the observed particle phase reactivity and especially the formation of short oligomers. In addition, in the ambient atmosphere high-mass oligomers are rarely observed. Thus the oxidation schemes of maleic where only a limited degree of oligomerisation is observed might be more representative of particle phase oxidation reactions occurring in the complex mixtures of ambient particles.

Pope, F.D. et al. (2010) Environ. Sci. Technol. 44, 6656.
Gallimore, P.J., et al. (2011) Atmos. Chem. Phys., 11, 12181.
Lee, J., et al. (2012), Phys. Chem. Chem. Phys., submitted.

Composition, Reactivity, and Energetics of Sulphuric Acid Clusters Containing Ammonia and Amines

Bryan R. Bzdek[1], Joseph W. DePalma[1], Julia Laskin[2], Douglas P. Ridge[1] and Murray V. Johnston[1]

[1]Department of Chemistry and Biochemistry, University of Delaware, Newark, Delaware, 19716, USA
[2]Pacific Northwest National Laboratory, Richland, Washington, 99352, USA
Keywords: aerosol kinetics, ambient nuclei, new particle formation, nucleation.
Presenting author email: bbzdek@udel.edu

New particle formation (NPF) may affect cloud albedo and climate by influencing global cloud condensation nuclei levels. To properly model the climate effects of NPF, its underlying mechanisms need to be fully understood. This work examines the composition, reactivity, and energetics of sulphuric acid clusters containing ammonia and amines.

The first portion of this work investigates the role of cluster size and charge on ammonium bisulphate cluster reactivity. Positively and negatively charged ammonium bisulphate clusters were analysed by Fourier transform ion cyclotron resonance mass spectrometry (FTICR-MS). Positively charged clusters differed significantly in composition from negatively charged clusters. Positively charged clusters exhibited enhanced neutralization to bisulphate, whereas negatively charged clusters were very acidic. With increasing cluster size, both polarity clusters converge towards ammonium bisulphate. Negatively charged cluster reactivity with dimethylamine (DMA) was also investigated by FTICR-MS. A specific cluster was selected and reacted with a constant pressure of DMA. As illustrated in Fig. 1, a plot of ion abundance as a function of trapping time was fit to the pseudo-first order rate law to determine the reaction kinetics and uptake coefficients. Two reaction types were observed: ammonia displacement by DMA and DMA addition to neutralize sulphuric acid to bisulphate. The displacement reaction was nearly collision-limited, whereas the addition reaction was very slow relative to exchange. These observations suggest: 1) amine-ammonia chemistry will only be evident and important in large ambient negative ions but will be evident in small ambient positive ions; 2) bisulphate is favored over sulphate at small cluster sizes; and 3) small (1-2 nm) ammonium salt clusters should easily exchange with amine to form aminium salts (Bzdek *et al*, 2011).

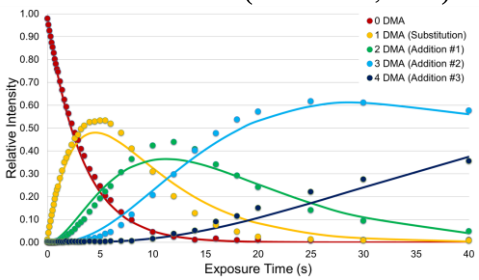

Figure 1. Reaction profile for exposure of $[(NH_4)(HSO_4)_2(H_2SO_4)_3]^-$ to DMA. Symbols are experimental values. Lines are fits to pseudo-first order kinetics.

The second portion of this work focuses on cluster growth mechanisms. Charged clusters were extracted into a FTICR-MS equipped with surface induced dissociation (SID), a method to fragment ions by impacting them onto a surface at known collision energy. Fig. 2 presents time- and collision energy-resolved fragmentation efficiency curves for dissociation of $[(NH_4)_6(HSO_4)_5]^+$. Upon collision, this cluster immediately dissociates to $[(NH_4)_3(HSO_4)_2]^+$, which further dissociates to $[(NH_4)_2(HSO_4)(H_2SO_4)]^+$ and $[(NH_4)_2(HSO_4)]^+$ with increasing collision energy. The experimental data were modeled using RRKM theory to determine the dissociation energetics (Laskin *et al*, 2000). Two other ammonium bisulphate clusters were also studied to determine the size dependence of cluster decomposition. Assuming that growth mechanisms are the reverse of decomposition mechanisms, association (growth) energetics can be determined from the decomposition energetics. Preliminary analysis suggests two cluster growth pathways exist: 1) stepwise growth by addition of sulphuric acid followed by ammonia; 2) growth by addition of an ammonium bisulphate monomer. The modeling suggests an activation barrier exists for the stepwise growth pathway, whereas none exists for the monomer growth pathway. The implications of these results will be discussed.

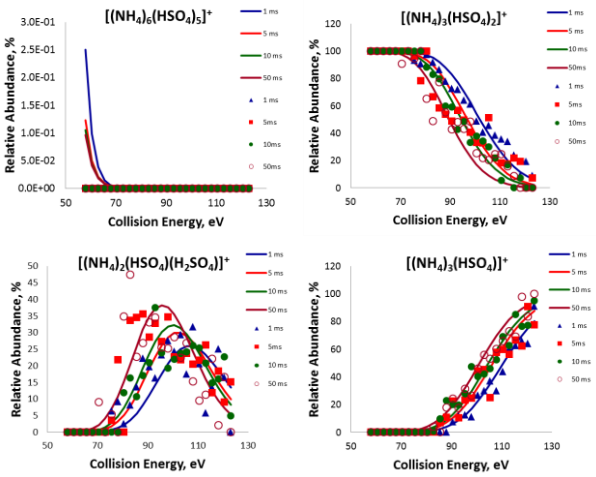

Figure 2. Fragmentation efficiency curves for $[(NH_4)_6(HSO_4)_5]^+$ decomposition. Symbols are experimental SID values. Lines are RRKM model fits.

This work was supported by NSF Grant CHE-1110554.

Bzdek *et al*, (2011) *Atmos. Chem. Phys.* **10**, 8735-8743.
Laskin *et al*, (2000) *Int. J. Mass Spectrom.* **195/196**, 285-302.

Monday, September 3, 2012

Session WG06S1O. Particle toxicity

Effects of different combustion conditions on the toxicological properties of PM_1 in adjustable biomass combustion reactor

O. Uski[1,2], J. Leskinen[1], P. Jalava[1], A. Virén[1], H. Lamberg[1], T. Kaivosoja[1],T. Kettunen[1], I. Nuutinen[1], M. Happo[1], T. Torvela[1], J. Tissari[1], O. Sippula[1], J. Jokiniemi[1,3], M.-R. Hirvonen[1,2]

[1]Univ. of Eastern Finland, Department of Environmental Science, P.O. Box 1627, FI-70211 Kuopio, Finland
[2]National Institute for Health and Welfare, Department of Env. Health, P.O. Box 95, FI-70701 Kuopio, Finland
[3]VTT Technical Research Centre of Finland, P.O. Box 1000, FI-02044 VTT, Espoo, Finland
Keywords: Biomass combustion, Health effects of aerosols, Chemical composition, Combustion particles.
Presenting author email: oskari.uski@uef.fi

Current levels of ambient air fine particulate matter are associated with mortality and morbidity in urban populations. Since large proportion of $PM_{2.5}$ emissions are derived from small scale combustion, it is important to reveal the possible health effects of the particle emissions from the combustion appliances. Especially there is a lack of knowledge concerning modern wood combustion systems. In this study, toxicological properties of PM_1 emissions from biomass combustion reactor operated by three different ways were examined.

Three different combustion conditions, efficient, erratic and poor, were generated in combustion reactor using wood chips as fuel. The efficient conditions corresponded to optimal biomass combustion and the poor conditions approach to conventional batch combustion. Instead, the erratic conditions represented malfunctioning of combustion appliance. The demanded combustion conditions were achieved by adjusting fuel feeding, air flows and air staging. (Table 1).

PM samples for toxicological analysis were collected on PTFE-filters from diluted flue gas by using Dekati® gravimetric impactor. Samples were extracted from filters using methanol. Mouse macrophage cells (RAW264.7) were exposed for 24 h to four doses (15, 50, 150 and 300 mg ml^{-1}) of emission samples.

The studied emission samples by all doses induced a statistically significant dose-dependent decrease in cell viability (MTT assay) when compared to control (Fig.1). However, the efficient combustion caused clearly more cytotoxicity than the other samples.

When cells cell cycle phases were analyzed (dose 150 mg ml^{-1}) statistically significant apoptosis was detected with erratic and poor combustion (Fig.2). All samples caused statistically significant decrease of G_1-phase when compared to control. Interestingly, only efficient combustion caused statistically significant increase in S-G2/M-phase which is considered as sign of cell cycle arrest caused by DNA damage.

The results indicated that even modern wood combustion appliances and optimal burning conditions may have health impact. Efficient combustion was causing highest cytotoxicity and clear cell cycle arrest. However, emissions from efficient combustion were negligible compared to two other situations and that is even more important when the aim is to reduce human exposure to PM.

Table 1. Emission parameters in averaged values.

Parameter	Efficient	Erratic	Poor
Number Conc.(1/MJ)	1.4E+14	5.5E+13	2.7E+13
PM_1 Mass Conc. (DGI)(mg/MJ)	8 ± 3	61 ± 47	135 ± 22
CO(mg/MJ)	7 ± 37	303 ± 633	2300±3300
CH_4 (mg/MJ)	0.3 ± 0.3	4 ± 21	115 ± 190
OGC (mg/MJ)	3.6 ± 1.4	7.1 ± 25	180 ± 340

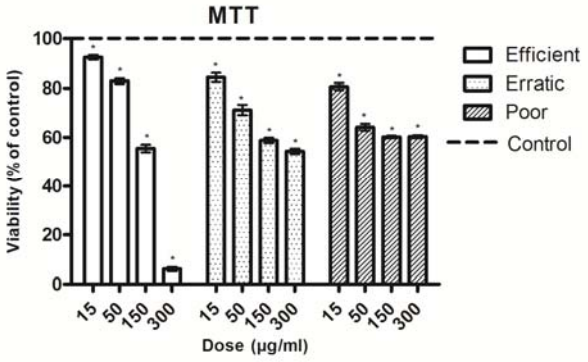

Fig.1. Viability of RAW264.7 macrophages after exposure to four doses (15, 50, 150 and 300 mg ml^{-1}) of cell medium suspended particles emitted from a biomass combustion reactor (the mean ±SEM). Asterisks (*) indicate a statistically significant difference from control cells as presented 100 % ($p < 0.05$, Dunnett's test). n=6 in total.

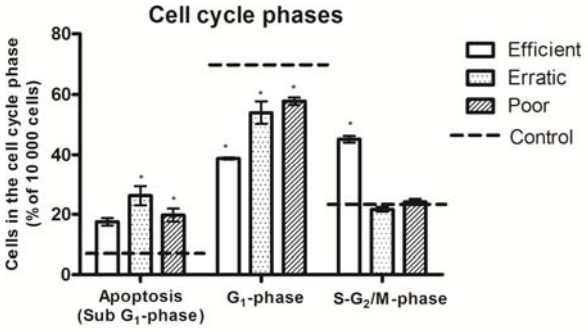

Fig. 2. Apoptosis and phases of the cell cycle in RAW264.7 macrophages after exposure to the particles emitted from a biomass combustion reactor. Bars represents the mean response (n=3±SEM) to dose 150 mg ml^{-1} of the emission particles. Asterisks (*) indicate a statistically significant difference from control cells ($p < 0.05$, Dunnett's test).

Characterization of an Air-Liquid Interface Cell Exposure system for Cigarette Smoke ($ALICE_{CS}$) using fluorescence imaging and a quartz crystal microbalance

Majeed Shoaib, Anke G. Lenz, Friedrich Prade, Bernd Lentner, Martina Schmidmeir, Tobias Stoeger, Oliver Eickelberg, Otmar Schmid

Comprehensive Pneumology Center, Institute of Lung Biology and Disease, University Hospital, Ludwig-Maximilians-University and Helmholtz Zentrum München, Ingolstädter Landstrasse 1, 85764 Neuherberg, Germany

Keywords: particle toxicity, nanotoxicity, aerosol dosimetry, quantitative cell deposition
Presenting author email: otmar.schmid@helmholtz-muenchen.de

Tobacco smoke is recognized as causal factor in various lung diseases. Both assessment of the toxicity and research into treatment options for smoke-related diseases require *in vitro* cell exposure systems for cigarette smoke. We have developed such a system (referred to as $ALICE_{CS}$) for cells cultured at the air-liquid interface using a combination. In this paper the $ALICE_{CS}$ is described and characterized with a combination of aerosol, photometric and biological measurement techniques.

Kentucky research cigarettes (prehumidified for at least 24h; RH = 60-70%) were smoked in a continuous flow mode (ca. 40 sec per cigarette) and the smoke was delivered via a stagnation point flow system to cells cultured at the air-liquid interface. The system is a scaled version of the one described by Tippe et al. (2002), where the cells are residing in up to 6 transwell inserts of a standard 6-well plate for cell cultures. The number size distribution of the smoke particles was determined with a scanning mobility particle sizer. The total aerosol mass generated per cigarette was determined by filter sampling and subsequent gravimetric analysis. The mass deposited on the cells and on other parts of the exposure system was measured using a combined gravimetric-photometric method. In addition, the cell-deposited mass was determined by a quartz crystal microbalance. Furthermore, the spatial homogeneity of the cigarette smoke on the cells was quantitatively investigated with a fluorescence imaging technique. Finally, the cytotoxicity and viability of a human epithelial cell line (A549) was investigated.

The total number and mass concentration of the cigarette smoke particles was about $1.5x10^7/cm^3$ and $380mg/m^3$, respectively. The CMD and σ_g was about 350 nm and 1.5, respectively. The average aerosol mass per cigarette was 38 mg and about 1% of this (0.36 mg) was deposited onto the 6 inserts. The corresponding cell-delivered dose of 14 $\mu g/cm^2$ per cigarette agreed to within 15% with the values obtained with the quartz crystal microbalance. The insert-to-insert variability of the dose was less than 10%. In addition, we determined the spatial uniformity of the cigarette smoke on the cells by placing a quartz fiber filter into the insert (instead of the cells). The exposed filter was imaged with a fluorescence imaging device (Caliper, Lumina II; excitation: 430nm; emission: 515-575nm) and analyzed quantitatively by evaluating the emitted light intensity along 36 radial trajectories (each shifted by 10 degrees). An example for the obtained fluorescence image of the filter and the corresponding light intensity profile along the trajectories is presented in Figure 1. This analysis revealed that the dose is uniformly distributed onto the cells with a pixel-by-pixel ($0.1x0.1\ mm^2$) variability of less than 7% (for the accumulated smoke of 4 cigarettes).

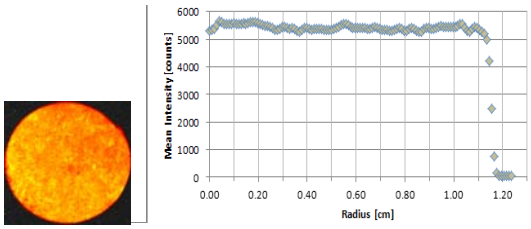

Figure 1. Left: Fluorescence image of a quartz fiber filter placed in a transwell insert where the cells are located (excitation: 430nm; emission: 515-575nm). Right: Emitted light intensity along a radial trajectory, where 0 represents the center of the spherical filter.

Finally, the $ALICE_{CS}$ was validated with human epithelial cells (A549). Cell viability (WST-1) and cytotoxicity (LDH) were measured for exposures with up to 6 cigarettes. No adverse effects on these parameters were observed for control experiments with clean air. However, exposure to 1 cigarette reduced the cell viability to about 30% and the cytotoxicity was increased to about 10%.

The $ALICE_{CS}$ is a viable tool for toxicity and health studies with highly concentrated aerosols such as cigarette smoke. To put the cell-delivered dose into perspective, we note that the estimated *in vivo* dose in the human lung is about $2x10^{-4}\mu g/cm^2$ per cigarette (assumed 60% deposition efficiency and 140 m^2 of exposed lung surface area). Thus, in spite of the relative small fractional *in vitro* deposition of about 1%, the $ALICE_{CS}$ delivers about 5 orders of magnitude more cigarette smoke onto the cells than encountered in a human lung.

Tippe, A., Heinzmann, U. and Roth, C. (2002). *J. Aerosol Sci.* 33, 207-218.

Analysis of the Dosimetric Properties of a Novel Thermal Precipitator for Cell Exposure to Nanoparticles at Air-Liquid Interface

Dirk Broßell[1, 4], Sabine Plitzko[1], Gunter Linsel[1],
Nkwenti Azong-Wara[2], Christof Asbach[2], Heinz Fissan[2, 3], Andreas Schmidt-Ott[4]

[1] Federal Institute for Occupational Safety and Health (BAuA), Berlin, Germany
[2] Institute of Energy and Environmental Technology (IUTA) e.V., Duisburg, Germany
[3] Center for Nanointegration Duisburg-Essen (CeNIDE), Duisburg, Germany
[4] Delft University of Technology, Delft, Netherlands
Keywords: nanoparticle, thermal precipitator, toxicity, in vitro.
Presenting author email: brossell.dirk@baua.bund.de

The so called “Cyto-TP” is a thermal precipitator (TP) (Azong-Wara, 2009) for the exposure of living human epithelial lung cells to airborne nanoparticles for toxicity screening studies. It combines the advantages of nanoparticle settling aided by thermophoretic deposition with the features of a cell culture system at air-liquid interface (ALI), which makes it possible to deposit nanoparticles directly from the gas phase.

Thermophoresis is the motion of particles in gas phase within a temperature gradient towards the cold region (Hinds, 1999). The Cyto-TP establishes different temperatures on two parallel plates with 1 mm spacing. Particles entering the gradient will migrate onto the colder plate, where the cells are located. The cold plate’s temperature is kept at constant 37°C to not affect the cells negatively. The gradient (and the particle deposition) is controlled by setting the temperature of the warmer plate in the range of 42°C to 52°C. Thermophoresis causes a very low velocity and particles are deposited smoothly onto the cell surface. Cells are therefore not damaged by particle impaction. Unlike in similar concepts using electrophoresis for particle deposition, particles bear their natural charge level. Additionally the physicochemical properties of the particles are not affected like in suspensions. The concept of thermal precipitation and the cell hosting at Air-Liquid Interface is shown in figure 1.

A model was developed for the motion of nanoparticles within the Cyto-TP to simulate the deposition on the cells. The deposition density is homogeneous when temperature gradient and flow rate are in the optimal range. The simulation calculates the deposition efficiency on the cells. The Cyto-TP hosts two cell cultures, one for exposure and one for negative control, so two deposition efficiencies are determined where the latter should be zero.

To verify this model we deposited spherical fluorescent polystyrene latex (PSL) primary nanoparticles on the cells. The model becomes simple for spherical primary particles. By using fluorescent particles we could locate and count the deposited particles using a fluorescence microscope. We deposited PSL primary particles of four different sizes (50 nm, 100 nm, 500 nm, 1000 nm).

In this work we compare the simulated deposition efficiencies with the experimental results obtained by counting the particles after exposure. We analysed twenty areas of 100x100 µm on each cell culture for statistical reasons. We also determined the deviation of the total number of deposited nanoparticles in each area to gain a parameter of homogeneity. Good homogeneity is necessary to calculate the effective dose, deposited particles per cell, since the deposition density must be consistent on the whole surface of the cell culture. These measurements contribute to the validation of the Cyto-TP as a cell exposure system with a representative and controllable dosimetry.

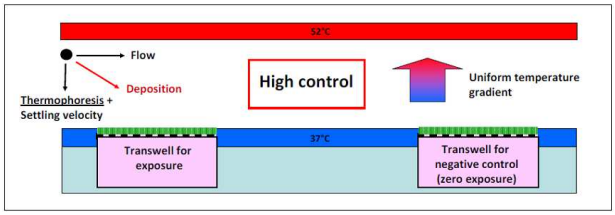

Figure 1. Overview of the concept of the Cyto-TP and cell hosting at Air-Liquid Interface. Deposition occurs due to thermophoresis and gravitational settling.

This presentation will focus on the dosimetric properties of the system. Technical aspects of the Cyto-TP will be discussed and the simulation model and first experiments for its verification presented.

The research leading to these results has received funding from the European Community's Seventh Framework Programme (FP7/2007-2013) under grant agreement n°211464-2.

Azong-Wara. N., Asbach, C., Stahlmecke, B., Fissan, H., Kaminski, H., Plitzko, S., Kuhlbusch, T. A. J. (2009), *Journal of Nanoparticle Research*, 11, 1611-1624

William C. Hinds (1999), *Aerosol Technology*, John Wiley, p. 171-174.

Estimation of biodurability of smectite particles in (synthetic) lung fluids

M.E. Ramos[1], C. Cappelli[1], M. Rozalén[1], S. Fiore[2] and F.J. Huertas[1]

[1]Instituto Andaluz de Ciencias de la Tierra, CSIC-Universidad de Granada, Granada, 18002, Spain
[2]Laboratory of Environmental & Medical Geology, IMAA-CNR, Tito Scalo, 85000, Italy
Keywords: mineral dust, lung/particle interaction, solubility, organic acids.
Presenting author email: elenaramos@ugr.es

Smectite together with kaolinite and illite, constitute the main part of the fine and ultrafine fraction in soils and sediments, as well as in airborne natural dust. Smectite has been identified by the World Health Organization as having the potential to produce moderate fibrosis in the lungs following long-term exposure (WHO, 2005). Harmful effects may be dependent on the dissolution rate in lung fluids. The aim of this study is to determinate the smectite dissolution rates in saline solutions that mimic synthetic lung fluids (SLF) to gain knowledge about the residence time of the inhaled clay particles in the human body.

Dissolution rates of K-montmorillonite were measured in modified Gamble's solutions at pH 4 (macrophages) and 7.5 (interstitial fluids) at 37ºC in stirred flow-through reactors. The particle size, measured by transmission electron microscopy, was of 500 nm in diameter. The effect of organic acids was investigated through the addition of 3 organic compounds present in the interstitial lung fluids: lactate, citrate and glycine. The effect of each organic compound was investigated separately through the addition of 3 different concentrations: 0.15, 1.5, 15 mmol L^{-1}.

The results showed that the addition of lactate or glycine does not markedly affect the montmorillonite dissolution rates at pH 4 irrespective of their concentration. However, at pH 7.5 there exists a slight inhibitory effect of lactate on the dissolution, probably due to a reduction in the number of reactive surface sites caused by lactate adsorption onto the montmorillonite surface. However, citrate enhances the dissolution rate by 0.5 orders of magnitude at pH 4 and more than one order of magnitude at pH 7.5, thus indicating the prevalence of the ligand-promoted over the proton-promoted dissolution mechanism under these experimental conditions. The enhancement of the dissolution rate in acidic citrate solution likely comes from the formation of surface complexes between the ligand and the edge surface of montmorillonite. In neutral conditions the effect may be also due to the decrease of the activity of Al^{+3} by formation of aqueous Al-Citrate complexes.

The kinetic data were used to estimate the reduction in size of an inhaled clay particle, by using a simple model (disk morphology of thickness *h* and radius *r*) and applying the following equation:

$$r^2 = r_0^2 - \frac{Rate_v}{\pi h} t$$

where *r* is the radius of the reacted particle at time *t*, r_0 is the inicial radius (250 nm), $Rate_v$ is the volumetric rate ($cm^3\ s^{-1}$) and *h* is the particle thickness.

The model showed that at pH 7.5 a particle of 500 nm in diameter could be reduced 25% in presence of citrate, whereas the reduction in saline solution would only be 10% after 10 years (Fig. 1).

We could conclude that the chemical clearance of inhaled phyllosilicates is limited in lung conditions and several years are necessary to halve the particles size, even in the presence of organic ligands.

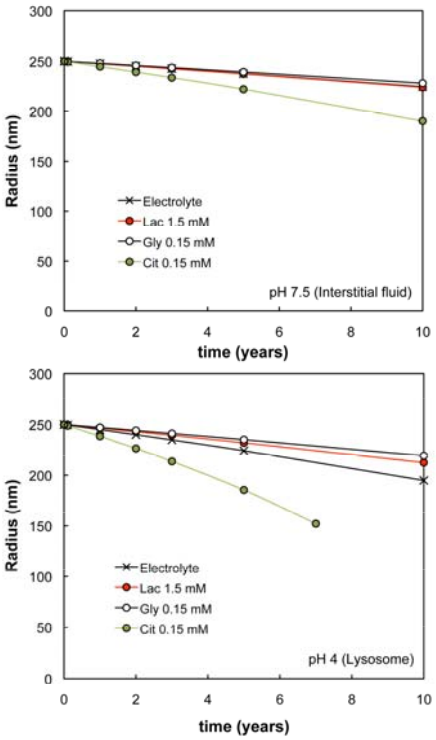

Figure 1. Decrease in the radius of a smectite particle during the dissolution in synthetic lung fluids.

Acknowledgement.- This work was supported from projects CGL2005-00618 and CGL2008-01652 (Ministerio de Ciencia e Innovación), P07-RNM-02772 and Group RNM-264 (Junta de Andalucía), with contribution of FEDER funds.

WHO (2005) *Bentonite, kaolin and selected minerals.* Environmental Health Criteria **231**, 1-174.

Toxicity testing of domestic wood combustion aerosols

S. Mülhopt[1], S. Gauggel[2], D.R. Dietrich[2], T. Schröder[3], B. van der Burg[4], H.-R. Paur[1]

[1]Institute for Technical Chemistry, Karlsruhe Institute of Technology, 76021 Karlsruhe, Germany
[2]Department of Human- and Environmental Toxicology, University of Konstanz, 78457 Konstanz, Germany
[3]Department Thermo-Chemical Conversion, German Biomass Research Centre, 04347 Leipzig, Germany
[4]BioDetection Systems b.v. Science Park 406, 1098 XH Amsterdam, The Netherlands

Keywords: Exposure, Deposition efficiency, Health effects of aerosols, Human lung cell, Nanoparticles
Presenting author email: muelhopt@kit.edu

Background:

Epidemiological studies show an association between the concentration of fine and ultrafine particles (PM10, PM2.5, PM0.1) in the atmosphere and the rate of mortality or morbidity due to respiratory and cardiovascular disease (Wichmann et al, 2000). The European Union therefore regulates the mass of ultrafine particle immissions, irrespective of their source, their chemical composition or their potential for adverse health effects, despite that the latter would be of utmost importance. Responsible for one third of the ultrafine particle emissions, domestic heaters are in the focus of interest. Especially the emissions of wood stoves containing a high amount of organic substances should be characterized regarding to their toxicological potential and thus adverse health effects in humans.

Material and Methods:

For the quantitative assessment of the toxicity of airborne particle emissions from domestic wood stoves the dose–response relationship is tested by *in-vitro* test systems using bioassays of cell cultures as sensor (Paur et al, 2011). Reproducible exposure of human lung cell cultures to aerosols at the air-liquid interface was achieved with the Karlsruhe Exposure System (Figure 1).

Figure 1. Karlsruhe Exposure System for Air-Liquid-Interface Testing of wood combustion aerosols (Mülhopt et al, 2007; Paur et al, 2008).

The bioavailability of particle bound Polycyclic Aromatic Hydrocarbons (PAH) (Gauggel et al., 2011) was tested using Ah-CALUX cells, i.e. a Ah-receptor transactivation assay, and two wood combustions runs.

Results:

Exposure of CALUX cells to wood combustion aerosol (Figure 2) in the KES was carried out during a 2.5 hours burn-off of 10 kg of beech logs and following dilution in a DEKATI dilution tunnel. Three cultures of the CALUX assay were exposed and compared to two cultures exposed to filtered aerosol. Upon exposure to biologically available PAH on wood combustion aerosol particles, CALUX cells presented with an increased luciferase activity and testimony of increased Ah-receptor activation.

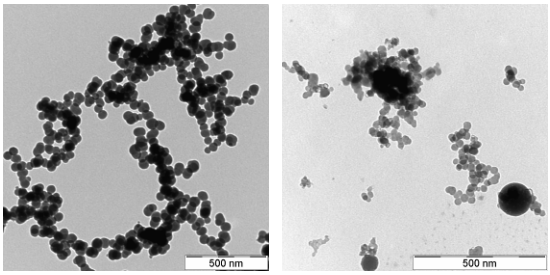

Figure 2. TEM images of particle emissions from a wood stove fired with 10 kg of beech logs.

Acknowledgement:

This work was supported by the Federal Ministry for the Environment, Nature Conservation and Nuclear Safety under grant 03MAP144.

References:

Gauggel, S., Wiese, J., Pieterse B., Dietrich D.R. (2011). EAC 2011, 05.-09.09.2011, Manchester, England

Mülhopt, S., Diabaté, S., Krug, H.F. Paur, H.-R., (2007) *Advanced Environmental Monitoring*, Kim Y J and Platt U (eds.), Springer Netherlands 402-414

Paur, H.-R., Cassee, F.R., Teeguarden, J., Fissan, H., Diabate, S., Aufderheide, M., Kreyling, W.G., Hänninen, O., Kasper, G., Riediker, M., Rothen-Rutishauser, B., Schmid, O. (2011) *Journal of Aerosol Science*, 42, 668–692

Paur, H.R., Mülhopt, S., Diabaté, S., Weiss, C. (2008) *Journal für Verbraucherschutz und Lebensmittelsicherheit*, 3, 319-329

Wichmann H.E., Peters A. (2000). *Phil. Trans. R. Soc. London A* 358:2751-2769.

An experimental comparison of dust resuspension due to human walking

Yilin Tian[1], Kyung Sul[2], Jing Qian[2] and Andrea Ferro[2]

[1]Institute for a Sustainable Environment, Clarkson University, Potsdam, NY, 13699, USA
[2]Department of Civil and Environmental Engineering, Clarkson University, Potsdam, NY, 13699, USA
Keywords: resuspension, dust, indoor air quality, respirable aerosols.
Presenting author email: tian@clarkson.edu

Resuspension is believed to contribute a considerable portion of human particulate matter exposure indoor (Yakovleva et al. 1999). In order to mitigate inhalation exposure of house dust, walking-induced particle resuspension was characterized as a function of flooring type (FT), surface dust loading (SDL), relative humidity (RH) and particle size. Distinct from previous studies, a consistent test mechanism was utilized instead of human participant to eliminate the impact of varied walking style, improve experimental reproducibility and facilitate a systematic comparison of the influencing factors mentioned above (Qian and Ferro 2008).

Developed by the Lawrence Berkeley National Laboratory, the resuspension mechanism is comprised of heel and toe plates controlled by electric actuators to simulate the human foot step. The resuspension mechanism is surrounded by a $0.13m^3$ plexiglass chamber with controlled temperature, relative humidity and filtered air supply. Air exchange rate inside the chamber was 1.38 ± 0.05 hr^{-1}.

Five types of flooring, including hardwood, vinyl, high density cut pile carpet, low density cut pile carpet and high density loop carpet were tested with two levels of RH (30-40% and 70-80%) and surface dust loading ($2g/m^2$ and $8g/m^2$), respectively. With a full factorial design, 60 randomized runs were conducted with 3 replicates for each treatment. The resuspension mechanism was equipped with a men's size ten tennis shoe and was operated for 30 continuous steps in each run with a consistent stepping frequency of 0.55 ± 0.03 Hz.

A portable laser particle counter was used to measure the particle size distribution between 0.4 μm and 10 μm. Resuspension rate coefficient r (1/h) was estimated based on the change in concentration of airborne particles following stepping motion of the resuspension mechanism using the method described in Qian and Ferro (2008).

Resuspension rate coefficients for house dust were found to vary from 10^{-4} h^{-1} to 10^{-1} h^{-1}, which is within the range of previous studies with actual humans walking (Manthena et al. 2008; Qian and Ferro 2008). Resuspension rate coefficients increase with the increase in particle size. Analysis of variance (statistic package: Minitab 16) results of main effects and two-factor interactions for each particle size bin with confidence level of 95% (α=0.05) are listed in Table 1 and Table 2, respectively.

Table 1. P-values for main effects of r

Particle size (μm)	Flooring type	RH	Surface dust loading
0.4-0.5	**0.004**	**0.054**	**0.000**
0.5-1.0	**0.005**	0.319	**0.000**
1.0-3.0	**0.000**	**0.025**	**0.003**
3.0-5.0	**0.000**	0.071	0.396
5.0-10.0	**0.000**	0.165	0.96

Table 2. P-values for two-factor interactions of r

Particle size (μm)	FY&RH	FY&SDL	RH&SDL
0.4-0.5	**0.019**	0.651	0.083
0.5-1.0	0.115	0.310	**0.014**
1.0-3.0	**0.007**	0.163	**0.008**
3.0-5.0	**0.000**	0.120	**0.004**
5.0-10.0	**0.000**	0.092	0.122

The statistical analysis results show that flooring type has a significant effect on resuspension rate coefficient for all particle size bins involved, while surface dust loading is influencing for particles less than 3.0μm in size. When the results for all floorings are combined, RH itself shows little effect on particle resuspension because the direction of effect of RH is opposite for carpet and hard flooring. The interactions between RH and flooring type as well as RH and surface dust loading verify that RH should be taking into account.

This work was funded by the US Department of Housing and Urban Development Healthy Homes Technical Studies Program Grant NYLHH0168-08 and U.S. National Science Foundation Grant Number CBET 0846704. Any opinions, findings, and conclusions or recommendations expressed in this material are those of the authors and do not necessarily reflect the views of the agencies.

Manthena S., Qian J. and Ferro A. (2008) *American Association for Aerosol Research 27th Annual Conference*, Orlando, FL.

Qian J. and Ferro A. (2008) *Aerosol Science and Technology*, **42**, 566-578.

Yakovleva E., Hopke P.K. and Wallace L. (1999) *Environmental Science & Technology*, **33**, 3645-3652.

Identification of plant DNA in air: DNA analysis and relevance for human health

I. Müller-Germann[1,2], J. Fröhlich-Nowoisky[1], U. Pöschl[1],and V. R. Després[3]

[1]Biogeochemistry, Max Planck Institute for Chemistry, P.O. Box 3060, D-55020 Mainz, Germany
[2]Geosciences, Johannes Gutenberg University, Joh.-Joachim-Becher-Weg 21, D-55128 Mainz, Germany
[3]General Botany, Johannes Gutenberg University, Saarstraße 1, D-55099 Mainz, Germany

Keywords: Bioaerosols, DNA analysis
Presenting author email: i.germann@mpic.de

Biogenic aerosols are ubiquitous in the Earth's atmosphere, where they influence atmospheric chemistry and physics, the biosphere, climate, and public health. They play an important role in the spread of biological organisms and reproductive materials, and they can cause or enhance human, animal, and plant diseases (Després *et al* 2007).

Mainly pollen, as the reproductive units of plants can cause allergies. Plant debris circulated in air play a role for human health as they may contain toxic or contact-dermatitis causing components as reported for several plants from the *Euphorbiaceae* and *Astaraceae* plant family (Schempp *et al* 2002).

A genetic analysis method was chosen as it works successfully for analyzing bioaerosols (Després *et al* 2007). Filter samples were collected over a period of 1 year (March 2006–April 2007) with a High Volume Sampler separating fine and coarse particles at a total flow rate of ~ 300 L min^{-1}, corresponding to a nominal cut-off diameter of ~3 µm. The average sampling time was 7 days, corresponding to a sampled air volume of approximately 3,000 m^3, in central Europe (see also Fröhlich-Nowoisky *et al* 2009).

Altogether the extracted deoxyribonucleic acid (DNA) of 42 coarse and 42 fine particle filter samples were analyzed with 2 plant specific primer pairs. Positive PCR products were cloned and sequenced. For comparison with known sequences, databank queries using the Basic Local Alignment Search Tool (BLAST) were performed via the website of the National Center for Biotechnology Information (NCBI). Sequences were furthermore analyzed with the program Mothur, a comprehensive software package for community analysis.

Preliminary results show that ~1600 sequences could be attributed to ~50 plant families. ~1200 of them were analyzed with the program Mothur, and grouped into operational taxonomic units (OTUs), which correspond to around 300 species.

Figure 1 shows the distribution of the OTUs during the sampling seasons of the air filter samples. Within fall and summer there are a number of OTUs exclusively present in these seasons while only very few species are shared between the seasons. In spring species from the *Betulaceae* family containing the highly allergenic birches and other tree species dominate, in summer the grasses and herbs belonging to the *Convolvulaceae*. In autumn mainly weeds belonging to the *Euphorbiaceae* family are present, which contain plants with contact allergens. In winter late flowering weeds from the *Asteracea*e plant family, containing the highly allergenic mugwort and ragweed and trees from the *Betulaceae* plant family dominate the sequences. Thus, the DNA analysis of plants in the air displays mainly the flowering of the different plants, often allergenic plants, whose pollen release plays a big role for human health.

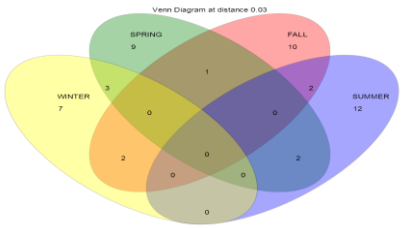

Figure 1: Venn Diagramm at distance 0.03 (97% sequence identity) created with Mothur. Numbers reflect the OTUs which are either unique for a season or shared between seasons

The Max Planck Society (MPG), the German Research Foundation (DFG, DE1161/2-1), and the LEC Geocycles Mainz are gratefully acknowledged for funding. We thank D. Pickersgill, J. Cimbal, S. Mayanna, and N. Knothe for technical assistance, M.O. Andreae, and H. Paulsen for helpful discussions and support.

Després, V.R., Nowoisky, J.F., Klose, M., Conrad, R., Andreae, M.O. and Pöschl, U. (2007) *Biogeosciences* **4**, 1127–1141.

Fröhlich-Nowoisky, J., Pickersgill, D.A., Després, V.R. and Pöschl, U. (2009). *Proc. Natl Acad. Sci.* **106**, (30), 12814 -12819.

Schempp, C.M., Schöpf, E. and Simon, J.C. (2002) *Hautarzt* **53**, 93-97.

Effective density of particles in an urban environment – measured with a DMA-APM system for lung dose estimations

J. Rissler[1], P.T. Nilsson[1], J. Pagels[1], A. Eriksson[2], E. Nordin[1], E. Swietlicki[2], B. Svenningsson[2], M. Frosch[2], E. Ahlberg[2], C. Wittbom[2], J. Löndahl[1], A. Wierzbicka[1], J.G. Hemmingsen[3], S. Loft[3], S. Sjögren[2]

[1]Division of Ergonomics and Aerosol Technology, Lund University, Box 118, 22100, Lund, Sweden, [2]Division of Nuclear Physics, Lund University, Box 118, 22100, Lund, Sweden, [3]Section of Environmental Health, Dept. Of Public Health, University of Copenhagen, Denmark

Keywords: effective density, urban environment, health, aggregated particles

Presenting author email: jenny.rissler@design.lth.se

Since the deposition fraction of particles in the human respiratory tract is size dependent, lung dose estimations requires size resolved particle distributions, with respect to number, surface are or mass. Often the number size distributions are measured by DMA-techniques (Differential Mobility Analyzer) such as the SMPS, FMPS, DMPS, EEPS, DMS, etc. The DMA is sizing particles according to their electrical mobility diameter (d_m), which has been shown to determine the deposition probability also for agglomerated particles (Rissler et al., 2012), <400 nm. The surface area or mass size distributions are often estimated from the number distribution. Particle mass is believed to be a crucial parameter for the health effects of airborne particles. When converting number to mass, or vice versa, the effective density of the particles is needed, defined as:

$$\rho_{eff} = m_{APM}(d_m) / \left(\frac{\pi d_m^3}{6}\right).$$

For aggregated or agglomerated particles assuming spherical particles may lead to overestimation of the mass dose by several times (Rissler et al., 2012).

In this study, measurements of the effective density in an urban environment were performed, using a DMA–Aerosol Particles Mass analyzer (DMA-APM) technique (McMurry et al., 2002). In a DMA-APM system, the mass of individual particles of a population of a certain mobility diameter is measured. During the study the chemical and physical properties of the particles were further characterized with an SMPS, an Aerosol mass spectrometer, TEM images, OC/EC and hygroscopic growth. The characterization was part of a study of the health effect of urban particulate matter, where elderly (>55 yrs) volunteers with moderate obesity (body mass index >25 kg/m^2) were exposed to the aerosol from a busy street in Copenhagen, Denmark.

The effective density measurement revealed that the particles of the same d_m consisted of an external mixture containing one group of particles with effective density of ~1.5 g/cm^3 and another group of agglomerate particles of lower effective densities. The group of particles with higher effective densities increased in number fraction with increasing particle size. The low-density group of particles had densities that decreased with increasing size (from 0.25 g/cm^3 for 350 nm particles to 0.9 g/cm^3 for 75 nm). This is typical for particles with an agglomerated structure, such as soot. In several previous studies it was shown that for newly emitted agglomerate particles the relation between d_m and the mass often is well described by a power law function (Sorensen 2011; Rissler et al., 2012). This was also the case for the agglomerate particles in this study, showing that the soot particles did not restructure, at least not within a few hours after emission, despite the high humidity in the atmosphere.

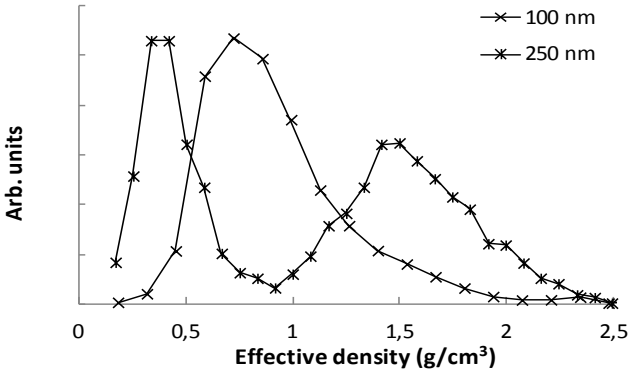

Figure 1. Two examples of DMA-APM spectra.

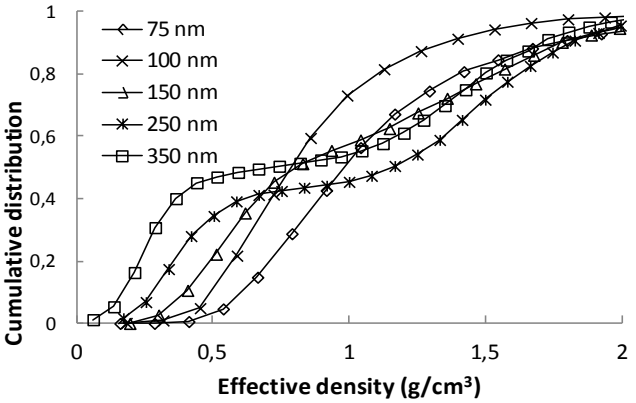

Figure 2. Cumulative distributions of effective densities.

By introducing a thermo denuder between the DMA and the APM it was showed that over 95% (by number) of the particles with high effective density evaporated at 300 °C, losing >85% of their mass. A closer study of the AMS data is needed to draw any further conclusions about the chemical composition or origin of these particles.

This work was supported by the Swedish Research Council FORMAS, the Swedish Governmental Agency for Innovation Systems VINNOVA.

McMurry P.H., et al. (2002), Aerosol Science and Technology 36: 227–238.

Rissler et al., 2012, Journal of Aerosol Science, DOI: 10.1016/j.jaerosci.2012.01.005.

Sorensen, C.M. (2011), Aerosol Science and Technology, 45, 765-779.

Monday, September 3, 2012

Session WG08S1O. New Instrumentation I

A new device for fast measurements of nanoparticle size distributions

Hans Grimm[1], Lothar Keck[1,] Markus Pesch[1], Matthias Richter[1], Hans-Joachim Schulz[1]

[1]Grimm Aerosol Technik GmbH & Co. KG, 83404 Ainring, Germany
Keywords: Instrumentation, Aerosol size distribution, Combustion particles, Vehicles emissions
Presenting author email: hjs@grimm-aerosol.com

Grimm has re-engineered the Fast Aerosol Particle Emission Spectrometer (FAPES) for fast measurements of nanoparticle size distributions in the range of 6.3 – 474 nm. The instrument comprises an integrated hot diluter and is particularly designed for measurements of combustion particles and for automotive applications.

The FAPES system has three unique features (Fig. 1). Firstly, it employs a strong bipolar charger (241-Am α-emitter) for establishing a well defined equilibrium charge distribution. Unlike for unipolar chargers, even the larger particles feature a low apportion of multiple charged particles and the different size fractions have well distinguishable mobilities. These two features are the base for an accurate reconstruction of the particle size distribution.

Secondly, the charged particles are classified with twelve individual Differential Mobility Analyzers (DMAs) of Vienna type design operated in parallel. The signal of each size channel originates from a single DMA and corresponds thus to a well defined and narrow size range. This well proven principle of size classification makes the FAPES a reference for fast particle sizers. Unlike for SMPS systems, each DMA voltage is kept constant and thus the sampling frequency is no longer limited by the scan-time for the DMA voltage. The 12 DMA voltages cover the broad range of 5 to 10000 V and the voltages of adjacent DMAs differ by a factor two to ease the correction of remaining multiple charged particles.

Thirdly, the detection of particles is accomplished with twelve Faraday Cup Electrometers (FCEs), one FCE for each DMA, and spatially separated from the mobility analyzing section. Therefore, the detected currents are unaffected from any variations of the high voltage and the FCEs feature a very low noise level. Due to the rinse air, the FCEs have a fast response time of T10-90 = 200 ms, which is the base of the fast overall response time of the FAPES (T10-90 = 0.7 s). The use of rinse air has a second advantage, namely to prevent contaminations on the isolation of the detection electrodes and thus leakage currents. In other products for fast measurements of nanoparticle size distributions, leakage currents between electrodes can degrade the size resolution in the course of the measurements, and cleaning of the surfaces is required. Such leakage current can be a major problem particularly for the measurement of engine exhaust because the soot particles are conducting. The FCE signals are insensitive to mechanical shocks and vibration.

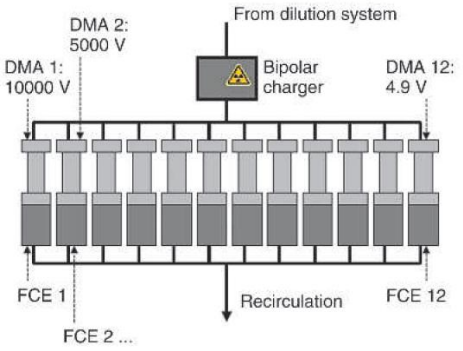

Figure 1: Principle of the FAPES

The concept of the sampling system is too "freeze" the state of the particles in the exhaust gas and to stabilize their condition for the analysis. This is achieved with a special integrated sample conditioning system with a heated dilution (temperature up to 500°C) right after the sample inlet. The diluter uses recycled sample air to achieve a variable dilution ratio of 1:5.7 – 1:40 in 7 steps. The recycled sample air is filtered, dried, and purified from organic gases with active carbon.

The main application of FAPES is measuring the particle size distributions in engine exhaust gas with high time resolution. As particle formation is connected to the fuel combustion process, such investigations can be used to optimize the efficiency of car engines. Moreover, they may assist the achievement of compliance with the new EURO5/6 regulations, which include a limit for particle number concentrations emitted by diesel and gas engines. The system is, however, also suitable for the fast measurements of size distributions at other applications. Monitoring the size of engineered nanoparticles in airborne state, nucleation events in industrial processes, or measurements in turbine exhaust are just examples.

Results for different applications are presented.

LOAC (Light Optical Particle Counter): a new small balloon-borne aerosol counter/sizer with some particle characterization capabilities

J.-B. Renard[1], G. Berthet[1], F. Dulac[2], J. Sciare[2], J. Nicolas[2], M. Mallet[3], P. Durand[3], C. Thaury[4], S. Salles[4], J.-L. Mineau[4], T. Tonnelier[4] and N. Verdier[5]

[1]LPC2E, 3A avenue de la recherche scientifique, F-45071 Orléans cedex 2, France
[2]LSCE, UMR 8212 CEA-CNRS-UVSQ, IPSL, CEA Saclay 701, F-91191 Gif-sur-Yvette, France
[3]LA, 14 avenue Edouard Belin, F-31400 Toulouse, France
[4]Environnement SA, 111 Boulevard Robespierre, BP 4513, F-78304 Poissy cedex, France
[5]CNES, 18 avenue Edouard Belin, 31000 Toulouse, France
Keywords: instrument, balloon, troposphere, stratosphere
Presenting author email: jbrenard@cnrs-orleans.fr

The determination of the size distribution of tropospheric and stratospheric aerosols with conventional optical counters is difficult when different natures of particles are present (droplets, soot, mineral dust, secondary organic or mineral particles...). Also, a light and cheap aerosol counter that can be launched (and lost) under all kinds of atmospheric balloons can be very useful during specific events as volcano plumes or local pollution episodes.

These goals are achieved with a new generation of aerosol counter, called LOAC (Light Optical Aerosol Counter). The instrument was developed in the frame of cooperation between French scientific laboratories (CNRS) and the Environnement-SA company. LOAC (Figure 1) is light particle counter/sizer of ~500 grams, having a low electric consumption. The main difference with already existing optical counters is its geometry of observation. The measurements are conducted at two scattering angles: the first one, at 10°, is used to determine the aerosol particle concentrations in 20 size classes within a diameter range of 0.4-100 μm. With such an angle close to forward scattering, the signal is much more intense and the measurements are not strongly sensitive to the nature of the particles (Renard *et al.*, 2010). The second angle is at 60°, where the scattered light is strongly dependent on the particle refractive index and thus on the nature of the aerosols. The ratio of the measurements at the two angles is used to discriminate between different types of particles dominating the nature of the aerosol particles in the different size classes.

Since 2011, LOAC have performed flights under different kinds of balloons: Zero pressure stratospheric balloon, tropospheric balloons, and meteorological balloons. For the last case, the total weight of the gondola, including batteries, is ~1.5 kg.

The results obtained during these flights will be presented, as well as projects in which LOAC is already involved: ChArMEx, (low altitude flights above Mediterranean Sea), and Strateole (long duration flights in the tropical stratosphere).

The scientific flights were performed by the French Space Agency (CNES). Commercial flights under meteorological balloons (coupled with meteorological measurements) can be conducted using the telemetry system of the MeteoMODEM Company.

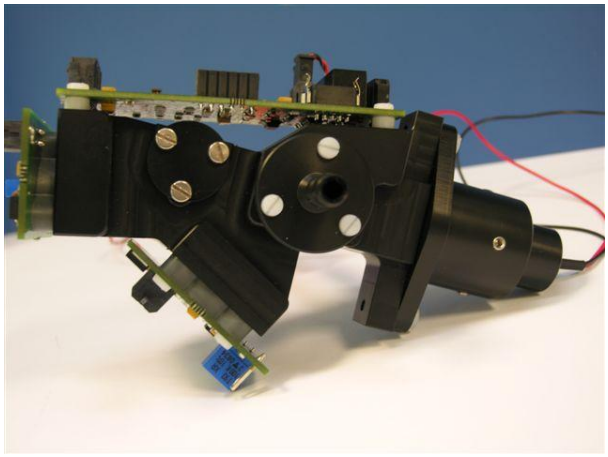

Figure 1: The LOAC instrument

This work was supported by the French ANR ECOTECH program and by CNES

Renard, J.-B., G. Berthet, V. Salazar, V. Catoire, M. Tagger, B. Gaubicher and C. Robert (2010), In situ detection of aerosol layers in the middle stratosphere, *Geophys. Res. Lett.*, **37** L20803, doi:10.1029/2010GL044307, 2010.

Aerosol detection with induced currents

M. Fierz[1,2], D.Meier[2], P.Steigmeier[1] and H. Burtscher[1]

[1]Institute for Aerosol and Sensor Technology, University of Applied Sciences Northwestern Switzerland, Windisch, 5210 Switzerland
[2]Naneos Particle Solutions GmbH, Windisch, 5210 Switzerland
Keywords: Particle charging, instrument development, personal exposure, electron microscopy.
Presenting author email: martin.fierz@fhnw.ch

Many aerosol instruments are based on unipolar charging followed by the detection of charged particles with electrometers. In instruments with multiple detection stages, charged particles can induce currents when passing through the initial stages of the instruments – this has been reported for example for the Dekati ELPI, the Cambustion fast particle analyser and for an electrical diffusion battery, leading to measurement artefacts (Fierz et al. 2009). These artefacts can be minimized or at least reduced through various techniques, such as guarding electrodes, dummy stages or data correction in software. In all these cases, however, the induced currents are a nuisance.

Here, we propose a new measurement technique which makes use of such induced currents to measure aerosols: We deliberately generate induced currents by switching the unipolar charger on and off at a well-defined frequency, thereby producing clouds of charged particles, which will induce currents in the instrument. The basic setup is shown in figure 1:

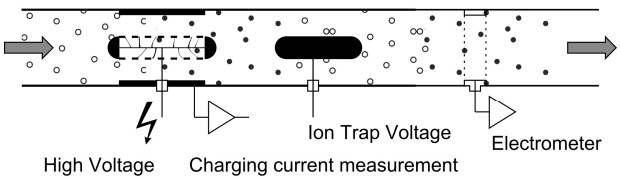

Figure 1: Scheme of an induced-current aerosol sensor; open circles represent uncharged particles, full circles represent charged particles.

The uncharged aerosol enters the sensor, and is charged in a unipolar charger whose high voltage is pulsed. Excess ions are removed after the charging zone in an ion trap, and thus, clouds of charged and uncharged particles are generated that flow through an empty Faraday cage, which can be either a real cage or simply an open tube. The electrometer amplifier will attempt to keep the Faraday cage at zero potential, and for any net charge Q inside the cage, it will thus produce a charge of equal magnitude but opposite sign, thus -Q, on the Faraday cage. The advantages of this principle compared to the traditional detection in particle filters are that (1) the charged particles are measured without contact, i.e. there is no (or much less) need for cleaning and filter exchanges, (2) the charged particles are still available after the measurement for further purposes and (3) there is practically no pressure drop over this type of measurement. This basic principle of operation allows multiple types of instruments to be constructed that make use of these advantages, for example:

1. Aerosol dosimeter: An instrument based on the principle shown in figure 1 is built in the smallest possible package (see figure 2), measuring a signal which is proportional to the lung-deposited surface area of the aerosol (Wilson, 2007).

Figure 2: dosimeter prototype with a volume of just 300cm^3.

2. Extended dosimeter with size and number determination: In this embodiment, two Faraday cages are used in succession, with a size-selective particle trap between them. The second Faraday cage then measures only the particles that passed the trap; and the comparison of the two signals allows a determination of particle size and number, similar to the algorithms used in the Matter Aerosol DiSC, or the Grimm nanoCheck.

3. Electron microscopy sampler with automatic determination of the necessary sampling time: in this embodiment, the charged particle stream leaving the Faraday cage is deposited in an electric field on a TEM grid. Because the amount of charge flowing to the grid is continually measured, the sampling time necessary for a sensible coverage of the grid can be determined

We have constructed the embodiments (1) and (3) described above, and will show results obtained with these devices in our presentation.

Fierz M., Weimer S., and Burtscher H. (2009), *J. Aerosol Sci.* **40**, 152-163.
Wilson W.E. et al. (2007) *J. Air & Waste Manage. Assoc.* **57**:211-220.

Remote sensing of atmospheric aerosols with the spectropolarimeter SPEX

J. de Boer[1], G. van Harten[1], F. Snik[1], O. P. Hasekamp[2], H. Volten[3], A. Apituley[4], C. U. Keller[1], J. H. H. Rietjens[2], J. M. Smit[2], D. M. Stam[2], and P. Stammes[4]

[1]Leiden Observatory, Leiden University, Leiden, 2300 RA, The Netherlands

[2]Earth and Planetary Science Division, SRON Netherlands Institute for Space Research, Utrecht, 3584 CA, The Netherlands

[3]Centre of Environmental Monitoring, National Institute for Public Health and the Environment (RIVM), Bilthoven, 3720 BA, The Netherlands

[4]Koninklijk Nederlands Meteorologisch Instituut (KNMI), De Bilt, 3730 AE , The Netherlands

Keywords: Polarization, Instrumentation, Aerosol Spectrometry, Aerosol instrumentation, Aerosol characterization.

Presenting author email: jozuadeboer@iSPEX.nl

Remote sensing of atmospheric aerosols is still an underdeveloped technique, despite the significant influence of aerosols on public health, climate and economy. Current methods are local, time consuming, expensive, and cannot determine macro- and microphysical aerosol properties simultaneously. Spectropolarimetry is a promising remote sensing method for the detection and characterization of aerosols. It is unique in its capability to unambiguously retrieve microphysical aerosol parameters such as size distribution, chemical composition and shape. Existing polarimetric instrumentation either uses a few broad spectral bands, a limited number of viewing angles, or is not accurate enough to fully exploit the polarization measurements.

SPEX, the Spectropolarimeter for Planetary EXploration, is designed to characterize aerosol and cloud particles in the atmospheres of Solar System planets from orbiting satellites, by measuring both the flux and the degree and direction of linear polarization across the visible spectrum with a spectral resolution of 2 nm (flux) to 20 nm (polarization). SPEX measures the polarization using the spectral modulation technique by Snik et al. (2009), which allows both the flux and the full linear polarization information to be measured simultaneously, across all wavelengths. Thanks to this technique, SPEX has no moving components, except for pointing purposes, is very robust and small, and also accurate.

This study aims at testing whether a ground-based version of SPEX is able to characterize aerosols by reaching a high polarimetric accuracy. It furthermore aims at assessing how SPEX would function autonomously within an air quality network. The ground-based SPEX instrument measures the polarized spectrum of the sky across the visible at a range of scattering angles.

The wavelength dependent intensity and degree of linear polarization for different scattering angles offer a large data dimensionality in a SPEX measurement, which is needed to retrieve all free parameters of our atmospheric aerosol models. The algorithm we use for retrieval of the aerosol properties is based on the POLDER retrieval code of Hasekamp et al. (2011). This algorithm fits intensity and polarization spectra computed with a radiative transfer model for an atmosphere containing gas molecules and aerosols to measured spectra, using a range of aerosol properties (e.g. size distribution, aerosol optical depth, refractive index).

The instrument is stationed at CESAR, the Cabauw Experimental Site for Atmospheric Research. Measuring at this location allows us to compare our measurements with the aerosol optical depth provided by the AERONET sun photometer, and our size distributions with the in-situ aerosol measurements performed at CESAR. Aerosol height distributions are provided by (Raman) lidar measurements.

We will present the concept and design of SPEX, the first blue sky observations, the retrieved aerosol properties and a comparison with aerosol properties derived from simultaneous measurements by other instruments.

References

Hasekamp, O. P., Litvinov, P., & Butz, A. 2011, J. Geophys. Res.-Atmos., 116, 14204

Snik, F., Karalidi, T., & Keller, C. U. 2009, Appl. Opt., 48, 1337

Evaluation of the Cavity Attenuated Phase Shift (CAPS) Extinction Monitor

A.Petzold[1], T. Onasch[2], P. Kebabian[2], A. Freedman[2]
[1] Institut für Physik der Atmosphäre, DLR, 82234 Oberpfaffenhofen, Germany
[2] Aerodyne Research Inc., 45 Manning Road, Billerica, MA 01821-3976, USA
Keywords: Soot particles, Optical properties, Extinction, Instrumentation.
Presenting author email: andreas.petzold@dlr.de

The measurement of the complete set of aerosol optical properties by means of closure studies is still demanding because it requires the simultaneous measurement of aerosol extinction, scattering and absorption coefficients. Particularly the in-situ measurement of the aerosol single-scattering albedo (= ratio of aerosol scattering to aerosol extinction) is identified as a key challenge in atmospheric sciences.

Among new methods for the measurement of aerosol extinction the Cavity Ring-Down (CRD) method yields the aerosol extinction coefficient by measuring the time constant for light decay in a high-finesse cavity containing the absorbing and scattering particles. A detailed introduction to the CRD technique for aerosol extinction measurement is given by Strawa et al. (2003) whereas Moosmüller et al. (2005) provide an overview over the various CRD approaches.

The Cavity Attenuated Phase Shift (CAPS) technique, similar in its basic principle to cavity ring-down, relies on the use of a sample cell employing high reflectivity mirrors (Kebabian, et al., 2007). Square-wave modulated light emitted from a light emitting diode (LED) at a wavelength $\lambda \cong 630$ nm is directed through one mirror into the sample cell. The distortion in the square wave caused by the effective optical path length within the cavity (approx. 1 km light path) is measured as a phase shift in the signal as detected by a vacuum photodiode which is located behind the second mirror. A detailed description of the method including first results from laboratory characterization and field deployment is given by Massoli et al. (2010).

Our study characterizes the CAPS instrument for both laboratory test aerosols and ambient aerosol. The CAPS instrument was evaluated against a combination of the 3-wavelength Integrating Nephelometer (TSI Model 3563), and the 3-wavelength PSAP (Virkkula, et al., 2005). Triggered by successful direct measurements of the single-scattering albedo (Massoli, et al., 2010) using CAPS-based extinction coefficients and absorption coefficients measured by a Multi-Angle Absorption Photometer (MAAP) (Petzold and Schönlinner, 2004) we included a MAAP instrument in our studies.

We used spherical polystyrene latex particles for instrument calibration, and black carbon, ammonium sulfate and mixtures of both components for the instrument evaluation. Aerosol light absorption was measured by a 3-wavelength particle soot absorption photometer (PSAP) and a Multi-Angle Absorption Photometer (MAAP), aerosol light scattering was measured by a 3-wavelength integrating nephelometer. Instrument calibration and evaluation was then tested by an instrument intercomparison for ambient aerosol.

The calibration studies yielded a linear instrument response over the investigated dynamical range from 20 to 450×10^{-6} m^{-1} (Mm^{-1}) with a linear correlation coefficient of $R^2 > 0.98$. Correlating CAPS extinction to extinction measured by the Integrating Nephelometer – PSAP combination provided a linear regression line with slope m = 0.986 ($R^2 = 0.996$) for single-scattering albedo values (λ = 660 nm) ranging from 0.35 (black carbon, BC) to 1.00 (ammonium sulfate, AS); see Fig.1 for details. For ambient aerosol, light extinction measured by CAPS was highly correlated ($R^2 = 0.995$) to extinction measured by Integrating Nephelometer – PSAP with slope m = 0.95.

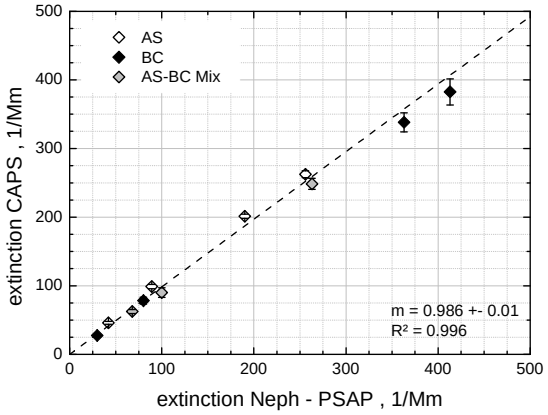

Figure 1. Intercomparison of extinction measured by CAPS and extinction obtained from the combined Neph – PSAP analysis for polydisperse laboratory aerosols; all data are adjusted to λ = 660 nm. The dashed line represents the 1:1 ratio.

This study was conducted during a DLR-sponsored research stay of A. Petzold at Aerodyne Research Inc.

Kebabian, P. L., Robinson, W. A. & Freedman, A. (2007) *Rev. Sci. Instrum.* **78**, 063102.
Massoli, P., Kebabian, P. L., Onasch, T. B., *et al.* (2010) *Aerosol Sci. Technol.* **44**, 428-435.
Moosmüller, H., Varma, R. & Arnott, W. P. (2005) *Aerosol Sci. Technol.* **39**, 30-39.
Petzold, A. & Schönlinner, M. (2004) *J. Aerosol Sci.* **35**, 421-441.
Strawa, A. W., Castaneda, R., Owano, T., *et al.* (2003) *J. Atmos. Oceanic Technol.* **20**, 454-465.
Virkkula, A., Ahlquist, N. C., Covert, D. S., *et al.* (2005) *Aerosol Sci. Technol.* **39**, 68-83.

Improvement of the nanoparticle charging efficiency by using sheath air flow in a single-wire corona unipolar charger

C.L. Chien[1], C.J. Tsai[1], V. Wattanmekhinkul[1]

[1] Institute of Environmental Engineering, National Chiao Tung University, Hsinchu, 300, Taiwan.
Keywords: unipolar aerosol charger, charging efficiency, nanoparticles, aerosol instrumentation.
Presenting author email: clchien.ev91g@nctu.edu.tw

The extrinsic charging efficiency of the unipolar aerosol charger designed with a sheath air by Chien et al. (2011) was shown to be higher than those of other corona-based unipolar chargers, except lower than those of Kimoto et al. (2010) for particles smaller than 10 nm in diameter. To improve the design of the previous charger, a single-wire corona unipolar charger was developed to enhance the extrinsic charging efficiency of nanoparticles by using radial sheath air through the grounded porous wall to avoid charged particle losses. The charger has a stainless steel porous tube (Mott Corp., MA, USA) of 6.35 mm in inner diameter in which a gold wire of 50 μm in diameter and 6 mm in length is used as the discharge electrode. A filtered sheath airflow with the flow rate (Q_{sh}) of 0.7–2.1 L/min was introduced through the porous wall while the aerosol flow (Q_a) was varied from 0.3 to 1 L/min. Currently, the performance of the present charger is being experimentally evaluated to determine an optimum operation condition.

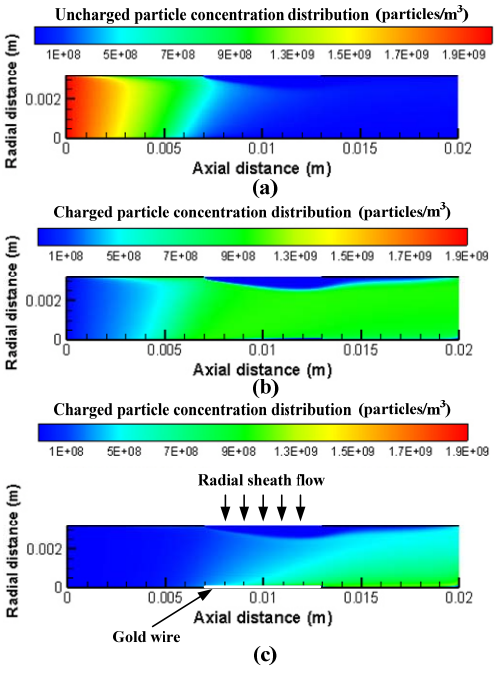

Figure 1. Number concentration field of 20 nm particles carrying 0–2 charges at the applied voltage of +2.9 kV at Q_a = 1 L/min at Q_{sh} = 0.7 L/min. (a) 0 charge, (b) 1 charge, (c) 2 charges.

A 2-D numerical model developed by Chien (2011) was first used to predict the charging efficiency of the present charger by simulating the simplified calculation domain. The analytical solution for the equation of unipolar diffusion charging incorporating the wire-in-tube electrostatic precipitator theory was calculated to examine the relationship between the fraction of charged particles and charging parameter, $\alpha_0 N_i t$ (α_0: combination coefficient between ion and uncharged particle, N_i: ion concentration, t: charging time). An example is shown for 20 nm particles carrying 0–2 charges at the applied voltage of +2.9 kV at Q_a = 1 L/min at Q_{sh} = 0.7 L/min in Figure 1. It shows that using the radial sheath air the charged particles migrating toward the wall are forced to move toward the core of the tube and the electrostatic loss is reduced. Major charged particle loss is seen to occur on the wall surface on the left-hand-side in the charging zone. Numerical results showed the advantage of using the radial sheath air to minimize charged particle loss. At the applied voltage of +2.9 kV, the predicted extrinsic charging efficiency of the present charger was 7.2%–71.1% for particles ranging from 2.5 to 20 nm, as shown in Figure 2. Using the current design, both aerosol and sheath air flow rate can be adjusted further to maximize the extrinsic charging efficiency.

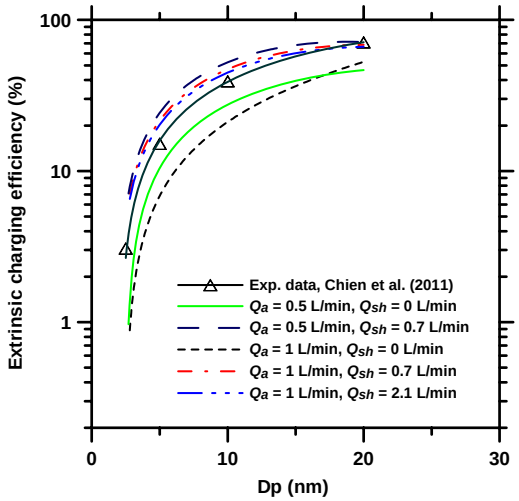

Figure 2. Predicted extrinsic charging efficiencies of the present charger.

This work was supported by the Taiwan National Science Council under grant no. NSC 96-2628-E-009-008-MY3 and NSC99-2221-E-009-038-MY3.

Chien, C. L., Tsai, C. J., Chen, H. L., Lin, G. Y., and Wu, J. S. (2011) *Aerosol Sci. Technol.* **45**, 1468-1479.

Kimoto, S., Saiki, K., Kanamaru, M., and Adachi, M. (2010) *Aerosol Sci. Technol.* **44**, 871-880.

An optical set-up for the multi-wavelength characterization of carbonaceous particulate matter

D. Massabò[1], M.C. Bove[1], E. Cuccia[1], P. Prati[1], V. Bernardoni[2], G. Valli[2], R. Vecchi[2]

[1] Department of Physics and I.N.F.N., University of Genoa, Genoa, Italy
[2] Department of Physics and I.N.F.N., Università degli Studi di Milano, Milan, Italy
Keywords: Black Carbon, Optical Instrumentation, Multi-wavelength optical analysis.
Presenting author email: massabo@ge.infn.it

Carbonaceous aerosol is a major component of urban particulate matter (PM), in particular of its finer fractions (PM2.5, PM1). The elemental part, often referred to as EC, is strongly light absorbing: when determined by optical methods it is usually called "black carbon" (BC). The two quantities, EC and BC, do not exactly define the same PM component.

PM samples are routinely collected in urban areas to monitor PM10 and PM2.5 levels. Low volume sequential samplers (LVS) are often equipped with 47 mm filters and operated on a daily basis. PTFE (Teflon®) membranes are very appropriate for gravimetric and compositional analyses of PM and currently 47 mm filters with 2 μm pores are often used to collect PM samples on daily basis (LVS). We have developed a simple, fully automatic and non-destructive new optical system to measure off-line the light absorption and hence the BC content in the PM on the PTFE filters routinely used for PM studies and on other collecting substrates. This gives the opportunity to measure in each sample the concentration of total PM by gravimetric analysis, BC, metals by, for instance, X Ray Fluorescence, and ions by Ion Chromatography. All these pieces of information can be obtained with just one filter being sure to analyze the same PM. The set-up we realized is composed by a collimated laser source and three low-noise photodiodes (PD) placed at 0, 125 and 160 degrees with respect to the laser beam direction. The PDs active surface is about 65 mm^2 and a large fraction of the forward scattered radiation is collected by the 0-degree PD positioned just behind the sample. Samples can be analyzed in sequence and in an automatic and controlled way in about 15 minutes thanks to a wheel which can host up to 16 47-mm filters. The wheel is connected to a stepping motor to change the filter under analysis and to two linear translator which allow the scanning of the whole deposition area. All the movements and the acquisition of the photodiode signals are controlled by a PC using a Labview 8.5 home-made software. The set-up is completed by three different interchangeable laser sources: 4 mW - red (λ = 635nm), 4 mW - blue (λ = 405nm) and 20 mW - IR (λ = 850nm). For the calculation of BC we have adopted and extended the method, based on the radiative transfer scheme proposed by Hänel (Hänel, 1987 and 1994), used by the MAAP (Petzold and Schönlinner, 2004). Furthermore, thanks to the computer control, the analysis of non-homogeneous PM samples, as those collected by multi-stage cascade impactors, is also possible.

Our new instrument has been validated in different campaigns and, for the first time, has been employed in a long campaign realized in the frame of the MED – APICE program (Common Mediterranean strategy and local practical Actions for the mitigation of Port, Industries and Cities Emissions, http://www.apice-project.eu/). In this case, a 6-month PM2.5 sampling campaign was organized between spring and summer 2011, at three sites in the urban area of Genoa (Italy). A LVS (TRC-Tecora, Italy) was used to collect daily PM2.5 alternatively on quartz fiber and on PTFE filters. All the samples (about 250 per each medium) were first analyzed with the optical set-up and quartz fiber filters only were subsequently analyzed by a SUNSET EC/OC thermal-optical instrument adopting the EUSAAR_2 protocol in order to obtain the EC load on each sample. Comparing the results obtained from the two different techniques it is possible to find the aerosol light absorption cross-section σ_{abs} for the different sites (in Figure 1 the results for one of the three sites). In this way we are able to calculate the BC concentration also for the days in which PTFE filters were used.

We will briefly describe the optical method providing details on the set-up and on its components. Results of the analysis on different set of samples will be also presented, with particular attention to the results obtained from measurements at the three different wavelengths with the two different kinds of filters.

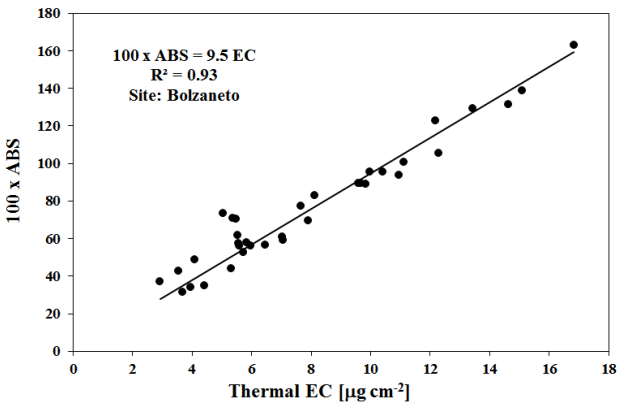

Figure 1. Regression study between ABS values given by the optical analysis and the EC concentration on quartz fiber filters measured by SUNSET using the EUSAAR_2 protocol.

Hänel, G., 1987. Contrib. Atmos. Res., **60**, 241–247.
Hänel, G., 1994. *Appl. Optic*s, **33**, 7187-7199.
Petzold, A., Schölinner, M., 2004. *J. Aerosol Sci.* **35**, 421-441.

A new expansion chamber CPC applicable to atmospheric measurements

T. Pinterich[1], P.M. Winkler[1,2], P.E. Wagner[1] and A. Vrtala[1]

[1]Faculty of Physics, University of Vienna, Vienna, Boltzmanngasse 5, A-1090, Austria
[2]Advanced Study Program, National Center for Atmospheric Research, 1850 Table Mesa Drive, Boulder, Colorado, 80305, USA
Keywords: CPC, nanoparticles, heterogeneous nucleation.
Presenting author email: tamara.pinterich@univie.ac.at

In the past few years the influence of atmospheric aerosols on the evolution of the global climate has received considerable attention. In this connection the formation of nanoparticles in the atmosphere is a major though not well understood process. Thus accurate determination of aerosol properties particularly in the size range above ~1nm diameter is of great importance.

Therefore we developed a new expansion chamber CPC – the versatile Size Analysing Nuclei Counter (vSANC). Using this device experiments on nucleation and condensational growth of nanoparticles in supersaturated vapours can be performed under well defined conditions. The measuring principle was adopted from the Size Analyzing Nulcei Counter and can be found elsewhere (see P. E. Wagner *et al* (2003)). During the development of the vSANC, care was taken to ensure its applicability to atmospheric conditions.

It is well known that sulphuric acid plays an important role in atmospheric nucleation (see e.g. M. Sipilä *et al* (2010)). Therefore great care was taken to ensure the chemical inertness of all parts in contact with the aerosol. The expansion chamber, for example, consists of stainless steel with black bronzed surface, a coated glass ring and FEP (fluorinated ethylene propylene) coated O-rings. Moreover the usage of any adhesives was avoided for all parts with aerosol contact.

So far a drawback of common CPCs was the limitation to positive temperatures only (see e.g. Kirkby *et al* (2011)). However the vSANC can operate at temperatures ranging from -20°C to +40°C. In order to prevent evaporation losses or changes of the aerosol during sampling the connection between inlet and expansion chamber is temperature controlled. The wide variability in temperatures is implemented by means of Peltier elements and an associated thermostating liquid. The thermoelectric modules control aerosol temperature in the aerosol pre-thermostating unit (APT, connection between sample inlet and expansion chamber), both humidifiers and the expansion chamber. The associated thermal fluid is used to increase the efficiency of the Peltier elements. This special temperature regulation permits fast changes and precise settings of any temperature within the range noted.

Another typical difficulty of expansion type CPCs is the detection of particles at comparatively low number concentrations as encountered, e.g., in atmospheric background measurements. Thus another focus in development was on decreasing the lower concentration limit to ~50/cc.

Therefore diffusion losses were minimized by designing the connection between inlet and expansion chamber short and straight. In this context hydraulically operated pinch valves with a complete and true full bore are applied. In other words, the inside diameter of the sampling line stays constant for aerosols flowing towards the expansion chamber.

Additionally the optical arrangement and the observed scattering light volume are optimized to obtain better data statistics even at comparatively low number concentrations.

A further, and decisive, point when performing field measurements are fast and unexpected changes in aerosol properties. Accordingly, it is necessary to have an instrument with high time resolution. Therefore the vSANC has a special designed flow shaper installed at the outlet of the expansion chamber. Its application guarantees fast and complete flushing of the measuring chamber after expansion. Thus the measuring frequency can be decreased down to a minimum of 6 seconds per expansion.

However, for the characterisation of atmospheric aerosols not only short-term changes but also long-lasting processes must be taken into account. Thus for future long term measuring campaigns all consumables such as filters, driers etc. were implemented redundantly. Thus they can be exchanged without stopping the experimental cycle.

By its special design we expect that the vSANC will bring new findings on the role of nanoparticles in atmospheric processes. With this aim the instrument will likely participate at the CLOUD campaigns at CERN.

This work was supported by the Austrian Science Fund (Proj. No. L00593 and P19546)

M. Sipilä *et al* (2010) Science **328** (5984):1366-7
P. E. Wagner *et al* (2003) Phys. Rev. E. **67**, 021605
J. Kirkby *et al* (2011) Nature **476**, 429-433

Monday, September 3, 2012

Session WG01S2O. New Particle Formation

Differences between Classes of Nucleation Events during the Summer Period in Thessaloniki, Greece: Kerbside versus urban background measurements

D. Siakavaras[1], C. Samara[2], M. Petrakakis[3], G. Biskos[1,4]

[1]Department of Environment, University of the Aegean, Mytilene 81100, Greece
[2]Department of Chemistry, Aristotle University of Thessaloniki, Thessaloniki 54124, Greece
[3]Environmental Department, Municipality of Thessaloniki, Paparigopoulou 7, Thessaloniki 54630, Greece
[4]Faculty of Applied Science, Delft University of Technology, Delft 2628-BL, The Netherlands

Keywords: nucleation events, number size distribution, SMPS, classification

Thessaloniki is a densely populated coastal city of northern Greece with high concentrations of atmospheric particulate matter (PM) frequently observed in the city centre. Several studies have investigated the concentration levels, the chemical composition of PM, as well as the size distribution of particle mass concentrations over the city (Voutsa *et al*., 2002; Petrakakis *et al*., 2007; Terzi *et al*., 2010;). Preliminary measurements of the size distribution of aerosol number concentration in Thessaloniki were conducted during winter-time at a kerbside site and an urban background site (Terzi et al., 2007). The size distribution of aerosol number concentration during the summer-time and the relationships with PM mass, photochemical pollutants and meteorological parameters was investigated in Siakavaras et al., (2008), while a classification of the nucleation events during the same period was recently reported (Siakavaras et al., 2011).

In this paper we analyse the differences between particle nucleation and growth events observed during the summer period at two monitoring stations (Venizelou – kerbside site, and Eptapyrgio – urban background site). Two identical Scanning Mobility Particle Sizers (TSI Model 3034) have been employed to measure simultaneously the size distributions of the particles having diameters in the range 10-487 nm at the two sites. Gaseous pollutants (CO, NO_x, SO_2 and O_3) and meteorological parameters (wind speed, wind direction, temperature and relative humidity) were also recorded during the measurements. The experiments were conducted during June to October 2009.

Nucleation events were classified in 5 categories based on their intensity. At Venizelou (kerbside site), 6% of the days were classified as class Ia events, 3% as class Ib, 10% as class II, 14% of the days exhibited no clear particle formation patterns and were considered as undefined and 67% of the days showed no event. At Eptapyrgio (urban background site) 8% of the days were class Ia events, 7% class Ib, 5% class II, 5% were undefined and 75% of the days showed no nucleation.

Characteristic differences between the classes can be seen in Fig. 1. For Class Ia the diurnal variation of the particle number concentration shows a significant increase starting at 07:00 at Venizelou and at 12:00 at Eptapyrgio, whereas for the non-event days, the diurnal variation is less pronounced for both stations. Nucleation events were more frequent during July, and for both stations correlated well with high concentrations of SO_2 and NO_x.

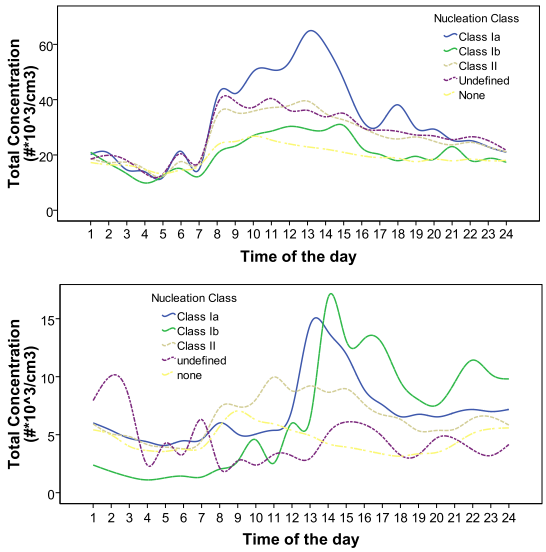

Figure 1. Average diurnal variation of particle number concentrations during nucleation event days of all classes at Venizelou (upper part) and Eptapyrgio (lower part)

References

Voutsa, D., Samara, C., Kouimtzis, Th., Ochsenkuehn, K. (2002). *Atmospheric Environment*, 36, 4453-4462.

Siakavaras, D., Samara, C., Pilinis, C., Kelesis, A. *European Aerosol Conference, Thessaloniki, Greece, 2008 (*Abstract T02A043P).

Terzi, E., Argyropoulos, G., Bougatioti, A., Mihalopoulos, N., Nikolaou, K., Samara, C. (2010). *Atmospheric Environment,* 44, 2231-2239.

Petrakakis, M.J., Kelessis, A.G., Samara, C., Tzoumaka, P., Zoumakis, N.M., Iosifidis, E. CEMEPE 07, *Skiathos, 2007* (Proceedings pp 2471-2477).

Dal Maso, M., Kulmala, M., Riipinen, I., Wagner, R., Hussein, T., Aalto, P., Lehtinen, E.J (2005) Boreal Environment Research 10: 323-336

The role of marine microcolloids in new particle formation over the Arctic Ocean

M. Karl[1], E. Coz[2] and C. Leck[3]

[1] Department for Urban Environment and Industry, Norwegian Institute for Air Research, NILU, NO-2027 Kjeller, Norway.
[2]CIEMAT, Department of Environment, E-28040 Madrid, Spain.
[3]Department of Meteorology, Stockholm University, S-10691 Stockholm, Sweden.
Keywords: MBL, nucleation, bubble bursting, climate effects.
Presenting author email: mka@nilu.no

The High Arctic summer atmosphere is of particular interest for the study of aerosol-cloud-climate interactions, since it is characterized by relatively few aerosol particles, usually less than 200 per cubic centimetre, available to form cloud droplets. The frequent occurrence of new particle formation events in the marine boundary layer (MBL) over the central Arctic Ocean is however difficult to explain because of the limited availability of low-volatile vapours, such as sulphuric acid (H_2SO_4), which can act as nucleating agents (Karl et al., 2012).

Spherical nanometre sized (~2-10 nm diameter) granules, hereafter termed nano-granules, have been discovered in surface micro layer (SML) samples of the open leads (openings in pack ice, 1-100 m wide and km long) in the High Arctic. These nano-granules form colloidal aggregates, classified as polymeric microgels, which are known to be exopolymer secretions (EPS) produced by phytoplankton and marine algae. Leck and Bigg (2010) recognized the significance of the very large numbers of airborne biogenic nano-granules and related their appearance to observed new particle formation events. Orellana et al. (2011) demonstrated that microgels found in cloud, fog and airborne aerosol sampled at 87°N during the Arctic Summer Cloud Ocean Study (ASCOS, www.ascos.se) cruise were material originating from the SML of the open leads.

An important observation is that the onset of inner Arctic nucleation events often occurred shortly after dissipation of fogs (Leck and Bigg, 1999; 2010; Karl et al., 2012). Fog droplets are proposed here to be a medium facilitating the collapse of the marine gels which enclosed the nano-granules. We postulate a novel pathway to new particle formation (illustrated in Fig. 1) which includes the following steps: 1) release of nano-granules from evaporating fog droplets, 2) nucleation of H_2SO_4 molecules to form stable clusters, 3) secondary production of condensing organic vapour (COV), 4) condensation of vapours onto nano-granules and H_2SO_4 clusters, 5) coagulation of nano-granules and H_2SO_4 clusters to form >3 nm diameter particles.

The novel pathway is supported by observational evidence from electron microscopy analysis and by model predictions obtained using the sectional multicomponent aerosol model MAFOR. The resolution of the field emission scanning electron microscopy (FESEM) allowed the quantification of native gels with sizes below 10 nm diameter. The morphology and structure of the microgels in cloud and fog samples from ASCOS showed high numbers of building blocks of the microgels, confirming that airborne nano-granules could in fact have been released from evaporating droplets.

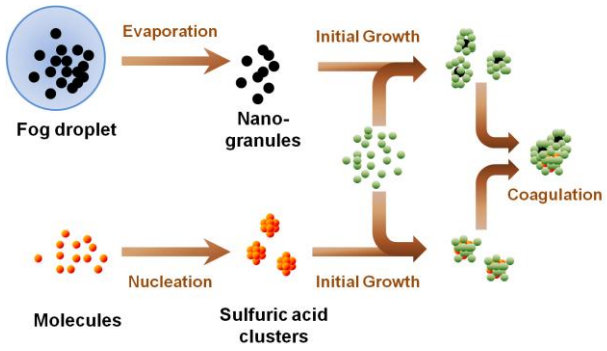

Figure 1. Schematic outline of the new nucleation route involving sulphuric acid (orange), organic vapour (green), and marine nano-granules (black).

Model simulations with MAFOR initialized with a pre-existing population of nm-sized clusters, representative for the novel pathway, showed much better agreement with the observed number enhancement of nucleation mode particles during selected new particle formation events than simulations that did not consider the presence of nano-granules.

The evident presence of nm-sized building blocks of microgels in surface waters of the Atlantic, Pacific, and central Arctic Ocean suggests that the proposed pathway, operative after the evaporation of cloud or fog, might be relevant worldwide and able to explain new particle formation events in the MBL of remote oceans.

This work was supported by the Swedish Research Council, the International Institute of Meteorology and the Knut and Alice Wallenberg Foundation.

Karl, M., Leck, C., Gross, A., and Pirjola, L. (2012) *Tellus B*, **64**, 17158, DOI: 10.3402/ tellusb.v64i0.17158.

Leck, C., and Bigg, E. K. (1999) *J. Geophys. Res.*, **26**, 3577-3580.

Leck, C., and Bigg, E. K. (2010) *Aerosol Sci. Technol.*, **44**, 570-577.

Orellana, M. V., Matrai, P., Leck, C., Rauschenberg, C. D., Lee, A. M., and Coz, E. (2011) *P. Natl. Acad. Sci.*, **108**(33), 13612-13617.

Response of Cloud Condensation Nuclei (> 50 nm) to changes in ion-nucleation

M. B. Enghoff,[1] H. Svensmark,[1] and J. O. P. Pedersen[1]

[1]National Space Institute, Technical University of Denmark, Copenhagen OE, dk-2100, Denmark
Keywords: Ion induced nucleation, Cloud condensation nuclei
Presenting author email: enghoff@space.dtu.dk

The role of ionisation in the formation of clouds and aerosols has been debated and investigated for many years. A substantial body of evidence exists that correlates cloud properties to galactic cosmic ray ionisation (e.g. Svensmark and Friis-Christensen 1997, Harrison and Stephenson 2006), however these results are still contested (e.g. Sloan and Wolfendale 2008). In recent years clear experimental evidence has also been produced showing that ionisation can promote the nucleation of small aerosols (1-3 nm) at atmospheric conditions (Svensmark *et al* 2007, Kirkby *et al* 2011).

The experiments initially showed that an increase in ionisation leads to an increase in the formation of ultrafine aerosols (~3 nm), but in the real atmosphere such small particles have to grow by coagulation and intake of condensable gases to become cloud condensation nuclei (CCN) (> 50 nm) in order to have an effect on clouds.

Theoretical doubts about the likelihood of such particle growth into CCN have arisen from consideration of (1) the competition between the additional ultra-fine aerosols for the limited supply of condensable gases leading to a slower growth and (2) the larger losses of the additional particles during the longer growth-time to larger particles by coagulation and by other loss mechanisms. Numerical studies using the current knowledge of aerosol dynamics predict that variations in the count of ultra-fine aerosols will lead only to an insignificant change in the count of CCN (Pierce and Adams 2009). It is even suggested that an increased production of ultra-fine particles as a result of GCR ionization leads to a reduction in the CCN count.

In order to study the growth of aerosols to CCN sizes, measurements were performed in an 8 m^3 reaction chamber made from electro-polished stainless steel. One side was fitted with a Teflon foil to allow ultraviolet light (253.7 nm) to illuminate the chamber, which was continuously flushed with dry purified air. Variable concentrations of water vapor, ozone, and sulphur dioxide could be added to the chamber, where the pressure was held a few Pa above atmospheric pressure, and the temperature at around 296 K. UV-lamps initiated photochemistry producing sulphuric acid. Ions were produced in the chamber by the naturally occurring GCR and by background radiation from radon, and the ionization could be enhanced with two Cs-137 gamma sources (30 MBq), mounted on each side of the chamber.

Figure 1 shows the evolution of the aerosols, following a nucleation event induced by the gamma sources. Previous to the event the aerosols were in steady state. Each curve represents a size bin: 3-10 nm (dark purple), 10-20 nm (purple), 20-30 nm (blue), 30-40 nm (light blue), 40-50 nm (green), 50-60 nm (yellow), and 60-68 nm (red). Black curves show a ~1 hour smoothing. In this event the initial increase in small aerosols persists all the way to the largest size bin.

Similar experiments where the aerosol burst was produced with either the ionisation source or an aerosol generator (neutralised aerosols) were made and compared with each other and model runs. The runs using neutral aerosol bursts agree with the model predictions, where the initial burst is dampened by increased losses such that there is little or no change in the largest sizes. Thus there seem to be a fundamental difference between the bursts produced by ionisation and those produced by the aerosol generator. One possible explanation is that the ionisation assists the growth of the aerosols, by catalytically producing additional sulphuric acid for growth (Svensmark *et al* 2012).

Figure 1. Growth of aerosols, nucleated by ionisation.

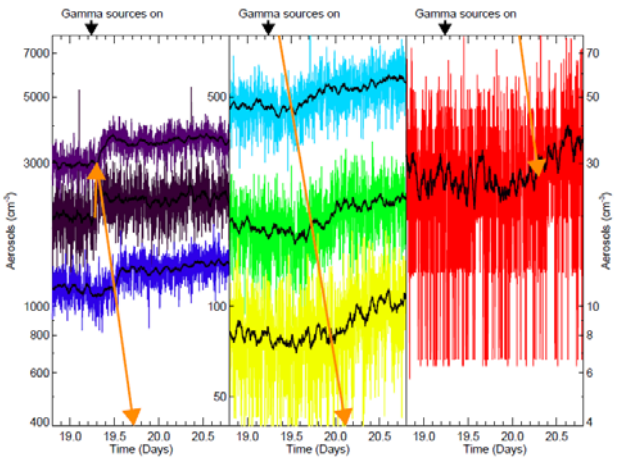

This work was supported by the Carlsberg Foundation and The Danish Council for Independent Research | Natural Sciences.

Svensmark, H. and Friis-Christensen, E. (1997), *J. Atmos. Sol-Terr. Phy*. **59**, 1225-1232.

Harrison, R. G. and Stephenson, D. B. (2006), *Proc. R. Soc. London, Ser. A* **462**, 1221-1233

Sloan, T. and Wolfendale, A. W. (2008), *Environ. Res. Lett.* **3**, 024001

Svensmark, H., Pedersen, J. O. P., Marsh, N. D., Enghoff, M. B. and Uggerhøj, U. I. (2007), *Proc. R. Soc. London, Ser. A* **463**, 385-396

Kirkby, J., Curtius, J., Almeida, J., Dunne, E., Duplissy, J. *et al* (2011), *Nature* **476**, 429 -433

Pierce, J. R. and Adams, P. J. (2009), *Geophys. Rev. Lett.* **36**, L09820

Svensmark, H., Enghoff, M. B., and Pedersen, J. O. P. (2012), http://arxiv.org/abs/1202.5156

Estimating the effect of gas-phase kinetics and nanoparticle dynamics on observed particle formation rate dependencies

M. Dal Maso[1], H. Korhonen[2], K. Lehtinen[2], H. Vehkamäki[1]
[1]Department of Physics, University of Helsinki, PO Box 48, 00014, Helsinki, Finland
[2]Finnish Meteorological Institute, Kuopio Unit, P.O.Box 1627, 70211 Kuopio
Keywords: nanoparticle formation, BVOCs, sulphuric acid, laboratory experiments
Presenting author email: miikka.dal@helsinki.fi

Atmospheric aerosol formation has been studied intensively due to its significance in adding to the tropospheric aerosol loading (e.g. Kulmala et al. 2004). A major problem in quantitatively explain atmospheric particle formation is the current inability to identify and quantitatively measure the actual vapors participating in particle formation Several studies make use of estimations of the logarithm of the nanoparticle formation rate as a function of the logarithm of vapour concentration to gain insight into the formation mechanism. however, there are suggestions that such analysis is inaccurate and the effect of this on the power-law fits is unknown (Vuollekoski et al., 2010). To estimate the importance of various gas phase precursors, correlation analysis of measured gas phase parameters and measured and estimated nanoparticle formation rates have also been performed. These analyses often simplify the chemical kinetics the precursor oxidation chemistry and omit various sink processes of the participating compounds. The results of these analyses are used to draw conlusions of the vapors participating in the particle formation process.

In this study, we investigate the most frequently used conceptual models for particle formation, such as oxidation of plant volatiles and the subsequent participation of the oxidation products in nanoparticle formation, or formation of stable clusters from sulphuric acid and oxidised plant emissions. We investigate the predictions of for the dependence of the particile formation rate on commonly measurable parameters, such as sulphuric acid concentration, probable volatile organic aerosol precursors, hydroxyl radical concentration, and the sink of nanoparticles and non-volatile vapours caused by pre-existing aerosol.

In addition to theoretical predictions derived from gas-phase kinetics analysis, we use a model that simulates the early stages of growing atmospheric nanoparticles on a resolution of a single molecule, similarly to the model described in Lehtinen and Kulmala, (2003). In practise, the model is given a formation rate and size of a stable condensation nuclei (CN); these nuclei then grow by colliding with either vapour monomers or other CN. This results in a size distribution of small CN. The coagulation coefficient for CN collisions and CN-monomer -collisions are calculated using the Fuchs coagulation kernel for the wet aerosol sizes assuming spherical particles (Lehtinen et al., 2007).

There are several phenomena affecting the detection of atmospheric particle formation rates. One of them is the loss of fresh particles due to coagulation to background, and also apparent losses due to change in the size distribution shape. This has been extensively studied theoretically (Lehtinen et al., 2007, Anttila et al., 2010).

Another process affecting the determination of the apparent particle formation rate is the intermodal coagulation affecting the shape of the just-formed particle mode. Our model simulations show that the new particle population shape quickly changes shape, starting to resemble a log-normal size distribution due to collisions between young clusters. This, in turn, affects the time derivative of CN measured at larger sizes than the nucleation size, as the edge of the fresh mode passes the detection threshold of the measuring instrument. We discuss the effect of these processes as well as the effect of different temporal behaviour of the temporal profile of the condensing vapour production rate.

We compare our measurements to real-world situations of actual measurements in field conditions and chamber experiments, and discuss the relevance of the studied processes for each.

We found that the magnitude of the reaction pathways leading to aerosol formation in comparison to non-aerosol forming pathways is a key factor determining the functional dependence of the observed formation rate on measurable parameters. In addition, nano-size aerosol dynamics add another layer of complexity to the analysis. We discuss these effects for various scenarios, including OH- or ozone-dominated environments, the presence of high sulphuric acid loading, and environments with either high or low background aerosol loadings.

This work was supported by the Academy of Finland.

Anttila, T., *et al* (2010*)*: Paramererizing the formation rate of new particles: The effect of nuclei self-coagulation, J. Aerosol Sci., 41, 621–636, doi:10.1016/j.jaerosci.2010.04.008, 2010. 18783, 18785

Kulmala, M.,et al (2004) Formation and growth rates of ultrafine atmospheric particles: A review of observations Aerosol Science 35, 143-176.

Lehtinen, K E J. and Kulmala, M. (2003): A model for particle formation and growth in the atmosphere with molecular resolution in size, Atmos. Chem. Phys., 3, 251-258

Lehtinen, K.E.J. *et al:* (2007) Estimating nucleation rates from apparent particle formation rates and vice versa: Revised formulation of the Kerminen–Kulmala equation J. Aerosol. Sci 38 (9), 988-994.

Vuollekoski, H., *et al* (2010) A numerical comparison of different methods for determining the particle formation rate Atmos Chem Phys Discuss, 10, 18781–18805

The role of amines in atmospheric nucleation

Almeida-Simões, João[1,2], Curtius, Joachim[1], Kirkby, Jasper[2], and the CLOUD collaboration

[1] Goethe-University of Frankfurt am Main, 60438 Frankfurt am Main, Germany
[2] Physics Department, CERN, CH1211, Geneva, Switzerland

Keywords: CLOUD experiment, cosmic rays, atmospheric nucleation, nucleation rate, amines.

Atmospheric sulphuric acid and water, together with other trace gases, can condense to form molecular clusters. These nucleated aerosol can grow to sufficient size to become cloud condensation nuclei. Thus understanding how aerosol form and what vapours participate is important to understanding climate and climate change. In the CLOUD experiment we have studied aerosol nucleation and early stages of growth from dimethylamine, sulphuric acid and water vapours at atmospheric concentrations.

The CLOUD experiment involves a 3m stainless steel aerosol chamber exposed to a pion beam from the CERN Proton Synchrotron. A suite of instruments continuously analyse the contents of the chamber via sampling probes. Each instrument has its own data acquisition system which delivers data in real-time to the CLOUD server. The CLOUD chamber is able to reproduce a wide range of well-controlled atmospheric conditions, including temperatures -90ºC to 100ºC, ion-pair concentrations 1-4000 cm^{-3} and relative humidities, RH, 0-100%.

The analysing instruments include the following: a Chemical Ionisation Mass Spectrometer (CIMS) for H_2SO_4 concentration, Atmospheric Pressure Interface Time Of Flight (APi-TOF) mass spectrometer for molecular composition of positive and negative ions, several particle counters with thresholds in the range 1.3–2.5 nm (2 Particle Size Magnifiers, PSM, of which one operated in a continuous scanning mode, 2 Di-Ethylene Glycol CPCs, DEG-CPC, and a TSI 3776), Neutral cluster and Air Ion Spectrometer (NAIS) and two instruments dedicated to NH_3 and DMA measurements (Ion Chromatograph, IC , and Proton Transfer Reaction Mass Spectrometer, PTR-MS).

A series of experiments have been performed in the CLOUD chamber with H2SO4 in the range 10^6-10^7 cm^{-3} at 278 K and 38% relative humidity. The experiments separate the contribution of neutral nucleation from ion-induced nulceation using the internal electric field of the CLOUD chamber (for neutral nucleation) and the CERN pion beam (for charged nucleation). To investigate the influence of amines, dimethylamine was added at mixing ratios between 1 and 65 pptv. Large enhancements were observed after adding dimethlamine. The results will be presented in this paper, including a comparison of amine-ternary with ammonia-ternary (reported in Nature Kirkby 2012) nucleation and with atmospheric boundary layer observations.

These data represent the first to measure amine-ternary nucleation at atmospheric conditions and the first to measure the molecular composition and nucleating mechanism of the amine-containing molecular clusters.

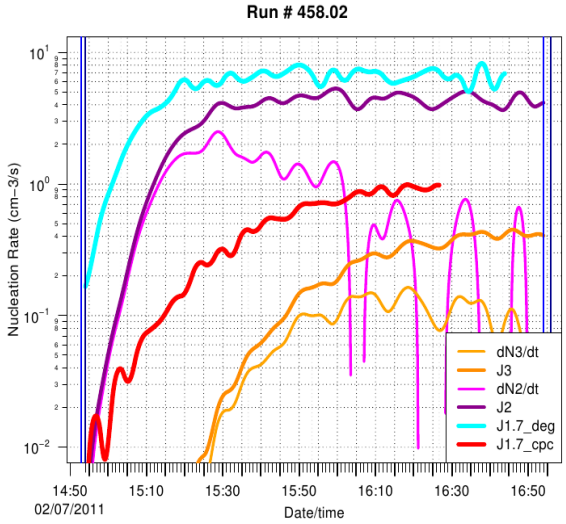

Figure 1. Typical nucleation rates in a CLOUD run with added DMA. The various lines represent observed rates provided by two independent counters with different cut-offs, with and without corrections applied. The corrected lines should plateau during the run if the loss mechanism is well known. Both counters are also scaled to the same small diameter of 1.7nm, which is taken as the critical stable cluster size.

We would like to thank CERN for supporting CLOUD with important technical and financial resources, and for providing a particle beam from the CERN Proton Synchrotron. This research has received funding from the EC Seventh Framework Programme (Marie Curie Initial Training Network "CLOUD-ITN" grant no. 215072, and ERC-Advanced "ATMNUCLE" grant no. 227463), the German Federal Ministry of Education and Research (project no. 01LK0902A), the Swiss National Science Foundation (project nos. 206621_125025 and 206620_130527), the Academy of Finland Center of Excellence program (project no. 1118615), the Austrian Science Fund (FWF; project no. P19546 and L593), the Portuguese Foundation for Science and Technology (project no. CERN/FP/116387/2010), and the Russian Foundation for Basic Research (grant N08-02-91006-CERN)

Atmospheric amine measurements with CI-APi-TOF

T. Jokinen[1], M. Sipilä[1], H. Junninen[1], M. Ehn[2], G. Lönn[1], J. Hakala[1], T. Petäjä[1], R. L. Mauldin III[1], M. Kulmala[1] and D.R. Worsnop[1,3]

[1]Department of Physics, University of Helsinki, Helsinki, 00014, Finland
[2] Institute for Energy and Climate Research, Forschungszentrum Jülich, 52425, Germany
[3] Aerodyne Research Inc., Billerica, MA 01821, USA

Keywords: amines, chemical ionization, mass spectrometry.
Presenting author email: tuija.jokinen@helsinki.fi

Nucleation of new particles is one of the main sources of cloud condensation nuclei (CCN) in the atmosphere contributing even up to 50% to the global CCN budget. The initial steps of nucleation require the presence of sulphuric acid (SA) (e.g. Sipilä *et al*. 2010) but additional vapours are needed because SA does not nucleate itself at typical atmospheric conditions. Kirkby *et al*. (2011) found ammonia and dimethylamine (DMA) from charged clusters formed by ion induced nucleation and concluded that amines are plausible candidates for stabilizing neutral clusters at lower atmospheric conditions. The enhancing effect of amines on new particle formation was observed also in laboratory studies by Berndt et al, (2010). Amines can bind the cluster much more strongly than ammonia and even ppt levels of amines can be enough to account for atmospheric nucleation rates (Petäjä *et al*., 2011).

In here we present the first ambient amine measurements using an acetone based Chemical Ionization Atmospheric Pressure interface Time-Of-Flight mass spectrometer (CI-APi-TOF). We previously used the exact same inlet for sulphuric acid measurements (Jokinen *et al*, 2011) but this time we used acetone for the proton transfer reaction and ran the APi-TOF in the positive polarity mode. In this experiment acetone + water in clean air was ionized using a ^{241}Am bipolar charger to create positively charged acetone ions and clusters. In the proton transfer reaction only compounds that have higher proton affinity than the reagent ions will get charged and detected by the APi-TOF.

The data analysis is still ongoing and these results must be considered preliminary. We identified amine clusters by their exact masses and isotopic patterns. So far two signals have been identified to correspond to the same chemical composition and exact mass as common aliphatic amines. These signals are $C_4H_{12}N^+$ (diethyl amine) and $C_6H_{16}N^+$ (triethylamine). Time series of these signals are shown in figure 1. Figure 1 also demonstrates SA concentration (divided by 10 000) and it's seen that during a nucleation event, when SA concentration reaches its maximum, we only see a minimum amine signal. This may indicate the role of surface source and boundary layer dynamics as factors controlling the concentrations or that amines are reacting and/or clustering with freshly forming SA molecules.

This setup has a few disadvantages that need to be further developed. First, one of the most interesting amine signals, trimethylamine (TMA), is overlapped with the acetone isotope signal and it is almost impossible to separate from the spectrum. Second, this instrument consumes high amounts of acetone. Also the purity of the air entering the ion source is crucial. The design of the inlet will be improved to consume less chemicals and the reagent ion may have to be changed before quantitative analysis of atmospheric amines can be done using the CI-APi-TOF.

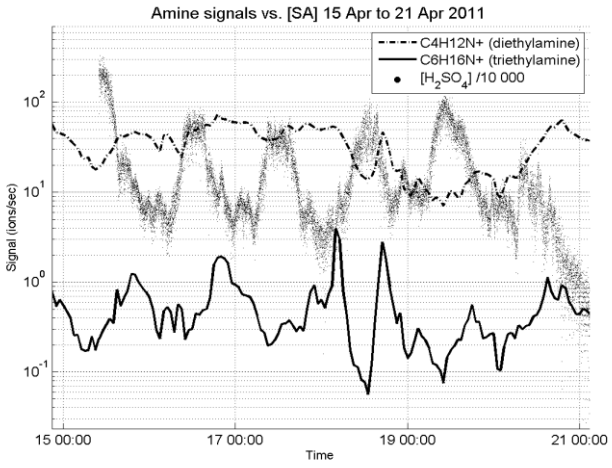

Figure 1. Diethyl and triethyl amine signals (ions/sec) and SA concentration (molec/cm^3) in Hyytiälä.

This work was supported by the EU Pegasos project and Academy of Finland projects 251427and 139656.

Sipilä M., Berndt T., Petäjä T., Brus D., Vanhanen J., Stratmann F., Patokoski J., Mauldin III R. L., Hyvärinen A.-P., Lihavainen H. and Kulmala M., *Science*, 327, 1243-1246, 2010.

Kirkby et al., *Nature*, 476, 429–433, 2011

Berndt T., Stratmann F., Sipilä M., Vanhanen J., Petäjä T., Mikkilä J., Grüner A., Spindler G., Mauldin III, R. L., Curtius J., Kulmala M., Heintzenberg J., *Atmos Chem Phys*, 10, 7101-7116, 2010.

Petäjä T., Sipilä M., Paasonen P., Nieminen T., Kurtén T., Ortega I. K., Stratmann F., Vehkamäki H., Berndt T., and Kulmala M., *Phys. Rev. Lett.*, 106, 228302, 2011.

Jokinen T, Sipilä M., Junninen H.,Ehn M., Lönn G., Hakala J., Petäjä T., Mauldin R.L. III, Kulmala M., Worsnop D.R., *Atmos. Chem. Phys. Discus*., 11, 31983–32002, 2011.

Lewis bases as the unifying concept for ion-induced and neutral H_2SO_4 nucleation

Theo Kurtén[1], Ismael K. Ortega[2], Oona Kupiainen[2], Tinja Olenius[2], Ville Loukonen[2] and Hanna Vehkamäki[2]

[1]Laboratory of Physical Chemistry, University of Helsinki, P.O. BOX 55, FI-00014 Finland
[2] Department of Physics, University of Helsinki, FI-00014, Helsinki, Finland
Keywords: nucleation, atmospheric aerosol, sulfuric acid, amines
Presenting author email: theo.kurten@helsinki.fi

Sulfuric acid is believed to be the main compound driving atmospheric new-particle formation. However, sulfuric acid (or sulfuric acid and water) alone cannot account for observed nucleation rates in the boundary layer. Three major groups of compounds have been proposed as ternary nucleation enhancing agents for H_2SO_4 or H_2SO_4- H_2O nucleation: ions (particularly anions), nitrogen-containing base molecules such as ammonia or amines, and non-basic oxygenated organic molecules such as diacids. Using the concept of Lewis acidity, the two first cases are actually examples of the same fundamental mechanism: enhancement of acid clustering by Lewis bases.

The textbook definition of a Lewis base is an electron pair donor. Ammonia and amines are moderately strong Lewis bases due to the lone electron pairs of the nitrogen atoms, which readily participate in hydrogen bonding. Anions such as HSO_4^- or NO_3^- are strong Lewis bases due to their excess electron. The different Lewis bases thus compete for the available sulfuric acid molecules, and the relative role of each base in enhancing nucleation depends both on the strength of its interaction with H_2SO_4, and on its concentration: typically around $10^{2,,4}$ cm^{-3} for anions, $10^{6...9}$ cm^{-3} for amines and $10^{8...11}$ cm^{-3} for NH_3. Anions interact much more strongly with the first few acid molecules in a nucleating cluster, but the differences between the Lewis bases with respect to acid addition free energies, and thus the acid saturation vapor pressures and evaporation rates, essentially disappear once the cluster contains more than two or three H_2SO_4 molecules (see Figure 1).

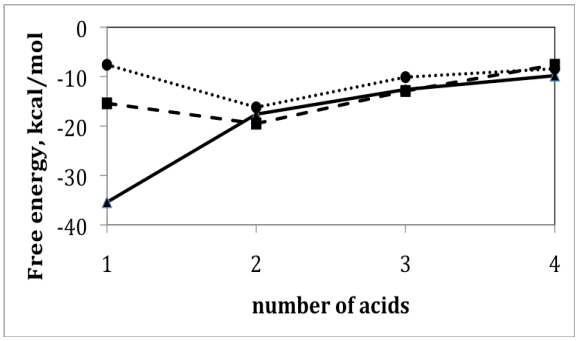

Figure 1. Free energies (kcal/mol) for the reactions $X•(H_2SO_4)_{n-1} + H_2SO_4 \Rightarrow X•(H_2SO_4)_n$, for n = 1…4 and $X = HSO_4^-$ (solid line), $(CH_3)_2NH$ (dashed line) and NH_3 (dotted line). Values correspond to 298 K and 1 atm, see Ortega et al. (2012).

There are two crucial differences between anions and other Lewis bases with respect to the growth dynamics of the base-stabilized sulfuric acid clusters. First, while self-coagulation of neutral acid-base clusters may efficiently promote cluster growth (while reducing total number concentrations), charged clusters cannot self-coagulate due to electrical repulsion. Second, the condensational growth rate of charged clusters is enhanced due to the attractive charge-dipole interaction with condensing molecules, which decays much more slowly with distance than the dipole-dipole interaction (see Figure 2 for representative numerical values).

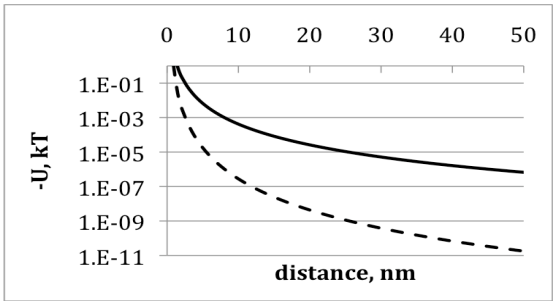

Figure 2. Potential energy (in units of k_bT) of H_2SO_4 interacting with a $X•H_2SO_4$ cluster, for $X = HSO_4^-$ (solid line), or $X = (CH_3)_2NH$ (dashed line). Computed using B3LYP/CBSB7 dipole moments on Gaussian 09 (Frisch et al, 2009), classical electrostatics and 298 K Boltzmann thermal averaging of interaction angles.

Using the concept of Lewis basicity, ternary neutral and binary ion-induced sulfuric acid nucleation are shown to be examples of the same fundamental process. The difference between the stabilizing effect of anions and neutral bases on the sulfuric acid clusters disappears rapidly with cluster size. Cluster growth is further enhanced by self-coagulation for the neutral base-containing clusters or by condensation enhancement for the anion clusters. Kinetic models (McGrath et al., 2011) will be used to determine the concentrations regimes at which the various bases are important for nucleation.

We thank the CSC IT Centre for Science in Espoo, Finland for computer time.

Frisch, M. J. *et al.* (2009) Gaussian 09, Gaussian, Inc., Wallingford CT, U.S.A.

McGrath, M. J., *et al*. (2011) *Atmos. Chem. Phys. Discuss*. **11**, 25263-25295.

Ortega, I. K., *et al*. (2012). *Atmos. Chem. Phys.* **12**, 225-235.

Monday, September 3, 2012

Session WG02S2O. Mineral Dust

CLIMARENO 2011 campaign: airborne characterization of a Saharan dust intrusion over the Iberian Peninsula

J. Andrey[1], J. Fernández-Gálvez[2,3], J.L. Guerrero-Rascado[2,3], M. Sorribas-Panero[2,3], G. Titos-Vela[2,3], A. Corrales-Sierra[4], M. Gil-Ojeda[1], V. Cachorro[5], B. de la Morena[1] F.J. Olmo[2,3] and L. Alados-Arboledas[2,3]

[1]Área de Investigación e Instrumentación Atmosférica (AIIA), INTA. 28850 Torrejón de Ardoz, Spain
[2]Departamento de Física Aplicada, Universidad de Granada, 1807106 Granada, Spain
[3]Centro Andaluz de Medio Ambiente (CEAMA), Universidad de Granada, 18006 Granada, Spain
[4]Plataformas Aéreas de Investigación (PAI), INTA. 28850 Torrejón de Ardoz, Spain
[5]Grupo de Óptica Atmosférica, Universidad de Valladolid, 47071, Spain

Keywords: Saharan dust, Airborne measurements, Aerosol optical properties, Aerosol physical properties.
Presenting author email: javier.andrey@gmail.com

Saharan dust is the major source of aerosols emitted yearly to the atmosphere. The Iberian Peninsula, located at the North of the Sahara desert, is frequently affected by Saharan dust intrusions, especially during the summer period (Toledano et al., 2007; Bennouna et al., 2011; Guerrero-Rascado et al., 2009).

In June 2011, an airborne campaign was conducted by INTA in collaboration with Granada University intended to study Saharan dust aerosols properties. Flights were carried out over INTA "El Arenosillo" sounding station (ARN, 37.1N 6.7W) and Granada (GRA, 37.2N, 3.6W) under dust (D) and non-dust (ND) conditions. The data under ND condition were used as a "clean" reference for the D measurements. Four flights were carried out during the airborne campaign, two of them over each station.

The INTA atmospheric research aircraft was equipped with two optical particle counters designed by Droplet Measurement Technologies (DMT): PCASP-100X (15 bins, 0.1-3.0 μm) and CAPS (30 bins, 0.51-50 μm). The CAPS was equipped with optional depolarization module allowing determinations of refractive index and particle shape of the sampled aerosols. The algorithm to determine both refractive index and particle shape are based on the Mie theory.

Several particle counters and two CIMEL sun-photometers were deployed at both stations or in the vicinity of them. The size distributions retrieved by the airborne instrumentation are compared with in-situ measurements of particle counters and AERONET retrievals from the particle counters and CIMEL sun-photometers respectively. Data from CIMEL stations within the studied area have been used to provide a global image of the Saharan dust episode. Refractive index retrieved by the optional depolarization module is also presented and compared with CIMEL retrievals in this work.

The AOD at 440 nm during the flight for D conditions reached values of 0.48 and 0.30 over ARN and GRA, while under ND conditions the AOD reached 0.10 and 0.11 respectively. The ceiling of the Saharan dust intrusions detected by the aircraft was located at 6 and 5 km asl over ARN and GRA respectively. In both cases the concentration of particles in the coarse mode was higher at lower levels (2-3 km asl) than in the intrusion top height.

An oversampling issue in the coarse mode was noted for the PCASP measurements during ND days. This may be related with the low particle concentration found in this range.

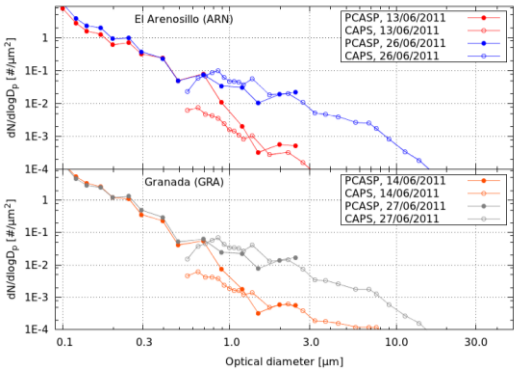

Figure 1: Columnar integrated SD from PCAPS and CAPS instruments

The authors are grateful to the crew of the C212 and people involved on the aircraft operation. We thank to P. Chazette, S. Wilbert, D. Mohammed and their staff for establishing and maintaining the Marbella_San_Pedro, Tabernas_PSA_DLR and Oujda sites used in this investigation. This work was supported by the Andalusia Regional Government through projects P08-RNM-3568 and P10-RNM-6299; by the Spanish Ministry of Science and Technology through projects CGL2010-18782, CSD2007-00067 and CGL2011-13580-E/CLI; and by EU through ACTRIS project (EU INFRA-2010-1.1.16-262254).

Bennouna et al (2011) *Remote Sensing of Environment*, pg. 1272-1284, doi: 10.1016/j.rse.201101.011

Guerrero-Rascado et al (2009) *Atmos. Chem, Phys.*, 9, 8453-8469, doi:10.5194/acp-9-8453-2009

Toledano et al. (2007) *J. Geophys. Res.* **112**, d21201, doi: 10.1029/2006JD008307

The importance of Nocturnal Low-level Jets for simulating mineral dust emission

S. Fiedler[1], K. Schepanski[1], B. Heinold[1], P. Knippertz[1] and I. Tegen[2]

[1]The University of Leeds, School of Earth and Environment, Leeds, LS2 9JT, United Kingdom
[2]Leibniz Institute for Tropospheric Research, Permoser Str. 15, 04318, Leipzig, Germany
Keywords: Aerosol emission, Modelling, Saharan/mineral dust
Presenting author email: eesfi@leeds.ac.uk

Mineral dust is important for the Earth system. The aerosols interact with short- and long-wave radiation, influence clouds and precipitation, and affect human health during atmospheric transport. Deposited desert dust fertilizes remote marine and terrestrial ecosystems. Modelling the atmospheric cycle and the impacts of dust depends on the accurate simulation of time, place and amount of mineral dust emission.

Dust emission in large scale atmospheric models is parametrised as a non-linear function of surface characteristics, and the momentum transfer of the wind to the ground. Particles are mobilised when the friction velocity exceeds the soil-specific threshold value. The nocturnal low-level jet (NLLJ) is one of the mechanisms that potentially generates a sufficient vertical momentum flux for dust emission. A NLLJ is a near-surface wind speed maximum developing over a surface-inversion at night. The air above the inversion-layer accelerates due to reduced dynamical friction. Momentum from the NLLJ is mixed towards the ground by both shear-induced turbulence at night and convection during the following morning. The latter, breakdown of NLLJs, has been suggested as important mechanism for dust emission based on observations covering weeks to a few years. However, a climatology of the NLLJ and its contribution to dust emission is missing.

This work presents the first statistical analysis of NLLJs and its importance for dust emission relative to other processes. A new and objective NLLJ detection algorithm for large-scale atmosphere models has been developed and is applied to 6-hourly data on 60 model levels from the European Centre for Medium-Range Weather Forecasts (ECMWF) ERA-interim re-analysis for 1979-2011. Re-analysis data are considered as the best estimate of atmospheric conditions for North Africa, where the observation network is sparse. The offline dust model by Tegen *et al* (2002) with updates described in Schepanski *et al* (2007) is driven by near-surface wind speed and soil moisture from ECMWF to calculate mineral dust emissions.

The spatially-averaged NLLJ frequency over North Africa ranges from 22% of nights per season in Northern Hemisphere summer and 20% in autumn, to 26% in winter and spring. Typical spatial standard deviations are 13-20% of NLLJ nights dependent on the season, reflecting the spatial variance. The areal distribution of the NLLJ highlights their frequent occurrence along the margins of the heat-low in summer, and in regions affected by mountain channelling, e.g. the Bodélé Depression, Chad, where NLLJs characterise 40-80% of the nights between December and February (Figure 1). Most frequent heights of NLLJs are 300-400m and the median core speed is 10m/s. The results point towards a relative contribution of NLLJs to dust emission of 28+/-22% (mean +/- standard deviation) at 06 UTC and 42+/-18% at 00 UTC in the annual-mean over North Africa. The relative importance of NLLJs increases to annual-mean values around 70% NLLJ nights in some regions, where the phenomenon is more frequent.

In future work, this first NLLJ climatology for North Africa enables an evaluation of the representation of this phenomenon in state-of-the-art atmosphere models. It therefore holds the potential for improving the diurnal cycle of wind speed and dust emission in numerical weather prediction and climate models.

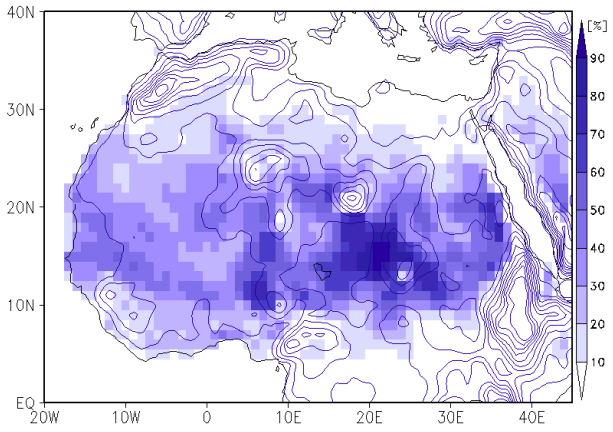

Figure 1. NLLJ frequency in % for north hemisphere winter (DJF) in North Africa. Contour lines show the topography in 200m steps (Fiedler *et al*)

The work is funded by the European Research Council as part of the project “Desert Storms” under grant number 257543.

Fiedler, S., Schepanski, K., Heinold, B., Knippertz, P. and Tegen, I., *in preparation for J. Geophys. Res.*

Tegen, I., Harrison, S., Kohfeld, K., Prentice, I., Coe, M. and Heimann, M. (2002) *J. Geophys. Res.*, **107**, D21, 4576.

Schepanski, K., Tegen, I., Laurent, B., Heinold, B. and Macke, A. (2007) Geophys. Res. Lett., **34**, L18803, 5.

Resuspension and wind erosion in semi-arid SE Spain: overview and key results from field campaigns in 2005 - 2012

J.A.G. Orza[1], M. Cabello[1], M.A. Barrero[2], L. Cantón[2], A. Berasaluce[2], A. Romero-Díaz[3], F. Belmonte-Serrato[3] V. Lidón[1] and J. Martínez[1]

[1]SCOLAb and Aeolian Erosion Research Group, Universidad Miguel Hernández, Elche, 03202, Spain
[2]Chemical Engineering Group, University of the Basque Country, San Sebastián, 20018, Spain
[3]Departamento de Geografía, Universidad de Murcia, Murcia, Spain
Keywords: mineral dust, aerosol size distribution, resuspension, meteorology.
Presenting author email: ja.garcia@umh.es

We present a summary of key results obtained in several field campaigns conducted from 2005 to 2012 mainly in the framework of two research projects. The RESUSPENSE project, 2005 – 2007, was aimed to quantify the contribution of resuspension to the airborne particulate levels in semi-arid Spain. The aerosol size distribution in the range 0.25 – 32 μm, PM10 concentration and chemical composition, as well as meteorological parameters, were studied at three measurement sites: a rural background location (R1), a rural site with influence of mineral industry (R2) and an urban background site (U). Another study was conducted from February to June 2008 in an agricultural plot previously cleared and leveled for future cultivation (R3). Aerosol size distribution was measured there at three heights above the ground. The field campaigns conducted since 2009 form part of the EroHondo project. *El Hondo* Nature Park is an area of ephemeral lakes that experiences cycles of flooding and desiccation with anthropic regulation. The sediments lying on the desiccated surface are susceptible to deflation. The objective of the project is studying the relationship between wind erosion and suspended particulate levels downwind, in relation to atmospheric and soil conditions. Two primary sampling sites (R4 and R5) were chosen for upwind – downwind measurement of suspended particulate concentrations (size distribution and PM10 levels). A number of sediment traps to collect saltating particles, as well as soil moisture and temperature sensors, were deployed. Top soil and saltating sediments were chemically analyzed, and granulometry was determined.

The crustal material in the PM10 fraction is elevated, 16.5, 12.5 and 9 μg m^{-3} at the U, R1 and R2 sites, respectively, which account for 54, 68 and 48% of the PM10 concentrations. Working days show a mean increase of the crustal material of 7 and 3.5 μg m^{-3} with respect to Sundays at R1 and R2, while days with African dust outbreaks increase that concentration by 9 μg m^{-3}. Daily PM10 concentrations, however, decrease with increasing wind speed at the typical situations of low to moderate winds. This holds also for the crustal component and any of the chemical elements in that fraction. Size-resolved measurements recorded with higher temporal resolution show, in turn, a net increase in the concentration of large particulates with higher wind speeds, while the smallest particles are dispersed by the wind action. Human activity in the surroundings may maintain moderate levels of particles lying in a broad intermediate size-range. These are dispersed with light winds although stronger winds increase their concentration due to resuspension.

The threshold wind speed from which particle concentration increases is higher for smaller particles. Results show that resuspension of the largest particles occurs just from very small wind speeds, convection being the facilitating mechanism.

The strong wind erosion episodes leading to dust storms in El Hondo Nature Park were associated to the passage of Atlantic frontal systems with no rainfall. Levanter (an easterly wind) promoted some moderate particle entrainment episodes. Winds larger than 9 m s^{-1} (at 2 m above the ground) and average friction velocity of 0.46 m s^{-1} triggered the erosion events. Such conditions were found in more than 40 occasions, but soil conditions limited deflation in some 80% of these situations by the existence of a large water sheet and near-surface water table, residual surface moisture or saline crusts.

As soil was getting drier, the concentrations of Na and Cl at the surface strongly increased and white saline crusts formed. The removal of the evaporite-rich top soil under erosion events led to a significant decrease in Na; correspondingly, both the saltating and the suspended particles were enriched in this element.

A clear indication of intense wind erosion is given by the concentration of suspended particles larger than 15 μm and by the relative abundance of sodium in the PM10 fraction. Streamwise fluxes of saltating particles in the range 0.5 to 85.5 kg through 1 m of field width and 0.35 m height have been registered in a single event. Suspended particulates, in turn, were lifted up to tens of meters while the dust plumes displaced over the eroding area, and the impact on a coastal village some 10 km downwind was registered.

We acknowledge financial support from the Spanish Ministry of Science and Innovation (RESUSPENSE project CGL2004-04419; EroHondo project CGL2008-05160) and from the Regional Government of Valencia (ACOMP2009/041; ACOMP/2011/088).

Long-term observations of mineral dust deposition to the Northeast Atlantic Ocean and hygroscopic properties at the Cape Verde Islands.

N. Niedermeier[1], T. Müller[1], A. Held[2], K. Kandler[3], and A. Wiedensohler[1]

[1]Leibniz Institute for Tropospheric Research, Leipzig, Germany
[2] Bayreuth Center of Ecology and Environmental Research, University of Bayreuth, Bayreuth, Germany
[3]Institute of Applied Geosciences, Technische Universität Darmstadt, Germany
Keywords: Mineral Dust, Mixing State, Dry Deposition, Hygroscopicity.
Presenting author email: nicole.niedermeier@tropos.de

Mineral dust is one of the most important aerosol types under investigation. Their impact on clouds (e.g. serving as ice nuclei) and radiation can differ depending on their chemical composition and aging state. Furthermore, the understanding of the global dust cycle is still incomplete (Mahowald et al., 2005). The removal of mineral dust is essential for bioactivity in the ocean, since dust serves as a source of nutrients (e.g. iron) for oceanic microorganisms such as phytoplankton. Long-term observations of Saharan dust layers spreading over the Northeast Atlantic Ocean do however not exist so far.

Within the project SOPRAN (Surface Ocean PRocesses in the ANthropocene), microphysical aerosol measurements at the Cape Verde Island Sao Vicente in the tropical North Atlantic Ocean are carried out since May 2007. Particle number size distributions (PNSD) using the combination of SMPS and APS and absorption measurements (MAAP) are available. Several intensive field experiments were performed to characterize optical and hygroscopic properties of mineral dust and sea salt particles. Together with micrometeorological measurements, dust mass deposition fluxes can be calculated. Since December 2011 mineral dust mass concentrations (Aethalometer) and high time resolved 3D wind velocities (sonic) are measured. Furthermore, number fractions (nf) and growth factors (GF) at a relative humidity of 90% of a mixture of mineral dust and sea salt at dry mobility diameters of 600, 800, 1000 and 1200 nm (H-DMA-APS, Leinert and Wiedensohler, 2008) are investigated.

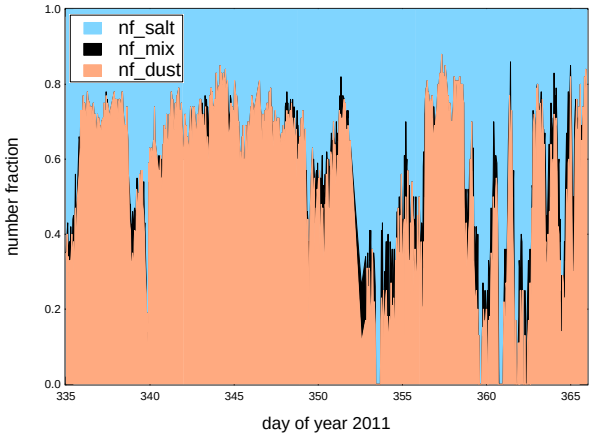

Figure 1: Number fractions of dust (brown), sea salt (blue) and a mixture of both (black) by hygroscopic growth measurements with an H-DMA-APS.

Hygroscopic growth measurements show an external mixing of dust and sea salt in most cases. However, in some cases, also an internal-external-mixture of both particle types is observed. This mixture was also detected by Kandler et al. (2012) at the same location by electron-microscopical single particle analysis of passive sedimentation samples. Figure 1 shows the number fractions of dust and sea salt at a dry mobility diameter of 800 nm for December 2011. Dust dominates the whole period with some exceptions having a mean value of 53%. In most cases nf_mix is lower than 10% and does not exceed 30%. Dust number size distributions and dust mass size distributions can be calculated from nf_dust at different diameters, the PNSD, and the particle density. Turbulence parameters obtained by the sonic measurements are used to calculate size-resolved particle deposition velocities. This data was combined to obtain the dust mass deposition fluxes (Held et al., 2006).

First calculations of the GF of mineral dust showed values below 1.1. This leads to the assumption that no or less aging occurs on mineral dust particles from the Saharan Desert to the Cape Verde Islands. Investigations of the GF of sea salt varied much more with values between 1.5 and 2.2. The highest values are consistent with that of pure sea salt. The lower values raise the question, whether organics and other insoluble material exist in internal mixture within the particles.

This work was supported by the Bundesministerium für Bildung und Forschung (BMBF) number **03F0611J**.

Held, A., et al. (2006), Field measurements and size-resolved model simulations of turbulent particle transport to a forest canopy, Journal of Aerosol Science, 37(6), 786-798.

Kandler et al. (2012): Aerosol deposition in the main African dust transport region: establishing a long-term time series at Sao Vicente, Cape Verde. *This conference*.

Leinert, S. and Wiedensohler, A. (2008), A DMA and APS based technique for measuring aerodynamic hygroscopic growth factors of micrometer-size aerosol particles, Journal of Aerosol Science, 39(5), 393-402.

Mahowald, N. M., et al. (2005), Atmospheric global dust cycle and iron inputs to the ocean, Global Biogeochemical Cycles, 19(4), doi:10.1029/2004GB002402.

Elemental Composition of Air Particulate Matter in Cape Verde

M. Almeida-Silva[1], S. M. Almeida[1], C.A. Pio[2], T. Nunes[2], J. Cardoso[2, 3]

[1]Technological and Nuclear Institute, URSN, E.N. 10, 2686-953 Sacavém, Portugal;
[2]Aveiro University, CESAM, P-3810193 Aveiro, Portugal;
[3]Cape Verde University, Campus do Palmarejo, Praia, Cape Verde
Keywords: Cape Verde, PM_{10}, chemical composition
Presenting author email: marinadealmeidasilva@itn.pt

Sahara desert is the most important source of mineral dust, contributing as much as 1900 million tons per year. Due to its localization, Cape Verde is ideal to quantify and to characterize the dust transported from Sahara desert. Cape Verde is an archipelago composed by 10 islands, localized in Atlantic Ocean, near African coast. Santiago's island is the biggest island of Cape Verde, with an area of 991 km^2 and it was the selected island to perform this study (Fig. 1), which was done within the project *Atmospheric aerosol in Cape Verde region: seasonal evaluation of composition, sources and transport* (*CV-Dust*) - that aims to assess the transport of dust from Sahara by using an integration of measuring and modelling tools.

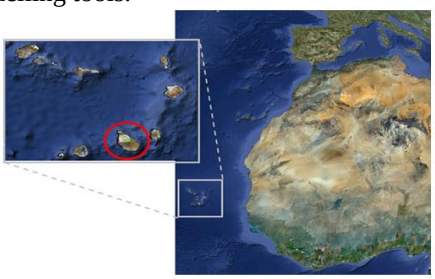

Figure 1 - Localization of the Cape Verde Islands

PM_{10} was collected in Praia city (14º94'N; 23º49'W) with a Tecora® sampler in order to characterize the chemical composition. The collected filters were weighted by gravimetry using a Mettler® Toledo balance with 0.1 µg readability, placed in a controlled clean room (class 10,000). All samples were irradiated at the Portuguese Research Reactor (RPI-ITN; nominal power: 1MW) during 5 h, and measured for 5-7 h after 2-5 days and 4 weeks of decay, in high-purity and high-resolution germanium detectors. A comparator – Al-0.1% Au alloy disk – was also irradiated and measured for application of the k_0-INAA methodology.

Fig. 2 shows the average element mass concentration in PM_{10}. The elements As, Sm, Co, Fe, Sc, K, Cr, Ce and Ba presented a similar behaviour throughout the sampling period, indicating a common source. Fig. 3 presents the relation between all the measured elements with Fe. Ratios for soil composition are presented and confirm a soil origin for these elements. Two periods with higher concentrations were achieved. Hysplit model indicated that these periods were associated with Sahara dust events. All these elements presented significantly higher concentrations in Cape Verde comparing with other studies performed in Lisbon by our research groups. The elements Na, Sb and Zn presented a different behaviour indicating the existence of other emissions sources, probably the sea salt for Na and anthropogenic emissions for Sb and Zn.

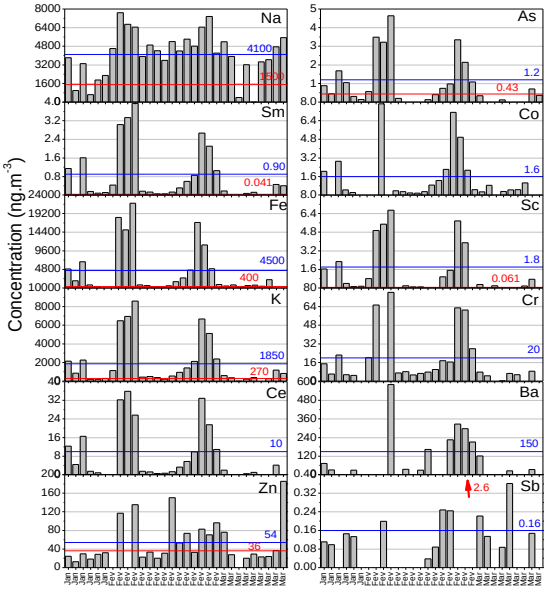

Figure 2 - Element mass concentration in PM_{10} sampled (average from CV-Dust and average from Lisbon)

The CV-Dust project is on-going which means that the results are being updated constantly.

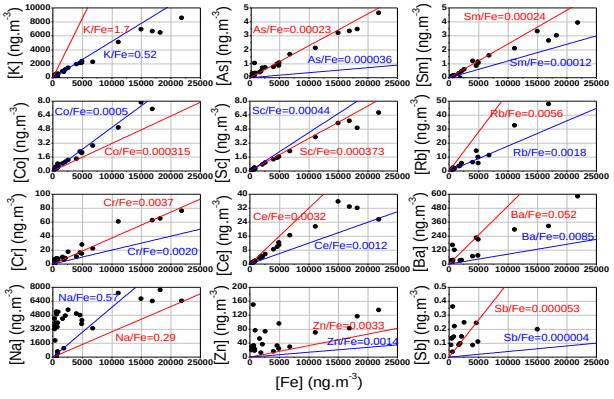

Figure 3 - Relation between composition of these particles and different types of soil (soil Mason composition[1] and Sahara desert soil[2])

We gratefully acknowledge FCT for funding the project PTDC/AAC-CLI/100331/2008 - Atmospheric aerosol in Cape Verde region: seasonal evaluation of composition, sources and transport (CV-Dust).

[1] B. Mason, C.B. Moore (1982). Principles of Geochemistry. Wiley, New York, pp. 46.
[2] N. Reguigui, J. Kucera and H. Ben Kraiem (2002) Determination of trace elements in Tunisian soil, desert and beach sand using Instrumental Neutron Activation Analysis, Proceedings of International Symposium on Environmental Pollution Control and Waste Management, 7-10 January 2002, Tunis (EPCOWM'2002), p.70-82.

Optical behaviour of mineralogical composition. A laboratory study

T. Ajtai, Á. Filep, N. Utry, M. Pintér, Z. Bozóki, G. Szabó
Department of Optics and Quantum Electronics, University of Szeged, Hungary

Keywords: minerals, photoacoustic, optical absorption, Ångström exponent.
ajtai@titan.physx.u-szeged.hu

One of the major contributions in uncertainties on climate forcing is associated to aerosol. These uncertainties are mostly governed by absorbing particles. Aerosol light absorption in the solar spectral region is dominated by the inorganic (BC) and organic carbon (BrC) particles emitted by anthropogenic and natural combustion process as well as mineral dust (MD) aerosol. Although the mass absorption efficiency of MD is much smaller than that of BC, it significantly influences the climate due to its remarkable global emission rate. MD aerosol is a complicated mixture of various minerals having versatile spectral behaviour. Absorption feature of dust strongly depends not only on relative abundance of its composition but also on details of how the minerals are mixed, as well as chemical and physical transformation during its transport in the atmosphere. The common approach used in model calculation on segregated MD radiative forcing relies on optical constant determined from bulk samples collected at specific geographical location (Sokolik and Toon 1999). This approach has serious limitations: (i) poor data quality, mainly due to the limitation of applied method and instrumentation, (ii) sample artefact, so the sample experienced specific atmospheric conditions and transformations during its transport from the source to the sampling site, therefore the deduced optical constant is not adequate for modelling time- and space varying optical properties, (iii) nonlinearity of optical properties on refractive indices, so optical constant determined from bulk including mixture of minerals is not adequate for modelling specific mineral optical behaviour. Finally, the reliability of optical coefficient of particles deduced from bulk material is also questionable. Therefore the measurement of optical behaviour of single composite, especially its absorption, of MD is one of the major concerns in modelling the net radiative forcing by dust.

In this work we present first, in-situ measurement of minerals aerosols such as illite, kaolinite, quartz, limestone, rutile, bentonite and hematite in the solar spectral region. Optical absorption coefficient of minerals was measured by our novel photoacoustic instrument (4λ-PAS) operating at four discrete wavelengths in the UV, VIS, near IR spectral region. The instrument applies wavelength independent calibration and provides a unique possibility for in-situ characterization of absorption behaviour of aerosol with high reliability (Ajtai et al, 2010). Other microphysical parameters of minerals, which affect the optical absorption coefficient such as size distribution and shape, were also measured parallel. Measured absorption spectra were compared with absorption spectra modelled with Mie-theory and T-matrix method to decide whether the absorption coefficient deduced theoretically from bulk can be transferred to airborne mineral particles or not (Fig. 1).

We demonstrated measurement data of optical absorption, mass specific optical absorption and wavelength dependent absorption Ångström exponent of the measured minerals. We also demonstrated experimentally that the absorption feature of minerals is source specific parameter. Finally, we demonstrated that the selectivity of composition identification is continuously increasing towards the shorter wavelengths.

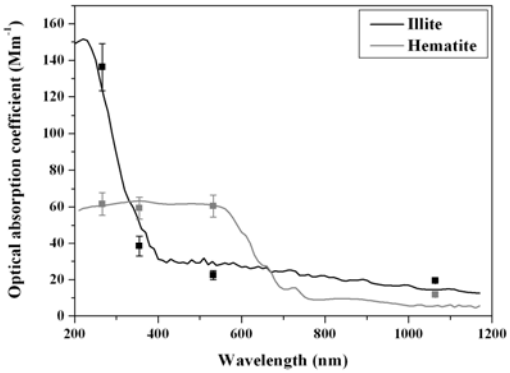

Figure 1: Optical absorption coefficient measured by the 4λ-PAS (symbols) and calculated with the Mie-theory (lines) of illite (labelled with black) and hematite (labelled with grey)

This work was supported by the Hungarian National Development Agency (JEDLIK_AEROS_EU) and OTKA foundation from the Hungarian Scientific Research Fund (project numbers: CNK 78549 and K 101905).

Sokolik, I.N. and Toon, O.B. (1999). Incorporation of mineralogical composition into models of the radiative properties of mineral aerosol from UV to IR wavelengths, Journal of Geophysical Research, 104, 9423-9444.

Ajtai, T., Filep, Á., Schnaiter, M., Linke, C., Vragel, M., Bozóki, Z., Szabó, G. and Leisner, T., 2010. A novel multi-wavelength photoacoustic spectrometer for the measurement of the UV-vis_NIR spectral absorption coefficient of atmospheric aerosols. Journal of Aerosol Science, 41, 1020-1029.

The Amsterdam-Granada Light Scattering Database

O. Muñoz[1], F. Moreno[1], D. Guirado[2], D.D. Dabrowska[1], H. Volten[3], J.W. Hovenier[4].

[1] Instituto de Astrofísica de Andalucía, CSIC. Granada, 18008, Spain.
[2]Netherlands Institute for Space Research, SRON, 3584 CA Utrecht, The Netherlands.
[3] Netherlands National Institute for Public Health and the Environment (RIVM), Centre for Environmental Monitoring, 3720 BA, Bilthoven, The Netherlands.
[4] Astronomical Institute "Anton Pannekoek", University of Amsterdam. 1098 XH, Amsterdam, The Netherlands.
Keywords: Light scattering matrix, Polarization, Mineral dust, Laboratory experiments.
Presenting author email: olga@iaa.es

In the last few decades, the Amsterdam light scattering setup (Hovenier 2000) fulfilled a unique position in producing a significant amount of experimental scattering matrices as functions of the scattering angle of samples of small irregular particles relevant for astronomy, and studies of the atmosphere, as well as coastal and inland waters of the Earth (see e.g. Volten et al. 1998, 2001; Muñoz et al. 2001, 2004). The measurements of aerosols were performed at two different wavelengths (441.6 and 632.8 nm) in the scattering angle range from 3-5 degrees (depending on the sample) to 174 degrees. The hydrosol measurements were done at 632.8 nm in the scattering angle range from 20 to 160 degrees. These experimental data are a powerful tool for properly interpreting space- and ground-based observations or for testing different computational approaches devoted to obtain the scattering behavior of small irregular particles (see e.g. Nousiainen 2009 and references therein). In addition, the light scattering results may also be applicable in the paper and paint industry, or in the fields of chemistry and biology.

Since September 2003, the Dutch experimental data are freely available in digital form in the Amsterdam Light Scattering Database (Volten et al. 2006). Many different research groups around the world made use of the experimental data (see e.g. Bi et al. 2010, Valenzuela et al. 2012). After the closing down of the Dutch scattering apparatus in 2007, a modernized and improved descendant, the IAA Cosmic Dust Laboratory (CoDuLab), has been constructed at the Instituto de Astrofísica de Andalucía (IAA) in Granada, Spain (Muñoz et al. 2010). In the new apparatus the scattering angle range at which the measurements are performed is 3-177 degrees. The measurements can be performed at five different wavelengths namely, 483, 488, 520, 568, and 647 nm. The first results of this instrument for water droplets and for a sample of green clay particles, that had also been studied in Amsterdam, demonstrate the excellent performance of the Granadian instrument (Muñoz et al. 2011). We proceed to make these and future data also available for the community in tabular form by constructing a new light scattering database, the Amsterdam-Granada Light Scattering Database available at the website (www.iaa.es/scattering). The particle samples included in the database comprise a wide range in origin and composition, and have relevance for different subjects. The typical diameters (or volume-equivalent diameters) of the particles measured with the experimental setups in Amsterdam and Granada range from sub-micron to about 200 micron. By combining the data from the two instruments in this database we ensure the continued availability of the Amsterdam data, and we prevent fragmentation of important data over different databases.

The purpose of this work is to introduce the new Amsterdam-Granada Light Scattering Database giving examples of applications of database data.

Hovenier, J. W. (2000) Measuring scattering matrices of small particles at optical wavelengths. In: Light scattering by nonspherical particles, ed. M.I. Mishchenko, J.W. Hovenier, L.D. Travis. Academic San Diego, CA, (2000): 355-365.

Volten, H., de Haan, J.F., Hovenier, J.W., Schreurs, R., Vassen, W., Dekker, A.G., Hoogenboom, H.J., Charlton, F., Wouts, R. (1998) *Limnol. and Oceanog.* **43**:1180-1197.

Volten, H., Muñoz, O., Rol, E., de Haan, J.F., Vassen, V., Hovenier, J.W., Muinonen, K., Nousianen, T. (2001) *J. Geophys. Res*. **106,** 17375-17401.

Muñoz, O., Volten, H., De Haan, J.F., Vassen, V., Hovenier, J.W. (2001) *J. Geophys. Res.* **106,** 22833-22844.

Muñoz, O., Volten, H., Hovenier, Veihelmann, B., van der Zande, W.J., Waters, L.B.FM., Rose W.I. J.W. (2004) *J. Geophys. Res*. **109,** D16201.

Nousiainen, T. (2009) *J. Quant. Spec. Radiat. Transfer* **110**, 1261- 1279.

Bi, L, Yang, P., Kattawar, G.W., Kahn, R. (2010) *Appl. Opt.* **49(3)**, 334–41.

Valenzuela, A., Olmo, F.J., Lyamani, H., Antón, M., Quirantes, A., Alados-Arboledas, L. (2012) *Atmosph. Res*. **104-105,** 292-301.

Volten, H. Muñoz, O., Hovenier, J.W., Waters, L.B.F.M. (2006) *J. Quant. Spec. Radiat. Transfer* **100**, 437-443.

Muñoz, O., Moreno, F., Guirado, D., Ramos, J.L., López, A., Girela, F., Jerónimo, J.M., Costill, L.P., Bustamante, I. (2010) *J. Quant. Spec. Radiat. Transfer* **11**, 187-196.

Monday, September 3, 2012

Session WG03S2O. Chemistry of Organic Aerosol: Laboratory Study (II)

Primary and Secondary Organic Aerosol from Road Vehicles

S. Platt[1], I. El Haddad[1], A.A. Zardini[2], M. Clairotte[2], C. Astorga[2], R. Wolf[1], J. G. Slowik[1], B. Temime-roussel[3], N. Marchand[3], I. Jezek[4], L. Drinovec[4], G. Mocnik[4], O. Möhler[5], U. Baltensperger[1] and A.S.H. Prévôt[1]

[1]Laboratory of Atmospheric Chemistry, Paul Scherrer Institut (PSI), Villigen, CH-5232, Switzerland
[2]Institute for Energy and transport, Sustainable Transport Unit, EC Joint Research Centre, 21027 Ispra, Italy
[3]Laboratoire Chimie Environment, Aix Marseille Université, Marseille, 13 331, France
[4]Aerosol d.o.o., SI-1000 Ljubljana, Slovenia
[5]Institute for Meteorology and Climate research, Karlsruhe Institute of Technology, 76021 Karlsruhe, Germany
Keywords: SOA, Vehicle emissions, Smog chamber, AMS
Presenting author email: stephen.platt@psi.ch

Vehicles are a major source of particulate matter (PM) in urban areas. A large fraction of ambient PM consists of organic aerosol (OA), either primary (POA), from direct emissions, or secondary (SOA), formed via gas-phase reactions. Therefore any attempt to mitigate the effect of on-road vehicle emissions on public health and the environment should consider not only primary aerosol emissions but also secondary aerosol production potential (SAPP). However, only the primary aerosol from on-road vehicles is currently subject to direct legislation.

SOA formation from diesel exhaust has been reported, (e.g. Robinson *et al.*, 2007), but SOA formation from other common vehicles including gasoline vehicles has not. The effect of different conditions, such as fuel type, engine technology and ambient temperature on SOA formation remains unknown.

Here we determine emission factors (EFs) (g kg^{-1} fuel) for primary PM and for SOA, from two- and four-stroke scooters, a gasoline car and a truck, all complying with the latest European emissions standards. We also quantified the effect of using alkylated gasoline in scooters, liquid petroleum gas (dual fuel) in trucks and the effect of ambient temperature on SOA formation from gasoline cars and from trucks.

Vehicle exhaust was introduced into the new PSI mobile smog chamber during regulatory driving cycles on chassis dynamometers at the European Joint Research Centre Ispra, Italy. A high-resolution time-of-flight aerosol mass spectrometer (HR-ToF-AMS) equipped with a $PM_{2.5}$ lens was used to quantify OA. Black carbon (BC) was measured using a multi angle absorption photometer (MAAP) and an Aethalometer (AE 33 prototype). A high resolution proton transfer time-of-flight mass spectrometer (PTR-ToF) was used to investigate volatile organic compounds and a suite of instruments was used to quantify CO, CO_2, CH_4, total hydrocarbon and other gases. EFs were calculated with a carbon mass balance applied to smog chamber data.

All gasoline vehicles showed significant SAPP. SOA/POA ratios were up to 27.1 for the gasoline car (Figure 1) vs. 1.4 from the truck. Average PM EFs, with the inclusion of SOA and BC, were higher from the gasoline car than from the diesel truck: 0.21 vs. 0.10 g kg^{-1} fuel, respectively. This large SOA formation is likely a consequence of higher gaseous hydrocarbon emissions from the gasoline car: 1.01 vs. 0.16 g kg^{-1} fuel for the truck.

OH exposure in smog chambers can be calculated from the decay rate of nine times deuterated butanol spiked into the chamber (Barmet *et al.*, 2011). Using this technique we show that SOA formation from gasoline exhaust would occur within 12-14 hours in the real atmosphere (colourscale, Figure 1).

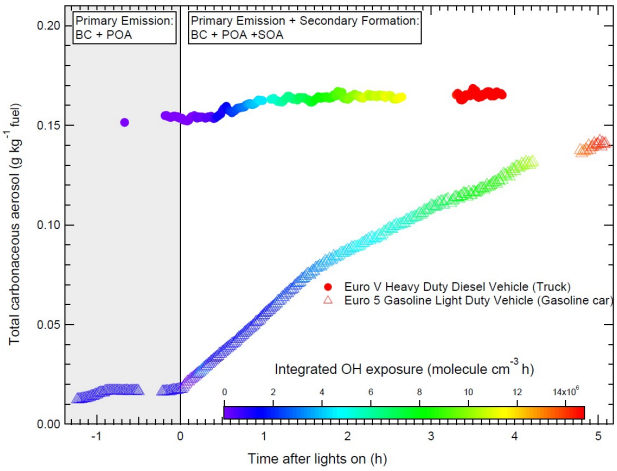

Figure 1: Carbonaceous aerosol and secondary aerosol formation emission factors from a gasoline car and a diesel truck vs. time in the PSI mobile smog chamber.

We demonstrate that aerosol emissions from gasoline vehicles can be significantly enhanced due to SOA formation and may match or even exceed those of diesel vehicles. This large SOA formation has substantial implications for emission controls which currently do not consider SAPP.

This work is supported by the Swiss Federal Office for the Environment (FOEN), the Federal Roads Office (FEDRO) and the the French environmental agency (ADEME); partly financed by the EU European Social Fund and EUROSTARS project E!4825 "FCAeth".

A. L. Robinson *et al.* (2007) *Science* **315**, 1259

P. Barmet *et al.* (2011) *Atmos. Meas. Tech. Discuss* **4**, 7471-7498

A source of oxygenated organic aerosol and oligomers from primary emitted gases

John Liggio[1], Shao-Meng Li[1] and Alexander Vlasenko[1]

[1]Atmospheric Science and Technology Directorate, Science and Technology Branch, Environment Canada, 4905 Dufferin Street, Toronto, Ontario M3H 5T4 Canada
Presenting author email: john.liggio@ec.gc.ca

It is well recognized that particulate organic matter (OM) often constitutes the largest fraction of the total particulate matter (PM) burden globally, and is an important factor with respect to climate change, and air quality issues. Despite its importance, the sources and formation mechanisms of OM remain poorly understood, due in part to the varied sources and complex mechanisms involved. Although SOA may comprise the largest OM fraction, a complete understanding of its formation mechanisms remains elusive, highlighted by the fact that traditional mechanisms involving the oxidation of precursors (via OH, O_3 and NO_3) are often unable to account for SOA observations. Recent evidence suggests that oligomer and high molecular weight (MW) species formed as a result of particle phase and heterogeneous chemistry mechanisms may also play an important role in SOA formation and potentially explain such discrepancies.

Although the relative importance of high MW compounds (via liquid phase reactions) and condensable species (via gas-particle partitioning) to the total SOA is not clear, both pathways are considered a result of the oxidation of biogenic or anthropogenic precursors on the time scale of hours in the atmosphere. As such, the degree of oxygenation in measured OM has been used as a metric to infer source types (POA vs SOA). Consequently, high OM oxygenation as represented by the atomic O:C ratio has been linked to varying degrees of aerosol aging and SOA formation, while conversely, POA is associated with a very low O:C.

In contrast, recent studies have suggested that the uptake of primary vehicle exhaust gases to pre-existing particles [Li et al., 2011] on very short timescales have the potential to increase OM mass in urban or suburban areas. In principle, this can lead to changes in the degree of aerosol oxygenation through the uptake of primary polar species to inorganic aerosol, or through subsequent particle phase reactions. From the standpoint of health impacts and atmospheric modeling, such a process occurring on a short time and spatial scale could lead to oxygenated OM and oligomers which will be indistinguishable from POA mass, and implies that POA in urban areas may be more oxygenated than previously considered.

In the present study the potential for primary hydrocarbon-like gases to partition and react on short timescales with inorganic seed particles is investigated by exposing urban ambient air influenced by vehicle emissions, to laboratory generated sulfuric acid particles and gas-phase ammonia in a smog chamber. The results demonstrate that the mixture and concentration of organic species in the ambient air is sufficient for a large organic uptake to particles to occur in less than 2 minutes. The resultant particulate organic mass spectra from the experiments were highly correlated to those of previous experiments exposing gasoline engine exhaust to neutral particles [Li et al., 2011], and concurrent with measured decreases in unsaturated hydrocarbons from the gas-phase. The initially added organics were considerably more oxygenated than that previously reported for primary organic aerosol, while the presence of numerous m/z fragments greater than 300 amu suggested that oligomer formation also occurred. Oligomerization was enhanced at high acidity but otherwise unaffected by subsequent particle neutralization. These results potentially represent a new source of oxygenated POA and high molecular weight species to the atmosphere, which may be similar or larger than the average POA (represented by HOA) measured in numerous regions worldwide. The results also suggest that a fraction of measured oxygenated OA, which correlate with secondary sulphate, may be of a primary source, formed prior to any gas-phase oxidation.

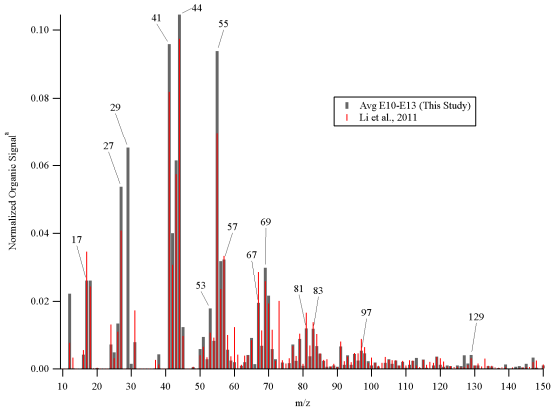

Figure 1. Average organic mass spectra in the first 3 minutes of experiments with the highest $(NH_3/SO_4)_i$ and that of Li et al, 2011.

Li, S.-M., Liggio, J., Graham, L., Lu, G., Brook, J., Stroud, C., et al. (2011). *Atmos. Chem. Phys., 11*(1), 3461-3492.

Uptake of glyoxal by organic and inorganic seed aerosols: Optical, physical and chemical properties of the product aerosols

M. Trainic,[1] A. A. Riziq,[1] A. Lavi,[1] J. M. Flores,[2,3] and Y. Rudich[1]

[1] Department of Environmental Sciences, Weizmann Institute, Rehovot 76100, Israel.
[2] Department of Particle Chemistry, Max Planck Institute for Chemistry, Mainz 55128, Germany
[3] University of Mainz, Institute for Atmospheric Physics, Mainz 55099, Germany
Keywords: Aerosol optical properties, aerosol coating, heterogeneous reactions, chemical properties
Presenting author email: miri.trainic@weizmann.ac.il

Constraining the optical properties of secondary organic aerosol (SOA) is a major challenge since they often consist of a mixture of several components with various internal structures, including homogeneous mixtures and core/shell structures. The importance in understanding the optical properties of aerosols is their effect on the magnitude and uncertainty of Earth's total radiative forcing and climate change. SOA form by the condensation of less-volatile gaseous compounds onto pre-existing aerosols, and by heterogeneous and multi-phase reactions.

The heterogeneous reaction between glyoxal gas and three atmospheric aerosol types; ammonium sulfate (AS), glycine and glycine-AS 1:100 was studied. The optical extinction cross section at λ=355nm and mobility size increased following the reaction under a broad range of RH values (30-90%), indicating that the reaction is relevant for a wide range of atmospheric conditions.

We propose that at low RH values, below the deliquescence point, the recations occur in interfacial monolayers of water, supporting previous findings about the importance of interfacial water in heterogeneous reactions.

The reactions exhibit a trend of increasing growth in physical and optical cross sections with decreasing seed aerosol size, as well as a clear dependence on ambient RH values (Figure 1). For small particles with near-zero extinction efficiency (Q_{ext}) values, the reaction induces the greatest increase in optical extinction cross section (up to 2 orders of magnitude enhancement) due to a combined effect of changes in optical properties and in size, resulting in a change in the location on the Mie curve.

AMS analyses of the reactions show that the main reaction products are glyoxal oligomers, and a small contribution from the formation of various C-N compounds, identified as imidazoles.

Our results suggest that unlike previously postulated, the reactions at RH values below deliquescence occur on interfacial water layers and their optical enhancement is mainly due to enhanced scattering and geometric cross section growth.

This study contributes to the understanding of the effect of the reactions on the optical properties of the aerosols in the atmosphere by demonstrating that the heterogeneous reactions between abundant atmospheric components may alter the aerosols' optical, physical and chemical properties on short timescales (~ 1 hour) and may have substantial implications on the radiative effects of these aerosols (Trainic et al. 2011; Trainic et al. 2012).

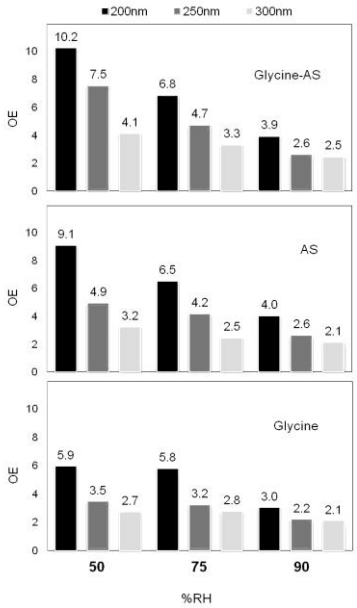

Figure 1: The optical enhancement (OE) of the extinction cross section due to reaction of glyoxal with pure glycine (bottom), AS (middle), and glycine-AS (top) at RH values of 50%, 75%, and 90% for initial sizes of 200nm (black columns), 250 nm (grey columns), and 300nm (light grey columns).

This work was supported by the Israel Science Foundation, FP7-ENV-2010-265148- PEGASOS, and the Helen and Martin Kimmel Award for Innovative Investigation.

References

Trainic, M., A. A. Riziq, et al. (2011). *Atmos. Chem. Phys.* **11**(18): 9697–9707.

Trainic, M., A. A. Riziq, et al. (2012). *J. Phys. Chem. A* **in press**: doi: 10.1021/jp2104837.

Secondary organic aerosol formation from glyoxal

J.G. Slowik[1], E.M. Waxman[2], C.J. Kampf[3], J. Timkovsky[4], B. Nozière[5], A.P. Praplan[1], L.Pfaffenberger[1], T. Hoffmann[3], T. Kuipers[4], R. Holzinger[4], J. Dommen[1], A.S.H. Prévôt[1], U. Baltensperger[1], and R. Volkamer[2,6]

[1]Laboratory of Atmospheric Chemistry, Paul Scherrer Institut, Villigen PSI, Switzerland
[2]Department of Chemistry and Biochemistry, University of Colorado, Boulder, CO, USA
[3]Inorganic and Analytical Chemistry, Johannes Gutenburg-Universität Mainz, Mainz, Germany
[4]Institute for Marine and Atmospheric Research Utrecht, Utrecht University, Utrecht, Netherlands
[5]IRCELYON, University of Lyon, Lyon, France
[6]Cooperative Institute for Research in Environmental Sciences, University of Colorado, Boulder, CO, USA
Keywords: secondary organic aerosol, glyoxal, aerosol mass spectrometry.
Presenting author email: jay.slowik@psi.ch

Conventional models for secondary organic aerosol (SOA) formation focus on the condensation of low-volatility products from gas-phase reactions. However, such models neglect aqueous-phase processing mechanisms, thereby excluding potentially important SOA formation pathways. These missing pathways may be an important factor in the inability of current models to fully explain SOA yields and oxidation states.

Glyoxal is an oxidation product of numerous organic gases and has recently been identified as an important SOA precursor (e.g. Ervens and Volkamer, 2010). Unlike traditional precursors, glyoxal partitions to the particle aqueous phase. Subsequent reactions can lead to low-volatility products that remain in the particle phase. Glyoxal partitioning and SOA formation have been observed to depend on numerous parameters, specifically aerosol water content, seed particle composition, and light exposure, which are explored in the present study.

Glyoxal SOA formation experiments were conducted in the PSI smog chamber. The chamber was filled by a mixture of seed particles (ammonium sulphate or internally-mixed ammonium sulphate/fulvic acid) with gas-phase HONO and acetylene (a glyoxal precursor) at controlled relative humidity (50 to 85%). Photochemistry was initiated by brief (i.e. a few minutes) exposure to UV light. Glyoxal was produced by the reaction of acetylene with OH radicals during brief (i.e. a few minutes) exposures to UV light. The reaction was then allowed to proceed undisturbed for several hours (under light or dark conditions), prior to another UV exposure. After several of these cycles, a dilution phase was initiated to investigate the reversibility of the produced SOA.

Gas-phase glyoxal was measured by a LED-CE-DOAS (Thalman and Volkamer, 2010), while additional gas-phase species were measured by ToF-PTR-MS. Aerosol composition was measured by an HR-ToF-AMS, thermal desorption PTR-MS, and offline filter measurements. Supporting measurements included gas-phase species (e.g. total hydrocarbons, CO, O_3, NO, NO_x), and particle number and size distributions.

The AMS organic mass spectral time series was analyzed by positive matrix factorization (PMF) to yield factors relating to reaction progress, including fulvic acid ("FA"), glyoxal ("GLY"), and glyoxal SOA ("GSOA"). Figure 1 shows a sample experiment, conducted at ~85% RH on a mixed ammonium sulphate/fulvic acid seed. All time series are normalized to SO_4 to correct for wall losses. Normalized GLY and GSOA both increase with each UV exposure. However, during the dilution phase there is a clear decrease in GLY while GSOA remains constant. This indicates that while GLY uptake is reversible, GSOA formation is irreversible. The GSOA factor mass spectrum has a strong contribution from mass fragments characteristic of imidazoles, which form irreversibly from reaction of hydrated glyoxal with several nitrogen-containing compounds (Ervens and Volkamer, 2010).

We will discuss glyoxal SOA yields and product distributions in terms of RH, seed composition, and visible light exposure. The effects of these parameters on glyoxal partitioning according to Henry's Law will also be explored.

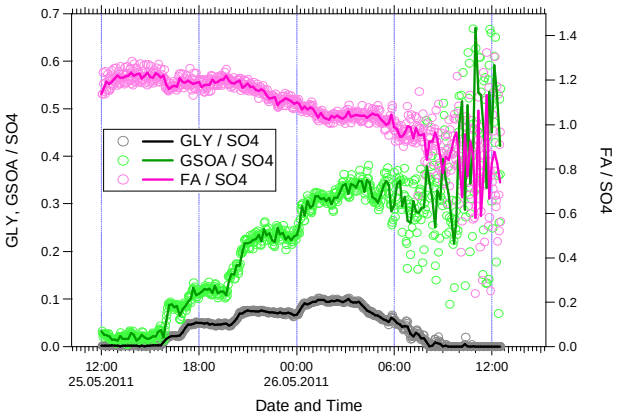

Figure 1. Sample time series of AMS PMF factors for glyoxal, glyoxal SOA, and fulvic acid, all normalized to particulate sulphate to account for wall losses.

Ervens, B., and Volkamer, R. (2010) *Atmos. Chem. Phys.* **10**, 8219-8244.

Thalman, R. and Volkamer, R. (2010) *Atmos. Meas. Tech.* **3**, 2681-2721.

Evolution of SOA chemical composition during ageing : impact of irradiation, cloud processing and presence of pre-existing seeds

N. Maurin[1], E.Perraudin[1,2], J. F. Doussin[1], P. Pardon[2], H. Budzinski[2]

[1]LISA, Universités Paris-Est-Créteil et Paris Diderot, CNRS UMR 7583, F-94010, Créteil, France
[2]EPOC, University of Bordeaux, CNRS UMR 5805, F-33400 Talence, France
Keywords: SOA (secondary organic aerosol), aerosol chemistry, chemical composition, chemical analysis
Presenting author email: e.perraudin@epoc.u-bordeaux1.fr

The investigation of atmospheric aerosol chemical composition and its evolution during ageing is necessary to document particle impact on climate and health. Chemical composition of secondary organic aerosol (SOA) is particularly complex. Hence, its chemical properties are often addressed using macroscopic parameters such as volatility, hygroscopicity or oxidation state. However, to investigate mechanisms occurring during ageing or to identify markers for specific processes, SOA chemical composition has to be elucidated at a molecular level. Most previous studies, which present SOA composition at a molecular level, were based on simulation chamber experiments and provided a "fixed" picture of SOA. Only very few of them have reported on the molecular composition evolution during aerosol ageing (Alfarra *et al*, 2012; Claeys *et al*, 2012).

In this context, the molecular composition of SOA formed from α-pinene ozonolysis (selected here as reference reaction system) and its evolution with time was investigated. Experiments were performed in CESAM facility, which allows not only to work in realistic and controlled conditions, but also to study aerosol ageing (Wang *et al*, 2011). Indeed, aerosol lifetime in CESAM ranges from 10 h to 4 days depending on particle size distribution. Moreover, CESAM is equipped with three high pressure xenon arc lamps which provide a very realistic artificial solar irradiation. Finally, being evacuable, it is possible to generate clouds by fast expansion in this chamber.

In the present work, SOA ageing was studied under four experimental conditions: (1) excess of ozone, (2) excess of ozone + irradiation, (3) excess of ozone + cloud generation and (4) excess of ozone + pre-existing seeds (acidified ammonium sulfate), and for 2 initial α-pinene concentrations (50 ppb and 200ppb). Experiments lasted for up to 20 hours. Gaseous phase composition was monitored using Fourier Transform InfraRed spectrometry. Ozone was measured using a commercial monitor instrument. Particle size distributions (20 - 980 nm in diameter) were measured with a scanning mobility particle sizer coupled to a condensation particle counter. Once generated in the chamber, SOA was sampled using glass fibre filters. An active charcoal denuder was used to trap reactive gases and reduce positive sampling artefacts. Filters were then stored in glass jars at -18°C.

Aerosol analyses were performed using two complementary techniques. Supercritical Fluid Extraction coupled to Gas Chromatography and Mass spectrometry (SFE-GC-MS) with in situ derivatisation using BSTFA allowed to identify and quantify oxidised products such as aldehydes, ketones, carboxylic acids and di- or tri-functional species. Liquid Chromatography coupled to triple quadrupole Mass Spectrometry (LC-MS) with a preliminary extraction step in methanol using Pressurised Fluid Extraction was chosen to investigate more specifically the presence of dimers and of organo-sulfates.

More than 25 compounds and, amongst them, four dimers, could be identified in the particulate phase and were quantified, either properly using corresponding standards or tentatively using surrogate standards. Mechanisms will be proposed to explain the formation of these compounds. The evolution of their concentrations along the different ageing experiments will also be presented. These results provide valuable information about mechanisms occurring within the aerosol during ageing processes and their potential atmospheric implications.

This work was supported by ADEME (French Agency for Environment and Energy Control) and by the EC within the I3 projects "Integrating of European Simulation Chambers for Investigating Atmospheric Processes" (EUROCHAMP, contract no. 505968).

Alfarra, R. M., Hamilton, J. F., Wyche, K. P., Good, N., Ward, M. W., Carr, T., Barley, M. H., Monks, P. S., Jenkin, M. E. and McFiggans, G. B. (2012) *Atmos. Chem. Phys. Discuss.* **12**, 2435-2482.

Yasmeen, F., Vermeylen, R., Maurin, N., Perraudin, E., Doussin, J. F. and Claeys, M. (2012) *Environ. Chem.*, submitted.

Wang, J., Doussin, J. F., Perrier, S., Perraudin, E., Katrib, Y., Pangui, E. and Picquet-Varrault, B. (2011) *Atmos. Meas. Tech.* **4**, 2465–2494.

Size dependence of growth rates: results of experiments in the CLOUD chamber

A. Franchin[1], S. Schobesberger[1], T. Nieminen[1] K. Lehtipalo[1], H.E. Manninen[1],
the CLOUD collaboration, T. Petäjä[1] and M. Kulmala[1]
[1]Department of Physics, University of Helsinki, P.O. Box 64, FI-00014, Helsinki, Finland
Keywords: growth , ions, sulfuric acid, organic compounds.
Presenting author email: alessandro.franchin@helsinki.fi

Secondary aerosol formation, via gas-to-particle conversion, happens extensively and frequently in the boundary layer of our planet (Kulmala et al., 2004); a portion of the nucleated particles manages to grow to Cloud Condensation Nuclei (CCN) size and therefore influences climate both directly, changing the way sunlight is scattered and absorbed by the atmosphere and indirectly, changing lifetime and optical properties of clouds. The number of nucleated particles that reaches big enough size to become a CCN is strongly dependent on the Growth Rates (GR), especially on the rate of growth of the particle when it is very small, at the early stage, right after the aerosol is created, when the probability of attaching to a pre-existing particle is higher. Sulfuric acid has been identified as a one of the key components for triggering nucleation (Weber et al., 1996) but it has been shown not to be enough to explain the growth of particles to CCN size. In fact most of the mass in ambient aerosol is found to consist of organic compounds (Tunved et al., 2006).

During the CLOUD (Cosmics Leaving OUtdoor Droplets) experiments, more than 500 nucleation bursts were produced in an aerosol chamber, at different conditions. The first results (Kirkby et al., 2011) were focusing on the charge enhancement of nucleation rates in pure sulfuric acid conditions; in this study we carried out the analysis of the GRs, for each of the nucleation experiments, and we retrieved information of size-dependent GR studied as function of sulfuric acid, ammonia, dimethyl amine and pinanediol concentration (e.g. Fig.1). The range of concentrations of trace gases used in the experiments was within the atmospheric variability. The main instrument used for retrieving the GRs was a Neutral cluster and Air Ion Spectrometer, (Kulmala et al., 2007), able to measure air ion number size distributions in the mobility equivalent diameter range of 0.8 to 42 nm and correspondingly neutral particle number size distributions from 2 to 42 nm mobility diameter; in this study we focused mainly on the ion mode. A comparison between GRs of neutral and of charged particles taken at same conditions will also be carried out to investigate a possible charge enhancement. Size dependent GRs can be also calculated in small sizes (1.0 - 2.5 nm) for electrically neutral and charged environment from a scanning Particle Size Magnifier, Airmodus A09 (PSM, Vanhainen et al., 2011) which can be then compared to the GRs retrieved with the NAIS.

A comparison among the size dependence of GRs at different condensible vapour concentrations and mixing ratios will give an interesting insight on the physics and chemistry of a growing freshly formed nano-particle in the CLOUD chamber under precisely controlled conditions, going from a pure sulfuric acid environment to an environment enriched with organic compounds, as well as with ammonia and nitrogen containing organics, such as amines.

We thank CERN for technical and financial resources. This research was funded by the EC 7th Framework Programme ("CLOUD-ITN" & "ATMNUCLE", grant nos. 215072 & 227463), the German Federal Ministry of Education and Research (no. 01LK0902A), the Swiss National Science Foundation (projects 206621_125025 & 206620_130527), the Academy of Finland Centre of Excellence program (project 1118615), the Austrian Science Fund (projects P19546 & L593), the Portuguese Foundation for Science and Technology (project CERN/FP/116387/2010), and the Russian Foundation for Basic Research (grant N08-02-91006-CERN).

Kirkby, J., et al. (2011). *Nature*, 476, 429–433.
Kulmala, M., et al. (2004). *J. Aerosol Sci.*, 35, 143–176.
Kulmala, M., et al. (2007). *Science*, 318: 89-92, 2007.
Merikanto, J., et al. (2009). *Atmos. Chem. Phys.*, 9, 8601–8616.
Tunved, J., et al. (2006). *Science*, 312, 261–263.
Weber, R. J., et al. (1996). *Chem. Eng. Commun.*, 151, 53–64.

Modelling study on the effect of salt formation on the atmospheric nanoparticle growth

T. Yli-Juuti[1], K. Barsanti[2], L. Hildebrandt Ruiz[3], A.-J. Kieloaho[1], T. Kurtén[4], U. Makkonen[5], T. Petäjä[1], M. Äijälä[1], M. Kulmala[1] and I. Riipinen[6]

[1]Department of Physics, University of Helsinki, Helsinki, 00014, Finland
[2]Department of Civil & Environmental Engineering, Portland State University, Portland, OR, 97201, USA
[3]Atmospheric Chemistry Division, National Center for Atmospheric Research, Boulder, CO, 80305, USA
[4]Department of Chemistry, University of Helsinki, Helsinki, 00014, Finland
[5]Finnish Meteorological Institute, Helsinki, 00101, Finland
[6]Department of Applied Environmental Science and Bert Bolin Center for Climate Research, Stockholm University, Stockholm, 10691, Sweden
Keywords: particle growth, atmospheric aerosols, organic aerosol, aerosol chemistry.
Presenting author email: taina.yli-juuti@helsinki.fi

Nucleation is a significant source of atmospheric aerosol particles. In order to have a climatic effect these nanoparticles need to grow several tens of nanometers in diameter and the growth needs to be fast enough to compete with the coagulational losses. While sulphuric acid is found to be the key compound in atmospheric nucleation, its contribution to nanoparticle growth is estimated to be small in many environments. The observations on atmospheric nanoparticle growth suggest that a large fraction of the growth is due to condensation of organic vapors, although the exact identification of these vapors is still unknown. To condense on atmospheric nanoparticles organic vapors must have very low-volatility (e.g., Pierce et al. 2011). While reversible condensation requires a very low saturation vapor pressure, particle phase processes like salt formation may enable also more volatile compounds to contribute to particle growth. In fact, evidence for the presence of organic salts in atmospheric nanoparticles has been observed by Smith et al. (2010).

We study the potential contribution of particle phase formation of organic and inorganic salts on particle growth rates. This is done by using a single particle condensation model for an atmospherically relevant system consisting of two acids (sulfuric acid and an organic acid) and two bases (ammonia and trimethylamine, TMA). The net mass flux of each of the compounds to the particle is calculated dynamically based on the gas phase concentrations and the evaporative fluxes, in which the salt formation in the particle phase is taken into account.

Initially in the conceptual model for particle growth, we assumed that there was no water in the particle phase and that the bases could exist in the particle phase only if they had formed salts with one of the acids (while the acids were allowed to exist in the particle also in their molecular form). All the salts were formed from an acid and a base in 1:1 molecular ratio. In this approach the evaporative part of the mass fluxes of the acids from the particle were calculated based on their saturation vapor pressures (p_{sat}) assuming unity mass accommodation coefficients. For bases we assumed p_{sat} to be zero and the evaporative flux was treated using effective mass accommodation coefficients estimated based on cluster evaporation rates (0.001 for ammonia and 1.0 for TMA). Results from this model (Fig. 1) suggest that in typical ambient conditions a large fraction of total acids in the particle phase may have formed salts with basic compounds, thereby highlighting the need for understanding the effects of salt formation on growth in further detail.

In this work we will modify the growth model by adding detailed thermodynamics of acid/base dissociation and by including water as one of the condensing compounds. With the modified growth model we will study the potential effect of particle phase salt formation on the growth rates of particles in various ambient conditions as well as the relative contributions of chemically distinct acids and bases. The results will be discussed in the context of atmospheric particle growth rates and their observed size dependence.

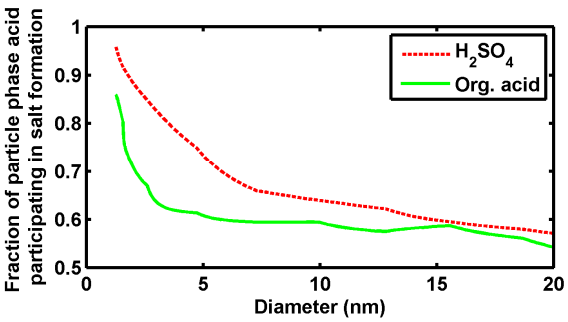

Figure 1. The fraction of the total mass of the acid in the particle phase that has formed salt with the bases as a function of particle size.

Financial support by the Academy of Finland Centre of Excellence program (project No. 1118615) is gratefully acknowledged.

Pierce, J. R., Riipinen, I., Kulmala, M., Ehn, M., Petäjä, T., Junninen, H., Worsnop, D. R. and Donahue, N. M. (2011) *Atmos. Chem. Phys.* **11**, 9019-9036.

Smith, J. N., Barsanti, K. C., Friedli, H. R., Ehn, M., Kulmala, M., Collins, D. R., Scheckman, J. H., Williams, B. J. and McMurry, P. H. (2010) *PNAS* **107**, 6634-6639.

Monday, September 3, 2012

Session WG06S2O. Particle lung deposition

Personal daily exposure of children to ultrafine particles and black carbon

C. Vargas Trassierra[1,2], S. Marini[1], L. Stabile[1], A. Russi[1], F. Fuoco[1], G. Buonanno[1],

[1]Dept. of Civil and Mechanical Engineering, University of Cassino and Souther Lazio, Cassino (FR) 03043, Italy
[2]INMRI, Istituto Nazionale di Metrologia delle Radiazioni Ionizzanti, ENEA Casaccia, Roma, 00123 Italy
Keywords: children exposure, personal monitoring, ultrafine particles, black carbon
Presenting author email: c.vargas@unicas.it

Epidemiologic evidence indicates a relationship between particle pollution exposure and adverse respiratory and cardiovascular health effects, including decreased lung function, asthma, myocardial infarction and all-cause mortality (Brunekreef and Holgate, 2002). In general, the smaller the particle size, the greater its ability to penetrate into the lungs and thus to produce adverse effects on human health. For this reason, sub-micrometer particles and even more UFPs (diameter < 0.1 μm), show higher health care interest than other particle sizes. Anyway, while there is considerable toxicological evidence of potential harmful effect of UFPs on human health, epidemiological studies are still not sufficient for conclusions on the dose-response relationship concerning this aerosol fraction (WHO, 2005).

This study, which falls within the UPTECH international project, deals with the children's personal exposure assessment to UFPs and black carbon. BC was used as an indicator of exposure to diesel exhausts whose negative health effects (short and long-term cardiovascular, respiratory and neurodegenerative health effects) were reported in Baja et al., 2010; McCracken et al., 2010.

We considered children because they represent the most vulnerable group with regard to harmful effects of airborne particles exposure. This is due to: i) the higher dose of UFPs as function of the children lung size compared to adult one; ii) their developing organs and immunological system.

Air quality can be measured at four different spatial scales: i) “city scale”, the broadest and most common scale used to characterize air quality across several city blocks using remote measurements; ii) “outdoor scale”, representative of outside building grounds particle exposure; iii) “indoor scale”, within building rooms reflecting indoor-based exposure; iv) “personal scale”, using hand-held instruments carried as a personal monitor in order to assess their actual exposure.

The daily overall children exposure is dominated by particle concentration levels in three main microenvironments: home, school, and transport mode. Therefore, children attending the same school, can receive different doses.

In the present work personal exposure measurements were performed on a sample of about one hundred children aged 8 to 11 years who attend three schools (S_1, S_2, S_3) in Cassino (Italy). S_1 is a primary school located on traffic urban street; S_2 is a secondary school close to intersection of moderate and heavily trafficked urban street; S_3 is a primary school located in a rural area far away from urban traffic.

The personal exposure was monitored through: two hand-held particle counters (NanoTracer, Philips) and one BC monitor (Aethalometer-microAeth Model AE51, MageeScientific). These monitors have a high temporal resolution (1÷16 s for NanoTracer, 1 s ÷ 5 min for Aethalometer), are small and portable (750 g and 250 g, respectively) and do not require special training to use.

NanoTracer, which works by diffusion charging, is able to provide number concentration (in the range 10-300 nm), average particle diameter, and lung deposited surface area concentration measurements. An electrometer measures the current induced by previously charged particles collected on a filter inside a Faraday cage. The device is also able to evaluate the different fractions of the lung deposited surface area through a semi-empiric algorithm implemented by Marra *et al*., 2010.

The Aethalometer detects the changing optical absorption of light transmitted through an internal small teflon-coated borosilicated glass fiber filter where BC-particles are captured.

We monitored children for 24-h, they also filled in a diary reporting the main indoor and outdoor activities (such as studying, eating, transportation, sleeping), also indicating the length of each activity.

From data collected by NanoTracers it was found that school contribution on daily exposure to UFPs is about 15%-20%, with an average particle number concentration in the range $1.5\times10^4 – 5.3\times10^4$ part. cm^{-3}. The highest exposure intensity was measured during lunch time with a contribution of about 20% and particle number concentrations in the range 4.2×10^4-1.9×10^5 part. cm^{-3}.

For BC, as expected, the most contributing activity to personal exposure is transport with an average exposure of 12.4 μg m^{-3}, while lowest average exposure was found at home (4.4 μg m^{-3}).

Baja, E.S., Schwartz, J., Wellenius, G.A., Coull, B.A., Zanobetti, A., Vokonas, P.S., Suh, H.H., 2010. *Environmental Health Perspectives* **118**, 840-846.

Brunekreef, B., Holgate, S., 2002. *Lancet* **360**, 1233-1242.

Marra, J, Voetz, M., Kiesling, H.J. (2010) *J. Nanoparticle Res.* **12**(21).

McCracken, J., Baccarelli, A., et al. (2010). Environmental Health Perspectives **118**, 1564-1570.

WHO, 2005. Regional Office for Europe, Bonn, Germany.

Determining the regional deposition of tobacco smoke in the human respiratory system

C.J. Dickens[1], C.M. McGrath[1], J. Perkins[1], P. Biggs[1], R.A. Cabot[1], J.J. McAughey[1]

[1]British American Tobacco, Group R&D, Southampton SO15 8TL, UK

Keywords: Aerosol modelling, lung deposition, particle deposition

A study was conducted to determine the regional deposition of tobacco smoke aerosol in the respiratory system of volunteer smokers, using real-time measurement of respiration and puffed/exhaled smoke particulate, and a compartment model for particle deposition in the human respiratory system.

Nine current regular cigarette smokers were recruited for this study. The volunteers smoked a commercial King-Size cigarette with 7mg tar yield, as measured by machine smoking at the ISO smoking regime. Each volunteer smoked 3 cigarettes with no constraints on how they smoked them (free smoking). Additional measurements were made to help optimise the model where volunteers smoked at the self-perceived inhalation regimes of mouth hold only and shallow inhalation. Real time puffing behaviour and puffed optical tar (smoke mass concentration) were measured by a smoking analyser (SA7), and real time respiratory behaviour and exhaled optical tar were measured using a Breathe in Breathe out system (BIBO). Both devices recorded data at 25Hz, with smoke concentration determined using light obscuration.

Exhaled smoke was captured by a sampling system operating at a constant flow of 217 $l.min^{-1}$. A sub-sample was taken from the sampling system for analysis by a real-time particulate spectrometer, DMS-500 (Cambustion, UK) which measures particle size and concentration over a size range of 5 – 1000 nm at 10Hz resolution. Puffed smoke was characterised by replaying the recorded human puffing profiles, as measured by the SA7, on a Smoking Cycle Simulator/DMS-500 (Cambustion, UK). Assuming spherical particles of unit density allowed a calculation of aerosol mass. Puffed and exhaled smoke was also characterised by measuring solanesol, a tobacco-specific high boiling point alcohol (C45H74O : MW = 630) which is a good marker for the particulate phase of tobacco smoke

The ratio between solanesol and aerosol mass was constant for all tests and similar between puffed and exhaled smoke. The ratios of optical tar to both solanesol and aerosol mass were higher for exhaled smoke than for puffed smoke, implying that the exhaled smoke aerosol was different to the puffed smoke aerosol. The assumption was made that this difference is due to hygroscopic growth of the particles in the lungs, which would affect the optical signal, but not the solanesol content, and not the aerosol measurement as the DMS operates at a pressure of 0.1atm which may dry particles before measurement. This gave an estimated hygroscopic growth factor of 4.0 for smoke particles in the lungs.

The model split the respiratory system into 200 compartments of equal volume representing progressively deeper depths into the respiratory system from the mouth down to the alveoli. The sum of the compartments represents the vital capacity of the lungs. Equations allowed the movement of particles between each compartment due to diffusion and under the influence of respiratory airflow, and the deposition of particles due to sedimentation. Coagulation was assumed to occur instantly once the smoke entered the mouth, and hygroscopic growth was assumed to occur instantly and uniformly once the particles reached the bronchi. The model ran in incremental time steps of 0.04s.

The model was run for each test using puffing data (flow and optical tar) and respiratory data as input. Model parameters for deposition rate in compartments representing five main anatomical regions of the respiratory system were set to provide the best fit between measured and model predictions of exhaled optical tar across all tests, including mouth hold only and shallow inhalation tests.

There were good correlations between the measurements and the model predictions of exhaled optical tar for all tests (R^2=0.90) and for the free smoking tests only (R^2=0.95) (Figure 1). This good correlation gives confidence in the regional deposition predictions of the model.

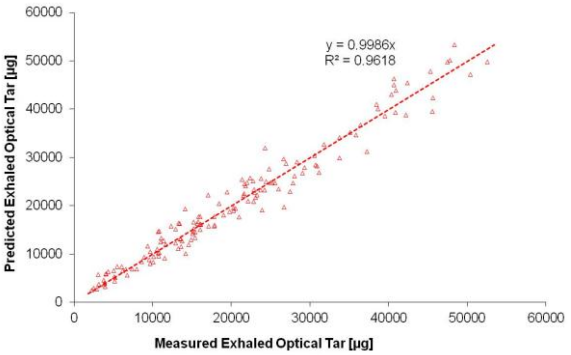

Figure 1. Predicted versus measured exhaled optical tar

It is hypothesised that the hygroscopic growth of the particles has a major effect on the deposition rate of the particles in the lungs. Future work will look to measure hygroscopic growth directly by measuring the particle size of exhaled smoke.

Phase transition of inhaled particles within the human respiratory system

L. Pichelstorfer and W. Hofmann

Department of Materials Research and Physics, University of Salzburg, 5020 Salzburg, Austria
Keywords: Condensation, relative humidity, lung deposition
Presenting author email: Lukas.Pichelstorfer@sbg.ac.at

To assess health risks due to airborne particle exposure, it is necessary to obtain information on regional and local deposition. Since the particle diameter is a key parameter of physical deposition mechanisms, the size distribution of an aerosol within the human respiratory tract is an important determinant of particle deposition.

During inhalation, particle size and composition may vary significantly due to various mechanisms such as deposition, coagulation or phase transition (i.e. condensation or evaporation). The latter also includes hygroscopic growth. Since relative humidity reaches nearly 100% within the human lung, growth due to condensation of water vapor has a considerable effect on hygroscopic particles. However, to describe the evolution of soluble particles within a vapor phase, the interaction of the constituents of the particles has to be taken into account. Thus, the objective of this work is to develop a numerical model for multi-component growth of a polydisperse aerosol within the human respiratory system which is independent of particle size.

The present model takes into account the interaction of various vapors (the case of unary growth may be considered as a limiting case). The condensation is assumed to be quasi-stationary. As a result, the temperature difference between the droplet and the ambient vapor phase adopts a constant value at each point in time. The same applies to the droplet composition. The present model is based on the work of Mattila et. al. (1997). Initially inhaled and newly formed particles are assumed to be spherical.

The inhalation of a “dry“, i.e. the particle does not contain substances from the vapor phase, cigarette smoke particle with a diameter of 150 nm was simulated with the model. Two cases were observed:

1) Water vapor as the only condensable vapor in the system
2) Water vapor and a constant 0.115% (of total vapor phase) nicotine fraction

Relative humidity of water and nicotine were adopted from Ferron (1987) and Lipowitz and Piadé (2004). According to Ferron, the initial relative humidity of water is 50% in the oral region. It increases to about 85% in the pharyngeal region and reaches its final value of 99.5% in the trachebronchial region. For the calculation we assumed a 1 s residence time of the particle in the mouth before it is inhaled.

Results from the calculation are plotted in Figure 1. The droplet growth can be segmented in four stages: In the first stage, in the case of pure water vapor the droplet does not grow since the saturation ratio of water is too low. The droplet situated in the binary vapor instantly starts to grow, though very slowly. In the second stage, which begins at about 0.75 s, the particle starts to grow faster until the soluble part of the cigarette smoke particle is totally dissolved. This stage lasts for about 0.1 s. In the next stage, which extends from 0.85 s to 1.25 s, particle growth is driven by the continuously rising relative water humidity. In the fourth stage of particle growth the relative water humidity reaches its final value. While the particle in the unary vapor reaches the equilibrium diameter rapidly, the particle in the binary vapor surrounding still grows, but very slowly.

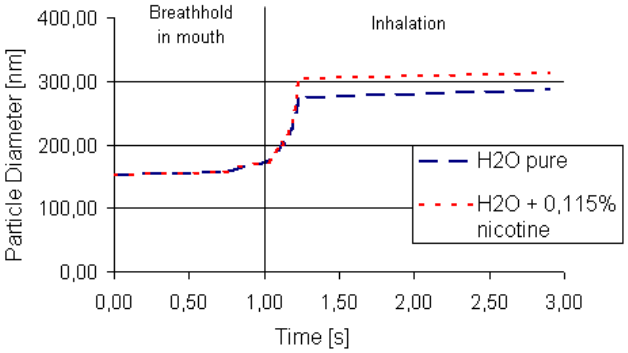

Figure 1. Particle diameter as a function of inspiratory time.

The time dependence of particle growth due to phase transition of the condensable vapors in the system is depicted in Figure 1. In case of an additional nicotine vapor in the system, very slow particle growth sets in immediately. However, the growth of the particles is quite similar. Interestingly, there is a significant difference in the final diameter of the droplet. In the case of binary growth, the particle reaches a diameter which is 8% greater than that in the vapor environment without nicotine. Note, that the mole ratio of nicotine to water is less than 1.9%.

This condensation/evaporation model will eventually be implemented into the stochastic deposition model IDEAL (Koblinger and Hofmann, 1990), considering dilution, deposition, coagulation and phase transition.

Ferron, G.A., Haider, B. and Kreyling, W.G. (1987) *J. Aerosol Sci.* **19**, 343-363.

Koblinger, L. and Hofmann, W. (1990) *J. Aerosol Sci.* **21**, 661-674.

Lipowitz, P.J. and Piadé, J.J. (2004) *J. Aerosol Sci.* **35**, 33-45.

Mattila, T., Kulmala, M. and Vesala, T. (1997) *J. Aerosol Sci*. **28**, 553-564.

Robinson, R.J. and Yu, C.P. (2007) *Aerosol Sci. Technol.* **28,** 21-32.

Particle deposition under transient high frequency ventilation air flow in a physiologically realistic bifurcation

E. Makris[1,2], M. Pilou[1,2] ,P. Neofytou[2],S. Tsangaris[1] and C.Housiadas[2].

[1]Department of Mechanical Engineering, Technical University of Athens, Athens, 15780, Greece
[2]Thermal Hydraulics & Multiphase Flow Laboratory of National Centre for Scientific Research "Demokritos", Agia Paraskevi, Athens, 15310, Greece
Keywords: Particle deposition, Mechanical Ventilation, CFD.
Presenting author email: vagmakr@ipta.demokritos.gr

The simulation of complex respiratory airflow fields coupled with particle dynamics may be a highly important tool for respiratory medical applications in terms of targeted drug delivery and inhalation toxicology.

High Frequency Ventilation (HFV) is a technique of mechanical ventilation assisting or replacing spontaneous breathing, with major application the adequate ventilation of neonates. High frequency ventilation is characterized by high flow oscillation frequency (5 – 50 hz) and small tidal volumes.

Alveolar delivery of inhaled aerosol drugs in critically ill neonates undergoing HFV is a highly interesting subject. However, pulmonary delivery of aerosol drugs during HFV has been rarely studied in - vivo due to the difficulty of in – vivo measurements and ethical concerns in conducting studies in neonates (Sood et al 2010).

The current study is a computational simulation of transport and deposition of inertial particles, under HFV flow field, inside a physiologically realistic bifurcation, modelling the third and fourth lung generation (G3 – G4).The simulation is a fully Eulerian approach, for both air and particle flow. Due to the small size of the particles, the influence of the particulate phase on the air flow field is considered negligible (one-way coupling).

The numerical simulation of the air HFV flow field is carried out by the commercial software Ansys CFX® .The inlet profile is assumed to be a sinusoidal velocity profile with frequency equal to 23 Hz and peak Reynolds number equal to 1250.

The aerosol particle dynamics simulation is carried out, also, using an in-house particle dynamics code developed for studying particle transport and deposition during internal flows (Pilou et al. 2011). The code is based on an Eulerian description of the particles General Dynamic Equation .The Eulerian approach offers significant advantages over the frequently chosen Lagrangian approach (Zhang Z. et al. 2002). Initially, it may be used for small particle diameters where the Lagrangian approach becomes highly demanding in terms of numerical implementation. Furthermore the Eulerian model is more accurate than passive tracer (Lagrangian) models as it can take into account simultaneous diffusive and inertial particle transport. The code is based on an Eulerian description of the particles General Dynamic Equation, and the particle velocity $\vec{v}_p$ is written as :

$$\vec{v}_p = \vec{u}_{fluid} + \tau_p(\vec{g} - \vec{u}_{fluid} \cdot \nabla \vec{u}_{fluid}) - D\nabla \ln c \quad (1)$$

Where τ_p is the particle relaxation time and D the Stokes – Einstein diffusion coefficient. The aerosol particles are assumed to be spherical with Stokes number ranging from 0.02 to 0.12. The particles are jetted at the beginning of the HFV operation and the particle concentration and deposition, inside the bifurcation, is calculated during several time periods.

The geometry of the study is a physiologically realistic bifurcation based on the geometrical characteristics of the bifurcation created by the third and fourth lung generation (G3 – G4). These generations are selected due to the peak particle deposition in this region that previous experimental studies have recorded.The computational grid of the study is created by an in - house structured grid generation code (Makris et al. 2012). The result is a multi-block high quality structured grid with the adoption of the "butterfly" topology.

In conclusion the study presents an application of aerosol particles deposition under HFV in a physiologically realistic bifurcation of the human lung. The Eulerian approach for the particles combined with a transient and strongly oscillating flow field, such as the HFV velocity profile, provides a valuable tool for the simulation of aerosols drug delivery under mechanical ventilation assistance.

Sood B., Shen Y., Latif Z., Galli B., Dawe E., Haacke E. (2010) Effective aerosol delivery during high-frequency ventilation in neonatal pigs. Resp. **15**, 551 – 555.

Pilou M., Tsangaris S., Neofytou P., Housiadsa H., Drossinos Y. (2011) Inertial Particle Deposition in a 90° Laminar Flow Bend: An Eulerian Fluid Particle Approach Aer.Sci. Tech. **45**,1376–1387

Zhang Z., Kelinstreuer C. (2002) Transient airflow structures and particle deposition transport in a sequqntially branching lung airway model Phys. Fluids. **14**, 862 – 880.

Makris E., Gkanis V., Tsangaris S., Housiadas C.(2012) A methodology to generate structured computational grids from DICOM data : application to a patient-specific abdominal aortic aneurysm (AAA) model. Computer Methods in Biomechanics and Biomedical Engineering **15(2),**173-183

Dynamics of exhaled aerosol with mixed composition

D. Katoshevski[1], D. Parienta[1], L. Morawska[2], G.R. Johnson[2], Z.D. Ristovski[2], M. Hargreaves[2], K. Mengersen[2], S. Corbett[3], C.Y.H. Chao[4], Y. Li[5],

[1]Biotecnology and Environmental Engineering, Ben-Gurion University of the Negev, Beer-Sheva, Israel
[2]Queensland University of Technology, Brisbane, QLD, Australia
[3]Centre for Public Health, Western Sydney Area Health Service, Sydney, NSW, Australia
[4]Mechanical Engineering, The Hong Kong University of Science and Technology, Hong Kong SAR, China
[5]Department of Mechanical Engineering, The University of Hong Kong, Hong Kong SAR, China

Keywords: Exhaled Aerosol, Droplets, Modelling
Presenting author email: davidk@bgu.ac.il

Aerosols are emitted from the respiratory tract during various activities such as coughing, speaking or sneezing. These aerosols play an important role in the transmission of airborne diseases such as influenza, tuberculosis and others. After evaporation droplets can form droplet nuclei which, in turn, can remain suspended for prolonged periods and constitute a health hazard.

The dynamics of droplets exhaled from the respiratory system during coughing or talking is addressed. A mathematical model is presented accounting for the motion of a droplet in conjunction with its evaporation. Droplet evaporation and motion are accounted for under two scenarios: (1) a well mixed droplet and (2) a droplet with inner composition variation. A multiple shells model was implemented to account for internal mass and heat transfer and for concentration and temperature gradients inside the droplet. The trajectories of the droplets are computed for a range of conditions and the spatial distribution and residence times of such droplets are evaluated.

Exhaled respiratory droplets, composing of saliva, mucus and several chemical species, are emitted during cough, sneeze or speak (Morawska et al., 2009). Small droplets can remain suspended in air for several minutes. Larger droplets can evaporate and form droplet nuclei that can remain suspended for a similar period of time. Droplet nuclei are composed of the non-volatile components (such as inorganic salts and glycoproteins) and a small amount of water. The size of the nuclei is determined by internal parameters such as initial droplet size and composition and environmental conditions such as temperature and relative humidity. Recent studies have also shown that relative humidity has an effect on the viability of viruses (Morawska, 2006).

In a recent study, Chao et al. (2009) conducted a series of experiments for measuring the size distribution and air velocity immediately at the mouth opening before evaporation occurs. Droplet size was determined using IMI (Interferometric Mie imaging) and the droplet velocity was determined using PIV (Particle Image Velocimetry). Measurements were taken at distances of 10mm and 60mm from the mouth. The estimated total number of droplets expelled ranged from about 1000 to 2000 per cough. The average expiration air jet velocity was about 12 m/s for coughing and 3 m/s for speaking. The velocity of air was found to be approximately constant at a distance of 100mm. The present calculations make use of data obtained in that study.

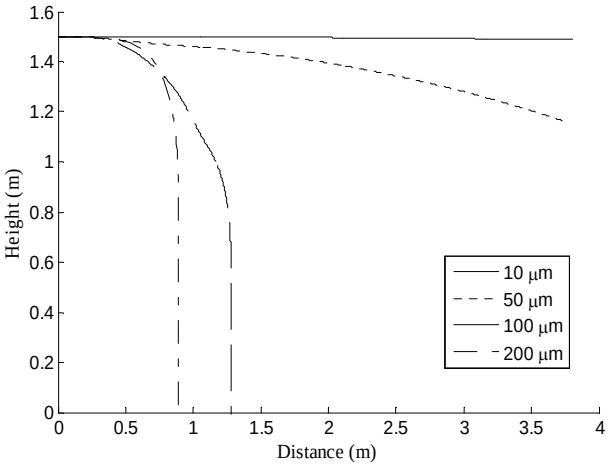

Fig. 1. Calculated trajectories of exhaled droplets during coughing, as a function of droplet size.

Fig. 1 presents examples of trajectories of droplets of various sizes. Smaller droplets are carried more effectively by the exhaled jet stream than larger ones. These trajectories are calculated as coupled with the change of composition and size of the droplets.

The model and results that will be elucidated, can serve together with the corresponding reported measurements in assessing the risk associated with the transmission of airborne diseases and assist in designing solutions to minimize this risk in controlled environments.

Chao, C.Y.H., Wan, M.P., Morawska, L., Johnson, G.R., Ristovski, Z.D., Hargreaves, M., Mengersen, K., Corbett, S., Li, Y., Xie, X., & Katoshevski, D. (2009) *J. Aerosol Sci.*, **40**, 122-133.

Morawska, L. (2006). *Indoor Air*, **16**, 335-347.

Morawska, L., Johnson, G. R., Ristovski, Z. D., Hargreaves, M., Mengersen, K., Corbett, S., Chao, C. Y. H., Li, Y., Katoshevski, D. (2009) *J. Aerosol Sci.*, **40**, 256-269.

In vivo regional deposition of submicron-sized airborne particles in the baboon respiratory model

J. Pourchez[1,2,3], I. Albuquerque-Silva[1,2,3], M. Durand[1,3,4], J. Avet[1,3,5,6,7], D. LePennec[8], M. De Monte[8], J. Montharu[8], M. Cottier [1,3,5,6,7], F. Dubois[1,3,5,6,7], L. Vecellio[8,9]

1 LINA, EA 4624, F-42023, Saint-Etienne, France
2 Ecole Nationale Supérieure des Mines, CIS-EMSE, LINA EA 4624, F-42023 Saint-Etienne, France
3 SFR IFRESIS, F-42023, Saint-Etienne, France
4 Centre Hospitalier Emile Roux, F-43012, Le Puy en Velay, France
5 Université Jean Monnet, Faculté de Médecine, F-42023, Saint-Etienne, France
6 CHU de Saint-Etienne, F-42055, Saint-Etienne, France
7 Université de Lyon, F-42023, Saint-Etienne, France
8 INSERM U618, Université Francois Rabelais, Tours, France
9 DTF Aerodrug – Diffusion Technique Française, Tours, France
Keywords: in vivo deposition, regional deposition, nano-aerosol.
Presenting author email: pourchez@emse.fr

Introduction

Deposition pattern of inhaled particles is a main parameter controlling target tissue, future clearance and potential adverse health effect. In this context the characterization and the estimation of risks to children from inhaled particles is complicated by the lack of reliable experimental data. Especially, a main challenge consists in measuring *in vivo* regional deposition within a child-like respiratory model of size-resolved particles in the submicron range. As a result, this work proposed to study the *in vivo* regional deposition of size-resolved radioactive particles in the 230nm-2.8µm range of AMAD within a baboon model (*i.e.* a child-like respiratory model).

Methods

Jet medical nebulizers were used to generate aerosols: an Atomisor NL11 (DTF Medical, France), a modified Sidestream (Philips Respironics, Ref 12NEB400, England), and a Nanoneb (DTF Medical, France). Nebulizers were loaded with 2 mL of DTPA solution containing 74 MBq Technetium 99m.. Particle size distributions and aerosol output of the analyzed radioactive aerosols were determined using gamma-camera detection coupled to an Electrical Low Pressure Impactor. *In vivo* experiments were realized with three healthy baboons weighing 10 kg to 14 kg. They were then kept awake while aerosol was administered through a tight-fitting face mask specifically designed for baboons. Each baboon inhaled twice an aerosol produced by the three different types of nebulizer selected for this study. The order of the nebulizers tested was randomized for each baboon, resulting in six inhalations per nebulizer.

Results

Particle size distributions are summarized in Table 1. Almost the totality of particles produced by the 230nm AMAD aerosol (98.6%) and the 550nm AMAD aerosol (98.3%) were smaller than 2.5µm. In contrast, less than a half (47%) of fines particles (FPs) were observed in the 2.8µm AMAD aerosol.

Table 1. Features of the aerosols inhaled by the baboons to assess the *in vivo* regional distribution.

AMAD	GSD	Aerosol output	FPs	UFPs
2.80µm	3.2	44.5 ± 1.5%	47.0%	0.4%
550nm	2.1	9.3 ± 3%	98.6%	1.7%
230nm	1.6	4.2 ± 1%	98.3%	7.3%

In the studied submicron-size range, results doubtless demonstrate that the total lung deposition decreases as the particles size increase (Figure 1). A huge deposition in the extrathoracic (ET) region was found for the 2.8µm AMAD aerosol (72 ± 17% of the total aerosol fraction deposited) whereas the 230nm AMAD aerosol showed the smallest ET deposition (only 16 ± 4% of the total aerosol fraction deposited). As a result, aerosols with smaller AMAD (*i.e.* 230nm) can be associated to an almost exclusively thoracic deposition (84 ± 4% of the total aerosol fraction deposited). Finally, airborne particles with an AMAD of 550nm showed an intermediate behaviour (49 ± 8% of the total aerosol deposition in ET region and 51 ± 8% of the total aerosol deposition in TH region).

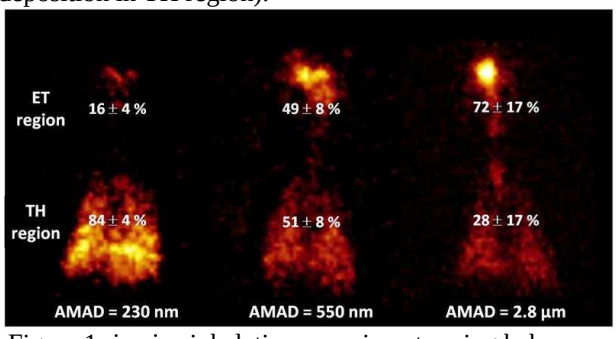

Figure 1. *in vivo* inhalation experiments using baboons.

Conclusion

We established that a diminution of the inter-subject variability and a targeted deposition in the thoracic region can be achieved by reducing the medium activity diameter (AMAD) of airborne particles around 230 nm.

Not only Asbestos exposure, but also inherited susceptibility, is responsible for the occurrence of mesothelioma in humans

F. Cetta [1], P. Paladini [2], C. Ghiribelli[2], M. Monti[3], F. Granato[1], R. Borrelli[2], V. Guercio[1], D. Stergiou[1] and G. Gotti[2]

[1] Dept. of Surgery and Thoracic Surgery, University of Siena, Siena, 53100, Italy
[2] Thoracic Surgery Unit, University Hospital of Siena, Siena, 53100, Italy
[3]Geriatric Institute "Pio Albergo Trivulzio" (PAT), Milan, 20146, Italy
Keywords: Mesothelioma, exposure, asbestos, individual susceptibility
Presenting author email: cetta_francesco@libero.it

Mesothelioma is a neoplasm with invariably dismal prognosis, which is strictly related with asbestos exposure and usually occurs 30-40 years after occupational or non occupational exposure. Recent reports have suggested that, although the incidence of mesothelioma (MM) is anticipated to decline in the coming decade, it may not decrease to background risk levels, because secondary asbestos exposure from the environmental will continue, Tse *et al* (2010).

During a 13 year- interval, a consecutive series of 80 subjects with MM was observed at the University of Siena. There were: 56 M, 24F , mean age 65 y, range 43-86 y. In particular, there were 66 pleural MM, 11 peritoneal MM, 1 MM of the pericardium and 2 MM of the tunica vaginalis testis. In particular, a genome wide analysis (array CGH analysis) performed in a small subset of these couples (husband occupationally exposed, but unaffected, and wife unexposed but affected), showed a panel of differently expressed genes, which were partly common and partly different from couple to couple.

Interestingly, common genes with diverse copy numbers included major histocompatibility genes, genes involved in the metabolism of xenobiotics and genes involved in the inflammatory response, Cetta (2011). It was shown that, analogously to what occurs for pollution related diseases, also concerning asbestos related diseases, clinical outcomes occur as the final result of host-fiber interaction. In particular, we showed that asbestos related MM occurred in the tonaca vaginalis testis (as primary site), i.e. in a distant site from the portal of entrance of asbestos fibers, and that asbestos fibers have been documented at this level (in other patients). In addition, we observed subjects developing MM more than 45 years after short-term exposure to asbestos (service in the Navy at age 18-20) without any additional occupational exposure. Finally, we observed some couples (husband-long-term occupationally exposed to asbestos and wife non occupationally exposed) with the interesting finding that the non exposed wife developed pleural MM (with asbestos fibers documented in the operative specimen), whereas the exposed husband had neither MM, nor lung cancer, or even overt asbestosis. This points dramatically to the crucial role of individual susceptibility in the occurrence of asbestos related diseases. In particular, after genome wide analysis of blood samples of these couples, we showed that they differed for a diverse expression of a panel of genes, including some of those responsible for major hystocompatibility system, drug metabolizing enzymes and host immune response, Cetta (2011). These findings dramatically suggest that, whereas most individuals do not develop MM or lung cancer even after a 30-year-occupational exposure to chrysotile, which is the most toxic variant of asbestos, other apparently normal, but highly susceptible people can develop pleural MM after indirect exposure to small quantities of asbestos of whatever structure and composition, or show a mesothelial tumor in a distant, but susceptible site, such as tonaca vaginalis testis. Further ecologic studies and analytical studies, but also pathophysiological and genetic studies are obviously required, before stating which is which, i.e. what is the relative potency of the various asbestos variants and what's the relative role of intrinsic toxicity fibers and of host susceptibility.

However, it is likely that, once that a powerful toxic agent as asbestos has been disseminated in a given community, the decrease to background risk levels is highly improbable, not only because of continuous asbestos use in other regions (imported as manufacts, even in small quantity), but also because secondary asbestos exposure from the environment will likely continue. In particular, this persistent exposure (after initial introduction) and the long-term persistency of asbestos fibers will be able, even at very low concentrations, to trigger the occurrence of MM. This evenience will be greater in predisposed people, as suggested by recent evidence that germ-line mutations in the gene encoding BRCA associated protein1 (BAP+1) are associated with an increased evidence of MM, Testa *et al* (2011). These observations further support the hypothesis that both asbestos exposure and inherited susceptibility are responsible for the occurrence of Mesothelioma in humans.

Tse, LA et al (2010) *Environ. Health Perspect.* **118**, 382–386.
Cetta, F. (2011) in Barbarisi A. Editor. *Biotechnology in Surgery. Springer Verlag* 169-190.
Testa, JR et al (2011) *Nat. Genet.* **43**, 1022-5.

Monday, September 3, 2012

Session WG08S2O. New Instrumentation (II)

Effect of particle diffusivity on DMAs with multiple monodisperse-particle outlets: theory validation and design optimization

M.Giamarelou[1], M. Stolzenburg[2], D.-R. Chen[3] and G. Biskos[1,4]

[1]*Dept. of Environment, University of the Aegean, Mytilene, Greece*
[2]*MRS Consulting, Sheboygan, WI, USA*
[3]*Dept. of Energy, Environmental and Chemical Eng., Washington University in St. Louis, St. Louis, MO, USA*
[4]*Faculty of Applied Science, Delft University of Technology, Delft, The Netherlands*

Keywords: MMO-DMA, Dual-DMA, transfer function, resolution.
Presenting author email: giamarel@env.aegean.gr

By simultaneously selecting aerosol particles having different sizes, Differential Mobility Analyzers (DMAs) with multiple monodisperse-particle outlets can have a number of advantages in aerosol metrology. When used in electrical mobility spectrometers, for instance, they can significantly reduce the time required to measure the particle size distributions. Depending on the relative location of the first and the last outlet from the inlet, one can also increase the dynamic mobility range of the measured particles in a single measurement.

Based on the approach proposed by Stolzenburg (1988), we have recently developed the theoretical framework for determining the transfer function and the resolution of DMAs with multiple monodisperse-particle outlets (cf. Giamarelou et al., 2011; 2012). To describe the spreading of the transfer function due to the Brownian motion of the particles, we divide the classifier into segments defined by successive monodisperse-particle outlets. The total diffusional broadening along the whole path of the particle that leads to the i^{th} sample exit can be approximated by

$$\sigma^2_{\Gamma_{i,total}} = \sum_{j=n}^{i} \sigma^2_{\Gamma_{i,j}} . \qquad (1)$$

Here $\sigma_{\Gamma_{i,j}}$ denotes the diffusional broadening of the particles classified through the i^{th} monodisperse-particle outlet during the time they travel through the j^{th} segment of the MMO-DMA.

Fig. 1a shows the comparison of the model to the measurements with the 3-monodisperse-particle-outlet DMA tested by Chen et al. (2007). The loss-corrected theoretical transfer functions for both sample outlets, at 2.54 cm and 15.24 cm, are in perfect agreement with the experimental values. The predicted resolution for each of the three outlets agrees well with the reported measurements (Fig. 1b), indicating that the theory captures well the broadening of the transfer function for particles having diameter smaller than 20 nm.

Using the validated transfer function model we provide design considerations for building a DMA with two monodisperse-particle outlets, and predict its performance under different operating conditions. A critical parameter when designing multiple-exit DMAs is the minimum distance between the entrance and the nearest sample exit as well as between the successive sample exits so that the flow profile remains laminar.

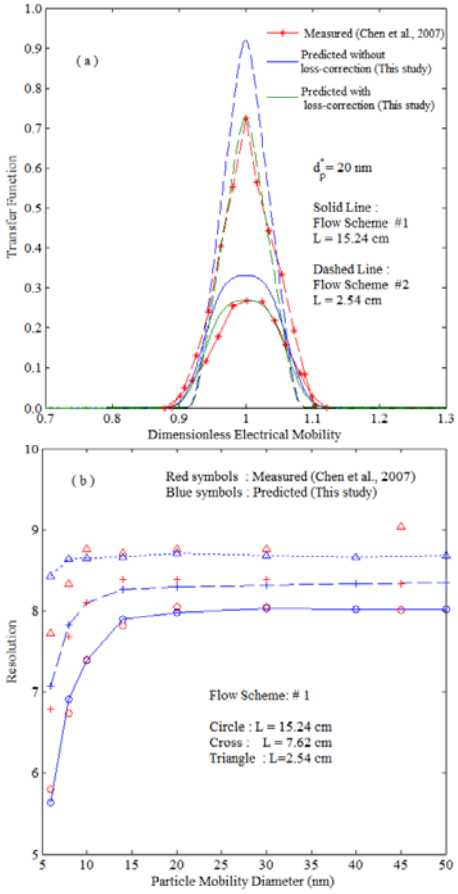

Figure 1 (a) Comparison between predicted and measured transfer function of the DMA with 3 monodisperse-particle outlets (measurements from Chen et al., 2007). The monodisperse-particle outlets are located 2.54, 7.62 and 15.24 cm downstream of the polydisperse aerosol inlet. Flow scheme #1 corresponds to 20 lpm sheath flow, 2.4 lpm polydisperse aerosol inlet flow, and 0.8 lpm for each monodisperse outlet flow. The respective values for flow scheme #2 are 20, 1.5 and 1.5 lpm. (b) Comparison between predicted and measured resolution of the DMA with 3 monodisperse-particle outlets.

References

Chen, D.-R., Li, W., Cheng, M.-D., 2007, *Aerosol Sci. & Technol.*, 41:217-230.

Giamarelou, M., Biskos, G., 2011, European Aerosol Conference, Manchester, Sept. 2011.

Giamarelou, M., Stolzenburg, M., Biskos, G., 2012, *Aerosol Sci. &Technol.*, (under revision).

Stolzenburg, M., 1988, PhD Thesis, University of Minnesota, Minneapolis, MN.

Characterization of the Airmodus A20 Condensation Particle Counter

K. Lehtipalo[1,2], J. Vanhanen[1], T. Toivola[1] , J. Mikkilä[1], T. Petäjä[2] and M. Kulmala[2]

[1]Airmodus Oy, 00560 Helsinki, FINLAND
[2]Department of Physics, University of Helsinki, 00560 Helsinki, FINLAND
Keywords: aerosol instrumentation, condensation particle counters
Presenting author email: katrianne.lehtipalo@helsinki.fi

Condensation particle counters (CPCs) are the basis of modern aerosol instrumentation in sub-micrometer range. CPCs can be used both as stand-alone instruments for measuring the total particle number concentration, and as counters in different kind of applications such as the differential/scanning mobility particle sizer (DMPS/SMPS).

A new laminar flow condensation particle counter, Airmodus A20, was launched in 2011. The A20 has a robust saturator design and uses butanol as condensing liquid. The aerosol flow rate is 1 LPM, achieved with a critical orifice and an external pump. Narrow pulse widths allow reaching high concentrations.

The performance of the A20 was verified in the University of Helsinki laboratory calibration setup (*e.g.* Petäjä *et al.,* 2006) using silver particles produced in a tube furnace and size selected by Hauke-type DMA. Nitrogen was used as carrier gas in the furnace, and the aerosol was neutralized with an Am241 source. Sheath flow of the DMA was 20 LPM and the aerosol flow 2 LPM, which corresponds to a size resolution of 0.3 nm. Figure 1 presents the results of the cut-off size calibration. The 50% cut-off diameter of the Airmodus A20 CPC for silver particles was 7.1 nm.

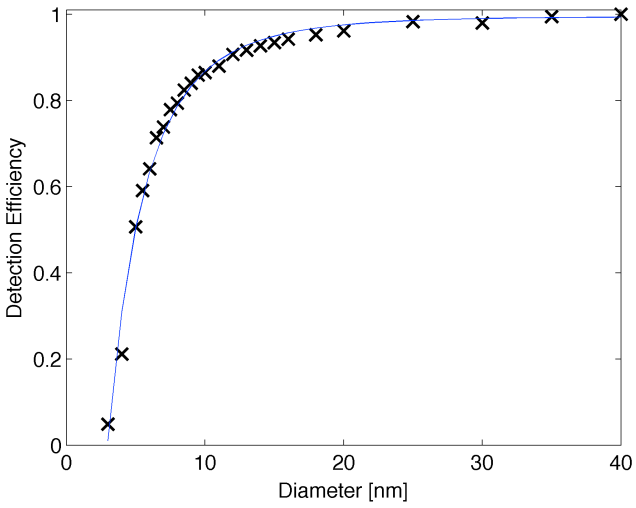

Figure 1. Cut-off size calibration of the A20, giving a cut-off size of about 7 nm for silver particles.

Concentration calibrations were conducted using 35 nm charged silver particles. The reference instrument used was an aerosol electrometer (TSI 3086B) with sample flow rate of 5 LPM. The single particle counting capability (< 10% co-incidence) of the A20 reached to about 25 000 #/cc. In higher concentrations the pulse rate started to decrease compared to the electrometer due to co-incidence in the optics. Based on calibrations, a 4th order polynomial correction function was determined for correcting the concentration. Using this correction function to the measured pulses the concentration matches with the electrometer even above 10^5 #/cc (Figure 2).

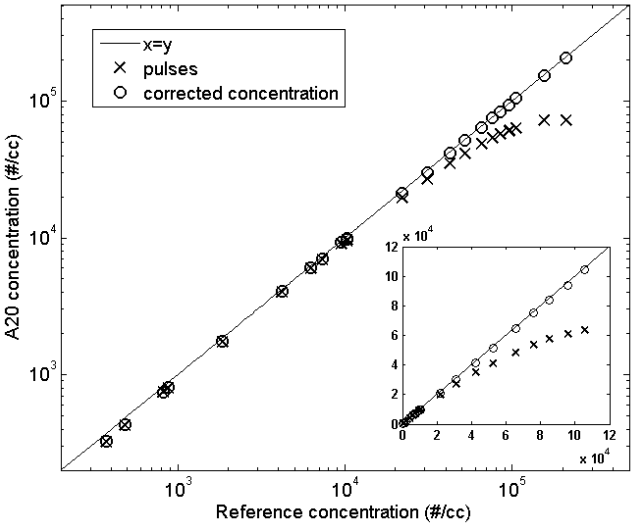

Figure 2. Concentration calibration of the A20 showing the pulse counts and the corrected concentration against the reference instrument.

The A20 bCPC was also tested in field conditions at the Hyytiälä SMEAR II measurement station (Hari and Kulmala, 2005). It proved to be suitable for long-term field measurements over large range of sizes and concentrations and compared well to other aerosol instrumentation.

Hari P., and Kulmala, M. (2005). *Boreal Environ. Res.* **10**, 315-322.

Petäjä, T. *et al.* (2006). *Aerosol Sci. Technol.* **40**, 1090-1097.

Broadband Aerosol Extinction Spectrometer, a new instrument for measuring the spectral dependence of aerosols.

R.A. Washenfelder[1], J.M. Flores[2], C.A. Brock[1], S.S. Brown[1] and Y. Rudich[2]

[1]National Oceanic and Atmospheric Administration, Boulder, CO, 80305, USA
[2]Weizmann Institute of Science, Environmental Science Department, Rehovot 76100, Israel
Keywords: optical properties, spectral dependence, refractive index, absorption, scattering
Presenting author email: flores@weizmann.ac.il

The interaction between aerosols and sunlight plays an important role in the radiative balance of Earth's atmosphere. Aerosols can both absorb and scatter solar radiation causing surface cooling and heating of the atmosphere. These interactions depend on the optical properties of the aerosols (e.g. complex refractive index), which are determined by measuring the removal (extinction), redistribution (scattering), and transformation into heat (absorption) of light by the aerosols. One of the largest uncertainties in assessing the direct effect of aerosols is the contribution of light absorbing organic compounds, such as brown carbon, where absorption increases towards the UV region (Andreae and Gelencser 2006). Approximately 33.9 Tg y^{-1} of organic carbon are emitted globally (Bond et al. 2004). Measuring and deriving their optical properties are critical in calculating the effects of aerosols on radiative transfer and on our understanding of the atmospheric system.

We describe a new Broadband Aerosol Extinction Spectrometer (BAES) to measure the extinction coefficient and derive complex refractive indices of purely scattering aerosols from 360 nm to 420 nm. The BAES consists of an LED light source that is coupled into a one meter optical cavity with two highly reflective mirrors opposite of each other. The spectrum of light exiting the cavity is recorded by a grating spectrometer with a charge-coupled device (CCD) array detector. The reflectivity of the mirrors is determined from the known Rayleigh scattering of He and N_2. The extinction coefficient ($\alpha_{ext}(\lambda)$) of the aerosols is then calculated using equation 1 (Washenfelder et al. 2008):

$$\alpha_{ext}(\lambda) = \left(\frac{1 - R(\lambda)}{d} + \alpha_{Ray}(\lambda) \right) \cdot \frac{I_o(\lambda) - I(\lambda)}{I(\lambda)} \quad (1)$$

where R is the mirror reflectivity, d is the length between the mirrors, α_{ray} is the Rayleigh scattering of the carrier gas, and I_o and I are the intensities recorded with an empty and filled cavity, respectively.

We measured polystyrene latex spheres (PSL) and ammonium sulphate aerosols (AS) at different sizes and concentrations to determine extinction cross sections between 360 – 420 nm with 0.5 nm resolution. We compare measurements made with the BAES with those made by a cavity ring down (CRD) at 407 nm. The extinction cross section measurements were used together with Mie theory to derive complex refractive indices (RI) using one diameter for PSL (Figure 1) and AS.

We further demonstrate how by measuring the extinction cross section for different sizes, we can determine the RI for each wavelength measured by the BAES, with 0.5 nm resolution.

The implications for determining the complex refractive index as a function of wavelength in the UV region for absorbing substances will be discussed with preliminary results of two different absorbing substances: Suwannee river fulvic acid (SFRA), which is a proxy for humic-like substances, and nigrosine dye, which is a proxy for highly absorbing aerosols.

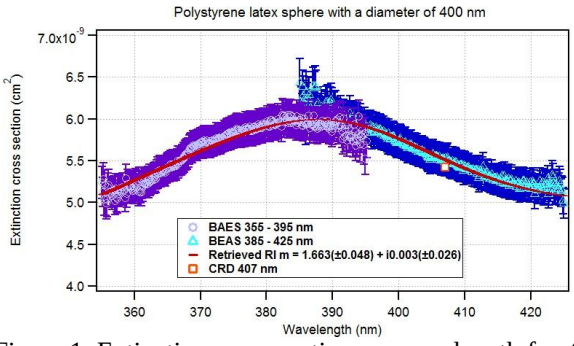

Figure 1. Extinction cross section vs. wavelength for 400 nm diameter PSL particles for two BAES channels, with spectral coverage from 355 – 395 nm (purple circles) and 385 – 425 nm (blue triangles). The red line represents the best Mie fit curve with a retrieved refractive index of m = 1.663 + i0.003. The orange square represents the measurement with a CRD at 407 nm.

This work was supported by the Israel Science Foundation (Grant #196/08) and by FP7-ENV-2010-265148-PEGASOS. Financial support at NOAA was provided by the NOAA Air Quality and NOAA Climate Research and Modeling programs. Y.R. acknowledges support by the Helen and Martin Kimmel Award for Innovative Investigation. J.M.F. is supported by a research grant from the Jinich Postdoctoral Fellowship.

Bond, T.C., Streets, D.G., Yarber, K.F., Nelson, S.M., Woo, J., and Kilmont, Z. (2004), *J. Geophys. Res.*, **109**(D14):

Washenfelder, R.A., Langford, A.O., Fuchs, H., Brown, S.S. (2008), *Atmos. Chem. Phys.*, **8**, 7779-7793.

M. O. Andreae and A. Gelencser (2006), *Atmos. Chem. Phys.*, **6**, 3131–3148.

Comprehensive Laboratory Characterization of a New Nano Water-based CPC and Performance Comparison to an Ultrafine CPC

A. Kupc[1], O.F. Bischof[2], M. Beeston[2], T. Tritscher[2], T. Krinke[2] and P.E. Wagner[1]

[1]Faculty of Physics, University of Vienna, Vienna, A-1090, Austria
[2]TSI GmbH, Research & Analytic, Aachen, 52068, Germany
Keywords: water-based condensation particle counter, lower size limit, counting efficiency, material sensitivity
Presenting author email: agnieszka.kupc@univie.ac.at

Ever since P.J. Coulier's experiments in 1875 the role of small particles acting as nuclei during the formation of cloud droplets has been studied. Only five years later John Aitken (1880) built the world's first instrument to measure particle concentrations of ambient air, today known as condensation particle counter (CPC). Yet it took until 2004 when Hering and Stolzenburg patented a method to use water as the condensing fluid in a laminar, thermally diffusive flow particle counting instrument.

The present study investigated the performance of a new Nano Water-based Condensation Particle Counter (N-WCPC, TSI 3788) to effectively measure airborne nanoparticles of various compositions. The N-WCPC's performance was assessed through comparison with the well established ultrafine CPC (TSI 3776), which was used as counting reference due to its identically specified lower cut size. In addition an aerosol electrometer (AE, TSI 3068B) was used as the primary reference for characterising aerosols over a mobility diameter range from 1.8 to 51 nm. An initial assessment of the urban aerosol in a light industrial area near a bus depot and motorway was carried out, followed by a comprehensive characterisation in the laboratory. The electrospray-based characterisation setup described by Liu et al. (2005) was used to produce particles from different materials such as sucrose, NaCl, proteins, and emery oil. Finally indoor air and a candle aerosol were assessed.

Size distributions of these aerosols were determined by a Nano Scanning Mobility Particle Sizer (nanoSMPS, TSI 3936N). Throughout the characterisation both counters and the AE always measured in parallel using a flow splitter (Figure 1).

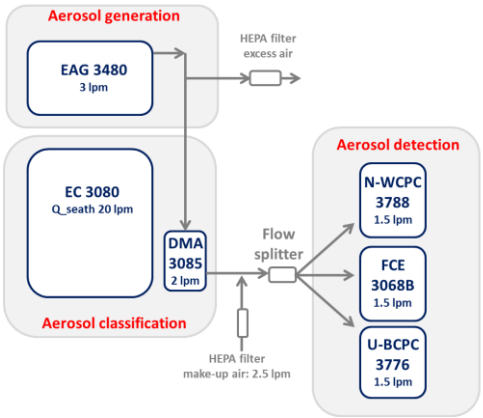

Figure 1. Schematic of the characterisation set-up

All measurements were performed at standard laboratory conditions with regards to operating temperatures. An inlet flow rate of 1.5 L/min was used by all three aerosol detection instruments.

The concentration linearity between the two CPC's with regards to a 64 hour urban background measurement is shown in Figure 2. This data was averaged over 5 min periods and demonstrates the excellent agreement between both particle counters for that aerosol, irrespective of the working fluid they use.

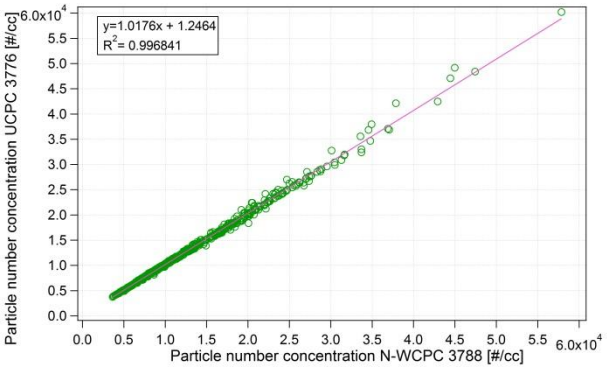

Figure 2. Linearity between particle number concentrations in urban background aerosol measured by the new N-WCPC and the UCPC

Size distributions of the urban aerosol observed were dominated mainly by particles below 150 nm in diameter, with a mode around 30 nm dependent on the actual traffic level.

Concerning the aerosol of different compositions generated in the laboratory, the counting efficiencies for the two CPC's were determined for each particle material using the ratio of the particle number concentration measured to the concentration determined by the aerosol electrometer.

This research has received funding from the EC's Seventh Framework Programme under the grant agreement no. 215072 (Marie Curie Initial Training Network "CLOUD ITN"), and from the Austrian Science Fund (project no. P 19546, L593)

Aitken, J. (1880). On dust, fogs and clouds. *Transactions of the Royal Society of Edinburgh*, **30**(1), 337–368

Hering, S. V., and Stolzenburg, M. R. (2005). *Aerosol Sci. Technol.* **39**:428–436.

Liu, W. et al (2005). Calibration of Condensation Particle Counters, *SAE Techn. Paper* 2005-01-0189

Calibration and performance of a novel particle sensor for automotive application

L. Ntziachristos[1], S. Amanatidis[1], A. Rostedt[2], J. Keskinen[2], K. Janka[3], J. Tikkanen[3]

[1]Aristotle University, Mechanical Engineering Dept, Lab of Applied Thermodynamics, P.O.Box 458, GR-54124, Thessaloniki, Greece
[2]Tampere University of Technology, Department of Physics, Aerosol Physics Laboratory, P.O.Box 692, FI-33101 Tampere, Finland
[3]PEGASOR Oy, Hatanpään valtatie 34c, FI-33100 Tampere, Finland
Keywords: combustion aerosol, automotive aerosol, calibration, real-time measurement
Presenting author email: samana@auth.gr

This paper presents the calibration and performance characteristics of a novel sensor designed to measure particulate concentration in the exhaust of engines and vehicles. The Pegasor Particle Sensor (PPS) operates by electrostatically charging particles drawn in its enclosure and then measuring the current produced by the charged particles as they leave the sensor. The basic principle of directly measuring the current escaping with charged particles was first described by Lehtimäki (1983). In the PPS the particles are charged by ions generated by corona discharge. Corona discharge is generated around a sharp tip at high voltage and is carried away as the pumping flow of an ejector. This charged flow mixes with the sample flow of the ejector pump and produces charged particles. After charging, the particles are neither collected on any filter nor accumulate on any part of the sensor. However, as charged particles leave the sensor, they produced an electrical current escaping the Faraday cup. Measurement of this current is proportional to the particle concentration.

In practical sensor realization and in addition of producing the electrically charged pump flow, clean air is used to cool and shield the critical insulators from soot deposition. As a result, all contamination-sensitive parts (corona tip, insulators) are shielded by clean air flow. The fact that the ion-containing pump flow is mixed extremely rapidly prior to the ejector nozzle enables efficient particle charging in minimal volume. This enables low internal gas volume in the sensor, and consequently, rapid response time. Those characteristics make the sensor ideal for automotive use, where rapid response time, high sensitivity and protection of sensitive components from a direct exposure to exhaust gases are required.

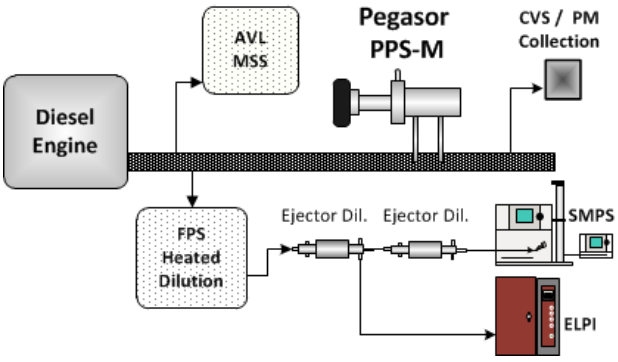

Figure 1. Setup used for the calibration of the PPS.

In this study the sensor is calibrated to measure the mass and number concentration of particles in the exhaust of diesel vehicles and engines, using the setup shown in Figure 1. A number of tests with a Euro 5 engine have been conducted under both steady-state and transient conditions and the signal of the sensor has been correlated to the mass and number of particles measured (Figure 2) by a gravimetric filter, an AVL micro-soot sensor and SMPS and ELPI instruments.

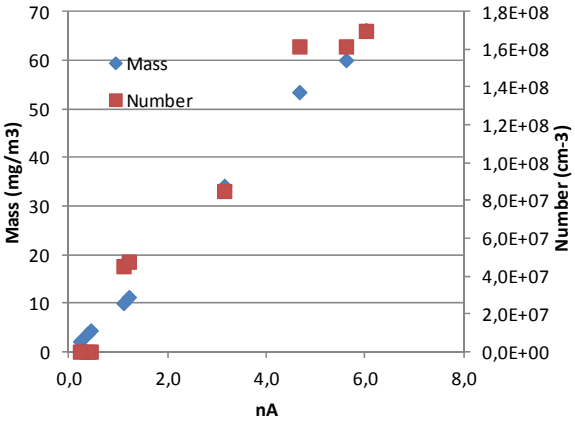

Figure 2. Correlation of sensor signal (x-axis) with diesel engine particle mass and number concentrations.

The calibration obtained with diesel measurements was compared to a laboratory calibration made with DOS test aerosol. The water CPC used as a reference instrument in the laboratory calibration was calibrated with single charged aerosol reference (SCAR, Yli-Ojanperä et al., 2010) to ensure the accuracy in the reference measurement.

Lehtimäki, M. (1983) Modified Aerosol Detector, in V.A. Marple and B.Y.H. Liu (Ed.), Aerosols in Mining and Industrial Work Environment., Vol. 3., 1135-1143. AnnArbor Science Publishers, Ann Arbor, Michigan, USA.

Yli-Ojanperä, J., Mäkelä, J.M., Marjamäki, M., Rostedt, A., Keskinen, J. (2010) “Towards traceable particle number concentration standard: Single charged aerosol reference (SCAR)” J. Aerosol Sci., 41, 719-728.

A novel portable instrument for exposure analysis in nanotechnology workplaces

C. Asbach[1], H. Kaminski[1], H. Fissan[1,2], T.A.J. Kuhlbusch[1,2], N. Azong-Wara[1], D. Broßell[3], R. Caldow[4], J. Scheckman[4], H.-G. Horn[5]

[1]Institute of Energy and Environmental Technology, 47229 Duisburg, Germany
[2]Center for NanoIntergration Duisburg-Essen, 47057 Duisburg, Germany
[3] Federal Institute for Occupational Safety and Health (BAuA), 10317 Berlin, Germany
[4]TSI Inc, Shoreview, MN, 55126, USA
[5]TSI GmbH, 52068 Aachen, Germany
Keywords: nanoparticle, exposure assessment, monitor, electrical mobility analysis
Presenting author email: asbach@iuta.de

The production and use of nanomaterials has risen at a constant pace over the recent years. Besides the tremendous beneficial properties of nanomaterials, they have also been reported to potentially cause adverse health effects. Inhalation is seen as the major uptake route and hence the assessment of exposure to airborne nanoparticles is of high relevance, particularly for workplaces where these particles are produced or processed. The established measurement technology for aerosol characterization is usually bulky and requires trained personnel for its operation and data evaluation. Easy-to-use, portable and battery operated devices are hence required. However, only a limited number of such devices exist.

The presentation will describe the development of a portable and battery operated instrument which allows for an extensive analysis of the workplace aerosol, but also limits the required effort for data evaluation. The developed instrument is based on electrical mobility analysis. Initially, larger particles are removed in a pre-separator with 450 nm cut-off and low pressure drop (Asbach et al., 2011). The remaining particle fraction then is charged to a known charge distribution (Kaminski et al., 2012) in a unipolar diffusion charger. The aerosol is then fractionated in a mobility classifier and the concentration of the classified aerosol measured in two sequential detectors. Due to the different particle size and morphology-dependent characteristics of the two sensors, this arrangement not only allows for the measurement of the particle number concentration but also provides insight into the size dependent particle morphology. Therefore, this measurement procedure may facilitate a first online distinction of engineered nanoparticles from background particles. In case of suspicion of the presence of engineered nanoparticles in the workplace air, an electrostatic precipitator (ESP) additionally can be enabled to sample aerosol particles onto substrates for consecutive SEM/EDX analysis that will provide a definitive proof for the presence or absence of engineered nanoparticles in the workplace air. The ESP is designed to deposit particles homogenously across the substrate when used along with the abovementioned charger and therefore also allows for a quantitative analysis. A thermal precipitator (Azong-Wara et al., 2009) can be used in addition to sample over a full work shift, i.e. 8 hours and provide averages of the size distribution, chemical composition and morphologies of the particles during the shift.

The presentation will cover the development of the instrument, experimental evaluation of its components and first results from the complete system.

Acknowledgement

The research leading to these results has received funding from the European Community's Seventh Framework Programme (FP7/2007-2013) under grant agreement n°211464-2.

References

Kaminski, H. et al. (2012) *Aerosol Sci. Technol.*, **46**:708-716.

Asbach, C., et al. (2011), *Aerosol Air Qual. Res.* **11**:487-496

Azong-Wara N., et al. (2009), *J. Nanopart. Res.* **11**: 1611-1624

Effect of particle diffusivity on DMAs with multiple monodisperse-particle outlets: theory validation and design optimization

M.Giamarelou[1], M. Stolzenburg[2], D.-R. Chen[3] and G. Biskos[1,4]

[1]*Dept. of Environment, University of the Aegean, Mytilene, Greece*
[2]*MRS Consulting, Sheboygan, WI, USA*
[3]*Dept. of Energy, Environmental and Chemical Eng., Washington University in St. Louis, St. Louis, MO, USA*
[4]*Faculty of Applied Science, Delft University of Technology, Delft, The Netherlands*

Keywords: MMO-DMA, Dual-DMA, transfer function, resolution.
Presenting author email: giamarel@env.aegean.gr

By simultaneously selecting aerosol particles having different sizes, Differential Mobility Analyzers (DMAs) with multiple monodisperse-particle outlets can have a number of advantages in aerosol metrology. When used in electrical mobility spectrometers, for instance, they can significantly reduce the time required to measure the particle size distributions. Depending on the relative location of the first and the last outlet from the inlet, one can also increase the dynamic mobility range of the measured particles in a single measurement.

Based on the approach proposed by Stolzenburg (1988), we have recently developed the theoretical framework for determining the transfer function and the resolution of DMAs with multiple monodisperse-particle outlets (cf. Giamarelou et al., 2011; 2012). To describe the spreading of the transfer function due to the Brownian motion of the particles, we divide the classifier into segments defined by successive monodisperse-particle outlets. The total diffusional broadening along the whole path of the particle that leads to the i^{th} sample exit can be approximated by

$$\sigma^2_{\Gamma_{i,total}} = \sum_{j=n}^{i} \sigma^2_{\Gamma_{i,j}} . \qquad (1)$$

Here $\sigma_{\Gamma_{i,j}}$ denotes the diffusional broadening of the particles classified through the i^{th} monodisperse-particle outlet during the time they travel through the j^{th} segment of the MMO-DMA.

Fig. 1a shows the comparison of the model to the measurements with the 3-monodisperse-particle-outlet DMA tested by Chen et al. (2007). The loss-corrected theoretical transfer functions for both sample outlets, at 2.54 cm and 15.24 cm, are in perfect agreement with the experimental values. The predicted resolution for each of the three outlets agrees well with the reported measurements (Fig. 1b), indicating that the theory captures well the broadening of the transfer function for particles having diameter smaller than 20 nm.

Using the validated transfer function model we provide design considerations for building a DMA with two monodisperse-particle outlets, and predict its performance under different operating conditions. A critical parameter when designing multiple-exit DMAs is the minimum distance between the entrance and the nearest sample exit as well as between the successive sample exits so that the flow profile remains laminar.

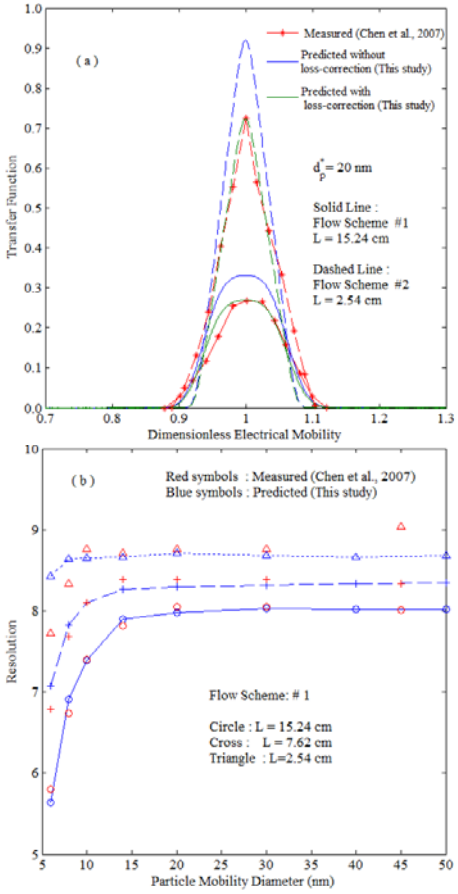

Figure 1 (a) Comparison between predicted and measured transfer function of the DMA with 3 monodisperse-particle outlets (measurements from Chen et al., 2007). The monodisperse-particle outlets are located 2.54, 7.62 and 15.24 cm downstream of the polydisperse aerosol inlet. Flow scheme #1 corresponds to 20 lpm sheath flow, 2.4 lpm polydisperse aerosol inlet flow, and 0.8 lpm for each monodisperse outlet flow. The respective values for flow scheme #2 are 20, 1.5 and 1.5 lpm. (b) Comparison between predicted and measured resolution of the DMA with 3 monodisperse-particle outlets.

References

Chen, D.-R., Li, W., Cheng, M.-D., 2007, *Aerosol Sci. & Technol.*, 41:217-230.

Giamarelou, M., Biskos, G., 2011, European Aerosol Conference, Manchester, Sept. 2011.

Giamarelou, M., Stolzenburg, M., Biskos, G., 2012, *Aerosol Sci. &Technol.*, (under revision).

Stolzenburg, M., 1988, PhD Thesis, University of Minnesota, Minneapolis, MN.

Monday, September 3, 2012

Poster session, Posters 1 - 327

Aerosol optical properties over East Asia: An integrating CMAQ-simulated and satellite-retrieved aerosol data using a data assimilation technique

C.H. Song, R.S. Park, K.M. Han and M.E. Park

Advanced Environmental Monitoring Research Center (ADEMRC), School of Environmental Science and Engineering, Gwangju Institute of Science and Technology (GIST), 1 Oryong dong, Buk-gu, Gwangju 500-712,Republic of Korea

Keywords: AOD, data assimilation, Direct Radiative Forcing, $PM_{2.5}$.
Presenting author email: chsong@gist.ac.kr

For a better estimation of direct radiative forcing by aerosols and particulate pollution (such as $PM_{2.5}$ or PM_{10}) over East Asia, the production of more accurate aerosol optical properties (e.g., Aerosol Optical Depth (AOD), Single Scattering Albedo (SSA), aerosol extinction coefficient (σ_{ext})) is of primary importance. For the purpose of producing the accurate aerosol optical properties, AOD, SSA and σ_{ext} over East Asia were first investigated in this study, based on US EPA Models-3/CMAQ v4.5.1 modeling. The CMAQ model simulations were improved in several ways, compared to the previous study (Song et al., 2008): (1) the wind fields from MM5 simulations were assimilated with QuikSCAT wind data; (2) the emission inventories of INTEX-B (for China and North Korea), REAS (for Japan) and CAPSS (for South Korea) were used for the year 2006 simulations; (3) for the NH_3 and BVOC (Biogenic BVOs) emissions, EDGAR and MOHYCAN emissions were adopted, respectively; (4) monthly variations for the NO_x, NH_3, NMVOCs and SO_2 were applied; (5) for the dust generation and transport in the domain, the operational ADAM (Asian Dust Aerosol Models) was used (Fig. 1); (6) all the MET/CMAQ simulations and emissions were carried out in a fine grid resolution of 30×30 km^2 for the entire year of 2006; (7) 4-D particulate species concentrations obtained from the CMAQ model simulations were converted into the 4-D AOD products, using Malm and Hand (2007)'s algorithm, which is evolved from the previous Malm (1994, 2000)'s algorithms; and (8) finally, the CMAQ-simulated AOD products were assimilated with MODIS-retrieved AOD.

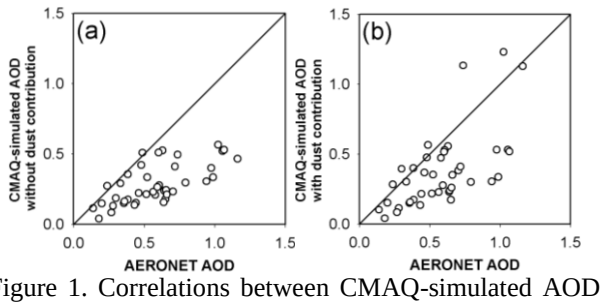

Figure 1. Correlations between CMAQ-simulated AOD and AERONET AOD in spring, 2006: (a) CMAQ-simulated AOD without dust contributions vs. AERONET AOD and (b) CMAQ-simulated AOD with dust contributions vs. AERONET AOD.

The results from the CMAQ model simulations (without assimilation) were improved greatly, compared to the previous study (Song et al., 2008) (e.g., from R=0.48–0.68 to R=0.77–0.89 for four seasons, R is correlation coefficient between CMAQ-simulated and MODIS-retrieved AODs). CMAQ-simulated SSA was also well matched with AERONET SSA, except for those near Honk Kong and Taipei, where biomass burning was strong from Jan. to Apr. It was also found that there were great matches between the vertical profiles of CMAQ-simulated σ_{ext} and LIDAR-derived σ_{ext}. The contributions of sulfate in summer, nitrate in winter, sea-salt in winter and dust in spring were large in East Asia. Especially, the large contribution of nitrate in winter to the AOD distribution over East Asia is remarkable compared to the previous study (Chung et al., 2010). In order to produce more accurate AOD products, the CMAQ-simulated AOD was assimilated with MODIS-retrieved AOD. Both the assimilated and AERONET AODs were better correlated with each other, compared to the correlation between CMAQ-simulated AOD and AERONET AODs (Table. 1). The obvious benefits for this study are that, with the improved aerosol optical properties, particulate pollution or PM forecasting over East Asia (e.g., AOD can be served as a proxy to $PM_{2.5}$) and direct radiative forcing by aerosols can be much better estimated in future.

Table 1. Statistical analysis among CMAQ-simulated and assimilated and AERONET AODs for four seasons, 2006.

AERONET vs.	period	R	RMSE	MNGE	MB	MNB
CMAQ	SPRING	0.59	0.31	45.24	-0.19	-29.88
	SUMMER	0.61	0.30	48.47	-0.13	-22.45
	FALL	0.69	0.24	61.08	-0.10	11.84
	WINTER	0.79	0.15	34.86	-0.07	-4.78
Assimilated	SPRING	0.71	0.20	26.41	-0.09	-8.69
	SUMMER	0.79	0.19	28.10	-0.06	-5.02
	FALL	0.77	0.20	63.15	-0.06	26.05
	WINTER	0.80	0.15	35.81	-0.07	-4.77

Chung et al. (2010) *Atmos. Chem. & Phys.*, **10**, 6007-6024.

Malm and Hand (2007) *Atmospheric Environment*, **41**, 3407-3427.

Song et al. (2008) *Atmos. Chem. & Phys.*, **8**, 6627-6654.

Temporal variations of the single scattering albedo in the southwestern Iberian Peninsula (Portugal)

S.N. Pereira[1], F. Wagner[1] and A.M. Silva[1]

[1]Évora Geophysics Centre, University of Évora, Évora, 7000, Portugal
Keywords: optical properties, single scattering albedo
Presenting author email: sergiopereira@uevora.pt

The direct effect of aerosol particles in terms of cooling or warming they can produce of the atmosphere depends, among other factors, on the single scattering albedo (ω_0) which is the ratio of the aerosol scattering to the extinction coefficients (σ_{sp} and σ_{ap} respectively).

This work presents an analysis of the temporal variations of the single scattering albedo, near the surface, at Évora, Portugal. Measurements of spectral scattering and absorption coefficients in the period of 2007 to 2009 were used. The scattering coefficients were measured at 450, 550 and 700 nm wavelengths with the three-wavelength integrating nephelometer (TSI, model 3563) (see e.g. Anderson et al., 1996) and the absorption coefficient was measured at 670 nm with the multi-angle absorption photometer (MAAP model 5012) (Petzold and Schönlinner, 2004).

The single scattering albedo was computed as $\omega_0(\lambda) = \sigma_{sp}(\lambda)/(\sigma_{sp}(\lambda) + \sigma_{ap}(\lambda))$ at the wavelength $\lambda = 670$ nm. Different temporal scales ranging from daily to seasonal scales were studied.

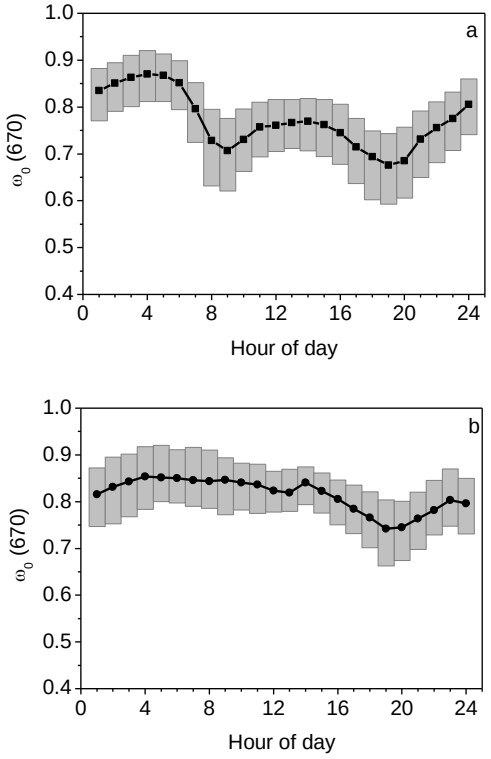

Figure 1. Median daily variation of the single scattering albedo considering (a) the working days (Sunday to Friday) and (b) Sundays in the period between 2007 and 2009. The grey bars stand for the P25 and P75 quartiles.

The mean value (± one standard deviation) of $\omega_0(670)$ for the whole period was found to be 0.77±0.11. The monthly mean values were in the range of 0.72 (November) and 0.81 (August) and a seasonal trend was observed which was characterized by lower values during winter/autumn and higher values during summer/spring seasons. The decrease in the single scattering albedo during the colder seasons corresponds to a relatively more absorbing aerosol population caused by the increase in anthropogenic production related to both traffic and wood burning for heating. Thus contributing to the increase of both scattering and absorption coefficients, but with the later increasing relatively more (Pereira et al., 2011a; Pereira, 2011).

The daily cycle of the single scattering albedo highlights the local particle production, namely related to traffic in the area. Figure 1 shows the daily variation of $\omega_0(670)$ considering the working days, from Monday to Friday (with the usual city activities being carried out) as well as Sundays, when the city activity is mainly suppressed, in particular during the morning hours.

This work was supported by Portuguese FCT under PhD grant SFRH/BD/29008/2006.

Anderson, T.L., Covert, D.S., Marshalll, S.F., Laucks, M.L, Charlson, R.J., Waggoner, A.P., Ogren, J.A., Caldow, R., Holm, R.L., Quant, F.R., Sem, G.J., Wiedensohler, A., Ahlquist, N.A., and Bates, T.S., "Performance characteristics of a high-sensitivity, three-wavelength total scatter/backscatter nephelometer," J. Atmospheric and Oceanic Technology, 13, 967-986, 1996.

Pereira, S. N., Wagner, F., and Silva, A. M.: Seven years of measurements of aerosol scattering properties, near the surface, in the south-western Iberia Peninsula, Atmos. Chem. Phys., 11, 17-29, 2011.

Pereira, S. N. Climate relevant characterization of different Aerosol types observed near the surface over Portugal. PhD Thesis. University of Évora, 2011.

Petzold, A. and Schönlinner, M.: Multi-angle Absorption photometry-A new method for the measurement of aerosol light absorption and atmospheric black carbon, J. Aerosol Sci., 35, 421–441, 2004.

Retrieval of Single Scattering Albedo values from Brewer spectrophotometer irradiance measurements at Uccle, Belgium

V. De Bock[1] and H. De Backer[1]

[1]Observations department, Royal Meteorological Institute of Belgium, Uccle, Belgium
Keywords: single scattering albedo, aerosol modelling, aerosol measurement, optical properties
Presenting author email: Veerle.DeBock@meteo.be

Aerosols can significantly affect the radiative balance of the Earth, both in a direct, semi-direct and indirect manner. Because of a lack of information concerning the temporal and spatial distribution of aerosols, they are key contributors to the uncertainties in current climate studies (Andreae, M. O. *et al*. 2005). The influence of aerosols is especially important in the UV spectrum, since the impact of UV radiation on human health, the biosphere and atmospheric chemistry depends strongly on the characteristics and quantity of aerosols in the atmosphere.

To gain a better understanding of the effect of aerosols in the UV, knowledge of the parameters that determine the optical and physical properties of aerosols is essential. More than 80% of the aerosol effect on UV radiation due to increasing turbidity is determined by the Aerosol Optical Depth (AOD) and the Single Scattering Albedo (SSA) (Petters, J.L. *et al*., 2003).

There are many studies on the retrieval of the SSA in the visible part of the spectrum, but less research has been done to determine the SSA values for the UV wavelengths (Petters, J.L. *et al*., 2003). The difficulty in estimating the SSA in the UV range is due to rather large uncertainties existing on ground based and space measurements in this wavelength range (Buchard, V. *et al.*, 2011). But since several studies (such as IPCC, 2007) indicate that significant uncertainties in global columnar SSA may constitute the largest single source of uncertainty in the current modeling estimates of aerosol climate forcing (Kazadzis, S. *et al*., 2010), it is necessary to improve our knowledge on the SSA in the UV.

It is possible to obtain SSA values with an reverse engineering procedure using UV irradiance measurements from the Brewer spectrophotometer, coupled with a Radiative Transfer Model (RTM). In such a procedure, the SSA value is changed until the modeled and observed UV irradiance are in agreement.

The RTM that will be used here is the Tropospheric Ultraviolet and Visible Radiation Model (TUV model version 3.0, Madronich 1993). This RTM can be used to model the UV irradiances for completely cloudless circumstances. The TUV model needs different input parameters, such as the ozone value, the AOD value, the cloud optical depth and the surface albedo. For the ozone value, the Direct Sun (DS) value (from the Brewer instrument) closest to the time of observation is used. At Uccle, we have developed different methods to retrieve the AOD from Brewer measurements at different wavelengths, using either the direct sun measurements (which lead to AOD at 306, 310, 313, 316 and 320nm) or the sun scan measurements (which enabled the retrieval of AOD at 340nm) (De Bock, V. *et al*., 2010). For this study, we will use the values retrieved from the DS measurements at the 5 different wavelengths to derive the SSA at the same wavelengths. We use 0.05 as surface albedo value and 0.0 as cloud optical depth.
The resulting SSA at the different wavelengths will be presented.

This work was supported by the Belgian Federal Science Policy Office under grant SD/CS/07A.

Andreae, M. O., Jones, C. D. and Fox, P. M.: Strong present-day aerosol cooling implies a hot future, *Nature*, **435**, 1187–1190, doi:10.1038/nature03671, 2005.

Buchard, V., Brogniez, C., Auriol, F. and Bonnel, B., Aerosol single scattering albedo retrieved from ground-based measurements in the UV and visible region, *Atmos. Meas. Tech*., **4**, 1-7, doi: 10.5194/amt-4-1-2011, 2011.

De Bock, V., De Backer, H., Mangold, A. and Delcloo, A., Aerosol Optical Depth measurements at 340nm with a Brewer spectrophotometer and comparison with Cimel sunphotometer observations at Uccle, Belgium, *Atmos. Meas. Tech*., **3**, 1577-1588, doi:10.5194/amt-3-1577-2010, 2010.

Kazadzis, S., Gröbner, J., Arola, A. and Amiridis, V., The effect of the global UV irradiance measurement accuracy on the single scattering albedo retrieval, *Atmos. Meas. Tech*., **3**, 1029-1037, doi: 10.5194/amt-3-1029-2010, 2010.

Petters, J.L., Saxena, V.K., Slusser, J.R., Wenny, B.N. and Madronich, S., Aerosol single scattering albedo retrieved from measurements of surface UV irradiance and a radiative transfer model., *J. Geophys. Res*, **108**, D9, 4288, doi: 10.1029/2002JD002360, 2003.

Constraining optical properties and refractive index of soot through combined experimental and modelling studies

J. Kim[1], H. Bauer[2], T. Dobovicnik[3], R. Hitzenberger[4], D. Lottin[5], D. Ferry[6] and A. Petzold[1]

[1]Institute of Atmospheric Physics, German Aerospace Centre (DLR), 82234 Oberpfaffenhofen, Germany
[2]Institute of Chemical Technologies and Analytics, Vienna University of Technology, 1060 Vienna, Austria
[3]Aerosol d.o.o, 1000 Ljubljana, Slovenia
[4]Institute for Experimental Physics, University of Vienna, 1090 Vienna, Austria
[5]ONERA - The French Aerospace Lab, F-92322 Châtillon, France
[6]CINaM-CNRS, Aix-Marseille University, 13009 Marseille, France
Keywords: Soot particles, Optical properties, Refractive index, Organic carbon.
Presenting author email: Jin.Kim@dlr.de

Soot particles generated from combustion processes are mixtures of elemental (black) and organic carbon. Because of their strong contribution to light absorption, many field and lab studies have been carried out to investigate their optical properties. However, a full characterisation including chemical and physical analyses is scarce. We present an optical closure study, which is complemented by chemical and physical characterisation of soot particles. Our main goals were a better understanding of the complex refractive index of the organic carbon fraction and the closure of modelled and measured soot optical properties.

Absorption and scattering coefficients of soot particles, generated from a propane diffusion flame under varying fuel-to-air (C/O) ratios, were measured with a three-wavelength nephelometer and a particle soot absorption photometer. Intensive optical properties such as single scattering albedos (SSA) and Ångström exponents were derived from the measured absorption and scattering coefficients. In addition to optical measurements, information on particle size distribution, morphology and elemental carbon to total carbon (EC/TC) ratio were obtained from scanning mobility particle sizer measurements, transmission electron microscopy analyses and thermal-optical analyses respectively. Based on these data, optical properties of soot particles were modelled and compared with the experimental data.

Particles generated under low C/O ratios had high elemental carbon fraction (EC/TC > 0.7) and were fractal-like aggregates (mobility diameter ~ 100 nm, fractal dimension = 1.74 ± 0.6, primary particle radius = 5 – 6 nm). Rayleigh-Debye-Gans (RDG) theory (Sorensen, 2001) could model their optical properties well as shown in Figure 1. In contrast, particles produced under high C/O ratios had low elemental carbon fraction (EC/TC < 0.2), were smaller (mobility diameter < 50 nm) and spherical in shape. Their optical properties were better modelled with Mie theory as can be seen in Figure 1.

By minimising the difference between the calculated and measured SSA and Ångström exponents for particles with high organic carbon (OC) content, refractive index of OC at different visible wavelengths were deduced as presented in Table 1. The estimated values are in close agreement with values previously reported by Kirchstetter *et al.* (2004) and Adler *et al.* (2010) and they show strong wavelength dependence. The OC component is speculated to be similar to polycyclic aromatic hydrocarbon (PAH) compounds, which have strong absorption in the ultra-violet spectral region (Schnaiter *et al.*, 2006). The OC refractive index inferred from this study is deemed valuable since there is still limited data on optical constants of OC.

Table 1. Estimated real (n) and imaginary (k) parts of organic carbon refractive index.

λ/nm	n	k
467	1.59 ± 0.02	0.11 ± 0.03
530	1.47 ± 0.03	0.04 ± 0.02
660	1.47 ± 0.03	0 + 0.01

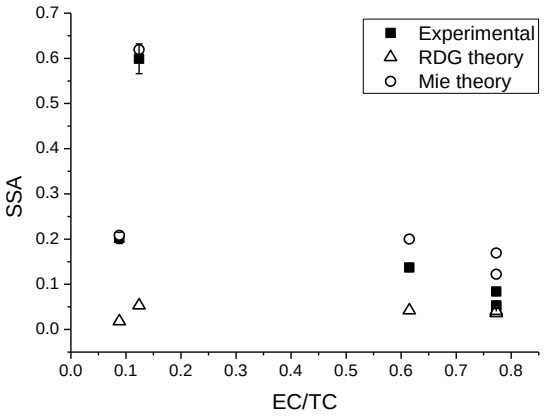

Figure 1. SSA at λ = 530 nm plotted as a function of elemental carbon to total carbon (EC/TC) ratio.

This work was supported by the European Aviation Safety Agency under the SAMPLE II Contract EASA.2009.OP.18. The authors are grateful for the valuable support from A. Ibrahim (DLR), M. Johnson (Rolls-Royce, UK), R. Marsh and A. Crayford (Cardiff University, UK).

Sorensen, C. M. (2001) *Aerosol Sci. Technol.*, **35**, 648-687.

Kirchstetter, T. W., Novakov, T. and Hobbs, P. V. (2004) *J. Geophys. Res.-Atmos.*, **109**, D21208.

Adler, G., Riziq, A. A., Erlick, C. and Rudich, Y. (2010) *Proc. Natl. Acad. Sci. USA*, **107**, 6699-6704.

Schnaiter, M., Gimmler, M., Llamas, I., Linke, C., Jaeger, C. and Mutschke, H. (2006) *Atmos. Chem. Phys.*, **6**, 2981-2990.

Modelling light scattering by mineral particles with small-scale surface roughness

M. Kahnert[1,2], T. Nousiainen[3], M. A. Thomas[1], and J. Tyynelä[3]

[1]Swedish Meteorological and Hydrological Institute, Research Department, SE-601 76 Norrköping, Sweden

[2]Chalmers University of Technology, Department of Earth and Space Science, SE-412 96 Gothenburg, Sweden

[3]Department of Physics, P. O. Box 48, FI-00014 University of Helsinki, Finland

Keywords: Mineral dust, scattering, surface roughness.

Presenting author email: michael.kahnert@smhi.se

Small-scale surface roughness is a morphological feature that is frequently encountered in mineral aerosols, ice-cloud particles that have experienced riming, as well as interplanetary and interstellar dust particles. Modelling the optical properties of such particles is notoriously difficult, since the particles' size parameters are often much larger than unity, while the surface roughness features typically vary on a scale smaller than the wavelength of light. To accurately model the light scattering process in the presence of subwavelength-scale surface structures requires the use of numerically exact methods for solving Maxwell's equations. However, for particles with large size parameters such methods are computationally highly demanding and can be plagued by ill-conditioning problems. To address these problems, a T-matrix approach has recently been proposed and tested which combines the use of group theory with a perturbation method for solving the light-scattering problem (Kahnert and Rother, 2011). This approach has been tailored to particles with small-scale surface perturbations.

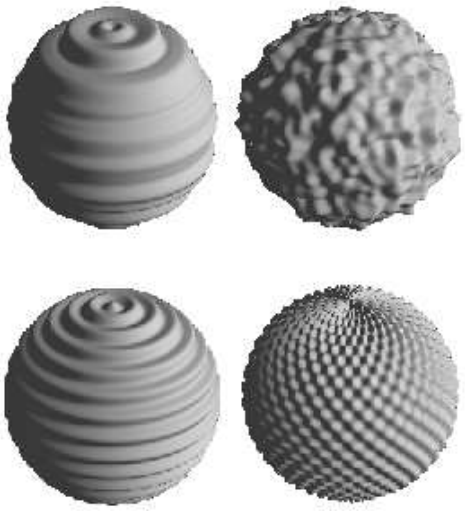

Figure 1: Example of model particle used in this study.

We apply this method to perform a comparative study of different models for small-scale surface roughness, as illustrated in Fig. 1. The emphasis is on comparing 2D- and 3D-roughness models, as well as regular and stochastic surface perturbations. The comparison are performed for size parameters of $x = 5$ and $x = 50$, as well as for refractive indices m=1.6+0.0005i and 3+0.1i. The former is taken as a proxy for silicate particles, and the latter is typical for hematite particles, both at visible wavelengths.

The results clearly show that the effect of small-scale surface roughness on the scattered intensity and polarisation is strongly dependent on the size parameter and the refractive index. 2D-roughness models predict a stronger impact of surface roughness on optical properties than 3D-roughness models. Stochastic surface perturbation cause a more pronounced modulation of the scattered polarisation and of the depolarisation ratio, while regular roughness structures can have a stronger impact on the scattered intensity and its angular distribution.

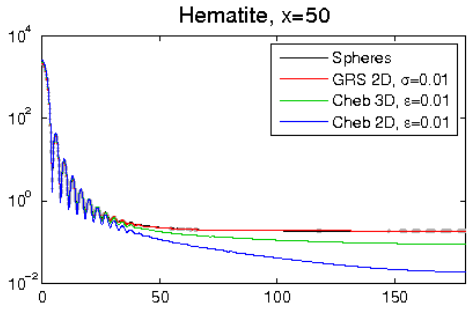

Figure 2: Phase function computed for hematite, x=50.

As an example, figure 2 shows the phase function computed for m=3+0.1i and x=50. In this case, particles with a 3D and, even more so, 2D regular surface perturbation deviate strongly from corresponding results for unperturbed spheres at scattering angles $> 50^\circ$. Particles with irregular surface perturbations scatter similarly to unperturbed spheres.

Kahnert, M., Rother, T. (2011) Opt. Express **19**, 11138-11151.

Physical and optical properties of atmospheric aerosol in Eastern Antarctica

A. Mangold[1], H. De Backer[1], V. De Bock[1], C. Hermans[2], I. Gorodetskaya[3] and W. Maenhaut[4]

[1]Royal Meteorological Institute of Belgium, Brussels, Belgium; [2]Belgium Institute for Space Aeronomy, Brussels, Belgium; [3]Catholic University of Leuven, Leuven, Belgium; [4]Ghent University, Ghent, Belgium
Keywords: atmospheric aerosol, optical properties, physical properties, AOD
Presenting author email: alexander.mangold@meteo.be

Aerosols play an important role in atmospheric physics and chemistry. They provide surfaces for photochemical reactions and they attenuate, scatter and absorb solar radiation and re-distribute in this way the energy coming from the sun, influencing photochemical reactions, the temperature at the surface and within the atmosphere and exerting a positive or negative radiative forcing. In addition, aerosols influence the formation, the properties and the lifetime of clouds. Aerosol measurements at several wavelengths are further important to derive information about aerosol type.

The Belgian Antarctic research station Princess Elisabeth, inaugurated in February 2009, is situated north of the Sor Rondane Mountains in Dronning Maud Land, East Antarctica, on the Utsteinen ridge (71°57'S, 23°20'E, 1390 m asl, Pattyn *et al.*, 2010). The station is designed as a zero-emission station with power supplied by wind turbines, solar panels and batteries. Two diesel-generators serve only as back-up. The station is manned only during austral summer. In winter, station and instruments operate in automatic mode with remote control. The station is located around 180 km inland, where aerosol concentration and composition can be different from coastal sites.

A Cimel 8-wavelength (UV-A to near-IR, measuring aerosol optical depth) Sun photometer belonging to the AERONET network (aeronet.gsfc.nasa.gov) has been installed since 2009 on the top of the station's roof with a perfect field of view. In 2010, a 7-wavelength (UV-A to near-IR) aethalometer (Magee Scientific, absorption coefficient, mass concentration of light-absorbing aerosol) and a Tapered Element Oscillating Microbalance with Filter Dynamics measurement system (TEOM-FDMS, total aerosol mass concentration) have been set up inside a container-size shelter about 60 m south of the research station, with the air inlet on the top of the shelter. In addition, a Brewer spectrophotometer (total ozone column, spectral UV radiation, UV-B aerosol optical depth) was installed at the end of 2010 on the roof of the main station. In February 2012, a 3-wavelength nephelometer (Aurora 3000, Ecotech, scattering coefficient), an ultrafine condensation particle counter (U-CPC, model 3776, TSI, total aerosol number concentration), and a Laser Aerosol Spectrometer (LAS, model 3340, TSI, aerosol size distribution) completed the instrument set-up in the aerosol shelter. Data of an automatic weather station (Van Den Broeke *et al.*, 2005), installed about 300 m away from the station are used for additional data interpretation.

The main wind direction at the location is ESE, connected with an average wind speed above 5 m/s. The aerosol measurements are thus most of the time not affected by the station's activities or emissions.

In addition to the austral summer measurements, the first two months of winter data from the TEOM-FDMS and the aethalometer could be collected during winter 2011. The winter measurements of light-absorbing aerosol mass concentration and of the absorption coefficient are especially interesting because the Antarctic background conditions could be measured.

The mean black carbon (BC) concentration (at 880 nm) was 2.6±6.1 ng/m^{-3}. The high standard deviation indicates that the averaging period (1 hr) might still be too short, causing negative values. The mean BC concentration detected at 370 and 470 nm together was 9.5±5.8 ng/m^{-3}, and the mean over all seven wavelengths was 5.9±4.8 ng/m^{-3}.

The mean absorption coefficient detected at 880 nm (BC absorbs strongest at this wavelength) was 5.3±4.8 Mm^{-1}. At 370 nm, the absorption coefficient was 23.9±12.4 Mm^{-1}, revealing that not only pure BC was present as absorber. The mean absorption Angstrom exponent (370 to 880 nm) was 2.0±1.3, reflecting that several absorbing aerosol types were present, as pure BC shows an absorption Angstrom exponent around 1.

During February 2012, the aethalometer and the nephelometer have been operated simultaneously. Therefore, both scattering and absorption coefficients have been measured, and a direct measurement of the single scattering albedo was possible. However, due to the very low aerosol concentrations in Antarctica, the instruments operate at their lower detection limit and careful data interpretation is necessary. E.g., the average aerosol optical depth (AOD) at 500 nm is only 0.02.

We will present data of the recent austral summer, when all instruments have been set up together for the first time. The measured aerosol size distribution and total number concentration will give further insight, which aerosol types were present.

This work was supported by the Belgian Federal Science Policy under grants EA/34/1A and EA/34/1B. Many thanks go to all expedition team members who helped in Antarctica to realise what has been done.

Pattyn, F., Matsuoka, K. and Berte, J. (2010), *Antarctic Science*, **22(1),** 79-85.

Van Den Broeke, M., Van As, D., Reumer, C. and De Wal, R. (2005), *J. Climatol*., **25**, 1081-1101.

Aerosol Scattering and Absorption Angström Exponents during desert dust events over Granada

A.Valenzuela[1], F.J. Olmo[1, 2], H. Lyamani[1, 2], M. Antón[1, 2], A.Quirantes[1], and L. Alados-Arboledas[1, 2]

[1] Dpto. Física Aplicada, Universidad de Granada, Fuentenueva s/n, 18071-Granada, Spain.
[2]Centro Andaluz de Medio Ambiente (CEAMA), Avda. del Mediterráneo s/n, 18006-Granada, Spain.
Presenting author email: avalenzuela@ugr.es

One of the largest uncertainties in the radiative forcing of climate is due to atmospheric aerosols. In fact, dust particles in the atmosphere play a relevant role in the climate system by altering the earth's energy budget through the scattering and absorption of solar radiation. The Absorption Angström Exponent (AAE) quantifies the absorption of solar radiation by atmospheric aerosols, being defined as the negative of the slope of a log-log plot of the aerosol absorption optical depth (AAOD) versus wavelength. Values of the AAE close to 1 are refered to urban aerosols (black carbon) while dust particles present AAE values larger than 2. However, AAE depends of the wavelength range (Bergstrom et al., 2007). On the other hand, the Extintion and Scattering Angström Exponent (EAE and SAE) are used to evaluating the extinction and scattering of solar radiation due to atmospheric aerosols. These two parameters depend primarily on the size of the particles, ranging from 4 for very small aerosols to 0 for large particles.

Simultaneous measurements of a passive remote sensor (sunphotometer CIMEL) and ground-based "in situ" instruments (integrating nephelometer and PSAP) are used to the characterization of the aerosol optical properties during desert dust events over Granada from 2005 to 2010. The main objective of this study is to analyze the wavelength dependence of aerosol optical properties, focusing on the aerosol absorption and scattering properties during these desert dust events.

Column-integrated characterization of the atmospheric aerosol has been performed by means of a sun-photometer CIMEL CE-318-4 included in the AERONET network (Holben et al., 1998). This sun-photometer makes direct sun measurements with a 1.2º full field of view at 340, 380, 440, 670, 500, 870, 940 and 1020 nm. In addition, the CIMEL instrument performs sky radiances, both in almucantar and principal plane configurations, at 440, 670, 870 and 1020 nm. At surface, we have measured the aerosol scattering coefficients (σ_{sp}) at three wavelengths (450, 550 and 700 nm) using a nephelometer (TSI model 3563). The aerosol absorption coefficients (σ_{ap}) were measured using a Particle Soot Absorption Photometer at three wavelengths (467, 531 and 650 nm).

We have computed SAE and AAE between 440-1020 nm wavelength ranges at the atmospheric column. At the surface, we have computed the SAE between 450-700 nm wavelength ranges while that AAE has been determinate between 467-650 nm wavelength ranges. During desert dust events high mean value of AAE and low mean value of SAE have been found at the atmospheric column. Simultaneously, these same parameters were determined at the surface. The SAE (AAE) showed slight higher (smaller) mean value at the surface than at the atmospheric column (Table1). These results could be related to two reasons: the different wavelength ranges used in the computation of the SAE and AAE at the column and at the surface, and the relatively high contribution of urban aerosol near the surface. In no-Dust conditions high mean SAE value and mean AAE value close to unity were found at the atmospheric column. This suggests the prevalence of the fine particles at the study site with an important contribution of absorbing aerosol at the atmospheric column in agreement with Lyamani et al. (2011) who showed that the aerosol over Granada contain a large fraction of absorbing particles. Additionally, the fine particles were dominant during no-dust conditions at the surface as indicated the high mean SAE value. However, the AAE showed a slight mean higher value in no-dust conditions than during desert dust events at the surface. This result could be due to resuspension processes of local mineral particles associated with anthropogenic activities.

Table 1. Scattering and Absorption Angström Exponent at surface and column-integrated over Granada.

	Dust		No-Dust	
	SAE	AAE	SAE	AAE
CIMEL	0.4±0.2	1.6±0.2	1.2±0.4	0.9±0.6
PSAP	--------	1.3±0.2	-------	1.4±0.3
NEPHE.	0.9±0.6	-------	1.6±0.4	-------

This work was supported by the Andalusia Regional Government through projects P08-RNM-3568 and P10-RNM-6299, by the Spanish Ministry of Science and Technology through projects CGL2010-18782, CSD2007-00067 and CGL2011-13580-E/CLI; and by EU through ACTRIS project (EU INFRA-2010-1.1.16-262254).

Bergstrom, R.W., Pilewskie, P., Russell, P.B., Redemann, J., Bond, T.C., Quinn, P.K., Sierau, B. (2007) *Atmos. Chem. Phys.,* **7**, 5937-5943.

Holben, B.N., Eck, T.F., Slutsker, I., Tanre, D., Buis, J.P., Setzer, A., Vermote, E., Reagan, J.A., Kaufman, Y.J., Nakajima, T., Lavenu, F., Jankowiak, I., Smirnov, A. (1998) *Remote Sens, Environ.,* **66**, 1-16.

Lyamani, H., Olmo, F.J., Alados-Arboledas, L. (2010) *Atmos. Chem. Phys.,* **10**, 239-254.

DIAPASON: A better assessment of the impact of Saharan dust on PM measurements

G.P. Gobbi [1], H. Wille[2], R. Sozzi[3], S. Frey[2], A. Bolignano [3], F. Costabile[1], F. Angelini[1], and F. Barnaba [1]
[1] ISAC-CNR,Via Fosso del Cavaliere 100, Rome, 00133, Italy
[2] Jenoptik ESW GmbH, Jena, Germany
[3] Latium Agency for Environmental Protection, ARPA Lazio, Rieti, Italy.
Keywords: dust, Mediterranean, aerosol, particulate matter.
Presenting author email: f.barnaba@isac.cnr.it

Introduction

Mineral particles from the North African deserts are among the natural contributions mostly affecting the PM levels in southern Europe (e.g., Gobbi et al., 2007). The EU Air Quality Directive 2008/50/EC allows Member States to subtract the contribution of natural sources before comparing the ambient PM concentrations to the relevant limit values set by the directive itself. It is therefore important to detect and characterize desert-dust advections by means of reliable, operational techniques.

Methodology

The EC LIFE+2010 DIAPASON Project (Desert dust Impact on Air quality through model-Predictions and Advanced Sensors ObservatioNs), intends to build on and upgrade the guidelines set by the EC to quantify the effects of Saharan advections (EC, 2011). At the core of DIAPASON stands the prototyping of affordable remote sensing devices (Polarization Lidar-Ceilometers, PLCs). These will be used in conjunction with optical particle counters to "certify" the presence of Saharan dust.

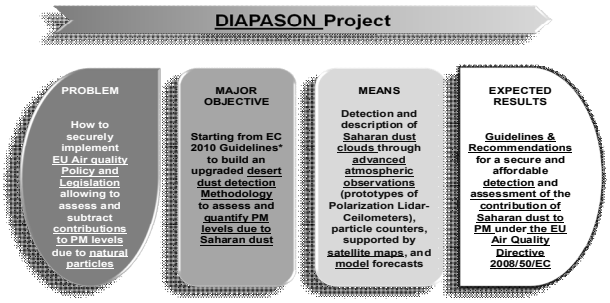

Figure 1. A snapshot of the DIAPASON project: Problems, Objectives, Means, and Expected Results

Results and discussion

An example of the DIAPASON approach is given in Figure 2, where EU guidelines' steps to identify Saharan advections (model forecast and PM levels at background sites) are "certified" by the actual observation of the dust cloud profile made by a research polarization lidar (e.g. Gobbi et al., 2000). This communication will discuss a one-year set of such comparisons.

Conclusion

DIAPASON aims at translating the results of research-based assessments into an operational, cost-effective, user-oriented methodology. It will be first implemented in Rome to be then easily transferable to the countries in Europe facing similar environmental problems. As an added value, the DIAPASON PLC-based approach will also be able to detect and monitor, with profiling capabilities, advections of other natural particulate matter as volcanic ash or wild-fire plumes, also considered in the EC 2011 Guidelines, bearing further benefits on civil protection and air traffic security.

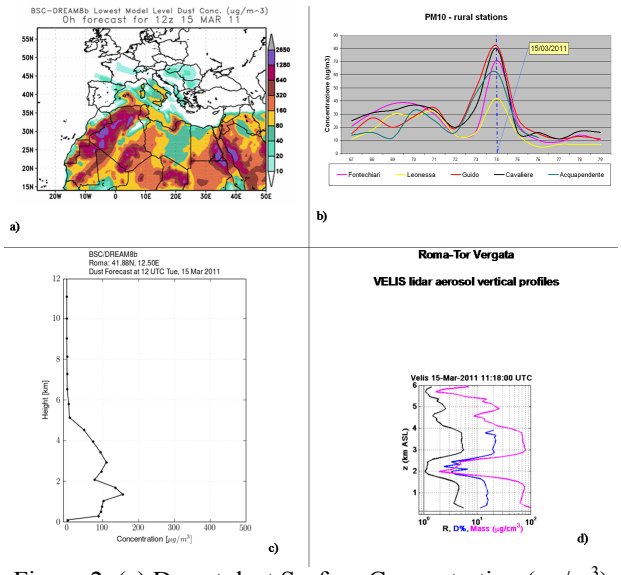

Figure 2. (a) Desert dust Surface Concentration (g/m^3) as forecast by the BSC DREAM Model for March 15, 2011. (b) PM10 measured at rural background stations surrounding Rome (Italy) in the period 8-20 March 2011 (Julian day 67-79). (c) Vertical profile of the desert dust concentration (g/m^3) as forecast by the BSC DREAM Model over Rome on 15 March 2011. (d) VELIS lidar profiles (0-6 km) of the aerosol backscatter ratio (R, black line), Depolarization Ratio (blue) and estimated dust mass (g/m^3, magenta), as observed in Rome on 15 March 2011.The retrieval of the dust mass from the lidar trace follows the dust volume estimation of Barnaba and Gobbi (2001), assuming a particle density of 2 g/cm^3.

Barnaba, F and G. P. Gobbi, 2001. Lidar estimation of tropospheric aerosol extinction, surface area and volume: Maritime and desert-dust cases. Journal of Geophysical Research, 106-D3, 3005-3018.

European Commission (EC), 2011. Establishing guidelines for demonstration and subtraction of exceedances attributable to natural sources under the Directive 2008/50/EC on ambient air quality and cleaner air for Europe. 38 pp., February, 2011.

Gobbi G.P., Barnaba F., Giorgi R., Santacasa A., 2000. Altitude-resolved properties of a Saharan-Dust event over the Mediterranean. Atmos. Env., 34, 5119-5127.

Gobbi, G. P., et al., 2007. Estimating the impact of Saharan Dust on the PM10 record in Rome (Italy) in 2001, Atmos. Environ., 41, 261-275.

Spatial variation of aerosol optical properties around the high-alpine site Jungfraujoch

P. Zieger[1], E. Kienast[2], M. Starace[3], von Bismarck[3], N. Bukowiecki[1], U. Baltensperger[1], F.G. Wienhold[2], T. Peter[2], T. Ruhtz[3], M. Collaud Coen[4], L. Vuilleumier[4], O. Maier[4], E. Emili[5], C. Popp[6], and E. Weingartner[1]

[1]Laboratory of Atmospheric Chemistry, Paul Scherrer Institut, 5232 Villigen, Switzerland
[2]Institute for Atmospheric and Climate Science, ETH Zürich, Switzerland
[3]Institute for Space Sciences, Freie Universität Berlin, Germany
[4]MeteoSwiss, 1530 Payerne, Switzerland
[5]Department of Geography, University of Bern, 3012 Bern, Switzerland
[6]Empa, 8600 Dübendorf, Switzerland

Keywords: optical properties, remote sensing, in-situ measurements, CLACE
Presenting author email: paul.zieger@psi.ch

We present results from the extensive field campaign CLACE 2010 (Cloud and Aerosol Characterization Experiment) performed in summer 2010 at the Jungfraujoch (JFJ) and Kleine Scheidegg (KLS) in the Swiss Alps. The main goal of this campaign was to investigate the vertical variability of aerosol optical properties around the JFJ and to show the consistency of the different measurement techniques considering explicitly the effects of relative humidity on the aerosol light scattering. Various aerosol optical and microphysical parameters were recorded using in-situ and by remote sensing techniques. The in-situ measurements of aerosol size distribution, light scattering, light absorption and scattering enhancement due to water uptake were recorded at the JFJ at 3580 m a.s.l. A unique set-up allowed remote sensing measurements of aerosol columnar and vertical properties from KLS located about 1500 m below and in the direct vicinity of JFJ (horizontal distance of approx.4.5 km, see Fig. 1). Two satellite retrievals from the Spinning Enhanced Visible and InfraRed Imager (SEVIRI) and the Moderate Resolution Imaging Spectroradiometer (MODIS) and back trajectory analysis were added to the comparison to account for a wider geographical context.

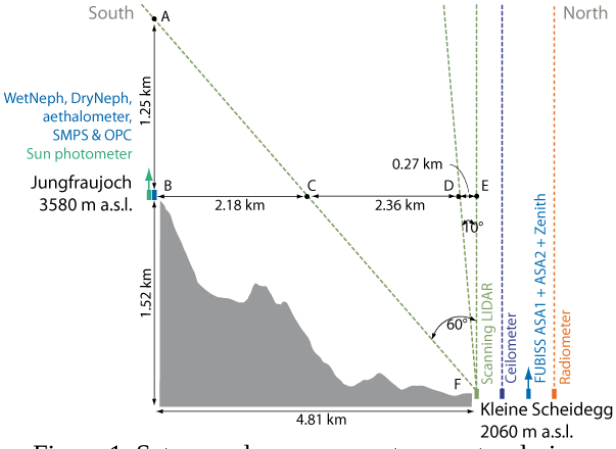

Figure 1. Set-up and measurement geometry during CLACE 2010

All in-situ and remote sensing measurements were performed in clear correspondence. The ambient extinction coefficient measured in-situ at the JFJ agreed well with the LIDAR (Light Detection and Ranging) retrieval at JFJ altitude, if certain assumptions on the unknown lidar ratio were taken. The comparison was clearly affected by the orography due to the exposed location of the JFJ on a saddle between two mountains and next to a large glacier. The local relative humidity (RH) around the JFJ was often larger than in the line of the LIDAR measurement, especially when the wind originated from South via the glacier. An example result is seen in Fig. 2, where the squared correlation coefficient of the ambient in-situ aerosol extinction coefficient vs. the LIDAR retrieved value is seen for different heights and RH data classes for an example lidar ratio of LR=75sr.

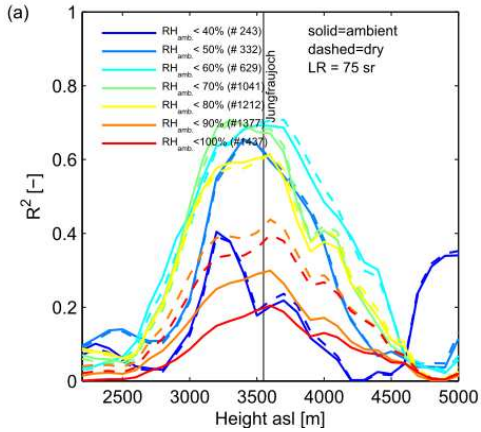

Figure 2. Squared correlation coefficient of the ambient in-situ extinction coefficient compared to the LIDAR retrieved value (at LR=75sr) at different heights above the LIDAR and for different ambient RH classes.

The dominance of long-range transported Saharan dust was observed in all measurements for several days, but for a shorter time period in the in-situ measurements due to the vertical structure of the dust plume. The columnar aerosol optical properties retrieved from SEVIRI and MODIS showed the same magnitude and a similar temporal evolution as the ground based measurements from KLS and JFJ. The remaining differences are attributed to the complex terrain and simplifications in the aerosol retrieval scheme in general.

Light scattering by ice-covered carbonaceous aerosol particles

S.S. Vlasenko[1],E.F. Mikhailov[1]

[1]Department of Atmospheric Physics, St.-Petersburg State University, Russia
Keywords: heterogeneous ice nucleation, hygroscopic growth, light scattering.
Presenting author email: Sergey.Vlasenko@paloma.spbu.ru

The formation of ice particles in the atmosphere has an appreciable impact on the radiation transfere, and hence on the Earth climate. The atmospheric clouds glaciation mainly happens via a variety of heterogeneous processes with involving of aerosol particles (ice nucleation, deposition freezing, immersion freezing, etc). Therefore the atmospheric ice particles certainly contain foreign inclusions and this can have some effect on their optical properties. The most interesting is a case when ice covers light-absorbing aerosol such as soot or smoke particles because multiple studies predict an increase of scattering and absorption cross section of absorbing core encapsulated into non-absorbing shell (Fuller 1999, Liu *et al.* 2008)

This study is a laboratory experiment aimed to quantify the effect of water crystallization on light scattering by water-covered smoke particles. To measure the optical properties of iced aerosol we improved the experimental setup designed for studying soot-water drop agglomerates (Mikhailov *et al.* 2006). This setup is schematically presented in Fig.1.

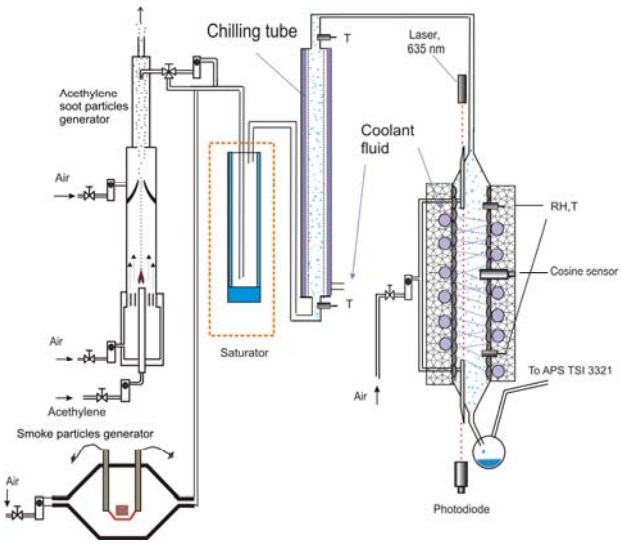

Figure 1. The experimental setup.

The carbonaceous aerosol was produced by combustion of acethylene (black soot) or wood (smoke). Then particles passed through saturator into chilling tube where aerosol flow can be gradually cooled down to -40^{0}C. The cooling led to vapour condensation and formation water shell on the particles. Depending on temperature in the tube this shell froze or kept liquid that made possible to observe the effect of phase transition on the optical properties of particles under consideration. After chilling tube the smoke particles entered optical cell which could be kept at temperature about -10^{0}C that guaranteed against ice fraction melting. A collimated laser beam at 635nm was used as a light source for the optical cell. The intensity of transmitted light was measured with a photodiode to calculate extinction volume coefficient and total light scattering was measured with an integral cosine sensor mounted in the middle of the cell. Provided the proper calibration the single scattering albedo of aerosol could be derived from the measuring data. The preliminary results are presented in the table 1.

Table 1. The single scattering albedo for carbonaceous aerosol particles covered with water or ice.

Soot type	Dry soot	Soot+water	Soot+ice
Acethylene soot	0,24±0.03	0,26±0.03	0,31±0.03
Wood smoke	0,74±0.03	0,80±0.03	0,88±0.03

Evidently the freezing of water shell leads to increase of the single scattering albedo for both types of examined soot aerosol

This work was supported by the RFBR under grant 10-03-00950-a and 11-05-00945-a.

K. A. Fuller. (1999) J. Geophys. Res. D **109**,15941-15954.

L. Liu, M.I. Mishchenko, and W.P. Arnott.(2008) *J. Quant. Spectrosc. RA.*, **109**: 2656–2663.

E.F. Mikhailov, S.S. Vlasenko, I.A. Podgorny, V. Ramanatan, C.E.Corrigan (2006) J. Geophys. Res. **111** doi:10.1029/2005JD006389

First ambient aerosol measurements with a polar nephelometer

M. Paixão[1], T. Müller[1] and A. Wiedensohler[1]

[1]Department of Physics, Leibniz Institute for Tropospheric Research, Leipzig, Germany
Keywords: aerosol optics, nephelometer, scattering coefficient, Saharan dust.
Presenting author email: paixao@tropos.de

In this work we present the first results of a campaign of measurements with a polar nephelometer of the angular scattering coefficient of ambient aerosol particles held on Cape Verde Islands, 2011. During the term of the campaign, the aerosol was dominated by marine and Saharan dust particles.

Aerosol particles are known to contribute to climate change (Forster, 2007). The asymmetry parameter or phase function of aerosol particles plays a key role in a proper evaluation of its radiative forcing effect. The polar nephelometer for aerosol monitoring comes to fill this lack of ambient aerosol measurements.

From the first designs of integrating nephelometers, introduced by (Beuttell and Brewer, 1949), several improvements have been made mostly regarding the detection limit and light source. That allowed the development of a larger number of applications other than measuring the horizontal visibility. Most of the studies rely on the spectral dependency of the scattering coefficient and its relation to the aerosol size distribution.

The Aurora4000 offers not only information about the total and backscattering coefficients of light by aerosols particles but also more detailed information about the angular characteristics in the forward hemisphere, measuring the scattered light for several illumination sectors by blocking part of the emitted light with a controllable shutter. For more details about the instrument please refer to (Müller, 2012). In this way, it's possible to evaluate a quasi-phase function from the differences of the scattering intensities, e.g. I(0°)-I(10°), I(10°)-I(20°), and so on, and by fitting the Henyey-Greenstein equation, determine the asymmetry parameter

Preliminary results

The data set of the campaign was divided in two periods according to date (end of November, and beginning of December 2011), due to dust load and calibration reasons.

The Figure 1 shows the time series from the first part of the campaign of the total scattering coefficient for the nephelometer wavelengths (450, 525, 635 nm) in the left, and the Ängstrom exponent, in the right axis. There is a clear change in the values of the Ängstrom exponent when the scattering values begin to increase due to the entry of continental air mass loaded with dust particles.

Comparing the dust concentration to the scattering coefficient for the second part of the campaign, in Figure 2, it's possible to identify two different correlations: the black cross shows the correlation when the aerosol is dominated by dust particles, from day 345 to 351, recalling that marine aerosol is always present, whereas the grey circle represents a more mixed state of aerosol particles.

In addition, the evaluation of a quasi-phase function in the forward hemisphere is in progress, and comparison with the results from Mie Theory will be performed. Future analysis includes the development of a reliable method to derive the asymmetry parameter together with size distributions measurements.

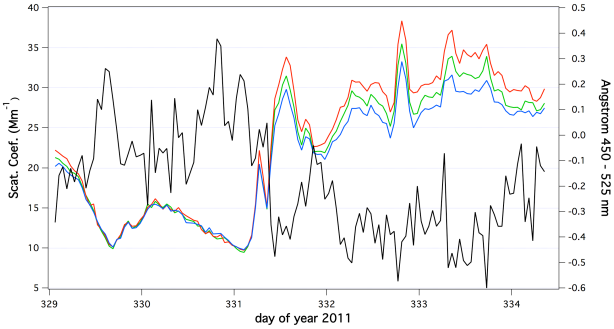

Figure 1. Time series of total scattering coefficient for blue, green and red channels (450, 525 and 635 nm, respectively) in left axis, and Ängstrom exponent (black line) in the right axis for the first part of the campaign.

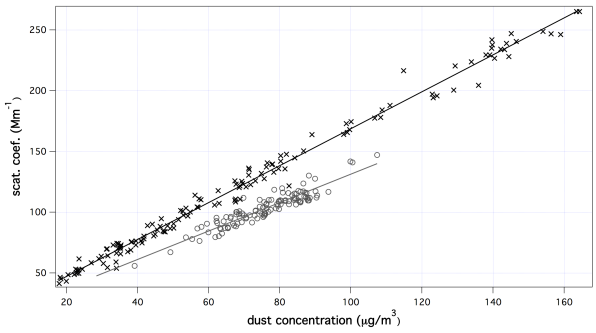

Figure 2. Correlation plot of total scattering coefficient (525 nm) and dust concentration in Cape Verde for the second part of the campaign.

Beuttell, R. G., and Brewer, A. (1949) *J. Sci. Instr. Phys. Ind.* **26**, 375-359.

Forster, P., Ramaswamy, V., Artaxo, P., Berntsen, T., Betts, T., and Fahey, D. (2007) *IPCC*, Cambridge University Press.

Müller, T., Paixao, M., Wiedensohler, A. (2012) *European Aerosol Conference*, Granada, Spain.

SPECTRAL DEPENDENCE OF IN-SITU AEROSOL OPTICAL PROPERTIES

F. Costabile[1], F. Angelini[1], F. Barnaba [1] and G.P. Gobbi [1],
[1] ISAC-CNR,Via Fosso del Cavaliere 100, Rome, 00133, Italy
Keywords: aerosol particles, Mediterranean, absorption, Angstrom exponent.
Presenting author email: f.barnaba@isac.cnr.it

Introduction

Aerosols play a significant role in the atmosphere from air pollution to climate. The Mediterranean is a unique area in terms of aerosol composition (e.g., Barnaba and Gobbi, 2004), climate (Giorgi and Lionello 2008), and interaction with urban emissions (e.g.:Costabile et al., 2010). Here, one-year in situ, multi-wavelength observations of aerosol absorption and scattering in the visible region will be discussed, with the objective to analyse optical impacts of aerosol populations, the focus on absorbing/ultrafine particles.

Methodology

Measurements, carried out in Rome in 2010-11, include scattering (σ_{sp}) and absorption (σ_{ap}) coefficients by 3-λ integrating nephelometer (Ecotech), and 3-λ PSAP (Radiance Research), total particle counts by CPC (TSI) and OPC (FAI).

Results and discussion

Distinctive diurnal and seasonal features of the aerosol properties and trends were observed (Fig. 1, Fig.2).

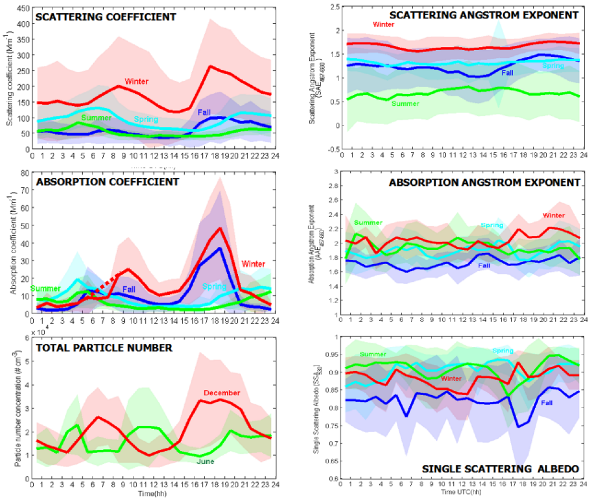

Figure 1. Seasonal change (color code) and diurnal cycles of absorption and scattering coefficients @530 nm, AAE and SAE (467-660 nm), SSA@467nm, and total particle number concentration.

An optical classification of different aerosol types was obtained by combining Single Scattering Albedo (SSA), Scattering Angstrom Exponent (SAE, 467-660 nm), and Absorption Angstrom Exponent (AAE, 467-660 nm), together with total particle number. The optically relevant aerosol populations include: dust, marine aerosols, inorganic and organic accumulation mode, biomass burning, organic condensation mode, soot mode, Aitken mode, and aged nucleation mode particles.

Conclusion

Results , indicate a strong impact of absorbing and UFP aerosols on the spectral dependence of both scattering and absorption properties. In general an enhanced absorption due to UFPs can increase the wavelength dependence of SSA, as well as decrease SAE.

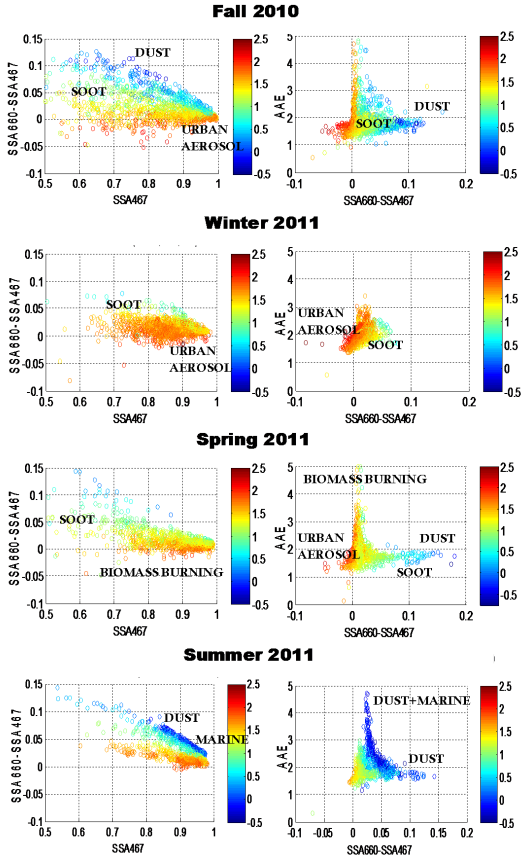

Figure 2. Seasonal Relationships linking SAE, AAE, and SSA @467 nm. Left column: SSA (x axis) and spectral variability (dSSA =SSA 660 nm - SSA 467 nm, y axis). Right column: dSSA (x axis) and AAE (y axis). (Color code=SAE).

Barnaba, F., and G. P. Gobbi, Aerosol seasonal variability over the Mediterranean region and relative contribution of maritime, continental and Saharan dust particles over the basin from MODIS data in the year 2001, Atmos. Chem. Phys., 4, 2367-2391, 2004.

Costabile, F., Amoroso, A., Wang, F., 2010. Sub- m particle size distributions in a suburban Mediterranean area. Aerosol populations and their possible relationship with HONO mixing ratios. Atmos. Environ., 44(39), 5258-5268.

Giorgi, F., Lionello, P., 2008. Climate change projections for the Mediterranean region. Global and Planetary Change, 63(2–3), 90-104.

Aerosol Characteristics and Radiative Forcing during summer and winter seasons over Pakistan

Khan Alam[1,3*], Thomas Trautmann[2], Thomas Blaschke[1]

[1]Department of Geography and Geology, University of Salzburg, Hellbrunnerstrasse 34, Salzburg 5020, Austria
[2]German Aerospace Centre, Remote Sensing Technology Institute, Oberpfaffenhofen, 82234 Wessling, Germany
[3]Institute of Physics and Electronics, University of Peshawar, Peshawar 25120, Khyber Pakhtunkhwa Pakistan
Key words: Aerosol optical depth; Ångström exponent; Radiative forcing; AERONET, Pakistan.
email: khanalamso@gmail.com

Very few studies have been published that focus on aerosols in Pakistan. Therefore, the present study has the potential to fill a geographic gap in our present knowledge of aerosol characteristics, radiative properties and the aerosols' impact on regional climate.

Aerosol Characteristics and radiative forcing have been analyzed through the ground-based Aerosol Robotic Network (AERONET) over the two megacities of Lahore and Karachi for summer (April-June) and winter (December-February) of 2010-11. The average AOD values in summer and winter are 0.66±0.30, 0.50±0.18 and 0.67±0.40, 0.34±0.12 in Lahore and Karachi respectively.

The relationship between the Absorption Ångström Exponent and the Extinction Ångström Exponent provided an indication of the relative proportions of urban-industrial and mineral dust aerosols over the two sites. The averaged aerosol ARF values over Lahore and Karachi for the entire period covered by the observations were −22.5±5.9 Wm^{-2} and −18±2.2 Wm^{-2} at the TOA and −96±13 Wm^{-2} and −60±6.8 Wm^{-2} at the surface, respectively, giving an averaged atmospheric forcing of 74.56±16.8 Wm^{-2} over Lahore and 41.85±6.4 Wm^{-2} over Karachi, which indicates significant heating of the atmosphere at both sites. The average heating rate during summer was 2.3±0.1 and 1.2±0.2 $Kday^{-1}$ and during winter was 1.8±0.4 and 1.1±0.1 $Kday^{-1}$ over Lahore and Karachi respectively.

Acknowledgment:
This work was suported by Higher Education Commission of Pakistan.

References:

Alam, K., Trautmann, T., Blaschke, T. (2011a). *Atmospheric Research 101, 773-782.*

Alam K., Blaschke, T., Madl, P., Mukhtar, A., and Hussain, M., Trautmann, T., Rahman, S. (2011b). *Journal of Environmental Monitoring13, 1944-1952.*

Alam, K., Qureshi, S., Blaschke, T. (2011c). *Atmospheric Environment 45, 4641-4651.*

Arola, A., Schuster, G., Myhre, G., Kazadzis, S., Dey, S., Tripathi, S.N. (2011). *Atmospheric Chemistry and Physics 11, 215-225.*

Russel, P. B., Hamill, P., Livingston, J. M., Shinozuka, Y., Strawa, A., Redemann, J., Omar, A., Clarke, A. D., Bergstrom, R. W., Holben, B., Ferrare, R., Burton, S. *American Geophysical Union Meeting 2010b; December 13-17,(2010); San Francisco, CA.*

Seasonal distinctions and temporal trends in frequency of different types of hygrograms in West Siberia

S.A. Terpugova, T.A. Dokukina, E.P. Yausheva and M.V. Panchenko

V.E. Zuev Institute of Atmospheric Optics, Tomsk 634021, Russia
Keywords: scattering coefficient, relative humidity, hygrogram
Presenting author email: swet@iao.ru

Transformation of the atmospheric aerosol under impact of the relative humidity modifies its scattering and absorbing properties and, hence, the climatic effects. Correct account for the aerosol in radiative and climatic models needs knowledge of the seasonal and regional peculiarities of the aerosol hygroscopicity.

In this paper we analyze the results of the 12-year long (2000-2011) study of transformation of aerosol particles at artificial humidification in the near-ground layer of the atmosphere near the city of Tomsk (56.5°N, 85.05°E). The parameter under investigation was the angular scattering coefficient at the angle of 45° and wavelength of 0.51 μm as function of relative humidity (hygrogram).

At the initial stage of our investigations we used the single-parameter representation of the angular scattering coefficient as a function of relative humidity:

$$\mu = \mu_0(1-Rh)^{-\gamma}, \quad (1)$$

where μ is the angular scattering coefficient, μ_0 is the angular scattering coefficient due to the dry matter of aerosol particles, γ is the parameter of condensation activity, and *Rh* is relative humidity. Parameter γ depends, first of all, on the ratio of soluble and insoluble species in the dry matter of aerosol particles.

As our data show, only about 70% of measured hygrograms can be satisfactory described by formula (1). Along with such a dependence, two other types of hygrograms are observed in the atmosphere (Terpugova et al, 2004).

Figure 1 shows the schematic plots of different types of hygrograms and their fraction in different years and seasons. The prevalent type of hygrograms in summer is G_0 (70-80% in all years). The fraction of hygrograms G_0 in winter and autumn is 50-70%, and in spring it does not exceed 40%. The number of situations with hygrograms of G_1 type diminished in all seasons since 2000 till 2011 from ~ 40% to ~ 10%. Respectively, the number of days with G_2 hygrograms has ascended. It is most noticeable in spring, when the type G_2 becomes prevalent (the quantity of hygrograms of this type increased up to ~ 60%). The values *Rh**, at which the derivative of the scattering coefficient upon 1- Rh (in logarithmic scale) rapidly changes, or has a break, are 60±5% in the case of hygrogram G_1 and 70±3% for G_2 type in all seasons.

Obviously, in the case of hygrogram G_0 we observe uniform water vapor uptake by particles, without explicit phase transition. In the case of hygrogram G_1, particles at low relative humidity weakly absorb water, but the particle substance is gradually dissolved. When some critical value *Rh** is reached, the concentration of solution becomes so that the saturated vapor pressure over the droplet decreases, and subsequent condensation of water vapor becomes more intensive. As for the hygrogram G_2, at the value of relative humidity *Rh** the particle substance is dissolved in the condensing water, so the droplet volume dramatically increases, and hence, the scattering coefficient also grows.

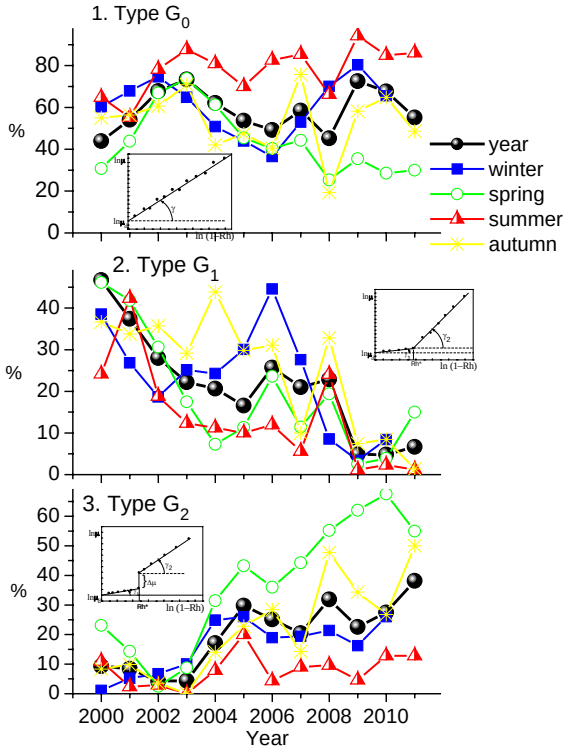

Figure 1. Different types of hygrograms and frequencies of their realization

Considering the shape of the dependence and the value of relative humidity at which the phase transition occurs, one can estimate the presence of different soluble salts in the aerosol particles. According to the data generalized by Martin (2000), the most close values to that observed in our experiments are NH_4NO_3, NaBr (60%); $(NH4)_3H(SO4)_2$ (69-70%); NaCl, KCl, $NaNO_3$ (73-75%).

This work was supported by Russian Foundation for Basic Researches under grant 10-05-00162.

Martin, S.T. (2000) *Chem. Rev*. **100**, 3403–3453.

Terpugova, S.A., Panchenko, M.V., Sviridenkov, M.A., and Yausheva, E.P. (2004) *J. Aerosol Sci*. **35**, suppl. 1, 1043–1044.

Trends in aerosol optical properties using AERONET surface observations

Aswathy V Nair and S. K. Satheesh
Centre for Atmospheric and Oceanic Sciences
Indian Institute of Science
Bangalore - 560012, India.
Tel: 080-22932505; Fax: 080-23600865
Email: aswathy.india06@gmail.com

The role of aerosols in the radiative forcing of the planet remain highly uncertain (IPCC 2007). Changes in the concentration and nature of aerosol cause serious concern since it affects the climate in regional and global scale. Trends in Aerosol Optical Depth (AOD) and Angstrom parameter over a regional scale have been reported earlier, but very few studies address the issues related to the changes in aerosol properties on a global scale. In this study, using AERONET surface observations, the trends in the fundamental aerosol properties like AOD, fine mode AOD, coarse mode AOD and Single Scattering Albedo (SSA) is analysed globally along with its effect on regional climate. The association of these aerosol trends with the decadal population rate of the sites are also investigated.

Trend analysis over 71 surface based observations showed a significant spatial inhomogenity. Asian continent shows a significant increasing trend in AOD compared to the other continents. Many of the Asian sites exhibit an alarming rate of increase in AOD from approximately 0.01 to 0.03/year. We have also observed that increasing trends in AOD not always coincide with the sites having increasing population rate. Simultaneous trend analysis of Fine AOD, Coarse AOD and SSA along with AOD present a comprehensive picture of the aerosol trend of each site under study.

In the current scenario of changing aerosols and its influence on the global climate, present study provides an opportunity to improve the understanding of the changing aerosol optical properties over the globe.

Optical properties of SiO_2 particles : inversion data from laboratory IR absorption spectra.

Denis PETITPREZ[1], Hervé HERBIN[2],

[1]Laboratoire de Physico-Chimie des Processus de Combustion et de l'Atmosphère (PC2A), UMR CNRS 8522, Université Lille 1, Cité Scientifique - Bâtiment C11, 59655 Villeneuve d'Ascq, France

[2]Laboratoire d'Optique Atmosphérique (LOA), UMR CNRS 8518, Université Lille 1, Cité Scientifique - Bâtiment P5, 59655 Villeneuve d'Ascq, France

Keywords: optical properties, SiO_2, refractive index
Presenting author email: Denis.Petitprez@univ-lille1.fr

Due to their ability to absorb and to scatter radiations, airborne particles play an important role in the energy budget of the earth-atmosphere system. It is assumed that aerosols are one of the atmospheric constituents participating to the cooling effect, but estimates are highly uncertain owing to the large spatial and temporal variability of aerosol concentration and physical properties.

The measurements from space-borne instruments are the only means for observing aerosol distributions from local to global scale. In particular, thermal infrared imagers such as MODIS or SEVIRI are routinely used to detect aerosols. Nevertheless, these broadband sensors are not suitable to distinguish the aerosol composition. Recent high spectral resolution sounders such IASI or Tanso-FTS are able to overcome these limitation. However, to fully exploit the hyperspectral instruments capabilities it is essential to have reference optical properties of various particles and mainly refractive indices.

Indeed, the knowledge of refractive indices is essential because it describe the proportioning of scattering and absorption of light by such particle matter. Moreover, the refractive index is strongly depending on the aerosol composition, size and shape.

The aim of this work is to measure high resolution transmittance spectra of model airborne SiO_2 particles in the infrared region and to use a Mie inverse algorithm to retrieve complex refractive indices. Refractive index measurements are generally performed by measuring absorbance or transmittance with bulk material of interest or particles diluted in solid pellets. In this study, we have recorded transmittance spectra of calibrated airborne particles by IRTF spectroscopy.

Aqueous solutions of calibrated SiO_2 microspheres (Bangs Laboratories, Inc.) were generated using an atomizer (TSI 3076). After drying, the continuous flow of aerosol particles was directed into a 10 m absorption length multipass cell within an IRTF spectrometer (Antaris Thermo Scientifique). The size distribution of the particles was measured at the exit of the multipass cell using an aerodynamic particle sizer spectrometer (TSI APS 3321). Concentration between 500 and 6000 particles per cubic centimetre were used for each 3 particle diameter: 0.5, 1 and 2 µm. 300 IRTF records were collected and averaged at a spectral resolution of 2 cm^{-1}. The IRTF spectra for SiO_2 microspheres (Ø = 2 μm) is displayed Fig1 showing an intense band around 1100 cm^{-1} .

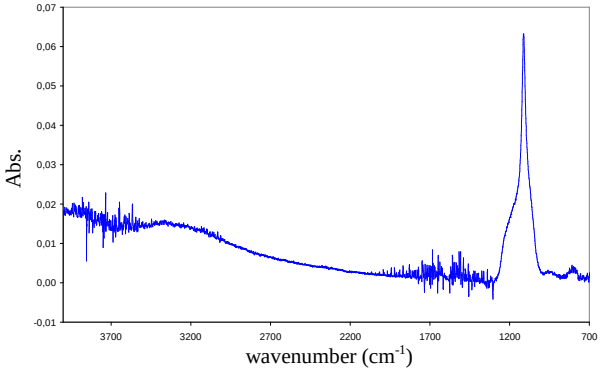

Fig. 1: Absorption spectra of calibrated SiO_2 particles Ø = 2 μm, [SiO_2] = 1430 particle.cm^{-3}.

The complex refractive indices of particles are obtained at each wavenumber by combining the Mie theory, the Kramers-Kronig relations, and a Levenberg-Marquardt algorithm. This inverse model allows avoiding some errors introduce by the extrapolated formulas of Kramers-Kronig relations. This methodology has the advantage to can be applied for any spherical particles.

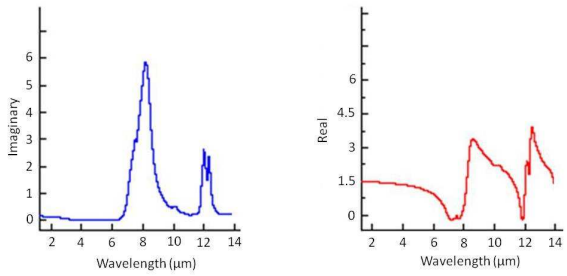

Fig. 2: Retrieved imaginary and real refractive indices of SiO_2 particles.

Experiments with particles (Ø = 0.5 μm and Ø = 1 μm) are currently in progress highlighting size dependence.

Climatlogy of aerosol optical properties with a synergy of remote sensing/altitude in situ measurements.

M. Hervo, K. Sellegri, J-C. Roger.

LaMP/OPGC, Université Blaise Pascal, Clermont-Ferrand, France.

Understanding spatial and temporal variability of aerosol particles in the atmosphere is important to characterize their contribution to health, visibility and climate. The aerosol vertical distribution is less documented than the horizontal variability because of the difficulty to make continuous altitude measurements compared to ground-based platforms.

For the first time to our knowledge, a long term in situ and co-located remote sensing study of optical aerosol properties has been realized at an elevated research station. The Puy de Dôme (1465m above sea level) is ideally situated to investigate aerosols vertical variability in both Planetary Boundary Layer and Free Troposphere.

We used a combination of in-situ (Nephelometer, MAAP, HTDMA, SMPS, OPC, AMS, TEOM) and remote sensing (LIDAR, Sun Photometer) instruments to realize a climatology of the optical aerosol properties. Mie calculation were computed from the size distribution measured by the SMPS and the OPC, grown at the ambient relative humidity from the HTDMA measurements. The synergy between the different instruments sampling in-situ allowed us to calculate a refractive index. During intensive field campaigns we also performed a complete optical closure to test the routine methodology of calculation of this refractive index. Aerosol mass vertical profile retrievals algorithms were then applied using the in-situ information.

Using the Lagragian model HYSPLIT we performed a classification of the air masses arriving at the Puy de Dôme and their corresponding aerosol properties. We found significant differences in the Angstrom coefficient, the single scattering albedo and the LIDAR ratio between, local, oceanic and Saharan air masses. We highlight the importance of a correct mass-extinction ratio and a well-known hygroscopicity to compute vertically resolved mass distribution from LIDAR extinction.

Combined observations with multi-wavelength Raman lidars and sun photometers on the southern Iberian Peninsula

J. Preißler[1], J.A. Bravo-Aranda[2,3], F. Wagner[1], M.J. Granados-Muñoz[2,3], F. Navas-Guzmán[2,3], J.L. Guerrero-Rascado[1,2,3], H. Lyamani[2,3], and L. Alados-Arboledas[2,3]
[1]Évora Geophysics Center, University of Évora, Évora, 7000, Portugal
[2]Andalusian Center for Environmental Research (CEAMA), University of Granada – Autonomous Government of Andalusia, Granada, 18006, Spain
[3]Department of Applied Physics, University of Granada, Granada, 18006, Spain
Keywords: Saharan dust, active and passive remote sensing.
Presenting author email: jana@uevora.pt

Objectives of this study were the combination of lidar and sun photometer data from different stations and consequently the determination of the vertical and horizontal distribution as well as the characterisation of free tropospheric aerosol layers.
Lidar measurements performed in Granada (37.16° N, 3.6° W, 680 m above sea level (asl)) and Évora (38.57° N, 7.91° W, 290 m asl) on the southern Iberian Peninsula were compared within this study. The distance between the two EARLINET stations (*Bösenberg et al.*, 2003) is about 410 km. The ground-based lidar systems in Granada and Évora both enable the determination of extinction coefficients at 355 and 532 nm, backscatter coefficients at 355, 532 and 1064 nm as well as the depolarisation ratio at 532 nm. Besides ground-based lidar measurements, sun photometer data from several AERONET stations (*Holben et al.*, 1998) and from two further sun photometers were used. Additionally, CALIOP data (*Winker et al.*, 2007) was compared to the data of the ground-based lidars.
A layer of Saharan dust was observed in the free troposphere over both lidar stations on 29 August 2011. In the evening the layer was detected between 2.6 and 3.7 km asl over Évora and between 2.9 and 3.4 km asl over Granada. Example profiles of extinction and backscatter coefficients as well as lidar ratios (LRs) and Ångström exponents (AEs) from ground-based lidar measurements in Granada and Évora are shown in Fig. 1. The data was averaged over 30 min. The layer mean backscatter and extinction-related AEs at the pair of wavelengths 355, 532 nm were larger over Granada than over Évora. Urban and industrial pollution from Granada or Moroccan sources might cause the higher values observed in Granada. The contribution of those sources is not evident in Évora. Throughout the whole period the AEs at both stations were clearly below 1. This indicates a strong contribution of large mineral dust particles. Differences were also found in δ_p from both stations. Over Granada δ_p is decreasing in the proximity of a small cloud that was observed within the dust layer around 21:10 UTC. The originally non-spherical dust particles, might have a spherical shape close to the cloud due to hygroscopic growth. This would lead to lower values of δ_p. To conclude, different processes suffered by the aerosol particles during their transport can be considered responsible for the observed differences.

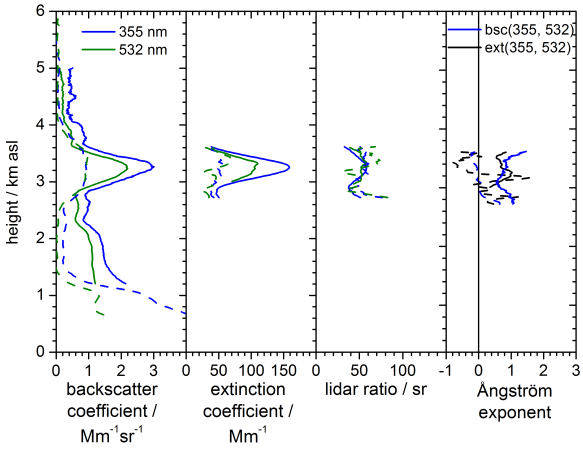

Figure 1: Profiles of extinction and backscatter coefficients, LRs and AEs from lidar measurements in Granada (solid) and Évora (dashed) from 20:00 to 20:30 UTC.

This work was funded by the FCT (Fundação para a Ciência e a Tecnologia) through projects PTDC/CTE-ATM/65307/2006 and REDE/1527/RNG/2007 and grant SFRH/BD/47521/2008; by the Andalusia Regional Government through projects P08-RNM-3568 and P10-RNM-6299; by the Spanish Ministry of Science and Technology through projects CGL2010-18782, CSD2007-00067 and CGL2011-13580-E/CLI; by the EU through ACTRIS project (EU INFRA-2010-1.1.16-262254); and by the Institute for Tropospheric Research, Leipzig, Germany.

References

Bösenberg, J., et al. (2003), *EARLINET: A European Aerosol Research Lidar Network to Establish an Aerosol Climatology, Report No. 348*, Max Planck Institute for Meteorology, Hamburg, Germany.

Holben, B. N., et al. (1998), AERONET - A federated instrument network and data archive for aerosol characterization, *Remote Sensing of Environment*, *66*, 1–16.

Winker, D. M., W. H. Hunt, and M. J. McGill (2007), Initial performance assessment of CALIOP, *Geophysical Research Letters*, *34*, doi:10.1029/2007GL030135.

Seasonal and regional variation of the vertical optical properties of aerosol from CALIPSO validated with aircraft in situ measurements

A. Cazorla[1], P.S. Praveen[2], K.A. Prather[1,2] and V. Ramanathan[2]

[1]Department of Chemistry and Biochemistry, University of California, San Diego. La Jolla, California, USA
[2]Scripps Institution of Oceanography, University of California, San Diego. La Jolla, California, USA
Keywords: vertical distribution, extinction coefficient, lidar, satellite, aircraft.
Presenting author email: cazorla@ucsd.edu

Optical properties of the aerosol and their spatial and temporal distribution have been investigated by means of passive remote sensing instruments aboard satellites such as MODIS, or ground-based sun photometers networks, e.g. AERONET. However, these instruments cannot provide information about the vertical layering of aerosol. The aerosol vertical distribution is of crucial importance in radiative transfer calculations and in the study of aerosol-cloud interaction (Forster *et al* 2007).

Satellite-borne Lidar CALIOP, aboard the CALIPSO, provides high vertical resolution profiles of aerosol and cloud optical properties on a global scale (Winker *et al* 2007). In this work, all the available Level 2 profiles, from 2006 to 2011, from night passes over California with a Cloud-Aerosol Discrimination (CAD) score smaller than -80 (80 % confidence of correct aerosol classification, i.e. cloud free) have been grouped into seasons and regions (north, central and south) in order to provide the extinction coefficient of aerosol and its variability in California as shown in Figure 1.

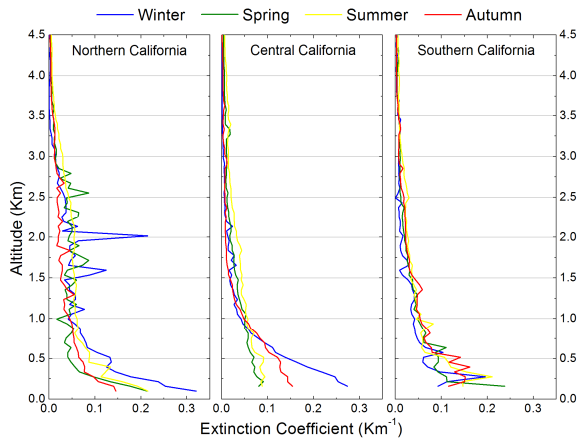

Figure 1. Seasonal variability of the mean extinction coefficient in the different regions of California.

On the other hand, we validated the CALIPSO vertical profiles with the vertical profiles retrieved from two aircraft field campaigns that took place in California. In May 2010 a total of 18 flights over the Los Angeles basin (southern California) under the frame of the CALNEX field campaign and, in June 2010, a total of 22 flights over Sacramento and the Sierra Nevada foothills (northern California) during the CARES field campaign. The extinction coefficient is derived from scattering and absorption coefficients measured on the aircraft and clouds are screened out from the data sets. Since CALIPSO profiles are night profiles, we matched them temporally with flights in the previous or next day, and spatially within the latitude/longitude region flown by the aircraft during that day. Thus, four aircraft profiles were compared with the CALIPSO profiles and they are show in figure 2.

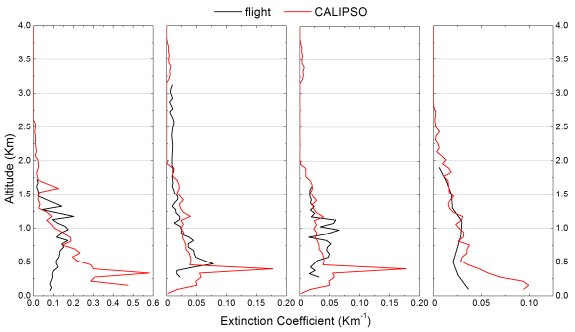

Figure 2. CALIPSO and aircraft profile comparison for 4 days

The comparison agrees well at altitude greater than 500 meters (750 meters in the May 6th case) but there are differences in the lower part, mainly due to the time difference between profiles and the changes in the boundary layer that the day/night difference implies.

The seasonal and regional profiles show differences in the lower part (the one that disagree with the aircraft profiles) showing larger extinction in northern and central California, especially in the winter. The other main difference is the layer of aerosol at about 2 Km in northern California during winter. This is probably due to long transport of aerosol (pollution and dust) coming from Asia.

Funding for this work was provided by CARB under agreement no. 08-323. The statements and conclusions in this report are those of the researchers and not necessarily those of the California Air Resources Board.

Forster, P., et al. (2007). *Changes in atmospheric constituents and in radiative forcing. Climate Change 2007: The Physical Science Basis*, S. Solomon et al., Eds., Cambridge University Press, 129–234.

Winker, D., Hunt, W. and McGill, M. (2007). *Geophys. Res. Lett.*, **34(19),** L19 803

Optical Characterization of Aerosols at a Rural Site in Southeast England During the Winter ClearfLo IOP

P. Massoli[1], A. Aiken[2], K. Gorkowski[2], S. Herndon[1], E. Fortner[1], J. Jayne[1], J. Franklin[1], W. Brooks[1], P. Chhabra[1], T. Onasch[1], L. Williams[1], M. Dubey[2], D. Worsnop[1] and A. Freedman[1*]

[1]Aerodyne Research, Inc, Billerica, MA 01821, U.S.A.
[2]Earth and Environmental Sciences Division, Los Alamos National Laboratory, Los Alamos, NM, 87545, U.S.A.
Keywords: extinction, absorption, single scattering albedo, field measurements
*Presenting author email: af@aerodyne.com

We present preliminary results on the optical characterization of aerosols during the ClearfLo (Clean Air for London) Intensive Operating Period from mid-January to mid-February, 2012 at a rural site southeast of London, England. The site, situated at the Kent Showground in Detling, is located approximately 50 km southeast of central London. Over the course of the campaign, sampled air masses appeared to be of local (A249 motorway proximate to the site), regional (Thames Estuary) or long range (continental Europe) origin depending on the direction and strength of the prevailing winds.

Aerosols were collected from two separate inlets mounted approximately 9 m above the ground that were outfitted with 2.5 micron cutoff impactors. The first inlet was routed to a number of instruments, including a CAPS PM_{ex} (Aerodyne Research) particle optical extinction monitor [Massoli, et al., 2010] and a Multi-Angle Absorption Photometer (MAAP) (ThermoFisher), both operated a nominal wavelength of 630 nm. The second inlet was routed to a CAPS PM_{ex} monitor operated at 450 nm and a Photo-Acoustic Soot Spectrometer (PASS-3) (Droplet Measurement Technologies) which provided particle absorption at three wavelengths (780 nm, 532 nm and 405 nm). The second inlet was equipped with a particle thermal denuder (Aerodyne Research) which could be operated at temperatures up to 250 ºC. [Huffman, et al., 2008] The sample flow was alternated between the denuder and a bypass line every 10 minutes.

Figure 1 shows optical extinction, absorption and the calculated single scattering albedo (SSA) measured at 630 nm shown as 1 hour averages as well as ambient carbon monoxide levels. Extinction levels varied from 7 to 230 Mm^{-1}; the absorption varied between 1 and 32 Mm^{-1}, corresponding to nominal black carbon levels of ~1 to 5 micrograms m^{-3}. The SSA averaged ~ 0.85 over this period. Peak extinction and absorption levels occurred over a two and a half day period starting at noon on January 30. Examination of carbon monoxide concentrations over this period indicates that the air mass responsible for these high readings was well mixed and not of local origin. HYSPLIT-based back-trajectory calculations indicate that these high extinction and absorption levels corresponded to outflow from continental Europe. The dramatic dropoff in particle extinction and absorption levels at the end of this period corresponded to an increase in wind speed (although not a change in direction) and a large decrease in carbon monoxide levels. Periods of low SSA corresponded to air masses dominated by emissions from local sources (e.g., exhaust from local traffic).

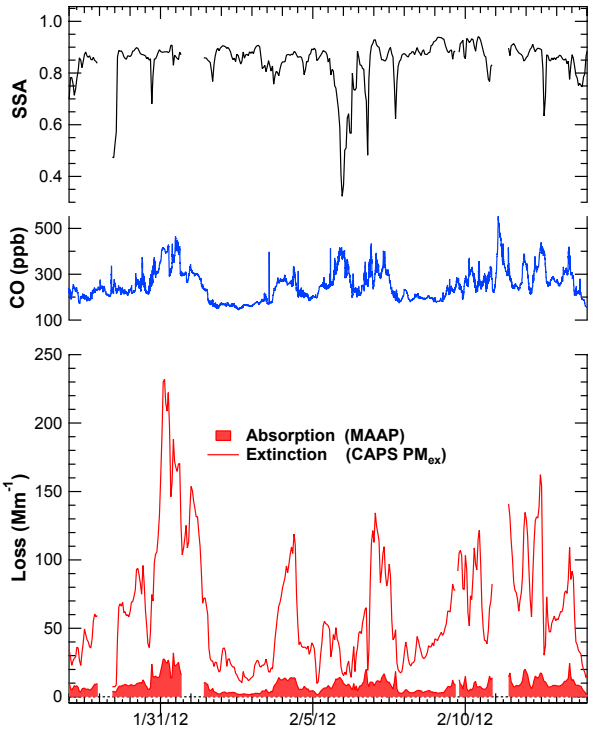

Fig. 1 (bottom) Plot of absorption and extinction levels (1 hour averages) at 630 nm measured using the MAAP and CAPS PM_{ex} monitors respectively. (middle) Carbon monoxide levels. (top) Single scattering albedo (SSA) calculated from data in bottom panel.

This work was supported by the U.S. Department of Energy, Atmospheric System Research Program and the U.K. Natural Environment Research Council.

Huffman, J.A, P.J. Ziemann, J.T. Jayne, D.R. Worsnop and J.L. Jimenez (2008) Aerosol Sci. Technol. **42**:395-407

Massoli, P., P.L. Kebabian, T. B. Onasch, F. Hills and A. Freedman (2010) Aerosol. Sci. Technol. **44**:428–435.

Long term measurements of aerosol optical depth in the UV range in central Poland

J. Jarosławski

Institute of Geophysics Polish Academy of Sciences, ul. Księcia Janusza 64, 01-452, Warsaw,
Keywords: aerosol optical thickness, Brewer spectrophotometer .
Presenting author email : januszj@igf.edu.pl

Aerosol optical thickness (AOT) is an important parameter describing the total content of aerosol in the atmosphere. The measurement of this parameter at different wavelengths allows to obtain additional information about atmospheric aerosols, such as particle size distribution. Most AOT measurements are performed in the visible and infrared part of the solar spectrum mainly because of the difficulty in measuring process (weak signal, atmospheric ozone and SO2 absorption bands). AOT in the UV range can't be obtained by simply extrapolation from the longer wavelengths range, because the dependence of AOT on the wavelength varies with the aerosol type. Knowledge of aerosol optical properties in the UV range is also very helpful in analysis of changes in the solar UV radiation intensity in the atmosphere. In certain circumstances the atmospheric aerosol can modify the intensity of solar UV radiation in the similar way as atmospheric ozone.

In this paper the results of nearly 20 years of measurements of AOT at 320 nm are presented. Measurements have been performed by the Brewer spectrophotometer, the instrument originally constructed to measure the total ozone content using the method described in Jarosławski *et al* (2003). Daily means of AOT measured during 1992-2011 period are shown on Fig. 1. Mean value of AOT is equal to 0.35. The measurement period is limited to the clear sky days (at least a part of the day)

A number of cases with the value of AOT exceeding several times the mean value is associated with episodes of long range transport of biomass burning or saharian dust aerosol in the region of measurement (Jarosławski, Pietruczuk 2010).

The lowest values of AOT are always greater than 0.1. The elevated low levels of AOT in 1992-1994 are associated with the remnants of Pinatubo eruption in 1991. An increase of minimum values of AOT can be also observed over the past few years. This increase is consistent with a similar increase of PM10 concentrations observed in the region.

When it comes to long-term changes in AOT, after a slight decrease in the nineties there is no significant change in n AOT after 2001.

Concerning the seasonal variation of AOT, a double maximum in spring and autumn and a minimum in the winter occurs. The main reason for this variability is seasonal biomass burning to the east and south of Poland. Winter minimum probably results from measurement conditions: sunny days in the winter occur when clean air from the north or north-east is transported to the measurement point.

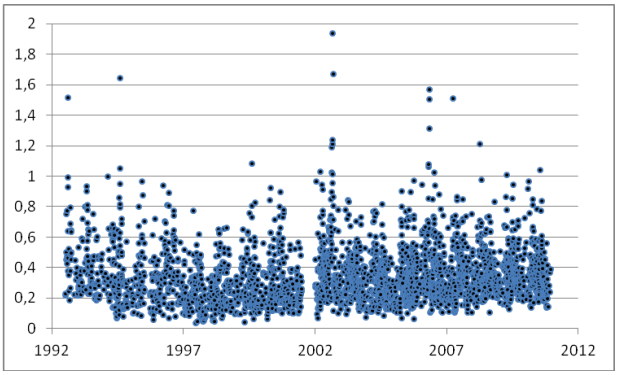

Figure 1. Aerosol optical thickness at 320 nm (daily means) measured at Belsk, Poland by the Brewer spectrophotometer No 064

Jarosławski, J., Krzyścin J.W., Puchalski S., Sobolewski P. (2003). On the optical thickness in the UV range: analysis of the ground-based data taken at Belsk, Poland, *Journal of Geophysical Research* **108** (D23), 4722, doi: 10.1029/2003JD003571.

Jarosławski, J., Pietruczuk, A. (2010) On the Origin of Seasonal Variation of Aerosol Optical Thickness in UV Range over Belsk, Poland Acta Geophysica vol. 58, no. 6, pp. 1134 - 1146

Retrieving aerosol properties over the Mediterranean basin with a climate model

N. Hatzianastassiou[1], P. Ginoux[2], V. Ramaswamy[2]

[1]Laboratory of Meteorology, Department of Physics, University of Ioannina, Ioannina, Epirus, 45110, Greece
[2]Geophysical Fluid Dynamics Laboratory/NOAA, Princeton, New Jersey, 08540, USA
Presenting author email: nhatzian@cc.uoi.gr

The broader Mediterranean basin is an ideal study region for aerosol physico-chemical, optical, radiative properties and climatic effects. This is because of: (i) the existence of a great variety of natural and anthropogenic aerosol types, such as dust, sea-salt, biomass burning, or urban, and (ii) the large magnitude of aerosol radiative and climatic effects in this world area, which is vulnerable to climatic changes (IPCC, 2007). The particularity of the greater Mediterranean basin with regards to aerosol properties arises from the fact that the area hosts various aerosol sources, as for example some of the world's largest deserts, i.e. Sahara and Middle-East, the Mediterranean Sea, or continental lands with environments ranging from pristine (e.g. alpine) to heavily polluted (megacities). The great magnitude of Mediterranean aerosol effects is due to the combination of significant aerosol loadings and large solar radiation amounts. In order to study the regional complex aerosol related properties, processes (micro-physical, chemical and radiative), and climatic effects, which exhibit a strong spatial and temporal variability, solutions enabling extended spatial coverage and consideration of multiple interactions between the various surface and atmospheric components are required. Such solutions are only ensured by aerosol and climate models, for which the Mediterranean basin is also a challenge to assess their ability to reproduce aerosol properties, processes and climate feedbacks.

In the present study, the state-of-the-art AM2 (Delworth et al., 2006) and AM3 (Donner et al., 2011) atmospheric model component of the NOAA Geophysical Fluid Dynamics Laboratory (GFDL) general circulation model (GCM) is used to estimate the composition and concentration of aerosols, and to quantify the contribution of the different sources to the Mediterranean aerosol burdens. The model results, from 1980s to 2000s, in terms of aerosol optical properties are evaluated against in-situ and remote sensing surface and satellite measurements, namely AERONET, AVHRR, MISR and MODIS. Aerosol concentrations at surface are compared against data from EMEP (Co-operative programme for monitoring and evaluation of long range transmission of air pollutants in Europe) as well as surface measurements. Emphasis is also given to the vertical distribution of Mediterranean aerosol, and model profiles are compared to version 3.0 CALIOP (Cloud-Aerosol Lidar with Orthogonal Polarization) and EARLINET (European Aerosol Research Lidar Network) data. Moreover, AM2 and AM3 aerosol properties are compared with each other and against measurements in order to evaluate the consequences of aerosol related changes/improvements made to the new version (AM3) of GFDL model (Donner et al., 2011).

In Figure 1, the AM3 aerosol optical depth (AOD) fractions contributed by sulfate, black carbon (BC), organic carbon (OC), sea-salt and dust aerosols on an annual basis are depicted. Sulfate aerosols (fractions from 29.6 to 79.2%) are by far dominating AOD over the European continent, especially its central parts. BC fractions do not exceed 3.9%, with maxima over central Europe, whereas OC contributions reach 15% over East Europe and maximize (up to 27%) in northern Russia and Scandinavia. Sea-salt dominates aerosol burdens over the Atlantic Ocean (AOD fractions of 20-62%) whilst dust contribution is major (20-58%) over North Africa and Middle-East. Therefore, aerosol contributions exhibit a strong spatial variability, which is further varying from one season to another (results not shown here). Thus, sulfate contributions are smallest/largest in winter/summer, while BC and OC fractions reach maximum values (21.3 and 32.6%, respectively) in winter and autumn. Fractions of sea-salt become largest in winter (maximum values of 91.2% off the coasts of British islands and Scandinavia) while dust fractions always dominate AOD over North Africa, taking maximum values (72.8%) during spring.

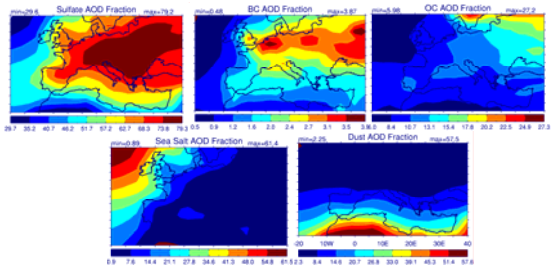

Figure 1. AOD fractions over the greater Mediterranean basin contributed by sulfate, black carbon, organic carbon, sea-salt and dust aerosols.

The performed comparisons against satellite and surface measurements reveal a reasonable agreement, and this is also valid for aerosol vertical distributions, while a significant improvement is evident from AM2 to AM3 model results. This diagnostic aerosol study will be followed by climate simulations tailored to address specific aerosol issues in the Mediterranean region.

Delworth, L., et al. (2006) *J. Climate*, 19, 643-674.
Donner, L., et al. (2011) *J. Climate*, 24, 3484-3519.
IPCC, 2007: Climate Change 2007: The Physical Science Basis, Solomon, S. et al (eds.), Cambridge University Press, Cambridge, United Kingdom and New York, NY, USA.

Day and night columnar aerosol properties at Granada (Spain) using sun and star photometry measurements.

D. Pérez-Ramírez[1,2,3], H. Lyamani[1,2], F.J. Olmo[1,2], D.N. Whiteman[3] and L. Alados-Arboledas[1,2].

[1]Centro Andaluz de Medio Ambiente (CEAMA), Universidad de Granada, 18006,Granada, Spain
[2]Departamento de Física Aplicada, Universidad de Granada, Campus de Fuentenueva s/n, 18071,Granada, Spain
[3] Mesoscale Atmospheric Processes Laboratory, NASA Goddard Space Flight Center, Greenbelt,Maryland, 20771, United States
Presenting author email: dperez@ugr.es
Keywords: Atmospheric Aerosols

Atmospheric aerosol is noted by the Fourth Intergovernmental Panel for Climate Change (IPCC 2007) as a key component to fully understand the climate change. Atmospheric aerosol particles scatter shortwave and longwave radiation and absorb radiation. Furthermore atmospheric aerosol particles can act as cloud condensation nuclei and thus they can modify cloud droplet size and cloud albedo.

In spite of the strong efforts in the last decade for aerosol characterizations by spaceborne missions and international networks, there are lacks of large observations of columnar aerosol properties at night-time. The knowledge of these properties will allow us to have a whole picture of the daily behavior of the atmospheric aerosol, covering the different stages in the evolution of the planetary boundary layer and pre-convection and pre-photochemistry processes that affect the atmospheric aerosol. The knowledge of AOD at night-time would also contribute to aerosol transport and chemistry models validation efforts, and can be also used as constraints for Lidar measurements.

Since March 2007 a star photometer is been operating on the rooftop of the Andalusian Centre for Environmental Research (37.16ºN, 3.60ºW, 680 m a.s.l; South-East of Spain). This works present the first analysis of long-term day- and night-time columnar aerosol optical properties from 2007 to 2010. To this end AERONET sun photometry measurements has been also used. Technical specifications of the star photometer are in Pérez-Ramírez et al., (2008), while calibration procedures and uncertainties are in Pérez-Ramírez et al., (2001).

For the whole study period, mean aerosol optical depth (AOD) at 440 nm (± standard deviation) is 0.18±0.10 and 0.19±0.11 for day- and night-time respectively, while the mean Angström exponent (α) is 1.0±0.4 and 0.9±0.4 for day- and night-time. The ANOVA statistical test reveals that there are no significant differences between the AOD and α obtained at day-time and those obtained at night-time. Additionally, the mean day-time values of AOD and α obtained during this period are within the values obtained in the surrounding AERONET stations. On the other hand, AOD presents an evident seasonal pattern characterized by large values in summer (mean values of 0.20±0.10 both at day and night) and low values in winter (mean values of 0.15±0.09 at daytime and 0.17±0.10 at nighttime), both at day- and night-time. The Angström exponent presents clear seasonal pattern (more remarkable at daytime) with low values in summer (mean values of 0.8±0.4 and 0.9±0.4 at day and night) and relatively large values in winter (mean values of 1.2±0.4 and 1.0±0.3 at day and night), These seasonal patterns are explained by the differences in the meteorological conditions and in the strength of aerosol sources between day and night. Additionally, the spectral analysis of the Angström exponent has revealed larger contribution of the fine mode particles to AOD and larger fine mode particle radius at night-time; The changes of meteorological conditions between day-and night, the aging processes and the changes in local aerosol sources may explain these changes in the fine mode characteristics between day and night.

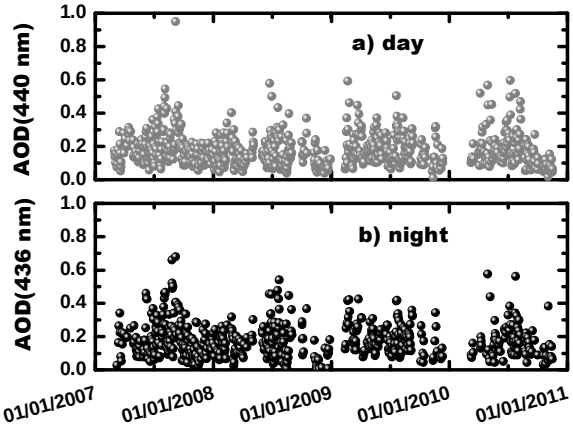

Figure 1: Temporal evolutions of (a) Day-time mean values of aerosol optical depth at 440 nm and b) Night-time mean values of aerosol optical depth at 436 nm.

This work was supported by the Spanish Ministry of Science and Technology through projects CGL2008-01330-E/CLI (Spanish Lidar Network), CGL2010-18782, CGL2011-13580-E/CLI and CSD2007-00067; by the Andalusian Regional Government through projects P10-RNM-6299 and P08-RNM-3568; and by the EU ACTRIS project (EU INFRA-2010-1.1.16-262254).

Pérez-Ramírez, D., et al., (2008) *Atmospheric Environment*, 42, 2739-2745.
Pérez-Ramírez, D., et al., (2010) *Journal of Aerosol Science*, 42, 737-735.

Absorption closure – filter-based absorption instruments compared to extinction-scattering measurements

E. Andrews[1,2], P. Massoli[3] , A.G. Hallar[4], A. Sedlacek[5], A. Freedman[3], J. A. Ogren[2] and P. Sheridan[2]

[1]CIRES, University of Colorado, Boulder, CO, 80305, USA
[2]NOAA/ESRL/GMD, Boulder, CO, 80305, USA
[3]Aerodyne Research Inc, Boston, MA, Billerica, 01821, USA
[4]Storm Peak Laboratory, Desert Research Institute, Steamboat Springs, CO, 80488, USA
[5]Brookhaven National Lab, Upton, NY, 11973, USA

Keywords: absorption coefficient, aerosol optics, in-situ measurements, instrumentation.
Presenting author email: betsy.andrews@noaa.gov

Filter-based aerosol light absorption (σ_{ap}) instruments are simple in concept and have been operated long-term at remote field sites since the 1980s (e.g., Bodhaine, 1995). Unfortunately, there are several issues with filter-based instruments that can lead to uncertainties in the reported σ_{ap}. Müller *et al.* (2011) and references therein summarize these issues, which include sensitivity to measurement conditions such as humidity and pressure, artifacts due to scattering aerosol depositing on the filter, discrepancies between manufacturer and actual instrument properties (such as flow rate, spot size, and wavelength) and changes in response as a function of filter loading, measurement biases due to the presence of organics/liquids. Corrections have been developed to account for many of these issues (e.g., Bond *et al.*, 1999), although the artifacts related to presence of organics/liquids are not yet well enough understood to parameterize (e.g., Lack *et al.*, 2008).

Aerosol absorption can also be obtained by utilizing non-filter-based measurements of aerosol extinction (σ_{ep}) and scattering (σ_{sp}) and taking the difference: $\sigma_{ap} = \sigma_{ep} - \sigma_{sp}$. The disadvantage of this approach is that it uses the difference between two large numbers to get a small number (σ_{ap} is typically a small fraction (~10%) of σ_{ep}). Also, until recently, measurements of σ_{ep} were typically made by prototype instruments requiring expert attention and thus not suited to long-term, remote monitoring.

Aerodyne Research Inc. has developed a new, commercially available instrument which uses Cavity Attenuated Phase Shift (CAPS) spectroscopy to measure extinction (Massoli *et al.*, 2010). Using this CAPS instrument in conjunction with a nephelometer to measure scattering, could provide a robust, long-term way of monitoring aerosol absorption, assuming instrument uncertainties for the difference method are less than the uncertainties associated with filter-based absorption measurements.

Here we present σ_{ep} and σ_{ap} closure results from five months of measurements made at Storm Peak Laboratory (SPL) in Steamboat Springs, CO in the winter/spring of 2011. A CAPS instrument, an integrating nephelometer and a particle soot absorption photometer (PSAP) sampled off a common inlet at SPL during the STORMVEx campaign. Figure 1 shows the relationship between extinction measured by the CAPS and extinction calculated from the sum of nephelometer scattering and PSAP absorption. The scattering and absorption measurements have been adjusted to 630 nm to match the CAPS extinction wavelength.

In addition to an analysis of the extinction closure (shown in Figure 1), we will (a) evaluate how absorption from the filter-based PSAP measurement compares with absorption derived from $\sigma_{ep,CAPS}$ - $\sigma_{sp,neph}$; explore potential causes of discrepancies between the measured and derived extinction and absorption; and finally look in more detail at a couple case studies involving biomass burning. A laboratory experiment utilizing a similar suite of instruments is planned for spring 2012 – pending successful completion of those measurements preliminary results from that experiment will also be presented.

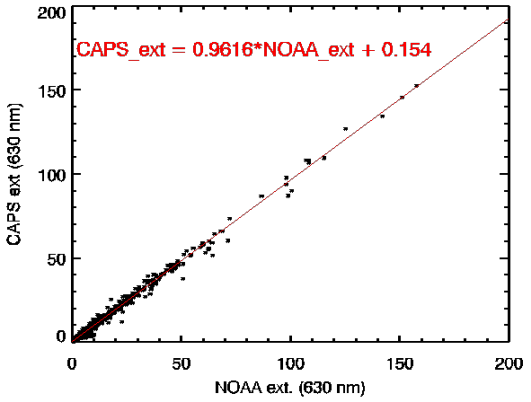

Figure 1. Comparison of $\sigma_{ep,CAPS}$ with $\sigma_{ep,neph+PSAP}$ ($\sigma_{ep,neph+PSAP}$ is called NOAA_ext on plot)

This work was supported by DOE/ARM for the StormVEx campaign and equipment, DOE/SBIR for the CAPS and the NOAA Climate Program.

Bodhaine, B.A. (1995) *J. Geophys. Res.* **100**, 8967-8975.
Bond, T.C., Anderson, T.L., and Campbell, D. (1999). *Aerosol Sci. Technol.* **30**, 582-600.
Lack, D.A., Cappa, C.D., Covert, D.S., Baynard, T., Massoli, P., Sierau, B., Bates, T.S., Quinn, P.K., Lovejoy, E.R., and Ravishankara, A.R. (2008) *Aerosol Sci. Technol.* **42**, 1033-1041.
Massoli, P., Kebabian, P.L., Onasch, T.B., Hills, F.B., and Freedman, A. (2010) *Aerosol Sci. Technol.* **44**, 428-435.
Müller, T. *et al.* (2011) *Atmos. Meas. Tech.*, **4**, 245–268.

Continuous measurements of aerosol size distribution at two Siberian stations: new particle formation bursts

M.Yu. Arshinov[1, 2], B.D. Belan[1], A.V. Kozlov[1] , P.N. Antokhin,[1] D.K. Davydov[1] and V.G. Arshinova[1]

[1]V.E. Zuev Institute of Atmospheric Optics, SB RAS, Tomsk, 634021, Russia
[2]Department of Meteorology and Climatology, Tomsk State University, Tomsk, 634050, Russia
Keywords: aerosol size distribution, atmospheric aerosols, boreal forest, in-situ measurements, monitoring.
Presenting author email: michael@iao.ru

The role of Siberia is of great importance to understand the climate change due to it covers about 10% of Earth's land surface. It extends longitudinally and latitudinally for several thousands of kilometres, so its ecosystems are represented by steppes, different types of forest, wetlands, tundra and arctic deserts. Assuming that increasing global temperature and CO_2 fertilization can likely lead to an extension of the annual photosynthesis period and forest growth, Kulmala *et al.* (2004) suggested a possible feedback mechanism linking forests, aerosols and the climate effect of CO_2 through the intensification of metabolic processes causing enhanced non-methane BVOC emission and organic aerosol production as well. Taking into account that the main part of boreal forests is located in Siberia, this possible feedback makes this region important not only because of studying GHG budget, but also because of it can be an important source of natural secondary aerosols. The most detailed data on new particle formation and growth in the troposphere over Siberian forests were reported by Dal Maso *et al.* (2008). In the overview done by Kulmala *et al.* (2011) authors arrived at a conclusion that continuous and comprehensive measurements of GHGs and aerosols over Siberia are still lacking, and, as a solution, they proposed a plan to carry out in the future a so-called Pan Siberian Experiment (PSE).

Understanding the importance of this problem, we decided to establish two monitoring stations for continuous measurements of aerosol and trace gas (CO_2, CH_4, O_3, NO_x, SO_2, CO) concentrations in order to fill up the gap in data. The first one is a so-called TOR-station (56°28'40"N, 85°03'14"E), and another one – Fonovaya Observatory (56°25'07"N, 84°04'27"E).

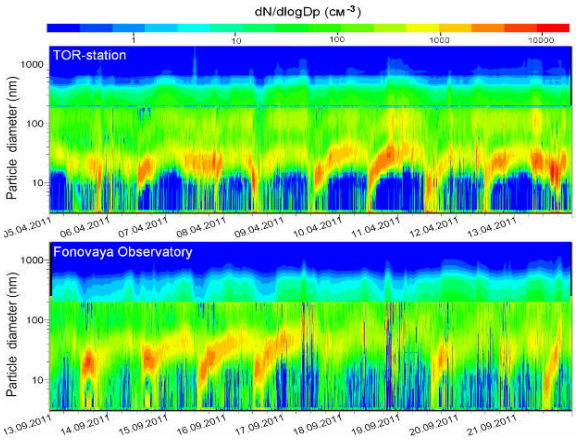

Figure 1. Golden day NPF events observed at TOR–station and Fonovaya Observatory.

Measurements of aerosol size distributions have been carrying out since March 2010 at TOR-station and since May 2011 at Fonovaya Observatory by means of the improved versions of Novosibirsk automated diffusion battery (Reischl *et al.*, 1991) and the GRIMM aerosol spectrometers (#1.109 and #1.108).

Analysis of the data obtained to date showed that new particle formation (NPF) happens frequently in the atmospheric boundary layer over Siberian boreal zone. A series of NPF bursts followed day after day were found in spring and early autumn (Fig. 1). Seasonal variation pattern of NPF event frequency is presented in Figure 2, which shows that the number of events in Siberia are more often observed during spring (from March to May) and autumn (secondary frequency peak in September).

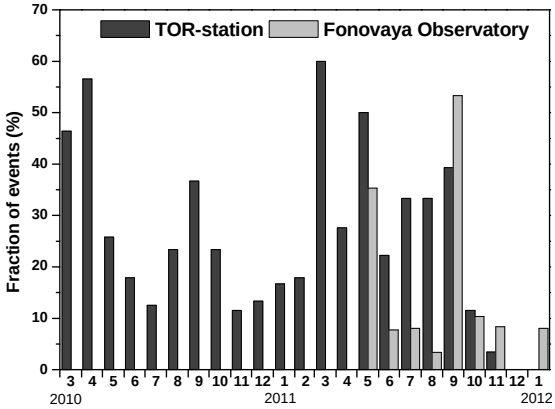

Figure 2. Seasonal variation of NPF events.

The most strong nucleation bursts occurred in March and April. The highest formation and growth rates of ultrafine particles reached values of 2.3 cm^{-3} s^{-1} and ≈25 nm h^{-1} in April. The observed seasonal pattern of event frequencies is similar to one observed in Hyytiälä (Kulama *et al.*, 2005). The fact of similarity between the NPF processes occurred in the boreal forests of Southern Finland and West Siberia allows a conclusion to be drawn that secondary aerosol formation in these regions may have a significant climatic effect in the temperate latitudes of the Northern Hemisphere.

This work was supported by Branch of Earth Sciences RAS (Program No5) and RFBR grant No 11-05-00516.

Dal Maso M. *et al.* (2008) *Boreal. Env. Res.* 13, 81-92.
Kulmala M. *et al.* (2004) *Atmos. Chem. Phys.* 4, 557-562
Kulmala M. *et al.* (2005) *Boreal. Env. Res.* 10, 323-336.
Kulmala M. *et al.* (2011) *Boreal. Env. Res.* 16, 337-362.
Reischl G.P. *et al.* (1991) *J. Aerosol Sci.* 22, 223-228

Insights into the nucleation by organic compounds involving oxidation products of pinanediol and sulphuric acid

F. Bianchi[1], S. Schobesberger[2], S. Ehrhart[3], H. Junninen[2], N. M. Donahue[4], J. Dommen[1], M. Kajos[2], S. Schallhart[2], T. Ruuskanen[2], M. Kulmala[2], D. R. Worsnop[2] U. Baltensperger[1] and the CLOUD collaboration

[1] Laboratory of Atmospheric Chemistry, Paul Scherrer Institut, Villigen, 5232, Switzerland
[2] Department of Physics, University of Helsinki, Helsinki, Finland
[3] Goethe-University of Frankfurt, Institute for Atmospheric and Environmental Sciences, Frankfurt am Main, Germany
[4] Department of Chemical Engineering, Carnegie Mellon University, Pittsburgh, PA, USA
Keywords: Nucleation, Chemical composition, Ion clusters, Organic compounds
Presenting author email: Federico.bianchi@psi.ch

Formation of new particles is an important process that can affect the concentration of cloud condensation nuclei and thus influence clouds and climate. Nucleation of new particles in atmosphere has been shown to correlate with sulphuric acid concentrations. Recent laboratory studies found that ammonia enhances the nucleation rate by a factor of 100-1000 compared to pure sulphuric acid. Despite this effect the nucleation rate observed in the atmosphere can still not be explained by just these two compounds (Kirkby et al., 2011).
There is evidence that organic compounds are involved in the nucleation process (Metzger et al., 2010). For a better understanding of the influence of organics on the nucleation, experiments with pinanediol were performed during the CLOUD 4 campaign. Pinanediol is produced during photooxidation of α-pinene thus mimicking a biogenic compound after an oxidation process in the atmosphere.

Pinanediol, SO_2 and ozone were added to the cloud chamber. Then UV lights induced OH formation from ozone photolysis leading to sulphuric acid production and OH radical reactions with pinanediol. The gas phase composition was measured by a Proton Transfer Reaction Time Of Flight Mass Spectrometer (PTR-TOF-MS). The cluster composition was retrieved by an Atmospheric Pressure interface Time Of Flight Mass Spectrometer (APi-TOF,). (Junninen et al., 2010) This instrument can determine the composition of ions in the CLOUD chamber in the mass/charge range up to 3300 Th.

During the nucleation experiments the APi-TOF revealed a large number of clusters formed by the interaction between sulphuric acid and oxidation products of pinanediol. The elemental composition of small ions and ion clusters was identified and the findings were compared with the gas phase organic composition retrieved from the PTR-TOF-MS. Since the concentration of oxidation products was very small in the CLOUD chamber, more experiments at a higher OH concentration were performed at the PSI smog chamber.
We will present the oxidation pathways of pinanediol and the observed oxidation products. The measurements of the gas phase composition will be related to the cluster composition and discussed.

We would like to thank CERN for supporting CLOUD with important technical and financial resources, and for providing a particle beam from the CERN Proton Synchrotron. This research has received funding from the EC Seventh Framework Programme (Marie Curie Initial Training Network "CLOUD-ITN" grant no. 215072, and ERC-Advanced "ATMNUCLE" grant no. 227463), the German Federal Ministry of Education and Research (project no. 01LK0902A), the Swiss National Science Foundation (project nos. 206621_125025 and 206620_130527), the Academy of Finland Center of Excellence program (project no. 1118615), the Austrian Science Fund (FWF; project no. P19546 and L593), the Portuguese Foundation for Science and Technology (project no. CERN/FP/116387/2010), and the Russian Foundation for Basic Research (grant N08-02-91006-CERN).

Junninen, H., Ehn, M., Petaja, T., Luosujarvi, L., Kotiaho, T., Kostiainen, R., Rohner, U., Gonin, M., Fuhrer, K., Kulmala, M., and Worsnop, D. R. (2010) Atmos. Meas. Tech. 3, 1039-1053.
Kirkby, J., Curtius, J., et al., (2011) Nature, 476, 429-U77.
Metzger, A., Verheggen, B., Dommen, J., Duplissy, J., Prevot, A. S. H., Weingartner, E., Riipinen, I., Kulmala, M., Spracklen, D. V., Carslaw, K. S., and Baltensperger, U. (2010) PNAS, 107, 6646-6651.

Differences between Classes of Nucleation Events during the Summer Period in Thessaloniki, Greece: Kerbside versus urban background measurements

D. Siakavaras[1], C. Samara[2], M. Petrakakis[3], G. Biskos[1,4]

[1]Department of Environment, University of the Aegean, Mytilene 81100, Greece
[2]Department of Chemistry, Aristotle University of Thessaloniki, Thessaloniki 54124, Greece
[3]Environmental Department, Municipality of Thessaloniki, Paparigopoulou 7, Thessaloniki 54630, Greece
[4]Faculty of Applied Science, Delft University of Technology, Delft 2628-BL, The Netherlands

Keywords: nucleation events, number size distribution, SMPS, classification

Thessaloniki is a densely populated coastal city of northern Greece with high concentrations of atmospheric particulate matter (PM) frequently observed in the city centre. Several studies have investigated the concentration levels, the chemical composition of PM, as well as the size distribution of particle mass concentrations over the city (Voutsa *et al*., 2002; Petrakakis *et al*., 2007; Terzi *et al*., 2010;). Preliminary measurements of the size distribution of aerosol number concentration in Thessaloniki were conducted during winter-time at a kerbside site and an urban background site (Terzi et al., 2007). The size distribution of aerosol number concentration during the summer-time and the relationships with PM mass, photochemical pollutants and meteorological parameters was investigated in Siakavaras et al., (2008), while a classification of the nucleation events during the same period was recently reported (Siakavaras et al., 2011).

In this paper we analyse the differences between particle nucleation and growth events observed during the summer period at two monitoring stations (Venizelou – kerbside site, and Eptapyrgio – urban background site). Two identical Scanning Mobility Particle Sizers (TSI Model 3034) have been employed to measure simultaneously the size distributions of the particles having diameters in the range 10-487 nm at the two sites. Gaseous pollutants (CO, NO_x, SO_2 and O_3) and meteorological parameters (wind speed, wind direction, temperature and relative humidity) were also recorded during the measurements. The experiments were conducted during June to October 2009.

Nucleation events were classified in 5 categories based on their intensity. At Venizelou (kerbside site), 6% of the days were classified as class Ia events, 3% as class Ib, 10% as class II, 14% of the days exhibited no clear particle formation patterns and were considered as undefined and 67% of the days showed no event. At Eptapyrgio (urban background site) 8% of the days were class Ia events, 7% class Ib, 5% class II, 5% were undefined and 75% of the days showed no nucleation.

Characteristic differences between the classes can be seen in Fig. 1. For Class Ia the diurnal variation of the particle number concentration shows a significant increase starting at 07:00 at Venizelou and at 12:00 at Eptapyrgio, whereas for the non-event days, the diurnal variation is less pronounced for both stations. Nucleation events were more frequent during July, and for both stations correlated well with high concentrations of SO_2 and NO_x.

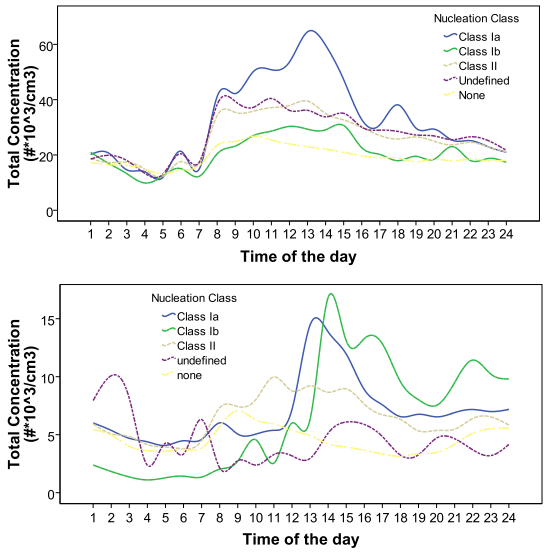

Figure 1. Average diurnal variation of particle number concentrations during nucleation event days of all classes at Venizelou (upper part) and Eptapyrgio (lower part)

References

Voutsa, D., Samara, C., Kouimtzis, Th., Ochsenkuehn, K. (2002). *Atmospheric Environment*, 36, 4453-4462.

Siakavaras, D., Samara, C., Pilinis, C., Kelesis, A. *European Aerosol Conference, Thessaloniki, Greece, 2008 (*Abstract T02A043P).

Terzi, E., Argyropoulos, G., Bougatioti, A., Mihalopoulos, N., Nikolaou, K., Samara, C. (2010). *Atmospheric Environment,* 44, 2231-2239.

Petrakakis, M.J., Kelessis, A.G., Samara, C., Tzoumaka, P., Zoumakis, N.M., Iosifidis, E. CEMEPE 07, *Skiathos, 2007* (Proceedings pp 2471-2477).

Dal Maso, M., Kulmala, M., Riipinen, I., Wagner, R., Hussein, T., Aalto, P., Lehtinen, E.J (2005) Boreal Environment Research 10: 323-336

Source apportionment of ultrafine and fine particles in Huelva industrial city

R. Fernández-Camacho[1], S. Rodríguez[1,2], J. de la Rosa[1], A.M. Sánchez de la Campa[1], Y. González-Castanedo[1].

[1]Associate Unit CSIC-University of Huelva "Atmospheric Pollution", CIQSO, University of Huelva, Campus El Carmen, E21071 Huelva, Spain.

[2]Izaña Atmospheric Research Centre, AEMET Joint Research Unit to CSIC "Studies on Atmospheric Pollution", La Marina 20, planta 6, Santa Cruz de Tenerife, E38071, Canary Islands, Spain.

Keywords: ultrafine particles, heavy metals, industrial emissions, vehicles emissions.

Presenting author email: rocio.fernandez@dgeo.uhu.es

Urban air quality impairment by ultrafine particles (diameter < 0.1 µm) has become a matter of concern due to the adverse effects on human health (Araujo and Nel, 2009). Most of the studies of ultrafine particles in urban air quality have focused on vehicle exhaust emissions. Thus, ultrafine particle emissions in vehicle exhaust have been subject to limit values in a recent stage of the EURO standards.

We present a study on how industrial emissions contribute to ultrafine particle concentrations in downwind urban ambient air. This research is based on experimental data collected in the ambient air of the industrial city of Huelva (SW Spain) over 18 months (particle number concentration, black carbon and levels and composition of $PM_{2.5}$ with daily resolution). This city is affected by emissions from the second largest Cu-smelter in Europe, phosphoric acid and fertilizer production plants and an oil refinery and petrochemical plant. In order to quantify the process contributing to ultrafine particles concentrations (N), two components (N1 and N2) were segregated by the methodology of Rodríguez and Cuevas (2007). N1 accounts for vehicle exhaust emissions and may also include compounds nucleating/condensing immediately after emission. N2 is correlated with SO_2 and accounts for new particle formation due to nucleation and rapid particle growth to detectable sizes (Fernández-Camacho et al., 2010b).

In order to identify the sources contributing ultrafine particles, Principal Component Analysis were performed to data for particle number concentration and $PM_{2.5}$ chemical composition. Three Principal Components were observed: APC-1, showing a high association with species linked to industrial emissions from the Cu-smelter (nss-$SO_4^=$, As, Sb, Pb, Zn and Sn), the phosphoric acid and fertilizer plant (nss-$SO_4^=$, P and NH_4^+) and the oil refinery (nss-$SO_4^=$, NO_3^-, NH_4^+, V and Ni). The presence of N2 in this PC is attributed to ultrafine sulphate particle formation in the plume during inland transport prompted by sea breeze from 09:00 to 17:00 GMT (Fernández-Camacho et al., 2010b); APC-2 associated with road traffic emissions: vehicle exhaust emissions (OM and N1) plus road dust (Al, Ca, Fe, Ti, Mn and K). The presence of N1 in this factor is in agreement with the weekly cycles of NO_x and N1 particles, which exhibits high values during working-day rush hours (view details in Fernández-Camacho et al. 2010b); APC-3 showing high factor loading for typical sea salt components (Cl, Na and Mg). As expected, neither of the particle number components, N1 or N2, was associated with this factor.

Only two sources contributed significantly to the particle number N: road traffic accounted for 50 ± 9%, whereas industrial emissions accounted for 44 ± 7% of N. Figure 10 shows the daily mean averaged values of the particle number N, classified from the highest to the lowest concentration (100^{th} to 1^{st} percentile), and the contribution of the identified sources. When vehicle exhaust is the main source, ultrafine particles typically show (24-h mean) concentrations within the range 14700 – 5000 cm^{-3} (50^{th} – 1^{st}), with 60% of these being linked to this source and 30% to industrial emissions. In contrast, when daily mean levels of N are within the range 50000 – 25500 cm^{-3} (100^{th} - 70^{th}) industrial and vehicle exhaust emissions accounted for 49 and 30%, respectively.

The results of this study show that industrial emissions are the main cause of ultrafine particles episodes in Huelva city.

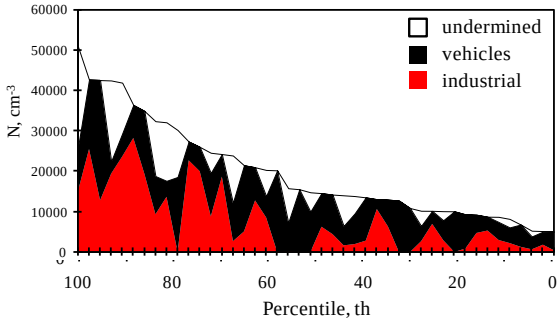

Figure 1. Daily averaged values of N classified from highest to lowest concentration highlighting the contribution of the industrial, vehicle exhaust and undetermined fraction contributions.

This work was supported by several research projects: P07-RNM-03125; P07-RNM-02729; CSD2007-00067; B026/2007/3-10.1; P11-RNM-7800.

Araujo, J.A., Nel, A.E. (2009) *Part Fibre Toxicol* **6**, 24, doi:10.1186/1743-8977-6-24.

Fernández-Camacho, R., et al. (2010b) *Atmos. Chem. Phys.* **10**, 9615-9630.

Rodríguez, S., Cuevas, E. (2007) *J. Aerosol Sci.* **38**, 1207-1219.

Basic Statistics of New Particles Formation Events at Kosetice Station

N. Zikova[1,2] and V. Zdimal[1]

[1] Department of Aerosol and Laser Studies, Institute of Chemical Process Fundamentals of the AS CR, v.v.i, Prague, 16502, Czech Republic (ICPF)
[2]Department of Meteorology and Environment Protection, Charles University in Prague, Prague, 180 00, Czech Republic
Keywords: nucleation, number size distribution, SMPS
Presenting author email: zikova@icpf.cas.cz

Introduction: Atmospheric aerosols have been studied extensively due to the confirmed influence of aerosols on global climate, aerosol – clouds interactions, atmospheric visibility, human health etc. (Kerminen *et al* 2005; IPCC, 2007; Wichmann *et al*, 2000). However, the uncertainties connected to the effects of aerosols on phenomena in the atmosphere are considerable – there are various sources of aerosol particles, having different chemical compositions and particle size distributions (PSD). Concerning changes of PSD, the most important processes are new particle formation events (NPF).

A NPF event, sometimes called a nucleation event, is characterized by a formation of ultrafine particles in the size range between 3 and 25 nm. The result of the NPF event is a new mode in the PSD. The formation of particles and their further growth by condensation and/or coagulation are key processes influencing the dynamics of the atmospheric aerosol PSD (Kulmala *et al* 2001).

In this work, we present a basic statistical evaluation of NPF at Kosetice background station in the region of middle Europe. The evaluation is based on the NPF classification according to Dal Masso et al. (2005). The individual days were classified into three categories – NPF event, Non-event and Undefined days.

Methods: The evaluated data were collected during the first three years of measurements (2008 - 2010) at Kosetice observatory, located in the Czech Highlands (49°35'N, 15°05'E, altitude 534 m a.s.l.). The observatory is a background meteorological station operated by the Czech Hydrometeorological Institute, and is a part of the national professional meteorological measurement network, specialized in the environmental quality monitoring. In 2008, the observatory became a part of the EUSAAR network and was equipped by an IfT-SMPS (Scanning Mobility Particle Sizer) provided by the Leibnitz Institute for Tropospheric Research (IfT) in Leipzig.

The SMPS samples every 5 minutes over the mobility size range from about 10 nm to 900 nm. Data in 5 minutes time resolution have been processed according to the EUSAAR standards into one-hour arithmetic means of particle number concentration.

Results: It has been found that the average annual cycle of NPF events (Fig. 1) has two maxima, the first in April and the second between July and September. The main minimum is located in the colder part of the year. The Non-event days follow an inverse annual cycle; Undefined days are approximately evenly spread over the year.

The variability between the three years is not high (Fig. 2), especially ratio of NPF events to all classifiable days varies only by several percent. What differs, however, is the ratio of Undefined and Non-event days to all classifiable days. While during the first two years there were slightly more Undefined than Non-event days, during the third year, the relationship is the opposite.

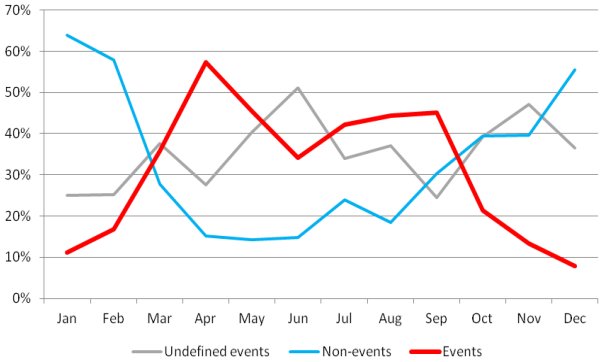

Fig 1. Annual cycles of ratios of NPF Events, Non-events and Undefined days to all classifiable days. Averaged from three years of measurement.

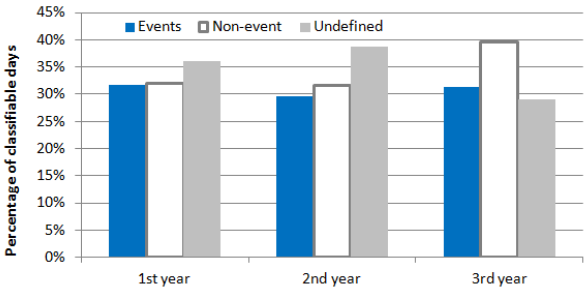

Fig 2. Ratio of NPF Events, Non-events and Undefined days to all classifiable days in the individual years.

We thank to the project CSF No. P209/11/1342 for financial support, and Dr. Milan Váňa and his colleagues from Kosetice Observatory for a valuable cooperation.

Dal Maso, M. *et al* (2005) *Boreal Env. Res.* **10**, 323-336.
IPCC (2007) *Climate Change 2007: The Physical Science Basis*, Cambridge University Press.
Kerminen, V.-M. *et al* (2005), *Geophys. Res. Lett.*, **32**, L14803, doi:10.1029/2005GL023130.
Kulmala, M. *et al* (2001) *Tellus* **53B**, 479 - 490
Wichmann H.-E. *et al* (2000) *Phil. Trans. R. Soc. Lond. A*, **358**, 2751-2769

Investigation of consecutive particle formation events in mixed residential and mining area in South Africa

A.Hirsikko[1], V.Vakkari[2], P. Tiitta[3], V.-M. Kerminen[2], J. Hatakka[1], J.P. Beukes[4], H.E. Manninen[2], M. Kulmala[2], D. Mabaso[5], and L. Laakso[2,4]

[1]Finnish Meteorological Institute, Research and Development, P.O. Box 503, 00101, Helsinki, Finland
[2]Department of Physics, University of Helsinki, P.O. Box 64, 00014 University of Helsinki, Finland
[3]Department of Environmental Science, University of Eastern Finland, PL 1627, 70211 Kuopio, Finland
[4]School of Physical and Chemical Sciences, North-West University, Potchefstroom, South Africa
[5]Rustenburg Local Municipality, Rustenburg, South Africa
Keywords: Particle formation.
Presenting author email: Anne.Hirsikko@fmi.fi

Aerosol particles are known to have several climate and health effects (IPCC, 2007). Therefore, aerosol particle formation and subsequent growth has been intensively investigated in a variety of environments (Kulmala *et al*, 2004; Hirsikko *et al*, 2011). Particle formation event frequency, formation and growth rates of freshly nucleated particles depend on several triggering and inhibiting factors, i.e. concentration and size of background aerosol particles, anthropogenic/natural sources of nucleating and condensing vapours, air mass trajectories and turbulent atmospheric mixing

Particle formation may take place several times a day, both during daylight and night-time (Hirsikko *et al*, 2011 and references therein). Hirsikko *et al* (2012a) observed that particle formation took place during several consecutive periods during the same day in a mining area with informal settlement in South Africa on 108 days. The aim of this work was to investigate driving factors behind the observed multiple daytime nucleation events (Hirsikko *et al*, 2012b).

The analysis was based on the observations of particle size distributions in diameter ranges 0.8-42 nm and 12-840 nm with an Air Ion Spectrometer (Mirme *et al*, 2007) and a Differential Mobility Particle Sizer, respectively. In addition, ancillary data were deployed, i.e. trace gas and meteorological parameters (Venter *et al*, 2012), as well as modelled air mass trajectories (www.arl.noaa.gov/archives.php) and boundary layer heights (www.ecmwf.int/research/ifsdocs/CY37r2/index.html). Temporal evolution of sulphuric acid concentration proxy was estimated based on SO_2 concentration, global radiation and condensation sink due to background aerosol particles (Dal Maso *et al*, 2005; Petäjä *et al*, 2009).

Days when the ancillary data were deficient or air mass origin, path and wind direction were changing notably between the particle formation events were rejected. Eventually, we were able to investigate multiple nucleation events followed by subsequent growth on 29 days. The results indicated that typically: 1) the first nucleation event took place between 06:00-09:00, 2) the second event was observed between 09:00-12:00 and 3) the third occurred late in the afternoon (approximately 15:00-18:00). Common to all of these particle formation events was that they occurred during day light hours, which allowed photochemical reactions and enhanced boundary layer mixing compared to night-time.

The first particle formation event of the day was associated with increasing sulphuric acid concentration, and sometimes also with very high condensation sink. These observations together with the timing of the event indicated that nucleation was observed with ground based instruments when a residual or inversion layer, influenced by emissions from the regional industry, mixed into the boundary layer. The particle formation was suppressed when the sulphuric acid concentration had decreased low enough.

The second particle formation event of the day was promoted by decreasing condensation sink and increasing concentrations of suitable vapours. Our results indicated that the sulphuric acid concentrations were insufficient to explain the second event. Therefore, it was probable that other vapours, such as oxidation products of monoterpenes, were involved in the particle formation and growth. The third particle formation event of the day was typically associated with different air mass paths or wind directions compared to the morning particle formation episode.

Our observations indicated that by investigating case study examples we were able to gain new information on the driving factor of multiple particle formation events. A similar investigational approach is also recommended for environments where multiple nucleation events might occur.

We would like to express our acknowledgements to Tshepo Lenake, Rustenburg Municipality, the Finnish Academy (project no 117505; no 132640), and the North-West University.

Dal Maso *et al* (2005) *Boreal Env. Res.* **10**, 323–336.
Hirsikko *et al* (2011) *Atmos. Chem. Phys.* **11**, 767-798.
Hirsikko *et al* (2012a) *Atmos. Chem. Phys. Discuss.* **12**, 1895-1934.
Hirsikko *et al* (2012b) *in preparation.*
IPCC (2007), *Fourth Assessment Report of the Intergovernmental Panel on Climate Change.*
Kulmala, M., *et al* (2004) *J. Aerosol Sci.* **35**, 143-176.
Mirme *et al* (2007) *Boreal Env. Res.* **12**, 247-264.
Petäjä *et al* (2009) *Atmos. Chem. Phys.* **9**, 7435-7448.
Vakkari *et al* (2011) *Atmos. Chem. Phys.* **11**, 767-798.
Venter *et al* (2012) *submitted to the S. Afr. J. Sci.*

New particle formation events in Hungarian background air at K-puszta, 2008-2011

Zs. Bécsi[1], Á. Molnár[2], K. Imre[1], T. Nieminen[3], J. Hakala[3], T. Petäjä[3] and M. Kulmala[3]

[1]Department of Earth and Environmental Sciences, University of Pannonia, Veszprém, P.O. Box 158, H-8201, Hungary
[2]Air Chemistry Group of the Hungarian Academy of Sciences, University of Pannonia, Veszprém, P.O. Box 158, H-8201, Hungary
[3]Department of Physics, University of Helsinki, Helsinki, P.O. Box 64, FI-00014, Finland
Keywords: nucleation, number size distribution, particle formation and growth, seasonal patterns.
Presenting author email: becsi.zsuzsanna@gmail.com

Studies with increasing number have been published in the last years due to the important role of fine particles in several atmospheric processes and effects on climate and human health. New particle formation events are observed all over the world both in polluted and clean, background air. Similarly, in Hungary NPF events can be detected in polluted cities like Budapest (Salma *et al* (2011) as well as in rural air at K-puszta. Our former results showed that in rural air these events can be frequently observed, NPF events are classified on 25-30% of the days (see Figure 1).

In this work we summarize our results on the particle formation at K-puszta station between Nov. 2008 and Dec. 2011. The size distribution of the particles between 3-800 nm is evaluated. On the basis of DMPS spectra the classification of particle formation events is carried out according to the recommendations of Yli-Juuti *et al* (2009). The event classification is studied with respect to the seasonal variation and the frequency of the particle formation event types (event, non-event and unclassified) is also discussed.

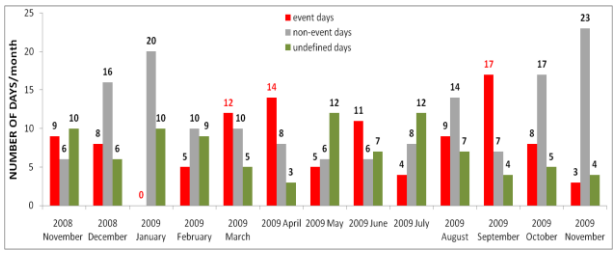

Figure 1. Event classification statistics (November 2008-November 2009), K-puszta.

Generally, in new particle formation (NPF) winter is the most inactive period (Figure 1), while the number of NPF events is found to be the highest in spring and in autumn. As a consequence of the seasonal variation of the NPF events, the frequency of the nucleation mode (3-25 nm) is the highest during spring and autumn. On the other hand, in winter the accumulation mode (100-800 nm) showed the highest, while in spring and summer the lowest frequency. This seasonality is also shown by the "typical" seasonal number size distributions. This means that in spring the freshly formed particles, while in winter the aged particles characterize the aerosol size distribution.

The growth rate (GR) of the freshly formed particles is also calculated (Hirsikko *et al* (2005), Yli-Juuti *et al* (2009). Our results show that at K-puszta the particle GR is highly variable; and has no significant seasonal variation. The rates were estimated between a few and 14 $nmhr^{-1}$ except one day with a growth rate of 18 $nmhr^{-1}$. The average GR was 5.67 $nmhr^{-1}$. On the other hand, the formation intensity of new nucleation mode particles (smaller than 25 nm) is also estimated. The calculation is based on the method considering the change of the particle number concentration in each size modes per unit time. According to our preliminary results the new particle formation rate varies in a wide range of values (e.g. the average formation rate for 10 nm particle size range was found between 2.31-21.8 particles $cm^{-3}sec^{-1}$.

This work was supported by the FP6 projects: European Integrated project on Aerosol Cloud Climate and Air Quality Interactions (EUCAARI, contract No: 036833-2) and European Super-sites for Atmospheric Aerosol Research (EUSAAR, contract No: RII3-026140).

Salma, I., Borsós, T., Weidinger, T., Aalto, P., Hussein, T., Dal Maso, M. and Kulmala, M. (2011) *Atmos. Chem. Phys.*, **11**, 1339–1353.

Yli-Juuti, T., Riipinen, I., Aalto, P.P., Nieminen, T., Maenhaut, W., Janssens, I.A., Claeys, M., Salma, I., Ocskay, R., Hoffer, A., Imre, K. and Kulmala, M. (2009) *Boreal Env. Res.* **14**, 683-698.

Hirsikko, A., Laakso, L., Hõrrak, U., Aalto, P., Kerminen, V.-M. and Kulmala, M. (2005) *Boreal Env. Res.* **10**, 357-369.

Continental source for secondary biogenic aerosols in Antarctica

E.-M. Kyrö[1], A. Virkkula[1,2], V.-M. Kerminen[1], M. Dal Maso[1], J. Parshintsev[3], J. Ruiz-Jimenez[3], L. Forsström[4], H. E. Manninen[1], P. Heinonen[5], M.-L. Riekkola[3], and M. Kulmala[1]

[1]Department of Physics, University of Helsinki, Helsinki, 00014, Finland

[2]Air Quality Research, Finnish Meteorological Institute, Helsinki, 00101, Finland

[3]Department of Chemistry, University of Helsinki, Helsinki, 00014, Finland

[4]Department of Biological and Environmental Sciences, University of Helsinki, Helsinki, 00014, Finland

[5]FINNARP logistics, Finnish Meteorological Institute, Helsinki, 00101, Finland

Keywords: Antarctic aerosols, Nucleation, Organic aerosols, Aerosol cloud interaction.

Presenting author email: ella-maria.kyro@helsinki.fi

Antarctica is very isolated continent, especially during the winter, and has had no known sources of secondary aerosol particles on its surface (Ito, 1989) until present. However, during the Finnish Antarctic Research Program (FINNARP) 2009 expedition, the first evidence of Antarctic particle formation due to continental biogenic precursors was observed.

The Finnish Antarctic Research Station Aboa ($73^{\circ}03'S$, $13^{\circ}25'W$) is build on a nunatak (mountaintop) Basen, 500 m a.s.l., some 130 km from the open ocean. During the Antarctic summer, lots of meltwater form close to the nunataks that are peaking out from the thick ice mass. These meltwater ponds hold a variety of biological activity in them (Jungblut *et al.*, 2005), e.g. cyanobacteria *Nostoc commune* (Vaucher), a species very tolerant for extreme conditions (Dodds *et al.*, 1995) and commonly found from Basen and the Antarctic mountains.

The concentrations of neutral $10-500$ nm and charged $0.8-42$ nm particles as well as their size distribution and quartz filter samples were taken from the atmosphere, about 3 m above the ground level. The measurement devices were kept inside a small container, approximately 200 m upwind from the main station. In addition, samples of the cyanobacterial mat of *N. commune* and water from the meltwater ponds were taken. The ponds were approximately 2.5 km upwind from the measurement site. Different chemical compounds from the filter as well as water and *N. commune* samples were analyzed later in Finland with a comprehensive two dimensional gas chromatography-time-of-flight mass spectrometry (GCxGC-TOF-MS).

During the campaign three periods of frequent new particle formation (NPF) and subsequent growth were observed - in the beginning of the campaign, in the beginning of January and in the end fo the campaign. The growth rate for the charged cluster ions as well as for neutral Aitken mode particles were high for Antarctica (Kulmala *et al.*, 2004), order of $1-10$ nm/h. The most intense and almost continuous nucleation happened after the melting of the ponds and the exposure of *N. commune* during the last two NPF periods; 1st to 3rd and 17th to 21st of January, 2010. The events started from the smallest cluster sizes and the particles grew very rapidly. In addition, the shape of the events was suggesting that the formation took place on a small scale, close to the station. To our knowledge, this has not been observed earlier in Antarctica.

We also estimated the contribution of the ponds to the aerosol budget at our measurement site. These calculations revealed that the ponds can be very important source areas for secondary aerosols during the summertime in Antarctica. In addition, we used HYSPLIT backtrajectories to estimate the origin of the growing Aitken mode particles during the same periods. The results showed that the particles originated from the inland mountains few hundred of kilometres away.

Even though the total surface area of the nunataks is quite small, they are important source regions for secondary organic aerosols during the summer in Antarctica. Furthermore, in a warming climate, it is likely that more meltwater ponds will open up during the summertime and they will exist longer. This could increase both the aerosol number concentrations and their condensational growth and finally CCN and cloudiness. Our results will help in estimating the climatic feedbacks of aerosols and future climate in Antarctica.

This work was supported by the Academy of Finland (project no. 127534 and 118780), the Academy of Finland Centre of Excellence program (project no. 1118615) and European Research Council (project no. 227463-ATMNUCLE). The atmospheric measurement group at the University of Helsinki is greatly acknowledged for their technical support before the expedition.

Dodds, W.K. *et al.* (1995) J. of Phycology **31(1)**, 123-126.

Ito, T. Ambio (1989) **18(1)**, 34-41.

Jungblut, A.-D. *et al.* (2005) Env. Microbio. **7(4)**, 519-529.

Kulmala, M. *et al.* (2004) J. Aerosol. Sci. **35**, 143-176.

NanoShip: Mapping of new particle formation events over the North Sea

N. Kelbus[1,2], A. Massling[3], M. Fiebig[4], B. Henzing[5], M. Glasius[6], M. Bilde[7], M. Moerman[5], G. de Leeuw[5,8,9], M. Dal Maso[8], and A. Kristensson[2]

[1]Dept. of Physical Geography and Ecosystem Sci., Lund University, P. O. Box 118, SE-221 00 Lund, Sweden
[2]Department of Physics, Lund University, P. O. Box 118, SE-221 00 Lund, Sweden
[3]Department of Environmental Science, Aarhus University, P. O. Box 358, DK-4000 Roskilde, Denmark
[4]Norwegian Institute for Air Research (NILU), NO-2007 Kjeller, Norway
[5]TNO, Princetonlaan 6, P.O.Box 80015, 3508TA Utrecht, the Netherlands
[6]Department of Chemistry, Aarhus University, Langelandsgade 140, DK-8000 Aarhus, Denmark
[7]Department of Chemistry, University of Copenhagen, DK-2100, Copenhagen, Denmark
[8]Department of Physics, University of Helsinki, P. O. Box 64, FI-00014, Helsinki, Finland
[9]Finnish Meteorological Institute FMI, P.O. Box 503, FI-00101 Helsinki, Finland

Keywords: SMPS, DMPS, nucleation, shipping emissions, sulphur dioxide
Presenting author email: natalia.kelbus@gmail.com

The secondary formation of atmospheric nanoparticles through gas-to-particle conversion occurs in many areas over the world. After subsequent condensational growth to sizes relevant for cloud formation, these particles become important for the global radiation balance. Potentially, the nanoparticle formation route might be responsible for up to 50% of world's cloud condensation nuclei (Merikanto et al., 2009), with a large uncertainty which stems from poor knowledge of formation routes. In this study, we seek to widen our knowledge in one of the formation routes. A basic question in this context is:

How frequent are ship-induced new particle formation events, and what conditions are favourable for their appearance?

In our NanoShip project, particle number size distribution measurements are carried out at a site at the Danish peninsula Jutland during 2012 to investigate if formation events are linked to winds from the North Sea. Also data from the Norwegian and Dutch EUSAAR sites Birkenes and Cabauw measured from late 2008 until present are used to infer the appearance and frequency of formation events during conditions with winds from south-east and north-west respectively.

By following the growth process of nanoparticles during the formation, and using back trajectories it is possible to infer where the formation of 1.5 nm diameter particles has taken place over the North Sea. This method is described by Kristensson et al. (2011).

Figure 1 shows an example of a formation event at Birkenes with a strong particle mode appearing larger than 15 nm in diameter around 10:00 local time, grown to around 25 nm in diameter at 12:00, and finally to sizes well above 50 nm in diameter in the evening. The growth rate suggests that the particles of around 25 nm in size have been formed as 1.5 nm diameter particles roughly 6 hours previously over the sea north of the Danish peninsula Jutland (thick line in Figure 2). Hence, formation events take place over densely trafficked ship lanes.

Maps will be superimposed for a full event probability distribution as function of geographical coordinates over the North Sea based on the data from the three sites.

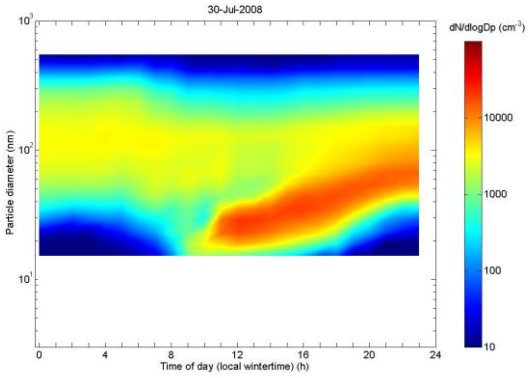

Figure 1. Particle number size distribution at Birkenes (Norway, rural site) during July 30, 2008.

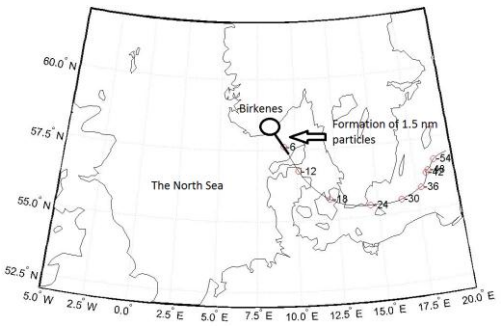

Figure 2. Back trajectory analysis recalculating the origin of a nucleation event observed at Birkenes at 100 m a.s.l at 12:00 July 30, 2008. Circles denote position of trajectory each 6 hours.

This work was supported by the Swedish Research council FORMAS under grant 2010-850.

Kristensson, A., Swietlicki, E., et al. (2011). EAC proceedings, Manchester, September 2011.

Merikanto, J., Spracklen, D. V., Mann, G. W., Pickering, S. J., and Carslaw, K. S. (2009) *Atmos. Chem. Phys.* **9**, 8601-8616.

Direct observations of atmospheric sub-2 nm neutral and charged clusters

J. Kontkanen[1], M. Kulmala[1], K. Lehtipalo[1], H.E. Manninen[1], T. Petäjä[1], M. Sipilä[1], H. Junninen[1], S. Schobesberger[1], P. Rantala[1], A. Franchin[1], T. Jokinen[1], E. Järvinen[1], M. Äijälä[1], J. Kangasluoma[1], T. Nieminen[1], J. Hakala[1], P.P. Aalto[1], P. Paasonen[1], J. Mikkilä[2], J. Vanhanen[2], J. Aalto[3], T. Ruuskanen[1], R.L. Mauldin III[1,4], J. Dublissy[1], J. Bäck[5], I. Riipinen[6], M. Johnston[7], J.N. Smith[8], V.-M. Kerminen[1] and D.R. Worsnop[1]

[1]Department of Physics, University of Helsinki, Finland, [2]Airmodus Oy, Helsinki, Finland, [3]SMEAR Station, Hyytiälä, Finland, [4]University of Colorado at Boulder, CO, USA, [5]Department of Forest Sciences, University of Helsinki, Finland, [6]University of Stockholm, Sweden, [7]University of Delaware, DE, USA, [8]National Center for Atmospheric Research, CO, USA,
Keywords: molecular clusters, ion clusters, nanoparticles, particle formation and growth
Presenting author email: jenni.kontkanen@helsinki.fi

Atmospheric new particle formation is proposed to happen via heterogeneous nucleation on molecular clusters or the activation of the clusters in the size range of 1–2 nm (Kulmala *et al*., 2000). There are numerous observations of sub-2 nm charged clusters and recent measurements have also proven the existence of neutral clusters (Lehtipalo *et al*., 2009). However, still many questions related to the exact particle formation mechanism remain. In this work we aim to shed light on these issues by using direct measurements of atmospheric sub-2 nm charged and neutral clusters.

Measurements were conducted from March 14th to May 16th 2011 at the SMEAR II station in Hyytiälä, southern Finland. The total nanoparticle concentration was measured with a particle size magnifier (PSM; Airmodus A09; Vanhanen *et al*., 2011) and ions were measured with a Neutral cluster and Air Ion Spectrometer (NAIS). In addition, sulfuric acid concentration was simultaneously measured using a Chemical Ionization Mass Spectrometer (CIMS). The total nanoparticle concentration and ion concentration were calculated for six size classes ranging from 0.9 nm to 2.1 nm in mobility diameter. The concentration of neutral clusters and particles due to the ion-ion recombination was estimated from the ion spectrometer data. The concentration of other neutral species was then calculated by subtracting the concentrations of ions and recombination products from the total concentration.

During the measurement period a continuous pool of sub-2 nm nanoparticles was observed (Kulmala et al., 2012, Kontkanen et al., 2012). This nanoparticle population was dominated by neutral clusters and particles not originating from the ion-ion recombination as their concentration exceeded the concentrations of ions and their recombination products most of the time. Particularly during new particle formation events the dominance of neutral species was clear. However, when the total concentration was low (typically at night), the ion concentration was often larger than the concentration of neutral clusters and nanoparticles. The typical concentration of neutral clusters was 1000–10000 cm^{-3}, the concentration varying stronger than the ion concentration.

To resolve atmospheric nucleation we studied the concentration of neutral clusters and ions in different size classes. During new particle formation events the concentration of neutral clusters seems to have its minimum at the size of 1.7–1.9 nm indicating that the growth from that size is clearly higher than the growth to that size. On the other hand, when the concentration of neutral clusters is normalized with the concentration of ions of the same size the minimum occurs at the size of 1.3–1.5 nm. These results indicate that the clusters smaller than 1.3 nm are subcritical clusters and clusters larger than 1.9 nm are growing clusters or nanoparticles. Thus, the critical size for nucleation seems to be 1.3–1.9 nm.

Several studies have shown that sulfuric acid has a crucial role in new particle formation. Our results support these observations as there is a strong correlation between the concentration of neutral clusters and nanoparticles and the concentration of sulfuric acid, especially during new particle formation. On an average new particle formation event day during our measurement period the growth rate of clusters from 1.3 nm to 1.7 nm was about 0.5 nm/h (determined from the PSM data) and from 1.7 nm to 3 nm about 1.5–2 nm/h (determined from the NAIS data). As the sulfuric acid concentration during the events was observed to be about $5 * 10^6$ cm^{-3}, the growth from 1.3 to 1.7 nm can be explained by sulfuric acid only. However, the growth from 1.7 to 3 nm needs a contribution of other, likely organic, compounds.

To conclude, our results suggest that 1) at least in Hyytiälä neutral clusters and nanoparticles dominate over small ions and their recombination products, 2) the critical size for the nucleation is 1.3–1.9 nm, and 3) sulfuric acid is responsible for the growth of clusters to the size of 1.7 nm. After that also other compounds are needed.

This work was supported by Finnish Centre of Excellence (FCoE), Cryosphere-Atmosphere Interactions in a Changing Arctic Climate (CRAICC), and European Research Council (ERC).

Kontkanen, J. *et al*. (2012), manuscript in preparation.
Kulmala, M. *et al.* (2000) N*ature*, 404, 66–69.
Kulmala, M., *et al.* (2012), manuscript in preparation.
Lehtipalo, K. *et al*. (2009) *Atmos. Chem. Phys*., 9, 4177–4184.
Vanhanen, J. *et al.* (2011) *Aerosol Sci. Technol.* 45, 533–542.

Cloud Condensation Nucleus Production from Nucleation Events at a Semi-Rural Environment: Puijo station, Eastern Finland

A. Hamed[1], M. Komppula[2], H. Portin[1,2], A. Leskinen[2], S. Romakkaniemi[1], K.E.J. Lehtinen[1,2], J. Smith[1,3], J. Joutsensaari[1] and A. Laaksonen[1, 4]

[1]Department of Applied Physics, University of Eastern Finland, P. O. Box 70211 Kuopio, Finland
[2]Finnish Meteorological Institute, Kuopio Unit, P.O. Box 1627, FIN-70210 Kuopio, Finland
[3]National Center for Atmospheric Research, Boulder, USA
[4]Finnish Meteorological Institute, P.O. Box 503, 00101 Helsinki, Finland

Keywords: CCN, Nucleation, New Particle Formation and Growth

New particle formation (NPF) in the atmosphere is a global phenomenon that has been shown to take place in a wide variety of environments (Kulmala et al., 2004). Particles grown from NPF can affect the Earth's radiation balance directly by scattering sunlight and indirectly by having the potential to grow large enough to act as cloud condensation nuclei (CCN), and moreover, can activate to cloud droplets, resulting in even greater scattering of radiation which leads to a cooling effect on the climate. However, the magnitude of aerosol indirect effects remains the single largest uncertainty in current estimates of anthropogenic radiative forcing and causes large uncertainties in the calculations of future climate change. The growth of NPF to reach CCN size may take several days, and since many aerosol dynamical as well as meteorological effects interact during such a time span, it has been difficult to determine CCN production rates on the basis of experimental observations.

Here, we address CCN production due to secondary particle formation based on the characteristics of NPF events observed in a semi-rural environment, Puijo station, Kuopio city, Eastern Finland. The station is on the top of the Puijo observation tower; 62° 54′ 32″ N, 27° 39′ 31″ E, 306 m a.s.l and 224 m above the surrounding lake and located about 2 km northwest of the center of Kuopio city, Eastern Finland. The surroundings of the station are different in each side. There are distinct sectors for cleaner and more polluted air, which give us a good opportunity to investigate the effects of local emission sources on aerosol particle formation. More detail of the station can be found in Leskinen et al. (2009). This study makes use of continuous 3 years of particle size distribution carried by Differential Mobility Particle Sizers with particle size ranges of 7-800 nm.

In order to estimate the production of potential CCN, we calculated the increases in concentrations of particles in the 50–800 nm, 80–800 nm size ranges on nucleation event days. We first determine visually the time t_1 when the leading edge of the growing nucleation mode reaches the lower limit of the size range in question (i.e. 50 & 80 nm), and denote by t_2 either the time the particle concentration in the given size range reaches a maximum, or midnight, whichever comes first. The concentration increase in the given size range is then determined from the difference of the concentrations between times t2 and t1 (Laaksonen et al., 2005). Moreover we compared CCN production (CCN_P) in Puijo station with CCN_P in Pallas station, Lapland, Northern Finland (Lihavainen et al., 2003).

For Puijo, the average increase of CCN_P in 50 and 80 nm size ranges were 5237 #cm^3 and 1375 #cm^3. We then compared the average CCN_P values from Puijo research station to the average CCN_P from sizes 50 and 80 nm in Pallas station in Northern Finland (table 1. in Lihavainen et al., 2003). The results show that the ratios of average CCN_P in Pallas to CCN_P in Puijo were 15.1 % and 14.3% for sizes greater than 50 and 80 nm, respectively. The obtained results implied that new particle formation events are a larger source of CCN in Eastern Finland as in Northern Finland. This is probably due to higher amount of anthropogenic contributions in Kuopio than in Lapland.

We will show a comprehensive statistical comparison of the Puijo data sets with respect to meteorological and trace gases of nucleation events to elucidate the different process govern new particle formation for this station.

Kulmala et al. (2004). *J. Aerosol Sci*., **35**, 143–176.
Laaksonen et.al., (2005). *Geophys Res Lett.*, **32**, 1-4.
Leskinen et al. (2009). *Boreal Env. Res.*, **14**, 576-590.
Lihavainen et al. (2003). *J. Geophys. Res*., **108**, doi:10.1029/2003JD003887.

Formation of halogen-induced secondary organic aerosol (XOA)

K. Kamilli[1], J. Ofner[2], C. Zetzsch[2], A. Held[1]

[1] Junior Professorship in Atmospheric Chemistry, University of Bayreuth, 95440 Bayreuth, Germany
[2] Atmospheric Chemistry Research Laboratory, University of Bayreuth, 95440 Bayreuth, Germany

Keywords: Smog chamber, SOA (Second. Organic Aerosols), Particle formation
Presenting author email: katharina.kamilli@uni-bayreuth.de

Caused by their potential of stratospheric ozone depletion and surface ozone destruction, reactive halogen species (RHS) are a very important topic of atmospheric research. Crucial sources for halogens in the troposphere are halogen-release from sea-salt aerosol (Finlayson-Pitts, 2003) and heterogeneous reactions on those aerosol surfaces (Rossi, 2003). RHS seem to interact with secondary organic aerosol (SOA) precursors similarly to common atmospheric oxidizing gases like OH radicals and ozone. Although aerosol formation from reaction of RHS with typical SOA precursors was previously studied, e.g. by Cai et al. (2006), no data are available on bromine-induced aerosol formation from organic precursors yet. The potential interaction of RHS with performed SOA has recently been studied (Ofner et al., 2012).

An aerosol smog-chamber was used to examine the halogen-induced secondary organic aerosol (XOA) formation under atmospheric conditions using simulated sunlight. With a concentration of 10 ppb for the organic precursor and 2 ppb for molecular chlorine and 10 ppb for molecular bromine the experimental setup is close to ambient conditions. By combined measurements of the aerosol size distribution, the ozone and the NOx concentrations, as well as the decay of the aerosol precursor, determination of aerosol yields and aerosol growth factors could be achieved. Thereby the decay of the aerosol precursor was analyzed by capillary gas chromatography coupled with flame-ionization detection (GC-FID) and the aerosol size distribution was measured using a Scanning Mobility Particle Sizer (SMPS). Additionally, with the decay rate of the precursor and the calculated photolysis rates of molecular halogen species, based on the well-known spectrum of the solar simulator, mechanistic details on the XOA formation pathways can be determined.

We observed XOA formation even at very low precursor and RHS concentrations with a diameter mode at about 20 nm and a number concentration up to 10000 particles cm^{-3}. While the XOA formation from chlorine is very rapid, the interaction of bromine with the organic precursors is about five times slower (see Figure 1).

These studies may be related to natural XOA formation in sea-salt dominated environments, where we find organic species as precursors from biogenic or anthropogenic sources and photolyzed RHS from the surface or the sea-salt aerosol.

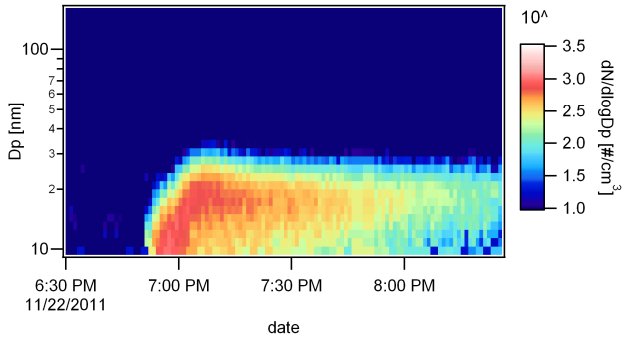

Figure 1. XOA formation from limonene and bromine in a 700 L aerosol smog-chamber.

This work was funded by German Research Foundation (DFG) under grant HE 5214/5-1.

References:

Cai, X., and Griffin, R. J.: Secondary aerosol formation from the oxidation of biogenic hydrocarbons by chlorine atoms, J. Geophys. Res., 111, D14206/14201-D14206/14214, 2006.

Finlayson-Pitts, B. J.: The tropospheric chemistry of sea salt: A molecular-level view of the chemistry of NaCl and NaBr, Chem. Rev., 103, 4801-4822, 2003.

Ofner, J. Balzer, N., Buxmann, J., Grothe, H., Schmitt-Kopplin, Ph., Platt, U., and Zetzsch, C., Halogenation processes of secondary organic aerosol and implications on halogen release mechanisms, Atmos. Chem. Phys. Discuss. 12, 2975-3017, 2012.

Rossi, M. J.: Heterogeneous reactions on salts, Chem Rev, 103, 4823-82, 2003.

Spectra of positive air ions up to 40 nm as a function of selected trace gases

T.-E. Parts, A. Luts, K. Komsaare, and U. Hõrrak

Institute of Physics, University of Tartu, Ülikooli 18, 50090 Tartu, Estonia
Keywords: Aerosol chemistry, Size distribution, Mass spectrometry, Ion-induced nucleation
Presenting author email: urmas.horrak@ut.ee

New results about aerosol particle formation in the atmosphere can be obtained applying air ion mobility distribution measurement technique together with traditional methods (e.g. Hõrrak et al., 2008). This work continues the recent study of negative air ions (Luts et al., 2011) and shows how enhanced concentrations of water vapor, iodine, ammonia, and diethylamine (DEA) modify the composition and mobility distribution of the positive ions at different age.

An advanced method to study the formation of secondary aerosol particles starting from gas phase reactions including trace gases and ions was examined for the positively charged particles. We produced new air ions in laboratory experiments and traced their evolution within the age interval from few tenths of a second up to few ten seconds. We investigated the changes in size and mass distribution of ions concurrently by means of two instruments: 1) Air Ion Spectrometer (AIS, Airel Ltd) and 2) mass spectrometer (MS, Sciex API-300).

The huge amount of different organic compounds in the background air complicates the interpretation of the data comparing to negative ions. Nevertheless, the results demonstrate the ability of the method to trace the temporal evolution of positive air ions. In all observed cases, the noticeable MS peaks are up to *m/z* 836. We modified the concentration of water vapor and trace gases in the reaction chamber by evaporation of water, liquid organics or sublimation of iodine. Iodine vapor was found to have a substantial effect in our previous study (Luts et al., 2011). DEA and ammonia as organic compounds with high proton affinity (PA) are expected to play substantial role in positive ion chemistry.

Mass spectra of the background air consist of a large number of peaks, the most prominent are at *m/z* 130, 294, 321, 378, 408. Water vapor tends to grow up the peaks at *m/z* 378 and 408. Diethylamine changes the spectra substantially; new peaks at *m/z* 189, 190, 210, 304 appear. Also, surprisingly iodine has an essential effect on MS – new peaks appear at *m/z* 482, 483, 619. Ammonia induces the new peaks at *m/z* 269 and 322. The distribution of all peaks and their intensity depends on the age of ions. The composition of positive air ions at an age of about 0.5 s was clearly different from that at about 20 sec.

Size distribution of positive ions at different age affected by trace gases demonstrated that iodine leads to enhanced concentration of the charged aerosol particles above 3 nm, which, in turn, decrease substantially the concentration of cluster ions due to ion-aerosol attachment (Figure 1). The burst of positive ions did not require any accompanying high concentration of water. Moreover, high relative humidity (RH) suppresses the ions between 3 and 20 nm. On the contrary, in the case of negative ions (studied previously), high RH strengthens the effect of iodine. It should be emphasized that in the case of positive ions the effect of iodine appears only at ion ages of about 20 seconds, when compared to the negative ions, where the effect was observed almost instantly.

Both diethylamine and ammonia induce new MS peaks. DEA does not evoke any substantial change in the AIS spectra. Ammonia induces moderate increase in the concentrations of the ions in the region 2 to 4 nm and in the region from 7 to 20 nm.

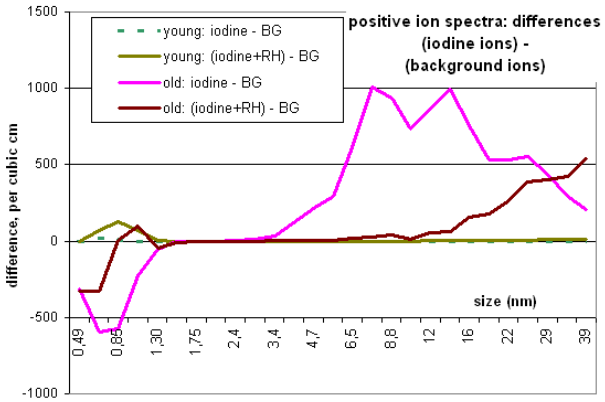

Figure 1. Differences in the AIS size distributions of positive ions induced by enhanced concentration of iodine and enhanced humidity.

This work was supported by the Estonian Science Foundation grant 8342 and by the research project SF0180043s08 of Tartu University. We thank Tapio Kotiaho and Alexey Adamov and Timo Maurila from the Helsinki University for help in MS experiments.

Hõrrak, U., Aalto, P. P., Salm, J., Komsaare, K., Tammet, H., Mäkelä, J. M., Laakso, L., and Kulmala, M. (2008) Variation and balance of positive air ion concentrations in a boreal forest. *Atmos. Chem. Phys.*, 8, 655-675.

Luts, A., Parts T.-E., Hõrrak, U., Junninen, H., Kulmala, M. (2011) Composition of negative air ions as a function of ion age and selected trace gases: mass and mobility distribution. *Journal of Aerosol Science*, 42, 820-838.

NanoMap: Methodology for geographical mapping of new particle formation events

M. Johansson[1], A. Kristensson[1], E. Swietlicki[1], M. Dal Maso[2], N. Kivekäs[3], T. Hussein[2,4], T. Nieminen[2], H. Junninen[2], H. Lihavainen[3], P. Tunved[5], and M. Kulmala[2]

[1]Department of Physics, Lund University, Lund, SE-221 00, Sweden
[2]Department of Physics, University of Helsinki, Helsinki, FI-000 14, Finland
[3]Finnish Meteorological Institute FMI, P.O. Box 503, FI-00101 Helsinki, Finland
[4]Department of Physics, University of Jordan, 11942, Amman, Jordan
[5]Department of Applied Environmental Science, University of Stockholm, SE-106 91, Stockholm, Sweden

Keywords: SMPS, DMPS, nucleation
Presenting author email: martin.epost@gmail.com

The formation of new nanometer sized particles around 1.5 nm diameter during so called new particle formation events is frequent in the atmosphere. After condensational growth to cloud condensation nuclei (CCN) sizes, the nanometer sized particles have a potential to influence the global radiation balance of the atmosphere. Potentially, up to 50 % of world's CCN come from formation events (Merikanto et al., 2009).

There are an increasing number of ground stations in Europe, where measurements of the particle size distribution are performed, and hence at these sites a full characterization of formation events can be performed. However, there is a lack of information where and when the formation events take place in between the stations. For example, in favourable regions we expect "hot-spots" with a higher frequency of events and conversely "cold-spots" where gaseous precursor concentrations necessary for the formation are low.

Fortunately, this information is possible to attain. In Kristensson et al. (2011) we explain briefly the methodology, which employs existing particle number size distribution data from field sites and meteorological back trajectories. With this methodology it is possible to calculate as an end product the probability of formation of 1.5 nm diameter particles during formation events in the boundary layer in grid cells with arbitrary horizontal resolution over a European geographical mesh.

We have chosen to develop this methodology in the NanoMap project for the EUSAAR site Hyytiälä in southern Finland, since there are over 15 years of size distribution data, which gives high geographical coverage and statistics.

In Figure 1 is shown an example of the applied methodology for Hyytiälä. Only 10 months of data are used for this plot, which gives a scattered impression in the different grid cells. However, it shows that the methodology can be extended to several years of data, and that we can calculate the probability of formation with a high horizontal resolution around the station.

The calculated probability further away from the Hyytiälä site needs to be validated with the observed probability of events at a different site than Hyytiälä. Since there are two stations where size distribution data is collected for many years rather close to Hyytiälä (Pallas in northern Finland and Aspvreten in southern Sweden), this is certainly possible to do.

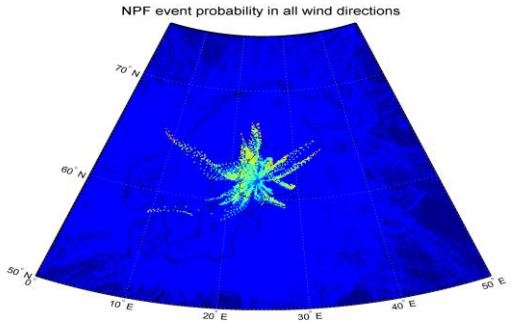

Figure 1. The probability (relative scale) of formation of 1.5 nm diameter particles during formation events around the Hyytiälä field site. Plot is based on data between Jan 1 2005 and Oct 31 2005 and the geographical grid box resolution is $0.2 \times 0.1^\circ$ in the latitudinal and longitudinal direction respectively.

The main deliverable of the NanoMap project is to make the methodology possible to apply at any site in Europe with a dense station network, where it is possible to validate the formation probability at nearby sites. With respect to the position of European sites, it is obvious that the methodology can be applied for the entire Nordic area and parts of Western Europe along a transect from Germany, Holland all the way down to northern Italy.

Simultaneously, we are trying the FLEXPART trajectory model (Stohl et al., 2005), which additionally incorporates estimates of particle dispersion. However, the development time needed is much longer, and in the meteorological back trajectory method, we already have a method up and running, which is evidently powerful and soon easily available to the scientific community

This work was supported by the Swedish Research council FORMAS under grant 2010-850.

Kristensson, A., Swietlicki, E., et al. (2011). EAC proceedings, Manchester, September 2011.

Merikanto, J., Spracklen, D. V., Mann, G. W., Pickering, S. J., et al. (2009) *Atmos. Chem. Phys.* **9**, 8601-8616.

Stohl, A., C. Forster, A. Frank, P. Seibert, and G. Wotawa (2005): Technical Note: The Lagrangian particle dispersion model FLEXPART version 6.2. *Atmos. Chem. Phys.* **5**, 2461-2474.

Trends in atmospheric new particle formation – 16 years of observations in boreal forest

T. Nieminen[1], M. Dal Maso[1], T.Petäjä[1], P. P. Aalto[1], V.-M. Kerminen[1, 2], P. Hari[3] and M. Kulmala[1]

[1]Department of Physics, University of Helsinki, Finland
[2]Finnish Meteorological Institute, Helsinki, Finland
[3]Department of Forest Sciences, University of Helsinki, Finland

Keywords: new particle formation, long-term trends

Presenting author email: tuomo.nieminen@helsinki.fi

Research on new particle formation (NPF) in the atmosphere has been very active during the last two decades. This phenomenon has been observed in various environments around the world (Kulmala *et al.*, 2004). One of the longest and most comprehensive data sets of atmospheric aerosol properties is available from the University of Helsinki SMEAR II station in Hyytiälä, southern Finland (Hari and Kulmala, 2005). Ambient aerosol size distributions have been measured at Hyytiälä since January 1996 with a DMPS system covering particle size range 3 – 1000 nm (3 – 500 nm until end of 2004; see Aalto *et al.*, 2001). Aerosol measurements are complemented by measurements of basic meteorological variables, trace gas concentrations (SO_2, O_3, CO, CO_2, NO, NO_x), and quantities related to the soil and forest surrounding the station.

Until end of 2011 we have observed 1337 days with regional NPF events, i.e. formation of new 3 nm particles followed by particle growth to sizes of 30 – 50 nm typically within 10 – 20 hours. Most of the events occur at spring time from March to May. The number of nucleation events detected at Hyytiälä varies from year to year in the range 60 – 120 per year. The reasons behind this quite substantial variation are not yet found. We have, however, established that the variation of the galactic cosmic ray intensity due to the 11 year solar cycle is not connected to the particle formation intensity at Hyytiälä (Kulmala *et al.*, 2010).

Mean values and observed trends in the quantities relative to NPF are listed in Table 1. There is no statistically significant trend in the formation rates of 3 – 25 nm particles. In contrast, the growth rates are increasing by 3% per year relative to their 16 year mean value. Concentrations of sulphuric acid, which is the most important precursor vapor in atmospheric NPF, can be approximated with a simple proxy model (Petäjä *et al.*, 2009). This proxy takes into account the source from SO_2 and the condensation sink by pre-existing particles. Both the SO_2 concentration and CS are decreasing in Hyytiälä, but the relative change in SO_2 is larger. This leads to a decreasing trend of 4% per year also in the H_2SO_4 proxy concentration, and suggests that the observed increase in the particle growth rates could be caused by increased concentrations of organic compounds and their oxidation products. As the emissions of these biogenic organic compounds are highly temperature dependent, increasing global temperatures can lead to a larger fraction of newly formed particles reaching cloud condensation nuclei sizes and this way NPF becoming more significant to climate.

This research was supported by the Academy of Finland Center of Excellence program (project number 1118615).

Aalto P. et al. (2001) *Tellus* 53B, 344–358.
Hari P. and Kulmala M. (2005) *Boreal Env. Res.* 10, 315–322.
Kulmala M. et al. (2004) *J. Aerosol Sci.* 35, 143– 176.
Kulmala M. et al. (2010) *Atmos. Chem. Phys.* 10, 1885–1898.
Petäjä et al. (2009) *Atmos. Chem. Phys.* 9, 7435–7448.

Table 1. Mean values and trends of gas and particle quantities related to new particle formation in Hyytiälä during 1996 –2011. Trend is calculated from linear least-squares fit to 30 min averaged values.

	1996 – 2011 mean value	**Trend**	
		absolute value	**relative to 1996 – 2011 mean**
SO_2	0.38 ppb	–0.02 ppb/year	–5.0%/year
Condensation sink	$5.1 \cdot 10^{-3}$ s^{-1}	$-1.5 \cdot 10^{-4}$ s^{-1}/year	–2.9%/year
H_2SO_4 proxy	$3.8 \cdot 10^{5}$ cm^{-3}	$-1.5 \cdot 10^{-4}$ cm^{-3}/year	–4.3%/year
Formation rate	0.84 cm^{-3} s^{-1}	no trend	-
Growth rate	3.1 nm/h	+0.1 nm/h	+3.2%/year

Characterization of new particles formation events at Izaña Mountain Observatory (Tenerife, Canary Islands): formation, growth rates and influencing atmospheric parameters

M.I. García[1], S. Rodríguez[1], R.D García[1] and Y. González[1]

[1]Izaña Atmospheric Research Centre, (IARC/CIAI), AEMet, Santa Cruz de Tenerife, E-38001, Spain
Keywords: Atmospheric aerosols, New Particle Formation Events, Growth, SMPS
Presenting author email: mgarciaa@aemet.es

We present a study of new particle formation events in the low free troposphere over Tenerife (Canary Islands). The study is based on 4 years (2008-2011) observations of particle number size distribution in the Izaña Global Atmospheric Watch Observatory. This site is placed at 2400 meters above the sea level. The site remains almost permanently above the marine stratocumulus layer typical of the subtropical oceans. The low troposphere is strongly inhibited, in such a way that the 'dry' troposphere is separated from the 'humid' marine boundary layer by the subtropical inversion layer (linked to trade winds). The study data set includes particle size distribution, measured with a Scanning Mobility Particle Sizer (10 – 500 nm), reactive gases (NOx, SO_2, O_3 and CO), meteorological parameters and radiation. The objective of this study is to identify the context in which New Particle Formation (NPF) events occur.

Ultrafine particle (<100 nm) concentrations showed a strong diurnal evolution, with a maximum during daylight. This evolution was prompted by the development of buoyant slope winds, which also resulted in increases in the concentrations of water vapour, reactive gases and nanoparticles (3 – 10 nm; Rodríguez et al., 2009). We observe that, in most of cases, the increases in the ultrafine particles were associated with burst in the nucleation mode particles (< 20 nm). In many cases these burst were followed by a subsequent particle growth up to diameters within the range 50 – 100 nm, resulting in New Particle Formation (i.e. banana type, Fig.1).

These NFP episodes were observed with any wind direction, being also associated with the arrival of polluted air from below due to the action of upslope winds. The frequency of NPF events showed a significant variability, within the range 2 - 14 events / year. The events are more frequent in summer. Growth rates of nucleation particles (diameter < 25 nm; Dal Maso et al., 2005) typically exhibits values within the range 1 - 5 $nm \cdot h^{-1}$. The frequency of NPF events, as well as the growth and formation rates is somewhat lower than those observed in the polluted continental boundary layer (Kulmala et al., 2004). This is attribute to the much lower concentrations of gas phase precursors in this free troposphere site (e.g. SO_2 concentrations are ~ tends to hundreds of ppt during daylight).

A day-to-day event classification was performed. Different subgroups were segregated, and the parameters that may influence on the NPF formation were studied.

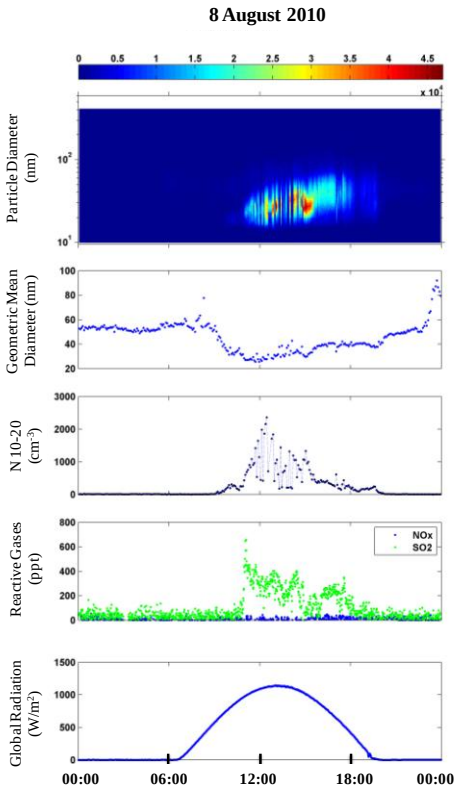

Figure 1. NPF and its comparison with atmospheric parameters

This study was performed within the context of projects REDMAAS (CGL2011-15008-E) and POLLINDUST (CGL2011-26259).The author is grateful to the Meteorological Sate Agency of Spain, Ministry of Agriculture, Food and Environment of Spain for the grant to carry out aerosol in-situ formation and studies.

Kulmala, M., Vehkamaki, H., Petaja, T., Dal Maso, M., Lauri, A., Kerminen, V.-M., Birmili, W. and McMurry, P.H. (2004) *Aerosol science.* **35**, 143-176.

Dal Maso, M., Kulmala, M., Riipinen, I., Wagner, R., Hussein, T., Aalto, P.P. and Lehtinen, K.E.J.(2005) *Boreal Env. Res.***10**, 323-336.

Rodriguez, S., González, Y., Cuevas, E., Ramos, R., Romero, P.M., Abreu-Afonso, J. and Redondas, A.(2009) *Atmos. Chem. Phys.* **9**, 6319-6335.

Influence of meteorological parameters and air mass history on new particle formation events at K-puszta, Hungary

A. Molnár[1] and Zs. Bécsi[2],
[1]Air Chemistry Group of the Hungarian Academy of Sciences, University of Pannonia, Veszprém, P.O. Box 158, H-8201, Hungary
[2]Department of Earth and Environmental Sciences, University of Pannonia, Veszprém, P.O. Box 158, H-8201, Hungary
Keywords: nucleation, particle formation, backward trajectory, meteorological parameters, seasonal variation.
Presenting author email: becsi.zsuzsanna@gmail.com

Atmospheric aerosol particles – the majority of them are formed in the atmosphere – have great importance in the environment. The ubiquitous secondary particles are produced from different precursor gases, they can be found in urban, background and remote air. The investigation of different processes leading to new particle formation is of great importance, since these particles play a key role in important atmospheric processes like in the formation of cloud and precipitation, in the control of shortwave radiation balance or in climate control.

It is well known that the physical characteristics of the atmosphere (meteorological parameters) also affect the occurrence of new particle formation (NPF) events; for this reason in this work this relationship is studied. The relationship between NPF and meteorological parameters such as temperature, wind speed and direction, relative humidity, precipitation, global radiation is presented. Besides, trajectory analysis (source regions, change of meteorological parameters (mixing height, precipitation, global radiation) is also involved in the evaluation. The backward air trajectories are calculated by Hysplit Trajectory Model (Draxler and Rolph, 2012; Rolph, 2012).

In this work we summarize our results on the influence of meteorological parameters on new particle formation at K-puszta, Hungary. Between November 2008 and November 2009 105 NPF events were classified (Yli-Juuti *et al.*, 2009): in winter 13, in spring 31, in summer 24 and in autumn (4 months) 37 NPF events were observed.

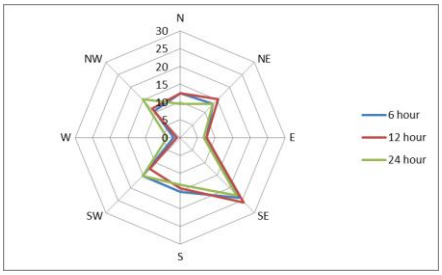

Figure 1. Direction of backward trajectories during NPF events (November 2008-November 2009), K-puszta.

The preliminary results of backward trajectory analysis are presented in *Fig. 1*. In the figure the frequency of NPF events as a function of 6, 12 and 24 hour backward trajectory directions is presented. One can see that from Nov. 2008 and Nov 2009 the contribution of southern trajectory directions was rather important. This contribution was the most definite in winter and autumn, while in summer NPF events are mainly occurred in northern air masses (*Table 1*).

Table 1: Summary of the seasonal occurrence of NPF events as a function of the direction of air trajectories.

		6 hour	12 hour	24 hour
Spring	Northern	29	39	42
	Southern	52	48	48
Summer	Northern	54	54	54
	Southern	38	38	38
Autumn	Northern	35	35	30
	Southern	59	57	57
Winter	Northern	23	23	23
	Southern	77	77	69

This work was supported by the FP6 projects: European Integrated project on Aerosol Cloud Climate and Air Quality Interactions (EUCAARI, contract No: 036833-2) and European Super-sites for Atmospheric Aerosol Research (EUSAAR, contract No: RII3-026140). The authors also gratefully acknowledge the NOAA Air Resources Laboratory (ARL) for the provision of the HYSPLIT transport and dispersion model and/or READY website (http://www.arl.noaa.gov/ready.php) used in this publication.

Draxler, R.R. and Rolph, G.D., 2012. HYSPLIT (HYbrid Single-Particle Lagrangian Integrated Trajectory) Model access via NOAA ARL READY Website (http://ready.arl.noaa.gov/HYSPLIT.php). NOAA Air Resources Laboratory, Silver Spring, MD.

Yli-Juuti, T., Riipinen, I., Aalto, P.P., Nieminen, T., Maenhaut, W., Janssens, I.A., Claeys, M., Salma, I., Ocskay, R., Hoffer, A., Imre, K. and Kulmala, M. (2009) *Boreal Env. Res.* 14, 683-698.

Rolph, G.D., 2012. Real-time Environmental Applications and Display sYstem (READY) Website (http://ready.arl.noaa.gov). NOAA Air Resources Laboratory, Silver Spring, MD.

Micrometeorological measurement of dry deposition of aerosols pollutants (PAH, PCB, metals) on a wetland (Seine river estuary)

O. Connan[1], M. Millet[2], D. Hébert[1], J.J Schwartz[2], F.Guéguen[2], P. Roupsard[1], R. Goujon[3], D.Maro[1], B. Letellier[1]

[1]Cherbourg-Octeville Radioecology Laboratory, IRSN, 50130 Cherbourg-Octeville, France
[2]Equipe Physico-Chimie de l'atmosphère LMSPC, UMR 7515 CNRS, 67084 Strasbourg, France
[3]Agence de l'eau Seine Normandie, 76000 Rouen, France
Keywords: Eddy Covariance Fluxes, Particle Deposition, Trace elements, Metal, PAH.
Presenting author email: olivier.connan@irsn.fr

A Natura 2000 protected wetland (Marais Vernier) located in the Seine estuary (West of France) was equipped with instruments in September 2010 to study dry and wet fluxes of pollutants on an annual scale. This site is located away from any nearby anthropic sources (the nearest road is 500 m away) and can be representative of medium and large scale atmospheric transport, with the possible very occasional influence of major industrial sites (oil refinery) during brief meteorological episodes. The IRSN (Institute for Radiological Protection and Nuclear Safety), studied the radiological and chemical pollutants (^{7}Be, PAH, PCB, and trace metals) in aerosols and rainwater on one year to obtain the dry and wet deposition fluxes separately. The dry deposition pollutants was quantified by combining chemical measurements performed in atmospheric aerosols with an eddy covariance technique, allowing deposition velocities to be obtained by turbulent correlation between fluctuation of vertical wind and airborne particles number. Eddy covariance allows to obtain a deposition velocity for aerosol (V_d in $m{\cdot}s^{-1}$), which will give the deposition flux for any atmospheric pollutants if concentrations are known.

The first objective of this study was to obtain the fluxes of chemical constituents over the wetland and to assess the atmospheric transfer of pollutants into the area considered. Particular attention was devoted in this study to accurately separating dry deposition from wet deposition; in fact, a better understanding of the dry deposition velocity parameter V_d and its dependence on meteorology (atmospheric turbulence, roughness length u*, and sensible heat flux H) is a major issue for the IRSN and scientific community (Fowler *et al*, 2009), in order to have available relevant data for better parameterization of dispersion and deposition models in the event of a radiological accident.

The second objective was to be able to establish relations between V_d, roughness length u* and sensible heat flux H in a sizeable data set. Being able to assess the relative importance of wet (rain) and dry deposition over a year also contributes to improve understanding transfer in case of radiological accident especially at large scale.

For this study, the site was equipped with an opening collector for rain (Eigenbrodt UNS 130/E), a partisol (FRM2000) for collecting trace metals Cd, Pb, Ni, Zn, and Hg, a partisol (FRM2000) equipped with a ChemComb cartridge to collect gaseous and particulate PAH and PCB, a particle counter (TSI 3010, 0.01 - 3 µm) and a sonic anemometer (YOUNG 81000V). Samples for chemical analysis were taken monthly to get integrated fluxes. For particles number, we used Particle Size Selector for measured particles above 0.1 µm (and then to be able to correlate dry deposition velocity with the atmospheric aerosol size).

The dry deposition velocities V_d measured over a year by eddy covariance have led to the establishment of reliable laws as a function of the meteorological parameters H (for H < and > 50 $W.m^{-2}$) and u* (Figure 1) thus allowing dry deposition fluxes to be recalculated precisely on a monthly scale. Dry velocity deposition from these rural area varying from 2.3 to 4.7 10^{-4} $m.s^{-1}$, which is lower than values commonly used in operational models (5 10^{-3} $m.s^{-1}$).

From Vd calculated precisely, we have estimated the dry fluxes of the chemical constituents PAH, PCB and metals.

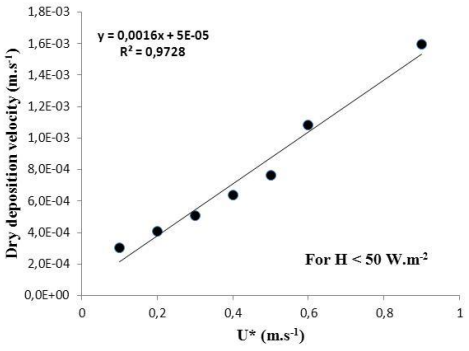

Figure 1. Dry deposition velocities Vd function of friction velocities U*, for H<50 $W.m^{-2}$.

Results from this study show HAP fluxes close to 44 $\mu g.m^{-2}.year^{-1}$, metal traces fluxes are 0.1-115 $\mu g.m^{-2}.year^{-1}$ depending of the element and PCBs indicate fluxes close to 10 $\mu g.m^{-2}.year^{-1}$.

This work allowed to use the eddy covariance over a long period to improve knowledge on Vd in function of micrometeorological, to clarify fluxes of pollutants on a rural particular site, to have a better understanding of the respective contribution of dry and wet deposition.

D. Fowler *et al.* (2009) *Atmos. Env.* 43, 5193-5267.

Experimental study of the submicron aerosol dry deposition in the urban canopy: original methodology and first results

P. Roupsard[1], D. Maro[1], A. Coppalle[2], V. Ruban[3], S. Percot[3], O. Connan[1], P. Laguionie[1], L. Solier[1], M. Rozet[1], D. Hébert[1] and M. Talbaut[2]

[1]Laboratoire de Radioécologie de Cherbourg-Octeville, IRSN, 50130 Cherbourg-Octeville, France
[2]COmplexe de Recherche Interprofessionnel en Aérothermochimie, 76801 Saint-Etienne du Rouvray, France
[3]Institut Français des Sciences et Technologies des Transports, de l'Aménagement et des Réseaux, 44341 Bouguenais, France
Keywords: dry deposition, deposition velocity, urban areas, submicron particles, 7Be
Presenting author email: pierre.roupsard@irsn.fr

In the case of an accidental or chronic atmospheric pollution by a nuclear plant, aerosols' deposition transfer coefficients must be known. A major issue is to determine the impact of aerosols contained in the radioactive plume on urban areas with the smallest uncertainties. In this case, local deposition must be known in urban canopy. In dry atmospheric conditions, transfer coefficients are defined by the dry deposition velocity V_d (m s^{-1}), the ratio between the aerosol dry deposition flux (particles m^{-2} s^{-1}) and the aerosol concentration (particles m^{-3}). Dry deposition depends on aerosol diameter, atmospheric turbulent conditions and deposit surface. Actually, only few dry deposition velocities were measured on urban surfaces and existing data are not linked to atmospheric conditions (Fowler *et al*, 2009). Thus, it is important to measure dry deposition velocities, associated with turbulence and local meteorological conditions to improve the knowledge and the models predictions for urban areas. In this study, a new three-step experimental methodology has been set up to approach the complexity of the urban canopy. The first step consists in a wind tunnel study and the second and third steps in *in situ* experiments with different time scales. This methodology allows to measure deposition velocities associated with turbulence and meteorological conditions, and to carry out a phenomenological study of dry deposition on urban surfaces.

Experiments are based on submicron aerosol's tracer deposition measurements: fluorescein submicron aerosol (d_p = 0.27 µm) and beryllium 7 (atmospheric aerosol, *dp* = 0.5 to 1.2 µm (Ioannidou, 2011)). The wind tunnel study was aimed at quantifying fluorescein aerosol dry deposition velocities and turbulence conditions for three urban surfaces (Roupsard *et al.*, 2011). Deposition on horizontal and vertical surfaces and thermophoresis effect by warmed horizontal surfaces were studied in the wind tunnel. The second step consists in short-time *in situ* experiments. Developed by Maro *et al.* (2010), these experiments were performed to measure fluorescein aerosol dry deposition on seven urban surface types in real urban turbulence conditions. Fluorescein aerosol was generated during 1 hour. Meteorological conditions were measured with a meteorological station and wind velocity with an ultrasonic anemometer near sampling surfaces. Surfaces' temperatures were measured to study thermophoresis effect on deposition in real conditions. Finally, submicron atmospheric aerosol's deposition under local meteorological conditions was measured on the seven surfaces by using beryllium 7 as a tracer of the accumulation mode (Maro *et al.*, 2010). This third step, named long-time *in situ* experiments, was carried out on a one year long period. Urban sampling surfaces are exposed to the atmospheric aerosol during one month and protected from precipitations. During this period, local meteorological conditions are measured by an ultrasonic anemometer and a meteorological station. Wind tunnel results are compared to short-time *in situ* results and short-time results are compared to long-time *in situ* results. With this method, physical parameters playing a role in aerosol dry deposition on urban surfaces are met, displayed and quantified. Furthermore, acute (wind tunnel and short-time *in situ* experiments) and chronic (long-time *in situ* experiments) pollution deposition conditions are met and studied.

First results give different values for V_d on same surfaces depending on experiment step (wind tunnel, *in situ* short- or long-time), with smaller values for the first and the second steps and larger values for the third step. Dependence of V_d on friction velocity and temperature gradient at the surface are quantified with few uncertainties in wind tunnel. For this range of diameter, interception and impaction prevail in isotherm conditions. Thermophoresis force is added in case of existing temperature gradient. Short-time *in situ* experiments give similar results than wind tunnel experiments. For glass surfaces, both dry deposition velocities are in good agreement with the Lai and Nazaroff model (2000), built for smooth surfaces without thermophoresis. Long-time *in situ* V_d are much larger than wind tunnel and short-time *in situ* V_d by a factor of 3 to 5. Several hypotheses will be tested to explain this difference, in particular atmospheric aerosol diameter variations with time due to condensation.

This work is supported by the INOGEV research program of the French National Research Agency.

D. Fowler *et al.* (2009) *Atmos. Env.* 43, 5193-5267.
A. Ioannidou (2011) *Atmos. Env.* 45, 1286-1290.
P. Roupsard *et al.* (2011) *Proc. 18th Eur. Aero. Conf.*, Manchester.
D. Maro *et al* (2010) *Proc. 8th Int. Aero. Conf.*, Helsinki.
A.C.K Lai and W.W. Nazaroff (2000) *J. Aero. Sci.* 31, 463-476.

First in situ measurements of atmospheric particle dry deposition velocity by eddy-correlation method using the the new 0.1 s time-response Pegasor Particle Sensor

P. Laguionie, D. Maro, D. Hébert and F. Sanson

Institute for Radiological Protection and Nuclear Safety, Cherbourg-Octeville, 50130, France
Keywords: atmospheric particle, dry deposition, eddy-correlation, time-response.
Presenting author email: philippe.laguionie@irsn.fr

During a nuclear accident, a radioactive aerosol, a gas and particles mixture, can be released into the atmosphere. Over short spatial ranges, *i.e.* distances less than about 10 km from the accident location, radioactive aerosol and atmospheric aerosol differ in terms of physicochemical properties. Beyond these short ranges, both aerosol particle granulometric spectra are undistinguishable. As a result, parameters constraining atmospheric particle deposition processes can be input into operational models to estimate surface radioactive contamination.

After release into the atmosphere, radionuclides scatter, then deposit on both natural (*e.g.* meadows, fresh water areas) and anthropogenic (*e.g.* building fronts, bituminous coating) surfaces. Radionuclide deposition can occur during either rain/snow falls or dry spells giving respectively wet or dry deposits. Wet deposition leads to high surface albeit short-duration radionuclide concentrations. By contrast, dry deposition lead to lower but persistent concentrations and so become dominant in mass balance over time. In this work, only dry-deposition has been considered. Currently, atmospheric particle dry-deposition velocity estimates encompass several orders of magnitude (Fowler *et al.*, 2009). Such a range is hardly explainable due to the lack of experimental micrometeorology data, especially regarding turbulences that drive particle deposition.

Currently, among the plethora of available estimation methods, only one directly estimates atmospheric particle deposition velocities in relation to turbulent processes occurring near surfaces: the eddy-correlation method. The latter accounts for turbulence created on a surface upstream from the measurement point (footprint concept). In practice, this method indirectly gives the dry deposition velocity ($m.s^{-1}$) by dividing the dry deposition flux ($particles.m^{-2}.s^{-1}$) by the measured particle concentration in the air ($particles.m^{-3}$). And the dry deposition flux is the outcome of the covariance between wind vertical velocity and atmospheric particle concentration. But, this method has hardly been carried out in situ because of measurement device technologic limitations. Indeed, the closer the measurement from the surface, the smaller the atmospheric eddy size and so, the shorter sampler device time-response to signal variations. In highly heterogeneous environments, measurements have to be done close to surfaces (less than 1 m) in order to discriminate particle deposition velocities with each surface. Being at less than one meter, a 10 Hz measurement frequency is necessary to characterise the whole atmospheric turbulence spectrum and concentration variations. Consequently it also requires measurement devices with time-response inferior or equal to 0.1 s.

So far, wind velocity has been measured using an ultrasonic anemometer (UA, 0.1 s time-response) and atmospheric particle concentration using an Electrical Low-Pressure Impactor (ELPI, 0.4 s time-response). ELPI advantage is to measure particle concentration for each granulometric class so that deposition velocity is a function of mean particle diameters. However ELPI time response is long, which precludes measurement at less than around 5 m above a surface as turbulence size is too small below 5 m (Damay *et al.*, 2009). In turn, a 5 m height cannot discriminate among several small surfaces and so measurements can only be done upstream of large (> 1000s m^2) homogeneous surfaces where air flow is stabilised. In addition, ELPI long time-response prevents from measuring in aerodynamic conditions shifting spectra towards high frequencies such as high wind speeds conditions (> 2 $m.s^{-1}$) or high atmospheric stability conditions (Horst, 1997).

Now, thanks to recent technologic breakthroughs, particle counter time-responses decrease. In particular, the Pegasor Particle Sensor (PPS) of Pegasor Oy (Ltd) can not only measure concentration with granulometric threshold sorting but also respond in 0.1 s. Consequently, for the first time, conjoint use of UA and PPS allows conducting in situ dry-deposition velocity determination method regardless of aerodynamic conditions and environmental heterogeneity.

This presentation is focused on dry-deposition velocity estimation results by eddy-correlation method conjointly using AU-PPS. Firstly, the conjoint use of AU-PPS is validated by comparing data obtained with AU-ELPI for measurements done at 5 m above a meadow with wind speeds less than $2m.s^{-1}$. Secondly, AU-PPA is used to estimate dry-deposition velocities at less than 5 m above a surface with non-constrained wind speeds. From then on, in situ dry-deposition velocity determination method by eddy-correlation can be generalised to highly heterogeneous environments and/or atmospheric conditions favouring small-scale eddies.

This work was supported by the French Institute for Radiological Protection and Nuclear Safety (IRSN).

Damay, P.E., Maro, D., Coppalle, A., Lamaud, E., Connan, O., Hebert, D. Talbaut, M. and Irvine, M. (2009). *Journal of Aerosol Science* **40**, 1050-1058.

Fowler D. *et al.* (2009). *Atmospheric Environment* **43**, 5193-5267.

Horst, T.W., (1997). *Boundary-layer Meteorology* **82**, 219-233.

Turbulent aerosol fluxes in a forest clearing measured with a fast mixing-type CPC

F. Kittler[1], F. Ditas[2], B. Wehner[2] and A. Held[1]

[1]Bayreuth Center of Ecology and Environmental Research, University of Bayreuth, Bayreuth, Germany
[2] Department of Physics, Leibniz Institute for Tropospheric Research, Leipzig, Germany

Keywords: Fluxes, Micrometeorology, Turbulence
Presenting author email: andreas.held@uni-bayreuth.de

Turbulent surface-atmosphere exchange of aerosol particles is a key control of the variability of the aerosol number concentration in the atmospheric boundary layer. A variety of micrometeorological techniques is available to quantify turbulent aerosol fluxes, e.g. eddy covariance or relaxed eddy accumulation. For eddy covariance flux measurements, fast sensors with a time resolution of 10 Hz or better are required. However, technical limitations of current aerosol instrumentation, in particular with respect to time resolution, constrain the application of direct eddy covariance for aerosol flux measurements.

Recently, a new fast mixing-type condensation particle counter (FCPC) with a time resolution of 20 Hz (Wehner et al., 2011a) has been applied successfully in the marine boundary layer near Barbados from the helicopter-borne platform ACTOS (Wehner et al., 2011b). Here, we present results of ground-based eddy covariance measurements using the new FCPC and a standard TSI CPC 3772 at the forest ecosystem research site "Waldstein" in the Fichtelgebirge mountains in south-east Germany in August 2011.

Wind and aerosol data were collected with a time resolution of 20 Hz. The particle inlet was co-located with a CSAT3 sonic anemometer at 2.5 m and 5.5 m above ground level in a forest clearing. The signal response to a change in particle number is not only due to the time constant of the particle counter, but also due to signal dampening in the sampling line. Fig. 1 shows typical response curves of the FCPC and the CPC 3772 (both sampling from the same inlet in the field) to a sudden change in particle number. With the sampling configuration used in this field experiment, evidently the FCPC adjusts to new particle concentrations within 0.2 s, whereas the CPC 3772 adjusts within ~2 s.

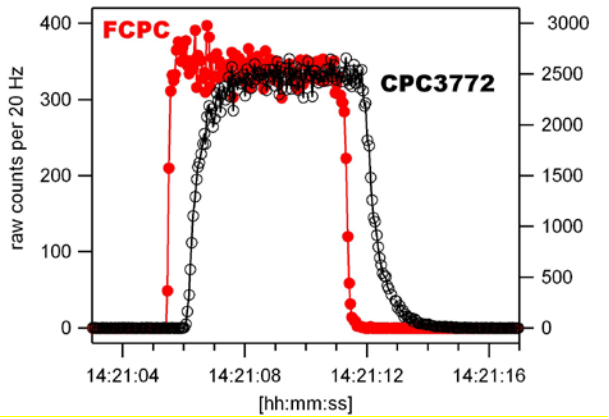

Figure 1: Response curves to step changes in particle number. Time steps from symbol to symbol are 0.05 s.

The fast response of the FCPC allows for a direct evaluation of the high-frequency contributions to the turbulent aerosol flux. So far, due to the lack of sufficiently fast sensors, this part of the frequency spectrum has been neglected, or corrected assuming spectral similarity of particle number and other atmospheric scalars. Now, the FCPC measurements can be directly evaluated at high frequencies with respect to spectral similarity with other atmospheric scalars.

We will present eddy covariance aerosol fluxes including directly measured high frequency contributions to the turbulent flux. The magnitude of these contributions will be assessed under various atmospheric conditions, and the applicability of spectral similarity with other atmospheric scalars will be evaluated. Our results will give additional insight into the process of turbulent aerosol transport, and challenge, or support, the current practice of eddy covariance aerosol flux measurement corrections.

Wehner, B., Siebert, H., Hermann, M., Ditas, F. and Wiedensohler, A. (2011a) Characterisation of a new Fast CPC and its application for atmospheric particle measurements. Atmos. Meas. Tech. 4, 823-833.

Wehner, B., Ditas, F., Wiedensohler, A. and Siebert, H. (2011b) Vertical transport of aerosol particles in the marine boundary layer near Barbados. Abstracts of the European Aerosol Conference 2011, Manchester, UK.

Highly size resolved particle fluxes: Results from biannual measurements using OPCs in an urban environment.

M.J. Deventer, O. Klemm and F.Grießbaum[1, 2]

[1]Climatology Working Group, University of Münster, Münster, 48149, Germany
[2]now at LI-COR Biosciences GmbH, Bad Homburg Germany
Keywords: fluxes, turbulence, optical particle counter, size-segregated aerosols
julian.deventer@uni-muenster.de

From Feb. 2012 onwards turbulent exchange of particles between the urban surface and the urban boundary-layer is measured above the city area of Münster (NW Germany). The scope of the study is to investigate and quantify the contributions of particles of various size classes to total urban particle fluxes and to study their seasonal variability.

According to the present knowledge, cities are both sources and sinks for atmospheric aerosol particles. The input of particulate material from the regional background is mostly established through aged accumulation range particles and can constitute a major fraction of the urban PM levels. On the other hand, emission mainly originates from combustion processes, yielding large numbers of nano-sized particles, and from re-suspension of coarse particles from the urban surfaces.

Results from preliminary studies support the following assumptions: Source apportionment analysis at urban street level sites in Münster (Gietl and Klemm, 2009) suggests that a considerable portion of the urban particle masss originates from distant sources. A first size-segregated flux approach, using an electrical low-preassure impactor (ELPI) and the disjunct eddy covariance (EC) technique, showed that emission of ultrafine particles may co-occur with deposition of particles in the micrometer range. This is equivalent to the simultaneous occurrence of positive (upward) number fluxes and negative (downward) mass fluxes (Schmidt and Klemm, 2008). A more recent study (Deventer *et al.*, 2011) validated these results with the employment of an optical particle counter (OPC) in direct EC. A tipping point between upward and downward oriented particle fluxes was found to be at 168 ± 20 nm (fig. 1). The authors showed that EC in combination with a fast OPC is an appropriate tool to study these bi-directional fluxes for multiple size classes.

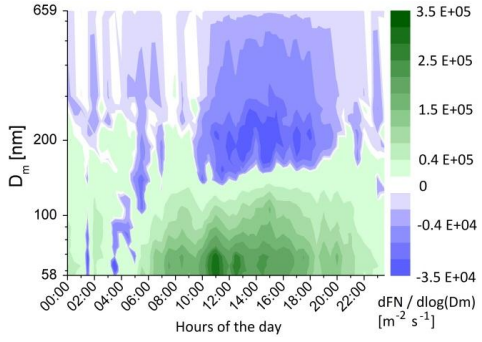

Figure 1. Contour plot of mean daily number fluxes (normalized) for all UHSAS channels. Log. Y-axis.

For this campaign, we expand the previous setup (consisting of the Ultra-High Sensitivity Aerosol Spectrometer (UHSAS)) with a Passive Cavity Aerosol Spectrometer Probe (PCASP-X2), both manufactured by Droplet Measurement Technologies, Boulder, Colorado (USA), now covering the aerosol particle size range between 0.6 – 10 µm diameters in up to 99 bins. In order to reach acceptable counting statistics and minimize random errors, we combine the initial 99 bins into 19 wider size bins. Despite this reduction of size information, the measurement yields a considerable improvement in comparison to that in previous studies. Furthermore, we will install an 11-stage electrical low pressure impactor (Outdoor ELPI, Dekati Ltd., 33700 Tampere, Finland) to collect hourly particle samples, which will be analysed with a TOF-MS in the lab. The eddy-covariance setup is placed on a 62 m above ground level (a.g.l.) high radio tower located in a military compound, southeast to the city center. For a more detailed site description see Schmidt and Klemm (2008), Griessbaum and Schmidt (2009) and Dahlkoetter *et al.* (2010).

The presentation will show results from biannual flux measurements resolved in 19 size classes for the PM_{10} range. Collected particles from the impactor stages will be used to calculate size resolved mass fluxes for numerous poly-aromatic hydrocarbons (PAHs). Furthermore, we will concentrate on the influence of atmospheric stability on fluxes as well as on the influence of varying weather conditions, wind directions, and seasons. Lastly we will locate the tipping point between upwards and downwards fluxes more precisely.

This work was supported by the Deutsche Forschungs-Gemeinschaft (DFG) through grant KL 623 -12.

Dahlkoetter, F., Griessbaum, F., Schmidt, A. and Klemm, O. (2010) *Meteorol. Z.* **19(6)**, 565–575.
Deventer, M. J., Griessbaum, F., and Klemm, O. (2011) *Abstract 10D3, European Aerosol Conference 2011, 4-9 Sept, Manchester (UK).*
Gietl, J.K. and Klemm, O. (2009) *Aerosol Science & Tech.* **43**, 828–837.
Griessbaum, F. and Schmidt, A. (2009) *Q. J. Roy. Meteorol. Soc.* **135**, 1603–1613.
Schmidt, A. and Klemm, O. (2008) *Atmos. Chem. Phys.* **8(24)**, 7405–7417.

Direct numerical simulation of aerosol growth processes in a turbulent mixing layer

Antonio Attili, Kun Zhou and Fabrizio Bisetti
King Abdullah University of Science and Technology
Keywords: turbulence, numerical simulation.
Presenting author email: antonio.attili@kaust.edu.sa

The complex interaction between turbulent mixing and aerosol growth processes is investigated in a canonical turbulent flow configuration by means of direct numerical simulation. A cold gaseous stream mixes with a hot stream of vapor in a developing mixing layer. Nanometer sized droplets nucleate at the turbulent interface and subsequently grow as more vapor condenses on their surface. As the droplet number density increases, coagulation processes become important. The simulation results show that the mean aerosol number density reaches a maximum on the lean vapor side across the mixing layer, while the average droplet diameter peaks on the rich vapor side, where growth is more intense. It is also found that the size distribution function of the droplets exhibits self-similarity along the streamwise direction.

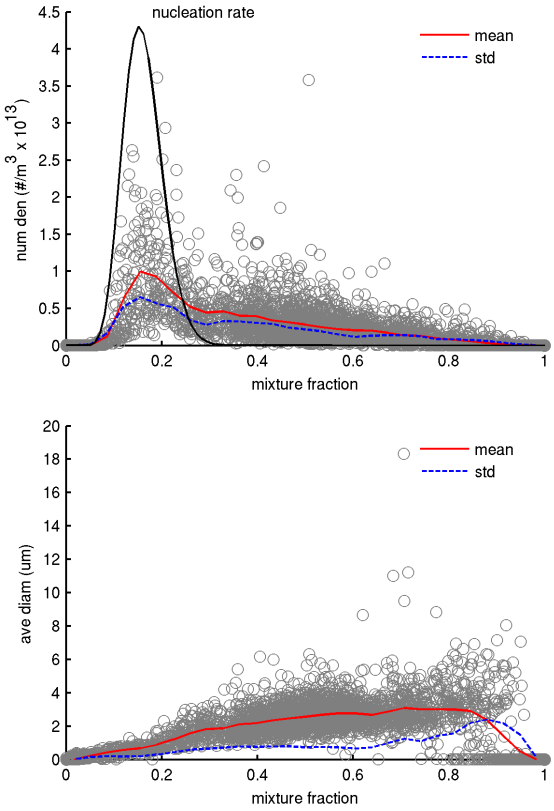

Figure 1: Scatter plots of number density and average diameter of condensing droplets in a turbulent mixing layer.

Motivation, scope, and methods

Nucleation, condensation and coagulation processes are typical of aerosols in a variety of fields, such as powder technology, cloud formation, and soot evolution. Turbulence greatly affects aerosol dynamics (Lesniewski and Friedlander, 1998; Bisetti et al., 2012). Yet, there exists little quantitative understanding about the complex interaction between turbulence and aerosols. This work investigates the evolution of a condensing aerosol in a turbulent mixing layer. The approach combines a Direct Numerical Simulation (DNS) for the flow field, the Quadrature Method of Moments (QMOM) for the statistical description of the aerosol (McGraw, 1997), and a Lagrangian particles method for the treatment of aerosol spatial transport (Koumoutsakos, 2005).

Differential transport of particles

The DNS data indicates that while particles are nucleated on the lean vapor side of the shear layer, droplets grow mostly on the rich side. The transport of particles from the lean to the rich side of the mixing layer is due to the high Schmidt Number flow typical of aerosols. Figure 1 illustrates the effects of differential transport on aerosol growth patterns. In this work, a detailed analysis of the differential transport of droplets across the layer is provided via Lagrangian and Eulerian statistics.

References

F. Bisetti, G. Blanquart, M.E. Mueller, and H. Pitsch. On the formation and early evolution of soot in turbulent nonpremixed flames. *Combust. Flame*, 159(1):317–335, 2012.

P. Koumoutsakos. Multiscale flow simulations using particles. *Annu. Rev. Fluid Mech.*, 37:457–487, 2005.

T.K. Lesniewski and S.K. Friedlander. Particle nucleation and growth in a free turbulent jet. *Proc. R. Soc. Lond. A*, 454(1977):2477, 1998.

R. McGraw. Description of aerosol dynamics by the quadrature method of moments. *Aerosol Sci. Tech.*, 27 (2):255–265, 1997.

Emission Factors for ultrafine particles obtained in Stockholm and Helsinki

Matthias Vogt[1], E Douglas Nilsson[1], Christer Johansson[1,2], Lena Järvi[3], Ivan Mammarella[3], Annika Nordbo[3], Timo Vesala[3]

[1]Department of Applied Environmental Science (ITM), Stockholm Univ., S-10691 Stockholm, Sweden
[2]City of Stockholm Environment and Health Administration, Stockholm Luft Buller analys (SLB), Stockholms stad, Box 8136, S-10420 Stockholm, Sweden
[3]Department of Physics, Division of Atmospheric Science, University of Helsinki, F-00560 Helsinki, Finland

Keywords: Aerosol Emissions, Traffic Aerosol, Traffic Activity, Emission Factors, Eddy Covariance
Presenting author email: Matthias.vogt@itm.su.se

Aerosol particles are ubiquitous in the atmosphere and they influence the quality of life on Earth in many ways; for example through air pollution, reduced visibility, climate modulation, material and ecosystem damage, and adverse health effects. In urbanized areas road traffic has been identified as the main aerosol source, especially for ultra-fine particles, which are either directly emitted or formed in secondary reactions from exhaust gases (e.g. Järvi et al., 2009).

Important quantitative information on particle sources can be obtained using micrometeorological methods such as eddy correlation however there are few direct emission measurements in cities to date (e.g Dorsey et al., 2002; Mårtensson et al., 2006, Järvi et al., 2010; Vogt et al., 2011). In this study we present direct measurements of ultrafine particle fluxes in combination with CO_2 in two North-European cities (Helsinki, Stockholm) in order to investigate similarities or differences in the processes governing these emissions.

Given that these two cities have comparable climate, living standards (e.g. the number of cars per household), and public transport systems and that emissions of both aerosols and CO_2 due to combustion of fossil fuels for cooking and heating are relatively small in both cities, comparison should provide valuable insight in to why emissions may differ (i.e. difference in engine type, fuel type etc.)

Ultrafine aerosol number fluxes were measured using the eddy covariance method from a 105 meter high communication tower over the city Stockholm, Sweden (Vogt et al., 2011) and from a 31m tall triangular lattice tower situated on a hill around 5 km north-east of Helsinki city centre (Järvi et al., 2009). Based on simultaneous measurements of the flux of CO_2, we have estimated emission factors in relation to vehicle fuel consumption, where the CO_2 emissions act as a proxy for the fuel consumption. If fleet composition and other factors are similar, this can be extrapolated to other cities since fuel statistics and/or CO_2 emission inventories are usually available. Figure 1 shows the total aerosol flux versus CO_2 flux and the resulting mean slope is $11.1*10^9$ particles/mmol CO_2 for Stockholm and $38.2*10^9$ particles/mmol CO_2. If we assume the mean fuel consumption and consider the vehicle fleet mix in Stockholm and Helsinki (mainly gasoline vehicles) we obtain an emission factor for ultrafine particles in Stockholm of $5.95*10^{13}$ particles veh^{-1} km^{-1} and Helsinki of $2.05*10^{14}$ particles veh^{-1} km^{-1}. These value is similar to the value ($4.6*10^{14}$ particles veh^{-1} km^{-1}) based on road tunnel measurements in Stockholm by Kristensson et al., (2004) and the value obtained in a street canyon ($2.86*10^{14}$ particles veh^{-1} km^{-1}) by Ketzel et al 2003. Further work will examine different possible explanations to the difference in emission factor between Stockholm and Helsinki.

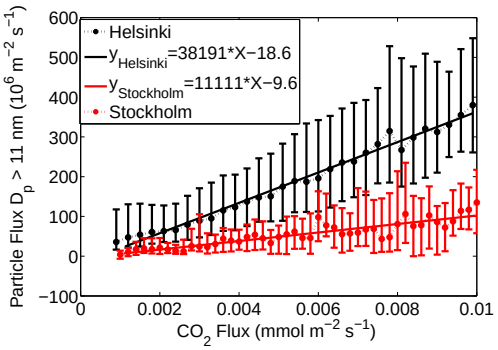

Figure 1. Median aerosol flux for $D_p > 11$nm v.s. CO_2 flux (red Stockholm, black Helsinki). Vertical bars represent 25 and 75 percentiles. Solid lines represent the linear fits.

Dorsey, J. R., Nemitz, E., Gallagher, M. W., Fowler, D., Williams, P. I., Bower, K. N., and Beswick, K. M.: , *Atmos. Environ., 36, 791–800, 2002*

Järvi, L., Rannik, U., Mammarella, I., Sogachev, A., Aalto, P.P., Keronen, P., Siivola, E., Kulmala, M. and Vesala, T. 2009. Annual particle flux observations over a heterogeneous urban area. *Atmos. Chem. Phys. 9*, 7847-7856.

Kristensson, A., Johansson, C., Westerholm, R. Swietlicki, E., Gidhagen, L., Wideqvist, U. & Vaclav Vesely, *Atmos Environ, 38, 657-673, 2004.*

Ketzel, M., Wåhlin, P., Berkowicz, R., and Palmgren, F.: Particle and trace gas emission factors under urban driving conditions in Copenhagen based on street and roof-level observations. *Atmospheric Environment*, 37, 2735–2749, 2003.

Mårtensson, E.M., Nilsson, E.D., Buzorius, G., Johansson, C., 2006.. *Atmospheric Chemistry and Physics* 6, 769–785

Vogt, M., Nilsson, E. D., Ahlm, L., Mårtensson, E. M., and Johansson, C.:2011. The relationship between 0.25–2.5 µm aerosol and CO_2 emissions over a city, *Atmos. Chem. Phys.*, 11, 4851-4859.

Analytical solution on the minimum scavenging efficiency particle size for below-cloud scavenging process using the harmonic mean method

S.Y. Bae[1], C.H. Jung[2], Y.P. Kim[3] and R.J. Park[4]

[1]Research Institute of Basic Sciences, Seoul National University, Seoul, 151742, Korea
[2]Department of Health Management, KyunginWomen's College, Incheon, 407740, Korea
[3]Department of Environmental Science and Engineering, Ewha Womans University, Seoul, 120750, Korea
[4]School of Earth and Environmental Sciences, Seoul National University, Seoul, 151742, Korea
Keywords: Minimum collection efficiency particle size, Scavenging gap, Minimum scavenging coefficient particle size.
Presenting author email: sooyabae@gmail.com

Removal of particle by precipitation is one of the most efficient particle sinks in the air. The scavenging process is largely divided into in-cloud and below-cloud processes (Bae *et al* 2006; 2010). Although the scavenging coefficient for in-cloud scavenging is larger than that for below-cloud scavenging, the latter is important for the removal of coarse and very fine particles from the boundary layer (Andronache, 2003).

Many previous studies showed the parameterization for important factors determining the efficiency of particle scavenging for the below-cloud scavenging process (Mircea *et al* (2000); Bae *et al* (2006); Croft *et al* (2009)).

One of the most important practical problems in scavenging studies is scavenging studies is determining the minimum scavenging efficiency particle size (most penetrating particle size), as well as the corresponding minimum efficiency. There is a particle size region where two or more mechanisms operate simultaneously and yet no one mechanism predominates. At the region, the penetration of particles through the collector is maximized and the collection efficiency is minimized. For this reason, the prediction of the most penetrating particle size in the scavenging gap is crucially important (Jung and Lee, 2006).

Jung *et al* (2011) calculated an approximated analytical solution for the scavenging gap for below-cloud scavenging process applied harmonic mean type approximation. They neglected the inertial impaction and consider only diffusion and interception in estimating most penetrating particle size.

For $0.01 < dp < 1$ μm, thermophoretic force increase about 0.5 order with the increase of particle diameter as shown in Pruppacher and Klett (1997). Andronache (2004) showed diffusion and electric charge mainly affected below-cloud wet removal for particles of $dp < 0.1$ μm. The below-cloud scavenging coefficients increase by almost one order of magnitude when the average charge on raindrops and particles exists, especially for particles of $0.01 < dp < 1$ μm. Bae *et al* (2009) showed relative contributions of thermophoresis and diffusiophoresis in the ambient condition.

Therefore it may need to include thermophoresis, diffusiophoresis, electrical effect and different expressions for inertial impaction may result different tendency (Jung and Lee, 2007).

In this study, we obtain an approximated solution of scavenging gap for the collection efficiency and scavenging coefficient adding thermophoresis, diffusiophoresis, and electrical forces. We also suggests an approximated analytical solution for the scavenging gap particle size which means the most penetrating particle size, during precipitation with harmonic mean method.

These results showed that the numerical results and approximated analytical solution were in good agreement without much loss of accuracy. The minimum collection efficiency and minimum scavenging coefficient were obtained using the currently suggested approach. The minimum scavenging coefficient diameter is a function of the geometric mean drop diameter, which becomes larger for wide drop size distributions. This study also estimated the minimum collection efficiency and minimum scavenging coefficient using the harmonic mean type approximation. The solution was compared with the numerically calculated results, which showed good agreement. The minimum scavenging coefficient increases with increasing falling velocity and drop geometric standard deviation.

Andronache, C. (2003) *Atmos. Chem. Phys.* **3**, 131-143.
Andronache, C. (2004) *J. Aerosol Sci.* **35**, 1467-1482.
Bae, S. Y., Jung, C. H. and Kim, Y. P. (2006) *J. Aerosol Sci.* **37**, 1507-1519.
Bae, S. Y., Jung, C. H. and Kim, Y. P. (2009) *J. Aerosol Sci.* **40**, 621-632.
Bae, S. Y., Jung, C. H. and Kim, Y. P. (2010) *J. Aerosol Sci.* **41**, 266-280.
Croft, B., Lohmann, U., Martin, R. V., Stier, P., Wurzler, S., Feichter, J., Posselt, R. and Ferrachat, S. (2009) *Atmos. Chem. Phys.* **9**, 4653-4675.
Jung, C. H. and Lee, K. W. (2006) *J. Environ. Eng.* **132**, 1381-1386.
Jung, C. H. and Lee, K. W. (2007) *Environ. Eng. Sci.* **24**, 257-266.
Jung, C. H., Bae, S. Y. and Kim, Y. P. (2011) *Atmos. Res.* **99**, 496-504.
Mircea, M., Stefan, S. and Fuzzi, S. (2000) *Atmos. Environ.* **34**, 5169-5174.
Pruppacher, H.R. and Klett, J. D. (1997) *Microphysics of clouds and precipitation*, Kluwer Academic Publishers.

The results of the coastal area of bitter-salty lakes in the Altai Territory in the summer of 2011 water and air samples study

A.S. Safatov[1], G.A. Buryak[1], S.E. Olkin[1], I.K. Reznikova[1], Yu.V. Marchenko[1], B.M. Desyatkov[1], N.A. Lapteva[1], I.S. Andreeva[1], A.S. Kozlov[2], S.B. Malyshkin[2], I.A. Sutorihin[3], V.I. Bukatyi[3], S.A. Litvinenko[3], B.S. Smolyakov[4], and M.P. Shinkorenko[4]

[1]FBRI SRC VB "Vector", Koltsovo, Novosibirsk rgn, 630559, Russian Federation
[2]IChK&C SB RAS, Novosibirsk, 630090, Russian Federation
[3]IWEP SB RAS, Barnaul, 656038, Russian Federation
[4]Acad. Nikolaev IIC SB RAS, Novosibirsk, 630090, Russian Federation
Keywords: Atmospheric aerosols, Bioaerosols, Aerosol emissions, Salt aerosol.
Presenting author email: safatov@vector.nsc.ru

Salty lakes present unique ecological systems. The results obtained in the study of chemical and biological composition of water of such lakes are presented in literature. The estimates of amounts of some chemical compounds getting into the lake from both the gas phase and aerosol are also given; however, the total aerosol emissions from the surface of bitter-salty lakes have not been evaluated previously. The goal of the study is estimation of the amounts of summer aerosol emissions by the surface of bitter-salty inland lakes in the western part of the Altai Territory.

In the summer of 2011, field works were conducted to assess the values of aerosol emissions by bitter-salty lakes of the Altai Territory – Bolshoye Yarovoye and Kuchukskoye Lakes. Lakes' areas are 53 and 181 km^2, respectively. A sampling network was deployed In the vicinity of each lake (1 point at the windward side, and 4 points at the leeward side), and simultaneous sampling was performed in all the points.

A complex for measuring the aerosol concentration and size distribution was situated in the point that was nearest to the lake at the leeward side. The complex included a diffusion aerosol spectrometer, DAS (ICCG RAS), and a photoelectric aerosol counter, Grimm 1.109 (Grimm Aerosol Technik GmbH, Germany).

The collected aerosol samples and brine samples from the lakes were studied for the ionic composition, the presence of total protein, culturable microorganisms and their diversity with the methods described in Safatov *et al* (2010).

The measured concentration values for each substance were used to solve the inverse problem - the flows of this substance from the land surface and water surfaces using a previously developed mathematical model of aerosol spread in the boundary atmospheric layer were calculated. The meteorological data required for the calculations were taken from the web site of the Air Resources Laboratory: http://ready.arl.noaa.gov/HYSPLIT.php.

The following weather conditions were recorded in the process of sampling at Kuchukskoye Lake on July 13, 2011: wind speed of 11 m/s, the angle of 33.7°, air temperature of 19.2°C and overcast of 5 points. At Bolshoye Yarovoye Lake on July 14, 2011 - the angle of 22.5°, wind speed of 5 m/s, air temperatures of 21.5°C and overcast of 5 points. Aerosol mass concentration was estimated by a number size aerosol distribution at an average particle density of 2 g/cm^3. The aerosol concentration and dispersity during the measurements at Bolshoye Yarovoye Lake slightly changed over time with an average of 13.23 ± 4.06 $\mu g/m^3$. The aerosol mass concentration during the measurements at Kuchukskoye Lake was significantly higher (due to wind-blown dust) and considerably decreased by the end of the measurements from approximately 200 - 500 to 6 - 10 $\mu g/m^3$ with an average of 157.1 ± 180.64 $\mu g/m^3$. PM_{10} during this measurement changed over time not so sharp with an average of 27.77 ± 24.26 $\mu g/m^3$.

The results of analyzing the ion composition of aerosol samples show that at the windward side of Kuchukskoye Lake aerosol contained an increased concentration of Na^+, SO_4^{2-} and Cl^- ions, and in the vicinity of Bolshoye Yarovoye Lake that of Na^+ и Cl^-. A typical dependence of concentrations of various substances in aerosol is as follows: at the windward side, an increasing concentration of the substance in the air is observed followed by passing a maximum and a gradual decrease in this concentration to the level determined for the leeward side. This indicates a significant emission of aerosol by the surface of the lakes. The coincidence of the list of the main substances present in the brine from the studied lakes with the composition of aerosol particles at the leeward side suggests that the lake brine is a precursor of aerosol found in the vicinity of Kuchukskoye Lake. For Bolshoye Yarovoye Lake containing lower concentrations of salts than Kuchukskoye Lake, this relationship is expressed to a lesser degree.

The results of mathematical simulation of aerosol emissions by the studied lakes allowed us to determine the power of flows of various substances from the surface of the lakes. Preliminary estimates show that aerosol emission by a unit of water reservoirs surfaces considerably exceeds the emission by a unit of land surface in the region of measurements. Consequently, it is the lakes that mainly contribute to air pollution in the vicinity of these lakes.

Safatov, A.S., *et al* (2010). In: *Aerosols – Science and Technology*. I. Agranovski (Ed.) Wiley – VCH, 407-454.

Spatial and Temporal Concentration of Ultrafine Particles in Rural and Urban Sites in the Po Valley (Bologna)

M. Rossi[1], L. Pasti[2], E. Sarti[2], E. Nava[3]

[1]Regional Agency for Prevention and Environment ARPA - Emilia-Romagna, Rimini, 47923, Italy
[2]Department of Chemistry, University of Ferrara, Ferrara, 44121, Italy
[3]Regional Agency for Prevention and Environment ARPA - Emilia-Romagna, Ferrara, 44124, Italy
Keywords: Ultrafine Particles, Air Quality, Monitoring, Cross-correlation Function
Presenting author email: marossi@arpa.emr.it

During the MONITER Project (Incinerator Monitoring in Emilia Romagna Area), the spatial and temporal variation of fine, ultrafine particles and gas phase parameters was assessed for the Bologna (Italy) area. Bologna is located in the south east of Po Valley, which is a well known atmospheric pollution critical area.

This assessment is based on measurements on selected days during different seasons in 2008/2009, covering urban, suburban and rural regions. Special focus was put on the investigation of particles in the fine (< 2.5 μm) and ultrafine (< 100 nm) size ranges, in particular the effect of meteorological parameters on the ultrafine (UFP) number concentration and size distribution was examined. The number concentrations of ambient particles in the size range of 5.6-560 nm were obtained from a Fast Mobility Particle Sizer, FMPS 3091, TSI. Meteorological parameters including ambient temperature, relative humidity, wind speed, wind direction, rainfall, and solar radiation flux, H-mixing were also monitored. The time series analysis reveals the 12 h periodicity of the particle number and significant seasonal and daily variations were observed: the morning peak is related to traffic. Significant differences were also observed in the UPF concentrations in the monitored sites depending on traffic and local conditions. A multilinear regression model of the day average concentration of UFP vs, the average meteorologic parameters was built . The models showed a good regression coefficients (adj-R^2: 0.79−0.89). However, this approach based on average values did not account for real time variations (Aggarwal, S., Jain, R., Marshall J. D. (2012)).

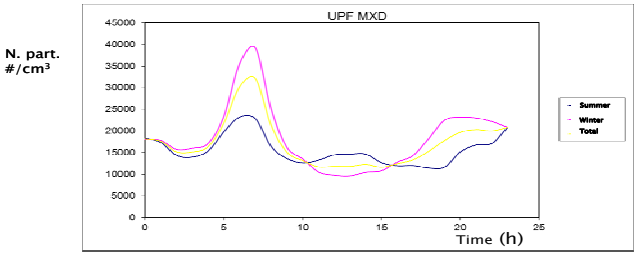

Figure 1. Averaged daily concentration of UFP at one monitored site (MXD): seasonal trend

Consequently, an approach based on cross-correlation functions between the concentration number of UFP and meteorological parameters was developed.

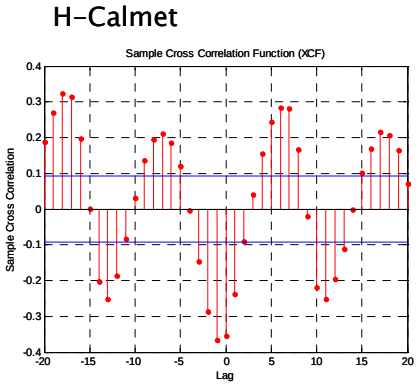

Figure 2: Cross-correlation function of instantanuos UPF concentration and mixing height (H-Calmet)

Analysis indicates that the influence of wind is probably related to stationary sources, which could be one of the contributors to elevated ultrafine particle concentration. Finally a transfer functions model was built, it was able to describe the observed temporal particle concentration. Model performance was evaluated.

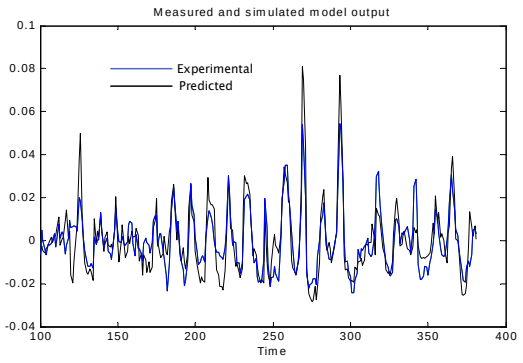

Figure 3. Concentration of UFP at one monitored site (MXD): predicted and experimental data

This work was supported by Regione Emilia-Romagna as part of the «Moniter Project». http://www.moniter.it

Aggarwal, S., Jain, R., Marshall J. D. (2012), *Environ. Sci. Technol., Real-Time Prediction of Size-Resolved Ultrafine Particulate Matter on Freeways,*

Attenuation of shock wave from a point blast in a dusty air

A.G. Girin

Odessa National Maritime University, Odessa, 65029, Ukraine
Keywords: aerosol dynamics, dust, aerosol impacts, ambient aerosol.
Presenting author email: club21@ukr.net

The problem of dynamics of shock wave initiated by point blast in a dusty air is solved numerically. Transient internal structure of wave and behavior of dynamic parameters at the wave front are investigated until the distances of hundred dynamic radii. Air is considered as a lean suspension of fine solid particles and equations of motion of two-phase two-velocity, two-temperature continuum are applied. Original three-stage calculation scheme is used, which is based on conservative difference schemes with adaptive grid. The discontinuity of leading shock is fitted and values of jumps of gas phase parameters at the shock are determined. Kinetics of interphase mechanical and thermal relaxation processes in the zone behind the shock are thus calculated with due accuracy. Comparison with known calculations of this problem for the blast in ideal air showed a good agreement.

The investigation shows that in the range of far asymptotics the behavior of blast wave in dusty air differs essentially from that in ideal. Despite small dust concentration, wave profile is transforming gradually under weak, but protracted friction and cooling of a huge amount of fine aerosol particles in the lengthy zone of interphase interaction and in large time interval, while shock propagates at large distances. The effect is most significant at the shock front, so, the jumps of gas-phase parameters bear additional decreasing there, with respect to acoustic in the case of ideal air. Difference of shock attenuation in ideal and heterogeneous air can be seen on fig. 1. Beginning from the length of three dynamic radii R_f, the redundant pressure Δp follows to another regularities in a dusty air, so, at a distances of ten dynamic radii the difference can exceed 60%. ***Blast wave with a front discontinuity disappears at finite distance from its origin and turns into dispersive wave without a shock***. Zone of maximum interphase

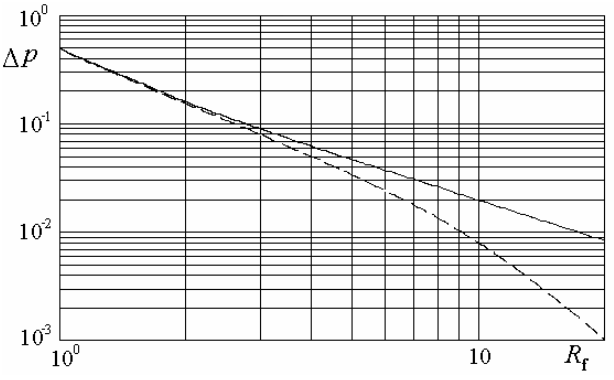

Fig.1. Shock attenuation dynamics as dependences $\Delta p(R_f)$ in ideal (solid) and in dusty (dashed) air.

interactions goes from the front inside wave. As a result, when the heterogeneity of air is taken into account, the ***total impulse of blast wave already cannot be determined by the value of redundant pressure on a distances greater than three dynamic radii***, i.e. over the whole range of far asymptotics.

An additional heterogeneous attenuation of shock wave can be seen on fig. 2, where the dependences $Z(R_f)=\frac{\gamma+1}{2\gamma}\Delta p(R_f)R_f\sqrt{\ln\left(R_f/R^*\right)}$, that were processed as a result of present calculations in accordance with far asymptotics law $\Delta p=\frac{2\gamma}{\gamma+1}\frac{C}{R_f\sqrt{\ln(R_f/R^*)}}$, are given. In ideal air Z must reach the asymptotic value $C\approx 0.270$, when the wave reaches the range of far asymptotics; vise versa, proximity of values Z and C manifests that wave has reached the range. In ideal air (upper curve) this occurs already at $R_f\approx 7\div 8$, which shows that blast wave has come into far asymptotics range. In dusty air (lower curve) blast wave undergoes strong dissipative heterogeneous action over the range $R_f>2$, which additionally diminishes shock amplitude. This curve clearly manifests, that at dust concentrations $\alpha_{d0}>3\cdot 10^{-3}$ ***blast wave never follows far asymptotic law in dusty air***.

If we take into account more strong, with respect to dust action, dissipative effect of rheological viscosity and heat conductivity of real air, the obtained results put doubts as for real blast waves would achieve the known regularities of far asymptotics valid for ideal gas model. The dissipative properties of real air begin to influence namely at early stage of far asymptotics, when the shock wave already has been weakened enough by expansion ($\Delta p<0.1$).

Similar investigation was done for the case of plane shock wave that confirms the conclusions.

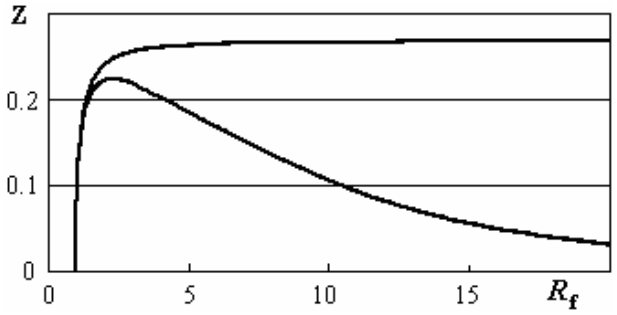

Fig.2. Additional heterogeneous attenuation of shock as dependencies $Z_3(R_f)$; $a_d=4\cdot 10^{-6}m$, $\alpha_{d0}=10^{-2}$.

The Variation of Aerosol Number Concentrations in Relation with 3-D Wind Components in the Ieodo Ocean Research Station

Sung-Hwa Park[1], Sang-Min Jang[2], Dong-In Lee[2*], Woon-Seon Jung[2] and Jong-Hoon Jeong[2]

[1]Interdisciplinary Program of Earth Environmental Engineering,
Pukyong National University, Busan, 608-737, Korea
[2]Department of Environmental Atmospheric Sciences, Pukyong National University, Busan, 608-737, Korea

Keywords: Aerosol number concentration, Laser particle counter, Ieodo Research Station.
Three-Dimesional wind speed, Marine boundary layer

Presenting author email: torch1407@pknu.ac.kr, leedi@pknu.ac.kr

To investigate variation of aerosol number concentration at each different size with three-dimensional (3D) wind components in ocean area, aerosol particles and 3D wind components were measured in the Ieodo Ocean Research Station, which is located to 419 km southwest from Marado, the southernmost island of Korea, from 25 June to 8 July 2010(Fig. 1).

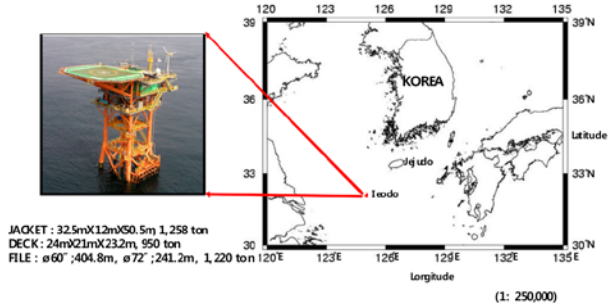

Figure 1. The location of study area.

The Laser Particle Counter (LPC) and ultrasonic anemometer were used to measure the size of aerosol particles and 3D wind components (zonal (u), meridional (v), and vertical (w) wind) respectively. Surface weather chart, NCEP/NCAR reanalysis data and sounding data were used to analyze the synoptic condition.

The distribution of aerosol number concentration had a large variation from bigger particles more than 1.0 ㎛ in diameter by wind direction during precipitation. In the number concentration of aerosol particles with respect to the weather conditions, particles larger than 1.0 ㎛ in size were decreased and sustained to the similar concentration at smaller particles during precipitation (Fig 2.).

The increase in aerosol number concentration was due to the sea-salt particles which was suspended by southwesterly and upward winds. In addition, the aerosol number concentration with vertical wind flow could be related with the occurrence and increasing mechanism of aerosol in marine boundary layer.

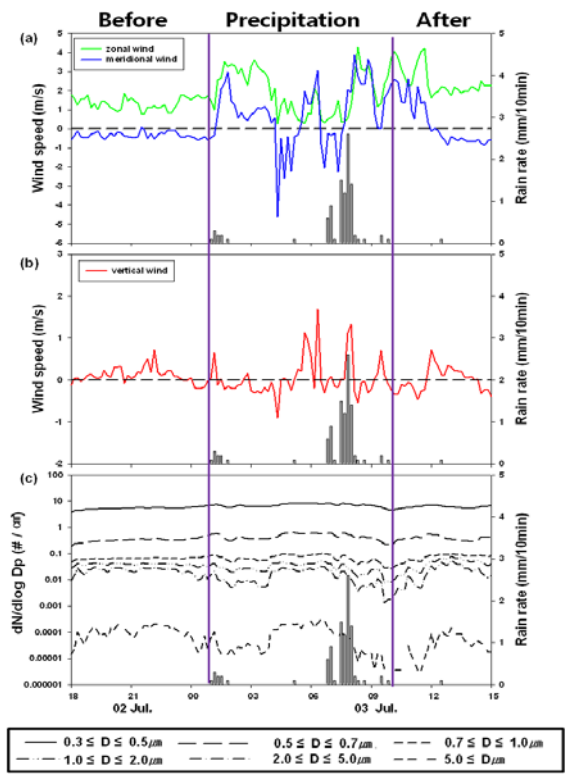

Figure 2. Time variation of (a) zonal and meridional wind speed, (b) vertical wind speed, and (c) the number concentration of aerosol particles at each channel and rain rate from 1800 LST and 1500 LST on 3 July 2010.

This work was supported by the National Research Foundation of Korea (NRF) through a grand provided by the Korea Ministry of Education, Science & Technology (MEST) in 2011 (No. 20607010000).

Time lag between the tropopause height and ^{7}Be activity concentrations on surface air

A. Ioannidou[1], A. Vasileiadis[1] and D.Melas[2]

[1]Aristotle University of Thessaloniki, Physics Department, Nuclear Physics & Elementary Particle Physics Division, Thessaloniki 54124, Greece.
[2] Aristotle University of Thessaloniki, Physics Department, Applied and Environmental Physics Division, Laboratory of Atmospheric Physics, Thessaloniki 54124, Greece.
Keywords: radioactive aerosols, ^{7}Be, tropopause height, time lag, 11-year solar cycle
Presenting author email: anta@physics.auth.gr, anta@auth.gr

The objective of this study is to define the time-lag between the elevation of tropopause and the concentration of ^{7}Be in near surface air. The concentration of ^{7}Be at surface air has been determined in the region of Thessaloniki, Greece at 40°N, over 52 weekly measurements covering the year 2009, a year of a deep solar minimum and of maximum concentration of ^{7}Be, where any fluctuation due to meteorological and seasonal variations are easily revealed.

Sampling of ^{7}Be aerosols was carried out by Staplex high-volume air sampler with glass-fiber filters, and a regulated airflow rate of 1.7-1.92 m^3 min^{-1} (60-68 ft^3 min^{-1}). The length of each collection period was 24 h. All samples were measured for ^{7}Be activity using an HPGe detector (42% relative efficiency). The tropopause height time series of daily values was obtained from the NCEP/NCAR Reanalysis data (Kalnay et al., 1996).

The positive correlations between the monthly activity concentrations of ^{7}Be and the tropopause height (0.94, $p<0.0001$) and also between ^{7}Be concentrations and the temperature T (°C) ($R=0.97$, $p<0.001$), confirm that the increased rate of vertical transport within the troposphere, has as a result the descent to surface of air masses enriched in ^{7}Be (Ioannidou, 2005; Zanis, 1999). However, the ^{7}Be concentration levels in near surface air are not expected to respond immediately to the change of elevation of the tropopause. The calculation of time lag is the next step in understanding the atmospheric procedures behind the correlation. This step will also reveal information about radioactive aerosols movement in the atmosphere's transfer cycles.

The time lag was found by holding the same column of data for ^{7}Be and calculating the correlation coefficient (R) for each new column of daily data of the tropopause height. The new columns are created by going back in time with a step of one day waiting for the best correlation in order to find how many days we have to wait until the concentration of ^{7}Be responds to the elevation of the tropopause height.

The correlation coefficient (R) between ^{7}Be and the tropopause height was successively calculated for different time lags starting with lag equal to zero (Figure 1). The analysis of the daily data revealed that the time delay between the elevation of tropopause and ^{7}Be concentrations in surface air is about 3days. The most striking feature of the data is the four day plateau (including the day of the measurement and the three previous days) revealing persistence in the state of the atmosphere.

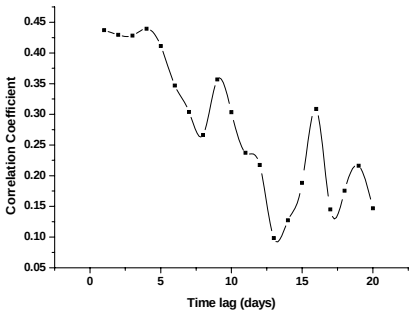

Figure 1. Correlogram between ^{7}Be surface concentration and tropopause height

In order to test our results and confirm that the correlation depends on the successive waves of air masses of a four day period a cumulative index should be calculated (Figure 2).

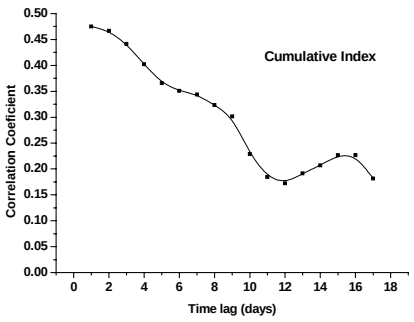

Figure 2. Cumulative index between ^{7}Be surface concentration and tropopause height

The results improved as the correlation coefficient hits a peak in the first calculation at 0.47 and 0.46 in the second one. This indicates that the time lag is 2 to 3 days as the first two calculations refer to the correlation between the ^{7}Be concentrations and 4day average (3 previous days and the day we measured ^{7}Be) measurements of tropopause heights.

Ioannidou, A., Manolopoulou, M. and Papastefanou, C. (2005) *Applied. Radiation. & Isotopes*, **63(2)** 277.
Kalnay, E., et al. (1996) *Bull. Amer. Meteor. Soc*., **77**, 437-470.
Zanis, P., Schuepbache, E., Gäggeler, H.W, Hübener, S., Tobler, L. (1999) Tellus **51B**, 789-805.

Aerosol Measurements Evaluating the Effects of the Red Mud Disaster in Hungary

A. Nagy, A. Czitrovszky, D. Oszetzky and A. Kerekes
Department of Laser Applications, Institute for Solid State Physics and Optics, Wigner Research Centre for Physics, Budapest, 1121, Hungary
Keywords: Red Mud Disaster, air pollution, size distribution
Presenting author email: oszetzky.daniel@wigner.mta.hu

As a result of the Red Mud Disaster in Devecser and Kolontár (Hungary) on October 4, 2010, the aerosol concentration -air pollution- increased at the region derived by the red mud sludge that flooded the area. Samples were collected and aerosol concentration and size distribution measurements were performed with a mobile environmental laboratory at the site right after the catastrophe. The results have been evaluated by different methods such as light scattering, airborne particle counting and sizing, optical- and electron-microscopy, micro Raman- and fluorescence-spectroscopy and EDAX micro analysis. The analysis of the composition, morphology and spectroscopy results show that the red mud dust under certain conditions causes health risk especially because of the high concentration of aerosols.

Figure 1. Image of the red mud spread over villages Kolontár and Devecser.

On October 4, 2010 a breach in the wall of the waste containment reservoir at the Ajka alumina plant in western Hungary sent a caustic flood of "red mud" pouring downhill. The villages of Kolontár and Devecser were caught in the path, and the ensuing deluge of alkaline waste spread over more than 40 square kilometres. Beside the death of 10 persons this disaster produced a considerable contamination of the area. After dehydration the re-suspending red mud dust exceeded the health limit and caused a long term health risk for the inhabitancies. Our aim was to determine the air contamination concentration on site and the physical and chemical parameters of the collected samples.

For the measurements at the site a mobile environmental laboratory was used, which had been developed previously for in situ measurements at different locations. The laboratory is installed in a van, has its own power supply system and is equipped with a wide range of optical particle counters such as the dual wavelength optical particle spectrometer developed by our department. This brode selection of instruments provides a variety of aerosol distribution and concentration measurements in a wide size range.

Both number- and mass distribution were measured at the site in two different measurement series. Mass distribution results are shown in Figure.2.

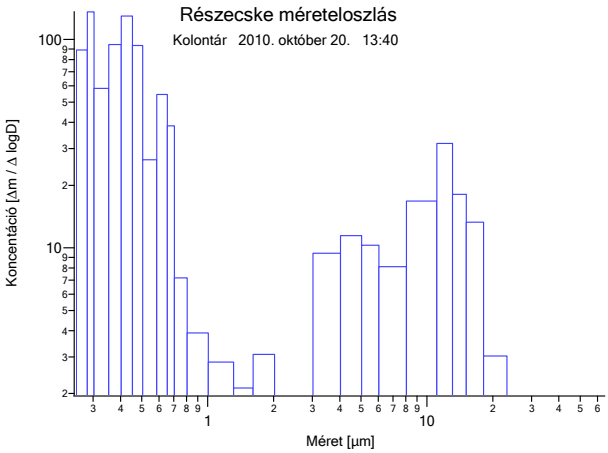

Figure 2. Mass distribution measurements

As we can see in the mass concentration diagram a peak near 10 µm is observable. Taking into account our other measurements at the site this peak is probably connected to the red mud aerosol. This peak is even more significant in measurements inside the mobile laboratory, where the red mud after dehydration was re-suspended and its concentration was high. In both cases the concentration values exceeded the health limit (50µg/m3). Because of the high concentration in indoor environment ventilation and washing is suggested to avoid health risk.

This work was supported by the Jedlik Ányos Program Proj. No. OM-00217/2007.

Szymanski, W.W., Nagy, A., Czitrovszky, A., Jani, P. (2002). A new method for the simultaneous measurement of aerosol particle size, complex refractive index and particle density, *Measurement Science and Technology*, 13, 303-307.

Nagy, A., Szymanski, W.W., Golczewski, A., Gál, P., Czitrovszky, A. (2007) Numarical and experimental study of the performance of the Dual Wavelength Optical Particle Spectrometer (DWOPS) (2007), *Journal of Aerosol Science*, vol. 38 issue 4. pp. 467-478.

Correlation between measurement results for three-type portable air purifiers: filter, ionizer and wet ones

Bangwoo Han, Hak-Joon Kim and Yong-Jin Kim

Environmental and Energy Systems Research Division, Korea Institute of Machinery and Materials, Daejoen, 305-343, Korea
Keywords: Clean air delivery rate (CADR), Particle collection efficiency, Gas reduction ratio, Ozone, Noise
Presenting author email: bhan@kimm.re.kr

The air purifiers can be classified to filter, ionizer and wet ones depending on their purification mechanism. Filter ones usually removes fine particles and harmful gases by using both fabric particle filters and gas-absorption activated carbon filters. Ionizer ones use a corona discharge to generate air ions and lead to the electrostatic effects on fine particles and harmful gases. Wet ones are water spraying scrubbers which lead to collision of sprayed water droplets with fine particles and gas molecules to collect the particles and absorb gas molecules in the water. Other type ones such as non-thermal plasma or photo catalytic oxidation have been disappeared in the portable air purifier markets probably due to their low performances. The correlation between the performances based on the type of air purifiers has not been understood clearly until now. In this study, the performances such as air flow rate (Q), particle collection efficiency (η), clean air delivery rate (CADR), gas reduction ratio of harmful gases and odors were tested for three-type air purifiers composed of 32 filter, 9 ionizer and 3 wet ones. Noise level and ozone emission were also compared based on the type of the purifiers. Their correlative relationship was then investigated. Filter air purifiers have much higher air flow rates compared to ionizer and wet ones and thus clean air delivery rates (CADRs) of filter air purifiers showed about 30-55 times higher than those of ionizer and wet ones when compared by their averaged values. Significant levels of ozone were emitted from the several ionizer air purifiers. Noises of filter ones were far higher than the other ones due to higher air flow rates. Gas reduction ratio of filter ones were around 50-85 % depending on the gas species. CADR was linearly increased with air flow rate, which indicates that air purifiers having higher air flow rates exhibit higher air purifying performances. Noise level was a little linear relationship with air flow rate and thus noise was slightly increased with air flow rate. Gas reduction ratios were also more than 60% for most filter ones irrespectively of air flow rate. CADR was very linearly correlated (R=0.94) with air flow rate and noise was also somewhat correlated (R=0.66) with the air flow rate. Particle collection efficiency and other gas reduction ratios were little correlated (R <0.35) with the air flow rate. Particle collection efficiency showed a relatively poor linear correlation (R=0.52) with the CADR compared to air flow rate. The product of air flow rate and particle collection efficiency was highly well correlated (R=0.99) with CADR as described in Fig. 1. Short-circuit factor, the ratio between CADR and the product of air flow rate and particle collection efficiency was about 0.85 in our study while it should be 1 for well mixed conditions. Acetic acid was considerably correlated with ammonia (R=0.76) and toluene gases (R=0.75) and somewhat with formaldehyde (R=0.61). Toluene was also somewhat correlated with formaldehyde gas (R=0.68). Acetaldehyde was little correlated with ammonia, formaldehyde and acetic acid (R<0.4). Ammonia was also little correlated with formaldehyde (R<0.4). Acetic acid seems to be the better indication gas for representing gas reduction performance for filter purifiers relatively compared to other gases.

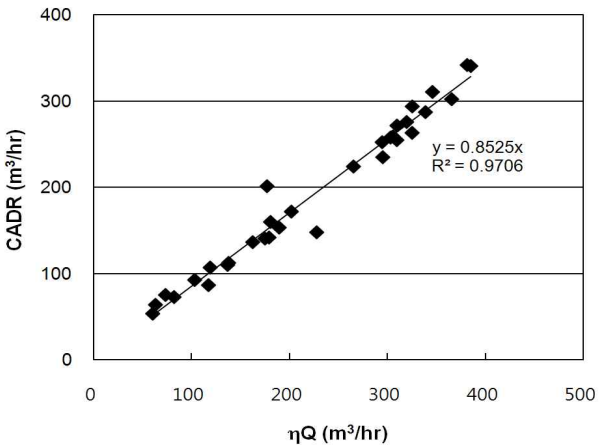

Figure 1. Clean air delivery rate (CADR) with the product of particle collection efficiency, η and air flow rate, Q.

Table 1. Correlation coefficient (R) between reduction ratios of different gases

	Ammonia	Acetaldehyde	Acetic acid	Toluene	Formaldehyde
Ammonia	1.00				
Acetaldehyde	0.30	1.00			
Acetic acid	**0.76**	0.37	1.00		
Toluene	0.52	0.59	**0.75**	1.00	
Formaldehyde	0.34	0.31	0.61	0.68	1.00

This work was supported by Korean Ministry of Environment as “The Eco- Innovation project”.

ANSI/AHAM AC-1-2006 (2006) Association of Home Appliance Manufacturers (AHAM)

JEM 1467 (1995) apanese Electrical Manufacturers’ Association (JEMA)

SPS-KACA002-132 (2006) orea Air Cleaning Association (KACA)

Drug-resistance and heavy metal tolerance of airborne microbes

O. Nikiforou[1], A. Kikna[1], M. Lazaridis[2], and E. Katsivela[1]

[1]Department of Natural Resources and Environment, Technological Educational Institute of Crete, Romanou 3, P.O. Box 89, 73103 Chania, Crete, Creece
[2]Department of Environmental Engineering, Technical University of Crete, Polytechneioupolis, 73100 Chania, Crete, Greece
Keywords: bioaerosols, bacteria, fungi, Indoor/outdoor particles, heavy metals, antimicrobial
Presenting author email: katsivela@chania.teicrete.gr

The growth and persistence of natural, airborne, viable microbes (heterotrophic bacteria and mesophilic fungi) was studied indoors/outdoors in the presence of drugs (streptomycin or cycloheximide) and heavy metals (mercury or lead).

Air samples were collected using a MAS 100 sampler for the determination of microbial concentrations. Duplicates of samples were collected during each campaign (15 campaigns in total) in a suburban, residential site of the coastal Mediterranean city of Chania (Crete, Greece). The sampling period was from December 2010 to June 2011. The heterotrophic bacteria were grown in Tryptone Soy Agar at 37^{o}C for 48 h, whereas the mesophilic fungi were cultivated in Malt Extract Agar at 20^{o}C for 72 h. The microbial resistance to heavy metal toxicity was studied using, separately, lead chloride or mercury chloride in concentrations varying from 200 to 1,500 μM and from 5 to 20 μM per growth medium, respectively. On the other hand, antibiotic and fungicide resistance was studied using, separately, Streptomycin or Cycloheximide in concentrations from 5 to 20 μg per mL growth medium. Respirable PM_{10} mass concentration and meteorological conditions were determined using portable monitors. The mean values of the ambient meteorological conditions during the measurement period were as follows: Temperature: 20.8 ± 5.3 ^{o}C; relative humidity: 49.7 ± 6.9 %; local wind speed: 0.25 ± 0.24 m/s; PM_{10}: 61 ± 33 μg/m^3. In parallel, the mean values of the meteorological conditions indoors (library; 384 m^3) were as follows: Temperature: 21.9 ± 1.8 ^{o}C; relative humidity: 50.9 ± 4.1 %; local wind speed: 0.04 ± 0.06 m/s; PM_{10}: 47 ± 23 μg/m^3.

Differences between heterotrophic bacteria and fungi were observed in relation to their abundance indoors/outdoors, heavy metal tolerance and drug resistance. Although, heterotrophic bacteria (433 ± 65 CFU/m^3) were more abundant than fungi (210 ± 212 CFU/m^3) indoors, airborne fungi showed significant higher concentrations (352 ± 370 CFU/m^3) than the airborne heterotrophic bacteria (106 ± 93 CFU/m^3) outdoors. In accordance, a higher heavy metal tolerance was observed for the heterotrophic bacteria indoors, whereas fungi possessed higher heavy metal resistance outdoors (Figures 1 and 2).

The highest heavy metal resistance was measured for lead in both taxonomic groups of microbes. However, heterotrophic bacteria were more tolerant to mercury (bacterial resistance to 20 μM Hg^{+2}: 64% indoors and 28% outdoors) than fungi (50% and 28%, respectively). In contrast, fungi were determined to be more tolerant to lead concentrations (fungal resistance to 1,500 μM Pb^{+2}: 100% indoors and 91% outdoors) in comparison to heterotrophic bacteria (28% and 24%, respectively).

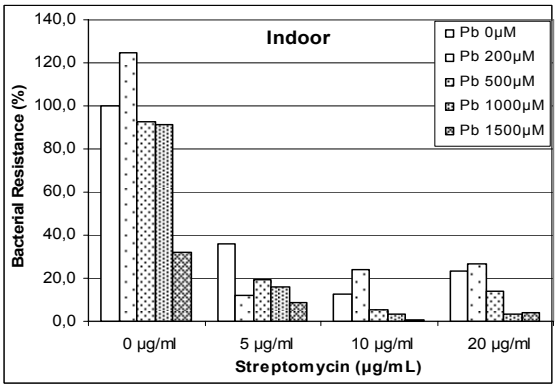

Figure 1: Percentage of viable, airborne heterotrophic bacteria, resistant to Pb^{+2} and Streptomycin indoors.

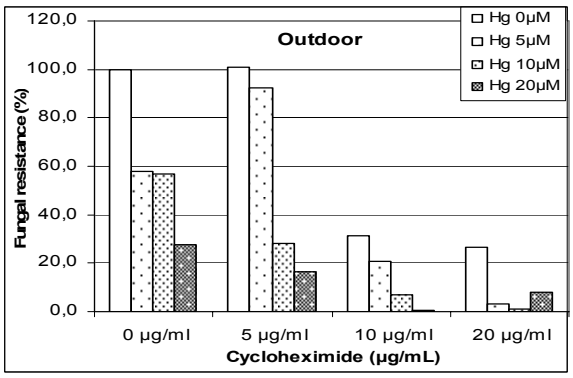

Figure 2: Percentage of viable, airborne mesophilic fungi resistant to Hg^{+2} and Cycloheximide outdoors.

A high percentage of drug and heavy metal tolerance, in the airborne, cultivable microbial community was obtained both indoors and outdoors (Figures 1 and 2). A percentage of 31% indoors and 9% outdoors of the heterotrophic bacteria were resistant, simultaneously, to 20 μM Hg^{+2} and 20 μg/mL Streptomycin. In addition, 18% indoors and 40% outdoors of the mesophilic fungi were resistant, simultaneously, to 20 μM Pb^{+2} and 20 μg/mL Cycloheximide.

Investigation of bioaerosols distribution in greenhouse for orchid growth

C.Y. Chuang[1], S. Yang[2], M.Y. Chang[3], C.H. Luo[4], Y.C. Huang[4], P.C. Huang[5] and W. Fang[1,*]

[1]Department of Bio-Industrial Mechatronics Engineering, National Taiwan University, Taipei, Taiwan
[2]Department of Environmental and Occupational Health, Toko University, Chiyai, Taiwan
[3]Department of Biomechatronics Engineering, National Ilan University, Ilan, Taiwan
[4]Department of Safety, Health and Environmental Engineering, Hungkuang University, Taichung, Taiwan
[5]Division of Occupational Hygiene, Institute of Occupational Safety and Health, New Taipei City, Taiwan
Keywords: bioaerosols, greenhouse, indoor.
Presenting author email: d97631001@ntu.edu.tw

Greenhouse provides physical environments suitable for the survival and growth for plants. The high density of biomass, including plant and soil inside the greenhouse is expected cause bioaerosols accumulation and dissemination; result in the distortion of environmental quality. Bioaerosols exposure in greenhouses among workers may lead various respiratory symptoms. (Hansen *et al*., 2012) In Taiwan, Orchid has the high economic value and becomes import commercial export in past decades. The growing process of Orchid depends on greenhouse facility to maintain the best quality. The objective of this study is investigating the bioaerosols distribution in the greenhouses designed for growing orchids.

Two greenhouses were selected as the target facility in the study. Greenhouse 1 was equipped with fan and pad system but different in area. In addition, Greenhouse 2 was fully-enclosed and equipped air conditioner without fresh air-intake. Sampling sites were set based on covering plant growing beds, aisles, near-pad fresh (sampling sites A~J for greenhouse 1) and outdoor (sampling sites K for greenhouse 1) to monitoring the bioaerosols distribution inside the space.

Viable bacteria and fungus were collected with collected in accordance with Taiwan Environmental Analysis Laboratory guideline (NIEA E301.11C). The BioStage single-stage viable cascade impactor (SKC Inc., USA), loaded with tryptic soya agar and melt extract agar were used to collect bioaerosols. The BioSatge impactor was operated at flow rate 28.3 L/minute for 30 seconds to obtain sample. For each sample, three replicates were performed. After incubation, the colonies formed on the plate samples were manually counted and convert to airborne bacterial concentration in CFU/m^3. The temperature and relative humidity was monitored with Q-trak (Model 8550, TSI Inc., USA).

Figure .1 shows the fungal bioaerosols distribution in the greenhouse 1. The concentration of indoor fungal bioaerosols is higher than outdoor can be found. In addition, higher fungal bioaerosols concentration reveal in the afternoon sampling section. It might be due to the increasing of relative humidity and plants irritation. Figure.2 shows the bacterial bioaerosols distribution in the greenhouse 1. No statically significantly difference was found between indoor and outdoor bacterial bioaerosols. The results can be explained by a generally more fungus was presented in the soil materials used for plant growth.

High concentration of fungus bioaerosols presented in the greenhouse indicates that workers' exposure should be further studies. Besides, Personal protecting equipments were also recommended to be used for protecting the respiratory systems of workers.

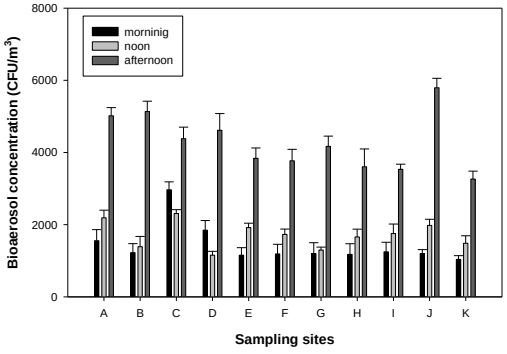

Figure 1. The fungal bioaerosols distribution in greenhouse 1.

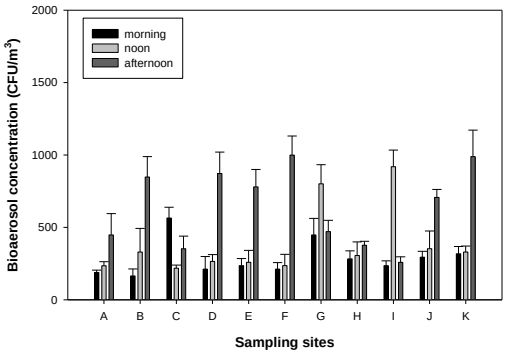

Figure 2. The bacterial bioaerosols distribution in greenhouse 1.

This work was supported by the Institute of Occupational Safety and Health of Republic of China for financially supporting this research under Contract No. IOSH100-H314

Hansen, V.M., Meyling, N.V., Winding, A., Eilenberg, J., Madsen, A.M. (2012) *Ann Occup Hyg*. 56, 170-81.

Adhikari, A., Gupta, J., Wilkins, J.R.[3rd], Olds, R.L., Indugula, R., Cho, K.J., Li, C., Yermakov, M. (2011) *Ann Occup Hyg*. 55, 272-85.

Hansen, V.M., Winding, A., Madsen, A.M. (2010), *Appl Environ Microbiol*. 76, 5874-81.

Autofluorescence of atmospheric bioaerosols – fluorescent biomolecules, biological standard particles and potential interferences

C. Pöhlker[1], J. A. Huffman[1,2], U. Pöschl[1]

[1]Biogeochemistry Department, Max Planck Institute for Chemistry, Mainz 55020, Germany
[2]Department of Chemistry and Biochemistry, University of Denver, Denver, Colorado 80208, USA
Keywords: Bioaerosols, Fluorescence, Bacteria, Fungal spores, Pollen.
Presenting author email: c.pohlker@mpic.de

Primary biological aerosol particles (PBAP) such as pollen, fungal spores, bacteria, biogenic polymers and debris from larger organisms are known to influence atmospheric chemistry and physics, the biosphere and public health. PBAP account for up to ~30% of fine and up to ~70% of coarse particulate matter in urban, rural and pristine environment and are released with estimated emission rates of up to ~1000 Tg/a (Elbert et al. 2007).

Continuous measurements of the abundance, variability and diversity of PBAP have been difficult until recently, however. The application of on-line instruments able to detect autofluorescence from biological particles in real-time has been a promising development for the measurement of PBAP concentrations and fluxes in different environments (Huffman et al. 2010; Pöschl et al. 2010). The detected fluorescent biological aerosol particles (FBAP) can be regarded as a subset of PBAP, although the exact relationship between PBAP and FBAP is still being investigated.

Autofluorescence of FBAP is usually a superposition of fluorescence from a mixture of individual fluorescent molecules (fluorophores). Numerous biogenic fluorophores such as amino acids (e.g., tryptophan, tyrosine), coenzymes (e.g., NAD(P)H, riboflavin) and biopolymers (e.g., cellulose) emit fluorescent light due to heterocyclic aromatic rings or conjugated double bonds within their molecular structures. The tryptophan emission peak is a common feature of most bioparticles because the amino acid is a constituent of many proteins and peptides. The influence of the coenzymes NAD(P)H and riboflavin on the autofluorescence of bacteria can be regarded as an indicator for bacterial metabolism and has been utilized to discriminate between viable and non-viable organisms (Lakowicz 1999). However, very little information is available about other essential biofluorophores in fungal spores and pollen.

In order to better understand the autofluorescence behavior of FBAP, we have used fluorescence spectroscopy and fluorescence microscopy to analyze standard bioparticles (pollen, fungal spores, and bacteria), atmospherically relevant chemical substances and ambient aerosol samples (Fig. 1). We found varying levels of fluorescent emission and significant differences in the spectral properties of major PBAP classes. The combination will support the quantitative interpretation of data obtained by real-time FBAP instrumentation (Pöhlker et al. 2012).

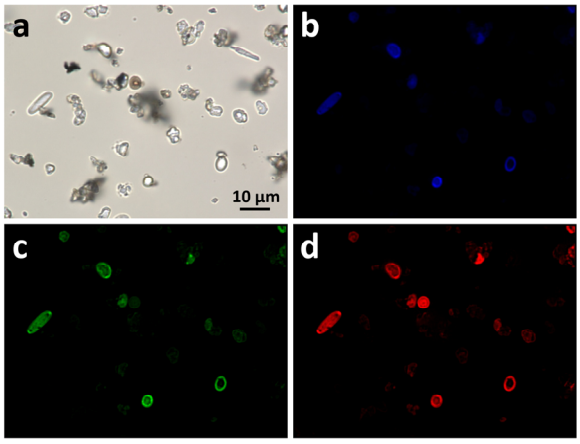

Figure 1. Microscopy pictures of ambient aerosol sample. Illumination source: (a) brightfield, (b-d) fluorescence in different spectral ranges.

This work has been supported by the Max Planck Society, the Max Planck Graduate Center and the LEC Geocycles Mainz. The authors gratefully acknowledge support by M. O. Andreae.

Elbert, W., Taylor, P. E., Andreae, M. O., & Pöschl, U. (2007). *Atmos. Chem. Phys.*, 7, 4569-4588.

Huffman, J. A., Treutlein, B., & Pöschl, U. (2010). *Atmos. Chem. Phys.,* 10, 3215-3233.

Lakowicz, J., Principles of fluorescence spectroscopy, Plenum publishers, New York, 1999.

Pöhlker, C., Huffman, J. A., & Pöschl, U., (2012). *Atmos. Meas. Tech.*, 5, 37-71.

Pöschl, U., et al. (2010). *Science*, 329, 1513-1516.

Fluorescent Biological Aerosol Particle (FBAP) Number Concentrations & Size Distributions Measured by the Waveband Integrated Bioaerosol Sensor (WIBS-4) at Environmental Research Station Schneefernerhaus (UFS)

Emre Toprak[1] and Martin Schnaiter[1]

Institute for Meteorology and Climate Research (IMK-AAF), Karlsruhe Institute of Technology (KIT), Karlsruhe, 76344, Germany
Keywords: Bioaerosols - monitoring, On-line measurements
Presenting author email: emre.toprak@kit.edu

Biological aerosol is one of the most important classes of the atmospheric aerosol. The occurrence and the abundance of the biological particles play a very important role in atmospheric processes. Diehl et al. (2001; 2002) investigated the ice nucleation (IN) ability of different pollens and found the IN activity up to -2°C temperatures. Although the potential relevance of biological aerosol has already been investigated by several groups (Matthias-Maser and Jaenicke, 2000; Matthias-Maser et al., 2000), there is still a lack of information about its regional abundance and release mechanisms.

In this study, we used the Wave Band Integrated Bioaerosol Sensor (WIBS-4) to detect and differentiate the biological aerosol at the high-altitude research station Schneefernerhaus (UFS) in Germany. The detection principle of the WIBS-4 is based on the UV Light-Induced Fluorescence (LIF) method (Kaye et al., 2005; Gabey et al., 2010; Huffman et al., 2010; Gabey et al., 2011). The LIF method assumes that all biological substances contain common fluorophores like tryptophan and NADH, which are used for detection and identification of biological aerosols. After excitation of the aerosol, emitted fluorescence signals from biological substances are stored as single particle data and used to identify biological aerosols. In addition to the fluorescence data the instrument also measures the optical particle size between 0.5 and 18 µm and performs a particle shape analysis based on the single particle scattering pattern.

WIBS-4 measures the emitted fluorescence signals in three channels: the emission following a 280 nm excitation is recorded at 310-400 nm (channel F1, tryptophan) and 420-650 nm (channel F2, NADH), and a 370 nm excitation is recorded at 420-650 nm (channel F3, NADH). The particles showing a simultaneous fluorescence signal in the F1 and F3 channels are accepted as fluorescent biological aerosol particles (FBAP).

As part of the UFS02 field campaign, we measured the biological aerosol at the UFS station, located 300m below the Zugspitze summit. A one week measurement period is presented in Fig. 1 to give an impression about the FBAP number concentrations and size distributions at UFS. Two distinct modes at ~ 3 µm and at ≥ 18 µm were essentially observed for all measurement periods. The ratio of the N_{FBAP} to the total aerosol number concentration N_T was found to be around 5.64% (median) and 7.67% (mean). Particle shape analysis for specific measurement periods was performed and two different trends were identified that are discussed in the contribution.

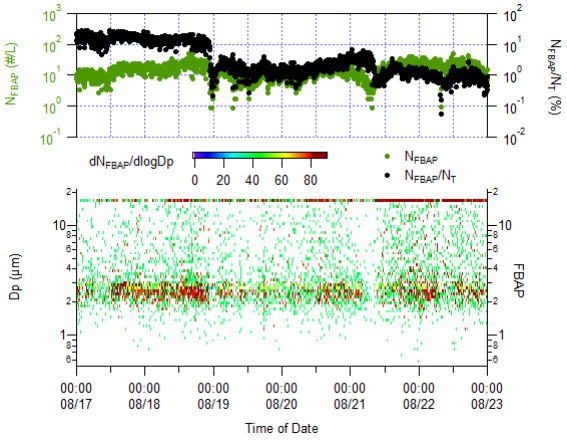

Figure 1. Upper panel: number concentration of fluorescent biological aerosol particles between 0.8 – 18 µm (green, left axis). Ratio of fluorescent particles to total aerosol particles (black, right axis). Lower panel: optical particle size distribution (dN/dlogDp) of the FBAP aerosol.

This work was supported by the Helmholtz Association in the framework of the Graduate School for Climate and Environment (GRACE).

Diehl, K., Quick, C., Matthias-Maser, S., Mitra, S. K., and Jaenicke, R. (2001) *Atmospheric Research*, **58**, 75-87.

Diehl, K., Matthias-Maser, S., Jaenicke, R., and Mitra, S. K., (2002) *Atmospheric Research*, **61**, 125-133.

Gabey, A. M., Gallagher, M. W., Whitehead, J., Dorsey, J. R., Kaye, P. H., and Stanley, W. R., (2010) *Atmospheric Chemistry and Physics*, **10**, 4453-4466.

Gabey, A. M., Stanley, W. R., Gallagher, M. W., and Kaye, P. H., (2011) *Atmospheric Chemistry and Physics*, **11**, 5491-5504.

Huffman, J. A., Treutlein, B., and Pöschl, U., (2010) *Atmospheric Chemistry and Physics*, **10**, 3215-3233.

Matthias-Maser, S., and Jaenicke, R., (2000) *Aerobiologia*, **16**, 207-210.

Matthias-Maser, S., Obolkin, V., Khodzer, T., and Jaenicke, R., (2000) *Atmospheric Environment*, **34**, 3805-3811.

P. H. Kaye, W. R. Stanley and E. Hirst, (2005) *Optic Express*, **13**, 3583-3593.

Ice Activity of Atmospheric Fungi

Janine Fröhlich-Nowoisky[1], Thomas C. J. Hill[2], Gary D. Franc[2] and Ulrich Pöschl[1]

[1]Biogeochemistry Department, Max Planck Institute for Chemistry, P.O. Box 3060, 55020 Mainz, Germany
[2]Plant Sciences Department, University of Wyoming, 1000 E. University Ave., WY 82071 Laramie, USA

Keywords: Fungi, Ice nuclei
j.frohlich@mpic.de

Primary biological aerosol particles (PBAP) are ubiquitous in the atmosphere (Fröhlich-Nowoisky, *et al* 2009). Several types of PBAP, including bacteria, fungi, pollen and lichen, have been identified as ice nuclei (IN) that can initiate the formation of ice at relatively high temperatures (e.g.; Pouleur et al., 1992; Georgakopoulos, *et al* 2009). The best-known biological IN are common plant-associated bacteria. The IN activity of these bacteria is due to a surface protein on the outer cell membrane that catalyzes ice formation, for which the corresponding gene has been identified and detected by DNA analysis (Georgakopoulos, *et al* 2009).

Fungal spores or hyphae can also act as IN, but the biological structures responsible for their IN activity have not yet been elucidated. So far, however, the abundance, diversity, sources, properties, and effects of fungal IN in the atmosphere have not yet been well characterized and quantified.

Recent studies have shown that airborne fungi are highly diverse (Fröhlich-Nowoisky, *et al* 2009), and that atmospheric transport leads to efficient exchange of species among different ecosystems (Burrows, *et al* 2009a/b). The results presented in Fröhlich-Nowoisky *et al* 2011 clearly demonstrate the presence of geographic boundaries in the global distribution of microbial taxa in air, and indicate that regional differences may be important for the effects of microorganisms on climate and public health (Figure 1).

Thus, the objective of this study is the identification and quantification of ice nuclei-active fungi and the unraveling of IN-active structures in fungi, including identification of relevant proteins and genes. Results will be essential for improving our understanding of the effects of microorganisms on climate and the hydrological cycle.

Results obtained from the analysis of various soil and air samples and the presence of new fungal ice active species will be revealed.

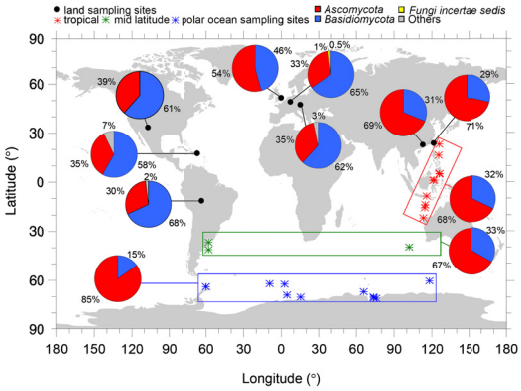

Figure 1. Geographical location and relative proportions of different phyla in continental, coastal, and marine (ocean) sampling locations.

Thanks for collaboration and support to M.O. Andreae, L.E. Hanson, I. Müller, and J. Odhiambo Obuya. The Max Planck Society (MPG), Ice Nuclei research UnIT (INUIT), and the German Research Foundation (PO1013/5-1) are acknowledged for financial support.

Burrows, S.M., *et al* (2009a) *Atmos. Chem. Phys.*, **9**, (23), 9281-9297.

Burrows, S.M., Elbert, W., Lawrence, M.G. and Pöschl, U. (2009b) *Atmos. Chem. Phys.*, **9**, (23), 9263-9280.

Fröhlich-Nowoisky, J., Pickersgill, D.A., Després, V.R., and Pöschl U. (2009) *Proc. Natl Acad. Sci.*, **106**, 12814-12819.

Fröhlich-Nowoisky, J., *et al* (2011) *Biogeosciences Discuss.*, **8**, 7071-7096.

Georgakopoulos, D.G., *et al* (2009) *Biogeosciences*, **6**, 721-737.

Pouleur, S., Richard, C., Martin, J.G. and Antoun, H. (1992) *Appl. Environ. Microbiol*. **58**, 2960–2964.

Characterization and validation of an easy-to-assemble kit of visible LED lights employed for inactivation of environmental bioaerosols

C.H. Luo[1*] and H.K. Chang[1]

[1]Department of Safety, Health and Environmental Engineering, Hungkuang University, Taichung, 43302, Taiwan

Keywords: LED, bacteria, bioaerosols, indoor air quality.

Presenting author email: andyluo@hk.edu.tw

The bactericidal and wound healing effects of visible lights with specific wavelengths have been identified by several researches (Lipovsky *et al*, 2010; Papageorgiou *et al*, 2000; Perricone, 2003). Light-induced phototoxicity was used to explain the inhibition of bacterial growth under the illumination exposure. Airborne bacteria are the major bio-pollutants in indoor environment. Furthermore, light-emitting diodes (LED) with visible wavelengths have become a popular and stable light source because of their high brightness, low energy consumption, small size and long lifetime. The relationship between light-induced inhibition of bacterial growth and visible wavelengths of commercial LED should be useful for bioaerosol control and lighting design of occupational workplaces and leisure facilities. An easy-to-assemble kit of LED arrays with visible wavelengths has been established in this study to evaluate inactivation of airborne bioaerosols (*E. coli* and *B. subtilis*) that are frequently bacterial species indoors.

LED wavelengths (visual colour) in the visible range, including 405nm (violet), 470nm (blue), 520nm (green), 589nm (yellow), and 640nm (red) were used for light exposure experiments. Domesticated bacteria in medium dishes were illuminated by LED arrays assembled on the powered kit. An array unit (10×10 cm) were installed by 100 5mm-sized LEDs of single or two-mixed wavelengths. Total light intensity of a unit is around 1—9 W/m^2 at the measurement distance. The setup is shown in Figure 1. Bacteria were illuminated for 24 hours at 37 ℃ until reaching a logarithmic phase. Controlled bacteria were kept under dark conditions.

The inactivation effect of illumination with individual colour LEDs of 405, 470, 520, 589, and 640nm on *E. coli* (*B. subtilis*) is 70.78±4.00% (12.30±4.16%), 12.34±6.24% (6.95±3.46%), 18.94±3.21% (8.43±2.52%), 8.81±2.65% (9.84±5.29%), and 7.96±6.34% (1.07±7.64%), respectively. The best sterilization for two kinds of bacteria was provided by the violet LEDs. There is a potential advantage of using violet light over antibiotic treatment for indoor spaces with high population density and infection risks. For five individual colour LEDs, the viability of *E. coli* was more inhibited than that of *B. subtilis*. Sometimes the growth of *B. subtilis* might be accelerated after illumination of red LEDs.

The inactivation effect of illumination with mixed LED arrays with two individual colours, violet/blue and yellow/red, on *E. coli* is 45.61±5.69% and 10.53±4.58%, respectively. The violet/blue mixed LEDs was more effective than the yellow/red mixed LEDs. Furthermore, a better inactivation of *E. coli* by the yellow/red mixed LEDs was than those by yellow or red individual LEDs. Moreover, the individual violet LEDs presented a better bactericidal effect than the violet/blue mixed LEDs.

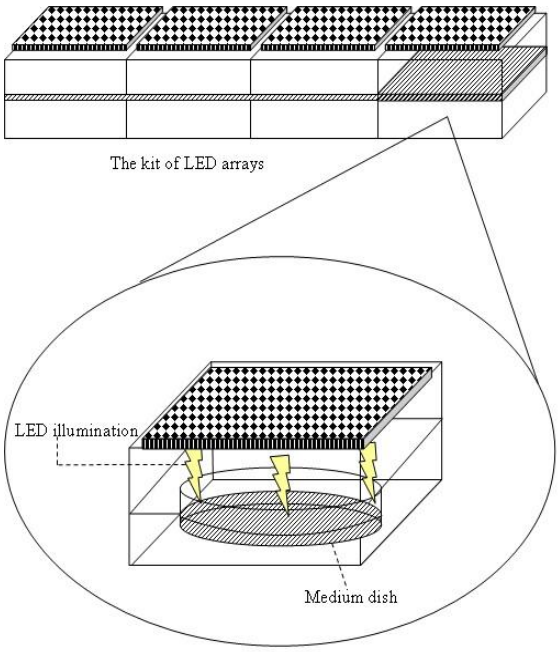

Figure 1. The setup for illumination measurements

This work was supported by the National Science Council of Taiwan under Contract No. NSC 100-2815-C-241-023-E.

Lipovsky, A., Nitzan,Y., Gedanken, A. and Lubart, R. (2010) *Laser. Surg. Med.* **42**, 467-472.

Papageorgiou, P., Katsambas, A. and Chu, A. (2000) *Brit. J. Dermatol.* **142**, 973-978.

Perricone, N.V. (2003) *Skin treatments using blue and violet light*, Thomson Delphion Patent Database.

Molecular genetic analysis of biological aerosol particles from African dust storms

Cristina Ruzene-Nespoli[1, 2], Janine Fröhlich-Nowoisky[1], T. Nunes[3], J. Cardoso[3, 4], S. M. Almeida[5] & Ulrich Pöschl[1, 2]

[1]Biogeochemistry Department, Max Planck Institute for Chemistry, 55020, Mainz, Germany
[2]Institute of Geosciences, Johannes Gutenberg University, 55128, Mainz, Germany
[3]CESAM & Department of Environment, University of Aveiro, 3810-193, Aveiro, Portugal
[4]University of Cape Verde, Praia, 279, Santiago, Cabo Verde
[5]ITN/MCTES , 2686-953, Sacavém, Portugal
Keywords: African dust, Bioaerosol, DNA
c.ruzene@mpic.de

There is a need to expand our knowledge of the diversity and biogeography of airborne microorganisms, since air connects all ecosystems at the Earth's surface. One of the most important phenomenon which can illustrate the role of the atmosphere as a dispersal mechanism for particulate matter is dust storms, that happen when the top soils from large deserts become airborne, and they can travel great distances through the atmosphere (Goudie and Middleton, 2001). More than half of the dust being transported in the atmosphere is believed to have originated from the Sahara-Sahel region in Africa (Kellog and Griffin, 2006). These dust storms are carrying microorganisms, some of them pathogens, along with the mineral particles (Griffin, 2007).

Studies have shown that the global microbial taxa are not homogeneously distributed in the air, and the regional differences and how they come to be needs to be further understood (Fröhlich-Nowoisky *et al*, 2011). It has been shown that atmospheric transport leads to efficient exchange of species among different ecosystems (Burrows *et al*, 2009a/b). In order to better understand the relationship between microorganism transport and dust, the present study aims to seek for a rhythm in the airborne contents found in African dust events.

Samples were collected between January 2011 and January 2012 in the Santiago Island from the Cape Verde archipelago. The sampling was done with a Hi-Vol with a PM10 head inlet (flow rate of 1,13 m^3min^{-1}). The sampling period was dictated by the data given by a continuous dust analyser (Grimm size dust analyser with 18 channels), with sampling periods ranging from less than 24 hours to 3 days.

Deoxyribonucleic acid (DNA) of filter sample aliquots were extracted, amplified and cloned according to protocol already established (Fröhlich-Nowoisky *et al*, 2009). The DNA extracts were used in several polymerase chain reaction (PCR) runs, using primer pairs targeting fungi and *Archaea*. For some samples, the colony PCR was followed by restriction fragment length polymorphism (RFLP) analysis to observe diversity in the clones. Selected positive products from the colony PCR were then sent to for sequencing, and the obtained DNA sequences were blasted in the National Center for Biotechnology Information (NCBI) database for taxonomic attribution to different phyla, classes, and species (Després *et al*, 2007, Fröhlich-Nowoisky *et al*, 2009).

Preliminary results for *Archaea* show a high diversity and the presence of members from the *Crenoarcheaota*, *Thaumarchaeota* and *Euryarchaeota*. It is also worth mentioning the finding of archeon clones belonging to the *Halobacteria*. As for the fungi, members of the *Agaricomycetes* are predominant for the *Basidiomycota*, with *Dothideomycetes* and *Sordariomycetes* appearing more often for the *Ascomycota*.

Further results will be obtained from sequences that are still being analysed, as well as new samples that will be processed, to expand the present data set.

Thanks for collaboration and support to M.O. Andreae, D. Jacob, N. Knothe, I. Müller, T. Pooya, the Max Planck Society (MPG), the LEC Geocycles in Mainz funded by the state Rheinland-Pfalz and the Portuguese Science Foundation through the project PTDD/AAC-CLI/100331/2008 (CV-Dust). J. Cardoso acknowledges the PhD grant SFRH-BD-6105-2009 from FCT.

Burrows, S.M., Butler, T., Jöckel, P., Tost, H., Kerkweg, A., Pöschl, U. & Lawrence, M.G. (2009a) *Atmos. Chem. Phys.* **9**, (23), 9281-9297.

Burrows, S.M., Elbert, W., Lawrence, M.G. & Pöschl, U. (2009b). *Atmos. Chem. Phys*. **9**, (23), 9263-9280.

Després, V.R., Nowoisky, J.F., Klose, M., Conrad, R., Andreae, M.O., & Pöschl, U. (2007) *Biogeosciences*, **4**, 1127–1141.

Fröhlich-Nowoisky, J., Pickersgill, D.A., Després, V.R., & Pöschl U. (2009) *Proc. Natl Acad. Sci*. **106**, 12814-12819.

Fröhlich-Nowoisky, J., et al (2011) *Biogeosciences Discuss.* **8**, 7071-7096.

Goudie, A.S. and Middleton, N.J. (2001) *Earth-Sci Rev* **56** (1–4), 179-204

Griffin, D.W. (2007) *Clin. Microbiol. Rev.* **20** (3), 459-477

Kellog, C.A. and Griffin D.W. (2006) *Trends Ecol Evol* **21** (11), 638-644

Survival of airborne influenza on surfaces

Cordonnier[1,2], Florian[1,2], Ha[1],Thi-Lan[1], Robine[1], Enric[1] and Gehin[2], Evelyne[2]

[1]Université Paris-Est, Centre Scientifique et Technique du Bâtiment (CSTB), Laboratoire de Recherche et d'Innovation pour l'Hygiène des Bâtiments, 84, avenue Jean Jaurès - Champs-sur-Marne, 77447 Marne-la-Vallée, France

[2]Université Paris Est,Centre d'Études et de Recherche en Thermique, Environnement et Systèmes (CERTES),; 61, avenue du Général de Gaulle, 94010 Créteil Cedex

Keywords: Airborne virus, influenza, virus survival, fomites

Florian.cordonnier@cstb.fr

In indoor environments, 80% of respiratory infections,have viral origin. Flu caused by *Myxovirus influenzae*, an unspecific virus of human, belongs to human pathologies with important morbidity and mortality rates. The transmission of the pathogenic agent is mainly interhuman : it occurs by direct contact with an infected person or through droplets expelled when coughing, sneezing or talking towardthe respiratory tract of a new host. The environment role (air and surfaces) in virus transmission remains unknown.

This research study aims to improve the knowledge of environmental mechanisms involved in the transport and the survival of flu viruses, and more particularly, the role played by fomites. In this context, an experimental device was set up in order to reproduce support contamination by an Influenza aerosol and to study survival of the flu virus.

The experimental device (Figure 1) is composed of an aerosol production line, a mixing chamber with hygrometry and temperature controlled, associated with a specific equipment to determine aerosol size, concentration and infectivity of airborne viruses. The device is also equipped with a contamination setup: different indoor typical media (office furniture, door handle, IPE…) are placed in a Single-stage Bioaerosol Impactor and contaminated by airborne viruses.

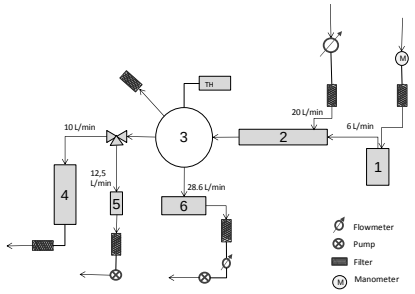

Figure 1. Representation of the experimental device

(1) Collison nebulizer, (2) Drying Column,(3)Mixing Chamber, (4) Electrical Low Pressure Impactor, (5)SKC Biosampler, (6)Single-stage Bioaerosol Impactor

The system produces, from the virus in a saliva substitute solution, a polydispersed aerosol (σ_g= 1.6) centered on 0.08 µm. The virus presence in aerosol was revealed by quantitative Polymerase Chain Reaction (quantification of total ARN) and Viral Plaque Assay (infectivity quantification) performed on particles collected on ELPI stages. The viral particle size ranges from 0.1 to 2 µm, with a bimodal distribution (modes at 0.25 and 0.8 µm) (Figure 2).

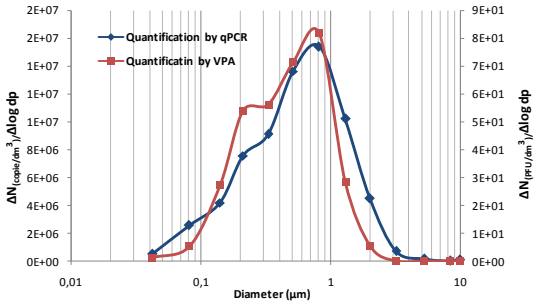

Figure 2. Virus size distribution

The experimental device permits to contaminate materials by airborne viruses and study effects of these materials on virus survival.

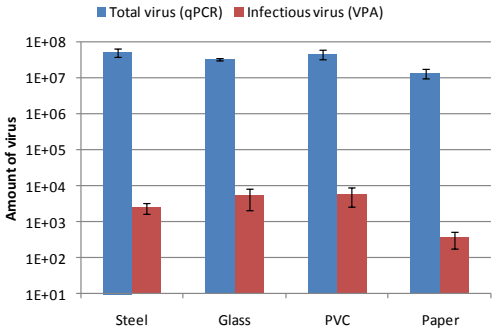

Figure 3. Virus survival just after material contamination

First results show (Figure 3) a viral contamination between materials comprised between 1.5×10^7 and 4.2×10^7 amount of virus/material. After contamination, virus survival is included between 2.5×10^3 and 5.8×10^3 infectious virus for steel, glass and PVC. The virus survival on paper is less of 1 log (3.7×10^2) compared to the other materials. These results of survival after contamination tend to be similar with Bean et *al.*,(1982) works on porous and non porous surfaces.

Bean, B., B. M. Moor, *et al.* (1982). "Survival of Influenza Viruses on Environmental Surfaces." The Journal of Infectious Diseases**146**(1): 47-51.

Internally controlled multiplex bioaerosol detection procedure

E.V. Usachev and I.E. Agranovski

Griffith School of Engineering, Griffith University, Brisbane, 4111 QLD, Australia
Keywords: Bioaerosol detection, personal sampler, internal control, multiplex real-time PCR.
Presenting author email: i.agranovski@griffith.edu.au

Detection of airborne pathogens has a crucial importance from health and safety prospects in many areas, including food industry, environmental quality, clinical diagnosis and others. Amongst growing areas of interest, usage of rapid methods for defense applications could be emphasized. Effective detection of biothreat agents requires a fast response with high sensitivity and specificity. More importantly, a detection system ought to be capable for simultaneous disclosure of many analytes in a sample, and have the ability of integration into a portable, miniaturized instrumentation.

Recently, we suggested a concept of portable fully automated "first alert" device combining personal bioaerosol sampler with miniature real-time PCR machine. The technology meets all requirements suggested for POC systems; it is portable (all modules could be located on a belt of security staff member), fully automated (consisting of sampling triggering devices, air sample collector, pumping station for aliquot delivery to a PCR machine, real time PCR/RT-PCR machine, and personnel alerting system), and capable of simultaneous detection of a range of targeted microorganisms in one reaction tube. In addition, a special PCR system, which does not require nucleic acid purification step has been developed and utilised by the new technology. This system enabled to eliminate bulky modules making the technology truly portable.

The aim of the current study was to develop an internally controlled system for bioaerosol detection by real-time PCR device combined with personal bioaerosol sampler. A recombinant phage fd (M13) was suggested for utilisation as internal amplification control (IAC). The main objective of this project was development of highly reliable and sensitive internally controlled on site detection of airborne viral strains.

The IAC was designed and optimized for use in multiplexed PCR with the aim to exclude false-negative results and to detect the presence of PCR inhibitors. Live virus based IAC has been chosen to match the sampling protocol for target microorganisms as the suggested "first-alert" concept presumes elimination of nucleic acids isolation and purification steps from the entire analytical procedure. The main advantages of this approach are related to low cost, simple maintenance and possibility of customising within wide spectrum of parameters. The IAC virus is simple to maintain, as it can be transfected or its double stranded phagemid transformed into appropriate bacterial strain. Then the virus can be easily recovered and harvested up to required titre. The fluorescence probe for the IAC detection can be synthesized with any fluorescent dye and appropriately paired quencher for particular optical settings of a PCR device used. Besides, the use of IAC in a format of full virion allows adding it directly into sampling liquid during aerosol collection and maintaining it along with a target pathogen at the same physical and biological conditions prior PCR amplification.

The IAC was tested individually in singleplex TaqMan reactions and also in multiplex reactions along with targeted T4 phage (commonly used virus surrogate for aerosol related studies) detection TaqMan assay. Amplification effects as a result of both high and low concentrations of T4 templates in the multiplexed assays were investigated to ensure that the IAC and the assay-specific reactions would not out-compete each other. No competitive effects were observed for target or IAC amplification within the concentration ranges from 3×10^1 to 3×10^6 PFU per reaction of T4 and 6.5×10^1 - 6.5×10^5 PFU per reaction of IAC. This demonstrated that the addition of IAC with concentrations of at least five orders of magnitude did not affect the amplification of as few as 30 copies (PFU) of T4 target. This outcome clearly shows the robustness of the amplification of our

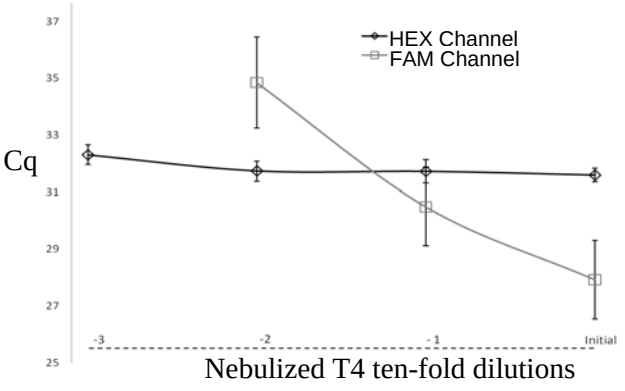

Figure 1. Internally controlled amplification of aerosolised T4 serial ten-fold dilutions. Error bars represent standard deviations of at least three measurements..

suggested IAC across wide range of target nucleic acid concentrations and the efficiency in which it can also be used to detect PCR inhibitors. The evaluation of use IAC in bioaerosol detection of T4 phage (Fig. 1) proves that it can be successfully utilised in real-time "first-alert" devices with multiple target detection, because of its non-competitive nature.

Usachev, E., Pankova, A., Rafailova, E., Pyankov, O. and Agranovski, I. (2011). Multiplex real time bioaerosol detection. *Proc IAC-2011, Manchester, UK*.

Could BFFB mode breath aerosol play a role in H5N1 transmission?

L. Morawska[1]; G.R. Johnson[1] and S.C. Bell[2,3]

[1]Queensland University of Technology, Brisbane, QLD, Australia
[2]Department of Thoracic Medicine, The Prince Charles Hospital, QLD, Australia
[3]Queensland Children's Medical Research Institute, Herston, QLD, Australia
Keywords: H5N1, influenza, exhaled aerosol, BFFB.
Presenting author email: l.morawska@qut.edu.au

Recent findings concerning exhaled aerosol size distributions and the regions in the respiratory tract in which they are generated could have significant implications for human to human spread of lower respiratory tract-specific infections. Even in healthy people, measurable quantities of aerosol are routinely generated from the Lower Respiratory Tract (LRT) during breathing(1-3).

We have found that there at least three modes in the exhaled aerosol size distribution of healthy adults(4) (see Figure 1). These modes each have a characteristic size and arise from different parts of the respiratory tract. The respiratory bronchioles produce aerosol during breathing, the larynx during speech and the oral cavity also during speech. The model of the resulting droplet size distribution is therefore called the Bronchial Laryngeal Oral (B.L.O.) tri-modal model of expired aerosol.

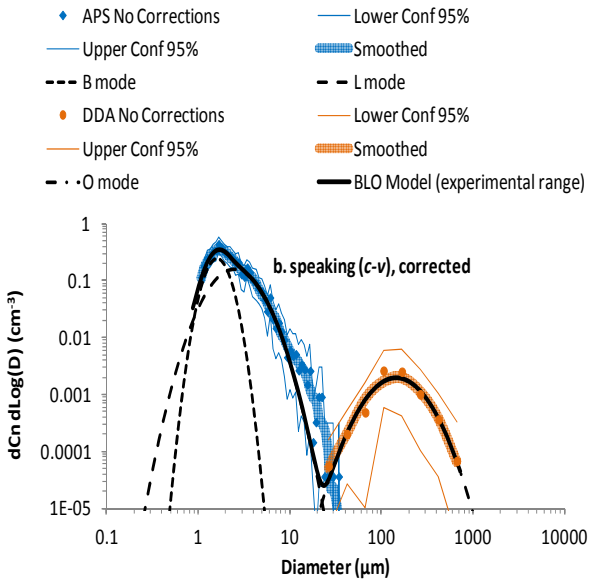

Figure 1: Breath aerosol number contribution compared to other modes during speech.

The bronchiolar fluid film burst (BFFB) mechanism (or simply B) mode is produced from fluid lining the respiratory bronchioles(1-3). The B mode droplets are produced in very large numbers by some individuals (see Figure 2). The small size of the B mode droplets means that they can remain in the air for prolonged periods, giving them the potential to travel large distances.

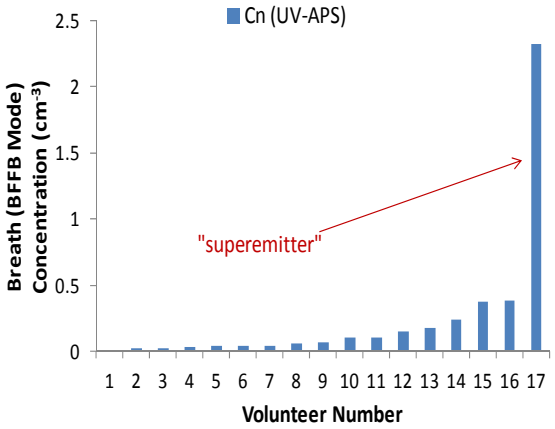

Figure 2: Example of super emitter of breath aerosol BFFB mode aerosol.

For a virus to be spread effectively between humans by aerosolisation, it must acquire the ability to infect cells in the upper respiratory tract and proliferate there so that high viral load can exist in the fluid that is aerosolised by sneezing and coughing(5).

We examine what role the B mode might play in the context of the news of the two research groups, who have independently demonstrated that H5 viruses including the much-hyped H5N1 avian influenza, can easily be modified to transmit between mammals (ferrets) and suggesting the potential in humans via exhaled aerosol.

1. Johnson GR, Morawska L. The Mechanism of Breath Aerosol Formation. *Journal of Aerosol Medicine and Pulmonary Drug Delivery* 2009;22:229-37.
2. Almstrand A-C, Bake B, Ljungström E, et al. Effect of airway opening on production of exhaled particles. *Journal of Applied Physiology* 2010;108:584-8.
3. Fabian P, Brain J, Houseman EA, et al. Origin of Exhaled Breath Particles from Healthy and Human Rhinovirus-Infected Subjects. *Journal of Aerosol Medicine and Pulmonary Drug Delivery* 2011.
4. Johnson GR, Morawska L, Ristovski ZD, et al. Modality of human expired aerosol size distributions. *Journal of Aerosol Science* 2011;42:839-51.
5. Shinya K, Ebina M, Yamada S, et al. Avian flu: Influenza virus receptors in the human airway. *Nature* 2006;440:435-6.

Recent advances in bioaerosol control methods

Byung Uk Lee[1]

[1]Department of Mechanical Engineering, Konkuk University, Seoul, Republic of Korea
Keywords: bioaerosols, control.
Presenting author email: leebu@konkuk.ac.kr

Bioaerosols are defined as aerosols of biological origin. Bioaerosols are one kind of aerosols, however they are different from non-biological aerosols in terms of viabilty and biological activity.

Historically, bioaerosols were studied as a part of researches for finding out the origin of life by the great French scientist, Louis Pasteur (1822-1895).

Currently, most of bioaerosol researches were conducted due to health effects of bioaerosols. There are three mechanisms regarding the health effects of bioaerosols, which are hypersensitivity, toxic reaction, and infection. These mechanisms are related to choosing correct methods for sampling, analyzing, and controlling bioaerosols.

As air infection outbreaks have received public attention, there are strong demands of studying of sampling and controlling of bioaerosols.

In controlling bioaerosols, there are several steps. First, the air flow containg bioaerosols should be controlled by fluid machineries. Second, aerosol particles inside the air flow should be controlled by typical aerosol control methods such as filters, impactors, and electrostatic precipitators. For bioaerosols, they can survive in the typical aerosol control devices, and somtimes they grow with producing rank odors and offsprings inside the aerosol control devices. Therefore, we need third step, which is to control bioaerosols in the control devices. Thermal energy, ultraviolet irradiation, unipolar ion emission, and hybrid methods have been studied for controlling bioaerosols (Lee, 2011).

Here, recent advances in bioaerosol control methods are reviewed and these methods are compared with each other. Each control method has advantages and weakness points. For example, a thermal energy system can be easily installed inside any ventilation system for controlling bioaerosols, however, thermal energy systems usally consume significant amount of energy which is an economical weakness point of the control method. To decrease the weakness points with maintaining advantages of an individual method is a key of hybrid control methods for bioaerosols.

Bioaerosol control methods have great potential to be applied in various research areas. Bioaerosol control methods with electrospraying have been studied for analysis tools for biological materials. Artificial generation of biological particles with bioaerosol control methods can be applied in articultural industry and health care medical industry.

This work was supported by a National Research Foundation of Korea (NRF) grant (‘Measurement of airborne microorganisms in public facilities and development of control methods against airborne pathogenic microorganisms’, No. 2012-0002857) funded by the Ministry of Education, Science, and Technology.

Lee, B.U. (2011) Aerosol Air Qual. Res. **11**, 921-927.

Study on the ventilation and air dispersion in a hospital Intensive Care Unit (ICU) using simulation techniques

J.H. Song, J.Y. Jang, M.Y. Cho, D.S. Park and S.-B. Kwon

[1]Subway IAQ Research Corp., Korea Railroad Research Institute, Uiwang-si, Gyeonggi-do, 437-757, Korea
Keywords: CFD, Diffusion, Ventilation system, Indoor air quality.
Presenting author email: songjihan@krri.re.kr

Infectious diseases such as influenza can be transmitted through respiratory droplets expelled from coughing or sneezing in indoor locations. Wan *et al.*, (2007) reported that the location of exhaust vents have significant impact on the dispersion pattern of expiratory droplets indicating that the airborne particles can be effectively controlled by air extraction from the exhaust air stream. There has been limited research on the air distribution system to improve the indoor environment (Tang *et al.*, 2007; Yau *et al.*, 2011). In this study, three possible types of ventilation systems in an intensive care unit (ICU) are tested using CFD simulation (Version 13.0) and the air flow pattern associated with the type of ventilation are discussed.

The isometric view of the simulated ICU room ($30m^3$) with a patient's bed is described in Figure 1. There are seven possible ventilation units that can be used for either supply or exhaust ventilation; ceiling-center, ceiling-division, ceiling-slit, side-center, side-division, Floor-center, Floor-division. Three cases of ventilation are considered for the simulation and the location of ventilation units for each case is described in Figure 2 (left). The ventilation rate for both inlet and outlet units are 0.1169 kg/s with the use of 12 ACH.

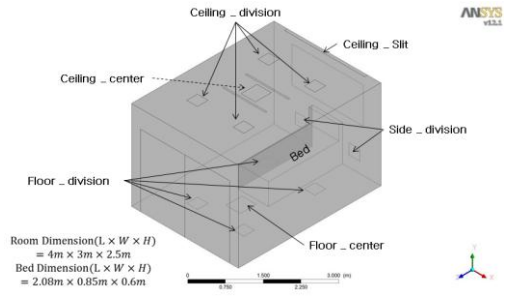

Figure 1. The isometric view of the simulated ICU room including interior bed location and ventilation systems.

The air flow vectors for three cases resulting from the CFD modelling are shown in Figure 2 (right) and the major air stream inside the room is described by a solid arrow. For both Case 1 and 2, the supply air flows from the slit at the side of the ceiling. It is less likely to have higher ventilation efficiency with the use of Case 1, since the exhaust units of Case 2 are at different four positions at the ceiling where air stream is distributed well than that of Case 1. For Case 3, rapid change in air speed is shown at the center part of the room and the air stream slows down near the bed to exit to the outlet located at the side wall. With the consideration of all values evaluated in this study such as air flow pattern, wind vectors, and mean age of air, Case 3 is chosen to be the most effective ventilation type in the simulated ICU room.

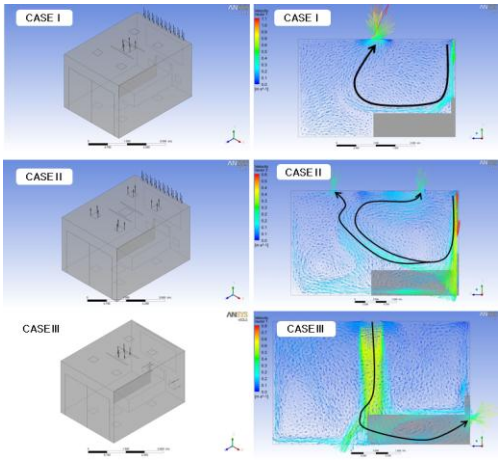

Figure 2. The geometry of model domain (left) and air flow vectors (right) for three cases of ventilation used in this study.

For further studies, environment variables such as the movement of a patient and the space of the room will be considered to study the air flow pattern inside the ICU room. Also, the dispersion and transmission mechanism of infectious particles expelled from the patient's cough in an ICU will be studied using CFD simulation based on the parameters obtained from previous study (Kwon *et al.*, 2012). Finally, ventilation performance will be tested depending on the various locations of supply and exhaust ventilation units to control the bio aerosol inside the ICU room effectively.

This work was supported by the National Research Foundation of Korea (NRF) funded by the Ministry of Education, Science and Technology (2009-0082056).

Kwon, S.-B., Park, J., Jang, J., Cho, Y., Park, D., Kim, C., Bae, G., and Jang, A. (2012) *Chemosphere*, in press.

Tang, J., Li, Y., Eames, I., Chan, P. and Ridgway, G. (2006) *Journal of Hospital Infection.* **64**, 100-114.

Wan, M., Chao, C., Ng, Y., Sze To, G. and Yu, W. (2007) *Aerosol Science and Technology.* **41**, 244-258.

Yau, Y., Chandrasegaran, D. and Badarudin, A. (2011) *Building and Environment.* **46**, 1125-1132

Real-time measurement of continuous thermal-inactivated bioaerosols by aerosol fluorescence sensor with dual UV- and Vis-channels

Jae Hee Jung[1], Gwi Byoung Hwang[1], Bo Mi Kwon[1], Jung Eun Lee[2], and Gwi Nam Bae[1]

[1]Center for Environment, Health and Welfare Research, Korea Institute of Science and Technology (KIST), Hawolgok-dong, Seongbuk-gu, Seoul 136-791, Republic of Korea
[2]Institute of Health and Environment, Graduate School of Public Health, Seoul National University, Gwanak-ro, Gwanak-gu, Seoul 151-742, Republic of Korea
Keywords: Bioaerosol, Real-time detection, Fluorescence, Measurement (Characterization).
Presenting author email: jaehee@kist.re.kr

Airborne particles, primarily bacteria, virus, and fungi, are a primary means of disease transmission in humans and other animals. Due to renewed concerns over biological airborne contaminants such as new strains of flu or anthrax, many researchers have investigated the real-time technique that can be continuously monitored for potentially harmful biological aerosols.

Recently, the focus on fluorescence-based optical sensors has been to improve characterization by individual fluorescence spectral analysis. The fluorescence spectrum varies from material to material, and the evidence obtained from laboratory measurements indicates that effective differentiation from likely interferents should be possible with broadband spectral differentiation (Pan *et al*., 2011; Kaye et al., 2005). There has also been a focus on developing simpler, more robust, and lower-cost real-time sensors for intelligent network deployments.

The aerosol fluorescence sensor (AFS; Biral, Bristol, UK) is a promising monitoring device for the continuous real-time detection of airborne microorganisms, which is based upon the principle of Ultra-violet light induced fluorescence (UV-LIF) targeting the intrinsic fluorescence response from common amino acids found in living matter. The sensor uses an UV optical excitation source of 280 (+20/-40) nm to illuminate an airstream flowing drawn continuously through the sensor detection volume. Fluorescence from all particles instantaneously present within a sensing volume is measured using two photomultiplier detectors optically filtered to detect radiation in the bands 305-385 nm (UV) and 415-550 nm (Vis), enabling a generic discrimination between different aerosol populations.

This study describes the continuous real-time fluorescence characteristics of bacterial bioaerosols (*E. coli, B. subtilis and S. epiderdmids*) with various cell viabilities using the AFS. To control cell viability, the test bacterial bioaerosols were continuously exposed at various surrounding temperature with very short-time in the thermal electric tube furnace and passed into the AFS (Jung *et al*., .2009).

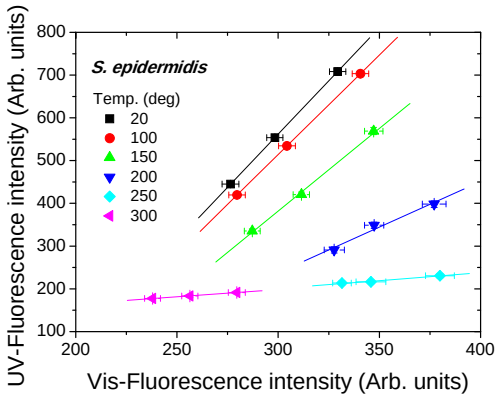

Figure 1. Variation of fluorescence characteristics of *S. epidermidis* bioaerosols under various thermal conditions.

Laboratory data show that these UV- and Vis-fluorescence intensities from the bacterial bioaerosols were decreased with increasing surrounding temperature following the decrease of bacteria viability.

In particular, this slope reduction value has statistically significant relationship ($p<0.05$) with the bacterial cell viability reduction. These experimental results provide basic information about the feasibility of AFS for real-time cell viability assessment of bacterial bioaerosols and may contribute in various applications such as indoor air quality, public health, and military defense against bioterrorism.

This research was supported by the Converging Research Center funded by the Ministry of Education, Science and Technology (2011K000750).

Pan, Y., Hill, S. C., Pinnick, R. G., House, J. M., Flagan, R. C., and Chang, R. K. (2011) *Atmos. Environ*. 45, 1555-1563.
Kaye, P. H., Baxter, K. L,. and Hirst, E. (2005) Opt. Express 13, 3583-3593.
Jung, J. H., Lee, J. E., and Kim, S. S. (2009) Sci. Total Environ. 407, 4723-4730.

The numerical pollen dispersion model COSMO-ART: model design and operational use at MeteoSwiss

A.Pauling[1], K. Zink[1], H. Vogel[2] and B. Vogel[2]

[1]Federal Office for Meteorology and Climatology MeteoSwiss
Kraehbuehlstrasse 58, CH-8044 Zuerich, Switzerland

[2]Karlsruhe Institute of Technology (KIT)
Institute for Meteorology and Climate Research – Troposphere Research
Hermann-von-Helmholtz-Platz 1, 76344 Eggenstein-Leopoldshafen, Germany
Keywords: Bioaerosols, Modelling (regional), Air pollution modelling, Health aspects of aerosols
Presenting author email: andreas.pauling@meteoswiss.ch

In Europe, about 15% of the population suffer from pollinosis. Pollen forecasts are a helpful tool for medical doctors to advise their patients. In addition, pollen forecasts can assist allergy sufferers to plan their leisure time and the medicine intake which reduces the symptoms. This highlights the need for regionally and temporally detailed pollen forecasts.

Model design of COSMO-ART

Numerical pollen dispersion models such as COSMO-ART (COnsortium for SMall-scale Modeling - Aerosols and Reactive Trace gases; Vogel *et al*, 2009) can provide spatially and temporally highly resolved pollen forecasts. COSMO is a non-hydrostatic mesoscale model that is used in operational weather forecasts in a number of European weather services including those of Switzerland and Germany. The ART module describes the chemical reactions and the aerosol dynamics as well as the pollen emission and dispersion processes.

We present the main features of the pollen module of COSMO-ART. A phenological heat sum model is used to predict the start and the end of the pollen season. This model performed very well in the verification process with an average accuracy of 2-3 days. The pollen season is described by various sigmoidal functions. The parameterization of the pollen emission is superposed on these seasonal factors and depends strongly on the meteorological conditions. The calculation of the settling velocity takes into account that the pollen grains can hydrate or dehydrate.

An important input to COSMO-ART is the source distribution. However, this input is not available for the allergy-relevant species such as hazel, alder, birch, grass or ragweed. Hence, plant distribution datasets need to be derived from suitable sources. For birch and grass we used the dataset by Pauling *et al* (2011). The source distribution for grass pollen was produced using a similar method.

Pollen forecasts using COSMO-ART

During the birch pollen season 2011, COSMO-ART was operational at MeteoSwiss for the first time using horizontal resolution of 7km. Figure 1 shows the observations at Zusmarshausen, Germany, and the modelled time series of the nearest grid point. Good agreement with the observations was achieved at many, though not all, observation sites. In addition, grass pollen were in a test phase in the same year.

We will present the results of the birch and grass pollen season 2012. Verification is done through rigorous comparison with observations and the calculation of skill scores. Moreover, the results of COSMO-ART are compared with statistically based pollen models and traditional man-made forecasts.

Future developments of COSMO-ART include the increase of the spatial resolution to 2km. This will significantly improve the results especially in complex terrains such as the Alps. Additionally, further allergy-relevant species such as ragweed will be modelled on a operational basis.

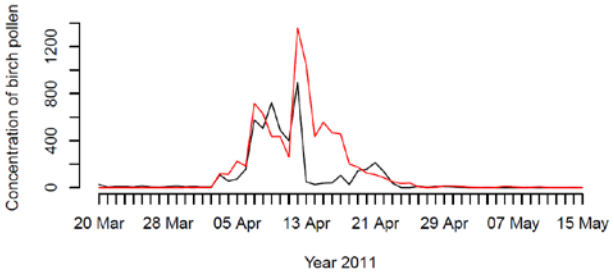

Figure 1. Time series of modelled (red) and observed (black) birch pollen concentration in m^{-3} at Zusmarshausen, Germany.

Pauling, A., Rotach, MW., Gehrig, R. and Clot, B. (2011) *Int. J. Biometeorol.* doi: 10.1007/s00484-011-0505-7.

Vogel, B., Vogel, H., Bäumer, D., Bangert, M., Lundgren, K., Rinke, R., Stanelle, T. (2009) *Atmos. Chem. Phys*. **9**, 8661–8680.

Rapid Inactivation of Biological Species in the Air using Atmospheric Pressure Non-thermal Plasma

Yongdong Liang[1,#], Yan Wu[2,#] , Ke Sun[1,], Qi Chen[2], Fangxia Shen[2], Jue Zhang[1,3,*], and Maosheng Yao[2,*], Tong Zhu[2], Jing Fang[1,3]

[1] Department of Biomedical Engineering, College of Engineering, Peking University, Beijing 100871,China ; [2] State Key Joint Laboratory of Environmental Simulation and Pollution Control, College of Environmental Sciences and Engineering, Peking University , Beijing 100871,China;

[3]Academy for Advanced Interdisciplinary Studies, Peking University, Beijing 100871,China

* Corresponding Author:

Maosheng Yao, Email: yao@pku.edu.cn, Ph: +86 01062767282

Jue Zhang, zhangjue@pku.edu.cn , Ph: +86 010 62755036

# Y. Wu and Y. Liang contributed equally to the work.

Abstract

Here, non-thermal plasma generated by a dielectric barrier discharge(DBD) system was applied to inactivating aerosolized *Bacillus subtilis* cells and *Pseudomonas fluorescens* as well as indoor and outdoor

bioaerosols. The culturability, viability, and diversity losses of the microorganisms in air samples treated by the plasma for 0.06-0.12 seconds were studied using culturing, DNA stain as well as polymerase chain reaction-denaturing gradient gel electrophoresis (PCR–DGGE) methods. In addition, the viable fraction of bacterial aerosols with and without the plasma treatment was also quantified using qPCR coupled with ethidium monoazide (EMA).

It was shown that less than 2% of *B. subtilis* aerosols survived the plasma treatment of 0.12 s, while none of *P. fluorescens* aerosols survived. Viability tests, EMA-qPCR results and Scanning Electron Microscopy (SEM) images demonstrated that both bacterial species suffered significant viability loss, membrane and DNA damages. Exposure of environmental bacterial and fungal aerosols to the plasma for 0.06 s also resulted in their significant inactivations, more than 95 % for bacteria and 85-98 % for fungal species. PCR-DGGE analysis showed that plasma exposure of 0.06 s resulted in culturable bacterial aerosol diversity loss for both environments, especially pronounced for indoor environment. The results here demonstrate that non-thermal plasma exposure could offer a highly efficient air decontamination technology.

Key words: Non-thermal plasma, *Bacillus subtilis*, *Pseudomonas*

fluorescens, Bioaerosols, Viability, Diversity, EMA-qPCR

Single-particle fluorescence spectroscopy of atmospheric relevant fungal spores and bacteria and potential interferences

S. Saari[1], M. Putkiranta[1] and J. Keskinen[1]

[1]Department of Physics, Tampere University of Technology, P.O. Box 692, FI-33101 Tampere, Finland
Keywords: fluorescence, bioaerosols, fungal spores, bacteria
Presenting author email: sampo.saari@tut.fi

Bioaerosols such as fungal spores and bacteria can act as CCN and IN in the atmosphere, so they have an impact on the global climate and precipitation. Bioaerosols contain usually alive micro-organism, which can have various health effects for humans and animals. For these reasons, information on the concentration, size distribution, sources and types of bioaerosols are needed in various environments. The development of real time measurement techniques is important for reliable bioaerosol classification.

Recently, laser induced fluorescence (LIF) has become a common way to detect bioaerosols. The LIF technique is an effective method for detecting biological molecules such as tryptophan, NADH and flavins that are present in bacterial cells and fungal spores. The focus on our previous studies was developing LIF based real time measurement technique for biological weapons detection (Manninen et al. 2008, 2009; Putkiranta et al. 2010). The idea is processed to use similar measurement technique for atmospheric relevant fungal spores and bacteria detection.

The idea in this study is to get information for effective fluorescence measurement parameters of airborne fungal spores and bacteria and also some fluorescent chemicals that can act as potential interferences in the atmosphere. The most important parameters are excitation wavelength and fluorescence emission spectrum and the best way to present these parameters is a fluorescence map. The fluorescence parameters depend on the state of biological origin and its environment. So it is important to measure fluorescence parameters in the natural aerosol phase. The fluorescence parameter studies are important for further instrumentation.

The experimental setup is represented by Manninen et al. (2008, 2009). The biological aerosol are generated with the ultrasonic nozzle (SNAG) and dried with the tube furnace and silica gel. The fluorescence spectrum is measured in the optical chamber and the size distribution of aerosol is measured with UVAPS (TSI Model 3314). A wavelength-tunable, pulsed solid-state optical parametric oscillator (OPO) laser (NT342/1/UVE, Ekspla UAB, Vilnius, Lithuania) is used to excite the fluorescence of individual aerosol particles. An image-intensified CCD (ICCD) camera (4 Quik E, Stanford Computer Optics, Berkeley, CA, USA). The ICCD camera acquires the fluorescence spectrum of individual aerosol particle through a grating spectrograph (250IS, Bruker Optics, Billerica, Massachusetts, USA). With this setup the fluorescence maps for single airborne bacteria and fungal spores and chemical particles can be measured.

The results of this study indicate that the fungal spores and bacteria have dissimilar fluorescence maps and the potential interference particles seems to have the similar fluorescence maps to common biological molecules. The bacteria and fungal spores are the common primary biological aerosol particles (PBAP) in the atmosphere. They have different emission sources and may have dissimilar properties when acting as CCN and IN. It may be possible to classify atmospheric bacteria and fungal spores through the dissimilar fluorescence properties, but influence of the potential interferences must be taken into account.

References:

Manninen, A., Putkiranta, M., Rostedt, A., Saarela, J., Laurila, T., Marjamäki, M., Keskinen, J., Hernberg, R. (2008) Appl. Opt., 47, 110

Manninen, A., Putkiranta, M., Saarela,J., Rostedt, A., Sorvajärvi, T., Toivonen, J., Marjamäki, M., Keskinen, J., Hernberg, R. (2009) Appl. Opt., 48, 4320

Putkiranta, M., Manninen, A., Rostedt, A., Saarela, J., Sorvajärvi, T., Marjamäki, M., Hernberg, R., and Keskinen, J. (2010) Applied Physics B: Lasers and Optics, pp. 1–11

Microbial and fungal bioaerosol concentrations in Lithuanian schools

I. Radziuniene, D. Martuzevicius, D. Ciuzas, E. Krugly, and T. Prasauskas

Department of Environmental Engineering, Kaunas University of Technology, Kaunas, LT-50254, Lithuania
Keywords: bioaerosol, indoor air quality, sedimentation method, microorganisms.
Presenting author email: inga.radziuniene@ktu.lt

Introduction

Indoor air quality is influenced by many different pollution factors, such as chemical components (e.g. carbon dioxide, formaldehyde, organic substances, radon), particles (asbestos, pollen, other particulate matter, etc.) and microbial contaminants (Jones, AP, 1999). It affects human health, comfort, performance and productivity. Since the majority of people spend most of their time in the indoor environment, it is very important to evaluate different risk factors' influence on people's health.

School children are very susceptible to adverse effects. They spend up to 30% of their day time in the school environment and are more sensitive to environmental pollutants (Kulkarni and Grigg, 2008). Large number of pupils generate high pollutants load inside the school buildings, therefore schools very often fail to comply with the indoor air quality standards (van Dijken, F., 2006).

In this study, microbial contamination in schools was investigated with respect to total viable microorganisms (TVM), fungal and Gram negative bacteria concentration in bioaerosol.

Methods

Five schools situated in Kaunas municipality, Lithuania, were participating in this study. Three classes in each of the schools were selected for this study. Measurements were performed during November and December of 2011. Microbial contamination in schools was measured using sedimentation method. The exposure time was one hour. Standard Petri plates (85x15 mm) loaded with Plate Count Agar (PCA), MacConkey agar and Sabouraud agar were used to indicate different bioaerosol contents. PCA was used to quantify TVM in bioaerosol, MacConkey agar – Gram-negative bacteria and Sabouraud agar – fungal contamination. A minimum of three sampling plates for each agar were taking simultaneously in each sampling place. Recorded concentrations of bacteria and fungi in bioaerosol were expressed as colony forming units per plate per hour (CFU/plate/h).

Results

Distribution of the mean concentrations of TVM and fungi are presented in Figure 1. The bacteria and fungi were not speciated. Number of Gram-negative bacteria (potential intestinal pathogens) colonies on the MacConkey agar was below reliable limit. The recorded CFU varied from 0 to 9 CFU/plate/h. Therefore these results were not evaluated. The presented results show microbial contamination, detected in the schools during classes. The observed contamination after the classes' period was considerably lower.

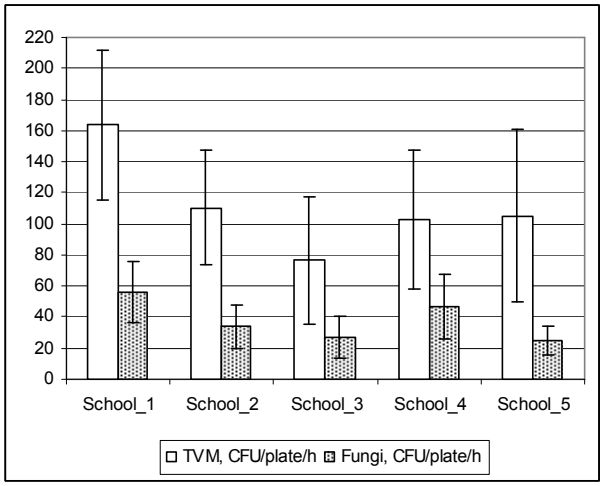

Figure 1. Average concentrations of TVM and fungi in schools, CFU/plate/h.

The results show that the observed microbial TVM contamination was above 100 CFU/plate/h in most of the schools. In each case the variation of the results was considerable. Recorded amount of total viable microorganisms cfu was varying from 14 CFU/plate/h (School_3) up to 224 CFU/plate/h (School_1), having average of 111,72±45,20 CFU/plate/h. Number of fungal CFU was lower in each case and was varying from 5 CFU/plate/h (School_3) to 90 CFU/plate/h (School_1), with an average 37,65±15,45 CFU/plate/h. The quality of indoor air varies depending on school. In each case the results are considerably dispersed, meaning that the bioaerosol concentration in the rooms varies depending on time and place. In summary it can be noted, that the bioaerosols concentration in the classrooms is relatively high. Fungi amounts about one third of the overall microbial contamination in schools.

More studies involving differentiation of bioaerosol concentration during different room occupation time and the results comparison with buildings parameters are needed (currently ongoing) to evaluate and find out the possible sources of indoor air contamination..

Jones, AP. (1999) *Atmospheric Environment*. 33 (28), 4535-4564.

Kulkarni, N. and Grigg, J. (2008) *Paediatrics. And Child Health*. **18**, 238-243

Van Dijken, F., van Bronswijk, J.E.M.H. and Sundell, J. (2006) *Building Res. and Inform.*, **34**(5), 437-446.

Airborne bacterial deposition in Sierra Nevada National Park

G. D´Orta [1], N. Mladenov [2] and I. Reche[1]

[1]Department of Ecology, Faculty of Sciences, University of Granada, Granada, 18071, Spain
[2]Department of Civil Engineering, Kansas State University, Manhattan, KS 66506, USA
Keywords: bioaerosols, African dust, dry and wet deposition
Presenting author email: ireche@ugr.es

The Sahara-Sahel region of Africa is the largest source of aerosolized soil dust on Earth, contributing as much as one billion metric tons of dust per year to the global atmosphere. Every year, massive airborne plumes of this Saharan dust are exported to the Mediterranean region influenced by the presence of cyclones mostly during spring and summer. These dust intrusions have a relevant impact on the chemistry and biology of the downwind ecosystems, in particular on the most pristine ones (Reche et al. 2009).

Bacteria are one of the many types of biogenic aerosol particles that are ubiquitous in the atmosphere. Airborne bacteria are typically transported <1 km from their source, however, dust-associated bacteria can be transported over 5000 km from Africa to the Caribbean coasts or Europe (Kellogg and Griffin, 2006). Therefore, these African dust intrusions could also have a role in expanding the biogeographical range of some microorganisms. Different approaches have been used to characterize the dust-associated microbial community. However, the total loading and the specific microbes associated with the dust intrusions remains poorly explored and highly imprecise.

Here, we tested a different procedure based on chemical and physical treatments to detach bacteria from the aerosol particles, similar to the technique proposed by Amalfitano and Fazi (2008) for benthonic bacteria. We determined the bacterial loadings in wet and dry collectors in Sierra Nevada National Park. This location is an ideal site to collect these aerosols because is close to the Sahara desert and has altitudes above 3000 m above sea level (asl) considering that the mainstream of Saharan dust transport occurs between 1500 and 4000 m asl. In Sierra Nevada National Park, there are also many pristine high mountain lakes submitted to this influence of Saharan dust intrusions.

Separate samples of dry and wet atmospheric deposition were collected, during the summers of 2007 and 2008, using two MTX1 ARS 1010 automatic deposition samplers located at about 2896 m asl at the Sierra Nevada Observatory (OSN) and at about 3000 m asl at Veleta peak. The bacterial loading in deposition samples were quantified in treated (detached) samples and in untreated samples (controls) using a flow cytometer. We examined the source of air masses over the Sierra Nevada, Spain, by computing daily backward trajectories (http://www.arl.noaa.gov/ready.html) using the HYSPLIT model with 120 h run time.

Detached bacteria from dust particles ranged from 2,77 x10^6 to 5,12 x10^7 with an average of 1,31 x10^7 cells m^{-2} day^{-1} (n = 51) whereas bacteria in the untreated samples ranged from 1,61 x10^4 to 3,03 x10^6 with an average of 1,58 x 10^5 cells m^{-2} day^{-1} (n= 49).

When data-set was split by the type (wet vs. dry) of deposition, a significant correlation ($p< 0.05$, $r = 0,57$) was found between the particulate matter (PM) and the bacterial loading in wet deposition whereas we did not obtain significant values for dry deposition.

Similarly, when PM deposition with a predominant Saharan source was related to the bacterial loadings, a significant correlation ($p <0.05$, $r=0,42$) was found (Figure 1). A non-significant relationship was found between PM with a predominant marine source and bacterial loading (not shown).

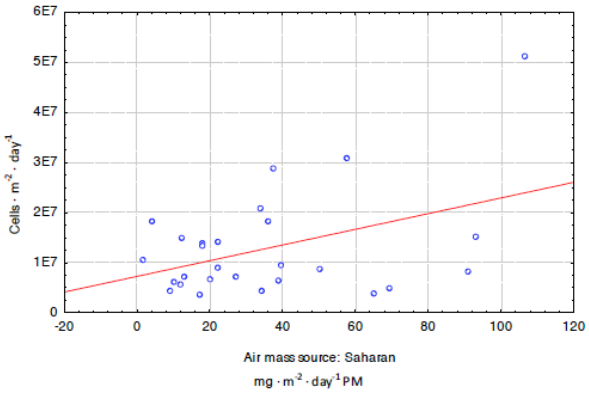

Figure 1. Relationship between Particulate Matter (PM) (mg m^{-2} d^{-1}) with a predominant Saharan source and bacterial loadings (cells $m^{-2}d^{-1}$).

Overall, we positively tested a bacterial detach procedure for aerosol deposition samples and we detected a high bacterial loading associated mostly with Saharan dust intrusions that should be taken into account to address ecological and biogeographical questions in the microbial realm.

This work was supported by the Fundación BBVA (BIOCON 04/009) and the Ministry of Environment (080/2007).

Amalfitano S. and Fazi S. (2008). Recovery and quantification of bacterial cells associated with streamed sediments *J. Microbiol. Met.* 75:237-243

Kellogg C.A. and Griffin D.W. (2006) Aerobiology and the global transport of desert dust. *TREE* 21: 638-644

Reche I et al. (2009) Effect of Saharan dust inputs on bacterial activity and community composition in Mediterranean lakes and reservoirs. *Limnol. Oceanogr.* 54: 869-879.

Neutralization of Viable Aerosolized Microorganisms due to Exposure to Combustion of Reactive Materials

S.A. Grinshpun[1], A. Adhikari[1], M. Yermakov[1], T. Reponen[1], E. Dreizin[2], M. Schoenitz[2], and V. Hoffmann[2]

[1]Center for Health-Related Aerosol Studies, University of Cincinnati, Cincinnati, Ohio, USA
[2]Department of Chemical, Biological, and Pharmaceutical Engineering, New Jersey Institute of Technology, Newark, New Jersey, USA

Keywords: bioaerosol, combustion, viability, neutralization.
Presenting author email: sergey.grinshpun@uc.edu

Neutralization of highly pathogenic aerosolized bio-threat agents is an important objective of bio-defense research programs. If a bio-weapon facility is accidentally or intentionally targeted, the bio-agent release should be prevented as some microorganisms (e.g., bacterial spores) may survive considerable heat and chemical stresses and, while remaining airborne, can represent a major health hazard. Various reactive materials are being currently developed with the added capability to "kill" (neutralize) viable microorganisms during their release to the atmosphere. A laboratory evaluation of these materials requires adequate experimental facilities and protocols. The main disadvantage of existing evaluation methods is that they do not differentiate between the effects caused by heat stress and by combustion products.

To address this gap, we have developed a two-configuration experimental approach, which allows establishing two sets of conditions for the bioaerosol exposure. In the first one, the challenge bioaerosol is supplied directly through the combustion zone so that the microorganisms are exposed to both the thermal and chemical inactivation. In the second one, the bioaerosol is supplied downstream from the combustion zone where the air temperature decreases to the levels, which do not cause significant thermal "killing" (Grinshpun et al., 2010), and thus the viability loss occurs primarily due to exposure to combustion products. Figure 1 schematically shows these configurations.

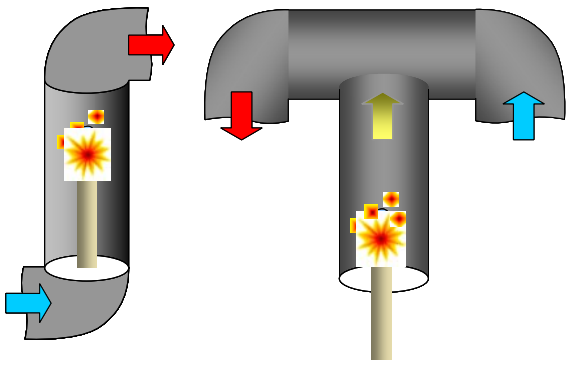

Configuration 1 **Configuration 2**

Figure 1. Exposure of a challenge bioaerosol to heat and chemical stresses associated with the combustion of reactive materials: two experimental configurations.

Two experimental setups were designed and built to implement these configurations. A hydrocarbon fuel flame seeded with three fuel additives, which were delivered to the burner from a powder disperser, represented the tested combustion environments. One of the powders contained aluminum with embedded iodine that was designed to be released at the aluminum melting temperature.

In experiments performed with both setups, endospores of *Bacillus subtilis var. niger* (also referred to as *Bacillus atrophaeus* or BG spores) as well as *Bacillus thuringiensis* (Bt spores) were exposed to the combustion environments, and the spore viability loss was quantitatively characterized using a culture-based enumeration of the exposed and non-exposed bioaerosol samples. Additionally, the first configuration was utilized to perform the tests, in which the burner was replaced with an axial heater providing specific temperature conditions for the challenge bioaerosol with no release of combustion products.

A separate set of experiments was conducted to evaluate different sampling techniques for collecting the aerosolized spores. These included four filter materials (Teflon, polycarbonate, membrane and gelatin) as well as a BioSampler (SKC, Eighty Four, PA, USA) with deionized water. The bioaerosol collection on the gelatin filter and into the BioSampler were found to be the most favorable sampling techniques for this study.

It was determined that the spore neutralization levels associated with the heat and chemical stresses may be comparable. It is anticipated that these factors may produce a synergistic effect, as a heat-induced damage of protein coats is likely to affect the spore outer membrane, cortex, and subsequently inner membrane, which enhances the penetration of the combustion-associated "lethal" chemical products. A systematic investigation is needed to test the above hypothesis.

The study was supported by the U.S. Defense Threat Reduction Agency (DTRA) and the U.S. Office of Naval Research. The authors are grateful for this support.

Grinshpun, S.A., Adhikari, A., Li C., Reponen, T., Yermakov, M., Schoenitz, M., Dreizin, E., Trunov M., and Mohan, S. (2010) *J. Aerosol Sci.* **41**, 352-363.

Carbonaceous compounds emitted from domestic biomass burning

M.A.C. Duarte, A.I. Calvo, L.A.C. Tarelho, T. Nunes, M. Evtyugina, C.A. Alves

Centre for Environmental and Marine Studies, Department of Environment and Planning, University of Aveiro, Aveiro, 3810-193, Portugal
Keywords: Biomass combustion, PM_{10}, OC, EC, chemical composition, emission factor
celia.alves@ua.pt

As in many other countries, biomass burning is a common practice in Portugal in order to obtain energy, especially for domestic heating. It has been estimated an annual wood consumption of 1.950 kton in domestic equipments in Portugal (Gonçalves et al. 2011). Besides gas emissions, biomass burning releases an important particulate matter fraction to the atmosphere that can represent up to 70% of particulate organic matter in rural regions of Europe during winter time (Puxbaum et al. 2007). This particulate emission is a major concern due to its impact on public health, indoor and outdoor air quality as well as its contribution to greenhouse gas (GHG) emissions. Emission factors (EF; $g_{\text{pollutant}}\,kg^{-1}_{\text{dry biomass burned}}$) for European biomass burning are scarce; the available EF were obtained for US, Alpine and Scandinavian biofuels (Fine et al., 2004, Johansson et al., 2004, Schmidl et al., 2004), which are uncommon in southern Europe. To better estimate the emissions of certain countries, it is necessary to burn biomass fuels commonly used in the country of study, as well as to use typical domestic heating equipments.

A set of tests was carried out to determine the gas and chemical composition of PM_{10} emitted from the combustion of three typical wood species in a stove and a fireplace. The species selected for this study were pine (*Pinus pinaster*), eucalyptus (*Eucalyptus globulus*) and Cork oak (*Quercus suber*) from Portuguese forest; common in Iberian Peninsula forests. The burning experiments were carried out in a fireplace and a wood stove; typical equipments used in Portugal for domestic heating.

The logs were cut in four small parts with weight variation between 0.3 and 0.7 kg and 0.3 and 0.4 m of length. The fireplace and woodstove were operated manually in batch mode. They heat the room air by a combination of natural convection and radiation. The woodstove has a combustion chamber with 0.093 m^3 of volume, while that of the fireplace has 0.15 m^3. Both equipments have a vertical exhaust duct with 0.2 m internal diameter and 3.3 m height. Each combustion cycle lasted between 45 and 60 minutes. The O_2 source was atmospheric air at a temperature between 20ºC to 25ºC and pressure from 101 kPa to 102 kPa.

The flue gas composition was monitored continuously at the exit of the chimney: i) total volatile hydrocarbons were determined using an automatic analyser with flame-ionisation detector and ii) CO_2 and CO were determined using a non-dispersive infrared analyser.

Particles (PM_{10}) were collected, under isokinetic conditions, on quartz filters using a low volume sampler in the dilution tunnel that was directly coupled to the chimney. Filters were analysed in order to determine the carbonaceous content (elemental - EC - and organic carbon - OC) by a thermal-optical transmission technique.

Higher EFs were obtained for the fireplace than for the wood stove, for the three tree species studied (Table 1). Carbonaceous compounds represent an important fraction of PM_{10}, with OC always remaining higher than EC.

This study points out the strong influence of the surrounding environmental conditions on fireplace emissions due to the open combustion chamber of this equipment. Changes in these conditions will influence the combustion process, affecting the combustion speed, temperatures and, hence, the emission profiles.

Table 1 - Emission factors for PM_{10}, OC and EC ($g.kg^{-1}$ biomass, dry basis).

		Pine	Eucalyptus	Cork oak
Woodstove	PM	4.42±1.89	7.75±3.30	6.96±2.12
	OC	1.93±0.78	4.05±2.08	3.68±1.38
	EC	1.54±0.56	0.58±0.23	0.53±0.06
Fireplace	PM	20.0±9.3	23.2±2.7	17.5±1.6
	OC	12.5±6.0	13.3±1.6	10.6±1.1
	EC	1.55±0.74	0.43±0.08	0.72±0.11

This work was supported by the Portuguese Science Foundation (FCT) through the project "Contribution of biomass combustion to air pollutant emissions", PTDC/AMB/65706/2006 (BIOEMI).

Fine, P.M., Cass, G.R. and Simoneit, B.R.T. (2004) *Environ. Eng. Sci.* 21, 705-721.

Gonçalves, C., Alves, C. and Pio, C., (2011) *Atmos. Environ.*, in press. http://dx.doi.org/10.1016/j.atmosenv.2011.12.013

Johansson, L. S. and Leckner, B. (2004). *Atmos. Environ.* 38(25): 4183-4195.

Schmidl, C., Marr, I.L., Caseiro A., Kotianová, P., Berner, A., Bauer, H., Kasper-Giebl, A. and Puxbaum, H. (2008) *Atmos. Environ*. 42, 126-141.

Puxbaum, H., Caseiro, A., Sánchez-Ochoa, A., Clayes, Gelencsér, M., Legrand, A. M., Preunkert S., Pio, C. (2007) *J. Geophys. Res*. 112, D23S05.

Inventory of emissions from residential wood combustion in Portugal

C. Gonçalves, C. Alves and C. Pio

Centre for Environmental and Marine Studies (CESAM), Department of Environment, University of Aveiro, 3810-193 Aveiro, Portugal.

Keywords: Survey questionnaire, wood species, burning appliances, emission factors, inventory.

catiagoncalves@ua.pt

Nowadays, most developed countries suffer from a nearly total dependence on fossil fuels for energy production, in economic and social activities. With the emergence of environmental politics and the imminent depletion of fossil fuels, there is a strong encouragement to change to renewable energy sources. The use of biomass for energy production is being promoted to decrease the dependence on fossil fuels. However, residential wood combustion (RWC) is one of the largest sources of fine particle emissions to the atmosphere in Portugal. Since wood burning practices and activities can vary geographically, residential wood combustion chemical composition profiles also differ by region.

In this study, data from a number of source burning tests conducted with several Portuguese wood species (Fernandes et al., 2011; Gonçalves et al., 2011) were used to assemble a national inventory of emissions. These emissions include $PM_{2.5}$, OC and EC, CO and CO_2 and various individual organic compounds (for example levoglucosan) that are released from RWC (fireplaces and woodstoves) in Portugal.

In addition to the emission factors, a comprehensive knowledge of RWC activity data and its spatial distribution, which are not available in national statistical databases, is required. The survey questionnaire was conducted by telephone calls between 21 September and 11 October 2010 by a market research company, working under contract for the University of Aveiro. The survey was based on 2387 effective respondents, from which a total of 806 positive answers were obtained, i.e., house owners who have declared the use of RWC.

The total amount of wood consumed in Portugal in the year 2010 was around 2 Mt for both heating (83%) and cooking (17%) purposes. In the households where wood is frequently burned, 43% use fireplaces, while 6% of respondents said that burn wood in barbecues fireplaces. Woodstoves and traditional ovens represent about 24% of the total number of appliances (Table 1). The largest percentage of wood (51%) is burned in fireplaces, while the lowest percentage of wood (0.30 %) is burned in furnaces (Table 1). The results of the questionnaire indicated an average of 1.3 wood combustion appliances per household.

Regarding wood species used, Holm oak and cork oak are the most common woods for residential combustion in the southern districts; maritime pine, Portuguese oak and eucalypt present a larger share in northern districts. Around 20% of the house owners burn mixtures of different types of woods.

The use of different appliances and wood species is of great importance because both affect the amount and type of emissions ($PM_{2.5}$, OC, EC and organic compounds).

Table 1 Appliance distribution (%) and wood consumption by appliance in mainland Portugal.

	(%) distribution	Wood Consumption (%)	Wood Consumption (t y^{-1})
Fireplace	43	51	954 652
Woodstove	20	22	411 646
Wood burning furnace	11	12	218 631
Salamander stove	7.8	7.6	143 125
Boiler	7.2	3.3	61 646
Barbecue	5.8	1.5	28 027
Oven	4.3	2.5	46 785
Wood burning water heater	0.57	0.58	10 839
Furnace	0.38	0.30	5 631

The emissions of $PM_{2.5}$ were estimated to be between 0.09 kt y^{-1} (Portalegre) and 1.30 kt y^{-1} (Aveiro), totalising 10.96 kt y^{-1} in Portugal. The national emissions of OC and EC were estimated to be 5.32 and 0.53 kt y^{-1}, respectively. It was estimated that the total CO_2 emissions from RWC in Portugal are 1.7 Mt y^{-1}. The levoglucosan emissions contribute with between 7.8% (Beja) and 16.1% (Vila Real) of $PM_{2.5}$ emissions from RWC. PAHs from RWC in Portugal represent approximately 6.5% of the total emissions from the main activity sectors.

This work was funded by the FCT through the PTDC/AMB/65706/2006 (BIOEMI) project and the PhD grant SFRH/BD/36540/2007.

Fernandes, A.P., Alves, C., Gonçalves, C., Tarelho, L., Pio, C., Schimdl, C., Bauer, H. (2011) J ENVIRON MONITOR. doi: 10.1039/C1EM10500K.

Gonçalves, C., Alves, C., Fernandes, A.P., Monteiro, C., Tarelho, L., Evtyugina, M., Pio, C. (2011) ATMOS ENVIRON 45, 4533–4545.

Aerosol aging during transport from Thailand to Taiwan

C.-T. Lee[1], M.-T. Chuang[1], N.-H. Lin[2], K. Sopajareepom[3], S.-Y. Chang[4], Y.-J. Chang[1]

[1]Graduate Institute of Environmental Engineering, National Central University, Jhongli, Taiwan
[2]Department of Atmospheric Sciences, National Central University, Jhongli, Taiwa
[3]Department of Environmental Engineering, Chiangmai University, Chiangmai, Thailand
[4]School of Public Health, Chung Shan Medical University, Taichung, Taiwan
Keywords: aerosol chemistry, biomass burning aerosol, aerosol transport, aerosol aging tracer.
Presenting author email: ctlee@cc.ncu.edu.tw

The transport of biomass burning (BB) aerosol from Indochina may affect climate change in the downstream Southeast Asia, East Asia, and West Pacific. Up to now, the investigation on BB aerosol aging during long-range transport is still very limited due to the lack of observation data. In this study, atmospheric aerosols were collected at the Suthep mountain site in Chiangmai, Thailand and the Lulin mountain site in central Taiwan from March to April 2010.

During the study period, five-day backward trajectories showed that the air masses originated from Indochina would transport to Taiwan. Therefore, these two sites (2,400 Km apart from each other) can be considered as the upstream and downstream sites under the prevailing westerlies. Comprehensive aerosol properties were resolved for $PM_{2.5}$ water-soluble ions (WSIs), carbonaceous content (from the U.S. IMPROVE protocol), water-soluble/insoluble organic carbons (WSOC/WIOC), low-molecular-weight dicarboxylic acids (C2-C5), and monosaccharide anhydrides.

By employing non-sea-salt potassium ion (nss-K^+) or low-temperature elemental carbon (EC1) after the correction for pyrolized organic carbon (OP) as the BB aerosol tracer, the aerosol is considered to be aged when the Aging Ratio (AR_X) exceeding unity as follows:

$$AR_{nss\text{-}K^+} = \frac{(\frac{C_i}{nss\text{-}K^+})_{Lulin}}{(\frac{C_i}{nss\text{-}K^+})_{Suthep}}$$

Table 1. Selected values of aerosol WSIs normalized to nss-K^+ or EC1-OP (in parenthesis) and the resulted AR_X values at the Suthep and Lulin sites.

	$\frac{NH_4^+}{nss\text{-}K^+}$	$\frac{NO_3^-}{nss\text{-}K^+}$	$\frac{nss\text{-}SO_4^{2-}}{nss\text{-}K^+}$
	$\frac{NH_4^+}{EC1\text{-}OP}$	$\frac{NO_3^-}{EC1\text{-}OP}$	$\frac{nss\text{-}SO_4^{2-}}{EC1\text{-}OP}$
Suthep (N=15)	0.96±0.20 (0.39±0.12)	0.49±0.16 (0.19±0.05)	3.92±0.99 (1.59±0.53)
Lulin (N=19)	3.17±1.15 (1.81±1.87)	1.78±0.88 (1.02±1.19)	8.12±2.83 (4.66±4.73)
$AR_{nss\text{-}K^+}$ ($AR_{EC1\text{-}OP}$)	3.31 (4.67)	3.61 (5.33)	2.07 (2.93)

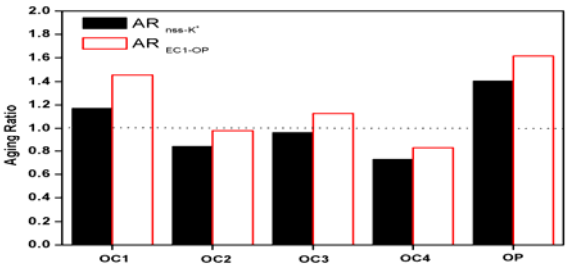

Figure 1. Aerosol AR_X values ($AR_{nss\text{-}K^+}$ or $AR_{EC1\text{-}OP}$) for the resolved OC fractions from the U.S. IMPROVE protocol.

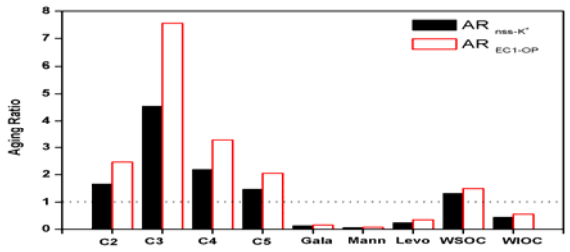

Figure 2. Aerosol AR_X values ($AR_{nss\text{-}K^+}$ or $AR_{EC1\text{-}OP}$) for the resolved organic fractions.

The computed AR_X values show that NH_4^+, NO_3^-, nss-SO_4^{2-}, the lowest volatility organic carbon (OC1), OP, C2-C5, and WSOC are all above unity which indicates that these fractions or species were enhanced and thus aged during transport. In contrast, the AR_X values of levoglucosan, galactosan, and mannosan are only in the range of 0.1 to 0.3 which indicates monosaccharide anhydrides would degrade during transport. Therefore, by comparing aerosol properties at the upstream and downstream sites, aerosol aging effect for different species or fractions can be evaluated.

With the observation of aerosol comprehensive compositions at the Suthep and Lulin sites and the development of an AR_X value, this study provides a quantitative method to assess the aging of BB aerosol species or fractions during long-range transport.

This work was supported by the National Science Council in Taiwan under grant NSC 98-2111-M-008 -023 -MY3.

Summer 2010 forest fires in central Portugal: characterisation of trace gases and aerosol emissions

A.M. Vicente[1], C.A. Alves[1], A.I. Calvo[1], A.P. Fernandes[1], T. Nunes[1], A.C. Monteiro[1], M. Evtyugina[1], L.A. Tarelho[1] and C.A. Pio[1]

[1]Centre for Environmental and Marine Studies, Department of Environment, University of Aveiro, 3810-193 Aveiro, Portugal

Trace gases and aerosol particle emissions from several wildfires occurring in Portugal were sampled in summer 2010 (Table 1).

Table 1. Wildfires episodes over Portugal in summer 2010, where smoke samples were collected.

Sampling locations	Date	Number of samples ($PM_{2.5}$+$PM_{2.5-10}$)	MCE(*)
Dornelas	26 Jul.	2	0.87
Rebordelo	27 Jul.	6	0.83-0.94
Albergaria-a-Velha	4 Aug.	2	0.92
Albergaria-a-Velha	6 Aug.	2	0.89
Junqueira (Vale de Cambra)	11 Aug.	4	0.87-0.91
Vila Nova de Tazem	13 Aug.	12	0.64-0.84

(*) modified combustion efficiency

Coarse ($PM_{2.5-10}$) and fine ($PM_{2.5}$) smoke particles were collected sequentially on pre-fired quartz fibre filters, using a portable high-volume sampler. Sampling was performed at 1.5 m above ground, downwind from the burning area, at distances of 10 e 200 m from the flame. Tedlar bags were used for the collection of gas samples in parallel with aerosol sampling. Total volatile hydrocarbons (THC) and carbon oxides (CO_2 and CO) in the Tedlar bags were measured using automatic analysers with flame ionisation and non-dispersive infrared detectors, respectively. The organic and elemental carbon content of particulate matter was analysed by a thermal-optical transmission technique (Alves et al., 2011a). The detailed speciation of organic compounds in smoke samples was carried out by gas chromatography-mass spectrometry. The water-soluble ions were obtained by ion chromatography.

Emission factors (EF) for some gaseous compounds and particulate matter were calculated. This parameter is usually defined as the amount of a compound released per amount of dry fuel consumed, expressed in units of g kg^{-1} (Alves et al., 2011a; Reid et al., 2005).

The CO emission factor (EF_{CO}) ranged between 67.1 and 364 g kg^{-1} biomass (dry basis) burned. The EF_{CO} obtained for wildfires in summer 2010 in Portugal (159±84 g kg^{-1}) are similar to those obtained in 2009, with values of 231±177 g kg^{-1} (Alves et. al. 2011b). The EF_{CO_2} obtained for wildfires in Portugal (2010) ranged between 1029 and a maximum of 1655 g kg^{-1} biomass (dry basis) burned. Total hydrocarbon emission factors (EF_{THC}) reached a maximum of 28.1 g kg^{-1} (dry basis), averaging 12.1±9.98 g kg^{-1}. $PM_{2.5}$ and PM_{10} particulate matter concentrations reached 11.6 mg m^{-3} and 12.2 mg m^{-3}, with average values of 3.72±3.60 mg m^{-3} and 4.01±3.80 mg m^{-3}, respectively. The EF ranged between 4.40 and 67.5 g kg^{-1} for $PM_{2.5}$ and between 4.80 and 72.1 g kg^{-1} (dry basis) for PM_{10}. A clear predominance of carbonaceous aerosol was observed, with OC concentrations always remaining much higher than EC in both size fractions. The EF_{OC}, on average, were 11.0±9.72 g kg^{-1} and 11.4±9.97 g kg^{-1}(dry basis) for fine and coarse particles, respectively. The EC emission factors (EF_{EC}) obtained for $PM_{2.5}$ and PM_{10} ranged between 0.07 and 2.26 g kg^{-1} (dry basis).

The concentration of water-soluble inorganic ions represented, on average, 3.9% and 2.8% of $PM_{2.5}$ and $PM_{2.5-10}$ mass, respectively. Focusing on average concentrations, highest values were registered for Cl^-, NH_4^+, K^+, SO_4^{2-} and Ca^{2+} in $PM_{2.5}$, and SO_4^{2-}, Ca^{2+} and K^+ in $PM_{2.5-10}$.

The chromatographically resolved organics included *n*-alkanes, *n*-alkenes, *n*-alkanoic acids, *n*-di-acids, unsaturated fatty acids, phenolic compounds, ketones, steroids, di- and triterpenoids, PAHs and anhydrosugars.

Levoglucosan was always present at higher concentrations than those of galactosan and mannosan. Ratios of OC to levoglucosan, galactosan and mannosan were similar to those registered during summer 2009 wildfires in Portugal (Alves, et al., 2011a; Vicente et al., 2011).

This work was supported by the Portuguese Science Foundation (FCT), through the project PTDC/AMB/65706/2006 (BIOEMI). Ana Vicente acknowledges the PhD grant SFRH/BD/48535/2008.

Alves, C., Vicente, A., Monteiro, C., Gonçalves, C., Evtyugina, M. and Pio, C. (2011a) *Sci. Total Environ.* 409, 1466-1475.

Alves, C., Vicente, A., Nunes, T., Gonçalves, C., Fernandes, A., Mirante, F., Tarelho, L., Sánchez De La Campa, A., Querol, X. and Caseiro, A. (2011b) *Atmos. Environ.* 45, 641-649.

Reid, J.S., R. Koppmann, T. F. Eck and Eleuterio, D.P. 2005) *Atmos. Chem. Phys.* 5**,** 799-825.

Vicente, A., Alves, C., Monteiro, C., Nunes, T., Mirante, F., Evtyugina, M., Cerqueira, M. and Pio, C. (2011) *Atmos. Environ.* 45, 5172-5182.

Contribution to $PM_{2.5}$ from domestic wood burning in a small community in Sweden

P. Molnár[1] and G. Sallsten[1]

[1]Occupational and Environmental Medicine, Sahlgrenska Academy at University of Gothenburg, Gothenburg, SE 405 30, Sweden

Keywords: Wood smoke, PM and source apportionment, PMF, XRF. Black carbon

Presenting author email: peter.molnar@amm.gu.se

Background: The use of wood stoves and fireplaces for heating is quite common in homes in many countries with cold climates. Biomass burning produces a number of gaseous and particulate pollutants which when released affects the ambient air (Fine et al., 2001; Hedberg et al., 2002; Lee et al., 2005; McDonald et al., 2000). The rising importance of biomass emissions in ambient air increases the demand to quantify the contribution in local settings.

The aim was to investigate and quantify the contribution to ambient air from domestic biomass burning for space heating in a residential area.

Methods: Daily 24 hours $PM_{2.5}$ samples during 151 days in the winter season 2007-08 were collected using the IVL weekly $PM_{2.5}$ sampler (IVL Swedish Environmental Research Institute, Gothenburg, Sweden) on 25 mm TF (PTFE) Membrane filters (Pall Corporation, USA) at two sampling places, one in a wood burning area and the other at a reference station without any houses with domestic wood burning nearby.

After determination of mass concentration, a subset of the filters (56 filters paired from 28 days) was selected for chemical analysis. Black carbon, BC, was analysed using Model OT21 Optical Transmissometer Magee Scientific Corporation, USA and elemental concentrations were determined using EDXRF. The 28 days were chosen based on trajectory analysis to be days with low regional contribution.

Source apportionment analysis was carried out by Positive Matrix Factorisation (PMF) technique using the US EPA software EPA-PMF 3.0.

Results: Statistically significant higher concentrations were found in the wood burning area compared to the reference area for the following variables; $PM_{2.5}$, BC, K, Zn, and Br. The concentrations for these variables were 22, 55, 58, 44, and 24 per cent higher in the wood burning area.

For the PMF analysis the two data sets from the wood burning and the reference area was put together into one data set. A five factor model was used for the PMF analysis and the following sources were identified; Long range transported (LRT), Biomass, Sea salt, Soil, and Traffic (Table 1).

The Biomass factor profile was identified by high percentage of the variables BC, K, Zn, and Cu being attributed to the factor.

Table1. Factor contributions and the ratios in the wood burning area and the reference area from the PMF analysis.

Factor	Wood burning area ($\mu g/m^3$)	Reference area ($\mu g/m^3$)	Ratio
LRT	1.65	1.57	0.93
Biomass	1.41	0.77	**1.84**
Sea Salt	0.90	0.85	1.06
Soil	0.47	0.51	1.10
Traffic	0.16	0.15	1.06

Discussion: All factors, besides the Biomass burning, are very similar in source strength at both places, indicating that the only real difference between the two areas was the presence of biomass burning. The reference area was not devoid of any biomass influence, but the contribution is only about half compared to the wood burning area.

The contribution from LRT in the current PMF model is smaller than in reality for the winter season since the analysis is performed only on a subset of the data without any influence from the more polluted regions of Europe. For all the other sources, including domestic biomass burning, the contribution is representative for the winter season.

Fine, P.M., Cass, G.R. and Simoneit, B.R.T., Chemical characterization of fine particle emissions from fireplace combustion of woods grown in the northeastern United States, *Environmental Science & Technology* **35**(2001), pp. 2665-2675.

Hedberg, E. *et al.*, Chemical and physical characterization of emissions from birch wood combustion in a wood stove, *Atmospheric Environment* **36**(2002), pp. 4823-4837.

Lee, R.G.M., Coleman, P., Jones, J.L., Jones, K.C. and Lohmann, R., Emission factors and importance of PCDD/Fs, PCBs, PCNs, PAHs and PM10 from the domestic burning of coal and wood in the UK, *Environmental Science & Technology* **39**(2005), pp. 1436-1447.

McDonald, J.D. *et al.*, Fine Particle and Gaseous Emission Rates from Residential Wood Combustion, *Environmental Science & Technology* **34**(2000), pp. 2080-2091.

Characterisation of regional ambient biomass burning organic aerosol mixing ratios

M. D. Jolleys[1], H. Coe[1], G. McFiggans[1], G. Capes[1], J. D. Allan[2], J. Crosier[2], P. I. Williams[2], G. Allen[1] and J. L. Jimenez[3]

[1] Centre for Atmospheric Science, University of Manchester, UK
[2] National Centre for Atmospheric Science, University of Manchester, UK
[3] Cooperative Institute of Research in Environment Sciences and Department of Chemistry and Biochemistry, University of Colorado, Boulder, Colorado, USA

Keywords: biomass burning, organic aerosols, emission ratios, field measurements

Presenting author email: matthew.jolleys@postgrad.manchester.ac.uk

No evidence for a regional additional source of secondary organic aerosol (SOA) has been identified in measurements of biomass burning-influenced ambient air masses. Measurements included in this study were obtained from the deployment of an Aerodyne Quadrupole Aerosol Mass Spectrometer during four field campaigns, involving both research aircraft flights and ground-based measurements. OA concentrations normalised to excess CO (OA/ΔCO) show strong regional and local scale variability, with a difference of almost a factor of five across fresh OA emissions between campaigns. Average OA/ΔCO is typically higher in the near-field than at a greater distance from source, indicating an absence of significant SOA formation, despite evidence to suggest OA becomes increasingly oxidized with age. This trend is in contrast with observations of anthropogenic OA in urban environments, where OA/ΔCO is consistently shown to increase with distance from source. There is no such agreement in the case of biomass burning OA (BBOA) amongst the literature base, with conflicting examples relating to the influence of SOA on aerosol loadings. A wide range of average initial emission ratios (ERs) close to source are observed both within the datasets analysed here and within the literature, together with considerable variability in individual OA/ΔCO values throughout fresh biomass burning plumes. The extent of this variability far outweighs any increase in OA/ΔCO in the few instances it is observed here, suggesting that source conditions are of greater importance for the propagation of BBOA loadings within the ambient atmosphere. However, the implications of ageing on OA/ΔCO variability appear to be highly uncertain, with little consistency between observed trends for different locations. Furthermore, the exact effects of the fire conditions influencing emissions from biomass burning events remain poorly constrained. These uncertainties regarding the evolution of biomass burning emissions emphasise the need for improved characterisation of BBOA to ensure accurate representation in global climate models.

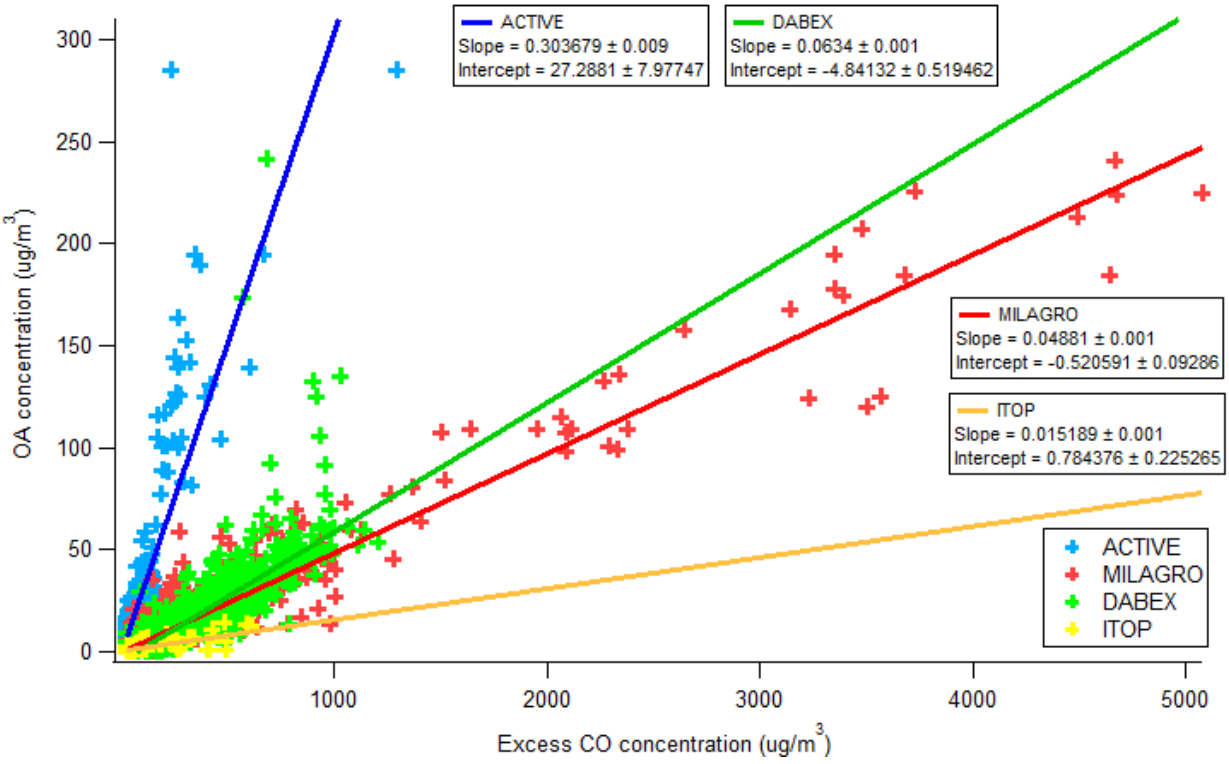

Figure 1. Organic aerosol mass concentration versus excess CO for all data meeting selection criteria throughout each campaign included in this study. Coefficients are for linear regressions applied to datasets, with uncertainties of ± 1σ.

Large use of wood combustion for domestic heating in France: impacts on the air quality in rural environments

C. Piot[1,2], J. Cozic[2], J.-L. Besombes[1] and J.-L. Jaffrezo[2]

[1]Université de Savoie-LCME, Le Bourget du Lac, France
[2]Université Joseph Fourier-CNRS-LGGE, St-Martin d'Hères, France
Keywords: organic tracers, Chemical Mass Balance, Positive Matrix Factorization.
Presenting author email: christine.piot@lgge.obs.ujf-grenoble.fr

France is the leading consumer of wood energy in Europe for domestic heating with an annual consumption of 7.3 million PET. This consumption is being increased due to the use of wood burning for domestic heating often considered by policy makers as an interesting source of renewable energy. Therefore, an increased impact of residential wood burning emissions on air pollution can be expected and a growing number of scientific studies have recently focused on the influence of these emissions on the ambient aerosol concentration. Indeed, biomass burning can represent an important source of Particulate Matter (PM) and carcinogenic compounds like Polycyclic Aromatic Hydrocarbons (PAH).

For example, biomass burning was found to account for 42% of PM2.5 in Grenoble during winter (Favez *et al.*, 2010) and for 41% of the organic aerosol in Zurich (Szidat *et al.*, 2006). However, there are few studies in the literature on the impacts of wood combustion on the air quality in rural environments in France. The need to study contributions of this source to the air quality in rural sites is increased since this type of emissions is very dependent of local fuel and practices (e.g. type of wood burned).

The Particul'Air program was proposed to investigate the chemical composition and sources of PM during one year: 9 week-long campaigns, from March 2009 to February 2010 simultaneously in 9 rural sites (3 rural background sites and 6 rural exposed sites) located along a West-East transect. A focus was put on the determination of biomass burning chemical tracers (levoglucosan and its isomers) and on the apportionment of this source. Additionally, detailed chemical composition of PM10 and source apportionment were also studied in 2 other rural background sites from the EMEP network (as part of the CAMERA program) since January 2011 (1 daily sample per week). In both programs, PM10 were collected by French air quality networks on quartz filters with high-vol. samplers (Digitel DA-80).

On average, levoglucosan represents a large part of organic matter (OM) in winter for rural sites, and its fraction tends to increase from West to East of France (Fig.1). It represents only a minor fraction in the summer season. For the two background sites from the EMEP network (BACK 4 and 5 on Fig.1), the concentrations are much lower than in other rural sites, indicative of a lower impact of biomass burning emissions in remote areas. Conversely, the contribution of biomass burning tracer to OM is very high for the exposed rural site "EXP5" located in an Alpine valley. This is valid both for winter and summer, and the contributions to OM are even larger than that measured by Favez et al. (2010) in Grenoble in winter (50 $mg.g^{-1}_{OM}$).

Source apportionment using the Chemical Mass Balance (CMB) method was performed for all these sites. It shows that in winter, biomass burning emissions accounts for between 10 and 60 % of PM10 in these rural sites. The presentation will discuss these results in detail, including limitations and uncertainties.

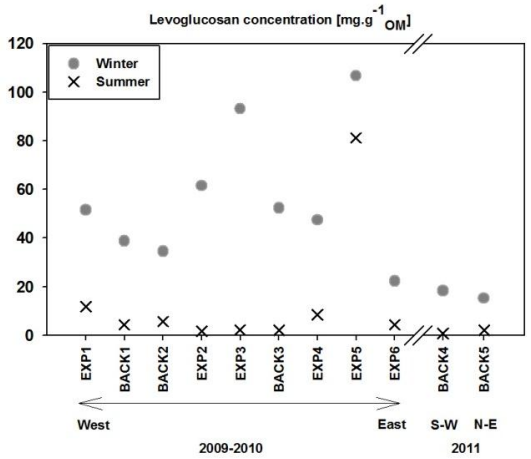

Figure 1. Average levoglucosan concentrations in rural sites background (BACK) and exposed (EXP) in winter and in summer in $mg.g^{-1}_{OM}$.

C. Piot thanks the Région Rhône-Alpes for her PhD grant. Campaigns were supported by the Particul'Air and CAMERA programs both funded by ADEME. Authors thank also the AASQA who have realized sampling: AIRBREIZH, AIRCOM, ATMO Poitou-Charentes, LIMAIR, LIGAIR, ATMO Auvergne, AIRAPS, ATMO Champagne-Ardennes and ORAMIP.

Favez, O., El Haddad, I., Piot, C., Boréave, A., Abidi, E., Marchand, N., Jaffrezo, J.-L., Besombes, J.-L., Personnaz, M.-B., Sciare, J., Wortham, H., George, C. and D'Anna, B. (2010) *Atmos. Chem. Phys.* **10**, 5295-5314.

Szidat, S., Jenk, T.M., Synal, H.A., Kalberer, M., Wacker, L., Hajdas, I., Kasper-Giebl, A. and Baltensperger, U. (2006) *J. Geophys. Res.* **111**, D07206.

http://www.atmo-poitou-charentes.org/2009-2010-Particul-air-etude-de-la.html

Burning of Olive Tree Branches: A Major Organic Aerosol Emission Source in the Mediterranean

E. Kostenidou[1], C. Kaltsonoudis[1,2], E. Louvaris[1,2], M. Tsiflikiotou[1,2], and S.N. Pandis[1,2,3]

[1]Institute of Chemical Engineering and High Temperature Chemical Processes, ICE-HT, Patras, 26504, Greece
[2]Department of Chemical Engineering, University of Patras, Patras, 26500, Greece
[3]Department of Chemical Engineering, Carnegie Mellon University, Pittsburgh, 15213, PA
Keywords: biomass burning, AMS, thermodenuder, levoglucosan.
Presenting author email: v_kostenidou@chemeng.upatras.gr

Burning of olive tree branches is a common agricultural waste management technique after the pruning of the olive trees during the months November to February. Almost 90% of the global olive trees are located around the Mediterranean Basin, so the emissions of olive tree branches burning in this area can be a significant source of fine aerosols during the cold months.

Organic aerosol produced by olive tree branches burning was characterized with both directed source-sampling (using the ICEHT smog chamber) and with ambient measurements during the burning season. A thermodenuder coupled with a High Resolution Aerosol Mass Spectrometer (HR-AMS) and a Scanning Mobility Particle Sizer (SMPS) were used for the particulate phase characterization, while the gas phase emissions were measured by a Proton Transfer Reaction Mass Spectrometer (PTR-MS), NO_x O_3, CO and CO_2 monitors.

The organic AMS mass spectrum changes with aging as the f_{44} increases while the f_{43} decreases (Figure 1). After the thermodenuder the organic mass fraction remaining at 80°C is around 50%, implying that the olive tree branches burning aerosol is semi-volatile. The thermodenuded mass spectrum is different from the original mainly at *m/z's* 44 and 43 which increase and decrease correspondingly for the less volatile OA components.

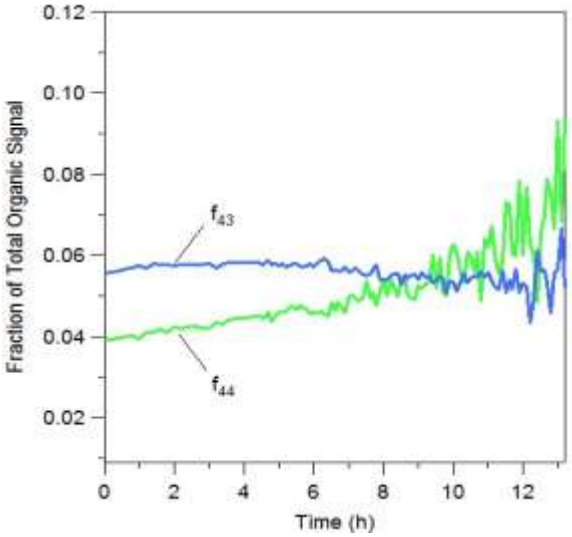

Figure 1. f_{44} and f_{43} of olive tree branches burning organic aerosol during aging.

The chamber organic AMS spectrum resembles the ambient mass spectrum during olive tree branches burning events (Figure 2).

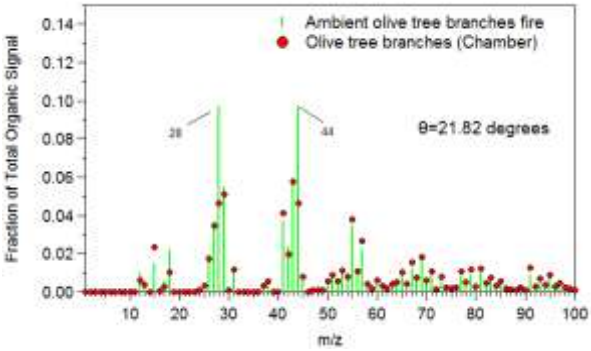

Figure 2. Mass spectrum of olive tree branches burning compared with ambient mass spectrum during olive tree branches fires event

The AMS mass spectrum of the olive tree branches burning differs from the other published biomass spectra. The levoglucosan tracer at *m/z* 60 is lower than in the most biomass burning sources. This may lead to an underestimation of the biomass burning in the Mediterranean Area, where the emissions of olive tree branches burning are high and levoglucosan is being used as a wood burning tracer.

Our estimates for the emissions from olive branch burning suggest that this is the most important fine aerosol emission source during the winter months in the Mediterranean countries in which this activity is prevalent.

Airborne measurements in the lower atmosphere in Finland during Russian wildfires in the summer 2010

K. Leino[1], R. Väänänen[1] , T. Pohja[1] , P.P. Aalto[1] , T. Petäjä[1] A. Virkkula[1,2] and M. Kulmala[1]

[1] Division of Atmospheric Sciences, Department of Physics, University of Helsinki, Finland.
[2] Finnish Meteorological Institute, Helsinki, Finland.

Keywords: Airborne aerosol, CPC, measurements.

Presenting author email: katri.paananen@helsinki.fi

Introduction

Atmospheric aerosol particles have both climate (IPCC, 2007) and health related effects (Vaclavik Bräuner et al., 2007). Particles are emitted into the atmosphere a multitude of sources. This study attends to wildfires in Russian forests and peat bogs and precisely emissions transported to Finland in summer 2010. In the end of July were made 4 flights overall to East and Central Finland because of Russian wildfire emissions. We measured total particle concentration and carbon dioxide as a function of altitude.

Methods and experimental setup

The flights were carried out in 29-30 of July 2010. We made profiles in the lower atmosphere from the ground level up to the 3.8 km altitude. The measurement flights were made using a small aircraft, Cessna FR172F. The plane was modified to a two-seater. Behind the pilot and operator there was a measurement rack with instruments. The measurement flights were operated from and to Tampere-Pirkkala airport. The flights were flown with 80 kn airspeed.

The particle concentrations were measured by TSI-3776 Ultrafine Condensation Particle Counter (UCPC) tuned and calibrated for 3 nm cut-off size (Mordas et al., 2008) and CO_2 concentration by CO2/H2O –gas analyzer (Li-COR LI-840). UCPC provided us the total number concentration of the sub-micron particles. The location was coordinated by GPS receiver. Backward airmass trajectories at two altitudes (in the boundary layer and free troposphere) were calculated using the Hybrid Single Particle Lagrangian Integrated Trajectory (HYSPLIT4) model (Draxler, 1999).

Results and discussion

In the preliminary result of this study we observed total number concentrations were high ($8 \cdot 10^3$ cm^{-3}) at the altitudes of 2.5 – 3.8 km over the Jämsä area. Air masses came to Finland from Southeast at the altitude of 3000 m and from Southeast or East at the altitude of 500 m. The particle total concentration was less than ($3 \cdot 10^3$ cm^{-3}) elsewhere. At July 30th we did not detected significant emissions any more. The CO_2 concentration was about 380-390 ppm during the flights. Even at the first flight in the smoky layers we did observed nothing of the ordinary.

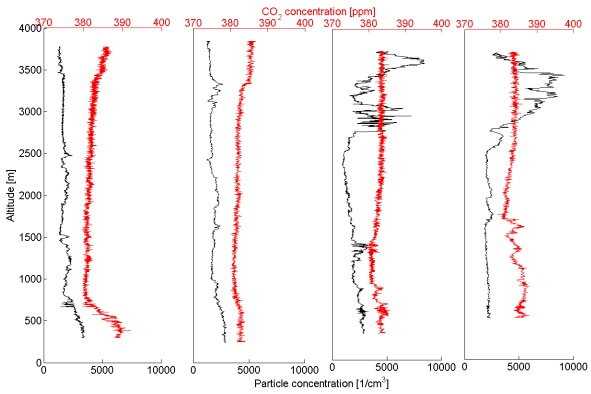

Figure 1. The total number concentration and CO_2 concentration during four altitudeprofiles on July 29th.

Acknowledgements

Funding via Academy of Finland (project nro 139656), Maj and Tor Nessling project 2010143, European Research Council and CRAICC are gratefully acknowledged.

Draxler, R.R. (1999). HYSPLIT4 user's guide. *NOAA Tech. Memo.* ERL ARL-230.

IPCC: Summary for Policymakers, in: Climate Change 2007: The Physical Science Basis, Contribution of Working Group I to the Fourth Assessment Report of the Intergovernmental Panel on Climate Change, edited by: Salomon, S., Qin, D., Manning, M., Chen, Z., Marquis, M., Averyt, K. B., Tignor, M., and Miller, H. L., Cambridge University Press, Cambridge, United Kingdom and New York, NY, USA, 2007.

Mordas et al., 2008. Nanometer Particle Detection by the Condensation Particle Counter UF-02proto. *Aerosol Sci. Tech.*, 42: 7, 521- 527.

Vaclavik . Bräuner, et al. (2007). Exposure to Ultrafine Particles from Ambient Air and Oxidative Stress–Induced DNA Damage. *Env. Health Perspect.*, Vol. 115, No.8: 1177-1182.

Measurement of fluorescence from ambient aerosol particles using WIBS-4 instrument

F. Taketani[1], Y. Kanaya[1], W. R. Stanley[2] and P.H. Kaye[2]

[1]Research Institute for Global Change, Japan Agency for Marine-Earth Science and Technology, 3173-25 Showa-machi, Kanazawa-ku, Yokohama, Kanagawa 236-0001, Japan
[2]Centre for Atmospheric & Instrumentation Research, University of Hertfordshire, AL10 9AB, UK

Keywords: fluorescence, particle shape, atmospheric aerosol.
Presenting author email: taketani@jamstec.go.jp

Among various optical techniques applied for the atmospheric particle detection, fluorescence is useful for detecting certain types of organic particles, especially those of biological origin. In this study, we employed a single-particle fluorescence sensor, WIBS-4 (Kaye et al, 2005), for the detection of fluorescence particles, to demonstrate the capability of the classification of organic particles in the ambient air.

The single-particle fluorescence sensor utilizes a continuous-wave 635 nm diode laser for the detection of particles and the determination of particle size. A quadrant photomultiplier tube (PMT) is used to detect spatial patterns of the forward scattering that can be related to the particle shape information. The scattering light signal derived from a single particle upon crossing the 635 nm-CW laser triggers two pulsed xenon UV lights (280 nm and 370 nm) for the excitation of compounds contained in the pertinent single particle. The fluorescence signals emitted from the particle are then detected by two PMTs, separately for the 310–400 nm and 420–650 nm wavelength windows.

We conducted ambient air measurements from April 21 to May 11, 2011 using the WIBS-4 instrument at our campus in Yokosuka city, facing Tokyo bay in Japan (35.32°N, 139.65°E). Figure 1 shows the temporal variations in the number concentrations of detected particles (ca. >0.8 μm, black line) and fluorescent particles (FL-particles, blue line). The "fluorescent particles" include those emitted fluorescence in either or both of the two wavelength windows. During the observation period, the ratio of the fluorescent particles to the total varied in the range of 3–53%. During May 2–4, high number concentrations were observed. From the features of the particle size and shape information, it was suggested that dust particles were mainly observed. From the fluorescence signals from individual particles, we found that some dust particles contain fluorescent compounds.

Figure 2 shows time series of number concentrations of FL-particles for different sizes. On April 26, fine particles (diameter < 2.5 μm) and coarse particles (diameter > 2.5 μm) showed peaks at different timings (in the morning and evening, respectively). The coarse particles emitted fluorescence only in the 420–650 nm wavelength range. These results suggested that the fluorescent species are different for the two cases. Further analysis (e.g., with respect to shape information) will be given in the presentation.

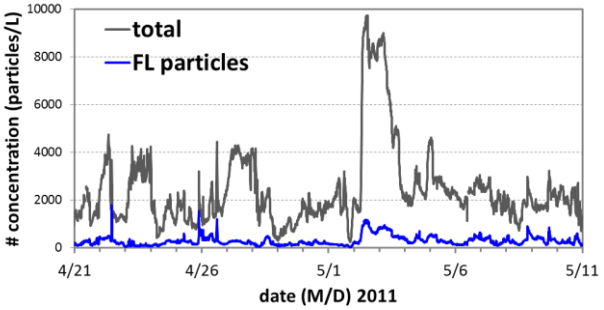

Figure 1. Temporal variations in the number concentrations (#/L) of particles measured by WIBS-4 instrument. Black and blue lines indicate total detected and florescent particles, respectively.

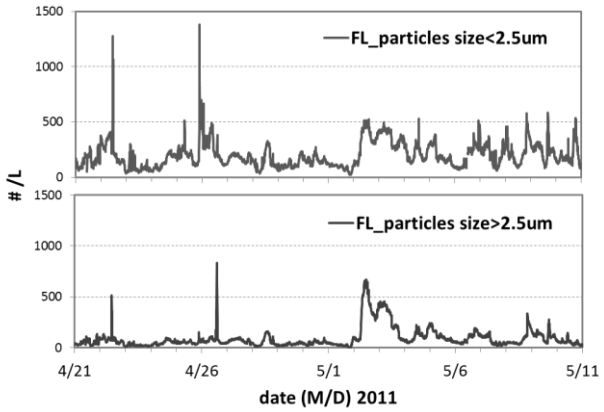

Figure 2. Temporal variations in the number concentrations (#/L) of fluorescent particles measured by WIBS-4 instrument. Upper panel shows concentration of detected fluorescent particles whose diameter is less than 2.5 μm. Lower panel shows concentration of detected fluorescent particles whose diameter is larger than 2.5 μm.

This work was supported by the SENTAN program of the Japan Science and Technology Agency (JST)

Kaye, P., Stanley, W. R., Hirst, E., Foot, E. V., Baxter, K. L., and Barrington, S. J.: Single particle multichannel bio-aerosol fluorescence sensor, *Opt. Express*, 13, 3583-3593, 2005.

Carbonaceous species and anhydrosugars measurements in coarse and fine aerosols size fractions at an urban area in the Po Valley, Italy

[1]T.M.G. La Torretta, [2]L.A. Stante, [1]A. Malaguti, [1]R. Nuzzi, [1]M. Berico

[1]Italian National Agency for New Technologies, Energy and Sustainable Economic Development (ENEA), Technical Unit for Environmental Assessment Models, Methods and Technologies (UTVALAMB), Air Quality Laboratory (AIR), 40129 Bologna – Italy
[2]ENEA – UTVALAMB-IDR, 40129 Bologna- Italy
Keywords: biomass burning, levoglucosan, HPAEC-PAD, organic carbon, elemental carbon, water soluble organic compounds
Presenting author email: teresa.latorretta@enea.it

Biomass burning contributes considerably to the atmospheric aerosol composition. As biomass burning markers both Potassium and Levoglucosan can be used.

It's undisputed fact that only the last one can be considered as biogenic univocal marker.

Levoglucosan and its isomers Mannosan and Galactosan are produced by cellulose and emicellulose degradation respectively. In addiction Levoglucosan has a good stability in atmosphere and it is detectable in fine fraction of particulate (Simoneit *et al*.,1999).

In order to assess the biomass burning contribute to the atmospheric pollution a measurements campaign was performed collecting PM10 and PM2.5 particulate samples. This campaign was conducted in winter, on February 2011, in an urban site situated in Bologna (44°31'30",63 N 11°20'40",92 E), in the Po Valley, one of the most polluted region in Europe.

Concentrations of PM, OC, EC, WSOC and anhydrosugars were compared.

Levoglucosan and its isomer concentrations were determined by Dionex ICS3000 instrument using High Performance Anion Exchange Chromatography (HPAEC) with Pulsed Amperometric Detection (PAD) (Piazzalunga *et al*.); WSOC was determined by TOC 5000-a Shimadzu; OC and EC concentrations were determined by OC/EC analyser (Sunset Lab.) using EUSAAR_2 thermal optical transmittance protocol (Cavalli *et al*., 2010).

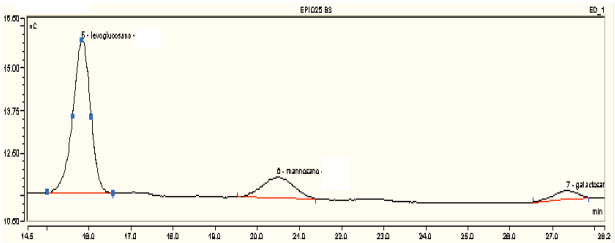

Figure 1. HPAEC-PAD chromatogram obtained from the analysis of winter PM2.5 sample collected on 19th February 2011

WSOC contributes for about 56% to OC in the fraction PM2.5 and for about 52% to OC in the fraction PM10. In the fraction PM2.5 the contribution of Levoglucosan-C to OC, of Levoglucosan-C to WSOC and of Levoglucosan-C to PM is respectively about 4% , 6.5 % and 0.7%. In the fraction PM10 the contribution of Levoglucosan-C to OC, of Levoglucosan-C to WSOC and of Levoglucosan-C to PM is respectively about 3%, 6.4% and 0.4%, confirming the most part of biomass burning is in the fine fraction.

Temporal variations of carbonaceous species and anhydrosugars contributions to fine and coarse aerosols are discussed.

Acknowledgments: This work is part of the EPIAIR 2 ("Inquinamento Atmosferico e Salute: Sorveglianza Epidemiologica ed Interventi di Prevenzione – Atmospheric Pollution and Health: Epidemiological Surveillance and Prevention Interventions) project, funded by the Italian Ministry of Health.

Simoneit, B.R.T., Schauer, J.J, Nolte, C.G., Oros, D.R., Elias, V.O., Fraser, M.P., Rogge, W.F., Cass, G.R. (1999) *Levoglucosan, a tracer for cellulose in biomass burning and atmospheric particles, Atmospheric Enviroment, 33, 173-182*.

Piazzalunga, A., Fermo,P., Bernardoni, V., Vecchi, R., Valli, G., De Gregorio, M.A. (2010) *A simpled method for levoglucosan quantification in wintertime atmosperic parti culate matter by high performance anion-exchange chromatography coupled with pulsed amperometric detection, International Journal of Enviromental Analytical Chemistry, 90, 934-947*.

Cavalli, F., Viana, M., Yttri, K.E., Genberg, J., Putaud, J.P. (2010), *Toward a standardised thermal-optical protocol for measuring atmospheric organic and elemental carbon, the EUSAAR protocol*, *Atmospheric Measurement Techniques*, 3, 79-89.

Mobile measurements for the detection of wood combustion: a case study in a rural environment

M. Van Poppel, N. Bleux, J. Peters, J. Van den Bossche P. Berghmans

VITO - Flemish Institute for Technological Research, 2400 Mol, Belgium

Presenting author email: martine.vanpoppel@vito.be

Wood combustion is a growing concern in rural environments. Recent studies show that wood combustion has a significant impact on PM concentrations and can result in increased numbers of exceedence of the PM_{10} limit value. In Flanders, residential wood combustion is responsible for 7 % of the PM_{10} emissions. Source apportionment studies suggest that wood combustion in rural areas is a larger contributor to PM_{10} as compared to traffic (Vercauteren et al., 2011). In addition, health impact might be significant since incomplete combustion can result in ultrafine particles (UFP), BC (black carbon) and other compounds such as benzene and PAHs (Tapanainen et al., 2011).
Local combustion sources will impact the local air quality. However, this implies knowledge of the exact location of the sources and this knowledge is limited so far. The feasibility of using time-resolved instruments installed at a mobile platform to identify hot spots of combustion aerosols in a rural residential setting is evaluated.

At VITO, a measuring bike – called Aeroflex – was developed for mobile measurements and mapping of UFP (P-trak, TSI), PM (Grimm Dust monitor) and BC (µ-Aethalometer, AethLabs). The tool is already extensively used in urban environments and industrial locations for respectively hot spot identification and source identification. In this study, a case study is presented to evaluate the tool for the detection of hot spots related to wood combustion, and to differentiate this from traffic related emissions.

A mapping was performed in a rural area where the use of wood combustion at different houses was known. Figure 1 shows an example of the mapping for UFP. Most peaks with high concentrations could be linked to wood combustion. Time profiles for BC, UFP and PM_{10} are presented in Figure 2. For BC a similar profile was observed. In this study, BC (1s) raw data were first processed using the Optimized Noise-reduction (ONA) algorithm to reduce noise (Hagler et al., 2011). PM_{10} concentrations were also observed to increase in the vicinity of wood combustion sources.

From this preliminary study, significant spatial heterogeneity both in BC and UFP concentrations was observed, due the presence of residential wood combustion particles. A further analysis of currently running experiments will be shown. hereby focussing on the correlations between different pollutants in order to distinguish between traffic related pollution and wood combustion.

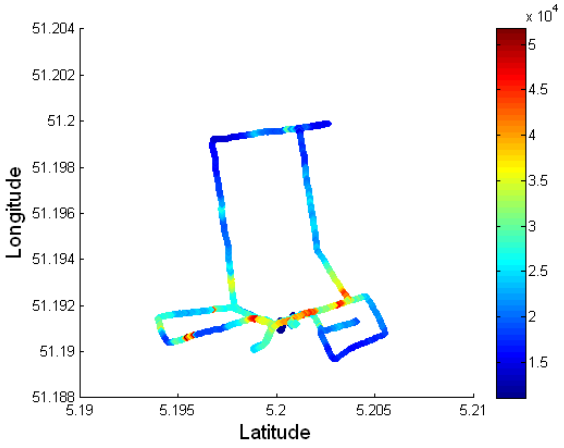

Figure 1: Result of mapping for the identification of wood combustion

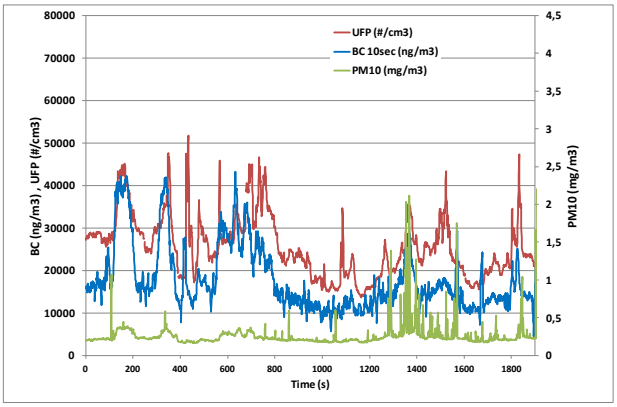

Figure 2: Time profile of UFP, BC and PM10 during the mobile measurements

Hagler, G.S.W., Yelverton, T.L.B., Vedantham, R., Hansen, A.D.A. and Turner, J.R.(2011) *Aerosol and Air Quality Research*, **11**: 539–546.

Tapanainen M., Jalayla P.I., Mäki-Paakkanen J., et al.(2011). Atmos. Environ. **45**,7546–7554

Vercauteren, J., Matheeussen, C., Roekens, E., et al. . (2011), *European Aerosol Conference* 2011, Manchester

An exceptional air pollution event in the southwest of Europe

J.A. Adame[1], M. Sorribas[2, 3], M.A. Hernández-Ceballos[4], J.P. Bolivar[4] and B.A. De la Morena[1]

[1]El Arenosillo-Atmospheric Sounding Station, INTA, Huelva, Mazagón, 21130, Spain
[2]Centro Andaluz de Medio Ambiente, Universidad de Granada, Junta de Andalucía, Granada, 18006, Spain
[3]Department of Applied Physic, University of Granada, Granada, 18071, Spain
[4]Department of Applied Physic, University of Huelva, Huelva, 21007, Spain

Keywords: Forest fires, biomass burning, air pollution event, ozone, CO, PM10, HYSPLIT, WRF-ARW
Presenting author email: sorribasmm@inta.es

Forest and vegetation fires are a relevant atmospheric source of both trace gases and aerosols (Crutzen and Andreae, 1990; Andreae and Merlet, 2001). Biomass burning has an important impact on the atmospheric chemistry, air quality, climate and on global biogeochemical cycles. Europe, and specially the Mediterranean area, is a region that suffers, mostly in warm seasons, the effects of wildfires. The aim of this work has been to study the relation between the wildfires occurred in summer 2006, which affected both Galicia (Spanish northwest) and the north of Portugal and an exceptional air pollution event observed in the southwest of the Iberian Peninsula (IP) which produced the increase of air pollutants to historical levels in some air quality stations of this region (Adame et al., 2012).

The air pollution event was recorded by several air quality stations located in this region, both inland and coastal zones. These stations belong to the Air Quality Network of the Environmental Council, Andalusia Government. Three stations are suburban background (San Fernando, Aljarafe and Santa Clara), two urban backgrounds (El Carmen and Jerez) and one rural background (El Arenosillo). Three are located close to the coastal line (El Carmen, El Arenosillo and San Fernando) and three inland (Jerez, Aljarafe and Santa Clara). In the stations mentioned have been recorded surface ozone, NO_2, CO, particle number concentration and PM10, but in all the stations not all the species are measured. To know the trajectory performed by the air masses that reach the event area, HYSPLIT model has been used whereas the WRF-ARW model has been used to achieve a detailed understanding of the mesoscale meteorological conditions.

The fires start on 2 August and were extinguished on 16 August. Air pollution event occurred in the southwest of the IP from 12 to 13 August. The air pollution event in the southwest starts approximately at 17:00 UTC on 12 August when an unexpected increase on surface ozone was observed in the two coastal stations of El Arenosillo and El Carmen. From 18:00 to 21:00 UTC, the 200 μg m^{-3} as hourly values of surface ozone in both monitoring sites are exceeded, with peaks of 271 and 200 μg m^{-3} at 19:00 UTC at El Arenosillo and El Carmen, respectively. At this time, particle number concentration in the accumulation mode, which was monitored at El Arenosillo, was 8380 cm^{-3}.

At El Carmen station a remarkable increase of CO was also measured. From 17:00 UTC on 12 August to 3:00 UTC on 13 August the 1500 μg m^{-3} was exceeded continuously, with a peak of 1870 μg m^{-3} at 23:00 UTC. PM10 concentrations were also increased at El Carmen from 18:00 UTC on 12 August with a peak of 243 μg m^{-3} at 23:00 UTC.

From 23:00 UTC on 12 August, surface ozone starts to increase at San Fernando and Jerez stations, remaining during the night with values up to 140 μg m^{-3}. At 00:00 UTC on 13 August, peaks of 157 and 191 μg m^{-3} are measured at Jerez and San Fernando respectively. Regards to the CO, at San Fernando a peak of 1558 μg m^{-3} was registered at 23:00 UTC on 12 August, while at Jerez 167 μg m^{-3} were collected at 2:00 UTC on 13 August.

From 00:00 to 13:00 UTC on 13 August the PM10 in both monitoring sites remain at 100 μg m^{-3}, with maximums of 184 μg m^{-3} at 00:00 and 162 μg m^{-3} at 08:00 UTC at San Fernando and Jerez respectively.
Thanks to the modelling tools, have been known that after travelling approximately 1000 kilometres along the Atlantic coast of Portugal, the fire plume went parallel to the Gulf of Cadiz, affecting from the coast line to almost 40-50 km inland. However, the urban stations located in the metropolitan area of Seville were not affected, since air masses from the north didn't reach this area.

Acknowledgements: Thanks to the Environmental Council of the Junta de Andalucía for supplying the air quality data from the Air Quality Network to perform this work. We acknowledge NOAA ARL for provision of the HYSPLIT transport. Mar Sorribas thanks Ministerio de Economía y Sostenibilidad (MICINN) for the award of a Juan de la Cierva post-doctoral grant.

References

Adame, J.A., Hernández-Ceballos, M.A., Bolívar, J.P. and De la Morena, B. (2012). Assessment of an air pollution event in the southwest of the Iberian Peninsula. *Atmos Environ* (Submitted).

Andreae, M.O. and Merlet, P. (2001). Emission of trace gases and aerosols from biomass burning. *Global Biogeochemical CyclesGlobal Biogeochem. Cycles* 15, 955–966.

Crutzen P.J. and Andreae, M.O. (1990). Biomass burning in the tropics: impact on atmospheric chemistry and biogeochemical cycles. *Science* 250, 1669 –78.

Identification of African dust influence to PM_{10} concentrations at the Athens air quality monitoring network during 2010

V. Aleksandropoulou and M. Lazaridis

Department of Environmental Engineering, Technical University of Crete, Chania, Polytechneioupolis, 73100, Greece

Keywords: urban aerosols, mineral dust, legislation and policy.

Presenting author email: vic.aleksandropoulou@enveng.tuc.gr

In the current study we analyse the concentrations of PM_{10} during 2010 at the Athens monitoring network with the objective to identify high PM_{10} events, exceeding the PM_{10} daily limit values (Air Quality Standard - AQS of 50μg/m^3), caused by natural particulate inputs produced by Sahara air mass intrusions. The day averaged PM_{10} concentrations used in the analysis were retrieved from the Hellenic Ministry for the Environment, Energy and Climate Change. In the Athens Metropolitan Area the concentrations of PM_{10} were recorded during 2010 at 3 traffic urban stations (Aristotelous - ARI, Marousi - MAR and Pireaus-1 - PIR-1) and at 4 background suburban stations (Lykovrisi - LYK, Agia Paraskevi - AGP, Thrakomakedones - THR and Koropi - KOR).

The methodology presented in EC (2002) was used to identify possible Saharan dust influences on PM_{10} concentrations. Initially simultaneous time series of different monitoring stations of the network and from a rural background area (Aliartos-ALI station; data were available only for the period 29/7/2010 – 31/12/2010) close to the monitoring sites were compared and coincident peaks in PM_{10} concentration were identified. To confirm the occurrence of desert dust events information were combined from the OMI aerosol index maps, satellite imagery from the NASA SeaWiFS Project (surface level); daily dust load maps over Europe and the Mediterranean (BSC-DREAM8b model, operated by the Barcelona Supercomputing Center), 5-day back-trajectories obtained using the HYSPLIT4 Model (Draxler and Rolph, 2012; at the coordinates of each station at 10 m above ground, at 00, 06, 12 and 18 UTC, isentropic), 6-h 3D trajectory data calculated using Flextra trajectory model for the Aliartos station (available from EMEP/CCC) and synoptic meteorological charts available every 6 h from the NCEP/NCAR Reanalysis Data Composites of the NOAA Earth System Research laboratory. Finally, in order to calculate the daily African PM load during dust outbreaks and estimate how many of the exceedences could be attributed to Saharan dust outbreaks or to anthropogenic sources the methodology presented by Escudero *et al.* (2007) was used (1/8/2010 – 31/12/2010). The daily rural background levels were obtained by applying a monthly moving 30th percentile (Querol *et al*, 2009 for rural background stations in the Mediterranean Basin) to the PM_{10} time series after a prior extraction of the days with African dust influence.

Descriptive statistics of PM_{10} concentrations at Athens monitoring stations and the rural background Aliartos station are shown in Table 1. It is observed that the current annual AQS was exceeded at the traffic urban stations, whereas the daily AQS for PM_{10} concentrations was exceeded at all the stations besides AGP. Most cases of non-attainment to AQS occur during the cold period. In particular, during February, November and December the meteorological conditions favour the transport of air masses loaded with dust from North Africa over the Eastern Mediterranean. Also in Table 1 are depicted the descriptive statistics of PM_{10} concentrations at Athens monitoring stations after prior extraction of the days with not attainment of the AQS coinciding with African dust outbreaks. It is observed that the current annual and daily AQS was still exceeded only at the ARI station. Finally, by subtracting the African net dust load during the period August to December it was found that only 48% to 67% of the exceedences can be attributed to the African dust influence.

Table 1. Daily averaged PM_{10} concentrations and days with not attainment of the AQS during 2010.

Station	Concentration (μg/m^3)*	Days with Exceedences*
MAR	40.6±19.5 (36.0±11.0)	63 (17)
THR	36.7±19.0 (31.8±11.6)	43 (9)
AGP	28.2±16.5 (24.9±9.5)	22 (1)
LYK	38.6±26.2 (32.6±10.4)	56 (12)
PIR-1	44.1±20.2 (37.2±11.7)	62 (18)
KOR	35.5±25.4 (30.0±11.7)	38 (7)
ARI	48.6±29.7 (40.7±12.2)	99 (36)
ALI	29.1±15.4	9

*The values in brackets correspond to the results after excluding the days with not attainment to the AQS coinciding with Saharan dust events.

This work was supported by the European Union's LIFE Programme under grant LIFE 09 ENV/GR/000289.

Draxler, R.R. and Rolph, G.D. (2012) *HYSPLIT Model, NOAA Air Resources Laboratory, Silver Spring, MD.*

EC (2002) *Guidance to member states on PM_{10} monitoring and intercomparisons with the reference method, Draft final report.*

Escudero, M., Querol, X., Pey, J., Alastuey, A., Perez, N., Ferreira, F., Alonso, S., Rodriguez, S. and Cuevas, E. (2007) *Atmos. Environ.* **41**, 5516-5524.

Querol, X., Pey, J., Pandolfi, M., Alastuey, A., Cusack, M., Perez, N., Moreno, T., Viana, M., Mihalopoulos, N., Kallos, G. & Kleanthous, S. (2009) *Atmos. Environ.* **43**, 4266-4277.

Identifying desert aerosols episodes in Cáceres (Spain)

M.A. Obregón[1], A. Serrano[1] and M.L. Cancillo[1]

[1]Department of Physics, University of Extremadura, Badajoz, Extremadura, 06006, Spain
Keywords: atmospheric aerosols, African dust, CIMEL, HYSPLIT.
Presenting author email: nines@unex.es

Atmospheric aerosols, in general, act upon cloud formation and modification, can be very harmful for human and animal health (Dockery and Pope, 1994), and play a substantial role in the Earth's radiation balance producing cooling or warming of the atmosphere depending on their physical characteristics. According to the Intergovernmental Panel on Climate Change 2007, the worldwide average aerosol direct radiative forcing is estimated to be about -0.5 [-0.9 to -0.1] W/m^2 and the worldwide indirect forcing about -0.7 [-1.8 to -0.3] W/m^2, thus contributing to the cooling of the planet. Furthermore than these average figures, there is still a large uncertainty concerning their climate effects. Thus, it is of particular interest to identify different types of aerosol and analyze the effects associated to each type. For this aim, the first step to take is to develop methodologies to achieve a reliable classification of aerosols.

One type of aerosol with a remarkable interest in the Iberian Peninsula is the "desert" one, corresponding to desert dust arriving from the near Sahara Desert in the North of Africa. The intrusions of these aerosols show a typical seasonal pattern driven by the annual latitudinal displacement of the general atmospheric circulation (Cachorro et al, 2005).

In order to properly identify desert aerosols reaching Cáceres (Western Spain), in this study a classification criterion is applied to measurements recorded at the Cáceres station by a CIMEL photometer. This station belongs to the AERONET (Aerosol Robotic NETwork) global aerosol network. The applied criterion is based on the analysis of 120-hour back-trajectories arriving at Cáceres during well-defined desert dust episodes. These trajectories were calculated using the HYSPILT (HYbrid Single-Particle Lagrangian Integrated Trajectory) model (Draxler and Hess, 1998). The trajectories calculated for this study correspond to an arriving time of 12:00 UTC and to heights of 1500 and 3000 m a.s.l.

For this purpose, seven well-defined desert episodes were selected analyzing the spectral optical depths, the Ångström α exponent and the air mass trajectories. Additionally, eight areas corresponding to possible origins of the air masses were establised: "Local", "Peninsula", "Rest of Europe", "Mediterranean Sea", "North Africa", "Tropical Atlantic", "Rest of the Atlantic", and "Arctic".

After analyzing the trajectories of air masses for these selected episodes, the number of hours that air masses spend on each region has been calculated. A common situation observed in all desert events is that the trajectories at 1500 or 3000 meters showed more than 40 hours over the region named Africa, and even in the case the trajectories spend less than 40 hours on this region, they circulate over the tropical Atlantic during more than 60 hours. This criterion for identifying desert events was applied to the whole set of trajectories during the period between July 2005 and July 2011, finding 99 trajectories that matched this criterion. More than 60% of these cases occur between April and August, in agreement with the seasonal pattern of desert dust events typical in the Iberian Peninsula. Figure 1 shows the trajectories of these 99 days at 3000 m a.s.l. It can be seen that most trajectories show similar path evidencing the transport of aerosols from Saharan Desert to the Iberian Peninsula. The desert character of the aerosol of the identified cases has been validated by analyzing the τ and α values measured by the CIMEL existing in Cáceres. Results indicate that 92% of cases were positively identified as desert while the remaining 8% correspond to other types. These results support the good performance of the proposed criterion.

Figure 1. 120 h back trajectories at 3000 m a.s.l. arriving at Cáceres during the days identified as desert aerosol according the new criteria proposed in this study.

This work was supported by the research projects CGL2008-05939-C03-02/CLI and CGL2011-29921-C02-01 granted by the "Ministerio de Ciencia e Innovación" from Spain.

Dockery, D., and Pope III, C. (1994) Annu Rev Public Health, **15**, 107-132.

Cachorro, V.E., Toledano, C., de Frutos, A.M., Sorribas, M., Vilaplana, J.M., and de la Morena, B. (2005) Geophys. Res. Abstract, **7(08559)**.

Draxler, R., and Hess, G.D. (1998) Aust. Met. Mag. **47**, 295–308.

Mineralogical composition and origin of airborne particles during dust events in the Eastern Mediterranean

I. Kopanakis[1], T. Glytsos[1], D. Pentari[2], V. Perdikatsis[2] and M. Lazaridis[1]

[1]Department of Environmental Engineering, Technical University of Crete, Chania, Greece
[2]Department of Mineral Resources Engineering, Technical University of Crete, Chania, Greece

Keywords: Sahara dust event, mineralogical composition, illite.

Every year, the vast area of Sahara and Sahel deserts, in North part of Africa, produce thousands of tones of airborne particles with considerable consequences in global climate, ecosystems and health. Produced particles from wind erosion can be transferred at long distances such as the Mediterranean Basin, Atlantic Ocean and Scandinavia.

Saharan particulates were found to be composed mainly of oxides and carbonates - principle constituents of the Earth's crust. The main aim of this study was: (1) to examine the origin of the eolian airborne particles during dust events and (2) to determine the mineralogical composition of different airborne Saharan dust samples which were collected during spring time in the period 2004-2009. The sampling of particulate matter took place at the Akrotiri station which is an urban background station on the island of Crete (Greece) (Lazaridis et al., 2008). In the current work, airborne dust samples measured in a period of 5 years were examined.

In total, five airborne dust samples were collected during intense Saharan dust events in canisters. Canisters were used in the sampling, which are a kind of precipitation samplers. The sampling was performed in the spring period during 2004, 2005, 2006 and 2009. The first 3 samples (S1, S2 and S3) were deposited in the canisters during wet deposition. Furthermore, during the year 2009, two other samples were collected (S4 and S5), one from dry deposition and the second, the same day, during wet deposition. The wind direction of the air masses during the sampling was from south directions. The transported air masses stayed at least one day above the African deserts before moving north to the island of Crete. Elevated $PM_{2.5}$ mass concentrations were recorded at the station in comparison to the time periods before and after the Saharan dust event, as it is depicted in Figure 1.

The bulk mineralogy of the collected dust was determined by X-ray powder diffraction (PXRD). Table 1 presents the dates of each sampling and the corresponding mineralogical composition. The results showed that Illite was the most abundant mineral identified in all samples. The mean percentage was 31.8% for the rain-collected samples and 30.0% for the airborne dust sample. It is believed that the percentage of illite is elevated when dust comes from the regions of Chad, compared to the Egyptian and Libyan deserts.

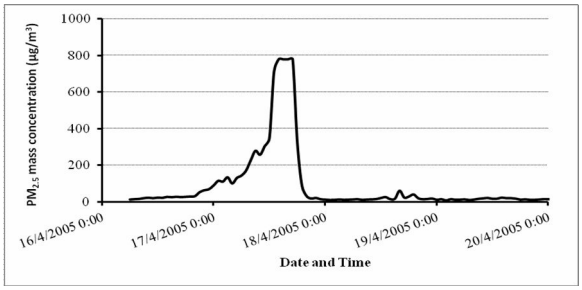

Figure 1: $PM_{2.5}$ mass concentration during an intense Saharan dust event on 17/4/2005.

Illite, quartz and calcite were the main components of mineral dust, in accordance with other XRD measurements on desert-derived dust (Blanco et al., 2003). Furthermore, the kaolinite percentage is much lower, in comparison to other measurements where kaolitine is found to be either the most abundant mineral in dust collected in the eastern Mediterranean Sea or represents a higher fraction (30%) of the minerals found in the dust originated from Libyan and Egypt**.**

Table 1: Mineralogical composition (%) of the eolian dust samples.

Sample	*S1 (rain)*	*S2 (rain)*	*S3 (rain)*	*S4 (rain)*	*S5 (air)*
Date	*5/5/04*	*17/4/05*	*21/4/06*	*5/3/09*	*5/3/09*
Illite	*30.0*	*29.8*	*38.6*	*28.7*	*30.0*
Quartz	*19.3*	*19.0*	*15.0*	*25.8*	*24.5*
Calcite	*21.2*	*28.7*	*17.0*	*12.7*	*13.0*
Kaolinite	*8.2*	*4.8*	*5.1*	*6.9*	*8.0*
Dolomite	*5.8*	*4.7*	*3.2*	*4.3*	*3.5*
Palygorskite	*6.3*	*4.9*	*3.5*	*3.5*	*3.0*
Albite	*9.3*	*7.4*	*12.0*	*14.0*	*10.0*
Chlorite	-	-	*4.6*	*4.5*	*3.0*
Gypsum	-	-	-	-	*5.0*

Acknowledgments: This work was supported by the European Union's LIFE Programme under grant LIFE 09 ENV/GR/000289.

References

Blanco A. et al., (2003). *Atmospheric Chemistry and Physics*, 3, 2147-2159.

Lazaridis M. et al., (2008). *Water Air Soil Pollut.*, 189, 85-101.

Aerosol deposition in the main African dust transport region: establishing a long-term time series at Sao Vicente, Cape Verde

K. Kandler[1], L. Mendes Neves[2], N. Niedermeier[3], and T. Müller[3]

[1]Institute of Applied Geosciences, Technische Universität Darmstadt, Germany
[2]Instituto de Nacional de Meteorologie e Geofisica, Mindelo, Cape Verde
[3]Institut für Troposphärenforschung, Leipzig, Germany
Keywords: mineral dust, deposition, electron microscopy, mixing state.
Presenting author email: kzk@gmx.de

Mineral dust is one of the dominating aerosol species in the atmosphere. Particularly, the tropical North Atlantic Ocean is heavily affected by dust, changing cloudiness, precipitation, nutrient fluxes into the ocean, radiation balance etc. A number of field experiments with different foci recently investigated dust properties (e. g., SAMUM, AMMA, SHADE, PRIDE, GERBILS). However, these experiments usually lasted a short time, usually a few weeks, some a season. As a result, they captured a low number of dust episodes only. Given the highly episodic nature of dust outbreaks and a potential inter-annual variation, the question arises, how these experiments should be rated with respect to an annual average, or how they can be compared to each other. This actual problem arises from the nonexistence of longer time series in the tropical North Atlantic Ocean (except at Barbados; Trapp *et al*, 2010).

While the shortcomings in the past can't be changed, a quasi-continuous measurement of aerosol deposition was installed in the middle of December 2012 at the Cape Verde Atmospheric Observatory (http://ncasweb.leeds.ac.uk/capeverde/), at the Island of Sao Vicente Island, Cape Verde. Aerosol deposition is measured by a passive aerosol sampler, modified from Ott and Peters (2008) "type A – flat plates" by introduction of a liquid trap and lowering the recipient position slightly below the level of the lower plate. 25 mm diameter aluminum stubs coated with standard electron microscopy carbon adhesives were used as sampling surface. The analysis was made with an acceleration voltage of 20 kV and a beam diameter of 2.6 nm. The particles were classified according to their chemical composition into eight classes (Fig. 1). For details on the materials and methods as well as the data processing refer to Kandler *et al* (2011).

Three samples in December 2011 could be analyzed as a start of the time series (total of 1841) particles. Trajectory calculations (HYSPLIT/GDAS) showed that during all period dust was transported straight from Mauritania and South Morocco to Cape Verde (about 24 to 30 h transport time from the coast), so the differences in dust abundance – also seen in the aerosol volume concentrations measured by Scanning Mobility Particle Sizer and Aerodynamic Particle Sizer (74, 33 and 48 cm^3/m^3 for SVS_101/2/3) – are most probably linked to dust emission variation.

The relative abundance of dust increases with the particle size between 1.5 and 10 µm (Fig. 1). The ratio of quartz to the silicate dust varies between 0.1 and 0.3. Sulfate plays a minor role during the more maritime periods and is absent during the dustier phase. Interestingly, the amount of mixed particles (internal mixtures of dust and sea-salt) is largely higher for particles of 5 – 10 µm diameter than for those with 2.5 – 5 µm. This points to an increased deposition flux of dust particles internally mixed with sea-salt, as proposed by Zhang (2008). It indicates that during the observed dust intrusions, larger pure particles have already been removed by sedimentation.

Kandler, K., Lieke, K., Benker, N. et al. (2011) Electron microscopy of particles collected at Praia, Cape Verde, during the Saharan Mineral dust experiment: particle chemistry, shape, mixing state and complex refractive index. *Tellus* **63B**, 475-496.

Ott, D.K., Peters, T. (2008) A Shelter to Protect a Passive Sampler for Coarse Particulate Matter, $PM_{10-2.5}$. *Aerosol Sci. Technol.* **42**, 299-309.

Trapp, J.M., Millero, F.J., Prospero, J.M. (2010) Temporal variability of the elemental composition of African dust measured in trade wind aerosols at Barbados and Miami. *Mar. Chem.* **120**, 71-82.

Zhang, D. (2008) Effect of sea salt on dust settling to the ocean. *Tellus* **60B**, 641-646.

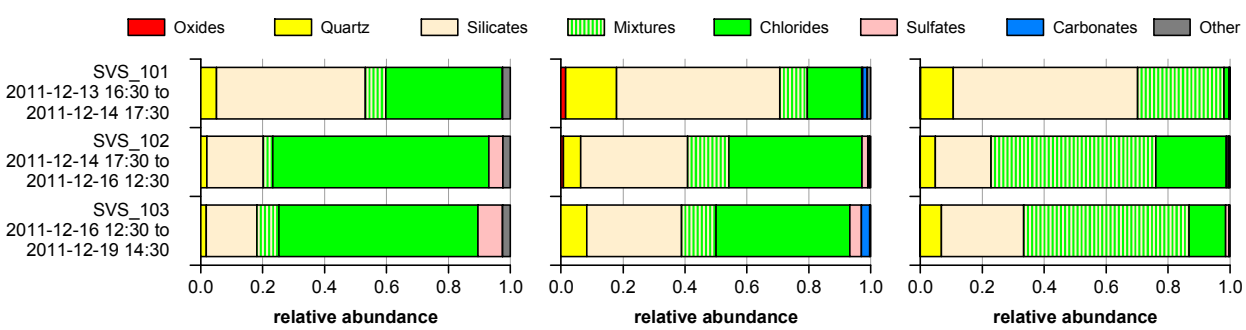

Figure 1: Relative abundance of different particle species in the aerosol sediment at Sao Vicente, Cape Verde. Left: 1.5 - 2.5 µm; center: 2.5 - 5 µm; right: 5 µm - 10 µm.

Influence of Saharan dust in deposition fluxes of nutrients in Spain

S. Castillo[1], X. Querol[2], A. Alastuey[2], A. Ávila[3], E. Cuevas[4], and J. de la Rosa[1]

[1]Unidad Asociada CSIC-Universidad de Huelva Contaminación Atmosférica, Universidad de Huelva, Spain
[2]Instituto de Diagnóstico Ambiental y Estudios del Agua (IDAEA), CSIC, Barcelona, Spain
[3]Centre de Recerca Ecològica y Aplicacions Forestals (CREAF), Barcelona, Spain
[4]Centro de Investigación Atmosférica de Izaña (AEMET), Santa Cruz de Tenerife, Spain
Keywords: deposition, Saharan dust, marine aerosol, soluble fraction
Presenting author email: sonia.castillo@dgeo.uhu.es

The mineral dust deposition, originated from the African dust outbreaks episodes, influences largely in deposition fluxes of metal nutrients in Southern Europe (Avila, 1996) and oceanic regions (Arimoto, 2001). The low precipitation in the Mediterranean basin favours the long residence time of dust in the atmosphere with the consequent impact on air quality and in atmospheric deposition. Recently, more studies are coming out about the impact of dust from deserts on health. An association between the increase of hospital admissions (respiratory and cardiovascular causes) and days with Saharan dust episodes (Perez et al., 2008) shows the evidence of the importance of these natural episodes in areas closely to Sahara desert.

Most studies that quantify the Saharan dust deposition have only measured the soluble fraction. In this study we compare the fluxes both in the soluble and insoluble fractions for the wet and dry deposition at two sites located at different distances from North Africa. One sampling site was in a rural area of the North-eastern of the Iberian Peninsula, in the Montseny Mountains (MSY) at 40km NNE from Barcelona. The other site was in the city of Santa Cruz de Tenerife (SCO) in Canary Islands.

The atmospheric deposition fluxes depend of the concentration of suspended particulate matter (SPM) in the atmosphere. In SCO where SPM levels were 3.3 times higher than in MSY, for the same period, the total annual deposition levels registered was up 29 g/m^2 while in MSY was up 20.9 g/m^2 (Table 1).

Table 1. Annual deposition levels (g/m^2) both in soluble and insoluble fractions in wet and dry deposition.

		soluble	insoluble	Total
MSY	DRY	2.9	4.3	7.2
	WET	8.0	5.7	13.7
	TOT			20.9
SCO	DRY	6.7	10.4	17.1
	WET	6.8	5.1	11.9
	TOT			29.0

It´s highly remarkable the dependence of climatology in the deposition fluxes. In MSY with an annual mean precipitation of 800-1000 l/m^2, 65% of SPM deposited was by wet deposition mode. In SCO with an annual mean precipitation of 200 l/m^2 was 41%. However, total wet deposition amounted to 13.7 g/m^2 in MSY and 11.9 g/m^2 in SCO (Table 1). The relatively high fluxes registered in SCO by wet deposition were accounted largely by the high sea spray contribution at this coastal site (being this 62% of the total mass, Na^+ and Cl^-) and the dust transported from Sahara and Sahel deserts (Ca^{2+} was 20% of the total mass). .

By contrast, dry deposition registered major annual levels in SCO than in MSY by a factor of 2.4, with 17.1 g/m^2 in SCO against 7.2 g/m^2 in MSY (Table 1). This is the result of the sea spray contribution (46% of total mass) and the high influence of the African dust outbreaks above the Islands (Ca^{2+} reaches 32%) under the quasi-permanent dry meteorological conditions in the Canary Islands. The vast amount of dust transported from Sahara and Sahel deserts into Atlantic Ocean generate elevated dry deposition fluxes of mineral dust to the surface.

Calcium presents the highest contribution in MSY and SCO. In MSY, with high precipitation and low levels of SPM, Ca^{2+} contribution is similar in wet and dry deposition and more elevated in the soluble fraction. In SCO, with low precipitation, high SPM levels and an elevated influence of African dust outbreaks, Ca^{2+} dominates in dry deposition, and is higher in the insoluble fraction.

Sodium content (originated by sea spray) is the second highest contribution in SCO (high sea spray emission rate in Atlantic Ocean) but not in MSY (low emission rate in Mediterranean Sea). Moreover, due to the high solubility of this species, the major contribution is in the soluble fraction, which is the dominant fraction (both in wet and dry deposition) at SCO.

This work was supported by the Spanish Ministry of Science and Innovation. The authors would also like to express their gratitude to the Izaña Atmospheric Research Center (AEMET) for their valuable collaboration in the deposition sampling.

Arimoto R. (2001). Aeolian dust and climate: relationships to sources, tropospheric chemistry, transport and deposition. Earth-Science Reviews 54, 29-42.

Ávila, A. (1996). Time trends in the precipitation chemistry at a mountain site in northeastern Spain for the period 1983– 1994. *Atmospheric Environment* **30**, 1363– 1373.

Pérez L., Tobias A., Querol X., Künzli N., Pey J., Alastuey A., et al. (2008). Coarse particles from Saharan dust and daily mortality. *Epidemiology* **19**: 800-7.

Laboratory investigations of contact and immersion freezing of mineral dust using two techniques: vertical wind tunnel and acoustic levitator

K. Diehl, H. Schmithüsen, M. Debertshäuser, S.K. Mitra, and S. Borrmann

Institute of Atmospheric Physics, Johannes-Gutenberg University, 55099 Mainz, Germany
Keywords: laboratory experiments, heterogeneous ice nucleation, mineral dust
Presenting author email: kdiehl@uni-mainz.de

According to model studies (e.g., Storelvmo *et al*., 2008) the type and quantity of atmospheric ice nuclei affect ice cloud microphysical and radiative properties as well as their precipitation efficiency. The role of mineral dust particles as ice nuclei is undoubted, however, information from laboratory experiments are available so far mainly for two mineral dust types, kaolinite and montmorillonite (e.g., Pitter and Pruppacher, 1973). Some most abundant minerals occurring in desert aerosols as e.g., quartz, calcite, mica, hematite, illite, and gypsum have not been investigated so far in immersion and contact freezing modes. New experimental results will serve as base for parameterizations to estimate the effects of new mineral dust types on cloud microphysics (Diehl *et al*., 2006).

Two methods are used in the laboratory: the Mainz vertical wind tunnel (e.g., v. Blohn *et al*., 2005), and an acoustic levitation technique (e.g., Diehl et al., 2009). In both cases drops are freely levitated, either at their terminal velocity in the wind tunnel updraft or around the nodes of a standing ultrasonic wave. Thus, heat transfer conditions are well approximated, and wall contact effects on freezing as well as electrical charges of the drops are avoided. Ambient temperatures reach -30°C in the wind tunnel and -40°C in the cold chamber where the acoustic levitator is placed. Drop radii are 180 to 400 µm and 0.5 to 3 mm, respectively. Immersion freezing is a volume-dependant process so that the results for different drop sizes allow deriving volume-dependant parameterizations for various types of ice nuclei. Contact freezing as it is not drop size dependant is investigated with the levitator technique only.

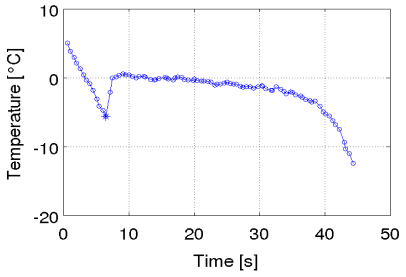

Figure 1. Temporal development of drop surface temperature during freezing in acoustic levitator.

Experiments are carried out either with drops containing a defined amount of ice nuclei (immersion freezing) or with pure water drops colliding with ice nuclei (contact freezing). In the wind tunnel, the onset of freezing is observed directly. The use of the acoustic levitator allows measuring the temperature of the drop surface by an in-situ calibrated Infrared thermometer as the drops are very stationary. Because of the release of latent heat the onset of freezing is indicated by a rapid rise of the drop surface temperature as shown in Figure 1. The time period needed to completely freeze the drops is indicated as the surface temperature again decreases afterwards.

Table 1. Freezing temperatures for various mineral dust types and freezing modes.

mineral dust type	**freezing mode**	T_{min} **(°C)**	T_{median} **(°C)**	T_{max} **(°C)**
montmorillonite	contact	-19.0	-8.7	-2.8
montmorillonite	immersion	-22.8	-18.0	-6.3
mica	contact	-20.0	-12.3	-2.2
mica	immersion	-22.0	-18.7	-4.2
illite	contact	-21.9	-15.4	-2.9
illite	immersion	-23.3	-19.9	-10.6

So far, experiments have been performed with montmorillonite to test the acoustic levitator set-up and with mica and illite as new samples. Results are given in Table 1. The median freezing temperatures of illite and mica are lower than the ones of montmorillonite which stands so far for the most efficient mineral dust type, but they are still somewhat higher than the ones of kaolinite (e.g., Pitter and Pruppacher, 1973) which might represent the lower limit for mineral dust. Additional wind tunnel experiments with illite and mica in the immersion mode will account for smaller drop sizes. Besides that, experiments with both techniques will be continued with hematite and results will be presented at the conference together with parameterizations based on the new data.

This work is supported by the German DFG research group INUIT.

v. Blohn, N., et al. (2005) *Atm. Res.*, **78,** 182-189.
Diehl, K., et al. (2006) *J. Geophys. Res.*, 111, D07202.
Diehl, K., et al. (2009) *Atm. Res.*, **94,** 356-361.
Pitter, R.L., and H.R. Pruppacher (1973) *Quart. J. Roy. Meteor. Soc.*, **99**, 540-550.
Storelvmo, T., et al. (2008) *J. Atmos. Sci.*, **60,** 3214-3230.

Long-term Chemical Characterization of Aerosol at the CVAO

K. Müller, K. W. Fomba, E. Brüggemann, T. Gnauk, G. Spindler, H. Herrmann
Department of Chemistry, Leibniz-Institute of Tropospheric Research, 03418 Leipzig, Germany

Keywords: Saharan dust, long-term observation, chemical constitution
Presenting author email: konrad@tropos.de

The Sahara and the North-East trade winds are responsible for the entry of enormous amounts of dust into the Tropical North Atlantic. The geographical location of the Cape Verde Islands makes the islands suitable for scientific investigations of ocean and atmosphere interactions. Starting during SOPRAN I in 2007, the collection and chemical characterization of PM_{10} particles by a high-volume filter sampler was carried out at a 30m tower near the north-eastern coastline of the island São Vicente. During intensive campaigns, size-segregated sampling of PM took place additionally. Seasonal and inter-annual variations of the transportation of Saharan dust have been observed. The observations show a maximum of Saharan dust entries during winters but episodes of high dust concentration were observed in other seasons, too (Fig. 1).

In the focus of the chemical characterization of PM_{10} aerosols was the iron concentration (Fig. 2) and their seasonal and interannular variation. Iron and other transition metals were analysed from impactor samples taken during intensive campaigns only on polycarbonate foils. Typically, the dust fraction was found in the coarse mode PM but in some samples strongly elevated concentrations were found in the fraction 0.14-0.42 µm.

Secondary inorganic species (non-sea-salt sulphate, nitrate and ammonium) and OC/EC were determined. During dust events highest concentrations of all anthropogenically emitted species were found as well. The transport of secondary ionic species, EC and OC from the African continent is combined with Saharan dust events.

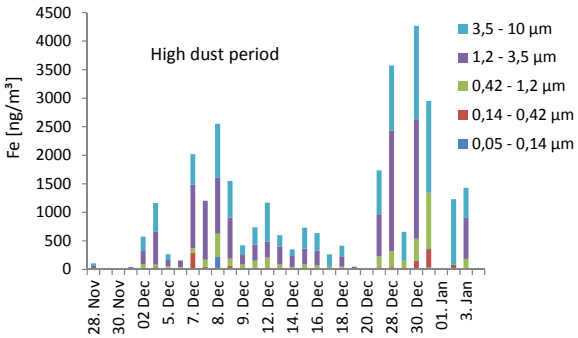

Figure 2. Iron concentration in size fractions of the impactor during dusty season in winter 2007/2008 (From a few samples not all size fraction have been analysed.).

This work was funded by the German BMBF under the grant No. FKZ 03F0611J. The authors have to thank Luis Mendes and Helder Timas from the INMG in Mindelo, CV, for their technical support.

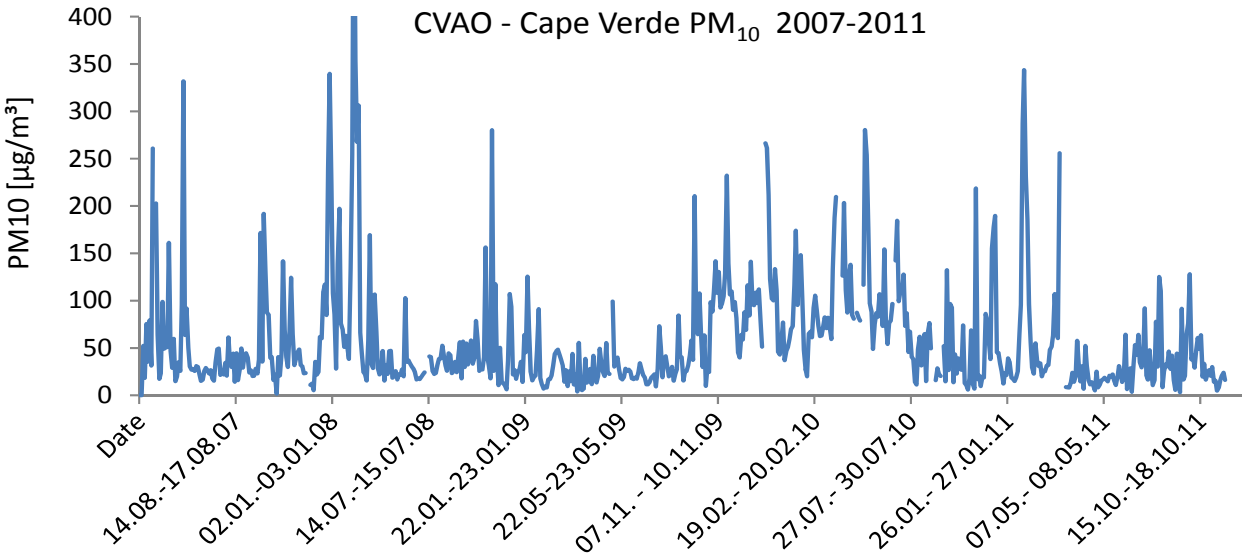

Figure 1. PM_{10} concentration at the research site CVAO at the island São Vicente. From October 2009 till June 2010 the sampler was operated not in 30 m but in 4 m above ground.

Effects of desert dust aerosols on surface UV radiation from OMI satellite instrument at Granada (Spain)

M. Antón[1,2], A. Valenzuela[1,2], R. Román[3], H. Lyamani[1,2], N. Krotkov[4,5], A. Arola[6], F.J. Olmo[1,2], L. Alados-Arboledas[1,2]

[1]Department of Physical Chemistry, University of Somewhere, City, Region, Postcode, Country
[1]Departamento de Física Aplicada, Universidad de Granada, Granada, Spain.
[2]Centro Andaluz de Medio Ambiente (CEAMA), Universidad de Granada, Granada, Spain
[3]Departamento de Física Aplicada, Universidad de Valladolid, Valladolid, Spain
[4]GEST Center, University of Maryland, Baltimore County, Maryland, USA
[5]Laboratory of Atmosphere, NASA/Goddard Space Flight Center, Greenbelt, Maryland, USA
[6]Finnish Meteorological Institute (FMI), Kuopio, Finland
Presenting author email: mananton@unex.es

The atmospheric aerosols affect the propagation of solar radiation through the atmosphere, modifying the values reaching the Earth's surface. The largest differences between the satellite and ground-based UV irradiance data are obtained in urban polluted areas, where UV-absorbing aerosols have a great relevance. Thus, it is expected that desert dust particles (with significant absorption properties in the UV range) may also produce large differences between the satellite-derived and experimental UV irradiance. This work focuses on the evaluation of the effects of desert dust intrusions (2006-2010) on surface UV erythemal irradiance (UVER) retrieved from the satellite Ozone Monitoring Instrument (OMI) at Granada (southern Spain).

The inventory of African desert dust events occurred at Granada from 2006 to 2010 is based on a supervised methodology using mixed information from models, back-trajectories analysis, synoptic meteorological charts, satellite and surface data. Detailed information about this desert dust's inventory can be found in the work of Valenzuela et al. (2012a, 2012b) which evaluated its aerosol optical properties and its dependence on source region and transport pathways.

The UVER data derived from the OMI satellite instrument strongly overestimate the ground-based UVER measurements during the desert dust cases (see Fig. 1) with a mean bias of 22%. The analysis of clear-sky cases shows that around eight percentages points of this large difference may be related to the fact that current OMI UV algorithm assumes no absorbing aerosols. Therefore, the effect of desert dust events on the UV irradiance derived from the OMI instrument cannot be neglected in regions like southern Spain, where the intrusions of the desert dust aerosols are frequent.

Those eight percentages points can be corrected by means of an off-line method which is tested using an independent dataset. Thus, the mean OMI bias change from ~21% for operational satellite UVER data to ~13% for corrected data, indicating this value the remaining bias associated with other sources of uncertainty different to the absorbing aerosols.

We would like to point out the great effects of desert dust aerosols over UV data retrieved from OMI, being essential to maintain routinely operative ground-based stations with high-quality instrumentation in order to validate the satellite data.

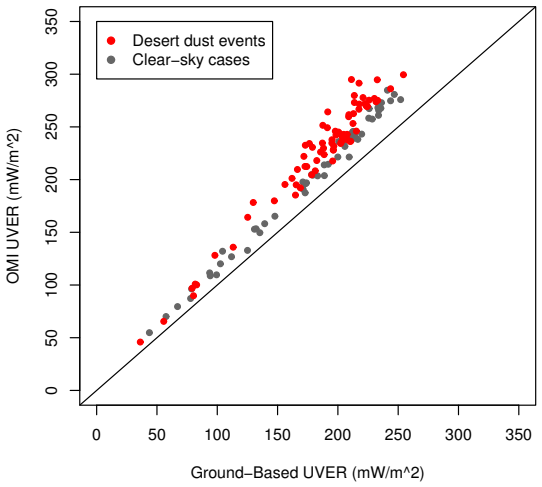

Figure 1. Correlation between OMI and ground-based UVER data for desert dust cases (in red) and clear-sky cases (in grey)

This work was supported by the Andalusia Regional Government through projects P08-RNM-3568 and P10-RNM-6299, by the Spanish Ministry of Science and Technology through projects CGL2010-18782, CSD2007-00067 and CGL2011-13580-E/CLI; and by EU through ACTRIS project (EU INFRA-2010-1.1.16-262254).This work was supported by the National Council for Aerosol Research under grant JB/005.

Valenzuela, A., Olmo, F.J., Lyamani, H., Antón, M., Quirantes, A., Alados-Arboledas, L. (2012a). *Atmos. Res.*, **104-105**, 292–301.

Valenzuela, A., Olmo, F.J., Lyamani, H., Antón, M., Quirantes, A., Alados-Arboledas, L. (2012b). *J. Geophys. Res.*, doi:10.1029/2011JD016885, in press

Aerosol sampling and coarse mode aerosol measurement of African mineral dust during Fennec 2011 field campaign

J.K.Brooke[1], M.Bart[1], J. Trembath[2], J.B.McQuaid[1], B.J.Brooks[3], P. Rosenberg[1], T. Malkin[1] and S.Osborne[4]

[1]Institute for Climate and Atmospheric Science, University of Leeds, LS2 9JT, UK
[2] Facility for Airborne Atmospheric Measurements, Cranfield, Bedford, MK43 0AL, UK
[3]National Centre for Atmospheric Science, University of Leeds, Leeds, LS2 9JT, UK
[4]Met Office Field Site, Cardington Airfield, Bedford, MK42 0SY, UK
Keywords: African mineral dust, aerosol sampling, cascade impactor, XRD
Presenting author email: eejkb@leeds.ac.uk

The Sahara desert is a major natural source of global mineral dust emissions, Forster *et al* (2007), through the mobilisation and lifting of dust particles into the atmosphere from dust storms. A significant fraction of this dust is in the aerosol coarse mode, Weinzierl *et al* (2009).

It is highlighted of the difficulty in making accurate and reliable measurements from an aircraft platform, particularly that of coarse mode aerosol, Wendisch *et al* (2004). To achieve the measurement of a representative aerosol sample an aerosol inlet, on an aircraft, is required for the delivery of the sample to the instruments making the measurements. Inlet design can modify aerosol size distribution through either underestimating due to aerosol losses or overestimation due to enhancements.

The Low Turbulence Inlet (LTI) was designed to improve inlet efficiency. This is achieved by reducing turbulence flow within the tip of the inlet, reducing impaction of particles to the walls of the inlet Wilson *et al* (2004). The LTI further maintains isokinetic sampling flow (free stream velocity, U_0 and sampling velocity, U are equal to 1).

Dust aerosol over the Sahara desert provides an excellent environment to test and quantify the capabilities of the LTI on the FAAM BAe 146, whilst enabling in-situ dust measurement. The LTI was operated during the Fennec field campaign in June 2011 with 11 flights during the campaign over Mauritania and Mali.

We are using the LTI to provide critical information on the sampling characteristics of the inlet used by nearly all aerosol instruments inside the aircraft (AMS, Nephelometer, PSAP, and CCN). Inlet experiments were performed with identical Optical Particle Counters (OPC) connected to the Rosemount and LTI with size distribution for each inlet measured and Rosemount enhancements determined. Rosemount inlet enhancements were determined to be 2 to 4.5 times for particles up to 3.0 μm.

A key parameter in aerosol measurement is size distribution, in which the LTI is a critical method of sampling quantifiably coarse mode aerosol up to 12 μm into the FAAM BAe 146 aircraft. Size distributions for the Fennec field campaign will be presented. Size distributions from the LTI are found to compare well with that of the externally mounted aircraft probes.

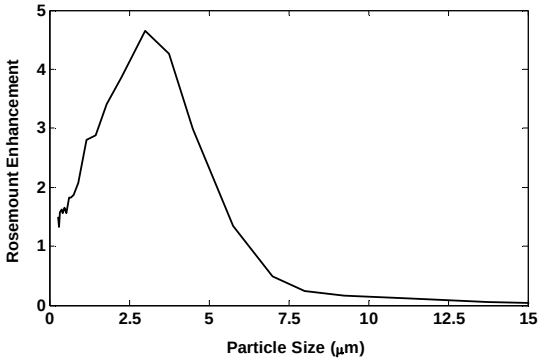

Figure 1. Rosemount inlet enhancement as a function of particle size

A Compact Cascade Impactor (CCI) was incorporated along the sample line and used to collect size segregated particle samples on polyurethane foam (PUF) substrates. X-Ray Diffraction (XRD) analysis is to be used to determine mineralogy of the dust samples. From known dust mineralogy it will be possible to infer the particles optical properties, specifically refractive index.

This work was supported by the Natural Environment Research Council and the Met Office. Acknowledgements include Dr J. Wilson, University of Denver, Fennec, FAAM, DLR and Avalon.

Forster *et al* (2007) *Intergovernmental Panel on Climate Change. Cambridge University Press.*
Weinzierl *et al* (2009). *Tellus B* **61**, 96-117.
Wendisch *et al* (2004) *Bulletin of the American Meteorological Society* **85**, 89-91.
Wilson *et al* (2004) *Aerosol Science and Technology* **38**, 790-802.

Optical properties and radiative impact of intense dust outflows in the Mediterranean basin, based on a synergistic use of satellite, ground-based measurements and modelling

A. Gkikas[1], N. Hatzianastassiou[1], S. Kazadzis[2], V. Amiridis[3], S. Basart[4], E. Marinou[3], J.M. Baldasano[4]

[1]Laboratory of Meteorology, Department of Physics, University of Ioannina, Ioannina, Epirus, 45110, Greece
[2]Institute of Environmental Research and Sustainable Development, National Observatory of Athens, Greece
[3]Institute for Space Applications and Remote Sensing, National Observatory of Athens, Greece
[4]Earth Sciences Department, Barcelona Supercomputing Center, Barcelona, Spain
Keywords: dust, episodes, Mediterranean, AERONET
Presenting author email: agkikas@cc.uoi.gr

Dust outflows frequently affect the broader Mediterranean basin, having significant impact on the radiation budget of the Earth-Atmosphere system of the region. The sources of dust outflows are located, primarily, in the North African deserts and secondarily, in the Arabian Peninsula. Given that desert dust episodes (DDEs) affect extended areas of the Mediterranean, implementation of satellite measurements is the appropriate tool to assess them. Their accuracy, however, should be validated and tested against ground measurements, e.g. by the AERONET network, which although being spatially limited are taken as the truth.

The main target of the present study is to describe the optical and radiative properties during DDEs in the Mediterranean. First, the DDEs are identified based on an objective and dynamic algorithm. In brief, the algorithm is based on quality optical properties from the MODerate resolution Imaging Spectroradiometer (MODIS-Terra), Earth Probe (EP) and Ozone Monitoring Instrument (OMI) databases, on a daily basis and upper and lower thresholds, defined according to the existing literature and several sensitivity tests enabled the identification of DDEs for each location and day, for the period 1 March 2000 – 28 February 2007. The optical properties which have been used are: aerosol optical depth (*AOD*), Ångström exponent (α), fine fraction (*FF*), effective radius (r_{eff}) and Aerosol Index (*AI*). The intensity of the DDEs has been calculated based on a methodology which has been presented by Gkikas et al (2009). Second, aerosol extinction profile information based on the CALIPSO satellite measurements is used for the determination of the aerosol layers, and finally the updated version of BSC-DREAM dust model is initiated (http://www.bsc.es/projects/earthscience/DREAM) in order to provide a link to the observed episodes using remote sensing techniques with in situ aerosol information.

Ground-truth data used for the evaluation of the algorithm performance include microphysical, optical and radiative properties from 9 selected AERONET stations across the Mediterranean. During study period, 58 DDEs with collocated satellite and ground measurements, have been sorted out and studied. Here, we present only AERONET retrievals (synergistic retrievals are presented on the EAC-related poster).

In Figure 1-i, the AERONET-resolved mean volume size distribution during DDEs is presented and compared to the general case of all days with common surface and satellite measurements (named as all period). During DDEs, a significant increase, by a factor of ~10, of the coarse mode and a peak of size distribution for particles radius centered at 2.24 μm are depicted. The $\alpha_{0.44\text{-}0.87\mu m}$ values during the DDEs vary between 0.03 and 0.47, and are significantly decreased, in all stations, compared with the all period values. Also, there is an increase, especially at the visible wavelengths, of the AOD (more intense loads), SSA (more scattering) and g (more forward scattering) spectral values. For the days with DDEs, the mean r_{eff} values range from 0.65μm to 1.1μm. Moreover, between 0.44μm and 1.02μm, the real part of the refractive index increases while the imaginary part decreases. Our results, as it concerns aerosol optical properties, are in line with the corresponding ones presented by Kim et al (2011).

The AERONET aerosol radiative forcing (RF) values at the bottom (BOA) and at the top (TOA) of the atmosphere are also given in Fig. 1-ii. During DDEs, there is an average surface radiative cooling equivalent to -92.2±21.2 Wm^{-2} and also a planetary cooling (at TOA) equal to -38±12.2 Wm^{-2}. Compared with the all period case, the DDEs RF values are increased in magnitude by about 150% at BOA and 190% at TOA, implying enhanced surface and planetary cooling over the Mediterranean. It should be noted, however, that this planetary cooling arises just because DDEs occur over sea or other than highly reflecting desert land surfaces, where a planetary warming can occur.

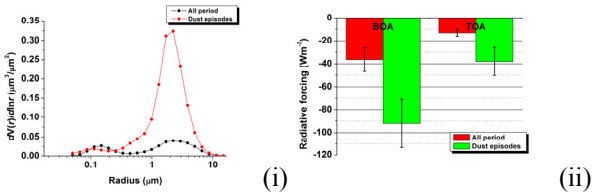

(i) (ii)

Figure 1. (i) Size distributions for the common period of ground-satellite measurements (all period) and during DD episodes, (ii) radiative forcing values (W/m^2) at BOA and TOA.

Gkikas, A., Hatzianastassiou, N., Mihalopoulos, N. (2009) *Ann. Geophys.*, 27, 3509-3522.

Kim, D., et al. (2011) *Atmos. Chem. Phys.*, 11, 10733-10741.

Combination of AERONET and CALIPSO data for the study of Saharan dust outbreaks over Valencia (Spain)

C.R. Marcos[1], R. Pedrós[1], J.L. Gómez-Amo[1], J.A. Martínez-Lozano[1], M.P. Utrillas[1]

[1]Department of Earth Physics and Thermodynamics, University of Valencia, Burjassot, 46100, Spain
Keywords: Satellites, Lidar ratio, Mediterranean, Saharan dust.
Presenting author email: Carlos.Marcos@uv.es

In this work a combination of CALIPSO level 1 data and sunphotometer measurements is performed to study the impact of Saharan dust over the metropolitan area of Valencia, in the Mediterranean coast of Spain.

The Cloud-Aerosol Lidar with Orthogonal Polarisation (CALIOP) is the main instrument on board the CALIPSO satellite, launched in April 2006 as part of the NASA A-Train constellation (Winker *et al*., 2007). Comparisons between the aerosol optical depth (AOD) derived by CALIOP and data from AERONET sunphotometers show little correlation (Bréon *et al.* 2011). To avoid the discrepancies found in level 2 data, a synergetic combination can be performed between level 1 data and the values of AOD obtained from an independent source (eg. Royer *et al*, 2010). This combination provides us with more accurate extinction profiles, which can be used to improve our understanding of the direct effect of aerosols in radiative forcing.

The CALIOP total attenuated backscatter at 532 nm (level 1 data) can be written as:

$$\beta'(z) = \left(\beta_m(z) + \beta_a(z)\right) \exp\left[-2\int_0^{r(z)} \left(\sigma_m(r') + \sigma_a(r')\right) dr'\right] \quad (1)$$

where β represents the backscatter coefficient, σ represents the extinction coefficient and the indices m and a point out the molecular and aerosol contribution respectively. The molecular terms can be calculated using atmospheric data from CALIPSO level 1 products. To retrieve the aerosol extinction coefficient from (1), a constant lidar ratio (LR), which is the relationship (σ_a/β_a) between the aerosol extinction and backscatter, is assumed. Finally, the value of LR is set so that the total integrated aerosol extinction coefficient match up the value of the AOD measured by a sunphotometer within a difference of 0.01.

The sunphotometer used in this study, belonging to the AERONET network since April 2007, is located in Burjassot (39.51N, 0.42W), a town of the metropolitan area of Valencia, in the Mediterranean coast of Spain. The values of AOD are averaged along one hour centred in CALIPSO overpass for daytime cases and linearly interpolated for night-time cases. The total attenuated backscatter cloudless data are averaged horizontally over the area within a distance of 25km from the sunphotometer (approximately, the metropolitan area of Valencia) to improve the signal-to-noise ratio.

A total of 57 cases (38 night-time cases and 23 daytime cases) could be used for this study. Among these events, 6 night-time and 2 day-time cases were classified as Saharan dust outbreaks by analysing the air masses backward trajectories given by HYSPLIT model.

The mean value of the lidar ratio obtained using the combination of AERONET and CALIPSO data (Table 1) is in agreement with the one retrieved by Pedrós *et al.* (2010) for Valencia. Remarkable differences can be seen in the mean extinction profile (Figure 1) above 1 km, since the extinction coefficient for the Saharan cases is greater than the one retrieved for the rest of the cases. This result show the notable influence of Saharan dust outbreaks in the vertical distribution of aerosols over Valencia, and the greater values for the extinction coefficient suggest the importance that these events have in the radiative forcing compared to the rest of cases.

Table 1. Mean value of LR (sr^{-1}).

	Saharan	Other
Night-time	45 ± 7	56 ± 24
Day-time	58 ± 10	67 ± 23
Pedrós *et al.* (2010)	55 ± 11	-

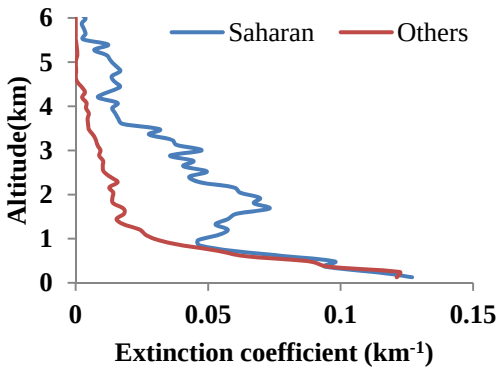

Figure 1. Mean extinction profile for Saharan dust outbreaks and for all other cases.

This work was funded by the Ministry of Economy and Competitiveness of Spain through projects CGL2009-07790 and CGL2011-24290, and the Valencian Autonomous Government through the project PROMETEO-2010-064.

Bréon, F.-M., Vermeulen, A. and Descloitres, J. (2011) *Remote Sensing of Environment.* **115**, 3102-3111.

Pedrós, R. et al (2010) IEEE *Transactions on Geoscience and Remote Sensing*, **48**, 237 – 249.

Royer, P., Raut, J.-C., Ajello, G., Berthier, S. and Chazette, P. (2010) *Atmos. Meas. Tech.* **3**, 893-907.

Winker, D. M., Hunt, W. H., and McGill, M. J. (2007) *Geophys. Res.Lett.* **34**, L19803.

Experimental study of hygroscopic properties of mineral dust particles.

T.I. Ryshkevich[1], E.F. Mikhailov[1] and S.S. Vlasenko[1]

[1] Institute of Physics, Department of Physics of Atmosphere, Saint-Petersburg State University, Saint-Petersburg, 198504, Russia

Keywords: Arizona test dust, hydroscopic growth, specific surface area.

Presenting author email: Ryshkevich_t@mail.ru

Despite extensive investigation of the processes of cloud formation and significant technological advances in this field the physical mechanisms that control the processes of cloud systems formation still cannot be fully understood (Pruppacher H.R. and Klett J.D., 2000). An important question is how ice forms in mixed-phase clouds. Various atmospheric observations of droplet freezing through heterogeneous ice nucleation show that mineral dust particles act effectively as ice nuclei (IN) (DeMott et al., 2003). Through their ability to nucleate ice, mineral dust particles influence microphysical and dynamical cloud properties, cloud life time, and therefore Earth's climate. As a result of different aging processes, the particle surface and therefore particles' IN ability may change. Several laboratory studies have been performed to investigate the hygroscopic properties of mineral dust particles.

The method of generating the initial particles with specified dispersed characteristics was worked out in the first stage of the experiment. This technique is based on the method of acoustic dispersion. This procedure is mainly used to generate a liquid aerosol. But it was optimized to get a narrow size fraction of Arizona test dust (ATD) particles. The result is shown in the fig.1. The range of particle sizes is the result of merging the measurement data obtained with a scanning mobility analyzer 3080 SMPS (TSI, USA) in the size range 20-800 nm, and the aerodynamic 3321 APS (TSI, USA) spectrometer in the range of 0.5 -20 microns.

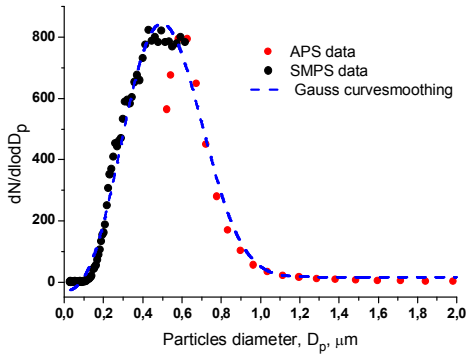

Figure 1. ATD particles size distribution.

Values of specific surface area of mineral dust particles were obtained based on nitrogen and water vapor adsorption using BET theory. These values are: $S_{sp}(N_2) = 5.6 \pm 0.2$ м^2/г and $S_{sp}(H_2O) = 5.6 \pm 0.5$ м^2/г, respectively. Moreover, the adsorption of nitrogen was investigated at a temperature of ~ 77K and the water adsorption at 295K. The effective radius (r) of ATD particles can be calculated as $r=3/S_{sp}\rho_{ATD}$, where ρ_{ATD} =2.65 g/cm^3, so it is equal to 201 nm. This is in agreement with *in-situ* measurements (see fig.1). This means that there are no aggregated clusters and selected ATD sample consist of single elementary particles.

We used a filter-based differential hygroscopicity analyzer for studying the hygroscopic properties of ATD particles based on a katharometric measurement of the amount of water vapor absorbed by an aerosol sample at temperature 295 K (E. F. Mikhailov et al, 2011). The results are shown in fig.2. It is shown that the number of water monolayers is about 6 at RH ~ 70% and a macroscopic liquid film has formed around the particles above this humidity. It is also important that the desorption branch coincides with the direct adsorption, indicating the absence of pores in the particles.

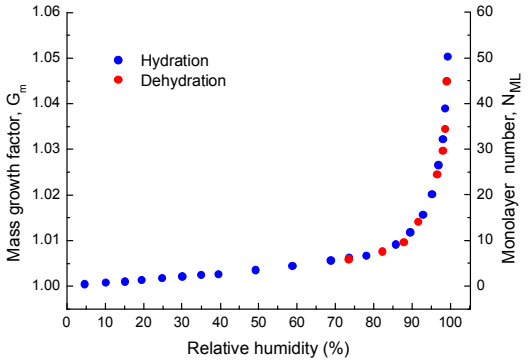

Figure 2. Mass growth factor G_m and the number of monolayers of water molecules N_{ml} depending on relative humidity.

This work was supported by the RFBR under grant 10-03-00950-a and 11-05-00945-a.

DeMott, P. J., Cziczo, D. J., Prenni, A. J., Murphy, D. M., Kreidenweis, S. M., Thomson, D. S., Borys, R., and Rogers, D. C.: Measurements of the concentration and composition of nuclei for cirrus formation, *P. Natl. Acad. Sci. USA*, **100 (25),** 14655–14660, (2003)

E. F. Mikhailov, V. V. Merkulov, S. S. Vlasenko, T. I. Ryshkevich and U. J. Pöschl: Filter-based differential hygroscopicity analyzer of aerosol particles, *Izvestiya Atmospheric and Oceanic Physics*, **47(6),** 747-759, (2011)

Pruppacher H.R. and Klett J.D.: Microphysics of cloud and precipitation, *2-d ed., Dordrecht*, 945 p., (2000)

Optical properties of a desert dust cloud after long-range transport using scattering matrix formalism and a polarization Lidar

G. David[1], B. Thomas[1], A. Miffre[1] and P. Rairoux[1]

[1]Laboratoire de Spectrométrie Ionique et Moléculaire, CNRS UMR 5579, Université Lyon 1, Villeurbanne, 69622, France

Keywords: remote sensing, scattering matrix, desert dust, number concentration

Presenting author email: amiffre@lasim.univ-lyon1.fr

Mineral dust particles are incriminated for their role on the Earth climate and radiative forcing. One of the main difficulties arises from the dust particles non-sphericity as Lorenz-Mie formalism is not applicable to highly irregularly-shaped particles (Nousiainen, 2009). Moreover, after advection over several thousands of kilometers, dust particles are highly dispersed and aged and the dust cloud is a complex mixture of both spherical (s) and non-spherical (ns) particles. To face this complexity, we have for the first time developed the scattering matrix formalism for a mixture of s and ns-particles (Miffre et al., 2011). We then applied this new formalism on a Saharan dust episode that occurred at Lyon (France) on 9th July 2010, by performing a polarization Lidar experiment. We hence provided a new methodology to remotely retrieve the dust particles number concentration (Miffre et al., 2011).

Starting from the **F**-scattering matrix definition (Mishchenko et al., 2002), we noticed that for a mixed aerosol cloud (a) = {s, ns}, $\mathbf{F} = \mathbf{F_s} + \mathbf{F_{ns}}$ since **F** is additive. By developing F_{11} and F_{22} matrix elements for s and ns-particles, we showed that, due to the presence of s-particles, the aerosol Lidar depolarization ratio δ_a differs from the ns-particles Lidar depolarization ratio $\delta_{a,ns}$ as follows:

$$1/\delta_a - 1/\delta_{a,ns} = 2F_{11,s}/(F_{11,ns} - F_{22,ns}) \quad (1)$$

Hence, while δ_s is always null, δ_a differs from $\delta_{a,ns}$, and in the presence of s-particles, δ_a is always below $\delta_{a,ns}$.

We then applied this new formalism to a Saharan dust episode that occurred at Lyon on 9th July 2010. Ns-particles were hence mostly attributed to desert dust particles while s-particles were most likely small-sized ammonium sulphates and aged carbonaceous particles (Kaaden et al., 2009). We separated backscattering from s and ns-particles by performing an accurate polarization Lidar experiment (providing the aerosol backscattering coefficient β_a for both {//,⊥}-polarization axes). This {s, ns}-partition is very efficient since laboratory measured polarization cross-talks are below 10^{-7}. Hence, by noting that dust particles are detected on both polarization channels, we retrieved the dust particles backscattering coefficient:

$$\beta_{dust} = \beta_{dust,//} + \beta_{dust,\perp} = \beta_{a,\perp}(1 + 1/\delta_{dust}) \quad (2)$$

The dust particles depolarization ratio [$\delta_{dust} = \delta_{a,ns}$ (dust) = (22.5 ± 2.0) %] is derived from the literature on T-matrix (Veselovskii et al., 2010). By using equation (2), we retrieved the dust particles number concentration N_{dust}, after numerical computation of the dust particles backscattering cross-section, assuming surface-equivalent spheres, or T-matrix computation to further reduce the N_{dust}-uncertainty. Vertical profiles of $\beta_{a,//}$, $\beta_{a,\perp}$, δ_a and N_{dust} are displayed in figure 1. In agreement with the newly developed scattering matrix formalism, at altitudes where the dust cloud is observed (z > 2 km), δ_a is below δ_{dust}, since, after long-range transport, the dust cloud is composed of both s and ns-particles. It is worth noting that the N_{dust}-vertical exhibit a different behavior from the δ_a-vertical profile, the latter being intensive and not dust particles specific, in contrary to $\beta_{a,\perp}$.

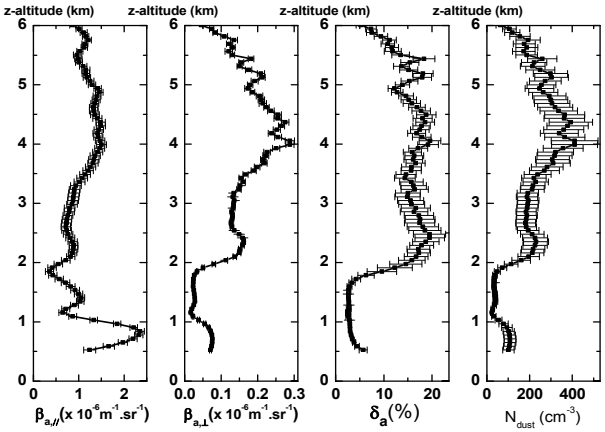

Fig. 1 Optical properties of a Saharan dust cloud at Lyon (France) measured with a UV-polarization Lidar.

The retrieved N_{dust}-values agree with recent in-situ measurements performed on dust particles over central Europe with optical counters (Klein et al., 2010). Moreover, dust particles specificity is here provided. The presentation will point out these new findings (Miffre et al., 2011), which concern the scattering matrix of a {s, ns}-dust cloud as well as its remote observation under real atmospheric conditions.

The authors thank Région Rhône-Alpes for research grant and CNRS for financial funding.

Kaaden et al. (2009), *Tellus B*, **61**, 51-63.
Klein H., et al., (2010), *Atm. Chem. Phys,* **10**, 10211-10221.
Miffre et al., (2011), *Geophys. Res. Lett*, **38**, L16804.
Mishchenko, M.I. et al., (2002), Scattering, absorption and emission of light by particles, Camb. Univ. Press.
Nousiainen, T., (2009), *J. Quant. Rad. Spect. Transf.* **110**, 1261-1279.
Veselovskii I., et al., (2010), *J. Geophys. Res.* **115**, D21203.

Desert-dust episodes over a background European environment: relationship between optical and physical properties by in-situ and columnar-integrated techniques

M. Sorribas[1,2,3], J.A. Ogren[4], F.J. Olmo[1,2], R. Fraile[5], B.A. de la Morena[3] and L. Alados- Arboledas[1,2]

[1]Centro Andaluz de Medio Ambiente, Universidad de Granada, Junta de Andalucía, Granada, 18006, Spain
[2]Department of Applied Physic, University of Granada, Granada, 18071, Spain
[3]El Arenosillo-Atmospheric Sounding Station, INTA, Huelva, Mazagón, 21130, Spain
[4]Earth System Research Laboratory, NOAA, Boulder, 80305, USA
[5]Department of Applied Physics, University of León, León, 24071, Spain
Keywords: desert-dust, particle size distribution, scattering coefficient, AOD, rural monitoring station.
Presenting author email: sorribasmm@inta.es

The wide variety of aerosol data sets from long-term monitoring programs can be used to analyze trends of aerosol properties and the synergy of aerosol products. Here we discuss the details of the desert-dust plumes (DDPs) aerosol properties in the South-west of Spain for improving the knowledge of aerosol properties and their interaction with solar radiation on regional scale.

The data sets used have been measured in El Arenosillo – Atmospheric Sounding Station (37.1N, 6.7W, 40 m a.s.l) , which is a multi-instrument platform located in a background rural-coastal site. In this observatory, aerosols are studied in great detail, using combinations of in-situ and remote sensing observations (Córdoba-Jabonero et al., 2011). Particle size distribution within (14 - 10000) nm was measured with a SMPS-APS system, scattering (SC) and back-scattering coefficients within PM_1 and PM_{10} size ranges were provided by an integrated nephelometer and optical columnar-integrated properties was monitored by a CIMEL sun-photometer. Levels of PM_{10} were measured in a nearby station 6 km away and they were supplied by the Andalusian Government.

Estimation of particle mass size distribution using a SMPS-APS tandem system was provided thanks to an intercomparison with the real-time monitor of PM10. A particle density was assumed depending on the analyzed period. In case of the desert-dust event which aerosol properties are shown in Figure 1, a particle density of 3.0 g/cm^{-3} was assumed. The correlation coefficient of the comparison was of 0.86.

To evaluate the aerosol effectiveness on solar light radiation, mass scattering coefficient efficiency (MSC), defined as the ratio of 1-hour SC^{550} to 1-hour PM1 or PM10 mass concentration, has been evaluated for several DDP events. In the example shown in Figure 1 (up), MSC for PM1 and PM10 were (0.9 ± 0.03) $m^2\ g^{-1}$ and (1.1 ± 0.04) $m^2\ g^{-1}$ respectively. In both cases high correlation coefficients (R) of 0.93-0.97 were obtained, indicating a good relation between optical and microphysical parameters.

The correlation based on coincident 1-hour PM1, PM10 and (PM1/PM10) mass concentrations from SMPS-APS system and the 1-hour AOD from Cimel during the selected DDP episode is shown in Figure 1 (down). High correlation between the two properties is found with correlation coefficient of 0.85-0.90. The best relationship is observed for AOD & PM10.

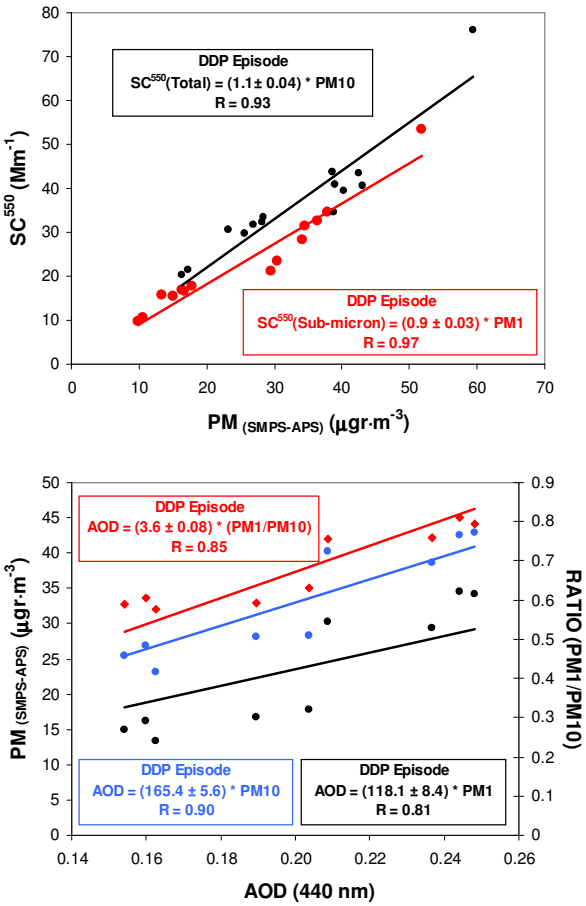

Figure 1. Relationship between (up) SC^{550} & (PM10 and PM1) and (down) AOD & (PM10, PM1 and ratio(PM1/PM10)) during a DDP episode.

Cordoba-Jabonero et al., 2011. Atmos. Chem. Phys. 11, 3067-3091.

Acknowledgments: Mar Sorribas thanks Ministerio de Economía y Sostenibilidad (MICINN) for the award of a Juan de la Cierva post-doctoral grant. This work was supported by MICINN through projects AEROMICROPRO (CGL2010-18782); by the Andalusian Regional Government through project TARTESOS (P10-RNM-6299). The authors thank the NOAA/ARL for the HYSPLIT back-trajectories and NOAA/ESRL for providing technical support. We also thanks the Andalusian Government for the data supplied.

Estimation of dust emission amount for spring in East Asia using WRF/Chem

Jung-Yoon Kang[1] and Soon-Chang Yoon[2]

[1]Atmospheric Environment and Applied Meteorology Research Department, Meteorological Research Institute, Tsukuba, Ibaraki, 305-0052, Japan
[2]School of Earth and Environmental Sciences, Seoul National University, Seoul, 151-747, Korea
Keywords: Mineral dust, Asian dust, Emissions, Modelling
Presenting author email: doosan8@snu.ac.kr

Mineral dust is one of the most important aerosols because it affects not only air quality and human health but also radiation budget by scattering and absorbing solar and terrestrial radiation. Taklimakan Desert and Gobi region are known to be one of significant source regions of airborne dust in the world, and dust phenomena frequently occur in the springtime in East Asia. It is important to estimate dust emission amount exactly in understanding the effect of dust particles, and dust model is a good means of obtaining dust emission amount. In this study, a new dust emission scheme proposed by Shao (2004) (hereinafter referred to as S04) was implemented in Weather Research and Forecasting with Chemistry (WRF/Chem) (Kang *et al.*, 2011) and numerical simulations were conducted to estimate dust emission amount for the springtime in East Asia.

The newly implemented dust emission scheme, S04 is a physically-based scheme and it considers two main dust emission mechanisms, called 'saltation bombardment', and 'aggregate disintegration'. The soil texture type data and vegetation cover data for East Asia were newly updated to improve the boundary condition.

A case study for a severe dust event that took place in the spring of 2007 was carried out to evaluate the new dust emission scheme. The model results show that WRF/Chem with S04 scheme has a capability to simulate dust phenomena reasonably; dust plumes are generated by strong wind over Mongolia and Gobi region and then transported to the Korean peninsula and Japan along the low-pressure system. The spatial distribution of dust plumes is also well matched with the Ozone Monitoring Instrument (OMI) Aerosol Index and World Meteorological Organization (WMO) synoptic data. The comparison between modelled dust concentration and observed PM_{10} data for several stations in Korea (Figure 1) reveals that model can capture the onset time of the dust event well and the estimated dust concentrations are quite well comparable to the observed data.

To calculate dust emission amount for the springtime in East Asia, the model simulation was conducted for March, April, and May from 2006 to 2010 for 5 years. The vegetation cover was updated every month and the horizontal grid size of the model domain was set to 100 km.

Figure 2 shows the 5-year-averaged dust emission amounts for the springtime for several regions. The Gobi region occupies the largest area and shows the highest dust emission amount. The dust emission amount per area is the highest for Badain Jaran Desert. The monthly and yearly changes of dust emission amount were also examined, and Taklimakan desert shows less variability than other regions while Loess region shows high variability because of the change of vegetation cover.

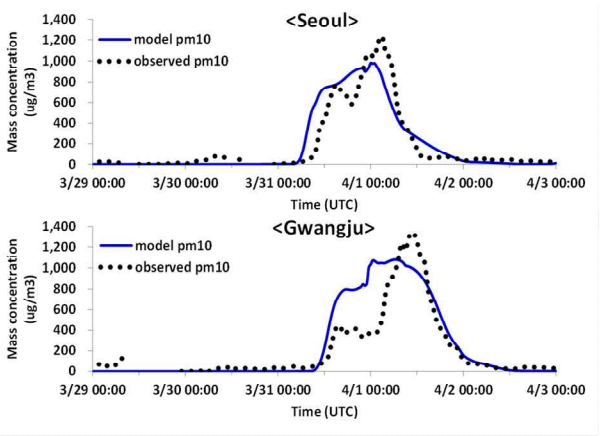

Figure 1. Comparison between model dust concentration (blue line) and observed PM_{10} concentration (black dot) at Seoul and Gwangju.

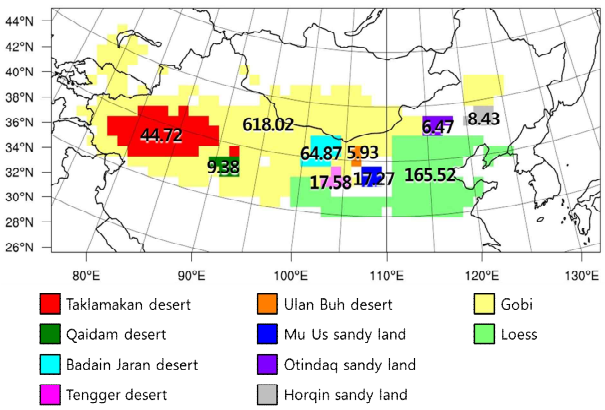

Figure 2. Total averaged dust emission amounts [Tg] for the springtime for several regions.

Kang, J.-Y., Yoon, S.-C., Shao, Y., and Kim, S.-W. (2011) *J. Geophys. Res.*, **116**, D09202, doi:10.1029/2010JD014649.

Shao, Y. (2004) *J. Geophys. Res.*, **109**, D10202, doi:10.1029/2003JD004372.

Carbonaceous and inorganic water soluble species in PM in Cape Verde atmosphere

Teresa Nunes[1], João Cardoso[1, 2], Danilo Custódio[1], Mário Cerqueira[1], Suzana Marta Almeida[3], M. Almeida-Silva[3] & Casimiro Pio[1]

[1]CESAM & Department of Environment, University of Aveiro, 3810-193, Aveiro, Portugal
[2]University of Cape Verde, Praia, 279, Santiago, Cabo Verde
[3]ITN/MCTES , 2686-953, Sacavém, Portugal
Keywords: Saharan dust, Carbonaceous aerosol, Sea salt
tnunes@ua.pt

The position of Cape Verde Islands in the Atlantic Ocean represents an important area to study and characterize Saharan/Sahel mineral dust transported over West Africa and the adjacent Tropical Atlantic Ocean. Sahara and Sahel regions are the most important contributors to the global dust emission (Goudi and Middleton, 2001). The atmosphere of Cape Verde Island is deeply marked by the contribution of these dust emission sources. At local level even the native population recognize the importance of this contribution, that occur mainly in the dry season (November / February), using a suggestive name "bruma seca" (dry haze). At Cape Verde islands, significant mixing of aerosols is expected due to the presence of desert mineral dust, sea salt and anthropogenic aerosol emissions. Uncertainties exist in the quantification of the highly variable distribution of this modified aerosol. In order to contribute for a better understanding and impact of mineral dust source, a year measurement campaign was performed at Santiago Island in the scope of CV-Dust Project. A surface field station was implemented in the surroundings of Praia City (14°55' N e 23°29' W, 98 m at sea level), where aerosol sampling, throughout different samplers, was performed.

Particulate matter were collected simultaneously with a Hi-Volume sampler (Tisch) and a low-volume sampler (Partisol), both with standard PM_{10} inlet heads, between January 2011 and January 2012, performing 115 parallel samples. Teflon filters with 0.45 µm pore size and quartz filters were used with low and high volume samplers, respectively. Teflon filters samples were used to quantify water inorganic soluble species by ion chromatography; instead quartz filter samples were used to quantify carbonaceous species. PM_{10} mass concentrations were quantified by gravimetric method. Carbonate fraction was determined by sample acidification with phosphoric acid and the CO_2 evolved measured with a NDIR gas analyzer. Organic and elemental carbon was determined by using a thermal-optical transmission technique after removing carbonate fraction by exposing the filters to HCl vapour (Castro et al., 1999). Complementary to PM_{10} samples, a set of 11 samples were performed along the year with a five stage cascade impactor and PM collected in quartz filters. The different species referred above were as well as quantified in these filters.

PM10 concentrations at Cape Verde Island shows a high variation, with concentrations ranging between <15µg m^{-3} up to more than 500 µg m^{-3}.

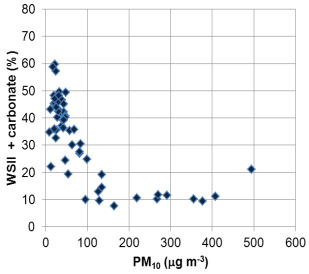

Figure 1 – Percentage contribution of WSII and carbonates for PM10.

Water soluble inorganic ions and carbonates, during mineral dust events, contribute around 10% of the PM10 mass concentration (Fig. 1), while out of this influence could increase up to 60%.

Carbonaceous particles, organic and elemental carbon account in average less than 1.02±0.82% of PM10, while Ca+Carbonates contribute with 2.47±1.60 %. Chloride, sodium and magnesium ions showed a high correlation among them (R^2>0.95), which denotes the strong sea salt source for the local observed aerosol. In average Na+Cl ions account 22.4±12.1 of the total PM mass.

Usually coarse particles, dominates the mass concentration of PM10 in Cape Verde, with the prevalence of particles between 3-7.2 µm (Fig. 2).

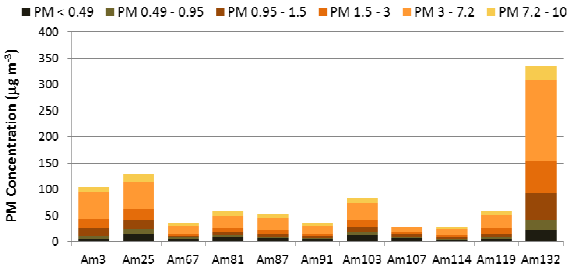

Figure 2 – Size distributions of PM mass concentration

We gratefully acknowledge FCT for funding the project PTDC/AAC-CLI/100331/2008 - CV-Dust. J. Cardoso acknowledges the PhD grant SFRH-BD-6105-2009 from FCT.

Castro, L.M., Pio, C.A., Harrison, R.M., Smith, D.J.T., (1999) *Atmospheric Environment* **33**, 2771–2781.

Goudie, A.S. and Middleton, N.J. (2001) *Earth-Sci Rev* **56** (1–4), 179-204.

Ground-based measurements of suspended and re-suspended volcanic ash in Iceland after the Grímsvötn eruption in 2011

S. von Löwis[1], C. Fischer[2], A. Vogel[2], K. Weber[2], R. Reichardt[2] and T. Jóhannsson[3]

[1]Icelandic Meteorological Office, Reykjavik, Iceland
[2]University of Applied Science, Environmental Measurement Techniques, Dusseldorf, Germany
[3]Environmental Agency, Reykjavik, Iceland
Keywords: volcanic particles, resuspension
Presenting author email: sibylle@vedur.is

In the evening of the 21st May 2011 an eruption started in Grímsvötn volcano, a sub-glacial volcano beneath the Vatnajökull glacier ice sheet in Southeast Iceland. The eruption plume exceeded 20 km in altitude during the first hours but decreased in the early hours of 22 May to 10-15 km altitude (Bjornsson, 2012). The eruption plume was observed until 25 May and the eruption was defined as deceased at 07 UTC 28 May. During the first hours of the eruption, ash fall was observed to the south and west of Vatnajökull glacier.

In the evening of the 22nd of May the volcanic ash cloud was advected over the South and Southwest part of Iceland due to strong north-easterly and easterly winds. Local ash fall was observed as well as severe reduced visibility and air quality.

The particle number concentrations were measured with optical particle counters at two different locations in South Iceland, in Skógar, 145 km southeast of Grímsvötn volcano, and in Hvolsvöllur, 160 km southeast of the volcano. The particle number concentrations were converted to mass concentrations assuming a density of volcanic ash of approximately 2600 kg/m^3.

During this event, high number concentrations were measured at both stations. The calculated mass concentrations are shown in Figure 1.

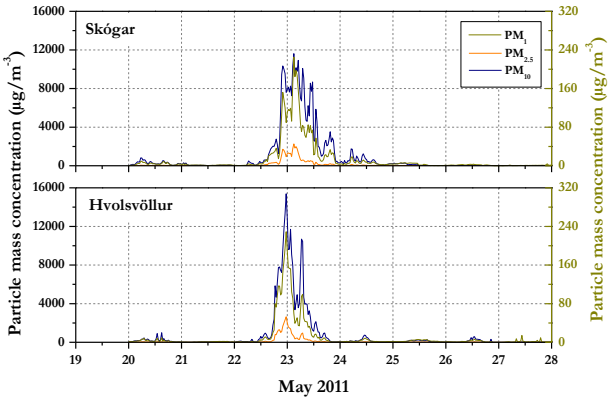

Figure 1. Calculated PM_1, $PM_{2.5}$ and PM_{10} mass concentrations of measured particle number concentrations (30 min average) at two different locations in S-Iceland.

In the aftermath of the eruption in Eyjafjallajökull volcano in 2010, volcanic ash was frequently remobilised by wind (Thorsteinsson, 2012). Those events were observed especially in South-Iceland and continued to occur into 2011 (Leadbetter et al., 2012). The Grímsvötn eruption added volcanic material in nearly the same region as the eruption one year before. And volcanic ash and dust resuspension was occasionally observed in summer and autumn 2011.

In September 2011, during a period of several days, heavy dust and sand storms were observed in the south part of Iceland. The dust cloud can clearly be seen on MODIS images of this time period. The PM_{10} concentrations, measured in Southeast Iceland, exceeded the European health limit value of 50µg/m^3 for several days (Figure 2).

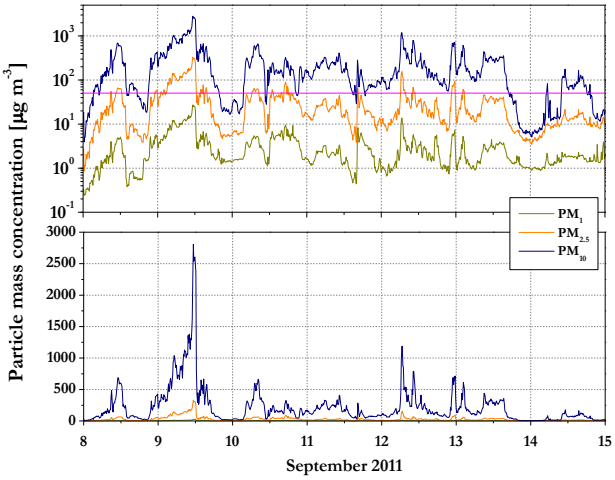

Figure 2. PM concentrations measured in Kirkjubæjarklaustur (SE-Iceland). The horizontal magenta line marked the European health limit value for PM_{10} of 50 µg/m^3 over 24 hours.

The PM_1 concentration was also significantly increased during this period. Strong northerly and north-easterly winds caused these events but when the wind direction turned to southeast, mineral dust and volcanic aerosols were also observed in the west part of Iceland including the capital region.

Bjornsson, H., G. N. Petersen and Þ. Arason (2012), *Geophysical Research Abstracts*, **14**, EGU2012-9706

Leadbetter, S. J., M. C. Hort, S. von Löwis, K. Weber, and C. S. Witham (2012), J. Geophys. Res., **117**, D00U10

Thorsteinsson, T., T. Jóhannsson, A. Stohl, and N. I. Kristiansen (2012), J. Geophys. Res., **117**, B00C05

Development of a certified reference material for Asian mineral dust (Gobi Kosa)

M. Nishikawa[1], I. Matsui[1], T. Sano[1], M. Ukachi[1], K. Nagano[1], K. Onishi[1], D.Batdorj[2], N. Enkhmaa[3] and I.Mori[4]

[1] Center for Environmental Measurement and Analysis, National Institute for Environmental Studies, Tsukuba, Ibaraki, 305-8506, Japan
[2]Institute of Meteorology and Hydrology of NAMEM, Gudamj-5, Ulaanbaatar, Mongolia,
[3]Meteolological Observatory of Sainshand, Sainshand, Dornogovi, Mongolia
[4]Analytical Research Division, Tokyo Metropolitan Research Institute for Environmental Protection, Koto-ku, Tokyo, 136-0075, Japan
Keywords: Asian dust, Gobi desert, certified reference material, element
Presenting author email: mnishi@nies.go.jp

Asian mineral dust is transported from the desert and loess areas of China and Mongolia to Japan, and even to transport around the world by the prevailing westerly winds. The mineral dust (well-known as kosa aerosol) generated from the northern Asia areas is estimated about several hundred million tons every year. The most deposition mounts of mineral dust surrounding Japan was reported to take account for that transported from Gobi desert, where is situated in Mongolia and the inner-Mongolia in China. Asian mineral dust has been interested by a wide range of scientific disciplines, such as meteorology, environmental science, medical science and precision engineering. We would like present to develop the new certified reference material, name of Gobi Kosa, available to use for various scientific experiments and quality control of chemical analyses.

We collected 1200 kg of surface soil (0-5cm) at four sites in southern Gobi desert area, Mongolia, where is located around 109°(east longitude) and 44°(north latitude). Heavy sand storms generate frequently at the sites area, in the springtime. The primary material of surface soil was sampled in May, 2011. The fine particle dust was collected by the cyclone separator with the 10 micro-meter for cut-off efficiency from the raw material, in the meteorological observatory, Sainshand, near Gobi Desert. The second material was obtained about 4kg, and then the material was transported to Japan. The final sieving and homogeneity procedure was performed, and then about 1kg. Two (g) of the final material was sealed into each of 600 brown glass bottles. There were sterilized by exposure to cobalt 60 irradiation.

The particle size distribution of Gobi Kosa was obtained by analyzing a microscopic image using image analysis software (OLS3500/SFT-3500, Olympus and Shimadzu) (Fig. 1). The detection limit of this method was 1 μm. About 1500 particles of Gobi Kosa was measured, almost particles were verified less than 10 micro-meter in diameter. The average of particle diameter was 2 micro-meter. The gravimetric density of the particles are about 2.5, therefore the aerodynamic diameter is calculated about 3.2 micro-meter. As the aerodynamic mean diameter of kosa aerosols observed in Japan has been reported 3-5 micro-meter range, this size of Gobi Kosa is consequently reasonable. Major components of Gobi Kosa exhibit in Table 1. Al, Fe, Ca, Ti are the primary indicator elements for Asian mineral dust. The concentration ratios of Fe, Ca, Ti to Al in kosa aerosols, were in the narrow ranges of 0.52-0.59 (Fe), 0.51-0.73 (Ca) and 0.049-0.082 (Ti), as shown in Table1. The ratios in the Gobi Kosa were very similar to those of kosa aerosols collected in Japan.

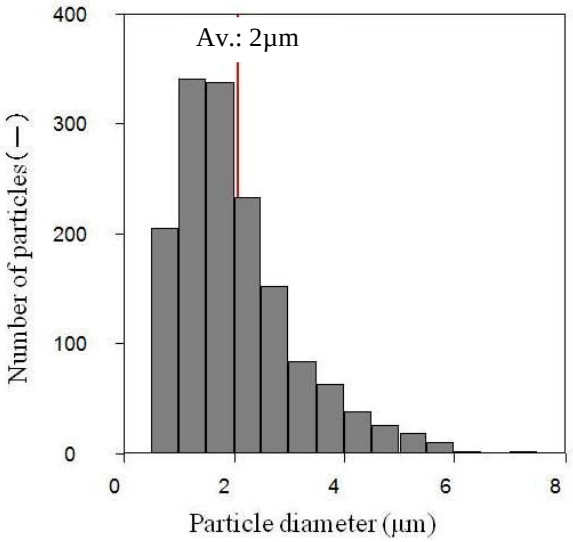

Figure 1 Size distribution of Gobi Kosa

Table 1 Elemental components of Gobi Kosa and comparison of the (X/Al) ratios with those in 4 examples of typical kosa aerosols collected in Japan

	Gobi Kosa		kosa aerosols (4examples)
	(mg/Kg)	(X/Al)	Range (X/Al)
Al	7.76	1	1
Ca	4.31	0.555	0.51 - 0.73
Fe	4.16	0.536	0.52 - 0.59
K	2.22	0.286	0.30 - 0.37
Mg	1.49	0.192	0.27 - 0.31
Na	0.936	0.121	0.17 - 0.50
Ti	0.454	0.0585	0.049 - 0.082
Mn	0.0801	0.0103	0.013 - 0.015

Acknowledgements
This study was partly supported by the Environmental Research and Technology Development Fund (B-1202) of MOE, Japan.

Planetary Boundary Layer and Saharan Air Layer top height determination using Ceilometer and Micro Pulse Lidar. Intercomparison for two case studies.

Y. Hernández[1], S. Alonso-Pérez[1,2], E. Cuevas[1], C. Camino[1], J. de Bustos[1], A.J. Gomez-Pelaez[1], R. Ramos[1], C. Córdoba-Jabonero[3] and M. Gil[3]

[1]Izaña Atmospheric Research Centre, Joint Research Unit to CSIC 'Studies on Atmospheric Pollution', La Marina 20, planta 6, 38071, Santa Cruz de Tenerife, Canary Islands, Spain
[2]Institute of Environmental Assessment and Water Research, (CSIC), Luis Solé i Sabarís, 08028, Barcelona Spain
[3]National Institute for Aerospace Technology (INTA), Atmospheric Research and Instrumentation Branch, Torrejón de Ardoz, 28850, Madrid, Spain
Keywords: Boundary Layer, Ceilometer, Lidar, Saharan Air Layer, Saharan dust
Presenting author email: chernandezp@aemet.es

Top heights of the Planetary Boundary Layer (PBL) and the Saharan Air Layer (SAL) during two Saharan dust events were compared by using both a Vaisala ceilometer CL51 (CL51; 910 nm) and a Micro Pulse Lidar (MPL; 523 nm) in Tenerife, Canary Islands.

Ceilometers were originally conceived for both cloud and PBL height detection, but not specifically to measure the dust layer. However, a previous study showed that the CL51 is capable of detecting mineral dust within the SAL (*Hernández et al., 2011*). That study was carried out in the Canary Islands in winter when Saharan dust intrusions occur within the Marine Boundary Layer, MBL, (*Viana et al., 2002; Alonso-Pérez, 2008*), with both the CL51 and the MPL located at the Santa Cruz Observatory (SCO; 28.5º N, 16.2º W, 52 m a.s.l.) a background urban station located in the metropolitan area of Santa Cruz de Tenerife that belongs to Izaña Atmospheric Research Centre.

Two case studies are presented in this work. From 14 October to 24 November 2011, the CL51 was installed at Izaña Observatory (IZO; 28.3º N, 16.5º W, 2373 m a.s.l.), which is representative of the free troposphere, and the MPL was located at SCO, within the MBL. In this period, an exceptional episode of Saharan dust intrusion at high altitude occurring from 15 to 17 October, 2011 was studied.

During the second period of the inter-comparison, both instruments have been located at SCO within the MBL. Our second case study is the Saharan dust episode occurred in December 5-11, 2011.

The PBL and SAL heights were determined using the gradient method. The PBL and SAL correspond respectively, to the first and subsequent measurable minima of the derivative of the CL51 and MPL backscatter signals. Also, we have developed a methodology for determining the SAL heights using relative humidity (RH) and temperature vertical profiles from radiosoundings.

Our results have been analysed using ancillary information: 1) analysis of airmass origin reaching the site, perfomed using both HYSPLIT 4 and ECMWF backtrajectories; 2) simulations of vertical profiles of dust concentrations using the BSC-DREAM8b dust model; 3) vertical profiles of temperature, RH and wind direction from radiosonde and ozonosonde stations, at Güímar and Jardín Botánico respectively, both in Tenerife 4) aerosol optical depth from Izaña and Santa Cruz de Tenerife AERONET stations; 5) Moderate Resolution Imaging Spectroradiometer (MODIS) and Meteosat Second Generation (MSG) satellite imaginery 6) ECMWF and the non-hydrostatic mesoscale meteorological MM5 models and 7) heights of PBL and aerosol layers and extinction coefficient measured at SCO provided by the Micro Pulse Lidar Network (MPLNET).

We have found a good agreement between the Vaisala CL51 ceilometer and the MPL in the determination of the PBL and SAL heights, noting that in winter season is more challenging for the MPL to detect dust layers because they travel at lower altitudes. The SAL heights determined by RH and temperature vertical profiles are also in good agreement with the results obtained by CL51 and MPL.

We would like to thank to Vaisala for providing the ceilometer CL51. Thanks to Reijo Roininen for the information about the ceilometer. Yballa Hernández enjoys a grant from the Meteorological State Agency of Spain, Ministry of Agriculture, Food and Environment of Spain to carry out studies in remote instrumental techniques.

Alonso-Pérez S. (2008) *Caracterización de las intrusiones de polvo en Canarias*, PhD Thesis, Universidad de la La Laguna, Centro de Publicaciones de la Secretaría general Técnica del Ministerio de Medio Ambiente, Madrid, ISBN: 978-84-8320-473-3.

Hernández, Y., Alonso-Pérez, S., Cuevas, E., Camino, C., Ramos, R., de Bustos, J., Marrero, C., Córdoba-Jabonero, C., and Gil, M. (2011) *Micro Pulse Lidar and Ceilometer inter-comparison during Saharan dust intrusions over the Canary Islands*, Proceedings of the V Reunión Española de Ciencia y Tecnología de Aerosoloes (RECTA 2011), Madrid (Spain), ISBN: 978-84-7834-662-2.

Viana, M., Querol, X., Alasstuey, A., Cuevas, E., and Rodruíguez, S. (2002), *Atmospheric Environment*, 36, 5861-5875.

An empirical relationship to estimate mineral dust concentration from visibility observations

C. Camino[1], S. Alonso-Pérez[1,2], E. Terradellas[3], S. Rodríguez[1], A.J. Gomez-Pelaez[1], P.M. Romero-Campos[1], Y. Hernández[1], S. Basart[4], J.M.Baldasano[4,5], E. Cuevas[1]
[1]Izaña Atmospheric Research Centre, AEMET, Santa Cruz de Tenerife, Spain
[2]Institute of Environmental Assessment and Water Research (CSIC) Barcelona, Spain
[3]Spanish Meteorological Agency, AEMET, Barcelona, Spain
[4]Earth Sciences Department, Barcelona Supercomputing Center-Centro Nacional de Supercomputación (BSC-CNS), Barcelona, Spain
[5]Environmental Modeling Laboratory, Technical University of Catalonia, Barcelona, Spain
Keywords: PM10, visibility, air quality, mineral dust, desert dust
Presenting author email: ccaminog@aemet.es

Northern Africa is the largest source of emission of mineral dust into the atmosphere. Mineral dust has a significant effect on human health and a strong interaction with the climate system. The main impact of mineral dust on the economy is related to visibility reduction, especially affecting air and ground transportation. It is necessary to characterize and quantify the mineral dust over the source regions to better understand the dust cycle and to assess its impacts.

Near dust source regions, there is a huge lack of PM10 (particulate matter with diameter less than 10 micrometers) measurements. Moreover, satellite remote sensing techniques have significant limitations over highly reflective surfaces, such as deserts, and therefore, provide limited performance over dust source regions. Due to all these limitations, given that meteorological stations provide a good spatial distribution and temporal resolution near dust source regions, we use visibility observations provided by meteorological stations as an alternative tool to characterize and quantify the concentration of mineral dust in Northern Africa.

The first goal is to derive an empirical relationship between PM10 concentration and horizontal visibility at Izaña Observatory (IZO, 28.30ºN, 16.49ºW, 2367 m a.s.l., under free troposphere conditions). The second goal is to assess whether this empirical relationship can be used to derive PM10 concentrations under desert conditions in North Africa.

In the first part of this work, summer data from the period 2005-2010 measured at IZO were used to determine the empirical relationship between PM10 concentration and visibility. The analysis was restricted to the summer months at IZO, because Saharan dust intrusions over IZO mainly occur during this season.

In an attempt to avoid fog or rain events, we excluded from calculations observations with relative humidity higher than 75% or any reported precipitation. Additionally, we used aerosol optical depth and Ångström exponent (α) from a collocated AERONET station to avoid events with dominant marine or anthropogenic aerosol, according to *Basart et al (2009)*.

A good empirical relationship to estimate PM10 at IZO from visibility data was found. Preliminary tests indicate that, in comparison with other equations found in the literature *D'Almeida (1986)* and *Shao et al (2003)* for visibility and PM10 and *Ben Mohamed et al (1992)* for total suspended particles and visibility, our empirical relation improves the quality of the fit.

In the second part of this work, in order to evaluate the performance of the derived empirical relationship in Northern Africa, the equation was tested for Sahelian stations reporting PM10 data: Baninzoumbou in Niger, Cinzana in Mali and M'Bour in Senegal, from the AMMA (African Monsoon Multidisciplinary Analysis) network, described by *Marticorena et al (2010)*.

Our resulting empirical relationship reproduces quite well the PM10 observations recorded at AMMA sites. It may be concluded that the empirical relationship found at IZO can be used as a new approach for estimating PM10 from horizontal visibility measurements from meteorological stations in Northern Africa.

The present work was carried out in the context of the MACC II project at the Spanish Meteorological Agency (AEMET). The authors would like to thank AERONET Network, AMMA Network and National Climatic Data Center (NCDC).

Ben Mohamed, A., Frangi, J.P., Fontan, J., Druilhet, A. (1992). Spatial and temporal variations of atmospheric turbidity and related parameters in Niger. *J. Appl. Meteorol., 31, 1286–1294.*

Basart, S., Pérez C., Cuevas E., Baldasano J.M., Gobbi G.P., (2009). Aerosol characterization in Northern Africa, Northeastern Atlantic, Mediterranean Basin and Middle East from direct-sun AERONET observations. *Atmos. Chem. Phys., 9, 8265-8282.*

D'Almeida, G.A., (1986). A model for Saharan dust transport. J. Clim. Appl. Meteorol., 25 (7), 903–916.

Marticorena B., Chatenet B., Rajot J. L., Traor´e S., Coulibaly M., Diallo A., Kon´e I., Maman A., NDiaye T., Zakou A., (2010). Temporal variability of mineral dust concentrations over West Africa: analyses of a pluriannual monitoring from the AMMA Sahelian Dust Transect. *Atmos. Chem. Phys., 10, 8899–8915.*

Shao, Y., L. Wang, (2003). A climatology of northeast Asian dust events. *Meteorol. Z., 12, 187–196.*

Particulate Matter Deposition Monitoring: Neglected Importance of Titanium?

G. Jereb[1], G. Dražič[2] and B. Poljšak[1]

[1] University of Ljubljana, College of Health Studies, Poljanska 26 a, 1000 Ljubljana, Slovenia
[2]Department for Nanostructured Materials, Jožef Stefan Institute, Jamova 39, 1000 Ljubljana, Slovenia
Keywords: particulate matter, deposition, monitoring, Titanium
Presenting author email: gregor.jereb@zf.uni-lj.si

Particulate matter deposition was measured at Slovenian coastal area in municipality of Koper. Three one year measurement campaign (2005-06, 2007-08 and 2009-10) were adopted in the vicinity of Port of Koper. Main reason for starting mentioned measurement was complaints from nearby inhabitants, who live near by the depot of coal and iron ore. For many years the inhabitants of Ankaran and its surroundings (the closest residential area is 1 km from the storage sites) have been complaining about the pollution of their residential area with emissions from the terminal EET in the Port of Koper. Port of Koper already introduced several dust control measures in order to reduce dusting to the environment from the EET terminal (coal and iron ore manipulation and storage place).

The amount of particulate matter deposition was determined gravimetrically using Bergerhoff deposition gauge for sampling and precise analytical weight for gravimetric analysis. Additionally samples were qualitative and quantitative analyzed using SEM EDXS. Chemical analysis on annual samples was also carried out in order to determine the amount of selected (Fe, Al, Cu, Zn, Cd, Pb, Cr, Ni, As) metals.

The study was designed to assess the dustiness in the region and determine the difference between vertical and horizontal (contribution of wind) deposition. Additionally the impact of background and correlation between dust deposition, the weather (especially extreme) and the activity at the Port of Koper was evaluated.

During the preliminary study (2005/06 - Figure 1) extreme values of particulate matter deposition in Port's surroundings were detected. During time period 2007/08 (Figure 2) and 2009/10 (Figure 3) elevated levels of suspended particles were not detected. Main reason for relatively lower values of dust deposition might be in rather good weather conditions and also in introduced precautionary "anti dust" measures taken by the Port of Koper.

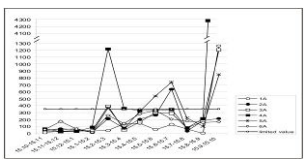

Figure 1: Particulate matter deposition - 2005/06

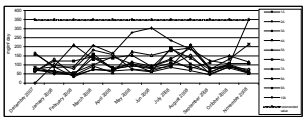

Figure 2: Particulate matter deposition - 2007/08

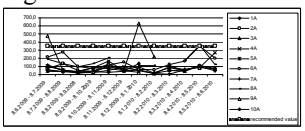

Figure 3: Particulate matter deposition - 2009/10

Main purpose of the study was to investigate the amount of particulate matter deposition and try to link it with the activities in the Port of Koper. Additionally also assessment of effectiveness of adopted "anti dust" measures was part of our interest. However, using SEM additionally interesting discovery was found. SEM/EDXS was employed to differentiate particles of coal and iron ore from other particles collected in the sampling device. An extremely large number of particles of titanium, all of which were present mainly in the smaller size fractions (less than 1 µm up to max 5 µm) were found during all three sampling intervals. Additional sampling sites were placed in Ljubljana (distance from Koper is 100 km) and also there particles of Titanium were found. According to SEM micrographs we can conclude that this particles are anthropogenic, however the main source of these particles remains unknown.

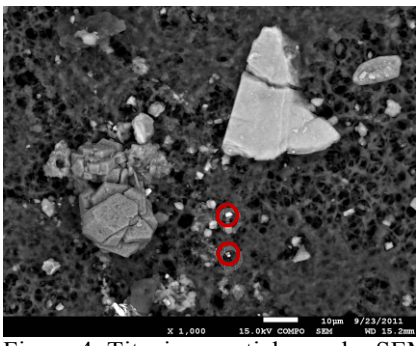

Figure 4: Titanium particles under SEM

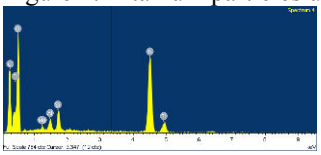

Figure 5: Typical spectrum of Titanium

Acknowledgements
Financial support to the study from Port of Koper is gratefully acknowledged.

Diurnal variation of particulate concentration by size and micrometeorology in semi-arid rural environments

M. Cabello[1], J.A.G. Orza[1], M.A. Barrero[2], L. Cantón[2], A.Berasaluce[2], V. Lidón[1] and J. Martínez[1]

[1]SCOLAb and Aeolian Erosion Research Group, Universidad Miguel Hernández, Elche, 03202, Spain
[2]Chemical Engineering Group, University of the Basque Country, San Sebastián, 20018, Spain
Keywords: mineral dust, aerosol size distribution, resuspension, meteorology.
Presenting author email: mcabello@umh.es

The diurnal variation of the concentration of suspended particulate matter in the range of 0.25-32 µm, segregated by size, is studied in relation to meteorological (solar radiation, wind speed, relative humidity, temperature) and top soil (moist content and temperature) parameters.

Measurements were made at two rural environments in the western Mediterranean (located 18 and 8 km inland), in the framework of two projects: RESUSPENSE and EroHondo. Aerosol spectrometers with 31 particle size channels (Grimm mod. 190 and 365) and meteorological stations were used.

The relationship between dust concentrations and wind speed has been recently addressed in detail. Overall, submicron particles show lower concentrations the higher the wind speed, and dilution is the dominant mechanism. In contrast, particles larger than 15 µm present a net increase with increasing wind, just from the first 1 m s^{-1}. Human activity in the surroundings may maintain moderate levels of particle in the size range 2-12.5 µm. These particles show a strong reduction in concentrations even with light winds, although higher wind speeds lead to a net increase in concentrations due to resuspension (Orza et al., 2011).

To reduce the number of the 31 particle size channels to a smaller number of uncorrelated variables, a varimax rotated principal components analysis (PCA) was performed. Then, one representative particle size was selected for each identified factor.

Soil and air parameters show inertia to solar radiation (Fig.1). Temperatures (of top soil and air) peak around one hour later of the maximum of solar radiation, while relativity humidity shows a minimum. Sea breeze increases wind speed later in the central hours of the day.

The diurnal patterns of each representative particle size concentration are totally different. While the smallest particles show an increase during the late afternoon and night hours, the concentration of the largest ones raises during the central hours. Photo-chemical processes during the afternoon and the dispersion of the pollutants from the surrounding cities lead to the increase of the smaller particles concentration, which are accumulated within a shallow nocturnal boundary layer. In the morning, they are dispersed by the wind and a higher boundary layer. Convection (topsoil temperature greater than air temperature at 2m) is found to be the mechanism that facilitates the entrainment of the largest particles even at light winds. This fact has direct implications for modelling and understanding air quality in semi-arid environments.

We acknowledge financial support from the Spanish Ministry of Science and Innovation (EroHondo project CGL2008-05160; RESUSPENSE project CGL2004-04419).

Orza, J.A.G., Cabello, M., Lidón, V. and Martínez, J. (2011) *J. Arid. Environ*. **75**, 545-554.

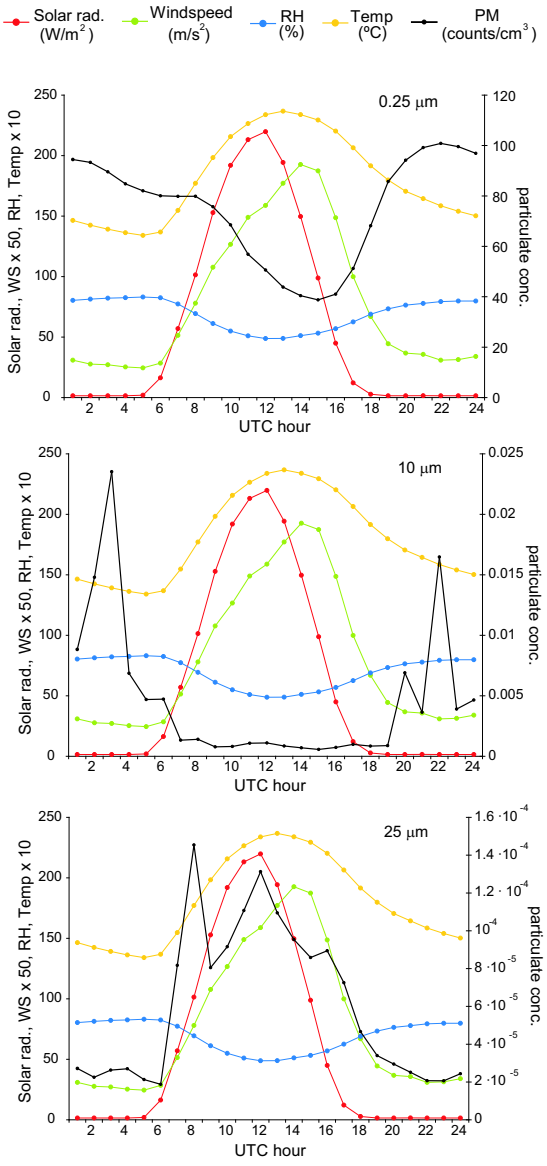

Figure 1. Diurnal variation of hourly mean particulate concentrations and meteo variables in *El Hondo*.

Mineralogy of Atmospheric Dust in Santiago island, Republic of Cape Verde: preliminary results

F. Rocha[1], A. Quintela[1], D. Terroso[1], C. Costa[1], J. Cardoso[2]; T. Nunes[2]; ; C.A. Pio[2], S. M. Almeida[3] and M.C. Freitas[3]

[1]Geobiotec Research Centre, Geosciences Dept., Univ. Aveiro, 3810-193 Aveiro, Portugal
[2]CESAM & Dep. Environment, Univ. Aveiro, 3810-193 Aveiro, Portugal.
[3]Instituto Tecnológico e Nuclear, 2686-953 Sacavém, Portugal
Keywords: mineralogy, atmospheric dust, Santiago island, Cape Verd.
Presenting author email: tavares.rocha@ua.pt

Mineral dust produced from windblown soils and deserts is one of the largest contributors to the global aerosol loading and has strong impacts on regional and global climates, long-term climate trends as well as marine and terrestrial ecosystems.

Knowledge of the compositions of atmospheric dust is pertinent to understanding its impact on human health and climate. Epidemiological studies have consistently shown an association between Air Particulate Matter pollution and the number of deaths from cancer and cardiovascular and respiratory diseases.

African dust is a special case in that it is comprised almost entirely of inorganic materials and the concentration of pollutant species is relatively low.

Cape Verde is located in an area of massive dust transport from land to ocean, and is thus ideal to set up sampling devices that will able the characterization and the quantification of the dust transported from Africa.

The main objectives of CV-Dust project are: 1) to characterize the chemical and mineralogical composition of dust transported from Africa by setting up an orchestra of aerosol sampling devices in the strategic archipelago of Cape Verde; 2) to identify the sources of particles in Cape Verde by using receptor models; 3) to elucidate the role Saharan dust may play in the degradation of Cape Verde air quality; 4) to model processes governing dust production, transport, interaction with the radiation field and removal from the atmosphere.

The project is a joint initiative of Aveiro University and Technological and Nuclear Institute (Lisbon, Portugal), together with the Cape Verde University and the support of the Cape Verde Atmospheric Observatory.

Almost all Cape Verde islands soils and sediments are from volcanic origin, but some islands, like Boavista, are covered by aeolian sands, composed by calcium carbonated minerals. So, it is expected to find some heterogeneities on the mineralogical composition of the atmospheric dusts.

Aerosol sampling is being performed at Praia airport during one year and mineralogical composition is being studied by X-ray diffraction, TEM and scanning electron microscopy.

PM10 sampling is being carried out since January 2011, and samples from the first 3 months are under studies.

Two subsamples were collected from each filter. Two diffractograms from each subsample were carried out, with and without spin. The four diffractograms were analyzed jointly, giving the mineralogical qualitative composition as well as the relative proportions for each identified mineral.

Iron hydroxides, such as lepidocrocite and goethite, and carbonates, such as calcite and siderite, are the most discriminating phases, allowing to differentiate 3 subsets:

- Iron hydroxides rich
- Calcite rich
- Siderite rich

Samples showing higher PM10conc. belong to first group, whereas those with lower PM10 conc. belong to second one.

On the contrary, silicates, such as quartz, feldspars and phyllosilicates (mainly micas), do not show any particular tendency, being ubiquitous and generally on small amounts. They show a trend to be more discrete in the carbonate-rich samples (also, with lower PM10 conc.), as expected.

The identification of the main sources and origins of the particles sampled in the archipelago will be carried out by integrating complementary tools such as Principal Component Analysis, Positive Matrix Factorization, Chemical Mass Balance, Multilinear Regression Analysis, Air Mass Back trajectories analyses, meteorological data and particle size segregate analysis.

This work was supported by the Portuguese Foundation for Science and Technology under CVDUST Project.

Modelling of long-range transport of mineral dust in Cape Verde

O. Tchepel[1], J. Ferreira[1], A.P. Fernandes[1], C. Gama[1], JM Baldasano[2], C. Borrego[1], J. Cardoso[1], S.M. Almeida[3], C. Pio[1]

[1]CESAM & Department of Environment and Planning, University of Aveiro, 3810-193 Aveiro, Portugal
[2]Earth Sciences Division, Barcelona Supercomputing Center, Barcelona, Spain
[3]ITN/MCTES, 2686-953, Sacavém, Portugal

Introduction

The mineral dust from deserts (e.g. Sahara) contributes largely to the content of tropospheric aerosols. Their long-range transport has impacts on air quality in several regions. To characterize 3D spatial and temporal variations of particulate concentrations and to establish a relationship between the emission sources and observed pollution levels dispersion models are used as valuable tools.

The present work aims to contribute to a better understanding of the role played by Saharan dust in the degradation of air quality in Cape Verde. For this purpose a modelling approach have been implemented and validated against the aerosol measurements.

Methodology

In the scope of CV-Dust project, the islands of Cape Verde, located in an area of massive dust transport from land to ocean, were chosen for air quality assessment.

The Dust REgional Atmospheric Model (DREAM) (Nickovic *et al*, 2001) designed to accurately describe the eroded desert dust cycle in the atmosphere has been used, in its updated version BSC-DREAM8b (Pérez *et al*, 2006) (www.bsc.es), to characterise long-range transport of mineral dust to Cape Verde. The model predicts 3D fields of dust concentration in the troposphere, taking into account all major processes of dust life cycle, such as dust production, horizontal and vertical diffusion and advection and wet and dry deposition. It includes 8-bin size distribution within the 0.1-10 µm radius range and dust-radiation interactions.

The simulation domain of BSC-DREAM8b covers North Africa, Europe and Middle East with an horizontal resolution set to 1/3ºx1/3º (~50kmx50km) and 24 z-vertical layers (up to ~15 km). Meteorological fields are initialized every 24h and boundary conditions updated every 6h with the NCEP/NCAR I global analysis (0.5ºx0.5º). USGS 1-km vegetation dataset and FAO 4-km global soil texture data are considered. In this study, 3-hour averages outputs were taken for the region of interest: 13ºN to 19ºN and 26ºW to 14ºW.

Measurements used for model evaluation have been provided by a field campaign (part of CV-DUST Project) performed during one year, from January 2011 to January 2012, at the former airport of Praia, Cape Verde.

Preliminary results

Figure 1 depicts the map of predicted PM10 concentrations for a day characterised by synoptic dynamics associated with dust uplift and transport till Cape Verde area (February 28, 2012).

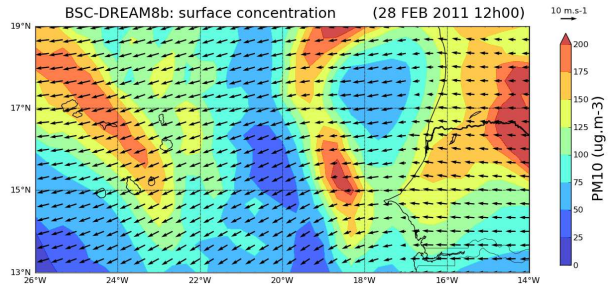

Figure 1. Map of predicted PM10 concentrations for 12 a.m. of February 28, 2012.

Figure 2 depicts the time series plot of predicted and observed PM10 concentrations in Praia, Cape Verde, during the field campaign period (when both predicted and observed data are available). It is possible to identify similarities between the annual behaviour of observed and predicted concentrations. However, it is clear the model shows a tendency to under predict the surface levels of PM10.

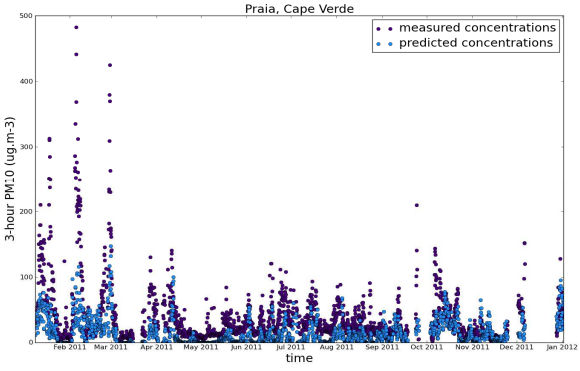

Figure 2. Time series plot of predicted and observed PM10 concentrations in Praia, (Jan 2011 - Jan 2012).

This work was supported by the Portuguese FCT through the PTDC/AAC-CLI/100331/2008 Project and the post doc grant of J. Ferreira (SFRH/BPD/40620/2007).The authors gratefully acknowledge the Barcelona Supercomputing Center for the provision of the BSC-DREAM8b modelling system.

Nickovic, S., Kallos, G., Papadopoulos, A. and Kakaliagou, O. (2001) *A model for prediction of desert dust cycle in the atmosphere*, J. Geophys. Res., 106(D16), 18113-18130.

Pérez, C., S. Nickovic, J. M. Baldasano, M. Sicard, F. Rocadenbosch, and V. E. Cachorro (2006) *A long Saharan dust event over the western Mediterranean: Lidar, Sun photometer observations, and regional dust modeling*, J. Geophys. Res., 111, D15214.

CLIMARENO 2011 campaign: airborne characterization of a Saharan dust intrusion over the Iberian Peninsula

J. Andrey[1], J. Fernández-Gálvez[2,3], J.L. Guerrero-Rascado[2,3], M. Sorribas-Panero[2,3], G. Titos-Vela[2,3], A. Corrales-Sierra[4], M. Gil-Ojeda[1], V. Cachorro[5], B. de la Morena[1] F.J. Olmo[2,3] and L. Alados-Arboledas[2,3]

[1]Área de Investigación e Instrumentación Atmosférica (AIIA), INTA. 28850 Torrejón de Ardoz, Spain
[2]Departamento de Física Aplicada, Universidad de Granada, 1807106 Granada, Spain
[3]Centro Andaluz de Medio Ambiente (CEAMA), Universidad de Granada, 18006 Granada, Spain
[4]Plataformas Aéreas de Investigación (PAI), INTA. 28850 Torrejón de Ardoz, Spain
[5]Grupo de Óptica Atmosférica, Universidad de Valladolid, 47071, Spain

Keywords: Saharan dust, Airborne measurements, Aerosol optical properties, Aerosol physical properties.
Presenting author email: javier.andrey@gmail.com

Saharan dust is the major source of aerosols emitted yearly to the atmosphere. The Iberian Peninsula, located at the North of the Sahara desert, is frequently affected by Saharan dust intrusions, especially during the summer period (Toledano et al., 2007; Bennouna et al., 2011; Guerrero-Rascado et al., 2009).

In June 2011, an airborne campaign was conducted by INTA in collaboration with Granada University intended to study Saharan dust aerosols properties. Flights were carried out over INTA "El Arenosillo" sounding station (ARN, 37.1N 6.7W) and Granada (GRA, 37.2N, 3.6W) under dust (D) and non-dust (ND) conditions. The data under ND condition were used as a "clean" reference for the D measurements. Four flights were carried out during the airborne campaign, two of them over each station.

The INTA atmospheric research aircraft was equipped with two optical particle counters designed by Droplet Measurement Technologies (DMT): PCASP-100X (15 bins, 0.1-3.0 μm) and CAPS (30 bins, 0.51-50 μm). The CAPS was equipped with optional depolarization module allowing determinations of refractive index and particle shape of the sampled aerosols. The algorithm to determine both refractive index and particle shape are based on the Mie theory.

Several particle counters and two CIMEL sun-photometers were deployed at both stations or in the vicinity of them. The size distributions retrieved by the airborne instrumentation are compared with in-situ measurements of particle counters and AERONET retrievals from the particle counters and CIMEL sun-photometers respectively. Data from CIMEL stations within the studied area have been used to provide a global image of the Saharan dust episode. Refractive index retrieved by the optional depolarization module is also presented and compared with CIMEL retrievals in this work.

The AOD at 440 nm during the flight for D conditions reached values of 0.48 and 0.30 over ARN and GRA, while under ND conditions the AOD reached 0.10 and 0.11 respectively. The ceiling of the Saharan dust intrusions detected by the aircraft was located at 6 and 5 km asl over ARN and GRA respectively. In both cases the concentration of particles in the coarse mode was higher at lower levels (2-3 km asl) than in the intrusion top height.

An oversampling issue in the coarse mode was noted for the PCASP measurements during ND days. This may be related with the low particle concentration found in this range.

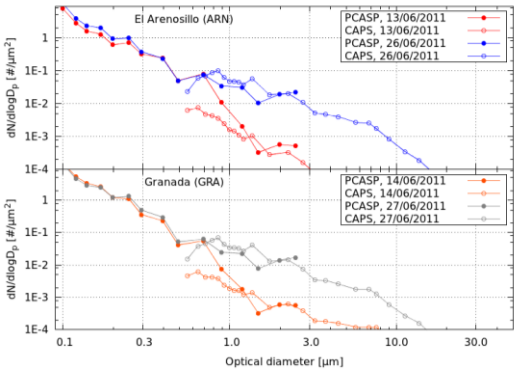

Figure 1: Columnar integrated SD from PCAPS and CAPS instruments

The authors are grateful to the crew of the C212 and people involved on the aircraft operation. We thank to P. Chazette, S. Wilbert, D. Mohammed and their staff for establishing and maintaining the Marbella_San_Pedro, Tabernas_PSA_DLR and Oujda sites used in this investigation. This work was supported by the Andalusia Regional Government through projects P08-RNM-3568 and P10-RNM-6299; by the Spanish Ministry of Science and Technology through projects CGL2010-18782, CSD2007-00067 and CGL2011-13580-E/CLI; and by EU through ACTRIS project (EU INFRA-2010-1.1.16-262254).

Bennouna et al (2011) *Remote Sensing of Environment*, pg. 1272-1284, doi: 10.1016/j.rse.201101.011

Guerrero-Rascado et al (2009) *Atmos. Chem, Phys.*, 9, 8453-8469, doi:10.5194/acp-9-8453-2009

Toledano et al. (2007) *J. Geophys. Res.* **112**, d21201, doi: 10.1029/2006JD008307

The influence of the Atlas Mountains and the meteorological situation on the impact of African dust outbreaks on the Iberian Peninsula

J.A.G. Orza, M. Cabello

SCOLAb, Universidad Miguel Hernández, Elche, 03202, Spain
Keywords: mineral dust, meteorology.
Presenting author email: ja.garcia@umh.es

In this work it is shown that the Atlas Mountains, under the appropriate meteorological conditions, may lead to the injection of dust-laden air masses directly into the atmospheric boundary layer in the Iberian Peninsula.

Satellite imagery, CALIPSO and radiosounding vertical profiles, meteorological records, synoptic charts as well as back-trajectories (ERA-Interim, 1-deg lat-long resolution) have been used to study a number of cases.

A good example is the most intense African Dust (AD) outbreak, in terms of impact at ground level, registered in southern Spain. A daily PM10 concentration of 309 µg m^{-3} was recorded on 11 Oct. 2008 at the Viznar background EMEP station. Hourly PM10 levels of 500 µg m^{-3} were recorded in Malaga, and concentrations remained quite high till the end of 13 Oct., 2008.

The interaction of an upper level cut-off low which formed on 9 October over the Strait of Gibraltar with the Atlas Mountains led to cyclogenesis in the lee (to the south) of the Moroccan Atlas. As shown by satellite imagery, large quantities of particles were mobilized as a massive haboob to Mauretania and Western Sahara, while a broad area north and east of the low was strongly sheared and mobilized a huge amount of dust northwards on 10 October. On 11 October the depression shifted northwestward to the Gulf of Cadiz at the time that a wide high pressure system concentrated over Tunisia and Italy. Such combination enhanced the south to north advection to the Iberian Peninsula (Cabello et al., 2012). Trajectories passed over the ridge descending the lee slope northward to the Alboran Sea and Spain (Fig. 1). Strong downward movement of air is found at the lowest heights (e.g. 1000m). Meteorological data registered a pressure decrease in the preceding hours of the AD outbreak, followed by a sharp increase just at the time of the dust impact on PM10 levels.

In contrast, the most intense AD outbreak in terms of aerosol optical depth (AOD) was registered in Granada on 4-7 September 2007 (Guerrero-Rascado et al., 2009). This event is classified as the second in intensity in southwestern Spain concerning AOD (Antón et al., 2012). Daily PM10 at the background EMEP stations, however, were lower than 35 µg m^{-3}; and hourly PM10 levels of 150 µg m^{-3} were recorded in Malaga with duration of a few hours. Mediterranean advection at low levels was induced by a strong high pressure system located over the British Isles and a deep low over southeastern Europe that extended to the central Mediterranean. A thermal low was present in all northern Africa and dust advection to the Iberian Peninsula was driven by a depression SW of the Gulf of Cadiz that intensified on 5 September (Fig. 1).

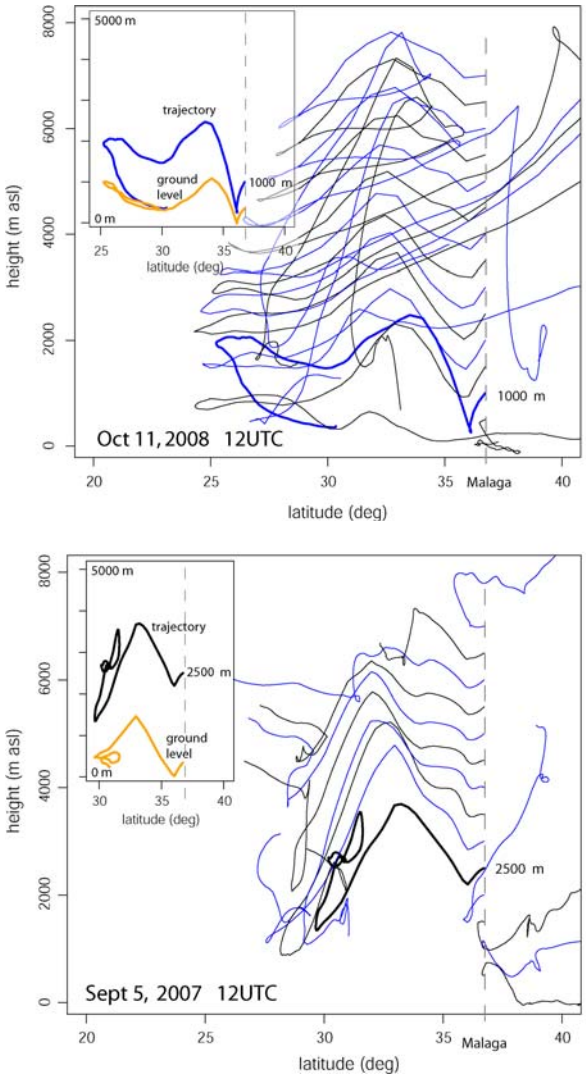

Figure 1. Plots of height vs. latitude of 96-hour trajectories arriving at Malaga (southern Spain) at 500 m steps. The insets depict the lowest trajectory with African origin and its corresponding ground level (peak is the Atlas; lowest point the Alboran Sea).

We acknowledge financial support from the Spanish Ministry of Science and Innovation (EroHondo project, CGL2008-05160).

Antón, M. et al. (2012) *J. Geophys. Res.* **117**, D03205.
Cabello, M. et al. (2012) *J. Geophys. Res.* (submitted)
Guerrero-Rascado, J.L. et al. (2009) *Atmos. Chem. Phys.* **9**, 8453–8469.

Computational investigation of vinylhydroperoxide dissociation: there is a barrier

Theo Kurtén[1], Neil M. Donahue[2]

[1] Laboratory of Physical Chemistry, University of Helsinki, P.O. BOX 55, FI-00014, Finland
[2]Dept. of Chemical Engineering, Carnegie Mellon University, Pittsburgh, PA 15213-3890, U.S.A.
Keywords: aerosol chemistry, SOA, ozone, vinylhydroperoxide
Presenting author email: theo.kurten@helsinki.fi

The oxidation of unsaturated hydrocarbons is one of the most important, yet least understood, aspects of the atmospheric component of the carbon cycle. Oxidation of terpenes (mainly by ozone) is one of the largest sources of secondary organic aerosols (SOA). The ozonolysis reaction is strongly exothermic, and proceeds via several intermediate steps, leading to a complex and variable product distribution even for relatively simple alkenes. The short lifetime and high energy of key intermediate species makes experimental characterization and separation of the individual reaction steps difficult. Many of the open issues in alkene ozonolysis concern the reactivity and fate of the Criegee Intermediates (CI), high-energy carbonyl oxides with partial biradical character. The reactivity of Stabilized Criegee Intermediates with key aerosol precursors such as SO_2 and NO_2 has recently (Welz *et al*, 2012) been experimentally shown to be significantly higher than previously measured – precisely as predicted by computational chemistry (Kurtén *et al*, 2011).

Besides leading to semivolatile or non-volatile products capable of forming SOA, ozonolysis also leads to the formation of OH radicals. This link between two of the three major atmospheric oxidants (the third being NO_3) is important, as it is one of the main routes by which OH can be formed at night, when direct photochemical sources are absent. In order to explain the pressure and time dependence of measured OH yields (OH radicals produced per consumed O_3 molecule), Drozd et al (2011) concluded that OH formation from ozonolysis proceeds via at least two intermediates, one of which is the vibrationally stabilized CI. The second intermediate was suggested to be the vinyl hydroperoxide (VHP), with a general structure $R_aR_bC=C(R_c)$-OOH where $R_{a,b,c}$ are hydrogens or alkyl groups. VHPs are formed from CIs via unimolecular isomerization. Unlike the highly reactive SCI, stabilized VHP is a relatively unreactive molecule (though one that decomposes rapidly to form OH). The atmospheric implications of stabilization data are thus dramatically different depending on which species – SCI or VHP – is produced. However, for VHP stabilization to be possible, that decomposition must involve a "tight" transition state with an energy barrier.

The dissociation of the simplest vinyl hydroperoxide CH_2=CH-OOH has been studied computationally, but with contradictory results. Richardson et al (1995) predicted that the dissociation reaction has a barrier, while some more recent studies (see e.g. Kuwata et al, 2003) have found - or assumed - the VHP decomposition to be barrierless. Common to all previous studies is their reliance on single-reference computational chemistry methods, which are unable to account for the static electron correlation associated with the resonance forms (CH_2=CH-O• and C•H_2-CH=O) of the vinyl oxide radical formed in the reaction.

We have reinvestigated the VHP dissociation using multireference methods more appropriate to the system (MRCISD(4,4)/cc-pVTZ, with energy corrections at higher levels), and found that the dissociation is indeed associated with a modest energy barrier. The corresponding transition state is shown in Figure 1. The transition state is connected by a reaction path to the reactant VHP on one side, and to a CH_2CHO•••HO radical – radical complex on the other side (see Figure 1). The transition state lies about 18 kcal/mol above the reactant and 3 kcal/mol above the product complex in enthalpy. Combining the MRCISD results with W1BD calculations for the overall reaction energetics indicates that the product complex is bound by about 7 kcal/mol with respect to free CH_2CHO + OH. Kinetic modeling will be performed in order to evaluate the impact of the computed reaction energetics on atmospheric ozonolysis chemistry.

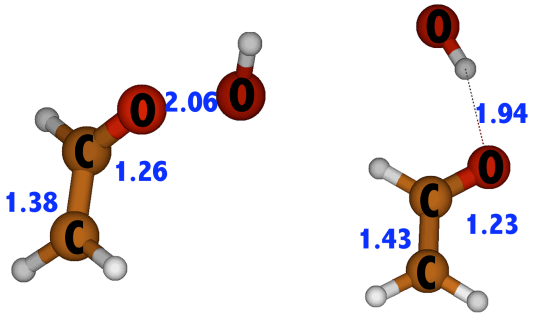

Figure 1. Transition state (left) and product complex (right) for the CH_2=CH-OOH → CH_2CHO + OH dissociation reaction, at the MRCISD(4,4)/cc-pVTZ level. Selected bond lengths are given in Ångström.

Calculations were performed using Gaussian 09 (Frisch et al, 2009) and Molpro 2010.1. (Werner et al, 2010). We thank the CSC IT Centre for Science in Espoo, Finland for computer time.

Drozd, G. T. *et al* (2011) *J. Phys. Chem. A* **115**, 161-166.
Frisch, M. J. *et al.* (2009) Gaussian 09, Gaussian, Inc., Wallingford CT, U.S.A.
Kurtén, T. *et al* (2011) *J. Phys. Chem A* **115**, 8669-8681.
Kuwata, K. T. *et al* (2003) *J. Phys. Chem. A* **107**, 11525-11532.
Richardson, W. H. (1996) *J. Org. Chem*. **60**, 4090-4095
Welz, O. *et al* (2012) *Science* **355**, 204-207.
Werner, H.-J. *et al.* (2010) MOLPRO, version 2010.1, http://www.molpro.net

Reaction of airborne allergenic protein with different nitrating agents

K. Selzle, C. Ackaert, S. Kofler, G.J. Oostingh and U. Pöschl

Department of Biogeochemistry, Max-Planck Institute for Chemistry, Mainz, 55128, Germany
Molecular Biology Department, University of Salzburg, 5020 Salzburg Austria
Keywords: protein nitration, NO_2, O_3, reactive oxygen species, aerosol chemistry, bioaerosols
k.selzle@mpic.de

Proteins account for up to ~5% of urban particulate matter, influence the physiochemical properties of atmospheric particles, and play a major role as airborne allergens (Franze et al. 2003)

Several studies indicated that proteins could be nitrated by NO_2 and O_3 gas in atmosphere and the nitration took place at the tyrosine residue (Franze et al. 2005). Moreover, studies have suggested that nitration can change the allergenicity of proteins (Gruijthuijsen et al. 2006, Untersmayr et al., 2010).

To get a better understanding of the nitration procedure, the reaction products and pathways of protein nitration were studied with three different nitration reactants. The recombinant major birch pollen allergen Bet v 1.0101 was nitrated by liquid tetranitromethane (TNM), by liquid peroxynitrite, and by gaseous nitrogen dioxide and ozone (NO_2+O_3) as illustrated in Fig 1. Each method was applied in multiple steps of titration to obtain proteins with different nitration degrees and to get information about reaction efficiency and site selectivity. The nitration degrees of individual nitrotyrosine residues (NDY) were determined by site-specific quantification with HPLC-MS/MS and compared to the total protein nitration degrees (ND) determined by photometric detection with HPLC-DAD.

The observed nitration patterns showed the site selectivity of protein nitration which depended on the nitrating agent, reaction conditions and molecular structure of the protein (Fig. 2). These findings suggest different nitration mechanisms as well as interesting insights in nitration pathways occurring under summer smog conditions in the atmosphere (NO_2 and O_3) or during inflammatory processes in the human body (peroxynitrite).

The chemical mechanisms and molecular processes that lead to adverse health effects of NO_2 and O_3 are, however, still poorly understood. We suggest that protein nitration by air pollutants plays a major role in the increase of allergies in the western countries besides nutrition effects and excessive hygiene practices.

This work was supported by the Max-Planck Society (MPG), the International Max-Planck Research School for Atmospheric Chemistry and Physics (IMPRS) and the Max-Planck Graduate School (MPGC) and by the FWF, the Austrian Research Funding Foundation (project P22236-B13).

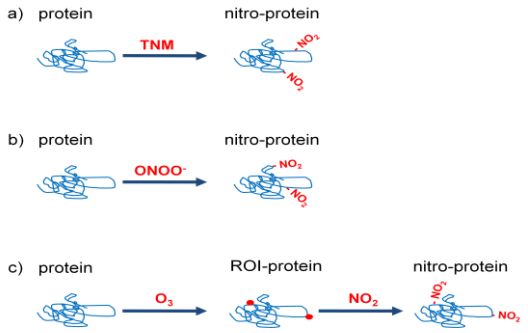

Figure 1: Protein nitration pathways. (Selzle et al., 2011)

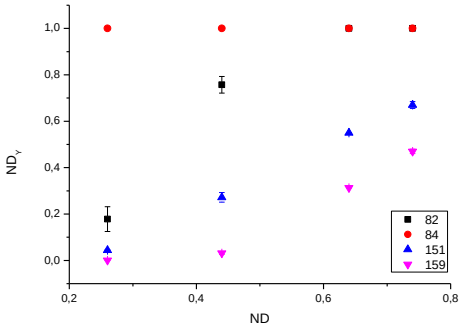

Figure 2: Site-selectivity of Bet v 1 nitration with TNM.

Franze, T., Weller, M. G., Niessner, R. and Pöschl, U. (2003) *Analyst*, 128(7): 824-831

Franze, T., Weller, M. G., Niessner, R. and Pöschl, U. (2005) *Environ. Sci. Technol.*, 39(6): 1673-1678

Gruijthuijsen, Y. K., Grieshuber, I. et al. (2006) *Int. Arch. Allergy Immunol.*, 141(3): 265-275

Untersmayr, E., Diesner, S. C. et al. (2010) *PLoS ONE* 5(12): e14210

Selzle K., Zhang Y. et al. (2011) *G.I.T. Laboratory Journal Europe* Issue 5-6

Shiraiwa M., Sosedova Y. et al. (2011) *Nature Chem.* Vol. 3, 291-295

Shiraiwa, M., Selzle, K. et al. (2012) *Free Radical Research, in press*

Zhang, Y., Yang, H. et al. *Anal. Bioanal. Chem.*, 399: 459-471

Temperature dependence of water activity in aqueous solutions of alcohols and organic acids

Gouri Ganbavale[1], Claudia Marcolli[1], U. K. Krieger[1], Greta Stratmann[1], Andreas Zuend[2], Thomas Peter[1]

[1]Institute for Atmospheric and Climate Science, ETH Zurich, Zurich, 8092, Switzerland
[2]Department of Chemical Engineering, California Institute of Technology, Pasadena, California, 91125, USA
Keywords: aerosols, vapour pressure, organics, temperature dependence.
Presenting author email: gouri.ganbavale@env.ethz.ch

The properties of tropospheric aerosols in terms of their hygroscopicity, phase transitions and light scattering are of great interest in view of their cloud forming and climatic characteristics. Aerosols are complex mixtures of organic and inorganic constituents. The organic aerosol fraction is expected to be present in liquid or amorphous state since a large number of organic compounds depress the temperature at which crystalline solids form (Marcolli et al 2004).

In the upper troposphere homogeneous ice nucleation and cirrus cloud formation occur on aqueous aerosol particles that grow into ice crystals by dissipating supersaturated water vapors. According to Koop et al. (2000) homogeneous ice nucleation in aqueous supercooled solutions does not depend on the nature of the solute but only on water activity, aw, the ratio between the water vapor pressure of the solution and of pure water under the same conditions. If aqueous aerosol particles are in equilibrium with the surrounding gas phase, aw and ambient relative humidity correspond. Thus aw of solutions at low temperatures is a crucial parameter for homogeneous ice nucleation.

Activity coefficients of organic solutions may exhibit a considerable temperature dependence that has to be explicitly parameterized in thermodynamic models in order to achieve accurate predictions at temperatures other than room temperature (Zobrist et al., 2008). However, most water activity data of aqueous organic solutions has been acquired at room or elevated temperatures. If temperature dependence of the activity coefficients is neglected, errors on the order of 10-15% in aw at the homogenous freezing temperature may result (Zobrist et al., 2008), which in turn would induce large uncertainties in estimating the direct and the indirect effects of aerosols.

To measure aw over a wide composition range while focusing on low temperatures, we use different measurement techniques. Direct aw measurements with an AquaLab dewpoint water activity meter (Model 3TE, Decagon devices, USA) cover the temperature range from 289-313K.Hygroscopicity measurements of single levitated aerosol particles with an electrodynamic balance cover dry conditions up to ice saturation from 200 to 300 K. The ice melting curves obtained from DSC measurements yield solid-liquid equilibria that can be directly related to the melting point depression as a function of aw.

To complement and validate these measurement techniques, we developed a setup to measure absolute vapor pressures of solutions at low temperatures and applied it to binary aqueous organic mixtures. Since we attribute measured absolute vapor pressures totally to water vapor pressures, we are restricted to binary mixtures with low organic vapor pressures that lie within the experimental uncertainty of the absolute vapor pressure. Moreover, we need an effective degassing procedure prior to the measurement to remove the air that is dissolved in the solutions.

Measurements were performed for alcohols/polyols and organic acids covering the –OH and –COOH functional groups which are commonly a part of tropospheric aerosols. Vapor pressure measurements are conducted for binary organic mixtures of water with namely 1,4-butandiol and the multi-component dicarboxylic acid mixture M5 composed of DL-malic, maleic, malonic, glutaric and methylsuccinic acid, counting among the most frequently detected in the atmosphere. Measurements were conducted over the concentration range of 10-90 wt % and temperature range of 223 to 290K. The measured vapor pressure values are used to calculate aw using the Murphy and Koop (2005) parameterization.

Results agree well within 2% of error with the aw measurements done at room temperatures and EDB measurements done at low temperatures. Strong temperature dependency was observed at low temperatures in case of 1,4-butanediol and M5 mixtures. Interestingly, binary M5 and water mixtures show a reversal of the trend of decreasing water activity with decreasing temperature at low temperature. This shows the need to measure water activities over a wide range of temperatures and compositions for various organic functional groups. We will conduct vapor pressure measurements for further interesting organic mixtures. This data will be implemented in the group contribution model AIOMFAC developed by Zuend et al. (2008) to improve the temperature dependency parameterization for low temperatures.

References:

Koop, T., Luo, B. P., Tsias, A. and Peter, T., Nature, 406, 611 - 614, 2000.

Marcolli, C., B. P . Luo, and Peter. T., J. Phys. Chem. A, 108, 2216 - 2224, 2004.

Murphy, D. M, Koop. T., Q. J. R. Meteorol. Soc., 131, 1539 - 1565, 2005.

B. Zobrist, Marcolli, C., Pedernera, D. A., and Koop, T., Atmos. Chem. Phys., 8, 5221–5244, 2008.

Zuend, A., Marcolli, C., and Peter, T., Atmos. Chem. Phys., 8, 4559 - 4593, 2008.

Heterogeneous Uptake of HO_2 Radicals onto Submicron Atmospheric Aerosols

P. S. J. Matthews[1], I. J. George[1], B. Brooks[2,3], A. Goddard[1], L. K. Whalley[1,3], M. T. Baeza-Romero[4] and D. E. Heard[1,3]

[1]School of Chemistry, University of Leeds, Woodhouse Lane, Leeds, LS2 9JT, UK
[2]School of Earth and Environment, University of Leeds, Woodhouse Lane, Leeds, LS2 9JT, UK
[3]National Centre for Atmospheric Chemistry, University of Leeds, Woodhouse Lane, Leeds, LS2 9JT, UK
[4]Escuela de Ingenieria Industrial de Toledo, Universidad de Castilla la Mancha, Toledo, 45071, Spain
Keywords: free radicals, aerosol-surface reactions, tropospheric aerosols, multiphase processes
Presenting author email: d.e.heard@leeds.ac.uk

The two radicals OH and HO_2, which are collectively known as HO_x, play crucial roles in tropospheric chemistry. The OH radical is responsible for the majority of the oxidation in the troposphere, whilst HO_2 is cycled back to OH. The OH radical is also responsible for controlling the concentrations of many reactive species, for example volatile organic compounds (VOCs). It is therefore important to be able to accurately predict OH and HO_2 concentrations in the troposphere.

Some recent field studies have measured significantly lower HO_2 concentrations than are predicted by constrained box models. Some of the differences between the model calculations and field measurements have been attributed to uptake of HO_2 by aerosols (Jaegle *et al.*, 2000; Sommariva *et al.*, 2006; Mao *et al*., 2010). However, there have been very few laboratory studies on HO_2 uptake by aerosols and the rates and mechanism of the HO_2 loss by aerosols are still uncertain. It is therefore essential to gain a better knowledge of the uptake of HO_2 by different aerosols under different conditions. If this is achieved then the uptake coefficients can be included within models to provide a better description of tropospheric processes involving HO_2.

The HO_2 uptake coefficients for a range of inorganic and organic aerosols were measured at room temperature (≈293 K) and atmospheric pressure (≈760 Torr) using an aerosol flow tube combined with the Fluorescence Assay by Gas Expansion (FAGE) technique. FAGE is a highly sensitive laser induced fluorescence based detection method which allows the experiments to be done with low HO_2 concentrations (≈10^8-10^9 molecule cm^{-3}). The HO_2 radicals were injected into the aerosol flow tube using a moveable injector which allowed position dependent HO_2 profiles to be created as a function of different aerosol concentrations. The aerosols were produced by placing a solution in an atomiser or by using homogeneous nucleation and HO_2 was formed by the photolysis of water vapour in the presence of trace amounts of oxygen. Particle size distributions were measured with a Scanning Mobility Particle Sizer (TSI).

The HO_2 uptake coefficients were measured and found to follow first order kinetics for a variety of aerosols. The HO_2 uptake coefficient was measured for dry inorganic aerosols (γ= 0.000- 0.001), wet inorganic aerosols (γ= 0.002- 0.005), wet copper doped ammonium sulfate aerosols (γ= 0.28) and ammonium sulfate aerosols doped with different molar amounts of iron (γ=0.003- 0.06). The pH dependence of the HO_2 uptake coefficient was also investigated, however, no dependence was observed. The HO_2 uptake coefficients onto a range of both wet and dry organic aerosols were measured and found to be small (γ<0.008) with the exception of humic acid aerosols which had a larger uptake coefficient that was also dependent on relative humidity (γ=0.008-0.13). However, humic acid was found to contain metals, which may explain the higher uptake coefficient. Finally, the temperature dependence of the HO_2 uptake coefficient is being studied for a range of aerosols.

This work was supported by the National Environment Research Council under grant number NE/F020651/1. PSJM is grateful to NERC for a research studentship.

Jaegle, L. *et al.* Photochemistry of HOx in the upper troposphere at northern midlatitudes. *Journal of Geophysical Research-Atmospheres* **105**, 3877-3892 (2000).

Sommariva, R. *et al.* OH and HO_2 chemistry during NAMBLEX: roles of oxygenates, halogen oxides and heterogeneous uptake. *Atmospheric Chemistry and Physics* **6**, 1135-1153 (2006).

Mao, J. *et al.* Chemistry of hydrogen oxide radicals (HO_x) in the Arctic troposphere in spring, *Atmospheric Chemistry and Physics* **10**, 5823-5838 (2010).

How do night-time oxidants affect the fate of an organic coated aerosol droplet?

F. Sebastiani[1,2], R.A. Campbell[1], I. Hoare[2] and C. Pfrang[2]
[1]Institut Laue-Langevin, 6 Rue Jules Horowitz, BP 156, 38042 Grenoble Cedex 9, France
[2]Department of Chemistry, University of Reading, P.O. Box 224, RG6 6AD Reading, UK
Keywords: organic aerosols, nitrogen oxides, neutron reflectometry
Presenting author email: sebastiani@ill.eu

Aerosols attract more and more the attention of the scientific community, because their impact on the Earth's radiative balance and on cloud formation is still largely unknown [*e.g.* Solomon *et al.*, 2007]. A key feature for aerosol behaviour is the presence of organic material both in the bulk and at the surface [Fuzzi *et al.*, 2006].

Our interest concerns the kinetics of oxidation reactions occurring on a surfactant monolayer at the air-water interface. Oleic acid is widely used as proxy for organic aerosols [Dennis-Smither *et al.*, 2012, Docherty & Ziemann, 2006, Hung & Tang, 2010], because of its presence in the atmosphere, for example due to meat cooking processes [Allan *et al.*, 2010]. Unlike the overwhelming majority of studies, we follow the fate of the oleic acid monolayer at the air-water interface. The reaction is driven by oxidising agents such as nitrogen oxides NO_y (NO_2, NO_3 and N_2O_5), present only during night-time, because they are rapidly photolysed by sunlight [Wayne *et al.*, 1991].

Thanks to the *in situ* production of NO_y from the reaction between NO_2 and O_3, a wide range of concentrations is accessible. Neutron reflectometry and deuterium labelling of molecules allow us to follow the reaction with high time resolution (less than 10 seconds per measurement).

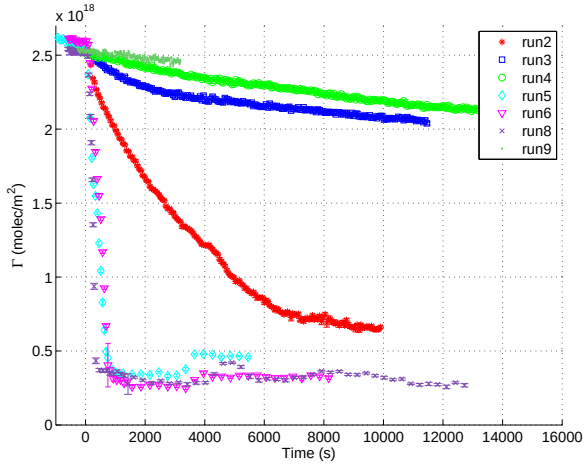

Figure 1: Decays of oleic acid surface excess as a function of time for different $[NO_3]$ and $[N_2O_5]$.

The monolayer is obtained by spreading a solution of chloroform and deuterated oleic acid on a subphase, made up by a mixture of H_2O and D_2O (8.1% by volume), in a Langmuir trough contained in a custom-built environmental chamber. The initial surface excess is controlled by changing the surface area by movable barriers; the surface pressure, which is directly related to the surface excess, is measured throughout the experiment.

In Fig.1 the decays of surface excess (Γ) are shown as a function of time for different ratios of $[NO_3]/[N_2O_5]$. At the end of the reaction the surface excess reaches a value substantially greater than the minimum Γ measurable, demonstrating that the reaction consistently leaves material at the interface. We found that once the layer is compressed again, the reaction restarts and the surface excess decays back to the previous minimum value.

The kinetic interpretation of these decays will give information on the rate coefficient specific to the reaction between the organic monolayer and the oxidant. Our aim is to understand this single component system in order to be able to move forward to multi-component systems, and investigate how the presence of different surfactants affects the rate coefficient. Complementary optical techniques, such as ellipsometry and Brewster angle microscopy, will be used to characterise the behaviour of multi-component monolayers, in order to optimise the use of neutron reflectometry and isotopic contrast variation to compare relative rate coefficients of the compounds in multi-component systems.

This work was supported by allocations of beam time at the Institut Laue-Langevin (Grenoble, France). The experiment was performed on FIGARO at the ILL. FS is grateful for support from ILL and the University of Reading in the framework of the NEATNOx studentship programme.

Allan, J. D. *et al.* (2010). *Atmos. Chem. Phys.,* **10** (2), 647–668.

Dennis-Smither, B. J. *et al.* (2012). *J. Phys. Chem. A,* ASAP, DOI: 10.1021/jp211429f.

Docherty, K. S. & Ziemann, P. J. (2006). *J. Phys. Chem. A,* **110** (10), 3567–3577.

Fuzzi, S. *et al.* (2006). *Atmos. Chem. Phys.,* **6** (7), 2017–2038.

Hung, H.-M. & Tang, C.-W. (2010). *J. Phys. Chem. A,* **114** (50), 13104–13112.

Solomon, S. *et al.* (2007). *Climate Change 2007 - The Physical Science Basis*, Cambridge University Press.

Wayne, R. *et al.* (1991). *Atmos. Environ.,* **25** (1), 1 – 203.

From free electrons to H_2SO_4 - assessing the efficiency of ion catalysed SO_2 oxidation

N. Bork[1,2] and H. Vehkamäki[1]

[1]Department of Physics, University of Helsinki, Helsini, 00014, Finland
[2]Department of Chemistry, University of Copenhagen, Copenhagen, 2100, Denmark
Keywords: Ion-induced nucleation, aerosol catalysis, air ions, sulfuric acid, chemistry
Presenting author email: nicolai.bork@helsinki.fi

Understanding the properties of clouds is one of the most challenging aspects within atmospheric chemistry. It is well known that a seed is needed to initiate nucleation and that the primary seeding is sulfuric acid (H_2SO_4). Understanding the properties of clouds is thus closely related to understanding the properties and in particular the atmospheric production of H_2SO_4 .

The most important source is UV induced oxidation of SO_2 , but recently, a number of studies have found evidence of a new synthesis mechanism, complimentary to this. This mechanism in known to invoke ions, but until now, no established mechanism can account for the observations (Kirkby *et al*, 2011).

We have initiated a line of studies dedicated to the discovery of this mechanism and the assessment of its importance. We have systematically investigated the very first interactions and reactions of a free atmospheric electron. Previously, we have established the size distributions of $O_2^-(H_2O)_n$ and $O_3^-(H_2O)_n$ clusters. Further, we have demonstrated that the rate of oxidation of SO_2 to $O_2SO_3^-$ by a $O_3^-(H_2O)_n$ cluster is collision limited (Bork et al, 2011). See also Fig. 1. This is particularly encouraging since the oxidation step of S(IV) to S(V) is known to be rate limiting of UV induced SO_2 oxidation (Loerting and Liedl, 2000).

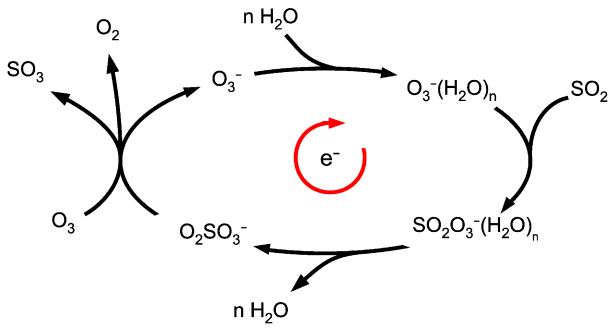

Fig. 1: The reactions involved in a simple catalytic cycle converting SO_2 to SO_3 . The catalyst is the electron.

We have continued these studies by considering the most likely chemical fate of $O_2SO_3^-$. Here, we report the reactions initiated by collision with O_3 . We have calculated the thermodynamic properties of all relevant species and complexes using density functional theory and statistical mechanics. Reaction rates were determined using transition state theory.

We find two major reaction channels,

$$O_2SO_3^- + O_3 \rightarrow \begin{cases} O_2 + O_3^- + SO_3 & (1) \\ O_2 + O_3SO_3^- & (2) \end{cases}$$

All ionic species in Reactions (1) and (2) have been observed in field studies and in experiments and are known products of ionizing radiation (Ehn *et al.*, 2010). However, until now the chemistry producing these otherwise rare species have been unknown.

We report and analyse the following results:

- The thermodynamics of Reactions (1) and (2) as well as several reactions of minor importance.
- The energy barriers and transition states, if any exist, of all reported reactions. See also Fig. 2.
- Reaction rates and rate constants at typical conditions.
- The relative rates of Reactions (1) and (2). This is of particular interest since Reaction (1) will close the catalytic cycle enabling the electron to catalyse the oxidation of another SO_2, whereas Reaction (2) stabilizes the electron and hence terminate its catalytic effect.
- The overall effects of this catalytic cycle at varying degrees of ionization, temperature, humidity and altitude and compare to experimental and field data.

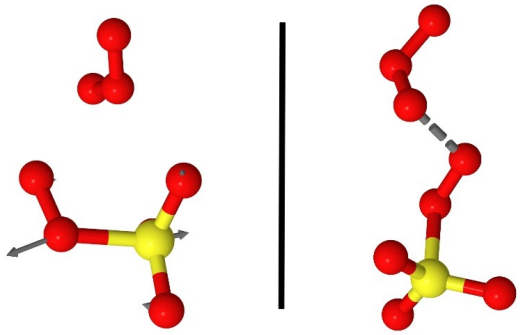

Fig. 2: Left: One of the vibrational modes leading to dissociation of the $O_2SO_3^-$ cluster and closing of the catalytic cycle, i.e. Reaction (1). Right: The transition state in the oxidation of $O_2SO_3^-$ to $O_3SO_3^-$, i.e. Reaction (2).

Kirkby, J. *et al. (2011) Science,476,429.*
Bork, N. *et al.* (2011), *Atmos. Chem. Phys. Discuss.* 11, 29647-29679.
Loerting, T., and Liedl. K.R. (2000) *PNAS*, 97,16
Ehn, M. *et al.* (2010) *Atmos. Chem. Phys.,* 10, 8513.

Simultaneous study of gas and particulate products formed from isoprene oxidation: laboratory and field measurements

C. Rio[1], S. Rossignol[1], S. Fable[1], L. Chiappini[1]

[1]Institut National de l'Environnement Industriel et des Risques (INERIS), 60 550 Verneuil-en-Halatte, France
Keywords: Isoprene, SOA, Gas-particle distribution, Smog chamber.
Presenting author email: caroline.rio@ineris.fr

Isoprene is one of the most abundant non-methane hydrocarbons emitted by vegetation into the troposphere. For a long time, it has been generally accepted that isoprene oxidation did not contribute to global SOA burden because of the volatility of its main oxidation products (methacrolein, methyl vinyl ketone…) (Pandis, 1991). It is only recently that isoprene oxidation contribution to SOA formation has been proven (Edney, 2005; Kroll, 2006).

There are still remaining uncertainties on the importance of isoprene contribution to atmospheric SOA and further studies combining ambient measurements of tracers, identified in laboratory experiments, coupled with atmospheric modeling are needed to better parameterize SOA yields and quantitatively model SOA production from isoprene oxidation (Carlton, 2009).

Therefore, the first part of this work focuses on laboratory experiments to study isoprene oxidation under realistic conditions in the EUropean PHOtoREactor (EUPHORE) in Valencia during the period 13–22 September 2010 (Figure 1(a)): seed aerosols (10 µg/m^3) were present in the chamber before isoprene and H_2O_2 introduction (70 ppb and 4 ppm respectively) under sunlight irradiation and a relative humidity close to 30 %. Moreover this study of the (isoprene + OH) reaction was performed under free-NOx condition.

A method recently developed in our laboratory (Rossignol, 2012) was used to investigate the chemical composition of both gas and particulate phases of SOAs formed.

This method consists in using stainless steel Tenax-TA adsorbent tubes previously coated with PFBHA (to specifically study carbonyl compounds) or MTBSTFA (to specifically study hydroxyl compounds) to collect the gas phase. Particulate sample are collected onto filters (quartz and Teflon-Quartz) subsequently exposed to PFBHA or MTBSTFA before analysis. These tubes and filters are subsequently analyzed by thermal-desorption coupled with gas chromatography and mass spectrometry (TD-GC-MS) analysis.

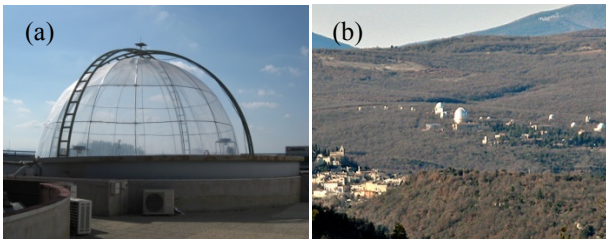

Figure1: (a) EUPHORE smog chamber, (b) St.Michel l'Observatoire with OHP in the background

About thirty compounds have been positively or tentatively identified in gas and/or particle phases. Some of these are monofunctionalized such as methacrylic acid or methacrolein, others are polyfunctionalized such as malic acid. These compounds have been quantified and for those identified in both gas and particulate phases, an experimental partitioning coefficient was calculated.

In a second time, these results will be compared to real atmosphere samples during a field campaign which will take place in June 2012 at the Observatoire de Haute provence (OHP; situated in southeast France) (Figure 1(b)) as a part of the CANOPEE field campaign. This work falls within the framework of a research program about the study of combined model-measurement of intra canopy chemistry. Not only gas and particles samplings will be realized but particles formation and isoprene emission will be observed at the same time.

Results obtained in both smog chamber and field campaign during isoprene oxidation will be presented and discussed.

Carlton A. G., Wiedinmyer C., and Kroll J. H. (2009) *Atmos. Chem. Phys.*, **9**, 4987–5005.

Edney, E. O., Kleindienst, T. E., Jaoui, M., Lewandowski, M., Offenberg, J. H.,Wang,W., and Claeys, M. (2005*) Atmos. Environ.*, **39**, 5281–5289.

Kroll, J. H., Ng, N. L., Murphy, S. M., Flagan, R. C., and Seinfeld,J. H. (2006) *Environ. Sci. Technol*., **40**, 1869–1877.

Pandis, S. N., Paulson, S. E., Seinfeld, J. H., and Flagan, R.C. (1991) *Atmos. Environ.* ; **25**, 997–1008.

Rossignol, S., Chiappini, L., Perraudin, E., Rio, C., Fable, S., Valorso, R., and Doussin, J. F (2012) *Atmos. Meas. Tech. Discuss.;* **5**, 1153-1231.

Aerosol yields from ozonolysis of α- and β-pinene in simulation chamber experiments with low precursor concentrations

H. Saathoff, K.-H. Naumann, and O. Möhler

Institute for Meteorology and Climate Research, Karlsruhe Institute of Technology, Hermann-von-Helmholtz-Platz 1, 76344 Eggenstein-Leopoldshafen, Germany
Keywords: aerosol chemistry, secondary organic aerosol, aerosol formation, low concentrations
Presenting author email: harald.saathoff@kit.edu

Secondary organic aerosols (SOA) from the oxidation of biogenic volatile organic compounds (BVOC) are a large fraction of the tropospheric aerosol especially over tropical continental regions. The dominant SOA forming compounds are monoterpenes of which pinene is the most abundant. The reactions of monoterpenes with OH radicals, NO_3 radicals, and ozone yield secondary organic aerosol mass in highly variable yields. Despite the various studies on SOA formation the influence of temperature and precursor concentrations on SOA yields are still major uncertainties in tropospheric aerosol models. In previous studies we observed a negative temperature dependence of SOA yields for SOA from ozonolysis α-pinene and limonene (Saathoff et al., 2009). However, this study as well as most of the literature data for measured SOA yields is limited to terpene concentrations of several ppb and higher, hence about an order of magnitude higher than terpene concentrations even near their sources. Monoterpene concentrations in and above tropical or boral forests reach values up to a few tenth of a ppb during daytime decreasing rapidly with altitude in the boundary layer (Kesselmeier et al. 2000; Boy et al., 2004).

Therefore we investigated the yield of SOA material from the ozonolysis of α- and β-pinene under simulated tropospheric conditions in the large aerosol chamber AIDA on time scales of several hours and for terpene concentrations between 0.1 and 1 ppb. The temperatures investigated were 243, 274, and 296 K with relative humidities ranging from 25% to 41%. The organic aerosol was generated by controlled oxidation with an excess of ozone (220-930 ppb) and the aerosol yield is calculated from size distributions measured with differential mobility analysers (SMPS, TSI, 3071 & 3080N) in the size range between 2 and 820 nm. On the basis of the measured initial particle size distribution, particle number concentration (CPC, TSI, 3775, 3776, 3022), and trace gas evolution model calculations were done using the aerosol model COSIMA supplemented by a SOA module (Saathoff et al., 2009).

As previously reported for higher SOA concentrations the overall SOA yields from ozonolysis of α- and β-pinene increase significantly with decreasing temperature. However, compared to the yields extrapolated from experiments done with higher terpene concentrations the SOA yields at ambient like concentrations are surprisingly high. They reach values of up to 20% at 243 K for organic aerosol mass concentrations of about 0.5 µg m^{-3} even without additional seed aerosol.

Figure 1 shows the evolution of integrated SOA mass and particle number during ozonolysis of 109 ppt and subsequently 377 ppt α-pinene by an excess of initially 282 ppb of ozone. Please note that OH radicals were not scavenged in this experiment.

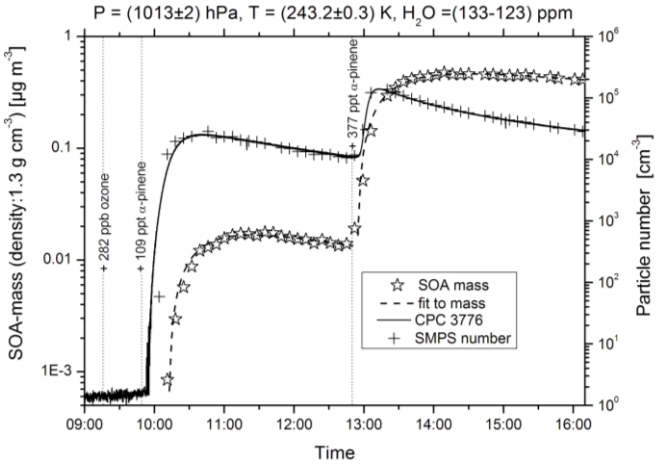

Figure 1 shows the evolution of the particle mass concentrations calculated by integration of the measured particle size distribution using a particle density of 1.3 g cm^{-3} as well as the particle number concentration for particles larger than 2.5 nm.

This paper discusses the temperature dependent SOA yields from the ozonolysis of α-pinene and β-pinene in comparison with data from literature.

Boy, M., Petäjä, T., Dal Maso, M., Rannik. Ü., Rinne, J., Aalto, P., Laaksonen, A., Vaattovaara, P., Joutsensaari, J., Hoffmann, T., Warnke, J., Apostolaki, M., Stephanou, E. G., Tsapakis, M., Kouvarakis, A., Pio, C., Carvalho, A., Römpp, A., Moortgat, G., Spirig, C., Guenther, A., Greenberg, J., Ciccioli, P., Kulmala, M. (2004) *Atmos. Chem. Phys.* **4**, 657–678.

Kesselmeier, J., Kuhn, U., Wolf, A., Andreae, M.O., Ciccioli, P., Brancaleoni, E., Frattoni, M., Guenther, A., Greenberg, J., De Castro Vasconcellos, P., Telles de Oliva, Tavares, T., Artaxo, P. (2000) *Atmos. Environ.* **34,** 4063-4072

Saathoff, H., Naumann, K.-H., Möhler, O., Jonsson, Å. M., Hallquist, M., Kiendler-Scharr, A., Mentel, Th. F., Tillmann, R., Schurath, U. (2009) *Atmos. Chem. Phys.* **9** (5), 1551-1577.

Phase-changes during oxidation of atmospheric aerosols: ozonolysis of levitated droplets containing oleic acid.

C. Pfrang,[1] A. M. Squires,[1] M. Rittman,[1] M. Ghosh,[1] F. Sebastiani,[1] and A. D. Ward.[2]

[1]Department of Chemistry, University of Reading, P.O. Box 224, RG6 6AD Reading, UK
[2]Research Complex at Harwell, Rutherford Appleton Laboratory, OX11 0FA Didcot, UK
Keywords: aerosol chemistry, ozone, organic aerosols, phase changes, laser tweezers
Corresponding author's email: c.pfrang@reading.ac.uk
Session: Multi-phase chemical processes and interactions involving aerosol

Self-assembled phase behaviour of surfactant molecules during atmospheric ageing may have a major impact on the fate of organic aerosols and thus on climate change. For direct quantification of phase changes, compositional changes and kinetic parameters we will perform studies of the oleic acid/ water/ ozone system using laser Raman tweezers combined with small- and wide-angle X-ray scattering, SAXS/WAXS, at the Diamond Light Source in August 2012. This work is complemented by off-line laser Raman tweezers and X-ray scattering investigations at RAL and Reading.

Atmospheric aerosols are key components of the climate system: they affect the climate directly, by scattering and absorbing solar radiation, and indirectly, by inducing cloud formation.[1] While atmospheric lifetimes of volatile compounds are largely determined by chemical kinetics,[2] phase-dependent mass transport parameters are important additional factors for organic aerosol components.[3] Nearly all atmospheric aerosols contain organic compounds that are often surface active, in particular fatty acids. These include stearic and palmitic acids found in marine aerosols and produced by biological degradation,[4] and oleic acid suggested as major component of cooking aerosols, mostly from seed oils.[5] Such surfactants would be expected to be present in their ionic form, where they would self-assemble into a range of aggregate structures including micelles, multi-lamellar vesicles, and other lyotropic phases. It has been

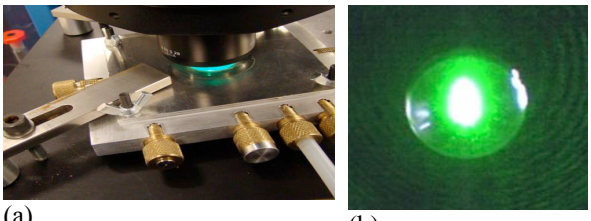

(a) (b)

Fig. 1 (a) Reading-built cell for laser Raman tweezers studies. (b) Image of levitated organic droplet.

proposed that this self-assembly would impact the properties of the aerosol,[4] potentially affecting its light scattering, and its atmospheric water uptake.[6] It has also been suggested as a mechanism for slowing down the rate of certain reactions involving the organic surfactant molecules themselves, potentially accounting for an unresolved discrepancy whereby their measured lifetimes in the atmosphere are much longer than those predicted from chemical kinetic parameters.[7,8] Feasibility of studies of atmospheric organic aerosol with laser Raman tweezers has been demonstrated at RAL.[9,10] Fig. 1(a) shows the laser-tweezing cell developed for experiments at RAL. Oxidation of organic droplets with O_3 and nitrogen oxides has been studied in this cell; a custom-made laser Raman tweezers aerosol reaction chamber has been designed at Reading, constructed at Diamond and tested successfully at RAL.

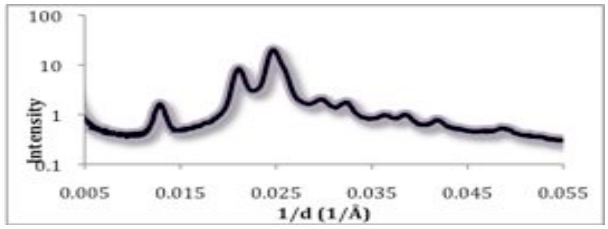

(a)

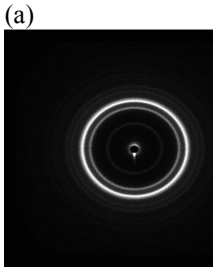

(b)

Fig. 2 Off-line XS results for ~ 50 wt % oleic acid / H_2O mixture at pH = 7. (a) Integrated intensities *vs.* 1/d obtained from diffraction pattern in (b). The sharp peaks indicate self-assembled structures on the nano-scale consistent with cylindrical micelles packed into a hexagonal array.

We levitated oleic acid/ water droplets at relative humidities controlled by balancing dry and wet O_2 flows. Once the droplet was stabilized, we initiated O_3 generation using a pen-ray ozoniser. We varied the conditions to achieve target mixtures and followed changes in composition by Raman spectroscopy. A 532 nm laser will be fibre-coupled for online Raman spectroscopy simultaneous with SAXS/WAXS studies at Diamond. A range of oleic acid/ water mixtures in bulk was studied in a Nanostar system at Reading to pin down key compositions leading to phase changes. Preliminary analysis of the Diamond experiment in August 2012 will be presented together with off-line work (see Fig. 2).

References

[1]Pöschl, *Angew Chem* **2005**, *44*, 7520; Stevens and Feingold, *Nature* **2009**, *461*, 607; Ziemann, *Nature* **2009**, *461*, 353; [2]Pfrang et al., *Atmos Environ* **2008**, *42*, 3018; [3]Virtanen et al., *Nature* **2010**, *467*, 824; [4]Tabazadeh, *Atmos Environ* **2005**, 5472; [5]Allan et al., *ACP* **2010**, *10*, 647; [6]King, et al., *PCCP* **2009**, *11*, 7699; [7]Shiraiwa, Pfrang and Pöschl, *ACP* **2010**, *10*, 3673; [8]Pfrang et al., *ACP* **2011**, *11*, 13003; [9]King, Thompson and Ward, *JACS* **2004**, 126, 16710; [10]King, Thompson, Ward, Pfrang and Hughes, *Faraday Discuss* **2008**, *137*, 173.

Characteristics of polymer blend particles produced by evaporation of binary solution droplets of incompatible polymers

V. Rajagopalan, E. A. Grulke and A. K. Ray

Department of Chemical Engineering, University of Kentucky, Lexington, KY 40506, USA
Keywords: droplet charge limit, evaporation, solute precipitation
Presenting author email: akray@engr.uky.edu

Polymer blend microparticles find wide range of applications in the field of opto-electronic devices, drug delivery systems, organic solar cells, and so on. These applications require generation of polymer blend microparticles with specifically tailored electrical, optical and mechanical properties. The final properties of these particles depend on the configuration (core-shell, hollow structures, etc.) and the degree of phase separation in the blend. The useful range of properties can be significantly expanded if uniformly blended polymer particles can be synthesized from arbitrary pairs of immiscible polymers. The precise control of the phase separation in polymer blends is difficult as there is inherent phase separation. The extent of phase separation in many polymer blends can by reduced by conventional methods that are limited to polymer pairs in certain property ranges. An approach based on evaporation of solution microdroplets, containing two immiscible polymers dissolved in a common solvent, has the potential for producing uniformly blended polymer microparticles. The production method based on solvent evaporation from solution droplets offers a number advantages such as high surface area, confinement effects (i.e., atto- to femto-liter volumes), and yields desirable nano- and micro-structures that are not achievable through conventional techniques. By limiting the timescale of solvent evaporation to less than that of polymer diffusion and self-organization, phase separation can be inhibited in a droplet, and thus homogeneous polymer-blend particles of immiscible polymers can be produced. The evaporation rate can be controlled by the judicious choice of solvent, temperature, and initial droplet size. In the present study we have examined characteristics of polymer blend particles produced from incompatible polymers pairs such as polyvinylcarbazol (PVK) and polystyrene (PS), polyvinyl chloride (PVC) and Poly(methyl methacrylate) (PMMA), PS and PMMA, under various conditions.

Experiments were conducted on highly mono-disperse microrddroplets that were generated using a modified vibrating orifice droplet generator. Microrddroplets were produced from a solution that was prepared by dissolving two incompatible polymers in a common volatile solvent. The effects of solvent, initial droplet size, temperature and airflow rate are studied by analyzing the final morphology of particles and the extent of phase separation. Final morphology of the particles was examined using a Scanning electron microscope (SEM) and the degree of phase separation was studied by using an Energy Dispersive X-Ray Analysis (EDS) on ultra-thin slices of produced particles and by Differential Scanning Calorimetry (DSC).

The results show that the droplet evaporation rate plays the most dominant role on the morphology of the final microparticles. The uniform polymer blend microparticles are produced by rapid evaporation of microdroplets, but the phase separation is observed when the droplet evaporation rate is reduced through solvent properties and environmental temperature.

This work was supported by the National Science Foundation (grant # ATM-0634789), and National Institute for Occupational Safety and Health (grant # 1R01OH009802-01).

An Inversion Method for Aerosol Particle Concentrations in the CERN CLOUD Experiment

C. Williamson[1], D Wimmer[1], K.Lehtipalo[2], J. Curtius[1] and the CLOUD collaboration

[1]Institute for Atmospheric and Environmental Sciences, Goethe University of Frankfurt, Frankfurt/M. Germany
[2]Department of Physics, University of Helsinki, Helsinki, Finland
Keywords: nucleation growth rates, ion-induced nucleation, size distribution, inverse problems, CLOUD experiment.
Presenting author email: williamson@iau.uni-frankfurt.de

A proposed link between galactic cosmic rays (GCRs) and cloud formation has been the subject of lively scientific debate (Marsh and Svensmark, 2000; Carslaw et al, 2002; Kirkby, 2007). One possible mechanism for this link is ion-induced nucleation, which is currently poorly understood. The role of ternary species, such as ammonia and organics, in aerosol nucleation has also not yet been fully characterized (Zhang, 2010).

A better understanding of the role of ions, amines and organics in aerosol nucleation can be achieved through analysis of aerosol particle growth rates under controlled conditions. The CLOUD-experiment (Cosmics Leaving OUtdoor Droplets) at CERN (European Organisation for Nuclear Research) has been set up to study the effect of GCRs on cloud formation (Kirkby et al 2011). It consists of an almost perfectly clean aerosol chamber containing synthetic air, controlled levels of sulphuric acid and negligible or controlled levels of amines and organics. Relative humidity and temperature are also controlled. The chamber can be run in a completely neutral mode (no ions present) by the application of a clearing field, with ambient surface levels of GCRs and with a high flux of simulated GCRs from the proton synchrotron beam. Conditions in the chamber are monitored by a number of instruments, including many measuring particle concentrations: two diethelene-glycol condensation particle counters (DEG-CPCs), two particle-size-magnifiers (PSMs), a CPC-battery, several Air Ion Spectrometers, a nano-differential mobility analyser, a laminar diffusion tube and a scanning mobility particle sizer.

This is the first time an integrated analysis of data from multiple instruments in the CLOUD experiment has been performed. Each instrument is sensitive to different sized particles with different efficiencies, with several of the instruments sensitive for particles in the 1-3 nanometre size range. These efficiencies were measured and the data was fitted using a four-parameter exponential function as described by Wehner et al. (2010). The results of this fitting are used to create a matrix describing the detection efficiency of each instrument for discretised diameter channels, which, along with the measured particle concentrations, forms the input for an inversion method based on that described by Fiebig et al. (2005). This produces smooth, non-negative size distributions without the use of any initial assumptions for the shape of the distribution, while taking into account the uncertainty of each of the instruments. Growth rates are calculated from the time development of these size distributions. The growth rates are important parameters for deriving the initial nucleation rates (at critical size) and for a detailed understanding of condensation, evaporation, coagulation, and wall loss processes in the 1-20 nm particle size range.

We would like to thank CERN for supporting CLOUD with important technical and financial resources, and for providing a particle beam from the CERN Proton Synchrotron. This research has received funding from the EC Seventh Framework Programme (Marie Curie Initial Training Network "CLOUD-ITN" grant no. 215072, and ERC-Advanced "ATMNUCLE" grant no. 227463), the German Federal Ministry of Education and Research (project no. 01LK0902A), the Swiss National Science Foundation (project nos. 206621_125025 and 206620_130527), the Academy of Finland Center of Excellence program (project no. 1118615), the Austrian Science Fund (FWF; project no. P19546 and L593), the Portuguese Foundation for Science and Technology (project no. CERN/FP/116387/2010), and the Russian Foundation for Basic Research (grant N08-02-91006-CERN).

Marsh, N. D. and Svensmark, H. (2000) Physical Review Letters, **85**, 5004-5007.
Carslaw, K. S. et al (2002) Science, **298**, 1732-1737.
Kirkby, J. (2007) Surveys in Geophysics, **28**, 333-375.
Zhang, R. (2010) Science **328**, 1366-1367.
Kirkby, J. et al (2011) Nature, 476, 429-433.
Fiebig, M. et al (2005) Journal of Aerosol Science, **36,** 1353-1372.

Development of an aqueous-phase mechanism for secondary organic aerosol formation

F. Couvidat[1], K. Sartelet[1] and C. Seigneur[1]
[1]CEREA, Joint Laboratory École des Ponts ParisTech/EDF R&D, Université Paris-Est, 77455 Marne-la-Vallée, France
Keywords: Aerosol model, Modelling (regional), SOA (Second. Organic Aerosols)
Presenting author email: couvidaf@cerea.enpc.fr

H^2O (Hydrophilic/Hydrophobic Organics) is a Secondary Organic Aerosol (SOA) model based on the molecular representation of SOA and on the partition of two types of compounds: hydrophilic species (which condense preferrentially on an aqueous phase) and hydrophobic species (which condense only on an organic phase). This model integrates the state of art knowledge and takes into account the condensation of semi-volatile compounds, formation of SOA from various precursors and several related processes. However, this model does not take into account the aqueous-phase chemistry of clouds and the formation of low-volatility compounds which can lead to SOA formation after cloud evaporation. The aim of this study is to take into account cloud chemistry and to estimate its impact on SOA formation. Impact of cloud chemistry on aerosols concentrations in Europe is estimated with the model from August 1st to August 15th 2002.

SOA formation from glyoxal, methylglyoxal, methacrolein, methylvynylketone and tetrols formation in an aqueous phase are included in the model. This new mechanism relies on published mechanisms and on recent experimental data. Fig. 1 shows the impact of cloud chemistry on ground concentrations. Only small quantities of SOA (between 2 and 14 ng/m^3) are formed in the model via the oxidation of Volatile Organic Compounds (VOC) in clouds. This seems to indicate that in-cloud oxidation of VOC has only a minor impact on SOA concentrations over Europe. However, impact of cloud chemistry could be higher in more humid areas with high emissions of biogenic emissions like Amazonia where high concentrations of tetrols were found [Claeys et al. (2004)].

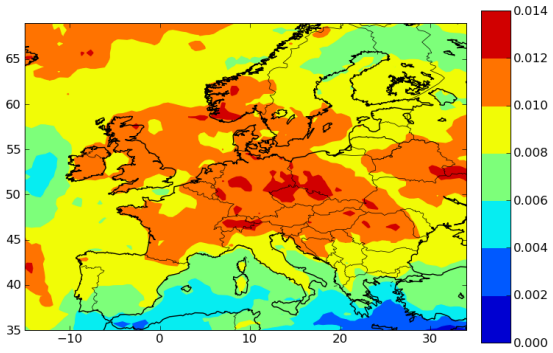

Figure 1: Ground concentrations (μg.m^{-3}) of SOA formed by aqueous-phase reactions over Europe from August 1st to August 15th 2002.

A simple aging mechanism of SOA in the aqueous phase of clouds was also developped and included in the model. This aging mechanism assumes that some Semi-Volatile Organic Compounds (SVOC) can be absorbed in clouds and be oxidised to form less volatile compounds. Clouds could then influence the oxidation and partitioning of existing aerosols. Impact of clouds on chemical aging will be studied to estimate whether or not clouds can contribute to organic aerosol formation over Europe.

This work was funded in part by ADEME, the French Agency for the Environment and Energy Management.

Claeys, M., Graham, B., Vas, G., Wang, W., Vermeylen, R., Pashynska, V., Cafmeyer, J., Guyon, P., Andreae, M.O., Araxo, P. and Maenhaut, W. (2004) *Science* **303**, 1173-1176.

Capturing of low-level CO_2 using AC particles

Y. H. Lim, Y. M. Jo†

Department of Applied Environmental Science, Kyung Hee University, Yongin, Gyeonggi-do, 446-701, Korea
Keywords: CO_2 adsorption, Activated carbon, MEA, Impregnation, Volume reduction
Presenting author email: ymjo@khu.ac.kr

Well insulation of modern buildings including residentials, industrial, schools, subways, etc deteriorates the public indoor air quality(IAQ)(Lim et al., 2010). Carbon dioxide level is one of the key indicators of IAQ as well as the main greenhouse gas of concern (Lee & Jo, 2008). Development of CO_2 capture and storage techniques using adsorption processes is of great interest due to their low energy requirement and low capital cost (Ranjani et al., 2005).

Nitrogen surface groups on particulate AC adsorbent, of which basis was coconut(WSC-470) was introduced from amine. In order to enhance the adsorption capacity, a commercial particulate AC was modified with MEA(monoethanolamine) by methods of impregnation and volume reduction. Impregnation method was a direct process to incorporate MEA onto the AC surface, whilest volume reduction method the solvent reduction by means evaporation till achieving the concentrated solution. The AC particles were immersed in an aqueous solution of 1.0M MEA with different solvents (distilled water, methanol and ethanol) at 40 ^oC and dried. Methanol and ethanol were chosen for their low boiling points(64.7 ^oC, 78.3 ^oC) comparing to water(100 ^oC) (Chatti et al., 2009). The completed adsorbents were analyzed by XPS and BET, and the adsorption capacity was evaluated in a fixed bed. The XPS proved chemical functionalities over the AC surface. Table 1 summarizes the elemental composition(at. %) for the prepared AC surface. The amount of nitrogen funtionalites over raw AC was 0.7%, and the modified samples were more than the raw AC. Volume reduction method was found to be better than the impregnation method.

Table 1. Elemental compositions of AC adsorbents by XPS

AC(WSC-470)		Atomic ratio(%)		
Method	Solvent	C	N	O
Imp.	H_2O	90.01	1.81	8.18
	C_2H_5OH	88.88	1.81	9.31
	CH_3OH	89.38	2.03	8.59
Vol. reduction	H_2O	86.55	2.37	11.08
	C_2H_5OH	88.18	2.53	9.29
	CH_3OH	88.26	2.51	9.24
Raw AC		93.30	0.70	6.00

The specific surface area of the prepared AC samples measured by BET is given in Table 2. It showed that grafting of nitrogen groups would decrease the surface area blocking tiny pores.

Table 2. BET surface area of raw and modified ACs

AC(WSC-470)		Surface area(m^2/g)
Raw AC		1369.60
Imp.	H_2O	954.53
	C_2H_5OH	1149.30
	CH_3OH	1071.41
Vol. reduction	H_2O	754.77
	C_2H_5OH	490.63
	CH_3OH	860.33

Figure 1 is the adsorption amount of raw and modified AC adsorbents. The CO_2 adsorption capacity of the modified ACs increased steadily with the increase of N-groups. According to the XPS analysis, the most N-groups were found in a samples of MM-AC prepared with volume reduction. In more details, the more NH_2-like N-groups as well as amine were distributed on the MM-AC adsorbent. The present study revealed the selective capability of dry capture of CO_2 in the atmosphere.

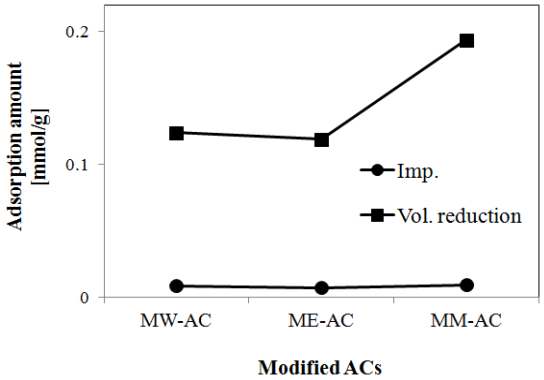

Figure 1. Adsorbed amount of CO_2 on the modified ACs (CO_2 conc. 3000ppm).

This research was supported by Basic Science Research Program through the National Research Foundation of Korea(NRF) funded by the Ministry of Education, Science and Technology(2012-0002485).

Lim, Y.H., Lee, K.M., Lee, H.S. and Jo, Y.M. (2010) *Journal of Korean Society for Atmospheric Environment*, **26**(3), 286-297.

Lee, K.M., and Jo, Y.M. (2008) *Journal of the Korean Industrial and Engineering Chemistry*, **19**(5), 533-538.

Ranjani , V.S., Shen, M.S. and Edward, P.F. (2005) *Energy & Fuel*, **19**, 1153-1159.

Chatti, R., Amit, K. and Sadhana, S.R. (2009) *Microporous and Mesoporous Materials*, **121**, 84-89.

SOA Formation from Acid Catalysed Rearrangement Reactions

Y. Iinuma[1], A. Kahnt[1,2], O. Böge[1] and H. Herrmann[1]

[1]Leibniz-Institut für Troposphärenforschung, Leipzig, 04318, Germany
[2]Present address: Department of Pharmaceutical Sciences, University of Antwerp, Antwerp, B-2610, Belgium
Keywords: SOA, Smog chamber, Aerosol characterisation
Presenting author email: yoshi@tropos.de

The influence of acidic seed particle on SOA formation has been received a significant attention in the past decade since Jang *et al.* (2002) have presented evidence for multifold increases in SOA formation through acid catalysed particle phase reaction. The enhanced SOA formation is attributed to the formation of accretion compounds from acid catalysed reaction of carbonyl compounds, peroxy compounds, or the formation of organosulfates from alcohols and epoxides.

Reactive uptake of gas-phase semi-volatile organic compounds has been reported to be an important pathway leading to the formation of organosulfates, and enhanced SOA formation (e.g. Iinuma *et al.*, 2009; Surratt *et al.*, 2010), though it does not explain increases in SOA production for some of VOC oxidation experiments in which no organosulfate formation is observed (e.g. α-pinene ozonolysis). In this study, we present a formation of highly reactive VOCs from acid catalysed multiphase reactions of monoterpene oxides. Subsequent oxidation of the highly reactive VOCs forms significantly more SOA than the precursor VOCs. The process involves both gas- and particle phase reactions and likely plays a role in SOA formation in the ambient atmosphere. Table 1 summarises experimental conditions used in the present study.

Table 1. Chamber experiment conditions used in this study

	α-Pinene oxide	*β-Pinene oxide*
Initial HC Conc. [ppbv]	100	100
Initial Ozone [ppbv]	0, 60	0, 60
RH%	0, 50	50
Temp [ºC]	20	20
Reaction Time [h]	~ 3	~ 3
Sampling [h]	1 (1.8 m^3)	1 (1.8 m^3)
Seed Particle	pH 0, 7	pH 0, 7

Figures 1 and 2 show the SOA mass increases as a function of experimental time for α-pinene oxide and α-pinene oxide, respectively. For both VOCs, almost no SOA mass increase was observed in the case of neutral seed aerosol experiments regardless of the ozone concentrations. On the other hand, significant increases in the SOA mass were observed for both VOCs in the presence of acidic seed aerosol and ozone. In the case of β-pinene oxide, acidic seed aerosol is sufficient to promote significant SOA formation from a reactive uptake process that forms organosulfates (Iinuma *et al.*, 2009).

In the presence of acidic seed aerosol, both α-pinene oxide and β-pinene oxide isomerise forming monoterpene aldehydes and alcohols that react rapidly with ozone, leading low volatile SOA compounds. This mechanisms partly explains the increased SOA formation in the presence of acidic seed particle.

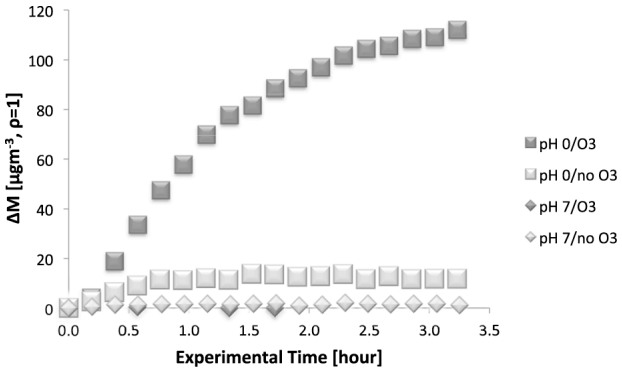

Figure 1. SOA mass increase as a function of experimental time for α-pinene oxide.

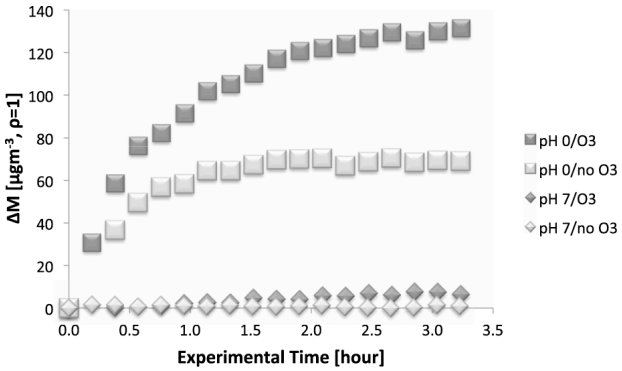

Figure 2. SOA mass increase as a function of experimental time for β-pinene oxide.

References

Iinuma, Y., O. Böge, A. Kahnt, and H. Herrmann (2009) *Phys Chem Chem Phys*, 7985-7997.

Jang, M. S., Czoschke, N. M., Lee, S., and Kamens, R. M. (2002) *Science*, **298**, 814-817.

Surratt, J. D., A. W. H. Chan, N. C. Eddingsaas, M. N. Chan, C. L. Loza, A. J. Kwan, S. P. Hersey, R. C. Flagan, P. O. Wennberg, and J. H. Seinfeld (2010) *PNAS*, **107**, 6640-6645.

Surface tension and aggregate formation in nanoaerosols containing model HULIS compounds

T. Hede[1]

[1] Department of Meteorology, Stockholm University, S-106 91 Stockholm, Sweden

The frequently used theory for water vapour condensation, water droplet growth and stability is Köhler theory (Köhler, 1936). This theory, however, is based on the assumption that the cloud condensation nuclei consist of inorganic salt and mineral dust. It has been shown that a large fraction of the CCN consist of organic compounds (Novakov and Penner, 1993). We have studied secondary organic aerosol compounds that are Humic-like substances (HULIS) (Hede *et al*, 2011). We focus on three compounds that make up model HULIS compounds. Cis-pinonic acid (CPA), pinic acid (PAD) and pinonaldehyde (PAL). These model HULIS compounds are amphiphilic and have surface active properties that can decrease the surface tension and thereby lower the supersaturation needed for water vapour condensation, according to Köhler theory.

In order to study nanoaerosols and to determine the molecular properties of these systems, we conducted molecular dynamics (MD) simulations. MD simulations use Newtonian laws of motions and apply this to a computer model of a system. From the trajectories, orientations of the individual molecules as well as surface tension was determined. In Fig. 1 the surface tension reduction dependent on the concentration of each model HULIS compound is shown. The data is fitted to the Szyszkowski equation (Szyszkowski, 1908).

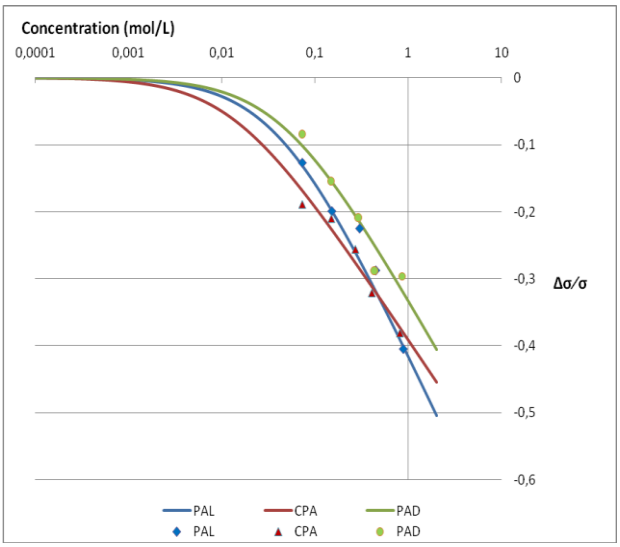

Figure 1. Szyszkowski curves for the model HULIS compounds CPA, PAD and PAL.

We could show that the surface tension reduction was high for these compounds, and that or simulated data was comparable to experimental data (Shulman *et al*, 1996)

We could also show that the model HULIS compounds not only accumulated at the surface, but also formed an aggregate inside the nanoaerosol. This is also reported in an experimental study by Virtanen *et al* (2011).

These results are of importance for the understanding of the structure and properties of organic compounds in nanoaerosols, and the use of MD simulations opens up for a new area of research in the field of aerosol science.

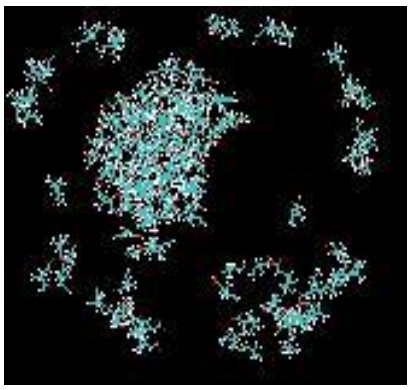

Figure 2. The system containing 162 CPA molecules. Cross-section picture. Water is removed for clarity.

Hede, T., Li, X., Leck, C., Tu, Y., Ågren, H. (2011) Model HULIS compounds in nanoaerosol clusters – investigations of surface tension and aggregate formation using molecular dynamics simulations, Atmos. Chem. Phys., **11**, 6549-6557, doi:10.5194/acp-11-6549-2011

Köhler, H. (1936) The nucleus in and the growth of hygroscopic droplets, T. Faraday Soc., **32**, 1152–1161

Novakov, T., Penner, J. E. (1993) Large contribution of organic aerosols to cloud condensation nuclei concentrations, Nature, **365**, 823–826

Shulman, M. L., Jacobson, M. C., Charlson, R. J., Synovec, R. E., Young, T. E. (1996) Dissolution behavior and surface tension effects of organic compounds in nucleating cloud droplets, Geophys. Res. Lett. **23**, 277-280

Szyszkowski, B (1908) Experimentelle Studien űber Kapilläre Eigenschaften der Wässrigen, Z. Phys. Chem., **32**, 1152-1161

Virtanen, A., Joutsensaari, J., Koop, T., Kannosto, J., Yli-Pirilä, P., Leskinen, J., Mäkelä, J. M., Holopainen, J. K., Pöschl, U., Kulmala, M., Worsnop, D. R., Laaksonen, A. (2010) An amorphous solid state of biogenic secondary organic aerosol particles. Nature, 824-827

Formation and aging of secondary organic aerosol through evaporation of aqueous phase processed isoprene reaction products

F. Siekmann, P. Renard, B. Temime-Roussel and A. Monod

Laboratoire Chimie Environnement, Aix-Marseille Université, Marseilles, 13003, France
Keywords: isoprene, SOA, clouds, evaporation, AMS, LC/MS
Presenting author email: frank.siekmann@uni-bayreuth.de

Reactive volatile organic compounds (VOC) emitted from biogenic sources, can be oxidized in the gas phase to transform into more water-soluble compounds that readily partition into atmospheric water droplets. Due to further oxidation in the liquid phase, higher molecular and less volatile compounds can be formed. Upon water evaporation, these less volatile products can remain at least in part in the particle phase, leading to secondary organic aerosol (SOA) formation (Carlton et al., 2009; Ervens et al. 2011).

In laboratory experiments, we investigated the ability of methyl vinyl ketone (MVK) and methacrolein (MACR), the two main gas phase atmospheric oxidation products of isoprene, to form secondary organic aerosol (SOA) through aqueous phase OH-oxidation and subsequent water evaporation.

In the first step, the oxidation products of MVK and MACR in the aqueous phase were studied by ESI-MS and LC-ESI-MS analysis. The aqueous phase chemical composition brought clear evidence for the formation of oligomer systems having a mass range up to 1400 Da (Liu et al., 2012). The intensity and masses of oligomers became increasingly important as precursor initial concentrations increased from 2 to 20 mM.

Subsequently, these aqueous phase oxidation products were studied in nebulization-evaporation experiments for their ability to generate organic aerosol. For these studies, AMS and SMPS analysis were used to determine the composition and mass of the dried aerosol. Furthermore, filter samples were taken to check for any chemical artifact due to the nebulization and drying steps.

The mass concentration of these SOA increased significantly with the reaction time. The evaluated SOA mass yield ranged from 2 to 12%, depending on the reaction advancement, for both precursors.

For both precursors, the oligomers were responsible for the SOA formation during nebulization experiments. The AMS results indicate differences, regarding the relative importance of oligomerisation and aging processes during aqueous phase photooxidation. The composition of the generated aerosol and the influence of initial precursor concentrations and reaction time will be presented and discussed.

This work was supported by the French embassy in Germany, the ANR CUMULUS and the CNRS INSU-LEFE-CHAT.

Carlton, A. G., Wiedinmyer, C., Kroll, J. H. (2009) Atmos. Chem. Phys. 9, 4987-5005.

Ervens, B., Turpin, B.J., Weber, R.J. (2011) Atmos. Chem. Phys. 11, 11069-11102.

Liu, Y., Siekmann, F., Renard, P., El Zein, A., Salque,G., El Haddad, I., Temime-Roussel, B., Voisin, D., Thissen, R., Monod, A. (2012) Atmos. Environ. 49, 123-129.

Influence of reaction conditions on the formation of dimers and peroxides originating from the ozonolysis of a-pinene and the OH reaction of nopinone

A.Mutzel, Y. Iinuma, O. Böge, A. Kahnt and H. Herrmann

Leibniz-Institut für Troposphärenforschung, Permoserstr. 15, Leipzig D-04318, Germany
Keywords: VOCs, SOA, Aerosol characterization
mutzel@tropos.de

The oxidation of biogenic volatile organic compounds (BVOC) leads to the formation of a wide range of products with multiple functional groups. The formed semivolatile products can partition into the particle phase and therefore they contribute significantly to the formation of secondary organic aerosol (SOA). Especially peroxides and dimeric compounds are suggested to make up a significant fraction of SOA (Docherty et al., 2005 and Kalberer et al., 2004). Although several studies exist about the formation of SOA originating from the monoterpene oxidation (see review by Hallquist et al., 2009) there is a gap in the knowledge about the involved species and the influence of the reaction conditions on the SOA formation.

The focus of the present study is to compare the formation of dimers and peroxides from the ozonolysis as well as from the OH radical reaction of monoterpenes and their related compounds. Two sets of chamber experiments were conducted for this purpose. The first set of experiments comprised the oxidation of α-pinene with ozone in the presence of carbon monoxide as OH scavenger. In the second set of the experiments the OH radical reaction of nopinone was examined. The OH radicals were generated using the ozonolysis of tetramethylethylene (TME). For both set-ups the influence of relative humidity (rh) and initial particle concentration (P_{ini}) were examined (Table 1).

Table 1. Reaction conditions for both experimental sets (temperature 20±1°C)

Relative humidity [%]	Initial Particle concentration P_{ini} [m^{-3}]
0	≈ 20 000
50	≈ 10 000, 20 000, 40 000
75	≈ 20 000

The formed particulate products were collected using a denuder/filter sampling device. One half of the filter was used for the analysis using HPLC/(-)ESI-TOFMS and the second half for the peroxide test. The peroxides were determined using an iodometric-spectrophotometric method developed based on the method described in Docherty et al., 2005.

The detected peroxides show a strong dependency on the reaction conditions. The peroxide content decreased with increasing particle concentration for both the OH radical reaction and the ozonolysis. In contrast to the ozonolysis samples, the peroxide content decreases with increasing relative humidity for the OH radical reaction. These strong dependencies can be caused by the influence of relative humidity on the partitioning behavior of the peroxides and their corresponding precursor (Seinfeld et al., 2001). Additionally, a direct influence of experimental conditions on the formation reactions cannot be excluded.

The further analysis of the particle-phase compounds revealed a number of monomeric and oligomeric compounds. The major monomeric products were detected at the mass to charge ratios (*m*/z) 157, 171, 185, 203 and 231 corresponding to terebic acid, terpenylic acid (Claeys *et al*., 2009), pinic acid, 3-methyl-1,2,3-butanetricarboxylic acid (Szmigielski *et al*., 2007) and diaterpenylic acid acetate (Iinuma *et al*., 2009). In addition pinonic acid with *m/z* 183 was detected from α-pinene. The detected monomeric compounds are also strongly influenced by relative humidity and seed particle concentration, which is explained by a change in partitioning behaviour.

Furthermore, among the detected dimers, one major dimer was identified from both α-pinene and nopinone. This compound with *m/z* 357 corresponds to $C_{17}H_{25}O_8$. The formation of this compound showed different response to the reaction conditions. In the ozonolysis experiments, the amount increased with increasing relative humidity and with particle concentration. Contrary, an influence of particle concentration was not seen during the OH radical reaction. This observation and the missing correlation between the formation behaviour of *m/z* 357 and the peroxide content give a hint that the observed dimer at *m/z* 357 likely contains no peroxide structure.

This work was supported by the Deutsche Forschungsgemeinschaft DFG under grant HE-3086/14-1 and code name FuProTer.

Claeys, M. *et al*., (2009), *Environ. Sci. Technol*. **53**, 6976-6982
Docherty, K.S. *et al.,* (2005) *Environ. Sci. Technol.* **39**, 4049-4059
Hallquist, M. *et al*., (2009) *Atmos. Chem. Phys*. **9**, 5155-5236
Iinuma, Y. *et al*., (2009), *Environ. Sci. Technol* **43**, 280-285
Kalberer, M. *et al.,* (2004), *Science* **303**, 1659-1662
Seinfeld, J.H. *et al*., (2001) *Environ. Sci. Technol*. **35**, 1806 – 1817
Szmigielski, R. *et al.,* (2007) *Geophys. Res. Lett.* **34**, L24811, DOI: 10.1029./2007GL031338

Comparison of sesquiterpene oxidation products in secondary organic aerosol from different vegetation zones

A. van Eijck[1], C. Kampf[1], T. Hoffmann[1]

[1]Institute for Inorganic and Analytical Chemistry, Johannes Gutenberg-University, Duesbergweg 10-14, 55128 Mainz, Germany

Keywords: Aerosol characterization, Atmospheric aerosols, Field measurements, Organic acids

Presenting author email: van.Eijck@uni-mainz.de

Secondary organic aerosol (SOA) has a huge impact on air quality and potentially climate change. It influences the Earth radiative budget through absorbing, scattering and reflecting radiation as well as the formation of clouds because the particulates can act as cloud condensation nuclei (CCN). Furthermore, SOA plays an important role for human health. SOA is formed from gaseous precursors which get oxidized by ozone, OH- and NO_3-radicals in the atmosphere. Due to their low vapor pressure these degradation products can nucleate to form new particles or they can condense on existing aerosol particles. Despite the major progress in research during the last few years the actual chemical composition as well as the contribution of various volatile organic compounds (VOCs) to the formation of secondary organic aerosol is still partially unknown.

Recent studies indicate that sesquiterpenes play an important role in the formation of SOA because of the low volatility of their oxygenated products (Lee *et al*., 2006). Their emission is estimated to be about 14,8 Tg per year (Henze *et al*., 2008), and some studies indicate that it can be as high as 30 or 40 % of the total monoterpene emission (Tarvainen et al., 2005; Helmig et al., 2007). However, these emission rates remain highly uncertain due to the lack of quantitative emission rate measurements. In addition, the knowledge about the actual atmospheric degradation mechanism and the main oxidation products of sesquiterpenes is quite limited. β-Caryophyllene, α-humulene, α-farnesene and β-farnesene are the most abundant sequiterpenes in many sesquiterpene emission profiles. But also aromadendrene, α-bergamotene and δ-cadinene and germacrene-D can contribute significantly to some emission profiles (Duhl *et al.*, 2008).

Furthermore the difference between the measured OH reactivity and the calculated OH reactivity indicates, that some undetected reactive biogenic volatile organic compounds emitted by vegetation are responsible for the excess of OH reactivity. Several studies suggest the assumption, that this excess of reactivity arises from sesquiterpene emissions (Kim et al., 2011).

To determine the major oxygenated products of sesquiterpenes in SOA, reaction chamber experiments with six different sesquiterpenes and ozone were performed in a 100 L reaction chamber. Their major oxidation products were determined. To measure the time dependent formation of initial oxidation products, an APCI-IT-MS was directly connected to the reaction chamber. After 2 hours the APCI-IT-MS was replaced by a filter holder and the generated aerosol was collected for 17 hours. In case of β-caryophyllene five different acidic oxidation products were synthesized and these acids were used for quantification. Atmospheric air samples taken during the HUMPPA campaign summer 2010 in Finland and during the BEACHON-RoMBAS campaign summer 2011 in Colorado, USA were analyzed for sesquiterpene oxygenated products. The major sesquiterpene oxidation products in the ambient air samples were quantified and compared to the amount of monoterpene oxidation products found in the filter extract. The mainly emitted sesquiterpenes in the two different vegetation zones were compared and the correlation with different meteorological data was analyzed.

This work was supported by the Max Planck Graduate Center, Mainz, Germany.

Duhl, T. R., Helmig, D. and Guenther, A. (2008) *Biogeosciences* **5**, 761-777.

Helmig, D., Ortega, J., Duhl, T., Tanner, D., Guenther, A., Harley, P., Wiedinmyer, C., Milford, J. and Sakulyanontvittaya, T. (2007) *Environmental Science and Technology* **41**, 1545-1553.

Henze, D.K., Seinfeld, J.H., Ng, N.L., Kroll, J.H., Fu, T.M., Jacob, D.J. and Heald, C.L. (2008) *Atmospheric Chemistry and Physics* **8**, 2405-2421.

Kim, S., Guenther, A., Karl, T. and Greenberg, J. (2011) *Atmospheric Chemistry and Physics* **11**, DOI: 10.5194/acp-11-8613-2011.

Lee, A., Goldstein, A.H., Kroll, J.H., Ng, N.L., Varutbangkul, V., Flagan, R.C. and Seinfeld, J.H. (2006) *Journal of Geophysical Research* **111**, D17305.

Tarvainen, V., Hakola, H., Hellén, H., Bäck, J., Hari, P. and Kulmala, M. (2005) *Atmospheric Chemistry and Physics* **5**, 989-998.

Ozonolysis of ultra fine particles of oleic acid: a detailed study mixing *on line* gas and condensed phase analyses.

Maxence Mendez[1], Vincent Crenn[2], Véronique Riffault[2], Sylvie Gosselin[1], Nicolas Visez[1], Denis Petitprez[1]

[1] Laboratoire de Physico-Chimie des Processus de Combustion et de l'atmosphère, PC2A, UMR 8522 CNRS/Lille 1, Université Lille1, Villeneuve d'Ascq, F-59655, France
[2] Département Chimie et Environnement, Ecole des Mines de Douai, Douai, F-59508, France

Keywords: Organic acids, Ozone, Multiphase processes, Marine aerosols
Presenting author email: Denis.Petitprez@univ-lille1.fr

Produced from biologic ocean activity, fatty acids are ejected into the atmosphere along with sea salt on their surface (Mochida, Kitamori et al. 2002). They are also emitted by cooking activity or biomass combustion. Once in the atmosphere, these compounds will be oxidized leading to the modification of their chemical and physical properties. Ozonolysis of oleic acid ($C_{18}H_{34}O_2$) is one of the most studied heterogeneous reactions as a model for aging of organic particle matter (Zahardis and Petrucci, 2007). Depending on experimental conditions and techniques used, the reactive uptake coefficient ranges between ~7×10^{-4} and ~10^{-2} . γ determination is also depending on the way where the kinetics is monitored (loss of ozone or oleic acid or appearance of reaction products). In this work, we fully characterize the reaction by measuring *in line* concentrations evolution of the products and of the reactants in the gas phase and in the condensed phase.

The heterogeneous ozonolysis of oleic acid particles have been studied in an aerosol flow tube (AFT). Ozone is generated by UV photolysis of O_2 and measured with a UV photometric analyzer (Thermo Scientific). Particles are generated by homogeneous nucleation of oleic acid vapors. Size distributions recorded by a scanning mobility particle sizer exhibit a monodisperse distribution centered at 130 nm. Particles are exposed to a large range of ozone concentrations from 30 to 650 ppb during 200 to 500 seconds. The originality of this study is to perform uptake experiments by measuring the loss of ozone as a function of the aerosol surface density. The later is modified by varying continuously the liquid oleic acid temperature leading to increase the aerosol concentration and, therefore, the aerosol surface density. Those measurements have been conducted by exposing particles concentrations (from 0 to 10^6 cm^{-3}) to stable ozone concentrations and monitoring the remaining ozone downstream the AFT.

The reactants and the products of the reaction have been measured in both gas and particle phase. The particle phase has been characterized online by an aerosol mass spectrometer (AMS) and collected on filters for Gas Chromatography – Mass Spectrometry (GC-MS) analysis. Gas-phase products have been measured by a Proton Reaction Transfer – Time of Flight – Mass Spectrometer (PTR-ToF-MS).

From the measurements, we derived the value of the uptake coefficient (γ_{obs}) as a function of the ozone exposure (10^{-5} to 3.5×10^{-4} Atm.s). It appears that γ_{obs} depends on the ozone exposure and decreases from 1.2×10^{-3} to 2.5×10^{-5} suggesting that the uptake kinetic could be limited by diffusion processes at the surface or inside the particle. The GC-MS analyses have allowed us to quantify the loss of oleic acid and the appearance of products as a function of the exposure of the particle phase to ozone. HR-Tof-AMS analysis are confirmed the GC-MS data (see Fig 1).

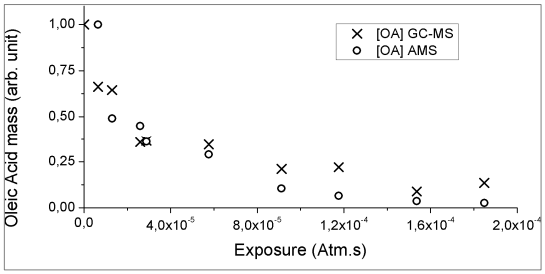

Fig 1: Normalized loss mass of oleic acid measured by AMS (m/z=264 amu) and by GC-MS as a function of ozone exposure.

Nonanoic acid, azelaic acid, 9-oxononanoic acid and nonanal reaction products have been quantified by GC-MS analysis. Moreover, under these specific conditions, it appears that there is up to 3 ozone molecules lost for only 1 oleic acid molecule consumed, which suggest that secondary ozonolysis takes place for high concentration of ozone.

Mochida, M., Y. Kitamori, et al. (2002). *J. Geophys. Res.* **107**(D17): 4325.

Zahardis, J. and G. A. Petrucci (2007). *Atmos. Chem. Phys*. 7(5): 1237-1274.

Effect of ions on the measurement of sulphuric acid at CLOUD

Rondo, Linda[1], Kürten, Andreas[1], Ehrhart, Sebastian[1], Curtius, Joachim[1] and the CLOUD collaboration
[1]Institute for Atmospheric and Environmental Sciences, University of Frankfurt am Main, Altenhöferallee 1, 60438, Frankfurt am Main, Germany
Keywords: CIMS, sulphuric acid, ternary nucleation, ions, CLOUD experiment

Atmospheric aerosols exert an important influence on clouds and climate. It has been well established that nucleation from gaseous precursors comprises an important source of particles in the atmosphere, and that sulfuric acid (H_2SO_4) plays a crucial role in atmospheric nucleation. In addition, recent studies indicate that ammonia (Kirkby *et al.,* (2011)) and oxidised organic compounds (Metzger *et al*., (2010)) can enhance the nucleation rate by order of magnitude for a given sulphuric acid concentration. However, it is not yet clear what ternary substances contribute in atmospheric nucleation and whether ions play an important role in this respect.

One goal of the CLOUD (Cosmics Leaving OUtdoor Droplets) experiment at CERN is to investigate to what extent the presence of atmospheric ions affects new particle formation (Kirkby *et al*., (2011)). Neutral and ion-induced nucleation experiments are carried out in an aerosol chamber under precisely controlled conditions. Trace gases are added into the CLOUD chamber in order to observe their influence on the ternary nucleation. The source of ions in the chamber is either Galactic Cosmic Rays (GCR) or CERN's proton synchrotron (PS) beam, respectively (Duplissy *et al.*, (2010)).

Highly accurate and precise measurements of gaseous [H_2SO_4] are required in order to interpret the data and for deriving parameterizations of the nucleation rate for certain conditions.
Therefore, for reliable sulphuric acid concentration measurement a Chemical Ionization Mass Spectrometer (CIMS) with a corona discharge ion source (Kürten, *et al*., (2011)) is used. The principle of this measurement is based on the reaction between H_2SO_4 and NO_3^- primary ions followed by the detection of HSO_4^- ions with a mass spectrometer (Tanner and Eisele *et al*, (1993)).

During ternary nucleation experiments, the addition of organic trace gases resulted in a cross-sensitivity of the CIMS H_2SO_4 measurements due to ions (ion enhancement effect). The ternary trace gases that were used were NH_3, DMA (dimethylamine) and oxidised products of pinanediol. The observed increase in bisulphate ion concentration due to ions occurred mainly during the introduction of pinanediol at a concentration of several ppbv into the CLOUD chamber. The enhancement of this effect was only observed during ion induced nucleation measurements by using either GCR or the PS beam, respectively. By applying a high voltage (HV) clearing field inside the CLOUD chamber the ion effect on the CIMS measurement is completely eliminated since, under these conditions, all small ions are swept from the chamber in about one second.

Using a corona ion source for the CIMS proved to be an advantage when measuring sulphuric acid in the presence of organic substances inside the CLOUD chamber. When switching off the corona ion source, the observed HSO_4^- can only be produced by the ionisation radiation inside the CLOUD chamber and is therefore a background signal which needs to be subtracted when present during normal operation (see Fig. 1). In the presentation the charge effect will be explained in detail as well as the method used to derive the representative numbers for [H_2SO_4] during the ternary nucleation experiments conducted at CLOUD. In addition, it will be discussed whether this effect could potentially affect atmospheric sulphuric acid measurements

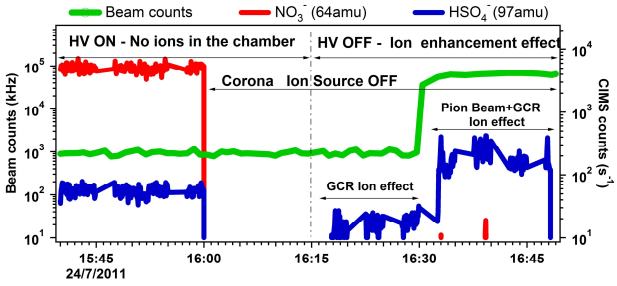

Figure 1. Example of the effect of charged pion beam to the monomer HSO_4^- concentration measured by CIMS during a nucleation run at the CLOUD chamber, when the corona ion source is being disabled.

We would like to thank CERN for supporting CLOUD with important technical and financial resources, and for providing a particle beam from the CERN Proton Synchrotron. This research has received funding from the EC Seventh Framework Programme (Marie Curie Initial Training Network "CLOUD-ITN" grant no. 215072, and ERC-Advanced "ATMNUCLE" grant no. 227463), the German Federal Ministry of Education and Research (project no. 01LK0902A), the Swiss National Science Foundation (project nos. 206621_125025 and 206620_130527), the Academy of Finland Center of Excellence program (project no. 1118615), the Austrian Science Fund (FWF; project no. P19546 and L593), the Portuguese Foundation for Science and Technology (project no. CERN/FP/116387/2010), and the Russian Foundation for Basic Research (grant N08-02-91006-CERN).

Kirkby, J., Curtius, J., *et al* (2011) *Nature* **476**,429- U77.
Metzger, A., *et al* (2010) *PNAS* **107**, 15, 6646 – 6651.
Duplissy, J., *et al* (2010) *Atmos. Chem. Phys*., **10**, 1635-1647
Kürten, A., *et al* (2011) *Atmos. Meas. Tech*., **4**, 437–443, 2011
Tanner, D., and F. Eisele, *et al* (1993) *J. Phys. Chem*. **104**, 830-836,

Characterisation of thin films on optically trapped single aerosols using broadband white light Mie spectroscopy

S.H. Jones[1,2], M.D King[1] and A.D. Ward[2]

[1]Department of Earth Sciences, Royal Holloway, University of London, Egham, Surrey, TW20 0EX, England
[2]Lasers for Science Facility, Central Laser Facility, Science and Technologies Facilities Council, Research Complex at Harwell, Rutherford Appleton Laboratory, Didcot, Oxfordshire, OX11 0FA, England
Keywords: Aerosol coating, Mie scattering, Aerosol characterisation, Optical instrumentation.
Presenting author email: stephanie.jones@stfc.ac.uk

For the first time, we have shown that thin films on an optically trapped aerosol can be probed and sized in real time. Optical trapping combined with white light broadband Mie Spectroscopy (Ward 2008, Schmitz 2011) has been used to determine the presence of a thin film on an aerosol droplet. This technique provides an ideal way to study the oxidation reaction of thin films on aerosol as it is non contact and therefore well represents atmospheric conditions. Initial results have been obtained that indicate the presence of a thin film of oleic acid on a sodium chloride aerosol.

The influence of aerosol on cloud formation and cloud radiative properties remains one of the largest uncertainties in aerosol radiative forcing as stated in the latest IPCC report, AR4 (IPCC 2007).

A major constituent of tropospheric aerosol is marine aerosol, which is often formed with a thin film of organic material present at the air/water interface (Tervahattu 2002). The interfacial films are made up of fatty acid molecules such as stearic and oleic acid, that originate from the breakdown of lipid membranes from ocean dwelling organisms such as phytoplankton. The fatty acids accumulate in the surface microlayer of the ocean, and can be incorporated as an organic coating at the air/water interface when marine aerosols are formed by wind action (Tervahattu 2002). As the thin film forms an encapsulating hydrophobic layer around the aerosol, it plays a central role in the chemistry and hygroscopic properties of the aerosol (Ellison 1999). Furthermore, this film also impacts on the ability of aerosol to form cloud condensation nuclei (CCN) and contribute to the aerosol radiative forcing of the climate (Ellison 1999).

Tropospheric chemical reactions of fatty acid thin films on aerosol, with ozone and atmospheric radicals have the ability to change aerosol properties. Such reactions can break down the hydrophobic thin film. It has been shown by King 2004, using an optical trapping technique, that the ozone oxidation of a thin film of oleic acid on sodium chloride aerosol alters the hygroscopic properties of the aerosol.

The subtle changes in Mie resonances between an uncoated sodium chloride aerosol and a sodium chloride aerosol coated with a thin film of oleic acid-highlighted by theoretical predictions in Figure 2, allow for size and refractive index characterisation of the aerosol.

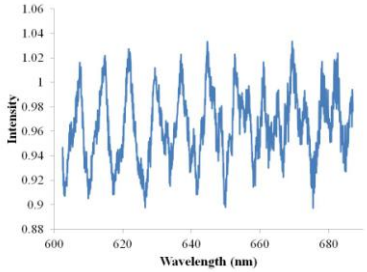

Figure 1. Experimental Mie resonances generated by an optically trapped sodium chloride aerosol with a thin film of oleic acid.

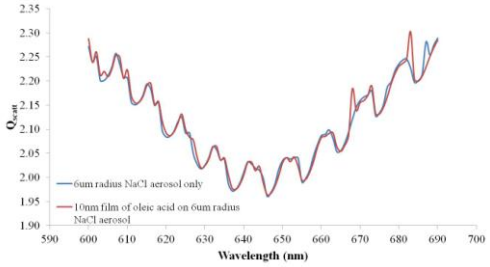

Figure 2. Theoretical Mie resonances for an uncoated 6µm radius sodium chloride aerosol and a coated 6µm radius sodium chloride aerosol with a 10nm thin film of oleic acid.

Future work will involve further fitting, modelling and refinement of the experimental technique.

This work was supported by the Natural Environment Research Council, NERC and the Science and Technology Facilities Council, STFC, Lasers For Science Facility, LSF1120015.

Ward, A., Zhang, M., and Hunt, O., (2008), *Opt.Express* **16**, 16390-16403.

Schmitz, M., Rothe, T., and Kienle, A., (2011) *Biomed. Opt. Express* **2**, (9), 2665-2678.

Climate Change 2007 - The Physical Science Basis *Contribution of Working Group I to the Fourth Assessment Report of the IPCC*, Cambridge University Press, 2007.

Tervahattu, H., Hartonen, K., Kerminen, V-H., Kupianen, K., Aarnio, P., Koskentalo, T., Tuck, A. and Vaida, V., (2002) *J.Geophys. Res.* **107**, 4053-4060.

Ellison, G., Tuck, A. and Vaida, V., (1999) *J.Geophys.Res.* **104**, 11633-11641.

King, M., Thompson, K., Ward, A., (2004), *J.Am.Chem.Soc*. **1**, 126, 16710-16711.

Study on the effect of CO_2 partial pressure on mechanism of sulfation of calcium carbonate sorbent particle

Seongha Jeong[1], Kang Soo Lee[1], Sang In Keel[2], Jin Han Yun[2], and Sang Soo Kim[1]

[1]Department of Mechanical Engineering, Korea Advanced Institute of Science and Technology, Daejeon, Republic of Korea
[2]Environmental Systems Research Division, Korea Institute of Machinery and Materials, Daejeon, Republic of Korea
Keywords: Sulfation, Oxy Combustion System, Calcium Carbonate, Calcination, Sintering
Presenting author email: jeongsh@kaist.ac.kr

Due to increasingly strict greenhouse gas emission regulations, Oxy combustion systems were introduced as a promising CO_2 recovery technique for use in power plants. In oxy-combustion, flue-gas recirculation creates an atmosphere that is primarily CO_2 with a small amount of O_2. Therefore, the phenomena of sorbent particles in an oxy atmosphere are different compared with those in an air atmosphere.

Direct sulfation of calcium carbonate sorbent particle which takes place under high CO_2 partial pressure atmosphere can be applied to Oxy combustion system. However, there's no apparent reaction mechanism about it in comparison with in-direct sulfation (Liu et al., 2000).

In this study, sulfation was performed by using a thermogravimetric analysis (TGA). Experiments were conducted at isothermal condition (1000ºC) with the gas stream of 20% O_2, 80% CO_2 for direct sulfation and 100% air for in-direct sulfation. In each case, SO_2 with concentration of 3000 ppm was injected. After reaction, the morphology of the surface and cross-section of the samples was observed using FIB-SEM. In addition, chemical compositions at the several positions were measured using EDS.

To determine the adsorption sites for SO_2 molecules, the spatial distribution of S-containing compounds was analyzed using EDS. Figure 1 shows that S-containing compounds (blue dots) were distributed over the entire particle in in-direct sulfation, whereas S-containing compounds were gathered around the surfaces of particles in direct sulfation.

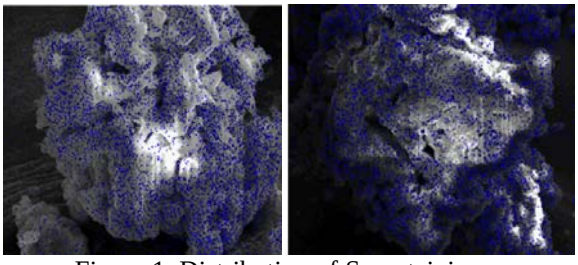

Figure 1. Distribution of S-containing compounds in cross-sectional images of $CaCO_3$ sorbent particles near the completion of in-direct sulfation (left) and direct sulfation(right).

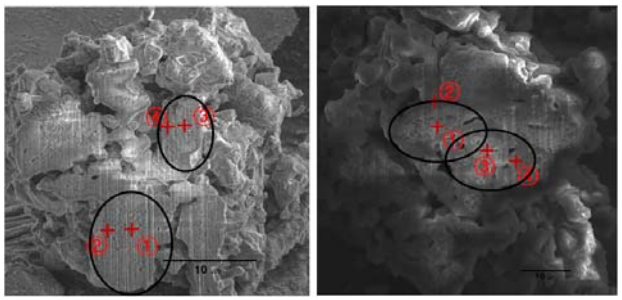

Figure 2. Cross-sectional SEM images of $CaCO_3$ sorbent particles near the completion of in-direct sulfation (left) and direct sulfation(right). Initial particle units are denoted by circles

Table 1. S/Ca ratio of the cross section of $CaCO_3$ sorbent particles

	S/Ca ration	
position	In-direct sulfation	Direct sulfation
①	0.72	0.058
②	0.34	0.047
③	0.64	0.12
④	0.40	0.88

Figure 2 and Table 1 show the quantitative distribution of S-containing compounds. Domains (circles) are the initial particle units. In in-direct sulfation, the S/Ca mole ratio at the surfaces of particles (denoted as ② and ④) was similar to that in the interior (denoted as ① and ③). In an direct sulfation, the S/Ca mole ratio at the surfaces of particles (denoted as ② and ④) was much greater than that in the interior (denoted as ① and ③). These results indicate that sulfation occurred over the entire interior of the particles in in-direct sulfation. In contrast, in direct sulfation, SO_2 molecules were absorbed into the interior through the surface of the particles.

This work was supported by Energy Resources Technology Development Project of the Korea Energy Management Corporation and by BK21 Program.

Liu H., Katagiri S., Kaneko U., & Okazaki K. (2000). Sulfation behavior of limestone under high CO2 concentration in O_2/CO_2 coal combustion, Fuel 79, 945-953

Pressure dependence of sulfuric acid induced SOA formation

P. T. M Carlsson, J. E. Dege, C. Keunecke, B. C. Krüger, J. L. Wolf and T. Zeuch

Institut für Physikalische Chemie, Universität Göttingen, 37077 Göttingen, Germany
Keywords: sulfuric acid, new particle formation, SOA, pressure dependence.
Presenting author email: tzeuch1@gwdg.de

Both mass balances of atmospheric aerosol and aerosol particle numbers are key issues in atmospheric science, since they are closely related to crucial processes like cloud formation and potential health effects of particles. Sulfuric acid (H_2SO_4) initiated new particle formation has been demonstrated in laboratory experiments to be able to account for nucleation events under ambient atmospheric concentrations (Sipilä et al. (2010)). Recently, it was shown that at least half of the observed particle growth rate in the 2-20 nm size range can be explained by condensation of products being produced from gas-phase chemistry (Donohue et al. (2011)).

In this work a new approach is presented for studying how sulfur and organic chemistry interact in the context of new particle formation. To the best of our knowledge the effect of pressure on this process has not been analysed until now. The ozonolysis of cyclohexene (CHEX) is used to generate condensable vapours. In the absence of SO_2 no H_2SO_4 is formed and very low particle number densities are observed. In the presence of SO_2 H_2SO_4 is produced by the reaction sequence

$$SO_2 + OH \rightarrow OHSO_2,\ OHSO_2 + O_2 \rightarrow HO_2 + SO_3,$$
$$SO_3 + H_2O \rightarrow H_2SO_4$$

The low particle number densities being generated during CHEX ozonolysis allow for an analysis of the sensitivity of the presence of H_2SO_4 in the gas mixture on new particle formation. Near the critical H_2SO_4 number density, where additional particle formation can be first observed, a similar sensitivity to recent near-atmospheric flow reactor experiments and atmospheric conditions is found. At higher H_2SO_4 concentrations the sensitivity is lower due to an increased loss of initial clusters by coagulation and condensation. The results are illustrated in figure 1. The similar sensitivity is striking considering our comparatively simple static reactor experiment (see Wolf et al. (2011)) and the difficulties in accurately determining the relation between sulfuric acid concentration and new particle formation in previous work. The dense vapour of condensable species being produced from CHEX ozonolysis seemingly takes over the role of the particle size magnifier in the Leipzig and Helsinki flow reactor experiments. H_2SO_4 number densities are derived by kinetic modelling using the well established rate coefficients for the reactions involved and the known OH yield for CHEX ozonolysis.

At low pressures (around 40 mbar) no significant new particle formation is observed even at high H_2SO_4 concentrations, which is shown in figure 2. These findings indicate that the collisional stabilisation of initial clusters is an important aspect for SOA formation processes involving sulfuric acid and organic compounds. The results may have implications for geo-engineering strategies based on stratospheric sulfur injection. However, at the moment caution is mandatory when room temperature laboratory results are extrapolated to stratospheric conditions.

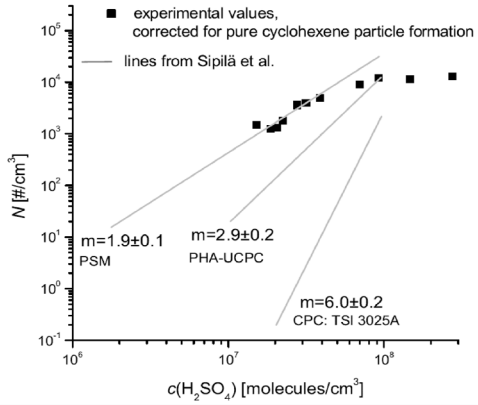

Figure 1. Additional particle formation during CHEX ozonolysis in the presence of SO_2 / H_2SO_4. T = 295±1 K, p_{tot}(synthetic air) = (450±10) mbar. The results are compared to slopes observed in flow reactor experiments using different CPCs, see Sipilä et al. (2010).

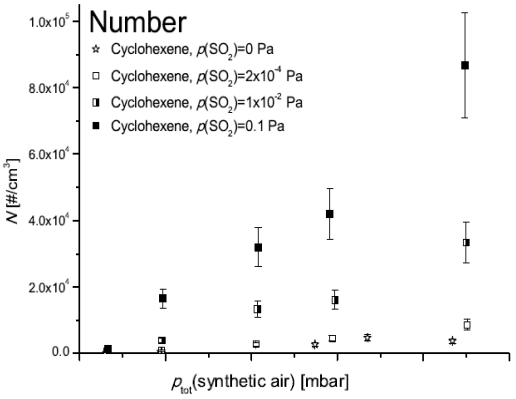

Figure 2. Pressure dependence of enhanced particle formation from CHEX ozonolysis in the presence of SO_2 / H_2SO_4.

Sipilä, M., Berndt, T., Petäjä, T., Brus, D., Vanhanen, J., Stratmann, F., Patokoski, J., Mauldin, R. L., Hyvärinen, A.-P., Lihavainen, H. and Kulmala, M. 2010, *Science*, **327**, 1243–1246.

Donahue, N. M., Trump, E. R., Pierce, J. R., and Riipinen, I. (2011) *Geophys. Res. Lett.*, **38**, L16801.

Wolf, J. L., Richters, S., Pecher, J. and Zeuch, T. (2011) *Phys. Chem. Chem. Phys.*, **13**, 10952–10964.

Changes in hygroscopicity and cloud-activation of diesel exhaust aerosols upon ageing

C.Wittbom[1], B. Svenningsson[1], J.Rissler[2], A. Eriksson[1], E. Swietlicki[1], E. Nordin[2], P. Nilsson[2] and J. Pagels[2]

[1]Department of Physics, University of Lund, P.O. Box 118 SE 221 00, Lund, Sweden
[2] Ergonomics and Aerosol Technology, Lund University, P.O. Box 118 SE-221 00 Lund, Sweden
Keywords: H-TDMA, CCN, AMS, Organic compounds.
Presenting author email: cerina.wittbom@nuclear.lu.se

Aerosol particles play an important role in cloud formation processes. There is a direct effect from primary particles as well as an indirect effect from secondary aerosol particles formed in the atmosphere via complex gas-particle conversion processes. Secondary organic aerosols (SOA) can be formed when volatile organic compounds (VOCs) are present. Then part of the oxidation products from the VOCs condenses on pre-existing particles and produce SOA. This alters the particle properties, via condensation of the oxidised VOCs, which may lead to a lowered critical supersaturation (SS_c). Though, organic compounds will typically not suppress the water activity as much as inorganic salts. In general, the understanding of the properties of the SOA is scanty relative to the understanding of the major inorganics and is thereby of great interest for investigation.

This study is a continuation of a previous campaign, where exhaust from light duty vehicles were transferred to a smog chamber and photochemically aged (Nordin *et al*., 2012). The aerosol properties were monitored using an extensive instrumental set-up, obtaining information on morphology, density, volatility, particulate and gas composition as well as hygroscopic growth and cloud droplet nucleation. The present study focus on experiments using soot (from a flame soot generator and diesel car exhaust) and different SOA precursors (Toluene and m-Xylene). During the ageing procedure, the transformation of the hygroscopic behaviour and its link to the effect on cloud droplet activation were related to the organic fraction in the particle as well as particle size and morphology.

Hygroscopic properties were analysed using a Hygroscopic Tandem Differential Mobility Analyser (H-TDMA; Nilsson et al., 2009), the cloud-activation properties were measured using a Cloud Condensation Nucleus Counter (CCNC; DMT 100), and a soot particle aerosol mass spectrometer (SP-AMS, Aerodyne research) to determine the composition of the cores and the coatings of the particles. The particle mass-mobility relationship was characterized using a Differential Mobility Analyser-Aerosol Particle Mass Analyzer (DMA-APM; McMurry et al., 2002; Kanomax Japan 3600). A thermodenuder was introduced in series between the DMA and the APM, used for quantification of the size dependent mass fraction condensed onto the non-volatile soot cores. The particles were first size selected by the DMAs, according to their mobility diameter. This was followed by measurements in the APM, the H-TDMA and CCNC. Furthermore, it was investigated whether the diameter growth factor (GF; Fig.1), derived from H-TDMA data, could be used to predict SS_c for particles of a certain mobility diameter. During the latter campaign, the CCNC was operating using a modified measurement procedure, i.e. Scanning Flow CCN Analysis (SFCA) (Moore & Nenes, 2009), enabling rapid measurements with high time resolution of the supersaturation spectra, revealing more detailed, accurate and continuous results.

Fresh diesel soot particles show no hygroscopic growth and require a higher SS_c than predicted when using a simple model, based on the Köhler theory. The model only take the Kelvin effect into account, using the mobility diameter and assuming wettable particles (Rissler *et al.,* 2010). This is probably due to the agglomerated structure of the soot particles (e.g. Khalizov et al. 2009). At 90% relative humidity (RH), the soot particles collapse when coating exceeds 15-40% condensed organic material. Moreover, the cloud droplet activation is improved long before the particles show any hygroscopic growth at all, at 90% RH (Fig.1).

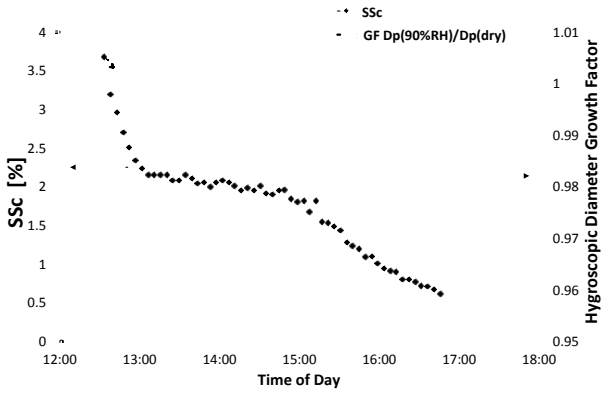

Figur 1. Preliminary SS_c decline for diesel soot particles (d_{dry}=150 nm) (data points), as well as the corresponding GF at 90% RH (solid black line) over time.

The Swedish Research Council (VR) and FORMAS supported this work.

Khalizov et al. (2009) *J. Geoph. Res.,* A 114, D05208
McMurry P.H., et al. (2002) *Aerosol Sci. and Technol.* 36: 227–238.
Moore, R. & Nenes, A. (2009) *Aerosol Sci. Technol*. 43:1192-1207.
Nilsson, E. et al. (2009) *Atmos. Meas. Tech.*, 2, 313-318.
Nordin, E.Z., et al. (2012) Smog chamber studies of SOA formation from Gasoline Vehicles & Aromatic precursors. *To be submitted to ACP* .
Rissler, J., et al. (2010) *J. Geoph. Res. A* 115, D22208

Hygroscopicity and optical properties of secondary organic aerosol formed in CESAM simulation chamber

C. Denjean[1], P. Formenti[1], B. Picquet-Varrault[1], Y. Katrib[1], E. Pangui[1], P. Zapf[1] and J.F. Doussin[1]

[1]Laboratoire Inter-Universitaire des Systèmes Atmosphériques (LISA UMR 7583), Université Paris Est Créteil – Val de Marne, Université Paris Diderot, 61 Avenue du Général de Gaulle, 94010 Créteil, France
Key-words: Hygroscopicity, optical properties, SOA (Secondary Organic Aerosols), Smog chamber
Presenting author email: denjean@lisa.u-pec.fr

Aerosol particles influence Earth's climate by scattering and absorbing light and by acting as cloud condensation nuclei. The impacts of organic aerosols on climate are poorly understood and require further understanding. To fill these gaps, the present work investigates the optical and hygroscopic properties of secondary organic aerosols (SOAs) generated from the ozonolysis of α-pinene at first and after having undergone atmospheric ageing reactions via an excess of ozone exposure or irradiation. Experiments have been performed in the atmospheric smog chamber CESAM, specifically designed to investigate multiphase processes and simulate atmospheric aerosol ageing (Wang *et al*, 2011). The chamber provides very realistic artificial solar irradiation and particle lifetime higher than two days.

The uptake of water of monodispersed SOA was measured using a Hygroscopicity Tandem Differential Mobility Analyser (H-TDMA) which was run at 90% RH and provided the hygroscopic growth factor (HGF). Parallel studies of hygroscopicity were done by varying linearly the relative humidity in the chamber from 0 to 100%. A Scanning Mobility Particle Sizer (SMPS, diameter range 20-800nm) and a Light Aerosol Spectrometer (WELAS, diameter range 0.2-10 µm) were used to directly follow the variation in size distribution as a function of relative humidity. The temporal evolution of the growth factor at 90% RH obtained with the H-TDMA for different ageing processes is shown in Figure 1. The hygroscopicity of α-pinene SOAs remained constant, with a growth factor around 1.05, during both ageing in dark conditions and ageing through ozone exposure. On the other hand, after ageing through irradiation exposure during 6h, SOAs exhibited a higher growth factor (HGF=1.15).

The investigation of optical properties of SOAs combined scattering and absorption measurements by a nephelometer and a spectral aethalometer directly connected to the chamber. The refractive indexes for the SOAs were derived from these measurements as well as from optical calculations using Mie scattering theory. As optical properties of atmospheric particles might depend on their affinity for water, the RH dependence of scattering coefficient and refractive indexes were also investigated. Results from absorption measurement of all experiments showed that α-pinene SOAs did not absorb in the visible region (imaginary part equal to zero). Figure 2 reports the temporal evolution of the real part of the refractive index at 525nm. We observed that the real part of the refractive index decreased during the α-pinene SOA formation. No trend was observed neither during ageing in dark conditions nor during ageing through excess ozone exposure. In contrast, significant increase of the real part of the refractive index was observed for SOAs exposed to irradiation. These observations are to be interpreted by observed concurrent changes in the particle bulk and surface chemical composition.

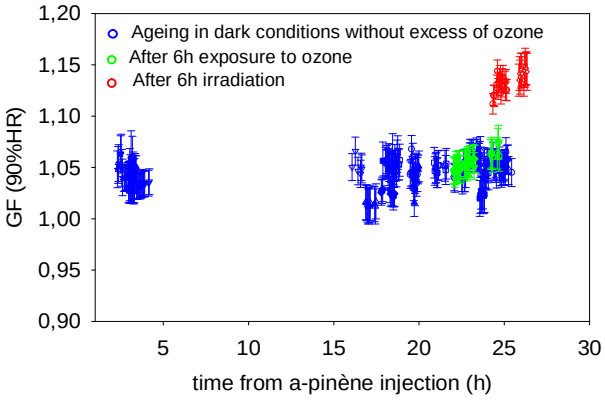

Figure 1. Temporal evolution of the growth factor at 90%RH for different ageing processes

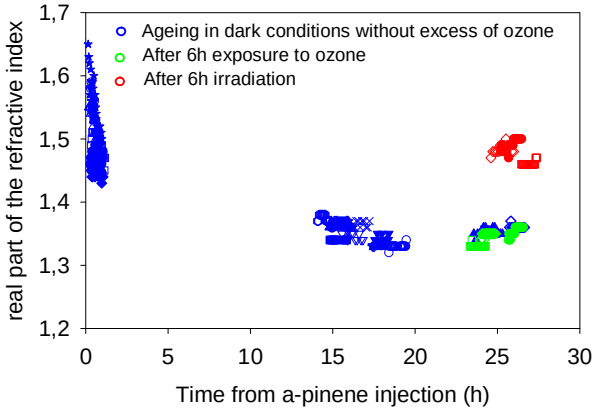

Figure 2. Temporal evolution of the real part of refractive index at 525nm for different ageing processes

Wang, J. et al (2011) *Atmospheric measurement techniques* **4**(11), 2465-2494

Secondary Organic Aerosol formation from isoprene photooxidation

L. Brégonzio[1], J.F. Doussin[1], E. Pangui[1], A. Monod[2], F. Siekmann[2], B. Temime[2], M. Camredon[1], B. Aumont[1]

[1]Laboratoire Inter-Universitaire des Systèmes Atmosphériques (LISA UMR 7583), Université Paris Est Créteil-Val de Marne, Université Paris Diderot, 61 Avenue du Général de Gaulle, 94010 Créteil, France
[2]Laboratoire Chimie Provence, Université de Provence, 3 place Victor Hugo, 13331 Marseille, France
Keywords: smog chamber, SOA (Second. Organic Aerosols), photochemical reaction, modelling.
Presenting author email: lola.bregonzio@lisa.u-pec.fr

Isoprene (2-methyl-1,3-butadiene, C_5H_8) is one of the most abundant non-methane hydrocarbons emitted into the troposphere. Its annual global emission has recently been estimated in the range of 440 to 660 TgC (Guenther *et al.*, 2006). Because of its large concentrations and high reactivity with the hydroxyl radical (OH), isoprene can have a strong influence on tropospheric photochemistry. It has been determined recently that isoprene also plays a role in secondary organic aerosol (SOA) formation in the ambient atmosphere even if isoprene leads to low SOA yields. The aim of the present work was to study isoprene photo-oxidation with OH radical in order to investigate its oxidation products and resulting aerosol production. A special care was taken to the realism of the experiment: light source, NOx level, OH source and aging time (around 10 hours).

To do so, experiments were performed in CESAM chamber at LISA, specifically designed to investigate multiphase processes with a highly realistic irradiation compared to solar radiation (Wang *et al.*, 2011). Connected to the chamber, a large panel of instruments was used to monitor the gas-phase and the particulate phase during experiments. Gas-phase composition was analysed in-situ via a Fourier Transform Infrared Spectrometer (FTIR) and a Proton Transfer Reaction Mass Spectrometer (PTR-TOF-MS) as well as NO_x and O_3 analyzers. A Scanning Mobility Particle Sizer (SMPS, diameter range 20-800 nm) measured SOA size distributions and total concentrations inside the chamber. An Aerodyne aerosol mass spectrometer (TOF-AMS) was also used to investigate aerosol composition. In each experiment, around 500 ppb of isoprene was injected in the chamber before irradiation. During all the experiment, a very low continuous flow of NO was injected in order to mimic atmospheric emission and maintain oxidation rate, thanks to its propagating role. It therefore allowed us to investigate not only isoprene chemistry but also the fate of its products. Some experiments were carried out with initial ammonium sulfate seed aerosols. The typical temporal evolution of gas-phase and SOA concentrations observed in experiments without seeds is shown in Figure 1.

The major gas-phase oxidation products of isoprene we measured, in low NO conditions, are formaldehyde, methacrolein and methyl vinyl ketone identified as first-generation products, and also methylglyoxal and peroxyacetyl nitrate (PAN), identified as second-generation products. NO_2 to NO ratios, yields of all measured oxidation products and carbon budget were calculated. In all experiments, we noted a SOA production at the end of isoprene oxidation i.e. exhibiting a clear secondary products type growth. Several results (including SOA densities and yields, and O/C ratios) were obtained using SMPS and AMS data allowing us to characterise SOA formation and composition during the experiments. The gas-phase composition as well as the aerosol yields obtained during these experiments have been compared to results simulated by a 0D photochemical box model. The goal of this work was to assess whether or not the processes contained in current chemical mechanisms enable to reproduce observations in the gas-phase. It is aiming also at assessing if the vapour pressure based parameterization of the aerosol production in the model is able to reproduce experimental data for the particle phase.

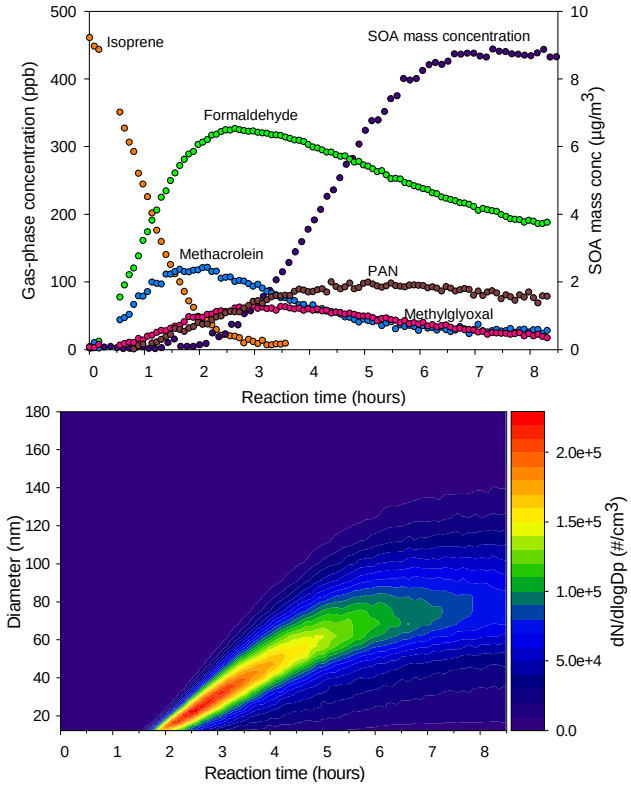

Figure 1. A typical temporal evolution of species in an experiment without seeds.

Guenther, A. et al. (2006).*Atmospheric Chemistry and Physics*, **6**, 3181–3210.

Wang, J. et al. (2011) *Atmospheric measurement techniques* **4**(11), 2465-2494.

AMISOC 2012: Multi-instrument campaign for assessment of trace gas-aerosol interactions

O. Puentedura[1], M. Gil[1], J.A. Adame[1], J. Andrey[1], C. Córdoba-Jabonero[1], L. Gómez[1], T. Hay[2], M. Navarro[1], C. Prados-Román[2], A. Saiz-López[2], M. Sorribas[3], D. Toledo[1] and B. de la Morena[1]

[1]Instituto Nacional de Técnica Aeroespacial (INTA), Atmospheric Research and Instrumentation Branch, Torrejón de Ardoz, 28850, Madrid, Spain
[2]Laboratory for Atmospheric and Climate Science (CIAC), Spanish National Research Council (CSIC) - Fundación General de Medio Ambiente of Castilla-La Mancha, Toledo, 45007, Spain
[3]Andalusian Center for Environmental Research (CEAMA), University of Granada - Autonomous Government of Andalusia, Granada, 18071, Spain
Keywords: Airborne and in-situ measurements, Saharan dust, Halogen chemistry, Remote sensing techniques.
Presenting author email: cordobajc@inta.es

AMISOC (Atmospheric MInor Species relevant to the Ozone Chemistry at both sides of the jet) is a research project, funded by the Spanish R&D programme, devoted to improving the knowledge of minor constituents playing a role in ozone chemistry. The core of the project is two coordinated campaigns to be performed at: 1) the Atmospheric Sounding Station (ESAt) "El Arenosillo", Huelva, in the southwestern Iberian Peninsula, during May-June 2012, and 2) Tenerife (Canary Islands) in July 2013, located at mid- and subtropical latitudes respectively.

AMISOC-El Arenosillo (AMISOC-ARN) is conceived as a multi-instrument campaign in order to study the behavior of minor trace gases under heavy aerosol loading. This situation is frequent in spring- and summer-time when Saharan dust intrusions arrive at the SW-IP (Toledano *et al.*, 2007; Córdoba-Jabonero *et al.*, 2011). Simultaneous measurements of gases and aerosols are proposed, making use of different platforms and techniques. Ground level (including a 100m tower) and airborne (aboard INTA aircraft C-212) in-situ (gases, aerosols and meteorology) measurements as well as aerosol lidar and columnar sun-photometry observations in addition to local radiosoundings will be performed. Table1 summarizes the main instrumentation and techniques to be used in AMISOC-ARN.

The study of halogens in the atmosphere is a hot research field due to its implications on ozone chemistry and because their concentration at different levels in the atmosphere and seasonal dependences are not yet well known (Saiz-Lopez *et al.*, 2011, and references therein). In this context, the principal objectives for this campaign are:

- Evaluation of the impact of Atmospheric Boundary Layer (ABL) air masses on the vertical distribution of halogen radicals.
- Analysis of the daily evolution of tropospheric NO_2 and IO.
- Study of the correlation between nanoparticles and halogens.
- Quantification of the O_3 vertical depletion observed during Saharan dust events and the changes experienced in other minor species (NO_2 and IO).
- Interpretation of the results in the frame of the current accepted chemistry.

Table 1. Instrumentation/techniques to be used in AMISOC-ARN (*).

Instrument / technique	Platform	Measurements	Species / particle parameters
GASES			
MAX-DOAS	Ground-level	Remote sensing, vertical profiles (inversion alg.)	NO_2, O_3, IO and O_4 concentration
O_3 monitor	Ground-level	Surface in-situ	O_3 concentration
NO_x analyzer	Ground-level	Surface in-situ	NO and NO_2 concentration
SO_2 analyzer	Ground-level	Surface in-situ	SO_2 concentration
O_3 monitor	Airborne	In-situ, vertical profiles	O_3 concentration
NO_x analyzer	Airborne	In-situ, vertical profiles	NO and NO_2 concentration
AMAX-DOAS	Airborne	In-situ, vertical profiles	NO_2, O_3 and IO concentration
AEROSOLS			
APS	Ground-level	Surface in-situ	SD (micrometer range)
SMPS	Ground-level	Surface in-situ	SD (sub-micron range)
Nephelometer	Ground-level	Surface in-situ	SC, AE, BSF
LIDAR (MPL)	Ground-level	Remote sensing, vertical profiles	EX, BS
Sun-photometer (CIMEL)	Ground-level	Remote sensing, columnar-integrated	AOD, AE, SD
PCASP (OPC)	Airborne	In-situ, vertical profiles	SD (accumulation mode: < 3 μm)
CAPS (OPC)	Airborne	In-situ, vertical profiles	SD (acc. + coarse modes: 0.5 μm - 50 μm)

(*) AE – Angstrom Exponent, AOD – Aerosol Optical Depth, BS – BackScattering coefficient, BSF – BackScattering Fraction, EX – EXtinction coefficient, MAX-DOAS – Multi AXis Differential Optical Absorption Spectroscopy, OPC - Optical Particle Counter, SC – SCattering coefficient, and SD – Size Distribution.

This work is supported by the Spanish Ministry for Research and Innovation (MICINN) under grant CGL2011-24891 (project AMISOC). MS thanks the 'Juan de la Cierva' post-doctoral grant support.

Córdoba-Jabonero *et al.* (2011) *Atmos. Chem. Phys.* **11**, 3067-3091.
Saiz-Lopez *et al.* (2011) *Chem. Rev.*, in press.
Toledano et al. (2007) *J. Geophys. Res.* **112**, D21201, doi:10.1029/2006JD008307.

Direct Surface Analysis of Size- and Time- Resolved Organic Aerosol

S.J Fuller[1], M. Kalberer[1], Y. Zhao[2], A.S Wexler[2]

[1]Department of Chemistry, University of Cambridge, Cambridge, CB2 1EW, UK
[2]Air Quality Research Center, University of California, Davis, CA 95616, USA
Keywords: Aerosol chemistry, mass spectrometry, air quality, organics.
Presenting author email: sjf53@cam.ac.uk

Ambient aerosol particles have been shown to have significant health and climate implications. Studies of the chemical composition of aerosol particles are important to establish the mechanisms of their reactivity. However the aerosol composition, especially the organic fraction is highly variable with both time and the size fraction concerned. Many previous organic aerosol studies involved filter or impaction collection with a limited time resolution of typically a day. Combining a rotating-drum impactor (RDI) with Liquid Extraction Surface Analysis (LESA) allowed the study of separate size fractions collected over a 2-week period to be analysed with a 3-hour resolution using a high-resolution mass spectrometer for organic species identification. Similar RDI studies have used X-ray fluorescence for elemental analysis (Richard *et al*, 2010).

An RDI was used to collect size segregated aerosol samples for approximately 2 weeks from 11 am 25/5/2011 to 11 am 7/6/2011 from a dairy farm in California. The RDI allows time resolved continuous collection of ambient particle impaction samples (Raabe *et al*, 1988). Ambient air is sampled (16.7 lpm) and aerosol particles are collected via impaction on greased mylar substrates. The RDI sampler consists of 8 stages collecting samples in 8 size ranges, however only the samples from 2 stages, stage 3 and stage 8, were investigated in this study; these corresponded to the size ranges 2.5-1.15 and 0.26-0.09 μm respectively.

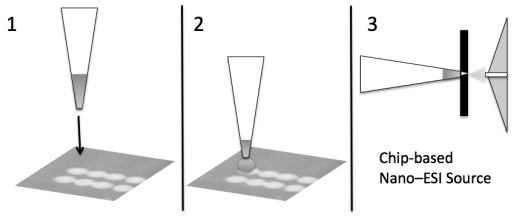

Figure 1. The LESA extraction process; a liquid junction is formed (2) before analysis by mass spectrometry (3).

The organic composition of stripes 3 and 8 were analyzed using a novel direct extraction technique - Liquid Extraction Surface Analysis (LESA). LESA is a mode of operation of the TriVersa NanoMate (Advion) chip-based Nano-ESI source (Kertesz *et al,* 2010). A small amount of solvent is dispensed with a pipette tip on the surface of the sample; the micro liquid junction is maintained to allow analytes present on the surface of the sample to dissolve. The droplet is aspirated and sprayed via an infusion method utilising the chip based electrospray ionsation (ESI). The size of the liquid junction translates to a time resolution of approximately 3 hours.

An ultra-high-resolution mass spectrometer (LTQ Velos – Orbitrap, Thermo-Scientific) was used to analyse the organic fraction following extraction by LESA. This data was used to determine the molecular formulae of the compounds found during the sampling period. For stage 3 a correlation was found between the N/C elemental ratio of species less that 150 Da in mass and the sample loading. This is shown in figure 2, the light areas of the black and white image correspond to high sample loadings that, following comparison with meteorological data, are due to wind blown dust from the local area. The higher N/C ratio found in these areas may be due to influence of fertilisers. In addition a number of amines, possibly from biomass burning, were found predominantly on stage 8.

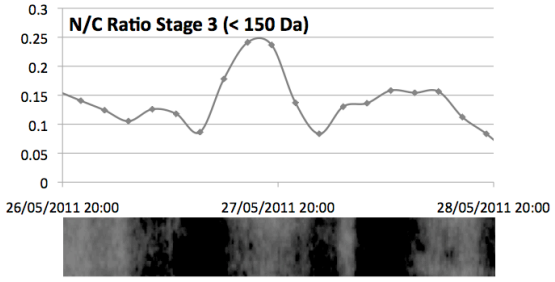

Figure 2. N/C elemental ratio, with stage 3 shown below. Variation with sample time and corresponds to sample loading.

This demonstrates that the combination of the RDI and LESA can be used for semi-quantitative analysis of organic trace components in ambient samples, with a high time resolution that can be easily compared to meteorological data.

This work was supported by the Natural Environment Research Council, UK.

Raabe *et al* (1988): Calibration studies of the drum impactor, *Journal of Aerosol.* **19**, *183-95*.

Kertesz *et al* (2010): Fully automated liquid extraction-based surface sampling and ionization using a chip-based robotic nanoelectrospray platform, *Journal of mass spectrometry*. **45**, *252-60*.

Richard *et al* (2010): Quantitative sampling and analysis of trace elements in atmospheric aerosols: impactor characterization and Synchrotron-XRF mass calibration, *Atmospheric Measurement Techniques*. **3,** *1473-85***.**

The Manchester Photochemical Aerosol Chamber: Formation, Transformation and Properties of Secondary Organic Aerosols

M.R Alfarra[1], A. Buchholz[2], W. Hesson[2], J.F. Hamilton[3], K.P. Wyche[4], I. White[4], P. Monks[4], A. Lewis[3], and G.B. McFiggans[2]

[1]National Centre for Atmospheric Science (NCAS), The University of Manchester, Manchester, M13 9PL, UK
[2]Centre for Atmospheric Sciences, The University of Manchester, Manchester, M13 9PL, UK
[3]Deparment of Chemistry, University of York, Heslington, York, YO10 5DD, UK
[4]Department of Chemistry, University of Leicester, Leicester, LE1 7RH, UK

Keywords: SOA, Smog Chamber, Chemical Composition, Hygroscopicity, Aerosol mass spectrometry
Presenting author email: rami.alfarra@manchester.ac.uk

Studies using photochemical aerosol chambers "also known as smog chambers" can provide valuable insights into the complex multiphase processes leading to the formation and transformation of atmospheric particulates. The Manchester aerosol chamber is an 18 m^3 photochemical batch reactor designed to study atmospheric processes of multicomponent aerosols under controlled and realistic conditions. Our research ranges from formation and transformation of secondary organic aerosols (SOA) under seeded and un-seeded conditions to investigations of the direct and indirect effects of multicomponent aerosols on climate. The facility enables us to evaluate and respond to hypotheses derived from field observations and provides a "test-bed" for evaluating (i) oxidation mechanisms of VOCs (e.g. Jenkin et al. (2012)) and (ii) processes in atmospheric models.

In order to enable this research, the facility is equipped with an array of state-of-the-art instruments measuring aerosol composition and properties as well as VOC precursors and their oxidation products. The chemical composition of the formed SOA is measured on-line using an Aerodyne Time-of-Flight Aerosol Mass Spectrometer (ToF-AMS). A hygroscopicity tandem differential mobility analyser (HTDMA) and a cloud condensation nuclei (CCN) counter are used to probe the hygroscopic properties and of the aerosols in the sub- and super-saturated regimes, respectively. A proton transfer mass spectrometer was used to study the evolution of the gas phase oxidation products.

In this poster, we will provide a technical description of the facility and discuss a number of scientific highlights obtained as part of the recently completed Aerosol Coupling in the Earth System (ACES) project, which focused on the formation and transformation of biogenic secondary organic aerosol (Hamilton et al., 2011; Alfarra et al., 2012). We will also present preliminary findings from a recently commissioned programme of research aiming to quantify remaining uncertainties related to the properties of aerosol particles determining their ability to form liquid droplets under ambient atmospheric conditions. Specifically, the programme aims to quantify (i) the impacts of semi-volatile components on aerosol water uptake; (ii) the impacts of aerosol phase on water uptake; and (iii) the impacts of aerosol phase on their IN behaviour.

This work was supported by the UK Natural Environment Research Council (NERC) through the APPRAISE and ACIDPRUF programmes.

Alfarra, M. R., Hamilton, J. F., Wyche, K. P., Good, N., Ward, M. W., Carr, T., Barley, M. H., Monks, P. S., Jenkin, M. E., and McFiggans, G. B. (2012), *Atmos. Chem. Phys. Discuss., 12*, 2435-248.

Hamilton, J. F., Rami Alfarra, M., Wyche, K. P., Ward, M. W., Lewis, A. C., McFiggans, G. B., Good, N., Monks, P. S., Carr, T., White, I. R., and Purvis, R. M. (2011), *Atmos. Chem. Phys., 11*, 5917-5929.

Jenkin, M. E., Wyche, K. P., Evans, C. J., Carr, T., Monks, P. S., Alfarra, M. R., Barley, M. H., McFiggans, G. B., Young, J. C., and Rickard, A. R. (2012), *Atmos. Chem. Phys. Discuss., 12*, 2891-2974.

COMPOUND SPECIFIC CONDENSATION TO SECONDARY ORGANIC AEROSOLS PROVIDING SIZE DEPENDENT INFORMATION

D. Mogensen[1,2], D. Lowe[3], G. Capes[3], D. O. Topping[3], G. B. McFiggans[3], S. Smolander[1], M. Kulmala[1] and M. Boy[1]
[1]Division of Atmospheric Sciences, Department of Physics, University of Helsinki, Finland
[2]Helsinki University Centre for Environment, University of Helsinki, Finland
[3]School of Earth, Atmospheric and Environmental Sciences, University of Manchester, UK
Keywords: Aerosol component composition, condensation, aerosol modelling, SOA
Presenting author email: ditte.mogensen@helsinki.fi

We are presenting the next version of the zero-dimensional model MALTE–BOX with implemented temperature depended saturation vapour pressures for atmospherically relevant organic compounds. We calculate size dependent secondary organic aerosol growth (from nucleation to accumulation mode), using a kinetic condensation approach, based on an open number of condensible organic vapours. We characterise the chemical composition of the formed aerosols and compare our results with atmospheric mass spectrometer (AMS) data.

As until now, modellers have mostly simulated the aerosol mass balance by using one or a few compounds (most often water, sulphuric acid and one or two organic compounds) as a representation for all condensing vapours or the Volatility Basic Set (VBS) (Donahue *et al.* (2006)). Those few studies that do take compound specific condensation into account, use a equilibrium partitioning approach for condensation, and generate a bulk aerosol, whereby all size information is lost. If we want to understand aerosol growth on a more process based level, we need to know what molecules contribute significantly to the aerosol mass in each size bin, and therefore compute the individual contributions from all possible candidates.

We are using the model MALTE-BOX for the implementation of saturation vapour pressures. MALTE–BOX is a zero–dimensional improved version of MALTE (Model to predict new Aerosol formation in the Lower TropospherE) (Boy *et al.* (2006)). It includes three parts; 1) emission, 2) chemistry, and 3) aerosol dynamics. The emissions of organic vapours from the canopy are calculated using MEGAN (Model of Emissions of Gases and Aerosols from Nature) (Guenther *et al.* (2006)). The chemistry is calculated using the Kinetic PreProcessor (KPP) (Damian *et al.* (2002)), with chemical reaction equations selected from the Master Chemical Mechanism v3.2 (Jenkin *et al.* (1997), Saunders *et al.* (2003)) via website: http://mcm.leeds.ac.uk/MCM/. The aerosol dynamic processes are simulated with UHMA (University of Helsinki Multicomponent Aerosol model) (Korhonen *et al.* (2004)).

For the calculation of the saturation vapour pressures, we use a script written by professor Gordon McFiggans' group at the University of Manchester. The script, which is written in the Python programming language, calculates the boiling temperature and following the saturation vapour pressures of any compound based on its molecular structure using Nannoolal's vapour pressure method (Nannoolal *et al.* (2008)). The saturation vapour pressures will be calculated for all the organic compounds listed on MCM's website. This includes 5707 chemicals. Following, the calculated saturation vapour pressures will be implemented in MALTE–BOX as look–up tables and tested together with and against the VBS code in comparison with certain selected chamber experiments including ozone – alpha-pinene.

The financial support by the Academy of Finnish Center of Excellence program (FCoE, project no. 1118615), the Helsinki University Centre for Environment (HENVI) and computational resources from CSC – IT Center for Science Ltd are all gratefully acknowledged.

Boy, M., Hellmuth, O., Korhonen, H., Nilsson, E. D., ReVelle, D., Turnipseed, A., Arnold, F. and Kulmala, M. (2006). Atmos. Chem. Phys. **6**, 4499-4517.

Damian, V., Sandu, A., Damian, M., Potra, F. and Carmichael, G. R. (2002) Comput. Chem. Eng. **26**, 1567-1579.

Donahue, N. M., Robinson, A. L., Stanier, C. O. and Pandis S. N. (2006) Environ. Sci. Technol. **40**, 2635-2643.

Guenther, A., Karl, T., Harley, P., Wiedinmyer, C., Palmer, P. I. and Geron, C. (2006). Atmos. Chem. Phys. **6**, 3181-321.

Jenkin, M. E., Saunders, S. M. and Pilling, M. J. (1997) Atmos. Environ. **31**, 81-104.

Korhonen, H., Lehtinen, K. E. J. and Kulmala, M. (2004) Atmos. Chem. Phys. **4**, 757-771.

Nannoolal, Y., Rarey, J, and Ramjugernath, D. (2008) Fluid Phase Equilibr. **269**, 117-133.

Saunders, S. M., Jenkin, M. E., Derwent, R. G. and Pilling, M. J. (2003) Atmos. Chem. Phys. **3**, 161-180.

Direct observations of surface/bulk partitioning and acid/base speciation in aqueous solutions of the atmospheric surfactant sodium decanoate using synchrotron X-ray photoelectron spectroscopy

N.L. Prisle[1], N. Ottosson[2], G. Öhrwall[3], J. Söderström[2], M. Dal Maso[1], and O. Björneholm[2]

[1]Department of Physics, University of Helsinki, P.O. Box 62, 00014 University of Helsinki, Finland
[2]Department of Physics and Astronomy, Uppsala University, P.O. Box 516, S- 751 20 Uppsala, Sweden
[3]MAX-lab University of Lund, Box 118, 22100, Lund, Sweden
Keywords: organic aerosol, surfactants, surface adsorption, synchrotron XPS.
Presenting author email: nonne.prisle@helsinki.fi

Surface active (surfactant) organic compounds are frequently observed in atmospheric aerosols. Long-chain fatty acids and their carboxylate anions constitute one important class of atmospheric surfactants. In aqueous solutions, such as aqueous aerosols and cloud droplets, surfactants preferentially adsorb at the air-water interface and can reduce the surface tension, compared to that of pure water. The aqueous surface activity is a central, but still not well constrained, property of organic aerosol components (Prisle *et al.*, 2010, and references therein).

We have investigated dilute aqueous solutions of the atmospheric surfactant sodium decanoate, using X-ray photoelectron spectroscopy (XPS) in combination with synchrotron radiation. We studied the chemical speciation in the aqueous surface, in terms of the relative abundances of the decanoate anion and the corresponding protonated form, decanoic acid, and the influence on these abundances of mixing in solution with some of the most common inorganic ions found in the atmosphere, the sodium and ammonium cations, and the chloride and sulfate anions (Seinfeld and Pandis, 2006). XPS is a highly surface and chemically sensitive spectroscopic technique (Hüfner, 1995) and in particular capable of resolving signals originating from the carboxylate and carboxylic acid groups of the decanoate/decanoic acid pair, respectively (Ottosson *et al.*, 2011). XPS has been adapted to the study of liquid surfaces by combination with the liquid-jet technique (Winter and Faubel, 2006).

We conducted liquid-jet photoelectron experiments at the Swedish national synchrotron facility MAX-lab in Lund, at the soft X-ray undulator beamline I411. The experimental setup and procedures have been described in detail by Bergersen *et al.* (2007). We investigated aqueous solutions of sodium decanoate (DecNa), as pure solute (binary) and in equimolar mixtures with one of the inorganic salts sodium chloride, sodium sulfate, ammonium sulfate, and ammonium chloride (ternary). Each solute composition was studied at concentrations corresponding to 10 and 25 mM DecNa. Results of these experiments are presented as core photo-electron spectra recorded in the carboxylate and carboxylic C1s energy region. At the X-ray photon energy used here (360 eV), the total experimental resolution in this energy region was better than 250 meV.

Adsorption of carboxylic compounds and their acid/base speciation from protonation/protolysis at the air-water interface may have significant implications for a number of atmospheric processes involving aqueous organic aerosols. Some of the process-level mechanisms that may be influenced are related to (i) heterogeneous reactivity of the aerosol surface, towards both gas and bulk aqueous phases, and thus to the formation of organic aerosol mass and the general chemical processing of atmospheric components, as well as to (ii) the thermodynamics of phase transformations in the atmosphere, such as organic aerosol hygroscopic growth, and cloud droplet and ice nucleation. These processes may in turn influence the overall atmospheric aerosol burden, composition, and properties, and thus affect various of the identified direct and indirect climate impacts of atmospheric aerosols (IPCC, 2007).

Directly probing the surfaces of the investigated aqueous solutions is greatly advantageous to conventional methods that rely on inferring surface composition and properties from those of the solution bulk phase, since no assumptions pertaining to the nature of molecular-scale interactions, phase equilibrium, or the applicability of specific adsorption isotherms are imposed on the system. Our presented results thus demonstrate the viability of the synchrotron XPS technique for studying properties of aqueous solution surfaces of immediate atmospheric relevance.

This work was supported by the NordForsk researcher network project 10160 NICITA, the Knut and Alice Wallenberg Foundation (KAW), the Swedish Research Council (VR), and the Carlsberg Foundation (N.L. Prisle personal grants 2009_01_0366 and 2010_01_0391).

Bergersen, H., et al. (2007) J. Phys.: Cond. Matt.**19**, 326-101.

Hüfner, S. (1995) Photoelectron spectroscopy, Springer Verlag, Berlin.

Intergovernmental Panel on Climate Change (2007) Climate Change 2007, Cambridge University Press.

Ottosson, N., *et al.* (2011) Phys. Chem. Chem. Phys. **13**, 12261-12267.

Prisle, N. L., *et al.* (2010) Atmos. Chem. Phys. **10**, 5663-5683.

Seinfeld, J.H. and Pandis, S.N. (2006) Atmospheric Chemistry and Physics, 2nd edn. John Wiley and Sons, Inc.

Winter, B. and Faubel, M. (2006) Chem. Rev. **106**, 1176–1211.

13-Carbon Isotopic Fractionation in Secondary Organic Aerosol Formation

C. Meusinger[1], U. Dusek[2], S.M. King[1], R. Holzinger[2], M. Bilde[1], T. Röckmann[2] and M.S. Johnson[1]

[1] Copenhagen Center for Atmospheric Research (CCAR), Department of Chemistry, University of Copenhagen, 2100 Copenhagen, Denmark
[2]Institute for Marine and Atmospheric research Utrecht (IMAU), Utrecht University, 3584 CC, Utrecht, The Netherlands
Keywords: SOA, isotopes, carbon, smog chamber.
Presenting author email: came@kiku.dk

Secondary organic aerosol (SOA) formed by oxidation of volatile organic compounds (VOC) is a main field of study in atmospheric research since its impact on climate, health and visibility is still not well understood. Given the vast amount of possible reactions involved in the oxidation of VOCs, reaction patterns are unclear and uncertainties of SOA yields are still large. Here, isotope measurements enable us to distinguish reaction pathways since they alter the isotopic composition of products and reactants (kinetic isotope effect, KIE). This in turn helps to establish chemical reaction schemes and to constrain budgets. Studied systems employing isotopes so far cover a wide range including atmospheric samples (Rudolph *et al*, 2002), gas-phase reactions (Iannone *et al*, 2010) and SOA generation (Irei *et al*, 2011; Fisseha *et al*, 2009).

The fundamental idea behind this research is to investigate the possible link between ^{13}C fractionation and oxidation state in organic aerosols. This poster presents an overview of (planned) experiments and initial results.

Our study is a first step in establishing a firm understanding of this complex link and aims to provide insight into SOA formation using stable carbon isotopes. Starting from precursors with natural isotopic abundance, aerosols will be created in chamber experiments by nucleation, i.e. without seeds present, from oxidation of volatile precursors using ozone. The resulting SOA will be collected on pre-treated quartz filters and subsequently analyzed for their carbon isotopic composition (^{13}C & ^{12}C.) KIEs will be presented for the following systems:

1) Single component organic aerosol generated using an atomizer and deposited on filters immediately after drying. Subsequently, the loaded filter is exposed to a flow of high ozone concentration.
2) Single component organic aerosol formed using an atomizer and introduced into a smog chamber together with ozone.
3) SOA from α-pinene ozonolysis created in a smog chamber.

Experiments 1 and 2 are designed to quantify the fractionation in filter handling and the potential ozonolysis of SOA only, while experiment 3 aims for the KIE of SOA formation from VOC.

The (dark) chamber experiments will be run at the Copenhagen Center for Atmospheric Research to generate the overall large amounts needed for the isotope analysis. Particle-size distributions are monitored continuously and GC samples are taken in intervals to keep track of precursor concentrations.

The isotopic measurements of the filters are done at the Institute for Marine and Atmospheric Research Utrecht using Isotope Ratio Mass Spectrometry. Here, the filters are heated stepwise (50-450 °C) in He to evaporate organic compounds that are subsequently converted to CO_2 for the isotope analysis. In parallel, the chemical composition is determined by Proton Transfer Ratio Mass Spectrometry at each heating step.

The setup will be presented in detail, along with first results and possible implications of the findings.

We thank IntraMIF and the Universities of Copenhagen and Utrecht for supporting this research. The research has received funding from the European Community's Seventh Framework Program (FP7/2007-2013) under grant agreement number 237890.

Rudolph, J., Czuba, E., Norman, A.L., Huang, L. and Ernst, D. (2002) *Atmos. Environ.* **36**(7), 1173–1181.

Iannone, R., Koppmann, R. and Rudolph, J. (2010) *Atmos. Environ.* **44**, 4135–4141.

Irei, S., Rudolph, J., Huang, L., Auld, J. and Hastie, D. (2011) *Atmos. Environ.* **45**, 856–862.

Fisseha, R., Spahn, H., Wegener, R., Hohaus, T., Brasse, G., Wissel, H., Tillmann, R., Wahner, A., Koppmann, R. and Kiendler-Scharr, A. (2009) *J. Geophys. Res.* **114**, D02304.

Sizing, Infrared Spectra and Phase Transitions of Neutral Water Clusters

C.C. Pradzynski[1], R.M. Forck[1], U. Buck[2] and T. Zeuch[1]

[1]Institut für Physikalische Chemie, Universität Göttingen, 37077 Göttingen, Germany
[2]Max-Planck-Institut für Dynamik und Selbstorganisation, 37077 Göttingen, Germany
Keywords: water, neutral clusters, IR spectroscopy, size selection, sodium doping.
Presenting author email: tzeuch1@gwdg.de

The characterisation of clusters in the nanometer size range is a key issue in aerosol science. Especially nanometer sized water particles play an important role in Earth's atmosphere and interstellar space (Kulmala (2003), Klemperer and Vaida (2006)). Huge progress has been made in recent years in the development of instruments for measuring ionic clusters (Kirkby *et al*. (2011)). However, particle sizing and size selective spectroscopic experiments with neutral clusters are much more difficult to conduct. In two very recent studies (Yoder *et al*. (2011), Forck *et al*. (2012)) it was shown that the difficulty of size selection can be mastered for neutral clusters by using the sodium doping technique. The experimental steps are:

1) the generation of a molecular beam by a supersonic expansion
2) sodium doping of clusters in a pick-up cell
3) soft single photon ionization of the clusters

Sodium doping allows for a soft ionization because the weakly bound 3s electron be easily removed in a single photon process. In the absence of fragmentation the particle mass distribution can be determined directly by analyzing the time of flight mass spectra, see Yoder et al. (2011).

The interaction of the clusters with infrared (IR) light prior to photoionization allows the generation of size selective IR spectra. This method is called IR excitation modulated photoionisation mass spectroscopy and demonstrated for methanol clusters by Forck *et al*. (2012).

In the present work we show that the method has been successfully employed for characterizing the evolution of the structure of water clusters containing a few up to a few hundred water molecules. Therefore it is now for the first time possible to examine the process of water micro-crystallization with a reliable control of cluster sizes. In figure 1 theoretically predicted infrared spectra in the OH stretching region are compared with our size selective measurements. In general, the simulations of Buch et al. (2004) are in good agreement with the measured spectra. The main difference is the spectrum for around 48 water molecules, which in the experiment resembles more the spectrum of the larger clusters. On the basis of the now available IR spectra the actual cluster structures can be unraveled using state of the arte quantum chemistry methods.

By changing the expansion conditions (He vs. Ar expansions) the cluster temperature can be changed. This allowed for the first time the distinction of water clusters in the solid state and an amorphous more glassy state on the basis of size selected IR spectra. This phase transition was previously characterized by calorimetric means for anionic water clusters by Hock *et al*. (2009). The two spectra are shown in figure 2. The region below 3400 cm^{-1} shows only in the Ar expansion the characteristic solid state pattern depicted in figure 1.

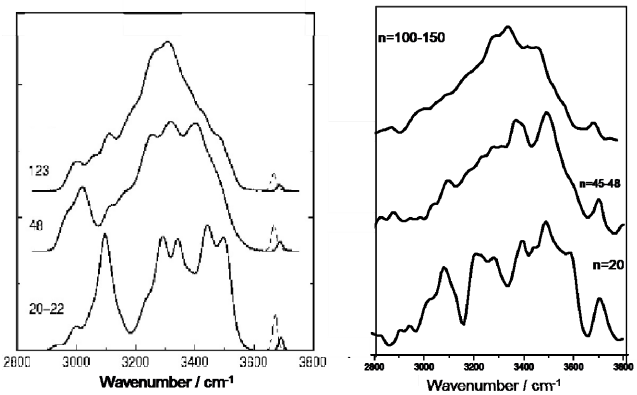

Figure 1. Predicted IR spectra for $(H_2O)_n$ (n=20-22,48, 123) (left panel, Buch et al. (2004)) compared with measured IR spectra of $Na(H_2O)_n$ (n=20,45-48, 100-150) (right panel).

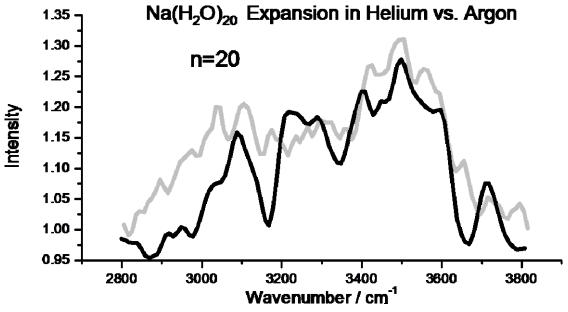

Figure 2. IR spectra for $Na(H_2O)_{20}$ in a cold Argon expansion (T <100 K, black line) compared with the warmer Helium expansion (T ~ 120-150 K, grey line).

Kulmala, M., (2003) *Science* **302**, 1000.
Klemperer, W. and Vaida, V. (20069 *Proc. Natl. Acad. Sci. U.S.A.* **103**, 10584.
Kirkby, J. *et al*. (2011) *Nature* **476**, 429.
Yoder, B. *et al*. (2011*) J. Phys. Chem. Lett*. **2**, 2623.
Forck, R. M. *et al*. (2012) *Phys. Chem. Chem. Phys*. **14**, 3004.
Buch, V. *et al*. (2004) *Int. Rev. Phys. Chem*. **23**, 375.
Hock, C. *et al*. (2009) *Phys. Rev. Lett*. **103**, 073401.

Growing clusters involving pinanediol oxidation products during nucleation experiments in the CLOUD chamber, observed by APi-TOF ion mass spectrometers

S. Schobesberger[1], A. Franchin[1], H. Junninen[1], F. Bianchi[2], J. Dommen[2], N. Donahue[3], S. Ehrhart[4], M. Ehn[1,5], K. Lehtipalo[1], T. Nieminen[1], G. Lönn[1], the CLOUD collaboration, T. Petäjä[1], M. Kulmala[1] and D.R. Worsnop[1,6]

[1]Department of Physics, University of Helsinki, Helsinki, 00014, Finland
[2]Laboratory of Atmospheric Chemistry, Paul Scherrer Institut, Villigen, 5232, Switzerland
[3]Department of Chemical Engineering, Carnegie Mellon University, Pittsburgh, PA 15213-3890, USA
[4]Institute for Atmospheric and Environmental Sciences, Goethe University, 60438, Frankfurt/Main, Germany
[5]Forschungszentrum Jülich GmbH, Jülich, 52428, Germany
[6]Aerodyne Research, Inc., MA 01821-3976, USA
Keywords: cluster ions, secondary organic aerosol (SOA), mass spectrometry, nucleation.
Presenting author email: siegfried.schobesberger@helsinki.fi

The CLOUD (Cosmics Leaving OUtdoor Droplets) experiment at CERN investigates a possible influence of cosmic rays on aerosol particles and clouds by providing exceptionally clean and well-defined experimental conditions in a stainless-steel chamber of 26.1 m^3. Cosmic rays can be simulated by exposing the chamber to a pion beam. So far, the research at CLOUD has focused on nucleation experiments, as nucleation from gaseous precursors is an important source of particles in the atmosphere. Sulfuric acid (H_2SO_4) was found to play a crucial role in this process. Other compounds hypothesized as important are water, ammonia (NH_3), and yet unidentified organic compounds (e.g. Metzger *et al.*, 2010). Therefore, the CLOUD experiment investigated nucleation for different conditions, including varying concentrations of H_2SO_4 and NH_3. In later experiments, dimethyl amine was added as well as pinanediol ($C_{10}H_{18}O_2$). The latter was expected to yield oxidation products similar to those of certain naturally abundant volatile organic compounds, such as α-pinene.

The APi-TOF (Atmospheric Pressure interface Time-Of-Flight) mass spectrometer is developed by Tofwerk AG, and Aerodyne Research, Inc. (Junninen *et al.*, 2010), typically obtaining resolutions between 4000 and 6000 Th/Th. Sampling occurs directly from atmospheric pressure. No ionization of the sampled aerosol is performed, and only naturally charged ions are detected by the setup in use.

During experiments at CLOUD, nucleation events were triggered in the chamber by switching on UV light. Depending on conditions, nucleation occurred mainly or partly by ions. Using the APi-TOF, the composition of ions could be determined based on their exact masses and isotopic patterns (Ehn *et al.*, 2012). Before adding any organics into the chamber, cluster ions were found to always contain H_2SO_4 (Kirkby *et al.*, 2011). They also contained NH_3 molecules, with the NH_3:H_2SO_4 ratio depending on cluster size and experimental conditions, and, to a lesser extent, organic contaminant compounds, mainly amines. The addition of organics altered nucleation, growth, and ion spectra. Clusters involving a wide range of pinanediol oxidation products were observed up to 1500 Th, and the elemental composition of the most important clusters could be identified (e.g. Fig. 1). Also, the growth of clusters was commonly observable at a time resolution of 30 s and up to 3300 Th, with the highest observable masses corresponding to mobility equivalent diameters between 1.8 and 2.1 nm. Correlations between the abundances of individual ion clusters and various experimental variables will give detailed insights into the early steps of new (charged) particle formation in the CLOUD chamber.

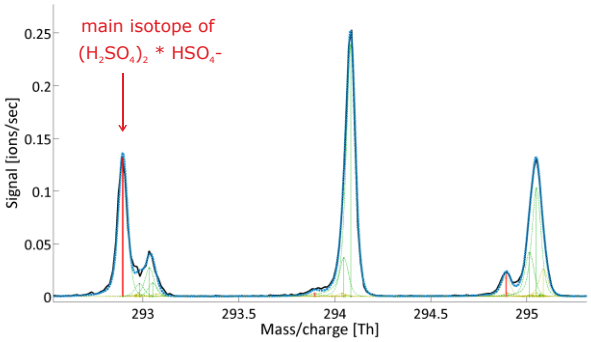

Figure 1. Section of a typical negative ion spectrum during nucleation. The isotopes of $(H_2SO_4)\bullet HSO_4^-$ are marked by red sticks. The sum of all identified compounds (blue dotted line), mostly including oxidized organics, explains well the signal (black line).

We thank CERN for technical and financial resources. This research was funded by the EC 7th Framework Programme ("CLOUD-ITN" & "ATMNUCLE", grant nos. 215072 & 227463), the German Federal Ministry of Education and Research (no. 01LK0902A), the Swiss National Science Foundation (projects 206621_125025 & 206620_130527), the Academy of Finland Centre of Excellence program (project 1118615), the Austrian Science Fund (projects P19546 & L593), the Portuguese Foundation for Science and Technology (project CERN/FP/116387/2010), and the Russian Foundation for Basic Research (grant N08-02-91006-CERN).

Ehn, M. et al. (2012) *Atmos. Chem. Phys. Discuss.* **12**, 4589-4625.
Junninen, H. et al. (2010) *Atmos. Meas. Tech.* **3**, 1039-1053.
Kirkby, J. et al. (2011) *Nature* **476**, 429-433.
Metzger, A. et al. (2010) *PNAS* **107(15)**, 6646-6651.

Aerosol mass spectrometer study of secondary organic aerosol formed during isoprene and methacrolein reaction chamber experiments - Composition and effect of humidity

F. Siekmann[1], L. Bregonzio[2], B. Temime-Roussel[1], S. Ravier[1], J.F. Doussin[2] and A. Monod[1]

[1]Laboratoire Chimie Environnement, Aix-Marseille Université, Marseilles, 13003, France
[2]LISA UMR 7583, Université Paris 12, Creteil, 94010, France
Keywords: isoprene, SOA, reaction chamber, AMS
Presenting author email: frank.siekmann@uni-bayreuth.de

This work investigates the composition of secondary organic aerosol (SOA) from the photooxidation of isoprene and methacrolein by HR-TOF-AMS measurements. The experiments were performed during the CUMULUS campaign at the CESAM reaction chamber (4.2m^3, stainless steel).

Both compounds were chosen because of their relevance in the atmospheric SOA formation. Isoprene is the most abundant volatile organic compound with a global emission of 500–750 Tg/yr. Methacrolein is one of its main first-generation gas phase oxidation carbonyl products, with a molar yield of 20–28% (Zimmermann and Poppe, 1995; Lee et al., 2005). Recent field and laboratory studies indicate that the oxidation of isoprene forms secondary organic aerosol (Carlton et al., 2009). Furthermore, Surratt et al. (2006) demonstrated a major contribution of methacrolein in the SOA formation through isoprene reactivity.

For both precursors, isoprene and methacrolein, reaction chamber runs were performed with initial concentrations of 500 ppb; the initial [NO] was approx. 100 ppb.

The study of these two compounds allowed us to report differences and similarities regarding the composition of SOA formed from the different precursors during the experiments.

Another task in this study is the influence of the humidity on the composition of the aerosol. The experiments started at dry conditions; after SOA formation, the relative humidity in the reaction chamber was increased up to 100%. This enabled us to simulate real atmospheric conditions, e.g. in terms of gas-droplet-aerosol interactions.

SOA derived from photooxodation under relative high NO_x conditions also has non-negligible content of organonitrates, which fragments in the AMS forming NO^+ and $NO2^+$ (Chhabra et al., 2010).

Time evolution of mass spectra and O/C-, H/C-, N/C and OM/OC ratios as well as the role of organonitrates, especially during high humidity periods, will be presented and discussed.

This work was supported by the French embassy in Germany and the ANR CUMULUS.

Zimmermann, J. and Poppe, D. (1995) Atmos. Environ., 30, 1255–1269.
Lee, W., Baasandorj, M., Stevens, P. S., and Hites, R. A. (2005) Environ. Sci. Technol., 39, 1030–1036.
Carlton, A. G., Wiedinmyer, C., Kroll, J. H. (2009) Atmos. Chem. Phys. 9, 4987-5005.
Surratt, J. D., Murphy, S. M., Kroll, J. H., Ng, N. L., Hildebrandt, L., Sorooshian, A., Szmigielski, R., Vermeylen, R., Maenhaut, W., Claeys, M., Flagan, R. C., and Seinfeld, J. H. (2006) J. Phys. Chem. A, 110, 9665–9690.
Chhabra, P. S., Flagan, R. C., Seinfeld, J. H. (2010) Atmos. Chem. Phys. 10, 4111-4131.

Pathways from aromatic aldehydes to aerosol in urban atmosphere: a competition between oxidation and photopolymerization

T.A. Maksimova[1], G.G. Dultseva[1,2] and S.N. Dubtsov[1]

[1]Institute of Chemical Kinetics and Combustion, SB RAS, Novosibirsk, 630090, Russia
[2]Novosibirsk State University, Novosibirsk, 630090, Russia
Keywords: aerosol formation, chemical composition.
Presenting author email: dubtsov@kinetics.nsc.ru

Aromatic aldehydes are considered as the markers of anthropogenic emission due to their presence in urban air as primary pollutants emitted from engines. However, aromatic aldehydes are also emitted by vegetation, which is a tremendous source of photonucleating compounds on the global scale. The atmospheric fate of aromatic aldehydes generally depends on the chemical nature of substituents and includes several pathways. The most important routes of gas-to-particle conversion of aromatic aldehydes are photooxidation and photopolymerization. To evaluate the details of these mechanisms, we studied photonucleation of benzaldehyde, as a representative of technogenic pollutants, and salicylic aldehyde, as a representative of the emissions of biological origin. The presence of the aldehyde group in both molecules makes them photochemically active, but the presence of OH group in salicylic aldehyde renders specific features to the mechanism of its photooxidation.

Aldehyde vapour was photolyzed in a flow reactor in the absence and in the presence of environmentally significant additives, such as ozone, water vapour, and nitrogen dioxide. Free radicals generated photolytically were studied using spin trapping technique with sampling directly from the reactor. Chemical analysis of the gas and aerosol products was carried out by means of high-performance liquid chromatography, UV, IR, NMR spectroscopy, and gas chromatography – mass spectrometry. The amount of photopolymer was determined with respect to the reference, benzaldehyde vapour in nitrogen. Water vapour was demonstrated to act as a clustering agent for aldehydes, simplifying intermolecular interactions participated by photoexcited species. The role of ozone is much more complicated. Reacting with aldehydes it adds its oxygen atoms into the organic molecule thus taking part in the formation of condensable products. Ozone hinders photo-polymerization almost completely, and the product is highly oxygenated, containing only a small amount of aromatic fragments.

Special attention was paid to the mechanism of the interaction of aromatic aldehydes with NO_x, in particular nitrogen dioxide. A combination of NO_x with aldehydes is an immediate route to peroxy nitrates, clear indicators of photochemical smog even nowadays, in spite of all the precautions against air pollution (Zhang, 2011). In addition to aerosol-forming capacity, nitrogen dioxide is a photoactive species giving rise to atomic oxygen. This is why NO_2 is a very efficient suppressor of photopolymerization of aromatic aldehydes. For example, the amount of photopolymer in benzaldehyde photolysis decreases with an increase in the concentration of NO_2, while the concentration of diphenyl peroxide increases. Here diphenyl peroxide is the product of chain termination in the interaction of O with phenyl radicals formed in photodissociation of benzaldehyde: $Ph + O \rightarrow PhO \rightarrow (PhO)_2$.

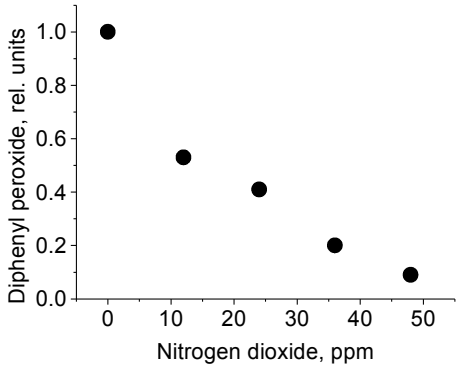

Fig. 1. Concentration of diphenyl peroxide *versus* NO_2.

No diaryl peroxides were detected in the products of photolysis of salicylic aldehyde. In addition, spin trapping studies failed to detect the formation of short-lived free radicals in the system, unlike for the case with benzaldehyde, when phenyl and phenoxy spin adducts were detected. The aerosol product exhibited the loss of the hydroxyl group at the aromatic ring. This allows us to suppose that the prevailing reaction route for the reaction of salicylic aldehyde with free radicals of any origin is detachment of the hydrogen atom of OH group. This example shows how substituents change reaction pathways even for the compounds of the same class.

Comparing the toxicity of products formed in photopolymerization and in oxidation, one can see that the latter route gives much more toxic intermediates and final products. Negative health effects of photochemical smog are in part due to the biological action of N- and O-containing aromatics formed under sunlight in urban atmosphere. So, chemical analysis of photonucleation products allows us not only to evaluate reaction pathways but also to predict environmental effects.

This work was supported by the Russian Foundation for Basic Research under project No. 11-05-00921-a.

Zhang, J. B.,Xu, Z., Yang, G., and B. Wang (2011)
Atmos. Chem. Phys. Discuss., 11, 8173–8206, 2011

Atmospheric Degradation of Oxygenated Volatile Organic Compounds on Mineral Aerosol Surfaces

Cristina Iuga[1], C. Ignacio Sainz-Díaz[2], and Annik Vivier-Bunge[3]

[1]Departamento de Ciencias Básicas, Universidad Autónoma Metropolitana-Azcapotzalco, México D.F.02200, México.
[2] Instituto Andaluz de Ciencias de la Tierra, CSIC-Universidad de Granada, Granada, Spain.
[3]Departamento de Química, Universidad Autónoma Metropolitana-Iztapalapa, México D.F. 09340, México.
Keywords: adsorption, mineral dust, density functional theory, oxalic acid
Presenting author: ciuga@xanum.uam.mx

Gas−solid interfacial phenomena play a key role in multiphase processes in atmospheric chemistry, affecting cloud and aerosol properties and influencing the radiation balance of the earth. In particular, mineral aerosols may be potential reactive surfaces for heterogeneous chemistry and a significant sink for many volatile organic compounds, as well as a vehicle for transportation of trace gases through the atmosphere. However, quantitative information on the gas/aerosol equilibrium of organic species is generally not available. In general, the fraction of organic compounds on aerosol surfaces is highly complex and variable, as it consists of a multitude of individual compounds from a variety of sources. Additional knowledge of heterogeneous processes, such as adsorption and reactions on the surface of mineral dust aerosols, could identify effective sinks and improve our understanding of global atmospheric chemistry.

In general, oxygenated organics with functional groups have a large tendency to be adsorbed on surfaces. Indeed, field measurements have shown that mineral atmospheric particles, such as aluminosilicate clays, often contain oxygenated organic components. Thus, it is interesting to study, at the molecular level, the adsorption of atmospheric volatile organic compounds (VOC) on model clay surfaces.

In this work, adsorption of formaldehyde, glyoxal, formic acid and oxalic acid on different silicate surface models is studied using quantum-mechanical methods. Both molecular clusters and a periodic crystal model of the (001) pyrophyllite surface have been employed, and all possible adsorption geometries have been considered. We find that silanol groups are always the most reactive adsorption sites, and adsorption at the cluster edges is favored. In the case of a periodic system hydroxyl groups on the octahedral phyllosilicate sheet are also reactive sites through the tetrahedral cavities (Figure 1). The effect of the studied VOC adsorption on the spectroscopic properties of the whole system is also analyzed in detail (Iuga et al. 2012). In all cases, significant frequency-shifts are detected in the vibration modes of both adsorbate and surface. The reactivity of these aerosol component with hydroxyl free-radical was investigated finding that these silicates are a good trap for free radicals.

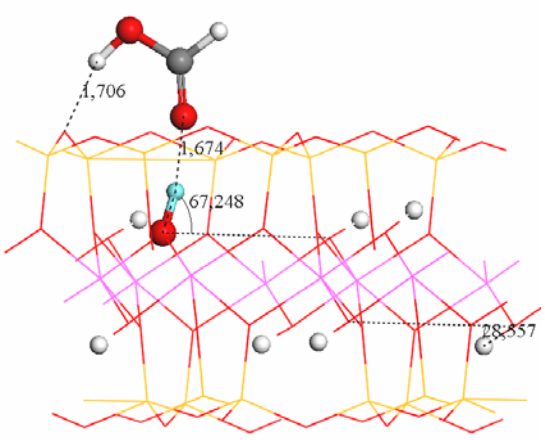

Figure 1. Adsorption complex ADS-1 of formic acid on the (001) surface of pyrophyllite.

Authors thank to RMAYS project funded by CONACYT-European Union.

Iuga, C., Sainz-Díaz, C.I., Vivier-Bunge, A. (2012) *J. Phys. Chem. C* (in press).

Primary and Secondary Organic Aerosol from Road Vehicles

S. Platt[1], I. El Haddad[1], A.A. Zardini[2], M. Clairotte[2], C. Astorga[2], R. Wolf[1], J. G. Slowik[1], B. Temime-roussel[3], N. Marchand[3], I. Jezek[4], L. Drinovec[4], G. Mocnik[4], O. Möhler[5], U. Baltensperger[1] and A.S.H. Prévôt[1]

[1]Laboratory of Atmospheric Chemistry, Paul Scherrer Institut (PSI), Villigen, CH-5232, Switzerland
[2]Institute for Energy and transport, Sustainable Transport Unit, EC Joint Research Centre, 21027 Ispra, Italy
[3]Laboratoire Chimie Environment, Aix Marseille Université, Marseille, 13 331, France
[4]Aerosol d.o.o., SI-1000 Ljubljana, Slovenia
[5]Institute for Meteorology and Climate research, Karlsruhe Institute of Technology, 76021 Karlsruhe, Germany
Keywords: SOA, Vehicle emissions, Smog chamber, AMS
Presenting author email: stephen.platt@psi.ch

Vehicles are a major source of particulate matter (PM) in urban areas. A large fraction of ambient PM consists of organic aerosol (OA), either primary (POA), from direct emissions, or secondary (SOA), formed via gas-phase reactions. Therefore any attempt to mitigate the effect of on-road vehicle emissions on public health and the environment should consider not only primary aerosol emissions but also secondary aerosol production potential (SAPP). However, only the primary aerosol from on-road vehicles is currently subject to direct legislation.

SOA formation from diesel exhaust has been reported, (e.g. Robinson *et al.*, 2007), but SOA formation from other common vehicles including gasoline vehicles has not. The effect of different conditions, such as fuel type, engine technology and ambient temperature on SOA formation remains unknown.

Here we determine emission factors (EFs) (g kg^{-1} fuel) for primary PM and for SOA, from two- and four-stroke scooters, a gasoline car and a truck, all complying with the latest European emissions standards. We also quantified the effect of using alkylated gasoline in scooters, liquid petroleum gas (dual fuel) in trucks and the effect of ambient temperature on SOA formation from gasoline cars and from trucks.

Vehicle exhaust was introduced into the new PSI mobile smog chamber during regulatory driving cycles on chassis dynamometers at the European Joint Research Centre Ispra, Italy. A high-resolution time-of-flight aerosol mass spectrometer (HR-ToF-AMS) equipped with a $PM_{2.5}$ lens was used to quantify OA. Black carbon (BC) was measured using a multi angle absorption photometer (MAAP) and an Aethalometer (AE 33 prototype). A high resolution proton transfer time-of-flight mass spectrometer (PTR-ToF) was used to investigate volatile organic compounds and a suite of instruments was used to quantify CO, CO_2, CH_4, total hydrocarbon and other gases. EFs were calculated with a carbon mass balance applied to smog chamber data.

All gasoline vehicles showed significant SAPP. SOA/POA ratios were up to 27.1 for the gasoline car (Figure 1) vs. 1.4 from the truck. Average PM EFs, with the inclusion of SOA and BC, were higher from the gasoline car than from the diesel truck: 0.21 vs. 0.10 g kg^{-1} fuel, respectively. This large SOA formation is likely a consequence of higher gaseous hydrocarbon emissions from the gasoline car: 1.01 vs. 0.16 g kg^{-1} fuel for the truck.

OH exposure in smog chambers can be calculated from the decay rate of nine times deuterated butanol spiked into the chamber (Barmet *et al.*, 2011). Using this technique we show that SOA formation from gasoline exhaust would occur within 12-14 hours in the real atmosphere (colourscale, Figure 1).

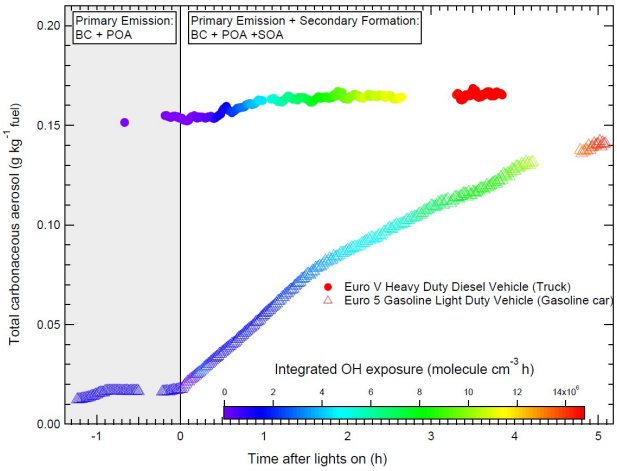

Figure 1: Carbonaceous aerosol and secondary aerosol formation emission factors from a gasoline car and a diesel truck vs. time in the PSI mobile smog chamber.

We demonstrate that aerosol emissions from gasoline vehicles can be significantly enhanced due to SOA formation and may match or even exceed those of diesel vehicles. This large SOA formation has substantial implications for emission controls which currently do not consider SAPP.

This work is supported by the Swiss Federal Office for the Environment (FOEN), the Federal Roads Office (FEDRO) and the the French environmental agency (ADEME); partly financed by the EU European Social Fund and EUROSTARS project E!4825 "FCAeth".

A. L. Robinson *et al.* (2007) *Science* **315**, 1259

P. Barmet *et al.* (2011) *Atmos. Meas. Tech. Discuss* **4**, 7471-7498

Optimization of a GC/MS method to analyse products from photo-oxidation of biogenic and anthropogenic mixtures of VOCs

O. Pindado Jiménez[1], R.Mª. Pérez Pastor[1], M. García Vivanco[2], M. Santiago Aladro[2]

[1]Chemistry Division, CIEMAT, Madrid, 28040, Spain
[2]Department of Environment, CIEMAT, Madrid, 28040, Spain
Keywords: Chemical analysis, GC-MS, SOA (Second. Organic Aerosols), Water soluble organic compounds.
Presenting author email: oscar.pindado@ciemat.es

Secondary organic aerosols (SOA) constitute a significant fraction of atmospheric particles. Much progress has been made in recent years concerning SOA formation, particularly due to experiments performed in smog chambers. Nevertheless there is still an important lack of knowledge about SOA composition.

The objective of this work is the development of an analytical methodology to quantify the composition of SOA and water soluble secondary organic aerosol produced as a result of the photo-oxidation of two different experiments performed in a smog chamber (EUPHORE, Ceam, Spain) by gas chromatography/mass spectrometry. Each experiment comprised the oxidation of a different mixture of volatiles organic compounds: an anthropogenic mixture in experiment 100609 (toluene, 1,3,5-trimethylbenzene, o-xylene and octane) and a biogenic one in experiment 240609 (α-pinene, limonene and isoprene).

The method consists in a double extraction with water & methanol jointly to a double derivatization with O-(2,3,4,5,6) pentafluorobenzyl hydroxylamine hydrochloride (PFBHA) and N,O-bis (trimethylsilil) trifluoroacetamide (BSTFA). Emphasis has been placed in developing a soft extraction to minimize losses of volatiles and a multistep derivatization technique to quantify the maximum number of compounds. Figure 1 shows the scheme of the whole methodology.

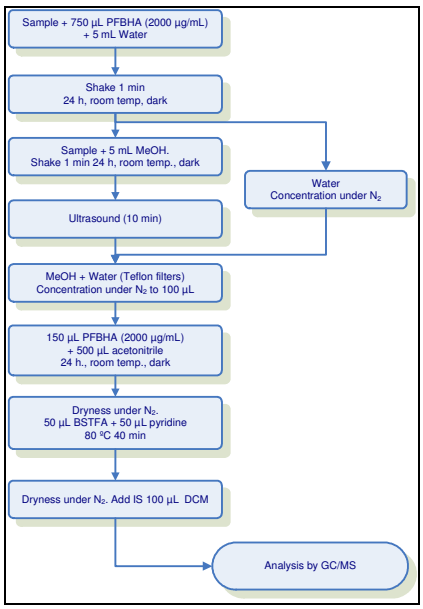

Figure 1: Scheme of analytical procedure to quantify components of SOA and WSOA.

Up to 20 compounds have been identified such as phenol, oxalic acid, malonic acid, benzoic acid, maleic acid, succinic acid, 2,3-butadione, citraconic acid, 4-etoxyphenol, glycolaldehyde, hydroxyacetone, glyoxilic acid, adipic acid, piruvic acid, norpinonic acid, pinic acid, 1,4-methylbenzoquinone, glyoxal, methylglyoxal and pinonic acid. Compounds were well separated in less than 25 minutes and identified through their mass spectra.

Figure 2 shows the collected mass of the compounds identified in each experiment.

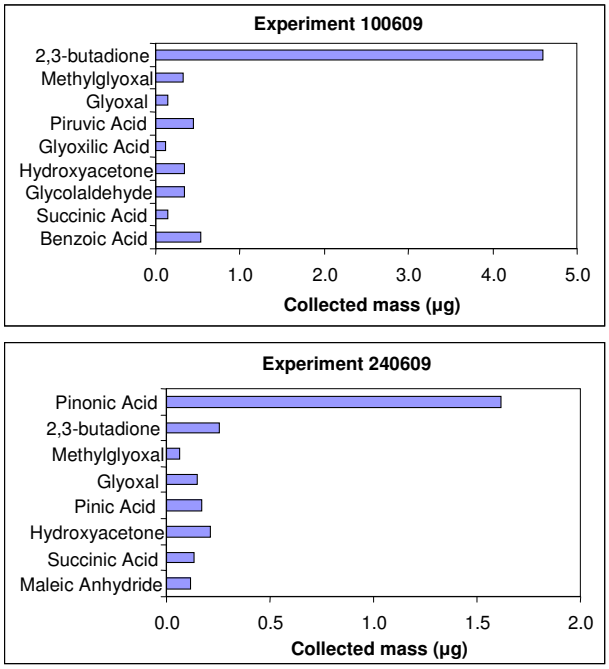

Figure 2: Collected mass of identified compounds in each experiment.

Adequate validation parameters such as applicability, selectivity, linearity, precision, recovery, detection limit, quantification limit and sensitivity have been found. However, this methodology was not suitable to analyze anhydrides, as they got hydrated during extraction, driving to the formation of dicarboxylic acids. In the light of these results, further research must be done.

This work has been financed by the Spanish Economy Ministry (project CGL2008-02260/CLI)

Development of a new tool to study atmospheric aerosol particles origin

L. Bourcier[1] and B. Geypens[1]

[1]Institute for Reference materials and Measurements - Joint Research Centre - European Commission, 2440 Geel, Belgium

Keywords: carbonaceous particles, source identification, isotopic ratio.

Presenting author email: laureline.bourcier@ec.europa.eu

Information on the atmospheric composition, from the local to the global scale, is of strategic value in particular for climate and air quality related studies. Stable isotope research for both compounds specific and bulk analysis finds its applications in various fields (Hoefs, 1987; Flanagan et al 2005). One of its applications is the source identification since the $^{13}C/^{12}C$ is highly dependent on its origin. This has been done by the study of the stable carbon isotopic composition ($^{13}C/^{12}C$) (Cachier et al 1989; Widory et al., 2004; Ceburnis et al., 2011).

In the literature, the simultaneous characterization of OC/EC and $\delta^{13}C$ is made with two different analyses (Huang et al., 2006). Our objective is to develop a method to obtain in one single analysis the OC and EC concentrations (instead of the total carbon, usually studied) and their isotopic ratios. For that purpose, we connected an Isotopic Ratio Mass Spectrometer (IRMS, Delta Plus, Thermo Scientific) behind a modified Sunset lab. instrument by using an open split coupling (Conflo II, Thermo Scientific). These data may allow a better linking of the particles to their origins.

The calibration of OC and EC is performed with known amount of sucrose, as usually used. For the isotopic ratio, since the standard VPDB is in very limited quantity, we used methionine to calibrate the analysis.

To test our instrumental set-up, sampling has been performed on the roof of the institute's building, located in forested area.

Results

We observed a pretty good repeatability for the analysis of specific compounds like beet sugar (± 0.90 ‰) or real samples (± 2.23 - 4.13 ‰ for OC and ± 1.11 – 1.23 ‰ for EC). Nevertheless, there is still a need of investigating closely the fractionation artefact since we observed a difference of 3.3 ‰ between the EA-IRMS (reference method) and the sunset-IRMS.

We cannot discuss yet about trends and origin but we can already notice a high $\Delta^{13}C_{OC\text{-}EC}$ ($\delta^{13}C_{OC}$-$\delta^{13}C_{EC}$), consistent with forested area and indicating the mixing of carbonaceous aerosol particles from different sources.

Cachier, H. (1989) *Isotopic characterization of carbonaceous aerosols*, Aer. Sci. Technol., 10 (2), 379-385.

Ceburnis, D., Garbaras, A., Szidat, S., Rinaldi, M., Fahrni, S., Perron, N., Wacker, L., Leinert, S., Remeikis, V., Facchini, M.C., Prevot, A.S.H., Jennings, S.G., Ramonet, M. and O'Dowd, C.D. (2011) *Quantification of the carbonaceous matter origin in submicron marine aerosol by ^{13}C and ^{14}C isotope analysis*, Atmos. Chem. Phys., 11, 8593-8606.

Flanagan, L. B., Ehleringer, J. R. and Pataki, D. E. (2005) *Stable Isotopes and Biosphere Atmosphere Interactions: Process and Biological Controls*, Elsevier, Great Britain.

Hoefs, J. (1987) *Stable Isotope Geochemistry*, third ed. Springer-Verlag, Berlin, Germany.

Huang, L., Brook, J.R., Zhang, W., Li, S.M., Graham, L., Ernst, D., Chivulescu, A. and Lu, G. (2006) *Stable isotope measurements of carbon fractions (OC/EC) in airborne particulate: A new dimension for source characterization and apportionment*, Atmos. Environ., 40, 2690-2705.

Widory, R., Roy, S., Le Moullec, Y., Goupil, G., Cocherie, A. and Guerrot, C. (2004) *The origin of atmospheric particles in Paris: a view through carbon and lead isotopes*, Atmos. Environ., 38, 953-961.

Aerosol chemical characterization by PMF analysis of single particle ATOFMS spectra

C. Giorio[1], A. Tapparo[1], M. Dall'Osto[2], R.M. Harrison[3], D.C.S. Beddows[3] and E. Nemitz[4]

[1]Department of Chemical Sciences, University of Padova, Padova, 35131, Italy
[2]Institute of Environmental Assessment and Water Research (IDÆA),
Consejo Superior de Investigaciones Científicas (CSIC), Barcelona, 08028, Spain
[3]Department of Geography, Earth and Environmental Sciences, University of Birmingham,
Birmingham, B15 2TT, United Kingdom
[4]Centre for Ecology & Hydrology, Bush Estate, Penicuik, Midlothian, EH26 0QB, United Kingdom

Keywords: ATOFMS, single particle analysis, PMF, K-means, ART-2a.
Presenting author email: chiara.giorio@unipd.it

Aerosol time of flight mass spectrometry (ATOFMS) is one of the most powerful state of the art techniques which allows both size and chemical characterization of single airborne particles (Gard *et al* 1997). Data analysis is still a challenge and in the present study three different data treatment techniques have been applied (PMF, K-means ART-2a) to a rural background dataset collected in Harwell, UK.

For the first time, PMF analysis was directly applied to single particle mass spectra as opposed to data previously clustered with another technique. The analysis was performed on a total of 56898 single particle mass spectra allowing the extraction of 10 factors. The results show that PMF analysis applied to single particles makes a deconvolution of their mass spectra and it extracts factors with very well defined and characterized chemical profiles, representing inorganic species, i.e. NIT (nitrate), SUL (sulphate), NaCl, and different elemental and organic carbon families including fresh EC, aged EC, oxidized organic aerosol, aromatic, and two organic nitrogen factors. In addition, for each extracted component (PMF factor), its temporal trend, both in terms of scores, equivalent number of particles and volume, is obtainable concurrently with its size distribution.

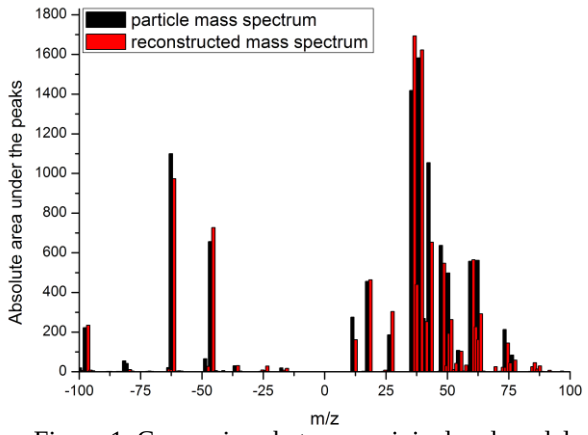

Figure 1. Comparison between original and model reconstructed mass spectrum of a particle made of 3% SUL, 10% NH4-OOA, 17% EC+, 8% OC-Arom, 2% EC-, 6% K, 7% NIT, 18% OC-CHNO, and 30% unexplained.

Moreover, a study of correlations among PMF factors could turn to be useful for study of the mixing state of particle components. In fact, it has been possible to identify two different elemental carbon contributions: fresh (EC-) and aged (EC+) elemental carbon internally mixed with secondary species.

The results of PMF analysis were compared to those obtained from K-means cluster analysis and ART-2a artificial neural network analysis. While K-means and ART-2a give broadly overlapping results by dividing the dataset into the different particle types, PMF makes a deconvolution of particle mass spectra and extracts their major contributing chemical species or important classes of components. In fact, from Figure 1 it may be seen that more than one factor is necessary to reconstruct a particle mass spectrum (Giorio *et al* 2012).

The joint deployment of factor and cluster analysis techniques, considering the different characteristic features, could be very promising to better understand particle properties and composition.

Moreover, temporal trends of factors and clusters were compared with independent ion and non refractory organic carbon measurements performed with a GRAEGOR (Thomas *et al* 2009) and an AMS (Drewnick 2005) in order to evaluate the performance of the data analysis. The results showed that the temporal trends of PMF factors are correlated to the corresponding species concentrations and thus PMF analysis could prove to be useful for quantification purposes.

Drewnick F., Hings S.S., DeCarlo P., Jayne J.T., Gonin M., Fuhrer K., Weimer S., Jimenez J.L., Demerjian K.L., Borrmann S. and Worsnop D.R. (2005) *Aerosol Sci. Technol.* **39**, 637-658.

Gard E., Mayer J.E., Morrical B.D., Dienes T., Fergenson D.P. and Prather K.A. (1997) Anal. Chem. **69**, 4083-4091.

Giorio C., Tapparo A., Dall'Osto, Harrison R.M., Beddows D.C.S. and Nemitz E. (2012) *Atmos. Environ.*, submitted for publication.

Thomas R.M., Trebs I., Otjes R., Jongejan P.A.C., Brink H.T., Phillips G., Kortner M., Meixner F.X. and Nemitz E. (2009) *Environ. Sci. Technol.* **43**, 1412-1418.

Analysis of surgical aerosols by on-line single particle and high resolution mass spectrometry

K.-P. Hinz[1], A. Fendt[1], K.-C. Schäfer[1], Z. Takats[1] and B. Spengler[1]

[1]Institute of Inorganic and Analytical Chemistry, Justus Liebig University Giessen, Giessen, D-35392, Germany
Keywords: Aerosol mass spectrometry, Chemical composition, Single particle analysis
Presenting author email: klaus-peter.hinz@uni-giessen.de

Analysis of single particles by online mass spectrometric instrumentation has been widely used for the investigation of aerosols. The method provides chemical and physical characterization of individual particles with high temporal resolution combined with a high level of specificity. Transportable instruments of this type can be operated directly at sites of interest during ambient measurements enabling in situ characterization of aerosols in various fields such as atmospheric science, homeland security, workplace control or medicine. During surgical interventions biological tissue is commonly treated by surgical lasers or electrosurgical instrumentation. These procedures generate large numbers of neutral or charged gas-phase biomolecules and aerosol particles. Surgical smoke can be harmful or infectious, but on the other hand it carries valuable chemical information about the tissue being dissected. For the latter reason, mass spectrometric methods were applied to tissue identification and differentiation and a mass spectrometry assisted surgery method was developed (Schäfer, 2009).

Application of mass spectrometric instrumentation in private homes or hospitals requires devices with reduced instrumental size and improved performance for a user friendly long-term operation. For this purpose, the compact mobile laser mass spectrometer LAMPAS 3 (19" rack, 150 cm in height) was developed (Hinz, 2011). All necessary components are arranged as compact as possible to reduce the overall size of the instrument. The highly robust instrument is designed for operation under field conditions and can be easily transported by only one operator. Particles are directly introduced into the instrument using an impact-free inlet system. After particle detection and sizing an actively triggered UV laser evaporates and ionizes the detected particles. Generated ions are analyzed by a bipolar time-of-flight mass spectrometer. During optimization several instrumental features (voltage settings, delayed ion extraction, use of a reflectron time-of-flight analyser) were integrated to significantly improve mass accuracy.

Several measurement series in the laboratory were performed to investigate surgical smoke generated during disintegration of biological tissues samples using standard electrosurgical equipment. The aim of these measurements was a comprehensive analysis of surgical aerosols with complementary methods for a better understanding of mechanistic aspects, advanced description of tissue dissection processes and improved tissue identification. For this purpose, the gaseous part of the smoke was analysed by a high resolution Orbitrap mass spectrometer (ThermoScientific GmbH, Germany) employing the REIMS method (rapid evaporative ionization mass spectrometry) for direct identification of biomolecules under atmospheric pressure conditions (Schäfer, 2009). Simultaneously, the LAMPAS 3 instrument and an optical particle counter (OPC) were operated to investigate the particle phase of the smoke. Statistical methods were used for tissue discrimination and allocation.

Spectra of both mass spectrometers showed characteristic patterns particularly in negative ion spectra. Orbitrap spectra were characterized by very high mass resolving power and high mass accuracies enabling direct identification of tissue components. Spectra were dominated by phospholipid signals and thermal decomposition products of phospholipids. LAMPAS spectra showed ion signals in a broad mass range for both ion polarities. Results of measurements during dissection of various tissue types will be presented. More detailed investigatons will be performed in the future to improve the analysis of surgical aerosols and to establish a reliable mass spectrometry-assisted surgery for improved medical treatments.

This work was supported by the Deutsche Forschungsgemeinschaft (DFG), Germany, Grant No. HI 857/4-1, and by the research program "Landes-Offensive zur Entwicklung Wissenschaftlich-oekonomischer Exzellenz - LOEWE", research focus "AmbiProbe", state of Hesse, Germany.

Schäfer, K.-C., Denes, J., Albrecht, K., Szaniszlo, T., Balog, J., Skoumal, R., Katona, M., Toth, M., Balogh, L. and Takats, Z. (2009) Angew. Chem. Int. Ed. **48**, 8240–8242.

Hinz, K.-P.; Gelhausen, E.; Schäfer, K. C.; Takats, Z.; Spengler, B. (2011) Anal. Bioanal. Chem. **401,** 3165-3172.

Artefacts Associated with ChemVol® Impactor Sampling of Semivolatile Organic Compounds (SVOCs)

E. Galarneau[1], M. Patel[1,2], G. Poole[3], J.-P. Charland[3], and J. Brook[1]

[1]Air Quality Research Division, Environment Canada, Toronto, Ontario, M3H 5T4, Canada
[2] *currently at* Departments of Biochemistry and Neuroscience, University of Toronto Scarborough, Scarborough, Ontario, M1C 1A4, Canada
[3]Air Quality Research Division, Environment Canada, Ottawa, Ontario, K1A 0H3, Canada
Keywords: semivolatile organic compound, SVOC, impactor, ChemVol®, sorption, polyurethane foam, PUF
Presenting author email: elisabeth.galarneau@ec.gc.ca

The ChemVol® is a high-volume cascade impactor air sampler aimed at separating airborne particles of different sizes. Polyurethane foam (PUF) rings are used conventionally as impaction substrates. The sampler was designed to capture involatile aerosols though it has subsequently been used to sample semivolatile organic compounds (SVOCs) (e.g., Sun et al., 2009).

Polyurethane foam is commonly used to capture the gaseous fraction of SVOCs in non-impactor high-volume filter-sorbent sampling. It is prone to breakthrough for more volatile compounds and/or at warm temperatures, but has nonetheless been used extensively for many years.

We hypothesize that PUFôs inherent sorption capacity makes it unsuitable as a ChemVol® substrate when SVOCs are among the target compounds. By extension, erroneous attributions of toxicity to particulate rather than combined (gaseous plus particulate) concentrations can occur if chemical methods capable of extracting SVOCs are used on ChemVol® PUF media. Tests of this hypothesis are described below as is a method that separates the sorbed gaseous compounds from those that are truly particulate.

Unsubstituted polycyclic aromatic hydrocarbons (PAHs) of molecular weight 178 to 228 g mol^{-1} were used as test compounds. First, the sorption of gaseous compounds was documented. The creation of a particle-free air stream was attempted by placing the after-filter upstream of the impactor stages rather than downstream as is typically the case.

This configuration was only partly successful in creating a particle-free stream of air. Deposits were observed on the three final stages of the sampler indicating that fine particles < 2.5 µm were flowing through the upstream after-filter and on to the impaction substrates. However, stages collecting coarser particles > 2.5 µm were largely deposit-free. As a result, the two coarsest ChemVol® stages (*viz*., 2.5-10 µm and > 10 µm) were chemically extracted and it was assumed that recovered PAHs had been collected on the PUFs exclusively from the atmospheric gas phase.

Results from the ChemVol® were compared to results from collocated and contemporaneous samples collected with a conventional high-volume filter-sorbent sampler. The ñparticle-freeò ChemVol® PUFs collected substantial quantities of PAHs that were found to be mostly gaseous in the high-volume samples (e.g., phenanthrene MW 178 g mol^{-1}, see Figure 1, and fluoranthene MW 202 g mol^{-1}). However, measured concentrations were less on the ChemVol® PUFs than on the filter-sorbent PUFs, indicating that the sorption on the ChemVol® media captured only a portion of the available gas-phase concentration. Very little chrysene (MW 228 g mol^{-1}) was found on the ñparticle-freeò ChemVol® PUFs and this is consistent with its phase distribution being overwhelmingly particulate as determined by filter-sorbent sampling.

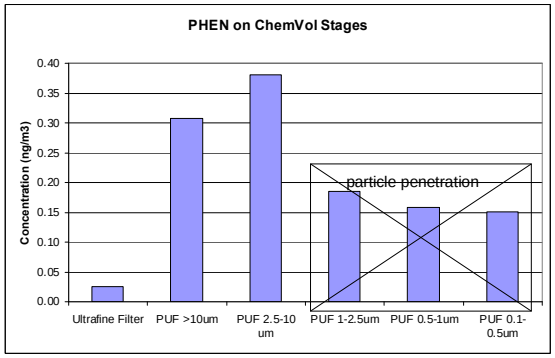

Figure 1: Phenanthrene Sampled by ChemVol® After Particle Removal

Previous reports in the literature (e.g., Becker et al., 2005) have suggested that collected particles can be separated from ChemVol® PUFs by sonication in water and/or alcohol. Microscopic examination of PUFs showed them to be largely particle-free after sonication preceded by wetting of the deposit area with alcohol. Subsequent extraction of the sonicated particles allowed for quantitation of collected particulate PAH without interference from sorbed gaseous compounds.

This work was conducted under the ALMITEE Project of Natural Resources Canadaôs Program for Energy Research and Development (PERD).

Becker, S., Dailey, L.A., Soukup, J.M., Grambow, S.C., Devlin, R.B. and Huang, Y.-C.T. (2005) *Environmental Health Perspectives* **113**:1032-1038.

Sun, Q., Alexandrova, O.A., Herckes, P. and Allen, J.O. (2009) *Talanta* **78**, 1115-1121.

In-situ methylation thermal extraction GC-MS method for the determination of anhydro-sugars in atmospheric aerosol samples

G. Matuschek, A. Wüst

Helmholtz Zentrum München, German Research Center for Environmental Health (GmbH), Ingolstaedter Landstr. 1, 85764 Neuherberg, Germany
Keywords: In-situ methylation, anhydro-sugars, WSOC, particulate matter, aerosols.
Presenting author email: matuschek@helmholtz-muenchen.de

The monosaccharide anhydrides levoglucosan (1,6-anhydro-b-D-glucopyranose), mannosan (1,6-anhydro-b-D-mannopyranose) and galactosan (1,6-anhydro-b-D-galactopyranose) are formed exclusively during combustion of cellulose and hemicelluloses, respectively. Therefore, they are source specific molecular markers for biomass burning and should be found in residues of incomplete combustion of fuels containing cellulose or hemicelluloses. Simoneit et al. (1999) were one the first who showed that levoglucosan and related degradation products from cellulose could be used as molecular markers for the presence of emissions from biomass burning in atmospheric fine particles (PM). Thus, during the last decade, the monosaccaride anhydrides, especially levogucosan, mannosan and galactosan have received increasing relevance as an important class of the water soluble organic compounds (WSOC) sub fraction of organic aerosols.

Although many studies reported on the monosaccharide's content of organic aerosols, a limited diversity of analytical methods is seen. The most frequently used methods are GC/MS methods, based on solvent extraction of the filter samples, followed by derivatisation using various silylating agents. Several studies, using this analytical technique have revealed that the WSOC fraction is dominated by oxygenated multifunctional polar compounds containing hydroxyl, carbonyl and carboxyl as well as amide and amino groups (Nolte et. al. 2002). Due to the time consuming derivatisation step, one of the key questions regarding reliable chemical analysis is the necessity of derivatisation. Some few studies, performing GC/MS analysis of non-derivative samples, either reported poor chromatographic behaviour or did not include detailed methodology description (Fraser 2000, Fine 2001).

Although a recently published study, using two dimensional GC-MS showed good results (Ma 2010), derivatisation seems to be necessary and a fast, simple and reliable derivatisation method is required.

In this work, a novel method for the determination of levoglucosan (1,6-Anhydro-β-D-glucopyranose) and its isomers galactosan and mannosan is described. The method is based on thermal extraction (thermal desorption) of filter samples of particulate matter under addition of tetramethylammonium hydroxide (TMAH). This in-situ methylation omits the use of hazardous silylation reagents as well as time and labour consuming reaction steps. Chemical analysis is performed by gas chromatography (GC) combined with quadrupole mass spectrometry. Evaluation of the in-situ tmethylation thermal extraction GC-MS method revealed low relative standard deviations (< 10 %), no carryover for the three analytes and detection limits of 0.6, 6 and 8 ng for levoglucosan, galactosan and mannosan respectively. The method was successfully applied to polar extracts of particulate matter samples as well as to original PM filter samples.

Simoneit, B.R.T., et al (1999) *Levoglucosan, a tracer for cellulose in biomass burning and atmospheric particles, Atmos Environ.* **33** (2) 173–182.

Nolte, C.G., et al. (2002) *Trimethylsilyl derivatives of organic compounds in source samples and in atmospheric fine particulate matter, Environ. Sci. Tech.* **36** (20) 4273–4281.

Fraser, M.P. and Lakshmanan, K (2000) *Using levoglucosan as a molecular marker for the long-range transport of biomass combustion aerosols, Environ Sci. Tech.* **34** (21) 4560-4564.

Fine, P. M., Cass, G. R. and Simoneit, B. R. T (2001) *Chemical characterization of fine particle emissions from fireplace combustion of woods grown in the northeastern United States, Environ. Sci. Tech.* **35** (13) 2665-2675.

Ma, Y., et al. (2010) *Technical Note: Fast two-dimensional GC-MS with thermal extraction for anhydro-sugars in fine aerosols, Atmos. Chem. Phys.* 10 4331-4341.

Studying Atmospheric Aerosols by Acoustic Levitation: Linking Head Space Solid-Phase Micro-Extraction (HS-SPME) with Gas Chromatography-Mass Spectrometry (GC-MS).

S. Almabrok, G. Marston and C. Pfrang

Department of Chemistry, University of Reading, P.O. Box 224, RG6 6AD Reading, Berkshire, UK
Keywords: Solid-Phase Micro-extraction, Acoustic Levitation, α-Pinene, Ozone.
Presenting author email: s.h.almabrok@reading.ac.uk

Climate change is one of the most important global environmental problems affecting natural ecosystems, food production, availability of fresh water as well as human health.(1) In acoustic levitation, a sound wave is generated between a piezoelectric transducer and a flat or concave reflector; therefore, by altering the distance between transducer and reflector a standing wave can be created and small samples of solids or liquids can be levitated.(2) This study has been conducted to improve our understanding of the reactions of O_3 and NO_3 with a range of terpenes found in the Earth's atmosphere and of the formation and properties of associated organic aerosols. For these investigations, a combination of acoustic levitation with gas chromatography-mass spectrometry (GC-MS) has been achieved by head space solid-phase micro-extraction (HS-SPME). The experimental set-up is illustrated in Fig. 1 (a-b).

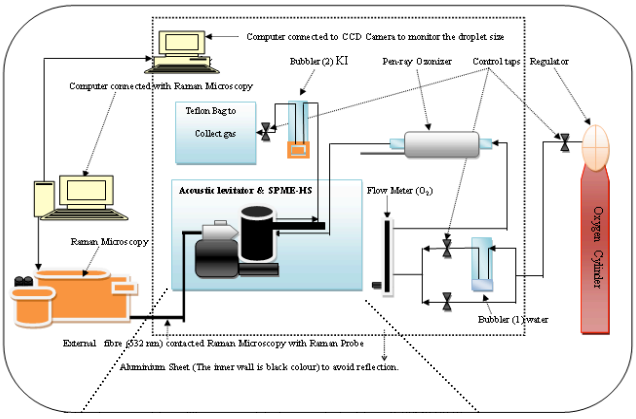

Figure 1 (a): Experimental set-up for the acoustic levitator with HS-SPME-GC-MS analysis.

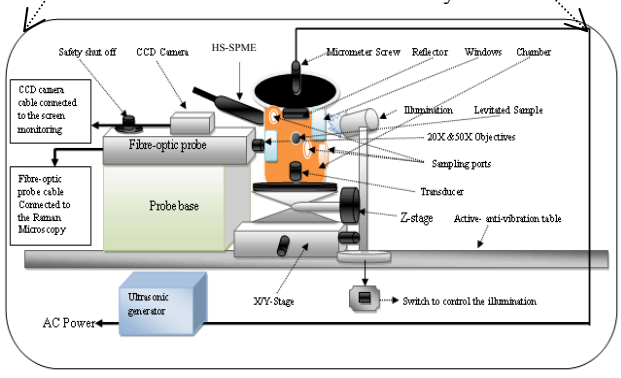

Figure 1 (b): Set-up for the combination of the acoustic levitator with HS-SPME (zoom into Fig. 1 (a)).

Fig. 2 shows the mass spectrum for a levitated droplet of pure α- pinene obtained by using HS-SPME-GC-MS under the following conditions: 174 ml/min flow of N_2, 5 min extraction time, and using a 100 µm polydimethylsiloxane (PDMS) coated fibre. Oxidation of acoustically levitated droplets of α-pinene and d-limonene has been studied in an environmental chamber that allowed control of the gas-phase surroundings and relative humidity. Several products could be identified mostly by comparison with reference samples in the same conditions including verbenone, verbenol, pinocarveol, carvone, carveol, norpinoaldehyde and pinonaldehyde (see example in Fig. 3).

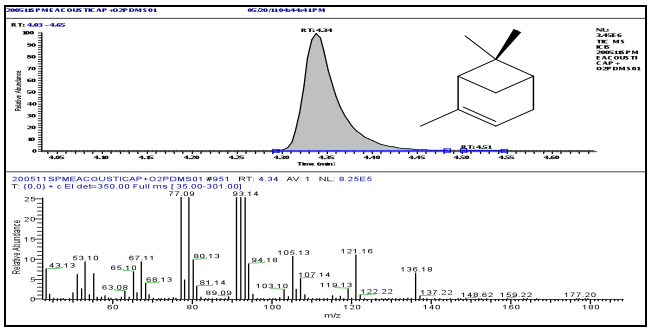

Figure 2: HS-SPME-GC-MS result for a levitated droplet of pure α-pinene (GC on top; MS below).

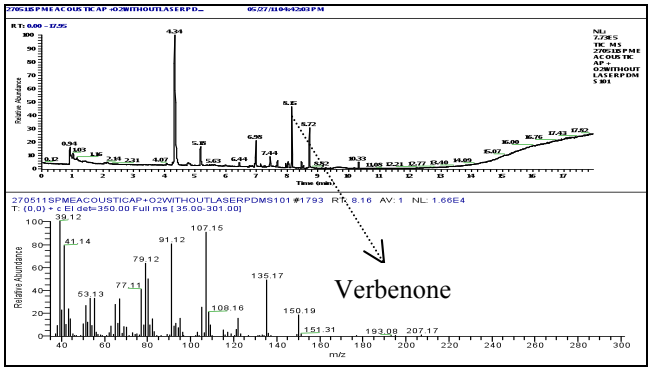

Figure 3: HS-SPME-GC-MS result for a levitated droplet of α-pinene after oxidative ageing (MS for the product verbenone).

References.

1- Ravindranath, N.H., and J. A. Sathaye, *Climate Change and Developing Countries*, 2003, Kluwer Academic Publishers.

2- Priego-Capote, F., and L. Decastro, *Trends in Analytical Chemistry*, 25, 9 (2006).

Calibration of CPCs at low temperatures using the CLOUD chamber

D. Wimmer[1], F.Kreissl[1], A. Kürten[1], J. Curtius[1], F. Riccobono[2], A. Kupc[3] K. Lehtipalo[4] and the CLOUD collaboration.

[1]Institute for Atmospheric and Environmental Sciences, Goethe University of Frankfurt, Frankfurt/M., Germany
[2] Laboratory of Atmospheric Chemistry, Paul Scherrer Institute, Villigen, Switzerland
[3] University of Vienna, Faculty of Physics, Vienna, Austria
[4]Department of Physics, University of Helsinki, Helsinki, Finland

Keywords: nucleation, nano particles, cut-off calibration, DEG-CPC, CLOUD experiment

One goal of the CLOUD (Cosmics Leaving OUtdoor Droplets) experiment at CERN is to investigate to what extent the presence of atmospheric ions affects new particle formation (Kirkby *et al*., (2011)). Neutral and ion-induced nucleation experiments are carried out in an aerosol chamber under precisely controlled conditions. For nucleation studies it is crucial to achieve very low and stable cut-off diameters in order to derive accurate nucleation rates. At the same time, however, significant auto-nucleation inside the particle counter as well as activation of pre-critical clusters should be avoided (Sipilä *et al.*, 2010). The so-called cut-off curve describes the detection efficiency of the particle counter as a function of particle size.

For the experiments at CLOUD two Diethylene Glycol-based CPCs (DEG-CPCs) have been set up and calibrated according to the design described by Iida *et al*. (2009). Operating temperatures and flows were chosen to realize cut-off diameters of 1.7 and 2.0 nm, respectively. To get a better understanding of the processes that lead to new particle formation in the middle and upper troposphere, the CLOUD campaign at CERN in autumn 2011 was dedicated to measure nucleation rates at temperatures well below 0°C. Therefore measurements at 3 different temperatures namely -25°C, -50°C and -65°C were carried out, respectively. The cut-off curves have to be determined for these low temperature sampling conditions. It is possible that a fraction of the freshly nucleated particles evaporates and shrinks to sizes with substantially lower detection efficiency while being transferred from the cold CLOUD chamber to the capillary and condenser of the DEG-CPC detection unit. Therefore, careful calibrations of the sampling and detection process have to be performed for the low temperature operating conditions. First exploratory studies were realized at CLOUD to determine the response and cut-off curves when low temperature aerosol samples enter the DEG-CPCs.

For these studies the CLOUD chamber is used as the particle generator. The advantage of the CLOUD chamber is that sufficient concentrations of nanometer-sized singly charged particles can be produced by ion-induced aerosol nucleation with the help of the ionizing beam from the Proton Synchrotron under very stable conditions. These particles can be directly classified using a nano-DMA (Differential Mobility Analyzer, model 5.710, Grimm Aerosol Technik).

To achieve a good resolution of the DMA a ratio between aerosol and sheath air flow of 1:10 was chosen As a reference instrument, a Faraday-Cup Electrometer could not be used because the particle concentrations at the nano-DMA outlet were too low. A Particle Size Magnifier (PSM, Vanhanen *et al.* (2011) was used instead because it realizes a very small cut-off diameter. By adjusting the instrument properly it is capable of counting 1nm particles with a high efficiency.

There is evidence that the detection efficiency curves are shifted to larger diameters for the low temperature condition. Reasons for the shift in detection efficiency will be discussed.

We would like to thank CERN for supporting CLOUD with important technical and financial resources, and for providing a particle beam from the CERN Proton Synchrotron. This research has received funding from the EC Seventh Framework Programme (Marie Curie Initial Training Network "CLOUD-ITN" grant no. 215072, and ERC-Advanced "ATMNUCLE" grant no. 227463), the German Federal Ministry of Education and Research (project no. 01LK0902A), the Swiss National Science Foundation (project nos. 206621_125025 and 206620_130527), the Academy of Finland Center of Excellence program (project no. 1118615), the Austrian Science Fund (FWF; project no. P19546 and L593), the Portuguese Foundation for Science and Technology (project no. CERN/FP/116387/2010), and the Russian Foundation for Basic Research (grant N08-02-91006-CERN).

Iida, Kenjiro, *et.al* (2009) *Aerosol Science and Technology* **43,**1, 81 — 96
Kirkby, J., Curtius, J., *et al* (2011) *Nature* **476**,429- U77.
Vanhanen, J. *et al,* (2011) *Aerosol Science and Technology*, **45,** 4, 533 — 542
Sipilä, M. *et al,* (2010)*, Science,* **327,** 1243–1246.

A method for assigning AMS measured nitrates and sulphates into molecular subgroups.

Äijälä, Mikko[1], Junninen, Heikki[1], Ehn, Mikael[1,2], Häkkinen, Silja[1], Hong, Juan[1], Petäjä, Tuukka[1], Kulmala, Markku[1] and Worsnop, Douglas[1,3]

[1]Department of Physics, University of Helsinki, P.O. Box 64, FI-00014 Helsinki, Finland
[2] Institute for Energy and Climate Research (IEK-8), Forschungszentrum Jülich, 52425 Jülich, Germany
[3]Aerodyne Research Inc, Billerica, MA 01821, USA

Keywords: aerosol mass spectrometry, AMS, chemical properties, inorganics

Presenting author email: mikko.aijala@helsinki.fi

The chemical composition of aerosols determines their physiochemical properties, which in turn affect *e.g.* their effects on climate and human health.

The Aerodyne Aerosol Mass Spectrometer (AMS, Canagaratna *et al.*, 2007) is a useful instrument for analysis of chemical composition and quantification of basic aerosol chemical species. However, this important ability of the AMS to quantitatively measure mass comes at a price: the 70 eV electron impact ionization fragments the sampled molecules, often leaving little trace of original molecular composition of the sample compound. The quality of AMS chemical analysis therefore depends significantly on data analysis methods, particularly on the reconstruction of a picture of the original molecular composition.

Typical AMS results provide concentrations of the main aerosol chemical species: nitrates, sulphates, ammonia, organics and chlorides. This classification is useful for many general purposes, but for studying aerosol physiochemical properties like particle hygroscopicity or volatility, additional molecular composition information is often required. In this study we present a simple method for assigning AMS main inorganic compounds – sulphates, nitrates and ammonia – into chemically more specific subgroups of sulphuric acid (SA), ammonium sulphate (AS), ammonium nitrate (AN) and organic nitrate. This can provide a way to better connect AMS measured aerosol chemical composition with observations of physiochemical properties from other aerosol instrumentation.

An estimate of ammonium sulphate and ammonium nitrate mass loadings can be derived using some basic chemical assumptions on acid-base reactions in forming salts, and assuming the aerosol is well mixed externally and internally. The latter assumption is often not fulfilled in ambient aerosol, but is a necessary first step in this type of analysis. Methods to account for incomplete mixing are an issue for further development. The calculation itself is inspired by, and closely related to, AMS collection efficiency (CE) estimations (Quinn *et al.*, 2006) and may prove to be of use in trying to better understand AMS CE dependencies on particle properties. Based on the relative molar amounts of ammonium and sulphate ions (NH_4^+ and SO_4^+) measured by the AMS, all observations can be divided into three distinct cases:

Case 1: the concentration of ammonium ions is lower than the concentration of sulphate ions ($[NH_4] < [SO_4]$). All available ammonia is taken up by sulphate to form ammonium bisulphate NH_4HSO_4. The rest of the sulphate ions are assigned to liquid phase sulphuric acid in particles. All nitrate signal is assumed to be from organic sources.

Case 2: $[SO_4] < [NH_4] < 2*[SO_4]$. All sulphate and ammonia is assigned to ammonium bisulphate or ammonium sulphate. All nitrate signal is attributed to organic nitrate.

Case 3: ($[NH_4] > 2*[SO_4]$). The leftover ammonium reacts with nitrogen condensed from gas phase to form ammonium nitrate NH_4NO_3. The rest of nitrate is assumed to be organic.

The estimate was tested on a month-long unit m/z resolution AMS dataset from the SMEAR II station in Hyytiälä, Southern Finland. The obtained inorganic-to-organic nitrate ratio was observed to correlate with the measured NO_2^+/NO^+ fragmentation ratio (Fig. 1), commonly used as a marker for the presence of inorganic nitrates. Further comparisons with instruments such as hygroscopicity and volatility tandem DMAs are ongoing to corroborate the results obtained using this method.

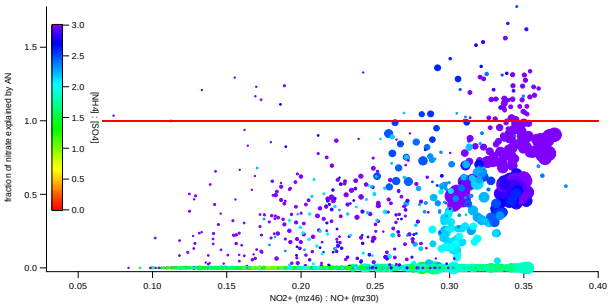

Figure 1. Fraction of nitrate signal explained by calculated ammonium nitrate loading, as a function of NO_2^+/NO^+ ion ratio. A high NO_2^+/NO^+ ratio is used as an indication of inorganic nitrate. Marker size describes AMS total nitrate concentration and colour the ratio of $[NH_4]$ to $[SO_4]$.

references:

Canagaratna, M. *et al.* (2007) *Mass Spectrom. Rev.* 26, 2, 185–222.

Quinn, P. *et al.* (2006) *J Geophys. Res.-Oc. Atm.* 111, D23S36.

Simplifying the complex nature of water-soluble organic matter from atmospheric aerosols: new insights from comprehensive two-dimensional liquid chromatography

R.M.B.O Duarte, A.C. Barros and A.C. Duarte

CESAM & Department of Chemistry, University of Aveiro, 3810-193 Aveiro, Portugal
Keywords: Carbonaceous aerosol, Water soluble organic compounds, Chemical properties, Molecular weight.
Presenting author email: regina.duarte@ua.pt

Water soluble organic matter (WSOM) from fine atmospheric aerosols is inherently complex (Duarte *et al.*, 2005,2007,2008), and detailed information regarding its major structural components, or even its individual structures, still remains indiscernible. It is clear that the substantial heterogeneity of aerosol WSOM limits the quality of structural data obtained by high-resolution instrumental techniques (e.g. nuclear magnetic resonance or mass spectrometry), thus making their interpretation extremely difficult. In this sense, the synergistic application of any chromatographic separation protocol prior to a structural inquiry can be of particular value for unfolding the molecular complexity of WSOM from fine aerosols and, therefore, further advance the current understanding on this organic component. Comprehensive two-dimensional liquid chromatography (LC x LC) presents itself as an excellent choice to dramatically improve the separation efficiency of WSOM. This technique provides enhanced separation by combining two liquid chromatographic modes with different separation mechanisms.

Therefore, and for the purpose of resolving the chemical heterogeneity of WSOM from fine particles, comprehensive LC x LC was employed for the first time to map the polarity *versus* molecular weight (MW) distribution of a WSOM sample collected during a winter season. The specific objectives of this research include: 1) evaluating the potential of comprehensive LC x LC as a novel methodology for WSOM separation; 2) determining how size-distinguished fractions differ in polarity; and 3) reassessing the MW properties of the studied WSOM sample. For accomplishing these objectives, a method has been developed using a mixed-mode hydrophilic interaction column in the first dimension and a size-exclusion column in the second dimension. The LC x LC fractions were screened on-line by UV at 254 nm.

Findings suggest that the combination of two independent separation mechanisms is promising in extend the range of WSOM separation. The comprehensive LC x LC system allowed the fractionation of the aerosol WSOM sample into two clusters of fractions with apparently different polarity and MW distribution (Figure 1). It seems that smaller Mw group fractions are related to a more hydrophobic nature. The complete range of MW distribution provided by the comprehensive LC x LC method was found to be within the range of those reported in the literature (Kiss *et al.*, 2003, Samburova *et al.*, 2005).

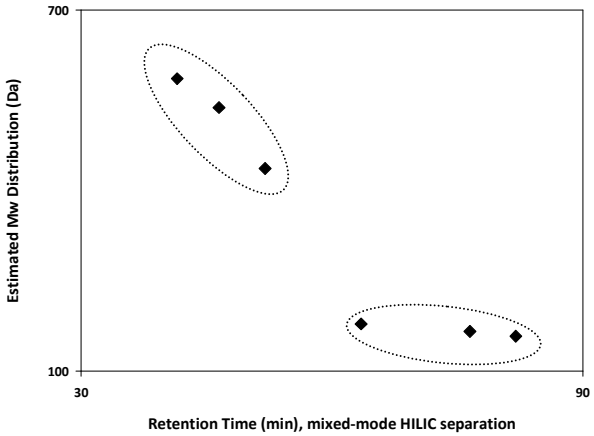

Figure 1. Mapping the polarity *versus* estimated MW distribution of the WSOM from fine particles.

Centre for Environmental and Marine Studies (University of Aveiro, Portugal) and the Portuguese Science and Technology Foundation (FCT), through the European Social Fund (ESF) and "Programa Operacional Potencial Humano – POPH", are acknowledged for financial support. This work was also funded by FEDER under the Operational Program for Competitiveness Factors – COMPETE and by National funds via FCT within the framework of research project ORGANOSOL (References FCOMP-01-0124-FEDER-019913 and PTDC/CTE-ATM/118551/2010).

Duarte, R.M.B.O., Pio, C.A. and Duarte, A.C. (2005) *Anal. Chim. Acta* **530**, 7-14.

Duarte, R.M.B.O., Santos, E.B.H., Pio, C.A. and Duarte, A.C. (2007) *Atmos. Environ.* **41**, 8100-8113.

Duarte, R.M.B.O., Silva, A.M.S. and Duarte, A.C. (2008) *Environ. Sci. Technol.* **42**, 8224-8230.

Samburova, V., Szidat, S., Hueglin, C., Fisseha, R., Baltensperger, U., Zenobi, R. and Kalberer, M., (2005) *J. Geophys. Res.* **110**, doi:10.1029/2005JD005910.

Kiss, G., Tombacz, E., Varga, B., Alsberg, T. and Persson, L. (2003) *Atmos. Environ.* **37**, 3783–3794.

Characterization of a thermal desorption mass spectrometer for freshly nucleated secondary aerosol particles

S. G. Gonser[1] and A. Held[1]

[1] Junior Professorship in Atmospheric Chemistry, University of Bayreuth, 95440 Bayreuth, Germany
Keywords: Aerosol mass spectrometry, Nucleation mode, SOA (Second. Organic Aerosols), Chemical composition.
Presenting author email: stefan.gonser@uni-bayreuth.de

Secondary aerosol formation introduces new particles to the atmosphere and is thereby relevant for human health and the global climate. Chemical reactions leading to atmospheric secondary aerosol formation are not yet fully understood. At the same time, analysing the chemical composition of freshly nucleated particles is still a challenging task.

We are currently finishing the development of a field portable aerosol mass spectrometer for nucleation particles with diameters smaller than 30 nm. The instrument consists of a custom-built aerosol sizing and collection unit coupled to a time-of-flight mass spectrometer (TOF-MS). The aerosol sizing and collection unit is composed of three major parts: (1) a unipolar aerosol charger, based on corona discharge from carbon fibres (e.g. Han *et al*, 2008), with an extrinsic charging efficiency of 32 % for 20 nm particles; (2) a compact radial differential mobility analyser (Zhang *et al,* 1995) for particle size separation in the range from 1 nm to 100 nm (geometric standard deviation of 1.09); and (3) an electrostatic precipitator where the aerosol is collected on a high-voltage biased metal filament, while a He counterflow protects the sample from contamination (see Fig. 1).

After collection, the aerosol sample is thermally desorbed, and the resulting gas sample is transferred to a Tofwerk CTOF mass spectrometer for chemical analysis.

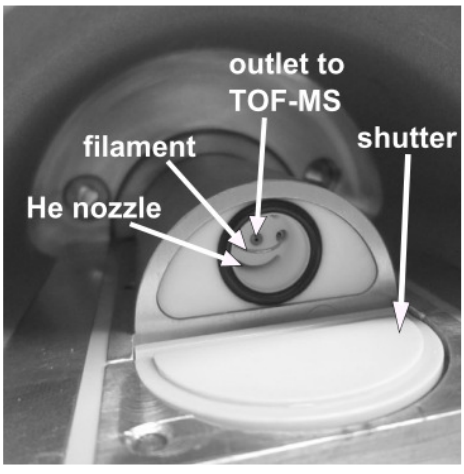

Figure 1. Photograph of the electrostatic precipitator. After collection, the filament is heated with the shutter closed, avoiding contamination of the gas sample.

Resistive heating of the filament allows temperature-controlled desorption of compounds of different volatility, thus facilitating the interpretation of the measured mass spectra.

We will present results of preliminary laboratory measurements performed in our aerosol smog chambers for calibration of the instrument. Secondary organic aerosol (SOA) is produced from photooxidation as well as dark ozonolysis of alpha-pinene. Particles with diameters below 30 nm are separated from the generated polydisperse particle population, collected in the electrostatic precipitator and subsequently analysed by the TOF-MS. The resulting mass spectra are compared to the chemical composition of laboratory generated SOA from published literature (e.g. Shilling *et al*, 2009), with alpha-pinene as precursor.

To date, the major part of published SOA mass spectra are measured with the Aerodyne aerosol mass spectrometer (AMS), determining the chemical composition of particles larger than 40 nm in diameter. The spectra measured with our instrument provide chemical information of freshly nucleated particles, extending the size range to the nucleation mode.

To evaluate the performance of our instrument in the field, we plan to conduct first measurements at the Waldstein research site of the University of Bayreuth before the end of this year.

This work is funded by the Deutsche Forschungsgemeinschaft (DFG) under grant DFG HE 5214/3-1.

Han, B., Kim, H. J., Kim, Y. J. and Sioutas, C. (2008) *Aerosol Sci. Technol.* **42**, 793-800.

Shilling, J. E., Chen, Q., King, S. M., Rosenoern, T., Kroll, J. H., Worsnop, D. R., DeCarlo, P. F., Aiken, A. C., Sueper, D., Jimenez, J. L., and Martin, S. T. (2009) *Atmos. Chem. Phys.* **9,** 771–782.

Zhang, S. H., Akutsu, Y., Russell, L. M., Flagan, R. C. and Seinfeld, J. H. (1995) *Aerosol Sci. Technol.* **23**, 357-372.

Comparison of two Laser Ablation Time-Of-Flight Aerosol Mass Spectrometers

S. R. Zorn[1], K.-P. Hinz[2], P. Croteau[3], B. Spengler[2], D. R. Worsnop[3], J. T. Jayne[3] and A. M. Trimborn[1]

[1]AeroMegt GmbH, Verbindungsstr. 27, 40723 Hilden, Germany
[2]Institute of Inorganic and Analytical Chemistry, University of Gießen, 35392 Gießen, Germany
[3]Aerodyne Research, Inc., 45 Manning Road, Billerica, MA 01821, United States

Keywords: aerosol mass spectrometry, single particle analysis, laser ablation
Presenting author email: s.zorn@aeromegt.com

Mass spectrometry has become a very powerful tool for the analysis of the atmospheric aerosol. Modern on-line instruments offer not only a very high time resolution with sampling intervals down to seconds and essentially real-time analysis of the chemical and physical parameters of aerosol particles but can also be deployed with little effort at very remote locations.

Currently, two types of aerosol mass spectrometers are commonly used. Instruments based on thermal desorption electron ionization offer a bulk analysis of the chemical composition of the non-refractory aerosol. Laser desorption ionization mass spectrometers can analyze the composition of single aerosol particles including soot, sea salt and mineral dust that cannot be vaporized using thermal desorption methods.

Most aerosol mass spectrometers using thermal desorption electron ionization are based on a common instrument platform and because of this, results from these instruments can generally be easily compared (Canagaratna et al., 2007).

For laser ablation instruments the situation is more complex. Many such instruments are individual builds. Even the few commercial instruments in existence differ slightly in details.

Besides the differences in construction the lasers used for the ablation of particles in the individual instruments differ in wavelength as well as in pulse energy. This makes a comparison of results from various laser desorption ionization instruments more difficult.

Here we present a comparison of two different laser ablation instruments (Table 1). A newly developed, very compact single particle mass spectrometer (LAAPTOF; AeroMegt GmbH) that is commercially available is compared to a custom built system (LAMPAS 3; Hinz et al., 2011).

For the comparison of the two instruments we used a test set of aerosols comprised of several different chemicals including sodium chloride, ammonium sulfate, ammonium nitrate, soot and mineral dust as well as different sizes of polystyrene latex particles. The measurement setup for both instruments was identical, using the same constant output atomizer (TSI 3076) and diffusion dryer (TSI 3062).

Aerosols having different composition were either atomized, nebulized or suspended in air. All test aerosols were dried prior to sampling. The whole range of chemicals was measured by both instruments. Additionally, spectra for each chemical makeup were recorded at different pulse energies for the ablation laser, to investigation the variability as well as the wavelength and energy dependence of the resulting ions and spectra.

Table 1. Specifications of LAMPAS 3 and LAAPTOF.

	LAMPAS 3	***LAAPTOF***
sizing laser, λ	532 nm	405 nm
ablation laser, λ	337 nm	193 nm
max. irradiance	$5 \cdot 10^9$ W/cm^2	$1 \cdot 10^9$ W/cm^2
mass resolving power	400 M/ΔM	800 M/ΔM

The results allow not only a direct comparison of both instruments for the tested compounds but can be also applied to field measurements as well as show the best instrument configuration for inter-comparison. Further investigations of the spectra collected at different pulse energies might be helpful for investigation of aerosol particles at different locations, e.g., to select the best energy for measurements at marine, rural or urban locations.

This work was supported by the German Federal Ministry of Economics and Technology under grant EP100853, by the Deutsche Forschungsgemeinschaft (DFG, HI 857/4-1) and by the research program "LOEWE", research focus "AmbiProbe", state of Hesse, Germany. AeroMegt GmbH acknowledges the Institute of Energy and Climate Research, Troposphere (IEK-8) for their collaboration and the possibility to use their laboratories.

Canagaratna, M. R., Jayne, J. T., et. all (2007) *Mass Spectrom. Rev.*, **26**, 185-222.

Hinz, K.-P., Gelhausen, E., Schäfer, K. C., Takats, Z., and Spengler, B. (2011) *Anal. Bioanal. Chem.* **401**, 3165-3172.

Complexation of transition metal ions by organic and inorganic ligands in size-segregated atmospheric aerosol particles in Melpitz, Germany

S. Scheinhardt[1], K. Müller[1], D. van Pinxteren[1], K. Fomba[1], A. Grüner[1], G. Spindler[1], H. Herrmann[1]

[1]Leibniz Institute for Tropospheric Research, 04318 Leipzig, Germany
Keywords: Aerosol chemistry, Atmospheric Aerosols, Trace metals, Carboxylic acids
Presenting author email: scheinhardt@tropos.de

Transition metal ions (TMI) like Fe, Cu and Mn are important species in atmospheric liquid phase reactions since they can take part in various redox reactions. Notably, they influence aqueous HO_x chemistry and participate in photochemical oxidation processes of organics. The chemical form under which TMIs are present has a huge influence on their photochemical properties, but so far their speciation remains unclear.

Therefore, size-segregated aerosol samples have been taken at a well-characterised rural background site in central Europe (Melpitz; Spindler, 2010) by means of a five-stage Berner impactor. After sampling, the impactor foils were extracted with water and the resulting aqueous extracts were chemically analysed (cf. Figure 1): TMIs were determined by totalreflection X-ray fluorescence (TXRF), inorganic ions by ion chromatography (IC) and capillary electrophoresis (CE), and small mono- and dicarboxylic acids by capillary electrophoresis. Additionally, the pH of the extracts was measured.

Together with meteorological parameters like humidity and temperature, these measurements allowed us to calculate the aerosol water content using the E-AIM Model (Wexler, 2002). Thus, the molar concentrations of dissolved TMIs, potential ligands and H^+ in the aqueous phase of atmospheric particles could be obtained.

Next, sampling days have been allocated into four case groups, depending on the season and the air mass origin during sampling: Summer West (SW), Winter West (WW), Summer East (SE) and Winter East (WE). In each category, the mean composition of the aqueous

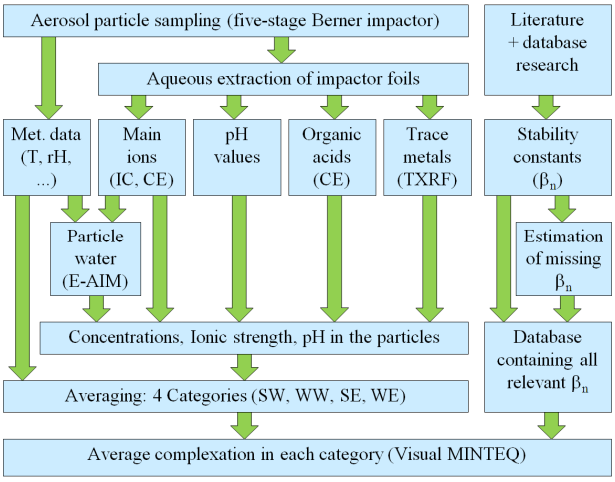

Figure 1. Scheme illustrating the strategy of the present study.

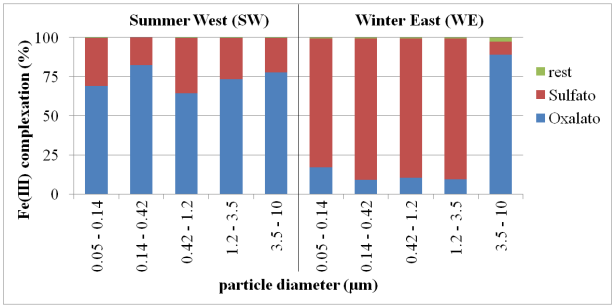

Figure 2. Calculated average complexation of Fe(III) in aerosol particles collected in Melpitz.

particle phase has been calculated (average of the corresponding sampling days). These average molar concentrations have finally been used as an input for the chemical speciation model Visual MINTEQ (Gustafsson, 2011), which allowed us to calculate the equilibrium complexation of TMIs by organic and inorganic ligands in the aqueous particle phase. Stability constants were ionic strength corrected using the Davies equation.

In this way, the mean TMI complexation in Melpitz has been calculated for the 4 categories. The results show that TMI complexation by organic compounds is important even in very acidic particles (pH~1). As an example, Fig. 2 shows that, in the SW case, Fe(III) is mostly present in the form of oxalato complexes, while in the WE case, Fe(III) is rather complexed by sulphate ions (due to higher sulphate loadings in this case). Mn(II) and Fe(II) are mainly complexed by sulphate and nitrate, while Cu(II) is, like Fe(III), complexed by oxalate, sulphate and additionally by nitrate (data not shown).

This is the first time that the complexation of TMIs in size-segregated aerosol particles is determined.

This work was supported by the German Federal Ministry for Education and Research under grant 01LR0802 (REGKLAM) and by the German Federal Environment Ministry grant F&E 370343200 (GUAN).

Gustafsson, J. P. (2011) *www.lwr.kth.se/english/OurSoftWare/Vminteq/index.htm*

Spindler, G., Brüggemann, E., Gnauk, T., Grüner, A., Müller, K. and Herrmann, H (2010) *Atm. Env.* **44**, 164-173.

Wexler, A. S., Clegg, S. L. (2002) *J. Geophys. Res.* **107**, No. D14, art. no. 4207, *www.aim.env.uea.ac.uk/aim/aim.php*

The organic carbon and total protein concentrations in atmospheric aerosol of Southwestern Siberia boundary atmospheric layer

A.S. Safatov[1], G.A. Buryak[1], S.E. Olkin[1], I.K. Reznikova[1], V.I. Makarov[2] and S.A. Popova[2]

[1]FBRI SRC VB "Vector", Koltsovo, Novosibirsk rgn, 630559, Russian Federation
[2]IChK&C SB RAS, Novosibirsk, 630090, Russian Federation
Keywords: Atmospheric aerosols, Organic carbon, Bioaerosols, Monitoring.
Presenting author email: safatov@vector.nsc.ru

Literature data show that atmospheric aerosol always contains a certain amount of organic (OC) and elemental carbon (EC) as well as components of biological origin. The aim of this study was to analyze long-term data on ground level concentrations of atmospheric aerosol in Southwestern Siberia and those of OC and total protein (TP, universal marker of components of biological origin).

Aerosol sampling was performed by pumping the air at the volumetric rate of 13 m^3/h for a day through fiber filters of AFA-HA-20 type and glass fiber filters. A series of observations for each season lasted for 30 days (4 series per year).

The weight of deposited aerosol was determined by the gravimetric method.

The concentrations of OC and EC were determined by the thermal method (reaction gas chromatography) as described in (Popova *et al*, 2007). The method of reaction gas chromatography allows us to determine the concentrations of OC and EC by their high-temperature separation in an inert atmosphere. Each component is oxidized to CO_2, converted into CH_4 and recorded by a flame ionization detector. The organic substances that are vaporized at heating the sample (to 700 ° C) in an inert atmosphere are defined as organic carbon, and when all substances are burned in an oxidizing atmosphere - as elemental carbon.

The weights of total protein in the samples were determined using a fluorescent dye (You *et al*, 1997).

Tables 1 and 2 show the results of measurements carried out in 2001-2010. The analysis of results demonstrates that, as a whole, the average annual concentration of aerosol tends to increase with a slight reduction during recent years of observations. The average annual concentration of OC in the atmosphere also tends to increase, whereas the average annual concentration of TP remains nearly constant, Table 1. At the same time, the portion of OC in the total mass of aerosol particles also tends to increase during the observation period, while the portion of TP remains practically constant.

Normalization of the values by the corresponding average annual values reveals their seasonal variation. In the cold season, the concentrations of aerosol, the OC and TP are lower than in the warm one. Aerosol concentrations and OC reach their maximums in spring, and TP does it in summer, Table 2.

Table 1. Average annual concentrations of aerosol, OC and TP (all in μg/m^3) in Southwestern Siberia (mean values ± 95% confidence interval).

Year of observation	Values		
	Aerosol	OC	TP
2001	38.6 ± 4.7	4.79 ± 0.90	0.11 ± 0.02
2002	31.4 ± 4.3	5.27 ± 0.98	0.31 ± 0.06
2003	28.9 ± 3.0	4.58 ± 0.74	0.59 ± 0.09
2004	35.2 ± 5.5	4.00 ± 0.63	0.78 ± 0.20
2005	32.2 ± 3.0	4.13 ± 0.47	0.35 ± 0.06
2006	52.1 ± 6.8	6.50 ± 1.14	0.89 ± 0.21
2007	47.9 ± 6.4	4.94 ± 0.68	0.69 ± 0.15
2008	49.6 ± 4.2	7.01 ± 1.20	0.39 ± 0.06
2009	44.6 ± 5.7	8.20 ± 2.25	0.49 ± 0.08
2010	36.8 ± 3.1	6.68 ± 0.91	0.35 ± 0.06

Table 2. Seasonal variation of the concentrations of aerosol, OC and TP normalized by the corresponding average annual values. Averaging over 2001 - 2010, the mean values are presented in increments of 1 ± their 95% confidence interval.

Year of observation	Values		
	Aerosol	OC	TP
Весна	1.41 ± 0.11	1.62 ± 0.19	1.40 ± 0.15
Лето	0.86 ± 0.04	0.80 ± 0.04	1.62 ± 0.12
Осень	0.80 ± 0.05	0.83 ± 0.07	0.72 ± 0.07
Зима	0.91 ± 0.04	0.73 ± 0.05	0.18 ± 0.02

The comparison of these data with those published in Safatov *et al* (2010) for the altitudes of 500 - 7000 m reveals an essential difference between them. For the atmospheric layer at 500 - 7000 m during the same period, aerosol concentrations and those of TP in it tend to decrease, while the portion of TP in the total mass of aerosol increases during the same period. This is probably explained by the influence of local bioaerosol sources, and the difference in the movement of air masses in the boundary atmospheric layer at the altitudes of 500 - 7000.

Popova, S.A., Makarov, V.I., Bashenkhaeva, N.V., and Khodzher, T.V. (2007) *Chem. Sustain. Develop*. **15**, 97-103.

Safatov, A.S., *et al* (2010) In: *Aerosols – Science and Technology*. I. Agranovski (Ed.) Wiley – VCH, 407-454.

You, W.W., Haugland, R.P., Ryan, D.K. and Haugland R.P. (1997) *Annal. Biochem.*, **244**, 277-282.

$PM_{2.5}$ and PM_{10} composition in São Paulo city Atmosphere – Summer and Winter campaigns

P.C. Vasconcellos[1], B. Oraggio[1], P.V. Veiga[1], A. Soreira[1], E. G. Alves[1], J.B De Andrade[2]

[1]Department of Chemistry, University of São Paulo, São Paulo, Cidade Universitária,05508-000, Brazil
[2]Department of Chemistry, Federal University of Bahia, Salvador, Campus de Ondina, 40170-290, Brazil
Keywords: air pollution, aerosols, organic and inorganic pollutants.
email: perola@iq.usp.br

PM_{10} and $PM_{2.5}$ samples were collected in São Paulo city (Brazil) at a site located into the University of São Paulo (SPA site). This site is impacted by miscellaneous emissions sources, including biogenic emissions from a local small forest. Summer campaign took place from October 2009 to March 2010, and the intensive winter campaign in June 2010. Polycyclic aromatic hydrocarbons (PAH) and n-alkanes were determined by gas chromatography after extraction by Soxhlet and fractionation in silica column. The water soluble ions were determined by ion chromatography.

In the summer campaign (wet and warm season) total water soluble ions concentration averaged 7266 ng m^{-3} for $PM_{2.5}$.

In the winter campaign, when events of air pollution were observed, these species averaged 9039 ng m^{-3} for $PM_{2.5}$ and 10307 ng m^{-3} for MP_{10}. The most abundant species were sulphate, nitrate and ammonium in both PM_{10} and $PM_{2.5}$ samples. Sulphate and oxalate didn't present good correlation indicating different formation processes and emissions sources of the precursors. In the winter back trajectories showed air masses coming from regions where sugarcane burning occurs. Except fumarate, all species are more abundant in the fine particulate. $PM_{2.5}$ contributed from 50 to 100% to PM_{10} (Figure 1). According to World Health Organization, the ratio of 0.5 is characteristic of the urban areas of developing countries and corresponds to the lower limit of the range found in urban areas of developed countries (0.5 - 0.8).

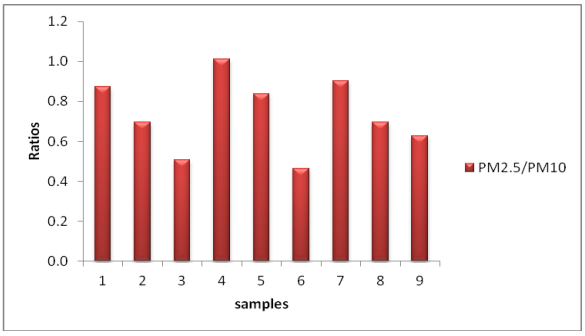

Figure 1. $PM_{2.5}/PM_{10}$ ratios during winter campaign.

The average SO_4^{2-}/NO_3^- ratio were about two times higher in the summer campaign (2.5) than at winter one (1.2). The volatilization of nitrate in the aerosol has been reported in the literature and the winds bringing sulphate derived from sea salt can increase these ratios.

Fourteen PAH (from phenanthrene to indenopyrene) and C_{16}-C_{30} range alkanes were determined. In summer, the most abundant PAH were pyrene, chrysene and benzo(e)pyrene; BeP/BaP ratios (<1) indicated that local emissions are more important than the transport of pollutants. On the other hand, in the winter samples, the lighter compounds were more abundant (phenanthrene, anthracene and fluoranthene). Retene, compound present in biomass burning smokes (Vasconcellos et al., 2011) was present in all samples (av. 20 ng m^{-3}) and BeP/BaP ratios (2.3) indicate transport of air masses and photochemical activity influencing the PAH concentrations.

Between the n-alkanes, the odd-even distribution of the higher n-alkanes shows the biogenic influence and pristane and phytane, the fossil fuel contribution in both campaigns. Figure 2 show the alkanes distribution in a sample collected in the summer campaign.

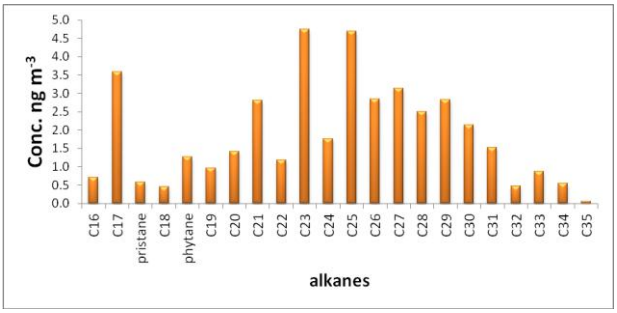

Figure 2. Mean concentrations of n-alkanes, pristane and phytane in samples collected during the wet campaign.

Conclusions

At SPA site, local emissions seem are more important to influence the air quality during the summer campaign, and transport of pollutants from areas with agriculture activities and local vehicular emission can impact the site during the winter time. $PM_{2.5}$ presented a large contribution to PM_{10}.

This work was supported by FAPESP and CNPq.

Vasconcellos, P. C. et al., (2011) *Atmos. Environ.* **45**, 5770-5777.

Aliphatic and aromatic amines in atmospheric aerosol particles

J. Ruiz-Jimenez[1], J. Parshintsev[1], T. Laitinen[1], K. Hartonen[1], T. Petäjä[2], M. Kulmala[2], M.–L. Riekkola[1]

[1]Laboratory of Analytical Chemistry, Department of Chemistry, P.O. Box 55, FI-00014 University of Helsinki, Finland;
[2]Division of Atmospheric Sciences, Department of Physics, P.O. Box 64, FI-00014 University of Helsinki, Finland

Keywords: Aliphatic amines, aromatic amines, aerosol particles, LC-MS, SMEAR II
Presenting author email: jose.ruiz-jimenez@helsinki.fi

Although the chemical composition of atmospheric aerosols has been extensively studied during the last decades, only a few papers have focused on the determination of chemical composition of ambient nanometer sized particles. Recent studies have demonstrated the relevance of the nitrogen compounds in the aerosol chemistry and their participation in particle growing processes.

The most common and abundant nitrogen containing organic compounds found in the atmosphere are the low-molecular weight aliphatic amines with one to six carbon numbers, and from aromatic amines especially aniline, amino acids and amides with biogenic and anthropogenic sources. The most common biogenic sources are the degraded biomolecules and biopolymers, and the cellular metabolism. Waste combustion, sewage treatment, automobile exhaust, vulcanization fumes, fish processing plants, fish stands of city markets and industrial animal farms can be regarded as the main anthropogenic sources.

The sampling of atmospheric aerosol particles is a highly challenging task, especially in the case of size segregated ultrafine particles. Two different devices such as, impactors and differential mobility analyzers (DMA) can be utilized, but unfortunately the collection efficiency of the former tend to be poor for particles significantly smaller than 100 nm due to evaporation processes.

The size-separated particles can be collected on the impactor plate or on a suitable filter, extracted and analyzed with chromatographic techniques utilizing mass spectrometric detection or directly transferred to a mass spectrometer. It is well known that a significant amount of gaseous compounds can be adsorbed on the filter, causing overestimation of particulate concentration of compounds, especially in the case of nanometer-size aerosols. Two different approaches can be used in order to avoid or limit the presence of these artefacts. The first one is based on the removal of gas phase compounds before the collection of the particles in the filter using classical denuders. The second involves the use of new sampling systems based on particle size separation using a DMA and simultaneous collection of gas-phase zero samples allowing the quantification of these artefacts.

The determination of nitrogen containing compounds in aerosol particles is mainly based on chromatographic techniques such as gas chromatography (GC), ion chromatography (IC) and high performance liquid chromatography (HPLC), although other separation techniques such as capillary electrophoresis (CE) has also been employed. However, the derivatization is generally mandatory in the case of GC and LC to improve the separation efficiency and the detection sensitivity of the analytes.

A tedious derivatization step is also almost mandatory for the sensitive analysis of amines by liquid chromatography. An adequate optimization procedure and/or the use of an auxiliary energy such as, ultrasound can minimize the time needed for the derivatization, the amount of expensive reagents, and analyte losses. Unfortunately the derivatizations reagents are suitable only for primary and secondary amines but not for tertiary amines. Fortunately the hyphenation of LC to mass spectrometry (MS) allows the analysis of the underivatized analytes, although most of the methods reported in the literature include a derivatization step in order to facilitate the separation and improve the sensitivity. The selection of the most suitable MS ion source in terms of sensitivity, linearity, repeatability and reproducibility is a key factor in the method development.

In this study, a complete LC-MS methodology was developed for the determination of aliphatic and aromatic amines in atmospheric aerosol particles after dansyl chloride derivatization. This new method was applied for the determination of 19 amines (ten aliphatic and nine aromatic amines) in 16 ambient aerosol particle samples collected at the SMEAR II station.

Several relevant aspects related to the performance of the developed method such as (1) the use of ultrasounds to avoid analyte losses due to evaporation and to hinder the formation of reaction by-products during the derivatization process; (2) the advantages and drawbacks of the use of different approaches in order to limit or avoid gas phase artefacts; and (3) the selection of the more adequate ionization source in terms of sensitivity, linearity, repeatability and reproducibility will be described.

Finally, the developed method was fully characterized and validated using different sample matrices. The results obtained from its application to atmospheric air samples were in a good agreement with those provided by other methods found in the literature.

This work was supported by the Academy of Finland Centre of Excellence program (project no 1118615).

Organic composition of fog: transformation between liquid and interstitial phase

S. Schüttauf[1], J. Matschullat[1], D. van Pinxteren[2], Y. Iinuma[2], H. Herrmann[2]

[1]Institute of Mineralogy, Technical University Bergakademie Freiberg, Freiberg, 09599, Germany
[2]Chemistry Department, Leibnitz Institute for Tropospheric Research, Leipzig, 04318, Germany
Keywords: aerosol chemistry, dicarboxylic acids, fog water, interstitial phase, SOA, VOC (s)

e-Mail: stephanie.schuettauf@ioez.tu-freiberg.de

Fog and cloud water may significantly alter the organic composition of aerosols. The liquid phase enables chemical reactions that do not exist in the gas phase. Furthermore, fog and cloud water are media for new particle formation and reformation. The extended residence time of fog near ground level supports several chemical reactions. Hence, fog and cloud water are important media, which considerably influence aerosols, their composition and properties in the atmosphere.

There is a large demand in understanding the transformation of organic compounds by fog and cloud water. We report measurements of the chemical composition of fog and interstitial aerosol samples from two different sites at the Erzgebirge summit: a) Zinnwald, 877 m asl, eastern Erzgebirge, and b) Fichtelberg, 1,214 m asl, highest elevation of the German Erzgebirge. The Erzgebirge (Ore Mountains) was chosen because it was one of the most polluted forested mountain ranges in Central Europe. The most important source of pollution was the highly-industrialized Northern Bohemian Basin (200–300 m asl) with a major concentration of Czech Republic's lignite power plants, petrochemical and heavy industry.

Passive string collectors were used for fog water sampling, as described in Lange *et al.* (2003). Interstitial aerosol was collected using an aerosol sampler, based on impaction principles and operating with quartz fiber filters. We determined pH-values, electrical conductivity and the concentration of major ions, trace metals and carbonaceous material. TOC (OC-/EC), carboxylic acids, sugar and sugar derivatives and nitrophenols were in focus of the organic analysis.

First results showed nine different sugars and sugar derivatives in the fog water. While levoglucosan and arabitol were the most prominent compounds at both sites, Fichtelberg was dominated by mannosan and Zinnwald was dominated by mannitol (Figure 1). The observed concentrations at both sampling sites were relatively low: 0.02 to 0.2 mg L^{-1}. This is surprising, especially for levoglucosan. Twenty-two carboxylic acids were detected, belonging to six different groups (aliphatic functionalized, aromatic and nitric aromatic monocarboxylic acids and aliphatic non-functionalized, aliphatic functionalized and aromatic dicarboxylic acids). The chemical composition of fog water differs considerably between the two sites. Zinnwald, a "polluted" site with high concentrations of sulphate, nitrate and ammonium, was dominated by levulinic, benzoic, adipic and 7-oxoocatanoic acid (0.98 µmol L^{-1}, 0.25 µmol L^{-1}, 0.15 µmol L^{-1}, 0.09 µmol L^{-1}). Fichtelberg, much less influenced by air pollution and dominated by chloride and sodium, showed the highest concentrations for 2-isopropylmalic, azelaic and suberic acid (0.08 µmol L^{-1}, 0.06 µmol L^{-1}, 0.05 µmol L^{-1}). Photochemical processes are the most expected sources for these carboxylic acids. Other possible sources remain uncertain and need further investigation.

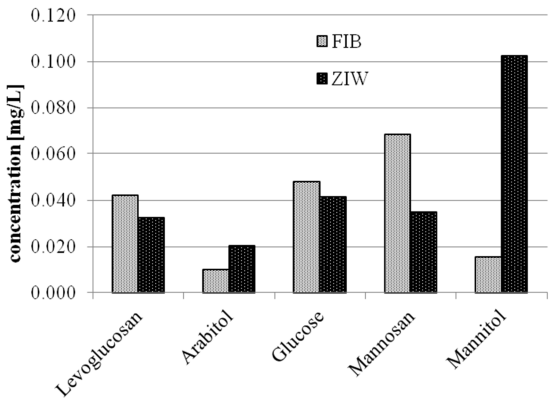

Figure 1. Sugar concentrations in Zinnwald (ZIW) and Fichtelberg (FIB)

This work was supported by the Deutsche Bund Umwelt (DBU) and the Leibniz Institute for Tropospherical Research.

Lange, C.A., Matschullat, J., Zimmermann, F., Sterzik, G., Wienhaus, O. (2003) *Fog frequency and chemical composition of fog water – a relevant contribution to atmospheric deposition in the eastern Erzgebirge, Germany*, Atmos Environ **39** 3731-3739

Secondary particulate matter formation during foggy days

A.Piazzalunga[1,2], M.Anzano[2], V.Bernardoni[3], P.Fermo[1], M.Urbani[1], G.Valli[3] and R.Vecchi[3]

[1]Department of Inorganic, Metal-organic and Analytical Chemistry, Università degli Studi di Milano, Milano, 20133, Italy
[2] Department of Environmental Sciences, Università degli Studi di Milano-Bicocca, Milano, 20126, Italy
[3]Department of Physics, Università degli Studi di Milano, Milano, 20133, Italy
Keywords: SOA (Second. Organic Aerosols), Water soluble compounds, particulate nitrate, sulphate.
Presenting author email: andrea.piazzalunga@unimib.it

In Milan, one of the largest cities in Italy, strong atmospheric stability conditions cause prolonged periods with high pollution levels exceeding the EU threshold limits. In many winter episodes secondary aerosol prevails on primary aerosol (Vecchi et al., 2004) but the mechanisms which cause secondary aerosol formation are not completely clear yet.

In this work, we present the results obtained in two different winter campaigns (2006 – 2007). PM10 was sampled in parallel on quartz fibre and PTFE filters with 4 hour and 8 hour time-resolution.. A detailed chemical characterisation (with quantification of elements, inorganic ions, OC/EC fractions, WSOC, and levoglucosan) was carried out on the samples.

The data analysis presented here is mainly focused on the secondary aerosol formation occurring during foggy days.

In the first campaign (November/December 2006 – 4 hour resolution) we used the Hydroxymethanesulfonate (HMS) as a tracer for heterogeneous chemical reactions (Dall'Osto et al., 2009) as it is a product of the aqueous reaction between dissolved SO_2 and HCHO. HMS was detected in more than 90% of our samples. HMS concentration ranged between 12 ng m^{-3} and 3500 ng m^{-3} and increased during the fog events as shown in figure 1. HMS concentrations resulted well correlated with sulphate values. This shows that sulphate is probably formed in cloud droplets (Choularton and Bower, 2001).

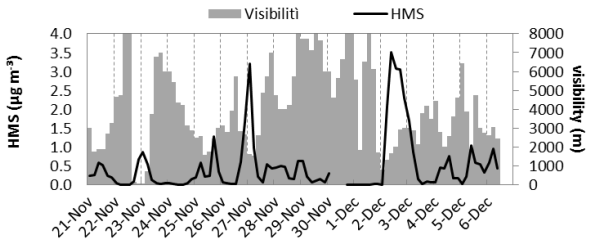

Figure 1. comparison between trend of HMS and visibility.

During the second field campaign (February 2007 – 4 and 8 hour resolution) we investigated the secondary nitrate formation. As shown in figure 2, the nitrate concentration increased from 20 to 110 µg m^{-3} in about 36 hours during the fog event. In the same period, an increase in WSOC (water soluble organic compounds), concentration and relative humidity levels was also detected. During the fog event, we also observed an increase of HMS concentration (concentration up to 700 ng m^{-3}), which was fostered by the low solar radiation. This day was also characterised by a high OC/EC ratio.

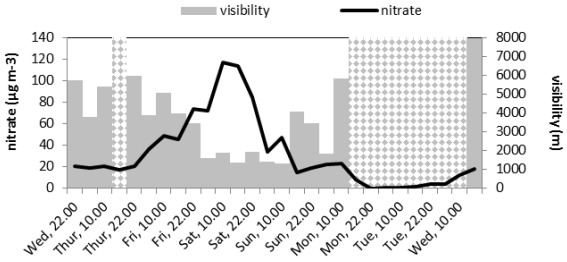

Figure 2. comparison between trend of nitrate and visibility.

In order to evaluate the acidity of the WSOC, we also quantified the organic carbon extracted at two different pH values (2.5 and 5.5). The concentration trend of the compounds extracted at lower pH is well correlated to the K^+ concentrations. K^+ is known to be related to wood burning. Therefore, this source is probably an important source of organic acid compounds too. On the other hand, the concentration of compounds extracted in less acidic solution increased during the night. The insoluble organic compounds are well correlated to the primary components of particulate matter.

Choularton, T., Bower, K. (2001) Water, Air, & Soil Pollution: **1** 365-372.

Dall'Osto, M., Harrison, R. M., Coe, H., Williams P., (2009) Atmos. Chem. Phys. **9** 2459-2469

Vecchi, R., Bernardoni, V., Fermo, P., Lucarelli, F., Mazzei, F., Nava, S., Prati, P., Piazzalunga, A., Valli, G. (2009) Environmental Monitoring and Assessment, **154** 283-300.

Fingerprint of shipping emissions on PM_{10} at Barcelona

J. Pey[1], N. Pérez[1], A. Alastuey[1], X. Querol[1], J. Cortés[2]

[1]Institute of Environmental Assessment and Water Research (IDAEA-CSIC), Barcelona, E-08034, Spain
[2]Autoritat Portuaria de Barcelona
Keywords: chemical composition, trace elements, source profile
Presenting author email: jorge.pey@idaea.csic.es

The Barcelona metropolitan area has a serious environmental problem concerning air quality. In the last years, new Directives on Air Quality are becoming more restrictive, requesting for a lowering in atmospheric pollutants. In the case of Barcelona, a serious problem is observed for NO_2 and particulate matter, with a high number of exceedences of the Air Quality standards across most of the metropolitan area. Estimations of contributions from different sources show that road transport in the main pollution source increasing the loads of atmospheric pollutants (NO_x and particles) in this region, but also an important contribution is coming from the harbour area (8-9%). The APICE (Common Mediterranean strategy and local practical Actions for the mitigation of Port, Industries and Cities Emissions) project pretends to reduce harbour emissions to the atmosphere by adopting mitigation strategies. In the harbour area, a number of emission sources are polluting the atmosphere, being ships one of them.

In this work we show the results from an intensive sampling campaign (7th November 2011 to 5th January 2012) carried out in the harbour area. During this campaign we deployed two low volume samplers for collecting PM_{10} every day (from 10 to 10), resulting in 59 consecutive days of successful campaign. The monitoring site was in the terrace of the 8th floor in the World Trade Center, a business building located in the northern border of the harbour area, just few meters from the cruise area. The aim of the study was to capture, as much as possible, fresh shipping emissions. This would happen when winds blow from the south (which is relatively usual) and there are cruises in the harbour. The fingerprint of these fresh shipping emissions may serve as inputs for subsequent receptor modelling that will be carried out in order to determine the contribution from ships to ambient PM_{10} levels in the Barcelona city.

Before and after sampling, quartz fibre filters were conditioned and weighted to determine PM_{10} concentrations. Thereafter, filters were treated in laboratory following procedures described in Pey *et al* (2010). Finally, concentrations of major and trace elements and compounds were determined (OC, EC, SO_4^{2-}, NO_3^-, NH_4^+, Cl^-, Al, Fe, Ca, Na, K, Mg, P, Ti, Mn, Sr, Rb, Zn, Cu, Sb, Sn, Pb, V, Ni, Co, among others, including typical tracers of shipping emissions.

Mean PM_{10} concentration was 33 $\mu g/m^3$: carbonaceous particles (33%), unaccounted material (30%, mostly water), mineral matter (15%), sea spray (10%), sulphate (6%), nitrate (4%) and ammonium (2%). At the beginning of the campaign, extremely high levels of PM_{10} were recorded owing to typical winter pollution episodes. PM_{10} composition during these events was dominated by secondary aerosols, both organic and inorganic. After these few polluted days, Mediterranean cyclones provoked heavy rains and strong winds over Barcelona area, which diminished secondary pollutants in the atmosphere in opposition to sea spray, which increased drastically. Sporadic and low-intense African dust episodes were also registered before and after autumn storms. Finally, from end November to the end of the campaign, sunny and warm days prevailed, which favoured the development of weak sea breezes during the day. Thus, Southern winds blown over the monitoring site bringing, a number of days, fresh emissions from ships. As seen in Figure 1a, V and Ni (typical tracers of shipping emissions) levels increased a number of days. Because shipping plumes are usually mixed with urban and industrial emissions, the identification of these fresh plumes is not direct. We have used the ratio V/Cu (Cu is a typical urban tracer – traffic- coming from tires and breaks abrasion) to distinguish which shipping emissions are fresh (with low Cu levels) and which are mixed with urban pollution (Figure 1b). As seen in Figure 1, the highest record of V, on 4th December 2011, was coincident with very low Cu levels, which is assumed to be of a dominant ship origin. Thus, the chemical profile of PM_{10} for that day may be deduced as a typical ship-signature.

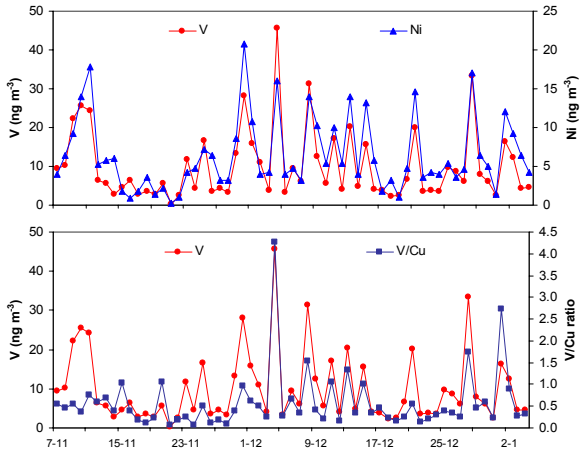

Figure 1. Daily variation of: a) V and Ni (ng m^{-3}); b) V and V/Cu, in PM_{10} during the campaign

This work has been supported by the MED programme (FEDER, CE) 2889, 2G-MED09-026.

Pey, J. Pérez, N. Querol, X. Alastuey, A. Cusack, M. Reche, C. (2010). *Sci. Tot. Env.* **408,** 1951-1959.

Characteristics of surface ozone over Qinghai Lake area in Northeast Tibetan Plateau, China

Zhenxing Shen[1], Xin Wang[1], Junji Cao[2], Zhuzi Zhao[2]

[1]Department of Environmental Sciences and Engineering, Xi'an Jiaotong University, Xi'an, China
[2]SKLLQG, Institute of Earth Environment, Chinese Academy of Sciences, Xi'an, China
Key words: Ozone formation, meteorological factor, NO_x, back trajectory
Presenting author E-mail: zxshen@mail.xjtu.edu.cn

One year continuous measurements of surface ozone over Qinghai lake area (36°58′37″N, 99°53′56″E) in Northeast Tibetan Plateau, China was presented in this study. Daily average O_3 ranged from 11.1 ppbv to 33.3 ppbv with an annual average of 20.9 ppbv. Seasonal average of O_3 followed a decreasing order of summer > autumn > spring > winter. The diurnal variation in O_3 shows low concentrations during daytime and high concentrations during late night and early morning.

Table 1 O_3 level in Qinghai Lake area

	O_3 level (ppbv)	
	Average	Range
Spring	19.8	12.7-28.9
Summer	24.9	3.1-33.3
Autumn	22.2	14.2-30.8
Winter	17.7	11.1-25.6

An intensive campaign on Aug 13 to 31, 2010 was conducted to investigate the correlation among meteorological factors and chemical condition with surface ozone. It was noted that solar radiation had a poor relationship with ozone level. Moreover, high wind speed was always coincided with the high ozone level. In addition, insufficient NO_x in atmosphere was observed in Qinghai Lake area. Such results revealed that local photochemical reaction process contributed limitedly to surface ozone, while intrusion of stratospheric O_3 and distance transport should be the main sources of surface ozone in this rural area. Back-trajectory analysis further indicated the contribution of long distance transport of air mass from northwest to the surface ozone in Qinghai Lake area. Moreover, transport of ozone-rich air masses from the stratosphere to the troposphere is also important.

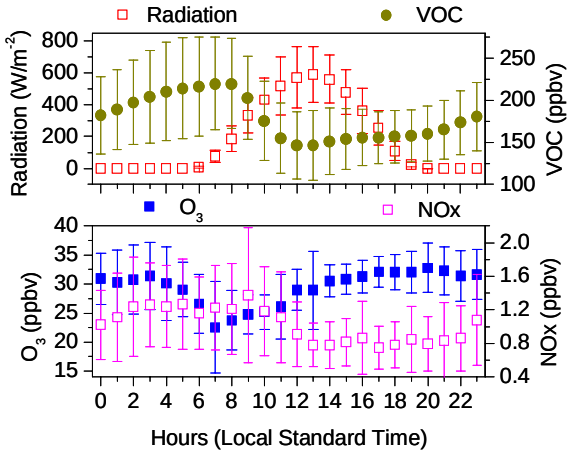

Figure 1 Diurnal cycle of solar radiation, NO_x, VOC, and O_3 levels in Qinghai Lake area during the strengthen campaign period

Brankov, E., Henry, R., Civerolo, K., Hao, W., Rao, S.T., Misra, P.K., Bloxam, R., Reid, N. (2003). *Environ. Pollut.* 123: 403–411.

Chan, C.Y., Chan, L.Y., Cui, H., Zheng, X.D., Zheng, Y.G., Qin, Y., Li, Y.S. (2003). *Tellus.* 55B: 982–992.

Wang, T., H. L. A. Wong, J. Tang, A. Ding, W. S. Wu, and X. C. Zhang. (2006). *J. Geophys. Res.* 111: D08303, doi:10.1029/2005JD006527.

Seasonal and diurnal variations of mono- and di-carbonyls in Xi'an, China

W.T. Dai[1], S.S.H. Ho[1,2], K.F. Ho[1], W.D. Liu[3], J.J. Cao[1], S.C. Lee[3]

[1] SKLLQG, Institute of Earth Environment Chinese Academy of Sciences, Xi'an, 710075, China
[2] Division of Atmospheric Sciences, Desert Research Institute, Reno, NV 89512, United States
[3] Research Center of Urban Environmental Technology and Management, Department of Civil and Structural Engineering, The Hong Kong Polytechnic University, Hung Hom, Kowloon, Hong Kong, China

Keywords: Carbonyl compounds; Seasonal and diurnal variation; Correlation; Xi'an.
Presenting author email: daiwt@ieecas.cn

Seventeen carbonyls in urban ambient air were quantified in summer (June 2009) and winter (January 2010) in an urban site located in Xi'an, China. Formaldehyde, acetaldehyde and acetone were the three most abundant carbonyls in the atmosphere with the concentration 6.54±2.38 ppbv, 2.08±1.07 ppbv and 2.74±1.14 ppbv in summer (from 14th to 24th June, 2009), respectively. In winter, the concentrations were 4.46±1.74 ppbv, 6.52±3.88 ppbv and 3.87±2.33 ppbv respectively from 4th January, 2010 to 10th January, 2010. Most carbonyls had higher concentrations in winter than in summer. And majority of the species had higher concentrations in daytime than in nighttime, indicating photochemical oxidation/human activities played an important role in diurnal variation. Formaldehyde/acetaldehyde ratios (F/A) in summer of 2.14 was much higher than 0.47 in winter, showing significant effect of photochemical oxidation in the urban air during summer. Acetaldehyde/propionaldehyde (A/P) average ratio was 12.2 in wintertime, implying anthropogenic emission was the major source of carbonyls in Xi'an. In addition, the ratio of acetone to methylglyoxal (A/M) is used to determine the impact of photochemistry in the atmosphere. The average acetone/methylglyoxal ratio (10.3±2.3) in summer was lower than that in winter (21.3±5.1) in Xi'an. Strong correlations among some carbonyls imply that they came from the same pollution sources. Formaldehyde and acetaldehyde play a very important role in photochemical smog formation. Methylglyoxal and glyoxal also have significant contribution to ozone formation potential.

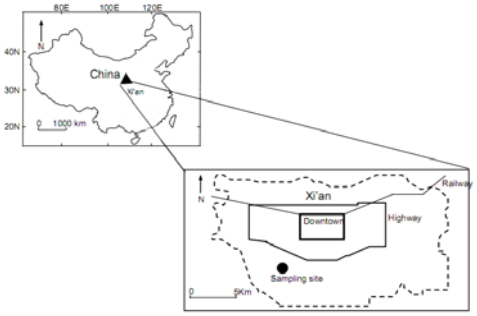

Fig. 1. A geographical map showing the location of Xi'an in China (upper plot) and sampling site IEECAS (black spot in bottom plot).

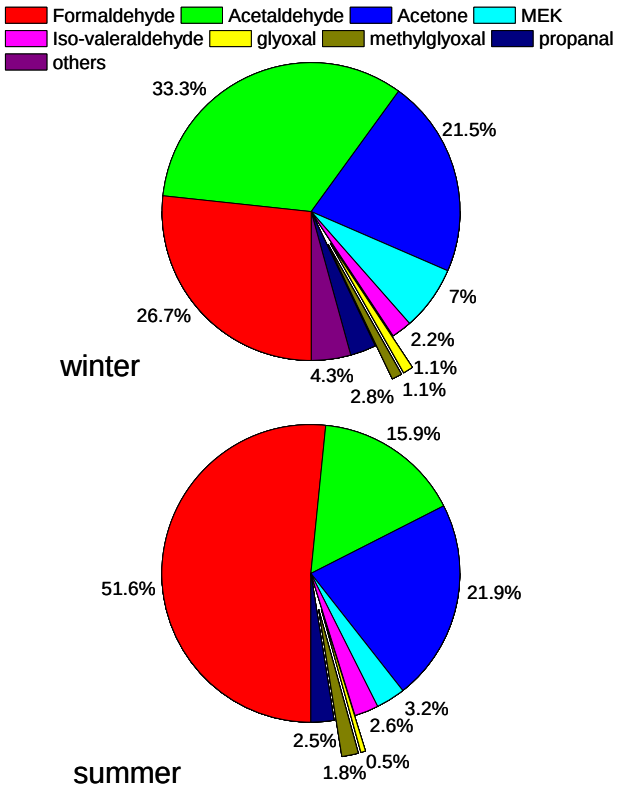

Fig. 2. Molar compositions for carbonyls in summer and winter in Xi'an.

This study is in part supported by projects from the Chinese Academy of Sciences (KZCX2-YW-BR-10).

Gas conversion to sulfate and nitrate in fine particulate matter at southern Taiwan

J.H. Tsai[1,2], J.H. Lin[1] and L.P. Chang[1]

[1]Department of Environmental Engineering, National Cheng Kung University, Tainan, 701, Taiwan
[2]Research Center of Climate Change and Environmental Quality, National Cheng Kung University, Tainan, 701, Taiwan

Keywords: MOUDI, conversion ratios, episode day, non-episode day.
Presenting author email: jhtsai@mail.ncku.edu.tw

Ions species in airborne fine particulate matter was investigated in southern Taiwan during episode event and non-episode periods. A Micro Orifice Uniform Deposit Impactor (MOUDI) and a nano-MOUDI were employed to take PM samples. Ambient concentrations of HNO_3 and SO_2, and particulate NO_3^- and SO_4^{2-} were determined in daytime and nighttime. Conversion of these inorganic species into airborne particulate matter, especial in the accumulation mode, was discussed in this study. High humidity atmosphere was observed in this study area.

NO_3^- partition between gas and particulate phases strongly depends on temperature, relative humidity, and ammonia concentration. The conversion ratios of Fn and Fs for NO_2 to nitrate and SO_2 to sulfate in particulate matter, respectively, are defined as follows (Kadowaki, 1986; Khoder, 2002; Lin et al., 2006):

$$F_n = \frac{[PNO_3^-]+[GNO_3^-]}{[NO_2]+[PNO_3^-]+[GNO_3^-]}$$

where $[PNO_3^-]$ is the particulate-nitrate concentration in the accumulation mode ($\mu g/m^3$ NO_2), $[GNO_3^-]$ is the gaseous-nitric acid concentration ($\mu g/m^3$ NO_2), and $[NO_2]$ represents the ambient NO_2 concentration ($\mu g/m^3$).

$$F_s = \frac{[PSO_4^{2-}]}{[PSO_4^{2-}]+[GSO_2]}$$

where $[SO_4^{2-}]$ is the particulate-sulfate concentration in the accumulation mode ($\mu g/m^3$ SO_2), and $[SO_2]$ is the ambient SO_2 concentration ($\mu g/m^3$). Atmospheric H_2SO_4 is neglected in this work.

Table 1 shows the information of NO_2, SO_2, PNO_3^-, GNO_3^- PSO_4^{2-}, Fn and Fs during the sampling periods. The NO_2 conversion factor at daytime and nighttime during the episode days was about 1.4 and 4 times higher than that during the non-episode days, respectively. The daytime data are higher than that reported in winter in Japan and Egypt, and are similar to those observed in autumn and winter in central Taiwan. Results of the non-episode nighttime were consistent with what were observed in the other studies in winter (Kadowaki, 1986; Khoder, 2002; Lin et al., 2006). On the other hand, the highest value of Fn during the episode nighttime was higher than that found by previous studies, and the Fn values during episode days were higher than those during non-episode days. In addition Fs of both daytime and nighttime during episode periods were about 1.5 times higher than that of non-episode periods.

High Fn and Fs in episode days indicated that ratio of SO_2 oxidation to sulfate and ratio of NO_2 oxidation to nitrate were relative high. Mass of sulfate and nitrate in accumulation mode particle during episode days were higher than those in non-episode days. This result suggests that the effect of gas-to-particle conversion plays an important role in the increment of airborne fine particulate matter concentration in southern Taiwan during air pollution episode days.

Table 1 Conversion of NO_2 to NO_3^- and SO_2 to SO_4^{2-} in Southern Taiwan

Compounds	Episode day		Non-episode day	
	Daytime (n=7)	Nighttime (n=8)	Daytime (n=12)	Nighttime (n=11)
NO_2 ($\mu g/m^3$)	49.35±4.90* (43.86-55.16)	61.04±9.64 (45.48-77.03)	15.73±14.33 (3.39-44.96)	20.38±14.80 (7.40-60.38)
SO_2 ($\mu g/m^3$)	34.09±8.02 (23.02-43.07)	21.54±8.09 (8.95-33.11)	10.98±9.83 (1.79-30.69)	6.49±5.56 (1.60-20.29)
PSO_4^{2-} ($\mu g/m^3$)	17.61±5.57 (12.78-28.91)	16.93±5.29 (7.23-22.87)	2.93±2.30 (0.32-6.76)	3.94±3.14 (0.86-9.82)
PNO_3^-($\mu g/m^3$)	9.94±4.24 (4.85-17.50)	26.03±6.98 (17.54-36.81)	1.33±2.21 (0.12-6.13)	1.31±1.10 (0.24-3.87)
GNO_3^-($\mu g/m^3$)	7.19±2.64 (3.73-10.34)	0.89±0.36 (0.42-1.54)	2.79±1.47 (1.44-5.92)	0.30±0.18 (0.09-0.69)
F_n	0.20±0.02 (0.16-0.24)	0.24±0.04 (0.21-0.31)	0.19±0.07 (0.09-0.35)	0.07±0.05 (0.02-0.16)
F_s	0.26±0.05 (0.20-0.32)	0.37±0.04 (0.30-0.41)	0.23±0.09 (0.09-0.45)	0.29±0.08 (0.19-0.46)

*The data indicates the mean value±standard deviation and the parenthesis presents the range of data.

This work was supported by the National Science Council, Taiwan, Republic of China under grants NSC95-2221-E-006 -287 and NSC 96-2211-E-006-004.

Kadowaki, S. (1986) *Environ. Sci. Technol.* **20**, 1249–1253.
Khoder, M.I. (2002) *Chemosphere* **49**, 675–684.
Lin, Y.C., Cheng, M.T., Ting, W.Y., and Yeh, C.R. (2006) *Atmos. Environ.* **40**, 4725–4733.

Regional contributions of arsenic species in Southwestern Spain

González-Castanedo Y[1], Sánchez-Rodas D.[2], Sánchez de la Campa A.M.[1], Fernández-Camacho R. [1] de la Rosa J. D[1]

[1]Associate Unit CSIC-UHU "Atmospheric Pollution", CIQSO, Campus El Carmen, 21071 Huelva, Spain
[2] Department of Chemistry and Materials Science, Campus El Carmen, Univ. of Huelva, 21071 Huelva, Spain
Keywords: regional background, heavy metals, arsenic speciation
Presenting author email: yolanda.gonzalez@dgeo.uhu.es

In the last decade, aerosols have been intensively studied in Southwestern Spain (SWS) for the purpose of assesing the air quality in Huelva. These studies indicate that the local population of the city is exposed to high concentration of a trace metal cocktail (As, Cu, Zn, Ti, Bi and Pb) related to the impact of several industrial emissions situated in the surroundings (Sánchez de la Campa, 2011). The presence of the arsenic in the samples is related to the influence of the near-by copper smelter considered the largest one in Spain (Fernández-Camacho, 2010). Arsenic is recognised to be a carcinogenic element which toxicity depends on the oxidation state and molecular form in which this element is included.

The present work is the first one reporting total mass and chemical composition PM2.5, arsenic speciation included, from a regional background site in SWS. For achieve this aim, simultaneous sampling of PM10 and PM2.5 were carried out at two stations (an urban background station (UB, Campus) situated in Huelva city and in a regional background station (RB, El Arenosillo) placed about 30 Km to the NW) in order to compare results of the same days and evaluate the influence of local and regional sources in the background PM composition.

Trace metal content of 71 and 54 synchronic samples, of PM10 and PM2.5 respectively, taken during 2006-2007 was determined by Inductively Coupled Plasma Mass Spectrometry (ICP-MS). Moreover, speciation analysis was performed using High Performance Liquid Chromatography coupled to Hydride Generation and Atomic Fluorescence Spectrometry (HPLC-HG-AFS) with those samples (34 filters) with total arsenic content higher than 2 $\mu g/m^3$ so as to characterize the distribution of arsenic species in this area. This methodology has previously employed for determination of inorganic As (III) and As (V) species in airborne particles (Sánchez-Rodas, 2007).

According to the chemical composition of PM (Table 1), high levels of metals (e.g. As, Se, Bi, Cu, Zn, Pb) were found in PM10 and especially in PM2.5 at RB and UB. This fact indicates that there is an industrial contribution in both stations which will depend on the meteorological sceneries. The impact of the industrial sources emissions plumes on the city of Huelva occurs with wind directions from the third quadrant (34% during whole sampling period) while fourth quadrant winds (30% during whole sampling period) will bring metal-rich plumes at RB station.

Table1.Trace metal and arsenic species concentration in PM_{10} and $PM_{2.5}$ at regional (RB) and urban background (UB) station during 2006-2007.

	PM_{10}		**$PM_{2.5}$**		**$PM_{2.5}$ /PM_{10}**	
	UB	**RB**	**UB**	**RB**	**UB**	**RB**
$\mu g/m^3$	40	31	20	17		
ng/m^3						
Cu	49.0	15.0	37.5	8.42	0.8	0.6
Zn	39.0	37.6	28.5	33.6	0.7	0.9
As	7.03	4.89	5.38	4.45	0.8	0.9
Se	1.76	1.29	1.10	0.87	0.6	0.7
Pb	13.9	11.9	14.0	11.4	1.0	1.0
Bi	0.86	0.53	0.63	0.49	0.7	0.9
As	11.4	6.64	9.79	6.04	0.9	0.9
AsIII	0.43	0.39	0.41	0.25	1.0	0.7
AsV	13.1	7.83	12.4	6.76	0.9	0.9

The behaviour of arsenic species is akin to that of total arsenic and the rest of the trace metals. The speciation analysis (Table 1) show that arsenate (As (V)) is the main arsenic species found in both stations, urban (13.1 $ngPM10/m^3$ y 12.4 $ngPM2.5/m^3$) and regional background (7.83 $ngPM10/m^3$ and 6,76 $ngPM2.5/m^3$). In spite of the low mean concentrations of arsenite (As (III)), the proportion of the most toxic specie, is similar at UB and RB ambient. As (III) varies between 3-5% in PM10 and 3-4% in PM2.5. In the same way, the mean As (V) contribution varies between 95-97 % in PM10 and 96-97% in PM2.5. The results indicate that arsenic species as well as trace elements (PM2.5/PM10=0.7-1) accumulate in the finer particles which may be transported long distance from the source emission.

This work was supported by several research projects: 2007-RNM027329, CGL2005-05693-C03-01, C2007-0067, P07-RNM-03125, P07-RNM-02729.

Fernández-Camacho R. et al (2010). *Atmos. Res.* **96**, 590-601.

Sánchez de la Campa, A.M. et al (2011) *J. Environ. Monit.*, **13**, 1276-1287.

Sánchez-Rodas, D. et al (2007) *Chemosphere*, **66**, 1485-1493.

Water soluble compounds in Arctic aerosols (Ny Alesund, Svalbard).

R. Zangrando[1*], C. Turetta[1], E. Barbaro[1,2], P. Zennaro[1,2], N. M. Kehrwald[1], J. Gabrieli[1], A. Gambaro[1,2], C. Barbante[1,2]

[1]Institute for the Dynamics of Environmental Processes-CNR, Venice, 30123 Italy
[2]Dept. of Environmental Sciences, Informatics and Statistics-University Cà Foscari, Venice, 30123 Italy
(I)Keywords: Biomass burning, Artic aerosols, HPLC-MS, ICP-MS.
Presenting author email: roberta.zangrando@idpa.cnr.it

A significant percentage of organic matter (between 40 and 60%) in atmospheric aerosols consists of a numerous but still poorly understood class of hydrosoluble compounds known as water soluble organic carbon (WSOC). WSOC can significantly decrease the surface tension of aqueous solutions, affect the hygroscopicity of aerosols, and may be important in determining the ability of particles to serve as cloud condensation nuclei (CCN), with consequences for climate, optical properties of the atmosphere and air quality. The scientific activity performed at Ny Alesund during the 2010 campaign had the aim of better understanding the formation, the chemical composition and the transport processes of aerosol towards the arctic zone.

Eighteen samples were collected from March to September 2010, sampling was performed using an high volume cascade impactor (TE 6000 series, Tisch Environmental Inc.) at the Gruvebadet supersite (78 55 07 N, 11 53 30E) (stage parameters: 10.0 – 7.2 µm (Stage 1), 7.2 – 3.0 µm (Stage 2), 3.0 – 1.5 µm (Stage 3), 1.5- 0.95 µm (Stage 4), 0.95 – 0.49 µm (Stage 5), < 0.49 µm (back up)).

The following analytes were determined: levoglucosan (Bourcier et al 2010) and methoxy phenols (vanillic acid VA, isovanillic acid IVA, homovanillic acid HA, syringic acid SyA, conyferil aldehyde CAH, ferulic acid FA, syringaldehyde SyAH, p-coumaric acid PA) (paper in preparation) as biomass burning tracers, acrylamide (antropogenic) (Zangrando et al 2011) and trace elements (TE) were analysed to better understand transport processes. Seasonal trends were obtained.

Instrumental analysis in WSOC employed an Agilent 1100 series HPLC system (Agilent, Waldbronn, Germany) coupled to an API 4000 triple quadrupole mass spectrometer (Applied Biosystems/MDS SCIEX, Toronto, Ontario, Canada).

For levoglucosan the highest levels were observed in back up filters in a range of concentration between 4 pg/m^{-3} and 682 pg m^{-3} (average 71± 166 pg m^{-3}). The analysis of slotted filters revealed in stage 4 the highest levels at 5.8 pg m^{-3}.

The presence of acrylamide in arctic aerosols was episodic. Significant concentrations were determined in ultrafine aerosols (< 0.49 µm) in some samples that range from 32 fg m-^{3} to 127 32 fg m^{-3}, average concentration was 37 ± 50g fg m^{-3}. In fine and coarse aerosols (stage 1 to 5) in general acrylamide was not detected, except in some samples, but with a very low concentration. Moreover we noticed that the atmospheric concentrations were highest in ultrafine particles, so we can attribute the presence of acrylamide mainly to long range transport although for some samples we can hypothesized a local source.

The determination of methoxyphenols in fine and ultrafine aerosols (< 0.49 µm) was performed on back up filters. In Arctic particulate matter total concentration of methoxyphenols determined range between 16554 and 1998 fg m^{-3}, average 5469 ± 3376 fg m^{-3}. The compounds mainly present are VA, HA and PA, average percentage 28.4%, 27.0% and 38.6% respectively. While SyA (3.5%), SyAH, IVA, CAH and FA are presents only in minor concentration, globally at average percentage of 6%. The analysis of slotted filters showed that in stages 3 and 4 are present the highest levels of methoxyphenols similar to that observed in the back up filter.

TE analyses were carried out using a Sector Field Inductively Coupled Plasma-Mass Spectrometer (SF-ICP-MS, Element2 Finnigan-MAT, Bremen, Germany), coupled with a cooled cyclonic spray chamber (ESI-PC3). Samples were acidified with 2% ultrapure nitric acid and directly analysed. The quantification of TE was carried out by external calibration method. Preliminary results of TE analyses in two back up filters (GB9 and GB15) have highlight higher concentrations in GB9 sample for all the elements analysed probably due to a local burning event.

This work was supported in part by the PRIN 2007L8Y4NB Project, funded by Italian MURST and in part by the European Project EARLYhumanIMPACT - How long have human activities been affecting the climate system? - “Ideas” Specific Programme - European Research Council - Advanced Grant 2010 - Grant Agreement n° 267696 - ERC-2010-AdG_20100224. The authors gratefully acknowledge the help of ELGA (High Wycombe, U. K.) in providing ultrapure water used in these experiments.

L. Bourcier, K. Sellegri, O. Masson, R. Zangrando, C. Barbante, A. Gambaro, J.-M. Pichon , J. Boulon , P. Laj, (2010), *Atmos. Environ.*, **44**, 2280-2286.

R. Zangrando, A. Gambaro, S. De Pieri, J. Gabrieli, E.Barbaro, C. Barbante, P. Cescon., (2011) *Int. J. Environ. An. Ch.*, i-First, 1-11.
http://dx.doi.org/10.1080/03067319.2010.520130

Aerosol-fog chemical interactions: a case study in the Po Valley (Northern Italy)

L.Giulianelli[1], S. Gilardoni[1], M. Rinaldi[1], S. Decesari[1], M. Paglione[1], C. Carbone[1], S. Fuzzi[1] and M.C. Facchini[1]

[1] Institute of Atmospheric Science and Climate (ISAC), CNR, Bologna, Italy
Keywords: aerosol chemistry, aerosol cloud interaction, chemical composition, droplets, multiphase processes.
Presenting author email: l.giulianelli@isac.cnr.it

Fog represents a multiphase system that play a significant role in the formation, distribution and removal of trace atmospheric components. Fog droplets form by condensation of water vapour onto condensation nuclei in supersaturation conditions, therefore the chemical composition of the aerosol particles acting as condensation nuclei influences the initial chemical composition of the fog droplets. Particles scavenging and the chemical reactions occurring in the aqueous phase determine changes in the composition of both fog droplets and residual aerosol particles resulting after fog dissipation. Since fog forms at the ground level, the interactions between fog droplets and particulate matter by the chemical and physical processes mentioned above can have a deep impact on the local air quality.

The frequency of the fog events and the high level of particulate matter in the air makes the Po Valley (Northern Italy) the perfect place to observe the relations between fog droplets and aerosol particles, Facchini *et al* (1999).

In order to investigate these processes fog samples were collected within the ARPA-Supersito Project field campaign (15^{th} - 30^{th} November 2011). The measurements took place in the field station of San Pietro Capofiume, a rural place in the Eastern Po Valley. Aerosol samples were collected before, during and after fog events that frequently occurred during the campaign, as well as fog droplets. Samples were collected with a day/night frequency for aerosol and bulk samples for each fog event. During two very dense fog events (15^{th} and 17^{th} of November) the sampling strategy changed in order to have higher time resolution samples: one fog sample every hour and one aerosol sample every 4 hours. The purpose is to investigate the evolution in the chemical composition of both fog droplets and size segregated aerosol particles during the whole fog event.

The campaign provided both online measurements by Aerosol Mass Spectrometer (AMS) and aerosol size segregated samples on tedlar and quartz substrates for offline analysis. An automated string collector was used to collect fog droplets, Fuzzi *et al* (1997). Ionic composition of the samples was determined by Ion Chromatography. Carbon and nitrogen analysis were performed to determine the amount of organic compounds (soluble and insoluble) and soluble organic nitrogen content. The distribution of the main species (NH_4^+, $SO_4^=$, NO_3^-, soluble organic compounds, etc.) between fog and aerosol particles and the variation in the chemical composition of aerosol samples allow us to investigate the partitioning process occurring into this multiphase system.

Scavenging of PM1 particles during fog formation is well illustrated in Fig.1, where the different trends of liquid water content (LWC) and particle mass concentration are reported. Detailed results of the chemical characterization of the multiphase system and the study of interactions occurring between particulate matter and fog droplets will be presented.

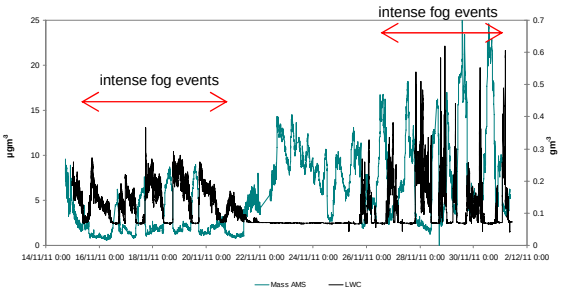

Fig. 1. Submicron particle mass concentration (μgm^{-3}, green line) measured by AMS and LWC (gm^{-3}, black line) trend during the field campaign.

This research was conducted as part of the Supersito Project, which was supported and financed by Emilia-Romagna Region and Regional Agency for Prevention and Environment under Deliberation of Regional Government n. 428/10.

Facchini, M.C., et al. (1999) *J. Geophys. Res.*, **104**, D21, 26821-26832.

Fuzzi, S., et al. (1997) *Water, Air and Soil Pollut.* **93**, 383-394.

Sulfur containing Polycyclic Aromatic Hydrocarbons (PASHs): new perspectives of tracers for source apportionment of aerosols

B. Golly[1], C. Piot[2], J.L. Jaffrezo[2], D. Chapuis[3], J.L. Besombes[1]
[1]Université de Savoie-*LCME, Le Bourget du Lac, France*
[2]Université Joseph Fourier-CNRS-*LGGE, St-Martin d'Hères, France*
[3]Air Rhône-Alpes, *Bron, France*
Keywords: Source apportionment models; Alpine Valley; Molecular Markers; Thiophenes
Presenting author email: benjamin.golly@univ-savoie.fr

For several decades, control of air quality is a main concern of public health. Further, the determination of chemical composition of Particulate atmospheric Matter (PM) is increasingly important in order to understand their atmospheric behavior and their impact on climate change. With this respect, the interest in the individual organic constituents of PM has grown, all the more since most of them can also be used as tracers in source apportionment models.

Particularly, the Sulfur containing Polycyclic Aromatic Hydrocarbons (PASHs) are considered as both pollutants and as markers of many sources emissions. Indeed these compounds are emitted in the atmosphere by combustion processes and they have already been identified on particulate organic matter. Due to their chemical stability, they are also distributed to other environmental compartments. In recent years, several studies have identified thiaarene in exhausts from combustion processes (Lemieux et al., 2004), in aquatic environments (Ni et al., 2008), and in ambient air (Becker et al., 1999).

Usually, PASHs have been used to distinguish emissions from exhaust diesel and coal tar. In fact thiophenes and benzothiazoles derivatives are mainly used respectively as molecular markers of diesel emissions and tire wear.

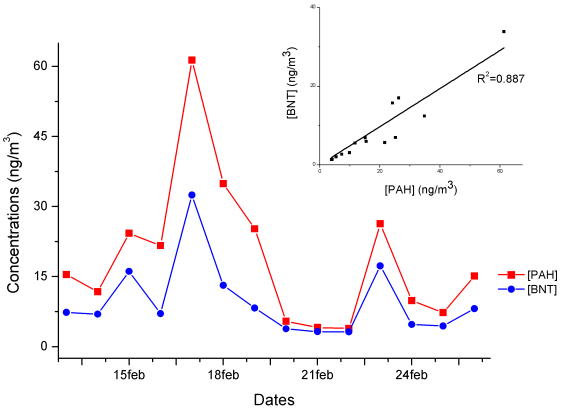

Figure 1: Temporal evolution and correlation between concentrations of PAHs and BNT in the particulate phase of aerosols in winter 2010 in Passy.

In this study, the identification of thiophenes and benzothiazoles has been achieved on aerosol samples from several experimental sites. The first sampling site is largely influenced by traffic, due to its localization near a highway around Grenoble; (Echirolles-Grenoble, France). A second sampling site was located in an Alpine valley with a strong industrial activity and crossed by an important main highway (Passy, France). At both sites, PM10 were collected on quartz filters and the gas phase was trapped on PUF with a high-vol sampler ($30.m^3.h^{-1}$). Each daily sample was analysed for EC-OC and organic speciation. Thiophenes and benzothiazoles were quantified by GC-MS analysis, together with several other source tracers (levoglucosan, hopanes, PAHs...).

Benzothiazole, as a tire wear tracers, has been detected next to the highway and mainly in the gas phase but not at the Alpine industrial valley site. Thiophenes were not identified on the kerbside site despite the proximity of vehicular emissions. The highest concentrations of thiophenes in particulate phase of aerosols were found in the Alpine industrial valley site. Benzo[b]naphtha(2,1-d)thiophene (BNT(2,1)) concentrations ranged from 1.32 to 33.84 ng/m^3 in winter 2010 and 1.30 to 16.40 ng/m^3 in spring 2011. Figure 1 shows that thiophenes and PAH's concentrations are rather well correlated with in the particulate phase at this site.

These results show that BNT(2,1) cannot be considered as marker of vehicular emissions. This result can be related to the decrease of sulfur concentrations in fuel. Measurements on bench test of vehicular emissions will allow to confirm it (test forseen within the PM Drive program funded by ADEME in France). Moreover, their presence on the Alpine industrial valley site indicates their potential as markers of industrial activity.

The new interest of these compounds as tracers will be discussed, focusing on their application in several receptor models such as Chemical Mass Balance (CMB) for aerosol source apportionment and multivariate regression model for HAP source apportionment.

References

Becker, G., Colmsjö, A. and Östman, C. (1999) *Env. Sci.Tech*., 33, 1321-1327.
Lemieux, P. M., Lutes, C. C. and Santoianni, D. A. (2004) *Prog. in Energy and Comb. Sci.,* 30, 1-32.
Ni, H.-G., Lu, F.-H. and Zheng, E. Y. (2008) *Env. Sci. Tech*., 42, 1892-1897.

Physical-chemical characterization and origin of atmospheric particulate material in Cordoba City – Spain

E. García-Lorenzo[1], J.D. de la Rosa[1], A.M. Sánchez de la Campa[1,2], Y. González-Castanedo[1] and R. Fernández-Camacho[1].

[1]Associate Unit CSIC-University of Huelva "Atmospheric Pollution", CIQSO, University of Huelva, Campus El Carmen E21071 Huelva, Spain
[2] Estación Experimental del Zaidín, CSIC, C/ Profesor Albareda 1, E18008 Granada, Spain
Keywords: PM10, Atmospheric pollution, brass smelting, Ag, Source contribution.
Presenting author email: elisagarcialorenzo@gmail.es

The city of Cordoba is one of the most populated cities of the Guadalquivir Valley (Andalusia, South of Spain), exhibiting an admissible air quality as stated by the Regional Environmental Agency of Junta de Andalusia. In this work, we focuses on the Geochemistry and source contribution on PM10, in the Lepanto monitoring station (urban background) of the Air Quality Network of Andalusia.

Tourism is considered one of the most important economical activities in Córdoba. Moreover, Zn-Cu smelter and jewellery industry is localized in the western part of the city. Also, domestic furnaces of jewellery are placed in downtown of Córdoba.

Mean total mass and chemical composition of PM10 were obtained by sampling on filter using EU reference methods between 2007 and 2010. Sixty-five inorganic chemical compounds and elements were analyzed by ICP-MS (trace elements), ICP-OES (major elements), Ion Chromatography (ions) and Elemental Analysis (Ctotal) techniques. Geochemical results of PM10 in Lepanto were compared with others monitoring stations of Spain and Andalusia referenced by Querol et al (2007) and de la Rosa et al (2010). Chemical analysis of Ag were performed in PM10 at Córdoba, and compared with another urban background monitoring station (Principes) of the city of Seville. Ag can be used as a tracer of jewellery industry emissions.

The highest annual average PM10 was obtained in 2007 (44 µg/m³). This value is higher than the average value limit proposed by 2008/50/CE Directive. In the same way, the daily limit value (VLD) for this year was exceeded 26 days. During the rest of the study period, the levels decreased to meet the Directive acceptability criteria (40 µgPM10/m³ and 35 VLD, respectively).

Since annual PM10 levels and chemical composition point of view, Lepanto can be considerer as a urban background monitoring station, compared with other monitoring station of Spain (Querol et al 2007) and Andalusia (de la Rosa et al 2010). However, high geochemical anomalies of Zn (206 ng/m³), Cu (83.3 ng/m³) and Cd (0.81 ng/m³) suggest as the Córdoba is influenced by the impact of Zn-Cu smelters emissions.

Also, Ag high concentrations of Ag have been analyzed in the city of Córdoba compared with the city of Seville (urban monitoring station of Príncipes). SEM-EDS images show the presence of irregular particles of 1.5 µm size.

The contribution of the main sources to PM10 in the monitoring station was quantified by receptor modelling techniques (Thurston & Spengler, 1985) (Fig. 1). The major contributor to the total mass for PM10 (54%, 20.3 µg/m³) is the crustal source (mainly Rb, La, Li, Ca, Al_2O_3, Mg, K, Mn, C total and V), which are considered a mixture of natural and anthropogenic mineral material that is deposited in urban areas and continuously suspended by the traffic and the wind. The traffic (NH_4^+, NO_3^-, Ti, Ni and Sb) and the industrial source contribute the same mass proportion (6%, 2.2 µg/m³). The composition of the industrial source is Cu, Zn, Cd, Bi, which is coincident with the composition of Zn-Cu smelter emissions. The fourth factor that defines the PCA is the Regional, mainly composed by sulphate and V (4%, 1.4 ng/m³). And last, there is a fifth source characteristic of this zone that accounts for a 3% (1.3 µg/m³) of PM10 total mass, composed mainly of Ag and Cd. This source presents a chemical profile related with emissions from silver smelting of the jewellery industry.

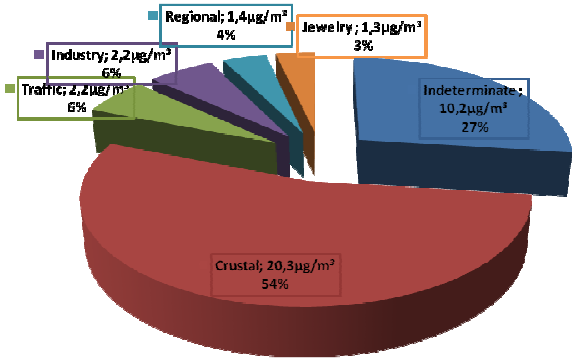

Figure 1. Source contribution to PM10 in Lepanto (city of Cordoba) during 2007-2008.

Acknowledgment
This study was supported by the Department of Innovation, Research and Enterprise of Junta de Andalusia (Projects P07-RNM-03125; P07-RNM-02729 and P11-RNM-7800).

De la Rosa et al (2010). *Atmos. Environ.* 44, 4595-4605

Querol et al (2007). *Atmos. Environ.* 41, 7219-7231.

Thurston, G. D., & Spengler, J.D. (1985). *Atmos. Environ.* 19, 9-25.

Chemical composition and microphysical parameters of fog samples in a 27 year long study in the Po Valley (Italy)

L.Giulianelli[1], M. Rinaldi[1], C. Carbone[1], S. Decesari[1], M.C. Facchini[1] and S. Fuzzi[1]

[1] Institute for Atmospheric Science and Climate (ISAC), CNR, Bologna, Italy
Keywords: chemical composition, droplets, multiphase chemistry, multiphase processes.
Presenting author email: l.giulianelli@isac.cnr.it

Fog is a multiphase system in which water droplets, aerosol particles and atmospheric gaseous species interact. This phenomenon occurs at the ground level, close to all the anthropogenic emissions which are involved in the chemical and physical transformations within the system.

The study of the fog multiphase system is an interesting topic in the area of the Po Valley (Northern Italy) due to several factors, first of all the frequency of this phenomenon during the fall-winter season. Furthermore the Po Valley is a densely inhabited region characterized by high level of pollution due to industrial and agricultural activities and intense vehicular traffic. High aerosol loading is often registered in this area. The field station of San Pietro Capofiume in the Eastern Po Valley thus represents a perfect point for the fog droplets sampling and characterization and possibly for the observation of particulate matter - fog droplets interactions.

The collection and study of fog samples began in the early 80s, Fuzzi *et al*. (1983). Initially fog droplets were sampled occasionally, then, at the beginning of the 90s field campaigns through all the fog season were carried out, Fuzzi *et al* (1992, 1996). During these field campaigns an automated sampling procedure was set up, Fuzzi *et al* (1997), and from 1997/98 the same sampling procedure has been carried out each fall-winter season until today. All these measurements allowed the collection of a nearly 30 years long database which is now available to investigate possible time trends of physical and chemical parameters, as frequency of fog events, liquid water content (LWC), acidity, chemical composition (NH_4^+, $SO_4^=$, NO_3^-, soluble organic compounds, etc.). Concentration ranges found in the Po Valley fog samples are 0.03-27.87, 0.02-16.90, 0.04-25.04 µeq/l and 2.70-163.00 mgC/l for NO_3^-, $SO_4^=$, NH_4^+ and water soluble organic Carbon (WSOC) respectively. pH values are very variable, ranging from 2.44 to 8.83.

Preliminary results of the database elaboration suggest a decreasing trend of the $SO_4^=$ concentration in the fog samples from the 80s up to now. This is consistent with the policy of reducing SO_2 emissions. Another trend regards the acidity of the samples: mean pH values are higher now than twenty years ago. During the 90s mean pH values ranged from 4.7 to 6.2, while values ranged from 5.7 to 7.1 from 2000 to 2011. Connections between these two trends will be investigated. No evident trends have been pointed out for NO_3^- and NH_4^+. Fig.1 shows the increasing trend of $NO_3^-/SO_4^=$ ratio due to the decreasing amount of $SO_4^=$ in the fog samples. WSOC and WSON (Water Soluble Organic Nitrogen) data are available since season 1997/98 and 2004/2005 respectively. The results of the elaboration of these data will be presented.

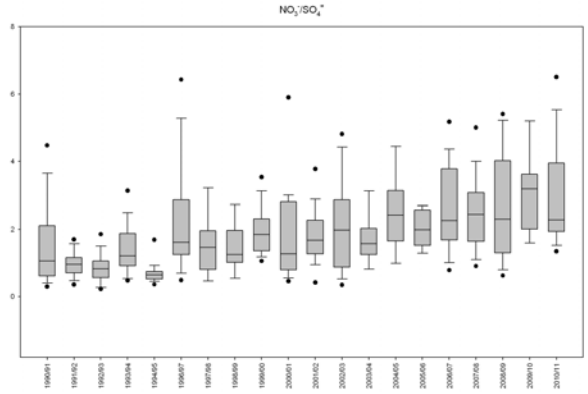

Figure 1. Increasing trend in the $NO_3^-/SO_4^=$ ratio from 1990/91 to 2010/11, due to the decreasing concentration of sulphate in fog samples.

Fuzzi, S., Orsi, G. and Mariotti, M. (1983) *J. Aerosol Sci.* **14**, 2, 135-138.

Fuzzi, S., et al. (1992) *Tellus*, **44B**, 448-468.

Fuzzi, S., et al. (1996) *Atmos. Environ.* **30**, 201-213.

Fuzzi, S., Orsi, G., Bonforte, G., Zardini, B. and Franchini P.L. (1997) *Water, Air and Soli Pollut.* **93**, 383-394.

Determination of Molecular Composition in Boreal Forest Aerosols (PM1.0), Hyytiälä, Finland using Ultra-High Resolution Mass Spectrometry

I. Kourtchev[1*], S. Fuller[1], J. Aalto[2], T. Ruuskanen[2], W. Maenhaut[3], M. Kulmala[2], and M. Kalberer[1]

[1]Department of Chemistry, University of Cambridge, Cambridge, CB2 1EW, UK
[2]Department of Physics, University of Helsinki, P.O.Box 64, Helsinki, Finland
[3]Dept. of Pharmaceutical Sciences, University of Antwerp (UA), Universiteitsplein 1, 2610 Antwerpen, Belgium

Keywords: BVOC, SOA, Ultra-High Resolution Mass Spectrometry, Elemental composition.

Presenting author email: ink22@cam.ac.uk

Biogenic volatile organic compounds (BVOCs) play an important role in atmospheric chemistry and give rise to secondary organic aerosols (SOA), which have effects on climate and human health. On a global scale, BVOCs account for about 90% of VOC emissions (Guenther *et al.*, 1995). A substantial fraction (20-90%) of atmospheric fine particulate matter is comprised of organic compounds (Kanakidou *et al.*, 2005), which cover a wide range of polarities, volatilities and masses. Our knowledge on the organic chemical composition of atmospheric aerosols is rather limited; only about 20-30% of the organic matter has been characterised at the molecular level. Because of this limitation, recent efforts have focused on methods that classify bulk organic aerosols. For instance, ultra high resolution mass spectrometry (UHR-MS) allows determination of thousands of individual organic aerosol constituents at once, providing their elemental formulae from accurate mass measurements (Nizkorodov *et al.*, 2011).

In this study, we applied UHR-MS for the analysis of the separate day and night PM_1 aerosol samples that were collected during a two week summer period (August, 2011) at a boreal forest site, SMEAR II station in Hyytiälä, southern Finland. Prior to mass spectral analysis, all aerosol samples were analysed for organic carbon (OC) and elemental carbon (EC) using a thermal optical transmittance (TOT) technique. Depending on the OC load of the aerosol sample, a portion of the filter was extracted in methanol, filtered, evaporated to dryness and resuspended in methanol – water (20:80 v/v) or acetonitrile – water (20:80 v/v) mixtures. The extracts were analysed using an LTQ Orbitrap Velos fitted with a chip-based electrospray ion source, TriVersa NanoMate®. In addition, pooled day and night samples were analysed using liquid chromatography/mass spectrometry (LC/MS). The mass spectra were recorded in positive and negative modes over the mass range *m/z* 50-1200 with a mass resolving power of 100,000 (m/Δm). Background peaks were subsequently eliminated by subtraction of peaks present in blank samples. The remaining peaks were assigned probable empirical formulae assuming that ions contain only ^{12}C, ^{1}H, ^{16}O, ^{14}N, ^{32}S and ^{23}Na (only in the positive mode).

Almost for all samples negative ionisation spectra contained significantly more ions than those of positive, and the majority of these ions were found below 350 Da. More than 1000 elemental formulae were assigned in both modes, and no apparent diel variations in the elemental compositions were observed. The majority of the peaks were attributed to oxygenated or nitrogen containing compounds. The peak assignments were examined using van Krevelen approach, which allows describing the evolution of functional groups in organic aerosol (OA). Figure 1 shows a van Krevelen diagram for a typical daytime sample from Hyytiälä, Finland.

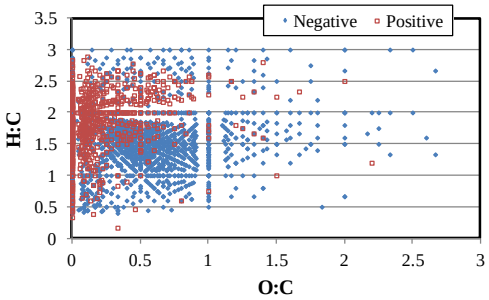

Fig. 1. Van Krevlen diagram for a typical sample collected at Hyytiälä, on 24 August, 2011. Blue and red markers corespond to data from negative and positive ion modes, respectively.

On average O:C ratio was found to be around 0.5 and 0.2 in the negative and positive modes, respectively and stayed constant throughout the sampling campaign. During two days an increased O:C ratio was observed, which could be explained by a change in the air mass back trajectories. In general, the O:C ratio was within the range obtained for SOA generated in laboratory experiments with a number of BVOCs, e.g., α-pinene (Shilling *et al.*, 2009) and isoprene (Nguyen *et al.*, 2011). The LC/MS analysis revealed more than 30 species mainly attributed to oxidation products of BVOCs (i.e., α-,β-pinene) supporting the results from the analysis of the bulk OA.

The work at the University of Cambridge was supported by a Marie Curie Intra-European fellowship (project # 254319).

Guenther, A., *et al.* (1995). *J. Geophys. Res.*, **100**, 8873-8892.

Kanakidou, M., *et al.* (2005). *Atmos. Chem. Phys.*, **5**, 1053–1123.

Nguyen, T.B., Laskin, J., Laskin, A., and Nizkorodov, S.A. (2011). *Environ. Sci. Technol.*, **45**, 6908-6918.

Nizkorodov, S.A., Laskin, J., and Laskin, A. (2011). *Phys. Chem. Chem. Phys.*, **13**, 3612-3629.

Shilling, J.E., et al. (2009). *Atmos. Chem. Phys.*, **9**, 771–782.

Nucleation and Aitken mode atmospheric particles in relation to O_3 and NO_X at semirural background in Denmark

Q.T. Nguyen[1,2], J.K. Nøjgaard[1], M. Glasius[2] and L.L. Sørensen[1]

[1]Institute for Environmental Science, Aarhus University, Roskilde, DK-4000, Denmark
[2]Department of Chemistry, Aarhus University, Aarhus, DK-8000, Denmark
Keywords: atmospheric particles, oxidants, nucleation mode, Aitken mode, source apportionment
Presenting author email: quynh@chem.au.dk

In order to study the formation, transformation and loss of atmospheric particles, it is beneficial to examine particle size distributions in relation to atmospheric oxidizing species. Atmospheric oxidants (O_3, NO and NO_2) and particle size distributions (6-700 nm) were studied at Lille Valby, a semi-rural background location in Denmark during 2009 to evaluate the sources of particulate matter. Particles were grouped into different size bins, including lower Aitken mode (< 30 nm), upper Aitken mode (30-110 nm) and accumulation mode (110-700 nm). The lower Aitken mode also covered the nucleation mode (6-19 nm).

Both upper Aitken mode particles (30-110 nm) and accumulation mode particles (110-700 nm) either showed no correlation O_3 or anti-correlated with O_3. In contrast, the lower Aitken mode particles (<30 nm), which typically peaked around noon from April to September correlated positively with O_3. This indicated that photochemistry was likely to be responsible for most of the nucleation mode particles in this period of the year (Hamed *et al.*, 2007).

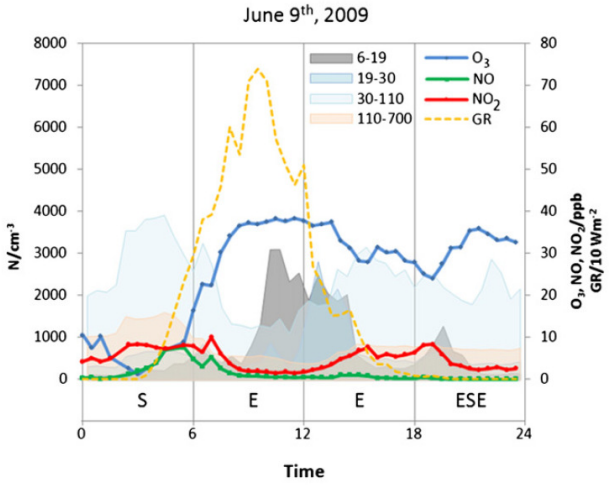

Figure 1. Diurnal plot example of atmospheric oxidants, particle number concentration according to particle mode, global radiation and wind direction.

In the months with lower global radiation (October-March), the lower Aitken mode correlated positively with NO_2, which typically showed peaks in the morning and afternoon on working days, indicating that traffic is the most important source of nucleation mode particles in that period of the year. A strong correlation was observed for Aitken mode particles and NO_2 throughout the year, which suggested a common traffic source (Hussein *et al.*, 2004; Ketzel *et al.*, 2007). Growth of Aitken mode particles was also observed during high NO_X episodes.

While photochemistry and traffic were major sources to Aitken mode particles, an additional source apportionment analysis using Constrained Physical Receptor Model (COPREM) (Wåhlin, 2003) identified Secondary Inorganic Aerosols (SIA) as the largest source to PM_{10} (36% including secondary marine aerosols) in the semi-rural background troposphere in Denmark. It was found that ammonium nitrate was a larger source than ammonium sulfate to the SIA mass fraction, where particulate nitrate exceeded that of sulfate by 2.6 times on a molar basis. Such results indicated that NO_2, as a precursor for e.g. ammonium nitrate is probably more important than SO_2, as a precursor for ammonium sulfate, in the formation of SIA. Subsequently, NO_2 from anthropogenic emissions and its following conversion to particulate nitrates thus appeared to influence semi-rural atmospheric particulate matter in both the Aitken mode and mass wise in PM_{10}.

This work is based on data from the Danish Air Quality Monitoring program and the Particle Project 2008-2010, which are financially supported by the Danish EPA.

Hamed, A., Joutsensaari, J., Mikkonen, S., Sogacheva, L., Dal Maso, M., Kulmala, M., Cavalli, F., Facchini, M.C., Decesari, S., Mircea, M., Lehtinen, K.E.J., Laaksonen, A., (2007). *Atmospheric Chemistry and Physics* **7**, 355-376.

Hussein, T., Puustinen, A., Aalto, P.P., Makela, J.M., Hameri, K., Kulmala, M., (2004). *Atmospheric Chemistry and Physics* **4**, 391-411.

Ketzel, M., Wåhlin, P., Kristensson, A., Swietlicki, E., Berkowicz, R., Nielsen, O.J., Palmgren, F., (2004). *Atmospheric Chemistry and Physics* **4**, 281e292.

Wåhlin, P., (2003). *Atmospheric Environment* **37**, 4861-4867.

Preliminary results on the characterisation of organic aerosols in urban schools by Aerosol Mass Spectrometry

L. Crilley, G. A. Ayoko, E.R. Jayaratne, L. Morawska

International Laboratory for Air Quality and Health, Queensland University of Technology, Brisbane, QLD, 4001, Australia

Keywords: Vehicle emissions, Schools, Organic aerosols

Presenting author email: leigh.crilley@qut.edu.au

Vehicle emissions have been linked to detrimental health effects with children thought to be more susceptible (See e.g., Ryan et al 2005). In an urban environment a major source of organic aerosols (OA) are vehicle emissions. The ambient concentration of OA is dynamic in nature and the use of an aerosol mass spectrometer can achieve the necessary temporal resolution to capture the daily variation of OA (Jimenez et al 2009). Currently there is a limited understanding of effects of long term exposure to traffic emissions on children's health. In the present study, we used an aerosol mass spectrometer to monitor OA and determine children's potential exposure at school to traffic emissions.In this paper, we present the preliminary results of this investigation. The study is a part of a larger project aimed at gaining a holistic picture of the exposure of children to traffic related pollutants, known as UPTECH (www.ilaqh.qut.edu.au/Misc/UPTECH%20Home.htm).

A compact time-of-flight aerosol mass spectrometer (AMS) was operated at four schools in different suburbs in Brisbane, Australia (S01, S04, S11 and S12). The AMS was housed within a classroom and the outdoor air was sampled using a minimum length of tubing. Sampling was carried out for 2 weeks at S01, S11 and S12 and for 3 weeks at S04. Sampling interval was 5 minutes alternating equally between PTOF and MS modes. The AMS was calibrated for ion efficiency (IE) and particle size at the beginning of the sampling and the IE calibrations also done in the middle and at the end of sampling. AMS data analysis was conducted using the standard software (Squirrel v1.51 in IGOR Pro v6.22).

The average diurnal variation of the total organic concentration for each school was determined. In general during school hours (9am – 3pm) the concentrations were lower compared to the rest of the day at all four schools. Peaks in the concentration of OA were observed in the morning around 6-8am and in the evening around 8pm at each school with varying intensities.

The diurnal variation observed at S04 (Figure 1) and S11 showed a large peak in morning and a smaller peak in the evening. The morning peak would suggest a traffic influence as it coincides with peak morning traffic. The average mass spectrum at this time for both schools more resembled the hydrocarbon-like organic aerosol (HOA) as described in Ng et al (2010). However, the m/z 44 was found to have a mass similar to that for m/z 41 and 43, which meant that the aerosols were partially oxidised and so were not fresh traffic emissions. Notably, there was no peak observed at around 5-6pm as would be expected due to peak evening traffic. Instead the evening peak was observed later and with different oxidation levels. At S04 it had a similar spectrum to the morning peak, which further suggests that this was due to slightly aged traffic emissions. At S11 the spectra was more like low-volatility oxygenated organic aerosols (LV-OOA) (Ng et al. 2010) meaning that this peak can be attributed to an increase in aged and highly oxidised OA concentration.

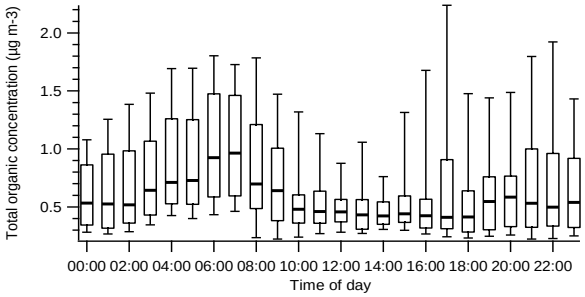

Figure 1: Average diurnal variation of total organic concentrations for S04.

In S12 the dominant peak was in the evening and these OA were LV-OOA in nature and so were highly aged and oxidised. The presence of m/z 60 and 73, which are attributed to levoglucosan, a marker for biomass burning (Ng et al 2011) means that the origin was biomass burning. At S01, there was little variation observed apart from a very large peak that was observed at 7am and we suspect that this was due to the use of fuel powered gardening equipment, possibly a leaf blower at the school.

At each school the lowest concentrations of OA were observed during school hours with peaks associated with traffic occurring outside school hours, which would indicate that, at these schools, children had limited direct exposure to traffic emissions during the sampling period.

The authors would like to acknowledge all the members of the UPTECH team, especially Dr Mandana Mazaheri. This work was supported by the Australian Research Council, Department of Transport and Main Roads (DTMR) and Department of Education, Training and the Arts (DETA) through Linkage Grant LP0990134.

Jimenez, J.L., et al., (2009) *Science*, 326, 1525-1529.

Ng, N.L., et al., (2010) *Atmos. Chem. Phys.*, 10, 4625-4641.

Ng, N.L., et al., (2011) *Environ. Sci. Technol.*, 45, 910-916.

Ryan, P.H., et al., (2005) *J Allergy Clin Immunol*, 116, 279-284.

Pb isotope of atmospheric aerosols in the Iberian Pyrite Belt, SW Spain

J. de la Rosa[1], A.M. Sánchez de la Campa[1], Y. González-Castanedo[1], J.C. Fernández Caliani[1], A. Romero[2], I. González-Díez[2]

[1]University of Huelva, Joint Research Unit to CSIC "Atmospheric Pollution", CIQSO, Campus El Carmen, E21071 Huelva, Spain.

[2]Departamento de Cristalografía, Mineralogía y Química Agrícola. Universidad de Sevilla, Sevilla, Spain.

Keywords: Pb isotope, PM10, Geochemistry, Iberian Pyrite Belt

Presenting author email: jesus@uhu.es

Pb isotopes have been using as an interesting tool in order to trace the sources and distribution of atmospheric aerosols and their impact in the environment (Chow and Johnstone 1965). Combustion of leaded gasoline, mining and smelting are the main sources of Pb in the air.

In this work, we present preliminary analyses of Pb isotopes ($^{206}Pb/^{207}Pb$ and $^{208}Pb/^{206}Pb$) of atmospheric aerosols (PM10) in the Iberian Pyrite Belt (IBP, SW Spain), in which isotope ratios can be used as a fingerprint of sources, and may discriminate the impact of the abandoned mining waste in the air.

IBP is considered as one of the most important mining district of the world, displaying geochemical anomalies of Cu, Zn, Pb and As among other toxic elements.

Since March 2009, a sampling of PM10 is performed using MCV high-volume captors (1-2 samples every week) in the town of Nerva (IBP) (3,000 inhabitants). Sampling and geochemical analysis of major and trace elements and compounds are described in Sánchez de la Campa et al. (2011).

Geochemical analyses of PM10 (op.cit.) have permitted the quantification of the contribution of resuspended particles from mining waste in the air, which can contribute toxic elements (e.g. Bi, As, Cu, pb, Cd, Zn and Sb). Town placed around the abandoned mining centres can receive the impact of those toxic elements.

The lead isotope analyses were done using ICP-MS (Agilent 7700) technique. Previously, filters were digested using a mixing of HF and HNO3 (see details Querol et al. 1999). Calibration of the ICP was done using a standard solution of NIST-981. During the calibration the masses 206, 207 and 208 were determined, with a R.S.D better than 1%. To monitor the drift of the ICP-MS, the standard solution (NIST-981) was analysed between batches of samples..

Marcoux (1998) has analyzed Pb isotope ratios from the main sulphide deposits in the Iberian Pyrite Belt. These analyses have been plotted in a $^{208}Pb/^{206}Pb$ vs $^{206}Pb/^{207}Pb$ diagram of PM10 with representative samples of atmospheric aerosols of Nerva, Iberian Peninsula aerosols (Bollhöfer and Rosman, 2001) and petrol aerosols (Erel et al., 1997). We have classified the aerosols from Nerva taking in account the air masses origin using backtrajectory analysis of HYSPLIT software (Draxler and Rolph, 2003). Under the influence of saharian air masses, the aerosols display an isotope signature similar to petrol aerosols. However, under scenarios of Atlantic air masses, the aerosols show similar isotope ratios than IPB rocks.

Atmospheric aerosols can be incorporated in the water by precipitation, modifying the isotope composition of water (Fernández et al. 2005). This conclusion is supported by the similar isotope composition of groundwater samples (op. cit.) and PM10 in the IPB.

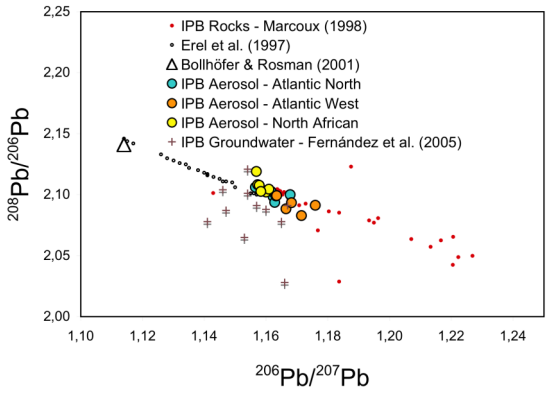

Fig. 1.- Pb isotopes diagram of IPB samples.

This work was supported by Spanish Ministry of Science and Innovation (Projects CGL2008-06270-C02-02/CLI and CGL2011-28025) and the Department of Innovation Research and Enterprise of Junta de Andalucia (Project 2009-RNM5163).

Bollhöfer, A., Rosman, K.J.R. (2001) *Geochim. Cosmochim. Acta* **65**, 1727-1740.

Chow, T. J., Johnstone, M.S. (1965) *Science* **147**, 502-503.

Draxler, R.R. and Rolph, G.D. (2003). HYSPLIT Model Access via NOAA ARL READY Website. available at. http://www.arl.noaa.gov/ready/hysplit4.html

Erel, Y.l., Veron, A., Halicz, L. (1997) *Geochim. Cosmochim. Acta* **61**, 4495-4505.

Fernández, I., Olías, M., Cerón, J.C., and de la Rosa, J.D. (2005) *Env. Geol.* **47**, 197-204.

Marcoux, E. (1998) *Min. Dep.* **33**, 45-58.

Querol, X, Alastuey, A., Puicercus, J.A., Mantilla, El, Miro, J.V., López Soñer, A, Plana, F., Artiñano, B. (1999) *Atm. Env.* **32**, 1963-1978.

Sánchez de la Campa, A.M., de la Rosa, J.D., Fernández-Caliani, JlC., González-Castanedo, Y. (2011) *Env. Res.* **111**, 1018-1023.

Metals and trace element characterization of weather condition - air quality relationships due to event based measurements of particulate matter

Silvia Leise, Frank Zimmermann, Jörg Matschullat

Interdisciplinary Environmental Research Center, Technische Universität Bergakademie Freiberg, Brennhausgasse 14, D-09599 Freiberg, Germany
Keywords: Aerosol chemistry, air quality, weather conditions, trace elements
Presenting author email: silvia.leise@ioez.tu-freiberg.de

The chemical composition of the atmosphere and the involved processes depend partly on temperature and humidity besides other meteorological conditions like mixing layer height. Consequently, climate change will affect the future composition of the atmosphere (Hedegaard et al. 2008). Atmospheric circulation has a major effect on air quality by controlling local meteorological conditions (Flocas et al. 2009). One of the most relevant air pollutants is particulate matter (PM). The effect of changing meteorological parameters on aerosols furthermore depends on the PM component (Jacob et al. 2009). PM from natural sources such as secondary organic aerosol or crust material is believed to be influenced much more by changing weather conditions (Carslaw et al. 2010) than by anthropogenic aerosols. We already showed the relation of air quality in Eastern Germany to large scale weather patterns in a study of a ten year time series of PM data (EAC 2011),. The intensity of the relationship strongly seems to depend on the type of air pollutant.

The ongoing study aims to characterize the aerosol composition at three different sites (DD (112m asl.): urban background, M (87m asl.) and OBB (735m asl.): rural) in Eastern Germany. Three five-stage LPI cascade impactors are used to collect size segregated aerosol samples on an event basis. At all three sites 24 hour samples are taken concurrent depending on the large scale synoptic weather conditions. Samples are analyzed by ICP-MS on metals and trace elements. This study focuses on crust elements and trace metals.

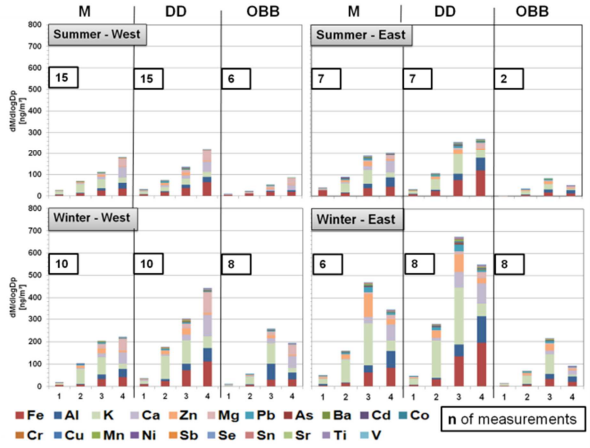

Fig. 1: Overview of element concentrations for the three sites M, DD and OBB. Four stages are taken into account (0.049 – 3.5 µm). Categories are based on the calculation of 96 hour backward trajectories

First results show that the magnitude of the correlation of PM compounds and weather patterns differs. Similar characteristics can be seen for all three sites (Fig. 1). In general, the summer categories are less polluted than the winter categories, due to more stable weather conditions (inversions) and due to additional sources in winter half year (heating period). Categories with air masses from eastern directions (continental air masses) are more polluted. The winter-east category shows higher concentrations for the third stage, which is likely due to a longer residence time of the aerosols in the atmosphere during this category.

Yet, particles in the accumulation mode show a stronger differentiation between the different weather patterns than fine or coarse particles. Large-scale synoptic weather patterns have a stronger influence on particles affected by long-range transport. The dependency of PM components to weather patterns is strongly related to sources and transport pathways of the components. Compounds that are dominated by local sources such as Ni or Cr, demonstrate almost no segregation between the weather patterns. Compounds like As, Zn or Pb demonstrate a stronger dependency. Crustal elements like Al, Fe or Ti are also influenced by air mass origin.

Carslaw K.S., Boucher O., Spracklen D.V., Mann G.W., Rae J.G.L., Woodward S., Kulmala M. (2010) A review of natural aerosol interactions and feedbacks within the Earth System. Atmos. Chem. Phys.10: 1701-1737

Flocas H., Kelessis A., Helmis C., Petrakakis M., Zoumakis M. and Pappas K. (2009) Synoptic and local scale atmospheric circulation associated with air pollution episodes in an urban Mediterranean area. Theoretical and Applied Climatology 95: 265-277

Hedegaard G.B., Brandt J., Christensen J.H., Frohn, L.M., Geels C., Hansen K.M., Stendel M. (2008) Impacts of climate change on air pollution levels in the Northern Hemisphere with special focus on Europe and the Arctic. Atmos. Chem. Phys. 8: 3337-3367

Jacob D.J. and Winner D.A. (2009): Effect of climate change on air quality. Atmos. Environ. 43: 51-63

EAC 2011: Leise S., Hoy A., Zimmermann F., Matschullat J.: Weather condition – air quality relationships in Eastern Germany (1999 – 2009). Manchester

Acknowledgement: We are very thankful to BMBF for their support of the authors within the REGKLAM project (support code: 01LR0802C).

Characterization of humic-like substances (HULIS) in size segregated atmospheric aerosol

G. Kiss[1], N. Törő[2], A. Hoffer[1], J. Dautovic[3], S. Frka[3], Z. Kozarac[3], M. Harir[4], P. Schmitt-Kopplin[4,5]

[1]Air Chemistry Group of Hung. Acad. Sci. at University of Pannonia, Egyetem 10, 8200 Veszprém, Hungary
[2]University of Pannonia, Dept. Earth and Environmental Sciences, Egyetem 10, 8200 Veszprém, Hungary
[3]Rudjer Bošković Institute, Division for Marine and Environmental Research, Bijenička 54, 10000 Zagreb, Croatia
[4]Helmholtz Center Munich, German Research Center for Environmental Health, Analytical BioGeoChemistry, Ingoldstädter Landstraße 1, D-85764 Neuherberg, Germany
[5]Lehrstuhl für Chemische-Technische Analyse und Chemische Lebensmitteltechnologie, Technische Univ. München, Weihenstephaner Steig 23, 85354 Freising-Weihenstephan, Germany

Keywords: aerosol, HULIS, size distribution, chemical properties
Author email: kissgy@almos.uni-pannon.hu

Humic-like substances (HULIS) constitute a considerable fraction (often the majority) of the water-soluble organic matter present in atmospheric aerosol. Consequently, this complex organic mixture significantly influences the physical and chemical properties of the aerosol particles as well as their biological effects. Several studies have dealt with the sources and characterisation of humic-like substances leading to considerable knowledge on their potential formation mechanism, elemental composition, molecular weight range, spectroscopic features, higroscopicity, CCN ability, etc. However, information on the size distribution of HULIS is very limited (Peng et al., 2010) although knowledge of this feature provides important information on possible sources and formation mechanisms in the atmosphere.

In this work humic-like substances isolated from aerosol particles of different size ranges were characterized. Aerosol samples were collected in the 0.0625-16 μm size range with an 8-stage Berner impactor at a rural site (K-puszta) in Hungary, an urban site (Zagreb) and a coastal site (Martinska) in Croatia. Humic-like substances were isolated from the aqueous extracts of each stage and their carbon content was determined by TOC analysis. The UV absorbance and fluorescence properties as well as the mass spectra of the constituents of the aqueous extracts and those of the isolated HULIS were studied. Approximately 90% of fluorescing compounds (EX=235nm/EM=410nm) were found in the 0.0625-1 μm size range which indicated that humic-like substances occurred in the fine fraction. This was confirmed by the results of carbon analysis and mass spectrometric investigations: the mass spectrum of the organic matter isolated from the particles in the 0.0625-1 μm size range resembled that of humic-like substances while the mass spectrum of the low amount of organic matter isolated from bigger particles differed significantly. Specific UV and fluorescent properties indicated that the chemical composition of particles within the 0.0625-1 μm size range is diverse. In order to confirm this finding the isolated humic-like substances were analyzed by ultra high resolution mass spectrometry (FT-ICR-MS). Elemental composition (obtained from FT-ICR-MS), UV absorbance and fluorescent properties of HULIS isolated from aerosol particles of different sizes will be shown for aerosol samples collected at different sites.

Peng L., Xiao-Feng H., Ling-Yan He., Jian Z. Yu (2010) J. Aerosol Sci., 41 (1), 74-78.

This research was partially funded by the bilateral intergovernmental Croatian – Hungarian research project “Complex investigation of organic aerosols in rural, urban and marine environment“ and the EU FP 6 project EUSAAR (Contract No RII3-CT-2006-026140).

A multi-tracer approach to better understand Secondary Organic Aerosol sources and (trans)formation processes in the Mediterranean region

J. B. Nicolas[1], J. Sciare[1], R. Sarda-Estève[1], N. Mihalopoulos[2], G. Kouvarakis[2] and F. Dulac[1]

[1]Laboratoire des Sciences du Climat et de l'Environnement (LSCE), CNRS-CEA, Gif-sur-Yvette, 91191, France
[2]Environmental Chemical Processing Laboratory (ECPL), Univ. of Crete, Heraklion Voutes, Greece
Keywords: SOA, oxalate, methanesulfonate, Aethalometer model, Mediterranean region.
Presenting author email: jose.nicolas@lsce.ipsl.fr

The Mediterranean region exhibits amongst the highest Particulate Matter (PM) loadings in Europe (Putaud *et al.*, 2010), inducing complex effects on regional climate, air quality and possibly on human health. Thus, a better understanding of PM sources and properties in this area is compulsory, since recent studies have shown it is one of the most sensitive regions to world climate changes.

Secondary Organic Aerosol (SOA) represents one of the major part of fine PM. Its origins and concentrations are still hardly predictable, pointing out the need for a better characterization of SOA in the Mediterranean, focusing on their sources and (trans)formation processes.

A 2-month field experiment (Sept-Oct 2011) was performed in the Eastern Mediterranean at the Finokalia atmospheric station (Crete Island, Greece), within ChArMEx (the **Ch**emistry-**Aer**osol **M**editerranean **Ex**periment) and ACTRIS (**A**erosols, **C**louds, and **T**race gases **R**esearch **I**nfra**S**tructure network) projects. A multi-tracer approach was carried out during this campaign, when photochemistry offers conditions to investigate different oxidation states of SOA.

Methodology

Fine aerosol ($PM_{2.5}$) real-time measurements of Organic Carbon (OC) and Water-Soluble Organic Carbon were performed by EC-OC Sunset field (every 2 hours) and PILS-TOC (every 4 min) instruments. Submicron measurements of major anions (sulfate, nitrate, chloride) and specific organic tracers (oxalate, methanesulfonate) were obtained every 12 min by a PILS-IC technique.

Co-located Black Carbon (BC) measurements were conducted with a 7-λ Aethalometer (Magee Scientific) enabling to separate the BC of wood burning origin from the fossil fuel fraction.

Filter samples (R&P Partisol Plus; every 6 hours) and liquid vials (BMI-PILS; every 30 min) were also collected in order to provide complementary organic speciation (by LC-MS/MS), tracing in particular wood burning and biogenic emissions.

Results

Co-variations were observed between oxalate and sulfate (Fig.1), and between oxalate and OC (Fig.2), indicating the major role of in-cloud processing in the formation of SOA (Yu *et al.*, 2005).

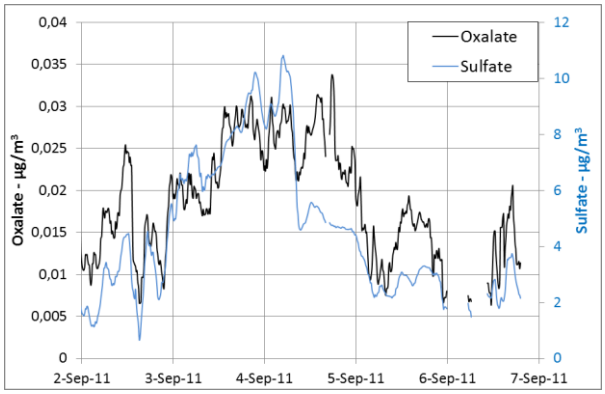

Figure 1. Co-variations between oxalate and sulfate.

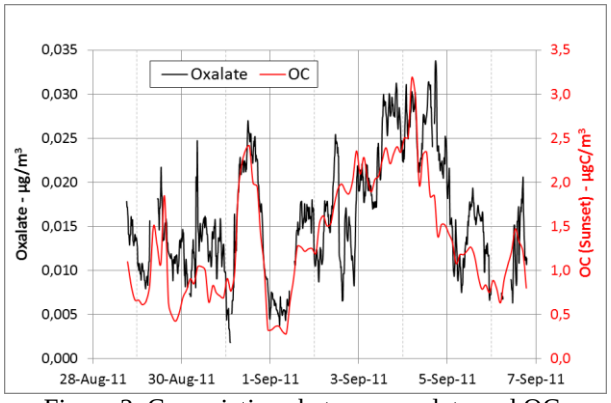

Figure 2. Co-variations between oxalate and OC.

These results will be compared with those from similar observations to be performed in the Western Mediterranean (Corsica Island) in summer 2012. It will allow us to investigate the differences between the two basins in terms of biogenic/anthropogenic sources and atmospheric processes, which are expected to be significant providing the major discrepancies observed in their fine aerosol compositions (Nicolas *et al.*, 2011).

This research was funded by ChArMEx, EU-FP7-ACTRIS (2011-2015), ADEME, CNRS and CEA. The FORTH (Heraklion and Patras) teams are thanked for their help and collaborative work during the campaign.

Nicolas J. B., Loÿe-Pilot M.-D., Cachier H., Sciare J., Oikonomou K., Mihalopoulos N. and Dulac F. (2011) *EAC Manchester*.

Putaud J.-P. *et al* (2010) *Atmospheric Environment* **44,** 1308-1320.

Yu J. Z., Huang X.-F., Xu J. and Hu M. (2005) Environ. Sci. Technol. **39**, 128-133.

Size-resolved measurement of the mixing state of soot in the megacity Beijing, China: diurnal cycle, aging and parameterization

Y. F. Cheng[1,2,7], H. Su[3], D. Rose[3], S. S. Gunthe[3], M. Berghof[2], B. Wehner[2], P. Achtert[2], A. Nowak[2], N. Takegawa[4], Y. Kondo[5], M. Shiraiwa[3], Y. G. Gong[6], M. Shao[1], M. Hu[1], T. Zhu[1], Y. H. Zhang[1], A. Wiedensohler[2], M. O. Andreae[3], and U. Pöschl[3]

[1]College of Environmental Sciences and Engineering, Peking University, Beijing 100871, China
[2]Leibniz Institute for Tropospheric Research, Leipzig, Germany
[3]Biogeochemistry Department, Max Planck Institute for Chemistry, Mainz 55020, Germany
[4]Research Center for Advanced Science and Technology, the University of Tokyo, Tokyo, Japan
[5]Department of Earth and Planetary Science, Graduate School of Science, the University of Tokyo, Tokyo, Japan
[6]Research Institute of Chemical Defence, Beijing 102205, China
[7]Center for Global and Regional Environment Research, University of Iowa, IA 52242, USA
Keywords: Black carbon, condensation, emissions
Presenting author email: h.su@mpic.de

Soot particles are regarded as the most efficient light absorbing aerosol species in the atmosphere, playing an important role as a driver of global warming. Their climate effects strongly depend on their mixing state, which significantly changes their light absorbing capability and cloud condensation nuclei (CCN) activity. Therefore, knowledge about the mixing state of soot and its aging mechanism becomes an important topic in the atmospheric sciences.

The size-resolved (30–320 nm diameter) mixing state of soot particles in polluted megacity air was measured at a suburban site (Yufa) during the CAREBeijing 2006 campaign in Beijing, using a Volatility Tandem Differential Mobility Analyzer (VTDMA). Particles in this size range with non-volatile residuals at 300 ℃ were considered to be soot particles. On average, the number fraction of internally mixed soot in total soot particles (*F*in), decreased from 0.80 to 0.57 when initial *D*p increased from 30 nm to 320 nm. Further analysis reveals that: (1) *F*in was well correlated with the aerosol hygroscopic mixing state measured by a CCN counter. More externally mixed soot particles were observed when particles showed more heterogeneous features with regard to hygroscopicity. (2) *F*in had pronounced diurnal cycles. For particles in the accumulation mode (*D*p at 100–320 nm), largest *F*in were observed at noon time, with apparent turnover rates ($k_{ex \rightarrow in}$) up to 7.8% h^{-1}. (3) *F*in was subject to competing effects of both aging and emissions. While aging increases *F*in by converting externally mixed soot particles into internally mixed ones, emissions tend to reduce *F*in by emitting more fresh and externally mixed soot particles. Similar competing effects were also found with air mass age indicators. (4) Under the estimated emission intensities, actual turnover rates of soot ($k_{ex \rightarrow in}$) up to 20% h^{-1} were derived, which showed a pronounced diurnal cycle peaking around noon time (Fig. 1). This result confirms that (soot) particles are undergoing fast aging/coating with the existing high levels of condensable vapors in the megacity Beijing. (5) Diurnal cycles of *F*in were different between Aitken and accumulation mode particles, which could be explained by the faster size shift of smaller particles in the Aitken mode.

To improve the *F*in prediction in regional/global models, we suggest parameterizing *F*in by an air mass aging indicator, i.e., $F\text{in} = a + bx$, where *a* and *b* are empirical coefficients determined from observations, and *x* is the value of an air mass age indicator. At the Yufa site in the North China Plain, fitted coefficients (*a*, *b*) were determined as (0.57, 0.21), (0.47, 0.21), and (0.52, 0.0088) for *x*(indicators) as $[NO_z]/[NO_y]$, [E]/[X] ([ethylbenzene]/[m,p-xylene]) and ([IM] + [OM])/[EC] ([inorganic + organic matter]/[elemental carbon]), respectively. Such a parameterization consumes little additional computing time, but yields a more realistic description of *F*in.

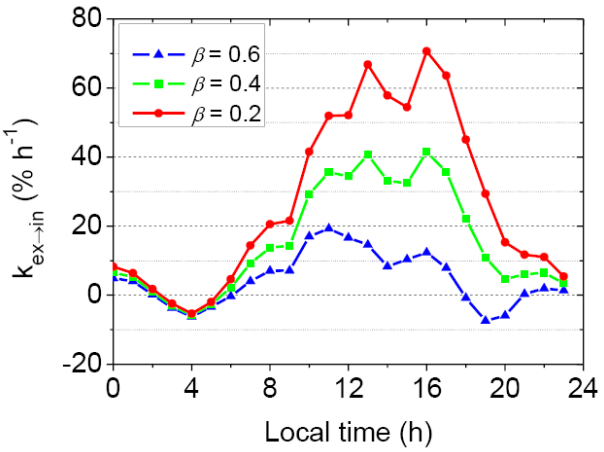

Fig. 1: The actual turnover rate of soot, $k_{ex \rightarrow in}$, under different emission factor β (number fraction of internally mixed soot particles to total soot particles).

This work was supported by PEGASOS (No. 265148) and EUCAARI (No. 036833-2).

Cheng et al (2012) Size-resolved measurement of the mixing state of soot in the megacity Beijing, China: diurnal cycle, aging and parameterization, *Atmos. Chem. Phys. Discuss.*, 11, 32161-32204, doi:10.5194/acpd-11-32161-2011, 2011.

Impact of urban atmospheric aerosols on cultural heritage objects of Granada, Southern Spain

C. Cardell[1], M. Urosevic[1], B. Horemans[2], V. Kontozova-Deutsch[2], S. Potgieter-Vermaak[2], E. Sebastián-Pardo[1] and R. Van-Grieken[2]

[1]Department of Mineralogy and Petrology, University of Granada, Campus Fuentenueva s/n, 18071 Granada, Spain
[2]Department of Chemistry, Environmental Analysis Group, University of Antwerp, Universiteitsplein 1, BE-2610 Antwerp, Belgium
Keywords: aerosol chemistry, air pollution, indoor/outdoor particles, carbonaceous particles.
Presenting author email: cardell@ugr.es

This research aimed to identify major atmospheric pollutant risks on selected cultural heritage items (limestone, polychromes) in the city of Granada (Southern Spain) with respect to their *preventive conservation*. This nowadays popular approach to safeguard our cultural heritage involves to characterize the historical item itself, monitoring its microclimatic and atmospheric exposure conditions, and to study the interactions at the interface aerosol-item substrate. In this context we have performed two types of field measurements: a) indoor and outdoor air quality was assessed in La Alhambra and Generalife located on top of the Sabika hill overlooking the city of Granada, and the monastery of San Jerónimo placed in the city center of Granada and surrounded by busy streets; b) a two-year term ageing test performed on a building limestone used in monuments and civil buildings in Granada, under different urban conditions to assess its cultural heritage sustainability with respect to its black soiling process.

Valuable information about concentrations of atmospheric gaseous pollutants as well as chemical and mineralogical composition, size, and morphology of particulate matter, their concentration, trends, major sources and the threatening effects on the artwork items is provided and discussed. Complementary micro- and nano-analytical techniques were applied to chemically characterize the pollutants: ion chromatography (IC) and UV-Vis spectrophotometry for analyzing gases, and electron probe microanalysis (EPMA), scanning electron microscopy with energy-dispersive X-ray analyzer (SEM-EDX), transmission electron microscopy (TEM), X-ray Fluorescence (XRF), X-ray diffraction (XRD), Raman microscopy (RM) and the novel tandem technique EPMA-RM for characterizing bulk and single particles. The soiling process (surface blackening) was monitored through lightness and chroma changes using colorimetry and spectrophotometry techniques.

Results reveal that soil dust particles (aluminosilicates, calcite, dolomite, quartz and clay minerals from the surrounding geological materials) and soot particles (black carbon) are the most abundant particles in the Granada air, intensifying stones and paintings darkening. Sea salts (chlorides) reacting with the urban atmosphere produce a mixture of particulates with diverse chemical composition (aged salt particles such as Na-nitrates, sulfates and ammonium-rich salts) that further promote discoloration of polychromes through mineral transformation, as noticed in the Alhambra artworks. Also fly ash particles (Si-Al rich) were found and the contribution of Saharan dust events to the composition of the mineral aerosol content. Blackening of surface decorative materials is fostered by particle re-suspension due to improper cleaning habits in the monastery of San Jerónimo, and cultural events and detailed curvatures and relief in the Alhambra polychromed artworks which results in uneven blackening (more offensive than a gradual blackening). Heave metals were found to originate from diesel exhaust (V and Ni) and tire tread emissions (Cu, Cr, Pb and Zn). High summer concentrations for O_3 (up to 229 $\mu g.m^{-3}$) were detected at the Alhambra differently to lower O_3 levels in the monastery of San Jerónimo in winter. Here average NO_2 concentration (32 $\mu g.m^{-3}$) is higher than in the Alhambra monument (15.4 $\mu g.m^{-3}$).

Black carbon (BC) concentration is around an average of 2$\mu g.m^{-3}$ (ranging from 0 to 15$\mu g.m^{-3}$) inside the Alhambra and the Gate of Pomegranates, the original access to the monument closed to traffic at present. BC concentration is expected to rise up to 8$\mu g.m^{-3}$, as found at a similarly steep and nearby street, with dense traffic in the Albayzín (values = 1 to 23$\mu g.m^{-3}$).

On limestones exposed to the Granada urban air, black soiling and gypsum crust formation were noticed after the first year of exposure. The effective area coverage, EAC, surpassed the 2% value considered to be the limit perceptible for the human eye (values ranging from 7.8 to 20.4%). The calculated soiling coefficient based on BC concentration was $8.0–9.9\times10^{-3}$ $days^{-1/2}$ $\mu g^{-1/2}m^{3/2}$, which are comparable to values obtained for other limestones placed in urban conditions in Atlantic and continental climates. This type of research should help restorers to be aware of the most vulnerable areas for architectural stones and polychromed artworks in polluted cities. Also these data can be potentially used as a first approximation for planning efficient cleaning policies and to define targeted strategies with respect to traffic access.

This work was supported by research group RNM-179 (CICE, JA, Spain), bilateral Hispano-Flemish project BOF-UA, 2008-2013 and 'Patronato de la Alhambra y Generalife'.

Characterisation of nasal spray drug delivery

K.Inthavong[1], M.C.Fung[1], W.Yang[2] and J.Y. Tu[1]

[1]School of Aerospace, Mechanical, Manufacturing Engineering, RMIT University, Bundoora VIC, 3065, Australia
[2]Division of Minerals, CSIRO, Clayton, 3168, VIC, Australia
Keywords: drug delivery, atomisation, nasal spray.
Presenting author email: kiao.inthavong@rmit.edu.au

A commercial nasal spray device was tested under a constant flow in order to better understand its spray formation and characteristics. External characteristics such as the spray cone angle define the shape of the atomized spray that exits from the device, while the internal characteristics such as the droplet size distribution help to determine the likelihood of inertial impaction within the nasal cavity. The experimental method makes use of particle image velocimetry (PIV) and particle/droplet image analysis (PDIA) to obtain droplet diameters and spray velocities in different spray regions. Image processing techniques were applied to enhance visualization and a droplet concentration field.

Figure 1 shows an image at the near-nozzle region. The liquid is forced through the nozzle orifice under the action of a swirling centrifugal force. The interaction between the swirling liquid sheet and the surrounding air creates instabilities in the form of rapidly propagating waves produced on the liquid surface.

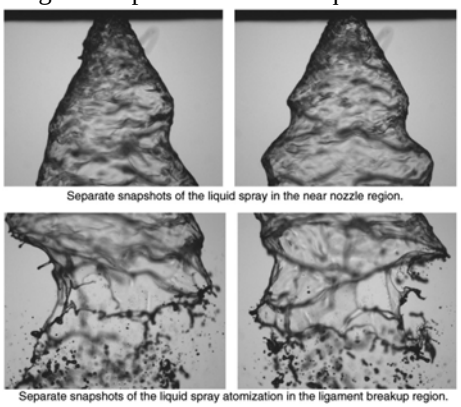

Figure 1. Two sets of images separated by in time showing the spray particle formation at the near-nozzle region and at the ligament breakup region

The spray outline shows the liquid oscillating in a sinusoidal pattern. Also on the surface, the liquid has sinusoidal wave patterns, suggesting the movement of the liquid '*rolling*' downstream in waves. The growth and amplitude of these waves are thought to be a function of the surface tension, aerodynamic forces, and liquid viscosity (Dombrowski and Johns 1963), and the sheet disintegrates into ligaments once the unstable waves reach a critical amplitude.

Time dependent spray formation was also captured which shows the swirling action of the spray as it is atomised (Figure 2) and the four modes described by Lefebvre (1989) can be seen.

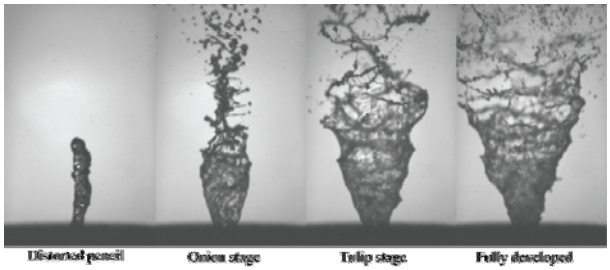

Figure 2 Spray development stages of nasal spray device

The results can be applied through Computational Fluid Dynamics (CFD) for a practical pharmaceutical application. A computational model of a human nasal cavity is used and initial conditions of the droplets described based on the shape of the measured spray plume are applied. By tracking the droplets, the wall deposition patterns and the spatial locations of the droplets as they pass through cross-sectional slices labeled A to D can be shown. Injection angles, 90 , and 45, are evaluated. The results in Figure 3 showed that the spray plume maximum length reached 47 mm for an injection angle of 30.

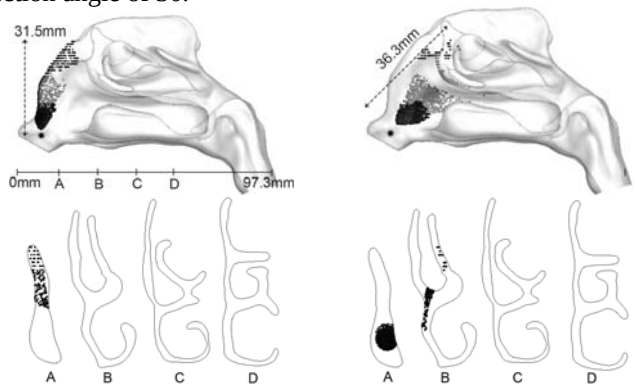

90° spray injection 45° spray injection

Figure 3 Visualisation of the unaffected experimental spray placed inside a human nasal cavity model. 100µm particles are delivered just inside the nasal cavity. Subsequent particle deposition onto nasal cavity walls are marked with small black dots.

This work was supported by the Australian Research Council under the Discovery Project ID: DP120103958.

Dombrowski, N. and W. R. Johns (1963). "The aerodynamic instability and disintegration of viscous liquid sheets." Chemical Engineering Science 18(3): 203-214.

Lefebvre, A. H. (1989). Atomization and Sprays, Hemisphere Publishing Corporation.

Evolution of droplet size distribution during nebulization of liposomes

T.R. Sosnowski

Faculty of Chemical and Process Engineering, Warsaw University of Technology,
Waryńskiego 1, 00-645 Warsaw, Poland
Presenting author email: t.sosnowski@ichip.pw.edu.pl

Aerosolized liposomes can be used as drug carriers in inhalation drug delivery to improve drug transfer to the cells and/or provide a method for the sustained drug release (e.g., Zaru et al. 2007). The droplets of colloid which contain drug encapsulated in liposomes can be generated by a variety of nebulizers, providing that the vesicles are not considerably destructed by atomization.

This study is focused on analysis of the evolution of size distribution of droplets released from liposome colloids using selected pneumatic and vibrating-mesh nebulizers.

Multilamellar liposomes were prepared by hydration of lipid film formed after solvent evaporation from lecithin/chloroform solution (10 mg/ml). The lipid film was hydrated with water (15 ml) to form large multilamellar vesicles (up to a few μm in size as observed microscopically). The resulting colloid was sprayed using MP1 pneumatic nebulizer (Medbryt, Poland) with RF6 nebulizing head (Flaemnouva, Italy) or using two types of vibrating-mesh devices: Aeroneb-Pro (Aerogen Inc., Ireland) and e-Flow Rapid (Pari, Germany). Droplet size distribution and its evolution with the nebulization time was measured using Spraytec diffraction spectrometer (Malvern, UK) with the inhalation cell operated at the 10 L/min airflow. The results obtained for liposome colloid were compared to the distributions measured for water. All experimental runs were triplicated.

Temporal evolution of the volume median diameter (VMD, i.e. Dv50) of droplets emitted from tested nebulizers are shown in Figure 1a-1c. For each vibrating-mesh device, the aerosol produced from liposome colloid is composed of smaller droplets than the aerosol formed of pure water. It can be explained by the fact that the colloidal system contains lecithin which is surface active while a decrease of surface tension promotes formation of finer droplets in such atomization systems (Sosnowski & Żołądkowicz, 2011). Size of droplets produced by Aeroneb from the liposome colloid is slightly decreasing with time, probably as a result of partial disruption of large vesicles what increases the concentration of free lecithin in the liquid and further lowers the surface tension. Such effect is not observed for e-Flow nebulizer, where the dominating effects may be attributed to droplet coalescence at the mouthpiece of this high-output device. In case of pneumatic nebulizer, VMD of water droplets slightly increases with time due to liquid cooling which is related to the rise of liquid viscosity and surface tension.VMD remains stable for the liposome colloid atomized with jet device as cooling effects may be compensated by the surface tension reduction due to increased content of lecithin liberated from vesicles. Observed differences in the quality of aerosol produced from liposome colloids by various nebulizers may be useful in the optimization of the inhalation delivery of liposome-encapsulated drugs.

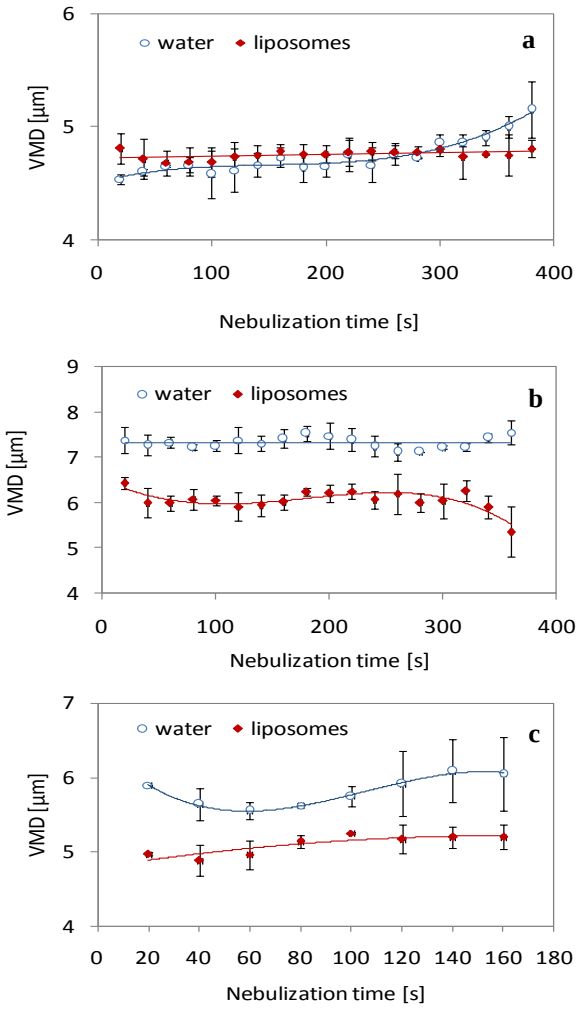

Figure 1. Evolution of droplet size distributions of water and liposome colloid emitted from different nebulizers: MP1-RF6 (a), AeroNeb Pro (b) and e-Flow Rapid (c).

This work was supported by the governmental funds for science in the years 2010-2013 under grant NN 209 0233 39.

Sosnowski, T.R. and Żołądkowicz J. (2011) *Inz. Aparat. Chem.* **50(5)**, 100-101 – *in Polish.*

Zaru, M., Mourtas, S., Klepetsanis, P., Fadda, A.M. and Antimisiaris, S.G. (2007) *Eur. J. Pharm. Biopharm.* **67**, 655-666.

Bipolar Charge Analyzer for inhaler particles

J. Kannosto[1], V. Niemelä[1], H. Isherwood[1], J. Yli-Ojanperä[2], J. Keskinen[2], R. Hillamo[3], A. Frey[3] and A. Ukkonen[1]

[1] Dekati Ltd., FIN-33700 Tampere, Finland
[2] Tampere University of Technology, Department of Physics, P.O.Box 692, FIN-33101 Tampere, Finland
[3] Finnish Meteorological Institute, P.O.Box 503, FIN-00101 Helsinki, Finland

Keywords: Bipolar charge, Dekati® Bipolar Charger Analyzer, impactor, natural charge, inhaler
Presenting author email: jonna.kannosto@dekati.fi

Recently, delivery of various drugs to lungs has been of increased scientific interest and it has become a more and more common way to treat different diseases, not only respiratory diseases like asthma. According to computer simulations, electrostatic deposition of inhaler drug particles dominates in the lower lung regions (Balachandran et al. 1997), particularly in the alveoli where the most efficient systemic absorption exists. Earlier charge studies have focused on particle net charge measurements (Telko et al. 2007) since a method for measuring bipolar charge has not been available.

The Dekati® Bipolar Charge Analyzer is the first commercial instrument available for measuring aerosol particles' bipolar electrical charge as a function of particle size. The instrument consists of two main components: flow divider and electrical collection tubes. The flow divider divides the aerosol evenly to 6 branches. Each branch has an electrical collection tube consisting of an impactor which separates the particles based on particle size and two nested cylinders which measure the electrical bipolar charge of particles. The particles with different polarity drift to inner or outer tubes due to the electric field between the tubes. The bipolar charge of particles is measured as a current from the inner and outer tubes using electrometers. After the measurement the electrical collection tubes can be uncoupled and positive and negative particles can be covered and analyzed separately. Hence, the Dekati® Bibolar Charge Analyzer measures the electrical bipolar charge of different sized particles but if the particles are also analyzed, the bipolar charge in respect of mass can be assigned as well as the particles' composition in different size ranges.

Table 1. The particle sizes collected to the branches in the Dekati® Bipolar Charge Analyzer.

Tube	Particle size, µm
1	$D_p < 0.94$
2	$0.94 < D_p < 2.84$
3	$2.84 < D_p < 4.47$
4	$4.47 < D_p < 8.07$
5	$8.07 < D_p < 12.79$
filter	collects all the particles

Each one of five branches has a different impactor cutpoint and therefore different sized particles pass through the impactors (Table 1.) and the bipolar charge of different particle sizes are gained from the tubes. In the sixth branch, there is no tube or impactor but a filter instead. The filter is used to check the net charge of the particles but also the quality of the successful flow dividing. The nominal cut-sizes of the impactors match with the corresponding stages in the NGI-impactor at 60 lpm flow rate (Virgil. et al. 2003).

The electrical bipolar charge distribution of lactose particles is presented in Figure 1. Also the net charge of the particles is shown. The bipolar charge measurement has much more information compared to net charge of particles.

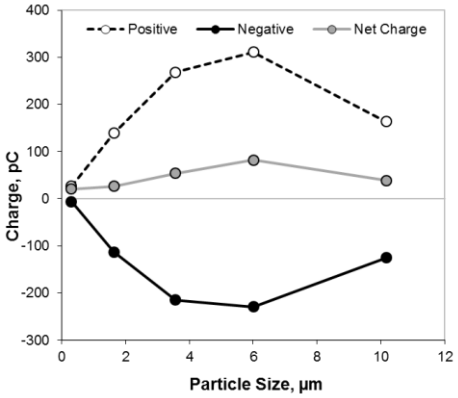

Figure 1. Positive, negative and net charge of lactose particles as a function of particle size

Each component of the instrument is calibrated separately: impactor stage collection efficiencies, the flow divider penetration and the tube particle collection efficiencies as a function of charge level and particle size (Yli-Ojanperä et al. 2012). The size distribution and net charge of Dekati® Bipolar Charge Analyzer are compared with the ELPI. The results are very comparable. The quality of flow dividing has been studied by net charges and analyzing the amount of particles in each branch. Particle deposition (losses) in different parts of the instrument has also been studied in detail.

Balachandran, W., Machowski, W., Gaura, E., Hudson, C., Control of drug aerosol in human airways using electrostatic forces, *J. Electrostat.* 40-41, 579, 1998

Virgil A. Marple, Daryl L. Roberts, Francisco J. Romay, Nicholas C. Miller, Keith G. Truman, Michiel Van Oort, Bo Olsson, Michael J. Holroyd, Jolyon P. Mitchell, and Dieter Hochrainer, Next Generation Pharmaceutical Impactor (A New Impactor for Pharmaceutical Inhaler Testing). Part I: Design, *Journal of Aerosol Medicine*, 16, 3, 283-299, 2003

Telko, Martin J., Kujanpää J., Hichey A. J., Investigation of triboelectric charging in dry powder inhalers using electrical low pressure impactor (ELPI™), *International journal of pharmaceutics*, 336, 352-360, 2007

Yli-Ojanperä J.et al., the paper under preparation.

Characterizing the Time-Dependant Hygroscopic Response of Aerosols Generated From Commercially Available Nebuliser Formulations

A.E. Haddrell[1], J.F. Davies[1], L.A. Dailey[2], D. Murnane[3] and J.P. Reid[1]

[1]School of Chemistry, University of Bristol, Bristol, UK, BS8 1TS
[2]Institute of Pharmaceutical Science, King's College London, UK, SE1 9NH
[3]University of Hertfordshire, Hatfield, UK, AL10 9AB
Keywords: Pulmonary drug delivery, nebuliser, particle size.
Presenting author email: A.haddrell@bristol.ac.uk

The use of the respiratory tract for drug delivery has been proven highly successful for treating not only diseases of the lung, such as delivering bronchodilators to treat asthma, but also in the treatment of systemic diseases, such as delivering insulin to treat diabetes. The three main delivery systems currently available are metered-dose inhalers (MDIs), dry powder inhalers (DPIs) and nebulisers, where the mechanism by which each generates an aerosol is unique. Although each method is different, the aim is to be able to deliver the appropriate drug dose to the desired location within the lung. This is accomplished through tailoring the excipients in the starting formulation as a means to affect the size of the aerosol, thus allowing delivery it to the desired location in the lung. Although the correlation between aerosol size and deposition site in the lung are well studied, the rapid change in size of an aerosol in the humid environment of the lung is not. In this study, we examine the thermodynamic and kinetic factors that regulate the time-dependant size of droplets generated from commercial nebuliser formulations.

The hygroscopic properties of various nebuliser formulations were studied using two different electrodynamic balances, the standard double ring EDB (DR-EDB) (Hargreaves el al., 2010) and a concentric cylinder EDB (CC-EDB) (Davies et al., 2012). The DR-EDB was used to study the relative size change of the droplets as a function of relative humidity (RH), where time was given for the droplets to reach a thermodynamic equilibrium at each RH. The CC-EDB was used to study the rapid change in size of the droplet from the point of its generation to the point where it reaches equilibrium, with a time resolution on the ms time scale.

The formulations utilised in this study were saline (as a control), Flixotide, Salbutanol, Tobramycin and Ventaris. The rapid evaporation of droplets of each formulation was measured under relative humidity conditions of >90%, ~50% and dry.

The results for Flixotide are shown in figure 1, the data collected using the DR-EDB is shown in figure 1A while the data collected using the CC-EDB is shown in figure 1B.

In looking at the relative size change as a function of RH (figure 1A), the shape of the hygroscopic curve was found to be similar to that of NaCl - both have deliquescence and efflorescence points of 75% and 50% respectively, which is not surprising given that the formulations are primarily a saline solution. However, the overall mass change of the aerosol was found to be far lower than that of pure NaCl (data not shown), suggesting that the excipients in the formulation play a major role in the uptake of water by the droplet.

The size of the droplet as a function of time (figure 1B) clearly demonstrates the necessity in undertaking these studies; for most inhaled particles, the equilibrium size of the aerosol is never reached.

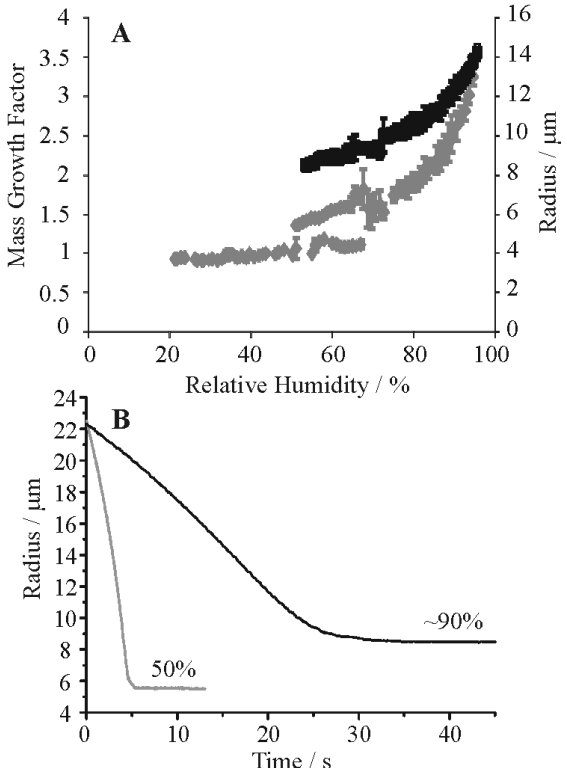

Figure 1. The relative size of droplets generated from a Flixotide formulation as a function of relative humidity (A) and time (B).

Additionally, the use of the two different EDBs was found to generate complimentary data. The ratio of the radii of the droplets at equilibrium between an RH of 95% and 50% for both instruments was ~1.5.

Davies, J.F., Haddrell, A.E. and Reid, J.P. (2012) *Aerosol Sci. Tech.*, **46**, 666-677.
Hargreaves, G., Kwamena, N. O. A., Zhang, Y. H., Butler, J. R., Rushworth, S., Clegg, S. L. and Reid, J. P. (2010). *J Phys Chem A,* **114**, 1806-1815.

Using the carbon-nanotube plasma for removal of indoor bioaerosols

S. Yang[1,*], C.H. Luo[2], Y.C. Huang[2], C.Y. Chuang[3], H.Z. Chen[4], P.C. Hung[5]

[1]Department of Environmental and Occupational Health, Toko University, Chiayi, Taiwan
[2]Department of Safety, Health and Environmental Engineering, Hungkuang University, Taichung, Taiwan
[3]Department of Bio-Industrial Mechatronics Engineering, National Taiwan University, Taipei, Taiwan
[4]Department of Animation and Game Design, Toko University, Chiayi, Taiwan
[5]Institute of Occupational Safety and Health, Council of Labor Affairs, Taipei, Taiwan

Keywords: carbon-nanotube, plasma, indoor, bioaerosol.
Presenting author email: shinhaoyang@ntu.edu.tw

Individuals spend an average of 87.2 % of their time indoors in the USA (Lance, 1996) and an average of 90 % of their time indoors in Taiwan, highlighting the increasing importance of indoor air quality. Bioaerosols induce various respiratory diseases and significantly impact indoor air quality (Eduard *et al*., 1993; Melbostad *et al*., 1994). Therefore, an increasing number of air-cleaning technologies remove indoor bioaerosols.

This work aimed to apply the carbon nanotube corona discharge plasma to remove bioaerosols. The nanotube carbon plasma device included two carbon nanotube discharge electrodes, a high voltage power supply, and a stainless steel mixing column. The carbon nanotube discharge electrodes were made by coating carbon nanotube on the stainless steel needles. Two carbon nanotube discharge electrodes connected with the positive and negative electrodes of the power supply.

The E-coli bioaerosols were chosen as the tested aerosols. The test bioaerosols were generated by using a Collison three-jet nebulizer (BGI Inc., Waltham, MA). The bioaerosol survival was measured by an Andersen single-stage impactor sampler (Andersen Samplers, Inc., Atlanta, GA) supplied with TSA plates. Figure 1 shows the components of the testing system. The test chamber made of stainless steel is 80 × 80 × 80 cm^3. Before experiments started, the chamber was well stabilized for 6 hr to achieve the demanded conditions. Two fans and a pump were utilized to retain a stable airflow and control the number of ACHs. The ACH is equal to the total airflow per volume of the tested chamber. Two ACHs, 0.5 and 1.0 (1/hr), were selected in this study. The air stream RH was modified by changing the ratio of flow rate of a dry gas stream to that of a humidified gas stream generated by a water vapor saturator.

Figure 2 plots the decay curves of *E-coli* bioaerosols in the testing system at a total ACH of 1.0 hr^{-1}, and RH of 30%. In the absence of the plasma system, the natural decay constant (kn) approached 0.135 min^{-1}. When the tesing system was equipped with a carbon-nanotube plasma system of 6 kV, the decay constant (ka) was 0.291 min^{-1}. The carbon-nanotube plasma system improved *E-coli* bioaerosols removal efficiency. This was due to the effects of inactivating of the carbon-nanotube plasma system. The plasma system using carbon nanotube electrodes had higher bioaerosol inactivation efficiency than the corona discharge system using stainless steel electrodes. The results further demonstrated that the inactivation efficiency increased as ACH and operating voltage increase.

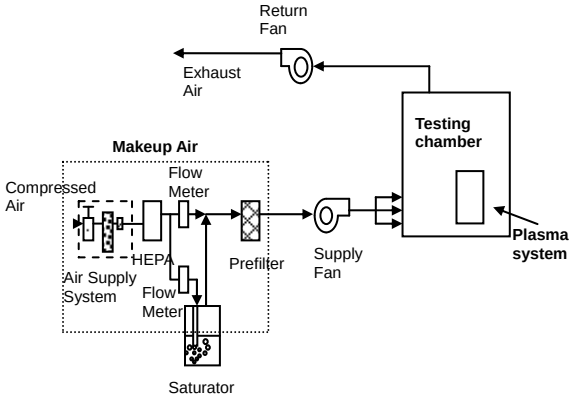

Figure 1. Schematic diagram of a small-scale testing system

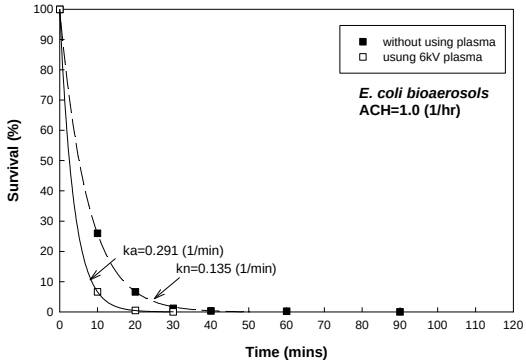

Fig. 2 Decay curves of the *E-coli* bioaerosols in the HVAC system with or without using plasma at ACH of 1.0 (1/hr).

The authors would like to thank the Institute of Occupational Safety and Health of Republic of China for financially supporting this research under Contract No. IOSH98-H313.

Eduard, W., Sandven, P., & Levy, F. (1993). *Am. J. Ind. Med.*, 24, 207-222

Lance, W. (1996). *Journal of Air and Waste Manage. Assoc.*, 46, 98-126.

Melbostad, E., Eduard, W., Skogstad, A., Sandven, P., Lassen, J., Sostrand, P., & Heldal, K. (1994). *Am. J. Ind. Med.*, 25, 59-63.

Periodical interruption of chronic exposure to PM in metropolitan areas could be of benefits to prevent chronic alterations of respiratory function in humans

G. Schiraldi [1], F. Cetta [2], P. Paladini [2], J. Martellucci [2], F. Granato[2], B. Lorenzi[2], R. Zangari [2], V. Guercio [2], E. Bolzacchini [3], M. Monti [4], G. Gotti [2] and L.Allegra[1]

[1]Toracopulmonary and Cardiovascular Dept., University of Milan, Milan, 20122, Italy
[2]Dept. of Surgery and Thoracic Surgery, University of Siena, Siena, 53100, Italy
[3]Dept. of Environmental Sciences, University of Milan, Milan, 20126, Italy
[4]Geriatric Institute "Pio Albergo Trivulzio" (PAT), Milan, 20146, Italy
Keywords: PM, COPD, urban areas, remote alpine sites.
Presenting author email: gianfranco.schiraldi@gmail.com

Increased concentration of particulate material (PM), mainly due to urban traffic, heating and industrial pollutants is likely to be responsible for a different incidence of respiratory complications and/or reduction of pulmonary function.

198 patients were recruited, on a casual and voluntary basis: 99 were recruited in Milan, Italy, i.e. a densely populated and polluted metropolitan area, the 99 in Aprica, a remote alpine site (1181 m.a.s.l), with low pollution, due to traffic or other pollution sources. PM_{10} (<10 μm)and $PM_{2,5}$ (<2,5μm) were measured by PM detection units during two 2 week-campaigns. Each group was classified in 2 subgroups. The former, aged 30 to 64 years, (n=72) the latter over 65 (n=27). All subjects, well matched for cigarette smoke, sex and age were in good health conditions, asymptomatic and with no previous history of respiratory chronic diseases. All of them underwent spirometry, with evaluation of the following parameters: FVC (forced vital capacity), FEV_1 (forced expiratory volume in 1 second), PEF (peak expiratory flow) and MEF_{50} and MEF_{25}, i.e. maximum forced expiratory flow at 50% and 25% of FVC, respectively. Data were expressed as the percentage ratio between measured and theoretical values (m/t%).

Results: m/t% of FEV_1 (index of bronchial patency), both in under 65 and over 65 subjects, was lower in Milan that in Aprica subjects (**Table 1** and **Table 2**).

Table 1: m/t% in subjects age 30-65 years

	Milan	Aprica	p (t test)
FEV_1 m/t%	96	103	<0.01
MEF_{50} m/t %	75	97	<0.0001
MEF_{25} m/t%	54	78	<0.0001

Table 2: m/t% in subjects age 65-89 years

	Milan	Aprica	P (t test)
FEV_1 m/t%	69	88	NS (p=0.052)
MEF_{50} m/t %	68	86	NS (p=0.073)
MEF_{25} m/t%	44	66	<0.0001

In particular, FEV_1 was <80% (value borderline between normal and abnormal data) in 20 out of 99 subjects in Milan (20,2%), whereas it was < 80% in only 8 out of 99 in Aprica (8,08%).

Evident differences were also observed in subgroups of different age: FEV1 resulted <80% in 8 out of 72 subjects under 65 years in Milan (11,1%) and in 2 out of 72 in Aprica (2,8%); and in 12 out of 27 (44,4%) and 6 out of 27 (22,2%) in subjects over 65 years, respectively (p<0,05), Allegra *et al* (2008).

Consistently, MEF_{50} and MEF_{25}, suggestive of the "smaller airway diseases", i.e. of a sub-clinical pathological entity somehow preceding chronic obstructive pulmonary diseases (COPD), were found (m/t%), both in under 65 and over 65 subjects, higher in Aprica than Milan inhabitants (**Table 1** and **Table 2**). In particular, in 30 out of 85 Milan subjects vs 18 out of 85 Aprica subjects, they were below the threshold (<65% for MEF_{50} , and <50% for MEF_{25}), which are considered borderline between normal and abnormal values (p<0,001) (**Table 3**).

Table 3: MEF_{50} and MEF_{25} changes (<65% and 50% respectively) Milan vs Aprica

MEF_{50}<65%, MEF_{25}<50%	Milan	Aprica
Total subjects	30 (35 %)	18 (21 %)
Subjects < 65y	17 (27 %)	3 (5 %)
Subjects >65y	13 (56 %)	15 (65 %)

Conclusion: Present data, even if preliminary, suggest that in the polluted metropolitan area of Milan, inhabitants are more prone to a progressive alterations of the respiratory function than in Aprica, a low pollution alpine site. In particular, not only in severely symptomatic subjects with evident respiratory diseases, but also in clinically asymptomatic individuals, it is possible to detect significant difference in respiratory function because of different levels of air pollution. Since PM related alterations are partly reversible because of repair and defense mechanisms of the host, Cetta *et al* (2009), periodical interruption of chronic exposure to metropolitan pollutants with exposure to a better environment (such as an Alpine site) could be of benefit.

This work was supported by the PROLIFE Project, City of Milan, Italy.

Allegra, L et al (2008) *GIMT* **62**, 389-396.
Cetta, F. et al (2009) *Environ. Health Perspect.* **117**, A190.

A 4-years follow-up study of traffic related respiratory changes in school children in Milan , Italy

M. Sala[1], F. Cetta[2], S. Argirò[1], P. Ballista[1], R. Zangari[2], V. Guercio[2], E. Bolzacchini[3], M. Monti[4] and M. Mandelli[1]

[1]Dept. of Pediatrics, University of Milan, Milan, 20122, Italy
[2]Dept. of Surgery and Thoracic Surgery, University of Siena, Siena, 53100, Italy
[3]Dept. of Environmental Sciences, University of Milan-Bicocca, Milan, 20126, Italy
[4]Geriatric Institute "Pio Albergo Trivulzio" (PAT), Milan, 20146, Italy
Keywords: air pollution, PM, traffic emissions, health effects of aerosols
Presenting author email: marco.sala@unimi.it

Important adverse effects on children health can be caused by exposure to air pollution, namely during the peculiar "susceptibility window" occurring during the first years of life, Clark *et al* (2010). In particular, traffic related pollution adversely affects lung function development.

Between 2007 and 2008, 228 children, mean age 8 years, were enrolled from 2 primary schools, located in different sites, in order to study pollution related respiratory symptoms and/or diseases in different places of Milan with a different traffic-related exposure. The former (School 1) was located near a large park, the latter was located downtown, close to main crossroads (School 2). Daily levels of PM10 and PM2,5 (diameter <10µm and 2,5µm) were measured both outdoor and indoor outside the schools (in the school garden) and within common places (corridors), for 7 consecutive days during 2 different campaigns (winter and spring-summer). Children underwent skin prick testing for inhaled allergens, analysis of exhaled nitric oxid (FeNO) and spirometry.

The distribution of FeNO values was significantly different (p=0,02) between the two schools. In particular, the percentage of children with FeNO values <5ppb in school 1 was higher (almost double) than in school 2. In 73% of children attending the school located downtown FeNO concentration was between 5 and 20ppb.

The percentage of asthma exacerbations in the previous 12 months was higher in children from school 2 (p=0.05). On the contrary, the prevalence of persistent allergic rhinitis in children allergic to grass pollen was higher in school 1 (p=0.03). In particular, the latter children also had a greater activity limitation, due to rhinitis and concomitant conjunctivitis (p=0.03). Interestingly, the highest recorded peak for PM10 occurred between 8:15 and 9:15 a.m., for 3 consecutive days, and was related to children arrival. This peak (>1000µg/m^3) (figure 1) didn't seem to produce specific health effects, likely because of the usual PM10 composition in a park site, with a lower content of toxic or reactive components.

Hospital admissions, because of lower respiratory tract diseases (bronchitis, bronchiolitis, pneumonia) were more frequent during the winter campaign and in school 2, whereas otitis and allergic rhinitis or conjunctivitis, together with asthma, were more severe during the spring-summer period and in school 1 (p<0,05).

Continuous monitoring for 3 years of both children and PM showed that: 1) short duration pollution peaks, even reaching concentrations 20 folds above the fixed limits, have no consequences on children health and were likely induced by children's arrival or movement; 2) there was an enormous daily variability in PM10 concentration, among the daily mean value results, from the average of values, with a very high standard deviation (+30,+1000µg/m^3) and with various peaks; 3) prolonged follow-up for 3 years in this selected group of children didn't show any evident difference in the occurrence of clinically relevant respiratory diseases. On the basis of FeNO values, different degrees of respiratory function and bronchial inflammation were found in the 2 groups.

Traffic could be responsible at least in part for the different air quality, but individual susceptibility and seasonal changes are also major determinants of clinical outcomes. In particular, early exposure during the first years of life could be responsible for future diseases occurring later, during adult life.

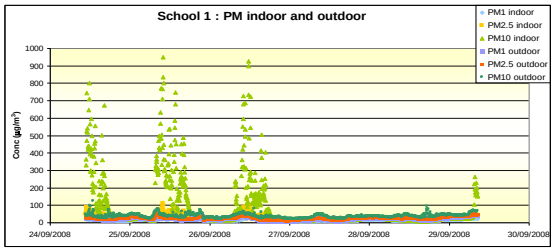

Figure 1. Concentration of PM10, indoor and outdoor, in School 1.

This work was supported by the PROLIFE Project, City of Milan, Italy.

Clark, N.A. et al. (2010). *Environ. Health Perspect.* **118**, 284-290.

Spirometric and laboratory assessment of the respiratory function as an effect of PM exposure in asymptomatic subjects living in a metropolitan area (Milan, Italy) and in a remote alpine site (Aprica)

L.Allegra[1] F. Cetta[2], G. Schiraldi[1], R. Zangari[2], V. Guercio[2], D. Stergiou[2], C. Ghiribelli[2], P. Paladini[2], L. Luzzi[2], E. Bolzacchini[3], M. Monti[4] and G. Gotti[2]

[1]Toracopulmonary and Cardiovascular Department University of Milan, Milan, 20126, Italy
[2]Dept. of Surgery and Thoracic Surgery, University of Siena, Siena, 53100, Italy
[3]Dept. of Environmental Sciences, University of Milan, 20126, Milan, Italy
[4]Geriatric Institute "Pio Albergo Trivulzio" (PAT), Milan, 20146, Italy
Keywords: air-pollution, traffic emissions, exposure, health effects of aerosols.
Presenting author email: luigi.allegra@unimi.it

Urban traffic and environmental pollution are responsible for a different air quality in metropolitan areas vs less polluted sites and for a different incidence of respiratory complications and/or alteration of pulmonary function.

In the 2008 two groups of 99 subjects were recruited (n=198), on a casual and voluntary basis: the former in Milan, Italy, i.e. a polluted metropolitan area, the latter in Aprica, a remote alpine site (1181 m.a.s.l), with low pollution. PM_{10} (<10 μm) and $PM_{2,5}$ (<2,5μm) were measured by PM detection units during two 2 week-campaigns. Each group was classified in 2 subgroups. The former, aged 30 to 64 y (n=72) , the latter over 65y (n=27). All subjects, well matched for cigarette smoke, sex and age were in good health conditions, asymptomatic and with no previous history of respiratory chronic diseases. All of them underwent spirometry, with evaluation of the following parameters: FVC (forced vital capacity), FEV_1 (forced expiratory volume in 1 second), PEF (peak expiratory flow) and MEF_{50} and MEF_{25}, i.e. maximum forced expiratory flow at 50% and 25% of FVC, respectively. In addition, the thiol redox status, which is crucial to balance oxidative stress and ROS generation, facilated by air pollution, was also evaluated in 2 subgroups of subjects,: the former (n=38, age 82±9y) living in Milan, and the latter (n=42, age 70±8y) living in Aprica. HPLC analysis was performed on blood samples for the evaluation of thiols in plasma and erythrocytes (total and reduced forms PT, PR; ET, ER) and also in exhaled breath concentrate (EBC). In fact, thiol redox status contributes to contrast oxidative stress and ROS generation promoted by air pollution. Namely cystein (Cys), cysteinylglycine (CG), homocysteine (Hcy) and glutathione (GSH) were evaluated both in blood and in EBC.

FEV_1 resulted <80% in 20 out of 99 subjects in Milan (20,2%), whereas it was < 80% in only 8 out of 99 in Aprica (8,08%). Evident differences were also observed in subgroups of different age: FEV1 resulted <80% in 8 out of 72 subjects under 65 y in Milan (11,1%) and in 2 out of 72 in Aprica (2,8%); and in 12 out of 27 (44,4%) and 6 out of 27 (22,2%) in subjects over 65 y, respectively (p<0,05), Allegra *et al* (2008). Concerning thiol analysis, there was no evident difference in the GSH levels between the two populations. In fact, GSH alteration is usually a late event, occurring in severe imbalances and no subject in both groups had clinically evident diseases, Cetta *et al* (2009). On the contrary, PT Cys was 459,8 ±152,2 vs 286,3 ±74,8 (p<0,001) and ER Cys 2,5±0,8 vs 1,5 ±0,6 (p<0,001), respectively. Finally, data concerning thiol balance analysis from EBC showed: 1) a striking individual variability of the various chromatographic peaks; 2) low concentration of reduced species.

Conclusion: inhabitants of areas with different traffic volumes showed significantly different Cys, CG and Hcy levels, even if GSH remains unchanged, suggesting a greater- pro-oxidant effect in more exposed populations, affecting Cys, CG and Hcy levels, before GSH alterations. Analysis of thiol redox balance in plasma and erythrocytes is able to distinguish between more and less exposed subjects and could be a useful diagnostic tool for early detection of subjects at higher risk of health effects from environmental pollution. In particular, thiol analysis in EBC could be a very early marker of redox imbalance, and be used to detect early alterations in predisposed subjects. Air pollutants are weak pollutants, which at usual concentration in Western countries, in the absence of increased individual predisposition to respiratory or cardiovascular diseases do not determine clinically evident health effects after short-term exposure. In particular, PM related diseases are likely due to progressive accumulation of biological and tissue damage, because of oxidative stress and other injuries to human cells. These alterations are likely to be reversible and could be repaired by endogenous repair and defense mechanisms of the host.

Periodical interruption of chronic exposure to metropolitan pollutants with exposure to a better environment (such as an Alpine site), could be of benefit in all subjects with prolonged exposure to PM.

This work was supported by the PROLIFE Project, City of Milan, Italy.

Allegra, L. et al (2008) *GIMT* **62**, 389-396.
Cetta, F. et al (2009) *Environ. Health Perspect.* **117**, A286-7.

Cryo-imaging as a quantitative pre-clinical method to determine the amount and spatial distribution of drugs in lung tissue: A feasibility study for fluorescent substances

Friedrich Prade[1], Nikolaos C. Deliolanis[2], Katie Dextraze[1], Nirav Barapatre[1], Vasilis Ntziachristos[2], Oliver Eickelberg[1], Otmar Schmid[1]

[1]Comprehensive Pneumology Center, Institute of Lung Biology and Disease, University Hospital, Ludwig-Maximilians-University and Helmholtz Zentrum München; Ingolstädter Landstrasse 1, 85764 Neuherberg Germany

[2] Institute of Biological and Medical Imaging, Helmholtz Zentrum München and Technische Universität München; Ingolstädter Landstrasse 1; 85764 Neuherberg; Germany

Keywords: Pulmonary drug delivery, cryoimaging, lung, quantitative dose determination, fluorescence.

Presenting author email: otmar.schmid@helmholtz-muenchen.de

Many therapeutic approaches for lung diseases rely on delivery of drugs directly to lungs via inhalation. The efficacy of the therapy will depend on the amount of the delivered drug, the location of its deposition and its bioactivity. Hence, quantification of drug amount and its spatial distribution in lungs are indispensable factors in the validation of any drug in pre-clinical research.

Fluorescence and bioluminescence imaging in the visible range is a promising method for *in vivo* determination of dose, spatial distribution and bioactivity of drug dose in the lungs. However, the biological tissue interacts strongly with the visible light. Due to absorption and especially scattering of the light, quantification and mapping of the drug dose is difficult. We, therefore, use Cryo-Imaging (Steyer et al, 2009) of fluorescent substances in an excised lung as the experimental method for determining the factors like, attenuation coefficient of the lung tissue and as a reference method for the pulmonary drug dose and distribution.

Cryo-Imaging involves imaging and slicing of the specimen in an alternate manner. It requires a conventional cryomicrotome to be fitted with an imaging unit capable of recording fluorescence signals at multiple wavelengths (fig. 1). The specimen block is first imaged then sliced by a defined thickness. This procedure is repeated until the whole specimen is recorded.

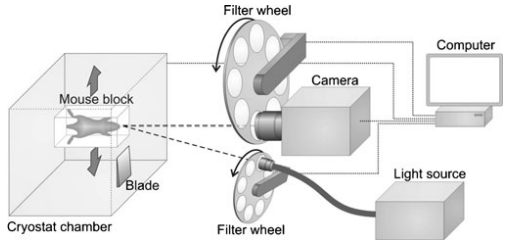

Figure 1. Schematic depiction of the Cryo-Imaging setup. As a first step the whole mouse instead of the excised lung is used. After each block face image the slicing takes place. The excitation light is provided by a filtered light source and the emission light is captured with a camera (Sarantopoulos et al, 2011)

Since each block face image not only contains light from a single slice, but also contains the fluorescence signal emanating from deeper layers of the specimen. The net fluorescence for a given slice is derived by taking into account the fluorescence images of deeper slices, modelling light propagation, and correcting for their contribution on the top layer. The corrected slices are stacked together to reconstruct a 3D distribution of the fluorophore. The sum of the net fluorescence from all the slices gives the total amount of fluorophore present in the specimen. The advantage of this method lies in its ability to obtain quantitative images with high spatial resolution and high sensitivity for the fluorescent signal.

A known amount of fluorescent polystyrene particles (diameter 450nm, excitation @ 670nm; emission @ 710nm) was instilled intratracheally to the lungs of a mouse, which was sacrificed immediately after the application. The lung was removed, fixed in an OCT solution (for fixation of the tissue) and snap frozen. The frozen block was then cryo-imaged with a slice thickness of 100 µm. A 3D distribution of the fluorophore in the lungs was reconstructed with an image processing routine written in MATLAB. Figure 2 shows a single slice of the reconstructed volume of three separated lobes of a mouse lung containing fluorescent polystyrene particles.

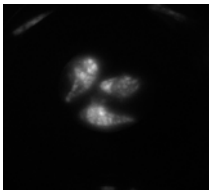

Figure 2. A fluorescence image of three separated lobes of a mouse lung taken with the Cryo-Imaging setup. The lungs contained fluorescent polystyrene particles (diameter 450nm, excitation @ 670nm; emission @ 710nm)

Steyer, G. J., Roy, D., Salvado, O., Stone, M. E. and Wilson, D. L. (2009) *Ann. Biomed. Eng.* **37**, 1613-1628.

Sarantopoulos, A., Themelis, G. and Ntziachristos, V. (2011) *Mol. Imaging Biol.* **13**, 874-885.

Stochastic rat lung dosimetry for radon progeny: A surrogate for the human lung

M.Hussain[1,2], R. Winker-Heil[1], and W. Hofmann[1]

[1]Department of Materials Research and Physics, University of Salzburg, 5020, Salzburg, Austria
[2]Higher Education Commission of Pakistan, 44000, Islamabad, Pakistan

Keywords: lung deposition, stochastic analysis, radon decay products

Experimental data on lung cancer risk in rats (Cross 1988; Chameaud et al. 1984) indicate that the mean lifetime risk coefficients per unit exposure are consistent with the epidemiological findings for uranium miners under various exposure conditions. The laboratory rat as a human surrogate to assess the associated risk following exposure to radon progeny has shown promising results (Monchaux et al. 2002), indicating that the rat is a suitable animal for lung cancer risk assessment.

Studies by Hofmann et al. (1999) have shown that airway diameters are more appropriate morphometric parameters to classify local particle deposition patterns and hence dose distributions across the human and the rat lung. In our present study, dose distributions from inhaled radon progeny are therefore computed by previously developed stochastic morphometric models of the human and rat lungs.

Dose estimation for inhaled radon progeny in mine environments are based on one percent of unattached fractions characterized by an activity median diameter (AMD) of 1 nm and attached fractions of 0.3µm (AMD) with a mean density of 2.7 g cm^{-3} and a geometric standard deviation (GSD) of 2.2. For dose calculations, the breathing parameters for the rat are derived from the data collected by Costa and Tepper (1988) with an average tidal volume of V_T = 2.0 mL and a breathing frequency of f = 117 min^{-1}.

Deposition patterns and hence doses delivered to bronchial airways as a function of airway diameter for radon progeny are shown in Figs 1 and 2.

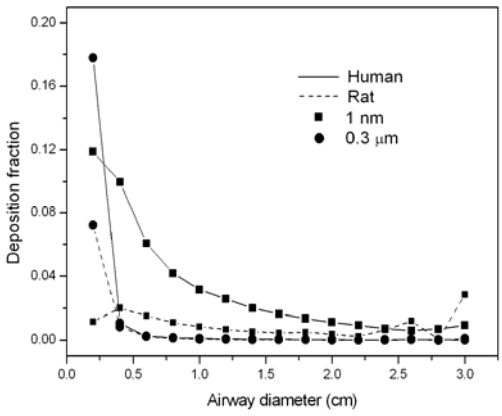

Fig 1: Deposition fractions of unattached and unattached radon progeny in the human and rat lungs.

Deposition in the trachea of the rat lung for the unattached fraction is higher than for the human lung, but is consistently lower in most of the conductive airways. However, doses delivered by the unattached fraction in both lungs do not show significant variations. In contrast to unattached fraction, attached fractions penetrate deeper into the lung with higher deposition fractions. The deposition distributions for the attached fractions in both species are nearly identical with relatively higher deposition in the trachea of rat lung. The doses delivered to the rat lung by the attached fraction are relatively higher in the deep lung. The average bronchial doses per unit exposure in the rat lung are 0.43 and 11.3 mGy WLM^{-1}, whereas in the human lung the corresponding doses are 0.55 and 7.1 mGy WLM^{-1}.

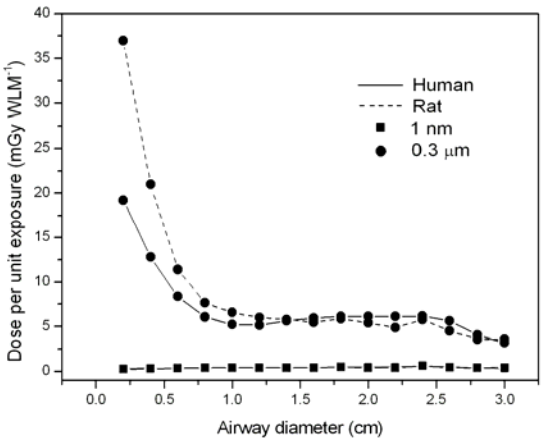

Fig 2: Doses per unit exposure for unattached and unattached radon progeny in the human and rat lungs.

The results presented above suggest that the rat lung diameters are an appropriate human surrogate model for human radon lung dosimetry.

This work was funded in part by EU contract no. 516483 and by the Higher Education Commission of Pakistan.

Chameaud, J., Masse, R. and Lafuma, J. (1984) *Radiat. Prot. Dosim.*, **7**, 385-388.

Costa, D.L. and Tepper, J. (1988) *Approaches to lung function assessment in small mammals*. New York, Raven Press.

Cross, F.T. (1988) *Radiat. Prot. Dosim.* **24**, 463-466.

Hofmann, W., Bergmann, R. and Koblinger, L. (1999) *J. Aerosol Sci*. **30**, 651-667.

Monchaux, G. and Morlier, J.P. (2002) *J. Radiol. Prot.* **22**, 81-87.

Aerosol infection of chickens by avian influenza virus A/H5N1

Ar.A. Sergeev[1], O.K. Demina[1], O.V. Pyankov[1,2], O.G. Pyankova[1,2], A.P. Agafonov[1], S.A. Kiselev[1], I.E. Agranovski[2], Al.A. Sergeev[1], A.N. Shikov[1], L.N. Shishkina[1], A.S. Safatov[1] and A.N. Sergeev[1]

[1]Federal Budgetary Research Institution State Research Center of Virology and Biotechnology "Vector", Novosibirsk Region, 630559, Koltsovo, Russia
[2]School of Environmental Engineering at Griffith University, Nathan Campus, Qld 4111, Brisbane, Australia
Keywords: Avian influenza virus, bioaerosols, aerosol infectivity, epidemiology.
Presenting author email: safatov@vector.nsc.ru

Avian influenza virus (AIV) A subtype H5N1 is an object of researches conducted worldwide in connection with frequent cases of mass death of wild birds and poultry as a result of influenza spread in recent years and high fatality of some strains of this pathogen for humans.

According to some authors, chickens are infected via the fecal-oral route i.e. through gastrointestinal tract. Recently Kwon and Swayne, 2010 reported that chickens and ducks were more susceptible to the H5N1 virus when exposed by intranasal as compared to alimentary routes of inoculation. Some authors also do not exclude the aerosol way of transmission of this disease in chickens (Antarasena *et al* 2006; Shortridge *et al* 1998). Previously we also demonstrated the possibility of the aerogenic way of AIV transmission for these avian species (Safatov *et al*, 2007).

The goal of the work was to study the infectious properties of different AIV strains A subtype H5N1 for chickens, the degree of sensitivity of respiratory and gastrointestinal tracts of this avian species to the given pathogen as well as the dynamics of AIV dissemination in the organism of chickens infected via respiratory route.

Eight highly-pathogenic AIV strains A/H5N1 (intravenous pathogenicity index, IVPI - from 2.7 to 3.0) isolated in Russia and CIS countries were used in this work. All the strains at the 2nd -3rd passages (from the source of isolation) were cultivated on chicken embryos to the concentration of 7.5 – 8.5 Log_{10} 50% embryonic infective doses in 1 ml (EID_{50}/ml) and stored in a refrigerator at -70 °C before they were used in experiments.

Hisex Brown cross chickens of Rhode-Island genetic line 1 weighing 280-340 g were used in the studies. All chickens used were free from antibodies to H5 influenza virus.

Experiments were conducted according to the procedures similar to one described in detail in Agranovski *et al* (2010) and Sergeev *et al* (2002).

Comparative studies of the chickens' susceptibility to different highly pathogenic AIV strains at aerosol infection were performed, Table 1.

For comparison, the ID_{50} of AIV (by the example of A/Chicken/Suzdalka/Nov-11/2005 strain) were determined at infecting chickens with 3 more different routes of infection. It was noted that the virus displayed a considerably higher virulence for chickens at the intranasal way of infection as compared with those at oral (by 15 times) and intragastral ones (by 300 times). The aerosol way to infect birds with this AIV strain had a higher efficiency as compared with intranasal one (by 30 times).

Table 1. Data on the virulence of AIV strains at aerosol way of infecting chickens. Averages ± confidence interval with the probability of 95%

AIV A subtype H5N1 strains	AID_{50}, $Log_{10}EID_{50}$
A/Turkey/Suzdalka/Nov-1/2005	1.0 ± 0.4
A/Chicken/Suzdalka/Nov11/2005	1.2 ± 0.5
A/Chicken/Kurgan/05/2005	0.9 ± 0.4
A/Duck/Kurgan/08/2005	0.8 ± 0.4
A/Chicken/Crimea/04/2005	0.8 ± 0.5
A/Chicken/Omsk/06	1.0 ± 0.4
A/Chicken/Krasnodar/02/06	1.2 ± 0.5
A/Chicken/Dagestan/06	0.3 ± 0.6

Note: AID_{50} = 50 % Aerosol Infecting Dose.

Data on AIV A/Chicken/Kurgan/05/2005 dissemination in chickens infected via aerosol and intranasal routes in the course of infection showed simultaneous appearance of the virus 30 hours post infection in blood, lungs and cloaca indicates that it most probably penetrates into these organs from nasal mucous membrane by hematogenic way, for example, through fenestrated endothelium of blood vessels in olfactory region. Later detection of the virus in trachea than in the lungs also confirms this supposition and demonstrates a low level of the probability of existence of a descending way of pathogen spread from nasal cavity along the chicken's respiratory tract.

The results obtained showed that aerosol of AIV strains A subtype H5N1 is very infective for chickens. It is much more infective than inoculation via other routes of infection studied. It is confirmed also by data on virus dissemination in infected via various routes chickens.

This work was partially supported by RF Government grant #820-R.

Agranovski, I.E., *et al* (2010) *J. Aerosol Sci.* **41**, 161-169.
Antarasena, C., *et al* (2006) *Avian Pathol*. **35**, 250-253.
Kwon, Y.K. and Swayne, D.E. (2010) *Avian Diseases* **54**, 1260-1269.
Shortridge, K.F., *et al* (1998) *Virology* **252**, 331-142.
Safatov, A.S., *et al* (2007) *Abst. European Aerosol Conf., 10-14 Sept., Salzburg, Austria*, T04A012.
Sergeev, A.N., *et al* (2002) *Vopr. Virusol.* **47**, 44-46.

A better knowledge of causative pathophysiological mechanisms, in addition to proper markers of effects, as key tools for a deeper insight into health effects of air pollution

F. Cisternino[1], V. Guercio[1], M. Monti[2], F. Granato[1], B. Lorenzi[1], J. Martellucci[1], R. Zangari[1] and F. Cetta[1]

[1]Dept. of Surgery and Thoracic Surgery, University of Siena, Siena, 53100, Italy
[2]Geriatric Institute "Pio Albergo Trivulzio" (PAT), Milan, 20146, Italy
Keywords: PM, markers of exposure and effect, causative mechanisms, transient and persistent alterations.
Presenting author email: cisternino2@unisi.it

Aim of the study: To focus on possible markers of effect and susceptibility and pathophysiological mechanisms for a better understanding of the health effects of air-pollution.

Methods: Between 2007 and 2011, a comprehensive approach to health effects of air pollution in Milan, Italy was designed (Prolife Project). In particular, the following studies were performed : 1) PM concentration measurement; 2) comparison between daily concentration of PM or other pollutants and acute hospital admission for respiratory or cardiovascular diseases (n= 53.514); 3) longitudinal studies in frail subpopulations, such as children attending primary school (n=440) and elderly people living in nursing homes (n=198); 4) "*in vitro"* and "*in vivo"* experiments concerning host particle interactions.

Results: Transient or persistent and severe alterations of respiratory or cardiovascular districts were observed, either in children or in old people, in addition to alterations of other system such as sperm-cell function or osteoarticular function. However, in people with similar exposure to pollutants, they depended at a greater extent on individual susceptibility of the host than on intrinsic toxicity of the pollutants. In particular, more severe alterations were observed in subjects with chronic infection, COPD, rheumatoid arthritis or varicocele. It was found that PM determines multiple effects, that cannot be explained by "pure" toxic mechanisms. Therefore, a single marker is insufficient to capture the complexity of host particle interactions. In fact, an ideal marker should reflect at least 2 different mechanisms: 1) the former, that is pollution related (i.e. due to concentration, composition or other intrinsic properties of PM). 2) the latter, that is host susceptibility related. However, pollution-related diseases are a no-threshold phenomenon, i.e. there is no threshold of PM concentration above which the effect is detectable in all individuals, and no level below which there is no effect. Therefore, to capture these complex interactions, other markers should be chosen, partly related, but also partly not related to the presumed intrinsic toxicity of pollutants. These markers should measure individual susceptibility, vulnerability and the overall response of the human being as a whole.

Discussion: 1) A "stepwise approach", based on levels or degrees of evidence in the mechanistic causative role of PM and other airborne pollutants for the occurrence of clinically evident diseases or death in humans; 2) the need for markers of effect, which should be graded, on the basis of the level or degree of possible, transient, persistent or definitive damage. These markers can be classified as phase 1 or molecular markers (molecular alteration, or biological changes such as oxidative stress, ROS production, DNA adduct formation, which should be repaired by usual cellular mechanisms); phase 2, or cellular markers; phase 3, or markers of permanent tissutal damage and phase 4, or markers of clinically evident disease, or permanent function impairment of one organ or apparatus. Finally, a cumulative score is required, which takes into account both these mechanisms: particle related and host related. The measurement of this final score will also be variable, because it is arbitrary the weight that is given to each end-point and marker: oxidative stress, genetic mutation, inflammation, individual ability to repair damage, risk for autoimmune response. The weight of the various components should also be compared with current knowledge concerning the various diseases of interest. The weight will be greater for the "particle related toxic mechanism".

When evaluating diseases with low to no evidence for autoimmunity in their pathogenesis. And for the "host related mechanism", when dealing with clinical outcomes or diseases, for the occurrence of which (rheumatoid arthritis, asthma) autoimmunity is a well known causative factor. Markers of the toxic mechanism will be the following molecules related with oxidative stress and ROS generation or genetic polymorphisms in drug metabolizing enzymes (GSMT, NADH), which can be responsible for repair capacity. In addition to these markers we have to select markers expressing host cellular immunity and general markers of good health, in addition to specific markers for each function or district of interest.

The final picture of the various markers of interest will be more complicated, and to provide a proper model will be more complex. But, it will be more adherent to what actually occurs in real world. In particular, misleading inferences from epidemiological studies could be prevented.

Aerosolization system for experimental inhalation study of metal oxides nanoparticules

Presumé[1], M, Attoui[2], M., Lanone[1], S.

[1] IRMB-INSERM-UPEC Créteil France
[2] LISA UPEC-Diderot, Créteil France

Keywords: nanoparticules, inhalation,
attoui@univ-paris12.fr

Respiratory effects of nanoparticles (NP) represent a major concern. However, no current data is available in the literature regarding health effects in human beings. Welders are a population of workers susceptible to be exposed to NP. Indeed, welding fumes are a complex mixture of particles and gases that is highly variable. It is estimated that 90% of welding is performed with mild steel, which is composed of mostly iron (Fe) and some manganese (Mn) to strengthen the steel (Antonini et al.2005; Morini & Viti 2009). In terms of particles number per cubic centimetre, 80 % of the generated particles are below 30 nm.

We therefore designed a study aimed to expose mice to aerosols of NP representative of that found in welding fumes, in order to assess the respiratory effects of such NP. In this paper we describe the aerosolization system with particles 20 nm particles size of Iron and Manganese produced with a home made spark generator. Filtered dried and compressed air is used as carrier gas to produce oxides in the hot plasma. Electrodes (6 mm OD) of Mn and Fe from Goodfellow (99.99 % purity) are used. The aerosol produced by the spark generator is pushed in an inhalation chamber with a flowrate of 10 lpm. Two SS spark generators and two inhalation chambers have been designed for each metal to prevent contamination. Each spark chamber and each inhalation chamber is used for one metal aerosol.

The spark generator is characterized in terms of size distribution and stability with a TSI SMPS with a long DMA column. Morphology and chemical analysis of the particles are performed with TEM deposition system. A high resolution TEM equipped with a field emission gun and Xray energy was used. For chemical composition XEDS and Electron Energy Loss Spectrometry EELS measurements are programmed. The figures 1 and 2 gives the size distribution of Fe and Mn particles produced by our spark generator in air.

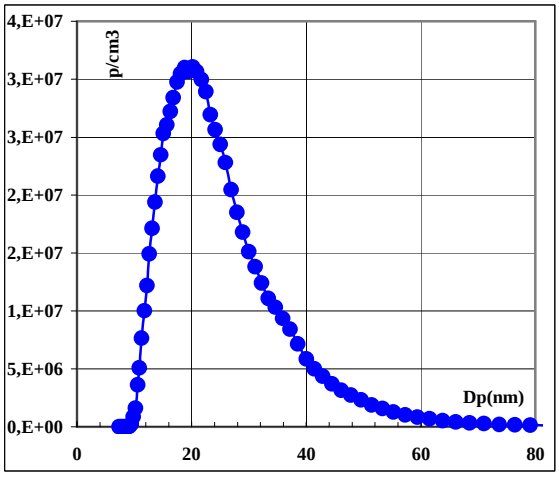

Fig.1
Size distribution of iron particles with a C=8800 pF and 10 lpm air

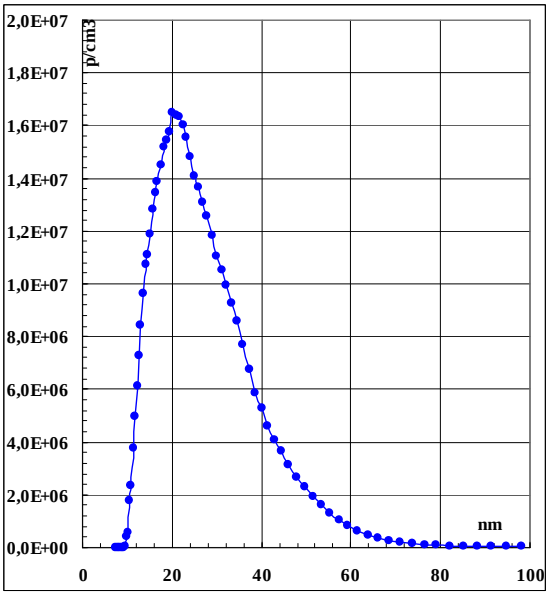

Figure 2
Size distribution of Mn particles with 13200 pF and 30 lpm air

Antonini,J.M.,Santamaria,A.B.,Jenkins,N.T.,Albini, E.,&Lucchini,R.(2006). NeuroToxicology, 27, 304–310

Moronia,B. And Viti, C. J. Aerosol Sci. 40 p 938-949 2009

Comparison of methods for measurement of surface area for six different nanomaterials.

M. Levin[1], I. K. Koponen[1], S. Bau[2], O. Witschger[3], E. Jankowska[4], C. Guiot[5], O. Spalla[5], K. A. Jensen[1]

[1]National Research Centre for the Working Environment, Copenhagen, DENMARK
[2]National de Recherche et deSécurité, Vandoeuvre, FRANCE
[3]Institut National de Recherche et de Sécurité, Vandoeuvre, FRANCE
[4]CentralInstitute fot Labour Protection - National Research Institute, Warszawa, POLAND
[5]Commissariat a l'Energie Atomique et aux Energies Alternatives, Sacley, FRANCE.
Keywords: Aerosol instrumentation, Nanoparticles, Respirable aerosols, Particle surface area
Presenting author email: mle@nrcwe.dk

It has been proposed that the toxicity of low-solubility nanomaterials is mainly dependent of the specific surface area of the particles (Oberdörster *et al* 2005). There has also been an increased availability in instrumentation for measuring the surface area of small-sized airborne particles. There is, however, still questions on to what extent the surface area of structurally complex dust particles from powders can be measured and how these measurements differ from data converted from size distributions from mobility and aerodynamic particle classification. Finally it is uncertain whether there is a reliable link between specific surface area of bulk powders and the surface area of the airborne particles as well as filter-collected respirable dust. Such a link would be crucial for the potential use of data on powder materials as well as future strategies in work-place monitoring and procedures in risk assessment.

Dustiness test using the small rotating drum (Schneider and Jensen, 2008) has been used in order to simulate industrial use of powders and thereby classifying them for risk assessments. This method was used with six chemically and structurally different materials stretching over a range of specific surface area from 0.03 to 225 m^2/g to produce test aerosols. Direct measurements on surface area were done using a Nanoparticle Surface Area Monitor (NSAM 3550, TSI) and an Aerotrak (9000, TSI). Additional size distribution measurements were done using a Fast Mobility Particle Sizer (FMPS 3091, TSI) and an Electric Low Pressure Impactor (ELPI+, Dekati). All size distribution data was recalculated with alveolar deposition to fit surface area instruments before being changed into surface area concentration assuming spherical shape. Respirable dust was collected for gravimetric measurements and analysis of surface area by off-line Small Angle X-ray Scattering (SAXS). Additional sampling of collection plates were done for analysis with Scanning Electron Microscopy.

Initial experiments showed a good agreement over the whole range of surface area concentrations for the two different surface area measurement instruments used. Figure 1 shows the calculated surface area measured using FMPS plotted against that measured using the surface area monitors. Despite some important deviations from 1:1 correlation, the dust surface area measured using FMPS generally appears to correlate well with that of the surface area monitors, throughout the whole surface area concentration range. The general disagreement between the methods increases slightly at lower surface areas, e.g., for TiO_2 measured using NSAM. It can also be noted that the Aerotrak seems to compare best against the FMPS, with the NSAM systematically giving slightly lower measurements, especially for higher levels of surface area concentrations. Similar comparisons between instruments for surface area measurements and ELPI initially show a systematic error and feeble agreement.

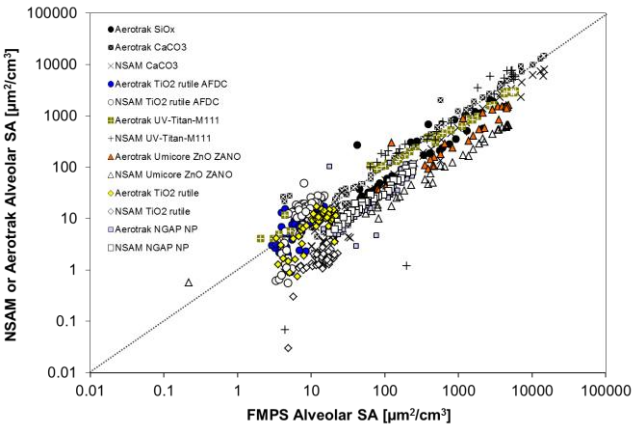

Figure 1. Correlation plot of time-series data on measured surface area using surface area monitors and FMPS. Dotted line indicates one-one correlation.

This work was sponsored by the EU FP7 project NANODEVICE contract NMP4-LA-2009-211464.

Oberdörster G, Oberdörster E, Oberdörster J. 2005 Nanotoxicology: an emerging discipline evolving from studies of ultrafine particles. *Environ Health Perspect* 113:823-839.

Schneider T and Jensen K.A. 2008 Combined single-drop and rotating drum dustiness test of fine to nanosize powder using a small drum. *Ann Occup Hyg* 52:23-34.

Medical effect from nanoparticlate hypotensive drugs inhaled by male rats

A. A. Onischuk[1,2], T. G. Tolstikova[3], M. V. Khvostov[3], I. V. Sorokina[3],
A.M. Baklanov[1], O. V. Borovkova[1], V. V. Boldyrev[4,5], V. M. Fomin[6]

[1]Institute of Chemical Kinetics & Combustion, RAS, Novosibirsk, 630090, Russia
[2] Novosibirsk State University, Novosibirsk, 630090, Russia
[3]Institute of Organic Chemistry, RAS, Novosibirsk, 630090, Russia.
[4]Scientific and Education Centre "Molecular design and ecologically safe technologies"
Novosibirsk State University, 630090, Russia.
[5]Institute of Solid State Chemistry & Mechanochemistry, RAS, Novosibirsk, 630090, Russia
[6] Institute of Theoretical and Applied Mechanics, RAS, Novosibirsk, 630090, Russia
Keywords: aerosol drug administration, particle lung deposition, non-steroid anti-inflammatory drugs, mice.

Presenting author email: onischuk@kinetics.nsc.ru

The administration of drugs directly into the respiratory tract has been used in a number of therapeutic area, including treatment of both lung and systemic diseases. The respiration of nano-sized particles gives some advantages with respect to the inhalation of micron-sized ones. First of all, the particles 10 to 20 nm in size deposit to the alveolar region about 4 times more efficiently than those of several microns in diameter. Moreover, the nanoparticles are easily transported across the membranes. In this paper we study the medical effect from inhalation of nanopaticulate nisoldipine (hypotensive drug) synthesized via the evaporation-condensation route. The male rats WISTAR and ISIAH were used as laboratory animals. The nose-only and whole body exposure chambers were used to study the inhalation effect. The chambers were designed and created in the Institute of Chemical Kinetics and Combustion, Russian Academy of Sciences.

The inhalation scheme includes a flow aerosol generator, inhalation chambers, filters, diluters, flow control equipment and aerosol spectrometer (Fig. 1). The evaporation - condensation aerosol generator consisted of a horizontal cylindrical quartz tube with an outer heater. Argon flow was supplied to the inlet and the aerosol was formed at the outlet. The particle mean diameter and number concentration were varied in the ranges 3 to 200 nm and 10^3 to 10^7 cm^{-3}, respectively, as measured by an Automatic Diffusion Battery. The Liquid Chromatography and X-Ray Diffraction methods were used to control the particle composition. The nose-only exposure chambers were used to determine the lung deposited dose and the particle deposition efficiency as a function of the mean particle diameter.

The medical effect was determined as the relative decrease of blood pressure P_i-P_f/P_i, where P_i and P_f are the blood pressures before and after inhalation (Fig. 2). The groups of five animals were used in each inhalation experiment. The inhalation time was 40 min. The mean diameter of inhaled particles is shown for each inhalation experiment.

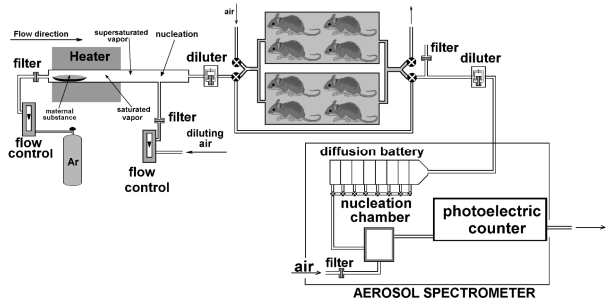

Fig. 1. Experimental set-up for inhalation experiments.

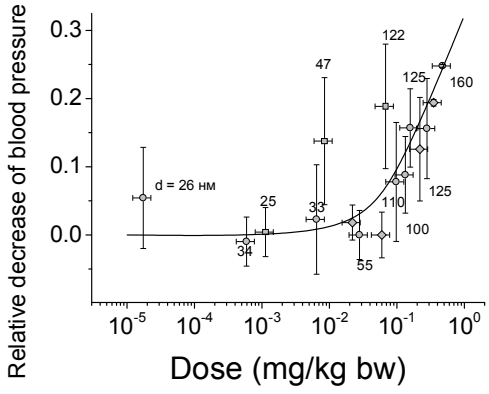

Fig. 2. Relative decrease of blood pressure vs. the inhaled or injected dose. Circles - inhalation (WISTAR), squares - inhalation (ISIAH), diamonds - injection (WISTAR).

Financial support for this work was provided by the Siberian Branch of Russian Academy of Sciences (Interdisciplinary Integration Project No. 108) and RFBR project no. 11-08-01204-a.

Aerosol Particles in Different Types of Museum Environment

L. Mašková[1,2], J. Smolík[2], and M. Ohlídalová[3]

[1]Charles University in Prague, Faculty of Science, Institute for Environmental Studies, Benátská 2, 12 801, Prague 2, Czech Republic
[2]Department of Aerosol and Laser Studies, Institute of Chemical Process Fundamentals AS CR, v.v.i., Rozvojová 135, 165 02, Prague 6, Czech Republic
[3]National Museum, Václavské náměstí 68, 115 79 Prague 1, Czech Republic
Keywords: Indoor/outdoor particles, mass size distribution, chemical composition
Presenting author email: maskova@icpf.cas.cz

Aerosol particles are one of the major pollutants in outdoor and indoor air. They may negatively influence health, but also have negative effects on ecosystems and cultural heritage. Particulate matter (PM) can be harmful for works of art by causing soiling and chemical damage, depending on particle size and chemical composition (Hatchfield, 2005). The aim of this study was to investigate concentrations and sources of airborne PM in two types of indoor environment of the National Museum (NM): a) in an exhibition hall in the centre of Prague and b) in a depository in a small town Terezin.

The measurements have been done during two intensive campaigns and included particle number concentrations and size distributions determined by a Scanning Mobility Particle Sizer (SMPS 3936, TSI, USA) and an Aerodynamic Particle Sizer (APS 3321, TSI, USA). Both instruments sampled alternately from indoor and outdoor, covering the size range 14 – 20,000 nm. In NM Prague visiting hours took place every day from 10 am to 6 pm and the depository in NM Terezin is closed for public.

In the NM Prague the results showed visitors as a source of coarse particles and traffic in the outdoor environment as the most probable source of fine particles. In the NM Terezin the results indicated smoking in an adjacent office as an important source of fine particles. Average value for the indoor/outdoor ratio of the submicron particle number concentration had a maximum between particle diameters of 0.1 – 1 μm for both museums, which indicates a maximum penetration factor and low indoor deposition velocity of these particles. During a day windows in Prague were mostly opened which resulted in a higher penetration than in Terezin. During the visiting hours in Prague the average indoor concentration of coarse particles was even higher than outdoors, which confirmed visitors as a source of these particles (Fig. 1).

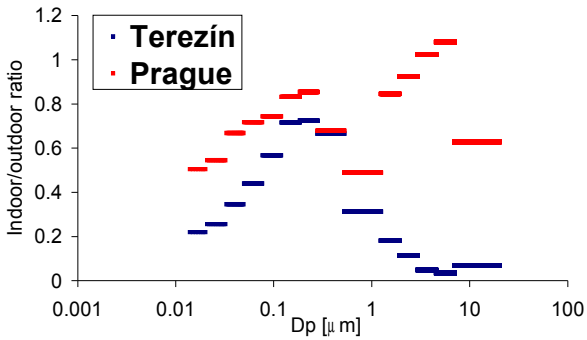

Figure 1. Indoor / outdoor ratios of particle number Concentration versus particle size in the NM Prague and Terezin.

This work was supported by the Grant Agency of the Charles University under grant 307111.

Hatchfield, P. B. (2005) *Pollutants in the Museum Environment*, Archetype Publications Ltd.

Transport of particulate matter in the indoor environment of the National Library in Prague

J. Smolík[1], L. Mašková[1,2]

[1]Department of Aerosol and Laser Studies, Institute of Chemical Process Fundamentals ASCR, v.v.i.
[2] Charles University in Prague, Faculty of Science, Institute for Environmental Studies
Keywords: transport, particulate matter, indoor environment, brownian diffusion
Presenting author email: smolik@icpf.cas.cz

In order to determine sources of particulate matter (PM) inside the National Library in Prague, transport between indoor and outdoor environment, transport inside the Library and deposition on books and manuscripts, we measured size resolved particle number concentrations of PM using Scanning Mobility Particle Sizer (3936L, TSI, USA) and Aerodynamic Particle Sizer (3321, TSI, USA), sampling alternately indoors and outdoors of Baroque Library Hall. In parallel spatial distribution of PM was measured by four DustTrak instruments (8520, TSI, USA), located at different positions and heights inside the Hall. During the sampling air exchange rate was measured by Indoor Air Quality Monitor PS 32 (Sensotron, Poland) and size resolved PM was sampled with two Berner type Low Pressure Impactors (BLPI, 25/0.018/2, Hauke, Austria) for subsequent analysis. The deposition of particles on indoor surfaces was examined using Whatman filters located on the free shelf of the Library. All measurements were performed during three intensive campaigns in 2009.

The results showed, that visitors were the main source of coarse particles and atmospheric PM, penetrating from the outdoor environment, the main source of submicron particles. The average concentrations of size fractions 10 - 100 nm and 100 nm-1 μm of indoor PM were of the order 10^3 particles/cm^3 with quite uniform concentrations. The I/O concentration ratio had maximum at about 300 nm with the highes values observed during the winter probably due to higher air exchange rate caused by larger temperature difference between indoor and outdoor environment. The Ion Chromatography revealed that the major water-soluble inorganic component of indoor submicron particles was ammonium sulphate with maximum concentration also centred at 300 nm (Andělová *et al,* 2010).

The deposition experiments were focused predominantly on test if submicron particles can penetrate by diffusion between pages. For this purpose twelve bunches of Whatman filters, fixed in open Petri dishes, were placed on free shelf of Library. Bunches were gently loosed to increase the distance between filters and exposed for three, six, nine, and twelve months. Exposed filters were examined by Scanning Electron Microscopy (SEM) and Ion Chromatography (IC).

To estimate penetration of particles between filters and subsequent deposition on inner surfaces we modelled transport of particles as nonsteady Brownian diffusion between two parallel discs, put into the environment with constant particle number concentration 10^3 particles/cm^3. The diffusion equation was solved numerically for particle sizes 10, 100, and 1000 nm and gap between filters 1 and 5 mm. Simple model showed that submicron particles can penetrate by diffusion between two parallel sheets of filter, followed by deposition on filter surfaces. The particle penetration and deposition depended on particle size and width of the gap, with the depth of the penetration limited by parallel diffusional deposition on filter surfaces. Smaller particles penetrated faster and deeper resulting in higher particle number concentration of deposited particle but higher mass was transported by larger particles (Smolík *et al* 2011). SEM investigations of exposed filters showed variety of particles of all sizes deposited uniformly on the surface of the top (first) filters, and smaller particles deposited on subsequent filters with concentrations decreasing with the distance from the filter edge. Since up to 60% of mass of water-soluble part of indoor submicron particles was formed by ammonium sulphate (Andělová *et al* 2010), sulphate anion was used as a marker for deposited particles. Results of IC analyses, corrected for blank values, showed that the sulphate concentrations on all filters increased with time. Higher concentrations were found on top filters due to larger exposed area.

Conclusions

Measurements of indoor PM, performed in the National Library in Prague showed the main source of coarse particles were visitors and main source of submicron particles was atmospheric PM, penetrating indoors from the outdoor environment. The particles were uniformly distributed indoors and contained ammonium sulphate. Deposition experiments showed that submicron particles can penetrate into gaps between pages of books by Brownian diffusion.

This work was supported by the Ministry of Culture of the Czech Republic under grant DF11P01OVV020.

Andělová, L.,Smolík, J.,Ondráček, J.,López-Aparicio, S., Grøntoft, T. and Stankiewicz, J. (2010) *e-Preservation Science* **7**, 141-146.

Smolík, J., Mašková, L., Zíková, N. and Ondráček, J. (2011) *Proc. 12nd Ann. Conf. of the Czech Aerosol Soc.*19-24.

Temporal evolution of pyrethroid aerosol concentrations after insecticide spray treatment in indoor atmosphere using a High Resolution Aerosol Time-of-Flight Mass Spectrometer (HR-ToF-AMS)

Aude Vesin, Nicolas Marchand, Etienne Quivet, Brice Temime-Roussel, Henri Wortham
Aix-Marseille Univ, CNRS, FRE 3416, Laboratoire Chimie Environnement, 13331 Marseille cedex 3, France
Keywords: pyrethroids, indoor atmospheres, HR-ToF-AMS, insecticide sprays.
Presenting author email: Nicolas.Marchand@univ-amu.fr

Providing high-time resolved monitoring of pesticide aerosol concentrations in the indoor atmosphere is necessary to accurately characterize the active substances behaviour after the use of household insecticide sprays. Due to the high time variability of the concentrations during these applications, the use of a high time-resolution instrument is relevant to supplement the state-of-the-art off-line methods (Berger-Preiss *et al*, 2009). Data on peak concentrations and kinetics are actually significant information in a perspective of human exposure evaluation.

The analytical method is based on the utilization of a High Resolution Aerosol Time-of-Flight Mass Spectrometer (HR-ToF-AMS) (Aerodyne Research), providing high-time resolved as well as size- and chemically-resolved on-line measurements of aerosols (Jimenez *et al*, 2003).

Materials/Methods

The HR-ToF-AMS, originally designed to measure the aerosol composition outdoors, provides chemical composition information about nitrate, sulphate, chlorine and total organic fractions. However, due to their known harmful health effects, it is found relevant to dissociate the contribution from the active substance relative to the additives to obtain precise concentration profiles of the pesticides alone. For that, the fragmentation tables were modified to follow pesticide concentrations alone instead of total organics.

Validation of this innovative data treatment is realized *via* the intercomparison of the HR-ToF-AMS pesticide concentrations obtained after fragmentation table modification with a more classical off-line sampling and analysis. Statistical analyses using the Chemical Mass Balance technique are also realised to validate data treatment.

Field measurements

Spraying experiments involving 5 different commercial insecticides containing permethrin, cypermethrin, tetramethrin, prallethrin, and/or piperonyl butoxide (PBO), mixed or not, were carried out under air exchange rate (AER) controlled conditions (around 0.5 h^{-1}) in a full-scale room, located in the "Mechanized house for Advanced Research on Indoor Air" (MARIA) experimental house, at the Scientific and Technical Center of Building (CSTB) research centre in Marne-la-Vallée, France. The insecticides were manually sprayed for 3 s. The air was monitored during and after application.

The presented concentration temporal profile (Fig.1) concerns a commercial spray containing permethrin, tetramethrin and PBO for which the peak concentrations are shown in Table 1.

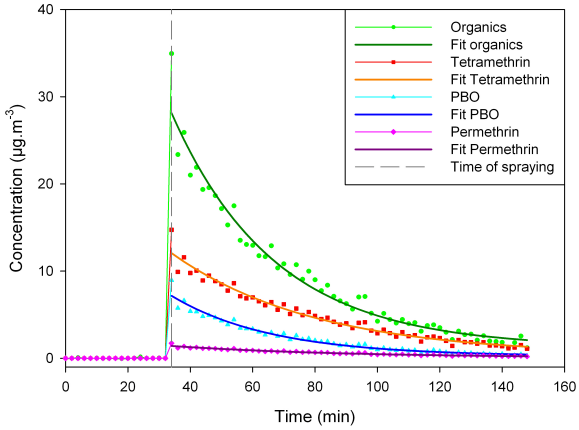

Figure 1. Concentration profiles after spraying

The time-dependent pesticide elimination kinetics is described in Eq. (1), assuming a well-mixed volume:

$$C(t) = C_{max}.e^{-K.t} \quad (1)$$

With t is the time (h), C(t) is the pesticide concentration (µg.m^{-3}), C_{max} is the maximum concentration (µg.m^{-3}), K is the elimination rate constant (h^{-1}).

Table 1. Characteristics of the temporal concentration profiles

	Peak concentration (µg.m^{-3})	Elimination rate constant (h^{-1})
Organics	35±6	1.8±0.2
Permethrin	1.7±0.3	1.1±0.2
Tetramethrin	15±3	1.3±0.2
PBO	9±2	1.9±0.2

The overall elimination rate constants (Table 1) are found to be far higher than the theoretical AER, therefore indicating that significant other elimination processes occur, such as particle deposition.

This work was supported by the French Environment and Energy Management Agency (ADEME) and the French National Centre for Scientific Research (CNRS).

Berger-Preiss, E., Koch, W., Gerling, S., Kock, H., Appel, K.E. (2009) *Int. J. Hyg. Environ. Health*. **212**, 505-518.

Jimenez, J.L., Jayne, J.T., Shi, Q., Kolb, C.E., Worsnop, D.R., Yourshaw, I., Seinfeld, J.H., Flagan, R.C., Zhang, X., Smith, K.A., Morris, J.W., Davidovits, P. (2003) *Aerosol Sci. Technol*. **33**, 49-70.

Particulate matter in school classrooms and outdoor air

C. Alves, T. Nunes, J. Silva, M. Duarte, C. Borrego

Centre for Environmental and Marine Studies (CESAM), Department of Environment, University of Aveiro, 3810-193 Aveiro, Portugal.

Keywords: indoor air quality, schools, PM_{10}, $PM_{2.5}$, OC/EC, water soluble ions.

celia.alves@ua.pt

EPA studies of human exposure to air pollutants indicate that indoor air levels of many pollutants may be 2-5 times, and occasionally more than 100 times, higher than outdoor levels. These levels of indoor air pollutants are of particular concern because it is estimated that most people, including children, spend as much as 90% of their time indoors. Over the past several decades, the exposure to indoor air pollutants is believed to have increased due to a variety of factors, including the construction of more tightly sealed buildings, reduced ventilation rates to save energy, the use of synthetic building materials and furnishings, and the use of chemically formulated personal care products, household cleaners, etc.

In January 2011, one kindergarten and eight elementary school classrooms were monitored (Table 1). The campaign included simultaneous measurements, indoors and outdoors, of comfort parameters, CO, CO_2 and particles. Automatic monitors using a light scattering technique were employed to measure PM_{10} continuously. During occupied periods, low volume samplers were used to daily collect $PM_{2.5}$ onto quartz fibre filters, which were subsequently analysed for carbonates, organic carbon (OC), elemental carbon (EC) and water soluble inorganic ions.

Table 1 School classrooms selected for the indoor air quality monitoring campaign in Aveiro, Portugal.

School	Characteristics	Nº of classrooms
Glória Elementary	Traffic City centre	3
Esgueira Elementary	Urban Residential	2
Esgueira Kindergarten	Urban Residential	1
Eixo Elementary	Rural	3

The daily average $PM_{2.5}$ concentrations obtained during the occupancy periods ranged from 44±5.0 μg m^{-3} to 111±16 μg m^{-3}. The highest values were obtained in the school with the highest occupancy rates. In addition, this school, located in a residential area, is the only one surrounded by an unpaved playground. Soil particles are tracked in on shoes or clothing from the outdoors, contributing to indoor-to-outdoor ratios (I/O) ranging from 1.8 to 3.2. I/O ratios between 1.5 and 2.0 were obtained in the other two schools, where comparable $PM_{2.5}$ concentrations have been measured. In the classroom with highest occupancy rates, the average PM_{10} levels for daytime and night-time periods were, respectively 362±84 and 111±36.9 μg m^{-3}. The corresponding $PM_{10}/PM_{2.5}$ ratios were 7.51±0.98 and 3.12±0.45. This suggests that high PM_{10} levels found in classrooms are probably due to resuspension of soil material or other coarse particles. The maximum concentrations coincided with the cleaning activities (Fig. 1).

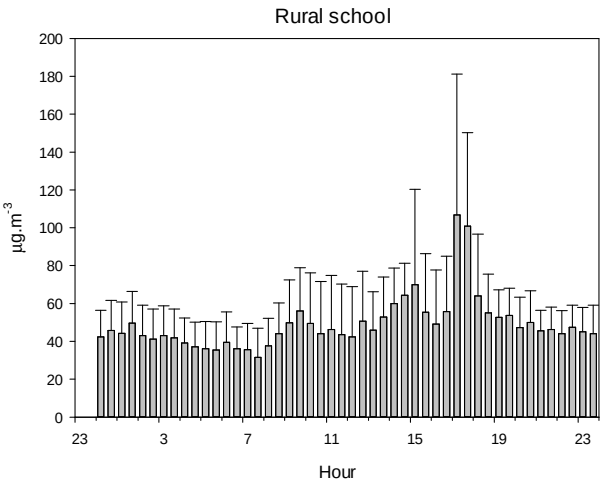

Fig. 1. Diurnal PM_{10} pattern in one of the classrooms.

The total of EC, OC and ions amounted to around 50% of the $PM_{2.5}$ in indoor air. A substantial contribution of calcium carbonate from chalk and/or soil dust to total particle mass was observed. Comparatively, the carbonate mass fraction in outdoor air is much lower.

CO_2 concentrations during school hours at a given day and classroom varied from 1300 ppm up to 7000 ppm, largely exceeding the limit of 1000 ppm stipulated in legislation. Regardless of classroom, the air exchange rates were not higher than 0.2 h^{-1}, showing an effective building tightness with closed windows that is responsible for the high levels of CO_2 and the extremely low outdoor air infiltration of not more than 0.4 L/s per person. The Portuguese legislation recommends a minimum outdoor airflow of 8.3 L/s per person.

This work was funded by the Directorate General for Health and Consumer Affairs (DG SANCO) through the "SINPHONIE - Schools Indoor Pollution and Health: Observatory Network in Europe" project.

Indoor and outdoor ultrafine particle characterisation in primary schools in Barcelona

M. Viana[1], I. Rivas[2], J. Sunyer[2], L. Bouso[2], M. Álvarez[2], Sioutas C[3], A. Alastuey[1] and X. Querol[1]

[1] Institute for Environmental Assessment and Water Research (IDÆA-CSIC), Barcelona, 08034, Spain
[2]Centre for Research in Environmental Epidemiology, Barcelona, 08003, Spain
[3]University of Southern California, Los Angeles, CA 90089, U.S.
Keywords: ultrafine particles, chemical characterisation, indoor air, I/O ratios
Presenting author email: mar.viana@idaea.csic.es

Major knowledge gaps exist currently regarding the health hazardous effects of exposure to fine and ultrafine atmospheric particles of outdoor and indoor origin, in indoor environments. This is especially true for specific risk groups such as children. The early school years are considered an important window for brain development, but also a long period of vulnerability given that susceptibility to environmental threats is elevated.

Recently, research interest has been directed towards ultrafine particles (UFPs, particulates with aerodynamic diameter <0.1 μm). Epidemiological studies (Donaldson *et al.*, 2001) indicate that UFPs may have an even greater potency to cause adverse health effects than larger particles, given that they have increased deposition rates in the lower respiratory tract. UFP are enriched in organic carbon content as well as prooxidative polycyclic aromatic hydrocarbons (PAH) that promote oxidative stress and inflammation. There is little information on the trend in UFP in European urban atmospheres, but the increased load of diesel vehicles and recent data (Wichmann, 2000) suggest an upward trend.

Population exposure to both supra- and sub-micron particulate concentrations is usually considered to take place in outdoor environments. However, it is estimated that on average adults spend 60-90% of their time indoors. In the case of children, already 30% of their time is spent indoors during school hours, independently of other indoor environments.

While most of the available studies on UFP focus on particle mass, there is still very little information on the indoor/outdoor relationship for other parameters such as chemical composition and emission sources. The main goal of the present work is to characterise child exposure to chemically-characterised ultrafine particles of outdoor and indoor origin in schools, with special attention to the influence of outdoor emission sources (e.g., vehicular traffic) on indoor air.

To this end, indoor and outdoor sampling of UFP concentrations is currently being carried out at 38 primary schools in Barcelona, within the framework of the ERC Advanced Grant BREATHE. UFP are sampled by means of PCIS impactors (Sioutas Personal Cascade Impactors), using 37mm and 25 mm Pall quartz-fibre filter substrates. Three cut-off sizes are used: >$PM_{2.5}$, $PM_{0.25\text{-}2.5}$, and $PM_{0.25}$. The sampling duration is 8 hours per day (9-17h, school hours) over 4 consecutive days, amounting to a total of 32 hours per filter. The flow is set to 9 lpm. The cascade impactors will provide detailed information on the chemical composition of ultrafine particles (particle size <0.25 microns). The chemical characterisation will be complete (>65 elements and components determined). The meteorological variations between sampling days at different schools will be accounted for by analysing indoor/outdoor ratios, in addition to absolute particle concentrations. The ventilation conditions (e.g., open or closed windows) will also be taken into account.

Because of the large number of schools targeted (38 schools), preliminary results available at this moment refer mainly to the optimisation of the experimental setup (the results on the chemical characterisation of indoor and outdoor UFPs will be presented at the conference). Numerous sampling durations were tested in order to determine the minimum number of hours necessary to achieve enough UFP mass for the analytical determinations (32 hours). A custom-made mobile sampling unit was devised (Figure 1), to ensure instrument mobility and minimise noise-effects (sampling is carried out inside the classrooms filled with children). Laboratory procedures were also optimised and adjusted to the low UFP mass collected on the filters.

Figure 1. Mobile sampling unit for indoor and outdoor environments.

This work was carried out in the framework of the European Research Council (ERC) Advanced Grant BREATHE. It was supported by national projects IMPACT (CGL2011-26574) and VAMOS (CGL2010-19464/CLI).

Donaldson, K.; MacNee, W. (2001). International Journal of Hygiene and Environmental Health. 203:411-415.

Wichmann, H.E.; Peters, A. (2000) Phil T Roy Soc. A 358:2751-2769.

Variations of PM concentrations in Lithuanian multifamily buildings: Preliminary results from INSULAtE study

Tadas Prasauskas[1,*], Dainius Martuzevicius[1], Edvinas Krugly[1], Darius Ciuzas[1], Ulla Haverinen-Shaughnessy[2], Mari Turunen[2], Virpi Leivo[3], Anu Aaltonen[3] and the INSULAtE Project Group

[1] Department of Environmental Engineering, Kaunas University of Technology, Kaunas, LT-50254, Lithuania
[2] National Institute for Health and Welfare (THL), Kuopio, FI-70701, Finland
[3] Tampere University of Technology (TUT), Tampere, FI-33101, Finland
Keywords: Particulate matter, Indoor/outdoor particles, Optical particle counter
Presenting author email: tadas.prasauskas@ktu.lt

Introduction

Buildings in the developed countries are becoming increasingly airtight as a response to more strict energy efficiency requirements. These changes are likely to have impacts on exposure to indoor air pollutants in residential buildings. The indoor/outdoor (I/O) particulate matter (PM) ratios vary considerably due to the difference in size-dependent indoor PM emission rates, the geometry of the cracks in building envelopes, and the air exchange rates.

INSULATE project aims to assess of the impacts of building renovation on indoor air quality (IAQ). In the first stage of the project activities, the concentrations of PM together with other parameters were assessed before building renovation. In this study, the variations of particulate matter were presented as an average PM2.5 and PM10 mass and number concentrations in five buildings (Table 1).

Methods

Field studies are in process in two European countries (Finland and Lithuania), including 20 multi-family buildings per country. Five multifamily buildings have been measured in Kaunas city so far (approximately five apartments per building).

Measurements of size segregated PM were performed using the Lighthouse Handheld 3016 IAQ Optical Particle Counter (OPC, 6 channels, in a range of 0.3-10 µm). PM measurements were carried out both inside (preferable living room) and outside of the residence (e.g., balcony), OPC units were located at the same location during entire measurement period. Sampling duration in one apartment was approx. 24 hours, with a 1-minute measuring resolution for both indoor and outdoor PM measurements. Particle mass concentrations were calculated based on particle density of 1.5 g/cm^3.

Results

The calculated average PM2.5 and PM10 levels revealed substantial difference among different buildings (Table 1). The outdoor PM2.5 and PM10 concentrations were approximately 2 and 1.5 times higher compared to indoor concentrations. In 3rd and 4th building the highest PM concentrations were observed compared to the other buildings. This was likely influenced by changes in outdoor climatic conditions, namely, decreased temperature. Therefore, PM concentrations were likely to be influenced by biofuel burning in residential homes. During this measurement campaign outdoor PM2.5 mass concentration for each of the five buildings (outside of five apartments) ranged from 10.2±2.4 to 20.8±5.5, 10.2±4.3 – 19.9±4.8, 18.5±5.2 – 40.3±19.9, 29.5±5.7 – 49.2±14.8 and from 7.3±3.2 to 11.4±5.2 µg/m^3, respectively. PM10 mass concentrations varied in a similar pattern to PM2.5. Based on these data, spatial distribution of outdoor PM2.5 and PM10 mass concentrations were observed depending on the location of each apartment in the building, taking into account the proximity of streets.

Table 1. Daily indoor and outdoor particle mass concentrations of PM2.5 and PM10 in five Lithuanian multifamily buildings (average of 5 apartments).

	IN, µg/m^3		OUT, µg/m^3	
Building	**PM2.5**	**PM10**	**PM2.5**	**PM10**
1	9.8±1.7	19.6±2.6	15.9±4.5	20.8±5.3
2	4.9±1.7	17.4±13.5	14.6±4.5	27.4±1.7
3	12.9±4.1	22.0±8.9	30.0±10.3	36.0±12.1
4	18.1±9.6	23.1±9.5	37.0±9.9	55.8±19.4
5	6.4±4.5	14.3±8.6	9.4±2.1	13.1±2.8

Similarly to mass concentration, the highest number concentrations (PNC2.5) were assessed during measurement campaigns of buildings 3 and 4. Outdoor particle number concentrations ranged from 97.1±27.2 to 271.2±72.1 #/cm^3 for buildings 5 and 3, respectively.

Table 2. PNC2.5 number concentrations variation in five multifamily buildings (indoor and outdoor), expressed as # of particles per cm^{-3}.

Building	IN, #/cm^3	OUT, #/cm^3
1	95.4±20.2	159.2±39.6
2	51.6±17.8	130.9±58.5
3	135.7±22.7	271.2±72.1
4	204.6±115.4	264.2±35.2
5	58.0±24.1	97.1±27.2

Acknowledgement. This work is being carried out as a part of INSULAtE (Improving energy efficiency of housing stock: impacts on indoor environmental quality and public health in Europe) project, co-financed by EU Life+ programme. Homepage: www.insulateproject.eu

Personal daily exposure of children to ultrafine particles and black carbon

C. Vargas Trassierra[1,2], S. Marini[1], L. Stabile[1], A. Russi[1], F. Fuoco[1], G. Buonanno[1],

[1]Dept. of Civil and Mechanical Engineering, University of Cassino and Souther Lazio, Cassino (FR) 03043, Italy
[2]INMRI, Istituto Nazionale di Metrologia delle Radiazioni Ionizzanti, ENEA Casaccia, Roma, 00123 Italy
Keywords: children exposure, personal monitoring, ultrafine particles, black carbon
Presenting author email: c.vargas@unicas.it

Epidemiologic evidence indicates a relationship between particle pollution exposure and adverse respiratory and cardiovascular health effects, including decreased lung function, asthma, myocardial infarction and all-cause mortality (Brunekreef and Holgate, 2002). In general, the smaller the particle size, the greater its ability to penetrate into the lungs and thus to produce adverse effects on human health. For this reason, sub-micrometer particles and even more UFPs (diameter < 0.1 μm), show higher health care interest than other particle sizes. Anyway, while there is considerable toxicological evidence of potential harmful effect of UFPs on human health, epidemiological studies are still not sufficient for conclusions on the dose-response relationship concerning this aerosol fraction (WHO, 2005).

This study, which falls within the UPTECH international project, deals with the children's personal exposure assessment to UFPs and black carbon. BC was used as an indicator of exposure to diesel exhausts whose negative health effects (short and long-term cardiovascular, respiratory and neurodegenerative health effects) were reported in Baja et al., 2010; McCracken et al., 2010.

We considered children because they represent the most vulnerable group with regard to harmful effects of airborne particles exposure. This is due to: i) the higher dose of UFPs as function of the children lung size compared to adult one; ii) their developing organs and immunological system.

Air quality can be measured at four different spatial scales: i) “city scale”, the broadest and most common scale used to characterize air quality across several city blocks using remote measurements; ii) “outdoor scale”, representative of outside building grounds particle exposure; iii) “indoor scale”, within building rooms reflecting indoor-based exposure; iv) “personal scale”, using hand-held instruments carried as a personal monitor in order to assess their actual exposure.

The daily overall children exposure is dominated by particle concentration levels in three main microenvironments: home, school, and transport mode. Therefore, children attending the same school, can receive different doses.

In the present work personal exposure measurements were performed on a sample of about one hundred children aged 8 to 11 years who attend three schools (S_1, S_2, S_3) in Cassino (Italy). S_1 is a primary school located on traffic urban street; S_2 is a secondary school close to intersection of moderate and heavily trafficked urban street; S_3 is a primary school located in a rural area far away from urban traffic.

The personal exposure was monitored through: two hand-held particle counters (NanoTracer, Philips) and one BC monitor (Aethalometer-microAeth Model AE51, MageeScientific). These monitors have a high temporal resolution (1÷16 s for NanoTracer, 1 s ÷ 5 min for Aethalometer), are small and portable (750 g and 250 g, respectively) and do not require special training to use.

NanoTracer, which works by diffusion charging, is able to provide number concentration (in the range 10-300 nm), average particle diameter, and lung deposited surface area concentration measurements. An electrometer measures the current induced by previously charged particles collected on a filter inside a Faraday cage. The device is also able to evaluate the different fractions of the lung deposited surface area through a semi-empiric algorithm implemented by Marra *et al*., 2010.

The Aethalometer detects the changing optical absorption of light transmitted through an internal small teflon-coated borosilicated glass fiber filter where BC-particles are captured.

We monitored children for 24-h, they also filled in a diary reporting the main indoor and outdoor activities (such as studying, eating, transportation, sleeping), also indicating the length of each activity.

From data collected by NanoTracers it was found that school contribution on daily exposure to UFPs is about 15%-20%, with an average particle number concentration in the range $1.5\times10^4 – 5.3\times10^4$ part. cm^{-3}. The highest exposure intensity was measured during lunch time with a contribution of about 20% and particle number concentrations in the range 4.2×10^4-1.9×10^5 part. cm^{-3}.

For BC, as expected, the most contributing activity to personal exposure is transport with an average exposure of 12.4 μg m^{-3}, while lowest average exposure was found at home (4.4 μg m^{-3}).

Baja, E.S., Schwartz, J., Wellenius, G.A., Coull, B.A., Zanobetti, A., Vokonas, P.S., Suh, H.H., 2010. *Environmental Health Perspectives* **118**, 840-846.

Brunekreef, B., Holgate, S., 2002. *Lancet* **360**, 1233-1242.

Marra, J, Voetz, M., Kiesling, H.J. (2010) *J. Nanoparticle Res.* **12**(21).

McCracken, J., Baccarelli, A., et al. (2010). Environmental Health Perspectives **118**, 1564-1570.

WHO, 2005. Regional Office for Europe, Bonn, Germany.

Assessing workers inhalation exposure and dose during production TiO_2 particles

A.J. Koivisto[1], J. Lyyranen[2], J. Jokiniemi[2,3], T. Tuomi[1] and K. Hämeri[4]
[1]Nanosafety Research Center, Finnish Institute of Occupational Health, Helsinki, Topeliuksenkatu 41 a A, 00250, Finland
[2]Fine&Nano Particles, Technical Research Centre of Finland (VTT), Espoo, P.O.Box 1000, 02044 VTT, Finland
[3]Department of Environmental Science, University of Eastern Finland, P.O. Box 1627, 70211 Kuopio, Finland
[4]Department of Physics, University of Helsinki, Helsinki, PO Box 64, 00014, Finland
Keywords: industrial aerosols, exposure, nanoparticle, measurements.
Presenting author email: joonas.koivisto@ttl.fi

Abstract

In conventional inhalation risk assessment, risk is assumed to be a function of hazard and exposure, where the potential hazard is expressed as a function of exposure in mass concentration. However, ultrafine particles (UFPs) are considered to be the most harmful fraction as concerns inhalation uptake (Seaton *et al* 1995). Thus, in the inhalation exposure assessment, size-fractioned concentrations fanging from around 10 nm to 10 μm are needed to estimate quantitative exposure. The exposure data should cover also particle number and surface area dose estimates so that dose-response relations of UFPs can be estimated.

Methods

In this study, we measured with airborne particle concentrations in TiO_2 production plant from following processes: jet milling, hammer milling, pelletizing, and packing. The concentrations were measured with mobility analyzers (SMPS, SMPS+C), aerodynamic analyzers (ELPIs), particle counters (CPCs), real-time mass analyzer (TEOM), and optical instrument (Dust Monitor 1.109). Particle samples were collected from air for electron microscopy analysis. The workers inhalation doses were analyzed as described in Koivisto *et al* (2012), where the workers regional inhalation dose rates was estimated by using the ICRP lung deposition model, and active surface area and mass concentrations were defined from the measured particle size distributions by using the particle mobility diameter and effective density.

Results

By interpreting particle size distribution time series and activity, we identified concentrations originating from combustion sources (soot) and manufacturing processes (H_2SO_4, TiO_2). Converted values were compared with the measured mass and active surface area concentrations. Figure 1b shows that forklifts and pressurized cleaning caused peak particle and mass concentrations respectively over 10^5 cm^{-3} and 1 mg m^{-3}. Mass concentration in Figure 1b correlates nicely with high coarse particle concentrations (Figures 1a and 1c). The workers total dose rates without use of respirator varied in particle number, active sirface area and mass form $0.2 \cdot 10^9$ to $5 \cdot 10^9$ particles min^{-1}, $0.8 \cdot 10^6$ to $20 \cdot 10^6$ μm^{-2} min^{-1}, and 1 to 50 μg min^{-1} (Figure 1d).

Conclusions

This study helps us understand the magnitude of the dose occurring in industry. It provides fundamental data for inhalation exposure risk assessment, regulations, dose metrics, the basis for defining metrics of dose-biological response. For risk assessment, the toxicity of particles should be known.

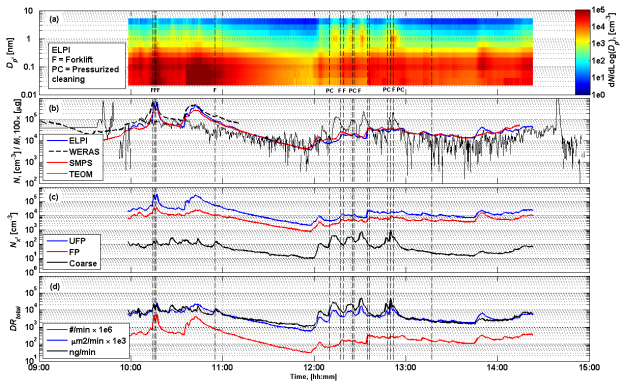

Figure 1: Packing of TiO_2 material: particle size distributions (a), particle and mass concentrations (b), fractions of UFP, FP and coarse particles (c), and dose rates (d). Figures (c) and (d) were calculated from particle size distributions in (a). Effective density was assumed to be 1 g cm^{-3}.

This work was supported by the Finnish Funding Agency for Technology and Innovation, Sachtleben Pigments Oy, Beneq Oy, Amroy Europe Ltd. and The Federation of Finnish Technology Industries.

Seaton A, MacNee W, Donaldson K & Godden D (1995). Lancet **345**, 176-178.

Koivisto, A.J.,Aromaa, M., Mäkelä, J.M., Pasanen, P., Hussein, T. and Hämeri, K. (2012). ACS Nano **6**, 1195–1203.

Semi-volatile partitioning effect on indoor PM: inorganic ions and PAHs.

G. Sangiorgi[1], M.G. Perrone[1], L. Ferrero[1], C. Lo Porto[1], B. Ferrini[1], S. Petraccone[1]

[1]Department of Environmental Sciences, University of Milan - Bicocca, Milan, I-20126, Italy
Keywords: indoor aerosols, gas-particulate partitioning, PM1, PM2.5.
Presenting author email: giorgia.sangiorgi1@unimib.it

The toxicity of PM is stronger for the fine particles and when are present species like PAHs and elements (Delfino *et al*, 2008; Saldiva *et al*, 2002). A little attention has been dedicated to the study of PM in offices, despite they are one of the most common workplaces all over the world.

The aim of the research was to investigate the PM1 and PM2.5 in four offices of Milan (Italy) and in the corresponding outdoor air, in order to highlight the changes of PMx composition. The offices were chosen because of their few and weak indoor sources of PM (i.e. computers, printers and photocopier machines). Smoking was forbidden, air supply systems were absent and the people movement was limited.

24-h PM1 and PM2.5 samples were collected simultaneously indoor and outdoor during two sampling campaigns (aug-oct 2007, jan-mar 2008). The concentration of inorganic ions and Polycyclic Aromatic Hydrocarbons (PAHs) were determined.

The indoor PMx level was 50-70% of the outdoor one: the indoor concentrations were always lower than outdoor, as expected from the low contribution of PM indoor sources.

The indoor (C_{in}) and outdoor (C_{out}) concentrations of PMx and of a particle-bound compound can be linearly related to roughly separate the indoor contributions due to 1) the outdoor fraction that enter indoor (infiltration factor, F_{INF}) and 2) the indoor-generated particle concentration C_{ig} (Hänninen *et al*, 2004):

$$C_{in} = F_{INF} * C_{out} + C_{ig} \qquad \text{(eq.1)}$$

For the analyzed chemical species, C_{ig} produced always negative or near zero values; comparing to the average indoor concentrations, it was <20%.

Table 1. Data of the measured infiltration factors, F_{INF}.

Season	PM1	PM2.5	NO_3^-	SO_4^{2-}	NH_4^+	4-ring PAHs	5-ring PAHs	6-ring PAHs
warm	0.49	0.50	0.19	0.95	0.45	0.92	0.88	1.17
cold	0.60	0.58	0.15	0.86	0.46	0.44	0.46	0.72

F_{INF} (Table 1 and Figure 1) showed the following patterns: I) the non-volatiles (i.e., SO_4^{2-}, present in the form of $(NH_4)_2SO_4$) had about the same F_{INF} during the two campaigns (~0.90); II) the semi-volatile inorganic compounds (i.e., NH_4NO_3) had always very low F_{INF} (NO_3^- ~0.17, NH_4^+ ~0.45); III) the semi-volatile organic compounds (PAHs) had a strong decreasing F_{INF} passing from the warm (~0.96) to the cold (~0.51) season.

When passing from outdoor to indoor, typically the temperature increases, most of all during winter. A semi-volatile molecule will tend to partition more on the gas phase, a process also favoured by the adsorption of the gaseous compounds onto the indoor surfaces (Weschler and Nazaroff, 2008). This effect was observed during the described campaigns.

It is likely that the real F_{INF} of the three inorganic ions was the same and close to the one of SO_4^{2-}, but once indoor a high portion of NH_4NO_3 rapidly had passed in the gaseous phase, thus reducing its particulate concentration and F_{INF}. Since the high vapor pressure of NH_4NO_3, a large fraction of NO_3^- suffered this process, whereas only the particulate NH_4^+ present as NH_4NO_3 passed in the gaseous phase.

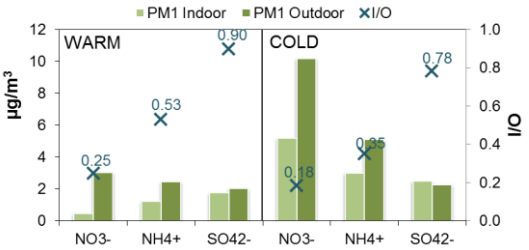

Figure 1. PM1 concentrations and indoor to outdoor concentration ratios of inorganic ions.

For all the PAHs, it was observed a decreasing F_{INF} passing from the warm to the cold season. This was likely due to the stronger difference of temperature between outdoor and indoor during winter.

The different seasonal trend of F_{INF} for the inorganic ions and PAHs could be explained by considering the very high vapor pressure of NH_4NO_3 ($3x10^{-3}$ mmHg) compared with the PAHs ($<4.5x10^{-6}$ mmHg): a very little increasing in the temperature could affect the ammonium nitrate, but not the PAHs partitioning equilibrium.

The results of the research confirm that a semi-volatile compound tend to redistribute in favor of the gas phase when entering indoor, where the conditions are warmer. Taking into account the semi-volatile partitioning effect, a change of the eq.1 is proposed.

Delfino, R.J., Staimer, N., Tjoa, T., Polidori, A., et al. (2008) *Environ. Health Persp.* **116**, 898-906.

Hänninen, O.O., Lebret, E., Ilacqua, V., Katsouyanni, K., et al. (2004) *Atmos. Environ.* **38**, 6411-6423.

Saldiva, P.H.N., Clarke, R.W., Coull, B.A., Stearns, R.C. et al. (2002) *Am. J. Resp. Crit. Care* **165**, 1610-1617.

Weschler, C.J., Nazaroff, W.W. (2008) *Atmos. Environ.* **42**, 9018-9040.

Variation of Wintertime $PM_{2.5}$ and PM_{10} in Primary Schools of Kaunas, Lithuania

E. Krugly[1], T. Prasauskas[1], L. Kliucininkas[1], D. Ciuzas[1], D. Martuzevicius[1]

[1]Department of Environmental Engineering, Kaunas University of Technology, Kaunas, LT-50254, Lithuania
Keywords: $PM_{2.5}$, PM_{10}, Optical particle counter, Indoor particles.
Presenting author email: edvinas.krugly@ktu.lt

Introduction

Children spend significant part of their time in schools. Therefore, indoor air quality affects children's health and ability to learn (Heinrich, J., 2011). Indoor air pollution and its control receiving increasing attention from scientists, health specialists, administrators and policy makers (Mejia et al., 2011).

Particulate matter (PM) is one of the most important air pollutants in indoor air. PM concentrations are regulated by mass concentrations in fractions $PM_{2.5}$ and PM_{10}. Diurnal variations of PM concentrations usually represent the daily school activities, while nighttime concentrations may represent the contribution of PM from outdoor environment.

Methods

The particulate matter was analyzed in indoor air in Kaunas primary school during winter time of 2011/2012. The indoor particulate matter were measured at five schools: School #1 representing residential multi-family apartment building area; School #2 representing residential multifamily apartment building area with heavy industrial influence; School #3 representing residential area, School #4, representing city center with heavy traffic, School #5, representing single family building residential area. All of these sampling sites representing different areas of Kaunas city. $PM_{2.5}$ and PM_{10} concentrations of indoor PM fractions were investigated during analysis period.

PM concentrations were measured using the Lighthouse Handheld 3016 IAQ Optical Particle Counter (OPC, 6 channels, in a range of 0.3-10 μm). PM measurements were carried out inside the classrooms, for five days in one sampling site. PM concentrations were logged with 1-minute resolution.

Results

The calculated 12 hour (6 am-6 pm) mean $PM_{2.5}$ and PM_{10}concentration in Schools are presented in Table 1. During the daytime $PM_{2.5}$ concentration comprised 12-16% of PM_{10} concentration, while during nighttime this contribution has reached 30-50%. The highest difference between $PM_{2.5}$ and PM_{10} concentrations was observed in School #4.

The concentration of $PM_{2.5}$ during day time was 2 – 3 times higher than night time. For PM_{10} differences between day time and night time was about 4 – 12 times. The highest differences were observed in School #5.

Table 1. The calculated 12 hour (6 am. - 6 pm.) mean $PM_{2.5}$ and PM_{10} concentrations in schools.

	Day time		Night time	
	PM2,5	PM10	PM2,5	PM10
School #1	13,28±2,80	38,88±33,30	16,35±4,14	19,63±4,78
School #2	6,88±3,88	50,95±47,62	4,62±20,7	13,87±10,28
School #3	11,19±2,19	78,69±47,89	6,32±0,96	10,22±8,72
School #4	23,11±6,17	178,86±99,76	11,99±4,04	31,68±29,48
School #5	9,70±3,98	58,14±40,27	3,15±0,79	4,67±1,61

5-day averaged $PM_{2.5}$ and PM_{10} concentrations in investigated schools during the sampling period are presented in Fig. 1.

The highest PM concentration in both fractions was measured in sampling site #4, which represents city center. Short-term PM_{10} concentration in schools #3, #4, #5 reached more than 100 $\mu g/m^3$.

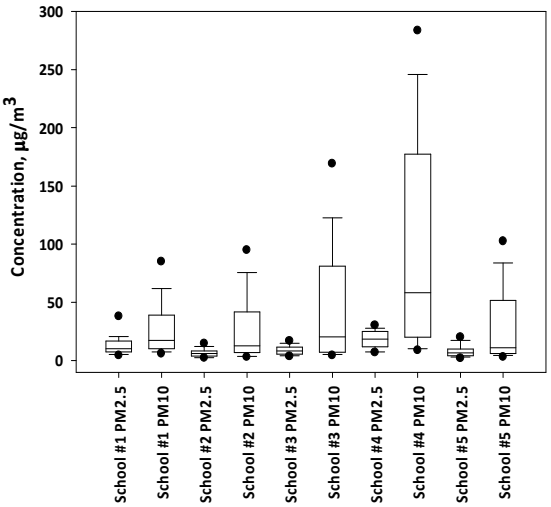

Fig. 1. Daily $PM_{2.5}$ and PM_{10} concentrations in schools of Kaunas, Lithuania. Median, interquartile range, 5th and 95th percentille and extremes are presented of 5-day data registered with 1-minute resolution.

Heinrich, J., (2011) *International Journal of Hygiene and Environmental Health 214 1–25*

Mejia, F. J., Choy, S. L., Mengersen, L. Morawska, K., (2011) *Atmospheric Environment, 45 813-823.*

Biomass burning source: Indoor - Outdoor comparison

Andriani E. [1], Dambruoso P. [1], de Gennaro G. [1], Demarinis Loiotile A[1], Di Gilio A. [1], Marzocca A.[1], Mazzone A. [1], Palmisani J. [1] and Tutino M. [1]

[1]Department of Chemistry, University of Bari, Bari, Apulia Region, 70126, Italy
Keywords: biomass burning, indoor, outdoor, particulate matter
Presenting author email: annalisa.marzocca@uniba.it

On the global scale, biomass burning represents an important source of atmospheric aerosols and greenhouse gases and, in recent years, the growing interest about biomass burning is due to its adverse effects on human health. In fact extensive studies (Nussbaumer, 2003) show that biomass combustion is responsible for high emissions of fine and ultrafine particles which are associated with increased morbidity and mortality. Therefore, more attention should be direct to the indoor biomass burning emissions. Exposure to indoor air pollution, especially to particulates, resulting from biomass burning (wood, charcoal, crop residues) has been implicated as a casual agent of respiratory and eye diseases. These effect are attributed to biomass burning sources, in particular to high levels of pollutants detected in indoor air when there is a fireplace.

The aims of this study are the chemical characterization of PM10 aerosols under the influence of biomass burning emissions and the assessment of the impact of this source on the levels and chemical composition of PM10, both outdoor and indoor environments. In particular, the impact of biomass burning source on the levels and chemical composition of PM has been evaluated in terms of PM10, metals, Polycyclic Aromatic Hydrocarbons (PHAs) and organic and elemental carbon (OC and EC) concentrations, by analysis of samples collected at a few meters from plume of a bonfire. The results of this monitoring have shown that the PM10 concentration (2164 ug/m^3) was about fifty times higher than PM10 collected at background site in no event conditions, and high concentrations of OC, K and PAHs, were observed. The analysis of collected data showed the relevance of organic and inorganic tracer species for interpreting the impact of biomass burning source on PM levels and allowed to determine diagnostic ratio for biomass burning sources. Moreover, higher OC, K and PAHs concentrations were determined in outdoor environments when combustion sources there were. In fact during an outdoor monitoring campaign in Apulia Region it can be possible to confirm that a little town in Apulia region denominated Torchiarolo and characterized by only agricultural activities, was not a regional background site such as it was defined by air quality network. The analysis of the sample collected at Torchiarolo site and trends of PM10, OC, EC, BaP and K concentrations (Fig.1) suggested the presence of an important local pollution sources. Moreover, as shown in Fig 2, PM10, OC and EC, K and PHAs concentrations at Torchiarolo were much higher than an other regional background site in Apulia Region; suggesting the relevance of biomass-burning sources in this area (Amodio et al, 2011), probably due to the presence of a great number of fireplaces used to domestic energy.

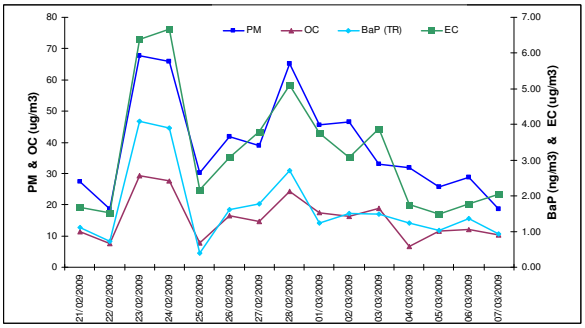

Fig.1: PM10, OC, EC, BaP concentration at Torchiarolo site

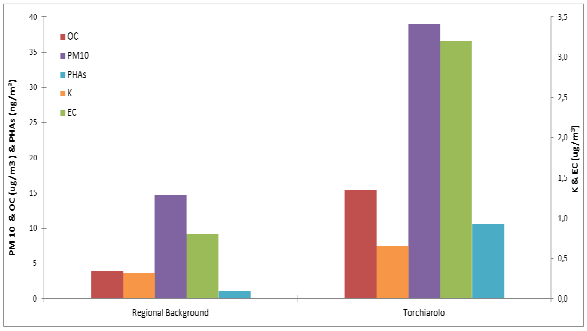

Fig.2 Comparison between two regional background sites in Apulia Region

Finally, the air quality of five houses where there was a fireplace, has been monitored. Every monitoring campaign was performed for three days and PM2.5 and PM10 concentrations have been determinated. The number concentration of fine and ultrafine particles has been detected by a optical particle counters (OPC) and a FMPS (Fast mobility Particle sizer), in order to obtain their dimensional distribution. The chemical characterization of samples was performed in order to determine elements, PAHs, OC and EC.

The preliminary information collected during these monitoring campaigns has allowed to evaluate the impact of biomass burning sources and in particular of fireplaces, on indoor air quality and the chemical composition of PM which people is mainly exposed.

Nussbaumer, T., 2003. Energy and Fuels 17 (6),1510–1521.

Amodio et al., 2011. Boreal Environment Research

Comparison of nasal deposition efficiency between Taiwanese and Caucasian adults

Y.M. Sun[1], C.W. Lee[2] and D.J. Hsu[2]

[1] Department of Occupational Safety and Health, Chung Hwa University of Medical Technology, Tainan 717, Taiwan

[2] Department of Safety, Health and Environmental Engineering, National Kaohsiung First University of Science and Technology, Kaohsiung 811, Taiwan

Keywords: Deposition efficiency, Human nasal passage, Nanoparticles.

Presenting author email: swimming@mail.hwai.edu.tw

Numerous studies on the removal efficiency of inhaled particles in the nasal region have been performed in the past decades, by using either replicate casts or human volunteers (Hsu and Chuang, 2012). Many empirical equations were also developed to characterize the deposition efficiency in this region. However, most of those studies were primarily based on a limited number of white male subjects (Kim and Hu, 2006). Kesavanathan and Swift (1998) pointed out that nasal anatomic and dimensional factor are important in determining the amount of deposition in the nasal passage and that particle deposition data from a demographically diverse group is important. An anthropometric study in Taiwan indicated that Taiwanese have a shorter craniofacial depth (i.e., distance between glabella and occiput) and longer craniofacial width (i.e., distance between two tragi) than Americans (Yu et al., 1996). Another US study suggested that Chinese workers have shorter face length, longer face width and smaller nose protrusion than Americans (Du et al., 2008). These differences in facial features are likely to affect the anatomical structure of the upper respiratory tract and, consequently, the characteristics of particle deposition in this region between the two ethnic groups. Thus, the experimental data of particle deposition in the respiratory tract reported previously will be less applicable to the Asians if the nasal particle deposition is different between two ethnic groups.

Four Taiwanese and two Caucasians adults were recruited to obtain the computed tomography (CT) scans of their respiratory tract extending from nostril/mouth to trachea. The images of the CT scans were used to build the 3D computer model. Then, based on the 3D computer models, the airway models were constructed with epoxy by a rapid prototyping machine (Sony Manufacturing Systems America, Inc., Lake Forest, CA, USA, Model SCS-8000). The human respiratory flow rates of 5, 10, 15, and 20 LPM were used and the particle sizes studied ranged between 14~500 nm. The particle size and number concentrations were measured by a Scanning Mobility Particle Sizer (SMPS) (TSI Inc., Shoreview, MN, USA).

Our results showed the deposition efficiency decreased with the increasing flow rate, and this trend conforms with the published data. Additionally, Figure 1 shows the deposition efficiency of both ethnic groups and Taiwanese adults had higher deposition efficiency than Caucasians. An empirical equation for Taiwanese adults was developed and is shown as follows:

$$\eta = 1 - \exp\left(-12.51 D^{2.970917}\, Q^{-0.40598} \right)$$

where D is the diffusion coefficient and Q the respiratory flow rate. The present study concludes that nasal structures is critical for nasal deposition and in vivo studies on Taiwanese adults should be conducted in the future, so as to provide the basis for the health risk assessment of exposure to particles

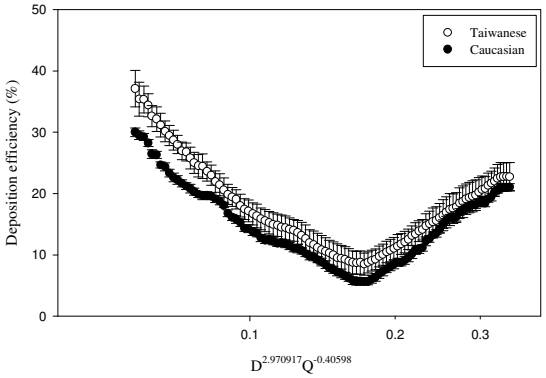

Figure 1. Comparison of nasal particle deposition efficiency between Taiwanese and Caucasian adults.

This work was financially supported by the National Science Council, Taiwan under NSC99-2314-B-327-001-MY2.

Du, L., Zhuang, Z., Guan, H., Xing, J., Tang, X., Wang, L., Wang, Z., Wang, H., Liu, Y., Su, W., Benson, S., Gallagher, S., Viscusi, D. and Chen, W. (2008) *Ann. Occup. Hyg*. 52, 773-782.

Hsu, D.J. and Chuang M.H. (2012) *Aerosol Sci. Technol.* 46, 631-638.

Kesavanathan, J. and Swift, D.L. (1998) *Aerosol Sci. Technol.* 28, 457-463.

Kim, C., and Hu, S.C. (2006) *J. Appl. Physiol.* 101, 401-412.

Yu, C.Y., Yeh, W.Y., Yang, Y.X., and Chang, P.H. (1996) *J.Occup. Safety Health* (in Chinese). 4, 31-46.

Lung deposition of charged aerosol particles – particle characterisation and experimental setup for a human volunteer study

M.D. Wright[1], M.F. Biddiscombe[2], J.C. Matthews[1], S.R. Underwood[2], D.L. Henshaw[1], O.S. Usmani[2] and D.E. Shallcross[1]

[1]Atmospheric Chemistry Research Group, School of Chemistry, University of Bristol, Bristol BS8 1TS, UK
[2]National Heart & Lung Institute, Imperial College London & Royal Brompton Hospital, London SW3 6NP, UK
Keywords: Charged particles, submicron particles, inhalation, lung deposition.
Presenting author email: matthew.wright@bristol.ac.uk

Electrostatic charge may increase particle deposition in the lung upon inhalation (Melandri *et al*, 1983), possibly leading to increased health risks associated with particulate matter. This study seeks to determine whether 100 nm and 200 nm particles which carry excess electric charge, compared to ambient charge-neutralised particles, show enhanced lung deposition efficiency in healthy human volunteers. The outcomes will help to determine the viability of the 'corona ion hypothesis' linking proximity to overhead high-voltage power lines with increased risk of childhood leukaemia (Fews *et al*, 1999) and will also provide important results relevant to the delivery of charged aerosol drugs to the lung.

The study comprises a characterisation stage, currently underway, and a human volunteer clinical study, planned for mid-2012. Figure 1 shows the basic experimental setup. We produce carbonaceous particles radiolabelled with ^{99m}Tc with Technegas (Cyclopharm) using the preparation method of Möller *et al* (2006), and apply increased charge using a corona charger. Enhanced deposition, or a change in the location of deposition, due to particle charge will be identified in a human volunteer study (8 volunteers, 4 study visits each) by direct comparison of inhaled and exhaled particle concentration using Mobility Particle Sizers (Grimm) and Electrical Low Pressure Impactor (Dekati), and via gamma scintigraphy (Usmani *et al*, 2005). We focus on particles of size 100-200 nm, since this is below the size range used in previous volunteer studies of charged particle deposition (Melandri *et al*, 1983). It is also the size range in which particles ordinarily deposit least efficiently within the lung, therefore the potential for electrostatic effects to enhance deposition is maximised.

The Technegas particle size distribution and charge at the output of the device and in the delivery system must be properly characterised to determine the expected dose (number and activity) received by volunteers. Typical number and mass size distributions, and total number concentration and mean particle diameter obtained each minute after actuation of the Technegas generator, are shown in Figure 2. To obtain the smaller particles, the generator chamber must be flushed into a dilution chamber soon after actuation, whereas for larger particles a holding period inside the generator is required to allow the particles to grow through coagulation, although number concentration drops significantly. Number concentration varies from run to run, with typical peak concentrations in the range 1-2 × 10^7 cm^{-3} (mass 1.5-5.0 mg m^{-3}) but the shape of the distribution is similar. The repeatability of the Technegas generator in producing particles of a given size distribution shape is good, but there is some variability in particle number concentration, with implications for possible received ^{99m}Tc dose to patients. Particle size distributions and electric charge states throughout the delivery system, including for the first time the incipient charge state of Technegas particles, along with further details of the clinical study, will be presented.

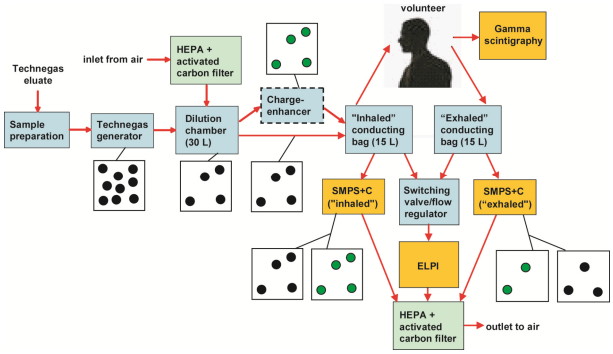

Figure 1. Schematic outlining the experimental setup for the human volunteer clinical study.

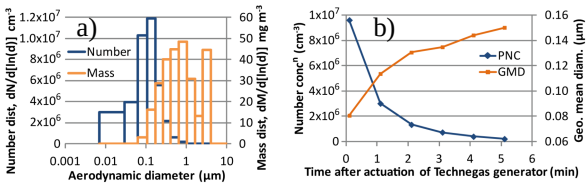

Figure 2. a) Number and mass distributions for Technegas particles, and b) number concentration and mean diameter evolution with holding time.

This work is supported by Children with Cancer UK, Registered Charity No. 298405. MDW acknowledges additional support from EPSRC (Grant EP/J501426).

Fews, A.P., Wilding, R.J., Keitch, P.A., Holden, N.K. and Henshaw, D.L. (1999). *Int. J. Radiat. Biol.* **75**, 1523-1531.

Melandri. C., Tarroni, G., Prodi, V., De Zaiacomo, T., Formignani, M. and Lombardi, C.C. (1983) *J. Aerosol Sci.* **14**, 657-669.

Möller, W., Felten, K., Seitz, J. *et al* (2006). *J. Aerosol Sci.* **37**, 631-644.

Usmani, O.S., Biddiscombe, M.F. and Barnes, P.J. (2005). *Am. J. Resp. Crit. Care Med*. **172**, 1497-1504.

Theoretical and experimental investigation of aerosol deposition in realistic human airway model

A. Kerekes, A. Nagy, A. Czitrovszky

Wigner Research Centre for Physics of the H.A.S., Institute for Solid State Physics and Optics, Budapest, 1121 Hungary

Keywords: laser Doppler anemometry, aerosol deposition, human airway, breath simulator.

Presenting author email: kerekes.attila@wigner.mta.hu

In vivo measurement of the parameters related to transport and deposition of inhaled aerosols within the airways is quite problematic. Although some imaging techniques (MRI, CT, gamma camera, SPECT) can provide useful information regarding particle deposition there are both ethical issues and technical barriers (insufficient resolution, inappropriate size etc.) that hamper their systematic and efficient use. In contrast, in vitro experiments are more suitable, holding less risk and being more cost effective. Similarly, computational techniques are available to anybody. Imre Balásházy's research group has conducted computer simulations to study the fate of the particles after their inhalation. They have participated in the development of the Stochastic Lung Model, which is one of the best known whole respiratory deposition models in the world. They have applied the model to compute regional and generation number specific particle deposition fractions for different breathing parameters and particle characteristics [1-4].

In addition to the advances in the field of simulation of aerosol transport and deposition there is a constant improvement of measurement devices and techniques. Early attempts of aerosol measurements consisted in the measurement of airflow profiles and particle deposition in simplified airway geometries (pipes or simple smooth walled bifurcations). Idealized upper airway measurements have also been performed. For this purpose PIV (Particle Image Velocimetry) and LDV (Laser Doppler Velocimetry) methods can be applied. The development and spread of rapid prototyping techniques has opened new perspectives in this field. Nowadays it is possible to manufacture realistic replicas of the airways by digitally reconstructing them from CT images, then printing them with a 3D printer. A key element of the usage of such replicas for experimental purposes regards their optical transparency.

Numerical modeling of aerosol deposition in the stochastic lung model and the application of the CFD code for various respiratory tracts were performed. The results of the simulations were compared with the experimental results obtained from measurements with the realistic hollow airway model made by rapid prototyping.

Aim of the measurement

In case of aerosol drug administration it is important to deliver the right amount of medication to the right place [5]. In this way drug efficiency can be maximized and side effects minimized. Both computational and experimental efforts were spent to examine how drug deposition sites depend on breathing modes and parameters, especially breathing pattern. The measurements were performed with realistic aerosol drugs administrated by inhalers existing on the market.

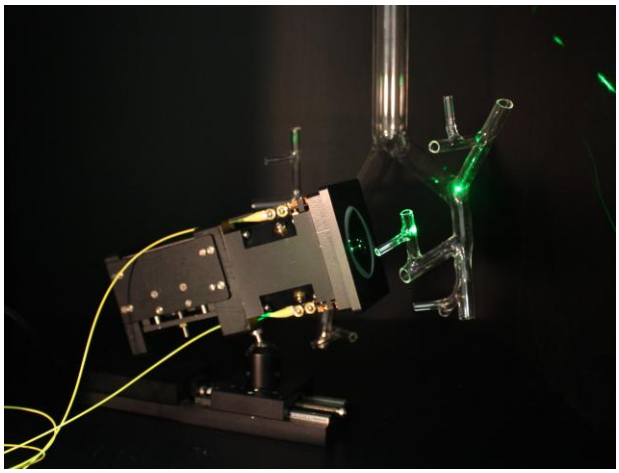

Figure 1. Laser Doppler Anemometer measurement in glass airway model.

.

[1]. Salma I, Balásházy I, Winkler-Heil R, Hofmann W, Záray Gy; Effect of particle mass size distribution on the deposition of aerosols in the human respiratory system; J AEROSOL SCI; 33: 119-132; (2002)

[2]. Imre Balásházy, Bálint Alföldy, Andrea J. Molnár, Werner Hofmann, István Szőke and Erika Kiss; Aerosol Drug Delivery Optimization by Computational Methods for the Caracterization of Total and Regional Deposition of Therapeutic Aerosols in the Respiratory System; Current Computer-Aided Drug Design; 3, 13-32; (2007)

[3]. Hegedűs Cs, Balásházy I, Farkas Á; Detailed mathematical description of the geometry of airway bifurcations. RESPIR PHYSIOL NEUROBIOL 141, 99-114 (2004)

[4]. Balásházy I, Hofmann W, Heistracher T; Local particle deposition patterns may play a key role in the development of lung cancer J APPL PHYSIOL 94, 1719-1725 (2003).

[5]. Farkas Á, Balásházy I, Szőcs K; Characterization of regional and local deposition of inhaled aerosol drugs in the respiratory system by computational fluid and particle dynamics methods. J AEROSOL MED 19, 329-343 (2006).

Computational study of aerosol flow in a physiologically realistic bifurcation under the influence of an external magnetic field

M. Pilou[1,2], E. Makris[1,2], P. Neofytou[1], S. Tsangaris[2] and C. Housiadas[1]

[1]Thermal Hydraulics & Multiphase Flow Laboratory, NCSR "Demokritos", Agia Paraskevi, 15310, Greece
[2]Laboratory of Biofluid Mechanics & Biomedical Engineering, School of Mech. Engineering, NTUA, Zografou, 15780, Greece
Keywords: Aerosol modelling, magnetophoresis, deposition, CFD, PRB.
Presenting author email: pilou@ipta.demokritos.gr

In the last decade, medical aerosols have been employed for the treatment of lung cancer (Rao et al. 2003, Ally et al. 2005). In order to improve therapeutic efficiency and decrease side effects, magnetisable aerosol particles are guided to specific sites of the lung using an external magnetic field (Plank 2008).

In the present study, a preliminary computational study of the flow of magnetic aerosol particles in a physiologically realistic bifurcation (PRB) (Figure 1) under the influence of an external magnetic field generated by a cylindrical superconducting magnet is presented. The aerosol particles, in particular, are composites of magnetite nanoparticles dispersed in a polymer matrix (polysterene).

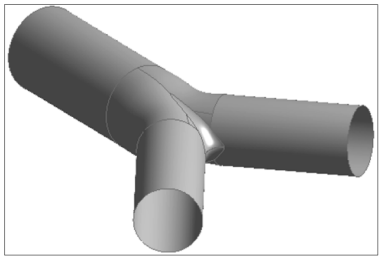

Figure 1. Physiologically realistic bifurcation of G3-G4 lung generations.

The PRB geometry is chosen, because it can be considered as a building block of the lung. The specific PRB in the present work is based on the geometrical characteristics of the bifurcation created by the third and fourth generation of the human lung. The in-house code developed by Makris et al. (2011) is used in order to obtain a high quality, multi-block, structured grid that describes the PRB. The airflow velocity and pressure fields in the PRB are, consequently, calculated through an in-house computational fluid dynamic (CFD) code (Neofytou & Tsangaris 2006).

The transport and deposition of aerosol particles under the influence of a magnetic field is described by the following steady-state population balance equation (neglecting aerosol internal processes):

$$\nabla \cdot \left[c \left(\vec{\upsilon} + \vec{v}_s + \vec{u}_m - \tau_p \, \vec{\upsilon} \cdot \nabla \vec{\upsilon} \right) \right] = \nabla \cdot \left(D \nabla c \right) \quad (1)$$

where c is the particles concentration, $\vec{\upsilon}$ the air velocity, $\vec{v}_s$ the particle settling velocity, τ_p particle relaxation time and $\vec{u}_m$ the velocity that a particle acquires due to the influence of the external magnetic field. Equation (1), thus, describes particle convective diffusion taking also into consideration the effects of particle inertia, gravity and magnetic force field in an Eulerian formulation. Total deposition fraction, particle concentration profiles and deposition sites are obtained under different conditions by solving Equation (1) numerically using a CFD-based code (Pilou et al. 2011). The parameters taken into account in the present study are the following:

- airflow Reynolds number,
- particles size,
- particles magnetic mass fraction,
- magnetic field flux density, and
- relative position of the PRB and the magnet.

Ally, J., Martin, B., Behrad Khamesee, M., Roa, W., and Amirfazli, A. (2005) *J Magnetism Magnetic Materials* 293, 442-449

Makris, E., Gkanis, V., Tsangaris, S. and Housiadas, C. (2011) *Comput Methods Biomech Biomed Engin* In press

Neofytou, P. and Tsangaris S. (2006) *Int J Num Methods Fluids* 51, 489-510

Pilou, M., Tsangaris, S., Neofytou, P., Housiadas, C. And Drossinos, Y. (2011) *Aerosol Sci Technol* 45,1376-1387

Plank, C. (2008) *Trends Biotechnol* 26, 59-63

Rao, R.D., Markovic, S.N. and Anderson, P.M. (2003) *Current Cancer Drug Targets* 3, 179-188

Cytotoxicity of organic extracts of particles emitted from a soy-biodiesel fuelled generator

J.H. Tsai[1], S.J. Chen[1,*], K.L. Huang[1], C.C. Lin[1] and W.Y. Lin[2]

[1]Department of Environmental Science and Engineering, National Pingtung University of Science and Technology, Pingtung County, Nei Pu, 91201, Taiwan
[2]Institute of Environmental Engineering and Management, National Taipei University of Technology, Taipei City, 10608, Taiwan

Keywords: diesel exhaust particles, soy-biodiesel, macrophage, cytotoxicity.
Presenting author email: chensj@mail.npust.edu.tw

Diesel engines play an important role in industry, agriculture, and transportation because of their simple and strong mechanical structures, low fuel costs, and high thermal efficiencies. However, diesel engines are commonly responsible for the emission of large amounts of gaseous and particulate pollutants, which adversely affect health (Lin *et al.*, 2008; Tsai *et al.*, 2011). Many studies have shown that the use of biodiesel as an alternative fuel in diesel engines may improve combustion efficiency and reduce the emissions of carbon monoxide (CO), hydrocarbons (HC), particulate matter (PM) and polycyclic aromatic hydrocarbons (PAHs) (Lin *et al.*, 2006; Wu *et al.*, 2009; Tsai *et al.*, 2010). Although the use of biodiesel may significantly reduce PM emission from diesel engines, it is necessary to evaluate the potential cytotoxicity of diesel exhaust particles (DEPs) and their effects on health when using biodiesel.

In this study, the DEPs from a biodiesel-fuelled generator operated at stable energy output (110 V/60 Hz, 1800 rpm) loads (unload (0 kW) and 3 kW) were investigated. We tested two types of fuels: D100 (pure petroleum diesel) and S20 (v/v = 20% soy-biodiesel/80% D100). A micro-orifice uniform deposit impactor (MOUDI) and a Nano-MOUDI (with 0.01–18 μm aerodynamic diameters) were used to collect PM samples. Each sample was extracted in a *Soxhlet* extractor with a mixed solvent (n-hexane and dichloromethane 1:1 vol/vol) for 24 hr. Subsequently, human male macrophage/monocyte cell strains (U937) were exposed to various extract samples for 24 hours after various organic solvents had been replaced by DMSO (dimethyl sulfoxide). The MTT (3-(4,5-dimethyl-thiazol-2-yl)-2,5-diphenyltetrazolium bromide) assay was adopted to analyze the cell viability rates of various DEP extracts.

Figure 1 shows the unit mass cytotoxicity (cell death rate per unit mass) of DEPs emitted from the diesel-engine generator fuelled with D100 and S20 under 0 kW and 3 kW loads. The DEPs with aerodynamic diameters of less than 0.1 μm (ultrafine particles and nanometer-particle) were found to have noticeably higher unit mass cytotoxicity than the DEPs with particles of other sizes (for D100, 4.92–5.60 times; for S20, 2.70–6.56 times). Additionally, under no load, the distribution pattern of unit mass cytotoxicity for particles of various DEPs obtained using S20 was similar to that obtained using D100. At 3 kW load, the unit mass cytotoxicity values of the extracts of nano/ultrafine DEPs (0.010–0.018, 0.018–0.032, 0.032–0.056, and 0.056–0.1 μm) were clearly lower when S20 was used than when D100 was used (by 47.7%, 46.5%, 63.3% and 52.8%, respectively), while those of larger DEPs (0.1–18 μm) were similar. The above results suggest that replacing D100 (petroleum diesel) with S20 (a mixture of 80% petroleum diesel with 20% soybean biodiesel) helped to reduce the bio-toxicity of DEPs that were emitted from the power generator.

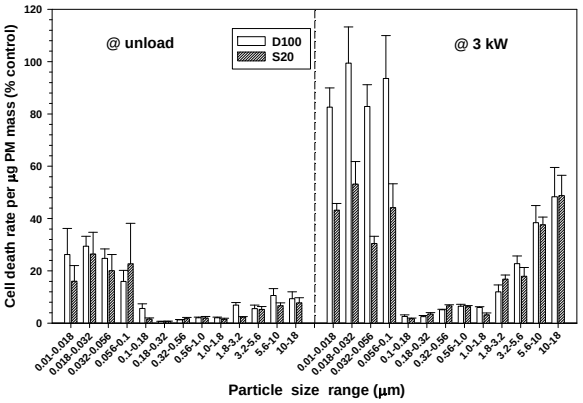

Figure 1. Unit mass cytotoxicity (cell death rate per unit mass) of DEPs emitted from the diesel-engine generator fuelled with D100 and S20 under unload and 3 kW loads.

Lin, C.C., Chen, S.J., Huang, K.L., Lee, W.J., Lin, W.Y., Tsai, J.H. and Chaung, H.C. (2008) *Environ. Sci. Technol.* **42**, 4229–4235.

Lin, Y.C., Lee, W.J. and Hou, H.C. (2006) *Atmos. Environ.* **40**, 3930–3940.

Tsai, J.H., Chen, S.J., Huang, K.L., Lee, W.J. and Lin, W.Y. (2011) *J. Environ. Sci. Health. Part A Toxic/Hazard. Subst. Environ. Eng.* **46**, 204–213.

Tsai, J.H., Chen, S.J., Huang, K.L., Lin, Y.C., Lee, W.J., Lin, C.C. and Lin, W.Y. (2010) *J. Hazard. Mater.* **179**, 237–243.

Wu, F., Wang, J., Chen, W. and Shual, S. (2009) *Atmos. Environ.* **43**, 1481–1485.

Toxicological effects of indoor PM_{10} in primary schools under different street traffic intensities

T. Moreno[1], A. Langford[2], K. BéruBé[2], T. Jones[3], W. Gibbons[4] and BREATHE participants

[1]Inst. of Environmental Assessment & Water Research (IDÆA-CSIC), Jordi Girona 18, 08034 Barcelona, Spain
[2] School of Biosciences, Cardiff University, Museum Avenue, Cardiff CF10 3AX, UK.
[3]School of Earth and Ocean Sciences, Cardiff University, Main Building, Cardiff CF10 3YE, UK.
[4]AP 23075, Barcelona 08080, Spain

Keywords: air pollution, PM10, toxicology, indoor, schools, traffic
Presenting author email: teresa.moreno@idaea.csic.es

Particulate matter (PM) present in suspension in the air we breathe has a complex composition which includes silicates, sulphates, nitrates, chlorides, carbonaceous particles and trace metals. The long-term exposure to elevated levels of this aerosol mixture has been linked epidemiologically to increased mortality from respiratory and cardiovascular diseases. Recent research has increasingly focused not only on the health impact of PM levels (legislated by the EU), but more especially on specific components within the aerosol chemical cocktail which may be causing much of the biological damage. In this context, metals, although generally low in mass, are prime suspects because of their known bioavailability. Although the source of many of these metals in the urban environment can be natural (such as volcanic eruptions or intrusions of air masses from desert areas), most are of anthropogenic origin and are mainly related to combustion-derived industrial and traffic emissions.

Air pollution due to vehicular traffic in ~~our~~ cities is a global problem. The exposure of sensitive individuals, such as children, to traffic-related PM is dependent on several factors, including the distance to the emission source (in this case the road), the number and type of vehicles, and subsequent processes during transportation that can transform PM characteristics. Therefore, different traffic densities within a given city will create zones with significant variations in the chemical composition of ambient inhalable PM.

The study of the risk that air pollution poses to the neuro-development and behavioural patterns of children is a challenge in the modern research environment. The BREATHE project funded by the European Union and led by the Research Centre of Environmental Epidemiology (CREAL, Spain) is currently measuring aerosols over both winter and summer of 2012 in primary schools located in the city of Barcelona. The schools are separated into high and low-traffic areas with the primary aims being to recognize if differences in ambient traffic emissions affect the neurological system of children and if there is a relationship between their behaviour at school and the levels of air pollution in their environment.

Within the BREATHE project the Complementary Action CECAT is considering the toxicological aspect of the problem by investigating the toxicity of PM by means of its ability to induce a systemic oxidative stress which damages cells and DNA molecules, and thus, create subsequent inflammation to produce a disease.

To achieve this, a total of 20 schools built in environments with highly contrasting variations in traffic conditions (10 with high density and 10 with low) have been selected and are being currently sampled. This sampling is being carried out inside the classrooms for 4 consecutive days at two different times a year (winter and summer of 2012) to take into account the effect of changes of air pollutants in different climatic conditions. For the determination of particle oxidative capacity, PM_{10} in the classrooms is being collected using an Airborne Sample Analysis Platform system (ASAP; Model 2800 Thermo, USA) on polyurethane foam substrates (PUF) with a high sample flow-rate of 200 l/min. The genotoxicity, inflammatory potential and cytotoxicity of the PM_{10} samples will be elucidated using three different but complementary biological assays::

- Plasmid Scission Assay (PSA) - genotoxicity
- DCFH ROS Assay - potential pro-inflammatory
- F-actin polymerisation Assay - cytotoxicity

These three assays are being performed routinely in the School of Biosciences, University of Cardiff and their application will allow the identification of PM component/s responsible for the toxicity of the sample. Determination of the toxic PM component/s will assist in identifying the related pollutant emitting source. The results that are currently being obtained and presented in this congress are helping us i) to reveal the effect of traffic emissions on air quality in school indoor environments, ii) to identify the inorganic components that may have an adverse effect on health, iii) to quantify the biological responses that subsequently cause health effects through measurements of both reactive species of oxygen and inorganic components (as well as their synergistic effects) and iv) to characterise and analyse the global response to different hierarchical levels (biochemical, and toxicological) of biological test systems, in order to reveal exposure dependent alterations.

This work is supported by the Spanish Ministry of Economy and Competitiveness with a Complementary Action (CECAT: CTM2011-14730-E) and by the BREATHE EU Advanced Grant ERC (Seventh Framework Programme).

Layered silicate nanofillers and their influence on the pulmonary surfactant

D. Kondej[1] and T.R. Sosnowski[2]

[1]Department of Chemical, Aerosol and Biological Hazards, Central Institute for Labour Protection – National Research Institute, Czerniakowska 16, 00-701 Warsaw, Poland
[2]Faculty of Chemical and Process Engineering, Warsaw University of Technology, Waryńskiego 1, 00-645 Warsaw, Poland
Keywords: lung/particle interaction, nanocomposites, industrial minerals, surfactant.
Presenting author email: dokon@ciop.pl

Polymer nanocomposites acquired special significance in recent years and they are of interest to researchers in nanotechnology. These are two-phase materials containing the polymer matrix and nanofillers (NF) added to improve the physical, thermal and resistance properties of nanocomposites. Layered silicates are an important group of NF due to their availability and relatively low price. Wide application of NF creates a potential hazard during manufacturing polymer nanocomposites as NF can be inhaled by workers involved in the production process.

The aim of this study was to evaluate the impact of selected layered silicate NF used in the production of polymer nanocomposites on the surface activity of the pulmonary surfactant (PS). Herewith, we present results regarding the layered silicates containing montmorillonite predominantly: a) PGV - bentonite, b) I.30E - nanoclay, surface modified contains 25-30 wt. % trimethyl stearyl ammonium, c) I.31PS - nanoclay, surface modified contains 15-35 wt. % octadecylamine and 0.5-5 wt. % aminopropyltriethoxysilane.

Observations of the NF morphology were conducted with the use of a scanning electron microscope - Fig. 1.

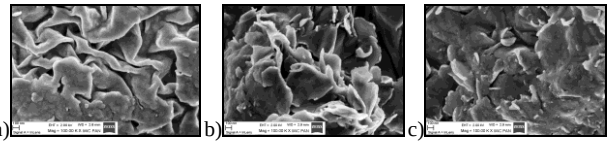

Figure 1. SEM picture of nanofiller particles: a) PGV, b) I.30E, c) I.31PS.

Specific surface area measurements were performed with the use of BET method - Table 1.

Table 1. Specific surface area of nanofillers.

Specific surface area (m^2/g)		
PGV	I.30E	I.31PS
67.3	14.0	13.5

The study of changes in the activity of PS after contact with NF particles was performed by using pulsating bubble tensiometer (PBS, Electronetics Corp., USA) with a dynamic tensiometric method (Kondej and Sosnowski, 2012). Pharmaceutical preparation Survanta (Abbott, France) was used as a model PS after dilution with sterile saline to obtain phospholipid concentration of 1.25 mg/ml.

Fig.2 and 3 show values of the relative surface tension hysteresis area, HA_R, and the relative minimum surface tension, σ_{Rmin}, found for different concentration of NF in the model PS: control (no NF), 0.5 mg/ml and 1 mg/ml. The decrease of HA_R and the increase of σ_{Rmin} for natural NF (PGV) were observed. The presence of surface-modified NF (I.30E and I.31PS) caused the increase of HA_R and the reduction of σ_{Rmin}. The results indicate altered surface activity of pulmonary surfactant caused by the presence of the particles of the layered silicate nanofillers.

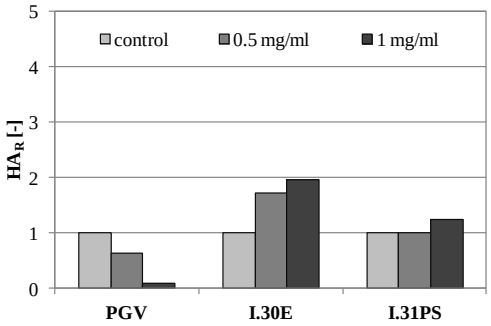

Figure 2. Comparison of the relative hysteresis area (HA_R) for PS/NF systems.

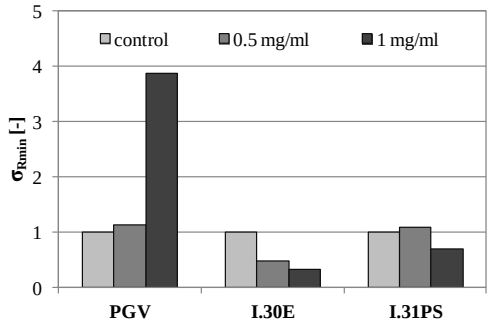

Figure 3. Comparison of the relative minimum surface tension (σ_{Rmin}) for PS/NF systems.

This paper has been prepared on the basis of the results of research project No. I.B.10 carried out within the National Programme "Improvement of safety and working conditions" partly supported in 2011-2013 within the scope of research and development by the Ministry of Science and Higher Education. CIOP-PIB has been the Programme main coordinator.

Kondej, D. and Sosnowski, T.R. (2012) *PiMOŚP*. **1(71)**, 5-11.

The increasing importance of " perinatal susceptibility window" to PM exposure in the pathogenesis of cardiovascular and respiratory diseases occurring later in life

F. Granato[1], M. Sala[2], E. Riva[2], V. Guercio[1], R. Zangari[1], B. Lorenzi[1], J. Martellucci[1] M. Monti[3], O. Caratozzolo[3], E. Bolzacchini[4] and F. Cetta[1]

[1]Dept. of Surgery and Thoracic Surgery, University of Siena, Siena, 53100, Italy
[2]Dept. of Pediatrics, University of Milan, Milan, 20122, Italy
[3]Geriatric Institute "Pio Albergo Trivulzio" (PAT), Milan, 20146, Italy
[4]Dept. of Environmental Sciences, University of Milan-Bicocca, Milan, 20126, Italy
Keywords: PM, perinatal susceptibility, spirometric values, FeNO
Presenting author email: felicegranato@yahoo.it

Aim of the study: to compare hospital admissions to a referral pediatric service of Milan with daily and seasonal variations in PM concentration, during 4 consecutive periods: winter/summer 2007, winter/summer 2008.

Methods: during 2007-2008, there were in total 440 pediatric admissions for respiratory diseases; 226 (132 M, 94 F) during the winter semester, and 214 (100 M, 114 F) during the summer semester. There were 12.7% asthma or asthma related admissions; 55.8% due to lower respiratory illness, and 31.5 % due to upper respiratory disease. The daily average of PM10 concentration during the 1st semester 2007 was 48.3+/- 17.9 mcg/m^3. There were 107 (59.1%) days with at least one hospital admission. The mean daily concentration of PM was higher in days with (n=107) than without (n=74) hospital admissions (p=0.032 or <0.05). Accordingly, children acute admissions were significantly affected by pollution data, with increased admission during winter, namely for upper air tract infections, whereas lower tract inflammation and acute admission for asthma were more frequent during spring-summer.

Between 2007-2008, 228 children, older than 7 y, were enrolled from 2 primary schools, in order to study pollution related respiratory symptoms and/or diseases in different places of Milan with a different traffic-related exposure. The former (S1) was located near a large park, the latter downtown (S2). Daily levels of PM10 and PM2.5 were measured both outdoor (garden) and indoor (corridors) for 7 consecutive days during 2 different campaigns (winter and spring-summer). Children underwent skin prick testing for inhaled allergens, analysis of exhaled nitric oxid (FeNO) and spirometry.

Results: the distribution of FeNO values was significantly different (p=0,02) between the two schools: the percentage of children with FeNO values <5ppb was almost double in S1; FeNO was 5- 20ppb in 73% of children from S2. The percentage of asthma exacerbations (previous 12 months) was higher in S2 (p=0.05). The prevalence of persistent allergic rhinitis in children allergic to grass pollen was higher in S1 (p=0.03). The latter children also had a greater activity limitation, due to rhinitis and concomitant conjunctivitis (p=0.03).

Discussion: air pollutants, at usual concentration in the atmosphere, are weak pollutants, with low intrinsic toxicity. Newborn exposure could be one the most relevant events determined by PM. Epidemiological studies evaluating concomitantly PM concentration and detectable diseases or hospital admissions usually miss this perinatal damage in foetuses and newborns. This damage is not immediately detectable, but is a delayed manifestation. Perinatal damage not only includes fetal malformations, birth defects or developmental alterations, but could also be responsible for the increased proportion of individuals who, because of the exposure to pollutants during the "perinatal susceptibility window", and because of epigenetic alterations, due to environmental factors, will turn from previously "unsusceptible" into "susceptible" individuals. The latter could also transfer this susceptibility to future generations, and develop not only asthma at age 4, but also respiratory, cardiovascular or systemic diseases, 20 or 40 y later.

Since peculiar pathophysiological mechanisms based on individual susceptibility play a major role in the occurrence of pollution related diseases, it is necessary to improve current epidemiological models, adding pathophysiological variables, which could account for tissutal damage, duration and type of exposure, or susceptibility markers.

Not only a better knowledge of the "particle side" of the interaction is required, but also a deeper insight into cause and effect relationships and pathophysiologic mechanisms or pathways, i.e. a deeper understanding of the "host side" of the host-particle interaction. A critical re-evaluation could open new avenues, including the design of new models, in which the increasing role of host reactivity will be properly considered. In particular, the possibility that autoimmune or inflammation related mechanisms, instead of purely toxic ones, could better explain clinical outcomes should be taken into account.

Clark, N.A. et al. (2010) *Environ. Health Perspect*. **118**, 284-290.
Cetta, F. et al. (2010) *Environ. Health Perspect*. **118**, A283-284.

Cytotoxicity and genotoxicity of emission particles from heavy EURO4 engine operated with conventional and biobased diesel fuels and compressed natural gas

P.I. Jalava[1], M.S. Happo[1], T. Murtonen[3], P. Yli-Pirilä[1], P. Hakulinen[2], P. Aakko-Saksa[3], J. Mäki-Paakkanen[2], J. Jokiniemi[1,3] and M-R. Hirvonen[1,2]

[1]University of Eastern Finland, Department of Environmental Science, FI-70211, Kuopio, Finland
[2]National Institute for Health and Welfare, Department of Environmental Health, FI-70701, Kuopio, Finland
[3] VTT Technical Research Centre of Finland, Fine Particles, FI-02044 VTT, Espoo, Finland
Keywords: Health effects of aerosols, Biofuels, Diesel emissions, Particulate matter.
Presenting author email: mikko.happo@uef.fi

Traffic related air pollution is associated with a large variety of adverse health effects, including both cardiac and respiratory symptoms. Diesel engine emissions are considered to be probably carcinogenic in humans, as well as cause pulmonary and systemic inflammation. However, the old diesel emission particle studies are at low relevance in comparison to more modern engines. The effects of new fuels are largely unknown, and their effects need to be characterized in details, especially when new generation fuels are introduced to wider use.

In this study, a direct injected turbocharged Scania truck engine that fulfilled EURO4 emission class requirements was used. The conventional diesel fuel (EN590), and two biobased fuels; rapeseed methyl ester (RME) and hydrotreated vegetable oil (HVO) were used with different blends as well as combinations of particle oxidation catalyst, including also compressed natural gas powered bus. The mouse RAW 264.7 macrophages were exposed to several doses of emission particles from each situation for 24 hours. Thereafter, viability of cells was measured with MTT test and genotoxicity with comet assay method.

All the samples evoked dose dependent increase in the cell death (Figure 1A). With the emission samples of EN590, HVO cat and CNG bus, also the smaller doses were cytotoxic. The smallest emissions seemed to have the largest cytotoxic potential when the same mass dose was compared. However, the overall harmfulness of the emissions from catalyst and HVO combination or the CNG powered bus can be considered as the smallest since the very low emissions.

All the samples increased dose-dependently the DNA damage measured in the Comet assay (Figure 1B). There were substantial differences between the different samples in their ability to cause DNA-damage. Emission particles from the engine operated with EN590 and 30% HVO/EN590 blend were the most potent and those from CNG bus clearly the least harmful in this parameter. EN590 sample differed statistically significantly from all the samples. Moreover, all samples except 100% RME were more genotoxic than CNG bus derived sample. Catalyst reduced the genotoxic responses of particulate mass both with EN590 and HVO. From the plain liquid fuels, methyl ester biodiesel was the least potent in inducing genotoxic responses after the macrophages were exposed to the emission particles.

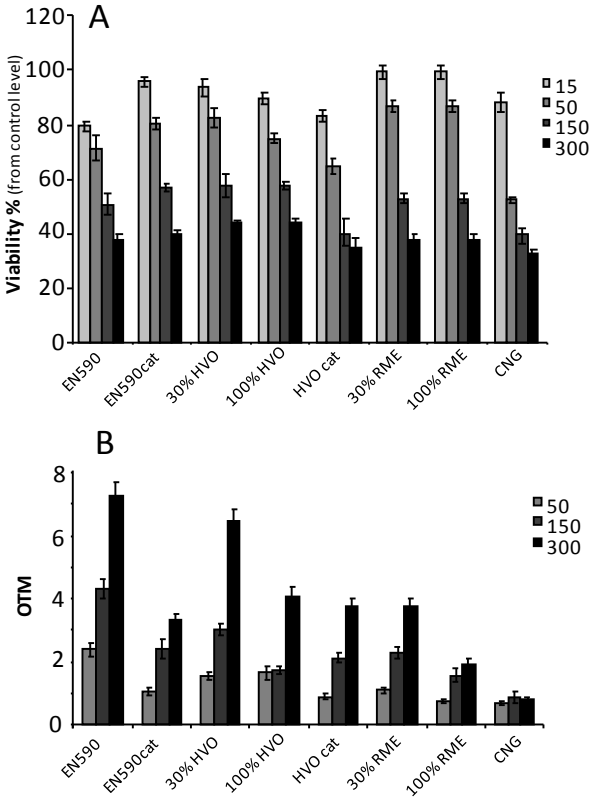

Figure 1. Cell viability assessed with MTT-test (A) and genotoxicity assessed with comet assay (B) after 24h exposure to PM_1 emission samples from EURO4 engine. Bars present control and four doses (15, 50, 150 and 300µg/ml) and whiskers the standard error of mean (SEM).

This study was funded by the Finnish Funding Agency for Technology and Innovation (Tekes). This conducted study belongs to lead program of University of Eastern Finland (Sustainable Bioenergy, Climate Change and Health).

Experimental study of aerosol transport in semi-realistic human airway model

J. Jedelsky[1], F. Lizal[1], J. Elcner[1] and M. Jicha[1]

[1]Department of Thermodynamics and Environmental Engineering, Brno University of Technology, Brno, 616 69, Czech Republic

Keywords: Lung model, aerosol transport, phase Doppler anemometry.

Presenting author email: jedelsky@fme.vutbr.cz

In vitro studies of aerosol transport in human airway models give considerable information for advancement of targeted drug delivery and serve for validation of numerical simulations where more accurate turbulence models are needed. We applied a semi-realistic transparent model of human airways for a study of flow of micron-sized spherical particles dispersed in air using Phase Doppler Anemometry (PDA).

Geometry of the model is based on CT scans of human lungs. The model encompasses mouth cavity, realistic glottal geometry and three to four generations of bronchi with three-dimensional branching. To allow optical measurement with air, certain degree of simplification of the complex realistic geometry was needed. Cylindrical tubes were used to replace original rough and warped walls of airway channels. But all other original characteristic such as asymmetric and three-dimensional branching angles were preserved. Tube dimensions were set to keep original volume as well as mean perimeter of the tubes (Fig. 1 a). Physical semi-realistic model is composed of cylindrical glass tubes connected by Rapid prototyping made bifurcation segments (Fig. 1 b).

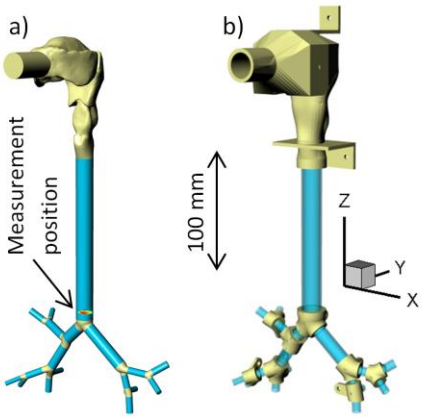

Figure 1. Airway geometry (a) and model (b) with system of coordinates.

1D PDA (Dantec Dynamics) with classical optics was used for measurement of time-resolved flow velocity and diameter of particle-laden air in multiple points of the optically transparent model for three steady breathing regimes. The PDA used focal length of both the transmitter and receiver of 310 mm, 1st order light refraction and scattering angle 45°. Aerosol particles of di-2-ethylhexyl Sebacate (DEHS) with 3 μm in diameter were produced by condensation monodisperse aerosol generator (CMAG TSI 3475), mixed in a static mixer with air and resulting dilute dispersed two-phase mixture was led to the lung model. We simulated three inspiration breathing regimes (Table 1).

Table 1. Breathing regimes

Activity	Flowrate (l/min)	*Re*	*Stk*
Resting cond.	15	1404	3.6E-03
Deep breathing	30	2809	7.1E-03
Light activity	60	5618	1.4E-02

Arbitrary results of the flow measurements are documented in Fig. 2. The particles flow in laminar or turbulent regime depending on Reynolds number (*Re*) with Stokes number *Stk* << 1, which suggests the particles follow the air flow closely (Table 1). The velocity profile is only very roughly parabolic. Maximum axial velocity is found near the centreline. Symmetry of the velocity profile along the X-axis is disturbed by the flow history, mainly by the complex structures of larynx. Symmetry along the Y-axis is harmed by the unlike distribution of the flow into main bronchi (past the bifurcation). Turbulence intensity (TI) reaches similar values in the centreline for all three regimes but spatial distribution varies significantly and also changes with regime. Particle deposition could increase in high TI regions as an effect of turbulent dispersion. Relation of the TI with deposition "hot spots" is a topic for our ongoing research.

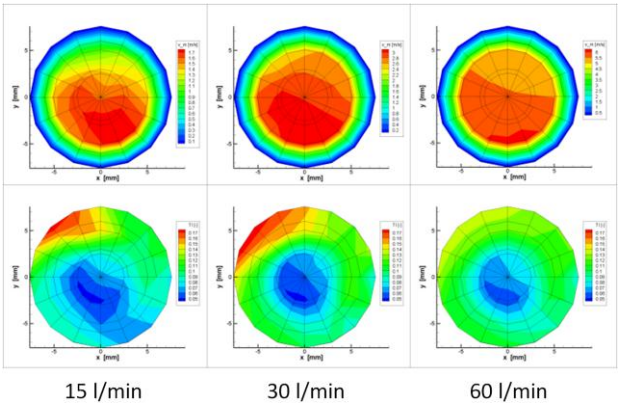

Figure 2. Mean axial velocity (top) and TI (bottom).

This work was supported by the project OC10052 (COST Action Particles No. MP0806) and project ME 09030 (program KONTAKT), funded by the Ministry of Education, Youth and Sports, CR.

Hygroscopic particle deposition in the human lung – a model comparison

W. Hofmann[1], R. Winkler-Heil[1], G.A. Ferron[2] and B. Asgharian[3]

[1]Department of Materials Research and Physics, University of Salzburg, 5020 Salzburg, Austria
[2]Comprehensive Molecular Analytics, Helmholtz Center Munich, 8576 Neuherberg/Munich, Germany
[3]Health Effects and Medical Response, Applied Research Associates, Raleigh, NC 27615-2963, USA
Keywords: hygroscopic growth, inhalation, lung deposition, modelling
Presenting author email: werner.hofmann@sbg.ac.at

Most aerosol particles used in medicine and occurring in ambient air are hygroscopic. Hence these particles will absorb water vapour from the air at the high relative humidity present in the human respiratory tract during respiration. As a consequence, inhaled aerosol particles grow in size and thus change their deposition properties.

The primary objective of the present study is to compare total deposition patterns of hygroscopic particles computed with different hygroscopic growth and morphometric lung models. Such a comparison will allow us to investigate the specific roles of particle growth and lung morphology for particle deposition in the human lung.

First, the hygroscopic particle growth model proposed by Ferron *et al.* (1988a,b) was implemented into the stochastic lung deposition model IDEAL (Koblinger and Hofmann, 1990; Hofmann and Koblinger, 1990) (IDEAL&Ferron), which is based on a stochastic, asymmetric lung morphology. The theoretical results published by Ferron *et al.* (1988a,b) employed the same hygroscopic growth model, but applied to a symmetric, deterministic lung geometry (Weibel, 1963). On the other hand, Asgharian (2004) developed a different hygroscopic growth model, while applying an asymmetric though deterministic airway geometry similar to the stochastic lung model. The most significant difference between the two hygroscopic growth models is the time a particle needs to reach its equilibrium diameter. For an additional comparison, the hygroscopic growth model of Asgharian (2004) was also implemented into the stochastic IDEAL model (IDEAL&Asgharian).

The comparison of total deposition fractions for inhaled NaCl particles obtained by the different hygroscopic growth and deposition models is illustrated in Figure 1 for a wide range of particle sizes under defined breathing conditions (flow rate Q = 250 cm^3 s^{-1} and tidal volume V_T = 1000 cm^3, assuming symmetric breathing). While the general trends are the same among all models, differences for ultrafine and very large particles may be attributed to the use of different deposition equations for the extrathoracic region.

Since the stochastic deposition model uses the hygroscopic growth model of Ferron *et al.* (1988a,b), differences with their theoretical predictions may be attributed to differences in lung morphometry. Except for the smallest particle diameters, both models predict very similar deposition fractions, indicating that lung morphometry is not a major determinant of total deposition of hygroscopic particles.

The results reported by Asgharian (2004) are significantly lower than the IDEAL predictions for submicron and significantly higher for very large particles. The same tendency can be observed if the hygroscopic growth model of Asgharian (2004) is implemented into the IDEAL code. This systematic underprediction for submicron particles and overprediction for micrometer-sized particles is caused by a growth curve which starts rising earlier during the inhalation phase than that in the modified Ferron *et al.* model (1988a,b), thereby reducing deposition by diffusion and increasing deposition by impaction and sedimentation. This model comparison indicates that the starting point of the hygroscopic growth curve significantly affects the resulting deposition curves.

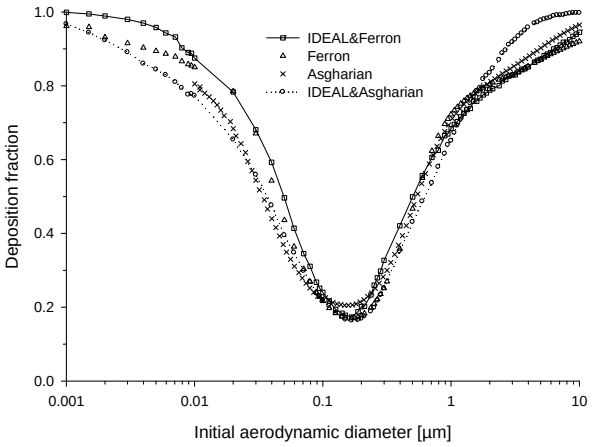

Figure 1. Comparison of total deposition fractions for orally inhaled NaCl aerosols predicted by the IDEAL&Ferron, modified Ferron (1988a,b), Asgharian (2004) and IDEAL&Asgharian models for defined breathing conditions (Q = 250 cm^3 s^{-1}, V_T = 1000 cm^3).

Asgharian, B. (2004) *Aerosol Sci. Technol.* **38**, 938-947.
Ferron, G.A., Haider, B. and Kreyling, W.G. (1988a) *J. Aerosol Sci.* **19**, 343-363.
Ferron, G.A., Kreyling, W.G. and Haider. B. (1988b) *J. Aerosol Sci.* **19**, 611-631.
Hofmann, W. and Koblinger, L. (1990) *J. Aerosol Sci.* **21**, 674-688.
Koblinger, L. and Hofmann, W. (1990) *J. Aerosol Sci.* **21**, 661-674.
Weibel, E.R. (1963) *Morphometry of the human lung*. Berlin Springer Verlag.

Effects of different combustion conditions on the toxicological properties of PM_1 in adjustable biomass combustion reactor

O. Uski[1,2], J. Leskinen[1], P. Jalava[1], A. Virén[1], H. Lamberg[1], T. Kaivosoja[1],T. Kettunen[1], I. Nuutinen[1], M. Happo[1], T. Torvela[1], J. Tissari[1], O. Sippula[1], J. Jokiniemi[1,3], M.-R. Hirvonen[1,2]

[1]Univ. of Eastern Finland, Department of Environmental Science, P.O. Box 1627, FI-70211 Kuopio, Finland
[2]National Institute for Health and Welfare, Department of Env. Health, P.O. Box 95, FI-70701 Kuopio, Finland
[3]VTT Technical Research Centre of Finland, P.O. Box 1000, FI-02044 VTT, Espoo, Finland
Keywords: Biomass combustion, Health effects of aerosols, Chemical composition, Combustion particles.
Presenting author email: oskari.uski@uef.fi

Current levels of ambient air fine particulate matter are associated with mortality and morbidity in urban populations. Since large proportion of $PM_{2.5}$ emissions are derived from small scale combustion, it is important to reveal the possible health effects of the particle emissions from the combustion appliances. Especially there is a lack of knowledge concerning modern wood combustion systems. In this study, toxicological properties of PM_1 emissions from biomass combustion reactor operated by three different ways were examined.

Three different combustion conditions, efficient, erratic and poor, were generated in combustion reactor using wood chips as fuel. The efficient conditions corresponded to optimal biomass combustion and the poor conditions approach to conventional batch combustion. Instead, the erratic conditions represented malfunctioning of combustion appliance. The demanded combustion conditions were achieved by adjusting fuel feeding, air flows and air staging. (Table 1).

PM samples for toxicological analysis were collected on PTFE-filters from diluted flue gas by using Dekati® gravimetric impactor. Samples were extracted from filters using methanol. Mouse macrophage cells (RAW264.7) were exposed for 24 h to four doses (15, 50, 150 and 300 mg ml^{-1}) of emission samples.

The studied emission samples by all doses induced a statistically significant dose-dependent decrease in cell viability (MTT assay) when compared to control (Fig.1). However, the efficient combustion caused clearly more cytotoxicity than the other samples.

When cells cell cycle phases were analyzed (dose 150 mg ml^{-1}) statistically significant apoptosis was detected with erratic and poor combustion (Fig.2). All samples caused statistically significant decrease of G_1-phase when compared to control. Interestingly, only efficient combustion caused statistically significant increase in S-G2/M-phase which is considered as sign of cell cycle arrest caused by DNA damage.

The results indicated that even modern wood combustion appliances and optimal burning conditions may have health impact. Efficient combustion was causing highest cytotoxicity and clear cell cycle arrest. However, emissions from efficient combustion were negligible compared to two other situations and that is even more important when the aim is to reduce human exposure to PM.

Table 1. Emission parameters in averaged values.

Parameter	Efficient	Erratic	Poor
Number Conc.(1/MJ)	1.4E+14	5.5E+13	2.7E+13
PM_1 Mass Conc. (DGI)(mg/MJ)	8 ± 3	61 ± 47	135 ± 22
CO(mg/MJ)	7 ± 37	303 ± 633	2300±3300
CH_4 (mg/MJ)	0.3 ± 0.3	4 ± 21	115 ± 190
OGC (mg/MJ)	3.6 ± 1.4	7.1 ± 25	180 ± 340

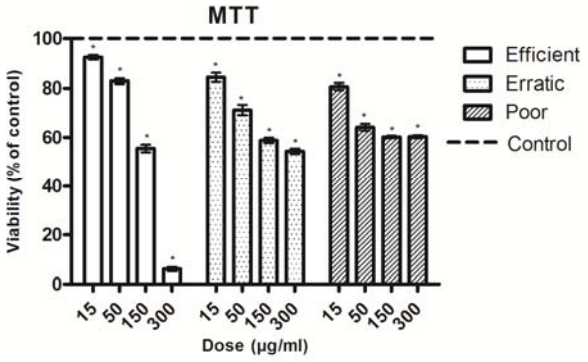

Fig.1. Viability of RAW264.7 macrophages after exposure to four doses (15, 50, 150 and 300 mg ml^{-1}) of cell medium suspended particles emitted from a biomass combustion reactor (the mean ±SEM). Asterisks (*) indicate a statistically significant difference from control cells as presented 100 % ($p < 0.05$, Dunnett's test). n=6 in total.

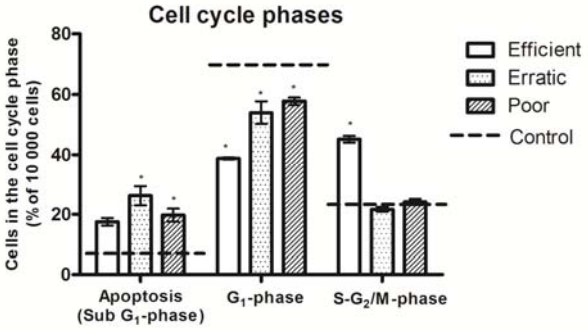

Fig. 2. Apoptosis and phases of the cell cycle in RAW264.7 macrophages after exposure to the particles emitted from a biomass combustion reactor. Bars represents the mean response (n=3±SEM) to dose 150 mg ml^{-1} of the emission particles. Asterisks (*) indicate a statistically significant difference from control cells ($p < 0.05$, Dunnett's test).

Aircraft Engine Soot Emissions and Smoke Number Uncertainties

M.E.J. Stettler[1] and A.M. Boies[1]

[1]Department of Engineering, University of Cambridge, Cambridge, UK, CB2 1PZ
Keywords: aerosol emissions, aerosol sampling, soot particles, generation of combustion aerosols
Presenting author email: ms828@cam.ac.uk

We describe how the current method to estimate aircraft particulate matter (PM), relying on measured engine smoke number (SN), shows significant discrepancies with recent published measurements. Flexibility within the SN measurement standard procedure is potentially a significant contributing factor. We describe results from a recent experimental study to examine the influence of changing filter diameter, sampling line temperature and sample line length within the prescribed ranges. These results are important to quantify the error associated with current estimation methods used in airport emissions inventories and motivate the development of alternative methods independent of SN.

Aircraft gas turbine engines emit particles with a geometric mean particle diameter less than 100nm (Kinsey et al., 2010) consisting of non-volatile and volatile particles. The non-volatile component is primarily black carbon soot (BC) (Timko et al., 2010). Emissions indices (EIs) of pollutants from aircraft engines are generally described in terms of mass of pollutant emitted per mass of fuel burned.

Currently, regulation is concerned with the visibility of aircraft exhaust, quantified via the SN. Each engine type in service has been measured for SN according to a standard procedure detailed in Aerospace Recommended Practice (ARP) 1179C (SAE, 1997). The SN is a dimensionless quantity related to the darkening of particle-loaded filters through the transmission of a given quantity of exhaust gas per unit of filter area.

Growing awareness of climate and air quality impacts of PM led to the development of an approximation method to estimate PM mass EIs. The non-volatile EI is estimated by relating the measured SN to a soot mass concentration in the exhaust sample via an empirical correlation. The latest version of this method is called the First Order Approximation v3.0 (FOA3) and is endorsed by ICAO and the US Federal Aviation Authority (ICAO, 2007; Wayson et al., 2009).

Current efforts by the SAE E-31 committee are directed towards specifying a new standard for aircraft exhaust non-volatile PM measurement (SAE, 2009), however in the absence of a campaign to enforce any new measurement standard on existing engines, PM emissions from engines currently in service will continue to be estimated.

Figure 1 shows that there is a factor of ten discrepancy in 40% of cases between FOA3 estimated and measured emissions index of black carbon EI(BC). For the real engine data (open symbols) two issues are clear: (a) a significant number of $EI(BC)_{FOA3}$ are zero even though $EI(BC)_{Measured}$ is non-zero, and (b) there is a significant underestimation of EI(BC), especially for the higher thrust setting of 85% rated thrust (F_{00}). Potential reasons for the discrepancy are discussed and the likely candidate of the observed discrepancy is identified as the correlation between SN and mass concentration and the potential for inconsistency in the SN measurement technique due to flexibility within ARP1179C.

We present results from an experimental study and quantify the error introduced to the SN as a result of the flexibility within ARP1179C with respect to flow velocity incident on the filter surface (a function of filter diameter), sampling line temperature and sampling line length. We discuss a potential alternative estimation method that is independent of SN and shows improved agreement with measured values.

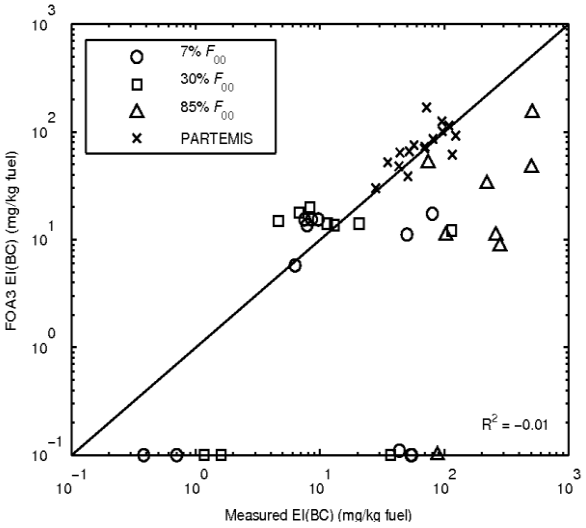

Figure 1: Comparison between FOA3 estimated and measured EI(BC) for real engines (open) and PARTEMIS combustor experiments (x). Calculated R^2 refers only to the engine data.

This work was supported by the UK Engineering and Physical Science Research Council (EP/H004505/1).

ICAO, 2007. Airport Air Quality Guidance Manual, Doc 9889.

Kinsey, J.S., Dong, Y., Williams, D.C., Logan, R., 2010. Atmos. Env. 44, 2147-2156.

SAE, 1997. Aerospace Recommended Practice 1179C.

SAE, 2009. Aerospace Information Report 6037

Timko, M.T., Onasch, T.B., Northway, M.J., Jayne, J.T., Canagaratna, M.R., Herndon, S.C., Wood, E.C., Miake-Lye, R.C., Knighton, W.B., 2010. J. Eng. Gas Turbines and Power 132, 061505.

Wayson, R., Fleming, G., Iovinelli, R., 2009. J. Air & Waste Manag. Assoc. 59, 91-100.

Estimation of uncertainty of elemental concentration in PM_1

G. Valotto[1], E. Pecorari[1], G. Rampazzo[1], F. Visin[1] and D. Zannoni[1]

[1]Department of Environmental Science Informatics and Statistics, University Ca' Foscari, Dorsoduro 2137, I-30123 Venezia, Italy

Keywords: measurement errors, chemical composition, PM1

Presenting author email: valotto@unive.it

In environmental studies, precision and accuracy of measurement are of considerable importance since they must be often compared to the existing legislation. Usually, laboratories minimize the data uncertainty by following measurement protocols that often need of a reference certificate standard. Unfortunately, there are not available standards for all matrix types, and existing ones are not certified for all their components (e.g., organic and inorganic). Furthermore, the error evaluation becomes difficult when the sample is handled several times before the analysis. This is the case of the elemental composition of atmospheric particulate, sampled on quartz filter, when it is characterized by ICP-OES (Inductively Coupled Plasma - Optical Emission Spectroscopy).

The aim of this research is at estimating the precision of elemental concentration of PM_1 sampled near the Venice airport and presenting a method simple and adaptable to other matrices for the evaluation of uncertainty associated to the data. It is worth noting that literature not always reports errors associated with environmental measures.

From November 2011 to June 2011, 200 samples of PM_1 were collected every 48 hours on a quartz filter (47 mm in diameter) at two site located at the start and the end of Venice airport airstrip (45°30'40''N, 12°20'38''E) by two Tecora Skypost PM HV at low volume (2.3 m^3 h^{-1}). PM_1 air concentration was determined gravimetrically: all filters were weighted before and after sampling with analytical balance after stabilization (48 hours at 20°C and 50% relative humidity). Filters were decomposed by microwave digestion with a mixture of HNO_3, HF and H_2O_2, and then diluted to 25 ml with high purity water. Before characterizing the elemental composition by ICP-OES, each sample was further diluted with calibrated micropipette by using high purity water (1:2). All these operations contribute to enhance the uncertainty associated to the determined concentration values. We used eq. 1 (quadratic formula of error propagation) to assess the error associated to the calculated concentration (PM_1 in air and elemental concentration of PM_1), and to identify the most critical sample processing steps, which we should focus to for improving the detection accuracy.

$$\delta F(x_1, x_2, \dots x_i, \dots x_n) = \sqrt{\sum_{i=1}^{n} \left(\frac{\partial F}{\partial x_i}\right)^2 \cdot (\delta x_i)^2} \quad (1)$$

where $\frac{\partial F}{\partial x_i}$ is the partial derivative of an F function over the x_i variable, and δx_i is the corresponding x_i uncertainty.

Field blank filter were used to correct the systematic errors and to evaluate measurement uncertainty of PM_1 air concentration and elemental concentration of PM_1.

This research shows that second dilution and ICP-OES analysis are the processing steps that most contribute to increase the error associated to PM_1 elemental concentration (as shown in figure 1).

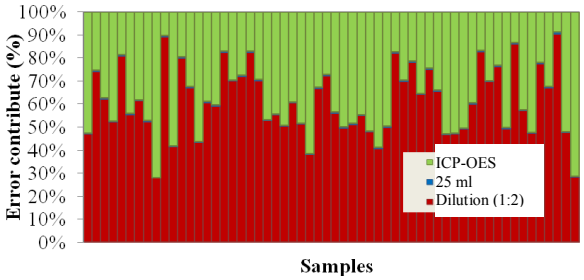

Figure 1. Error contribution of processing steps

Finally, for all detectable elements (Fe, Zn, Mn, K, S - whose concentrations are higher than the limit of detection of ICP-OES and are not highly concentrated in the quartz filter) was estimated the percentage error of element concentration as a function of PM_1 concentration and element concentration in PM_1. Table 1 shows the Fe example.

PM_1 concentration ($\mu g\ m^{-3}$)	Fe concentration in PM_1 ($\mu g\ \mu g^{-1}$)	Error (%)
0–10	$<2.5 \cdot 10^{-3}$	14
	$2.5 \cdot 10^{-3}$–$4.0 \cdot 10^{-3}$	10
	$>4.0 \cdot 10^{-3}$	7
10-50	$<2.5 \cdot 10^{-3}$	12
	$2.5 \cdot 10^{-3}$–$4.0 \cdot 10^{-3}$	5
	$>4.0 \cdot 10^{-3}$	4
>50	$<2.5 \cdot 10^{-3}$	7
	$2.5 \cdot 10^{-3}$–$4.0 \cdot 10^{-3}$	-
	$>4.0 \cdot 10^{-3}$	-

Table 1. Fe concentration and relative error

Collection efficiency and interstage nanoparticle loss in MOUDI

A. Awasthi, C. N. Liu, B. Gumgamsetty and C.J. Tsai

Institute of Environmental Engineering, National Chiao Tung University No. 1001, University Road, Hsinchu, 30010, Taiwan
Keywords: Collection efficiency, MOUDI, nanoparticle, particle loss
Presenting author email: awasthitiet@gmail.com

The performance of 13-stage MOUDI-II cascade impactor (MSP Model 122, 30 L/min) was studied for the collection efficiency and particle loss. Monodisperse test particles in the aerodynamic size range between 17 to 450 nm were used for experiments, which were generated by a constant output atomizer (TSI Model 3076) using solutions of Oleic Acid (OA) or Dioctyl Sebacate (DOS) of different concentrations. Particles generated by atomizer pass through the evaporation and condensation process before entering an electrostatic classifier (TSI 3080). Finally, a scanning mobility particle sizer (SMPS, TSI 3936); a combination of EC and Ultra-Fine Condensation Particle Counter (UCPC, TSI 3776) was used to scan the size distribution of classified particles and check their monodispersity.

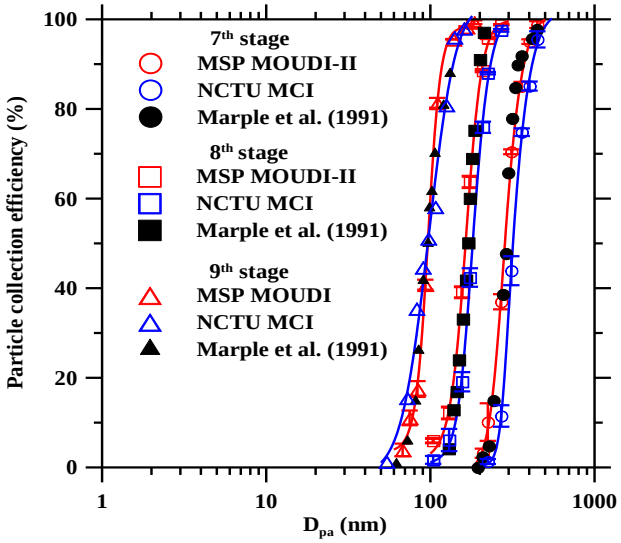

Figure 1: Particle collection efficiency curve of the 7, 8 and 9th stage of the MSP MOUDI-II and NCTU MCI.

From the particle collection efficiency curve (Figure 1) and experimental data, it was observed that the cutoff aerodynamic diameter (d_{pa50}) of 7, 8 and 9th stage of the MOUDI-II were 10, 8 and 3% lower than the nominal values given by Marple et al. (1991) and particle loss (Figure 2) increased from 13.85 to 31.96 % as the particle diameter was decreased from 83.5 to 17 nm for the inlet to the 8th stage (cutoff diameter is 180 nm). The loss is may be due to the high velocity jet from the nozzles, which creates a flow field recirculation region behind the impaction plate or near the rear end of the nozzles leading to diffusional deposition of nanoparticles. To increase the accuracy of the cutoff diameters, a NCTU MCI (micro-orifice cascade impactor) was designed using new micro-orifice nozzles with a smooth round nozzle shape for the 7th to 10th stages, which were fabricated using a semiconductor technique to reduce possible clogging inside the nozzles. The S/W values (S: jet to plate distance, W: nozzle diameter) of these lower stages were adjusted so that d_{pa50} values were close to the nominal values of the MOUDI-II. Results showed that S/W values, 3.5 (7th stage), 3.6 (8th stage) and 13.8 (9th stage) were different from those specified by Marple et al. (1991), which were 4.1 (7th stage), 6.4 (8th stage) and 10.6 (9th stage).

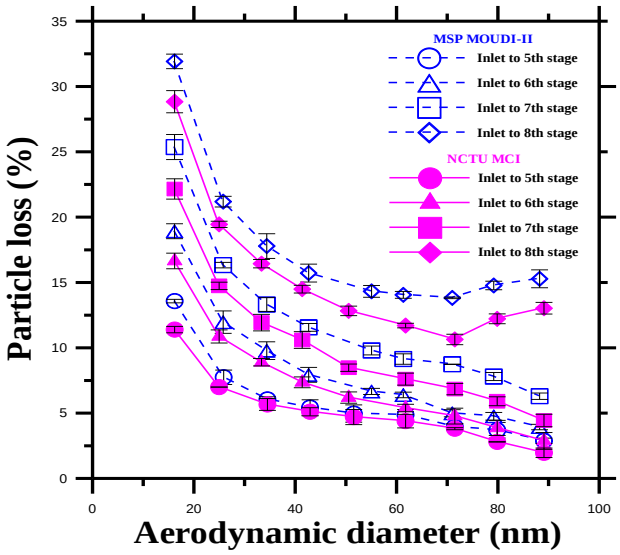

Figure 2: Particle loss for inlet to different stages of the MSP MOUDI-II and NCTU MCI.

Figure 2 shows that the particle loss of 31.96% was observed in the MSP MOUDI-II whereas the NCTU MCI with new nozzles shows maximum particle loss up to 28.87%. Newly designed smooth nozzles reduced the particle loss in MOUDI due to its smooth curved surface geometry. It is expected that the NCTU MCI with new micro-orifice plates are able to obtain more accurate mass distributions of ambient aerosols.

Acknowledgment:
This work was supported by the Taiwan National Science Council under contract number (NSC 98-2221-E-009 -020 -MY3).

Reference:
Marple, V. A., Rubow, K. L. and Behm, S. M. (1991) *Aerosol Sci. Technol*. **14,** 434-446.

On the calibration of the Single Particle Soot Photometer (SP2)

M. Gysel, M. Laborde, P. Mertes, P. Zieger, J. Dommen, and U. Baltensperger

Laboratory of Atmospheric Chemistry, Paul Scherrer Institut, 5232 Villigen PSI, Switzerland
Keywords: black carbon, diesel soot particles, SP2, single particle analysis.
Presenting author email: martin.gysel@psi.ch

Atmospheric black carbon (BC) particles are known to contribute to global warming and to cause adverse health effects. Therefore BC emission reductions have been suggested for simultaneously mitigating near-term climate change and improving human health and food security, as BC particles have a very short atmospheric life-time (Shindell *et al.*, 2012).

An emerging method for quantitative measurements of BC mass concentration in atmospheric aerosols is the single particle soot photometer (SP2; Stephens *et al*, 2003), using laser-induced incandescence. The SP2 has many advantageous features, but also disadvantages, such as the need for empirical calibration for quantitative detection of BC mass. Furthermore, Moteki and Kondo (2010) have shown that the SP2's sensitivity to BC mass differs between different BC types, including SP2 calibration materials and ambient BC, and they identified the need for further investigations on ambient BC.

In this study we compare the SP2's sensitivity to Aquadag and fullerene soot, the most common SP2 calibration materials, with that to BC from diesel car exhaust, log wood stove exhaust and ambient air.

"Atmospheric" BC calibration aerosol was obtained by thermo-denuding the soot particles sampled from a diesel car, a wood stove or ambient air at 400 °C. Aquadag and two batches of fullerene soot were nebulised from aqueous dispersions and dried. An aerosol particle mass analyzer (APM) was then used to select the "pure" BC particles by their mass, prior to measurement of the corresponding SP2 incandescence signal amplitude.

The results of the SP2 calibration are shown in Fig. 1 for all BC samples, presented as absolute calibration curves (Panel A) and as relative sensitivity compared to that of diesel car BC (Panel B). Diesel car BC is chosen as a reference calibration for two reasons: first, diesel exhaust is the dominant source of atmospheric BC in many locations and, second, the non-BC components could readily be removed by thermo-denuding the fresh diesel soot particles. The ambient BC calibration is ~10% below the diesel car BC calibration. However, at least part of this difference is caused by incomplete removal of non-BC components from the ambient soot particles prior to mass selection. The SP2's sensitivity to wood burning BC is ~10-20% below that of diesel car BC, again somewhat biased due to incomplete removal of non-BC components. The two batches of fullerene soot agree within ±10% with the diesel car BC calibration, whereas Aquadag produces 20-40% higher incandescence signal at equal BC mass. In summary, fullerene soot can, in agreement with Moteki and Kondo (2010), be considered as a favourable SP2 calibration material resulting in ~10% uncertainty of measured ambient BC mass concentrations. In contrast Aquadag-based SP2 calibrations will result in substantial over-estimation of BC mass concentrations.

Above results will be presented in the context of general strength and limitations of the SP2 technique. Further insight will be given into the calibration of the scattering detector and the interpretation of these signals to derive particle mixing state information.

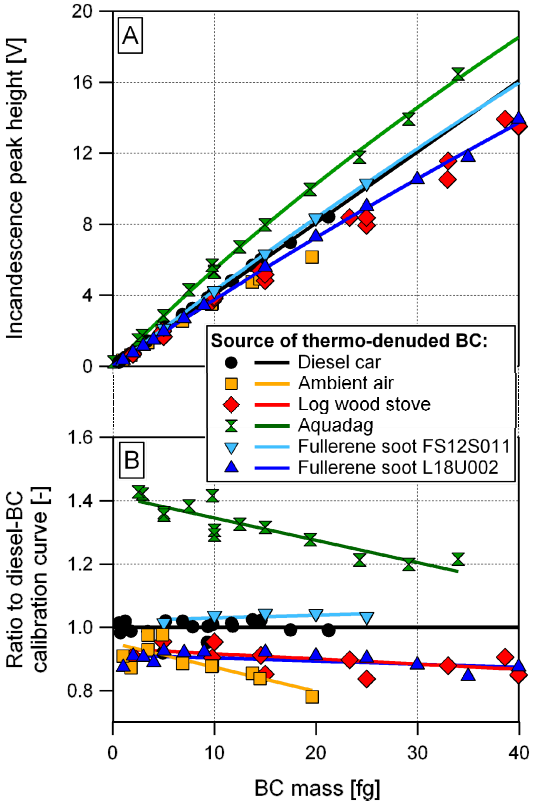

Figure 1. SP2 calibration: Absolute sensitivity to different types of BC (A) and relative sensitivity compared to BC from a diesel car (B).

This work was supported by the Swiss National Science Foundation (SNSF).

Laborde, M., Mertes, P., Zieger, P., Dommen, J., Baltensperger, U. and Gysel, M. (2012) *Atmos. Meas. Tech. Discuss.* **5**, 663-690.

Moteki, N. and Kondo, Y. (2010) *Aerosol Sci. Technol.* **44**, 663-675.

Shindell, D., *et al.* (2012) *Science* **335**, 183-189.

Stephens, M., Turner, N. and Sandberg, J. (2003) *Appl. Opt.* **42**, 3726-3736.

Using a CPMA-Electrometer System as a Suspended Mass Standard

T.J. Johnson[1], J.P.R. Symonds[2], K.St.J Reavell[2], J.S. Olfert[1]

[1]Department of Mechanical Engineering, University of Alberta, Edmonton, Alberta, T6G 2G8, Canada
[2]Cambustion Ltd., J6 The Paddocks, 347 Cherry Hinton Road, Cambridge, CB1 8DH, U.K.
Keywords: Mass concentration, Particulate mass, Instrumentation, Measurement errors.
Presenting author email: tjjohnso@ualberta.ca

Many different methods have been developed to measure aerosol mass concentration and each system has measurement errors that are difficult to quantify. Gravimetric methods do not account for gas-phase material filter absorption or the evaporation of semi-volatile material. This method is also dependent on the relative humidity and temperature during measurement. Optical methods, such as Laser Induced Incandesce (LII) or MultiAngle Absorption Photometry (MAAP), are sensitive to particle morphology, composition or optical properties, such as refractive index.

The Centrifugal Particle Mass Analyzer (CPMA), which classifies particles by their mass-to-charge (Olfert *et al.*, 2005), can be used with an electrometer to calibrate these instruments. Since the CPMA classifies by mass-to-charge ratio, particles with multiple charges are also classified through the device (Symonds *et al.*, 2011). For example, a particle with one charge is classified the same as a particle with two charges and twice the mass as shown in Figure 1.

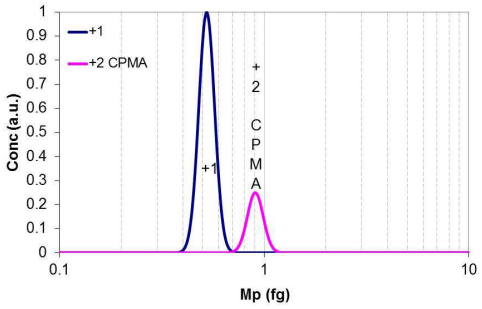

Figure 1. Effect of multiple charges on particle classification in the CPMA

Symonds *et al.* (2011) developed the theory of using a CPMA-electrometer system for a suspended mass standard. By using an electrometer to measure the charge of the particles, particles with *i* charges will be measured *i* times by the electrometer. The proposed setup is shown below in Figure 2.

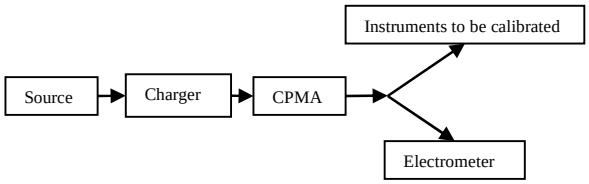

Figure 2. Experimental setup to account for multiply charged particles

The post-CPMA mass concentration (m_{total}) can be found by considering the total mass concentration of each particle charge level as shown in Equation 1.

$$m_{total} = m_{+0} + Mn_{+1} + 2Mn_{+2} + 3Mn_{+3} + \ldots \quad (1)$$
$$m_{total} = m_{+0} + M(n_{+1} + 2n_{+2} + 3n_{+3} + \ldots),$$

where m_{+0} is the mass concentration of neutrally charged particles, M is the mass set-point of the CPMA and n_i is the number concentration of particles with i charges.

Only the mass of positive particles is considered because the CPMA removes negatively charged particles. The current of the aerosol (I) is measured with the electrometer and is shown in Equation 2.

$$I = Qe(n_{+1} + 2n_{+2} + 3n_{+3} + \ldots), \quad (2)$$

where Q is the volumetric flow rate of the aerosol, e is the value of the elementary charge and n_i is the number concentration of particles with i charges.

Therefore by combining Equations 1 and 2, the post-CPMA mass concentration is given by,

$$m_{total} = m_{+0} + \frac{MI}{Qe}, \quad (3)$$

where the last term is simply the assumed singly charged number concentration displayed on the electrometer multiplied by the CPMA set-point. The zero-charge mass correction can be minimized or eliminated by: (1) minimizing small particles (of which many may be uncharged), (2) using a unipolar corona charger, and/or (3) using a DMA to remove zero-charged particles before the CPMA. A corona charger also increases system sensitivity as particles have more charges and the electrometer will measure a higher current.

The proposed system measures the mass concentration of an aerosol, while overcoming the uncertainties of other mass measurement methods.

This work was supported by the Green Aviation Research and Development Network (GARDN) and MDS Aero.

Olfert, J.S. and Collings, N. (2005). New Method for particle mass classification- the Couette centrifugal mass analyzer. *Journal of Aerosol Science*, **36**, 1338-1352.

Symonds, J.P.R., Rushton, M.G., Reavell, K.St.J., Lowndes, C. (2011). Behaviour of Non- and Multiply-Charged Aerosols in the Centrifugal Particle Mass Analyzer. *American Association for Aerosol Research Conference*, Orlando, FL, Oct. 3-7.

First field application of a thermal desorption resonance-enhanced multiphoton-ionisation single particle time-of-flight mass spectrometer for on-line measurements of particle bound polycyclic aromatic hydrocarbons and source identification

M. Oster[1,2], G. Dragan[1,2], M. Elsasser[1,2], J. Schnelle-Kreis[1] and R. Zimmermann[1,2]

[1]Joint Mass Spectrometry Centre, Cooperation Group Comprehensive Molecular Analytics, Helmholtz Zentrum München, Ingolstädter Landstr. 1, 85764 Neuherberg, Germany
[2]Joint Mass Spectrometry Centre, University Rostock, Institut für Chemie, Lehrstuhl für Analytische Chemie, Dr.-Lorenz-Weg 1, 18059 Rostock, Germany
Keywords: Aerosol mass spectrometry, Single particle analysis, Polycyclic aromatic compounds, Source identification.
Presenting author email: markus.oster@helmholtz-muenchen.de

Laser based mass spectrometric methods became a very important tool for the on-line analysis of single aerosol particles. There is a special focus on the detection of particle substances that may be responsible for adverse effects on human health. These organic molecules are often very difficult to detect due to the high degree of fragmentation. Therefore, an analytical tool that uses soft ionisation techniques is necessary.

The results of a first field application during a measurement campaign of a system affording these features will be presented. This setup consists of a differentially pumped inlet system to create a particle beam, a sizing unit for velocimetry and determination of the aerodynamic diameters of single particles (SP), an ion source for soft ionisation and a reflectron time-of-flight mass spectrometer (TOFMS) for ion analysis and detection. The ion source consists of a heating rod (T = 550 °C) for thermal desorption (TD) of particle bound molecules. A KrF-excimer laser (λ = 248 nm) is triggered according to the individual velocity of the detected particles for the selective ionisation of desorbed polycyclic aromatic hydrocarbons (PAH) via a resonance-enhanced multiphoton-ionisation (REMPI) process. By separating desorption and ionisation in two different steps, a soft ionisation with reduced fragmentation is provided (Bente, 2008).

This TD-REMPI-SP-TOFMS setup was tested for the first time in the field during a measurement campaign in Augsburg, Germany in winter 2010 with the scope to estimate the impact of particles deriving from wood combustion on ambient aerosol with an urban background (Oster, 2011).

About 360.000 particle events could be detected with the TD-REMPI-SP-TOFMS setup during the campaign. Analysis of the acquired mass spectra showed, that PAH could be found on 15.7 % of the analysed particles. On 13.5 % of the PAH-containing particles (2.1 % of all particle events), retene (m/z = 234) could be detected, a marker for the combustion of coniferous wood. 84.3 % of the particles showed no peaks that could be dedicated to PAH. It could be shown, that there are differences in the time series and diurnal variation of the occurrence of the separated particle classes (Fig 1). The differentiated particle classes also show differences in the size distributions of the measured aerodynamic diameters (Fig 2).

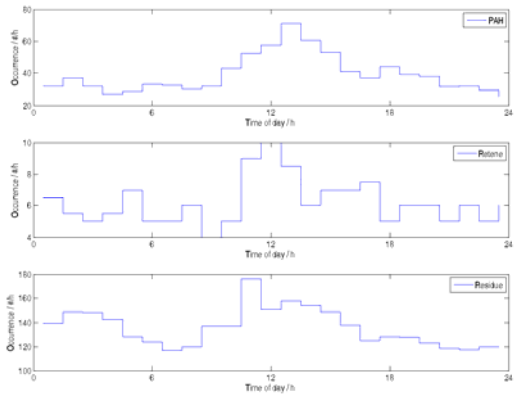

Figure 1: Diurnal variations of the PAH class (top), retene class (middle) and residue class (bottom)

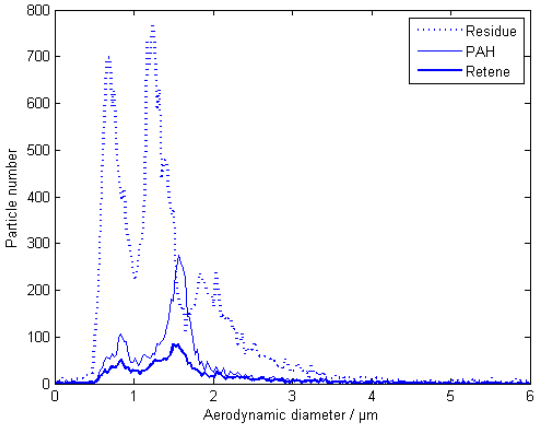

Figure 2: Size distributions of the PAH class particles (thin line), retene class particles (bold line) and residue class particles (dotted line)

The experimental setup for this work was enabled by the financial support of the Deutsche Forschungsgemeinschaft (DFG), grant ZI 764/1 and ZI 764/1-2.

Bente, M, Sklorz, M., Streibel, T. and Zimmermann, R. (2008) *Anal.Chem.* **80**, 8991-9004.

Oster, M, Elsasser, M., Schnelle-Kreis, J. and Zimmermann, R. (2011) *Anal.Bioanal.Chem.* **401**, 8991-9004.

A Study of the Shape and Fluorescence of SOA using ASPECT combined with AFS

M.V.Ghosh[(a)], I. Hoare[(a)], S. Almabrok[(a)], L. Chen[(b)], J.M. Clark[(b)], G.Cartwright[(b)], G. Marston[(a)] and C. Pfrang[(a)]

[(a)]Department of Chemistry, University of Reading, Reading, RG6 6AD, UK
[(b)]Biral, Bristol, Portishead, BS20 7JB, UK
Keywords: SOA, AFS, ASPECT, Fluorescence
Presenting author email: m.v.ghosh@reading.ac.uk

In this study, experiments are described that are aimed to measure simultaneously the particle shape and fluorescence of secondary organic aerosol (SOA) produced from the reaction of α-pinene with ozone using an ASPECT aerosol size and shape analyser combined with an aerosol fluorescence sensor (AFS).

There is a considerable and growing interest in the detailed mechanism of the atmospheric oxidation of complex biogenic molecules, such as isoprene, terpenes and sesquiterpenes.[1-6] These volatile organic compounds (VOCs) are emitted from a wide range of vegetation[2] and their emission rate is estimated at around 1000 Tg yr^{-1}, *ca*. a factor of ten greater than the rate of release of anthropogenic VOCs.[3] There have been a large number of studies investigating the link between chemical mechanism and particle formation from the ozonolysis of terpenes, and how size and number of particles varies with reaction conditions. Such particles are likely to have severe health implications, since their size allows them to be easily inhaled. While the number density and size distribution are clearly important properties of SOA, the physical nature of the individual particle also has a major impact on SOA behaviour, affecting e.g. the interaction with radiation, its atmospheric lifetime and chemical processing. It is therefore important to employ techniques to investigate the physical properties of the aerosols.

The ASPECT aerosol size and shape analyser is the only commercial instrument which simultaneously measures the shape of an airborne particle in real time, as well as its size and total particle concentration. Many particle characterisation systems measure only particle size and base their measurements on the assumption that the particles are perfect spheres. [7] Both natural and man-made particles have a very wide variety of shapes and this non-sphericity may be an important parameter in classifying them. The ASPECT particle analyser uses Biral's Aerosol Size and Shape (ASAS) technology to simultaneously measure the size and shape of single particles at a high output rate.[7]

Samples were prepared in the following way at the University of Reading: A 100L inert Teflon bag is used as the sample chamber. A known pressure of the terpene is introduced into a 1L glass bulb attached to a vacuum line. The terpene is then diluted with synthetic air: the bulb is brought to atmospheric pressure and then evacuated slowly until the desired pressure is reached. The diluted sample is then blown into the bag using synthetic air. We can thus accurately determine the terpene concentration in the sampling bag.

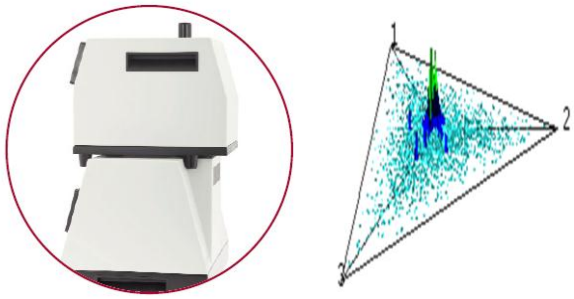

Figure 1: a) Image of AFS and ASPECT instruments for measuring particle size and shape in real time.[7] b) The triangular centroid plot illustrates the shape distribution of the SOA particles at 0% RH. The colour of each point denotes the number of particles at that location. Spherical particles can be seen close to the centre of the plot. Particles with flat surfaces such as cubic particles have a random orientation, therefore the display shows a three-point shaped distribution.[7]

Signal	UV Fluorescence	Visible Fluorescence
Minimum	187.00	768.00
Maximum	3219.00	4095.00
Average	1330.31	2309.18

Table 1. Summary of fluorescence data from the 100L sampling bag of SOA formed from the reaction of α-pinene (2 ppm) with ozone (1 ppm) at 0% RH recorded by two detection channels covering the UV and visible bands.

Conclusion: Our pump-priming study gives clear evidence for fluorescence in SOA formed in the reaction of α-pinene with ozone at 0% RH. The SOA generated in this study was predominantly of spherical shape.

References

1. Kanakidou *et al.*, *Atmos. Chem. Phys.*, **5**, 1053 (2005).
2. Calogirou *et al.*, *Atmos. Environ.*, **33**, 1423 (1999)
3. Glasius *et al.*, *Environ. Sci. Technol.*, **34**, 1001 (2000).
4. Johnson and Marston, *Chem. Soc. Rev.*, **37**, 699 (2008).
5. Ma and Marston, *Phys. Chem. Chem. Phys.*, **10**, 6115 (2008)
6. Ma *et al.*, *Phys. Chem. Chem. Phys.*, **10**, 4294 (2008)
7. Aspect User Manual, Part No: 104125.03, Doc100125.03A

Rupture event scanning: a novel procedure based on QCM to measure particle size within the nanometer range

F.N. Dultsev[1], S.N. Dubtsov[2]

[1]Institute of Semiconductor Physics, Novosibirsk, 630090, Russia
[2]Institute of Chemical Kinetics and Combustion, Novosibirsk, 630090, Russia
Keywords: Aerosol size distribution
Presenting author email: dubtsov@kinetics.nsc.ru

Determination of particle size is necessary in aerosol chemistry, in surveying health effects of particulate matter and in many other applications. The method based on QCM proposed by us previously (Dultsev, 2009) is a useful tool also in testing the reactivity of airborne particulate matter, because the chemical properties of the QCM surface affecting its affinity to the particles may be modified The necessary bonding of a particle with the surface may be achieved by coating the QCM surface with the appropriate agent. Provided that physical adsorption occurs (i.e. weak bonding), it is possible to analyze the particles several tens nanometers in size. We used particle generator described previously (Ankilov, 2002). It generates tungsten oxide nanoparticles 20–30 nm in size, depending on air flow rate at a given temperature of the tungsten filament.
The flow ratio through channels 1 and 2 was 1:30. Total flow rate into the reactor was kept constant in our experiments. The generator was calibrated with the diffusion spectrometer of aerosol (DSA). Particle size distribution obtained with the help of DSA is shown in Fig. 1.

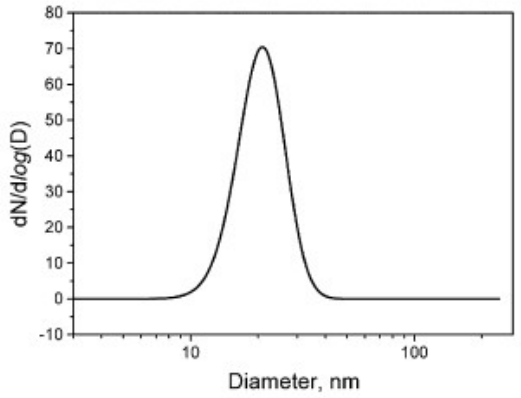

Fig. 1. Particle size distribution determined with the diffusion spectrometer of aerosol (DSA).

Filament temperature and flow rate were chosen so that the particles with the mean size of 20 nm were generated. The particles in air flow arrive from the generator to the chamber where the QCM is placed. The results of the measurements made with the help of QCM are presented in Fig. 2. One can see how the acoustic signal changes with an increase
in the voltage on QCM in the presence of nanoparticles in the gas phase, for different air flow rates through the particle generator.

The QCM (sensor) used in this experiment was a quartz strip with metal electrodes. The electrodes were coated with silicon dioxide. Thus prepared surfaces provide physical adsorption of nanoparticles (weak bonding). One can see that an increase in the flow rate causes a decrease in particle size. Such behaviour was previously observed with the help of DSA. With a decrease in tube length, an increase in particle concentration occurs due to the smaller particles. The signal from these smaller particles appears at a voltage of about 2V, while the major signal for particles 20nm in size appears at a voltage of 1.5 V..

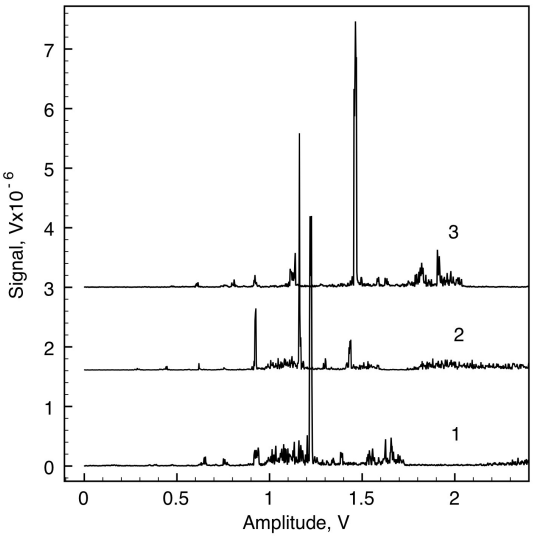

Fig. 2. Acoustic signal from rupture event scanning.

Thus, the application of a quartz resonator in the active mode allows us to obtain particle size distribution for the particles having similar interactions with the surface. This allows one to use this method in environmental monitoring and in aerosol measurements Frequency scanning simplified the adjusting procedure and allowed us to obtain amore complete picture of nanoparticle rupture from the surface. Integrated functioning of a single quartz strip both as an active resonator and a microphone registering the acoustic signal allows the development of simple and cheap procedures for detecting and identifying the particles with different bonding strengths.

Dultsev, F.N., and Kolosovsky, E.A. (2009) *Langmuir* 25 (20) (2009) 12195–12200.
Ankilov, A., Baklanov, A., Colhoun, M. et al., (2002) *Atmos. Res.* 62 177–207.

Nanoparticle counting efficiency with photon correlation LDA

P. Jani, L. Vámos, A. Nagy, P. Schlosser

Research Institute for Solid State Physics and Optics, Konkoly-Thege str. 29-33. H-1121. Budapest, Hungary
Keywords: nanoparticle, sizing, photon correlation, LDA
Presenting author email: pjani@sunserv.kfki.hu

Field measurements with the dual wavelength optical particle analyzer

A. Nagy[1], A. Czitrovszky[1], A. Kerekes[1], W.W. Szymanski[2], Z. Bozóki[3], T. Ajtai[4], Á. Filep[4]

[1]Department of Laser Applications, Institute for Solid State Physics and Optics, Wigner Research Centre for Physics, Budapest, 1121, Hungary
[2]Faculty of Physics, University of Vienna, A-1090 Vienna, Boltzmanngasse 5, AUSTRIA
[3]Hilase Ltd., Szeged, 6720, Hungary
[4]Faculty of Physics, University of Szeged, Szeged, 6720, Hungary
Keywords: elastic light scattering, multiple detectors, particle size, complex refractive index.
Presenting author email: nagy.attila@wigner.mta.hu

We have developed a new optical method for the determination of different physical properties of aerosol particles suspended in the ambient air based on elastic light scattering on single particles (Szymanski et al. 2002). Comprehensive numerical analysis and laboratory tests were performed to study the reliability of the method (Nagy et al. 2007). A mobile prototype instrument were built so that we can study the method in field measurement campaigns and compared the results with other devices (TL-APC, Grimm-OPC, Magee Sc. Aethalometer, etc.).

In the frame of Jedlik Ányos project the Dual Wavelength Optical Particle Spectrometer (DWOPS) was utilized in 3 different longer measurement campaigns that aims to develop a new method/model for identification of different aerosol sources having different origin (anthropogenic - industrial, combustion/traffic, agricultural, etc.) (Fig. 1.). The main advantage of the new method is that with a short (several minutes) sampling time the contamination sources could be determined without further time consuming and expensive laboratory analyses. Fig. 2 shows the results obtained using DWOPS and Aethalometer instruments where the data from different instruments are presented. We have extracted and presented the number concentration and the absorbing fraction of particles (absorbing - imaginary refractive index are larger then 0.1) from the DWOPS data.

Figure 1. The measurement site at Gilice sqr, in Budapest.

The results of the measurement campaigns show that the counting efficiency of the instrument is similar to the counting efficiency of other commercially available instruments. The time series of the absorbing fraction of the particles behave differently in different size ranges.

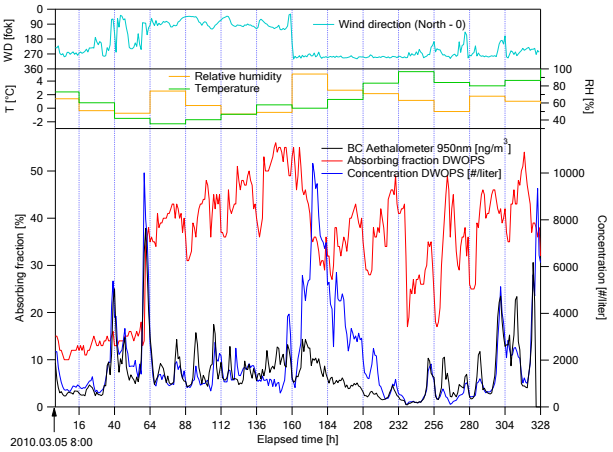

Figure 2. Some results of the measurement campaign

This work was supported by the Jedlik Ányos Program Proj. No. OM-00217/2007.

Szymanski, W.W., Nagy, A., Czitrovszky, A., Jani, P. (2002). A new method for the simultaneous measurement of aerosol particle size, complex refractive index and particle density, *Measurement Science and Technology*, 13, 303-307.

Nagy, A., Szymanski, W.W., Golczewski, A., Gál, P., Czitrovszky, A. (2007) Numarical and experimental study of the performance of the Dual Wavelength Optical Particle Spectrometer (DWOPS) (2007), *Journal of Aerosol Science*, vol. 38 issue 4. pp. 467-478.

Atmospheric Aerosol Sampling using All-in-one Balloon System

Kang Ho Ahn[1] , Hong Ku Lee, Eun Hee Ram, Gun Ho Lee
[1]Department of Mechanical Engineering, Hanyang University
1271, Sa 3-dong, Sangrok-gu, Ansan, Kyunggi-do, 426-791, KOREA, Rep. of
Keywords: Atmospheric aerosols, Monitoring, Impactor, Aerosol sampling
Presenting author email: khahn@hanyang.ac.kr

It is very important to measure atmospheric aerosols and analyze the characteristics of them since they have great effect on environment and human body. Satellite, aircraft, radio sonde have usually been used to measure vertical distribution of aerosols and its conditions such as temperature, humidity and atmospheric pressure (Daniel R. *et al*., 2008; Wenying H. *et al*., 2009). The common method of aircraft sampling takes that extracts collected particle on sampler filter and carries chemical analysis. Although, the method is favorable to measure the distribution of atmospheric aerosol, problems caused by fast flight speed; fragmentation of aerosol droplet and dispersion of collected particle (Hermann *et al*, 2001), legal limit; flight altitude, prohibited airspace and flight time, and economical limit; frequency of sampling, have been restricted the measurement. These restrictions can be resolved by our all-in-one balloon system applying custom-made polyurethane balloon controlled by electrical winch. The system is composed of developed mini-impactor of 56g weight, several sensors, pump and its data processing board. It can not only collect atmospheric aerosol depending on each altitudes and particle sizes at low cost, but also monitor the atmospheric conditions; temperature, humidity, wind velocity, atmospheric pressure, GPS data, during the measurement.

In this research, we performed the atmospheric aerosol measurement using all-in-one balloon particle sampler system at altitude of 300m and 900m. Figure 1. shows the atmospheric conditions profile depending on its altitude and Figure 2. shows the TEM images of collected particle. Figure 3. EDS analysis of Fig 3. samples

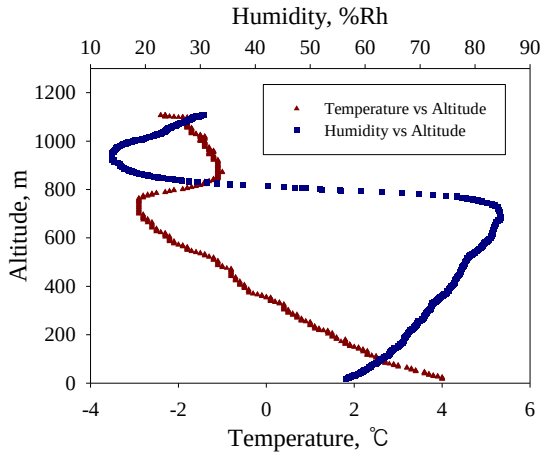

Figure 1. Temperature and Humidity profile.

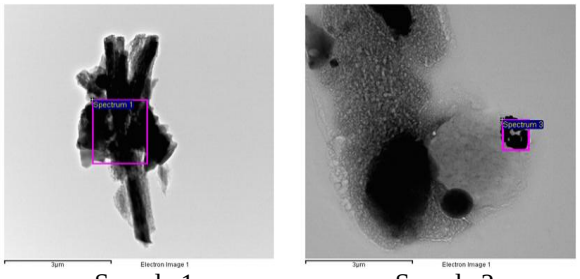

Sample 1 Sample 2

Figure 2. There are TEM images of collected particle.

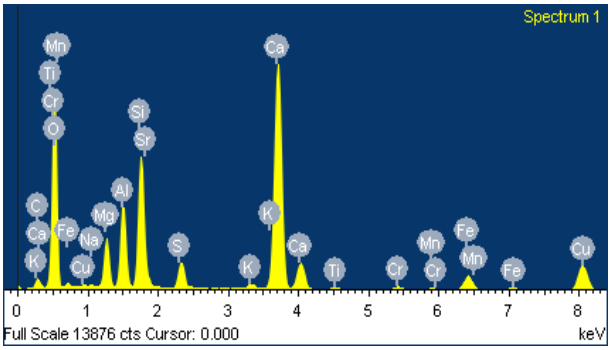

Sample 1

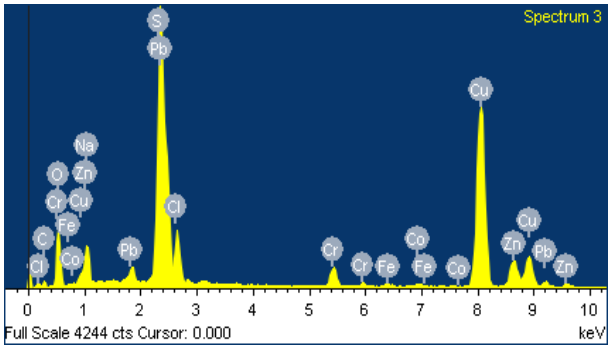

Sample 2

Figure 3. EDS analysis of Fig. 2. samples.

This subject was supported by Korea Environmental Industry & Technology Institute as “The Eco-Innovation Project”

Daniel R., William L., D.A. (2008) *Journal of Geophysical Research*, VOL.113, D15203.
Wenying He, Shu-peng Ho, H.C., X.Z., Doung H., Ying-Hwa Kuo (2009) *Geophysical Research Letters*, VOL.36, L17807.
Hermann, M., F. Stratmann, M. Wilck, A. Wiedensohler (2001). *J. Atmos. Oceanic Technol.*, 18, 7–19.

Atmospheric Aerosol Sampling using All-in-one Balloon System

Kang Ho Ahn[1] , Hong Ku Lee, Eun Hee Ram, Gun Ho Lee
[1]Department of Mechanical Engineering, Hanyang University
1271, Sa 3-dong, Sangrok-gu, Ansan, Kyunggi-do, 426-791, KOREA, Rep. of
Keywords: Atmospheric aerosols, Monitoring, Impactor, Aerosol sampling
Presenting author email: khahn@hanyang.ac.kr

It is very important to measure atmospheric aerosols and analyze the characteristics of them since they have great effect on environment and human body. Satellite, aircraft, radio sonde have usually been used to measure vertical distribution of aerosols and its conditions such as temperature, humidity and atmospheric pressure (Daniel R. *et al*., 2008; Wenying H. *et al*., 2009). The common method of aircraft sampling takes that extracts collected particle on sampler filter and carries chemical analysis. Although, the method is favorable to measure the distribution of atmospheric aerosol, problems caused by fast flight speed; fragmentation of aerosol droplet and dispersion of collected particle (Hermann *et al*, 2001), legal limit; flight altitude, prohibited airspace and flight time, and economical limit; frequency of sampling, have been restricted the measurement. These restrictions can be resolved by our all-in-one balloon system applying custom-made polyurethane balloon controlled by electrical winch. The system is composed of developed mini-impactor of 56g weight, several sensors, pump and its data processing board. It can not only collect atmospheric aerosol depending on each altitudes and particle sizes at low cost, but also monitor the atmospheric conditions; temperature, humidity, wind velocity, atmospheric pressure, GPS data, during the measurement.

In this research, we performed the atmospheric aerosol measurement using all-in-one balloon particle sampler system at altitude of 300m and 900m. Figure 1. shows the atmospheric conditions profile depending on its altitude and Figure 2. shows the TEM images of collected particle. Figure 3. EDS analysis of Fig 3. samples

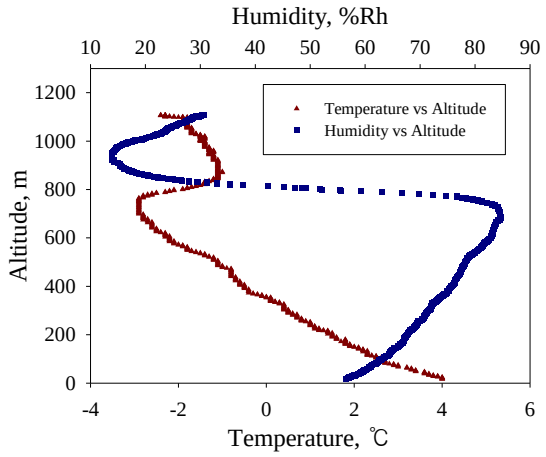

Figure 1. Temperature and Humidity profile.

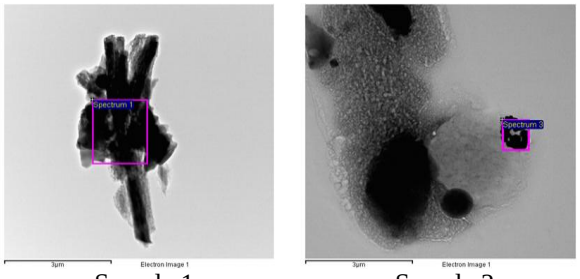

Sample 1 Sample 2

Figure 2. There are TEM images of collected particle.

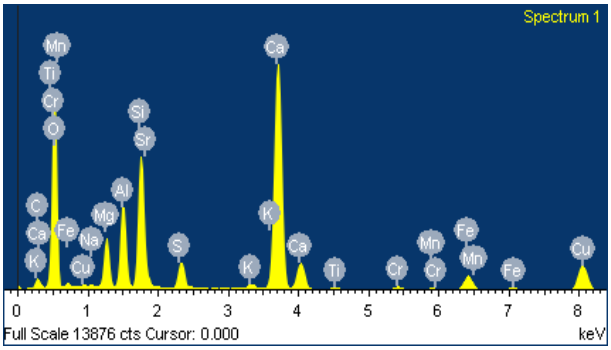

Sample 1

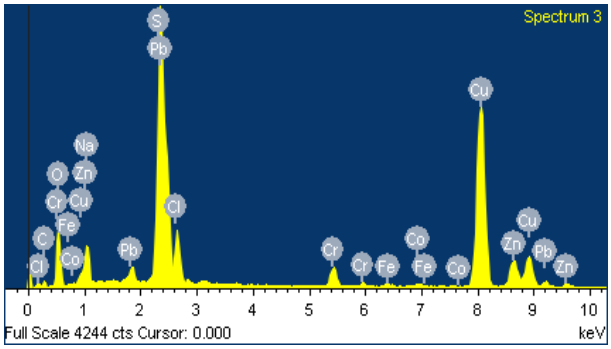

Sample 2

Figure 3. EDS analysis of Fig. 2. samples.

This subject was supported by Korea Environmental Industry & Technology Institute as “The Eco-Innovation Project”

Daniel R., William L., D.A. (2008) *Journal of Geophysical Research*, VOL.113, D15203.
Wenying He, Shu-peng Ho, H.C., X.Z., Doung H., Ying-Hwa Kuo (2009) *Geophysical Research Letters*, VOL.36, L17807.
Hermann, M., F. Stratmann, M. Wilck, A. Wiedensohler (2001). *J. Atmos. Oceanic Technol.*, 18, 7–19.

Sampling test of particle concentration for single-nozzle impactor with collection trap

C-H Huang[1], S-W Shen[1], C-J Wu[1], C-Y Tai[1] and M. Alonso[2]

[1]Department of Environmental Engineering and Health, Yuanpei University, 30015 Hsinchu, Taiwan
[2]National Center for Metallurgical Research (CENIM-CSIC). Gregorio del Amo, 8. 28040 Madrid, Spain

Keywords: impactor, particle concentration, collection trap
Presenting author email: chhuang@mail.ypu.edu.tw

The aerosol sampler using an impactor with collection trap was applied to determine particle concentration in the air stream. Due to the solid particle may bounce off from the surface of the impactor plate to change the particle size distribution; the porous substrate within the collection trap in the impactor has been used. The particle collection efficiencies of porous foam substrate within the collection trap in the impactor with larger porosity and thickness was found to be higher than those with smaller thickness and porosity (Huang & Lin 2010).

In this study, the collection characteristics of particles by separating the particles from the air stream that impacts on the porous substrate within the collection trap in the impactor were studied experimentally at different flow rates. Oleic acid particles were generated as liquid particles by utilizing an ultrasonic atomizing nozzle. An aerodynamic particle sizer was applied to determine the particle number concentrations at the inlet and outlet of a test sampler including a circular jet and collection substrate. Porous foams were used as the collection substrates with foam thicknesses of 3 mm and foam porosity of 100 ppi.

In the test, samples of particle concentration for single-nozzle impactor with collection trap were obtained from a titanium dioxide factory and a classroom. The sampling tests used a cyclone, a Multi-orifice Uniform Deposit Impactor, and an impactor with collection trap. In the sampling, two collocated IOSH cyclones used polytetrafluoroethylene and mixed cellulose ester filters to obtain samples for weight measuring and metal concentration measuring, respectively.

When particles went into the IOSH cyclone, those over the size of 4.0 μm were collected by cyclone, while those less than 4.0 μm were collected by the bottom filter of the device. The concentration of the particles collected by polytetrafluoroethylene is equal to the weight concentration of respirable particulate matter. The samples collected by the mixed cellulose ester filter were then processed according to standard digestion procedures; afterwards, they were analyzed for metal content using inductively coupled plasma - optical emission spectrometer.

Fig. 1 displays the penetration characteristics of particles for single-nozzle impactor with collection trap at the flow rates of 1.3 LPM and 1.9LPM. The figure shows that the particle collection efficiencies of the single-nozzle impactor with collection trap at the flow rates of 1.3 LPM are lower than those for 1.9 LPM. It indicates that the cutoff aerodynamic diameter of the penetration curve for the single-nozzle impactor with collection trap at flow rate of 1.9 LPM is found to be near 4.0 μm. This study will evaluate particle concentration based on the use of IOSH cyclone, Multi-orifice Uniform Deposit Impactor and the impactor with collection trap in different places.

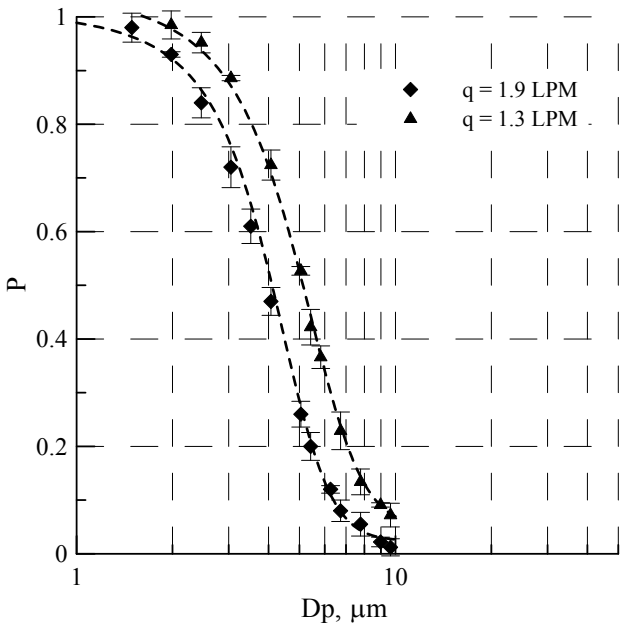

Fig. 1 Penetration characteristics of particles for single-nozzle impactor with collection trap at different flow rates

Huang, C.H. and Lin, Y.C. (2010) *J Aerosol Sci.*, **41,** 364-372.

Environmental monitoring of ultrafine particles in NW Europe (Joaquin project)

J. Staelens[1], G.P.A. Kos[2], E.P. Weijers[2], D. de Jonge[3], E. Frijns[4], P. Berghmans[4], C. Matheeussen[1] and E. Roekens[1]

[1]Unit Air, Flemish Environment Agency (VMM), Antwerp, 2000, Belgium
[2]Dept of Air Quality, Energy Research Centre of the Netherlands (ECN), Petten, 1755ZG, the Netherlands
[3]Dept of Air Quality, Municipal Health Service Amsterdam, Amsterdam, 1000CE, the Netherlands
[4]Flemish Institute for Technological Research (VITO), Mol, 2400, Belgium
Keywords: urban pollution, ultrafine particles, number size distribution, SMPS.
Presenting author email: j.staelens@vmm.be

Ambient air pollution constitutes a risk to human health and can cause a significant reduction in life expectancy. Despite considerable improvements in air quality over the last decades, ambient aerosol concentrations remain high, particularly in areas where urban development is concentrated. A major part of the North-West European (NWE) region is considered as one of the two European hot spot zones for particulate matter. Research shows that pollutant metrics not often measured in air quality monitoring networks such as the number and characteristics of airborne ultrafine particles (UFP) constitute better links to human health effects than e.g. nitrogen dioxide and particulate matter (PM_{10}). However, there is little understanding of the spatial distribution of these metrics (Hoek *et al* 2011) and their relationship with health aspects. This hampers decision makers from taking effective measures.

Therefore, the primary aim of the Joint Air Quality Initiative (Joaquin) is to facilitate the development of health-relevant air quality policies in the NWE region. To achieve this, three work packages are carried out: (1) measuring health-relevant air pollutants such as UFP and elemental carbon, (2) evaluating measures to reduce human exposure to these pollutants and (3) raising awareness of policy makers, stakeholder groups and the general public on health effects of air pollution. The Joaquin project is a cooperation of nine partners and four sub-partners from four NWE countries (Belgium, the Netherlands, France and the United Kingdom), including research institutes and universities as well as regional and local public authorities.

Within the monitoring package of Joaquin (WP1), the most suitable air quality monitoring infrastructure for ultrafine particles will be selected based on a literature review and laboratory testing. This infrastructure will be set up in four of the partner cities (Amsterdam, Antwerp, Brighton and Leicester) to provide real-time information on the UFP number concentration and size distribution on a continuous and multi-annual basis, in combination with the monitoring of other air quality parameters such as PM_{10} and black carbon. The transnational character of the infrastructure and the use of equal devices and operational control will be a clear benefit for the data analysis. This fixed infrastructure will be complemented by a mobile station with identical equipment as the fixed stations, allowing validation and harmonization of the instrument operation. Furthermore, this mobile van will allow expanding the coverage of the fixed locations and testing the representativeness of these sites (Weijers *et al* 2004). Second, the composition and sources of PM_{10} will be studied during 1-2 years for all sites. Filter samples collected every 6th day (Vercauteren *et al* 2011) will be analyzed for elemental content, water-soluble ions, elemental and organic carbon, levoglucosan and reactive oxygen species. Third, to improve public availability of health-relevant air pollution information, all data of the Joaquin project will be gathered within a NWE air pollution observatory and information centre. In this way the data from the novel network and of the source characterisation studies will be collectively analyzed, assessed and distributed. Using data from other European networks and earth observing satellites, air quality data will be visualized within an open access on-line geographical information system.

In addition to the description of the monitoring work package of the Joaquin project, we will present results from a recent intercomparison study of UFP monitors. Eight different UFP monitors that measure size distribution were tested, differing in sample flow rate, differential mobility analyzer and type of aerosol charger (radioactive vs. corona discharge). After classification particles were counted using the condensation technique or an electrometer. The monitors were compared using generated aerosols consisting of several monodisperse polystyrene latex sizes (diameters ranging from 20 to 600 nm) and ammonium sulphate particles (~70 and ~150 nm). They were also challenged with ambient indoor and outdoor air, the latter with and without exhaust air. These results, together with the literature review, were used as a guidance to select the UFP monitor that is most appropriate for the fixed and mobile monitoring network of the Joaquin project.

The Joaquin project is supported by INTERREG IVB North-West Europe (http://www.nweurope.eu).

Hoek, G., Beelen, R., Kos, G., Dijkema, M. *et al* (2011) *Environ. Sci. Technol.* **45**, 622-628.
Vercauteren, J., Matheeussen C., Wauters E., Roekens *et al* (2011) *Atmos. Environ.* **45**, 108-116.
Weijers, E.P., Khlystov, A.Y., Kos, G.P.A. and Erisman J.W. (2004) *Atmos. Environ.* **38**, 2993-3002.

A seven Aethalometer correction algorithm intercomparison

J. Backman[1], A. Virkkula[1,2], A. Hyvärinen[2], A. Dell'acqua[3]

[1] Department of Physics, University of Helsinki, Finland
[2] Finnish Meteorological Institute, Helsinki, Finland
[3] European Commission, Joint Research Center, Climate Change Unit, 21020 Ispra, Italy
Keywords: light absorption, black carbon, in-situ measurements
Presenting author email: john.backman@helsinki.fi

Tropospheric aerosols are abundant and they both scatter and absorb solar irradiance. Therefore, they have the ability to affect the radiative budget of the atmosphere. Aerosols remain one of the uncertainties in atmospheric modelling (Jacobson 2001). Light scattering by aerosols is strongly size dependent while light absorption is dependent on the area of the light absorbing species, commonly referred to as light absorbing carbon (LAC) or black carbon (BC, Bond & Bergstrom 2006).

Airborne LAC can alter the temperature profile in the atmosphere by absorbing solar irradiance in the atmosphere and reducing it at the surface. An altered temperature profile can suppress convection and cloud formation.

Filter-based absorption measurements are a popular means of measuring light absorption coefficients or BC mass concentrations since they are cheap and suited for unattended use. The method relies on the deposition of aerosol particles onto a filter matrix in a known volume of air while light transmittance trough the filter is monitored.

There are a variety of issues associated with this method which have been addressed by the scientific community (Collaud Coen et al., 2010 and references therein) mainly focusing on the transmission correction function. The transmission correction function is intended to correct for the samples change in the radiative transfer of light in the aerosol-laden filter matrix.

Different correction algorithms have different approaches to deal with the issue as the filter gets loaded. These artefacts are due to the shadowing effect by pre-deposited particles, increased optical path by light scattering particles, the asymmetry of the particles using back scattering fractions, and the single-scattering albedo of the pre-deposited aerosols. Furthermore, it has been shown that the instrument response of filter-based absorption measurements is sensitive to the penetration depth of the sample particles (Moteki et al., 2010). Ideally, a correction algorithm would be able to compensate for all of these effects and the change from an aerosol-laden filter to a pristine one would go unnoticed. By comparing data before and after a filter-spot change we get an indication on how well the algorithms are able to compensate for these artefacts at different atmospheric conditions (Fig 1).

Seven Aethalometer correction algorithms were evaluated in comparison to reference absorption (MAAP) for two different data sets from Pallas in Finland (Fig. 1a) and Ispra, Italy (Fig. 1b). The data used is 9 and 18 months long respectively.

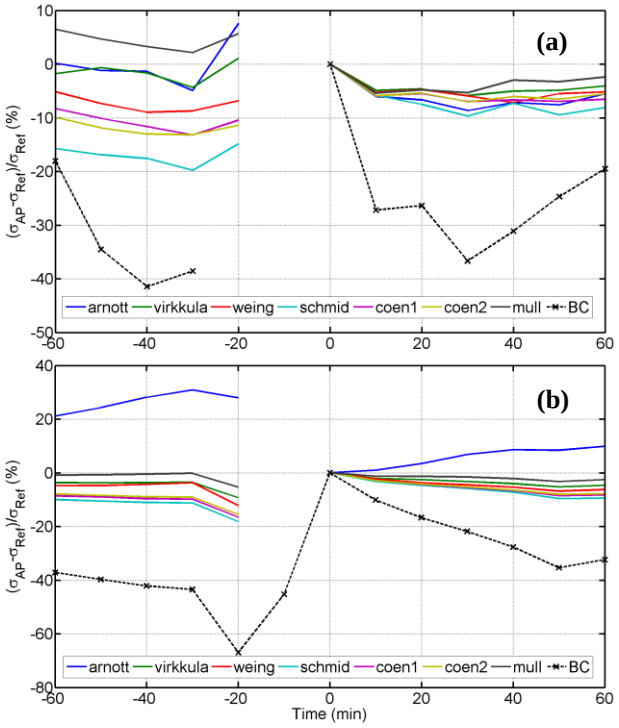

Figure 1. Aethalometer absorption coefficients calculated using seven different correction algorithms before and after filter change for Pallas, Finland **(a)** and Ispra, Italy **(b)**.

This work was supported by the Academy of Finland (project No. 1133603).

Bond T.C. and Bergstrom R.W. (2006). *Aerosol Sci. Technol., 39:1-41*

Collaud Coen, M., Weingartner, E., Apituley, A., Ceburnis, D., Fierz-Schmidhauser, R., Flentje, H., Henzing, J. S., Jennings, S. G., Moerman, M., Petzold, A., Schmid, O. and Baltensperger, U. (2010). *Atmos. Meas. Tech., 3:457-474*

Jacobson M.Z. (2001). *Nature. 409:695-697*

Moteki, N., Kondo, Y., Nakayama, T., Kita, K., Sahu, L.K., Ishigai, T., Kinase, T., and Matsumi, T. (2010). *J. Aerosol Sci., 41(4):401-412*

Water Soluble Organic Carbon (WSOC) Measurement: A Theoretical Analysis

M. Psichoudaki[1,2], S.N. Pandis[1,2,3]

[1]Department of Chemical Engineering, University of Patras, Patras, 26500, Greece
[2]Institute of Chemical Engineering and High Temperature Chemical Proccesses (ICE-HT), Foundation of Research and Technology Hellas, Patras, 26500, Greece.
[3]Department of Chemical Engineering, Carnegie Mellon University, Pittsburgh, PA 15213, USA.

Keywords: organic aerosols, water soluble organic compounds, measurement characterization
Presenting author email: mpsichoudaki@chemeng.upatras.gr

Organic aerosol represents one of the least understood fractions of atmospheric aerosol, although it typically comprises a large fraction of ambient particulate matter. Due to the large number of sources each emitting hundreds of compounds and their subsequent atmospheric oxidation, thousands of semi-volatile organic species exist in the atmosphere, ranging from highly water-soluble to insoluble (Sullivan et al., 2006). The water soluble fraction of the organic particulate matter (usually referred to as WSOC) influences the interactions of aerosols with water and thus alters their hygroscopicity and their ability to act as cloud condensation nuclei. Additionally, WSOC is an indicator of the age of organic aerosol, since atmospheric oxidation of organic species generally leads to more water soluble species. However, WSOC is operationally defined and there is a variety of methods that are used for its measurement.

A typical off-line WSOC sampling technique includes sample collection on quartz fibber filters followed by extraction and total organic carbon analysis. The volume of water used for the extraction of the water soluble organic compounds per unit of area of the filter analyzed (V/A) ranges from 0.3 to 15 mL cm^{-2}. In this work we quantify theoretically the impact of the method used for the WSOC measurement on its results.

The fraction of an organic aerosol compound that will contribute to the WSOC depends not only on its solubility, but also on its concentration, the concentration of the aerosol components, and the method used for the WSOC measurement. We investigate two rather extreme cases: an organic aerosol phase that behaves like an ideal solution and in the other organics that act independently of each other. We also assume that the method used allows the organic aerosol-water system to equilibrate and that aqueous solution after the extraction is dilute.

In the ideal organic solution case the fraction of an organic compound that will be dissolved in the water after the extraction does not depend on its atmospheric concentration. On the other hand, it depends not only on the solubility of the compound, but also on the concentration of the other organic aerosol species (Figure 1). For higher organic aerosol concentrations the extracted WSOC fraction decreases.

If, on the other hand, an organic compound is assumed to be independent of the other organics (not dissolving in the organic aerosol phase) its fraction dissolved in the WSOC depends on its concentration in the particulate phase, its solubility and the water used for the WSOC extraction (Figure 2).

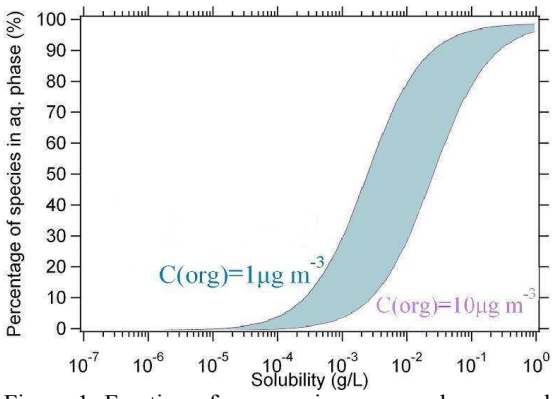

Figure 1: Fraction of an organic compound measured as WSOC for total organic aerosol concentrations 1 and 10 μg m^{-3} and V/A = 0.3 mL cm^{-2}.

In Figure 2 if the concentration and solubility of the compound are such that the corresponding point lies below the 100% line of a method, then 100% of the compound's mass will be measured as WSOC by this method. If a compound is in the upper triangle less than 10% of its concentration will be measured as WSOC.

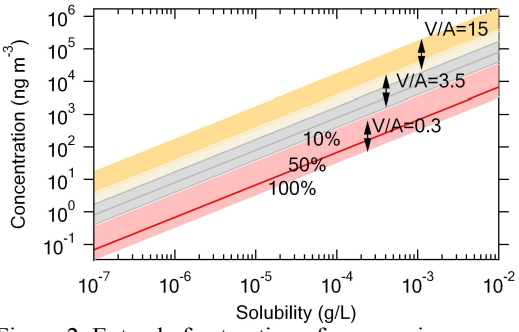

Figure 2: Extend of extraction of an organic compound as a function of its concentration, solubility and the extraction method.

The implications of these theoretical insights for the measurement of compounds as WSOC in different situations (ambient, laboratory, source characterization) will be discussed.

Sullivan, A., Peltier, R., Brock, C., de Gow, J., Holloway, J., Warneke, C., Wollny, A., Weber, R. (2006) *J. Geophys. Res.* 111, D23S46.

Insights on BC determination on quartz-fibre and PTFE filters: results of two field experiments in Milan (Italy)

R. Vecchi,[1] G. Valli[1], V. Bernardoni[1], C. Paganelli[1], and A. Piazzalunga[2,3]

[1]Department of Physics, Università degli Studi di Milano, Milan, 20133, Italy
[3]Department of Inorganic, Metallorganic and Analytical Chemistry, Università degli Studi di Milano, Milan, 20133, Italy
[3]Department of Environmental Sciences, University of Milan – Bicocca, 20126, Milan, Italy
Keywords: polar photometer, MAAP, mass absorption coefficient, denuder, TOT
Presenting author email: roberta.vecchi@unimi.it

Many measurement methods have been developed for Black Carbon (BC) measurements based on light absorption and a lot of inter-comparisons among different methods have been conducted so far. Nevertheless, at the state of the art, a reference methodology and a clear definition of black carbon does not exist (Bond and Bergstrom, 2006).

In this presentation, we will show results obtained with a home-made polar photometer suitably set up to measure light-absorption by BC particles collected on quartz-fibre and Teflon filters. Parallel measurements by a Multi Angle Absorption Photometer (MAAP) were also performed. Thermal optical transmittance analysis was carried on quartz fibre filters to obtain $\sigma_{abs,BC}$ values by different thermal protocols.

Two field experiments were carried out in Milan in 2009/2010 and in 2011 performing sampling campaign during winter and summer periods in each experiment.

The first campaign was mainly devoted to the validation of our experimental set-up, which was demonstrated to give b_{abs} values (in Mm^{-1}) fully comparable to those obtained by a MAAP when using quartz fibre filters to collect atmospheric particles ($b_{abs,\ polar\ ph.} = 0.96\ b_{abs,\ MAAP}$ R^2=0.96). On the contrary, b_{abs} values (in Mm^{-1}) determined with the same set-up and radiative transfer scheme resulted significantly lower (about a factor 2) when collecting the aerosol on PTFE filters and – even if at a less extent – the same behaviour was detected on quartz fibre filters where the water soluble component was removed by washing the filter.

The second experiment was planned to investigate the potential role of volatile organic compounds on the differences observed on quartz fibre and PTFE filters. In this case, the sampler collecting on the quartz-fibre filter was equipped with an activated carbon monolith denuder to remove organic gases from the incoming air stream. Results obtained by our polar photometer showed a fairly good agreement between the absorption coefficients measured on quartz fibre and PTFE filters ($b_{abs,\ PTFE} = 0.90\ b_{abs,\ quartz\ denuded}$ R^2=0.97).

According to our results, the use of a denuder on optical systems collecting particle on quartz/glass fibre filters would give a more accurate b_{abs} value and, therefore, a better BC estimate.

In methods based on light-absorption measurements a crucial parameter is the BC mass absorption coefficient ($\sigma_{abs,BC}$ in $m^2\ g^{-1}$) defined as the ratio of aerosol absorption coefficient (m^{-1}) to the BC mass concentration ($\mu g\ m^{-3}$). Depending on the size distribution and refractive index, $\sigma_{abs,BC}$ can range between 2 and 25 $m^2\ g^{-1}$ (Bond and Bergstrom, 2006) and the absorption properties due to the internally mixed BC particles can be enhanced as compared to those in the externally mixed BC particles (Naoe et al. 2009). In particular, a problem arises when converting aerosol absorption properties to BC concentration as generally mass absorption coefficients are derived from the TOT/TOR analysis of EC, which is not standardised yet. During the field experiments carried out in Milan we determined the BC mass absorption coefficients using three different thermal protocols (NIOSH, EUSAAR_2, IMPROVE-like) on untreated quartz fibre filters and water washed fibre filters (first experiment) and the NIOSH protocol was used on denuded quartz fibre filters collected during the second experiment.

Results show that there is a very large variability in the $\sigma_{abs,BC}$ as reported in table 1.

Table 1. Comparison between BC mass absorption coefficients ($\sigma_{abs,BC}$ in $m^2\ g^{-1}$) obtained with the TOT method and different thermal protocols

	NIOSH	EUSAAR_2	IMPROVE-like
Untreated	16.0	10.7	10.1
Water washed	8.7	6.9	6.3
Denuded	9.6		

These results clearly show that the BC concentration given by optical systems using conversion coefficients based on EC values will always be affected by a certain degree of inaccuracy. Methods to overcome this problem are therefore mandatory as this practise is widely used by the scientific community using optical systems.

Bond, T.C. and Bergstrom, R.W. (2006) *Aerosol Sci. Technol.* **40**, 27-67.

Naoe, H., Hasegawa, S., Heintzenberger, J., Okada, K., Uchiyama, A., Zaizen, Y., Kobayashi, E., Yamazaki, A. (2009). *Atmos. Environ.*, **43**, 1296-1301

Comparison of methods for measuring black carbon in medium speed diesel engine exhaust

S. Saarikoski[1], S. Carbone[1], M. Happonen[2], A. Rostedt[2], T. Rönkkö[2], J. Ristimäki[3], J. Keskinen[2] and R. Hillamo[1]

[1]Air quality, Finnish Meteorological Institute, Helsinki, Finland
[2]Aerosol Physics Laboratory, Tampere University of Technology, Tampere, Finland
[3]Wärtsilä Finland Oy, Vaasa, Finland
Keywords: black carbon, diesel engine exhaust.
Presenting author email: sanna.saarikoski@fmi.fi

Black carbon (BC) is a by-product of anthropogenic (e.g. fossil fuel) and natural incomplete burning (wild fires). Being a strong absorber of solar radiation it is a key component in global warming, and due to its health effects, an important factor of air pollution. Diesel engines are one anthropogenic source of BC. E.g. the contribution of marine diesel engines on global BC emission and arctic ice retreat are being studied with theoretical models. However, there is a gap of knowledge between the parameters required by the models and the current measurement results of ship derived BC. A link between the climate model parameters and measurement methods commonly used in engine laboratories is needed.

Filter smoke number (FSN) is a common filter-based absorption method that detects the filter blackening caused by engine exhaust smoke. FSN requires substantial empirical corrections to derive BC mass (Northrop et al., 2011). Multi-angle absorption photometer (MAAP) is a filter-based instrument that measures the aerosol black carbon concentration at the wavelength of 670 nm. MAAP utilizes a combination of reflection and transmission measurements together with a radiative transfer model to yield the BC concentration (Petzold and Schönlinner 2004). The aim of this study was to compare the two filter-based methods in measuring black carbon concentration of diesel exhaust.

The measurements were performed in the emission laboratory of Wärtsilä Finland Oy in October 2011. The tested engine was a medium speed diesel engine and the used fuel was ultra-low sulphur diesel fuel. Eight engine load points were tested in two consecutive days. Each load point was tested for approximately 30 min. The data averaging time for the MAAP was 1 min and the flow rate was 10 lpm. A default absorption cross-section of 6.6 m^2 g^{-1} was used for the MAAP. The dilution ratio was in range 38–604. FSN was measured directly from the undiluted samples. In addition to BC, particle size distributions of diesel exhaust were measured with two scanning mobility particle sizers (SMPS), particle chemical composition with soot particle aerosol mass spectrometer (SP-AMS; http://www.aerodyne.com/products/soot-particle-aerosol-mass-spectrometer-sp-ams) and particle mass concentration with Tapered element oscillating microbalance (TEOM).

The measured BC concentration from the MAAP varied from 1 to 30 µg m^{-3} corresponding to the undiluted BC concentrations of 0.2–2.1 mg m^{-3}. BC from the MAAP and FSN correlated very well for the whole concentration range (Figure 1). On average the MAAP gave 27% lower values than the FSN. Black carbon constituted 43% of the particle mass measured by the TEOM on average, with the BC fraction ranging from 14 to 77% depending on the engine load. Organic compounds composed slightly lower fraction of the particle mass than BC; the mass percentage of organics was 33% on average. The rest of the particle mass either chemical components not measured by the AMS, or particles larger than ~1 µm in diameter that were included in the TEOM mass concentration but not in that of the AMS because of different cut-offs in AMS and TEOM sampling inlets.

The results obtained in this study indicated that the FSN method is comparable with the MAAP for measuring BC emission of medium speed diesel engine.

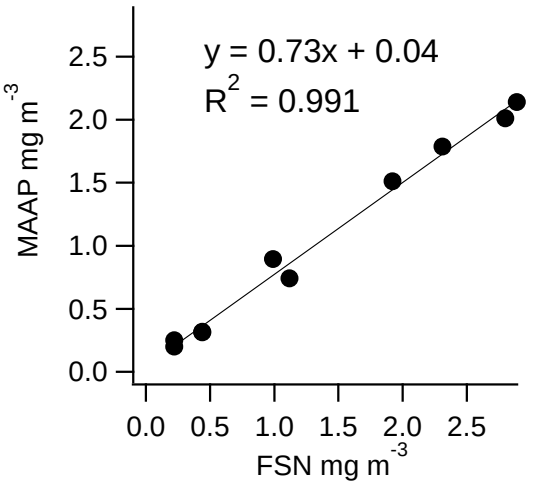

Figure 1. The comparison of black carbon concentrations measured by the MAAP and FSN.

This work was supported by the the Cluster for Energy and Environment (CLEEN Ltd) Measurement, Monitoring and Environmental Assessment (MMEA) Work package 4.5.2.

Northrop, W. F., Bohac, S. V., Chin, J.-Y. and Assanis, D. N. (2011) *J. Eng. Gas Turbines Power*, **133**, 102804-102806.

Petzold A. and Schönlinner M. (2004) *J. Aerosol Sci*. **35**, 421-441.

Efficiency of portable counters in measuring particle number and lung deposited surface area concentrations

C. Vargas Trassierra[1,2], G. Buonanno[1], P. De Felice[2], L. Stabile[1], F. Cardellini[2], A. Russi[1]

[1]Dept. of Civil and Mechanical Engineering, University of Cassino and Southern Lazio, Cassino 03043, Italy
[2]INMRI, Istituto Nazionale di Metrologia delle Radiazioni Ionizzanti, ENEA Casaccia, Roma, 00123 Italy
Keywords: particle counter, calibration, SMPS, aerosol generator
Presenting author email: c.vargas@unicas.it

Aerosol exposure is of great concern for medical and air-quality experts due to the particles' ability in crossing human respiratory system, depositing in its deepest and defenceless regions and carrying condensed toxic compounds. In particular, epidemiological, toxicological and environmental researchers are trying to understand what is the particle property mainly related to negative effect on human health. About the size the interest of such experts is moving from particle mass concentrations to particle number and surface area concentrations mainly characterized in terms of sub-micrometer and ultrafine particles (UFPs). Particle number concentrations are usually measured through condensation particle counters (CPCs) which are able to count particles down to few nanometers by optical methods after their growth by condensation of a working fluid onto the particles. Several CPC models were designed having different minimum detectable particle diameter (cut-off size) as function of the working fluid, the aerosol losses in the inlet of the CPC, the efficiency of the optical system, and the particle activation efficiency (Petaja *et al.* 2006). Due to their operation methods, such CPCs were mainly used for laboratory purposes. Anyway, in order to perform UFP exposure assessments on personal scale, hand-held, battery powered devices are needed. To this purpose a particle counter (NanoTracer, Philips) based on diffusion charging technique was developed. It does not require working fluid to growth the particles, and it is able to provide number concentration (in the range 10-300 nm), average particle diameter, and lung deposited surface area concentration measurements. Shortly, aerosol accurately charged is captured by fibrous filter in a Faraday cage producing a current signal proportional to the amount of charged particles, and their average diameter. Through a semi-empiric algorithm the device is also able to evaluate the different fractions of the lung deposited surface area (Marra *et al*. 2010).

In the present work a calibration method of two NanoTracers in terms of total number concentration, average diameter and total alveolar deposited surface area is proposed and applied. In order to perform such calibration an aerosol generation system (3940 TSI Inc.) was used. It is able to generate particles with a specific mode and total concentration. The first step was the calibration of a CPC 3775 (TSI Inc.) making a comparison with an Aerosol Electrometer 3068 (TSI Inc.) according the procedure reported in Hameri *et al.* (2002). In order to calibrate the NanoTracers a buffer volume (about 20 L) was used. Monodisperse and polidisperse aerosols accurately produced was flown in the volume where two NanoTracers were placed. Simultaneously, particles were sampled from the volume through a CPC3775, a Nanoparticle Surface Area Monitor (NSAM 3550, TSI Inc.) and a Scanning Mobility Particle Sizer spectrometer (SMPS 3936, TSI Inc.) in order to measure total particle number concentration, total alveolar deposited surface area concentration and particle number distribution, respectively. The following ranges are investigated: 10^4-10^5 part. cm^{-3} in terms of particle number concentrations and 30-200 nm for the mean diameter. Preliminary results obtained at a diameter of 50 nm and low concentrations ($8.4\times10^3 \pm 51$ part. cm^{-3}) are encouraging: maximum differences of 10% were found in terms of particle number and alveolar deposited surface area concentrations, as well as of 4% in terms of mean diameter (Figure 1).

Hameri, K., Koponen, I.K, et al. (2002) *J. of Aerosol Science* **33**, 1463–1469

Marra, J, Voetz, M., and Kiesling, H.J. (2010) *J. Nanoparticle Res.* **12**(21)

Petaja, T., Mordas, G., et al. (2006) *Aerosol Science and Technology*, **40**,1090–1097.

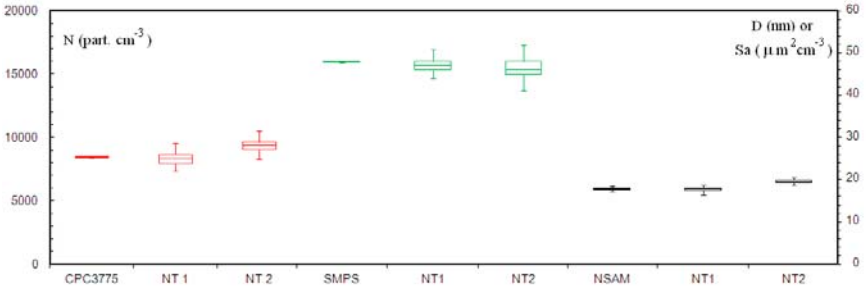

Figure 1. Statistics at D=50 nm. Red, green and black box plots represent number, alveolar deposited surface area concentrations and mean diameter for reference instruments and two Nanotracers under comparison.

Comparison between offline and semi-continuous analyzers for aerosol organic and elemental carbon detection.

G. Belz[2], A. Cinieri[2], P.R. Dambruoso[1], B.E. Daresta[1], G. de Gennaro[1], A. Giove[2], G. Miglietta[2], R.M. Nacci[2] and C. Tortorella[2]

[1]Department of Chemistry, University of Bari, Bari, Apulia, 70126, Italy
[2] Research Technical Area, ENEL Engineering and Research, Brindisi, Apulia, 72100, Italy
Keywords: Organic carbon, Elemental carbon, Instrumentation, Online measurements
Presenting author email: barbara.daresta@chimica.uniba.it

Carbonaceous material in atmospheric particulate matter can be classified as elemental carbon (EC), organic carbon (OC) and carbonate carbon (CC) (Birch and Cary, 1996). OC is associated with organic compounds either directly emitted from the sources or formed by the condensation of products formed via the atmospheric photooxidation of organic species. Emissions of EC are dominated by primary emissions from combustion sources.

Traditionally, organic and elemental carbon measurements have been made by collecting particulate matter on quartz fibre filters that are subsequently analyzed by offline thermal evolution and combustion techniques. For OC end EC speciation a thermal – optical method is used. In this method He-Ne laser light passed through the filter allows continuous monitoring of filter transmittance. A flame ionization detector is used for quantification of evolved carbon. (Birch and Cary, 1996).

In recent years, a semi-continuous OC/EC analyzer has become available (Sunset Laboratory - Forest Grove, OR). In a first stage it provides the sampling of atmospheric particles on quartz fibre filter and in the second stage the thermal analysis and the detection are carried out. An infrared detector is used for quantification of evolved carbon.

This work presents the results of the intercomparison among the offline instrumentation (Sunset Laboratory) of the Department of Chemistry, University of Bari (offline 1) and the offline (offline 2) and the semi-continuous analyzers (online) (Sunset Laboratory) of ENEL - Research Technical Area of Brindisi.

PM_{10} samples were collected at different times (2, 4, 8, 12 and 24 hours) in order to assess the analytical agreement over a wide range of OC, EC and total carbon (TC) concentration.

Five replicates of the same filters were analyzed by the offline instruments and three replicates were analyzed by the semi-continuous analyzer. Student's *t*-test showed that 64% of the OC, EC and TC average data were not significantly different ($\alpha = 0.05$) when analyzed by different instruments and 22% of the significantly different data were referred to EC.

Good linear correlations were found between the OC, EC and TC data obtained by the offline analyzers. As example, in Figure 1 the linear correlation between the OC data sets from the offline 1 and offline 2 instruments is reported.

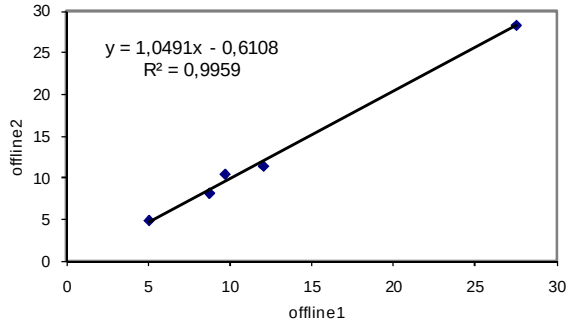

Figure 1. Comparison between OC data from offline instruments

However, a worse agreement was found from comparison among the offline analyzers and the online instrument data, in fact in these cases slopes deviate from the unit value. Such results showed a different response when samples at the lowest and highest concentration were analyzed by offline and online analyzers. This bias does not occur at the intermediate OC, EC and TC concentrations.

In Figure 2 the linear correlation between the OC data sets from the offline 1 and online analyzers is reported.

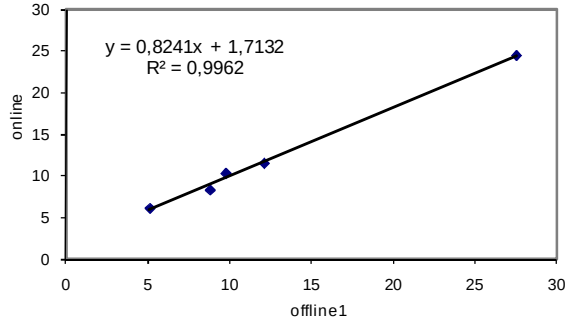

Figure 2. Comparison between OC data from offline 1 and online instruments

Birch, M.E. and Cary, R.A. (1996) *Aeros. Sci. And Techn.* **25**, 221–241.

Investigating aerosol functionalization using HRMS: inputs, advantages, validation in controlled environment and comparison with AMS.

G. Salque-Moreton[1], D. Voisin[1], N. Marchand[2], F. Siekmann[2], A. Monod[2], B. Nozières[3], B. D'Anna[3], J.-L. Jaffrezo[1], J.-L. Besombes[4] and R. Thissen[5]

[1] UJF / CNRS, Laboratoire de Glaciologie et Géophysique de l'Environnement, Grenoble, France

[2] Aix-Marseille Université – CNRS, Laboratoire Chimie Provence, 3 place Victor Hugo, Marseille, France

[3] CNRS, Institut de Recherches sur la Catalyse et l'Environnement de Lyon, Villeurbanne, France

[4] Université Savoie, Laboratoire de Chimie Moléculaire et Environnement, Chambéry, France

[5] UJF / CNRS-INSU, Institut de Planétologie et d'Astrophysique de Grenoble, Grenoble, France

Keywords: SOA, multiphase chemistry, AMS, ESI-HRMS.

Presenting author email: guillaume.salque@lgge.obs.ujf-grenoble.fr

Global estimates of secondary organic aerosol (SOA) formation flux show that current descriptions miss a large fraction of the sources (Goldstein and Galbally, 2007). This gaping underestimation has been linked to a poor understanding of aerosol functionalization in the atmosphere (Volkamer *et al*., 2006) and lead to the formation of a new conceptual framework for the description of the aerosol, based on volatility versus polarity plots (Jimenez *et al*., 2009). This new framework is almost exclusively based on High Resolution Time of Flight Aerosol Mass Spectrometer (HR-Tof-AMS) data, as this instrument gives access to average H:C, N:C and O:C ratios for the bulk aerosol.

Electrospray ionization coupled with high-resolution linear ion trap Orbitrap™ (Thermo Corp.) mass spectrometry (ESI-HRMS) provides an alternative for retrieving such elemental information on the aerosol organic fraction.

The highest resolving power of HR-ToF-AMS reaches Δm/m=4300 at m/z 200, with mass range ranging from 10 to 500 amu. The AMS estimates for O:C and H:C ratios are thus based on heavy fragmentation of organics followed by stoichiometry attribution on those fragments. Given the resolution of the HR-ToF-AMS, such an attribution is not feasible above a certain mass, making fragmentation a necessary aspect of the measurement. On the other hand, Orbitrap-HRMS provide a resolution of 100,000 at m/z 400, with a mass range 50 – 2000 amu, enabling stoichiometry retrieval up to higher masses than the AMS. Coupled to a "soft" electrospray ionization method, Orbitrap-HRMS gives O:C and H:C ratios on entire molecules in the analysed mixture. In order to cross-validate the measured O:C and H:C ratios, we applied both methods on different types of atmospherically relevant samples: two surrogates of secondary organic aerosol, obtained from controlled aqueous phase photochemistry experiments, and samples from two different field experiments.

The first photochemistry experiment investigated the aqueous phase photooxidation of methacrolein (MACR) and methylvinyl-ketone (MVK), the two main oxidation products of isoprene, the volatile organic compound (VOC) that is mostly emitted on the global scale. Photolysis of H_2O_2 provided OH radicals whose reaction with MACR and MVK initiated the production of oligomers that extended up to 1400 amu (Liu *et al.,* 2012). Taking advantage of the regularities observed in the oligomer systems, the ESI-HRMS data were used to propose stoichiometries for more than 75% of the observed signal. The observed stoichiometries and their evolution during the reaction are compared with HR-ToF-AMS data obtained from the nebulized content of the aqueous phase photoreactor.

The second photochemistry experiment investigated the photosentitized reaction of selected VOCs in an aerosol flow tube, where the resulted AOS was analyzed online by HR-Tof-AMS, and collected for off-line Orbitrap analysis.

Finally, we used samples from two contrasted field campaigns: the first at an urban kerbside site (Grenoble, France) and the second at an urban site impacted by harbor activities and regional photochemistry (Marseille, France).

The French Région Rhône-Alpes is acknowledged for GSM PhD grant. The MOCOPO and APICE programs kindly provided the field samples. The photochemistry experiments were conducted analysis were conducted under the CUMULUS and Atm-Orbitrap projects.

Allan, J.D., Jimenez, J.L., Williams, P.I., Alfarra, M.R., Bower, K.N., Jayne, J.T., Coe, H., Worsnop, D.R., (2003). *J. Geophys. Res*. **108**, 4090.

Gelencsér, A., May, B., Simpson, D., Sánchez-Ochoa, A., Kasper-Giebl, A., Piot, C., Legrand, M., (2007). *J. Geophys. Res*. **112**, D23S04.

Goldstein, A.H., Galbally, I.E., (2007). *Environmental Science & Technology* **41**, 1514–1521.

Jimenez, J.L., Canagaratna, M.R., Donahue, N.M., Prevot, A.S.H., Zhang, Q., et al., 2009. *Science* **326**, 1525–1529.

Liu, Y., Siekmann, F., Renard, P., El Zein, A., Salque, G., El Haddad, I., Temime-Roussel, B., Voisin, D., Thissen, R., Monod, A., 2012. *Atmospheric Environment* **49**, 123–129.

Volkamer, R., Jimenez, J.L., San Martini, F., Dzepina, K., Zhang, Q., Salcedo, D., Molina, L.T., Worsnop, D.R., Molina, M.J., 2006. *Geophys. Res. Lett* **33**, L17811.

Determination of site specific correction parameters for Aethalometer using multi-wavelength photoacoustic data.

Á. Filep, T. Ajtai, N. Utry, Z. Bozóki, G. Szabó
Department of Optics and Quantum Electronics, University of Szeged, Hungary

Keywords: photoacoustic spectroscopy, optical absorption, Ångström exponent.
afilep@titan.physx.u-szeged.hu

Light absorption by aerosols strongly influences the global radiation balance and visibility. Additionally, absorption feature of aerosol is characteristic to its constituent, therefore on-line investigation of absorption provides unique possibility for identification of its chemical composition or its changes. The most frequently used instrument for on-line measurement of light absorption by atmospheric aerosols in the visible and the upper UV region is the 7λ-Aethalometer (Magee Scientific), which obtains aerosol absorption coefficient from the real time measurement of light transmission on filter accumulated aerosol at seven wavelengths. The absorption coefficient deduced from changes in light transmission is suffering from serious measurement artefacts. When the filter is relatively unloaded with aerosol, multiple scattering, when the filter gets more polluted, shadowing effect influences the deduced absorption. To increase the reliability of deduced absorption the additional correction of measured data is necessary. Although numerous efforts have been made to correct these artefacts, no generally valid correction procedure is available, due to the fact that the complex interaction between filter and aerosol depends not only on relative abundance of the sampled analyte, but also on its microphysical (size distribution, single scattering albedo, shape irregularity) properties (Collaud Coen et al. 2010). Although the only method that can measure the light absorption by aerosol in-situ, without sampling artefact is the photoacoustic spectroscopy, it is not as widespread in its application as the filter-based technique yet. In the last decades several promising technical realization of the photoacoustic method for measurement of light absorption by aerosol has been published, but most of them is operating only at one wavelength in the visible, limiting their selectivity. We have introduced recently a novel multi wavelength photoacoustic instrument for the measurement of absorption behaviour of the ambient aerosol in the UV, VIS, and near-IR spectral region. The instrument operates at four discrete wavelengths (266 nm, 355 nm, 532 nm, 1064 nm) and applies wavelength independent calibration procedure providing a unique possibility on sensitive and selective measurement of the absorbing fraction of the ambient (Ajtai et al. 2011).

We present the results of optical absorption measurements on atmospheric aerosols carried out in different meteorological conditions at different seasons and sites using a conventional 7λ-Aethalometer and the 4λ-PAS. Optical absorption determined by the two instruments was thoroughly inter-compared in the overlapped wavelength region and out of the common wavelength range, especially focusing on UV region, where measured (4λ-PAS) and extrapolated (7λ-Aethalometer) results were compared. We also present a possibility on determining site-specific, wavelength dependent correction parameters using concurrently measured absorption by photoacoustic spectroscopy.

We demonstrate that by using site specific correction parameters optical absorption deduced from measurement data of the Aethalometer are reliable in its operational wavelength range; but extrapolated absorption coefficients towards the shorter wavelengths need further correction. We also demonstrate that the correction towards the shorter wavelengths strongly depends on the absorption Ångström exponent (Fig. 1).

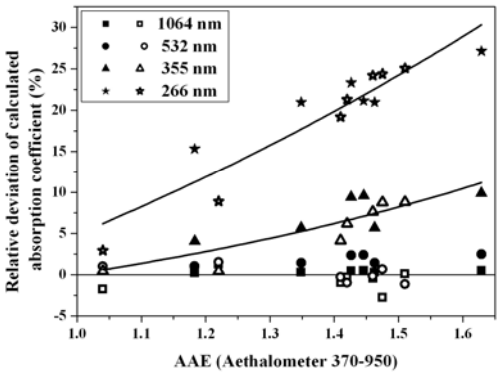

Figure 1: Average relative deviations of the 4λ-PAS and the 7λ-Aethalometer as a function of the average absorption Ångström exponent of the 7λ-Aethalometer.

This work was supported by the Hungarian National Development Agency (JEDLIK_AEROS_EU) and OTKA foundation from the Hungarian Scientific Research Fund (project numbers: CNK 78549 and K 101905).

Collaud Coen, M., Weingartner, E., Apituley, A., Ceburnis, D., Fierz-Schmidhauser, R., Flentje, H., Henzing, J. S., Jennings, S. G., Moerman, M., Petzold, A., Schmid, O. and Baltensperger, U., 2010. Minimizing light absorption measurement artifacts of the Aethalometer: evaluation of five correction algorithms. Atmospheric Measurement Techniques, 3, 457-474.

Ajtai, T., Filep, Á., Utry, N., Schnaiter, M., Linke, C., Bozóki, Z., Szabó, G. and Leisner, T., 2011. Inter-comparison of optical absorption coefficients of atmospheric aerosols determined by a multi-wavelength photoacoustic spectrometer and an Aethalometer under sub-urban wintry conditions. Journal of Aerosol Science, 42, 859-866.

Comparison of new UFP monitor with SMPS system in urban sites, in Athens, Greece

E. Diapouli[1], S. Vratolis[1], V. Vasilatou[1], M. Gini[1], G. Habilomatis[2], S. Cheristanidis[2], A. Chaloulakou[2], S. Pothos[3] and K. Eleftheriadis[1]

[1]Institute of Nuclear Technology and Radiation Protection, Environmental Radioactivity Laboratory, National Centre of Scientific Research "Demokritos", 15310 Ag. Paraskevi, Attiki, Greece
[2] School of Chemical Engineering, National Technical University of Athens, Zographos, 15773, Athens, Greece
[3]TSI GMBH, Aachen, Germany
Keywords: ultrafine particles, size distribution, SMPS, urban aerosols.
Presenting author email: elefther@ipta.demokritos.gr

Recent toxicological studies have demonstrated that ultrafine particles (UFPs), that is particles less than 100 nm in diameter, may have a greater impact on human health than larger particles. These findings highlight the need to complement monitoring of traditional parameters (such as PM_{10} and $PM_{2.5}$) with UFPs measurements, when studying associations with health effects and developing mitigation measures. Ultrafine particles contribute very little to particle mass concentration but account for the bulk of the number concentration. In this framework it has become apparent that there is a need for reliable particle counters and sizers that may be used for long-term monitoring and require less maintenance and experienced personnel than traditional instrumentation. The aim of this work was to assess the performance of a new UFP monitor designed by TSI Inc. for long-term, air quality monitoring networks, against a reference system such as a Scanning Mobility Particle Sizer (SMPS).

Measurements were conducted in Athens, Greece, during June and July of 2010 and covered in total a period of one month. Two sites were selected: the N.C.S.R. "Demokritos" urban background monitoring station (DEM) and a heavy-trafficked site located in a central residential urban area (CRU). Particle number size distributions were monitored by an SMPS (DMA, Model 3081 and CPC, Model 3776, TSI, Inc.) and an Ultrafine Particle Monitor (UFP, Model 3031, TSI, Inc.). The logging intervals were 5 and 15 min for the SMPS and UFP, respectively. SMPS measured in the size range 5.9 – 224.7 nm. In order to compare results with the UFP, the SMPS data were grouped in the UFP's size bins. In addition to particle counters, a DustTrak DRX (Model 8533, TSI, Inc.) was employed in CRU, in order to monitor short-term variation of PM_1, $PM_{2.5}$ and PM_{10} concentration.

Temporal variation of the number concentrations obtained by the two instruments showed in general good agreement for all size bins. The 15-min time-series of the number concentration in the size range 20 – 200 nm, measured by UFP and SMPS during the whole measurement period is shown in Fig. 1. SMPS was more effective in capturing short-term peak concentrations which may be attributed to the longer time needed by the UFP to scan the measured size range (15 versus 5 min). Mass and number concentrations variation patterns were dissimilar most of the times, indicating that different sources contributed to the levels measured by each metric parameter.

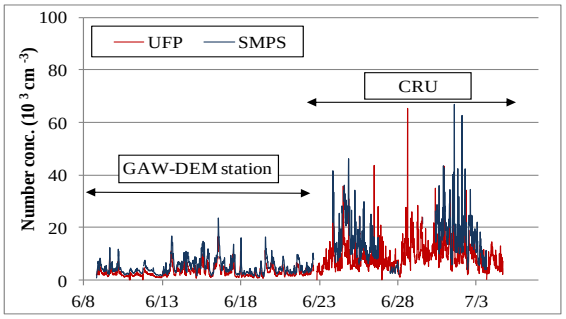

Figure 1. 15-min variation of number concentration in the size range 20 – 200 nm.

Mean 1-hr concentrations at each size bin obtained by the two instruments were linearly correlated for both sites (Table 1). The data were highly correlated but UFP showed a constant underestimation of the concentration by a factor of two approximately, in relation to SMPS. Similar results have been reported by Bae et al .(2009) and Wehner et al. (2007). This underestimation was more pronounced in lower size bins and higher concentrations. Based on these initial results, TSI, Inc. has proceeded to re-calibration of the UFP, using polydisperse, ambient aerosol and SMPS systems as reference.

Table 1. Linear correlation of UFP versus SMPS mean 1-hr data: Coefficient of correlation (r), slope (a) and intercept (b) [10^3 cm^{-3}].

	r	a	b	r	a	b
Site	***20 – 30 nm***			***30 – 50 nm***		
DEM	0.83	0.49	0.09	0.83	0.54	0.10
CRU	0.73	0.45	0.48	0.61	0.35	1.00
	50 – 70 nm			***70 – 100 nm***		
DEM	0.79	0.67	0.02	0.80	0.54	0.08
CRU	0.60	0.38	0.63	0.68	0.40	0.36
	100 - 200 nm			***20 – 200 nm***		
DEM	0.87	0.59	0.04	0.85	0.57	0.28
CRU	0.84	0.51	0.02	0.80	0.41	2.88

Bae, M.-S. et al. (2009) *Proc. AAAR 29th Annual Conference.*
GAW-DEM (2007) http://gaw.empa.ch/gawsis/reports.asp?StationID=20 76202728
Wehner, B., et al. (2007) *Proc .European Aerosol Conference 2007.*

A dry high altitude astronomical observatory in continental Europe

A. Gardini[1], E. Pérez[1] and J.A. Quesada

[1]Instituto de Astrofísica de Andalucía (CSIC), Glorieta de la Astronomía s/n, Granada 18008, Spain
Keywords: columnar water vapour, modelling (regional).
Presenting author email: gardini@iaa.es

Summary. A study of the precipitable water vapour (PWV) above the observatories in Sierra Nevada, the southernmost high altitude location in continental Europe with a dry climate, indicates that Sierra Nevada is a very competitive location for MIR-submm, with PWV<0.2mmH2O, and a 25% quartile of PWV=2.3 mm(H2O) as compared with 2.1 for Mauna Kea.

Method. We use four independent methods to measure PWV: (i) radiometer opacity at 225 GHz located at the 30m IRAM observatory; (ii) on- off- narrow band photometry at 940 nm; (iii) spectroscopic monitoring in the band 800-1000 nm; and (iv) bi-daily balloon-borne atmospheric soundings (retrieved from the University of Wyoming database, fig.1). We use the radiative transfer code SCIATRAN to model the local atmosphere and calibrate the on-site spectroscopic data which measure with high precision the very dry epochs.

Results. **Balloon-borne atmospheric soundings.** The statistical calibration of the results between the IRAM taumeter, the narrow band photometry and the balloon soundings for Gibraltar all agree extremely well, which indicates that the Gibraltar soundings are a reliable proxy. The outcome is shown in figure 2. Sierra Nevada compares very favourably with Hawaii, even though its altitude is 1260m less. The dotted probability line gives the values for an altitude of 3400m, the highest available in Sierra Nevada, where the statistics is similar to or better than Hawaii at 4160m.

We are now able to characterize the statistics of very low PWV epochs.

Results. **Radiative transfer model atmosphere and spectroscopic data.** We obtain direct solar irradiance spectra with an array spectrometer (BWspec) operating in the 700-1020 nm range (0.25 nm spectral resolution). The Wyoming radiosounding data is used to provide profiles of Temperature (T), Pressure (P) and H_2O mixing ratio (mr) as a function of the geopotential height. The Radiative Transfer Model (RTM) incorporated in the SCIATRAN 2.2 package developed at the Institute of Remote Sensing/Institute of Environmental Physics of Bremen University (Germany), allows to simulate radiance/irradiance spectra in the 240-2400 nm range. The RTM was used to simulate the direct solar irradiance spectra at OSN and to compare them with those measured with the spectrometer. After testing the RTM we fixed the parameters: aerosols, spectral albedo, profiles of line-absorbers and continuum-absorbers gases.

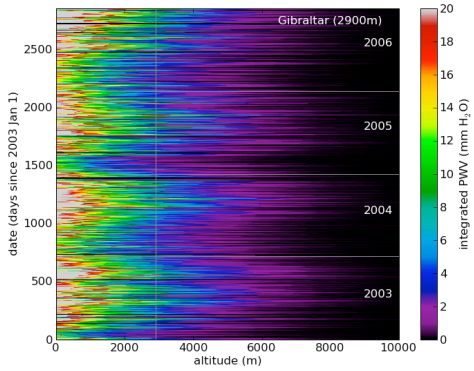

Figure 1. Bi-daily balloon sounding profiles of PWV integrated above the given altitude.

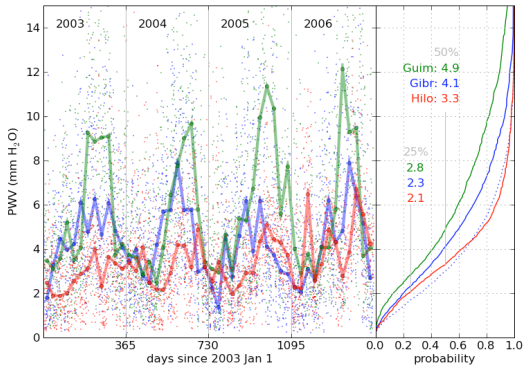

Figure 2. Statistics for Granada, Hawaii and Canary Is.

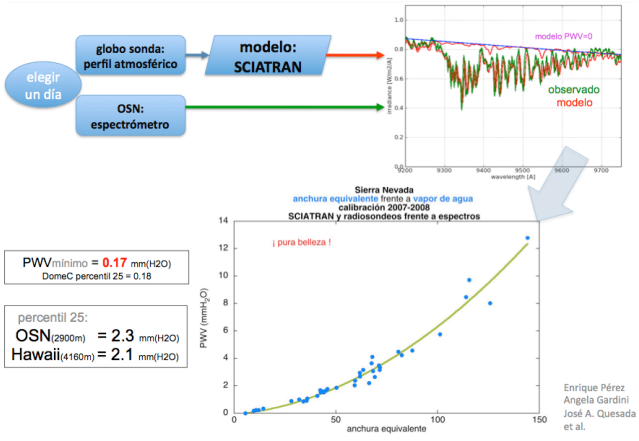

Figure 3. Calibration for Granada, down to 0.18mmH2O.

Batch-to-Batch-Variability of Stöber synthesized SiO2 nanoparticles – Comparison of DLS and SMPS data within Q-NANO

S. Mülhopt[1], M. Hauser[1], E. Mahon[2], Reinhard Schneider[3], H.-R. Paur[1]

[1]Institute for Technical Chemistry, Karlsruhe Institute of Technology, 76021 Karlsruhe, Germany
[2]Centre for Synthesis and Chemical Biology, University College Dublin, Belfield, Dublin 4, Ireland
[3]Laboratory for Electron Microscopy, Karlsruhe Institute of Technology, 76021 Karlsruhe, Germany

Keywords: Nanoparticles, Stöber synthesis, silica, DLS, SMPS
Presenting author email: muelhopt@kit.edu

Background:

QNano is a European Union-funded infrastructure for nanomaterial safety testing. This four year project which has begun in February 2011 comprises 27 top European analytical and experimental facilities in nanotechnology, medicine and natural sciences. It aims to create an integrated hub to support Europe's nanosafety research community. It also covers research themes about nanoparticle production and characterization. In WP 5 one aspect is to define the sources for batch-to-batch-variability of nanoparticles within one production route.

Material and Methods:

Particle production:

The only variable is the amount of aqueous ammonia present in the system which was used to determine resultant particle size. To a defined amount of aqueous ammonia (28%) in a polypropylene container was added EtOH (99.9%) to a volume of 50 ml and stirred at 25^{0}C (for SilNP007 and SilNP009) or 55^{0}C (for SilNP008 and SilNP010) and 600 r.p.m on a plate stirrer. To this rapidly stirring solution was then added Tetraethylorthosilicate (TEOS) (1670 µl) in one aliquot. The solution was then sealed under N_2 and stirred for a further 20 hours at 25^{0}C. The resulting nanoparticle suspension was divided in fractions and centrifuged down at 14,000 rpm for 20 minutes with the pellet then resuspended in fresh ethanol aided by bath sonication. This washing procedure was repeated twice more with ethanol followed by 3 pure water washes and a final resuspension in pure water to a concentration of 10 mg/ml.

Size Measurements

The silica nanoparticles were size characterized by different methods: in suspension by dynamic light scattering with a Malvern Zetasizer Nano ZS and for comparison it was aerosolized by electrospray (Model 3480, TSI, USA) and measured with SMPS (Model 3934, TSI, USA) in the range of 7 – 350 nm.

Results:

The analysis shows a very similar behaviour but depending on method and suspension medium there is a difference in number mean size of about 10 nm. The batches SilNP007 and SilNP009 show a modal value at about 43 nm by DLS (Table 1) but 50 and 53 nm in the SMPS measurements in aerosol phase (Figure 1). The batches SilNP008 and SilNP010 were determined to be 20 nm in liquid suspension and 33 nm in the gas phase.

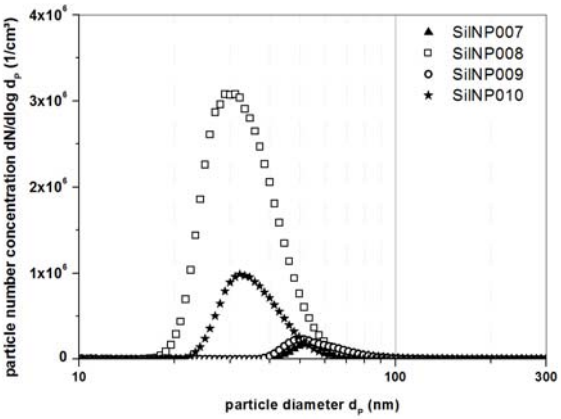

Figure 1. SMPS measurements of the 4 batches SilNP007 – SilNP010 of Stöber synthesized silica suspended in air by electrospray.

Table 1. Comparison between different methods of size measurements. DLS: number mean in nm. SMPS: Modal diameter of number size distribution in nm.

	DLS	SMPS
SilNP007	43	53
SilNP008	20	33
SilNP009	44	50
SilNP010	21	33

Acknowledgement:

This work is part of the European Research Infrastructure for nanosafety assessment QNano. http://www.qnano-ri.eu/

Field experiment with ozone scrubber for monitoring of PAHs

L. Hejkrlík, I. Nikolova, H. Plachá

Czech Hydrometeorological Institute, Branch office in Ústí nad Labem, Czech Republic
Keywords: PAH(s), ozone, denuder
Presenting author email: hejkrlik@chmi.cz

It has been demonstrated that determination of benzo(a)pyrene (BaP) in ambient air may be influenced by the presence of oxidants such as ozone. The losses can be reduced by adding an ozone removing device (denuder) into the sampling line.

Here we present preliminary results of testing the ozone MnO_2-coated ceramic ozone denuder by Digitel in the process of monitoring 15 select PAHs at the measuring station Ústí nad Labem – Kočkov of the Czech Hydrometeorological Institute in period from February to June 2011.

Samples were collected every third day on a quartz filter and a polyurethane foam cartridge using two parallel low volume (2.3 m^3/h) samplers, one of them was equipped with the ozone scrubber (D+), the other was without it (D-).

The laboratory tests of denuder with synthetic air with known concentration of ozone at flow rate 10 l/h (Table 1) confirmed high efficiency of the scrubber even after both 4 and 7 months of use.

Table 1. Efficiency of the ozone denuder

	O_3 (µg.m^{-3}) D-	O_3 (µg.m^{-3}) D+	Efficiency
12/5/2011	60	2	96.7 %
	200	6	97.0 %
	858	36	95.8 %
31/8/2011	58	0	100.0 %
	259	0	100.0 %
	856	2	96.7 %

The fine dust losses were investigated by weighing D+ and D- filters, the mean values were about 10%, maximal weight losses reached as much as 41%.

Regarding the relation between the concentrations measured with/without the denuder, the PAHs were separated into three groups. The concentration of BaP, and similarly of all particle associated PAHs, were underestimated when denuder was not present (Group 1, Figure 1). Second group was formed by PAHs with 4 rings, which were mostly in gas phase in the samples. It is evident from Figure 2 that their concentrations decreased in the case of denuder, probably due to adsorption at the active centres of the catalyst. The third group (Figure 3) was represented by the PAHs that demonstrate unpredictable behaviour related in 75 % of events to Group 1 and in the rest to Group 2.

We have found that the denuder effectively decomposes the ozone and minimizes the decay of PAHs bound to the particles. The application for lighter PAHs in the gas phase is questionable because of possible oxidation.

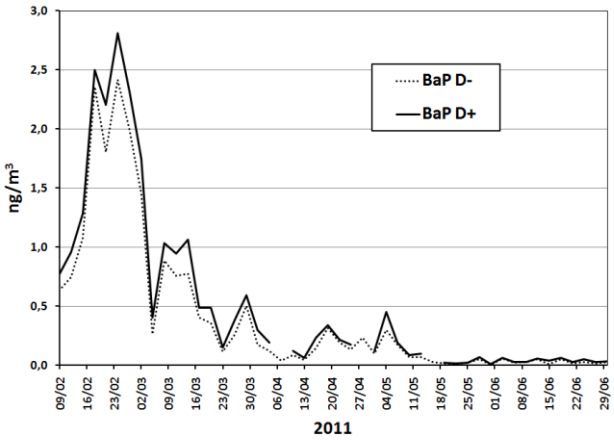

Figure 1. Concentrations of BaP (Group 1, similar behaviour exhibit particle associated PAHs)

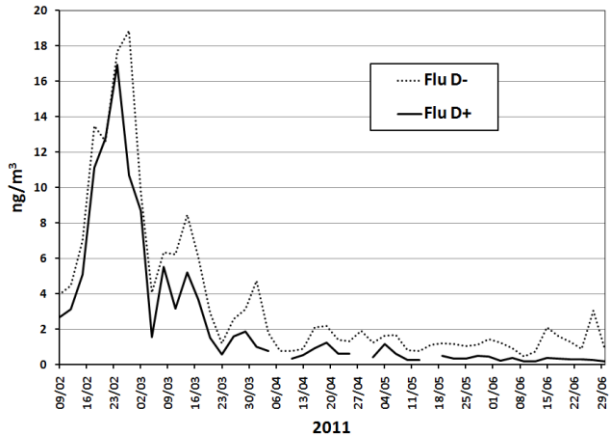

Figure 2. Concentrations of fluoranthene (Group 2, similar behaviour was found for pyren)

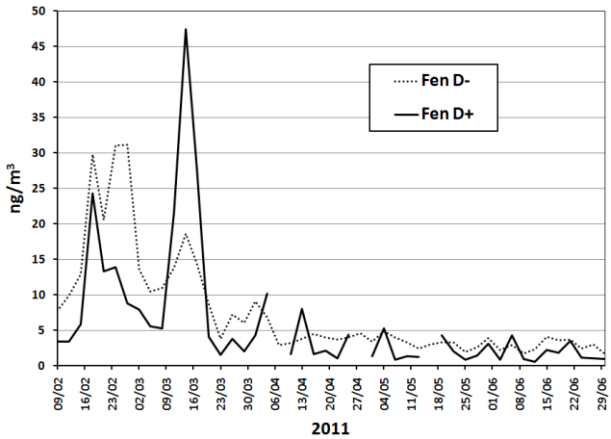

Figure 3. Concentrations of phenanthrene (Group 3, similar random behaviour exhibit anthracene and fluorene)

Retrieval of sky radiance at three wavelengths using a sky camera

R. Román[1], M. Antón[2], A. Cazorla[2,3,*], A. de Miguel[1], F.J. Olmo[2,3], J. Bilbao[1] and L. Alados-Arboledas[2,3]

[1] Laboratorio de Atmósfera y Energía, Department of Applied Physics, University of Valladolid, Valladolid, 47011, Spain
[2] Centro Andaluz de Medio Ambiente (CEAMA), Granada, 18006, Spain
[3] Department of Applied Physics, University of Granada, Granada, 18071, Spain
[*] Now at: Department of Chemistry and Biochemistry, University of California, San Diego, California 92093, USA

Keywords: sky radiance, sky camera, Radiative transfer model, CIMEL.
Presenting author email: robertor@fa1.uva.es

Several columnar aerosol properties can be retrieved from sky radiance measurements using inversion codes. Dubovik *et al* (2006) and Olmo *et al* (2008) derived the columnar aerosol size distribution, the single scattering albedo, the phase function and the asymmetry parameter from sky radiance measurements (using a CIMEL sunphotometer) in the almucantar and in the principal plane configurations, respectively.

The principal aim of this work is to develop a method to retrieve radiance measurements using images from a sky camera. For this goal we use a radiative transfer model combined with aerosol properties retrieved from sun/sky photometer. There are some advantages in the proposed method. Thus sky cameras are less expensive than sky photometers. Furthermore, a sky camera can take a measurement of the full sky (including almucantar and principal plane) in a few milliseconds, while the sun/sky radiometer requires a few minutes.

The measurements used in this work were taken on the rooftop of the Andalusian Center for Environmental Studies (CEAMA, 37.17º N, 3.61º W, 680 m a.s.l). The All-Sky Imager consisting of a digital color CCD camera with a fish eye lens encapsulated in an environmental housing that is temperature regulated with a peltier cell. The system is installed in a sun tracker which blocks the direct solar radiation by a shadow ball. Images are taken every 5 minutes and are composed of three images at three channels: red, green and blue. All information about All-Sky Imager is detailed in Cazorla (2010). A sunphotometer CE-318 (CIMEL Electronic, France) was installed next to the sky imager in the same rooftop. This instrument (included in the AERONET network) provides sky radiance measurements and optical properties of aerosol like aerosol optical depth at different wavelengths.

The UVSPEC model, included in the LibRadtran library developed by Mayer and Kylling (2005), was used to estimate sky radiance under cloud-free conditions. First, the UVSPEC simulations were tested with almucantar radiance measurements (CIMEL): finding a great agreement when all aerosol properties were included as inputs in the model. The model showed the worst results for the estimations near to the sun. The effective wavelengths of each channel of the camera (464, 534 and 626 nm) were calculated using the UVSPEC radiative transfer model and the spectral response of the camera.

Then, a set of cloudless images were chosen, and the radiances at the effective wavelengths were simulated for these images. The signal of each pixel was linearly correlated with its corresponding radiance. Therefore, for each spectral channel a matrix, which ij-element converts the signal of the ij-pixel in the radiance viewed by the ij-pixel, was developed. An image is transformed in three radiance images when the matrices are applied.

The calibration procedure was tested using an independent set of images. The radiances in the principal plane and almucantar were compared with the radiances measured side by side by the CIMEL radiometer,. After considering the spectral differences we obtain average bias smaller than 15% for scattering angles larger than 10º for the three wavelengths.

In conclusion, a method to obtain sky radiance measurements at three wavelengths (which can be used to obtain columnar aerosol properties using inversion codes) is developed. The proposed method provides a tool with higher temporal and spatial resolution than sun/sky photometers. The differences between the estimated (camera) and measured (CIMEL) radiance are lower than 15% for all channels.

This work was partially supported by the Spanish Ministry of Science and Technology through projects CGL2011–25363, CGL2010-12140E, CGL2010-18782, CGL2011-13580-E/CLI and CSD2007–00067. This work was also partially supported by the Andalusian Regional Government through projects P08-RNM-3568 and P10-RNM-6299, and by the European Union through ACTRIS project (EU INFRA-2010-1.1.16–262254).

Cazorla, A. (2010) *Development of a sky imager for cloud classification and aerosol characterization*, Ph.D. thesis, University of Granada, Spain.

Dubovik, O. et al. (2006) *J. Geophys. Res. Atmos.*, **111**, D11, D11208.

Mayer, B. and Kylling A. (2005) *Atmos. Chem. Phys*., **5**, 1855–1877.

Olmo, F. J., Quirantes, A., Lara, V., Lyamani, H. and Alados-Arboledas, L. (2008) *J Quant. Spectrosc. Radiat. Transfer.*, **109**, 1504-1516.

Correlating the extinction-based dustiness to the morphology of particles

S. Bach, E. Schmidt

Department of Safety Engineering / Environmental Protection, University of Wuppertal, Germany
Keywords: Dust, Air quality, Optical instrumentation, Respirable aerosols, Shape factors
Presenting author email: sbach@uni-wuppertal.de

It is still widely unknown which material-specific properties lead to special dustiness behaviours of powders and/or bulk solids. The topic is especially complex, because it is not only due to the nature of the material but also to the energy induced to the powder by the test apparatus used to measure the dustiness.

The present research project employed an approach with a single-drop apparatus, the "DustView" from the Palas GmbH in Karlsruhe, Germany (see fig. 1). This dustiness testing method measures the laser beam attenuation (opacity) caused by a dust cloud. The material falls down a tunnel into a dust chamber (total drop height: 70 cm) and is then dispersed inside the chamber through the impact forces. The relatively low mechanical stress the material is exposed to usually leads to lower measured dustiness indices then with other testing principles (Lyons and Mark, 1992). On the other hand, the material does not alter significantly during the process (Burdett et al., 2000).

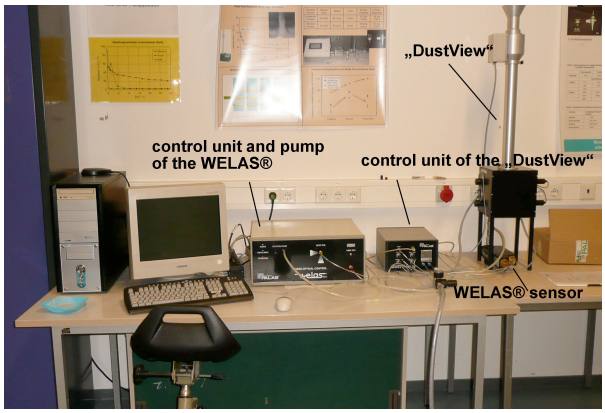

Figure 1. Modified version of the Palas DustView, including single-drop apparatus and OPC "WELAS®"

With the new laboratory set-up, it is possible to measure the opacity every 10 ms as well as the particle number concentration and size distribution with an Optical Particle Counter (OPC) simultaneously. The main question of the project is, do these variables, opacity and number concentration resp. size distribution, correlate in a way that enables the user to gain information about health- and safety-related dustiness – for example about the contingent of the inhalable or respirable aerosol fraction in the dispersed particles – from the opacity values.

Additionally, other material-specific properties have been eaxmined, to ensure the best possible knowledge of the examined powders. Bulk density, relative humidity and particle density have been analysed as well as the particle size distribution of the original material (with laser diffraction spectrometry) and particle morphology (with scanning electron microscopy).

This presentation will focus on the coherence between the dustiness behaviour (i.e. caused opacity, particle number concentration and size distribution of the dispersed powder) and the obtained shape factors.

A total of 15 materials has been examined with the "DustView" and analysed for their particle morphologies. Nine of those were calcium carbonates (limestones) of different particle size distributions. Figure 2 shows an example for a calculated correlation coefficient according to Pearson (r_{xy}), only considering the limestones. Here, the circularity is displayed over the opacity-value after 30 seconds.

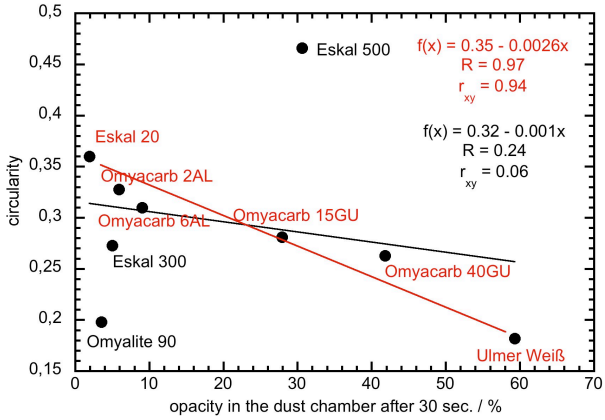

Figure 2. Circularity over 30-sec.-value of the opacity for nine calcium carbonates. Black line and curve fit parameters: all limestones, red line and parameters: six out of nine

The three materials displayed in black characters have two things in common; they only consist of relatively small particles (< 5 µm), whereas the other materials all contain one or more bigger size modes. And secondly, they show comparatively narrow mass- and number-based density distributions.

The present work will try to connect more similarities and peculiarities of powders to the dustiness behaviour of a material, leading to a better understanding.

This work was supported by the German Federation of Industrial Research Associations (AiF).

Burdett G.J., Chung K.Y.K., Mark D. et al., *Development of a method for dustiness testing*, EU contract SMT4-CT96-2074, HSE report, Sheffield, UK, 2000

Lyons, C.P., Mark, D., *An Evaluation of the Roaches Dust Particle Apparatus Testing Equipment*, HSE Contract, Research Report No. 40, 1992

Indoor aerosols sampling and analysis using personal aerosol sampler and filters

A. Akachat[1], H. Rebbah[1]

[1] URMPE, Université Med Bougara, Avenue de l'Indépendance, 35000 Boumerdes, Algérie.
Keywords: particles, isocyanates, PU,
Presenting author email:a.akachat@yahoo.fr

Workplace atmosphere is an important distribution of various pollutants, resulting from the handled products and concerned processes. The fate of these pollutants in the air (transport, deposition, degradation), is determined by their distribution between atmospheric particles and gas phase (Lohmann et al. 1998). Harmfulness of particles in workplace atmosphere and the disease hazards that they present are related to their chemical nature and size. The production of one kilogramme rigid polyurethane foam releases nearly 7362 milligrams of solid particles in air.

In this work, we used the personal aerosol sampler CIP10-R (Courbon et al. 1988) and filters for evaluation of alveolar (Gorner et al. 1996) and inhalable fractions of particles during clean of casts after injection of the polyurethane foam (PU) (fig 1). HPLC was used for detection of MDI in different post (fig 2).

Obtained Results reveal that MDI in alveolar fraction prevail the total collected particles, this can be allotted to the process used for cleaning and to the quality of formulated foam.

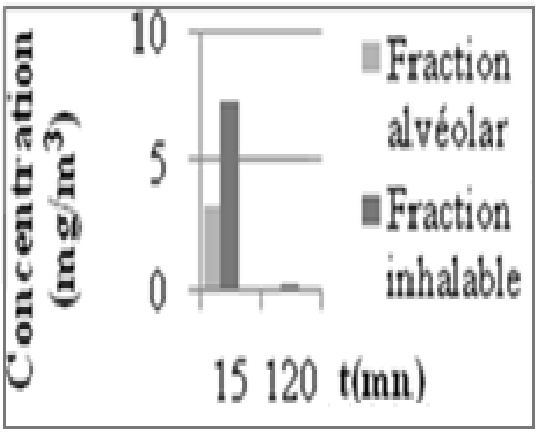

Fig. 1 : Concentration in 15 et 120 mn.

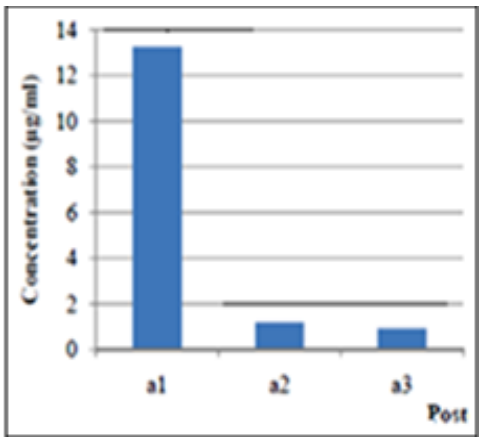

Fig. 2: Alveolar concentration by post

Lohmann, R., Jones, K.C. (1998). Dioxins and furans in air and deposition: a review of levels, behaviour and processes. Science of the Total Environment 219, 53-81.

Courbon P., Wrobel R., Fabries J.F. (1988). Anew individual respirable dust sampler: the Cip 10. Annals of Occupational Hygiene, 32pp. 129 - 143.

Gorner P., Fabries J.F. (1996). Industrial aerosol measurement according to the new sampling convention. Occupational Hygiene, 3, pp 361 – 376.

Chemical composition of commonly used CPC calibration ions in the sub 2nm range

J. Kangasluoma[1], J. Mikkilä[2], K. Lehtipalo[1,2], J. Vanhanen[2], H. Junninen[1], M. Sipilä[1], M. Kulmala[1], T. Petäjä[1]

[1]Department of Physics, University of Helsinki, 00560 Helsinki, Finland
[2]Airmodus Oy, 00560 Helsinki, Finland
Keywords: CPC, mass spectrometry, nanoparticles, characterization
Presenting author email: juha.kangasluoma@helsinki.fi

Recent development of condensation particle counters (eg. Vanhanen et al. 2011) has led to a need of generating monodisperse ion samples that are smaller than 2 nm in mobility diameter in order to calibrate the counters. Apart from electrospray experiments there are no reports on the ion composition in the sub 2 nm range and no reports related to the problems that might arise for example due to impurities, charger ions and relative humidity in the calibration experiments. We present here the first step towards reliable CPC calibrations, which is the analysis of mass spectra of the commonly used calibration ions, ammonium sulphate, sodium chloride, silver and tungsten oxides.

Airmodus A09 PSM is a turbulent mixing type CPC that is able to detect particles down to 1 nm in mobility diameter by condensing diethylene glycol on to the particles. It is possible to choose the cut-off diameter between approximately 1 and 2 nm by changing the flow in the saturator. APi-TOF (Junninen et al. 2010) is a time of flight mass spectrometer with a mass resolution of 5000, which therefore allows measuring the mass defect of a molecule which increases the possibility to solve the chemical composition.

Excluding tungsten oxides, which were generated with a hot wire generator, the sample ions were evaporated to a nitrogen flow with a tube furnace, cooled down in a water bath, charged with a bipolar Am241 neutralizer and finally classified with a high resolution, closed loop Herrmann DMA (Herrmann 2000) with resolution of 20. After the DMA the sample was then led to the mass spectrometer and after its inlet to the PSM and the electrometer without any dilution or disturbances from the room air. Before the experiments all sample lines were chemically cleaned, and the tube in the oven and tungsten wire were heated for several hours to minimize the impurities.

Ammonium sulphate consisted mainly of series $(HSO_4)_x(NH_3)_y$(mass 112)$_z SO_4$-, where mass 112 is an unknown organic impurity most probably coming from the sample, as it was not present in all ammonium sulphate experiments. In the sodium chloride spectrum there were two series: $(NaCl)_xCl$- and $(NaCl)_x$mass- 141, where again mass 141 is some unknown impurity. In the tungsten oxide spectrum the peaks were of series $H_xW_yO_z$(mass 88)$_i$-, where the ratio y/z was about 1/3. In addition to the pure tungsten oxide peaks in some of them was also impurity molecule of mass 88 present. The silver spectrum was full of unidentified peaks without any regular series, although some silver peaks were found, for example Ag_x, where x=3, 5, 7, 9, 13, 17 or 19. However at the moment silver is not in good enough level to be used in calibrations due to high amount of impurities. In spite of some impurities in the mass spectra, the first three can be considered rather clean and usable for calibration experiments.

References:

Junninen et al. (2010), *Atmos. Meas. Tech.*, **3**, 1039–1053.
Herrmann, et al. (2000). *Abstract AAAR Conference*, 15B5.
Vanhanen et al. (2011), *Aerosol Sci. Tech.*, **45**, 533–542.

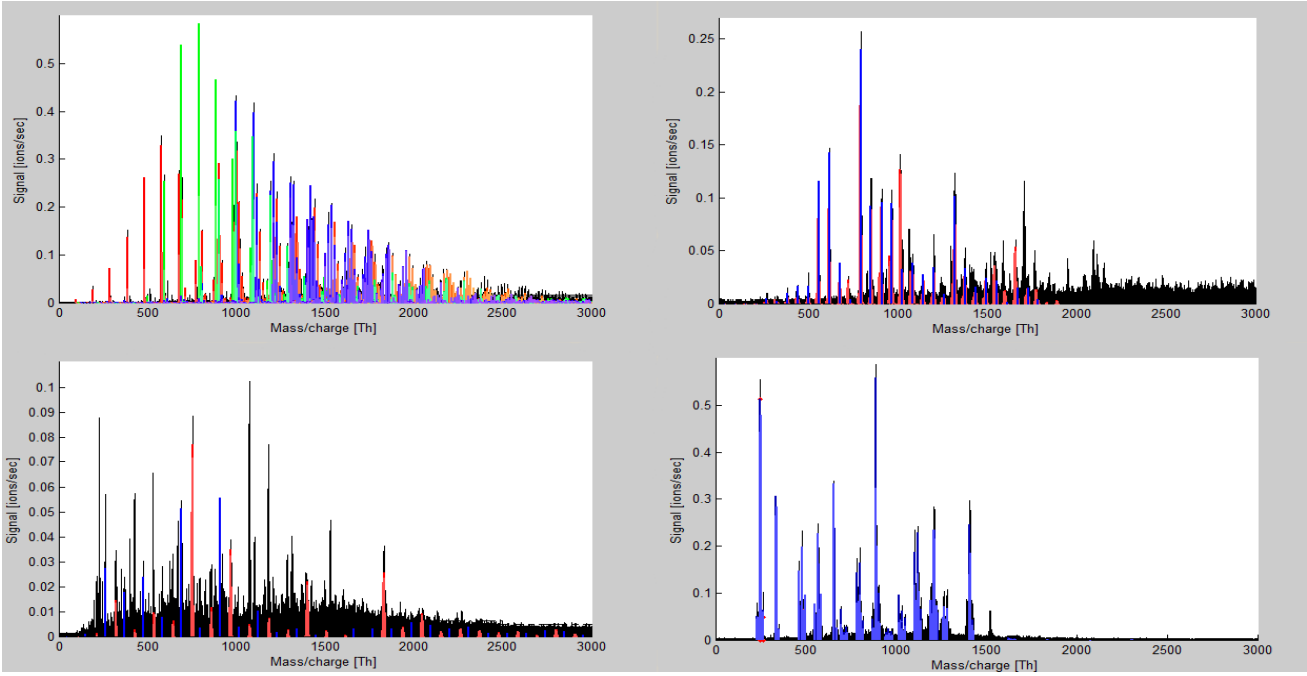

Figure 1. Mass spectra for negative ammonium sulphate (up left), sodium chloride (up right), silver (down left) and tungsten oxides (down right). Identified peaks are marked with color.

Methodology for mapping air pollution in an urban environment: the background issue

M. Van Poppel, J. Peters, N. Bleux.

VITO - Flemish Institute for Technological Research, 2400 Mol, Belgium

Presenting author email: martine.vanpoppel@vito.be

Traffic related air pollution is one of the major concerns in urban environments. Fixed air quality monitoring stations have limitations when used to assess spatial patterns of traffic related pollutants (UFP, $PM_{2.5}$, BC) in urban environments.

Mobile platforms are increasingly used to acquire high level temporal and spatial resolution measurement in a complex urban environment. As such, mobile measurements provide a solution to assess spatial variation of pollutants with a limited number of instruments and in a confined timeframe. In this way, mobile measurements can be used for air quality mapping, hot spot identification and exposure assessment. However, issues related to representativeness of repeated runs and variation in background concentrations are not yet solved.

At VITO, a measuring bike – called Aeroflex – was developed for mobile measurements and mapping of UFP (P-trak, TSI), PM (Grimm Dust monitor) and BC (µ-Aethalometer, AethLabs). A method to take into account differences in background concentrations and to compare repeated runs is discussed in this paper. In addition, a method to compare street-by-street variation based on repeated runs is presented. The developed method was applied on a case study.

A case study was performed in Mol, Belgium (a city with 34,000 inhabitants). The 10 km long sampling route was repeated 20 times on 10 different days and includes roads characterized by different amounts of traffic. The sampling route comprises 6 different zones characterised as: (1) access road outside the city centre, (2-3) major road in the city, (4) road with restricted traffic, (5) green space, (6) road in the city centre. The different zones are also characterised by differences in the surroundings: more 'open' zones (1, 5) and 'street canyon'-like (2, 3 and 6).

Significant differences between different zones for UFP and BC, however not for $PM_{2.5}$ were found (Kruskal-Wallis test, $p<0.05$). Urban concentrations contain a background component in addition to the street level contribution. When trying to assess spatial variation in an urban environment by repeated mobile measurements, we are confronted with differences in background that hamper the averaging over different runs.

Therefore a background correction should be applied. A common practice is to subtract a background concentration from the mobile measurements, resulting in the local component of the pollutant concentration. To determine a background concentration based on the mobile measurements, different percentile concentrations were calculated for the entire run and for the green zone (5) only. The green zone is considered to give a good estimate of the variable background concentration and represents 10% of the entire data volume in this study.

As an example, average UFP concentrations of one run for the different zones are compared to different percentile concentrations for the green zone . The results show that the local contribution of UFP was 2 to 3 times higher than the background concentrations. In contrast, for $PM_{2.5}$ 80% or more could be attributed to background.

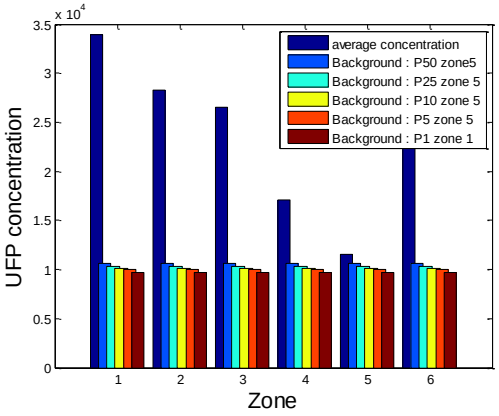

Figure 1: Average concentrations of UFP compared to different percentile concentrations (P1, P5, P10, P25 and P50) for the green zone.

A background correction, by subtracting the 1st quartile concentration of the green zone resulted in a higher similarity of pollutant concentrations over the different runs. The P25 for the green zone corresponds to the P5 over the entire run in this study. The advantage of using a percentile concentration of a green zone as background value is that the number of measurements made in the green zone is not important and will not influence the result. Whereas, if a lower percentile concentration of the entire run is chosen, more care must be taken in selecting the route.

This analysis showed the potential of mobile measurements to assess spatial variation of traffic related pollutants in an urban environment. However data-processing accounting for background concentrations is important for interpretation and comparison. The background correction presented in this paper can be easily integrated in the mobile mapping methodology, without the need for data from fixed AQ monitors.

On the use of Direct Analysis in Real Time/Quad-Time of Flight (DART/Q-TOF) for the analysis of Organic Aerosol

A. Sylvestre[1], S. Ravier[1] and N. Marchand [1]

[1]Aix-Marseille Univ., CNRS, Laboratoire Chimie Environnement, 13331, Marseille, France.
Keywords: DART, organic aerosol, organic markers.
Presenting author email: alexandre.sylvestre@etu.univ-provence.fr

In the last ten years, ambient mass spectrometry creates a lively interest for sample analysis. Many ambient ion sources have been designed such as Extractive Electrospray Ionization (EESI) (Chen et al., 2005), Desorption Electospray Ionization (DESI) (Cooks et al., 2004) or Direct Analysis in Real Time (DART) (Cody et al., 2005) which allow direct analysis from surfaces. Thus the sample preparation step is simplified as much as possible avoiding analyte losses and reducing the length of the analytical procedures.

DART source can be used to analyse gases, liquids, solids and materials on surfaces. A gas (helium or nitrogen), cross a chamber (figure 1) where an electrical discharge produces ions, electrons, metastable atoms and molecules. Perforated lenses remove charge particles, and only metastable species and neutral gas molecules remain. Then, those species can be heated and the grid electrode focuses them through the insulator cap to the sample surface, containing an analyte M. In positive mode, when helium is used, $[MH]^+$ ions are formed by proton transfer reaction :

$$He(2^3S) + H_2O \rightarrow H_20^{+\cdot} + He(1S) + e^-$$
$$H_20^{+\cdot} + H_2O \rightarrow H_3O^+ + OH^\cdot$$
$$H_3O^+ + n\,H_2O \rightarrow [(H_2O)nH]^+$$
$$[(H_2O)nH]^+ + M \rightarrow MH^+ + nH_2O$$

In negative ionisation mode, $[MH]^-$, $M^{-\cdot}$ and $[MO_2]^{-\cdot}$ ions formation occur according to the following reactions:

$$\text{Excited gas} + \text{surface} \rightarrow \text{Gas} + \text{surface} + e^-_{fasr}$$
$$e^-_{fast} + \text{atmospheric pressure gas} \rightarrow e^-_{slow}$$
$$e^-_{slow} + O_2 \rightarrow O_2^-$$
$$O_2^- + M \rightarrow MH^- + OH^\cdot$$
$$O_2^- + M \rightarrow M^{-\cdot} + O_2$$
$$O_2^- + M \rightarrow MO_2^{-\cdot}$$

DART source enables soft ionization and produces simple mass spectra in a few seconds. What it can be suitable for complex matrix like biological matrix (Jagerdeo et al., 2009), food matrix (Vaclavik et al., 2010) or warfare agent (Nilles et al., 2009).

DART source has been used in many fields, and while this technique offers great perspectives in field of organic aerosol analysis, DART source has not been applied on aerosol filter samples, for now. Thus, this study aims to test the ability the DART source to analyse organic aerosol deposited onto filters. The DART source is coupled to Q-ToF mass spectrometer (Synapt G2 HDMS, Waters) with a mass resolution up to 40 000. Our first objective was to test the ability of this analytical setup to quantify organic markers such as levoglucosan, PAHs, hopanes and fatty acids. To do so, different parameters like gas temperature, gas flow, sample position, etc., have been tested on standard solutions. Matrix effects have also been studied by the addition of ammonium nitrate and ammonium sulfate. In a second step, various ambient and smog chamber samples have been analysed (urban samples collected during the APICE field campaign, cooking samples and Kerbside samples). Results obtained have then been compared with traditional GC/MS technique, if any.

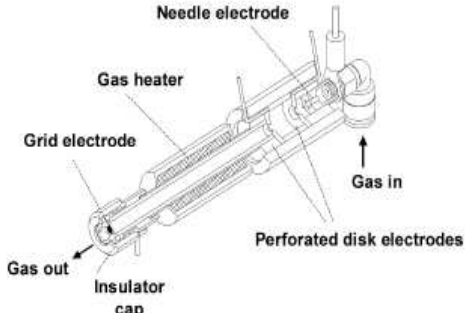

Figure 1. Schematic diagram of the DART ion source (source Cody et al, 2005)

Cody, R. B., Laramée, J. A., Nilles, J. M. and Durst, H. D., (2005) *JOEL News*, **40**, 8-12.

Chen, H. W., Talaty, N. N., Takats, Z., Cooks, R. G., (2005) *Analytical Chemistry*, ***77***, 6915–6927.

Chen, H. W., Lai, J. H., Zhou, Y. F., Huan, Y. F., Li, J. Q., Zhang, X.,Wang, Z. C., Luo, M. B., (2007) *Chinese Journal Anaytical. Chemistry*, ***35***, 1233–1240

Jagerdeo, E. and Abdel-Rehim, M., (2009) *Journal of the American Society for Mass Spectrometry*, **20**, 891-899.

Nilles, J. M., Connell, T. R. and Durst, H. D., (2009) *Analytical Chemistry*, **81**, 6744-6749.

Cooks, R. G., Takats, Z., Wiseman, J. M., and Gologan, B., (2004) *Science*, **306**, 471-473.

Vaclavik, L., Rosmus, J., Popping, B. and Hajslova, J., (2010) *Journal of Chromatography A,* **1217**, 4204–4211.

Using a Single Particle Soot Photometer to detect and distinguish different absorbing aerosol types

K. Heimerl[1], B. Weinzierl[1], M. Gysel[2], D. Baumgardner[3], G. Kok[4], C. Linke[5], M. Schnaiter[5], J. Schwarz[6], P. Sheridan[6], R. Subramanian[4] and J. Walker[4]

[1]Institut für Physik der Atmosphäre, Deutsches Zentrum für Luft- und Raumfahrt, 82234 Oberpfaffenhofen, Germany
[2]Laboratory of Atmospheric Chemistry, Paul Scherrer Institut, CH-5232 Villigen PSI, Switzerland
[3]Centro de Ciencias de la Atmósfera, Universidad Nacional Autónoma de México, Mexico City 04510, D. F., Mexico
[4]Droplet Measurement Technologies, Boulder, CO, 80301 USA
[5]Institute for Meteorology and Climate Research, Karlsruhe Institute of Technology, 76021 Karlsruhe, Germany
[6]Earth System Research Laboratory, National Oceanic and Atmospheric Administration, Boulder, CO, 80305 USA

Keywords: SP2, volcanic particles, hematite particles, soot particles, aerosol characterization
Presenting author email: Katharina.Heimerl@dlr.de

The Single Particle Soot Photometer (SP2) was originally designed to measure (refractory) black carbon, but also absorbing materials different from black carbon can be detected. This presentation shows results from experiments with volcanic ash and hematite, performed during two laboratory studies, and introduces a method to distinguish these materials from black carbon.

The SOOT11 campaign at the KIT AIDA (Aerosol Interaction and Dynamics in the Atmosphere) chamber in November and December 2010 was dedicated to compare the performance and efficiency of six different SP2s (Laborde *et al*. 2012). During one experiment of the SOOT11 campaign, a ground sample of ash from the Eyjafjallajökull volcano was brought into the AIDA chamber to test the SP2's sensitivity to absorbing materials different from black carbon. The volcanic ash aerosol remained in the AIDA chamber for several hours and was mixed externally with black carbon later in the experiment. Experiments with pure hematite and an external mixture of hematite and black carbon were performed as part of the Boulder light absorption intercomparison study (BLAC09) in January and February 2009.

The SP2 uses laser-induced incandescence to measure the mass of individual absorbing particles which are heated in a continuous laser beam with Gaussian intensity distribution such that they emit thermal radiation and evaporate. This radiation is detected at two different visible wavelength bands. The ratio of the signals from the two incandescence channels, the color ratio, provides a relative measurement of the incandescence temperature of the particle (Moteki & Kondo 2010). While a particle passes the laser beam, also the scattered laser light is recorded. Initially, this scattering signal allows to derive the optical size of the whole particle before evaporation started. In contrast, the scattering signal at the point of maximum incandescence corresponds to the optical size of the incandescing particle core.

Both volcanic ash and hematite were found to be detectable in the SP2 incandescence channels with low efficiency only, as they absorb light less efficiently than black carbon. About 5-10% of all measured particles were detected in the incandescence channels, with the percentage rising with size.

Comparisons between the different materials show that the color ratio is larger for black carbon than for both volcanic ash and hematite, because the incandescence temperatures of those materials are lower. For both mixtures, the color ratio shows two peaks: one at the level of black carbon, and one at a lower level corresponding to the less absorbing material. This method is difficult to apply for single particles, because the color ratio may be noisy, especially for small particles.

A more precise distinction between the materials can be made by using the differences in both optical and physical properties. Volcanic ash and hematite particles with similar incandescence signals will have scattering signals different to those of black carbon particles at the point of incandescence, as they have different incandescence temperatures and refractive indices. Therefore, the ratio between the signals in the scattering and incandescence channels at the point of incandescence shows a strong dependence on material. Figure 1 shows this ratio for the volcanic ash experiment of the SOOT11 campaign. The data points separate into two clusters: the lower one represents the black carbon particles, while volcanic ash particles have higher values with a distinct gap between the two materials. This makes it possible to distinguish materials on a particle-by-particle basis.

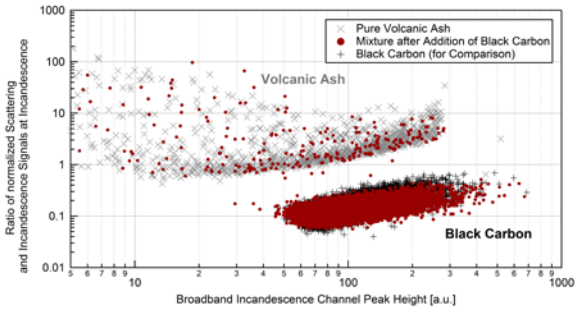

Figure 1: Signal ratio at incandescence for volcanic ash before and after the addition of black carbon (SOOT11 experiment). Pure black carbon data from another experiment are added for comparison

Laborde, M, *et al*. (2012) Single Particle Soot Photometer intercomparison at the AIDA chamber, manuscript in preparation.
Moteki, N & Kondo, Y (2010) *Aerosol Science & Technology*, **44** (8), 663–675.

Detection efficiency of a TSI Environmental Particle Counter 3783 particle counter: experimental and simulated results

J. Hakala, H.E. Manninen, T. Petäjä and M. Sipilä

Department of Physics, University of Helsinki, PL 64, 00014 University of Helsinki, Finland
Keywords: CPC, Aerosol instrumentation
Presenting author email: jani.hakala@helsinki.fi

Monitoring the number concentration of aerosol particles is one of the basic measures to characterize the air quality for health and climatological purposes. The Condensation Particle Counters (CPCs), which include the new water based TSI Environmental Particle Counter (EPC) 3783 under the study, are widely used for this purpose. In this study we present the experimental and simulated results of the performance of the EPC 3783 for hygroscopic and hydrophobic materials.

The detection efficiency and cut-off diameter D_{50} for a TSI model 3783 were determined by particles produced by evaporating silver (Ag), ammonium sulphate ($(NH_4)_2SO_4$) and sodium chloride (NaCl) to passing nitrogen flow in a tube furnace. As the flow cooled down after exiting the furnace, the vaporized material nucleated forming polydisperse aerosol particles. A monodisperse fraction of a certain diameter was selected with a Differential Mobility Analyzer, and the detection efficiency of the EPC was determined by comparing the number concentration measured by EPC 3783 to the number concentration measured by an electrometer. The cut-off diameters for different materials with default saturator and growth tube temperatures (20°C and 60°C respectively) are presented in table 1.

Table 1. The EPC 3783 cut-off diameters for particles of different chemical composition.

Particle material	D_{50} [nm]
Ag	6.4
$(NH_4)_2SO_4$	4.8
NaCl	4.3

The supersaturation inside the growth tube is the key element affecting the detection efficiency of the laminar flow water based CPCs (Hering and Stolzenburg, 2005). It was calculated using Comsol Multiphysics 3.5a simulation software. Knowing the supersaturation, it was possible to calculate the contact angle best suited to replicate the detection efficiency curve for non-soluble particles using the heterogeneous nucleation theory (Fletcher, 1958). The contact angle for silver particles retrieved from the simulation was 36°, which is in good agreement with experimental results from Porstendörfer et al., 1985. In figure 1 are presented the simulated and experimental results for the detection efficiency of the EPC 3783 for silver particles. It can be seen from the figure that the contact angle alone can not be the only parameter for predicting the detection efficiency.

The Kohler-theory was used to simulate the detection efficiency for hygroscopic and water soluble salts. It turned out that the simulations overestimated the detection efficiency for NaCl and $(NH_4)_2SO_4$ particles. It seems that there are no experiments published that study the hygroscopic growth and activation of NaCl and $(NH_4)_2SO_4$ particles below the diameter of 8 nm to compare our results with.

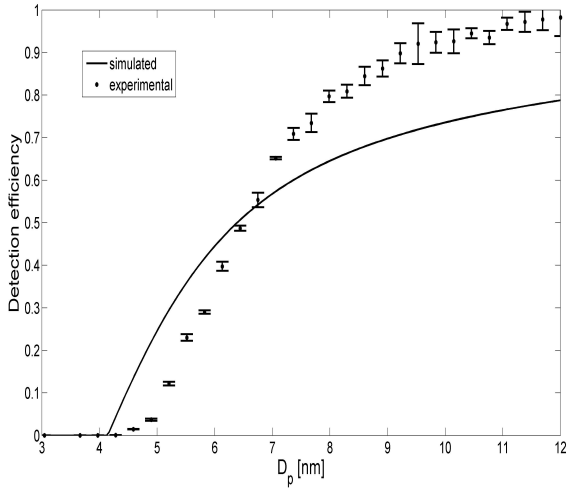

Figure 1. The simulated and experimental detection efficiency of the TSI EPC 3783 for silver particles.

This work was supported by the Academy of Finland (projects 251427 and 139656).

Fletcher, N. H. (1958) *J. Chem. Phys.* **29**, 572-577.
Hering, S. V. and Stolzenburg M. R. (2005) *Aerosol Sci. Technol.,* **39**, 659-672.
Porstendörfer, J. et al. (1985) *Aerosol Sci. Technol.,* **4**, 65-79.

Evaluation of collection efficiency for the Aerodyne Aerosol Chemical Speciation Monitor using long-term ambient air data

M. Maasikmets[1,2,3], F. Canonaco[3] J.G. Slowik[3], A.S.H. Prévôt[3], U. Baltensperger[3]

[1]Estonian Environmental Research Centre (EERC), Marja 4d, 10617 Tallinn, Estonia, [2]Institute of Agricultural and Environmental Sciences, Estonian University of Life Science (EULC), Kreutzwaldi 5, 51014 Tartu, Estonia; [3]Laboratory of Atmospheric Chemistry, Paul Scherrer Institut, 5232 Villigen PSI, Switzerland
Keywords: collection efficiency, ACSM, AMS.
Presenting author email: marek.maasikmets@klab.ee

Atmospheric aerosols play important roles in human health, visibility, acid deposition, and global climate. The Aerodyne Aerosol Chemical Speciation Monitor (ACSM) provides robust, low-maintenance measurements of non-refractory submicron particulate matter in real-time, making it well-suited for long-term monitoring applications. The ACSM is based on the widely used Aerodyne Aerosol Mass Spectrometer (AMS) and combines an aerodynamic lens for particle focusing with high-vacuum particle thermal vaporization, electron impact ionization, and mass spectrometry (Ng, et al. 2011). A critical parameter for quantitative ACSM (and AMS) measurements is the "bounce collection efficiency" (E_b), defined as the probability that a particle impacting the ACSM/AMS vaporizer does in fact vaporize, rather than bouncing off the vaporizer surface and remaining undetected.

E_b depends strongly on particle phase, with solid particles more likely to bounce than liquid ones. An E_b of ~0.5 has been found to be appropriate for many ambient measurements, and this value is assumed to be correct in many published AMS datasets. However, E_b > 0.5 has been observed in previous laboratory and field studies with increasing particle acidity, nitrate content, relative humidity (at the instrument inlet) and coatings of pure liquid organic material (Matthew et al., 2008; Middlebrook et al., 2012).

Here we investigated the effect of different parameters (meteorological data, gas-phase pollutants e.g., CO, NO_x, O_3, NMVOC, O_x and aerosol species) on E_b. E_b was estimated as the volume ratio between ACSM and SMPS. It was assumed that ACSM and SMPS have same transmission efficiency. For the volume calculation it was assumed that Org, SO_4, NO_3, NH_4 and Chl have density of 1.27, 1.78, 1.72, 1.75, 1.4 g/cc respectively. For the SMPS volume calculation the particle density was assumed 1.5 g/cc. The measurements were conducted from February 2011 to January 2012 in Zürich Kaserne (urban background) station. This long-term dataset provides a more statistically robust sampling of E_b-influencing parameters than is possible with short-term intensive campaigns. The ACSM measured non-refractory PM1 chemical composition with a time resolution of 15 to 30 min. The SMPS measured submicron particle number size distributions between 13 and 615 nm mobility diameter with a time resolution of 5 min. For the ACSM and SMPS the same inlet (4m above ground) with Nafion dryer (Perma-Pure, length 100 cm) was used.

The CE analysis showed that the mean E_b results are with 0.62 somewhat higher compared to default E_b. Three main periods according to daily mean temperature were identified – warm (mean +16.9±6.35°C), cold (mean +7.2±4.32°C) and mixed period (mean +15.85±5.02). CE rose during the summer when f43, f55, temperature and O_x were high. This can be explained by the fact that freshly emitted organic aerosols (cooking, BVOC) are detected by the ACSM with minor losses or/and there are evaporative losses of semi-volatile species in the SMPS. During the colder period the f44, f57 and BC were high, which indicates that more primary aerosols were available during those periods. Rather low E_b (< 0.5) were found for periods with intermediate temperatures but higher f44 than in the warm summer periods.

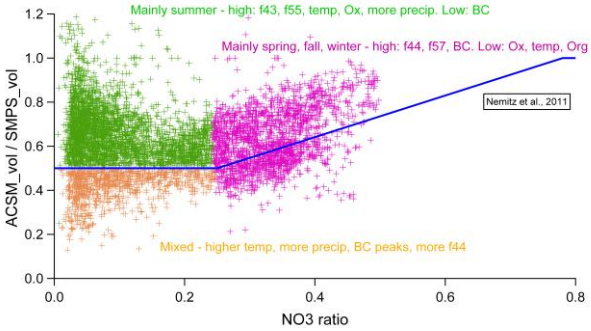

Figure 1. CE analysis based on ACSM and SMPS ratio

This work was supported by the Swiss Federal Office for the Environment (FOEN) and Scientific Exchange Programme NMS-CH (Sciex-NMS[ch]).

Matthew et al. (2008) Collection Efficiencies in an Aerodyne Aerosol Mass Spectrometer as a Function of Particle Phase for Laboratory Generated Aerosols. Aerosol Sci. Technol. 42:884–898.

Middlebrook et al. (2012) Evaluation of Composition-Dependent Collection Efficiencies for the Aerodyne Aerosol Mass Spectrometer using Field Data. Aerosol Science and Technology, 46, 258–271.

Nemitz et al. (2011). Aerosol Mass Spectrometer Network Measurements During the EUCAARI/EMEP Intensive Measurement Campaigns. Atmos. Chem. Phys. Disc. in prep.

Ng et al. (2011) An Aerosol Chemical Speciation Monitor (ACSM) for Routine Monitoring of the Composition and Mass Concentrations of Ambient Aerosol, Aerosol Science and Technology, 45: 7, 770 — 784.

An innovative and efficient method for the analysis of levoglucosan in ambient air particulate matter by thermal desorption coupled with GS/MS.

E. Grandesso, P. Pérez Ballesta, K. Valler, K. Kowalewski

European Commission. Joint Research Centre, Ispra (VA), 21027, Italy

Keywords: Levoglucosan, thermal desorption, air monitoring.
P. Pérez Ballesta: pascual.ballesta@jrc.ec.europa.eu

Levoglucosan (1,6-anydro-β-D-glucopyranose) is an important constituent of particulate matter emitted in large quantities during biomass burning (Simoneit, 1999). Due to its atmospheric stability and high concentrations, it has been used as a tracer for the long-range transport of biomass aerosol (Nolte *et al*. 2002; Fraser and Lakshmanan, 2000; Lee *et al*. 2008; Caseiro *et al*. 2009). For these reasons determination of levoglucosan is becoming an important issue, in particular, for source apportionment modelling that requires concentration values on daily bases.

In this work, a quick and sensitive method for analysis of levoglucosan in PM filters using thermal desorption (TDU/CIS4, Gerstel, GmbH) coupled with GC/MS (Agilent Technologies) is presented. Analysis results by this new method are compared with previously reported data from certified reference material (CRM) 1649a. The method consists on the derivatisation of levoglucosan directly on the liner used for thermal desorption.

The optimisation of the method was done by means of standard solutions (STD) prepared with known amount of levoglucosan and Levoglucosan-d7 (98%). The STD were spiked on a quartz filter placed inside the liner on top of a glass wool plug. 5 µL of derivatising agent (N,O-bis(trimethylsilyl) trifluoroacetamide with 1% of trimethylchlorosilane, BSTFA+TMCS) was then added. Reaction conditions of 5, 15, 30 and 45 min at 60°C and of 5 min at ambient temperature (22°C) were tested. The reaction was complete in all cases, with no significant difference in the total yields and peaks abundances. Therefore, the derivatisation occurred almost instantaneously even at ambient temperature.

Thermal desorption parameters were critical for levoglucosan determinations. For primary thermo desorption (TDU) temperatures of 120, 150, 170, 200 and 300°C were tested with holding times of 10 minutes. The transfer line temperature was kept equal to the primary desorption temperature. The cryogenic trap (CIS) was hold at -15°C during the primary desorption step and subsequently ramped to a final temperature of 50°C over the primary desorption temperature for injection into the column. Flow parameters were set as previously reported (Van Drooge, 2009). These parameters were tested not only on STD, but also on CRM.

CRM analysis was performed by different techniques: a) by liquid extraction, as refereed in bibliography (Simoneit, 1999; Larsen, 2006.) and b) by suspension and deposition on the TDU liner filter to simulate sample filter analyses. While no difference in response was found on varying desorption temperature when analyzing STD or liquid extracts, significant differences were observed for the CRM suspension.
Liquid extraction technique resulted in an average concentration of 85 ± 11 mg/kg. Such a value was in accordance to the concentration reported for CRM 1649a and to those reported by Larsen, (2006). On the other hand, the analysis of the CRM suspension resulted in 90 mg/kg at a TDU desorption temperature (T) of 120°C, 86 ± 2 mg/kg (n=2) at T = 150°C, 95 ± 2 mg/kg (n=2) at T = 170°C, 143 ± 15 mg/kg (n=4) at T = 200°C and 1265 ± 179 (n=2) at T = 300°C.

The high amounts of levoglucosan detected at 300°C could be due to artefacts produced during sample heating in the TDU under nitrogen stream. Since at TDU temperature lower than 170°C levoglucosan determinations were not varying significantly and were comparable to the concentration reported by the CRM certificate of analysis the recommended desorption temperature was fixed at 150° C.

This method has been applied for analysis of PM10 samples on quartz filters at the JRC Ispra site during winter 2010. The low volume sample filters were cut at an optimal section of 2.5 mm, placed in the liner on top of the quartz filter and spiked with 3 µL of internal standard. The addition of 5 µL of BSTFA+TCMS was sufficient to cover completely the filter with the reagent. The method provided good reproducibility results (generally better than 15 %). Moreover, this new method presents the advantages of providing quick analyses, by eliminating the use of solvent and tedious extraction steps, improving in this way the limit of detection (Van Drooge, 2009).

Caseiro, A., Bauer, H., Schmidl, C., Pio, C. A., Puxbaum, H. (2009) *Atmos. Environ*. **43**, 2186-2195,

Fraser, M.P. and Lakshmanan, K. (2000) *Environ. Sci. Technol*. **34**, 4560–4564.

Larsen, R.K., Schantz, M.M., Wise S.A. (2006) *Aerosol Science and Technology*, **40,** 781–787

Lee, J. J., Engling, G., Lung, S.-C. C. and Lee, K.-Y. (2008) Atmos. Environ. **42**, 8300–8308.

Nolte, C.G., Schauer, J.J., Cass, G.R.,. Simoneit, B.R.T (2002) *Environ. Sci. Technol*. **36**, 4273–4281

Simoneit, B.R.T., Schauer J.J., Nolte, C.G., Oros, D.R., Elias, V.O., Fraser, M.P., Rogge, W.F., Cass G.R. (1999) *Atmos. Environ.* **33**, 173-182

Van Drooge B. L. and Ballesta P. P. (2009) *Environ. Sci. Technol*. **43**, 7310–7316.

The use of quartz filters as reference material for analysis of PAHs in particulate matter ambient air samples

P. Pérez Ballesta, E. Grandesso, K. Kowalewski

European Commission, Joint Research Centre, Ispra (VA), 21027, Italy

Keywords: PAH, standard reference material, particulate matter, intercomparison exercise.
P. Pérez Ballesta: pascual.ballesta@jrc.ec.europa.eu

The use of an appropriate reference material for PAH analyses in air particulate matter (PM) is a very relevant issue for the data quality and control. Although desirable, a PAHs reference material from real ambient air sampled on filter is currently not available. The objective of this work is to demonstrate the feasibility of producing certified reference concentrations for PAHs on real PM ambient air filters by using a methodology that allows: i) A rapid and accurate analysis on tiny pieces of filter; ii) testing homogeneity and stability of the filter composition; iii) the selection of filters based on custom laboratory requests. The feasibility of the proposed methodology is supported from the results obtained in an inter-laboratory comparison (Grandesso *et al*., 2012).

PM10 was sampled in background areas of Madrid (Spain) and Prague (Czech Republic) on quartz filters (QM-A, 20.3 mm x 25.4 mm, Whatman International Ltd., England) using a Anderson high volume sampler (HVS). Those filters were cut in twenty circles of 39 mm diameter, corresponding to low volume filter samples. The circles were systematically cut by means of a pattern specifically designed for this purpose. The low volume dimension filters were than accurately packed for distribution and storage.

The filters were analyzed using a thermal desorption unit coupled with a cryogenic trap (TDU/CIS4, Gerstel GmbH) according to previously reported method (Van Drooge, 2009). This system allows for the direct introduction in the TDU of glass liners in which small filter sections were deposited and pre spiked with an internal standard mixture containing deuterated PAHs. After desorption the compounds were analyzed by means of a GC/MS.

To verify the homogeneity of the PAHs distribution in the filter, a minimum of four small filter sections were randomly taken from each filter for analysis. Figure 1 reports for two different HVS filters, the analytical repeatability standard deviation (RSD) obtained from liquid standard injections and the homogeneity RSD derived from the real sample analysis. The sum of both RSD was lower than 10% except for some compounds with concentrations close to the detection limit or with co-elution problems. It was noted that instrumental variability had a high contribution to the overall analytical uncertainty especially for filters with low PAH concentration levels. The calculated "RSD homogeneity" values were in any case low enough to guarantee the use of these filters in an intercomparison exercise.

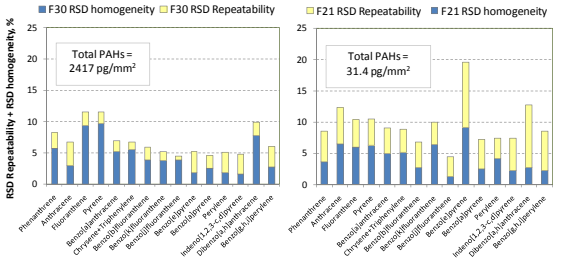

Figure 1 – Repeatability and homogeneity standard deviation for PAHs determination in HVS PM10 filters.

Stability of filters over more than a year of storage time was tested at temperatures of 20°C (ambient temperature) and -18°C. At -18°C all the filters showed insignificant variations with respect to the initial concentration values. A significant decrease in concentration of the more volatile PAHs (i.e., Phenanthrene, Fluoranthene, Pyrene) was observed for filters kept sealed at ambient temperature for long periods, i.e., one year. Nevertheless, this was not when the storage time was shorter than one month.

PAH concentrations determined by thermal desorption were in agreement with the intercomparison reference value, with overall expanded uncertainties better than ± 20%.

Therefore, by means of this methodology it is possible to select, characterise and certify PAH concentration levels in PM filters in accordance with laboratory or sampling needs, *i.e.* concentration levels, matrix characteristics or PM origin with a minimum use of filter surface.

ISO/IEC guide 43-1:1997(E) *Proficiency testing by interlaboratory comparisons-Part1: Development and operation of proficiency testing schemes*, Geneva (CH).

Van Drooge B. L. and Ballesta P. P. (2009) *Environ. Sci. Technol*. **43**, 7310–7316.

Grandesso, E., Kowalewski, K., Pérez Ballesta, P. *First EC-JRC PAHs inter-laboratory comparison on PM10 quartz filters*. 2012. JRC Scientific and Technical Reports DOI 10.2788/63064.

Deposition chamber for in vitro toxicity tests of nanoparticles

N. Jeannet[1], D. Egli[2], P. Steigmeier[2], M. Geiser[1], M. Fierz[2], Zs. Juranyi[2], M. Kalberer[3], and H. Burtscher[2]

[1]Institute of Anatomy, University of Bern, 3012 Bern, Switzerland
[2]Institute of Aerosol and Sensor Technology, University of Applied Sciences Northwestern Switzerland, 5210 Windisch, Switzerland
[3]Department of Chemistry, University of Cambridge, Cambridge CB2 1EW, UK

Keywords: nanoparticles, toxicity, in vitro test, aerosol deposition.
Presenting author email: heinz.burtscher@fhnw.ch

Safe application of the promising and quickly growing nanotechnology requires a comprehensive clarification of the effects on person and environment. Inhalation of engineered nanoparticles (ENP) in industrial processes and in consumer products poses a potential and largely unknown risk. Individuals with chronic lung diseases, as well as children and the elderly are expected to be more vulnerable than healthy adult subjects. Safety testing needs to include studies in the susceptible population. Furthermore, for efficient, economical, and ethically sound evaluation of health hazards by inhaled nanomaterials, as well as for regulatory toxicity testing, animal-free in vitro test systems that mimic real situations are needed.

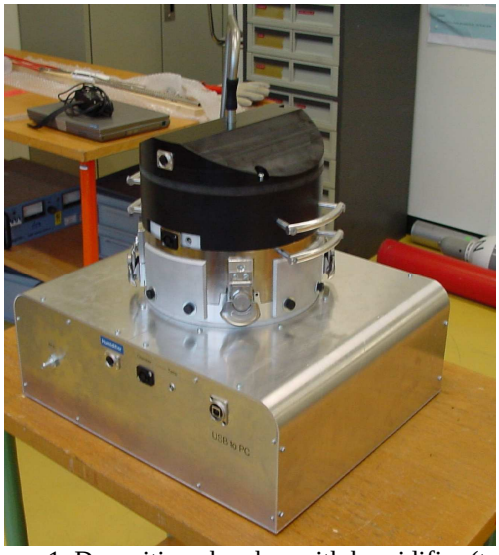

Figure 1. Deposition chamber with humidifier (top), insert holder and control box

Based on previous work (Savi et al. 2008), an aerosol deposition chamber for efficient and quantitative deposition of nanoparticles out of a continuous air-stream on cell cultures has been developed. It allows the parallel deposition of particles on 24 cell cultures in standard inserts. The particles are first charged by a unipolar diffusion charger. Then the particle containing gas is first humidified to an adjustable RH (typically 90%). The whole chamber is temperature controlled. Particles are precipitated on the cells by electrostatic deposition.

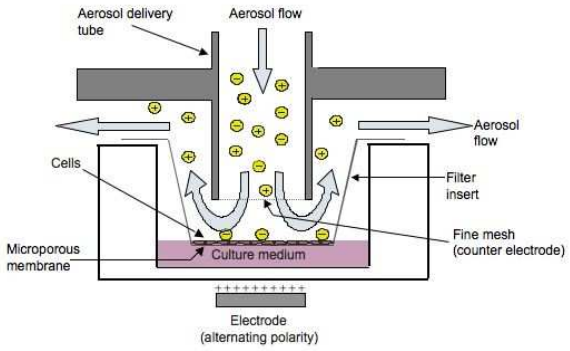

Figure 2. Electrostatic particle deposition on cell culture

To determine the amount of particles deposited, the flow is split after the charger and a part is passed through an electrostatic precipitator, having the same deposition characteristics as the inserts. The current produced by the particles precipitated there is measured and integrated.

First tests show that the deposition efficiency on all 24 inserts is very.

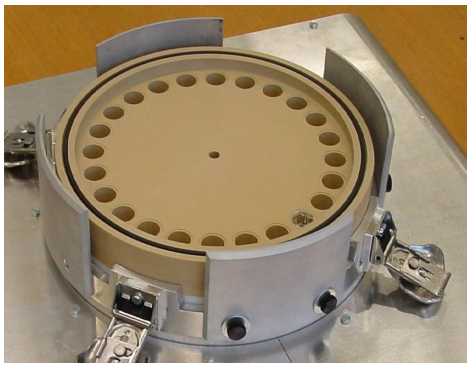

Figure 3. Disc with 24 holes for the inserts

This work was supported by the Swiss National Science foundation.

Savi M, Kalberer M, Lang D, Ryser M, Fierz M, Gaschen A, Rička J, Geiser M. (2008) A novel exposure system for the efficient and controlled deposition of aerosol particles onto cell cultures. *Environ Sci Techn* 42: 5667-5674.

Developments towards an NO_2 denuder for elevated temperatures

J. C. Wolf and R. Niessner

Chair for Analytical Chemistry, Technische Universität München, Marchioninistr. 17, 81377, Munich, Germany

Keywords: NO_2, Diesel exhaust, coatings, diffusion denuder, ionic liquids.
Presenting author email: jan.wolf@mytum.de

The occurrence of artefacts during aerosol measurement and sampling is a known problem in analytical chemistry. Especially reactive gases like ozone, SO_2 and NO_2 can cause degradation of several analytes of interest. Ozone and NO_2 for instance are known to cause negative sampling artefacts for polycyclic aromatic hydrocarbons (PAH). In contrary several authors (e.g. Samy et al.; Carrara et al.) reported positive sampling artefacts for nitrated polycyclic aromatic hydrocarbons (NPAH) due to NPAH formation out of PAH and NO_2 during filtration.

Usually diffusion based denuding techniques are used to remove such interfering reactive gases prior to sampling or measurement. There have been several approaches to optimize the geometry and the coatings for each individual target gas at room temperature. Since 1984, several coatings for selective stripping of NO_2 have been proposed (e.g. MnO_2, alkaline guiacol, potassium iodide, cobalt oxide).

However, PAH and NPAH are formed during incomplete combustion and are therefore monitored in various combustion processes. For example, in the case of automotive exhaust, PAH and especially NPAH might be formed due to the incomplete combustion and the high NO_2 levels present in the aftertreatment system. Here the question arises, whether these newly formed NPAH are in the gaseous state or adsorbed on particles. To give an answer on such questions a NO_2 denuding system is required that can withstand the temperatures of automotive exhaust and thus avoid condensation of water or analytes.

For this reason, we investigated and improved common coatings for NO_2 stripping, with focus on heat stability. Besides of that, we developed a new coating based on an ionic liquid. We used the ionic liquid Butyl-methyl-imidazolium iodide $[BMIm]^+[I]^-$ as coating in a newly designed heatable 13 channel annular denuder. The denuder was then passed by 50 ppm of NO_2 in nitrogen at a flow of 5 l/min. The breakthrough curves were recorded by a chemiluminescence analyzer (*CLD 700-Al, Eco Physics*). In comparison with the polyethylenglycole/ potassium iodide (PEG + KI) coating we found a three fold higher capacity for $[BMIm]^+[I]^-$ (see figure 1) at room temperature.

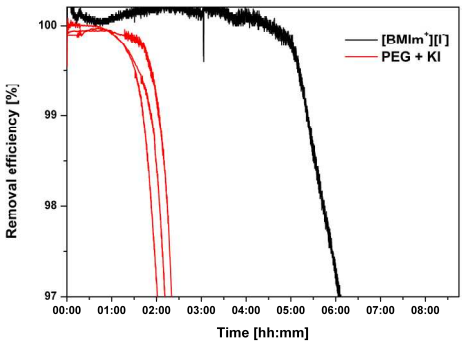

Figure 1.: Breakthrough curves of polyethylenglycole/potassium iodide (PEG+KI) and $[BMIm]^+[I]^-$ coating (25°C; 5 l/min; 0% RH; 50 ppm NO_2 in N_2)

With increasing temperature the NO_2 binding capacity of both coatings decreases rapidly. For potassium iodide, we additionally found a PEG aerosol formation at temperatures above 423K. This was not the case for $[BMIm]^+[I]^-$ due to the low vapour pressure. Nevertheless, the potassium iodide coating was more efficient at elevated temperatures.

Table 1. Comparison of NO_2 denuding capacity of potassium iodide and $[BMIm]^+[I]^-$ at different operation temperatures.

Capacity	KI (ppmh)	$[BMIm]^+[I]^-$ (ppmh)
298 K	112	300
373 K	38	17
423 K	13	11

Our investigations revealed two coatings suitable for denuding NO_2 at temperatures up to 423K. In addition, the ionic liquid coating $[BMIm]^+[I]^-$ showed extraordinary NO_2 removal and binding efficiency at room temperature, indicating its use in other fields e.g. ambient sampling.

Carrara M., Wolf J.-C., Niessner R. (2010), *Atmospheric Environment*, **44**, 3878-3885.

Samy S., Zielinska B., Sagebiel J. C., McDonnald J. D. (2011), *Journal of Air & Waste Management Association*, **61**, 319-323.

Wolf J.-C., Niessner R. (2012), *Analytical and Bioanalytical Chemistry* (submitted).

Development of a portable instrument to determine the fractal dimension from angular light scattering meaurements

Zs. Jurányi, A. Keller and H. Burtscher

Institute of Aerosol and Sensor Technology, University of Applied Sciences Northwestern Switzerland, Windisch, 5210, Switzerland
Keywords: soot agglomerates, light scattering, fractals, optical instrumentation.
Presenting author email: zsofia.juranyi@fhnw.ch

Introduction

Black carbon is a major constituent of the atmospheric aerosols and has most of the time anthropogenic origin. It is produced during incomplete combustion processes, and forms usually fractal-like particles through aggregation. Fractal aggregates are scale invariant, which means that within limits they appear the same when viewed over a range of scales. An important property of aggregates is the fractal dimension which connects the number of primary particles (N, proportional to the mass) in the aggregate to the radius of gyration (R_g, measure of the overall radius):

$$N = k_0 \cdot \left(\frac{R_g}{a} \right)^D$$

Where k_0 is a constant in the order of unity, a is the radius of the primary particle and D is the fractal dimension.

The angular light scattering of fractal aggregates depends on the wavelength of the incident light, the complex refractive index, the shape of the particle and the scattering angle. According to the scaling approach of angular light scattering by fractals from Sorensen and Oh (1998) the measured scattered light intensity as function of the magnitude of the scattering vector (q, proportional to the sinus of the half of the scattering angle) contains the information on D: the logarithm of the intensity versus the logarithm of q has a slope of D in a specific q range. This q regime is called the power law regime.

Results

At the University of Applied Sciences Northwestern Switzerland a portable instrument is being developed in order to measure the angular scattering of aerosols. The goal is to be able to measure the scattering signal simultaneously at several angles and to derive the fractal dimension of fractal-like particles. The aerosol is brought into a closed chamber where a laser diode illuminates the particles that can be found in the sampling volume. The scattered light is then detected by avalanche photodiodes at different angles.

Now, the chamber is built, and ready for the first tests. These tests aim for the better understanding of the instrument's performance and therefore are performed using almost spherical salt particles. The nebulized salt particles were size selected by a differential mobility analyser (DMA) before entering the chamber. The number size distribution of the nebulized aerosol was also measured. Figure 1 shows the measured results along with theoretical calculations at two different (35 and 150 degrees) scattering angles. The calculations were done using Mie theory (Bohren and Huffmann, 2004) and the refractive index of 1.54+0i. The effect of the different concentrations at the different diameters was taken into account by weighing the theoretical differential cross section with the normalized size distribution. The DMA transfer function and the effect of the multiple charged particles were also considered.

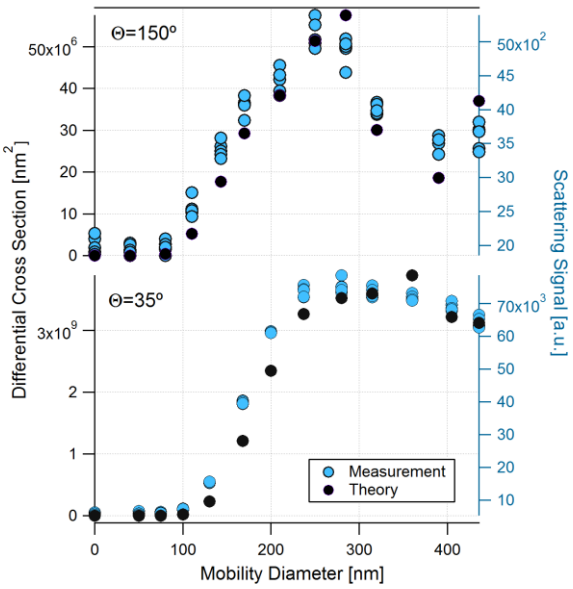

Figure 1. Theoretical and measured scattering signal of 660 nm laser light as function of the nominal mobility diameter from the DMA, see the text for more details

The curves of the measured and the calculated values show a very good agreement. The small differences can be associated with measurement errors and with the fact that the number size distribution was not measured simultaneously with the scattering. We can state that the instrument is ready for further tests and measurements.

Sorensen, C. M. and Oh, C. (1998) *Phys. Rev. E* **58**, 4666–4672

Bohren C. and Huffman D. (2004) *Absorption and Scattering of Light by Small Particles*, Wiley-VCH.

iSPEX: Measure aerosols with your smartphone!

H. Volten[1] representing the iSPEX team[1,2,3,4]

[1]Centre of Environmental Monitoring, National Institute for Public Health and the Environment (RIVM), Bilthoven, 3720 BA, The Netherlands
[2]Netherlands Research School for Astronomy (NOVA), Leiden, 2300 RA, The Netherlands
[3] Earth and Planetary Science Division, SRON Netherlands Institute for Space Research, Utrecht, 3584 CA, The Netherlands
[4]Koninklijk Nederlands Meteorologisch Instituut (KNMI), De Bilt, 3730 AE , The Netherlands
Keywords: polarization, aerosol characterization, aerosol instrumentation, air quality network.
Presenting author email: hester.volten@rivm.nl

An increasing number of people carry a smartphone with internet connection, a camera and considerable computing power in their pocket almost all the time, wherever they go. iSPEX, a spectropolarimetric add-on with complementary App makes use of this opportunity, and instantly turns a smartphone into a scientific instrument to measure dust and other aerosols in our atmosphere (Figure 1). A measurement involves scanning the blue sky, which yields the angular behavior of the degree of linear polarization as a function of wavelength, which can unambiguously be interpreted in terms of size, shape and chemical composition of the aerosols in the sky. The measurements are automatically tagged with location and pointing information, and submitted to a central database where they will be interpreted. Together with observations from other users at random locations, the data is compiled into an aerosol map. Through crowd sourcing, the general public will thus be able to contribute to a better assessment of the presence of different types of aerosols in the atmosphere. It may also improve the understanding of the relationship between atmospheric aerosols and health issues or climate change.

iSPEX is based on our new ground-based SPEX instrument which will also be presented at the conference [see contribution of J. de Boer et al.]. With SPEX (Spectropolarimeter for Planetary Exploration) we perform multi-angle, multi-wavelength measurements of the intensity and polarization of sunlight scattered by aerosols in the atmosphere (Snik et al. 2009). It will be deployed at CESAR, the Cabauw Experimental Site for Atmospheric Research, which is also host to complementary aerosol measurement equipment, including PM_{10} and $PM_{2.5}$ monitors, sunphotometers and lidar instruments. Both for the ground-based SPEX and iSPEX, we interpret the data using a modified version of the POLDER algorithm (Hasekamp, 2010). The data from the SPEX instrument add significantly to the current suite of aerosol measurement equipment, but they are restricted to the Cabauw site. By distributing many iSPEX units, an air quality measurement network can be created that has both large coverage and the potential for detecting localized effects. Such a smartphone spectropolarimeter is less accurate than its official counterpart at a meteorological site, but we show how many measurements allow for suppression of errors through averaging.

We will give a live demonstration of the first iSPEX prototype. We hope to convince you that iSPEX is not only a great outreach tool to engage the public in issues pertaining to atmospheric aerosols, but that it may also contribute to the solution of several urgent social and scientific problems.

Hasekamp, O. P., (2010): Capability of multi-viewing-angle photo-polarimetric measurements for the simultaneous retrieval of aerosol and cloud properties. *Atmos. Meas. Tech.* **3**, 839–851.

Snik, F., Karalidi, T., and Keller, C. U. (2009) Spectral modulation for full linear polarimetry, *Appl. Opt.* **48**, 1337-1346.

Figure 1. Observing with a smartphone

The iSPEX team consists of the following people:

Frans Snik, Stephanie Heikamp, Christoph Keller, Jos de Boer, Gerard van Harten, Lars Einarsen, Maria de Juan Ovelar (NOVA)
Daphne Stam, Otto Hasekamp, Jeroen Rietjens, Arjen Stap, Theodora Karalidi (SRON)
Hester Volten (RIVM)
Piet Stammes, Arnoud Apituley, Bas Mijling (KNMI)

Near-ground hyperspectral imaging for urban scale remote sensing of aerosols, during nighttime –laboratory and upscaling study

Y. Etzion[1], D.M. Broday[1]

[1] Department of Environmental and Water Resources Engineering, Technion - Israel Institute of Technology, Haifa 32000, Israel

Keywords: remote sensing, urban pollution, fine PM, aerosol measurement, hyperspectral imaging

Spatiotemporal variations of fine ambient aerosols near the ground are important indicators for air pollution events and public health risk assessment, especially the diurnal variations of aerosol size resolved concentrations and composition at urban-scale resolution.

Aerosol remote sensing is an accepted methodology to retrieve aerosol size distributions in vertical atmospheric columns, based on PM interactions with radiation in the visible-NIR range that are measured at multiple wavelengths or multiple angles. Both satellite and ground remote sensing (RS) platforms mostly rely on solar radiation, and therefore they are limited by sun elevation angle and the cloud cover, and also by the revisit periods and variability of surface albedo for satellite-borne sensors.

Current RS procedures can provide estimates of bi-modal size distributions in vertical atmospheric columns (Wang *et al.*, 1996; Dubovik *et al.*, 2002). However, the correlation between the vertical aerosol profiles and ground-level particulate matter (PM) distribution at the urban-scale resolution is highly influenced by the geo-site specific seasonality and the corresponding mixing layer height (Schäfer *et al.*, 2008).

The aim of this study was to apply ground hyperspectral imaging in order to extract the size attributes of fine PM along horizontal open paths of 1-4km. A camera that acquires high resolution spectral signatures in the visible-NIR range (VDS Vosskühler Cool-1300Q, λ=400-1100nm, 160-180 wavelengths) was used for that purpose. A dedicated procedure was developed by exploiting nocturnal illumination sources as a novel concept for urban scale horizontal RS, as well as an innovative solution for nighttime when solar radiation cannot be used.

Validation of the hyperspectral response to fine PM was obtained as a first step in a controlled laboratory chamber, for bimodal mixtures of PSL standards, using halogen illumination. Analysis of the hyperspectral sensor response showed highest sensitivity to AOT in 550-900nm wavelength range, which encompasses signatures of fine modes above ~0.2 μm, based on Mie calculations. The retrieval of modal concentrations was demonstrated by applying random search. The HS imaging procedure was next applied during time series release of tri-ethylene glycol aerosol (urban-like) in ambient conditions, and demonstrated correlated spectral signatures to the measured size distributions of that aerosol.

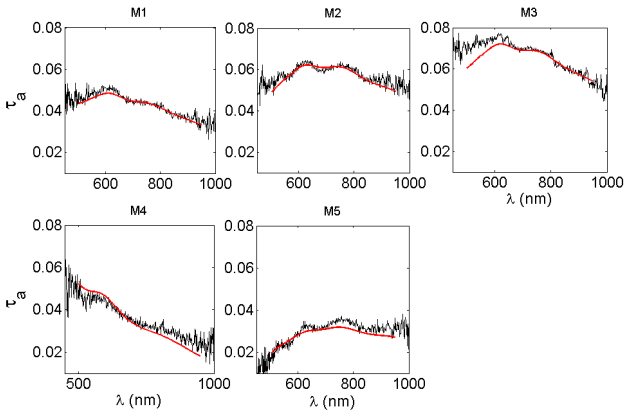

Figure 1. Experimental (black) vs. computational (red) hyperspectral signatures of bimodal PSL aerosols in a laboratory chamber. The computed attenuated spectral signature is based on simultaneously measured aerosol size distributions.

Schäfer, K., Harbusch, A., Emeisa, S., Koepke, P., & Wiegner, M (2008). *Atmospheric Environment* 42, 4036–4046.

Wang, P., Kent, G. S., McCormick, M. P., Thompson, L. W., & Yue, G. K. (1996).*Applied Optics* 35, 433-440.

Dubovik, O., Holben, B., Eck, T. F., Smirnov, A., Kaufman, Y. J., King, M. D., Tanré, D., & Slutsker, I. (2002). *Journal of the Atmospheric Sciences*, 59, 590-608.

New instrument to investigate size-resolved chemical composition of nano-particles

A. Kürten, J. Hoker, C. Fuchs and J. Curtius

Institute for Atmospheric and Environmental Sciences, University of Frankfurt, Frankfurt, 60438, Germany
Keywords: nucleation, nano aerosol, mass spectrometry, CIMS.
Presenting author email: kuerten@iau.uni-frankfurt.de

Determining the speciated chemical composition of sub-20 nm particles remains a major challenge in atmospheric chemistry. There are only very few instruments available which can perform such an analysis in real-time for atmospherically relevant concentrations of aerosol particles. The TD-CIMS (Thermal Desorption-Chemical Ionisation Mass Spectrometer) is a unique instrument (see Voisin *et al* (2003) and Smith *et al* (2004)) which has given valuable information about the composition of particles in that size range. However, additional experimental studies are required to further elucidate the mechanisms how freshly nucleated particles can overcome the gap between their initial size of ~2 nm and ~20 nm. This step is crucial for the fate of the particles. It decides whether they are scavenged out by larger particles or if they eventually reach sizes where they can act as cloud condensation nuclei and thereby exert a substantial effect on the Earth's climate.

In this study, a new instrument is introduced which allows collecting aerosol particles on a small substrate. The particles are electrically charged before they enter a DMA-like geometry where they are separated from their carrier gas and classified according to their electrical mobility diameter. After the classification they are electrostatically precipitated inside the DMA on a short stainless steel wire. Following appropriate collection times, the wire can be translated into the sampling line of a Chemical Ionisation Mass Spectrometer (CIMS) by means of a linear motor. This CIMS (THS Instruments, LLC) is used to measure gaseous sulphuric acid through the reaction of H_2SO_4 with NO_3^- primary ions. However, the instrument can in principle also be used with other primary ions, e.g. when it is intended to analyse organic compounds. Before their chemical analysis, the collected aerosol particles are evaporated by applying a heating current to the wire. During these periods ultrapure nitrogen is introduced further upstream into the CIMS sampling line in order to measure only the particulate constituents of the sample (Figure 1). The distance between the wire and the CIMS ion source is minimized which prevents substantial wall loss of the evaporated material.

The main advantages of this method are the following: (1) The same instrument (CIMS) can be used to study gas phase compounds as well as aerosol particles in the sample gas. No measurement time is lost despite the rather long collection times for the aerosol particles. (2) A size-resolved analysis is possible. The accessible size range is roughly between 5 and 50 nm. The size range of the classified aerosol particles which are subsequently chemically analyzed is adjustable. (3) The particle collector is compact and modular. In principle it can be combined with any other analytical instrument, e.g. with a PTR-MS or even with GC-MS systems.

The set-up of the new instrument will be introduced in detail. First results on its performance for test measurements in the laboratory will be presented. For these, aerosol particles of known chemical composition and size are generated and collected over specified time intervals. From the collected mass detection limits for various compounds can be derived. Other studies which will be presented include the characterisation of the size accuracy of the classifier and its collection efficiency with respect to different particle sizes.

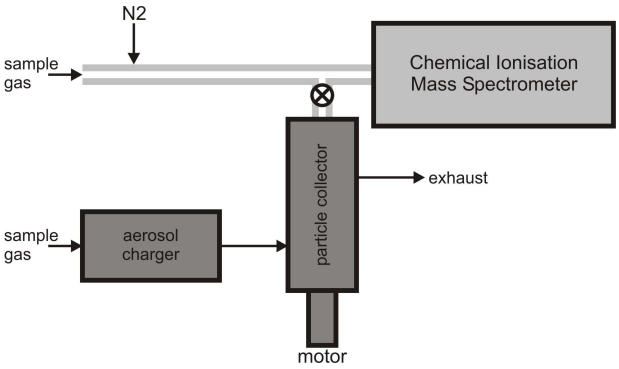

Figure 1. Schematic set-up of the new particle collector combined with a chemical ionisation mass spectrometer (CIMS) for chemical analysis of nano-aerosol particles.

Smith, J. N., Moore, K. F., McMurry, P. H. and Eisele, F. L. (2004) *Aerosol Sci. Technol.* **38**, 100–110.

Voisin, D., Smith, J. N., Sakurai, H., McMurry, P. H. and Eisele, F. L. (2003) *Aerosol Sci. Technol.* **37**, 471–475.

Development of New Particle Size Magnifier Using Cooling Nucleation Tube

T. Yamamoto and M. Adachi

Department of Chemical Engineering, Osaka Prefecture University, 1-1 Gakuen-cho, Sakai, 599-8531 , Japan
Keywords: Nanoparticles, Heterogeneous nucleation, Condensation
tyamamoto@chemeng.osakafu-u.ac.jp

Introduction

The 1 nm-range particles have been one of hottest topics in the atmospheric aerosol research field[1]. A particle size magnifier (PSM) is one of strong candidate for the measurement of the 1 nm-range particles. Vanhanen et al. have developed a new PSM using low temperature nucleation tube[2]. We have also investigated the same concept PSM; called the cooling type PSM, for 5 years.

New PSM using cooling nucleation tube

In the PSM, the mixing of nanoparticle aerosol and condensed vapour is very important for the performance. Therefore, we have proposed and developed the novel mixing unit which has a critical orifice. Figures 1 (a) and (b) show our PSM and vertical cross-section view of the developed mixing unit, respectively. The mixing unit consists of upper disk wall and under disk wall. The center of under disk wall has a critical orifice with a hole of 0.3 μm in the diameter. DBP vapor is expanded at exit of the orifice and makes lower pressure space in the mixing unit. Therefore, the nanoparticle flow is sucked in the mixing unit by the pressure lower than the atmosphere. As the results, particle losses are prevented.

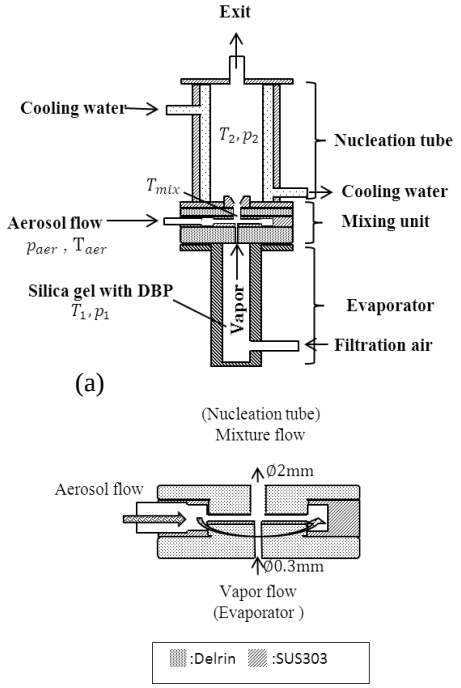

Fig.1 (a) cooling type PSM (b) vertical cross-section view of mixing unit.

Results

Monodisperse 5nm Ag particles were used as the test aerosol. Number concentrations at inlet and exit of PSM were measured by condensation particle counter (TSI Model 3025A). Figure 2 shows the result at various nucleation tube temperatures. The penetration ratio becomes equal to 1.0 at the nucleation tube temperature of 288K and the evaporator temperature of 353K.

Particle size distributions after the growth of the test aerosol were measured by the optical particle counter (Rion Model, KC-01E). The PSM was operated at the evaporator temperature of 353K, nucleation tube temperature: of 288K and ratio of DBP vapor flow rate to total flow rate of 0.3. Figure 3 shows the particle sizes distribution in size range larger than 0.3μm. The 68 % of 5 nm Ag particles was magnified to size lager than 0.3 μm by the DBP vapor of 353 K.

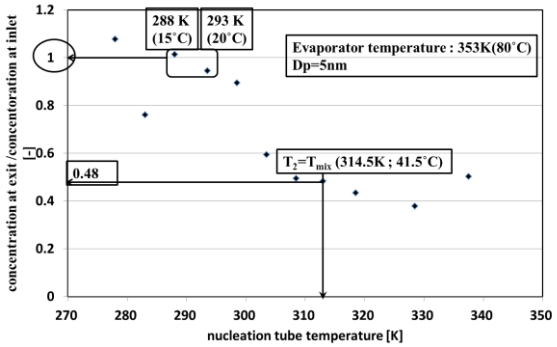

Fig.2 Penetration ratios of 5 nm Ag particles

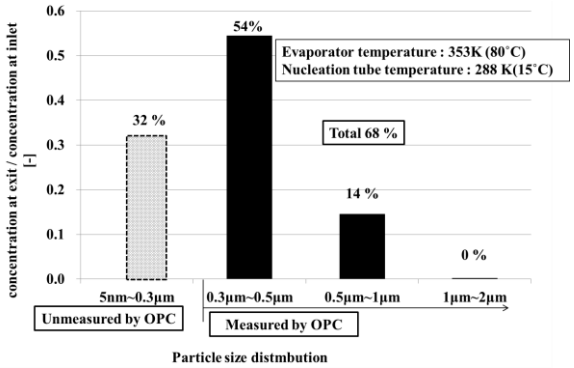

Fig .3 Particle size distribution after growth at PSM

References

1) J. Jiang et al., (2011). *Aerosol Sci. Technol.*45.ii-v
2)J. Vanhanen et al., (2011). *Aerosol Sci. Technol.* 45:533-542

High Temperature Condensation Particle Counter

K. Rongchai and N. Collings

Department of Engineering, University of Cambridge, Cambridge, CB5 1QH, UK
Keywords: Particle Concentration, CPC, Aerosol Instrumentation, Instrument development, High Temperature
Presenting author email: kanchit.rongchai@gmail.com

Condensation Particle Counters (CPCs) are commonly used to measure the number concentration of airborne nanoparticles in various applications. A typical CPC consists of three major stages. They are: a saturation stage where an aerosol sample is saturated with vapour of a fluid e.g. butanol; a supersaturation stage where the nanoparticles grow to optically detectable sizes by condensation of the vapour on particle surfaces; and an optical particle counter (OPC). The working temperature of a typical CPC is around ambient or slightly higher.

This work is connected with the development of a CPC that operates at such a high temperature that volatile material is not measured, due to it being evaporated or prevented from condensing. The obvious application is measurement from internal combustion engines, where the European legislated particle number method (PMP) requires a complex system for the removal of volatile material, prior to measurement by a conventional CPC.

The study involves theoretical modelling, design, construction and testing of a high temperature CPC. Di-Ethyl-Hexyl-Sebacat (DEHS) has initially been chosen as the working fluid because it is non-toxic, is a liquid at room temperature and has a high boiling point. The supersaturated region in the condenser where particles are grown, is modelled by numerically solving the heat and mass transfer equations based on the finite difference method. The model was found to be in good agreement with an alternative model due to Stolzenburg and McMurry (1991).

The simulations suggest that the high-temperature CPC will be able to grow and detect fine particles. The saturator and condenser would be held at approximately 210˚C and 190˚C respectively. For a likely embodiment, the saturation ratio in the condenser is shown in Figure 1. Particle growth was modelled by the mass and heat balance at the droplet surface, following the approach of Ahn and Liu (1990). The growth profile of a 23 nm particle is shown in Figure 2.

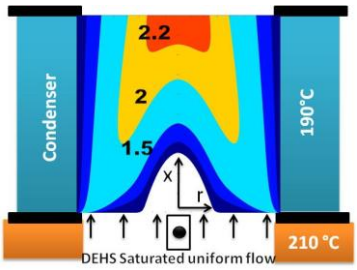

Figure 1. Supersaturation contour in the condenser.

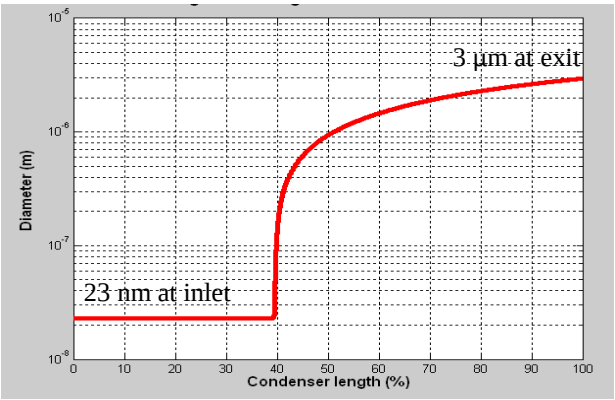

Figure 2. Particle growth along the condenser.

Experimental Study

A step decrease in particle concentration was introduced at the aerosol inlet. Particle pulses in the optical signal were counted over periods of 20 ms. The particle number vs. time is shown in Figure 3.

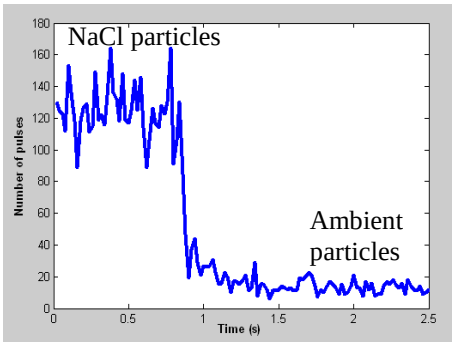

Figure 3. Testing of the high-temperature CPC Particle counts vs. time

The high-temperature CPC has been shown to successfully grow and detect NaCl particles and ambient particles.

Stolzenburg, M. R, and McMurry, P. H. (1991) *An Ultrafine Aerosol Condensation Nucleus Counter*, Aerosol Science and Technology, 14: 1, 48 - 65.

Ahn, K.-H., and Liu, B. Y. H. (1990) *Particle Activation and Droplet Growth Processes in Condensation Nucleus Counter. I. Theoretical Background*, J. Aerosol Sci. 21: 2, 249 - 261.

Effect of particle diffusivity on DMAs with multiple monodisperse-particle outlets: theory validation and design optimization

M.Giamarelou[1], M. Stolzenburg[2], D.-R. Chen[3] and G. Biskos[1,4]

[1]*Dept. of Environment, University of the Aegean, Mytilene, Greece*
[2]*MRS Consulting, Sheboygan, WI, USA*
[3]*Dept. of Energy, Environmental and Chemical Eng., Washington University in St. Louis, St. Louis, MO, USA*
[4]*Faculty of Applied Science, Delft University of Technology, Delft, The Netherlands*

Keywords: MMO-DMA, Dual-DMA, transfer function, resolution.
Presenting author email: giamarel@env.aegean.gr

By simultaneously selecting aerosol particles having different sizes, Differential Mobility Analyzers (DMAs) with multiple monodisperse-particle outlets can have a number of advantages in aerosol metrology. When used in electrical mobility spectrometers, for instance, they can significantly reduce the time required to measure the particle size distributions. Depending on the relative location of the first and the last outlet from the inlet, one can also increase the dynamic mobility range of the measured particles in a single measurement.

Based on the approach proposed by Stolzenburg (1988), we have recently developed the theoretical framework for determining the transfer function and the resolution of DMAs with multiple monodisperse-particle outlets (cf. Giamarelou et al., 2011; 2012). To describe the spreading of the transfer function due to the Brownian motion of the particles, we divide the classifier into segments defined by successive monodisperse-particle outlets. The total diffusional broadening along the whole path of the particle that leads to the i^{th} sample exit can be approximated by

$$\sigma^2_{\Gamma_{i,total}} = \sum_{j=n}^{i} \sigma^2_{\Gamma_{i,j}} . \qquad (1)$$

Here $\sigma_{\Gamma_{i,j}}$ denotes the diffusional broadening of the particles classified through the i^{th} monodisperse-particle outlet during the time they travel through the j^{th} segment of the MMO-DMA.

Fig. 1a shows the comparison of the model to the measurements with the 3-monodisperse-particle-outlet DMA tested by Chen et al. (2007). The loss-corrected theoretical transfer functions for both sample outlets, at 2.54 cm and 15.24 cm, are in perfect agreement with the experimental values. The predicted resolution for each of the three outlets agrees well with the reported measurements (Fig. 1b), indicating that the theory captures well the broadening of the transfer function for particles having diameter smaller than 20 nm.

Using the validated transfer function model we provide design considerations for building a DMA with two monodisperse-particle outlets, and predict its performance under different operating conditions. A critical parameter when designing multiple-exit DMAs is the minimum distance between the entrance and the nearest sample exit as well as between the successive sample exits so that the flow profile remains laminar.

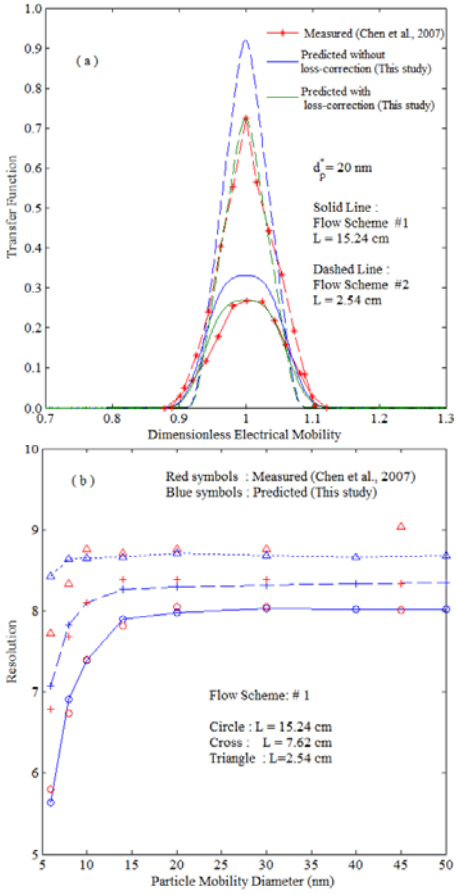

Figure 1 (a) Comparison between predicted and measured transfer function of the DMA with 3 monodisperse-particle outlets (measurements from Chen et al., 2007). The monodisperse-particle outlets are located 2.54, 7.62 and 15.24 cm downstream of the polydisperse aerosol inlet. Flow scheme #1 corresponds to 20 lpm sheath flow, 2.4 lpm polydisperse aerosol inlet flow, and 0.8 lpm for each monodisperse outlet flow. The respective values for flow scheme #2 are 20, 1.5 and 1.5 lpm. (b) Comparison between predicted and measured resolution of the DMA with 3 monodisperse-particle outlets.

References

Chen, D.-R., Li, W., Cheng, M.-D., 2007, *Aerosol Sci. & Technol.*, 41:217-230.

Giamarelou, M., Biskos, G., 2011, European Aerosol Conference, Manchester, Sept. 2011.

Giamarelou, M., Stolzenburg, M., Biskos, G., 2012, *Aerosol Sci. &Technol.*, (under revision).

Stolzenburg, M., 1988, PhD Thesis, University of Minnesota, Minneapolis, MN.

Influence of Turbulent Diffusion in an Electrical Mobility Spectrometer

J. Salm[1], P. Intra[2], A. Yawootti[2], N. Tippayawong[3] and U. Hõrrak[1]

[1]Institute of Physics, University of Tartu, Tartu 50090, Estonia
[2]College of Integrated Science and Technology, Rajamangala University of Technology Lanna, Chiang Mai 50220, Thailand
[3]Department of Mechanical Engineering, Faculty of Engineering, Chiang Mai University, Chiang Mai 50300, Thailand
Keywords: aerosol, particles, electrical mobility, diffusion, turbulence.
Presenting author email: jaan.salm@ut.ee

The spectrometer had one long column of coaxial, cylindrical electrodes (Intra and Tippayawong, 2009; 2011). The inner electrode of the spectrometer was maintained at a high DC voltage while the outer chassis of the spectrometer was grounded. The charged particles were collected on a series of electrically isolated electrometer rings positioned at the inner surface of the outer chassis of the spectrometer column. The inputs of highly sensitive electrometers were connected to these electrometer rings. In this spectrometer, the 22 electrometer rings used resulted in the classification of aerosols into 22 mobility ranges. The entire size range of particles collected on the electrometer rings could be varied by adjusting the aerosol and sheath airflow rates and the voltage applied to the inner electrode.

For approximate estimations, consider a model of the differential mobility classifier of second order with parallel plain electrodes and a uniform gas flow. Such a simplified classifier model has a characteristic (limiting) mobility (Tammet, 1970; Salm, 2000):

$$Z_C = \frac{ud^2}{VL}, \qquad (1)$$

where u is the gas flow velocity, d is the gap width between the electrodes, V is the central rod voltage, and L is the distance from aerosol inflow section to the corresponding electrometer ring (collector). Charged aerosol particles with a mobility of Z reach the electrometer ring with a characteristic or central mobility of Z_c, if $Z = Z_c$. The distance L determines a particular electrometer ring.

According to the theory proposed by Salm (2000), the mobility resolution can be expressed as:

$$R_d = \frac{Z_C}{\Delta Z_{\min}} = \frac{\sqrt{ud/D}}{2\sqrt{2}\sqrt{L/d + d/L}}, \qquad (2)$$

where ΔZ_{min} is the least distinguishable interval of the mobility spectrum and D is the diffusion coefficient of charged particles.

Molecular diffusion and turbulent diffusion share attributes. However, turbulent diffusion has two essential peculiarities. First, the coefficient of turbulent diffusion does not depend on the mobility of a particle. Secondly, in general the correlation between successive random displacements of a particle cannot be neglected.

In the case of small-scale turbulence ($\lambda << d$, where λ is the Eulerian length scale of turbulence), the coefficient of turbulent diffusion may be defined in its first approximation as:

$$D_T = u' \lambda, \qquad (3)$$

where u' is the root-mean-square pulsation velocity of gas flow.

Neglecting the evolution and the decay of turbulence in the classifier, the resolution R_d may be approximately estimated from Eq.2 when substituting D_T for D. The root-mean-square pulsation velocity u' inside the classifier depends on the intensity of turbulence of the inflowing gas and on the flow conditions in the classifier. Usually the pulsation velocity is roughly proportional to the average velocity u and considerably less than u. The turbulence intensity is calculated as u'/u. A turbulence intensity of 1% or less is generally considered low and turbulence intensities greater than 10% are considered high. If the spectrometer is operated in a still environment, low turbulence intensity is expected. The length scale of turbulence, λ, is a physical quantity related to the size of the large eddies that contain the energy in turbulent flow. In ducts or channels, λ is restricted by the size of the duct, since the turbulent eddies cannot be larger than the duct. In the classifier, it is rational to assume that usually $\lambda << d$.

An example with low and small-scale turbulence: the velocity $u = 0.25$ ms^{-1}, the gap width $d = 1.5$ cm, the turbulence intensity 1% and the length scale $\lambda = d/15$, i.e. $u' = 0.0025$ ms^{-1} and $\lambda = 0.001$ m. For the electrometer ring No. 22, $L_{22} = 0.45$ m. These numbers when substituted into Eq.3 yielded $D_T = 2.5\times10^{-6}$ m^{2}s^{-1} for turbulent diffusion, and the resolution for the electrometer ring No. 22 was $R_{d,22} = 2.5$. As Eq.2 showed, a relatively short, $L \approx d$, classifier is advisable for increasing the resolution.

The authors wish to express their gratitude to the National Electronic and Computer Technology Center, Thailand for their support (contract no. NT-B-22-SS-11-50-18). The Estonian Science Foundation through grant 8342 and 8779, and the Estonian Research Council Project SF0180043s08 also supported this research.

Intra, P. and N. Tippayawong (2009) *Korean Journal of Chemical Engineering* **26**, 269-276.
Intra, P. and N. Tippayawong (2011) *Korean Journal of Chemical Engineering* **28(1)**, 279-286.
Salm, J. (2000) *Aerosol Sci. Technol.* **32**, 602-612.
Tammet, H. (1970) *The Aspiration Method for the Determination of Atmospheric Ion Spectra*, Israel Program for Scientific Translations, Jerusalem.

A Micro-Orifice Volatilization Impactor (MOVI) coupled to an ion trap mass spectrometer with a soft ionization source (APCI-IT/MS) for the analysis of secondary organic aerosols

M. Brueggemann, A. Vogel and T. Hoffmann

Institute of Inorganic and Analytical Chemistry, Johannes Gutenberg-University, Mainz, Germany

Keywords: Instrumentation/chemical char., SOA (Second. Organic Aerosols), Inertial impactor, Mass spectrometry.
Presenting author email: brueggemann@uni-mainz.de

We describe the development and characterization of a Micro-Orifice Volatilization Impactor (MOVI) which is coupled to an ion trap mass spectrometer with atmospheric pressure chemical ionization (APCI-IT/MS), and its application in laboratory and field measurements. The MOVI-APCI-IT/MS allows the quantification of organic acids and other oxidation products of volatile organic compounds (VOCs) in secondary organic aerosols (SOA) on a semi-continuous basis. Furthermore, the vapour pressure and saturation concentration of the particle components can be estimated.

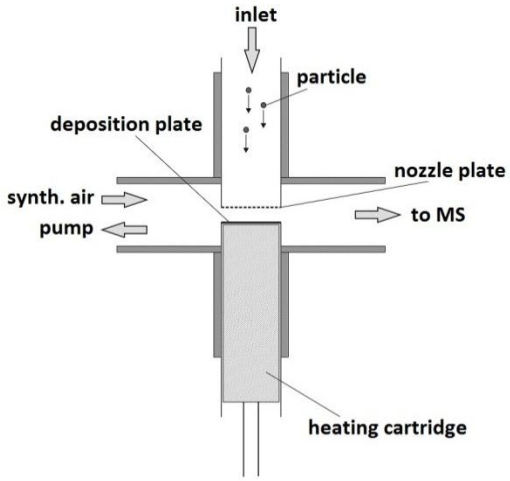

Figure 1: Cross section through the Micro-Orifice Volatilization Impactor (MOVI).

The MOVI was first described in 2010 by Yatavelli and Thornton. It is a single stage, multi-nozzle impactor with 100 nozzles, each having a diameter of 150 µm. At a flow-rate of 10 L•min^{-1} air is drawn through the MOVI and particles are collected on a deposition plate. The cut-point diameter (d_{50}, diameter of 50% collection efficiency) is at 130 nm. A low pressure-drop of only 5.3% of atmospheric pressure behind the nozzles allows collecting not only low-volatile but even semi-volatile compounds, which are an important part of SOA. After collecting particles hydrocarbon-free synthetic air is led over the collection surface into the APCI-IT/MS and the collection surface is heated up to 120 °C in less than 200 s, volatilizing the sampled SOA. The vaporized compounds are transferred into the ion source and subsequently analysed by mass spectrometry. Due to the soft ionization at atmospheric pressure the obtained mass spectra show only low fragmentations and can easily be interpreted.

In laboratory experiments the MOVI-APCI-IT/MS was used for the chemical analysis of SOA generated from α-pinene-ozonolysis in a smog chamber. The limit of detection was found at 7.3 ng for pinic acid. The vapour pressure $\log p^0$ and the saturation concentration C_{25}^* for pinic acid were calculated from the desorption temperature using the method presented by Faulhaber *et al* (2009). Furthermore, in summer 2011 the MOVI-APCI-IT/MS was successfully tested in field measurements during the „Bio-hydro-atmosphere interactions of Energy, Aerosols, Carbon, H_2O, Organics and Nitrogen – Rocky Mountain Biogenic Aerosol Study" (BEACHON-RoMBAS) in a ponderosa pine woodland in the southern Rocky Mountains of North America. The study was focused on understanding the formation, growth and properties of biogenic organic aerosol. We measured the composition of the aerosol particles and determined the concentration of pinic acid and isobaric substances. By means of intercomparison studies with other instruments like an aerosol mass spectrometer (AMS) and a MOVI coupled to a chemical ionization mass spectrometer (CIMS) we could validate our measurements.

Faulhaber, A. E., Thomas, B. M., Jimenez, J. L., Jayne, J. T., Worsnop, D. R., Ziemann, P. J. (2009), *Atmos. Meas. Tech.* **2**, 15–31.

Yatavelli, R. L. N. and Thornton, J. A. (2010), *Aerosol Sci. Technol.* **44**, 61–74.

A Novel Compact Aerosol Mass Spectrometer - the ToF-ACSM: Instrument Performance and First Field Deployment

R. Fröhlich[1], M. J. Cubison[2], J. G. Slowik[1], A. S. H. Prévôt[1], U. Baltensperger[1], U. Rohner[2], M. Gonin[2]
J. R. Kimmel[3], D. R. Worsnop[3] and J. T. Jayne[3]
[1]Laboratory of Atmospheric Chemistry, Paul Scherrer Institute, CH-5232 Villigen PSI, Switzerland
[2]TOFWERK AG, CH-3600 Thun, Switzerland
[3]Aerodyne Research, Inc., Billerica, MA-01821, United States
Keywords: AMS, Aerosol mass spectrometry, Instrument development, Instrumentation, Free troposphere.
Presenting author email: roman.froehlich@psi.ch

The Aerodyne Aerosol Mass Spectrometer (AMS) (Jayne, 2000) provides quantitative, highly time-resolved mass spectra of non-refractory, submicron particles. These data have been widely used to quantify inorganic species and organic material, segregate primary and secondary aerosol, and identify certain primary sources. The Aerosol Chemical Speciation Monitor (ACSM) (Ng, 2011) is a low-cost version of the AMS designed for long-term operation and stability, and thus requires minimal user maintenance. Its small size also makes it well-suited for integration into existing monitoring stations, or other locations where space is limited. However, the quadrupole-based ACSM (hereafter denoted "Q-ACSM") is much less sensitive than the standard AMS, constraining both detection limits and achievable measurement time resolution. Here we present the testing and initial deployment of a new Time-of-Flight ACSM (ToF-ACSM).

In the ToF-ACSM the quadrupole mass spectrometer in the conventional Q-ACSM is replaced with the new Tofwerk E-ToF mass spectrometer. This modification yields a higher mass spectrometer duty cycle and hence improved sensitivity. Preliminary results indicate a hardware dependent improvement of the detection limits compared to the Q-ACSM of a factor of 4 - 18 (organics), although the instrument was not yet fully optimized. This means that the detection limits lie between the ones of the W-mode and the V-mode HR-ToF-AMS. In Fig. 1, a subset of the raw ToF-ACSM spectrum of aerosols in ambient laboratory air averaged over 1 min is shown, while Fig. 2 depicts a background subtracted mass spectrum of NH_4NO_3 particles. The air peaks and the instrument background were subtracted using a filtered measurement, and the peak signals were integrated, converted to ions / s and illustrated as UMR sticks. With a resolving power of 300 - 500 Th / Th, isobaric mass peaks are easily resolved, and even the mass excess of ions is discernible.

We will report instrument performance, including detection limits, short- and long-term stability and amount of maintenance required. An intercomparison of the ToF-ACSM with Q-ACSM and a high resolution (HR-) ToF-AMS will be presented. Furthermore we will present first ToF-ACSM field data from deployment at the high-altitude Jungfraujoch station, which resides in the free troposphere for most of the year (Baltensperger, 1997). The low aerosol concentrations at this site provide an ideal test case for the ACSM. Finally we will demonstrate the application of the positive matrix factorization (PMF) (Ulbrich, 2009) source appointment method to the ToF-ACSM data.

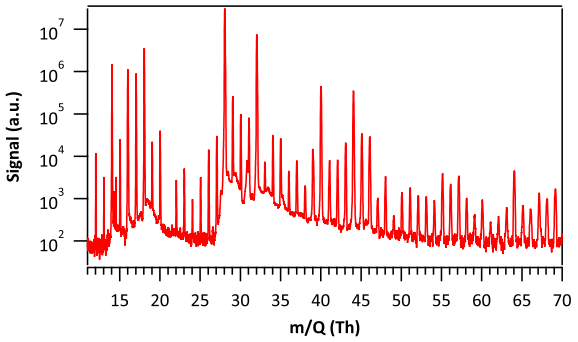

Figure 1: Excerpt from a mass spectrum of ambient laboratory air with 1 min averaging time, recorded with the ToF-ACSM.

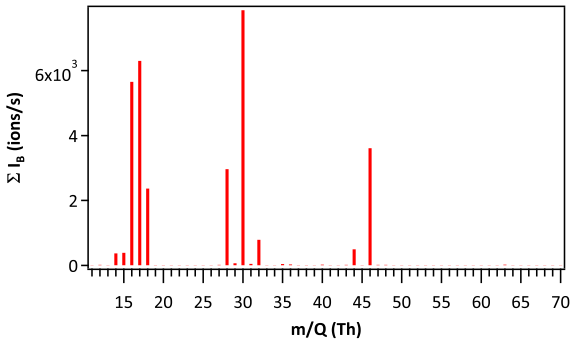

Figure 2: Excerpt from a background subtracted stick difference spectrum of NH_4NO_3 particles ($d = 300$ nm, $N = 7.5 \cdot 10^3$ cm^{-3}, $Q = 1.52$ cm^3/s), recorded with the ToF-ACSM.

This work was supported by the Swiss Commission for Technology and Innovation as well as the European FP-7 project ACTRIS.

Jayne, J. T. et al. (2000) Aerosol Sci. Tech., **33**, 49-70.
Ng, N. L. et al. (2011) Aerosol Sci. Tech., **45**, 770-784.
Baltensperger, U. et al. (1997) J. Geophys. Res., **102**, 707-719.
Ulbrich, I. M. et al. (2009) Atmos. Chem. Phys., **9**, 2891-2918.

Novel Polar Nephelometer for the Measurement of the Particle Asymmetry Parameter

Paul L. Kebabian, Timothy B. Onasch, Joda C. Wormhoudt and Andrew Freedman

Aerodyne Research, Inc., 45 Manning Road, Billerica, MA 01821, U.S.A.
Keywords: polar nephelometer, particle asymmetry parameter
Presenting author email: af@aerodyne.com

Radiative transfer models use the particle asymmetry parameter, *g*, as a measure of scattering angle because it is far more computationally efficient than including the entire scattering phase function. A number of other parameters, such as backscatter fraction and hemispheric backscatter fraction, are also used because comparatively simple instruments exist which can provide estimates of these parameters.[Ogren, et al, 2006] However, linking these measured parameters with *g* requires various assumptions and/or use of supporting data, especially the aerosol size distribution of particles below 1 micron diameter and their refractive indices. While using these approximations appears to produce values of *g* which agree with one another to a reasonable degree, it raises the question of how accurate these values really are. Calculations indicate that a 10% change in the assumed value of *g* (which is typically in the range of 0.5-0.7) can have a 20% effect on radiative forcing at the top of the atmosphere and only a somewhat lesser effect at the earth's surface. [Andrews, et al, 2006]

We present a proof-of-principle demonstration of an apparatus capable of directly measuring the aerosol scattering phase function and aerosol asymmetry parameter without the need for calibration or adjustment of data. The measurement technique utilizes a technique which allows for the collection of scattered light at all angles simultaneously and thus offers the potential for more rapid acquisition of scattering data from ambient polydisperse aerosols compared to polar nephelometers which measure scattered light from one angle at a time.

Figure 1 shows the measured asymmetry parameter of polystyrene latex particles of known diameter and a comparison to Mie theory. The illumination wavlength is 532 nm. Figure 2 presents the measured scattering phase function of a polydisperse distribution of ammonium sulfate particles. The Mie scattering calculation is based on the measured size distribution of the generated particles. The agreement between experiment and theory in both cases is excellent.

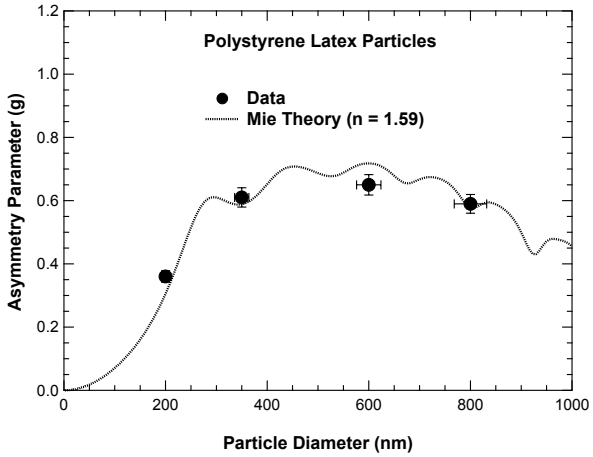

Fig. 1 Plot of asymmetry parameter obtained for four sizes of polystyrene latex particles at 532 nm.

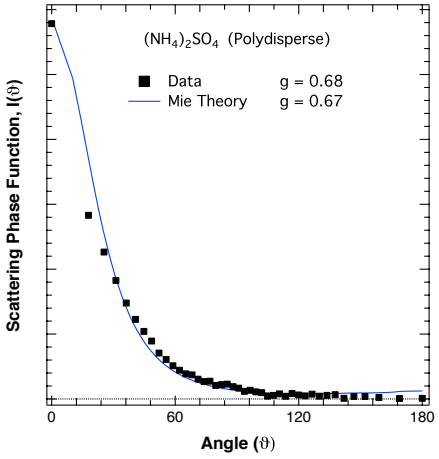

Fig. 2 Scattering phase function obtained from a polydisperse distribution of ammonium sulfate particles at 532 nm.

This work was sponsored by NASA under the Small Business Innovation Research Program.

Andrews, E., P.J. Sheridan, M. Fiebig, et al. (2006), J. Geophys. Res. 111, D05S04, doi:1029/2004JD005734

Ogren, J.A., E. Andrew, A. McComiskey, et al., (2006) 16th ARM Science Team Meeting Proceedings (Albuquerque, NM, March 27-31)

Scattering Coefficients and Asymmetry Parameters derived from the Polar Nephelometer Aurora4000

T. Müller, M. Paixão and A. Wiedensohler
Department of Physics, Leibniz Institute for Tropospheric Research , Leipzig, Germany
Optical properties, Light scattering, Optical instrumentation
Presenting author email: Thomas.mueller@tropos.de

Since decades integrating nephelometers are in widespread use for measuring the particle scattering coefficient. Integrating nephelometers are easy to operate, calibrate and long-term stable what makes this instrument favourable device for monitoring and laboratory purposes.

Drawbacks of the nephelometer design are the *truncation error* and the *non-Lambertian* illumination by the light source. Truncation error means that light scattered by particles in small angular ranges in forward and backward directions are not detected by the instrument because of limitations of the design. Truncation angles of the nephelometer of type Aurora4000 (Ecotech Pty Ltd.) are from 0° to 10° and 170° to 180°. Ideally, the light source should have a Lambertian light emission pattern proportional to sin(θ). For the Aurora4000, the light source characteristics was determined to be proportional to $\sin(\theta)^{1.109}$. A correction of measured scattering intensities because of the truncation error and the non-Lambertian illumination is given in Anderson and Ogren (1998) for multi-wavelength nephelometers. This correction is a function of the spectral run of the scattering coefficient, which is described by the scattering Ångström exponent. However, corrections using the Ångström exponent are sensitive to the particles refractive index (c.f. Figure 2).

The new polar nephelometer of type Aurora4000 (Ecotech Pty Ltd.) measures the scattered light for several illumination sectors by blocking a part of the emitted light in forward direction with a controllable shutter. The shutter allows to block light from 0° to a user controlled angle α in the range 0°<α<90. Measured illumination functions are shown in Figure 1.

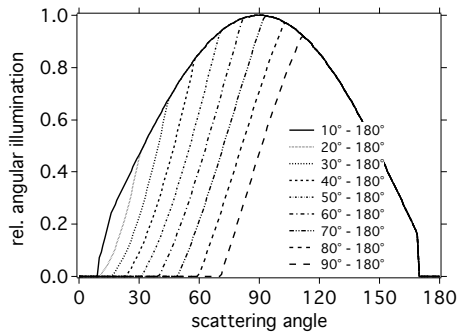

Figure 1: Angular illumination functions of the Aurora4000 for different illumination sectors by changing the shutter position in steps of 10°.

Correction for truncation errors, defined by the ratio of the scattering measured with nephelometer and the true scattering coefficients, were calculated using Mie theory. Also the relative scattered intensity I(α) for different angles of the shutter position were calculated. A quasi-phase function was determined from differences of scattering intensities calculated for pairs of shutter positions, e.g. I(0°)-I(10°), I(10°)-I(20°), etc. Mie-calculations were done for a range of particle size distributions with mode diameters from 0.1 to 1.0 µm and a standard deviation of 1.5. The real and imaginary parts of the complex refractive index ranged from 1.5 to 1.6, and 0.0 to 0.1, respectively. The Mie-simulated nephelometer signals were used as a test data set to develop methods for correction of the truncation error and for retrieval of the particle asymmetry parameter.

Henyey-Greenstein phase functions were fitted to the simulated quasi-phase functions and permit to derive an asymmetry parameter g_{HG}. A good correlation between the nephelometer truncation error and g_{HG} was found and a correction function for the truncation error was derived. Figure 2 shows values of the corrected nephelometer scattering coefficient $\sigma_{neph,cor.}$, calculated using the new correction based on the polar measurements and the correction from Anderson and Ogren (1998).

Values of the Henyey Greenstein asymmetry parameter g_{HG} differ from values of the asymmetry parameters calculated with Mie theory g_{Mie}. However a good correlation between g_{HG} and g_{Mie} was found.

Use of polar scattering measurements can significantly reduce the uncertainties for correction of the truncation error of nephelometers and allows to determine the asymmetry parameter.

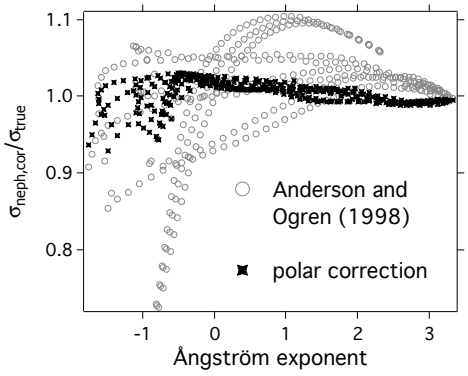

Figure 1: Ratios of truncation corrected and true scattering coefficient for a variety of particle sizes and refractive indices. Shown are results for the Anderson and Ogren (1998) and the new polar correction.

Anderson, T. L. and J. A. Ogren (1998). Determining aerosol radiative properties using the TSI 3563 integrating nephelometer. *Aerosol Science and Technology* **29**(1): 57-69.

Feasibility study of a Differential Aerodynamic Diameter Analyzer

D. Kiesler and F.E. Kruis
Institute for Technology of Nanostructures and Center for Nanointegration Duisburg-Essen (CENIDE),
University Duisburg-Essen, Duisburg, 47057, Germany
Keywords: Aerodynamic focusing, Nanoparticles, CFD, DMA, ELPI, Instrument development, Size Measurement.
Presenting author email: Dennis.Kiesler@uni-due.de

The aerodynamic diameter is an important property in studies of particle deposition, or agglomerate structure. But still no instrument exists, which has a differential transfer characteristic and can separate particles by their aerodynamic diameter like a DMA does for the mobility. Current measurement methods like the low-pressure impactor or ELPI have an integral transfer characteristic, or time of flight measurements like the APS do not separate the particles at all.

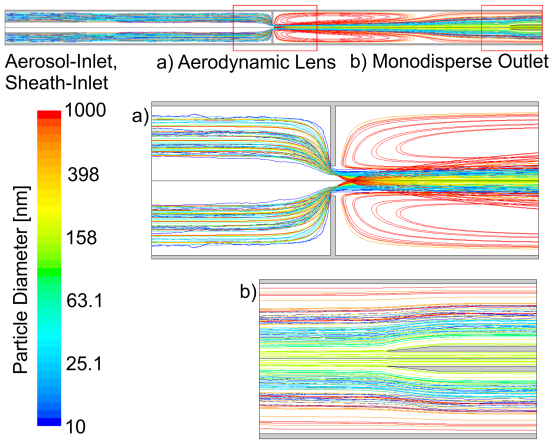

Figure 1: *Setup for the differential aerodynamic diameter analyzer tube. The polydisperse particles and the central sheath gas are introduced in the left. The aerodynamic lens a) sorts the particles by their aerodynamic diameters. Sampling at the tube center b) leads to a monodisperse particle distribution.*

In this work we want to combine the working principle of a DMA with the properties of an aerodynamic lens. Figure 1 gives an overview of the setup. The inlet on the left is designed like a DMA: The insertion of additional sheath air in the center of our tube creates a particle free zone. The polydisperse aerosol is inserted on the outer ring. But instead of applying an electric field, we use an orifice plate of an aerodynamic lens to apply a well defined force on the particles. This needs to be done in a low pressure environment in a laminar flow. The theory of the aerodynamic lens developed by Liu *et. al* (1995) shows, that particles in an accelerated gas stream can be separated from the gas streamlines due to their inertia. They showed, that one Stokes-Diameter d_f of the particles exists, which is focused to the center line. Particles smaller than d_f follow the streamlines and leave the center again. If the particles are too heavy, they overshoot the center and get defocused again (see figure 1 a). Downstream of the orifice we find only one diameter on the centerline. These particles can be sampled as monodispersed aerosol(see figure 1 b).

First, the aerodynamic lens orifice plate was designed with the aerodynamic lens calculator (Wang *et. al*, 2005, 2006). A further evaluation of this setup has been done by CFD simulations with particle tracking in a Lagrangian frame. A transfer function could be evaluated, which shows a clear differential characteristic. Figure 2 shows these transfer functions for titanium particles and different pressures behind the orifice plate. The selected diameter can be shifted by changing the pressure behind the orifice plate. The system can separate aerodynamic diameters from around 45nm to 1000nm, for pressures between 200Pa to 1200Pa.

While these first transfer functions are quite wide and have a broad geometric standard deviation of around $\sigma_g =$ 1.2 to 1.15 the design needs to be optimized. Based on a better evaluation of the aerodynamic lens, we tried different geometries in the simulation and found a design that leads to a σ_g of 1.04 which is clearly monodisperse.

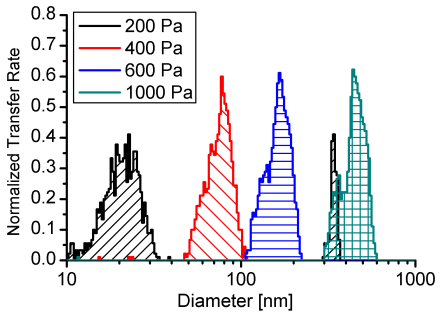

Figure 2: *The simulation results show a clear differential transfer characteristic. Different pressures behind the aerodynamic lens shift the sampled particle diameter.*

This work was supported by the Deutsche Forschungsgemeinschaft in the framework of the collaborative research program "Nanoparticles from the gas phase" (SFB 445).

Liu, P., Ziermann, P.J. Kittelson, D.B., McMurry, P.H. (1995) Aerosol Sci. Technol. **22**, 293

Wang, X., McMurry, P.H., Kruis, F.E. (2005) Aerosol Sci. Technol. **39**, 611

Wang, X., McMurry, P.H. (2006) Aerosol Sci. Technol. **40**, 320

Experimental comparison of two Very Long DMAs

J. Uin, E. Tamm
Laboratory of Environmental Physics, Institute of Physics, University of Tartu, Tartu, Estonia
Keywords: Aerosol instrumentation, DMA, transfer function, laboratory experiments.
Presenting author email: janek.uin@ut.ee

The Very Long DMA is a Vienna-design based DMA, developed in University of Tartu, which can be used for experiments involving aerosol particles with sizes up to 10 µm (Uin and Tamm, 2011). It's main characteristics are: inner and outer diameters of the electrodes - 84 and 100 mm, working length - 1200 mm. Due to the instrument's size, the cylindrical electrodes of the DMA could not be made out of single piece of metal and instead a sectional design was implemented. This can cause some geometrical non-idealities that can distort the transfer function of the DMA. As there are now two VLDMAs in existence, a question arises, whether the working parameters of the two instruments are similar enough that the two DMAs can be treated as identical and used as such in the experiments.

To compare the two VLDMAs, two sets of experiments were done. First, a simple measurement of an aerosol size distribution was done with both instruments. Here silver + DOP particles with mean diameter around 800 nm were generated using the setup that avoids multiply charged particles (Uin et al., 2009). The results are shown in Fig. 1. As can be seen, the measurement results of the two DMAs are very similar. The minor visible differences can be attributed to the dissimilar length of the input tubing (and thus different particle losses) and to the small errors in setting the sheath flows of the DMAs.

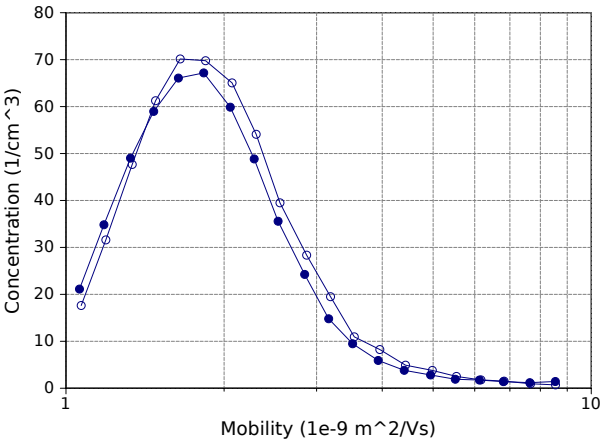

Figure 1: Aerosol distribution measurement results of the two VLDMAs in similar experimental setup.

Next, the two VLDMAs were paired with a known instrument – a TSI Long DMA and the transfer functions of the VLDMAs were measured using a tandem DMA setup (Stratmann et al., 1997; Birmili et al., 1997). In this setup, the known instrument was set to separate particles with a given modal diameter (around 800 nm in this case) and the aerosol distribution produced was measured with both VLDMAs. From the measurement results, the relative half-width β of the VLDMA transfer function was calculated for both instruments (due to technical reasons, it was not possible to accurately determine the transfer function height). The results for both instruments are identical with $\beta = 0.40$. This value, however, differs from the theoretical $\beta = 0.1$ (given by the airflows used) and from the experimental result $\beta = 0.17$ obtained with latex particles (Uin and Tamm, 2011).

The most likely reason for this is the presence of the electric wind between the electrodes of any of the three DMAs. The TSI Long DMA was operated using voltages > 9 kV and, considering the very high particle concentrations required by a tandem DMA experiment, the presence of the electric wind in that instrument is very likely.The voltages for the VLDMAs were around 5 kV and previous experiments show, that electric wind can readily arise in such conditions. However, as the experimental setup for both VLDMAs was the same, the effect of the electric wind on the registered aerosol distribution is also the same (regardless whether the electric wind was in the TSI Long DMA or in both of the VLDMAs). Thus, if any difference between the results for the two VLDMAs would have been detected it would have only been due to the differences between the actual instruments.

There is a very good agreement between the experimental results obtained using both VLDMAs, despite the potential non-idealities coming from the methods of their manufacturing. The conclusion of this investigation is, that the two VLDMAs can be considered identical and thus can be used in the experiments that require identical instruments. This opens up new possibilities for experimental work, as both VLDMAs are capable of operating in the particle size range of up to 10 µm.

This work was supported by the Estonian Science Foundation under grant 8779 and by the Estonian Research Council Targeted Financing Project SF0180043s08.

Birmili, W., F. Stratmann, Wiedensohler, A., Covert, D., Russell, L. M., and Berg, O. (1997). *Aerosol Science and Technology*, 27:215–223.

Stratmann, F., Kauffeldt, T., Hummes, D., and Fissan, H. (1997). *Aerosol Science and Technology*, 26:368–383.

Uin, J. and Tamm, E. (2011). *Aerosol and Air Quality Research*, 11(5):531–538.

Uin, J., Tamm, E., and Mirme, A. (2009). *Aerosol Science and Technology*, 43(8):847–853.

Applying Particle Size Magnifier to nano-particle measurements

J. Mikkilä[1], K. Lehtipalo[1,2], J. Kangasluoma[2], J. Vanhanen[1], T. Petäjä[2] and M. Kulmala[2]

[1]Airmodus Oy, Gustaf Hällströmin katu 2a, 00560, Helsinki, Finland
[2]Department of Physics, University of Helsinki, P.O. Box 64, 00014, Helsinki, Finland
Keywords: nano-particle, nano-CN, instrumentation, CPC
Presenting author email: jyri.mikkila@airmodus.com

The Airmodus A09 particle size magnifier (PSM) was developed for detection of nano-CN as small as ~1nm in mobility diameter (Vanhanen *et al.*, 2011). Being able to measure even the smallest particles is crucial for example when studying atmospheric new particle formation. Inside the instrument a high super-saturation is achieved by mixing cooled sample flow Q_a turbulently with heated clean air flow saturated with working fluid Q_s. Diethylene glycol was chosen as the working fluid in order to activate nano-CN without homogeneous nucleation (Iida *et al.*, 2009). With the selected working fluid, the particles grow to a mean diameter of 90 nm, after which they can be easily counted with any conventional condensation particle counter (CPC) (McMurry, 2000). The instrument combining the functionality of the PSM and a CPC is called a nano condensation nucleus counter (nCNC).

Besides the relatively high inlet flow rate and low diffusion losses compared to laminar flow type CPCs, the mixing type nCNC benefits of its capability to rapidly change the saturation ratio at the point of activation. This is done simply by controlling the flow rates inside the instrument, so that the mixing ratio

$$\frac{Q_s}{Q_s + Q_a}$$

is changed. The sample flow rate Q_a is always kept constant at 2.5lpm. The *Figure 1* shows an example how the 50% activation diameter changes with the saturator flow Q_s i.e. with the mixing ratio. Thus the particle size distribution between 1 and 3.5nm can be determined by comparing the results with different mixing ratios. Generally, size information from about 1 to 3nm can be obtained with this method.

The results in *Figure 1* were obtained by using ammonium sulphate particles generated in a tube-furnace (Petäjä *et al.*, 2006). The composition was verified measuring simultaneously with APi-TOF mass spectrometer (Junninen *et al.*, 2010). Also the chemical composition plays a role in the activation of nano-CN. For example the mobility standards (ammonium halide salts) (Ude & Fernández de la Mora, 2005) and silver particles have somewhat different size dependence. This needs to be kept in mind when comparing ambient measurements to calibration results, which give the mobility equivalent diameter for a certain composition. On the other hand the possibility to tune Airmodus A09 to detect even some large molecules, such as ammonium halide salts, can give an alternative way to monitor and develop industrial processes.

To some extent the composition effect can be overcome by using a nano-DMA in front of a fixed flow nCNC when they work together as a nano-DMPS. Then the size of the particles is definitely mobility equivalent but the concentration data in the smallest sizes can still have some uncertainty, and thus the detection efficiency curve of the nCNC might vary according to the composition of the nano-CN. Below about 1.5nm the charger ions start to dominate the sample aerosol in a DMPS system. However with correct selection of the mixing ratio, the nCNC does not detect the charger ions, but can still have for example detection efficiency of 20% for negatively charged 1.2nm NaCl particles and 50% detection efficiency at 1.35nm. On the other hand the losses inside the sampling and DMA section might be too high at some occasions, so that scanning of the saturation ratio is the only way to get size information of the smallest particles.

Using a switchable ion filter in front of the inlet the nCNC can be used to measure the amount of charged versus neutral particles, which is interesting especially in nucleation studies. Thus by combining different applications of the nCNC it's possible to study not only the effect of charge but also the chemical composition in sub-3nm size range.

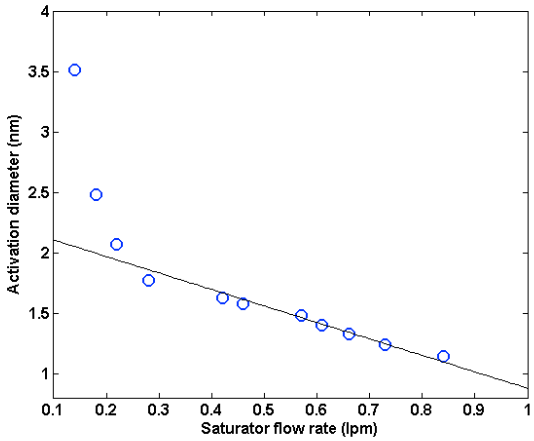

Figure 1. Activation diameter for ammonium sulphate given by 50% activation efficiency as a function saturator flow rate Q_s.

Iida, K., Stoltzenburg, M. R. & McMurry, P. H. (2009). *Aerosol Sci. Technol.*, **43**, 81-90.

Junninen, H. *et al.* (2010) *Atmos. Meas. Tech.*, **3**, 1039-1053.

McMurry, P. H. (2000). *Aerosol Sci. Technol.*, **33** 297-322.

Petäjä, T. *et al.* (2006). *Aerosol Sci. Technol.* **40**, 1090-1097.

Ude, S. & Fernández de la Mora, J. (2005), *J. Aerosol Sci.*, **36**, 1224-1237.

Vanhanen, J. *et al.* (2011). *Aerosol Sci. Technol.*, **45**, 533-542.

Novel continuous ambient air quality monitoring system that simultaneously reports multiple PM-fractions, number concentration and size distribution

M. Weiss, J. Spielvogel

Palas GmbH, Karlsruhe, 76229, Germany
Keywords: aerosol instrumentation, air quality network, fine particulate matter, particulate mass, particle size
Presenting author email: weiss@palas.de

Real time continuous and accurate measurements of atmospheric particles are important when complying with regulation or in the context of source apportionment; e.g in determining how much is contributed by traffic, industry or residential heating. If the time resolution is high enough it allows reliable transport modelling based on actual data. A lack of this information was causing the closure of the European air space when the Iceland volcano Eyjafjallajökull erupted in April 2010.

We will present the Fidas®, a new fine dust monitoring system based on optical light scattering. The Fidas® is equipped with a white light LED as stable light source with long lifetime and an integrated filter holder. A Sigma-2 sampling inlet (described in detail in VDI 2119-4) and intelligent aerosol drying system leads to representative sampling. The Fidas® allows the continuous recording of the particle number and particulate mass (simultaneously PM_1, $PM_{2.5}$, PM_4, PM_{10}, TSP) with a time resolution of two minutes providing the opportunity to monitor dynamic changes. Also recorded is the particle size distribution that can provide additional information for health related risk assessments.

We will report on a number of comparison measurements and compare results with other monitoring techniques. In the context of these comparisons we will also show the first results from the on-going European aptitude and equivalency test.

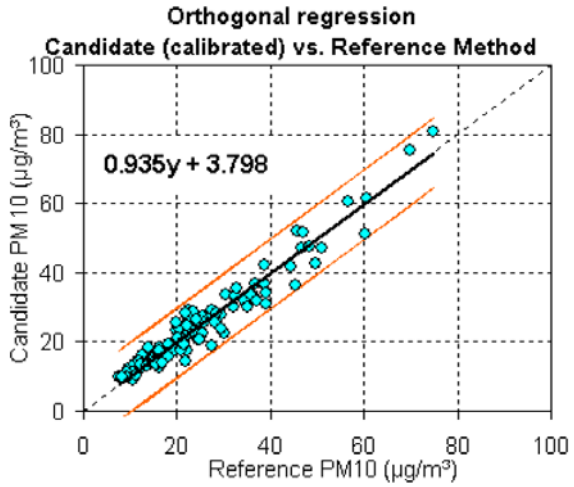

Figure 1. Orthogonal regression of the Candidate Method against the Reference Method. Confidence interval (99 %) indicated in orange.

In a second part we will show an example where the additionally provided information on particle size distribution is used to analyse special events (here in this abstract only one example is mentioned briefly).

Figure 2 shows the particulate mass and particle number distributions corresponding to before, during and after fireworks. As can be seen, the mass concentration of small particles increases significantly and is caused by a factor of 10 increase in particle number. These small particles (< 400 nm) are primarily caused by the combustion process of the rockets and explosives.

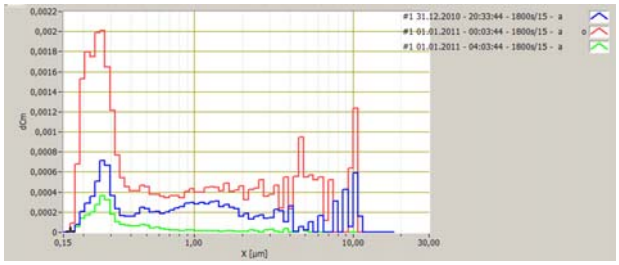

Figure 2. Particle mass distributions in mg/cm^3 before (blue), during (red) and after (green) new year 2011

Due to the implemented filter holder in the Fidas®, a gravimetric filter can be used to analyse the sample further, e.g. by chemical analysis, and to verify the optically measured data.

DIN EN 12341: Air quality. Determination of the PM10 fraction of suspended particulate matter. Reference method and field test procedure to demonstrate reference equivalence of measurement methods.; EN 12341:1999 (March 1999)

Directive 2008/50/EC of the European Parliament and of the Council of 21 May 2008 on ambient air quality and cleaner air for Europe (ABI.EU: 11.06.2008 No. L 152/1

Guide to the demonstration of equivalence of ambient air monitoring methods, Report by an EC working group for demonstration of equivalence, January 2010 http://ec.europa.eu/environment/air/quality/legislation/pdf/equivalence.pdf

Direct probing of aerosol surfaces by synchrotron-radiation-based XPS

J. Werner[1], Y. Cai[1], N. L. Prisle[2], G. Öhrwall[3], J. Söderström[2], M. Dal Maso[2] and O. Björneholm[1],
[1]Department of Physics and Astronomy, Uppsala University, P.O. Box 516, S- 751 20 Uppsala, Sweden
[2]Department of Physics, University of Helsinki, P.O. Box 48, 00014 University of Helsinki, Finland
[3] MAX-lab, University of Lund, P.O. Box 118, S-22100 Lund, Sweden
Keywords: Aerosol characterization, Surface activity, Instrumentation/chemical char.
Presenting author email: olle.bjorneholm@fysik.uu.se

Aerosols are complex finite systems, with properties determined by the interplay between their size, structure and stoichiometry. The microscopic spatial distributions of the chemical species is important; the three aerosol particles composed of yellow and red species, schematically illustrated in fig. 1, have different radial distribution of the component species. Even with the same total composition, their properties would be different.

Fig. 1. Three different radial distributions in aerosols with the same total stoichiometric composition

Many of the compounds, both inorganic and organic, identified in atmospheric aerosol particles are from studies of macroscopic aqueous systems known to have either positive or negative surface propensity. This means that the composition of the surface will be different than in the bulk. Since the surface fraction increases with decreasing aerosol size, such surface phenomena will become increasingly important for the properties of the system, and in the small-size limit determine the properties. In contrast to macroscopic systems with a virtually infinite bulk, the finite size of microscopic aerosols means that surface segregation phenomena also will affect bulk composition. Enrichment of a species at the surface means depletion of the same species in the bulk.

We have developed a novel laboratory set-up for direct probing of the surface propensity and speciation of aerosols. As schematically shown in fig. 2, we produce aerosols in an atomizer, dry them and use an aerodynamic lens system to focus them into a beam. Further downstream, the aerosols are exposed to x-rays from a synchrotron radiation (SR) beamline, allowing core-level X-ray Photoelectron Spectroscopy (XPS), which is well-established and very successful technique to characterize solids, surfaces, molecules, clusters and liquids (Hüfner 1995). Some key advantages of XPS are that the measurement process is virtually instantaneous, meaning that the interpretation is not complicated by fragmentation upon ionization, and its chemical and surface sensitivity, implying that both the chemical state and the microscopic spatial distribution of the component species are probed. We have already used these properties of XPS to study how the surface composition of atmospherically relevant aqueous systems such as inorganic ions and carboxylic acids varies with factors such as pH, concentration and co-solvation (Ottosson N *et al* 2009, 2010, 2011, 2011).

The set-up will be taken into operation during spring 2012, and we will present the first results on how surface composition and speciation for model systems of both marine and continental aerosols vary with factors such as pH, concentration and co-solvation.

Hüfner, S. (1995) Photoelectron spectroscopy, Springer Verlag, Berlin
Ottosson N *et al* (2009) J. Chem. Phys **131**, 124706
Ottosson N *et al* (2011) Phys Chem Chem Phys **12**, 10693 (2010)
Ottosson N *et al* (2011) J. Phys. Chem. Lett **2**, 972
Ottosson N *et al* (2011) Phys Chem Chem Phys **13**, 12261

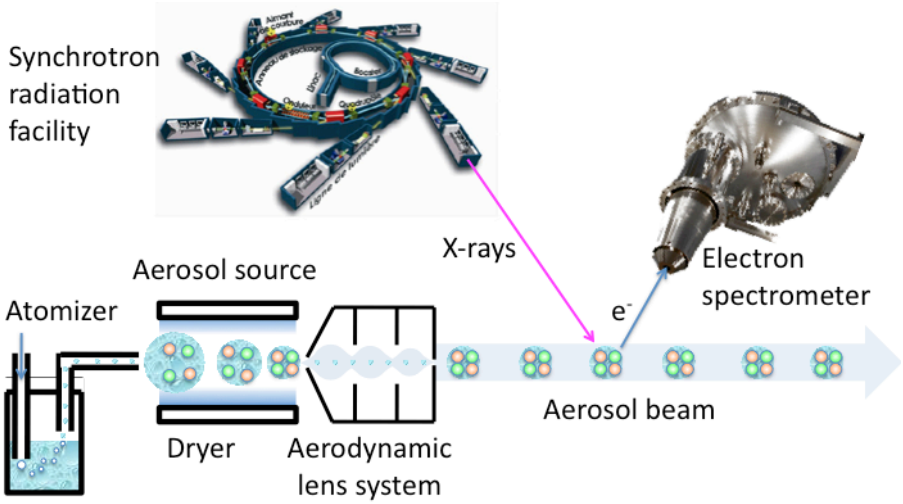

Fig. 2. Schematic experimental setup

Liquid sample nanoparticle sizing system

J.E. Farnsworth[1], K. Erickson[1], B.L. Osmondson[1], and R. Caldow[1]

[1]TSI Incorporated, Shoreview, MN, 55126, USA
Keywords: nebuliser, SMPS, electrospray, nanoparticles characterization
Presenting author email: jim.farnsworth@tsi.com

Nanotechnology-based industries today require real-time and quantitative sizing of nanoparticles. Commonly, light scattering techniques such as dynamic light scattering (DLS), laser diffraction, and optical particle counting are used to size nanoparticles suspended in liquids. These techniques have limited size resolution, sensitivity, and accuracy, since results are dependent on the optical properties of the sample. This is a critical shortcoming of real-time, liquid phase sizing instrumentation.

Aerosol particle technology is an enabling discipline for these applications. By converting the sample from liquid phase to gas phase, one can take advantage of the high resolution sizing and single particle sensitivity afforded by Differential Mobility Analysis (DMA) based sizing. This paper presents two options for liquid sample particle sizing using aerosol instrumentation.

The first configuration (TSI LiquiScan NP) combines a new nanoparticle nebulizer with a Scanning Mobility Particle Sizer spectrometer (SMPS). This system configuration allows size distribution measurements to be made from 5-500 nm with higher resolution and sensitivity than can be obtained from liquid phase sizers (Figure 1), and avoids sub-100 nm residue interference issues experienced by traditional nebulizers by controlling the median droplet diameter to ~300 nm and by using ultrapure water for sample dilution (Grant and Beuscher, 2009). The nebulizer comprises a peristaltic pump for 0.3-1.5 mL/min sample introduction, 20:1-20000:1 liquid sample dilution, ultrafine nebulization under controlled temperature and pressure conditions, and an internal dryer to remove solvent from solute. The dried aerosol is pulled from the nebulizer by the SMPS at 0.6-1.5 L/min. Software is used for system control, data inversion, calibration and statistical analysis. Additionally, the nebulizer-SMPS system provides quantitative hydrosol concentrations, accomplished via calibration to a standard solution of known particle volume concentration.

The second configuration (TSI LiquiScan ES) combines an electrospray with an SMPS. The electrospray creates droplets ~150 nm median diameter with a narrow size distribution ~1.2 geometric standard deviation (σ_g). The small, uniform droplets make the system well suited to measuring small nanoparticles. Additionally, electrical mobility has shown excellent correlation to molecular mass from 4MDa to 12 MDa (Allmaier et al, 2008) for large molecules (macromolecules such as proteins or lipids). Therefore using the electrospray/SMPS system, data distributions can be displayed as particle diameter or molecular mass (using a correlation constant). Software is used for data inversion and analyses.

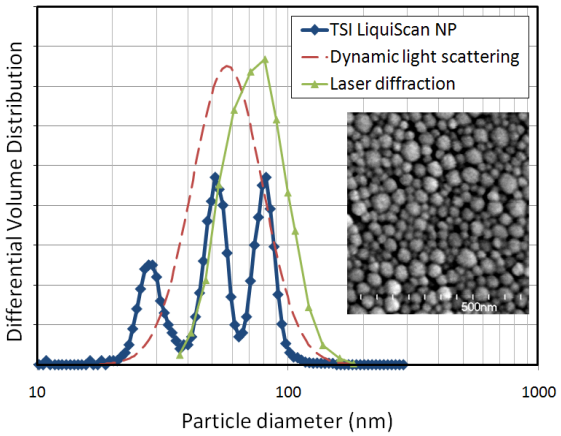

Figure 1. Size distribution data of a tri-modal polishing slurry measured via 1) nanoparticle nebulizer/SMPS, 2) Dynamic Light Scatter (DLS) and 3) Laser Diffraction. A SEM micrograph of the slurry is shown as a reference. As can be seen, the nanoparticle nebulizer/SMPS is able to resolve all three modes of the slurry, while the two optical techniques indicate only a mean diameter.

Liquid sizing via aerosol technology has proven useful for a wide array of applications such as nanoparticle size characterization, colloidal solution kinetic investigations, nanoparticle coating evaluation, characterization of chemical mechanical planarization (CMP) slurries (Figure 1), water purity investigations, particle retention of liquid filters, macromolecule characterization, and virus identification.

Data from both system configurations is presented. Advantages and disadvantages of each technique are discussed.

Grant, D. and Beuscher, U. (2009) *Ultrapure Water J.* **26**, 34-40.

Allmaier G, Laschober C, Szymanski WW. (2008) *J Am Soc Mass Spectrom*. **19(8)**:1062-8.

Approximate relationship between mobility and voltage for Brownian particles in a cylindrical DMA

M. Alonso[1], F.J. Alguacil[1] and C.H. Huang[2]

[1]National Center for Metallurgical Research (CENIM-CSIC). Gregorio del Amo, 8. 28040 Madrid, Spain
[2]Department of Environmental Engineering and Health, Yuanpei University, 30015 Hsinchu, Taiwan

Keywords: DMA, Brownian diffusion, central mobility, applied voltage
Presenting author email: malonso@cenim.csic.es

In the case of non-diffusing particles, the relationship between mobility and voltage in a concentric cylindrical DMA is given by the well known expression $Z = Q_c \ln(R_2/R_1)/2\pi LV$ for balanced flows (aerosol = classified; sheath = excess). When particle diffusion can not be neglected, the mobility of the classified aerosol is a bit smaller. An approximate expression for a more correct relationship between *Z* and *V* will be given here.

Consider a Brownian particle moving in the radial direction, starting from a given point R_i, and let us determine the mean time $\tau(r)$ required for a particle placed at *r* to reach a specified location R_f for the first time. This definition implies that, obviously, $\tau(R_f) = 0$. During a time interval Δt, the particle travels a deterministic distance $ZE\Delta t$ and also suffers a superimposed random displacement which, for simplicity, will be considered of constant length Δr and equal probabilities in both the positive and negative radial directions. For the particle to be at *r* at time *t* it is necessary that, at an earlier time $t - \Delta t$, it was at either $r_1 = r - ZE\Delta t + \Delta r$ or $r_2 = r - ZE\Delta t - \Delta r$. Therefore,

$$\tau(r) = \Delta t + \tfrac{1}{2}\left[\tau(r - ZE\Delta t + \Delta r) + \tau(r - ZE\Delta t - \Delta r)\right].$$

Expanding in Taylor's series up to second order, dividing through by Δt and taking the limit $\Delta t \to 0$ yields

$$\beta \frac{d^2\tau}{dr^2} - 2ZE\frac{d\tau}{dr} + 2 = 0, \qquad (1)$$

where

$$\beta = \lim_{\Delta t \to 0} \frac{\Delta^2 r}{\Delta t} = 2D\left[1 + h(r)\right]. \qquad (2)$$

In the last expression, *D* is the particle diffusion coefficient, and $h(r)$ takes into account the non uniformity of the electric field, $E = -V/r\ln(R_2/R_1)$. For the conventional cylindrical DMA, where the particles travel toward the inner electrode, $h(r) > 1$, so that the "effective" diffusion coefficient is larger than *D*. Since no analytical expression is available for the function $h(r)$, we will take, as a first approximation, $h(r) = 0$ thus assuming that the particle spreading rate occurs as if the field were uniform (or as if there were no field at all acting on the particle).

With this approximation, the solution of (1) with boundary condition $\tau(R_f) = 0$ is

$$\tau(r) = \frac{r^2 - R_f^2}{2\left[D + VZ/\ln(R_2/R_1)\right]}. \qquad (3)$$

The particle of central mobility enters the DMA at position $r = R_i$, where

$$R_i^2 - R_f^2 = Q_c/\pi\bar{u}. \qquad (4)$$

In the last equation, Q_c is the sheath air flow rate, and $\bar{u}$ the mean axial flow velocity. Equation (3) for the particle of central mobility can be written as

$$\frac{L}{\bar{u}} = \frac{R_i^2 - R_f^2}{2\left[D + VZ_c/\ln(R_2/R_1)\right]}. \qquad (5)$$

From expressions (4) and (5) we arrive at the approximate equation relating central mobility and applied voltage:

$$Z_c = \frac{Q_c \ln(R_2/R_1)}{2\pi LV} - \frac{D}{V}\ln(R_2/R_1). \qquad (6)$$

The first term in the r.h.s. of (6) is the classical expression for non diffusing particles, and the last one is the approximate correction accounting for the effect of diffusion. Finally, using the relation $D = kTZ_c/pe$, where *kT* is twice the thermal energy of the particle and *pe* its charge, one finds

$$Z_c = \frac{Z_{c,nd}}{1 + \dfrac{kT}{peV}\ln\dfrac{R_2}{R_1}}, \qquad (7)$$

where the subscript *nd* refeers to no diffusion. For a typical DMA with electrode radii R_1 = 0.937 cm and R_2 = 1.958 cm, the $Z_c/Z_{c,nd}$ ratios are 0.9817, 0.9981 and 0.9998 for applied voltages of 1, 10 and 100 volts, respectively. The differences are thus very small, but it must be noted that these figures have been obtained using the approximate equation (7), derived from the assumption that the function *h*(*r*) in (2) is zero. As said before, *h*(*r*) is actually larger than unit for the cylindrical DMA, that is $\beta > 2D$ and, furthermore, since β depends on *r*, the solution of (1) is not (3). In the absence of an analytical expression for *h*(*r*), the actual values of $Z_c/Z_{c,nd}$ will be determined by computer simulations.

Evaluation of Size Selective PM_{10} Sampling Inlets in Aerosol Wind Tunnel

Sangil Lee*, Miae Yu, Hyun Ho Kim
Center for Gas Analysis, Division of Metrology for Quality of Life, Korea Research Institute of Standards and Science, 305-340, Republic of Korea
Corresponding to Sangil Lee (slee@kriss.re.kr)

Size selective particulate matter (PM) sampling inlets play an important role in PM measurement system. Improper designs of the sampling inlets result in collecting PM in undesired size, leading to significant errors in the measurement of PM mass concentrations. Therefore, the performance of PM inlets should be carefully evaluated in a proper environment prior to their field application.

In this study, a new aerosol wind tunnel system is designed and evaluated for the uniformity of wind speed distribution and aerosol concentration in the test section of the aerosol wind tunnel. Results for the wind speed distribution show that the deviation from the mean (DOM) at three different wind speeds is less than 10 % with turbulence intensity less than 5 %. Results for the aerosol concentrations show that DOM at three different wind speeds is less than 10 %. A PM_{10} sampling inlet is designed according to the U.S. Environmental Protection Agency (40 CFR Part 53 Appendix L) and its performance is evaluated in the newly developed aerosol wind tunnel. Results show that the PM_{10} inlet is characterized to meet the performance specifications for PM_{10} inlets in the 40 CFR Part 53.

Enhanced multiple charge inversion algorithm for mobility size spectrometers

S. Pfeifer[1], T. Müller[1] and A. Wiedensohler[1]

[1]Leibniz Institute for Tropospheric Research, Leipzig, 04318, Germany
Keywords: Charged particles, DMA, SMPS, DMPS, Coarse particles, Size distribution
Presenting author email: pfeifer@tropos.de

Differential or scanning mobility size spectrometer (DMPS/SMPS) are often used to measure the particle number size distribution in the sub-micron range. Due to the measuring principle, particles are classified by their size to charge ratio. To obtain a “true” size distribution with the particles diameter as the independent variable, an inversion algorithm to account for single and multiple charged particles is used

Many inversion algorithms are operating with explicit interpolation and discretization of the particle number size distribution (PNSD). This numerical step is an unnecessary calculation and a reduction of physical information content of the raw data. Furthermore, possible multiply charged particles in the largest size bins as well as possible aerodynamic shape factors are often ignored. We present a new algorithm without these mentioned limitations.

improvements of the new algorithm:

- based on operation with the measured grid points of the continuous PNSD, therefore an explicit interpolation and integration isn't necessary
- the algorithm only consists of an inversion of a clever occupied matrix, therefore it is a strict linear problem with the potential to transform the variance of the counting statistics of the raw data for the inverted size distribution
- the algorithm is able to consider an aerodynamic shape factor for the particles, both a linear value and a dynamic course over the whole range of the size distribution
- we can also consider multiply charged particles in the upper range of the DMPS/SMPS for the inversion using information of an additional size distribution for larger particles, e.g. aerodynamic particle sizer (APS) or optical particle sizer (OPC)

Results

The new multiply charge inversion algorithm was compared to other codes in Wiedensohler et al (2011). A good agreement over the whole size range with deviations smaller than 5% was found.

Figure 1 shows the necessity for using information from other instruments to simulate the multiple charged distribution for larger size bins of the SMPS. The data of that example were measured with a SMPS and an APS at the Cap Verde Islands during an event with high Saharan dust concentrations. We used a density of 2.5 g/cm³ and an aerodynamic shape factor of 1.2 to describe the mineral particles. Ignoring the multiply charged particles in the upper SMPS bins leads to erroneous results and even to negative concentrations.

In contrast to this, the result of enhanced multiply charge inversion is much smoother without these implausible peaks. There are no negative concentrations and the SMPS and the APS data fits together in the overlap range.

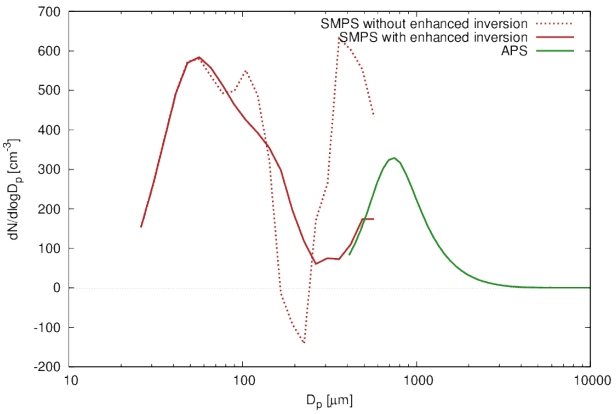

Figure 1. Comparison between the results without and with the enhanced multiply charge inversion algorithm using additional information from coarse mode size distribution measured with an APS.

There are still few open questions and limitations. We used the approximation by Wiedensohler (1988) for the charge probability distribution, with its upper limit for the particle size of 1µm. Although a mathematical deconvolution of the DMA transfer function has a negligibly influence for measurements under natural conditions, it would be useful for laboratory condition, e.g. for calibrations purpose using particle with a narrow size distribution, e.g. PSL spheres.

Wiedensohler, A. (1988) *An approximation of the bipolar charge distribution for particles in the sub-micron size range*, J. Aerosol Sci., 19, 387–389

Wiedensohler, A., et al (2011) *Particle mobility size spectrometers: harmonization of technical standards and data structure to facilitate high quality long-term observations of atmospheric particle number size distributions* , Atmos. Meas. Tech. Discuss., 3, 5521–5587

Thermodynamic characterization of the atmosphere during a Saharan dust intrusion over South Spain with onboard and remote sensing instrumentation: CLIMARENO

N. Seoane-Vieira[1], J. Andrey-Andrés[2], M.J. Granados-Muñoz[3,4], J. Fernández-Gálvez[3,4], R. González-Armengod[1], J.A. Adame[2], J. Tabrizi Sirvani[1], F. Lahoz-Pequerul[1],O. Serrano[1], M. Marco-Saurín[1].

[1]Laboratorio de Telemedida e Instrumentación, Área de Ensayos en Vuelo y Armamento (AEVA), Instituto Nacional de Técnica Aeroespacial (INTA), 28850 Torrejón de Ardoz, Madrid, Spain
[2]Área de Investigación e Instrumentación Atmosférica (AIIA), Instituto Nacional de Técnica Aeroespacial (INTA), 28850 Torrejón de Ardoz, Madrid, Spain
[3] Centro Andaluz de Medio Ambiente (CEAMA), Universidad de Granada, 18006 Granada, Spain
[4]Departamento de Física Aplicada, Universidad de Granada, 18071 Granada, Spain
Keywords: Aerosol instrumentation, Airborne measurement, Saharan dust.
Presenting author email: nevesseoane@gmail.com

The occurrence of Saharan dust intrusions over the Iberian Peninsula is well known. This work characterizes the thermodynamic atmospheric conditions prevailing during the CLIMARENO campaign carried out in June 2011. This campaign combined remote sensing and aero-transported instrumentation aiming to measure atmospheric variables in the presence and absence of a Saharan dust outbreak.

Measurements were taken at two sites in South Spain: "El Arenosillo" (37.1N, 6.7W in Huelva) and CEAMA (37.2N, 3.6W in Granada). Selected dates for the campaign were chosen based on an atmospheric dust alert system using information from different models (BSC/Dream, UoA/SKIRON and NRL/NAAPS). Dates 13 and 14 June 2011 were representative of no atmospheric dust while 26 and 27 June 2011 were representative of Saharan dust intrusion.

The characterization of the air masses was done by the use of a new and recently acquired CAPS atmospheric probe (Droplet Measurements Technology, Boulder, CO). The CAPS probe measures temperature, pressure, relative humidity, aerosols (0.5-50 mμ) and other miscellaneous data. This probe was installed on the CASA C-212 aircraft, instrumented for airborne atmospheric measurements and owned by the "Instituto Nacional de Técnica Aerospacial" (INTA). Additionally, radio sondes were launched from "El Arenosillo" Atmospheric Sounding Station, and humidity and temperature profiles from a ground-based passive microwave radiometer (RPG-HATPRO, Germany) were used at Granada.

Two distinct conditions were clearly identified due to the presence or absence of Saharan dust at both sites. The sample collection was made during the ascendant profiles of the C-212 aircraft. Atmospheric profiles, with or without Saharan dust, were characterized for temperature, relative humidity and aerosols. Data from the CAPS probe were compared with a radio sonde (Huelva) and the passive microwave radiometer (Granada). Temperature profiles showed higher gradient on days with intrusion (average 7º per 1000 m) compared to no-intrusion (average 5º per 1000 m) at both sites. Moreover, the temperature gradient increases further from around 1800 m asl on day without intrusion. It is noteworthy that the temperature profiles have better agreement at lower altitudes but the discrepancies at higher altitudes are close to the error limits.

The number of aerosol particles measured by the CAPS probe is low for both scenarios due to the relatively high lower limit of the probe in relation with the type of aerosol present in the atmosphere during these days. On the dates without intrusion there were traces of particles (fire smoke from North America) at high altitudes (around 6000 m asl) when a completely clear profile was expected. Figure 1 shows particles and temperature profiles during the campaign at both sites.

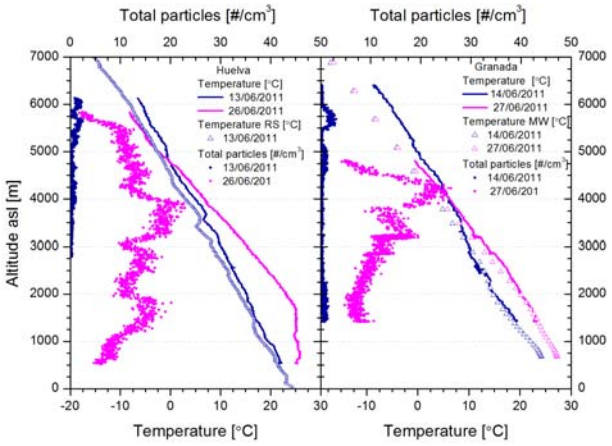

Figure 1: Temperature and total number of particles profiles during the CLIMARENO campaign. The left hand side shows details for Huelva and the right hand side for Granada. Temperature from both the CAPS and the radio sonde (RS) at Huelva as well as temperature from the CAPS and the passive microwave radiometer (MW) at Granada are also shown.

The authors of this study are grateful to the CLAEX unit of the Spanish Air Force for operating the C-212.

This work was supported by the Andalusia Regional Government through projects P08-RNM-3568 and P10-RNM-6299; by the Spanish Ministry of Science and Technology through projects CGL2010-18782, CSD2007-00067 and CGL2011-13580-E/CLI; and by EU through ACTRIS project (EU INFRA-2010-1.1.16-262254).

Integrated instrument data and control for CLOUD chamber

J. Almeida[1,2], A. Amorim[1], A. David[3], P. Pereira[2], A. Tomé[4]
and Cloud Collaboration
[1]SIM, University of Lisbon, Lisboa, 1749-016, Portugal
[2]Goethe-University of Frankfurt, Germany
[3]CERN, Geneve, Switzerland
[4]IDL, Universidade da Beira Interior, Covilhã, Portugal
Keywords: Instrumentation, Laboratory experiments.
Presenting author email: jalmeida@mail.cern.ch

Aerosol experiments large chambers like CLOUD motivate the gathering of several different measurement instruments during special data taking periods. The cloud team has developed an integrated data acquisition and control system that address the challenges of online monitoring and data plotting while providing a centralized data repository with unified tools for data access and visualization.

The system is optimized for rapid instrument integration and flexible data format processing. It was developed using several open architecture components including a computing cluster monitoring and a open database management system.

Supervisory control and data acquisition (SCADA) systems have been around for long time with the traditional hardware being increasingly replaced by software components. While industrial systems use mainly PLC controllers or Real Time Systems according to the performance requirements, laboratory equipment and control systems have seen in recent years a predominance of LabView based systems from National Instruments. During the last decade with the CERN LHC development a common effort between the LHC control and the experiments resulted in the use a common framework that was chosen to be PVSS from ETH. The described systems are proprietary, tend to behave as complete independent frameworks and are strictly incompatible in terms of modular development.

The CLOUD monitoring and control implementation has in fact delivered a high performance scada system, much like PVSS, but based on an open source system: ZABBIX (www.zabbix.com). Some trigger programs were made to connect the ZABBIX interfaces with the instruments. Specific patches were applied to zabbix to include an advanced scientific plotting capabilities.

Alongside with the low level components of the CLOUD DAQ integration toolkit, that includes open sources components, Zabbix extensions for monitoring and control, web based configuration toolkit for Mysql database tables and partitions, tuned for aerosol instrument data and a modular data access API, a high level gui interface was developed for data retrieval, data visualization and basic aerosol data analysis.

The Cloud data retrieval GUI interface is a Qt based application that directly interfaces with the central databases and it is designed to allow the development to became a general application for atmospheric aerosol analysis.

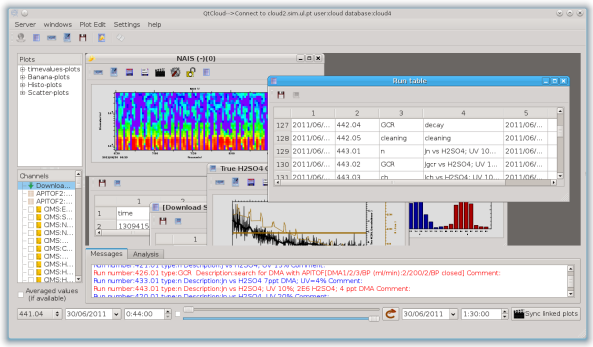

Figure 1. Screenshot of the Cloud Gui tool for data retrieval and data visualization. This is a comparison between theory and experimental data.

The developed CLOUD DAQ toolkit is released under GPL public license and is freely available. It was developed with the aim of making it easy to be used in any type of aerosol experiment that brings together several instruments.

Acknowledgments: We would like to thank CERN for supporting CLOUD with important technical and financial resources, and for providing a particle beam from the CERN Proton Synchrotron. This research has received funding from the EC Seventh Framework Programme (Marie Curie Initial Training Network "CLOUD-ITN" grant no. 215072, and ERC-Advanced "ATMNUCLE" grant no. 227463), the German Federal Ministry of Education and Research (project no. 01LK0902A), the Swiss National Science Foundation (project nos. 206621_125025 and 206620_130527), the Academy of Finland Center of Excellence program (project no. 1118615), the Austrian Science Fund (FWF; project no. P19546 and L593), the Portuguese Foundation for Science and Technology (project no. CERN/FP/116387/2010), and the Russian Foundation for Basic Research (grant N08-02-91006-CERN).

Reducing measurement error of Cloud Droplet Probe with a statistical smoother

S.Mikkonen[1], H. Portin[1,2], M. Komppula[2], A. Laaksonen[1,3] and S. Romakkaniemi[1]

[1]Department of Applied Physics, University of Eastern Finland, POB 1627, FIN-70211 Kuopio, Finland
[2] Finnish Meteorological Institute, Kuopio unit, P.O.B. 1627, FIN-70211 Kuopio, Finland
[3]Finnish Meteorological Institute, P.O. Box 503, 00101 Helsinki, Finland
Keywords: Cloud Droplet Probe, Measurement error, Statistical smoothing.
Presenting author email: santtu.mikkonen@uef.fi

In order to find the relationships between cloud properties and different meteorological parameters and aerosols we need reliable measurements on cloud droplet concentration. One of the instruments that can be used to measure cloud droplet concentration is Cloud Droplet Probe (CDP) manufactured by Droplet Measurement Technologies, Inc., Boulder, CO, USA.

Cloud droplet measurements can be subject to a wide variety of instrument biases, uncertainties and limitations (Lance at al., 2010). These biasing factors cause additional uncertainties in further analysis of the measurement data, e.g. computing the liquid water content or finding correlations between cloud droplet concentrations and the factors assumed to influence into the cloud formation. Our main goal is to find the factors affecting to the cloud droplet concentration and thus we have to reduce the bias of the measurements.

The cloud droplet measurements were made in Puijo measurement station in the town of Kuopio in central Finland. The station is located on the top of an observation tower (306 m a.s.l.) and the station is detected to be in-cloud approximately 15% of the time. The station has produced continuous data on aerosol cloud interactions since June 2006 (Portin et al., 2009). An intensive measurement period was conducted between 14 October and 7 March 2009. Within this period the CDP was measuring concentrations in 1Hz frequency and in total 16 cloud event days were detected.

Lance et al. (2010) found out that the CDP underestimates high cloud droplet concentrations due to coincidence, when two or more droplets pass through the CDP laser beam within a very short time. In addition our results indicate that measured cloud droplet concentration time series contains random bias, which affects the interpretation of the time series.

The method used in reducing the bias in the measured data is called “Time series decomposition using eigenvector filtering” (EVF). The eigenvector filtering decomposes the signal by applying a principal component analysis (PCA) on the original signal and a certain number of copies of it incrementally lagged, collected in a multivariate matrix. Reconstructing the signal using only the most representative eigenvectors allows filtering it (Ibanez and Grosjean, 2009).

Figure 1 shows a 30 minute sequence of a measured time series within a cloud event which took place in March 6th 2009. The original measured time series in presented in the top panel, the filtered time series is in the middle and the residual time series, presenting the random bias, is shown in the lowest panel. The results indicate that the bias in a single observation may be as high as 50% of the measured cloud droplet concentration. The average bias of the measurements was around 10%.

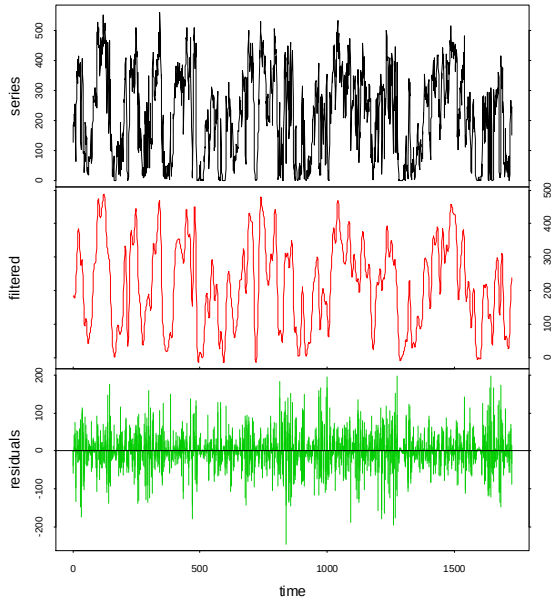

Figure 1. Original series in topmost panel, filtered series in the middle and the residual series in the bottom panel.

Proper filtering of the time series was found to increase the correlations between cloud droplet concentration and meteorological parameters suggested to influence in the cloud droplet concentration (e.g. wind conditions). The residual time series was found to be uncorrelated with these other parameters, which indicates that no information was lost in the filtering but all the information contained in the measured time series was passed to the filtered series. This indicates that the filtered time series can be used for example studying the effect of aerosol particles on the cloud formation.

The Academy of Finland Center of Excellence program (project number 1118615) is acknowledged.

Ibanez, F. and Grosjean, P. (2009) http://CRAN.R-project.org/package=pastecs
Lance, S. et al. (2010) Atmos.Meas.Tech., 3, 1683–1706
Portin, H et al. (2009) Boreal Env. Res. 14: 641-653.

Off-line organic aerosol analyses of filter samples using aerosol mass spectrometry

I. El Haddad[1], J. Slowik[1], U. Baltensperger[1], A.S.H. Prévôt[1]

[1]Laboratory of Atmospheric Chemistry, Paul Scherrer Institut, Villigen, Switzerland

Keywords: Source apportionment, innovative analysis method

Presenting author email: andre.prevot@psi.ch

Organic aerosol (OA), emitted directly from primary sources (primary OA, POA) or formed in-situ in the atmosphere from the oxidation of trace gas precursors (secondary OA, SOA), makes up a major component of submicrometer particulate matter (PM). Development of effective air quality control strategies intended to mitigate adverse effects is hampered without an accurate knowledge of the main sources and evolution processes of OA.

Field deployments of the Aerodyne Aerosol Mass Spectrometer (AMS) in the last years have advanced the real-time measurement of PM. Statistical methods like positive matrix factorization and multi-linear engine 2 applied on OA spectra demonstrate that these contain sufficient information to differentiate several OA sources and/or components (e.g. Lanz et al., 2010). These components include primary emissions from traffic, biomass burning, cooking and oxygenated OOAs interpreted to be mostly secondary. The high cost of the AMS and the complexity of its deployment in certain environments greatly limit the spatial coverage of AMS measurements and make the collection of long-term, continuous datasets not easily achievable. Recently, a new, moderately expensive, aerosol chemical speciation monitor (ACSM) was developed to overcome these shortcomings. However, the low mass resolution of this instrument prevents the assessment of OA elemental ratios and hence the assessment of the oxidation state.

These limitations motivated us to explore the application of laboratory AMS measurements on aerosol filter samples. Such samples are relatively easy and inexpensive to collect and store, and are already routinely collected at many air quality stations worldwide. In the meantime, Mihara and Mochida (2011) have described a similar method as used here.

The approach consists of water or organic solvent extraction of the particulate matter from the filter samples (here quartz Pall filters) and subsequent atomization of resulting solutions into the AMS. Using only water, we found typically an extraction efficiency of about 70%.

The obtained mass spectra from the off-line analyses were compared to average mass spectra taken from on-line mass spectrometer measurements. We found very similar mass spectra (Fig. 1), with correlation coefficients (R^2) higher than 97% (Fig. 2). These comparisons were done for both summer and winter samples. Both online and offline methods show for instance higher contributions from m/z related to biomass burning organic aerosol (e.g. m/z 60, 73) and hydrocarbon-like organic aerosol (e.g. m/z55, 57, 69) for the winter sample and higher contributions from OOA-related m/z ratios (e.g. m/z 43, 44) for the summer samples.

Further, we will present the first application of this method on filter samples collected at different stations in Switzerland with different exposure characteristics. Source apportionment results using these data will be discussed.

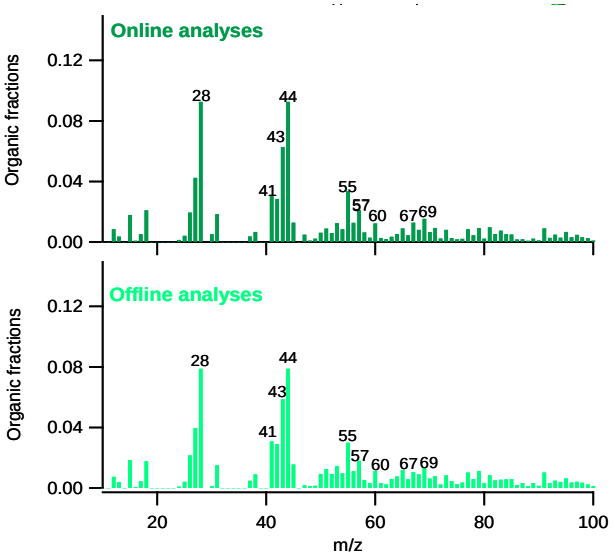

Fig. 1 Organic mass spectra of on-line versus off-line measurements of a sample during winter in Zurich.

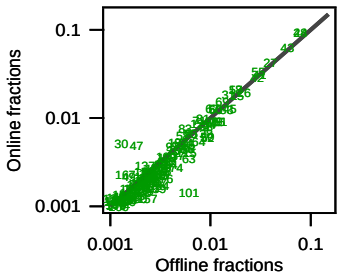

Fig. 2 Correlation of online versus offline measured organic mass fractions at unit mass resolution

This work was supported by the Swiss Federal office for the Environment and the Swiss National Science Foundation.

Lanz, V. et al. (2010) Atmos. Chem. Phys., 10, 10453-10471.

Mihara, T., and M. Mochida (2011) *Environ. Sci. Technol.*, **45**, 9168-9174.

Tuesday, September 4, 2012

Plenary 2

ACTRIS Research Infrastructure for coordinated long-term observation of aerosols, cloud-aerosol interactions, and trace gases in Europe

Gelsomina Pappalardo[1] and Paolo Laj[2]

[1]Consiglio Nazionale delle Ricerche-Istituto di Metodologie per l'Analisi Ambientale (CNR-IMAA), Tito Scalo, Potenza, Italy
[2]Laboratoire de Glaciologie et Géophysique de l'Environnement, CNRS-Université J. Fourier, Grenoble, France
Keywords: in-situ measurements, lidar, remote sensing
Presenting author email: pappalardo@imaa.cnr.it

Climate change is for a large part governed by atmospheric processes, in particular the interaction between radiation and atmospheric components (e.g. aerosols, clouds, greenhouse, and trace gases). Some of these components are also those with adverse health effects influencing air quality. Strengthening the ground-based component of the Earth Observing System for these key atmospheric variables has been unambiguously asserted in the IPCC Fourth Assessment Report and Thematic Strategy on air pollution of the EU. However, a coordinated research infrastructure for these observations is presently lacking.

ACTRIS (Aerosols, Clouds and Trace gases Research InfraStructure Network) aims to fill this observational gap through the coordination of European ground-based network of stations equipped with advanced atmospheric probing instrumentation for aerosols, clouds and short-lived gas-phase species (Figure 1). ACTRIS will have the essential role to support building of new knowledge as well as policy issues on climate change, air quality and long-range transport of pollutants.

The main objectives of ACTRIS are:

- To provide long-term observational data relevant to climate and air quality research on the regional scale produced with standardized or comparable procedures throughout the network.
- To provide a coordinated framework to support trans-national access to large infrastructures strengthening high-quality collaboration in and outside the EU and access to high-quality information and services for the user communities (research, Environmental protection agencies, etc.).
- To develop new integration tools to fully exploit the use of multiple atmospheric techniques at ground-based stations, in particular for the calibration/validation/integration of satellite sensors and for the improvement of the parameterizations used in global and regional-scale climate and air quality models.
- To enhance training of new scientists and new users in particular students, young scientists, and scientists from eastern European and non-EU developing countries in the field of atmospheric observation.
- To promote development of new technologies for atmospheric observation of aerosols, clouds and trace gases through close partnership with EU SMEs.

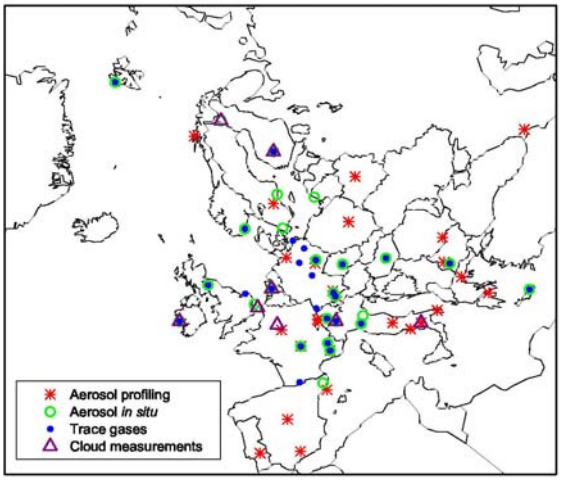

Figure1. Map of measurement sites contributing to ACTRIS.

A key for ACTRIS success is to build a new research infrastructure on the basis of a consortium joining existing networks/observatories that are already providing consistent datasets of observations and that are performed using state-of-the-art measurement technology and data processing. In particular the ACTRIS consortium merge two existing research infrastructures funded by the European Commission under FP6: EUSAAR (European Supersites for Atmospheric Aerosol Research) and EARLINET (European Aerosol Research Lidar Network). ACTRIS also includes the distributed infrastructure on aerosol – cloud interaction existing from a previous EU Research project CLOUDNET and by grouping the existing EU ground-based monitoring capacity for short-lived trace gases which is, at present, not coordinated at any level, besides EMEP (European Monitoring and Evaluation Programme) and GAW (Global Atmosphere Watch) caring for a few specific compounds. Therefore, ACTRIS represents an unprecedented effort towards integration of a distributed network of ground-based stations, covering most climatic regions of Europe, and responding to a strong demand from the atmospheric

research community. ACTRIS will be a step towards better integration of aerosol, cloud and trace gases communities in Europe necessary to match the integration of high-quality long-term observations of aerosol, clouds and short-lived gas-phase species and for assessing their impact on climate and environment. ACTRIS outcomes will be used for supporting decisions in a wide range of policy areas, including air quality but also health, international protocols and research requirements.

ACTRIS is organized in Networking Activities, Transnational Access and Service Activities, and Joint Research Activities as reported in Figure 2.

The data provision structure in ACTRIS involves four networking activities (NAs) that will feed the data centre:
WP2: Remote sensing of vertical aerosol distribution
WP3: In-situ chemical, physical and optical properties of aerosols
WP4: Trace gases networking: Volatile organic carbon and nitrogen oxides
WP5: Clouds and aerosol quality-controlled observations

These networking activities are completed by a fifth networking activity aimed at integrating information from *WP2-5* into a higher level of products required by users in the modelling and satellite-validation communities: *WP6: Integration, outreach, and sustainability.*

The activities of the research infrastructure will be oriented to a rigorous quality assurance program addressing both instruments and evaluation algorithms, and a standardized data exchange format. ACTRIS will also found and strongly sustain effective partnership between users and data providers and will pursue innovative initiatives to address the need of users. Moreover, standardization of procedures for the different measurement techniques and best practices across all stations and all European climatic regimes are paramount to facilitate the coordinated expansion of the network in a sustainable and efficient way.

Transnational access activities and service activities will enable users to conduct high-quality research by:

- Offering access to infrastructures with an excellent combination of instruments and expertise. This gives the opportunity to perform experiments using the state-of-art equipment in atmospheric research which could be used for measurement campaigns or instrument tests (*WP7-17*: *Trans-National Access*).

- Training a new generation of scientists. ACTRIS activities are aimed at enhancing the accessibility to the observatories and the exploitation of technical resources and knowledge. This is organized through *WP6* and *WP7-17*.

- Offering to the whole scientific community the use of a unique sun photometer calibration facility currently operational in the frame of PHOTONS/AERONET. This is performed in WP18: AERONET-EUROPE Calibration Service.

- Enhancing access to information on advanced aerosols, clouds and trace gases high-quality data in Europe through a Service Activity (*WP19: The ACTRIS Service Centre: Access to observations and service products of the infrastructure). The data centre* integrates measurement data from the ACTRIS infrastructure and other highly relevant networks. In addition to free access to atmospheric high-quality data, the data centre will provide tools and applications for end users to facilitate the use of all measurements for broad user communities, offer a direct interface towards external users (e.g., MACC, GMES in-situ), and take into account the principles outlined in SEIS, INSPIRE, WIS and GEOSS.

Joint research activities are intended to support and promote the ACTRIS infrastructure by taking advantage of the synergistic effects of coordinating different observation capabilities. WP20 and WP22 address novel techniques and algorithms using a multi-sensor approach to improve observation performances and define new data products. WP21 focuses on investigating technological and methodological aspects of simultaneously networking real-time chemical composition of aerosols and trace gases. These JRAs are topically connected with networking activities and in cooperation with WP6 to ensure their results are assimilated for the whole ACTRIS infrastructure benefit.

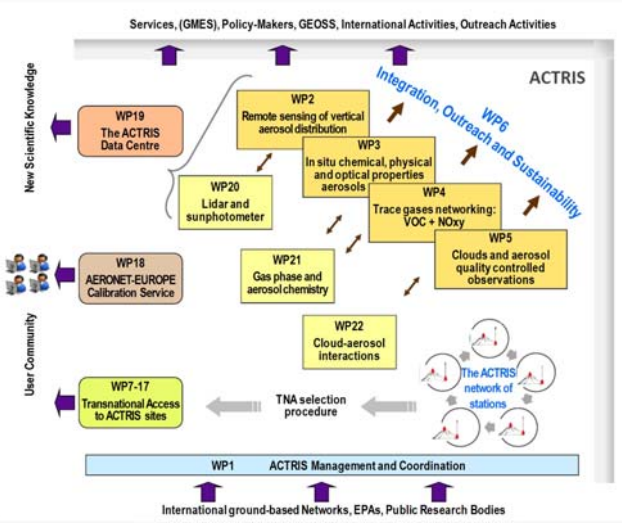

Figure 2. Interdependence of activities and tasks within ACTRIS.

At international level ACTRIS operates in strong cooperation with the Global Atmospheric Watch Program of the WMO, the ARM Climate Research Program and all the relevant research networks as (i.e. AERONET, GALION, NDACC, etc.) for the establishment of the ground-based component of the Global Earth Observation System of Systems.

ACTRIS is supported by the the European Union Seventh Framework Programme (FP7/2007-2013) under grant agreement n° 262254.

Tuesday, September 4, 2012

Session SS01S1O. ACTRIS

Long-term trends of aerosol number concentrations at GAW stations

A. Asmi[1], M. Collaud Coen[2], E. Andrews[3], M. Fiebig[4], A. M. Fjaeraa[4], P. Laj[5], J.A. Ogren[3], P. Sheridan[3], A. Virkkula[1], U. Baltensperger[6] and E. Weingartner[6]

[1]Department of Physics, University of Helsinki, P.O. Box 64, Helsinki, Finland
[2]MeteoSwiss, 1530 Payerne, Switzerland
[3]NOAA, Earth Systems Research Laboratory, Boulder, Colorado, 80305, USA
[4]Norwegian Institute for Air Research, Instituttveien 18, 2027 Kjeller, Norway
[5]Laboratoire de Glaciologie et Géophysique de l'Environnement, University of Grenoble, 38 402 St Martin d'Hères Cedex, France
[6]Laboratory of Atmospheric Chemistry, Paul Scherrer Institut, 5232 Villigen, Switzerland

Keywords: Long term trends, number concentration, GAW stations
Presenting author email: ari.asmi@helsinki.fi

Aerosol number concentration (CN) measurements provide a unique view of the sources of ultrafine particles and on the processes affecting aerosol indirect effects in the climate system. CN trends can thus provide information of changes in aerosol and aerosol precursor emissions, give opportunity to test aerosol model ability to produce realistic changes in aerosol concentrations on decadal time scales and provide important insight into the uncertainties related to indirect aerosol climate effects.

The global network of long-term aerosol number concentration measurements is concentrated in the northern hemisphere, especially in Europe and North America (Figure 1). The longest continuous time series of aerosol number concentrations start in the late 1970s, with the majority starting in the 2000s. Long-term aerosol size distribution measurements series are scarcer, with all long period (over 10 years of data) measurements done in or near Europe. Most of the stations are involved in the Global Atmospheric Watch (GAW) partnership.

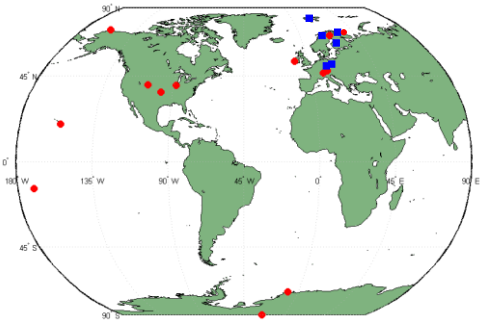

Figure 1: Locations of stations with long-term (>10 years of data) of aerosol number concentration (red circles) and aerosol size distribution (blue squares).

High variability of aerosol number concentrations creates additional challenges for trend detection, especially for significance testing (see the accompanying abstract by Collaud Coen, *et al.*, 2012). The trend analyses of aerosol optical properties and number size distributions are done with the same methodology, taking into account instrumental differences.

Figure 2 shows an example of aerosol number concentration trends in the 100-500 nm diameter range indicative of cloud condensation nuclei (CCN), measured at Värriö in Northern Europe. The CCN-sized particles exhibit a downward trend, likely connected to decreases of SO_2 emissions in Europe. The decreasing trend is steeper during summer, suggesting that a decrease of secondary aerosol formation could be a significant factor in this process. This is in agreement with earlier studies showing significant reduction in the occurrence of new particle formation in central Europe resulting from a decrease in anthropogenic SO_2 emissions (Hamed et al., 2010). This kind of trend analysis illuminates possible adverse climate side effects of air pollution control policies in the past and in the future (Makkonen et al., 2012).

Collecting the available measurements together and analyzing them in a consistent way will give a comprehensive view of decadal variability of aerosol number concentrations. Together with aerosol optical properties (Collaud Coen et al., 2012), these results provide a previously unavailable spatial and temporal description of aerosol variability in a changing climate.

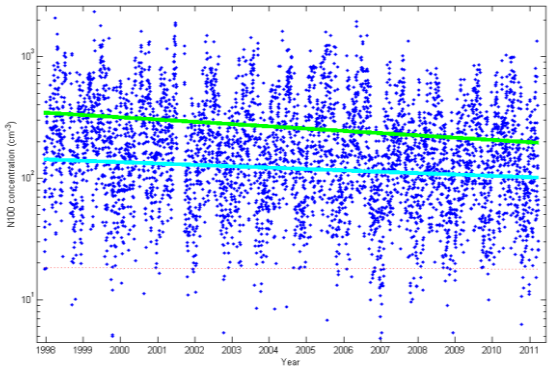

Figure 2: Particle number concentrations between 100 and 500 nm of diameter (N_{100}) at Värriö (preliminary data), showing summertime decreasing N_{100} trend of approximately 4%/year in summer time (green line) and smaller decreasing trend (~2 %/year) in wintertime.

Collaud Coen, M. *et al*. (2012) this abstract book.
Hamed, A., *et al*., *Atmos. Chem. Phys.*, 10, 1071-1091, 2010.
Makkonen, R., *et al*., *Atmos. Chem. Phys*., 12, 1515-1524, 2012

Long-term trend analysis of aerosol optical variables at GAW stations

M. Collaud Coen[1], E. Andrews[2], A. Asmi[3], M. Fiebig[4], A. M. Fjaeraa[4], P. Laj[5], C. Lund Myhre[4], J. A. Ogren[2], J.-P. Putaud[6], P. J. Sheridan[2], A. Virkkula[3], A. Wiedensohler[7], U. Baltensperger[8], and E. Weingartner[8]

[1]MeteoSwiss, 1530 Payerne, Switzerland
[2]NOAA, Earth Systems Research Laboratory, Boulder, Colorado, 80305, USA
[3]Department of Physics, University of Helsinki, P.O. Box 64, Helsinki, Finland
[4]NILU-Norwegian Institute for Air Research, Instituttveien 18, 2027 Kjeller, Norway
[5]Lab. de Glaciologie et Géophys. de l'Environ., University of Grenoble, 38 402 St Martin d'Hères Cedex, France
[6]European Commission, Joint Research Centre, 21027, Ispra, Italy
[7]Leibniz Institute for Tropospheric Research, 04318 Leipzig, Germany
[8]Laboratory of Atmospheric Chemistry, Paul Scherrer Institut, 5232 Villigen, Switzerland

Keywords: Long-term trends, optical properties, atmospheric aerosol
Presenting author email: martine.collaud@meteoswiss.ch

Since the 1970s, aerosols have been considered as an important atmospheric parameter and operational measurements first began at several locations including the South Pole, Mauna Loa, Point Barrow [*Bodhaine, 1983*], Cape Grim and Mace Head [*Junker et al.*, 2006]. Awareness of the impact of aerosols on climate radiative forcing led to the extension of measured variables and to an increase of measurement sites in the 1990s. Currently many stations include measurements of aerosol physical and optical properties, resulting in more than 30 long-term aerosol measurement sites on five continents. Most of these sites measure the aerosol number concentration, the wavelength dependent scattering and backscattering coefficients and the absorption coefficients. The existence of these long-term datasets enables the analysis of trends in aerosol optical properties as described here.

Since the aerosol variables are approximately lognormally distributed, a non-parametric trend test and slope estimator, the seasonal Mann-Kendall test and the Sen's slope estimator, were applied to detect the long-term trends and their magnitudes for each month. The global trend was also estimated by a least-mean square (LMS) fit of the data logarithms [*Collaud Coen et al., 2007*, and references therein]. With these statistical tools, a global picture of the aerosol long-term variability can be obtained.

To allow a comparison among measurement sites with varying length of data records, trends of 5, 10 and 15 years periods are calculated. As an example, Figure 1 presents the Mann-Kendall monthly trends for the light scattering coefficient at the mountaintop sites Jungfraujoch (JFJ, 1995-2010) and Mauna Loa (MLO, 2000-2011) research stations. Over these time periods the two datasets do not contain significant break points. The 5-year trend slopes have a very high variability in comparison with longer time periods, which can lead to statistically significant but unrealistic trends of more than 20% per year. The longer periods (10 and 15 years) lead to smaller and more consistent trends.

The 2001-2010 and 1996-2010 trends of the scattering coefficient at the JFJ are consistent, with a statistically positive trend in April and negative trends in June and August. The JFJ LMS trend analysis shows no statistically significant trends for the considered periods. Compared to the former 1995-2004 analysis [*Collaud Coen et al., 2007*], the negative summer trends become statistically significant, whereas the positive fall trends are no more statistically significant.

The MLO scattering coefficient has statistically significant positive trends for most months, but particularly for October to April. The yearly trend can be considered as homogeneous with a positive slope of 3.8%/yr. This is confirmed by the LMS analysis which shows a statistically significant positive trend of 3.3%/yr for the 2000-2010 period.

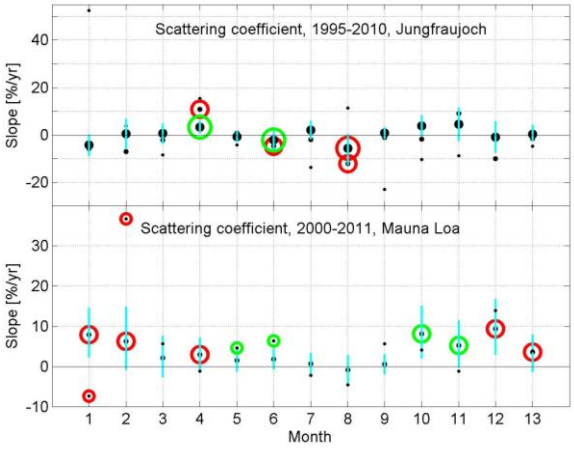

Figure 1: Long-term trends of the scattering coefficient at λ=450 nm at the JFJ and at MLO. Black dots correspond to Sen's slopes, cyan bars to their confidence limits and red and green circles to statistically significant Mann-Kendall trends at 95% and 90% confidence intervals, respectively. The size of the dots and circles is proportional to the length of the analyzed periods (5, 10 and 15 years).

Collaud Coen, M., et al. (2007), J. Geophys. Res., 112, D13213, doi:10.1029/2006JD007995.
Junker, C. et al. (2006), Atmos. Chem. Phys., 6, 1913-1925.
Bodhaine, B. (1983). J. Geophys. Res., 88, 753-768.

Soot absorption over Europe combining observations and models

E. Vignati[1], M. Schulz[2], F. Cavalli[1], T. Mueller[3], A. Virkkula[4], C. Lund Myhre[5], A. Wiedesohler[3] and P. Laj[6]

[1] European Commission, Joint Research Centre, Ispra, 21027, Italy
[2] Norwegian Meteorological Institute, Oslo, 0313, Norway
[3] Leibniz Institute for Tropospheric Research, Leipzig, 04318, Germany
[4] Finnish Meteorological Institute, Helsinki, 00014, Finland
[5] NILU-Norwegian Institute for Air Research, Kjeller, 2027, Norway
[6] Lab. de Glaciologie et Géophysique de l'Environnement- CNRS, St Martin d'Hères, 38402, France
Keywords: absorption, measurements, modelling, ACTRIS
Presenting author email: elisabetta.vignati@jrc.ec.europa.eu

An accurate estimate of the atmospheric aerosol direct effect on radiation is very important for the evaluation of the particle effect on climate. In particular, aerosol absorption contributes to the atmospheric warming and its quantification is still affected by high uncertainties. The principal light absorbing component is soot heating the atmosphere and thus playing an important role in the global climate system. The calculation of its radiative forcing strongly depends on absorption which in turn is a function of the spatial-temporal distribution of the aerosol mass, as well as the vertical distribution and the used radiative transfer scheme (Stier *et al*. 2007).

The aim of this work is to use *in-situ* measurements collected at European ground stations in the framework of the EU EUSAAR and ACTRIS projects to assess surface modeled concentrations and absorption coefficients from the global aerosol models participating in the AeroCom aerosol model inter-comparison (http://aerocom.met.no/Welcome.html). This is done using long-term elemental carbon (EC, as proxy for soot) concentrations and absorption coefficient measurements collected during 2008-2010 in the network of stations. The inter-comparison studies of instrumentations used for EC concentrations and absorption coefficient measurements allow determining uncertainties in the data sets in a homogeneous way (Müller *et al*., 2011).

The absorption coefficients were measured using MAAPs, aethalometers and PSAPs. Modeled absorption coefficients are given at 550 nm, therefore MAAP values (at 637 nm) had to be corrected for wavelength.

A preliminary comparison of model results to measurements shows a tendency of the models to overestimate EC concentrations in the remote stations in North Europe as well as in the more continental sites. The only exception is Ispra, a site at the edge of the polluted Po Valley (Italy) where the models do not capture the high concentrations in winter, most probably due to a wrong meteorological characterization in the models for this site. This European analysis confirms an evaluation of modelled black carbon prediction at global scale using previous versions of these models (Koch *et al*, 2009).

A novelty of this work is the evaluation of the schemes used in the models to compute the optical properties; it is done by looking at the ratio between the absorption coefficient and EC concentrations at the site were both are available, thus separating the model capability in predicting mass concentrations from the ability to calculate the absorption. The EUSAAR-ACTRIS dataset (available at http://ebas.nilu.no) is a unique collection that allows such an analysis with eight stations where this evaluation can be done. In Figure 1 some model results (green lines with symbols) are shown with the ratio observed in Ispra (blue line) for different seasons. The measured ratio has a seasonal variation with a maximum in summer. The models predict lower ratios up to a difference of a factor of 3-4 and this is independent from the modeled underestimation of EC concentrations at the site.

Such an analysis will be conducted for the eight stations to understand which factors in the calculations of the optical properties are responsible of the model behaviour.

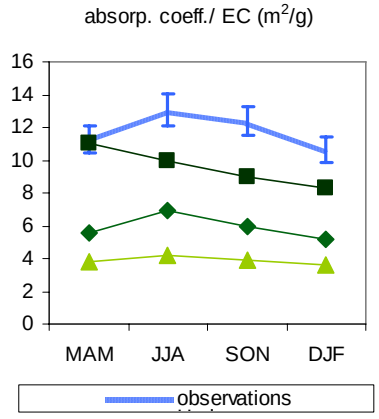

Figure 1. Seasonal ratio of absorption coefficient to EC at Ispra: observed and modelled (green lines) values

The research leading to these results has received funding from the EU 7th Framework Programme (FP7/2007-2013) under grant agreement n° 262254. The data providers of the stations and the AeroCom modelers are acknowledged for their contributions.

Koch et al, (2009) *Atmos. Chem. Phys* **9**, 9001-9026
Müller et al. (2011) *Atmos. Meas. Tech.* **4**, 245-268
Stier, P., Seinfeld J.H., Kinne S. and Boucher O. (2007) *Atmos. Chem. Phys.* **7**, 5237-5261

Merging air ion spectrometer and particle mobility size spectrometer measurements

H.E. Manninen[1], T. Petäjä[1], P. Aalto[1], W. Birmili[2], M. Kulmala[1] and A. Wiedensohler[2]

[1]Department of Physics, University of Helsinki, P.O. Box 64, 00014, University of Helsinki, Finland
[2] Leibniz Institute for Tropospheric Research, Permoserstraβe 15, 04303 Leipzig, Germany
Keywords: Aerosol instrumentation, Nucleation mode, Number size distribution, ACTRIS project.
Presenting author email: hanna.manninen@helsinki.fi

We investigate the possibility to study sub-10 nm number size distributions using a Neutral cluster and Air Ion Spectrometer (NAIS, Manninen et al. 2010) together with Mobility Particle Size Spetrometers (MPSP, Wiedensohler et al. 2010). Our objective within the ACTRIS project (WP3, Task 3.1) is to ensure the implementation of the existing standardized protocols for high-quality-assured and -controlled aerosol number size distributions in the network and to develop procedures for its extension to the nucleation mode range.

The most common method to measure ultrafine particle number size distribution is Differential Mobility Particle Sizer (DMPS) and Scanning Mobility Particle Sizer (SMPS) in the size range of 10-800 nm. In laboratory verifications, the number size distribution from 20 to 200 nm determined by mobility size spectrometers of different design are within an uncertainty range of ±10% after correcting internal particle losses, while below and above this size range the discrepancies increased (Wiedensohler et al., 2010). Prior to the NAIS measurements, the particle number size distribution was typically measured with MPSPs. The ion spectrometers are widely used in atmospheric nucleation studies in sub-10 nm size ranges due to their ability to measure down to molecular sizes. With the NAIS, ions are measured in the size range of 0.8–42 nm, whereas total (i.e. charged plus neutral) particles are detected in the range of ~2–42 nm.

The electrical detection of sub-10 nm particles is a challenging task due to small concentrations, transport losses, and insufficient charging efficiency of small neutral particles. Thus, electrical instruments need to be sensitive enough to distinguish the minuscule signal brought in by the small particles from the instrument background. To tackle the difficulties in the electrical techniques, high flow rates are used to minimize the ion diffusion losses and also increase the sensitivity to the ion concentrations. By utilizing a unipolar charger, the charging efficiency can be improved by employing high ion concentrations. However, high particle loss within the charger, resulting in a small percentage of charged particles exiting the chargers, is typically the case for unipolar chargers.

The NAIS was calibrated and intercompared, and found to be in good agreement with the reference instruments both in the laboratory and in the field (Asmi et al., 2009). It was concluded that NAIS can be reliably used to measure small atmospheric ions and particles directly at the sizes where nucleation mode begins. Several NAIS systems have already been deployed simultaneously at 12 European measurement sites in parallel with MSP's within the EUCAARI project (Manninen et al., 2010) to quantify the spatial and temporal distribution of particle formation events. New Particle Formation (NPF) occurs when nucleated particles grow to detectable size range. Typical MSP particle size distributions together with NAIS derived ion distributions from Hyytiälä during NPF are presented in Fig. 1 which shows the particle and ion size distributions in the size range of 2-1000 nm and 0.8-40 nm, respectively, during 8–13 April 2007 in Hyytiälä, Finland. Our aim is to write a standard operating procedure for sub-10 nm particle number size distribution measurments.

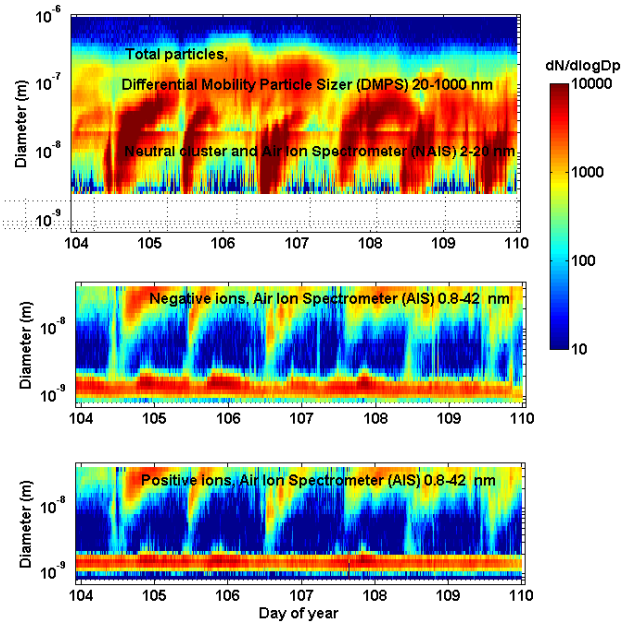

Figure 1. Particle number size distribution measured with the NAIS in the size range 0.8–20 nm and with a DMPS in the size range 20–1000 nm (top). Negative (middle) and positive (bottom) ion distributions were also measured with the NAIS (0.8–42 nm). NB: no fitting applied when merging the NAIS and DMPS data.

This work was supported by the Research Infrastructure for Atmospheric Research program under the EU FP7, ACTRIS Contract No.262254.

Asmi, E. et al. (2009) *Atmos. Chem. Phys*., 9, 141-154.
Manninen, H. E. et al. (2010) *Atmos. Chem. Phys.*, 10, 7907-7927.
Wiedensohler, A. et al (2010) *Atmos. Meas. Tech. Discuss.*, 3, 5521-5587.

Retrieval of aerosol microphysical properties profiles by combination of Lidar and sun photometer measurements. Application to mineral dust and volcanic aerosols.

M.J. Granados-Muñoz[1,2], J.A. Bravo-Aranda[1,2], F. Navas-Guzmán[1,2], J.L. Guerrero-Rascado[1,2], H. Lyamani[1,2], A. Chaikovsky[3], J. Wagner[4], U. Wandinger[4], F.J.Olmo[1,2] and L. Alados-Arboledas[1,2].

[1]Centro Andaluz de Medio Ambiente, Junta de Andalucía, Universidad de Granada, Avda. del Mediterráneo s/n, 18006-Granada, Spain.
[2]Departamento de Física Aplicada, Universidad de Granada, Avda. Fuentenueva s/n, 18071- Granada, Spain.
[3]Institute of Physics National Academy of Sciences, 68, Scaryna ave., 220072, Minsk, Belarus.
[4]Leibniz Institute for Tropospheric Research, Permoserstraße 15, D-04318 Leipzig, Germany.

Keywords: lidar, sun photometer, microphysical profile.
Presenting author email: mjgranados@ugr.es

Sun photometers are a widespread tool to retrieve column integrated values of aerosol optical, microphysical and radiative properties. Lidars are powerful systems that allow for the vertical profiling of aerosols in the atmosphere. However, microphysical properties profiles are not easy to derive from lidar data. Within the frame of the European project ACTRIS (Aerosols, Clouds, and Trace gases Research InfraStructure Network) there are several working packages. Particularly WP20 includes the objective of developing tools that combine AERONET sun photometers measurements and EARLINET multiwavelength lidar data to obtain vertical profiles of aerosol microphysical properties. The retrieval algorithm developed in the National Academy of Sciences of Belarus is used in this study (Chaikovsky *et al.*, 2008).

The CEAMA station, in Granada (37.2ºN, 3.6ºW, 680 m a.s.l.), is equipped with a multiwavelength Raman lidar LR331D400 (Raymetrics S.A., Greece) and a collocated sun photometer (CIMEL Electronique). This station is part of the EARLINET and AERONET networks. It presents the advantage that during summer, an additional sun photometer is placed in Sierra Nevada, near the station, but at higher altitude (1800 m a.s.l.).

In this work, the combined retrieval algorithm is applied to lidar and sun photometer data to obtain vertical profiles of aerosol concentration in fine and coarse (spherical and spheroid) modes. The results are compared with simultaneous columnar size distributions obtained from the Cimel radiometers at two different height levels, for this purpose the retrieval algorithm proposed by Olmo *et al* (2006) has been used.

Several cases have been analyzed. Thus, vertical profiles of volume concentrations for fine and coarse modes are obtained during a Saharan dust outbreak on 30 June 2011(Figure 1). During this event, a plume from the Nabro volcano is also observed at 17 km a.s.l. A clear predominance of the coarse spheroid mode has been detected along the column, except for the volcanic plume, where the retrieval procedure determines a mixture of fine and coarse particles. Size distributions provided by the sun photometer at the high mountain place shows agreement with the retrieved concentration profiles. The retrieval procedure has also been applied to some backscatter profiles acquired during the arrival of the Eyjafjallajökull volcanic plume at Granada. Evolution of the retrieved profiles of fine and coarse concentration illustrates the changing contribution of ashes and sulphates to the volcanic plume during 7-8 May 2010.

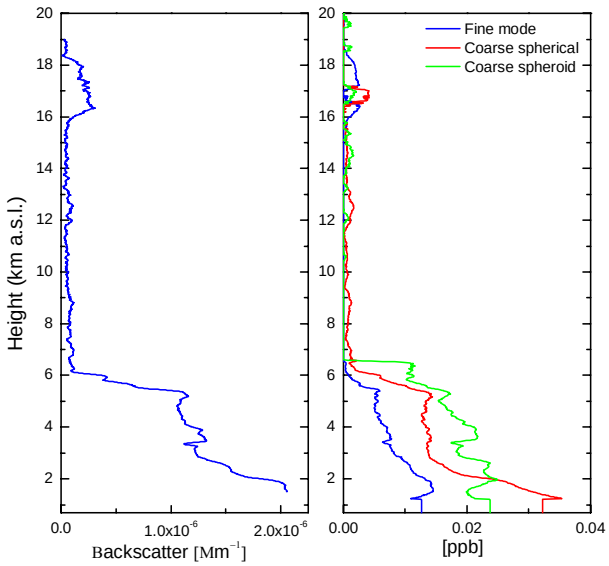

Figure 1. (left) Backscatter profile at 532 nm for 30 June 2011 between 20:00 and 20:30. (right) Vertical profile of the aerosol volume concentration in the fine, coarse spherical and spheroid modes for the same period.

This work was supported by the Andalusia Regional Government through projects P08-RNM-3568 and P10-RNM-6299, by the Spanish Ministry of Science and Technology through projects CGL2010-18782, CSD2007-00067 and CGL2011-13580-E/CLI; and by EU through ACTRIS project (EU INFRA-2010-1.1.16-262254). Mrs. Granados-Muñoz is funded by the Spanish Ministry of Education under grant AP2009-0552.

Chaikovsky, A., Dubovik, O., Goloub, P., Balashevich, N., Lopatsin, A., Karol, Y., Denisov, S., and Lapyonik, T. (2008). Technical report, Institute of Physics, National Academy of Sciences of Belarus, Minsk, Belarus.

Olmo, F.J., Quirantes, A., Alcántara, A., Lyamani, H., and Alados-Arboledas, L. (2006). J. Quant. Spectros. Radiat. Transfer, 100 (1-3), pp. 305-314.

Optical and microphysical characterization of volcanic sulphate particles in the lower troposphere by Raman lidar

F. Navas-Guzmán,[1,2] D. Müller,[3,4,*] J. A. Bravo-Aranda,[1,2] D. Pérez-Ramírez[1,2], F.J. Olmo[1,2], J.L. Guerrero-Rascado[1,2], U. Wandinger[4] and L. Alados-Arboledas[1,2]

[1]Centro Andaluz de Medio Ambiente, University of Granada, Junta de Andalucía, Granada, 18006, Spain
[2] Department of Applied Physic, University of Granada, Granada, 18071, Spain
[3]Gwangju Institute of Science and Technology (GIST), 1 Cheomdan-Gwagiro (Oryong-dong), Buk-Gu, Gwangju 500-712, Republic of Korea
[4]Leibniz Institute for Tropospheric Research (IfT), Permoserstrasse 15, 04318, Leipzig, Germany
* now at: Science Systems and Applications, Inc, 1 Enterprise Parkway, Hampton, VA 23666, USA
Keywords: Raman lidar, microphysical properties, volcanic sulphate particles.
Presenting author email: fguzman@ugr.es

The Eyjafjallajökull volcanic particles have been characterized with remote sensing techniques at different locations in Europe. A unique combination of Raman lidar, sun- and star-photometer is used in this work in order to characterize the optical and microphysical properties of the volcanic plume that was observed over Granada (Spain, 37.16º N, 3.6º W, 680 m height above sea level (asl)) from 5 to 8 May 2010. Our study reveals that mainly sulphate and sulphuric-acid particles were at least episodically present over Southwest Europe. Previous studies of volcanic plumes (*Mattis et al.*, 2010; *Wandinger et al.*, 1995) dealt with the characterization of sulphuric-acid droplets in the lower stratosphere and upper troposphere only. Additional importance of our study therefore arises from the fact that, to our knowledge, this is the first time that an optical and microphysical characterization of these particles has been performed in the lower troposphere with a multiwavelength Raman lidar.

Particle effective radius was derived with an inversion algorithm (Müller *et al.*, 1999). The methodology used to retrieve microphysical properties is based on the spectral information contained in the backscatter and extinction data at multiple wavelengths and its change with particle size. Actually, an important effort is being made within the frame of the European project ACTRIS (Aerosols, Clouds, and Trace gases Research InfraStructure Network) in order to retrieve microphysical properties from lidar techniques.

On 7 May, an increase in the AOD at 440 nm was observed, reaching maximum values (around 0.45) during night time. The corresponding Ångström exponent (AE) was in the range of 1.2-1.3, indicating a predominance of the fine-mode particles. An increase in the accumulation mode was also observed between the morning of 7 May and the morning of 8 May. Lidar observations allowed us to characterize the volcanic layers during the night from 7 to 8 of May 2010. Lidar ratio values were around 55 sr at 355 and 532 nm in the volcanic layers decoupled of the Planetary Boundary Layer. The large Ångström exponents and low linear particle depolarization ratios (4-7%) indicate the presence of small and spherical particles. The particle effective radii ranged between 0.30-0.55 μm. In situ instrumentation confirmed an increase of sulphate particles at ground level during this period.

Figure 1 shows effective radius versus the lidar ratio at 355 nm retrieved for different layers during this volcanic event. They are compared with fresh smoke particles measured at Granada and stratospheric volcanic particles observed over Leipzig (Mattis *et al.*, 2010). We can see that effective radii of the volcanic particles observed at our station are bigger than the effective radii of fresh smoke and stratospheric volcanic particles. A large variability of the lidar ratio at 355 nm is observed for the volcanic particles observed at Granada, ranging from 34 to 67 sr. These values are very similar to those observed for volcanic aerosol coming from different eruptions over Leipzig.

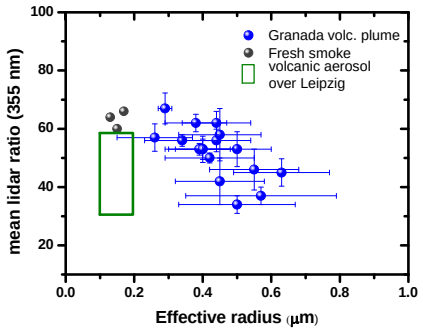

Figure 1. Effective radius versus lidar ratio at 355 nm for different types of aerosols.

Aknowledgments: This work was supported by the Andalusia Regional Government through projects P08-RNM-3568 and P10-RNM-6299, by the Spanish Ministry of Science and Technology through projects CGL2010-18782, CSD2007-00067 and CGL2011-13580-E/CLI; and by EU through ACTRIS project (EU INFRA-2010-1.1.16-262254)

Mattis, I. *et al.*(2010), *Journal Geophysical Research*, **115**, D00L04.
Müller, D. Wandinger, U. and Ansmann, A. (1999), *Applied Optics*, **38** (12), 2346-2357.
Wandinger, U., Ansmann, A. Reichardt, J. and Deshler, T. (1995), *Applied Optics*, **34** (36), 8315-8329.

ACTRIS Data Centre: An atmospheric data portal

Cathrine Lund Myhre[a], Aasmund Fahre Vik[a], Robert Logna[a], Kjetil Tørseth[a], Holger Linné[b], Ewan O'Connor[c]
[a]NILU - Norwegian Institute for Air Research, P.O. Box 100, N-2027 Kjeller, Norway
[b] Max-Planck Institute for Meteorology, Hamburg, Germany
[c] Department of Meteorology, University of Reading, Reading, United Kingdom

Keywords: measurements, data access, ACTRIS
Presenting author email: clm@nilu.no

The ACTRIS data centre (ACTRIS DC) provides free and open access to all data resulting from the ACTRIS infrastructure network, complemented with data from other relevant networks and data bases. The ACTRIS activities result in improved atmospheric measurement and data from more than 60 European sites, from numerous instruments and includes variables measured by ground based *in situ* and remote sensing technologies. Core variables are *in situ* aerosol optical, physical and chemical properties, short-lived trace gases (volatile organic carbon and nitrogen oxides), aerosol scattering and extinction profiles, and various cloud properties.

The backbone of the ACTRIS DC is the three core data bases:

- EARLINET Data Base hosting aerosol lidar data from more than 30 European sites
- EBAS hosting ground based atmospheric *in situ* data from more than 1000 sites globally
- Cloudnet hosting remote sensing cloud data and products from 5 European sites

A joint data portal is developed to combine information from various data sources to gain new information not presently available from standalone databases or networks. The data centre will also provide tools and services to facilitate the use of measurements for broad user communities. Higher level and integrated products will be developed stage-by-stage during the project, based on user requirements, interactions and feedbacks.

The first version of the ACTRIS DC allows users to search for atmospheric composition data from a multitude of data archives through a single user interface. Examples of data bases and frameworks included are EMEP, the GAW- world data centres, EARLINET, NDACC, CARIBIC-GEOmon, HTAP, AMAP amongst others. Currently the portal provides an overview of more than 800 000 data sets from almost 1700 different locations and more than 20 data bases/frameworks globally. For some of the databases included in the portal, the interface allows you to download data directly through the portal. A map functionality is implemented facilitating the identification of data and making it possible to search for collocation of observations, variables and sites both in time and space. The upper panel of Figure 1 shows the front page of the data portal, and the lower panel shows location of absorption coefficient (violet), scattering coefficient (green), and where both is available at same site (light blue).

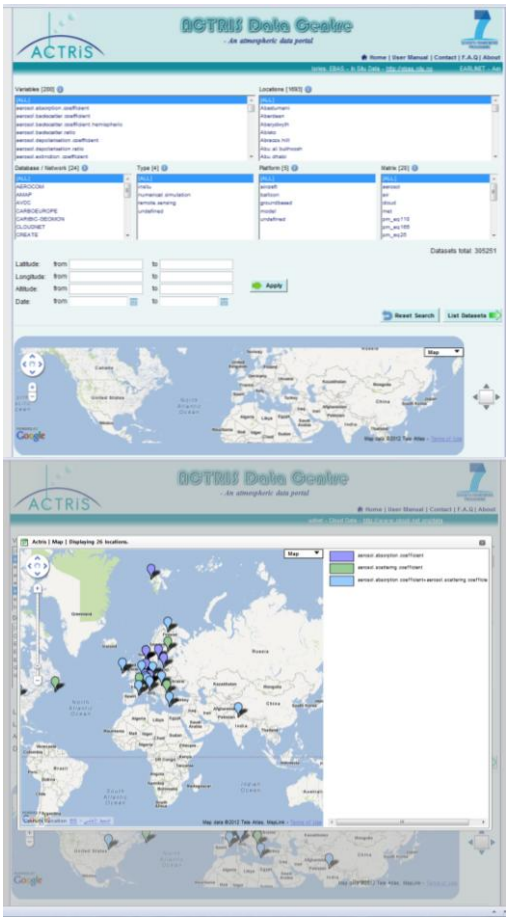

Figure 1: Examples from the ACTRIS joint data portal. Upper panel: front page, Lower panel: available absorption and scattering coefficient collocation of sites.

The data portal can serve as "one-stop-shop" of atmospheric high-quality data, also for larger data volumes. The portal will also offer a direct interface towards external users like the MACC II project and GMES in-situ. The data dissemination will take into account the principles outlined in SEIS, INSPIRE, WIS and GEOSS.

The presentation will explain and demonstrate the ACTRIS DC with the goal to strengthen the dialog with users for further development of the data centre in ACTRIS.

The research leading to these results has received funding from the European Union Seventh Framework Programme (FP7/2007-2013) under grant agreement n° 262254."

Tuesday, September 4, 2012

Session WG02S3O. Urban Aerosol in Large Cities (I)

Spatial distribution of particle number concentrations measured with the AERO-TRAM

B. Vogel, R. Hagemann, R. Rinke, A. Wieser, U. Corsmeier, Ch. Kottmeier
Institute for Meteorology and Climate Research, Karlsruhe Institute for Technology,
Hermann-von-Helmholtz-Platz 1, 76344 Eggenstein-Leopoldshafen, Germany
Keywords: urban aerosols, mobile measurements, air quality.
Presenting author email: bernhard.vogel@kit.edu

The spatial and temporal variation of selected aerosol and gas phase parameters is assessed in long term measurements for the Karlsruhe (Germany) area with an automated self calibrating mobile laboratory. As measurement platform a tramway (AERO-TRAM) operating in the public transport is used. Beside the gas phase components O_3, CO, CO_2, NO, and NO_x particle number density and particle number distributions are measured. For the year 2010 measurements on more than 2300 runs are obtained resulting in an extraordinary dataset for ground based mobile applications. The AERO-TRAM operates on two selected lines. Both lines connect the rural and suburban hinterland of Karlsruhe with the city centre. They are crossing areas with high concentrations of particles and trace gases and areas where only background concentrations are expected. Therefore, the obtained comprehensive dataset is useful for determining regional variation of particles and trace gases as well as for the identification of source areas.

The analysis of the measured number densities gives a concentration gradient between the city centre and the suburban areas of only 30 %. In comparison the NO_x concentrations are about 50 % lower in the suburban.

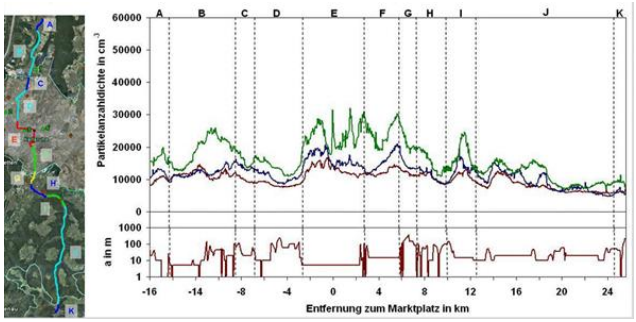

Figure 1. Median of the running mean of the particle number density for 2010 at different stability conditions. Green = stable stratification, blue = neutral stratification, red = unstable stratification (upper panel). Distance of the track to the next road (lower panel).

Figure 1 shows the distribution of the median of a running mean of number density for the year 2010 along the track and its dependence on the turbulence conditions. It can be seen that there is no remarkable gradient of the number densities between the distinct regions but the concentration level differs up to a factor of 2 in depending on the turbulence state of the atmosphere. This shows the difficulty of measuring an effect of emission reduction measures. Figure 2 gives the median values as a function of the wind velocity. As expected these concentrations are lower for the higher wind speeds but there is no uniform behaviour for the different areas. In the city centre there is almost no effect visible whereas in the northern vicinity the concentration level is considerable higher for the lower wind speeds.

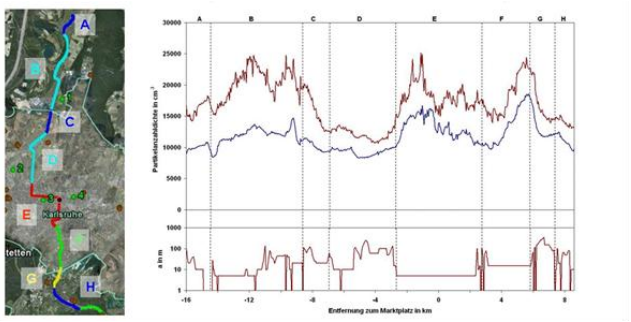

Figure 2. Median of the running mean of the particle number density for 2010 at different ranges of wind velocity. Red = 1-5 m s^{-1}, blue = > 5 m s^{-1} (upper panel). Distance of the next road (lower panel).

The investigation of the influence of the wind directions shows the impact of elevated single sources in the area on the number densities that so far could not be detected by the standard monitoring stations in that area.

SAPUSS: Solving Aerosol Problems by using synergistic strategies in Barcelona, Spain

Manuel Dall'Osto[1,2,4], A. Alastuey[1], M. A. Pedemonte[1], B. L. van Drooge[1], M. Pandolfi[1], M. C. Minguillon[1], F. Amato[1], T. Moreno[1], J. Pey[1], C. Reche[1], M. Cusak[1], M. Viana[1], A. Roca[1], J . Gietl[2], D. Beddows[2], Roy M. Harrison[2], J. Wenger[3], E. Mc Gillcuddy[3], J. Sudou[3], R. Healy[3], D. Ceburnis[4], G. Martucci[4], C. O'Dowd[4], F. Lucarelli[5], S. Nava[5], J. L. Jimenez[6], F. Gomez Moreno[7], B. Artinono[7], A. S. H. Prevot[8], L. Pfaffenberger[8], S. Frey[9], F. Wilsenack10, S. Ng[11], D. Worsnop[11], D. Casabona Fina[12], P. Jiménez Guerrero[13] and X. Querol[1]

(1) IDAEA-CSIC, Barcelona (Spain), [IDAEA-CSIC, C/ LLuis Solé i Sabarís s/n 08028 Barcelona, Spain. Tel: +34 93 409 5410, Fax: +34 93 411 0012, e-mail: manuel.dallosto@gmail.com] **(2)** University of Birmingham (UK), **(3)** University of Cork (Ireland), **(4)** NUIG Galway (Ireland), **(5)** University of Florence (Italy), **(6)** University of Colorado (USA), **(7)** CIEMAT, Madrid (Spain), **(8)** PSI (Switzerland), **(9)** Jenoptic (Germany), **(10)** Wehrwissenschaftliches Institut für Schutztechnologien (Germany), **(11)** Aerodyne inc (USA), **(12)** Area de Medi Ambient, Diputació de Barcelona (Spain), **(13)** Universidad de Murcia (Spain)

Keywords: chemical composition, hourly resolution, $PM_{2.5}$, urban aerosols.

Compared to other European regions, the metropolitan area of Barcelona sees relatively high particulate matter due to high anthropogenic emissions, a dry and warm Mediterranean climate and low dispersive conditions due to a unique topographical situation. State-of-the-art instruments such as particle mass spectrometers have been only recently deployed in the Southern and Western European regions. During the autumn of 2010, the SAPUSS experiment took place, involving measurements of aerosols with multiple techniques occurring simultaneously in order to deduce point source characteristics and to understand the atmospheric processes responsible for their modifications. Five sites were used: a main road, an urban background site, a regional background site and two towers within the city (150m and 450m above sea level, respectively, Figure 1). The use of the synergy of highly time-resolved instruments (such as 2 Aerosol Time-of-flight Mass Spectrometer and 2 HR-Aerosol Mass Spectrometer – ATOFMS and AMS) was coupled with traditional off-line techniques (11 high-volume samplers) in order to deduce all the information provided by them. The about 600 filters obtained during SAPUSS were analyzed by GC-MS, ICP-MS, ICP-AES and EC/OC analysis. A vast number of instruments were also deployed to characterize simultaneously all five sampling sites at hourly resolution, including black carbon, particle number and mass concentrations and size-resolved concentrations. Two cielometers were used simultaneously horizontally and vertically in order to get close to the full picture of the dynamics of the urban boundary layer.

This presentation aims: to present 3D distribution of PM_1, $PM_{2.5}$ and PM_{10} across Barcelona under different boundary layer conditions; to elucidate the fate of nanoparticles in the urban atmosphere – focusing on the evaporation of freshly traffic generated particles and the nucleation occurring at different altitudes within the urban boundary layer; to quantify the contribution of exaust and non-exaust traffic generated particles in the road site relative to the urban background; to understanding the physical and chemical differences of the aerosols detected at ground level and above the city. PMF results of co-located HR-TOF-AMS and ATOFMS mass spectrometers results are also shown, trying to elucidate further insights on cooking aerosols sources.

Simultaneous Single Particle Mass Spectrometry Measurements at Two Different Urban Sites and Comparison with Quantitative Techniques

Eoin McGillicuddy [1], Manuel Dall'Osto [2], Franco Lucarelli [3], Silvia Nava [4], Xavier Querol [2], Roy M. Harrison[5], Johanna K. Gietl[5], David C. S. Beddows[5], Deborah Gross [6], Robert Healy [1], John Wenger [1], John Sodeau [1].

[1] Department of Chemistry and Environmental Research Institute, University College Cork, Ireland
2Institute for Environmental Assessment and Water Research (IDAEA-CSIC), Barcelona, Spain
[3] Dipartimento di Fisica e Scienze dello Spazio, Universita degli Studi di Firenze, Via Sansone 1, 50019 Sesto Fiorentino, Italy
[4] INFN, Istituto Nazionale di Fisica Nucleare, Sezione di Firenze, Via Sansone 1, 50019 Sesto Fiorentino,Italy
[5]National Centre for Atmospheric Sciences, Division of Environmental Health and Risk Management, School of Geography, Earth & Environmental Sciences, University of Birmingham, United Kingdom
[6] Department of Chemistry, Carleton College, 1 N. College Street, Northfield, MN 55057, USA

Keywords: Aerosol mass spectrometry, Single particle analysis, Urban aerosols, PIXE.
Presenting author email: e.j.mcgillicuddy@mars.ucc.ie

Two Aerosol Time-of-Flight Mass Spectrometers (TSI ATOFMS) were deployed in Barcelona (Spain), during the SAPUSS (Solving Aerosol Problems by Using Synergistic Strategies) field campaign in autumn 2010. One ATOFMS, operated with a nozzle inlet, was deployed at an Urban Background (UB) site while the second one, operated with an aerodynamic lens, was located at a Roadside site (RS)

During the SAPUSS campaign the ATOFMS at UB and RS collected 274,974 and 1,042,331 single particle dual ion mass spectra respectively. The single particle mass spectra were subsequently analysed by using the ART-2a algorithm. Single particle mass spectra from the UB ATOFMS were also imported into ENCHILADA (Environmental Chemistry through Intelligent Data Analysis), a freeware single particle data analysis software package (Gross, Atlas et al. 2010) and clustered using the *K*-means algorithm, (*K*=80).

Several particle types were identified at both sites and assigned to both transported and local sources, including biomass burning, fossil fuel combustion, industrial processes, wind-blown dust, and sea salt. During the clustering analysis it was found that RS had a higher number of particle types (19) relative to the UB one (14). Along with the mass spectra, size ranges, temporal trends, wind direction and HYSPLIT back trajectories were also used to assist with source identification of each particle type.

Both ATOFMS datasets obtained were inter-compared with hourly average concentrations of numerous elements present in $PM_{2.5}$ collected with streaker samplers which were also simultaneously located at both sites. The $PM_{2.5}$ fraction was subsequently analysed using Particle-Induced X-ray Emission (PIXE) (Chiari, Lucarelli et al. 2005). Na, K, Ca, Ti, V, Cr, Mn, Fe, Zn and Pb measured by The PIXE data was used to validate the metal ion intensity temporal trends produced by the ATOFMS. Following the approach of Snyder el al (2009) we extend it for both type of instruments, and we extensively expand the number of data point with a data point for each hour of the campaign. The dual ion mass spectra measured by the ATOFMS provide information on the mixing state of the metal-containing particles and can thus facilitate identification of the particle sources. It was observed from the inter-comparison of the two techniques at the UB site that iron had inputs from both crustal and industrial sources. Manganese and lead occur with a similar temporality and the peaks in both elements belong to the same particle class, and are internally mixed. The source of vanadium appears to be from the combustion of heavy fuel oil such as that used in shipping.

Chiari, M., F. Lucarelli, et al. (2005). "Characterization of airborne particulate matter in an industrial district near Florence by PIXE and PESA." X-Ray Spectrometry **34**(4): 323-329.

Gross, D. S., R. Atlas, et al. (2010). "Environmental chemistry through intelligent atmospheric data analysis." Environmental Modelling & Software **25**(6): 760-769.

Hourly elemental concentrations at two different urban locations in Barcelona, Spain

F. Lucarelli[1], S. Nava[1], G. Calzolai[1], M. Chiari[1],
M. Dall'Osto[2], X. Querol[2]
[1]Department of Physics and Astronomy, University of Florence & INFN, Sesto Fiorentino, 50019, Florence, Italy
[2]Institute for Environmental Assessment and Water Research (IDAEA-CSIC), Barcelona, Spain

Keywords: chemical composition, hourly resolution, $PM_{2.5}$, urban aerosols.
Presenting author email: lucarelli@fi.infn.it

The present study aims at evaluating the impact on PM chemistry of the emission sources present in the urban area of Barcelona. The vast majority of results in literature are limited to time resolution of the input samples typically 12 or 24 h. However, source emissions can heavily affect air quality with very high loading of toxic elements during a few hours: the knowledge of the timing and the intensity of certain episodes may be important for the assessment of human exposure as well as for source identification and apportionment. The novelty of this study stands on the hourly-resolved PM speciation data which can be a powerful tool to determine the source origin of atmospheric pollutants in urban environments.

Two different sites (a road site and an urban background site; RS and UB, respectively) were used within the SAPUSS (Solving Aerosol Problems by Using Synergistic Strategies) project, a European Union project involving measurements of aerosols with multiple techniques occurring simultaneously.

During SAPUSS campaign, PM2.5 samples with 1-hour resolution were collected between September 27, 2010 and October 19, 2010 for a total of 528 hours by a streaker sampler (PIXE International Corporation). Data coverage during this period was 80% at the UB and 57% at the RS. The overlap between the two sites was higher than 98%, making 57% of the time having simultaneous measurements. The PIXE analysis of these samples was done with the external beam set-up at the INFN LABEC laboratory in Florence; it allowed the assessment of hourly resolution elemental time trends of 17 elements: Na, Mg, Al, S, Cl, K, Ca, Ti, V, Cr, Mn, Fe, Ni, Cu, Zn, Sr, Pb.

Several results will be discussed, for example: Cu diurnal profiles exhibited daily variations with peaks during traffic rush hours; Al showed a peak from October 8 till October 10, due to a Saharan dust intrusion; Zn showed peaks both in the morning and in the night, typical of an industrial source.

Positive Matrix Factorisation (PMF) was applied to the whole data set. Input data were prepared using the procedure suggested by Polissar and PMF results for multiple values of FPEAK were systematically explored to find out the most reasonable solution. Nine factors were found in both sites (in parenthesis the specific markers):

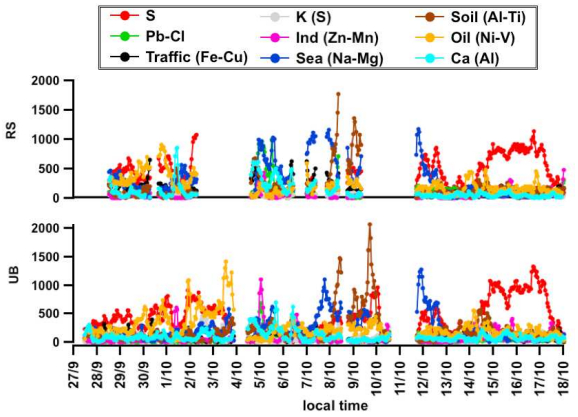

Figure 1: Hourly resolution time trend of the aerosol sources identified by PMF.

Regional sulphates (S); *two industrial sources*, one with Zn, Mn and a bit of Pb, a second one with Pb-Cl (also supported by concomitant single particle ATOFMS measurements); *traffic* (Fe-Cu and some Ca), as primary non exhaust particles; *Biomass burning* (K); *aged marine aerosol* (Na-Mg); *oil combustion* (V-Ni) with a small contribution from combustion (S); *two soil sources*, one characterized by Al-Ti (Saharan dust) and some Ca, whose temporal pattern clearly reflects a strong Saharan influence, the other characterized by Ca with small contribution of Al and Ti, with a time pattern which is a combination of traffic in the morning at RS, yet spiking in the afternoon at the UB, reflecting higher wind speed and contribution from construction activity. Strong correlation among RS and UB sites for some of the nine different PM sources supports the validity of the PMF solution, as well as regionality fingerprint associated with some of the sources.

The three different dust sources (Saharan dust, soil and primary non-exhaust particles) have an important contribution on the total measured mass of the 17 elements (12%, 6% and 7% of the total elements measured, respectively). However, neither primary non-exhaust traffic dust nor soil dust was found correlated with wind speed or with traffic counts, suggesting the resuspension of dust may have more complex relations linked to both wind speed, wetness conditions and traffic counts altogether.

Seasonal comparison of comprehensive aerosol measurements in London during ClearfLo

D.E. Young[1], J.D. Allan[1,2], P.I. Williams[1,2], M.J. Flynn[1], D. Liu[1], J.D. Whitehead[1], N.H. Robinson[1], A.S.H. Prevot[3], S. Visser[3], M. Furger[3], M.W. Gallagher[1], and H.Coe[1]

[1]School of Earth, Atmospheric and Environmental Sciences, University of Manchester, Oxford Road, Manchester, M13 9PL, UK
[2]National Centre for Atmospheric Science, University of Manchester, Oxford Road, Manchester, M13 9PL, UK
[3]Laboratory of Atmospheric Chemistry, Paul Scherrer Institut, 5232 Villigen, Switzerland
Keywords: urban aerosols, air quality, seasonal characteristics, Aerosol Mass Spectrometer.
Presenting author email: dominique.young@postgrad.manchester.ac.uk

Elevated aerosol concentrations are frequently associated with atmospheric pollution and have serious implications for air quality, particularly in cities (Mayer, 1999). At present, the dominant source of primary particulates is the transport sector although there are many other causes of air pollution including solid fuel burning and cooking. The effects of aerosols on health and the mechanisms by which they occur are not well understood. The size distribution, chemical composition, and mixing state of atmospheric aerosols also influence their effect on climate (Forster *et al*, 2007), however the exact impacts of aerosols are difficult to determine due to their complex nature. Examination of various aerosol properties and how aerosols change spatially and temporally is essential for refining the quantification of aerosol effects in climate models, health policies, and legislations.

A suite of state-of-the-art instrumentation, measuring aerosols, gases, radicals and meteorological parameters was deployed as part of the Clean Air for London (ClearfLo) campaign for two major intensive observation periods (IOPs) during 2012 at a number of sites in and near London. One of the major aims of ClearfLo is to characterise the spatial and temporal evolution of boundary layer pollution in London. Here we report aerosol composition measurements from the main ClearfLo urban background supersite located in the grounds of a school in North Kensington, London for both of the four-week IOPs, which took place during different seasons. The winter IOP took place between 11 January and 8 February, a time when primary emissions dominate the aerosol loading, and the summer IOP took place between 18 July and 22 August, covering the 2012 Summer Olympic period. Measurements took place during both clean westerly conditions and more polluted conditions when transported European plumes influenced the site.

Comprehensive measurements of size segregated aerosol chemical composition, microphysical properties, and optical properties were taken to obtain high-resolution data sets on aerosol composition in conjunction with black carbon properties and hygroscopicity. Instrumentation included a 7-wavelength Aethalometer, Aerosol Particle Sizer (APS), Aerosol Particle Spectrometer with Depolarization (APSD), Condensation Cloud Nucleus counter (CCNc), Differential Mobility Particle Sizer (DMPS), GRIMM dust monitor, Hygroscopicity Tandem Differential Mobility Analyser (HTDMA), Multi Angle Absorption Photometer (MAAP), PhotoAcoustic Soot Photometer (PASS), Single Particle Soot Photometer (SP2), and a Soot Photometer Aerosol Mass Spectrometer (SP-AMS). In addition, a GRIMM dust monitor, a Wide Issue UV Fluorescence Bioaerosol Spectrometer (WIBS) and a Rotating Drum Impactor (RDI) were located on the container's exterior. The RDI samples were subjected to Synchrotron Radiation induced X-Ray Fluorescence Spectrometry (SR-XRF) analysis to determine trace elemental composition. A compact Time-of-Flight Aerosol Mass Spectrometer (cToF-AMS) was housed in the permanent monitoring station from January until August covering both IOPs providing long term measurements of aerosol chemical composition.

Preliminary data from both ClearfLo IOPs along with data from the long-term cToF-AMS measurements will be presented (Fig. 1), highlighting diurnal and seasonal characteristics of London urban background pollution. These data will be used to quantify the contribution by different urban activities in London to both local and regional air pollution.

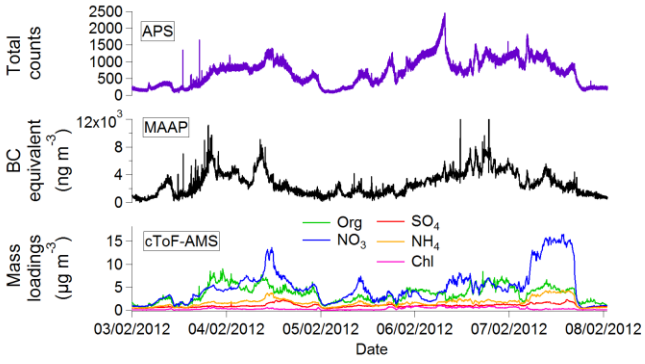

Figure 1. Preliminary data from the cToF-AMS, MAAP, and APS covering six days during the winter IOP with both relatively high and low aerosol concentrations.

This work was supported by the UK Natural Environment Research Council under grants NE/H003150/1 and NE/H008136/1.

Mayer, H. (1999), *Air pollution in cities*, Atmospheric Environment, **33**, 4029-4037.

Forster, P. *et al* (2007), *Changes in Atmospheric Constituents and in Radiative Forcing. In: Climate Change 2007:The Physical Science Basis.* Cambridge University Press, Cambridge, United Kingdom and New York, NY, USA.

A mobile measurement network for ultrafine particulate matter in the city of Zürich

A. Richard, P. Steigmeier, H. Burtscher and M. Fierz
University of Applied Sciences and Arts Northwestern Switzerland, Institute of Aerosol and Sensor Technology, 5210 Windisch

Keywords: Ambient aerosol measurement, Air quality network, Fine particulate matter, Number concentration
Presenting author email: agnes.richard@fhnw.ch

A mobile measurement network with ten miniDiSC devices is set up in the city of Zürich, Switzerland to assess the spatial and temporal evolution of ultrafine particle number concentrations. MiniDiSCs (Fierz, 2011) measure the number concentration of ultrafine particulate matter (size range 10-300nm), its average particle diameter and the lung deposited surface area with a time resolution of one second. The devices are installed on trams frequenting the main streets in Zürich as well as carried by deliverymen on bicycles, which drive along narrower streets.

A GPS/GPRS extension of the devices enables the transmission of measured data as well as its current location to a central web-server, where it is available online in real time. Measurement data in combination with the location can be viewed in Google Earth and are made publicly available on the project homepage: https://feinstaub.cs.technik.fhnw.ch/feinstaubmessnetz/.

In contrast to stationary measurements such a moving measurement network allows for capturing a more complete picture of different pollution scenarios within a city.

The project is a cooperation with the openSense network of ETH Zürich (Aberer, 2010), which is part of the Nano-Tera program, dealing with wireless sensor networks and publishing of sensor data on the internet. In the framework of this project CO, NO_2 and O_3 sensors are also positioned on the trams, which will finally complement the particle number concentration data.

Data will be divided into subsets to assess diurnal, weekly and seasonal variations as well as changes due to different meteorological situations. For this purpose the miniDiSC data will be compared to meteorological data such as temperature, wind direction, wind speed and precipitation. With measurements throughout the year 2012, seasonal variations can be examined.

Through the combination of the information about the position of the devices and the number concentration, pollution maps can be generated. Since concentrations rapidly change over relatively small distances a large repetitive data set is needed. The measurement period will last for approximately one year, such that enough data will be available to obtain a representative mean for each point along the paths.

Eventually, the measurements will be used to generate such a pollution map. This pollution map will be based on calculations with the Kriging algorithm (Pebesma, 2004) and will possibly also include information about the urban road system.

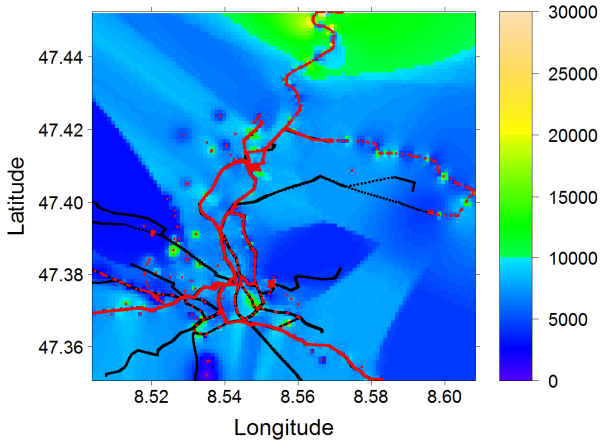

Figure 1.: First Kriging calculations with particle number concentration data obtained from tram rides on two different tram lines (data from Sept 2011 – Jan 2012). The red lines depict the two tram lines and the black ones show all tram lines in Zürich, which will also be frequented in a later stage of the project.

Figure 1 shows an example of a first Kriging calculation with the first particle number concentration data obtained during test rides on two tram lines in the city of Zürich from Sept 2011 – Jan 2012.

This work is kindly supported by the Lunge Zürich.

Fierz, M., Houle, C., Steigmeier, P., and Burtscher, H. (2011) *Design, Calibration and Field Performance of a Miniature Diffusion Size Classifier*, Aerosol Science and Technology, 45, 1-10.

Aberer, K., Sathe, S., Chakraborty, D., Martinoli, A., Barrenetxea, G., Faltings, B., and Thiele, L. (2010) *OpenSense: Open Community Driven Sensing of Environment*, IWGS '10, November 2, 2010, San Jose, CA, USA.

Pebesma, E.J. (2004) *Multivariable geostatistics in S: the gstat package*. Computers and Geosciences 30, 683–691.

High-resolution mobile monitoring of traffic emissions in an urban area in Finland

L. Pirjola[1,2], T. Lähde[1], A. Malinen[1], J.V. Niemi[3], A. Kousa[3], T. Rönkkö[4], P. Karjalainen[4], J. Keskinen[4], A. Frey[5], and R. Hillamo[5]

[1]Department of Technology, Metropolia University of Applied Sciences, P.O. Box 4021, FI-00180 Helsinki, Finland
[2]Department of Physics, University of Helsinki, P.O. Box 64, FI-00014 Helsinki, Finland
[3]Helsinki Region Environmental Services Authority HSY, P.O. Box 100, FI-00066 HSY, Finland
[4]Aerosol Physics Laboratory, Tampere University of Technology, P.O. Box 527, FI-33101 Tampere, Finland
[5]Finnish Meteorological Institute, P.O. Box 503, FI-00101 Helsinki, Finland
Keywords: size distribution, black carbon, mobile laboratory, microenvironment.
Presenting author email: liisa.pirjola@metropolia.fi, liisa.pirjola@helsinki.fi

Traffic emissions significantly contribute to regional air pollution. Meteorology, traffic characteristics, road design and side structure affect near-road air quality by modifying dispersion of emissions (Hagler et al., 2010). Urban areas typically consist of street canyons where pollutant concentrations can be several times higher than in open areas due to reduced exchange of air and dispersion of pollutants inside the canyon. To obtain more detailed assessment of physical and chemical characteristics and source contributions of fine-particles in urban environment, an advanced measurement method was developed as part of the MMEA (Measurement, Monitoring and Environmental Assessment) program.

Three weeks street canyon campaign was performed in December 2010 in Helsinki. Mobile laboratory Sniffer (Pirjola et al., 2004) was driven on a 20 km route in the city center during the morning and afternoon rush hours, occasionally also at noon. The main street Mannerheimintie was driven back and forth always 5 times. Similarly, the measurements were carried out in side streets and background locations up to the shore. A special attention was given for the urban microenvironments close to the high traffic density street. Stationary measurements were conducted in four measurement stations by HSY, along the driving route.

The spatially and temporally high-resolution data included number concentration and size distribution of particles larger than 3 nm (ELPI, CPC and SMPS) as well as black carbon (Aethalometer) in PM_1 size fraction. Also continuously measured were NO, NO_2, NOx, CO, CO_2, PM_1, $PM_{2.5}$, meteorological and geographical parameters. A thermodenuder was used for volatility studies of particles.

Figure 1 shows the contour plot of the average total number concentration during the rush hours on 2 Dec, 2010. Temporal concentrations were highly variable. Meteorological conditions as well as traffic characteristics and urban planning was shown to have strong effect on the measured air quality.

Within a microenvironment where Mannerheimintie can be considered as an avenue canyon, the wake interference flow is produced (Vardoulakis et al., 2003). The windward concentrations of NO_x were around 26-59% of the leewind concentrations. Rather similar results (55%) were also predicted by a street canyon model OSPM (Berkowicz, 2000).

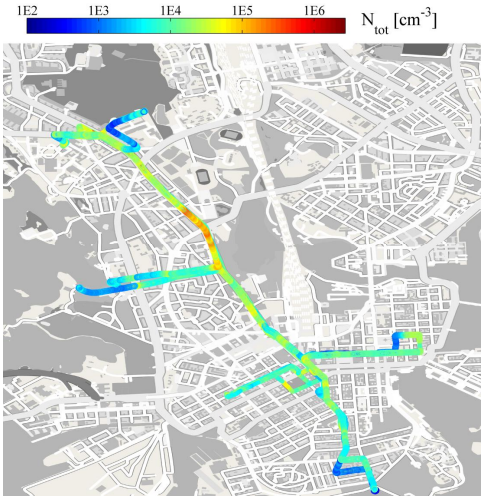

Figure 1. The map of downtown of Helsinki. The colour bar indicates the particle number concentration on Mannerheimintie and on the nearby streets.

More detailed analysis showed that the surrounding built environment combined to the predominant wind conditions changed the dispersion around the high traffic density streets markedly. The comparison of the stationary measurements to mobile measurements corresponded well promoting the mobile measurement method in an urban air quality studies.

MMEA is supported by Tekes (the Finnish Funding Agency for Technology and Innovation) and coordinated by the Finnish energy and environment cluster - CLEEN Ltd.

Berkowicz R. (2000). Environ, Monit. Ass. 65, 323-331.
Hagler G.S.W, Thoma E.D. and Valdauf R.W. (2010). *J. Air &Waste Manage. Assoc.* 60, 328-336.
Pirjola L., Parviainen H., Hussein T., Valli A., Hämeri K., Aalto P., Virtanen A., Keskinen J., Pakkanen T., Mäkelä T., Hillamo R (2004). *Atmos. Environ.* 38, 3625-3635.
Vardoulakis S., Fisher B.E.A., Pericleous K., and Gonzalez-Flesca N. (2003). *Atmos. Environ.* 37, 155-182.

Spatial and Seasonal Variations of Black Carbon and NO_2 Concentrations in an Urban Environment and correlation with UFP concentrations at selected locations

Martine Van Poppel[1], Christina Matheeussen[2], Patrick Berghmans[1]

[1]VITO - Flemish Institute for Technological Research, 2400 Mol, Belgium
[2]Flemish Environmental Agency, 2000 Antwerp, Belgium

Keywords: Black Carbon, NO2, UFP, traffic.
Presenting author email: martine.vanpoppel@vito.be

Traffic is one of the main sources of BC (black carbon), UFP (Ultrafine Particles) and NO_2 in urban environments. In addition, BC and UFP are considered to have a larger health impact (per mass) as compared to PM (Particulate Matter). Therefore, it is important to know the spatial variation in order to assess people's exposure and related health impact.

The results presented in this paper are part of a larger multidisciplinary study dealing with health impact of traffic related air pollution (UFP, BC, NO_2) on school children. To assess the exposure of the children, air quality measurements were performed at two school locations, at 40 home location and during 'in transport'. This paper focuses on the seasonal and spatial variation of UFP, BC and NO_2 at school and home locations.

Monitoring of UFP, BC and NO_2 was performed during summer (May – June 2011) and winter (November – December 2011). At two school locations BC, NO_2 and UFP were measured. BC and NO_2 measurements were performed at 8 locations simultaneously during 5 consecutive weeks resulting in 40 locations sampled. During each week, UFP measurements were performed at one of these locations. The locations represent the home locations of the children. In addition, measurements were performed during the entire monitoring campaign at an urban location of the AQ monitoring network. These data were used to rescale BC and NO_2 concentrations that were measured consecutively. The locations are characterised by different exposure to traffic. Two rural locations were included to estimate the regional background contribution. NO_2 was monitored using diffusive sampling tubes. BC was measured using µ-Aethalometer (AethLabs). UFP number concentrations were measured using CPC (TSI type 3783 and 3786) and Nanocheck (Grimm). During a limited period of the monitoring campaign at the school locations, BC concentrations were compared to EC analysed on filter samples using TOT (Thermo Optical Transmission).

BC concentrations measured in summer are less than 1 µg/m^3 at rural location and range from 1 to 3 µg/m^3 at the urban locations. Highest concentrations are measured at locations with more traffic. Similar trends are observed for NO_2. Weekly average concentrations of NO_2 measured in the urban locations range from 17 – 48 µg/m^3.

Weekly average NO_2 and BC concentrations show a good correlation (Figure 1) and a spatial variation of a factor 3 during summer. Correlation of BC with UFP are higher at street locations as compared to background locations.

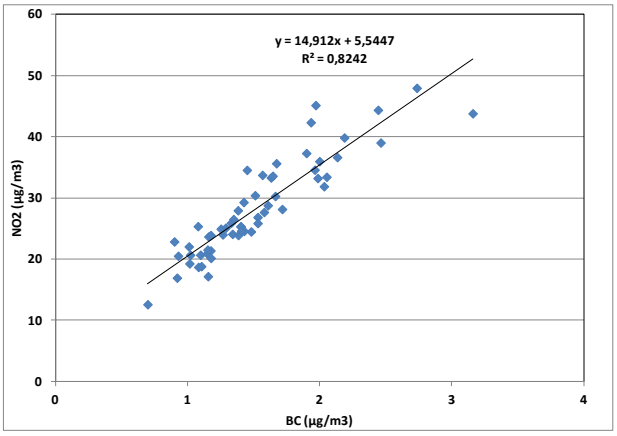

Figure 1. Weekly average BC and NO_2 concentrations at different locations in Antwerp in summer.

Preliminary results of the summer campaign show a high spatial variation for BC and NO_2 and the added value of a dense (temporary) monitoring network to asses more accurate real exposure in health-related studies.

Results of the winter campaign will be further discussed in the paper.

This work was funded by the Flemish Environmental Agency.

Tuesday, September 4, 2012

WG03S3O. Characterisation Techniques for Organic Aerosol

Studying Atmospheric Aerosols by Acoustic Levitation: Linking Head Space Solid-Phase Micro-Extraction (HS-SPME) with Gas Chromatography-Mass Spectrometry (GC-MS).

S. Almabrok, G. Marston and C. Pfrang

Department of Chemistry, University of Reading, P.O. Box 224, RG6 6AD Reading, Berkshire, UK
Keywords: Solid-Phase Micro-extraction, Acoustic Levitation, α-Pinene, Ozone.
Presenting author email: s.h.almabrok@reading.ac.uk

Climate change is one of the most important global environmental problems affecting natural ecosystems, food production, availability of fresh water as well as human health.(1) In acoustic levitation, a sound wave is generated between a piezoelectric transducer and a flat or concave reflector; therefore, by altering the distance between transducer and reflector a standing wave can be created and small samples of solids or liquids can be levitated.(2) This study has been conducted to improve our understanding of the reactions of O_3 and NO_3 with a range of terpenes found in the Earth's atmosphere and of the formation and properties of associated organic aerosols. For these investigations, a combination of acoustic levitation with gas chromatography-mass spectrometry (GC-MS) has been achieved by head space solid-phase micro-extraction (HS-SPME). The experimental set-up is illustrated in Fig. 1 (a-b).

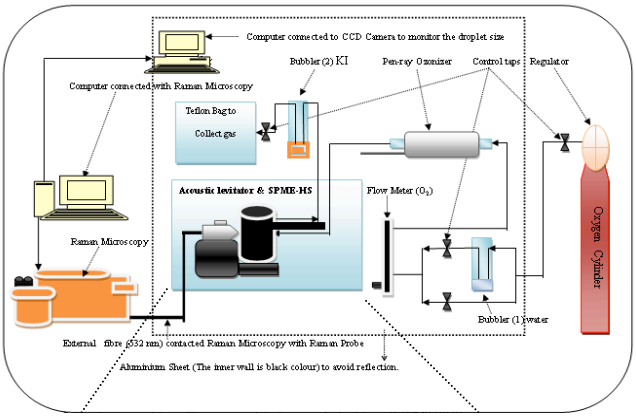

Figure 1 (a): Experimental set-up for the acoustic levitator with HS-SPME-GC-MS analysis.

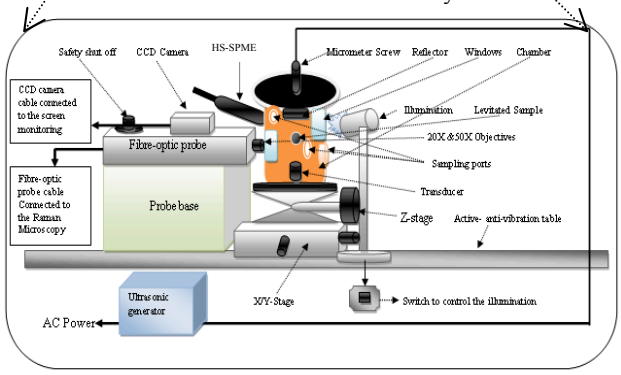

Figure 1 (b): Set-up for the combination of the acoustic levitator with HS-SPME (zoom into Fig. 1 (a)).

Fig. 2 shows the mass spectrum for a levitated droplet of pure α- pinene obtained by using HS-SPME-GC-MS under the following conditions: 174 ml/min flow of N_2, 5 min extraction time, and using a 100 µm polydimethylsiloxane (PDMS) coated fibre. Oxidation of acoustically levitated droplets of α-pinene and d-limonene has been studied in an environmental chamber that allowed control of the gas-phase surroundings and relative humidity. Several products could be identified mostly by comparison with reference samples in the same conditions including verbenone, verbenol, pinocarveol, carvone, carveol, norpinoaldehyde and pinonaldehyde (see example in Fig. 3).

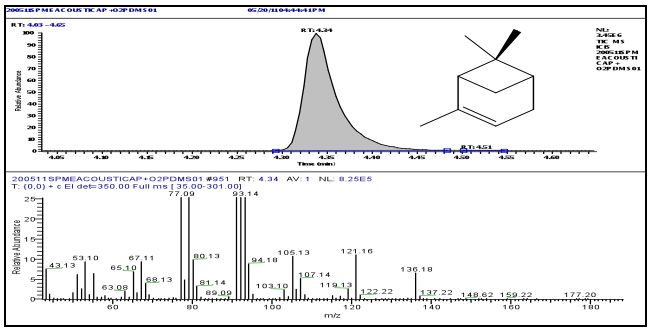

Figure 2: HS-SPME-GC-MS result for a levitated droplet of pure α-pinene (GC on top; MS below).

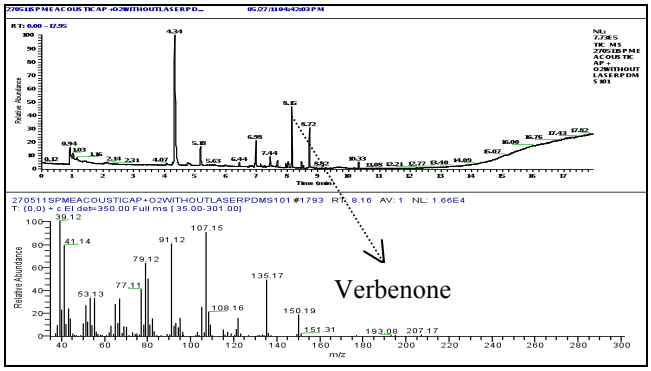

Figure 3: HS-SPME-GC-MS result for a levitated droplet of α-pinene after oxidative ageing (MS for the product verbenone).

References.

1- Ravindranath, N.H., and J. A. Sathaye, *Climate Change and Developing Countries*, 2003, Kluwer Academic Publishers.

2- Priego-Capote, F., and L. Decastro, *Trends in Analytical Chemistry*, 25, 9 (2006).

Single particle mass spectrometry of bacteria – laboratory measurements as reference for the identification of ambient "bioaerosols"

B. Sierau[1], F. Freutel[2], A. Roth[2], J. Schneider[2], C. Oehm[3], O. Möhler[3], and A. A. Mensah[1]

[1]ETH Zurich, Institute for Atmospheric and Climate Science, Universitätsstr. 16, 8092 Zürich, Switzerland
[2]Particle Chemistry Department, Max Planck Institute for Chemistry, Hahn-Meitner-Weg 1, 55128 Mainz, Germany
[3]Karlsruhe Institute of Technology, Institute for Meteorology and Climate, Hermann-von-Helmholtz-Platz 1, 76344 Eggenstein-Leopoldshafen, Germany
Keywords: bioaerosols, aerosol mass spectrometry, single particle analysis, aerosol-cloud interactions.
Presenting author email: berko.sierau@env.ethz.ch

Aerosols of biological origin such as bacteria and spores are gaining increasing attention in the research field of cloud microphysics. Their ability to act as heterogeneous ice nuclei has been shown in various laboratory studies; however, their atmospheric relevance in aerosol-cloud interactions is debatable. This is partly due to the lack of understanding of the actual processes driving water and ice nucleation on biological particles (e.g. Möhler *et al.*, 2008), but also to the challenging identification of these particles in the field (Pratt *et al.*, 2009). Both objectives were tackled in the framework of the BIO05 and BIO06 campaigns at the AIDA facility at the Karlsruhe Institute of Technology, Germany. The ice nucleation behavior of bacterial species such as *Pseudomonas syringae* and *Pseudomonas fluorescence* was studied with focus on differences in the physico-chemical properties between the individual, intact cells, bacteria strains and their residuals. The latter are a product of the aerosol generation process and smaller in size than the intact cells.

This study focuses on mass spectrometric measurements of the chemical composition of the laboratory generated bacterial cells and their residues. Three different aerosol mass spectrometers were applied featuring the analysis of single particles: a TSI Aerosol Time-of-Flight Mass Spectrometer (ATOFMS), Aerodyne's C-ToF-AMS with Light Scattering Probe (LSP) for single particle detection, and the Aircraft-based Laser ABlation Aerosol MAss spectrometer (ALABAMA), developed by MPI Mainz (Brands *et al.*, 2011). The ATOFMS and ALABAMA both use laser ablation to evaporate and ionize the particles for mass spectrometric detection (LDI), whereas the C-ToF-AMS uses thermal vaporization with subsequent electron impact for ionization. All three instruments allow a size resolved analysis of the particles' chemical composition, i.e. mass spectra from intact cells and their residues are separated. Both were represented as two distinct modes in the measured size distribution.

The elaboration of mass spectrometric "fingerprints" usable for the identification of bacteria by aerosol mass spectrometry is a key aspect of this study. *Fig. 1* exemplarily depicts an ATOFMS mass spectrum of *Pseudomonas syringae* cell of strain 13b2. The ions representing phosphate, potassium, and nitrogen-containing organic compounds are clearly visible and have been detected by both LDI instruments. However, unidentified peaks remain which have also been observed in ambient aerosols.

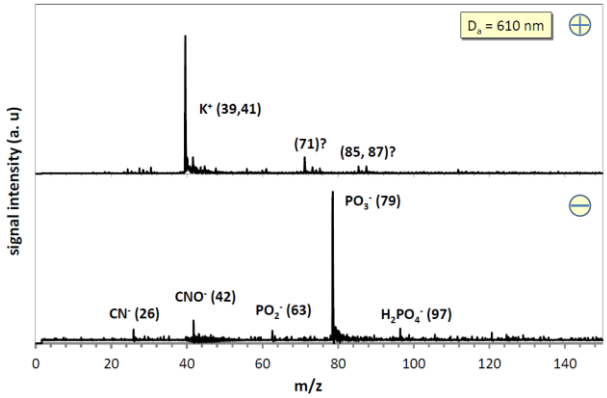

Figure 1. Mass spectrum of *Pseudomonas syringae* bacteria cell recorded by the ATOFMS. The most prominent, identified ion peaks are marked.

Similarities and differences in the ion peaks obtained from all three instruments will be highlighted. The findings are referenced to ambient spectra collected by the identical instruments in the field, and also to spectra referred to as "bioaerosols" in the literature (e.g. Fergenson *et al.*, 2004). The study provides valuable reference spectra for the mass spectrometric community which is of high importance as single particle instruments are widely used for the online, in situ detection and identification of aerosols as well as ice crystal and cloud droplet residuals in field studies.

M. Brands *et al.* (2011) *Aerosol Sci. Technol.*, **45**, 1, 46-64.
D. P. Fergenson *et al.* (2004) *Anal. Chem.*.**76**, 373.
O. Möhler *et al.* (2008) *Biogeosciences*, **5**, 1425-1435.
K. A. Pratt *et al.* (2009) *Nature Geosci.* **2**, 398-401.

On-line analysis of organic aerosols with an ion-trap aerosol mass spectrometer

S.J. Gallavardin[1,2], J. Fachinger[1], F. Helleis[1], F. Drewnick[1], and S. Borrmann[1,2]

[1]Particle Chemistry Dept., Max Planck Institute for Chemistry, Mainz, 55128, Germany
[2]Institute for Atmospheric Physics, Johannes-Gutenberg University, Mainz, 55099, Germany
Keywords: Instrument development, organic aerosols, aerosol mass spectrometry
Presenting author email: johannes.fachinger@mpic.de

Organic aerosols in the atmosphere are a complex matter due to the large amount of different compounds. For a better understanding of the evolution of the particle composition and its effect on its environment, a more detailed characterization, in particular of the chemical functionality and/or molecule structures, is necessary (Hallquist et al., 2009).

Compared to time-of-flight mass spectrometers, ion-trap mass spectrometers allow for more detailed chemical analysis due to their unique features: specific ion fragmentations and ion-molecule reactions can be induced to access molecule or ion structural information (Gross, 2011).

We report here on the recent improvements and operation of the Ion-Trap Aerosol Mass Spectrometer (IT-AMS) initially developed by Kürten et al (2007). The IT-AMS is similar to the Aerodyne AMS instrument with the exception of the mass spectrometer module that is replaced by a home-built 3D quadrupole ion-trap mass spectrometer. A home-written software controls the ion-trap mass spectrometer through the definition of series of measurement cycles. Each measurement cycle controls the ion manipulation allowing thereby for specific analyses. By combining successively in time different measurement cycles, one can obtain different structural information related to the different molecules in the aerosol particles.

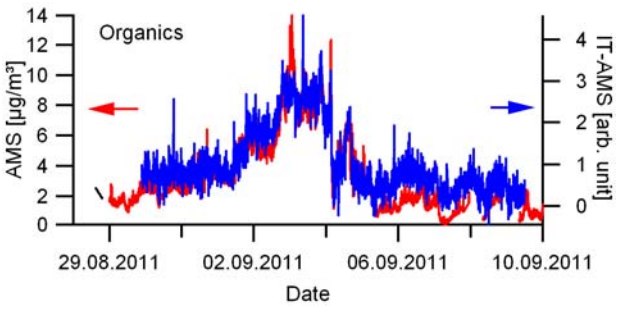

Figure 1. Detection of organics in atmospheric aerosol particles using a standard AMS instrument (left, red) and IT-AMS (right, blue).

Figure 1. shows comparative measurements of IT-AMS with a standard AMS instrument during 10,5 days at the Kleiner Feldberg (Germany) in summer 2011 probing atmospheric aerosols. A good correlation of the temporal evolution of the concentrations of total organics as well as of nitrate and sulphate (not shown here) was observed for both instruments.

In the laboratory, measurement cycles were tested to explore the different features of IT-AMS. As an example, pure aerosol particles of tryptophan and glutathione, considered as markers of primary biological particles, can be distinguished from each other by the fragmentation of one common ion (m/z=130). The used measurement cycles also reveal details of the ion structure and fragmentation pathways (see Figure 2.).

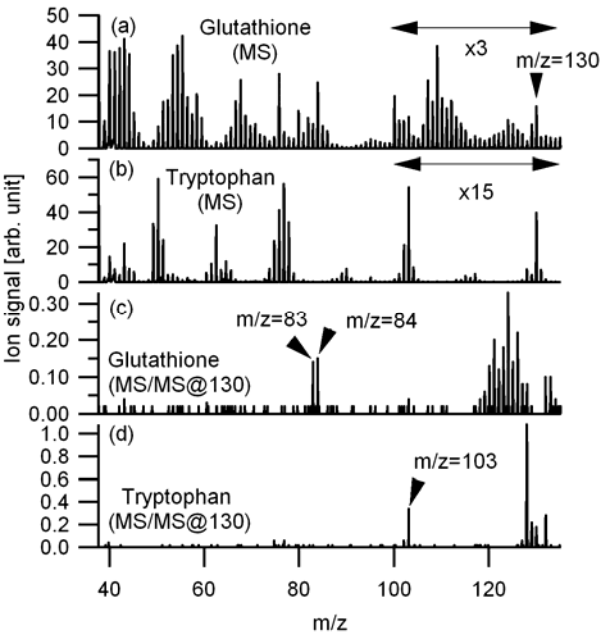

Figure 2. IT-AMS Mass spectra (MS) of glutathione (a) and tryptophan (b). Removal of ions (m/z=40-115) and fragmentation of ions (m/z=130) (MS/MS@130) (c), (d).

Thus, by the choice of appropriate measurement cycles applied to frequently found ions in classic aerosol mass spectrometric analyses with AMS, it is possible to gain on-line more insights into the composition complexity of atmospheric organic aerosols.

Hallquist, M., et al., (2009) *Atmos. Chem. Phys.* **9**, 5155-5236.

Kürten, A., et al., (2007) *Int. J. Mass. Spectrom.* **265**, 30-39.

Gross, J. (2011) *Mass Spectrometry*, 2nd ed., Springer-Verlag Berlin Heidelberg.

Organic particle and gas phase measurements with a new MOVI-CI-TOF-MS

C. Mohr[1], F. Lopez-Hilfiker[1], J. D. Wargo[1], R. L. N. Yatavelli[1,2], and J. A. Thornton[1]

[1]Department of Atmospheric Sciences, University of Washington, Seattle, WA, 98195, USA
[2]Department of Chemistry and Biochemistry/Cooperative Institute for Research in the Environmental Sciences (CIRES), University of Colorado, Boulder, CO, 80309, USA
Keywords: Organic aerosol, VOC, mass spectrometry, partitioning
Presenting author email: cmohr@u.washington.edu

Organic compounds are ubiquitous in the atmosphere and present in both gas and particle phase. Their evolution in time is determined by emissions, oxidation, deposition, and gas/particle partitioning especially for semi-volatiles (SVOCs). A fundamental understanding of this highly dynamic system thus requires quantitative measurements of organic compounds in both gas and particle phases.

Here we present laboratory and field data from an improved version of the Micro Orifice Volatilization Impactor Chemical Ionization Time-of-Flight Mass Spectrometer (MOVI-CI-ToF-MS, Yatavelli and Thornton, 2010). While particles are impacted on a post for subsequent thermal desorption and analysis using chemical ionization mass spectrometry (CIMS), gases are drawn into the MOVI and analyzed in real time using CIMS. Particle collection/gas phase analysis and temperature-programed desorption for particle phase analysis are alternated ~every 15 min.

The current version of the MOVI incorporates modifications done to (a) minimize the adsorption of gases and thus the loss of semi and low volatility compounds on to the MOVI surfaces, (b) rapidly return the collection post to ambient temperature after a desorption step, and (c) provide a means of robust calibration. Moreover, the instrument continuously switches between positive and negative ion proton transfer chemical ionization, allowing the detection of organic compounds with a variety of functional groups. We demonstrate mass accuracies better than ± 20 ppm and sensitivities in the range of 5 - 15 counts s^{-1} per ppt for gas phase measurements. For particle phase, the detection limit is a few nanomoles per m^3.

The instrument was recently deployed in a month-long field campaign (ClearfLo) in Detling, UK, from January 16 to February 15, 2012. The measurement site is influenced by local emissions from nearby roads and villages, but also by continental air masses or the London plume. Preliminary analysis shows that a high number of organic acids, as well as other compounds such as organonitrates and organosulfates, in both gas and particle phase up to a m/Q of ~500 Th could be detected and quantified (Figure 1). Diurnal patterns of ions with mass-to-charge ratios consistent with levoglucosan, syringic acid (m/Q 197) and tentatively nitrophenols (m/Q 138) indicate the presence and importance of wood smoke in England during cold ambient temperatures (Figure 2). Moreover, the intensity of a number of ions in the thermal desorption steps are well correlated with the organic aerosol time series.

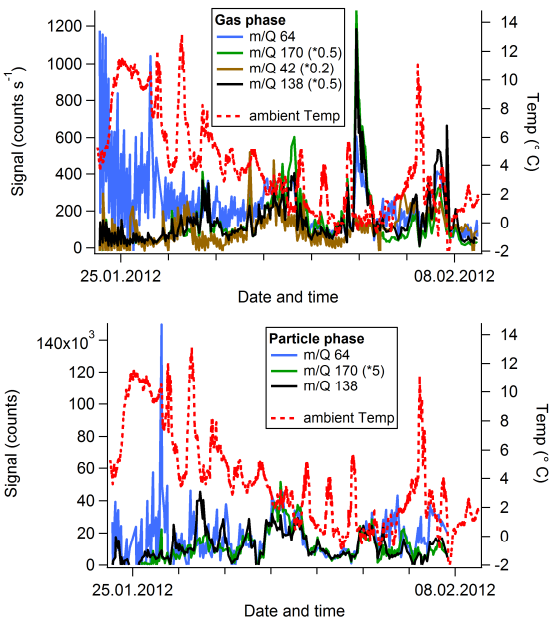

Figure 1. Time series of gas and particle phase species measured in negative mode, as well as ambient temperature.

Overall instrument performance in the field, relative to laboratory characterizations, and initial statistical pattern analysis of the multi-dimensional field data set are also discussed.

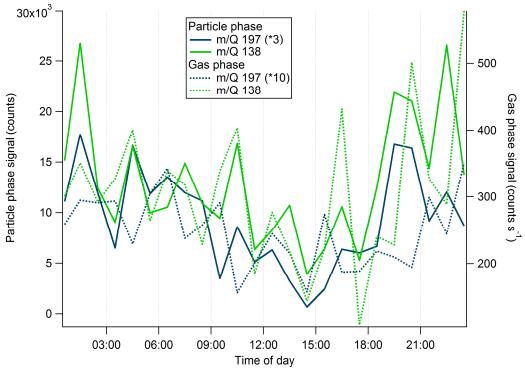

Figure 2. Diurnal pattern of gas and particle phase of m/z 197 (syringic acid) and m/z 138 (nitrophenols), related to biomass burning emissions.

Funding provided by a grant to J. A. Thornton from the U.S. Department of Energy, DE-SC0006036.

Yatavelli, R. L. N. and Thornton, J. A. (2010) *Aerosol Sci. Tech.* **44**, 61-74.

Urban organic aerosols composition measured by ultra-high resolution mass spectrometry

A.G. Rincón[1], A.I. Calvo[2], M. Dietzel[3], M. Kalberer[1]

[1]Department of Chemistry, University of Cambridge, Cambridge, CB2 1EW, UK
[2]Centre for Environmental and Marine Studies, Department of Environment, University of Aveiro, Aveiro, Portugal
[3]Institute of Nano and Microfluidics Center of Smart Interfaces, Technical University Darmstadt, Darmstadt, Germany
Keywords: Water-soluble organic fraction, SOA, urban aerosol, Ultra-high resolution mass spectrometry
Presenting author email: agr36@cam.ac.uk

Organic compounds are major constituents of atmospheric aerosol particles. The understanding of their chemical composition, their properties and reactivity are important for assessing aerosol effects upon both global climate change and human health. Among organic aerosols, secondary organic aerosols (SOA) are predominant especially in summer due to intense photochemical activity.
Here we describe the chemical composition of aerosols with particle diameters <1µm collected on filters at an urban site in Cambridge, UK, during summer 2009 (Rincón *et al*., 2012).

The water-soluble organic fraction of the filters was separated from inorganic ions by a solid phase extraction step and re-dissolved in acetonitrile-water prior to analysis. Ultra-high resolution mass spectrometry (UHRMS) analyses were performed using an LTQ Orbitrap Velos, with an accuracy bellow 2ppm, using an electrospray ionisation source. Mass spectra were measured by direct infusion, in negative and positive polarities and recorded within the range of 50-500m/z. Molecular formulas were assigned to the exact masses of the more than 5000 compounds in a single sample using the Xcalibur™ software. After data processing, visualization schemes, such as van Krevelen diagrams and Kendrick mass defect plots were used for data interpretation.

The identified elemental formulas are classified into six compound categories, including CHO, CHN, CHON, CHOS, CHS, and CHONS compounds. CHONS compounds refer to compounds that contain carbon, hydrogen, oxygen, nitrogen and sulfur. Other compound categories are defined analogously. 80% of the data contains compounds with OS or N heteroatoms; only 20% of the data contains compounds with CHO. The overall average O/C ratios of the all sub-groups are about 0.55 - 0.60 in negative and 0.43 - 0.47 in positive polarity which compares well with other UHRMS studies of urban aerosols, where an average O/C of 0.37 was observed (Roach *et al*., 2011).

Of all N-containing compounds only about 20% can be detected in both polarities emphasizing the need to characterize complex samples like organic aerosols in both modes. Figure 1 shows van Krevelen plots of H/C versus N/C of the CHN subgroup, detected in negative and positive polarity. More CHN compounds are measured in positive mode than in negative mode, which is mainly due to amine functional groups in these compounds. Accordingly, CHN compounds in positive mode have high H/C (>1) and on average a lower N/C than in negative mode. In addition, more CHON components were measured in negative mode especially at N/C > 0.5 and only about 23% of the formulas were detected in both modes, indicating the variety of functional groups in this sub-group.

A large number of highly unsaturated reduced nitrogen-containing compounds were detected, corresponding likely to cyclic amines. Homologous series with mass differences of CH_2 were found, especially pronounced in the CHO sub-group. Both, amines and long-chain aliphatic acids are likely signatures of biomass burning and other primary biological sources.

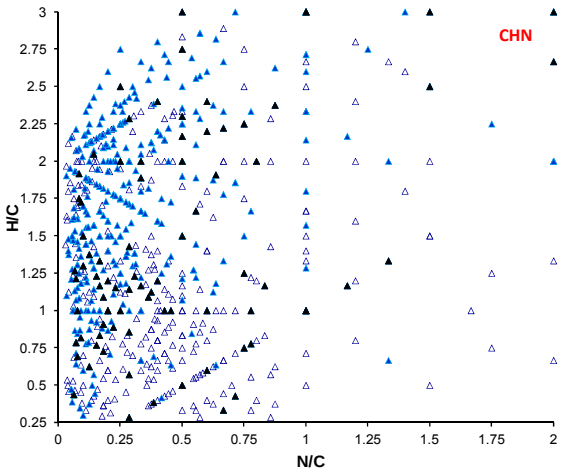

Fig 1. H/C elemental ratio vs. N/C for the CHN sub-group, measured in negative (Δ) and positive (▲) polarity. Black full signs shows compounds measured in both polarities.

Roach, P. J., Laskin, J., Laskin, A. (2010) *Anal. Chem.* **82**, 7979-7986.
Rincón, A. G., Calvo, A.I., Dietzel, M., Kalberer, M. (2012) *Environ. Chem.* **Submitted**.

Unravelling the molecular organic signature of the EC/OC fractions of PM: Coupling of an EC/OC-carbon analyzer to photo-ionization mass spectrometry

J.Grabowski[1], T.Streibel[1,2], M.Sklorz[1], J.Chow[3], J.Watson[3] and R.Zimmermann[1,2]

[1] Joint Mass Spectrometry Centre, Chair of Analytical Chemistry, University of Rostock, Rostock, Germany
[2] Joint Mass Spectrometry Centre, Comprehensive Molecular Analytics, Helmholtz Zentrum München, Germany
[3] Desert Research Institute, Reno, Nevada, USA

Keywords: PM, EC/OC-Carbon analyzer, Photo-ionization mass spectrometry, evolved molecular signature,
Presenting/corresponding author email: ralf.zimmermann@helmholtz-muenchen.de

Carbonaceous material in airborne particulate matter (PM) is of increasing interest due its adverse health effects and its potential influence on the climate. Its analytical ascertainment on a molecular level is still challenging. Hence, analysis of carbonaceous fractions for many studies is often solely carried out by determining sum parameters such as the overall content of organic carbon (OC) and elemental carbon (EC) as well as the total carbon content, TC (sum of OC and EC). The used thermal procedure, however, allows to get additional interesting information: By defining different thermal OC fractions (i.e temperature steps) also information on the refractory properties of the carbonaceous material is obtained. In this context it is particularly interesting to investigate the release and formation behaviors of the molecular species responsible for the different OC and EC fractions. Thus after initial promising results of a pre-study [1] in the current work an EC/OC carbon analyzer (Model DRI 2000) and a homebuilt photo-ionization time-of-flight mass spectrometer (PI-TOFMS) were hyphenated [2] to investigate individual organic compounds especially from the different OC fractions The carbon analyzer enables the stepwise heating of filter samples loaded with PM and provides the sum values of the carbon release (Used steps – "Improve protocol" [2]: OC1 - 120 °C, OC2 - 250°C, OC3 - 450°C OC4 - 550°C). With the on-line coupled PI-TOFMS now in addition the organic compounds which are released during the thermal profile are detectable in real time. This is possible by the soft photo ionization methods (SPI - single photon ionization and REMPI - resonance-enhanced multi photon ionization) which suppress fragmentation upon ionization. The two instruments were coupled by a newly developed interface and characterized with standard substances. The final EC/OC-analyzer - PI-TOFMS instrument then was applied to several types of PM samples, such as ambient aerosol, gasoline/diesel emissions and wood combustion emission. Ambient filter samples e.g. showed a strong impact of wood combustion markers. This was revealed by comparison to the thermal OC signatures of pure cellulose, lignin and wood combustion PM with the ones of ambient air PM. At higher temperatures (450 °C) often a shift to smaller molecules occurs. This is due to the thermal decomposition of larger oligomeric or polymeric molecular structures comparable to lignocelluloses and similar oxygenated humic-like substances. Finally, PM from vehicle exhaust (gasoline and diesel with 10% biodiesel) was analyzed (Fig. 1 and 2). Gasoline PM exhibited large polycyclic aromatic hydrocarbons, whereas diesel PM showed a much higher total organic content in the REMPI measurements. The detected pattern (SPI) revealed a strong influence of the biodiesel content on the nature of the organic PM material.

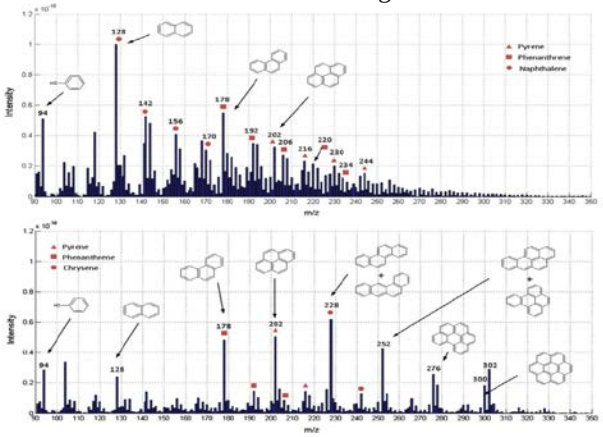

Figure 1. REMPI/TOF-MS spectrum of OC3 (450° C) of diesel (top) and gasoline PM (bottom). REMPI selectively detects aromatic compounds at the chosen ionization wavelength.

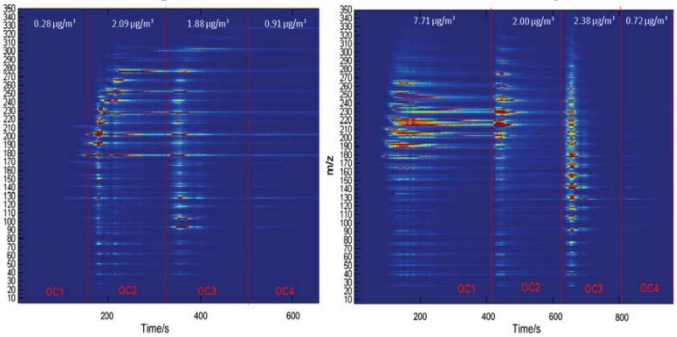

Figure 2. Two-dimensional EC/OC-analyzer - REMPI/TOF-MS signature of filters from car emissions using gasoline (left) and diesel (right). The abscissa reflects the time of the thermo-optical measurements (s), the ordinate shows the molecular masses (m/z).

The health effects of organic fractions in aerosols are currently further investigated in the framework of the Helmholtz Virtual Institute of Complex Molecular Systems in Environmental Health, HICE (www.hice-vi.eu).

[1] T. Streibel, J. Weh, S.Mitschke, R. Zimmermann (2006). *Anal. Chem.* ***78, 5354-5361***

[2] J. Grabowsky, T. Streibel, M. Sklorz, J. Chow, J. Watson, A. Mamakos and R. Zimmermann (2011). *Anal Bioanal Chem* 401, 3153–3164

A long pathlength absorbance photometer for the determination of peroxide content and brown carbon in primary and secondary organic aerosol

J. Dommen[1], P. Mertes[1], S.M. Platt[1], I. El Haddad[1], L. Pfaffenberger[1], A.S.H. Prévôt[1], M. Kalberer[2], and U. Baltensperger[1]

[1]Laboratory of Atmospheric Chemistry, Paul Scherrer Institut, 5232 Villigen PSI, Switzerland
[2]Centre for Atmospheric Science, Department of Chemistry, University of Cambridge, United Kingdom
Keywords: peroxide, SOA, light absorption, particle composition.
Presenting author email: josef.dommen@psi.ch

Organic aerosols are chemically still poorly characterized as they are composed of thousands of different organic molecules. These compounds have low vapour pressures and must therefore contain many functional groups, e.g. alcohols, carbonyls, carboxylic acids and peroxides. Of these groups, organic peroxides are the least understood. They are difficult to measure and they have been quantified in only few studies (e.g. Docherty et al., 2005; Surratt et al., 2006). Furthermore it is assumed that they contribute to adverse health effects because of their high reactivity and high oxidation potential.

Not only black carbon but also many organic compounds are light absorbing. The occurrence of such compounds in organic aerosols has been referred to as brown carbon (Andreae and Gelencsér, 2006). Incomplete combustion, especially associated with biomass burning has been shown to produce particulate brown carbon. However, brown carbon formation and its removal by photochemical oxidation is not well understood.

Here we present an instrument for the quantification of peroxides in aerosol particles based on iodometry and long pathlength absorption photometry (Peroxide-LOPAP). Extraction, chemical conversion and subsequent measurement of the aerosol samples is performed in a closed, oxygen-free environment. The limit of detection is 0.1 µM peroxide, which is orders of magnitude lower than previously obtained.

Figure 1 shows the instrument calibration for various hydroperoxides. The method measures quantitatively all peroxides except for very stable compounds like *tert*-butyl hydroperoxide. Thus, with this instrument the total concentration of peroxides in the aerosol is effectively measured.

Since the measurement technique relies on absorption we also measured the light absorbance of other species extracted from the aerosols. Thus, all aerosol samples were divided into two fractions. From one fraction we determined the absorbance due to peroxides after addition of KI, from the second the absorption due to none peroxide species. The following systems were investigated: SOA from ozonolysis and photooxidation of α-pinene, POA and SOA of emissions from wood burning, a diesel car, a two-stroke scooter and cooking.

The highest amount of peroxides with 34% (assuming a molecular weight MW of 300 g/mol) was found in freshly generated SOA from α-pinene ozonolysis, in agreement with measurements of Docherty et al. (2005). Peroxide contents in POA were low while increased levels were observed in the SOA after photo-oxidation of the emission mixtures. Peroxide contents decreased with increasing NO concentration in the photo-oxidation experiments. Generally, a decrease of the peroxide content was observed with aging of the aerosol, indicating a decomposition of peroxides in the particles. Particles from wood combustion showed at 365 nm the highest bulk mass absorption efficiency (0.3-0.5 m^2g^{-1}) followed by diesel, while scooter and cooking emissions exhibited only small mass absorption efficiencies.

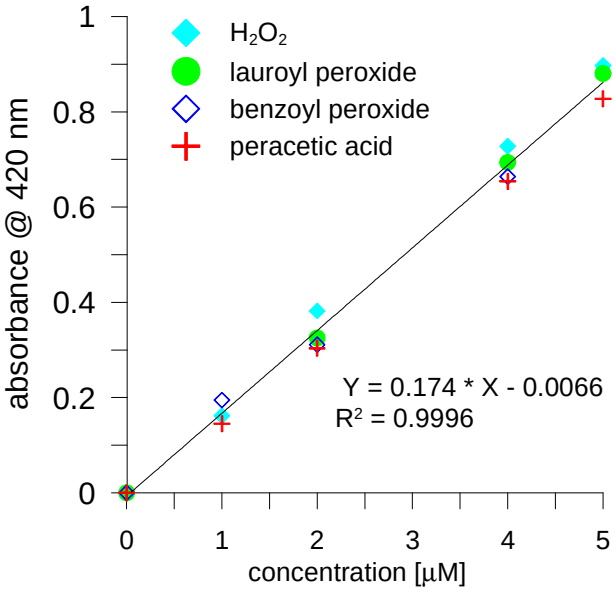

Figure 1. Peroxide-LOPAP calibration with various hydroperoxides.

This work was supported by the Swiss National Science Foundation (SNSF).

Andreae, M. O. and Gelencsér, A. (2006) *Atmos. Chem. Phys.* **6**, 3131-3148.

Docherty, K. S., Wu, W., Lim, Y. B., and Ziemann, P. J. (2005) *Environ. Sci. Technol.* **39**, 4049-4059.

Surratt, J. D., Murphy, S. M., Kroll, J. H., Ng, N. L., Hildebrandt, L., Sorooshian, A., Szmigielski, R., Vermeylen, R., Maenhaut, W., Claeys, M., Flagan, R. C., and Seinfeld, J. H. (2006) *J. Phys. Chem. A* **110**, 9665-9690.

Investigation of Free Radicals Formed in the Oxidation of Acoustically Levitated α-Pinene Droplets by Electron Spin Resonance

M.V.Ghosh[1], P.Ionita,[2] S. Almabrok,[1] G. Marston[1], and C. Pfrang[1]
[1]Department of Chemistry, University of Reading, Reading, RG6 6AD, UK
[2]Department of Organic Chemistry, University of Bucharest, 050663, Romania
Keywords: EPR, DMPO, Free Radicals, α-pinene
Presenting author email: m.v.ghosh@reading.ac.uk

Free radicals control the lifetime of gases important for the Earth's radiative balance (e.g. CH_4), the budget of O_3 in all parts of the atmosphere, as well as the production of acidic species. Understanding the behaviour of free radicals in the atmosphere is of paramount importance for establishing the lifetime and hence spatial scales of pollutant transport. Assessment of the variability of free radical formation from reactions of ozone with terpenes is important for understanding the health effects associated with the particulate matter (Johnson and Marston, 2008). Studies showed that a significant amount of reactive oxygen species is associated with secondary organic aerosol (SOA) formed under laboratory conditions during the reaction of α-pinene with ozone (Pavlovic and Hopke, 2009).

The α-pinene oxidation by ozone has been studied in individually levitated aerosol droplets using an acoustic levitator at 100 kHz encased in a custom-built environmental chamber allowing control of the gas-phase surroundings and relative humidity (Ghosh et al, 2011).

Figure 1: Images of a α-pinene droplet levitated in an ultrasonic trap.

In order to determine the chemical composition of free radical species from the oxidation of levitated α-pinene droplets with ozone by Electron Spin Resonance, a spin trap was employed to stabilize the radicals and increase their lifetimes for characterisation (Ghosh et al, 2008).

The EPR spectra were recorded at ambient temperature on a JEOL FR30EX spectrometer using the following settings: centre field 3360 G, frequency 9.42 GHz, power 4 mW, sweep time 60 s, time constant 0.1 s, modulation frequency 100 kHz and modulation width 1G. The EPR hyperfine coupling constants (due to the interaction of unpaired electron with the nitrogen atom) were extracted from the simulation of the experimental spectra.

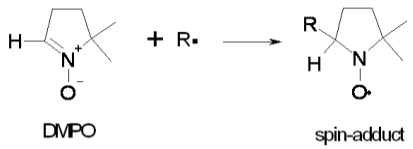

Figure 2. The spin-trapping technique: DMPO (5,5-dimethyl-1-pyrrolidine-N-oxide) spin-trap scavenges a short-lived radical R· by forming a persistent spin-adduct.

Figure 3: Spin adducts spectra from the levitation of α-pinene in Ozone by Spin Trapping Methodology by EPR in DMPO.

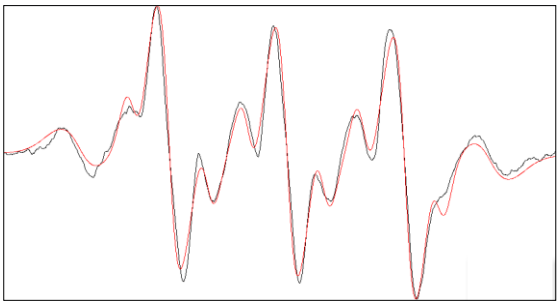

Figure 3 displays the experimental EPR spectrum (in black) together with a computer simulated spectrum (in red). The fitting was achieved with the following simulation parameters based on a mixture of three species: one oxygen-centred radical (5% of the total), with hyperfine couplings a_N=13.54 G and a_H=8.73 G, one carbon centred radical (~20%) with a_N=14.37 G and a_H=19.41 G and a decomposition spin-adduct (~75%) with a_N=13.85 G.

Our study demonstrates that it is possible to analyse free radicals by Electron Spin Resonance formed from the oxidation of α-pinene in a containerless environment with applications to studies of reaction mechanisms in atmospheric science and beyond.

Acknowledgements:
We would like to thank Prof. F. Hartl and JEOL for enabling us to access the EPR instrument used for radical detection. This work was supported by NERC (grant numbers NE/G000883/1 and NE/G019231/1)) and the Royal Society. We are also grateful for essential access to the Chemical Analysis Facility, CAF, at the University of Reading.

References:

M. Ghosh, S. Almabrok, I. Hoare, D. Stewart, G. Marston, C. Pfrang, Study of terpenes by Raman Acoustic Levitation, *European Aerosol Conference Handbook* , 12E2, 272, 2011

M. Ghosh, P. Ionita, J McAughey and F. Cunningham, *Journal of Organic Chemistry ARKIVOC*, Volume 2008, Part (xii): General Papers: 08-2886HP

D. Johnson and G .Marston, *PCCP*, 2008, 10, 37, 39

J. Pavlovic and P. K. Hopke, *Atmos. Chem. Phys. Discuss.*, 9, 23695-23717, 2009

Tuesday, September 4, 2012

WG07S1O. Application of engineered nanoparticles

Electrospray deposition of graphene nanosheets

L. B. Modesto-Lopez[1], O. V. Bilousov[2], J. J. Carvajal[2], F. Díaz[2] and J. Rosell-Llompart[1,3]

[1]Department of Chemical Engineering, Universitat Rovira i Virgili, Tarragona, Catalonia, E-43007, Spain
[2] Física i Cristal·lografia de Materials and EMaS, Univ. Rovira i Virgili, Tarragona, Catalonia, E-43007, Spain
[3]Catalan Institution for Research and Advanced Studies (ICREA), Barcelona, Catalonia, E-08010, Spain
Keywords: electrospray, graphene, coatings.
Presenting author email: luis.modesto@urv.cat

Graphene, a 2-D nanomaterial with unique properties (Zhu et al, 2010) is an attractive optically transparent conductor for optoelectronic applications (Blake et al, 2008). Particularly, graphene thin coatings may be used as saturable absorbers, to develop ultrafast pulsed laser technology (Cho et al, 2011). Recently, Chu et al (2010) electrospray-deposited single walled carbon nanotubes, a close relative of graphene, for use as saturable absorbers in the 1.5 μm region, although they can also be used in the 2 μm emission range (Cho et al, 2009). Electrospray is a liquid atomization method that leads to highly charged, nearly monosized micro- and nano-droplets, which has been applied to create thin films and coatings (Jaworek, 2007; Modesto-Lopez & Biswas, 2010). The small droplet size combined with the low flow rate characteristic of electrospray may be ideal to control the film thickness. In addition, the electrostatic control implies a virtual 100 % deposition efficiency. To our knowledge, however, no reports exist yet on the use of electrospray for depositing graphene films.

Therefore, the purpose of this study is to characterize the deposition patterns of graphene onto flat substrates as a function of electrospray operating parameters and to identify conditions leading to layer-by-layer deposition.

Graphene oxide (GO) was synthesized by oxidizing graphite with potassium chlorate in an acidic medium. GO was filtered and washed several times with HCl and distilled water until reaching a neutral pH of the filtrate. Graphene was then prepared by reduction of GO with iron. The obtained graphene nanosheets were filtered and washed with distilled water and ethanol, and then dried at 100 ºC for over 12 h in vacuum. Figure 1a shows a SEM image of a multi-layered graphene particle. Each layer is formed by hundreds of graphene nanosheets, which cannot be observed by SEM. The nanosheets exfoliate individually when suspended in ethanol, as can be seen by TEM (Figure 1b). Graphene was also characterized by Raman spectroscopy and XRD (Figures 1c and d, respectively).

In the electrospray-deposition experiments, graphene nanosheet powder suspensions were prepared in dimethylformamide (DMF). The suspensions were stable over many hours, allowing for sufficient time to carry out depositions. Electrospray was performed solely in the cone-jet mode. Highly stable spraying was obtained at a liquid flow rate of 1 μL/min and applied voltage of 4.4 kV for suspensions of < 0.5 wt % (relative humidity 39 %, temperature 24 ºC).

Electrosprayed graphene nanosheets were collected onto quartz substrates, and their optical characteristics (including linear and nonlinear transmission, nonlinear response dynamics for saturable absorption, saturation fluences, modulation depths and nonsaturable losses) are studied as a function of electrospray-deposition time and initial suspension concentration.

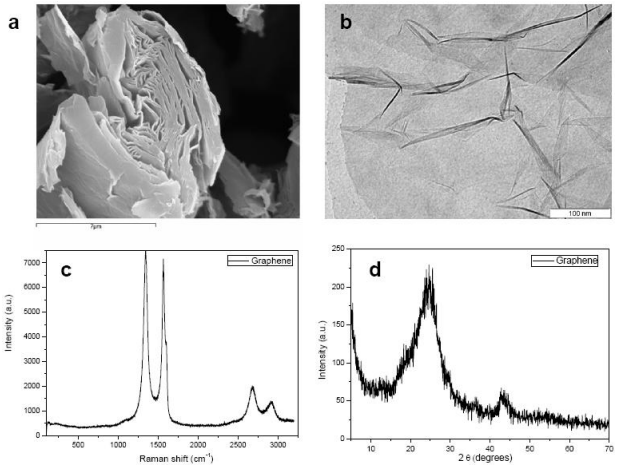

Figure 1. a) SEM of dry graphene layered structure, b) TEM of two superimposed graphene nanosheets, c) and d) Raman and XRD spectra of graphene, respectively.

This work was supported by the Spanish Ministry of Science and Innovation (Grants CTQ2008-05758/PPQ, MAT2011-20255-C02-02, TEC2010-21574-C02-02 and PI09/90527), the Government of Catalonia (Grants 2009SGR1529 and 2009SGR235), and the European Union (Grant FP7-SPA-2010-263044).

Blake, P., et al. (2008) *Nano Lett.* **8**(6), 1704-1708.
Cho, W.B., et al. (2009) *Opt. Express* **17**(13), 11007-11012.
Cho, W.B., et al. (2011) *Opt. Lett.* **36**(20), 4089-4081.
Chu, S., et al. (2010) *Appl. Phys. Lett.* **96**, 051111.
Jaworek, A. (2007) *J. Mater. Sci.* **42**(1): 266-297.
Modesto-Lopez, L. B., Biswas P. (2010) *J. Aerosol Sci.* **41**, 790-804.
Zhu, Y., et al. (2010) *Adv. Mater.* **22**, 3906-3924.

Tailoring Single-walled Carbon Nanotube Diameters in Aerosol Synthesis Method

Albert G. Nasibulin[1], Ying Tian[1], Marina Timmermans[1], Antti O. Kaskela[1], Kimmo Mustonen[1], Toma Susi[1], Ilya V. Anoshkin[1], Esko I. Kauppinen[1]

[1] NanoMaterials Group, Center for New Materials and Laboratory of Physics, Aalto University, Finland;
[2] Laboratory of Carbon NanoMaterials, Kemerovo State University, 650043, Kemerovo, Russia;
Keywords: Carbon Nanotube, Synthesis, saturable absorber
Presenting author email: albert.nasibulin@aalto.fi

Single-walled carbon nanotubes (SWCNT) have been widely explored in attempts to take advantage of their outstanding electronic, mechanical and optical properties for many applications, and extensive efforts have been made to develop various fabricating techniques to optimize the growth of SWCNTs. Aerosol chemical vapor deposition (CVD) approach, in particular, has potential for large scale SWCNT growth since it is a continuous process involving both catalyst particle formation and SWCNT growth. Recently, SWCNTs have been reported as excellent saturable absorbers used in solid state and fiber lasers because of their fast recovery time, low saturation intensity, large flexibility and environmental robustness. However, one bottleneck for their widespread applications is the limited control of diameter and chiral angle of the produced SWCNTs, and these physical variations lead to striking changes in their electronic and optical behaviors.

In this work, we report an effective and simple approach to address the above mentioned issue by producing SWCNTs on the surface of iron catalyst nanoparticles formed by decomposition of ferrocene vapor in CO atmosphere in the aerosol CVD reactor. The introduction of the controlled amount of CO_2 is found to be a key factor for the efficient, selective growth of SWCNTs using the aerosol method. Figure 1 shows the absorption spectra of the as-synthesized SWCNT thin film samples grown at different CO_2 concentrations. The intensity of absorption peaks from van Hove transitions of semiconducting and metallic SWCNTs are noticeably pronounced compared to the background absorption, indicating the high purity of the as-synthesized SWCNTs. Moreover, the absorption peaks steadily shift to longer wavelengths from 1450 to 2300 nm as the CO_2 concentration increases from 0.25 to 1.00%. This significant up-shift of absorption peaks implies the increase of SWCNT diameter with the CO_2 concentration. The diameter distributions of SWCNTs calculated based on optical absorption spectra are shown in Figure 1 (Tian *et al.*, 2010). A Gaussian fit shows that the mean diameter of SWCNT samples increases from 1.2 to 1.9 nm with the CO_2 concentration. The diameter distribution mainly ranging from 0.8 to 1.4 nm is obtained for the SWCNT samples synthesized at 0.24 and 0.50% CO_2 concentration. For the SWCNT samples collected at the concentration of 0.75 and 1.00%, the diameter distribution shift to larger diameter range of 1.2~2.0 nm. Increasing the diameter of SWCNTs with CO_2 concentration can be explained by the etching effects of CO_2. When CO_2 is present in the system, the CNT embryos of high curvature can be etched due to the inverse Boudouard reaction, consequently suppressing the growth of small diameter tubes (Tian *et al.*, 2011).

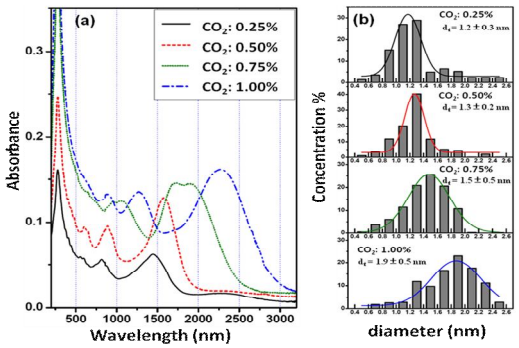

Figure 1. (a) The absorption spectra of SWCNT samples synthesized at 880 °C with different CO_2 concentrations. (b) The evaluated diameter distributions of SWCNT samples with different CO_2 concentrations based on absorption spectra.

This result opens up a route towards the diameter-controlled synthesis of SWCNTs. Using the simple dry-transfer technique, the as-deposited SWCNT films with desirable diameters are stamped onto the highly reflecting Ag-mirrors forming a saturable absorber mirror (SAM). The SAMs with deposited SWCNTs are ready for use without any additional purification and processing steps. Such as-deposited SWCNT thin films with optimized diameters show promising applications as saturable absorbers in mode-locked fiber lasers, due to the adequate control of their absorption properties which ensure the self-starting short-pulse operations. The effect of nanotube diameter distribution on nonlinear absorption characteristics and fiber laser mode-locking behaviour has been studied.

This work was supported by the Academy of Finland (Project No. 128445), ’08 NEDO Grant, by Aalto University MIDE program via CNB-E project.

Tian, Y., Jiang, H., Pfaler, J.v., Zhu, Z., Nasibulin, A.G., Nikitin, T., Aitchison, B., Khriachtchev, L., Brown, D.P., & Kauppinen, E.I. (2010). *The Journal of Physical Chemistry Letters*, **1**, 1143-1148.

Tian, Y., Timmermans, M., Kivistö, S., Nasibulin, A., Zhu, Z., Jiang, H., Okhotnikov, O., & Kauppinen, E. (2011). *Nano Res.*, **4**, 807-815.

Aerosol-derived antimony doped-tin oxide nanoparticles and studies on the influence of organic and inorganic shells in nanoparticle assemblies on the overall conductance

S.B. Bubenhofer[a], C.M. Schumacher[a], G.A. Sotiriou[b], R.N. Grass[a] and W.J. Stark[a]

[a]Institute for Chemical and Bioengineering, ETH Zurich, Zurich, 8093, Switzerland
[b]Institute of Process Engineering, ETH Zurich, 8092 Zurich, Switzerland
Keywords: flame spray pyrolysis, oxide nanoparticles, core-shell particles, coatings, surfactants.
Presenting author email: s.bubenhofer@chem.ethz.ch

Transparent conductive oxides are of high interest for transparent electrodes in solar cells or liquid displays and for infrared-reflecting applications. The most common material is indium doped tin oxide showing a high conductivity and transparence. Nevertheless a change to other doped tin or zinc oxides was driven in the last years by the low abundance of indium on earth.[1] Furthermore, the need to overcome the traditional vacuum deposition methods for more cost efficient and moreover even flexible devices, led to intensive investigation on nanoparticle film processing.

Good film forming behavior in nanoparticle deposition methods, as spin coating or dip coating, is based on highly stabilized dispersions, where normally surfactant molecules are added or a functionalization of the particles is necessary. The introduction of such impurities in the films, which cannot always be removed by heat post-treatment (flexible polymer substrates: temperature sensitive) mostly leads to an decrease in conductivity in the overall nanoparticle assembly.[2]

We therefore present the high temperature, aerosol synthesis of antimony doped tin oxide nanoparticles and a systematic study on the influence of organic and inorganic shells on the overall conductivity of assembled nanoparticles.[3] Flame spray synthesis was used as scalable and cost efficient process to produce high purity antimony doped tin oxide with a highly controlled dopant content.[4] The as-prepared particles were coated with three different organic surfactants using common dispersing processes. For comparison to well-known insulating shell thickness, additionally particles with in-situ coating of SiO_2 were produced.[5]

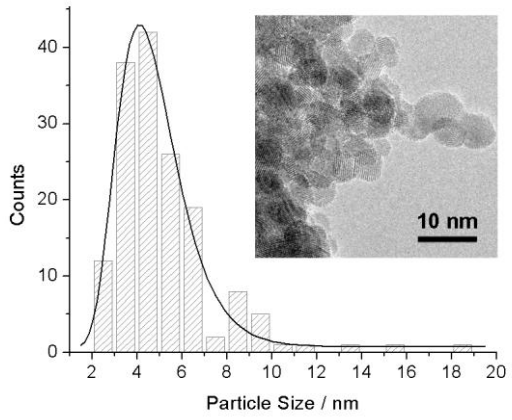

Figure 1. Antimony doped tin oxide nanoparticles produced by high temperature, aerosol flame spray synthesis.

The electron transport through the nanocomposites was tested for both organic and inorganic shell materials by measuring the electrical resistivity of pressed pills. Pure conducting nanoparticles, thin organic shells as well as thin, probably only partially coated SiO_2 shells showed a clear decrease in resistivity under pressure load due to irreversible compaction of the powder. However, thick polymer shells showed a relaxation of the resistivity when the pressure was decreased. For insulating SiO_2 shells of similar thickness the same reversible behavior in resistivity was observed and we could therefore describe this effect by electron tunneling through the insulating shell. The compression of the shell led to a decrease in thickness and therefore a higher electron tunneling probability.[6]

These findings on the influence of impurities such as surfactants or processing aids on the electron transport in assembled nanoparticle systems are important for improving the production of low cost, high performance electronics.

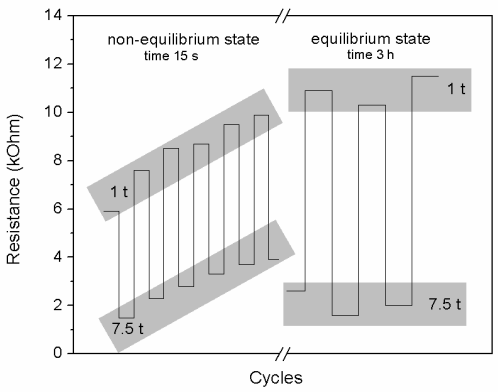

Figure 2. Reversible resistivity of polymer coated antimony doped tin oxide nanoparticle due to electron tunnelling probability changes under pressure cycles.

(1) Ginley, D. S.; Bright, C. (2000) *MRS Bull.* **25**, 15-18.
(2) Buhler, G.; Tholmann, D.; Feldmann (2007) C. *Adv. Mater.* **19**, 2224-2227.
(3) Bubenhofer, S. B.; Schumacher, C. M.; Koehler, F. M.; Luechinger, N. A.; Sotiriou, G. A.; Grass, R. N.; Stark, W. J. *submitted*.
(4) Stark, W. J.; Strobel, R.; Guenther, D.; Pratsinis, S. E.; Baiker, A. (2002) *J. Mater. Chem.* **12**, 3620-3625.
(5) Teleki, A.; Heine, M. C.; Krumeich, F.; Akhtar, M. K.; Pratsinis, S. E. (2008) *Langmuir* **24**, 12553-12558.
(6) Athanassiou, E. K.; Krumeich, F.; Grass, R. N.; Stark, W. J. (2008) *Phys. Rev. Lett.* **101**, 166804

Synthesis of well-structured Pt catalysts on spherical SiO_2 support by a CVS/CVD process using novel metal-organic precursors

M. Faust[1], K. Gao[1], M. Enders[2], S. Bräse[2], W. Gerlinger[3] and M. Seipenbusch[1]

[1]Institute for Mechanical Process Engineering and Mechanics, Karlsruhe Institute of Technology, Karlsruhe, 76131, Germany
[2]Institute of Organic Chemistry, Karlsruhe Institute of Technology, Karlsruhe, 76131, Germany
[3]Joint Lab IP3, BASF SE, Ludwigshafen, 67056, Germany
Keywords: chemical vapor deposition, platinum nanoparticles, catalyst
Presenting author email: matthias.faust@kit.edu

Introduction

Platinum on metal oxide support is a widely used catalyst in chemical synthesis and environmental technology. The dependency of activity and selectivity on surface structure and modification of catalysts is a research topic of growing interest. Continuous chemical vapour synthesis (CVS) of gas-borne support particles combined with chemical vapour deposition (CVD) of noble metal dots gives ordered, defined nanocatalysts with high surface area. Previous investigations show narrowly distributed, highly dispersed palladium nanoparticles with median sizes between 3 and 9 nm on SiO_2 (figure 1) produced by the CVS/CVD process at atmospheric pressure (Binder *et al.*, 2010). In this study Pt nanoparticles are deposited on spherical SiO_2 substrates by metal organic chemical vapour deposition (MOCVD) using commercial and newly synthesized precursors. The surface chemistry of the support particles has a great influence on the Pt deposition. It is proposed that the Pt precursor interacts with the surface hydroxyl group (OH) of SiO_2 and decomposes to form Pt on the surface (Xue *et al.*, 1992). Afterwards autocatalysis takes place on local Pt clusters and catalyses nucleation and deposition. Thereby platinum acts as a hydrogenation catalyst on the surface during the deposition mechanism (Kumar *et al.*, 1989). We propose that the precursor formulation is the decisive factor for controlled and highly dispersed Pt dot concentration on the support.

Experimental

For support particle production alkoxide tetra-ethylorthosilicate ($Si(OC_2H_5)_4$,TEOS) is evaporated at 60 °C and mixed with oxygen and nitrogen. Subsequently spherical SiO_2 nanoparticles with mean particle size of about 80 nm are generated by homogeneous nucleation, followed by sintering at 1500 °C. Commercially available Methylcyclopentadienyl-(trimethyl)Platinum(IV) ($MeCpPtMe_3$) or three synthesized organometallic precursors are sublimated at 100 °C. Directly in the aerosol, Pt is deposited on SiO_2 support particle surface in CVD reactor at 380 °C and atmospheric pressure. Afterwards nanoparticles are characterized by SMPS measurement and TEM images.

Results and discussion

According to TEM images (figure 2) the difference between Pt particles deposited on SiO_2 using the commercial precursor $MeCpPtMe_3$ and using newly synthesized precursors are significant. In contrast to the particles produced by the commercial precursor, the Pt dots are homogeneously dispersed with narrow size distributions between 2 and 4 nm. Our observations show that the suitable stability of the new precursors under vaporization and the adequate decomposition under CVD conditions play an important role in the synthesis of these well-structured Pt catalysts.

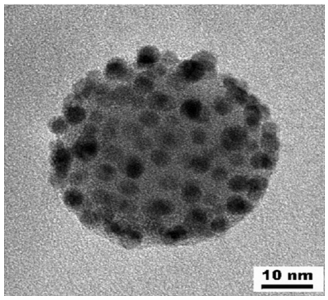

Figure 1: TEM image of Pd deposited on SiO_2.

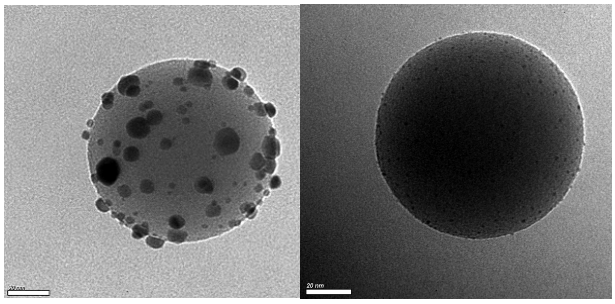

Figure 2: TEM image of Pt deposited on SiO_2 using commercial $MeCpPtMe_3$ (left) and using newly synthesized precursor (right).

This work was supported by the state Baden-Württemberg, Germany and Joint Lab IP3, BASF SE.

References

Binder, A., Seipenbusch, M. and Kasper, G. (2010) *J. Phys. Chem. C.* **114**, 7816-7821.

Xue, Z., Thridandam, H., Kaesz, H., Hicks, R., (1992) *Chem. Mater.* **4**, 162-166.

Kumar, R., Roy, S., Rashidi, M. and Puddephatt, J. (1989) *Polyhedron.* **8**, No. 4, 551-553.

Different hybrid and single-phase nanoparticles by aerosol-photopolymerization

E. Akgün[1], W. Gerlinger[2], M. Wörner[1], B. Sachweh[2], J. Hubbuch[1]

[1]Process Engineering in Life Sciences, Karlsruhe Institute of Technology, Karlsruhe, 76131 Germany
[2]BASF SE, Ludwigshafen, 67056, Germany
Keywords: dielectric barrier discharge, photoinitiation, nanocomposites, inorganics, molecular weight
Presenting author email: ertan.akguen@kit.edu

Polymeric hybrid nanomaterials containing inorganic nanoparticles find a variety of applications in optical, magnetic and electronic components as, for example, UV-protecting transparent polymers and magneto-optical storage elements. Depending on the inorganic and organic materials, the polymer matrix could serve as the low-cost printing agent onto a surface for the inorganic content to fulfill its function within such multifunctional nanocomposites (Althues *et al*, 2007). Such nanomaterials are also used in nanomedicine. In drug delivery, for instance, they can be used as carrier vehicles (Shi *et al*, 2010).

Different methods are available to produce nanoscale polymer particles or polymeric hybrid structures. Among wet methods, the mini-emulsion polymerization is a widely used technique. Based on particle generation methods in aerosols, Esen and Schweiger (1996) and Gao *et al* (2007) performed photopolymerization for the generation of spherical microscale polymer particles. These authors used multiacrylate mixtures as monomer solutions and finally obtained low-concentrated particles in aerosols. In our work, we demonstrate the aerosol-photopolymerization not only for the production of concentrated and spherical nanoscale polymer particles, but also for hybrid particles. There are many advantages of photoinitiated polymerization in aerosols compared to other methods. The polymerization reactions in each single monomer droplet can be started instantaneously due to photoinitiation via UV irradiation. Furthermore, the initiation rate can be adjusted by the photoinitiator concentration in monomer solution and by UV photon flux. In comparison to wet methods, there is no need of surfactant addition in the aerosol process, which results in higher product purity. Additionally, photochemistry allows a continuous experimental set-up.

Main components of the set-up are an aerosol generator and an in-house constructed flow-through photoreactor. The aerosol generator, which is an atomizer, produces nitrogen-carried submicron monomer droplets from the monomer solution containing at least one monomer type and photoinitiator. Additives like cross-linker or inorganic nanoparticles can also be added into the monomer solution. The produced droplet aerosol is passed through the photoreactor, where polymeric particles are formed from nanoscale droplets by UV-initiated free radical polymerization. Irradiation in the photoreactor starts the polymerization reactions in each single monomer droplet, which in turn leads to the formation of solid polymers. For characterization, the produced particles in the aerosol leaving the photoreactor may be collected on a filter membrane, on a TEM grid, or transferred into a liquid phase.

The resulting particles were characterized by Fourier Transform Infrared Spectrometry with an attenuated total reflection unit (FTIR-ATR), Scanning Mobility Particle Sizer (SMPS), Transmission Electron Microscopy (TEM), Scanning Electron Microscopy (SEM), and Gel Permeation Chromatography (GPC). In addition, simulation has been performed to support the experimental results and to illustrate the power of photoinitiated polymerization for homopolymer and organic-inorganic hybrid nanostructure synthesis.

Figure 1 shows on the left side a SEM picture of on purpose agglomerated single-phase spherical nanopolymers. On the right side, a TEM picture of a hybrid nanoparticle can be seen. In this type of hybrid nanoparticles, where the inorganic nanoparticles are distributed in the polymer matrix, the concentration of the inorganic phase can be varied broadly ranging from 0.5 to 20 mass percent.

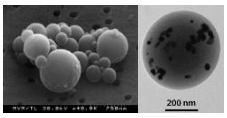

Figure 1. On left: spherical single-phase particles; on right: a spherical hybrid particle composed of organic and inorganic phases.

Other types of hybrid nanoparticles are generated as well and will be demonstrated.

This project is part of the JointLab IP3, a joint initiative of KIT and BASF. Financial support by the ministry of science, research and the arts of Baden-Württemberg (Az. 33-729.61-3) is gratefully acknowledged.

Althues, H., Henle, J., Kaskel, S. (2007) *Chem. Soc. Rev.* **36**, 1454-1465

Shi, J., Votruba, A., R., Farokhzad, O., C., Langer, R. (2010) *Nano Lett.* **10**, 3223-3230

Esen, C., Schweiger, G. (1996) *J. Colloid Interface Sci.* **179**, 276-280

Gao, Z., Grulke, E. A., Ray, A., K. (2007) *Colloid Polym. Sci.* **285**, 847-854

Continuous, electrostatic controlled synthesis of organic-inorganic composite particles

S. Sigmund[1], E. Akgün[2], J. Meyer[1], M. Wörner[2], W. Gerlinger[3] and G. Kasper[1]

[1]Institute of Mechanical Process Engineering and Mechanics, Karlsruhe Institute of Technology, 76131 Karlsruhe, Germany
[2]Institute of Process Engineering in Life Science, Karlsruhe Institute of Technology, 76131 Karlsruhe, Germany
[3]BASF SE, 67056 Ludwigshafen, Germany
Keywords: Composite nanoparticles, electrostatic particle coating
Presenting author email: stephanie.sigmund@kit.edu

An electrostatic controlled process will be described to generate organic-inorganic composite particles, consisting of an inorganic core, and a polymeric shell. Depending on the respective application, either a porous or a closed shell is desired.

Mostly, a polymeric shell serves as protection for core particles. This protection can keep the core particle from changing its chemical conditions, for example from oxidizing. A polymeric shell can ensure defined spacing between the core particles. Other applications of organic-inorganic composite materials can be found in medicine. A modified organic shell is applied for specific transport of the core material into cells, where it is used either for diagnostics, or therapy. But there are other applications as well. The shell affords the printability of every desired core material on a surface, which can serve as a low cost manufacturing method of semi-conductor technology. Therefore a polymeric shell turns the core particle into a versatile applicable and processable product while preserving its characteristics.

The coating process which we use is an electrostatic controlled process. The core material is charged, while the coating material is charged with inverse polarity. The attractive forces between negative and positive charges cause an increase in coagulation rate, compared to diffusive coagulation, which has been described by Zebel (1959). Additionally, repulsive forces between unipolar charges decrease coagulation rate of two coating particles, or two core particles, respectively. This effect of selective coagulation, controlled by surface charges is capitalized for the generation of composite particles. The method of charge supported agglomeration has been used before (Maisels et al. 2000) to generate particle doublets, but not to generate a core-shell structure. The charge controlled coating process is a purely physical process and thus independent of the core and the coating material. The coating thickness is conditioned by the amount of polymer material. The charges on the core particles surface locate themselves homogeneously due to repulsive forces and this leads to homogeneous allocation of the polymer material onto the core particle. The generation of composite particles in liquid phase has been investigated by Nabih et al. (2011) but a liquid phase process cannot provide the product pureness, process control and short time scales an integrated gas phase process does.

For our experiments a model system of SiO_2 core particles and polystyrene coating particles is used. The spherical, monodisperse core particles are 250 nm in size. An aqueous suspension of core particles is atomized and the water is removed by a diffusion-dryer. Afterwards the core particles are charged by a corona charger. Every core particle carries several ten positive elementary charges after leaving the charging system. The polymer particles, used to form a porous shell around the core particle, are also suspended in water and dispersed into air. These spherical polystyrene particles of 34 nm in diameter get charged negatively by passing a second corona charging system. Subsequently, charged core particles and charged coating particles are mixed and passed through a variable residence time volume ensuring selective coagulation. The attachment of negative polymer particles to the positive silica surface leads to equalization of positive charges. While using a mobility scan via SMPS for monitoring the number of positive elementary charges per core particle, one can follow the coating process progress. After the completion of surface coating several analyses were done. Samples were taken for control of coating thickness and structure via electron microscopy. Results from offline analysis were compared to those from online coating thickness measurements by SMPS.

Also presented will be a modified process to generate a continuous polymer shell of variable thickness around a core particle. This process cannot be described yet due to patent law reasons.

This project is part of the JointLab IP3, a joint initiative of KIT and BASF. Financial support by the ministry of science, research and the arts of Baden-Württemberg (Az. 33-729.61-3) is gratefully acknowledged.

Nabih, N., Landfester, K., Taden, A.,(2011). *Water-Based Inorganic/Polymer Hybrid Particles Prepared Via a Multiple Minieemulsion Process.* Journal of Polymer Science Part A, Polymer Chemistry, 49, 5019.

Maisels, A., Kruis, F.E., Fissan, H., Rellinghaus, B., Zähres, H.(2000) *Synthesis of Tailored Composite Nanoparticles in the Gas Phase.* Applied Physics Letters, 77, 4431

Zebel, G.(1959). *Zur Theorie der Koagulation disperser Systeme aus elektrostatischen und magnetischen Dipolen,* Staub 19, 381.

Room temperature ultraviolet nanophosphor of geometrical MgO nanoparticles

P.V. Pikhitsa[1], C.H. Kim[2], S. Chae[1], S. Shin[3], S. Jung[4] and M. Choi[1]

[1] Global Frontier Center for Multiscale Energy Systems, School of Mechanical and Aerospace Engineering, Seoul National University, Seoul 151-744, Korea

[2] Department of Mechanical Engineering, The University of Minnesota, Minneapolis, Minnesota 55455, United States

[3] Department of Mechanical Engineering, The University of Michigan, Ann Arbor , Michigan 48109-2125, United States

[4] Automotive Research & Development Division, Hyundai Motor Group, Yongin-si, Gyeonggi-do 446-912, Korea

Keywords: MgO nanoparticles, flame metal combustion, cathodoluminescence.
Presenting author email: peter@snu.ac.kr

We report a novel type of MgO nanoparticles that we named “geometrical” smoke which appeared to be a room-temperature ultraviolet nanophosphor.

Unlike usual MgO nanocubes that are generated during a Mg metal particle self-burning in air “geometrical” smoke is characterised by an abundance of pure spherical and terraced nanoparticles yet preserving the perfect cubic lattice of MgO. The generation of “geometrical” smoke follows the violent burning of Mg powder assisted by oxy-hydrogen flame Yang *et al* (2010) or by applying a cw CO2 laser to the self burning Mg particle. The dramatic intensification of the combustion process leads to switching to another nanoparticle growth mechanism leading not only to spherical shapes of MgO nanoparticles but also to creation of new types of structural defects in “geometrical” smoke.

These novel di-vacancy defects named P-centers may appear in the perfect cubic MgO structure when a whole MgO molecule is omitted. The P-center looks formally as a close pair of other well-known defects F (oxygen vacancy) and V (Mg vacancy) centers both of which are optically active in MgO Gibson *et al* (1994). We performed cathodoluminescence (CL) measurements and interpreted two strongly correlated bands (at ultraviolet (UV) 260 nm and at 490 nm) shown in Fig. 1 as the optical response from the P-center. For ordinary MgO smoke the cathodoluminescence revealed only the band from F^+ centers at 420 nm depicted in Fig. 2.

Finding room temperature strong UV in pure MgO looks unusual as far as all UV bands found above 5 eV and at low temperatures previously were due to impurities like Al, Si etc. Kalder *et al* (1976). Yet in our case we found no correlation with the impurity levels as far as the same low level of impurities existed in both UV and non-UV emitting samples.

We also checked the robustness of the P-centers by treating the powder with immersing in water, with hydrogen plasma and outgassing at high temperatures only to find out that the UV activity remained intact.

As far as such a well-distinguished UV CL makes it possible to indicate the “violent” history of the nanoparticle generation we foresee possible applications of the reported phenomenon in geosciences, planetology and astrophysics. Other application for nanooptics are possible as well.

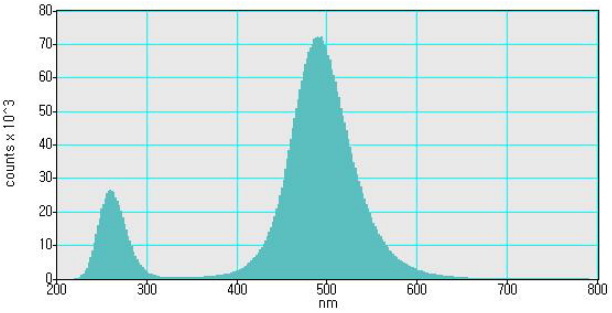

Figure 1. Typical CL spectrum from “geometrical” smoke with P-centers.

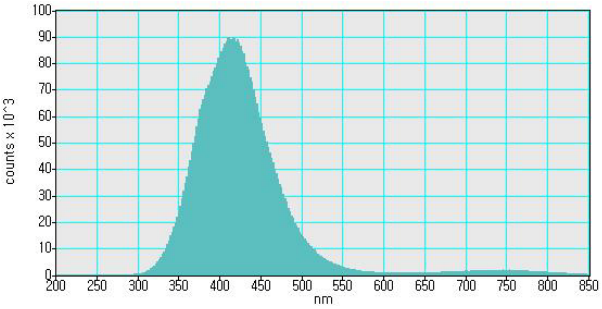

Figure 2. Typical CL spectrum from ordinary smoke with F^+ centers.

This work was done by financial support from the Global Frontier Center for Multiscale Energy System supported by the Korean Ministry of Science and Technology..

Yang, S. *et al.* (2010) *Powder Technol* **197**, 170-176.

Gibson, A., Haydock, R. and LaFemina, J. P. (1994) *Phys Rev B* **50**, 2582-2592.

Kalder, K. A., Kyarner, T. N., Lushchik, C. B., Malysheva, A. F. and Milenina, R.V. (1976) *Zhurnal Prikladnoi Spektroskopii* **25**, 1250-1255.

Tuesday, September 4, 2012

Session WG08S3O. Measurement Methods

Batch-to-Batch-Variability of Stöber synthesized SiO2 nanoparticles – Comparison of DLS and SMPS data within Q-NANO

S. Mülhopt[1], M. Hauser[1], E. Mahon[2], Reinhard Schneider[3], H.-R. Paur[1]

[1]Institute for Technical Chemistry, Karlsruhe Institute of Technology, 76021 Karlsruhe, Germany
[2]Centre for Synthesis and Chemical Biology, University College Dublin, Belfield, Dublin 4, Ireland
[3]Laboratory for Electron Microscopy, Karlsruhe Institute of Technology, 76021 Karlsruhe, Germany

Keywords: Nanoparticles, Stöber synthesis, silica, DLS, SMPS
Presenting author email: muelhopt@kit.edu

Background:

QNano is a European Union-funded infrastructure for nanomaterial safety testing. This four year project which has begun in February 2011 comprises 27 top European analytical and experimental facilities in nanotechnology, medicine and natural sciences. It aims to create an integrated hub to support Europe's nanosafety research community. It also covers research themes about nanoparticle production and characterization. In WP 5 one aspect is to define the sources for batch-to-batch-variability of nanoparticles within one production route.

Material and Methods:

Particle production:

The only variable is the amount of aqueous ammonia present in the system which was used to determine resultant particle size. To a defined amount of aqueous ammonia (28%) in a polypropylene container was added EtOH (99.9%) to a volume of 50 ml and stirred at 25^{0}C (for SilNP007 and SilNP009) or 55^{0}C (for SilNP008 and SilNP010) and 600 r.p.m on a plate stirrer. To this rapidly stirring solution was then added Tetraethylorthosilicate (TEOS) (1670 µl) in one aliquot. The solution was then sealed under N_2 and stirred for a further 20 hours at 25^{0}C. The resulting nanoparticle suspension was divided in fractions and centrifuged down at 14,000 rpm for 20 minutes with the pellet then resuspended in fresh ethanol aided by bath sonication. This washing procedure was repeated twice more with ethanol followed by 3 pure water washes and a final resuspension in pure water to a concentration of 10 mg/ml.

Size Measurements

The silica nanoparticles were size characterized by different methods: in suspension by dynamic light scattering with a Malvern Zetasizer Nano ZS and for comparison it was aerosolized by electrospray (Model 3480, TSI, USA) and measured with SMPS (Model 3934, TSI, USA) in the range of 7 – 350 nm.

Results:

The analysis shows a very similar behaviour but depending on method and suspension medium there is a difference in number mean size of about 10 nm. The batches SilNP007 and SilNP009 show a modal value at about 43 nm by DLS (Table 1) but 50 and 53 nm in the SMPS measurements in aerosol phase (Figure 1). The batches SilNP008 and SilNP010 were determined to be 20 nm in liquid suspension and 33 nm in the gas phase.

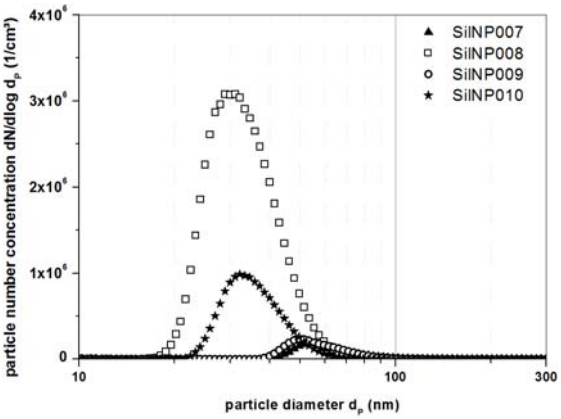

Figure 1. SMPS measurements of the 4 batches SilNP007 – SilNP010 of Stöber synthesized silica suspended in air by electrospray.

Table 1. Comparison between different methods of size measurements. DLS: number mean in nm. SMPS: Modal diameter of number size distribution in nm.

	DLS	SMPS
SilNP007	43	53
SilNP008	20	33
SilNP009	44	50
SilNP010	21	33

Acknowledgement:

This work is part of the European Research Infrastructure for nanosafety assessment QNano. http://www.qnano-ri.eu/

The use of Nuclear Reaction Analysis technique for the determination of Nitrogen in aerosol samples collected on Teflon filters

I. García Orellana[1,2], S. Becagli[3], G. Calzolai[4], M. Chiari[4], J. García López[2], S. Nava[4], F. Lucarelli[4], M. Respaldiza[2], R. Vecchi[5]

[1] Departamento de Física Aplicada 1, EPS, Universidad de Sevilla,E-41011 Seville, Spain
[2] Centro Nacional de Aceleradores, E-41092 Sevilla, Spain
[3] Department of Chemistry, University of Florence, and INFN, I-50019, Sesto Fiorentino (FI), Italy
[4] Department of Physics and Astronomy, University of Florence, and INFN, I-50019, Sesto Fiorentino (FI), Italy
[5] Department of Physics, University of Milan, and INFN, I-20133, Milan, Italy

Keywords: Ion beam analysis, NRA, deuteron, EBS, Nitrogen, PM2.5, PM10, Teflon
Presenting author email: iorellan@us.es

Ion Beam Analysis (IBA) techniques are very suitable for non-destructive characterization of atmospheric particulate matter. The most used for this purpose is Particle Induced X-ray Emission (PIXE) thanks to its ability to detect a wide range of elements (Z>10) simultaneously with higher sensitivity than other IBA techniques. Nevertheless, the determination of light elements content, as C, N, O and H, is of crucial interest, as these elements constitute a big amount of the aerosol composition. These elements are not detectable by PIXE because of the self-absorption of their characteristic X-rays in the sample itself and in the detector window. A method has been developed to measure light elements in aerosol particulate matter collected on Teflon (CF_2) filters by Elastic Backscattering Analysis (EBS) and Particle Elastic Scattering Techniques (PESA) with proton beams (Chiari, 2004, Chiari, 2005). Quantitative results have been obtained for these light elements with very satisfactory accuracies for C, and some less for O and especially for N.

In this work, Nuclear Reaction Analysis (NRA) has been used as an alternative IBA technique for N determination in aerosol samples collected on Teflon, namely exploiting the reactions $^{14}N(d,\alpha_0)^{12}C$ and $^{14}N(d,\alpha_1)^{12}C$. The high Q-values of these reactions avoid the interferences between the reaction products and the backscattered beam particles. NRA measurements have been performed at the 3 MV Pelletron accelerator of the CNA in Seville on a set of PM10 and PM2.5 samples with beams of deuterium of 1.9 MeV energy and a detection angle θ = 150º, which corresponded to the optimal measurement conditions. As can be seen in Figure 1, the signal peak from the $^{14}N(d,\alpha_0)^{12}C$ reaction appears in a background-free region of the spectrum thus allowing Nitrogen determination without interferences from filter or other aerosol components. Absolute N concentrations were obtained by normalization to thin reference standards containing known areal density of Nitrogen, with an overall uncertainty of about 4-8%. Typical minimum detection limit (MDL) for N is 0.1 μg/cm^2, corresponding to 0.02 μg/m^3 considering a 47 mm diameter Teflon filter and sampling for 24 hours at 2.3 m^3/h (EN12341 European standard).

The samples have been analysed also by EBS at the 3 MV Tandetron accelerator of the LABEC laboratory of INFN in Florence, using proton beams of 3.6 MeV energy and a scattering angle of 150°. The total N content obtained by the different IBA techniques is comparable, nevertheless EBS provides about 20% more Nitrogen concentration than NRA.

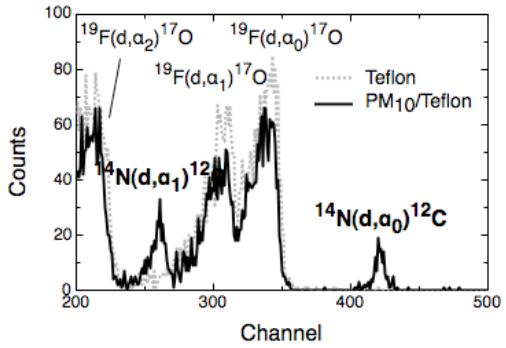

Figure 1. Comparison of NRA spectra of blank and loaded (PM10) Teflon filters obtained with 1.9 MeV deuterons.

Ion Chromatography measurements have been performed on a portion of the same samples for the determination of ammonium (NH_4^+) and nitrates (NO_3^-). Then the organic component of Nitrogen can be obtained from the total N concentrations measured by NRA as the amount in excess of "ammonium N" and "nitrate N", being in our situation negligible the contribution from nitrites. In PM10 samples "organic N" resulted about 40% of total Nitrogen, while this fraction decreased to about 25% for PM2.5 samples.

This work has been supported by INFN (NUMEN project) and by the Spanish Ministry of Education and Science (MEC).

Chiari, M., Del Carmine, P., Lucarelli, F., Marcazzan, G., Nava, S., Paperetti, L., Prati, P., Valli, G., Vecchi, R., Zucchiatti,A.,2004. *Atmospheric aerosol characterisation by Ion Beam Analysis techniques: recent improvements at the Van de Graaff laboratory in Florence.* Nucl. Instr. and Meth. B 219–220, 166-170

Chiari, M., Lucarelli, F., Mazzei, F., Nava, S., Paperetti, L., Prati, P., Valli, G., Vecchi, R.,2005. *Characterization of airborne particulate matter in an industrial district near Florence by PIXE and PESA.* X-Ray Spectrometry 34, 323-329

Laser Vaporizer-AMS for exposure assessment and detection of airborne engineered metal nanoparticles

P.T. Nilsson[1], A. C. Eriksson[1], M. E. Messing[2], C. Isaxon[1], M. Hedmer[3], H. Tinnerberg[3], B. O. Meuller[2], C. R. Svensson[1], K. Deppert[2], M. Bohgard[1] and J. Pagels[1]

[1]Ergonomics and Aerosol Technology, Lund University, P.O. Box 118, SE-22100, Lund, Sweden
[2]Solid State Physics, Lund University, P.O. Box 118, SE-22100, Lund, Sweden
[3]Occupational and Environmental Medicine, Lund University, SE-22100, Lund, Sweden

Keywords: LV-AMS, SP-AMS, metals, engineered nanoparticles, exposure
Presenting author email: patrik.nilsson@design.lth.se

The production of materials containing engineered nanoparticles (ENPs) is a rapidly growing industry and emissions of such particles can occur any time during the materials lifetime.

The aim with this work was to utilize and to explore the potential of the Aerodyne Laser Vaporizer Aerosol Mass Spectrometer (LV-AMS) as a tool to investigate and characterize exposure levels of metal ENPs. In contrast to the regular AMS technique, that uses a heated plate (600 ^{o}C) for vaporization of the sampled particles, the LV-AMS has an Nd-YAG laser (λ = 1064 nm) installed in the vaporization zone (Onasch, 2012). This vaporisation technique is selective for absorbing particles, e.g. black carbon and metals. Vaporized molecules are then ionised using electron ionization (70 eV) and detected in a high resolution time of flight mass spectrometer.

Two methods for production of metal ENPs were used in a clean room laboratory, a spark discharge generator (SDG) and a high temperature furnace (HT). For particle size selection a tandem-DMA set-up was used with intermediary sintering furnace. The LV-AMS was used in parallel with an electrometer and a CPC to measure directly on the particles formed by the generators. One type of particles was generated at a time and the generated metals were Au, Ag, Pd, PdAg, FeO and CuO.

Emission measurements were performed in the ambient air during the cleaning of the generators. The sampling point for the LV-AMS and a photometer sensor (Dusttrak, TSI Inc.) was located a few centimeters away from the expected emission zone.

The vacuum aerodynamic diameter (d_{va}), given by the AMS, can together with the mobility diameter (d_m) be used to calculate effective densities as:

$$\rho_{eff} = \frac{d_{va}}{d_m}\rho_o \qquad (1)$$

Information on particle effective density is crucial when particle mass is to be determined from number concentrations. Often, for instance during dose estimations in exposure studies, a unit density has to be assumed which may induce significant errors. For Au particles the effective densities from the LV-AMS could be compared to values obtained with a DMA-Aerosol Particle Mass Analyzer (DMA-APM).

It was deduced that all the generated metals, except CuO, could be vaporized by the laser and detected in the mass spectrometer. The calculated mass based relative ionization efficiency (Onasch, 2012) were similar (0.01-0.02) for all detected compounds.

In figure 1 LV-AMS and Dusttrak times series, obtained during the cleaning process of the generator setup, are presented. Only the Au (m/z 197) and one Fe (m/z 56) isotope signal is shown. Each detected metal showed a unique time series.

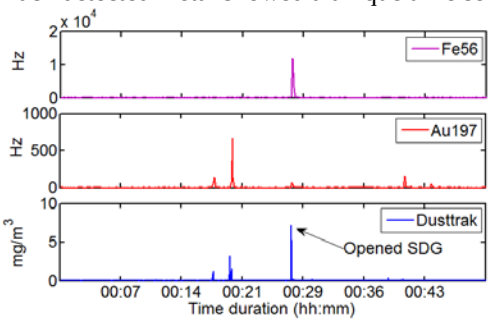

Figure 1. Time series of Au and Fe signal and Dusttrak during cleaning of the generator setup

The effective densities for Au agglomerates, determined by DMA-LVAMS, showed the same trend as those determined with DMA-APM, with slightly lower values from the DMA-LVAMS.

Table 1. Effective densities for Au agglomerates

d_m (nm)	DMA-LVAMS (g/cm^3)	DMA-APM (g/cm^3)
60	1.8	2.4
100	1.3	1.5

The LV-AMS is a promising tool for highly time-resolved studies of airborne exposures to engineered metal nanoparticles.

This work was performed within the Consortium for Aerosol Science and Technology (CAST) and supported by the Nanometer Structure Consortium at Lund University (nmC@LU), the Swedish research council FAS and the FAS-centre METALUND

Onasch T. et. al., 2012, *Aerosol Science and Technology*, In press, DOI: 10.1080/02786826.2012.663948

Size and surface area characterization of Carbon nanoparticle aggregates by means of a cascade epiphaniometer

M.I. Gini[1,2], K. Eleftheriadis[1], S. Vratolis[1], C. Helmis[2], K. Giannakopoulos[3], D. Papanastasiou[4], G.Orfanopoulos[4] E. Raptakis[4]

[1]E.R.L., Institute of Nuclear Technology & Radiation Protection, NCSR "Demokritos", Ag. Paraskevi, Greece
[2]National and Kapodistrian University of Athens, Department of Physics, Division of Environmental Physics and Meteorology, University Campus, Athens, Greece
[3]Institute of Microelectronics, NCSR "Demokritos", Ag. Paraskevi, Greece
[4]Fasmatech Science & Technology, Lefkippos Attica Technology Park, Athens

Keywords: aerosol size distribution, epiphaniometer, surface area, spark source
gini@ipta.demokritos.gr

It has been generally accepted that the physical properties of engineered nanoparticles can be important with respect to the industrial usage of these particles, the potential hazardous health effects when inhaled and their fate when they are released in the environment. The objective of this work was to demonstrate results of a novel technique regarding size and surface area characterization of generated nanoparticles by spark generation.

Nanoparticles synthesis by spark discharge is based on the evaporation of the electrode material used to produce the spark, and the subsequent cooling of the vapor stream that initiates nucleation of the vapors to clusters and primary nanoparticles. Further coagulation of the primary nanoparticles can lead to particles of versatile size and shape. In this study Carbon nanoparticles (CNps) were generated by a Novel Spark Generator operating under a controlled spark mode providing modulated pulses of chosen frequency between the two graphite electrodes.

The characterization of the generated nanoparticles was performed by Scanning Mobility Particle Sizer spectrometry (SMPS). The surface area of the generated particles was measured in parallel by the SMPS described above and the Cascade Epiphaniometer (CEPI) (Gini et al., 2010) which measures the surface area for different size fractions. Further information on the shape and structure was also obtained by low voltage scanning electron microscopy (SEM).

The cascade epiphaniometer was thoroughly calibrated against mono- and poly-disperse aerosols of known properties. The results show that SMPS and CEPI size distributions in the case of spherical or almost spherical particles are in reasonable accord. The average root mean square deviation of the total surface area measured with the CEPI from the theoretically estimated total surface area was about 15%.

In fig.1a, the calculated surface area of the generated CNps from SMPS data assuming equivalent spheres of measured mobility diameter (d_m) is depicted. Another approach for idealized loose agglomerates was also adopted for calculating aggregate surface area from SMPS data, estimating the number of the primary particles that compose the aggregate of a given mobility diameter (Lall et al., 2004). The primary particles were spheres with a typical diameter between 18nm and 20nm, which was estimated from SEM micrographs. In fig.1b, the surface area size distribution from CEPI is shown. The size distribution of CEPI is a function of aerodynamic diameter (d_a) whereas the distribution from SMPS is a function of mobility diameter.

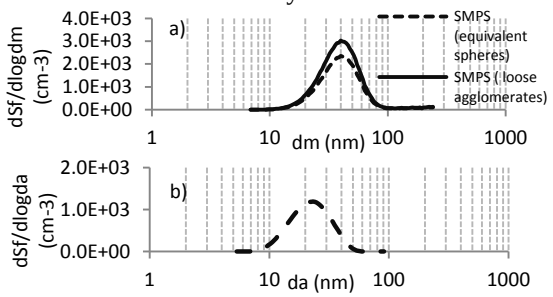

Fig.1. Surface area size distribution of CNps estimated from SMPS data (a) and measured with CEPI (b).

The results of the comparison between the calculated and the measured surface area demonstrate the importance of surface area measurements for non-spherical nanoparticles, since the calculated total surface area showed an overestimation, by a factor of 2, in relation to the measured one. This discrepancy cannot be explained by the uncertainty of the measurement. Fig.2. shows the estimated and the measured surface area as a function of the mobility diameter after accounting for the relationship between the particle mobility diameter and its aerodynamic diameter. The best fit value for the shape factor was 2.42.

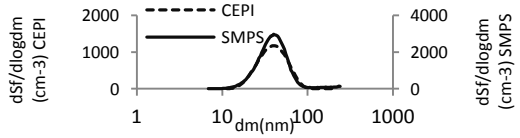

Fig.2. 'Fuchs' surface area distribution of CNps calculated from SMPS data and measured with the CEPI.

References

Gini, M I.; Helmis, C; Eleftheriadis, K: Development of a Cascade a-impactor epiphaniometer for aerosol surface size distribution measurements, International Aerosol Conference 2010, 29th Aug-3rd Sep., Helsinki.

A. A. Lall, S. K. Friedlander." On-line measurement of ultrafine aggregate surface area and volume distributions by electrical mobility analysis: I. Theoretical analysis". Aerosol Science 37 (2006) 260–271

TwinPAS – a photoacoustic instrument for the parallel, time-resolved analysis of soot and NO_2 in exhaust gas

C. Haisch and R. Niessner

Chair for Analytical Chemistry, Technische Universität München, Marchioninistr. 17, 81377, Munich, Germany

Keywords: photoacoustic, NO_2, soot, Diesel exhaust.
Presenting author email: Christoph.Haisch@ch.tum.de

Photoacoustic (PA) spectroscopy earned its merits in aerosol analysis on many occasions. In automotive industry, a PA-based instrument is routinely to monitor the mass concentration of soot in exhaust gas. An extension of our PA soot sensor, which had been the basis of the commercial soot sensor, allows for parallel detection of NO_2 and soot.

The PA effect is the conversion of absorbed optical energy to thermal energy, which results in thermal expansion. This effect is well suitable for aerosol analysis, as it allows for an artefact-free absorption analysis in the presence of light scattering particles. The direct correlation between excitation light intensity, optical absorption, and the resulting PA signal makes it a very sensitive tool with a dynamic concentration range of several orders of magnitude and time resolution in the range of seconds.

Beyond soot, NO_2 is one of the major hazardous engine emissions. Parallel quantification of these two components is particularly relevant due to their anticyclical behaviour in modern exhaust aftertreatment systems. Up to now, there is no routine instrument allowing for the parallel detection of both compounds. Current instrumentation for NO_2 analysis in exhaust gas requires for the filtration of the sample gas before the sampling cell in order to avoid contamination by the soot. Adsorption and chemical reactions of the NO_2 on the soot loaded filter surface can inflict artefacts, particularly in the case of transient analyses.

Consequently, the new TwinPAS system allows for a parallel detection of both components without filtration. The core components of the system are two PA cells, one for soot detection and one for the quantification of NO_2. While soot is detected at a laser wavelength of 806 nm, NO_2 is monitored at 532 nm. Both wavelengths are generated by a single semiconductor laser source with an emission wavelength of 806 nm. The 532 nm radiation is generated by a set of non-linear optical crystals, thus making the system compact and limiting the costs.

For exhaust gas monitoring, heating of the whole sampling and analysis system is desirable in order to prevent condensation in the system. A special PA cell design has been developed, which is heated to 80 °C, while the sensitive microphones are kept at a temperature of 45 °C. To achieve high signal stability for a wide range of gas conditions, a low-Q acoustical resonator was designed which is a combination of a longitudinal and a Helmholtz-type resonator. The data recording rate is 5 Hz; however, the time resolution (10/90 rise and fall times) are in the range of a second. In order to increase temporal resolution, a special design of the gas flow system is required. On the one hand, high flow rates result in high gas exchange rates as required for high temporal resolution, on the other hand, high-velocity gas flows may generate significant flow noise, which is picked up by the PA microphone and thus limits the signal to noise ratio.

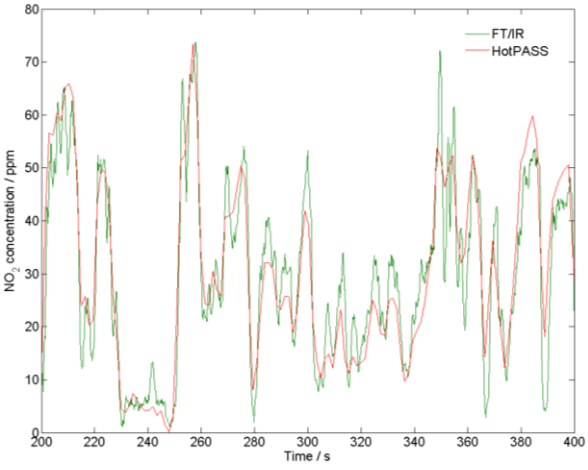

Figure 1.: NO_2 emissions of a typical driving cycle analysed by a FT/IR spectrometer and the TwinPAS system.

In the current configuration, the system features detection limits of 0.6 ppm for NO_2 and 1.2 µg m^3 for soot, determined by the common $6s_B$ criterion and on a 0.2 s time basis. A typical transient measurement is presented in Fig. 1, where the TwinPAS results are compared to the NO_2 concentrations determined by FT/IR. Further results, highlighting the key features of the new system will be presented. Future developments will be devoted to the extension to further gas components and to an improved tolerance to sample gas pressure and temperature fluctuations.

Investigation of Fast Scanning SMPS Measurements: 16s and Below

K. Erickson, F. Quant, J. Farnsworth and R. Caldow

TSI Incorporated, Shoreview, MN, 55126, USA
Keywords: SMPS, CPC, Particle Size
Presenting author email: kerickson@tsi.com

The concept introduced by Wang and Flagan (1990) of scanning the voltage in an electrical mobility based sizing instrument (SMPS) resulted in a dramatic improvement in the time resolution of the technique. Practically, moving from a voltage stepping approach to a scanning approach also increases size resolution above a minimum scan time. However, as would be expected, at some point shortening the voltage scan time will result in reduced resolution compared to the ideal resolution of the instrument defined by the DMA transfer function.

The reduced resolution is thought to be primarily a function of the response time of the CPC and the non-ideal flow laminarity between the DMA and the CPC. Now, two decades after Wang and Flagan's original work, CPCs are available which have significantly faster response times and higher sample flow rates, opening the door to faster SMPS size measurements. Tubing lengths between the DMA and CPC have also been substantially reduced. We have investigated SMPS sizing scans at 16 seconds and below using a TDMA technique. CPCs used had varying response times and sample flow rates and are detailed in Table 1.

Table 1. CPCs used in fast scanning study.

Feature	3788 N-WCPC	3787 GP-WCPC	3776 UCPC
Sample Flow (LPM)	0.3	0.6	0.05
Sheath Flow (LPM)	0.3	N/A	0.25
Time Constant τ_s (s)	0.043	0.13	0.069
Working Fluid	H_2O	H_2O	C_4H_9OH

Russell et al 1995 investigated resolution limitations to fast scanning and determined that the transfer function widened with increasing time constant (τ_s) and decreasing scan time (τ_r).

Table 2. Theoretical lower limit for scan time. τ_s/τ_r ratio >0.1 corresponds with decreased resolution.

Scan Time (s)	3788 τ_s/τ_r	3787 τ_s/τ_r	3776 τ_s/τ_r
1	0.297	0.896	0.476
2	0.145	0.440	0.233
3	0.098	0.297	0.157
5	0.059	0.178	0.094
7	0.042	0.128	0.068
10	0.029	0.088	0.047
30	0.010	0.030	0.016

The CPC response time to a step function change in concentration can be described by an exponential function. The time constant (τ_s) is the denominator of the natural logarithm exponent. The exponential voltage ramp used in scanning mobility measurements can be described with a time constant of (τ_r). It was noted that if the ratio of τ_s to τ_r was less than 0.1, that the rise of the transfer function of the scanning system was nearly as sharp as the ideal transfer function of the DMA. Table 2 details the τ_s/τ_r ratios for the scan times and CPC used in this study.

The effect of scan time on SMPS resolution was measured for a variety of scan times using monodisperse and polydisperse aerosol. Experimental conditions and results will be discussed.

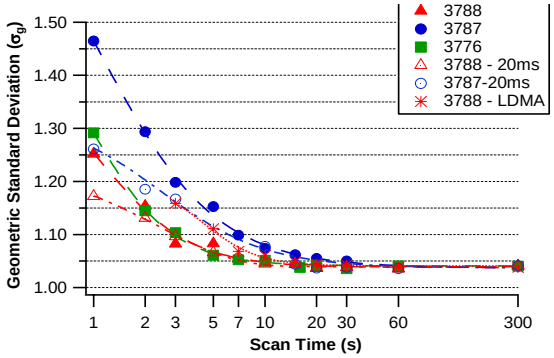

Figure 1. Geometric standard deviation (σ_g) of the size distribution of DMA classified aerosol measured using a variety of scan times. As scan time decreases, the monodisperse peak widens.

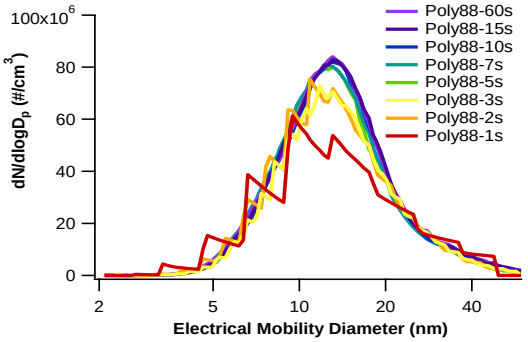

Figure 2. Polydisperse silver aerosol taken using a 3788 N-WCPC. As shown, little difference is seen in polydisperse size distributions as a function of scan time. Below 3 seconds, data reporting rate became a limiting factor even though a 20ms data reporting rate was used.

Wang SC, Flagan RC. (1990) *Journal of Aerosol Science*, 13:230-240.

Russell, LM, Flagan, RC, Seinfeld, JH. (1995) *Aerosol Science & Technology*, 23:491-509.

New portable device for high time resolved measurements of particle size distributions

Hans Grimm[1], Daniel Huhn[1], M. Pesch[1], M. Richter[1] and Friedhelm Schneider[1]

[1]Grimm Aerosol Technik GmbH & Co. KG, 83404 Ainring, Germany
Keywords: aerosol instruments, Nano particles, particle size distributions, work place measurements
Presenting author email: mp@grimm-aerosol.com

Measurements of particle size distributions for Nano particles and particles in the µ-meter size range generally requires a combination of separate devices as SMPS and optical particle counters (OPC) or aerodynamic particle sizers (APS). The company GRIMM developed in the frame of the EU founded Project NANODEVICE a new compact and portable (pre)-prototype that consists of an optical and electrical sensor in one device. It allows a wide range of particle size detection between approx. 10 nm and 20 µm in over 30 size channels with a time resolution of only 1 minute for one complete scan. Thus very short-lived as well as highly time-varying particle sources can be examined. Figure 1: shows the new prototype.

Figure 1: New prototype for particle size distributions

The measured values of the two sensors are combined internally by special electronics and firmware, such that the user receives measurements, which do not differ from the output of a single sensor in the nature and structure. The calculation of the derived measurands as particle surfaces and particle volumes is done online and the output as data telegram is send via the interfaces Bluetooth or RS232. A special control software was developed, which allows full operation with a small Netbook. Figure 2 shows a typical measurement example.

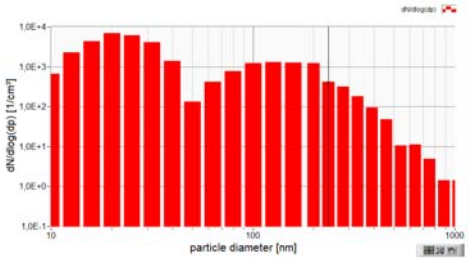

Figure 2: Measurement example

The optical module is a newly designed particle spectrometer, which detects each individual particle and classifies its size accordingly (single particle counting). A powerful laser diode is used as light source. An internal monitor diode monitors the power of the laser diode and keeps it constant. A pin diode generates the detection signal, which turned out to be the best compromise between reliability and performance. The number of particles is determined by the number of stray light pulses per period, the particle size determines the amplitude of the scattered light. These measurements require a precisely controlled flow rate which is determined continuously via aperture and pressure sensors.

The electrical module consists of three main components, the unipolar corona charger, a precipitation electrode and a Faraday Cup Electrometer (FCE). Once the aerosol particles (each single particle) are counted by the optical sensor and classified, they pass a short tube connected directly to the electrical sensor. Here all Nanoparticles can be detected reliably. Initially the particles are charged unipolar (negatively) in the electric sensor with a negative corona charge. Then the particles enter a collecting electrode, where they are separated according to their electrical mobility. A portion of the aerosol stream passes through the collecting electrode and is recorded in the Faraday Cup Electrometer (FCE). Based on the current measured at the FCE, the volume flow, the geometry of the sensor and the charge efficiency of the particles, the size of the particles can be determined. The electrical sensor offers the possibility to determine the number of particles in each size distribution of particles similar to the optical sensor: A change of the electrode voltage in 10 steps classifies the particle size between 10 nm to approximately 300 nm in 10 classes.

When measuring particles, humidity plays an important role. On the one hand, increased air humidity leads to a swelling of particles, which alters their diameter, on the other hand charges of particles change with air humidity. In addition, the determination of currents with an FCE is very sensitive to moisture and cause changes in the offset. To ensure reliable operation at varying humidity levels and to permit very high humidity (up to 90%), an internal drying cycle was designed. The FCE is continuously purged with dry air, dried by dint of a cartridge filled with silica gel.

The calibration and validation is based on parallel SMPS measurements with latex particles of different sizes.

Experimental aerosol characterization for the evaluation of source term from RDE's (Radiological Dispersion Events)

F.G. Di Lemma[1, 2], J.Y. Colle[2], H. Thiele[2] and R.J.M. Konings[1, 2]

[1]Department of Radiation, Radionuclides & Reactors, Faculty of Applied Physics, Delft University of Technology, Delft, 2629JB, The Netherlands.
[2]European Commission, DG Joint Research Centre, Institute for Transuranium Elements, P.O. Box 2340, D-76125, Karlsruhe, Germany.
Keywords: Radioactive aerosol, High temperature aerosols, Laser ablation, Laboratory experiments.
Presenting author email: fidelma.DI-LEMMA@ec.europa.eu

In the recent years, following the 9/11 terrorist attack in the U.S., an increased focus has been posed on the threat of malicious attacks involving radioactive materials. In view of this, evaluation of the source term related to RDE's and especially to the detonation of "dirty bombs" has become relevant. The descriptions of the aerosols formed during these events (both in dimension and chemical composition) are the input for modelling studies to "quantify respirable hazards, the associated radiological risk assessments and vulnerability assessments" (Molecke *et al.* (2006)). Dedicated experiments in this field could also reduce the uncertainties on the source terms applied in software codes (e.g. HOTSPOT), which assess the extension of the contaminated area after a radioactive fallout.

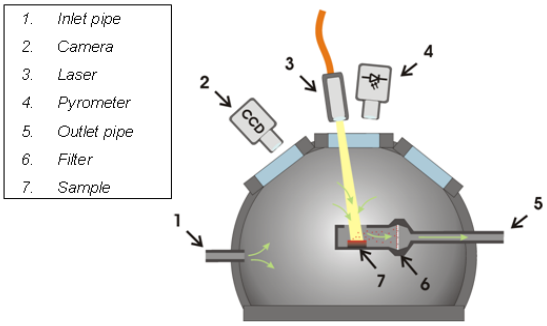

Figure 1. A scheme of the experimental set-up.

A new experimental set-up was created for these purposes. The laser heating pulse technique was applied for the first time to simulate RDE's. Different samples which could simulate widely used radioactive material are tested, in their no-radioactive form (CsCl, Co, ZrO_2 and ZrO_2 with simulated fission products). ZrO_2 was selected as a ceramic material to simulate UO_2. Samples were heated through a focused Nd-YAG laser beam. The laser can be controlled in a very flexible way, applying pulse from ms to minutes and power from 0 W to several kW, thus producing a broad variety of thermal transients. The sample surface temperature was measured by a 650 nm pyrometer. The set-up offers also the possibility to test different environments, and in our tests atmospheric conditions were established in order to assess the interaction between the aerosols and a real environment. The aerosols formed are collected by means of filters, to which they are transported by air flow created by a vacuum pump and pressurized air inlet. The filter are subsequently analysed by SEM and EDX.

From the first tests two types of aerosols were generally collected: spherical individual particles with a diameter >1 μm and "string" structures formed by particles in the range of 50-300 nm. The micrometer sized particles may be related to the ejection of liquid particles by mechanical process due to boiling. These spherical particles usually were present in a small fraction (0.1-1% of the covered filter surface). The nanometre sized particles instead may have formed by condensation processes from the vapour (Friedlander (2000)). These particles formed cluster structures, which could have been produced by agglomeration during the transport phase to the filter. Of particular interest were the doped ZrO_2 samples; the EDX analysis of the aerosols showed that low volatile elements (as Ba, Zr) were present in the bigger particles, while high volatile elements (Cs and I) were enriched in smaller aerosols. Through these last results on ZrO_2 the hypothesis on aerosol formation could be confirmed. Finally SEM analyses suggested that particles are mostly formed in the inhalable fraction (<10 μm), with potential health risk.

A relation between the thermo-physical properties of the samples and the aerosols is investigated. Experimental results suggest that the vapour pressure, surface tension and viscosity may be important parameters; these will be further studied with a wider class of materials.

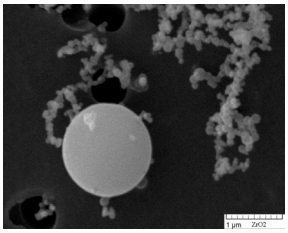

Figure 2. An example of aerosols collected showing: on the left a >1 μm particle and on the right cluster structures.

This work was supported by the 7th Framework Program of the European Commission.

Friedlander, S. K. (2000) *Smoke, Dust and Haze* Oxford University Press.
Molecke, M.A, Brockmann, J.E., Lucero D.A. et al. (2006) *47th Annual Meeting of the INNM*.

Tuesday, September 4, 2012

Session WG01S3O. Remote Sensing of Aerosol Properties

Aerosol vertical distribution and its variability over Sweden during nighttime: A view from the CALIOP-CALIPSO and AIRS instruments

M.A. Thomas[1], A. Devasthale[1] and M. Kahnert[1,2]

[1]Swedish Meteorological and Hydrological Institute, Research Department, Norrköping, SE-60176, Sweden
[2]Chalmers University of Technology, Department of Earth and Space Science, SE-412 96 Gothenburg, Sweden
Keywords: Atmospheric aerosols, Satellites, Vertical distribution
Presenting author email: manu.thomas@smhi.se

An accurate knowledge of aerosol properties is a key to understand its direct and indirect radiative effects. Especially the vertical distribution of aerosols determines the degree with which it would interact with clouds, influence air quality and the atmospheric heating profiles, among others. Most of the passive satellite imagers have difficulties in retrieving accurate aerosol properties over Sweden due to large solar zenith angles during most part of the year, snow and ice covered surfaces etc. CALIPSO offers a viable alternative to overcome this difficulty. It also has a distinct advantage of providing vertical structure and nighttime observations [1]. Furthermore, the orbital track of CALIPSO is aligned very well with the semi-major axis of Sweden's elongated topography during nighttime (Fig. 1), thus making it extremely appealing for generating statistics of aerosol properties. Here, we use 5 years of Aerosol 5km Layer product from CALIPSO and investigate statistics of aerosol properties. We further investigate the role of temperature inversions in influencing vertical distribution of aerosols.

For the present study we use the standard CALIPSO 5km Aerosol Layer Product (Version 3.01) [1], specifically the aerosol retrievals of aerosol layer base and top heights, and optical depth at the 532nm wavelength. A rigorous quality control is applied while selecting the data for analysis. For example, if a feature is classified as aerosol and the classification quality flag is set to "high", only then are the results used for the analysis. The aerosols are further categorized into six different types, based on their integrated attenuated backscatter and volume depolarization ratio along with ancillary information on surface type and altitude [2]. The six aerosol types analyzed are "clean continental", "polluted continental", "dust", "polluted dust", "clean marine", and "smoke".

The data used in the present study cover the period from June 2006 through May 2011 and is analyzed for four seasons separately, winter (December, January, and February; DJF), spring (March, April, and May; MAM), summer (June, July, and August; JJA), and autumn (September, October, and November; SON).

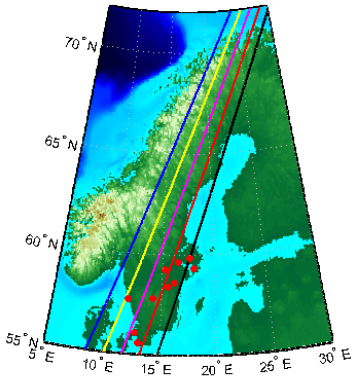

Fig. 1: CALIPSO track over Sweden during nighttime. The red dots show top 10 populated cities.

We investigate the seasonality of:

1) The vertical distribution of aerosols along five selected curtains over Sweden shown in Fig. 1.
2) Aerosol layer optical thickness.
3) Number of aerosol layers present.
4) Relative distribution of aerosol types.
5) Aerosol verticality with respect to temperature inversions derived from AIRS [3,4].

References

[1] Winker, David M., Mark A. Vaughan, Ali Omar, Yongxiang Hu, Kathleen A. Powell, Zhaoyan Liu, William H. Hunt, Stuart A. Young, 2009: Overview of the CALIPSO Mission and CALIOP Data Processing Algorithms. J. Atmos. Oceanic Technol., 26, 2310–2323. doi: http://dx.doi.org/10.1175/2009JTECHA1281.1

[2] Omar, A., D. Winker, C. Kittaka, M. Vaughan, Z. Liu, Y. Hu, C. Trepte, R. Rogers, R. Ferrare, R. Kuehn, and Hostetler C. 2009. The CALIPSO Automated Aerosol Classification and Lidar Ratio Selection Algorithm. J. Atmos. Oceanic Technol., 26, 1994-2014, doi:10.1175/2009-JTECHA1231.1.

[3] Devasthale, A., U. Willen, K.-G. Karlsson, and C. G. Jones, Quantifying the clear-sky temperature inversion frequency and strength over the Arctic Ocean during summer and winter seasons from AIRS profiles, Atmos. Chem. Phys., 10, 5565-5572, 2010.

[4] Devasthale, A., M. Tjernström and A. H. Omar, The vertical distribution of thin features over the Arctic analysed from CALIPSO observations. Part II: Aerosols, Tellus B, 63, 1, 86-95, 2011.

In situ aerosol measurements for the validation and improvement of CALIPSO lidar extinction retrievals

P.J. Sheridan[1], J.A. Ogren[1], E. Andrews[2], J.L. Tackett[3], and D.M. Winker[4]

[1]NOAA Earth System Research Laboratory, Boulder, Colorado, 80305, USA
[2]CIRES, University of Colorado/NOAA, Boulder, Colorado, 80309, USA
[3]Science Systems and Applications, Inc., Hampton, Virginia, 23681, USA
[4]NASA Langley Research Center, Hampton, Virginia, 23681, USA
Keywords: ambient aerosols, optical properties, A-Train satellite, extinction coefficient.
Presenting author email: patrick.sheridan@noaa.gov

Between June 2006 and September 2009, an instrumented light aircraft (the NOAA Airborne Aerosol Observatory, AAO) measured over 400 vertical profiles of aerosol and trace gas properties over eastern and central Illinois. The primary objectives of this program were to 1) measure the *in situ* aerosol properties and determine their vertical and temporal variability and 2) compare these aircraft measurements with concurrent surface and satellite measurements. The satellite comparisons were accomplished by coordination of aircraft activities with A-Train satellite overflights. The satellite sensors require "air truth" *in situ* measurements to identify and constrain systematic errors in the retrievals of aerosol physical properties. Improvements in these algorithms will improve the quality of height dependent information from CALIPSO and other satellites that measure vertical aerosol profiles.

Aircraft profiles were conducted near the NOAA/ESRL surface aerosol monitoring station near Bondville, Illinois, with each profile location within 10 km of an A-Train satellite track. Of the 401 research profiles, 63 were conducted during an overpass of the CALIPSO satellite. Of these 63 profiles, CALIPSO was able to retrieve extinction in the nearest 35-km path of the satellite track for 28 cases. The aircraft sampled at 10 levels at each profile location, starting at an altitude of ~4.6 km above sea level (asl) and finishing at ~0.5 km asl. About half of the levels were conducted in the free troposphere (10 minute legs) while the remainder were flown in the boundary layer (5 minute legs). Flight times were chosen so that the aircraft was sampling in the boundary layer when the satellite passed overhead.

The primary aerosol optical property measurements made on the aircraft were the aerosol light scattering coefficient (σ_{sp}), the aerosol hemispheric backscattering coefficient (σ_{bsp}), and the aerosol light absorption coefficient (σ_{ap}). Each of these was made at three visible wavelengths. Measurements of the light scattering coefficient in the mid-visible at elevated relative humidity were made for determination of the aerosol hygroscopic growth factor. The primary measurements permitted calculation of the aerosol light extinction coefficient (σ_{ep}) at ambient conditions at 532 nm at each level, for direct comparison with the CALIPSO lidar extinction retrieval. Other optical properties calculated were the single scattering albedo, scattering and absorption Ångström exponents, hemispheric backscatter fraction, submicron scattering ratio, and aerosol radiative forcing efficiency.

Figure 1 shows the statistical comparison of all 28 collocated *in situ* (AAO) and satellite-derived (CALIPSO) extinction profiles. The comparisons suggest that CALIPSO tends to overestimate extinction in the boundary layer and underestimate it at higher altitudes. The overestimation of extinction at lower altitudes appears to be related to problems associated with cloud screening. Our *in situ* aerosol data suggest extinction thresholds for the likelihood of aerosol layers being detected by the CALIPSO sensor. In this study, 71% of the aerosol layers CALIPSO did not detect had aerosol extinction values <20 Mm^{-1}, and 95% of the undetected layers were <50 Mm^{-1}. These statistical data offer guidance as to the likelihood of CALIPSO's ability to measure aerosol extinction at various locations around the globe.

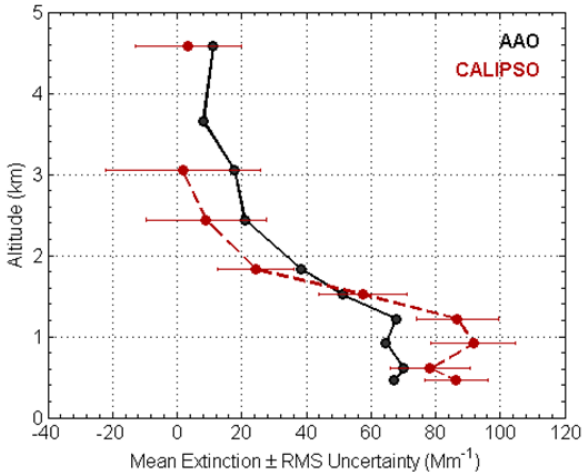

Figure 1. Median in situ and satellite-derived extinction profiles.

This work was supported by the NOAA Climate Program.

Sheridan, P.J., Andrews, E., Ogren, J.A., Hoff, R.M., Tackett, J.L. and Winker, D.M. (2012) Atmos. Chem. Phys. Disc., in review.

CLIMARENO-GRA 2011 campaign: Aerosol optical properties characterization from ground-based instrumentation

J.A.Bravo-Aranda[1,2], F. Navas-Guzmán[1,2], J. Andrey[3], M.J. Granados-Muñoz[1,2], J.L. Guerrero-Rascado[1,2], M. Gil[3], H. Lyamani[1,2], A. Valenzuela[1,2], G. Titos[1,2], J. Fernández-Gálvez[1,2], F.J. Olmo[1,2] and L. Alados-Arboledas[1,2]

[1] Andalusian Center for Environmental Research (CEAMA), Granada, 18006, Spain
[2]Department of Applied Physics, University of Granada, Granada, 18071, Spain
[3]Área de Investigación e Instrumentación Atmosférica (AIIA), INTA. Torrejón de Ardoz, 28850, Spain
Keywords: Atmospheric aerosols, lidar, optical properties.
Presenting author email: jabravo@ugr.es

It is well known that aerosol particle effects play an important role in the radiative balance of the Earth-Atmosphere system. According to the forth assessment of the IPCC (Forster et al., 2007) there are still uncertainties in the role of atmospheric aerosols on climate change predictions. In this sense, one of the main objectives of the European project ACTRIS (Aerosols, Clouds, and Trace gases Research InfraStructure Network) is to improve the observations of the vertical aerosol distribution. Particularly, working package WP2 intends to define new aerosol parameters to improve its study, as the aerosol depolarization ratio.

CLIMARENO campaign was developed during June 2011 with the main objective of studying the Saharan dust impact on the Earth radiative forcing (J. Andrey et al., 2012; Guerrero-Rascado et al., 2012, submitted to this conference). Particularly, two flights were performed under non-dust (14th June) and dust (27th June) conditions over Granada (37.2ºN, 3.6ºW, 680 m a.s.l.) where ground-based instrumentations were deployed.

Two lidar systems were operating during CLIMARENO campaign. The multiwavelength Raman lidar (Raymetrics S.A.) is a system with detection of elastic signals at 1064, 355 and 532 nm (in parallel and perpendicular components) and three Raman signals at 607, 408 and 387 nm. The scanning Raman lidar (Raymetrics S.A.) allows for detecting elastic signals at 355 (in parallel and perpendicular components) and one Raman signal at 387 nm. The synergic use of both lidar allows dual aerosol depolarization ratio study. Column-integrated characterization of the atmospheric aerosol has been done by means of a sun-photometer CE-318-4 included in the AERONET network. Additionally, surface measurements have been obtained at the Granada station by means of an integrating nephelometer (TSI3563), a Multiangle Absorption Particle, (MAAP) and an Aerosol Particle Sizer (APS).

In this work, the aerosol optical properties obtained from ground based active and passive remote sensing and in-situ instrumentation are analyzed and compared with height-resolved information retrieved from airborne instrumentation. On 14th June fine and coarse modes present similar contributions (Fig.1 Top) and a lofted aerosol layer was detected around 5 km asl with backscattered-related Angström Exponent, $å_{\beta}$(355/532nm) around 1.7 Fig. 1(bottom). According to HYSPLIT backward trajectories analyses (http://wwww.arl.noaa.gov/ready/hysplit4.html) and MODIS Fire (http://firefly.geog.umd.edu/firemap/), this layer was a smoke layer originated in North America. On 27th June, coarse particle mode predominance (Fig.1 Top) and low $å_{\beta}$ (0.3, averaging range 2-4.5 km asl), (Fig.1 Bottom), showed up the dust conditions.

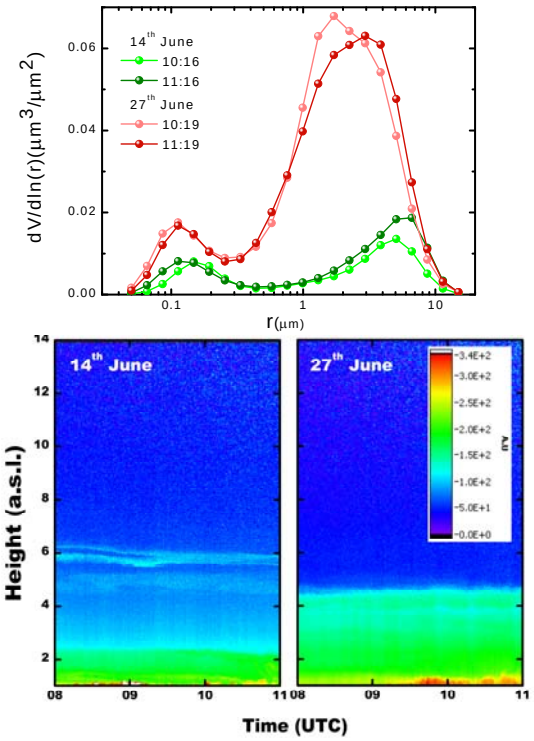

Figure 1. Top: Aerosol volume size distributions obtained during non-dust (green) and dust (red) events Bottom: temporal evolution of the range corrected signal

This work was supported by the Andalusia Regional Government through projects P08-RNM-3568 and P10-RNM-6299, by the Spanish Ministry of Science and Technology through projects CGL2010-18782, CSD2007-00067 and CGL2011-13580-E/CLI; and by EU through ACTRIS project (EU INFRA-2010-1.1.16-262254).

Forster P, et al. (2007). Changes in Atmospheric Constituents and in Radiative Forcing. In: Climate Change 2007. Cambridge University Press, Cambridge.

Tropospheric aerosols remote sensing with a sensitive and accurate UV-VIS polarization Lidar

G. David[1], B. Thomas[1], A. Miffre[1] and P. Rairoux[1]

[1]Laboratoire de Spectrométrie Ionique et Moléculaire, CNRS UMR 5579, Université Lyon 1, Villeurbanne, 69622, France

Keywords: tropospheric aerosols, polarization, optical properties: remote sensing.

Presenting author email: gdavid@lasim.univ-lyon1.fr

Tropospheric aerosol is a very complex mixture of particles having different sizes, shapes and chemical composition. In this paper, to study the tropospheric aerosols morphology, we built, optimized and used an UV-VIS polarization Lidar to remotely measure the tropospheric aerosols backscattering and polarization properties, under real atmospheric conditions of temperature and humidity. Our 2λ-polarization detector has been designed to detect very small changes in the tropospheric aerosols morphology, corresponding to a measured detection limit of 0.6 % for the aerosol depolarization ratios δ_a, comparable to the molecular depolarization. Hence, to our knowledge for the first time, the non-sphericity of tropospheric aerosols is addressed in the UV spectral range with a calibrated time-altitude map (while UV-molecular scattering is strong). Very small aerosols depolarization ratios are hence measured, enhancing the non-sphericity of these aerosols, which is new (David et al., 2012).

Our new and home-built 2λ-polarization Lidar detects tropospheric backscattered photons as a function of their wavelength (λ = 355, 532 nm) and their polarization ($\boldsymbol{\pi}$ = {//, ⊥} with respect to the laser linear polarization). UV-light has been chosen to increase our sensitivity to aerosols in the fine particle mode (Mishchenko et al., 2002), while VIS-light is more sensitive to coarse particles. Monitoring δ_a-values in the percent range requires sensitive and accurate polarization measurements. Hence, we carefully analyzed any possible system bias affecting δ_a: imperfect laser linear polarization, presence of possible polarization cross-talks, role of the dichroic beamsplitter used for the λ-separation, misalignment between the laser and the polarization axes. We hence specified each optical component separately, on a laboratory test-bench to achieve the best possible sensitivity and accuracy in the UV and the VIS. The measured polarization cross-talks were found to be fully negligible (below 10^{-7}). Moreover, by introducing controlled amounts of polarization cross-talks (Alvarez et al., 2006), we calibrated the 2λ-polarization Lidar experiment with better than 2% accuracy. Range averaging and high frequency noise filtering lead to a 75 m-altitude resolution.

Figure 1 displays the measured parallel and perpendicular tropospheric aerosols backscattering coefficient ($\beta_{a,//}$, $\beta_{a,\perp}$) and the aerosols depolarization ratio δ_a, in the form of UV, VIS time-altitude maps. To our knowledge, such a calibrated time-altitude map is new in the UV. The achieved sensitivity and accuracy allows distinguishing different layers having different polarization backscattering properties and revealing the presence of small non-spherical tropospheric aerosols.

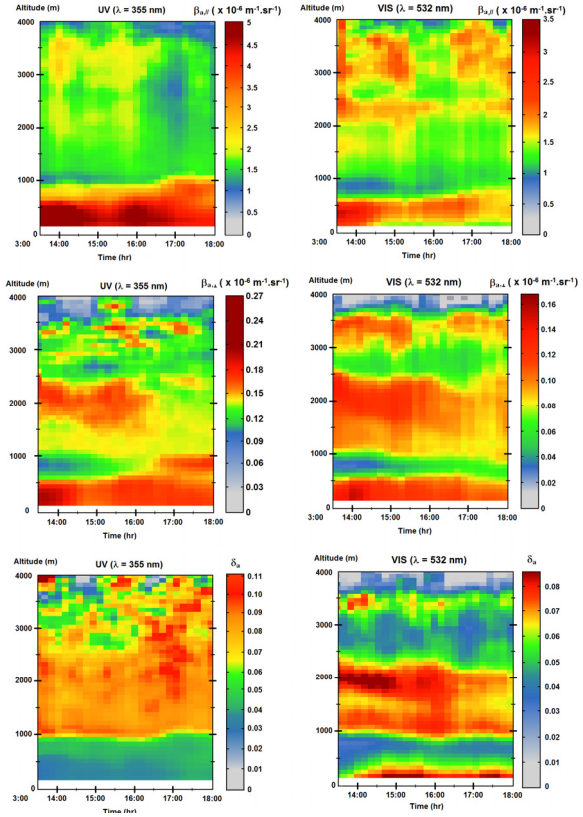

Figure 1. UV, VIS ($\beta_{a,//}$, $\beta_{a,\perp}$, δ_a) time-altitude maps for tropospheric aerosols on October 18th 2011 at Lyon.

The different behavior UV / VIS can be interpreted by considering the higher scattering efficiency of fine particles in the UV. Hence, fine and coarse particles are addressed in the PBL (where a smog episode is observed) and in the free troposphere (where expected sea-salt particles are observed). The presentation will explicit the achieved sensitivity and accuracy of our home-built 2λ-polarization Lidar and further detail the optical properties of tropospheric aerosols, derived from the above time-altitude maps. The methodology associated to this work is currently under review in Appl. Phys B (David et al., 2012).

We thank CNRS and Région Rhône-Alpes for financial funding of this work and research grant.

Alvarez J.M., et al., (2006), *J. Atm. Ocean. Tech.,* **23**, 683-699.

David G. et al., (2012), submitted to *Appl. Phys. B.*

Mishchenko, M.I. et al., (2002), *Scattering, absorption and emission of light by particles,* Camb. Univ. Press.

Study on the influence of different error sources on sky radiance measurements and inversion-derived aerosol products in the frame of AERONET

B. Torres[1], C. Toledano[1], A.J. Berjón[2], O. Dubovik[3], V. E. Cachorro[1], Y. Bennouna[1], D. Fuertes[1], R. González[1], P. Goloub[3], T. Podvin[3], L. Barel[3], A. M. de Frutos[1]

[1]Group of Atmospheric Optics, Valladolid University, Valladolid, Spain

[2]Izaña Observatory, Spanish Meteorological Agency, Tenerife, Spain

[3]Laboratory of Atmospheric Optics, University of Lille, Lille, France

Presenting author email: benjamin@goa.uva.es

The remote sensing of the atmospheric aerosol is a well-established technique that is currently used for routine monitoring of this atmospheric component, both ground-based and from satellite. The AERONET program, initiated in the 90's, is the most extended network and the data provided are currently used by a wide community for aerosol characterization, satellite and model validation and synergetic use with other instrumentation (lidar, in-situ, etc.). However there are still open questions and inconsistencies in the modeling of the aerosol optical properties. For example, there are known limitations in the inversion of sky radiances, especially related to the large uncertainty of the retrieved products from almucantar scans at low solar zenith angles (SZA) or at low aerosol optical thickness conditions. Another topic of especial interest is the analysis of desert dust, which is by far the most problematic aerosol type regarding the adequate modeling of optical properties. Within AERONET, sky radiances are acquired in two geometries: almucantar and principal plane. Principal plane inversions were provided together with the almucantar inversion products at the beginning of the AERONET version 2 direct Sun and inversion algorithm, released in 2006. However the principal plane retrievals were later removed from the AERONET database, keeping only almucantar retrievals considered more stable and reliable, although only at large solar zenith angles. Two problems arise from this situation: first, the monitoring of inversion-derived properties such as size distribution, refractive index and single scattering albedo, which are necessary for the evaluation of the aerosol, cannot be retrieved in the middle of the day. Second, there is a need to find out the reason for the inconsistency between principal plane and almucantar retrievals.

We have investigated to what extent the discrepancies can be a consequence of the measurement procedure. In particular, three systematic errors in the radiance observations were analyzed in order to quantify the effects on the inversion-derived aerosol properties: calibration, pointing accuracy and finite field of view. The aim of this work is to determine how each of the analyzed errors affects the aerosol retrievals in both geometries and try to provide criteria for quality assurance and product error estimations. For this purpose, sky radiances were simulated with the forward module of the Dubovik's algorithm using several aerosol types (desert dust, oceanic, urban and biomass burning), described by the volume size distribution and the complex refractive index. Then the systematic errors were induced and we applied the inversion module to the erroneous radiances in order to compare the retrieved aerosol properties with the original ones.

The results of the analysis show that only the pointing error can cause these discrepancies, since it affects more the principal plane than almucantar (less affected at least from the typical pointing errors considered: 0.2° y 0.4°).

On the other hand, self-consistency test demonstrated that, even for simulated measurements without error, aerosol retrievals at low SZA are distorted due to the lack of information of scattering angles larger than 2·SZA in the almucantar measurements. And what's more, the insertion of the calibration errors presents more influence on the retrievals at low SZA, therefore they can amplify the differences between retrievals at low and large SZA.

Finally we want to remark that most of the investigated errors are more relevant for the desert dust aerosol type: the coarse mode has the worst behaviour in the self-consistency test; the least sensitive to the inversion procedure; and the most affected by calibration errors. These facts, together with the particle non-sphericity, can explain why this aerosol type presents the largest complications in the retrieval of properties from sky radiances.

Financial support from the Spanish MICINN under projects with ref. CGL2009-09740, CGL2011-23413, CGL2010-09480-E and CGL2011-13085-E is gratefully acknowledged.

Dubovik, O. and King, M. (2000). A flexible inversion algorithm for retrieval of aerosol optical proper- ties from Sun and sky radiance measurements. J. Geophys. Res. **105(D16)**, 20673–20696.

Dubovik, O., Smirnov, A., Holben, B., King, M., Kaufman, Y., Eck, T. and Slutsker, I. (2000). Accuracy assessments of aerosol optical properties retrieved from Aerosol Robotic Net- work (AERONET) Sun and sky radiance measurements. J. Geophys. Res. **105(D8)**, 9791–9806.

Holben B, Eck T, Slutsker I, Tanre D, Buis J, Setzer A, Vermote E, Reagan J, Kaufman Y. (1998). AERONET - a federated instrument network and data archive for aerosol characterization. Remote Sens. Environ. **66**, 1-16.

Evaluation of aerosol OC / BC estimations derived from AERONET data, using in-situ ground measurements.

D. Paraskevopoulou[1,2], S. Kazadzis[1], N. Mihalopoulos[2], A. Arola[3], K. Eleftheriadis[4], C. Theodosi[2], A. Bougiatioti[2], E. Diapouli[4] and E. Gerasopoulos[1]

[1]Institute for Environmental Research and Sustainable Development, National Observatory of Athens, I. Metaxa and Vas. Pavlou, 15236, P. Penteli, Athens, Greece
[2]Environmental and Analytical Chemical Division, Department of Chemistry, University of Crete, P.O. Box 2208, 71003 Heraklion, Greece.
[3]Finnish Meteorological Institute, P. O. Box 1627, 70211 Kuopio, Finland
[4]Environmental Radioactivity Laboratory, National Centre of Scientific Research Demokritos, Athens, Greece
Keywords: black carbon, organic carbon, remote sensing.
Presenting author email: dparask@meteo.noa.gr

Carbonaceous material constitutes a major fraction of atmospheric aerosol, and is considered a significant parameter for global climatic change and for public health. Therefore, several studies have focused worldwide on the estimation of aerosol organic carbon (OC) and elemental (EC) or black carbon (BC) composition.

This study provides a first long term comparison of the estimated AERONET (AErosol RObotic NETwork) (Arola *et al* 2011) OC and BC concentrations with in-situ measurements in the southern Europe, in order to validate the particulate matter OC/BC composition from remote sensing techniques.

Multiyear surface PM_1 measurements performed on Crete Island and $PM_{2.5}$ performed on Athens, Greece, were compared to ground-based remote sensing measurements (AERONET FORTH-Crete and Athens-NOA station).

The quality assured (level 2.0) FORTH-Crete and Athens-NOA Aeronet data, were processed for columnar mass concentration of absorbing organic carbon and OC/BC ratio using the innovative retrieval procedures developed by Arola et al (2011). On Crete aerosol PM_1 fractions were collected from 2004 to 2011 at Finokalia station (35°32'N, 25°67'N; http://finokalia.chemistry.uoc.gr) and were analysed for OC and EC concentration according to the analytical procedure described by Theodosi et al 2010; while, PM2.5 were collected from 2008 to 2011 at Demokritos urban background station in Athens (GAW-DEM, 2007), by a Semi-Continuous OCEC Field Instrument (Sunset Laboratory Inc.).

The monthly mean seasonality of OC/BC ratio and the yearly seasonality of EC or BC concentration for Finokalia and for AERONET data is presented in Fig.1a, and 1b, respectively. The whole period average OC/EC ratio from in situ measurements was 12.26 compared to AERONET columnar OC/BC ratio found of 0.97. The difference could be attributed to that in our AERONET approach not all OC species are estimated as "organic carbon" but only those species that cause enhanced absorption at the shortest wavelengths.

The comparisons between AERONET data and in situ measurements suggested that for the majority of the study (sampling period 2004-2011) OC/BC ratio presented similar monthly seasonality while, the same similarity was observed concerning the yearly and monthly seasonality of OC and EC concentrations (not shown). The ground based measurements of OC/BC ratio and in situ OC/EC ratio were well correlated (R^2 0.33).

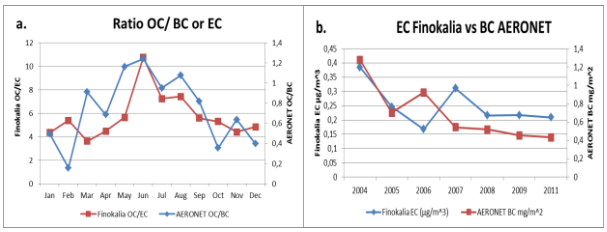

Figure 1 a. Monthly mean value of OC/EC or BC ratio and b. Yearly mean values of EC or BC concentration, for PM_1 collected fraction at Finokalia and for AERONET data, from 2004 to 2011.

All the aforementioned data indicate that for most of our sampling period, remote sensing data from AERONET could provide a reasonable estimation of the OC and BC seasonality at the ground level. We plan to extend this comparison to additional data from other southern European locations.

This work was supported by EU funded projects EUSAAR and ACTRIS. DP acknowledges the support of Research Funding Program: Heracleitus II.

Arola, A., Schuster, G., Myhre, G., Kazadzis, S., Dey, S., and Tripathi, S. N. (2011) *Inferring absorbing organic carbon content from AERONET data*, Atmos. Chem. Phys., 11, 215–225.

GAW-DEM (2007) http://gaw.empa.ch/gawsis/reports.asp?StationID=20 76202728

Theodosi, C., Im, U., Bougiatioti, A., Zarmpas, P., Yenigun, O., Mihalopoulos, N., (2010) *Aerosol chemical composition over Istanbul.* Sci Total Environ, in press. doi: 10.1016/j.scitotenv.2010.02.039

Retrieving MODIS Aerosol Optical Depth in real time at 500 m resolution: urban-scale evaluation over Hong Kong

Muhammad Bilal[1], Janet E. Nichol[1], Max P. Bleiweiss[2], David Dubois[3]

1.Department of Land Surveying & Geo-Informatics, The Hong Kong Polytechnic University, Hung Hom, Kowloon, Hong Kong
2. Center for Applied Remote Sensing in Agriculture, Meteorology, and Environment, New Mexico State University, Las Cruces, New Mexico, USA
3. Department of Plant and Environmental Sciences, New Mexico State University, Las Cruces, New Mexico State, USA
Keywords: AOD, MODIS, AERONET, Hong Kong, Urban
Presenting author email: muhammad.bilal@connect.polyu.hk

Satellite remote sensing with nadir scanning radiometer provides quantitative measurements of spectral Aerosol Optical Depth (AOD) from local to global scales (Kaufman et al., 2002). Monitoring and understanding the behavior of the atmospheric aerosols on local scales over complex urban terrain like Hong Kong requires aerosol retrieval algorithms that support high spatial resolution (Wong et al., 2010; Nichol et al., 2008). In the current study, a Real Time Fine Spatial Resolution (RTFSR) algorithm is developed to retrieve the AOD using MODerate resolution Imaging Spectroradiometer (MODIS) Level-2 Swath data (MOD02HKM) of 500 m spatial resolution over the complex and bright surfaces of Hong Kong. This study employs a novel approach to high-resolution AOD retrieval because it does not rely on an empirical AOD lookup table generated using a Radiation Transfer Model (RTM). Instead, AOD is retrieved on real-time basis by applying RTM's equations directly on the MODIS data.

The RTFSR algorithm is evaluated with AOT from the PolyU AERONET station in Hong Kong. Comparison between RTFSR AOD at 3x3 spatial region and AERONET AOT at $\pm$ 30 min of MODIS overpass times in November and December 2007 is shown in Table 1. The RTFSR AOD algorithm also successfully detected biomass burning over mainland China on 30th November 2007 that was also detected by the MODIS Web Fire Mapper but was not detected by the MOD04-V05 Level-2 Aerosol Product at 10 km spatial resolution (Figure 1).

Table 1. Comparison of RTFSR AOD with AERONET AOT over Hong Kong

Date	PolyU_AOT	RTFSR _AOD
04:11:2007	0.29	0.29
10:11:2007	0.39	0.32
11:11:2007	0.41	0.33
12:11:2007	0.39	0.37
17:11:2007	0.28	0.29
01:12:2007	0.25	0.24
10:12:2007	0.36	0.33
12:12:2007	0.34	0.32
21:12:2007	0.30	0.34
26:12:2007	0.23	0.27
28:12:2007	0.23	0.28

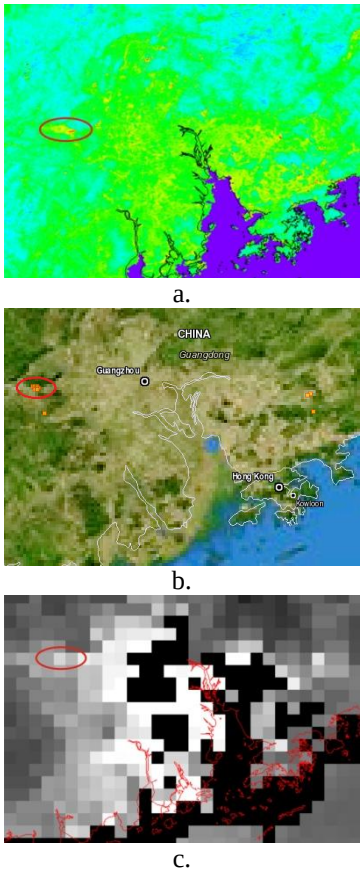

a.
b.
c.

Figure 1. Biomass burning inside the red circle as detected by a-RTFSR AOD, b-MODIS Fire Mapper but not by c-MOD04 level-2 AOD

Kaufman, Y.J., Tanre, D., and Boucher, O. (2002) A satellite view of aerosols in the climate system, *Nature*, 419, 215-223.

Nichol, J.E. and Wong, M.S. (2009) High Resolution Remote Sensing of Densely Urbanised Regions: a Case Study of Hong Kong, *Sensors*, 9, 4695 4708.

Wong, M.S., Lee, K.H., Nichol, J.E., Li, Z. (2010) Retrieval of Aerosol Optical Thickness Using MODIS 500 x 500 m^2, a Study in Hong Kong and the Pearl River Delta Region, *IEEE Transactions on Geoscience and Remote Sensing*, vol., 48, 3318-3327.

Tuesday, September 4, 2012

Session WG02S4O. Marine and Carbonaceous Aerosol

New Findings on Submicron Sea Salt Source Flux

J. Ovadnevaite, D. Ceburnis, H. Berresheim and C. O'Dowd

School of Physics and Centre for Climate and Air Pollution Studies, Ryan Institute, National University of Ireland Galway, University Road, Galway, Ireland

Keywords: sea salt, sea spray source function, marine aerosol, HR-ToF-AMS.
Presenting author email: jurgita.ovadnevaite@nuigalway.ie

Sea spray aerosol is a significant component of the aerosol population in the marine environment, and given that 70% of the Earth's surface is oceanic, sea spray contributes significantly to the global aerosol budget (Vignati et al., 2010). In order to better understand and quantify these effects, detailed information on the chemical composition, along with size distribution and abundance, is required.

The high-time resolution sea salt measurement by a High Resolution Time of Flight Aerosol Mass Spectrometer (HR-ToF-AMS) enabled the quantification of sea salt mass in both increasing and decreasing wind speed regimes up to 26 m s^{-1}. A mass flux source function was also derived and found to have a power-law wind speed dependency with an exponent of 3.1 for increasing winds and 2.3 for decreasing winds. Whereas, submicron aerosol particles are expected to be uniformly mixed in the marine boundary layer, an effective sea spray aerosol production flux was estimated from the sea spray concentration divided by a filling time and multiplied by the marine boundary layer height.

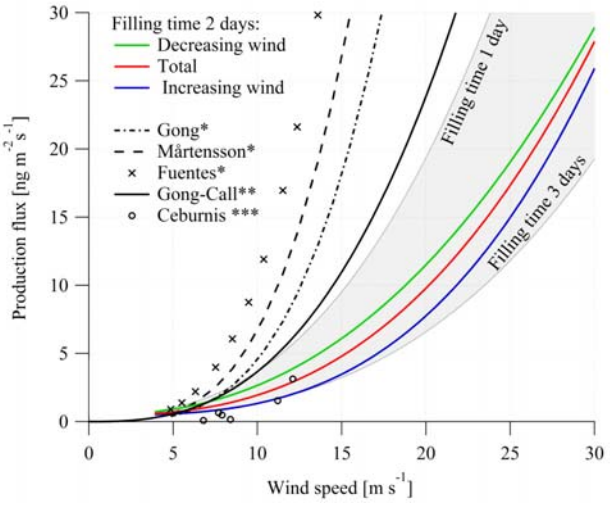

Figure 1. Production flux dependence on the wind speed. Color lines represent the flux derivations from the AMS sea salt measurements at different wind speed regimes. Grey area represents the flux variability due to the different time of filling. Black lines illustrates fluxes derived from the parameterizations by Gong (2003), Mårtensson et al. (2003) , Callaghan et al. (2008), Ceburnis et al. (2008) and Fuentes et al. (2010).
*number flux presented in the original work was recalculated to the mass flux; **includes differential whitecap - to - aerosol productivity derived by Gong (2003), ***fluxes calculated from the data presented.

A comparison with already existing source functions derived from the whitecap method is presented in Figure 1. It suggests that previous schemes based on the Monahan whitecap - wind speed approach significantly over-estimate the submicron mass flux. There could be several reasons for that: one is the whitecap area - to - wind speed parameterization and another is the parameterization of differential whitecap - to - aerosol productivity. The former parameterization has recently improved by applying a digital image processing of sea-state photographs and removing the subjectivity in determining the intensity threshold. Replacing the Monahan component of the source flux with the more recent Callaghan et al. (2008) whitecap – wind speed relationship brings the Gong (2003) source function closer to the ones presented in this study; however, the comparison also points to an over-estimation of the differential whitecap - aerosol productivity component of the source flux function.

This work was supported by the SFI, HEA-PRTLI4, EC IP EUCAARI, EPA Ireland and ESA STSE.

Callaghan, A., G. de Leeuw, L. Cohen & C. D. O'Dowd (2008) *Geophysical Research Letters*, 35, L23609

Ceburnis, D., C. D. O'Dowd, G. S. Jennings, M. C. Facchini, L. Emblico, S. Decesari, S. Fuzzi & J. Sakalys (2008) *Geophysical Research Letters*, 35, L07804

Fuentes, E., H. Coe, D. Green, G. de Leeuw & G. McFiggans (2010) *Atmos. Chem. Phys.*, 10, 9295-9317.

Gong, S. L. (2003) *Global Biogeochemical Cycles*, 17,1097-1104.

Martensson, E.M., E.D. Nilsson, G. de Leeuw, L.H. Cohen & H.C. Hansson (2003) *Journal of Geophysical Research-Atmospheres*,108, 4297.

Vignati, E., M. C. Facchini, M. Rinaldi, C. Scannell, D. Ceburnis, J. Sciare, M. Kanakidou, S. Myriokefalitakis, F. Dentener, and C. D. O'Dowd (2010) Atmos. Environ, 44(5), 670-677.

Radiocarbon analysis on organic and elemental carbon in aerosol samples and source apportionment at an urban site in Northern Italy.

V. Bernardoni[1], G. Calzolai[2], M. Chiari[2], M. Fedi[2], F. Lucarelli[2], S. Nava[2], A. Piazzalunga[3,*], F. Riccobono[1,#], F. Taccetti[2], G. Valli[1], R. Vecchi[1]

[1]Department of Physics, Università degli Studi di Milano and INFN, Milan, 20133, Italy
[2]Dept. of Physics and Astrophysics, Università degli Studi di Firenze and INFN, Sesto Fiorentino, 50019, Italy
[3]Dept. of Inorganic, Metallorganic, and Analytical Chemistry, Università degli Studi di Milano, Milan, 20133, Italy
* now at: Dept. of Environmental and Territorial Sciences, University of Milan-Bicocca, Milan, 20122, Italy
[#]now at: Laboratory of Atmospheric Chemistry, Paul Scherrer Institut, Villigen PSI, 5232, Switzerland

Keywords: Carbonaceous Aerosol, Radiocarbon, OC/EC, thermal protocols.
Presenting author email: vera.bernardoni@unimi.it

Carbon is one of the main constituents of atmospheric aerosol. The study of carbonaceous aerosol is important because of its adverse effects on health, air quality, visibility, and Earth's radiation balance. In this context, the development of analytical and modelling techniques aiming at the identification of natural and anthropogenic contributions gains great importance.

^{14}C measurement on total carbon (TC) is a good tool for fossil/non fossil sources separation (Hildemann et al., 1994). However, wood burning has to be considered mainly of anthropogenic origin at mid-latitudes. Therefore, ^{14}C measurements on TC do not allow the complete natural/anthropogenic contributions separation.

^{14}C measurements on organic and elemental carbon (OC and EC, respectively) allow a distinction between the wood/biomass burning and the biogenic source, provided that the OC/EC emission ratio for wood/biomass burning is known. This model is limited by the difficulty in the assessment of the secondary contribution from wood/biomass burning (Szidat et al., 2009), as the OC/EC emission ratio measured at the source cannot correctly account for secondary aerosol formation. Moreover, ^{14}C measurements for the fraction of modern carbon (f_m) determination must be carried out on each carbon fraction after a suitable isolation. At the state of art EC and OC are operationally defined. Therefore, a key point of ^{14}C measurements on carbon fractions is the thermal separation of OC and EC.

This work aimed at gaining information on the effects of different thermal treatments on ^{14}C measurements of organic (OC) and elemental (EC) carbon fractions in the atmospheric aerosol. Improvements to the traditional approaches for the determination of the f_m(OC) and f_m(EC) are proposed and tested using a devoted sample preparation line (Calzolai et al., 2011).

f_m(EC) determination is usually carried out after EC isolation using a single oxygen combustion step. In this work, we show that the most refractory OC fraction cannot be efficiently removed by the oxygen treatment alone without significantly affecting the EC recovery. Therefore, we propose to use a Helium combustion step at high temperature in addition to the oxygen treatment. Our tests demonstrate that the addition of a high temperature He step (optimised temperature setting: 750 °C) to the oxygen treatment (375°C, 40 min) is effective in removing the refractory OC.

The direct determination of f_m(OC) can be difficult because of possible OC pyrolysis, which can be reduced by water soluble components removal. Therefore, here we propose to determine f_m(OC) measuring either the fraction of modern carbon of TC and EC or the fraction of modern carbon of water soluble (f_m(WSOC)) and water insoluble (f_m(WINSOC)) organic carbon. Tests on the equivalence of the approaches have shown good agreement.

Our tests were carried out on PM10 samples collected in a heavily polluted urban area (Milan, Italy) during wintertime. f_m(OC), f_m(EC), and f_m(TC) values obtained in our tests were then used to attempt a preliminary source apportionment using ^{14}C measurements (Figure 1).

The wood burning primary contribution to OC was evaluated from both ^{14}C and levoglucosan using tailored emission factors (Piazzalunga et al., 2011). A good agreement between the approaches was found and wood burning primary contribution accounted for about 18% of OC in Milan during wintertime. Secondary OC from biomass burning and the contribution from other urban sources were tentatively identified following literature approaches, with the aim of evaluating the biogenic contribution to OC, which was estimated to be about 18%.

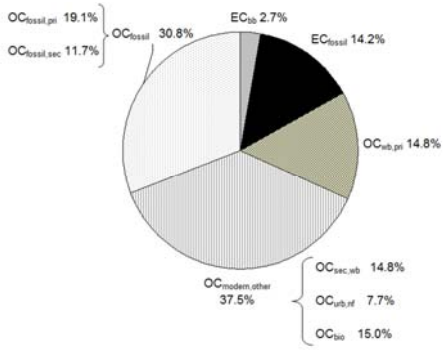

Figure 1. TC source apportionment in Milan – Italy.

Hildemann, et al. (1994). Environ. Sc. Technol., **28**, 1565-1575
Szidat, et al. (2009). *Atmos. Chem. Phys.* **9**, 1521-1535.
Calzolai, et al. (2011). *Nucl. Instr. and Meth.* **B269**, 203-208.
Piazzalunga, et al. (2011). *Atmos. Environ.* **45**, 6642-6649

Results of a monitoring campaign from a cruise ship in the Western Mediterranean

M.C. Bove[1], G. Calzolai[3], F. Cavalli[2], M. Chiari[3], E. Cuccia[1], J. Hjorth[2], D. Massabò[1], A. Piazzalunga[4], P. Prati[1], C. Schembari[2]

[1] Department of Physics, University of Genoa, and INFN, 16146, Genoa, Italy
[2] Institute for Environment and Sustainability, European Commission, JRC , I-21027, Ispra (VA), Italy
[3] Department of Physics and Astronomy, University of Florence, and INFN, 50019, Sesto Fiorentino (FI), Italy
[4] Department of Chemistry, University of Milan, 20133, Milan, Italy

Keywords: Mediterranean Sea, PM2.5, ships cruise, MSA.
Presenting author email: mcbove@ge.infn.it

In order to fill in the gap of observation in the Mediterranean basin and to obtain more information about sources of air pollutants and atmospheric dynamical and chemical mechanisms, the Joint Research Centre of the European Commission (JRC, EC) has started a long-term monitoring program over the Mediterranean Sea in collaboration with the cruise line Costa Crociere. In this framework, in a joint experiment with the Department of Physics of the University of Genoa, an intensive PM2.5 sampling campaign was organized in summer 2011, on a cruise ship following a regular route in the Western Mediterranean with continuous measurements of BC, NO_x, CO, SO_2 and O_3 by the monitoring station, placed in a cabin of the top deck of the ship.

During this campaign the route of the ship was Civitavecchia-Savona-Barcelona-Palma de Mallorca-Malta (Valletta)-Palermo-Civitavecchia (see Figure 1).

From July 18 to 25, August 15 to 22, and September 12 to 19, 2011, PM samples were collected on Quartz and Teflon filters (47mm diameter, flow rate 2.3 m^3/h) using in parallel two Sven Leckel Ingenieurburo sequential samplers, placed on the top of the cabin where the monitoring station itself was located. The samplers were switched on after the departure from each harbor and stopped before the arrival in the next port. Each leg was then divided in periods of about 5 hours with one filter for each sampler collected per period, thus resulting in a variable number of filters per leg and in a total of about 100 filters for all the sampling campaigns during summer 2011. Information about meteorological parameters (wind speed and direction, temperature, humidity) was available with 10 min intervals from the meteorological station of the ship, together with information about the ship position, speed and sailing direction.

Samples were analyzed with different techniques: Energy Dispersive X-Ray Fluorescence at the Department of Physics of Genoa (Ariola et al, 2006); Ion Chromatography (Chow and Watson, 1999) at Department of Chemistry of University of Milan; Thermo-optical analysis (Birch and Cary, 1996) at the JRC laboratory. Ion Beam Analysis measurements of the Teflon filters sampled during the week of September 2011, using simultaneously PIXE, EBS and PESA techniques (Chiari, 2005), were performed at the 3 MV Tandetron accelerator of the LABEC laboratory of INFN in Florence.

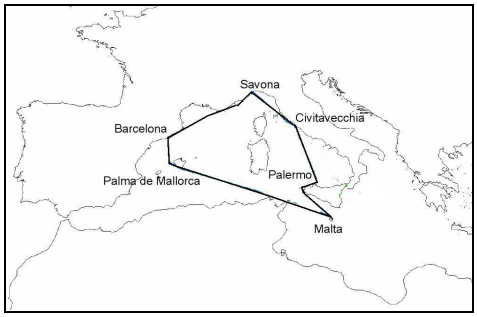

Figure 1. Route of the ship during the sampling campaigns in the summer 2011.

Positive Matrix Factorization, PMF (Paatero et al, 1994), was used to identify and characterize the major PM2.5 sources along the ship route. Particular attention was given to the evidence of emissions from heavy fuel oil combustion by ships, known to be an important source of secondary sulphate aerosol. The biogenic contribution to sulphate concentration along the route was estimated from the measurement of the MSA (methanesulfonic acid) concentrations.

This work has been partially supported by INFN (NUMEN project) and by Costa Crociere.

Ariola, V., D'Alessandro, A., Lucarelli, F., Marcazzan, G., Mazzei, F., Nava, S., Garcia-Orellana, I., Prati, P., Valli, G., Vecchi, R., Zucchiatti, A. 2006. *Elemental characterization of PM10, PM2.5 and PM1 in the town of Genoa (Italy).* Chemosphere 62, 226-232.

Birch, M. E., Cary, R. A. 1996. *Elemental carbon-based method for monitoring occupational exposures to particulate diesel exhaust.* Aerosol Science and Technology 25, 221-241.

Chow, J. C., Watson, J. G. 1999. *Ion chromatography.* In: Landsberger, S., Creatchman, M. (Eds.), Elemental Analysis of Airborne Particles. Gordon and Breach Publishers, Newark, NJ, pp. 97-137.

Chiari, M., Lucarelli, F., Mazzei, F., Nava, S., Paperetti, L., Prati, P., Valli, G., Vecchi, R. 2005. *Characterization of airborne particulate matter in an industrial district near Florence by PIXE and PESA.* X-Ray Spectrometry 34, 323-329.

Paatero, P., Tapper, U. 1994. Positive matrix factorization: a non-negative factor model with optimal utilization of error estimates of data values. Environmetrics 5, 111-126.

Organic Carbon detection in crude-oil plant emissions in South Italy

M. Calvello[2], F. Esposito[1] , G. Pavese[2], M. Lovallo[3], L. Mangiamele[3]

[1] DIFA- Università della Basilicata, C. da Macchia Romana, 85100, Potenza, Italy
[2] CNR-IMAA, C. da S. Loya, 85050, Tito Scalo (PZ), Italy
[3] ARPAB, Via della Fisica C/D, 85100 Potenza, Italy
Keywords: Carbonaceous aerosol, black carbon, organic carbon.
Presenting author email: calvello@imaa.cnr.it

The possibility to evaluate Organic Carbon (OC) presence in carbonaceous aerosol by a 7-wavelenghts Aethalometer has been tested in a site with intensive extraction activities of crude oil in South Italy (Agri Valley, 40.33°N, 15.92° E, 582 m a.s.l).

In the measurements site a crude oil pre-treatment plant is present and the area is characterized by continuous and controlled smokes emissions.

In-situ measurements of Black Carbon (BC) content have been continuously carried out by a Magee AE31 aethalometer (7 wavelenghts from 370 to 950 nm) from January to April 2011 . Usually, when dealing with aethalometer data, the difference between BC computed at 370 nm and BC computed at 800 nm is used to detect the presence of organic compounds (Hansen, 2005). For all data collected in Agri Valley a prevailing 370-UV component was found indicating the presence of organic compounds among carbonaceous absorbing particles. An example is shown in Figure 1.

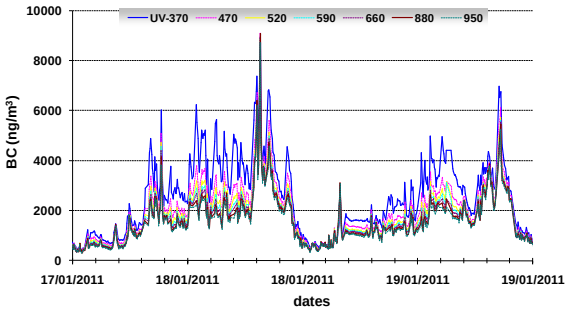

Figure 1. Temporal variation of BC content in Agri Valley near the oil plant as estimated at the 7 wavelenghts for the period January 17th-19th 2011.

These results have been compared to those obtained after three years (2008-09-10) of BC content measurements carried out in a rural site (Tito Scalo) always in South Italy where no particular BC emission sources are present a part from vehicular traffic. In this case a prevailing 370-UV component of BC has never been detected (Calvello *et al*., 2010, Pavese et al. Submitted).

Going back to data collected in Agri Valley, in Figure 2 the time dependence of the difference between 370-UV component and 880-BC component as estimated by Magee Aethalometer is reported together whit that of benzene concentration as measured by ARPAB (Basilicata region environmental protection agency).

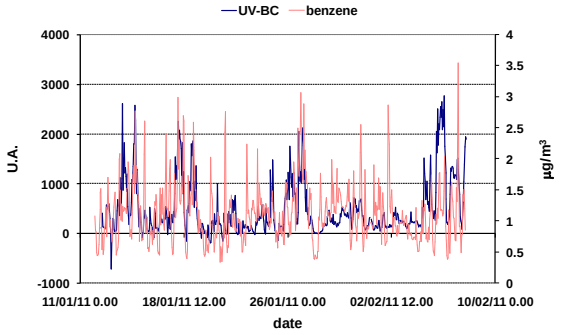

Figure 2. Time dependence of the difference between 370-UV component and 880-BC as estimated by Magee Aethalometer and of benzene concentration as measured by ARPAB.

As it is possible to see, a good agreement is found showing the goodness of Aethalometer data to qualitatevely determine OC presence.

It must be pointed out, anyway, that the attenuation at 370 nm as measured by the Aethalometer cannot give a quantitative estimate of OC content. Moreover, if Brown Carbon (BrC) is one of the particulate component, the standard Magee algorithm, based on the hypotesis of a mass absorption coefficient inversely proportional to the wavelength, can give wrong information on OC detection. Thus a novel algorithm has been tested on Agri valley BC content data to improve the standard Magee algorithm. This new algorithm is able to verify the carbonaceous particles spectral absorption behavior thus distinguishing between BC and BrC and to better detect OC component (Esposito *et al.*, 2012).

Calvello, M., Esposito, F., Pavese, G., and Serio, C., (2010). *Atmos. Chem. Phys.,10*, 2195-2208.

Esposito, F., Calvello, M., and Pavese, G. (2012). *Atmos. Meas. Tech. Discuss.*, 5, 1003-1027

Hansen, A. D. A. (2005). *The Aethalometer manual*, Magee Scientific.

Pavese, G., Calvello, M., Esposito, F., submitted to . *AAQR.*

The Seasonal Cycle of Sea Spray Emissions: Long term Eddy Covariance Aerosol Flux measurements from Östergarnsholm, Baltic Sea (57°27`N ,18°59` E)

E. Douglas Nilsson[1] and Monica E. Mårtensson[2]

[1]Department of Applied Environmental Science, Stockholm University, S-10691 Stockholm, Sweden
[2]Department of Earth Sciences, Uppsala University, S-752 36 Uppsala, Sweden
Keywords: Sea spray, eddy covariance, aerosol fluxes, marine aerosol
Presenting author email: douglas.nilsson@itm.su.se

On the island Östergarnsholm (57°27`N ,18°59` E) in the Baltic Sea we have measured turbulent fluxes of aerosols, CO_2, H_2O, heat and momentum using Eddy Covariance (EC). The measurements were conducted from a tower at the southern tip of the island, with an asymmetric ultrasonic anemometer (Gill HS-50) and a CO_2+H_2O sensor (LICOR 7500) and aerosol air inlets at ~12m above sea level, see Figure 1. The aerosol was counted with an Optical Particle Counter (OPC) (Grimm 1.109), with 15 size bins from 0.25-2.5 μm Diameter (D), and a Condensational Particle Counter (CPC) (TSI 3772), for particles >10 nm D. Fluxes were de-trended, rotated, and corrected for tube effects etc., and calculated over 30 minutes periods. Power were provided by solar panels and a wind power generator. More than a decade of research on CO_2 air-sea-exchange, has characterized the site as representing open sea conditions within a wide wind sector to the south-east and south.

Figure 1. To the left, the new Stockholm University aerosol flux tower, to the right, mast with CO_2 fluxes at several levels operated by Uppsala University.

So far all existing in situ flux measurements are limited to short campaigns of at the most a few months (e.g. Nilsson et al., 2001, 2007; Geever et al., 2005). The strongest driving physical parameter, the wind speed, usually experience seasonal variations. For example, in the North-Atlantic we expect stronger wind in winter than in summer. Strong seasonal cycles in the organic fraction of the sea spray has been found on both southern and northern hemisphere and attributed to the seasonal cycle in marine biology (Yoon et al., 2007; Sciare et al., 2009). The current project was therefore initiated in order to provide the first long term direct measurements of sea spray emissions. This should allow us to determine the importance of seasonal changes in physical parameters (wind, water temperature etc.) and marine biology, and to better judge the effect of climate driven changes in these parameters.

Preliminary evaluation of the data suggest that the magnitude of the sea spray emissions exceed that which can be explained by sea salt only, which leaves room for a substantial organic sea spray fraction, see Figure 2. There is evidently, as expected, as strong wind dependency, and several severe storms during the winter season have resulted in record levels of sea spray emissions. At the time of the EAC2012 we will have more than a year of data, and we will be able to present the first ever full seasonal cycle in sea spray emissions based on direct emission measurements.

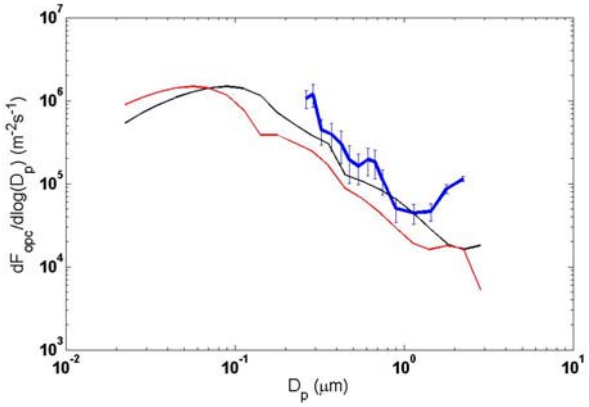

Figure 2. Winter season median aerosol emission fluxes in the OPC size range (blue curve) with the 25-75 percentile, compared to the Mårtensson et al. (2003) sea salt source parameterisation (black curve), corrected for the lower salinity of the Baltic Sea (red curve).

This work was supported by the Swedish Research Council for the Environment (FORMAS).

Geever, M., C. O'Dowd, S. van Ekeren, R. Flanagan, E. D. Nilsson, G. de Leeuw, and Ü. Rannik (2005) *Geophys. Res. Lett.* **32** (15), Art. No. L15810

Mårtensson, E.M., E.D. Nilsson, G. de Leeuw, L.H. Cohen, H.C. Hansson (2003) *J. Geophys. Res.* **108**, 4297

Nilsson, E.D., Ü. Rannik, E. Swietlicki, C. Leck, P.P. Aalto, J. Zhou, and M. Norman (2001) *J. Geophys. Res.* **106**, 32,139-32,154.

Nilsson, E. D., E.M. Mårtensson, J. S. Van Ekeren, G. de Leeuw, M. Moerman, C. O'Dowd (2007), *Atmos. Chem. Phys. Discuss.* **7**, 13345–13400

Sciare, J., O. Favez, R. Sarda-Este`ve, K. Oikonomou, H. Cachier, and V. Kazan (2009) *J. Geophys. Res.* **114**, D15302

Yoon, Y. J., et al. (2007) *J. Geophys. Res.* **112**, D04206

Diurnal cycle of fossil and non-fossil carbon using ^{14}C analyses during CalNex

P. Zotter[1], A.S.H. Prévôt[1], I. El-Haddad[1], Y. Zhang[2], S. Szidat[2], L. Wacker[3], X. Zhang[4], R. Bahreini[5], P. Hayes[6], J.B. Gilman[5], J.A. de Gouw[5], J.L. Jimenez[6], R. Weber[4], U. Baltensperger[1]

[1]Laboratory of Atmospheric Chemistry, Paul Scherrer Institut, Villigen, Switzerland
[2]Department of Chemistry and Biochemistry & Oeschger Centre for Climate Change Research, University of Bern, Switzerland
[3]Laboratory of Ion Beam Physics, Swiss Federal Institute of Technology, Zürich, Switzerland
[4]School of Earth and Atmospheric Sciences, Georgia Institute of Technology, Atlanta, GA, USA
[5] Cooperative Institute for Research in Environmental Sciences, University of Colorado, Boulder, CO, USA
[6]Department of Chemistry and CIRES, University of Colorado, Boulder, CO, USA
Keywords: Source apportionment, carbonaceous aerosols, environmental radiocarbon, megacity
Presenting author email: peter.zotter@psi.ch

The Sum of carbonaceous particles (total carbon, TC) is a major fraction of the fine aerosol and affects climate and human health. TC is classified into the sub-fractions elemental carbon (EC) and organic carbon (OC). EC originates only from fossil fuel combustion and biomass burning. OC can be emitted directly as primary organic aerosol (POA) from biogenic emissions, wood burning and fossil fuel combustion or can be formed in-situ in the atmosphere (secondary organic aerosol, SOA) (Szidat et al. 2006). Radiocarbon (^{14}C) analysis is a direct and quantitative tool for distinguishing fossil and non-fossil sources, since ^{14}C in fossil fuels is completely depleted whereas other sources have a contemporary ^{14}C level.

Previous ^{14}C analyses have been performed on aerosol filter samples with a sampling time ≥6h, hindering clear and time-resolved assessment of the sources and processes emitting TC. This study presents unprecedented ^{14}C measurements performed on high time resolution (3-4h) PM_1 filter samples collected during the CalNex-LA 2010 campaign at the California Institute of Technology in Pasadena located about 20 km northeast of downtown Los Angeles (LA). Separation of OC and TC was carried out using the THEODORE system (Szidat et al. 2004) and a Sunset EC/OC analyzer. The resulting CO_2 was cryo-trapped and sealed in glass ampoules for ^{14}C measurements, performed with the mini radiocarbon dating system MICADAS (Ruff et al. 2007).

Results for several days show a consistent and distinct diurnal cycle with a fossil peak for TC and OC (Fig.1, top panel) in the early afternoon after the plume of the western LA basin is transported to Pasadena with the sea breeze. The non-fossil fractions of TC and OC (Fig. 1, bottom panel) show no daily cycles and stay constant throughout all days. The EC concentrations are low (max. 1.0 µg/m^3) and show only weak daily cycles. Likewise, the traffic related factor HOA (hydrogen like organic aerosol) (see Fig. 1, bottom panel) calculated with positive matrix factorisation (PMF) from aerosol mass spectrometry (AMS) data and measurements of benzene, a tracer for anthropogenic POA, show also only a weak diurnal variation.

In contrast, the semi-volatile oxygenated organic aerosol (SV-OOA) found by PMF shows a strong diurnal cycle with a peak in the afternoon and correlates well with the fossil OC for all days (r^2 = 0.74 ± 0.1 on average). In addition, acetaldehyde, a tracer for photochemical processing, shows a clear daily cycle with a peak around the same time as SV-OOA, and non-fossil OC and TC. These results indicate that the increase of fossil OC and TC in the early afternoon is mainly attributed to fossil SOA formed from anthropogenic precursor gases in the LA plume, suggesting that anthropogenic emissions can substantially influence the SOA formation in urban areas, especially in megacities.

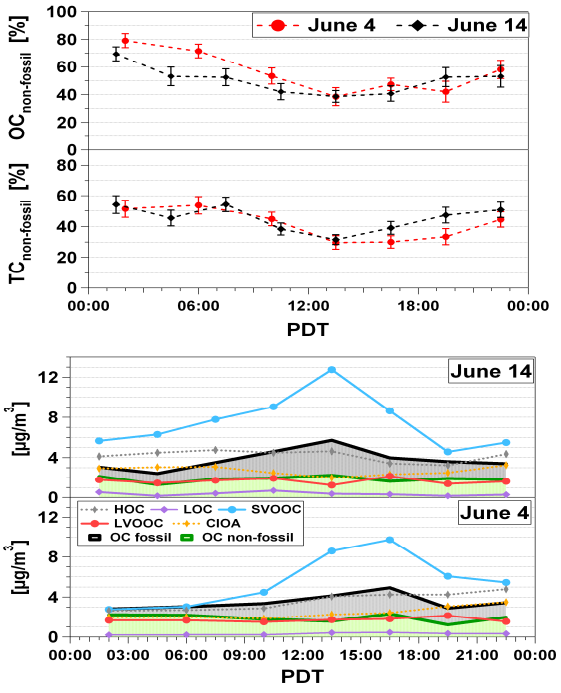

Figure 1. Diurnal cycle of non-fossil OC and TC (top) and comparison with PMF factors (bottom).

This work was supported by CALTECH (J. Seinfeld) CARB, NOAA (J. de Gouw), the University of California, Los Angeles (J. Stutz) and the US NSF.

Ruff, M. et al (2007) Radiocarbon 49(2), 307-314
Szidat, S. et al. (2004) Nuclear Instruments and Methods in Physics Research Section B: Beam Interactions with Materials and Atoms 223-224: 829-836
Szidat, S. et al. (2006) J. Geophys. Res. 111, D07206

A new sea-salt module implemented within the NMMB/BSC Chemical Transport Model

M. Spada[1], O. Jorba[1], C. Pérez[2], Z.I. Janjic[3] and J.M. Baldasano[1,4]

[1]Department of Earth Sciences, Barcelona Supercomputing Center, Barcelona, Spain
[2]NASA Goddard Institute for Space Studies, New York, USA
[3]National Centers for Environmental Prediction, Camp Springs, Maryland, USA
[4]Environmental Modeling Laboratory, Universitat Politècnica de Catalunya, Barcelona, Spain
Keywords: Sea salt, Aerosol modelling.
Presenting author email: michele.spada@bsc.es

A new sectional module for the forecasting of sea-salt aerosol has been implemented within the NMMB/BSC Chemical Transport Model (NMMB/BSC-CTM) (Pérez *et al*, 2011; Jorba *et al*, 2011), currently under development at the Barcelona Supercomputing Center. While most of the global aerosol models are not capable to reproduce meso-β or smaller scale phenomena, NMMB/BSC-CTM can simulate from global to regional scales, with a fully on-line coupling of atmospheric physics and aerosol processes.

The major uncertainities in sea-salt modeling at global scale are related to the comparison with observations: in effect, surface measurements could be affected by surf-zone production and it is difficult to separate the sea-salt contribution from measured total aerosol optical depths. Moreover, since the short lifetime of large sea-salt articles, comparisons between models and measurements may be very sensitive to the model resolution, especially when complex terrains and/or land-ocean interfaces occurr. Thus, the NMMB/BSC-CTM capability to downscale may be very useful.

The sea-salt module uses 8 bins in the dry radius interval $[0.1 - 15]\mu$m to properly describe mass concentrations and optical depth. Ultrafine particles are not considered. A sub-bin lognormal approach is assumed to calculate the optical properties of the particles. Different open-ocean emission schemes are implemented, accounting both for bubble-bursting and spume production, such as the combined Monahan *et al* (1986)/Smith *et al* (1993) (M86/SM93) and Gong (2003) (G03). SST-dependent emissions of sea-salt bubbles have been also implemented by merging with the scheme of Martensson *et al* (2003) (MA03/M86/SM93). The water uptake is taken into account by using prescribed growth factors for different relative humidity values. The parameterizations of the aerosol processes affected by the water-uptake (i.e. sedimentation, dry deposition, wet deposition, etc.) have been extended to wet particles from those implemented in the dust module (Pérez et al, 2011).

We describe the new module and we present its results vs observations, climatologies, and spatial patterns from different datasets, e.g. the University of Miami Network, the AERONET Sunphotometers Network, cruise measurements, and satellite data. Global simulations of the year 2006 have been performed at different resolutions (ranging from 2 x 2.8 to 0.333 x 0.469 degrees). The coarse part of the optical depth has also been taken into consideration in order to avoid the influence of other fine particles, such as sulfate. The dust contribution to the optical depth is provided from the dust module of NMMB/BSC-CTM. Evaluation and influence of horizontal resolution are discussed, also by the performing of regional simulations. Figure 1 shows the resulting surface concentration at Bermuda for different emission schemes.

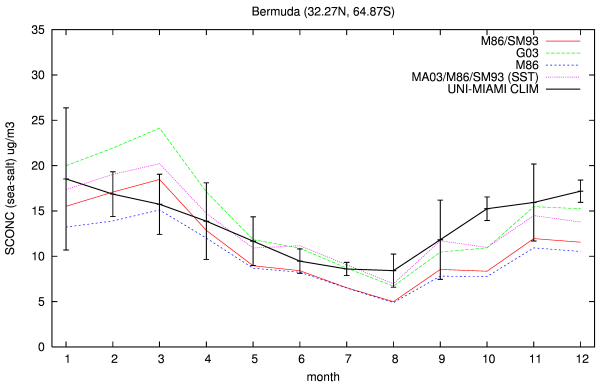

Figure 1: Sea-salt surface concentration: modeled monthly means of year 2006 vs UNI-MIAMI network climatology (means+stdevs) at Bermuda. Model res.=1x1.4

This work is funded by grants CGL2008-02818-CLI and CGL2010-19652 of the Spanish Ministry of Economy and Competitiveness. All the numerical simulations were performed with the MareNostrum Supercomputer hosted by the Barcelona Supercomputing Center.

Pérez, C. *et al* (2011) *Atm. Chem. and Phys.* **11**, 13001-13027

Jorba, O. *et al* (2011) *14th Conf. on Harmonisation within Atm. Disp. Modelling for Reg. Purp.* **14**, 345-349

Monahan, E.C. *et al* (1986) *in: Oceanic whitecaps and their role in air-sea exch. proc.*, Reidel, 167-174

Smith, M.H. *et al* (1993) *Q. J. Roy. Meteor. Soc.* **119**, 809-824

Gong, S.L. (2003) *Global. Biogeochem. Cy.* **17**, 1097

Martensson, E.M. (2003) *J. Geophys. Res.* **108**, 4297

Tuesday, September 4, 2012

Session WG03S4O. Chemistry of Organic Aerosol: Field Study

Characterization of humic-like substances (HULIS) in size segregated atmospheric aerosol

G. Kiss[1], N. Törő[2], A. Hoffer[1], J. Dautovic[3], S. Frka[3], Z. Kozarac[3], M. Harir[4], P. Schmitt-Kopplin[4,5]

[1]Air Chemistry Group of Hung. Acad. Sci. at University of Pannonia, Egyetem 10, 8200 Veszprém, Hungary
[2]University of Pannonia, Dept. Earth and Environmental Sciences, Egyetem 10, 8200 Veszprém, Hungary
[3]Rudjer Bošković Institute, Division for Marine and Environmental Research, Bijenička 54, 10000 Zagreb, Croatia
[4]Helmholtz Center Munich, German Research Center for Environmental Health, Analytical BioGeoChemistry, Ingoldstädter Landstraße 1, D-85764 Neuherberg, Germany
[5]Lehrstuhl für Chemische-Technische Analyse und Chemische Lebensmitteltechnologie, Technische Univ. München, Weihenstephaner Steig 23, 85354 Freising-Weihenstephan, Germany

Keywords: aerosol, HULIS, size distribution, chemical properties
Author email: kissgy@almos.uni-pannon.hu

Humic-like substances (HULIS) constitute a considerable fraction (often the majority) of the water-soluble organic matter present in atmospheric aerosol. Consequently, this complex organic mixture significantly influences the physical and chemical properties of the aerosol particles as well as their biological effects. Several studies have dealt with the sources and characterisation of humic-like substances leading to considerable knowledge on their potential formation mechanism, elemental composition, molecular weight range, spectroscopic features, higroscopicity, CCN ability, etc. However, information on the size distribution of HULIS is very limited (Peng et al., 2010) although knowledge of this feature provides important information on possible sources and formation mechanisms in the atmosphere.

In this work humic-like substances isolated from aerosol particles of different size ranges were characterized. Aerosol samples were collected in the 0.0625-16 μm size range with an 8-stage Berner impactor at a rural site (K-puszta) in Hungary, an urban site (Zagreb) and a coastal site (Martinska) in Croatia. Humic-like substances were isolated from the aqueous extracts of each stage and their carbon content was determined by TOC analysis. The UV absorbance and fluorescence properties as well as the mass spectra of the constituents of the aqueous extracts and those of the isolated HULIS were studied. Approximately 90% of fluorescing compounds (EX=235nm/EM=410nm) were found in the 0.0625-1 μm size range which indicated that humic-like substances occurred in the fine fraction. This was confirmed by the results of carbon analysis and mass spectrometric investigations: the mass spectrum of the organic matter isolated from the particles in the 0.0625-1 μm size range resembled that of humic-like substances while the mass spectrum of the low amount of organic matter isolated from bigger particles differed significantly. Specific UV and fluorescent properties indicated that the chemical composition of particles within the 0.0625-1 μm size range is diverse. In order to confirm this finding the isolated humic-like substances were analyzed by ultra high resolution mass spectrometry (FT-ICR-MS). Elemental composition (obtained from FT-ICR-MS), UV absorbance and fluorescent properties of HULIS isolated from aerosol particles of different sizes will be shown for aerosol samples collected at different sites.

Peng L., Xiao-Feng H., Ling-Yan He., Jian Z. Yu (2010) J. Aerosol Sci., 41 (1), 74-78.

This research was partially funded by the bilateral intergovernmental Croatian – Hungarian research project “Complex investigation of organic aerosols in rural, urban and marine environment“ and the EU FP 6 project EUSAAR (Contract No RII3-CT-2006-026140).

Observations of monoterpene organosulfates in wintertime aerosols

A.M.K. Hansen, K. Kristensen, F. Cozzi, A. Zare, M.F. Lauridsen and M. Glasius

Department of Chemistry, University of Aarhus, Langelandsgade 140, DK-8000 Aarhus C, Denmark
Keywords: Biogenic Secondary Organic Aerosols, Monoterpene Oxidation Products, Chemical Analysis
Presenting author email: glasius@chem.au.dk

Organosulfate derivatives of isoprene and monoterpenes, as well as their oxidation products, have been identified in both laboratory and field studies where they are formed through heterogeneous reactions involving sulphur compounds (e.g. Surratt *et al*., 2008), primarily emitted to the atmosphere from anthropogenic sources. Organosulfates of biogenic oxidation products thus provide a coupling between air pollution and formation of low-volatility secondary organic aerosols (SOA), contributing to anthropogenically enhanced biogenic SOA (ABSOA) as suggested in recent studies (e.g. Hoyle et al., 2011).

Particles ($PM_{2.5}$) were collected using a high-volume sampler at an urban background site in Aarhus, Denmark in January 2011. After extraction, the samples were analysed by HPLC coupled through an electrospray inlet to a quadrupole time-of-flight mass spectrometer (qTOF-MS) (Kristensen, Glasius, 2011). Organosulfates and nitrooxy organosulfates were identified from their characteristic MS-fragments (HSO_4^-, SO_3^- and HNO_3) and the isotopic patterns of sulphur and nitrogen and quantified using a standard.

Molecular formula, MW	Suggested molecular structure	Suggested precursors
$C_{10}H_{18}O_5S$, 250		α-pinene, β-pinene
$C_{10}H_{16}O_7S$, 280	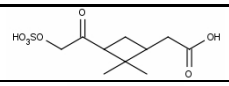	α-pinene β-pinene
$C_{10}H_{17}NO_7S$, 295	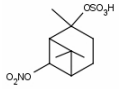	α-pinene β-pinene
$C_9H_{15}NO_8S$, 297	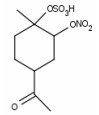	Limonene
$C_{10}H_{17}NO_{10}S$, 343	Unknown	α-pinene, α-terpinene

Table 1. Organosulfates identified in $PM_{2.5}$ samples collected during winter (January 2011)

Organosulfates of α -pinene and β -pinene were identified in the samples together with nitrooxy organosulfates of monoterpenes (see examples in Table 1). All of these compounds have previously been observed in aerosol samples from Denmark during spring and summer (Kristensen and Glasius, 2011), as well as Norway, Sweden and Finland during summer (Yttri *et al*., 2011), but not during winter.

Concentrations of most of the classical monoterpene oxidation products were generally much lower than during springtime, while some, such as terpenylic acid, where observed at comparable levels.

The ground was snow-covered during the study period, so local, as well as regional, emissions of monoterpenes are expected to be minimal.

The results thus point towards regional-scale processes affecting formation of ABSOA during winter, in accordance with the study by Frossard *et al*. (2011) in the Arctic. This will be further investigated by use of air mass back-trajectories and modelling of monoterpene emissions in source regions.

We thank the VILLUM Foundation and the Nordic Top-level Research Initiative (CRAICC) for funding of this work.

Frossard, A. A., Shaw, P. M., Russell, L. M., Kroll, J. H., Canagaratna, M. R., Worsnop, D. R., Quinn, P. K., and Bates, T. S.: (2011) *J. Geophys Res* **116**, D05205.

Hoyle, C.R., M. Boy, J.L. Fry. M. Glasius, A. Guenther, A.G. Hallar, K. Huff Hartz, M.D. Petters, T. Petäjä, T. Rosenoern, A.P. Sullivan (2011) *Atmos Chem Phys* **11**, 321.

Kristensen, K., M. Glasius (2011) *Atmos Environ* **45**, 4546.

Surratt, J. D., Gomez-Gonzlez Y., Chan A. W. H., Vermeylen R., Shahgholi M., Kleindienst T. E., Edney E. O., Offenberg J. H., Lewandowski M., Jaoui M., Maenhaut W., Claeys M., Flagan R. C. and Seinfeld, J. H. (2008) *J. Phys Chem A* **112**, 8345.

Yttri K. E, Simpson D., Nøjgaard J.K, Kristensen K., Genberg J., Stenström K., Swietlicki E., Hillamo R., Aurela M., Bauer H., Offenberg J. H, Jaoui M., C. Dye, Eckhardt S., Burkhart J. F, Stohl A., and Glasius M. (2011) *Atmos Chem Phys* **11**, 13339.

Simultaneous study of gas and particulate products formed from limonene oxidation: smog chamber and citrus fruit field measurements

L. Chiappini[1], S. Rossignol[1], C. Rio[1], S. Fable[1], G. Grignion[2], J.L. Savelli[2]

[1]Institut National de l'Environnement Industriel et des Risques (INERIS), 60 550 Verneuil-en-Halatte, France
[2] Qualit'Air Corse, Lieu-dit Lergie RN 200, 20250 Corte, France
Keywords: SOA, gas-particle partitioning, nucleation event
Presenting author email: laura.chiappini@ineris.fr

Limonene is a significant contributor to monoterpenes emissions that accounts for around 11 % of global VOCs emissions (Guenther 1995). Its two double bonds enhance its reactivity making it display a higher SOA yield (around two times,Griffin 1999) compared to mono-unsaturated monoterpenes, such as α- and β-pinene, more emitted at a global scale (Geron 2000). Limonene can therefore be considered as a significant contributor to SOA.

To accurately evaluate secondary organic aerosol climate and health impacts from limonene oxidation, and provide models with data obtained under real atmospheric conditions, the evaluation of gas/particle partitioning behaviour of secondary organic matter semi-volatile fraction and the associated multiphase chemistry is needed.

To that purpose, smog chamber experiments and field measurement campaign to be provided with partitioning coefficients obtained under real conditions, have been combined.

In order to describe multiphase chemistry involved in SOAs formation and to take into account gas/particles partitioning phenomena, a new analytical approach has been employed (Rossignol 2012). Both gas and particulate phases are simultaneously collected, respectively on sorbent tubes and filters, and molecular composition is investigated using PFBHA and MTBSTFA derivatization prior to thermal-desorption coupled with gas chromatography and mass spectrometry (TD-GC-MS) analysis.

For each experiment, chemical data are coupled with ozone and limonene concentrations evolution monitoring and physics characterisation of formed particles: mass, size and number distribution evolution.

Simulation chamber experiments

Simulation chamber experiments were performed at the EUPHORE European chamber (Figure 1, Valencia, Spain) under close to reality conditions: ozone and limonene concentrations around 80 ppb, seeds introductions and humidity ratio close to 50 %. In mean 75 µg of SOAs are formed.

Chemical characterisation of both gas and particulate phases allowed identification of limonene ozonolysis tracers, such as limononaldehyde or limonaketone, and evaluation of gas/particles partitioning of these species for a better understanding of physico-chemical mechanisms and processes involved in the limonene SOAs formation.

Figure 1: EUPHORE European atmospheric simulation chamber (left) and the INRA citrus fruits field (right)

Field campaign

A field campaign was performed in the French National Institute for Agricultural Research (INRA) citrus fruits filed in Northern Corsica during a week in June 2011.

Episodic $PM_{2.5}$ number concentration increases could be observed when limonene concentrations were rising during the day, and have been tentatively attributed to SOA formation from limonene oxidation.

Indeed, among the thirty compounds which have been positively or tentatively identified in gas and/or particle phases, some can be specifically attributed to limonene ozonolysis such as ketolimonene, Limononaldehyde and ketonorlimonic acid. These limonene oxidation specific tracers, have been quantified and for those identified in both gas and particulate phases, an experimental partitioning coefficient is proposed.

This study provides an insight into particulate and gaseous phase secondary products formation from limonene ozonolysis .

Geron, C., R. Rasmussen, et al. (2000). "A review and synthesis of monoterpene speciation from forests in the United States." Atmospheric Environment **34**(11): 1761-1781.

Griffin, R. J., D. R. Cocker, III, , et al. (1999). "Estimate of global atmospheric organic aerosol from oxidation of biogenic hydrocarbons." Geophys. Res. Lett **26**: 2721-2724.

Guenther, A., C. N. Hewitt, et al. (1995). "A global-model of natural volatile organic-compound emissions." J.Geophys. Res.-Atmos **100**: 8873-8892.

Rossignol, S., L. Chiappini, et al. (2012). "Development of parallel sampling and analysis for the elucidation of gas/particle partitioning of oxygenated semi-volatile organics: a limonene ozonolysis study." Atmos. Meas. Tech. Discuss. **5**: 1153-1231.

Quantification of nitrocatechols and related aromatic compounds in atmospheric aerosols

Zoran Kitanovski[1], Irena Grgić[1], Magda Claeys[2], Reinhilde Vermeylen[2] and Willy Maenhaut[2]

[1]Laboratory for Analytical Chemistry, National Institute of Chemistry, Hajdrihova 19, SI-1000 Ljubljana, Slovenia

[2]Department of Pharmaceutical Sciences, University of Antwerp, Universiteitsplein 1, BE-2610 Antwerp, Belgium

Keywords: aerosol characterization, biomass burning, HPLC-MS, PM10, SOA (Secondary Organic Aerosol)

Presenting author email: irena.grgic@ki.si

In the last decade, it was demonstrated that organic aerosol (OA) represents a significant fraction of ambient aerosol, and further a substantial portion of it is secondary organic aerosol (SOA) (Hallquist *et al.*, 2009). However, there are still large uncertainties in evaluation of their role in the chemistry and physics of the atmosphere.

Biomass burning (BB) emits huge amounts of organic aerosols in the atmosphere (Laskin *et al.*, 2009). Many different compounds can be present in BB aerosol (Simoneit, 2002). Some of these compounds are very specific to biomass burning; hence, they can be used as markers, e.g., levoglucosan for primary BBA (Fine *et al.*, 2002). An important class of compounds of SOA are nitrocatechols known as very strong absorbers of UV and Vis light. Very recently, methyl-nitrocatechols were proposed as suitable tracers for highly oxidized secondary BBA (Iinuma *et al.*, 2010).

The objective of the present study was to characterize nitrocatechols and related compounds in ambient aerosols using liquid chromatography/negative ion electrospray ionization mass spectrometry [LC/(-)ESI-MS]. A new method for the separation and identification of these compounds has just been developed (Kitanovski *et al.*, 2012), and further validated for quantitative analysis.

For this purpose, an HPLC system (Agilent 1100) coupled with a linear ion trap (4000 QTRAP, Applied Biosystems/MDS Sciex) was used. The separation of nitrocatechol and related nitro-aromatic compounds was achieved using an Atlantis T3 column. PM10 samples were collected on quartz fiber filters at an urban background location in Ljubljana, Slovenia. The deposits on the filters were extracted with methanol in an ultrasonic bath. The extracts were evaporated to dryness and dissolved in methanol/water with ammonium formate buffer pH 3 prior to LC/MS^2 analysis.

Several nitro-aromatic compounds were detected in the wintertime PM10 (Figure 1). The most intense peaks were found for 4-nitrocatechol and the methyl-nitrocatechols. In comparison with the summertime PM10 samples (August 2010), the concentration of these compounds was found to be 100 – 500 times higher; for example, for 4-nitrocatechol the winter concentrations were in the range of 20-135 ng/m^3. Furthermore, the targeted nitro-aromatic compounds were well correlated with levoglucosan, but less with the organic carbon (OC) levels.

These measurements, for the first time, give information about the real concentrations of the nitro-aromatics in ambient aerosols, and without doubt support the proposed role for 4-nitrocatechol and methyl-nitrocatechols as tracers for BB SOA.

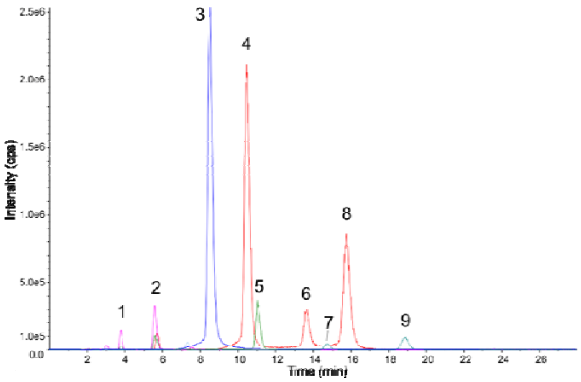

Figure 1. Extracted ion chromatograms of a PM10 sample from the city of Ljubljana, Slovenia (December 2010). **1**: 3-nitrosalicylic acid; **2**: 5-nitrosalicylic acid; **3**: 4-nitrocatechol; **4**: 4-methyl-5-nitrocatechol; **5**: 4-nitrophenol; **6**: 3-methyl-6-nitrocatechol; **7**: 3-methyl-4-nitrophenol; **8**: 3-methyl-5-nitrocatechol; **9**: 2-methyl-4-nitrophenol.

This work was supported by the Slovenian Research Agency (Contract no. P1-0034-0104 and BI-BE/11-12-F-012). The PM samples were provided by the Environmental Agency of the Republic of Slovenia.

Hallquist, M. *et al.* (2009) *Atmos. Chem. Phys*. **9**, 5155-5236.

Fine, P.M., Cass, G.R. and Simoneit, B.R.T. (2002) *J. Geophys. Res.* **107(D21)**, 8349, doi: 10.1029/2001JD000661.

Iinuma, Y., Böge, O., Gräfe, R. and Herrmann, H. (2010) *Environ. Sci. Technol*. **44**, 8453-8459.

Kitanovski, Z., Grgić, I., Yasmeen, F., Claeys, M. and Čusak. A. (2012) *Rapid Commun. Mass Spectrom.* **26**, in press.

Laskin, A., Smith, J.S. and Laskin, J. (2009) *Environ. Sci. Technol*. **43**, 3764-3771.

Simoneit. B.R.T. (2002) *Appl. Geochem*. **17**, 129-162.

Contribution of Cooking Emissions to Primary and Secondary Organic Aerosol in Urban Atmospheres

I. El Haddad[1], S.M. Platt[1], J. Slowik[1], C. Mohr[1,‡], M. Crippa[1], B. Temime-roussel[2], A. Detournay[2], N. Marchand[2], U. Baltensperger[1], A. S. H. Prévôt[1]

[1]Laboratory of Atmospheric Chemistry, Paul Scherrer Institut, Villigen, CH-5232, Switzerland
[2]Aix Marseille Univ.-CNRS, Laboratoire Chimie Environnement, Marseille, 13 331, France
[‡]Now at: Department of Atmospheric Sciences, University of Washington, Seattle WA 98195, USA
Keywords: cooking emissions, non-fossil SOA, smog chamber, AMS
Presenting author email: imad.el-haddad@psi.ch

Long before the industrial evolution and the era of fossil fuels, high concentrations of aerosol particles were alluded to in heavily populated areas, including ancient Rome and medieval London. Recent radiocarbon measurements (^{14}C) conducted in modern megacities came as a surprise: carbonaceous aerosol (mainly Organic Aerosol, OA), itself a predominant fraction of particulate matter (PM), remains overwhelmingly non-fossil despite extensive fossil fuel combustion. Such particles are directly emitted (Primary OA, POA) or formed in-situ in the atmosphere (Secondary OA, SOA) via photochemical reactions of volatile organic compounds (VOCs). Urban levels of non-fossil OA exceed several folds the levels measured in pristine environments strongly impacted by biogenic emissions, suggesting a contribution from unidentified anthropogenic non-fossil sources to urban OA.

Positive Matrix Factorization (PMF) techniques applied to ambient aerosol mass spectrometer (AMS, Aerodyne) data identified primary cooking emissions (COA) as one of the main sources of primary non-fossil OA in major cities like London (Allan et al., 2010), New York (Sun et al., 2011) and Beijing (Huang et al., 2010). Cooking processes can also be associated with VOCs that can act as SOA precursors, explaining potentially in part the high levels of oxygenated OA (OOA) identified by the AMS in urban areas. However, at present, the chemical nature of these VOCs and their secondary aerosol production potential (SAPP) remain virtually unknown.

The approach adopted here is multi-dimensional, involving ambient measurements of the COA contribution in European megacities, as well as laboratory quantification of PM and VOC emission factors from the main primary COA emitting processes and their SAPP. Primary emissions from deep-fat frying, vegetable boiling, vegetable frying and meat cooking were analysed under controlled conditions after ~100 times dilution for different oils, meats and vegetables. A high-resolution time-of-flight aerosol mass spectrometer (HR-ToF-AMS) and a high resolution proton transfer time-of-flight mass spectrometer (PTR-ToF-MS) were used to quantify OA and VOC emissions, respectively. SOA production potential of the different emissions was quantified by introducing them into the new PSI mobile smog chamber where they were photochemically aged.

Our AMS measurements in Paris (Jan. 2010) and Barcelona (Mar. 2009) showed that cooking emissions constitute a predominant source of urban OA. In the case of Barcelona for example (Mohr et al., 2012), primary cooking emissions contributed, on average, 17% to total OA and 28% to total non-fossil OA (Fig.1a). Laboratory measurements of primary emissions suggest that the COA factor identified in ambient atmospheric aerosols is mostly related to fat release from frying with vegetable oils or grilling fatty-meats (Fig.1b). In contrast, vegetable cooking (boiling and frying) was associated with significant VOC emissions. Emission factors and SAPP from all these processes and their potential contribution to non-fossil carbon in urban areas will be discussed.

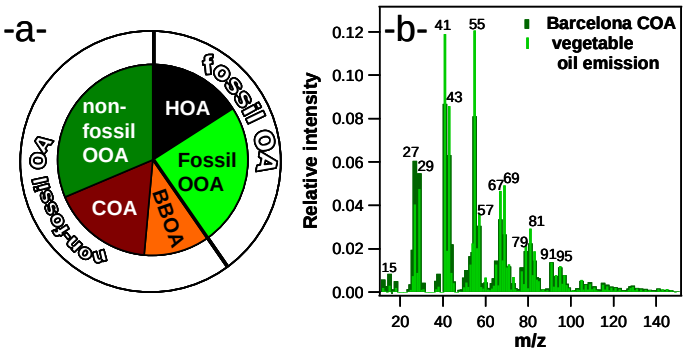

Figure 1: **-a-** Source apportionment of OA in Barcelona based on ^{14}C data (Minguillón et al., 2011) and PMF analysis of AMS data (Mohr et al., 2012). **-b-** AMS spectrum of COA factor deconvolved using PMF analysis on the Barcelona data *vs.* an AMS spectrum recorded for heated vegetable oil direct emissions.

This work was supported by the Swiss National Science Foundation as well as the Swiss Federal Office for the Environment.

J. Allan et al, Atmos. Chem. Phys. 10, 647-668 (2010)
X.-F. Huang et al, Atmos. Chem. Phys. 10, 8933-8945 (2010)
M.-C. Minguillón et al, Atmos. Chem. Phys. 11, 12067-12084 (2011)
C. Mohr et al, Atmos. Chem. Phys. 12, 1649-1665 (2012)
Y.-L. Sun et al, Atmos. Chem. Phys. 11, 1581-1602 (2011)

Interpretation of Sources and Formation Processes of Sub-micron Aerosols near Denver, Colorado from Tower Measurements during NACHTT 2011

Öztürk, F.[1,2], Bahreini, R.[2,3], Wagner, N. [2,3], Dubé, W. [2,3], Young, C. [2,3], Brown, S.S.[2] , Brock, C.[2], Ulbrich, I.M.[3,4], Jimenez, J.[3,4] and Middlebrook, A.M.[2]

[1]Abant Izzet Baysal University, Faculty of Engineering and Architecture, Environmental Engineering Department, Bolu, Turkey
[2] Earth System Research Laboratory, Chemical Sciences Division, NOAA, Boulder, CO, USA
[3]Cooperative Institute for Research in Environmental Sciences (CIRES), University of Colorado, Boulder, Colorado, USA
[4]Department of Chemistry and Biochemistry, University of Colorado, Boulder, CO, USA
Keywords: Aerosol Mass Spectrometer (AMS), Secondary Organic Aerosol (SOA), Positive Matrix Factorization (PMF), Aerosol Vertical Profiles
Presenting author email: ozturk_fatma@ibu.edu.tr

The Nitrogen, Aerosol Composition, and Halogens on a Tall Tower (NACHTT) field campaign was carried out at Erie (40.0500°N, 105.0039°W), CO between February 17 and March 14, 2011. An Aerodyne Compact Time-of-Flight Aerosol Mass Spectrometer (C-ToF-AMS, henceforth it will be called AMS) was deployed to measure the non-refractory PM_1 (NR-PM_1) composition. The AMS was installed in a moving carriage, obtaining vertical profiles along a 300 m tall tower during the study period. Complementary data such as meteorological parameters (wind speed and direction, temperature, and RH), nitrogen oxides, ozone, and aerosol size distributions were simultaneously determined on this carriage. To our knowledge, this study is unique since it represents for the first time the vertical profile of NR-PM_1 composition determined by the AMS during wintertime in a suburban environment.

Ten-second-resolved measurements of the AMS data were analysed and the average total mass concentration was 4.64±5.71 μg/m^3. The average contributions of nitrate, organics, sulphate, ammonium, and chloride to the total NR-PM_1 mass were 35, 26, 20, 17, and 1 %, respectively.

Average vertical profiles of NR-PM_1 during day (07:00-18:00 local time) - and night (20:00-05:00 local time) are depicted in Figure 1. It is clear from Figure 1 that aerosol concentrations were low above 120 m while higher values were observed from the surface up to 120 m. Based on the temperature and NR-PM_1 mass profiles, we evaluated data for two layers: Layer I ranges from the ground up to 40 m and Layer II ranges from 40 to 120 m. Wind sector analysis was performed to find the immediate sources affecting the chemical composition of NR-PM_1 in Layer I. Forty-eight-hour HYSPLIT backward trajectories were calculated to use as input for cluster

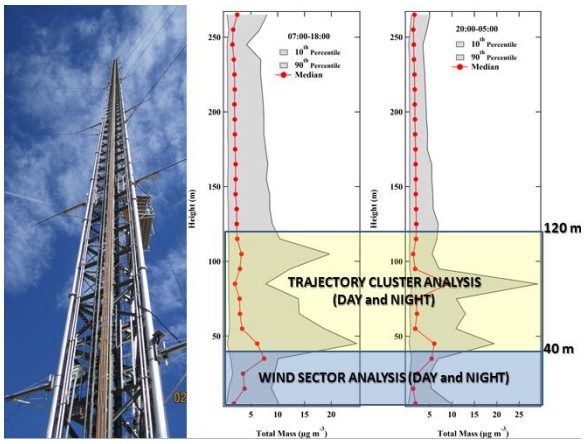

Figure 1: Average vertical profiles of total mass during day (left) and night (right) along the tower

analysis to find the long range transported sources influencing the data collected in Layer II. In addition, variations in the mass distributions of AMS measured parameters for each layer were investigated in this study. Positive Matrix Factorization (PMF) was applied to the organic aerosol (OA) data to characterize contributions of different types of OA. PMF identified three factors: (1) OOA-I (Oxygenated Organic Aerosol, a surrogate for secondary and highly aged OA), (2) OOA-II, and (3) HOA (Hydrocarbon-like Organic Aerosol). OOA-I and OOA-II represent the low-volatility and semi volatile components of OA, respectively, based on the contribution of m/z 43 and 44. HOA represents primary organic aerosol from combustion sources. Average contribution of OOA-I, OOA-II and HOA to total organic mass was 52, 32, and 16 %, respectively. Correlations between the PMF factors, air mass types, and inorganic aerosol components were evaluated.

Composition and formation of organic aerosol particles in the Amazon

C. Pöhlker[1], K. T. Wiedemann[2,3,4], B. Sinha[5,6], M. Shiraiwa[1], S. S. Gunthe[1,7], M. Smith[3], H. Su[1], P. Artaxo[2], W. Elbert[1], M. K. Gilles[8], A. L. D. Kilcoyne[8], R. C. Moffet[8,9], M. Weigand[10], S. T. Martin[3], U. Pöschl[1], M. O. Andreae[1]

[1]Biogeochemistry Department, Max Planck Institute for Chemistry, Mainz 55020, Germany
[2]Institute of Physics, University of São Paulo, São Paulo 05508-900, Brazil
[3] Department of Earth and Planetary Sciences, Harvard University, Cambridge, MA 02138, USA
[4]University of Arizona, Tucson, AZ 85721, USA
[5]Particle Chemistry Department, Max Planck Institute for Chemistry, Mainz 55020, Germany
[6]IISER Mohali, Department of Earth and Environmental Science, S.A.S. Nagar, Manauli PO, India
[7]Indian Institute of Technology Madras, Chennai 600036, India
[8]Lawrence Berkeley National Laboratory, Berkeley, CA 94720, USA
[9]Department of Chemistry, University of the Pacific, Stockton, CA 95211, USA
[10]Max Planck Institute for Intelligent Systems, Stuttgart 70569, Germany
Keywords: Organic aerosols, STXM-NEXAFS, Aerosol formation, Aerosol chemistry.
Presenting author email: c.pohlker@mpic.de

We applied scanning transmission X-ray microscopy with near edge X-ray absorption fine structure (STXM-NEXAFS) analysis to investigate the morphology and chemical composition of aerosol samples from a pristine tropical environment, the Amazon Basin. The samples were collected in the Amazonian rainforest during the rainy season and can be regarded as a natural background aerosol (Martin et al. 2010; Pöschl et al. 2010). The samples were found to be dominated by secondary organic aerosol (SOA) particles in the fine and primary biological aerosol particles (PBAP) in the coarse mode. Lab-generated SOA-samples from isoprene and terpene oxidation as well as pure organic compounds from spray-drying of aqueous solution were measured as reference samples. The aim of this study was to investigate the microphysical and chemical properties of a tropical background aerosol in the submicron size range and its internal mixing state.

The lab-generated SOA and pure organic compounds occurred as spherical and mostly homogenous droplet-like particles, whereas the Amazonian SOA particles comprised a mixture of homogeneous droplets and droplets having internal structures due to atmospheric aging. In spite of the similar morphological appearance, the Amazon samples showed considerable differences in elemental and functional group composition. According to their NEXAFS spectra, three chemically distinct types of organic material were found and could be assigned to the following three categories: (1) particles with a pronounced carboxylic acid (COOH) peak similar to those of laboratory-generated SOA particles from terpene oxidation; (2) particles with a strong hydroxy (C-OH) signal similar to pure carbohydrate particles; and (3) particles with spectra resembling a mixture of the first two classes.

In addition to the dominant organic component, the NEXAFS spectra revealed clearly resolved potassium (K) signals for all analyzed particles. During the rainy season and in the absence of anthropogenic influence, active biota is regarded to be the major potassium source (Artaxo and Hansson 1995; Andreae and Crutzen 1997). In addition a strong size dependence of the K mass fraction in the SOA particles has been found, with highest K content in small particles. We suggest that K-rich biogenic salts act as a template for condensational growth by low-volatility organic compounds from atmospheric isoprene and terpene oxidation. The presence of K-rich salts in SOA particles has been confirmed by scanning electron microscopy (SEM) and secondary ion mass spectrometry (NanoSIMS) techniques. Seeding of SOA particles by biogenic salts may explain the absence of new particle formation events in pristine boundary layer air over the Amazonian rainforest.

This work has been supported by the Max Planck Society, the Max Planck Graduate Center, the LEC Geocycles Mainz and the Office of Science (BES), U.S. Department of Energy, Grants No. DE-FG02-08ER6452, and No. DE-AC02-05CH11231.

Andreae, M. O., Crutzen, P. J., *Science* **276**, 1052 (1997).
Artaxo, P., Hansson, H. C., *Atmospheric Environment* **29**, 393 (1995).
Martin, S. T. *et al.*, *Rev. Geophys.* **48**, RG2002 (2010).
Pöschl, U. *et al.*, *Science* **329**, 1513 (2010).

Tuesday, September 4, 2012

Session WG05S1O. Physical and chemical analysis of PMx

Personal monitoring of ambient particulate matter – online monitoring and offline filter sample analysis

J. Schnelle-Kreis[1] G. Abbaszade[1], J. Cyrys[3,4], J. Gu[3], M. Pitz[4], A. Peters[3], R. Zimmermann[1,2]

[1]Joint Mass Spectrometry Centre, Comprehensive Molecular Analytics, Helmholtz Zentrum München, Germany
[2]Joint Mass Spectrometry Centre, Chair of Analytical Chemistry, University of Rostock, Rostock, Germany
[4]Environmental Science Centre (WZU),University of Augsburg, Germany
Keywords: Personal sampling, $PM_{2.5}$, black carbon, organic markers,
Presenting author email: juergen.schnelle@helmholtz-muenchen.de

Several epidemiological studies have shown adverse health effects of ambient particulate matter (PM). Many epidemiological studies on effects of air pollutants use data from a central measurement station as a surrogate for exposure. However, exposure assessment studies have demonstrated that individual personal exposure to PM is poorly correlated with ambient concentrations. Here we report data from a pilot study investigating personal exposure to ambient PM in differently characterised outdoor micro environments.

Measurements were performed in May 2011 in Augsburg, Germany. Exposure data were collected by a researcher equipped with personal monitors and a sampler walking along roads with high traffic volume (traffic) or walking in residential areas with little traffic (residential). Particle number concentration (PNC) in the size range of 10 nm – 1 µm was measured with a Condensation Particle Counter (Model 3007, TSI). Black carbon (BC) was measured by an Aethalometer (microAeth® Model AE51, Magee Scientific), $PM_{2.5}$ mass was determined with a personal aerosol monitor (Model DataRAM pDR-1500, Thermo). $PM_{2.5}$ samples (PEM-10-2.5, MSP) were collected on pre-fired quartz fibre filters at a flow of 10 l min^{-1} (Leland Legacy Pump, SKC). Average sampling times were 60 minutes. Samples were analysed by IDTD-GC-TOFMS (Orasche et al., 2011). Results were compared with the stationary monitors for PNC, BC and $PM_{2.5}$, operated at a central aerosol measurement station located at an urban background site (Cyrys et al., 2006).

High correlations were found for variables measured at the fixed site and the personal monitors, but the personal monitors generally showed the higher values. On average 1.5 fold higher $PM_{2.5}$ mass was found in personal samples (traffic 1.5, residential 1.4). PNC on average showed 2.1 higher values (traffic 2.7, residential 1.2) in the personal measurements. Walking near roads with dense traffic resulted in 4.3 fold higher BC values compared to the fixed background site. In the residential area the increase in BC levels compared to the fixed background site was similar to the increase in PNC (1.3 fold).

Differences of the personal monitoring results from the differently characterised sampling areas were less pronounced. $PM_{2.5}$ mass showed no significant differences whereas PNC and BC showed much higher values in the traffic area. About three times higher BC concentrations were found near the busy street compared to the residential area.

The differences in concentration of organic compounds were less pronounced than BC and PNC. The highest differences were found for hopanes, which are discussed as molecular markers for traffic emissions. On average, 1.9 fold higher values were found in the highly traffic-influenced area. Compounds coming from different sources showed lesser differences. The polycyclic aromatic hydrocarbons showed varying differences ranging from almost equal average concentrations (bezofluoranthenes, crysene) to about 2 fold higher values (bezo[ghi]perylene) in the traffic area. Compounds which have a more uniform emission within the city area, like levoglucosan which is discussed as marker for biomass (in this case wood) combustion, did not show significant differences amongst the investigated areas.

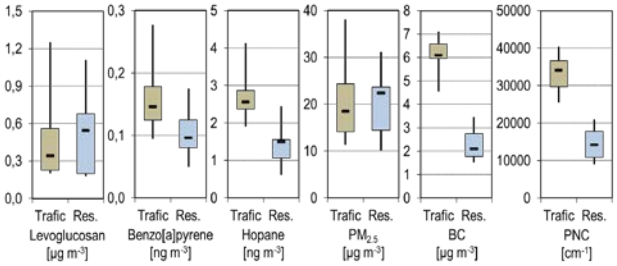

Figure 1. Box plots of concentrations of selected variables determined from personal monitoring near highly traffic influenced roads (Traffic) and in residential areas with little traffic (Res.)

This pilot study clearly indicates the variability in personal exposure to ambient PM and its constituents or source contributions when walking in a city.

The Health effects of organic compounds in aerosols are currently investigated in the framework of the Virtual Helmholtz Institute HICE (www.hice-vi.eu)

Cyrys J, Pitz M, Soentgen J, Zimmermann R, Wichmann HE, Peters A. 2006. *Epidemiology* **17**: S250-S251.
Orasche J, Schnelle-Kreis J, Abbaszade G, Zimmermann R. 2011. *Atmos Chem Phys* **11**: 8977-8993.

Inhalable aerosol chemistry of transboundary particulate intrusions into western Japan

T. Moreno[1], T. Kojima[2], X. Querol[1], A. Alastuey[1], F. Amato[3], F. Lucarelli[4], J. de la Rosa[5] and W. Gibbons[6]

[1]Inst. of Environmental Assessment & Water Research (IDÆA-CSIC), Jordi Girona 18, 08034 Barcelona, Spain
[2]Dept. of Earth & Environmental Sciences, Kumamoto University, Kurokami, Kumamoto 860-8555, Japan
[3]TNO Climate, Air and Sustainability, Princetonlaan 6, PO Box 80015, 3508 TA Utrecht, The Netherlands
[4]Dept. of Physics, University of Florence, and INFN, Sesto Fiorentino, Florence I-50019, Italy
[5]University of Huelva, University Campus El Carmen, E21071 Huelva, Spain
[6]AP 23075, Barcelona 08080, Spain

Keywords: Transboundary aerosols, SW Japan, *Kosa*, metalliferous sulphate PM_{10}, coal emissions.
Presenting author email: teresa.moreno@idaea.csic.es

The eastward transport of aerosols exported from mainland Asia strongly influences air quality in the Japanese archipelago. The bulk of the inhalable particulate matter (PM_{10}) in these intrusions comprises either natural, desert-derived minerals or anthropogenic pollutants, in various states of mixing. In this context we analyse PM_{10} collected in Kumamoto, SW Japan, during contrasting types of aerosol intrusions involving different PM mixtures. In addition to analysing the daily chemistry of PM_{10} using 24-hour filter samples, an elemental characterization of PM was performed by a Streaker sampler collecting hourly aerosol samples in two size ranges (0.1-2.5µm and 2.5-10µm) that were then analyzed by Particle Induced X-Ray Emission (PIXE).

Whereas the chemistry of the natural mineral component is characterised by "crustal" elements (Si, Al, Fe, Mg, K, Li, P, Sc, V, Rb, Sr, Zr, Th, lanthanoids), the anthropogenic component is rich in secondary inorganic compounds and more toxic metallic elements (NH_4^+, SO_4^{2-}, As, Pb, Cd, Cu, Zn, Sn, Bi, Sb, and Ge). Some desert-dust (*Kosa*) intrusions are more calcareous than others, implicating geologically different source areas, and contain enhanced levels of NO_3^-, probably as supermicron $Ca(NO_3)_2$ particles produced by chemical reaction between NOx pollutants and carbonate during atmospheric transport. The overall trace element chemistry of aerosol intrusions into Kumamoto shows low V/Rb, low NO_3^-/SO_4^{2-}, enhanced As levels, and unfractionated La/Ce values, which are all consistent with anthropogenic sources including coal emissions rather than those derived from the refining and combustion of oil fractionates.

On Figure 1 we introduce a ternary AsCeLax2 diagram to illustrate the As-enrichment in our samples. The Kumamoto samples, displaying no lanthanoid fractionation, lie on a mixing line between the Izaña (located in the free troposphere, Canary Islands) and Wuhan samples (up to 70ngAs/m^3 attributed to a mixture of metallurgical and coal emissions), with the most crustal compositions corresponding to the arrival of dust waves. The most anthropogenically contaminated Kumamoto samples plot close to the As apex. For comparison, we also plot the natural composition of coal compared with its different constituents separated into different densities. The lightest coal fraction, mostly silicate mineral matter, plots close to crustal compositions (UCC). In contrast, the heaviest coal fraction, representing the volatile material released during combustion and thus including the bulk of the heavy metal content as sulphides, plots adjacent to the As apex. For comparison we also add PM_{10} samples contaminated by La during FCC oil refining, and by Ce in ceramic industrial emissions.

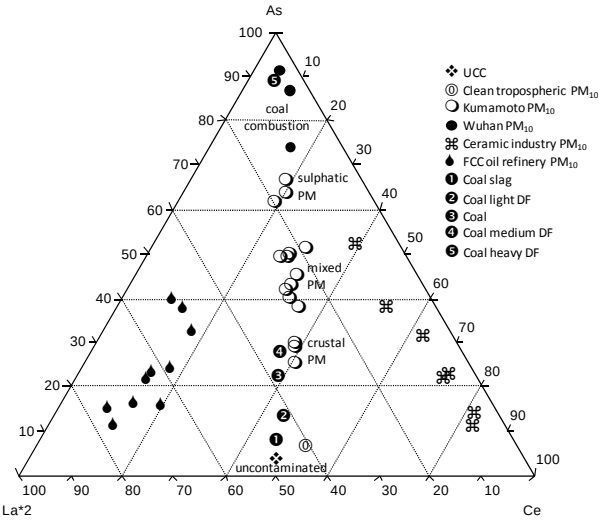

Figure 1. Ternary diagram depicting the mixing line between uncontaminated crustal compositions (UCC) and urban PM contaminated by coal/industrial emissions in Wuhan, China.

Our data clearly demonstrate the great chemical differences between the natural and anthropogenic aerosol components arriving in Japan from China. It is unlikely that the inhalation of coarse silicate mineral dust during a *Kosa* event has the same chronic health impact as a persistent haze of finely respirable sulphatic aerosol containing enhanced amounts of toxic metals. Finally, as we can also see in many other studies of ambient aerosol chemistry, the Kumamoto dataset highlights the limitations associated with legal air quality standards based only on PM mass rather than chemical composition.

This work was supported by the Generalitat de Catalunya (CUR- DIUE: BE-DGR 2010), the Grant-in-Aid for Scientific Research (No. 17684026), and the Invitation Fellowship Program for Research of the Japan Society for the Promotion of Science (No. 11019).

Size-segregated Characterization of PM_{10} in German low lands (EMEP site Melpitz) using a five-stage Impactor: A six year study

G. Spindler, A. Grüner, Y. Iinuma, K. Müller, S. Scheinhardt, H. Herrmann

Leibniz-Institut für Troposphärenforschung e.V., Permoserstrasse 15, 04318 Leipzig, Germany
Keywords: Berner impactor, Aerosol size distribution, organic matter, long-range transport, trajectory
Presenting author email: spindler@tropos.de

Particle sampling took place at the IfT-research station and EMEP-site Melpitz (12°56' E, 51°32' N, 86 m asl.). This site is located about 50 km northeast of Leipzig and 120 km west from the Polish border in a rural region in the German low-lands (EMEP, 2007). Particle samples were collected on ring–like aluminium foils using a BERNER impactor (van Pinxteren *et al.*, 2009) for five size classes (stages 1-5: aerodynamic cut-off diameters 0.05-0.14-0.42-1.2-3.5-10 µm, duration 24 hours, sampled air volume 108 m³). Sampling was planned following the weather forecast. Days without precipitation and with a continuous airflow from either the West or the East were preferred. Air-mass origin was rechecked after sampling based on 96-h backward trajectories (NOAA-Hysplit-Model). Between June 2004 and September 2009, 169 daily samples were taken (8.9 % of the total number of days). The sorting criteria were (i) the distinction between winter (W, November to April) and summer (S, May to October) and (ii) a distinction between air mass inflow from a sector West (W, 210° - 320°) and from sector East (E, 35° - 140°). Four categories (WW, WE, SW and SE) with 48, 18, 42 and 29 days were established. For every sampling day and all stages the mass concentrations of gravimetric mass (weighing of equilibrated aluminium foils before and after sampling), the water soluble ions (cations: ion chromatography, anions: capillary electrophoresis), the organic (OC) and elemental carbon (EC) (two-step thermographic method VDI 2465 part 2) and the PAH and n-alkanes (CPP-GC-MS, Curie point 510°C) were determined. The water content was calculated using the extended Aerosol Thermodynamics Model (E-AIM). OC was converted to organic matter (OM) using different conversion factors (1.4 for stage 1, 1.7 for stage 2 and 2 for stages 3-5).

The lowest mean particle mass concentrations have been found for SW and the highest for WE with relative mass concentration distributions (stages 1-5) of 5.9, 28.2, 36.5, 18.0, and 11.4% and 3.5, 22.7, 52.6, 16.7, and 4.5%, respectively. The mean mass closure for water soluble ions, water, OM and EC accounts for 81 to 99% in summer and 60-81 % in winter (depending on the stage). The fractions of nitrate are relatively high for WW; in contrast, sulphate is high for WE. The estimated mean concentrations of secondary organic carbon (SOA) (Castro *et al.*, 1999) on stage 3 for WW, WE, SW and SE are 0.32, 1.25, 0.27 and 0.58 µgm^{-3}, respectively. The highest difference in the percentages of SOA in OC was found between winter (WW 55%, WE 59%) and summer (SW and SE 74%), indicating photochemical processes. The mean Carbon Preference Indices (CPI) are the highest for SE (stage 4: 7.57 and stage 5: 9.82), resulting from plant wax abrasion in the surrounding forests. The mean PAH concentration for WE on stage 3 is 9.7 ngm^{-3} which is more than 4 times higher than for WW. PAHs account for about 610 and 310 ppm of the particle mass concentration for WE and WW, respectively. This indicates long range transport from emissions of domestic heating and other combustion processes (Figure 1) especially for WE.

These results are in agreement with former findings of higher fractions of sulphate, organic and black carbon during air mass transport from E (especially in winter) in particles of different size ranges at the Melpitz site (Spindler *et al.*, 2010).

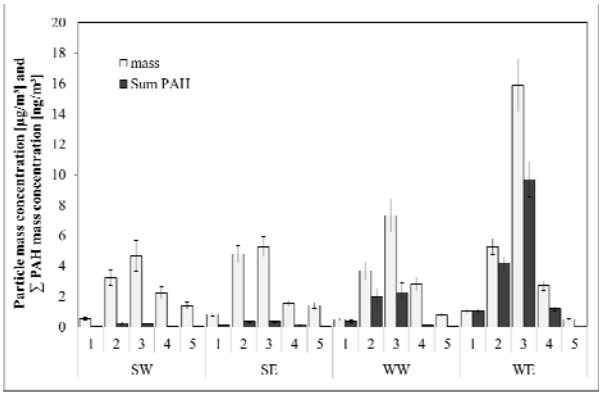

Figure 1. Sum of individual PAH and particle mass concentration for stages 1 to 5 of the BERNER-impactor in Melpitz. Means for the four categories WW, WE, SW and SE.

Castro, L.M., Pio, C.A., Harrison, R.M., Schmith, D.J.T. (1999) *Carbonaceous aerosol in urban and rural European atmospheres: estimation of secondary organic carbon concentrations. Atmos. Environ.*, 33, 2771-2781.

EMEP (2007) *Transboundary particulate matter in Europe.* Status report 4/2007 Ed.: Yttri, K.-E., Aas, W., Tarrason, L., Vestreng, V., Tsyro, S., Simpson, D., Putaud, J.,P., Cavalli, F., NILU reference O-98134, ISSN: 1504-6109 (http://www.emep.int/publ/common_publications.html).

Spindler, G., Brüggemann, E., Gnauk, T., Grüner, A., Müller, K., Herrmann, H. (2010) *A four-year size-segregated characterization study of particles PM_{10}, $PM_{2.5}$ and PM_1 depending on air mass origin at Melpitz. Atmos. Environ.*, 44, 164-173.

van Pinxteren, D., Brüggemann, E., Gnauk, T., Iinuma, Y., Müller, K., Nowak, A., Achtert, P., Wiedensohler, A., Herrmann, H. (2009) *Size- and time-resolved chemical particle characterization during CAREBeijing-2006: Different pollution regimes and diurnal profiles. J. Geophys. Res.*, 114D, doi:10.1029/2008JD010890.

Ultrafine particles and PM1 measurements in a hot-spot pollution area: size distribution, mass closure and source apportionment.

R. Vecchi[1], V. Bernardoni[1], A. Bigi[2], M. Elser Fritsche[1], P. Fermo[3], G. Ghermandi[2], A. Piazzalunga[3,4], Raquel Gonzales Turrion[3], M. Urbani[3],, G. Valli[1]
[1]Department of Physics, Università degli Studi di Milano, Milan, 20133, Italy
[2]Department of Mechanical and Civil Engineering, University of Modena and Reggio Emilia, Modena, 41125, Italy
[3]Department of Inorganic, Metal-organic and Analytical Chemistry, Università degli Studi di Milano, Milano, 20133, Italy
[4]Department of Environmental Sciences, Università degli Studi di Milano-Bicocca, Milano, 20126, Italy
Keywords: sub-micron sized particles, size distributions, chemical characterisation, source apportionment
Presenting author email: roberta.vecchi@unimi.it

In urban areas, ultrafine particles and PM1 are of great concern because can deeply enter the respiratory system strongly affecting human health.

Hot-spot pollution areas are peculiar sites where source emissions and meteorological conditions foster particulate matter accumulation and very high aerosol concentrations are often registered. The Po Valley is one of the main hot-spot pollution areas in Europe, especially during wintertime. Despite the high levels of PM registered in the area, little knowledge on PM1 and ultrafine particles composition and sources is available, apart from a couple of studies carried out by our group in 2002 and 2004 in the same area.

This work aimed at a detailed physical and chemical characterisation of PM1 and ultrafine particles and at singling out major sources contributing to the high concentrations observed in the urban area. A critical comparison to the results obtained during the previous PM1 campaigns will be also shown.

PM1 was sampled at an urban background station in Milan, Italy, during winter 2011-2012. Parallel PM1 sampling was carried out twice a day (07-16, 19-04) on PTFE and quartz fibre filters using two low-volume samplers for a total of about 300 samples. Mass concentration was determined by the gravimetric technique and all the PM1 samples were chemically characterised for elements, inorganic ions, levoglucosan, EC/OC and water soluble organic compounds. BC determination was also carried out on both PTFE and quartz fibre filters by a polar photometer (Vecchi et al., 2010; Vecchi et al., 2012). Moreover, BC concentrations in PM1 were monitored with a 5 minute resolution by a MAAP.

The ultrafine fraction was characterised for number size distribution by an optical particle counter (range 0.25-32 μm in 31 size bins) and a differential mobility particle scanner (8-700 nm in 31 size bins). Moreover, parallel samplings using multistage cascade impactors (Dekati-SDI and nanoMOUDI) were collected on different substrates (polycarbonate membranes and quartz fibre filters) to gain information on the size-segregated chemical composition (elements, ions, and carbonaceous components). It is noteworthy that the detailed characterisation of size-segregated PM required the optimisation of the analytical techniques because of the small quantities of material to analyse and of the peculiarities of the PM deposits.

Ancillary information on atmospheric dispersion conditions was available by ^{222}Rn measurements and the main meteorological parameters (temperature, pressure, RH, solar radiation, wind speed and direction) were also monitored at the sampling site.

PM1 data will be used to resolve the main sources in the area using Positive Matrix Factorization. This is important to develop suitable and efficient abatement strategies in an area heavily affected by high PM levels.

Results obtained for size-segregated samples will be analysed using the MICRON inversion model aiming at the identification of the size-distribution modes for the different chemical components. These modes can track different formation processes adding useful information to the results obtained by PMF on the PM1 samples.

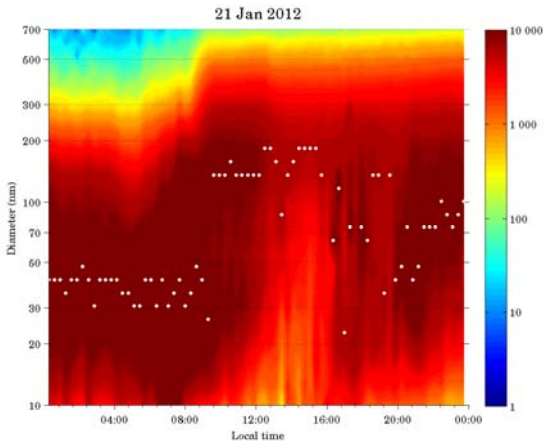

Figure 1: example of DMPS data (Milan, 21 Jan 2012)

Vecchi, R., Bernardoni, V., Broccoletti, S., Canepa, P., Cuccia, E., Massabò, D., Paganelli, C., Piazzalunga, A., Prati, P., and Valli, G. (2010). *Abstract 11E2, International Aerosol Conference 2010*, Helsinki, August 29 - September 3, 2010.

Vecchi, R., Valli, G., Bernardoni, V., Paganelli, C., and Piazzalunga, A. (2012). *Abstract, European Aerosol Conference 2012*, Granada, 2 – 7 September, 2012.

Factors influencing levels and composition of PM in the Barcelona's city subway system

Querol X.[1], Moreno T.[1], Karanasiou A.[1], Reche C.[1], Alastuey A.[1], Viana M.[1], Font O.[1], Gil J.[1], de Miguel E.[2], Capdevila M.[2]

[1.]Institute of Environmental assessment and Water Research, IDAEA, CSIC, C/ Jordi Girona 18-24, 08034 Barcelona, Spain
[2.]Transports Metropolitans de Barcelona, Barcelona, Spain
Keywords: PM, metro system, air quality, train, indoor, exposure
Presenting author email: xavier.querol@idae.csic.es

An assessment of indoor air quality and passenger exposure in the Barcelona metro focusing on PM levels and their metal contents is presented.

Summer and winter measurement campaigns are carried out in platforms and trains to measure levels of PM10, PM2.5 and PM1. Furthermore, sampling of PM10 and PM2.5 and subsequent analysis of around 40 major and trace components is carried out. The impact of a new and advanced ventilation system, as well as of the platform screen door systems (automated systems consisting of closed rail track and platforms) on indoor air quality are evaluated, to determine whether these systems reduce passenger exposure to PM when compared with conventional systems (open tracks and platforms). To this end measurements were carried out in July 2011 and February-March 2012.

Results show summer PM levels inside the trains amongst the lowest reported for worldwide metro systems (11-32 µPM2.5/m3). This is most probably due to the air conditioning system working in all carriages of the Barcelona metro during the whole year. On the platforms, levels were considerably higher, reaching mean levels of 59 and 88 µgPM2.5/m3 in the new (L9) and old (L3) lines, respectively. PM10 data are also reported in the present study, but comparison with other metro systems is more difficult due to the scarcity of data compared with PM2.5.

The elements with the highest enrichment are those associated with wheel or brake abrasion products (Ba, Fe, Cu, Mn, Cr, Sb, As, Mo, Co, Sr, among others). Laminar hematite (Fe2O3) was the dominant particle type, being mainly originated by mechanical abrasion of the rail track and wheels.

Regarding passenger exposure to PM inside the metro system, the contribution of commuting by metro was estimated to account for around 10% of the daily exposure. Finally, we conclude that the implementation of platform screen door systems results in reductions of both PM levels and metal concentrations, but in addition an advanced optimized ventilation system gave even a much higher efficiency in reducing PM exposure to metro commuters. Combining these two features PM exposure levels in the platforms may be reduced down by a factor of 7 with respect the old subway lines in Barcelona. Thus, full summer ventilation set up implemented from 13th July at S-L9 produces a high air renovation rate, but also higher convective dynamics may cause the resuspension of dust. The ventilation system is very complex and with the data available is not possible to identify the specific features causing the large differences in PM levels measured. In any case, during the first 8 days of measurements, without this summer ventilation set up being fully implemented, the reduction of ambient PM with respect to the conventional L3 line reached a factor of 7.2, but also of 4.2 with respect to the full summer ventilation operation settings at the same S-L9.

Subsequent tests carried out in February 2012 yield similar results concerning the influence of the ventilation system.

The different composition of brake pads of the braking systems of the new lines is responsible for much higher levels (by factors from 5 to 200) of specific metals, such as Ba, As, Sr, Mo, Cu, among others, in the conventional line 3. Low metal specifications for brake pads would reduce considerably exposure to metals of commuters.

The chemical speciation of PM allowed identifying 3 major sources of particles in the metros system: a) Brake wear; b) Outdoor air introduced into the metro; c) Metal wear.

The mineralogical characterization by means of SEM and XRD permitted to identify the presence of laminar hematite (Fe2O3) as the dominant particle, being mainly originated by mechanical abrasion of the rail track and wheels.

Acknowledgements
This study has been supported by the Ministry of the Environment of Spain. The authors would like to thank the TMB staff who contributed to this study: Jordi Mitjà, Oscar Oliva, Francisco Sánchez and David Carulla form Gerència L3; Olga Cerezo, Antonio Pérez, Alfons Andreu and Marc Calzada from Gerència L9; Ferran Gràcia, Sergio Estepa, David Álvarez and Ivan Noguera form Manteniment Baixa Tensió i Instal•lacions Electromecàniques; Oscar Playà from CCM; Ricardo Ortega from Seguretat i Protecció Civil; Javier Robles from Material Mòbil L9; Xavier Llauradó form Àrea de Manteniment i Projectes; Sònia Centelles from Departament de Medi Ambient.

Chemical characterization and source apportionment of oxidized organic aerosol components by advanced spectroscopic techniques in the Po Valley, Italy

M. Paglione[1], S. Decesari[1], M. Dall'Osto[2], R. Hillamo[3], S. Carbone[3], S. Saarikoski[3], R. Harrison[4], C. O'Dowd[5], and M.C. Facchini[1]

[1]Institute of Atmospheric Sciences and Climate, National Research Council, Bologna, I-40129, Italy.
[2] Consejo Super Invest Cient, Inst Environm Assessment & Water Res, E-08034 Barcelona, Spain.
[3] Finnish Meteorological Institute, Air Quality Research, Helsinki, Finland
[4] Univ Birmingham, Natl Ctr Atmospher Sci, Sch Geog Earth & Environm Sci, Birmingham B15 2TT, W Midlands, England.
[5]Natl Univ Ireland, Sch Phys, Ryan Inst, Galway, Ireland

Keywords: HNMR spectroscopy, Source apportionment, Factor analysis, PMF, AMS.
Presenting author email: m.paglione@isac.cnr.it

Outside urban areas, oxidized organic aerosols (OOA) dominate composition of organic atmospheric particulate matter. In the frame of the EC project EUCAARI and of the Italian project SUPERSITO, the submicron aerosol chemical composition in rural background site of S. Pietro Capofiume, Po Valley, Italy, was characterized by means of proton-Nuclear Magnetic Resonance (^{1}H-NMR) spectroscopy and Aerosol Mass Spectroscopy (AMS) used in parallel with aim of organic aerosol characterization and source apportionment.

The experiments were conducted in 3 different intensive campaigns in different seasons: spring 2008, summer 2009 and fall 2011, representative of very different atmospheric conditions and active sources contributions. Sets of PM_1 filter samples for each of these 3 IOPs were analysed by **^{1}H-NMR spectroscopy** and the resulting collection of spectra was processed using a suite of **Factor Analysis** techniques (Positive Matrix Factorization or PMF, Non-negative Matrix Factorization or NMF, Multivariate Curve Resolution or MCR) aiming to identify recurrent spectral profiles. The contributions of the identified factors to total NMR-detected organics with the help of additional chromatographic measurements of organic and inorganic ions were used to trace the temporal variations of the various organic aerosol types at the sampling location and to identify different prevalent sources. The analysis was applied to water-soluble organic aerosols (WSOA), which is a proxy for OOA.

The comparison of NMR results with those of Positive Matrix Factorization (**PMF**) applied to parallel **HR-Tof-AMS** datasets showed that the NMR factors broadly match with chemical classes already identified by AMS.

On the basis of their spectral profiles and their correlation with organic or inorganic tracers, the identified factors can be characterized as follows: (a) wood burning products, with clear signatures from aromatic phenolic compounds and polyols and showing a good correlation with levoglucosan; (b) one or more WSOA factors showing spectra having less distinguishing features but reflecting a high functionalization degree, similar to those of Humic-Like substances (HULIS); (c) semi-volatile WSOA associated to low-molecular weight alkyl-amines and correlated with nitrate, probably linked with biogenic sources from anaerobic processes and agriculture activity; (d) minor contribution from WSOA associated to Methanesulphonic Acid (MSA), with probable marine origin; (e) compounds bearing oxygenated linear aliphatic structures.

Biomass burning products were clearly major constituents of WSOA in spring and fall seasons. Levoglucosan/OC ratios suggest that more than one factor is needed to account for the whole BB fraction. The best match between total biomass burning fraction of OC estimated from AMS and NMR is found when including an oxygenated fraction of possible secondary origin together with the primary component. Overall, the biomass burning fraction reached 40% of total water-soluble organic carbon during the spring and fall campaigns.

During the summer campaign, the wood burning factor could not be found, whereas the alkyl-amines were still present and the "HULIS" factors increased their contributions (about 60-70% of total WSOC). The latter were clearly enriched in daytime and were present in both polluted and more background conditions indicating that they are mainly associated to low-volatility organic compounds (i.e., AMS OOA1-type) forming from photochemical activity and accumulating in regional pollution.

Another factor which was found to occur in summertime was that of aliphatic compounds, possibly originating from photochemical degradation of unsaturated fatty acids and also linked to a AMS factor with a strong peak at m/z 55, reminding the "cooking organic aerosols" (COA) detected at the site mainly during night time. Concomitant ATOFMS measurements also revealed a unique particle type internally mixed with nitrate and OOA.

Therefore factor analysis applied to NMR atmospheric datasets complement AMS in lumping the complex oxidized organic mixtures into chemical classes characterized by specific sources or ageing states.

This work is supported by EC project EUCAARI and by Emilia-Romagna Region "Supersito" Project.

Towards an identification of sources of HUmic LIke Substances (HULIS) by statistical analysis

J. Guilhermet[1], C. Piot[1], J. Vessaire[1], C. Baduel[1], J.-L. Jaffrezo[1] and D. Voisin[1]

[1]UJF-Grenoble 1 / CNRS, LGGE UMR 5183, Grenoble, F-38041, France
Keywords: HULIS, source apportionment, PCA, Positive Matrix Factorization.
Presenting author email: guilhermet@lgge.obs.ujf-grenoble.fr

Chemical composition of aerosol can be described with three fractions: inorganic, elementary carbon (also called black carbon) and organic carbon (OC). The radiative effects of inorganic aerosol composed of sulfate, sea salt or mineral dust, and black carbon begin to be reasonably well-known and are now included in several climate models (Carslaw *et al.*, 2010). Conversely, composition and effects on the climate of the Particulate Organic Matter (POM) is still largely unknown.

Until recently, studies of POM failed to assign more than half of the organic carbon measured globally to individual organic compounds (Turpin *et al.*, 2000), suggesting that a significant fraction of OC may be present as oligomeric or polymeric matter. These substances, commonly named HULIS (Humic Like Substances) are oligomeric material with strong polar, poly-acidic, and chromophoric properties. Potential origins of HULIS in the atmosphere are primary sources (e.g. biomass burning) for the winter season and secondary sources for the summer (Baduel *et al.*, 2010). HULIS may strongly affect the radiative properties of aerosol by absorbing light and might have a significant impact on the radiative budget of aerosol (Dinar *et al.*, 2008). Despite their potential impact on climate and the physical and chemical properties of aerosol, HULIS are still poorly documented in terms of concentration, temporal evolution and sources.

Source apportionment of aerosols can be achieved by using statistical analysis like Principal Component Analysis (PCA) or multivariate statistical models such as Positive Matrix Factorization (PMF) both commonly applied to the main chemical components of aerosols or to detailed organic speciation (Viana *et al.*, 2008). In this work, these statistical tools are used with HULIS concentrations and physical characterization, in order to explore their sources.

In a first step, PCA and PMF analysis are applied on the chemical characterization of aerosols for a large database obtained in different environment (urban or rural) and seasons (winter and summer). These chemical data include the main components, organic tracers of sources like levoglucosan (biomass burning tracer), together with HULIS concentrations. In second step, physical characterization of HULIS (UV absorbance at several wavelengths) is also integrated in statistical analysis. Specific absorbance and ratios of particular wavelengths give indications on the chemical structure (aromatic and/or aliphatic) of HULIS (Fig.1) and can also be considered as indicator of the origin of HULIS (Baduel *et al.*, 2010).

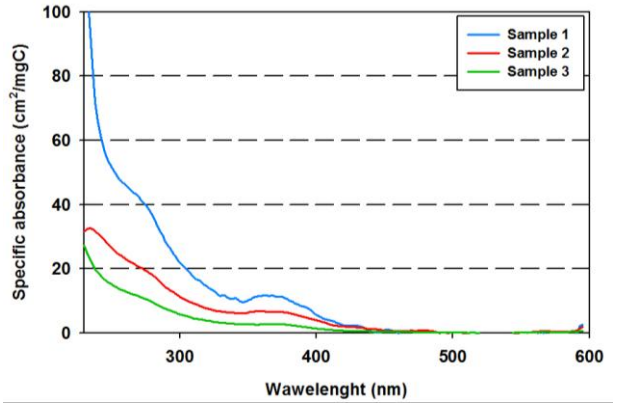

Figure 1. Specific absorbance for three different HULIS ice core samples.

The first results of the statistical analysis indicate very large changes in the associations between the various chemical indicators and HULIS, depending upon the season and location. For exemple, changes in the aromaticity of the HULIS are linked with the levoglucosan content, a good indication of the impact of biomass burming emissions on this type of complex organic matter.

In the presentation, results obtained for the complete set of statistical analyses on data of chemical composition and physical characteristics of HULIS in the different environments and seasons will be detailed and discussed. A comparison between PCA and PMF results will also be presented.

The authors would like to acknowledge the support of several funding agencies, including ADEME, LCSQA, Région Rhône Alpes, for the funding of programs that allowed the construction of this data base.

Baduel, C., Voisin, D. and Jaffrezo, J.L. (2010) *Atmos. Chem. Phys.* **10**, 4085-4095.

Dinar, E., Abo Riziq, A., Spindler, C., Erlick, C., Kiss, G. and Rudich, Y. (2008) *Faraday Discuss.* **137**, 279, doi:10.1039/b703111d.

Carslaw, K. S., Boucher, O., Spracklen, D. V., Mann, G. W., Rae, J. G. L., Woodward, S., and Kulmala, M., Atmos. Chem. Phys., 10, 1701-1737

Turpin, B.J., Saxena, P. and Adrews, E. (2000) *Atmos. Environ.* **34**, 2983-3013.

Viana, M., Pandolfi, M., Minguillon, M.C., Querol, X., Alastuey, A., Monfort, E. and Celades, I. (2008) *Atmos. Environ.* **42**, 3820-3832.

Tuesday, September 4, 2012

Session WG07S2O. Fundamentals and measurement of nanoparticles

A MEMS sensor based personal sampler for ultrafine particles

S. Merzsch[1], H.S. Wasisto[1], E. Peiner[1], I.Kirsch[2] and E. Uhde[2]

[1] Institute of Semiconductor Technology (IHT), TU Braunschweig, Braunschweig, Germany
[2] Dep. Material analysis and indoor chemistry, Fraunhofer Wilhelm-Klauditz-Institut, Braunschweig, Germany
Keywords: Airborne particles, measurements, ultrafine particles, MEMS.
Presenting author email: erik.uhde@wki.fraunhofer.de

In the production of consumer goods and building materials the use of nanomaterial as additives becomes more and more common. High-tech applications like printed electronics and solar-cells as well as daily life products like toothpaste and cosmetics are enhances by addition of e.g. TiO_2, ZnO, carbon spheres or tubes, and silver particles. Especially in the production environment, where large amounts of nanomaterial is handled and substantial exposure is possible, monitoring of the air quality is an important issue in respect to further use of this technology. In the production industry, a demand for personal monitors to assess the exposure of workers towards these particles undoubtedly exists (Tsai et al, 2011). Unlike a conventional particle counter, such a device must be small and lightweight, and the sensor and the electronics must be simple enough to allow a mass production at low costs.

Simple collection of the particles on filters or impactors offers an affordable solution to this, but requires complex laboratory analysis and can cannot provide timely warning in case of increased concentrations in the surrounding environment.

A MEMS (micro-electromechanical system) based approach was proposed to weigh extremely small particles (Hajjam 2010). This concept was developed further to design a particle detector for use in personal monitors. A joint project (NANOEXPO) examines the possibility of use thermally excited cantilevers as sensors for ultrafine particles. The project aims towards developing a small personal dosimeter-like sampler that collects and weighs ultrafine particles over a work shift.

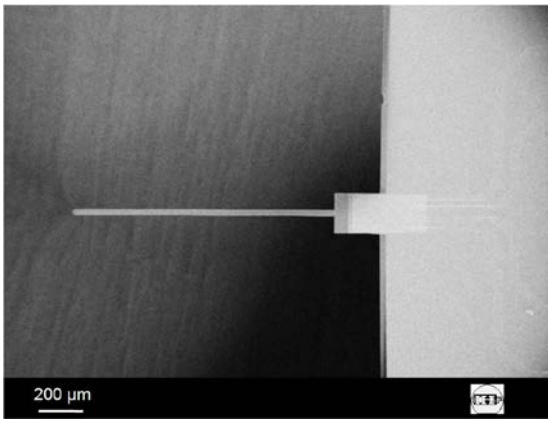

Figure 1. The cantilever sensor.

A slender geometry (Figure 1) allows for a very sensitive detection of particles impacting on the cantilever. After manufacturing the first prototypes of the sensor, and providing proof-of-principle measurements, work is on-going to further improve the sensitivity of the microbalance, to integrate part of the excitation and sensing electronics, and to construct a sampler case with defined flow field around the sensing cantilever.

The following section highlights a number of achievements of the project at the current state.

Results

Cantilevers of different sizes and geometries were tested in regard to their particle collection and sensing efficiencies. Current experiments are carried out with silicon-based cantilever-type resonators with fully integrated Wheatstone bridge piezo-resistors for signal read out.

To test the microbalances, test aerosols were generated in a 1 m³ environmental test chamber by nebulizing a suspension of e.g. carbon nanoparticles (< 30 nm) in water/butanol using a constant output atomizer (TSI 3076), followed by a dryer. Particle number concentration and size distribution is controlled by a fast mobility particle sizer (FMPS, TSI 3091). To improve the collection efficiency, the sensor was mounted on a nanometer aerosol sampler (TSI 3089) – at later stages, the collection voltage will be supplied by the sampler electronics.

Using the second resonant mode, a mass sensitivity of 32.7 Hz/ng was found. Detection limits of less than 1 ng can be achieved with current prototypes under climatic standard conditions and normal pressure.

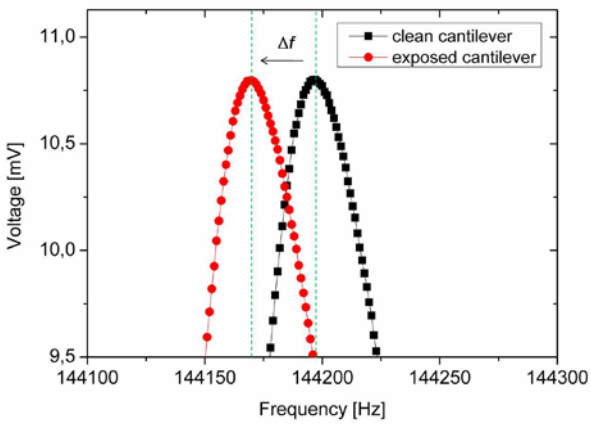

Figure 2. Frequency shift measured with a prototype cantilever (black line: clean cantilever; red line: exposed to carbon aerosol (5000 #/cm³) for 15 min.

Particles were collected predominantly at the tip and along the edges of the cantilever (Figure 3). An improved design of the field around the cantilever will be used to increase the sampling efficiency and to focus the particles deposition to the tip of the cantilever.

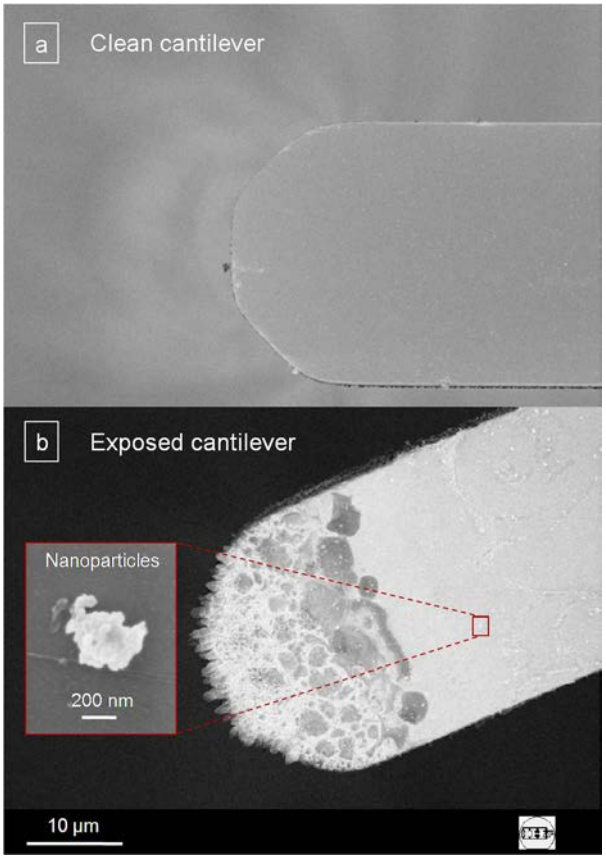

Figure 3. Cantilever tip (a) before and (b) after exposure to airborne carbon particles.

In a next step possible climatic interferences on particle sensing were studied: Temperature and relative humidity were expected to impact on the performance of the sensor. Variation of pressure, temperature and relative humidity during operation of the sensor revealed a minor cross sensitivity: Temperature changes of 2 K, pressure changes of 20 kPa, and relative humidity changes of 10 % during the measurement cycle would lead to an uncertainty of 15% with the current prototypes (Wasisto et al., 2012). Slower climatic changes that extend over several measurement cycles are less critical. Considering a measurement cycle time of only 15 to 30 min, the cross sensitivity is not critical for the workplace environment.

Currently, a sensor case with integrated fan is designed and tested. The main development targets are an optimized air supply to the sensor and a defined electrical field to improve particle collection (Figure 4).

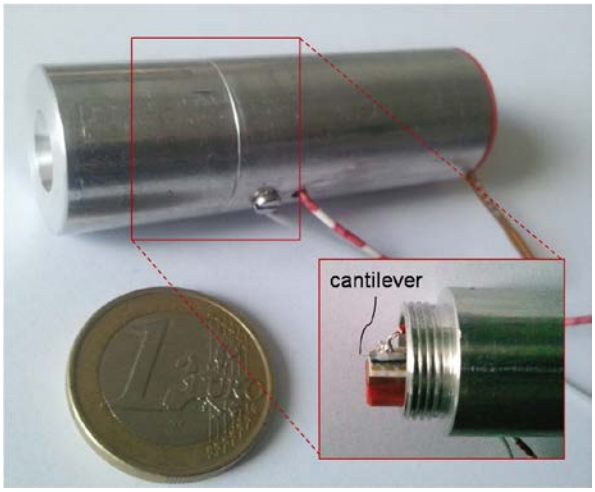

Figure 4. The sensor case with integrated fan.

Conclusion

At the current development stage the microbalance-detector prototypes show a mass-sensitivity sufficient to allow for 15-minute measurement cycles if the (preferred) second resonant mode is used for sensing. A mass resolution below 1 ng can be reached under typical indoor conditions, and the cross-sensitivity in regard to environmental changes is in an acceptable range. Evaluation the performance of the sensor towards a selection of industrially relevant nanoparticles (TiO_2, Silver, Carbon, SiO_2, PTFE) is still on-going, and a number of integration steps have to be finished before the sensor/sampler can be tested under more realistic conditions.

Acknowledgement

The authors greatly acknowledge funding by the German Federal Ministry of Education and Research (BMBF) under grant no. 03X0098A/B.

References

Hajjam A, Wilson J.C, Rahafrooz A, and Pourkamali S. 2010 Fabrication and characterization of resonant aerosol particle mass sensors. *Proc. IEEE-MEMS 2010*, 863-866.

Tsai CJ, Huang CY, Chen SC, Ho CE, Huang CH, Chen CW, Chang CP, Tsai SJ, Ellenbecker MJ, (2011) "Exposure assessment of nano-sized and respirable particles at different workplaces", *J Nanopart. Res*. 13, 4161–4172.

Wasisto H. S., Merzsch S., Waag A., Kirsch I., Uhde E., Salthammer T., Peiner E. (2012) Determination of exposure to engineered carbon nanoparticles using a self-sensing piezoresistive silicon cantilever sensor, *Microsyst. Technol.*, DOI 10.1007/s00542-011-1405-9.

Physical defect formation in few layer graphene-like carbon on aerosol-made metal nanoparticles

C.M. Schumacher[1], R.N. Grass[1], M. Rossier[1], E.K. Athanassiou[1] and W.J. Stark[1]

[1]Institute for Chemical- and Bioengineering, Department of Chemistry and applied Biosciences, ETH Zurich, Wolfgang-Pauli-Strasse 10, 8093 Zurich, Switzerland

Keywords: Core-shell nanoparticles, composite nanoparticles, flame spray synthesis, carbon
Presenting author email: ch.schumacher@chem.ethz.ch

Magnetic nanoparticles are used in a multitude of research areas. Comparably high and readily available specific surfaces combined with the ease of separation (Grass 2007) due to very high saturation magnetizations make aerosol-derived carbon-metal nanomagnets promising candidates as precious metal extraction agents (Rossier 2009) and in magnetic chemistry where a reagent is linked to a nanomagnet (Schaetz 2010). Furthermore, the feasibility as cleaning agents of complex liquids such as blood has been demonstrated (Herrmann 2010). The chemical stability in conjunction with a high saturation magnetization is a decisive parameter for a broad range of practicability.

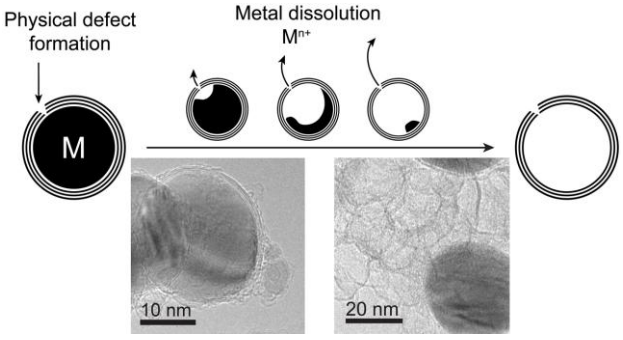

Figure 1. Physical defect formation on a metal-carbon nanoparticle leads to fast release of core-material into the surrounding solution. The prevalent mechanism results in empty graphene-like carbon-nanoshells with possibly one specific shell defect in the size of a few carbon atoms.

A systematical examination of the chemical stability of cobalt metal nanomagnets with a graphene-like carbon coating was used to study the otherwise rather elusive formation of nanometer sized physical defects in few layer graphene as a result of acid treatments (Schumacher 2012). The release of metal into the solutions over time offered a simple tool to monitor the progress of particle degradation and therefore to determine the prevalent mechanism of physical defect formation. The suggested mechanistic insight was further confirmed by the covalent chemical functionalization of the particle surface with chemically inert aryl species, which leads to an additional thickening of the shells. The possibility to prepare well-defined shells or containers combined with the new findings may provide attractive tools to material sciences.

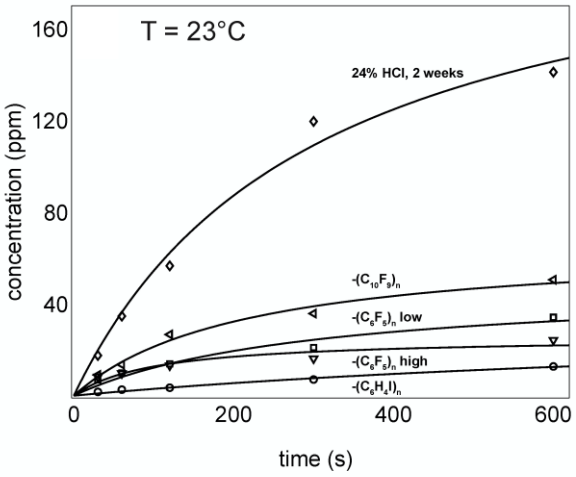

Figure 2. Metal release rates into acidic solutions at pH = 2 as a simple tool to observe the physical defect formation rate. Compared to non-functionalized particles (washed in 24% HCl, 2 weeks) the physical defect formation rate shows a strong dependence on the carbon-shell thickening when inert chemical aryl species (pentaflurobenzene, nonafluorobiphenyl and iodobenzene) are attached to the graphene-like surface by the use of aqueous diazotation.

Grass R.N., Athanassiou E.K., Stark W.J. (2007) *Chem. Int. Ed*. **46**, 4909-4912.

Rossier M., Koehler F.M., Athanassiou E.K., Grass R.N., Aeschlimann B., Günther D., Stark W.J. (2009) *J. Mater. Chem.* **19**, 8239-8243.

Schaetz A., Grass R.N., Stark W.J. (2010) *Nachrichten aus der Chemie* **58**, 857.

Herrmann I.K., Urner M., Koehler F.M., Hasler M., Roth-Z'Graggen B., Grass R.N., Ziegler U., Beck-Schimmer B., Stark W.J. (2010) *Small* **6(13)**, 1388-92.

Schumacher C.M., Grass R.N., Rossier M., Athanassiou E.K., Stark W.J. (2012) *Langmuir*, in press.

Measurement of the velocity of nanoparticles in a molecular beam of a particle mass spectrometer

W. Baumann, H. Mätzing, J. Seibold, M. Hauser, H.-R. Paur and H. Seifert

Institute of Technical Chemistry (ITC), Karlsruhe Institute of Technology (KIT)
Hermann-von-Helmholtz-Platz 1, 76344 Eggenstein-Leopoldshafen, Germany
Keywords: Nanoparticle measurement, Particle mass spectrometer, Gas phase synthesis of nanoparticles
Presenting author email: w.baumann@kit.edu

The size distributions of primary nanoparticles synthesized in plasmas (Paur, 2005) or flames (Mätzing, 2012) were measured using a particle mass spectrometer (PMS), which was developed for low and atmospheric pressure applications. The size range of the spectrometer is from 1 to 25 nm and for number concentrations between 10^9 and 10^{13} cm^{-3}. The microwave plasma burns under low pressure conditions in the range between 10 to 150 mbar. The maximum process pressure depends on the carrier gas. Silica nanoparticles were generated in a microwave plasma discharge, using Silane as precursor. Further, the microwave plasma with Argon and Helium as carrier gas with a flow rate of 4 slpm and 50 ppm Silane were operated.

The particles were sampled without prior dilution, 40-140 ms behind the plasma region with a molecular beam technique of a two-stage nozzle arrangement. With this sampling technique the inlet stream is rapidly quenched and, in particular, all particle–gas interactions are minimized which allows the measurement of particles with high concentration. A high fraction of the nanoparticles are charged in the microwave plasma, therefore, it is not necessary to ionise particles in the spectrometer. The charged particles are deflected according to the m/z ratio by an electric field in the spectrometer. The deflection voltage (U) is proportional to the ratio of the kinetic energy of the particles and the number of charges ($U \sim ½\ m\ v^2/z$). For positively and negatively charged particles Faraday cups are located symmetrically left and right of the centre line at the end of the detection chamber with defined deflection angle. By varying the deflection voltage, particles of different energy-to-charge ratio are collected at Faraday cups. The current detected at the Faraday cup is proportional to the incoming number of particles times their total charge, which is measured with a highly sensitive amplifier. The raw data give the energy distribution and can be converted with knowledge of the particle velocity and the material density. Primary particles from flames and plasmas are usually singly charged with a narrow particle size distribution.

The advantage of PMS is the simultaneous measurement of the signal intensity and the flight time of the particle with a lock-in amplifier. The PMS works with an electrostatic chopper technique to get a chopped particle beam and the deflected particle beam hits the Faraday cups periodically with a known frequency. The lock-in amplifier measures the flight time difference between triggering of the capacitor voltage and the detection of the particle signal at the Faraday cup as a phase shift. The phase shift grows proportional with the frequency of the particle beam modulation and to get a good resolution for the simultaneous measurement of the phase shift and the signal intensity, the particle beam is chopped with a frequency in the range of 1 kHz.

In this study, we report about our investigations of measuring the velocity of nanoparticles in the molecular beam of the PMS. The particle size of the silica nanoparticles generated in the microwave plasma discharge depends on the pressure in the plasma zone and the precursor concentration. Figure 1 shows the velocity and mean particle diameter of SiO_2 nanoparticles in the molecular beam of the PMS as function of the pressure with Argon and Helium as carrier gas. Our investigations show that the particle velocity depends mainly on the pressure (p_o) in front of the inlet nozzle. SiO_2 nanoparticles synthesised in microwave plasma with 4 nm, operated at 25 mbar have particle velocity of 400 m s^{-1} with Argon, whereas 650 m s^{-1} with Helium. With Argon as carrier gas the particle velocity and the particle diameter increases nearly linear with the pressure. With Helium as carrier gas the particle velocity was higher than with Argon and nearly independent from the particle diameter.

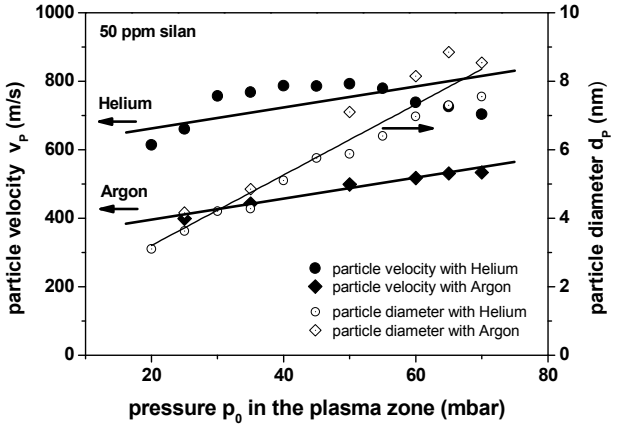

Figure 1. Particle velocity and particle diameter as function of the pressure (p_0)

Paur et al. (2005) *Nanotechnology 16,* 354–361.
Mätzing et al. (2012) *Combustion and Flame 159,* 1082–1089.

Scaling-up the production of monodisperse nanoparticles by means of a high-flow rate parallel plate DMA

M. Rouenhoff[1], E. Hontañón[2], A. Azabal[2], E. Ramiro[2] and F. E. Kruis[1]

[1]Institute for Nanostructures and Technology and CENIDE (Centre for Nanointegration Duisburg-Essen), University of Duisburg-Essen, Bismarckstr. 81, 47057, Duisburg, Germany
[2]RAMEM S.A., Sambara 33, 28027 Madrid, Spain
Keywords: plasma reactor, differential mobility analysis, monodisperse, scaling up.
Presenting author email: esther.hontanon@uni-due.de

There are many possibilities for generating aerosols containing particles between 5 and 100 nm at production rates around 1 g/hr. Characteristic for these processes it is that the particles are polydisperse due to Brownian motion, leading to a theoretic lower limit for the geometric standard deviation around 1.45. Thus, size fractionation is needed for applications requiring a narrower distribution than given by this theoretical limit.

The scalability of the particle-size selection technique based on Differential Mobility Analyzer (DMA) was demonstrated before (Hontañón and Kruis, 2008 and 2009) for aerosol and sheath flow rates as large as 0.1 and 1 m^3min^{-1}, respectively. In this work we describe a pilot plant (BigMAG - Big Monodisperse Aerosol Generator) for high-yield delivery of size-selected nanoparticles. Basically the facility consists of a plasma reactor for the generation of bipolarly charged nanoparticles up to 100 nm, a novel DMA of parallel plate electrodes (MegaDMA) developed by RAMEM, a particle collector, recirculation lines with cooling units for the aerosol flow (up to 1 m^3min^{-1}) and sheath flow (up to 10 m^3min^{-1}) and precision laminar flow elements (LFE) for monitoring the flow rates (figure 1).

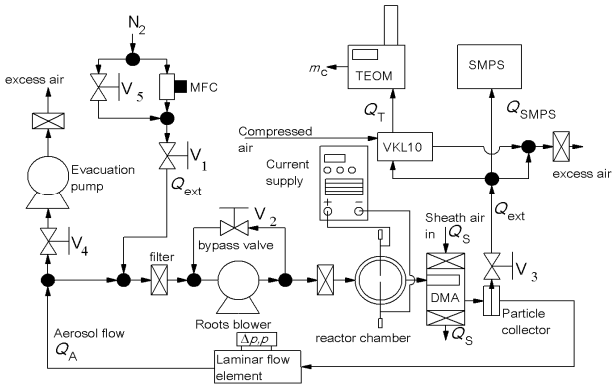

Figure 1. Layout of the aerosol recirculation line.

The quality of the size fractionation is monitored by means of a SMPS and mass production rate is recorded online by a TEOM. We were able to realize geometric standard deviations σ_g less than 1.10 after size classification with aerosol flow Q_A to sheath air flow Q_S ratios of 1/3 and 1/5 (figure 2). Monodisperse silver nanoparticles were delivered at a flow rate of 200 slm. With a Q_A/Q_s ratio of 1/3, the number concentration of particles in the gas was of about 10^5 cm^{-3} (table 1), while the mass yield varied from 10 µg/h to 1 mg/h, depending upon the particle size.

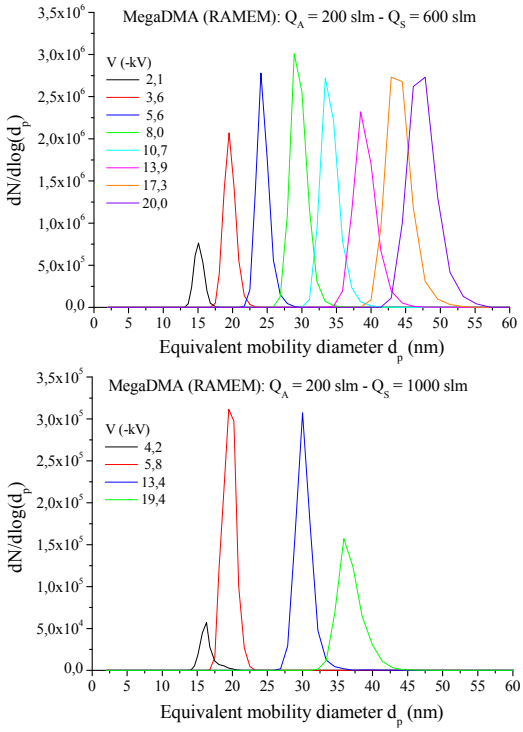

Figure 2. Number size distributions of size-selected silver nanoparticles at Q_A/Q_s ratios of 1/3 and 1/5.

Table 1. Number concentration, mean diameter and standard deviation of size-selected silver nanoparticles.

Q_A = 200 slm Q_S = 600 slm			Q_A = 200 slm Q_S = 1000 slm		
d_g (nm)	N (cm^{-3})	σ_g	d_g (nm)	N (cm^{-3})	σ_g
15,1	3,8E+04	1,05	16,6	3,0E+03	1,09
19,5	9,6E+04	1,05	19,6	1,7E+04	1,08
24,1	9,9E+04	1,04	30,1	1,2E+04	1,08
28,9	1,3E+05	1,04	36,6	7,4E+03	1,08
33,4	1,1E+05	1,04			
38,5	1,1E+05	1,04			
42,9	1,3E+05	1,04			
47,8	1,3E+05	1,05			

This work is financially supported by the Deutsche Forschungsgemeinschaft (DFG) in the framework of the collaborative research program “Nanoparticles from the gas phase: formation, structure, properties” (SFB 445).

Hontañón, E., Kruis, F.E. (2008). *Aerosol Sci. Tech.* **42**, 310-323.
Hontañón, E., Kruis, F.E. (2009). *Aerosol Sci. Tech.* **43**, 25-37.

Direct Transfer and Stabilization of Aerosol Particles into Liquid Suspensions by Means of a Wet Electrostatic Precipitator

C. Anderlohr[1], K. Schaber[1], W. Gerlinger[2]

[1]Institute of Technical Thermodynamics and Refrigeration, Karlsruhe Institute of Technology, Karlsruhe, 76131, Germany
[2]BASF SE, Ludwigshafen, Germany
Keywords: Combustion Synthesis, Wet Electrostatic Precipitation, Dispersion, Stabilization, Nanoparticle Deagglomeration
Presenting author email: christopher.anderlohr@kit.edu

Nanoparticles produced by gas phase processes are usually precipitated in (baghouse-) filters forming a more or less agglomerated powder.

However, in many cases the final application of these particles is not as a powder but as a liquid suspension, i.e. printable electronics, heterogenous catalysis, paints etc. This necessitates the dispersion of the particles into a liquid before use.

Due to the increase of inter-particle forces with increasing specific surface area and decreasing particle size, dispersing and deagglomerating these powders become more and more energy consuming, as particle size is reduced. In some cases complete deagglomeration is nearly impossible (Mandzy, 2005). Furthermore, handling of fine powders is somewhat difficult since unlike liquids distribution of powders through pipes is quite complex. In addition there is always the danger of exposure to particle aerosols due to dusting.

In this work the direct transfer and stabilization of SiO_2 and TiO_2 nanoparticles generated by a lab scale flame reactor into stable liquid suspensions by means of a wet electrostatic precipitator (WESP) is studied.

Wet electrostatic precipitation is an energy efficient possibility for gas cleaning with high removal efficiencies. WESPs are employed in numerous industrial applications, i.e. the control of acid mist, the precipitation of sticky or high resistivity aerosol particles, or when fire hazard is an issue. Recently, there have also been approaches of using WESPs for emission control of diesel particulate matter from stationary diesel generators. Other than in dry type electrostatic precipitators particles collected on the precipitation electrode are not removed by intermittent rapping, but are washed off by a liquid flushing the electrode. In these processes the precipitated particles are usually removed from the flushing liquid before it is redistributed onto the collection electrodes (Parker, 1997; Saiyasitpanich, 2007).

The aim of our approach, rather than removing the particles from the liquid, is to produce a stable suspension of product particles, which can be used directly for its later application.

Before the precipitation onto a filter the aerosol particles in the gas phase in our setup show little to no agglomeration. Thus, if the single particles can be precipitated directly into the liquid, no additional energy for dispersion and deagglomeration is necessary. During the transfer into suspension particles can be stabilized and protected against agglomeration and other degrading effects.

This makes the step of dispersing powders unnecessary and eliminates the need of powder handling. Also, the risk of exposure is greatly reduced, since the nanoparticles are contained within a liquid.

Stabilization is investigated by means of adjusting the pH-value of the circulated liquid as well as by addition of different stabilizing agents. The Particle size distributions (PSD) in the liquid phase are measured by Photon Correlation Spectroscopy (PCS) and compared to the SMPS-measurements of the aerosol size distributions (Fig. 1). In order to evaluate the process' effectiveness, the suspensions obtained from the WESP are compared to suspensions from the respective particles in powder.

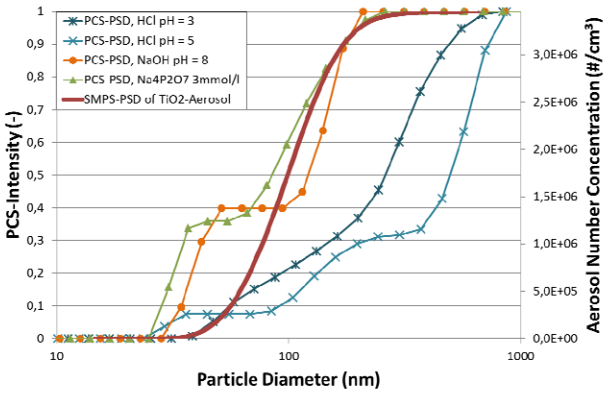

Figure 1: PCS-PSDs of TiO_2 nanoparticles in liquid suspension with different stabilizing agents and the SMPS-PSD of the corresponding aerosol before precipitation.

Mandzy, N, Grulke, E, Druffel, T (2005)
Breakage of TiO_2 agglomerates in electrostatically stabilized aqueous dispersions, Powder Technology **160**, 121-126

Parker K. (1997)
Applied Electrostatic Precipitation, Blackie Academic & Professional

Saiyasitpanich, P, Keener, T, Khang, S, Lu, M (2007)
Removal of diesel particulate matter (DPM) in a tubular wet electrostatic precipitator, Journal of Electrostatics **65**, 618-624

An Aerosol Process for Fabrication of a Carbon NanoTube Membrane with Tuneable Pore Size

M. Valenti[1], A.C. Zonnevylle[2], V. Vons[1], C.W. Hagen[2], R. van Ommen[1] and A. Schmidt-Ott[1]

[1] Chemical Engineering, Delft University of Technology, Delft, 2628 BL, The Netherlands
[2] IST, Delft University of Technology, Delft, 2628CJ, The Netherlands
Keywords: Metal nanoparticles, Carbon Nanotubes, Membrane
Presenting author email: M.Valenti@tudelft.nl

We introduce an aerosol process combined with Chemical Vapour Deposition (CVD) for fabrication of membranes with equal-sized and size controllable Carbon NanoTubes (CNTs) forming the pores. Membranes have various applications, e.g. in separation processes in chemical industry. A CNT membrane is of special interest for water desalination in a reverse osmosis process, as CNTs around 2 nm in diameter have shown the highest H_2O permeabilities by far with respect to both porous and non-porous membranes (Humplik, 2011). The low salt rejection (~ 60%) achieved to date is due to the non-uniformity of the CNT pores, and it is a goal of the present project to improve this behaviour by gaining full control over the CNT diameter using aerosol processes.

We produce equally sized metal nanoparticles, which serve as catalysts for CNT growth in a CVD reaction. We demonstrated that the CNT diameter is fully controlled by the catalyst diameter under suitable conditions.

Methodology

A monodisperse aerosol of positively charged Pd nanoparticles is generated by means of a Glowing wire (Peineke et al.), and this nanoparticle source is coupled to a Differential Mobility Analyser (DMA). The size selected aerosol of unipolarly charged particles is forced through a porous alumina membrane, and the particles deposit inside the pores. Separate experiments on depositing unipolarly charged particles on insulating material show that there is no agglomeration of particles on the substrate. The deposited particles keep their charge for a while, and Coulomb repulsion avoids that other particles deposit on top of them. This effect is essential for production of uniform CNT diameters. The nanoparticles are typically 20-30 times smaller than the diameter of the alumina pores. The membrane is then transferred to a CVD reactor where each deposited Pd nanoparticle catalyzes the growth of one CNT inside the alumina pores. The alumina pores guide the CNTs to align in the same direction. Subsequently, all gaps inside the alumina pores are filled with low-pressure chemical vapour–deposited Si_3N_4 and etched to expose the CNT's tips and to remove the catalyst nanoparticles.

Results

As shown in Figure 1, nanoparticles of 20 nm were successfully deposited inside the alumina pores with a penetration depth of about 1 µm. Using smaller particles, CNTs with an approximate internal diameter of about 3 nm were grown and vertically aligned.

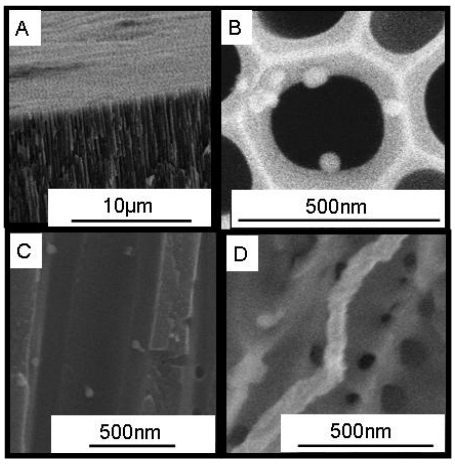

Figure 1. SEM images of A) Edge of the alumina membrane. B) Top view of a single alumina pore with deposited nanoparticles. C) Lateral view of the cross section of a single alumina pore with deposited nanoparticles. D) Vertically aligned CNT.

Conclusions

We have demonstrated that gas phase production of catalyst particles followed by non-agglomerated deposition within alumina pores enables aligned growth of the CNTs within these pores and fabrication of a membrane. The results presented here are seen as a decisive step towards a scalable fabrication of a CNT membrane with a uniform tuneable CNT inner diameter (pore size).

Humplik, T, Lee, J, Hern, S, Fellman, B, Baig, M, Hassan, S, Atieh, M, Rahman, F Laoui, T, K B. (2011) *Nanotechnology*, **22**, 292001-292020.

Peineke, C.; Attoui, M. B.; Schmidt-Ott, A. *Journal of Aerosol Science* (2006), **37**, 1651-1661.

Structural determination of charged nanoparticles in a Polarizable Gas

C. Larriba[1] and C. Hogan[1]
[1] Department of Mechanical Engineering, University of Minnesota, Minneapolis, MN, USA
Keywords: Aerosol fundamental, nanoparticles, Ion Mobility, Polarization
Presenting author email: clarriba@umn.edu

In both, field and laboratory settings, the most ubiquitously employed technique for the physical characterization of sub 10-nm aerosol particles is the separation of particles by their electrical mobilities, Z_p. Such particles fall within the momentum transfer free molecular regime, for which the electrical mobility can be expressed as (Mason & McDaniel, 1988):

$$Z_p = \sqrt{\frac{\pi m_{red}}{8kT}}\frac{3ze}{4\rho_{gas}\Omega} \qquad (1a)$$

where m_{red} is the reduced mass for the gas molecule and particle, k is Boltzmann's constant, T is the temperature, z is the net number of excess (positive or negative) charges on the particle, e is the unit electron charge, ρ_{gas} is the gas volumetric density, and Ω is the particle's collision cross section. In the examination of aerosol particles with the common approximation that particles are spherical, following Epstein (Epstein, 1924) and Fernandez de la Mora et al (Fernandez de la Mora et al., 2003), the collision cross section is in turn expressed as:

$$\Omega = \frac{\pi}{4}\xi\left(d_p + d_g\right)^2 \qquad (1b)$$

where d_p is the particle mobility diameter, d_g is the gas molecule diameter (also assumed spherical), ξ is a gas molecule-particle momentum transfer coefficient, and electrical mobility measurements are used to infer mobility diameter with (1b). From mobility measurements in air and N_2, and for varying particle chemical compositions, use of (1b) with ξ = 1.36 and d_g = 0.3 nm leads to inferred d_p values in excellent agreement (within 1-2%) of the particles' volume equivalent diameters (Larriba et al., 2011), down to $d_p \approx 1.3$ nm.

In spite of near-universal observed applicability of (1b), there are pending issues to be resolved with this equation. First, a theoretical basis for ξ = 1.36 is necessary. Deriving from Epstein (1924), the origin of ξ has been attributed to two modes of gas molecule scattering upon impinging on the surface of a particle: (1) specular reflection (deterministic angle and conserved gas molecule kinetic energy) collisions with the assumption that the particle surface is completely smooth, and (2) diffuse/inelastic scattering (random angle with the gas molecule energy resampled from a Maxwell-Boltzmann distribution at the particle temperature as in a perfect thermal conductor). Completely specular collisions lead to ξ = 1.00, while the diffuse model leads to $\xi = 1+\pi/8$. In line with these two collision types, to the present day it has been assumed that $\xi = 1+\pi\alpha_t/8$, where α_t, the accommodation coefficient (i.e. the percent of collisions which are diffuse in nature), must equal 0.91 to lead to the correct ξ (Friedlander, 2000). As ξ = 1.36 is found to apply for particles of all chemical compositions without exception, however, we posit here that the two type collision model of Epstein is only a fit to experimental results; on the contrary, we propose that there is a single description of gas molecule-particle collisions which leads to ξ = 1.36. This description relies on the vibrational modes of freedom of the molecule itself. The fact that it is constantly vibrating allows for an accommodation equivalent to (2) but where all collisions are considered elastic in nature. At the same time, the translational kinetic energy close to the particle is lowered due to an increase in the number of collisions and thus an increase in internal energy. This effect, reminiscent and opposite of the Joule-Thomson effect, causes a decrease in the momentum of the emitted particles and thus leads to a universal 1.36.

The second concern with (1b) is the origin of the deviation between the mobility diameter and the volume diameter for d_p < 1.3, particularly given the recent interest in particles in this size range. Below this size, the mobility diameter is consistently found to be larger than the volume diameter, i.e. there is more drag on the particle's than anticipated with (1b). The most likely origin of this deviation is an enhanced number of collisions with gas molecules due to the attractive polarization (induced dipole) potential between gas molecules and particles. (1b) applies only for hard-sphere interactions, and despite some theoretical effort to calculate particle mobility accounting for potentials (Tammet, 1995), an analytical expression analogous to (1b) but accounting for gas molecule polarization (enabling its use for particles with sizes 1.3 nm) remains undeveloped. We derive such an expression analytically here and confirm its validity through trajectory calculations of gas molecule-particle scattering accounting for polarization as shown in Figure 1 for ξ=1:

$$Z_{pol} = Z_p/\left(\xi\left(1+\frac{U_p(d_p)}{6kT}(1+1/\xi)\right)\right) \qquad (1c)$$

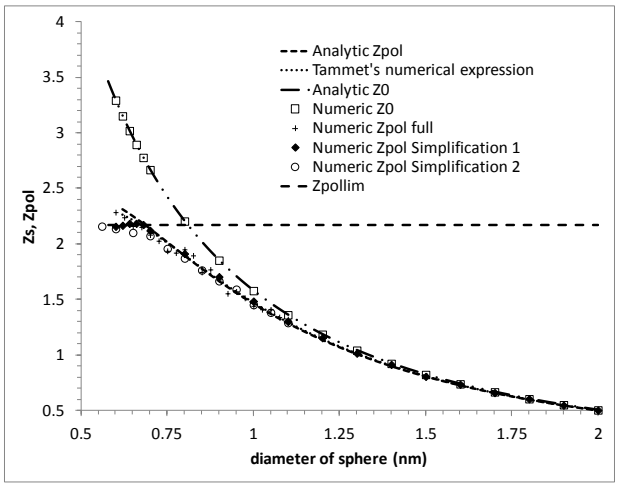

Figure 1. Analytic and Numerical prediction of a particle with and without Mobility for ξ=1. Mobility is shown in cm^2/Vs

Epstein, P. S. (1924). On the Resistance Experienced by Spheres in their Motion through Gases. *Physical Review*, **23**, 710-733.
Fernandez de la Mora, J., de Juan, L. et al. (2003). Mass and size determination of nanometer particles by means of mobility analysis and focused impaction. *Journal of Aerosol Science*, **34**(1), 79-98.
Friedlander, S. K. (2000). *Smoke, Dust, and Haze*. Oxford University Press, New York.
Larriba, C., Hogan, C. J. et al. (2011). The Mobility-Volume Relationship below 3.0 nm examined by Tandem Mobility-Mass Measurement. *Aerosol Science and Technology*, **45**, 453-467.
Mason, E. A. & McDaniel, E. W. (1988). *Transport Properties of Ions in Gases*. Wiley, New York.
Tammet, H. (1995). Size and Mobility of Nanometer Particles, Clusters and Ions. *Journal of Aerosol Science*, **26**(3), 459-475.

Tuesday, September 4, 2012

Posters Session B, Posters P001 to P299

Estimation of the aerosol optical depth in the UV region at Cáceres (Spain) by the Ångström formula

M.A. Obregón[1], A. Serrano[1] and M.L. Cancillo[1]

[1]Department of Physics, University of Extremadura, Badajoz, Extremadura, 06006, Spain
Keywords: atmospheric aerosols, UV, CIMEL, optical depth.
Presenting author email: nines@unex.es

In recent years, the interest in studying the aerosol properties (such as aerosol optical depth, τ) in the ultraviolet range (UV) has notably increased. This interest is enhanced by the importance of atmospheric aerosols in the atmosphere attenuation of solar UV radiation (Liu et al., 1991). Thus, in certain cases, the variation in UV radiation caused by changes in aerosol optical depth can be of similar magnitude than that due to changes in ozone content (Jaroslawski and Krzyscin, 2005). In spite of its high interest, there are no measurements of aerosol properties in the UV range until very recent times. These measurements have been notably rare because they require an accurate calibration which has not been always available. Currently the τ at ground level is widely measured at visible and infrared wavelengths but not in the UV range. Therefore, the purpose of this work is to estimate aerosol optical depth values in the UV range based on the spectral measurements of aerosol optical depth in the visible and infrared range at Cáceres, Spain, given by the CIMEL sunphotometer installed at the AERONET station of Cáceres. This instrument also measures the optical depth in the UV range (specifically at 340 and 380 nm), which will allow for the validation of the estimated τ values.

Thus, the aerosol optical depth at 340 and 380 nm is estimated by extrapolating the measurements obtained for the channels in the visible and infrared ranges, i.e. 440, 550, 675, and 870 nm. The extrapolation is performed following the well-known Ångström formula $\tau_a(\lambda)=\beta\,\lambda^{-\alpha}$. The α and β coefficients are calculated by a least-square fit on a log-log plot scale of the experimental optical depth in the visible and infrared range versus the wavelength. According to the recommendations by Cachorro et al., (2000), the range of wavelengths between 440 and 870 nm has been used.

This procedure has been applied to the spectral measurements of τ in the visible and infrared range at Cáceres, during the period from July 2006 - July 2008. The estimated τ (340 and 380 nm) values have been compared with those measured by CIMEL at the same wavelengths (Figure 1 and 2, respectively). In addition to the generally good performance shown by the estimations, the results indicate that at 340 nm, estimated τ values are generally higher than those measured by the CIMEL. The reason is the dependence of Ångström coefficient with wavelength, since decreases towards the shorter wavelengths (Jaroslawski et al., 2003).

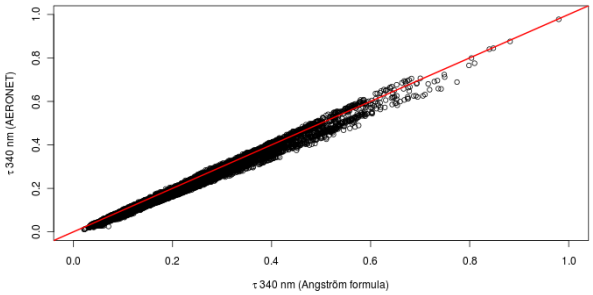

Figure 1. Comparison of τ at 340 nm measured by the CIMEL and estimated by Ångström formula.

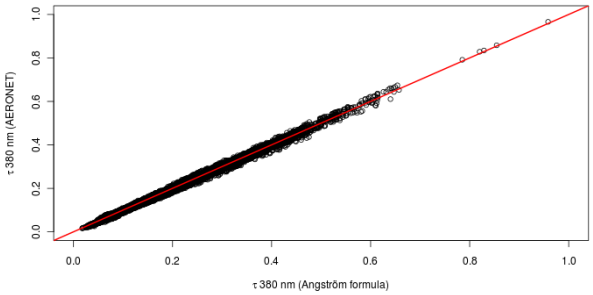

Figure 2. Comparison of τ at 380 nm measured by the CIMEL and estimated by Ångström formula.

The above mentioned results suggest that Ångström turbidity coefficients calculated by a least-square fit in the visible-infrared range can be successfully used to estimate the optical depth at the UV range in Cáceres.

This work was supported by the research projects CGL2008-05939-C03-02/CLI and CGL2011-29921-C02-01 granted by the "Ministerio de Ciencia e Innovación" from Spain.

Cachorro, V. E., Durán, P., Vergaz, R., Frutos, A.M. (2000). *J. Aerosol Sci.* **31**(6), 687–702.

Jaroslawski, J., Krzyscin, J.W., Puchalski, S. and Sobolewski, P. (2003) J. Geophy. *Res.* **108**, 4722.

Jaroslawski, J., and Krzyscin, J.W. (2005) J. Geophy. *Res.* **110**.

Liu, S.C., McKeen, S.A., and Madronich, S. (1991) *PGeophys. Res. Lett.* **18**, 2265-2268.

Calculation of aerosol microphysical properties by neural network inversion of ground-based AERONET data

M. Taylor[1] , S. Kazantzis[1], A. Tsekeri[2], A. Gkikas[3] and V. Amiridis[2]

[1]Institute of Environmental Research and Sustainable Development, National Observatory of Athens, Greece.
[2]Institute of Space Applications and Remote Sensing, National Observatory of Athens, Greece.
[3]Physics Department, University of Ioannina, Greece

Keywords: aerosol optical properties, remote sensing, neural networks
Presenting author email: patternizer@gmail.com

Radiative-forcing by aerosols is the most important and most uncertain of all Earth climate, direct radiative-forcing estimates (IPCC Report, 2001). Reducing this uncertainty calls for the expansion of worldwide aerosol measurements and studies in order to characterize different types of aerosols and sources. Aerosols are characterized by their microphysical properties (AMPs): the aerosol size distribution a_i (in each i^{th} size bin) and complex refractive index Z (Hansen and Travis, 1974), which are accurately retrieved from ground-based instruments (Holben et al., 1998). Unfortunately, their global resolution is very uneven – being densely-situated in industrialized areas and sparsely-located elsewhere.

We report on the initial phase of *AEROMAP* - a new EU-funded project designed to map the global distribution of aerosol microphysical and optical properties (AOPs) by capitalising on the full-Earth coverage provided by satellite remote sensing instruments like MODIS in conjunction with the accuracy provided by ground-based AMP and AOP retrievals provided by AERONET. Figure 1 shows the 5 steps adopted for implementation of *AEROMAP*.

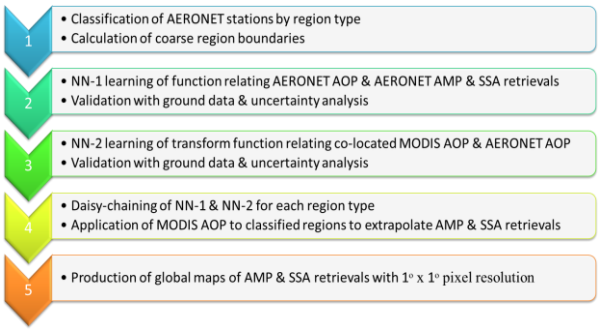

Figure 1. The stepwise implementation of *AEROMAP*.

In step 1, data pre-processing involves the application of a cluster analysis algorithm (Omar et al 2000) to AERONET data and the use of Gobbi coordinates (Gobbi et al., 2007) to classify aerosol regions by type. A nearest neighbour algorithm is used to establish regional boundaries. In step 2, multiple-input multiple-output (MIMO) universal function-approximating artificial neural networks (NN) are trained at selected sites for each aerosol region type. The NN inputs include: the aerosol optical depth (*AOD*) at four wavelengths in the visible wavelength range, the Ångström Exponent (*AE*) at visible wavelengths, and the fine mode fraction (η). The NN outputs include the AMP and SSA retrievals. An indicative NN architecture is shown in Figure 2. To train the NN, AERONET level 2 AOP and AMP products are used, as this data is cloud-screened and available daily.

NNs trained for each aerosol region type are evaluated by: a) analysing uncertainties using the AERONET AMP and SSA retrievals for the training periods, b) validating NN-derived AMPs and SSA for non-training periods using the corresponding AERONET products, c) validating NN results against AERONET products at different sites of the same aerosol type. The results allow assessment of the potential of such NN-derived AMP and SSA retrievals for each aerosol region type.

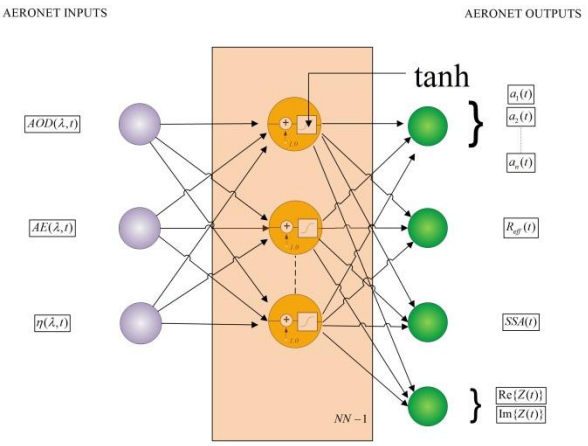

Figure 2. The architecture of the NN in step 2.

This work is supported by a Marie-Curie IEF funded project "*AEROMAP: Global mapping of aerosol properties using neural network inversions of ground and satellite based data".*

Gobbi, G.P., Kaufman, Y.J., Koren, I. and Eck, T.F. (2007) *J. Atmos. Chem. Phys.* **7**(2), 453-458.
Holben, B.N., Eck, T.F., Slutsker, I., Tanré, D., Buis, J.P. et al. (1998) *J. Rem. Sens. Environ.* **66**, 116.
Intergovernmental Panel on Climate Change (IPCC) (2001) *Climate Change 2001*. Cambridge University Press (New York).
Hansen, J.E., and Travis, L.D. (1974) *Space Sci. Rev*., **16**, 527-610.
Omar, A.H., Won, J.G., Winker, D.M., Yoon, S.C., Dubovik et al (2005) *J. Geophys. Res*. **110**, D10S14.

Aerosol fine fraction characterization by integrated in-situ and columnar measurements.

M. Calvello[2], F. Esposito[1] and G. Pavese[2]

[1] DIFA- Università della Basilicata, C. da Macchia Romana, 85100, Potenza, Italy
[2] CNR-IMAA, C. da S. Loya, 85050, Tito Scalo (PZ), Italy
Keywords: black carbon, fine fraction mass, columnar properties.
Presenting author email: calvello@imaa.cnr.it

Atmospheric aerosol optical and physical properties have been studied in a semi-rural site in Southwest Italy (Tito Scalo, 40° 35' N, 15° 41' E, 750m a.s.l), not continuously, during 2008, 2009 and 2010 by integrating surface and columnar measurements.

In-situ measurements have been carried out by a 13 stages DLPI impactor (0.03 to 10.0 μm) and an AE31 aethalometer (7 wavelenghts from 370 to 950 nm), while columnar ones by a high resolution (1.5 *nm*) spectroradiometer Ocean Optics (spectral range 400*nm*-800*nm*).

The measurements site belongs to the Mediterranean basin, a very complex area to investigate due to the mix of aerosols originating from different sources as such as marine particles from both Mediterranean Sea and Atlantic Ocean , dust particles from Sahara desert, polluted and smoke aerosols from continental Europe.

The combined use of impactor mass-size distributions, Black Carbon (BC) concentrations from aethalometer and optical parameters from radiometer, could deeply describe all these different aerosol types (Calvello *et al*., 2010). Focusing the attention on the particulate fine fraction, BC is an important component at ground as shown in Figure 1 where surface fine fraction mass M_1, as obtained from DLPI measurements, has been compared with values of BC (surface Black Carbon concentration, 880nm) for the entire period.

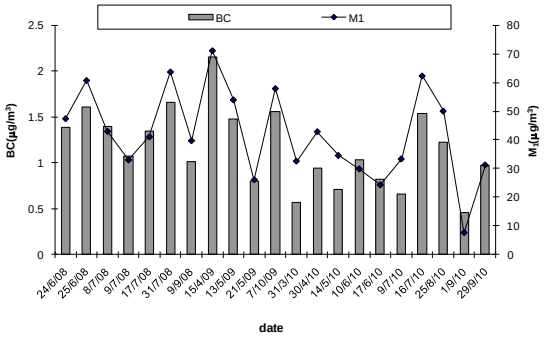

Figure 1. Temporal variations of M_1(daily averaged surface fine fraction mass), and of BC (surface black carbon concentration, 880nm, averaged out over contemporary measurements hours).

The BC concentration daily trend for working days is characterised by two peaks coinciding with rush hours. A less regular behaviour has been found for week-end days without definite modes and with lower concentrations on the whole. This suggests the local traffic to be the main source of black-carbon at the site. But BC concentrations enhancement has been found for pollution long-range transport events (25 June and 31 July 2008, and 15 April 2009 in Fig. 1) when daily trends are lost and minimum concentration threshold is shifted to higher values also for week-end days.

These pollution events, associated with air mass transport from continental Europe, have been identified from radiometric measurements too, with an increase of α parameter and of AOD @ 500 nm. Moreover, even columnar volume size distributions from inverted direct solar radiance, show a prevailing fine mode in all these cases.

Looking at all the measurements dataset, a better agreement has been found, between in-situ and columnar data, in the case of anthropogenic transported and local produced fine particle loading, than in the case of Saharan dust intrusions. In this last case, coarse dust particles seem to affect columnar data in a more intense way than surface ones, thus revealing an underestimate in coarse particle detection at ground level (Lyamani *et al*., 2008). Good agreement for anthropogenic and back-ground aerosols suggests that in these cases, surface aerosols optical properties dominate columnar integrated data.

Calvello, M., Esposito, F., Pavese, G., and Serio, C., (2010). *Atmos. Chem. Phys.*, 10, 2195-2208.

Lyamani, H., Olmo, F., J., Alados-Arboledas, L., (2008). *Atmos. Envir.*, 42, 2630-2642.

SPEX: Multi-Angle Spectro-Polarimetry for Aerosol and Cloud Characterization from the ISS

O.P. Hasekamp[1], M. Smit[1], J. Rietjens[1], F. Snik[2], G. van Harten[2] & the SPEX team*

[1] SRON Netherlands Institute for Space Research, Sorbonnelaan 2, 3584 CA Utrecht, the Netherlands
[2]Sterrewacht Leiden, Universiteit Leiden, Niels Bohrweg 2, 2333 CA Leiden, The Netherlands;
Keywords: aerosols &clouds, climate, remote sensing, polarimetry.
Presenting author email: O.Hasekamp@sron.nl

We present the SPEX instrument that is designed to perform multi-angle spectro-polarimetric observations from a low earth orbit satellite in order to derive aerosol and cloud properties in the Earth atmosphere. The effect of anthropogenic aerosols represents the most uncertain factor in the climate system. Aerosols affect the climate directly by scattering and absorption of solar radiation and indirectly by changing the properties of clouds. Here, the effect of aerosols on cloud properties is considered the largest yet most uncertain aerosol climate effect. To improve the estimate of the aerosol effect on clouds and climate, accurate satellite based measurements of aerosol microphysical and optical properties, as well as cloud properties, are required. The SPEX instrument is designed to provide these measurements. SPEX has been proposed in response to the Announcement of Opportunity for International Space Station Experiments relevant to the study of Global Climate Change.

Instrument description

In order to derive the relevant aerosol and cloud properties with accuracy sufficient for climate research, multiple-viewing-angle, multiple wavelength measurements of the intensity as well as the Degree of Linear Polarization (DoLP) of the light reflected by the Earth atmosphere are essential. SPEX will measure intensity, degree- and angle of linear polarization of scattered sunlight between 400 and 1600 nm, sampling each ground pixel with 25-30 viewing angles. SPEX' novel polarimetric technique allows for achieving the extremely high polarimetric accuracy (0.001+0.005DoLP) needed to derive aerosol properties with sufficient accuracy for climate research [Hasekamp and Landgraf, 2007]. SPEX' relatively high spectral resolution enables resolving the spectral feature of the O2-A absorption band, which is important for deriving aerosol and cloud height. SPEX' large number of viewing angles enables resolving the angular features resulting from light scattering by aerosol and cloud particles, and to distinguish between these types of particles.

The novel polarimetric measurement approach works as follows [Snik et al., 2009]: Incoming linearly polarized light passes through a set of birefringent polarizing crystals which, combined, result in an intensity spectrum that has the degree of polarization coded onto it as an amplitude modulated signal. The depth of the modulation is proportional to the degree of linear polarization of the incoming light, and the phase is proportional to the angle of linear polarization. This measurement approach, that uses no filter wheels or multiple apertures to determine the state of polarization, allows for simultaneous measurements of both radiance and polarization for a given ground scene. This is essential to reach the required accuracy. The SPEX geophysical data product will consist at least of: aerosol effective radius, effective variance, number concentration, refractive index of the fine and coarse mode of the aerosol size distribution, aerosol height, cloud effective radius, droplet number concentration, cloud top/base height, and cloud phase.

References:

Hasekamp, O. P., and J.Landgraf, *Appl. Opt.* (2007), Vol. 46, No. 16, P. 3332

Snik, F., Karalidi, T., and Keller, C. U. (2009), *Appl. Opt*. **48**, 1337-1346.

* **SPEX Science Team**:

O. Hasekamp[1], M. Smit[1], A. Kokhanovsky[3], F. Snik[2], I. Koren[4], GJ Roelofs[5], J. Rietjens[1], G. van Harten[2], Jozua de Boer[2] J. Riedi[6], M. Mishchenko[7], P. Stammes[8], R. Boers[8], P. Veefkind[8], A.Segers[9], P.Builtjes[9], H.Volten[10], J. Landgraf[1], D. Stam[1], M. Krol[11], T. Li[12], Z. Chen[13], C. Keller[3], G. de Leeuw[14], J. Lelieveld[15]

[3]IUP, Bremen, Germany, [4] Weizman Institute of Science, Rehovot, Israel, [5] IMAU, Utrecht, the Netherlands, [6] LOA, University of Lille-1, France,[7] NASA GISS, New York, USA, [8] KNMI, De Bilt, The Netherlands, [9]TNO B&O, Utrecht, The Netherlands, [10] RIVM, Bilthoven, The Netherlands [11]Wageningen University, Wageningen, the Netherlands [12] Univ. of Science and Tech. of China, Anhui, China [13] Institute of Atm. Physics, CAS, Beijing, China [14] Finnish Meteorological Institute, Helsinki, Finland [15] Max-Planck-Institute for Chemistry, Mainz, Germany

***SPEX Industry Team**:

J-F Bos[a], L. Meijer[a] , R. Voors[a], E. Boom[a], A. Verlaan[b], O. v.d. Togt[b], F. Draaisma[b], A. Court[b], M. Beijersbergen[c], E. Kroesbergen[d], B-J Volmöller[e]

[a] Dutch Space B.V., Leiden, the Netherlands, [b] TNO, Delft, the Netherlands, [c] Cosine, Leiden. the Netherlands [d] Mecon, Mecon Engineering B.V., the Netherlands, [e] National Aerospace Laboratory NLR, Amsterdam, The Netherlands

Intercomparison of lidar aerosol backscatter and in-situ size distribution measurements

A. Held[1], T. Seith[1], I.M. Brooks[2], S.J. Norris[2] and S.D. Mayor[3]

[1]Bayreuth Center of Ecology and Environmental Research, University of Bayreuth, Bayreuth, Germany
[2]Institute for Climate and Atmospheric Science, University of Leeds, Leeds, UK
[3]Departments of Geoscience and Physics, California State University, Chico, CA, USA

Keywords: Aerosol size distribution, Backscatter, In-situ measurements, Lidar, Remote sensing
Presenting author email: andreas.held@uni-bayreuth.de

The atmospheric aerosol is highly variable in time and space with respect to particle size, number, and chemical composition. In-situ observations with point sensors cannot fully represent the spatial variability of aerosol particles in the atmospheric boundary layer. Thus, in-situ observations yield spatially averaged data or disjunct information which may, for example, misrepresent the available aerosol surface area for heterogeneous chemical reactions, or the small-scale effect of aerosol optical properties.

Direct observation of the spatial variability of aerosol concentration with high time resolution is possible through remote sensing techniques. For example, the Raman-shifted Eye-safe Aerosol Lidar (REAL; Mayor et al., 2007) can safely transmit high energy laser pulses in order to visualize small-scale atmospheric motions and changes in the structure of the lower atmosphere through aerosol scattering. However, knowledge of the sensitivity of the lidar to small changes in the microphysical characteristics of aerosol particles is a prerequisite to extract information about the spatial and temporal evolution of the atmospheric aerosol from the backscatter signal.

There is a lack of direct intercomparison studies of lidar and high-time-resolution in-situ aerosol measurements. Here, we compare aerosol backscatter data of the REAL with in-situ measurements of aerosol size distributions during two different field campaigns. The REAL backscatter signal is compared with aerosol size distribution measured with a LASAIR optical particle sizer during the Canopy Horizontal Array Turbulence Study (CHATS; Patton et al., 2011) in Dixon, CA, USA, in May 2007, and with a MetOne optical particle counter and a Compact Lightweight Aerosol Spectrometer Probe (CLASP; Hill et al., 2008) during a field experiment at the Chico State University Farm in Chico, CA, USA, in October 2011.

From an intercomparison of the CHATS field data, preliminary results about the sensitivity of the REAL towards particle size were obtained. Figure 1 shows the time series of the REAL backscatter signal and the aerosol surface concentration in the diameter range from 0.5 to 10 µm during a five-day measurement period. Obviously, the two time series do not trace each other perfectly at all times. In part, this may be due to the spatial separation of the remote sensing volume and the in-situ sensor. However, the influence of particles smaller than 0.5 µm on the backscatter signal was found to be negligible at all times.

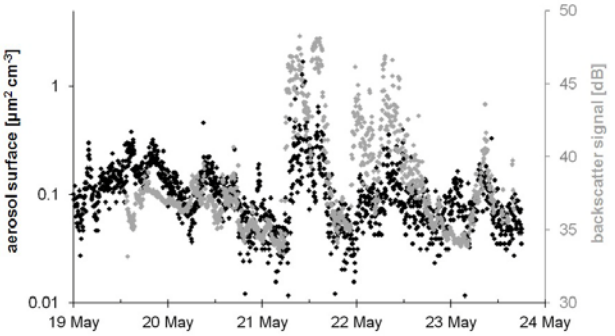

Figure 1: Time series of REAL backscatter signal (grey) and aerosol surface concentration (diameter > 0.5 µm; black) during five days of CHATS 2007.

In 2011, a dedicated intercomparison experiment was carried out. The REAL laser beam was directed horizontally across a very flat field at the Chico State University Farm and passed the inlets of two optical particle counters located approximately 1.3 km away from the REAL within 1 m or less.

We will present additional results from a detailed analysis of the CHATS intercomparison data, and from the Chico intercomparison experiment. After characterization of the sensitivity of the REAL backscatter signal to changes in aerosol size and concentration, this signal can be analyzed for a better representation of the spatial variability of aerosol particles in the atmospheric boundary layer.

Support from the Bavaria California Technology Center (BaCaTeC 9[2010-1]), NSF AGS Awards 0924407 and 1104342, CSU Chico Research Foundation, and NCAR EOL is gratefully acknowledged.

Hill, M.K., Brooks, B.J., Norris, S.J., Smith, M.H., Brooks, I.M. and DeLeeuw, G. (2008) A compact lightweight aerosol spectrometer probe (CLASP). J. Atmos. Ocean Technol. 25, 1996-2006.

Mayor, S.D., Spuler, S.M., Morley, B.M., Loew, E. (2007) Polarization lidar at 1.54-microns and observations of plumes from aerosol generators. Opt. Eng. 46, 096201.

Patton, E. G., et al. (2011) The Canopy Horizontal Array Turbulence Study (CHATS). Bull. Amer. Meteorol. Soc. 92, 593-611.

SEVIRI based aerosol optical depth and type retrieval

S. Nevens, N. Clerbaux, A. Velazquez Blazquez, E. Baudrez, I. Decoster, S. Dewitte, A. Ipe
Royal Meteorological Institute of Belgium (RMIB), Section Remote Sensing from Space,
Avenue Circulaire 3, B-1180 Brussels, Belgium
Keywords: remote sensing, tropospheric aerosols, optical depth, climate change
Presenting author email: stijn.nevens@meteo.be

Tropospheric aerosol particles form a major uncertainty in predicting climate change due to three main mechanisms. First there is the direct radiative forcing effect of the aerosols which occurs when radiation is scattered or absorbed by the aerosols. Next we have indirect radiative forcing which has its origin in the influence of the aerosols on cloud microphysics. And last, the presence of aerosols can modify the concentration of climate-influencing constituents such as greenhouse gases trough heterogeneous chemistry. Global observations from space are required due to short lifetime and a high spatial variability in aerosol optical and radiative properties.

In the autumn of 2012 the Climate Monitoring SAF (CM SAF) will release an aerosol product of climate quality for which the RMIB is responsible. This will be a retroactively produced data set covering the whole MSG (Meteosat Second Generation) period. The main components of the product are the aerosol optical depth (AOD) and the aerosol type over ocean.

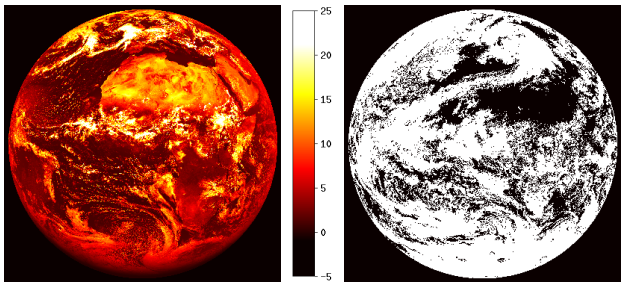

Figure 1: Input data for the algorithm for midday on the 22nd of June 2004. Left: radiance (units = W/m^2sr) from the SEVIRI solar channel at 600 nm. Right: cloud mask where white equals cloudy.

The solar and thermal SEVIRI channels (multichannel imager aboard the MSG satellite) together with the CM SAF cloud mask and wind speed over ocean from ERA-Interim reanalysis (Dee et al, 2011) form the input for the AOD and aerosol type retrieval algorithm.

The heart of the algorithm consists of look up tables for the AOD at 550 nm and all SEVIRI solar channels generated using LIBRADTRAN (Mayer and Kylling, 2005). These have as parameters the wind speed, all relevant angular information and 6 aerosol types. The aerosol types consist of 3 spherical and 3 non-spherical classes taken from (Govaerts et al, 2010) and where originally derived from an analysis of AERONET retrievals.

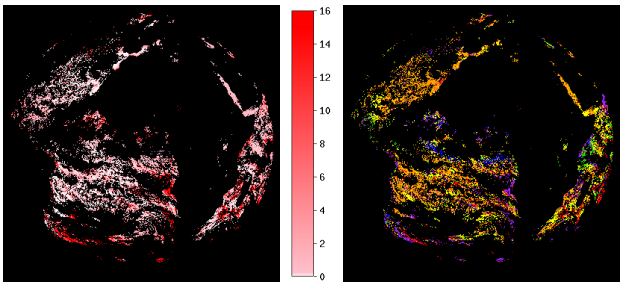

Figure 2: Output found using the input from figure 1. Left: AOD (no units). Right: aerosol type (6 colors to represent the 6 types).

Having all necessary inputs we use our algorithm to retrieve the AOD and aerosol type over ocean in the MSG field of view. The method is inspired by the method developed for AVHRR (Ignatov and Stowe, 2002) which was later adapted for SEVIRI (Brindley and Ignato, 2006). It is currently deployed within the GERB (Geostationary Earth Radiation Budget) processing chain (De Paepe et al, 2007). By doing a least least squares fit on 6 families of curves we can determine which aerosol type and corresponding AOD give the best agreement between the observed and simulated reflectance in all SEVIRI solar channels given the specific solar/observation geometry.

The authors are supported by EUMETSAT and the Belgian Science Policy Office under the contract EUMETGERB and by CM-SAF.

Dee D.P. et al, 2011, *Quarterly Journal of the Royal Meteorological Society*, **137**, 553—597.

Mayer B. and Kylling A., 2005, *Atmos. Chem. Phys.*, **5**, 1855–1877.

Govaerts Y. et al, 2010, *J. Geophys. Res.*, **115**, D02203.

Ignatov A. and Stowe L., 2002, *J.Atm.Sci.*, **59, 3(1)**, 313–334.

Brindley HE. and Ignatov A., 2006, *Remote Sensing of Environment*, **102**, 344–363.

Brindley HE. and Russell JE., 2006, *Remote Sensing of Environment*, **104**, 426–446.

De Paepe B. et al, 2007, *Remote Sensing of Environment*, **112**, 2455–2468.

Lidar observations of stratospheric aerosol over the Northern Hemisphere from Nabro volcano: MPLNET, EARLINET, CALIPSO, NDACC synergy

P. Sawamura[1], J.P.Vernier[2], J. E.Barnes[3], T.A. Berkoff[4], E.J. Welton[5], L.Alados-Arboledas[6], F. Navas-Guzmán[6], L.Mona[7], D. Lange[8], M.Sicard[8], S. Godin-Beekmann[9], G. Payen[9], Z. Wang[10] and R.M. Hoff[1,4]

[1]Department of Physics, University of Maryland Baltimore County, Baltimore, MD 21250, USA.
[2]NASA Langley Research Center, Hampton, VA 23666, USA.
[3]NOAA/ESRL/Mauna Loa Observatory, Hilo, HI 96720, USA.
[4]Joint Center for Earth Systems Technology, Baltimore, MD, USA.
[5]NASA Goddard Space Flight Center, Greenbelt, MD 20771, USA.
[6]CEAMA, Junta de Andalucía-Univerdad de Granada, Granada, Spain.
[7]CNR – IMAA, 85080 Tito Scalo, Potenza, Italy.
[8]Remote Sensing Laboratory, Universitat Politècnica de Catalunya, E-08034 Barcelona, Spain.
[9]Laboratoire Atmosphères, Millieux, Observations Spatiales, UPMC, France.
[10]Key Laboratory of Atmospheric Composition and Optical Radiation, Anhui Institute of Optics and Fine Mechanics, Chinese Academy of Sciences, Hefei, Anhui 230031, China.

Keywords: Nabro, lidar, stratospheric aerosols.
Presenting author email: psawamura@umbc.edu

On June 12th, 2011 Nabro volcano, situated in the border between Ethiopia and Eritrea, started a series of eruptions that lasted until September 2011. It released approximately 1.5 - 2 Tg of SO_2 to the atmosphere in the first days - one of the largest SO_2 emissions measured since Nyamuragira volcano in Congo, 1994 and Mt. Pinatubo eruption in 1991, which injected about 20 Tg of SO_2 into the stratosphere. Nabro left a trace of stratospheric aerosols that circulated the globe in both directions, heading eastward and westward at different altitudes and staying in the atmosphere for a couple of months.

Lidars are important tools that help assess the vertical distribution of aerosols in the atmosphere. In this study we report on stratospheric aerosols that were observed over the Northern Hemisphere with the aid of multiple lidar networks such as MPLNET, EARLINET and NDACC, and satellite (CALIOP – Cloud-Aerosol Lidar with Orthogonal Polarization). Measurements in Hefei, China were provided by the Key Laboratory of Atmospheric Composition and Optical Radiation.

Figure 1 shows the average aerosol optical depth (AOD) retrieved from CALIOP over the globe from July 16 to July 31, 2011.

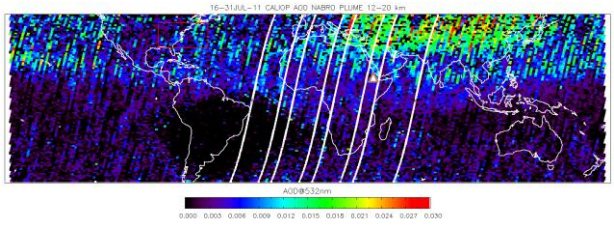

Figure 1. Global CALIOP AOD retrieval from July 16 to July 31 between 12 and 20 km of altitude.

This type of study is important to many remote sensing communities. In the stratospheric trace gases community, being able to determine how volcanic eruptions may affect the load of background aerosols in the stratosphere is very valuable. In other cases, such as in comparative studies of satellite and/or column measurements versus ground-based measurements it is also important to determine the stratospheric contribution of aerosols. During the DISCOVER-AQ mission that took place in the Baltimore-Washington corridor in the United States in July 2011, an offset of approximately 0.03 between AOD measurements from sun-photometer (total column) and airborne high-spectral resolution lidar (down-looking HSRL at ~6km) was observed and we believe that stratospheric aerosols due to Nabro might have contributed with AOD=0.01.

In this study the AOD retrieved from lidar measurements in the stratosphere ranged between 0.01 to 0.04 at 532 nm and from 0.04 to 0.08 at 355 nm. The measurements spanned a good area over the Northern Hemisphere: East and West Coast of the US (Maryland and California, respectively), Hawaii, Canary Islands, Israel, India, Spain, Italy, France and China.

It is unlikely that the aerosols generated by Nabro's eruption would have a significant effect on the radiative balance of the atmosphere like Pinatubo did. However, we show with this study how the synergy of lidar measurements across the globe - as proposed by GALION (GAW Aerosol Lidar Observation Network) - could aid the scientific (and also aviation control) community to rapidly assess the outcome of future, and possibly more explosive, volcanic eruptions.

The NASA Micro-Pulse Lidar Network is funded by the NASA Earth Observing System and Radiation Sciences Program. Lidar work in Hefei site was funded by the National Key Basic Research Project of China under Grant No. 2007FY110700. Lidar work at Universidad de Granada was funded by grants CGL2010-18782 and P10-RNM-6299 and EU ACTRIS project.

Detection of the stratospheric volcanic aerosol plume from the Nabro eruption in summer 2011 in the framework of SPALINET

J.L. Guerrero-Rascado[1,2,3], J.A. Bravo-Aranda[1,2], F. Wagner[3], C. Córdoba-Jabonero[4], F. Molero[5], D. Lange[6,7], M. Granados-Muñoz[1,2], J. Preißler[3], D. Toledo[4], A.J. Fernández[5], M. Sicard[6,7], F. Navas-Guzmán[1,2], Y. Hernández[8], A.M. Silva[3], M. Pujadas[5], A. Comerón[6], S. Pereira[3], F. Rocadenbosch[6,7], and L. Alados-Arboledas[1,2]

[1]Andalusian Center for Environmental Research (CEAMA), University of Granada – Autonomous Government of Andalusia, Av. del Mediterráneo s/n, 18006, Granada, Spain
[2]Department of Applied Physics, University of Granada, Fuentenueva s/n, 18071, Granada, Spain
[3]Évora Geophysics Centre (CGE), University of Évora, Rua Romão Ramalho 59, 7000, Évora, Portugal
[4] Instituto Nacional de Técnica Aeroespacial (INTA), Atmospheric Research and Instrumentation Branch, Torrejón de Ardoz, 28850, Madrid, Spain
[5]Centro de Investigaciones Energéticas, Medioambientales y Tecnológicas (CIEMAT), Av. Complutense 40, 28040, Madrid, Spain
[6]Department of Signal Theory and Comunications, Remote Sensing Lab., Universitat Politécnica de Catalunya/Institut d'Estudis Espacials de Catalunya, Barcelona, Spain
[7]Institut d'Estudis Espacials de Catalunya – Aeronautics and Space Research Center (IEEC-CRAE), Universitat Politécnica de Catalunya, Barcelona, Spain
[8]Agencia Estatal de Meteorología, Atmospheric Research Centre of Izaña, Sta. Cruz de Tenerife, Spain
Keywords: lidar, Nabro eruption, remote sensing, stratospheric aerosol.
Presenting author email: rascado@ugr.es

During the night of 12 June 2011 the Nabro volcano (13.37ºN, 41.70ºE) in the state of Eritrea (Horn of Africa) started its eruption generating large amounts of ashes, water vapour and sulphur dioxide gas that intermittently blocked the air traffic over Eastern Africa. Besides the human and economical factors, the Nabro episode was relevant from the climate point of view by injecting a layer of sulphur aerosol particles, which persisted for months in the stratosphere and was detected over several continents.

The stratospheric aerosols generated from the Nabro's eruption were detected over southern Europe by five stations of SPALINET (the Spanish and Portuguese aerosol lidar network, www.lidar.es/spalinet/en) (Sicard et al., 2009; 2011), namely (m asl):

- GR: Granada (37.16ºN, 3.58ºW, 680 m)
- EV: Évora (38.57ºN, 7.91ºW, 290 m)
- SC: Sta. Cruz de Tenerife (28.47ºN, 16.25ºW, 52 m)
- MA: Madrid (40.46ºN, 3.72ºW, 665 m)
- BA: Barcelona (41.39ºN, 2.11ºE, 115 m)

The capabilities of SPALINET for volcanic aerosol characterization have been demonstrated previously during the Eyjafjallajökull eruption in 2010 (Guerrero-Rascado et al., 2010; Sicard et al. 2011). This study is focused on both geometrical and optical properties of the volcanic particles. On the one hand, the zero-crossing method is used to determine the minimum and maximum heights and geometrical thickness. On the other hand, the transmittance method (i.e. Young, 1995) is applied to pre-processed elastic lidar signals for deriving the aerosol optical depth (AOD) in those isolated volcanic layers. In a further analysis, this information could be used to constrain the retrieval of the Klett's algorithm to estimate a layer-effective lidar ratio.

The first volcanic aerosol particles from the Nabro volcano could be detected over Spain and Portugal after a relatively short time (within the first two weeks after the eruption). All the stations considered in this study observed the first layers on 26 to 27 June and a few of them detected the volcanic layer until the middle of July. Besides the stratospheric volcanic layer, another coupled layer was detected over several stations in the uppermost troposphere during some periods (notice the minimum altitude values in Table 1).

Table 1. Dates when the Nabro volcanic plume was mainly observed between the minimum (z_{min}) and maximum (z_{max}) and AOD at 532 nm (± st. dev.).

Station	Period	[z_{min},z_{max}] km asl	AOD_{532nm}
GR	26/06-30/06	12.6-18.8	0.044±0.013
EV	26/06-02/07	9.1-19.7	0.048±0.016
SC	26/06-10/07	10.5-19.7	0.021±0.011*
MA	27/06-01/07	14.0-18.6	0.042±0.014
BA	27/06-30/06	15.8-18.2	0.057±0.023

* At 523 nm

This work was supported by the Andalusia Regional Government through projects P08-RNM-3568 and P10-RNM-6299, by the Spanish Ministry of Science and Technology through projects CGL2010-18782, and CSD2007-00067; Spanish Ministry of Science and Innovation and FEDER funds under the Complementary Action CGL2011-13580-E/CLI; and by EU through ACTRIS project (EU INFRA-2010-1.1.16-262254).

Guerrero-Rascado, et al. (2010) Proc. Cuarta Reunión Española de Ciencia y Tecnología de Aerosoles, C15-1-6, ISBN: 978-84-693-4839-0.
Sicard, M., et al. (2009) *IEEE Trans. Geosci Remote Sens.*, 47, 3547-3559.
Sicard, M., et al. (2011) *Atmos. Chem. Phys. Dis.*, 11, 29681–29721.
Young, S. (1995) *Appl. Opt.*, 34, 7019-7031.

CLIMARENO-GRA 2011 campaign: retrieval of vertically-resolved aerosol microphysical properties by lidar at daytime

J.L. Guerrero-Rascado[1,2], M. J. Granados-Muñoz[1,2], F. Navas-Guzmán[1,2], J. A. Bravo-Aranda[1,2], F. J. Olmo[1,2], J. Andrey[3], M. Gil[3], A. Chaikovsky[4], U. Wandinger[5] and L. Alados-Arboledas[1,2]

[1]Andalusian Center for Environmental Research (CEAMA), University of Granada – Autonomous Government of Andalusia, Av. del Mediterráneo s/n, 18006, Granada, Spain
[2]Department of Applied Physics, University of Granada, Fuentenueva s/n, 18071, Granada, Spain
[3] Department Earth Observation, Remote Sensing and Atmosphere, Instituto Nacional de Técnica Aeroespacial, Torrejón de Ardoz, Spain
[4]Institute of Physics National Academy of Sciences, 68, Scaryna ave., 220072, Minsk, Belarus.
[5]Leibniz Institute for Tropospheric Research, Permoserstraße 15, D-04318 Leipzig, Germany.
Keywords: aerosol types, lidar, microphysical properties, sun-photometer.
Presenting author email: rascado@ugr.es

Microphysical properties, along with optical ones, play a key role for the understanding of the aerosol radiative effect in climate. Particularly interesting, and however poorly investigated, is the vertical distribution of aerosol microphysical properties. Since last years, several algorithms in the framework of EARLINET try to address this issue based on the analysis of multiwavelength Raman lidar signals, which are mainly restricted to night time. Nowadays, new tools based in the combination of elastic lidars and sun-photometers have been developed within the working package WP20 of the European project ACTRIS (Aerosols, Clouds, and Trace gases Research InfraStructure Network). This work focuses on the application of the retrieval algorithm developed by Chaikovsky et al. (2008) for microphysical properties profiling under two different scenarios that took place at Granada (Spain) during the CLIMARENO field campaign.

The CLIMARENO field campaign allowed for the study of atmospheric aerosol particles from a multi-instrumental approach. For further details see Andrey et al. (2012) and Bravo-Aranda et al. (2012). On 14th June 2011 aerosol particles advected from North America and the northernmost part of South America were monitored over Granada especially between 4.0 and 6.5 km asl. The columnar values (derived from sun-photometer, AERONET level 1.5 data) of aerosol optical depth (AOD) at 500 nm were 0.07-0.12, and Angström Exponent (AE) at 440-870 nm were 0.82-1.41 during the morning. The microphysical properties profiling indicated a clear predominance of the fine mode and the spherical-coarse mode in these layers (Figure 1, left). This agrees with the low linear particle depolarization ratios (not shown here) detected by lidar and an expected particle growth during the long-range transport. In contrast, on 27th June there is a clearly marked signature of Saharan dust mineral particles, which were observed up to 5.0 km asl. For this case daily mean AOD (500 nm) was 0.30±0.02 and daily mean AE (440-870 nm) was 0.48±0.06, indicating a dusty scenario. The predominance of both spherical- and spheroid-coarse mode (Figure 1, right) also evidences this fact.

Additionally, the coherence of the results from this algorithm is checked against independent datasets:

(i) simultaneous and co-located microphysical properties measured by in-situ instrumentation aboard aircraft.
(ii) non-simultaneous (night time) and co-located microphysical properties retrieved from Raman lidar through algorithms based on the analysis of Raman signals.

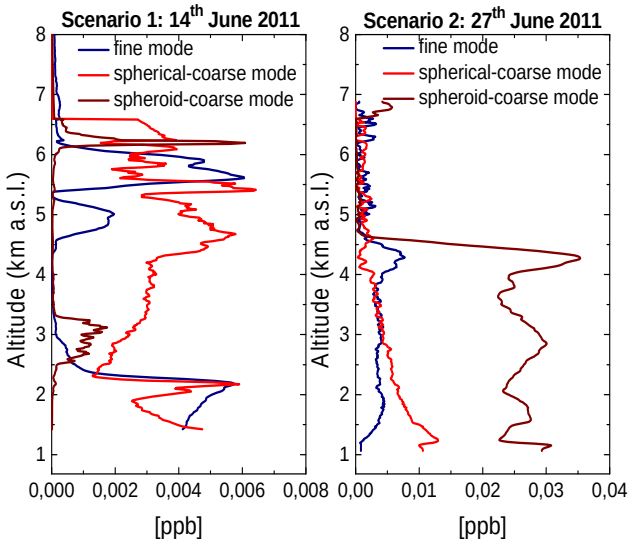

Figure 1. Vertical profiles of aerosol volume concentration for fine, spherical-coarse and spheroid-coarse modes for trans-Atlantic aerosols on 14th June (left) and Saharan dust particles on 27th June (right).

This work was supported by the Andalusia Regional Government through projects P08-RNM-3568 and P10-RNM-6299, by the Spanish Ministry of Science and Technology through projects CGL2010-18782, CSD2007-00067 and CGL2011-13580-E/CLI; and by EU through ACTRIS project (EU INFRA-2010-1.1.16-262254).

Andrey, J., et al. (2012), abstract submitted to this conference.
Bravo-Aranda, J. A., et al. (2012), abstract submitted to this conference.
Chaikovsky, A., et al. (2008). Technical report, Institute of Physics, National Academy of Sciences of Belarus, Minsk, Belarus.

First profiling of aerosol microphysical properties from combination of multiwavelength lidar (EARLINET) and sun-photometric (AERONET) data at Évora (Portugal)

J.L. Guerrero-Rascado[1,2,3], A. M. Silva[1,4], M. J. Costa[1,4], J. Preißler[1], S. Pereira[1], A. Chaikovsky[5]and F. Wagner[1]

[1] Évora Geophysics Centre (CGE), University of Évora, Rua Romão Ramalho 59, 7000, Évora, Portugal
[2]Andalusian Center for Environmental Research (CEAMA), University of Granada – Autonomous Government of Andalusia, Av. del Mediterráneo s/n, 18006, Granada, Spain
[3]Department of Applied Physics, University of Granada, Fuentenueva s/n, 18071, Granada, Spain
[4]Department of Physics, University of Évora, Rua Romão Ramalho 59, 7000 Évora, Portugal
[5]Institute of Physics National Academy of Sciences, 68, Scaryna ave., 220072, Minsk, Belarus
Keywords: aerosol types, lidar, microphysical properties, sun-photometer.
Presenting author email: rascado@ugr.es

The key for a comprehensive understanding of atmospheric aerosols regarding air quality and climatic relevant processes lies in the research of their chemical composition and microphysical properties. In spite of their relevance, their temporally and vertically resolved microphysical properties are yet only poorly understood. In order to achieve a deeper knowledge of these properties, the analysis of systematic measurements like those performed in the framework of EARLINET (European Aerosol Research lidar Network) is needed.

During the last decades, multiple inversion techniques have been used for retrieving microphysical properties by means of multiwavelength measurements of optical properties. In this study we present the application of a software that allows for retrieving aerosol microphysical properties through the combination of lidar and sun-photometric data obtained at the Évora station (Portugal, 38.6ºN, 7.9ºW, 290 m asl). It was developed by Chaikovsky et al. (2008) and recently disseminated in the EARLINET community. The novelty of this study is based on the features offered by the AERONET+EARLINET station at Évora. On one hand, the privileged location of Évora allows for studying the aerosol particles advected from different sources. On the other hand, the multi-instrumental capabilities of the Évora station (active/passive remote sensing and in-situ techniques) enable a thorough characterization of the aerosol particles.

The method is based on constructing the vertical distribution of aerosol volume concentrations matching both the integrated aerosol properties derived by sun-photometer and the vertical variability of the multispectral lidar signals. Thus, the method provides the fine and coarse fractions with a cutoff radius of 0.5µm. Refractive index is considered to be independent on the altitude. Information in the incomplete overlap range height is modeled as a constant profile.

As an example of the first vertically resolved aerosol microphysical retrievals, a case of long-range transported particles from America to Évora on 23/01/2012 is selected. Aerosol particles were detected up to 7.4 km (agl) (Figure 1). The reference height was selected at 8 km (agl). Noise prevented retrievals in higher altitudes. The microphysical retrieval indicated a clear predominance of the fine mode in the free troposphere in contrast to a predominance of the coarse mode in the lowermost part of the troposphere.

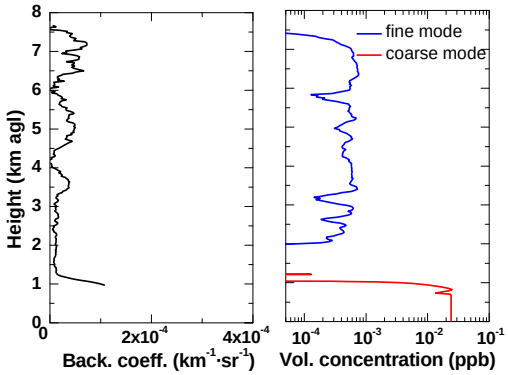

Figure 1. Profiles of aerosol backscatter coeff. at 532 nm (left) and aerosol volume concentrations for fine and coarse modes (right) on 23/01/2011 at 12:00-12:30 UTC.

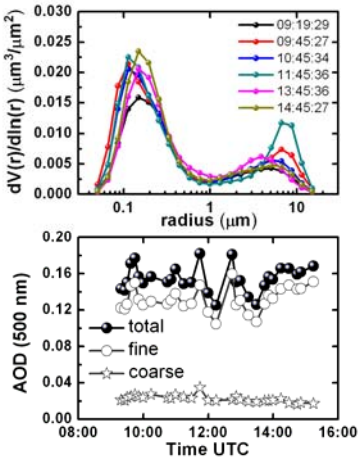

Figure 2. Columnar volume size distributions and AODs, including fine and coarse discrimination, at the same day obtained from AERONET (Évora).

This work was supported by the Andalusia Regional Government through projects P10-RNM-6299, by EU through ACTRIS project (EU INFRA-2010-1.1.16-262254), FEDER (COMPETE) and FCT under project FCOMP-01-0124-FEDER-007122 (PTDC / CTE-ATM / 65307 / 2006), and grant SFRH/BD/47521/2008.

Chaikovsky, A., et al. (2008). Technical report, Institute of Physics, National Academy of Sciences of Belarus, Minsk, Belarus.

A case study of a strong aerosol load over Heraclion Crete (Greece), detected with ground-based lidar and in situ airborne measurements

P. Kokkalis[1], G. Tzeremes[2], A. Papayannis[1], V. Amiridis[3], E. Armandillo[2], and
[1]National Technical University of Athens, Laser Remote Sensing Unit, Physics Department, Zografou, Greece
[2]European Space Agency, Noordwijk, Netherlands
[3]National Observatory of Athens, Palaia Penteli, Greece
Keywords: aerosol, lidar, dust.
Presenting author email: panko@central.ntua.gr

During September-October 2011 the ESA Mobile Raman Lidar (EMORAL) was operating at the complex environment of the large urban coastal city of Herkleion (Crete, Greece).This city combines high aerosol loads originating from different distant (e.g. Saharan desert, biomass burning areas, etc.) and local sources (local sources, such as traffic and industrial activities).

During 7 of September 2011 the handheld sun photometer Microtops II indicated rather coarse particles (AE=0.93±0.12, with AOD at 500 nm=0.41±0.10) at 12:00 UTC. EMORAL operated from 09:30 to 13:00 UTC and detected, indeed, high aerosol loads, and the evolution of this event was monitored over the operational site (Fig. 1). The vertical profiles of the aerosol optical properties (backscatter coefficient at 355 nm and 532 nm, backscatter-related (bp355/bp532) Ångström exponent and the volume linear depolarization ratio) obtained by EMORAL (Fig. 2) delineate two distinct aerosol layers of about 1 km thickness, each (1.5-2.5 km and 3-3.8 km height). The first aerosol layer is probably composed by a mixture of dust and biomass burning aerosols, as demonstrated by air mass back-trajectory analysis (not shown) and by single scattering albedo (SSA) and CO values, obtained in situ (Fig. 3). The backscatter-related Ångström (bp355/bp532) exponent ranged from 1 to 2 (with a mean value of 1.52±0.25) indicating the presence of rather small particles with a large variability of the aerosol type, inside this layer. At this height the volume linear depolarization ratio at 355 nm was of the order of 8.5±0.1%.

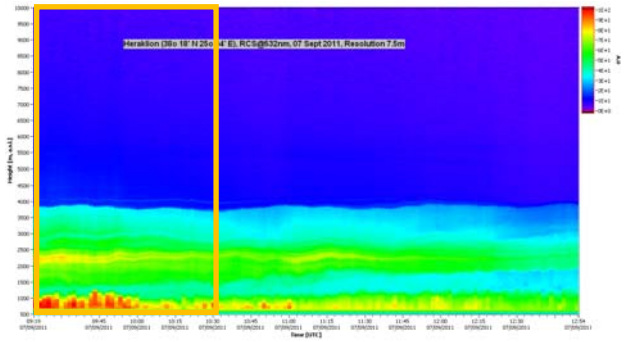

Figure 1. Spatio-temporal evolution of the range-corrected lidar signal, obtained by EMORAL (in a.u.) at 532 nm (7 September 2011).

The second aerosol layer was probably composed by Saharan dust as previously discussed. The backscatter-related Ångström exponent was found to decrease with height, having a mean value of the order 0.3 inside the aerosol layer (indicating the presence of rather big particles), while the volume linear depolarization ratio was found to be ~ 9.2 %.

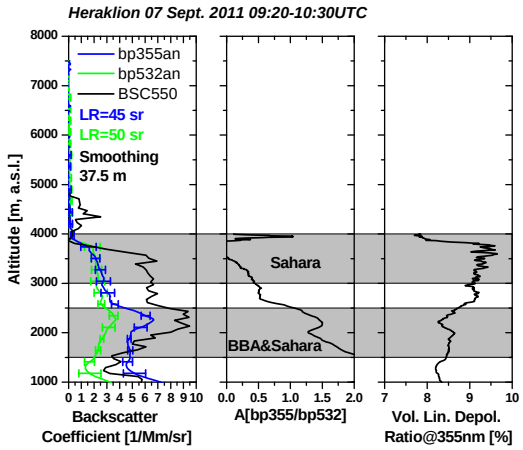

Figure 2. The aerosol backscatter coefficient at 355 nm and 532 nm, the backscatter-related Ångström exponent and the volume linear depolarization ratio at 355 nm of aerosols retrieved by EMORAL over Herakleion, Crete (7 September 2011: 09:20 UTC-10:30 UTC). The aerosol backscatter coefficient at 550 nm (BSC550) was obtained by FAAM in situ instrumentation.

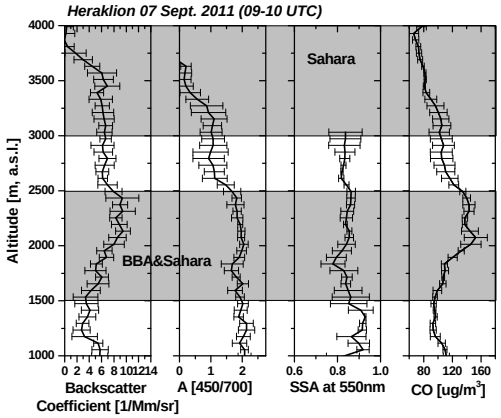

Figure 3. Aerosol backscatter coefficient profile at 550 nm retrieved on board by FAAM aircraft, along with the scattering-related Ångström exponent and the SSA and the CO concentration during the flight of 7 September 2011 (09:00 UTC-10:00 UTC).

Acknowledgements: This work was supported by the European Space Agency (ESA) (ESTEC Contract No. 4200022921/10/NL/PA). We acknowledge the support of the technical personnel of the EUFAR fleet.

PBL determination from ground based lidar over Herakleion-Crete Greece

P. Kokkalis[1], G. Tzeremes[2], A. Papayannis[1], and E. Armandillo[2]
[1]National Technical University of Athens, Laser Remote Sensing Unit, Physics Department, Zografou, Greece
[2]European Space Agency, Noordwijk, Netherlands
Keywords: aerosol, lidar, planetary boundary layer.
Presenting author email: panko@central.ntua.gr

Based on the ESA's mobile lidar system (EMORAL) lidar signals analysis and by calculating the minimum value of the first derivative of the range-corrected signal (RCS) profiles, obtained over the Herakleion, Crete, we were able to determine the mean daily value of the Planetary Boundary Layer (PBL) height, for the first time over Crete, as well as its mean value during September and October 2011 (Fig. 1). According to that Figure, the PBL height for the studied period varied from 1563 to 1079 m, while the mean value for the whole period was of the order 1266±135 m. Moreover, in Table 1 we summarize the monthly diurnal (mean, morning-to-noon and afternoon hours) variation of the PBL height obtained by EMORAL over Herakleion. The mean PBL height value for September 2011 was found to be 1252 m, while that of the cooler month October, was 1101 m. The corresponding mean values for the morning-to-noon hours (<10:00 UTC) were 1159 m and 1037 m, while those for the afternoon hours (>10:00 UTC) were 1267 m and 1152 m, respectively.

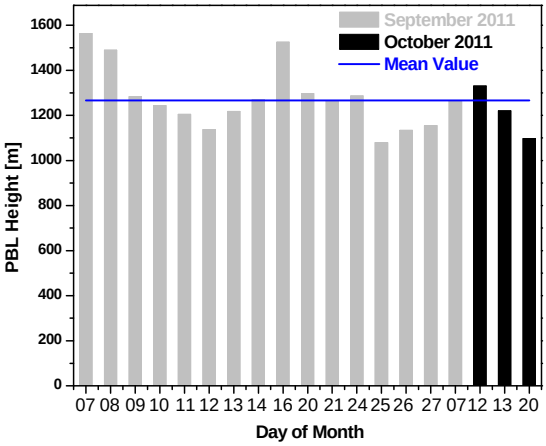

Figure 1. PBL height variation as determined by the analysis of the first derivative of the RCS obtained by EMORAL at the city of Herakleion, Crete, during September and October 2011.

Table 1. Monthly, mean, morning-to-noon and afternoon variation of the PBL height obtained by EMORAL over Herakleion, Crete (September to October 2011).

PBL Height (m)	Mean	Morning	Noon
September 2011	1252	1159	1267
October 2011	1101	1037	1152

Analyzing in more detail the values of the PBL height given in Fig. 2 and Table 2, since the PBL height - due to uprising thermals - is increasing near local noon, we estimated the rate of the relative increase (comparing the PBL height at 12:00 UTC to that at 09:00 UTC) to be of the order of 9.3 % in September and 9.9% in October. In Figures 1 and 2, we present the spatio-temporal evolution of the PBL height obtained during 20 October 2011. During the morning hours (~ 09:00 UTC), when the land is still quite cold, thus no intense updrafts exist, the PBL height is around 1100 m, which keeps strong aerosol loads near ground. During the hotter hours of the day, more intense thermals appear (around 11:00 UTC), thus transferring heat upwards; In this case the PBL height increases up to nearly 1300 m. Later on, the PBL height starts decreasing around the local sunset. Finally, a typical example is given in Figure 2, where the mean PBL height is found at 1096 m height, as retrieved by height minimum of the first derivative of the RCS signal, obtained from approximately 10.000 laser shots averaged from 09:156 UTC to 13:07 UTC at 532 nm on 20 October 2011 (see insert in Fig. 2).

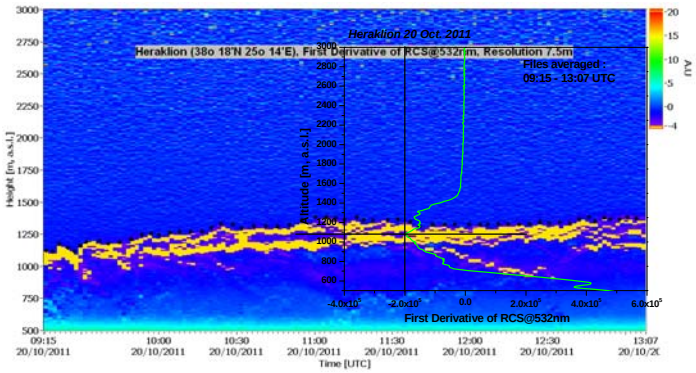

Figure 2. Spatio-temporal variation of the first derivative of RCS, obtained by EMORAL at 532 nm over Herakleion (Crete), from 09:15 UTC to 13:07 UTC (20 October 2011). The black dots show the position of the top of the PBL height. The insert figure shows the averaged first derivative of RCS (green line).

Acknowledgements: This work was supported by the European Space Agency (ESA) (ESTEC Contract No. 4200022921/10/NL/PA).

Amiridis, V., et al. (2007). *Atmos. Chem. Phys*., 7, 6181–6189.
Menut, L., et al. (1999). *Appl. Opt*., 38, 945–954.

Saharan Air Layer (SAL) over Tenerife: Summertime statistic analysis from lidar measurements

C. Córdoba-Jabonero[1], D. Toledo[1], J.A. Adame[1], Y. Hernández[2], E. Cuevas[2] and M. Gil[1]

[1]Instituto Nacional de Técnica Aeroespacial (INTA), Atmospheric Research and Instrumentation Branch, Torrejón de Ardoz, 28850, Madrid, Spain
[2]Agencia Estatal de Meteorología (AEMET), Atmospheric Research Centre of Izaña, Sta. Cruz de Tenerife, Spain
Keywords: Aerosol extinction, Dust events, Micro Pulse Lidar, Saharan Air Layer.
Presenting author email: cordobajc@inta.es

The vertical distribution of dust is a key parameter on aerosol-ozone-UV interactions (i.e., Bonasoni *et al.*, 2004) for atmospheric radiative forcing assessment and climate-related studies (IPCC, 2007). Despite of a great attention has been paid in last years to the aerosols in a global scale and, in particular, to the Saharan dust, a large uncertainty on the sign of the radiative forcing still remains. In addition, height-resolved information of the dust properties is also required in other frameworks as for aerosol forecast modeling (i.e., Pérez *et al.*, 2006) and satellite data validation (i.e., Pappalardo *et al.*, 2010).

Canary Islands offer the most promising site as located downwind of the Saharan outbreaks sources for dust monitoring. The arrival of dust plumes to that area is a common feature, more frequently observed in summertime and extended up to high altitudes, resulting from strong convective activity over the Sahara desert under favorable meteorological conditions. The vertical characterization of individual dust events is significant for the determination of the so-called Saharan Air Layer (SAL), identified as a mass of warm, dusty and dry air which forms over the Saharan desert, in order to evaluate the climate impact of such phenomena, even at local scales.

In general, the synergy between lidar and sun-photometry observations is also widely used for dust research (i.e., Müller *et al.*, 2003; Mona *et al.*, 2006; Papayannis *et al.*, 2008; Córdoba-Jabonero *et al.*, 2011). Since 2005 height-resolved measurements are routinely performed at the AEMET/Santa Cruz de Tenerife subtropical station (SCO, 28.5ºN 16.2ºW, 52 m a.s.l.) by using a Micro Pulse Lidar v. 3 (MPL-3) within the NASA/MPLNET (Micro Pulse Lidar NETwork). SCO is also an AERONET (Aerosol Robotic NETwork) site.

In this work we present the statistical results of the SAL characterization in summertime over SCO from routine lidar measurements. This study focuses on vertical features (single/multi-layered structure, top height, among others) of the dusty episodes, in addition to other optical properties (Free-Tropospheric dust contribution to the total AOD, Lidar Ratio frequency, etc.). Air masses backtrajectory analysis completes this study. For instance, the SAL is examined for a strong dust intrusion occurring on 21 July 2009 over SCO (see Figure 1). Extinction coefficients are retrieved considering a pure dust scenario (Córdoba-Jabonero *et al.*, 2010) and a Lidar Ratio of 55 sr is found. In this case, daily SAL top is ranging between 5.3 and 5.7 km, and a FT dust contribution of 88.3% is calculated.

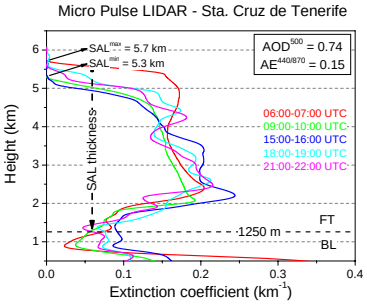

Figure 1. Dust extinction coefficients on 21 July 2009, for instance, over SCO site.

This summertime statistic analysis represents a relevant advance on SAL characterization in aerosol stations fairly close to dust emissions. Moreover, these results can be directly applied to the evaluation of the ozone vertical depletion observed under Saharan dust events (Andrey *et al.*, 2010) and the changes experienced by minor halogen species involved in ozone chemistry.

This work is supported by the Spanish Ministry for Research and Innovation (MICINN) under grant CGL2011-24891 (project AMISOC).

Andrey *et al.* (2010) *International Aerosol Conference*, 29 August-3 September, 2010, Helsinki, Finland.
Bonasoni *et al.* (2004) *Atmos. Chem. Phys.* **4**, 1201-1215.
Córdoba-Jabonero *et al.* (2010) *IV Spanish Meeting on Aerosol Research and Technology*, Abstract extended, G31-G35.
Córdoba-Jabonero *et al.* (2011) *Atmos. Chem. Phys.* **11**, 3067-3091.
IPCC 2007 *Intergovernmental Panel on Climate Change*, Geneva, 210 pp., 2008.
Mona *et al.* (2006) *J. Geophys. Res.* **111**, D16203, doi:10.1029/2005JD006569.
Müller *et al.* (2003) *J. Geophys. Res.* **108**, 4345, doi:10.1029/2002JD002918.
Papayannis *et al.* (2008) *J. Geophys. Res.* **113**, D10204, doi:10.1029/2007JD009028.
Pappalardo *et al.* (2010) *J. Geophys. Res.* **115**, D00H19, doi:10.1029/2009JD012147.
Pérez *et al.* (2006) *J. Geophys. Res.* **111**, D15214, doi:10.1029/2005JD006579.

Polar Stratospheric Clouds observations in coastal Antarctica based on Micro Pulse Lidar measurements. I. Depolarization ratio comparison with CALIOP

C. Córdoba-Jabonero[1], J.L. Guerrero-Rascado[2,3], D. Toledo[1], M. Parrondo[1], M. Yela[1], M. Gil[1] and H. Ochoa[4]

[1]Instituto Nacional de Técnica Aeroespacial (INTA), Atmospheric Research and Instrumentation Branch, Torrejón de Ardoz, 28850, Madrid, Spain
[2]Andalusian Center for Environmental Research (CEAMA), University of Granada - Autonomous Government of Andalusia, Granada, 18071, Spain
[3]Department of Applied Physics, University of Granada, Granada, 18071, Spain
[4]Dirección Nacional del Antártico (DNA), Buenos Aires, Argentina
Keywords: CALIPSO, Depolarization, Micro Pulse Lidar, Polar Stratospheric Clouds.
Presenting author email: cordobajc@inta.es

The use of lidar depolarization is a key tool for climate-related cloud and aerosol studies because depolarization measurements provide information about the shape and/or the thermodynamic phase of the particles in the atmosphere.

In particular, the Polar Stratospheric Clouds (PSCs) depolarization ratio (δ) obtained from lidar observations is usually used as a PSC-type discriminator together with the lidar backscattering ratio (i.e., Maturilli *et al.,* 2005; Pitts *et al.,* 2009). Indeed, this PSC-type identification is critical on polar ozone depletion research, and directly linked to the stratospheric temperature variability. Therefore this δ parameter must be accurately estimated.

Since January 2009 PSC observations are performed over the coastal Antarctica in Belgrano II station (Argentina, 77.9ºS 34.6ºW) by using an improved version of the standard NASA/Micro Pulse Lidar, the MPL v.4 (MPL-4), which includes a built-in depolarization module unlike other MPLs. This study focuses on the analysis of MPL-4 two-channel data, i.e. both parallel (p-) and perpendicular (s-) MPL signals, in order to retrieve the PSC lidar depolarization ratio δ values. Antarctic 2009-2011 winter data, from May to September periods, are used for that purpose.

From the practical point of view, the most general expression to calculate the linear volume depolarization ratio δ in terms of lidar signals is:

$$\delta(z) = K\frac{P^{\perp}(z)}{P^{\parallel}(z)} + \chi \qquad (1)$$

where $P^{\perp}(z)$ and $P^{\parallel}(z)$ are the s- and p- components of the measured MPL signals, respectively, once corrected for intrinsic instrumental factors (see Campbell *et al.* (2002) for details); K is a calibration constant that accounts for the differences of the receiver channel gains; and χ is a correction to account for any slight mismatch in the transmitter and detector polarization planes and any impurity of the laser polarization state (Sassen, 2005). Optimal K and χ values are found by using fitting procedures with molecular backgrounds.

MPL-4 depolarization retrieval is compared to the PSC depolarization ratio reported from the space-borne lidar CALIOP to test the degree of agreement. CALIOP is on board of CALIPSO (Cloud-Aerosol Lidar and Infrared Pathfinder Satellite Observation, www-calipso.larc.nasa.gov), whose closest ground-track overpasses to Belgrano II station are selected. A few examples are shown in this work to illustrate such a comparison analysis. For instance, δ-profiles comparison on 30 and 31 July 2009 is shown in Figure 1.

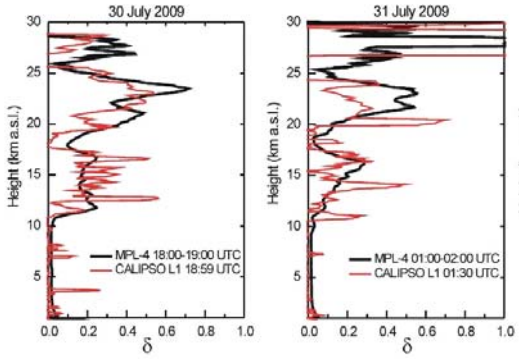

Figure 1. δ-profiles comparison on 30 and 31 July 2009 at the closest CALIPSO overpass distance from Belgrano II station: 25.6 km and 48.9 km, respectively.

Results indicate that there is a good correlation between both linear volume depolarization ratio δ profiles once MPL-4 calibrated depolarization parameters are calculated. This correlation is based on the height range match of the layered structure as well as the δ values found for each layer. As expected, this agreement is much better when the CALIPSO ground-track overpass is much closer to the Belgrano II station.

This work is supported by the Spanish Ministry for Research and Innovation (MICINN) under grant CGL2010-20353 (project VIOLIN). CALIPSO data were obtained from the NASA Langley Research Center Atmospheric Science Data Center. Authors specially thank the DNA/IAA team at Belgrano II station for their valuable assistance and support.

Campbell *et al.* (2002) *J. Atm. Ocean. Tech.* **19**, 431-442.
Maturilli *et al.* (2005) *Atmos. Chem. Phys.* **5**, 2081-2090.
Pitts *et al.* (2009) *Atmos. Chem. Phys.* **9**, 7577-7589.
Sassen (2005) Polarization in Lidar, in *Lidar: Range-Resolved Optical Remote Sensing of the Atmosphere*, Ed. C. Weitkamp, Springer Ser., Singapore.

Polar Stratospheric Clouds observations in coastal Antarctica based on Micro Pulse Lidar measurements. II. PSC-type discrimination assessment

D. Toledo[1], C. Córdoba-Jabonero[1], J.L. Guerrero-Rascado[2,3], M. Parrondo[1], M. Yela[1], M. Gil[1] and H. Ochoa[4]

[1]Instituto Nacional de Técnica Aeroespacial (INTA), Atmospheric Research and Instrumentation Branch, Torrejón de Ardoz, 28850, Madrid, Spain
[2]Andalusian Center for Environmental Research (CEAMA), University of Granada - Autonomous Government of Andalusia, Granada, 18071, Spain
[3]Department of Applied Physics, University of Granada, Granada, 18071, Spain
[4]Dirección Nacional del Antártico (DNA), Buenos Aires, Argentina
Keywords: Micro Pulse Lidar, PSC backscattering ratio, PSC depolarization ratio, Stratospheric temperature.
Presenting author email: toledocd@inta.es

Polar Stratospheric Clouds (PSCs) have been identified as determinant elements for the ozone depletion processes occurring at high latitudes during spring time. In Polar regions PSCs start to form during winter at stratospheric temperatures below the condensation threshold of the Nitric Acid Trihydrate (NAT), which depends on the water vapor and nitric acid partial pressure (Hanson and Mauersberger, 1988). PSCs are classified in two groups (i.e., Toon *et al.*, 1990) depending on the temperature formation threshold: PSC type I (PSC-I) are nitric acid clouds formed above the frost point (T_{NAT} = 194 K at 30 hPa), and PSC type II (PSC-II) are water ice clouds (T_{ice}=185 K at 30 hPa). Therefore, the PSC-type identification is directly linked to the stratospheric temperature.

Lidar measurements have been usually used for PSC classification (PSC-I and PSC-II) on the basis of two lidar parameters: both backscattering (R) and depolarization (δ) ratios (i.e., Adriani *et al.*, 2004; Maturilli *et al.*, 2005; Pitts *et al.*, 2009). According to those R and δ values found, PSC-II present rather higher R and δ values respect to those found for PSC-I.

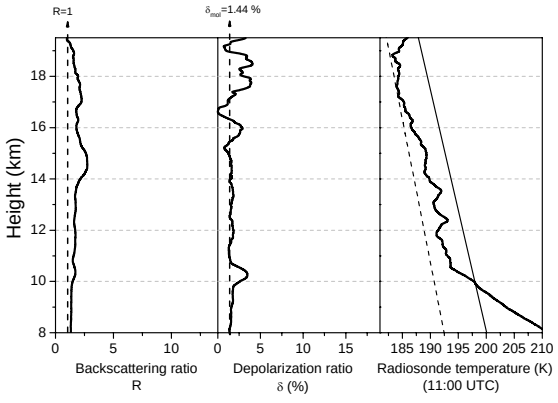

Figure 1. PSC-I backscattering ratio for 1-h averaged profile (11:00-12:00 UTC) (left); volume depolarization ratio (centre), with the molecular value (δ_{mol}=1.44%) also indicated; and the radiosonde temperature profile (right) with the 2-ppmv H_2O and 2-ppbv HNO_3 threshold temperatures for NAT (solid line), and ice (dotted line), on 23 September 2009.

In this work, an improved version of the standard NASA/Micro Pulse Lidar (MPL v.4, MPL-4) deployed in the continental Antarctica Belgrano II station (Argentina, 77.9ºS 34.6ºW) since January 2009 for PSC observations is used to obtain these two parameters. The degree of performance of this kind of micropulse lidars for PSC discrimination is evaluated. An example of each PSC-I and PSC-II as identified by the MPL-4 parameters is shown in Figures 1 and 2, respectively. Radiosonde temperature profiles are also shown on each day. Results show that MPL-4 retrievals are reliable for PSC discrimination between PSC-I and PSC-II over Antarctica. In particular, a more detailed PSC-I discrimination into Ia and Ib, NAT and liquid PSC subgroups, respectively, according the criteria adopted from Adriani *et al.* (2004), requires a more accurate lidar data processing.

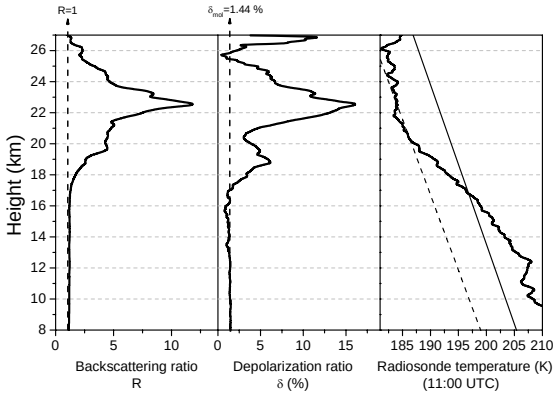

Figure 2. The same as Fig. 1, but for PSC-II on 29 June 2009, and with 5-ppmv H_2O and 8-ppbv HNO_3 threshold temperatures for NAT (solid line) and ice (dashed line).

This work is supported by the Spanish Ministry for Research and Innovation (MICINN) under grant CGL2010-20353 (project VIOLIN). Authors also wish to thank the DNA/IAA team at Belgrano II station for their valuable assistance and support in lidar and radiosounding measurements.

Adriani *et al.* (2004) *J. Geophys. Res.*, **109**, D24211, doi:10.1029/2004JD004800.
Hanson and Mauersberger (1988) *Geophys. Res. Lett.*, **15**, 855-858.
Maturilli et al. (2005) *Atmos. Chem. Phys.*, **5**, 2081-2090.
Toon et al. (1990) *Geophys. Res. Lett.*, **17**, 393-396.

Multiwavelength Raman lidar observations of aerosols at Gual Pahari, India

E. Giannakaki[1,2], T. Mielonen[1], K. Korhonen[1], H. Lihavainen[3], A.-P. Hyvärinen[3], D. Müller[4,5,6], H. Baars[4], R. Engelmann[4], D. Althausen[4], T.S. Panwar[7], R.K. Hooda[3,7], V.P. Sharma[7], K.E.J. Lehtinen[1,8], Y. Viisanen[3] and M. Komppula[1]

[1]Finnish Meteorological Institute, Kuopio Unit, P.O.Box 1627, FI-70211, Kuopio, Finland
[2]Laboratory of Atmospheric Physics, Aristotle University of Thessaloniki, Thessaloniki, 54124, Greece
[3]Finnish Meteorological Institute, P.O.Box 503, FI-00101, Helsinki, Finland
[4]Leibniz Institute for Tropospheric Research, Permoserstr. 15, D-04318, Leipzig, Germany
[5] Gwangju Institute of Science and Technology, Korea
[6] now at: Science and Systems Applications, Inc. NASA Langley Research Center, Hampton VA, USA
[7]The Energy and Resource Institute, Dabari Seth Block, IHC Complex, Lodhi Road, 110 003, New Delhi, India
[8]University of Eastern Finland, Department of Applied Physics, P.O.Box 1627, FI-70211, Kuopio, Finland
Keywords: aerosol characterization, lidar, microphysics
Presenting author email: eleni.giannakaki@fmi.fi

High quality case studies characterizing vertically resolved aerosol optical properties of specific aerosol types have been made world-wide with ground-based Raman lidars (e.g. Müller *et al.*, 2007). During the past decade, sophisticated computational procedures have been developed and successfully tested for multiwavelength Raman lidar observations that permit the retrieval of particle microphysical properties (Müller *et al.*, 1999).

Figure 1 shows one such measurement taken on 13th of July 2008 at Gual Pahari site, India (28.43° N, 77.15° E, 243 m) from 20:00 to 20:50 UTC. The measurement was conducted with a seven-channel Raman lidar called "POLLYXT–POrtabLe Lidar sYstem eXTended" (Althausen *et al.*, 2009). A detailed description of the site can be found in Hyvärinen *et al.*, 2011.

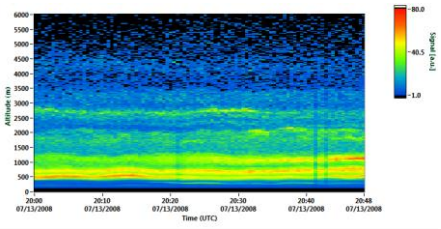

Figure 1. Range corrected signal at 1064 nm measured at Gual Pahari, India on 13th July 2008.

Distinct aerosol layers are observed throughout the atmosphere and reached top heights of approximately 4.5 km height above sea level. Vertically resolved lidar measurements of aerosol extensive parameters (extinction and backscatter coefficients) as well as intensive parameters (lidar ratio, depolarization, Ångström exponent) are calculated. No significant spectral behavior between lidar ratio values was found. The mean lidar ratio is 96± 29 sr and 94 ± 65 sr at 355 and 532 nm respectively. The extinction-related Ångström exponents (355/532 wavelength pair) vary between 0.9-1.9. The profile of the linear depolarization ratio indicates that the particles observed are nearly spherical.

The HYSPLIT trajectory model (Draxler and Hess, 1999) is used to identify the source regions of the plumes that are observed over Gual Pahari (Figure 2). According to the backward trajectory analyses the air masses that arrived over Gual Pahari at 500 m and 1000 m height had crossed over the Arabian sea. The signature of a strong thin particle layer at 500 m is evident during the whole observation time and is probably related with maritime aerosols. Nevertheless, aerosol layers observed at heights between 1500 and 4500 m have different origins. The air masses were rising during their travel in central India carrying probably anthropogenic aerosols before their arrival at Gual Pahari.

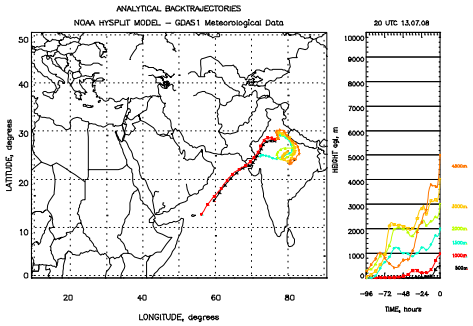

Figure 2. Four-days backtrajectories obtained from HYSPLIT on 13th July 2008 at 20:00 UTC for arrival height of 0.5, 1.0, 1.5, 2.0, 3.0 and 4.5 km.

To retrieve the microphysical properties at different altitudes, lidar profiles are separated into distinct aerosol layers. The mean values of optical properties calculated within the defined layers are then used as input in the inversion algorithm.

This work was supported by the EUCAARI project.

Althausen *et al.*, (2009) *J. Atmos. Oceanic Technol.*, **26**, pp. 2366–2378.
Draxler, R. R., and Hess, G. D. (1998) *Australian Meteorological Magazine*, **47**, pp. 295–308.
Hyvärinen, A.P., *et al.* (2011) *Atmos. Chem. Phys*, **11**, 8283-8294.
Müller, D., Wandinger, U. and Ansmann, A. (1999) *Appl. Opt.*, 38, 2346–2357.
Müller, D., *et al.* (2007), *J. Geophys. Res.*, **112**, D16202, doi:10.1029/2006JD008292.

Preliminary results from the new portable backscatter aerosol lidar in Turkey

K. R. Allakhverdiev[1, 2], A. Secgin[1], M. F. Huseyinoglu[1] and Z. Salaeva[1]

[1]TUBITAK, Marmara Research Center, Materials Institute, P.K. 21, 41470 Gebze/Kocaeli,Turkey
[2]Azerbaijan National Academy of Aviation, Bina 25th km, Baku 1045, Azerbaijan
Keywords: aerosol measurement, aerosol characterization, aerosol size distribution, depolarization
Presenting author email: alper.secgin@mam.gov.tr

Aerosols are recognized to have various effects on the earth on different levels. They increase air pollution and thus reduce airspace visibility, and have hazardous effects to human health when inhaled. By altering the radiative properties of the atmosphere, aerosols also affect global warming and cooling, even though they are one of the biggest uncertainties of the climate system (Salomon *et al*, 2007).

Lidars have been used for the past few decades to have better and efficient remote study of the aerosols in the atmosphere and the instrumentations for these studies have been extremely sophisticated in time. It is also possible to have *in situ* information about the properties of atmospheric particles without disturbing their microphysics. A portable backscatter lidar using Nd:YAG laser with its harmonics has become an significant device for the measurement of aerosols in the lower atmosphere with the advantage of being easily transported to various locations (Veselovskii *et al*, 2002).

In Gebze region there are different types of aerosols related to industrial pollution, urban development, marine and desert dust. A stable multiwavelength Raman lidar using an Nd:YAG laser with its second and third harmonics has been built in the Scientific and Technological Research Council of Turkey (TUBITAK), Marmara Research Center (MRC), KA09 Laser and Lidar Laboratory to get information about atmospheric particle parameters for different seasons and meteorological conditions in different regions. This lidar (EARLINET name, MRC K09) measures aerosol backscattering, extinction coefficients and polarization, and from the obtained data, the particle microphysical parameters such as volume, surface area and number concentrations, effective radius, size distribution, particle and volume polarization, and complex refractive index are retrieved through inversion with regularization, principal component analysis and linear estimation techniques (Veselovskii *et al*, 2011).

A portable backscatter lidar has been built in the same laboratory to obtain information about the aerosol parameters at heights within the Planetary Boundary Layer (PBL) and slightly above. It has an Nd:YAG laser transmitter with its second harmonic emitting 10 GHz pulses with 4 W average power. Receiver is a 20 cm aperture Cassegranian telescope. Licel TR20-160 is used with Newport LP-1A Avalanche Photo Diode (APD) at 1064 nm and with PMT's for polarization measurements at 532 nm. Figure 1 illustrates the above mentioned portable backscatter lidar.

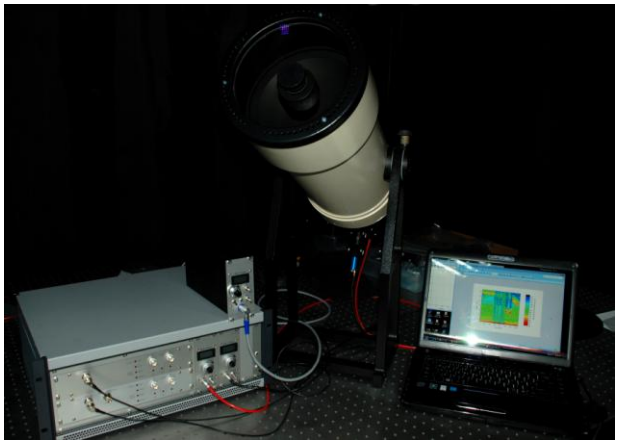

Figure 1. Portable backscatter lidar at MRC, Scientific and Technological Research Council of Turkey (TUBITAK).

The aim of this paper is to describe the experimental details and to demonstrate the first results of the new portable backscatter lidar sounding over the industrial zone of Gebze, Kocaeli district, Turkey located at the shore of Marmara Sea, Gulf of Izmit, about 40 km East from Bosphorus, Istanbul.

This work was supported by State Planning Committee of Turkey.

Salomon, S., Qin, D., Manning, M., Chen, Z., Marquis, M., Averyt, K. B., Tignor, M., Miller, H. L., (eds) (2007) *Contribution of Working Group I to the Fourth Assessment Report of the Intergovernmental Panel on Climate Change*, Cambridge University Press.

Veselovskii, I., Kolgotin, A., Griaznov, V., Müller, D., Wandinger, U. and Whiteman, D. (2002) *Appl. Opt.* **41**, 3685-3699.

Veselovskii, I., Dubovik, O., Kalgotin, A., Korenskiy, M., Whiteman, D. N., Allakhverdiev, K., Huseyinoglu, M. F., (2011) *Atmos. Meas. Tech. Disc* **4** (2011), 1-31.

Aerosol vertical distribution and its variability over Sweden during nighttime: A view from the CALIOP-CALIPSO and AIRS instruments

M.A. Thomas[1], A. Devasthale[1] and M. Kahnert[1,2]

[1]Swedish Meteorological and Hydrological Institute, Research Department, Norrköping, SE-60176, Sweden
[2]Chalmers University of Technology, Department of Earth and Space Science, SE-412 96 Gothenburg, Sweden
Keywords: Atmospheric aerosols, Satellites, Vertical distribution
Presenting author email: manu.thomas@smhi.se

An accurate knowledge of aerosol properties is a key to understand its direct and indirect radiative effects. Especially the vertical distribution of aerosols determines the degree with which it would interact with clouds, influence air quality and the atmospheric heating profiles, among others. Most of the passive satellite imagers have difficulties in retrieving accurate aerosol properties over Sweden due to large solar zenith angles during most part of the year, snow and ice covered surfaces etc. CALIPSO offers a viable alternative to overcome this difficulty. It also has a distinct advantage of providing vertical structure and nighttime observations [1]. Furthermore, the orbital track of CALIPSO is aligned very well with the semi-major axis of Sweden's elongated topography during nighttime (Fig. 1), thus making it extremely appealing for generating statistics of aerosol properties. Here, we use 5 years of Aerosol 5km Layer product from CALIPSO and investigate statistics of aerosol properties. We further investigate the role of temperature inversions in influencing vertical distribution of aerosols.

For the present study we use the standard CALIPSO 5km Aerosol Layer Product (Version 3.01) [1], specifically the aerosol retrievals of aerosol layer base and top heights, and optical depth at the 532nm wavelength. A rigorous quality control is applied while selecting the data for analysis. For example, if a feature is classified as aerosol and the classification quality flag is set to "high", only then are the results used for the analysis. The aerosols are further categorized into six different types, based on their integrated attenuated backscatter and volume depolarization ratio along with ancillary information on surface type and altitude [2]. The six aerosol types analyzed are "clean continental", "polluted continental", "dust", "polluted dust", "clean marine", and "smoke".

The data used in the present study cover the period from June 2006 through May 2011 and is analyzed for four seasons separately, winter (December, January, and February; DJF), spring (March, April, and May; MAM), summer (June, July, and August; JJA), and autumn (September, October, and November; SON).

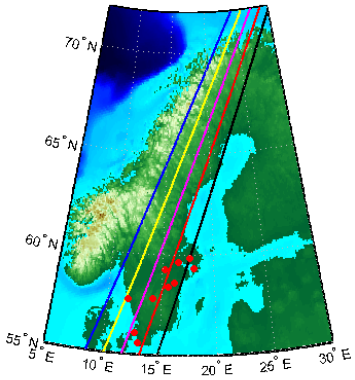

Fig. 1: CALIPSO track over Sweden during nighttime. The red dots show top 10 populated cities.

We investigate the seasonality of:

1) The vertical distribution of aerosols along five selected curtains over Sweden shown in Fig. 1.
2) Aerosol layer optical thickness.
3) Number of aerosol layers present.
4) Relative distribution of aerosol types.
5) Aerosol verticality with respect to temperature inversions derived from AIRS [3,4].

References

[1] Winker, David M., Mark A. Vaughan, Ali Omar, Yongxiang Hu, Kathleen A. Powell, Zhaoyan Liu, William H. Hunt, Stuart A. Young, 2009: Overview of the CALIPSO Mission and CALIOP Data Processing Algorithms. J. Atmos. Oceanic Technol., 26, 2310–2323. doi: http://dx.doi.org/10.1175/2009JTECHA1281.1

[2] Omar, A., D. Winker, C. Kittaka, M. Vaughan, Z. Liu, Y. Hu, C. Trepte, R. Rogers, R. Ferrare, R. Kuehn, and Hostetler C. 2009. The CALIPSO Automated Aerosol Classification and Lidar Ratio Selection Algorithm. J. Atmos. Oceanic Technol., 26, 1994-2014, doi:10.1175/2009-JTECHA1231.1.

[3] Devasthale, A., U. Willen, K.-G. Karlsson, and C. G. Jones, Quantifying the clear-sky temperature inversion frequency and strength over the Arctic Ocean during summer and winter seasons from AIRS profiles, Atmos. Chem. Phys., 10, 5565-5572, 2010.

[4] Devasthale, A., M. Tjernström and A. H. Omar, The vertical distribution of thin features over the Arctic analysed from CALIPSO observations. Part II: Aerosols, Tellus B, 63, 1, 86-95, 2011.

Aerosol variability over Lemesos, Cyprus: Use of ground based data, satellite observations and model simulations.

RE Mamouri[1], S. Kleanthous[2], S. Basart[3], V. Amiridis[4], Nisantzi[1], A., D.G Hadjimitsis[1], A. Agapiou[1] and J.M.Baldasano[3]

[1] Department of Civil Engineering and Geomatics, Cyprus University of Technology, Lemesos, Cyprus
[2]Department of Labour Inspection, Air Quality Sector, Nicosia, Cyprus
[3]Barcelona Supercomputing Center-Centro Nacional de Supercomputacion (BSC-CNS), Earth Sciences Department, Barcelona, Spain
[4]Institute for Space Applications and Remote Sensing, National Observatory of Athens, Athens, Greece

Keywords: aerosols, optical depth, PM10, satellite sensors.
Presenting author email: rodanthi.mamouri@cut.ac.cy

Aerosols play a very important role for the Earth-atmosphere energy budget as they modify it through various atmospheric processes. Aerosols found in the Mediterranean are due to a superimposition of a marine component, a mineral dust component (Saharan dust outbreaks and local dust suspension) and the local and long range transported anthropogenic component (Lelieveld *et al.*, 2002).

Lemesos is an Eastern Mediterranean seaside city, located in Southern coast of Cyprus. Under favorable meteorological conditions (sea breeze and calms) and due to the trans-boundary pollution (forest/biomass burning fires, dust from Desert regions, etc.), the concentration of air pollutants at ground may exceed the air quality standards of the European Union and the World Health Organization (WHO).

Sunphotometric measurements that have been conducted at the ground based AERONET station of Lemessos (34°67' N, 33°04' E) from April 2010 to December 2011, depict the strong variability of aerosol optical properties at this site. Figure 1 presents the temporal variability of aerosol optical depth (AOD) at UV, Vis and IR as well as the Ångström exponent (a) at 380/500nm over Lemesos. The seasonal variability of the aerosol optical properties is strongly related to the seasonal characteristics of aerosol production and transportation processes over specific regions.

In this study, the aerosol variability over Lemessos is examined, using longer AOD records than the ones available from the AERONET station, taken from the satellite-based MODerate resolution Imaging Spectro-radiometer (MODIS) on-board Terra and Aqua satellites. The optimum spatial resolution of the MODIS AOD product has been depicted by Mamouri et al., (2012), using the available ground-truth AERONET data. In this study, the AERONET derived aerosol optical properties are compared with those calculated from MODIS products, using various spatial resolutions. MODIS-Terra platform, with 50km diameter spatial resolution with respect to CUT-AERONET station, showed the highest correlation coefficients for the AOD (Mamouri *et al* 2012).

Based on the good correlation between the two instruments a climatology before 2010 is presented here using MODIS.

Additionally, BSC-DREAM8b model simulations are used in order to provide information on the dust contribution in Cyprus region both, at surface level and atmospheric column. Model's simulations for PM10 at surface are compared also with PM10 measurements available at Lemesos site. Several case studies have outlined the good performance of BSCDREAM8b (e.g. Pérez *et al.*, 2006a,b; Amiridis *et al.* 2009) concerning both the horizontal and vertical extent of the dust plume in the Mediterranean Basin. The model simulations are used in this study complementary with the MODIS aerosol products and in situ measurements of PM10, from the air quality monitoring network operated by Department of Labour Inspection (DLI), Ministry of Labour and Social Insurance of Cyprus.

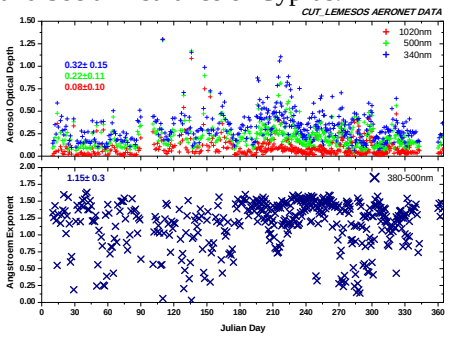

Figure 1. : Mean daily AOD in UV-Vis-IR and Ångström exponent from CIMEL sunphotometer, over Lemessos Cyprus.

This work was supported by "WebAir-2"-EUREKA project funded by the Cyprus Promotion Research Foundation. Thanks are given to the Remote Sensing Laboratory of the Department of Civil Engineering & Geomatics at the Cyprus University of Technology for the support (http://www.cut.ac.cy/).

Lelieveld, *et al* (2002) Global Air Pollution Crossroads over the Mediterranean, *Science*, 298, 794–799.
Mamouri R.E, *et al* (2012) *Proc. Int. Conf. of Air Quality, 19-23 March, Athens, Greece*.
Amiridis,V. *et al* (2009) *Annales Geophysicae*, 27, 3155-3164, 2009.
Pérez, C., *et a.* (2006a) *J. Geophys. Res.*, 111, D16206.
Pérez, C, *et al* (2006b) *J. Geophys. Res.*, 111. D15214.

Nine years of aerosol optical depth measurements over north-central Spain from ground (AERONET-RIMA) and their comparison with satellite (MODIS) observations

Y.S. Bennouna[1], V.E. Cachorro[1], B. Torres[1], R. Rodrigo[1], C. Toledano[1], A. Berjón[2] and A.M. de Frutos[1]
[1]Atmospheric Optics Group (GOA), University of Valladolid (UVA), Valladolid, 47071, Spain
[2]Izaña Atmospheric Research Center, Meteorological State Agency of Spain (AEMET), Santa Cruz de Tenerife, 38071, Spain
Keywords: remote sensing, aerosol, AERONET, MODIS, Aerosol Optical Depth (AOD).
Presenting author email: yasmine@goa.uva.es

The present study establishes the first long-term characterization of aerosol seasonal variability over the northern continental region of the Iberian Peninsula, based on remotely sensed aerosol optical properties, with a focus on the Aerosol Optical Depth (AOD) and Ångström exponent (Alpha) parameters. This work uses direct Sun data from the AERONET-RIMA (Aerosol Robotic NETwork - Iberian Network for Aerosol Measurements) site of Palencia (Spain, 42N, 4.5W). This site can be considered as representative of the background atmospheric conditions of the "Castilla y León" region, and has one of the longest AERONET time series in Europe, starting back in 2003.

In this work, which is similar to that carried out for the AERONET-RIMA site of El Arenosillo (Bennouna et al., 2011), the annual cycle of the two parameters was built for the period 2003-2011, and the interannual variability during the whole period was also examined. The ability of satellite data to reproduce the seasonal patterns and anomalies was investigated using MODIS (Moderate Resolution Imaging Radiometer) aerosol products for Terra and Aqua corresponding to the same period. MODIS instantaneous fields were validated against ground-based sun photometer data, and the differences between monthly values were estimated.

The Palencia site is characterized by a mean daily AOD(440 nm) of 0.15±0.10 and an Alpha(440-870 nm) of 1.25±0.35, thus presenting values typical of a clean continental background. The seasonal pattern correspond to mid-high AOD values during a period starting in mid-spring to the end of the summer (max 0.19), and to a lower AOD during fall and winter months (min 0.09). Although the Alpha parameter is nearly constant throughout de year, the latter shows a slight increase in summer, which is correlated with the high AOD values. This might be explained by the frequent occurrence desert dust intrusions and recirculation processes that have the effect to trap pollutants and aged desert dust aerosols.

When using MODIS data, the overall results for Palencia give a higher AOD(470 nm) with 0.19±0.15 and a much lower Alpha (470-660 nm) of 0.70±0.20. The aforementioned numbers reflect substantial differences, with overestimations of the monthly means that can be almost double those of AERONET in the summer months. However MODIS satisfactorily reproduces the increase-decrease cycle in the AOD. These large differences tend to be more attributed to the aerosol models used in the MODIS algorithm rather than to the sampling difference between ground and satellite in this season. Despite the poor sampling in winter and the small AOD (<0.1) observed over the area, the best agreement between satellite and ground is found during this period. The seasonal pattern of the Ångström exponent derived from MODIS was found to be very different from that of AERONET, the former showing apparently no consistency with the latter. Given the aforementioned results and the fact that the AERONET Alpha value for 470-660 nm is 1.41±0.37 (wavelengths used in the comparison with MODIS), we can conclude that the Alpha derived from MODIS is not representative of the aerosol type characterizing this region of the globe.

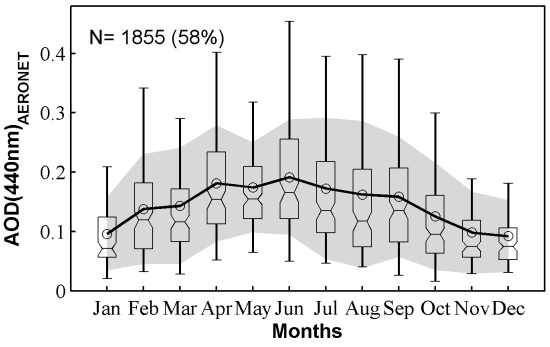

Figure 1: Monthly statistics of the daily AERONET AOD (440 nm) for 2003-2011. N is the total number of days with measurements.

Financial supports from the Spanish MICIIN (projects of ref. CGL2008-05939-CO3-01/CLI, CGL 2009-09740, and "Acción Complementaria" CGL2010-09480-E and CGL2011-13085-E), and from the Environmental Council of the CyL Regional Government (Consejería de Medio Ambiente, Junta de Castilla y León) are gratefully acknowledged.

Bennouna, Y. S., Cachorro, V. E., Toledano, C., Berjón, A., Prats, N., Fuertes, D., Gonzalez, R., Rodrigo, R., Torres, B., de Frutos, A., (2011) Comparison of atmospheric aerosol climatologies over southwestern Spain derived from AERONET and MODIS. *Remote Sensing of Environment* **115**, 1272–1284.

A first approach to study the aerosol indirect effect over Madrid by means of multiwavelength Raman lidar

A.J. Fernández, F. Molero and M. Pujadas
Department of Enviroment, CIEMAT, Madrid, 28040, Spain
Keywords: Lidar, Aerosol, Water vapour, Indirect effect
Presenting author email: alfonsoj.fernandez@ciemat.es

Atmospheric aerosols and water vapour play key roles in the atmospheric radiation budget as recent studies have shown (Wang et al., 2010). Water vapour is one of the most important absorbers of infrared radiation in the atmosphere, responsible for about sixty percent of the natural greenhouse effect. As regards atmospheric aerosols and according to the Intergovernmental Panel on Climate Change (IPCC), a cooling effect quantified by -0.5 W m^{-2} has been found when they act as scattering and absorption center of the incoming solar radiation, (the so-called direct effect) (Forster et al. 2007). In addition, aerosols also play an important role as cloud condensation nuclei which produce a latent heat exchange in the condensation process as well as an increase of the earth's albedo by clouds. This latest effect is known as indirect effect and quantified by -0.7 Wm^{-2}, nevertheless the IPCC still considers the indirect effect of aerosol the most uncertain component in forcing of climate change over the industrial period. Therefore further studies are required in order to improve the level of understanding of the interaction between aerosols and water vapour.

As the indirect effect occurs at altitudes where the atmospheric parameters reach cloud formation conditions, remote sensing systems are required to study this effect. Lidar techniques represent a powerful tool because of their capability to provide aerosol and water vapour profiles with high resolution both in time and vertical dimension. In this work we present the results obtained by the CIEMAT-Madrid Lidar system (Madrid Lidar station is integrated in EARLINET since 2005). This multiwavelength Raman Lidar system is based on a monostatic biaxial configuration and emits the fundamental, second and third harmonic of a Nd:YAG 30 Hz laser. The receiver is a 30-cm-diameter telescope with a multiwavelength detection module for the three elastic channels at 355, 532 and 1064 nm and three Raman channels at 387 and 607 nm (nitrogen Raman-shifted signals) and 408 nm (water vapour Raman-shifted signal). This experimental configuration has been designed for retrieving water vapor and aerosols properties with maximum accuracy in a maximum vertical range. The water profiles are determined by the ratio between the water vapour 355 nm-Raman-shifted signal and the nitrogen 355 nm-Raman-shifted signal (Whiteman et al., 1992) and are provided in mixing ratio units.

The calibration methodology has been based on the comparison between lidar profiles and radiosoundings launched from Barajas Airport, 15 km east of the lidar site. The influence of different synoptic situations occurred during these measurements are discussed.

Additional information on aerosol characteristics can be provided by multiwavelength lidars because the wavelength dependence of the backscatter and extinction coefficients allows to retrieve vertical profiles of microphysical properties of the aerosols (Müller et al., 2001). Backscatter-related and extinction-related Angstrom exponents provide information of the size of the observed particles. Lidar ratio, the ratio between the extinction and the backscattering coefficients obtained independently by the Raman lidar, characterizes the type of aerosol. Quantification of these aerosol microphysical and optical properties and their dependency on relative humidity is needed to reduce the large uncertainty associated with radiative forcing calculations.

Tropospheric aerosol microphysics and water vapour profiles are simultaneously investigated with unprecedent temporal and vertical resolution in different atmospheric situations. Several features of the profiles are discussed in this work, especially in situations when low-level water clouds are present. In these synoptic situations, the measurements provide relevant information about the role of aerosol properties in cloud-formation processes in the lower atmosphere.

The research leading to these results has received funding from the EU 7th Framework Programme (ACTRIS project, grant agreement n° 262254) and also from the MICINN (Spanish Ministry of Science and Innovation) under project CGL2010-17777.

Forster, P. *et al.* (2007) *Climate Change 2007: The Physical Science Basis*. Contribution of Working Group I to the Fourth Assessment Report of IPCC, edited by S. Solomon, 129–234, Cambridge Univ. Press. New York, USA.

Müller, D., U. Wandinger, D. Althausen, and M. Fiebig (2001) *Appl. Opt.* 40(27), 4863–4869

Wang, J., Cubison, M. J., Aiken, A. C., Jimenez, J. L., and Collins, D. R. (2010) *Atmos. Chem. Phys.*, 10, 7267-7283, doi:10.5194/acp-10-7267-2010

Whiteman, D. N. *et al*. (1992). *Appl. Opt*. 31 3068-3082.

Single scattering albedo and fine mode faction retrieved with AATSR satellite instrument

E. Rodríguez[1], P. Kolmonen[1], A-M Sundström[2], L. Sogacheva[1], T. Virtanen[1], G. de Leeuw[1,2,3]

[1]FMI, Climate Change Unit, Erik Palmen Aukio 1, 00101, Helsinki, Finland
[2]University of Helsinki, Dept. of Physics, Helsinki, Finland
[3]TNO, Utrecht, The Netherlands
Keywords: FMF. SSA, Satellite retrievals
Presenting author email: edith.rodriguez@fmi.fi

The Single Scattering Albedo (SSA) and the Fine Mode Fraction (FMF) are new retrieval products using the Advanced Along Track Scanning Radiometer (AATSR) satellite instrument. In addition to the Ångström Exponent (AE) which is a very sensitive parameter to measurement and modeling errors in the AOD retrieval, AATSR retrieves include now the FMF which is the contribution of the fine particles in the total AOD. We consider the FMF to be a more robust aerosol size describing parameter than the AE. The SSA and the FMF are obtained with a new method, based on Lookup Tables (LUT), for selected aerosol size distribution, with given refractive index. The LUTs are used together with the contribution in the AOD retrievals of absorbing and not absorbing aerosol particles. The SSA is retrieved at 659 nm. To validate the results two years of retrievals are compared with the SSA and the FMF retrieved from AERONET at level 2.0. The results are compared as well with the results obtained using some other satellite product like MODIS-Terra FMF and the fine mode AOD over land from Parasol. The SSA is compared with the Ozone Monitoring Instrument (OMI) products.

The Advanced Along Track Scanning Radiometer (AATSR), on board the ENVIronmental SATellite (ENVISAT), the successor of ATSR-2 (on board ERS-2), is designed mainly for monitoring land and sea surface temperatures. The special feature of the AATSR instrument is that it provides measurements at two viewing angles, a 55° forward one and about two minutes later a nadir one. This feature is used in the AATSR dual view (ADV) algorithm for aerosol retrieval over land to eliminate the surface contribution from measurements at the top of the atmosphere (TOA) reflectance. The ADV aerosol retrieval algorithm is based on the ATSR-2 algorithm that was initially developed by (Veefkind et al 1998, Veefkind et al 2000) and is described in Curier et al 2009. Hence, an additional surface reflectance model is not needed. The spatial resolution is approximately 1x1 km^2 at nadir and the swath width is 512 km. The AATSR instrument has seven wavelengths in the visible and infra-red regions, centered nominally at 0.555, 0.659, 0.865, 1.61, 3.70, 11.00, and 12.00 µm. At mid-latitudes the return time of AATSR is about three days, and to reach the global coverage takes about five days.

Preliminary results shows predominance of fine particles over Europe with influence of large particles over Spain and North Africa mainly related with dust events. The SSA from AERONET and AATSR has a good agreement between them when the particles are not strongly absorbing.

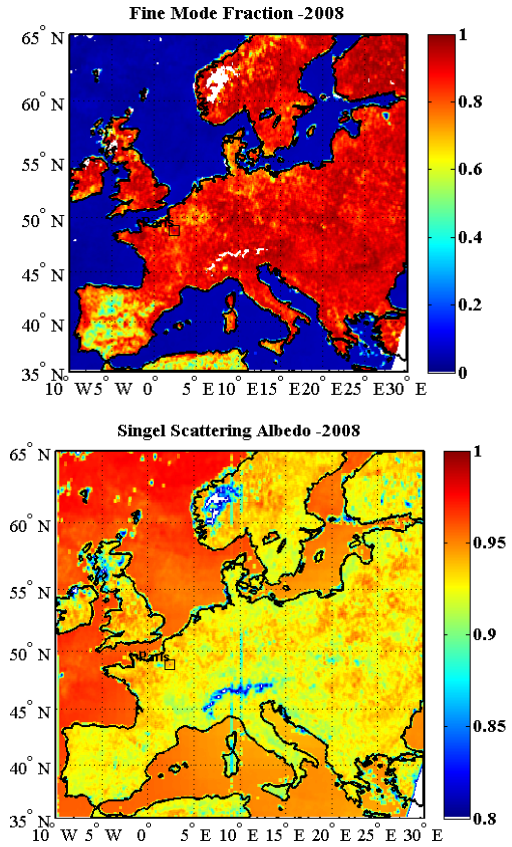

Figure 1. FMF (top) and SSA (bottom) retrieve with the AATSR satellite instrument over Europe in 2008 .

Curier, R.L., de Leeuw G., Kolmonen P., Sundström A-M., Sogacheva L., and Bennouna Y.S. (2009): *A.A. Kokhanovsky, G. de Leeuw Editors,Springer-Praxis pages, UK, 135--160.*

Veefkind, J.P., de Leeuw, G.D., and Durkee, P.A. (1998) *Geophys. Res. Lett., 25, 3135-3138.*

Veefkind, J.P., de Leeuw, G.D., Stammes, P., and *Koelemeijer, R.B.A. (2000) Sens. Environ., 74, 377—386.*

Optical and Microphysical properties from Raman lidar and depolarization data

F. Navas-Guzmán[1,2], L. Osterloh[3], C. Böckmann[3], M.J. Granados-Muñoz[1,2], and L. Alados Arboledas[1,2]
[1] Centro Andaluz de Medio Ambiente, Universidad de Granada, Junta de Andalucía, Granada, 18006, Spain
[2]Applied Physics Department, Universidad de Granada, Granada, 18071, Spain
[3]Institute of Mathematics, University of Potsdam, Potsdam, 14469, Germany
Keywords: Saharan dust aerosol, lidar, depolarization, microphysics
Presenting author email: fguzman@ugr.es

Studying the influence of non-spherical cloud and aerosol particles on the radiation budget of Earth's atmosphere is of growing importance in remote sensing. Saharan dust storms and volcanic eruptions, e.g., are main sources of non-spherical aerosol particles which are of importance for a better understanding of the direct and indirect climate effects of such global events. There exist essential differences in the light scattering behavior between spherical and non-spherical particles. For this purpose, we consider an ensemble of spheroidal particles characterized by the complex refractive index m, the aspect ratio a and the size parameter r of volume equivalent spheres. I.e., the aspect ratio is the additional microphysical parameter which goes beyond the conventional Mie theory. Such spheroidal particles are used as microphysical model in recent measurement campaigns like EARLINET, SPALINET and SAMUM to study the effect of non-spherical particles on different measurement scenarios and to estimate their influence on the radiative forcing, e.g. [1].

The inversion will be performed with the following data Γ_j : direct-polarization at 355, 532 and 1064 nm and cross-polarization backscatter at 532 nm as well as extinction at 355 and 532 nm (3+1+2 wavelengths λ). We can write this with the particular efficiencies Q_j and surface S as

$$\Gamma_j(\lambda) = \int_{a_{\min}}^{a_{\max}} \int_{r_{\min}}^{r_{\max}} \frac{3S}{16\pi r^3} Q_j(r,\lambda,m,a) v(r,a) \mathrm{d}r\mathrm{d}a.$$

Thus, we are looking at two-dimensional distributions. In this work we present an analysis of a Saharan dust event detected from 2 to 8 April 2011 over Granada, Southern Iberian Peninsula. The event has been monitored with both active and passive remote sensing instrumentation. Back-trajectories analysis indicates air masses coming from North Africa fundamentally. In addition, NAAPS and DREAM models forecast the presence of a mineral dust plume over Southern Iberian Peninsula. Extensive and intensive vertically resolved aerosol properties were obtained from multiwavelenght Raman lidar during the night on 7 April 2011. Particle volume depolarization ratio at 532 nm reached values around 15 % (Fig. 1). Angström exponent values were close to zero.

Note that we are implying spheroidal particles here, with moderate aspect ratios between 0.67 and 1.5. We do not have a physical or meteorological justification for that; the results do look promising though, as in our experience, data not fitting the model will neither lead to

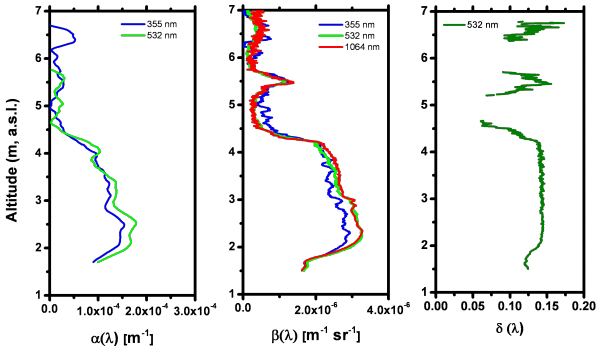

Figure 1: Optical profiles, April 07, 2011, 20:30 UTC.

diagonal structures in the refractive index grids nor to roughly lognormal distributions in the particles. The retrieval of the refractive index grid resulted in a distinct diagonal structure with a sharply defined minimum around $m = 1.4 + 0.01\mathrm{i}$ (not shown here). In the distribution retrieved, there seem to be two distinct modes; first, there is a mode of roughly spherical particles of about 0.5 μm in size, and another mode of larger prolate particles, [2]. The retrieved microphysical properties can be found in Table 1. A total effective radius around 1 μm was found for this layer. This value is higher than the obtained during late afternoon by means of sun-photometer inversion (0.6 μm). This discrepancy could be explained by the fact that whole column sun-photometer measurements could be affect by anthropogenic particles at lower altitudes, this will cause a shift of columnar total effective radius to smaller sizes.

$\Re(m)$	$\Im(m)$	r_{eff} μm	a_t $\mu\mathrm{m}^2\mathrm{cm}^{-3}$	v_t $\mu\mathrm{m}^3\mathrm{cm}^{-3}$
1.4	0.01	1	249	85
v^{oblate}	v^{sphere}	v^{prolate}	mean: μ_a	width: σ_a
22%	34%	44%	1.06	0.27

Table 1: Microphysical properties of layer 2000-2500 m.

This work was supported by the Andalusia Regional Government through projects P08-RNM-3568 and P10-RNM-6299, by the Spanish Ministry of Science and Technology through projects CGL2010-18782, CSD2007-00067 and CGL2011-13580-E/CLI; and by EU through ACTRIS project (EU INFRA-2010-1.1.16-262254).

[1] Otto, S., Bierwirth, E., Weinzierl, B., Kandler, K., Esselborn, M., Tesche, M., Schladitz, A., Wendisch, M., and Trautmann, T., (2008) Tellus B **61(1)**, 270-296.

[2] Osterloh, L. (2011), PhD thesis Potsdam University.

Towards a remote sensing tool for aerosol hygroscopicity studies combining lidar and passive microwave radiometry

F. Navas-Guzmán[12], J. Bravo-Aranda[12], M.J. Granados-Muñoz[12], J.L. Guerrero-Rascado[12], J. Fernández-Gálvez[12] , A.J. Fernández[3] and L. Alados-Arboledas[12]

[1] Centro Andaluz de Medio Ambiente, Universidad de Granada, Junta de Andalucía, Granada, 18006, Spain
[2] Department of Applied Physic, University of Granada, Granada, 18071, Spain
[3]Centro de Invest. Energéticas, Medioamb. Y Tecn. (CIEMAT), Avda. Complutense, 22. Madrid, 28040, Spain
Keywords: Relative humidity, Raman lidar, microwave radiometer.
Presenting author email: fguzman@ugr.es

The importance of atmospheric aerosols for the Earth's climate has been widely recognized. They affect solar radiation and hence climate directly by scattering radiation back to space, but also indirectly by acting as cloud condensation nuclei (Twomey, 1974). An important factor affecting the role aerosols play in climate change is their hygroscopicity. Although numerous studies have investigated the relationship between aerosol scattering and relative humidity (RH) from in-situ techniques (e.g., McInnes et al. 1998) remote sensing techniques provide the opportunity to investigate hygroscopic growth of aerosols beyond this RH range, under ambient atmospheric conditions and without perturbing the sampled air.

By virtue of its ability to provide both high spatial and temporal resolution measurements of water vapour throughout much of the troposphere, Raman lidar has emerged in recent years as a potential tool for providing the detailed water vapour profiles required for modelling the complicated processes occurring in the troposphere. However, most of these systems are unable to provide RH profiles due to necessity of simultaneous temperature and water vapour mixing ratio profiles.

This work presents an alternative procedure to obtain RH profiles from two instruments, microwave radiometer and Raman lidar. The study has been developed at Andalusian Center for Environmental Studies (CEAMA), located in South-eastern Spain in the urban area of Granada (37.18ºN, 3.58ºW and 680 m asl). A Raman lidar LR331D400 (Raymetrics S.A.) included in EARLINET was used to retrieve mixing ratio profiles during night time. This information was combined with continuous tropospheric temperature profiles measured by a ground-based multifrequency passive microwave radiometer (RPG-HATPRO, Radiometer Physics GmbH). Additionally, air pressure profiles were estimated assuming standard atmospheric conditions. All these information allowed us to retrieve RH profiles.

A radio-sounding campaign was carried out in our station during summer and autumn in 2011. A total of six launches performed during night-time were used to calibrate lidar water vapour vertical profiles. Besides, these data allowed us to compare the RH profiles derived from Raman lidar and microwave radiometer and those retrieved from radiosondes.

Figure 1 shows an example where RH and temperature profiles are presented. The result shows a good agreement between the RH profile retrieved from lidar and microwave radiometer and that obtained by radiosonde. The biggest discrepancies were found around 3.4 m (asl), where radiosonde reaches RH values around 15% bigger than those retrieved from Raman lidar and microwave radiometer. These bigger differences in RH are due to the deviation between the temperature measured with the radiosonde and those retrieved from microwave radiometer. However, the agreement in the rest of the RH profiles is quite good and the relative differences are below 10 %. These results show the capacity to obtain RH profiles from Raman lidar and microwave radiometer with a high temporal and spatial resolution allowing us perform hygroscopic growth studies.

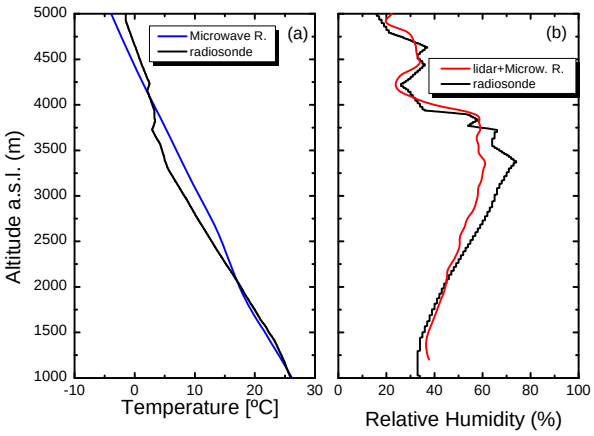

Figure 1. Nighttime measurements performed on 25 July 2011. (a) Temperature profiles from microwave radiometer and radiosonde. (b) RH profile obtained from lidar-microwave radiomenter and radiosonde.

Aknowledgments: This work was supported by the Andalusia Regional Government through projects P08-RNM-3568 and P10-RNM-6299, by the Spanish Ministry of Science and Technology through projects CGL2010-18782, CSD2007-00067 and CGL2011-13580-E/CLI; and by EU through ACTRIS project (EU INFRA-2010-1.1.16-262254)

McInnes, L. *et al*. (1998), *Geophys. Res. Lett.*, **25**, 513-516.
Twomey, S. (1974), *Atmos. Environ.*, **8**, 1251-1256.

A first estimation of aerosol radiative forcing at Málaga (Spain) through the direct method

I. Foyo-Moreno[1,2], I. Alados[1,3], H. Lyamani[1,2], F.J. Olmo[1,2] and L. Alados-Arboledas[1,2].

[1]Centro Andaluz de Medio Ambiente, Universidad de Granada, Junta de Andalucía, Granada, 18006, Spain.
[2]Department of Applied Physic, University of Granada, Granada, 18071, Spain.
[3]Department of Applied Physic, University of Málaga, 29071, Spain.
Keywords: aerosol, aerosol radiative forcing, aerosol radiative forcing efficiency
Presenting author email: ifoyo@ugr.es

In this work we study the aerosol radiative forcing (ARF) at Málaga, a coastal location in the Western Mediterranean (36.72ºN, 4.5ºW, 40 m a.s.l) using the direct method (Satheesh and Ramanathan, 2000). In this method the knowledge of the net flux free of aerosols is not required. Others authors have also employed this method recently (Di Biagio et al., 2010; Antón et al., 2011). The analysis uses measurements gathered from January 2009 to December 2010. Columnar aerosol properties were measured by a CIMEL sun photometer included in the AERONET network (Holben et al., 1998). Measurements of global irradiance to calculate the surface net flux have been provided by AEMET.

The aerosol optical depth (AOD) at 440 nm shows values ranging from 0.21 ± 0.10 in summer to 0.11 ± 0.07 in winter, indicating larger aerosol loading during summer than in winter. The seasonal variation of the Angström exponent (α) also shows an evident seasonal cycle but opposite to that of AOD, ranging from 1.1 ± 0.4 in winter to 0.8 ± 0.3 in summer, indicating the dominance of fine particles during winter.

In order to classify additional aerosol properties using AOD measurements, we have followed the framework considered by Gobbi et al. (2007). Figure 1 shows the results. It can be seen the low variability of radius for fine mode (average value close to 0.11 μm), contributing less than 70% by AOD for cases with low AOD. Values with high AOD (AOD>0.7) and lowest α (α<0.5), corresponding to r_f~0.2 μm, showed AOD contributions of the fine mode lower than 35%. This fact indicates the predominance of coarse particles at the site for high AOD. So, it is evident the great influence of the Sahara dust particles at Málaga.

ARF estimations have been done using the direct method to compute the aerosol surface shortwave forcing efficiency (AFE), which is the ARF produced by atmospheric aerosol with AOD equal to 1. Direct measurements of A at Málaga are not available. Taking into account estimates obtained by AERONET network for the two years we have used an average value of 0.14 independently of solar zenith angle (θ_o).

Table 1 shows the retrieved values of AFE for the solar zenith angle intervals considered. We have observed a lower efficiency as increasing solar zenith angle. At 500 nm, the AFE show values close to -(210±20) W/(m^{2}δ) for low solar zenith angles. At Lampedusa, a Mediterranean island, Di Biagio et al. (2009) found AFE values (θ_o= 20º, 495.7 nm) ranging from -250 to -170 W/(m^{2}δ) -rely on the aerosol type-, with a mean value of -210 W/(m^{2}δ).

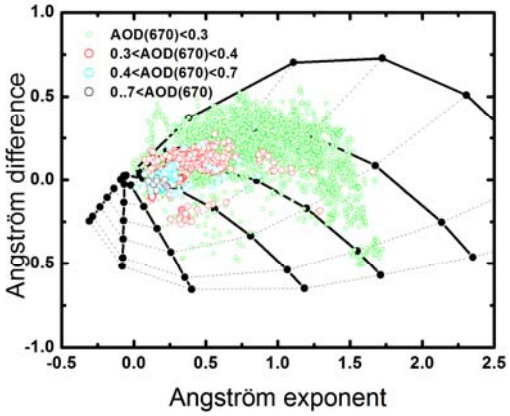

Figure 1. Angstrom exponent difference, α=(440, 675)−α(675, 870), as a function of α (440–870 nm) and AOD at Málaga

Then the value of ARF is derived multiplying AFE by the corresponding value of AOD.

Table 1. Values of AFE for different solar zenith angles

Solar zenith angle (º)	AFE ± σ (Wm^{-2}δ^{-1})
15º≤θ_o<25º	(-210±20)
25º≤θ_o<35º	(-150±20)
35º≤θ_o<45º	(-120±20)

Aknowledgments: This work was supported by the Andalusia Regional Government through projects P08-RNM-3568 and P10-RNM-6299, by the Spanish Ministry of Science and Technology through projects CGL2010-18782, CSD2007-00067 and CGL2011-13580-E/CLI; and by EU through ACTRIS project (EU INFRA-2010-1.1.16-262254). The global solar irradiance values were kindly provided by AEMET.

Antón, M., et al. (2011). *J. Geophys. Res.*, 116, D20214.
Di Biagio, C., et al. (2009). *J. Geophys. Res.*, 114, D06211. doi: 10.1029/2008JD011037.
Di Biagio, C., et al. (2010). *J. Geophys. Res*., 115, D10209. doi:10.1029/2009JD012697.
Gobbi et al., 2007. Atmos. Chem. Phys.,7, 453-458.
Holben, B.N., et al. (1998). *Remote Sens. Environ*., 66 (1), 1-6.
Satheesh, S.K, and V. Ramanathan (2000), *Nature* 405, *60-63,* doi: 10.1038/35011039.

Cloud screening and quality control algorithms for star photometry.

D. Pérez-Ramírez[1,2,3], H. Lyamani[1,2], F.J. Olmo[1,2], D.N. Whiteman[3], F. Navas-Guzmán[1,2] and L. Alados-Arboledas[1,2].

[1]Centro Andaluz de Medio Ambiente (CEAMA), Universidad de Granada, 18006,Granada, Spain
[2]Departamento de Física Aplicada, Universidad de Granada, Campus de Fuentenueva s/n, 18071,Granada, Spain
[3] Mesoscale Atmospheric Processes Laboratory, NASA Goddard Space Flight Center, Greenbelt,Maryland, 20771, United States
Presenting author email: dperez@ugr.es
Keywords: Atmospheric Aerosol

The fourth Intergovernmental Panel on Climate Change notes the importance of studying the atmospheric aerosol radiative effects to fully understand its role on climate change. To characterize aerosol columnar effects, passive remote sensing techniques are widely used. This techniques take advantage of the modification of the radiative field due to the atmospheric aerosol.. During the last decades, sun photometry has been developed considerably, and the international network AERONET has been established to study day-time columnar aerosol properties worldwide. This last network has established and standardized the measurement protocol, data processing and quality control of data (Smirnov et al., 2000). Currently, columnar aerosol properties at night-time are poorly known, and their studies are taking an ongoing interest, which include the development of appropriate instrumentation to fill the night-time gaps in large temporal observations that rely on the sun. In this sense, different approaches have been developed using the moon (Berkoff et al., 2011) or the stars (Perez-Ramirez et al., 2008).

As for sun photometry, one of the critical points of star photometry measurements for aerosol characterization is the separation between cloud-affected and cloud-free data. In principle, human observers can detect clouds based on subtle textural and spatial patterns. But the development of automatic instruments posed the problem of defining an effective and automatic cloud-screening procedure.

This work present the development and set up of a cloud screening and data quality control algorithm for a star photometer based on CCD camera as detector. This kind of algorithms is necessary for passive remote sensing techniques to retrieve the columnar aerosol optical depth, $\delta_{Ae}(\lambda)$, and precipitable water vapor content, W, at night-time. This cloud screening procedure consists of calculating moving averages of $\delta_{Ae}(\lambda)$ and W under different time-windows combined with a procedure for detecting outliers. Additionally, to avoid undesirable $\delta_{Ae}(\lambda)$ and W fluctuations caused by the atmospheric turbulence, the data are averaged on 30 minutes. The algorithm is applied to the star photometer deployed in the city of Granada (37.16°N, 3.60°W, 680 m a.s.l; South-East of Spain) for the measurements acquired between March 2007 and September 2009.

The algorithm is evaluated with correlative measurements registered by a lidar system and also with all-sky images obtained at the sunset and sunrise of the previous and following days. Figure 1 shows an example of the cloud screening procedure presented. After applying the moving averages procedure for all-night-window, many data are eliminated (Figure 1a). Figure 1b shows the final day and night time evolution for $\delta_{Ae}(\lambda)$ and the Angström parameter. Some all-sky images are shown at sunrise.

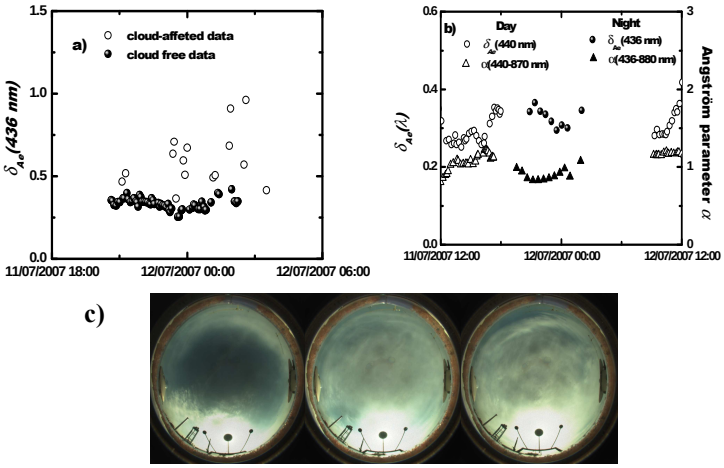

Figure 1: Application of the cloud screening algorithm proposed for the data acquired on 11 and 12 July 2007. All-sky images are also presented.

Promising results are obtained detecting cloud-affected data. Additionally, the cloud screening algorithm has been evaluated under different aerosol conditions including Saharan dust intrusion, biomass burning and pollution events.

This work was supported by the Spanish Ministry of Science and Technology through projects CGL2008-01330-E/CLI (Spanish Lidar Network), CGL2010-18782, CGL2011-13580-E/CLI and CSD2007-00067; by the Andalusian Regional Government through projects P10-RNM-6299 and P08-RNM-3568; and by the EU ACTRIS project (EU INFRA-2010-1.1.16-262254).

Berkoff, T.A. et al., (2011), Journal of Atmospheric Ocean and Technology, 28, 1294-1306.
Pérez-Ramírez, D., et al., (2008) *Atmospheric Environment*, 42, 2739-2745.
Smirnov, A., et al., (2000), *Remote Sensing of Environment,* 73, 337-349.

Mixing height from passive remote sensing at high temporal resolution

J.Fernández-Gálvez[1,2], M.J. Granados-Muñoz[1,2], F.J. Olmo[1,2] and L. Alados-Arboledas[1,2]

[1]Centro Andaluz de Medio Ambiente (CEAMA), Universidad de Granada, 18006 Granada, Spain
[2]Departamento de Física Aplicada, Universidad de Granada, 18071 Granada, Spain

Keywords: mixing height, ground-based microwave radiometry, monitoring
Presenting author email: jesusfg@ugr.es

Inputs of aerosol particles and gases from the surface into the atmosphere disperse horizontally and vertically. The mixing height determines the available volume for pollutant dispersion and therefore plays an important role in climate modelling and air pollution. It depends on meteorological parameters, surface turbulent fluxes and physical parameters, and follows a diurnal cycle. Determination of the mixing layer height is not direct but indirect estimates are possible from atmospheric profile measurements. A number of methodologies are already developed depending on the available information (Holzworth, 1964; Vogelazang et al., 1976; Morille et al., 2007) but due to limitations in atmospheric monitoring, continuous values of the mixing height are not easily available. This work shows first results from continuous high temporal resolution estimates of the mixing height over Granada.

Passive microwave remote sensing allows continuous temperature and humidity profiles for nearly all weather conditions under no supervision, representing an advantage to active sensors from the operational point of view. Although temporal resolution is high, passive remote sensing has lower vertical resolution than both radiosounding and active remote sensing.

A ground-based passive microwave radiometer (RPG-HATPRO, Radiometer Physics GmbH) has been used for continuous mixing height estimates under conditions established by the parcel method (Holzworth, 1964). The methodology determines the mixing height as the equilibrium level of a hypothetical rising parcel of air representing a thermal. Surface temperature is independently monitored from a meteorological station located next to the microwave radiometer. Continuous profile measurements are available since October 2010 and an automatic algorithm is capable for monitoring mixing height automatically. Nevertheless, a high uncertainty in the mixing height may result in situations without a pronounced inversion at the convective boundary layer top.

The vertical resolution of the microwave radiometer decreases with height then, when the determination of the mixing height is possible, the maximum error in its estimate is lower than 100 m. Profile data are available every 15 minutes and also the mixing height. Figure 1 shows the temporal evolution of the mixing layer height together with the surface temperature for two representative days in summer and winter. In summer, strong convective conditions promote the growth of the mixing height from early morning to late afternoon, with maximum mixing height about 1800 m agl between 10:30 and 16:30 UTM. During winter time, temperature inversions dominate the rate of growth of the mixing layer and maximum heights are lower than in summer time. Particularly for 8 February 2011 the mixing height rises from around 10:00 to 17:00 UTM with a maximum height of 1500 m agl. After surface temperature start to decrease convective conditions disappear and the mixing layer drops.

The capability of this methodology allows a detailed analysis of the daily evolution of the mixing layer height with applications in a large number of disciplines.

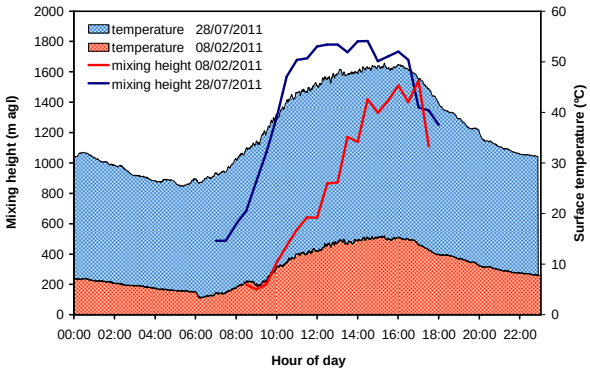

Figure 1. Temporal evolution of the mixing height and surface temperature for two representative days in summer and winter 2011.

This work was supported by the Andalusia Regional Government through projects P08-RNM-3568 and P10-RNM-6299; by the Spanish Ministry of Science and Technology through projects CGL2010-18782, CSD2007-00067 and CGL2011-13580-E/CLI; and by EU through ACTRIS project (EU INFRA-2010-1.1.16-262254).

Holzworth, C.G. (964) *Mon. Weather Rev.* **92**, 235–242.
Morille, Y., Haeffelin, M., Drobinski, P. and Pelon, J. (2007) *J. Atmos. Ocean. Tech.* **24**, 761–775.
Vogelezang, D.H.P. and Holtslag, A.A.M. (1976) *Bound. Lay. Meteorol.* **81**, 245-269.

EARLINET and the international ChArMEx and PEGASOS measurement campaigns in summer 2012

L. Mona[1], M. Sicard[2], A. Amodeo[1], A. Apituley[3], L.Alados- Arboledas[4], D. Balis[5], C. Böckmann[6], A. Chaikovsky[7], A. Comeron[2], G. D'Amico[1], F. De Tomasi[8], V. Freudenthaler[9], A. Giunta[1], I. Grigorov[10], M. Haeffelin[11], M. Iarlori[12], H. Linnè[13], M. McAuliffe[14], F. Molero[15], V. Mitev[16], D. Nicolae[17], N.Papagiannopoulos[1], A. Papayannis[18], M.R. Perrone[8], A. Pietruczuk[19], M. Pujadas[15], J.-P. Putaud[20], V. Rizi[12], F. Rocadenbosch[2], V. Simeonov[21], N. Spinelli[22], K. Stebel[23], T. Trickl[24], U. Wandinger[25], X. Wang[22], F. Wagner[26], M. Wiegner[9] and G. Pappalardo[1]

[1]Istituto di Metodologie per l'Analisi Ambientale, CNR, Tito Scalo, Potenza, I-85010, Italy
[2]RSLab – IEEC-CRAE, Universitat Politècnica de Catalunya, Barcelona, Spain
[3]KNMI - Royal Netherlands Meteorological Institute, De Bilt, The Netherlands
[4]Universidad de Granada, Granada, Spain
[5]Aristoteleio Panepistimio, Thessalonikis, Greece
[6]Institut für Mathematik der Universität Potsdam, Germany
[7]Institute of Physics, National Academy of Sciences, Minsk, Bjelarus
[8]Università del Salento, Department of Physics, Lecce, Italy
[9]Ludwig-Maximilians-Universität, München, Germany
[10]Institute of Electronics, Bulgarian Academy of Sciences, Sofia, Bulgaria
[11]Université Pierre et Maris Curie-Institut Pierre Simon Laplace, Paris, France
[12]Università degli Studi dell'Aquila - Dipartimento di Fisica - CETEMPS, L'Aquila, Italy
[13]Max-Planck-Institut für Meteorologie, Hamburg, Germany
[14]Physics Department University College Cork, Cork, Ireland
[15]Centro de Investigaciones Energéticas, Medioambientales y Tecnológicas, Madrid, Spain
[16]CSEM, Centre Suisse d'Electronique et de Microtechnique SA, Neuchâtel, Switzerland
[17]National Institute of R&D for Optoelectronics, Magurele-Bucharest, Romania
[18]National Technical University of Athens, Department of Physics, Athens, Greece
[19]Institute of Geophysics, Polish Academy of Sciences, Warsaw, Poland
[20]EC Joint Research Centre, Ispra, Italy
[21]Ecole Polytechnique Fédérale de Lausanne, Switzerland
[22]Consorzio Nazionale Interuniversitario per le Scienze Fisiche della Materia, Napoli, Italy
[23]Norwegian Institute for Air Research (NILU), Kjeller, Norway
[24]Karlsruher Institut für Technologie, Garmisch-Partenkirchen, Germany
[25]Institut für Troposphärenforschung, Leipzig, Germany
[26]Universidade de Évora, Centro de Geofísica de Évora, Évora, Portugal

Keywords: profiling, remote sensing, optical properties.
Presenting author email: mona@imaa.cnr.it

Two international measurement campaigns are planned for the summer 2012: ChArMEx (The Chemistry-Aerosol Mediterranean Experiment) pre-campaign planned from June 8 to July 12 and PEGASOS (Pan-European Gas-AeroSOls-climate interaction Study) campaign using the Zeppelin airship planned in two phases from June 8 to July 2 in Po-valley and France and possibly Eastern Europe and 3-9 July over Bologna and surrounding regions [http:// http://charmex.lsce.ipsl.fr/; http://pegasos.iceht.forth.gr/].

On the one hand, the main objective of the ChArMEx pre-campaign is the characterization of dynamic processes of exportation of contaminated air masses from source regions around the Mediterranean coast and the quantification of the exchanges between the boundary layer and the free troposphere above the Mediterranean Basin. On the other hand, PEGASOS campaign goal is to provide detailed measurements of HO_x, trace gases and aerosols throughout the PBL in certain regions. The main focus of the campaign is the boundary layer chemistry (0-3000 m). EMEP (European Monitoring and Evaluation Programme) is also planning an intensive measurement campaign from June 8 to July 17 in coordination with the PEGASOS campaign. The main focus of the EMEP intensive campaign in 2012 is aerosols in terms of PM and chemical speciation (EC/OC, inorganic aerosols and minerals).

Besides measurements performed by EARLINET (www.earlinet.org) stations accordingly to EARLINET schedule, additional measurements will be performed at certain sites during these international campaigns accordingly to specific atmospheric conditions and in support to aircraft measurements. EARLINET lidar measurements will provide the needed additional information about aerosol vertical profiling and aerosol typing. Furthermore some EARLINET stations will participate in an exercise of lidar data assimilation in an air quality model.

The financial support by the European Community through the ACTRIS Research Infrastructure Action under the 7th Framework Programme under ACTRIS Grant Agreement n° 262254 is gratefully acknowledged.

Climatology of aerosol optical properties over a tropical –urban location in western India

G. R. Aher and G. V. Pawar

Physics Dept., Nowrosjee Wadia College, Pune (India), 411 001, +91(020) 26162944, +91(020) 26163108,

Keywords: Aerosol optical thickness, Angstrom Exponent, turbidity coefficient.
Presenting author: aher.g.r@gmail.com.

Atmospheric aerosols of natural and anthropogenic origin contribute substantially to global climate variability (IPCC, 2007). Changes in the columnar content of aerosols constitute a major forcing mechanism affecting the radiative balance of the climate system. Understanding of the regionally dependent aerosol optical properties and their spatio-temporal distribution is required for the accurate evaluation of aerosol effects in the climate system. Long term measurements of aerosol optical thickness and Angstrom exponent were analyzed and compiled into aerosol optical properties climatology for tropical–urban location, Pune in western India. Monitoring of aerosol parameters have been made by operating multiple wavelength solar radiometer (MWR) and MICROTOPS-II Sunphotometer on cloudless clear sky days during the period 1998- 2011. The observing season normally spans over December to May months in a year. This formed the core source of database in the present study.

Results show that the seasonal variation of the aerosol optical thickness at 500 and 1020 nm are characterized by low values during winter and high values during pre-monsoon (Fig.1). It is found that the long term mean AOT at 500 nm ranged between 0.61±0.13 during winter and 0.67±0.14 whereas the corresponding range for AOT values at 1020 nm is found to 0.36±0.12 and 0.51±0.17. The pre-monsoon increase is found to be due to the high wind speed producing larger amount of wind driven dust particles. The winter AOT values decrease more at larger wavelengths indicating a general reduction in the number of bigger particles. The quantity of AOT values in pre-monsoon is higher (low during winter) for wavelength, such as near infra-red (NIR), which shows that coarse particles contribute more compared with sub-micron particles.

The Angstrom exponent (α), which represents the particle size distribution and the turbidity coefficient (β), which represents the aerosol loading, are almost opposite to each other which implies higher values of β are associated with smaller value of α (Kumar et al., 2009). In the present case, inverse relationship between α and β is found with a correlation coefficient assuming a value equal to 0.99. Thus, low exponent α values are associated with high β values and vice versa. This indicates that as aerosol loading increases, the relative dominance of fine-mode aerosol decreases. In other words, the increase in loading is due to more increase in coarse-mode aerosol loading. The overall mean value of the Angstrom size exponent (α) at this location is 0.47 and the mean turbidity coefficient is 0.48. The value of α is higher in winter season compared to the pre-monsoon season which indicates the presence of coarse-mode aerosol particles.

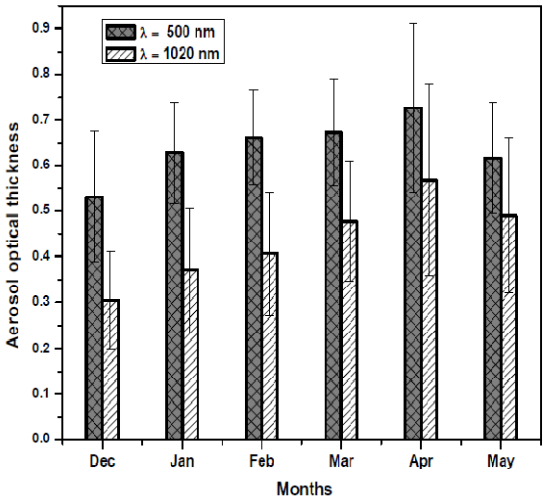

Fig. (1): Multiyear monthly mean variation of aerosol optical thickness during 1998-2011 at Pune

This work was supported by the Indian Space Research Organization under the joint programme of ISRO and Pune University.

IPCC, 2007. Climate change 2007: The Physical Science Basis. Contribution of Working Group 1 to the Fourth Assessment Report of the IPCC, Cambridge University Press, Cambridge, UK.

Kumar, K.R et al., (2009a). *Science of the Total Environment,* **407**, 2673-2688.

Calibration and intercomparison results in the Spanish network on environmental DMAs

F. J. Gómez-Moreno[1], B. Artíñano[1], V. Juncal Bello[2], M. Piñeiro Iglesias[2], P. López Mahía[2], N. Pérez[3], J. Pey[3], A. Alastuey[3], B. A. de la Morena[4], M. I. García[5], S. Rodríguez[5], M. Sorribas[6,7], G. Titos[6,7], H. Lyamani[6,7] and L. Alados-Arboledas[6,7]

[1]Department of Environment, CIEMAT, Madrid, E-28040, Spain
[2]Institute of Environment, University of A Coruña (IUMA-UDC), A Coruña, E-15179, Spain
[3]Institute of Environmental Assessment and Water Research (IDAEA-CSIC), Barcelona, E-08034, Spain
[4]Atmospheric Sounding Station 'El Arenosillo', INTA, Mazagón-Huelva, E-21130, Spain
[5]Izaña Atmospheric Research Centre, (IARC/CIAI), AEMet, Santa Cruz de Tenerife, E-38001, Spain
[6] Andalusian Environmental Centre (CEAMA), University of Granada, E-18071 Granada, Spain
[7]Applied Physics Department, University of Granada, E-18071 Granada, Spain
Keywords: Atmospheric aerosols, Particle size distribution, DMA, SMPS
Presenting author email: fj.gomez@ciemat.es

There are currently six groups in Spain involved in the measurement of atmospheric particle size distributions by means of Differential Mobility Analyzers (DMAs). These groups are: IUMA-UDC, IDÆA-CSIC, INTA, IARC-AEMET, University of Granada and CIEMAT. All the groups have to solve many common problems related with the instrumentation required for this type of measurements. For this reason, the Spanish network on environmental DMA (Red Española de DMAs Ambientales, REDMAAS) has been working during 2010-2011 (Gómez-Moreno et al., 2011). The REDMAAS has as main objective the cooperation between the groups, which will lead to solve common problems and to optimize their facilities and protocols. In this work, the main results obtained during these two years will be discussed.

The main activities developed in the network include: DMA calibration; CPC, SMPS and UFP intercomparison; measurement quality control program; losses in sampling lines; support for the radioactive facility license; webpage; and new DMA applications. In the current work, we show the results obtained in the calibrations and intercomparison performed this last year 2011.

Four DMA calibrations have been checked. First, it was necessary to check the DMA (sample, sheath and excess) and CPC (monodisperse) flow rates and then, a monodisperse aerosol, latex, was introduced into the DMA to calibrate the electrical mobility. Two particles sizes have been selected: 80 and 190 nm. In the case of the first particle size, the instruments measured 80 nm, with a -2.3-0.6% deviation, except one of the instruments with 5.8%. The second particle size gave a deviation of 0-2.8%, with the same exception again 9.3%. There is a clear shift in the calibration of one of the instruments. This result shows the need for an environmental DMA network.

A field intercomparison exercise was performed during October 2011 in the INTA facilities (El Arenosillo, Huelva). There were 4 complete SMPS systems, an UFP and two additional CPCs. After calibrating all the flow rates and the DMAs, a CPC intercomparison was performed, see figure 1. The main result obtained was that the CPC3022 was measuring properly concentrations below 10^4 cm^{-3}, but above this value the counter uses the photometric mode which was clearly uncalibrated.

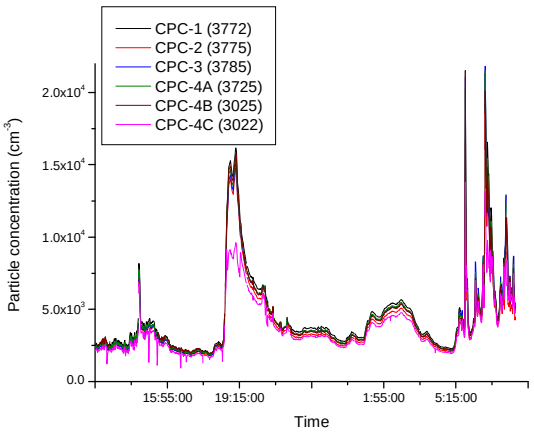

Figure 1. CPC intercomparison

The four SMPS systems and an UPF were compared. As during the 2010 field intercomparison, different concentrations were measured for the nucleation mode, depending on the sheath flow rate. Taking into account the diffusion correction included in the TSI software, these differences were reduced very much.

This network is financed by the Ministry of Science and Innovation (CGL2011-15008-E).

Gómez-Moreno, F. J., Sastre, M., Artíñano, B., Juncal Bello, V., Piñeiro Iglesias, M., López Mahía, P., Pey, J., Ripoll, A., Alastuey, A., Sorribas, M., Fernández, M., de la Morena, B. A., Trujillo de Cabo, J. L. and Rodríguez, S. (2011) *European Aerosol Conference,* 4P291, Manchester.

Influence of the thermophoresis on aerosol deposition on warm urban surfaces

P. Roupsard[1], D. Maro[1], A. Coppalle[2], H. Branger[3], O. Connan[1], D. Hébert[1] and B. Letellier[1]

[1]Laboratoire de Radioécologie de Cherbourg-Octeville, IRSN, 50130 Cherbourg-Octeville, France
[2]COmplexe de Recherche Interprofessionnel en Aérothermochimie, UMR 6594, 76801 Saint-Etienne du Rouvray, France
[3]Institut de Recherche sur les Phénomènes Hors Equilibre, UMR 7342, CNRS, 13384 Marseille, France
Keywords: dry deposition, deposition velocity, thermophoresis, urban areas, submicron particles
Presenting author email: pierre.roupsard@irsn.fr

In the case of an accidental or chronic atmospheric pollution by a nuclear plant, aerosols' deposition transfer coefficients must be known. A major issue is to determine the impact of aerosols contained in the radioactive plume on urban areas with the smallest uncertainties. In this case, deposition must be determined locally in urban canopy. In dry atmospheric conditions, transfer coefficients are defined by the dry deposition velocity V_d (m s^{-1}) which is defined by the ratio between the aerosol dry deposition flux (particles m^{-2} s^{-1}) and the concentration of aerosols (particles m^{-3}). Commonly, dry deposition is considered dependent on aerosol diameter, atmospheric turbulent conditions and deposit surface type. Recently, Maro *et al.* (2010) have observed diminution of submicron aerosol deposition on urban surfaces warmed by the sun during the French Salifa-Primequal experimental campaign. Their results show clearly, and for the first time, the influence of thermophoresis on dry deposition on urban surfaces. Thus, in the frame of our *in situ* submicron aerosol deposition experiments on urban surfaces, a particular interest falls on the quantification of the thermophoresis effect for different surfaces and atmospheric conditions. In parallel, a wind tunnel study has been conducted. Dry deposition velocity of a submicron aerosol has been measured both in wind tunnel and *in situ*, in function of temperature difference between air and warmed surface and wind speed.

Studied submicron aerosol was a monomodal polydispersed fluorescein aerosol (d_p = 0.27 µm), already used by Roupsard *et al.* 2011. This aerosol was taken for both wind tunnel and *in situ* experiments. Wind tunnel experiments were conducted in the IRPHE closed-circuit wind tunnel (8.7 m x 0.7 m x 0.3 m). The tunnel was equipped with a heating board (1.8 m x 0.7 m) at its centre. The bottom of the tunnel was alternatively recovered with each studied surface from the entrance of the tunnel to the end of the heating board. Studied surfaces were horizontal glass (smooth) and horizontal cement facing (rough). Deposition fluxes were sampled with squares substrates (200 mm x 200 mm) made in the studied surface. We used two filter sampling units to measure aerosol concentration in the wind tunnel. One was located 10 mm above substrates and the other was located at the centre of the wind tunnel section. Air temperature was measured at the top of this section, above sample units. Substrates surface temperature was measured with thermocouples. Deposition velocities were measured for four temperature difference ΔT between air and surface (2, 5, 10 and 30 K) and at three wind speeds u_{ref} (1.3, 5.0 and 10 m s^{-1}). Vertical temperature profiles were measured with a rack of thermocouples with the aim of determining temperature gradients to compare experimental results to models. *In situ* experiments were realized at IRSN laboratory (Cherbourg-Octeville). Aerosol deposition was measured on vertical glass and on cement facing, horizontal asphalt, and oblique (30°) zinc, tile and slate. Surfaces were exposed to atmospheric conditions from the day before the experiment to be in real temperature conditions. Fluorescein aerosol was generated and dispersed by wind over the studied surfaces. Surface temperature was measured with thermocouples. Wind speed was measured near surfaces with an ultrasonic anemometer. Ambient temperature and other meteorological parameters were measured with a meteorological station.

Wind tunnel results for heated surfaces are compared with results for the same non-heated surfaces from Roupsard *et al.* (2011). Significant thermophoresis effects were measured from the lowest temperature gradient (ΔT = 2 K) onwards at all wind speeds with minimum decreasing of 40 % of V_d for all surfaces. Deposition velocity appears to be a decreasing logarithmic function of increasing air/surface temperature difference. Impact of thermophoresis is not the same for smooth and rough surfaces. For glass, V_d does not vary with u_{ref} for the same ΔT, except for ΔT = 2 K. For cement facing, V_d decreases in the same way for increasing ΔT and increases with u_{ref}. Temperature profiles have logarithmic patterns with decreasing temperatures for increasing vertical position above the surface. Temperature gradient must be taken near the surface to compare experimental results and physical models. *In situ* deposition velocities present some variations for same wind speed conditions, depending on sunshine conditions. Obviously thermophoresis plays a major role on aerosol deposition on urban surfaces.

The results of this study confirm Maro *et al.* (2010) preliminary observation. In addition, our measurements show that thermophoresis is one of the most important physical phenomenon that should be taken into account in urban area aerosol deposition models.

D. Maro *et al.* (2010) *Proc. 8th Int. Aero. Conf.*, Helsinki.
P. Roupsard *et al.* (2011) *Proc. 18th Eur. Aero. Conf.*, Manchester.

Long Term Trends in Arctic Aerosol Composition at Kevo, Finland

P.K. Hopke[1], J.R. Laing[1], L. Hussain[2,3], V.A. Dutkiewicz[2], J. Paatero[4], and Y. Viisinen[4]

1Department of Environmental Health Sciences, School of Public Health, SUNY, Albany, NY. 12201, USA
2Wadsworth Center, NYS Department of Health, Albany, NY 12201-0509
3Center for Air Resources Engineering and Science, Clarkson University, Potsdam, NY 13699
4Finnish Meteorological Institute, Helsinki, Finland

Keywords: black carbon, Arctic, time series, Kevo
Presenting author email:hopkepk@clarkson.edu

Introduction

Carbon, primarily a byproduct of incomplete combustion of fossil fuel and biomass burning constitute only a few % of the total PM mass, but disproportionately affect the global climate by absorbing the incoming sunlight and directly warm the atmosphere. BC coated with sulfate is even more effective than externally mixed BC and SO4 particles. Recent studies have indicated that substantial radiative forcing in the Arctic is due to the indirect impact of BC on the albedo of snow and ice surfaces. We are determining the concentrations of BC, EC, MSA, SO_4, and selected trace elements in weekly samples collected at Kevo, Finland from 1964-2010 to assess the impact of aerosols on (1) radiative forcing, (2) source regions that have contributed to the burden of BC/EC and SO4 in the Arctic region, and (3) how the regional emissions impacting Arctic have changed with time.

Methods

Samples were collected over 7 day periods beginning in October 1964 through the present in Kevo [Yli-Yuomi et al., 2003a,b], Finland in an automated system to measure airborne radioactivity. The filters from 1964-1978 have been analyzed for trace metals by neutron activation (INAA) and inductively coupled plasma mass spectrometry (ICP-MS), major ions and methane sulfonate (MSA) by ion chromatography, black carbon, and elemental carbon [Yli-Tuomi 2003a,b]. Filters after 1978 have been analyzed for total and soluble trace elements by inductively coupled plasma mass spectrometry (ICP-MS), and major ions and methane sulfonate (MSA) by ion chromatography. Black carbon, and elemental carbon were analyzed using the approach developed by Li et al. [2002]. The light absorption of each new filter was measured with a Magee OT21 transmissometer. EC was measured using a Sunset Analyzer and the NIOSH protocol [Birch and Cary, 1996].

Results and Conclusions

Figure 1 shows the annual average BC values for 1965 to 2000. The concentrations of BC aerosols during 1965 were 430 ng m^{-3}. From 1966 thru 1987 it varied from ~250 to 430 ng m^{-3}. Beginning in 1989, concentrations showed a systematic decrease to about 150 ng m^{-3}. From 1989 to 2002, the concentrations have remained between 150 and 230 ng m^{-3}. The data from 2003 to 2010 is not yet available. These data show that there was a substantial decrease in BC concentrations around the time of the collapse of the Soviet Union and the change in political systems in eastern Europe.

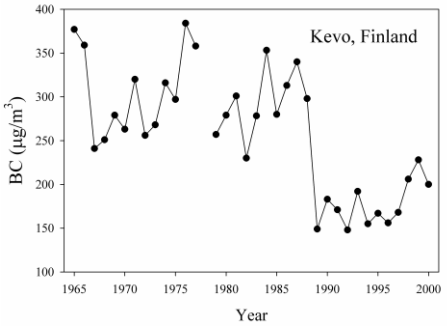

Figure 1. Time series of annual average concentrations of BC at Kevo, Finland

. The solubility of certain elements can provide information about the origin of the aerosol and formation processes. Trend analysis will be performed on individual species. The complete data set will be analyzed by Positive Matrix Factorization (PMF). The receptor modeling results will be connected with back trajectory data in a Potential Source Contribution Function (PSCF) analysis to determine possible source areas. Future work includes complete chemical analysis of the weekly filters through 2010 for trace elements and soluble trace elements by ICP-MS, major ions and methane sulfonate (MSA) by ion chromatography, and black carbon by light-absorption and thermo-optical techniques. This complete dataset will be able to provide insight into the long term trend of Arctic aerosol chemical species and the possible implications of global climate change in the Arctic.

Li, J., et al., 2002, Atmospheric Environ. 36, 4699–4704.
Yli-Tuomi, T., et al., 2003a. Atmospheric Environ. 37, 2355-2364.
Yli-Tuomi, T., et al., 2003b, .Atmospheric Environ. 37: 4381-4392.

Hygroscopicity of organic/inorganic internally mixed particles by infrared spectroscopy

Lorena Miñambres, Estíbaliz Méndez, María N. Sánchez, Fernando Castaño and Francisco J. Basterretxea[1]

[1]Departamento de Química Física, University of the Basque Country, UPV/EHU,
B. Sarriena, s/n, 48940 Leioa, Bizkaia, Spain
Keywords: tropospheric aerosol, hygroscopicity, deliquescence.
Presenting author email: lorena.minambres@ehu.es

Tropospheric aerosols are composed of inorganic and/or organic material and elemental carbon in varying proportions [Seinfeld and Pandis, 1998]. Among the inorganic fraction, sulfates are important components of continental aerosol. The organic fraction, which can be made up of an enormous variety of compounds, is found either in the surface of the inorganic particles or internally mixed. Organic compounds can alter the hygroscopic and optical properties of the inorganic particles and their chemical reactivity. Much information is still needed to construct more detailed atmospheric models that include the influence of organic compounds in the properties of inorganic particles.

In this work we present a laboratory study of the influence of several dicarboxylic acids (oxalic, malonic, maleic, glutaric and pimelic) in the water uptake properties of submicrometer ammonium sulfate (AS) particles monitored by infrared extinction spectroscopy. Dicarboxylic acids (DA) have been identified at a variety of sources, urban and remote [Prenni et al., 2001]. Infrared spectroscopy is a sensitive technique to characterize aerosol composition, water content and particle phase, and has been used to study other internally mixed organic/inorganic particles [Brooks et al., 2003].

Aerosols are prepared by atomizing aqueous solutions of desired concentrations to yield submicrometer aerosol particles. The relative humidity (RH) of aerosols is controlled by mixing dry and humid flows of nitrogen. The extinction spectra of particles flowing through an aerosol cell are recorded from 800 to 4000 cm^{-1} with a FTIR spectrometer. Particle phase, composition and water content can be monitored by measuring the absorption bands of the various species.

Deliquescence curves of the mixed particles at various solute mass fraction ($0 \le f(DA) \le 1$) have been recorded. The results show that water uptake behavior of internally mixed particles changes noticeably with the organic acid, in some cases favoring the uptake of liquid water at lower RH values than in the pure components. The results are qualitatively explained in terms of intermolecular/interionic forces in the internally mixed solids, which are evidenced in their infrared spectra in terms of shift and broadening of the ν_3 spectral band of sulfate. When the Gibbs free energy of the internally mixed organic/inorganic solid is similar to the sum of Gibbs free energies of the pure solids ($G_{mix} \approx G_{DA} + G_{AS}$), the deliquescence properties are simply intermediate between those of the pure components. However, for the systems where $G_{mix} > G_{DA} + G_{AS}$ (malonic, maleic and oxalic), the intermolecular interactions raise the energy of the mixed solid (as evidenced by intense spectral band broadening) and makes it more unstable than the pure solids, favoring the admittance of water molecules in the net in order to energetically stabilize the system. These results can be of interest to scientists working in atmospheric modelling to be able to predict more accurately the physico-chemical behavior and chemical reactivity of organic/inorganic atmospheric aerosols.

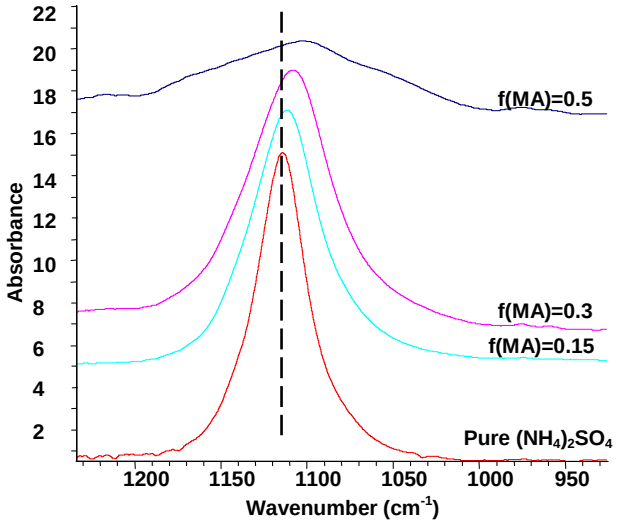

Figure 1. Infrared $\nu_3(SO_4^{2-})$ absorption band of internally mixed dry particles of malonic acid and ammonium sulfate at several f(DA) compositions, showing the changes in bandwidth and band center with solute composition. The spectra have been shifted in the vertical scale.

This work was supported by Ministerio de Ciencia e Innovación via grant-in-aids (CGL2008-06041/CLI and CSD-2007-00013), Gobierno Vasco/Eusko Jaurlaritza and Universidad del País Vasco through general support.

Brooks, S. D., Garland, R. M., Wise, M. E., Prenni, A. J., Cushing, M., Hewitt, E., Tolbert, M. A. (2003) *J. Geophys. Res*. **108** (D15), 4487-4497.

Prenni, A. J.; DeMott, P. J.; Kreidenweis, S. M.; Sherman, D. E.; Russell, L. M.; Ming, Y. (2001) *J. Phys. Chem. A* **105**, 11240-11248.

Seinfeld, J. H., Pandis, S. N. (1998) *Atmospheric Chemistry and Physics*; John Wiley; New York.

General assessment of the main factors governing the particle concentrations in urban and regional background environments

J.F. Nicolás[1], J. Crespo[1], E. Yubero[1], N. Galindo[1], J. Moltó[2] and E. Mantilla[3].

[1]Atmospheric Pollution Laboratory, Miguel Hernández University, Avda. Universidad, 03202, Elche, Spain
[2]Department of Chemical Engineering, University of Alicante, P.O. Box 99, 03080, Alicante, Spain
[3]Centro de Estudios Ambientales del Mediterráneo (CEAM), c/ C. R. Darwin, 14, 46980, Paterna, Spain
Keywords: Number size distribution, Mixed layer depth, Optical particle counter, Regional background.
Presenting author email: j.nicolas@umh.es

During the autumn of 2011 particle number concentrations were simultaneously measured in two different environments. The first one represented a regional background site (RS). The sampling point (38°39´N; 0°16´W; 1558 m a.s.l) was located on top of a mountain range, in a military area (EVA nº 5) of the Ministry of Defence, 25 km from the Mediterranean coast. The second monitoring site, about 60 km SE of RS, represented an urban background environment (US). The station was placed in the city of Elche (38°16´N; 0°41´W; 95 m a.s.l), 12 km from the coast.

The study aims to obtain the main factors affecting the particle number concentrations measured at each station and analyse the degree of anthropogenic influence on RS. Anthropogenic emissions from the major coastal cities could reach RS under the appropriate meteorological conditions (e.g. sea breezes).

The instruments used to measure particle concentrations were two optical counters: Grimm 365 (US) and Grimm 190 (RS). These instruments determine particle number concentrations in 31 particle size channels from 0.25 to 32 µm. Previously to the measurement campaign, an intercomparison between the two counters was performed: $N_{360}=1.04 \cdot N_{190}+21$ (Part./l) / $R^2=0.996$; where N is the total particle number concentration.

At the RS site, meteorological data were obtained from a weather station located about 5 m from the ground. For the US site, the data provided by one station of the air quality network of the Government of Valencia, located ~ 2 km south of the measurement site, were used. Meteorological maps from the Spanish Meteorological Agency (AEMET) were consulted. A data base related to Saharan dust intrusions and other differential events affecting the Iberian Peninsula and Canary Islands (http:www.calima.ws) was also used.

For an initial analysis of the hourly variations of particle number concentrations, we selected five consecutive labour days (from 10 to 14 October 2011) without differential events. The synoptic situation during these days was mainly anticyclonic. Table 1 shows the average values of meteorological parameters and total particle number concentrations obtained at each station. As can be calculated from the data shown in Table 1, N at RS represented ~ 30% of that measured at US.

The predominant wind direction in RS during the study period (SE) was appropriate to identify a possible anthropogenic influence from the coastal urban nuclei on the RS site.

Table 1. Average values of meteorological data and particle number concentration

Station	T (°C)	v (m/s)	Wind direction	HR (%)	N (Part./l)
Regional	15.7	2.8	SE	46.7	17218
Urban	22.7	0.5	NW	74.3	63485

Figure 1 presents the average hourly evolution of the total particle concentration N(t) at each station.

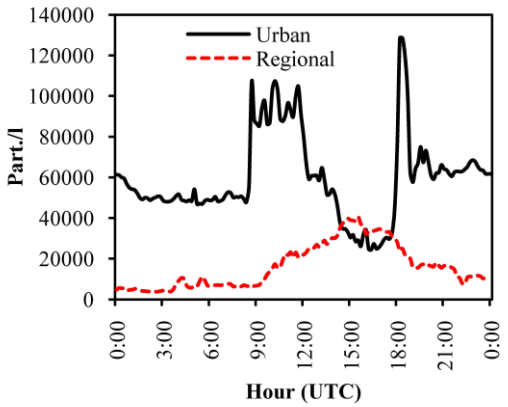

Figure 1. N(t) at both stations

$N(t)_{US}$ presented a similar pattern to that of road traffic intensity in the city, with a peak in the morning and a maximum between 18-20 h (UTC), when people come home from work. On the other hand, $N(t)_{RS}$ showed a wide peak coincident with the hourly variations of solar radiation. Thus, no urban influence on RS was initially observed. Another evidence supporting this assertion is the shape of the particle size distribution obtained at each station. For all particle sizes, the number concentration was higher in US than in RS. However, the relative difference between concentrations measured at both locations was not constant. So, in RS particles belonging to the accumulation mode represented 25% of those measured at US, while this percentage rises to 75% for the coarse mode. This could be due to RS being situated above the mixing layer (ML) (~700 m during the study period). This situation could change if RS is located within the ML, but this scenario is more frequent during spring and summer.

This work was supported by the Spanish Ministry of Science and Innovation under the CGL2009-08036 (PASSE) project. We would like to thank the military area (EVA nº 5) for its assistance in this work.

Non-volatile aerosol in the Arctic Winter Stratosphere and its role for PSC formation.

R. Weigel[1], M. Ebert[2], K. Kandler[2], S. Molleker[3], W. Frey[3], M. Klingebiel[1], C. M. Volk[4], G. Günther[5], H. Schlager[6], F. Cairo[7], S. Kaykin[8], S. Borrmann[1,3]

[1]Johannes Gutenberg Universität Mainz, Institut für Physik der Atmosphäre, Mainz, Germany
[2]Institut für angewandte Geowissenschaften, Technische Universität Darmstadt, Germany
[3]Partikelchemie, Max Planck – Institut für Chemie, Mainz, Germany
[4]Fachbereich C - Abteilung Physik, Bergische Universität Wuppertal, Germany
[5]Institut für Energie- und Klimaforschung – Stratosphäre (IEK-7), FZ Jülich, Germany
[6]Institut für Physik der Atmosphäre, DLR, Oberpfaffenhofen, Germany
[7]Istituto di Scienze dell'Atmosfera e del Clima, Consiglio Nazionale delle Ricerche, Rome, Italy
[8]Central Aerological Observatory, Moscow, Russia

Keywords: Stratospheric aerosol, Arctic Winter Vortex, non-volatile particles, PSC
Presenting author email: weigelr@uni-mainz.de

In-situ measurements with a 4-channel condensation particle counter (COPAS, Weigel et al., 2009) with different d_{p50} (50 % detection efficiency cut-off particle diameter) were conducted in the altitude range of 12.0-20.5km on board the M-55 *Geophysica*. One of four channels has a heated aerosol inlet line (at 250°C) which additionally allows for counting non-volatile particles.

Kiruna, North Sweden, was the operations base from where research flights towards the Arctic Winter Vortex (AWV) were performed during three scientific missions: EUPLEX (Jan.-Mar. 2003, 15 flights); RECONCILE, (Jan.-Mar. 2010, 13 flights); and ESSENCE, (Dec. 2011, 2 flights).

For potential temperatures $\Theta > 400$K the progression of the vertical profiles strongly depends on whether the measurements occurred in- or outside the AWV (Figure 1, left). Outside the AWV the particle mixing ratio N remains nearly constant with altitude while inside the AWV N increases with ascent.

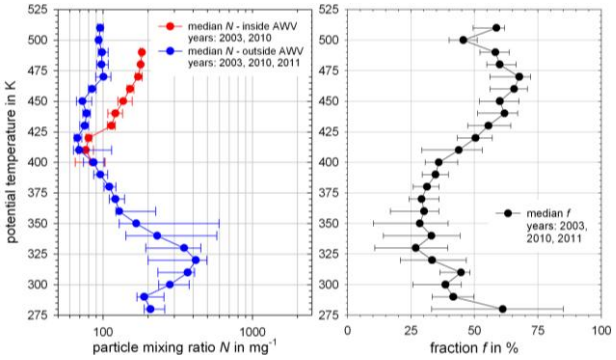

Figure 1. Vertical median profiles with 25- and 75-percentiles of particle mixing ratio N and the fraction f of non-volatile particles.

The fraction f of non-volatile aerosol in the AWV region is generally increasing at altitudes with $\Theta > 400$K from about 35% up to 70% at $\Theta = 475$K (Figure 1, right), which is high compared to f measured elsewhere in the stratosphere at same altitudes (cf. Borrmann et al., 2010). Hence, subsiding air masses inside the AWV entrain particles into the Arctic lower stratosphere from aloft. Up to 7 of 10 of these particles contain solid, not vaporizable material and were previously assumed to mainly stem from meteoritic ablations at mesospheric altitudes (Curtius et al., 2005).

During RECONCILE and ESSENCE particles were collected with an impactor at altitudes of $\Theta > 410$K. The chemical analysis of these aerosols with Environmental Scanning Electron Microscopy (ESEM) and Energy Dispersive X-ray (EDX) analysis techniques yields (apart from found residuals of the volatile nitric- and sulfuric acid compounds):

A) Non-volatile particles with $d_p < 500$nm mainly consist of soot, sometimes with bearings of lead.

B) Particles with $d_p > 500$nm (and $d_p < 6$µm) are partly amorphous, most likely of crustal material. In the same size range also molten spheres were found, alloy particles, metals or metaloxides and silicates.

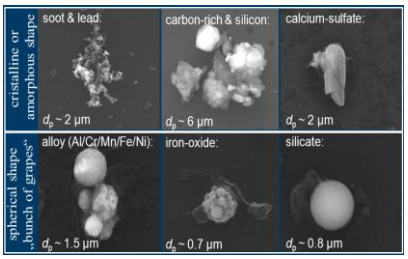

Figure 2. ESEM images of collected particles in the AWV region.

The fly-ash habit indicates that some particles were exposed to high temperatures for a sufficient duration.

These non-volatile particles in the AWV region provide condensation surfaces and thus could contribute to the formation of Polar Stratospheric Clouds (PSCs).

Geophysica missions were funded by the EC within the FP5 and FP7 (EVK2-CT-2001-00119and 226365-FP7-ENV-2008-1) and by the European Space Agency (ESA). Further support was provided by the Universities of Mainz and Darmstadt and the Max-Planck-Institute for Chemistry.

Borrmann, S., et al., (2010), Aerosols in the tropical and subtropical UT/LS: In-situ measurements of ultrafine particle abundance and volatility, *Atmos. Chem. Phys. 10*, 5573–5592.

Curtius, J. et al. (2005), Observation of meteoritic material and implications for Aerosol nucleation in the winter Arctic lower stratosphere derived from in situ particle measurements; *Atmos. Chem. Phys*., 5, 1-25.

Weigel, R., et al. (2009), Experimental characterization of the COndensation PArticle counting System for high altitude aircraft borne application; *Atmos. Meas. Tech.*, 2, 243-258.

Chemical Characterization of Impactor Samples from seven Sites in Germany

K. Müller, G. Spindler, T. Gnauk, Y. Iinuma, H. Herrmann

[1]Department of Chemistry, Leibniz Institute for Tropospheric Research, 04318 Leipzig, Germany
Keywords: aerosol, chemical size distribution, seasonality, spatial distribution
Presenting author email: konrad@tropos.de

Within the German Ultrafine Aerosol Network (GUAN) the collection of size-segregated PM was carried out simultaneously at seven sampling sites in Germany by identical equipment. The seven sites were distributed between one traffic site (Leipzig), two urban sites in residential areas (Augsburg, Leipzig), two rural sites (Bösel, Melpitz), and two mountain background sites (Hohenpeißenberg, Schauinsland). Using weather forecast days with a mainly uniform air mass inflow to Germany and without precipitation were selected to collect PM. After collection of five size fraction in BERNER-LPI 80/0.05 the samples were stored and transported frozen to Leipzig.

All chemical analyses were carried out at the IfT. The main interest was directed to OC/EC distribution and the concentration of single organic species as well as the major ionic constituents. During a period of two years (2009-2010) 48 sampling events of 24 hours took place. At the both sampling sites in Leipzig at fall 2010 five events were applied to test ten-stage LPI. Seasonality and air mass origin were major criteria of the selection of sampling days (Tab.1).

Table 1. Sampling days selected by season and air mass origin.

Season	continental	maritime
Summer	4	22
Winter	12	10

With the exception of the mountain background sites a clear difference between Winter-continental and Winter-maritime air masses was found in all samples. In the long-range transport fractions (0.14-0.42 and 0.42-1.2 µm) highest mass concentrations were determined for OM (Organic Matter), EC (Elemental Carbon), and secondary inorganic compounds. The percentage of carbonaceous material (EC+OM) in the size fraction mass is decreasing from ultrafine to coarse mode particles from 60 to 13 % as a mean for the traffic site and from 55 to 24 % for a rural site (Fig.1). Highest relative concentrations were found in ultrafine particles during summer at the traffic site and in Augsburg.

For the secondary ions sulphate and nitrate the maximum was observed in winter samples in the submicron fractions with a concentration gradient from East to West, depending on long range transports from Eastern Europe. The seasonal variation of nitrate and ammonium is more pronounced than for other ions because of the volatility of ammonium nitrate.

Winter concentrations of PAH were found highest in Melpitz, Leipzig and Augsburg depending on long range transports and emissions of wood burning in the major cities. According to previous works (Poulain et al., 2011) the amounts of PAH are well correlated to the levoglucosan concentrations, which were found to be highest during winterly days with air mass origin in Eastern Europe.

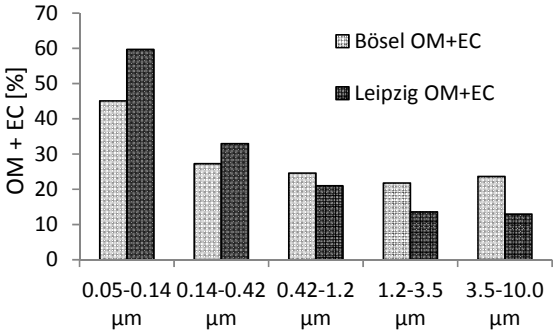

Figure 1. Percentage of carbonaceous material in size fractions of PM at traffic site in Leipzig and at rural site in Bösel (mean values for summer).

During the summer measurement days the OM concentrations at the background mountain sites are comparable to winter measurements while at all other sites in winter samples the submicron particles show higher concentrations than in summer samples. In coarse mode PM higher summer concentrations of OM were observed depending on higher emissions of biogenic material. Fig. 2 shows results from Bösel as an example.

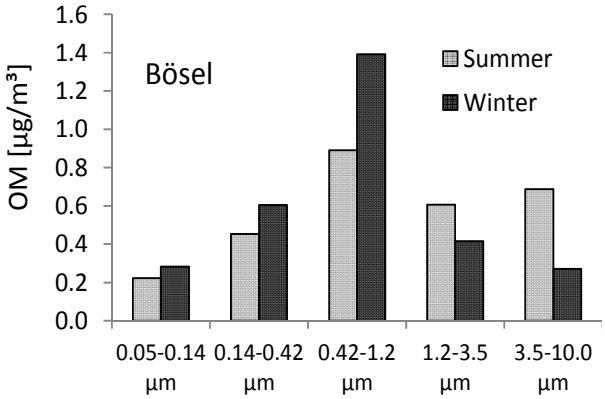

Figure 2. OM concentration in Bösel depending on season

This work was funded by BMU F&E 370343200.

Poulain, L., Iinuma, Y., Müller, K., Birmili, W., Weinhold, K., Brüggemann, E., Gnauk, T., Hausmann, A., Löschau, G.,Wiedensohler, A., Herrmann, H. (2011), Atmos. Chem. Phys. 11, 12687-12713

Physicochemical Properties of Ultrafine Aerosol Particles in the North Aegean during the AEGEAN_GAME Field Campaign

E. Triantafyllou[1], M.Giamarelou[1], S. Bezantakos[1], K. Barmpounis[2], E. Bossioli[3], Ch. Theodosi[4], M. Tombrou[3], N. Mihalopoulos[4], K. Eleftheriadis[5], G. Biskos[1,2]

[1]Department of Environment, University of the Aegean, Mytilene 81100, Greece
[2]Faculty of Applied Science, Delft University of Technology, Delft 2628-BL, The Netherlands
[3]Department of Physics, University of Athens, Athens 15784, Greece
[4]Department of Chemistry, University of Crete, Heraklion 71003, Greece
[5] ERL, Inst. of Nuclear Tech. & Rad. Protection, N.C.S.R. Demokritos, 15310 Ag. Paraskevi, Attiki, Greece

Keywords: PM, Aerosol Sampling, Chemical Composition, Scattering Coefficient.
Presenting author email: etriantaf@env.aegean.gr

The Aegean Sea is a region of the globe that is influenced by maritime and continental aerosol sources. Very often the dominance of summer northerlies transport polluted air masses from the main continental Europe to the region, thereby affecting the physicochemical properties of the aerosol particles and thus their impacts on regional climate (e.g., Lelieveld et al. 2002; Bougiatioti et al. 2009). The objective of the AEGEAN_GAME field campaign that took place from 25 August to 10 September 2011 was to investigate the properties of aerosol particles in the region and identify their sources. One of the two ground monitoring points of the campaign was at Vigla, a remote location on the NorthWest of Lemnos island.

Dry particle size distributions and scattering coefficients were measured with a Scanning Mobility Particle Sizer (TSI Model 3034) and a Nephelometer (TSI Model 3563), respectively. For the chemical composition of the particles (inorganic species and organic/elemental carbon) we collected size segregated samples using a cascade impactor (MOUDI Model 110 MSP) and a TSP sampler. Concentrations of O_3, SO_2 and NO_x were also measured using gas analyzers (Model 400A for O_3, Model 100A for SO_2, and Model 200A for NO_x).

Time-series of the average number concentration, the scattering coefficients at three wavelengths and the concentrations of elemental and organic carbon are shown in Fig. 1. The average number concentration of particles having diameter from 10 to 487 nm ranged from ca. 500 to 12.5×10^4 particles/cm^{-3} with an average value of around 2093×10^3 particles/cm^{-3} (Fig. 1a). The concentrations observed where at similar levels with those observed at Finokalia station at the South Aegean (Pikridas et al. 2010). The peaks of average number concentration observed on 29/08 and 30/08 were correlated with air masses originating from Eastern Europe, while on 9/9 from Northern Europe as indicated by back-trajectory analysis (HYSPLIT model; Eleftheriadis et al. 2006). The average values of ambient aerosol scattering coefficients measured at three wavelengths (λ = 450, 550 and 700 nm) were 27.5±19.5, 15.7±12.9, and 6.7±7.2 Mm^{-1}, respectively (Fig. 1b). The mean values were in average two times lower than other studies at coastal sites (Bryant et al., 2006).

The chemical analysis of organic and elemental carbon (OC and EC) shows that the ratio OC/EC ranged from 5.9 to 21.94 with an average value of 11.6±4.8 during the total sampling period (Fig. 1c). The mean concentrations of organic and elemental carbon were 1.53±0.92 and 0.17±0.15 μg/m^3, respectively. The mean concentration of OC was on average 9 times higher than EC, indicating the dominant contribution of secondary organic matter.

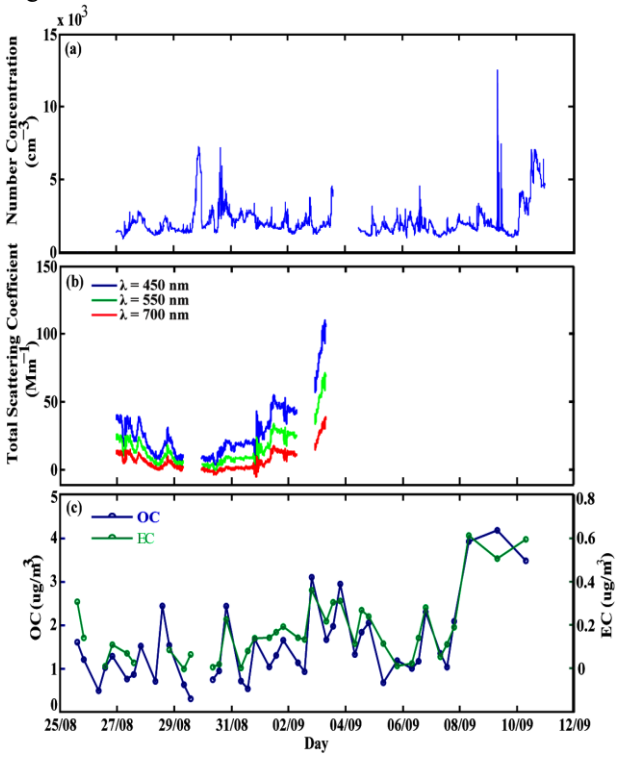

Figure 1. Time series of (a) the total number concentrations of particles having diameter from 10 to 487 nm, (b) the total scattering coefficient 450nm (blue), 550nm (green) and 700 nm (red), and (c) the concentrations of organic (blue line) and elemental carbon (green line) from 25/08/11 to 10/09/11.

References

Eleftheriadis, K., et al. (2006) *Atmos. Environ.,* **40**, 6245–6260.
Lelieveld, J., et al. (2002) *Science*, Vol. **298,** no. 5594, 794-799.
Bougiatioti, A., Fountoukis, C., Kalivitis, N., Pandis, S. N., Nenes, A., and Mihalopoulos, N. (2009) *Atmos. Chem.Phys.*, **9**, 7053-7066.
Bryant, C., et al. (2006) *Atmos. Environ.*, **40**, 6229-6244.
Pikridas, M., et al. (2010) *Atmos. Chem. Phys.*, **10**, 6793–6806.

Physico-chemical characterization of HULIS from different environments

T.B. Kristensen[1], L. Du[1], Q.T. Nguyen[2,3], H.G. Kjærgaard[1], C.B. Koch[1], J.K. Nøjgaard[3], A.G. Hallar[4], D.H. Lowenthal[5], B. Nekat[6], D. van Pinxteren[6], M. Glasius[2] and M. Bilde[1]

[1]Department of Chemistry, University of Copenhagen, Copenhagen, DK-2100 Ø, Denmark
[2]Department of Chemistry, Aarhus University, Aarhus, DK-8000 C, Denmark
[3]Department of Environmental Science, Aarhus University, Roskilde, DK-4000, Denmark
[4]Desert Research Institute, Storm Peak Laboratory, Steamboat Springs, CO-80488, USA
[5]Desert Research Institute, Reno, NV-89512, USA
[6]Leibniz Institute for Tropospheric Research, Leipzig, 04318, Germany
Keywords: HULIS, FTIR, Raman, LC-MS.
Presenting author email: thomas@chem.ku.dk

Humic-Like Substances (HULIS) have been proven to comprise a significant fraction of the aerosol particle organics in various environments. HULIS have attracted a lot of attention because of their ability to efficiently lower surface tension of water solutions and thereby influence hygroscopic growth and cloud condensation nuclei (CCN) activity (Graber and Rudich, 2006).

We have previously presented CCN-activity and growth factors of HULIS from three different environments. Our results from the three sites were almost identical and similar to what has been observed for Suwannee River Fulvic Acid (SRFA) (Kristensen *et al*, 2011). Filter samples from the rural continental background site Melpitz ($PM_{2.5}$), from a street canyon in Copenhagen (PM_{10}) and from Storm Peak Laboratory (SPL) located 3.2 km a.s.l. in Colorado ($PM_{2.5}$) were used. In this study SRFA and the three HULIS samples were characterized by use of HPLC-QTRAP-MS, Fourier transform infrared (FTIR), ultraviolet-visible (UV/Vis) and Raman spectroscopy. It is to our knowledge the first time Raman spectroscopy has been used for characterization of atmospheric HULIS samples.

The extraction of HULIS was carried out by applying the one-step protocol described by Varga *et al* (2001) with minor modifications. A VERTEX 70 (Bruker) FTIR spectrometer was used to measure the absorbance of HULIS samples with 1.0 cm^{-1} resolution. The samples were prepared on a CaF_2-window by drying the HULIS-methanol-solution in a gentle stream of N_2. The spectrometer was purged with N_2 to minimize the interference by H_2O and CO_2 during measurements. The Raman spectra of the dried samples were measured using a Bruker RFS 100 FT-Raman spectrometer. The exciting laser is a Nd:YAG laser with a wavelength of 1064 nm, and spectra were measured at a resolution of 1 cm^{-1}.

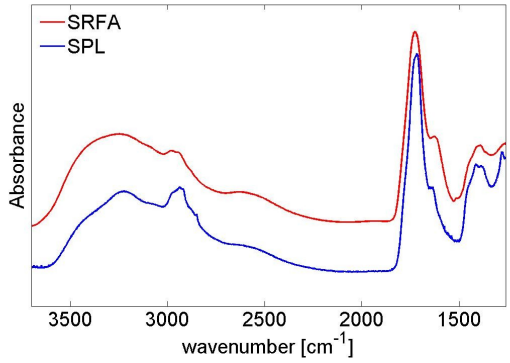

Figure 1. FTIR spectra of SRFA and HULIS from SPL

The UV/Vis spectra were measured with a PerkinElmer Lambda 1050 UV/Vis/NIR spectrometer. The spectrometer was operated with a reference sample in a double beam mode and the resolution was 0.4 nm. The HPLC-QTRAP-MS consisted of a liquid chromatograph (Agilent 1200) interfaced to a ion trap mass spectrometer (AB Sciex QTrap 5500, AB Applied Biosystem - MDS Analytical Technologies) that employed Turbo Ionspray (TIS) ionization.

The FTIR and Raman spectra of HULIS from SPL and SRFA are depicted in Figure 1 and 2 respectively. Many spectral features of the two samples are similar, implying similarities of functional groups. However, distinct differences in spectra obtained by the different techniques indicate characteristic differences of the three HULIS samples.

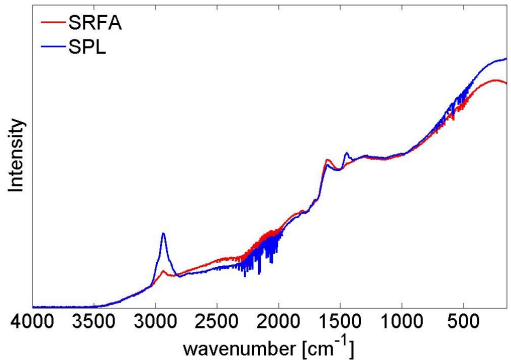

Figure 2. Raman spectra of SRFA and HULIS from SPL.

This work was in part supported by the National Science Foundation under Grant Number AGS-0931431.

Graber, E.R. and Rudich, Y. (2006) *Atmos. Chem. Phys.* **6**, 729-753.

Kristensen, T.B., Wex, H., Nekat, B., Van Pinxteren, D., Mildenberger, K., Stratmann, F., Nøjgaard, J.K., Koch, C.B., Hallar, A.G., Mentel, T.F. and Bilde, M. (2011) *European Aerosol Conf. 2011*, Manchester.

Varga, B., Kiss, G., Ganszky, I., Gelencsér, A. and Krivácsy, Z. (2001) *Talanta* **55**, 561-572.

Photophoresis of soot aerosols in the atmospheric radiation field

L.B. Kochneva* and S.A. Beresnev

Aerosol Physics Laboratory, Ural Federal University, Ekaterinburg, 620083, Russia
Keywords: fundamental aerosol physics, stratospheric aerosols, photophoresis, soot aerosol
Presenting author email*: louisa.letfulova@usu.ru

This report continues and summarizes analysis and estimations of the photophoretic effects for soot aerosols in stratosphere. One of possible mechanisms of aerosol transport in the thermally and mechanically stable stratosphere can be well-known radiometric photophoresis as the regular factor of aerosol vertical motion on the synoptic and global temporal scales. It can lead, for example, to the uncontrollable accumulation of soot particles at the certain altitudes in stratosphere from aircraft engines and biomass burning.

At the first stage of studies the estimations of transport opportunities of negative "solar" (motion of particles in the field of short-wave solar radiation against gravity) and positive "thermal" (motion in the field of thermal outgoing radiation) photophoresis of soot particles have been given at the assumptions of the highest possible intensities of atmospheric radiation fluxes (Beresnev *et al,* 2003). In this report we present updated and expanded calculations of the photophoretic motion characteristics according to the advanced radiation block of the model. Firstly, the results for "solar" photophoretic motion are calculated in the framework of advanced model for short-wave solar radiation (Beresnev *et al*, 2012). Secondly, the characteristics for "thermal" photophoresis are specified taking into account the downward flux of the long-wave thermal radiation (Beresnev *et al.*, 2011).

The results of theoretical analysis of photophoretic motion of soot particles in the short-wave solar radiation field for stationary atmosphere are presented. The integrated fluxes of solar radiation were calculated by the Monte Carlo method with approximation of a plane-parallel, horizontal-homogeneous molecular-aerosol atmosphere. The analysis confirms again an opportunity essential photophoretic effects for soot aerosol particles in stratosphere: the "sun" photophoresis can be considered as the effective mechanism of vertical transport of well-absorbing sub-micrometer particles up to heights of the middle stratosphere. The forces of "sun" photophoresis can compete to gravities up to heights 30-35 km for particles of sub-micrometer and micrometer sizes. On other hand, the estimations have shown again the small efficiency of radiometric photophoresis for weakly-absorbing, dense and high-conducting particles of atmospheric aerosol. The results for photophoretic motion of soot particles in the field of the Earth' thermal radiation in a stationary atmosphere are also presented. In calculations the up- and down-fluxes of thermal radiation are taken into account. It is shown that positive "thermal" photophoresis potentially can be the effective mechanism of vertical transport for micron-sized soot particles at stratospheric altitudes.

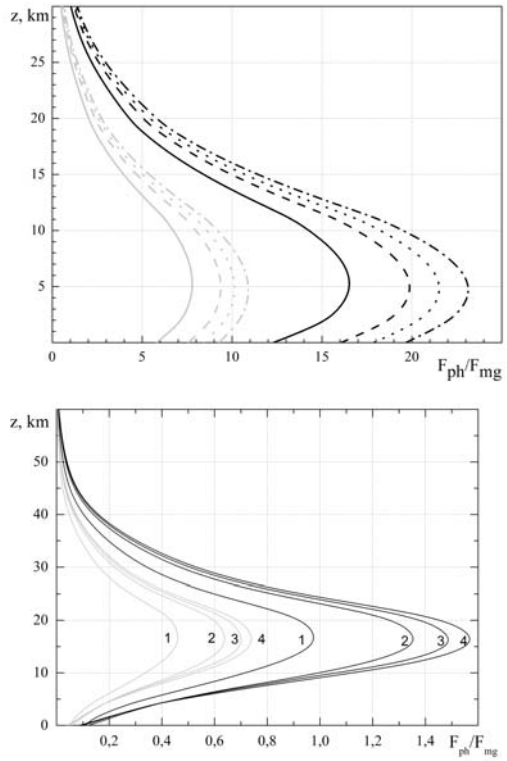

Figure 1. Ratio F_{ph}/F_{mg} as function of altitude z for soot particles in stratosphere. The top panel: the negative "sun" photophoresis; $R_p = 0{,}2$ μm; $m = 1{,}95 + 0{,}1i$; $\Lambda = \lambda_p / \lambda_g = 5$, middle latitudes – summer, solar angle 30^0, surface albedo 0.0(solid), 0.1(dash), 0.2(dot), 0.4(dash-dot); black lines $\rho_p = 165$ kg/m^3; grey lines $\rho_p = 350$ kg/m^3. The bottom panel: the positive "thermal" photophoresis; $R_p = 1{,}5$ μm; $m = 2{,}42 + 1{,}02i$; black lines $\rho_p = 165$ kg/m^3; grey lines $\rho_p = 350$ kg/m^3; 1 – subarctic–summer; 2 – USA standard atmosphere; 3 – middle latitudes – summer; 4 – tropical atmosphere.

This work was supported by the Ministry of Education and Science of the Russian Federation (research project implemented by leading scientist at Russian institution of higher education, agreement No.11.G34.31.0064).

Beresnev, S.A., Kochneva L.B. and Suetin, P.E. (2003) *Thermophys. and Aeromech*. **10(2)**, 287–301.
Beresnev, S.A., Kochneva L.B., Zhuravleva, T.B. and Firsov, K.M. (2012) *Atmos. Oceanic Opt.* **25(2)**, 175-180 (in Russian).
Beresnev, S.A., Kochneva L.B., Zakharon, V.I. and Gribanov, K.G. (2011) *Atmos. Oceanic Opt.* **24(7)**, 597-600 (in Russian).

Chemistry of Size Separated Aerosols over the Indian Arctic Station, Himadri

M.P. Raju, S. M. Sonbawne, P.D. Safai, P.S.P. Rao and P.C.S. Devara

Indian Institute of Tropical Meteorology, Pune, Maharastra, 411 008, India
Keywords: Size seperation, Arctic region, Chemical composition, fine and coarse mode particles
Presenting author email: mpraju@tropmet.res.in

Abstract:

During the 20th Indian Scientific Expedition to Arctic a detailed study of aerosol mass size distribution was made during July 2010. In order to establish the sources of aerosols, it is necessary to monitor their physical and chemical properties. Low volume aerosol air sampler (Andersen 2000 Inc., USA) was installed at the Indian Arctic site, Himadri. The sampler is operated at a constant flow rate 30 LPM for about one week period to get sufficient aerosol load. Two set of samples were collected. Size distribution of aerosols showed bimodal distribution during both the periods. The coarse mode particles during 13-19 July 2010 period (Set 1) and 24-29 July 2010 period (Set 2) contributed 78.8% and 79.8%, respectively as compared to the fine size aerosol which contributed 21.2% and 20.2%, respectively. The residence time of aerosols in the atmosphere mainly depends upon the size of the particles. Percentage contribution of aerosol for set 1 in nucleation, accumulation and coarse mode was 2.8%, 18.3% and 78.8%, respectively where as in set 2 it was 1.5%, 18.6% and 79.8%, respectively.

Chemical composition of aerosols have also shown a peak each in fine and coarse size for all the components with maximum concentration observed in the coarse mode. Concentration of Na, Cl and Ca was found to be higher indicating dominence of the marine source, but the concentration of F, NO_3, SO_4, NH_4, K and Mg were comparatively less during the study period. Marine source contributed about 48.5% to total measured composition of aerosols where as crustal and anthropogenic sources contributed about 30.0% and 33.6%, respectively. Similarly, in set 2 maximum contribution was from marine (17.8 $\mu g/m^3$), followed by crustal (1.0 $\mu g/m^3$) and anthropogenic (5.2 $\mu g/m^3$). Thus, the site at Indian Arctic station, Himadri is not highly enfluenced by anthropogenic activities.

Two years of measurements of atmospheric aerosols at a remote mountain site in NE Spain

A.Ripoll[1], M.C. Minguillón[1], J. Pey[1], X. Querol[1], A. Alastuey[1],

[1]Institute of Environmental Assessment and Water Research (IDAEA-CSIC);
Presenting author email: anna.ripoll@idaea.csic.es

Investigation of atmospheric aerosols at mountain sites permits to perform ground measurements in the free troposphere without the interference of local pollution, and consequently to better characterize background aerosols, source origins and atmospheric processes. This paper summarizes preliminary results on the interpretation of the time variation of levels of physico-chemical parameters of tropospheric aerosols measured at the Montsec (MSC, 1570 masl) remote background station located in NE of Spain, since November 2009.

PM_{10}, $PM_{2.5}$ and PM_1 concentrations were recorded on a semi-hourly basis by an optical counter (Grimm Labortechnik GmbH & Co. KG, model 1107). Aerosol absorption coefficients at 637 nm (from which black carbon (BC) concentrations were calculated) and particle number (N) concentrations were measured on a 1-5 minutes basis by means of a Multi Angle Absorption Photometer (MAAP, model 5012, Thermo) and a Condensation Particle Counter (CPC, Model TSI 3776, 3-1000nm), respectively. PM_{10} and PM_1 24h samples were collected on quartz fibre filters at a ratio of 1 sample out of 4 days by means of sequential high-volume samplers (MCV CAV-A/MSb), equipped with PM_{10} and PM_1 cut-off inlets. Filters were treated and analysed following the methodology described by Querol et al. (2008), for the determination of the concentrations of major PM components (Al, Ca, Fe, K, Mg, Na, NO_3^-, NH_4^+, SO_4^{2-}, Cl^-, OC and EC) and trace elements (V, Ni, Ti, Cu, Zn, As, among others). In addition to the routine measurements, an intensive field campaign was performed during summer 2011, focused on the investigation of the summer regional recirculation episodes and Saharan dust outbreaks. To this end additional parameters were monitored: size distribution of submicron particles by using a SMPS 3080TSI; NH_3 hourly concentrations by AIRRMONIA; particles scattering (σ_{sp}) and hemispheric backscattering (σ_{bsp}) coefficients by means of a LED-based integrating nephelometer (model Aurora 3000, ECOTECH Pty, Ltd, Knoxfield, Australia); hourly concentrations of non refractory compounds (SO_4^{2-}, NO_3^-, NH_4^+, Cl^- and organics) by means of an Aerosol Chemical Speciation Monitor (ACSM, Aerodyne Research).

Local meteorology was studied by using the data from the Montsec d'Ares station (Catalan Autonomous Meteorological Service). The calculation of back-trajectories ending at MSC at 1500 and 2500 m a.s.l were made in order to classify the origin of the air masses reaching this site. Furthermore, the interpretation of aerosol maps for the identification of long range transport of atmospheric aerosols, including African dust, biomass burning and anthropogenic pollution plumes, were made by using BSC/DREAM8b, SKIRON and NAAPS models.

Low average concentrations of particle matter (PM) and BC were recorded for 2010-2011 (11.5 µg m^{-3}, 8.5 µg m^{-3}, 5.9 µg m^{-3} and 192 ng m^{-3} for PM_{10}, $PM_{2.5}$, PM_1, and BC, respectively), which is typical of the continental background sites,. On the contrary, the mean level of N for the same period (3588 # cm^{-3}) can be considered as relatively high for remote sites.

Concentrations of PM, BC, N, and PM components varied markedly according to the origin of the air masses. Lowest levels for most pollutants were recorded during winter stagnating conditions and the Atlantic advections, when the MSC site is located above the boundary layer. High absorption coefficients and levels of PM_{10} and mineral matter were obtained during Saharan dust outbreaks. Summer regional recirculation episodes (Rodriguez et al., 2003) are characterized by high levels of PM_1, SO_4^{2-}, OC, EC, absorption coefficients (BC) and N. The European episodes, occurring typically in winter, showed high concentrations of NO_3^- and EC. The maximum N was usually recorded in summer at midday, associated to winds from the SWS sector, and are interpreted as the new formation of particles by photochemistry nucleation episodes (Figure 1).

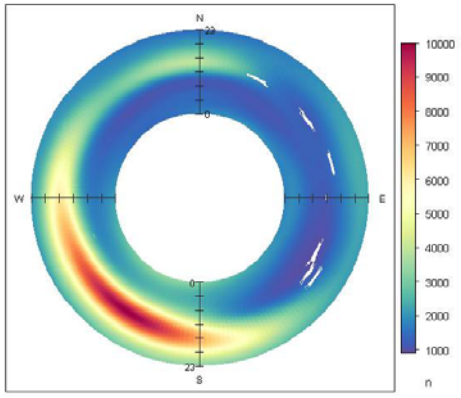

Figure 1. Daily variation of particle number concentration as a function of the wind direction

This work was supported by the MICINN (Spanish Ministry of Science and Innovation) and FEDER funds under the project CARIATI (CGL2008-06294/CLI).

Querol, X., Alastuey, A., Moreno, T., Viana, M.M., et al. (2008) *Atmos. Environ.*, **42**, 3964-3979.

Rodríguez, S., Querol, X., Alastuey, A., Viana, M., and Mantilla, E. (2003). *Environ. Sci. and Tech.*, **37**, 216-222.

Investigating physicochemical properties of marine aerosol over the Atlantic Ocean

S. Huang, L. Poulain , Z. Wu, F. Höpner, H. Herrmann, A. Wiedensohler

Leibniz Institute for Tropospheric Research, Leipzig, 04318, Germany

Keywords: Atlantic aerosol, Marine sulphate, Methane sulfonic acid, Hygroscopicity, Polarstern.
Presenting author email: huang@tropos.de

Marine aerosol plays an important role in global climate regulation and marine biogenic system. For a better understanding of its importance, much research was performed to investigate its physical and chemical properties by ship campaigns, but mostly focused on coastal regions or part of ocean areas. In our study the physicochemical properties of marine boundary layer aerosol were measured on board of the research vessel Polarstern during a series of cruises from North Atlantic to South Atlantic.

The primary results of chemical composition and hygroscopic properties of Atlantic aerosols for the first cruise, Polarstern Expedition ANT-XXVII/4 from Cape Town (South Africa) to Bremerhaven (Germany) in April and May of 2011 were presented. During this cruise, a large suite of on-line instrumentation including a High Resolution Time of Flight Aerosol Mass Spectrometer (HR-ToF-AMS), a Scanning Mobility Particle Sizer (SMPS), a Cloud Condensation Nuclei counter (CCNc), a Hygroscopicity Tandem Differential Mobility Analyzer (H-TDMA), an Integrating Nephelometer, and a Multi Angle Absorption Photometer (MAAP) were deployed, as well as 24-hour DIGITEL filter samples (PM_1).

HR-ToF-AMS provided high time resolution and size-resolved chemical compositions for marine aerosol. Since Methane sulfonic acid (MSA) is considered as an important tracer for marine aerosol and sulphur cycle, but mainly contained in sulphate and organic compositions when detected by AMS, we extracted MSA from the standard AMS compositions by the method described by Zorn *et al* (2008).

AMS Unit Mass Resolution (UMR) results showed that sulphate is the dominant species of non-refractory submicron marine aerosol in marine boundary layer(-9 ng/ m^3 - 11.95µg/m^3), averagely taking 61% of total measured mass fraction during the whole measuring period (excluding periods with ship exhausts contamination). Figure 1 provided a full picture of the sulphate mass concentration along the ship track. The outflow from Gibraltar and continents seems have strong influence when ship passed by. However, a clearer understanding could be achieved after detailed back trajectory analysis.

The organic is the second important species accounting for 22% in average over the whole period. Ammonium shows an obvious concentration (-5 ng/ m^3 - 2.13µg/m^3) in most measurement period. But the mass concentrations of nitrate and chloride are very low all over the cruise. The same situation happened to the marine aerosol tracer MSA. However, it presented a visibly similar trend with sulphate.

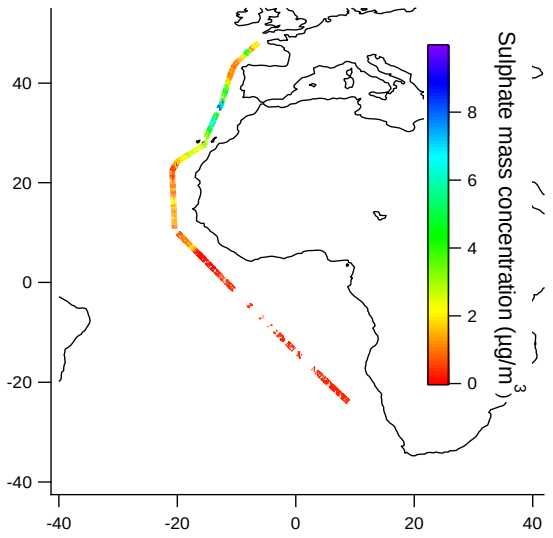

Figure 1. Sulphate concentration along the ship track

In addition, we performed a closure study of hygroscopicity of the size-resolved particles using the Zdanovskii–Stokes–Robinson (ZSR) method based on H-TDMA measurements and AMS data. The theoretically predicted GFs, which were calculated from chemical compositions, showed a good consistence with the measured GFs derived from HTDMA measurements. The high time resolution and size-resolved particle chemical composition provided a significant insight into the influence of the aerosol chemical composition on the aerosol hygroscopicity.

Zorn, S. R., Drewnick, F., Schott, M., Hoffmann, T., and Borrmann, S.(2008) *Atmos. Chem. Phys.*, **8,** 4711–4728

Evaluation of aerosols properties using ground based instruments in Magurele, Romania

J. Vasilescu[1], L. Marmureanu[1], A. Nemuc[1] and L. Belegante[1]

[1]National Institute of Research and Development for Optoelectronics, Magurele, RO 77125, Romania
Keywords: organic aerosols, refractive index, aerosol size distribution
Presenting author email: jeni@inoe.inoe.ro

The aim of this study is to characterize local and biomass burning long-range transported aerosols influences at Magurele site (44.35 N, 26.03 E), using collocated ground based instruments. Chemical composition and size distribution of submicronic aerosols at ground level have been studied using an Aerodyne C-TOF aerosol mass spectrometer (AMS) (Allan et al, 2003). Inversion products (Angstrom exponent, single scattering albedo, refractive indexes and integrated aerosol size distributions) from an eight wavelengths CIMEL Electronique spectral sun photometer, part of AERONET-Aerosol Robotic Network (Holben et al, 2001), have been also used. Long range transported aerosols cases have been confirmed by Hysplit-Hybrid Single Particle Lagrangian Integrated Trajectory Model (Draxler et al, 2012) and MODIS (Moderate Resolution Imaging Spectroradiometer) global fire maps.

In order to assess the influence of local organic aerosols we have been chosen measurements data in cases of nearby fires (spring 2010) and local heating (winter 2011, 2012). Two cases of long range transported biomass burning aerosols (summer 2010) are taken into consideration as well. The age of organic aerosols was assessed from mass spectrum values of m/z 57, 43 and respectively 44 (Hildenbrandt et al, 2010) and from percentage of the *m/z* 44 fraction from the total organics (Adler et al, 2011). Even though the instruments measured different air samples, AMS at the ground level and sunphotometer on integrated column, some correlations between optical and chemical retrieved parameters were observed.

According to AMS measurements, main species at ground level are organics, nitrate, sulphate, and ammonium. Organics concentrations five times higher than other species in some particular cases have been noticed. Small values of the percentage of the m/z 44 from the total organics indicate less oxygenated organic aerosols. The spring cases with percentage around 0.02±0.001 are fresh organics, in contrast with summer cases, with higher percentage (0.18 ±0.003) considered aged aerosols transported from Ukraine region.

The aerosols refractive indexes, real (mR) and imaginary (mI) part, are related to the particles chemical composition and to the internal mixture of species. As it was expected in the cases with local aerosols influence the sunphotometer retrieved refractive indexes values are different from those measured nearby sources indicated by literature (mR: 1.49-1.53; mI 0.01-0.02) (Adler et al, 2011). The local ground aerosols don't influence too much the data sensed by instruments which measure an integrated column. In Figure 1 real and imaginary part of refractive indexes from sunphotometer are plotted versus normalized organics concentration from AMS to show the correlations of these parameters for nearby fires (green), house heating related organics (white) and long range transported biomass burning (grey). The mR values sensed by sunphotometer are not influenced by local aerosols, but the mI is more sensitive to these events. Size distributions of submicronic aerosols during heating period presented in general two peaks (at 200 and 500 nm diameter) and during biomass burning influence only one peak (at 400 nm diameter). The AMS and sunphotometer data are in good agreement regarding the size distribution of aerosols.

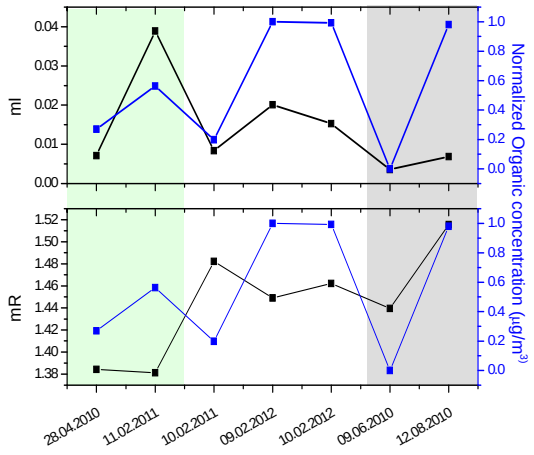

Figure 1 Comparison between sunphotometer refractive indexes (imaginary and real) and normalized organic aerosols concentration derived from AMS measurements

This work was supported by a grant of the Romanian National Authority for Scientific Research, CNCS – UEFISCDI, project number PN-II-RU-PD-2011-3-0082.

Adler G. et al, (2011), *Atmos. Chem Phys* **11**, 1491-1503
Allan J.D. et al, (2003), *J. Geophys. Res.* **108**, 4091-4105
Draxler, R.R. and Rolph, G.D., (2012) HYSPLIT (HYbrid Single-Particle Lagrangian Integrated Trajectory) Model access via NOAA ARL READY Website (http://ready.arl.noaa.gov/HYSPLIT.php). NOAA Air Resources Laboratory, Silver Spring, MD
Hildebrandt L. et al, (2010), *Atmos. Chem. Phys.* **10**, 4167–4186
Holben B. N. et al, (2001), *J. Geophys. Res.* **106**, 12 067–12 097

Size-segregated inorganic aerosol compounds during different meteorological scenarios

M. A. Revuelta, F. J. Gómez-Moreno, L. Núñez, M. Pujadas, B. Artíñano

Department of Environment, Centro de Investigaciones Energéticas, Medioambientales y Tecnológicas (CIEMAT), Madrid, 28045, Spain
Keywords: sulfate, particulate nitrate, hygroscopic growth, size distribution
Presenting author email: b.artinano@ciemat.es

Secondary inorganic compounds (SIC) represent a significant fraction of particulate matter in urban environments. They are formed from precursor gases through different processes that define the chemical and physical state of the particulate compound. Photochemical oxidation through the OH radical and aqueous-phase reactions – and thus meteorological conditions - play a key role in these processes. SIC generation produces acidic nitrate and sulfate that in the urban atmosphere are usually neutralized mainly by ammonium (Bari et al, 2003).

In an urban background site in the Madrid Metropolitan Area measurements have been taken for three different meteorological scenarios during winter 2011. A severe fog episode (E1) was compared to a typical intense winter accumulation situation (E2). E3 was intermediate between E1 and E2.

During the three events, size-distributed particle ion composition was obtained by a micro-orifice deposit impactor (MOUDI) and a nano-MOUDI attached. This impactor collected fourteen size fractions that were chemically analyzed for soluble ions (sulfate, nitrate, ammonium, calcium and others). Total size distribution spanned from 18 µm to particles smaller than 0.01 µm. Samples were taken on a 24 h time basis. Near real-time measurements of particulate sulfate, nitrate and precursor gases concentrations were continuously monitored, as well as meteorological variables. In addition, for E2 the particle size distribution from 20 to 0.015 µm was measured by the combined use of an optical particle counter GRIMM1108 and a Scanning Mobility Particle Sizer.

During E1, ion analysis showed a very pronounced accumulation mode of 1-1.8 µm of both sulfate and nitrate. Aerosol was acidic below 0.18 µm. Time series shows production of these compounds during day and night and relative humidities always above 85%.

During E2 the prevailing aerosol mode was also in the accumulation range, but the highest concentrations were found in smaller sizes. A minor nitrate coarse mode was found. Aerosol was acidic in the range 0.32-1.8 µm and also below 0.18 µm. Total concentrations were one order of magnitude lower than in E1. Time series shows daily SIC generation correlating with solar radiation and related to precursor gases. A comparison between the ion size distributions and the aerosol volume distribution was performed.

During E3, ion distributions and time evolution parameters show intermediate characteristics between E1 and E2. However, ion concentrations are only slightly higher than in E2, and very far from those found in E1. (See Fig. 1). This indicates that aqueous-phase is more efficient than photochemical-dominated SIC production.

This study was conducted in Madrid as an extension of Plaza et al (2011). In that case the efficiency of sulfate formation by aqueous phase oxidation and further ammonia uptake was stated. In the present work this efficiency is evaluated for a severe fog event and also for nitrate.

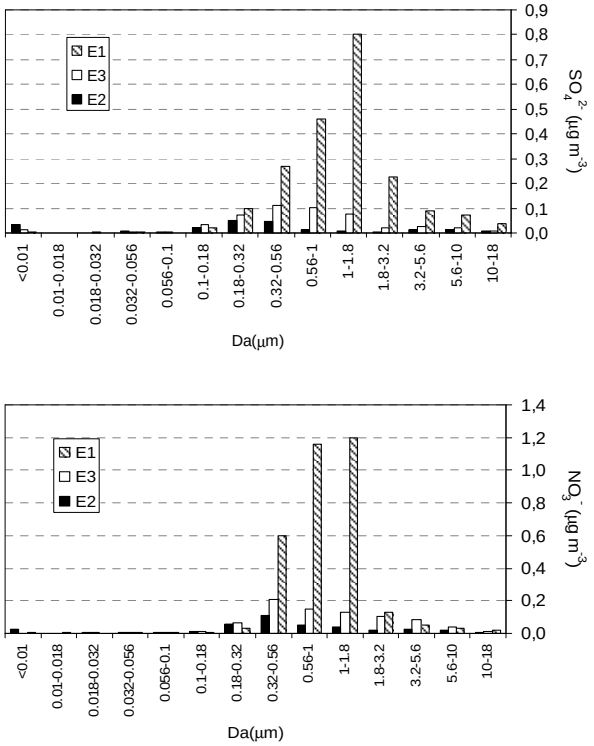

Figure 1. Sulfate (top) and nitrate (bottom) size distribution for E1, E2 and E3.

This work was supported by the National R&D Plan, through the project MICROSOL (CGL2011/CLI-27020). M. A. Revuelta acknowledges the Ministry of Science and Innovation for their economical support through the FPI predoctoral grant BES-2008-007079.

Bari, A., Ferraro, V., Wilson, L.R., Luttinger and D., Husain, L. (2003) *Atmospheric Environment* 37, 2825–2835.

Plaza, J., Pujadas, M., Gómez-Moreno, F.J., Sánchez, M., Artíñano, B. (2011). *Atmospheric Environment* **45**, 4966-4976

Ionization of the atmosphere induced by cosmic rays: Full model and practical applications

I.G. Usoskin[1]
[1]Sodankylä Geophysical Observatory and Dept. of Physics, University of Oulu, Finland
Keywords: atmosphere, ionization, cosmic rays
Presenting author email: ilya.usoskin@oulu.fi

An important physical characteristic of the atmosphere is its degree of ionization. Although it is usually very low, viz. the atmosphere is essentially neutral, the small amount of mobile ions can play an important role in atmospheric chemistry. Ionization in the atmosphere is grossly defined by the cosmic ray energetic particles either of galactic or solar origin. A direct effect of atmospheric ionization on aerosol formation and growing is not confirmed by field experiments (Kulmala et al., 2010) and is shown to be small by laboratory experiments (e.g., Kirkby et al., 2012). On the other hand, a case study of an extreme solar energetic particle event of January 20, 2005 suggest that barely noticeable effect in polar stratospheric aerosols may exist (Mironova et al., 2008, 2011), probably via indirect way.

In order to study the role of ionization, one needs a reliable numerical model. Here we present a full 3D numerical model of cosmic ray induced ionization in the atmosphere which can be applied in all conditions. The model CRAC:CRII (Cosmic Ray induced Atmospheric Cascade: application for Cosmic Ray Induced Ionization) is a full 3D physical model based on a full Monte-Carlo simulation of the cosmic ray induced atmospheric cascade (Usoskin and Kovaltsov, 2006; Usoskin et al., 2010). We note that most of earlier models (including semi-empirical) do not consider the full atmospheric cascade and/or limited in energy of incoming energetic particles and thus have strict limitation to be valid only in the upper polar atmosphere. The CRAC:CRII model is applicable in the entire neutral atmosphere, from poles to equator and from ground level to the mesosphere. It has been tested versus fragmentary measurements to show agreement within 10%. The model output is given either as a pre-calculated look-up tables or a simple parametrization, and is easy to apply in practice. The CRAC:CRII model is used to evaluate the ionization background in many atmospheric models, and also in the CLOUD experiment.

We present the physical background of the ionization processes, and discuss practical implications.

Kulmala, M., I. Riipinen, T. Nieminen, et al., (2010), Atmos. Chem. Phys. **10**, 1885-1898.

Kirkby, J., J. Curtius, J. Almeida et al. (2011), Nature, **476**, 429–433.

Mironova, I.A. et al. (2008) Geophys. Res. Lett., **35**, L18610.

Mironova, I.A., I.G. Usoskin, G.A. Kovaltsov, and S.V. Petelina (2012) Atmos. Chem. Phys. **12**, 769-778.

Usoskin, I.G., G.A. Kovaltsov (2006) J. Geophys. Res., **111**, D21206.

Usoskin, I. G., G. A. Kovaltsov, and I. A. Mironova (2010), J. Geophys. Res., **115**, D10302.

Long term observations of aerosol light absorption and particle volatility properties in the lower tropical free troposphere

T. Hamburger[1], R. Krejci[1], M. Matisans[1], J. Ström[1], P. Tunved[1], G. Hoschild[2], J. Gross[2], S. Calderon[3] and P. Hoffmann[3]

[1]Department of Applied Environmental Science (ITM), Stockholm University, Stockholm, 106 91, Sweden
[2] Karlsruhe Institute of Technology, Institute for Meteorology and Climate Research (ASF), 76344 Eggenstein-Leopoldshafen, Germany
[3]Universidad de Los Andes, Merida 5101, Venezuela
Keywords: absorption, aerosol measurement, biomass burning, tropospheric aerosols, volatility.
Presenting author email: thomas.hamburger@itm.su.se

The tropics comprise an important source region of aerosol particles, most notably desert dust, biomass burning and biogenic aerosols. However, long-term measurements of aerosol properties in the tropical free troposphere are sparse. Aerosol measurements were conducted between March 2007 and May 2009 at the Pico Espejo Atmospheric Research Station Alexander von Humboldt (Schmeissner *et al*, 2011). The Pico Espejo (8.51° N, 71.05° W, 4765 m a.s.l.) is located on the top of the Sierra Nevada mountain ridge close to the city of Mérida, Venezuela.

Particle number concentration, size distribution, volatility and light absorption were observed at the high altitude research station. The aerosol instrumentation contained a Particle Soot Absorption Photometer (PSAP) and two Differential Mobility Particle Sizer (DMPS). Particle number concentrations were measured using Condensation Particle Counters (CPC). A thermodenuder was used to heat the sampled aerosol to 300°C. It was combined with one DMPS to retrieve information on volatile particle number and volume. Case studies using different thermodenuder settings were performed to analyse the temperature dependency of volatile and semi-volatile particle compounds.

The location of the Pico Espejo allows for observations of air masses within the lower free troposphere as well as air masses from the planetary boundary layer reaching the high altitude station through shallow convection. Observed air masses frequently originate from the Amazon Basin. The Amazon is a rich source of biomass burning aerosol during the dry season from December till April (Guyon *et al*, 2003). In addition to the influence from regional and continental aerosol sources episodes of long-range intercontinental transport were observed. Results retrieved from the Lagrangian Particle Dispersion Model FLEXPART (Stohl *et al*, 2005) show that air masses originating in Africa are a very likely source of aged biomass burning plumes observed at Pico Espejo station.

The seasonal cycles of particle absorption and ambient and heated (300°C) particle concentrations follow a well-defined pattern reaching their maxima in the end of the dry season around March and April. Besides the seasonal cycle, there is also a distinct diurnal cycle at Pico Espejo. Free tropospheric air dominates during night time until midday. Air influenced by the planetary boundary layer often reaches the station from midday until evening hours due to increased surface heating and shallow convection induced by the orography.

Fig. 1 shows diurnal cycles of the absorption coefficient (a) and heated (300°C) particle volume concentration (b). Both diurnal cycles are divided into dry (red) and wet (blue) seasons. Median values (lines) and Quartiles (shades) are shown in both panels. The median values of both parameters increase during the wet season by a factor 2-3 from night time to daytime. An increase by a factor of 10 was observed for both parameters during the dry season. The third quartile of the absorption coefficient reaches 1.3 Mm^{-1} during the dry season. However, single events of absorption coefficients up to 8 Mm^{-1} were observed.

Further, aerosol light absorption and aerosol volatility seasonal cycles in the tropical free troposphere will be discussed with respect to meteorological conditions, transport, general circulation and source regions.

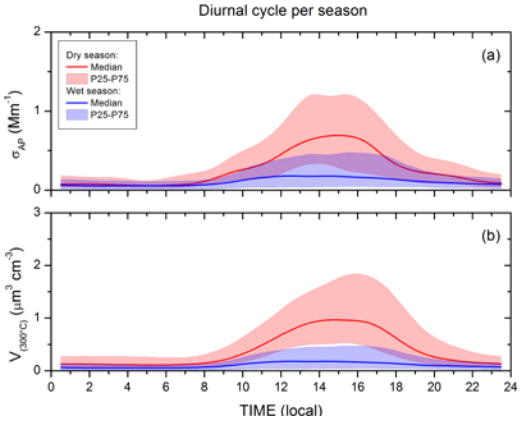

Figure 1. Diurnal cycle of the absorption coefficient (a) and non-volatile (300°C) particle volume concentration (b) for dry (red) and wet (blue) season.

This work has been funded by Swedish Research Council (VR) and Swedish International Development Cooperation Agency (SIDA).

Guyon, P., et al (2003) *Atmos. Chem. Phys.* **3**, 951-967.
Schmeissner, T., et al (2011) *Atmos. Chem. Phys.* **11**, 3319-3332.
Stohl, A., et al (2005) *Atmos. Chem. Phys.* **5**, 2461-2474.

Aerosol long-term volatility measurements in a boreal forest environment

S.A.K. Häkkinen[1], M. Äijälä[1], K. Lehtipalo[1], H. Junninen[1], J. Backman[1], A. Virkkula[1, 2], T. Nieminen[1], M. Vestenius[2], H. Hakola[2], M. Ehn[3], D. R., Worsnop[1, 4], M. Kulmala[1], T. Petäjä[1] and I. Riipinen[1, 5]

[1]Department of Physics, University of Helsinki, 00014 Helsinki, Finland
[2]Finnish Meteorological Institute, 00560 Helsinki, Finland
[3]Institute for Energy and Climate Research (IEK-8), Forschungszentrum Jülich, 52425 Jülich, Germany
[4]Aerodyne Research, Inc., Billerica, Massachusetts, USA
[5]Department of Applied Environmental Science and Bert Bolin Centre for Climate Research, Stockholm University, 10691 Stockholm, Sweden

Keywords: fine particles, volatility, black carbon
Presenting author email: silja.hakkinen@helsinki.fi

Climate and health effects of atmospheric aerosols are determined by their properties such as their chemical composition. Aerosol chemical composition can be studied indirectly by measuring volatility of the aerosol particles. The volatility of submicron aerosol particles (15-500 nm) was studied in a boreal forest site at SMEAR II (Station for Measuring Ecosystem-Atmosphere Relations II) station (Vesala *et al.*, 1998) in Hyytiälä, Finland, during 01/2008-05/2010. The instrument used for the measurements was a VDMPS (Volatility Differential Mobility Particle Sizer), which consists of two separate instruments: a DMPS (Differential Mobility Particle Sizer, Aalto *et al.*, 2001) and a TD (Thermodenuder, Wehner *et al.*, 2002).

Aerosol evaporation was examined by heating aerosol and comparing the total aerosol mass before and after heating. In the VDMPS system ambient aerosol sample was heated to temperatures ranging from 80 ºC to 280 ºC. The higher the heating temperature was the more aerosol material was evaporated. There was a non-volatile residual present in aerosol particles when heated to 280 ºC. This residual explained on average 19% of the total aerosol mass. The aerosol non-volatile mass fraction had a clear negative correlation with ambient temperature: aerosol mass fraction remaining was the highest during winter and the smallest during the summer months.

The role of black carbon in the observed non-volatile residual was determined. Black carbon explained on average 55 to 90% of the non-volatile mass. However, especially during colder months noticeable fraction of non-volatile material, something else than black carbon, was observed. According to Kalberer *et al.* (2004) some atmospheric organic species can form polymers that have high evaporation temperatures. Also low-volatile organic salts may contribute to the non-volatile aerosol (Smith *et al.*, 2010).

Aerosol mass composition measured directly with AMS (Aerosol Mass Spectrometer, Jayne *et al.*, 2000) was analyzed in order to examine the properties of the non-volatile material (other than black carbon). The AMS measurements were performed during spring and autumn 2008. Results from the aerosol mass spectrometry indicate that some nitrate and organic compounds may be found in the non-volatile aerosol residual, especially during autumn. During the winter and spring months the non-volatile core (black carbon removed) correlated markedly with carbon monoxide and sulfur dioxide, which are tracers of anthropogenic emissions. Due to this, the non-volatile residual may also contain other pollutants in addition to black carbon. Thus, it seems that the volatility of submicron aerosol particles is affected by both anthropogenic and biogenic factors as well as by the meteorological conditions.

This work was financially supported by the University of Helsinki three-year research grant (No. 490082), Academy of Finland, Finnish Center of Excellence grant (No. 141135), European Research Council grant ATMNUCLE (No. 227463) and ATMOGAIN (No. 278277), and Maj and Tor Nessling Foundation (No. 2010143),which are gratefully acknowledged.

Aalto *et al.*, (2001). Physical characterization of aerosol particles during nucleation events. *Tellus B*, 53, 344-358.

Jayne *et al.*, (2000). Development of an aerosol mass spectrometer for size and composition analysis of submicron particles. *Aerosol Sci. Technol.*, 33(1-2), 49-70.

Kalberer *et al.*, (2004). Identification of Polymers as Major Components of Atmospheric Organic Aerosols. *Science*, 303, 1659-1662.

Smith *et al.*, (2010). Observations of aminium salts in atmospheric nanoparticles and possible climatic implications. *P. Natl. Acad. Sci., 107(15).*

Vesala *et al.*, (1998). Long-term field measurements of atmosphere-surface interactions in boreal forest combining forest ecology, micrometeorology, aerosol physics and atmospheric chemistry. *Trends Heat, Mass Mom. Trans.*, 4, 17-35.

Wehner *et al.*, (2002). Design and calibration of a thermodenuder with an improved heating unit to measure the size-dependent volatile fraction of aerosol particles. *J. Aerosol Sci.*, 33, 1087-1093.

Aerosol water soluble organic matter: Characterization of surface active substances by electrochemical method

Z. Kozarac[1], B. Ćosović[1], S. Frka[1], J. Dautović[1], G. Kiss[2], A. Hoffer[2]

[1]Ruđer Bošković Institute, Division for Marine and Environmental Research, Bijenička 54, 10000 Zagreb, Croatia
[2]Air Chemistry Group of Hung. Acad. Sci. at University of Pannonia, Egyetem 10, 8200 Veszprém, Hungary

Keywords: Aerosol, water soluble organic matter, surface active substances, electrochemical method
Author email: kozarac@irb.hr

The composition of the organic part of the atmospheric aerosol and the respective source contributions are far less known than those of the inorganic part. Significant proportion (30-80%) of the organic carbon is water-soluble (WSOC) and made up of polymer-type substances of higher molecular weight. Surface active substances (SAS) are the most reactive part of organic matter in natural environmental systems which accumulate at the interfaces and are present in aerosols and atmospheric precipitations. They form the surface film at the rain drop/air interface in which persistent organic pollutants accumulate, making long distance transmission possible. Surface active organic constituents can influence the surface tension of nucleating cloud droplets and thereby modify the critical supersaturation necessary to activate aerosol particles. The electrochemical methods offer an elegant way of SAS qualitative and quantitative characterization based on the measuring of electrode double layer capacity changes at mercury electrode surface. The method is applicable for the analysis of SAS in different aquatic systems, both freshwater and marine, which is very convenient for comparative studies.

Aerosol samples (PM 2.5) were daily collected at Middle Adriatic station influenced by marine, regional and continental air masses inputs as well as from urban (Zagreb, Croatia) and rural (K-puszta, Hungary) areas during late spring-early autumn period and SAS were analysed by the electrochemical method.

The highest SAS concentrations, expressed in equivalents of Triton-X-100, ranging from 0.34-0.91µg m^{-3} (mean 0.55± 0.21µg $m^{-3,}$ n=10) were detected in urban samples. The surfactant activities of marine, regional and continental samples were in the narrow ranges from 0.14-0.31µg m^{-3}(mean 0.25±0.06µg m^{-3},n=10), 0.18-0.42µg m^{-3} (mean 0.27±0.07 µg $m^{-3,}$ n=18) and 0.07-0.28µg m^{-3} (mean 0.17±0.075 µg m^{-3}, n=10), respectively. The SAS concentrations in K-puszta aerosol samples ranged from 0.13-0.46 µg m^{-3} (mean 0.29±0.11 µg m^{-3}, n=6). Investigation of isolated humic-like substances (HULIS) confirmed that HULIS material exhibit strong surface activity. On the basis of the normalized surface activity we recommend that the surface activity of non-urban samples can be modeled by C9 fatty acid.

This work was funded by the bilateral Croatian –Hungarian research project "Complex investigation of organic aerosols in rural, urban and marine environment" and by the grant from the Croatian Ministry of Science, Education and Sports project "Nature of organic matter, interaction with traces and surfaces in environment" (098-0982934-2717).

Hygroscopic Properties of Ultrafine Aerosol Particles over the Aegean Sea

S. Bezantakos[1,2], K. Barmpounis[3], E. Bossioli[4], M. Tombrou[4], N. Mihalopoulos[5], K. Eleftheriadis[2], J. D. Allan[6], H. Coe[6], A. Bacak[6], G. Biskos[1,3]

[1]Department of Environment, University of Aegean, Mytilene 81100, Greece
[2]ERL, Inst. of Nuclear Tech. & Rad. Protection, NCSR Demokritos, 15310 Ag. Paraskevi, Attiki, Greece
[3]Faculty of Applied Sciences, Delft University of Technology, Delft 2628-BL, The Netherlands
[4]Department of Physics, National and Kapodistrian University of Athens, Athens 15784, Greece
[5]Department of Chemistry, University of Crete, Heraklion 71003, Greece
[6]School of Earth, Atmospheric and Environmental Science, The University of Manchester, Manchester, United Kingdom

Keywords: Aerosol Measurement, Particle size, Particle growth, H-TDMA, Mediterranean
Presenting author email: bezantakos@env.aegean.gr

Ultrafine aerosol particles in the atmosphere can absorb and scatter radiation, thereby affecting the climate of the Earth at a local and a global scale (IPCC 2007). The scattering and absorption efficiency of these particles strongly depends, among other factors, on their water content. It is therefore important to have information on their ability to take up water (i.e., particle hygroscopicity) when exposed to conditions of different relative humidity (RH) in order to understand their impacts on climate.

In this work we report in situ measurements of the hygroscopicity of the particles observed in the atmosphere over the Aegean Sea during the end of summer (from 25 August to 10 September 2011) when the composition of the atmosphere in the region is affected by northern winds (Etesians). For the measurements we employed a Hygroscopic Tandem Differential Mobility Analyzer (HTDMA; Rader & McMurry, 1986) located at Vigla station on the island of Lemnos, and high time-resolution particle composition measurements obtained by an Aerosol Mass Spectrometer (AMS; Jayne et al. 2000) that was onboard the BAe146-FAAM aircraft that was also operational in the region during the measuring period. The hygroscopic growth of the particles over the Aegean Sea was then estimated using the k-Köhler theory (Petters & Kreidenweis, 2007) in combination with the AMS measurements

Fig. 1 shows the HTDMA measurements of particles having dry diameter from 50 to 170 nm at Vigla station. The hygroscopic growth factors ranged from 1.0 to 1.8 with an average value of ca. 1.2 when the operating RH within the HTDMA was set to 85%. The relatively low hygroscopic growth factors indicate that the particles had a substantial amount of organic species. This conclusion is corroborated by the airborne AMS measurements when the aircraft flew over Lemnos at a height ± 300 meters higher/lower from the station. Using the k-Köhler theory and the AMS measurements when the aircraft was flying close to the station the predicted hygroscopic growth factors showed good agreement with those measured by HTDMA (cf. inset in Fig. 1).

Fig. 2 shows the particle growth factors calculated using k-Köhler theory using as input the AMS measurements during flight from Crete to Lemnos of 1 September. The predicted growth factors ranged from 1.0 to 1.8 with an average value ca. 1.3. Similar behaviour was observed for all the flights of the aircraft indicating that particles of low hygroscopicity due to a high fraction of organic species is characteristic for that period over the Aegean Sea.

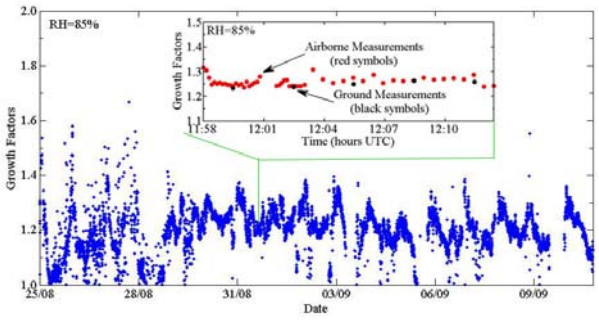

Figure 1. Hygroscopic growth factors of aerosol particles having dry diameter between 50 and 170 nm when exposed to 85% RH at Vigla station from 25/8/2011 to 11/9/2011. Inset: comparison between growth factors measured by the HTDMA (black symbols) and predicted by k-Köhler theory using the chemical composition measurements from the airborne AMS (red symbols) when the aircraft was flying over the station on 1/9/2011.

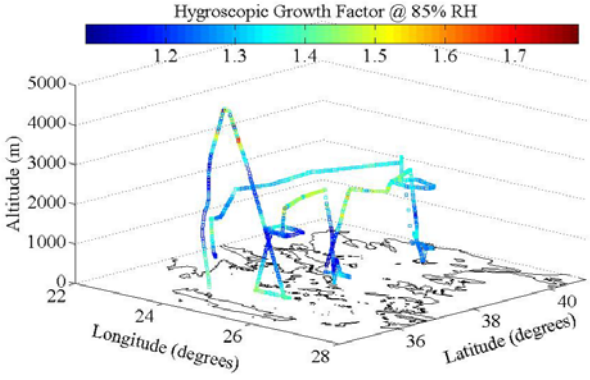

Figure 2. Hygroscopic growth factors of aerosol particles at 85% RH over the Aegean Sea on 1/9/2011. The GFs are calculated by the k-Köhler theory using the chemical composition measurements from the airborne AMS.

References

IPCC (2007), Fourth Assessment Report

Jayne T. J., Leard, D. C., Zhang, X., Davidotis, P. (2000) , *Aerosol Science & Technology*, 33, 49-70.

Petters, M. D. & Kreidenweis S. M. (2007), *Atmospheric Chemistry and Physics*,7, 1961-1971.

Rader, D. and McMurry,P. (1986), *J. Aerosol Sci*,17,771-787.

Hygroscopic Properties of Fine and Ultrafine Aerosol Particles over an Urban Background Site in Athens, Greece

S. Bezantakos[1,2], S. Vratolis[2], L. Diapouli[2], K. Eleftheriadis[2], G. Biskos[1,3]

[1]Department of Environment, University of Aegean, Mytilene 81100, Greece
[2]ERL, Inst. of Nuclear Tech. & Rad. Protection, NCSR Demokritos, 15310 Ag. Paraskevi, Attiki, Greece
[3]Faculty of Applied Sciences, Delft University of Technology, Delft 2628-BL, The Netherlands

Keywords: Aerosol Measurement, Particle size, Particle growth, H-TDMA, Mediterranean
Presenting author email: bezantakos@env.aegean.gr

In planetary scale, fine and ultrafine aerosol particles contribute to the planet's global radiative balance through direct and indirect effects (IPCC 2007). In regional scale, the same particles affect human health by infiltrating the lower respiratory system (Brunekreef & Holgate, 2002), and visibility (Cababa et. al., 2004). Quantitative measurement of particle hygroscopicity can help us understand the ability of the particles to act as Cloud Condensation Nuclei (CCN) and their efficiency to infiltrate the respiratory system, thereby providing valuable information for estimating their potential impacts on global climate and human health.

In situ measurements of particle hygroscopicity were conducted at the NCSR Demokritos Global Atmosphere Watch (GAW) urban background site in Athens from 13 October to 6 November 2011 using a Hygroscopic Tandem Differential Mobility Analyzer (HTDMA; Rader & McMurry, 1986). HTDMA scans over a period of 180 s each were processed by a curve fitting algorithm that was designed to fit up to three lognormal distributions depending on the spread of the selected monodisperse size distributions. By doing that we were able to identify different particle hygroscopic behaviour and the aerosol mixing state. Fig. 1 shows a characteristic example where two distinct modes are identified when dry monodisperse particles having 100 nm mobility diameter are exposed to 85% relative humidity (RH), indicating that the sampled aerosol is externally mixed.

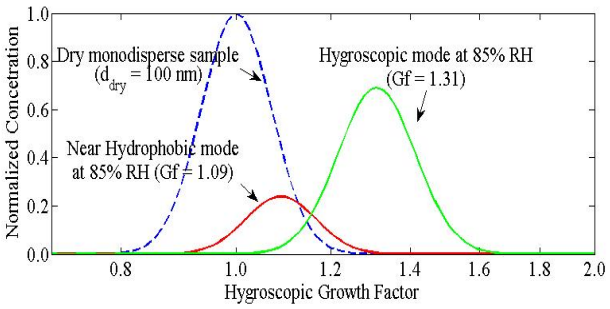

Figure 1. HTDMA measurements of particles having dry mobility diameter of 100 nm when exposed to < 10% RH (blue line) and 85% RH. Two modes are revealed when the particles are exposed to 85% RH indicating that the aerosol is externally mixed. The first population is almost hydrophobic having a hygroscopic growth factor of ca. 1.10 (red line) and the second is more hydrophilic having a hygroscopic growth factor of ca. 1.31 (green line).

Table 1 shows aggregate statistical results of particle hygroscopicity observed in the Demokritos site during the period of our study. Monodisperse particles having dry mobility diameters from 60 to 170 nm were selected using the first DMA of the system. More than half of the measurements (58.1%) indicated internally mixed aerosols, with an average growth factor ca. 1.2. More than one third of the measurements indicated externally mixed particles with one hydrophobic mode having a growth factor of ca. 1.1, and one more hydrophilic of ca. 1.3. Less than 5% of the measurements indicated externally mixed particles, with three distinct hygroscopicity modes: one hydrophobic mode with an average growth factor of ca. 1.1, one less hygroscopic with an average growth factor ca. 1.3, and one more hygroscopic with an average growth factor ca. 1.6. The variability of growth factors and modes observed was statistically evaluated against other important aerosol parameters (e.g., scattering coefficients, concentration of organic and elemental carbon, etc.).

Table 1: Aggregate statistical results of particles hygroscopicity in Athens from 13 Oct. to 6 Nov. 2011. Key: N is the number of modes of each sample, P is the relative frequency of occurrence for unimodal (1), bimodal (2) and trimodal (3) samples, Gf 1, 2, and 3 are the average growth factor ± one standard deviation of mode 1, mode 2, and mode 3, respectively, whereas C1, 2, and 3 are the ratios of particle number concentration of each mode with respect to the total particle number concentration of the selected dry fraction

N	P (%)	Gf 1	C1 (%)	Gf 2	C2 (%)	Gf 3	C3 (%)
1	58.1	1.23 ±0.12	100				
2	37.0	1.10 ±0.09	47.4	1.34 ±0.13	52.6		
3	4.9	1.08 ±0.07	36.0	1.31 ±0.09	46.8	1.59 ±0.14	17.2

References

IPCC (2007), Fourth Assessment Report

Brunekreef, B. & Holgate, S. (2002), *The Lancet*, 360, 1233–1242

Cabada, J., Khlystov, A., Wittig, A., Pilinis, C., Pandis, S. (2004), *J. Geophys. Res.*, 109, D16S03, doi:10.1029/2003JD004155

Rader, D. & McMurry,P. (1986), *J. Aerosol Sci*,17,771-787

Determination of the parameters of the critical nucleus that is formed on the seed particles during heterogeneous nucleation

S.V. Valiulin[1], V.V. Karasev[1], S.V. Vosel[1,2], A.A. Onischuk[1,2], A.M. Baklanov[1], S. di Stasio[3]

[1]Institute of Chemical Kinetics and Combustion, Novosibirsk, 630090, Russia
[2]Novosibirsk State University, Novosibirsk, 630090, Russia
[3]Istituto Motori CNR-IM Aerosol and Nanostructures Lab, Napoli, 80125, Italy
Key words: heterogeneous nucleation, nanoparticles, sulfur, critical nucleus
Presenting author email: valiulin@kinetics.nsc.ru

Method of the heterogeneous nucleation investigation in the laminar flow chamber is developed. This method give the relationships between the main process parameters: the critical nucleus size *d*, size of the seed particle *D*, supersaturation ratio, temperature and contact angle. The efficiency of this approach is demonstrated for the heterogeneous nucleation of sulfur vapor on tungsten oxide nanoparticles.

The experimental setup is shown in Fig. 1. The installation consists of three main parts: the generator of seed aerosol particles of tungsten oxide, the laminar flow chamber and the diffusion spectrometer of aerosol (DSA). The sulfur vapor was generated inside the chamber with the concentration below of the homogeneous nucleation limit. Clean air was used as a carrier gas. Number concentration and size distribution of aerosol particles at the outlet of reactor were measured by DSA.

Fig. 2 shows the size distributions of the incoming seed particles and the particles at the exit of chamber after the heterogeneous nucleation. During the experiments we varied the vapor pressure of sulfur without changing the size distribution seed nanoparticles. At low vapor pressure the size distribution of the particles before and after the chamber is identical (Fig. 2*a*), i.e. the size of the particles that were filed into the chamber lie below the minimal size to start the heterogeneous nucleation. When the pressure is high enough (Fig. 2*b*), the bimodal size distribution at the output is recorded. Left peak is a part of the spectrum of original particles which is smaller than the size required for the start of heterogeneous nucleation. The right peak corresponds to the particles on which critically nucleus were generated followed by condensation growth. The comparison of the outlet and inlet spectra gives the threshold diameter from which heterogeneous nucleation was started.

The approximate location of the heterogeneous nucleation region was determined experimentally using the "supersaturation cut-off" method. For this purpose round metallic grid with diameter equal to the inner diameter of the tube was inserted into the chamber perpendicularly to the flow (Fig. 1). Sulfur vapor and small seed particles of tungsten oxide were partially deposited on the grid. Particles on which nucleation and condensation growth occurred are large enough for penetration through the grid.

The temperature radial and axial profiles inside the chamber were measured by a chromel-alumel thermocouple. The rate of sulfur evaporation in the saturation zone and the axial profile of wall vapor deposition rate were measured experimentally. The difference between these two quantities gave the vapor concentration *n* averaged over the tube cross section vs the axial coordinate *Z*. Based on function *n(Z)* the radial profiles of sulfur vapor concentration were determined solving the mass transfer equation. The supersaturation profiles were calculated from the concentration and temperature profiles.

Based on these experimental data and theoretical approaches [1-3] it were determined the parameters of sulfur critical nucleus (size, contact angle) which formed on the surface of the seed particle, Fig. 3. Contact angle of sulfur critical nucleus on the surface of tungsten oxide seed particle is $\Theta \approx 41$ °.

1. J. Frenkel Kinetic Theory of Liquids (Oxford University Press, New York, 1946), P. 403.
2. N.H. Fletcher // J. Chem. Phys., V. 29. (1958) P. 572.
3. M. Lazaridis // Journal of Colloid and Interface Science 155 (1993) P. 386.

Financial support for this work was provided by the Siberian Branch of Russian Academy of Sciences (SBRAS): Interdisciplinary Integration Project No. 3 and SBRAS-Taiwan Collaboration Project No. 7; RFBR project no. 11-08-01204-a and the cooperation Agreement between CNR (Italian National Research Council) and RAS (Russian Academy of Science) years 2011-2013.

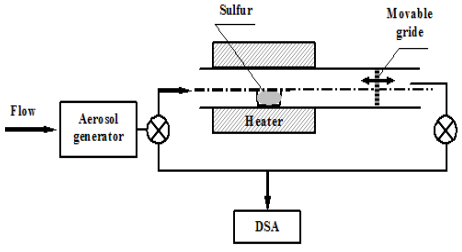

Fig. 1.

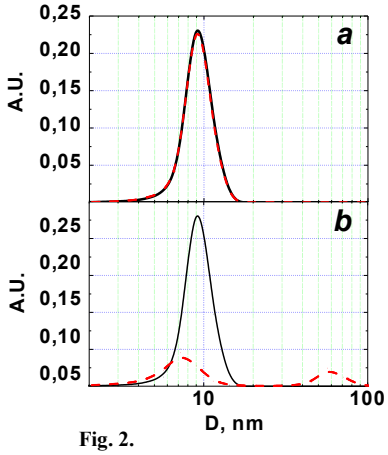

Fig. 2.

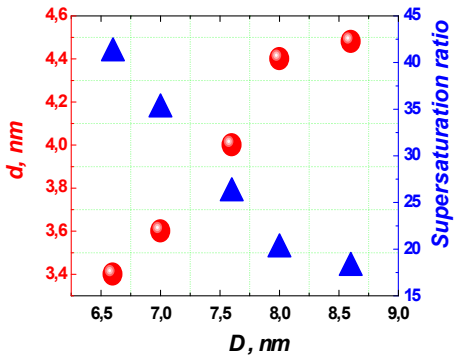

Fig. 3.

A Tandem DMA study on selected sugars and sugar alcohols

N.Zannoni[1], J.Hong[2], A.A. Zardini[3], K.Lieke[1], M. Bilde[1]

[1]Department of Chemistry, University of Copenhagen, Copenhagen 2100 Ø, Denmark
[2]Department of Physics, University of Helsinki, Helsinki 00014, Finland
[3]European Commission- Joint Research Center, Institute for Energy and Transport, Sustainable Transport Unit, Ispra 21027, Italy
Keywords: aerosol, sugars, vapour pressure.
Presenting author email: norazannoni@gmail.com

Sugars and sugar alcohols constitute an important component of the organic fraction in atmospheric particles. They have been detected in high concentrations in ambient aerosols during field campaigns (Graham et al., 2003; Facchini et al., 2000). They are found to be mainly in the coarse mode fraction of ambient particles, with a diurnal variation associated to the class of compounds. Biogenic sources are: pollen, fern spores and insects for sugars, yeasts and small fungal spores for sugar alcohols. The hydroxyl groups on these compounds make them particularly interesting for their behaviour in aqueous droplets, e.g. they can alter the water activity and surface tension of the aqueous solution. In order to clarify their behaviour in the particle phase and hence their effect on climate, the volatility and physical state of laboratory generated particles was investigated through a Tandem Differential Mobility Analyzer (TDMA) coupled with a laminar flow tube.

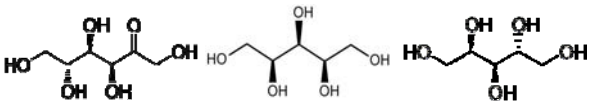

Figure 1. Chemical structures of Fructose, Xylitol and Arabitol.

Methods

A modified TDMA set up combined to a laminar flow reactor was used to measure the size distributions of laboratory generated particles (Bilde et al., 2003; Koponen et al., 2007, Zardini et al., 2010) of three compounds: Fructose, Xylitol and Arabitol. Aqueous solutions of ~$1*10^{-4}$ M of Fructose, Xylitol and Arabitol were prepared and atomized to obtain a polydisperse aerosol flow. The flows were then dried, and size selected with a Differential Mobility Analyzer coupled with a neutralizer. Particles entered a laminar flow reactor 3.5 m long, with four sampling ports along its length. A sheath flow of dry air was used to assure laminar conditions along the tube, and a water recirculating bath was used to control the temperature during each experiment. The particles initial and final diameter was sampled with a Scanning Mobility Particle Sizer (SMPS) at different sites along the set up. A lognormal function was used to fit the measured size distributions and from mass transfer theory we could infer a value of the vapour pressures for the three investigated compounds.

To obtain deeper information about the particles physical state, we repeated the experiments by varying the relative humidity at the last step of the set up.
The growth factors of the particles of a given compound were used to assess if the particles were either solids or liquids.

Results

The estimated growth factors obtained from the wet particles experiments suggest that the particles of Fructose, Xylitol and Arabitol were in the metastable liquid phase also when dried low to RH~2%, as in these experiments (Table1).
The obtained values of vapour pressure in the order of 10^{-6}-10^{-5} Pa, indicate that the compounds in the investigated conditions are semivolatile, hence they can continuously partition between the particle and the gas phase.

Table 1. Particles diameter in nm at the DMA and at Port 2 of the reactor, at different values of the SMPS RH and corresponding growth factors.

Compound	Dp RH=2%	Dp RH=45%	Dp RH=76%	Gf 45%	Gf 76%
Fructose	107.2	110.7	113.0	1.03	1.05
	108.1	109.0	112.8	1.01	1.04
Xylitol	105.4	109.7	114.6	1.04	1.09
	107.0	110.1	113.0	1.03	1.06
Arabitol	98.7	101.4	104.7	1.03	1.06
	97.8	101.2	103.9	1.03	1.06

Conclusions

The experiment on wet particles showed that under the investigated conditions particles were liquid. The results of vapour pressures indicate that studies on the effects of these compounds on the atmosphere are needed.

Graham, B. et al., (2003), *J.Geophys.Res*. **108**,4766.
Facchini, M.C. et al., (2000), *Atmosph. Environ*., **34**, 4853-4857.
Bilde, M. et al., (2003), *Environ. Sci.Technol*., **37**, 1371-1378.
Koponen, I. et al., (2007), *Environ. Sci.Technol.*, **41**, 3926-3933.
Zardini, A.A. et al., (2010), *J. Aeros. Sci*., **41**, 760-770.

Acknowledgments

This work was supported by the Danish Agency for Science Technology and Innovation, under the NaKIM project.

Vertical Profiles of Aerosol Properties and Black Carbon in the Arctic during spring and summer 2011: relationship with nucleation events and ship plumes

L. Ferrero[a], D. Cappelletti[b], B. Moroni[b], V. Vitale[c], R. Udisti[d], G. Sangiorgi[a], M.G. Perrone[a], M. Busetto[c], C. Lanconelli[c], M. Mazzola[c], A. Lupi[c], S. Becagli[d], R. Traversi[d], D. Frosini[d], M. Maturilli[e], R. Neuber[e], C. Ritter[e], J. Graeser[e], M. Fierz[f], G. Mocnik[g] and E. Bolzacchini[a]

[a]POLARIS research centre, DISAT, University of Milano-Bicocca, Piazza della Scienza 1, 20126, Milano, Italy.
[b]DICA, University of Perugia, Via G. Duranti 93, 06125 Perugia, Italy.
[c]ISAC CNR Viale Gobetti 101, 40129, Bologna, Italy.
[d]University of Florence, Via della Lastruccia 3, 50019, Sesto Fiorentino, Florence Italy.
[e]Alfred-Wegener Institut für Polar- und Meeresforschung (AWI), Forschungsstelle Potsdam, Telegraphenberg 43A, 14473 Potsdam, Germany.
[f]University of Applied Sciences Northwestern, Switzerland, Windisch, Switzerland.
[g]Aerosol d.o.o., Kamniska 41, SI-1000 Ljubljana, Slovenia

Keywords: Vertical distribution, Artic Aerosol, Black Carbon, Nucleation, Shipping emissions
Presenting author email: luca.ferrero@unimib.it

Aerosols are fundamental for understanding climate change (IPCC, 2007). The knowledge on size, distribution, chemical composition (especially Black Carbon, BC) and the vertical distribution of aerosols is vital to explain the effect of aerosols on climate (Corrigan et al., 2008). In the Arctic aerosol properties are typically obtained at ground while they are scarce along the vertical profile. Thus, systematic aerosol vertical profile measurements over Svalbard (Ny-Ålesund) were performed in the frame of the CICCI (Cooperative Investigation of Climate-Cryosphere Interaction) program (http://ny-niflheim.nilu.no/cicci//).
Vertical profiles (up to 1 km height) were carried out in the periods 30 March – 30 April and 30 June – 15 July 2011 at the Gruvebadet station (Ny-Ålesund).
A tethered balloon was fitted with an instrumentation package consisting of: 1) an Optical Particle Counter (OPC)-tandem system (2 OPCs GRIMM *1.107*; 31 size classes between 0.25 to 32 µm); the first OPC measured aerosol number size distribution at ambient relative humidity (RH), the second one used a drier; 2) a miniaturized electrical nanoparticle detector (miniDiSC); 3) a novel micro-Aethalometer (AE51 and AE52 prototype, Magee Scientific) to measure BC aerosol and the absorption coefficient; 4) a miniaturized cascade impactor (Sioutas SKC with 2 impaction stages: <1 µm, >1 µm) to collect samples of particulate matter; 5) a meteorological station (Vaisala Tethersonde TTS 111).
During the spring and summer we measured 84 and 18 aerosol profiles respectively to study the vertical structure of aerosol over Ny-Ålesund (Fig. 1a). Multilayered structures, homogeneous profiles and transport events were observed. The Multilayered structures were detected in ~75% of profiles. Each aerosol stratification was characterized by a change in aerosol concentration. Balloon profiles measured a concentration drop with increasing height in 80% of cases. The frequency distributions of the 1st and the 2nd aerosol stratifications with height are shown (Fig. 1b). The ratio between the aerosol concentrations measured across each aerosol stratification for three broadsize ranges (d_p<250 nm, 250 nm<d_p<1000 nm, d_p>1000 nm) are resumed in Tab. 1. Finest particles (d_p<250 nm) experienced a higher concentration decrease at the first aerosol stratification than larger particles (Tab. 1). This behavior, found essentially in the nanoparticle size, was accompanied by a decrease of BC concentration (Fig. 1a). Thus it may be related to early nucleation events close to the ground level.

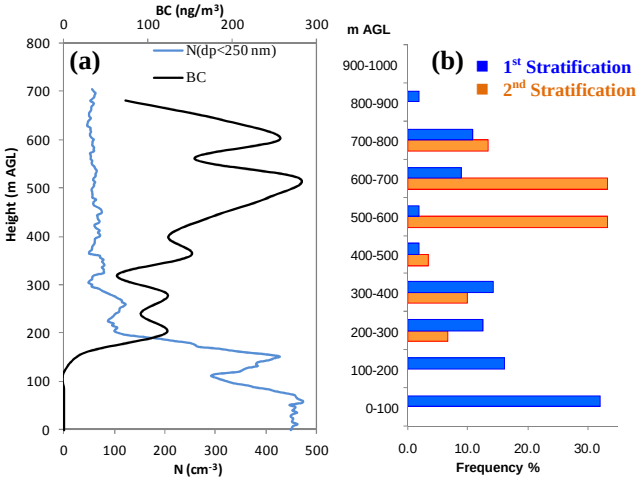

Figure 1. (a) Vertical profiles of N(d_p<250 nm) and BC on 6th April 2011 19.00 UTC (b) Frequency distributions of the 1st and the 2nd aerosol stratifications with height.

Aerosol ratio	N(dp<250 nm)	N(250 nm<dp<1000 nm)	N(dp>1000 nm)
1° Stratification	0.63(±0.27)	0.82(±0.16)	0.69(±0.21)
2° Stratification	0.81(±0.16)	0.67(±0.19)	0.43(±0.15)

Table 1. The ratio between the aerosol concentrations measured across each aerosol stratification.

In summer, vertical profiles allowed to study the impact of ships anchoring in Ny-Ålesund harbour.
Particularly on 6th July 2011 the ship plume affected the whole Ny-Ålesund. As a result the aerosol concentration reached values up to $2*10^4$ cm^{-3}, and BC up to 2000 ng/m^3. In the same day vertical profiles of both parameters were measured and were not affected by the ship plume. They were 534 cm^{-3} and 81 ng/m^3 respectively, underling the immense impact of ship emissions in the Arctic.

This work was supported by the Italian National Research Council (CNR) and the German Alfred-Wegener-Institut (AWI).

Corrigan et al. (2008). Atmos. Chem. Phys., 8, 737–747.
IPCC: Climate Change 2007.

Influence of adsorbed organic films on ice particle growth under conditions relevant to the upper troposphere

X. Kong[1], E.S. Thomson[1], P. Papagiannakopoulos[1], N. Markovic´[2] and J.B.C. Pettersson[1]

[1]Department of Chemistry and Molecular Biology, Atmospheric Science, University of Gothenburg, SE-412 96 Gothenburg, Sweden
[2]Department of Chemical and Biological Engineering, Physical Chemistry, Chalmers University of Technology, SE-412 96 Gothenburg, Sweden
Keywords: surfactant, ice, alcohol, cirrus
Presenting author email: xiangrui.kong@chem.gu.se

Surface-active organic compounds influence water uptake on atmospheric aerosol and cloud particles. The efficiency of water uptake by such particles contributes to cloud development and growth in the atmosphere with implications for the Earth's water cycle and climate.

Here, we investigate the influence of organic coatings on ice's water uptake. Methanol and *n*-butanol are used as alcohol surfactants with different carbon numbers and miscibilities in water. Water interactions with ice are probed using a recently developed environmental molecular beam (EMB) technique that allows for experiments at vapour pressures up to 10^{-2} mbar (Kong *et al.* 2011; Thomson *et al.* 2011). When probing alcohol-coated ice, a micrometer thick water ice layer is first condensed onto a graphite substrate, upon which an alcohol monolayer is subsequently grown (Kong *et al.* 2012). The application of a large range of alcohol partial pressures confirms the stability of the adsorbed monolayer. A pulsed molecular beam consisting of D_2O and helium is directed at the ice surface over a range of temperatures (165-200 K). A quantitative analysis of time-of-flight distributions of the scattered and desorbed D_2O illuminates molecular kinetics (Figure 1), including water uptake efficiency. No HDO is detected above the noise threshold, eliminating it as a sink of D_2O.

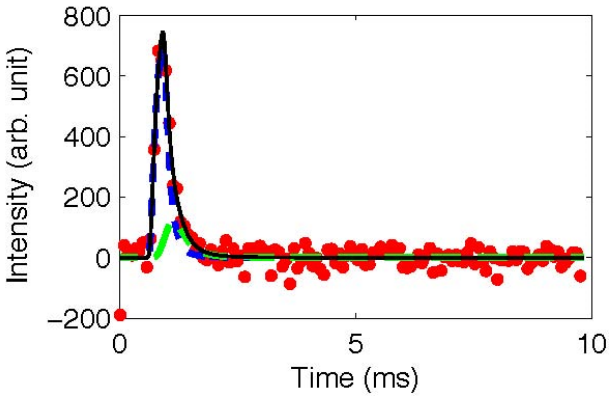

Figure 1. Time-of-flight distribution for D_2O scattering from butanol-covered ice at 180 K: Experimental data (red points), and fit to the data (black line) including indirect scattering (blue line) and trapping-desorption (green line) components. The incident angle and kinetic energy were 45° and 30 kJ/mol.

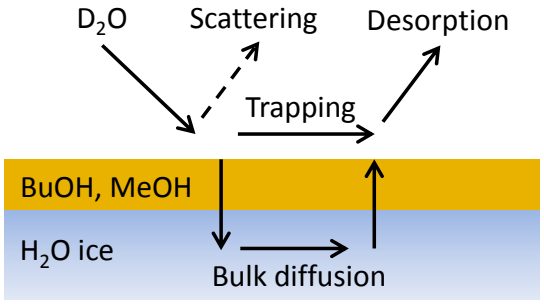

Figure 2. Pathways for heavy water molecules colliding with water ice covered with a surfactant monolayer of either methanol or *n*-butanol. In case of *n*-butanol, the surface layer provides a barrier that partially blocks incorporation of molecules into the ice structure and desorption of bulk water.

The results illustrate that on pure ice surfaces uptake of impinging D_2O molecules is almost unity. However, the presence of alcohol surfactants attenuates sticking in a manner that depends on the carbon chain length. Molecules colliding with the butanol-coated ice scatter and thermally desorb (Figure 2) more efficiently than from ice coated by methanol. The butanol layer is concluded to provide a substantial barrier for water desorption and for water adsorption and incorporation into the water ice structure. The temperature dependence of water uptake is also investigated.

These results provide a quantitatively constrained demonstration that adsorbed volatile organic compounds fundamentally alter ice surfaces and thus have the potential to be important in cloud processes ranging from formation to gas-phase scavenging.

This work was supported by the Swedish Research Council and by the Nordic Top-level Research Initiative through the program CRAICC (Cryosphere-Atmosphere Interactions in a Changing Arctic Climate).

Kong, X., Andersson, P. U., Markovic´, N. and Pettersson, J. B. C. (2011) *Physics and Chemistry of Ice 2010*, Eds. Furukawa, Y., Sazaki, G., Uchida, T. and Watanabe, N., Hokkaido University Press, 79-88.

Thomson, E., Kong, X., Andersson, P. U., Markovic´, N. and Pettersson, J. B. C. (2011) *J. Phys. Chem. Lett.* **2**, 2174–2178.

Kong, X., Thomson, E., Andersson, P. U. and Pettersson, J. B. C. (2012) *J. Phys. Chem. C*, submitted.

Continuous multiple-year atmospheric nitrate record from East Antarctic plateau

R. Traversi[1], S. Becagli[1], D. Frosini[1], M. Severi[1], M. Mazzola[2], C. Lanconelli[2], V. Vitale[2] and R. Udisti[1]

[1]Department of Chemistry "Ugo Schiff", University of Florence, Sesto F.no (Florence), I-50019, Italy
[2] ISAC CNR, Bologna I-40129, Italy,

Keywords: aerosol, Antarctica, nitrate, stratosphere-troposphere exchange.
Presenting author email: rita.traversi@unifi.it

Since 2005, a continuous, all-year-round aerosol sampling has been carried out at Dome C (Central East Antarctica, 3233 m a.s.l., about 1100 km far from the coastline), in the framework of "Station Concordia", an Italian PNRA – French IPEV joint program.

Size-segregated aerosol samples were collected in summer and winter periods by low- and medium-volume systems, including pre-selected cut-off samplers and multi-stage impactors.

Here we report the first multi-year record (2005-2008) of nitrate content in the atmospheric aerosol collected at Dome C, which can be considered as representative of the Antarctic background aerosol in the high central plateau.

A preliminary data analysis of nitrate concentration in PM10 aerosol shows a characteristic pattern for all the annual sampling campaigns with relatively low and constant background values throughout the year and some marked concentration maxima in early summer, namely November and, to a lesser extent, December (Fig. 1).

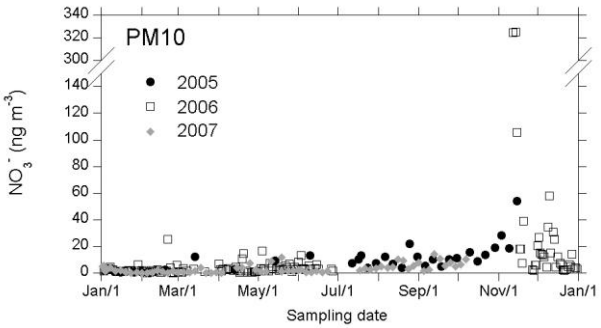

Figure 1. Nitrate concentration in PM10 aerosol collected at Dome C in the 2005-2007 period.

As shown in Fig .2, such maxima are related to both super-micrometric and sub-micrometric fractions but are particularly evident in the aerosol size classes ranging from 0.4 to 2.1 μm, with concentration up to 80 ng m^{-3} in the 1.1-2.1 μm size class (stage 5).

The availability of a complete aerosol chemical composition will allow establishing if nitrate concentration spikes (accounting for a significant part of total nitrate budget) are linked to common transport processes or neutralization reactions with sea spray or crustal aerosol components or rather due to nitric acid deposition. Considering the results reported by Frey *et al* (2009), we suppose the early summer nitrate peak is of stratospheric origin.

Such a result is particularly relevant in order to help in the assessment of the relative contribution and seasonal behaviour of nitrate sources in central Antarctica, not yet fully understood. In fact, nitrate deposition onto the Antarctic ice sheet has been attributed to various sources (stratospheric N_2O oxidation, low latitude lightning activity, polar stratospheric cloud precipitation and solar activity) but their extent and temporal evolution have not been disentangled so far.

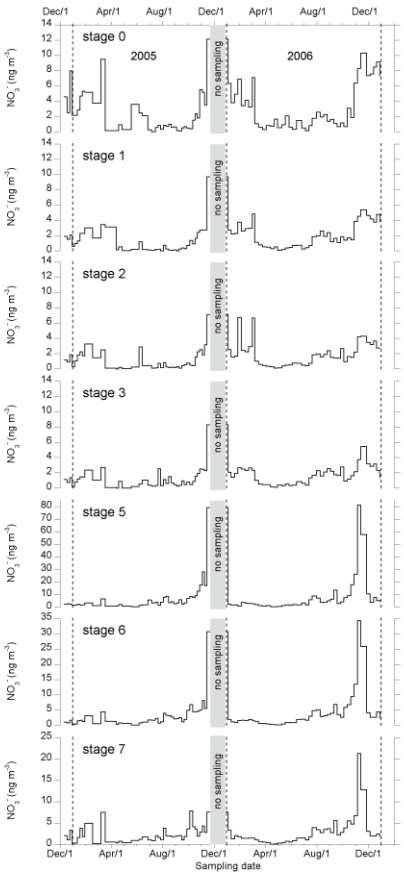

Figure 2. Nitrate distribution in 8 aerosol size classes collected at Dome C in 2005-2006.

This work benefited of Concordia Station logistic and personnel facilities.

Frey, M.M., Savarino, J., Morin S., Erbland, J., and Martins, J.M.F. (2009) *Atmos. Chem. Phys*. **9**, 8681–8696.

Volume-based κ-interaction model, hygroscopicity parameters and solute interaction coefficients

E. Mikhailov[1,2], S. Vlasenko[2], D. Rose[1] and U.Pöschl[1]

[1]Max Planck Institute for Chemistry, Biogeochemistry Department, 55128 Mainz, Germany
[2]St. Petersburg State University, Atmospheric Physics Department, Institute of Physics, 198504 St. Petersburg, Russia

Keywords: aerosol hygroscopicity, volume-based theory, interaction parameters.
Presenting author e-mail: Eugene.Mikhailov@paloma.spbu.ru

In this study we have presented an volume-based version of κ -interaction model (KIM) (Mikhailov et al.,2011) to describe hygroscopic properties by pure and mixed aerosol particles. Likewise mass-based model the volume-based analogue (KIM_v) describes the particles hygroscopic behavior including early stage of particles growth where all solutes are in solid state and final stage where all solutes are completely dissolved. Non-ideal behavior of the concentrated particle solution is accounted for cross-($i \neq j$) and self ($i=j$) – interaction coefficients ($\chi_{i,j}$) in hygroscopicity parameter, κ_v:

$$\kappa_v = \sum_i \kappa_{v,i,\infty} \varepsilon_i + \sum_{i,j} \chi_{i,j} c_i c_j \ , \qquad (1)$$

where εi is the dry volume fraction of the solute i and and ci its volume concentration in solution. In Eq.(1) first term is based on additive ZSR relation, and second term accounting for interaction effects. In contrast to rigorous thermodynamic models the interaction coefficient consider only binary interactions between all forms of the solutes. For example, for dissociated salt, MX and nondissociated organic, O, these pair interactions are M-O, X-O, M-X, and only one coefficient $\chi_{MX,O}$ responsible for all of them. As a result the final expression for hygroscopicity κ_v is simpler than for osmotic coefficient (Clegg et al., 2001).

In this work the experimental growth factors, g_b obtained from humidified tandem differential hygroscopicity analyzer (HTDMA) (Mikhailov et al. 2004) were used to test the theory approach. As an example Fig. 1 shows experimental data (a) and fit results based on KIM_v model (b) for mixed particle containing ammonium sulfate and levoglucosan with 1:3 mass ratio. By application of KIM_v to the measurement data we can distinguish two different regimes of hygroscopicity: gradual deliquescence at low relative humidity (RH<78%, blue model curve), where solute undergo gradual dissolution in aqueous phase, and a dilute regime, where solutes are fully dissolved including high concentrated metastable solution (gray model curve). The observed gradual deliquescence of the mixed particles can be attributed to an amorphous (semi-solid) state of organic species (Mikhailov et al., 2009).

The volume-based KIM_v theory model provides a good fit on the all stages of mixed particle evolution. We suggest that κ_v-model may be useful in describing particle hygroscopicity both in under- and in super-saturated water vapor.

If the chemical composition, interaction parameters and solubilities of the multicomponent aerosol particles are known the hygroscopicity κ_v can be determined over the all water activity range. In the absence of information on these characteristics, experimental data for complex particles can be fitted to obtain the volume hygroscopicity parameter.

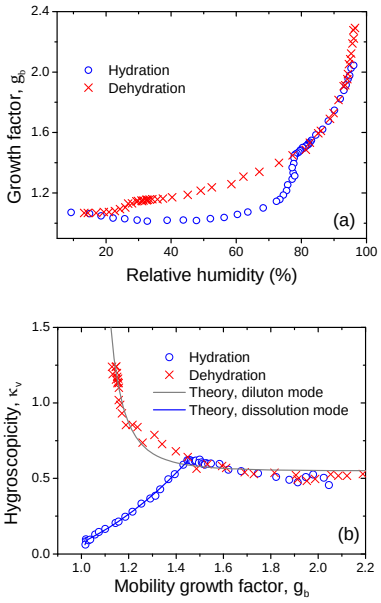

Figure 1. Hygroscopic properties of ammonium sulphate and levoglucasan mixed particles with 1:3 mass ratio: **(a)** - HTDMA derived growth factors ; **(b)** – a comparison between KIM_v theory predicted particle hygroscopicity and experimental data.

This work was supported by the Russian foundation for basic research, under grant No. 12-05-00945-a, and European integrated project on aerosol cloud climate and air quality interactions (EUCAARI), No.036833-2.

Clegg, S., Seinfeld, J., and Brimblecombe, P., (2001), Aeros. Sci., 31, 713-738.

Mikhailov, E., Vlasenko, S., Niessner, R., and Pöschl,U., (2004), ACP., 4, 323-350.

Mikhailov, E., Vlasenko, S., Martin, S., Koop, T., and Pöschl,U., (2009), ACP, 9, 9491-9522.

Mikhailov, E., Merkulov, B., Vlasenko, S., Rose, D, and Pöschl,U., (2011), ACPD, 11, 30877-30918.

Aerosol optical properties at Santiago Island, Cape Verde

M. Cerqueira[1], C. Pio[1], P. Fialho[2], J. Cardoso[1,3], T. Nunes[1] and S. M. Almeida[4]

[1]CESAM & Department of Environment, University of Aveiro, 3810-193, Aveiro, Portugal
[2]Department of Agrarian Sciences, University of the Azores, São Pedro, 9700-042 Angra do Heroísmo, Portugal
[3]University of Cape Verde, Praia, 279, Santiago, Cape Verde
[4]Instituto Tecnológico e Nuclear, Reactor, Apartado 21, 2686-953, Sacavém, Portugal

Keywords: atmospheric aerosol, African dust, optical properties, size distribution.
Presenting author email: cerqueira@ua.pt

Huge amounts of mineral dust are emitted every year from the Sahara desert and the Sahel to the atmosphere. A significant amount of this mineral dust is exported towards the Caribbean, North America and Europe under the prevalent synoptic scale air mass circulations. Optical parameters of mineral aerosols, e.g. scattering and absorption coefficients, the particle size distribution and spatial distribution of mineral aerosols determine the direct interaction of solar and terrestrial radiation in the atmosphere through scattering and absorption. Mineral dust also has a great impact on cloud formation leading to additional indirect radiation effects. The dense haze from dust events is also known to affect visibility.

The Cape Verde islands are ideally located to study mineral dust properties since they are under the pathway of trade winds, which transport dust from sources in North Africa to the northern tropical Atlantic Ocean. Aerosol measurements were performed at the outskirts of Praia, Santiago Island, Cape Verde (14º55'N, 23º29'W, 98 m above sea level), between January 2011 and January 2012, within the framework of CV-Dust project (Atmospheric aerosol in Cape Verde region: seasonal evaluation of composition, sources and transport). Aerosol size distribution was measured with a GRIMM EDM164 optical dust monitor from 0.25 um to 32 µm in 31 channels. The aerosol light absorption was measured with a Magee Scientific AE31 Aethalometer at seven wavelengthts (370, 470, 520, 590, 660, 880 and 950 nm).

The time variation of daily average $PM_{2.5}$, PM_{10} and TSP concentrations is presented in Fig. 1. The highest aerosol mass concentrations were observed in January and February 2011, during periods of air mass transport from northern Africa, and the lowest during November 2011, under the influence of marine air masses.

The aerosol size distribution measurements revealed three modes (fine, coarse and giant). An increase of the aerosol mass concentration was observed for the three modes during dust advection from Africa, but much more significantly in the coarse mode (around an aerodynamic diameter of 2 µm).

The seven wavelength spectra of equivalent black carbon concentration generated with the aethalometer during dust event periods revealed similar profiles but with different amplitudes of variation. These results suggest that mineral constituents in aerosol particles transported from the African continent may give a significant contribution to aerosol absorption properties. Iron oxides, mainly in the form of hematite, are known to explain this effect (Fialho et al., 2006) and high concentrations of iron were already observed after the chemical analyses of aerosol samples collected in Santiago Island during dust events, also as part of CV-Dust project research activities.

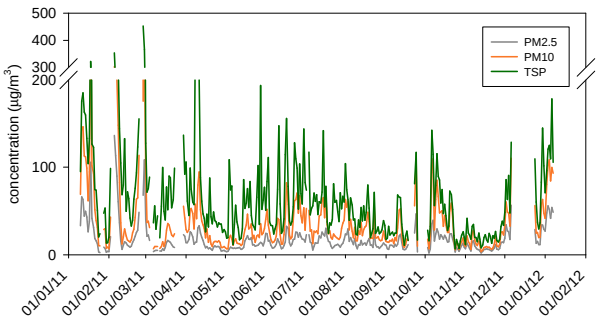

Figure 1. Daily average $PM_{2.5}$, PM_{10} and TSP concentrations at Santiago island.

This work was supported by the Portuguese Science Foundation (FCT) through the project PTDD/AAC-CLI/100331/2008 and FCOMP-01-0124-FEDER-008646 (CV-Dust). J. Cardoso acknowledges the PhD grant SFRH-BD-6105-2009 from FCT.

Fialho, P., Freitas, M.C., Barata, F., Vieira B., Hansen A.D.A. and Honrath R.E. (2006) Journal of Aerosol Science, 37, 1497-1506.

Mass scattering efficiency and chemical composition of different aerosol types at a coastal area of the Gulf of Cadiz (SW Spain)

J.F. López[1], V.E Cachorro[1], Y. González-Castanedo[2], J.D. de la Rosa[2] and A.M. de Frutos[1]

[1]Atmospherics Optics Group (GOA), University of Valladolid, Valladolid, 47071, Spain
[2]Associate Unit CSIC-UHU "Atmospheric Pollution", Center for Research in Sustainable Chemistry (CIQSO), University of Huelva, Spain
Keywords: aerosol, scattering, nephelometer, chemistry.
Presenting author email: juanfran@goa.uva.es

Atmospheric light extinction, scattering and absorption by aerosol depend on the particle load, size and chemical composition. The latter in particular determines the particle refractive index which is the most important optical property in the interaction processes of radiation and particles. Since the nineties the sensitivity of radiative forcing to the nature of aerosol has been discussed (Charlson, et al., 1992). Therefore, aerosol studies require the measurement and analysis of scattering and absorption coefficients together with chemical analysis of particle composition in a wide and multidisciplinary task.

Simultaneous measurements of the aerosol scattering coefficients σ_{sp} (López, 2011) and daily sampling of PM10 and PM2.5 were carried out during 2006 and 2007 at El Arenosillo-ESAT station belonging to INTA (Spanish Aerospace National Institute). These measurements allow the determination of the mass scattering efficiency α_{sp}, through the slope of the linear correlation between both magnitudes σ_{sp} and PMx. In addition, the PMx chemical analysis is also used to calculate the specific scattering efficiency for the main particle aerosol components. The σ_{sp} was measured using a 3-λ integrating nephelometer of TSI Company, and the aerosol samples were collected on quartz fiber filters with two high-volume sampling system (MCV). The filter weight and its chemical analysis were carried out in CIQSO of the University of Huelva.

A total of 30 and 34 days for PM2.5 and PM10 respectively under dry σ_{sp} measurements conditions have been selected for this study. The mass scattering efficiency α_{sp} at 550 nm ranges from 1.33 to 5.20 m^2g^{-1} with an average of 3.02±0.09 m^2g^{-1} and a correlation coefficient of R=0.82 (see Figure 1).

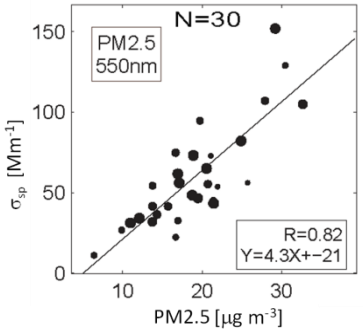

Figure 1 Correlation between daily scattering coefficient and PM2.5 value.

The composition of the dominant particulate matter obtained in the chemical analysis as $(SO_4)^{-2}$, $(NH_4)^+$, $(NO_3)^-$, C, and other minor species were grouped in anthropogenic, marine, desert types and a class representing "not-determinated" mass components. The best agreement was found for $(NH_4)^+$ component with a correlation coefficient of R=0.92 for PM10 and 0.88 for PM2.5 taking σ_{sp} at 450 nm. Using a least square fit multivariable regression:

$$\sigma_{sp} = \alpha_0 + \alpha_i M_i$$

the specific mass scattering efficiency α_i of the mainly aerosols components were obtained which are summarized in Table 1.

Despite the high relative efficiency of anthropogenic contribution , the presence of low efficiency scatters as marine and mineral aerosol, is in agreement with the average mass efficiency close to 3 m^2g^{-1} obtained at this rural-coastal site.

Aerosol Component	Mass scattering efficiency (m^2g^{-1})
Anthropogenic	4.86 (*)
Sulphate	3-7 (McMurry, et al., 1996)
Marine	0.05 (*)
Mineral	0.30 (*)
	0.77 (Li, et al., 1996)

Table1. Mass scattering efficiency of different aerosol types. (*) refer to this study.

We gratefully acknowledge the support and scientific collaboration of INTA-ESAT team. Financial support was provided by the Spanish CICYT (CGL2008-05939-CO3-01/CLI, CGL2009-09740 and CGL2011-13085-E)

Charlson, R. J. et al (1992). Climate forcing by anthropogenic aerosols.. *Science,* Volumen 256, pp. 423-430.

Li, X. et al (1996). Dominance of mineral dust in aerosol light-scattering in the North Atlantic trade winds. *Nature,* Volumen 380, pp. 416-419.9

López et al. (2011). Medidas y análisis del coeficiente de scattering de aerosoles en un área de la costa Atlántica de Huelva. *Universidad de Valladolid. Dpto de Física Teórica, Atómica y Óptica*.

McMurry, P. H., Zhang, X. & Lee, C.-T. (1996). Issues in Aerosol Measurement for Optics Assessments. *J. Geophys. Res.,* Volumen 101, pp. 19189-19197.

Long-term atmospheric aerosol deposition in Southern Portugal: first results on chemical and morphological characterization of particles by VP-SEM+EDS

F. Wagner[1], N. Schiavon[1,2], K. Kandler[3], L. Tobias[1,2] and J.Mirão[1,2]

[1]Centro de Geofísica, Universidade de Évora, Évora, 7000-671, Portugal
[2]HERCULES Laboratory – Universidade de Évora, Portugal
[3]Institut für Angewandte Geowissenschaften, Technische Universität Darmstadt, 64287, Germany

Keywords: aerosol mineralogy, aerosol chemistry, sedimentation sampling.
Presenting author email: frankwagner@uevora.pt

Introduction

Atmospheric aerosol particles play an important role in climate and air quality. In Portugal, long time series on the chemistry and morphology of atmospheric aerosol particles as well as on their seasonal dependency are still relatively scarce and mostly confined to the North of the country. To assess the relative contribution of several aerosol particle sources, a 1 year quasi continuous aerosol sampling is currently under way, which started on 10 August 2011 at a sampling site in Evora, Southern Portugal. In the first month an intensive field measurement campaign was carried out, providing additional data for summer (Wagner et al. 2012).

Experimental

Particulate matter was collected using a modified version of the aerosol passive sampler Type A "flat plates" by Ott and Peters (2008). This collector consists of 2 brass plates at a distance of about 1.6 cm and it was modified by the introduction of a liquid trap. The air could freely flow and particles deposited by gravitation. Aluminium stubs coated with carbon adhesives were used as deposition substrates. The sampler was placed at the top of a university building about 15m above ground level. As the gravitational settling of particles is slow the sampling was run on a weekly basis. Single particle automated analysis was performed using an HITACHI VP-SEM interfaced with a Bruker EDS QUANTAX automatic ESPRIT software. Analytical conditions were as follows: 20 kV accelerating voltage; 10 mm working distance; 120 mA emission current; 70 mA probe current. The particles were classified according to their chemical composition into eight classes and into 3 classes according to their size.

Results

First results (Fig. 1) of the SEM automated particle analysis on a selected sample of 1000 particles collected during a dust episode in August (whose provenance could be ascribed to Northern Africa as deduced from trajectory calculations (HYSPLIT/GDAS) show that the relative abundance of dust-related aerosols (oxides+quartz+silicates) increases with particle size reaching a maximum in the > 10 µm class. Within this size range, larger particles commonly are formed by agglomeration of heterogeneous particles. Sulphate containing particles are mainly concentrated in the smaller particles.

It is interesting to note the presence of significant amounts of phosphorus-bearing particles whose origin is currently under investigation but could perhaps be due to the semi-rural location of the sampling site and its nearby agricultural activities.

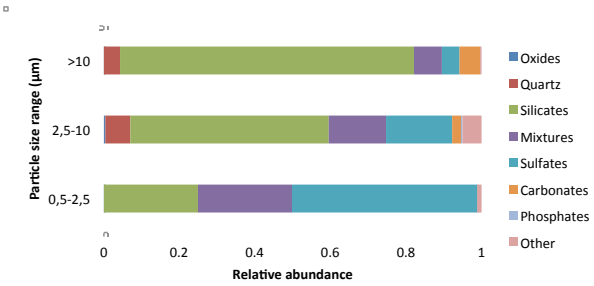

Figure 1. Classification according to chemical composition and particle size. Sampling period: 18-21 August 2011.

Summary and Conclusions

For the first time a fully automated VP-SEM+EDS single particle characterization was performed in Portugal. By the time of the conference the collection of aerosol particles by gravitational settling will have completed its first year. The annual cycle of particle sizes, morphology and elemental chemical composition will be shown.

This work was supported by the Fundação para a Ciencia e a Technologia.

Ott, D.K., Peters, T. (2008) A Shelter to Protect a Passive Sampler for Coarse Particulate Matter, PM10-2.5. *Aerosol Sci. Technol*. 42, 299-309.

Wagner, F., K. Kandler, N. Schiavon, L. Tobias, S. Pereira, J. Preißler, A. Candeias, and J. Mirão (2012): Summer Campaign on Aerosol Optics, Microphysics, Chemistry and Mineralogy in Portugal – Overview, *this conference*.

Arctic aerosol sampled at Ny Ålesund: results from size-segregated samples

G. Calzolai[1], S. Becagli[2], C. Ghedini[2], F. Rugi[2], D. Frosini[2], S. Nava[1], M. Chiari[1], F. Lucarelli[1], R. Traversi[2] and R. Udisti[2]

[1]Department of Physics and Astronomy, University of Florence and INFN Sez. Firenze, Sesto Fiorentino, Florence, I-50019, Italy
[2]Department of Chemistry, University of Florence, Sesto Fiorentino, Florence, I-50019, Italy
Keywords: size distribution, chemical composition, arctic aerosols.
Presenting author email: calzolai@fi.infn.it

The chemical characterization of size-segregated aerosol samples can help in the identification of the main aerosol sources and can give information on the atmospheric processes occurring during atmospheric transportation and modifying the aerosol properties. Moreover, both size distribution and chemical composition play a crucial role in the interaction aerosol-solar radiation, in the aerosol ability to induce cloud and fog formation and to modify the microphysical cloud properties (thus affecting the Earth's radiation budget), in the long-range transport processes and in the deposition patterns of anthropogenic pollutants over the polar areas.

In this work, we report the results on size distribution and bulk chemical composition of the Arctic aerosol sampled at Ny Ålesund (78.6°N, 11.6°E, Svalbard Islands, Norway) in March – September 2010, at the recently installed Gruvebadet station.

Svalbard Islands are an ideal site for the study of the interaction between the climate changes and the atmosphere, ocean and land variations, since they are located in the northernmost point influenced by the warm West Spitsbergen Current. Furthermore, in Ny Ålesund, the international cooperation ensures the continuous study and monitoring of a large number of physical and chemical parameters characterizing the Arctic ecosystem.

The sampling site is located sufficiently far from the village (about 800 m) and in a sector usually not affected by winds coming from the village direction, in order to minimize contamination. Anyway, a meteo-trigger system turns off the long-term samplers if wind direction or too low wind velocity make possible the transport or the diffusion of pollutants from the village.

The presented data regard the samples collected with a PM10 sampler (24-h resolution), with Teflon filters, and a 12-stages impactor (4-days resolution, Dekati Small Deposit area Impactor (SDI) [1], stages with cut points in the range from 45 nm to 8.5 μm), with polycarbonate filters.

PM10 samples were analyzed for cations, inorganic anions and selected organic anions (acetate, formate, oxalate and methanesulphonate) composition in the clean room at the Department of Chemistry of Florence by means of Ion Chromatography (IC), taking care to avoid any contamination during filters handling and analysis.

Size segregated samples were analyzed for elemental characterization by means of Particle Induced X-ray Emission – Particle Induced γ -ray Emission (PIXE-PIGE) measurements at INFN-LABEC laboratory in Florence. PIXE is unrivalled for the direct measurement of the mineral dust fraction in the aerosol, as it is highly sensitive to all the crustal elements except oxygen and carbon. PIGE was coupled to PIXE in order to get a more accurate estimate of light elements. Moreover, both the techniques do not need any sample pre-treatment, thus minimizing contaminations.

Results on the chemical compositions of the daily PM10 samples will be shown (Figure 1). Such results were also used to identify interesting and representative events to be deeply characterized by means of the analysis performed on the multi-stage impactor samples.

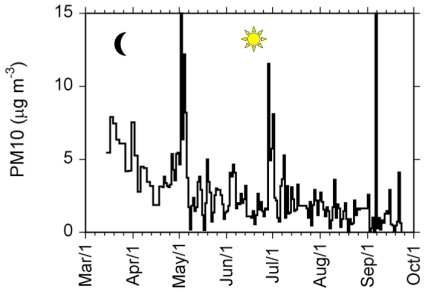

Figure 1. Daily PM10 concentrations.

The measurements on size-segregated samples have demonstrated to be an important tool for aerosol source identification, as they give information on the elemental mass size distributions. In particular, they allowed the identification of both local and long-range transport episodes, evidencing contributions from dust, sea spray and anthropogenic aerosol (Figure 2).

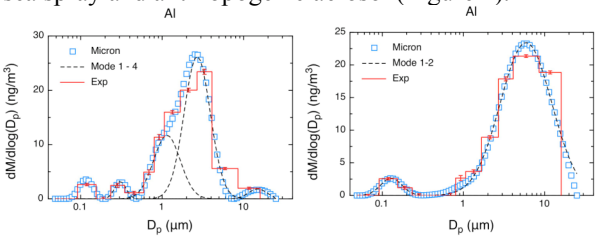

Figure 2. Mass size distributions for Al during a long-range transport (left) and a local dust event (right).

Some preliminary results on seasonal trends were also assessed, showing, as an example, that coarse modes are more important during summer.

Maenhaut, W., Hillamo, R., Mäkelä, T., Jaffrezo, J.-L., Bergin, M.H. and Davidson, C.I., (1996) *Nucl. Instr. & Meth. B* **109-110**, 482-487.

Carbonaceous aerosol characterization in Piacenza (Italy)

M. Calvello[2], F. Esposito[1], G. Pavese[2], G, Lonati[3], S. Ozgen[3] and G. Ripamonti[3]

[1] DIFA - Università della Basilicata, C. da Macchia Romana, 85100, Potenza, Italy
[2] CNR-IMAA, C. da S. Loya, 85050, Tito Scalo (PZ), Italy
[3] DIIAR – Politecnico di Milano, P.za L da Vinci 32, 20133, Milano, Italy

Keywords: ultrafine aerosol, carbonaceous aerosol, urban areas
Presenting author email: pavese@imaa.cnr.it

The UPUPA project (Ultrafine Particles in Urban Piacenza Area) is currently running in Piacenza (45.03 °N, 9.41 °E, 67 m a.s.l), a medium-sized city (about 100.000 inhabitants) located in the middle of the river Po Valley in Northern Italy.

In the framework of the UPUPA project an integrated measurements campaign was devoted to the investigation of the presence of carbonaceous particulate species in the urban atmosphere. In particular, the campaign was intended to collate information on different parameters tracing the carbonaceous aerosols.

A large set of instruments were concurrently employed during the monitoring campaign, including filter-based instruments measuring the optical absorption coefficient of the aerosol at different wavelengths, a radiometer in the visible spectra, a single-particle laser photometer, particulate matter impactors, condensation particle counters and spectrometers, and gravimetric samplers for PM1 samples speciation.

Measurements started on September 20th 2011 and lasted ten days at the LEAP laboratory site in Piacenza, located between the river Po bank and the main railway station, close to a flyover connecting two heavy traffic motorways.

Preliminary data analyses focused on aethalometer data: Black Carbon (BC) concentration have been derived from the Magee AE31 aethalometer (7 wavelenghts) data collected with a 5-minute time resolution. The resulting estimated BC time pattern over the entire monitoring campaign is presented in Figure 1.

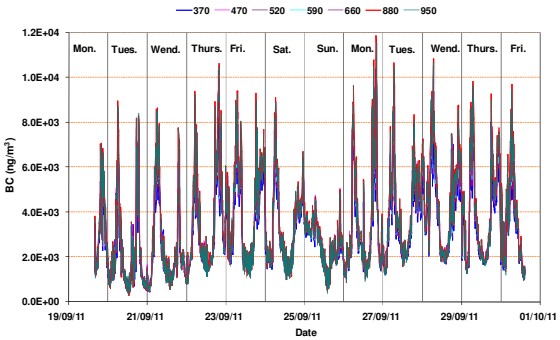

Figure 1. Time pattern of BC content in PM2.5 in Piacenza as estimated based on the 7-wavelenght aethalometer data. September 19th-30th 2011.

According to the regular daily pattern of BC content (two peaks per day on morning and evening rush hours) vehicular traffic can be considered as the main source of carbonaceous particles at the site. Due to the anthropogenic activities fine particles contribution is expected to be prevailing over the coarse one. This is confirmed by the information on the particle size distribution derived from radiometric measurements: Figure 2 displays the daily mean volume size distributions for three days during the campaign. Despite the different PM levels measured on these days all the size distributions display a bi-modal structure essentially dominated by submicron particles.

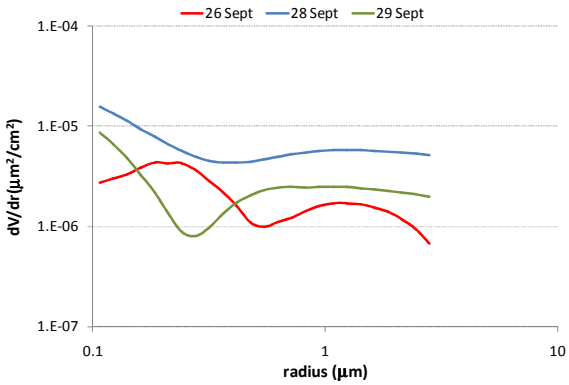

Figure 2. Daily mean volume size distributions as retrieved from radiometric measurements on September 26th, 28th and 29th.

These preliminary findings are to be further analysed concurrently with the piece of information provided by the other instruments for carbonaceous species monitoring and with the concurrent particle number concentration and related size distribution data.

Saharan vs. local influence on atmospheric aerosol deposition in the southern Iberian Peninsula: significance for N and P inputs

R. Morales-Baquero[1], C. Pérez-Martínez[1]

[1]Departmento de Ecología and Instituto del Agua, Universidad de Granada, 18071 Granada, Spain
Keywords: Saharan dust, nutrients, ecosystems, aerosol chemistry.
Presenting author email: rmorales@ugr.es

Atmospheric deposition is recognized as a significant input of both gaseous (e.g. nitrogen) and soil-derived (e.g. phosphorus) elements to ecosystems. Nitrogen deposition in the Northern hemisphere has increased due to anthropogenic activity and its impact on diverse ecosystems has intensely been studied. In particular, a considerable scientific effort has been made to assess its impact on lake chemistry and lake recovery after emission reduction. On the other hand, atmospheric inputs of phosphorus derived from Saharan dust deposition and its impact on ecosystems are receiving growing attention.

The southern Iberian Peninsula is an area strongly influenced by Saharan dust deposition. Previous results indicate that atmospheric contribution of P and Ca is essential to explain the functioning of oligotrophic lakes (Morales-Baquero et al, 2006; Pulido-Villena et al, 2006), and that atmospheric input of organic matter partially supports the pelagic food web of these ecosystems (Pulido-Villena et al, 2005). Nevertheless, the importance of Saharan dust contribution to atmospheric deposition in relation to local sources it is not well established. The goal of this work was to assess the relative importance of the Saharan dust vs. local sources in the atmospheric aerosol deposition in the southern Iberian Peninsula. Moreover, we studied its relevance to atmospheric inputs of N and P in this area.

To achieve this goal, during spring and summer of the years 2004 and 2005, we obtained simultaneous weekly series of wet and dry atmospheric deposition of particulate matter, total nitrogen (TN) and total phosphorus (TP), at three locations in the province of Granada, spaced apart by up to 40 Km. Common variability between sites tens of kilometers distant, it is recognized to be caused by a factor as climate that affects them equally.

Figure 1 shows the time series of total atmospheric deposition of particulate matter. As can be seen the series presents simultaneous maximum depositions at the three sites, which coincide with the weeks in which there was significant Saharan intrusions over Iberian Peninsula. As a result, the three series show significant positive correlations with each other and, through a principal component analysis, we obtain that 75% of the variability in the deposition of the three sites is common. The deposition of TN and TP is also studied in relation with the particulate matter deposition and Saharan dust intrusions

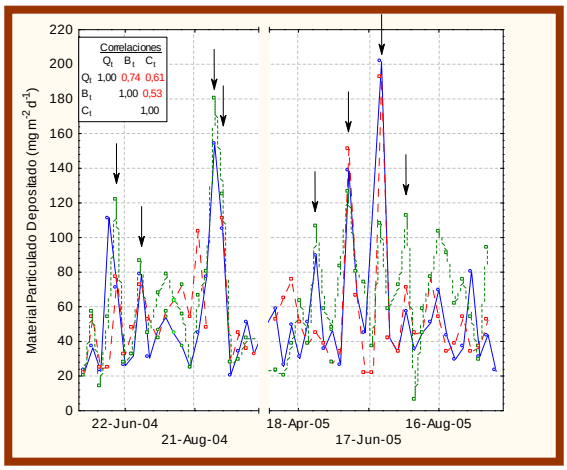

Figure 1.- Deposition of particulate matter (dry + wet) during spring and summer at three locations: (Qt), (Bt) and (Ct,) during the two years studied. Arrows indicate weeks in which the Saharan intrusions were more important. Box shows the correlations, all significant, between the corresponding series.

This work was supported by the MEC Grant REN2003-03038.

References

Morales-Baquero, R., E. Pulido-Villena, and I. Reche (2006), Atmospheric inputs of phosphorus and nitrogen to the southwest Mediterranean region:Biogeo-chemical responses of high mountain lakes, **Limnol. Oceanogr.,** 51(2), 830– 837

Pulido-Villena, E., I. Reche, and R. Morales-Baquero (2005), Food web reliance on allochthonous carbon in two high mountain lakes with contrasting catchments: A stable isotope approach, **Can. J. Fish. Aquat. Sci.,** 62, 2640–2648, doi:10.1139/f05-169.

Pulido-Villena, E., I. Reche, and R. Morales-Baquero (2006), Significance of atmospheric inputs of calcium over the southwestern Mediterranean region: High mountain lakes as tools for detection, **Global Biogeochem. Cycles,** 20, GB2012, 9/2005GB002662.

Observations of aerosol of different origin by Siberian - Far Eastern lidar network and photophoresis

A.A. Cheremisin[1], V.N. Marichev[2], V.V. Bychkov[3], B.M. Shevtsov[3], P.V. Novikov[4], I.S. Shnipov[5]

[1]Scientific Research Department, Siberian Federal University, Krasnoyarsk, 660041, Russia
[2]Laboratory of Lidar Methods, V.E. Zuev Institute of Atmosphere Optics SB RAS, Tomsk, 634021, Russia
[3]Institute of Cosmophysical Researches and Radio Wave Propagation FEB RAS, Paratunka, Kamchatka, 684034, Russia
[4] Department of Computer Science, Krasnoyarsk Railway Institute, Krasnoyarsk, 660028, Russia
[5] Department of Mathematics, Krasnoyarsk Railway Institute, Krasnoyarsk, 660028, Russia
Keywords: atmospheric aerosols, long-range transport, lidar, photophoresis.
Presenting author email: aacheremisin@gmail.com

Now a network of stratospheric lidar stations operates in Siberia and Far East: in Institute of Atmosphere Optics, Tomsk, in U.G. Shafer Institute of Cosmophysical Iinvestigations and Aeronomy, Yakutsk, and in Institute of Cosmophysical Researches and Radio Wave Propagation, Kamchatka. Monitoring of vertical aerosol structure in the upper troposphere, in the stratosphere, and in the mesosphere is one of the main goals of these stations.

In this work we present systematization of lidar observations of aerosol layers in the middle atmosphere registered by this network. To a great extent, identification of different types of aerosols results from analysis of air masses transfer by backward trajectories method. Trajectory calculations were carried on the basis of software package which we have developed. We used UK MetOffice assimilated data on wind velocities and temperature. Results of our calculations were complemented by calculations using GDAS data and HYSPLIT software package available on NOAA site.

Such combined data of local lidar observations of the atmosphere and global satellite data enables to identify certain correlations of aerosol formation with structure of dynamic, thermal and chemical processes in the atmosphere.

For explanation of some types of aerosol layers in the stratosphere and mesosphere we employed gravito-photophoresis theory. This is the result of our investigation on photophoretic phenomenon.

Photophoresis can be responsible for aerosol layer formation at altitudes of 20, 30, 50, 70 and 85 km. The layers form in specific geographic regions and at certain seasons (Cheremisin et al., 2011a). The equality of the average gravito-photophotetic force and gravity force has been taken as the main condition of layer formation. This requirement has been supplemented by the condition of mechanical stability, that ensures return of the particle to the equilibrium position when an accidental shift in altitude occurs. Laboratory observations of photophoresis are available in the literature, obviously for the laboratory conditions.

Several types of aerosol layers were detected.

1. Appreciable aerosol content of the upper troposphere and the stratosphere at altitudes of up to 30 km was observed in winter-spring period.

2. Several cases of polar stratospheric clouds (PSC) were registered in winter time. The facts of PSC observations were confirmed by backward trajectory analysis.

3. Aerosol scattering peaks were observed in the stratosphere episodically at altitudes about 20 km in summer time. Aerosol at these altitudes has been associated with its transport from tropical aerosol reservoir described by Hitchman.

4. Volcanic activity in the northern hemisphere has increased over the last few years. After various powerful eruptions aerosol layers of volcanic origin were observed in Tomsk. Volcanic origin of aerosol was confirmed by backward trajectory calculations (Cheremisin *et al*., 2011b).

5. Lidar observations of the upper stratosphere and the mesosphere above Kamchatka were started in 2007, and aerosol layers at altitudes 35-50 km and 60-75 km were found (Bychkov *et al.*, 2011). Noctilucent clouds were registered above Kamchatka and Tomsk as well.

This work was supported by the Russian Fund of Basic Research under grant 10-05-00907a, Presidium of Russian Academy of Science under programme No.16, Ministry of Science and Education of Russian Federation under state contract No. 16.518.11.7048.

Authors are grateful to the British Atmospheric Data Centre and UK MetOffice for providing the Stratospheric Assimilated Data, National Oceanic and Atmospheric Administration for providing software and data.

Cheremisin, A.A., Shnipov, I.S., Horvath, H. and Rohatschek, H. (2011a) *Geophys. Res.* **116**, D19204, 15 pp.

Cheremisin, A.A., Marichev, V.N. and P. V. Novikov (2011b). *Rus. Meteorol. and Hydrol.* **36**, 600-607.

Bychkov, V.V., Perezhogin, A.S., Shevtsov, B.M., Marichev, V.N., Novikov, P.V. and Cheremisin, A.A. (2011) *Izvestiya, Atm. and Ocean. Phys.* **47**, 603-610.

Direct observations and model simulations of long-range transported aerosols over Northeast Asia inferred from ground, airborne and satellite measurements

M.G. Cayetano[1], Y.J. Kim[1], J.S. Jung[1a], K.Y. Lee[1], K.C. Kim[1], R. S. Park[1], C.H. Song[1], M. Koike[2] and Y. Kondo[2]

[1] School of Environmental Science and Engineering, Gwangju Institute of Science and Technology (GIST), Gwangju 500712, South Korea

[2]Division of Global Atmospheric Environment, RCAST, University of Tokyo, Tokyo, Japan

[a]*now at*: Institute of Low Temperature Science, Hokkaido University, Sapporo, Japan

Keywords: $PM_{2.5}$, aircraft measurements, long-range transport, Northeast Asia.

Presenting author email: yjkim@gist.ac.kr

Asian mineral dust and anthropogenic pollutants (long-range transported pollutants, LTP) are usually transported long distance in the lower troposphere. Results from ground based measurements in Deokjeok island (Cayetano, *et al.*, 2011) and aircraft measurements (A-FORCE Campaign) were used for direct observations of LTP aerosols. In order to identify the air mass origin, HYSPLIT (Draxler and Rolph, 2011) air parcel back trajectory model was used. An algorithm (Lee, *et al.*, 2006) to retrieve aerosol optical depth (AOD) using the NASA moderate resolution imaging spectroradiometer (MODIS) data was used to map the transport of LTP aerosols during the Spring of 2009. A three-dimensional aerosol transport model (CMAQ 4.5) was also used to simulate the transport of aerosols over the region of interest. Level flights to measure fine mode SO_4^{2-} and NO_3^- have been conducted over Deokjeok Island on clean (April 2-4) and LTP days (April 5).

Table 1. Comparison between ground and airborne measurements in Deokjeok island on April 4-5, 2009.

Date	$PM_{2.5}$ ($\mu g/m^3$)	NO_3^-($\mu g/m^3$)	SO_4^{2-}($\mu g/m^3$)
April 2G	23.0 ± 2.9	1.1 ± 0.5	2.2 ± 0.4
April 3G	14.9 ± 3.0	0.5 ± 0.2	2.1 ± 0.5
April 4G	24.6 ± 1.4	1. 3 ± 0.2	4.3 ± 0.1
A		2.7 ± 2.0	8.9 ± 1.9
April 5G	83.5 ± 5.1	5.7 ± 0.2	15.9 ± 0.6
A		0.1 ± 0.1	2.5 ± 2.0

Airborne measurement on April 4 showed that elevated layer SO_4^{2-} was observed around 2km altitude. It was found that transported fine mode SO_4^{2-} aerosols reached the ground on April 5 resulting in three-fold increase in SO_4^{2-} concentration (Figure 1) compared to previous day (Table 1). CMAQ model predicted relatively well the column integrated SO_4^{2-} concentration for both days. Evidence of aerosol transport was confirmed by satellite retrieved AOD data showing plume of thick aerosol (AOD>2.0) observed near the Shandong area of China on April 4, and moved over the Korean peninsula the next day, passing over Deokjeok island on April 5 (Figure 2).

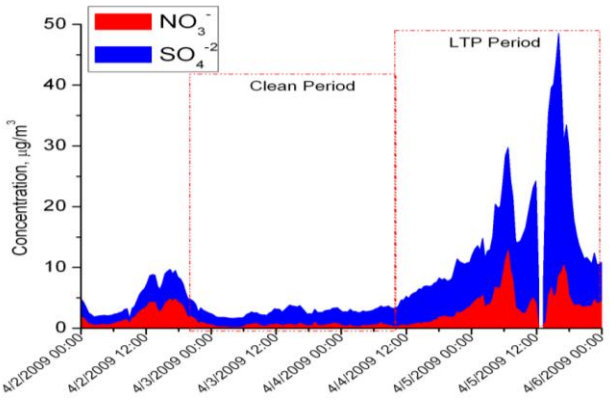

Figure1. Temporal plot of SO_4^{2-} and NO_3^- concentrations at the surface

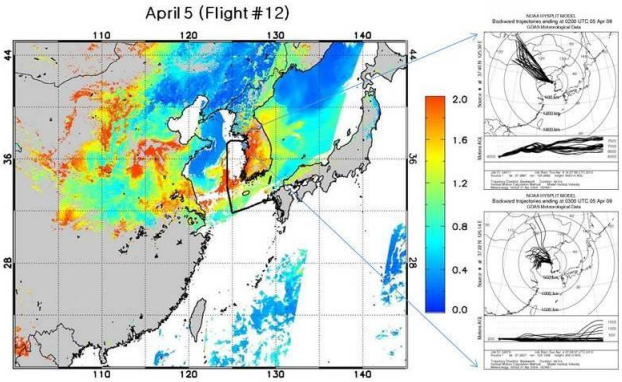

Figure2. Satellite retrieved AOD and Hysplit back trajectory plots at ground and aircraft levels on April 5.

This work was supported by National Research Foundation of Korea (NRF) grant funded by the Korean government (MEST) (Project No. 2008-0060618).

Cayetano, M. G., *et al.* (2011) *Journal of the Air & Waste Management Association* **61**(11): 1192-1203.

Draxler,R.R.and Rolph G.D.(2011) *http://ready.arl.noaa.gov/HYSPLIT.php.*

Lee, K. H., *et al.* (2006) *International Journal of Remote Sensing* **27**(14): 2813 - 2830.

Analysis of particle size distribution on urban and rural sites with connection to meteorological conditions

B. Kotlík[1], J. Keder[2], L. Černikovský[2]

[1]Department of Environmental Hygiene, National Institute of Public Health, Prague, Czech Republic
[2]Czech hydrometeorological Institute, Prague, Czech Republic
Keywords: aerosol, size spectra, temperature, source identification
Presenting author email: b.kotlik@szu.cz

Continuous weekly particle counts from four selected stationary AIM stations in the North Moravia region were conducted during 2. 2. to 9. 2. 2011.

The aim of this study was to identify the spectra of those particle distribution counts that would enable description of effects caused by sources and meteorological conditions. Four measuring stations were selected - 2 urban-industrial (Ostrava-Fifejdy and Karvina) and 2 rural (Studenka and Vernovice) all of which are suitable for representing measured fractions from local sources during the heating season and particularly during prevailing south-westerly winds.

The monitoring periods characterize favorable dispersion conditions associated with prevailing south-westerly zonal winds over the targeted areas. The mean wind speed during 1 hour in the urban collection sites was 1 - 4 m/s on 8. 2 - 9. 2. 2011 (except at night) and 2 - 7 m/s at the rural stations.

Thanks to favorable dispersion conditions the 1 hour PM_{10} concentrations were very low, largely far below 50 ug/m^3.

This abstract presents preliminary analysis results from the rural station in Studenka.

Particle counts within the separate size bins were normalized by the bin width and assigned to the bin centre size (fig. 1).

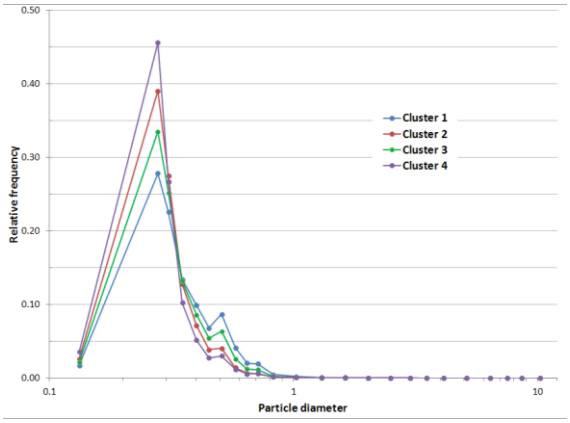

Figure 1. The typical distributions are presented in rural station (in µm).

For each measuring time period a particle size distribution has been obtained by this procedure. With the aim to find some typical structures among the particle size distributions a cluster analysis has been applied. Using hierarchical clustering approach a number of four distinct clusters has been estimated in the size distribution data. Applying the K-means clustering method the particular size distributions were sorted into 4 clusters. For each cluster a typical size distribution has been obtained as a mean of all distribution within the particular cluster.

An analysis of the link to the meteorological conditions prevailing during the measuring period has been provided. With this goal air temperature histograms categorized by the particle size distribution clusters were constructed (fig. 2). This made apparent that temperature values distribution differs significantly among particular clusters.

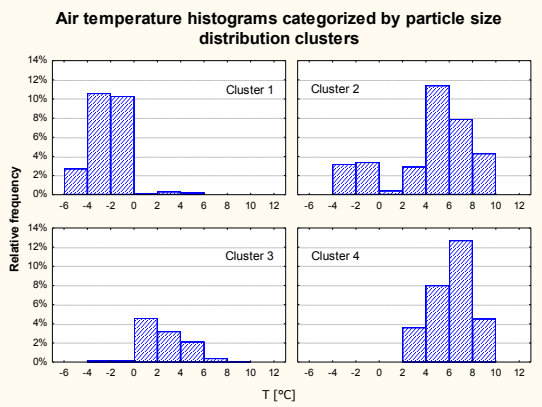

Figure 2. Air temperature histograms categorized by particle size distribution clusters

The expected dependence on wind speed in excess of 4 m/s was not proven.

The most significant difference between the clusters 1 and 4 might be observed: for cluster 4 with prevailing small-sized particles air temperatures above 2^{0}C were typical whilst cluster 1 in which the small particle share decreases in favour of coarser ones is mainly connected with negative air temperatures.

The detected clusters have a characteristic distribution pattern and their incidence corresponds to recorded temperatures. The reason for this is the probable influence of various ratios of local sources such as traffic and domestic heating.

The reason for this will be a subject of further analysis.

Temperature influence on the natural aerosol budget over boreal forests

L. Liao[1], H. Junninen[1], M. Kulmala[1] and M. D. Maso[1]

[1] Division of Atmospheric Sciences, Department of Physics, University of Helsinki, P.O.Box 48, 00014, Helsinki, Finland

Keywords: aerosol, temperature, VOCs

Presenting author email: li.liao@helsinki.fi

Atmospheric aerosol has climatic influence, and affects air quality and human health. The source of atmospheric aerosols includes both natural and anthropogenic origins. Secondary aerosol formed via the oxidation of biogenic volatile organic compounds accounts for the most significant fraction among the global aerosol budget. The boreal forest emitted VOCs, in particular terpenes, have shown to be one of the important aerosol precursor sources linking to the secondary aerosol production in northern hemisphere (Tunved et al., 2006). The emission of biogenic VOCs is temperature dependent, thus it may influence the secondary aerosol production as well as the CCN loading (Tunved et al., 2008), which further forms the vegetation, aerosol and climate interaction system (Kulmala et al., 2004).

In this work, we investigate the potential and the order of magnitude of the temperature influence to the natural aerosol budgets; we discuss the natural aerosol growth at different size ranges in different temperature bins from back trajectory analysis.

The research and data analysis were based on the observations at the SMEAR II station (61º51'N, 24º17'E, 170 m asl, Figure 1), Hyytiälä, Finland. 15 year dataset from 1996 to 2010 has been used, including continuously DMPS measurements, temperature and backward trajectory data. The DMPS particle size spectrums were divided into three size modes: the nucleation mode in the particle size range of 3--25 nm, Aitken mode (25--100 nm), and accumulation mode (100--1000 nm). Particle number concentrations at each mode were calculated every one hour. Hourly particle volume concentrations were integrated from the DMPS size distribution assuming spherical particles. The hourly 96 hour backward trajectories arriving at 100 m a.g.l over the Hyytiälä station were calculated from the HYSPLIT4 model (Draxler et al., 1997).

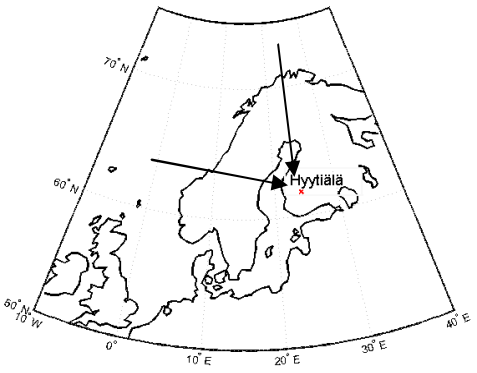

Figure1. The transport zone of the back trajectories.

Trajectories transporting 90% of time in an 80° North-West sector over land were extracted from the whole dataset. The travelling time over land for each trajectory was estimated from topographical data. The temperature along each trajectory was equally separated to 6 bins from 0 to 30 Celsius degrees.

Figure 2 depicts the integrated aerosol volume concentrations against time over land at the SMEAR II station. The colours indicate the range of temperatures. It is visible that the fitting slopes of the particle volume concentrations in relation to time over land increased when the temperature range elevated.

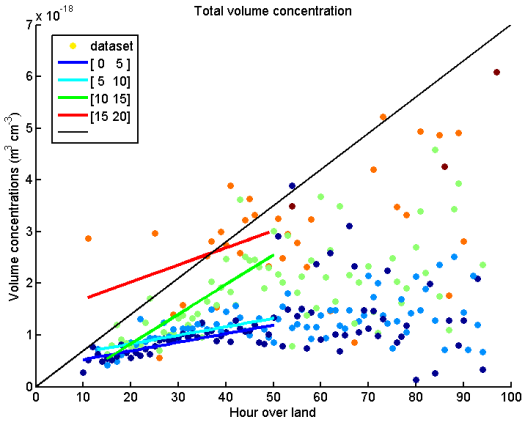

Figure 2. The integrated aerosol volume vs. time over land at four temperature bins.

The preliminary results suggest that temperature plays a strong role on controlling the growth of aerosol particles. In other word, temperature controls the precursor emissions of secondary aerosols, which will directly link to the volume (and mass) growth of aerosol particles. However, temperature has various influences on aerosol particles at different modes.

The Authors wish to thank the Maj and Tor Nessling foundation for financial support (grant No 2009362), as well as the Academy of Finland (Project No. 128731).

Draxler, R. R. and Hess, G. D. (1997). Description of the Hysplit_4 modelling system. (NOAA Tech Memorandum, ERL ARL-224.

Tunved, P., Hansson, H.-C., et al., (2006). *Science*, 312, 261-263.

Tunved, P., Ström, J. et al., (2008). *Tellus B*, 473-484.

M. Kulmala *et al.*, (2004). *Atmos. Chem. Phys.*, 4, 557–562.

Large particle climatology in Finland – Estimating the effect of aerosols in extinction of infrared radiation

N. Kivekäs[1], T. Mielonen[2], H. Portin[2,3], T. Kaurila[4], I. Rajakallio[4], K.E.J. Lehtinen[2,3] and H. Lihavainen[1]

[1]Research and Development, Finnish Meteorological Institute, Helsinki, PO.Box 503, 00101 Finland
[2]Research and Development, Finnish Meteorological Institute, Kuopio, PO.Box 1627, 70211 Finland
[3]Department of Applied Physics,University of Eastern Finland, ,Kuopio, PO Box 1627,70211 Finland
[4]Technical Research Center of Finnish Defense Forces, Lakiala, Finland
Keywords: Extinction, Aerosol impacts, Infrared visibility.
Presenting author email: niku.kivekas@fmi.fi

Automatic measurements of visibility are often based on the scattering or extinction of infrared radiation in ambient air. Infrared radiation can also be used passively to detect signals caused by motors or electrical devices. In these applications it is crucial to know the rate of extinction of the signal in air to be able to estimate the distance to the signal source.

Shettle and Fenn (1979) have developed a model for estimating the extinction of radiation in atmosphere due to aerosols. The model was developed in military use. In their model there are four different shapes for the aerosol particle size distribution: Urban, rural, marine with continental origin, marine with oceanic origin and tropospheric. The logarithmic mean diameter of the mode depends on both distribution type and ambient relative humidity. Finally the number concentration of aerosol particles is parameterized by the distribution type and the ambient visibility.

In some cases this model greatly underestimates the aerosol effect on extinction in Scandinavian conditions (Kaurila et al., 2006; Mielonen et al., 2008). The work presented here aims to improve the estimation by taking a prescribed source region dependent shape of the dry aerosol size distribution and then scaling it by PM10 aerosol concentration and relative humidity.

We have analysed continuous dry aerosol size distribution data from three stations in Finland: Hyytiälä (61º 51' N, 24º 17' E), Puijo (62º 54' N, 27º 31' E) and Pallas (67º 58' N, 24º 07' E) from years 2007-2011. The data was measured from dried flow of ambient air using DMPS and APS, giving the aerosol size range 0.01 – 15 µm. The number size distributions were converted to volume size distributions and normalized by the total volume concentration. The aerosol data was combined with FLEXTRA air mass back trajectories (Stohl et al., 1995).

Different combinations of marine and continental source areas were studied, but the differences between different continental areas as well as those between different marine areas were so small that in the end two simple source areas were used: marine and continental. The size distributions for these areas were somewhat different than those by Shettle and Fenn (1979) for the corresponding maritime and rural areas. For both size distributions extinction was calculated using Mie theory and assuming spherical $(NH_3)_2SO_4$ particles. There were significant differences in extinction between the new and S&F size distributions, especially in the case of continental air, where the new extinction was much larger due to larger fraction of large particles (fig 1).

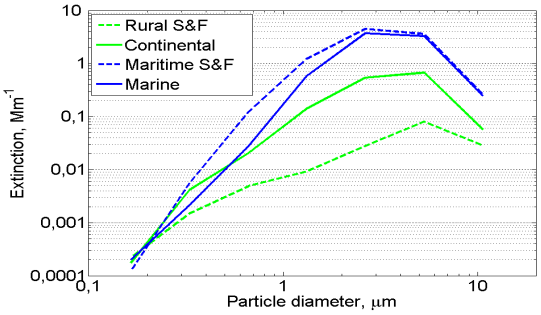

Figure 1. Extinction of 1 µm radiation caused by 1000cm^{-3} aerosol concentration in Shettle and Fenn (S&F) 1979 and in this work

For each trajectory the normalized aerosol size distribution was parameterized by taking a weighted average of the continental and marine size distributions based on the weighted fraction of time the air had spent over land or ocean, respectively.

The accuracy of this method was tested by scaling each parameterized aerosol size distribution by the measured total volume concentration (representing PM10). These were compared to real measured number-size distributions. Extinction in infrared wavelengths was calculated to both type of distributions, and these were compared to each other. The parameterized and "real" extinction values agree on average, but in individual cases the values can be significantly different.

In future the values will be compared to measured extinction values to see if the new size distributions improve the accuracy of the estimation. Also aerosol chemical properties will be included.

This work was supported by The Finnish Scientific Advisory Board for Defence (MATINE).

Kaurila, T., Hågård, A. and Persson, R. (2006), *Appl. Opt*. **45**, 6750-6761.
Mielonen, T., Kaurila, T., Arola, A., Lihavainen, H., Komppula, M. & Lehtinen K. E. J. (2008) *Atmospheric Environment* **42**, 2603-2610.
Shettle, E. and Fenn, R. (1979), *Environmental Research Papers* **676**, AFGL-TR-79-0214.
Stohl, A., Wotawa, G., Seibert, P. and Kromp-Kolb, H. (1995) *J. Appl. Meteor*. **34**, 2149-2165.

Comparison of new particle formation events and an analysis of aerosol dynamics between three sites in northern Scandinavia

R. Väänänen[1], T. Nieminen[1], M. Dal Maso[1], A. Virkkula[1,2], B. Svenningsson[3,4], N. Kivekäs[2], T. Holst[4], A. Arneth[5], V-M. Kerminen[1], M. Kulmala[1]

[1]Department of Physics, University of Helsinki, P.O. Box 64, FIN-00014 University of Helsinki, Finland
[2]Finnish Meteorological Institute, P.O. Box 503, FIN-00101 Helsinki, Finland
[3]Department of Physics, Lund University, Box 118, SE-221 00 Lund, Sweden
[4]Division of Physical Geography and Ecosystems Analysis, Sölvegatan 12, 223 62 Lund, Sweden
[5]Karlsruhe Institute of Technology, Institute of Meteorology and Climate Research/Atmospheric Environmental Research, Kreuzeckbahn Str. 19, 82467 Garmisch-Partenkirchen, Germany

Keywords: nucleation, atmospheric aerosols, airmass, trajectory
Presenting author email: riikka.vaananen@helsinki.fi

New particle formation (NPF) events and growth of the new particles has been observed frequently in different locations globally (Kulmala et al., 2004). Since the growth of the new particles can last from hours up to a couple of days, regional airmasses need to be considered atop of more local processes, when studying this phenomenon.

We examined the new particle formation in three measurement sites at Northern Scandinavia, and also analyzed how particle size distribution evolves when airmasses travel hundreds of kilometers.

Two of the measurement sites, Värriö SMEAR I station and Pallas GAW stations are situated in Finland and the last one, Abisko in Sweden near the border of Norway. The sites are located roughly along a straight line from west to east on latitudes 67-68 °N. The distance from Abisko to Värriö is 440 km. The Abisko area is dominated by subarctic mires surrounded by birch woodland and mountain tundra, whereas Pallas and Värriö are surrounded by boreal forest. The Pallas itself is situated above the tree line.

Our aerosol size distribution data were collected between Aug-2005 - Dec-2007. The data was measured using Differential Mobility Particle Sizers (DMPS) with a cutoff sizes of 3 and 7 nm in Värriö and Pallas, respectively, and using a Scanning Mobility Particle Sizer (SMPS) with a cutoff size of 10 nm in Abisko. The measurements at Pallas and Värriö are continuous, whereas the Abisko data were collected during campaigns of several months.

We analyzed and compared NPF events from each site according to the schema created by Dal Maso et al. (2005). The days are classified as events, non-events and undefined days. For event days we fitted the particle number-size distribution data to sum up to three lognormal distributions, and calculated the growth and formation rates of the nucleating particles.

Tunved et al. (2006) have shown that boreal forests are a source of secondary organic aerosols via emission of biogenic volatile organic compound precursors. Here we repeated and broadened their analysis to cover also Abisko, and compared the growth of particles as a function of time the corresponding airmass has spend over land for all three measurement station. We used the HYSPLIT trajectory model (Draxler and Hess, 1998) was used to calculate the passing-times over-lands. In Fig. 1 is shown the growth of the particle diameter when the airmasses arrive from sea to over land. As a comparison, during the NPF events the observed growing rate is about 3-4 times larger than these rates, which includes all data, not only the data from NPF days.

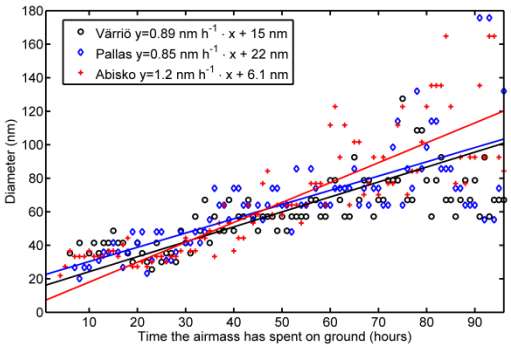

Figure 1: Particle diameters as a function of time the corresponding airmass has spent on-land. Coefficients calculated from time values of <80 h.

Three measurement sites located in a row enabled us to use a pseudo-Lagrangian approach to examine the dynamics of the aerosol during transport. Among other features, we discuss shifts in the modes of the particle size distributions, when the airmasses are drifting between a measurement site pair.

This research was supported by the Academy of Finland Center of Excellence program (project number 1118615).

References:

Dal Maso, M., Kulmala, M., Riipinen, I., Wagner, R., Hussein, T., Aalto, P. P., and Lehtinen, K. E. J. (2005), *Boreal Environ. Res*., **10**, 323–336.

Draxler, R.R. and G.D. Hess (1998), *Aust. Meteor. Mag.* **47**, 295-308.

Kulmala, M., Vehkamäki, H., Petäjä, T., Dal Maso, M., Lauri, A., Kerminen, V.-M., Birmili, W., and McMurry, P. H. (2004*), J. Aerosol Sci.*, **35**, 143-176.

Tunved, P., Hansson, H.-C., Kerminen, V.-M., Ström, J., Dal Maso, M., Lihavainen, H., Viisanen, Y., Aalto, P.P., Komppula, M, Kulmala, M. (2006) *Science***, 312**, 261-263.

The Impact of Meteorological Conditions on PM air pollution in Tartu, Estonia

E.-S. Kerner[1], M. Eller[1]

[1]Institute of Physics, University of Tartu, Tartu, 51007, Estonia
Keywords: air quality, meteorological conditions
Presenting author email: stinkin@ut.ee

We study in the meteorological phenomena which impact the presence and accumulation of PM in the near-ground air and thus worsening air quality. Our study is based on the EAS and NAIS measurements in the city of Tartu. Most influentially, these unfavourable conditions appear to be (i) in case of the smallest PM fractions but also in case of new particle formation – the presence and prevailing of high air pressure systems (Fig. 1) on one hand, but the strength of turbulent motion in the air on the other hand (Fig. 2) – the two phenomena which generally work against each other. (ii)Thermal stratification – in terms of PM NC fractions around 100 nm (Fig. 3).

The role of turbulence in new particle formation has not been under thorough investigaion up to now. The role of thermal stratification and inversions in PM accumulation is interesting in terms of local climate and topography.

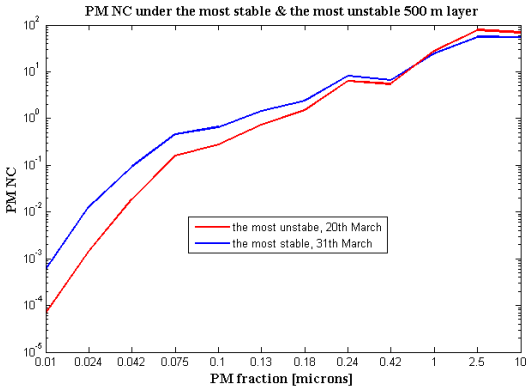

Figure 1. Examples of the number of particles in the air on days with very stable/unstable stratification.

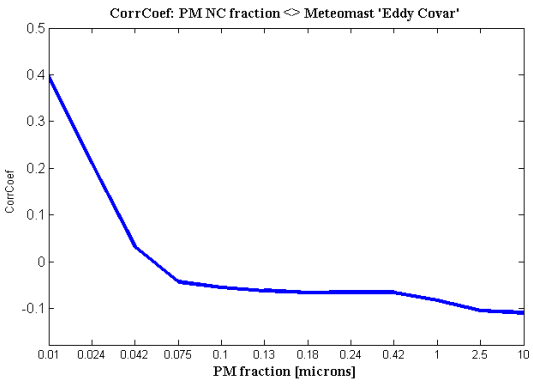

Figure 2. The correlation of EAS PM fractions [NC] with wind speed eddy covariance.

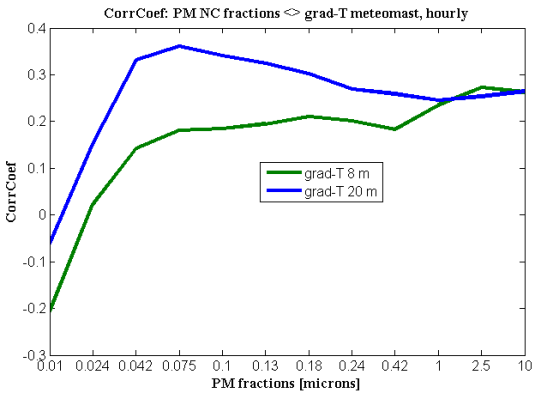

Figure 3. The correlation of PM fractions [NC] with the stratification of near-ground air.

Data

We use the measurements of NAIS and EAS in Tartu during the spring 2011 and since October 2011 till now, in comparison with measurements of night-time radiosondings and a 24 m high meteomast for vertical profiles of meteorological variables near Tartu.

We have observed the accumulation of particles measured with EAS under strong and shallow surface-based inversion rather than under high and long-lasting high air pressure systems. On the other hand, we have found dependence of the formation of new particles on the strength of turbulent motion present in the air as based on the measurements of NAIS.

This work was supported by the Estonian Research Fouocation under grant ETF8523.

Wehner, B. et al(2010) Observations of turbulence-induced new particle formation in the residual layer. *Atm. Chem. Phys* 10, 4319–4330

Aerosol investigations with light aircraft during the Grímsvötn eruption and during Etna volcanic activities in the year 2011

Weber, K.[1], Reichardt, R.[1], Elíasson, J.[2], Vogel, A.[1], Fischer, C.[1], Moser, H.M. [1], Palsson, A.[3], Palsson, T.[4], Sturm, K.[5]

1University of Applied Sciences Duesseldorf, Josef-Gockeln-Str. 9, 40474 Duesseldorf, Germany
[2] Earthquake Engineering Research Centre, University of Iceland, Austurvegur 2a, 800 Selfoss, Iceland
3 ISAVIA, Reykjavik, Iceland
4 Air Navigation Technology, Reykjavik University, Iceland
5 German Weather Service, Aeronautical Meteorology, Frankfurter Straße 135, 63067 Offenbach, Germany
Keywords: volcano, research aircraft, Eyjafjallajökull, Grimsvötn, Etna, aerosol, size distributions
Presenting author email: konradin.weber@fh-duesseldorf.de

Volcanic activities posed certain thread to the aviation in Europe during the last two years. European airspace was closed throughout most part of Europe because of the eruption of Eyjafjallajökull 2010. Moreover in 2011 airspace was temporarily closed in different parts of Europe because of the Grimsvötn eruption. Several paroxysms of Etna in 2011 resulted in a closure of the international airport of Catania (Sicily). During the eruption periods of all these volcanoes the Duesseldorf University of Applied Sciences performed a large number of research flights with light aircraft in close cooperation with the University of Iceland. The light aircraft were equipped with optical particle counters (OPCs) and, dependent on the flight mission, with additional instrumentation for ultrafine particles and volcanic gases.

Whereas the results of the research flights during the Eyjafjallajökull eruption are published elsewhere [1], this presentation will focus on the investigations during the Grimsvötn and Etna volcanic activities.
During the Grimsvötn eruption in May 2011 the airport of Keflavik in Iceland as well as airports in England, Scotland and Scandinavia were closed for some time, because of ash plume forecasts of the VAAC London. Even in Germany the airports of Bremen, Hamburg and Berlin were closed for several hours on 25 May 2011.

During this eruption period of Grimsvötn a team of the Duesseldorf University of Applied Sciences, the University of Iceland, the University of Reykjavik and the IMO has performed airborne in-situ measurements over Iceland and Germany as well as ground-based measurements in the south of Iceland.

The research flights on Iceland were started already one day after the beginning of the eruption (twelve in-situ measurement flights) and investigated the spatial and temporal spread of volcanic ash in the atmosphere. During all the flights TSP (total suspended particles) was recorded. These flights focused on the western part of Iceland in the region of Reykjavik and Keflavik and were mostly coordinated by ISAVIA. The measurement flights helped to keep Keflavik International Airport open for many additional hours despite of adverse predictions by the London VAAC model, because it was possible to observe the particle concentration on-line during the flights.
In Germany a research flight was performed on 25 May 2012 over the northern part of Germany where the volcanic ash cloud was forecasted from the dispersion model of the London VAAC. This flight was performed on the behalf of the German Weather Service (DWD).

Over western Iceland the research flights revealed most time relative low airborne ash concentrations, although the ground-based measured ash concentrations in the south of Iceland nearer to the Grimsvötn were very high.

In Germany the measured concentrations during the flight were low enough to be consistent with the re-opening of the airports Bremen, Hamburg and Berlin, which were closed by the authorities for several hours on 25 May 2011 because of high concentration predictions by the VAAC-model. During the research flight in Germany TSP, PM10, PM2.5, PM1 and aerosol size distributions were measured.

Whereas the airborne measurements during the Grimsvötn eruption were focused on the question, if the airspace was safe, the research flights at Etna concerned the investigation of the aerosol formation, change and dispersion within the volcanic plume. These investigations comprised the measurement of ultrafine aerosols as well as the full variety of aerosols in a size distribution between 250 nm and 32 µm. Moreover, volcanic gases as SO2 and gas fluxes were measured.

This work was supported in parts by the German Weather Service DWD, AIRBUS and German Federal Ministry of Transport, Building and Urban Environment. The support is greatly acknowledged

[1] Weber, K., et al. (2012) *Airborne in-situ investigations of the Eyjafjallajökull volcanic ash plume on Iceland and over North-Western Germany with light aircrafts and optical particle counters*, Atmospheric Environment 48, 9-21, doi:10.1016/j.atmosenv.2011.10.030
[2] Eliasson, J.; Palsson, A.; Weber, K. (2011) *Monitoring ash clouds for aviation*; Nature 475, S. 455 28 Jul 2011, doi: 10.1038/475455b

Indoor and Outdoor Particle Concentrations and Elemental and Organic Carbon at 17 Primary Schools

L. Morawska[1], M. Mazaheri[1], F. Salimi[1], R. Laiman[1], L. Crilley[1], G. Ayoko[1]

[1]International Laboratory for Air Quality and Health, Institute of Health and Biomedical Innovation, Queensland University of Technology, Brisbane, Queensland 4001, Australia
Keywords: urban aerosols, ambient air monitoring, indoor aerosols, schools.
Presenting author email: l.morawska@qut.edu.au

The focus of this paper is on the measured particle number concentrations (PNC) as well as elemental and organic carbon in 17 primary schools. This study is part of the "Ultrafine Particles from Traffic Emissions and Children's Health (UPTECH)", which aims to determine the relationship between exposure to traffic related ultrafine (UF) particles and children's health (http://www.ilaqh.qut.edu.au/Misc/UPTECH%20Home.htm). To achieve this, air quality and health data are being collected at 25 schools within Brisbane Metropolitan Area in Australia over two years. This paper presents the general aspects of UF particles data and preliminary results from the first 17 schools (S01 to S17), tested from Oct 2010 to Dec 2011.

Air quality data are being collected continuously at 5 sampling locations (3 outdoor and 2 indoor sites) within the school grounds for two weeks at each school. Particle number concentration (PNC) is measured at all sites. At one of the outdoor sites, which is in a central location within the school grounds, a range of particle and gaseous parameters are measured, including UF particle size distribution (10 - 400 nm); particle surface area; elemental and organic carbon (EC/OC) components in particle emissions; particle elemental composition; volatile organic compounds (VOC); polycyclic aromatic hydrocarbons (PAH); carbonyls; particle mass (including PM_{10}, $PM_{2.5}$ and PM_1); NO_x; CO; SO_2; ions; airborne pollen grains; culturable moulds; and meteorological conditions (wind speed and direction, relative humidity and temperature). Indoor sites (2 classrooms) are also sampled for particle chemical composition (carbonyls, VOC); CO_2; culturable moulds; endotoxins; total bacteria and exposure to persistent organic pollutants (POPs).

Figure 1 demonstrates the 25th, 50th (Median), and 75th percentile of the PNC at the central location for the first 17 schools during the weekdays. The whiskers illustrate the 10th and 90th percentiles. The variations in PNC at each school can be seen in this graph, showing the outdoor PNC is highest in S03 and lowest in S01.

Figure 2 shows the daily average indoor to outdoor (central location) PNC ratios (I/O) at schools. The I/O ratios of PNC greater than 1 show presence of an indoor source and this is more pronounced in S01, S10, S12 and S17.

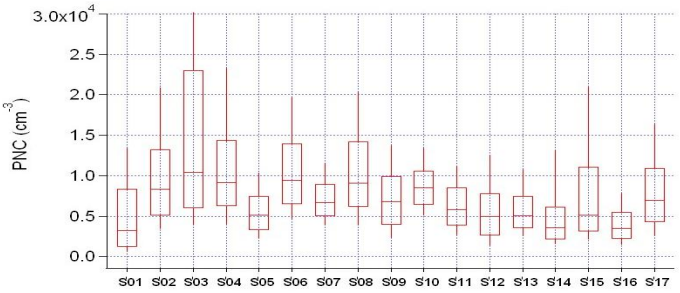

Figure 1: PNC in the central site at 17 schools.

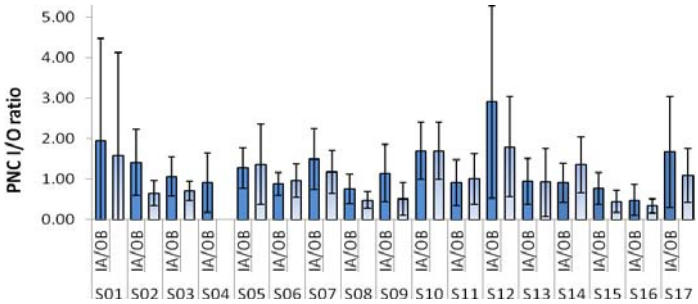

Figure 2: Daily I/O PNC ratios in 17 schools.

Figure 3 shows the average OC/EC ratio at each school, which was above 2, indicating the presence of secondary organic aerosols (SOA) (Chow et al. 1996) in addition to organic aerosols emitted from primary sources. The schools with the highest ratio had higher proportion of SOA while the schools with lower ratio showed more influence from primary sources (likely vehicle emissions).

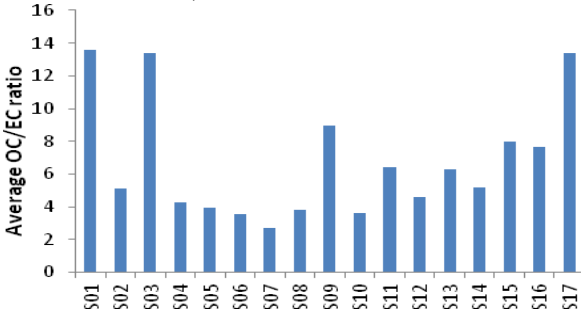

Figure 3: Average OC/EC ratio in the first 17 schools.

This work has been supported by the ARC, DTMR and DET through Linkage Grant LP0990134.

Chow, J. C., J. G. Watson, et al. (1996). "Descriptive analysis of PM2.5 and PM10 at regionally representative locations during SJVAQS/AUSPEX." Atmospheric Environment **30**(12): 2079-2112.

Carbonaceous aerosols in Barcelona during the SAPUSS campaign

A. Karanasiou[1,2], M. Dall'Osto[1], M. Viana[1], A. Alastuey[1], X. Querol[1]

[1] Institute of Environmental Assessment and Water Research (IDAEA-CSIC), Barcelona, Spain
[2]Centre for Research in Environmental Epidemiology (CREAL), Barcelona Biomedical Research Park, Dr Aiguader, 88, 08003 Barcelona, Spain
Keywords: elemental carbon, organic carbon, EC tracer method, secondary organic aerosol.
Presenting author email: angeliki.karanasiou@idaea.csic.es

Organic carbon (OC) and elemental carbon (EC) constitute an important component of the atmospheric aerosol forming typically 10 to 50% of the total PM_{10} mass (Jimenez et al., 2009). EC is exclusively of primary origin (mainly traffic in urban agglomerates) while OC can be of both primary and secondary origin, associated to particulate organic compounds emitted directly into the atmosphere or formed by the condensation of compounds produced by the atmospheric photo-oxidation of volatile organic species.

The contribution of primary and secondary organic aerosol sources is rather difficult to quantify. This is due to the vast number of organic compounds with a variety of chemical and physical properties. However, it is possible to use an indirect method for the quantitative assessment of secondary organic aerosols (SOA), as the EC trace method (Pio et al., 2001). Nevertheless some limitations exist related to the capability of this method to represent the primary ratio between the OC and EC, $(OC/EC)_p$ resulting from fossil fuel combustion (Pio et al., 2011).

OC and EC concentrations were determined during the SAPUSS (Solving Aerosol Problems by Using Synergistic Strategies) campaign on September 2010 in Barcelona, Spain. Five monitoring sites were used: Road Site (RS), Urban Background (UB), Tower Mapfre (TM), site Tower Collserola (TC) and Regional Background (RB). The sites TM and TC were 154 and 445 m a.s.l respectively. Here we present the results of PM_{10} collected simultaneously with high volume samplers (MCV) using 12h intervals.

The concentrations of OC and EC were determined by a thermal analysis method using the Sunset Laboratory OCEC Analyzer and the EUSAAR-2 thermal protocol. As it was expected EC concentrations in RS were higher than those determined at all sites attributed to the considerable amount of primary emissions by traffic. OC concentrations had a similar behavior, Figure 1. The ratio of the ambient concentrations of OC to EC includes information about the extent of secondary OC formation. The fact that the average OC/EC ratio (~4.5) during SAPUSS exceeded significantly the $(OC/EC)_p$ measured at typical traffic sites (0.3-0.4) (Pio et al., 2011) shows significant contribution of secondary organic aerosol that is rapidly formed. Consequently the EC tracer method could not accurately assess the input of the secondary organic aerosol.

Figure 2 shows the regression of OC to EC concentrations in PM_{10} at the sampling sites. The intercept of the regression represents the non combustion OC. The intercept was similar for all sampling sites at ground level: RS, UB, RB and also for the two towers TC and TM at 154 and 445 m a.s.l respectively, suggesting a uniform horizontal and vertical distribution of this non combustion OC. Significant differences were observed in the intercept only during days with intense regional air mass recirculation. During normal conditions non combustion OC accounted for 48% of OC while during regional episodes reached 68% of total organic aerosol mass. This fact implies that the non combustion OC is mainly emitted by regional and not local sources, consistent with its relatively homogeneous spatial distribution.

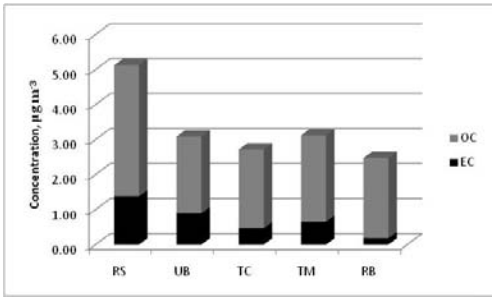

Figure 1. EC and OC concentrations during SAPUSS in the five sampling sites

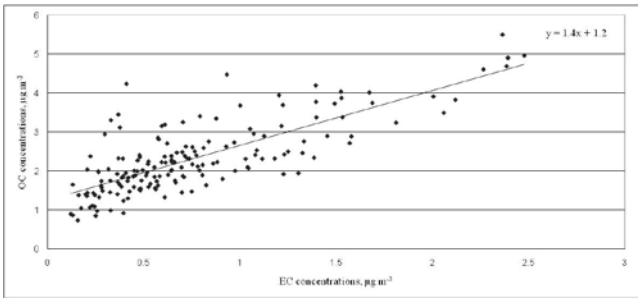

Figure 2. Regression of OC to EC concentrations during SAPUSS

This work was supported by the Marie Curie Actions – Intra European Fellowships (FP7-PEOPLE- 2009-IEF, Project number 254773: Researcher M. Dall'Osto.

Jimenez, J.L., Canagaratna, M.R., Donahue, N.M., et al., 2009. *Science*, **326**, 1525–1529.

Pio, C., Alves, C., Duarte, A., 2001. *Atmos. Environ.*, **35**, 1365–1375.

Pio CA, Cerqueira M, Harrison RM, Nunes T, Mirante F, Alves C, et al. 2011. *Atmos Environ*, **45**, 6121–6132.

Carbonaceous content of PM_{10} and $PM_{2.5}$ in urban-traffic and urban background sites within the Thessaloniki Major Area (TMA), northern Greece

C. Samara[1], D. Voutsa[1], A. Kouras[1], Th. Maggos[2]

[1]Aristotle University of Thessaloniki, Department of Chemistry,
Environmental Pollution Control Laboratory, University Campus, 54124 Thessaloniki, Greece
[2]National Centre of Scientific Research "Demokritos", Institute of Nuclear Technology and Radiation Protection, Environmental Research Laboratory, 15310 Ag. Paraskevi, Attiki, Greece

Keywords: Carbonaceous particles; elemental carbon; organic carbon, PM10/PM2.5; urban aerosols
Presenting author email: csamara@chem.auth.gr

Thessaloniki (40°62´E, 22°95´N) is a densely populated Greek city suffering from high concentrations of airborne particulate matter (PM), particularly in the city center. Several studies have been carried out to determine the chemical composition of ambient PM at various sites within the Thessaloniki Major Area. However, the organic and elemental carbon content of PM_{10} (OC and EC) has only recently started to be studied (Flarountzou *et al*., 2008; Chrysikou *et al*., 2009; Terzi *et al*., 2010). In a PM_{10} mass closure (Terzi *et al*., 2010), at an urban-industrial and an urban-traffic site, organic matter constituted a significant fraction of PM_{10} (18% and 23%, respectively), while EC had a lower contribution at both sites (3.6 % and 6.3%).

The aim of the present study was to investigate the OC and EC content of PM_{10} and $PM_{2.5}$ at two sites within the Thessaloniki Major Area (TMA), UT (urban-traffic) and UB (urban-background) (Figure 1). At both sites, PM_{10} and $PM_{2.5}$ samples were concurrently collected during the warm season of 2011 according to EN-12341 and EN14907, respectively. Low Volume Samplers (Ingenieur Derenda, Berlin) equipped with PM_{10} and $PM_{2.5}$ inlets were employed operating at constant flow rate 2.3 m^3/h. PM_{10} and $PM_{2.5}$ fractions were collected on Φ 47 mm high purity quartz filters (Tissuquartz^{TM}, Pall) prefired at 500 ^oC for 4 hours. Each sampling had a 24-h duration starting at 00:00. Organic carbon (OC) and elemental carbon (EC) were determined by the Thermal Optical Transmission method in a Sunset Laboratory OCEC Analyzer.

Summary statistics for OC and EC concentrations associated with $PM_{2.5}$ and PM_{10} are given in Table 1. These values are in general agreement with those previously found in Thessaloniki during the warm period (Flarountzou *et al*., 2008; Chrysikou *et al*., 2009; Terzi *et al*., 2010). As seen, both PM fractions were higher in the UT site, which exhibited lower $PM_{2.5}/PM_{10}$ ratio (Table 2) suggesting stronger impact of traffic induced resuspension of road dust.

Table 1. Mean±SD for mass concentrations of PM_{10}, $PM_{2.5}$ and associated OC and EC (μg/m^3)

	PM_{10}	OC_{10}	EC_{10}	$PM_{2.5}$	$OC_{2.5}$	$EC_{2.5}$
UT	48±10	8.4±2.9	7.7±1.4	26±6	6.2±2.3	6.0±1.3
UB	28±9	4.1±1.7	0.7±0.2	17±6	3.2±1.3	0.5±0.2

Daily concentrations of OC and EC associated with the PM_{10} and $PM_{2.5}$ particle fractions are illustrated in Fig. 2.

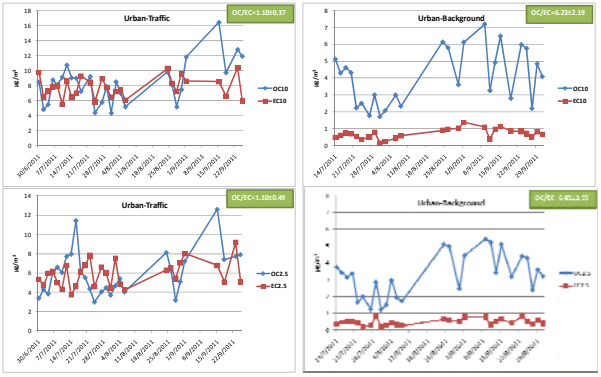

Figure 2. Daily variation of OC and EC concentrations associated with the PM_{10} and $PM_{2.5}$ particle fractions

EC, considered as a tracer of primary emissions mostly derived from traffic, was higher at the UT site, while both sites exhibited similar $EC_{2.5}/EC_{10}$ ratios averaging 0.81, indicative of EC distribution mainly in fine particles (Table 2). OC, that may originate from secondary aerosol formation processes as well, was also higher at the UT site**.** The relatively lower $OC_{2.5}/OC_{10}$ ratio at UT (0.77) suggests inputs of organic matter in the coarse fraction, whereas the high value of this ratio at UB (0.92) implies secondary organic aerosol formation.

Table 2. $PM_{2.5}/PM_{10}$ ratios for PM mass, OC and EC

	$PM_{2.5}/PM_{10}$	$OC_{2.5}/OC_{10}$	$EC_{2.5}/EC_{10}$
UT	0.54±0.10	0.77±0.26	0.81±0.26
UB	0.64±0.10	0.92±0.46	0.81±0.41

As seen in Fig. 2, the OC/EC ratio at the UT site was 1.1 in both particle fractions, in contrast to the significantly higher values observed at the UB site (6.23 in PM_{10}, 6.85 in $PM_{2.5}$), which reveal increased secondary organic particle formation (Duan et al., 2005).

References

Chrysikou, L.P., Samara, C., Bougiatioti, A., Mihalopoulos, N., EAC2009, Carlsruhe, Germany, Abstract T022A22.

Duan, F., He, K., Ma, Y., Jia, Y., Yang, F., Lei, Y., Tanaka, S., & Okuta, T., (2005). *Chemosphere* 60, 355-364.

Flarountzou, A., Terzi, E., Samara, C., Bougatioti, A., Mihalopoulos, N., Nikolaou, K., EAC2008, Thessaloniki, Greece, Abstract T02A053P.

Terzi, E., Argyropoulos, G., Bougiatioti, A., Mihalopoulos, N., Nikolaou, K., Samara, C. (2010). *Atmos. Environ.*, 44, 2231-2239.

Aknowledgements

This work was supported by the European Community (LIFE + Environment Policy and Governance).

Characteristics of fine carbonaceous aerosol at a coastal rural site in the Central Mediterranean as given by OCEC online measurements

Antonella Malaguti[a], Mihaela Mircea[a], Teresa M.G. La Torretta[a], Chiara Telloli[b], Massimo Berico[a]
[a]Italian National Agency for New Technologies, Energy and Sustainable Economic Development (ENEA), Technical Unit for Environmental Assessment Models, Methods and Technologies (UTVALAMB), Air Quality Laboratory (AIR), 40129 Bologna (Italy).
[b]Department of Earth Science, Ferrara University - Italy
Keywords: Carbonaceous aerosol, Organic carbon, Elemental carbon, Particle number, rural background site
Presenting author email: antonella.malaguti@enea.it

In Europe, the carbonaceous aerosol is a major fraction of atmospheric aerosol even at rural background sites (Yttri *et al*., 2007) with possible exceptions at coastal sites and at sites located in the Mediterranean area where the contribution of Saharan dust can be high. The Mediterranean area is one of the most susceptible areas to climate changes, yet with large uncertainties regarding the fine-scale climate processes associated to the complex physiography of the region (Diffenbaugh *et al*., 2007).

This work shows the OC and EC concentrations at coastal rural site in the in the South of Italy (ENEA-Trisaia Research Centre (44°30'N, 11°21'E)) during a two months (May and June 2010) field campaign. The measurements were performed with a semi-continuous OC/EC analyzer (Model-4 Field analyzer, Sunset Lab.) using the EUSAAR_2 thermal optical transmittance protocol (Cavalli *et al*., 2010).

In order to better understand the OC/EC aerosol mass concentration in relation to number concentration of particles with different sizes, real-time particle concentration measurements performed with a dust monitoring system (Mobile Enviro Check GRIMM EDM107) are shown.

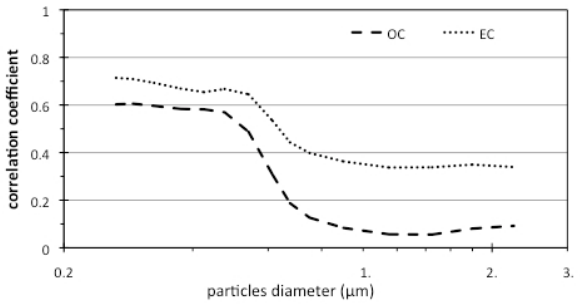

Fig. 1 Correlation coefficient between the OC and EC mass concentrations and the number concentration of aerosol particles with diameters contained in the following ranges: 0.25- 0.28- 0.3- 0.35- 0.4- 0.45- 0.5- 0.58- 0.65-0.7- 0.8- 1- 1.3- 1.6- 2.0-2.5 µm.

Temporal variations of carbonaceous aerosols, gaseous pollutants such as carbon monoxide (CO) and nitrogen dioxide (NO_2), and meteorological variables over the days of the week are also examined.

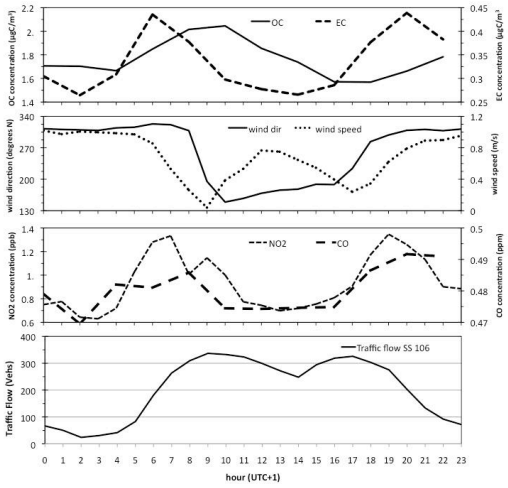

Fig. 8 Daily cycle of wind speed and direction, OC and EC concentrations, NO_2 and CO concentrations, and traffic flow on SS106 freeway.

Acknowledgments: This work is part of the MINNI (Integrated National Model in support to the International Negotiation on Air Pollution) project, funded by the Italian Ministry of the Environment and carried out by ENEA.

Cavalli, F., Viana, M., Yttri, K.E., Genberg, J., Putaud, J.P. (2010), *Toward a standardised thermal-optical protocol for measuring atmospheric organic and elemental carbon, the EUSAAR protocol*, *Atmospheric Measurement Techniques*, 3, 79-89.

Diffenbaugh, N. S., J. S. Pal, F. Giorgi, and X. Gao (2007), Heat stress intensification in the Mediterranean climate change hotspot, *Geophysical Research Letters*, 34, L11706, doi:10.1029/2007GL030000.

Yttri, K. E., Aas, W., Bjerke, A., Cape, J. N., Cavalli, F., Ceburnis, D., Dye, C., Emblico, L., Facchini, M. C., Forster, C., Hanssen, J. E., Hansson, H. C., J ennings, S. G., Maenhaut, W., Putaud, J. P., and Tørseth, K.: *Elemental and organic carbon in PM10: a one year measurement campaign within the European Monitoring and Evaluation Programme EMEP*, *Atmospheric Chemistry and Physics*., 7, 5711–5725, doi:10.5194/acp-7-5711-200

Black carbon optical properties measured in Pasadena, Los Angeles during CalNex

J.W.Taylor[1], J.D. Allan[1,2], M.J. Flynn[1], Patrick Hayes[3], Jose Jimenez[3,4], Barry Lefer[5] and Hugh Coe[1,2]

1Centre for Atmospheric Science, School of Earth, Atmospheric and Environmental Science, University of Manchester, Manchester, M13 9PL, United Kingdom
[2]National Centre for Atmospheric Science, University of Manchester, Manchester, M13 9PL, United Kingdom
[3]University of Colorado at Boulder, Boulder, CO 80309, USA
[4]Cooperative Institude for Research in Environmental Sciences, University of Colorado at Boulder, Boulder CO 80309, USA
[5]University of Houston, Houston, TX 77004, USA

Keywords: Black carbon, Soot particles, SP2, Optical Properties, Photoacoustic
Presenting author email: jonathan.taylor@postgrad.manchester.ac.uk

Black carbon is the second biggest contributor to current global warming, second only to carbon dioxide in global radiative forcing (Ramanathan and Carmichael, 2008). Optical absorption is commonly modelled using Mie theory, assuming a concentric sphere core-shell configuration, however this is sensitive to the physical size and complex refractive index of the particles(Bond and Bergstrom, 2006). As nonrefractory species condense to form a thicker coating, the amount of light absorbed per unit mass of black carbon is increased, analogous to a lensing effect focusing light onto the core.

This effect has been studied in detail theoretically (Lack and Cappa, 2010) and has been seen in numerous laboratory studies (e.g. Schnaiter *et al.*, 2005; Shiraiwa *et al.*, 2010). Many ambient measurements of mass absorption cross-section (MAC) are available, though most used filter-based methods, which are subject to artefacts when nonrefractory material is present. Several measurements of core-shell diameters have also recently been published since the introduction of the single-particle soot photometer (SP2). Ambient studies of this effect are however extremely limited, and no study has compared SP2 core-shell measurements to changes in measured absorption.

We present results from the CalNex study, which took place in Pasadena, Los Angeles in summer 2010 in an attempt to provide a real-world assessment of the validity of models and parameters used to represent black carbon optical properties. The BC at this site was believed to be dominated by diesel emissions. An SP2 was deployed alongside a 3-wavelength photoacoustic soot spectrometer (PASS) measuring absorption. Combining both measurements yields the MAC in high time-resolution, free from filter-based artefacts.

We compare measured MAC to that calculated from SP2 core-shell measurements using Mie theory under a range of different atmospheric conditions, to test the applicability of the core-shell model in an urban environment. A thermal denuder (Huffman *et al.*, 2005) was also used to assess the optical properties and model performance of the BC cores in isolation, allowing the effect of the coatings to be quantified.

This work was supported by UK Natural Environment Research Council (NERC) under grant NE/H008136/1 and a NERC doctoral training grant.

We thank Jim Smith for loan of the thermal denuder.

Bond, T. C., and R. W. Bergstrom (2006) *Aerosol Science and Technology*, **40**(1), 27-67.
Huffman, J. A., J. T. Jayne, F. Drewnick, A. C. Aiken, T. Onasch, D. R. Worsnop, and J. L. Jimenez (2005) *Aerosol Science and Technology*, **39**(12), 1143-1163.
Lack, D. A., and C. D. Cappa (2010) *Atmospheric Chemistry and Physics*, **10**(9), 4207-4220.
Ramanathan, V., and G. Carmichael (2008) *Nat. Geosci.*, **1**(4), 221-227.
Schnaiter, M., C. Linke, O. Mohler, K. H. Naumann, H. Saathoff, R. Wagner, U. Schurath, and B. Wehner (2005) *Journal of Geophysical Research-Atmospheres*, **110**(D19), 11.
Shiraiwa, M., Y. Kondo, T. Iwamoto, and K. Kita (2010) *Aerosol Science and Technology*, **44**(1), 46-54.

FTIR-ATR spectroscopy of water-soluble organic matter from atmospheric aerosols

S.M.S. Freire, R.M.B.O Duarte and A.C. Duarte

Department of Chemistry &CESAM, University of Aveiro, Aveiro, 3800-193, Portugal
Keywords: Atmospheric aerosols; Water-soluble organic matter; FTIR-ATR spectroscopy.
Presenting author email: sandra.freire@ua.pt

Water-soluble organic matter (WSOM) in fine aerosols (i.e., aerosols particles with aerodynamic diameter <2.5 µm, and also called $PM_{2.5}$ fraction) is in the forefront of atmospheric research. Aerosol WSOM play an important role in the physical and chemical properties of atmospheric aerosols and therefore on climate effects (Facchini *et al* 1999; Gysel *et al* 2004). However, a sensitive methodology for the detailed characterization of such component of atmospheric aerosols is lacking on the current literature. Such lack may be due to the complex nature of WSOM.

In this work, $PM_{2.5}$ samples were collected during four different seasons (autumn, spring, summer, and spring/winter) in an urban North Western European coastal region (40°38'N, 8°39'W). Aqueous extracts of the $PM_{2.5}$ samples were fractionated through a DAX-8 resin resulting into two different fractions: a) a more hydrophobic fraction, and b) a more hydrophilic fraction. Figure 1 show typical images of the isolated hydrophobic fraction of WSOM from fine aerosols obtained at autumn and winter/spring seasons. Since the hydrophobic fraction represents more than 60% of the WSOM, this study began by the characterization of its structural features using Fourier transform infrared - attenuated total reflectance (FTIR-ATR) spectroscopy.

The results obtained show the presence of various functional groups in the different aerosols samples, which were collected at different environmental conditions. The hydrophobic acids fraction from autumn and winter/spring aerosols seems to contain lignin derived structures. The winter/spring samples also reveal signals typical of carbohydrate structures. All these structures are commonly found in biomass burning emissions (Duarte *et al* 2005; Duarte *et al* 2007).

Furthermore, this work can contribute to the comprehension of the influence of different seasonal events on the chemical nature of WSOM, as well as to assess the usefulness of a sensitive analytical technique such as FTIR-ATR for the characterization of WSOM.

Figure 1. Isolated hydrophobic fraction of WSOM obtained from fine aerosols collected at: a) autumn, and b) winter/spring seasons.

The Portuguese Institute for Development (IPAD) is acknowledged for financial support through a PhD grant attributed to S.M.S. Freire. Centre for Environmental and Marine Studies (University of Aveiro, Portugal) and the Portuguese Science and Technology Foundation (FCT), through the European Social Fund (ESF) and "Programa Operacional Potencial Humano – POPH", are also acknowledged for financial support. Finally, this work was also funded by FEDER under the Operational Program for Competitiveness Factors – COMPETE and by National funds via FCT within the framework of research project ORGANOSOL (References FCOMP-01-0124-FEDER-019913 and PTDC/CTE-ATM/118551/2010).

Duarte, R. M. B. O., Pio, C. A. and Duarte, A. C. (2005) *Anal. Chim. Acta* **530**, 7-14.

Duarte, R. M. B. O., Santos, E. B. H., Pio, C. A. and Duarte, A. C. (2007) *Atmos. Environ.* **41**, 8100-8113.

Facchini, M. C., Fuzzi, S., Zappoli, S., Andracchio, A., Gelencser, A., Kiss, G., Krivacsy, Z., Meszaros, E., Hansson, H. C., Alsberg, T. and Zebuhr, Y. (1999) *J. Geophys. Res-Atmos.* **104**, 26821-26832.

Gysel, M., Weingartner, E., Nyeki, S., Paulsen, D., Baltensperger, U., Galambos, I. and Kiss, G. (2004) *Atmos. Chem. Phys.* **4**, 35-50.

Seasonal and diurnal observations of black carbon and trace gases in the north suburb of Nanjing influenced by industiral areas

L.L Tang[1,2,3], X.Z Zhang[1], D.T. Liu[2], J. Allan[2], Hugh Coe[2]

[1] The Center of Jiangsu Environmental Monitoring, Nanjing,210016,China
[2] University of Manchester, SEAES, Manchester, M13 9NL,United Kingdom
[3] Jiangsu Key Laboratory of Atmospheric Environment Monitoring and Pollution Control, NUIST, Nanjing, 210044 ,China

Keywords: black carbon; trace gases; observational; north suburb of Nanjing.
Presenting author email: lily3258@163.com

Black carbon (BC) in atmospheric particulate is composed of amorphous carbon, which is a by-product of incomplete combustion (Bond and Bergstrom, 2006). Emissions from natural sources such as forest fires are localized and incidental in China (Bai and Wang, 2005), whereas anthropogenic emissions are widespread and continuous (Liu et al., 2010). The increasing demand for energy in the past century has led to a great increase in the rate of BC emissions resulting from fossil fuel combustion. Black carbon particles have received increased interests. Nanjing is one of the mega cities in China. The high population density and rapid industrialization lead to an increase of primary emission of pollutants. Combination of primary and secondary pollutants results in high concentrations of fine particles.

The experiment presented in this paper was conducted at north suburb of Nanjing which is located in the center of the Yangtze River Delta of China during November 2008 to April 2010. Twelve-hour integrated samples of $PM_{2.5}$ were collected on quartz filters. These samples were analyzed for elemental carbon (EC) using a Thermo/Optical Reflectance (TOR) method. Aerosol black carbon (BC) was determined using an Aethalometer, a continuous optical absorption method. Twelve-hour average concentrations were calculated from the continuous BC measurements to temporally match the EC/OC integrated quartz filter samples. BC and EC concentrations are highly correlated over the study period (R^2=0.9492). In this paper, the seasonal and diurnal variation characteristics of black carbon (BC) in $PM_{2.5}$ and the effects of heterogeneous reactions of traces gases within BC were studied. The results showed that daily averaged concentrations of BC ranged from 1114 to 19408 ng · m^{-3}. The diurnal variabity in BC mass was characterized by a double peak, which can be attributed to local anthropogenic emission and atmospheric boundary layer diurnal changes. The background concentration of black carbon in $PM_{2.5}$ is 2920ng/m^3 during observation period, which was higher than that of most cities in China. Observations of SO_2, NO_2, HNO_2 and O_3 by differential optical absorption spectroscopy were used to investigate the relationships between trace gases and BC. During very hazy days, there were positive correlations between BC and SO_2, NO_2 and HNO_2, with correlation coefficients of 0.290, 0.615 and 0.676, respectively. In contrast, negative correlation was found between BC and O_3, with the correlation coefficient of -0.455.

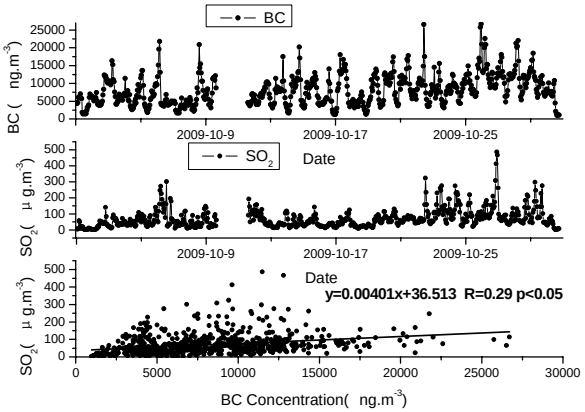

Fig. 1 Hourly mean variation series of SO_2 concentration in the north suburb of Nanjing during Oct.2009 and correlation character between SO_2 and BC

This work was supported by the Natural Science Key Research of Jiangsu Province High Education of China (Grant No. 11KJA170002).

Bond Tami C., Bergstrom Robert W., （2006）. *Aerosol Science and Technology***40,** 27-67.

Bai J H, Wang B C, (2005). *Science Technology and Engineering***5**, 585-591.

Liu D., Allan J., Corris B., Flynn M., Andrews E., Ogren J., Beswick K., Bower K., Burgess R., Choularton T., Dorsey J., Morgan W., Williams P., Coe H.,(2010). *Atmospheric Chemistry and Physics Discussions* **10**, 25243-25286.

Organic, elemental and water-soluble organic carbon in size segregated aerosols in the Eastern Mediterranean.

A. Bougiatioti[1], P. Zarmpas[1], E. Koulouri[1], M. Antoniou[1], C. Theodosi[1], G. Kouvarakis[1], S. Saarikoski[2], T. Mäkelä[2], R. Hillamo[2] and N. Mihalopoulos[1]

[1] Environmental Chemical Processes Laboratory, Department of Chemistry, University of Crete, 71003, Heraklion, Greece
[2] Finnish Meteorological Institute, Air Quality Research, 00101, Helsinki, Finland
Keywords: size distribution, organic carbon, chemical composition, Eastern Meidterranean
Presenting author email: kbougiatioti@chemistry.uoc.gr

Size-segregated aerosol measurements were carried out at the Finokalia measuring site of the University of Crete during a three-year period using a 12-stage Small-Deposit-area low-volume-Impactor for particles with aerodynamic diameters between 0.01 and 13.6 μm. 111 samples were collected in total and were subsequently analyzed in order to determine, for the first time in the area, the size distribution of organic, elemental, and water-soluble organic carbon.

All three carbonaceous constituents exhibit a unimodal distribution with a prominent maximum in the Accumulation mode particles (D_a ~0.45 μm) which sometimes exhibits a second, less pronounced peak in the Coarse fraction (D_a 1.66-4.08 μm). OC and EC occasionally show a minor, secondary peak in the lower particle range (D_a 0.04-0.06 μm), especially for anthropogenic emission-laden (traffic/heating) air masses coming from Central-Eastern Europe (Figure 1). Maximum concentrations for OC and WSOC occur during summer, while for EC during spring, summer and autumn. In general, it was found that almost 2/3 of OC and EC concentrations are found in the PM_1 fraction of the aerosol.

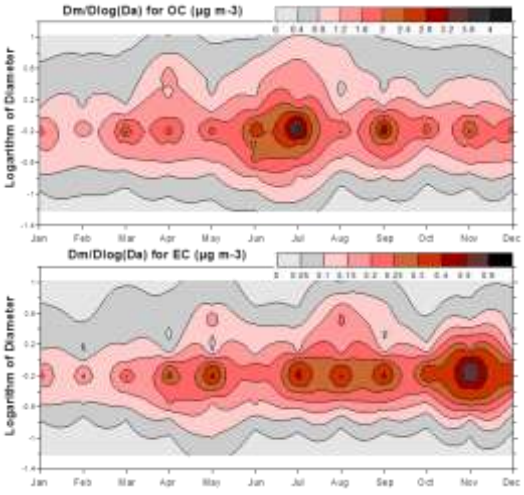

Figure 1. Contour plots of monthly averages for OC, EC.

Using the majority of samples for all 12 stages of the SDI, an OC/EC ratio of 5.13 is obtained, with this ratio being slightly higher for the PM_1 fraction. This ratio is similar to other ratios found for marine background sites (e.g. Aveiro-Portugal). Using the EC-tracer method, it was found that 64.6±17.6% of the PM_{10} organic carbon is secondary, with the percentage reaching ~70% for the PM_1 fraction. Having in mind that high secondary organic aerosol concentrations result principally via photochemical oxidation, adding oxidized functional hydrophilic groups and increasing the solubility of organic carbon in water, we studied the WSOC/OC relationship in the samples. It occurred that a grand majority (~70%) of the OC in the fine fraction is water-soluble, with the ratio increasing, as expected, during summer.

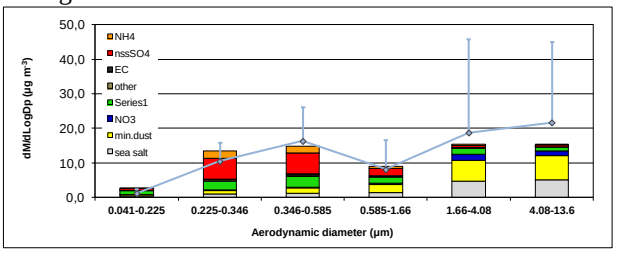

Figure 1. Mass closure of size-segregated aerosol.

Finally, we concurrently established the size distribution of major water-soluble inorganic aerosol components. SO_4^{2-} and NH_4^+ also exhibit a pronounced maximum in the fine fraction (0.45-0.67 μm), with ammonium sulphate accounting for 59.4±17.9% of the total inorganic mass fraction and 82.8±12.8% of the total sulphate being in the submicron mode. Together with ammonium and organic matter, they constitute the largest part of this aerosol faction. NO_3^-, Na^+ and Cl^-, on the other hand, show a maximum in the coarse fraction (aerodynamic diameters 3.31-5.85 μm). Using the median size segregated concentrations, a mass closure study was successfully performed (Figure 2). It was estimated that sea salt and mineral dust account for 32.9% and 44.5% of the coarse inorganic mass fraction, respectively. Our results represent a valuable long-term measurement dataset of size-segregated aerosol measurements in the area.

This research project (PENED) is co-financed by E.U.-European Social Fund (75%) and the Greek Ministry of Development-GSRT (25%).

A yearly cycle of radiocarbon in organic and elemental carbon at a rural site in the Netherlands

U. Dusek[1], M. Monaco[1], S. Szidat[2], H. A. J. Meijer[3], J. van der Plicht[3], T. Röckmann[1]

[1]IMAU, Utrecht University, Utrecht, the Netherlands
2Department of Chemistry and Biochemistry, University of Berne, 3012, Switzerland
[3]Center for Isotope Research, Groningen University, Groningen, the Netherlands

Keywords: organic carbon, elemental carbon, 14C, fossil fuel.
Presenting author email: u.dusekt@uu.nl

Measurement of the radioactive carbon isotope ^{14}C in aerosols can provide a direct estimate of the contribution of fossil fuel sources to aerosol carbon. In aerosol science, measurements of $^{14}C/^{12}C$ ratios are usually reported as fraction modern (f_m). The radiocarbon signature gives a clear distinction between 'modern' carbon sources (f_m around 1.1-1.2 for biomass burning and around 1.05 for biogenic secondary organic aerosol) and 'fossil' carbon sources (f_m =0 for primary and secondary formation from fossil fuel combustion).

High volume filter samples have been collected since February 2011 at the Cabauw site, situated in a small rural area in the Netherlands, surrounded by some major urban centers. We report measurements of f_m for total carbon (TC), organic carbon (OC), water insoluble OC (WIOC) and thermally refractory carbon (RC) as a proxy for elemental carbon. The carbon fractions are isolated by combusting TC at 650 °C, OC and WIOC at 360 °C. Refractory carbon is defined as the carbon remaining on the filter after water extraction, combustion at 360 °C for 15 min and at 450 °C for 2 minutes. The method has been tested with test substances and real aerosol filters and indicates little charring for water-extracted filters.

First results of 7 filter samples taken from February – Mai 2011 show f_m(OC) generally larger than 0.86, except for one case, when a strongly polluted air mass originating in Eastern Europe reached the site. This indicates a strong contribution of natural sources to OC, even in the Netherlands, a very densely populated country with one of the highest levels of aerosol pollution in Western Europe. In particular, water soluble OC in the rural springtime aerosol seems to originate almost entirely from contemporary sources.

Refractory carbon also showed relatively high f_m, generally between 0.3-0.5, except in two cases, when marine air masses reached the site from the west and f_m(RC) dropped to around 0.1. This could mean that biomass combustion plays a significant role around the Netherlands even in springtime. It is also possible that there exists a biogenic, organic component of the aerosol that evolves at such high temperatures that it is virtually inseparable from elemental carbon.

Figure 1 shows a first estimate of the contribution of biomass burning sources to EC, under the assumption that all non-fossil EC comes from biomass burning and that biomass burning aerosol has f_m = 1.2. During our campaign, biomass burning sources account for 10 to 40% of EC. The contribution of biomass burning to EC in Cabauw is lower than the contribution measured in two winter campaigns at rural sites in Switzerland and Sweden (Szidat *et al.,* 2007; Szidat *et al.,* 2009). However, a significant part of our campaign was held in Spring and air pollution from fossil sources is likely higher in the densely populated Netherlands than in rural Switzerland or Sweden. Therefore, the significant contribution from biomass burning sources to EC was somewhat unexpected.

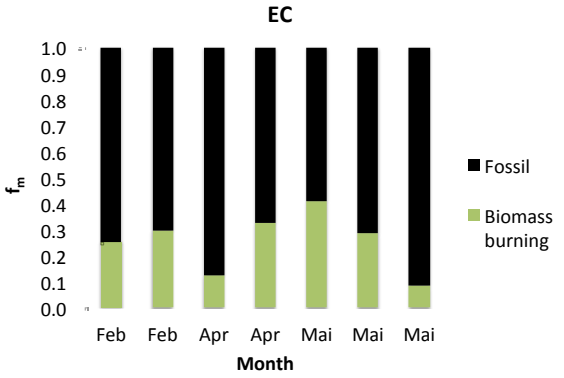

Figure 1. The fraction of EC from fossil and biomass burning sources, assuming no primary biological contribution to EC, and fm = 1.2 for biomass burning

Currently, filter samples from other seasons are prepared for radiocarbon analysis and a full yearly cycle of ^{14}C measurements in various fractions of the carbonaceous aerosol will be presented.

This work was supported by the Netherlands Organization for Scientific Research (NWO, grant nr. ALW820.01.001).

Szidat, S., Prevot, A. S. H., Sandradewi, J., Alfarra, M. R., Synal, H.-A., Wacker, L., and Baltensperger, U., (2007) *Geophys. Res. Lett.,* **34**, L05820, doi:10.1029/2006GL028325.

Szidat, S. M. Ruff, N. Perron, L. Wacker, H.-A. Synal, M. Hallquist, A. S. Shannigrahi, K. E. Yttri, C. Dye, and D. Simpson (2009) *Atmos. Chem. Phys., **9***, 1521–1535, 2009.

Characterisation of trace metals in airborne carbonaceous aerosols by single-particle EDX - Scanning Electron Microscopy

A. Pietrodangelo[1], S. Pareti[1] and C. Perrino[1]

[1]Institute for Atmospheric Pollution Research, National Research Council (C.N.R.), Monterotondo (Rome), 00016, Italy

Keywords: carbonaceous aerosol, trace metals, scanning electron microscopy, backscatter analysis.

Presenting author email: pietrodangelo@iia.cnr.it

Different types of carbonaceous aerosols have been identified in airborne particulate matter (PM) samples collected during a two years extended field campaign in Central Italy. Airborne PM to be investigated by scanning electron microscopy (SEM) was collected in parallel at three sites (two sub-urban and one regional background) by 8-stage cascade impactors (Moudi 100); 3 days and 24 h sampling was performed, respectively, for size fractions above and below 1 µm aerodynamic diameter (a.d.).

Identified carbonaceous formations include char particles, soot single-chains and aggregates, cenospheres, carbon-with-secondary sulphates combined aerosol and silicon-rich carbonate particles.

Aerosol aggregates and single particles were characterised by morphology and elemental microanalysis by energy dispersive X-ray spectroscopy (EDX). Backscatter analysis was employed to investigate the presence of metal particles included in each type of carbonaceous aerosol and X-rays mapping was also performed to gain information about the chemical species contributing to element composition.

Char and soot aggregates, cenospheres and Si-rich carbonate particles were mostly observed in the >1 µm (a.d.) fraction, while mixed carbon-sulphates materials mainly distribute in the finer fractions; moreover the latter type is hardly distinguishable as single particles or aggregates.

Metal particles observed were in the 1 – 0.05 µm physical size range, although the presence of smaller particles should be reasonably considered. Iron-rich particles were found in large number, showing rounded shape and average physical diameter ranging 0.8 - 1 µm. EDX spectra of smaller metal particles show Fe, Mn, Cu, Cr and Zn in different proportion, with either rounded or elongated shapes. All these particles were found associated mainly to char aggregates and Si-rich carbonate particles. The presence of Pb, in some cases combined with Zn, has been observed in a large number of nano-sized metal particles particularly identified in mixed carbon-sulphates materials, while these particles were not observed in char and Si-rich carbonate types. Moreover, EDX spectra put on evidence the presence on Ni, V and Ce in nano–sized particles included in cenospheres. Conversely, no evidence of metal particles was generally observed in soot; nevertheless, metal particles, mostly Fe-rich and in the 0.8 - 1 µm have been found included in the structure of large soot aggregates, mainly together with Si-rich particles (silicates and silica spheres) and inorganic salts.

Figure 1 show a cenosphere where metal nano-particles are evidenced by backscatter electron detector (BSE); the EDX spectrum of a Ni,V,Fe particle included in the cenosphere is showed in Figure 2..

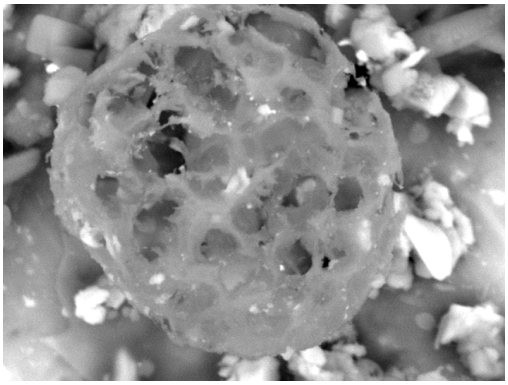

Figure 1. Cenosphere. Metal nano-particles are evidenced by backscatter electron detector (BSE).

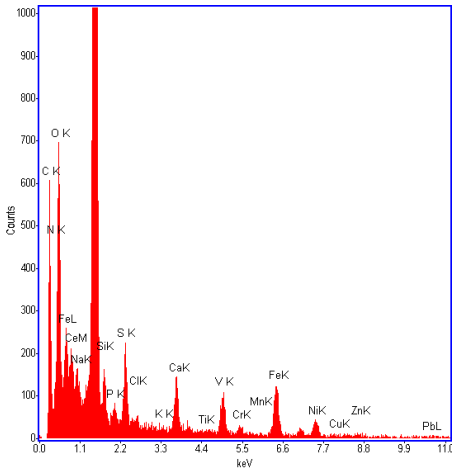

Figure 2. EDX spectrum of a Ni, V, Fe particle included in the cenosphere of Figure 1.

$\delta^{13}C$ values of TC, EC+CC and OC in size segregated aerosol particles

A. Garbaras, R. Bariseviciute, K. Kvietkus, R. Skipityte, I. Garbariene, A. Masalaite and V. Remeikis

[1]Institute of Physics, Centre for Physical Sciences and Technology, Vilnius, LT-02300, Lithuania
Keywords: Carbonaceous aerosol, Organic carbon, PM and source apportionment.
Presenting author email: garbaras@ar.fi.lt

Stable carbon isotopes have been used in source apportionment studies of atmospheric aerosols where two or more sources have a distinct isotopic composition. It has been shown that areal and temporal isotopic variabilities of aerosol samples are related to the diversity of the sources (Cahier, 1989). The stable C isotope signature of individual PAHs has been used to determine the contribution of different sources to the PAH content of soils and sediments. Glaser et al. (2005) concluded that compound-specific $\delta^{13}C$ analysis in PAHs failed for source apportionment, probably due to the low differences between their stable carbon isotope signature.

We think size spectrometry can help to follow aerosol transformation in the atmosphere, but there is a lack of studies of size segregated aerosol carbon isotope values (Garbaras et al., 2009).

We report $\delta^{13}C$ values of TC, EC+CC and OC in size segregated aerosol particles. Aerosol samples were collected at Preila (Baltic sea coast), Rugsteliskis (forested area) background stations and Vilnius city (0.5 mill inh.) during winter 2010, spring and summer 2011. MOUDI impactor had 11 size intervals, from 0.056 to 18 μm.

MOUDI foils were analyzed with EA-IRMS (FlashEA 1112 coupled to ThermoFinnigan Delta Plus Advantage). Half of the foil was measured directly (TC $\delta^{13}C$ values). The rest was baked in the oven (400 °C) to remove organic part and measured EC+CC δ13C values (carbonates were not removed with acid). OC $\delta^{13}C$ values were calculated using isotopic balance equation.

There is differences in $\delta^{13}C$ values and carbon concentration in each size interval in different locations and time of the year. In overall, in Aitken and in accumulation mode EC+CC had $\delta^{13}C$ values ranging from -25 to -28 ‰; OC from -25 to -32 ‰.

The variation of carbon isotopic ratio values clearly reflects the different sources of size segregated aerosol particles and ongoing processes in the atmosphere. Isotopic ratio mass spectrometry, when combining with other analysis methods, can be used not only in source apportionment, but also for aerosol evolution studies.

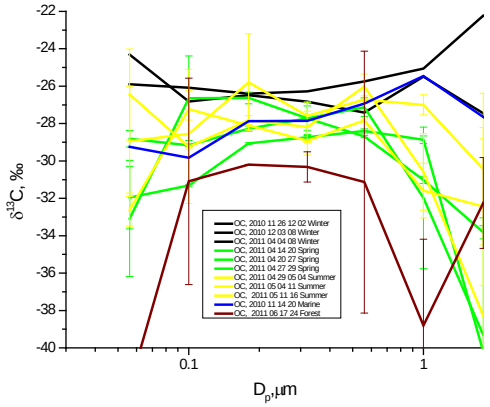

Figure 1. $\delta^{13}C$ values of OC in size segregated aerosol particles in spring, summer and winter.

This work was supported by the Research Council of Lithuania under project No. MIP-105/2010.

Cachier H. (1989) *Aerosol Science and Technology*, Vol. **10**, 379-385.

Garbaras, A., Rimšelytė, I. Kvietkus, K. and Remeikis V. (2009) *Lithuanian Journal of Physics*, Vol. **49**, 229-236.

Glaser B., Dreyer, A., Bock, M., Fiedler, S., Mehring M., and Heitmann, T. (2005) *Environmental Science and Technology*, Vol. **39,** 3911-3917.

Comparison of PM1 Organic and Elemental carbon between an urban and a regional background station

E. Yubero[1], J.F. Nicolás[1], Crespo J[1], M. Chiari[2], S. Nava[2], G. Calzolai[2], F. Lucarelli[2]

[1]Department of Physics, Miguel Hernández University, Avda. Universidad, 03202, Elche, Spain
[2] Physics Department, University of Florence and INFN, Via Sansone 1, I-50019 Sesto Fiorentino, Italy
Keywords: PM1, OC, EC,regional background.
Presenting author email: eyubero@umh.es

The present study was performed in two locations. The first one is located in the city centre of Elche (235,000 inhabitants), approximately 12 km from the Spanish Mediterranean coast. The sampling point is placed in a busy canyon street with a lot of traffic. The device was located 3 m above ground level on the first floor of a City Hall building. The other one is located at the top of Aitana mountain range (38°38'56.50"N, 0°15'55.23"W, ▲1558 amsl.). It is located approximately 60km from the city of Elche and 20 km from the Mediterranean coast in an east westerly direction. Twenty-four hour PM1 samples were collected approximately every three days from February to October 2011 using a low volume sampler (2.3m/h). The set of samples (around 70 samples in each site) collected was analysed for EC and OC at INFN of Florence with a Sunset Laboratory Thermal-Optical Carbon Aerosol analyser using the NIOSH protocol.

Period mean and daily maximum values were compared at both sites during the study period (Table 1), for the PM1, OC, EC, TC (calculated as the sum OC+EC), OM (calculated as 1.4*OC) and the OC/EC ratio.

Table 1. Concentrations for PM1 related carbonaceous species measured in Elche and Aitana (µg/m^3)

	Elche		Aitana	
	Mean	Max	Mean	Max
PM1	19.0	41.7	3.9	12.1
OC	3.6	7.7	1.6	6.3
EC	1.6	3.3	0.1	0.3
TC	5.2	10.0	1.7	6.6
OM	5.0	10.8	2.2	8.8
OC/EC	2.7	8.6	19.2	101

As can be seen, the difference between values in both stations is huge. The traffic station presents very high values for concentration of particles under 1µm. Organic matter and elemental carbon represent 26% and 8% of the bulk mass respectively. OC/EC ratio varies between 8.6 and 1.4, highlighting the presence of secondary aerosol. This secondary aerosol is not constant during the year and does not have any seasonal pattern. The PM1 concentrations measured in the Aitana station are remarkably low, despite being located close to important cities (Benidorm, a coastal city which is highly populated during summer months, is located less than 20km away). It is not observed that the urban aerosol reaches this urban background location during the entire year. That is confirmed with the EC data, with values close to the method detection limit in every sample. On the other hand, OC values are not negligible and represent more than 56% of the concentration PM1. In this case, either the organic aerosol has a secondary origin or it is bio-aerosol or biomass burning primary aerosol

A simple and low cost method for the indirect evaluation of secondary OC in atmospheric particles is based on the minimum values of OC/EC ratios, considering that those represent samples containing exclusively primary carbonaceous aerosol from fossil fuel combustion. In this approach the concentration of secondary OC was estimated from the following equation: $OC_{sec}=OC_{total}-(OC/EC)_{minimum}\times EC$.

The $(OC/EC)_{minimum}$ has been estimated for the traffic data by means of the ten values with a fewer ratio (squares in Figure 1). A lineal adjustment is shown in the graph. The slope of this straight line is our estimation of the primary carbon fossil fuel emission ratio. This value is $(OC/EC)_{ff}$.=1.4

Figure 1. OC and EC concentrations in PM1 aerosol samples collected in Elche (Traffic)

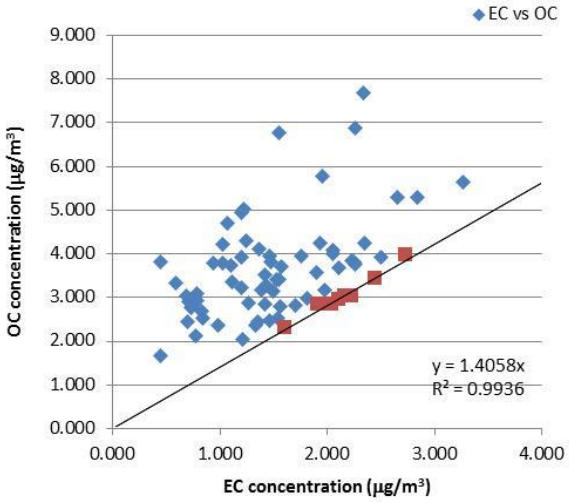

The concentration of primary fossil fuel OC is around 60%, with the remaining 40% being secondary. This secondary aerosol is due to the high photochemical activity in the city of Elche.

This work was supported by CGL2009-08036 (PASSE) project.

Organic matter and non-refractory aerosol over the remote Pacific: oceanic and combustion sources

L. M. Shank[1], S. Howell[1], A. D. Clarke[1], S. Freitag[1], V. Brekhovskikh[1], V. Kapustin[1], C. McNaughton[1], T. Campos[2], R. Wood[3]
[1]Dept. of Oceanography, University of Hawaii, Honolulu, HI, USA
[2]National Center for Aerosol Research, Boulder, CO, USA
[3]Dept. of Atmospheric Sciences, University of Washington, Seattle, WA, USA
Keywords: organic aerosol, black carbon, marine source
Presenting author email: tclarke@soest.hawaii.edu

Organic aerosol (Org) is now recognized as an important component of the atmospheric aerosol with both natural and anthropogenic sources. Recent studies have indicated oceanic emissions constitute an important natural source to the global atmosphere (O;Dowd et al, 2004; Spracklen et al., 2008). However, many studies have focussed upon the North Atlantic Ocean and most have had limited or uncertain criteria for exluding the influence of non-marine sources linked to combustion. Here we report on submicron aerosol physical and chemical properties in remote marine air measured from aircraft over the Southeast Pacific (SEP) during VOCALS-REx in 2008 and the North Pacific during IMPEX in 2006, and aboard a ship in the Equatorial Pacific in 2009. Black carbon (BC) measurements from a single particle soot photometer (SP2) and carbon monoxide (CO) concentrations over the Southeast Pacific provided sensitive indicators of combustion influence. As BC is in the particle phase and only derived from combustion it provides a direct indicator of the presence of combustion aerosol. In clean air over the Pacific we find lower organic mass fraction in the aerosol than most other studies and over the SEP we see little evidence of a significant marine source in air from South Pacific (Shank et al., 2012).

A High Resolution – Particle Time of Flight Aerosol Mass Spectrometer (HR-ToFAMS) measured non-refractory submicron aerosol composition during all campaigns. Sulfate (SO4) and Org measured during VOCALS off the coast of Chile and the TAO cruise in the equatorial Pacific show lower absolute values than those reported for previous "clean air" studies. In the marine boundary layer, average concentrations for SO4 were 0.52 μgm−3 for the VOCALS region and 0.85 μgm−3 for the equatorial region while average Org concentrations were 0.10 and 0.07 μgm−3, respectively. Campaign average Org/SO4 ratios were 0.19 (VOCALS) and 0.08 (equatorial Pacific).

CO and BC were used to identify the least polluted air, which had average concentrations of SO4 and Org of 0.14 and 0.01 μgm−3, respectively, with an average Org/SO4 of 0.08. Data from IMPEX was constrained to similar clean air criterion, and resulted in an average Org/SO4 ratio of 0.19. Under the cleanest MBL conditions during VOCALS, identified by CO below 61 ppbv, a robust linear relationship between Org and BC concentrations (Fig. 1) revealed that even at very low BC concentrations (< 10 ng m^{-3}) levels, combustion sources dominated organic aerosol, suggesting little to no marine source of submicrometer Org to the atmosphere over the eastern South Pacific.

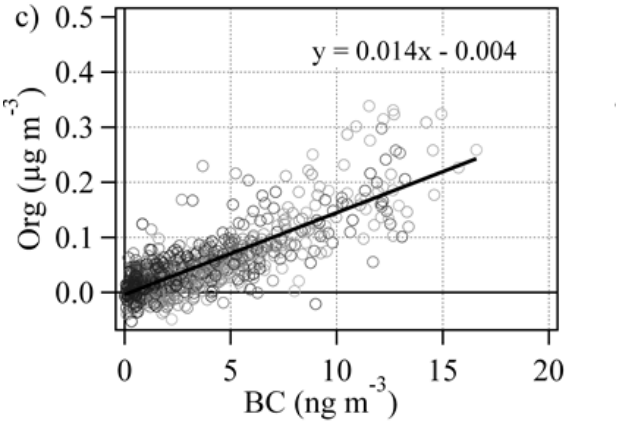

Figure 1. Organic aerosol mass (AMS) vs. BC from SP2 for clean MBL over SEP where CO is < 63ppb. Symbol shaded by CO ranging from 50ppb (black) to 61 ppb (light grey).

Note that all BC values plotted are generally much lower than BC criteria for "clean air" (often inferred BC from light absorption) in other studies. Many other studies use an arbitrary particle concentration or trajectory assessment over a few days to "screen" for pollution. Our observations imply that marine organics cannot be identified by merely setting a standard for background conditions below which anthropogenic influence can be disregarded. Other methods must be used to exclude non-marine sources.

We also examined the relation of sulphate concentrations to BC for CO<61ppb. Many values trended with BC even under this restriction. However, for CO restricted to <56ppb we found marked variation in sulphate to be independent of BC for BC< 1.8 ng m^{-3}. This SO4 is likely to be of marine origin, so any correlation of these data with Org may represent Org with a similar marine origin. A linear fit to the raw data between Org and SO4 mass, yielded a slope of 0.08±0.02, possibly indicative of an oceanic source for this Org. Our data argues for a weaker source of marine Org than currently used in many models.

O'Dowd et al., Nature, 431, 676-680, 2004.
Shank et al., ACP, 12, 557-576, 2012.
Spracklen et al., Geophys, Res. Lett., 35, L12811, 2008.

Organic export from the ocean to the atmosphere - first investigations

M. v. Pinxteren[1], C. Müller[1], Y. Iinuma[1], C. Stolle[2] and H. Herrmann[1]

[1] Leibniz Institute for Tropospheric Research (IfT), Leipzig, D-04318, Germany
[2] Leibniz-Institute for Baltic Sea Research Warnemuende (IOW), Rostock, 18119, Germany
Keywords: sea surface microlayer, marine aerosol, chemical characterisation, organic compounds
e-mail: manuela@tropos.de

Marine aerosols contain, besides sea salt, a significant amount of organic material. As the composition of aerosols may influence their physiochemical properties, their chemical characterization and the identification of the source of the organic content is an important task [*Chan et al.*, 2005]. Recent investigations suggest that the organic content of marine aerosols, especially of particles in the sub-micron range, is strongly connected to the biological activities of the ocean [*Cavalli et al.*, 2004]. In this context, the sea surface microlayer (SML), i.e. the physical boundary layer between oceans and atmosphere plays an important role. The SML is operationally defined as the first 1000 micrometers of the ocean and often enriched with organic and inorganic matter. To study the interaction processes, a detailed chemical investigation in terms of organic material of the oceanic water and atmospheric phase above the mandatory.

Our first investigations dealt with the chemical analysis of the SML that is a challenging analytical task as seawater is quite a complex matrix and the high salt content is often problematic to analytical instruments. Moreover, the organic compounds are present in trace levels and some of them, like aliphatic amines, are very polar and reactive species and difficult to extract from the seawater. Therefore, appropriate sample preparation methods with the aim of enrichment of the target analytes and elimination of the matrix, especially the high salt content, in combination with hyphenated analytical techniques were developed [*van Pinxteren et al. submitted*].

Our results of sea water analysis (SML and bulk water) from the southern Baltic Sea suggest that different compound groups within the broad chemical class of nitrogen containing organic compounds and carbohydrates show very different behavior with respect to water concentrations and enrichment in the SML (Fig.1). Generally amines and amino acids tend to be enriched in the sea surface microlayer, whereas for dissolved carbohydrates a trend towards depletion was observed. The characteristics of the different compound classes were found to be in strong correlation to bacterial activity and meteorological conditions [*Stolle et al. 2010*; *van Pinxteren et al. submitted*].

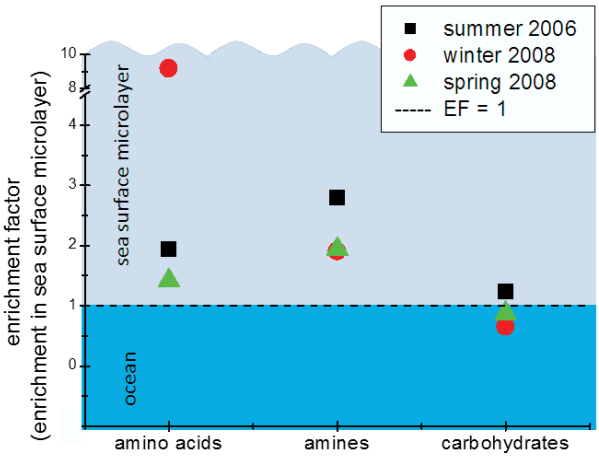

Figure 1. Enrichment factor of organic compound groups in the SML.

Our recent chemical analyses of seawater and the corresponding marine aerosol sampled in different field campaigns will help to reveal the connection of organic matter in these two compartments to address the question of net effluxes of organic matter between oceans and atmosphere.

This work was supported by the Federal Ministry of Education and Research (BMBF), SOPRAN phase II.

Cavalli, F., M. C. Facchini, S. Decesari, M. Mircea, L. Emblico, S. Fuzzi, D. Ceburnis, Y. J. Yoon, C. D. O'Dowd, J. P. Putaud, and A. Dell'Acqua (2004), *J. Geophys. Res. - Atmos.*, *109*(D24), -, doi: Artn D24215 Doi 10.1029/2004jd005137.

Chan, M. N., M. Y. Choi, N. L. Ng, and C. K. Chan (2005), *Environ. Sci. Technol.*, *39*(6), 1555-1562

Stolle, C., Nagel, K., Labrenz, M., and Juergens, K. (2010), *Biogeosci.*, *7*(9), 2975-2988.

van Pinxteren, M., Müller, C., Iinuma, Y., Stolle, C., Herrmann, H. (submitted), *Environ. Sci. Technol.*

Investigating primary marine aerosol properties: CCN activity of sea salt and mixed inorganic-organic particles

S.M. King[1], A.C. Butcher[1], T. Rosenoern[2], E. Coz[3], K. I. Lieke[1], G. de Leeuw[4], E. D. Nilsson[5], M. Bilde[1]

[1]Department of Chemistry, University of Copenhagen, 2100 Copenhagen, Denmark
[2]FORCE Technology, 2605 Copenhagen, Denmark
[3]Departamento de Medio Ambiente, CIEMAT, 28040 Madrid, Spain
[4]Climate Change Unit, Finnish Meteorological Institute, 00560 Helsinki, Finland
[5]Department of Applied Environmental Science, Stockholm University, 11418 Stockholm, Sweden
Keywords: sea spray, aerosol generation, sea salt, CCN, aspect ratio.
Presenting author email: stephanie@chem.ku.dk

Sea spray particles ejected as a result of bubbles bursting from artificial seawater containing salt and organic matter in a stainless steel tank were sampled for size distribution, morphology, and cloud condensation nucleus (CCN) activity. The artificial seawater solution consisted of a salt (NaCl or sea salt) and one organic compound in deionized water. Bubbles were generated in the tank either by aeration through a diffuser or by water jet impingement on the seawater surface.

The ability of sea spray tanks to serve as proxies for aerosol generation from bubble bursting is addressed in this study. One concern is the effect of bubble residence time, which is much shorter in a tank than in the oceans. Bubble residence time was controlled by varying the depth of the diffuser in the water column of the tank. The effect of varying bubble residence time on particle size and CCN activity was found to be insignificant for the organic compounds studied. Moreover, at typical oceanic salinities, the CCN activity of particles from diffuser-generated bubbles is nearly indistinguishable from that of the salt component, which is not surprising since theoretical and experimental evidence show that small amounts of salt can dominate CCN activity (Bilde and Svenningsson, 2004).

Although sea salt consists largely of NaCl, and is therefore assumed to have similar properties, the minor constituents may alter its aerosol properties. Furthermore, the measurement of CCN activity of salt is complicated by the variations in its morphology as a function of size and rate at which it was processed from a droplet to a crystalline particle (Biskos *et al*, 2006; Wang *et al*, 2010). In this study, the CCN activity of solely inorganic artificial sea salt was measured and was found to differ from that of pure NaCl and from model predictions (Fig. 1). The possibility that the discrepancy could be explained by morphology was investigated by analyzing scanning and transmission electron microscopy images of salt particles for their aspect ratios (Table 1).

The effect of different bubble production methods (i.e., jet impingement and diffuser aeration) on particle physicochemical properties was also probed. CCN activities of particles produced from jet impingement on seawater containing sodium laurate, an organic surfactant, were much lower than those from diffuser aeration. Analyses indicate a considerable amount of organic enrichment in the jet-produced particles relative to the bulk seawater composition. The production of a thick foam layer during impingement may explain the difference in activation and supports hypotheses that particle production from the two methods of generating bubbles is not equal (King *et al*., submitted 2012).

Table 1. Mean aspect ratios of salt particles.

Sample description	Mean aspect ratio
Atomization	
60-nm PSL spheres	1.09 (SEM)
Polydisperse NaCl	1.20 (SEM) 1.28 (TEM)
100-nm NaCl	1.24 (SEM)
Artificial seasalt (SS)	1.21 (TEM)
Bubble-bursting from 35‰ seawater (SS)	1.28 (SEM)

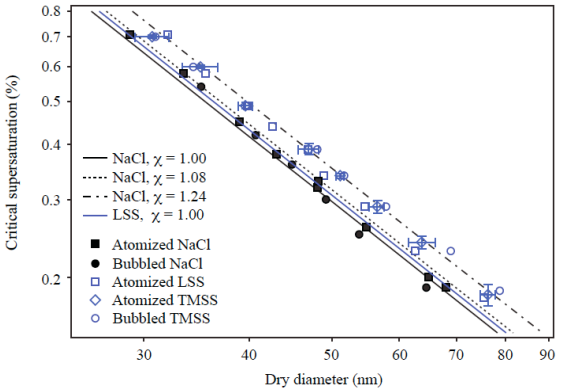

Figure 1. CCN activity of NaCl and sea salt. Model curves are calculated using Köhler theory for particles having different shape factors (χ).

This work was supported by the Carlsberg Foundation, the Swedish Research Council, and the CRAICC project.

Bilde, M. and Svenningsson, B. (2004) *Tellus* **56B**, 128-134.
Biskos, G. *et al*. (2006) *Geophys. Res. Lett.* **33**.
King, S. M. *et al*., submitted to *Env. Sci. Tech.*
Wang, Z. *et al*. (2010) *Aerosol Sci. Tech.* **44**, 939-953.

Aerosol particle distribution in the Baltic Sea marine boundary layer with the enlarged continental outflows and ship exhaust emissions

K. Plauškaitė[1], N. Špirkauskaitė[2], S. Kecorius[1], T. Petelski[3], T. Zielinski[3,4] and V. Ulevicius[1]

[1]Department of Environmental Research, SRI Center for Physical Sciences and Technology, Savanoriu 231, 02300 Vilnius, Lithuania
[2]Department of Nuclear Research, SRI Center for Physical Sciences and Technology, Savanoriu 231, 02300 Vilnius, Lithuania
[3]Physical Oceanography Department, Institute of Oceanology PAS, Powstańców Warszawy 55, PL-81-712 Sopot, Poland
[4]Department of Physics, University of Szczecin, Wielkopolska 15, PL-70-451 Szczecin, Poland
Keywords: marine aerosols, aerosol size distribution, aerosol formation.
Presenting author email: kristina@ar.fi.lt

The aim of this study was to analyse the potential circumstances controlling the variability of the aerosol number concentration over the south-eastern Baltic Sea with respect to the investigations of the Lithuanian coastal zone. In result of overview of several European campaign-type projects have provided information on the atmosphere submicron aerosol properties in Europe, showed that the measurement data of the Preila Environmental pollution research station, located in the south-eastern coast of the Baltic Sea, had partially similar characteristics to the Northern European region (Plauškaitė *et al*, 2010) with both aerosol concentration and size distributions showing influence from multiple source areas of particles and some similarities in concentration levels with Central European aerosol.

Measurements were performed during five cruises of r/v "Oceania" (Institute of Oceanology of Polish AS) in 2005 – 2010 mostly in southern and south-eastern parts of Baltic Sea. The data of the total aerosol particle concentration was compared with measurements at the Preila station during the same periods. The total aerosol particle concentration was measured by using CPC (size-cut 4.5 nm) at both investigation sites. Over the same period the measurements of the aerosol particle number concentration and size distribution were performed at the Preila station using DMPS (10 – 200 nm) in the year 2005 – 2008 and SMPS (9 – 840 nm) in 2009 – 2010. The series of HYSPLIT (NOAA) 72 hours air mass backward trajectories for the entire period at several altitudes above sea level which processed long-range transport of air mass at investigation sites (open sea or Preila station) were used for the analysis to determine source regions of atmospheric aerosols or precursor gases leadings to new particle formation (NPF) as well. The results indicated that the total aerosol particle concentrations over the open sea during all cruises despite different seasons (spring and autumn) or air mass transport directions was higher than at the Preila coastal station and showed influence both of cleaner (Atlantic ocean) and more polluted (continental outflow) air masses as well as the ship exhaust emissions, regional or lokal NPF and breaking waves during storm (Fig. 1). The analysis showed that the new particle formation (short-term "bump" type events; Figs. 1 and 2) both in marine boundary layer and coastal zone was observed during transport of air mass originating from the Atlantic Ocean and travelled upwind over Baltic Sea to Preila station. The change of air mass transport direction from western to eastern (from polluted continental regions) resulting the sharp increase of the total aerosol particle concentration in the coastal zone (8 – 9 April 2010). Especially high influence of ship emissions to increase of aerosol particle and chemical ingredients concentration (from 3 to 6 times) was determined in the marine boundary layer of harbours regions (Tallin, Tartu, Kaliningrad, Klaipėda, Gdansk Bay).

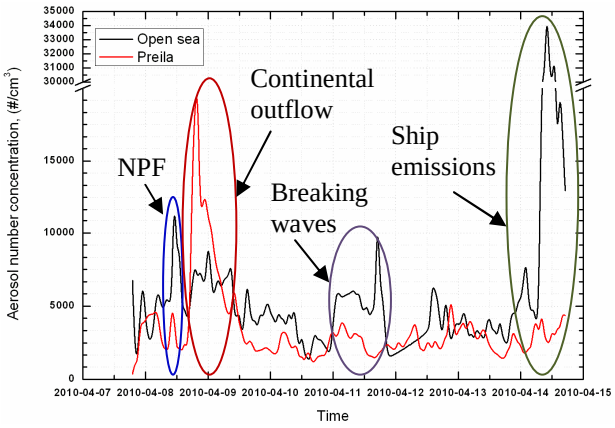

Figure 1. The CPC data as function of time in the marine boundary layer and at the Preila station during 7-14 April 2010.

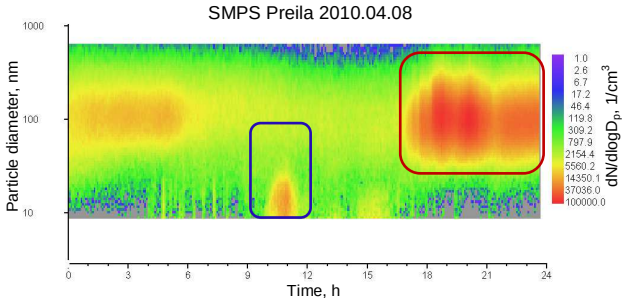

Figure 2. Aerosol size distribution during regional NPF and influence of polluted continental outflow.

Plauškaitė, K., Ulevičius, V., Špirkauskaitė, N., Byčenkienė, S., Zielinski, T., Petelski, T., Ponczkowska, A. (2010) *Oceanologia* **52(1)** 53-75.

Sub-Antarctic marine aerosol: Significant contributions from biogenic sources

J. Schmale[1,2], J. Schneider[1], E. Nemitz[2], S.Y. Tang[2], U. Dragosits[2], T.D. Blackall[3], P.N. Trathan[4], G. Phillips[1] and C.F. Braban[2]

[1]Max Planck Institute for Chemistry, Mainz, 55128, Germany
[2]Centre for Ecology and Hydrology, Edinburgh, EH26 0QB, UK;
[3]Kings College London, London, WC2R 2LS, UK; [4]British Antarctic Survey, Cambridge, CB3 0ET, UK;
Keywords: marine aerosols, aerosol mass spectrometry, biogenic particles, source apportionment
Presenting author email: Julia.schmale@gmail.com

In recent years significant efforts have been made to investigate marine particles, principally through ship-based and stationary methods; however, many questions concerning their sources, chemical nature and evolution in the atmosphere remain. Indeed, there are even suggestions that not all drivers of marine aerosol production, especially of secondary nature, are fully understood yet (Lapina *et al* 2011). This is partly due to the low spatial and temporal data coverage and the seasonality of oceanic emissions associated with biological activity, among other factors (Decesari *et al* 2011). Here we present a preliminary detailed analysis of organic aerosol derived from stationary online mass spectrometric measurements in the Sub-Antarctic Atlantic Ocean during spring/summer 2010.

Eight weeks of measurements were performed at the remote Sub-Antarctic Bird Island (54°00'S, 38°03'W), which is approx. 4 km in length, 800 m wide, and lies about 1400 km east of the Falkland Islands. At Bird Island emissions are mainly influenced by the marine environment and local seabirds and seals. A set of instruments was used to characterize the ambient aerosol comprising among others a scanning mobility particle sizer (SMPS), and an Aerodyne high-resolution time-of-flight aerosol mass spectrometer (HR-ToF-AMS). The non-refractory chemical composition of submicron aerosol was determined with the AMS with a temporal resolution of 5 minutes and a collection efficiency of 50 %.

On average, the submicron particle concentration was 0.76 µg m^{-3}. Particulate sulphate, originating mainly from DMS emissions, contributed 40 %, while organics made up 34 % of the mass. The median particle number concentration was 377 cm^{-3}, ranging from around 180 to 1100 cm^{-3} between the 10^{th} and 90^{th} percentiles.

Based on the statistical method of positive matrix factorisation (PMF, Ulbrich *et al* 2009) applied to the organic aerosol (OA) data, five factors were determined (see Figure 1): (1) Methane sulfonic acid (MSA), a secondary marine aerosol component, was observed to contribute 25 % of the OA. (2) Organics associated with the sea salt primary marine aerosol (Sea Salt OA) were found to contribute 7 %, which correlated well with the local wind speed. It should be noted that quantifying this factor with the AMS is highly uncertain due to the refractory properties of sea salt. (3) In addition, a factor AA, strongly resembling the signatures of amino acids and amines (Schneider *et al* 2011, Hildebrandt *et al* 2011) was present and accounts for 18 % of the OA mass. The N:C ratio of 0.13 is very high compared with, e.g., 0.02 of the marine oxygenated OA (M-OOA). There are indications that the AA factor is of biogenic origin and not directly associated with marine emissions, as it is slightly anti-correlated to MSA. Thus, it may potentially originate from the local fauna (birds and seals). (4) A dominant fraction of 40 % was classified as M-OOA which is characterized by highly oxygenated ion fragments whose exact origins, however, are still under investigation. The last factor (5) is composed of hydrocarbon-like OA (HOA, 9 %) which originated from the local generator of the research station on the island.

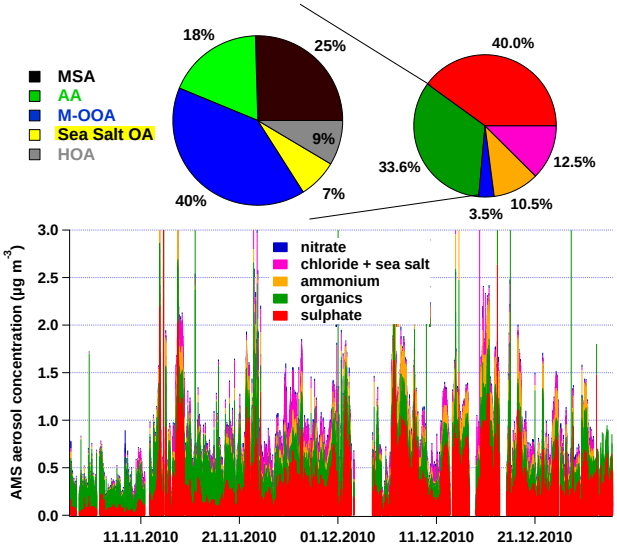

Figure 1. Time series of the submicron particle chemical composition, including the average composition (right pie chart), and the average contribution of 5 factors derived from positive matrix factorisation to the organic aerosol (left pie chart, see text for abbreviations).

This work was supported through the NERC AFI-CGS-69 project, Centre for Ecology & Hydrology and the Max Planck Institute for Chemistry.

Decesari, S. et al. (2011) *J. Geophys. Res.* 116, D22210.
Hildebrandt, L. et al. (2011) *Atmos. Chem. Phys.* 11, 12499-12515.
Lapina, K. et al. (2011) *Atmos. Chem. Phys.* 11, 8847-8860.
Schneider, J. et al. (2011) *Atmos. Chem. Phys.* 11, 11415-11429.
Ulbrich et al. (2009) *Atmos. Chem. Phys.* 9, 2891-2918.

Amino acids in Arctic aerosols

A. Gambaro[1,2], E. Scalabrin[1,2], R. Zangrando[2], E. Barbaro[1] and C. Barbante[1,2,3]

[1] Department of Environmental Sciences, Informatics and Statistics, University of Venice, Ca' Foscari, 30123 Venice, Italy
[2] Institute for the Dynamics of Environmental Processes-CNR, University of Venice, 30123 Venice, Italy
[3] Accademia Nazionale dei Lincei, Centro "B. Segre", 00165, Roma, Italy
Keywords: Water soluble organic compounds, aerosol chemistry, Arctic aerosol, long range transport, HPLC/MS

Andrea Gambaro: gambaro@unive.it

Amino acids are ubiquitous compounds with an integral role in atmospheric aerosol compositions (Ge *et al.*, 2011). Despite their atmospheric abundance, the amino acids fate and properties are poorly understood; they could be involved in cloud formation or act as ice-forming nuclei due to their hygroscopicity (Szyrmer and Zawadzki, 1997), affect atmospheric radiation balance (Chan *et al*., 2005), lead to secondary aerosol formation (De Haan *et al*., 2009) and influence air pollutants scavenging (McGregor and Anastasio, 2001). As amino acids have a wide range of reactivities, they can help determine atmospheric transport of particles and drops (McGregor and Anastasio, 2001). Several sources affect atmospheric amino acids complicating the possibility of identifying their origin. Due to their distance from emission sources and their naturally low aerosol concentrations, Polar Regions are excellent natural laboratories to conduct source apportionment studies of such compounds.

In order to better understand the importance of amino acidic compounds for the global atmosphere, we analyzed twenty free amino acids (FAAs) in seventeen size-segregated aerosol samples collected in a polar station in the Svalbard Islands from April 19 until September 14, 2010. Samples were processed and analyzed using a previous developed method (Zangrando *et. al*, 2010); Total FAAs concentration ranged between 592 fmol m^{-3} and 4593 fmol m^{-3} with serine and glycine being the most abundant compounds in almost all samples and accounting for 45-60% of the total amino acid relative abundance. The other compounds had an average concentration between 0.3 and 98 fmol m^{-3}. The higher amino acids concentrations were found in the ultrafine aerosol fraction (<0.49 µm) which in most cases accounted for the major part of the total amino acid content. Some samples showed a more complex distribution in the different aerosol size fractions, evidencing the presence of local-derived aerosol. Local aerosol sources such as neighboring volcanic activity and human-induced fires influenced FAAs concentrations in the large (10-7.2 µm) and medium (3.0-1.5 µm) size distributions of samples collected during these events. Back trajectory analysis determine marine derived aerosol as the major amino acids source in the rest of samples.

A cluster analysis and a factor analysis identify possible aerosol and amino acids sources influencing the study site, demonstrating the contribution of both long-range aerosol transport and a local marine source.

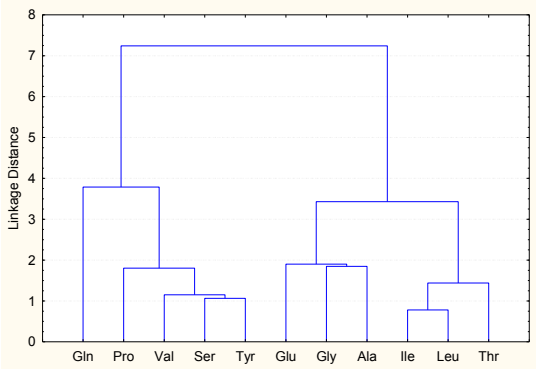

Figure 1: Cluster analysis results

This work was financially supported by the National Research Council of Italy (CNR). The authors also gratefully acknowledge the help of ELGA LabWater in providing the PURE- LAB Option-R and Ultra Analytic, which produced the ultra-pure water used in these experiments.

Chan, M. N., Choi, M. Y., Ng, N. L., and Chan, K. C. (2005). *Environ. Sci. Technol. ,* **39**, 1555-1562.

De Haan, D., Corrigan, A., Smith, K., Stroik, D., Turley, J., Lee, F., Tolbert, M.A., Jimenez, J.J., Cordova, K.E. and Ferrell, G.R (2009). *Environ Sci Technol,* **43**, 2818-2824.

Ge, X., Wexler, A. S., and Clegg, S. L. (2011). *Atmos Environ,* **45**, 524-546.

McGregor, K. G., and Anastasio, C. (2001). *Atmos Environ ,* **35**,1091-1104.

Szyrmer, W., and Zawadzki, I. (1997).. *Bull Amer Meteor Soc,* **78**, 209-228.

Zangrando, R., Piazza, R., Cairns, W., Izzo, F. C., Vianello, V., Zendri, E., and Gambaro, A. (2010). *Anal Chim Acta ,* **675**, 1-7.

Oceanic energy dissipation and the relationship to laboratory generated SSA

A.C. Butcher[1], S.M. King[1], E.D. Nilsson[2], and M. Bilde[1]
[1]Department of Chemistry, University of Copenhagen, DK-2100 Copenhagen, Denmark
[2]Department of Applied Environmental Science, Stockholm University, S-10691 Stockholm, Sweden
Keywords: sea spray, MBL, turbulence, aerosol size distribution.
Presenting author email: andrew@chem.ku.dk

Sea spray aerosols (SSA) represent large uncertainty in models of aerosols flux from the oceans. The physico-chemical processes producing these aerosols may play an important role in their emissions, size, and chemical composition.

SSA are generated from wind-steepened breaking waves. As the wave breaks the peak of the wave curls forming a plunging jet, entraining air which causes bubbles to form, rise and burst, releasing aerosols. SSA have been generated in the laboratory using different techniques including frits, diffusers, and plunging jets. Despite limitations of replicating an oceanic process in the laboratory, such that all variables can not be satisfied, plunging jets appear to reproduce sea-spray generation mechanics.

Despite the extensive literature on the subject of SSA, there is no consistent method to compare laboratory generated SSA and their production methods. This may contribute to the uncertainty in the flux parameterizations, particularly in the sub-micrometer size range (de Leeuw *et al*, 2011). In this work we attempt to determine key jet parameters that are essential for reproducing the physical system of air entrainment, bubble bursting, and subsequent aerosol production in the open ocean and across various experimental configurations.

The plunging jet used most commonly in laboratory experiments can be characterized in many ways, but only some parameters may be important for the production of aerosols. The jet flow rate, entrained air flow rate, and turbulence generated in the flow field of the jet appear to be relevant. These factors provide clues of the characteristics of the underwater bubble cloud as well as the bursting characteristics of bubbles that reach the surface.

D_{Jet}	Flow Rate ($L min^{-1}$)	E_{diss} (W/m^2)	$\#/cc$
4 mm	3.2	11	872
	4.8	37	6.39×10^3
	6.3	88	1.09×10^4
16 mm	14	4.5	382
	15.5	6.3	-

Table 1: Jet energy dissipation and aerosol concentration

The energy dissipation rate of wind generated breaking waves over the ocean scales with the square of the wind friction velocity, however the energy transfer from wind to wave diminishes depending on the age of the wave or fetch. Gemmrich *et al* (2008) indicate that the wave energy dissipation rate varies with the effective wave speed, C_{eff}, a function of wave age, over three orders of magnitude from 10^{-1} to 10^2 W/m^2.

Following the work of Garret *et al* (2000), we calculate the energy dissipation rate within a laboratory SSA tank using bubble spectra and compare this with the calculated energy dissipation rate from the kinetic energy of the jet, $E_J = \frac{1}{2}\rho_w V_{jet}^2 Q_w$. Assuming that all incoming energy from the jet is dissipated, the average energy dissipation rate of the system can be determined. It is found that the dissipation rate calculated from the bubble spectra are several orders of magnitude higher than the energy that is added to the system via the plunging jet. Due to the nature of the bubble spectra measurement, energy dissipation calculated from the bubble spectra may represent fluctuations in energy dissipation rate due to the turbulent flow field produced by the jet.

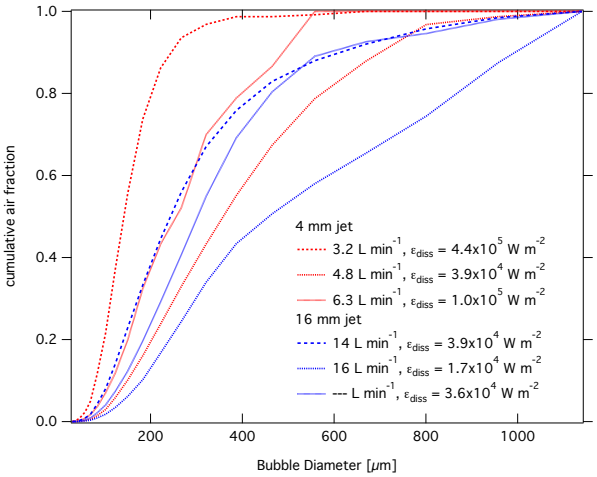

Figure 1: Cumulative air fraction of bubbles, flow rate, and energy dissipation

This work was supported by the Carlsberg Foundation, the Swedish Research Council, and the CRAICC (Cryosphere-Atmosphere Interactions in a Changing Arctic Climate) project.

de Leeuw, G., et al. (2011) Reviews of Geophysics **49(2)**.

Gemmrich, J.R., et al. (2008) Journal of Physical Oceanography **38(6)**: p. 1296-1312.

Garrett, C., M. Li, and D. Farmer. (2000) American Meteorological Society **30**: p.2163-2171

Shipboard characterization of a wet scrubber system: Influence on particle number concentration, particle size distribution and chemical composition

A.G. Hemmersam[1], M.K. Lykkegaard[1], K. Fuglsang[2], T. Rosenoern[2], J.B. Markussen[2], J.P. Hansen[3], K.I. Lieke[4] and M. Bilde[4]

[1]Chemistry and Biotechnology, Danish Technological Institute. Kongsvang Allé 29, 8000 Aarhus, Denmark
[2]FORCE Technology, Park Alle 345, 2605 Brøndby, Denmark
[3]Alfa Laval Aalborg, Gasværksvej 24, 9100 Aalborg, Denmark,
[4]University of Copenhagen, Denmark
Keywords: Combustion aerosols, shipping emissions, number concentration, number size distribution, SMPS
Presenting author email: agh@dti.dk

Ultrafine particles are generally recognized to have a severe impact on human health and an increasing focus is turned towards particle emissions from marine engines. Although regulations on NOx emission from ships have been implemented and sulfur content in marine fuel is now limited to 1.0 % in emission control areas, emissions from ship traffic is still an important factor especially in harbor cities. Mainly two ways for limiting the emissions from ships are presently being exploited: 1) lowering of the fuel sulfur content and 2) implementation of emission reducing technologies such as filters and scrubbers.

In this study emission data from a ship with a wet scrubber system installed is presented. The main engine is a MAN B&W 9L60 MC-C 2 stroke Diesel engine. Maximum continuous rating was 88-90 % during measurements. The effect of the scrubber operating in seawater mode on particle emission was tested during two days in February 2011using two different heavy fuels (1.0 % and 2.3 % sulfur). The main focus was on measuring the particle number concentration and size distribution before and after the scrubber system.

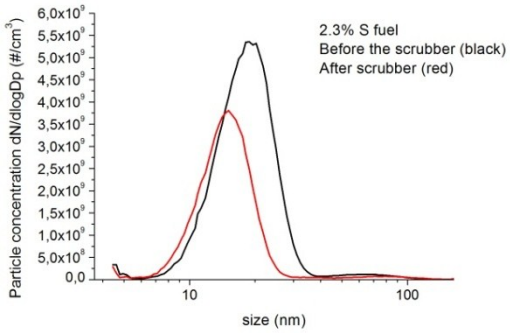

Figure 1. Particle size distributions measured by SMPS before and after the scrubber using 2.3 % S fuel.

Particle measurements were performed in this study using an SMPS and an ELPI. The results show that combustion particles from the ship have a bimodal size distribution, both before and after the scrubber system (figure 1). The two peaks in the bimodal particle size distributions measured by the SMPS system were found at 8-10 nm and 50-60 nm respectively for 1.0 % S fuel and at 15-20 nm and 70 nm respectively for 2.3 % S fuel. Upon changing from 1.0 % S fuel to 2.3 % S fuel the total particle number concentration was found to increase by a factor of 4.8-6.4 when measuring before the scrubber system. Particle number concentrations measured in the size interval 20-1000 nm using SMPS, ELPI, and CPC were found to be in generally good agreement. It was found that the scrubber system decreases the emitted particle number concentration (#/cm^3) by 30-55 % averaged over a 1 hour measurement period for specific operating conditions (figure 2). SMPS diameters are electrical mobility diameters and ELPI diameters are aerodynamic diameters, no conversion between the two has been applied yet.

Elemental analyses of particles collected on the top six ELPI impactor stages (particles >200 nm aerodynamic diameter) by SEM/EDX, show that the carbon content of the particles was reduced by 50-60 % by the scrubber. Increase in the percentage of sulfur, sodium, silicon, iron, nickel, chromium, vanadium, and magnesium in the particle mass was observed. The chemical composition of the salt containing particles measured after the scrubber resembles that of the fuel oil better than that of sea water, indicating that the salt particle formed in the scrubber are condensates of the fuel.

In conclusion, nanoparticles were characterized in the ship exhaust gas before and after a wet scrubber system.

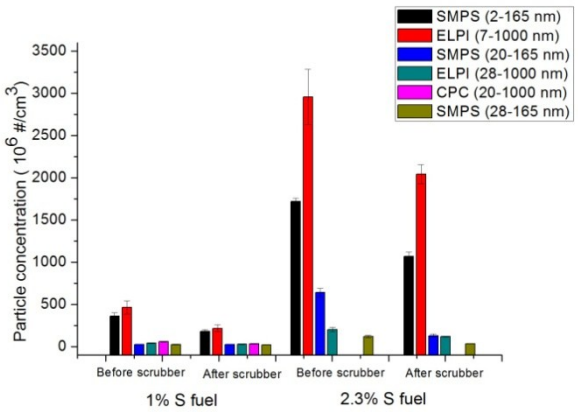

Figure 2. Comparison of PN concentration measured by SMPS, ELPI and CPC for 2.3 % S fuel and 1.0 % S fuel.

This work was supported by the Danish Agency for Science, Technology and Innovation, and part of collaboration between Danish Technological Institute, FORCE Technology and Alfa Laval Aalborg.

New Findings on Submicron Sea Salt Source Flux

J. Ovadnevaite, D. Ceburnis, H. Berresheim and C. O'Dowd

School of Physics and Centre for Climate and Air Pollution Studies, Ryan Institute, National University of Ireland Galway, University Road, Galway, Ireland

Keywords: sea salt, sea spray source function, marine aerosol, HR-ToF-AMS.
Presenting author email: jurgita.ovadnevaite@nuigalway.ie

Sea spray aerosol is a significant component of the aerosol population in the marine environment, and given that 70% of the Earth's surface is oceanic, sea spray contributes significantly to the global aerosol budget (Vignati et al., 2010). In order to better understand and quantify these effects, detailed information on the chemical composition, along with size distribution and abundance, is required.

The high-time resolution sea salt measurement by a High Resolution Time of Flight Aerosol Mass Spectrometer (HR-ToF-AMS) enabled the quantification of sea salt mass in both increasing and decreasing wind speed regimes up to 26 m s^{-1}. A mass flux source function was also derived and found to have a power-law wind speed dependency with an exponent of 3.1 for increasing winds and 2.3 for decreasing winds. Whereas, submicron aerosol particles are expected to be uniformly mixed in the marine boundary layer, an effective sea spray aerosol production flux was estimated from the sea spray concentration divided by a filling time and multiplied by the marine boundary layer height.

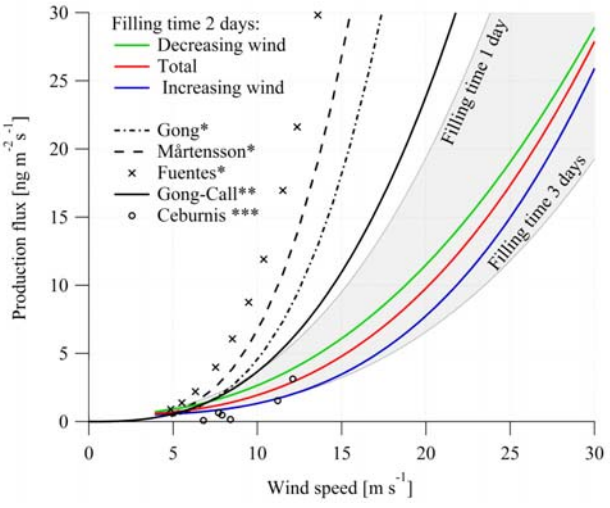

Figure 1. Production flux dependence on the wind speed. Color lines represent the flux derivations from the AMS sea salt measurements at different wind speed regimes. Grey area represents the flux variability due to the different time of filling. Black lines illustrates fluxes derived from the parameterizations by Gong (2003), Mårtensson et al. (2003) , Callaghan et al. (2008), Ceburnis et al. (2008) and Fuentes et al. (2010).
*number flux presented in the original work was recalculated to the mass flux; **includes differential whitecap - to - aerosol productivity derived by Gong (2003), ***fluxes calculated from the data presented.

A comparison with already existing source functions derived from the whitecap method is presented in Figure 1. It suggests that previous schemes based on the Monahan whitecap - wind speed approach significantly over-estimate the submicron mass flux. There could be several reasons for that: one is the whitecap area - to - wind speed parameterization and another is the parameterization of differential whitecap - to - aerosol productivity. The former parameterization has recently improved by applying a digital image processing of sea-state photographs and removing the subjectivity in determining the intensity threshold. Replacing the Monahan component of the source flux with the more recent Callaghan et al. (2008) whitecap – wind speed relationship brings the Gong (2003) source function closer to the ones presented in this study; however, the comparison also points to an over-estimation of the differential whitecap - aerosol productivity component of the source flux function.

This work was supported by the SFI, HEA-PRTLI4, EC IP EUCAARI, EPA Ireland and ESA STSE.

Callaghan, A., G. de Leeuw, L. Cohen & C. D. O'Dowd (2008) *Geophysical Research Letters*, 35, L23609

Ceburnis, D., C. D. O'Dowd, G. S. Jennings, M. C. Facchini, L. Emblico, S. Decesari, S. Fuzzi & J. Sakalys (2008) *Geophysical Research Letters*, 35, L07804

Fuentes, E., H. Coe, D. Green, G. de Leeuw & G. McFiggans (2010) *Atmos. Chem. Phys.*, 10, 9295-9317.

Gong, S. L. (2003) *Global Biogeochemical Cycles*, 17,1097-1104.

Martensson, E.M., E.D. Nilsson, G. de Leeuw, L.H. Cohen & H.C. Hansson (2003) *Journal of Geophysical Research-Atmospheres*,108, 4297.

Vignati, E., M. C. Facchini, M. Rinaldi, C. Scannell, D. Ceburnis, J. Sciare, M. Kanakidou, S. Myriokefalitakis, F. Dentener, and C. D. O'Dowd (2010) Atmos. Environ, 44(5), 670-677.

The composition of Sea Spray Aerosol (SSA) produced from coastal Baltic seawaters

K. Plauskaite[1], V. Ulevicius[1], J. Ovadnevaite[2], M. Rinaldi[3], M.C. Facchini[3], C. O'Dowd[2] and D. Ceburnis[2]

[1]Environmental Research Department, SRI Center for Physical Sciences and Technology, Vilnius, Savanoriu 231, 02300, Lithuania
[2]School of Physics and Centre for Climate and Air Pollution Studies, Ryan Institute, NUI Galway, University Road, Galway, Ireland
[3]Istituto di Scienze dell'Atmosfera e del Clima - CNR, Bologna, Italy
Keywords: aerosol generation, marine aerosols, chemical composition, organic matter.
Presenting author email: kristina@ar.fi.lt

The chemical composition of Sea Spray Aerosol (SSA) consists of both an inorganic and organic fraction which depends on biological activity, trophic level interactions and wind speed regime. Organic matter may be internally mixed with the sea salt particles or be a part of bacteria, viruses and transparent-exopolymer-gels, all of which are enriched in aggregate SSA (Ovadnevaite *et al*, 2011)

The aim of this study was to investigate the size resolved SSA composition of the Baltic Sea water with a special emphasis on the water soluble and water insoluble organic matter (WSOM and WIOM, respectively) and salinity of the water. Thus the marine aerosol generation chamber was built and the comparison of the seawater to the freshwater and the mixture of water from these two was made to better understand the influence of water salinity on the seaspray particle composition and formation processes. The water for the chamber measurements was collected from two separate coastal locations: the Baltic Sea and the Curonian Lagoon near Preila, Lithuania.

The WSOM and WIOM fraction of the aerosol generated from the Baltic seawater sample increased with the decreasing particle size measured as the aerodynamic particle diameter (Fig. 1). The WIOM significantly contributed to the three smallest impactor stages while WSOM most significantly contributed (50 – 86%) to the larger particle stages (0.32 – 3.2 μm) using fresh water sample and the relative concentrations of the OM were considerably higher using fresh water than the corresponding values using seawater. However, a closer inspection reveals that the absolute OM (WIOM + WSOM) concentrations for the two samples were actually quite similar. The higher OM fraction of the fresh water sample was due to much lower absolute salt concentration, as expected for the aerosol generated from the fresh water. Despite that fact, some low salt concentration was measured in the composition of the generated particles and confirmed that salt is an important component of the particle generation from the water. Another prominent feature of the fresh water lagoon sample is the large concentrations of the WSOM observed on all size ranges, except the first stage corresponding to the smallest particles and can be related to the large cyanobacteria blooms which are common in the Curonian Lagoon during this period of the year creating highly eutrophic conditions due to anthropogenic pollution.

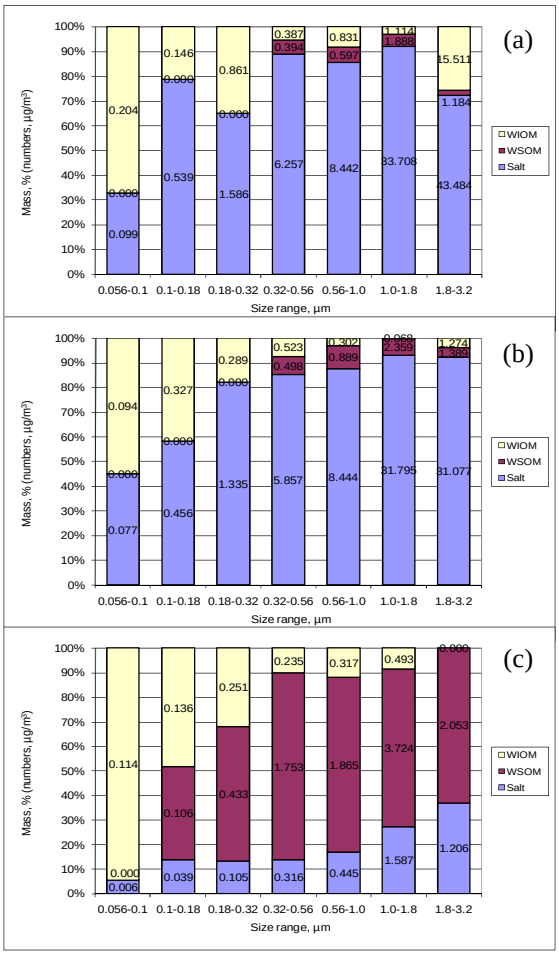

Figure 1. Size-resolved relative concentrations of the sea salt, WIOM and WSOM in the SSA generated from (a) the Baltic seawater, (b) the 50:50 mixture and (c) the fresh lagoon water.

This work was supported by the European Commission project ACCENT subproject Access to research infrastructures (3rd call) and by the Research Council of Lithuania under grant LYMOS-2011-3.

Ovadnevaite, J., Ceburnis, D., Martucci, G., Bialek, J., Monahan, C., Rinaldi, M., Facchini, M.C., Berresheim, H., Worsnop, D.R., and O'Dowd, C. (2011), *Geophys. Res. Lett.*, 38, L21806, doi:10.1029/2011GL048869.

Laboratory based studies of primary sea-spray generation in plankton-enriched sea-water

D. Ceburnis, J. Ovadnevaite, M. Zacharias, J. Bialek, S. Connan, M. Rinaldi, C. Monahan, M.C. Facchini, H. Berresheim, D.B. Stengel and C. O'Dowd

[1]School of Physics and Center for Climate and Air Pollution Studies, Ryan Institute, National University of Ireland Galway, Galway, Ireland.
[2]Botany and Plant Science, School of Natural Sciences, Ryan Institute, National University of Ireland Galway, Galway, Ireland.
[3]Institute of Atmospheric Sciences and Climate, National Research Council, Bologna, 20129, Italy.

Keywords: sea spray, primary marine aerosol, phytoplankton, HR-ToF-AMS.
Presenting author email: darius.ceburnis@nuigalway.ie

Marine aerosol enrichment by biogenic organic matter (OM) has been linked to phytoplankton activity (O'Dowd et al., 2004), thus having a strong seasonal impact on both the Earth's albedo and climate. In addition to a seasonal cycle, sea-spray generation and its enrichment with OM is a very dynamic process producing regular OM plumes over N.E. Atlantic (Ovadnevaite et al., 2011). Plankton-enriched seawater contains a complex mixture of dissolved and particulate organic carbon components (POC and DOC) producing both water soluble and insoluble organic aerosol species (Facchini et al., 2008; Russell et al., 2010); this warrants detailed laboratory studies aimed at establishing a link between observed ambient aerosol OM and its very primary form (e.g. Fuentes et al., 2010).

Laboratory studies using the microalgal species *Emiliania huxleyi, Leptocylindrus danicus* and *Cylindrotheca closterium* were performed by on-line and off-line analytical techniques using a sea spray production chamber and an ageing chamber with day-light and ozone. Under controlled conditions a sea spray highly enriched in OM was produced with levels similar to Facchini et al. (2008) (Figure 1) over a period of 48 hours.

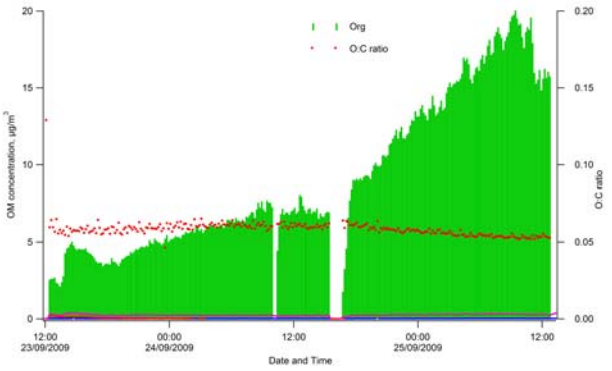

Figure 1. OM concentration and O/C ratio evolution in *Emiliania huxleyi* enriched sea water.

HR-ToF-AMS, [1]HNMR and HTDMA techniques confirmed OM composition of highly hydrocarbon-like, water insoluble OM characteristic of unsaturated lipids exhibiting low hygroscopic growth factor (Figure 2). Freshly produced OM, while largely insoluble, was far less oxidised (less sugars) than the OM reported by Facchini et al. (2008). The HTDMA measurements revealed a gradual change in physical properties as contribution of OM increased along with a certain degree of external mixture.

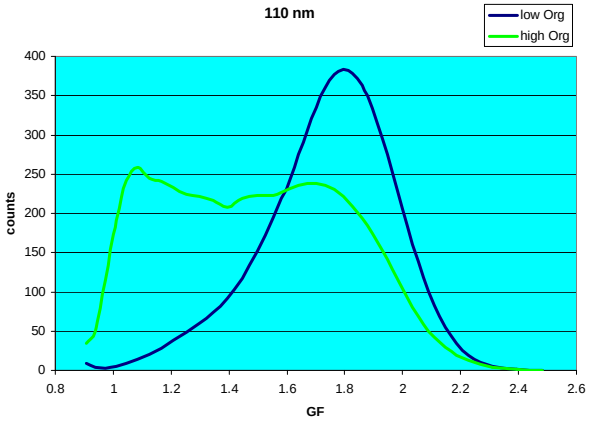

Figure 2. Change in hygroscopic growth factor of 110nm particles during *Emiliania huxleyi* experiment.

Processing primary sea spray with light and/or ozone caused a gradual change in chemical composition (preserving low GF and slowly increasing O/C ratio) supporting primary origin and atmospheric evolution of observed ambient OM while not excluding trophic level interactions.

This work was supported by the EPA Ireland EASI-AQCIS project, SFI, HEA-PRTLI4, EC IP EUCAARI.

Facchini, M.C., et al. (2008) *Geophys. Res. Lett.*, 35(17), L17814.
Fuentes, E., et al. (2010) *Atmos. Chem. Phys.*, 10, 9295-9317
O'Dowd, C.D., et al. (2004) *Nature*, 431, 676-680.
Ovadnevaite, J., et al. (2011) *Geophys. Res. Lett.*, 38(2), L02807.
Russell, L.M., et al. (2010) *P. Natl. Acad. Sci.*, USA 107(15), 6652-6657.

Characterization of PM_1 sampled in the "Marco Polo" airport area (Tessera-Venice)

G. Valotto[1], D. Bassano[2], E. Pecorari[1], E. Rampado[3], G. Rampazzo[1], S. Sollecito[2], F. Visin[1] and D. Zannoni[1]

[1]Department of Environmental Science Informatics and Statistics, University Ca' Foscari, Dorsoduro 2137, I-30123 Venezia, Italy
[2]SAVE S.p.A., Marco Polo Venice airport viale G. Galilei 30/1, I-30173 Tessera-Venezia, Italy
[3]Ente Zona Industriale di Porto Marghera, via dell'Elettricità 39, I-30175 Porto Marghera-Venezia, Italy
Keywords: aircraft plumes, PM1, chemical composition, air quality network
Presenting author email: valotto@unive.it

Ca' Foscari University in collaboration with SAVE S.p.A. and Ente Zona Industriale (EZI) has been studying the "Marco Polo" airport (45°30'40''N, 12°20'38''E – Tessera, Venice - Italy) emissions since June 2009, by monitoring the main atmospheric variables and the major pollutants concentration revealed in the study area. Specifically, the chemical species monitored every hour are: SO_2, PM_{10}, O_3, NO, NO_X NO_2, CO, methane and non-methane hydrocarbons, while meteorological variables sampled are wind speed and direction, solar radiation intensity, precipitation rate, and temperature. The sampling site (a parking area near the airstrip – site 1 in figure 1) was chosen estimating the main fallout points of aircraft emissions below 1000 m and neglecting the other sources. This was done by processing the air traffic data provided by SAVE SpA, using a Lagrangian model SPRAY (Tinarelli et al., 1994) that is part of the SCAIMAR modeling system, managed by EZI. Moreover, from November 2011 to June 2011, 200 samples of PM_1 were collected every 48 hours on a quartz filter by two Tecora Skypost PM HV at low volume (2.3 m^3 h^{-1}), at two sites located at the start and the end of Venice airport airstrip as shown in figure 1 (site 2, 3). The major components were analyzed by ICP-OES (Inductively Coupled Plasma - Optical Emission Spectroscopy). These sites were chosen to estimate the airport emission contribution by studying the different concentration of PM_1 and elemental concentration in the PM_1 as a function of the wind direction.

Results show that i) the concentration of PM_1, PM_{10} and the ratio PM_1/PM_{10} increase with the environmental temperature decrease (as shown in figure 2), likely due to the emission increase from several different sources, as well as by the changes in climate conditions that favor their concentration; ii) there is no significant difference in PM_1 concentration between two sites, suggesting a low contribution of the airport; iii) some samples exhibit different elemental concentration in PM_1 suggesting that the two sites are contaminated by several sources, contributing differently; iv) statistical analysis of atmospheric concentration revealed in three sites a significant contribution of the vehicular traffic source.

Figure 1. Sampling sites in Marco Polo airport and prevailing wind direction

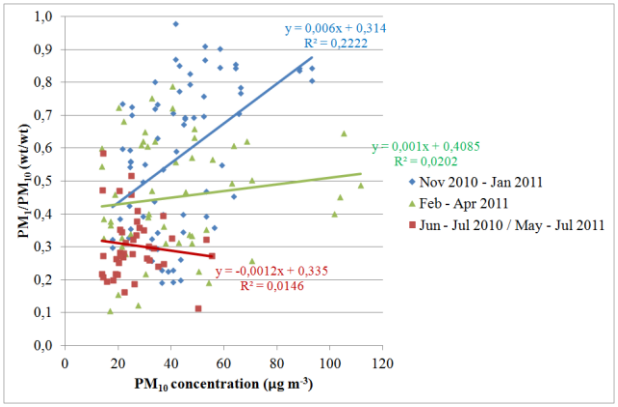

Figure 2. PM_1/PM_{10} ratio as a function of PM_{10} concentration

References

Tinarelli G., Anfossi D., Brusasca G., Ferrero E., Giostra U., Morselli M.G., Moussafir J., Tampieri F., Trombetti F. (1994). Lagrangian particle simulation of tracer dispersion in the Lee of a schematic two-dimensional hill. Journal of Applied Meteorology, 33, pp. 744–756.

Monitoring of ultrafine particles at an urban environment in southern Europe

G. Titos[1,2], H. Lyamani[1,2] , M. Sorribas[1,2], I. Foyo-Moreno[1,2] and L. Alados-Arboledas[1,2].

[1]Centro Andaluz de Medio Ambiente, Universidad de Granada, Junta de Andalucía, Granada, 18006, Spain.
[2]Department of Applied Physic, University of Granada, Granada, 18071, Spain.
Keywords: urban aerosols, ultrafine particles, BC, PM_{10}.
Presenting author email: gtitos@ugr.es

In this work we study the influence of road traffic emissions on urban air quality and the relationship between particle matter, PM_{10}, gaseous pollutants and aerosol number concentration at an urban environment in southern Europe (Granada, 37.18ºN, 3.58ºW and 680 m a.s.l.). Levels of PM_{10} and gaseous pollutants were supplied by the Andalusian Government (Department of Environment, www.juntadeandalucia.es/medioambiente) from a nearby station (0.5 km). Furthermore, black carbon (BC) mass concentration was measured with a Multi-Angle Absorption Photometer (MAAP) using a mass absorption efficiency of 6.6 m^2g^{-1} and fine particle number concentration (N) in the size range 20-450 nm was measured with a UFP-3031 from TSI. Both instruments are run side by side at the CEAMA station (Lyamani et al., 2010). The UFP-3031 is able to run continuously with little maintenance and does not require radioactive source. This fact in conjunction with the growing interest in studying ultrafine particles due to their harmful effect on human health (Araujo and Nel, 2009) make this instrument suitable for air quality monitoring networks.

The diurnal variability of all parameters analyzed was strongly influenced by road traffic activity. CO, NO_2, BC and N increased during traffic rush hours (6-8 GMT), decreased during the day due to dispersion owing to a higher PBL height and the reduction of traffic emissions, and increased again during the afternoon rush hours showing a second peak around 17-19 GMT (Figure 1). The increase in N and BC levels during rush hours was more pronounced than for the other pollutants denoting direct exhaust of traffic emissions. PM_{10} presented a peak a little bit later in the morning (around 9-10 GMT) mainly due to formation of secondary aerosols. During the weekends, lower peaks were observed as a consequence of traffic reduction.

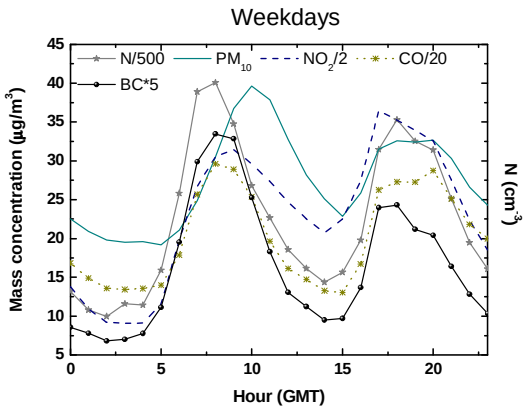

Figure 1. Diurnal evolution of N, PM_{10}, NO_2, CO and BC.

The diurnal pattern of the number of particles obtained in Granada is characteristic of urban environments. In this sense, a completely different pattern was observed at the rural background station El Arenosillo where the UFP-3031 was operating during two weeks. The total number concentration at El Arenosillo was considerably lower than in Granada being the diurnal pattern characterized by a single peak around midday. A different behaviour depending on the size range considered was also observed.

There is a recent interest in studying the representativeness of different metrics (Pey et al., 2008) in order to establish appropriate strategies in monitoring networks. In this sense, the relationships between number concentration and PM_{10} and BC mass concentration have been analyzed. A significant correlation between daily averages of PM_{10} and N (R^2 = 0.51) and between BC and N (R^2 = 0.72) have been obtained. The correlation between mass concentration and N in the size ranges 20-30, 30-50, 50-70, 70-100 and 100-200 nm is shown in Figure 2. As can be observed, the correlation coefficients change significantly depending on the size range considered, being higher for larger particle size.

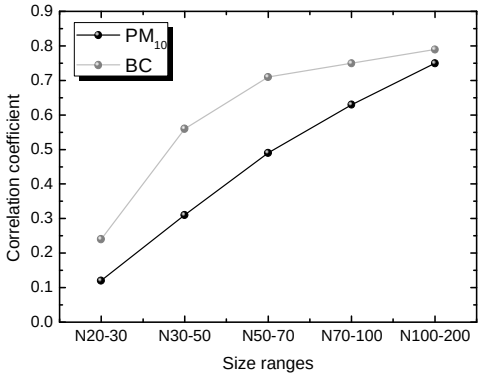

Figure 2. Correlation coefficient between daily mean PM_{10} and BC versus number concentration in different size ranges.

Aknowledgments: This work was supported by the Andalusia Regional Government through projects P08-RNM-3568 and P10- RNM-6299, by the Spanish Ministry of Science and Technology through projects CGL2010-18782, CSD2007-00067 and CGL2011-13580-E/CLI; and by EU through ACTRIS project (EU INFRA-2010-1.1.16-262254).We also thanks the Andalusian Government for the data supplied.

Araujo, J.A. and Nel, A.E., (2009). Part. Fibre Toxicol., 6(24).
Lyamani, H., et al (2010). Atmos. Chem. Phys., 10, 239-254.
Pey, J., et al (2008). Atmos. Environ., 42, 9052-9062.

Short term control efficiencies of dust suppressants to reduce fugitive dust

Sehyun Han, Yoonho Seo and Yongwon Jung

Department of Environmental Engineering, Inha University, 253 Yonghyun-Dong, 402-751, Incheon, Korea
Keywords: PM_{10}, fugitive dust, suppressants, wind erosion, control efficiency.
Presenting author email: jungyw@inha.ac.kr

Fugitive dust is a typical air pollution source generated by wind erosion of exposed area or construction activities. There are many control measures to prevent the fugitive dust emitted from exposed area, such as windscreens, shelters, confinement, and wet suppression. Wet suppression can be considered the most effective method among them. Water and chemicals are the two major suppressants used in the wet suppression. Watering without chemical binders is usually used as a temporary measure. The application of chemical binders is the most commonly used and cost-effective method for controlling dust emissions by binding particles together to enhance the resistance to wind erosion and physical disruption. Certain benefits and advantages can be obtained by the addition of chemical binders to the water used for dust suppression. The available chemical binders include bituminous-asphaltic compounds, polymers, resins, surfactants, calcium lignosulfonate, and others.

Estimation studies on the long-term control efficiencies of dust suppressants have been conducted by some researchers (Gillies *et al*, 1999). However, the studies on control efficiencies of chemical binder in the initial short-term stage have not received much attention, although some data has been published (Chang *et al*, 2003).

This study focuses on investigating the short-term control efficiencies of dust suppressants. To estimate them with minimum efforts and time, we made a lab-scale wind tunnel, which made it possible to carry out experiments in a laboratory with a test soil bed of small size. Control efficiencies of dust suppressants were estimated using the data of dust concentrations simultaneously measured from both upstream and downstream of the test soil beds treated with chemical binders. Dust concentrations were measured using Dusttrak (TSI, Model 8520). To investigate how control efficiencies of dust suppressant vary depending on wind speed, chemical spraying intensity, chemical mass concentration in water, and the duration of test, test runs were carried out for the four suppressants including water. Test soil beds were dried at least for five days to have equilibrium moisture of the test day.

As shown in Figure 1, preliminary results show that polymer and cellulose type dust suppressants have higher control efficiencies than $CaCl_2$ type dust suppressant at the test conditions used in this study. It also shows that during 10 minute test runs control efficiency of $CaCl_2$ type dust suppressant gradually decreases with time, whereas those of polymer and cellulose type dust suppressants remain relatively constant. As shown in Figure 1, water has the lowest dust control efficiencies among the dust suppressants. It is also clear that dust control efficiency of water decreases with time more rapidly than those of the other chemical binders do.

All the results showing the effect of wind speed, chemical spraying intensity, and chemical mass concentration in water on dust suppression efficiencies will be presented and discussed.

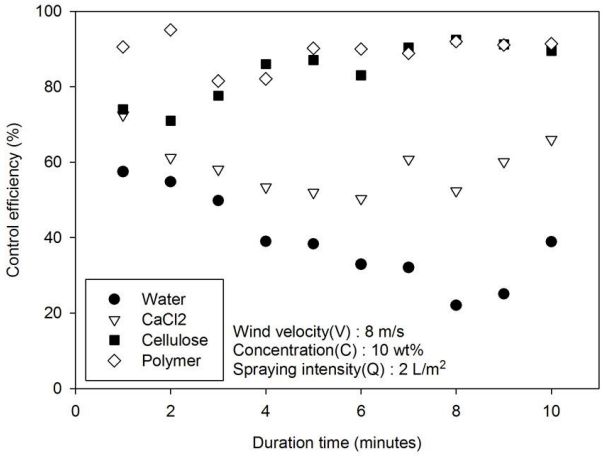

Figure 1. Dust control efficiency vs. duration time.

This work was supported by the Korea Environmental Industry & Technology Institute

Gillies, J., Watson, J., Rogers, C., DuBois, D. and Chow, J. (1999) *J. of the Air & Waste Management Association* **49**, 3-16.

Chang, Y., Hwang, J. and Chou, C. (2003) *Environmental Engineering Science* **20**, 265-280.

Source apportionment of PM-bound PAHs, *n*-alkanes and inorganic ions in an urban environment in southeastern Spain

J. Gil-Moltó, N. Galindo, M. Varea and C. Chofre

Department of Physics, Miguel Hernández University, Avda. de la Universidad s/n, 03202, Elche, Spain
Keywords: PM, PAH, alkanes, water-soluble ions, PMF.
Presenting author email: j.gil@umh.es

Aerosol concentrations and chemical composition have been extensively studied during the last years due to their known adverse health effects on humans. The magnitude of these effects can significantly vary depending on the study location, primarily due to differences in air pollution sources and meteorological conditions. Therefore, source apportionment is a crucial exercise in determining environmental pollution control strategies. Among the different available techniques, PMF is a powerful and valuable multivariate statistical tool for source identification.

PM1, PM2.5 and PM10 low volume samples (2.3 m^3/h) were collected from October 2008 until July 2009 in the city of Elche (southeastern Spain). The samples were analysed to determine the concentrations of 17 polycyclic aromatic hydrocarbons (PAHs), *n*-alkanes from C_{16} to C_{40} and major water-soluble ions (Na^+, NH_4^+, K^+, Mg^{2+}, Ca^{2+}, Cl^-, NO_3^- and SO_4^{2-}). The sampling site, classified as urban background, was located on the roof of a building at the Miguel Hernández University, adjacent to a major city avenue, in a highly ventilated area.

PMF analyses were performed on each PM fraction concentration data. The spring-summer and autumn-winter periods were considered separately because of the different organic and inorganic compound behaviour with temperature and solar radiation.

Mean concentrations of particulate matter, total PAH (TPAH), *n*-alkanes (T*n*-A) and ions (TIons) for the spring-summer (S-S) and autumn-winter (A-W) seasons are shown in Table 1.

Table 1. Mean concentrations during the study period.

Fraction	PM (μg/m³)		TPAH (ng/m³)		T*n*-A (ng/m³)		TIons (μg/m³)	
	S-S	A-W	S-S	A-W	S-S	A-W	S-S	A-W
PM1	10.8	8.66	0.42	1.03	9.71	13.02	6.02	4.07
PM2.5	12.8	14.76	0.56	1.22	11.96	18.31	6.37	6.5
PM10	41.36	23.79	0.61	1.28	19.02	18.89	17.72	8.42

In the western Mediterranean basin, PM10 levels are strongly affected by Saharan dust intrusions (Galindo *et al* 2008), as shown by the higher concentrations obtained in spring-summer with respect to those measured in the autumn-winter period. TPAH were predominantly associated with fine particles, as reported in previous studies (Cecinato *et al*, 1999), meanwhile *n*-alkanes size distributions were seasonally dependent.

PMF studies were carried out in a trial to discriminate different potential sources. As an example, figure 1 presents the results of the PMF analysis for PM1-bound PAHs and *n*-alkanes in the spring-summer period.

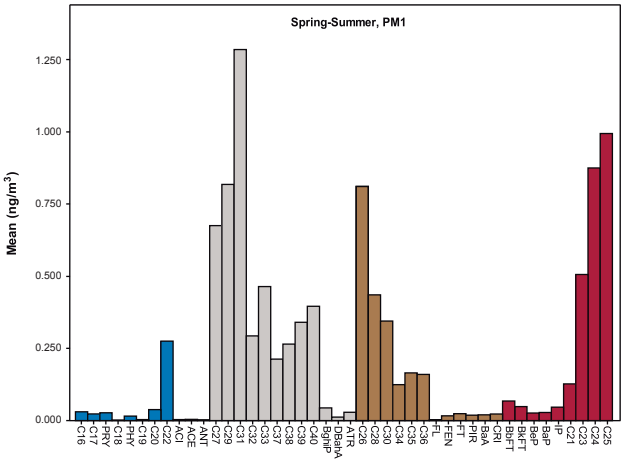

Figure 1. PMF factors for PM1 in the spring-summer period.

Four factors explained 95% of the total variance. The outcomes suggest that different sources account for odd-carbon (C27-39) and even-carbon (C26-C36) *n*-alkane emissions. These factors can be related to biogenic and anthropogenic sources, respectively (Abas and Simoneit, 1996).

Bivariate correlations among ions, PAH and *n*-alkanes were also carried out. Statistically significant relationships between TPAH and Ca^{2+} in PM1, PM2.5 and PM10 were found for the autumn-winter period. This can be explained considering that traffic exhaust is the primary PAH source, while Ca^{2+} is mainly emitted by traffic-induced resuspension during autumn and winter.

This work was supported by the Ministerio de Educación y Ciencia under the CGL2007-63326 (DAPASE).

Galindo, N., Nicolas, J. F., Yubero, E., Caballero, S., Pastor, C. and Crespo, J. (2008) *Atmos. Res.* **88**, 305-313.

Cecinato, A., Marino, F., Di Filippo, P., Lepore, L. and Possanzini, M. (1999) *J. Chromatogr. A* **846**, 255-264.

Abas, M. R. B. and Simoneit, B. R. T. (1996) *Atmos. Environ.* **30**, 2779-2793.

An original device for the measure of aerosol deposition. Results of a one year survey period on the Pin Sec catchment in Nantes, France

Stéphane Percot[1*], Véronique Ruban[1], Pierre Roupsard[2], Denis Maro[2] and Maurice Millet[3]
[1] Institut Français des Sciences et Technologies des Transports, de l'Aménagement et des Réseaux
[2] Institut de Radioprotection et de Sûreté Nucléaire
[3] Université de Strasbourg/CNRS
Keywords: ^{7}Be, Deposition, Aerosol size distribution, Urban aerosols, Heavy metals, PAH(s)
*Tel : +33(0)2 40 84 57 73 ; fax : +33(0)2 40 84 59 98 ; E-mail : stephane.percot@ifsttar.fr

Pollutants associated to atmospheric particles in urban areas have been characterized in many studies throughout the world. Pollutant sources are either natural (e.g. volcanoes, forest fires) or of anthropogenic origin (traffic, industries, domestic heating). The nature of surfaces as well as weather conditions and atmospheric turbulence influence the aerosol deposition. Previous studies in Nantes (France) on the Pin Sec catchment allowed the chemical characterization of total atmospheric deposition. In order to improve our knowledge of aerosol dry deposition on this catchment an original approach has been developed.
Our objective here is to present the instruments set up in the district of the Pin Sec to measure dry and wet atmospheric deposits and to show the results of a one- year survey.

The original approach carried out in this long-term study (September 2010 to October 2011) combines particle collectors (Partisol 2000 FRM), a covered pluviometer and frames on which test samples of different urban materials are fixed (tiles, glass, bitumen etc…). A meteorological station and an ultrasonic anemometer supply meteorological and micrometeorological data. Measuring instruments have been installed on the roof of a 4-store building in the Pin Sec catchment; the data should be representative of the global quality of atmospheric deposition on this catchment. Pollutants analysed are heavy metals, pesticides and Polycyclic Aromatic Hydrocarbons.
The analysis of deposited airborne particles on test samples was performed through beryllium 7 (^{7}Be) used as a tracer. Aerosol concentration is given by the Partisol. This methodology will allow calculating a monthly dry deposition velocity of particles and determining deposition fluxes. The percentage of the different surfaces (glass, bitumen, tiles, etc.) on the Pin Sec catchment was estimated in order to calculate an annual dry deposition flux.
Regarding monthly wet deposition, the flux is calculated as the ratio of the mass of pollutants collected in the covered pluviometer to the active surface of the catchment.

Finally, in order to validate the use of ^{7}Be as tracer of atmospheric deposition, a Low Pressure Impactor (LPI) was used allowing the measurement of aerosol size.

The medium diameter (D50) of ^{7}Be atmospheric on particles varies from 0.50 to 0.59 µm. These values are in good agreement with the literature (Ioannidou, 2011). It confirms the fixation of ^{7}Be on accumulation mode of atmospheric aerosol. A good correlation between the distribution of Pb mass and ^{7}Be activity tends to appear. The same pattern is observed for Zn. As a whole, metals are mainly distributed in the fine fraction (0.47<D50<0.62 µm). The same is observed for the detected PAH (Benzo[a]pyrene; Benzo[b]fluoranthene; Benzo[ghi]perylene; Benzo[k]fluoranthene; Fluorene), (0.41<D50<0.67 µm). This affinity of pollutants for the accumulation mode was observed in other studies for PAH (Sanderson *et al.* 2005) and for heavy metals (Song, 2011). Therefore, ^{7}Be seems to be representative of the distribution of particulate trace metals and PAH. Thanks to those results, concentration of pollutants measured on air particle will be combined with the data of the one-year survey of ^{7}Be deposit (Roupsard *et al* 2012) in order to get the dry deposition flux.
Concerning wet deposition, concentration of heavy metals, PAH and pesticides were measured during the whole sampling period allowing to calculate the annual wet deposition flux.

In the future, this original approach of the dry deposition taking into account urban parameters such as the type of surface, the atmospheric turbulence and the meteorological conditions will be compared with a classical method using boxes to collect total atmospheric deposition.
This work is supported by the INOGEV research program of the French National Research Agency.

A.Ioannidou (2011) *Atmos. Env.* 43, 1286-1290.
E. Sanderson *et al.* (2005) *Environ. Sci. Technol.,* 39, 7631-7637.
F. Song *et al.* (2011) *Atmos. Env.* 45, 6714-6723.
P. Roupsard *et al.* (2012) *Proc.* 19th *Eur. Aero. Conf.* Granada.

Evidence of regional-scale biomass burning contributions to urban aerosols in the Western Mediterranean

M. Viana[1], C- Reche[1], F. Amato [1], A. Alastuey[1], T. Moreno[1], F. Lucarelli[2], S. Nava[2], M. Rico[3], J. Gracia[3] and X. Querol[1]

[1] Institute for Environmental Assessment and Water Research (IDÆA-CSIC), Barcelona, 08034, Spain

[2] Department of Physics and Astronomy, University of Florence, and INFN, I-50019, Sesto Fiorentino (FI), Italy

[3]Agència de Salut Pública de Barcelona,Barcelona, 08012, Spain

Keywords: biomass burning, residential, recreational, streaker, black carbon, K^+

Presenting author email: mar.viana@idaea.csic.es

Recent studies evidence that carbonaceous aerosols emitted during biomass burning processes (natural or anthropogenic) may contain high amounts of carcinogenic compounds (Lewtan, 2007) as well as black carbon particles with a potentially high impact on health and air quality in urban environments (Andreae & Gelencsér, 2006). The main source of biomass burning aerosols in European urban environments is regional-scale transport (from rural areas towards cities), and in central and Northern European regions the use of this fuel for residential purposes (mainly heating) may also be a relevant source. However, major knowledge gaps remain regarding the quantification of the contributions from this source in major European cities. Paris is one of the first to have quantified the impact of biomass burning on urban air quality (up to 20% of $PM_{2.5}$ at an urban background site in winter, Favez et al., 2009). Biomass burning emissions are significant contributors to air quality degradation, and they are especially relevant due to their SOA-generating potential. Recent works point out to a high contribution of SOA to the ultrafine particle size range, thus stressing the higher hazardous potential of SOA (which penetrates thus deeper into the respiratory tract).

In Southern Europe, biomass burning is a much less frequent practice than in central and Northern Europe due to the characteristic Mediterranean climatology. It takes place mainly in rural areas, and its purpose is residential heating and/or agricultural (e.g., burning of agricultural residues). However, as a consequence of meso-scale air mass circulation biomass burning aerosols originated in rural areas may be detected in urban areas. The proportion of SOA in these cases is generally enhanced through transport. Within Mediterranean urban areas, biomass is only rarely used as a fuel for residential heating purposes, and mostly in high-income residential area (recreational use).

The aim of this work is to detect the presence and assess the potential contribution of biomass burning aerosols to $PM_{2.5}$ mass and composition in Barcelona. Two main sources were targeted: regional-scale emissions (reaching Barcelona through meso-scale transport), and local-scale emissions (for heating and recreational purposes).

To this end, a 2-week dedicated monitoring campaign was devised at two locations in Barcelona: the university campus, and a high-income residential area where residential/recreational biomass burning emissions were expected. The campaign was carried out in January 2011. Two sets of identical instruments were set up: one high-volume $PM_{2.5}$ sampler (MCV, S.A), one Streaker (analysing only the fine PM fraction), one laser spectrometer (GRIMM), and one absorption photometer (MAAP at the university site, and microAeth AE51 at the residential area). A detailed chemical characterisation (up to 65 elements and components) of the 24-hour $PM_{2.5}$ filter samples was carried out. The hourly and daily time variation of black carbon (BC) and PM chemical components were analysed, with special attention to hourly BC and K levels. An estimation of K^+ was obtained with a daily time resolution.

Source apportionment analysis allowed us to detect regional-scale biomass burning contributions to urban aerosols in Barcelona. Regional-scale biomass burning aerosols were mixed with secondary aerosols as a consequence of transport in the meso-scale, and showed a characteristic hourly trend with night-time maxima, coinciding with the land-to-sea breeze (Figure 1). We conclude that residential biomass burning emissions were not detectable in neither of the monitoring stations, possibly due to the fact that their contribution is too short in time (only a few hours/day).

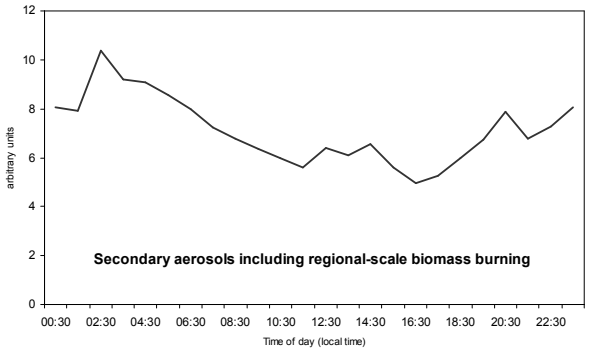

Figure 1. Mean hourly evolution of the secondary aerosol source (including regional-scale biomass burning tracers).

This work was supported by national project VAMOS (CGL2010-19464/CLI).

Andreae, M. O.; Gelencsér, A. (2006) Atmos. Chem. & Phys. 6, 3131-3148.

Favez, O.; Cachier, H.; Sciare, J.; Sarda-Estève, R.; Martinon, L. (2009) Atmos. Environ. 43, 3640-3644.

The effect of size, location, occupancy and microclimatic factors on air quality of university lecture rooms

M. Braniš[1] and K. Stupková[1]

[1] Charles University in Prague, Faculty of Science, Institute for Environmental Studies, Albertov 6, 128 43 Prague 2, Czech Republic

Keywords: indoor air quality, school, particulate matter, microclimate

Presenting author email: brains@natur.cuni.cz

As has been repeatedly documented in scientific literature, one of the most polluted indoor microenvironment can be found at schools. School buildings and classrooms suffer from poor air quality from two reasons: (1) Schools in cities are frequently situated in quarters or near streets with dense traffic and the infiltration of freeway particles into the school buildings represents an important source of pollutants (Janssen et al. 2001; Green et al. 2004) and (2) High levels of particulate matter in schools are frequently attributed to human activity and insufficient frequency of cleaning which is not capable in removing deposited particles (Branis et al., 2005; Fromme et al., 2007). Since these particles are only partly removed, they can be resuspended again and again. To ascertain the effect of infiltration and resuspension under various conditions (such as position of the classroom with respect to outdoor sources, its size and occupancy) we performed a year long project in three university lecture rooms situated in the centre of Prague.

Twenty-four hour mass concentrations of size-segregated aerosol were measured simultaneously in three university lecture rooms and outdoors in the central part of Prague (Czech Republic) by a five-stage A - F (<0.25µm, 0.25-0.5µm, 0.5-1.0µm, 1.0-2.5µm and 2.5-10µm) Personal Cascade Impactor Sampler (PCIS). Identical sets of instruments were deployed at the outdoor and indoor sites. Other variables such as CO_2, ventilation, temperature, relative humidity, occupancy were monitored as well. The measurements were performed during all seasons of the year during 11 three to four-day long campaigns involving working days as well as weekends and holidays.

The results documented that finer indoor size fractions (below 500nm) were significantly affected by outdoor concentrations while coarse particulate matter levels ($PM_{2.5-10}$) were predominantly dependent on the number of students in the lecture rooms. Nevertheless, some effect of human presence on the PM below 500nm was recorded as well, indicating a possible effect of the so called personal cloud (Table 1; Figure 1). The level of particulate matter concentrations corresponded to the proximity to the adjacent street (the closer the lecture room the higher the average PM concentration) and to the size of the size of the lecture room (the smallest was the space the highest PM concentrations were recorded).

In addition, concentrations of carbon dioxide frequently reached values over 1500ppm and higher. One of the common problems in all the three lecture rooms was very low relative humidity (around 30-35%). The results of the study not only confirmed previous results but also showed that measurements in one classroom per school may be insufficient because differences in position, size and occupancy may affect the concentrations of aerosol from which the estimates of exposure are made for the whole population of students in a particular school.

Table 1. The effect of occupancy on size resolved aerosol. OC - occupied; UOC - unoccupied periods; A, B, C, D, F - impactor stages; CPM ($PM_{10-1.0}$). B11, B12, B14 - lecture rooms.

	B11		B12		B14	
	OC	UOC	OC	UOC	OC	UOC
A	2.18	0.78	2.56	0.49	2.88	0.50
B	1.50	0.66	1.32	0.56	1.45	0.78
C	1.14	1.01	1.01	0.61	1.07	0.88
D	4.64	4.03	5.13	3.50	4.24	4.49
F	10.15	10.02	10.06	6.22	9.96	7.79
PM_{10}	18.30	15.78	20.08	11.38	20.03	11.77
CPM	3.68	1.44	3.88	1.05	4.33	1.29

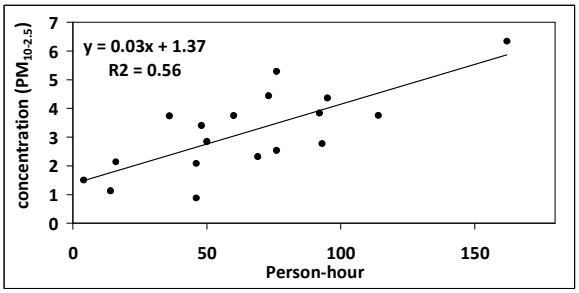

Figure 1. The relationship between coarse PM ($PM_{10-2.5}$) and occupancy (in person-hours) in one lecture room.

This work was supported by Ministry of Education, Youth and Sports of the Czech Republic under program NPV II, project No. 2B08077.

Branis, M., Rezacova, P., Domasova, M. (2005) *Environ. Res.* **99(2)**:143–149.

Green, R.S., Smorodinsky, S., Kim, J.J,, McLaughlin, R., Ostro, B. (2004) *Environ. Health. Perspect.* **112**:61–66.

Janssen, N.A.H., van Vliet, P.H.N., Aarts, F., Harssema, H., Brunekreef, B. (2001) *Atmos. Environ.* **35**:3875–3884.

Fromme, H., Twardella, D., Dietrich, S., Heitmann, D., Schierl, R., Liebl, B., Ruden, H. (2007) *Atmos. Environ.* **41**:854–866.

Impact of port activities on urban air quality at a Mediterranean coastal city

N. Pérez[1], J. Pey[1], C. Reche[1], X. Querol[1], A. Alastuey[1] and J. Cortés[2]

[1] Institute of Environmental Assessment and Water Research (IDAEA-CSIC), Barcelona, Spain
[2] Autoritat Portuaria de Barcelona, Spain
Keywords: PM_{10} and $PM_{2.5}$ chemical speciation, port emissions
Presenting author email: noemi.perez@idaea.csic.es

Important ports in the Mediterranean represent a significant impact on air quality. The APICE Project (Common Mediterranean strategy and local practical Actions for the mitigation of Port, Industries and Cities Emissions; www.apice-project.eu) pretends to reduce harbour emissions to the atmosphere by adopting mitigation strategies, that will be taken at local (specific abatement measures for each harbour) and transnational (common strategies to be applied in the five harbours involved in the project) scales. In the framework of this project long monitoring campaigns were carried out during one year (2011) at five Mediterranean ports: Barcelona (Spain), Genoa (Italy), Marseille (France), Thessaloniki (Greece) and Venice (Italy). With the objective to assess the impact of harbour activities on urban air quality, simultaneous measurements were also carried out at the urban areas.

In the urban area of Barcelona the main source of atmospheric pollution is road traffic (Amato et al., 2009), although emissions from industry, power generation, construction, and harbour activities are also relevant. Owing to the location of the harbour and the wind regime (with high frequency of sea breezes), harbour pollution affects the urban area.

We present here an intercomparison study of atmospheric particulate matter levels and composition measured simultaneously at the Barcelona port and at an urban background monitoring site (Palau Reial) from February to June 2011.

Daily 24-hour ambient PM_{10} and $PM_{2.5}$ samples were collected on quartz fibre filters using high volume samplers for gravimetric determination and, for a selection of these filters, the chemical analysis of carbonaceous components (OC and EC), soluble ions (Cl^-, NO_3^-, SO_4^{2-} and NH_4^+), and major and trace elements was performed, following the procedure described in Pey et al. (2010).

Available results (February-June 2011) show that daily average PM_{10} levels during this period were higher at the port (34 µg/m^3) than at the urban site (30 µg/m^3). For $PM_{2.5}$, similar levels were obtained, with average levels of 21 and 22 µg/m^3 at the port and the urban site, respectively. The daily PM_{10} limit value (50 µg/m^3) was exceeded during 3 days at the port and 2 days at the urban site.

Regarding the chemical composition of PM_{10} and $PM_{2.5}$ (Figure 1) the main difference was found for mineral matter, being more than 50% higher at the port in both fractions (12 vs. 6 µg/m^3 in PM_{10}), probably reflecting emissions from the new port extension works, but also handling of materials. Elemental carbon (EC) was more than 50% higher at the port in $PM_{2.5}$ (2 vs. 1 µg/m^3), probably due to the heavy truck transport. Sulphate was more than 20% higher at the port in PM_{10} (4 vs. 3 µg/m^3) reflecting ship exhaust and local industrial emissions (oil refinery).

Trace element levels were in general higher at the port for both PM_{10} and $PM_{2.5}$. Differences higher than 50% were found for road traffic tracers (Cu, Zn, Sb, Sn) and higher than 40% for fuel oil combustion tracers (V, Ni), reflecting emissions from the oil refinery and ship exhausts. Tracers of industrial emissions, such as As, Cd, Pb and Mn, presented also differences higher than 40% at the port with respect to the urban area.

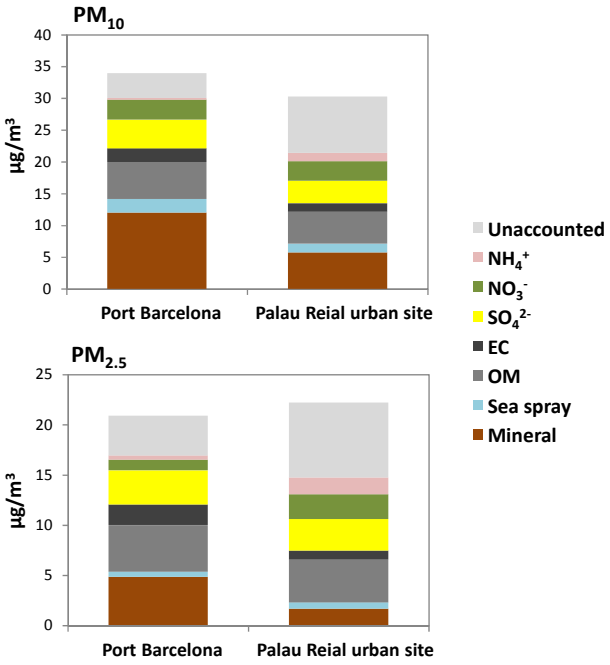

Figure 1. Comparison between main PM_{10} and $PM_{2.5}$ components measured at the port of Barcelona and Palau Reial urban site.

This work has been supported by the MED (FEDER, CE) programme (2889 2G-MED09-026), the Spanish Ministry of Science and Innovation (CGL2010-19464) and the Departament de Territori i Sostenibilitat of the Generalitat de Catalunya, in collaboration with the Autoritat Portuaria de Barcelona.

Amato, F., Escrig, A., Querol, X., Alastuey, A., Pey, J., Pérez, N. and Hopke, P.K. (2009). *Atm. Env.* **43,** 2770-2780.

Pey, J., Pérez, N., Querol, X., Alastuey, A., Cusack, M. and Reche, C. (2010). *Sci. Tot. Env.* **408,** 1951-1959.

Comparative study of ultrafine aerosol within a city

I. Salma[1], T. Borsós[1], Z. Németh[1], P. Aalto[2] and M. Kulmala[2]

[1] Institute of Chemistry, Eötvös University, H-1525 Budapest, P.O. Box 32, Hungary
[2] Department of Physical Sciences, University of Helsinki, FIN-00014 Helsinki, P.O. Box 64, Finland
Keywords: DMPS, urban aerosol, number concentration, diurnal variation, atmospheric nucleation.
Presenting author email: salma@chem.elte.hu

Particle number size distributions were determined in the near-city background, city centre, street canyon and road traffic tunnel environments in Budapest. Measurements were performed by a flow-switching type differential mobility particle sizer (DMPS) in an electrical mobility diameter range of 6–1000 nm in 30 channels, with a time resolution of ca. 10 min.

Daily average particle number concentrations are shown in Table 1. Median daily concentrations varied by a factor of 33 from the background to the tunnel. The median and maximum number concentrations increased monotonically and substantially with the intensity of road traffic, which implies that the major source of particles is vehicular emission. The maximum measured concentration of 465×10^3 cm^{-3} was obtained in the tunnel. Mean contribution of ultrafine particles to the total particulate number and its standard deviation for the listed environments were (76±9)%, (79±6)%, (86±3)% and (85±2)%, respectively, which indicates that the combination of the primary emissions and atmospheric nucleation maintains more or less constant ultrafine contribution.

Mean diurnal variation of particles averaged by the time of day for the different environments exhibited similar structure. They contained three concentration peaks. The first peak occurred between 7:00 and 10:00 local time, and it was explained by vehicular emissions during morning rush hours. The third peak showed up in the evening between 19:00–22:00, and it was also related to traffic emissions but it was shifted from afternoon rush hours (that occurs between 16:30 and 18:00 in Budapest), mostly as a result of the daily cycling in meteorological parameters. The second peak appeared around midday for residential environments, and it was related to new particle formation and consecutive growth. The importance of atmospheric nucleation was clearly revealed by the diurnal variation of the mean ratio of ultrafine particles to the total particulate number, which exhibited a huge midday peak for the nucleation days, and no peak for the days without nucleation.

Table 1. Minimum (N_{min}), median (N_{med}) and maximum (N_{max}) daily number concentrations of aerosol particles in various environments in Budapest. The unit is 10^3 cm^{-3}.

Environment	N_{min}	N_{med}	N_{max}
Near-city background	1.25	4.3	10.1
City centre	2.7	11.8	20
Street canyon	4.9	23	41
Road tunnel	3.7	143	392

New particle formation occurred on 27% of all days in the city centre on a yearly scale. Its frequency showed an apparent seasonal variation. There were significant differences between the environments as far as nucleation frequency is concerned. It was the largest for the near-city background, and it was the smallest for the street canyon. No nucleation event was observed at all in the tunnel. Particle growth was usually finished within 1 day. Growth processes that were developing for two days were identified in the background. One of them is shown in Fig. 1. Special types of banana curves were also identified.

This work was supported by the Hungarian Scientific Research Fund under grant K84091.

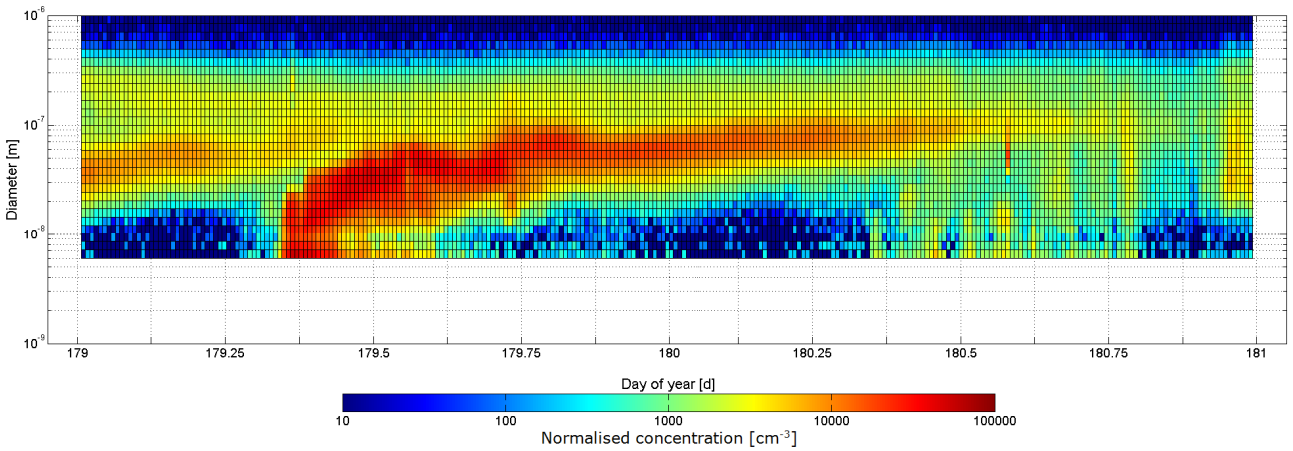

Figure 1. New particle formation event and consecutive growth developing for two days in the near-city background of Budapest on 28–29 June 2011 (Tuesday–Wednesday).

Black carbon mixing state in Paris megacity

M. Laborde[1], M. Gysel[1], T. Tritscher[1], M. Crippa[1], Zs. Jurányi[1], P.F. DeCarlo[2], A. Prévot[1], U. Baltensperger[1]

[1]Laboratory of Atmospheric Chemistry, Paul Scherrer Institut, Villigen, 5232, Switzerland
[2] Department of Civil, Architectural, and Environmental Engineering, Drexel University, Philadelphia, 3141, USA
Keywords: Black carbon, mixing state, hygroscopic growth, MEGAPOLI.
Presenting author email: marie.laborde@psi.ch

Black carbon (BC) is the result of incomplete combustion and is nowadays mainly of anthropogenic origin. BC is the main light absorbing material in atmospheric particulate matter and is therefore of interest for climate studies. It is usually non-hygroscopic upon emission and becomes hygroscopic with time via the condensation of secondary aerosol thereby forming a water-soluble coating (Stier et al., 2006).

Such aging of BC dramatically changes its role in climate forcing. Hydrophilic coating will enhance its cloud condensation nuclei activity, lower its lifetime and increase its light scattering and absorption efficiency.

Presently, only a few studies have performed ground based measurements of BC's mixing state and hygroscopicity in urban areas (Healy et al., 2011; McMeeking et al., 2011). This study aims at filling up this gap by investigating aerosol hygroscopicity and mixing state in Paris with a particular focus on BC particles.

A Single Particle Soot Photometer (SP2, Droplet Measurement Technology) was used along with a Hygroscopicity Tandem Diameter Mobility Analyzer (HTDMA) and an Aerosol Mass Spectrometer (HR-ToF-AMS). The SP2 allows the determination of the number concentration of BC containing particles (>0.4 fg BC/particle), their BC core size and their coating thickness along with the number concentration of purely scattering particles (<0.4 fg BC/particle). The HTDMA was used to determine the growth factor probability distribution function (GF-PDF) defined as the ratio of wet (90 % RH) over dry particle mobility diameters.

The positive matrix factorisation (PMF) method was applied to the organic trace of the AMS in order to identify their sources (Fig. 1a). We will here focus on three time periods when either traffic, biomass burning or background aerosol were the most prominent organic aerosol components, distinguished by a respective dominant contribution of hydrocarbon-like organic aerosol (HOA), biomass burning organic aerosol (BBOA) and oxidized organic Aerosol (OOA) in the PMF (Fig. 1a).

The air mass influenced by background aerosol contains the highest number fraction of thickly coated BC particles (Fig. 1b) which is consistent with the lowest non-hygroscopic mode at GF=1 (Fig. 1c). A mode of more hygroscopic particles (GF>1.5) dominates, indicating the presence of purely scattering particles or coated BC particles (Fig. 1b). The air mass influenced by traffic shows the lowest number fraction of coated BC, consistent with the distinct non-hygroscopic mode at GF=1. The background aerosol can also be seen in the presence of a more hygroscopic mode and a high fraction of purely scattering particles (Fig. 1b). The air mass influenced by biomass burning shows a higher number fraction of coated BC particles than the traffic influenced one, and the less hygroscopic mode is shifted from GF=1 to GF~1.1, indicating that the soot particles from biomass burning contain substantial organic coating. On the other hand, the very hygroscopic mode of the background aerosol at GF~1.6 is not as strongly seen as for the other two cases.

Further experimental results corroborating the above observations as well as results on the importance of BC mixing state on its CCN activation behaviour will be provided.

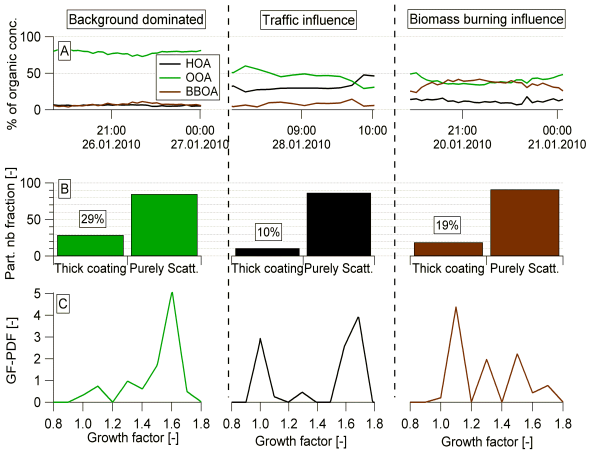

Figure 1. a) AMS: Organic aerosol factors retrieved by PMF b) SP2: Number fraction of BC containing particles with a thick coating and number fraction of purely scattering (both at optical diameter between 250 – 280 nm) c) HTDMA: Growth factor distribution (GF-PDF) of 265 nm particles.

This work was supported by the Swiss National Science Foundation (SNSF) and the European Community's Framework Program FP/2007-2011, in the context of the MEGAPOLI project.

Healy, R. M. et al., Atmos. Chem. Phys. Discuss., 11, 30333–30380, 2011.
McMeeking,G. R. et al., Atmos. Chem. Phys., 11, 9037-9052, 2011.
Stier, P. et al, J. Geophys. Res., 111, D18201, doi:10.1029/2006JD007147, 2006.

Seasonal variations of saccharides in PM2.5 aerosols in urban area

K. Křůmal[1], N. Kubátková[1,2], P. Mikuška[1] and Z. Večeřa[1]

[1] Institute of Analytical Chemistry of the ASCR, v.v.i., Veveří 97, 602 00 Brno, Czech Republic
[2] Faculty of Chemistry, Brno University of Technology, Purkyňova 464/118, 612 00 Brno, Czech Republic
Keywords: saccharides, organic compounds, PM2.5, urban aerosols.
Presenting author email: krumal@iach.cz

Saccharides are the most abundant group of the natural molecules, produced in large quantities by photosynthesis by plants and microorganisms. They form also a major part of cellular structure of plants and animals (Lindhorst, 2007). Saccharides are sources of energy for living organisms and basic structural unit of plant tissues – cellulose (glucose) and hemicellulose (xylose, arabinose, mannose and galactose) (Ek, 2009). Cellulose is the most abundant biopolymer, representing 40 – 50 % of dry weight of wood while hemicellulose represents 20 – 30 % of dry weight of wood. Another type of plant biopolymer is lignin which represent 20 – 30 % of dry weight of wood (Simoneit, 1999). Saccharides could be emitted to the atmosphere during burning of biomass, resuspension of soil particles, wind abrasion of leaf surfaces and sea spray (Wan, 2007) and they are present in biological aerosol particles (spores, pollens, fungi, algae, protozoa, bacteria, viruses and fragments of plants and animals) (Jia, 2010). Microorganisms, plants and animals can release into the atmosphere primary saccharides (monosaccharides and disaccharides) while fungi, lichens and bacteria produce saccharidic polyols (sugar alcohols; arabitol, mannitol and sorbitol) (Caseiro, 2007).

The concentrations of saccharides (monosaccharides, disaccharides and sugar alcohols) in the atmospheric aerosols were measured in Brno in the Czech Republic in spring, summer, autumn and winter of 2010 and in winter of 2011. The concentrations were measured in PM2.5 aerosol samples, over one week in each season. Measured monosaccharides included D(-)fructose, D(+)glucose, D(+)mannose, D(+)galactose and D(+)xylose. Disaccharides included D(+)maltose, D(+)sucrose and D(+)trehalose. Sugar alcohols included arabitol, sorbitol, manitol and myo-inositol.

The mean mass concentration of PM2.5 aerosols was in the range from 13.9 μg m^{-3} in summer to 39.3 μg m^{-3} in winter. The highest concentrations of monosaccharides and disaccharides were measured in spring of 2010. The most abundant saccharide in this season was sucrose. Disaccharides represent 65 %, monosaccharides 12 % and sugar alcohols 23 % of the total sum of measured saccharides in spring 2010. Contributions of sugar alcohols increase in the other seasons (53 – 59 %). Sucrose as a dominant disaccharide was determined in the range from 7.7 ng m^{-3} (winter 2010) to 85.4 ng m^{-3} (spring 2010). The most abundant monosaccharide was glucose in the range from 5.3 ng m^{-3} (winter 2010) to 11.4 ng m^{-3} (summer 2010). From the group of sugar alcohols, dominant myo-inositol was determined in the range from 23.1 ng m^{-3} (spring 2010) to 55.9 ng m^{-3} (autumn 2010).

Figure 1 shows the mean concentrations of the sum of saccharide compounds in individual seasons. Results including detailed concentrations of individual saccharides and optimalization of extraction from QMA filters with different solvents will be presented.

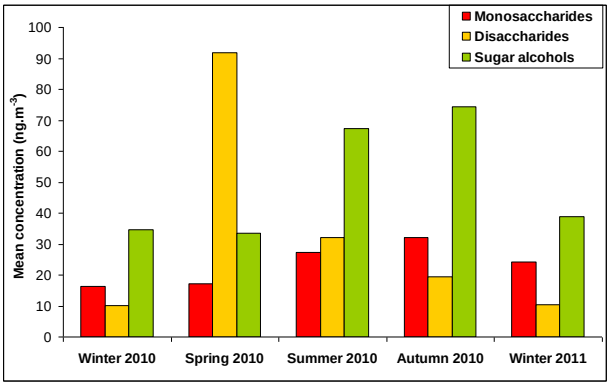

Figure 1. The mean concentrations of the sum of the saccharide compounds in individual seasons.

This work was supported by Grant Agency of the CR under grant No. P503/11/2315, by Ministry of Culture of the Czech Republic under project NAKI DF11P01OVV028 and by Institute of Analytical Chemistry of ASCR under an Institutional research plan No. AV0Z40310501.

Lindhorst, K. (2007) *Essentials of Carbohydrate Chemistry and Biochemistry*, Wiley-VCH.

Ek, M., Henriksson, G. (2009) *Wood chemistry and biotechnology*, Walter de Gruyter.

Simoneit, B.R.T., Schauer, J.J., Nolte, C.G., Oros, D.R., Elias, V.O., Fraser, M.P., Rogge, W.F., Cass, G.R. (1999) *Atmos. Environ.* **33**, 173-182.

Wan, E., Yu, J. (2007) *Environ. Sci. Technol.* **41**, 2459-2466.

Jia, J., Clements, A., Fraser, M. (2010) *J. Aerosol Sci.* **41**, 62-73.

Caseiro, A., Marr, I.L., Claeys, M., Kasper-Giebl, A., Puxbaum, H., Pio, C.A. (2007) *J. Chromatogr. A* **1171**, 37-45.

Source apportionment of the organic aerosol fraction by comparing positive matrix factorization, EC-tracer-method and ^{14}C-analysis

Wagener, Sandra[1,2], Langner, Marcel[1], Perron, Nolwenn[3], Hansen, Ute[1], Moriske, Heinz-J[2], and Endlicher, Wilfried[1]

[1] Humboldt-Universität zu Berlin, D-12489 Berlin, Germany
[2]German Federal Environmental Agency, D-14195 Berlin, Germany
[3]Lunds Universitet, S-22363 Lund, Sweden
Keywords: biogenic particles, biomass burning, urban aerosols, SOA
Presenting author email: sandra.wagener@geo.hu-berlin.de

Source apportionment of organic aerosol can be performed using several techniques. The positive matrix factorization (PMF) is a multivariate receptor model to determine potential sources of any origin. ^{14}C measurements allow distinguishing between non-fossil (biogenic or biomass burning (BB)) and fossil carbon. The EC tracer method distinguishes between primary and secondary organic aerosol (POA and SOA), assuming that fossil POA and EC have the same sources (Turpin and Huntzicker, 1995).

From Feb 2010 to Oct 2010, PM_{10} and PM_1 24 hr samples were taken at a traffic site, a park and a background site in Berlin. Tracers for SOA and POA and biomass burning were determined by GC-MS, whereas organic and elemental carbon (OC and EC) were measured by an OC/EC-Sunset analyzer. Additional samples for ^{14}C- and corresponding OC and EC analysis were taken in Jan, Jun, Jul and Oct 2010 at the traffic site and the park. Analysis was performed with a Single Stage Accelerator Mass Spectrometer.

PMF produced two biogenic SOA and four POA factors, with major contribution of biomass burning (Wagener *et al.* 2012). The SOA fractions at all stations varied between 9-47% in PM_{10} and 11-72% in PM_1, with higher values in the warmer months. For the EC-tracer-method, the sampling period was divided into periods with high and low biomass burning contributions (conform to warmer and colder months), as levoglucosan clearly influenced the OC/EC-ratio (correlation > 5). The EC tracer method yields SOA estimations comparable to PMF for the traffic site, but lower ones for the park, in the non-BB-period also for the urban background (table 1). This deviation is all the

Table 1: PM_{10} SOA contribution to OC, in %, from PMF and EC-tracer, calculated by scenario.1: excluding samples with SOA events; scenario.2: using the lowest OC/EC ratio.

	BB-period		Non-BB-period		
	sc.1	PMF	sc.1	sc.2	PMF
Park	11	18	17	22	41
Traffic	14	9	17	26	18
Urb. backgr.	15	15	30	32	47

bigger that EC-tracer-derived SOA also includes the fossil fraction. This is assumedly due to little traffic at these sites and the (relatively) large contributions of biogenic primary OC compared to fossil OC, which are falsely counted to the $[OC/EC]_p$ ratios.

The biogenic contribution to OC determined from ^{14}C-analysis on total carbon (TC) was 27-100% at the traffic site and the park, with higher values occurring in the warmer season, but even between PM-fractions. Calculated values of biogenic SOA (OC_{bioSOA}) reached up to 93%. These high values have not been expected and exceed clearly the values calculated by PMF, leading to the question whether the ^{14}C method overestimates the biogenic contribution to OC. Besides the measured biogenic contribution to TC, OC_{bioSOA} is also dependent on the levels of biomass-burning OC (OC_{bb}), which are determined by measurements of levoglucosan and lev/OC_{bb} ratios at the respective areas. Lower lev/OC_{bb} ratios lead to lower OC_{bioSOA}. This ratio, often not available, needs to be taken from literature and varies strongly with wood types. Thus, calculations have been performed with varying lev/OC_{bb} ratios (fig. 1), the lowest one stemming from PMF results. The latter leads to closer, but still lower OC_{bb} than calculated with PMF, resulting in higher OC_{bioSOA}. This raises the question whether PMF

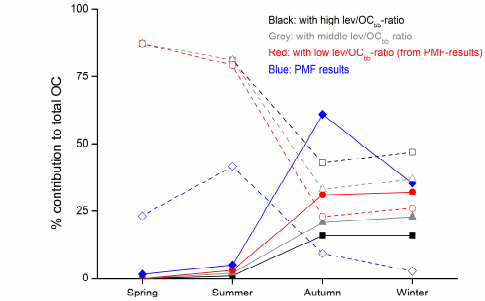

Figure 1: %contribution of OC_{bb} (continuous) and OC_{bioSOA} (dotted) to OC from PMF results (traffic site, PM_{10}) and ^{14}C-analysis with varying lev/OC_{bb}-ratios;

overestimates OC_{bb} or if lev/OC_{bb} ratios in this area are much lower than in other areas. Summarized, biogenic SOA in urban areas makes up a substantial fraction of OC, over all in warm months, whereas wood burning contributes strongly in the colder seasons. Variations with different apportion techniques indicate that the EC tracer method seems to fit better to areas with higher contributions of fossil combustion and for ^{14}C-analysis, measurements of the actual lev/OC_{bb}-level are utile. It turns out that comparisons are important to revise the results and may give hints to possible information gaps and future investigation approaches.

This work was supported by the DFG.

Turpin, B. J.; Huntzicker, J. J. (1995) *Atmos. Environ.* **29,** 3527-44.
Wagener, S., Langner, M., Hansen, U., Moriske, H.-J[2], and Endlicher, W. (2012), submitted in Env. Sci. & Techn.

Chemical and optical characterization of aged fossil fuel aerosol

L. Marmureanu[1], J. Vasilescu[1], A. Nemuc [1], D. Nicolae[1] and L. Belegante[1]

[1] National Institute of Research and Development for Optoelectronics, Magurele, 077125, Romania
Keywords: scattering coefficient, aerosol component composition, fossil fuel
Presenting author email: mluminita@inoe.inoe.ro

The atmospheric load of anthropogenic aerosol species is determined by factors such as emission, aging, convective transport and deposition processes, the level of scientific understanding being recognized to be medium and low. The optical parameters estimations have uncertainties linked with emission sources, optical properties, mixing and separation from natural background aerosol, state of mixing, method of mixing, and asphericity (IPPC 2007).

This study aims to characterize suburban aerosol during winter (2012) when soil dust influence is reduced due to snow coverage, and to investigate chemical, physical and optical properties of the aerosol during day time. Most frequent aerosol type investigated is the one resulted from traffic and from different types of fuel for domestic use such as wood or fossil fuel.

For this study were used three different types of equipments in order to obtain a detailed characterization of the aerosol load. Aerosol Mass Spectrometer (AMS) was used to characterizes submicron particles from the chemical point of view. AMS has a measurement size range of $0.04 < 2r <\sim 1000$ nm, and can deliver size-resolved particle composition using electron impact ionization. (Allan et al., 2004). The AMS is capable of deriving volatile and semi-volatile nitrate, sulphate, ammonium, organics and chloride (Takegawa et al., 2005). A Nephelometer (model 3563) designed for long-term monitoring of visual range and air quality at ground-based was used to continuously monitor the light scattering coefficient of airborne particles (Anderson et al, 1996). Aerodynamic Particle Sizer (APS) more sensitive to micron particle give information of size range between 0.5 and 20 µm (Peters. et al, 2003)

The AMS and APS results are in good correlations related to size distributions of submicron particle measured.

From the AMS output the presence of ions with m/z 44, 57, 60 and 73 were analyzed in order to identify the age of organic aerosols and their possible source (Adler et al, 2011). Higher concentrations of m/z 44 indicates the presence of oxygenated organic aerosols (OOA). During the entire period of measurements f 44 were between 0.0946 ± 0.00519 and 0.0987±0.019, values that characterize semi volatile OOA as defined by Ng et.al (2010) (f 44=0.07±0.04). The prominent peaks of the OOA were found at m/z 28, 43, 44, 55, 69 series characteristic to alkenes and alkanes (Slowik et al. 2010).

We have been observing correlation between oxygenated organic aerosol and NOx as previously observed by Zhang et al.(2005), Herndon et al.(2008). NO is emitted into the atmosphere also during fossil fuel use; in Magurele and Bucharest this type of fuel is used for heating. The data analyzed showed that NO_3 is internally mixed with NH_4 (ammonium nitrate) and in a very low proportion internally mixed with SO_4 like ammonium sulfate. Phenomena is explained by availability of ammonia, low temperature (~-10^{0}C) that causes ammonium nitrate to be stable and with high relative humidity (~ 80% measured at 10 m altitude-near the place of measurements).

Optical properties of the aerosol were extracted from nephelometer that gives real part refractive index (scatter and backscatter). The three wavelengths of the nephelometer were used to characterize the aerosol type related to scatter coefficient. The scatter coefficient was analyzed for different type of chemical species SO_4, Chl or NH_4. The suitable wavelength for this is at 700 nm and it showed association with total organics and NO_3 (fig.1)

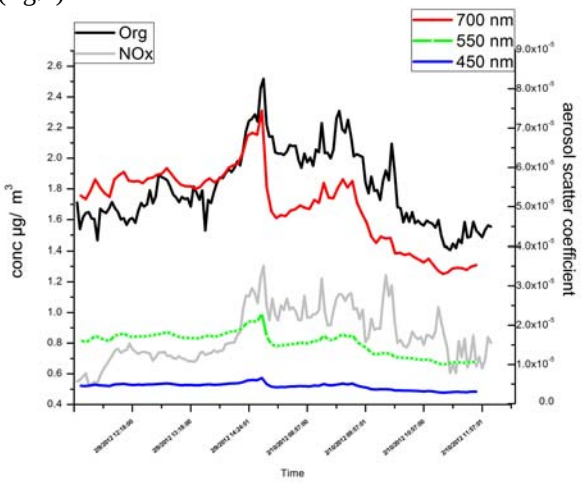

Figure 1 Distribution of chemical composition and aerosol scatter coefficient

This work was partially supported by the Romanian National Authority for Scientific Research, CNCS – UEFISCDI, project number PN-II-RU-PD-2011-3-0082.

Adler G. et al, (2011), *Atmos. Chem Phys* **11**, 1491-1503
Allan J. et al.(2004) *J. Aerosol. Sci*, **34**, 909-922
Anderson et al, 1996, *Journal of Atmospheric and oceanic Technology*, **13**, 967-985
Herndon S. C. et al.(2008), *Geophys. Res. Let*,**35**
Ng N. L. et.al (2010), *Atmos Chem. Phys*. **10,** 4625-4641
Peters M.T. & Leith D. (2003), *J. Aerosol Sci.*, **34**, 627-634
Slowik J.G. et al. (2010), *Atmos. Chem Phys*,**10**,1969-1988
Takegawa et al. (2005) *Aerosol Sci. technology*, **39**, 760-770
Zhang Q. et al.(2005), *J. of Geophys. Res.*, **110**

Influence of Meteorological Variables on Particle Number Concentration in Madrid

E. Alonso-Blanco[1*], A. Hidalgo[2], F.J. Gómez-Moreno[1], and B. Artiñano[1]

[1] Dept. Medio Ambiente, CIEMAT, Av. complutense, 40, Madrid, Spain
[2] Dept. Química Analítica e Ingeniería Química, Universidad de Alcalá, Alcalá de Henares, Madrid, Spain

Keywords: Fine particles, Meteorology, Particle concentration, SMPS, Urban aerosols
*E-mail: elisabeth.alonso@ciemat.es

One of the most important contributors to air pollution is the content of particulate matter. The characterization of atmospheric particles is necessary to know their potential effects in human health because the particle size-area ratio establishes its deposition in the respiratory system and the interaction with biomolecules (Oberdörster *et al*, 2005). Particle number concentration in the atmosphere and its time of permanence are highly dependent of the meteorological variables in each moment. Besides, particle number concentration influences the radiative balance, because of dispersion and absorption processes of the solar radiation (IPCC, 2007; Calvo *et al*, 2010).

In this work, we have analyzed the influence of the meteorological variables in the particle number concentration and in the particle size distribution in the period 2007-2011, continuing the studies of Gómez-Moreno *et al* (2011). The annual, seasonal, monthly and weekly averaged patterns have also been studied.

The measurements have been carried out at the CIEMAT facilities, located northwest of Madrid (Spain). It has a population density greater than 5000/km^2, heavy traffic and light industrial activity, this allows studying its plume as a typical urban plume.

A Scanning Mobility Particle Sizer (TSI-SMPS; DMA 3081 with CPC 3022 or CPC 3775) for the size range 15-600nm was installed. The meteorological parameters have been measured in a permanent tower. For this study, we have used those months with more than 50% of available data.

In Madrid, during the last 5 years, there was a slightly decreasing tendency of the particle number concentration (Fig.1). During the first 2 years (2007-2008), the average particle number per year was 9918 and 7325 particles cm-3 respectively, meanwhile during 2009-2011 it was around 6000 particles cm-3. During the last 3 years, there was an increase in the average wind speed per year, with a slight decrease during 2011, meanwhile during 2007 and 2008 the average wind speed was the lowest of the studied period. By the end of 2011, when the wind speed starts to have low values there is an increasing tendency in the particles number concentration.

It is necessary to emphasize that during 2009 it was incorporated to the SMPS a nafion drier. At the same time, a European Directive reducing permitted sulphur contents in fuel was adopted. Therefore, both changes could have influenced in the measurements performed from this date. During the studied period it was observed an increase of the particle number concentration from November to January. It was produced by a highest atmospheric stability, due to the presence of thermal inversions. During spring there is a lower particle concentration associated to the presence of strong winds that dilute the contaminants in the area closest to the surface.

During all the period, the Aitken mode is the predominant, while the accumulation and nucleation modes maintain similar concentrations. However, by the end of 2010 and the beginning of 2011, while the averaged wind speed per month suffers a remarkable decrease, this tendency changes and the accumulation mode predominates over the nucleation mode. This is due to the highly atmospheric instability, the winds are strong and dilute the gaseous precursors capable of forming particles corresponding to that mode.

Hence, the conclusion is that during the period of the study there is a decreasing tendency in the particle number. The concentration of the matter particulate in the atmosphere depends not only on the emission sources, but also on the meteorological variables that control the atmospheric dynamics.

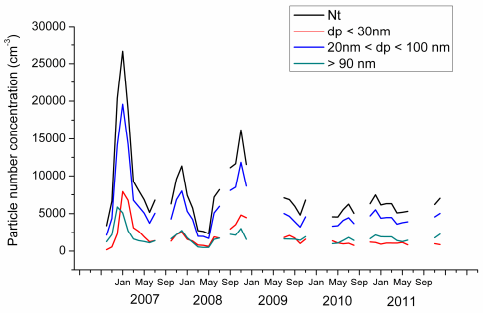

Figure 1. Evolution of the total particle number concentration and the different modes for the last five years in Madrid.

This work was supported by the Spanish Ministry MICINN through the projects MICROSOL (CGL2011-27020) and PHAESIAN (CGL2010-1777)

Calvo, A.I., Pont, V., Castro, A., Mallet, M., Palencia, C., Roger, J.C., Dubuisson, P., Fraile, R., 2010. *J. Geophys Res.* **115**, D08206.

Gómez-Moreno F.J., Pujadas M., Plaza J., Rodríguez-Maroto J.J., Martínez-Lozano P., Artinaño B. (2011) *Atmos. Environ*. 45 (**18**), 3169-3180.

IPCC (2007) *Climate change 2007: synthesis report*. IPCC, Geneva, Switzerland.

Oberdörster, G., Oberdörster, E., Oberdörster, J. (2005) *Environ. Health Perspect*. **113**, 823-839.

Characterization of Particulate-phase High Molecular Weight Mono-carbonyls and Dicarbonyls in Urban Atmosphere of Xi'an, China

Kin-Fai Ho[1,2], Wen-Ting Dai[1], Steven Sai Hang Ho[1,2], Jun-Ji Cao[1]

[1] SKLLQG, Institute of Earth Environment, Chinese Academy of Sciences, Xi'an, 710075, China

[2] School of Public Health and Primary Care, The Chinese University of Hong Kong

[3] Division of Atmospheric Sciences, Desert Research Institute, Reno, NV 89512, United States

Tel.: 86-29-88329320 ; fax:.86-29-88320456; E-mail:hejh@ieecas.cn

ABSTRACT:

Analytical method to quantify particulate-phase high molecular weight mono-carbonyls (C#>5) and di-carbonyls has been developed by adopting 2,4-dinitrophenylhydrazine (DNPH) derivatization followed by high performance liquid chromatography/ultra-violet (HPLC/UV) detection. Satisfy reproducibility and precision of the measurements were achieved. This method was applied for measuring the carbonyls in PM2.5 collected on quartz-fiber filters, sampled in Xi'an, China from 2008 to 2009. Nonanaldehyde was the most abundant compound, followed by octanaldehyde, hexanaldehyde and heptaldehyde, accounting for 40%, 20%, 12% and 11% in the total quantified carbonyls. For dicarbonyls, the concentrations of methylglyoxal were much higher than that of glyoxal. The seasonal variations of the particulate-phase mono-carbonyls and dicarbonyls were similar with those in the gas-phase, namely winter > autumn > spring > summer (except octanaldehyde). Strong correlation among those carbonyls was observed in winter, resulting from low temperature partitioning, weaker photochemical reaction, and more primary emission sources. On the contrary, vehicle emission, cooking emission and photochemical reactions are the major pollution source in Xi'an in summer.

Spatial patterns of high-resolution AOD and PM over Israel

Sorek-Hamer M.[1], Broday D.M[1], and Levy R.C[2]

[1]Department of Civil and Environmental Engineering, Technion, Haifa, 32000, Israel
[2]NASA/Goddard Space Flight Center, Greenbelt, MD, USA
Keywords: Remote sensing, aerosols, AOT, PM
Presenting author email: dbroday@technion.ac.il

The aerosol retrieval algorithm of the Moderate Resolution Imaging Spectroradiometer (MODIS) has been developed to retrieve aerosol properties globally. Under favorable conditions (clear sky over dark surfaces), MODIS provides a daily global coverage of its standard 10x10 km^2 aerosol products. This spatial resolution is useful for analysing the regional aerosol distribution and for studying events that show spatial extent (e.g. transboundary aerosol transport) but is too coarse for assessing the aerosol variation at the local scale. Li *et al.* (2005) have modified the MODIS algorithm to retrieve the aerosol optical depth (AOD) at a 1x1 km^2 resolution over Hong Kong, and found that relative to the standard 10x10 km^2 aerosol products the 1x1 km^2 aerosol products correlated better with the ground PM_{10} measurements and accounted for their spatial distribution. Recently, a new algorithm - Multi-Angle Implementation of Atmospheric Correction (MAIAC) - was developed for MODIS (Lyapustin *et al.* 2011), which also provides aerosol products at a 1 km resolution. The 1x1 km^2 MAIAC data may offer a clear advantage over the 10x10 km^2 standard MODIS aerosol products by improving our ability to characterize air quality at ground level using satellite-borne aerosol products, thus reducing exposure estimation errors.

It can be expected that as the spatial resolution of the aerosol products improves, their spatial coverage will increase. However, it is not clear if the added resolution provides higher noise or whether it represents improved aerosol signal. In this study we analyzed high-resolution (1x1 km^2) AOD data over Israel from two models: a new MODIS product obtained using a modification of the benchmark dark target algorithm and output of the new MAIAC algorithm.

In general, as the resolution of the aerosol product improved more data points were retrieved over the study area, with a ratio of ~85:8:1 between the number of the retrieved data points for the 1x1 km^2, the 3x3 km^2, and the 10x10 km^2 products, respectively. Moreover, as the resolution improved, the range of the AOT values became wider and the STD and the variance slightly increased (Table 1).

In order to find relationships between high resolution AOD and ground PM concentrations, we analyzed the AOD and PM data from several representative days using two parameters: their pertinent mean and coefficient of variation (CV=STD/mean). The CV of the AOD increased as the resolution increased (Fig. 1), with the highest CV obtained at the 1x1 km^2 resolution, close to the CV of the ground PM_{10}.

Table 1. Range and variance of AOD over Israel at different spatial resolutions in two days.

	AOD 17.1.07			**AOD 20.10.10**		
	10x10 km^2	**3x3 km^2**	**1x1 km^2**	**10x10 km^2**	**3x3 km^2**	**1x1 km^2**
Range	0.062 - 0.305	0.056 - 0.644	0.041 - 0.714	0.243 - 0.506	0.231 - 0.673	0.203 - 0.848
Variance (x 10^{-3})	2.96	3.8	4.7	2.9	3.6	3.9

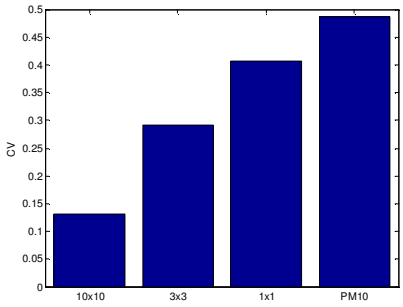

Figure 1. CV of AOD at different spatial resolutions, and of ground PM_{10} observations across all Israel on 17.1.07.

A comparison between the MODIS and the MAIAC 1x1 km^2 products suggests that the spatial patterns of the 1x1 km^2 AOD data partially represent one or more of the following (GIS) layers: roads, land use, and observed PM_{10} and $PM_{2.5}$ concentrations.

We expect that the 1x1 km^2 AOD product will enable improved correlations between ground PM and satellite-borne aerosol products, and help in assessing the true spatial variability of ambient PM, thus enabling to estimate reliably exposure to fine PM for public health applications.

This work was supported by the EHF Doctoral fellowship.

Li C.C., Lau A.K.H., Mao J.T., and Chu D.A., (2005). IEEE Trans. Geosci. Remote Sens., 43 (11)., 2650-2658

Lyapustin A., Wang Y., Laszlo I., Kahn R., Korkin S., Remer L., Levy R.C., and Reid J.S., (2011). J. Geophys. Res., 116.

Real time characterization of ambient aerosol at Prague suburban site during wintertime

P. Vodička, O. Makeš, J. Ondráček and J. Schwarz

Institute of Chemical Process Fundamentals of the AS CR, Prague, Czech Republic
Keywords: urban aerosol, high time resolution, OC/EC, AMS
Email: vodicka@icpf.cas.cz

Wintertime behavior of ambient aerosol was studied at Suchdol urban background site in Prague, Czech Republic in December 2010. The semi-online field OC/EC analyzer (Sunset Inc.) and the C-ToF aerosol mass spectrometer (AMS; Aerodyne Inc.) were used for measurements. The instruments were sampling using a common inlet equipped with a $PM_{2.5}$ cyclone. The AMS measured ca PM_1 fraction due to technical parameters. Samples were collected in two-hour intervals by ECOC instrument and analyzed by modified EUSAAR_2 protocol (Cavalli *et al*, 2010). The AMS measured in one-minute time resolution and results were averaged as required. Measurements covered 99% of the period.

In Fig. 1 the diurnal patterns of selected aerosol components are shown. It is well visible that the organic carbonaceous aerosols prevailed. If we take into account elements bound with carbon in organics, concentrations of organic matter (Org.) measured by the AMS are in good agreement with concentrations of organic carbon (OC) determined by the OC/EC analyzer (Takegawa *et al*, 2005). These two parameters are well correlated; the Spearman correlation coefficient of all time series between OC and Org. that was found to be 0.97.

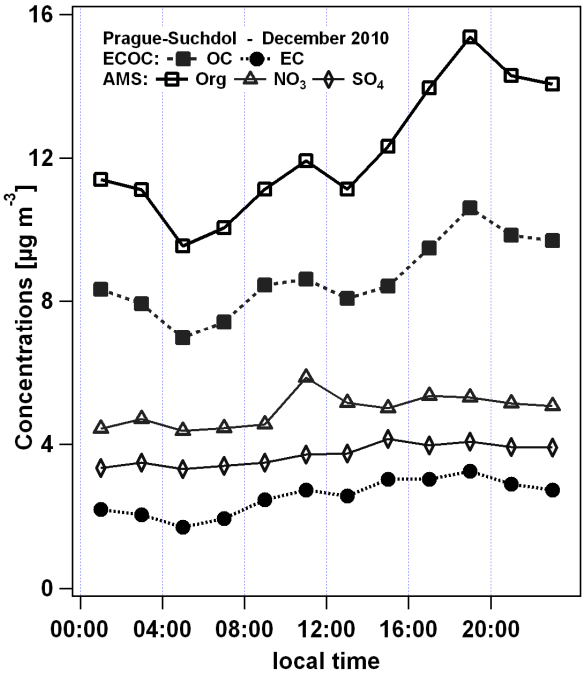

Fig.1. Averaged diurnal cycles of selected aerosol fractions

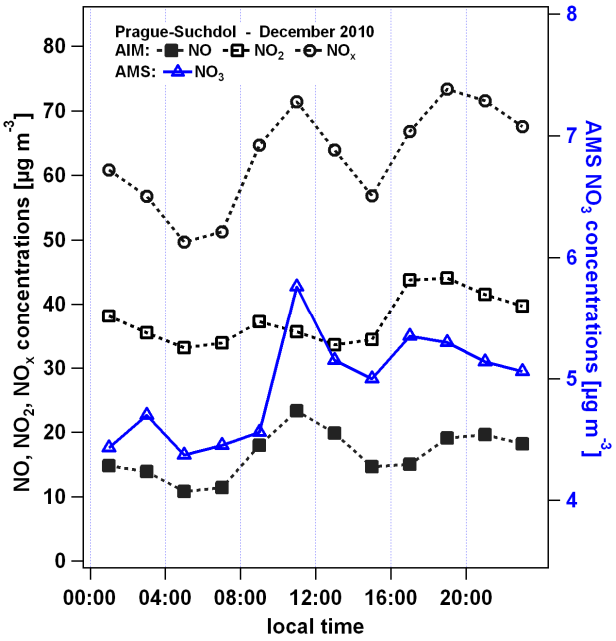

Fig.2. Comparison of averaged diurnal cycles of NO_3 aerosol fraction with nitrogen trace gases

AMS and ECOC data are also compared with meteorological (temperature, humidity, wind speed and direction, global radiation) and air quality (PM_{10}, SO_2, NO, NO_2, NO_x, O_3) data obtained from automated immission monitoring (AIM). For example, in Fig. 2 averaged diurnal variations of nitrogen trace gases are compared with NO_3. Spearman correlation coefficients were counted from all time series averaged into 2 hour means. Correlations between NO_3 and NO, NO_2, NO_x has found to be 0.50, 0.65 and 0.64, respectively. Similar analyses provide insight into the possible mechanism of aerosol formation and behavior at this site.

This work was supported by the Grant Agency of the Czech Republic under grant P209/11/1342.

Cavalli, F., Viana, M., Yttri, K. E., Genberg, J. and Putaud, J.-P. (2010) *Atmos. Meas. Tech.*, **3**, 79-89.

Takegawa, N., Y. Miyazaki, Y. Kondo, Y. Komazaki, T. Miyakawa, J.L. Jimenez, J.T. Jayne, D.R. Worsnop, J. Allan, and R. J. Weber (2005) *Aerosol Science and Technology*, **39**, 760-770.

Levels and chemical composition in airborne particulate matter (PM10) of eastern Andalusia (SE Spain)

A.M. Sánchez de la Campa[1], R. Fernández-Camacho[1], Y. González-Castanedo[1] and J.D. de la Rosa[1]

[1]Associate Unit CSIC-University of Huelva "Atmospheric Pollution", University of Huelva, Campus El Carmen E21071 Huelva, Spain

Keywords: Eastern Andalusia, PM10, traffic, trace element.

Presenting author email: ana.sanchez@pi.uhu.es

Andalusia is the second largest region in Spain, representing the 17% of the territory, with more of 8 M inhabitants. It's located in the boundary between two continents (Europe and Africa) being the place where the Mediterranean meets the Atlantic across the Strait of Gibraltar. Andalusia displays a complex orographic, with very different climatic and topographic patterns.

Seven representative monitoring sites (urban background, traffic hot-spot and urban with industrial influence) of eastern Andalusia have been selected to characterize levels and chemical composition of atmospheric particulate matter (PM10) during four years (2007-2010) (Table 1). These studies may supply relevant information for the air quality management (Putaud et al. 2004; Querol et al. 2004a,b; Hueglin et al. 2005), and also identify and quantify the different anthropic and natural contributions to PM in eastern Andalusia areas.

1161 filters were sampled and analysed for major and trace elements, water soluble ions (NH_4^+, SO_4^{2-}, NO_3^-, Cl^-) and total carbon, a total of 65 elements and compounds, using Inductively Coupled Plasma (ICP-MS and ICP-OES), Ion Chromatography and LECO instrumentation, respectively.

A study of air mass origin has been performed for one ideal monitoring station located at 37ºN 3ºW, using HYSPLIT4 model (Draxler and Rolph, 2003). We have used this model to gain insight on the influence of long-range transport to air pollutant levels (e.g. air masses from North Africa).

The mean concentration of PM10 of eastern Andalusia monitoring stations are in the range described at other sites urban-industrial (28-57 µg/m^3) and heavy traffic hot spots (46-50 µg/m^3) of Spain (Querol et al. 2004a). PM10 levels show simultaneous concentrations peak coinciding with maximum in summer when the North African dust outbreaks are more frequent. A decreasing trend of North African dust outbreak frequency is observed from 2007 to 2010, while the Atlantic air masses manifest an opposite tendency.

The highest concentrations of crustal components were measured in eastern Andalusia, compared to western Andalusia (de la Rosa et al. 2010). Also, the highest concentrations of anthropogenic sulphate were recorded in Bailén and traffic hot-spot monitoring stations. Cnm concentrations were highest in Granada Norte monitoring station.

Peak concentrations of V, Ni and Rb are registered in Bailén, derived mainly from the combustion of coke in brick factories, while the Rb is related with the emissions of K in the combustion of olive husk. Also, peak concentrations of V were registered in the traffic stations. On the other hand, hot-spot traffic sites in Granada and Málaga display the highest concentrations of Sn and Sb of Andalusia.

Table 1. Location and mean concentration PM10 (µg/m^3) of the monitoring stations selected for the study.

Station	Province	type	Latitude	Longitude	PM10 (µg/m^3)
Ronda del Valle	Jaén	Urban background	37º 47' 0.9"N	3º 46' 50,9"W	28
Carranque	Málaga	Traffic	36º 43' 12.8"N	4º 25' 45.8"W	43
Mediterráneo	Almería	Traffic	36º 50' 42"N	2º 27' 24.9"W	38
Granada Norte	Granada	Traffic	37º 11' 50,8"N	3º 36' 28" W	46
Plza. Castillo	Almería	Urban + Ind	36º 59' 47.91"N	1º 53' 41.91"W	28
Torredonjimeno	Jaén	Urban + Ind	37º 45' 48.8"N	3º 56' 46"W	37
Bailén	Jaén	Urban + Ind	38º 5' 34"N	3º 47' 1.6"W	43

This work was funded by the Projects 2007-RNM027329 and 2011-RNM7800: Department of Innovation Science and Enterprise, Andalusian Autonomous Government and the Project CGL2011-28025: Spanish Ministry of Science and Innovation (MINECO).

De la Rosa, J.D. et al. (2010). *Atmos. Environ*. **44**, 4595-4605.

Draxler, R.R. and Rolph, G.D. (2003). HYSPLIT (Hybrid Single-Particle Lagrangian Integrated Trajectory) Model Access via NOAA ARL READY Website. available at. NOAA Air Resources Laboratory, Silver Spring, MD. http://www.arl.noaa.gov/ready/hysplit4.html.

Hueglin, C. et al. (2005) *Atmos. Environ.***39**, 637-651.

Putaud, J.P. et al. (2004). *Atmos. Environ*. **38**, 2579-2595.

Querol, X. et al. (2004a) *Sci. Total Environ*. **334-335**, 359-376.

Querol, X. et al. (2004b) *Atmos. Environ*. **38**, 6547-6555.

PM level in Seoul metropolitan subway cabin indoor during the rush hour

S.-B. Kwon[1], J.B. Kim[1], J.H. Song[1], Y. Cho[1], D.S. Park[1], W. Jeong[1] and C.H. Shin[2]

[1]Subway IAQ Research Corp., Korea Railroad Research Institute, Uiwang, Gyeonggi, 437-757, Korea
[2]Seoul Metro, Seoul, 156-080, Korea
Keywords: PM10, PM2.5, subway cabin, rush hour
Presenting author email: sbkwon@krri.re.kr

In the modern society various types of transportation mode are utilized, among them the subway system is the one of the main transportation mode in which more than 7.21 million people ride a day in Korea. Also, there are increasing concerns on air quality of subway system including platform, tunnel and cabin indoors. Since the indoor air of subway system contains particulate matters (PM) of heavy metals generated from frictions of wheels, break-pads, and pantographs. The air cleaning of subway cabin is important since the cabin indoor is the most time spent space by passengers of subway. In our previous study conducted on the morning rush hour showed the average level of PM10 was about 142 μg/m^3 in Seoul subway (Kwon *et al.*, 2008). In this study, we measured PM concentrations in a subway cabin during the rush hour. Coarse mode particles defined as the particle sizes of 2.5~10 μm and fine mode known as PM2.5 (smaller than 2.5 μm in size) were monitored by real time optical particle sizer and indoor concentration was compared with outdoor concentration.

The size distribution of cabin indoor particulate matters (PM10 and PM2.5) were measured by the optical particle sizer (OPS, TSI model 3330) during the morning rush hour (07:00~10:00) for 4 weekdays between September to November 2011. In order to perform the on-board measurement, the OPS was installed on the cabin shelf at the Sinjeong subway depot before its departure. Figure 1 shows the transient PM10 and PM2.5 concentration levels in a cabin during the rush hour. All data were averaged from four days measurement. Averaged PM10 concentration was 95.7 μg/m^3 and PM2.5 was 57.7 μg/m^3. Approximately 60% of fine mode particles were found among PM10 in a subway cabin.

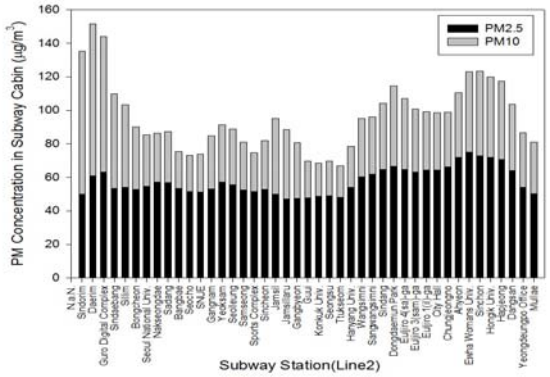

Figure 1. Transient PM10 and PM2.5 concentrations in a subway cabin.

Since the Seoul metro Line 2 is a loop lane circulating the boundary of central Seoul (total length = 60.2 km), we referred the outdoor PM concentration of averaged monitoring results from Air Quality-Climate Change Information of Seoul (AQCCI, 2011). During the 4 week days of on-board measurement, PM10 and PM2.5 of subway cabin indoor and outdoor concentrations were correlated as shown in Figure 2. It reveals that subway indoor PM is linearly correlated with outdoor PM concentration (R^2 = 0.94 for PM10, 0.99 for PM2.5). The ratio of indoor to outdoor (I/O) was 1.53 for PM10 and 1.43 for PM2.5. It is obvious that the indoor PM concentration of subway cabin is significantly affected by outdoor PM concentration and the indoor concentration is higher than that of outdoor by 48%.

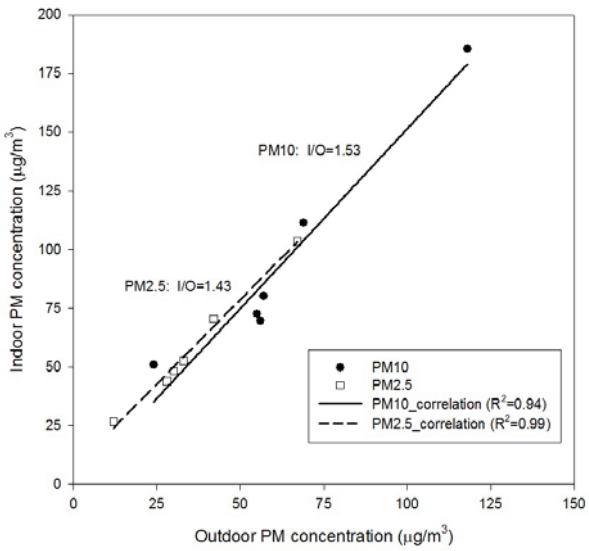

Figure 2. The ratio of indoor to outdoor PM concentration.

This work was supported by a grant (IAQ Research of Urban Transit) funded by Ministry of Land, Transport and Maritime Affairs of Korean government

AQCCI (2011) http://cleanair.seoul.go.kr
Kwon, S.-B., Cho, Y., Park, D. and Park, E.-Y. (2008) *Indoor Built Environ.* **17**, 361-369.

School Children's Personal Exposure to Ultrafine Particles in Urban Environments

M. Mazaheri[1], M. Mokhtar[1], R. Jayaratne[1] and L. Morawska[1]

[1] International Laboratory for Air Quality and Health, Institute of Health and Biomedical Innovation, Queensland University of Technology, Brisbane, Queensland 4001, Australia
Keywords: ultrafine particles, personal exposure, Nano Tracer, schools.
Presenting author email: m.mazaheri@qut.edu.au

This work was motivated by the limited knowledge on personal exposure to ultrafine (UF) particles, and it quantifies school children's personal exposure to UF particles, in terms of number, using Philips Aerasense Nano Tracers (NTs). This study is being conducted in conjunction with the "Ultrafine Particles from Traffic Emissions and Children's Health (UPTECH)" project, which aims to determine the relationship between exposure to traffic related UF particles and children's health (http://www.ilaqh.qut.edu.au/Misc/UPTECH%20Home.htm). To achieve this, air quality and health data are being collected at 25 schools within the Brisbane Metropolitan Area in Australia over two years. The school children's personal exposure to UF particles in the first 17 schools are presented here. These schools were tested between Oct 2010 and Dec 2011. Data collection is expected to be complete by mid 2012.

Four NTs were available for this project, 3 of which were used for data collection and one was the reference unit. The NT is a hand-held battery-operated instrument that measures particle number concentration up to 10^6 cm^{-3} and particle size in the range of 10-300 nm within the breathing zone. At each school, three to six 8 to 11 years old school children, who gave consent to participate in the study, were asked to carry the NT and a global positioning system (GPS) all the times for a total period of 24 hours. The children were instructed to wear the NT around the waist using a dedicated belt and were requested to have it in his or her close proximity during the 24 hours of measurements when it was not being worn (e.g. during sports activities, when using the bathroom and sleeping). Each child and their parents or guardians were asked to record their travel times and activities, during non-schooling and schooling hours, and the time and duration when the sampler was not with the child at any particular time.

63 children in the 17 schools (S01 – S17) participated in this study. Time series of the UF particle number data during the 24 hours of measurements for each child were used to identify the peak concentrations in the first instance. Each child's exposure was quantified over a total of 24 hours, as well as for school hours only, non-school hours, and commuting.

Figure 1 shows the children's' average exposure to UF particles during schooling activities (indoors and outdoors) over the 24 hours of data collection at each individual school. These preliminary results show that children's exposures during indoor and outdoor activities were lowest at S09 and highest at S03 and S02, respectively.

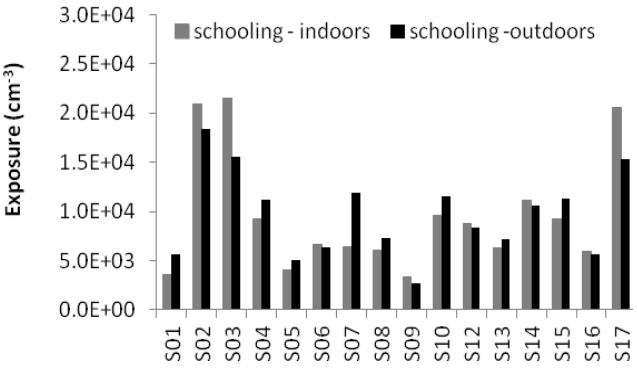

Figure 1. Average children's exposure to UF particles during school hours (indoors and outdoors) at each school.

Figure 2 shows the children's average exposure to UF particles during after school hours and transport over the 24 hours of measurements. The non-schooling hours also include commuting and are affected by many factors relating to different children activities during after school hours. Children attending S07 and S08 had higher exposures during commuting and S01 had the lowest.

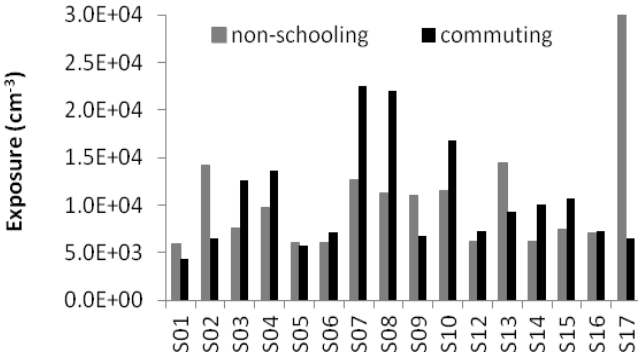

Figure 2. Average children's exposure to UF particles during after school hours and transport at each school.

Preliminary analysis indicates that the results are consistent with the general characteristics of the schools and local traffic conditions during the data collection.

This work was supported by the ARC, DTMR and DET through Linkage Grant LP0990134.

Distribution characteristics and trends of $PM_{2.5}$ and PM_1 -bound polycyclic aromatic hydrocarbons (PAHs) over an urban Mediterranean area

St. Pateraki[1,2], D.N. Asimakopoulos[2], Th. Maggos[1], and Ch.Vasilakos[1]
[1]Environmental Research Laboratory/INT-RP, National Centre for Scientific Research "DEMOKRITOS", 153 10 Aghia Paraskevi Attikis, P.O.B. 60228 Athens, GREECE
[2]Department of Environmental Physics and Meteorology, Faculty of Physics, University of Athens, University Campus, building PHYS-5, 157 84, Athens, GREECE

Keywords: PM, PAHS, Meteorology, Urban Pollution

Presenting author email: stella@ipta.demokritos.gr

Airborne particulate matter (PM) is one of the most important markers of the urban air quality, especially with respect to a number of chronic respiratory diseases. On one hand, epidemiology suggests that especially the smaller diameter particles which are able to reach deeper lung regions, have considerable impact on health even at concentrations below the present ambient air quality standards. On the other hand, Polycyclic Aromatic Hydrocarbons (PAHs), are ubiquitous constituents of urban aerosols and of major and well justified health concern since some of them are thought to be among the strongest known toxic, mutagens and carcinogens. 17 PAHs have been classified as priority pollutants by the USEPA based on their toxicological profile with benzo(a)pyrene (BAP) being considered as the most toxic and known to induce lung cancer and DNA binding ((Ravindra et al. (2008)). Sources, emitted amounts, gas/particulate partitioning coefficient of PAHS, atmospheric loss mechanisms such as long range transport and photolysis are potential factors affecting the seasonal variability of atmospheric PAHs (Kume et al. (2007)).

Five daily $PM_{2.5}$ and PM_1 measurements were deployed simultaneously, with the use of low volume gravimetric samplers, in two different environments within the Athens basin, during the period 20/3-2/8/2008. The sampling stations were selected carefully, taking into consideration their pollution characteristics and sources: Aegina is a coastal background monitoring station located in the countryside at some distance from anthropogenic PM emission sources while Votanikos is an urban-industrial monitoring station generally dominated by traffic, under the influence of industrial particulate matter emissions. The whole procedure which was followed for the determination of the PM concentration was according to EN14321. Sampling and analysis of Polyaromatic Hydrocarbons (26 PAHs) performed according to ISO 12884. The meteorological data (temperature, wind speed, relative humidity) for Aegina and Votanikos were provided by the Agricultural University of Athens and the Hellenic National Meteorological Service, respectively.

This work addresses three different tasks: (i) to record the $PM_{2.5}$ and PM_1 levels (ii) to characterize chemically the collected samples in connection with the associated PAHs (iii) to investigate the trends for both PM mass and PAHs (molecular weight, number of rings, carcinogenicity) during the different prevailing meteorological cases (wind, temperature, humidity, atmospheric circulation) and most importantly (iv) to explore the pathways of aerosols transportation (mass and composition) from and towards the Greater Athens Area (G.A.A.).

The daily concentration levels of $PM_{2.5}$ and PM_1 did not exceed 38.0 and 32.5 $\mu g/m^3$, respectively. The recorded $PM_{2.5}$ values appeared to exceed the E.U. daily limit (25 $\mu g/m^3$) three and two sampling days in Votanikos and Aegina, respectively. Irrespectively of the type of the environment, PM_1 appeared to constitute the most significant part of the $PM_{2.5}$ mass (61%-95%). It is of great importance to mention the equal $PM_{2.5}$ levels at the different environments on 25/3, 2/7 and 2/8 as well as the significant associations between $PM_{2.5}$ (r: 0.76) and PM_1 (r:0.80).

As far as polyaromatic hydrocarbons are concerned, they were mainly accumulated at the center station and more specifically at $PM_{2.5}$.The same assumption can be also made for the $PAHs_{Cancer}$ (Fig. 1). It is of great importance to mention not only the higher AvgΣPAHs concentrations at PM_1 of the coastal station than those at $PM_{2.5}$ but also the higher $Avg\Sigma PAHs_{Cancer}$ concentrations (Fig. 1). Generally, B(ghi)P was the most abundant PAH at Aegina and B(b)F at Votanikos station.

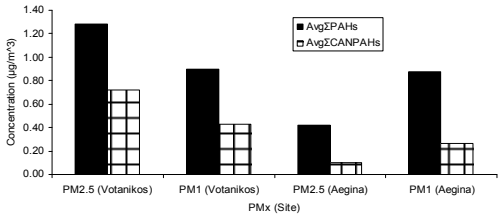

Figure 1. Average ΣPAHs and $\Sigma PAHs_{CAN}$ for each PM fraction and station

Investigating each day separately, with the only exception being 21/7/08, 2-methylnaphthalene prevailed in Aegina. At the city center the PAHs distribution was more complicated with uniform trends for both fractions being registered only at 20/3 and 25/3 with the B(b)F and B(ghi)P prevalence, respectively.

Ravindra, K., Ranjeet, S., Van Grienken, R. (2008) *Atmos. Environ.* **42**, 2895-2921.
Kume, K., Ohura, T., Noda, T., Amagai, T., Fusaya, M. (2007), J. Hard. Mater. **144**, 513-521.

Particle number size distribution characteristics in the urban background in Helsinki

B. Mølgaard[1], H. Hannuniemi [2], G. Ripamonti[1,3], T. Wegner[4,5]
S. Weber[4], L. Järvi[1], T. Vesala[1], K. Hämeri[1], T. Hussein[1,6]

[1]Department of Physics, University of Helsinki, Helsinki, FI-00014, Finland
[2]Finnish Meteorological Institute, Helsinki, FI-00101, Finland
[3]DIIAR Environmental Engineering Section, Politecnico di Milano, Milano, 20133, Italy
[4]Institute of Geoecology, Technische Universität, Braunschweig, D-38106, Germany
[5]Department of Applied Climatology and Landscape Ecology, University of Duisburg-Essen, Essen, D-45141 Germany
[6]Department of Physics, University of Jordan, Amman, 11942, Jordan
Keywords: urban aerosol, particle number size distribution, cluster analysis
Presenting author email: tareq.hussein@helsinki.fi

Health effects of aerosols are particle size dependent. In cities the particle concentration is often elevated due local sources. These sources have different temporal and size characteristics. In addition to the local sources, also long rang transport and local weather conditions affect the particle number size distributions in the urban atmosphere.

We have investigated how the particle number size distribution at an urban background location in Helsinki is affected by local sources and weather conditions. One year of particle number size distribution data along with meteorological data was used. To reduce the complexity of the data set we used cluster analysis (Beddows *et al*, 2009). In this way the number size distributions were separated into six groups. For each of these six groups the mean particle number size distribution is shown in figure 1.

Clusters 1 and 2 were common when the air was affected by fresh road traffic emissions. Cluster 3 was frequent when the wind came from downtown Helsinki, probably due to aged traffic emissions or ship emissions. Cluster 4 and 5 were characteristic for clean air and for air containing many long range transported particles.

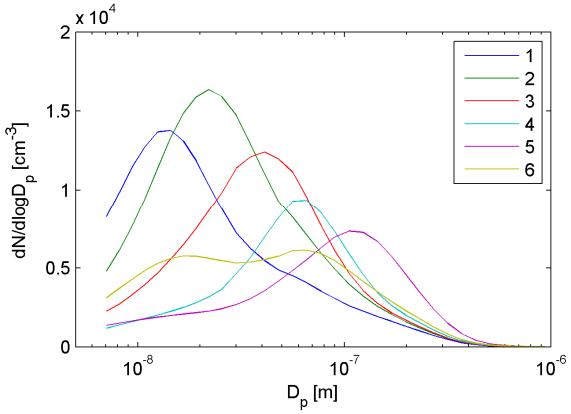

Figure 1. Mean size distributions of the six clusters.

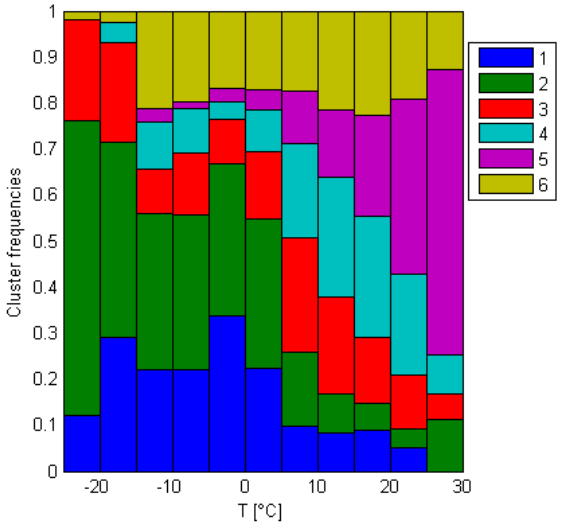

Figure 2: Frequencies of clusters as a function of temperature.

Figure 2 shows that cluster 1, 2, and 3 are most common at low temperatures. Comparison to figure 1 shows that the particles number size distributions are often dominated by particles with diameters below 50 nm when temperatures are low. One reason for this is probably increased vehicular emissions at low temperatures (Olivares *et al*, 2007). Another probable reason is less vertical dilution in winter.

At high wind speeds the particle number size distribution was more often dominated by nucleation mode particles.

Beddows, D.C.S., Dall'Osto M., Harrison, R.M., (2009) *Environ. Sci. Technol.* **43**, 4694-4700

Olivares, G., Johansson, C., Ström, J., Hansson, H-C. (2007) *Atmos. Environ.* **41**, 2145-2155

Ionic composition of PM_{10} and $PM_{2.5}$ in urban-traffic and urban background sites within the Thessaloniki Major Area (TMA), northern Greece

E. Gounari, D. Lazarou, E. Manoli, D. Voutsa, C. Samara

Environmental Pollution Control Laboratory, Department of Chemistry,
Aristotle University of Thessaloniki, University Campus, 54124 Thessaloniki, Greece
Keywords: chemical composition, PM10/PM2.5, sulfate, urban aerosols
Presenting author email: dvoutsa@chem.auth.gr

Thessaloniki is a densely populated Greek city constantly exceeding the EU limits for PM_{10}, particularly at traffic impacted sites in the city centre. Previous studies have investigated the ionic composition of ambient PM, and the size distribution of major anions and cations (Voutsa *et al*., 2002; Tsitouridou *et al.*, 2003; Terzi *et al*., 2010). Recently, the analysis of PM_{10} at two urban sites within the city indicated that ionic species were major components of PM_{10} mass with average contributions 14% and 16%, respectively. The dominant anion was SO_4^{2-} followed by NO_3^-, while the dominant cations were Ca^{2+} and NH_4^+ (Terzi *et al*., 2010). Nevertheless, further understanding of the ionic composition of atmospheric particles, particularly those in the fine fraction, is required.

The aim of the present study was to investigate the ionic composition of PM_{10} and $PM_{2.5}$ at two sites within Thessaloniki, UT (urban-traffic) and UB (urban-background) (Figure 1). PM_{10} and $PM_{2.5}$ samples were concurrently collected during the warm season of 2011 according to EN-12341 and EN-14907, respectively. Low Volume Samplers (Ingenieur Derenda, Berlin) equipped with PM10 and PM2.5 inlets were employed operating at constant flow rate 2.3 m^3/h. PM_{10} and $PM_{2.5}$ ionic fractions were collected on Φ 47 mm Teflon filters (Zefluor™ membranes, Pall 2μm). Each sampling had a 24-h duration starting at 00:00. PM_{10} and $PM_{2.5}$ samples were analyzed by ion chromatography for major ions according to previously standardized procedures (Terzi *et al*., 2010).

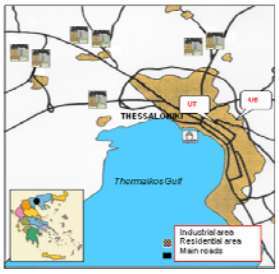

Figure 1. Map of the TMA showing the locations of sampling sites (UT: urban traffic site, UB: urban background site)

Similarly to previous findings, both PM fractions were significantly higher in the UT site (Table 1). This site exhibited lower $PM_{2.5}/PM_{10}$ ratio suggesting stronger impact of traffic induced resuspension of road dust.

Table 1. Mean±SD for PM_{10} and $PM_{2.5}$ mass concentrations (μg/m^3) and $PM_{2.5}/PM_{10}$ ratios

	PM_{10}	$PM_{2.5}$	$PM_{2.5}/PM_{10}$
UT	48±10	26±6	0.54±0.1
UB	28±9	17±6	0.64±0.1

The average concentrations of anions associated to PM_{10} and $PM_{2.5}$ are presented in Figure 2. These values are in general agreement with those previously found in the same area during the warm period (Samara and Tsitouridou, 2000; Terzi et al., 2010; Tsitouridou et al., 2003; Voutsa et al., 2002). The PM_{10} fractions of all anions were similar at the two sampling sites. The concentrations of SO_4^{2-} and Cl^- associated to $PM_{2.5}$ were slightly higher at the UB site, whereas the $PM_{2.5}$ fraction of NO_3^- was significantly higher at the UT site suggesting photochemical formation of nitrate aerosol from vehicular NOx emissions. Correspondingly, the $PM_{2.5}/PM_{10}$ ratios of Cl^- and SO_4^{2-} (Table 2) did not exhibit remarkable spatial difference in contrast to those of NO_3^- that was significantly higher at the UT site designating its strong affection by traffic emissions. Very high $PM_{2.5}/PM_{10}$ ratio values, close to unity, were found for SO_4^{2-} at both sites and for NO_3^- at the UT site suggesting total distribution in the fine particle fraction in contrast to Cl^- that exhibited a significant coarse fraction.

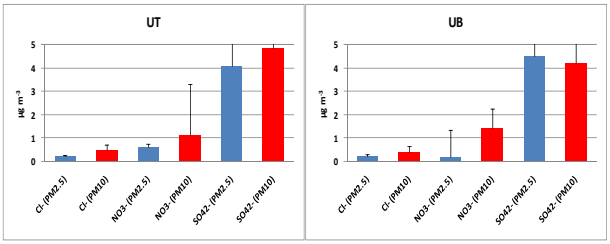

Figure 2. Average concentrations of anions associated with the PM_{10} and $PM_{2.5}$ particle fractions at two sampling sites.

Table 2. $PM_{2.5}/PM_{10}$ ratios for ionic concentrations

	Cl^-	NO_3^-	SO_4^{2-}
UT	0.61±0.33	0.99±1.91	0.92±0.24
UB	0.72±0.35	0.24±0.32	1.09±0.24

References

Samara, C. and Tsitouridou, R. (2000) *Wat., Air Soil Pollut.* **120**, 71-88.

Terzi, E., Argyropoulos, G., Bougiatioti, A., Mihalopoulos, N., Nikolaou, K., Samara, C. (2010) *Atmos. Environ.* **44**, 2231-2239.

Terzi, E., Gemenetzis, P., Petrakakis, M., Samara, C. (2007) 10th Intern. Conf. on Environ. Sci. and Technol., Kos, Greece, Proceeding A-1415-1422.

Tsitouridou, R., Voutsa, D., Kouimtzis, Th. (2003) *Chemosphere* **52**, 883-891.

Voutsa, D., Samara, C., Kouimtzis, Th., Ochsenkuehn, K. (2002) *Atmos. Environ.* **36**, 4453-4462.

Aknowledgements

This work was conducted under the project ACEPT-AIR supported by the European Community (LIFE 09 ENV/GR/000289).

Particle size distribution of *n*-Alkanes and PAHs in urban and industrial areas of Algiers, Algeria

R. Ladji[a], S. Khedidji[a], A. Lemou[b], L. Rabhi[b] an d N. Yassaa[a,b]
[a]Centre de Recherche Scientifique et Technique en Analyses Physico-Chimiques (C.R.A.P.C), BP 248, Alger RP 16004, Algeria.
[b]Laboratoire d'Analyse Organique Fonctionnelle, Faculté de Chimie, Université des Sciences et de la Technologie Houari Boumediene, USTHB, BP32 El-Alia, Bab-Ezzouar, 16111, Algiers, Algeria.

Keywords: PAHs, n-alkanes, size distribution, Aerosol.
Presenting author email: nyassaa@usthb.dz

Atmospheric particulate organic matter (POM) contains a wide variety of constituents that may induce adverse effects to human health and/or can be used as markers for the emission sources. Thus, the deep understanding of the POM composition is a suitable tool whenever the source identification is attempted with the purpose of pollution control or toxicants abatement. Anthropogenic *n*-alkanes are associated to fossil fuel utilization and are derived from both incomplete fuel combustion and lubricant oil evaporation. On the other hand, biogenic sources of *n*-alkanes include particles derived from epicuticular waxes of vascular plants (e.g., leaf debris) and direct suspension of pollen, micro-organisms and insects (Yassaa et al., 2001 and references therein). The percentage distributions of *n*-alkanes are source-specific and therefore provide useful information about their origin. PAHs are emitted from a number of sources (e.g. fossil fuel combustion, waste incineration, oil refining, steel and iron manufacturing, or coke and asphalt production), however the release from motor vehicles has been identified as the predominant source in urban areas (Rogge et al., 1993 and references therein). Both mutagenicity and carcinogenicity of PAHs released concurrently to emission exhausts or adsorbed on ambient aerosols have been conclusively demonstrated through bacterial and in-vivo/in-vitro mammalian cell assays as well as through epidemiological studies. The potential health effects of PAHs are usually attributed to the number of aromatic rings and structure; in particular, many congeners having four to six rings, such as benzo(a)pyrene and indeno(1,2,3,-cd)pyrene, are carcinogenic or genotoxic. Since particles varying in aerodynamic diameters display different capabilities of entering the human respiration system, information on the particle size distribution of particulate matter components is essential to estimate their aftermaths on health.

In this study, the size distribution of ambient air *n*-alkanes and polycyclic aromatic hydrocarbons (PAHs) associated to particles, was investigated at an urban and industrial sites of Algiers, Algeria. Size-resolved samples (<0.49 µm, 0.49-0.95µm, 0.95–1.5 µm, 1.5–3 µm, 3–7.2 µm and 7.2-10 µm) were concurrently collected from the two sampling sites using five-stage high volume cascade impactors. After extraction and cleanup PAHs were analyzed by gas chromatography/mass spectrometry with electron impact ionization (GC/EI-MS) while n-alkanes were analyzed by gas chromatography/ flame ionization detector (GC/FID).

At both site, *n*-Alkanes and PAHs were primarily associated with small particles. Generally, more than 85 % of the total concentrations of *n*-alkanes and PAHs were accumulated in particles <1.5 µm. The size distribution diagram of *n*-alkanes indicates the existence of a bimodal distribution, which can be explained by non-equilibrium.

The size distributions of total *n*-alkane concentrations and biogenic *n*-alkanes derived from epicuticular waxes of vascular plants in an urban area of Algiers are shown in Fig. 1. Both alkanes showed similar distributions indicating that these pollutants are mostly generated from combustion of fossil fuels and biomass burning.

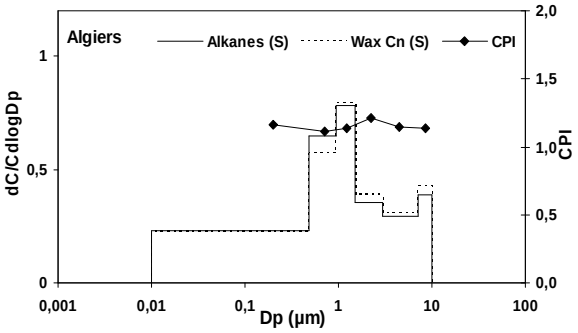

Figure 1. Differential distribution curves of total *n*-alkanes and biogenic *n*-alkanes recorded in urban area of Algiers.

Unimodal distribution of high molecular weight PAHs basically reflects the gas-to-particle conversion after their emission, whereas the low molecular weight PAHs were distributed in bimodal distributions, which can be interpreted by partitioning to larger particles by vaporization and sorption processes.

Rogge, W. F., Hildemann L. M., Mazurek, M. A., Cass, G. R., Simoneit, B. R. T., Environ. Sci. Technol. 27, 636–651, 1993.

Yassaa, N., Meklati B.Y., Cecinato, A., Marino, F., Environ. Sci. Technol.35, 306 –311, 200.

The air pollutants emitted from biomass burning in North Korea to the air quality in Seoul, South Korea

In Sun Kim [1], Yong Pyo Kim [1], Ji Yi Lee [2], Lan Jin [1]

[1] Departent of Environmental Science and Engineering, Ewha Womans University, 11-1 Daehyun-Dong, Seodaemun-Gu, Seoul, 120-750, Korea
[2] Department of Environmental Engineering, BK21 Team for Biohydrogen Production, Chosun University, 375 Seosuk-Dong, Dong-Gu, Gwangju, 501-759, Korea
Keywords: North Korea, PAHs, levoglucosan, CMB, backward trajectory analysis
Presenting author email: supidang@gmail.com

South Korea is contiguous to China, Japan and North Koreas, so air pollutants transported from outside South Korea should be investigated. Kim (2010) identified that air pollutants emitted from out of South Korea effect on approximately 30% of the ambient PM 10 concentrations in the SMA based on the modelling results.

Energy consumption in North Korea is less than in other countries (Table 1). North Korea might emit a small amount of air pollutants compared to China. However, North Korea is next to Seoul Metropolitan Area (SMA) and the air quality in North Korea is considered inferior to in neighbour countries.

Table 1. Total primary energy consumption for 2008 (unit: quadrillion Btu (%)) (EIA, 2011)

China	85.06	(17.25%)
Japan	21.87	(4.44%)
South Korea	9.88	(2.01%)
North Korea	0.88	(0.18%)
World	493.01	

In this study, the chemical mass balance (CMB) model and the backward trajectory analysis were conducted to understand the influences of air pollutants' emission from North Korea to South Korea, especially Seoul. CMB model were applied to analyze the source apportionment of particulate polycyclic aromatic hydrocarbons (PAHs) at Seoul between 2006 and 2007. In order to strengthen the uncertainty of CMB result, the trend of levoglucosan (1,6-anhydro-b-D-glucopyranose) concentration at Seoul is also discussed.

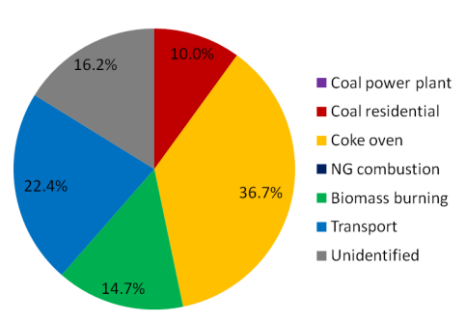

Figure 1. The fraction of the source contributions for particulate PAHs at Seoul for the whole sampling period.

To understand the transport of air pollutants emitted from North Korea, the backward trajectories in the sampling days were estimated and classified to four cases depending on which area the trajectories predominantly passed through.
Based on the contribution of biomass burning calculated by the CMB and the trajectories, the influence of air pollutants from North Korea to Seoul is quantified. Furthermore, statistical analysis was applied to supplement those results.

This work was supported by the National Research Foundation of Korea (NRF) grant funded by the Korea government (MEST) (2011-0016297)

Kim Y.P. (2010) Analysis of the trend of atmospheric PM10 concentration over the Seoul Metropolitan Area between 1999 and 2008, Korean Society of Environmental Impact Assessment, 19(1), 69-74.
EIA (US Energy Information Administration) (2011) http://www.eia.doe.gov/

Analysis of PM_{10} concentrations in the urban area of Volos, Greece

G.T. Proias[1], S. Katartzis[2], P.T. Nastos[3], A.G. Paliatsos[4]

[1]Department of Planning and Regional Development, University of Thessaly, Volos, Thessaly, 38334, Greece
[2]Municipal Organisation for Water - Sewage in Greater Area of Volos, Volos, Thessaly, Greece
[3]Laboratory of Climatology and Atmospheric Environment Department of Geology and Geoenvironment, University of Athens, Panepistimiopolis, Athens, Zografou, 15784, Greece
[4]General Department of Mathematics, Technological Education Institute of Piraeus, Athens, Aegaleo, 12244, Greece
Keywords: urban pollution, air particles, PM10, Volos.
Presenting author email: giproias@prd.uth.gr

Abstract review

Several epidemiological studies have shown an association between particulate air pollution and health effects. It of great consensus among the scientific community that suspended particulate matter is considered as one of the most harmful pollutant, particularly the inhalable particulate matter with aerodynamic diameter less than 10 micrometers (PM_{10}) causing respiratory health effects and heart diseases. The effects of aerosols on human health are significant and are determined by both their size and their chemical composition. The critical level is the exceeding average daily concentration appearing among other cases, during Sahara dust episodes, a natural phenomenon that degrades the air quality in the urban area of Volos.

The city of Volos is a coastal city of medium size in the Thessaly region and extends along the northern Gulf of Pagasssitikos, on the east coast of Central Greece. The case of Volos is an interesting example, where in recent decades urbanization and increased industrialization have resulted in deterioration of air quality in the region. The meteorological factors play an important role in the development of air pollution, and the complex topography of Volos exacerbate air pollution episodes.

The main objective of the present work is the study of suspended particulate matter temporal evolution in the city of Volos. For this purpose, concentration measurements of the particulate matter with an aerodynamic diameter less than 10 μm (PM_{10}), for a 5-year period (2007–2011) are analyzed.

Table 1. Descriptive statistics for PM_{10} daily concentrations ($\mu g/m^3$) in the city of Volos.

	2007	2008	2009	2010	2011
Mean ($\mu g/m^3$)	46.5	44.6	36.3	38.8	46.4
St. Deviation ($\mu g/m^3$)	21.6	20.5	17.1	26.9	33.0
Median ($\mu g/m^3$)	44.0	42.9	33.8	35.1	37.9
Minimum ($\mu g/m^3$)	5.1	3.3	2.4	6.7	8.4
Maximum ($\mu g/m^3$)	157.5	158.0	132.2	325.0	285.0
Number of exceedances	**123**	**114**	**49**	**66**	**96**

Air pollution data were obtained by a monitoring station, fully automated, which was established by the Municipal Water Supply - Sewage in Greater Area of Volos, located in the centre of Volos. The analysis shows that the PM_{10} concentration levels remain higher than corresponding thresholds for human health protection set by the European Union, during the examined period (Table 1).

Moreover, from the statistical analysis of the 5-year measurements of daily PM_{10} concentrations it is showed that the mean seasonal variability of the examined concentrations presents a minimum during the warm period of the year 2009, against a maximum during the cold period of the year 2007 (Figure 1).

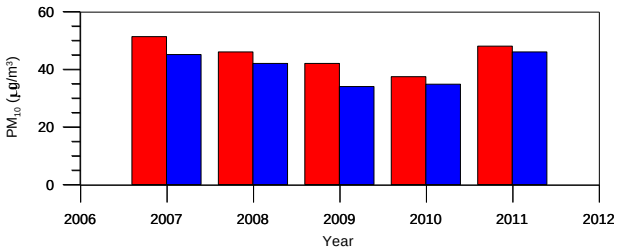

Figure 1. Temporal evolution of average seasonal PM_{10} concentrations at the city of Volos during the cold (red color bars) and the warm (blue color bars) period for 2007-2011.

Larissi, I.K., Koukouletsos, K.V., Moustris, K.P., Antoniou, A. and Paliatsos, A.G. (2010) *Fresen. Environ. Bull.*, **19**, 226-231.

Larissi, I.K., Antoniou, A., Nastos, P.T. and Paliatsos, A.G. (2010) *Fresen. Environ. Bull.*, **19**, 1989-1996.

Nastos, P.T., Paliatsos, A.G., Anthracopoulos, M.B., Roma, E.S., Priftis, K.N. (2010) *Environ. Health*, **9:**45, doi:10.1186/1476-069X-9-45.

Paliatsos, A.G. and Amanatidis, G.T. (1994) *Sci. Total Environ.*, **144**, 137-144.

Proias, G.T., Nastos, P.T., Larissi, I.K. and Paliatsos, A.G. (2009) *AIP Conf. Proc., vol. 1203, 7th Int. Conf. of the Balkan Physical Union*, American Institute of Physics.

Samoli, E., Nastos, P.T., Paliatsos, A.G., Katsouyanni, K., Priftis, K.N. (2011) *Environ. Res.*, **111**, 418-424.

Proias, G.T., Moustris, K.P., Larissi, I.K., Nastos, P.T. and Paliatsos, A.G. (2012) *Fresen. Environ. Bull.*, **21**, (in press).

Preliminary results of first intensive observation program campaign of "Supersite" Project in Emilia-Romagna region (Italy)

S. Ferrari[1*], I. Ricciardelli[1], C. Maccone[1], A. Trentini[1], F. Scotto[1], C. Sartini [1], D. Bacco[3], S. Gilardoni[2], M.C. Facchini[2] and V. Poluzzi[1]

[1] Regional Agency for Prevention and Environment (ARPA), Bologna, Italy
[2] Institute of Atmospheric Sciences and Climate, Italian National Research Council (CNR), Bologna, Italy
[3] University of Ferrara, Chemical Department, Ferrara, Italy
Keywords: ultrafine aerosol, AMS, particles chemical composition**,** nanoparticle number size distribution.
Presenting author email: sferrari@arpa.emr.it

"Supersite" project is a detailed study of some chemicals, physical and toxicological parameters in the atmosphere of Emilia-Romagna region (Italy) and their assessments by epidemiological, environmental and health models. The project rises from the necessity to improve knowledge about environmental and health aspects of fine and ultrafine aerosol, in primary and secondary components, in atmosphere.

Some field campaigns (intensive observation program) are defined and measures are carried out with a high time resolution and detailed chemical speciation. The aim of this paper is to supply an overview of preliminary results in the two monitoring sites, combing chemical, physical measures and meteorological parameters.

The first field campaign was from 15th November up to 7th December 2011. During the campaign different measures were carried out in two sites: urban background station (MS) of Bologna (Italy) and rural site (SPC) about 30 Km north-east of Bologna in the Po Valley.

The activities performed in two sites were:

- real time chemical speciation (organic, sulphate, nitrate, ammonium, chloride) in range 40-600 nm, by aerosol mass spectrometer (W-ToF High Resolution Aerosol Mass Spectrometer System, Aerodyne),
- PM2.5 and PM1 β-absorption measures,
aerosol size distribution (5.6-560 nm) using Fast mobility particle spectrometer (FMPS, TSI-3091),
- number concentrations by optical particle counter (OPC monitor, FAI Instruments),
- ions, metals, EC/OC and organic speciation (PAH, Nitro-PAH, Oxi-PAH sugars, carboxylic acids).

Some preliminary results are discussed. PM1 and PM 2.5 mass concentrations show an evident common trend for the two sites as shown in fig. 1. Divergences seen in some days (principally on 28th November) can be attributed to the fog formation in the SPC site, occurrence not evident in Bologna MS site. It is evident a change of chemical composition passing from 27th to 28th November as shown in fig. 2.

AMS speciation data confirm values observed in urban and rural sites in the Po Valley (Carbone *et al.*, 2010).

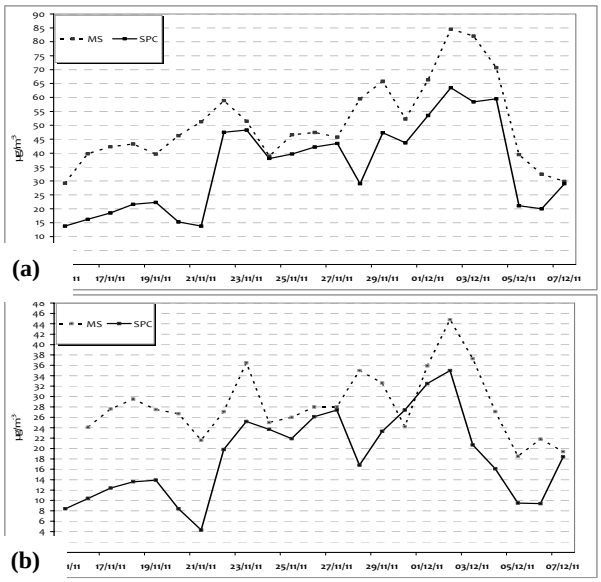

Figure 1. PM2.5 (a) and PM1 (b) mass concentration trend in MS and SPC.

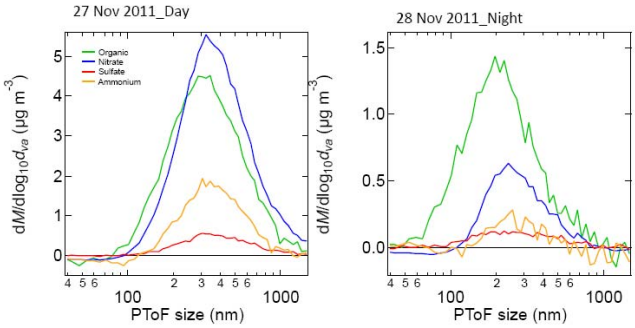

Figure 2. Mass speciation distribution on 27th November and on 28th November in SPC.

This research was conducted as part of the "Supersite" Project, which was supported and financed by Emilia-Romagna Region and Regional Agency for Prevention and Environment under Deliberation of Regional Government n. 428/10.

Carbone C., Decesari S., Mircea M., Giulianelli L., Finessi E:, Rinaldi M., Fuzzi S., Marinoni A., Duchi R., Perrino C., Sargolini T., Vardè M., Sprovieri F., Gobbi G.P., Angelini F., Facchini M.C. *Size-resolved aerosol chemical composition over the Italian Peninsula during typical summer and winter conditions.* Atm. Env., 44, 5269-5278, 2010

Bias caused by adsorbed water in standard gravimetric PM10 measurements

K. Imre[1], A. Gelencsér[2] A. Molnár[1] and V. Dézsi[3]

[1]Air Chemistry Group of the Hungarian Academy of Sciences, Veszprém, 8200, Hungary
[2]Department of Earth and Environment Sciences, University of Pannonia, Veszprém, 8200, Hungary
[3]Hungarian Meteorological Service, Air Quality Reference Center, Budapest, 1024, Hungary
Keywords: air quality, water content, urban aerosol, PM10, dry mass
Presenting author email: kornelia@almos.uni-pannon.hu

Water is a highly variable but very often predominant constituent of atmospheric aerosol particles. The interaction between aerosol particles and water vapor plays a crucial role in many fundamental atmospheric processes. Adsorbed water may significantly increase the size of the particles which in turn enhance the extinction (mainly scattering) of visible light in the atmosphere. This is manifested in strongly reduced standard visibilities at high relative humidities.

The online measurement of PM10 mass concentration is carried out worldwide with instruments using the β-ray attenuation method (BAM). As a reference the gravimetric method (GMM) is widely accepted. The biggest uncertainty in the measurement of the PM10 mass concentration is caused by the fact that atmospheric water may significantly influence the mass and size of the aerosol particles.

In Europe, monitoring of PM10 is regulated by CEN standard (EN 12341), the β-ray absorption and gravimetry are the most widely used. Gravimetry is the reference method in the PM10 measurements. This method gives information about the aerosol concentration only after 48h, while beta-attenuation method provides data in high time resolution. According to the regulations, the gravimetric mass measurements are carried out at RH=50±5% and T=20±1°C. In both cases the water vapour content of the air and consequently the absorbed water can cause positive artefact during the sampling. This is the result of the hygroscopicity and hysteresis of the aerosol particles. As it is well known, at higher RH the particles can absorb the water vapour, therefore their size and mass can grow. On the other hand, when RH decreases the particles begin to lose the absorbed water. In the most cases this weight loss is less than the previous mass growth, due to hysteresis.

The aim of this work is to study the effect of water vapour on the aerosol mass measurement by both methods. First we tested the gravimetric method. Each filter (Whatman) was weighted before and after sampling to determine the aerosol mass on the filter. The sampling was carried out by a Hi-vol (Digital DH-80) sampler and a FH 62 IN (FAG) beta monitor. The experimental period was between 4 November 2008 and 18 March 2010 in a residential site in Budapest, Hungary. The hygroscopic behaviour of the aerosol particles were investigated in a chamber, where the RH was adjusted between RH=20% and RH=90%.

First we studied the water uptake of the aerosol particles from RH=50% to RH=90%. After the humidification, the RH was reduced back to 50%, and on the basis of the "remaining water mass" the effect of hysteresis was estimated.

Our results show that because of the hysteresis of the aerosol mass concentration can be overestimated by up to 16%. From these results we can conclude that the aerosol mass at RH=50% cannot be considered as dry mass. In order to verify it, the mass measurements were continued at lower (<20%) RH, this reduction resulted in further loss in the aerosol mass. The average aerosol mass deficit was 4.56%, while its maximum value reached 16.8%.

Finally, we concluded that the PM10 mass concentration measured at 50% RH can be overestimated by 2% to 17%. In Fig. 1 the degree of this overestimation is presented for the time interval of this study.

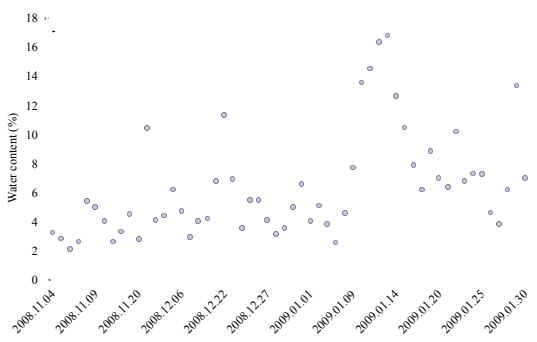

Figure 1. The water content of aerosol samples at RH=50% relative to RH=20%

Beta-attenuation is an online method and the sampling is usually carried out at ambient relative humidity. During the online measurement the aerosol particles are usually not conditioned and, as a consequence, most of their water content taken up from the atmosphere distorts the measurement. Heating of the sampling line is a possible solution to eliminate the error caused by the water content but this may lead to loss of volatile compounds. Therefore humidity correction should be applied on these data. The water uptake of the particles from the same period was measured between RH=20% and RH=95% and the mass growth factors were calculated ($GF=mass_{wet}/mass_{dry}$).

The authors acknowledge to AEROS_EU project (project number OM-00218/2007).

EN 12341:1998, (1998) CEN

Chemical characterization of fine particulate matter collected in Budapest

T. Szigeti[1], V.G. Mihucz[1,2,3], M. Óvári[1,2,3] and Gy. Záray[1,2,3]

[1]Department of Analytical Chemistry, Eötvös Loránd University, Budapest, Hungary
[2]Cooperative Research Center for Environmental Sciences, Eötvös Loránd University, Budapest, Hungary
[3]Hungarian Satellite Center of Trace Element Institute for UNESCO, Budapest, Hungary
Keywords: urban aerosol, PM2.5, chemical composition, seasonal patterns
Presenting author email: tamas.szigeti@yahoo.com

Increasing amounts of harmful gases and particles emitted from different pollutant sources into the atmosphere represents a risk for human health and local environment. Recently, the increasing concern about air pollution in populated cities has required the monitoring of pollutants in atmospheric particles.

In the present work, a comprehensive chemical characterization of fine particulate matter (PM2.5) collected in Budapest (Hungary) was carried out. During the two-year-long sampling period, a high-volume aerosol sampler equipped with a PM2.5 head was used for the collection of the aerosol samples.

The monthly collected samples were taken onto quartz fiber filters. Seven parameters – PM2.5 mass, total carbon (TC) and water soluble carbon (WSC), occurrence of total and water–soluble trace elements, major anions and NH_4^+ – were used to characterize PM2.5 aerosol fractions.

Two types of sample preparation were applied: microwave-assisted *aqua regia* extraction and water extraction by sonication. In both cases, an inductively coupled plasma sector field mass spectrometer was used for the determination of the concentration of twenty-one trace metals (Bi, Cd, Co, Cr, Cu, Fe, Ga, Li, Mn, Mo, Ni, Pb, Pt, Rb, Sb, Sn, Te, Tl, U, V, Zn). Beside the trace metal content, the concentration of seven water-soluble anions (SO_4^{2-}, NO_3^-, Cl^-, CH_3COO^-, F^-, Br^-, NO_2^-) were determined by ion chromatography. A spectrophotometric method was used for the quantification of water-soluble NH_4^+. In order to get information about the organic content, the concentration of total and water-soluble carbons were determined by a C/N analyzator.

The mean PM2.5 mass concentrations was 23.0 μg/m^3, meanwhile the target value for this parameter set by the European Commission as annual mean value is 25.0 μg/m^3 to enter into force in January 2015.

The highest concentration values were observed for total carbon, which accounted for 20-50% of the total PM2.5 mass. The water-soluble part of TC was about 25%, thus about 10% of the PM2.5 fractions consisted of WSC compounds.

The highest average concentrations for the investigated trace elements were observed for Fe, accounting for about 75% of the total measured trace element content in Budapest. Trace metal concentrations in Budapest are similar to concentration data measured in other European cities. On average, the measured water–soluble part of trace elements typically constitutes about 20% of the total trace element concentration obtained. In the aqueous extracts, the highest concentrations were registered for Fe and Zn. Seasonal change of trace element concentrations was found in the case of crustal elements and some trace metals connected to anthropogenic source such as Cd and Pb in the total concentration and water-soluble fractions.

Sulphate and nitrate ions were the dominant anions in both cities. Seasonal changes in the NO_3^- and SO_4^{2-} were observed. Stoichiometric calculations demonstrated the contribution of sea salt–SO_4^{2-} to the PM2.5 aerosol fractions.

Monitoring of PM2.5 urban aerosol fractions is necessary because finer particles have a stronger impact on human health. This work can be considered a pilot study in Hungary since the PM2.5 aerosol fractions are not as regularly investigated as the PM10 fractions. Moreover, health limit values have not been yet set by the decision makers of the EU for the investigated elements. Therefore, the results of the present work obtained especially for trace elements are important because they could be useful for the EU decision makers in order to establish health limit values for the elements found in PM2.5 urban aerosol fractions. Comparing the obtained PM2.5 mass and concentration of the measured components with the results reported in other European cities, it can be concluded that Budapest is a moderately polluted city in Europe.

This work was supported by the National Innovation Office under grant No. OMFB-00582/2009.

Spatial distribution of particle number concentrations measured with the AERO-TRAM

B. Vogel, R. Hagemann, R. Rinke, A. Wieser, U. Corsmeier, Ch. Kottmeier
Institute for Meteorology and Climate Research, Karlsruhe Institute for Technology,
Hermann-von-Helmholtz-Platz 1, 76344 Eggenstein-Leopoldshafen, Germany
Keywords: urban aerosols, mobile measurements, air quality.
Presenting author email: bernhard.vogel@kit.edu

The spatial and temporal variation of selected aerosol and gas phase parameters is assessed in long term measurements for the Karlsruhe (Germany) area with an automated self calibrating mobile laboratory. As measurement platform a tramway (AERO-TRAM) operating in the public transport is used. Beside the gas phase components O_3, CO, CO_2, NO, and NO_x particle number density and particle number distributions are measured. For the year 2010 measurements on more than 2300 runs are obtained resulting in an extraordinary dataset for ground based mobile applications. The AERO-TRAM operates on two selected lines. Both lines connect the rural and suburban hinterland of Karlsruhe with the city centre. They are crossing areas with high concentrations of particles and trace gases and areas where only background concentrations are expected. Therefore, the obtained comprehensive dataset is useful for determining regional variation of particles and trace gases as well as for the identification of source areas.

The analysis of the measured number densities gives a concentration gradient between the city centre and the suburban areas of only 30 %. In comparison the NO_x concentrations are about 50 % lower in the suburban.

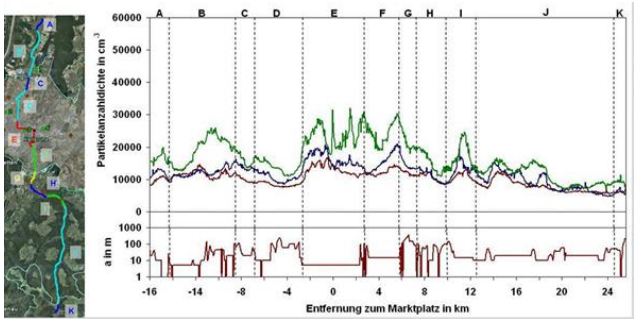

Figure 1. Median of the running mean of the particle number density for 2010 at different stability conditions. Green = stable stratification, blue = neutral stratification, red = unstable stratification (upper panel). Distance of the track to the next road (lower panel).

Figure 1 shows the distribution of the median of a running mean of number density for the year 2010 along the track and its dependence on the turbulence conditions. It can be seen that there is no remarkable gradient of the number densities between the distinct regions but the concentration level differs up to a factor of 2 in depending on the turbulence state of the atmosphere. This shows the difficulty of measuring an effect of emission reduction measures. Figure 2 gives the median values as a function of the wind velocity. As expected these concentrations are lower for the higher wind speeds but there is no uniform behaviour for the different areas. In the city centre there is almost no effect visible whereas in the northern vicinity the concentration level is considerable higher for the lower wind speeds.

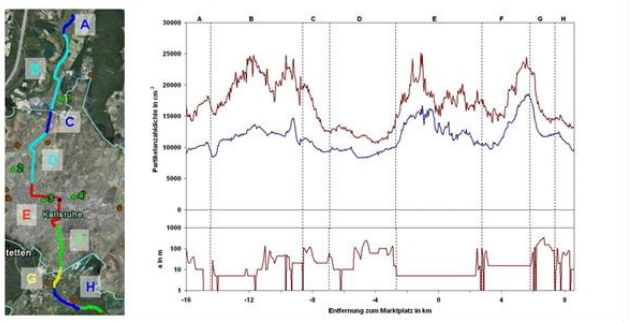

Figure 2. Median of the running mean of the particle number density for 2010 at different ranges of wind velocity. Red = 1-5 m s^{-1}, blue = > 5 m s^{-1} (upper panel). Distance of the next road (lower panel).

The investigation of the influence of the wind directions shows the impact of elevated single sources in the area on the number densities that so far could not be detected by the standard monitoring stations in that area.

Short-term variation in near-highway air pollutant gradients.

P. Berghmans, E. Frijns, M. Van Poppel

VITO - Flemish Institute for Technological Research, 2400 Mol, Belgium

Keywords: UFP, PM2,5, Black Carbon, traffic
Presenting author email: patrick.berghmans@vito.be

Aerosol particles emitted from road traffic significantly contribute to high levels of air pollution and, at the same time, the population exposed to these particles is very large. Today, these particles represent one of the main sources of air pollution in the urban environment. Recent interest has focused on the health effects of ultrafine particles because of the documented toxicity and the larger concentration contrast near motorways of UFP than for PM10 or PM2.5. Air pollution due to vehicle exhaust at urban areas is known as local hot-spot pollution phenomena. Some previous studies reported the decreasing trends of particle concentrations within a few hundred meters apart from highways or freeways (Hitchins et al., 2000; Zhu et al., 2002). The Netherlands introduced guidelines, to prohibit siting new schools within 200 m of a busy road for protecting the health of students. Levels of UFPs are strongly influenced by traffic emissions and meteorological factors downwind of a highway (Zhu et al., 2002; Hagler et al., 2009). However, little is known about the relationship between traffic-generated UFPs and meteorological factors, such as wind speed, on highways. Studies have shown that concentrations of UFP as well as other primary vehicular emissions are elevated near highways but then decrease to background within several hundred meters primarily as a result of dilution.

As part of a study to assess the exposure risks related to particulate matter in the outdoor environment of a childcare centre nearby a highway in the centre of Antwerp city, particle mass concentration and number concentration were measured at both sides of the highway. One of the objectives of this study was to compare the contrast of UFP, PM(2.5) and soot (BC) measured simultaneously at 2 near-highway locations, in order to gain more insights in the causes of variations in the magnitude and extent of traffic-related pollutant gradients near highways. The results were compared with datasets from previous studies on urban monitoring where measurements were performed on several urban locations, a street location and a background location and data from the local air quality network at an urban background station.

The measurements at both locations included UFP (CPC 3783 and 3786, TSI), number concentration (Nanocheck, Grimm), black carbon (Aethalometer, Magee Scientific AE-42) and PM2.5 (Partisol, Thermo Instruments). Moreover, the meteorological conditions were also measured at one high-way location. During the campaign one measurement location was placed directly at the north side of the highway at about 100 m and one measurement location was placed about 50 m south of the highway. In this way it was possible to determine the air pollution from the highway traffic during periods with southerly wind direction. During southerly wind subtraction of the results from the two sites can be used to evaluate the concentrations resulting from the highway traffic alone.

The mean PNC at the high-way locations and the street location was significant higher than at a background location, indicating that vehicles exhaust considerable amounts of UFPs. For the entire measurement campaign the average particle number per cm^3 was a factor of 3 higher at the highway locations and a street location compared to a background location. The contrast was similar for soot concentrations. In PM(2,5) concentrations less contrast was found. Particle mass of PM2.5 originating from the highway traffic were estimated to be less than 10%. This is in agreement with other studies, which have shown that the long range transported fraction of the particle mass is relatively high. Consequently, the fraction of PM2.5 originating from the highway traffic is low.

Mean PNC concentrations were poorly correlated with PM(2,5) and soot. At the street location, higher temporal variation of PNC concentrations occurred within each sampling day compared to the highway sampling locations, probably related to variations in traffic volumes, high-emission of individual vehicles, wind direction and distance to the traffic. Temporal variation was smaller at the background locations.
According to the measurement results, high levels of UFP were observable at low wind speeds and high traffic volumes. For example, UFP levels can be $>5*10^5$ particles cm^3 during rush hours when wind speed is <0.5 m/s.

Hagler, G. S. W., Baldauf, R. W., Thoma E. D., Long, T. R., Snow, R. F., Kinsey, J. S., Oudejans, L., and Gullett, B. K, Atmos. Environ., 43, 1229–1234, 2009.

Hitchins, J., Morawska, L., Wolff, R. and Gilbert, D. (2000) Atmos. Environ. 34, 51-59.

Zhu, Y., Hinds, W.C., Kim, S. and Sioutas, C. (2002) J. Air & Waste Manage. 52, 1032-1042.

Effect of the shutdown of a coal-fired power plant on urban mercury species

Yungang Wang[1], Philip K. Hopke[2], Jiaoyan Huang[3] and Thomas M. Holsen[3]

[1]Lawrence Berkeley National Laboratory, Berkeley, CA 94720 USA
[2]Center for Air Resource Engineering and Science, Clarkson University, Potsdam, NY 13699 USA
[3]Department of Civil and Environmental Engineering, Clarkson University, Potsdam, NY 13699 USA
Keywords: Aerosol modeling, ambient aerosols, air quality, positive matrix factorization (PMF)
Presenting author email: phopke@clarkson.edu

Continuous atmospheric measurements of speciated mercury (Hg) (elemental mercury (GEM), reactive gaseous mercury (RGM), and particulate mercury (Hg_p)) were conducted in Rochester, NY from Dec 2007 to May 2009. A large coal-fired power plant (CFPP) on the northwest side of the city was shutdown in the spring of 2008. This shutdown resulted in a significant reduction in observed concentrations of the mercury species, ultrafine particle (UFP) number and other pollutants (Wang et al., 2011a, 2011b).

Figure 1 shows the quarterly concentrations of the three mercury species over the measurement period. It can be seen that the concentrations in the winter of 2007-08 (December 2007 and January-February 2008) show higher concentrations than the subsequent quarters. These decreases are statistically significant and suggest that the shutdown beginning in late February 2008 resulted in a decline in measured Hg concentrations.

In this study, positive matrix factorization (PMF) model and conditional probability function (CPF) were then used to identify the CFPP source effects based on Dec 2007 to May 2009 hourly concentration mercury species, particles, gaseous species and meteorological variables. The impacts of the CFPP on mercury species were quantified as a part of an extensive project assessing the contributions of CFPP and traffic to air quality in Rochester, NY.

This work was supported by the New York State Energy Research and Development Authority (NYSERDA) through Contracts 8650 and 10604; the United States Environmental Protection Agency (US EPA) through Science to Achieve Results (STAR) grant RD83241501; a Syracuse Center of Excellence Collaborative Activities for Research and Technology Innovation (CARTI) project award, which is supported by a grant from the US EPA (Award No: X-83232501-0); and the Electric Power Research Institute underAgreementW06325.

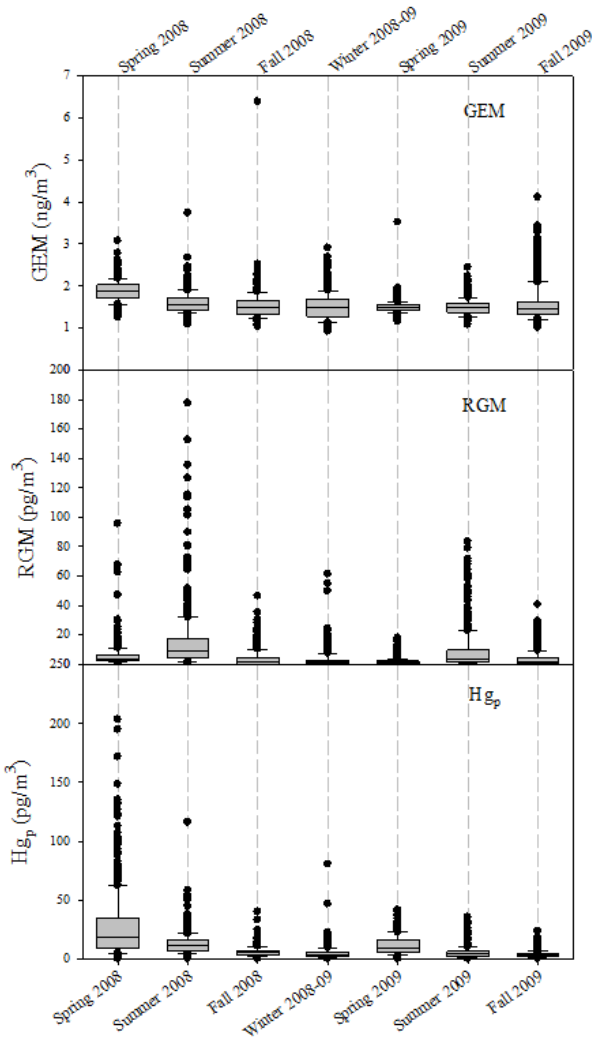

Figure 1. Seasonal variations of concentrations the three mercury species. Box-Whisker plot indicates median and 25/75% quartiles (boxes), 10/90% quartiles (whiskers).

Wang, Y., Hopke, P. K., Chalupa, D. C. and Utell, M. J. (2011a) *Aerosol Sci. Technol*. **45**, 1245-1249.
Wang, Y., Hopke, P. K., Chalupa, D. C. and Utell, M. J. (2011b) *Atmos. Environ*. **45**, 7672-7680.

^{7}Be and ^{210}Pb in both bulk deposition and atmospheric aerosols from Southwest Spain

R.L. Lozano*, E.G. San Miguel and J.P. Bolívar

Department of Applied Physic, University of Huelva, Huelva, 21071, Spain
Keywords: ^{7}Be, ^{210}Pb, deposition velocity
*Presenting author email: rafa.lozano@dfa.uhu.es

Activity concentrations of ^{210}Pb and ^{7}Be in aerosols in surface air were measured at Huelva, (37°16'07" N, 6°55'27"W), from July 2004 to April 2010. Additionally, bulk surface depositional fluxes of both ^{7}Be and ^{210}Pb were determined over a period for 16 months (April 2009 - July 2010).

The sampling station was chosen at an urban site, at the border of the city of Huelva (population ~ 150000). Aerosol samples were collected from ~ 10 m above ground at the El Carmen campus of the University of Huelva. In addition, four drums were deployed for collection of the bulk deposition.

Aerosol samples (PM10 < 10 μm) were collected onto quartz fiber filters (QF20 Schleicher & Schuell, 25.4 cm x 20.3 cm) with high volume samplers at a flow rate of 40 cfm (68 m^3 h^{-1}). Samples were taken for 48 hours every fifteen days. The whole procedure applied to atmospheric filters can be seen elsewhere (Lozano et al., 2011).

Bulk depositional samples were collected by using 4 drums with a total surface area of 4120 ± 30 cm^2. Data of the precipitation were recorded from a meteorological station close to the sampling site.

^{210}Pb and ^{7}Be were determined by gamma spectrometry through their 46.5 and 477 keV photons, respectively. Gamma spectrometry measurements were performed using an XtRa coaxial Ge detector (Canberra), with 38% relative efficiency and FWHM of 0.95 keV at the 122 keV (^{57}Co) and 1.9 keV at the 1333 keV (^{60}Co). The detector is coupled to a set of standard electronics components, including a multichannel analyzer, and was shielded with 15 cm thick Fe shield.

The ^{7}Be monthly depositional flux ranges from 5.6 up to 186 Bq m^{-2} $month^{-1}$ (Figure 1), with the lowest deposition value occurring during the summer months (June and July) when there is no precipitation. On the contrary, ^{210}Pb monthly depositional fluxes were one order of magnitude lower than ^{7}Be, ranging from 0.8 to 10.9 Bq m^{-2} $month^{-1}$.

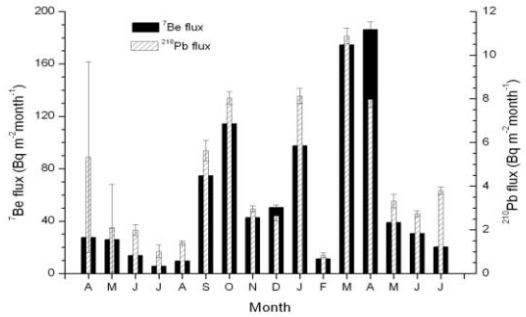

Figure 1: Monthly depositional flux of ^{7}Be and ^{210}Pb in Huelva, Spain

PM10 concentration ranged from 4.8 to 80.5 μg m^{-3} with a mean value of 34.9 μg m^{-3}. ^{7}Be in surface air ranged from 0.6 to 11.7 mBq m^{-3} with a mean of 5.1 mBq m^{-3}. The concentration of ^{210}Pb in aerosol samples ranged from 0.04 to 2.9 mBq m^{-3}, and a mean of 0.59 mBq m^{-3} (Figure 2). These ranges are comparable to those found in other coastal regions (McNeary and Baskaran, 2003).

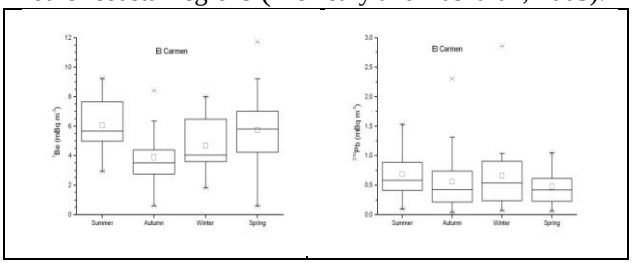

Figure 2: Concentrations of ^{7}Be and ^{210}Pb box diagram in Huelva, Spain.

The depositional fluxes and the atmospheric activity concentrations of ^{210}Pb and ^{7}Be have been used to determine the called "aerosol deposition velocity" at Huelva, which can be determined through the equation (e.g., McNeary and Baskaran, 2003):

$$V_d = F/C_s$$

F is the total flux of a nuclide to the Earth´s surface and C_s is the activity concentration of that nuclide in the surface air. The total deposition velocity for ^{7}Be ranges from 0.05 cm s^{-1} (July 2009) to 1.77 cm s^{-1} (April 2010), with a mean value of 0.50 ± 0.15 cm s^{-1}. Values for the total deposition velocity for ^{210}Pb vary between 0.06 cm s^{-1} (August – 09) and 1.33 cm s^{-1} (January – 10), with a mean value of 0.51 ± 0.12 cm s^{-1}. Deposition velocities obtained using these nuclides are quite similar. These data suggest that the ^{7}Be and ^{210}Pb have to be attached onto the aerosol particles by similar mechanisms.

Lozano R.L., Bolívar J.P., San Miguel E.G., García-Tenorio R., and Gázquez M.J., 2011b. An accurate method to measure alpha-emitting natural radionuclides in atmospheric filters: application in two NORM industries. Nuclear Instrument and Methods in Physic Research A, doi: 10.1016/j.nima.2011.08.006.

McNeary D. and Baskaran M., 2003. Depositional characteristics of ^{7}Be and ^{210}Pb in southeastern Michigan. Journal of Geophysical Research, Vol. 108, NO. D7, 4210, doi:10.1029/2002JD003021.

The effect of winter salting on PM_{10} concentrations in the Rhine-Ruhr area

D. Gladtke, A. Olschewski, Th. Retny and P. Risthaus
North Rhine Westphalia State Agency for Nature, Environment, and Consumer Protection
45133 Essen, Germany
Key words: PM_{10}, winter salting, sea salt
Presenting author email: dieter.gladtke@lanuv.nrw.de

The winters 2009/2010 and 2010/2011 were relatively cold in central Europe. Even in the plains low temperatures and heavy snowfall caused massive traffic problems. Chemical analysis of PM10 samples from these winters was used to study the influence of winter salting on air quality and to determine how many days with exceedances of the limit values for PM10 could be neglected due to winter salting as it is described in EU Air Quality Directive 2008/50/EC (EC 2008).

A working paper of the European Commission (EC 2011) suggests to analyse the chloride concentration to identify the contribution of winter salting to PM10, if the composition of the chemicals used for salting is known. This method could well be applied in the Rhine Ruhr region because only sodium chloride was used for road salting in this area. Thus the contribution of winter salting to PM_{10} was calculated from the concentration of chloride in PM_{10}, after non salt chloride, estimated as the average chloride concentration during summer at days without a significant contribution of sea salt, was subtracted. Multiplication of the so evaluated salt derived chloride concentration by 1,65 resulted in the contribution of winter salting to PM_{10}. To check interferences caused by other sources of chloride the concentrations of calcium, potassium and trace metals as marker compounds for crustal material, combustion and industrial aerosols (Beuck et al. 2011) were also measureded. Only at three days these sources caused high chloride concentrations. Episodes with a high contribution of sea salt could be identified by back trajectories (Draxler et al. 2003). This made the separation of winter salting and sea salt possible.

Lists of days when roads were salted in 2009, 2010 and 2011 were provided by the municipal authorities. As figure 1 (see below) shows for a station at a highly frequented street canyon (Düsseldorf-Corneliusstrasse), the connection between these days (black squares) and salt concentrations (red line) is not clearly evident. The formation of sodium chloride aerosols after salting is a slow process strongly depending on meteorological conditions like temperature (green interrupted line) and precipitation (blue line).

Figure 1: Course of chloride concentration, precipitation, temperature and salt application days at Düsseldorf-Corneliusstrasse in December 2010

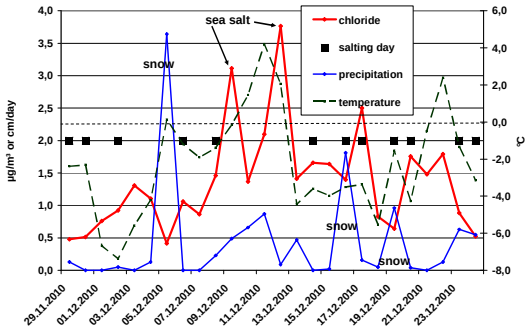

Aerosols from winter salting can spread several hundred metres, leading to slightly elevated salt concentrations also at background stations in the whole Rhine-Ruhr area. At these sites the annual contribution of winter salting to PM10 was 0,2 µg/m³ or lower, at traffic influenced sites it was about 0,5 µg/m³ in 2010. Even if these values are rather low compared with results from other areas (Diemer et al. 2011), 4 days with exceedances of the daily limit value of 50 µg/m³ for PM_{10} could be attributed to of the contribution of winter salting at 2 traffic influenced stations.

References

EC (2008): Directive 2008/50/EC of the European Parliament and the Council relating to Air Quality and Clean Air for Europe

EC (2011): Working paper establishing guidelines for determination of contributions from the resuspension of particulates following winter sanding or salting of roads under the Directive 2008/50/EC on ambient air quality and cleaner air for Europe

Beuck, H., Quass, U., Klemm. O., Kuhlbusch, T. A. J., (2011) *Atmospheric Environment* **45** , 5813-5821

Draxler, R., Rolph, G. (2003) Hysplit Model access via NOAA ARL READY Website. http://ready.arl.noaa.gov/HYSPLIT_traj.php

Diemer, J., Ott, H. (2011) Auswirkungen des Winterdienstes auf die PM 10 Konzentration an Straßen. Bayrisches Landesamt für Umweltschutz, Augsburg, Germany

Composition and Source Identification of Ambient Single Particles on Haulbowline Island, Cork Harbour.

J. Arndt[1], R.M. Healy[1], D. Healy[1], L. Hacker[1], J.R. Sodeau[1] and J.C. Wenger[1]

[1]Department of Chemistry and Environmental Research Institute, University College Cork, Cork, Ireland
Keywords: Single particle analysis, source identification, anthropogenic aerosols, metal
Presenting author email: 104531485@umail.ucc.ie

Haulbowline, an island in the centre of Cork Harbour, Ireland, has been the subject of much environmental concern for the past two decades; until 2002 the island was the home of Ireland's heaviest industrial activity as the site for the Irish Steel plant. A 9 ha. (0.09 km^2) area on the eastern part of the island remains as a landfill for almost 500,000 tonnes of heavy metal-rich slag and other by-products of steel manufacturing (White Young Green, 2005). The island's location in Cork Harbour subjects it to marine, shipping and urban influences. The town of Cobh (over 11,000 inhabitants) is less than 1 km to the north and Cork City (over 200,000 inhabitants) is approximately 10 km to the north-west. Also in close proximity are a number of pharmaceutical plants and an oil refinery. The aims of this study were to investigate single particle composition and sources in this environment, with a particular interest in possible airborne particulate matter (PM) from the Irish Steel waste site.

To this end, an aerosol time-of-flight mass spectrometer (ATOFMS, TSI model 3800) was deployed on the island where it sampled ambient air for seven weeks in August and September 2011. Over 700,000 individual particle spectra were generated and then classified using the *K*-means algorithm. Based on their mixing state, size distribution and temporality, 14 major particle types were identified including; domestic coal, peat and wood combustion, shipping, sea salt, soil, traffic and several organic carbon types. Mass concentrations for each particle type were reconstructed using data from a Scanning Mobility Particle Sizer (SMPS, TSI model 3081). Also operating at the site was a Waveband Integrated Bioaerosol Sensor (WIBS-4) used for the detection and quantification of ambient fluorescent biological aerosol particles (FBAP) in the size range: ~0.5 - 13μm (Healy *et al*, 2012; Kaye *et al*, 2005). Where overlap was observed between the size measurement ranges of the WIBS-4 and ATOFMS techniques, comparisons were made to define the detected FBAP according to their chemical signatures/spectra obtained by the ATOFMS.

To establish if PM from the landfill was impacting the site, ion intensities for several metals, including As, Cd, Cr, Cu, Ni, Pb and Zn (White Young Green, 2008), were examined in terms of their temporality, wind dependence and correlation with the *K*-means particle types (Snyder *et al*, 2009). The majority of the metals exhibited dependences on wind directions associated with Cobh and Cork City, as well as similar temporality to several domestic combustion classes. This suggests that the metals detected by the ATOFMS were not associated with airborne PM from the Irish Steel landfill site. However, the ATOFMS was operated using an aerodynamic lens (TSI model AFL100) exhibiting relatively poor transmission efficiency for particles > 1 μm and therefore resuspended dust (a likely source of metals from the waste site) may not be detected as efficiently as submicron combustion particles.

This work was supported by the Irish Research Council for Science, Engineering & Technology. The authors would like to thank the Irish Naval Service on Haulbowline for access to the site and Met Éireann for providing the meteorological data.

White Young Green (2005) *Haulbowline SI Factual Geo-Environmental Report*, Cork City Council.

White Young Green (2008) *Environmental Assessment of the East Tip area of Haulbowline Island*, Department of the Environment, Heritage and Local Government.

Healy, D., O' Connor, D. and Sodeau, J.R. (2012) *J. Aerosol Sci*. **47**, 94-99.

Kaye, P., Stanley, W. R., Hirst, E., Foot, E. V., Baxter, K. L. and Barrington, S. J. (2005) *Opt Express,* **13**, 3583-3593.

Snyder, D.C., Schauer, J.J., Gross, D.S. and Turner, J.R. (2009) *Atm. Env.* **43,** 4033-4042.

Characterization of aerosols released from agricultural operations in the Po Valley

Antonella Malaguti[a], Chiara Telloli[b], Massimo Berico[a], Carmela Vaccaro[b], Mihaela Mircea[a]

[a]Italian National Agency for New Technologies, Energy and Sustainable Economic Development (ENEA), Technical Unit for Environmental Assessment Models, Methods and Technologies (UTVALAMB), Air Quality Laboratory (AIR), 40129 Bologna (Italy).
[b]Department of Earth Science, Ferrara University - Italy
Keywords: Scanning electron microscopy, ICP-MS, chemical composition, crustal species, organic aerosol, agricultural aerosols.
Presenting author email: antonella.malaguti@enea.it

The aerosol produced by agricultural operations has significant contribution to the atmospheric aerosol loadings and, therefore, its impacts on visibility, climate forcing and human health should be considered.

This work shows the chemical composition and the morphology of agricultural aerosols produced during wheat harvest threshing, plowing, and wheat sowing. The aerosol was sampled with an 9-stage Andersen-Marple impactor with quartz filter and with a modified Millipore Swinnex 47 Polypropylene holder within the dust plume generated by the agricultural machines with teflo filter.

The aerosol sampling was carried out in three different periods: summer on 25 June 2009 for wheat harvest threshing, autumn on 7 and 8 October 2009 for plowing and winter on 17 November 2009 for wheat sowing. The sampling area is located near Comacchio Valleys (44 ° 36' 40.79" N - 12° 04' 10:52" E,-1m), in the Po Valley, in the north east of Italy, near Adriatic Sea.

The chemical composition of sampled aerosol was analyzed by the dissolution of the aerosol and the quartz filter in an acid mixture and analyzed by Inductively Coupled Plasma Mass Spectrometry (ICP-MS) (X Series spectrometer from Thermo Electron Corporation collision/reaction cell CCTED). The surface morphology and the elemental composition of the particles was studied on teflo filter by Scanning Electron Microscopy with an Energy Dispersive X-ray Spectrometer (SEM-EDS) (CARL-ZEISS EVO 40). The comparison of these two methodologies has allowed determining the markers of the natural sources of the aerosol.

The aerosol mass size distribution is different for the three agricultural operations under investigation: for plowing, the aerosol mass increases with the increase of aerosol size while for sowing and threshing has a second peak on the second and first impactor stage, respectively. Overall, the amount of aerosol produced is one order of magnitude higher during harvest threshing and plowing than during sowing.

The agricultural aerosol are mainly composed by organic particles and dust.

This work is part of the MINNI (Integrated National Model in support to the International Negotiation on Air Pollution) project, funded by the Italian Ministry of the Environment and carried out by ENEA.

ATMOSPHERIC FLUXES OF RADIONUCLIDES AT MALAGA (SPAIN)

C. Dueñas, M.C. Fernández, S. Cañete, E. Gordo and M. Pérez
Department of Applied Physics I, Faculty of Sciences, University of Málaga. 29071 Málaga (SPAIN)
E-mail: mcduenas@uma.es
Keywords: atmospheric aerosol, deposition, ^{7}Be, ^{210}Pb, precipitation

ABSTRACT.- Bulk atmospheric deposition of gamma radionuclides (^{7}Be, ^{210}Pb and ^{40}K) has been measured at Málaga (4º 28′ 80″ W; 36º 43′ 40″ N) a coastal Mediterranean station in the south of Spain, from January 2005 through December 2011 for monthly periods.

INTRODUCTION Berylium-7 is one of the radionuclide produced by spallation reactions of cosmic rays with light atmospheric nuclei.^{7}Be rapidly associates primarily with submicron-sized aerosol particles. Lead-210 which is one of the natural radionuclide of the ^{238}U decay series is widely used as a tracer. ^{210}Pb depositional pattern gave us information on continental aerosols in lower troposphere. These two radionuclides with their different sources and therefore are useful to understand the mechanisms of aerosol removal from the atmosphere. These radionuclides have measured routinely in many places of the word in order to study the description of environmental processes such as aerosol transit and residence times in the troposphere and aerosol deposition velocities . ^{40}K is found in most types of soil and can easily be transported by re-suspended material. Potassium is an important constituent of fertile soil and is an essential nutrient for plant growth and in the human diet. This nuclide have been previously associated with the arrival of coarse re-suspended material (PM10, particulate matter with diameter below 10 µm) from the African continent (Hernández et al., 2005b).

MATERIAL AND METHODS.- The sampling site is one of the environmental radioactivity monitoring network stations operate by the Spanish Nuclear Security Council (CSN). The sampling point was located above the ground, on the roof of the Faculty of Sciences, University of Málaga.
Monthly precipitation and dry fallout samples were routinely collected using a steel tray 1m^2 in area as a collecting system and polyethylene vessels of 50 l capacity for rainwater samples reservoirs. Measurements by gamma spectrometry were performed to determine the ^{7}Be and ^{210}Pb activities of the samples using an intrinsic REGe detector. The peak analysis of ^{7}Be (I= 10.52 %, 477.7 KeV) and ^{210}Pb (I = 4%, 45 KeV) was done using GENIE 2000 peak analysis software. The counting time was 172800s

RESULTS. The results from fluxes of ^{7}Be , ^{210}Pb and^{40}K were correlated with four parameters: rainfall amount, rainfall duration, number of dry days and number of wet days. The next table provides the correlation coefficients between the fluxes and the mentioned parameters.

	Flux ^{7}Be	Flux ^{210}Pb	Flux ^{40}K
Rainfall (mm)	0.81	0.88	0.66
Rainfall duration (min)	0.71	0.82	0.59
Nº of dry days	-0.45	-0.63	0.55
Nº of wet days	0.47	0.65	0.61

The fig. show the monthly fluxes of ^{7}Be and ^{210}Pb with precipitation. The depositions of ^{7}Be and ^{210}Pb were well correlated with the amount of rainfall. Such relations have been commonly observed and explained by the fact that rainfall constitutes the major depositional pathway of these radionuclides. As previously observed, correlation of rainfall with ^{210}Pb seems better than with ^{7}Be (Caillet el al., 2001) likely due to a relatively greater contribution of ^{210}Pb from dry deposition.

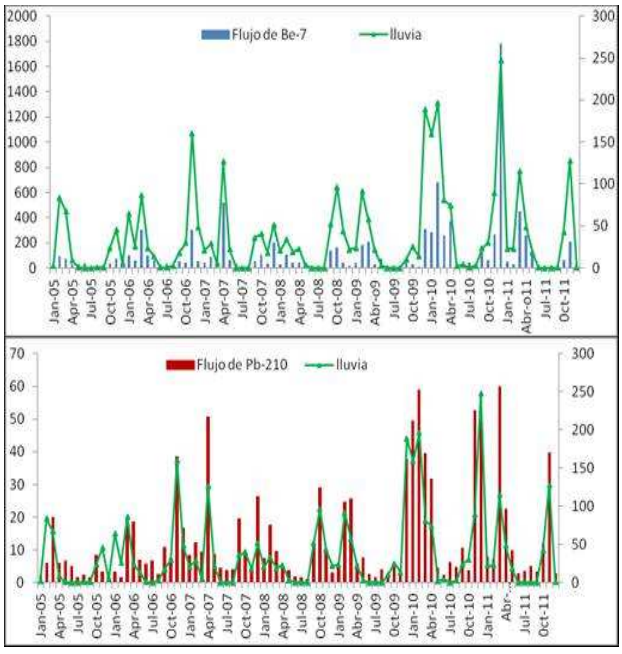

BIBLIOGRAPHY

Caillet, S., P. Arpagaus, F. Monna and J. Dominik (2001). Factors controlling ^{7}Be and ^{210}Pb atmospheric deposition as revealed by sampling individual rain events in the region of Geneva, Switzerland.J. Environ. Radioactivity 53, 241-256

Hernandez, F. Hernández Armas Catalán A., Fernández Aldecoa, J.C. andKarlson,L. 2005.Gross alpha, gross beta activities and gamma emitting radionuclides composition of airborne particulate samples in an oceanic island .Atmospheric Environment,39,4057-4066.

The importance of forest fires and dust on aerosol over Portugal's background

J.V. Monjardino, A.C. Carvalho, L. Mendes and F. Ferreira

Centre for Environmental and Sustainability Research - CENSE, Faculdade Ciências e Tecnologia, Universidade Nova de Lisboa, Almada, 2829-516 Caparica. Portugal

Keywords: Particulate matter exceedances, forest fires, dust, measurements, MACC reanalysis.

Presenting author email: jvm@fct.unl.pt

The determination of dust intrusions and forest fires emissions contribution to particulate matter (PM) concentration in the atmosphere is of great importance in all European Member States. In Southern European countries that is particularly important, due to their proximity to dust sources and to the high number of forest fires and area burned. These act as "grey sources" because the emitted amount of pollutants are strongly dependent on uncontrolled factors such meteorological, biological, and climatic.

The European Commission (SEC(2011) 208 final) accepted a methodology in order to quantify the natural sources contribution and to subtract exceedances attributable to them. Since 2005, Portugal and Spain have been jointly applying a common methodology to quantify daily African PM load during dust outbreaks (Escudero *et al.*, 2007), in the Iberian Peninsula, providing to their Environment Ministries reports that identify possible exceedances to the PM10 daily limit value caused by natural episodes. However, forest fires contributions' methodologies to account for their role in measured PM are still being refined.

The quantitative methodology presented in this paper is based on the analysis of time series of PM_{10} levels from regional background (RB) stations, representing Iberian Peninsula zones. In this sense, this work investigated the correlation between the RB stations and the remaining air quality network of the same zone for five Portuguese regions, for the year 2005. The authors started to study 2005, because it was the second highest year for area burned over Portugal in the last decade, and also due to the greater availability of PM measurements at the Portuguese RB stations.

Results have shown a good correlation for PM_{10} measured at RB stations and the rest of the monitoring network of each region, in dust events days (Figure 1). This allows the application of the quantification methodology. For cases where doubts were raised relating the origin of the air mass and the presence of dust influence the HYSPLIT back trajectory and cluster analysis were used at 500 m and 1000 m (Figure 1).

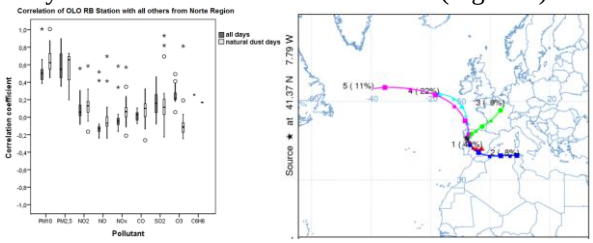

Figure 1: Correlation coefficients for OLO RB station for several pollutants, for all days and dust outbreak days, and HYSPLIT back trajectory cluster analysis.

In this work, the MACC reanalysis product of the global atmospheric composition (both on reactive gases and aerosols) was used to investigate which chemical species may be considered as predictors of aerosol large mode when all the biogenic and anthropogenic species are included into the MACC model (Stein et al., 2011; and Kaiser et al., 2011) over the area corresponding to the rural background station representativeness. The time series model results for CO, SO_2, NO_x, formaldehyde, organic, and black carbon into the two forms (hydrophobic and hydrophilic terms), large bin for dust and sea aerosol, over the MACC points near the rural backgrounds stations, were used in a step-wise regression, by month and MACC point, as possible estimators for the model aerosol large mode.

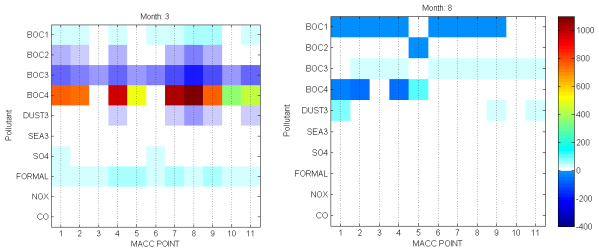

Figure 2: Step-wise regression coefficients for the MACC reanalysis over points near the RB air quality stations over Portugal, in March and August. Explanation: hydrophilic black carbon aerosol (BOC4), hydrophilic organic matter aerosol (BOC2), hydrophobic black carbon aerosol (BOC3) and hydrophobic organic matter aerosol (BOC1)).

As expected, different pollutants are considered as statistical significant estimators for the step-wise regression in different months. As an example, although formaldehyde could be considered an indicator for forest fire, it may not be an interesting indicator during months for high biological activity, as in Spring (March). During August, the more southern part of the country (points 9, 10 and 11) show positive coefficients for the larger dust bin, whereas in March the polynomial coefficient is negative over these areas. Higher values for the coefficients are obtained for the hydrophilic black carbon aerosol (BOC4), except for months were forest fires were active and devastating.

Escudero, M.; X. Querol, J. Pey, A. Alastuey, N. Pérez, F. Ferreira, S. Alonso, S. Rodríguez, and E. Cuevas (2007b). A methodology for the quantification of the net African dust load in air quality monitoring networks. *Atmos. Env.*, 41, 5516–5524.

Kaiser, J. W., Heil, A., Andreae, M. O., Benedetti, A., Chubarova, N., Jones, L., Morcrette, J.-J., Razinger, M., Schultz, M. G., Suttie, M., and van der Werf, G. R. (2011) Biomass burning emissions estimated with a global fire assimilation system based on observed fire radiative power. *Biogeosciences Discuss.*, 8, 7339-7398.

Stein, O.; M. Schultz, J. Flemming, A. Inness, J. Kaiser, L. Jones, A. Benedetti, J-J Morcrette (2011) MACC Global air quality services – Technical Documentation. MACC Deliverable D_G-RG_3.8. ECMWF Reading.

Primary and secondary marine aerosol at Station Concordia (East Antarctica). Seasonal pattern and implications for atmospheric transport from a multi-year continuous data-set.

R. Udisti[1], S. Becagli[1], M. Busetto[2], M. Chiari[3], U. Dayan[4], D. Frosini[1], C. Lanconelli[2], F. Lucarelli[3], S. Nava[3], C. Scarchilli[5], M. Severi[1], R. Traversi[1], V. Vitale[2]

[1]Dept. of Chemistry, University of Florence, Sesto Fiorentino, Florence, I-50019, Italy
[2] ISAC CNR, Bologna I-40129, Italy,
[3]Department of Physics, University of Florence and INFN Sez. Firenze, Sesto F.no, Florence, I-50019, Italy
[4]Department of Geography, Hebrew University of Jerusalem, Jerusalem 91905, Israel
[5]ENEA/UTMEA-TER, S. Maria di Galeria, Roma I-00123, Italy

Keywords: sea salt, sulphate, methanesulphonate, Antarctic plateau,.
Presenting author email: udisti@unifi.it

In the period Nov 2004- Nov 2007, all-year-round aerosol was collected by PM10 and PM2.5 samplers and multi-stage impactors (4 and 8 stages, from 0.7 to 10 um) at Station Concordia (Dome C, East Antarctica, 75° 60' S, 123° 200' E, 3220 m a.s.l. and 1100 km away from the nearest coast).

Sea spray (marked by sea-salt Na) is a major component at DC, especially in winter, when it contributes 80-90% to the aerosol ion mass. In summer (Dec-Mar), ssNa is mainly in the coarse fraction (2.1-1.1 μm) at concentrations around 2-3 ng m^{-3}. In winter (Apr-Nov), the values are about 10 times higher, with a size-distribution shifted towards the sub-um fraction. The seasonal pattern of ssNa is explained by changes in the large-scale atmospheric circulation evaluated by synoptic-field analysis for the last 62 years. The 20 highest sea-spray events along the 3-year record were characterized by a weakening of the Polar High centre including DC (favouring advection of marine air masses), in relation with a deepening of the major sub-polar low over Ross Sea and its further expansion towards Vostok and DC. Such deepening resulted in a strengthening of the zonal winds along the coasts of east Antarctica, enhancing sea spray production. Back-trajectory analyses carried out for 8 major sea spray events revealed that size distribution is a function of air masses origin and lifetime over the Antarctic Plateau.

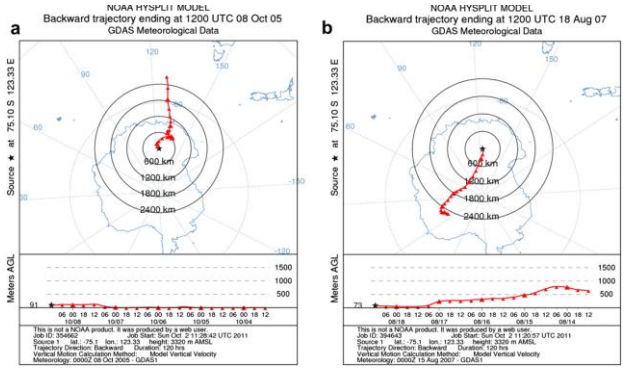

Figure 1. Backward trajectories for extreme ssNa concentration events with particulate distributed in the 2.5-1μm (a) and in the <1 μm (b) fractions.

Coarse sea spray is coming from the Indian-Pacific sector and their pathway over the Plateau is shorter. Sub-um particles are related to the transport over South Pole, probably coming from the Atlantic Sector and with longer Plateau trajectories (figure 1).

The different sea spray origin (from open sea areas or from sea ice surface) was also evaluated.

MSA and $nssSO_4^{2-}$, as markers of oceanic biogenic emissions, exhibit a seasonal cycle with summer maxima, but they show a different size distribution in early and late summer. In November, particles are distributed both in the accumulation mode (0.4-0.7 μm), and in the micrometric mode (1.1-2.1 μm). On the contrary, only the finest mode is present in February.

The two modes reflect a different speciation: acidic forms dominate in the finest mode, whereas MSA and $nssSO_4^{2-}$ are related to Na^+ or NH_4^+ salts in the micrometric particles. Such differences are related to different transport pathways. In the early summer, air masses arise mainly from Indian Ocean, where the sea ice margin is close to the coast and DMS is emitted at the interface air/sea. DMS is easily oxidised to H_2SO_4 and MSA by gas-phase reactions. In November, high velocity zonal winds over the coastal areas injects micrometric sea spray aerosol at high elevation, where it constitutes condensation nuclei for newly formed gas-phase H_2SO_4 and MSA, that form sodium salts. In February, by contrast, the gas to particle conversion of H_2SO_4 and MSA is dominant during the fast transport at high elevation of air masses coming from highly bio-productive oceanic sectors located as far north as 50 °S. This phenomenon leads to the highest concentrations of the acidic species over the whole year, with a distribution mode in the fine fraction of aerosols reaching Dome C.

This work benefited of Concordia Station logistic and personnel facilities.

Aerosol and gas concentrations at the Finnish Antarctic station Aboa in Queen Maud Land and comparisons with the Norwegian station Troll

A.Virkkula[1,2], S.Begagli[3], X.Chi[4], W.Maenhaut[4], M.Fiebig[5], H.Hellén[1], H.Hakola[1], E.Asmi[1], S. Häkkinen[2], J.Backman[2], T.Vihma[1], T.Valkonen[1], S.Kirkwood[6] and M.Kulmala[2]

[1]Finnish Meteorological Institute, Research and Development, FI-00560, Helsinki, Finland
[2]Department of Physics, University of Helsinki, FI-00014, Helsinki, Finland
[3]Dept. of Chemistry, University of Florence, Sesto Fiorentino (FI), I-50019, Italy
[4] Ghent University, Department of Analytical Chemistry, Gent, Belgium
[5]Department of Atmospheric and Climate Research, NILU N-2027 Kjeller, Norway
[6]Swedish Institute of Space Physics, Kiruna, Sweden
Keywords: Antarctic, Scattering coefficient, Volatility, Chemical composition
Presenting author email: aki.virkkula@fmi.fi; aki.virkkula@helsinki.fi

Aerosols and trace gases have been measured at the Finnish Antarctic research station Aboa (73°03'S, 13°25'W) in Queen Maud Land during several summer campaigns but no comparisons with simultaneous measurements at the other stations in the region have been made. In this work we present data collected from Aboa during an International Polar Year campaign in December 2007 – January 2008 and compare them with data from the Norwegian station Troll (72°01′S, 2°32′E), approximately 540 km east of Aboa. At Troll there is a long-term monitoring program for aerosols and trace gases. Of these data we have here used the aerosol number size distributions, scattering coefficients, and surface ozone concentrations.

At Aboa aerosol number size distributions and volatility were measured in the size range 10 – 700 nm with a DMPS connected to a thermodenuder. Aerosol scattering and absorption were measured with 3-λ in situ instruments. PM1 filter samples and 12-stage impactor samples were taken for aerosol chemical composition. Gas-phase measurements were conducted with an ozone monitor and by taking daily canister samples. Ion concentrations were analyzed from the impactor and filter samples by ion chromatography at the University of Florence. Elemental and organic carbon and water-soluble organic carbon concentrations were analyzed from the quartz filter samples at Ghent University, Belgium. The canister air samples were analyzed for volatile organic compounds (VOCs) with gas chromatography at the Finnish Meteorological Institute.

Transport route calculations were done with trajectory models and more accurately by using a Weather Research and Forecasting model (WRF) model, modified for use in the Polar Regions. 3D wind data were measured with the Movable Atmospheric Radar for Antarctica (MARA) near the aerosol laboratory.

Light scattering coefficient showed similar temporal variation at both Aboa and Troll (Figure 1). Detailed analyses show that there are episodes when the peak first appears at Troll and 12-24 hours later at Aboa. Surface ozone concentrations at the two stations vary analogigally. Particles were clearly more volatile than ammonium sulfate in laboratory calibration and ambient aerosols at the SMEAR II forest site in Hyytiälä, Finland (Figure 2). The relationship between volatility and chemical composition will be discussed.

The MARA data and WRF model showed consistently that high wind speeds create turbulence and downward wind that brings gases and particles from upper atmospheric levels to the surface. This observation may probably be generalized to other Antarctic mountains and mountain ranges as well.

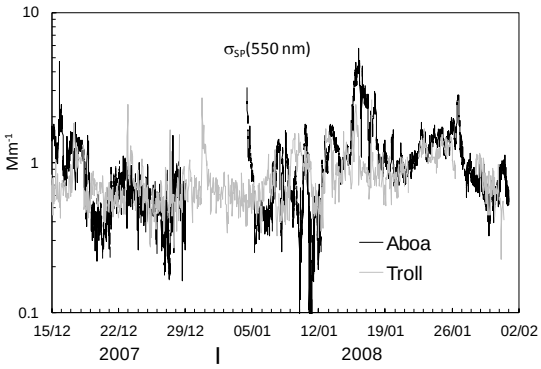

Figure 1. Light scattering coefficient at λ=550 nm at Aboa and Troll in 15 Dec 2007 to 30 Jan 2008.

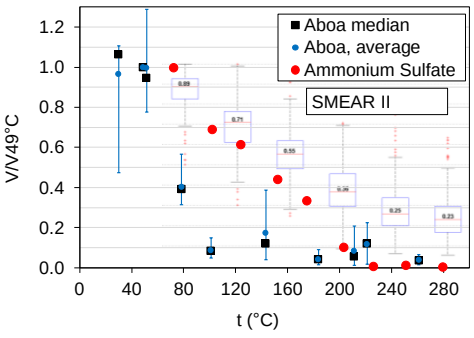

Figure 2. Aerosol volatility at Aboa and a comparison of the same instrument used for ammonium sulfate measurements in the laboratory and for ambient aerosol measurements at SMEAR II.

This work was supported by the Academy of Finland, Contract no. 210998

In situ aerosol measurements at Dome C, Antarctica, in 2007 - 2011

A.Virkkula[1,2], E. Järvinen[2], T.Nieminen[2], R.Väänänen[2], H. Manninen[2], P.P. Aalto[2], E. Asmi[1], J.Backman[2], M. Busetto[3], C. Lanconelli[3], R. Schioppo[4], A. Lupi[3], V. Vitale[3], R. Hillamo[1] and M.Kulmala[2]

[1]Finnish Meteorological Institute, Research and Development, FI-00560, Helsinki, Finland
[2]Department of Physics, University of Helsinki, FI-00014, Helsinki, Finland
[3]Institute of Atmospheric Sciences and Climate of the Italian National Research Council, Bologna, Italy
[4]ENEA Area Sperimentale di Monte Aquilone, Manfredonia (FG), Italy
Keywords: Antarctic, Number size distribution, Absorption
Presenting author email: aki.virkkula@fmi.fi; aki.virkkula@helsinki.fi

Aerosol number concentrations, size distributions and chemical composition have been studied at several stations around Antarctica. There exist long-term records of aerosol number concentrations, for instance from Neumayer and South Pole but aerosol number size distributions have been measured mainly during campaigns both at coastal stations and in the upper plateau at South Pole. The Norwegians recently started long-term size distribution measurements at the Troll station in Queen Maud Land (Hansen et al. 2009) but there are no long-term size distribution measurements from the upper plateau. The measurements presented here are the first step towards filling in this gap: particle number size distributions have been measured at the Dome C station (75˚S, 123˚E) in the upper plateau at about 3200 m amsl since December 2007. The size distributions in the size range 10 – 600 nm are measured with a differential mobility particle sizer (DMPS) and in the size range 0.3 – 15 µm with a Grimm Model 1.108 optical particle counter. They were first stopped at the end of year 2009 due to technical problems but they were continued again in December 2010, and the goal is to continue these measurements. In December 2010 also a new instrument, an Air Ion Spectrometer (AIS), that measures charged particle size distributions in the size range of about 0.4 – 40 nm, was installed at the station. The AIS produced good data until May 2011.

In addition to the size distributions, light absorption by particles has been measured at Dome C with a Radiance Research 3λ Particle Soot Absorption Photometer (PSAP). The PSAP reports absorption coefficients with a 0.1 Mm^{-1} accuracy. This is not good enough since most of the time absorption coefficients are below that at Dome C. Therefore all absorption coefficients were calculated from the raw signal and reference counts of the PSAP by taking long enough integration time between subsequent measurements of signal and reference. This makes it possible to get essentially indefinitely low detection limits – at the cost of time resolution, however (Springston and Sedlacek, 2007). The PSAP data processing also needs scattering coefficients. These are not being measured at Dome C. However, the measured size distributions in the size range 0.01 – 15 µm have been used to calculate light scattering coefficients in the same wavelengths as the PSAP measures. To do this a Mie code has been used, assuming spherical particles and varying refractive indices from that of sulfuric acid to ammonium sulfate and sea salt.

In this work we will present seasonal variation of the particle number and mass concentrations, modal structure of the size distributions, estimated light scattering and absorption, particle formation and growth and connections with the air masses. The modal structure of the size distributions was studied a with an automatic mode-fitting algorithm. Growth rates during the particle formation episodes were calculated.

There was a clear seasonal cycle in the number concentration data. The concentrations were at their lowest around July and August and at highest around January, which is in agreement with the data from all other stations in Antarctica. In the sunlit seasons there were from one to three modes in the size distributions, in the darkest period mainy only one. Strong new particle formation events were rare and only happened in summer when there is plenty of solar radiation available. However, a careful analysis of the size distribution data shows that these events did occur all year round, even in the darkest and coldest months June and July. These events were weak but not nonexistent, which is a new and interesting phenomenon, not reported earlier from the upper plateau of Antarctica.

The median scattering and absorption coefficients in the period when the DMPS, the OPC and the PSAP were all operational are presented in Table 1. The scattering coefficients and thus also the absorption coefficients in Table 1 were calculated using the refractive index of sulphuric acid (n_r = 1.426).

Table 1. Median scattering (σ_{sp}) and absorption (σ_{ap}) coefficients at the PSAP wavelengths in Dome C in December 2007 to November 2009.

	467 nm	530 nm	660 nm
$\sigma_{sp}(Mm^{-1})$	0.31	0.25	0.17
$\sigma_{ap}(Mm^{-1})$	0.019	0.017	0.015
ω_0	0.94	0.94	0.92

Hansen, G., Aspmo, K., Berg, T., Edvardsen, K., Fiebig, M., Kallenborn, R., Krognes, T., Lunder, C., Stebel, K., Schmidbauer, N., Solberg, S. and Yttri, K. E. (2009) *Polar Research*, **28**, 353–363.

Springston, S.R. and Sedlacek A.J. (2007) *Aerosol Sci. Technol.*, **41**, 1110 – 1116.

Advanced gas-phase synthesis of LTO nanocomposites for Li-ion battery applications

T. Karhunen[1], A. Lähde[1], J. Leskinen[1], T. Torvela[1], E. Pohjalainen[2], M. Karppinen[2], O. Waser[3], R. Büchel[3], U. Tapper[4], J. Jokiniemi[1,4]

[1]Fine Particle and Aerosol Technology Laboratory, University of Eastern Finland, 70210 Kuopio, Finland

[2]Laboratory of Inorganic Chemistry, Aalto University, 00076 Aalto, Finland

[3]Particle Technology Laboratory, ETH Zürich, 8092 Zürich, Switzerland

[4]Fine Particles, VTT Technical Research Centre of Finland, 02044 VTT, Finland

Keywords: Nanocrystalline materials, Nanopowders, Chemical synthesis methods, Lithium-ion batteries.

Presenting author email: tommi.karhunen@uef.fi

Li-ion secondary cells are one of the most advanced energy storage systems currently available as it provides one of the highest energy-to-weight ratios. Due to the high energy density of Li-ion batteries, they offer the best route for many advanced storage applications related to clean electricity (Hall and Bain, 2008). However, new commercial applications, such as hybrid and full electric vehicles, place increasing demands on specific capacity, power density, rate capacity and cycle life of the energy storage devices (Du Pasquier *et al.*, 2003; Wen *et al.*, 2008).

Lithium titanium oxide ($Li_4Ti_5O_{12}$, LTO) is recognized as a promising material for the negative electrode of Li-ion batteries as it is cheap and safe, and has an excellent cycle life (Du Pasquier *et al.*, 2003; Ohzuku *et al.*, 1995). However, the major drawback of LTO is its low electronic conductivity. To overcome this problem the particle size can be reduced to the nanoscale increasing the specific surface area, and decreasing the diffusion lengths within particles and the local current density (Arico *et al.*, 2005). For LTO an optimum size of about 17 nm has been reported (Kavan *et al.*, 2003). However, the current method of solid-state chemical reaction typically produces LTO particles with a diameter of the order of 1 μm. Another solution is to use metal dopants (e.g. Cu, Ag) (Wang *et al.*, 2009; Huang *et al.*, 2006). Currently the doping is typically carried out in a separate process which increases the complexity and costs of the production.

Here, pure and doped LTO nanoparticles are prepared in the gas phase with flame spray pyrolysis (FSP). It is a fast, dry, and single-stage process that enables the preparation of materials with high-purity (Mädler *et al.*, 2002). The precursor solution used for the studies contained lithium acetyl acetonate and titanium isopropoxide in mixture of toluene and 2-ethyl hexanoic acid (1:1). The silver and copper doping was performed by adding, respectively, silver and copper 2-ethyl hexanoic acid directly into the precursor solution. Finally, a vertical flow aerosol reactor was used to increase the high-temperature residence time and thus the crystallinity of the particles.

The resulting particles were found to be high-purity (99%), single crystalline nanoparticles with a primary particle size down to 10 nm. A uniform dopant distribution was observed in the doped LTO nanoparticles. The silver dopant nucleated independently and deposited on the surface of the LTO particles. The copper doping, on the other hand, reacted chemically with the LTO forming a double spinel structure (Karhunen *et al.*, 2011). Both dopants were found to improve the electrochemical performance of the LTO at high C-rates.

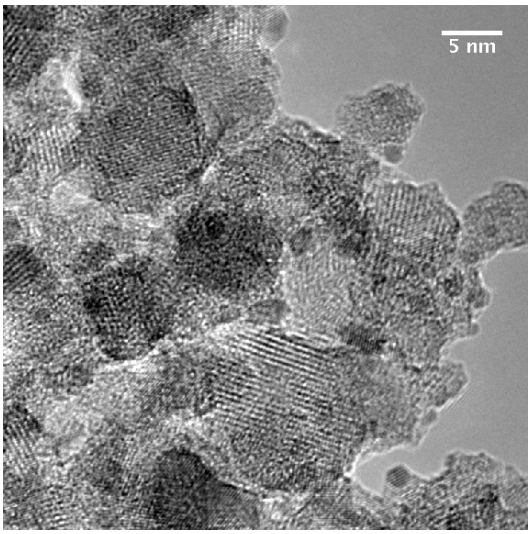

Figure 1: HRTEM figure of $Li_4Ti_5O_{12}$/Ag nanocomposite.

This work was supported in part by the Finnish Funding Agency for Technology and Innovation (40051/09), the strategic funding of the University of Eastern Finland (Namber) and by the Fortum foundation (10-136, 12-072).

Arico *et al.*, 2005. Nature Mater. **4**, 366–377.

Du Pasquier *et al.*, 2003. J. Power Sources, **115**, 171–178.

Hall and Bain, 2008. Energy Policy, **36**, 4352–4355.

Huang *et al.*, 2006. Solid State Ion., **177**, 851–855.

Karhunen *et al.*, 2011. ISRN Nanotechnology, **2011**, Article ID 180821.

Kavan *et al.*, 2003. J. Electrochem. Soc., **150** (7), A1000–A1007.

Mädler *et al.*, 2002. Aerosol Science, **33**, 69–389.

Ohzuku *et al.*, 1995. J. Electrochem. Soc., **142** (5), 1431–1435.

Wang *et al.*., 2009. Electrochem. Commun., **11**, 50–53.

Wen *et al.*, 2008. Solid State Ionics, **179**, 1800–1805.

Flame-spray pyrolysis of copper-based p-type semiconducting oxide nanoparticles and their application in printable electronics

D. Kilian[1], B. Meyer[2], M.P.M. Jank[3], M. Voigt[1], S. Polster[2], L. Frey[2,3] and W. Peukert[1]

[1] Institute of Particle Technology, University of Erlangen-Nuremberg, Erlangen, Bavaria, 91058, Germany
[2] Chair of Electron Devices, University of Erlangen-Nuremberg, Erlangen, Bavaria,91058, Germany
[3] Fraunhofer Institute for Integrated Systems and Device Technology, Erlangen, 91058, Germany

Keywords: flame spray pyrolysis, nanoparticles, oxides
Presenting author email: d.kilian@lfg.uni-erlangen.de

Flame spray pyrolysis (FSP) is a versatile, easy to handle and cost-effective way for the production of nanoscale materials. Especially the synthesis of oxide materials can be carried out under atmospheric conditions. The high product purity and the possibility of mixing of several precursors for easy doping or production of compound materials (Teoh et al., 2010) makes FSP a promising technique for the production of electronic materials, namely insulator and semiconductor nanoparticles.

One application for semiconducting materials are low cost printable electron devices like thin-film transistors (TFTs) deposited from nanoparticulate dispersions. For the fabrication of TFTs, the synthesized nanoparticles are suspended into a liquid used for coating or printing the active semiconducting thin films, which are then integrated into TFT devices. To date, only n-type semiconductors have been reported for solution processed inorganic oxide semiconductors in TFTs. Therefore, the development of p-n junctions and thus p-type TFTs is a major goal, as this would lead to the fabrication of complementary metal oxide semiconductor (CMOS) structures. Fortunato presented results based on sputtering deposition of cuprous oxide Cu_2O (Fortunato et al., 2010) at room temperature leading to p-type TFTs. As sputtering is a cost-intensive technique alternative ways as described above for TFT processing are of special interest.

In this work the synthesis of p-type semiconducting CuO and mixed-phase Cu_2O/CuO is carried out by flame spray pyrolysis. After synthesis, the particles are collected by a filter unit and particle size, crystallinity and phase composition are analyzed by SEM, TEM, XRD and gas sorption methods as a function of process parameters. The focus of the work lies especially on formation of Cu_2O nanoparticles under atmospheric conditions. Copper Oxide in oxidation state Cu (I) is favored for electronic applications due to its lower intrinsic charge carrier concentration minimizing leakage current in TFTs. Furthermore, Cu_2O shows a higher charger carrier mobility than CuO favoring this material for transistor applications.

By properly adjusting the process conditions, it is possible to achieve either pure CuO or a mixed phase of Cu_2O/CuO nanoparticles. The phase diagram suggests that the flame temperature significantly influences the oxidation state of copper. In Fig. 1 a scanning electron microscopy (SEM) picture of copper oxide is shown. As typical for flame processes the particles show strong sintering.

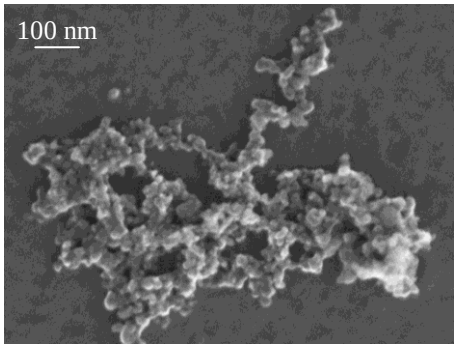

Fig. 1. SEM picture of CuO nanoparticle aggregate synthesized by flame spray pyrolysis

By gas sorption analysis of different samples specific surface areas between 40 – 140 m²/g can be achieved. Furthermore we could successfully synthesize mixed phases of CuO/Cu_2O under atmospheric conditions as it can be seen in the XRD diffractogram (Fig. 2).

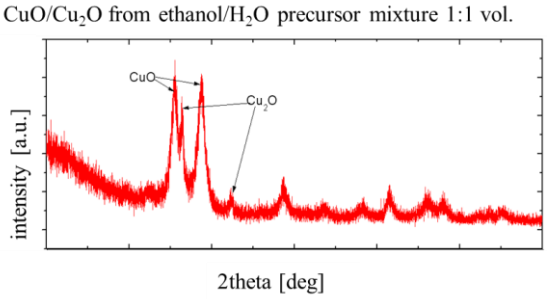

Fig. 2. XRD diffractogram of a mixed phase Cu_2O/CuO thin film on a SiO_2/Si substrate

First electric performance tests show significant p-type gating at low current levels and moderate off-state leakage.

This work was supported by the German Research Council and Evonik Industries within the RTG/GRK 1161/2 Disperse Systems for Electronic Applications.

Teoh, W.Y., Amal, R. and Mädler, L. (2010) *Nanoscale* **2**, 1324-1347.

Fortunato, E., et. al., (2010) *Appl. Phys. Lett.* **96**, 192102.

Aerosol-derived antimony doped-tin oxide nanoparticles and studies on the influence of organic and inorganic shells in nanoparticle assemblies on the overall conductance

S.B. Bubenhofer[a], C.M. Schumacher[a], G.A. Sotiriou[b], R.N. Grass[a] and W.J. Stark[a]

[a]Institute for Chemical and Bioengineering, ETH Zurich, Zurich, 8093, Switzerland
[b]Institute of Process Engineering, ETH Zurich, 8092 Zurich, Switzerland
Keywords: flame spray pyrolysis, oxide nanoparticles, core-shell particles, coatings, surfactants.
Presenting author email: s.bubenhofer@chem.ethz.ch

Transparent conductive oxides are of high interest for transparent electrodes in solar cells or liquid displays and for infrared-reflecting applications. The most common material is indium doped tin oxide showing a high conductivity and transparence. Nevertheless a change to other doped tin or zinc oxides was driven in the last years by the low abundance of indium on earth.[1] Furthermore, the need to overcome the traditional vacuum deposition methods for more cost efficient and moreover even flexible devices, led to intensive investigation on nanoparticle film processing.

Good film forming behavior in nanoparticle deposition methods, as spin coating or dip coating, is based on highly stabilized dispersions, where normally surfactant molecules are added or a functionalization of the particles is necessary. The introduction of such impurities in the films, which cannot always be removed by heat post-treatment (flexible polymer substrates: temperature sensitive) mostly leads to an decrease in conductivity in the overall nanoparticle assembly.[2]

We therefore present the high temperature, aerosol synthesis of antimony doped tin oxide nanoparticles and a systematic study on the influence of organic and inorganic shells on the overall conductivity of assembled nanoparticles.[3] Flame spray synthesis was used as scalable and cost efficient process to produce high purity antimony doped tin oxide with a highly controlled dopant content.[4] The as-prepared particles were coated with three different organic surfactants using common dispersing processes. For comparison to well-known insulating shell thickness, additionally particles with in-situ coating of SiO_2 were produced.[5]

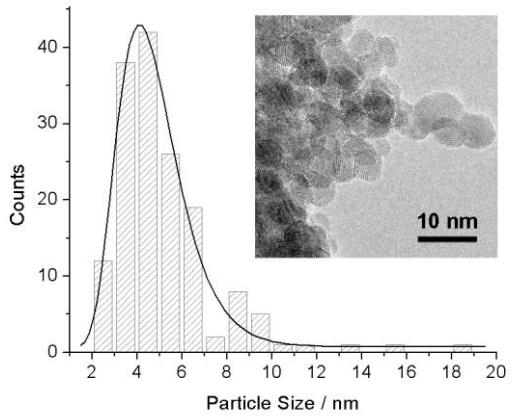

Figure 1. Antimony doped tin oxide nanoparticles produced by high temperature, aerosol flame spray synthesis.

The electron transport through the nanocomposites was tested for both organic and inorganic shell materials by measuring the electrical resistivity of pressed pills. Pure conducting nanoparticles, thin organic shells as well as thin, probably only partially coated SiO_2 shells showed a clear decrease in resistivity under pressure load due to irreversible compaction of the powder. However, thick polymer shells showed a relaxation of the resistivity when the pressure was decreased. For insulating SiO_2 shells of similar thickness the same reversible behavior in resistivity was observed and we could therefore describe this effect by electron tunneling through the insulating shell. The compression of the shell led to a decrease in thickness and therefore a higher electron tunneling probability.[6]

These findings on the influence of impurities such as surfactants or processing aids on the electron transport in assembled nanoparticle systems are important for improving the production of low cost, high performance electronics.

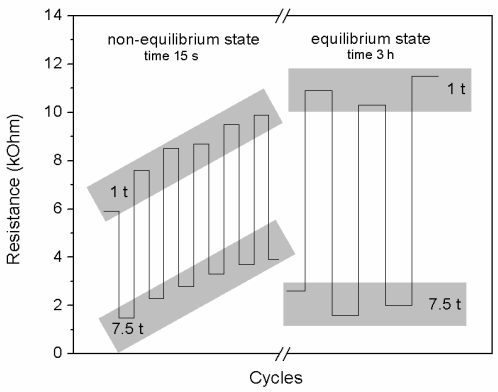

Figure 2. Reversible resistivity of polymer coated antimony doped tin oxide nanoparticle due to electron tunnelling probability changes under pressure cycles.

(1) Ginley, D. S.; Bright, C. (2000) *MRS Bull.* **25**, 15-18.
(2) Buhler, G.; Tholmann, D.; Feldmann (2007) C. *Adv. Mater.* **19**, 2224-2227.
(3) Bubenhofer, S. B.; Schumacher, C. M.; Koehler, F. M.; Luechinger, N. A.; Sotiriou, G. A.; Grass, R. N.; Stark, W. J. *submitted*.
(4) Stark, W. J.; Strobel, R.; Guenther, D.; Pratsinis, S. E.; Baiker, A. (2002) *J. Mater. Chem.* **12**, 3620-3625.
(5) Teleki, A.; Heine, M. C.; Krumeich, F.; Akhtar, M. K.; Pratsinis, S. E. (2008) *Langmuir* **24**, 12553-12558.
(6) Athanassiou, E. K.; Krumeich, F.; Grass, R. N.; Stark, W. J. (2008) *Phys. Rev. Lett.* **101**, 166804

Size controlled flame synthesis of CuO nanoparticles for Li-ion batteries

O. Waser[1], A. Güntner[1], M. Heß[2], P. Novák[2] and S.E. Pratsinis[1]

[1]Particle Technology Laboratory, Department of Mechanical and Process Engineering, ETH Zurich, CH-8092 Zurich, Switzerland
[2]Electrochemistry Laboratory, Paul-Scherrer-Institute, CH-5232 Villigen PSI, Switzerland
Keywords: Nanoparticle production, Flame spray pyrolysis, Oxides nanoparticles, Copper$^{(II)}$oxide, Li-ion battery
Presenting author email: oliver.waser@ptl.mavt.ethz.ch

Recent developments in Li-ion batteries (e.g. $LiMn_2O_4$, $LiFePO_4$ or $LiCo_{1/3}Ni_{1/3}Mn_{1/3}O_2$) lead to enhanced performance or safety compared to the most commonly used $LiCoO_2$. All these insertion type materials, however, show an intrinsic barrier towards higher specific capacity, as their accessible Li-sites are limited before irreversible crystal structure changes occur. It is therefore believed that a substantial breakthrough in battery energy density necessitates a different concept of Li-ion storage materials (Cabana et al., 2010). Conversion type materials are considered as such a higher energy density alternative since lithium directly undergoes electrochemical reaction with a transition-metal compound, allowing multi-electron redox reactions with the general reaction equation (Li et al., 2011):

$$CuO + 2\ Li \rightarrow Cu + Li_2O$$

Copper oxide is thereby an attractive active material as it is inexpensive, relatively non-toxic, and offers about 2-fold higher theoretical energy density (1010 Wh/kg) than the currently used cobalt oxide (540 Wh/kg).

Flame spray pyrolysis (FSP) is a versatile and scalable technique for synthesis of mixed oxides, metal salts and even pure metals in the form of nanoparticles or porous films with closely controlled characteristics (Strobel & Pratsinis, 2007) including active materials ($LiMn_2O_4$, $Li_4Ti_5O_{12}$, $LiFe_5O_8$) for batteries (Ernst et al., 2007) and recently also in-situ acetylene carbon black coated $LiFePO_4$ (Waser et al., 2011). Characteristically for FSP synthesis, the primary-particle size can be easily controlled, offering ideal conditions for size-effect analysis in various applications.

In this work, pure CuO (copper$^{(II)}$oxide) nanoparticles of closely controlled primary particle diameter are made by the continuous and scalable FSP technique. The resulting particles were analyzed by X-ray diffraction (XRD), nitrogen adsorption (BET), transmission electron microscopy (TEM) and electrochemical performance testing as Li-ion battery material in composite electrodes vs. Li-metal.

The BET equivalent diameter (d_{BET}) of the CuO primary particles grows from 6 to 20 nm by increasing the ratio between precursor solution feed rate and dispersion O_2 flow rate. Enclosing the FSP flame with a quartz tube inhibits flame quenching by air entrainment, hence, increasing the particle diameter to 50 nm as a result of intensified sintering at higher temperature and higher precursor concentration (Teleki et al., 2006). Size control by precursor solution to dispersion gas flow rate variation, however, is not significant anymore, underlining the importance of air entrainment for size variation in open-FSP.

The FSP-made CuO particles show high initial discharge capacity (Fig. 1, diamonds) that scales inversely with CuO size and reaches a maximum of 1450 mAh/g for the smallest 6 nm CuO (d_{BET}). Outstanding reversible capacities of 930 and 800 mAh/g are obtained for intermediate CuO sizes of 20 and 50 nm, respectively, where larger (commercial) CuO of 670 nm (d_{BET}) shows only 450 mAh/g. The smallest particles (6 and 11 nm), however, encounter pronounced capacity degradation within few cycles only that may be attributed to electrical contact loss due to the strong volume changes upon conversion reaction.

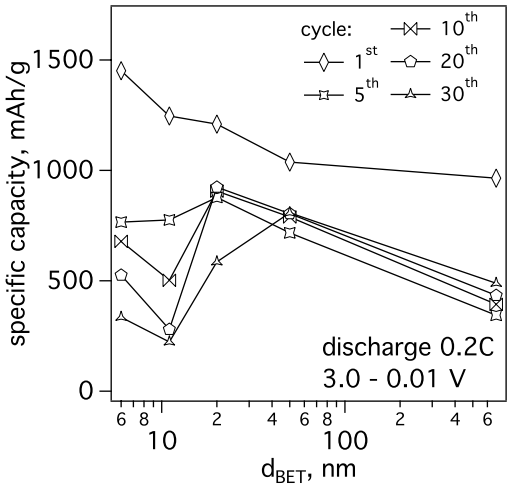

Fig. 1 Specific discharge capacity of FSP-made CuO nanoparticles of 6, 11, 20 and 50 nm in comparison to commercial CuO of 670 nm (d_{BET}).

Cabana, J., Monconduit, L., Larcher, D., & Palacin, M.R. (2010) *Adv. Mater.,* ***22*****,** E170-E192.

Ernst, F.O., Kammler, H.K., Roessler, A., Pratsinis, S.E., Stark, W.J., Ufheil, J., & Novák, P. (2007) *Mater. Chem. Phys.,* ***101*****,** 372-378.

Li, T., Ai, X.P., & Yang, H.X. (2011) *J. Phys. Chem. C,* ***115*****,** 6167-6174.

Strobel, R., & Pratsinis, S.E. (2007) *J. Mater. Chem.,* ***17*****,** 4743-4756.

Teleki, A., Pratsinis, S.E., Kalyanasundaram, K., & Gouma, P.I. (2006) *Sens. Actuator B-Chem.,* ***119*****,** 683-690.

Waser, O., Buchel, R., Hintennach, A., Novák, P., & Pratsinis, S.E. (2011) *J. Aerosol. Sci.,* ***42*****,** 657-667.

$Ir_xRu_yO_z$ particles for hydrogen generation

J. Forsman[1], U. Tapper[1], A. Auvinen[1], A. Pasanen[1], M. Johansson[2], T. Karhunen[3], J. Jokiniemi[1,3], P. Kauranen[1]

[1]Fine Particles, VTT Technical Research Centre of Finland, P.O. Box 1000, FI-02044 VTT, Finland
[2]Laboratoty of Inorganic Chemistry, Åbo Akademi Univeristy, FIN-20500 Åbo, Finland
[3]Department of Environmental Science, University of Eastern Finland, P.O. Box 1627, FI-70211 Kuopio, Finland

Keywords:gas phase nanoparticle production, nanoparticle applications, CVD, flame spray synthesis
Presenting author email: johanna.forsman@vtt.fi

IrO_2 is routinely used as oxygen evolution catalyst in proton exchange membrane (PEM) water electrolyzers. The commercially available Ir catalysts may have nanosized grains, but the overall particle size is in the micron scale. Since iridium is rare and very expensive, producing the catalyst in nanosize could reduce costs by enabling lower catalyst loadings.

In this work, IrO_2 and $Ir_xRu_yO_z$ nanoparticles were produced by two aerosol methods; chemical vapour deposition (CVD) and flame spray synthesis (FSP). Previously Ir catalysts have been manufactured by wet methods. (Marshall et al. 2006, 1134-1140).

For characterisation of the catalyst material, the onset potential of oxygen evolution was measured with a rotating disk electrode setup (RDE). The limiting current was measured by voltammetric sweeping in 0,5M H_2SO_4 at room temperature. For the electrolyzer, an ink is made of the catalyst powder which is then printed on Ti felt. This step may be overcome with the FSP technique as the catalysts may be directly collected on Ti felt.

In the CVD method, $IrCl_3$ and $RuCl_3$ were dissolved in dilute HCl in various proportions. The liquid was sprayed with atomiser to air flow in tubular furnace (500-1100°C). The precursors evaporated and reacted with air to form Ir, Ru, their oxides and mixtures of these. The flow was quenched with nitrogen and analysed with scanning mobility particle sizer (SMPS) and Fourier transform infrared spectroscopy (FTIR). All catalysts were studied by transmission electron microscopy (TEM) and X-ray diffraction (XRD). Particles were collected on gold substrates by electrostatic precipitation for measurement of the onset potential and limiting current.

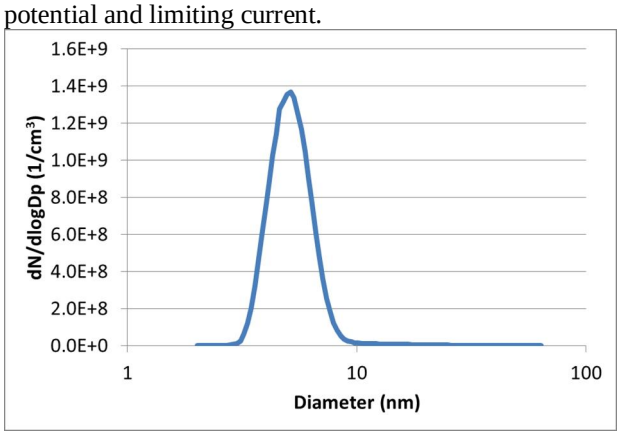

Figure 1: The DMA size distribution of IrO_2 particles produced by CVD.

The CVD IrO_2 particles had number average diameters of 5-10 nm (Figure 1 and Figure 2). The onset potential was 1450 mV and limiting current 27 mA. Ihe Ir-Ru mixture particles were significantly larger, 10-40 nm and had crystal size of 14 nm. Ruthenium species with higher vapour pressure caused the ruthenium

For FSP, $Ir(acac)_3$ and $Ru(acac)_3$ precursors were dissolved in ethanol-acetic acid mixture in several proportions. The liquid precursor was sprayed to methane flame. The formed particles were collected directly on quartz substrates and Ti-felts. The Ti-felt was well covered by the particles and could be directly used in electrolyzer experiments. The flow was also analysed by fast mobility particle sizer (FMPS).

The size distribution of the FSP catalysts was relatively wide and particle size was 10-100 nm (Figure 2). The particles were amorphous as collected and were heat-treated before catalyst tests. After heat treatment, the crystal size of the particles was 5 nm. The onset potential was 1460-1490 mV and limiting current 27-29 mA.

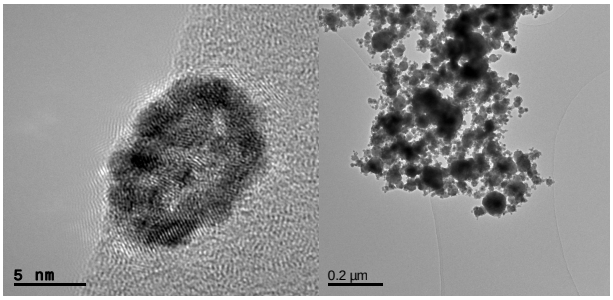

Figure 2: Left: IrO_2 particle produced by spray pyrolysis. Right: Ir_3RuO_8 particles produced by FSP .

Acknowledgements
This research was funded by The Fuel Cells and Hydrogen Joint Undertaking (FCH JU, Contract 245228) and Tekes- the Finnish Funding Agency for Technology and Innovation

Marshall, A., B. Borresen, G. Hagen, S. Sunde, M. Tsypkin, and R. Tunold. (2006). *Russian Journal of Electrochemistry* **42** (10), 1134-1140.

Multimineral supplementation with nano-CaO as carrier matrix

J.T.N. Knijnenburg[1], F.M. Hilty[1,2], M.B. Zimmermann[2] and S.E. Pratsinis[1]

[1] Department of Mechanical and Process Engineering, ETH Zurich, Zurich, CH-8092, Switzerland
[2] Department of Health Sciences and Technology, ETH Zurich, Zurich, CH-8092, Switzerland
Keywords: FSP, iron deficiency, supplementation, solid solution.
Presenting author email: jesper.knijnenburg@ptl.mavt.ethz.ch

Iron deficiency (ID) is a health problem affecting approximately 2 billion people worldwide (Zimmermann and Hurrell, 2007). It is one of the most common micronutrient deficiencies, not only in developing countries but also industrialized countries are affected. ID adversely affects cognition and may cause fatigue and reduce work performance. Supplementation of iron was shown to be cost-effective to relieve ID (Wieringa *et al*, 2007).

Solubility (and therefore bioavailability) of iron compounds can be improved by increasing its specific surface area (SSA), i.e. decreasing its particle size to the nm range. Recently Rohner *et al* (2007) have prepared nanostructured $FePO_4$ by flame spray pyrolysis (FSP), where the SSA was as high as 195 m^2/g (~11 nm particle size). This iron phosphate has high solubility i.d.a. (a good predictor of potential in-vivo bioavailability) and is as bioavailable as $FeSO_4$ (the "gold standard") in rats.

Zinc deficiency (ZD) negatively affects growth and immune function, and ZDs often exist in the same areas as ID. Thus Hilty *et al* (2009) developed nanostructured iron/zinc compounds with nutritionally valuable amounts of zinc by FSP. The addition of zinc increased iron solubility i.d.a. and (as shown recently) bioavailability comparable to $FeSO_4$ (Hilty *et al*, 2010).

Very recently we have shown that the incorporation of calcium into nanostructured iron oxide increases iron solubility (Hilty *et al*, 2011) and potentially also bioavailability (Hilty *et al*, 2010) compared to pure iron oxide. For high dopant contents the solubility was comparable to $FeSO_4$. The increase in iron solubility is a result of the formation of a solid solution, decreasing the average bond energy of the crystal.

Here, nanostructured calcium oxide-based supplements are developed as carriers for iron/zinc fortification. Calcium oxide doped with nutritionally relevant amounts of iron and/or zinc was produced in one step with FSP. The mineral composition of the supplements was based on their Recommended Dietary Allowance (RDA) values, given for iron (8 mg), zinc (11 mg) and calcium (1000 mg) for males 19-50 years (Otten *et al*, 2006). Since significantly more calcium is required than iron or zinc, materials with a composition based on these RDA values mainly have the properties of calcium.

Solubility i.d.a. was very high for each of the elements, indicating these compounds should have very high in-vivo bioavailability. Particle size was found not to affect dissolution (Figure 1), in strong contrast to pure Fe_2O_3 where the solubility is strongly size-dependent. Calcium/zinc oxides showed the formation of a solid solution by measuring the unit cell volume. This is in contrast to the CaO-ZnO phase diagram where no such solid solutions are found.

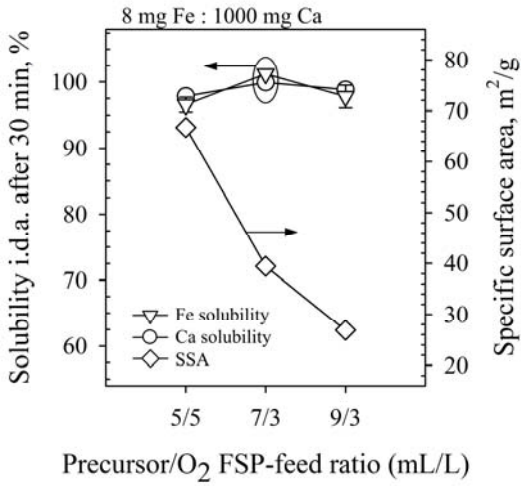

Figure 1. Specific surface area (diamonds), and iron (triangles) and calcium (circles) solubility as function of precursor/O2 FSP-feed ratio, of Ca/Fe oxide. Increasing the precursor/O_2 FSP-feed ratio decreases SSA, which does not influence calcium and iron solubility i.d.a.

This work was supported by ETH Research Grant ETH-06 10-1.

Hilty, F.M., Teleki, A., Krumeich, F., Buchel, R., Hurrell, R.F., Pratsinis, S.E. and Zimmermann, M.B. (2009). *Nanotechnology*, **20**, 475101.

Hilty, F.M., Arnold, M., Hilbe, M., Teleki, A., Knijnenburg, J.T.N., Ehrensperger, F., Hurrell, R.F., Pratsinis, S.E., Langhans, W. and Zimmermann, M.B. (2010). *Nature Nanotechnology*, **5**, 374-380.

Hilty, F.M., Knijnenburg, J.T.N., Teleki, A., Krumeich, F., Hurrell, R.F., Pratsinis, S.E. and Zimmermann, M.B. (2011). *J. Food Sci.* **76**, N2-N10.

Otten, J.J., Hellwig, J.P., Mayers, L.D. (2006) *Dietary Reference Intakes: The Essential Guide to Nutrient Requirements.* Institute Of Medicine of the National Academies, Washington DC.

Rohner, F., Ernst, F.O., Arnold, M., Hilbe, M., Biebinger, R., Ehrensperger, F., Pratsinis, S.E., Langhans, W., Hurrell, R.F. and Zimmermann, M.B. (2007). *J. Nutr.*, **137**, 614-619.

Wieringa, F.T., Berger, J., Dijkhuizen, M.A., Hidayat, A., Ninh, N.X., Utomo, B., Wasantwisut, E. and Winichagoon, P. (2007). *J. Nutr.*, **137**, 466-471.

Zimmermann, M.B. and Hurrell, R.F. (2007). *Lancet*, **370**, 511-520.

Flexible superparamagnetic-plasmonic nanocomposite films with flame-made fillers

Georgios A. Sotiriou, Christoph Blattmann and Sotiris E. Pratsinis

Particle Technology Laboratory, Institute of Process Engineering, Department of Mechanical and Process Engineering, ETH Zurich, Sonneggstrasse 3, CH-8092 Zurich, Switzerland
Keywords: polymers, nanoparticles, iron oxide, silver.
Presenting author email: blattmac@student.ethz.ch

Polymer composites combine the desired functionalities of the host matrix and the inorganic fillers in sensors, optoelectronics, artificial muscles, optical components [1], to name a few applications. The addition of the filler may enhance a certain property of the matrix such as increased Young's modulus [2] and thermal stability or introduce new ones like luminescence and magnetism [3]. This class of materials is not new; polymer composites exist for many years, with perhaps the most well-known ones the automobile tires reinforced with carbon-black, giving them their characteristic color and durability. The superior performance of composite materials has prompted extensive research on both the invention of new types that exhibit unprecedented functionalities, and methods to improve and optimize their manufacturing [4].

When the dimensions of inorganic fillers are reduced to nanoscale, composite properties improve significantly and typically, much less filler is needed to achieve superior performance [1]. For example, the mechanical strength of silicone rubber improves progressively for smaller fillers [2]. The use, however, of nanosized fillers involves a major pitfall; they are difficult to be dispersed homogeneously in a polymer matrix without filler agglomeration [4].

An attractive functionality that can be induced to polymers by filler particles, is superparamagnetism [5]. Such polymers are typically made by embedding superparamagnetic iron oxide nanoparticles in the matrix. The resulting nanocomposites capitalize on the polymer flexibility and can be actuated by an external magnetic field with potential applications in biosensing (lab-on-a-chip) [6], controlled drug-release [7]. For most of these applications a homogeneous dispersion of nanoparticles in the polymer is crucial since formation of large agglomerates can deteriorate the final performance.

Here, a novel fabrication technique of inorganic/polymer nanocomposites is developed by flame-synthesis of nanofillers [8]. This technique allows for fabrication of free-standing multilayer films with tunable thickness composition and functionalities (e.g. superparamagnetic-plasmonic and -phosphorescent), surface smoothness at high filler-contents without formation of large agglomerates. The present fabrication technique can employ a large variety of nanoparticles [8,9] and polymers. In addition it is fast, highly reproducible and scalable [10], facilitating the commercialization of such nanocomposites.

References

[1] Camenzind, A., Caseri, W. R. & Pratsinis, S. E. Flame-made nanoparticles for nanocomposites. *Nano Today* **5**, 48-65 (2010).

[2] Camenzind, A., Schweizer, T., Sztucki, M. & Pratsinis, S. E. Structure & strength of silica-PDMS nanocomposites. *Polymer* **51**, 1796-1804 (2010).

[3] Lu, A. H., Salabas, E. L. & Schuth, F. Magnetic nanoparticles: Synthesis, protection, functionalization, and application. *Angew. Chem.-Int. Edit.* **46**, 1222-1244 (2007).

[4] Twardowski, T. E. *Introduction to Nanocomposite Materials: Properties, Processing, Characterization*. (DEStech Publications, Inc., 2007).

[5] Oh, J. K. & Park, J. M. Iron oxide-based superparamagnetic polymeric nanomaterials: Design, preparation, and biomedical application. *Prog. Polym. Sci.* **36**, 168-189 (2011).

[6] Suter, M., Ergeneman, O., Zürcher, J., Moitzi, C., Pané, S., Rudin, T., Pratsinis, S. E., Nelson, B. J. & Hierold, C. A photopatternable superparamagnetic nanocomposite: Material characterization and fabrication of microstructures. *Sens. Act. B-Chem.* **156**, 433-443 (2011).

[7] Hoare, T., Timko, B. P., Santamaria, J., Goya, G. F., Irusta, S., Lau, S., Stefanescu, C. F., Lin, D. B., Langer, R. & Kohane, D. S. Magnetically triggered nanocomposite membranes: A versatile platform for triggered drug release. *Nano Lett.* **11**, 1395-1400 (2011).

[8] Strobel, R. & Pratsinis, S. E. Flame aerosol synthesis of smart nanostructured materials. *J. Mater. Chem.* **17**, 4743-4756 (2007).

[9] Teoh, W. Y., Amal, R. & Madler, L. Flame spray pyrolysis: An enabling technology for nanoparticles design and fabrication. *Nanoscale* **2**, 1324-1347 (2010).

[10] Pratsinis, S. E. Aerosol-based technologies in nanoscale manufacturing: from functional materials to devices through core chemical engineering. *AIChE J.* **56**, 3028-3035 (2010).

Electrospray deposition of graphene nanosheets

L. B. Modesto-Lopez[1], O. V. Bilousov[2], J. J. Carvajal[2], F. Díaz[2] and J. Rosell-Llompart[1,3]

[1]Department of Chemical Engineering, Universitat Rovira i Virgili, Tarragona, Catalonia, E-43007, Spain
[2] Física i Cristal·lografia de Materials and EMaS, Univ. Rovira i Virgili, Tarragona, Catalonia, E-43007, Spain
[3]Catalan Institution for Research and Advanced Studies (ICREA), Barcelona, Catalonia, E-08010, Spain
Keywords: electrospray, graphene, coatings.
Presenting author email: luis.modesto@urv.cat

Graphene, a 2-D nanomaterial with unique properties (Zhu et al, 2010) is an attractive optically transparent conductor for optoelectronic applications (Blake et al, 2008). Particularly, graphene thin coatings may be used as saturable absorbers, to develop ultrafast pulsed laser technology (Cho et al, 2011). Recently, Chu et al (2010) electrospray-deposited single walled carbon nanotubes, a close relative of graphene, for use as saturable absorbers in the 1.5 μm region, although they can also be used in the 2 μm emission range (Cho et al, 2009). Electrospray is a liquid atomization method that leads to highly charged, nearly monosized micro- and nano-droplets, which has been applied to create thin films and coatings (Jaworek, 2007; Modesto-Lopez & Biswas, 2010). The small droplet size combined with the low flow rate characteristic of electrospray may be ideal to control the film thickness. In addition, the electrostatic control implies a virtual 100 % deposition efficiency. To our knowledge, however, no reports exist yet on the use of electrospray for depositing graphene films.

Therefore, the purpose of this study is to characterize the deposition patterns of graphene onto flat substrates as a function of electrospray operating parameters and to identify conditions leading to layer-by-layer deposition.

Graphene oxide (GO) was synthesized by oxidizing graphite with potassium chlorate in an acidic medium. GO was filtered and washed several times with HCl and distilled water until reaching a neutral pH of the filtrate. Graphene was then prepared by reduction of GO with iron. The obtained graphene nanosheets were filtered and washed with distilled water and ethanol, and then dried at 100 ºC for over 12 h in vacuum. Figure 1a shows a SEM image of a multi-layered graphene particle. Each layer is formed by hundreds of graphene nanosheets, which cannot be observed by SEM. The nanosheets exfoliate individually when suspended in ethanol, as can be seen by TEM (Figure 1b). Graphene was also characterized by Raman spectroscopy and XRD (Figures 1c and d, respectively).

In the electrospray-deposition experiments, graphene nanosheet powder suspensions were prepared in dimethylformamide (DMF). The suspensions were stable over many hours, allowing for sufficient time to carry out depositions. Electrospray was performed solely in the cone-jet mode. Highly stable spraying was obtained at a liquid flow rate of 1 μL/min and applied voltage of 4.4 kV for suspensions of < 0.5 wt % (relative humidity 39 %, temperature 24 ºC).

Electrosprayed graphene nanosheets were collected onto quartz substrates, and their optical characteristics (including linear and nonlinear transmission, nonlinear response dynamics for saturable absorption, saturation fluences, modulation depths and nonsaturable losses) are studied as a function of electrospray-deposition time and initial suspension concentration.

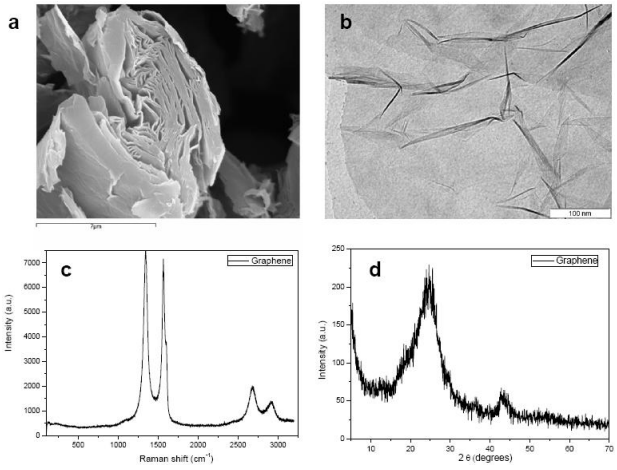

Figure 1. a) SEM of dry graphene layered structure, b) TEM of two superimposed graphene nanosheets, c) and d) Raman and XRD spectra of graphene, respectively.

This work was supported by the Spanish Ministry of Science and Innovation (Grants CTQ2008-05758/PPQ, MAT2011-20255-C02-02, TEC2010-21574-C02-02 and PI09/90527), the Government of Catalonia (Grants 2009SGR1529 and 2009SGR235), and the European Union (Grant FP7-SPA-2010-263044).

Blake, P., et al. (2008) *Nano Lett.* **8**(6), 1704-1708.
Cho, W.B., et al. (2009) *Opt. Express* **17**(13), 11007-11012.
Cho, W.B., et al. (2011) *Opt. Lett.* **36**(20), 4089-4081.
Chu, S., et al. (2010) *Appl. Phys. Lett.* **96**, 051111.
Jaworek, A. (2007) *J. Mater. Sci.* **42**(1): 266-297.
Modesto-Lopez, L. B., Biswas P. (2010) *J. Aerosol Sci.* **41**, 790-804.
Zhu, Y., et al. (2010) *Adv. Mater.* **22**, 3906-3924.

A MEMS sensor based personal sampler for ultrafine particles

S. Merzsch[1], H.S. Wasisto[1], E. Peiner[1], I.Kirsch[2] and E. Uhde[2]

[1] Institute of Semiconductor Technology (IHT), TU Braunschweig, Braunschweig, Germany
[2] Dep. Material analysis and indoor chemistry, Fraunhofer Wilhelm-Klauditz-Institut, Braunschweig, Germany
Keywords: Airborne particles, measurements, ultrafine particles, MEMS.
Presenting author email: erik.uhde@wki.fraunhofer.de

In the production of consumer goods and building materials the use of nanomaterial as additives becomes more and more common. High-tech applications like printed electronics and solar-cells as well as daily life products like toothpaste and cosmetics are enhances by addition of e.g. TiO_2, ZnO, carbon spheres or tubes, and silver particles. Especially in the production environment, where large amounts of nanomaterial is handled and substantial exposure is possible, monitoring of the air quality is an important issue in respect to further use of this technology. In the production industry, a demand for personal monitors to assess the exposure of workers towards these particles undoubtedly exists (Tsai et al, 2011). Unlike a conventional particle counter, such a device must be small and lightweight, and the sensor and the electronics must be simple enough to allow a mass production at low costs.

Simple collection of the particles on filters or impactors offers an affordable solution to this, but requires complex laboratory analysis and can cannot provide timely warning in case of increased concentrations in the surrounding environment.

A MEMS (micro-electromechanical system) based approach was proposed to weigh extremely small particles (Hajjam 2010). This concept was developed further to design a particle detector for use in personal monitors. A joint project (NANOEXPO) examines the possibility of use thermally excited cantilevers as sensors for ultrafine particles. The project aims towards developing a small personal dosimeter-like sampler that collects and weighs ultrafine particles over a work shift.

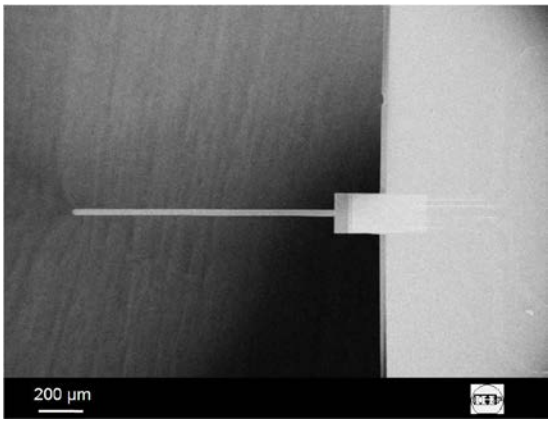

Figure 1. The cantilever sensor.

A slender geometry (Figure 1) allows for a very sensitive detection of particles impacting on the cantilever. After manufacturing the first prototypes of the sensor, and providing proof-of-principle measurements, work is on-going to further improve the sensitivity of the microbalance, to integrate part of the excitation and sensing electronics, and to construct a sampler case with defined flow field around the sensing cantilever.

The following section highlights a number of achievements of the project at the current state.

Results

Cantilevers of different sizes and geometries were tested in regard to their particle collection and sensing efficiencies. Current experiments are carried out with silicon-based cantilever-type resonators with fully integrated Wheatstone bridge piezo-resistors for signal read out.

To test the microbalances, test aerosols were generated in a 1 m³ environmental test chamber by nebulizing a suspension of e.g. carbon nanoparticles (< 30 nm) in water/butanol using a constant output atomizer (TSI 3076), followed by a dryer. Particle number concentration and size distribution is controlled by a fast mobility particle sizer (FMPS, TSI 3091). To improve the collection efficiency, the sensor was mounted on a nanometer aerosol sampler (TSI 3089) – at later stages, the collection voltage will be supplied by the sampler electronics.

Using the second resonant mode, a mass sensitivity of 32.7 Hz/ng was found. Detection limits of less than 1 ng can be achieved with current prototypes under climatic standard conditions and normal pressure.

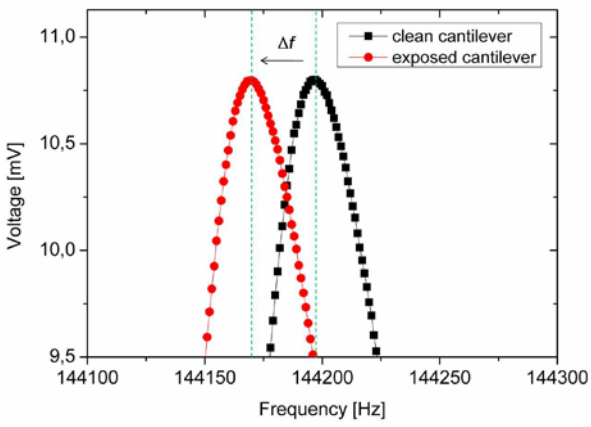

Figure 2. Frequency shift measured with a prototype cantilever (black line: clean cantilever; red line: exposed to carbon aerosol (5000 #/cm³) for 15 min.

Particles were collected predominantly at the tip and along the edges of the cantilever (Figure 3). An improved design of the field around the cantilever will be used to increase the sampling efficiency and to focus the particles deposition to the tip of the cantilever.

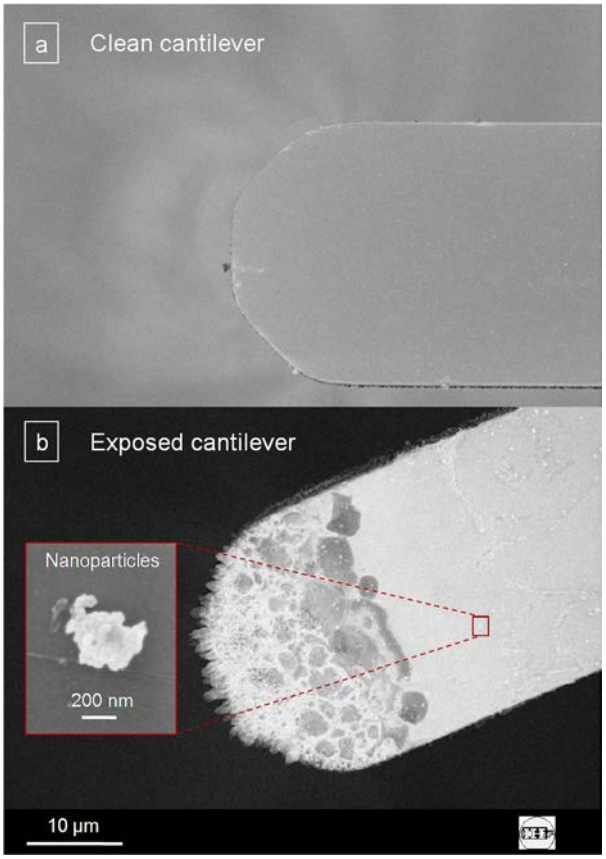

Figure 3. Cantilever tip (a) before and (b) after exposure to airborne carbon particles.

In a next step possible climatic interferences on particle sensing were studied: Temperature and relative humidity were expected to impact on the performance of the sensor. Variation of pressure, temperature and relative humidity during operation of the sensor revealed a minor cross sensitivity: Temperature changes of 2 K, pressure changes of 20 kPa, and relative humidity changes of 10 % during the measurement cycle would lead to an uncertainty of 15% with the current prototypes (Wasisto et al., 2012). Slower climatic changes that extend over several measurement cycles are less critical. Considering a measurement cycle time of only 15 to 30 min, the cross sensitivity is not critical for the workplace environment.

Currently, a sensor case with integrated fan is designed and tested. The main development targets are an optimized air supply to the sensor and a defined electrical field to improve particle collection (Figure 4).

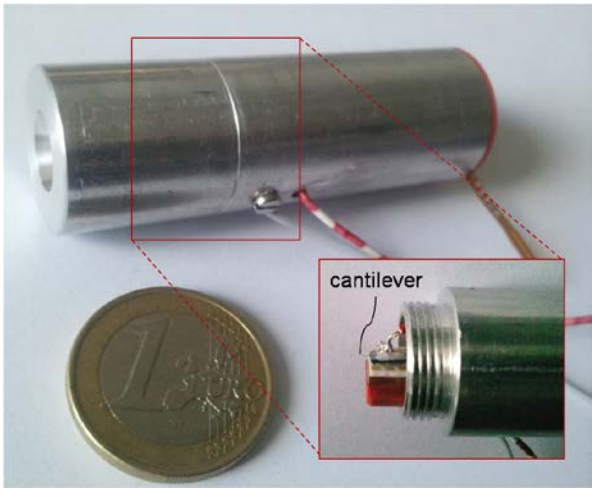

Figure 4. The sensor case with integrated fan.

Conclusion

At the current development stage the microbalance-detector prototypes show a mass-sensitivity sufficient to allow for 15-minute measurement cycles if the (preferred) second resonant mode is used for sensing. A mass resolution below 1 ng can be reached under typical indoor conditions, and the cross-sensitivity in regard to environmental changes is in an acceptable range. Evaluation the performance of the sensor towards a selection of industrially relevant nanoparticles (TiO_2, Silver, Carbon, SiO_2, PTFE) is still on-going, and a number of integration steps have to be finished before the sensor/sampler can be tested under more realistic conditions.

Acknowledgement

The authors greatly acknowledge funding by the German Federal Ministry of Education and Research (BMBF) under grant no. 03X0098A/B.

References

Hajjam A, Wilson J.C, Rahafrooz A, and Pourkamali S. 2010 Fabrication and characterization of resonant aerosol particle mass sensors. *Proc. IEEE-MEMS 2010*, 863-866.

Tsai CJ, Huang CY, Chen SC, Ho CE, Huang CH, Chen CW, Chang CP, Tsai SJ, Ellenbecker MJ, (2011) "Exposure assessment of nano-sized and respirable particles at different workplaces", *J Nanopart. Res*. 13, 4161–4172.

Wasisto H. S., Merzsch S., Waag A., Kirsch I., Uhde E., Salthammer T., Peiner E. (2012) Determination of exposure to engineered carbon nanoparticles using a self-sensing piezoresistive silicon cantilever sensor, *Microsyst. Technol.*, DOI 10.1007/s00542-011-1405-9.

Detecting the Morphology of SiO_2 Aerosols using the Universal NanoParticle Analyzer (UNPA)

R. Wernet[1], A. Gutsche[1], B. Sachweh[2], G. Kasper[1], M. Seipenbusch[1]

[1]Institute for Mechanical Process Engineering and Mechanics,
Karlsruhe Institute of Technology (KIT), 76131, Karlsruhe, Germany
[2]BASF SE, Fine Particle Technology and Particle Characterization, 67056 Ludwigshafen, Germany
Keywords: Measurement (characterization), Particle shape, Aerosol characterization.
Presenting author email: Ruth.Wernet@kit.edu

In a collaboration of the University of Minnesota, TSI Inc. and BASF, the Universal NanoParticle Analyzer (UNPA) was recently developed (Zhun et al., 2012) with the goal of providing an instrument for the analysis of the structure of nano-sized particles. In order to obtain information about the morphology of gas-born particles, the dependence of diffusion charging on the particle structure is utilized. According to Chang's theory for non-spherical particles (1981), the mean charge per particle can be calculated and compared to the mean charge of a spherical particle. This comparison gives evidence about the particle structure. The UNPA contains a DMA classifying particles according to their mobility diameter. The screened aerosol is split into two flows which pass a CPC and a NSAM in parallel. Therefore the particle number concentration and a current, depending on the particle charge which is linked to the particle structure, are measured. The ratio of both is termed "sensitivity" and allows conclusions regarding the particle morphology. Once the sensitivity and size is known, the theories of Lall and Friedlander (2006) and Wang et al. (2010) can be applied to calculate the primary particle size of loose agglomerates. Potential s of the UNPA are accelerating new ENP product development process monitoring. Due to its short measurement time, sensitivity data can be obtained quasi-online.

The aim of the studies was to test UNPA's structure detecting capability. The test particles were made of SiO_2 synthesized by chemical vapor synthesis which would optionally be followed by chemical vapor deposition in tube furnaces.

Three experimental setups were utilized. The purpose of the first approach was the investigation of the primary particle size of agglomerates. For this agglomerates were generated and fed into the UNPA. From the sensitivity data of differently sized agglomerates, the UNPA software was able to calculate the primary particle size. In order to verify the results delivered by the UNPA, small angle x-ray scattering measurements on filter-collected agglomerates were carried out. Furthermore TEM images were analyzed. Good agreement between the three independently determined values was found. In a second approach, spherical particles and agglomerates were mixed and analyzed with UNPA to examine the impact of mixed structures on the sensitivity. To get an idea of the measured particles and to support the interpretation of the sensitivity data, TEM images of sampled particle were taken. Since the sensitivity data of a mixture of particles can be distinguished from those of spheres and agglomerates, an effect of mixture on sensitivity was detected. In a third set of experiments Pt-coated SiO_2 spheres were analyzed to investigate whether the UNPA is able to detect even small surface textures, indicating that particles are not completely spherical. Here different degrees of coating were compared, starting from pure spheres, to lightly and heavily coated supports. Again TEM pictures of the coated particles were consulted. The measurements allow for a correlation between the sensitivity and the degree of coating. The flow patterns of the second and third experimental setups are shown in figure 1.

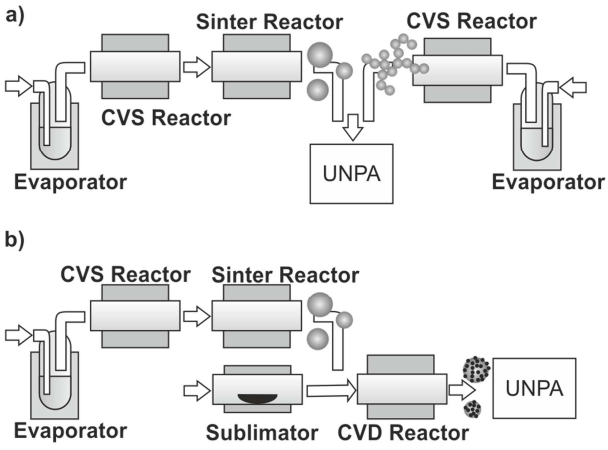

Figure 1: a) Flow pattern of the spherical particles and agglomerates mixing experiment b) Flow pattern of the coating experiment

References

Chang, J.-S. (1981) *J. Aerosol Sci.* **12**, 19-26.

Lall, A.A. and S.K. Friedlander (2006) *J. Aerosol Sci.* **37**, 260-271.

Wang, J., Shin, W. G., et al. (2010) *Aerosol Sci. Technol.* **44**, 97-108.

Zhun, L., et al. (2012) *Aerosol Sci. Technol.* **46**, 333-346.

Acknowledgment

The authors are grateful to TSI Inc. who made the measurements at KIT possible and gave UNPA operating advice.

Mass-Mobility Characterization of Flame-made ZrO_2 Aerosols: the Primary Particle Diameter

M.L. Eggersdorfer[1], A.J. Gröhn[1], C.M. Sorensen[2], P.H. McMurry[3] and S.E. Pratsinis[1]

[1] Department of Mechanical and Process Engineering, ETH Zurich, CH-8092 Zürich, Switzerland
[2] Department of Physics, Kansas State University, Manhattan, Kansas 66506-2601, USA
[3] Department of Mechanical Engineering, University of Minnesota, Minneapolis, Minnesota 55455, USA
Keywords: Agglomerates, Aerosol Particle Mass Analyzer, DMA, Particle Surface Area.
Presenting author email: meggers@ptl.mavt.ethz.ch

Gas-borne nanoparticles generated at high temperatures undergo coagulation forming agglomerates (physically-bound particles) and aggregates (chemically- or sinter-bound particles). The structure of such particles influences their transport, light scattering, effective surface area and density. Significant advances have been made in characterization of agglomerates (physically – bonded particles) by employing fractal theory and relating agglomerate structure to its generation pattern through the mass fractal dimension, D_f. The D_f values have been developed for agglomerates of *monodisperse* primary particles. For coagulating aerosols, however, this needs to be carefully examined as Brownian coagulation leads to polydisperse particles (Eggersdorfer and Pratsinis, 2012). Furthermore, once coalescence or sintering starts between these primary particles, sinter necks are formed between them converting the agglomerates to aggregates.

Real-time characterization of nanoparticles is necessary for continuous monitoring of aerosol manufacturing and airborne pollutant particle concentrations, but is still challenging (Scheckman *et al.*, 2009). Mostly ex-situ methods have been used to characterize such structures in terms of agglomerate mass, mobility and radius of gyration, D_f, primary particle diameter and number and specific surface area (SSA). Figure 1 shows a sphere, an aggregate (Eggersdorfer *et al.*, 2011) and agglomerate (Eggersdorfer and Pratsinis, 2012) having the same mobility diameter, d_m, but different mass and surface area. So measuring only one particle property is not sufficient to characterize those structures.

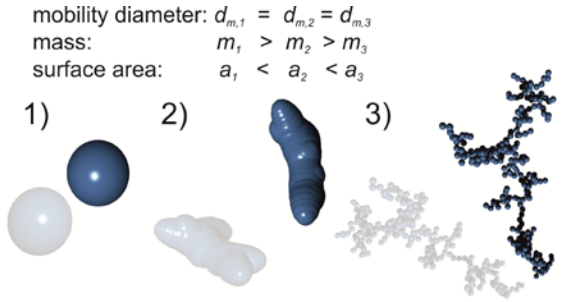

Figure 1. Snapshots of simulated nanoparticle structures: 1) sphere, 2) aggregate & 3) agglomerate.

Here, zirconia nanoparticles are generated by a scalable flame spray process and are characterized in almost real-time with their mass and mobility diameter. The mobility diameter is measured by a differential mobility analyser (DMA) and the mass by an aerosol particle mass (APM) analyser to determine the mass-mobility exponent (D_{fm}). Additionally, a new relation (Eggersdorfer *et al.*, 2012) between surface area mean primary particle diameter, aggregate/agglomerate mass and mobility diameter is used to extract the surface area mean primary particle diameter or SSA from these data. The effect of oxygen flow (Fig. 2) and precursor feed rate as well as precursor concentration on agglomerate/aggregate structure and primary particle diameter are investigated. Good agreement between ex-situ nitrogen adsorption (BET), transmission electron microscopy (TEM) and on-line DMA-APM is found for all investigated process conditions.

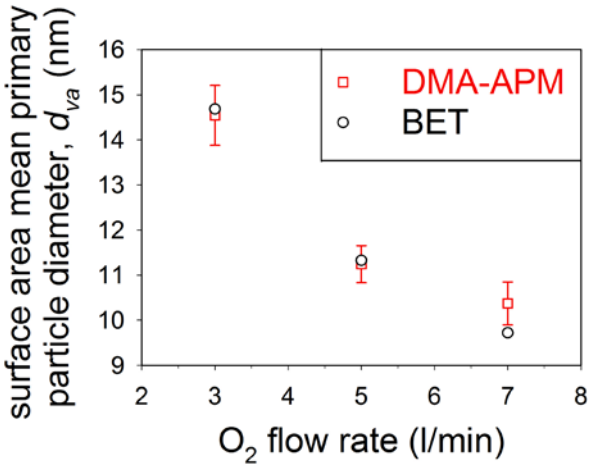

Figure 2. Effect of oxygen flow rate on the surface area mean primary particle diameter measured by ex-situ BET and on-line DMA-APM measurements using a new correlation (Eggersdorfer *et al.*, 2012b).

Financial support by ETH Research Grant (ETHIIRA) ETH-11 09-1 and the European Research Council is gratefully acknowledged.

Eggersdorfer, M.L., Kadau, D., Herrmann, H.J. and Pratsinis, S.E. (2011) *Langmuir* **27**, 6358-6367.
Eggersdorfer, M.L. and Pratsinis, S.E. (2012) *Aerosol Sci. Technol.* **46**, 347-353.
Eggersdorfer, M.L., Kadau, D., Herrmann, H.J. and Pratsinis, S.E. (2012) *J. Aerosol Sci.* **46**, 7-19.
Scheckman, J.H., McMurry, P.H. and Pratsinis, S.E. (2009) *Langmuir* **25,** 8248-8254.

Determination of soot size distributions from spectra extinction measurements: a feasibility study

C. Caumont-Prim[1], J. Yon[1], A. Coppalle[1] and K.F. Ren[1]

[1]UMR 6614 CORIA, Avenue de l'université, BP 8, 76801 Saint Etienne du Rouvray, France
Keywords: soot particles, fractals, soot size distribution, extinction.
Presenting author email: chloe.caumont@coria.fr

The size of nanoparticles in aerosol is currently monitored by using low pressure impactor (ELPI) or differential mobility analysis (SMPS / DMS…). These techniques are expensive and need an aerosol's sampling. Optical techniques under development can also be used to infer size distribution in situ by interpreting scattered light (DLS or SLS). These techniques are generally difficult to implement in industrial applications (car exhaust, control of nanomaterial processes of production…).

A simple and cheap method consists in analyzing measurements of the spectrally resolved extinction of the light by particles. This last method has been successfully used for determining size distributions for polystyrene spherical particles using a commercial spectrometer and a white light source in the visible range (Ren, et al., 2009). For non-spherical particles, extinction spectrum must be interpreted thanks to an adapted light-particle interaction theory. For example, in case of soot particles (which are fractal aggregates (Jullien and Botet, 1987)), the Rayleigh Debye-Gans theory for Fractal Aggregates (RDG-FA (Dobbins and Megaridis, 1991)) can be used. This has been done to determine the soot optical properties (Yon, et al., 2011) knowing the soot size distribution. We propose to test the potential of extinction spectral measurements as a mean to determine soot size distributions.

The RDG-FA theory uncouples absorption and scattering effects for the calculation of light extinction by soot particles:

$$K_{ext} = C_{abs} M_{abs} E(m) + C_{sca} M_{sca} F(m), \qquad \text{(Eq. 1)}$$

Where $M_{abs} = \int_0^\infty N_p N^{agg}(D_g) dD_g$

And $M_{sca} = \int_0^\infty N_p^2 g(R_g, \lambda, D_f) N^{agg}(D_g) dD_g$.

In these expressions, the research size distribution is expressed by $N^{agg}(D_g)$; *E(m)* and *F(m)* are respectively absorption and scattered functions, which depend on *m*, the optical index of soot ($m = n(\lambda) - ik(\lambda)$). D_g, N_p and D_f are parameters which describe size and morphology of the soot; finally C_{abs} and C_{sca} are functions of the primary sphere diameter and wavelength.

The RDG-FA model is incorporated into the inversion procedure developed by Ren (Ren, et al., 2009) in order to find size distribution of non-spherical particles. Spectra extinction measurements have been done on an ethylene diffusion flame, at different height above the burner. The measured extinction spectral was determined applying the Beer-Lambert law on measured transmitted light, $K_{ext} = -\frac{1}{L}\ln\frac{I}{I_0}$ (where L is the length of the extinction bench, I_0 the reference intensity without particles, and *I* the measured light intensity with particles). From these measured extinction spectra, the new inversion procedure is applied allowing determination of a soot size distribution. Figure 1 presents soot size distributions at 8 cm above the burner determined by two ways: inversion of spectrum extinction measurements and Transmission Electron Microscopy pictures analysis (TEM analysis).

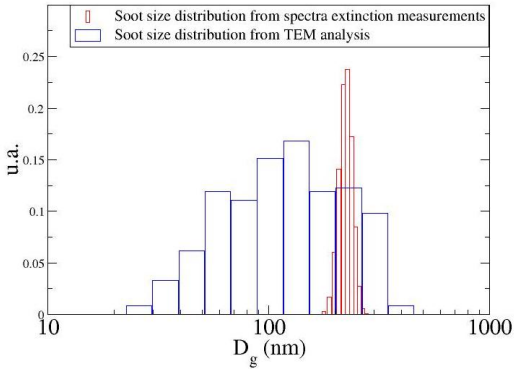

Figure 1 Soot size distributions at 8 cm above the burner in an ethylene diffusion flame

The two results seem very different especially for standard deviation. Soot size distribution found by inversion of the extinction signal is very thin in comparison with the one found by TEM analysis. As shown in Eq. 1, interpretation of extinction spectra needs the knowledge of morphological parameters and spectral optical index. Literature gives a lot of different values and expressions for *E(m)* and *F(m)* (Yon, et al., 2011). Furthermore, information about size distribution is contained in scattering contribution whereas absorption is devoted to the global volume fraction of the aerosol and the absorption term is often more important than the scattered term. That could explain the difficulty to invert and so the difference between the two soot size distributions.

So, a parametric study on optical index and morphological parameters will be presented in order to show if aggregates soot size distributions found from the extinction spectra measurements are reliable.

This work was supported by the French Nat. Res. Agency ANR-09-BLAN-023-02.

Dobbins, R.A. and Megaridis, C.M. (1991) *Applied Optics*, **30**, 4747-4754.

Jullien, R. and Botet, R. (1987) *Aggregation and fractal aggregates*. Word Scientific.

Ren, K., Xu, F., Cai, X. and Dorey, J.-M. (2009) *Chemical Engineering Communications*, **197**, 250-259.

Yon, J., *et al.* (2011) *Applied Physics B*, **104**, 253-271.

Conductivity for Soot Sensing: Possibilities and Limitations

B. Grob[1], J. Schmid[1], N. P. Ivleva[1] and R. Niessner[1]
[1]Chair for Analytical Chemistry, Technical University of Munich, Munich, Bavaria, 81377, Germany
Keywords: electrical conductivity, raman microscopy, soot reactivity, real-time detection
Presenting author email: benedikt.grob@mytum.de

It is a matter of common knowledge that aerosol particles have a significant influence on the climate, environment and human health. Especially in urban areas soot particles emitted by diesel engines, pose a health risk. Current and upcoming limits require a removal of diesel soot particles, which is mainly accomplished by ceramic wall-flow diesel particle filters (DPF). Due to increasing back-pressure the DPF has to be regenerated periodically by gasification of the deposited soot. Thereby the efficiency of the regeneration step is affected by the oxidation reactivity of the deposited soot, which mainly depends on the microstructure of the soot particles. Since the DPF has to be controlled to avoid malfunctions, cheap and reliable tools are demanded for an on-board diagnostic system (OBD). A very promising attempt is the detection of particles by a conductometric sensor (Malik, 2010). Moreover, the conductance is strongly affected by the microstructure, which opens the possibility to use the conductometric sensor method also as a simple cheap and rapid analytical tool for characterization of soot structure.

In our study we want to give a perspective about the possibilities and the limitations of the electrical conductivity measurement for soot sensing. The sensor principle is based on measuring the electrical resistance of deposited particles between interdigitated electrodes. Therefore we developed a thermophoretic precipitator to deposit the particles on an oxidized silicon substrate with a structured 1µm thick AlSiCu layer (Figure 1). The thermophoretic precipitation system could be already tested under real-world conditions in a serial car with a Euro VI diesel engine. Thereby the sensor was validated by a AVL Micro Soot Sensor (photoacoustic aerosol sensor), which has been installed parallel in the car. As shown in Figure 2 the signals of the Micro Soot Sensor and the interdigitated electrodes agreed very well.

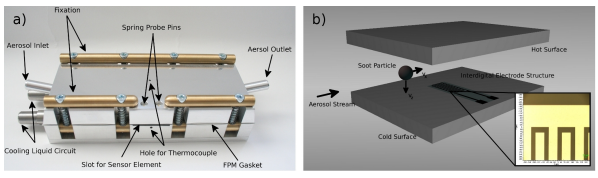

Figure 1: Thermophoretic precipitator with a cooled and heated plate (a) and a slot for a conductometric sensor with interdigitated electrodes (b).

Beside the on-road tests various basic laboratory experiments have been performed. Different commercial available carbon blacks and spark discharge soot were pressed into pellets and the electrical conductivity was determined by a van der Pauw arrangement (van der Pauw, 1958). The results were compared with the standard methods for structural (Raman microspectroscopy) and reactivity (temperature programmed oxidation) analysis (Sadezky, 2005, Schmid, 2011, Grob, 2012). It was shown that the conductivity of carbon materials varies over four orders of magnitude and is strongly influenced by the microstructure.

Moreover the influence of inorganic impurities in the soot matrix was investigated by mixing different materials (which can be found probably in the emitted particles of a combustion engine, i.e. $Fe_2O_3, TiO_2, SiO_2, (NH_4)SO_4, CaO, CaSO_4, MgSO_4, ZnO$) with graphite powder. The samples with varying mass concentrations were milled and compressed to get a thinly dispersed mixture. The composites showed a percolation behaviour with a sharp increase of the conductivity at a critical mass fraction of several orders of magnitude.

With this study we open the way for further research to use a conductometric sensor as a cheap, simple and rapid analytical tool for soot real-time detection and soot structure and reactivity characterization.

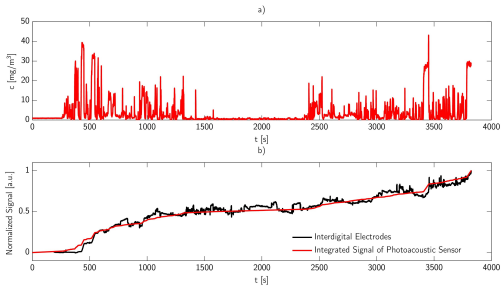

Figure 2: Soot concentration measured by Micro Soot Sensor (AVL List GmbH, Graz, Austria) (a) and correlation between integrated soot mass concentration and the signal of the conductometric sensor with interdigitated electrodes (b).

Grob, B., Schmid, J., Ivleva, P. N., Niessner, R. (2012) submitted to *Anal. Chem.*
Malik, A. *et al.* (2010) *Aerosol Science & Techonology* **45**, 284-294.
Sadezky, A., Muckenhuber, H., Grothe, H., Niessner, R., Pöschl, U. (2005) *Carbon* **43**, 1731-1742.
Schmid, J., Grob, B., Niessner, R., Ivleva, N. P. (2011) *Anal. Chem.* **83**, 1173-1179.
van der Pauw, L. (1958) *Philips Res. Rep.* **13**, 1-9.

Concentrations of particles emitted during spraying of product with silver nanoparticles

Jankowska E. and Łukaszewska J.

Department of Chemical and Aerosol Hazards, Central Institute for Labour Protection – National Research Institute, Czerniakowska 16, 00-701 Warsaw, Poland
Keywords: silver nanoparticles, emission, number and surface concentrations, mass concentration.
Presenting author email: joluk@ciop.pl

The aim of the investigation was to determine the parameters of particles emitted to the air during spraying commercially available Product for Glass Cleaning (PGC) from Nano SILVER.

Investigation were done in the chamber with diameters 3x4,7x2,3m with ventilation switch-off. Before measurements ventilation was switch-on (from 12:25 to 12:37) for the time in which quite stabile background concentrations of particles were received. Spraying of PGC were conducted (from 12:38 to 15:34) seven times for the 10s on the surface located in the distance 52cm from the sampling points. After spraying of PGC ventilation was switch-on (from 15:35 to 15:53) for removing from the chamber air particles emitted during spraying PGC.

A following parameters of particles were determined: number concentrations (P-TRAK and GRIMM), surface concentration (AERO-TRAK) and mass concentration (DUST-TRAK).

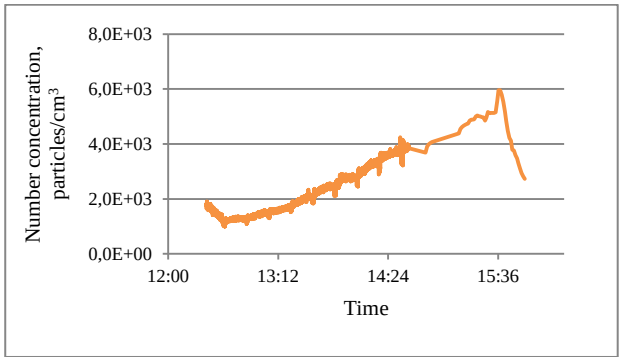

Figure 1. Number concentration of particles 20-1000nm (P-TRAK results).

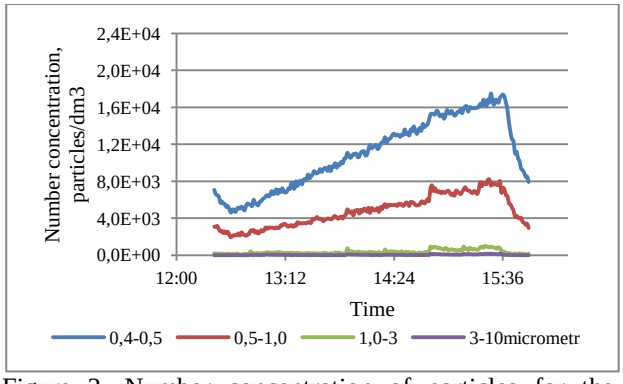

Figure 2. Number concentration of particles for the ranges 0,4-0,5µm, 0,5-1,0µm, 1,0-3µm and 3-10µm (GRIMM results).

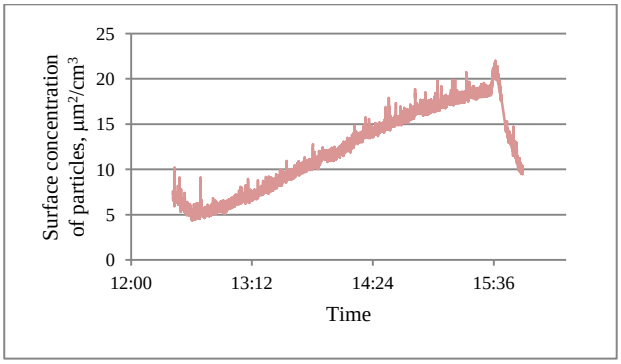

Figure 3. Surface concentration of particles 10-1000nm (AERO-TRAK results – fraction "A" alveolar).

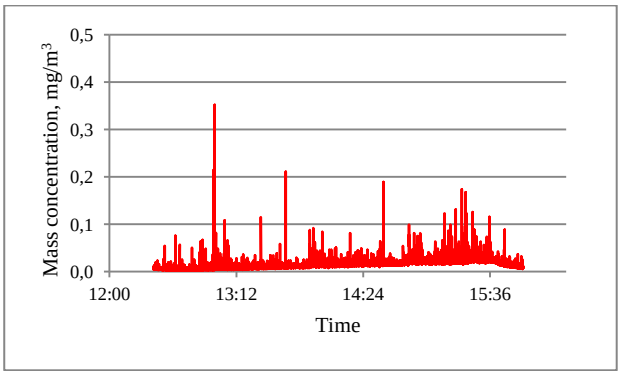

Figure 4. Mass concentration of particles 0,1-10µm (DUST-TRAK results).

It results from the analysis of data presented on Figures 1-3 that number and surface concentrations of particles increased evenly and the visible maxima of the concentration associated with the spraying products didn't appear. Switch-on of ventilation before spraying (from 12:25 to 12:37) an after spraying (from 15:35 to 15:53) with airflow 2000m^3/h significantly influenced on the decrease of number and surface concentrations. Above discussed changes weren't observed in case of mass concentrations determined with DUST-TRAK for particles 0,1-10µm (Figure 4).

This study has been prepared within RP CIOP-PIB (No. I-30) and NANODEVICE project (number FFP7 211464). The views and opinions expressed in this presentation do not necessarily reflect those of the European Commission.

Continuous tandem DMA determination of the mass and charge distribution of electrosprayed nanometer polystyrene particles

M. Attoui[1], J. Fernandez-García[2], J. Cuevas[3], G. Vidal[3] and J. Fernandez de la Mora[2]
[1]M. Attoui, Universty de Paris 12, 94010 Creteil, Paris, France; Presenting author: attoui@univ-paris12.fr
[2]Department of Mechanical Engineering, Yale University, New Haven, CT 06520-8286, USA
[3] SEADM, Parque Tecnológico de Boecillo, 205; 47151 Boecillo, Valladolid, Spain.
Keywords: nanoparticle, size, charge, tandem DMA.

Nanoparticle studies based on a differential mobility analyzer followed by a mass spectrometer (DMA-MS) produce informative two-dimensional (2D) maps which have revealed unusual transitions such as shape changes at critical sizes and charges (Larriba et al. 2012), single molecule evaporation activated by the Kelvin effect on presumably involatile materials (Hogan et al 2010), charge loss transitions of apparently stable clusters (Rus et al, 2010), etc. However, these transitions are difficult to study quantitatively by DMA-MS due to uncontrolled heating of the particles by confining radiofrequency fields as they enter the MS. In order to investigate these phenomena controlling temperature and residence time during the transit between two analyzers we have assembled a tandem DMA (DMA^2) system (Rader & McMurry 1986) where the voltages V_1, V_2 of both DMAs are scanned in an effectively continuous fashion.

Experimental. The two nano-DMAs used were of the Half-Mini type (Fernandez de la Mora 2011). The computer control program was developed at SEADM. It scans the two DMAs over a 2-dimensional (2D) grid of voltages and measures the corresponding nanoparticle current I exiting the second DMA. The resulting 3D data set (V_1, V_2, I) is stored as a single file and can be represented via 2D graphics

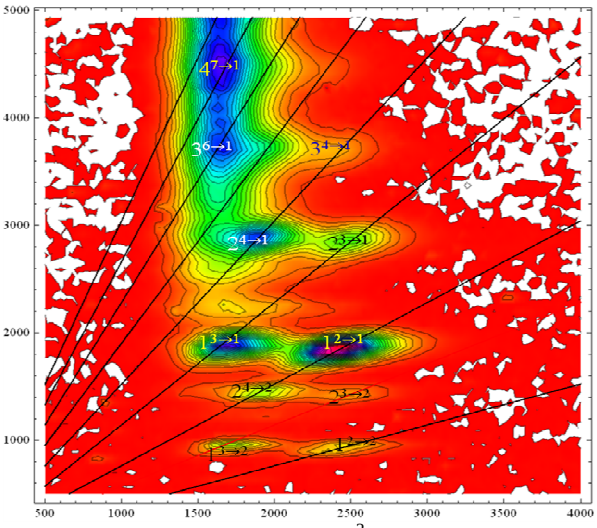

Figure 1: 2D continuous DMA^2 spectrum of multiply charged polystyrene particles 4.7 to 7.5 nm in diameter.

The system has been tested by studying aerosols of nanoparticles electrosprayed from a 1 mM solution of polystyrene (Psty) dissolved in l-methyl-2-pyrrolidone (NMP) seeded with 10% (vol) dimethylammonium formate (Ude *et al*, 2006). DMA_1 analyzes the Psty particles in their natural charge state, as electrosprayed. The aerosol is then charge-reduced on its way to DMA_2 by flowing through a tube internally coated with Ni^{63} (10 mCi).

Results. Figure 1 shows the 2D mobility spectrum from a spray of Psty with a relatively narrow size distribution and average molecular weight M_w=34.5 kDa. The line labelled 1 corresponds to particles having the same mobility (same charge state) on both DMAs. Its slope will be denoted k. Lines labelled 2, 3, .. have slopes 2k, 3k,... The peaks labelled $n^{z\to z'}$ correspond to aggregates of n chains (n-mer) of Psty 34.5 kDa having passed with z and z' charges through DMA_1 and DMA_2, respectively. They can be identified unambiguously (i) because they lie over lines of slope k(z/z'); (ii) Because the charge reduction process is relatively efficient, the most abundant peaks correspond to z'=1, so that peaks $n^{z\to 1}$ of given n fall on horizontal lines whose abscissa give the (known) mobility of the singly charged n-mer. The monomer, dimer, trimer and tetramer carry primarily 2, 4, 6 and 7 charges, respectively. The larger aggregates are less efficiently discharged, whence the greater number of surviving charge states crowd together on the upper left region of the plot, precluding clear peak assignment. The present approach is limited by the poor transmission of high mobility multiply charged particles through the tandem DMA, particularly due to space charge losses from the ES chamber to the inlet of the first DMA. These losses are moderated at the relatively large sample flow rates used here, though this reduces the efficiency of the neutralizer and the resolving power of the DMA. The acquisition (typically 10^4 points) is also slow due to the ~1s response time of most aerosol instruments. These limitations will hopefully be alleviated by use of a planar DMA on the first stage, whose high transmission will permit moderate sample flow rates and the use of a faster electrometer.

Fernandez de la Mora, J. (2011) pp. 697-721 in *Aerosol Measurement*; P. Kulkarni, P.A. Baron, K. Willeke editors, John Wiley & Sons, Inc. 2011
Hogan, C. J. *et al* (2010), J Am. Soc. Mass Spectrom. 21, 1382-1386
Larriba, C. *et al.* (2012), *J. Phys. Chem. B*, 116, 593-598
Rader, D.J., McMurry P.H. (1986) J. Aerosol Sci. 17(5) 771-787
Rus, J. et al. (2010), *Int. J. Mass Spectrom*, **298**, 30-40
Ude, S. *et al.* (2006), *J. Coll. Int. Sci.*, **293**, 384-393.

A carbon nanotubes suspension study by vortex shaker : Sampling and mass analysis

A.Ustache[1], D. Bernard[2], O. Le Bihan[1], E. Peyret[1], O. Aguerre-Chariol[1]

[1]Institut national de l'environnement industriel et des risques (INERIS), Parc Technologique Alata BP 2, 60550 Verneuil-en-Halatte, France
[2]ARKEMA, France
Keywords: Nanotubes, Nanoparticles, characterization, generation, TEM, TEOM
Presenting author email: aurelien.ustache@ineris.fr

New materials based on nanotechnology are reaching the market in a wide variety of consumer products. Since these nanostructured materials can be in powder form, a suspending powder system is essential for many purposes:

- For in vivo inhalation toxicological studies
- For dustiness evaluation

Different powders suspending systems have been developed like the rotating drum or the single drop. They are used as a reference method to evaluate bulk materials dustiness. Usually cumbersome, these systems need a huge amount of powder (a few hundred grams) and require time-consuming cleaning processes which could be even more tedious when a nanostructured material and/or a toxic powder is used. The vortex shaker is proposed as a solution. Quite easy to handle, this system requires a very small amount of powder (a few grams) in a tube. It has been set up to study the dustiness of any type of powder under controlled and reproducible conditions.

The aim of this work is to aerosolize Multiwalled carbon nanotubes Graphistreght C100 and characterise the generated aerosol. The set up is designed to aerosolize, observe and quantify the carbon nanotubes mass.

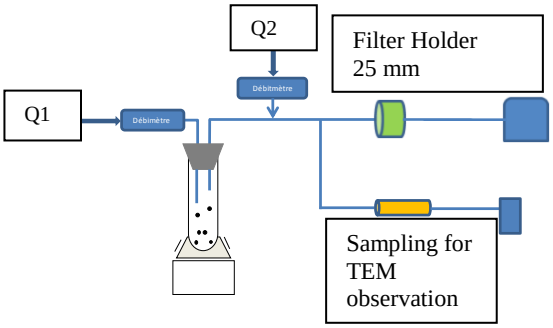

Figure 1 : Set up
Q1,Q2: Respectively clean and dry air in the tube and for dilution

In order to observe the generated particles with a Transmission Electronic Microscope giving information on size distribution, particle shape and composition, a TEM grid sampler was operated. This sampler, coupled with a Gilian LFS-113DC pump, allows the aerosol trapping through a copper grid whose pictures are shown on figure 2. The observed aerosol display different type of shape: agglomerate on the left picture, single nanotube on the right.

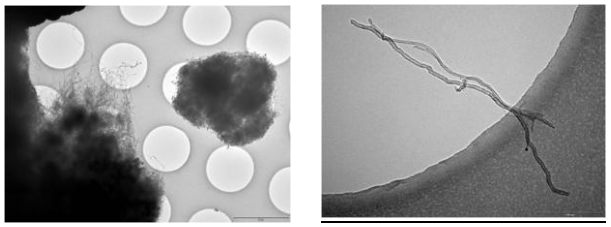

Figure 1:TEM picture at two different scales

In parallel, to measure the aerosol mass, samples have been performed on a 25 mm quartz filter. The carbon nanotubes deposited on the filter are oxidized by combustion at 980°C in the module SSM 5000A (Solid Sample Modul). The melting point is lowered by addition of V_2O_5. Platinum is used as catalyzer. The carbon is then released in CO_2 measured by non dispersive infrared analysis by a Shimadzu detector. To lower the quantification limit, a second infrared detector, the MIR6000 was added in series to the first one. This assembly allows to obtain a limit of quantification of 5 µg / filter.

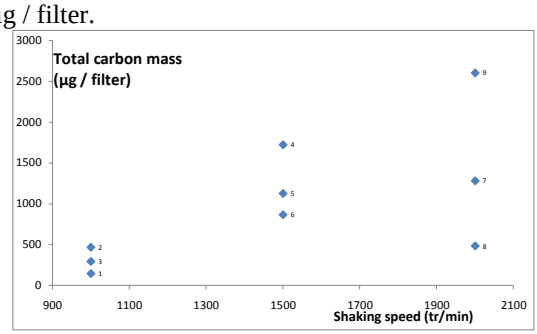

Figure 2: Correlation between the total carbon mass and the shaking speed.

An hour sampling time was repeated three times at three different shaking speeds. The mass and the standard deviation increase with the shaking speed.

A continuous mass measurement with TEOM will be added in the set up in order to determine the stability of the aerosols concentrations.

This work is supported by ARKEMA France

Baron *et al 2008 ; Aerosolization of Single-Walled Carbon Nanotubes for an Inhalation Study ;*
Maynard *et al 2004 ; Exposure to carbon nanotube material: aerosol Release during the handling of unrefined singlewalled Carbon nanotube material*
EN 15051-3, *2008; Workplace atmospheres - Measurement of the dustiness of bulk materials*
Isamu Ogura *et al, 2009. Nanosafe 2008, Journal of Physics: Conference Series 170 (2009)*

Influences on nanoparticle size distributions generated by the spark principle

J. Spielvogel, R. Joachim, M. Schmidt

Palas GmbH, Karlsruhe, 76229, Germany
Keywords: aerosol generation, nanoparticles, agglomerates, particle size distribution
Presenting author email: spielvogel@palas.de

In various fields of study a defined and well characterized nano particle source is essential to creating precise and reproducible measurements. The Palas defined nano particle (DNP) generators that generate aerosol particles by electrode atomization in a spark discharge are widely used in the fields of toxicology and automotive. In the latter the particle generators are used to calibrate the emission measurement systems that were defined in the framework of the particle measurement programme (PMP) and put into regulation in the EURO 5b emission standard.

These types of aerosol generators have unique advantages. They can generate a steady stream of high concentrations of particles over a wide mobility range. When this is used in combination with a differential electrical mobility classifier (DEMC) a very well defined calibration aerosol is obtained. By changing the electrode material a large number of materials can be aerosolized.

In this presentation we will present a thorough comparison of submicron particle size distributions resulting from the use of different aerosol materials e.g. carbon, gold, copper, stainless steel and the use of different carrier gases e.g. nitrogen, argon. By adjusting instrument parameters such as the spark frequency the sizes of the formed agglomerates can be tuned to the region of interest (see figure 1). These particle size distributions are measured and characterized using the U-SMPS.

Figure 1 shows an example of the influence of spark frequency on the generated size distribution.

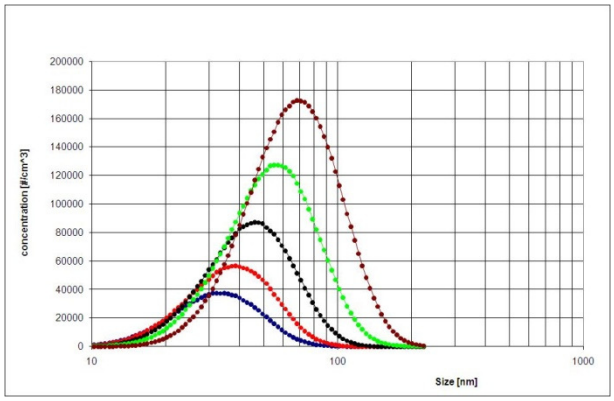

Figure 1. Size distributions of particle agglomerates at different spark frequencies.

In the second part of the presentation the underlying process will be examined theoretically. Correlations between spark frequency, evaporation temperature, and particle size and number concentration are examined and presented.

Bau S. Witschger O. Gensdarmes F. Thomas D. Borra J.P. (2010) Electrical properties of airborne nanoparticles produced by a commercial spark-discharge generator *J. of Nanoparticle Research*, Vol. 12, Issue 6, 1989-1995

Tabrizi N.S. Xu Q. Van Der Pers N.M. Lafont U. Schmidt-Ott A. (2009) Synthesis of mixed metallic nanoparticles by spark discharge *J. of Nanoparticle Research*, Vol. 11, Issue 5, 1209-1218

Nanoparticle Emission Measurement during Polymer Extrusion Experiments

Yu-Ying Kuo,[1,2] Jelena Buha,[1,2] Haijun Zhang,[3] Andreas Gerecke,[2] Giuseppino Fortunato[2] and Jing Wang*[1,2]

[1] Institute of Environmental Engineering, ETH Zürich, CH-8093 Zürich, Switzerland
[2]Swiss Federal Laboratories for Materials Science and Technology, Empa, Switzerland
[3]Dalian Institute of Chemical Physics (DICP), Chinese Academy of Sciences, Dalian 116023, China
Keywords: chemical properties, particle characterization, size analysis, TiO_2 nanoparticles.
Email: yu-ying.kuo@empa.ch

Pilot melt spin-tester has been widely used in the research of polymer composites for years, due to its capability of producing bi- and tri-component composite fibres, and relatively small requirement of materials. Recently, this technique is frequently applied in many fields such as the development of carbon fibre composites (Shaffer *et al*, 2004) and biodegradable materials (Hufenus *et al*, 2012). The safety assessment of the operating environment, however, has not been conducted extensively. The effect of the potential nano-scale bi-products generated by the heating extruding procedure is still unclear while researchers and operators have been working in this environment for long time-durations without suitable protective equipment. Based on the known damage by micro-particles to human being, the increasing interest about nanotoxicology, and potential work-place nanoparticle emission (Wang *et al*, 2011, 2012, and Walser *et al*, 2012), safety in melt spinning plants could be a serious topic.

We measured the emitted aerosol particles in the working environment of a fibre melt spinning production, which features mixing of polyester (PET) and P25 TiO_2 nanoparticles. The setup was built under a ventilation hood for isolating workers from the emissive particles. Measurement was performed in both the case of pure PET extrusion and the case of extrusion of the mixture of PET and nanoparticles. A fast mobility particle sizer (FMPS) and a nano-micro-orifice uniform-deposit impactor (MOUDI) were employed to measure aerosol particle distribution. Samples for SEM and TEM were prepared in order to directly measure the structural properties. The usage of a thermo-denuder (TD) enabled separation of the volatile components of the particles and further characterization of the chemical composition was performed by a GC-MS with a Thermal Desorption Unit (TDU) using impactor samples.

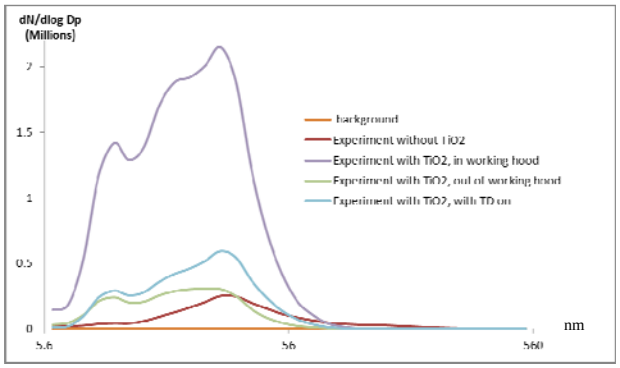

Figure 1. Size distribution of particles analysed in different experiments based on FMPS.

Based on the measurements in the hood by FMPS, the total concentration was $3*10^5$ #/cm^3, ten times as the background value in the experiment without TiO_2. The concentration increased up to around $6*10^5$ #/cm^3 when TiO_2 was added but then down to 10^5 #/cm^3 when it was sampling outside of the ventilation hood. Even the total concentration fluctuated, the size distribution did not change substantially, not even with the change of mixing ratio between the polymer and nanoparticle material. The particle sizes were in the range of 10-100 nm in all tests and the majority were smaller than 30 nm (Fig 1).

With the operation of the TD, the total concentration dropped to 150,000 #/cm^3 in TiO_2 experiment. This indicates that non-volatile particles existed since the heating of air stream in the TD removed volatile particles. SEM and TEM images (Fig 2) showed both polymer and TiO_2 particles. Agglomerates of TiO_2 nanoparticles were observed in the size range from 200 nm to a few microns. The analysis by GC-MS provided further information about the composition in both particle and gas phases. Fragments of broken PET chain, the terephthalate esters, were found in the full-field scanning analysis.

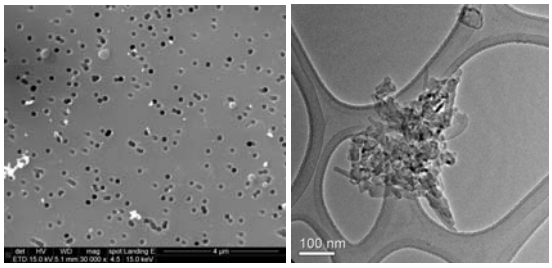

Figure 2. SEM (left) and TEM (right) images of mixture of polymer and TiO_2.

Hufenus, R., Reifler, F. A., Maniura-Weber, K. Spierings, A., and Zinn. M. (2012) *Macromol. Mater. Eng.*, **297**, 75–84.

Sandler, J.K.W., Pegel, S., Cadek, M., Gojny, F., van Es, M., Lohmar, J., Blau, W.J., Schulte, K., Windle, A.H., Shaffer, M.S.P. (2004) *Polymer* **45**, 2001–2015.

Wang, J., Asbach, C., Fissan, H., Hülser, T., Kuhlbusch, T.A.J., Thompson, D., Pui, D.Y.H. (2011) *J. Nanopart Res*, **13**, 1373 – 1387.

Walser, T., Hellweg, S., Juraske, R., Luechinger, N.A., Wang, J., Fierz, M. (2012) *Sci Total Environ*, doi:10.1016/j.scitotenv.2012.01.038.

Wang, J., Asbach, C., Fissan, H., Hülser, T., Kaminski, H., Kuhlbusch, T.A.J., Pui, D.Y.H. (2012) *J. Nanoparticle Res*, DOI: 10.1007/s11051-012-0759-y.

Dissociation rates of Fe_2^+, Fe_2^-, and Fe_2

M. Noppel

Institute of Physics, University of Tartu, Ülikooli 18, 50090 Tartu, Estonia
Keywords: iron dimers, dissociation rate.
madis.noppel@ut.ee

Iron nanoparticles have a wide field of technical applications due to their magnetic, electronic and catalyst properties. They are extensively used in synthesis of carbon nanotubes, where the uniformity and controllable size of particles plays essential role. One way for the generation of particles is their gas-phase synthesis. For a better understanding and description of gas-phase formation processes, kinetic data are necessary. Giesen et al (2003) found that the major initial reactions for the understanding of the condensation of iron vapour are the formation and the decomposition of Fe_2. In the following we present the preliminary results of calculations of the dissociation rate coefficients of ionic and neutral iron dimers.

Dissociation rate coefficients are calculated by RRKM theory. Experimental dissociation energies, vibration frequencies, equilibrium bond lengths of dimers and electronic level values of iron atoms and atomic cations are taken from literature as well as the density functional theory values of higher electronic energy levels of dimers. As ab initio calculation results are still uncertain, experimental dissociation energies are used to estimate energy barrier value for dissociation reactions. Available experimental and theoretical results refer that there is an energy barrier for reverse association reaction of neutral iron atoms. Therefore, in calculations, the moments of inertia of activated complex and dimer are taken approximately equal. For the activated complex of ionic dimers the "apparent" moment of inertia is used (Waage *et al*, 1970).

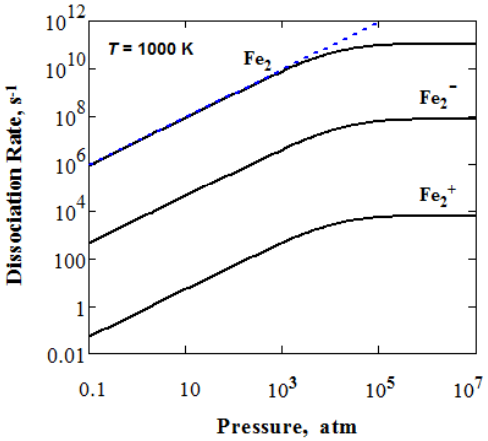

Figure 1. The pressure dependence of dissociation rates of Fe_2^+, Fe_2^-, and Fe_2 at temperature T=1000 K. Dashed curve represents rate of Fe_2 by Giesen *et al* (2003).

Figure 1 shows that at common experimental pressures calculated dissociation rates are located in the fall-off regime. In Figure 2 the temperature dependence of dissociation rates in low-pressure region are presented.

The obtained dissociation rate of Fe_2 is close to the result by Giesen *et al* (2003) at temperatures of their experiments, but the dependence on temperature is weaker. Ionic dimers, especially cations, are remarkably more stable than neutral dimers Fe_2.

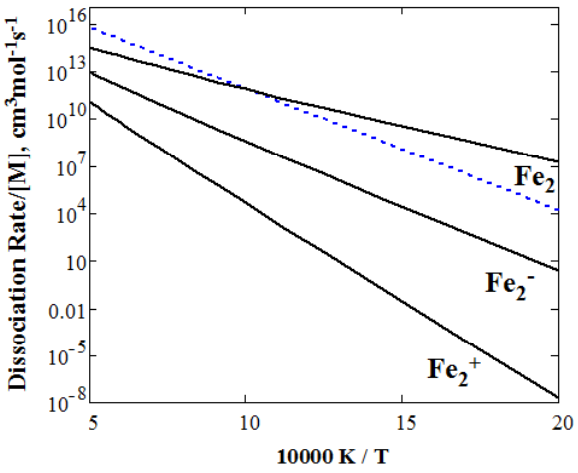

Figure 2. Arrhenius plot of the dissociation rate coefficients. Dashed curve represents rate of Fe_2 by Giesen et al (2003). At low pressure unimolecular reaction rates become proportional to buffer gas concentration [M].

This work was supported by the Estonian Science Foundation under grant 8806 and the Estonian Research Council Project SF0180043s08.

Giesen, A., Herzler, J. and Roth, P. (1970) *J. Phys. Chem. A,* **107**, 5202-5207.

Waage, E. and Rabinovitch, B. (1970) *Chem. Rev.* **70**, 377-387.

Surface concentration of particles emitted during burning of foams with nano-objects

Jankowska E., Sobiech P., Łukaszewska J. and Zatorski W.

Department of Chemical and Aerosol Hazards, Central Institute for Labour Protection – National Research Institute, Czerniakowska 16, 00-701 Warsaw, Poland
Keywords: nano-objects, foams, emission, surface concentration.
Presenting author email: pisob@ciop.pl

The aim of the investigation was to determined surface concentration of particles emitted during burning of two types of foams with ca. 9% of nano-objects: foam (TT) with titanium dioxide and foam (MMT) with Nanomer I.34TCN nanoclay which is a surface modified montmorillonite.

Investigation were done during burning of each foam for 30s. Surface concentrations of particles with size 10-1000nm were measured with AERO-TRAK for the scenarios described in Table 1.

Table 1. Scenarios of measuring surface concentration of emitted particles.

Abbreviations	Description of scenarios/time(s)
1. BB-TT/4800	Before burning of TT foam/4800s
2. JBB-TT/30	Just before burning of TT foam/30s
3. DB-TT/30	During burning of TT foam/30s
4. JAB-TT/30	Just after burning of TT foam/30s
5. BB-TT/MMT /6240	Between burning of TT and MMT foams/6240s
6. JBB-MMT/30	Just before burning of MMT foam/30s
7. DB-MMT/30	During burning of MMT foam/30s
8. JAB-MMT/30	Just after burning of MMT foam/30s
9. AB-MMT/7380	After burning of MMT foam/7380s

Table 2. Surface concentration of particles presented in the air during different scenarios.

Scenarios	Surface concentration of particles ($\mu m^2/cm^3$)			
	Min	Max	Median	ArMean
1. BB-TT/4800	26	33	30	29
2. JBB-TT/30	27	28	28	28
3. DB-TT/30	35	13422	1370	2943
4. JAB-TT/30	1281	5105	2682	2712
5. BB-TT/MMT /6240	166	5105	331	375
6. JBB-MMT/30	166	174	169	170
7. DB-MMT/30	320	2632	757	1111
8. JAB-MMT/30	506	1867	737	975
9. AB-MMT/7380	27	1867	175	182

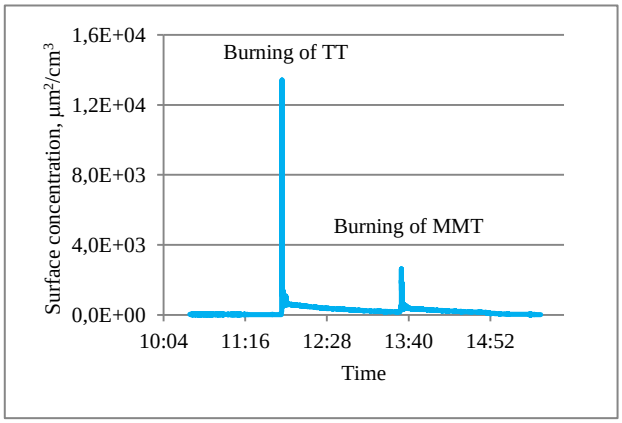

Figure 1. Surface concentration of particles 10-1000nm (AERO-TRAK results for fraction "A").

It results from the analysis of data presented in Table 2 and Figure 1 that depending of the type of foam during burning can be emitted particles with different surface concentrations: higher for TT foam with mean concentration 2943$\mu m^2/cm^3$ and lower for MMT foam 1111$\mu m^2/cm^3$. Maximum value of surface concentration of particles emitted during burning of TT foam was 13422$\mu m^2/cm^3$, when during burning of MMT foam 2632$\mu m^2/cm^3$. Measured values of surface concentrations were higher than that recommended to measured with AERO-TRAK for the fraction "A" (alveolar).

Process of burning can significantly influenced on the increase of surface concentration of particles presented in the air, especially just after burning. During the period of 30s after burning of foams mean surface concentrations of particles were very high (2712$\mu m^2/cm^3$ for TT foam and 975$\mu m^2/cm^3$ for MMT foam).

Particles emitted during burning can presented in the air log time. In the period of 6240s mean surface concentration after the burning of TT foam was 375$\mu m^2/cm^3$, when in the period of 7380s after burning of MMT foam 182$\mu m^2/cm^3$. The surface concentration of particles achieved the value similar to the mean concentration obtained before burning (28-29$\mu m^2/cm^3$) only 7380s after burning of MMT foam.

This study has been prepared within RP CIOP-PIB (No. I-39) and NANODEVICE project (number FFP7 211464). The views and opinions expressed in this presentation do not necessarily reflect those of the European Commission.

Real-time measurement of airborne nanoparticles released to a windtunnel and filtration test

I.M. Kammenou[1,2], J. Wang[1,2]

[1]Department of Civil, Environmental and Geomatic Engineering, Institute of Environmental Engineering, Swiss Federal Institute of Technology, ETH Zürich, Zürich, 8093, Switzerland
[2]Laboratory of Analytical Chemistry, Swiss Federal Institute for Materials Testing and Research, EMPA, Zürich, Dübendorf, 8600, Switzerland
Keywords: Aerosol generation, aerosol measurement, filtration, nanoparticles.
Presenting author email: ikammenou@ethz.ch

Nowadays there is an intense concern about the health hazard posed to humans exposed to inhalation of toxic nanoparticles [1]. It is supported that engineered nanomaterials are released at high mass and/or number concentrations only under unusual circumstances and the particles are also present in air as agglomerates of several hundred nm [2, 3, 4].

Airborne nanoparticles are released to the windtunnel located at EMPA Dübendorf and a series of experiments are performed to measure them. Specifically, the nanoparticles are released via a nozzle into a DIN EN 779 windtunnel at different injection flow rates and carried downstream by controlled air flow. The nanoparticles are monitored at two different sampling points, upstream and downstream of the filter. Sampling probes capable of isokinetic sampling are used to transport nanoparticles from the windtunnel to the measuring instruments, with the aim to obtain information on nanoparticle size and number concentrations. The filtration efficiency is also studied under different experimental conditions based on DIN EN 779.

Standard aerosol instruments, including SMPS, OPC, and FMPS are used for the measurement of generated airborne nanoparticles. The particle concentration can be controlled by adjusting the flow rates of the aerosol and the windtunnel flow. An Atomizer Aerosol Generator (TSI 3079), a 6-Jet-Atomizer (TSI Model 9306A) and a furnace have been adopted for generation of the aerosols in various experiments. The temperature and humidity of the clean air can be controlled using a heater and a humidifier upstream of the flow straightener. NaCl and KCl solutions in different concentrations (% w/t) and silver powder purchased from Sigma Aldrich are experimented for the aerosol generation.

The following figure (figure 1) depicts the filter efficiency in all the cases studied. It is observed that the initial efficiency for 0.35 μm is generally higher than 72.2 % (observed at 1000 m^3/h) and the maximum level of efficiency achieved is 100% under all windtunnel flow rates. The standard airflow rate for F7 filter used in these studies is 3400m^3/h. In figure 2, it is observed that the higher the temperature, the bigger the peak of the particle number-size distribution. Furthermore, the nanoparticle size is increased at elevated aerosol flow rate when the temperature remains the same.

Future studies will be oriented in analyzing the transport characteristics of nanomaterials after their release, as well as their morphology and structural properties.

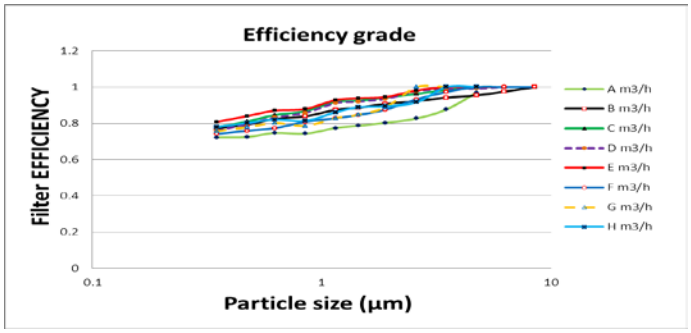

Figure 1. F7 (DIN EN 779) Filter efficiency under A-H windtunnel airflow rates (m^3/h), A<H, 6% w/t NaCl.

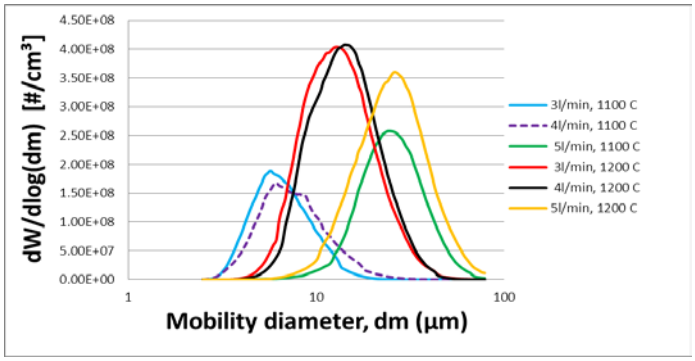

Figure 2. Size distribution of silver nanoparticles generated by a furnace under 1100 and 1200 ^{0}C and 3 to 5 l/min airflow rate.

1. Mostofi, R., Wang, B., Haghighat, F., Bahloul, A., Jaime, L. (2010), *Industrial Health* **48**, 296-304.
2. Kuhlbusch, T.A.J., Neumann, S., Fissan, H. (2004) *Journal of Occupational and Environmental Hygiene* **1:10**, 660–671.
3. Kuhlbusch, T.A.J. and Fissan, H. (2006) *Journal of Occupational and Environmental Hygiene*, **3:10**, 558-567.
4. Seinfeld, J. and Pandis, S. (1998) *Atmospheric Chemistry and Physics*, J. Willey INC.

Structure deformation of Ag nanoparticle clusters induced by deposition onto carbon nanotubes

T. Shinohara, N. Nishida, H. Tanaka

Institute of Science and Engineering, Chuo Univ. 1-13-27 Kasuga, Bunkyo-ku, Tokyo, 112-8551, Japan

Keywords: Ag nanoparticle cluster, carbon nanotube, size selection, deformation

Presenting author email: hnznshubiduba1354@yahoo.co.jp

Nanoparticles have been considered to be expected as building blocks to construct nanocomposites with surprisingly unique properties. Especially, Ag nanoparticles are good candidates for this purpose because they have specific chemical and optical properties. While it is relatively easy to produce these nanoparticles in the gas phase using gas-aggregation technique, it is not easy to avoid aggregation each other because of their surface activity. In this regard, we have synthesized Ag nanoparticle clusters previously, which are composed of surface-active Ag nanoparticles and surface-inactive C_{60} nanoparticles [1]. In this study, we have investigated the deposition of the Ag nanoparticle clusters onto carbon nanotubes. Structure changes of the deposited clusters were analyzed by scanning transmission electron microscope (STEM).

Ag nanoparticles were produced by a gas aggregation method and were passed through C_{60} vapor. The nanoparticles thus produced were admitted into an ionizer equipped with a radioactive ^{241}Am and were size-selected at 20 nm by a differential mobility analyzer (DMA). The selected nanoparticles were electrically collected onto CNT deposited on a Cu grid, and were analyzed by STEM.

Fig.1 shows STEM image for size-selected Ag nanoparticle cluster deposited on a CNT. The deposited cluster is observed to be composed of 9 Ag nanoparticles with high contrast. In addition, these nanoparticles are superposed on areas with low contrast. Because these high- and low-contrast features resemble those for the nanoparticle clusters observed previously [1], the cluster produced in the gas phase is considered to be deposited on the CNT.

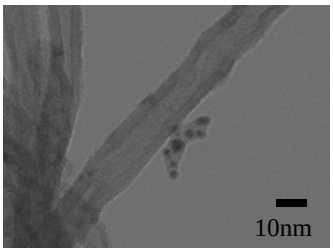

Fig.1. STEM image for
Ag nanoparticle cluster size-selected at 20 nm on a CNT

The number of Ag nanoparticles is found to be quite close to that for the previous report. This indicates that the no fission occurs on the deposition process.

On the other hand, although the shape of the cluster seems drastically deformed, the constituent Ag nanoparticles are well isolated each other. The deformation implies shape conversion induced by the impact energy. The isolation suggests that aggregation of the Ag nanoparticles is probably restricted by existence of C_{60} molecules. In fact, the distance between adjacent Ag nanoparticles was estimated to be approximately 2.2 nm, and this distance is close to the diameter of a few C_{60} molecules. In other words, C_{60} molecules work as effective isolator for Ag nanoparticles.

[1] H.Tanaka, H.Maeda, *Chem. Phys. Lett.*, 484 (2009) 37.

Reactant depletion in chemical reactions inside nanoscale particles

V.V. Levdansky[1], J. Smolik[2], V. Zdimal[2] and P. Moravec[2]

[1]Heat and Mass Transfer Institute NASB, 15 P. Brovka Str., 220072 Minsk, Belarus
[2]Institute of Chemical Process Fundamentals AS CR, v.v.i., Rozvojova 135, 165 02 Prague 6, Czech Republic
Keywords: nanoparticles, chemistry, size effect.
Presenting author email: vlev5@yahoo.com

It is known that physicochemical processes occurring in aerosol systems with nanoscale particles and in the particles themselves can depend on the particle size. Some problems related to phase transitions in aerosol systems with nanoparticles in the dependence of the condensation coefficient on the particle size were studied in (Levdansky *et al*., 2010). Here we consider the influence of the size effect on reactant depletion in nanoparticles due to a chemical reaction.

The rates of chemical reactions in nanoparticles can be higher than in a bulk matter. This is related to the size dependence of activation energies for diffusion of reactants in nanoparticles and intrinsic activation energies of chemical reactions. The size dependence of the mentioned activation energies leads to the size dependence of rate constants of chemical reactions as well as the size dependence of reactant depletion. Let us consider a decrease in the number density of the reactant component A in the nanoparticle n_A with time due to a bimolecular chemical reaction of components A and B inside the particle. For simplicity, we assume further that concentrations of reactants are uniform throughout the nanoparticle, the diffusivity of the component A in the particle D_A is much greater than the diffusivity of the component B (D_B) and the number density of the component B in the particle n_B is much greater than n_A. Under the above-mentioned assumptions, we can suppose that the value of n_B is independent of time t and $n_B = n_B(t = 0) = n_{B0}$ (Connors, 1990). In this case the value of n_A in a diffusion-controlled chemical reaction can be found from the equation

$$\frac{dn_A}{dt} = -4\pi D_A R_0 n_A n_{B0}, \qquad (1)$$

where R_0 is the effective radius at which a reaction can occure.

It is known that the cohesive energy decreases with a reduction in the nanoparticle size (Vanithakumari and Nanda, 2008). In turn, it leads to a decrease in the activation energy for diffusion of reactants inside the particle and to an increase in the rate of a chemical reaction.

Taking into account the relation between the activation energy for diffusion of components in nanoscale particles and their melting temperature by analogy with (Vanithakumari and Nanda, 2008) and allowing for the size dependence of the nanoparticle melting temperature according to (Rekhviashvili and Kishtikova, 2006), we can obtain the following equation for n_A:

$$n_A = n_{A0} \exp\left\{-t^* \exp\left[\frac{E_{A\infty}}{kT}\left(1-\exp\left(-\frac{4\delta}{\delta+d}\right)\right)\right]\right\}, \qquad (2)$$

where $n_{A0} = n_A(t = 0)$, $t^* = 4\pi R_0 n_{B0} D_{A\infty} t$, $E_{A\infty}$ and $D_{A\infty}$ are respectively the activation energy for diffusion and the the diffusivity of the component A without considering the size effect, k is the Boltzmann constant, T is the temperature, d is the particle diameter, δ is the Tolman length.

Figure 1 shows the dependence of the dimensionless number density of the component A in the nanoscale particle $n^* = n_A/n_{A0}$ on t^* for different values of $d^* = d/\delta$.

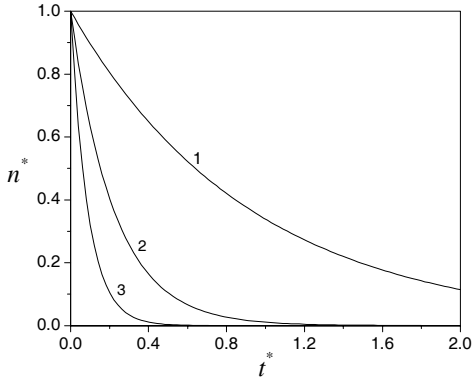

Figure 1. Dependence of n^* on t^* at $E_{A\infty}/kT = 20$. 1: $d^* = 1000$, 2: $d^* = 50$, 3: $d^* = 30$.

It follows from Fig. 1 that the value of n^* decreases with an increase in t^* and in a decrease in d^*.

This work was supported by GAAVCR project IAA200760905 and GACR project 101/09/1633.

Connors, K.A. (1990) *Chemical kinetics: the study of reaction rates in solution*, New York: VCH Publishers, Inc.

Levdansky, V.V., Smolik, J. and Moravec, P. (2010) *Int. Commun. Heat Mass Transfer*, **33**, 56-60.

Rekhviashvili, S.Sh. and Kishtikova, E.V. (2006) *Tech. Phys. Lett.* **32**, 439-441.

Vanithakumari, S.C. and Nanda, K.K. (2008) *Phys. Lett. A* **372**, 6930-6934.

Monitoring a CVD process for the synthesis of nanostructured particles by means of low-pressure impaction

F.Weis, M. Seipenbusch and G. Kasper

Institute for Mechanical Process Engineering and Mechanics, Karlsruhe Institute of Technology (KIT), Karlsruhe, 76131, Germany
Keywords: aerosol coating, impactor, nanoparticle, CVD.
Presenting author email: frederik.weis@kit.edu

Nanoparticles synthesized by gas phase processes like flame spray pyrolysis, spark discharge generation or chemical vapour synthesis (CVS) show great potential in gas sensing, catalytic or electrical applications. In order to optimize and simplify screening for the required synthesis parameters online monitoring of the process is desirable. In this work an integrated CVS/CVD aerosol process[1] at atmospheric pressure was adapted to synthesize core-shell structured nanoparticles composed of SiO_2 support particles coated with a bismuth and molybdenum oxide shell. These nanoparticles are active catalysts for selective oxidation of hydrocarbons like methanol or propene. The whole process can be monitored online by the use of a single stage low pressure impactor (LPI) in the pressure scanning mode in combination with a differential mobility analyzer (DMA). The SiO_2 support particles were synthesized by thermally activated Chemical Vapour Synthesis (CVS) in a hot wall reactor using tetraethyl(ortho)silicate (TEOS) as precursor and a nitrogen-oxygen mixture as carrier gas. A sintering furnace was used to adjust particle morphology and the resulting change in effective particle density was measured by the use of the LPI. The values given in table 1 for a particle with a mobility diameter of 130nm show that after the CVS reactor agglomerates with a low effective density are formed. After the sintering furnace a density close to the bulk value of silica (2200 kg/m^3) is determined, indicating complete coalescence of the particle. This is in agreement with TEM images, showing the spherical shape of the particles.

Table 1 Effective particle density of SiO_2 particles measured by low pressure impaction.

	ρ_{eff} (kg/m^3)
CVS reactor (1000°C)	310
Sintering furnace (1500°C)	2145

In a second step the support particles were directly coated downstream in the aerosol state with Mo- and Bi-oxide by Chemical Vapour Deposition (CVD) using molybdenum hexacarbonyl and bismuthtriphenyl as precursors and oxygen as reactive gas. Since the resulting shells of molybdenum and bismuthoxide have a higher density, the coating of the particles can be monitored online. If the particles are coated successfully, the penetration curves of the LPI for a constant mobility diameter shift to higher pressures as shown in figure 1 for a subsequently coated particle. From this shift the coating thickness in the nanometer range can also be determined online. Figure 2 shows the growth of the molybdenum oxide shell with increasing residence time in the CVD reactor. Since the density of the film is not exactly known the values resulting from the LPI measurements are given by the grey band, showing good agreement with the coating thickness determined by TEM-image analysis. The presentation will show how a low pressure impactor can be used to study the coating step online and possibilities to increase the resolution for the determination of coating thickness will be discussed.

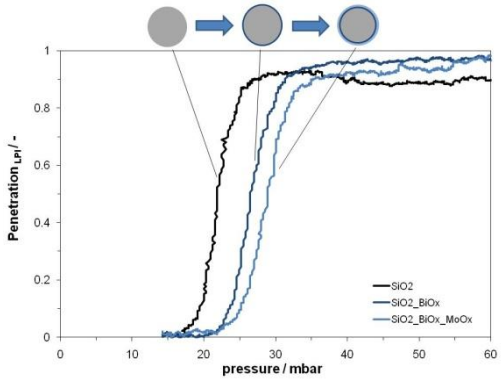

Figure 1 Penetration curves of LPI for coated silica

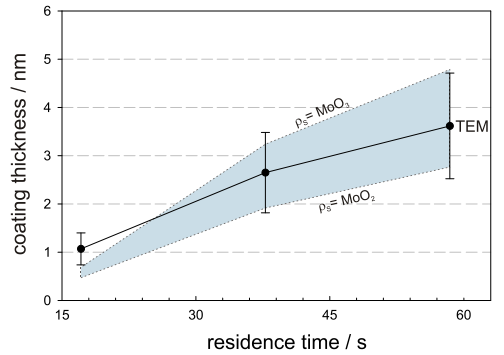

Figure 2 Coating thickness of silica particles coated with molybdenum oxide as function of residence time

This project is part of the JointLab IP3, a joint initiative of KIT and BASF. Financial support by the ministry of science, research and the arts of Baden-Württemberg (Az. 33-729.61-3) is gratefully acknowledged.

Weis F., Gao K., Seipenbusch M., Kasper G. (2011)
An Aerosol-Process for the synthesis of nanostructured molybdenum oxide catalysts by integrated CVS/CVD at atmospheric pressure
J. Nanoscience and Nanotechnology, Vol. 11 (9), 8313-8317

Electro-hydrodynamic atomization of solutions with strongly electrolytic behaviour – governing parameters and applications

A. Maißer[1], M.B. Attoui[2], A.M. Ganan-Calvo[3] and W.W. Szymanski[1]

[1]Faculty of Physics, University of Vienna, Vienna, 1090, Austria
[2]LISA, UPEC-Diderot, Créteil, 94010 ,France,
[3]ESI, Universidad de Sevilla, Sevilla, 41092, Spain
Keywords: electrospray, aerosol generation, nanoparticles, salt aerosol.
Presenting author email: anne.maisser@univie.ac.at

Electro-hydrodynamic atomization (EHDA) is a widely applied tool for aerosol generation and can be applied to produce aerosols of various sizes and chemical composition.

In this work EHDA has been applied to produce airborne sub 10 nm nanoparticles from salt solutions of strongly electrolytic behaviour (sodium chloride NaCl and potassium chloride KCl). The goal of the investigation was to find the relationship between molar concentration and solution conductivity to the particle size produced. The results have been compared to existing scaling laws under the assumption that the chemical composition is preserved during the spraying process. The quality of the generated aerosol and their possible applications have been investigated.

For EHDA a commercial TSI electrospray aerosol generator (EAG, 3480 TSI Inc.) has been used. This device includes a ^{210}Po radioactive alpha radiation to produce a high concentration bipolar ion cloud for neutralization of the highly charged droplets emerging from the tip of the electrospray capillary.

The generated aerosol has been investigated using a custom-made differential mobility analyzer (Vienna type nanoDMA) in combination with a Faraday cup electrometer for particle detection. For investigations of the charge state and monodispersity of the generated particles a tandem DMA experiment has been performed using two identical Vienna type nanoDMAs in series. The applications of the monodisperse particles for further investigations has been tested by measuring the detection efficiency of the sub 10 nm particles with a commercial ultrafine water condensation particle counter (WCPC, 3786 TSI Inc.).

Experimental Results

NaCl and KCl salts have been dissolved in various concentrations in either pure water or in an aqueous ammonium acetate buffer liquid of varying molarities. The solutions have been sprayed in stable cone-jet mode.

Because of the strongly electrolytic behaviour of the salts used the change in concentration strongly affects the conductivity of the solutions.

Figure 1 shows the compiled results for NaCl sprayed from solutions in pure water and for constant electrical fields applied to the liquid at the capillary tip and constant liquid flow rates through the capillary. It can be seen that there is a linear relationship between the concentration of salt in solution and the conductivity. The dry particle diameter has been measured and the droplet diameter has been derived from the particle diameter under the assumption that the residue particles consist of pure NaCl or KCl, respectively.

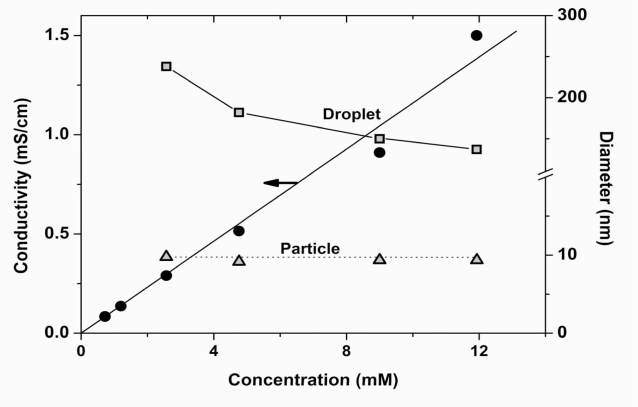

Figure 1. Measured dependency of particle and droplet diameter to the molar concentration and conductivity of the solution for NaCl.

It can be seen that the variation of the dry particle size is small for solutions in pure water and thus strong variations of conductivity.

The experimental results have been compared to two different theoretical approaches so called scaling laws introduced by Fernandez de la Mora and Loscertales (1994) and Ganan-Calvo (1997), respectively.

It has been found that the electrolytic behaviour of the solutions needs to be taken into account for scaling the droplet diameter and particle size. Apparently, the particle size can be scaled solely by the 1/3rd power of the liquid flow rate as far as the hypothesis of non-altered chemical composition holds (Maißer *et al.* 2012). However, the experimental results and comparison to the scaling law by Ganan-Calvo indicate a possibility of some electrochemical effects that could affect the chemical composition; this issue still requires some further experimental studies.

Fernandez de la Mora, J., Loscertales, J., (1994), *Fluid Mech.,* **260**, 155-184

Ganan-Calvo, A.M., (1997), *Phys. Rev. Lett.,* **79**, 217-220

Maißer, A., Attoui, M., Ganan-Calvo, A.M., Szymanski, W.W., (2012) *Phys. Rev. E*. submitted

The effect of charge on ultrafine particle deposition: an experimental pilot study

L.L. Guo[1], L.Morawska[1], G.Johnson[1,] R. Jayaratne[1] and W.Hofmann[1, 2]

[1] International Laboratory for Air Quality and Health (ILAQH),
Queensland University of Technology (QUT), 4000, Brisbane, Australia
[2]Division of Physics and Biophysics, Department of Materials Research and Physics,
University of Salzburg, 5020 Salzburg, Austria
Keywords: ultrafine particles, charged particles, lung deposition.
Presenting author email: l.guo@student.qut.edu.au

Eepidemiological studies have linked exposure to ultrafine particles (UFPs, <100 nm) to a variety of adverse health effects. To understand the mechanisms behind these effects, it is essential to measure aerosol deposition in the human respiratory tract. Electrical charge is a very important property as it may increase the particle deposition in human respiratory tract (Melanderi et al., 1983). However, the effect of charge on UFP deposition has seldom been investigated. The aim of this study is to investigate the effect of charge on UFP deposition in human lung, by conducting a pilot study using a tube-based experimental system.

A nebuliser (Model CN241, BGI Inc., US) was used to generate polydisperse diethyl-hexyl-sebacate (DEHS) particles. A Scanning Mobility Particle Sizer (SMPS) was used to measure particle size distribution and particle number concentration (PNC) was measured by both an SMPS and a TSI 3010 Condensation Particle Counter (CPC). The SMPS is comprised of a CPC and a 3071 Electrostatic Classifier (EC). An ioniser (AH-202, Aironic, US) inside the chamber was used to charge the DEHS particles, and an Aerosol Electrometer (AE, TSI Model 3068) was used to measure particle charge. In order to investigate the effect of charge on particle deposition in the tube, three aerosols were compared: charged (generated by nebuliser, then charged by an ioniser), non-charged (generated by nebuliser), charge neutralised (generated by nebuliser and then passed through an ^{85}Kr bi-polar charger). A sampling box (9 L) was connected to the end of the tube (L: 85 cm; D: 1.7 cm), which acted as a reservoir to avoid measuring the artefacts produced by flow fluctuation. The aerosols were drawn through the tube from the large chamber ($1m^3$) into the sampling box at a flow rate of 7.5 L/min. Particle number concentration and charge were measured by the CPC and AE, respectively, both before and after the aerosols were drawn through the tube. For each of the three aerosols, particle deposition was determined by comparing the particle number concentration difference before and after the aerosol passed through the tube. The average of three to five measurements was taken as the final deposition value.

Only the comparison between the deposition fraction of charged and non-charged particles is reported here. As can be seen form Table 1, the deposition fraction of charged particles increased 78% compared with non-charged particles. The increase in deposition for UFPs was generally higher than those of submicron particles. However, it is too early to conclude that charge has a greater effect on lung deposition for UFPs than for larger particles, since the difference could be a result of conducting in vitro experiments (i.e. the plastic tube used this study or the metal cast used by Cohen et al., 1998) versus in vivo experiments (i.e. the rats studies in Ferin et al., 1983 and the humans studied in Melandri et al., 1983). Further in vivo experiments are needed to confirm this hypothesis and therefore, the focus of our future work will be to measure the deposition of charged UFPs directly in the human lung.

Table 1. Comparison of deposition increase

DFI	Subject	Particle	Literature
1.78 Charged/ Non-charged	PE tube	DEHS Polydisperse (CMD 90nm)	Current study
2.3 Singly charged/ neutralised	Metal cast	FAH Monodisperse 125 nm	Cohen et al., 1998
1.15-1.3 29-66e/3e	Human lung	Carnauba wax Monodisperse 0.33-1 um	Melanderi et al., 1983
1.25 Non-charged/ Neutralised	Rat lung	TiO2 Polydisperse 0.5 um	Ferin et al., 1983

DFI: Deposition fraction increase, ratio of deposition fraction between particles with different charges **PE**: polyethylene **FAH**: Fluorescein-ammonium hydroxide

This work was supported by a PhD Scholarship funded by Dr Greg Wren.

Ferin J., Mercer T. T. and Leach, L. J.(1983). *Environ Res* **31**(1): 148-151.
Melandri, C., Tarroni, G., Prodi, V., Dezaiacomo, T., Formignani, M. and Lombardi, C. C. (1983) *Journal of Aerosol Science*, **14**(3): 184-186.
Cohen, B. S., Xiong, J. Q., Fang, C. P. and Li, W. (1998) *Health Phys* **74**(5): 554-560.

A new method for characterizing bounce and charge transfer properties of nanoparticles

H. Kuuluvainen[1], A. Arffman[1], E. Saukko[1], A. Virtanen[2] and J. Keskinen[1]
[1] Tampere University of Technology, Department of Physics, P.O. Box 692, FIN-33101 Tampere, Finland
[2] University of Eastern Finland, Department of Applied Physics, P.O. Box 1627, 70211 Kuopio, Finland
Keywords: bouncing, charge transfer, nanoparticles, ELPI
Presenting author email: heino.kuuluvainen@tut.fi

Introduction

Bouncing and charge transfer has previously been studied mainly for aerosol particles larger than one micrometer. Furthermore, studying particle bounce in impactors has often focused on means to reduce the bounce, not to explore the phenomenon itself. Recently, however, a new method was established in which the particle bounce in an electrical low pressure impactor (ELPI) was used to verify the physical phase state of newly formed SOA particles (Virtanen et al., 2010). To be able to use the method for more accurate and quantitative analysis in the future, both modelling and laboratory measurements are required.

Methods

A new model for bouncing particles and charge transfer in the ELPI is presented. The model is based on previous theories of Dahneke (1971) and John et al. (1980), which were originally developed and verified for larger particles. Along with these theories, it is very important to know the impact velocities of the particles at different impactor stages. For the estimation of these velocities, a recently published flow field model of the ELPI by Arffman et al. (2011) is used.

The bounce and charge transfer model covers the process in the ELPI stage by stage starting from the top and ending finally to the filter stage. At a single stage, the size distribution and the charge distribution of incoming aerosol change through impaction, bouncing and charge transfer. The modelled ELPI current distribution is calculated as a result of impacted particles and charge transfer from bouncing particles. In the model, there are basically three parameters describing the properties of the aerosol: material coefficient of bouncing, contact charge and effective density.

Laboratory measurements were conducted for sodium chloride and levoglucosan particles with polydisperse distributions and average mobility sizes below 100 nm. The ELPI current distribution was measured both charger on and charger off. In addition, as an approximation of the bounced fraction and bounced particles without charge transfer, so called bounce current can be defined, which is the difference of the two measured current distributions.

Finally, the model was fitted into the two measured currents and the bounce current for each measured aerosol distribution. Three parameter values were defined for each distribution minimizing the difference between the modelled and measured currents. The results are seen in Fig. 1 as a function of particle size distribution GMD. Substrate roughness and particle size seem to have only minor effect on the results. In the case of contact charge, substrate loading during the measurement is a problem and, for material coefficient, the theoretical size dependence may require further studies.

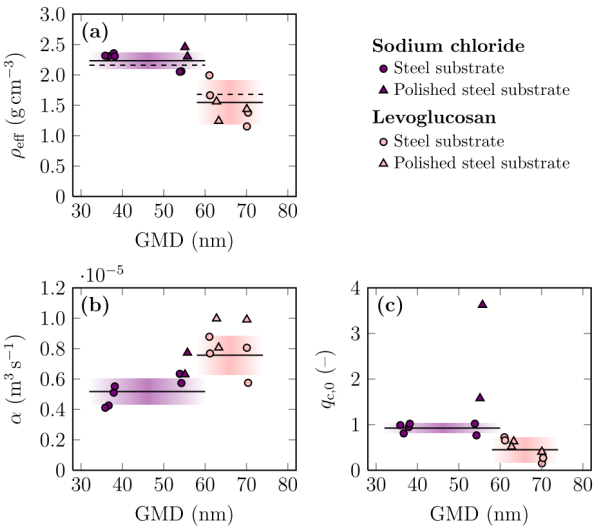

Figure 1: The values of (a) effective density, (b) material coefficient of bouncing and (c) contact charge as a function of particle size distribution GMD. In the subfigure (a), the dashed lines represent bulk densities.

Conclusions

The new method based on the bouncing and charge transfer model in the ELPI is shown to be a promising tool for measuring bounce and charge transfer properties of nanoparticles. The good agreement between the model and the experiment also shows that the previous theories for larger particles are to some extent relevant for particles below 100 nm.

Arffman, A., Marjamäki, M. and Keskinen, J. (2011). J. Aerosol Sci., 42, 329–340.

Dahneke, B. (1971). J. Colloid Interface Sci., 37, 342–353

John, W., Reischl, G. and Devor, W. (1980). J. Aerosol Sci., 11, 115–138

Virtanen, A. et al. (2010). Nature, 467, 824–827.

Influence of flow conditions and process parameters on the production rate and characteristics of nanoparticles produced by spark discharging

M. Wagner[1], M. Wild[1], F. Weis[1] and M. Seipenbusch[1]

[1]Karlsruhe Institute for Technology KIT, IMVM, Straße am Forum 8, 76139 Karlsruhe, Germany

Keywords: Aerosol size distribution, Metal nanoparticles, Nanoparticle production, SMPS.
Presenting author email: moritz.wagner@kit.edu

Spark discharge generators are widely used for the synthesis of metallic, mixed-metallic and oxidic nanoparticles at the laboratory scale. They are flexible with respect to electrode material and enable the production of high purity particles without employing hazardous precursors.

During particle production, the electrodes are being consumed since they constitute the particle feedstock, thus constantly increasing the width of the inter-electrode gap. As the electrode distance influences the production process, it is necessary to continuously readjust the gap width. This is especially important for the high production rates necessary for an industrial-scope application of the spark discharge generator. Consequently, two manual or automatic electrode feed mechanisms are usually employed to keep the electrodes at a constant distance (Helsper, Mölter et al. 1993), as can be seen in figure 1.

However, as ablation rates are dependent on polarity, the electrode gap is prone to displacement even if held at constant width (Tabrizi, Ullmann et al. 2009). This leads to a change in flow conditions in the vicinity of the gap, which in turn influences the removal of particles and residual ions from the gap as well as the dilution in the electrode wake (Schwyn, Garwin et al. 1988).

In order to allow for stable flow conditions even in case of high electrode ablation, we constructed a spark discharge generator with coaxial configuration as shown in figure 2. In contrast to the conventional setup, the gas flows alongside the electrodes, thus reducing the influence of spark gap displacement. As a side effect, it is possible to operate the coaxial spark discharge generator using only one feed mechanism by fixing one electrode to the housing. The failure rate in comparison to the conventional setup is therefore lower, as the number of moving parts is essentially halved.

We investigated the influence of the spark gap position on the production rate and properties of particles from spark discharge generators both with coaxial and traditional configuration. An SMPS was used to determine the size distributions of the aerosol, while the mass production rate was examined by gravimetric analysis. The measurements were conducted with different parameter constellations, including a variation of the gas flow rate.

Helsper, C., W. Mölter, et al. (1993). *Investigations of a new aerosol generator for the production of carbon aggregate particles*. Atmospheric Environment. Part A. General Topics **27**(8): 1271-1275.

Schwyn, S., E. Garwin, et al. (1988). *Aerosol generation by spark discharge.* Journal of Aerosol Science **19**(5): 639-642.

Tabrizi, N., M. Ullmann, et al. (2009). *Generation of nanoparticles by spark discharge.* Journal of Nanoparticle Research **11**(2): 315-332.

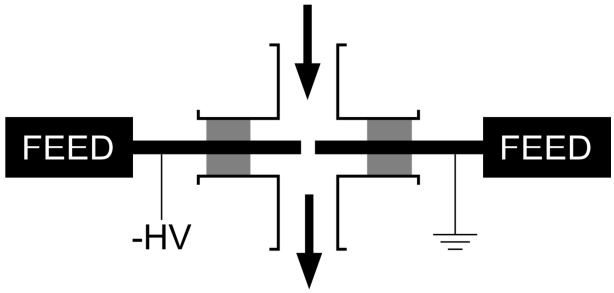

Figure 1: Schematic of a conventional spark discharge generator. After (Schwyn, Garwin et al. 1988).

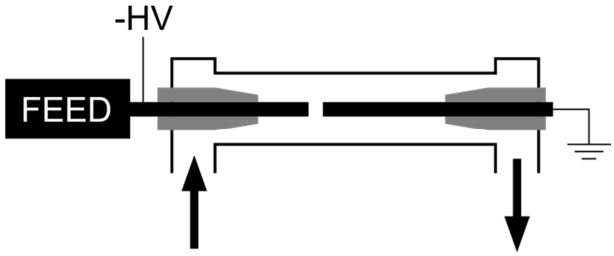

Figure 2: Schematic of the coaxial spark discharge generator.

The research leading to these results has received funding from the European Community's Seventh Framework Programme (FP7 2007-2013) under grant agreement n° 280765 (BUONAPART-E).

Variability of nanoparticles number concentration during summer in a humid region

V. Juncal-Bello[1], S. Iglesias-Samitier[1], M. Piñeiro-Iglesias[2], P. López-Mahía[1,2], S. Muniategui[1] and D. Prada[1,2]

[1]Department of Analytical Chemistry, University of A Coruña, Campus da Zapateira, 15071, A Coruña, Spain
[2]Institute of Environment, University of A Coruña, Pazo de Lóngora, 15179, Oleiros, A Coruña, Spain
Keywords: particle size distributions, nanoparticles
Presenting author email: purmahia@udc.es

Size distribution measurements have been a recent focus of field campaign studies at several places around the world including urban, rural and remote sites (Zdímal *et al*., 2011).

Atmospheric particles are the object of a rising concern from environmental agencies, public opinion and scientific community. Excessive concentration of airborne particles is known to have detrimental effects on human health on global heat balance and possibly on precipitation patterns (Bigi and Ghermandi, 2011).

Measurements of number size distributions of submicron aerosols during summer 2011 have been performed at the Western part of Spain as part of an extensive measurement campaign to study volatile organic compounds and aerosols (NANOVOC Project). The measurements were made at the Institute of Environment station in Galicia.

This area is characterized by an Atlantic climate, with an accumulated precipitation of 33 l/m^2, 85 l/m^2 and 26 l/m^2 and a relatively humidity of 65%, 67% and 64% for July, August and September, respectively. Average temperature was around 22ºC during the measurements.

The data collection system used was a scanning mobility particle sizer with particle distributions measured in the range between 7,37 < Dp < 289 nm, where dp is the mobility particle diameter. The SMPS consisted of TSI 3081 Electrostatic Classsifier and TSI 3785 Water Condensation Particle Counter. The SMPS was set to the sheath and polydisperse aerosol flow rates of 10.0 and 1 l/min, respectively, to scan the size range 7,37–289 nm. A pre-impactor with nozzle 0,457 cm was used. The SMPS sampled periodically every 10 minutes with two scans per sample and 120 seconds scan up. The distributions were corrected for multiple charging and diffusion.

Particle size distributions during three months were different. The highest monthly average concentrations in all size distributions occur in August. July showed a bimodal distribution with two maximum, between 17,5-25 nm and 44,5-59,4 nm respectively. On the other hand, August showed only one maximum between 31,1 and 44,5 nm. September showed a bimodal distribution as occurs in July but particle number concentration with diameter between 17,5-25 nm was higher (figure 1).

The full range of the SMPS (N_{SMPS}, 7,37-289 nm) was integrated and the total particle number concentration showed different weekly patterns between different months: in July and September, number concentration was the lowest during weekend days but in August no differences were observed between weekdays due to an increase in the traffic flow generated by the proximity of the sampling point to the beach (figure 2).

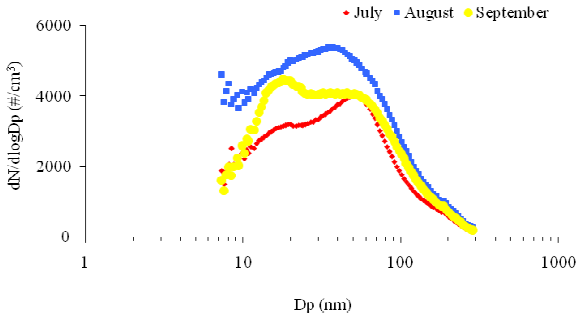

Figure 1. Average number size distributions during the measurements.

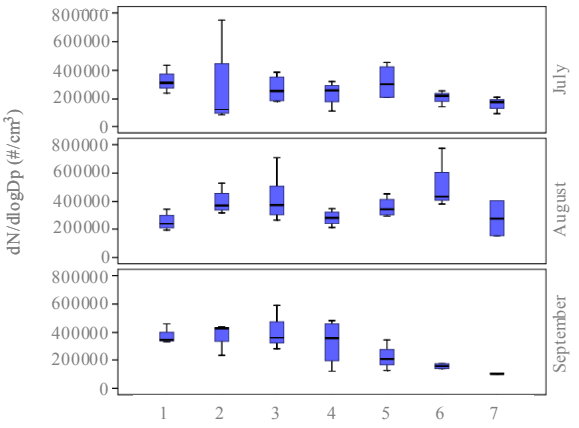

Figure 2. Weekly variations of total number concentrations during sampling months (1: Monday; 2: Tuesday; 3: Wednesday; 4: Thursday; 5: Friday; 6: Saturday; 7: Sunday).

This work was supported by the Spanish Ministry of Science and Innovation under grant CGL2010-18145 (NANOVOC project). The authors also express thanks to P. Esperon for her valuable help.

Ždímal, V., Smolík, J., Eleftheriadis, K., Wagner, Z., Housiadas, C., Mihalopoulos, N., Mikuška, P., Večeřa, Z., Kopanakis and I., Lazaridis, M. (2011) *Water Air Soil Pollut.* **214**, 133–146.

Bigi, A. and Ghermandi, G. (2011) *Water Air Soil Pollut.* **220**, 265–278.

Characterization of different CNT using a thermo-optical elemental carbon / organic carbon analyzer in view of workplace aerosol measurements

A.C. John[1], M. Renker[1] and T.A.J. Kuhlbusch[1]

[1]Air Quality & Sustainable Nanotechnology Unit, IUTA e.V., 47229 Duisburg, Germany
Keywords: nanotubes, CNT, nanoparticles (characterization), occupational exposures.
Presenting author email: johnas@iuta.de

Introduction

In the last few years, applications involving carbon nanotubes (CNT) have been experiencing enormous growth because of the material's unique properties. Besides these promising opportunities, however, potential risks of these new materials for human health and the environment have to be assessed. In view of exposure assessment during CNT production and the processing of CNT-containing products, a method for the detection and quantification of carbon nanotubes in ambient and workplace air is needed.

Methods and Materials

Thermo-optical carbon analysis is a standard to determine exposure to soot at workplaces (NIOSH method 5040). This method determines total carbon (TC=OC+EC) and uses a specific thermal protocol to fractionate different types of "organic carbon" (OC) during a first analysis step in pure helium. Similarly, "elemental carbon" (EC) is analyzed in a second step in a helium/oxygen atmosphere. An optical correction can be applied to account for artefact formation during analysis.

In our study, 13 different CNT (SWCNT= single walled CNT, MWCNT= multi-walled CNT, functionalised MWCNT) having different lengths and diameters were analyzed to determine similarities and differences in their thermal behaviour. In addition to the above mentioned NIOSH protocol, other generally applied methods for ambient air analyses (EUSAAR 2, IMPROVE A, quartz.par) were tested. These protocols last between about 10 and 30 minutes and apply different temperatures in the OC and EC analysis step.

Results and discussion

The results of the 13 different CNT showed that they could be successfully analyzed with the thermo-optical EC/OC analyzer. However, only 11 CNT were analysed with all 4 above mentioned "standard protocols", whereas two out of the 13 CNT showed higher thermal stability and needed a modification of the helium/oxygen step for all 4 protocols (increase of last temperature step, extension of analysis time) to be converted completely.

As expected, the carbon nanotubes were mostly analyzed as elemental carbon, with an EC/TC- ratio ranging from 85% to 100%. However, differences in the fractionation into organic and elemental carbon did not only depend on the type of CNT, but also on the applied temperature protocol. The latter ones can be (amongst others) explained by the different temperatures in the helium step. Protocols with high temperatures in this first step (NIOSH 850°C, quartz.par 870°C) convert some of the material that is only released in the second step in the other protocols (EUSAAR2 650°C, IMPROVE A 580°C in the first step).

When looking for the "best protocol" to analyze CNT, we did not only pay attention to the OC/EC fractionation, but also to the possible distinction of CNT from other carbonaceous substances. Figure 1 and figure 2 show the thermograms of the different materials using the NIOSH protocol and the quartz.par protocol, respectively. Whereas in the first example most of the thermograms overlap, the thermograms of the second figure are better separated, and three groups of CNT can be distinguished.

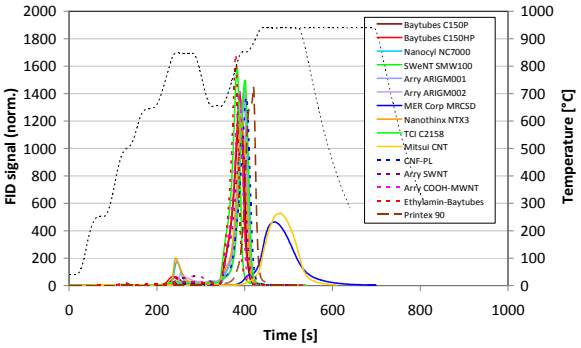

Figure 1. Thermograms of different CNT and carbonaceous materials using the NIOSH protocol.

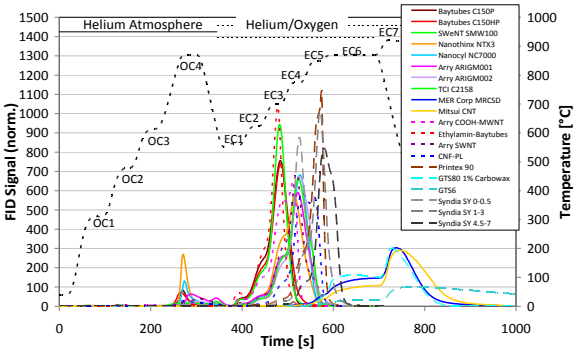

Figure 2. Thermograms using the quartz.par protocol.

The thermograms indicate that CNT seem to be distinguishable from other carbonaceous materials, but that the established temperature protocols might not be suitable for this purpose.
Based on these findings, we currently investigate methods to specifically detect CNT for workplace and environmental measurements.

This work was supported by the German Bundesministerium für Bildung und Forschung (BMBF) under grant 03X0114D.

(Quasi) Real-time detection of catalytically active nanoparticles in presence of a background aerosol

N. Neubauer[1], M. Seipenbusch[1] and G. Kasper[1]

[1]Institut für Mechanische Verfahrenstechnik und Mechanik, Karlsruhe Institute of Technology (KIT), 76131 Karlsruhe, Germany

Keywords: background distinction, catalytically active nanoparticles, (quasi) real-time detection

Presenting author email: nicole.neubauer@kit.edu

Introduction

Workers involved in the production or handling of engineered nanoparticles are likely to be at a high exposure risk. The isolation of this additional contribution to the total background particle concentration at the workplace still remains a challenge. Especially small particles can quickly attach to the background aerosol of the workplace due to coagulation (Seipenbusch, 2008). Because of the resulting disappearance in the size distribution, the on-line measurement devices currently used during exposure studies are not capable to discriminate them from the background particles of the workplace. In a recent publication (Neubauer, 2011) we introduced a new measurement technique based on catalysis for the material-specific detection of nanoparticles with a high sensitivity. We now present further details of this method, especially with regard to the discrimination of catalytically active nanoparticles from a non-active background aerosol.

Experimental

To investigate the specificity of our method, the detection of palladium nanoparticles both directly after their production by spark discharge and after mixing them with SiO_2 background particles was studied. At first the particles were sampled onto a filter for a fixed time interval. Afterwards they were exposed to gaseous reaction educts which initiate the catalytic reaction. The hydrogenation of ethene was chosen as a specific catalytic test reaction for the detection of palladium. The conversion of ethene to ethane due to the catalytic activity of the palladium nanoparticles is measured online by infrared spectroscopy.

In addition, the palladium and the background particles as well as their mixture were characterized by an electrical mobility spectrometer and by electron microscopy. The specific surface area of the catalytically active palladium nanoparticles was determined by nitrogen BET.

Results

Electron microscopy analysis resulted in a median primary particle size of 3.2 nm for the palladium nanoparticles. They are arranged in agglomerates with a mode of the mobility equivalent diameter of 74 nm. The SiO_2 background particles also form agglomerates ($x_{mob,mod}$ 163 nm) of primary particles with a median size of 48 nm. The nitrogen BET analysis of the palladium nanoparticles gave a specific surface area of 87 g/m^2.

The catalytic experiments showed a proportional dependence of the catalytic activity of the pure palladium nanoparticles on their BET surface. In addition, the influence of the temperature and the contact time between the reaction gases and the particles were studied in order to find ideal conditions for the substance-specific detection of palladium.

After the addition of the background aerosol, the smaller palladium agglomerates attach to the SiO_2 particles due to coagulation (cf. Figure 1) and disappear from the particle size distribution. Nevertheless, it was possible to detect them via their catalytic behaviour – even in the attached state.

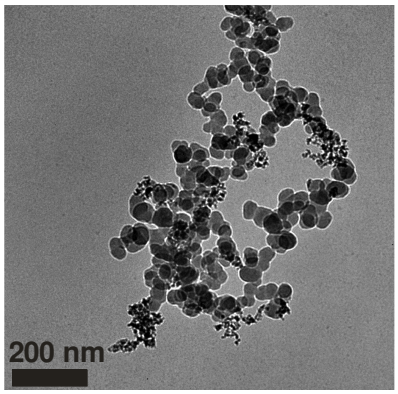

Figure 1: Palladium agglomerates attached to a background agglomerate of SiO_2

Conclusion

The presented measurement technique enables the detection and quantification of palladium nanoparticles based on their catalytic activity. Besides, the method is suitable for a discrimination of catalytically active particles from a non-active background aerosol in (quasi) real-time. The used setup is already a compact and portable version which allows measurements directly at workplaces.

The research leading to these results has received funding from the European Commission's Seventh Framework Programme (FP7/2007-2013) under grant agreement n° 211464-2 (Nanodevice).

Seipenbusch M, Binder A and Kasper G (2008) *Ann. Occup. Hyg. 52(8)*

Neubauer N, Weis F, Binder A, Seipenbusch M and Kasper G. (2011) *Journal of Physics: Conference Series 304 (1)*

Release of carbon nanotubes from an epoxy-based nanocomposite during an abrasion process

L. Schlagenhauf[1,2,3], B.T.T. Chu[1], J. Buha[3], F. Nüesch[1] and J. Wang[2,3]

[1]Laboratory for Functional Polymers, Swiss Federal Institute for Materials Testing and Research, Dübendorf, ZH, CH-8600, Switzerland

[2]Laboratory for Analytical Chemistry, Swiss Federal Institute for Materials Testing and Research, Dübendorf, ZH, CH-8600, Switzerland

[3]Institute of Environmental Engineering, Swiss Federal Institute of Technology Zurich, Zurich, ZH, CH-8093, Switzerland

Keywords: nanoparticle release, nanocomposites, carbon nanotubes, particle size distribution.

Presenting author email: Lukas.Schlagenhauf@empa.ch

Epoxy /carbon nanotubes (CNTs) nanocomposites exhibit excellent mechanical properties. Compared to the pure epoxy, they have additional properties like electrical conductivity and thermal conductivity. They are used for applications where low weight, high strength, and high conductivity are required. The potential hazard of such materials has become a significant concern to researchers, manufacturing industries and customers. The exact environmental and health impact of nanoparticles released into the ambient either during manufacturing or in applications is still unknown and a matter of debate. Most of the literature on the toxicity related to CNTs has so far focused on raw CNTs in a finely granulated form to assess their potential health and environmental risks (Helland et al. 2007, Pulskamp et al. 2007). However few studies report on the toxicology of CNT reinforced nanocomposites (Wohlleben et al. 2011).

This study investigated the release of CNTs from the nanocomposite during abrasion. Therefore, three samples containing 0 wt%, 0.1 wt%, and 1 wt% of CNTs were produced and an experimental set-up has been established to perform abrasion, particle measurement, and collection all in one. The particle size distribution of the abraded particles was measured in the size range from 10 nm to 20 µm by a scanning mobility particle sizer (SMPS) and an aerosol particle sizer (APS). Additionally, collected particles were investigated by scanning electron microscopy (SEM), energy dispersive X-ray spectroscopy (EDX), and transmission electron microscopy (TEM).

The measured particle size distributions showed four size modes for all measured samples. The mode corresponding to the smallest particle sizes of 300-400 nm showed a trend of increasing size with increasing nanofiller content. The three measured modes with particle sizes from 0.6 to 2.5 µm were similar for all samples. In contrary to other release studies, the imaging by TEM revealed that free standing individual CNTs and agglomerates were emitted during abrasion as is shown in Fig. 1.

To our knowledge, the present study is the first to show release of free standing individual CNTs from CNT-embedded composites. The discovery indicates that in environmental, and safety studies, single CNTs should be considered as well as CNT bundles and agglomerates.

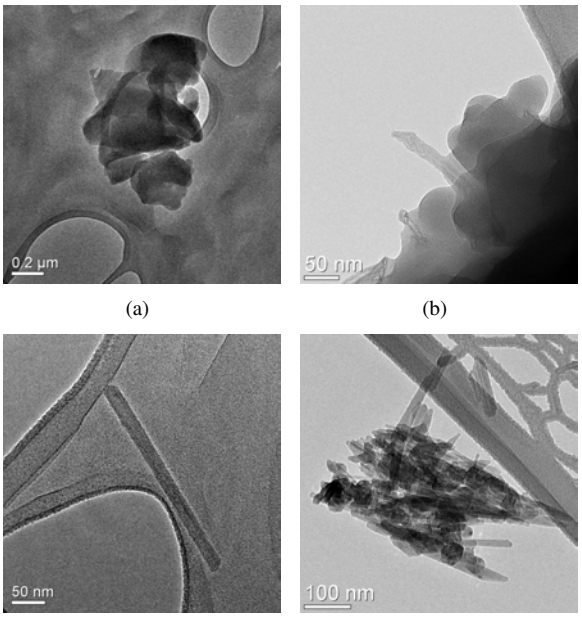

Figure 1: TEM images of abraded particles. a) Agglomerated particles from the pure epoxy sample; b) protruding CNTs from abraded particles of the 1 w% CNT composite; c)-e) free standing individual CNTs; f) an agglomerate of CNTs with a couple of individual CNTs scattered nearby.

This study was financed by the Swiss National Science Foundation (NFP 64), "Evaluation platform for safety and environment risks of carbon nanotube reinforced nanocomposites", 406440_131286.

Helland, A., Wick, P., Koehler, A., Schmid, K., and Som, C. (2007) Environmental Health Perspectives **115**, 1125-1131.

Pulskamp, K., Diabate, S., and Krug, H. F. (2007) Toxicology Letters **168**, 58-74.

Wohlleben, W., Brill, S., Meier, M. W., Mertler, M., Cox, G., Hirth, S., von Vacano, B., Strauss, V., Treumann, S., Wiench, K., Ma-Hock, L., and Landsiedel, R. (2011) Small **7**, 2384-2395.

Enabled Aerosol-based Methods for Assessing the Toxicity of Engineered Nanoparticles

A. Kourmouli[1], P. Kavarnoy[1], K. Barmpounis[2], O.I. Kalantzi[1], G. Biskos[1,2]

[1]Department of Environment, University of Aegean, Mytilene 81100, Greece
[2]Faculty of Applied Sciences, Delft University of Technology, Delft 2628-BL, The Netherlands

Keywords: Cytotoxicity, AgNPs, Aerosol, Blood cell
Presenting author email: env08036@env.aegean.gr

The increasing penetration of products containing engineered nanoparticles (ENPs) has raised many concerns with respect to their environmental impacts (Scown et al, 2010). Due to the high variability of ENPs (i.e., in size, morphology, and composition), attempting such an assessment requires standardized methods for measuring potential nanoparticle spills in the environment, as well as techniques for assessing their toxicity on living cells. With respect to the latter, to date there is lack of universal technique for assessing nanoparticle toxicity (Oberdörster, 2005). This is reflected by the vast number of works which in many cases report measurements that are contradicting with one another (Hamouda et al, 2000; Sondi and Salopek-Sondi, 2004).

In this paper we demonstrate the use of aerosol-based techniques for assessing the toxicity of ENPs on living cells. Compared to wet-chemistry techniques, generating test nanoparticles by aerosol-based methods has the advantage of higher purity, as well as of better control over their size, morphology and composition. For our study we generated Ag nanoparticles with mobility diameter of 15, 22, 30 and 50 nm using vaporization condensation. The particles were then collected on filters and were placed on Columbia ANC + 5% sheep's blood (CAN) dishes containing the tested cells. After 3 hours of incubation inhibition zones were evident as a result of the absorption of the ENPs by the cells and their subsequent death. After the growth of the inhibition zones was stabilized, the test plates were held in front of a desk lamp and the zones were measured using a ruler held against the back of the Petri dish. The diameter was measured to the nearest millimeter.

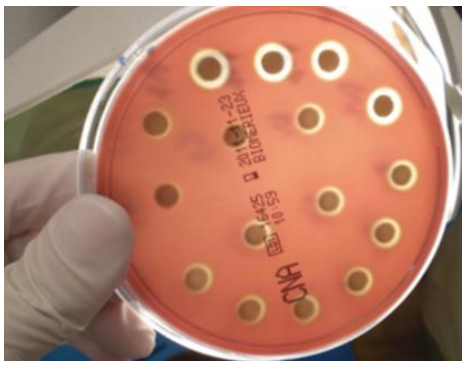

Figure 1: Inhbition zones observed around the nanoparticle-laden filters (brown spots) placed on Columbia ANC + 5% sheep's blood (CAN) medium.

The size of the inhibition zones increased progressively from the start of the experiment until they became stable after ca. 48 hours of incubation. Fig. 2 shows the growth of the inhibition zones (expressed as the diameter of the zone over the diameter of the filter) for the different particle size tested. As expected, increasing the concentration of nanoparticles, the inhibition zone was greater, indicating that the technique provides meaningful results with respect to nanoparticle toxicity. Although no apparent nanosize effect is observed with particle diameters investigated, the method can be easily extended for testing particles of other diameters and morphologies.

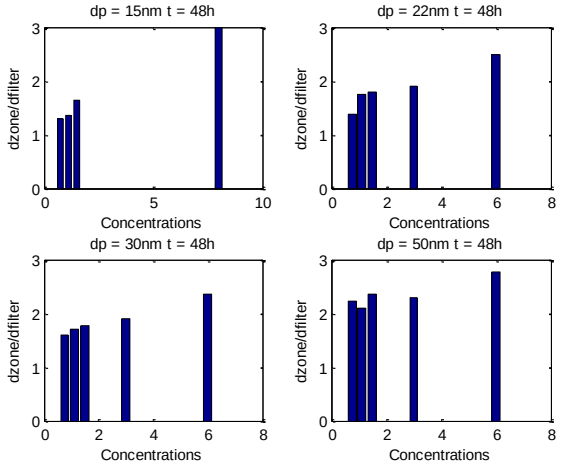

Figure 2: Normalized size of the inhibition zone's with respect to the diameter of the filter as a function of ENP surface concentration expressed in 10^{14} #/m^2.

References

Scown T.M, R. van Aerle, Tyler C.R, 2010 *Do engineered nanoparticles pose a significant threat to the aquatic environment?*, Crit. Rev. Toxicol., 40, 653-670

Oberdörster G, Oberdörster E, Oberdörster J, 2005 *Nanotoxicology: An Emerging Discipline Evolving from Studies of Ultrafine Particles*, Environ. Health Perspect., 113, 823-840.

Hamouda T, Myc A, Donovan B, Shih A, Reuter JD, Baker Jr JR, 2000, *A novel surfactant nanoemulsion with a unique non – irritant topical antimicrobial activity against bacteria, enveloped viruses and fungi*, Microbiol. Res., 156,1-7

Sondi I, Salopek-Sondi B, 2004, *Silver nanoparticles as antimicrobial agent: a case study on E. coli as a model for Gram-negative bacteria*, J. Colloid Interface Sci., 275,177-82

Nanoparticle Balancing from Release to Dose

H. Fissan[1,2], B. Stahlmecke[1], C. Asbach[1], T.A.J. Kuhlbusch[1,2]

[1]Institute of Energy and Environmental Technology, 47229 Duisburg, Germany
[2]Center for NanoIntergration Duisburg-Essen, 47057 Duisburg, Germany
Keywords: nanoparticle release, exposure pathway, nanoparticle concentration balances, dose estimation
Presenting author email: heinz.fissan@uni-due.de

The production and use of nanomaterials in form of products has risen over the recent years. Besides the expected beneficial properties of nanomaterials, they have also been reported to potentially cause adverse (health) effects, especially if engineered nanoobjects are released into the air and cause exposure of humans. Inhalation is seen as the major uptake route. The starting point for balancing is the amount of released nanoparticles per mass unit of nanostructured material. It can be considered to be a material property. Techniques that have the capability of being standardized, based on different stress (energy input) situations have to be developed (Fissan and Horn, 2012) to reduce the tremendous variability of stress cases. Besides defined stress cases, measurement techniques allowing for quantitative determination of nanoparticle release have to be used. The measures of interest (number, surface area, volume (mass)) depend on the physical and chemical processes occurring during the transport of the nanoparticles in the environment (air) and in the effect system, and the kind of effect considered to be risky. Release is followed by the changes occurring during transport, described by the nanoparticle release-exposure relationship (mainly dilution), then followed by the description of the changes during transport in the effect system (lung deposition), described by the exposure-dose relationship. Balancing should finally allow the determination or at least the estimation of the dose. These processes can be modeled taking into account different exposure scenarios. From thereon it is the task of, for instance toxicologists, to determine the possible hazard for different health endpoints.

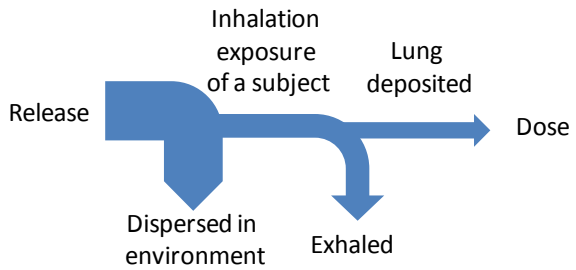

Figure 1. Balancing a metric from release to dose

Modeled balances can be evaluated or controlled by measurements at different points of the exposure pathway. For aerosol balancing, measurement techniques for number size distributions of spherical particles and loose agglomerates are available (SMPS, UNPA). For aggregates correction procedures for multiple charge effects still have to be developed. For transformation into number, surface area and volume distributions as function of volume per aggregate, calibration methods are developed (Fissan et al., 2012).

Another difficult problem for measurements is the in the real world especially in the environment always existing background of nanoscale particles.

We will report about first steps towards measuring nanoparticle release properties of nanostructured materials. We will set up a balance for number, surface area and volume concentration in an exposure scenario for inhalation to determine the expected dose. We will describe the possible control measurements along the exposure pathway.

Acknowledgement

Thanks for support from the European Community's Seventh Framework Program (FP7/2007-2013) under grant agreement n°211464-2.

References

Fissan H. and Horn H-G. (2012) Pan Stanford Publishing Pte.Ltd – in print
Fissan H. et al. (2012) Chemie Ingenieur Technik (CIT) – in print

Cytotoxicity of nanosilver with different sizes: Effect of Ag^+ ion release

A.Pratsinis[1], P. Hervella[2], S. E. Pratsinis[1], J-C. Leroux[2] and G. A. Sotiriou[1]

[1]Particle Technology Laboratory, Institute of Process Engineering, Department of Mechanical and Process Engineering, ETH Zurich, Sonneggstrasse 3, CH-8092, Zurich, Switzerland
[2]Drug Formulation and Delivery Laboratory, Department of Chemical and Applied Biosciences, ETH Zurich
Keywords: silver nanoparticles, toxicity, surface area concentration, dissolution.
Presenting author email: panna@student.ethz.ch

Nanosilver is used in heterogeneous catalysis and has promising applications in textiles [1], biomedical applications, biodegradable polymer films for food packaging [2], biological labeling [3], photonics, coloristic (plasmon)[4], optoelectronics and surface enhanced Raman scattering (SERS). At the same time, the use of nanosilver raises concerns for its toxicity against aquatic micro-organisms when disposed and therefore draws public attention. In fact, nanosilver is one of the first nanomaterials to be regarded toxic and petitions had been filed to the U. S. Environmental Protection Agency (EPA) to regulate it as pesticide. Therefore to safely employ nanosilver, correct risk and dose relations assessments need to be made.

There are several studies on the antibacterial activity of nanosilver made by wet-methods, co-condensation, and flame spray pyrolysis. Smaller nanosilver particles are more toxic than larger ones [5] especially when oxidized. Additionally, even though silver metal is practically insoluble in water, when present in nanometer size range Ag^+ ions are released (leached) [6-8] from its surface. It has been shown recently [9] that the antibacterial activity of small (<10 nm) nanosilver particles is dominated by Ag^+ ions, while for larger ones (>15 nm) the antibacterial contribution by Ag^+ ions and particles is comparable. Such a behavior implies a surface area dependency of the antibacterial activity especially for small nanosilver sizes since the Ag^+ ion release is proportional to the exposed nanosilver surface area [9]. Additionally, when a nanothin silica coating on the surface of nanosilver is applied, this antibacterial activity can be minimized [10].

Here, the toxicity of nanosilver against mammalian cells is investigated by immobilizing nanosilver on nanostructured silica particles and closely controlling Ag content and size. These Ag/SiO_2 nanoparticles were characterized by S/TEM, EDX spectroscopy, X-ray diffraction, N_2 adsorption. Furthermore, the fraction of dissolved nanosilver was determined by measuring the released (leached) Ag^+ ion concentration in aqueous suspensions of such Ag/SiO_2 particles. The toxicity of Ag^+ ions was distinguished from that of nanosilver particles by monitoring the growth of cell populations in the presence and absence of Ag/SiO_2 particles. The toxicity of nanosilver was dominated by Ag^+ ions when fine Ag nanoparticles (less than about 10 nm in average diameter) were employed that release high concentrations of Ag^+ ions. In contrast, when relatively larger Ag nanoparticles were used, the concentration of the released Ag^+ ions was lower. Then the toxicity of the released Ag^+ ions and nanosilver particles was comparable.

References

[1] Sotiriou, G. A. & Pratsinis, S. E. Engineering nanosilver as an antibacterial, biosensor and bioimaging material. *Curr. Opin. Chem. Eng.* **1**, 3-10 (2011).

[2] Loher, S., Schneider, O. D., Maienfisch, T., Bokorny, S. & Stark, W. J. Micro-organism-triggered release of silver nanoparticles from biodegradable oxide carriers allows preparation of self-sterilizing polymer surfaces. *Small* **4**, 824-832 (2008).

[3] Sotiriou, G. A., Hirt, A. M., Lozach, P. Y., Teleki, A., Krumeich, F. & Pratsinis, S. E. Hybrid, silica-coated, Janus-like plasmonic-magnetic nanoparticles. *Chem. Mater.* **23**, 1985-1992 (2011).

[4] Quinten, M. The color of finely dispersed nanoparticles. *Appl. Phys. B-Lasers Opt.* **73**, 317-326 (2001).

[5] Lok, C. N., Ho, C. M., Chen, R., He, Q. Y., Yu, W. Y., Sun, H., Tam, P. K. H., Chiu, J. F. & Che, C. M. Silver nanoparticles: partial oxidation and antibacterial activities. *J. Biol. Inorg. Chem.* **12**, 527-534 (2007).

[6] Benn, T. M. & Westerhoff, P. Nanoparticle silver released into water from commercially available sock fabrics. *Environ. Sci. Technol.* **42**, 4133-4139 (2008).

[7] Gunawan, C., Teoh, W. Y., Marquis, C. P., Lifia, J. & Amal, R. Reversible antimicrobial photoswitching in nanosilver. *Small* **5**, 341-344 (2009).

[8] Navarro, E., Piccapietra, F., Wagner, B., Marconi, F., Kaegi, R., Odzak, N., Sigg, L. & Behra, R. Toxicity of silver nanoparticles to *Chlamydomonas reinhardtii*. *Environ. Sci. Technol.* **42**, 8959-8964 (2008).

[9] Sotiriou, G. A. & Pratsinis, S. E. Antibacterial activity of nanosilver ions and particles. *Environ. Sci. Technol.* **44**, 5649-5654 (2010).

[10] Sotiriou, G. A., Sannomiya, T., Teleki, A., Krumeich, F., Vörös, J. & Pratsinis, S. E. Non-toxic dry-coated nanosilver for plasmonic biosensors. *Adv. Funct. Mater.* **20**, 4250-4257 (2010).

Investigations on nanoparticle release from artificially weathered coatings and composites that experience different treatment processes

D. Göhler, A. Nogowski, P. Fiala and M. Stintz

Research Group Mechanical Process Engineering, Institute of Process Engineering and Environmental Technology, Technische Universität Dresden, 01062 Dresden, Germany
Keywords: nanoparticle release, exposure, artificial weathering, sanding, dynamic friction, wind erosion, EHS.
Presenting author email: daniel.goehler@tu-dresden.de

Possible risk to health, safety and environment, associated with the use of engineered nanomaterial, is determined by whose hazard potential and exposure level. Exposure studies in laboratory as a consequence of the tiered approach of exposure measurements (Kuhlbusch *et al.*, 2011) can provide basic data about the ability and/or the quantity of nanoparticle release due to simulated treatment processes.

Currently, only few studies have analyzed the release of engineered nano-objects (ENO) from composites and coatings in the air. Vorbau *et al.* (2009), Guiot *el al.* (2009) and Wohlleben *et al.* (2011) simulated weak, but long-term abrasion processes and found only a slight release of coarse particles containing embedded ENO. Total abrasion by sunlight, wind and human contact (Hsu & Chein, 2007) led to similar results. The nanoparticle release from coatings due to sanding were studied by Koponen *et al.* (2011), Göhler *et al.* (2010) and Wohlleben *et al.* (2011), while cutting and drill processes on composite material were simulated by Bello *et al.* (2009 & 2010). Sanding, cutting and drilling based on high energy input, that led in each case to a considerable generation of nanoparticles, whether ENO were added to the matrix material or not. Free ENO were only observed by Bello *et al.* (2010), which can maybe explained by thermal degradation of the matrix material.

External impacts like sunlight, moisture or temperature fluctuations can destruct the matrix material of coatings and composites, what can lead to an open laying of ENO and is probably associated with a higher release risk.

Based on an extended test apparatus (Göhler *et al.*, 2010) artificially weathered samples of numerous coatings and composites with and without nanoscaled pigments were exposed to different treatment processes (wind erosion, dynamic friction and sanding). Concerning the process-specific amount of released particles different experimental setups with suitable aerosol measurement devices (e.g. EEPS, APS, CPC) were chosen to determine particle size distributions and particle number concentrations. Additionally, electrostatic precipitation was used for preparing samples analyzed by scanning electron microscopy, transmission electron microscopy and energy dispersive X-ray spectroscopy.

Results based on the sanding of artificially weathered coatings show an increase of the nanoparticle release in comparison to the non-weathered samples, while the weathering of the composites led to a decrease in the particle release. In some cases the addition of nanoscaled pigments to the matrix material results in a decrease of released particles, for both non-weathered and weathered coatings. Some coatings based on non-nanoscaled pigments show a higher release of nanoparticles in comparison to the non-doped ones.

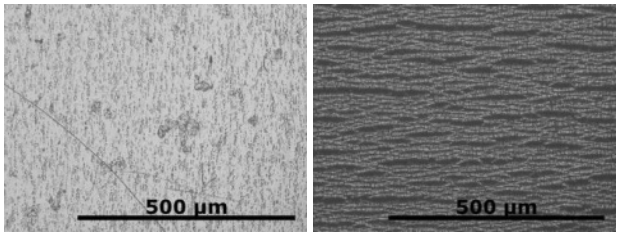

Figure 1: Example of changes on the sample surface due to artificial weathering (initial state left)

In addition to the results of particle release, the presentation will also show the process simulations, the evaluation of measurement data for the quantification of the particle release and the possibility to determine emission factors for the comparison of different treatment processes.

This work was supported by the German Federal Ministry of Economics and Technology (BMWi) under grant 01FS10004. The pigments were provided by the companies of the Verband der Mineralfarbenindustrie e.V. (VdMi), Germany.

Bello, D., Wardle, B.L., Yamamoto, N., deVilloria, R.G. et al. (2009) *J. Nanopart. Res.* **11**, 231-249.

Bello, D., Wardle, B.L., Zhang, J., Yamamoto, N. et al. (2010) *Int. J. Occup. Environ. Health* **16**, 434-450.

Göhler, D., Stintz, M., Hillemann, L. and Vorbau, M. (2010) *Ann. Occup. Hyg.* **54**(6), 615-624.

Guiot, A., Golanski, L. and Tardif, F. (2009) *J. Phys.: Conf. Ser.* **170**, 012014.

Hsu, L. Y. and Chein, H. M. (2007*) J. Nanopart. Res.*, **9**, 157-163.

Koponen, I.K., Jensen, K.A. and Schneider, T. (2011) *J. Expo. Sci. Env. Epid.* **21**(4), 408-418.

Kuhlbusch, T.A.J., Asbach, C., Fissan, H., Göhler, D. and Stintz, M. (2011) *Part. Fibre Toxicol.* **8**: 22.

Vorbau, M., Hillemann, L. and Stintz, M. (2009) *J. Aerosol Sci.* **40**(3), 209-217.

Wohlleben, W., Brill, S., Meier, M.W., Mertler, M., Cox, G., et al. (2011) *Small* **7**(16), 2384-2395.

Assessment of exposure to airborne nanomaterials using a pragmatic, tiered approach

C. Asbach[1], D. Dahmann[2], M. Voetz[3], B. Stahlmecke[1], H. Kaminski[1], Thomas A.J. Kuhlbusch[1,4], U. Götz[5], S. Engel[5], S. Plitzko[6]

[1]Institute of Energy and Environmental Technology (IUTA) e.V. 47229 Duisburg, Germany
[2]Institute for the Research on Hazardous Substances (IGF), 44789 Bochum, Germany
[3]Bayer Technology Services GmbH, 41368 Leverkusen, Germany
[4]Center for NanoIntegration Duisburg-Essen, 47057 Duisburg
[5]BASF SE, 67063 Ludwigshafen, Germany
[6] Federal Institute for Occupational Safety and Health (BAuA), 10317 Berlin, Germany

Keywords: nanoparticles, exposure assessment, strategy, tiered approach
Presenting author email: asbach@iuta.de

The number of nanotechnological products, particularly those using nanoparticles has risen constantly over the recent years. Besides the tremendous advantages these products provide over conventional products, a discussion about possible adverse effects especially to human health has been initiated. Since a risk may only arise from nanoparticles if an exposure coexists with a potential hazard of the substance, exposure assessment is a substantial element of risk analysis. The highest probability for release of and consecutive exposure to engineered nanomaterials exists in workplaces where these materials are produced, handled or used. The assessment of exposure to nanoparticles requires a differentiation of the engineered nanomaterials from ubiquitous background particles. While a definitive online differentiation of engineered nanomaterials from other background particles is usually impossible, we here present a more pragmatic approach, used in the German project nanoGEM. The approach is tiered and based on a suggestion by the German Chemical Industry Association (VCI). The first tier comprises data gathering for the considered workplace to obtain information if nanomaterials may be released. If exposure to nanomaterials cannot be excluded from tier 1, the second tier comes into play, which foresees a simplified assessment of the particle concentrations in the workplace and comparison with the common average background concentration. Tier 2 assessment can either be carried out as a short term measurement or as a long-term monitoring. Monitoring instruments can either permanently be installed in workplaces to allow for a continuous monitoring of the particle concentrations in the workplace, or only temporarily, e.g. if a first assessment revealed indications for a potential particle release. If the assessment in the second tier provides evidence that particles may be released, tier 3 needs to be followed that foresees a detailed analysis of the workplace aerosol. In tier 3 the particle size distributions are measured in a wide size range and particle samples taken for consecutive chemical and morphological analysis. Two sets of measurements are conducted to differentiate between background particles from those stemming from nanomaterials. This can be achieved by either measuring with two sets of equipment simultaneously in a background location and a workplace location or by using a single set and measuring during periods before/after and during the use of nanomaterials. Consecutive electron microscopic analysis of the sampled particles can provide clear evidence for the presence or absence of engineered nanomaterials. All measurements within nanoGEM are conducted in accordance to standard operation procedures (SOPs). The strategy and SOPs will be presented along with first measurement results.

Acknowledgement

This work is funded by the German Ministry for Education and Research (BMBF) under grant number 03X0105 (NanoGEM). The Financial support is gratefully acknowledged.

References

VCI (2011): https://www.vci.de/Downloads/ Tiered-Approach.pdf

Aerosol particle emissions from sanding coated plates: effect of the sanding paper and filtering method to the human exposure.

I.K. koponen[1], M. Levin[2] and K.A. Jensen[2]

[1]National Research Centre of Working Environment, Copenhagen, Denmark
Keywords: Occupational exposures, Occupational health
Presenting author email: ikk@ikkopone.fi

There are several safety concerns with consumer products were engineered nano materials (ENM) have been used. However, there is a vast amount of products in the everyday use which have embedded ENMs. Production lines where ENMs are handled are usually controlled; therefore exposure to nanoparticles is more likely to happen after the manufacturing process itself. One common product group where ENMs have been used for decades are e.g. paints and lacquers.

Studies of dust released performing sanding to coated plates have been published by e.g. Koponen et al, 2010; Gohler et al., 2010. Both studies were focused on investigating differences in dust emission depending what kind of ENMs were used in the coating. On this study aim is to investigate what could be the real exposure for the worker or end user when sanding coated plates.

Exposure experiments were conducted inside a 20.6 m3 human exposure chamber made with an inner wall of stainless steel (a nominal air exchange rate of 9.2 ± 0.8 h-1). HEPA-filtering of the supply air to exposure chamber assured low total background particle concentrations (<300 cm-3).

To compare emission rates we made an attempt to measure emission source strength more precisely. These experiments were performed in the small 0.66 m^3 stainless steel chamber.

Number size distribution measurements were conducted using a TSI Fast Mobility Particle Sizer (FMPS; 5.6-560 nm) and a GRIMM Dust monitor Model 1.109 (0.28-30µm) for the aerosol size and number distribution. For background measurements, we used a TSI Condensation Particle Counter (CPC) Model 2022 and GRIMM Dust monitor Model 1.109 (0.28-30µm). The particulate mass of particles smaller than 1 µm (PM1) was sampled with Triplex cyclones Model SC.1.106 mounted with cellulose-filters for electron microscopy and Teflon filters for gravimetric analysis. Humidity and temperature were monitored using Gemini sensors.

Test plates were coated with paints, fillers and lacquers. Paints were manufactured for indoor, outdoor and metal use. Some of them had ENM embedded like e.g. Nano-Silicasol (SiO2; 7 nm). One of the filler were with CaCO3 and other one with CaCO3+perlite. We had two types of lacquers; UV-hardcoat and another with 5% Nano-SiO2 (SiO2; <50 nm) added.

Previously in our study Koponen et al.,2011, we presented aerosol particle emission data for sanding different paint products. Main focus was to compare the difference between the products where ENMs have been used to enhance paint quality and paints were ENMs were not used. In that study we used closed system to make sure that we would characterize released dust as good as possible.

Here focus was to estimate real exposure risk while using sanding machine to sand coated plates. We compared different paint products using two different kind of filter paper with grin sizes 120 and 240. In addition three different kind of filtering methods were used to estimate possible exposure.

Figure 1 presents aerosol number size distribution spectra measured from human exposure chamber during sanding indoor wall paint without ENPs added. Small particles under 50 nm are originating from the sanding machine electrical motor as reported in our previous study. Figure 1 illustrates how filtering is effecting the particle emissions and the possible exposure to the user.

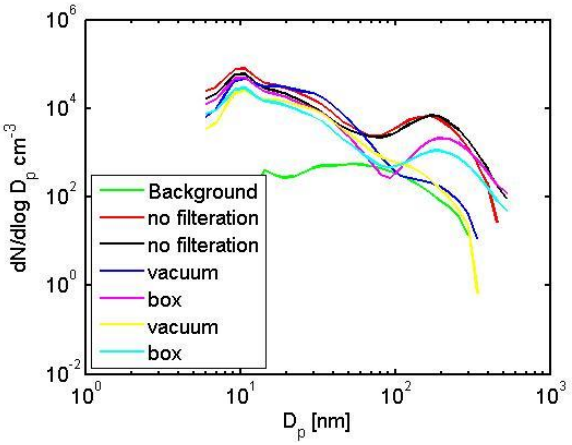

Figure 1. Measured size distribution spectra during sanding experiment.

This work was supported by the. Danish Working Environment Research Fund (Nanokem), Grand Number 20060068816 and EU FP7 project NanoSustain.

Koponen, IK., Jensen, KA., Schneider, T., (2010) *Comparison of dust released from sanding conventional and nanoparticle-doped wall and wood coatings*. J. Exp Sci. and Env. Epid,21,4,pp409-418.

Gohler, D., Stintz, M., Hillemann, L.,Vorbau, M.,(2010), *Characterization of Nanoparticle Release from Surface Coatings by the Simulation of a Sanding Process,*. Annals of Occ. Hyg.,54, 6, pp: 615-624

Exposure and Risk Assessment during Production of Nanoparticles by Plasma Synthesis

Jelena Buha[1,2], Drew Thompson[3], Marc Leparoux[4], Christian Jäggi[4], David Y.H. Pui[3] and Jing Wang[1,2]

[1]Institute of Environmental Engineering, ETH Zurich, Zurich, 8093, Switzerland
[2] Swiss Federal Laboratories for Materials Science and Technology, ETH Zurich, Dubendorf, 8600, Switzerland
[3]Particle Technology Laboratory, University of Minnesota, Minnesota, 55455, USA
[4]Swiss Federal Laboratories for Materials Science and Technology, ETH Zurich, Thun, 3602, Switzerland
Keywords: exposure, risk, nanoparticles, ICP
Presenting author email: jelena.buha@empa.ch

Environmental health and safety of nanomaterials are of growing concern as it becomes more common for consumer goods to utilize nanomaterials. For a risk to be posed by nanomaterials both hazard and exposure need to be present. The hazard is determined by toxicology studies, whereas the exposure is determined by exposure assessments.

The few reports (Wang et al. 2011, Walser et al. 2012) of workplace exposures suggest that engineered nanomaterials are released at high mass and/or number concentrations only under unusual circumstances. However, there still exists the need for study of exposure levels to different engineered nanomaterial types in occupational and environmental settings. Herein we present emission measurements of airborne nanoparticles performed at EMPA Thun, during the process of nanoparticle production.

Assessments of potential occupational exposure to nanoparticles were conducted at a pilot facility where nanoparticles were synthesized by inductively coupled plasma (ICP) (Leparoux, et al. 2005, 2010). The nanoparticles plasma synthesis is based on rapid condensation, also called quenching, of a supersaturated gas phase. The quenching dynamics influence the nanoparticles properties such as size, size distribution and eventually the final chemical composition. The synthesis procedure is taking place in the plasma reactor and the process itself is based on the evaporation-condensation method. Numerous view ports for process observation, monitoring, and in-situ characterization were analysed.

Regarding the emission studies, the filtration unit was used to collect small quantities of nanoparticles on the surface of a filter. The filter cartridge contained metal filters which were backpulsed to removed caked nanoparticles. This system was used to collect larger quantities of nanoparticles.

Further on, real-time aerosol instruments were used to monitor particle concentration and size distribution. By looking for relative changes in size and concentration, while also considering particle sources, it was possible to monitor a nanoparticle release. Instrumentation that was included was: fast mobility particle sizer (FMPS), handheld condensation particle counter (CPC), nanoparticle surface area monitor (NSAM) and aerodynamic particle sizer (APS). Area sampling with track-etched polycarbonate filters was done for particle identification by scanning electron microscopy (SEM).

The P-Trak and DustTrak were placed in front of the ventilation exhaust. This placement likely resulted in elevated concentrations. Dust was visible when filter was blown with compressed air. The cleaning of the cartridge resulted in a significant increase in particle concentrations. During this process the particle concentrations increased by 20 times. The blowing of the cartridge with compressed air resulted in elevated particle concentrations which subsided after approximately five minutes. The particle concentration returned to that which was present before cleaning began (background level).

A particle release was not detected during the synthesis of SiC nanoparticles. Particles were released when nanoparticles or nanoparticle contaminated equipment were handled in the open air. Compressed air was found to resuspend nanoparticles when it was used in inadequately ventilated areas. The use of compressed air in workplaces containing nanoparticles should be avoided or methods recommended by ASTM and NIOSH standards should be used instead.

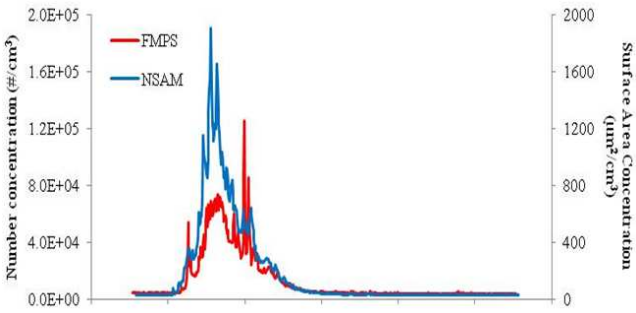

Figure 1. Number concentration and surface area concentration measurements performed during the process of cartridge filter cleaning

Wang, J. et al. (2011) *J. Nanopart Res*, **13**, 1373 – 1387.
Walser, T. et al. (2012) *Exposure to engineered nanoparticles: Model and measurements for accident situations in laboratories*, *Sci Total Environ*, accepted.
Leparoux, M. et al. (2005) *Advanced Engineering Materials*, **7**, (5), 349-353.
Leparoux, M. et al. (2010) *Plasma Chemistry and Plasma Processing*, **30**, (6), 779-793.

Analysis of aerosol solid nanoparticles produced during soldering using metal alloys

Virginia Gómez, Silvia Irusta, Francisco Balas and Jesús Santamaría
Instituto de Nanociencia de Aragón (INA), Edificio I+D, c/ Mariano Esquillor s/n, 50018 Zaragoza (Spain)
Keywords: Nanoparticles ;Soldering ; Occupational exposure
virgomez@unizar.es

In the recent years, there has been an increasing concern about the toxicological effect of airborne particles. Several factors as size, shape, charge, aggregation state and material have capital importance in the toxicological effects of particles with diameters below 100 nm. Among the different exposure routes to particles, the most worrying are inhalation and ingestion. In order to prevent worker exposure to harmful aerosols, different industrial processes has been studied as welding, sanding and grinding.

Soldering is a broadly used process in electronica industry and also in investigation process. This process involved join two electronic components by using a filler tin-based metal alloy. Moreover, solder wires also contains a small amount of flux based in colophony rosins in order to prevent solder oxidation. Continuous exposure to colophony fumes can lead in harmful effects as bronchial asthma [1-3] and dermatitis [4]. Another concern about soldering is the use of lead bases solders. Despite the development in latest years of lead-free solders, soldering with lead alloys is still common in a wide variety of occupational environments.

In the present work, aerosol particles generated during soldering process has been characterized. Two solder wires have been chosen one lead-free (SnAgCu) and the other with lead (SnPbCu). The soldering wires have been characterized by X-ray photoelectron spectroscopy (Axis Ultra DLD, Kratos Tech.) and scanning electron spectroscopy, secondary electron image and energy dispersive X-ray spectroscopy (FESEM, Inspect form FEI).

Experiments have been performed inside an especially-designed globe box chamber in order to avoid the presence of background nanoparticles. The aerosol formation is alternatively online monitored with a condensation particle counter (CPC, Grimm) and an optical particle counter (OPC, Grimm). As the CPC and OPC take the aerosol from the chamber at 0.3 and 1.2 l/min, the same flow of HEPA-filtered clean air is added during the experiment to keep constant air pressure. Offline analysis of the aerosol particles has been performed using transmission electron microscopy (T20 – FEI), scanning transmission electron microscopy (STEM) and energy dispersive X-ray spectroscopy (TEM-EDX) (F30 – FEI) using holey-carbon coated copper grids placed in a stainless steel filter holder. Aerosol nanoparticles have been also filtered through polycarbonate filters and subsequently observed by scanning electron microscopy (SEM) and SEM-EDX

Figure 1 shows the SEM image of nanoparticles and aggregates collected on the surface of polycarbonate filters. Online aerosol analysis shows also the generation of primary nanoparticles with average diameters below 100 nm and aggregates with diameters below 1 μm consisting of metallic nanoparticles in a flux matrix. The EDX analysis of the particles and aggregates show lead and tin signals.

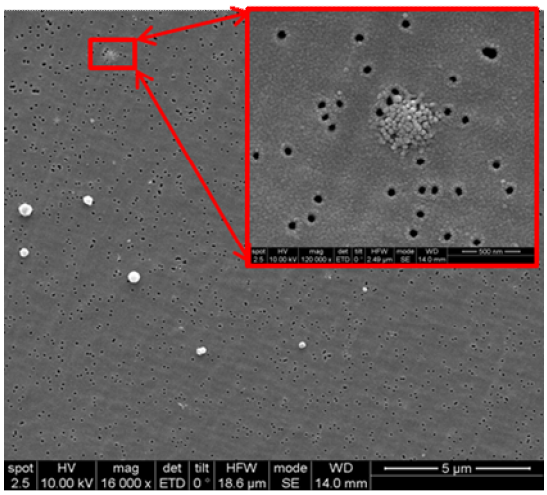

Figure 1. SEM image of aggregates and some nanoparticles collected on the surface of a polycarbonate filter after soldering with SnPbCu at 250 ºC.

The chemical analysis soldering fumes show the presence of tin and lead-containing nanoparticles. This study points to the possible harmful impact of soldering due to the presence of nanoparticle-laden aerosols with variable contains of metals.

This work was supported by Spanish MICINN through research projects MAT2008-01319/NAN and PSE-2008-420000-3. Financial support of the FP7 European project NanoValid (#263147) is also acknowledged. V.G. acknowledges the FPU scholarship AP2008-02067

Burge, P.S. et al., *Occupational asthma in a factory making flux-cored solder containing colophony.* Thorax 1981. **36**(11): p. 828-834.

McDonald, J.C. et al., *Incidence by occupation and industry of acute work related respiratory diseases in the UK, 1992-2001.* Occup. Env. Med. 2005. **62**(12): p. 836-842.

Perks, W.H. et al., *Work-related respiratory disease in employees leaving an electronics factory.* Thorax, 1979. **34**(1): p. 19-22.

Downs, A.M.R. and Sansom, J.E. *Colophony allergy: a review.* Contact Dermat. 1999. **41**(6): p. 305-310.

Particle characterisation from reducing Cl-process producing Cu and Cu-CNT like nanoparticles - safety issues to consider for scale-up

J. Lyyränen[1], J. Hokkinen[1], U. Backman[1], A. Auvinen[1], J. Jokiniemi[1,2]

[1]VTT Technical Research Centre of Finland, P.O. Box 1000, FI-02044 VTT, Finland
[2]Univ. of Eastern Finland, Department of Environmental Science, P.O. Box 1627, FI-70211 Kuopio, Finland
Keywords: Nanoparticle, characterisation, Cl-process, particle removal.
Presenting author email: jussi.lyyranen@vtt.fi

The increased use of nanoparticles and nanomaterials to produce different kind of products has increased concern on the possible health effects of these products. Also the processes used to manufacture these products have raised interest. In this study Cu and carbon nanotube (CNT) like containing Cu-particles produced by hydrogen reduction reaction from copper chloride precursor vapour and H_2O + ethene (for CNT production) in nitrogen carrier gas (Forsman, et al., 2008) were studied. The aim was to characterise the produced particles with aerosol measurement devices to help to design the scale-up of the Cl-process as well as possible both technically and occupationally safe. In addition, a custom-made electrostatic precipitator (ESP) was installed to the measurement system to determine its particle removal efficiency.

The particle number concentration was measured with a TSI 3775 CPC and the number size distribution with a TSI 3080 electrostatic classifier with a TSI 3081 DMA connected with a TSI 3775 CPC and controlled by the SMPS software. The mass concentration was measured with a TEOM 1400a. The gas composition was monitored with a Fourier-Transform Infrared spectrometer (FTIR). Individual particle samples for electron microscopy (EM) analyses were collected with an aspiration EM sampler.

The particle number concentration with CuCl and H_2 feed only varied between 0.4-1.0·10^9 1/cm^3 and the CMD 35-47 nm. The average mass concentration was 450 mg/m^3. When the ESP was switched on the number concentration dropped down to 1.0-2.0·10^3 1/cm^3 producing particle removal efficiency of 99.999 %. The produced particles were almost smooth spherical particles up to about 150 nm in diameter (Fig. 1a). The HCl concentration measured by FTIR indicating the reduction of CuCl to Cu was approximately 200 ppm.

With CuCl and H_2 feed together with and H_2O + ethane (for CNT production) the particle number concentration varied between 0.2-0.6·10^9 1/cm^3 and the CMD 66-74 nm. The average mass concentration was 370 mg/m^3. When the ESP was switched on the number concentration dropped down to a few hundred particles 1/cm^3 producing particle removal efficiency of 99.99999 %. The produced particles were carbon nanotube like cords or wires with very small spherical Cu particles at the end of the wires (Fig. 1b). The width of the wires was approximately 25 nm or less. The HCl concentration measured by FTIR indicating the reduction of CuCl to Cu was approximately 100 ppm.

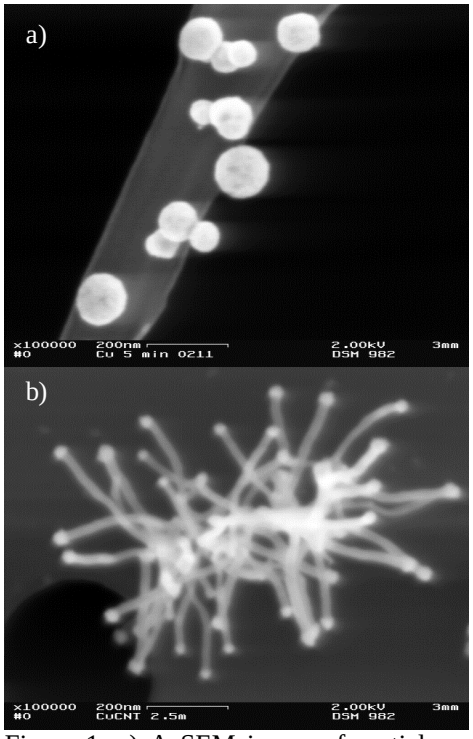

Figure 1. a) A SEM image of particles produced with CuCl and H_2 feed only.
b) A SEM image of particles produced with CuCl and H_2 together with H_2O + ethene (for CNT production).

The results indicated that even in very aggressive environments, i.e. reducing and HCl containing atmospheres, the ESP was able to remove practically all the produced particles. For the final scale-up a large enough back-up filter after the ESP would be recommended to remove the particles possible penetrating the ESP.

The research leading to these results has received funding from the European Union Seventh Framework Programme (FP7/2007-2013) under grant agreement 24789 (NanoSustain).

Forsman, J., Tapper, U., Auvinen, A., & Jokiniemi, J. (2008). *J. Nanopart. Res.*, 10, 745-759.

Particle characterisation during melting of nanoparticle containing coated and uncoated window glass

J. Lyyränen[1], J. Hokkinen[1], U. Backman[1], A. Auvinen[1], J. Jokiniemi[1,2] and A. Kurz[3]

[1]VTT Technical Research Centre of Finland, P.O. Box 1000, FI-02044 VTT, Finland
[2]Univ. of Eastern Finland, Department of Environmental Science, P.O. Box 1627, FI-70211 Kuopio, Finland
[3]Nanogate Indisutrial Solutions GmbH, Zum Schacht 3, 66287 Göttelborn, Germany
Keywords: Nanoparticle, characterisation, glass, melting, recycling.
Presenting author email: jussi.lyyranen@vtt.fi

The increased use of nanoparticles and nanomaterials may set new demands for the recycling of the products containing these materials. In this study the possibly emitting nanoparticles during heating and melting of window glass coated with pro.Glass Barrier 401 (containing ZnO nanoparticles) and only with sol-gel binder matrix were investigated. As a reference, a plain window glass sample without any surface treatment was heated/melted. The glass sheets were provided by Nanogate. The particle number and mass concentration as well as the number size distribution were measured during the heating/melting, i.e. mimicking the established recycling process of the product. The heating/melting was carried out in an induction furnace and the temperature range studied was 700-1500 °C.

The particle number concentration was measured with a TSI 3775 CPC and the number size distribution with a TSI 3080 electrostatic classifier with a TSI 3081 DMA connected with a TSI 3775 CPC and controlled by the SMPS software. The mass concentration was measured with a TEOM 1400a. Individual particle samples for electron microscopy (EM) analyses were collected with an aspiration EM sampler.

The first traces of particles appeared in the number concentration for coated window glass at approximately 700 °C, but the mass concentration was very low, close to 0 (MC≈0-5 mg/m^3). The primary particles from sol-gel binder matrix coated glass were almost perfect spheres, with a diameter of approximately 50 nm or smaller. The primary spheres had not formed aggregates by adhering to each other. For pro.Glass Barrier 401 coated glass the primary particles were also almost perfectly shaped single spheres at 700 °C, but the diameter was much smaller, less than 15 nm.

At the highest temperature of 1500 °C the number of the primary spheres and nanoparticles seemed to have decreased, and the number of larger particles (>100 nm) increased. This indicated the further growth of the nanoparticles by condensation and aggregation. At 1500 °C the number concentration for sol-gel binder matrix coated glass was somewhat lower than for pro.Glass Barrier 401 coated glass, 1.0-1.6·10^9 1/cm^3 and 1.4-2.0·10^9 1/cm^3, respectively. However, the mass concentration for the sol-gel binder matrix coated glass was clearly higher than for the pro.Glass barrier 401 coated glass, 135-150 mg/m^3 and 84-93 mg/m^3, respectively. The particles emitted from the plain window glass were mainly rod-like and asymmetrical (Fig. 1a) compared to almost spherical ones for coated glass (Fig. 1b).

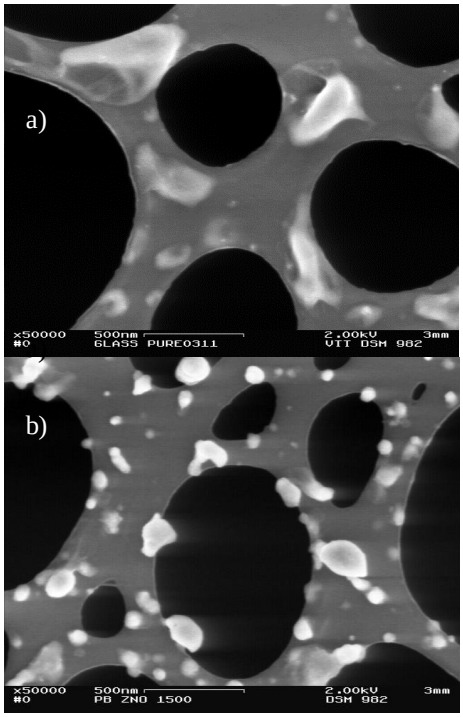

Figure 1. a) A SEM image for particles emitted at 1500 °C for plain window glass.
b) A SEM image for particles emitted at 1500 °C for pro.Glass Barrier 401 coated glass.

The number and mass concentration of the emitted particles from the glass samples did not depend on whether coating was applied or not, nor on the type of coating. A relatively larger amount of the particles emitted from plain window glass seemed to be larger than nanoparticles (>100 nm) than the ones emitted from coated glass samples. A notable increase in the number concentration begun at > 1000 °C and in the mass concentration > 1300 °C for all samples. In the emitted particles Na was enriched whereas the amount of Si was decreased in all of the glass samples. Zn was found only in particles emitted from the pro.Glass Barrier 401 coated glass.

The research leading to these results has received funding from the European Union Seventh Framework Programme (FP7/2007-2013) under grant agreement 24789 (NanoSustain).

Atmospheric new particle formation in the Central European boundary layer: A long-term study using Neutral Cluster Air Ion Spectrometer (NAIS) data

J. Größ[1], W. Birmili[1], A. Hamed[2], A. Sonntag[1], A. Wiedensohler[1], G. Spindler[1], H. E. Maninnen[3], M. Kulmala[3], U. Hõrrak[4], C. Plass-Dülmer[5]

[1]Leibniz Institute for Tropospheric Research, Permoserstrasse 15, 04318 Leipzig, Germany
[2]Department of Applied Physics, University of Eastern Finland, P.O. Box 1627, 70211 Kuopio, Finland
[3]Department of Physics, University of Helsinki, P.O. Box 64, 00014, University of Helsinki, Finland
[4]Institute of Physics, University of Tartu, Ülikooli 18, 50090 Tartu, Estonia
[5]German Meteorological Service DWD, Albin-Schwaiger-Weg 10, 82383 Hohenpeissenberg

Keywords: Nucleation, New Particle, Sulphuric acid, Formation and Growth

New particle formation (NPF) from supersaturated vapors (nucleation) has been show to occur almost everywhere in the atmosphere. According to current understanding, NPF is controlled mainly by gaseous sulphuric acid (H_2SO_4), a species that has a low vapor pressure and is therefore easily condensable. However, there numerous observations in the literature imply that ambient H_2SO_4 concentrations are not sufficient to explain the observed nucleation rates and subsequent particle growth by H_2SO_4 alone. Organic compounds represent a large fraction of secondary aerosol mass and are therefore considered to play an important role for the growth of the freshly formed particles.

NPF events were experimentally detected at the research station Melpitz (Germany) for the time period 2008-2011 using the following instruments:

- NAIS (Neutral Cluster Air Ion Spectrometer), measurement range 2-20 nm
- TDMPS (Twin Differential Mobility Particle), measurement range 3-800 nm
- APS (Aerodynamic Particle Sizer), measurement range 0.5-10 µm

A new method has been devised to identify and classify NPF events. It is based on the convolution integral (CI) of time series of freshly nucleated particles (2-20 nm). First, outstanding NPF events, which amounted to about 20% of all measurement days, were selected manually from the data set. An average diurnal cycle $N^*_{[2\text{-}20nm]}$, in which time series were normalised relatively to the beginning of the NPF event, was computed for those days. $N^*_{[2\text{-}20nm]}$ represents the "idealistic" behaviour of a new particle formation event. In a second step, the time series of the convolution function between $N^*_{[2\text{-}20nm]}(t)$ (defined for a 15 hour interval) and $N_{[2\text{-}20nm]}(t)$ was calculated. This time series is illustrated in Fig. 1a. Next, the peak values of the convolution integral were evaluated. High values in CI indicate an objective measure of significant particle formation. Fig. 1b illustrates the classification of NPF events into three classes. The CI method was also compared against the widely used method by Dal Maso et al. (2005). The comparison shows basically a good agreement between the methods for the strongest NPF events. However, the new CI method was, at least for this data set, able to detect weak NPF days more accurately than based on a visual inspection of contour diagrams of particle size distributions.

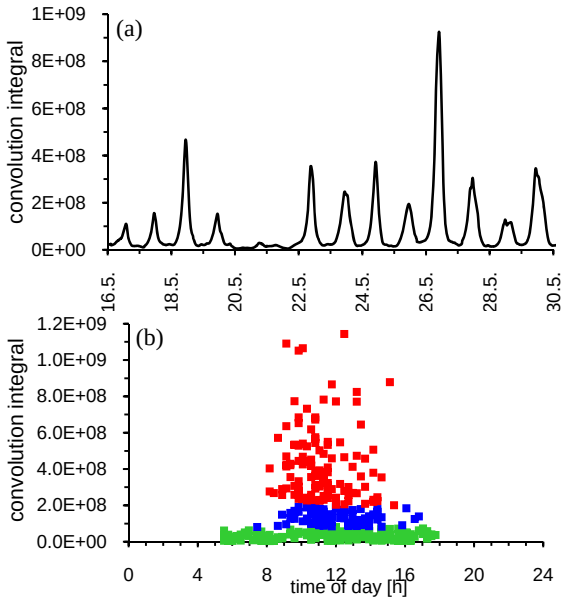

Fig. 1. (a) time diagram of the convolution integral from 16th to 30th May 2011, (b) daytime diagram of the daily maximum of the convolution integral for all observation days. Event classes are as follows: red: class I (intense new particle formation), blue: class II (new particle formation occurs but at low intensity), green: class III (NPF below significance level).

The presentation will conclude with the analysis of the relationship between NPF events and precursor concentrations, such as a H_2SO_4 proxy and a calculated ternary nucleation rate.

References

Dal Maso M., Kulmala M., Riipinen I., Wagner R., Hussein T., Aalto P.P. and Lehtinen K.E.J., 2005: Formation and growth of fresh atmospheric aerosols: eight years of aerosol size distribution data from SMEAR II, Hyytiälä, Finland. Boreal Env. Res., 10, 323-336.

Nanostructured catalytic layers for fuel cell electrodes prepared by electrospray

S. Martin, B. Martinez-Vazquez, P.L. Garcia-Ybarra and J.L. Castillo

Dept. Fisica Matematica y de Fluidos, Facultad de Ciencias UNED, Madrid, Spain
Keywords: Electrospray, Deposit morphology, Nanoparticles, Fuel cell
Presenting author email: smartin@dfmf.uned.es

The electrohydrodinamic atomization or electrospray has demonstrated to be a suitable technique for micro- and nano-thin-film deposition (Martin *et al*., 2005; Jaworek and Sobczyk, 2008). In our laboratory, the electrospraying of liquid suspensions containing catalytic nanoparticles is being successfully used in the production of porous catalytic layers for proton exchange membrane fuel cell (PEMFC) electrodes (Martin *et al*., 2010a, 2010b). One of the factors limiting the wide use of PEMFCs is the cost of the catalyst (platinum) in the electrodes. The goal of this study is to determine the electrospraying working conditions for obtaining electrodes with a low catalyst loading without compromising the fuel cell performance.

The electrospray deposition method enables the generation of nanostructured catalytic layers whose building blocks are clusters (of a few catalyst particles each) with a characteristic size of approximately 100 nm disposed in a dendritic arrangement (see Fig. 1).

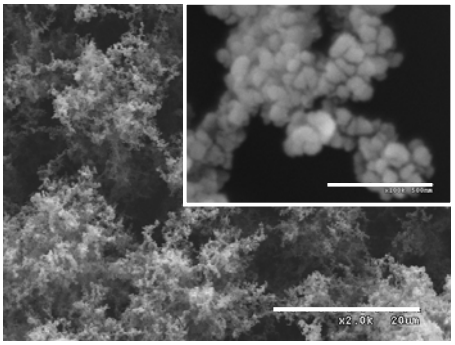

Figure 1. Dendritic structure of a catalyst layer with 0.01 $mg_{Pt}cm^{-2}$ Pt loading. The micron bar is 20 μm long for the main image and 500 nm for the inset.

This arrangement produces catalytic deposits with the appropriated morphology for PEMFC electrode preparation. On the one hand, the small size of the catalyst clusters leads to a high dispersion of the catalyst. On the other hand, the dendritic arrangement of the catalyst clusters results in a highly porous deposit with an enhanced permeability and increased electrochemical active surface area (Castillo *et al*., 2012).

The electrospray technique allows the preparation of efficient PEMFC electrodes with ultra-low platinum loadings (0.01 $mg_{Pt}cm^{-2}$). The conditions for achieving uniformly thin layers with the electrospray working in a stable cone-jet mode will be discussed. Figure 2 shows the fuel cell performance for several electrodes prepared under the same electrospraying parameters. The catalyst utilization (power per gram of platinum) delivered by these electrodes lies in the interval 30-35 kW g_{Pt}^{-1} what, to the best of our knowledge, represents the maximum platinum utilization reported up to now for any catalyst deposition method. Indeed, these results overcome in more than 50% the highest utilization achieved by sputtering (Cavarroc *et al*., 2009) and it is 3 times the Pt-utilization in our previous work (Martin *et al*., 2010b).

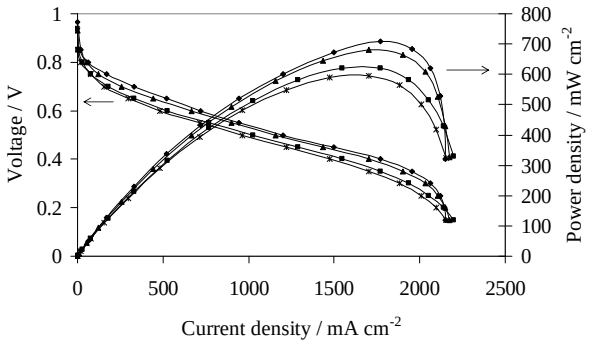

Figure 2. Fuel cell current-voltage and power density curves for electrodes with a Pt loading of 0.01 $mg_{Pt}cm^{-2}$.

The latter results were achieved using a fuel cell with small (5 cm^2) square electrodes. The scaling up to get 50 cm^2 square electrodes (delivering the same power density) will be discussed. In this way, the electrospray deposition method may be used to cover the entire range of required electrode sizes: from automotive or stationary applications down to portable units.

Work supported by Ministerio de Ciencia e Innovacion (Spain) (grants ENE2011-26868 and CSD2010-00011), and by Comunidad de Madrid (grant S2009ENE-1597).

Castillo, J.L., Martin. S., Rodriguez-Perez, D., Perea, A. and Garcia-Ybarra, P.L. (2012). *KONA Powder and Particle Journal*, **30** (2012), in press.

Cavarroc, M., Ennadjaoui, A., Mougenot, M., Brault, P., Escalier, R., Tessier, Y., Duran, J., Roualdès, S., Sauvage, T. and Coutanceau, C. (2009). *Electrochem. Comm.*, **11**, 859-861.

Jaworek, A. and Sobczyk, A.T. (2008). *Journal of Electrostatics*, **66**, 197-219.

Martín, S., Galán, D., Rodríguez-Pérez, D., Loscertales, I.G., Castillo, J.L., Barrero, A., García-Ybarra, P.L. (2005), in *Proceedings of the EAC*, Ghent, p. 637.

Martin, S., Garcia-Ybarra, P.L., and Castillo, J.L. (2010a). *J. Power Sources*, **195**, 2443-2449.

Martin, S., Garcia-Ybarra, P.L., and Castillo, J.L. (2010b). *J. Hydrogen Energy*, **35**, 10446-10451.

Control of phase composition of $LiFePO_4$ prepared with spray pyrolysis

A. Lähde[1], T. Karhunen[1], T. Torvela[1] and J. Jokiniemi[1,2]

[1]Department of Environmental Science, University of Eastern Finland, Kuopio, 70211, Finland
[2]Department of Chemical Physics, University of Elsewhere, City, Region, Postcode, Country
Keywords: $LiFePO_4$, spray pyrolysis, phase composition, crystallinity.
Presenting author email: anna.lahde@uef.fi

The structure of global energy supply is changing rapidly towards sustainable energy solutions. However, all forms of sustainable and intermittent energy production (e.g. wind power, photovoltaics) and sustainable transportation (e.g. hybrid and full electric vehicles) require excellent energy storage systems in order to increase their effectiveness (Hall and Bain 2008). Li-ion secondary cells are one of the most advanced battery energy storage systems currently available due to their high energy density. However, new higher capacity materials are urgently required in order to address the need for greater energy density, cycle life, lower cost and charge lifespan, among other issues faced by Li-ion batteries.

Iron-based cathode materials are ideal for future Li-ion batteries in terms of cost and environmental friendliness. In particular, olivine phase $LiFePO_4$ is an attractive material due to its high cycle stability, low toxicity and affordable precursor materials. However, $FePO_4$ is known to crystallize at least in four different polymorphs in addition to olivine that could also be electrochemically active (Voβ et al. 2012, Arroyo-de Dompablo et al. 2005).

In this paper, we present the preparation of $LiFePO_4$ with controlled phase composition using a spray pyrolysis. The precursors were dissolved in water and atomized using an ultrasonic nebulizer (RBI Pyrosol 7901). The produced droplets were then carried to the heated zone of the reactor. Experiments were carried out at temperatures between 200 and 800 ºC. The aerosol exiting the heat zone was rapidly cooled with a large volume of dilution gas (air or N_2) at ambient temperature. The particle size was controlled by precursor solution concentration. The particle properties were analyzed with electron microscopy, XRD and Raman.

The particles were spherical, soft agglomerates, see Figure 1. The particle size was around 0.5 µm based on SEM images.

Figure 2 shows the XRD patterns of particles produced at 800 ºC. Based on the XRD the particles contained two different crystalline phases, i.e. high pressure and olivine polymorphs. By controlling the conditions, the desired crystalline phase can be obtained.

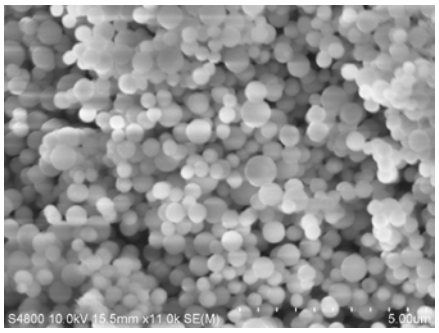

Figure 1. SEM image of the $LiFePO_4$ particles prepared with spray pyrolysis.

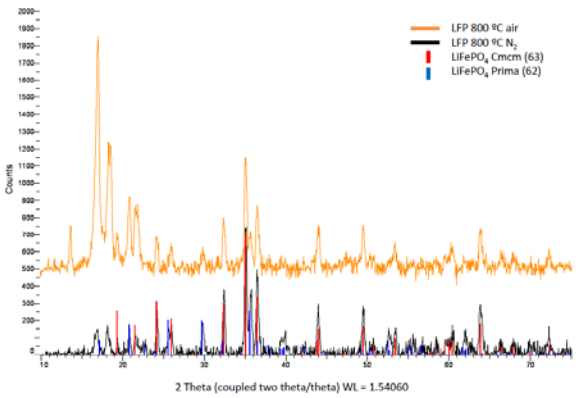

Figure 2. XRD data of $LiFePO_4$ nanoparticles produced at different processing conditions.

This work was supported by the Suomen Luonnonvarain Tutkimussäätiö under grant 1749/12 and by the Finnish Funding Agency for Technology and Innovation (TEKES).

Arrooyo-de Dompablo, M.E., Galardo-Amores, J.M. and Amador, U. (2005) *Electrochem Solid St.* **8**, A564-A569.

Hall, P.J. and Bain, E.J. (2008) *Energy Policy* **36**, 4352-4355.

Voβ, B., Nordmann, J., Kockmann, A., Piezonka, J., Haase, M., Taffa, D.H. and Walder, L. (2012) *Chem. Mater.*, DOI: 10.1021/cm202015g.

Two-component aerosol nanoparticle coating for paperboard on roll-to-roll process

J. Haapanen[1], M. Aromaa[1], H. Teisala[2], M. Tuominen[2], M. Stepien[3], J.J. Saarinen[3], M. Toivakka[3], J. Kuusipalo[2] and J.M. Mäkelä[1]

[1] Aerosol Physics Laboratory, Dept. of Physics, Tampere Univ. of Technology, P.O.Box 692, FI-33101, Finland

[2] Paper Converting and Packaging Technology, Tampere Univ. of Technology, P.O.Box 589, FI-33101, Finland

[3] Laboratory for Paper Coating and Converting, Abo Akademi Univ., Porthansgatan 3, FI-20500 Turku, Finland

Keywords: Liquid flame spray, Flame spray synthesis, Coatings, Nanoparticles, applications

Presenting author email: janne.haapanen@tut.fi

Introduction

Liquid Flame Spray (LFS) is an aerosol synthesis method for nanoparticles. LFS generated nanoparticles are deposited onto paperboard surface on roll-to-roll process. Functional nanoparticle coating is produced on paperboard surface in order to modify the surface properties. Main focus is to modify paperboard wetting properties. Coating is applied in laboratory conditions, demonstrating roll-to-roll process with line speed of 50 m/min. Functional properties like hydropohobicity and hydrophilicity are demonstrated. (Mäkelä et al. 2011, Stepien et al. 2011 and Teisala et al. 2010) In this study, different mass ratios of Ti/Si on the coatings were analysed.

Methods

In LFS method, liquid precursor is sprayed into a turbulent H_2/O_2-flame. The material evaporates, reacts, nucleates and grows inside the flame. Liquid precursors were prepared by solving titanium(IV) i-propoxide (TTIP) and tetraethoxysilane (TEOS) to isopropanol. All liquid precursors contained total concentration of 50 mg/ml of Ti+Si combined. Produced nanoparticles are mixture of TiO_2 and SiO_2. Coating of the paperboard can be carried out in laboratory scale with the coating track, demonstrating the roll-to-roll process or in a pilot scale roll-to-roll process. Line speed can be varied between 0-200 m/min. Coated paperboard surfaces were analysed using water contact angle (WCA) measurement and mean mobility particle sizes were measured with SMPS.

Results

WCA measurements (Figure 1) show that Ti/Si ratio in the used precursor has a significant effect on the water contact angle. Coatings with high Ti/Si ratio are superhydrophopic, water contact angles exceeding 160°. Coatings with low Ti/Si ratio are superhydrophilic with contact angle below 10°. Water contact angle of the non-coated reference paperboard is around 90°. Ti/Si ratio has a clear effect on mean mobility particle size, as shown in Figure 2.

Further studies will focus on the composition of the nanocoating as well as morphology and deposited size of the nanoparticles.

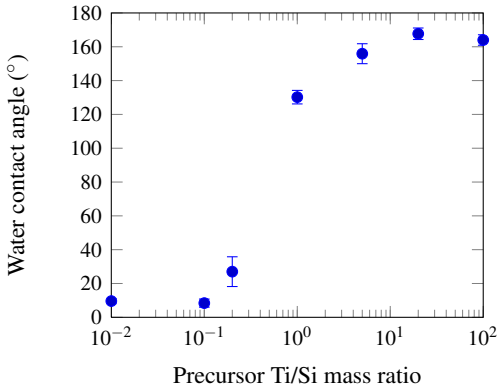

Figure 1. WCA with different Ti/Si mass ratios.

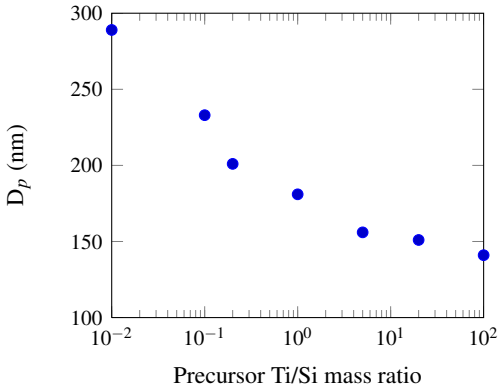

Figure 2. Mean mobility particle size (D_p) measured with SMPS with different Ti/Si mass ratios.

This work was supported by the Finnish Funding Agency for Technology and Innovation (Tekes) project "Nanorata 2".

Mäkelä, J.M., Aromaa, M., Teisala, H., Tuominen, M., Stepien, M., Saarinen, J.J., Toivakka M. and Kuusipalo, J. (2011). Aerosol Sci. Technol., 45, 827-837.

Stepien, M., Saarinen, J.J., Teisala, H., Tuominen, M., Aromaa, M., Kuusipalo, J., Mäkelä, J.M. and Toivakka, M. (2011). Appl. Surf. Sci., 257, 1911-1917.

Teisala, H., Tuominen, M., Aromaa, M., Mäkelä, J.M., Stepien, M., Saarinen, J.J., Toivakka, M. and Kuusipalo, J. (2010). Surf. Coat. Technol., 205, 436-445.

Plasmonic properties of size-selected spherical silver nanoparticles

J. Harra[1], J. Mäkitalo[2], R. Siikanen[2], M. Virkki[2], G. Genty[2], T. Kobayashi[3], M. Kauranen[2] and J.M. Mäkelä[1]
[1]Aerosol Physics Laboratory, Department of Physics, Tampere University of Technology, Tampere, Finland
[2]Optics Laboratory, Department of Physics, Tampere University of Technology, Tampere, Finland
[3]Advanced Ultrafast Laser Research Center, University of Electro-Communications, Tokyo, Japan
Keywords: aerosol synthesis, silver nanoparticle, localized surface plasmon resonance.
Presenting author email: juha.harra@tut.fi

Introduction

Optical properties of noble metal nanoparticles are dominated by coherent oscillations of conduction electrons which give rise to localized surface plasmon resonances (LSPR). The wavelength of the resonance depends on the particle size, shape and dielectric environment. Materials with plasmonic properties can be utilized in, e.g., biosensors and plasmonic solar cells.

Plasmonic materials containing silver or gold nanoparticles can be prepared with, e.g., ion implantation, sputtering or wet chemical techniques. These techniques usually offer rather restricted size control of spherical nanoparticles. However, the size range of spherical silver particles generated with aerosol techniques extends from a few nanometers to over 100 nm. Thus, aerosol synthesis gives the opportunity to tune the wavelength of the LSPR more extensively.

In this study (Harra *et al*, 2011), size-controlled aerosol synthesis was used to prepare plasmonic samples consisting of spherical and monodisperse silver nanoparticles deposited on a glass substrate. The particle coverage was varied between approximately 2 and 8 %.

Experimental

Silver agglomerates were generated in a tube furnace using an evaporation-condensation technique. The generation was followed by a size selection with a differential mobility analyzer and a sintering step with an additional tube furnace to obtain spherical particles. Finally, the nanoparticles were collected on a glass substrate with an electrostatic precipitator. The optical extinction spectra of the prepared samples were measured with a UV-VIS spectrophotometer, and the measured spectra were compared to a simple theoretical model.

Results and conclusions

Figure 1 shows high extinction near 400 nm for 90 nm particles, which is typical for silver. The spectrum also displays some fine structure: the peaks 1 and 2 near 400 nm and the peak 3 at longer wavelength. In order to analyze the spectrum, theoretical calculations were carried out using refractive indices of 1.0 and 1.3 for the dielectric environment. The calculations suggest that the peak 1 is caused by a dipolar resonance and the peak 2 is at least contributed by a quadrupolar resonance. The peak 3 is most likely caused by dimer particles formed during the collection process.

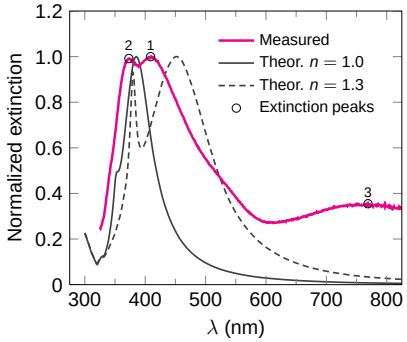

Figure 1: Extinction spectrum of 90 nm silver particles.

In Figure 2, the wavelengths of the peaks 1 and 2 are presented as a function of the particle size and compared to the theoretical peak wavelengths of dipolar and quadrupolar resonances. Some discrepancies occur most likely because the theoretical model neglects, e.g., effects caused by the dielectric substrate.

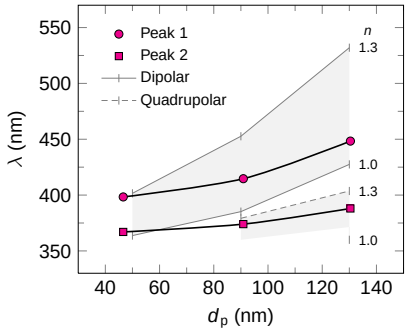

Figure 2: The wavelenghts of the extinction peaks as a function of the particle size.

All in all, aerosol techniques can be successfully used to prepare plasmonic nanoparticle samples for optical studies. Furthermore, the wavelength of the LSPR can be tuned by controlling the size of the deposited particles.

This work was supported by the Academy of Finland.

Harra, J., Mäkitalo, J., Siikanen, R., Virkki, M., Genty, G., Kobayashi, T., Kauranen, M. and Mäkelä, J.M. (2011) J. Nanopart. Res., Submitted.

Synthesis of germanium nanoparticles in an aerosol reactor

C. Mehringer[1], R. Körmer[1], B. Butz[2], E. Spiecker[2] and W. Peukert[1]

[1]Institute of Particle Technology, Friedrich-Alexander-University Erlangen-Nuremberg, Cauerstr. 4, 91058 Erlangen, Germany
[2]Center for Nanoanalysis and Electron Microscopy (CENEM), Friedrich-Alexander-University Erlangen-Nuremberg, Cauerstr. 6, 91058 Erlangen, Germany
Keywords: nanoparticles, material synthesis, silicon, germanium.
Presenting author email: c.mehringer@lfg.uni-erlangen.de

Nanocrystalline germanium (Ge) is a promising material for the application in printable electronics. Dispersed in organic liquids and deposited as thin functional film, e.g. as a thin film transistor, the electronic properties of the nanocrystals (NCs) can be investigated (Holman et al, 2010). The synthesis of freestanding Ge NCs is challenging and can for example be achieved in a nonthermal plasma reactor (Gresback et al, 2007). We report on our progress in synthesizing Ge NCs in a reactor system with two consecutive hot-wall reactors.

In this setup the first reactor is used to produce, silicon nanoparticle (Si NP) seeds from monosilane pyrolysis in argon atmosphere. Those seeds influence the particle growth in the subsequent reactor, as known from literature (Alam et. al, 1986). After the first reactor stage the aerosol is quenched by additional argon. Prior to the second reactor stage, monogermane is fed into the system. In the second reactor stage the Si seeds serve as nuclei for Ge NP growth at temperatures of 700°C to 900°C. At the reactor exit the aerosol is quenched by nitrogen. The particles are collected with a membrane filter or sampled via a low pressure impactor by deposition on TEM grids or silicon wafers.

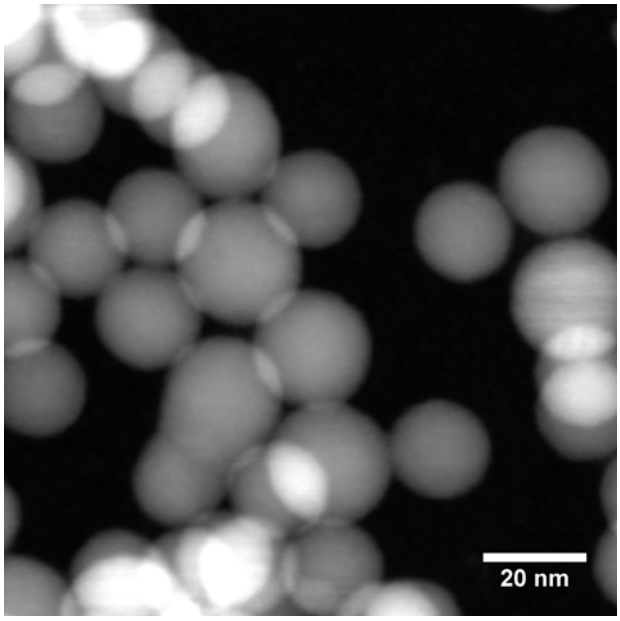

Figure 1. STEM image of Ge NPs

It is found, that monogermane pyrolysis in the absence of any seed particles leads to too high nucleation rates and subsequently to a growth mechanism, which is dominated by agglomeration and sintering. Therefore undesired particle structures are obtained, meaning strongly branched hard aggregates of very small primary particles around 9 nm in size. By addition of small amounts of monosilane however, nanoparticles with a mean particle size of 26 nm are accessible. The geometric standard deviation of their number density distribution is 1.25. Analysis with XRD and EDX shows almost pure germanium particles. STEM images prove, that the initial Si seed is completely dissolving in the evolving particle, as can be seen in figure 1. The monocrystallinity is also proven by HRTEM analysis (figure 2). The influence of monosilane addition and process parameters on particle formation, morphology and composition will be discussed.

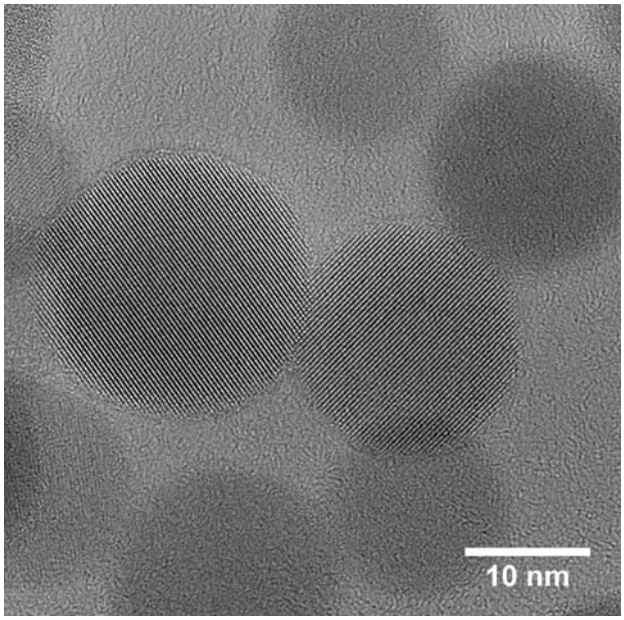

Figure 2. HRTEM image of Ge NPs

This work was supported by the German Research Council (DFG) and the Cluster of Excellence “Engineering of Advanced Materials” (EAM).

Holman, Z. C., Liu, C.-Y., Kortshagen, U. R. (2010) *Nano Lett.* **10**, 2661-2666.
Gresback, R.; Holman, Z.; Kortshagen, U. (2007) *Appl. Phys. Lett.* **91**, 093119.
Alam, M. K., Flagan, R. C. (1986) *Aerosol Sci. Tech.*, **5:2**, 237-248

Gas-Phase Synthesis of Metal-Decorated Titanium Dioxide Nanoparticles

N. Alam[1] and A.M. Boies[1]
[1]Department of Engineering, University of Cambridge, Cambridge, UK, CB2 1PZ
Keywords: catalyst, particle synthesis, self assembly and particle charge
Presenting author email: a.boies@eng.cam.ac.uk

Metallic catalysts are critical components in technologies for renewable energy generation and pollution mitigation. As catalysts are often the most costly and rate-limiting components in many devices, advances in catalytic performance have the potential to make technologies such as fuel cells viable for widespread use. In order for nanoparticles to be viable for devices, methods must be developed to control their surface properties and assembly. In particular, the controlled spatial orientation of nanoparticles composed of different metals allows for the design of materials with better performance and increased durability. Studies of bimetallic nanoparticle combinations of gold (Au), platinum (Pt) and palladium (Pd) have demonstrated that each material catalyzes different reactions and when located in close proximity can lead to significant reductions of carbon monoxide, a harmful pollutant and fouling agent in fuel cells.

Research on the effects of substrates has shown that titanium dioxide (TiO_2) enhances the activity of catalytic oxidation reactions of carbon monoxide. Gas-phase processes offer practical benefits for catalytic nanoparticle synthesis as they allow for production in inert or non-reacting environments where particle size and charge can be manipulated. These continuous throughput processes can achieve high production rates at low cost, and are "green" as they do not require the use of environmentally hazardous solvents. Recent work has shown that nanoparticle surface properties can be controlled in the gas phase through both coating [1] and decoration [2].

This study demonstrates the production of TiO_2 nanoparticles decorated with catalytically active metals collocated on the surface. A conceptual schematic of the gas-phase synthesis system is shown in Figure 1. Core TiO_2 particles were synthesized by thermally decomposing a gas-phase precursor, titanium tetraisopropoxide ($C_{12}H_{28}O_4Ti$) in a temperature-controlled (~700°C) reaction chamber at atmospheric pressure. Titanium particle size and morphology were controlled by varying the temperature, precursor concentration and residence time within the reaction chamber. In-situ monitoring of the nanoparticle size and concentration were conducted using tandem differential mobility analysis (TDMA).

Metallic nanoparticles (<5 nm) were synthesized concurrently with TiO_2 particles in parallel hot-wire evaporators. Hot-wire evaporators produce metal vapors by resistively heating a metallic wire in an inert gas flow. Upon cooling the vapor nucleates forming particles. The size, morphology and charge state of the metallic nanoparticles were controlled by selecting the gas velocity, applied voltage, and voltage bias of the hot-wire generator. As depicted in Figure 1, the charge state of the two metallic nanoparticle aerosols was modified to ensure that they are charged to opposite polarities. By setting the particle charges to opposite polarities, the assembly of the agglomerates composed of different metals is encouraged while like-particle collisions are suppressed. Modification of the metallic particle charge state using corona and x-ray sources was used to ensure unipolar charge distribution. Preferential agglomeration between the opposite-charged materials occurs as the two flow streams are joined. The metallic agglomerates were then mixed with the larger (~30 nm) TiO_2 particles where the collision frequency between particles of different sizes dominates like-sized collisions.

The change in nanoparticle size and charge as a result of the surface decoration was monitored using a DMA, CPC and an electrometer. We measured and controlled the charge state of the nanoparticles to direct their synthesis. The fundamental dynamics of small particle charging and agglomeration were experimentally measured and compared to theoretical calculations. Ex-situ analysis of the particles was conducted by collecting the particles on TEM substrates for microscopy and elemental analysis. Further catalytic analysis of the particles was conducted using infrared spectroscopy analysis.

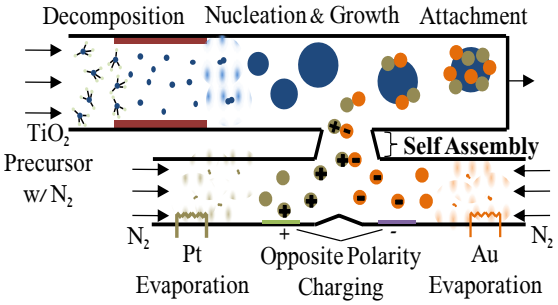

Figure 1: Schematic of heterogeneous nanoparticle synthesis reactor.

This research was sponsored in part by the Engineering and Physical Sciences Research Council (EPSRC) and the University of Cambridge Strategic Grant initiative.

[1] A. M. Boies, J. T. Roberts, S. L. Girshick, B. Zhang, T. Nakamura, A. Mochizuki, *Nanotechnology* **2009**, *20*, 295604.
[2] A. M. Boies, P. Lei, S. Calder, S. L. Girshick, *Nanotechnology* **2011**, *22*, 8.

Spark Generated Intermetallic Mg-Ti Nanoparticles for Hydrogen Storage

R. J. Canales-Perez[1], T. V.Pfeiffer[1], A. Anastasopol[2], J. Middelkoop[3], S.W.H. Eijt[2], and A. Schmidt-Ott[1]

[1]Nanostructured Materials, Department of Chemical Engineering, Faculty of Applied Sciences, Delft University of Technology, 2628 BL 136, Delft, the Netherlands
[2] Fundamental Aspects of Materials and Energy, Department of Radiation, Radionuclides & Reactors, Faculty of Applied Sciences, Delft University of Technology, 2629 JB 15, Delft, the Netherlands
[3] Materials for Energy Conversion and Storage, Department of Chemical Engineering, Faculty of Applied Sciences, Delft University of Technology, 2628 BL, Delft, the Netherlands
Keywords: spark discharge, hydrogen storage, nanoparticles, generation, nanoparticles, composition
Presenting author email: r.j.canalesperez@student.tudelft.nl

Metal hydrides are one of the most promising materials for hydrogen storage given their high volumetric capacity when compared to gas or liquid storage, and their high hydrogen content when compared to carbon materials (Sakintuna, Lamari-Darkrim, & Hirscher, 2007). Nanostructured magnesium is one of the most promising materials for creating these metal hydrides. It has also been shown that 20-40 at.% of titanium can enhance the sorption kinetics of magnesium (Danaie, Mauer, Mitlin, & Huot, 2011).

Instead of ball milling or roll-bonding, we chose to use the techniques described by Tabrizi *et al* (2010) to create intermetallic Ti-Mg nanoparticles. We used two metal rods as electrodes, one made from magnesium and the other from titanium. By creating a spark the metals vaporize and later condense to form nanoparticles. Non-alloyed intermetallic nanostructures are formed by the rapid co-condensation of both vapour species. In this study, we attempt to control the composition of the nanoparticles by varying the polarity and distance of the rods.

The resulting nanoparticles were analysed using XRD, STEM/EDX and ICP-OES to determine the composition of the samples, their structure and the distribution of elements. Tests were also made regarding the hydrogen absorption and desorption capabilities.

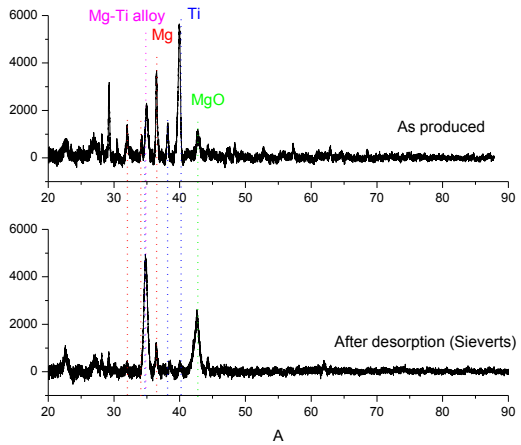

Figure 1. XRD before and after cycling.

Samples produced with a titanium anode (+) and a gap spacing of 2 mm show a Ti content of 33 at.%, as measured by ICP. XRD shows the existence of an intermetallic Mg-Ti phase, in addition to MgO and metallic Mg and Ti. STEM elemental mapping shows primary particles with nanometer sized Mg and Ti domains, as expected from the results of Tabrizi (2010) for non-alloying metals.

The hydrogen absorption and desorption isotherms were used to create Van't Hoff plots for two samples of $Mg_{0.67}Ti_{0.33}$. Significantly lower enthalpies of formation were found, lower than reported in previous studies (Gross, Spatz, Züttel, & Schlapbach, 1996). 2.5 %wt of H_2 was reversibly ab- and desorbed at 473K.

By using a spark discharge generator it was possible to synthesize Mg-Ti nanoparticles of the desired composition. These nanoparticles were not mixed on an atomic level, but rather showed distinct domains but nevertheless showed good hydrogen storage properties.

We thank Q. Xu and U. Lafont for STEM analyses. Funding by Agentschap NL, grant EOSLT07052.

Danaie, M., Mauer, C., Mitlin, D., & Huot, J. (2011). *Int. J. Hydrogen Energy, 36*(4), 3022-3036.

Gross, K. J., Spatz, P., Züttel, A., & Schlapbach, L. (1996). *J. Alloys Compd., 240*(1), 206-213.

Sakintuna, B., Lamari-Darkrim, F., & Hirscher, M. (2007). *Int. J. Hydrogen Energy, 32*(9), 1121-1140.

Tabrizi, N., Xu, Q., van der Pers, N., & Schmidt-Ott, A. (2010). *J. of Nanopart. Res., 12*(1), 247-259.

Generation of sub 10 nm self charged particles with a spark generator in positive and negative mode

Michel ATTOUI
University Paris Est Creteil France
attoui@univ-paris12.fr
Keywords : nanoparticles, spark, generation, mobility,

Schwyn et al., (1988) introduced the spark method between 2 electrodes as generator of metallic particles. The spark generator (SPG) is made mostly of standard stainless steel ultra high vacuum (UHV) parts. The electrodes are mounted in a five way cross by a high voltage feedthrough with an embedded gas inlet. One of the remaining flanges of the SS cross is equipped with a viewport. All the parts of the generator are in SS to avoid desorption of surface contaminants inside the generator. Cylindrical electrodes of 6 mm diameter of Al, Cu, Ag are used. The mounting enables precise adjustment of the spacing of 1 mm, used in this study, between the electrodes. A high voltage capacitors are continuously charged by a high voltage power supply mounted in constant current mode (+/- 5 kV – 10 mA). The accumulated energy in the capacitors is then sent to the spark during the discharge. The frequency of charge or discharge of the capacitors is measured with an oscilloscope through a high voltage divider.

Helium or argon is required to produce clean metallic aerosols. The inert shield is required to f1ow over the arcing region, removing the aerosol and ions produced by the previous spark.

The aerosol particle size distributions from the spark generator have been measured recently by Tabrizi et al. (2009) using a home made DMA-Electrometer system for different electrodes and flowrates values. They detected a minimum diameter of 3 nm. The DMA used in their study (short cylindrical TSI) is not designed for small particles in terms of minimum diameter nor for high resolution.

The present paper gives the size distributions in different conditions obtained with a high flow, high transmission and high resolution DMA. This DMA is designed for particles smaller than 10 nm with a very high resolution and very high transmission. Ions in positive and negative mode are produced by the spark when the flowrate is very high (> 10 lpm) in the chamber. These ions has been seen with different metals (Ag; Cu; Al; Ni etc…)

Figure 1 gives the size distribution of positive silver particles. The small peak on the left at 1.2 nm is given by the silver ions. Figure 2 gives the size distribution of the small ions seen in the fig 1 in positive mode. In the other hand the charge distribution of the particles with a tandem high resolution DMAs has been measured.

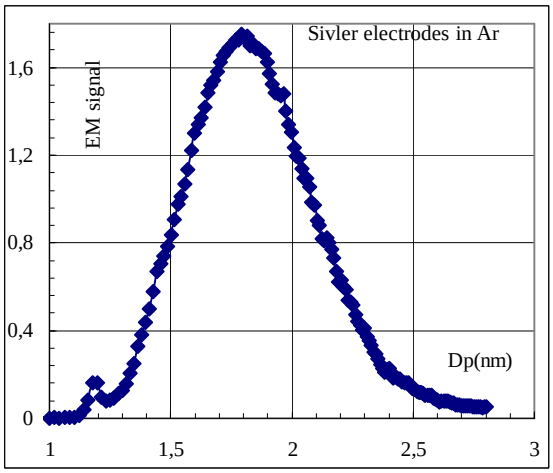

Figure 1
Size distribution of self singly charged positive silver particles in the hypothesis of singly charged particles

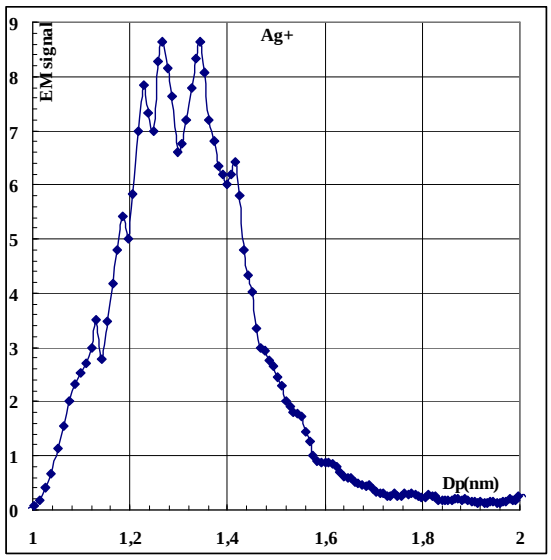

Figure 2
Size distribution of silver positive ions

References:

Schwyn, S., Garwin, E., & Schmitt-Ott, A. (1988). J. of Aerosol Sci, 19, 639–642.

Tabrizi,N.S., Ullmann,M., Vons,V.A., Lafont,U., Schmidt-Ott, A., (2009) : J. Nanoparticles Res. 11 p 315-332

Morphology dependency of electrospray-generated polymer particles and coatings on ambient humidity

E. Bodnár[1], P. Kiselev[1], J. Grifoll[1] and J. Rosell-Llompart[1,2]

[1]Department of Chemical Engineering, Universitat Rovira i Virgili, Tarragona, Catalonia, E-43007, Spain
[2]Catalan Institution for Research and Advanced Studies (ICREA), Barcelona, Catalonia, E-08010, Spain
Keywords: electrospray, particle formation, relative humidity, microstructure.
Presenting author email: eszter.bodnar@urv.cat

The functionality of structures (particles, coatings) made from electrosprays of dilute polymer solutions depend critically on their morphology, which we have recently found to be strongly influenced by ambient relative humidity (RH). We have investigated the influence of RH on the morphology (shape and microstructure) of polymer particles from various polymer-solvent systems which differ in how strongly polymer solubility is lowered by the presence of water. The polymers studied include ethyl cellulose (EC), polystyrene (PS), and poly(methyl methacrylate) (PMMA). Water miscible solvents (isopropanol, acetone), one water soluble solvent (2-butanone) and one water-immiscible solvent (dichloromethane) were used.

At dry ambient conditions compact smooth particles are collected, which often carry single nanofilaments (as shown for PS in Figures 1a, 1b). The globular part of these particles is shaped as a deflated capsule, an indication that polymer precipitation starts near the surface of the droplet, producing a shell that grows in time from within. Nanofilaments are likely to be a signature of the last Coulomb explosions as the polymer solution was sufficiently concentrated to electrospin a fiber that dried up at the same time. However, at high ambient RH (Figures 1c, 1d) the filaments disappear and porous particles are obtained. In this case, water from the ambient is absorbed by the droplet and becomes a non-solvent, triggering the precipitation of the PS, which happens early on when the solution is still dilute, thus precluding the formation of filaments, leading to porous particles instead. The lower polymer concentration solution (Figure 1c) at high RH produced flat irregular particles on the collection substrate (see Figure 1c inset), which may be the relics of globular thin shell-like particles that have undergone compressive failure upon impingement with the collection surface (Hogan et al, 2007), but remain cohesive.

Under dry conditions, EC in isopropanol leads to collapsed capsules, whose wall is thicker at higher polymer concentration as expected. At 1.0 wt %, the effect of RH on EC in every solvent is to wrinkle the particle surface, which may reflect a partial loss of polymer chain entanglement and mechanical strength, and non uniform distribution of this effect. At low polymer concentration (0.1 wt %), the precipitation due to ambient water is delayed. Instead, droplets arrive wet at the collector surface giving rise to dense films, suggesting that ambient water slows down solvent evaporation from these droplets. The topography of these films is not flat, suggesting some fraction of precipitated polymer phase in the arriving droplets. Dense films were also obtained with PMMA in water miscible solvents. In these systems, water slows down solvent evaporation or increases the solvent fraction held by the polymer precipitate, or both.

In dry ambient, EC-dichloromethane solution at 1.0 wt % leads to disc shaped particles with a smooth-wall. At high humidity, a reticular structure on the surface of the particles is encountered, which resembles those found in some electrospinning systems, as well as "breath figure" patterns.

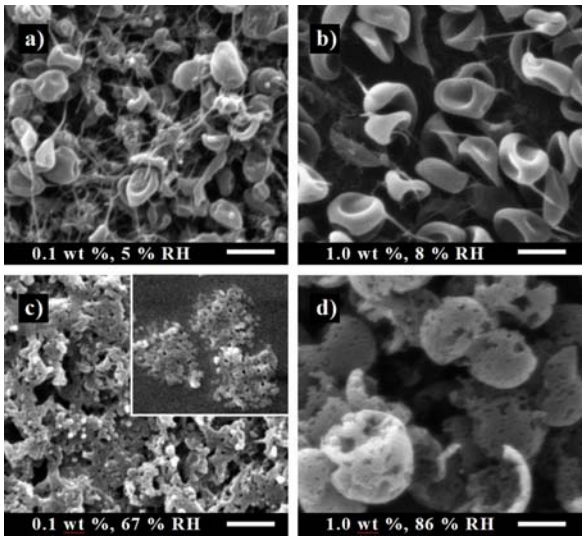

Figure 1. Particles formed from PS-butanone solutions at different initial concentrations (0.1 wt % left; 1.0 wt % right) and RH (dry at top; humid at bottom). Inset shows individual particles from a short collection time sample. Scale bar = 1 μm.

This work was supported by Grant CTQ2008-05758/PPQ from the Spanish Ministry of Science and Innovation, and Grant 2009-SGR-1529 from the Government of Catalonia, Spain.

Hogan, C.J., Yun, K. M., Chen, D.-R., Lenggoro, I. W., Biswas P., Okuyama K. (2007) *Coll. Surf. A: Physicochem. Eng. Asp.* **311**, 67–76.

Formation of rutile nanoparticles from the condensed disperse phase at a surface of high-temperature particles of the titanium

N.Kh. Kopyt[1], K.I. Semenov[1], N..N. Kopyt[1] and A.K. Semenov[2]

[1]Research laboratory for Aerosol systems, Odessa I.I. Mechnikov National University, Odessa, Region, 65052, Ukraine
[2]Department of Physics, Odessa I.I. Mechnikov National University, Odessa, Region, 65052, Ukraine
Keywords: nanoparticles, nanotechnologies, particles of the titanium.
Presenting author email: semenovki@rambler.ru

Formation of the condensed disperse phase (CDP) round a metal particle, with a size 10 - 100 microns, warmed up to temperature in some thousand degrees is one of ways to produce nanoparticles. Depending on a chemical compound, environment round a particle, it is possible to receive both nanoparticles of pure metal, and nanoparticle of metal oxides. We conduct researches on reception and studying of characteristics of rutile nanoparticles which are widely used in light protective structures, at influence on bacterial endospores, in semiconductors for creation of the forbidden zone in width 3,23 and 3,06 eV. Particles of the fused titanium with the size about one hundred micron produced by electrical discharge from the pure titanium. After formation the drop of the titanium was deposited in the rectangular cell which walls could be used as a condenser facing in the corresponding atmospheric environment. As results of the chemical analysis have shown, about 7 discrete phases of a rutile homological number were formed in the air. Only in the oxygen environment at pressure 101 kPa oxide nanoparticles (rutile) were formed.

As a result of thermionic emission from a particle surface, both the particle, and a CDP of nanoparticle get electric charges. Expected concentrations of nanochastic and electrons in resulted on pictures 1 and 2 (Lyalin *et el*, 2008). Research of

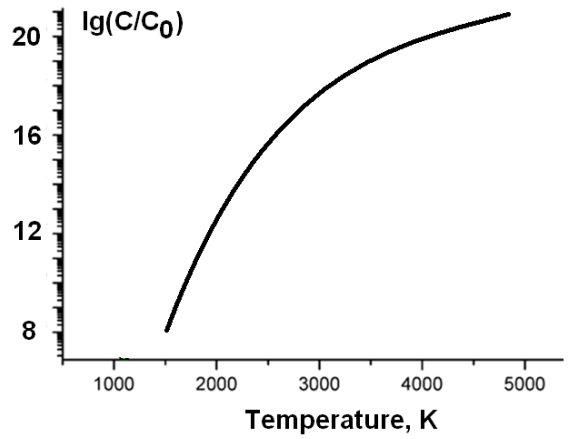

Figure 1. Dependence of logarithm of concentration C of nanoparticles of CDP near a particle from the temperature of particle ($C_0 = 1m^{-3}$).

parameters of the CDP was spent with application of x-ray diffractometer DRON - 3.0 which allowed us to

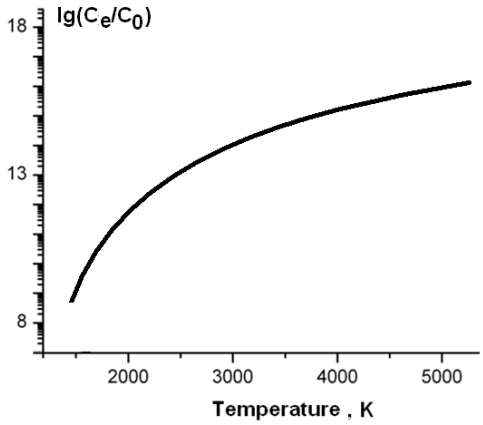

Рисунок 2. Dependence of logarithm of concentration of electrons C_e in CDP from the temperature of particle.

determine phase, chemical transformations and size intercalates crystals lattice constant. Photographing has shown that the nanoparticles representing the CDP around moving in environment metal particle have cylindrical symmetry. Sedimentation in an electrostatic field has revealed distinctions in signs on charges of nanoparticles depending on their distance from a parent particle. The density of nanoparticles in CDP "tail" falls in 3-6 times, concentration of nanoparticles depends on initial temperature of a parent particle. Researches of the nanoparticles deposited on a substrate have shown that their size lies in limits from 5 to 100 nanometers and depends on entry conditions.

The equation of thermionic emission charge of the parent particle surrounded with nanodisperses particles in the field of its positive and negative charges are received.

The equation of charging balance of a parent particle with a nanodisperse phase surrounding it in the field of its positive and negative charges is presented. It has allowed to receive the decision of system of the equations defining dependence of an equilibrium charge of a parent particle from its temperature.

Lyalin, L.A., Semenov, K.I., Kalinchak, V.V. and Kopyt, N.Kh. (2008) Ukrainian journal of physics. №11, 1075 - 1079.

Obtaining of nanoparticles near moving heated metal particle

K.I. Semenov[1], N.Kh. Kopyt[1], A.K. Semenov[2] and N..N. Kopyt[1]

[1]Research laboratory for Aerosol systems, Odessa I.I. Mechnikov National University, Odessa, Region, 65052, Ukraine
[2]Department of Physics, Odessa I.I. Mechnikov National University, Odessa, Region, 65052, Ukraine
Keywords: nanoparticles, nanotechnologies.
Presenting author email: semenovki@rambler.ru

Further development of nanoscience and nanotechnologies connected among the other factors with search of new methods of nanoparticles production, which can have new interesting properties based on specification of concrete method.

Existing methods and technologies, for example precipitation of vapor in vacuum, explosion of wire, et al., are carried out without presence of powerful electric fields. That's why organization of process of nanoparticles production in conditions of large temperature gradients and electric field is of interest as new direction of search. Such process can be carried out in vicinity of heated metallic particle using applied by us method of developed of monodisperse particles in impulse electric arch. Received heated particle in cold gas creates large gradient of temperature around itself. In addition, at the expense of thermoemission from the surface of particle, the particle itself gets certain electric charge in its vicinity. Intensive evaporation of metal goes on a surface of particle, vapors condense in certain vicinity of particle, react with active components of gas environment, creating nanoparticles.

The experimental arrangement consisted of monodisperse particle generator, airtight vessel, which could be filled with different gas. Movement of particle under the action of force of gravity took place in the vessel. Control of particle temperature was carried out with the help of digital method (Semenov, 2010). Measurement of charge was conducted by deviation of particle in external homogeneous electric field (Semenov K.I. *et al* , 2008). After some time of moving in gas, particle hit the surface of glass bottom layer. Herewith particle melted into the bottom layer, nanoparticles, consisting of chemical compounds of metal with components of employed gas, precipitated around the particle. Figure 1 shows a photograph of copper particle with precipitated around it nanoparticles. After removing the bottom layer with the particle from the airtight vessel, the analysis of obtained products was conducted. Figure 2 shows one of the photographs of nanoparticles of condensed phase at the distance 10 micrometers from the particle. Size of nanoparticles near the surface of the particle was about 10 nanometers, and at the distance – about 100 nanometers. Thereby, the increasing of particle size with the increasing of distance to the particle can be seen.

Particles from tungsten, molybdenum, copper, and tantalum were studied in air environment under normal conditions. The calculation scheme for evaluating the charge of particles was developed, the calculation of their charge and intensity of electric field was made. The analysis of possible mechanisms of electric (Lyalin L.A. *et al*, 2011) field influence on characteristics of nanoparticles, which are being generated, particularly on their agglomeration, was made. The formation of aerogel from linked nanoparticles was revealed experimentally for the particles of tungsten and molybdenum, oxides of which are prone to polymerization.

Figure 1. Photograph of particle with surrounding it nanoparticles on the bottom layer (diameter of the particle is 346 micrometers).

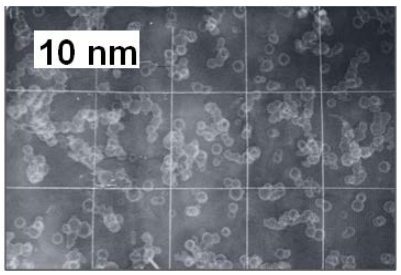

Figure 2. Photograph of nanoparticles of cupric oxide near the copper particle, made on transilluminate electron microscope.

As a result, it's shown that the proposed method can be used to obtain nanoparticles of sizes ranging from tens to hundreds of nanometers of different chemical composition which it is possible to vary.

Semenov K.I. (2010) Patent of Ukrain № 51576.
Semenov K.I., Lyalin L.A., Kalinchak V.V., Kopyt N.Kh. (2008) Ukrainian journal of physics. №11, 1075 - 1079.
Lyalin L.A., Semenov K.I., Kalinchak V.V., Kopyt N.Kh. (2011) Ukrainian journal of physics. №12, 1295-1299.

Investigation of the particle formation mechanism in flame spray pyrolysis of silica nanoparticles based on optical techniques

D. Kilian[1], M.Voigt[1], S. Engel[2,3], Y.Gao[2,3], A. F. Kögler[2], T.Seeger[3,4], A. Leipertz[2,3] and W. Peukert[1,3]

[1] Institute of Particle Technology, University of Erlangen-Nuremberg, Erlangen, 91058, Germany
[2] Institute of Engineering Thermodynamics, University of Erlangen-Nuremberg, Erlangen-Tennenlohe, 91058, Germany
[3] Erlangen Graduate School in Advanced Optical Technologies, University of Erlangen-Nuremberg, Erlangen, 91052, Germany
[4] Institute of Engineering Thermodynamics, University of Siegen, Siegen, 57076, Germany

Keywords: flame spray pyrolysis, nanoparticles, oxides
Presenting author email: d.kilian@lfg.uni-erlangen.de

For the production of nanoparticles at a commercial scale flame spray processes are most frequently used [Kammler *et al*., 2001]. Despite the simplicity of the set-up, the process control is rather complex. Consequently, a profound knowledge of the particle formation mechanism during combustion is required. As minor changes of the process parameters may have a huge impact on the product, there is a huge demand for non-invasive advanced optical measurement tools to understand the local formation mechanisms and to quantify particle formation kinetics.

In this work, silica particles are made from Hexamethyldisiloxane (HMDSO) / ethanol precursor solutions. For the characterization of the flame spray process the following optical techniques are employed (Table 1).

Table 1. Optical techniques used for characterization of the silica synthesis by flame spray pyrolysis

Technique	Information
Mie scattering	Spatial droplet distribution
OH* chemiluminescence	Post reaction zone
CH* chemiluminescence	Reaction zone
SiO* chemiluminescence	Precursor decomposition / Nucleation regime
Coherent anti-Stokes Raman scattering (CARS)	Temperature, rel. N_2/O_2 gas concentration

By systematic combination of these techniques we can identify the predominant mechanisms in regions of the flame. Based on these results we are able to classify the flame into different regions and propose a particle formation mechanism.

Due to limited space we highlight in this abstract an extract of our results regarding the identification of the particle nucleation regime, which is linked to the work of Glumac 2001: On the right hand side of Fig. 1 the measured SiO* chemiluminescence intensity is depicted. As reaction rate constants for the formation of SiO_2 from SiO* are very high, up to 10^{15} mol/cm*s (Chagger *et al.*, 1996), this is the predominant region of particle formation.

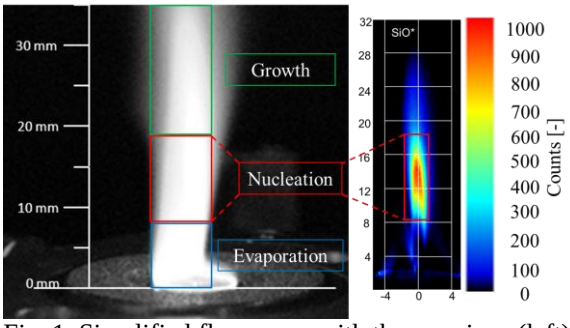

Fig. 1. Simplified flame map with three regions (left), SiO* chemiluminescence intensity (right)

The other zones in Fig. 1 (blue and green boxes) are determined by the combination and evaluation of the results from the other optical techniques. For example, combining the results of Mie scattering and OH* / CH* chemiluminescence measurements give an insight up to which height droplet evaporation is dominant before the early combustion reaction starts.

Based on the classification in different zones a particle formation mechanism is proposed in this work. By variation of process parameters the position of the regimes (evaporation, nucleation and growth) is shifted and the main influencing process parameters on particle formation are identified.

The authors gratefully acknowledge the funding of the German Research Council (DFG), which, within the framework of its 'Excellence Initiative' supports the Cluster of Excellence 'Engineering of Advanced Materials' and the Erlangen Graduate School in Advanced Optical Technologies at the University of Erlangen-Nuremberg.

Kammler, H.K., Mädler, L., & Pratsinis, S.E. (2001) *Chem. Eng. Technol* **24**, 583-596.
Glumac, N.G. (2001) *Comb. and Flame* **125**, 702-711.
Chagger, H.K., et al., (1996) *Twenty sixth Symposium (International) on Combustion/The Combustion Institute*, 1859-1865.

Formation of advanced SiC and carbon structures with controlled annealing of preceramic silicon-carbon nanoparticles

A. Lähde[1], M. Miettinen[1], J. Hokkinen[2] ,T. Karhunen[1], T. Torvela[1], U. Tapper[2]and J. Jokiniemi[1,2]

[1]Department of Environmental Science, University of Eastern Finland, Kuopio, 70211, Finland
[2]Fine Particles Team, Technical Research Center of Finland, Espoo, 02044 VTT, Finland
Keywords: preceramic silicon-carbon, induction heating, SiC and carbon structures
Presenting author email: anna.lahde@uef.fi

Silicon carbide (SiC) is an important high temperature structural material and high performance semiconductor, which can be operated at high temperatures, high power and high frequencies and in harsh environments (Legrand and Sénemaud 2003). Furthermore, SiC can be used as a precursor material for more advanced structures such as graphene layers (Emtsev et al. 2009).

The pre-ceramic Si/C synthesised with the aerosol method (Miettinen et al. 2011) was used as a precursor for induction heating, which enables the vaporization of metals at high temperatures. In this study, thermal treatments were performed on SiC nanoceramic particles in argon atmosphere at temperatures between 1900 and 2600 ^{o}C. The evolution of the particle structure and crystalline phases at different annealing temperatures was studied with SEM/EDS, XRD and Raman spectroscopy.

The annealing caused an increase in the crystallite size from few nanometers of the untreated precursor (Miettinen et al. 2011) to several micrometer crystals obtained in the annealed particles. In addition, the annealing temperature had an effect on the crystalline phase of the formed particles, see Figure 1. At lower temperature, i.e. below the melting temperature of amorphous silicon carbide (T_m = 2172 ºC, Baeri et al. 1999), the crystalline phase of SiC-3C was dominant (>96 w-%). Above the decomposition temperature (T_{dec} = 2577 ºC, Baer et al. 1999) a separation of carbon and silicon was observed, i.e. graphitic carbon (T=2600 ºC vessel) was formed in the sample vessel while SiC-3C and -6H was formed due to the cooling at the exit of the sample vessel (T=2600ºC exit), see Figure 1.

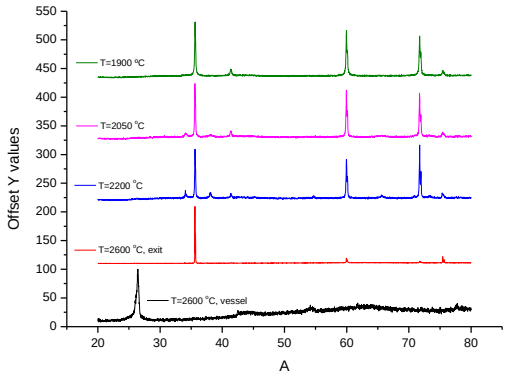

Figure 1. Normalized XRD diffraction patterns of crystalline phase of particles produced with induction heating of preceramic SiC

Figure 2 shows the SEM images of the particles produced at 2600 ºC. Leafy, graphitic carbon among the spherical particles was obtained in the sample vessel (Figure 2a) while silicon carbide was grown as large needles at the exit of the vessel (Figure 2b).

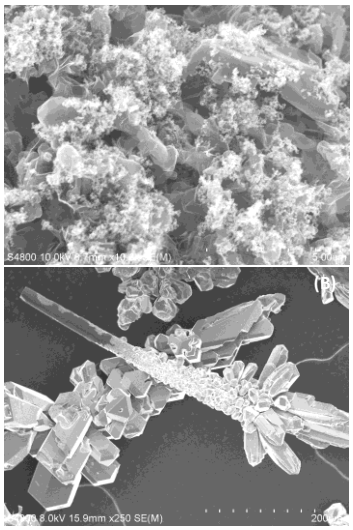

Figure 2. SEM image of Si/C particles formed with the induction heating at T=2600 ºC. The particles obtained from the sample vessel (A) and the exit of the vessel (B).

Induction heating of preceramic Si-C nanoparticles enables the preparation of advanced SiC and carbon structures. The preceramic precursor and high surface area of nanoparticles improve the formation of single layer graphenes by thermal decomposition of silicon carbide

This work was supported by the strategic funding of the University of Eastern Finland under the NAMBER spearhead project.

Baeri, P., Spinella, C. and Reitano, R. (1999) *Int. J. Thermophys.* **4**, 1211-1221.

Emtsev, K.V., Bostwick, A., Horn, K., Jobst, J., Kellogg, G.L., LEy, L., McChesney, J.L., Ohta, T., Reshanov, S.A., Röhrl, J., Rotenberg, E., Schmid, A.K., Waldmann, D., Weber, H.B. and Seyller, T. (2009) *Nat. Mater.* **8**, 203-207.

Legrand, A. P. and Sénémaud, C. (2003) *Nanostructured silicon-based powders and composites*, CRC Press.

Miettinen, M., Johansson, M., Suvanto, S., Riikonen, J., Tapper, U., Pakkanen, T.T., Lehto, V.-P., Jokiniemi, J. and Lähde, A. (2011) *J. Nanopart. Res.* **13**, 4631-4645.

In situ observation of sintering behavior of Pt particles supported on silica nanoparticles

Kun Gao[1], Philipp Müller[2], Matthias Faust[1], Reinhard Schneider[2] and Martin Seipenbusch[1]

[1]Institute for Mechanical Process Engineering and Mechanics, Karlsruhe Institute of Technology, Karlsruhe, 76131, Germany
[2]Laboratory for Electron Microscopy, Karlsruhe Institute of Technology, Karlsruhe, 76128, Germany
Keywords: in situ, TEM, contact angle, surface migration.
Presenting author email: kun.gao@kit.edu

Supported catalysts, such as Pt or Pd supported on different oxides, are widely used in chemical industry today, but sintering of the active phase, usually noble metal, is a serious mode of deactivation in this kind of catalysts. Therefore, it is significant to slow down the deactivation of them.

The present project deals with the stabilization of the noble metal supported nanoparticles. Three different mechanisms were proposed for this process (Binder and Seipenbusch 2011) and a theoretical description was developed by Wynblatt (Wynblatt 1975 and 1976). In order to study the sintering process, supported Pt nanoparticles were chosen as a model system. First of all, Pt/SiO_2 particles were prepared in the gas phase by a highly controlled chemical vapour synthesis (CVS) and metal organic chemical vapour deposition (MOCVD) process at atmospheric pressure. The size distribution and the number density of Pt nanoparticles can be controlled by the concentration of Pt precursor and O_2 in the gas phase in the CVD process.

The TEM grid, with Pt/SiO_2 nanoparticles on it by a low pressure impaction process, was heated up from the room temperature to 800°C at a constant rate of $5°C \cdot min^{-1}$ under ultra-high vacuum, and the surface migration, the collision and the sintering process of Pt nanoparticles on silica was observed in situ. Therefore, series of TEM images were taken at a frequency of approx. $1s^{-1}$ (Figure 1). The change of the Pt nanoparticle size distribution at different temperatures and the average surface migration velocity of Pt particle could be measured. Additionally, the contact angle between Pt and silica can also be measured in a high resolution TEM image.

The influence of the temperature on contact angle, surface migration velocity and the surface collision frequency of Pt nanoparticles will be investigated.

$$\beta = f(T, \alpha, v, n, d, x)$$

- β surface collision frequency
- T temperature
- α contact angle
- v average surface migration velocity
- n number density of Pt particle on carrier surface
- d size of supported nanoparticle
- x size of carrier nanoparticle

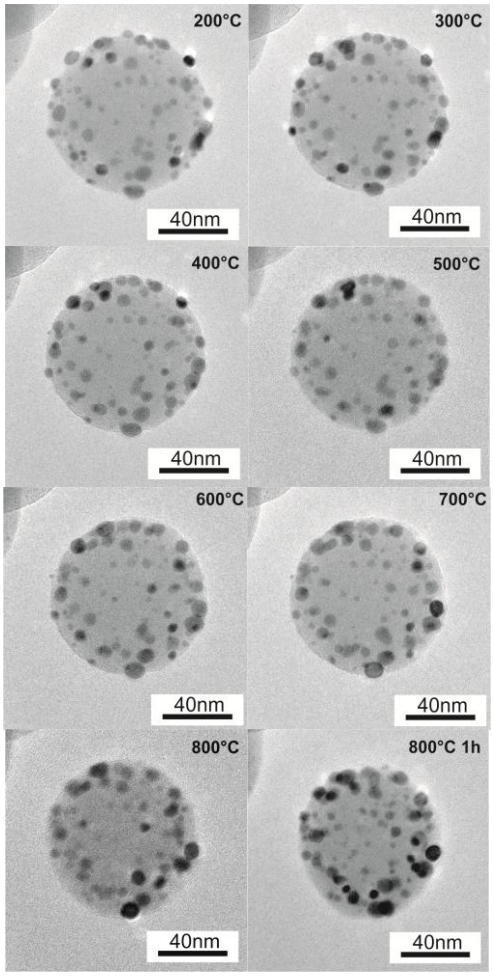

Figure 1. TEM photographs of the same spot of Pt/SiO_2 at different temperatures

This work was supported by Land Baden-Württemberg, Germany and Joint-Lab IP[3], BASF SE.

A. Binder and M. Seipenbusch (2011) *Applied Catalysis A: General* **396**, 1-7.
P. Wynblatt, N.A. Gjostein, in: J.O. McCaldin, G.A. Somorjai (Eds.) (1975) *Progress in Solid State Chemistry*, 21.
P. Wynblatt, N.A. Gjostein (1976) *Acta Metall* **24**, 1165-1174.
P. Wynblatt (1976) *Acta Metall* **24**, 1175-1182.
Kohji Narui et al. (1999) *Applied Catalysis A: General* **179**, 165-173.

Synthesis of copper nanoparticles formed on carbon nanotubes by photochemical process

N. Nishida, A. Miyashita, and H. Tanaka

Department of Applied Chemistry, Faculty of Science and Engineering, Chuo University,
1-13-27 Kasuga, Bunkyo-ku, 112-8551, Tokyo, Japan
Keywords: Copper nanoparticles, carbon nanotubes, photochemical process
Presenting author email: nnishida@kc.chuo-u.ac.jp

Metal nanoparticles have a variety of interesting spectroscopic, electronic, and chemical properties that arise from their small sizes and high surface-to-volume ratios. Especially, copper nanoparticles are the most desirable candidates for the replacement of precious materials because of their low price. In fact, various synthesis methods have been developed, although these methods usually use hazardous reagents and many chemical substances. Recently, we have succeeded the regenerative synthesis of copper nanoparticles by using photochemical reduction [1]. Herein, we have applied this method to the mixture of copper acetate solution and carbon nanotubes (CNTs) at room temperature. The structure and oxidation state of the products were analyzed by scanning transmission electron microscopy (STEM) and X-ray photoelectron spectroscopy (XPS), respectively.

The synthesis of copper nanoparticles by photoreduction was carried out using a similar method reported previously [1]. Copper acetate powder and CNTs powder were dissolved in ethanol. The mixed solution was photoirradiated using a high-pressure Hg lamp for 18 h at room temperature.

Figure 1 shows a typical STEM image for the as-prepared solution. The nanoparticles in the order of 10 nm diameter are observed on CNTs in the image. This suggests a direct evidence for nanoparticle formation by photoreduction. Two days later for exposed to fresh air, the nanoparticles were kept their shape and size. These indicate that the obtained nanoparticles were deposited and stabilized by CNTs. Furthermore, high concentrated nanoparticles were observed for area of CNTs aggregation. This result expected that, initially, nanoparticles deposited on CNTs evenly. Then these nanoparticles were concentrated by CNTs aggregation.

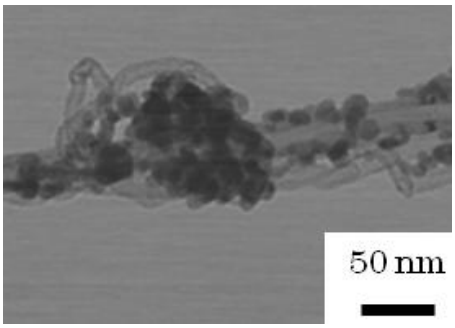

Figure 1. The STEM image of copper nanoparticles on CNTs

Additionally, when amount of CNTs were decreased, the observed diameter for the nanoparticles were increased. This result implies that growth of nanoparticles was inhibited by CNTs. Furthermore, the synthesized nanoparticles were identified as Cu metal by XPS spectrum and XRD patterns.

In summary, we have synthesized copper nanoparticles through the photoreduction of copper acetate and carbon nanotubes at room temperature.

[1] Nishida, N., Miyashita, A., Hashimoto, N., Murayama, H., Tanaka, H. (2011) *Eur. Phys. J. D.* **63**, 307-310.

Aerosol synthesis of building blocks for layered catalyst structures for Fischer–Tropsch reaction

Lintao Zeng and Alfred P. Weber

Institute of Particle Technology, TU Clausthal, Leibnizstrasse 19, 38678, Clausthal-Zellerfeld, Germany

Keywords: spray drying, porous layered structure, catalyst support, Fischer–Tropsch synthesis

Fischer–Tropsch synthesis (FTS) has become of interest for production of fuels and chemicals in recent years. Selectivity control is one the biggest challenges for getting an optimal product distribution. However, there is still no catalyst that demonstrates enough selectivity for the direct production of valued chemicals such as olefins from syngas. Therefore, the development of new novel catalysts that has a high selectivity to desired products is an important goal for academic research [1].

The utilization of porous nano-structured materials as FTS catalyst supports has provided new possibilities for optimizing the catalytic properties, for example, selectivity.

We present a novel aerosol approach towards the preparation of well-defined trimodal nano-porous layered structure as catalyst support for Fischer–Tropsch synthesis, which consists of two layers of SiO_2-building blocks and one layer of spherical glass particles (Fig. 1).

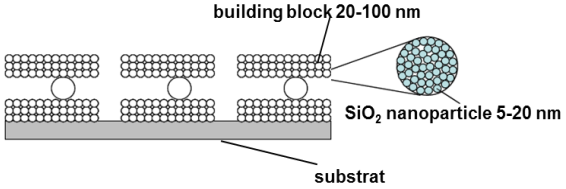

Fig. 1 Schematic representation of nanoporous structured layers of building blocks.

Porous SiO_2 building blocks (20-100nm) containing smaller pores (1-20nm) have been synthesized by spray drying of colloidal SiO_2 suspension (8 or 20nm) followed by tempering in an aerosol furnace at 500-700°C to control mechanical stability and porosity of the building blocks. Fig. 2 (left) shows a REM micrograph of porous SiO_2 building blocks. Then the building blocks were impregnated with cobalt (Fig. 2 right).

Two layers of building blocks were built through surface filtration of the aerosol and reinforced by pressure and thermal treatment. The middle pores (20-50nm) exist between the building blocks. The larger pores (100-200nm) were built by using spherical latex particles as template. The two layers were bound by partially melted glass particles (20-50µm).

The larger pores were designed for rapid transportation of products and reactants and the smaller and middle pores for the diffusions of reactants and products. It was possible to influence the product selectivity by varying pore size and structure of the catalyst support.

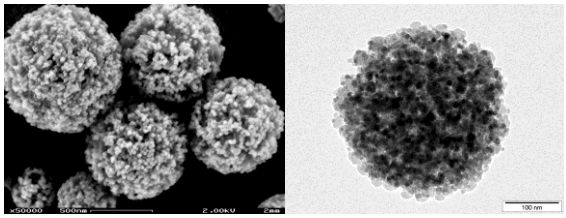

Fig. 2: REM image of porous SiO_2 building blocks (left), TEM image of Co_3O_4/SiO_2 building blocks, after impregnation (right).

The porosity of the building blocks was determined from impaction experiments using a single stage low pressure impactor. This method was particularly helpful when the cobalt catalyst was directly added to silica suspension before spray drying.

In this contribution the aerosol synthesis of the different building blocks will be outlined together with the results of the porosity characterization. In addition, first results for the influence of the impregnation procedure (impregnation of individual building blocks vs. impregnation of layered structure) on the resulting catalytic behavior will be presented.

This work was supported by the Deutsche Forschungs Gesellschaft (DFG) under grant DFG-We 2331/13-1.

[1] Q. Zhang, J. Kang and Y. Wang, ChemCatChem (2010), 2, 1030-1058

The Spark Generator as a Simple Source of sub-Nanometer Atomic Clusters

M.D. Barankin, K.Barmpounis, G. Biskos, T. Bosboom, A. Maisser, T.V. Pfeiffer, A. Schmidt-Ott

Nanostructured Materials, Chemical Engineering, Delft University of Technology, Delft, 2628-BL, The Netherlands

Keywords: Atomic Clusters, Spark discharge, Spark Generator

Presenting author email: A.Schmidt-Ott@tudelft.nl

Atomic clusters consisting of less than 100 atoms have been a subject of research since the 1970s, and it is agreed that the myriad number of possible properties they have are bound to play an important role in future technology. Nevertheless, they have, until now, scarcely found their way to application, which is, at least in part, a result of the limited production rates and the inflexibility of the state-of-the-art vacuum-based cluster beam technology.

The main purpose of the present paper is to call the attention to the fact that aerosol methods offer an interesting alternative. We believe that they will finally open the door to very interesting applications, e.g., in catalysis. Atomic clusters can arbitrarily be modified chemically, heat treated or charged while suspended in a gas. Size selection can be achieved with differential mobility analyzers (DMAs) suitable for this size range (Peineke et al., 2009). They can softly be deposited or positioned (Zonnevyle et al., 2009) on any desired surface, while this represents a major difficulty in connection with cluster beams.

The spark-discharge aerosol generator (Schwyn et al., 1988, Tabrizi et al., 2008) in connection with a DMA is a very versatile source of atomic clusters for any metallic or semiconducting material. In contrast to vacuum-based cluster beams, this method bears the potential of being scaled up for high mass production rates while being comparatively simple and inexpensive. Spark discharge generators are widely used for a controllable and stable production of high-purity aerosol nanoparticles. The present study shows that their range of application can be extended to atomic clusters in the size range below 1 nm. Peineke et al. (2009) had already shown that a glowing wire combined with a DMA produces equally sized atomic clusters, but the mass production rate of such a system is limited.

Microsecond sparks between two electrodes with an energy per spark between 0.05 mJ and 1 mJ produce Ga and Pt clusters with mobilities in the range of 1 Vs/cm^2, as shown in Fig. 1. In the case of Ga, the gas temperature was cooled to the temperature of boiling nitrogen to avoid melting of the electrodes. The broadness of the peak for 0.07 mJ roughly corresponds to the resolution of the DMA, which indicates that the clusters produced are highly monodisperse. Variation of the spark energy hardly changes the spectrum. In analogy with mass spectra that have been recorded for Al (Khanna et al., 1995), also a metal with 3 valence electrons, we believe that this peak corresponds to Ga_{13}, which exhibits electronically closed shells for the anion, thereby making it much more stable than clusters of different sizes.

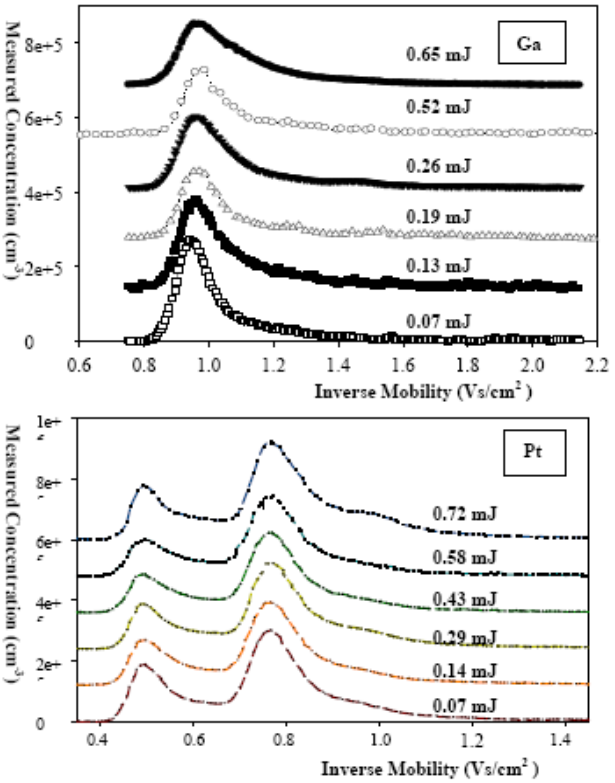

Fig. 1 Inverse mobility spectra of Ga and Pt clusters at different spark energies. In the case of Pt, which has 1 valence electron, 3 stable cluster sizes are seen for the conditions chosen.

References

C. Peineke, M. Attoui, R. Robles, A.C. Reber, S.N. Khanna, A. Schmidt-Ott, *J. Aerosol Science*, 40(5), 423 – 430 (2009)

Schwyn, S., Garwin, E. & Schmidt-Ott, A., *J. Aerosol Sci.*, 19(5), 639-642 (1998).

Tabrizi, N.S., Ullmann M., Vons V. A., Lafont U., Schmidt-Ott, A, *J. Nanopart. Res.*, 11(2), 315-332 (2008)

A. C. Zonnevylle, C. W. Hagen, P. Kruit, M. Valenti, and A. Schmidt-Ott, *Virtual Journal of Nanoscale Science & Technology*, 20 (24) (2009)

Khanna, S.N., Jena P., Phys. Rev. B 51, 13705 (1995)

Tabrizi, N.S., Ullmann M., Vons V. A., Lafont U., Schmidt-Ott, A, *J. Nanopart. Res.*, 11(2), 315-332

The analysis of size-segregated cloud condensation nuclei counter (CCNC) data from SMEAR II and its implications for aerosol-cloud relations.

M. Paramonov[1], T. Petäjä[1], P.P. Aalto[1], M. Dal Maso[1], N. Prisle[1], V.-M. Kerminen[1] and M. Kulmala[1]

[1]Department of Physics, University of Helsinki, P.O. Box 64, Helsinki, FI-00014, Finland
Keywords: CCN, cloud formation, critical diameter, hygroscopicity.
Presenting author email: mikhail.paramonov@helsinki.fi

Through a variety of microphysical processes aerosol particles influence the albedo, lifetime and precipitation patterns of clouds in what is known as indirect effects of aerosols on climate (Forster *et al*., 2007). The ability of aerosol particles to act as cloud condensation nuclei (CCN) is strongly linked to CCN number concentration N_{CCN}, aerosol critical diameter D_c and hygroscopicity parameter κ. Size-segregated CCNC measurements have been conducted in the boreal environment of the SMEAR II station (Hari and Kulmala, 2005) in Hyytiälä, Southern Finland since February 2009. The CCNC in question is a diffusion-type CCN counter, providing measurements across 30 size channels, with particle diameters ranging from 20 to 300 nm for five supersaturation levels SS.

Activated fractions A were calculated for each size channel in each CCN spectrum by dividing N_{CCN} by the corresponding N_{CN}. To determine the critical diameter D_c, which in this study is defined as the diameter at which half of the incoming particles are activated at a certain SS level, two methods were used, both based on Eq. 1 from Rose *et al*. (2008). The first fitting method was carried out as per Rose *et al*. (2008). The second fitting method used the observed, non-normalized A values, and allowed the upper plateau of the *s*-shaped function to vary in order to find the best fit. Hereafter, the two methods are referred to as Rose *et al*. (2008) and new methods, respectively. κ was calculated for each pair of D_c and SS using equation A30 from Rose *et al*. (2008) for both sets of critical diameters.

Rose *et al*. (2008) method produced consistently higher D_c values than the new method for all SS levels. Normalizing A values to unity forced the function to level out at A=1, which may not always be the case if aerosol is externally mixed. The Rose *et al*. (2008) method was particularly inappropriate for higher SS levels due to a large scatter of A values at higher sizes. The new method produced better fit to the data, as shown by the root mean square error (RMSE) analysis.

The analysis of monthly variation of D_c showed that a particle of the same diameter is more hygroscopic in the winter than in the summer. No diurnal variation of D_c was found. An overall average κ for aerosol particles at SMEAR II was determined to be 0.18 and 0.29 for Rose *et al*. (2008) and new methods, respectively, indicating the presence of organic species within the particles; κ of 0.18 is the same as was reported by Sihto *et al*. (2010) for the same location. While larger particles (> 100 nm in diameter) in the boreal environment of Southern Finland represent the global continental mean of κ well, smaller particles are highly non-hygroscopic (Fig. 1). κ is largest in February and smallest in July-August, corresponding well with the observed monthly variation of D_c. The annual trend in D_c and κ is mostly pronounced for larger particles, indicating that over the course of the year the chemical composition of smaller particles remains the same, while larger particles exhibit changes in their chemical composition. Considering typical SS levels inside the cloud, the variation in chemical composition of larger particles throughout the year plays a crucial role in cloud formation.

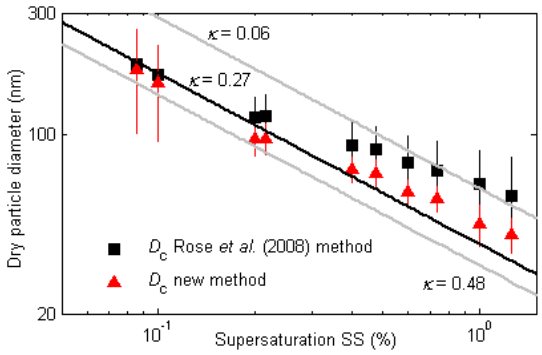

Figure 1. Particle dry size as a function of supersaturation SS. The black and grey lines correspond to the global continental mean of κ of 0.27±0.21, as reported by Pringle *et al*. (2010).

D_c did not correlate with black carbon concentration or with the wind direction, indicating that the chemical composition of CCN-sized aerosol particles in Southern Finland is most likely dominated by regional, non-combustion sources.

This work is supported by the Maj and Tor Nessling Foundation project nr. 2012443.

Forster, P. *et al*. (2007), in: *Climate Change 2007: The Physical Science Basis. Contribution of Working Group I to the Fourth Assessment Report of the Intergovernmental Panel on Climate Change*, Solomon, S. *et al*., Eds. (Cambridge University Press).

Hari, P. and Kulmala M. (2005). *Boreal Env. Res.* **10,** 315-322.

Pringle, K.J. *et al*. (2010). *Atmos. Chem. Phys. Discuss.* **10**, 6301-6339.

Rose, D. *et al*. (2008). *Atmos. Chem. Phys.* **8**, 1153-1179.

Sihto, S.-L. *et al*. (2010). *Atmos. Chem. Phys. Discuss.* **10**, 28231-28272.

Results of elemental and organic carbon (EC-OC) regular measurements within EUSAAR and ACTRIS projects 2009-2011 at the Košetice Observatory

M.Vana[1], J. Čech[1], A.Holubová Šmejkalová[1], E. Chalupníčková[2] and J.Schwarz[3]

[1] Czech Hydrometeorological Institute, Kosetice Observatory, 394 22 Kosetice, Czech Republic
[2] Czech Hydrometeorological Institute, Central Laboratories, 143 06 Praha4, Czech Republic
[3] Institute for Institute of Atmospheric Physics, Boční II 1401, 141 31 Praha 4, Czech Republic

Keywords: ACTRIS, elemental and organic carbon, regional background, Czech Republic
Presenting author email:milan.vana@chmi.cz

Atmospheric elemental carbon (EC) is a product of anthropogenic activities, especially incomplete combustion of fossil fuels by transport, heating, power plants, wood and biomass burning and agriculture activities. EC has negative effects on human health.

Regular EC-OC measurement has been implementing at the Košetice Observatory since February 2009 within the framework of EU-projects EUSAAR (European Supersites for Atmospheric Aerosol Research) and ACTRIS (Aerosols, Clouds, and Trace gases Research Infrastructure Network).

Long-term air quality monitoring and research at Kosetice Observatory, operated by the Czech Hydrometeorological Institute (CHMI), has been carried out since 1988. The observatory is located in free area outside of settlement (49°35´ N, 15°05´E, 534 m above sea level) and represents the Czech Republic in several international long-term monitoring programmes as EMEP (Co-operative Programme for Monitoring and Evaluation of Long-range Transmission of Air Pollutants in Europe), GAW (Global Atmosphere Watch) and International Co-operative Programme on Integrated Monitoring (ICP-IM) under the Convention of Long-Range Transport of Air Pollution (CLRTAP).

Sampling frequency is every 6th day in fraction $PM_{2,5}$ on 2 quartz-fibre filters. Since October 2011 (within ACTRIS) the sampling on filters has been implementing behind the denuder catching the organic vapor. Amount of organic carbon (OC) on back quartz fiber filter represents positive artifact by measurement without denuder and negative artifact by measurements with denuder.

The analytical method is thermal-optical analysis. The samples are analyzed in CHMI Central Laboratories in Prague-Libuš using EC-OC Sunset Lab Dual Analyzer. Charring correction is made by laser transmission monitoring.

Table 1. shows, that the mean annual concentration of total carbon in $PM_{2,5}$ in the period under review was 3,73 µg.m^{-3}. The figure for elemental carbon (0,51 µg.m^{-3}) represents the mean annual ratio of 14% on TC. EC-OC concentrations follow an annual course that reflects their emission levels, i.e. with maximums in winter and minimums in summer. The seasonal variation of EC/TC ratio is not significant and ranges between 12 to 15%.

Table 1. Mean annual and seasonal concentration of EC, OC and TC at Košetice Observatory in 2009-2011.

	EC (µg/m^3)	OC (µg/m^3)	TC (µg/m^3)	EC/TC
spring	0.53	3.27	3.80	0.14
summer	0.27	1.86	2.13	0.13
autumn	0.58	3.22	3.80	0.15
winter	0.76	5.44	6.20	0.12
total	0.51	3.22	3.73	0.14

Mean TC ratio on $PM_{2,5}$ total mass in the period under review was 26%, the highest ratios reached 50%. EC participated on $PM_{2,5}$ total mass by 4% in average.

3D trajectories were used for sector analysis of measured EC-OC data (NILU, 2011). The highest concentrations are recorded in situations when air masses reach the territory of the Czech Republic from the eastern directions or the local air masses prevailing. The difference between sectors is much larger in the cold period of the year.

The comparison with available data from other EUSAAR/ACTRIS sites (Cavalli et al., 2011) shows, that the Košetice EC-OC data are in very good agreement with similarly located central European stations (Melpitz, K-Puszta).

The research leading to these results has received funding from the European Union Seventh Framework Programme (FP7/2007-2013) under grant agreement n° 262254

Cavalli, F., Viana, M., Yttri, K-.E., Genberg, J., Putaud, J-P. (2010) *PAtmos.Meas. Tech., 3, 79-89.*

Cavalli, F., J., Putaud, J-P. (2011) *The EUSAAR carbonaceous aerosol phenomenology.* presentation on EUSAAR Symposium, Grenoble

3D trajectories, www.emep.int. Kjeller, NILU (2011).

Vana, M., Holoubek, I., et al., 2007, 2009. Kosetice Observatory – 20 years. Pt. 1 + 2. Praha: CHMU

Particle formation and growth in the boundary layer over boreal forest

L. Zhou[1], M. Boy[1], H. Vuollekoski[1], C. Watcharapaskorn[1], D. Mogensen[1], S. Smolander[1], A. Sogachev[2] and Markku Kulmala[1]

[1]Department of Physics, University of Helsinki, P. O. Box 48, 00014 Helsinki, Finland
[2]Wind Energy Division, Risø National Laboratory for Sustainable Energy, Technical University of Denmark Building 118,P.O. Box 49, 4000, Roskilde, Denmark
Keywords: boundary layer modelling, particle formation and growth, aerosol dynamics
Presenting author email: luxi.zhou@helsinki.fi

Natural and anthropogenic aerosols may have a great impact on climate as they can directly interact with solar radiation and indirectly affect the Earth's radiation balance and precipitation by modifying clouds. In order to quantify the direct and indirect effect, we must understand the complex processes that connect an aerosol particle to a cloud droplet. However, while modern measurement techniques are able to detect particle sizes down to nanometre all the way from ground up to the stratosphere, the data does not serve for all of our needs for understanding the processes. Hence we will demonstrate a modelling approach to investigate the complex processes of aerosols in the atmospheric boundary layer (ABL).

SOSAA (model to **S**imulate the concentration of **O**rganic vapours, **S**ulphuric **A**cid, and **A**erosol) was developed by adding an aerosol dynamics model UHMA (Korhonen, 2004) to an exiting chemistry – transport column model SOSA (Boy, 2011) . It was constructed to study the emissions, transport, chemistry, as well as aerosols in the ABL. Up to our knowledge, it is the first column model existing in the world with detailed chemistry and aerosol dynamics. Thanks to the parallel computing, the model can be used to study the aerosol processes in the ABL for a few days up to a year with high vertical resolution. As a first application of the model, we carried out simulations for the monoterpenes, OH, and H_2SO_4 during the HUMPPA – COPEC campaign in summer 2010 as well as the new particle formation events in March 2010 at a boreal forest site in Hyytiälä, Finland (Figure 1).

We simulated the particle nucleation with different nucleation theories. The results do not suggest us a single theory that works all the time. Instead, it once again emphasizes the complexity of the phenomenon that a combination of different parametrizations may give better fit to the observation. The model SOSAA has also turned out to be a good tool to study the vertical distribution of particles. Scavenging of background particles before a nucleation event has been observed regularly in the morning (Figure 2).

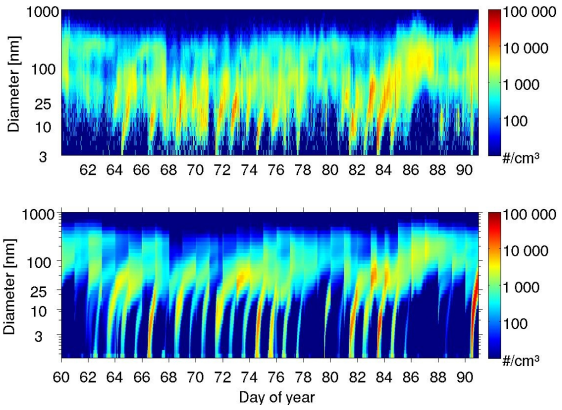

Figure 1. Measured (upper plot) and modelled (lower plot) particle number size distributions for March 2011.

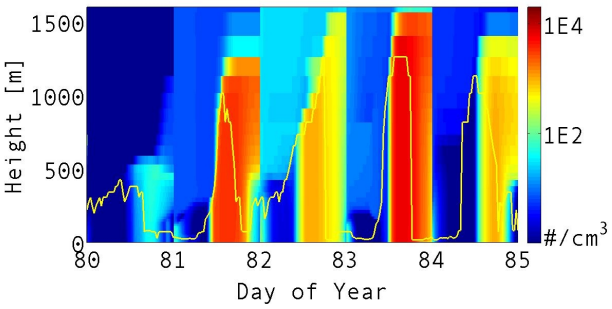

Figure 2. Simulated vertical distributions of particles in size range $3 < D_p < 10$ nm : 21 – 25 March, 2010.

The financial support by Helsinki University Centre for Environment (HENVI), the Academy of Finland Centre of Excellence program (project no. 1118615), and the European Commission 6th Framework program project EUCAARI is gratefully acknowledged.

Boy, M., Sogachev, A., Lauros, J., Zhou, L. and Smolander, S. (2011) *Atmos. Chem. Phys.* **11**, 43-51.

Korhonen, H. and Lehtinen, K. E. J. and Kulmala, M. (2004)) *Atmos. Chem. Phys.* **4**, 757-771.

Aerosol particle number concentration studies based on Fourier and wavelet analysis

S. Byčenkienė, S. Kecorius, K. Plauškaitė, J. Andriejauskienė and V. Ulevicius

Center for Physical Sciences and Technology, Vilnius, Savanoriu 231, LT-02300, Lithuania
Keywords: field measurements, aerosol formation, number concentration, statistical analysis.
Presenting author email: ulevicv@ktl.mii.lt

Recently, the numerous epidemiological and toxicological studies have addressed the association between the particulate matter (PM) concentration and the negative health risk to ultrafine particles (UFP, particle diameter $D_p < 0.1\mu m$) compared to particles of greater diameters. Some studies declare that the particle number concentration (PNC) might be a better indicator of health effects of the particulates than the mass-based method; there is a lack in aerosol number investigation studies. The spectral analysis based on Fourier and Wavelet transform (WT) is used to characterize the time series in the frequency domain and to study the periodicities hidden in the data (Sebald *et al*, 2000). The wavelet transform methods have found wide application in various fields of science including meteorology and oceanography (Torrence and Compo, 1998). The dissimilarity between these two kinds of transforms is that the individual wavelet functions are localized in space. The wavelet theory can be viewed as an extension of the Fourier theory and give a flexible alternative to the Fourier method in the non-stationary signal analysis.

The aerosol PNC measurements were performed at the EMEP Preila environmental pollution research station (55°55'N, 21°00'E, 5 m above the sea level) in the coastal/marine environment. This station is located on the Curonian Spit, which separates the Curonian Lagoon and the Baltic Sea, and thus can be characterized as a regionally representative background area.

For the 2008 – 2009 period, the aerosol PNC was continuously measured using a condensation particle counter (CPC) UF-02. The CPC was designed to detect the ultrafine aerosol particles of a few nanometres with the high detection efficiency. The design of the instrument is based on the swirling flow generated inside the saturator (43 ^{o}C) – condenser (10 ^{o}C). The instrument uses a high flow rate (1 $l \cdot min^{-1}$) of the carrier. From the carrier flow, the aerosol flow (0.27 $l \cdot min^{-1}$) is extracted by a capillary. This aerosol flow is divided into two. The first one (0.03 $l \cdot min^{-1}$) is directed to the condenser. The second flow (0.24 $l \cdot min^{-1}$) is circulated through a HEPA filter and a saturator block, in which the flow is saturated with respect to n-butanol and then mixed with the aerosol-laden air at a cooled condenser. This mixing generates a supersaturated region with respect to n-butanol. The butanol vapour condenses on the particles that act as condensation nuclei. This process increases the size of each individual nanoparticle. Such large droplets can be conveniently detected by light scattering.

The monthly mean variation of the PNC showed the high mean concentrations during the summer and early spring seasons and the low concentrations during the winter. The long-range or regional transported smoke emitted by wildfires had a strong impact on the total aerosol number concentrations in Lithuania over early spring period. The lowest monthly PNC values were observed during November 2008 (1500 ± 900 cm^{-3}) and the highest ones during June 2008 (4500 ± 900 cm^{-3}). The results of Fourier and WT analysis (Fig. 1) indicated that the most important variations in the data series are represented with period 4, 6 – 7, 11, 16 to 23 days, which are synoptic scale fluctuations typical for the synoptic weather systems, but also 80 – 120 days cycles were noticeable in period. For the entire period of the experiment the most significant is the diurnal variation of particle number concentration. However, when passing to the cold season the amplitudes of 1- and 2-day oscillations significantly decrease and become less pronounced.

The study also provided a wavelet covariance transformation technique which facilitated the development of adequate new particle formation identification by aerosol number concentration measurement strategy and contributed to a deeper insight into dynamics of aerosol particles. In this work we describe the new results obtained using the wavelet-based methodology to detect and characterize the new particle formation by aerosol number concentration. Mainly, we showed that the wavelet transforms allow us to untangle waves that otherwise would be mixed up in the Fourier decompositions.

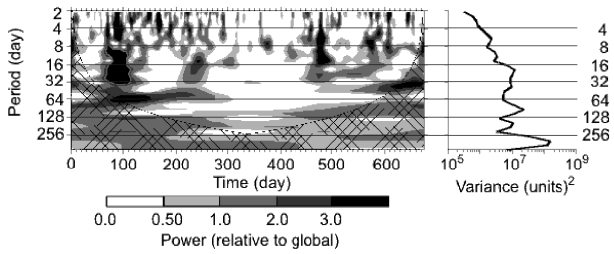

Figure 1. The wavelet power spectrum (left). The power has been scaled by the global wavelet spectrum (on the right). The cross-hatched region is the cone of influence (COI), where zero padding has reduced the variance.

This work was supported by the FP7 ACTRIS and FP7 TRANSPHORM projects.

Sebald, L., Treffeisen, R., Reimer, E. and Hies, T. (2000). *Atmos. Environ*. **34**, 3503–3509.

Torrence C. and G. P. Compo (1998). *Bull. Amer. Meteor. Soc.* **79**, 61–78

A Mediterranean Atmospheric Network for in-situ aerosol measurements: Motivation and Objectives

J. Sciare[1], A. di Sarra[2], R. Ellul[3], E. Gerasopoulos[4], H.C. Hansson[5], S. Kleanthous[6], N. Mihalopoulos[7], J. Pey[8], A. Alastuey[8], and N. Yassaa[9]

[1]Laboratoire des Sciences du Climat et de l'Environnement (LSCE), CNRS-CEA, Gif/Yvette, 91191, France
[2]ENEA, UTMEA-TER, Roma, 00123, Italy
[3]Atmospheric Research, Dept of Physics, Univ of Malta, Msida, 2080, Malta
[4]Institute for Environmental Research and Sustainable Development (IERSD), NOA, Athens, 15236, Greece
[5]Department of Applied Environmental Science (ITM), Stockholm University, Stockholm; 106 92, Sweden
[6]Department of Labour Inspection, Nicosia, 1493, Cyprus
[7]Environmental Chemical Processes Laboratory (ECPL), Univ. of Crete, Heraklion Voutes, 71003, Greece
[8]Institute of Environmental Assessment and Water Research (IDÆA), CSIC, Barcelona, 08034, Spain
[9] Laboratoire d´Analyse Organique Fonctionnelle(LAOF), Faculté de Chimie, USTHB, Algiers, 16111, Algeria

Keywords: Aerosol, Network, Mediterranean.
Presenting author email: jean.sciare@lsce.ipsl.fr

Scientific context. The Mediterranean region is characterized by a complex mixture of (mainly transported) aerosols having different origins (anthropogenic, biogenic, biomass burning, dust, sea spray), with strong east-west and north-south trends observed, both by means of concentrations and chemical composition (Querol et al., 2009). The Mediterranean holds among the largest atmospheric concentrations of aerosols at global scale (3 times more than over Europe) inducing locally important direct radiative forcing (Bergamo et al., 2008). Besides, this region is already facing important climatic changes with increasing numbers of forest fires and heat waves inducing significant changes in aerosol concentrations and properties that may, in term, affect regionally air quality and climate. These changes have been confirmed by recent projections (IPCC, 2007) which have designated the Mediterranean as one of the most vulnerable regions at global scale with an increasing occurrence of heat waves and profound changes in water cycle.

Motivation. Compared to the rest of Europe, the Mediterranean region suffers from the lack of a dense ground-based atmospheric network that will provide long term in-situ observations of aerosol properties. The maturity of existing atmospheric stations in the Mediterranean differs; some of them operating upon international standards for many years, whereas others are operational since very recently. They are monitoring various aerosol parameters, few of them being common to all sites. Beyond quality control guidelines and aerosol database supported following international standards (EU-FP7-ACTRIS; EMEP; GAW), there is a clear need to better coordinate experimental strategies in the Mediterranean, in order to ensure a minimum set of common (relevant) aerosol parameters to be monitored in each station. Such efforts are crucial in the context of international programs (such as The Chemistry-Aerosol Mediterranean Experiment, CHARMEX, initiative; http://charmex.lsce.ipsl.fr/), which will have to be fed by large and homogeneous aerosol database. These efforts may also promote intra-Mediterranean collaboration and dissemination, in particular within the non-EU countries bordering the Mediterranean.

Objectives. This presentation aims to provide a (non exhaustive) review of existing atmospheric stations in the Mediterranean (see Fig. 1). Namely, Montseny (Spain), Mallorca (Spain), Corsica (France), Bou Ismail (Algeria), Giordan (Malta), Lampedusa (Italy), NEO (Pylos-Greece), Finokalia (Greece), and Cyprus. It will identify common and relevant in-situ aerosol parameters that are (to be) monitored in most of the stations. Recent experimental efforts in emerging stations will be emphasized here with the objective to bring in-situ aerosol monitoring activities at these stations to an international quality standard level, as it is provided within the EU-FP7-ACTRIS program.

Figure 1. Mediterranean Atmospheric Network for in-situ aerosol measurements.

Bergamo, A.; Tafuro, A. M., Kinne, S., et al., Atmos. Chem. and Phys., 8, 6995-7014, 2008

IPCC: Climate Change 2007: The Physical Science Basis, Cambridge University Press, UK, 2007

Querol, X., Alastuey, A., Pey, J., et al., Atmos. Chem. Phys., 9, 4575–4591, 2009

OVOC – precursors for SOA: measurements within ACTRIS-WP4

J. Englert, C. Plass-Dülmer, E. Tensing, K. Michl and A. Werner

Hohenpeissenberg Meteorological Observatory, German Weather Service, 82383 Hohenpeissenberg, Germany
Keywords: SOA, VOC, GC-MS.
Presenting author email: jennifer.englert@dwd.de

Introduction

Work package 4 of the ACTRIS (Aerosols, Clouds and Trace gases Research InfraStructure Network) project focuses on the integration and harmonisation of European nitrogen oxides (NO_{xy}) and volatile organic compounds (VOC) measurements. VOC are subdivided into three groups: non-methane hydrocarbons (NMHC), biogenic hydrocarbons (terpenes) and oxygenated volatile organic compounds (OVOC). The latter include highly functionalised with low saturation vapour pressure and/or high polarity. Hence, they allow gas/particle partitioning and are important precursors for the formation of SOA (Secondary Organic Aerosols) (Camredon et al., 2007).

Generally, OVOC are difficult to measure because they are low concentrated polar compounds and highly sticky to surfaces in the sampling system. Further, they dissolve in water and form artefacts in combination with ozone and other oxidants. Hence a specific GC-MS system for high quality OVOC analysis was developed at the Hohenpeissenberg Meteorological Observatory, an institution of the German Weather Service (DWD). With further measurements of NMHC and terpenes at Hohenpeissenberg (Plass-Dülmer et al., 2002) a wide range of VOC is monitored. These measurements allow the consideration of the contribution of VOC to mass closure experiments (e.g. of the total organic carbon (TOC) budget, work package 21 of ACTRIS) or turn-over rates of trace gases with OH radicals (Figure 1).

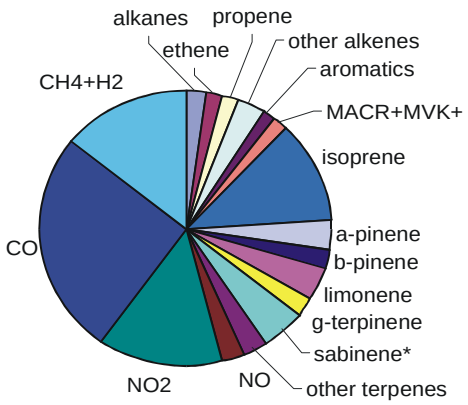

Figure 1. Turn-over of trace gases with OH radicals at Hohenpeissenberg between June to August 2004 (total = $10*10^6$ molecules/(cm³ s), noon time averages).

GC system for OVOC analysis

In the here presented OVOC system, ambient air samples are enriched on a 3-phase adsorbent tube. Water from the sample is frozen out by a cryogenic trap. Ozone is excluded by titration with nitrogen monoxide. After desorption of the analytes from the adsorbent tube, they are refocused cryogenically on a capillary. Subsequently, the sample is injected on a polar GC-capillary column and detected via a split with a flame ionisation detector (FID) and a mass spectrometer (MS).

Measurement campaigns

Campaign activities involving measurements of VOC, OH, RO_x and particles will be performed at Hohenpeissenberg in late spring and early summer 2012.

First results of the OVOC measurements performed during these campaigns will be presented together with a consideration of the TOC budget and a re-evaluation of the turn-over rates of trace gases with OH radicals.

Within the ACTRIS project it is possible to use the observatory's infrastructure for research and training activities in the field of trace gases and aerosol measurements (TransNational Access activity, TNA; http://www.dwd.de/mohp).

This work is supported by the European Union Seventh Framework Programme ACTRIS, FP7/2007-2013, under grant agreement n° 262254.

Camredon, M., Aumont, B., Lee-Taylor, J. and Madronich, S. (2007) *The SOA/VOC/NO_x system: an explicit model of secondary organic aerosol formation*, Atmos. Chem. Phys. 7, 5599-5610.

Plass-Dülmer, C., Michl, K., Ruf, R. and Berresheim, H. (2002) *C_2-C_8 Hydrocarbon measurement and quality control procedures at the Global Atmosphere Watch Observatory Hohenpeissenberg*, Journal of Chromatography A 953, 175-197.

The "Dual-Spot" Aethalometer: Improved measurement of Aerosol Black Carbon with real-time loading compensation

L. Drinovec[1], G. Močnik[1], P. Zotter[2], A.S.H. Prévôt[2], C. Ruckstuhl[3], A.D.A. Hansen[1,4]

[1]Aerosol d.o.o., SI-1000 Ljubljana, Slovenia
[2]Paul Scherrer Institute, CH-5232 Villigen, Switzerland
[3]inNET Monitoring AG, CH-6460 Altdorf, Switzerland
[4]Magee Scientific Corp., Berkeley, CA 94703, USA
Keywords: Instrumentation/physical characterization; black carbon; optical properties; absorption.
Presenting author email: luka.drinovec@aerosol.si

Filter-based measurements of aerosol optical absorption are widely used to determine Black Carbon ('BC') concentrations in real time. Measurements at multiple wavelengths make the separation of contributions of BC from different combustion sources possible. However, these methods can suffer from non-linearity due to the 'loading' effects of increasing aerosol deposit density on the filter (Gundel *et al.* 1984, Weingartner *et al.* 2003, Arnott *et al.* 2005, Virkkula *et al.* 2007). One model represents this non-linearity by a parameter $\boldsymbol{k}$, which is found to be highly dependent on the nature of the aerosol and is also a function of wavelength $\boldsymbol{\lambda}$. Consequently, a static algorithm to compensate for the effect, either by post-processing of the data or fixed in the instrument firmware, fails to capture the details and potential variability of these aerosol optical properties. When sampling ambient air over an extended period of time at any location, $\boldsymbol{k(\lambda)}$ is found to vary according to season and air-mass origin. The parameter may range from moderate values in winter to zero or opposite-sign values in summer, a behaviour also seen in the post-processing of data (Virkkula *et al*. 2007). Atmospheres dominated by local sources show higher values for fresher aerosols while lower values are seen for well-mixed aerosols exposed to aging and accretion.

We have developed a new Aethalometer® (model AE33), in which two parallel sampling channels are operated at loading rates that differ significantly. Combining the data from the two parallel analyses allow both an extrapolation to "zero density", i.e. the ideal measurement of BC in the absence of any loading effects, and additionally yields a dynamically-calculated value of the non-linearity parameter $\boldsymbol{k}$. These analyses are performed for multiple discrete optical wavelengths spanning the range from 370 nm to 950 nm and with a time resolution as rapid as 1 second.

The results show greatly improved analytical performance for the primary data output of BC versus time across the operational spectrum. The instrument is network-ready and is designed for both research and routine monitoring operations.

We present data examples from this new instrument showing the following:

- Continuity of data across filter tape advances demonstrating elimination of the 'loading effect' as the collection spot saturates.
- Absorption spectra illustrating the identifiable characteristics of diesel and biomass-burning (Sandradewi *et al*. 2008).

The data produced by this new instrument may be interpreted by models of aerosol optical properties in order to yield additional information applicable to studies of source apportionment; radiative forcing; and other impacts.

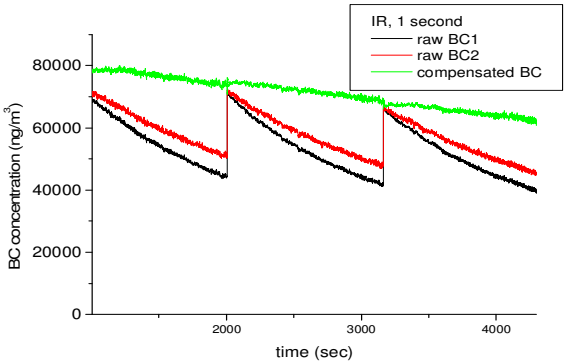

Figure 1. Time series of AE33 raw data with 1-second resolution. BC1 and BC2: raw data from two parallel aerosol spots on the filter. Compensated BC result calculated in real time by the instrument.

Arnott, W. et al. (2005), *Towards Aerosol Light-Absorption Measurements with a 7-Wavelength Aethalometer: Evaluation with a Photoacoustic Instrument and 3-Wavelength Nephelometer*, Aerosol Sci. Technol. **39**, 17-29.

Gundel, L.A., et al. (1984), *The Relationship between Optical Attenuation and Black Carbon Concentration for Ambient and Source Particles*, Sci. Total Environment **36**, 197-202.

Sandradewi, J. et al. (2008) *A study of wood burning and traffic aerosols in an Alpine valley using a multi-wavelength aethalometer*, Atmos. Environ., **42**, 101-112.

Virkkula, A. et al., (2007), *A Simple Procedure for Correcting Loading Effects of Aethalometer Data*, J. Air & Waste Manage. Assoc. **57**, 1214-1222.

Weingartner, E., et al. (2003), *Absorption of light by soot particles: determination of the absorption coefficient by means of Aethalometers*, J. Aerosol Sci. **34**, 1445-1463.

The work described herein was co-financed by the EUROSTARS grant E!4825 "FC Aeth - Fast and loading compensated Aethalometer – an instrument for real time measurement of light absorbing carbonaceous aerosol".

New particle formation in the western Mediterranean regional background.

M. Cusack[1], A. Alastuey[1], X. Querol[1], N. Pérez[1], A. Wiedensohler[2]

[1]Institute of Environmental Assessment and Water Research (IDAEA-CSIC)
[2]Leibniz Institute for Tropospheric Research (IfT), Leipzig, Germany
Presenting author email: michael.cusack@idaea.csic.es

The study of the formation of new particles and the factors influencing their subsequent growth in the western Mediterranean (WM) regional background (RB) is presented in this work, performed at the Montseny (MSY) ACTRIS site. The variability and comparison of size-segregated aerosols at RB sites in Europe has been well documented by Asmi et al, 2011. This study interpreted results on the harmonized dataset of submicron aerosols obtained during 2008-2009 at a number of ACTRIS and GUAN sites in Europe. However, no data from the WM was presented as the SMPS system at MSY was not yet in operation. Within the framework of the ACTRIS project, the MSY site was equipped with a Scanning Mobility Particle Sizer (SMPS) system (in operation since 2010), supplied by IfT in Leipzig. This paper summarizes data on submicron particle size distribution at MSY and compares the data obtained with other RB sites in Europe, with special focus on new particle formation.

New particle formation (NPF) is currently a topic of great interest and the processes controlling NPF are still not clearly understood. NPF is typically observed under clean atmospheric conditions, as the presence of pre-existing particles act as a condensation sink for gaseous precursors which could potentially nucleate. However some studies have observed NPF occurring under polluted conditions provided the growth rate of newly formed particles is sufficiently rapid to prevent scavenging by pre-existing particles. The condensation of VOCs emitted by vegetation upon newly formed particles is believed to play an important role in particle growth after initial clustering.

Measurements of sub-micron size distributions were performed at MSY from October 2010 to June 2011 by means of an SMPS system. The system provided a complete number size distribution of the number of particles between 9 and 850 nm every five minutes. Levels of gaseous pollutants, PMx, black carbon (BC) and meteorology were also continuously measured on site. Interpretation of time variation of pollutants permitted the identification of frequent nucleation events observed under the study period. These are highlighted in Figure 1, where the red arrows indicate NPF under clean atmospheric conditions (when PM levels are low). The green arrows indicate NPF occurring under polluted conditions (high PM). Note that NPF under polluted conditions occurs exclusively in summer.

Number size distribution of submicron particles has been investigated under different scenarios. As an example, Figure 2 depicts episodes of NPF recorded under low pollution conditions (8/12/2010) and relatively polluted conditions (25/05/2011). On the 8/12/2010, PM_{10} levels recorded a daily mean of 2.4 µg m^{-3}, mean temperature of 11ºC and relative humidity of 66%. NPF commences at 10:00 GMT and continues until 13:00, followed by subsequent growth into the Aitken mode. The growth rate (GR) of nucleation mode particles ($N_{9\text{-}20}$) on this day was 1.7 nm h^{-1}. Conversely, NPF on the 25/05/2011 occurred under relatively polluted conditions, with PM_{10} of 22.6 µg m^{-3} and average temperatures of 19ºC and relative humidity of 40%. The particle GR on this day was significantly higher, at 8 nm h^{-1}. Nucleation on this day is attributed to the condensation of VOCs emitted by surrounding vegetation on the newly formed particles, giving rise to much faster particle GR than that observed on 8/12/2010.

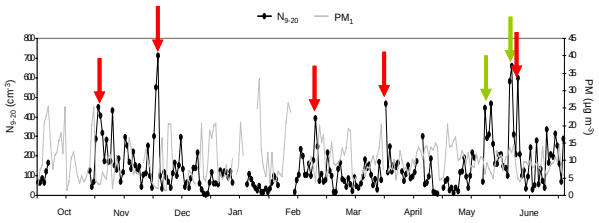

Figure 1. PM_1 and $N_{9\text{-}20}$ from Oct. 2010 – June 2011.

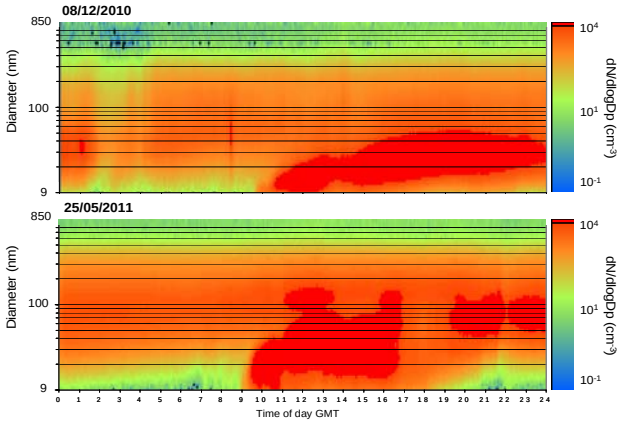

Figure 2. Particle size distribution ($N_{9\text{-}850}$) on 8/12/2010 and 25/05/2011

This work is supported by the MICINN (Spanish Ministry of Science and Innovation) and FEDER funds under the project CARIATI CGL2008-06294/CLI. The research leading to these results has received funding from the European Union Seventh Framework Programme (FP7/2007-2013) under grant agreement n° 262254.

Asmi, A., Wiedensohler, A., Laj, P. et al. (2011) *Atmos. Chem. Phys.*, **11**, 5505-5538.

A Finnish remote-sensing network for monitoring aerosol, clouds, and the boundary layer

A. Hirsikko[1], E.J. O´Connor[1,2], M. Komppula[3], M. Bauer-Pfundstein[4], A. Poikonen[1], M. Kurri[1], E. Giannakaki[3], T. Karppinen[1], H. Lihavainen[1], A. Laaksonen[1], Kari E.J. Lehtinen[3] and Y. Viisanen[1]

[1]Finnish Meteorological Institute, P.O. BOX 503, FI-00101, Helsinki, Finland
[2]Meteorology Department, University of Reading, UK
[3]Finnish Meteorological Institute, P.O.Box 1627, FI-70211, Kuopio, Finland
[4]Meteorologische Messtechnik GmbH (METEK), Elmshorn, Germany

Keywords: Aerosol-cloud interaction, Boundary layer, Mixed-layer depth, Remote sensing, Doppler lidar, cloud radar.
Presenting author email: Mika.Komppula@fmi.fi

The Earth's energy balance is affected by clouds, which absorb and reflect solar radiation (IPCC, 2007). As clouds also have an important role in the atmospheric hydrological cycle, their evolution, from a microphysical and dynamical point of view, is currently a key research topic.

Ash plumes from the 2010 volcano eruption in Iceland disrupted aviation throughout Europe and were responsible for huge economic losses in the airline industry. In addition, ash and smoke from forest fires are also a health threat for general population. Information on the elevation, thickness, transport and potential for dispersion of these ash and smoke layers is essential for aviation safety and the provision of emergency services. Air quality, atmospheric chemistry, clouds and atmosphere-ecosphere interaction are all influenced by the dispersion of pollutants, moisture, gases and aerosol particles from natural sources through turbulent mixing in the boundary layer.

In order to monitor aerosol layers, clouds and the boundary layer, the Finnish Meteorological Institute has established a network of Doppler lidars (Halo Photonics, Pearson et al., 2009) situated at the following stations, representing different environments

- Helsinki (60.12°N, 25.58°E, 45 m ASL), urban site with marine influence
- Kuopio (62,44°N, 27, 32°E, 190 m ASL), rural
- Sodankylä (67.37°N, 26.63°E, 171 m ASL), sub-arctic

All sites are equipped with standard meteorological, trace gas and aerosol instrumentation, together with Vaisala ceilometers operating at 905 nm wavelength.

Continuous measurements with Doppler lidars, operating at 1.5 μm wavelength and with scanning capability, have been performed at Helsinki and Kuopio since September 2011. Both sites have comprehensive surface in-situ measurements of the chemical, physical and optical properties of aerosols. Kuopio will participate in ACTRIS WP2 and WP3, with a POLLY^{XT} lidar (Althausen et al., 2009) due to restart operations in April 2012. A Doppler cloud radar (Mira-36 by Metek GmbH) and Doppler lidar will be operated continuously at Sodankylä from spring 2012. This site will participate in ACTRIS WP5 (clouds and aerosol quality-controlled observations).

In addition to announcing the new Finnish remote-sensing network, our aim here is to present results from an inter-comparison of three identical Doppler lidar during a short campaign in Helsinki (1 – 15 September 2011)), prior to their deployment in their stated locations. We have compared the backscatter, Doppler velocity and wind profile parameters obtained from the Doppler lidar's internal data processing algorithm. We will show, for example, that the wind profile parameters (i.e. horizontal components as well as speed and direction) obtained from each instrument, measured every 10 minutes, showed very good agreement. The profiles of vertical wind velocity, fluctuating around zero and subject to turbulence, are only comparable when the instruments are situated within a few metres of each other; otherwise the turbulent structures appear uncorrelated. However we will show that the variability is similar in a statistical sense.

We have also, for the first time, examined the capability of the Doppler lidars to operate in harsh winter conditions. During the previous winter, the lidars operated without problems even when the ambient temperature dropped below -20°C for several days. Due to the built-in heating system, the instruments were typically able to melt snow and evaporate any standing water from the surface of the lens and background calibration plate, ensuring reliable operation without additional intervention. However, during heavy snow in temperatures lower than -10°C, the internal heating was insufficient and manual snow removal was required. To rectify this in future winters, an additional blower system will be deployed for each Doppler lidar.

We are planning to extend the network to new stations, which already have comprehensive surface aerosol measurements.

Althausen, D., Engelmann, R., Baars, H., Heese, B., et al. (2009) *J. Atmos. Ocean. Tech*. **26**, 2366–2378.

IPCC (2007) Fourth Assessment Report of the Intergovernmental Panel on Climate Change.

Pearson, G., Davies, F., Collier, C. (2009) *J. Atmos. Ocean. Tech.* **26**, 240-250.

Long-term observation of time-resolved submicron aerosol chemical composition in the region of Paris (France)

J-E. Petit[1,2], R. Sarda-Estève[1], J. Sciare[1], O. Favez[2]

[1]Laboratoire des Sciences du Climat et de l'Environnement, Gif-sur-Yvette, F-91191, France
[2]INERIS, Parc Technologique ATALA, BP2, 60550 Verneuil-en-Halatte
Keywords: aerosol measurement, mass spectrometry, PM1, source identification
Presenting author email: jean-eudes.petit@lsce.ipsl.fr

In every major European cities, aerosol pollution is of great scientific, economic, health and social concern. Despite geographical disparities, the particulate phase in urban areas is complex by virtue of its chemical composition and the multitude of emission sources. Long-term and detailed chemical speciation studies are key variables to constrain atmospheric processes and local versus continental imports leading to urban pollution episodes; European standards and legislations however mainly focus on indiscriminate mass concentrations ($PM_{2.5}$ and PM_{10}). While Aerosol Mass Spectrometers (AMS) may provide valuable 'real-time' data for the chemical characterization of submicron particles, their cost and implementation as networking devices make them improper to be used for long-term measurements. Developed by Aerodyne Research Inc. (Billerica, MA), the Aerosol Chemical Speciation Monitor (ACSM) measures quantitative chemical composition for non-refractory sub-micron aerosol particles. Smaller, lower cost and more robust, the ACSM is designed for long-term unattended deployment and routine monitoring applications.

Experimental

In this context, the infrastructure EU-FP7-ACTRIS program has been promoting the use of ACSM for long-term observations at background stations, among which the SIRTA/LSCE site. This station, representative of PM pollution in the region of Paris, has been equipped with an ACSM since June 2011. Co-located multi-wavelength absorption measurements (AE-31, Magee Scientific) allow for Black Carbon source apportionment (Sciare et al. 2011). Reliable PM1 data (TEOM-FDMS 1405F, Thermo) are also available since February 2012.

Results

The ACSM has been providing continuous data since June 2011. This large dataset highlight raising important issues on data processing. Nevertheless, the two datasets (ACSM + BC versus PM1) show very good temporal agreement, with a slope close to 1 (slope=1.08, r^2=0.87), pointing out the very good consistency and long term stability of ACSM measurements.

First results enlighten the major role played by organics and ammonium nitrate on PM loadings in the region of Paris (Fig.1), especially during severe winter pollution episodes.

Statistical tools, such as Potential Source Contribution Function, reveal the strong influence of continental import on secondary species (nitrate and sulphate) highest concentrations (Fig.2). Such methodologies applied to Positive Matrix Factorization outputs will also help to better understand the sources and atmospheric processes of organic aerosols.

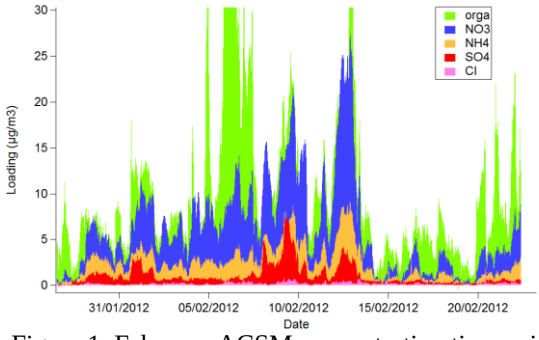

Figure 1. February ACSM concentration timeserie.

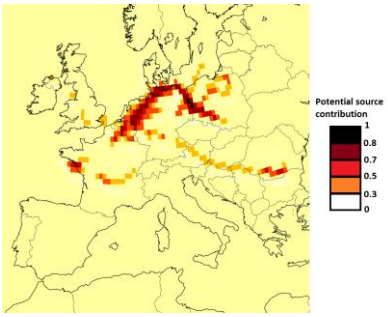

Figure 2. PSCF analysis from Jan. 1st to Feb. 22th 2012; sulphate concentrations; threshold at 75th centile.

Perspectives

For time-limited intensive campaigns, a substantial analytical fleet is engaged in order to investigate specific pollution sources. Since early February 2012, PILS-IC, PILS-TOC and PILS-MS/MS (for the anionic fraction, water-soluble organic carbon and levoglucosan, respectively) have been implemented to constrain wood burning emissions. Fertilizer spreading emissions will be investigated this spring, emphasizing on gaseous precursors of aerosol.

Sciare et al. (2011), *Large contribution of water-insoluble secondary organic aerosols in the region of Paris (France) during wintertime*, **JGR**, 116.

Characterize aerosol properties observed over Lemesos, Cyprus using passive and active remote sensing instruments.

A. Nisantzi[1], RE Mamouri[1], P. Kokkalis[2] and D. G. Hatzimitsis[1]

[1] Department of Civil Engineering and Geomatics, Cyprus University of Technology, Lemesos, Cyprus
[2] Physics Department, National Technical University of Athens, Greece
Keywords: aerosol, angstrom exponent, lidar
Presenting author email: argyro.nisantzi@cut.ac.cy

Atmospheric aerosols affect the Earth radiative budget by interacting with the solar and the Earth's long-wave radiation (Charlson et al., 1992). Cyprus is located in the eastern part of Mediterranean and the contribution of different aerosol sources comes from air masses originating in Europe and Africa (Sciare et al., 2003). Thus different meteorological patterns transport different aerosol types (Saharan dust, biomass burning) over Lemesos.

Remote sensing techniques have established a great number of records of aerosol measurements since 1970s by giving the opportunity of high spatial and temporal coverage. Daily lidar measurements of the aerosol vertical distribution have been performed over Lemesos (34.675ºN, 33.043ºE) using a backscatter lidar system since May 2010. In this work we selected to present two cases which have been identified as different aerosol types (Saharan dust, biomass burning). Additionally we calculated the back-trajectories in order to identify the origin of air masses ending over the lidar site of Cyprus. For a better characterization of aerosol types sunphotometric measurements retrieved from the ground based AERONET station of Lemesos are used.

For the first case study and according to the Range Corrected Signal (RCS) at 532nm on 30 August 2011 over Lemesos from 08:13 to 09:12UT (figure 1a) an enhanced aerosol layer between 1200 and 2500m height are shown. The same day the Angstrom exponent derived from the CIMEL sun-tracking photometer fluctuate from 1.2 to 1.42 during the day and clearly indicate the existence of small aerosols particles.

In the second case (figure 1b) the RCS at 532nm on 7 September 2010 depicts two distinct dust layers at 600-1500m and 1800-3500m respectively and the Angstrom Exponent has small values (0.2-0.45) similar to the values retrieved in case of Saharan dust episode in previous studies (Mattis et al., 2002).

In both cases the aerosol optical properties will be examined with the respect of the vertical backscatter profile at 532nm and the particle depolarization ratio at the same wavelength. Thus different depolarization ratios could give information of particles with nonspherical geometry. Specifically in this study the depolarization ratio with values greater than 10% characterize desert dust while for biomass burning aerosols depolarization values are lower than 10% and agree with previous studies (Cattrall et al., 2005).

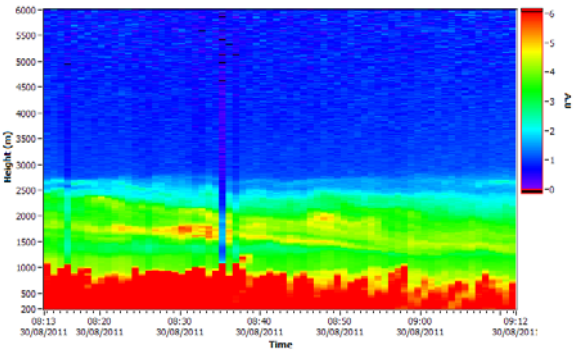

(a)

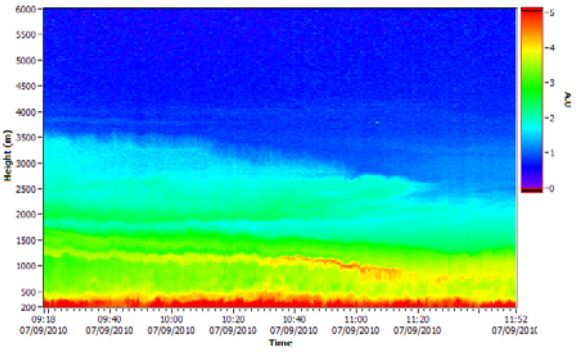

(b)

Figure 1. Temporal evolution of (a) biomass burning layer and (b) dust layer over the area of Lemesos

This work was supported by "PENEK" project funded by the Cyprus Promotion Research Foundation. Additionally thanks are given to the Remote Sensing Laboratory of the Department of Civil Engineering & Geomatics at the Cyprus University of Technology for the support (http://www.cut.ac.cy/).

Cattrall, A., Reagan, J., Thome, K., and Dubovik, O. (2005) *J. Geophys. Res.*, 110, D10S11,

Chalson, R.J, Schwartz, S.E., Hales, Cess, R.D., Coakley, J.A., Hansen, J.E., and Hoffman, D.J. (1992) *Science*, 255, 423-430

Mattis, I., Ansmann, A., Muller, D., Wandinger, U., and Althausen, D. (2004) *Geophys. Res.* Lett., 29, D1306

Sciare J., et al (2003) *Atmos. Chem. Phys*., 3, 291-302,

The AERONET-Europe calibration facility: access within the ACTRIS project

P. Goloub[1], V.E. Cachorro[2], E. Cuevas[3], L. Blarel[1], A. Berjón[3], C. Toledano[2], T. Podvin[1], A. Lapionak[1], C. Guirado[3], R. Ramos[3], R. González[2], D. Fuertes[2]
[1]Laboratory of Atmospheric Optics, University of Lille, Lille, France
[2]Group of Atmospheric Optics, Valladolid University, Valladolid, Spain
[2]Izaña Observatory, Spanish Meteorological Agency, Tenerife, Spain
Keywords: AERONET, ACTRIS, calibration, aerosol.
Presenting author email: chiqui@goa.uva.es

The Aerosol Robotic Network (AERONET, Holben et al., 1998) is a well established ground-based network for aerosol and water vapor content monitoring and characterization. This program, initiated in the 90's by NASA and the University of Lille, is currently greatly expanded, aiming at global coverage and long-term measurements. To enable the development of the network, alternative calibration centers (besides the headquarters in NASA) have been developed in Europe, primarily in France and then in Spain.

Within the European infrastructure project ACTRIS (Aerosols, Clouds, and Trace gases Research InfraStructure Network), access to the AERONET-Europe calibration facility is provided. The AERONET-EUROPE Calibration Service is a scientific infrastructure composed by three separate but complementary installations located in France and Spain (Figure 1).

Three institutions collaborate to form AERONET-Europe: the Laboratory of Atmospheric Optics (LOA), University of Lille-CNRS (France); the Group of Atmospheric Optics (GOA), Valladolid University (Spain); and the Izaña Atmospheric Research Center (CIAI), Spanish Meteorological Agency (Spain). Three outdoor platforms for calibration of AERONET-Cimel sun photometers are available: Carpentras from LOA and Autilla from GOA are devoted to inter-calibration of field instruments; a unique facility for calibration of master instruments is provided by CIAI at Izaña. The indoor platforms in Lille and Valladolid include NASA-NIST traceable integrating spheres for radiance calibration, polarized light sources, solar-simulator, maintenance and repair room, spectrometer for filter characterization, thermal chamber for response to temperature characterization and computers linked to AERONET/NASA database for calibration coefficients computation and data reprocessing.

Both new users that want to joint AERONET and institutions already participating in the network can apply to access to this facility and have their Cimel sun photometers calibrated and incorporated to the database. The access to the infrastructure is made under the modality of transnational access. The call for proposals is continuously open throughout the project duration. Visit http://www.actris.net/AERONETEurope/tabid/4321/Default.aspx for further information.

Figure 1: Location of the three calibration facilities of AERONET-Europe.

This work has received funding from the European Union Seventh Framework Programme (FP7/2007-2013) under grant agreement N. 262254. Financial support from the Spanish Ministry of Science (MICINN) under projects with ref. CGL2009-09740, CGL2011-23413, CGL2010-09480-E and CGL2011-13085-E as well as from Junta de Castilla y León are gratefully acknowledged.

Holben B, Eck T, Slutsker I, Tanre D, Buis J, Setzer A, Vermote E, Reagan J, Kaufman Y. (1998). AERONET - a federated instrument network and data archive for aerosol characterization. Remote Sens. Environ. **66**, 1-16.

Data interoperability solutions for the Finnish SMEAR station network

M. Dal Maso[1], P. Kolari[1], H. Junninen[1], P.P. Aalto[1], P. Keronen[1], P. Järveläinen[2], S. Sorvari[1] and M. Kulmala[1]

[1]Department of Physics, University of Helsinki, PO Box 48, 00014, Helsinki, Finland
[2]CSC - IT Center for Science Ltd., P.O. Box 405 FI-02101 Espoo, Finland
Keywords: data integration, measurements, infrastructure.
Presenting author email: miikka.dal@helsinki.fi

Today's aerosol and atmospheric scientists have at their disposal a wealth of observations of parameters affecting atmospheric aerosol processes; however, in practical scientific work much delay and frustration arises from lacking data interoperability, such as difficulties to find suitable datasets, unclear documentation, varying conventions for data processing and units, etc.

As the amount of observational data grows, so do the challenges of successful data interoperability. Worldwide, the scale of the storage needed for climate and environmental data is expected to grow to exabytes within next 10 years. Research with such data volumes needs robust, but adaptable and scalable IT infrastructure. It is an old truth that to foster innovation, the components needed – people, knowledge, and resources – must be brought as close to each other as possible.

A significant part of the atmospheric environmental data, including aerosol observations, in Finland is obtained from the SMEAR measurement station network (Hari and Kulmala, 2005). These stations measure weather conditions and interactions between ecosystems and the atmospheres aiming for a comprehensive picture of the matter, energy and momentum budgets and thus increasing the understanding of processes in the climate and Earth system.

Currently, a bottleneck in environmental sciences is often not the aquisition of environmental data itself, but answering interoperability challenges - the *processing, transport, storage* and *combining* of variable datasets that represent different aspects of our environment at different scales and complexities. As it often is the comparison and integration of these variable datasets that gives scientist the most powerful tools for scientific innovation, significant gains should be expected when existing data and computation bottlenecks can be resolved, and scientists can be allowed to focus more of their time to research instead of mechanical data processing.

As instrumentation constantly develops, for example with advances in atmospheric mass spectrometry (eg. measurement of organic compound concentrations and fluxes using time-of-flight mass spectrometry, ToF-MS), the sheer amount of data has grown to volumes that present significant new IT challenges for the integration.

Ongoing research activities lead to established data flows, in which scientists find their own optimized solutions for processing, transport, storage and comparison activities. Individual data flows can refer to individual data sets or time series (for example aerosol size distributions, solar irradiation, or carbon dioxide uptake by trees), or to whole groups of measurements from a single measurement station. The processing and analysis a data set undergoes involves usually several specialized processing steps performed by scientists focusing on this dataset. Currently, many of these steps are known to a small group of scientists. Linking and combining different data sets together requires knowledge of these processing steps, so that the scope and range of validity of the datasets can be verified. For this, the data and related information need to be collected together and described in a formalized manner.

We will discuss the solutions for data interoperability, workflow documentation and orchestration, and data distribution that we develop for the Finnish SMEAR station network. The data environment can be broken down into a data collection environment, data storage solutions, and a data processing and exploration environment. We discuss the challenges and existing (*eg*. Junninen et al., 2009) and future solutions for integrating these three domains, with focus on atmospheric aerosol and cluster data measured in the SMEAR network. We will also discuss solutions of integrating international field campaign data (eg. the European aerosol project PEGASOS) with the continuous measurements at field stations.

This work is supported by the Academy of Finland. The research leading to these results has received funding from the European Union Seventh Framework Programme (FP7/2007-2013) under grant agreement n° 262254, and the FP7 project ENVRI (FP7/2011-2014).

Hari, P. & Kulmala, M. 2005: Station for Measuring Ecosystem–Atmosphere Relations (SMEAR II). Boreal Env. Res. 10: 315–322

Junninen et al., 2009: Smart-SMEAR: on-line data exploration and visuzalization tool for SMEAR stations *Boreal Env. Res: 14: 447-457*

Using sulfur isotope analyses to understand in-cloud sulfate formation during HCCT 2010

E. Harris[1], B. Sinha[1,2], P. Hoppe[1], J. Schneider[1], D. van Pinxteren[3], W. Fomba[3], T. Gnauk[3], B. Fahlbusch[3], S. Mertes[3], T. Lee[4], S. Foley[5], S. Borrmann[1] and H. Herrmann[3]

[1]Particle Chemistry Department, Max Planck Institute for Chemistry, Mainz, 55128, Germany

[2]Department of Earth Sciences, IISER Mohali, Manauli, PO 140306, India

[3]Leibniz Institute for Tropospheric Research, Leipzig, 04318, Germany

[4]Department of Atmospheric Science, Colorado State University, Fort Collins, Colorado, 80523, USA

[5]Earth System Science Research Centre, University of Mainz, Becherweg 21, Mainz, 55128, Germany

Keywords: sulfate formation, cloud processing, aerosol radiative forcing.

Presenting author email: eliza.harris@mpic.de

Processing of aerosol by clouds has been shown to modify the cloud condensation nucleus spectrum, leading to important climatological effects (Hegg *et al.*, 2004). In-cloud SO_2 oxidation and uptake of sulfate play a large role in this processing, causing both hygroscopicity changes and mass increases. However, the in-cloud oxidation of SO_2 is not well understood. Measurements of stable sulfur isotopes can be used to investigate the chemistry of SO_2 in the environment, providing insight into sources, sinks and oxidation pathways. Due to the distinctive isotopic signature of the reaction, sulfur isotope measurements are particularly useful to quantify the importance of transition metal-catalysed oxidation of SO_2, which may be significantly underestimated in current models (Hegg *et al.*, 2004).

Sulfur isotopic compositions in SO_2 and H_2SO_4 gas and particulate sulfate were measured upwind, in-cloud and downwind of an orographic cloud during three cloud events as part of the HCCT 2010 campaign. Changes in the sulfur isotope composition of SO_2 between the upwind and downwind stations were used to determine the dominant SO_2 removal process occurring in the cloud, as shown in Table 1.

Event	LWC g m^{-3}	α_{cloud} ‰	Oxidant	α_{ox} ‰
FCE7.1	0.14	20.4±5.3	H_2O_2	15.1±1.3
FCE11.2	0.37	-12.7±2.3	TM-cat	-9.5±3.1
FCE11.3	0.32	-7.9±1.7	TM-cat	-9.5±3.1

Table 1: Comparison between isotopic fractionation factors measured during in-cloud SO_2 oxidation and fractionation factors for known reactions (Harris *et al.*, 2011a,b).

Changes in the isotopic composition of particulate sulfate were then used to show that the dominant SO_2 oxidation reaction, the transition metal catalysis pathway, was primarily occurring on coarse mineral dust particles (summarised in Figure 1). Sulfate produced from in-cloud SO_2 oxidation will therefore be removed relatively quickly from the atmosphere and will have a minor climatic effect. The reactive uptake coefficient for the transition metal catalysis reaction, γ_{obs}, was calculated to be between 0.02 and 0.11. This is close to the accommodation coefficient for SO_2 uptake, and shows the pathway is significantly underestimated in most global climate models. Improving our understanding of the extent and climatic effects of this reaction is particularly important considering the majority of future SO_2 emissions are predicted to be in the dust source regions of India and China (Solomon *et al.*, 2007).

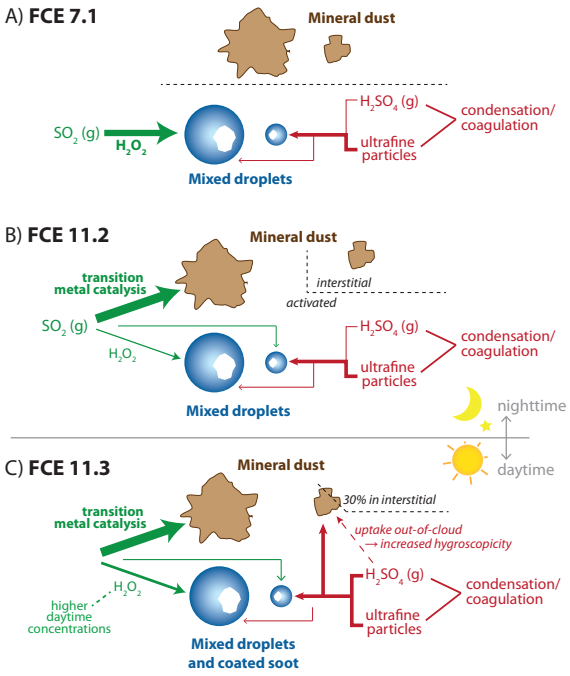

Figure 1: Major processes adding sulfate to particulate during passage through a cloud in HCCT 2010.

This research was funded by the Max Planck Society and the Max Planck Graduate Centre.

Hegg, D. A., Covert, D. S., Jonsson, H. *et al.* (2004) Tellus **56**, 285-293.

Harris, E., Sinha, B., Hoppe, P. *et al.* (2012a) Atmos. Chem. Phys., **12**, 407-423.

Harris, E., Sinha, B., Foley, S. *et al.* (2012) Atmos. Chem. Phys. Discuss., **12**, 2303-2353.

Solomon S., Qin, D., Manning, M. *et al.* (2007) Cambridge University Press, New York.

Inorganic cloud chemistry and its relation to the valley sites particle chemistry during HCCT

K. Müller[1], G. Spindler[1], D. T. Lee[2], J. Collett Jr.[2], van Pinxteren[1], H. Herrmann[1]

[1]Department of Chemistry, Leibniz Institute for Tropospheric Research, 04318 Leipzig, Germany
[2]Department of Atmospheric Science, Colorado State University, Ft. Collins, CO, 80523, USA
Keywords: size segregated aerosol, chemical interaction, cloud water
Presenting author email: konrad@tropos.de

During HCCT at the two valley sites in Goldlauter (upwind site) and Gehlberg (downwind site) aerosol collection by low-pressure impactors (Hauke, LPI 80/0.05) and high-volume filter samplers (Digitel, DHA-80) took place. At the mountain site Schmücke cloud water was collected by four bulk samplers, a three stage and a five stage sampler (Moore et al., 2004; Raja et al., 2008). Aerosol and cloud water samples were stored and transported frozen up to analysis.

During the six week campaign in September and October 2010 nine cloud events have been selected where a connected flow between the three sites was observed. Additionally three non-cloud events have been added for comparison to cloud events.

Water soluble ions, OC and EC were analysed from filter and impactor samples. Cloud water samples were analysed for the content of WSOC, H_2O_2, water soluble ions, and further species reported in other contributions.

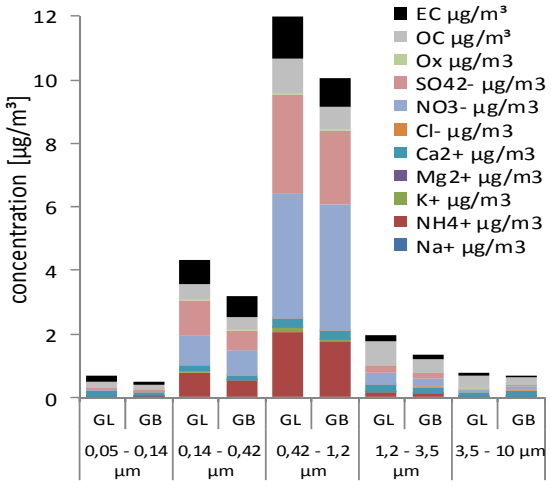

Figure 1. Mass concentration of OC, EC and ionic constituents of size segregated aerosol samples collected during cloud event 13.1 at both valley sites (GL: Goldlauter; GB: Gehlberg).

Ionic constituents are predominant components of the two fractions d_p = 0.14 to 0.42 and 0.42 to 1.2 µm. These fractions contain mainly the long range transported secondary material. The three other fraction were dominated by a high percentage of organic carbon (OC) and in the ultrafine mode of the stage 1 (0.05-0.14 µm) elemental carbon (EC) was found up to 30 % decreasing with PM size. OC from biogenic sources was reported up to 55 % in the coarse mode samples with higher concentrations typically at the upwind site. EC was found in all samples of the cloud events at the upwind site in all fractions in higher concentration than after the cloud passage at the downwind site. Not only the cloud but also the deposition on the humid forest surface influence the decrease in concentrations of nearly all components towards the downwind sampling station in Gehlberg in the mass rich fractions 2 to 4. For ultrafine and coarse mode particles some exceptions were reported.

The comparison between cloud water bulk samplers and the droplet size selective three- and five-stage sampler delivered comparable results. In nearly all samples the measured concentration of species is highest in the smallest droplet class (d<4 µm). The cloud water pH values were measured between 5.5 and 3.3.

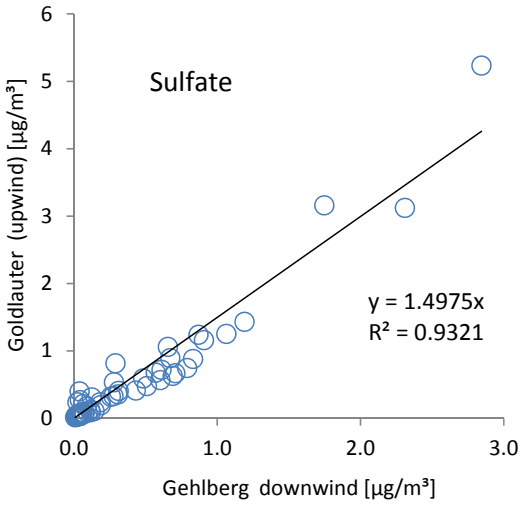

Figure 2. Comparison of sulphate content in impactor samples (all stages) during all cloud events between upwind site Goldlauter and downwind site Gehlberg.

For all major ionic species a decrease in particle concentration was observed between the valley sites in all size classes. Similar results according to Fig. 2 were found for other ions. The correlation coefficient was found to be lower for ammonium (R^2 = 0.879) and nitrate (R^2 = 0.724). Deposition and dilution of PM are the main causes.

Moore, K.F. et al. (2004), *Atmos. Environ.*, **38**, 1389-1402.
Raja, S. et al. (2008), *Atmos. Environ.*, **42**, 2048-2061.

Evaluation of PM_{10} and trace gas measurements with the MARGA during the HCCT 2010 campaign

B. Fahlbusch[1], G. Spindler[1], L. Poulain[1], A. Grüner[1], M. Wallasch[2] and H. Herrmann[1]

[1]Leibniz-Institut für Troposphärenforschung e. V., Permoserstr. 15, 04318 Leipzig, Germany
[2]Umweltbundesamt, Wörlitzer Platz 1, 06844 Dessau-Roßlau, Germany

Keywords: PM_{10}, Instrumentation, Tropospheric aerosols, Chemical composition
Presenting author email: fahlbusch@tropos.de

During the HCCT 2010 campaign (Hill Cap Cloud Thuringia) in September and October 2010 the online system MARGA (Monitor for Aerosols and Gases in ambient Air, Applikon Analytical, NL, *ten Brink et al., 2007*) was deployed at the upwind station in Goldlauter. The instrument was connected to a PM_{10} inlet to measure the mass concentrations of the water-soluble ions Cl^-, NO_3^-, SO_4^{2-}, Na^+, NH_4^+, K^+, Mg^{2+}, Ca^{2+} and their corresponding trace gases HCl, HNO_2, SO_2, HNO_3 and NH_3 at a time resolution of one hour.

The hourly PM_{10} MARGA measurements were analyzed with consideration of the meteorological conditions. The mean concentrations of the measured aerosols are shown in table 1.

Table 1. Summary of the measured concentrations between 11 Sep and 24 Oct 2010. The mean, the standard deviation (stdev) and the number of data points (N) are presented.

	Mean [µg/m³]	Stdev [µg/m³]	N
HCl	0.13	0.14	164
HNO_2	0.64	0.39	999
SO_2	0.67	1.34	1002
HNO_3	0.23	0.62	989
NH_3	0.81	0.84	1000
Cl^-	0.19	0.21	402
NO_3^-	1.94	2.08	1003
SO_4^{2-}	1.38	0.80	1003
Na^+	0.12	0.16	922
NH_4^+	1.12	3.27	1001
K^+	0.10	0.04	888
Mg^{2+}	0.14	0.15	981
Ca^{2+}	0.59	0.36	992

To evaluate the dataset obtained by the MARGA the measurements were compared with a SO_2 gas monitor (Thermo Environmental Instruments Inc., USA) and with a High Resolution Time of Flight Aerosol Mass Spectrometer (HR-ToF-AMS, Aerodyne, USA, *DeCarlo et al., 2006*).

The SO_2 concentration of the MARGA and the gas monitor are in good agreement (R^2: 0.82). But discrepancies can be seen during periods with low SO_2 concentrations.

A good correlation was observed between the MARGA and AMS measurements for nitrate, ammonium and sulphate with correlation coefficients (R^2) between 0.8 and 0.9 despite the different size cutting of the two instruments. This indicates that these three compounds were mainly present in the submicron fraction of particles during the HCCT campaign. Only during the first week of the campaign a significant higher NO_3^--concentration was measured by the MARGA compared to the AMS. This difference points out the presence of high nitrate concentrations in the particle coarse mode which was not observed during the rest of the campaign. Figure 1 shows the correlation between the MARGA and the AMS for NH_4^+ and SO_4^{2-}.

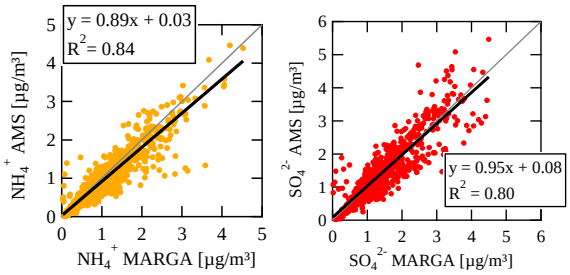

Figure 1. Comparison between MARGA and AMS measurements of ammonium (yellow) and sulphate (red).

The authors gratefully acknowledge financial support by the Umweltbundesamt in Dessau-Roßlau, Germany (grant no. 351 01 070).

DeCarlo, P. F., Kimmel, J. R., Trimborn, A., Northway, M. J., Jayne, J. T., Aiken, A. C., Gonin, M., Fuhrer, K., Horvath, T., Docherty, K. S., Worsnop, D. R., and Jimenez, J. L. (2006) *Field-deployable, high-resolution, time-of-flight aerosol mass spectrometer, Anal. Chem.*, **78**, 8281-8289.

ten Brink, H., Otjes, R., Jongejan, P., Slanina, Sjaak (2007) *An instrument for semi-continuous monitoring of the size-distribution of nitrate, ammonium, sulphate and chloride in aerosol. Atmos. Environ.* **41**, 2768-2779.

HOx measurements at the upwind site during HCCT

D. Amedro, C. Schoemaecker, C. Fittschen and Jean-François Pauwels

Laboratory "Physicochimie des Processus de Combustion et de l'Atmosphère," PC2A, University of Lille 1, Villeneuve d'Ascq, 59655 cedex, France
Keywords: radicals, gas removal, cloud, field measurements.
Presenting author email: coralie.schoemaecker@univ-lille1.fr

The oxidative capacity of the troposphere is mainly driven by OH radicals. They are at the origin of most of the oxidation processes that takes place in the gas phase. HO_2 radicals are closely related to OH (OH and HO_2 are called together HOx radicals) as they are a product of hydrocarbon reactions with OH radicals. In most of the studies, the characterization of the sources and sinks of OH and HO_2 focused mainly on the gas phase. Nevertheless, uptake coefficient of HO_2 on aerosols was the subject of several laboratory studies (Taketani, 2008) and was taken into account as an HO_2 sink in atmospheric chemical models (Sommariva, 2006). The impact of HOx uptakes on aerosols in the cloud formations needs to be understood.

The HCCT (Hill Cap Cloud Thuringia) field campaign was organised by the IfT (Leipzig) during the autumn 2010 (from September 14th until October 24th). The newly built UL-FAGE (University of Lille, Fluorescence Assay by Gas Expansion) was deployed during the entire campaign to measure OH and HO_2 at the upwind site in Goldlauter.

Ambient air is probed into a low pressure cell, where OH is measured by Laser Induced Fluorescence (LIF). HO_2 is measured in a second cell following its conversion to OH using NO (see Figure 1). The detection limit was 6×10^5 molecules.cm^{-3} for OH and 1×10^6 molecules.cm^{-3} for HO_2 for a one minute integration time.

Special attention was driven on the so-called Cloud Events (orographic cloud formation on top of the hill with connectivity between the sites) and Non Cloud Events (absence of cloud, connectivity between the sites). HOx radicals were measured at two different sites in order to characterise the oxidative budget of the gas phase upwind and on top of the hill where the University of Leeds FAGE instrument was installed. In this configuration, during a Cloud Event, the HOx radicals were measured in the cloud (Leeds) and before the cloud formation at the upwind site (Lille).

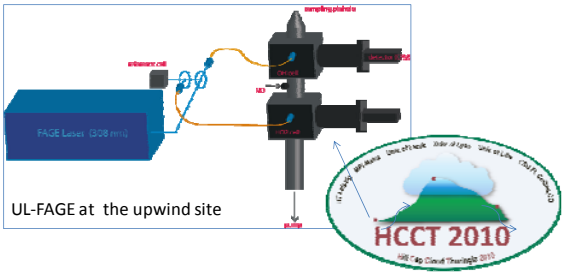

Figure 1. Deployment of the UL-FAGE during HCCT

Most of the cloud events occurred at night or under cloudy conditions, as a consequence the different photolytic sources of OH were diminished strongly. OH concentration was always under our detection limit and HO_2 concentration was measured at a very low level approximately $2.5.10^7$ molecules.cm^{-3} (~1 ppt).

During the entire campaign, maximum measured concentrations were 9×10^6 molecules.cm^{-3} for OH and 7×10^8 molecules.cm^{-3} for HO_2 (Figure 2).

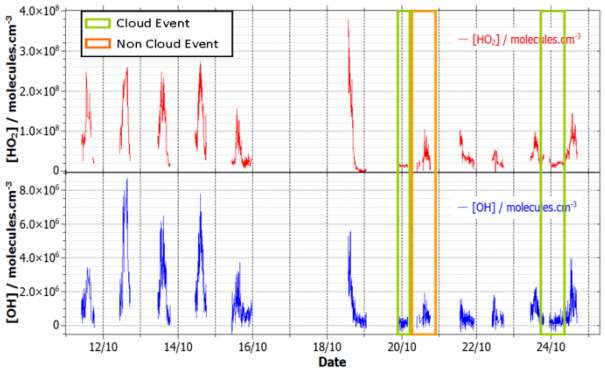

Figure 2. OH and HO_2 profiles during HCCT. Cloud Event and Non Cloud Event are highlighted.

HOx profiles were similar between the two sites, nevertheless significant differences between the HO_2 concentrations were observed, with systematic higher concentrations at the upwind site (UL-FAGE). HO_2 concentrations can be affected locally due to different chemical processes on the two different sites. However instrument interferences cannot be discarded: a recent work (Fuchs, 2011) has shown the interferences of several peroxy radicals on HO_2 signals. Further investigations need to be done in order to characterise the possible interferences for the principal Volatile Organic Compounds (VOCs) measured at both sites.

An atmospheric chemical model will be realised. Comparing the model with the measurements will be of importance in order to check how the cloud formation is affected by the local chemistry and also the long range transport of well characterized aerosols.

Taketani, F., Kanaya Y., Akimoto, H. (2008) *J. Phys. Chem. A* **112**, 2370–2377.

Sommariva R., Bloss W.J. et al. (2006) *Atmos. Chem. Phy.*, **6**, 1135-1153.

Fuchs, H., Bohn, B., et al. (2011). *Atmos. Meas. Tech. Discuss.* **4**, 1255-1302.

Characterisation of biological and biomass burning monosaccharides during Hill Cap Cloud Thuringia 2010 (HCCT 2010) campaign

Y. Iinuma and H. Herrmann

Leibniz-Institut für Troposphärenforschung, Leipzig, 04318, Germany

Keywords: Chemical composition, Aerosol cloud interaction, Biomass burning
Presenting author email: yoshi@tropos.de

Over the past few decades, substantial efforts have been made to study chemical properties of cloud and fog waters. Most of studies have reported similar chemical composition to that of ambient aerosol with sulphate, chloride, nitrate, ammonium and sodium as the dominant inorganic ions in cloud and fog waters. More recently, a wide variety of organic compounds have been identified in cloud and fog waters ranging from small carbonyl compounds such as glyoxal and methylglyoxal to macromolecules such as humic like substances (HULIS). Although the formation processes of these organic compounds in cloud and fog waters is not fully understood, an aerosol cloud interaction likely plays an important role in the occurrence of these compounds in cloud and fog waters. Furthermore, multiphase chemical mechanisms likely contribute to the formation of these compounds in the cloud and fog waters. In the present study, we present first results of size resolved biological and biomass burning originating monosaccharides concentrations in cloud water and aerosol between September and October 2010 as part of Hill Cap Cloud Thuringia 2010 (HCCT-2010) campaign. The focus of the campaign was to study aerosol cloud interaction through orographic cloud that formed at Mt. Schmücke, Germany. The samples collected during the campaign contained monosaccharides at non-negligible levels. A comparison of 5 stage Berner impactor aerosol samples taken at upwind and downwind sites indicates that more effective scavenging of PM10 bound biological monosaccharides (i.e. arabitol and glucose) than PM1 bound biomass burning originating levoglucosan (Figure 1).

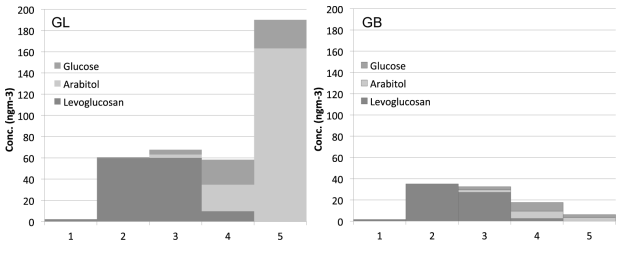

Figure 1. The composition of size resolved aerosol samples collected at the downwind site (Goldlauter, GL) and upwind site (Gehlberg, GB) on 14 September 2010 with a Berner type impactor with 50% cut-offs at 0.05, 0.14, 0.42, 1.2, 3.5 and 10 mm aerodynamic diameter (Dpa).

Similarly to the aerosol samples, the concentrations of arabitol and glucose were found at elevated levels in larger droplet fraction of the cloud water samples (Figure 2). Figure 3 shows the time series of size fractionated monosaccharide concentrations in the cloud water samples during 14 September 2010. The concentrations of all three monosaccharides increased steeply towards the night, especially arabitol and glucose in 20 μm droplet. This is consistent with earlier reports about inorganic ions that the chemical size distribution of aerosol is partly kept during the activation and growth processes (e.g. Collett *et al.*, 1993), with larger particles being more readily activated to cloud droplets.

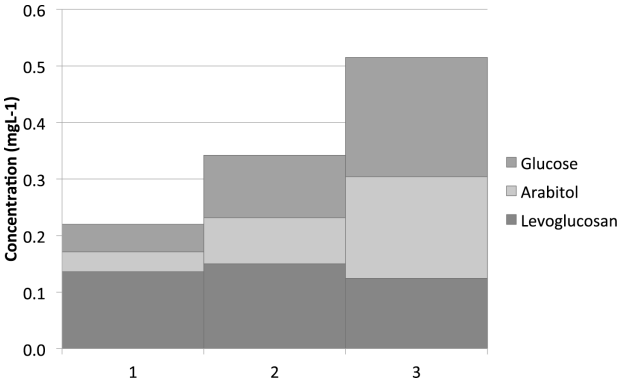

Figure 2. The composition of size resolved cloud water samples collected on 14 September 2010 at the Schmücke site with 50% cut-offs at 4, 16, and 20 mm aerodynamic diameter (Dpa).

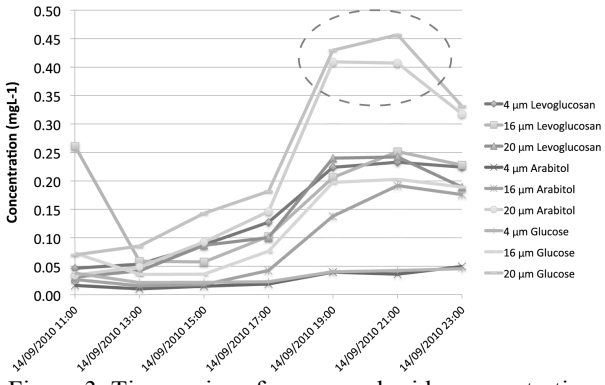

Figure 3. Time series of monosaccharide concentrations for the size fractionated cloud water samples collected on 14 September 2010 at the Schmücke site.

References

Collett, J., B. Oberholzer, and J. Staehelin (1993) *Atmos Env*, DOI: 10.1016/0960-1686(93)90068-A

Trace metal characterization during HCCT2010

K. Wadinga Fomba, K. Müller, T. Lee[2], J. Collett Jr.[2], H. Herrmann

[1]Leibniz-Institute for Tropospheric Research (IfT), permoserstr.15, 04318 Leipzig, Germany
[2]Department of Atmospheric Science, Colorado State University, Ft. Collins, CO, 80523, USA

Keywords: cloud water, TMI, iron
Presenting author email: Fomba@tropos.de

Trace elements in aerosols and cloud water are useful tools to study important processes that govern aerosol behavior. Soluble trace metals especially transition metal ions are known to influence the redox processes in atmospheric aqueous phase systems. Amongst others, they are known to strongly influence the HO_x cycle as well as the sulfur budget (Deguillaume, 2005).

To better understand the role these metals played during the Hill Cap Cloud Thuringia (HCCT) 2010 campaign in Thüringer Wald (Germany), trace metals and transition metal ions (TMI) analysis in aerosols and bulk and size resolved cloud water have been performed. The measured transition metals ions were Fe (III), Fe (II), Cu (II), Mn (II), Ni (II) and Zn (II), using a Dionex ICS 900 ion chromatography. The trace metals Al, Si, Ca, Ti, V, Co, Cd, Mn, Fe, Mo, Sr, Pb, Zn, Cu were analyzed using total reflection x-ray fluorescence spectroscopy (TXRF).

Figure 1 shows the hourly TMI concentration in cloud water observed during the first cloud events on the 14th of September 2010. The figure shows typical TMI concentrations observed throughout the campaign. The concentrations obtained during the whole campaign for the TMI's (iron 0.1 to 1.8 µM) where within expected range for cloud water (Deguillaume, 2005; K. Plessow, 2001).

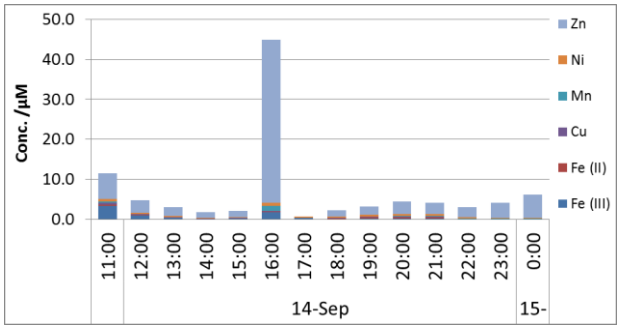

Figure 1. Hourly TMI concentration profile in cloud water during the first day of HCCT2010

Zinc was found to be the most abundant element in the cloud water with periods of high zinc concentration correlated with westerly air masses that traveled through regions of high industrial activities. The soluble iron was about 4 % of the total iron in the cloud water implying a significant amount of the iron was mobilized from the crust. Nevertheless, most of the observed soluble iron was present in the Fe (III) redox state compared to Fe (II) state except for some periods wherein the cloud was exposed to a high UV radiation during which higher Fe (II) concentrations compared to Fe (III) were observed.

Our results show indication of photochemical processes occurring during day time cloud events that influence iron processing. However, no strong correlation could be found between the HO_x cycling and the iron redox state processing.

Via estimation of crustal enrichment factors, the anthropogenic contribution to the cloud water concentration was obtained. Iron showed good correlation with other crustal elements such as Ti, Si and Al while no correlation with iron and higher enrichment factors were observed for elements like V, Co, Cd, Sr, Pb, Zn, Cu, indicating their likely anthropogenic origin.

The difference in the origin of the metals was further observed from the TMI measurements of the size resolved cloud water samples. Different size distributions were observed for Zn, Ni, and Cu which were mostly found in the second and third stages in comparison to iron species which were mostly found in the second and first stages. These differences in size distribution and enrichment factor comparison show that the observed metals during the campaign were of mixed origin.

K. Plessow, K. Acker, H. Heinrichs, D. Möller (2001), *Atmos. Environ.* **35**, 367-378
Deguillaume, L., M. Leriche, K. Desboeufs, G. Mailhot, C. George, and N. Chaumerliac. (2005). *Chem. Rev.***105**, 3388-3431.

Cloud influence on local aerosol chemical composition during the Hill Cap Cloud Thuringia 2010

L. Poulain [1], Z.J. Wu [1], A. Tilgner [1], D. van Pinxteren [1], B. D' Anna [2], C. George [2], J. Schneider [3], A. Wiedensohler[1] and H. Herrmann[1]

[1] Leibniz-Institut für Troposphärenforschung, 04318 Leipzig, Germany
[2] Université Lyon 1, CNRS, UMR5256, IRCELYON, Institut de Recherches sur la Catalyse et l'Environnement de Lyon, 69629 Villeurbanne, France
[3] Max Planck Institute for Chemistry, Particle Chemistry Department, 55128 Mainz, Germany

Keywords: AMS, Aerosol cloud interaction, particle characterization, PM1.
Presenting author email: poulain@tropos.de

The impact of orographic clouds to the local aerosol chemical composition was measured during the Hill Cap Cloud Thuringia 2010 (HCCT-2010) field campaign, which took place in September/October 2010 at the Schmücke mountain ridge in the Thuringia forest (Germany). The main objectives of the HCCT-2010 project were to assess the effects of clouds on particle composition, gas phase oxidant budget, changes of hygroscopic properties and activation of aerosol particles. Three sampling sites were equipped: one on the top of the Schmücke Mountain, where clouds were sampled, and two valley stations located upwind and downwind of the summit. In total, four Aerodyne ToF-AMSs were deployed during the campaign. One at each valley station and two at the summit station: one downstream of a Cloud Virtual Impactor (CVI) for droplet residual analysis and one to measure interstitial particles. Based on air mass trajectories, gas tracer experiments and meteorological parameters, it is possible to identify periods during which the air mass of the three stations were connected. The overflow periods were divided in two subsections corresponding to the presence of cloud at the summit station (Full Cloud Events, FCE) and to the absence (Non Cloud Events, NCE) of cloud at the summit station. For these two categories of connected flow, the AMS results were compared in order to follow the cloud induced modification of the aerosol chemical compositions as well as modification of the chemical size distribution.

AMS results were successfully compared according to instrumental uncertainties and possible particle loss and dilution effects between the stations during the NCE periods and to the bulk chemical composition measured at the three stations show similar mass fraction. The comparison of the two valley stations is presented in Figure 1. Because the results measured at the three stations during NCE events were comparable, the same approach could be directly used to investigate aerosol cloud interaction and influence of clouds to local particles. Figure 1 also shows the first results of the comparison between the upwind and downwind station during several FCE periods. The scatter plots suggest a possible change on the bulk chemical composition of the particles corresponding to a small decrease of the particulate nitrate fraction as well as a tiny increase of sulfate. Details on the aerosol changes during the different cloud events including a comparison of the organic components as well as chemical size resolved will be presented.

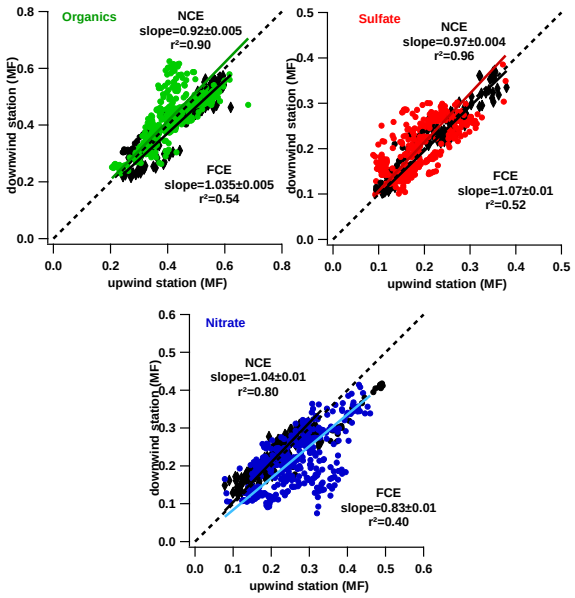

Figure 1: Scatter plots of the organics, sulphate and nitrate mass fraction measured at the upwind and downwind stations during NCE (black) and FCE (color). Regression slopes were calculated using orthogonal linear fitting.

Particle hygroscopicity during atmospheric new particle formation events: Implications for the chemical species contributing to particle growth

Z.J. Wu, W. Birmili, L. Poulain, M. Merkel, B. Fahlbusch, D. van Pinxteren, H. Herrmann, A. Wiedensohler
Leibniz Institute for Tropospheric Research (IfT) Leipzig
Keywords: New particle formation, hygroscopicity, HCCT
Presenting author email: wuzhijun@tropos.de

New particle formation (NPF) is an important source of atmospheric particles and likely contributes to the balance of optically active particles and cloud condensation nuclei. However, the mechanisms of atmospheric nucleation and particle subsequent growth still remain unclear. In this abstract, we will present the observations on NPF events at a mid-level mountain site in Germany during the field experiment HCCT-2010 (Hill Cap Cloud Thuringia 2010) to analyze the growth process of newly formed particles based on the hygroscopicity measurements.

During the HCCT campaign, a total of two NPF events with different features could be characterized in much detail. The particle number size distribution and meteorological parameters are shown in Fig. 1. The particle hygroscopic growth of nucleation mode was investigated to deduce the chemical species contributing to particle growth during NPF events. The results are given in Fig.2. A significant difference in particle hygroscopicity was observed between the two NPF events, indicating that the chemical species driving particle growing were not exactly the same. During both events, the hygroscopic growth of newly formed particles decreased with particle growing. This means that the condensing vapors changed during the particle growth process from more to less hygroscopic vapors.

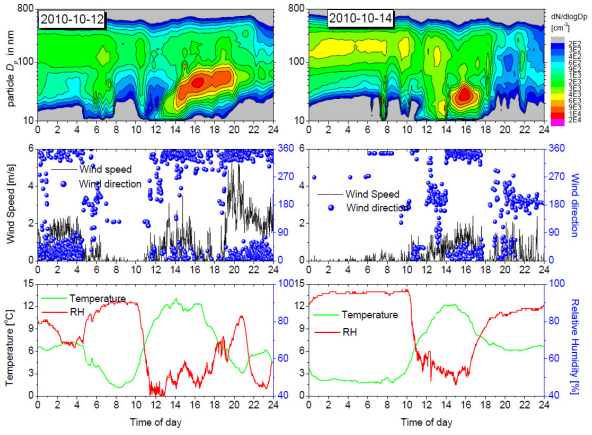

Fig. 1: The evolution of particle number size distribution and weather conditions during NPF events on 12 and 14 October, 2010.

An analysis of High Resolution-Time of Flight-Aerosol Mass Spectrum (AMS) data confirmed that sulfate may have played a more pronounced role in the first NPF case featuring a clear growth process. The contribution of sulfuric acid condensation to the soluble fraction was estimated. Result shows that a larger soluble fraction are failed to be explained by H_2SO_4 condensation, indicating that some other soluble compound contributing to the particle growth. Recently, Smith and coworkers (2010) have shown that alkylammoniumcarboxylate salts account for 20–50% of the mass of freshly nucleated particles in locations that include Atlanta, Mexico City, Boulder, and Hyytiälä, while sulfates account for only about 10%. That new finding may explain the miss source of the soluble fraction.

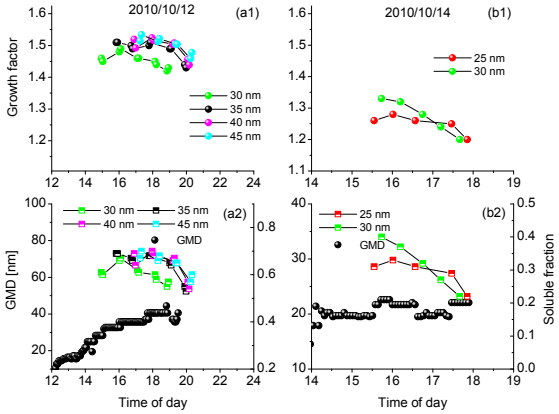

Fig. 2: The temporal evolution of geometric number mean particle diameter (GMD), growth factor, and the soluble equivalent fraction during the two NPF events. Time is indicated in CET.

This work was supported by German Research Foundation

Smith, J. N., Barsanti, K. C., Friedli, H. R., Ehn, M., Kulmala, M., Collins, D. R., Scheckman, J. H., Williams, B. J., and and McMurry, P. H.: Observations of aminium salts in atmospheric nanoparticles and possible climatic implications, Proceedings of the National Academy of Sciences of the United States of America, 6634-6639, 2010.

The effect of cloud processing on the chemical composition and mixing state of accumulation mode aerosol: A combined SEM-NanoSIMS study during HCCT 2010

B. Sinha[1,2], E. Harris[1], P. Hoppe[1], S. Mertes[3], T. Gnauk[3], J. Schneider[1], D. van Pinxteren[3] and H. Herrmann[3]

[1]Department of Particle Chemistry, MPI for Chemistry, Mainz, Hahn-Meitner-Weg 1, 55128, Germany
[2]Department of Earth Sciences, IISER, Mohali, Sector 81 SAS Nagar, 140306 Manauli PO, India
[3] Leibniz-Institute for Tropospheric Research, Leipzig, Permoserstrasse 15, 04318, Germany
Keywords: aerosol, single particle analysis, CCN properties, mixing state.
Presenting author email: baerbel.sinha@mpic.de

Clouds play a crucial role for physical and chemical processes in the atmosphere. During HCCT, a lagrangian-type field experiment, an orographic cloud is used as a natural flow-through reactor to study in-cloud aerosol processing. Three measurement sites were installed at Schmücke Mountain in Thuringia, Germany: An upwind site, which served for the characterisation of incoming air masses, an in-cloud site on the Schmücke summit, and a downwind site, where under appropriate meteorological conditions air masses after their passage through a hill cap cloud could be studied. Particles were collected at all three stations on gold coated Nuclepore filters mounted in a stacked filter unit. At the in-cloud site droplet residues and interstitial particles were collected separately.

Elemental composition, morphology and mixing states of aerosol particles were determined using SEM-EDX and NanoSIMS for one nighttime and one daytime cloud event using the methodology described in Sinha *et al* (2008) and Sinha *et al* (in prep.).

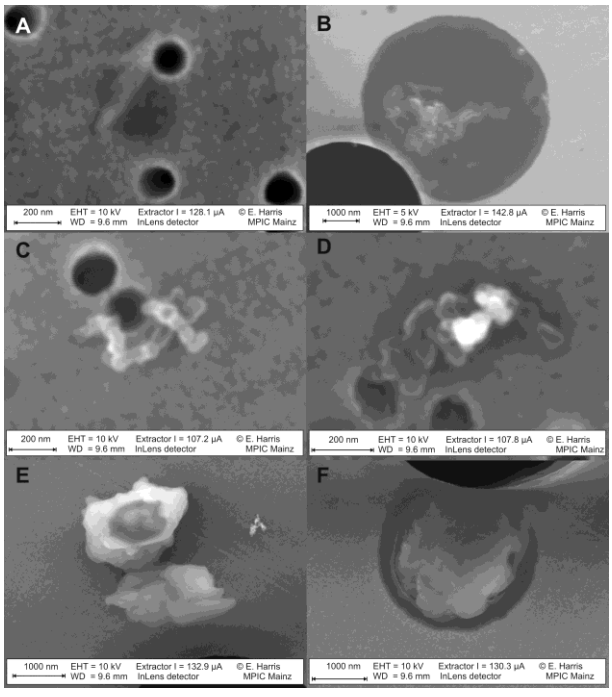

Fig.1: Particle types encountered during HCCT 2010. A) fine mixed SOA/SIA particles, B) coarse mixed SOA/SIA particles, C) soot, D) soot with SOA coating, E) mineral dust, F) mineral dust with SOA coating

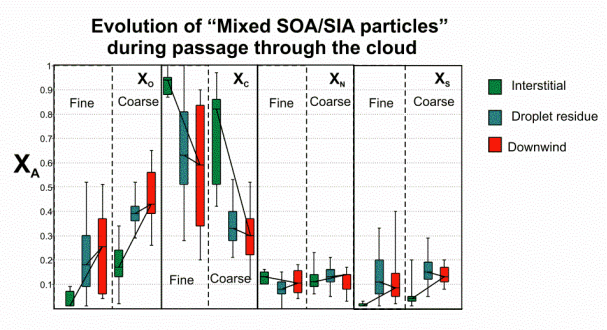

Fig. 2: Evolution of the composition of SOA/SIA particles from the in-cloud to the downwind station

The particle number distribution is dominated by secondary aerosol particles with a high fraction of organic aerosol (SOA). However, secondary aerosol particles are typically mixed in nature, i.e. they contain a secondary inorganic component (SIA). The inorganic fraction in secondary droplets is higher during the daytime event resulting in a smaller activation diameter of the mixed SOA/SIA particles during daytime (80±8 nm) compared to the nighttime event (116±12).

The inorganic fraction is larger in coarse compared to the fine mixed SOA/SIA particles and increases during the passage through the cloud while the organic fraction decreases. The SIA is added to the particles which activated (droplet residues).

Soot particles without coatings were not CCN active at night. During day all soot particles were coated with SIA. The CCN properties of coated soot depended on the amount of soluble material present in the coating and were independent of the size of the primary soot core. Once activated soot particles accumulated additional SIA during the passage of the cloud and coarse soot particles showed signs of repeated processing prior to reaching the site.

This work was supported by the Max Planck Society and by the Max Planck Graduate Center Mainz.

Sinha, B., Hoppe, P., Huth, J., Foley, S. and M. O. Andreae, M. O. (2008) *Atmos. Chem. Phys.*, 8, 7217–7238, 2008.

Sinha, B., Pöhlker, C., Wiedemann, K., Harris, E., Hoppe, P., Kilcoyne A. L. D., Andreae, M. O., Gunthe, S. S., Pöschl, U. and Borrmann, S. (in prep. for AMT, 2012)

Physico-chemical analysis of cloud drop residues and interstitial particles sampled inside clouds within the Hill Cap Cloud Thuringia (HCCT) Experiment 2010

S. Mertes[1], J. Schneider[2], R. Otto[1], K. Diekmann[1], W. Birmili[1], D. van Pinxteren[1], A. Roth[2], Frank Stratmann[1], and H. Herrmann[1]

[1]Leibniz Institute for Tropospheric Research, 04318 Leipzig, Germany
[2]Particle Chemistry Department, Max Planck Institute for Chemistry, 55128 Mainz, Germany
Keywords: Aerosol cloud interaction, Phase partitioning, Cloud processing, Counterflow virtual impactor.
Presenting author email: stephan.mertes@tropos.de

Activation, phase partitioning, and cloud processing of ambient aerosol particles in low continental clouds were investigated during the Hill Cap Cloud Thuringia field experiment (HCCT-2010) in central Germany during September and October 2010. The measurement area is located in the low mountain range "Thüringer Wald" and included the mountain ridge cloud site Schmücke (938 m asl) and an upwind and a downwind site, respectively.

Inside clouds that prevailed at the mountain ridge site, an interstitial inlet and two counterflow virtual impactors (CVI) were operated side by side in order to separate and collect interstitial particles (IP) and cloud drops (Mertes et al., 2005). Inside the CVI systems the collected cloud drops are evaporated releasing dry cloud drop residues (CDR), which are closely related to the original cloud condensation nuclei forming the clouds. Downstream the inlets, microphysical and chemical properties of IP and CDR were simultaneously determined by two sets of instruments connected to each inlet type.

Here we present results from measurements of IP and CDR number concentration (CPC), size distribution (SMPS and OPC), mass concentration of non-refractory substances (C- and HR-ToF-AMS, filter analysis), and black carbon (PSAP, MAAP). Moreover, cloud microphysical parameters like liquid water content, effective drop radius and drop concentration were detected by a PVM and a FSSP, respectively.

The phase partitioning of particle number concentration N_P and mass concentrations of chemical species is derived by the respective CDR concentration divided by the total concentration, CDR+IP. The obtained results are shown in Figure 1 for eight different cloud events, which are identified as periods of connected flow between upwind, summit, and downwind site. It was found that 10 to 30 % of the abundant particles were activated to cloud droplets. Concerning black carbon (BC) an equal distribution between both phases is observed (phase partitioning between 40 and 60 %), but two times more than 80 % of the BC mass was found in the CDR, which is surprisingly high for hydrophobic substances. Nitrate and ammonium have always the highest activated fractions, whereas for organic matter (OM) and sulphate this fraction varies substantially between 60 and 95 %. These findings are evaluated in more detail with respect to absolute concentrations, mixing states, cloud microphysics, air mass history and upwind/downwind measurements.

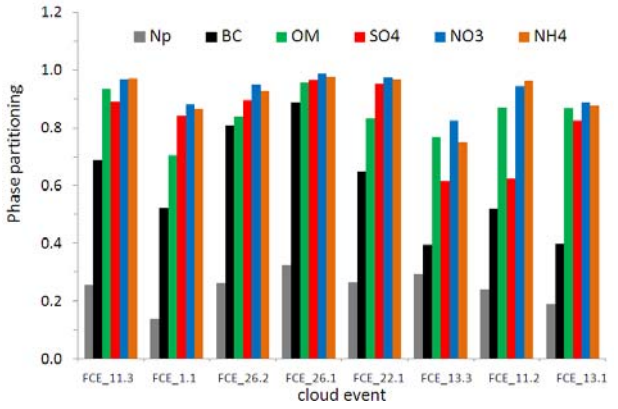

Figure 1. Partitioning between droplet and interstitial phase of particle number N_P and mass concentration of several chemical compounds indicated in the legend.

Typical number size distributions of CDR and IP measured with two SMPS are shown in Figure 2. From these results, the activation diameters of the cloud events are inferred ranging roughly between 100 and 200 nm.

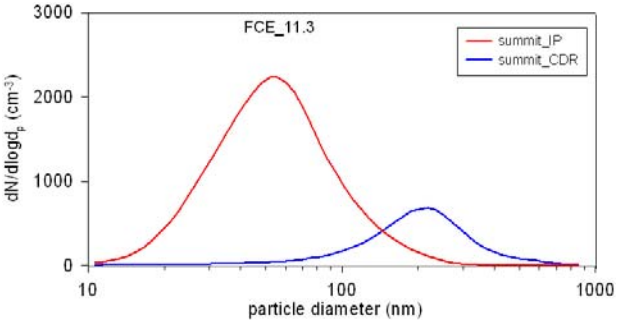

Figure 2. Mean IP and CDR number size distribution during cloud event FCE_11.3.

For the cloud events with connected flow between the three sites, the in-cloud particle number size distributions as well as the activation diameters will be compared to the total particle number size distributions (SMPS) and particle activation measurements (CCN counters) in the upwind and downwind site, which means in the inflow and outflow of the clouds.

Mertes, S., Lehmann, K., Nowak, A., Massling, A. and Wiedensohler, A. (2005). *Atmos. Environ.*, **39**, 4247-4256.

Meteorological characterisation of the HCCT-2010 hill cap cloud experiments: Synoptic and local meteorological conditions, tracer experiments and flow connectivity

A. Tilgner, L. Schöne, P. Bräuer, D. van Pinxteren, H. Deneke, W. Birmili, R. Otto, M. Merkel, K. Weinhold, A. Wiedensohler, G. Spindler, and H. Herrmann

Leibniz-Institut für Troposphärenforschung, Permoserstr. 15, Leipzig, 04318, Germany
Keywords: meteorology, aerosol cloud interaction
tilgner@tropos.de

To study aerosol-cloud interactions in more detail, Lagrangian-type field experiments, where an orographic cloud is used as a natural flow-through reactor, were performed. In Sept./Oct. 2010, the Lagrangian-type cloud passage experiment HCCT-2010 (Hill Cap Cloud Thuringia 2010) was conducted at Mt. Schmücke in Thuringia, Germany (see Figure 1) due to the utmost probability of the occurrence of warm orographic clouds and the south-westerly incoming flow perpendicular to the mountain range. These two conditions are essential for the experimental design (Herrmann et al., 2005). The philosophy is based on the connected flow between the two valley stations via Mt. Schmücke including an orographic hill cap cloud. Hence, the quality of such cloud passage experiments strongly depend on the meteorology and particularly on the flow connectivity between the measurement sites (see Tilgner et al., 2005; Heinold et al., 2005).

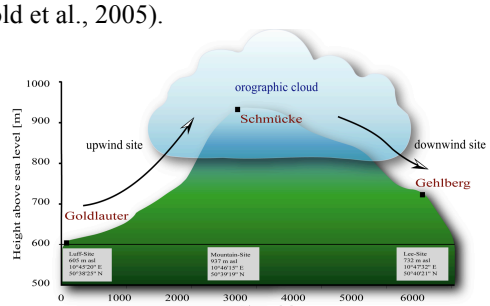

Figure 1. Schematic representation of the campaign area of the cloud passage experiment HCCT-2010.

At first, the meteorological characterisation was focused on the evaluation of large-scale conditions with particular emphasis on the incident flow conditions and on the separation of orographic and non-orographic clouds. In the case of the flow characterisation, weather charts and calculated backward trajectories are used to determine the horizontal wind pattern and the rawinsonde data for the vertical wind structure. Synoptic charts were analysed for detection of frontal processes, synoptic scale advection and air mass classification. Additionally, backward trajectories were used to identify the origin and characteristics of air masses reaching the experimental area, the sources for aerosols and constancy of the advection.

For the examination of the cloud conditions including the orographic character, satellite pictures of different spectral channels, rawinsonde observations of a nearby weather station as well as the measured liquid water content and cloud base height were evaluated. Furthermore, the meteorological and microphysical datasets of the three sites assisted the cloud analysis, the temporal detection of frontal-induced air mass change and the constancy of the local wind. Especially for the anticyclonic southwest weather-type (SWZAF), stable incoming flow conditions combined with orographic cloudiness were identified. In total, about 30% HCCT-2010 cloud event periods were characterised by orographic cloudiness and about 60% by clouds occurring associated to synoptic front systems.

In the following, the characterisation was devoted to further detailed local flow analyses. An analysis of the locally measured quasi-inert trace gas ozone and the measured aerosol particle distributions was intended to assure that measurements were performed in identical air masses and under connected flow conditions. By means of a comprehensive COD (Coefficient of Divergence) and cross-correlation analysis of the measured time series data of ozone and a selected particle number concentration interval, the links and the possible time delay between different measurement sites were investigated. The latter analysis was also done to characterise the typical flow times between the sites. Particularly, for days with constant south-westerly flow conditions, high wind speeds and less stable stratification strong link between the sites were found. Additionally to the above-mentioned investigations, relevant non-dimensional flow parameters such as the Froude number (Fr) were used to characterise the flow regime in mountainous terrain (Pierrehumbert and Wyman, 1985). By means of scale analysis of the calculated Fr, the limiting or supporting flow parameters such as synoptical flow and the thermal stratification conditions were investigated. Moreover, data from locally performed tracer experiments using the inert gas SF6 were used for studies on transport processes in the experimental site.

Finally, a qualitative classification results in 6 out of 10 cloud events, which relatively well conform the philosophy of the cloud passage experiment, and which provided the basis for subsequent investigations of the obtained HCCT-2010 dataset.

This work was supported by the German Research Foundation (DFG, He 3086/15-1).

References:

Herrmann, H. et al. (2005) *Atmos. Environ.* **39** (23-24), 4169-4183.
Heinold, B. et al. (2005) *Atmos. Environ.* **39** (23-24), 4195-4207.
Pierrehumbert, R.T., Wyman, B. (1985). *J. of Atmos. Sciences*. **42**, 977-1003.
Tilgner, A. et al. (2005) *Atmos. Environ.* **39** (23-24), 4185-4194.

Cloud chemistry during HCCT-2010: Mono- and dicarboxylic acids

Dominik van Pinxteren[1], Monique Teich[1], Stephan Mertes[1], Taehyoung Lee[2], Jeff Collett[2], Hartmut Herrmann[1]

[1]Leibniz-Institut für Troposphärenforschung, Permoserstr. 15, 04318 Leipzig, German
[2]Colorado State University, Department of Atmospheric Science, Fort Collins, CO 80523, USA

Keywords: cloud chemical composition, organic acids, field campaign
Presenting author email: dominik@tropos.de

Hill Cap Cloud Thuringia 2010 (HCCT-2010) was a complex field campaign on aerosol cloud interaction, performed at Mount Schmücke in central Germany in September and October 2010. Cloud water was sampled on a tower, 20 m above ground, using different cloud water collectors: The Caltech Active Strand Cloud Water Collector (CASCC2, [*Demoz et al.*, 1996]) sampled bulk cloud water with a 50 percent droplet size cut (D_{50}) of 3.5 µm and a one hour time resolution. A 3-stage version of the CASCC [*Raja et al.*, 2008] was applied to sample size-resolved cloud water with D_{50} of 22, 16, and 4 µm diameter for stages 1, 2, and 3, respectively. Additionally, a 5 stage collector [*Moore et al.*, 2002] was used with D_{50} of 30, 25, 15, 10, and 4 µm for stages 1 to 5. Due to the lower amounts of cloud water available in the different droplet size classes, the multistage collectors usually sampled 2-hourly (3-stage) and 4-hourly (5-stage) cloud water samples.

In addition to the liquid cloud water samples, droplet residuals and interstitial particles were collected on filters downstream of a counterflow virtual impactor (CVI) and an interstitial inlet (INT) [*Mertes et al.*, 2005]. The samples were analysed for short-chain mono- and dicarboxylic acids (C1-C5) using capillary electrophoresis with indirect UV detection. Additionally, a suite of longer-chain (C5-C10) functionalised carboxylic acids, i.e. acids with an additional functional group (hydroxy-, oxo-, or nitro-group) were determined by a relatively new technique based on hollow-fibre liquid phase microextraction and capillary electrophoresis – mass spectrometry.

The concentration ranges of short-chain carboxylic acids are given in Figure 1. Formic and acetic acid usually showed the highest concentrations, followed by oxalic acid. The concentrations of longer-chain functionalised acids are generally 1-2 orders of magnitude lower. Many of the compounds are reported for the first time in cloud water samples.

The dataset will be discussed with regards to cloud microphysical and meteorological parameters. For the short-chain acids, results from size-resolved cloud water sampling will be presented as well. Additionally, the phase partitioning of the most abundant short-chain diacids, obtained from the CVI and INT filters, will be discussed.

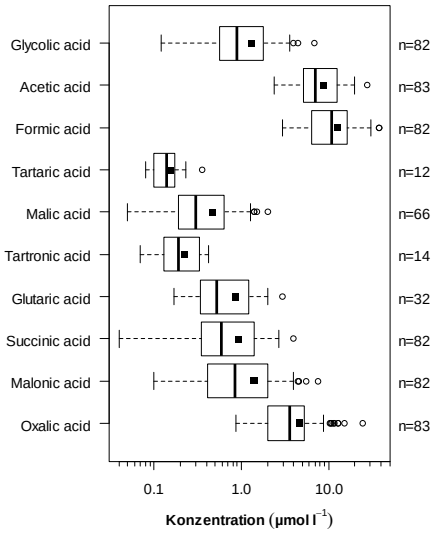

Figure 1: Concentrations of short-chain carboxylic acids

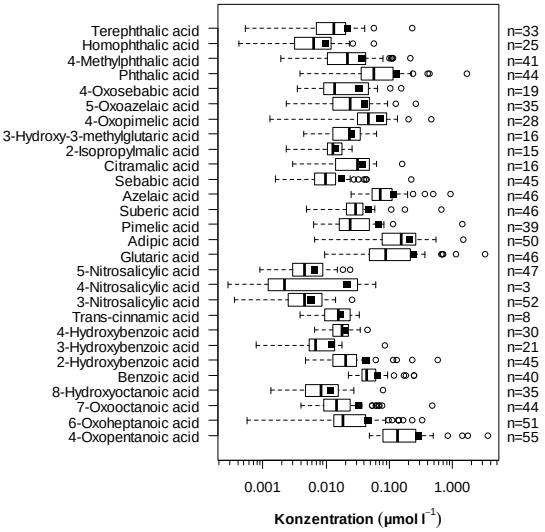

Figure 2: Concentrations of longer-chain acids

Demoz, B. B., J. L. Collett, and B. C. Daube (1996), *Atmos. Res.*, *41*(1), 47-62.

Raja, S., R. Raghunathan, X. Y. Yu, T. Y. Lee, J. Chen, R. R. Kommalapati, K. Murugesan, X. Shen, Y. Qingzhong, K. T. Valsaraj, and J. L. Collett (2008), *Atmos. Environ.*, *42*(9), 2048-2061

Moore, K. F., D. E. Sherman, J. E. Reilly, and J. L. Collett (2002), *Atmos. Environ.*, *36*(1), 31-44.

Mertes, S., D. Galgon, K. Schwirn, A. Nowak, K. Lehmann, A. Massling, A. Wiedensohler, and W. Wieprecht (2005), *Atmos. Environ.*, *39*(23-24), 4233-4245.

Cloud chemistry during HCCT-2010: Water soluble organic carbon

Dominik van Pinxteren[1], Stephan Mertes[1], Johannes Schneider[2], Stephan Borrmann[2], Taehyoung Lee[3], Jeff Collett[3], Hartmut Herrmann[1]

[1]Leibniz-Institut für Troposphärenforschung, Permoserstr. 15, 04318 Leipzig, Germany
[2] Max Planck Institute for Chemistry, Joh.-J.-Becherweg 27, 55128 Mainz, Germany
[3]Colorado State University, Department of Atmospheric Science, Fort Collins, CO 80523, USA

Keywords: cloud chemical composition, DOC, field campaign
Presenting author email: dominik@tropos.de

In September/October 2010 the ground-based cloud experiment “Hill Cap Cloud Thuringia 2010” took place at Mount Schmücke in the Thuringian Forest, Germany. The chemical composition of clouds was studied by means of different sampling and analytical techniques. Four Caltech Active Strand Cloud Water Collectors (CASCC2, [*Demoz et al.*, 1996]) were applied to sample large volumes (up to 640 ml) of bulk cloud water with a 50 percent droplet size cut (D_{50}) of 3.5 µm and a one hour time resolution. Additionally, two multistage versions of the CASCC were used. A 3-stage collector [*Raja et al.*, 2008] with D_{50} of 22, 16, and 4 µm diameter for stages 1, 2, and 3, respectively, and a 5 stage collector [*Moore et al.*, 2002] with D_{50} of 30, 25, 15, 10, and 4 µm for stages 1 to 5. Due to the lower amounts of cloud water available in the different droplet size classes, the multistage collectors usually sampled 2-hourly (3-stage) and 4-hourly (5-stage) cloud water samples. All cloud water collectors were installed on top of a 20 m high tower.

To complement the liquid cloud water samples, droplet residuals and interstitial particles were sampled downstream of a counterflow virtual impactor (CVI) and an interstitial inlet [*Mertes et al.*, 2005] using filters and an aerosol mass spectrometer (AMS).

Water soluble organic carbon (WSOC) was measured as non-purgable organic carbon (NPOC) with a commercial TOC analyser (Shimadzu TOC-V) after filtration of the samples through 0.45 µm syringe filters. The samples were stored frozen in pre-cleaned plastic bottles until analysis.

As can be seen in Figure 1, the bulk water concentrations of WSOC were between 1.2 and 34 mgC l^{-1} with an average concentration of 6.2 mgC l^{-1}. From the size-resolved sampling with the 3-stage CASCC (Figure 2) it can be observed, that the smalles droplets (stage 3) typically have higher concentrations than the larger ones (stages 1 and 2).

The cloud water concentration data will be discussed with regards to cloud microphysical parameters (liquid water content, droplet size spectrum), meteorology, and air mass origin. Additionally, a comparison of WSOC concentrations from cloud water and CVI filters will be given, as well as the fraction of organics measured by the AMS behind the CVI that can be explained by WSOC.

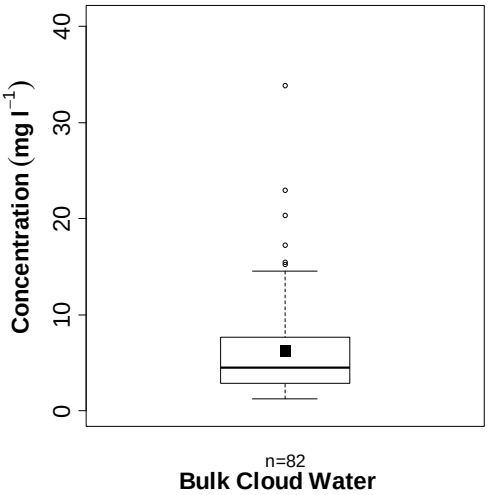

Figure 1: Bulk concentrations of WSOC in mg l^{-1}.

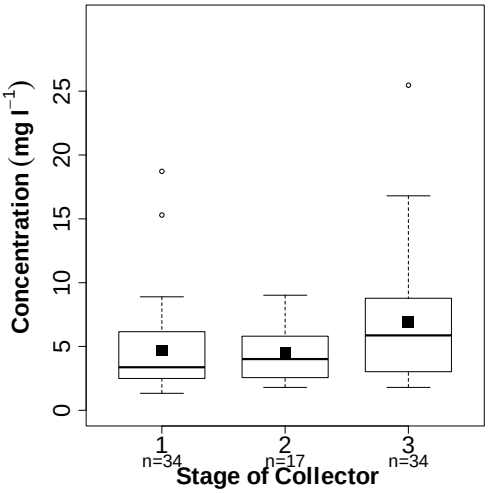

Figure 2: Size resolved concentrations of WSOC from 3-stage collector.

Demoz, B. B., J. L. Collett, and B. C. Daube (1996), *Atmos. Res.*, *41*(1), 47-62.

Raja, S., R. Raghunathan, X. Y. Yu, T. Y. Lee, J. Chen, R. R. Kommalapati, K. Murugesan, X. Shen, Y. Qingzhong, K. T. Valsaraj, and J. L. Collett (2008), *Atmos. Environ.*, *42*(9), 2048-2061

Moore, K. F., D. E. Sherman, J. E. Reilly, and J. L. Collett (2002), *Atmos. Environ.*, *36*(1), 31-44.

Mertes, S., D. Galgon, K. Schwirn, A. Nowak, K. Lehmann, A. Massling, A. Wiedensohler, and W. Wieprecht (2005), *Atmos. Environ.*, *39*(23-24), 4233-4245.

Concentrations of organic and trace element PM species and derivation of freeway-based emission rates in Los Angeles

J. Liacos[1], W. Kam[1], R.J. Delfino[2], J.J. Schauer[3] and C. Sioutas[1]

[1]Department of Civil and Environmental Engineering, University of Southern California, Los Angeles, CA, USA
[2]Department of Epidemiology, University of California-Irvine School of Medicine, Irvine, CA, USA
[3]Environmental Chemistry and Technology Program, University of Wisconsin-Madison, Madison, WI, USA
Keywords: Source apportionment, Emission rates, Sampling, Physico-chemical analysis
Presenting author email: sioutas@usc.edu

On-road particulate matter was collected during an in-vehicle sampling campaign in March-April of 2011 on two major Los Angeles freeways, 710 and 110. The 710 freeway is a major route for trucks traveling to and from the Ports of Long Beach and Los Angeles. The 110 freeway is a high-traffic route parallel to 710 but with a very low truck fraction. Two sets of samples were collected for each roadway, each set representing approximately 50 hours of on-road sampling. Concurrent sampling at a fixed site at the USC's downtown L.A. campus provided estimates of urban background levels.

Chemical analysis was performed for elemental carbon (EC), organic carbon (OC), polycyclic aromatic hydrocarbons (PAHs), hopanes and steranes. On-road concentrations (mass per m^3) and freeway-based emission rates (ERs) (mass per km of roadway per hour) are presented here. These ERs are presented such that freeways could be analyzed as a line source of emissions, with implications for population exposure models for nearby communities.

Concentrations are compared to previous studies of fixed sites near 710, while ERs are compared to previous freeway and tunnel studies. Concentrations and ERs were generally lower on 110 than 710, findings consistent with the former's significantly lower truck fraction. Compared to previously reported values, current 710 concentrations were largely comparable for PAHs and hopanes but significantly lower for steranes. Current trace metal concentrations on both freeways were significantly higher, especially for Fe, Cu, and Ba.

Current ERs for light molecular weight PAHs are much higher on 710 than 110, while ERs for heavy MW PAHs are more comparable. Compared to previously reported values, current 110 PAH ERs are significantly lower; current 710 PAH ERs are comparable; current 110 hopane and sterane ERs are generally comparable (with trisnorhopane significantly lower and homohompanes significantly higher); current 710 hopane and sterane ERs are comparable (but significantly lower for trisnorhopane, norhopane, bishomohopanes, and sitostane); both freeway metal and trace element ERs were lower for Mg, P, and K, but higher for Fe and Cu.

Table 1. Trace element emission rates from current and previous studies.

	110 (Current)	710 (Current)	710 (previous)
Mg	685.6	601.2	1042.0
P	162.3	123.6	589.0
S	1040.2	0.0	12821.5
K	624.0	146.8	860.8
Ca	2044.7	2346.3	2537.1
V	0.0	7.4	90.6
Mn	110.4	119.3	45.3
Fe	14787.2	16448.0	7611.4
Ni	5.6	7.4	45.3
Cu	1002.2	630.9	362.4
Zn	324.9	268.5	317.1
Mo	39.8	37.5	45.3
Ba	1444.7	1812.3	1268.6
Pb	9.8	0.4	90.6

Emission rates (ug/(km*hr)). Previous values from Ning et al. (2008)

This work was supported by the US EPA and the California Air Resources Board.

Ning, Z., Polidori, A., Schauer, J.J., and Sioutas, C. (2008) *Emission factors of PM species based on freeway measurements and comparison with tunnel and dynamometer studies,* Atmospheric Environment **42**, 3099-3114.

The impact of harbour activities on the air quality of the city of Genoa: source apportionment and simulation by dispersion models

P. Brotto[1], M.C. Bove[1], F. Cassola[1], E. Cuccia[1], D. Massabò[1], A. Mazzino[1], A. Piazzalunga[2] and P. Prati[1]

[1]Department of Physics & INFN, University of Genoa, Italy
[2]Department of Environmental and Territorial Science, University of Milan-Bicocca

Keywords: PM2.5, source apportionment, PMF, Eulerian dispersion modelling, harbour emissions,
Presenting author email: brotto@fisica.unige.it

In the framework of local and international projects, the Department of Physics of the University of Genoa is involved in the evaluation of the impact of on the urban air quality. Among the others, the Programme MED APICE project (http://www.apice-project.eu/) aims at the evaluation of the impact of harbor activities on urban air quality and the definition of strategies to reduce air pollution in port cities. In this frame, the year 2011 was devoted to monitoring campaigns, in particular addressing the Particulate Matter (PM) levels, composition and sources, in the five cities joining the project (Barcelona, Genoa, Marseille, Thessaloniki and Venice).

The monitoring activities were addressed to the source apportionment in each study area and to the set-up of numerical tools able to reproduce the experimental results. In Genoa, this turned out in a PM2.5 sampling campaign with daily samples collected in three sites for a 6-month period (May-October 2011). Subsequent compositional analyses (anions, cations, metals, EC/OC) produced a large database for a receptor model analysis through Positive Matrix Factorization (Paatero, 1994) and the comparison with numerical dispersion models. PM2.5 samples were collected on daily basis and in the same period in three sites in the urban area of Genoa (namely: Bolzaneto, C.so Firenze and Multedo) selected considering the direction of prevailing wind. Also, a meteorological and air quality modelling system was implemented, based on the mesoscale NWP model WRF (Skamarock 2008) and the Eulerian CTM CAMx (ENVIRON 2010) Through subsequent nestings, meteorological and pollutant concentration fields are obtained up to resolutions of order of 1 km.

A large amount of data has been collected and is now under analysis while simulations are running in order to get results over the whole monitoring period. Some discussion can be already done about what has been preliminary observed.

Despite of a distance of several kilometers and of the quite complex topography of the area, the time trends of PM2.5 daily concentration values measured in the three sites are very well correlated and have the same mean value over the six month period of sampling (see Figure 1). Interesting results has been obtained by analysing the correlation between the concentration values of V and Ni, typical tracers of heavy oil combustion and therefore of ship emissions, which have shown the same average ratio in the three monitoring sites, consistent with values previously observed in the urban area of Genoa (Mazzei *et al.*, 2008 and references therein).

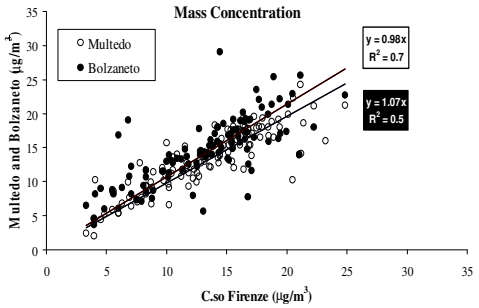

Figure 1. Correlation study among the PM2.5 data sets for the three sites in Genoa

The effect of transport phenomenon has been clearly evidenced by the comparison of concentration values observed in the two near-harbour sites (Multedo and C.so Firenze) with respect to Bolzaneto, a few km inlands. Furthermore, a strong correlation has been observed with wind directions while no correlation turns out between the time series of the concentration of one of the two elements measured in two different sites this suggesting that the dispersion of ships emission from the harbour is driven by meteorological conditions.

The full results of the source apportionment performed with PMF and with the Eulerian models will be given.

This work was supported by the Programme MED under the APICE grant.

ENVIRON 2010 *User's Guide, Comprehensive Air Quality Model with Extensions (CAMx). Version 5.30*, ENVIRON International Corporation, Novato, CA.

Mazzei, F., D'Alessandro, A., Lucarelli, F., Nava, S., Prati, P., Valli, G., Vecchi, R. 2008. *Characterization of particulate matter sources in an urban environment*. The Science of the Total Environment 401, 81-89.

Paatero, P., Tapper, U., 1994. *Positive matrix factorization: a non-negative factor model with optimal utilization of error estimates of data values.* Environmetrics 5, 111-126

Skamarock, W. C., Klemp, J. B., Dudhia, J., Gill, D. O., Barker, D. M., Huang, X. Z., Wang, W., Powers ,J. G. 2008. *A Description of the Advanced Research WRF Version 3. Technical report, Mesoscale and Microscale* Meteorology Division, NCAR, Boulder, Colorado

Assessment of vehicular profiles vis-à-vis real-world traffic emissions

Pallavi Pant[1] and Roy M. Harrison[1,2]

[1] Division of Environmental Health and Risk Management, School of Geography, Earth and Environmental Studies, University of Birmingham, Edgbaston, Birmingham, B15 2TT, United Kingdom
[2]Centre of Excellence in Environmental Studies, King Abdulaziz University, PO Box 80203, Jeddah (21589) Saudi Arabia
Keywords: Traffic, PM and source apportionment, PM 2.5, Receptor model
Presenting author email: r.m.harrison@bham.ac.uk

Road traffic emissions, both exhaust and non-exhaust contribute significantly to particulate matter concentrations in urban areas. In the current milieu, much attention is being paid towards an improved understanding of these emissions and their contribution to overall PM concentrations.

Receptor modelling, particularly the chemical mass balance model is one of the often-used tools for estimation of source contributions to concentrations of particulate matter in ambient air. Further, the chemical mass balance model relies to a large extent on the accuracy of the source profiles used as an input. However, in the absence of locally-relevant source profiles, the source contribution estimates can be prone to erroneous results. Further, in recent years, significant differences have been observed between laboratory-tested and real-world mixed source traffic emissions (Ancelet et al., 2011; Yan et al., 2009).

To achieve the twin goals of assessing existing source profiles with respect to the ambient traffic emissions data and preparation of a mixed-source traffic profile for London, samples were collected at two different urban sites (background and roadside) in London, United Kingdom and it was assumed that if all other sources contribute to the same extent at both sites, the increment in marker concentrations would be due to traffic emissions. This approach has been used in previously published studies (Gietl et al., 2010; Pey et al., 2010). The traffic increment thus obtained was assessed in relation to existing profiles using ratio-ratio plots (Figure 1).

It was observed that there were significant differences between the (mainly U.S.) source profiles and the ambient data which can be attributed to differences in local conditions and vehicular technology. A European mixed-source traffic profile (El Haddad et al., 2009) was found to correspond best with one of the diesel profiles also finding a good fit with ambient data.

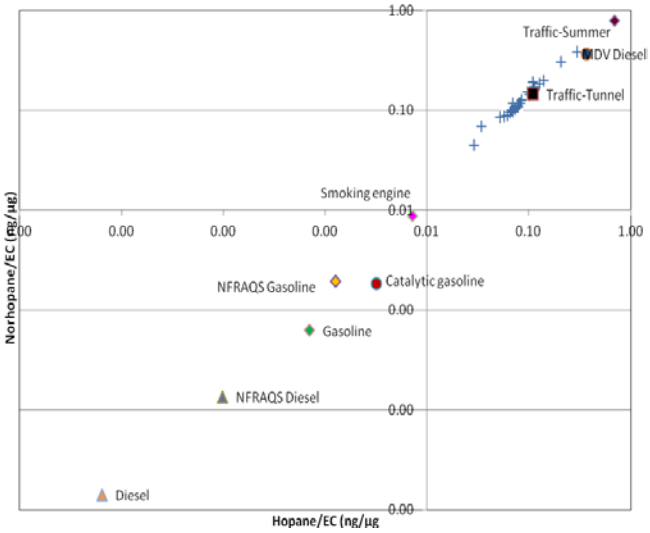

Figure 1. Ratio-ratio plot for ambient traffic increment data with published source profiles

Results indicate that mixed-traffic profiles might fare better for source apportionment using chemical mass balance. This might be due to their relative similarity to the real-world driving and emission conditions. The next step will be to use this mixed-traffic source profile to run the chemical mass balance model.

Pallavi Pant gratefully acknowledges financial support from the University of Birmingham.

Ancelet, T., Davy, P.K., Trompetter, W.J., et al. (2011) *Atmos. Environ.* 45(26), 4463-4469.
El Haddad, I., Marchand, N., Dron, J., Temime-Roussel, B., et al. (2009) *Atmos. Environ.* **43 (39)**, 6190-6198.
Gietl, J.K., Lawrence, R., Thorpe, A.J. & Harrison, R.M. (2010) *Atmos. Environ.* 44(2), 141-146.
Pey, J., Querol, X. & Alastuey, A. (2010) *Atmos. Environ.* 44(13), 1587-1596.
Yan, B., Zheng, M., Hu, Y., et al. (2009) *Environ. Sci. Technol*. 43(12) 4287-4293.

PMF vs CMB for source apportionment of PM: advantages, limitations, complementarity of the two models explored by applications at different types of environments

C. Piot[1,2], M.F.D. Gianini[3], J. Cozic[2], L. Polo[2,4], J.-L. Besombes[1], J.-L. Jaffrezo[2] and C. Hueglin[3]

[1]Université de Savoie-LCME, Le Bourget du Lac, France
[2]Université Joseph Fourier-CNRS-LGGE, St-Martin d'Hères, France
[3]EMPA, Materials Science and Technology, Duebendorf, Switzerland
[4]LTE, IFSTTAR, Bron, France
Keywords: source apportionment, Chemical Mass Balance, Positive Matrix Factorization.
Presenting author email: christine.piot@lgge.obs.ujf-grenoble.fr

Compliance with the tougher regulations of ambient particulate matter (PM) in the European Union will require detailed and quantitative information about the sources of PM. Such information can be provided by source apportionment studies based on determination of the chemical composition of PM and application of receptor models (RM). These RM can be applied to on-line measurements or off-line PM sampling. Off-line PM sampling is developing largely because of the ease of implementation, especially by air quality networks throughout Europe. From the off-line chemical characterization of PM, different RM have been proposed in the literature (see review of Viana *et al.*, 2008), including the Molecular Marker - Chemical Mass Balance (MM-CMB) and multivariate statistical models, e.g. Positive Matrix Factorization (PMF).

MM-CMB is commonly based on the organic speciation of PM while PMF is typically applied to major components, metals and traces elements. Given differences between the two models (mass balance or statistical analysis) and the chemical speciation used, identified sources and estimated contributions may be different and intercomparisons of these two models are necessary. Just a few of these intercomparisons have been published so far (Ke *et al.*, 2008 ; Shrivastava *et al.*, 2007). In this work, the two models were applied on the same set of PM10 samples collected in various types of environments and seasons, representing various sources and chemical composition of PM: urban background, urban kerbside, rural and alpine valley sites in France and in Switzerland.

Results obtained in the urban background site of Zurich (Switzerland) and in the rural site of Payerne (Switzerland) for the estimation of PM10 show a reasonable agreement between the two models (Fig. 1) particularly in winter and confirm the estimated contributions. Differences are observed in summer for vehicular emissions due probably to an underestimation of this source by CMB (organic tracers of this source are lower than limits of detection in this season). Estimations of secondary inorganic (sulphates and nitrates) and organic aerosols (SOA) are almost equivalent despite the method of estimation: in MM-CMB they are indirectly estimated while in PMF they represent some individual factors (containing inorganics and SOA in same factors).

The presentation will also cover comparisons of the estimation of OC and EC in various types of environments. From these comparisons, MM-CMB seems to be more adapted to primary organic sources and source apportionment of OC. PMF allows estimation of a greater number of inorganic sources but by reconstructing the total mass of PM it can overestimate the fraction of each source. All this will be discussed in the presentation focusing on the complementarity of the two models.

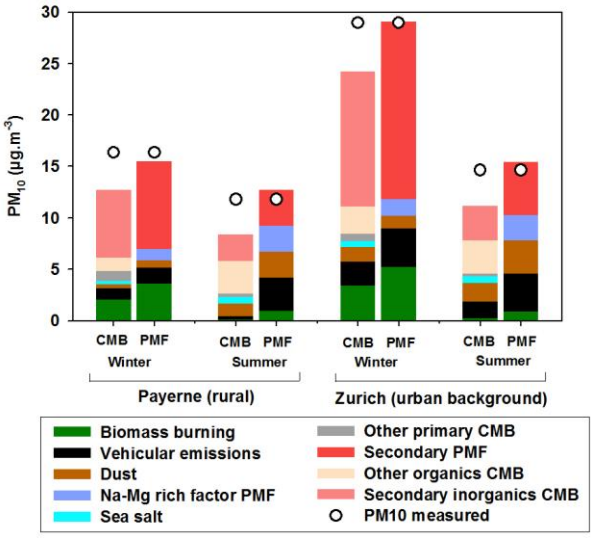

Figure 1. Contributions to PM10 estimated by PMF and MM-CMB in Zurich and Payerne.

C. Piot and L. Polo thank the Région Rhône-Alpes for their PhD grant. The activities at the Swiss sites were supported by the CCES- IMBALANCE and by the Swiss FOEN. Campaigns in France were supported by the MOCOPO program funded by the French Ministry in charge of Transport or studies of AASQA, and several activities were funded by ADEME.

Ke, L., Liu, W., Wang, Y., Russell, A.G., Edgerton, E.S. and Zheng, M. (2008) *Sci. Total Environ.* **394**, 290-302.

Shrivastava, M.K., Subramanian, R., Rogge, W.F. and Robinson, A.L. (2007) *Atmos. Environ.* **41**, 9353-9369.

Viana, M., Pandolfi, M., Minguillon, M.C., Querol, X., Alastuey, A., Monfort, E. and Celades, I. (2008) *Atmos. Environ.* **42**, 3820-3832.

Concentrations and source contributions of particulate organic matter before and after implementation of a low emission zone

R.M. Qadir[1,2], G. Abbaszade[1], J. Schnelle-Kreis[1] and R. Zimmermann[1,2]

[1]Joint Mass Spectrometry Centre, Comprehensive Molecular Analytics, Helmholtz Zentrum München, Ingolstädter Landstr. 1, 85764 Neuherberg, Germany
[2]Joint Mass Spectrometry Centre, Chair of Analytical Chemistry, University of Rostock, Dr.-Lorenz-Weg 1, 18059 Rostock, Germany
Keywords: Low emission zone, organic compounds, PMF
Presenting author email: raeed.qadir@helmholtz-muenchen.de

Low emission zones (LEZ) are areas in which vehicular access is restricted to vehicles that emit low levels of air pollutants only. In 2008 a low emission zone (LEZ) was established in the inner city of Munich, Germany, in order to pursue the reduction of pollution. Samples of $PM_{2.5}$ were collected at the monitoring site in Lothstrasse before and after the implementation of the LEZ every third day from October 2006 to February 2007 and from October 2009 to February 2010. The Lothstrasse is located within the LEZ, allowing for a thorough monitoring of the LEZ implementation effect upon the reduction of hazardous, particle associated organic substances and the different sources of PM pollution.

The samples were analyzed for particulate organic compounds (POC) by in-situ derivatization thermal desorption gas chromatography time of flight mass spectrometry (IDTD-GC-ToF-MS) (Orasche *et al.*, 2011).

The results of the measurements of the two sampling periods were compared. The implementation of LEZ has no significant reduction effect on the concentrations of the organic compounds. Moreover, a higher concentration of some organic compounds in the 2009-2010 sampling period was detected.

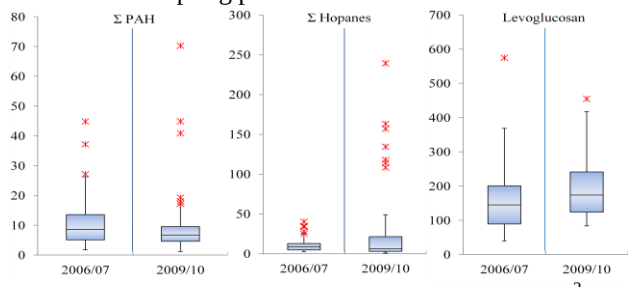

Figure 1. Box plots for the concentrations (ng m^{-3}) of some organic compounds before and after the LEZ

The main sources of POC were identified using positive matrix factorization (PMF) (Paatero and Tapper, 1994). More than 60 organic species were used for PMF analysis, including PAH, oxidized PAH, n-alkanes, iso & anteiso alkanes, hopanes, resin acids, fatty acids, anhydrous sugars and phenolic compounds. The PMF analysis with four factors afforded the most reasonable interpretation of the source profiles, which were related to primary PM emissions.

The factors are dominated by the pattern of a single source or groups of sources with similar time dependency of emissions.

In the first factor, the influence of the vehicular emission source is predominant. 55-85% of hopanes with mineral-oil-based pattern (homohopane index of 0.49) and n-alkanes (CPI of 0.78) are associated in this factor.

The second factor is characterized by compound patterns which represent a mix from tobacco smoke (iso & anteiso alkanes and n-alkanes with CPI of 2.13), cooking emissions (fatty acids) and traffic (homohopane index of 0.59).

In the third factor, about 10-85% of PAH and 15-45% of oxidized PAH are associated beside the hopane pattern (homohopane index of 0.22) what is similar to emissions from brown coal combustion.

The last factor is characterized by pattern which represents a wood combustion source. 60% of Levoglucosan, 59% of Dehydroabietic acid, 60% of Retene and 40-80% of the oxidized PAH are associated with this factor.

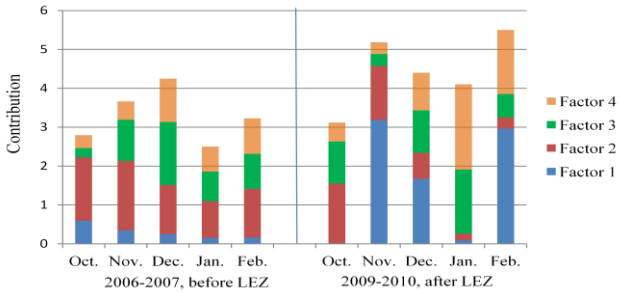

Figure 2. The monthly mean proportions of source factors

Differences in contributions are seen between the two sampling periods for all factors. For example, a high contribution of the first factor is noticed in the second sampling period and that most probably due to some construction activities near the sampling site.

The health effects of organic compounds in aerosols are currently investigated in the framework of the Helmholtz Virtual Institute of Complex Molecular Systems in Environmental Health, HICE (www.hice-vi.eu).

Orasche, J., Schnelle-Kreis, J., Abbaszade, G. and Zimmermann, R. (2011). *Atmos. Chem. Phys.* **11**, 8977–8993.

Paatero, P. and Tapper, U., (1994). Environmetrics **5**, 111–126.

Source apportionment of fine aerosol in Athens by positive matrix factorization and Unmix analysis

A.Karanasiou[1,2,3], M. Scoullos[4], K. Eleftheriadis[1]
[1] Institute of Nuclear Technology and Radiation Protection, Environmental Radioactivity Laboratory, National Centre of Scientific Research "Demokritos", 15310 Ag. Paraskevi, Attiki, Greece
[2] Institute of Environmental Assessment and Water Research (IDAEA-CSIC), Barcelona, Spain
[3]Centre for Research in Environmental Epidemiology (CREAL), Barcelona Biomedical Research Park, Dr Aiguader, 88, 08003Barcelona, Spain
[4]University of Athens, Department of Chemistry, Div. III, Laboratory of Environmental Chemistry, Zografou, Panepistimiopolis 157 71, Athens, Greece

Keywords: aerosol, tracers, PM_{10}, receptor models
angeliki.karanasiou@idaea.csic.es

The objective of this study was to identify the major pollution sources in Athens urban area by means of receptor models. Two different multivariable methods were used (Unmix and PMF) and compared for their effectiveness to apportion aerosol emission sources.

Two aerosol-sampling campaigns were performed in Athens urban area, covering the cold and warm period. PM_{10} and PM_2 were collected simultaneously at three typical urban sites. Black carbon concentrations (BC) were concurrently measured by means of an aethalometer (AE-9, Maggee Sci). After gravimetric analysis the loaded filters were analysed for major and trace elements Fe, Al, Ca, Na, Mg, K, Ni, Mn, Cr, Cu, Cd, Pb and V by atomic absorption spectrometry and for water soluble ions by ion chromatography.

PMF and Unmix models were used to identify the sources of fine PM_2 and coarse PM_{2-10} particles. Here we present the results for the fine aerosol fraction. PMF identified five sources: motor vehicles emissions, road dust, biomass burning, marine aerosol and fuel oil combustion (Karanasiou et al., 2009). In order to determine if certain species could act as unique tracers the Pearson correlation coefficients between source contributions and variable concentrations were calculated. In fine particles Na, BC and Fe were exclusively correlated to marine aerosol, motor vehicles and oil combustion respectively. These species were at the same time the predominant variable in the mass profile of these sources. Surprisingly, Ni is exclusively correlated to motor vehicles emissions although this element had a minor contribution in the mass profile of this source. It was concluded that for Athens urban area Ni could be a unique tracer of traffic.

The initial runs of the Unmix model identified only 3 sources: road dust, marine aerosol and a third source that appeared as a mixture of sources such as vehicles emissions, oil combustion and biomass burning. However, Unmix model has the option of selecting one variable as tracer (only emitted by one source). The pearson correlation coefficients between source contributions and variable concentrations (determined by PMF) allowed the consideration of various species to be introduced as tracers in Umnix model. When Ni was used as a tracer (Figure 1) four sources were resolved by Unmix with similar profiles to those resolved by PMF.

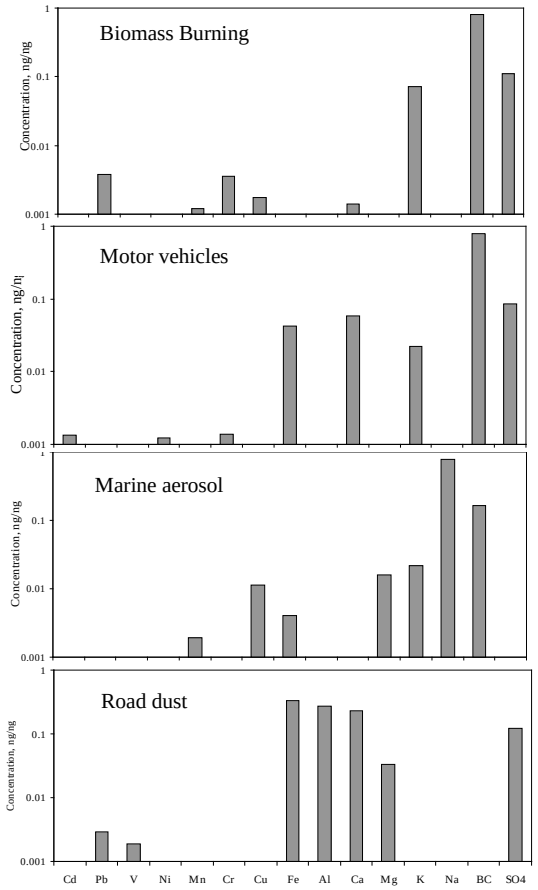

Figure 1. Source profiles for fine particles resolved from Unmix using Ni as a tracer.

PMF was proved to be powerful in resolving the sources of fine aerosol while Unmix could not separate the diverse combustion sources.

This work was supported by the the E.U. contract No EVK4-CT-2000-0018 under "Urban Aerosol".

Karanasiou A., Siskos P.A., Eleftheriadis K., 2009. *Atmos. Environ.* **43**, 3385-3395

Wintertime aerosol source apportionment in the metropolitan area of Paris by Chemical Mass Balance

E. Abidi[1], A. Monod[1], J. Cozic[2], J.L. Jaffrezo[2], M. Crippa[3] , J. Slowik[3], U. Baltensperger[3], A.S.H. Prévôt[3] and N. Marchand[1]

[1]Aix Marseille Univ., CNRS, Laboratoire Chimie Environnement, 13331 Marseille, France.
[2] Université Grenoble 1, Laboratoire de Glaciologie et Géophysique de l'Environnement, CNRS, 38402, Saint Martin d'Hères, France
[3] Laboratory of Atmospheric Chemistry, Paul Scherrer Institut, PSI Villigen, 5232, Switzerland
Keywords: Source Apportionment, Organic markers, CMB, AMS-PMF, MEGAPOLI
email: ehgere.abidi@etu.univ-provence.fr

Within the framework of the MEGAPOLI project, an intensive field campaign has been conducted in the Paris metropolitan area during winter, from 15 January to 15 February 2010. With 12 millions of inhabitants, Paris is one of the most populated areas in Europe and is relatively isolated from other urban areas. During this campaign, comprehensive chemical characterization of PM2.5 has been carried out including major ions, trace metals, OC/EC, and organic markers. Source apportionment has been performed using Chemical Mass Balance model (CMB). At the same time, High-resolution time-of-flight aerosol mass spectrometers (HR-ToF-AMS) was employed and PMF analysis was applied. The measurements were performed at two sites situated in the Paris region : one urban supersite (LHVP) and one suburban supersite (SIRTA) located 20 km southwest of the city center.

The contributions of seven primary fine particles sources were quantified in ambient air samples with the CMB approach, including some major primary anthropogenic sources. The obtained results show that among the 35% of the PM2.5 concentration apportioned to the primary sources, the biomass burning and vehicular emission contribute equally to the PM2.5 concentration (16 and 17%, respectively). Industrial emissions impacted also the atmosphere of Paris during a long range transport episode from Eastern Europe. Their contribution, characterized by the aggregate emissions from three industrial processes (heavy fuel oil combustion, coke production and steel manufacturing) remains very limited (2% on average) during the field campaign. A meat charbroiling source has also been apportioned, but these results need improvement.

Comparisons of the CMB approach with AMS-PMF (Crippa et al., 2012) have also been performed, with some first results presented in Figure 1 for the organic fraction. A very good agreement is observed for the traffic source (VEOM for CMB and HOA for AMS/PMF). Absolute contribution calculated by CMB are, however, slightly higher by a factor of 1.5. This difference could be explained by the different aerosol collection cut-off sizes (PM2.5 for CMB and PM1 for AMS/PMF) and/or oxidation and/or volatilization of the organic aerosol during its transport from the emission point to the receptor site. For biomass burning aerosol, we compare BBOM calculated by CMB and the sum of BBOA and OOA2-BBOA derived from AMS-PMF. The OOA2-BBOA profile is dominated by both the masses typical of the biomass burning and the semi volatile OOA (OOA2) spectra. The interpretation of this factor is not fully clear since it could be considered both as a BBOA SOA and/or processed BBOA POA, or alternatively as an atmospheric mixture of BBOA POA with OOA from another source (Crippa et al, 2012). Our results support the first two assumptions since differences between CMB and AMS/PMF increase for this source during the period dominated by long range transport episodes (Figure 1). The discrepancy observed between CMB and AMS-PMF approach may also be explained by the OC/levoglucosan used to apportion the CMB BBOA, as this ratio may be variable according to the source area.

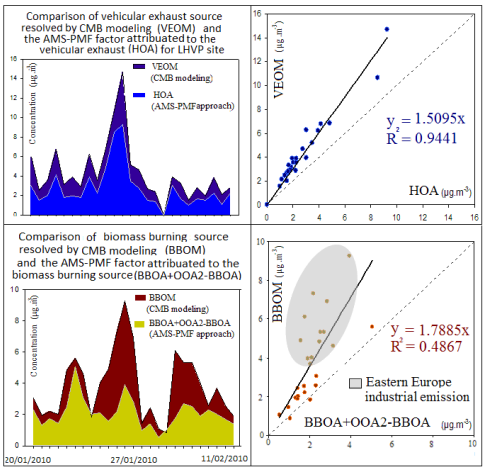

Figure1. Comparison of CMB modeling and AMS-PMF results in contributions from vehicular exhaust and biomass burning sources to PM concentrations at LHVP (PM2.5 for CMB modeling and PM1 for AMS-PMF approach).

A strong correlation in terms of mass loadings and temporal variability of the sources at the two sites is also observed. This result suggests that the particulate pollution from Paris is dominated by regional transport and the influences of local emissions from Paris itself do not significantly influence its surroundings.

This research was funded by the European Union's Seventh Framework program FP/2007-2011 within the project MEGAPOLI, grant agreement n°212520. E.A. gratefully acknowledges the ADEME and PACA region for their support.
Crippa, M. et al., (2012), *ACP* in prep.

Source Apportionment of Particles in London Paddington Station

U. Chong[1], J.J. Swanson[1], and A.M. Boies[1]

[1]Department of Engineering, University of Cambridge, Cambridge, UK, CB2 1PZ
Keywords: diesel exhaust, urban pollution, measurement (characterisation), source apportionment.
Presenting author email: uc211@cam.ac.uk

Exposure to airborne particles from combustion sources and industrial processes are a major health risk in the urban environment. The health impacts of particle emissions are exacerbated when emissions occur within densely populated areas with enclosed boundaries that do not allow for diffusive or convective dispersion. Enclosed train stations with diesel-powered locomotives, in particular, represent a health risk because of the close proximity of the emissions to the passengers. In order to reduce the impacts from diesel locomotives, particle emissions by mass for new EU diesel locomotive engines greater than 130 kW have been regulated by EU Directive 2004/26/EC since 2006. In January 2012, this PM mass emissions standard was lowered by 87.5% (0.200 g/kWh to 0.025 g/kWh) (EU, 2004). Locomotive PM emissions are also influenced by EU Directive 2003/17/EC, which has limited the fuel sulphur content of gas oil to 0.1% by mass since 2008 (Silver, 2007).

To evaluate the impact of diesel engine exhaust within a train station relative to other emission sources, particle measurements (PM mass, size, concentration, and composition) were taken at London Paddington Station, the 8th largest station in Great Britain serving 30 million passengers per year (ORR, 2010). Of the 14 lines in this station all but two host rail traffic powered by diesel engines. The purpose of this study is to determine the sources of particle emissions in Paddington Station and evaluate the potential impact of the new emission regulations. While a few air quality monitoring studies have been conducted inside and adjacent to the station, none provide an in depth apportionment of the sources of PM beyond a mass-based metric. We determine the relative contribution of PM from various emissions sources by measuring particles in different locations and analysing their chemical and size characteristics.

An initial survey was conducted with mobile measurement instruments from TSI, Inc. A P-TRAK 8525 Ultrafine Particle Counter was used to measure number concentration of PM below 0.1µm. An Optical Particle Sizer (OPS) was used to measure the concentration of particles between 0.3-10 µm. Figure 1 shows the averaged results of the P-TRAK measurements (<0.1 µm) sorted by activity.

Elevated levels of PM were observed during departing and arriving train activity, with departing engine acceleration causing higher levels of PM than braking from arriving trains. Beyond the locomotives, it was determined that other activities, such as food vendors, can contribute to elevated levels of PM.

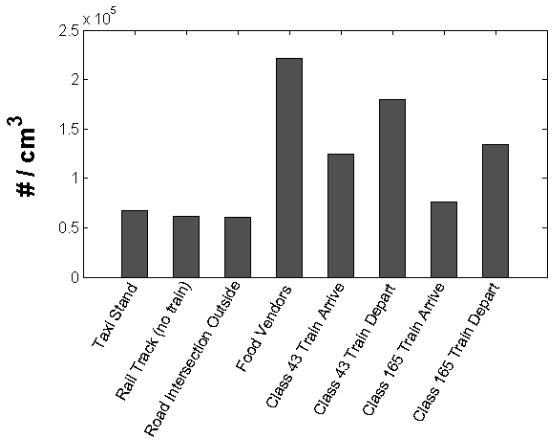

Figure 1: Results of initial survey of particle concentrations at different Paddington locations.

A subsequent measurement campaign was conducted in order to rigorously apportion the sources of PM. Six measurement locations were selected and are described in Table 1.

Table 1: Measurement locations

Location	Purpose
Hot food vendors	Cooking exhaust
Eastbourne Terrace	Taxi exhaust
Platform 1 Bridge	Class 43 Train exhaust
Platform 13 Stairs	Class 165 Train exhaust
The Lawn Shopping	Indoor; away from trains
Praed St. Intersection	Outside ambient location

PM mass concentration measurements were taken continuously at all locations using a TSI AM510 SIDEPAK monitor. A SMPS and an ELPI were rotated on a daily basis between the six locations. SMPS measurements were taken with and without a catalytic stripper to determine the EC/OC ratios of measurements, which allowed for source apportionment of PM emissions. Filtered PM samples from the ELPI were used to determine the chemical composition of particles. Ultimately, the results of this study will better inform policy decisions on improving air quality in Paddington by efficiently targeting the appropriate sources.

This work is supported by the Engineering and Physical Sciences Research Council and the Schiff Foundation.

EU (2004) *Directive 2004/26/EC of the European Parliament and of the Council*. Official Journal of the European Union L 146.

Silver, I. (2007) *Investigation into the use of sulphur-free diesel fuel on UK railways*, Rail Safety and Standards Board Report.

ORR (2010) *2009-2010 Station Usage Report and Data*, UK Office of Rail Regulation.

Chemical mass balance modelling for the source estimation of high PM2.5 concentrations in Milan, Northern Italy

Perrone M.G.[1], Larsen B.R.[2], Ferrero L.[1], Sangiorgi G.[1], De Gennaro G.[3], Udisti R.[4], Zangrando R.[5], Gambaro A.[5,6] and Bolzacchini E.[1]

[1]Research Center POLARIS, University of Milano-Bicocca, DISAT, P.zza della Scienza 1, 20126 Milan
[2]European Commission Joint Research Center, IHCP, Via E. Fermi 2749, Ispra (VA) 21020, Italy
[3]Department of Chemistry, University of Bari, Via Orabona 4, 70126 Bari, Italy
[4] Institute for the Dynamics of Environmental Processes-CNR, Dorsoduro 2137, 30123 Venice, Italy
[5]Department of Chemistry, University of Florence, Via della Lastruccia 3, 50019 Sesto F.no, Florence
[6]Department of Environmental Sciences, University of Venice, Santa Marta 2137, 30123, Venice, Italy

Keywords: PM2.5, receptor models, source apportionment
Presenting author email: grazia.perrone@unimib.it

Northern Italy is one of the most industrialized and populated regions in Western Europe and is characterized by high levels of fine particulate matter (PM2.5). Harmful health effects have been associated with exposure to PM2.5 and to associated toxic compounds.In Europe, the recent Air Quality Directive (2008/30/CE) establishes an annually averaged PM2.5 concentration of 25 μg m^{-3}, which will be the legal limit value from 2015 onwards. With the aim of designing effective PM2.5 reduction strategies, information on the strength of impacting sources is required.

In order to study PM2.5 mass concentrations and chemical compositions in Northern Italy, we conducted measurement campaigns at an urban site in Milan (MI) and a rural site in Oasi Le Bine (OB), over a three-year period (2006-2009) (Perrone et al., 2012).

Chemical mass balance modelling (CMB) was applied to PM chemical composition data in order to quantify the major PM2.5 sources during different seasons. 13 fitting species (EC, levoglucosan , C29 and C31 *n*-alkanes, five PAHs and four elements), comprised of compounds known to be good molecular markers, were used in CMB modelling with the aim of assessing contributions from five primary sources: traffic (TR), biomass burning (BB), natural gas combustion (NGC), plant debris (PD) and road dust (RD). A critical issue for CMB modelling is the availability of source profiles that represent the aggregate emissions from a given source at the considered receptor site. In the present study we used profiles representative of the region in question, where such were available (TR, BB and PD), and various composite profiles derived by literature data. The sensitivity of the CMB model to the selection of different profiles (TR and BB) was assessed .

From CMB calculations the contributions of primary sources to OC was estimated for seasonally averaged PM2.5 samples, and the PM mass from each source was reconstructed by applying a specific OM-to-OC conversion factor to each source and adding other primary components (e.g. EC; primary sulphate, nitrate and ammonium; major elements and their oxides) (El Haddad et al., 2011).

In MI, TR was found to be the strongest primary source (17-24%) for PM2.5 in all seasons, together with secondary inorganic and organic aerosol (21-54%) (Fig.1).In fall (F) and winter (W), BB was a major contributing primary source to PM2.5 concentrations at the MI urban site as well at the OB rural site, with a source contribution estimation (SCE) ranging from 8 to

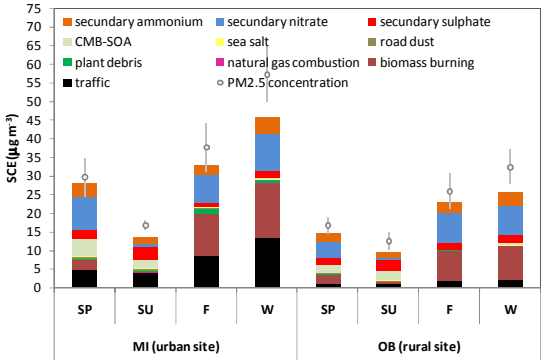

Figure 1. Source contribution estimation (SCE) to averaged seasonal PM2.5 concentrations in MI and OB.

15 μg m^{-3} at the MI urban site as well at the OB rural site. While TR is mainly a local source, and it has a stronger impact nearer the source, BB is a widespread source with a substantial regional contribution.

BB was also a contributing source to the high PAHs concentrations measured in the PM2.5 samples in the cold season. In figure 2 the ratio-ratio plot compares PAHs/EC ratios in the ambient air with those of sources. Winter data mainly cluster between a 50/50 and a 25/75 mix of BB and TR sources, thus suggesting a relative contribution of 25-50% for BB source to PAHs (BghiP and IcdP) ambient concentrations at the MI site.

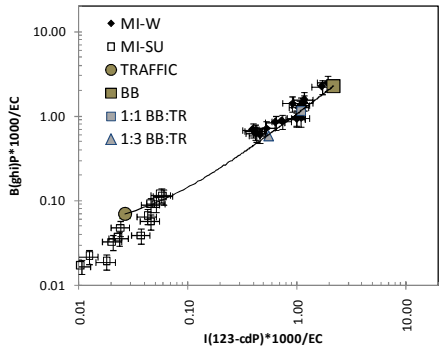

Figure 2. Ratio-ratio plot using PAHs and EC. Ambient data for MI site (W=winter; SU=summer) and source profiles for TR and BB.

El Haddad I, et al. (2011) *Atmos Chem Phys* **11**, 2039-2058
M.G. Perrone, et al. (2011) *Science of the Total Environ* **414**, 343-355

Impacts of industrial and harbor activities on fine particles over Marseille

D. Salameh[1], A. Detournay[1], H. Wortham[1], J.L. Jaffrezo[2], J. Cozic[2], A. Armengaud[3], D. Piga[3], J. Dron[4], P. Chamaret[4], M. Parra[5], M. Deveze[5] and N. Marchand[1]

[1]Université Aix Marseille, CNRS, Laboratoire Chimie Environnement, 13331 Marseille, France
[2]Université Joseph Fourier - CNRS - LGGE, 38402 St-Martin d'Hères, France
[3]AirPACA, Regional Air Observatory, 13006, Marseille, France
[4]Institut Eco-citoyen pour la Connaissance des Pollutions, 13270 Fos-sur-Mer, France
[5]Grand Port Maritime de Marseille, 13001, Marseille, France
Keywords: Source apportionment, organic markers, harbor and industrial activities, Marseille, APICE
Email: dalia.salameh@etu.univ-provence.fr

With traffic of about 97 million tons (Mt) (62.5% of crude oil and oil products) in 2007, the autonomous port of Marseille is the most important port of the Mediterranean Sea. A huge petrochemical area among other industrial plants (steel mill, coke plant…) is also located close to Marseille, the second most populated city in France with more than 1 million inhabitants. This area is also well known for its huge photochemical pollution.

Within the framework of the EU-MED APICE project (Common Mediterranean strategy and local practical Actions for the mitigation of Port, Industries and Cities Emissions ; www.apice-project.eu) a long monitoring campaign began in Marseille in July 2011, and will end in July 2012. Samples of fine particulate matter (PM2.5) are collected with a temporal resolution of 24 or 48 hours on two main sites. The first one is in an urban background environment ("Cinq avenues" site). This measurement site belonging to the air quality network AirPACA, is also equipped with instruments for continuous measurement of NOx, SO_2, O_3 and both PM2.5 and PM10. The second site is located in the eastern docks of Marseille harbor in the vicinity of ships emissions. These strategic locations allow, first, to characterize the physicochemical composition of the particulate matter emitted by the harbor activities, and secondly, to characterize and to quantify the contribution of these specific emission sources in the atmosphere of Marseille. A comprehensive chemical characterization of the collected samples is carried out including major fractions (OC/EC, ionic species), 33 elements and trace metals and about 100 organics markers (PAHs, levoglucosan, linear alkanes, hopanes…).

An intensive measurement campaign has also been conducted in the industrial area near Marseille in June 2011 (Fos-sur-Mer). High time resolved measurements have been performed for both submicron aerosol and VOCs (HR-ToF-AMS, PTR-ToF-MS, SMPS, MAAP, OPC) in addition to offline samples collection. Results from this intensive campaign are presented in figure 1. While PM10 and SO_2 concentrations were significantly lower than those usually observed in this environment at the same period of the year, we observed intense particle events reaching 140 000 cm^{-3}, most of the time associated with SO_2. This particles events are associated to ultrafine particles (D<50 nm). As well intense and sharp peaks of submicron organic aerosol up to 200µg/m3 are observed all along the campaign. These OA events are associated with particles in the 300-400 nm size range.

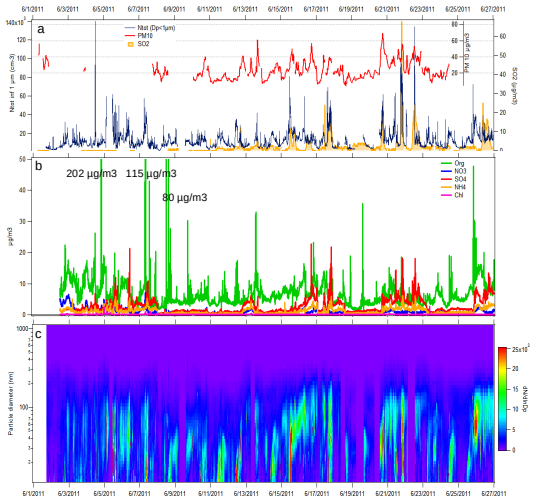

Figure 1. Results from a one month intensive campaign held in the industrial area of Fos-Berre (Juin 2011).

From these results two major lessons can be drawn. First, particle mass concentration (PM10 and PM2.5) do not constitute a totally relevant parameter to study the impact of industrial emissions and, second, these industrial particles events are associated to an important fraction of organic materials. Metals usually used to trace industrial emissions offer only a partial view of the complexity of industrial particles emissions.
In addition to the results obtained within this intensive campaign, preliminary results of source apportionment realized during the long monitoring campaigns carried out in Marseille will be presented.

This work is supported by the MED program under grant 2G-MED09-26. D.S. gratefully acknowledges ADEME and PACA region for her PhD Grant.

Absorption Ångström exponent, and its correlation with other aerosol variables such as number size distribution, gas phase- and trace elements of the atmosphere. A field study.

T. Ajtai, Á. Filep, N. Utry, M. Pintér, Z. Bozóki, G. Szabó
Department of Optics and Quantum Electronics, University of Szeged, Hungary

Keywords: source apportionment, photoacoustic, optical absorption, Ångström exponent.
ajtai@titan.physx.u-szeged.hu

One of the major contributions in uncertainties on climate forcing is associated to aerosol. Optical absorption coefficient of aerosol (OAC) is one of the most uncertain parameters associated to both direct and indirect effect on climate and is one of the most difficult quantities to measure Due to its strong influence on the climate and its adverse health effects, in-situ characterisation of light absorbing carbonaceous matter (LAC) is in the middle of scientific interest today. LAC is a mixture of graphite-like particles and light-absorbing organic matter having various origins. The term absorption Ångström exponent (AAE) is introduced to describe the wavelength dependence of OAC. Great many papers demonstrated that AAE of LAC is characteristic for its constituents, therefore its measurement can be a valuable tool for in-situ source apportionment (Andreae and Gelencsér, 2005). Although the only method that can measure OAC of LAC, in-situ, is photoacoustic spectroscopy, it is not widespread in its application yet. During last decades several promising photoacoustic instruments for OAC measurement with high reliability have been published, but most of them operate only at one wavelength. Recently multi-wavelength photoacoustic instruments become available and initial laboratory and field measurements demonstrate experimentally that AAE might be an indicator of the chemical composition of atmospheric bulk.

We present a study of OAC of ambient aerosol measured by our four wavelength photoacoustic instrument (4λ-PAS) in the UV, VIS, near IR spectral region (1064 nm, 532 nm, 355 nm and 266 nm) The instrument applies wavelength independent, non-site specific calibration with accuracy below 5%, therefore it provides unique and novel possibility for investigation of absorption spectra with high selectivity. Segregated AAEs were calculated at different wavelength pairs of the 4λ-PAS. Systematic daily fluctuation of AAE was identified with different dynamics. Correlation with other aerosol variables such as size distribution and elemental composition, as well as concentration of trace gases were revealed and quantified. Reliable correlation was found between $AAE_{532nm\text{-}266nm}/AAE_{1064\text{-}532nm}$ and N_{GMD20}/N_{GMD100} ratios. Similarity of volume size distributions measured at the two representative periods confirms that variations in AAE were not caused by variation in particle size, but by chemical composition. High correlation between $AAE_{532nm\text{-}266nm}/AAE_{1064\text{-}532nm}$ and CO/NO_x ratio further confirms that daily changes in absorption spectra are related to the changes in relative strength of emission sources most likely between traffic and residential heating. Finally, we have demonstrated and quantified the correlation between $AAE_{532nm\text{-}266nm}/AAE_{1064\text{-}532nm}$ and the ratio of source specific trace elements.

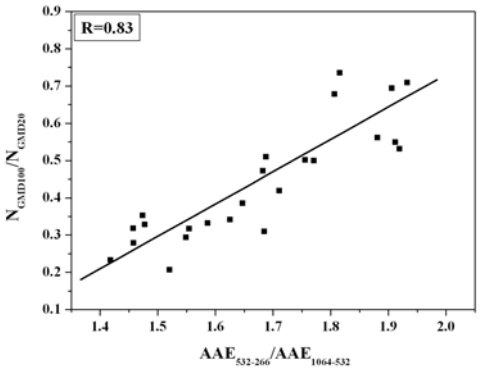

Figure 1: Correlation of the modal number concentration ratio and the ratio of AAE calculated from 532-266 nm and from 1064-532 nm.

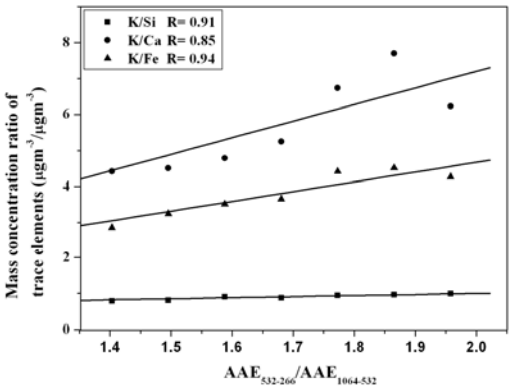

Figure 2: Correlation of ratio of K with Si (labelled with squares), Ca (circles), Fe (triangles) and AAE calculated from 532-266 nm and from 1064-532 nm.

This work was supported by the Hungarian National Development Agency (JEDLIK_AEROS_EU) and OTKA foundation from the Hungarian Scientific Research Fund (project numbers: CNK 78549 and K 101905).

Andreae, M.O., Gelencsér, A., (2006). Black carbon or brown carbon? The nature of light-absorbing carbonaceous aerosols, Atmos. Chem. Phys. 6, 3131–3148.
Andreae, M.O. (2005). The dark side of the aerosols, Nature 409, 671-672.

Source apportionment of indoor and outdoor $PM_{2.5}$ in an apartment situated in central Athens, Greece

D.E. Saraga[1], M. Seleventi[2], C.G. Helmis[2], Ch. Vasilakos[1] and Th. Maggos[1]

[1]Environmental Research Laboratory/INT-RP, National Centre for Scientific Research "Demokritos", Aghia Paraskevi Attikis, P.O.B. 60228, 15310 Athens, Greece
[2]Department of Environmental Physics and Meteorology, Faculty of Physics, University of Athens, University Campus, building PHYS-5, 157-84 Athens, Greece

Presenting author email: dsaraga@ipta.demokritos.gr

The role of the outdoor environment in indoor particles concentration presents special interest in cases where the house is situated in an aggravated urban atmosphere. The aim of the present study is to identify the main sources and estimate their contribution to the indoor and outdoor $PM_{2.5}$ levels measured in an apartment situated on a high-traffic street (Ch. Trikoupi), in central Athens. For the purpose of the study, Positive Matrix Factorization (PMF) model was applied on a set of indoor and outdoor $PM_{2.5}$ samples collected during a 2-week campaign (winter 2011).

Using two similar low volume controlled flow rate ($2.3m^3/h$) samplers (DERENDA), $PM_{2.5}$ samples were collected both indoors and outdoors of a $120m^2$ apartment situated on the 5^{th} store of a block of flats. The samples were analysed for 10 ionic species (F^-, Cl^-, K^+, Na^+, Mg^{2+}, Ca^{2+}, NO_3^-, PO_4^{3-}, SO_4^{2-}, NH_4^+) and organic/elemental carbon (OC/EC and organic carbon fractions). The chemical analysis for the ionic species was conducted with the use of ion chromatography and organic/elemental carbon analysis with the use of NIOSH Method 5040, IMPROVE methods. Occupants' activities were daily recorded on questionnaires.

Experimental results showed that particles concentration ranged between 9.0 and 65.4 $\mu g/m^3$ indoors and between 11.7 and 43.5 $\mu g/m^3$ outdoors. The maximum indoor concentration was noticed during the day that smoking took place. Furthermore, OC/EC ratio exceeded the value of 2 in all indoor samples and in the 77% of the outdoor samples, implying the presence of secondary organic aerosol (SOA). A strong correlation was observed between indoor and outdoor EC (R^2 =0.94), implying common (outdoor) origin. Finally, among the ions measured, Cl- and SO_4^{2-} presented the most significant variation. I/O ratio for NO_3^- and NH_4^+ was much lower than unity because of the presence of strong outdoor sources (intense vehicles circulation).

For the source apportionment analysis EPA PMF model (version 3.0) was used. Data pre-treatment included concentration data below the methods detection limit replacement with one-half of the detection limit and missing concentration data substitution with the median value. Correspondingly, uncertainty for data below the detection limit was set equal to 5/6 of the detection limit while uncertainty for missing data were set equal to 4 times the median concentration (Polissar et al., 2001). The model was run for 3 to 10 factors, in a random seed and the optimal number of factors ranged between three and five, depending on the species used in each run. Finally, bootstrap and Fpeak runs were conducted in order to examine the stability and the rotational ambiguity of the solutions, respectively.

Preliminary results indicate four main groups of sources contributing to both indoor and outdoor $PM_{2.5}$ levels: a combustions-related source (including smoking for indoor air), a traffic-related source (vehicles and road dust), a crustal source (soil dust) and a source connected with secondary aerosols. Representative quantitative results are presented in figures 1a,b. A preliminary conclusion underlines the different sources contributions in indoor and outdoor air. Smoking (combustion sources) and dust is the main sources indoors while traffic and soil dust contribute the most to outdoor particles.

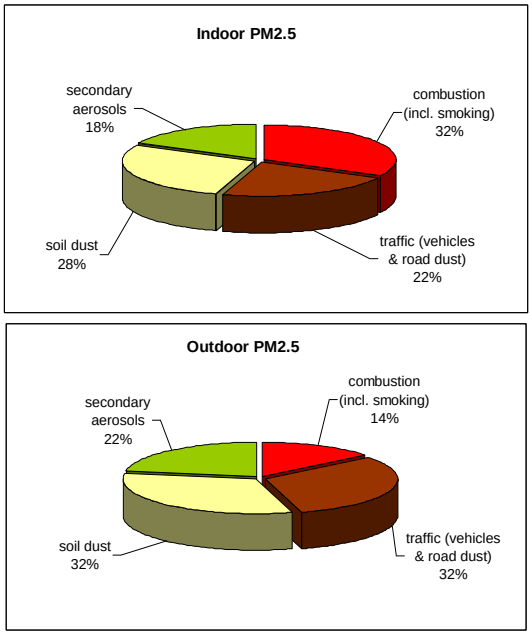

Figures 1a,b. Relative contribution of the four group of sources to indoor and outdoor $PM_{2.5}$ mass concentration..

Polissar A..V., Hopke P.K., and Poitrot R.L. *Atmospheric aerosol over Vermont: chemical composition and sources* (2001) Environ. Sci. Technol. 35 (23), 4604-4621.

Reff A., Eberly S., Bhave P. *Receptor Modeling of ambient particulate matter data using Positive Matrix Factorization: review of existing methods* (2007) J. Air & Waste Manage. Assoc. 57:146-154.

Source apportionment of PM during 2008-2010 at Station Nord, North East Greenland

J.K. Nøjgaard[1], H. Skov[1], L.L. Sørensen[1], B.J. Jensen[1], A.G. Grube[1], A. Massling[1], M. Glasius[2] and Q.T. Nguyen[1,2]

[1]Department for Environmental Science, Aarhus University, Roskilde, DK-4000, Denmark
[2]Department of Chemistry, Aarhus University, Aarhus, DK-8000, Denmark
Keywords: Arctic, PMF, COPREM, Atmospheric particles
Presenting author email: jakn@dmu.dk

Sources of particulate matter (PM) were evaluated at Station Nord (81°36'N, 16°40'W) in North East Greenland based on two-years of measurements of black carbon, elements and inorganic ions from March 2008 to February 2010. Particulate species were sampled on filters with weekly resolution, while the time resolution of gasses and black carbon were 30 and 15 min, respectively. Sources of PM were apportioned using Positive Matrix Factorization (PMF) and the Constrained Physical Receptor model (COPREM). COPREM is a hybrid receptor model, which unifies qualities from both Chemical Mass Balance (CMB) and PMF (Wåhlin, 2003).

Table 1. Analytical methods and analysed species

Elements (Proton Induced X-ray Emission) Al, Si, S, Cl, K, Ca, Ti, V, Cr, Mn, Fe, Ni, Cu, Zn, Ga, As, Se, Br, Rb, Sr, Zr, Pb
Inorganic ions (Ion Chromatography) SO_4^{2-}, Na^+, NH_4^+, NO_3^-, Br^-
Carbon (Particle Soot Absorption Photometer) Black carbon
Inorganic gasses (gas monitors) O_3, NO_2, NO, SO_2

In general, COPREM and PMF solutions agreed well as was expected since only the natural sources were constrained in COPREM. Five factors (sources) were chosen to describe the dataset, including a *Marine* and a *Soil* (crustal) factor of natural origin. Anthropogenic sources were heavily influenced by metal industry. *Metal (Zn)* was the largest source of Zn with a time profile different from the other anthropogenic sources. Significant peaks were observed during the summer in addition to typical high concentrations in the winter/spring. Most Cr was associated with this source, while most non-crustal elements and combustion related species were of low abundance, e.g. NO_3^-, SO_X=SO_2+SO_4^{2-} and black carbon (BC). *Metal (Cu/Ni)* was the predominant source of Cu. Furthermore, significant amounts of NH_4^+, NO_3^-, SO_4^{2-} and BC were apportioned to this source, which evidently was highly influenced by anthropogenic emissions, predominantly husbandry and combustion processes. The time profile of *Metal (Pb/As)* resembled *Metal (Cu/Ni)*, but the chemical composition was different. Most As, Pb and Br were apportioned to this source, in addition to combustion-related SO_X and BC. The comparable time profiles of *Metal (Pb/As)* and *Metal (Cu/Ni)* showed a typical *Arctic haze pattern* with low summer and high winter/spring concentrations. This suggest that both factors had a common origin, most likely an Eastern source to which Cu, Ni and As have previously been associated (Heidam *et al.*, 2004; Maenhaut *et al.*, 1989). Also, combustion has previously been associated with Pb and As in the high Arctic (Heidam et al., 2004).

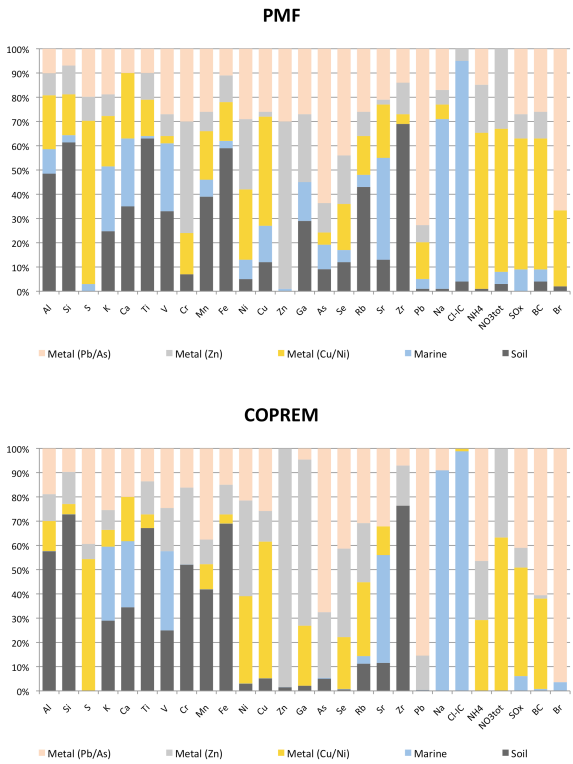

Figure 1. Comparison of PMF and COPREM

Se was present in all anthropogenic factors (21-41%), which suggests, that coal is important as energy carrier for the corresponding anthropogenic activities. With respect to climate issues, as much as 80-98 % of BC was apportioned to *Metal (As/Pb)* and *Metal (Cu/Ni)*.

This work was supported by the Arctic Monitoring and Assessment Programme (AMAP) and Short-Lived Climate Forcers (SLCF) granted by the Danish EPA.

Wåhlin, P., (2003). *Atmos. Environ.* **37**, 4861-4867.
W. Maenhaut, P. Cornille, J.M. Pacyna and V. Vitols, (1989). *Atmos. Environ*. **23**, 2551-2569.
N.Z. Heidam, J. Christensen, P. Wåhlin and H. Skov, (2004). *Science of the Total Environment* **331**, 5-28

Structural properties of mineral dust from vehicle resuspension

E. Coz[1], C. Barrios[1], C. Martín[1], A. Domínguez[1], and B. Artíñano[1]

[1]Department of Environment. CIEMAT, Madrid, 28040, Spain
Keywords: road dust, resuspension, morphology, CCSEM
Presenting author email: esther.coz@ciemat.es

Recent studies suggest that resuspension of road dust might represent a major source of particle matter (PM) in urban Spanish environments (Amato et al., 2011) A combined effect of PM accumulation in roads due to the absence of rainfall during long periods with extremely high vehicle densities in large cities are pointed out as the main cause (Amato et al., 2009). Quantifying this type of emissions and differentiating their properties from remote desert transports is a key to solve the natural/anthropogenic dust fluxes debate relating climate change. With this regard, direct comparisons of the different morphological properties of particles with similar mineralogy from the different sources might be determinant on the novel radiative transfer and cloud condensation nuclei models that include particle shape (Otto et al., 2011; Kurmar et al., 2011).

The aim of the study was to quantify the structural properties of the particles emitted by the disk brakes of road vehicles in absence of traffic (to isolate the emission). Previous urban campaigns in Madrid and Barcelona pointed out the presence of Fe-oxides from disk brake abrasion with a unique nanostructure forming aggregates of 20-30 nm monomers that highly differs from natural occurring ones (Coz et al., 2011). This might be associated to the high temperatures during abrasion. This fact is of special importance for health since the peak of maximum deposition in the alveolar region of human respiratory system is between 10-30 nm (Oberdörster et al., 2005).

Particle load density in the substrate (load density after here), size, shape and elemental chemical composition of 0.2-15 μm sized individual particles from vehicle resuspension in a test circuit were analyzed by Computer-Controlled Scanning Electron Microscopy coupled to Energy Dispersive X-ray Spectroscopy (CCSEM/EDS) (Coz et al., 2009). The samples were collected in a closed circuit inside the research centre (CIEMAT) of 5 minutes duration in the absence of traffic. Three passive samplers were strategically located and three types of samples were taken during the experiment: up and down sides of the fender ("up-fender" and "down-fender" sample notation) and next to the wheel tire ("wheel" sample) of an Audi A2 as testing vehicle. Direct samples from the break disk ("break" sample) and road deposited dust ("road dust" sample) were collected for comparison. Particles were classified in six main clusters based on their elemental ratios: Si-rich, Ca-rich, Ca/Si-rich, Fe-rich, other Metal-rich, and Miscellaneous particles.

As expected, the down-fender sample recovered most of the road resuspension with the highest efficiency (load density of $8.1 \cdot 10^4$ Np·cm-2, Np – particle number). Particles from down-fender and road dust samples are statistically equal in all the studied properties. Less than 5% (by number) of the particles can be associated to break abrasion. The dominating clusters is Ca-rich, mostly occurring as carbonates, followed by the Si-rich and Ca/Si-rich clusters, mostly comprised of quartz, phyllosilicates and feldspars. The up-fender sample presents 50/50 contribution from break/tyre abrasion and soil resuspension, and half load density than the down-fender sample. In the case of the wheel sample, the estimated ratio break abrasion to soil resuspension is of 80/20. Primary organic particles from the tyre were rare in sizes smaller than 10 μm. 5% of the particles in the sample were identified as a characteristic Si-rich subgroup from the tire. Fe-oxides comprise nearly 80% of the total particle number. Fe-oxides in the wheel sample presented higher contents of Mg, and Ca-Cr-Mn-Cu were fingerprints in the particles. P-S-Cl and Ti-Mn-Ba are typically associated to the Fe-oxides in the brake sample.

Fe-oxides are generally at smaller sizes than the rest of the mineral particles. They are mostly concentrated in sizes smaller than 2 μm. The PM2.5 from both wheel and tyre abrasion seem to be formed of the hypothesized aggregation of nanometer sized oxides. Quantification of these unique structural properties as well the associated AR (aspect ratio) values of the different clusters and sources will be discussed during the presentation.

CCSEM analyses were performed at RJLee Group, Inc. This study has been supported by the Spanish National Research Plan (CGL2011-27020) and AEROCLIMA project (Fundación Ramón Areces).

Amato, F., Pandolfi, M., Moreno, T., Furger, M., Pey, J., Alastuey, A., Bukowiecki, N., Prevot, A.S.H., U. Baltensperger, U. and Querol, X. (2011) Atmos. Environ. 45 (2011) 6777-6787.

Amato, F., Pandolfi, M.,Viana, M., Querol, X., Alastuey, A. and Moreno, T. (2009) Atmos. Environ. 43 1650–1659.

Coz, E., Gómez-Moreno, F. J., Pujadas, M., Casuccio, G. S., Lersch, T. L. and Artíñano, B. (2009) Atmos. Environ. 43, 1850-1863.

Coz, E., Casuccio, G., Lersch, T.and Artíñano, B. Geophys. Res. Abst., Vol. 13, EGU2011-4514, 2011.

Kumar, P., Sokolik, I. N. and Nenes, A. (2011) Atmos. Chem. Phys. 11, 3527-3541.

Otto, S., Trautmann, T. and Wendisch, M. (2011) Atmos. Chem. Phys. 11, 4469-4490.

Thermo-chemical properties of fleet ship emitted aerosols: relation to composition and structure

H. Bladt[1], J. Schmid[1], E. Kireeva[2], O. B. Popovicheva[2], J. Moldanová[3], N. P. Ivleva[1] and R. Niessner[1]

[1]Chair for Analytical Chemistry, Technische Universität München, Munich, 81377, Germany
[2]Skobeltsyn Institute of Nuclear Physics, Moscow State University, Moscow, 119991, Russia
[3]IVL, Swedish Environmental Research Institute, Gothenburg, 40014, Sweden
Keywords: shipping emission, chemical composition, inorganics, Raman microscopy, soot reactivity.
Presenting author email: bladt@tum.de

Transport-emitted aerosols are known to significantly impact air quality, the atmospheric radiative and chemical balance, cloud formation and human health. Especially emission by shipping is of major concern as it contributes to 0.4 -1.4 % to the total black carbon burden and an increment in the total particle number concentration of up to 25 % overseas (Lauer et al., 2007). In contrary to urban traffic, marine traffic is not subject to stringent emission control. In order to evaluate particulate emission from shipping, design appropriate exhaust particle filters and set limitations in consequence, a detailed characterization of the aerosol particle oxidation reactivity in relation to its chemical and structural properties is required.

For this purpose, the exhaust of 9 different seagoing transport ships was investigated in the frameworks of the QUANTIFY EU project in the Odessa port, Black Sea in 2008/2009 (Popovicheva et al., 2010) and the TRANSPHORM project on the Baltic Sea in 2010. The samples were analyzed by ICP-MS, Raman Microspectroscopy (RM), Infrared spectroscopy (IR) and Temperature-Programmed Oxidation (TPO). The water-soluble fraction was investigated by Ion Chromatography and Atomic Absorption Spectroscopy.

The quantification of specific elements and ions and the analysis of the particle surface chemistry revealed great variability in composition and structure between different ship emission samples. Concerning heavy metals, Fe is the most dominant element and accounts for up to 5.0 % (m/m) of the total particulate emission of a ferry (2 200 000 t) shipping across the Black Sea and fueled with light fuel oil in summer and gas oil in winter. In contrary, only traces of V, Ni and Pb were quantified (<1.3 % (m/m)). Ions of the alkaline metals, i.e. Na^+ and K^+, in the water extract were found to amount for less than 0.5 % (m/m). However, the earth alkaline metal ion Ca^{2+} was found in concentrations of up to 6.5 % (m/m). IR spectra of some ship particles demonstrate the presence of $CaSO_4$. Anions in the water extract are most dominantly SO_4^{2-} (up to 15 % (m/m)). Cl^-, NO_3^- and PO_4^{3-} are below 0.4 % (m/m).

Raman analysis of ~140 individual particles of each ship PM deposit revealed the presence of diverse inorganic salts and oxides. Specifically α-Fe_2O_3 and $CaSO_4$ were found in up to 20 and 12 % of all particles, respectively (Fig. 1). These species can be derived from engine corrosion or contaminations and additives in fuel or lubricating oil. Fe and Ca are known catalysts for soot oxidation (Bladt et al., 2012, Castoldi et al., 2009).

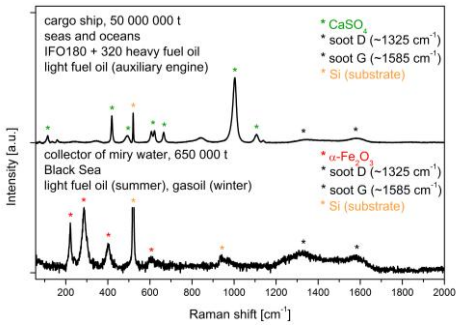

Fig. 1. Raman spectra of particles of different ship exhaust samples.

TPO shows the oxidation reactivity of emitted carbonaceous aerosols which depends on its microstructure as well as on the catalytic effect of present inorganic contaminations. The TPO profiles of the analyzed ship emitted particles show high diversity. The temperature of maximum CO and CO_2 emission T_{max} is a criterion for soot oxidation reactivity. It strongly depends on impurities and varies in a broad range from 343°C for very reactive particles to 630°C for rather unreactive particles. Furthermore, the emission profiles show from one up to three emission maxima (see Fig. 2).

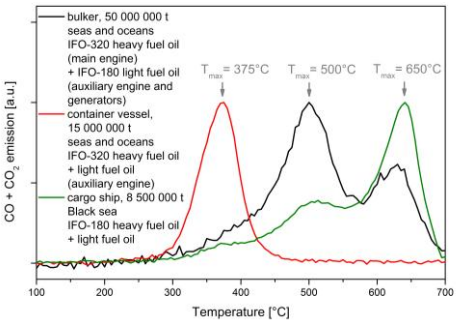

Fig. 2. TPO profiles of different ship exhaust samples.

This study reveals the relation of composition and structure of multicomponent fleet ship particulate emission to its thermo-chemical properties.

Financial support by the DFG, RFBR and the DAAD is gratefully acknowledged.

Bladt et al. (2012) *Aerosol Sci. Technol.* (submitted).
Castoldi et al. (2009) *Appl. Catal. B* **90**, 278-285.
Lauer et al. (2007) *Atmos. Chem. Phys. Discuss.* **7**, 9419-9464.
Popovicheva et al. (2010) *Izv. Atmos. Ocean Phy.+*, **46**, 339-346.

Detailed chemical characterization of ultrafine particles from vehicle exhaust

F. Donaz[1], L. Polo[1], C. Piot[1,2], J. Cozic[1], B. Golly[2], N. Marchand[3], J.L. Besombes[2] and J.L. Jaffrezo[1]

[1]Université Joseph Fourier-CNRS-LGGE, St-Martin d'Hères, France
[2]Université de Savoie-LCME, Le Bourget du Lac, France
[3] Aix Marseille Univ., LCE, Marseille, France
Keywords: Ultrafine particles chemistry, organic speciation, urban kerbside, France.
Contact email: jaffrezo@lgge.obs.ujf-grenoble.fr

The knowledge of the PM10 and PM2.5 chemical composition is now quite large, while just a few studies exist about that of ultrafine particles (UF-PM ; PM < 150 nm). However, because of its size, this PM fraction could be involved in regional and global climate changes, and also affect the human health. Further, their chemical composition can be largely different from that of larger particle and could significantly change their impacts for these two topics.

Few studies present the global composition of UF-PM. It is known that a major proportion is generally made of organic matter and others important components are EC, sulphate and ammonium (Kudo et al., 2011). Very few authors have studied the speciation of organic matter, but Di Filippo et al. (2010) showed higher percentage of PAHs, methyl-PAHs and nitro-PAHs in UF-PM than in PM_{10} and $PM_{2.5}$.

In this study, the chemical composition of UF-PM was investigated during 15 days in September 2011 in the course of the MOCOPO (http://mocopo.ifsttar.fr/) and PM-Drive programs, conducted along a highway in an urban environment (Grenoble-Echirolles, France). UF-PM were collected daily with a high volume cascade impactor BGI© (2008 BGI Incorporated, Waltham, USA). In order to compare with the chemical composition of larger PM, PM10 were also simultaneously collected at this site and at a nearby urban background site (Grenoble-Les Frênes, France) with high-volume samplers (Digitel DA80) in both cases. All of these samples were analysed for major ions, EC-OC, trace metals, and organic speciation with GC-MS analysis.

Significant differences in the global chemical composition of PM10 between samples from kerbside and urban background can be observed (Fig. 1). Vehicular emissions increase the contribution of elemental carbon whereas the major ions and organic matter (OM) concentrations decrease. The results obtained for the UF-PM fraction indicate that this feature is accentuated for this PM fraction, with a higher proportion of elemental carbon and a smaller proportion of ions and OM than in PM10. Further, with an average concentration of 2 µg.m^{-3}, the UF-PM fraction comprises one third of the total EC.

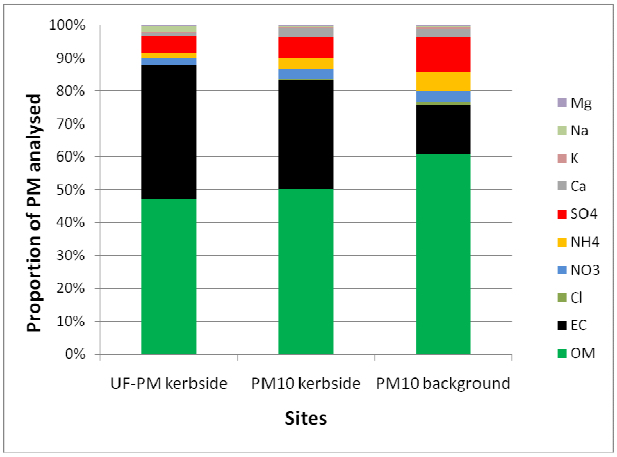

Figure 1. Comparison of the global chemical composition of UF-PM and PM_{10} at an urban kerbside site and PM_{10} at an urban background site. Results are the average of 12 daily samples.

The detailed chemical composition of PM measured at these three sites will be discussed in the presentation, focusing, on the trace metals and organic markers. UF-PM chemical composition from kerbside environment will also be compared with those obtain in urban sites highly impacted by biomass burning and during episodes influenced by photochemistry.

This work was supported by the Université Grenoble-1 Pole SMINGUE with a grant for the equipment. JL Jaffrezo would also like to acknowledge the general support of CNRS-INSU and that of ADEME for the PM Drive program.

Di Filippo, P., Riccardi, C., Pomata, D. and Buiarelli, F. (2010) *Atmos. Env.*, 44, 2742-2749.

Kudo, S., Sekiguchi, K., Kim, K.H. and Sakamoto, K. (2011) *Atmos. Env.*, 45, 6403-6413.

The field experiments on the HTO washout from the atmosphere.

A.V. Golubev, S.V. Mavrin, V.N. Golubeva, A.V. Stengach, Yu.S. Balashov, V.P. Kovalenko, I.I. Solomatin.

Russian Federal Nuclear Center - VNIIEF, 607190, Sarov, Russia.

Keywords: scavenging, wet removal, field measurements, atmospheric pollution, tritiated water(HTO)
Presenting author email: balashov.yu@gmail.com

The results of the field experiments of HTO washout with rainfall in the vicinity of the HT and HTO emission source are presented. The objective of the current study was to obtain the direct experimental data on the impact of raindrops characteristics (rate and spectrum of the drops) on HTO washout from the atmosphere.

The site of the scavenging experiments was around a 30 m emission source. The experimental site was a relatively flat one (the maximal height variations within the site were - ±5 m) covered with single buildings and individual trees whose height was from 10 to 30 m. The sampling arcs were chosen at 150 m from the base of the source to minimize dry deposition on the precipitation collectors (Fig.1).

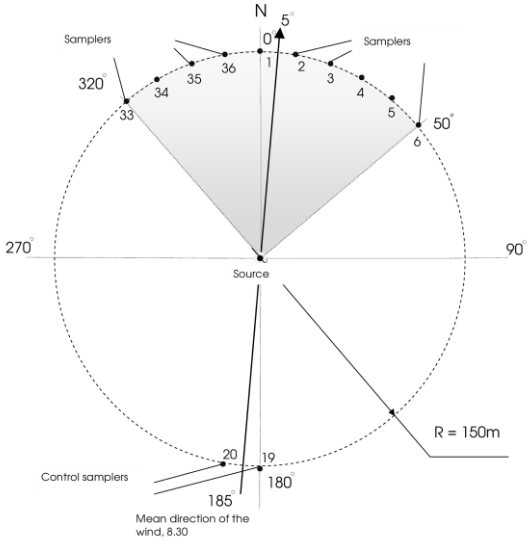

Figure 1. Experimental setup.

To study dependence of scavenging of tritium on raindrops characteristics, a laser optical device was constructed and used to measure the distribution of the drop radius and velocities during the period of experiment (Fig.2) (Hauser et al, 1984).

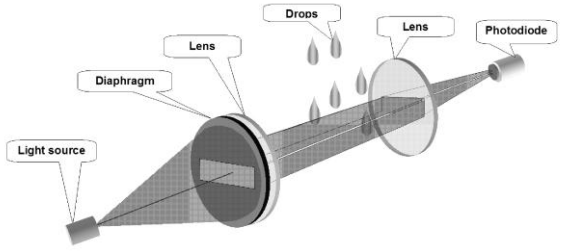

Figure. 2. The optical layout of the device to measure rain drops' parameters.

The following parameters were measured in every experiment: temperature and air humidity; HT and HTO activity in a stack gases; rain event parameters, including rain intensity, raindrop's size and falling down velocity (Fig.3); HTO activity in rainwater samples, activity of volatile tritiated organics in water samples.

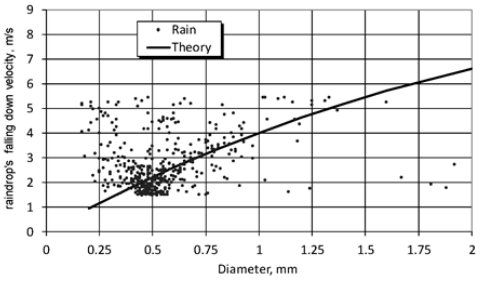

Figure. 3. Drops' sedimentation velocity vs. their diameter *V(D).*

Processing of the results of field experiments allowed evaluating the HTO wash-out factor with rain precipitation (Table 1).. The results are applied in (Piskunov, 2011) for the development and validation of various models of washout.

Table 1. Experimental values of the wash-out factor.

Exp. №.	$\tilde{\Lambda}, \text{sec}^{-1}$
1	13.5·10-5
2	18·10-5
4	12.4·10-5
5	14·10-5

The authors express their grateful acknowledgement to the International Science and Technology Center (ISTC, Moscow) for the support of the experimental research into tritium wash-out under project № # 654-99.

Hauser, D., P. Amayenc, B. Nutten, and P. Waldteufel, (1984) *A new optical instrument for simultaneous measurement of raindrop diameter and fall speed distributions*. J. Atmos. Oceanic Technol., Vol. 1, p. 256-269.

Piskunov V.N. (2011) *Rate determination for precipitation scavenging of HTO vapour*. LMC8 abstract, September 6-10, Wien, Austria.

Long-range transport of radionuclides released from Fukushima accident into the Iberian Peninsula

M.A. Hernández-Ceballos, R.L.Lozano*, E.G. San Miguel and J.P. Bolívar

[1]Department of Applied Physic, University of Huelva, Huelva, 21171, Spain
Keywords: Fukushima, Iberian Peninsula, air masses, radionuclides.
*Presenting author email: rafa.lozano@dfa.uhu.es

Massive amount of artificial radionuclides were released from the nuclear reactors located at Fukushima, northeast of Japan between 12th and 16th March 2011 following the earthquake and tsunami occurred on 11th March. The total atmospheric releases of ^{134}Cs and ^{137}Cs during this period were estimated to be around 15.6 and 13 PBq, respectively. The analysis of the 8 days air mass forward movements at 1000 m during 12th -16th March showed an eastward displacement of the plume from Fukushima (Figure 1), bifurcated in two branches outside of Japan during 12th-16th March: northern and southern branches, being in agreement with the simulation of the potential dispersion of the radioactive cloud after the nuclear accident of Fukushima.

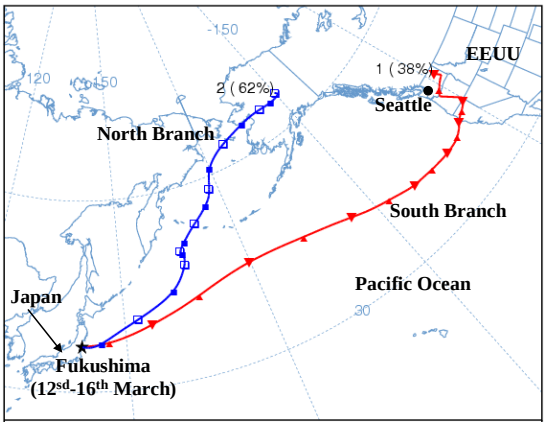

Figure 1. The two main air mass branches (centroids) from Fukushima Daiichi nuclear power plant from 12th to 16th March. Each centroid has a temporal coverage of 192 hours (8 days) and initial height of 1000 m.

The south branch air mass was displaced toward the western North America, located more than 7000 km, and arrived the western part of the North America on March 16 (Díaz-León et al 2011). Taking this fact into account, the analysis of backward trajectories over south-western Iberian Peninsula justified the connection of this south branch with the higher activity concentrations of several man-made radionuclides (such as 131I, 132I, 132Te, 134Cs and 137Cs) registered in Huelva city on 27th-28th March (Lozano et al 2011).

Trying to minimize the uncertainty calculation associated to each trajectory, the backward air mass analysis was carried out in two steps. In a first step, 8 days hourly backward trajectories at 1000 m were calculated at Huelva city from 27th-28th March, and secondly, taking the city of Washington DC as reference point of the east coast of North America, from 19th- 20th March. After that, the daily average path (centroid) was calculated for each day, representing the 8 day backward dynamic pattern over both sites, and, thus, joining both studies it was possible to analyze the dynamic of air mass over Huelva city with a temporal coverage of 16 days.

The results obtained (Figure 2) confirmed the relationship between the Fukushima release and the higher concentrations measured in Huelva 27th-28th March, defining an air mass movement throughout the Pacific Ocean–North America–Atlantic Ocean until finally reaching the South-western Iberian Peninsula. In addition, these results indicated the limited influence of the north branch in south Europe, which was responsible of the activity concentrations observed in central-north Europe (Masson et al 2011).

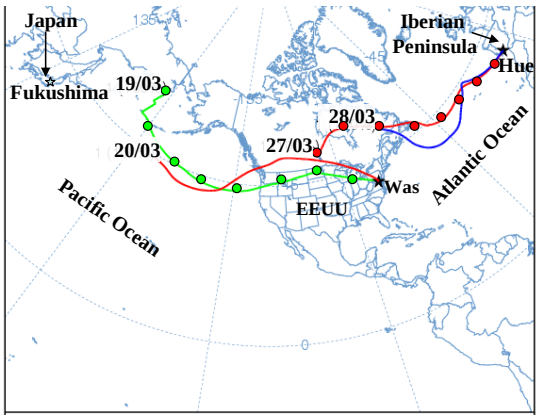

Figure 2. Horizontal displacement of the 8 days backward trajectories over Washington DC (Was) during 19th-20th March and Huelva (Hue) during 27th-28th March 2011 at a final height of 1000 m.

Diaz Leon, J., Jaffe, D.A., Kaspar, J., Knecht, A., Miller, M.L., Robertson, R.G.H. & Schubert, A.G. (2011). Arrival time and magnitude of airborne fission products from the Fukushima, Japan, reactor incident as measured in Seattle, WA, USA. J. Environ. Radioactiv 102, 1032-1038.

Lozano, R.L., Hernández-Ceballos, M.A., Adame, J.A., Casas-Ruíz, M., Sorbías, M., San Miguel, E.G. & Bolívar, J.P. (2011) Atmospheric routes involved in the radioactive impact of Fukuhima accident on the Iberian Peninsula. Environ. Int. 37, 1259-1264.

Masson, O., et al. Tracking of airborne radionuclides from the damaged Fukushima Dai-Ichi nuclear reactors by European networks. Environ. Sci. & Techno. 45, 7607-7677 (2011).

Atmospheric radioactivity in the High Arctic following the Fukushima nuclear accident

J. Paatero[1], J. Vira[1], J. Hatakka[1], K. Holmén[2], A.-P. Hyvärinen[1] and Y. Viisanen[1]

[1]Finnish Meteorological Institute, P.O.Box 503, FI-00101 Helsinki, Finland
[2]Norwegian Polar Institute, Fram Centre, Hjalmar Johansens gt. 14, NO-9296 Tromsø, Norway
Keywords: Radioactive aerosols, Arctic aerosols, Long-range transport, Modelling.
Presenting author email: antti-pekka.hyvarinen@fmi.fi

A huge earthquake with a magnitude of 9.0 occurred east of the Honshu Island, Japan (38.32°N, 142.379°E) on 11 March 2011 05:46 UTC. The earthquake and especially the resulting tsunami destroyed the nuclear power plant of Fukushima Dai-ichi. This caused releases of radioactivity to both the atmosphere and the ocean (International Atomic Energy Agency, 2011).

In this work we analysed the aerosol samples collected at Mt. Zeppelin Global Atmosphere Watch (GAW) station (78°58´ N, 11°53´ E), Svalbard to determine the Fukushima-related radionuclides in them. The exposed filters and the field blanks are measured for total beta activity with an automatic alpha/beta analyzer (Mattsson et al., 1996). The gamma emitter content of the filters is assayed with semiconductor gamma spectrometry.

Dispersion of the radioactive release was simulated with the SILAM model (Sofiev et al., 2006). The source term was based on the values reported by the Japan Nuclear Safety Commission, with a total ^{131}I release of 150 PBq. This was assumed to consist of equal fractions in gas and particulate phase.

Particle-bound iodine-131 was first detected at Mt. Zeppelin from a sample collected between 25 March 2011 10:11 UTC and 28 March 2011 13:04 UTC (Fig. 1; Paatero et al., 2012). The highest total beta activity concentration value, 1140 μBq/m³, can in rare cases be of natural origin, i.e. caused by lead-210 (Paatero et al., 2010).

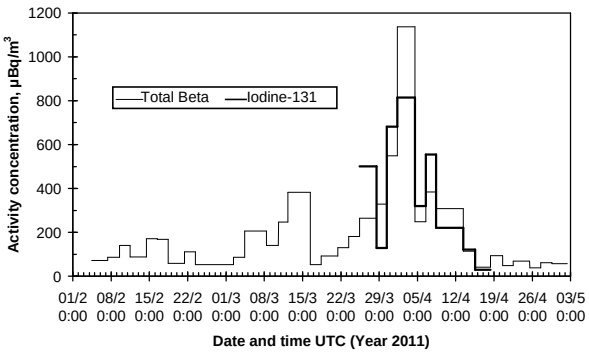

Figure 1. Activity concentrations of total beta and particle-bound ^{131}I (μBq/m3) at Mt. Zeppelin, Svalbard.

The modeled ^{131}I activity concentration at Mt. Zeppelin calculated with the SILAM model supports the time frame (Fig. 2). The calculated concentration levels are clearly lower than the measured ones. This may be related to the uncertainties in the source term. But the model predicts well the temporal behaviour of the ^{131}I activity concentration features. The maximum ^{131}I activity concentration observed at Svalbard was 810 ± 20 μBq/m3. For comparison, a leaking underground nuclear test at Novaya Zemlya, Soviet Union, caused an ^{131}I activity concentration of 5300 μBq/m^3 in northern Finland in August 1987 (Bjurman et al., 1990). It has to be emphasized that we have measured only the fraction of ^{131}I bound to aerosol particles.

The amounts of airborne fission products observed in the High Arctic are insignificant from the radiological point of view. The contribution of the Fukushima-related fission products to the airborne total beta activity is limited too. Similar variations can be found due to the fluctuations in the natural radionuclide content of the air.

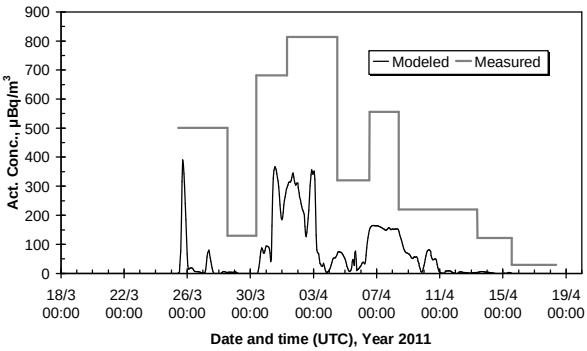

Figure 2. Observed and modeled particle-bound ^{131}I activity concentration (μBq/m^3) at Mt. Zeppelin, Svalbard. The model calculations were performed with the SILAM model.

Bjurman, B., De Geer, L.E., Vintersved, I., Rudjord, A.L., Ugletveit, F., Aaltonen, H., Sinkko, K., Rantavaara, A., Nielsen, S.P., Aarkrog, A. and Kolb, W. (1990). *J. Environ. Radioact.* **11**, 1-14.

International Atomic Energy Agency (2011). www.iaea.org/newscenter/focus/fukushima/missions ummary010611.pdf.

Mattsson, R., Paatero, J. and Hatakka, J. (1996). *Radiat. Prot. Dosim.* **63**, 133-139.

Paatero, J., Buyukay, M., Holmén, K., Hatakka, J. and Viisanen, Y. (2010). *Polar Res.* **29**, 345-352.

Paatero, J., Vira, J., Siitari-Kauppi, M., Hatakka, J., Holmén, K. and Viisanen, Y. (2012). *J. Environ. Radioact.* DOI 10.1016/j.jenvrad.2011.12.027.

Sofiev, M., Siljamo, P., Valkama, I., Ilvonen, M. and Kukkonen, J. (2006). *Atmos. Environ.* **40**, 674-685.

Airborne fission products from the Fukushima accident in the air over Milano, Italy

A. Ioannidou[1,4], E. Giannakaki[2,3], S.Manenti[4] , L.Gini[4] and F. Groppi[4]

[1]Nuclear Physics & Elementary Particle Physics Division, Aristotle University of Thessaloniki, 54124 Greece
[2]Laboratory of Atmospheric Physics, Aristotle University of Thessaloniki, Thessaloniki, 54124, Greece
[3]Finnish Meteorological Institute, Kuopio Unit, Kuopio, FI-70211, Finland
[4]L.A.S.A. Lab, INFN and Università degli Studi di Milano, Via Flli Cervi 201, I-20090 Segrate (MI), Italy
Keywords: nuclear accident, Fukushima accident, radioactive aerosols; radioactive fallout, ^{131}I, ^{134,}Cs, ^{137}Cs
Presenting author email: anta@physics.auth.gr, anta@auth.gr

An earthquake of magnitude 9.0 occurred on March 11, 2011 on the Pacific Ocean side of northern Honshu, Japan, followed by a tsunami that struck the east coast of the Tohoku region. A serious nuclear accident at the Fukushima Daiichi Nuclear Power Plant was caused and fission nuclides released since March 12, 2011. The contaminated air masses were transported up to Europe despite dispersion and washout along the trip (Masson et al., 2011).

Analyses of ^{131}I, ^{137}Cs and ^{134}Cs in airborne aerosols were carried out in daily samples in Milano, Italy (45°N) after the Fukushima accident during the period of March-April, 2011. The two maxima found in radionuclide concentrations (April 3, 2011 and April 7, 2011) were related to complicated long-range air mass transport from Japan across the Pacific to Central Europe. HYSPLIT backward trajectories and meteorological data were applied for interpretation of activity variations of measured radionuclides observed at the site of investigation.

The maximum ^{131}I activity concentration observed in Milano (467 μBq m^{-3}) was almost similar with the highest value (497 μBq m^{-3}) observed in Thessaloniki, Greece, 40°N, (Manolopoulou et al, 2011) and the highest observed value (490μBq m^{-3}) in Athens Greece, 37°, (Kritidis et al., 2012) but lower than that observed (810 μBq m^{-3}) in Svalbard, 78°, (Paatero et al., 2012) and in Lithuania, 54°, (3700 μBq m^{-3}, Lujaniene, 2012). The maximum ^{137}Cs activity concentration at Milano was 63 μBq m^{-3}, while in Thessaloniki, Greece was 145 μBq m^{-3} and in Svalbard was 675 μBq m^{-3}.

The ^{134}Cs/^{137}Cs activity ratio was about 1, related to the burn-up history of the damaged nuclear fuel of the damaged nuclear reactor. The presence of more than one peak of ^{131}I and $^{137,\ 134}$Cs indicates that the radionuclides were continuously transferred from Fukushima, Japan to Europe till the end of April, 2011. The large ^{131}I/^{137}Cs ratio, observed during the first days after the accident, as high as 18, followed by lower values during the next days, as low as 3, reflects not only the initial release ratio but also the different volatility, attachment and removal of the two isotopes during transportation due to their different physicochemical properties.

The NOAA HYSPLIT model (Draxler and Rolph, 2011) was used to assess the transport pattern and to explain the deviation in radionuclide activity concentrations found in Milano, Italy. Thirteen days (312) back-trajectories were calculated for 500, 3000 and 5000m arrival height and for 12 UTC time. The trajectories are labeled every 24 h by a filled symbol. The vertical projection of the trajectories with time is shown in the panel below the map. An example of transported air mass at 07 of April 2011 at Milano is presented in Fig. 1. The results showed a direct transfer from Fukushima across the Pacific Ocean, a transport through the North Pole and a pathway through the Greenland and Iceland at height of 500m to Milano. The air masses at higher altitudes were rapidly transported, while the air masses at 500m exhibited rather slow transport.

This work gives the extent of contamination in Northern Italy due to Fukushima fallout and interprets any measured activity at the site of investigation as these resulted from a complicated air mass transport, arrival time and height, meteorology and downward transport.

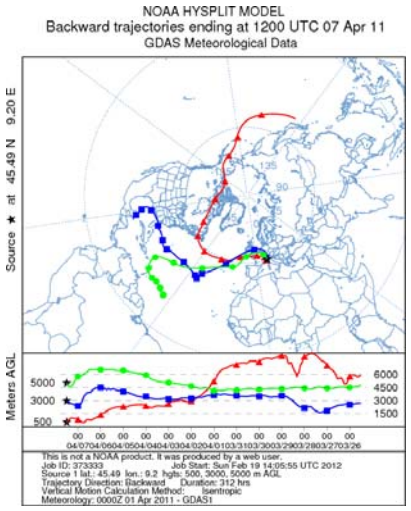

Figure 1. Thirteen-day back trajectories, arrival to Milano 7 April 2011, at heights 500, 3000 5000 m.

Draxler, R.R. and Rolph, G.D. (2011) HYSPLIT Model access via NOAA ARL READY Website (http://ready.arl.noaa.gov/HYSPLIT.php). NOAA Air Resources Laboratory, Silver Spring, MD.

Kritidis, P., Florou, H., Eleftheriadis, K., et al. (2012) *J. Envir.Radioac.* doi./10.1016/j.jenvrad.2011.12.006

Lujanienė,G., Byčenkienė,S., Povinec,P.,Gera M, (2012) *J.Envir .Radioact.* doi:10.1016/j.jenvrad.2011.12.004

Masson, O., et al. (2011) *Environ. Sci. Technology* **45**, 7670-7677.

Paatero, J., Vira, J., Siitari-Kauppi, M., Hatakka J., Holmen, K., and Viisanen Y. (2012) *J. Envir. Radioac.* doi/10.1016/j.jenvrad.2011.12.027

Modification of cloud properties by the Eyjafjallajökull eruption

H Vogel[1], M. Bangert[1], B. Vogel[1], A. Wintzen[1], D. Barahona[2], A. Nenes[3], and J. Förstner[4]

[1]Institute for Meteorology and Climate Research, Karlsruhe Institute of Technology (KIT), Germany
[2]Global Modeling and Assimilation Office, NASA GSFC, Greenbelt, MD, USA
[3]Georgia Institute of Technology, School of Earth & Atmospheric Sciences and Chemical & Biomolecular Engineering, USA
[4]Deutscher Wetterdienst (DWD, Germany

Keywords: activation, cloud, aerosol modelling, regional scale, volcanic ash.
Presenting author email: heike.vogel@kit.edu

After resting for 187 years the volcano Eyjafjallajökull, Island, woke up again at March 20th, 2010. Starting at April 14th massive emissions of volcanic ash occurred and finally lead to a shutdown of civil aviation over entire Europe. The emissions went on with variable strength until May 23rd, 2010. The volcanic eruption offers a unique field experiment for investigating atmospheric processes as transport, radiation and cloud formation on a large variety of scales applying both observations and numerical models.

We used the comprehensive online coupled model system COSMO-ART (Vogel *et al.*, 2009) to simulate the dispersion of the ash plume. COSMO-ART is the extension of the operational weather forecast model COSMO (Baldauf *et al.*, 2011) of the Deutscher Wetterdienst (German Weather Service). Six individual size distributions of the ash particles were simulated starting from 1 µm up to 30 µm. Deposition, sedimentation, and below cloud scavenging were taken into account. For the source heights we used data that were published by the volcanic ash advisory centre London (VAAC). During specific periods not only ash particles were emitted but also SO_2. Simulations taken into account these gas phase emissions additionally to all the other anthropogenic and natural emissions of gases and particles show the impact on the various aerosol concentrations. E.g. at the beginning of May 2008 due to strong northerly winds nucleation over the Iberian Peninsula is simulated leading to rather high number concentrations in that area (Fig.1).

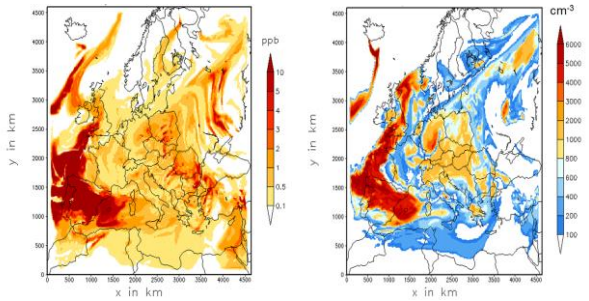

Figure 1. Simulated SO2 concentration (left) and number concentration of the Aitken mode particles (right) at 3 km height on 06/05/2010 at 23 CET.

For the investigation of the impact of the various aerosol particles on the cloud microphysics and therefore on cloud properties COSMO-ART was coupled with the two-moment cloud microphysics scheme of Seifert and Beheng (2006) by using comprehensive parameterisations for aerosol activation (Barahona *et al.*, 2010) and ice nucleation (Barahona and Nenes, 2009). The activation of the ash particles is based on FHH adsorption activation theory (Kumar *et al.*, 2009) and measurements of the activation behaviour of ash samples of the Eyjafjallajökull. Simulations were performed taking into account the anthropogenic and natural emissions of gases and particles to investigate the impact of the ash particles on cloud formation. Figure 2 shows a joint histogram of the difference of occurrence of grid points with a specific ice crystal number concentration at April 18th 2008. The ash particles cause an increase in ice crystal number concentration in the temperature range between 250 and 265 K. The implication on the microphysical cloud properties will be presented.

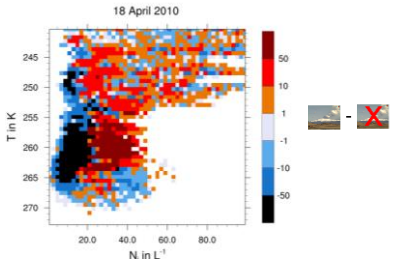

Figure 2. Joint histogram of the difference of occurrence of ice crystal number concentration.

Baldauf, M., Seifert, A., Foerstner, J., Majewski, D., Raschendorfer, M., and Reinhardt, T. (2011) *Mon Wea Rev*. doi:10.1175/MWR-D-10-05013.1 (e-view).

Barahona, D., West, R. E. L., Stier, P., Romakkaniemi, S., Kokkola, H., and Nenes, A. (2010) *Atmos. Chem. Phys*., **10**, 2467-2473.

Barahona, D. and Nenes, A. (2009) *Atmos. Chem.Phys*., 9, 5933-5948.

Kumar, P., Sokolik, I. N., and Nenes, A. (2009) Atmos. Chem. Phys., **9**, 2517-2532.

Seifert and Beheng (2006) *Meteorol. Atmos. Phys*., **92**, 45-66.

VACC, www.metoffice.gov.uk/aviation/vaac/.

Vogel, B., Vogel, H., Baeumer, D., Bangert, M., Lundgren, K., Rinke, R., and Stanelle T. (2009) *Atmos. Chem. Phys*. **9**, 8661–8680.

Comparison of three particle number concentration standards for CPC calibration in the particle size range from 10 nm up to 10 µm

Jaakko Yli-Ojanperä[1], Hiromu Sakurai[2], Kenjiro Iida[2], Jyrki M. Mäkelä[1], Kensei Ehara[2] and Jorma Keskinen[1]

[1]Tampere University of Technology, Aerosol Physics Laboratory, Korkeakoulunkatu 3, P.O. Box 692, FI 33101 Tampere, Finland
[2]National Institute of Advanced Industrial Science and Technology (AIST), 1-1-1- Umezono, Tsukuba, Ibaraki 305-8563, Japan
Keywords: CPC, Instrumentation, Measurement, Number concentration, Standard, Calibration
Presenting author e-mail: hiromu.sakurai@aist.go.jp

Aerosol particle measurement is widely applied for example in clean rooms of production facilities and in studying particulate emissions from traffic and industry. In these applications, measurements of particle number concentration is of particular interest because it is limited by standards and/or legislation. In these fields, the commonly applied instruments are optical and condensation particle counters (OPC/CPC). Calibration of OPCs/CPCs is, however, challenging for at least two reasons. Firstly, no internationally coherent number concentration standard (NCS) exists for this purpose. Secondly, no single standard can cover the whole measuring particle size range of these instruments, which extends to several orders of magnitude.

In our recent study, a comparison between three number concentration standards was conducted by calibrating the same CPC unit (Model 3772, TSI Inc.) with each standard (Yli-Ojanperä et al., 2012). The standards were: the primary NCS of the National Institute of Advanced Industrial Science and Technology (AIST, Japan), the Single Charged Aerosol Reference (SCAR, Finland) and the Inkjet Aerosol Generator (IAG) of AIST (Sakurai and Ehara, 2011; Yli-Ojanperä et al., 2010; Iida et al., 2010). All of the measurements were carried out at AIST in the same laboratory.

The first two standards are measurement instrument-type standards, in which the reference number concentration is measured with a Faraday cup aerosol electrometer simultaneously with the CPC concentration measurement. These standards use different approach for producing singly charged calibration aerosol. The third standard, the IAG, is a generator-type standard, in which the particle number concentration and the particle size at the inlet of the CPC can be derived directly from the operation parameters of the generator. The particle size ranges in the CPC calibration performed in this study were between 10 and 300 nm for the primary NCS of AIST, between 12 nm and 1 µm for the SCAR and between 200 nm and 10 µm for the IAG.

Regarding the comparison, the SCAR and two other standards had sufficient overlaps in the size axis. Comparisons were made in terms of the CPC detection efficiency which was the ratio of the concentration reported by the CPC to the concentration by a standard. The results obtained with the three standards were found to agree at all overlapping particle sizes within the uncertainty limits, which was for each standard ~ 0.01 – 0.02 in the expanded uncertainty with k = 2. From the metrological perspective, the agreement of the results is an important step towards internationally coherent number concentration standards.

As a result of this study, a traceable calibration from 10 nm to 10 µm, which covered the whole operating particle size range of the CPC, was carried out for the first time (Yli-Ojanperä et al., 2012). The calibration results are presented in Fig. 1. The results indicate that the detection efficiency was constant at the plateau efficiency of ~ 0.95 approximately from 30 nm to 3 µm.

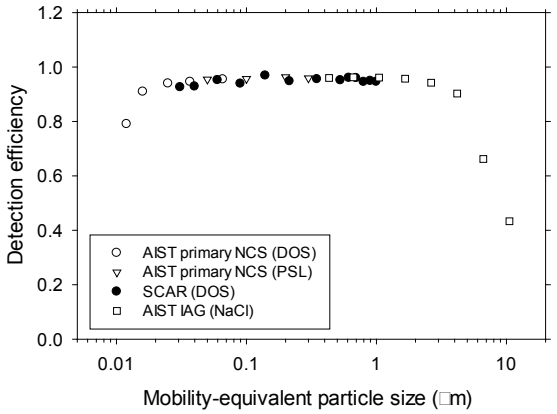

Figure 1. Calibration results obtained with the three standards for the same CPC unit (TSI Model 3772).

Iida, K., Sakurai, H., Saito, K., Ehara, K. (2010) An inkjet aerosol generator for calibrating particle counters. *Abstract book of International Aerosol Conference 2010 Helsinki*, Poster number P1E59.

Sakurai, H. and Ehara, K. (2011) Evaluation of uncertainties in femtoampere current measurement for the number concentration standard of aerosol nanoparticles. *Meas. Sci. Technol,*. **22** 024009

Yli-Ojanperä, J., Mäkelä, J. M., Marjamäki, M., Rostedt, A. and Keskinen, J. (2010) Towards traceable particle number concentration standard: Single charged aerosol reference (SCAR). *J. Aerosol Sci*., 41, 719–28.

Yli-Ojanperä, J., Sakurai, H., Iida, K., Mäkelä, J.M., Ehara, K. and Keskinen, J. (2012) Comparison of three overlapping particle number concentration standards through CPC calibration in a wide particle size range. Submitted to *Aerosol Sci. Technol.*

Large-scale modelling of polycyclic aromatic hydrocarbons and polychlorinated dibenzodioxins in open fire aerosols: On the contribution of biomass burning to POPs in air in Africa

G. Lammel [1,2], A. Heil [3] and I. Stemmler [1]

[1]Max Planck Institute for Chemistry, Mainz, Germany
[2]Masaryk University, Research Centre for Toxic Compounds in the Environment, Brno, Czech Republic
[3]Helmholtz Research Centre Jülich, Institute for Energy & Climate Research, Jülich, Germany
Keywords: persistent organic pollutants, aerosol model, biomass burning, gas-particle partitioning
E-mail contact: g.lammel@mpic.de

Biomass burning is a source for persistent organic pollutants (POPs), i.e. polychlorinated dibenzodioxins and -furanes (PCDD/Fs) and polycyclic aromatic hydrocarbons (PAHs) and may trigger secondary emissions of other POPs stored in soil.

Transport, transformation (OH and O_3 reactions in the gas-phase) and surface exchange are simulated using the global multicompartment chemistry-transport model MPI-MCTM (Semeena et al., 2006; Lammel et al., 2009) which includes the dynamic aerosol sub-model HAM. The atmospheric sub-model was nudged to ECMWF re-analysis data. Emissions were based on recommended (PCDDs; UNEP, 2005) and selected (PAHs) emission factors and daily real-time fire data (fire radiative power measured from MODIS; Heil et al., 2010). Gas-particle partitioning is determined by absorption in OM (PCDDs) or absorption and adsorption to BC (PAHs; Lohmann and Lammel, 2004). Reactions on particles were neglected in lack of data.

Continental half-year (Jan-June 2008) mean near-ground atmospheric concentrations are 0.0076, 0.52 and 3.32 fg m^{-3} of 2,3,7,8-TCDD, 1,2,3,4,6,7,8-HpCDD and OCDD, respectively, and 0.82, 0.48, 0.25 and 0.022 ng m^{-3} of phenanthrene, fluoranthene, pyrene and benzo(a)pyrene, respectively. Maxima are in the range 10-100 fg m^{-3} for HpCDD and OCDD, one order of magnitude lower for TCDD. High concentrations of PCDD and PAH are predicted in the free troposphere, stretching far into the Gulf of Guinea (Fig. 1). Based on comparison with observations (passive air sampling at 14 sites; Klánová et al., 2009) it is concluded that large open fires in Africa in 2008 have determined the observed PAH levels in the respective region, contributed up to ≈30% of observed PCDD levels, and accounted for typically 1-10% of the continental background of these POPs.

Exceedances of observed PAH levels indicate overestimated emission factors. The incomplete knowledge of chemical kinetics of gaseous and particle-associated PAHs is severely limiting source attribution and understanding of transport and fate (Lammel et al., 2009; Dvorská et al., 2011). Validation of passive sampling techniques by side-by-side sampling with active samplers needs to be extended to high temperatures, particularly for semivolatile species.

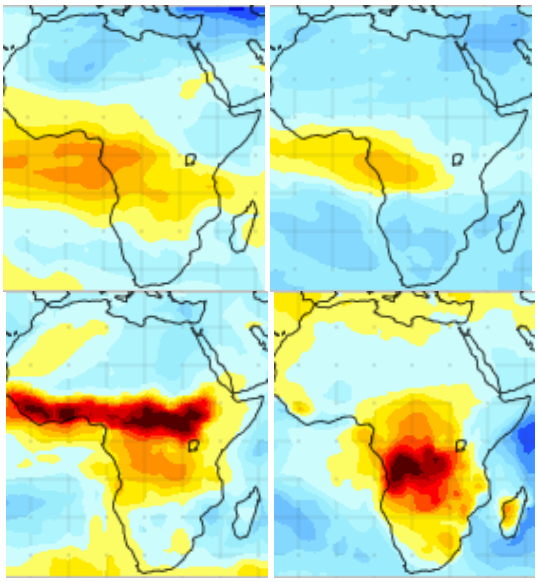

Figure 1. Model-predicted distributions of the dioxin HpCDD from open fires in January (left column) and June (right column) 2008 at 5000 m height (upper row) and ground-level (lower row).

This research was supported by the Granting Agency of the Czech Republic and the European Commission, European Structural Funds (project CETOCOEN) and 7th FWP R&D (project ArcRisk).

Dvorská, A., Lammel, G., and Klánová, J. (2011) *Atmos. Environ.* **45**, 420-427.

Heil, A., Kaiser, J.W., van der Werf, G.R., Wooster, M.J., Schultz, M.G., and Denier van der Gon, H. (2010) ECMWF Tech. Memo No. 628, Reading, UK.

Klánová, J., Čupr, P., Holoubek, I., Borůvková, J., Přibylová, P., Kareš, R., Tomšej, T., and Ocelka, T. (2009) *J. Environ. Monit.* **11**, 1952-1963.

Lammel, G., Sehili, A.M., Bond, T.C., Feichter, J., and Grassl, H. (2009) *Chemosphere* **76**, 98-106.

Lohmann, R., and Lammel, G. (2004) *Environ. Sci. Technol.* **38**, 3793-3803.

Semeena, V.S., Feichter, J., and Lammel, G. (2006) *Atmos. Chem. Phys.* **6**, 1231-1248.

UNEP Chemicals (2005) *Standardized toolkit for identification and quantification of dioxin and furan releases*, Genève, Switzerland.

Gas-particle partitioning and air-sea exchange of polycyclic aromatic hydrocarbons and polychlorinated biphenyls in the central and eastern Mediterranean

Marie D. Mulder[1], Jana Klánová[1], Petr Kukučka[1], Jan Kuta[1], Gerhard Lammel[1,2], Roman Prokeš[1]

[1]Masaryk University, Research Centre for Toxic Compounds in the Environment, Brno, Czech Republic
[2]Max Planck Institute for Chemistry, Mainz, Germany
E-mail contact: mulder@recetox.muni.cz

The marine atmospheric environment is a receptor for polycyclic aromatic hydrocarbons (PAHs) and polychlorinated biphenyls (PCBs) which are advected from combustion sources on land (power plants, biomass burning, road transport). Marine PAH sources may be significant near transport routes (ship exhaust). A number of PAHs and PCBs are semivolatile (saturation vapour pressures at 298 K in the range 10^{-6}-10^{-2} Pa) and, hence partition between the phases of the atmospheric aerosol, influenced by temperature, particulate phase chemical composition and particle size. Semivolatile substances may be subject to re-volatilisation from the sea surface. Net-deposition seems to prevail for PAHs wherever determined (e.g. Tsapakis et al., 2006).

Samples were collected along a cruise of RV Urania in the central and eastern Mediterranean, 27 August – 11 September 2010. The gaseous and particulate phases were addressed separately by sorption to polyurethane foam placed downstream a total high-volume filter or cascade impactor, respectively (e.g. Lammel et al., 2010). Analysis was by GC-MS (Holoubek et al., 2007).

The total concentration of 27 3-6 ring PAHs (24 were positively determined) was by average 1.8 ng m^{-3} and varied between 0.3 to 6.3 ng m^{-3} (Figure 1), with ≈10% in the particulate phase, i.e. particles <0.25 µm of aerodynamic diameter. The concentration of the sum of 7 indicator PCBs (PCB28, PCB52, PCB101, PCB118, PCB153, PCB138 and PCB180) was 3.5 (2.0-7.7) pg m^{-3} (Figure 1), with 0.5% in the particulate phase. For abundance aerosol loading and air mass trajectory were apparently less influential than mixing (diel variation of the marine boundary layer). Models to explain gas-particle partitioning models, such as K_{oa} (Finizio et al., 1997) and combined absorption and adsorption (Lohmann and Lammel, 2004) were tested. For chrysene (particle-associated mass fraction $\theta = 0.35$) the latter model predictions are in agreement with observations (given large input data uncertainties, i.e. unknown organic and black carbon concentrations), while the K_{oa} model underestimates for half of the samples, the latter one a small overestimation. For the PCBs in most of the samples, the K_{oa} model underestimates θ, even more so considering a possible sampling artifact (underestimated particulate mass fraction; Mandalakis and Stephanou, 2002).

The fugacity analysis suggests net volitalisation of retene from the sea surface for most of the samples, while for fluoranthene and pyrene a few samples suggest volatilisation, but most fugacity ratios were within the range of uncertainty.

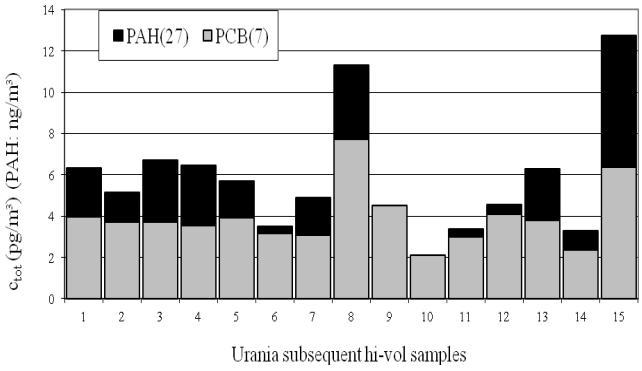

Figure 1. RV Urania high-volume samples total concentration (gas +particle) of 7 PCBs (pg/m^3) and 27 PAHs (ng/m^3), 27 August – 11 September 2010.

We thank the crew of RV Urania and the scientific support of Francesca Sprovieri and colleagues, CNR, Rende. This research was supported by the Granting Agency of the Czech Republic (GACR project No. P503/11/1230) and by the European Commission (European Structural Funds project No. CZ.1.05/2.1.00/01.0001, CETOCOEN).

Finizio, A., Mackay, D., Bidleman, T., and Harner, T. (1997) *Atmos. Environ.* **31(15)**, 2289–2296.

Holoubek, I., Klánová, J., Jarkovský, J. and Kohoutek, J. (2007) *J. Environ. Monitoring* **9**, 557-563.

Lammel, G., Klánová, J., Ilić, P., Kohoutek, J., Gasić, B., Kovacić, I., Lakić, N. and Radić, R. (2010) *Atmos. Environ.* **44**, 5015-5021.

Lohmann, R. and Lammel, G. (2004) *Environ. Sci. Technol.* **38**, 3965-3970.

Mandalakis, M., Tsapakis, M., Tsoga, A. and Stephanou, E. (2002) *Atmos. Environ.* **36**, 4023–4035.

Tsapakis, M., Apostolaki, M., Eisenreich S., and Stephanou E. (2006) *Environ. Sci. Technol.* **40**, 4922-4927.

Biothreat and distant detection of bioaerosol

P.Grzybowski and T.Ciach

Faculty of Chemical and Process Engineering, Warsaw University of Technology, Warsaw 00-645, Poland

Keywords: Bioaerosol, Biaerosol detectionfirst.
Presenting author email: grzybows@ichip.pw.edu.pl

Introduction

Bioterrorism is a potential thread nowadays. It is considered by terroristic groups and it is rather a matter of time when it happens. The spreading of knowledge and experience in biotechnology and accessibility of pathogen cultures increase the risk of terror acts with the use of pathogenic factors. The “natural” SARS epidemic in 2003 demonstrated how weak could be social services struggling with the quickly increasing number of infected individuals. The possibility of the rise of a global pandemic was also being taken into consideration then. It is necessary to work out testing techniques save for the personnel operating in a contaminated area.

Mobile sampling and detecting platform

In the case of bioattack suspicion or biological contamination of the area it is necessary to:

- confirm the contamination
- identify the genus of the pathogen applied
- determine the contaminated zone

A new concept of a wireless controlled mobile platform capable to fill the above outlined expectations is the subject of our study. The platform itself is based onto the IBIS robot (Fig.1). It is electrically driven vehicle operating in the range of 1000 m form the controlling unit. The robot itself plays the role of the carrier of the

Fig.1. Wireless robot IBIS from Industrial Institute for Automation and Measurements (PIAP), Warsaw.

analytical equipment, collects the samples of the air together with the samples of water and the soil, prepares the samples and provide them to the analytical units. It also drives the environment samples to the controlling station where they are additionally analyzed.

The measurements techniques applied

The main function of the mobile platform is the detection of the biothread. To fill this task the vehicle is equipped with the UV light detector operating based on effect of fluorescence of the biomaterial and helps the operator to lead the vehicle toward the most contaminated area where the bioaerosol concentration is increased. Being at the place the IBIS robot takes the samples of the environment and pack them tightly and safely for further analysis. At the same time IBIS prepares the sample of the bioaerosol and sample of the soil, transfers them into a liquid form as a water suspensions and deliver to the next apparatus where follows the analysis based on the surface plasmon resonance phenomenon (SPR). In this step a quick detection of selected types of pathogens is performed. In the case when the SPR test gives a positive result a radio signal is emitted to the control station.

During the whole mission the permanent control of the chemical and radiological threads is conducted thanks to the third detecting device mounted on the vehicle.

Samples of the environment return to the controlling station together with the robot and are additionally analysed with classical polymerase chain reaction (PCR) methods.

Results

A new concept of practical distant detection of biological contamination or bioterror attacks was achieved. The movable setup is able to undertake the mission in various day time and at various weather conditions. The procedures applied are safe for the person and effective in detection and identification steps.

This work was supported by the National Centre for Research and Development under grant 0031/R/ID1/2011/01.

Agranovski V. Ristovski Z.D. (2005) *Real time monitoring of viable bioaerosol*, J. Aerosol Sci. 36, 665-676

Chinowsky T.M. et al. (2012) *Portable 24-analyte surface plasmon resonance instruments for rapid, versatile biodetection* Biosensors and Bioelectronics **22**, 2268-2275

Mechanistic insights into the formation of 2-methyltetrols from the photooxidation of isoprene under low-NO_x conditions

W. Wang[1,*], Y. Iinuma[2], A. Kahnt[1], O. Ryabtsova[1], A. Mutzel[2], R. Vermeylen[1], P. Van der Veken[1], W. Maenhaut[1,3], H. Herrmann[2] and M. Claeys[1]

[1]Department of Pharmaceutical Sciences, University of Antwerp, Antwerp, BE-2610, Belgium
[2]Leibniz-Institut für Troposphärenforschung, Leipzig, D-04318, Germany
[3]Department of Analytical Chemistry, Ghent University, Gent, BE-9000, Belgium
*On leave from: Institute of Environmental Pollution and Health, Shanghai University, Shanghai, 200444, China
Keywords: Aerosol formation, GC-MS, Isoprene, SOA.
Presenting author email: wu.wang@ua.ac.be

Isoprene, a five-carbon diene, is a major contributor to non-methane hydrocarbon emissions in the atmosphere, where it is rapidly oxidised by the hydroxyl (OH) radical. Photooxidation of isoprene leads to volatile gas-phase products but also to secondary organic aerosol (SOA) products such as the 2-methyltetrols (2-MTs). These SOA tracers are known to be second-generation oxidation products but their formation mechanism is uncertain and an outstanding puzzle in atmospheric aerosol chemistry (Claeys et al., 2004, 2010; Surratt et al., 2006; Kleindienst et al., 2009; Paulot et al., 2009). Evidence is available for the formation of isomeric C_5-alkene diols, i.e., 1,2-dihydroxy-2-methyl-3-butene (DMB-1) and 1,2-dihydroxy-3-methyl-3-butene (DMB-2) in both laboratory-generated isoprene SOA and ambient denuder samples (Ruppert and Becker, 2000; Kleindienst et al., 2009). Here, we demonstrate that C_5-alkene diols play a role as intermediates in the formation of the 2-methyltetrols.

DMB-1 was prepared from 2-methyl-2-vinyl-oxirane as reported by Ruppert and Becker (2000), whereas DMB-2 was synthesised from 3,4-epoxy-tetrahydrofuran as described by Hodgson et al. (2001). Isoprene and the C_5-alkene diols were oxidised by OH generated through the photolysis of hydrogen peroxide (H_2O_2) in a Teflon bag. Known amounts of isoprene, DMB-1 or DMB-2 and H_2O_2 were introduced into the chamber before ultraviolet lights were switched on. For experiments with isoprene volatile gas-phase products (i.e., methacrolein, methylvinylketone and methylfuran) and unreacted isoprene were quantified off-line with thermal desorption – gas chromatography/mass spectrometry (TD-GC/MS). Isoprene SOA products were collected on Teflon filters and measured using GC/MS with prior trimethylsilylation (TMS-ation).

Figure 1 shows GC/MS data for isoprene SOA products, analysed directly and after leaving the TMS-ated reaction mixture for two days at room temperature. Upon direct analysis, it can be seen that in addition to the 2-MTs there are two abundant products (labelled with *) with retention times between those of the 2-MTs and 2-methylglyceric acid. These products are assigned to thermal degradation products of C_5-trihydroxyhydro-peroxides, which are unstable and are almost completely converted to the 2-MTs after two days at room temperature. The same products are also formed by photooxidation of DMB-1, whereas isomeric unstable products are formed from DMB-2. Close examination of the GC/MS data obtained for isoprene SOA reveals that the latter DMB-2-related unstable products are also present but at lower relative abundances than the DMB-1-related unstable products.

In conclusion, our results demonstrate that the isomeric C_5-alkene diols DMB-1 and DMB-2 can serve as gas-phase precursors for the 2-methyltetrols through unstable products, tentatively identified as intermediary C_5-trihydroxyhydroperoxides.

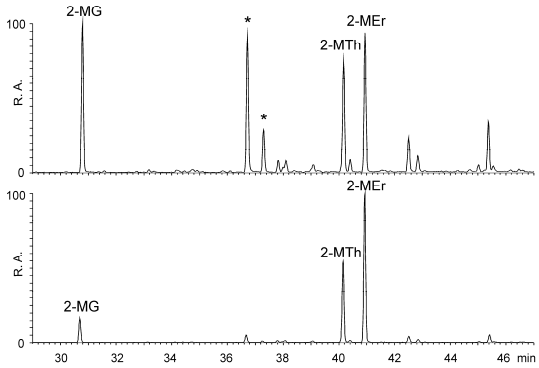

Figure 1. GC/MS data (*m/z* 219 extracted ion chromatograms) for isoprene SOA: TMS-ated extract analysed directly (top panel) and after two days at room temperature (bottom panel). The products labelled with * correspond to thermal degradation products of unstable intermediates that result in the 2-methyltetrols. Abbreviations: 2-MG, 2-methylglyceric acid; 2-MTh, 2-methylthreitol; 2-MEr, 2-methylerythritol; R.A., relative abundance.

Claeys, M. (2010) *Science* **327**; doi:10.1126/science.1180942.
Claeys, M., et al. (2004) *Science* **303**, 1173-1176.
Hodgson, D. M., et al. (2001) *Org. Lett*. **3**, 3401-3403.
Kleindienst, T. E., et al. (2009) *Atmos. Chem. Phys.* **9**, 6541-6558.
Paulot, F., et al. (2009) *Science* **325**, 730-733.
Ruppert, L. and Becker, K. H. (2000) *Atmos. Environ*. **34**, 1529-1542.
Surratt, J. D., et al. (2006) *J. Phys. Chem. A* **110**, 9665-9690.

A non-invasive method to sample exhaled endogenous particles from the respiratory tract

Susanna Lohman[1], Ann-Charlotte Almstrand[1], Anna Bredberg[1], Per Larsson1, Ekaterina Mirogrodskaya[1], Evert Ljungström[2], and Anna-Carin Olin[1]

[1]Occupational and Environmental Medicine, Sahlgrenska Academy at the University of Gothenburg, 405 30 Göteborg, Sweden
[2]Atmospheric Science, Department of Chemistry, University of Gothenburg, 412 96 Göteborg, Sweden
Keywords: particle formation, particle size distribution, particle characterization, lung/particle interaction
Presenting author email: susanna.lohman@amm.gu.se

Purpose

To develop a non-invasive method to monitor small airways

Background

Aerosol particles are generated in the human airways and leave the respiratory tract by exhaled breath. We have recently developed a non-invasive method to count and sample endogenously formed particles in exhaled air (PEx) by use of a cascade impactor. The method can provide important information on ongoing changes in the composition of respiratory tract lining fluid (RTLF) and be valuable for monitoring of ongoing pathological processes in the respiratory system.

Method

A special breathing maneuver is applied during the sampling procedure involving airway closure and re-opening. After inhalation of particle-free air, the subject exhales into the device. Particle concentration in exhaled air is measured with an optical particle counter (Grimm) and the surplus of exhaled air is drawn through a cascade impactor. Concentrations of particles (0.3-2.0 μm) are recorded by means of an optical particle counter. In a separate experiment a scanning mobility particle sizer was used to also measure particles in 0.01-0.43 μm range. The biochemical analyses of the samples are made by MALDI TOF MS (lipids), LC-MS (proteins) and ELISA.

Results

The number and size distribution of endogenous exhaled particles varies between tidal breathing and breathing with airway closure. The majority of exhaled particles are distributed as a broad maximum between 0.2-0.5 μm following re-opening of the airways while number of particles <0.05 μm does not increase with a breathing maneuver that promotes airway closure. The mechanisms of formation of these smaller endogenous particles in exhaled air are still unclear. Number of exhaled particles varies between individuals, but in average 100 L of exhaled air generates 150 ng particles, of which around 25% are proteins and the rest phospholipids. We have characterized the protein composition of PEx and identified 124 proteins. The protein amylase could not be detected, indicating the absence of saliva contamination with this sampling technique.

Conclusions

Our non-invasive method for sampling of exhaled endogenous particles from the respiratory tract represents a new approach for monitoring biochemical processes in the small airways.

Field-Performance of a new time-resolved sampler for the collection of dry aerosol particles

A. Eiguren-Fernandez[1], G.S. Lewis[1], S.R. Spielman[1] and S.V. Hering[1]
[1]Aerosol Dynamics Inc., 935 Grayson St., Berkeley, CA
Keywords: time-resolved PM sampler, anions, PAHs.
Presenting author email: arantza@aerosol.us

A versatile and compact sampling system has been developed to collect sequential time-resolved, dry aerosol particles down to 5 nm in diameter. Using the same technology as in the water-based condensation particle counters this system collects and deposits dry samples of ambient fine and ultrafine particles in small spots (300 um) (Figure 1). The size of the deposition area allows reducing collection times by increasing the concentration of particles in the 50-100ul volume of solvent used to extract the chemicals of interest.

Figure 1. Collection plate and sample spots

The sample collection plates have been designed to easily couple with commercially available autosamplers, reducing the extent of matrix and/or sample manipulation related artifacts, and automating the chemical analysis.

Laboratory testing was conducted at ADI (Berkeley, California, USA) and field performance was assessed by deploying the new system at Stockton, an inland area located in Northern California, and at San Gorgonio National Forest. $PM_{2.5}$ samples we collected for 1 hour for anion analysis (IC-ECD), and 12 hrs for polycyclic aromatic hydrocarbon (HPLC-FL). Parallel filter samples were collected for 48 hrs and used for comparison. System reproducibility and results comparison with a real-time EchoChem (PAS2000) were also evaluated.

Results

Experiments conducted in the laboratory with generated and ambient aerosols show particle collection efficiencies >95% down to 6nm.

System reproducibility was 4% and 5% for sulfate and nitrate measurements, respectively, and ambient concentration measured in the collected samples were comparable to the levels found on filters.

Anion concentrations varied significantly from day to day, with nitrate being the major component (Figure 2).

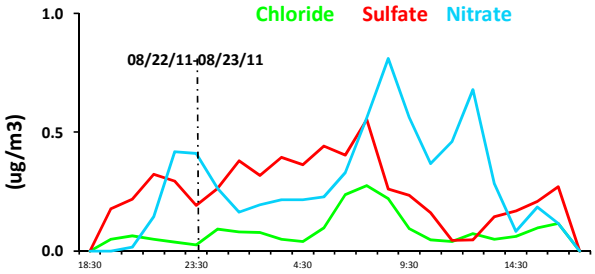

Figure 2. Hourly ambient concentrations of anions

Total PAH concentrations measured with the new collection system vary between 80-110% of those found on 48-hr filter collections. For individual PAHs, better agreement was observed for compounds mostly found in the particle-phase.

With a 12-hr time-resolution afforded by our sampler, we observed a clear day/night pattern in the ambient PAH concentrations. In general night time concentrations were higher than daytime values (figure 3).

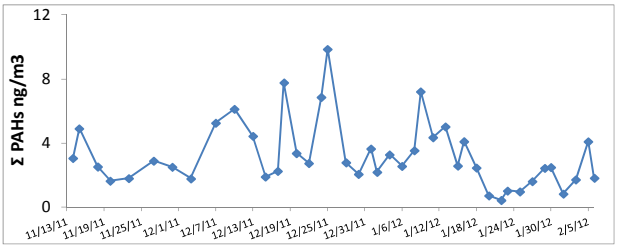

Figure 3. Temporal variability of particle-PAHs

An increase in ambient PAH concentrations was observed during the Christmas Holidays, when contributions from fireplaces added up to the common emission sources.

Diurnal and temporal variations are important when determining contribution of emission sources to ambient pollutants as well as assessing human exposure.

The temporal variability of total PAH concentrations observed with our collection system tracked the diurnal pattern measured simultaneously by an EcoChem PAS2000 sampler. This similarity with another widely used near-real system supports the validity of the new collector.

Acknowledgements

Funding: NIH Grant 1 RC3 ES019081-01
Dr. Jeffrey Collett and Dr. Amy Sullivan (Colorado State University)

High Resolution Ion Mobility Spectrometer (HRIMS): a new instrument for aerosol nucleation studies

E. Montoya, S. López-Vidal, P. Dohányosová, E. Ramiro
RAMEM, SA. Madrid, Spain
emontoya@ioner.eu, www.ioner.eu

High flow, high resolution DMAs able to classify particles, clusters and even ions in the sub-5nm size range have received considerable attention in the last ten years as prefilters for MS and nanoDMAs and even as alternatives to Ion Mobility Spectrometers. Some prototypes have been developed in the lab but to our knowledge no commercial, compact, robust, and user friendly instrument is available yet. We will present the IONER® HRIMS, a bench-top, planar-parallel DMA-based mobility spectrometer. This instrument includes ionization, classification with high resolution (RP 40-80) DMA and electrical detection with high sensitivity. Species such as free ions, VOCs, clusters and particles in the sub-3nm size range can be mobility-classified and detected. Moreover, this instrument allows for a high versatility by changing different measuring conditions such as sheath and sample flowrates and temperatures, ion source (UV, radioactive, corona, electrospray, DBD). Applications of this instrument range from gas-to-particle conversion studies, ion aging, ions source characterization, but also more applied ones such as chemical trace detection thanks to multivariate analysis algorithms.

Figure 1: IONER® HRIMS instrument

As a way to test the instrument, a solution of tetraheptylammonium bromide (THAB) was electrosprayed (IONER® ES-3020) and the inlet slit of the DMA of HRIMS and introduced with a flow of air. The corresponding mobility spectra of THAB are shown in Figure 2. The spectra were measured at different values of the sheath gas in order to optimize the resolving power (RP). The result is shown in Figure 3 for the monomer ion THA^+. As it can be seen, the maximum RP obtained is around 45 at 160 l/min.

As an application example, standards of vapours of toluene were generated in a closed chamber. Concentration was calibrated by GC-MS. Figure 4 shows the mobility spectra of toluene.

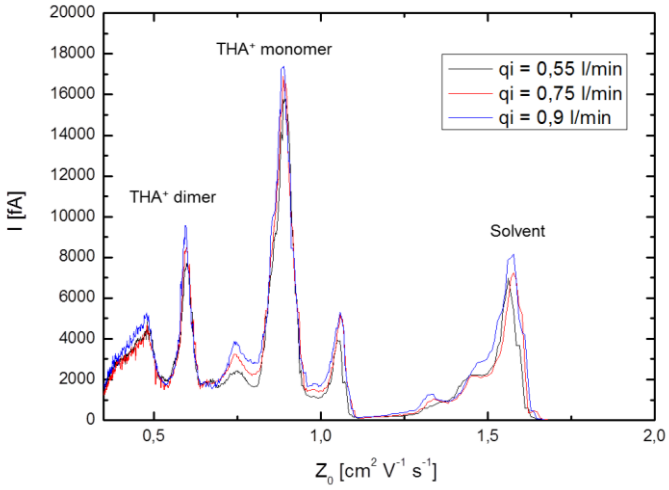

Figure 2: THAB mobility spectrum

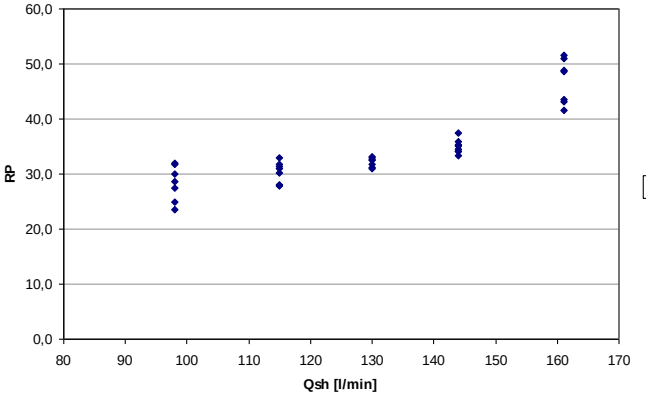

Figure 3: RP of HRIMS for the monomer ion THA^+

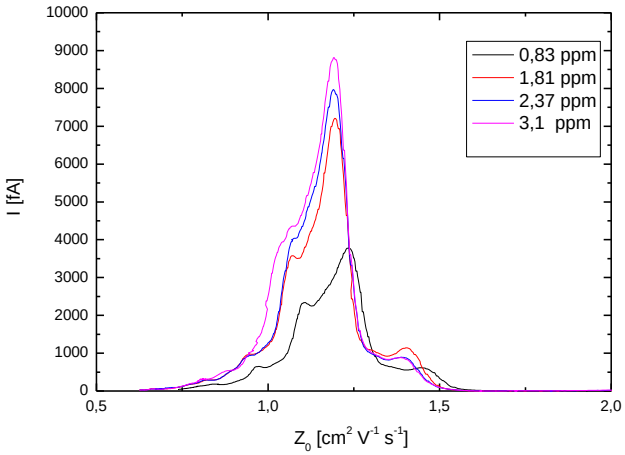

Figure 4: Measurement of different concentrations of toluene

This work was partially supported by the CENIT projects TECNOCAI and PROSAVE

Pre-industrial atmospheric elemental carbon concentrations

Tanveer Ahmed,[1] Akhtar Shareef,[1] Abdul Bari,[1] Liaquat Husain[1,2]

[1]Wadsworth Center, New York State Department of Health, Albany, NY, 12201-0509, USA
[2]Department of Environmental Health Sciences, School of Public Health, State University of New York at Albany, Albany, NY 12201-0509, USA.
Keywords: Elemental Carbon, Black Carbon, Climate Change, Carbonaceous Aerosols.
Presenting author email: lhusain@albany.edu

Elemental carbon, (EC), is directly emitted into the atmosphere during incomplete combustion of forest fires, fossils fuels and biomass burning. EC particles strongly absorb solar radiation, heat the atmosphere and contribute to the global warming (e.g., Seinfeld, 2008; Jacobson, 2001, 2002; Crutzen and Andreae, 1990). The bulk of EC particles are associated with $PM_{2.5}$ and are transported over long distances. When EC is deposited onto snow surfaces, it may initiate melting. Unlike CO_2, the radiative forcing, RF, estimates of EC aerosols are highly uncertain because EC measurements are spatially and temporally sparse. The pre-industrial atmospheric EC, $[EC]_{atm}$, data will provide a valuable baseline for comparison with the industrial period and help to establish the background $[EC]_{atm}$. Currently long-term trends of $[EC]_{atm}$ are estimated based on fuel consumption inventories using emission factors (i.e., how much BC is emitted per g or kg of fuel burnt). These estimates have large uncertainties, which in turn induce large uncertainties in calculating its RF estimates.

EC is removed from the atmosphere mainly by precipitation and deposited in lake sediment. Husain *et al* (2008) showed that in an undisturbed lake $[EC]_{sed}$, is related to $[EC]_{atm}$, through the equation

$$[EC]_{sed} = K*[EC]_{atm} \quad (1)$$

where K is the deposition rate. If K is known $[EC]_{sed}$ can be used to calculate past $[EC]_{atm}$. We determined annual $[EC]_{atm}$ from monthly composites of daily samples collected from 1978 to 2007 at Whiteface Mountain, NY.

We also collected lake sediments cores from two remote high altitude lakes, West Pine Pond, (WP), and Deer Pond, (DP), near Whiteface Mountain. The sediment cores were sliced, freeze dried, and ages determined using ^{210}Pb dating. EC was chemically separated (Husain *et al*, 2008) in individual samples, and quantified by the thermal-optical method. The $[EC]_{atm}$ and $[EC]_{sed}$ for the 1978- 2007 was used in equation (1) to determine K, which in turn was used to calculate back $[EC]_{atm}$ from the lake sediments. The comparison of EC flux in WP and DP between ~1700 and 2005 agreed well; however after ~1950 the EC flux in DP showed low values compared with WP. The mean pre-industrial EC flux in WP for the period ~1700-1850 was 0.05±0.02 $gm^{-2}yr^{-1}$, in excellent agreement with 0.07±0.02 $gm^{-2}yr^{-1}$ from DP for ~1000-1850 periods. Also the pre-industrial EC flux from WP and DP was in excellent agreement with that obtained by Elmquist *et al* (2007), 0.07±50% $gm^{-2}yr^{-1}$ from ~11^{th} century to ~1850. This is a very important conclusion, where two sites almost ~6400 km apart gave the same pre-industrial EC flux. The mean $[EC]_{atm}$ estimated from WP for the period ~1700-1850 was found to be 62±22 ng m^{-3}, in excellent agreement with the value of 68±19 ng m^{-3} found from DP for the ~1000-1850 period. From the results of $[EC]_{atm}$ estimated from WP and DP, it could be concluded that the pre-industrial $[EC]_{atm}$ was stable around 65±29 ng m^{-3}.

Crutzen, P.J., and Andreae, M.O. (1990) *Science* **250**, 1669-1678.

Elmquist, M., Zencak., Z., and Gustafsson, Ö. (2007) *Environmental Science and Technology* **41**, 6926-6932.

Jacobson, M.Z. (2001) *Nature* **409**, 695-697.

Jacobson, M.Z. (2002) *Journal of Geophysical Research* **107,** doi:10.1029/2001JD001376.

Husain, L., Khan, A.J., Ahmed, T., Swami, K., Bari, A., Webber, J.S., and Li., J. (2008) *Journal of GeophysicalResearch***113**, doi:10.1029/2007JD009398.

Nanoparticle synthesis from manganese(II) acetylacetonate

P. Moravec[1], J. Smolík[1], S. Bakardjieva[2] and V.V. Levdansky[3]

[1]Institute of Chemical Process Fundamentals AS CR, v.v.i., Rozvojová 135, Prague, 16502, Czech Republic
[2]Institute of Inorganic Chemistry AS CR, v.v.i., Husinec Řež 1001, 25068, Czech Republic
[3]Heat and Mass Transfer Institute NASB, 15. P. Brovka str., Minsk, 220072, Belarus

Keywords: nanoparticle generation, metal organic CVD, hot wall tube reactor.
Presenting author email: moravec@icpf.cas.cz

Over the last decade, Mn and MnO_x nanoparticles has been extensively investigated due to their great importance in catalysis, electrochemistry, ion exchange materials, batteries and other areas (Si *et al.*, 2005; Han *et al.*, 2006). This work describes preliminary experiments producing manganese nanoparticles by metal organic chemical vapor deposition (MOCVD) using manganese(II) acetylacetonate (MnAA) as a precursor.

Particles were synthesized in an externally heated tube flow reactor with i. d. 25 mm and the length of heated zone 1 m. Experiments were performed in an inert atmosphere using nitrogen as a carrier gas (pyrolysis) as well as in oxidizing atmosphere at 2 and 10 vol. % of oxygen in the reaction mixture (oxidation). Particle production and their characteristics were studied in dependence on reactor temperature (T_R), precursor vapor pressure (P_{MnAA}), oxygen concentration (c_O), and reactor flow rate (Q_R). P_{MnAA} was controlled by the variation of the saturator temperature (T_S). The particle production was monitored by scanning mobility particle sizer (SMPS, TSI model 3936) and samples for particle characterization were deposited onto TEM grids using nanometer aerosol sampler (NAS, TSI model 3089) and on Sterlitech Ag filters. Particle characteristics were studied by HRTEM, SAED, EDS, XRD and XPS.

The SMPS monitoring showed that the particle production depends in particular on precursor concentration and also on the chemistry of precursor decomposition. Number concentration and mean particle size increase with increasing P_{MnAA} and more and larger particles/clusters are generated by pyrolysis than by oxidation. Number concentration also slightly increases with T_R and Q_R, while mean particle size decreases.

Particles produced by pyrolysis were typically agglomerated into clusters with primary particle size between 5 and 10 nm, and with clusters size increasing with increasing P_{MnAA}. Mixture of spherical and facetted particles was formed by oxidation. Size of spherical particles varied between 10 and 30 nm, facetted particles were larger, 20 – 50 nm. Both spherical and facetted particles were partially agglomerated, see Figure 1. Portion of facetted particles increases with increasing T_R and c_O.

Particles prepared by pyrolysis were XRD amorphous and selected area electron diffraction (SAED) patterns were rather week. HRTEM images revealed lattice fringes in the cores of particles, which were mostly indexed as cubic Mn. Particles produced by oxidation, were much more crystalline. Electron diffraction patterns consist of spots, which are difficult to index, and lattice fringes were visible through the whole size of particles. EDS analysis discovered Mn, O and C in the samples with much higher oxygen concentration in the particles prepared by oxidation. XPS analysis of the 5 nm thick surface layer of the samples showed carbon present in bonds C-C, C-H and C-O and manganese in bonds Mn-O. From the above mentioned we can suppose formation of Mn nanoparticles encapsulated in partially decomposed MnAA by pyrolysis and MnO_x nanoparticles by oxidation.

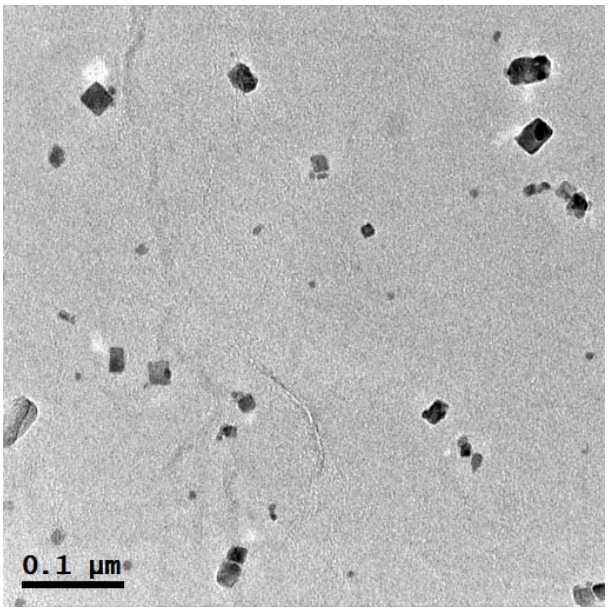

Figure 1. HRTEM image of particles prepared at T_R=800 °C, c_O=10 vol. %, P_{MnAA}=2.2 Pa, Q_R=800 cm^3/min.

This work was supported by the Grant Agency of the Czech Republic under grants 104/07/1093, P503/11/2315 and P503/12/G147. XPS analyses were performed by Dr. Josef Zemek, Institute of Physics AS CR, v.v.i. and XRD analyses by Dr. Jaroslav Maixner, Institute of Chemical technology, Prague.

Si, P.Z., Brück, E., Zhang, Z.D., Tegus, O., Zhang, W.S., Buschow, K.H.J. and Klaasse, J.C.P. (2005) *Mater. Res. Bull.* **40**, 29-37.

Han, Y.-F., Chen, F., Zhong, Z., Ramesh, K., Chen, L. and Widjaja, E. (2006) *J. Phys. Chem. B* **110**, 24450-24456.

Formation of secondary organic aerosol: OH initiated oxidation of dodecane in the presence of NOx

A. Gratien, M. Camredon, Y. Mohamed Yassin, B. Aumont, and J.F. Doussin

Laboratoire Interuniversitaire des Systèmes Atmosphériques, UMR-CNRS 7583, Université Paris-Est Créteil et Université Paris Diderot, Institut Pierre Simon Laplace, 94010 Créteil, France
Keywords: SOA, n-Alkanes, Atmospheric aerosols, Smog chamber, Aerosol formation, modelling
Presenting author email: aline.gratien@lisa.u-pec.fr

Secondary organic aerosols (SOA) are known to be harmful health and have an impact on the climate. Furthermore, the largest uncertainty in predicting climate change is the contribution of airborne particles, which impact climate in more complex ways.

However, the chemical transport models (CTM) fail in estimating SOA formation in the atmosphere. The main factors limiting the chemical accuracy of current and future models are limitations in our knowledge of processes involved in SOA formation and the development of parameterizations directly on the basis of experimental data.

This project aims at a better understanding of the processes involved in SOA formation in both gas and particle phase. The project aims also to build a SOA formation database by delivering parameterization that represents physical-chemical processes controlling SOA formation in CTM models.

The strategy put in place to achieve the objectives of this project is based a combination of explicit modeling with GECKO-A and smog chamber experiments with CESAM. Experiments adapted for the evaluation of models will be performed in CESAM. Comparisons at a molecular scale between GECKO-A and experiments performed in CESAM will be carried out to evaluate and ameliorate our understanding of SOA formation in the atmosphere. These comparisons will contribute to fill the lack of experimental data at the molecular scale for the evaluation of models, such as GECKO-A. GECKO-A will be updated and will then serve as a benchmark for the development of reliable SOA parameterizations for CTM.

A first step in the evaluation of models would consist in studying SOA formation from simplest structures, as alkanes (Presto et al. 2010; Chacon-Madrid and Donahue 2011; Ziemann 2011; Yee et al. 2012). The oxidations of dodecane by OH in the presence of NOx have been studied at 1 atm air in CESAM. The analytical device includes long path in-situ FTIR for the detection of gaseous secondary organic species. In addition, collecting air samples on Tenax solid adsorbent have been performed. The measurements of the SOA mass and SOA composition at the molecular level are performed by SMPS and gas chromatography – mass spectrometry, respectively. The figure 1 shows an example of experiment. Comparisons at a molecular scale between GECKO-A and experiments performed in CESAM will be presented and the atmospheric implications discussed.

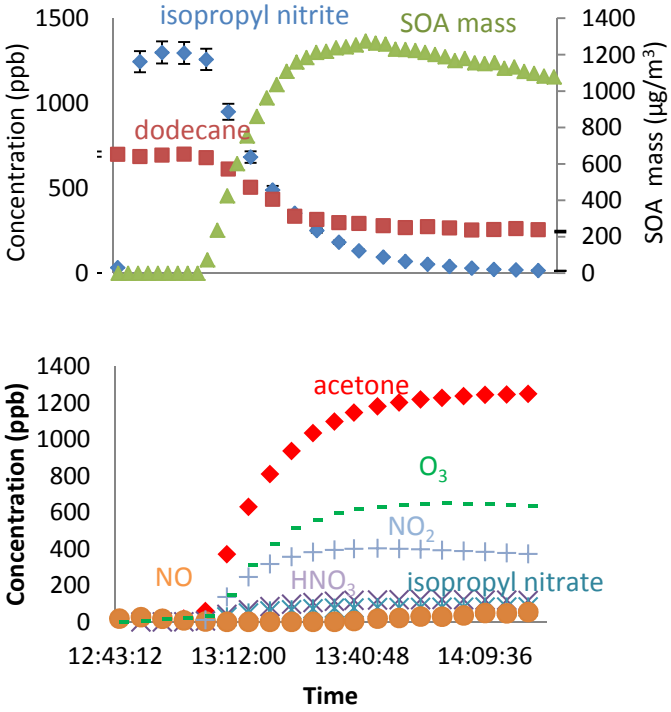

Figure 1. Time dependant concentrations and aerosol mass during an experiment of OH oxidation of dodecane

This work was supported by the European Community within the 7th Framework Programme, section “Support for Research Infrastructure – Integrated Infrastructure Initiative”: EUROCHAMP-2.

Chacon-Madrid, H. J. and N. M. Donahue (2011). *Atmospheric Chemistry and Physics* **11**(20): 10553-10563.

Presto, A. A., M. A. Miracolo, N. M. Donahue and A. L. Robinson (2010). *Environmental Science and Technology* **44**(6): 2029-2034.

Yee, L. D., J. S. Craven, C. L. Loza, K. A. Schilling, N. L. Ng, M. R. Canagaratna, P. J. Ziemann, R. C. Flagan and J. H. Seinfeld (2012). *The Journal of Physical Chemistry A.*

Ziemann, P. J. (2011). *International Reviews in Physical Chemistry* **30**(2): 161-195.

Some considerations about Langley method on the retrieval of spectral irradiance at the TOA and of the total atmospheric optical depth

M. Melgão[1], M.J. Costa[1,2] and A.M. Silva[1]

[1]Geophysical Centre of Évora, University of Évora, Évora, 7000, Portugal
[2]Department of Physics, University of Évora, Évora, 7000, Évora
Keywords: Remote Sensing, Optical Depth
Presenting author email: martamel@uevora.pt

Ground based instruments, soundings with atmospheric balloons and instruments on board of satellites are responsible for the monitoring of the atmosphere. Remote sensing is one of the techniques of measuring atmospheric quantities and it's used by several instruments. In this study we are concerned with a special instrument: spectral radiometer YES MFR-7 (MFR-7). This radiometer measures the diffuse and global spectral hemispherical irradiances. Also, the software instrument makes use of a method derived from the Beer-Bouguer-Lambert law (eq.1) – Langley method. The Langley method consists of using eq. 1 to compute the extra-terrestrial spectral irradiance at the top of the atmosphere ($I_{\lambda 0}$), providing the existence of some conditions: 1) clear sky, 2) low aerosol concentration and 3) a stable atmosphere. At the same time the total spectral optical depth (τ_λ) of the atmosphere can be obtained from the slope of the measured spectral irradiance at the surface, I_λ versus the relative air mass (effective path length), m, as shown in Fig.1.

$$I_\lambda = I_{\lambda 0}\, e^{-\tau_\lambda m} \qquad (1)$$

Optical depth retrieval via Langley regression is complicated due to cloud transits and other time varying interferences (Harrison, et al. 1994) and several conditions (presented above) limit the accuracy of the initial retrieval of the data.

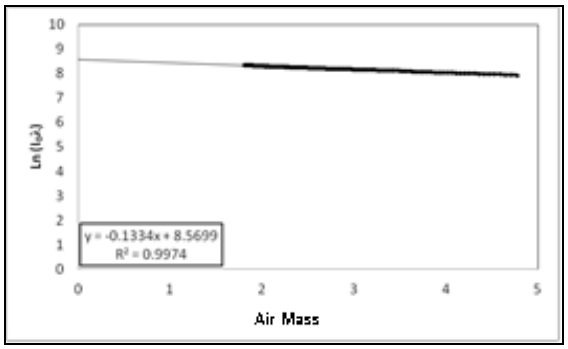

Figure 1. Example of Langley Method for the morning. Spectral channel: 415nm.

The aim of this study is to compare results of the Langley method obtained from the instrument's software with the ones calculated with our methodology (IDL software developed), which executes also a linear fitting of the data, as the one showed in fig.1. For this study we consider 6 years of data, 2003 to 2008 and 2010, although there are some missing data corresponding to periods where the instrument was disable. A particular motivation of the study is to check the reliability of the MFR-7 procedure; its associated error and several parameters associated to the method itself, for example if it's done for every available channel, in the morning or in the afternoon, when compared with the same results obtain independently.

In order to achieve those, we are analysing graphics as the one presented in fig.2, where the first results for the year 2010 can be observed, for the morning period and for channel 415nm. In this specific example, the afternoon period exists but it's very similar so it's not shown here.

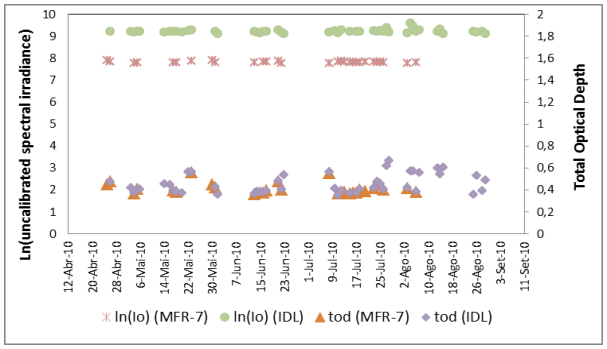

Figure 2. Time evolution series of total spectral optical depth (right axis) and the uncalibrated logarithm of the spectral irradiance derived at the top of the atmosphere (left axis), during the morning period, from the MFR-7 software and IDL software.

Figure 2 shows that $I_{\lambda 0}$ obtained with IDL software are superior to the one given by MFR-7 software and that the total spectral optical depth is similar in both cases. The differences observed probably rely on the used criteria. In the Langley method performed by IDL software, the condition imposed is that the linear correlation coefficient between $Ln(I_\lambda)$ and m (fig.1), was superior to 0.9. In the Langley method performed by the instrument software, several points are dismissed because, for example, cloud transit (could be corrected by speed up the time sampling), thus resulting in a lower number of points in the MFR-7. Considering this fact, a preliminary conclusion is that the filtering of the IDL routine is weaker than the one of the MFR-7 software, which can introduce greater error in the results. The difference between the two values of uncalibrated spectral irradiance is still open for discussion. Presently we still study those differences and which part of the MFR-7 algorithm is responsible for it.

L. Harrison et al (1994). *Objective Algorithms for the Retrieval of Optical Depths from Ground-Based Measurements. Appl. Opt.*, **33**,*5126-5132.*

Lenoble, J. (1993). *Atmospheric Radiative Transfer*. A. Deepak Publishing, USA.

Reduction of combustion alkali aerosols by addition of kaolin to pelletized biomass fuels

C. Boman, J. Fagerström, G. Gårdbro, E. Steinvall and D. Boström

Energy Technology and Thermal Process Chemistry, Umeå University, SE-901 87, Umeå, Sweden

Keywords: alkali, aerosols, combustion, biomass, kaolin, additive
Corresponding author e-mail: christoffer.boman@chem.umu.se

The use of new feedstocks for biomass fuels are pushing the market towards potentially more problematic raw materials with high ash content, e g forest logging residues, energy crops, cereals and industrial waste materials. Compared to stemwood fuels like sawdust, such raw materials generally contain higher concentrations of ash forming elements, where the alkali elements (K and Na), together with Cl, S and P, are of special relevance concerning the aerosol chemistry and formation of fine particles and deposits. The present focus on potential health related effects of combustion aerosols will lead to more stringent regulations of particle emission from small (residential) and medium scale (0.5-3 MW) stationary combustion sources within EU. Since these combustion units lacks advanced particle removal devices, cost effective primary measures (i.e. fuel and process related) will become more attractive to implement. Such fuel related measures (additives or co-combustion) may be used to change the ash transformation processes and the use of Al-silicates as additives during combustion of "problematic" biomass is rather extensively studied. Most common are studies of kaolin as an additive. Kaolin is a clay, mainly consisting of the mineral kaolinite, $Al_2Si_2O_5(OH)_4$. This mineral can remove gaseous alkali compounds by binding potassium and forming K-Al-silicates which have higher melting temperatures than the pure K-silicates and thereby reduce alkali release and aerosol formation [Boman *et al*., 2008; Boström *et al*., 2009; Bäfver *et al*., 2009; Tissari *et al*., 2008; Tran *et al*., 2004; Uberoi *et al*., 1990; Zeuthen *et al*., 2007]. Still, the effect on kaolin addition to different biomass fuels as well as a detailed understanding of suitable addition levels and the effects of different process parameters are still not elucidated. The objective of the present work was to determine the effect of the fuel additive sorbent kaolin on aerosol particle formation and emission during fixed bed combustion of two biomass fuels. In addition, the results will be discussed in comparison with data on alkali release from single pellet tests in a large-sample TGA set-up with same fuels and additive.

Two typical pelletized biomass fuel assortments were used; soft wood and wheat straw. Both fuels were co-pelletized with kaolin powder and the combustion experiments were performed in a typical underfed (fixed bed) residential burner (~10 kW) connected to a reference boiler. Combustion with one level of kaolin was compared to the pure fuels. The content of kaolin in soft wood was 3 wt-% and in wheat straw 7 wt-% (mixing proportions based on dry substance biomass). The kaolin levels were chosen based on earlier experience and chemical equilibrium calculations, and the levels should be enough to elucidate the reduction of alkali aerosols. The combustion performance was monitored by FTIR gas measurements (e.g. CO_2, H_2O, CO, NO/NO_2, HCl, SO_2 and CH_4) in flue gases to ensure good gas burnout and follow the effect of the fuel additive on relevant inorganic gas species. The temperature in the fuel bed (i.e. where the ash is formed) was measured by thermocouples, to better interpret relevant ash transformations on the grate. The aerosol particles were sampled in the flue gases at a temperature of ~150 °C and characterized regarding PM_{tot} mass concentration (standard filter sampling), mass size distribution (low pressure impactor, 0.03-10 µm), number concentration and size distribution (SMPS, 0.01-1 µm) as well as elemental composition (SEM/EDS) and inorganic phase distribution (XRD). In addition, the bottom ash and slag was collected and characterized regarding elemental, morphological and crystalline phase composition. This enables a more complete evaluation of the influence of the kaolin additive on the total ash transformation process.

Preliminary results indicate a clear reduction of alkali aerosol emissions by kaolin addition for both biomass fuels. Further detailed results on the effects on aerosol particle mass and number concentrations as well as ash transformation and aerosol chemistry will be presented from the combustion tests in the pellet burner and discussed in relation to data from single-pellet tests.

This work was supported by the Swedish Energy Agency within the ERA-NET Bioenergy project *FutureBioTec*.

Boman, C. *et al*., (2008) Proc. *16th European Biomass Conference & Exhibition*, Valencia, Spain.
Boström D. *et al*., (2009) *Energy Fuels*, **23**:5184-5190.
Bäfver L.S. *et al*., (2009) *Fuel Process. Technol*. **90**:353-359.
Tissari J. *et al*., (2008) *Energy Fuels* **22**:2033-2042.
Tran K.-Q. *et al*, (2004) *Energy Fuels* **18**:1870-1876.
Uberoi M. *et al.*, (1990) *Prog. Energy Combust. Sci*. **16**:205-211.
Zeuthen J.H. *et al*., (2007) *Energy Fuels* **21**:699-709.

Morphology-Controllable of Porous Hyaluronic Acid Prepared using A Spray-drying Method

Asep Bayu Dani Nandiyanto, Takashi Ogi, and Kikuo Okuyama

Department of Chemical Engineering, Graduate School of Engineering, Hiroshima University, 1-4-1 Kagamiyama, Higashi Hiroshima 739-8527, Japan
Keywords: porous material, aerosol technique, spray route, drug delivery.
Presenting author email: asepbayudn@gmail.com

Recently, production of both powder and solution formulations of pharmaceuticals, especially for inhalation application, has received considerable interest. However, although current methods for this drug fabrication has been well-known, there are significant difficulties: particle size distribution, insufficient process control, high cost, complexity of the process, loss of chemical activity, and problems associated with scaling-up the process (Iskandar, 2009). With this reason, production of specific particle that sufficient for this purpose, and certainly, using an effective method are required.

Based on our experience in the synthesis of porous particles (Iskandar et al,, 2009, Nandiyanto et al, 2009, Nandiyanto et al, 2012), here, we reported the new design porous material, consisted multi-pore types with a good arrangement, was prepared via aerosol route. As a model of drug, we used hyaluronic acid (HA). In the synthesis procedure, HA powder (Kewpie Corp., Japan) was used to prepare aqueous solutions (mass concentration: 0.005-0.5 wt%). Polystyrene particle (PS, JSR, Japan; size = 100, 200, and 300 nm) was added to the aqueous HA, forming the suspension that was then used in spray drying. The mass ratio of HA to PS in the suspension was fixed at 1 to 4. The suspensions were then sprayed using a two-fluid nozzle spray dryer (SD-1000, Eyela, Tokyo Rikakikai Co. Ltd., Japan) at 120 °C (using heated compressed air as carrier gas). The solid particles were collected using a cyclone separator. To obtain porous particles, the collected composite particles were etched with an organic solvent—toluene (Sigma Aldrich, USA)—for one minute to dissolve the PS template particles. The morphology of the prepared particles was examined using a scanning electron micrograph (SEM, Hitachi, S-5000, 20 kV)

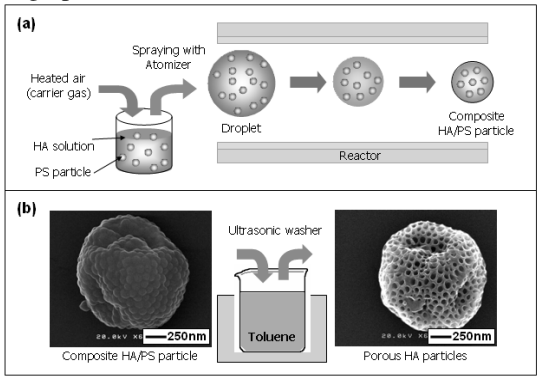

Figure 1. Schematic illustration diagram of the preparation method {(a) composite particle preparation and (b) etching process}

When the solution of HA and PS was spray dried, composite HA/PS particles were produced (Fig. 1a). In this process, heat was used to evaporate the solvent and template. To avoid the use of high temperature heating process, an advanced method that combines spray drying with template removal by dissolution was used to produce porous particles. Fig. 1b shows the morphology of the spray-dried particles before and after template removal. PS particles were arranged on the surface of the droplet, which formed as a result of spraying the solution, due to buoyancy and surface forces; HA solution filled the space. After drying, solid particles with raspberry-like arrangements were produced (Fig. 1b, left SEM figure). The effects of removal of the templating agent via etching that occurred when the primary particles were washed in toluene are shown in Fig. 1b, right SEM figure. PS particles were completely removed leaving holes, the diameters of which corresponded to those of the PS particles used in the process.

The effect of the changing parameters are shown in Fig. 2. The result showed that changing PS size led the production of particles with controllable pore size (Fig. 2a-c), while changing initial precursor resulted in the preparation of particles with controllable particle outer diameter (Fig. 2a,d,e).

Reference

Iskandar, F., A.B.D. Nandiyanto, W. Widiyastuti, L.S. Young, K. Okuyama and L. Gradon (2009) *Acta Biomater.* **5**, 1027-1034

Nandiyanto, A.B.D., S.-G Kim, F. Iskandar and K. Okuyama (2009) *Micropor. Mesopor. Mater.* **120,** 447-453

Nandiyanto, A.B.D., A. Suhendi, T. Ogi, T. Iwaki, and K. Okuyama (2012) *Colloid Surf. A* **396**, 96–105

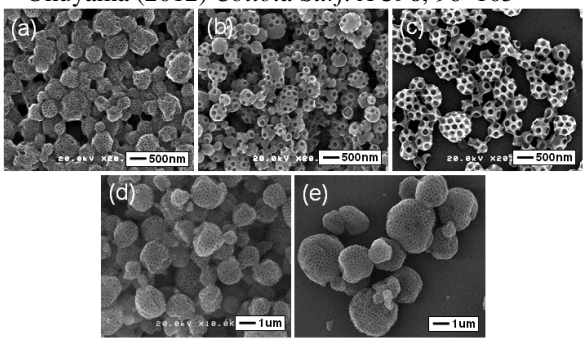

Figure 2. SEM images of HA porous particle as a function of PS size {(a) 100, (b) 200, and (c) 300 nm; using initial precursor of 0.005 wt%} and initial precursor concentration {(d) 0.05 and (e) 0.5 wt%; using PS of 200 nm}

Prague Aerosol Supersite, Suchdol (PASS, urban background)

V. Ždímal[1], J. Ondráček[1], N. Zíková[1], P. Vodička[1], O. Makeš[1], D. Řimnáčová[1], L. Štefancová[1], J. Šilhavý[2], J. Smolík[1] and J. Schwarz[1]

[1] Department of Aerosol and Laser Studies, Institute of Chemical Process Fundamentals, AS CR, v.v.i., Prague, 165 02, Czech Republic
[2] Central Laboratory of Air Quality, Czech Hydrometeorological Institute, Prague, 143 06, Czech Republic
Keywords: atmospheric aerosol, urban background.
Presenting author email: zdimal@icpf.cas.cz

Detailed knowledge of physical and chemical properties of atmospheric aerosol in the urban environment is becoming more important in last years as more adverse health effects of aerosol particles are known. According to the current Czech legislation, concentrations of selected gaseous pollutants and of $PM_{2.5}$ and PM_{10} aerosol fractions are monitored at selected sites. However, this monitoring gives only limited information on properties of measured aerosol, especially concerning the related health effects.

In order to improve this knowledge, a Prague Aerosol Supersite, Suchdol (PASS), has been completed during last years. Various instruments (see Table 1) have been added to the site during several EU and local projects. Recently, the instrumentation covers both physical and chemical properties of sampled atmospheric aerosol in a complex way.

The supersite is hosted by the Institute of Chemical Process Fundamentals (ICPF) located inside a Suchdol campus of the Academy of Sciences of the Czech Republic. This campus is placed in a suburban district of Prague, situated about 6 km NW from Prague's center and about 9 km NE from the airport on a plateau elevated 80 m above the Prague's downtown valley. There are no major sources of air pollution close to the campus except family houses (with local gas heating). The closest road with 10-15 thousands cars per day goes about 250 m eastward from the campus.

The PASS supersite includes aerosol equipment for on-line measurements and long term monitoring, as well as for short-period off-line measurement campaigns including impactor- and filter-based sampling followed by chemical analysis (IC, PIXE, RBS). Highly time-resolved elemental composition can be also measured using a 3DRUM impactor in three size fractions. Recently, the equipment has been extended by an HTDMA (ICPF home-made).

The PASS supersite is connected to the automated imission monitoring station AIM-ASUCA of the Czech Hydrometeorological Institute. The station provides basic information about meteorological conditions (temperature, wind speed and direction, relative humidity, UV intensity), concentrations of selected gaseous pollutants (NO, NO_2, NO_x, O_3, SO_2, CO), and $PM_{2.5}$ / PM_{10} concentrations.

Part of the long term data series obtained during completion of the PASS supersite were published in few papers (Schwarz et al. 2008, Putaud et al., 2010, and Řimnáčová et al., 2011). Results of few short term campaigns were published as well (Ondráček et al., 2011, Štefancová et al., 2010). These and other data files show advantages of such a site for investigations on contrasts between background and urban pollution levels, including various traffic and heating sources localized in different parts of the city.

Table 1. List of aerosol equipment at PASS.

Measured quantity	Measurement range	Instrument	Time resolution	Data available
Size distribution	10 – 470 nm now variable	SMPS 3034 (TSI) rebuilt at IfT	5 min	since 2007 since 2012
	0.52 – 10 μm	APS 3321 (TSI)	5 min	since 2007
Size distribution and chemical composition	50-800 nm	cTOF-AMS (Aerodyne)	1 min	since 2010
EC/OC	PM_{10}, $PM_{2.5}$, $PM_{1.0}$	EC/OC field analyser (Sunset)	2 hours	since 2009
Hygroscopicity	adjustable	HTDMA (ICPF)	about 1 hour	since 2012

Authors gratefully acknowledge support of this work by following projects: Czech Science Foundation – No. CSF P209/11/1342, Norwegian Financial Mechanism – No. MF CZ 0049, ERDF within the Central Europe Programme UFIREG - No. 3CE288P3.

Ondráček, J. et al. (2011) *Atmos. Environ.* **45(29)**, 5090-5100.
Putaud, J-P. et al. (2010) *Atmos. Environ.* **44(10)**, 1308-1320.
Schwarz, J. et al. (2008) *Atmos. Res.* **99(2-4)**, 287-302.
Štefancová, L. et al. (2010) *Atmos. Res.* **98(2-4)**, 237-248.
Řimnáčová, D. et al. (2011) *Atmos. Res.* **101(3)**, 539-552.

Synthesis and Characterization of Pt/WO_3 Nanoparticles Photocatalyst Prepared by Flame Spray Pyrolysis

Takashi Ogi, Asep Bayu Dani Nandiyanto, Agus Purwanto, Kikuo Okuyama

Department of Chemical Engineering, Graduate School of Engineering, Hiroshima University, 1-4-1 Kagamiyama, Higashi Hiroshima 739-8527, Japan
Keywords: nanoparticle, photocatalyst, aerosol technique, spray route
Presenting author email: ogit@hiroshima-u.ac.jp

Tungsten oxide (WO_3) is a visible-light-driven photocatalyst which has many potential applications: energy conversion devices, virus deactivation, and harmful pollutant degradation. Bare WO_3 shows very low photocatalytic activity under visible light irradiation. Many attempts have been made to improve the photocatalytic activity of WO_3. The addition of a co-catalyst, such as platinum (Pt), gold (Au), and silver (Ag), enhances the photodegradation activity of WO_3. Thus far, Pt has been the most powerful co-catalyst for high-activity WO_3 (Purwanto, 2011). However, the high cost of Pt is a primary impediment for a scale-up process.

Herein, in this study, the optimum condition of Pt amount was investigated for Pt/WO_3 nanocatalysts prepared by a flame spray pyrolysis (FSP) method (Widiyandari, 2012). This is a fast, continuous, and controlled aerosol process for the production of nanoparticles.

In this method, $H_2PtCl_6 \cdot 6H_2O$ was mixed with $5(NH_4)_2O \cdot 12WO_3 \cdot 5H_2O$ (ATP) in aqueous solution to produce a homogeneous precursor. A thorough mixing of the Pt and W components was expected to produce a better distribution of Pt in the Pt/ WO_3 nanocatalyst. The preparation of Pt/WO_3 was conducted with a CH_4 flow rate of 0.5 L/min, an O_2 flow rate of 1.1 L/min, and a nitrogen carrier gas flow rate of 2 L/min. The ATP concentration was 0.01 M, and the Pt content was varied from 0 to 0.5 wt.%.

Fig. 1 shows the concentration–time evolution of amaranth degradation by Pt/WO_3 at various levels of Pt content under solar simulated irradiation. The optimal level of Pt addition for high photocatalytic activity was 0.12 wt.%. This concentration was much lower compared with other methods (0.5–1 wt.%). From the XRD analysis, the spectra indicated that WO_3 was monoclinic. The characteristic peaks of Pt were not detected in the spectra due to the low fraction of Pt in the nanocatalyst.

Fig. 2(a) shows the TEM image of Pt/WO_3 (Pt = 0.12 wt.%). The prepared particles were nanorods with aspect ratios ranging from 2 to 5 (diameter 10–20 nm and length 20–50 nm). However, this image does not clearly represent the existence of Pt particles, which may have been due to the small amount of Pt. Further characterization indicated the stacking-fault in the HR-TEM images (Fig. 2(b)), which indirectly implied the existence of Pt. Pt serves as a pool for electrons which lead to the effective excited electron consumption. This results in an efficient charge separation and ensures high activity for Pt/WO_3. This investigation suggests that the optimal condition for Pt/WO_3 is reached at a Pt content of 0.12 wt.%.

Our results showed that FSP-made Pt/WO_3 nanocatalyst required a lower Pt fraction for an efficient photodegradation process compared to the well-known photodeposition method. This lower Pt fraction resulted from a stacking fault of Pt in the WO_3 matrix, as shown in Fig. 2(b). In the photodeposition technique, Pt was deposited onto the WO_3 surface. However, the reduced Pt was not all deposited onto the WO_3 surface. This implies that a higher concentration of Pt is needed for optimal photocatalytic activity. Thus, FSP offers a facile method to produce a Pt/WO_3 nanocatalyst which is a low fraction of Pt for efficient dye photodegradation.

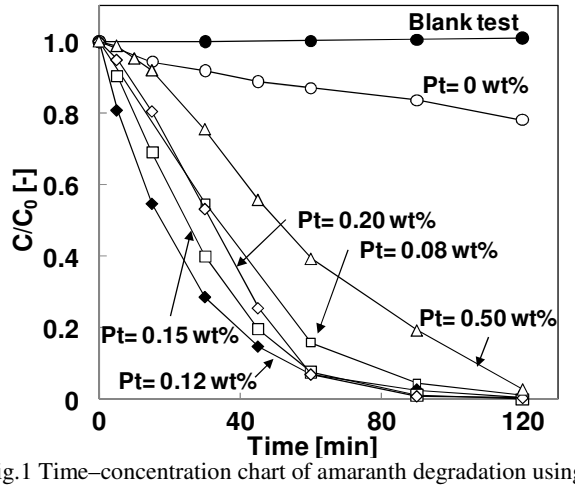

Fig.1 Time–concentration chart of amaranth degradation using Pt/WO_3 nanocomposite in different Pt concentrations.

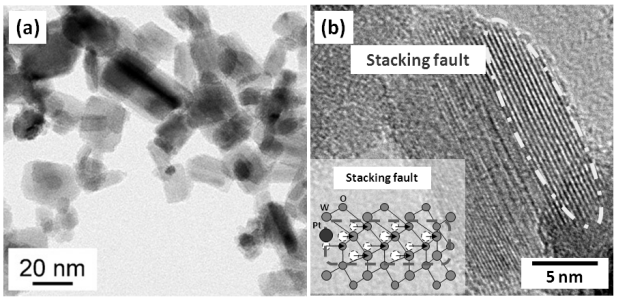

Fig.2 HRTEM image of Pt/WO_3 nanoparticle (Pt=0.12 wt.%)

Reference

Purwanto, A., H. Widiyandari, T. Ogi and K. Okuyama, (2011) *Catal. Commun.*, **12**, 525-529.

Widiyandari, H., A. Purwanto, R. Balgis, T. Ogi, K. Okuyama (2012) *Chem. Eng. J.*, **180**, 323–329.

TiO_2 Thin Film Morphologies Controlled by Aerosol Flame Deposition Process

Jinrui Ding and Kyo-Seon Kim*

Department of Chemical Engineering, Kangwon National University
Chuncheon, Kangwon-Do, 200-701, Korea
Keywords: Columnar Morphology, AFD Process, Photoelectrochemical Properties, TiO_2 Thin Films,
*E-mail: kkyoseon@kangwon.ac.kr

Nanostructured TiO_2 thin films have been extensively studied for use in solar energy applications, such as photosplitting of water and dye sensitized solar cells (Thimsen et al, 2008). The thin film morphology has been identified as an important, efficiency-limiting aspect of TiO_2 film characteristics. It is believed that TiO_2 thin films with one-dimentional morphology have potential to make a breakthrough in efficiency improvement for photoelectrochemical cell. Flame technology for material synthesis was highlighted recently by Strobel (2008) and Pratsinis (2010) to make "smart" nanoparticles for catalysts, sensors, biomaterials and so on. The Aerosol flame deposition process offers an inexpensive way to prepare nanostructured thin films from liquid precursor.

In this study, we prepared nanostructured TiO_2 thin films by aerosol flame deposition process. TiO_2 thin films with columnar morphology deposited on ITO conductive glasses were obtained. The influence of the various process parameters, such as precursor feed rate, depositon height, the total gas flow rate and substrate temperature, on morphology evolution of TiO_2 thin films were investigated, respectively. The structure properties were characterized by Scanning electron microscopy. The photoelectrochemical properties were tested by a Potentiostat (Pinceton Applied Research, Versastat 3).

This research was supported by the Basic Science Research Program through the National Research Foundation of Korea (NRF) grant funded by the Ministry of Education, Science, and Technology (No. 2009-0090428).

Thimsen, E. Rastgar, N. and Biswas, P. (2008) *J. Phys. Chem. C*, **112**, 4134-4140
Strobel, R. and Pratsinis, S.E. (2007) *J. Mater. Chem*., **17**, 4743-4756.
Camenzind, A. Caseri, W.R. and Pratisinis. S.E. (2010) *Nano Today*, **5**, 48-65

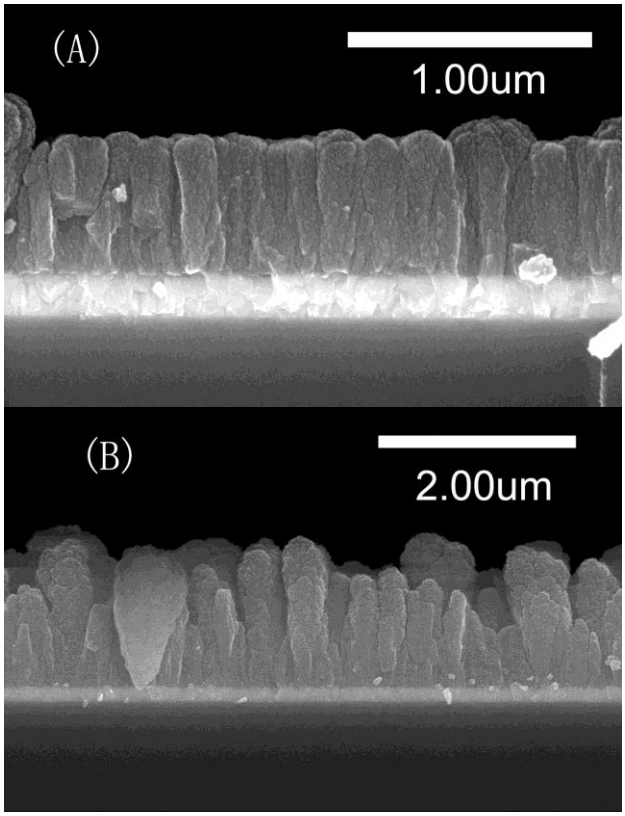

Figure 1: SEM images of TiO_2 thin films deposited with different process conditions: (A) TTIP feed rate: 2.0mmol/h, residence time (τ_{res}): 0.24ms, deposition height: 2cm, deposition time: 8mins, substrate temp.: 150 ℃; (B) TTIP feed rate: 3.5mmol/h, residence time (τ_{res}): 0.22ms, deposition height: 2cm, deposition time: 20mins, substrate temp. : 55±5℃.

Chemical Composition and Hygroscopic Properties of Ultrafine Aerosol Particles in the Atmosphere over an Urban Background Site in Patras, Greece

S. Bezantakos[1,2], E. Konstenidou[3], A. Bougiatioti[4],
K. Eleftheriadis[2], N. Mihalopoulos[4], A. Nenes[5], S. Pandis[3,6], G. Biskos[1]

[1]Dept. of Environment, University of the Aegean, Mytilene, 81100, Greece
[2]Inst. of Nuclear Tech. & Rad. Protection, NCSR Demokritos, 15310 Ag. Paraskevi, Attiki, Greece
[3]Institute of Chemical Engineering, ICE-HT, Patras, 26504, Greece
[4]Environmental Chemical Processes Laboratory, Dept. of Chemistry, University of Crete, Heraklion, 71003, Greece
[5]Schools of Earth & Atmospheric Sciences & Chemical & Biomolecular Engineering, GeorgiaTech, Atlanta, GA, USA
[6]Depts. of Chemical Engineering & Engineering & Public Policy, Carnegie Mellon University, Pittsburgh, PA, U.S.A

Keywords: Aerosol Measurement, Particle size, Particle growth, H-TDMA, Mediterranean
Presenting author email: bezantakos@env.aegean.gr

Ultrafine particles in the atmosphere can absorb and scatter radiation, thereby affecting the climate of the Earth at a local and a global scale (IPCC 2007). The scattering and absorption efficiency of atmospheric particles strongly depend on their ability to take up water (i.e., their hygroscopicity), which in turn is determined by their chemical composition.

In situ measurements of particle hygroscopicity and chemical composition were conducted at an urban background site in Patras from 8 to 27 June 2012. For the measurements we employed a Hygroscopic Tandem Differential Mobility Analyzer (HTDMA; Rader & McMurry, 1986) combined with a Cloud Condensation Nucleus Counter (CCNC; Roberts and Nenes 2005), and a High Resolution Aerosol Mass Spectrometer (HR-AMS; DeCarlo et. al., 2006). Dried aerosol particles having mobility diameter of 40, 60, 80, 100, and 120 nm were selected by the first DMA of the HTDMA system. Half of the monodisperse particle flow downstream of DMA-1 was conditioned at a relative humidity of 87±2%, while the other half was passed through the CCNC within which the supersaturation of the sample ranged from c.a 0.1 to 1%.. The HR-AMS measurements provided mass concentrations of ammonium, sulphate, chlorine, nitrate and organic ions. The volume fractions of common atmospheric chemical species were calculated using the ion mass measurements and the ion pairing algorithm described by Gysel et. al., (2007).

Table 1 provides a summary of the HTDMA measurements obtained over the entire period of our study. Most monodisperse-particle samples exhibited unimodal distributions following humidification, indicating that the particles are internally mixed. Almost a quarter of the samples corresponding to the smaller dry diameters selected by the first DMA (i.e., 40 and 60 nm) exhibited two modes of the growth factor distribution: one less and one more hygroscopic having growth factors of 1.07±0.03 and 1.11±0.04, respectively. As the dry mobility diameter of the particles increased the percentage of samples having bimodal distributions decreased, whereas the difference of the growth factors between the less and more hygroscopic populations increased (cf. Table 1).

Table 1: Summary of the HTDMA measurements performed at the suburban station in Patras from 8 to 27 June 2012. Key: d_{dry} is the mobility diameter selected by DMA-1; P_u and P_b are the relative frequencies of occurrence for unimodal and bimodal distributions, respectively; g_1, g_{21}, and g_{22} are the average growth factors ± one standard deviation for the measurements showing unimodal and two bimodal distributions, respectively.

d_{dry}	g_1	P_u (%)	g_{21}	g_{22}	P_b (%)
40	1.21 ±0.07	74.2	1.11 ±0.04	1.33 ±0.06	25.4
60	1.23 ±0.07	76.9	1.07 ±0.03	1.32 ±0.06	22.8
80	1.25 ±0.06	87.3	1.06 ±0.03	1.30 ±0.05	12.7
100	1.25 ±0.06	94.3	1.07 ±0.03	1.33 ±0.08	5.46
120	1.26 ±0.06	96.8	1.06 ±0.05	1.30 ±0.05	3.15

The HR-AMS showed that organic volume fractions accounted for almost half of the volume of the particles. The average fraction of ammonium sulphate volume fractions was of the order of 30%, whereas ammonium bisulphate volume fractions averaged at 12%. Considering the substantial amount of organic species present on the particles and assuming that they are hydrophobic, the particles predicted hygroscopic growth factor will be suppressed, as indicated by the HTDMA measurements.

Acknowledgement:
This research was co-financed by Greece and the European Union through the education and lifelong learning operational program Thales: "Sources and physicochemical properties of fine and ultrafine aerosol particles that affect the regional climate of Greece".

References

DeCarlo, P., Kimmek, J. R., Trimborn, A., Northway, M. J., (2006), *Anal. Chem,* 78, 8281 – 8289

Gysel. M., Crosier, J., Topping, D. O., Whitehead, J. D., (2007), *Atmospheric Chemistry and Physics,*7, 6131-6144.

IPCC (2007), Fourth Assessment Report

Rader, D. & McMurry, P., (1986), *J. Aerosol Sci,*17,771-787

Roberts, G. C., & Nenes, A., A., (2005), *Aerosol Sci. Technol.,* 39, 206–221.

Comparison of Chemical Characteristics of Diesel Particulates from a Euro 0, Japanese and US Engines

T.H. Gan[1], P. Hield[1], P.J. Hanhela[1], M. Leist[1], W. Mazurek[1] and R. Gillett[2]

[1]Defence Science and Technology Organisation, 506 Lorimer St, Fishermans Bend, Victoria 3207, Australia
[2]CSIRO Marine and Atmospheric Research, Station St., Aspendale, Victoria 3195, Australia
Keywords: diesel exhaust, elemental carbon, chemical properties, mass size distribution
Presenting author email : tiang-hong.gan@dsto.defence.gov.au

Introduction Diesel exhaust is classified as 'carcinogenic to humans' (Group 1) by the World Health Organisation. Characteristics defined for diesel particulate (DPM) exposure are complex, and include particle size, elemental carbon (EC), total carbon (TC) and other chemical species. In exposure regulations, EC content has been defined as 50% of TC, which is too simplistic, given the variation of EC and DPM with engine type, age, operating conditions, lubricants and fuel. Consequently EC in addition to other characteristics of DPM were investigated as chemical markers for a Euro 0, Japanese and several US built engines.

Experimental EC, DPM and particle size (0.3 μm – 20 μm), were monitored continuously in the personnel module of a Unimog truck powered by a Mercedes Benz OM 353.959 (Euro 0) engine. EC, organic carbon (OC), TC, inorganic ions and metals were also sampled using quartz and Teflon filters. Size fractionated characterisations were conducted using two Sioutas impactors under vehicle idling only. Field trials were conducted on test circuits in a rural area, free from vehicular pollution.

Results and Discussion Real time EC levels were found to correlate with DPM in the Unimog module for various vehicle operating modes, consistent with findings of filter and impactor samples. EC content of the Euro 0 engine was predominantly confined to particles < 0.25 μm size and mass averaged from 23% to 45% of TC (Fig 1), in agreement with the results of a 1986 Nissan engine (Kelly et al, 2003). A lower EC/TC is associated with incomplete oxidation of OC at lower exhaust temperatures (Ng et al, 2007).

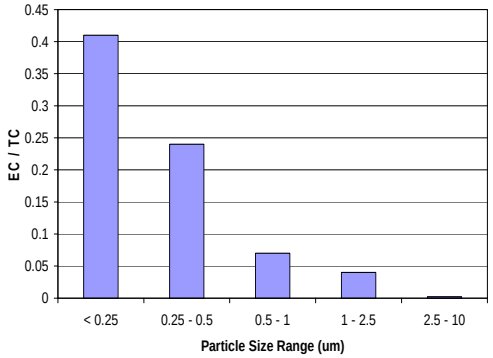

Fig. 1. EC/TC size distribution of Euro 0 diesel particulates under idling conditions.

EC/TC for the 1996 Cummins engine in a military Dodge Bobtail varied from 3% to 15% for various engine loads (Kelly et al, 2003). EC/TC for US commercial trucks fitted with Detroit, Cummins and Caterpillar engines (1996 - 2000) ranged from 3% to 83% for low and high engine loads respectively (Shah et al, 2004). Since EC is assumed as 50% TC for exposure compliance, these findings suggest DPM exposures can differ by up to an order of magnitude.

Toxicity of metals in diesel emissions are DPM size dependent especially in < 1μm and nanoparticles (Mayer et al 2010). Mass size distributions of the Euro 0 engine metals (Al, Fe, Mn and Ni) under idling conditions were found to be uniform from engine wear. By comparison unsized characterisation (Gautam et al, 2002) is less exposure informative.

Distribution of sulphate across the particle size range as the sole chemical marker of engine combustion (Kelly et al, 2003) has limited use, due to interference from other sources. In contrast, size distribution of lubricant minerals concentrated in the < 0.25 μm fraction (Fig.2) is definitive of diesel engine combustion.

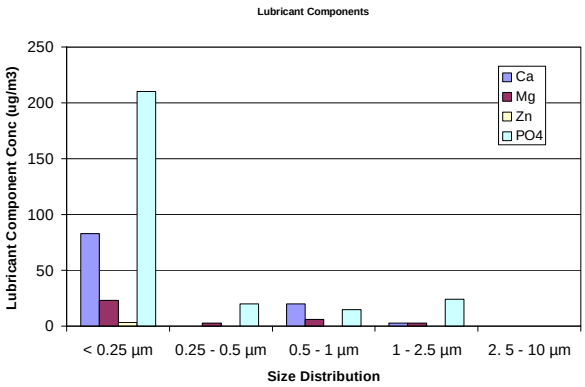

Fig. 2. Particle size distribution of Euro 0 engine lubricant minerals under idling conditions.

Conclusions Hence, in addition to elemental carbon (EC), DPM should be reintroduced as an exposure metric. For the Euro O engine localisation of DMP mass EC and lubricant minerals (<0.24 um size fraction) provides definitive evidence of diesel engine combustions.

Gautam, M., et al (2002) *Diesel Engine Emission Reduction Conference*, Aug 25 – 29, San Diego.
Ng I.P.,Ma H.B.,Kittelson D.B. and Miller A. (2007). *SAE Paper 2007-01-0334.*
Kelly, K.E. et al (2003) *J. Air & Waste Manage. Assoc.* **53**, 273-282.
Mayer, A., Czerwinski, J., Ulrich, A., Wischer, A., Kasper, M. and Mooney, J. (2010) *SAE 2010-01-0792*
Shah, S.D. et al (2004) *Environ. Sci. Technol.* **38,** 2544-2550.

Droplet formation via a 1.7 MHz ultrasonic droplet generator

K. Zhong[1], G. Peabody[1], A. Marshall[2], H. Glicksman[3], and S. Ehrman[1],
[1]Department of Chemical and Biomolecular Engineering, University of Maryland, College Park, MD, 20740, US
[2]Department of Fire Protection Engineering, University of Maryland, College Park, MD, 20740, US
[3] DuPont Electronic Technologies, Research Triangle Park, NC, 27709, US
Keywords: ultrasonic, droplet, viscosity, size distribution.
Presenting author email: sehrman@umd.edu

Ultrasonic atomization, developed for liquid atomization, plays an important role in applications including drug delivery, precursor transport and environmental improvement, with the advantages of tunable and relatively narrow droplet size distributions. In our experiment, copper nitrate/water/ethanol and copper nitrate/water/ethylene glycol precursor solutions were atomized by a 1.7 MHz ultrasonic nebulizer. The droplet size distribution and atomization rate were measured. The effects of nitrate concentration, cosolvent volume ratio and carrier gas flow rate on the droplet diameter and atomization rate were investigated. Results indicated that increasing either the concentration or the cosolvent volume ratio increased the viscosity and the droplet diameter, and at the same time decreased the atomization rate. Increasing the carrier gas flow rate increased the atomization rate, and had a limited effect on the droplet diameter.

Droplets with D50 around 5 µm were observed with a solution viscosity lower than 3 mm^2/s. Dimensionless diameter D and frequency Ω were defined as $D50/(\gamma^2\rho/\sigma)$ and $\omega/(\sigma^2/\rho^2/\gamma^3)$ separately, where ω is the ultrasonic frequency, γ is the kinematic viscosity of the solution, ρ is the solution density and σ is the solution surface tension. Linear behaviour of log(D) vs. log(Ω) indicated that droplets may be generated from periodic surface fluctuation on the wavelets formed by ultrasonic excitation of the fluid. As the viscosity became larger than 3 mm^2/s, a bimodal droplet size distribution was observed, with the first peak around 5 µm and the second one around 70 µm.

The formation process of droplets was also investigated using Shadowgraphy with a high-speed camera and laser illumination. Atomization process images of pure water and 40v% EG/water solution are shown in Figure 2-a, b. For the pure water system with low viscosity, all droplets were generated around the water cone, which was activated at the center of the generator. Droplets with diameters around 50 microns appeared to be generated by the breakup of water ligaments, while formation of the droplets with smaller sizes was likely due to the capillary waves on the solution surface. For the 40v% EG/water solution with a relatively larger viscosity, a cone at the center was activated, and droplets were mainly generated by the breakup of water ligaments with diameters around hundred microns. Investigation of the relationship between fluid viscosity and droplet formation mechanism is ongoing.

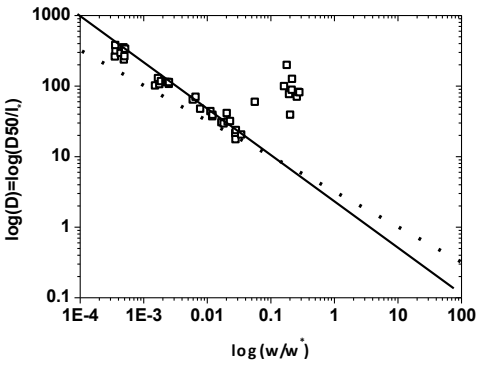

Figure 1. Correlation between dimensionless diameter and dimensionless frequency. Solid line corresponds to $D=2.79\Omega^{-0.602}$

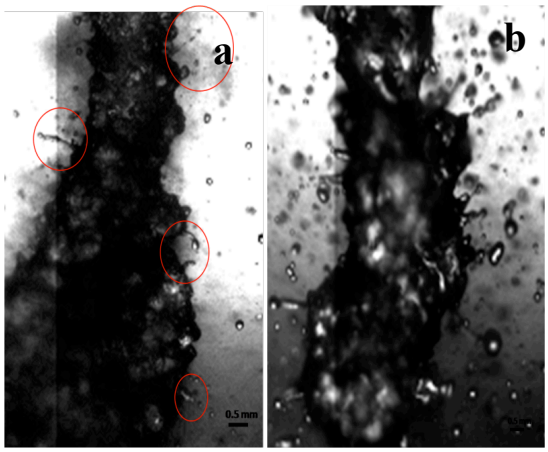

Figure 2. Images of the atomization process (a) water (b) 40v% EG water solution

This work was supported by the NSF (National Science Foundation CBET0755703) and by the DuPont Company.

Spatial distribution of the air quality in Portugal (rural, urban, and archipelagos)

A.M.J. Cruz[1], S.M. Sarmento[3], A.V. Silva[2], T. Verburg[3], S. Almeida[2], C. Alves[4], M.C. Freitas[2], H. Th. Wolterbeek[3]

[1]College of Technology and Management of Oliveira do Hospital, Polytechnic Institute of Coimbra, Portugal
[2]Instituto Tecnológico e Nuclear, Instituto Superior Técnico, Portugal
[3]Delft University of Technology; Nertherlands
[4]University of Aveiro, CESAM, Portugal
ana.cruz@estgoh.ipc.pt

Keywords: Aerosol emissions, monitoring, Statistical analysis

Abstract: The objective of this study is to perform a spatial distribution of atmospheric pollutants concentrations in Portugal (mainland and archipelagos) in a total of 78 stations for a period 2006-2008 and to compare these results with the EU Directive. The data were measured within the Portuguese Environment Agency (APA) Air Quality Monitoring Network. The latter consists on several stations distributed in Portugal providing hourly data of the main atmospheric pollutants such as particulate matter, SO_2, NO, NO_2, CO, and O_3. Particulate matter results shows that 25% of the sampling stations exceeded the PM_{10} limit value of 40 mg/m^3 in 2006; in 2007 and 2008, the limit value was exceeded in 13% and 7% of the stations. Concentrations were higher in littoral where the main urban and industrial areas are placed in Portugal. In Lisbon PM_{10} concentrations were exceeded in 40 % of the stations in 2006 and 20% of the stations in 2007 and 2008; the stations are in the center of Lisbon near important traffic street. In 2006, except in Madeira island, Vermoim – north of mainland Portugal and Estarreja - center of mainland Portugal, all the stations presented $PM_{2.5}$ concentrations lower than 20 mg/m^3 (EU limit value). In 2007, only Vermoim and Estarreja presented concentrations higher than 20 mg/m^3. In 2008 all stations presented concentrations lower than 20 mg/m^3. In general, PM_{10} and $PM_{2.5}$ concentrations decreased from 2006 to 2008. Statistical significant tests are applied to establish differentiation between rural, urban and archipelago stations. The Portuguese data are compared with other European published data or originated by European Monitoring and Evaluation Program (EMEP). Mass trajectories as given by HYSPLIT (Hybrid Single-Particle Lagrangian Integrated Trajectory) model will be studied for days were the concentrations of the pollutants are significantly higher than the European legislation.

An update on ChArMEx (the Chemistry-Aerosol Mediterranean Experiment) activities and plans for aerosol studies in the Mediterranean region

F. Dulac[1] and an international ChArMEx Team:
T. Agacayak, L. Alados Arboledas, A. Alastuey, Z. Ameur, G. Ancellet, E.-M. Assamoi, J.-L. Attié, S. Becagli, M. Beekmann, G. Bergametti, M. Bocquet, F. Bordier, T. Bourrianne, J.A. Bravo-Aranda, P. Chazette, I. Chiapello, P. Coddeville, A. Colomb, A. Comerón, G. D'Amico, B. D'Anna, K. Desboeufs, J. Descloitres, M. Diouri, C. Di Biagio, G. Di Sarra, P. Durand, L. El Amraoui, R. Ellul, L. Fleury, P. Formenti, E. Freney, E. Gerasopoulos, P. Goloub, M.J. Granados-Muñoz, J.-L. Guerrero Rascado, C. Guieu, D. Hadjimitsis, E. Hamonou, H.C. Hansson, M. Iarlori, S. Ioannou, E. Jaumouillé, M. Jeannot, W. Junkermann, C. Keleshis, S. Kleanthous, P. Kokkalis, D. Lambert, B. Laurent, J.-F. Léon, C. Liousse, M. Lopez Bartolome, R. Losno, M. Mallet, R.-E. Mamouri, N. Marchand, L. Menut, N Mihalopoulos, R. Morales Baquero, P. Nabat, F. Navas-Guzmán, D. Nicolae, J. Nicolas, G. Notton, C. Paoli, A. Papayannis, G. Pappalardo, S. Pandis, J. Pelon, J. Pey, V. Pont, X. Querol, F. Ravetta, J.-B. Renard, V. Rizi, G. Roberts, K. Sartelet, J.-L. Savelli, J. Sciare, K. Sellegri, D.M. Sferlazzo, M. Sicard, A. Smyth, F. Solmon, D. Tanré, A. Tovar Sánchez, N. Verdier, F. Wagner, Y. Wang, J. Wenger, N. Yassaa, *et al.*

[1]Laboratoire des Sciences du Climat et de l'Environnement, UMR 8212 CEA-CNRS-UVSQ, IPSL/LSCE, CEA Saclay 701, F-91191 Gif-sur-Yvette, France
Keywords: atmospheric aerosols, processes and properties, field campaigns, remote sensing, Mediterranean.
Presenting author email: francois.dulac@cea.fr

The objective is to present an update of the Chemistry-Aerosol Mediterranean Experiment project (ChArMEx) with a focus on on-going aerosol research activities and future campaign plans.

ChArMEx is a French initiative aiming at developing and coordinating regional research actions for a scientific assessment of the present and future state of the atmospheric environment in the Mediterranean Basin, and of its impacts on the regional climate, air quality, and marine biogeochemistry. The target of ChArMEx is short-lived particulate and gaseous tropospheric trace species.

Through seven work packages, ChArMEx addresses: emissions and source apportionment; chemical ageing of air masses with a focus on the formation of secondary organic aerosols; transport processes and their effect on air quality; direct radiative forcing by aerosols and its consequences on the water budget and regional climate; atmospheric deposition of nutrients and contaminants; recent trends and variability in atmospheric composition; and the future evolution of atmospheric chemistry at the horizon of 2030 and 2050.

ChArMEx proposes a multi-scale model-satellite-field observation integrated strategy. The field observation strategy combines continuous monitoring in a network of background stations, and intensive campaigns including airborne measurements.

We briefly illustrate recent ChArMEx activities that include aerosol remote sensing climatology (Nabat *et al.*, and Chiapello *et al.*, 2012), 3-D modelling of African dust aerosol radiative impact, developing monitoring networks for aerosol chemistry (Sciare *et al.*, 2012), aerosol optical properties (AERONET), and dust deposition, performing intensive aerosol chemistry measurement campaigns at Majorca (Pey et al., 2012) and the Finokalia observatory in Crete (Nicolas *et al.*, 2012) and at our new background station at Ersa, Cape Corsica (Fig. 1) in 2011 and 2012, and other intensive field measurements during the Pre-ChArMEx/TRAQA-VESSAER campaign (11 June-13 July 2012) including (i) soundings with a new balloonborne OPC (Renard *et al.*, 2012), (ii) tentative assimilation of aerosol lidar data from ACTRIS monitoring network in southern Europe, (iii) aircraft observations over the NW Mediterranean basin with drifting balloons for tentative Lagrangian re-flight, and (iv) ultralight aircraft measurements over Corsica in conjunction with lidar profiling.

Fig. 1. The ChArMEx/CORSiCA atmospheric chemistry background station at the wind mill of Santa Catalina at Ersa, Cape Corsica (42.97°N, 9.38°E, alt. 533 m).

We finally present plans for a large field campaign in summer 2013 with aircraft and balloons in the western Mediterranean, and ideas for a cruise across the Mediterranean in May 2015. Future plans will be discussed at the 3rd ChArMEx International Workshop in early Nov. 2012 in Cargese, Corsica Isl. (registration at *http://charmex.lsce.ipsl.fr/index.php/third-intern-workshop*).

Acknowledgements: ChArMEx (*http://charmex.lsce.ipsl.fr*) is part of the international multidisciplinary research programme MISTRALS (Mediterranean Integrated Studies aT Regional And Local Scales). ChArMEx-France activities are supported by ACTRIS, ADEME, ANR, CEA, CNES, CNRS/INSU, CTC, EGIDE/Campus France, EMD, EUFAR, IPSL, Météo-France, OMP, PHOTONS, Univ. of Clermont-Ferrand, Corse, Dunkerque, Lille, Paris-6, Paris-7, Paris-12, Provence and Toulouse.

Chiapello, I., *et al.*, (2012) *IRS-2012*, 06-10 Aug. 2012, Berlin.
Nabat, P., *et al.*, (2012) *EGU-2012*, 22-27 Apr. 2012, Vienna.
Nicolas, J. et al. (2012) *EAC-2012*, 2-7 Sept. 2012, Granada.
Pey, J., *et al.* (2012) *EAC-2012*, 2-7 Sept. 2012, Granada.
Renard, J.B., *et al.* (2012) *EAC-2012*, 2-7 Sept. 2012, Granada.
Sciare, J., *et al.* (2012) *EAC-2012*, 2-7 Sept. 2012, Granada.

TiO_2 thin film structures prepared by controlling the particle formation and deposition in PCVD system

Hoang Hai Nguyen and Kyo-Seon Kim

Department of Chemical Engineering, Kangwon National University,
Chuncheon, Kangwon-Do, 200-701 Korea
Keywords: Plasma chemical vapor deposition, Thin film growth, Particle coating, Titanium dioxide
Presenting author email: kkyoseon@kangwon.ac.kr

The titanium dioxide (TiO_2) is one of the most focally studied photocatalysts for environmental applications due to its nontoxicity, chemical stability, low cost and active reactivity. In recent years, many studies have focused on TiO_2 thin film which can be used as gas sensors, solar energy cells, and self cleaning effects. In addition, there have been many methods to improve the activity of TiO_2 thin films such as increasing the ratio specific surface area by controlled structure and morphology of thin films.

TiO_2 films can be prepared by various methods, such as chemical vapour deposition, sputtering, ionized cluster beam, aerosol chemical vapour deposition and plasma chemical vapour deposition.

In this work, TiO_2 thin films were deposited on silicon wafer by Plasma Chemical Vapor Deposition (PCVD) system. Figure 1 shows the schematic diagram of PCVD system, which consists of the RF generator, precursor supplying system, vacuum system and plasma reaction chamber. We used titanium tetra-isopropoxide (TTIP) as the precursor of TiO_2 films, and N_2 pure gas or N_2 mixed with O_2 gas as plasma gas. The important process variables in this PCVD system are gas flow rate, precursor temperature, power and substrate temperature and we investigated the effects of these process variables on the morphologies of resulting TiO_2 thin films. Table 1 shows the ranges of experimental variables we investigated in this work. The standard bubbler temperature was 80°C, and the TTIP/ N_2 gas line was heated to prevent condensation onto the tube. The N_2/TTIP mixture was delivered into the chamber (buffer) where it was mixed with oxygen. The operation pressure was 3 Torr and substrate temperature was 150°C for all deposition experiments. The TiO_2 thin films were prepared for 20 min. The influences of initial TTIP concentration, oxygen flow rate were examined in detail.

In this study, we demonstrate that a simple, one-step PCVD system can be applied to prepare TiO_2 thin films with different controlled morphologies. The morphologies of TiO_2 were characterized by scanning electron microscopy to study the morphology, by X-ray diffraction to study the structure and SEM cross section to deduce the film thickness.

Table 1. Ranges of experimental variables to prepare TiO_2 thin film in this study.

Experimental variables	Ranges
Pressure	3 Torr
Power	20-70 W
Substrate temperature	150 °C
Precursor temperature	80 °C
O_2 flow rate	10 sccm
Carrier gas flow rate	5-50 sccm
Total gas flow rate	80-100 sccm
Distance	40 mm

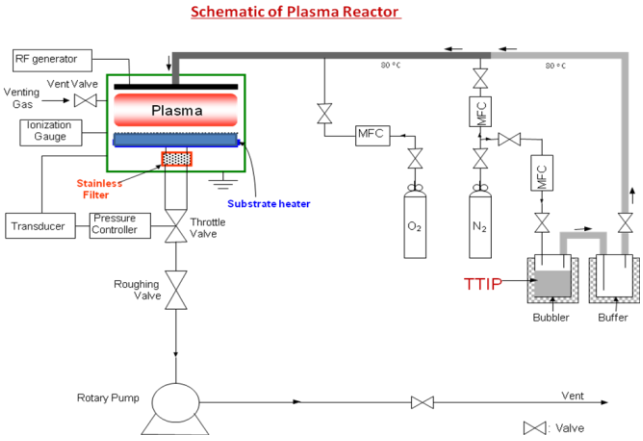

Figure 1. Experimental schematic of PCVD system to prepare thin film by controlling the particle formation and deposition.

Polarized Imaging Nephelometer for Field and Aircraft Measurements of Aerosol Phase Function

G. Dolgos[1,2], J.V. Martins[1,2]

[1]Joint Center for Earth Systems Technology, University of Maryland, Baltimore County, Baltimore, MD, 21250, USA
[2]Department of Physics, University of Maryland, Baltimore County, Baltimore, MD, 21250, USA

Keywords: Scattering matrix, Scattering coefficient, Optical instrumentation, In-situ measurements.
Presenting author email: gdolgos@umbc.edu

At the Laboratory for Aerosols, Clouds and Optics (LACO) at the University of Maryland, Baltimore County we have developed a new technique to directly measure the aerosol phase function and the degree of linear polarization of the scattered light. We designed and built a portable instrument called the Polarized Imaging Nephelometer (PI-Neph). The PI-Neph was successfully flown on dozens of flights as a part of the NASA Development and Evaluation of satellite ValidatiOn Tools by Experimenters (DEVOTE) project and the Deep Convective Clouds and Chemistry (DC3) project.

The LACO imaging nephelometer concept has been implemented as a portable instrument after laboratory proof of concept experiments (Dolgos et al, 2010). The aerosols that enter the PI-Neph are illuminated by laser light (wavelength of 532 nm) and scattered light is imaged by a stationary wide field of view camera in the scattering angle range of 2° to 178°. (in some cases stray light limited the range to 3° to 176°)

Figures 1 and 2 show data from the DEVOTE flight on 2011/10/17 aboard the NASA Langley B-200 aircraft. The aircraft was based at NASA Langley Research Center and flew over three AERONET stations that day.

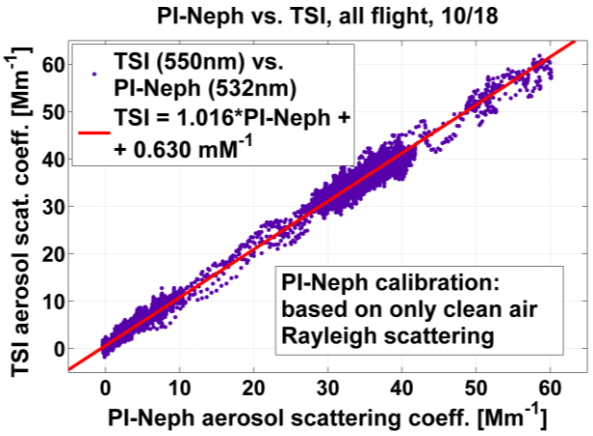

Figure 1. Scatter plot and the least squares linear fit showing the correlation between the independent measurements of the aerosol volume scattering coefficient by the PI-Neph and the TSI integrating nephelometer aboard the NASA Langley B200 aircraft.

The volume scattering coefficient is compared to parallel and independent TSI measurements and the spiral averaged phase function from the flight over NASA Wallops Flight Facility is compared to the ground based AERONET retrievals.

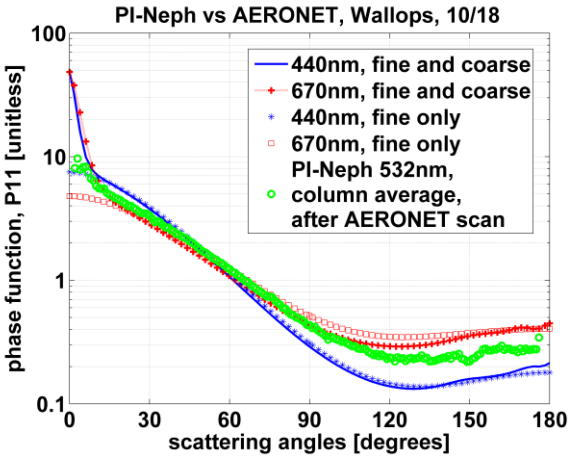

Figure 2. Comparison of the phase function measured by the PI-Neph aboard the NASA Langley King Air and retrieved from AERONET sky radiance measurements.

Results from this dataset showed good agreement between the PI-Neph measurements of volume scattering coefficient and the parallel TSI integrating nephelometer measurements, as well as between the PI-Neph measurement of phase function and the AERONET retrievals. The differences between the PI-Neph and the AERONET retrievals can be attributed to differences between the ambient size distribution and the one sampled inside the aircraft. Further analysis of the DEVOTE and DC3 flight data is underway.

At LACO our goal is to enable systematic in-situ and eventually inlet-free measurements of aerosol phase function that can be compared to AERONET and satellite retrievals to enhance the quality of our global view of aerosols from ground and space.

This work was supported by the Cloud-Aerosol Lidar and Infrared Pathfinder Satellite Observations (CALIPSO) mission, the NASA Langley Research Center DEVOTE project, and the DC3/SEAC4RS projects funded by NASA HQ.

Dolgos, G., J. V. Martins, L. A. Remer, A. L. Correia, M. Tabacniks, and A. R. Lima (2010) Proceedings of SPIE Vol. 7588

Water diffusion in glassy aerosol investigated using a new Raman isotope tracer method

H.C. Price[1], B.J. Murray[1], J. Mattsson[2] and L.G. Benning[1]

[1]School of Earth and Environment, University of Leeds, Leeds, LS2 9JT, UK
[2]School of Physics and Astronomy, University of Leeds, Leeds, LS2 9JT, UK
Keywords: Atmospheric aerosols, glassy aerosol, diffusion, Raman spectroscopy, water soluble compounds.
Presenting author email: eehcp@leeds.ac.uk

The properties of aerosol containing water soluble organic compounds is much more poorly understood than aerosol containing inorganic solutes. Recently it has been suggested that atmospheric aerosol may be present in the form of amorphous solids and semi-solids at low relative humidity and even at room temperature (Virtanen et al., 2010). These highly viscous particles are thought to have low diffusion coefficients, leading to very long equilibration times, with profound effects on their interactions with water vapour and other chemical species (Koop et al., 2011).

Water uptake by amorphous solids on increasing humidity occurs slowly at the surface of a particle, proceeding to the interior of the particle more rapidly when this outer layer has softened the solid and increased the rate of diffusion. This plasticizing effect leads to considerable difficulty in determining the diffusion coefficient of water in a particle undergoing hygroscopic growth due to the non-linearity of the diffusion problem (Zobrist 2011, Bones 2012). A method which involves observing a tracer diffuse into a particle without a corresponding change in viscosity or size would be advantageous.

A technique has been developed whereby Raman spectroscopy can be used to give a quantitative measure of water diffusion into an ultra-viscous aqueous solution or amorphous solid droplet. A disk of solution is placed in a temperature and humidity controlled cell, with its circumference (but neither face) exposed to the surrounding gases. The droplet is allowed to come to equilibrium with the surrounding H_2O vapour, before switching to D_2O vapour of the same dewpoint. Raman spectra are taken at various radial distances as the D2O diffuses into the droplet. The ratio of the OD to OH stretch peaks gives an indication of the concentration of each isotope at any one time and position. By solving Fick's second law for diffusion into a disk, the coefficient of diffusion of heavy water can be determined over a range of water activities.

Results will be presented for raffinose solution droplets. These data show that below 30% RH, the 150 µm disk remained out of equilibrium for a period longer than 48 hours and the diffusion coefficient was determined to be $5x10^{-15}$ m^2/s. Using this diffusion coefficient a 1 µm diameter aerosol particle would have a diffusion half-life of 7 seconds at 30% RH. The implications for water retention in atmospheric organic aerosol will be discussed.

Acknowledgments

This work was supported by the European Research Council under grant 240449 – ICE.

References

Virtanen, A. *et al.* (2010) Nature **467,** 824-827.
Koop, T. e*t al.* (2011) Phys. Chem. Chem. Phys. **13**, 19238-19255.
Zobrist, B. e*t al.* (2011) Phys. Chem. Chem. Phys., **13**, 3514–3526.
Bones, D.L. *et al.* (2012) PNAS **109**, 11613–11618.

Exploring the use of satellite-derived whitecap data to improve sea-spray emission estimates

M.F.M.A. Albert[1], M.D. Anguelova[2], G. de Leeuw[1,3,4], A.M.M. Manders[1], and M. Schaap[1]

[1]TNO, Utrecht, Princetonlaan 6, 3584 CB, The Netherlands
[2]Remote Sensing Division, Naval Research Laboratory, Washington DC, 20375, USA
[3]Climate Change Unit, Finnish Meteorological Institute, Helsinki, Erik Palménin aukio, FI-00101, Finland
[4]Department of Physics, University of Helsinki, Helsinki, Gustaf Hällströmin katu 2a, FI-00014, Finland
Keywords: sea spray, aerosol emissions, modelling, remote sensing.
Presenting author email: monique.albert@tno.nl

Sea-spray aerosol considerably affects the climate, both directly and indirectly. The emission rate of sea-spray droplets per unit area of the sea surface is implemented in climate models through a sea-spray source function (SSSF). Recent formulations of the SSSF include a contribution of organic matter based on satellite observations of ocean colour (Gantt *et al*, 2012) Organic material substantially contributes to the composition of sub-micron sea-spray aerosols, especially in biologically active regions, where small sea-spray particles may be mainly composed of organic matter (OM) with a decreasing contribution as particle size increases (Facchini *et al*, 2008). The amount and type of organics in sea-spray aerosol have an impact on their scattering potential (Randles *et al*, 2004) and their ability to act as cloud condensation nuclei (O'Dowd *et al*, 2004; Fuentes *et al*, 2010). Starting from a first estimate of the total annual global emission of OM, we have performed a sensitivity analysis on used parameterizations and input data and found variability to a factor of 50%, which could be mainly assigned to the sea-spray source function that was chosen (Albert *et al,* 2012).

The uncertainties in current sea-spray source functions are still large (de Leeuw *et al*, 2011). Conventional sea-spray source functions are expected to be improved by including factors, complementary to wind speed, which better account for the effects of a suite of meteorological and oceanographic factors. We are currently exploring the use of global satellite-retrieved whitecap fraction, W, data (Anguelova *et al,* 2006) Figure 1 shows an example of a global W distribution for one day. An advantage of satellite data over traditional observations (photographic or video images) of W data may be a better representation of open ocean conditions across the world's oceans as opposed to local observations from ships or platforms. It should be stressed that the W data as used in our study are research products and are therefore not yet available as operational type of data used in global models. Therefore our study additionally serves to validate the satellite derived W data.

The goal of our study is to find an alternative W parameterization which can be used to replace the commonly used relationship derived by Monahan and Muircheartaigh (1980). Once we have optimized our new parameterization for global application we will validate the outcome of our sea-spray emission tool through application in the regional chemistry transport model LOTOS-EUROS (Schaap *et al.*, 2008). The outcome of LOTOS-EUROS will be compared with in situ measurements of Sodium concentrations. Preliminary results will be presented.

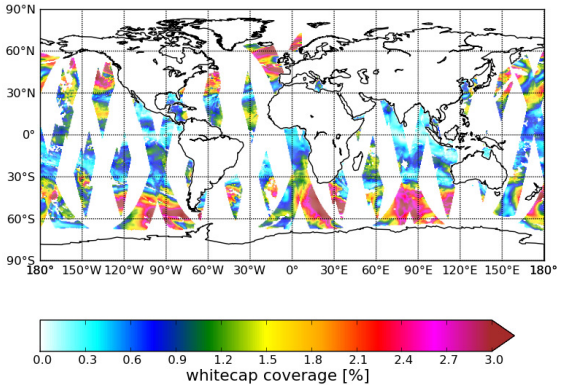

Figure 1. Satellite-derived W data for 1 March 2006.

This study is partly funded by SRON through the Dutch Users Support Programme GO-2, project EO-096.

Albert, M.F.M.A. *et al* (2012) *Atmos Environ.* DOI:10.1016/j.atmosenv.2012.04.009.

Anguelova, M., Bettenhausen, M. and Gaiser, P. (2006) *Proc. International Geoscience and Remote Sensing Symposium (IGARSS)*, Denver CO, USA, 3676-3679.

Clarke, A.D., Owens, S.R. and Zhou, J. (2006) *J. Geophys. Res.***111** (D06202).

de Leeuw G. *et al* (2011) Reviews of Geophysics **49**, (RG2001).

Facchini, M.C. *et al* (2008) *Geophys. Res. Lett.* **35** (L17814).

Fuentes, E. *et al* (2010) *Atmos. Chem. Phys* **10,** 9295-9317.

Gantt, B. *et al* (2012) *Atmos. Chem. Phys. Discuss*, **12**, 12853-12883.

Monahan E.C. and Ó Muircheartaigh I. (1980). *Journal of Physical Oceanography* **10**, 2094-2099.

Randles, C.A., Russell, L.M. and Ramaswamy, V. (2004) *Geophysical Research Letters* **31** (L16108).

Schaap, M. *et al* (2008) *Int. J. of Environ. and Pollution* **32**, No. 2, 270–290.

O'Dowd, C.D. *et al*. (2004) *Nature* **431**, 676-680.

Wednesday, September 5, 2012

Plenary 3

Aerosols, clouds and climate

U. Lohmann[1]

[1] Institute for Atmospheric and Climate Science, ETH Zurich, Switzerland
Keywords: indirect aerosol effect, climate modeling, ice nucleation
Presenting author email: ulrike.lohmann@env.ethz.ch

Aerosol particles modify the radiation budget directly by scattering and absorption of solar and longwave radiation and indirectly by acting as cloud condensation nuclei and ice nuclei. The cloud albedo or Twomey effect of warm clouds refers to an increase in the cloud droplet number concentration for a constant liquid water content that increases cloud albedo.

In addition, the more and smaller cloud droplets in polluted clouds decrease the precipitation formation, presumably increasing cloud lifetime (cloud lifetime effect). Both effects partially set off greenhouse gas warming. In cirrus clouds the same shortwave effects occur as for water clouds described above, but in addition changes in the particle concentration also affect the longwave radiation.

Because clouds in mid-latitudes originate predominately via the ice phase, changes of the properties of ice nuclei maybe of crucial importance for the hydrological cycle. An increase in ice nuclei can result in a rapid glaciation of a supercooled liquid water cloud due to the difference in vapor pressure over ice and water. Unlike cloud droplets, these ice crystals grow in an environment of high supersaturation with respect to ice, quickly reaching precipitation size, and with that can turn a non-precipitating cloud into a precipitating cloud (glaciation effect). But if ice nuclei are chemically modified by anthropogenic material such as sulfates or organics, they may de-activate ice nuclei, which has an opposite effect.

In order to estimate these effects, global climate model simulations with present-day aerosol emissions are contrasted to those driven with pre-industrial aerosol emissions. The results differ substantially as shown in Figure 1.

Recently more emphasis is placed on aerosols acting as IN as more laboratory data on ice nucleation and how it can be parameterized in global climate models have become available. Also the role of bioaerosols as ice nuclei receives more attention. In this talk, I will discuss some of these indirect aerosol effects with emphasis on processes occurring in mixed-phase and cirrus clouds.

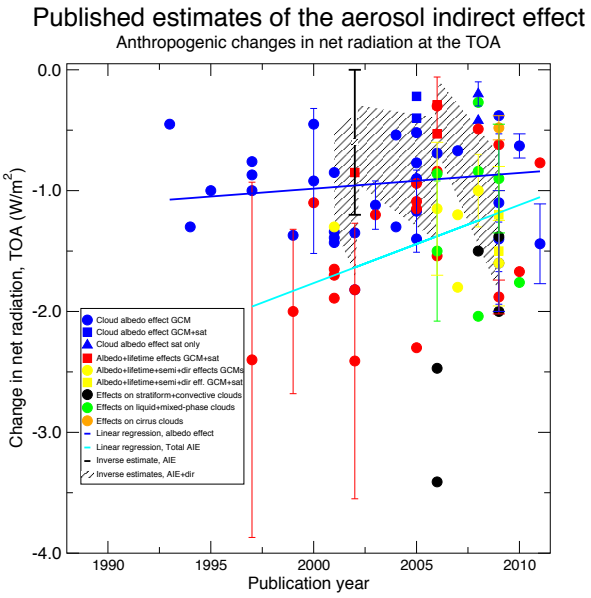

Figure 1. Model, satellite and inverse estimates of the aerosol indirect effects over the last two decades. For each method or effect considered, each symbol represents one published estimate (one paper one vote). Blue represents estimates of the cloud albedo effect from GCMs (dots), GCMs combined with satellite measurements (squares) and satellite estimates only (triangles). Red represents estimates of both the cloud albedo and cloud lifetime effect from GCMs (dots) and GCMs combined with satellite estimates (squares). The yellow dots represent estimates of the combined cloud albedo, lifetime, direct and semi-direct effects. Black dots represent the aerosol effects on stratiform and convective clouds and green dots represent estimates of aerosol effects on liquid and mixed-phase clouds. The black stippled area refers to inverse estimates. In case of multiple estimates per paper, the vertical bars denote the standard deviation. Updated from Lohmann et al, 2010.

Lohmann, U., L. Rotstayn, T. Storelvmo, A. Jones, S. Menon, J. Quaas, A. M. L. Ekman, D. Koch, and R. Ruedy (2010) *Atmos. Chem. Phys.* **10**, 3235-3246.

Wednesday, September 5, 2012

Session SS02S1O. A ground-based integrated study of chemical aerosol-cloud interaction (HCCT2010)

Cloud influence on local aerosol chemical composition during the Hill Cap Cloud Thuringia 2010

L. Poulain [1], Z.J. Wu [1], A. Tilgner [1], D. van Pinxteren [1], B. D' Anna [2], C. George [2], J. Schneider [3], A. Wiedensohler[1] and H. Herrmann[1]

[1] Leibniz-Institut für Troposphärenforschung, 04318 Leipzig, Germany
[2] Université Lyon 1, CNRS, UMR5256, IRCELYON, Institut de Recherches sur la Catalyse et l'Environnement de Lyon, 69629 Villeurbanne, France
[3] Max Planck Institute for Chemistry, Particle Chemistry Department, 55128 Mainz, Germany

Keywords: AMS, Aerosol cloud interaction, particle characterization, PM1.
Presenting author email: poulain@tropos.de

The impact of orographic clouds to the local aerosol chemical composition was measured during the Hill Cap Cloud Thuringia 2010 (HCCT-2010) field campaign, which took place in September/October 2010 at the Schmücke mountain ridge in the Thuringia forest (Germany). The main objectives of the HCCT-2010 project were to assess the effects of clouds on particle composition, gas phase oxidant budget, changes of hygroscopic properties and activation of aerosol particles. Three sampling sites were equipped: one on the top of the Schmücke Mountain, where clouds were sampled, and two valley stations located upwind and downwind of the summit. In total, four Aerodyne ToF-AMSs were deployed during the campaign. One at each valley station and two at the summit station: one downstream of a Cloud Virtual Impactor (CVI) for droplet residual analysis and one to measure interstitial particles. Based on air mass trajectories, gas tracer experiments and meteorological parameters, it is possible to identify periods during which the air mass of the three stations were connected. The overflow periods were divided in two subsections corresponding to the presence of cloud at the summit station (Full Cloud Events, FCE) and to the absence (Non Cloud Events, NCE) of cloud at the summit station. For these two categories of connected flow, the AMS results were compared in order to follow the cloud induced modification of the aerosol chemical compositions as well as modification of the chemical size distribution.

AMS results were successfully compared according to instrumental uncertainties and possible particle loss and dilution effects between the stations during the NCE periods and to the bulk chemical composition measured at the three stations show similar mass fraction. The comparison of the two valley stations is presented in Figure 1. Because the results measured at the three stations during NCE events were comparable, the same approach could be directly used to investigate aerosol cloud interaction and influence of clouds to local particles. Figure 1 also shows the first results of the comparison between the upwind and downwind station during several FCE periods. The scatter plots suggest a possible change on the bulk chemical composition of the particles corresponding to a small decrease of the particulate nitrate fraction as well as a tiny increase of sulfate. Details on the aerosol changes during the different cloud events including a comparison of the organic components as well as chemical size resolved will be presented.

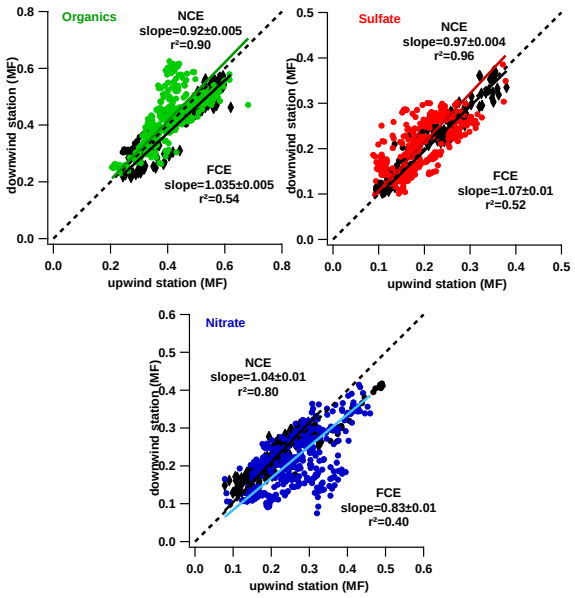

Figure 1: Scatter plots of the organics, sulphate and nitrate mass fraction measured at the upwind and downwind stations during NCE (black) and FCE (color). Regression slopes were calculated using orthogonal linear fitting.

Hill Cap Cloud Thuringia 2010 (HCCT-2010): Overview and highlight results

D. van Pinxteren[1], W. Birmili[1], B. Fahlbusch[1], W. Fomba[1], T. Gnauk[1], Y. Iinuma[1], S. Mertes[1], K. Dieckmann[1], M. Merkel[1], C. Müller[1], K. Müller[1], L. Poulain[1], G. Spindler[1], M. Schäfer[1], F. Stratmann[1], A. Tilgner[1], L. Schöne[1], P. Bräuer[1], K. Weinhold[1], A. Wiedensohler[1], W. Zhijun[1], S. Borrmann[2], E. Harris[2], A. Roth[2], J. Schneider[2], B. Sinha[2], I. George[3], D. Heard[3], L. Whalley[3], B. D'Anna[4], C. George[4], M. Müller[4], W. Haunold[5], A. Engel[5], A. Wéber[5], D. Amedro[6], C. Fittschen[6], C. Schoemaecker[6], J. Collett[7], T. Lee[7], and H. Herrmann[1]

[1]Leibniz-Institut für Troposphärenforschung, 04318 Leipzig, Germany
[2]Particle Chemistry Department, Max Planck Institute for Chemistry, 55128 Mainz, Germany
[3]School of Chemistry, University of Leeds, Leeds LS2 9JT, Great Britain
[4]Université Lyon 1, Lyon, F-69626, France; CNRS, UMR5256, IRCELYON, Institut de Recherches sur la Catalyse et l'Environnement de Lyon, Villeurbanne, F-69626, France
[5]Institut für Atmosphäre und Umwelt, Goethe Universität Frankfurt, 60438 Frankfurt, Germany
[6]University of Lille, UMR CNRS-USTL 8522, 59655 Villeneuve d'Ascq, France
[7] Department of Atmospheric Science, Colorado State University, Fort Collins, CO 80523, USA

Keywords: aerosol cloud interaction, physical and chemical properties, multiphase chemical processes.
Presenting author email: dominik@tropos.de

Clouds have a strong impact on physical and chemical processes in the atmosphere. Studying the interaction of aerosol and clouds under natural conditions is challenging, due to the height, as well as the spatial and temporal variability of clouds. Lagrangian-type field experiments, where a hill cap cloud is used as a natural flow-through reactor were successfully performed in the past to investigate different aspects of physical and chemical aerosol cloud interaction [*Bower et al.*, 2000; *Fuzzi, 1994; Fuzzi, 1997; Gallagher, 1999*; *Herrmann*, 2005].

In September/October 2010, the international cloud experiment "Hill Cap Cloud Thuringia 2010" (HCCT-2010) was performed at the Schmücke, which is part of a large mountain ridge in Thuringia, Germany. HCCT-2010 aimed at a better understanding of (i) the chemistry and microphysics within a cloud, (ii) chemical and physical modifications of aerosol particles by their passage through a cloud, (iii) the effects of clouds on the phase partitioning of oxygenated volatile organic compounds (OVOCs), and (iv) the effects of clouds on the budget of the main radical oxidants OH and HO_2.

In Figure 1 a scheme of the campaign area is given.

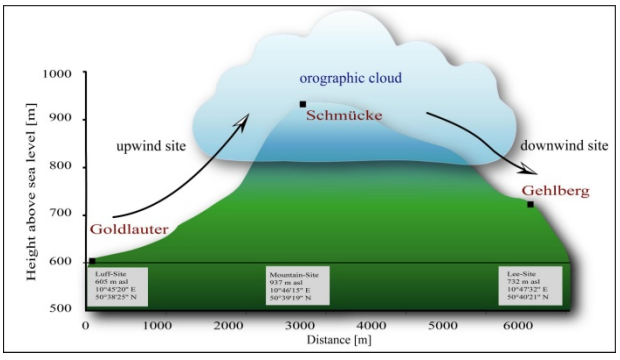

Figure 1: Scheme of the campaign area and the 3 sites.

Three measurement sites were set up: An upwind site to comprehensively characterize incoming air masses, an in-cloud site on the Schmücke summit to sample the different phases of a cloud, and a downwind site to study possible modifications of the aerosol after the cloud passage.

An extended pool of instruments was installed at the sites, including gas monitors, VOC and OVOC samplers, FAGE, SMPS, APS, HTDMA, CCNC, MAAP, CPC, filter samplers, impactors, MARGA, PILS, AMS, ALABAMA, a ceilometer, bulk and multi-stage cloud water collectors, CVI and interstitial inlet, PSAP, PVM, and FSSP.

A total of 370 hours of clouds could be captured at the summit station during the six weeks duration of the campaign. Certain offline samplers were operated only when meteorological observations predicted favourable flow connectivity between the sites, which was the case for a total of 73 hours during 12 so-called "full cloud events". A thorough investigation of meteorological conditions results from statistical analyses and several SF_6 tracer experiments revealed several top events, where a good flow connectivity between the three sampling sites can be assumed.

The study of physical and chemical parameters within these air masses led to interesting findings in scientific areas such as aerosol processing through clouds, chemical cloud composition, or the influence of clouds on the radical oxidants budget.

Within this contribution, an overview over the campaign will be given and some of the results will be highlighted.

Bower, B. K. N., T. W. Choularton, M. W. Gallagher, et al. (2000), *Tellus Ser. B-Chem. Phys. Meteorol.*, *52B*(2), 750-778.
Fuzzi, S. (Ed.) (1994), *J. Atmos. Chem.*, *19(1-2)*.
Fuzzi, S. (Ed.) (1997), *Atm. Env.*, *31(16)*.
Gallagher, M.W. (Ed.) (1999), *Atm. Res.*, *50(3-4)*.
Herrmann, H. (Ed.) (2005), *Atm. Env.*, *39(23-24)*.

Influence of Cloud Processing on CCN Activation Behavior in the Thuringian Forest, Germany

K. Dieckmann[1], M. Schäfer[1], P. Zedler[1], H. Wex[1], S. Henning[1], H. Herrmann[2], D. van Pinxteren[2], W. Birmili[1], M. Merkel[1], Z. Wu[1], A. Wiedensohler[1], Th. Mentel[3], and S. Stratmann[1]

[1] Department of Physics, Leibniz Institute for Tropospheric Research, 04318 Leipzig, Germany
[2] Department of Chemistry, Leibniz Institute for Tropospheric Research, 04318 Leipzig, Germany
[3]Forschungszentrum Jülich, ICG-II: Troposphere, Jülich, Germany

Keywords: CCN activation, cloud processing, HCCT.
Presenting author email: milde@tropos.de

Aerosol particles are known to influence the climate directly as well as indirectly. The indirect aerosol effect is amongst others determined by the efficiency of an aerosol particle to act as cloud condensation nucleus (CCN). The ability of a particle to be CCN active is a function of particle size, chemical composition and saturation ratio. In a cloud, interstitial particles and gases are entering the cloud droplets through in cloud scavenging and uptake. If the cloud evaporates, the scavenged mass (particles and gases) leads to larger, internally mixed and more hygroscopic particles. This mechanism is called cloud processing and is assumed to modify the chemical composition of CCNs during cloud passage.

A ground-based integrated study of chemical aerosol-cloud interaction was conducted in September and October 2010 in the Thuringian Forest in Germany in the frame of the Hill Cap Cloud Thuringia experiment (HCCT2010). Aim was to study possible cloud processing in the orographic clouds formed at Mount Schmücke. CCN measurements were performed at two study sites, i.e. upwind (station Goldlauter) and downwind (station Gehlberg), of the orographic clouds forming at Mount Schmücke. Measured were particle number and CCN size distributions, the latter for supersaturations (SS) between 0.07% and 0.4% utilizing a Cloud Condensation Nucleus Counter (DMT, USA).

From the size segregated CCN measurements, the critical diameter (D_{crit}), which is defined as the diameter at which 50% of the particles become activated to cloud droplets, was determined. From the resulting D_{crit}–SS-values, the hygroscopicity parameter κ was calculated (Petters and Kreidenweis, 2007). κ values were determined during so-called, full cloud (FCE) and non cloud events (NCE) at both sites, Goldlauter and Gehlberg. An event was defined as a time when the wind direction was such that an air mass from Goldlauter could be assumed to reach Gehlberg.

Table 1. Local meteorological parameters during FCEs.

Parameter	criterion
LWC	>0.1 g m^{-3}
wind direction	200°-250°
wind speed	2-12 m s^{-1}
Temperature	>0°C
Precipitation	0 mm

FCEs are characterized by the local meteorological conditions presented in Table 1 with an orographic cloud forming on Mount Schmücke, while there was no cloud/fog at the valley sites Goldlauter and Gehlberg. During NCE, no cloud/fog was present at any of the stations.

In Figure 1 κ values determined during the FCEs 11.3, 13.3, and 22.1 are shown. It can be seen that, downwind (Gehlberg) of the orographic clouds formed at Mount Schmücke, κ was higher for supersaturations between 0.07% and 0.2% than upwind of the clouds, i.e. in Goldlauter. This means, that while passing through the clouds, particles became more hygroscopic, respectively more CCN active during cloud passage. In contrast, in cases where no clouds were present at Mount Schmücke, κ featured the same values for both stations.

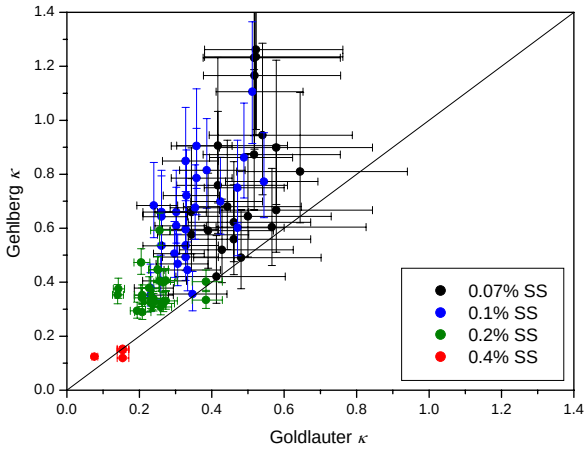

Figure 1. κ values during the FCEs 11.3, 13.3, and 22.1.

Interestingly, for 0.4% supersaturation, κ was found to be equal in Goldlauter and Gehlberg. The according D_{crit} ranged between 71 nm and 107 nm. This suggests that particles in this size range were not activated to cloud droplets, remained part of the interstitial aerosol, and were consequently not processed in the cloud. Hence, the supersaturation reached within the cloud was lower than 0.4% during the considered FCE. In connection with the findings described above, the supersaturation in the cloud at Mount Schmücke can be estimated to be between 0.2 % and 0.4%.

Petters, M.D. and Kreidenweis, S.M. (2007). *Atmos. Chem. Phys*., **7**, 1961-1971.

Relating particle hygroscopicity to chemical composition during HCCT-2010 field campaign

Z.J. Wu, L. Poulain, W. Birmili, M. Merkel, K. Dieckmann, M. Schäfer, D. van Pinxteren, S. Stratmann, H. Herrmann, A. Wiedensholer
Leibniz Institute for Tropospheric Research (IfT) Leipzig, Permoserstraße 15, 04318 Leipzig
Keywords: Hygroscopicity, AMS, HCCT
Presenting author email: wuzhijun@tropos.de

Particle hygroscopic growth, number size distributions, and chemical composition were measured simultaneously at a low mountain range in central Germany (Thüringer Wald), during the HCCT-2010 (Hill Cap Cloud Thuringia 2010) field campaign which took place in September and October 2010. The main objective of HCCT-2010 was to perform a ground-based Langrangian-type experiment for investigating the influences of clouds on aerosol chemistry. Three sampling sites were equipped: one at the top of the mountain and two valley stations located upwind and downwind of the summit. This abstract focusses on the interactions between sub-micrometer particles and water vapor, as well as the role of chemical composition in particle hygroscopicity at the upwind site.

The hygroscopic growths at 90% for size-resolved particles derived from HTDMA measurements are converted into the hygroscopicity parameters κ (Petters and Kreidenweis, 2007) in order to eliminate the effect of particle size. The statistics performed over the entire sampling time period is shown in Fig.1. We can clearly see that the smaller particles are less hygroscopic than larger particles. Such size dependence of particle hygroscopicity can most likely be explained by an increasing fraction of organic compounds with decreasing dry diameter, which are shown by AMS measurements (Not shown in this abstract).

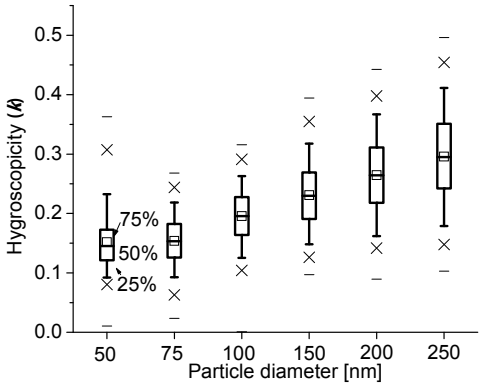

Figure 1: The size dependence of the hygroscopicity parameters κ

The predictions of particle hygroscopicity are performed using the detailed chemical composition provided by aerosol mass spectrometer (AMS) based on the Zdanovskii–Stokes–Robinson (ZSR) method. A good agreement between measured and predicted κ for 250 nm particle is found and illustrated in Fig. 2, indicating that the ZSR mixing rule combined with AMS data allows for accurate quantitative predictions of the mean growth factor of mixed atmospheric aerosol particles. We found that the agreement between prediction and measurement is very sensitive to the κ of organic fraction selected in the model due to the large contribution of organics to the total mass (lower panel of Fig. 2). Therefore, a further analysis on the relationship between finer organic structure and water vapor will be deployed in a hygroscopicity closure study. As a further topic, the relationship between the particle oxidation states and particle hygroscopicity will be also presented.

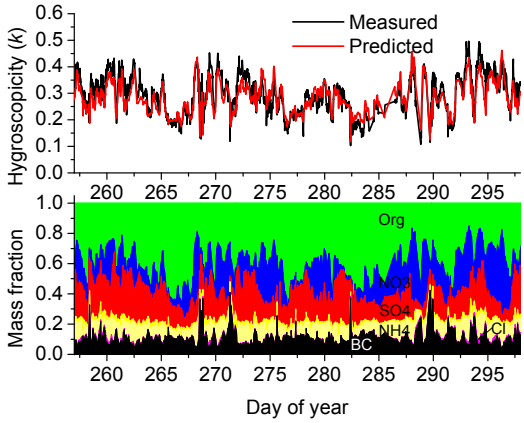

Figure 2: Time series of measured and predicted κ, as well as composition of non-refractory compounds as measured by AMS.

This work was supported by German Research Foundation

Petters, M.D. and Kreidenweis, S.M. (2007). Atmos. Chem. Phys., 7, 1961-1971.

Cloud residual analysis using two types of aerosol mass spectrometers within the Hill Cap Cloud Thuringia (HCCT) Experiment 2010

J. Schneider[1], A. Roth[1], S. Mertes[2], D. van Pinxteren[2], H. Herrmann[2], and S. Borrmann[1,3]

[1]Particle Chemistry Department, Max Planck Institute for Chemistry, 55128 Mainz, Germany
[2]Leibniz Institute for Tropospheric Research, Leipzig, Germany
[3]Institute for Atmospheric Physics, Johannes Gutenberg University, 55128 Mainz, Germany
Keywords: Aerosol cloud interaction, Chemical composition, Single particle analysis, Mass spectrometry.
Presenting author email: johannes.schneider@mpic.de

Aerosol-cloud interactions were studied during the Hill Cap Cloud Thuringia (HCCT) experiment which was conducted at the mountain "Schmücke" (938 m a.s.l.) located in the forest "Thüringer Wald" in Central Germany, in September and October 2010. Three sampling sites have been set up: one station upwind, one on the mountain top and one downwind. Here we report on results obtained at the mountain top station where cloud residual particles were sampled by a counterflow virtual impactor and subsequently their submicron fraction was analysed by two types of aerosol mass spectrometers: one Aerodyne C-ToF-AMS and one laser ablation single particle mass spectrometer (ALABAMA, Brands et al., 2011). The C-ToF-AMS was additionally equipped with a light scattering probe, enabling single particle analysis also with the AMS (Freutel et al., 2011). The interstitial aerosol was sampled through a 5-µm cut-off inlet and analysed by an Aerodyne HR-ToF-AMS.

Additional instrumentation included black carbon mass concentration (MAAP), particle size distributions (SMPS, OPC) and total number concentration (CPC) of the cloud residuals and the interstitial and out-of-cloud aerosol, as well as cloud liquid water content (PVM) and cloud droplet size distribution and concentration (FSSP).

During out-of-cloud periods, both AMSs were operated in parallel behind the interstitial inlet to ensure the comparability between the two instruments.

The results obtained with both instrument show an enhancement of nitrate in cloud residuals in comparison to the out-of-cloud aerosol sampled shortly before the or after the cloud event (Figure 1). The comparison of interstitial aerosol and cloud residuals from the same cloud events show the enhancement of nitrate even more pronounced. This nitrate enhancement might be due to a less efficient activation of small particles that contain a higher sulphate fraction, or possibly also to the uptake of nitric acid by the cloud droplets.

In general, most particles detected and analysed by ALABAMA were internal mixtures of organic and inorganic compounds. The ALABAMA data indicate a relative increase of soot-containing particle in the cloud residuals, which is confirmed a decrease of the interstitial black carbon mass concentrations during cloud events. The detected soot particles were always internally mixed with nitrate and/or organics, hence the activation can be explained by a inorganic or organic coating on the soot particles which initiates the activation. The laser ablation data also showed significant number of biological particles and of mineral dust, at least in certain cloud events.

The organic fraction of the out-of-cloud aerosol was found to have a slightly higher O:C ratio than the interstitial aerosol sampled during cloud events. This indicates that the more oxidized (aged) organic aerosol is preferably activated as CCN, but this effect on average was found to be rather small.

This presentation will summarize the results obtained with both types of mass spectrometers, with emphasis on particle mixing state, air mass origin and organic composition of the cloud residuals.

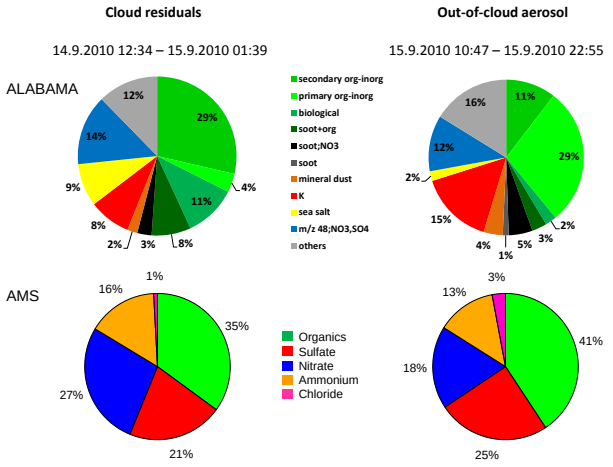

Figure 1. Comparison between composition of cloud residuals and out-of-cloud data for a selected cloud event (upper panel: ALABAMA, lower panel: AMS).

Brands, M., Kamphus, M., Böttger, T., Schneider, J., Drewnick, F., Roth, A., Curtius, J., Voigt, C., Borbon, A., Beekmann, M., Bourdon, A., Perrin, T. and Borrmann, S. (2011) *Aerosol Sci. Technol.*, **45**, 46-64.

Freutel, F., Klimach, T., Schneider, J., Drewnick, F., and Borrmann, S. (2011), *European Aerosol Conference*, Manchester, UK.

Composition analysis of cloud residual and aerosol particles by single particle mass spectrometry during the Hill Cap Cloud Thuringia Experiment 2010

A.Roth[1], S. Mertes[2], D. van Pinxteren[2], T. Klimach[1], J. Schneider[2] and S. Borrmann[1,3]

[1]Particle Chemistry Department, Max Planck Institute for Chemistry, 55128 Mainz, Germany
[2]Leibniz Institute for Tropospheric Research, Leipzig, Germany
[3]Institute for Atmospheric Physics, Johannes Gutenberg University, 55128 Mainz, Germany
Keywords: Single particle analysis, CCN, Mass spectrometry.
Presenting author email: a.roth@mpic.de

The chemical composition of cloud residual and background aerosol particles as well as the aerosol-cloud interaction was investigated during the field campaign Hill Cap Cloud Thuringia (HCCT) in September and October 2010 on the mountain site Schmücke (938m a.s.l.) in Central Germany. Either background aerosol was sampled by an interstitial inlet or orographic cloud droplets were sampled by a counterflow virtual impactor (CVI) which evaporates the cloud water. The remaining particles as well as the background aerosol particles were sized and analyzed by the bipolar Aircraft-based Laser Ablation Aerosol Mass Spectrometer (ALABAMA, particle size range 150 nm – 900 nm, Brands et al., 2011). Additionally the particle size distribution was measured by an optical particle counter (OPC) with a size range between 0.25 µm and 32 µm.

About 21 000 positive and negative mass spectra of cloud residual particles and about 239 000 of background aerosol particles were recorded. The size distributions measured by the OPC verify as expected, that the activated fraction shows a higher abundance of larger particles compared to the out-of-cloud aerosol.

A comparison of the averaged mass spectra shows a higher fraction of nitrate-containing particles as well as a lower fraction of organic and sulfate containing particles among cloud residuals. The mass spectra were separated by means of the fuzzy algorithm (Hinz et al., 2006) into clusters consisting of mass spectra with similar fragmentation patterns representing a certain particle type. This shows compared to the background aerosol composition that principally internally mixed particles containing secondary inorganic and secondary organic material and soot particles mixed with nitrate or organics serve as cloud condensation nuclei.

Depending on various meteorological conditions of cloud events and the air mass origin, cloud residual aerosol shows different composition (Figure 1). The main fractions are particles of organic and inorganic mixtures, potassium salts and internally mixed soot with nitrate. Furthermore variable fractions of mineral dust and sea salt particles are observable.

Difficulties arise in the case of mass spectra that contain only information on one polarity. These mass spectra, which amount to about 40% of the total recorded mass spectra, cannot be assigned definitely to one particle type.

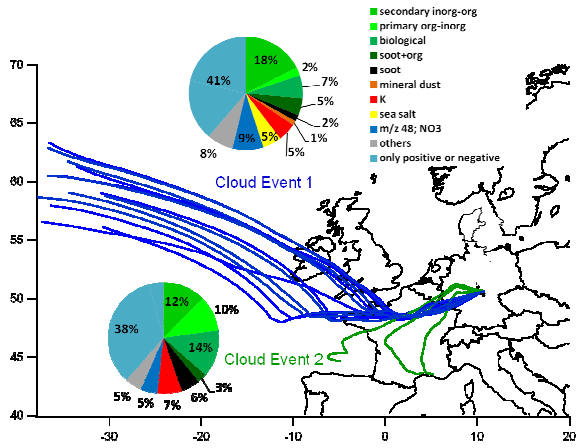

Figure 1. Comparison of cloud residual particle composition and HYSPLIT back trajectories (96 h, 500 m a.g.l., Draxler, 2012) for two different cloud events.

This work was supported by the Max Planck Society.

Brands, M., Kamphus, M., Böttger, T., Schneider, J., Drewnick, F., Roth, A., Curtius, J., Voigt, C., Borbon, A., Beekmann, M., Bourdon, A., Perrin, T. and Borrmann, S. (2011) *Aerosol Sci. Technol.*, **45**, 46-64.

Hinz, K.-P., Erdmann, N., Grüning, C., Spengler, B. (2006) *International Journal of Mass Spectrometry*, **258**, 151-166.

Draxler, R.R. and Rolph, G.D., 2012. HYSPLIT (HYbrid Single-Particle Lagrangian Integrated Trajectory) Model access via NOAA ARL READY Website (http://ready.arl.noaa.gov/HYSPLIT.php). NOAA Air Resources Laboratory, Silver Spring, MD.

The impact of clouds on radical concentrations: Observations of OH and HO_2 during HCCT-2010

L.K. Whalley[1,2], I.J. George[1], D. Stone[1] and D.E. Heard[1,2]

[1]School of Chemistry, University of Leeds, Leeds, West Yorkshire, LS2 9JT, United Kingdom
[2]National Centre for Atmospheric Science, University of Leeds, Leeds, LS2 9JT, United Kingdom
Keywords: free-radicals, cloud uptake, heterogeneous loss
Presenting author email: d.e.heard@leeds.ac.uk

Clouds play a crucial role in the chemistry of the atmosphere, occupying, on average, ~ 15 % of the volume of the lower atmosphere (Lelieveld & Crutzen, 1990). Modelling studies have shown that aqueous phase chemistry in clouds can influence gas phase radical chemistry and in turn can cause significant reductions in the oxidative capacity (e.g. Lelieveld & Crutzen, 1991; Kreidenweis et al., 2003) and, hence, removal rate of VOCs. A number of aircraft projects have identified significantly reduced HO_2 concentrations when flying through clouds that exceeds the depletion expected due to the reduction in radiation alone (Olson et al., 2004; Commane et al., 2010). These experimental observations are relatively sparse, however, and until recently a comprehensive study to validate model predictions has been lacking.

Here we report measurements of OH and HO_2 radicals made during the HCCT (Hill Cap Cloud Thuringia) project that took place at Mt. Schmücke, Thuringia in Germany during September/October 2010. The University of Leeds Fluorescence Assay by Gas Expansion (FAGE) instrument was located at the summit of Mt. Schmücke and made near-continuous measurements of the radicals at the top of a 22 m tower. The site was regularly influenced by clouds throughout the measurement period and co-located measurements of liquid water content were made at the site enabling the influence of this microphysical parameter on the radical budget to be determined. On average, the photolysis rate of O_3 to form $O(^1D)$, the primary daytime source of HO_x radicals, was ~ 65 % lower in-cloud relative to the out of cloud observations. The HO_2 concentrations were significantly depleted in cloud, with concentrations ~ 90 % lower relative to the out of cloud observations; an OH signal above the noise of the instrument was not observed during cloud events. These results suggest that heterogeneous processes in clouds do perturb the gas-phase radical chemistry. Using a simple steady state analysis, to replicate HO_2 in-cloud observations, a first order loss rate of HO_2 to clouds = 0.2 s^{-1} is needed, suggesting a reactive uptake coefficient, γ, equal to 0.0125 at a cloud droplet surface area of 1.5 x 10^{-3} cm^2cm^{-3}. This value is consistent with HO_2 uptake coefficients determined for relevant aerosols in the laboratory using an aerosol flow reactor combined with FAGE detection of HO_2 radicals.

This work was supported by the NERC National Centre for Atmospheric Science, and the Leibniz-Institut für Troposphärenforschung.

Lelieveld, J. and Crutzen P. J., 1990, Influences of Cloud Photochemical Processes on Tropospheric Ozone, Nature 343 (6255), 227-233.

Lelieveld, J. and Crutzen P. J., 1991, The Role of Cloud in Tropospheric Photochemistry, Journal of Atmospheric Chemistry, 12, 229-267.

Kreidenweis, S. M. et al., 2003, Modification of aerosol mass and size distribution due to aqueous phase SO_2 oxidation in clouds: Comparison of several models. Journal of Geophysical Research-Atmospheres, 108.

Olson, J. R. et al., 2004, Testing fast photochemical theory during TRACE-P based on measurements of OH, HO_2 and CH_2O. Journal of Geophysical Research-Atmospheres, 109.

Commane, R. et al., 2010, Observations of OH and HO_2 over West Africa. Atmospheric, chemistry and Physics, 10, 8783–8801.

SPACCIM model studies on the multiphase chemistry occurring in orographic hill cap clouds during the HCCT-2010 field campaign

A. Tilgner, P. Bräuer, R. Wolke and H. Herrmann

Department of Chemistry, Leibniz-Institut für Troposphärenforschung,
Permoserstr. 15, Leipzig, 04318, Germany

Keywords: aerosol modelling, multiphase chemistry, aerosol cloud interaction, organic aerosols
tilgner@tropos.de

Tropospheric clouds and deliquescent particles are a complex multiphase and multi-component environment with simultaneously occurring gas and aqueous phase chemical transformations. Such aqueous phase chemical processes in cloud droplets and deliquescent particles are expected to proceed very efficient on short timescales and hence they are able to alter the chemical aerosol composition and the deduced physical properties on a global scale (Ravishankara, 1997). Besides the physico-chemical aerosol processing, chemical aerosol cloud interactions have significant effects on the whole multiphase oxidation budget.

In order to improve the still limited understanding of the aerosol-cloud interactions, Lagrangian-type field experiments, where an orographic cloud is used as a natural flow-through reactor, are used for studying such processes in more detail. In Sept./Oct. 2010, the Lagrangian-type cloud passage experiment HCCT-2010 (Hill Cap Cloud Thuringia 2010) was conducted at Mt. Schmücke in Thuringia, Germany to study aerosol cloud interactions (see Figure 1). As known from former cloud passage experiments, particularly associated model investigations (see e.g. Tilgner et al., 2005) including comparisons of model results with observations have considerably contributed to the interpretation of the measured field data.

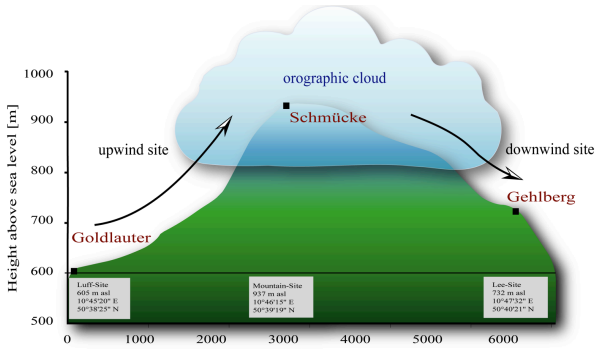

Figure 1. Schematic representation of the campaign area of the cloud passage experiment HCCT-2010.

In the present study, the parcel model SPACCIM (SPectral Aerosol Cloud Chemistry Interaction Model, Wolke et al., 2005) is applied to investigate the effects of multiphase cloud processing of tropospheric aerosol particles and trace gases resulting from a passage through an orographic cloud at Mt. Schmücke (Germany) during HCCT-2010. The applied model combines a complex microphysical and a detailed multiphase chemistry model with 11381 gas phase and over 3600 aqueous phase reactions. The chemical multiphase mechanism (MCMv3.1 (Master Chemical Mechanism; Saunders et al., 2003)/ CAPRAM3.0i-ext (Chemical Aqueous Phase RAdical Mechanism, Herrmann et al., 2005)) incorporates a detailed near-explicit description of the inorganic and organic multiphase chemistry based on time-dependent size-resolved aerosol/cloud spectra. The measured physical and chemical data at the upwind site provided the basis for the model initialisation under real environmental conditions.

First SPACCIM simulations have been carried out for few cloud events, which provided appropriate meteorological and overflow conditions fulfilling the cloud passage experiment requirements. Model results of the cloud passage simulation have been compared with experimental cloud water composition data at Mt. Schmücke (summit site) as well as gas and aerosol measurements at the downwind site in order to interpret the experimental data and to evaluate the model results. To this end, detailed analyses of the chemical multiphase system have been performed including chemical source and sink studies with special emphasis on radical and non-radical oxidants as well as important organic and inorganic chemical subsystems. For the fist time, modelled interstitial gas phase in-cloud HO_x concentrations were compared with measurements performed at the in-cloud summit site. Moreover, a central objective of the study was to assess in-cloud oxidations of important C2 and C3 organic compounds such as glyoxal and methylglyoxal.

This work was supported by the German Research Foundation (DFG, He 3086/15-1).

References:

Herrmann, H. et al. (2005) *Atmos. Environ.* **39** (23-24), 4351-4363.

Ravishankara, A. R. (1997) Science, **276** (5315), 1058-1065.

Saunders, S. M. et al. (2003) *Atmos. Chem. Phys*., **3**, 161-180.

Tilgner, A. et al. (2005) *Atmos. Environ.* **39** (23-24), 4389-4401.

Wolke, R. et al. (2005) *Atmos. Environ.* **39** (23-24), 4375-4388.

Wednesday, September 5, 2012

Session WG01S4O. Physical and chemical properties + Transport (I)

Non-volatile aerosol in the Arctic Winter Stratosphere and its role for PSC formation.

R. Weigel[1], M. Ebert[2], K. Kandler[2], S. Molleker[3], W. Frey[3], M. Klingebiel[1], C. M. Volk[4], G. Günther[5], H. Schlager[6], F. Cairo[7], S. Kaykin[8], S. Borrmann[1,3]

[1]Johannes Gutenberg Universität Mainz, Institut für Physik der Atmosphäre, Mainz, Germany
[2]Institut für angewandte Geowissenschaften, Technische Universität Darmstadt, Germany
[3]Partikelchemie, Max Planck – Institut für Chemie, Mainz, Germany
[4]Fachbereich C - Abteilung Physik, Bergische Universität Wuppertal, Germany
[5]Institut für Energie- und Klimaforschung – Stratosphäre (IEK-7), FZ Jülich, Germany
[6]Institut für Physik der Atmosphäre, DLR, Oberpfaffenhofen, Germany
[7]Istituto di Scienze dell'Atmosfera e del Clima, Consiglio Nazionale delle Ricerche, Rome, Italy
[8]Central Aerological Observatory, Moscow, Russia

Keywords: Stratospheric aerosol, Arctic Winter Vortex, non-volatile particles, PSC
Presenting author email: weigelr@uni-mainz.de

In-situ measurements with a 4-channel condensation particle counter (COPAS, Weigel et al., 2009) with different d_{p50} (50 % detection efficiency cut-off particle diameter) were conducted in the altitude range of 12.0-20.5km on board the M-55 *Geophysica*. One of four channels has a heated aerosol inlet line (at 250°C) which additionally allows for counting non-volatile particles.

Kiruna, North Sweden, was the operations base from where research flights towards the Arctic Winter Vortex (AWV) were performed during three scientific missions: EUPLEX (Jan.-Mar. 2003, 15 flights); RECONCILE, (Jan.-Mar. 2010, 13 flights); and ESSENCE, (Dec. 2011, 2 flights).

For potential temperatures $\Theta > 400$K the progression of the vertical profiles strongly depends on whether the measurements occurred in- or outside the AWV (Figure 1, left). Outside the AWV the particle mixing ratio N remains nearly constant with altitude while inside the AWV N increases with ascent.

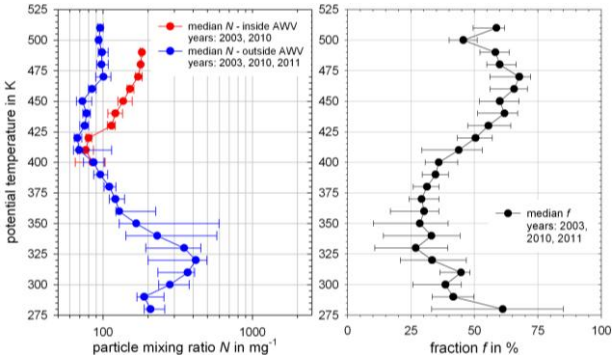

Figure 1. Vertical median profiles with 25- and 75-percentiles of particle mixing ratio N and the fraction f of non-volatile particles.

The fraction f of non-volatile aerosol in the AWV region is generally increasing at altitudes with $\Theta > 400$K from about 35% up to 70% at $\Theta = 475$K (Figure 1, right), which is high compared to f measured elsewhere in the stratosphere at same altitudes (cf. Borrmann et al., 2010). Hence, subsiding air masses inside the AWV entrain particles into the Arctic lower stratosphere from aloft. Up to 7 of 10 of these particles contain solid, not vaporizable material and were previously assumed to mainly stem from meteoritic ablations at mesospheric altitudes (Curtius et al., 2005).

During RECONCILE and ESSENCE particles were collected with an impactor at altitudes of $\Theta > 410$K. The chemical analysis of these aerosols with Environmental Scanning Electron Microscopy (ESEM) and Energy Dispersive X-ray (EDX) analysis techniques yields (apart from found residuals of the volatile nitric- and sulfuric acid compounds):

A) Non-volatile particles with $d_p < 500$nm mainly consist of soot, sometimes with bearings of lead.

B) Particles with $d_p > 500$nm (and $d_p < 6$µm) are partly amorphous, most likely of crustal material. In the same size range also molten spheres were found, alloy particles, metals or metaloxides and silicates.

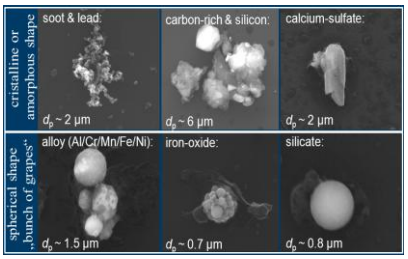

Figure 2. ESEM images of collected particles in the AWV region.

The fly-ash habit indicates that some particles were exposed to high temperatures for a sufficient duration.

These non-volatile particles in the AWV region provide condensation surfaces and thus could contribute to the formation of Polar Stratospheric Clouds (PSCs).

Geophysica missions were funded by the EC within the FP5 and FP7 (EVK2-CT-2001-00119and 226365-FP7-ENV-2008-1) and by the European Space Agency (ESA). Further support was provided by the Universities of Mainz and Darmstadt and the Max-Planck-Institute for Chemistry.

Borrmann, S., et al., (2010), Aerosols in the tropical and subtropical UT/LS: In-situ measurements of ultrafine particle abundance and volatility, *Atmos. Chem. Phys. 10*, 5573–5592.

Curtius, J. et al. (2005), Observation of meteoritic material and implications for Aerosol nucleation in the winter Arctic lower stratosphere derived from in situ particle measurements; *Atmos. Chem. Phys*., 5, 1-25.

Weigel, R., et al. (2009), Experimental characterization of the COndensation PArticle counting System for high altitude aircraft borne application; *Atmos. Meas. Tech.*, 2, 243-258.

Fluorescent lifetime imaging of aerosol viscosity and phase

F.D. Pope[1,2], N.A. Hosny[3] , C. Fitzgerald[1], M.Kalberer[1], and M.K. Kuimova[3]

[1]Centre for Atmospheric Science, Department of Chemistry, University of Cambridge, Cambridge, CB1 3HY, UK.
[2]School of Geography, Earth and Environmental Sciences, University of Birmingham, Birmingham, B15 2TT, UK.
3Department of Chemistry, Imperial College London, London, SW7 2AZ, UK.

Keywords: fundamental aerosol physics, aerosol chemistry, FLIM, instrumentation.
Presenting author email: fdp21@cam.ac.uk

The viscosity and phase of atmospheric aerosols are key properties that help define aerosol reactivity and hence aerosol aging (Virtanen et al, 2010). The viscosity and phase are strongly linked to the water content of aerosols and hence the aerosol hygroscopicity. The ability of chemical species to diffuse into the aerosol core, or be limited to surface reactions, is closely linked to the aerosol viscosity. In particular, the bulk reactivity of fast lived species with a limited lifetime is often diffusion limited (Pfrang et al, 2011).

At present, there are no analytical techniques that can directly measure the viscosity and phase of atmospheric aerosol. This greatly limits the physical chemical understanding of these important atmospheric systems. In particular, a measure of viscosity would allow for direct probing of the glassy state of aerosols (Koop et al, 2011).

We are developing the use of Fluorescence Lifetime Imaging (FLIM) techniques, which have previously been used for investigating cell viscosity (Kuimova et al, 2009), to probe the viscosity of atmospheric aerosol. The FLIM technique works by the insertion of novel fluorescent probes (molecular rotors) into the aerosol systems of interest (Kuimova et al 2008). The fluorescent lifetimes of these probes are dependent on the viscosity of the surrounding environment because the fluorescence competes with intramolecular rotation. In a highly viscous environment the rotation of the rotors is significantly hindered and hence the fluorescence is strongly perturbed. This technique allows the viscosity of model aerosols to be measured whilst varying the environmental conditions such as relative humidity and temperature.

The use of different molecular rotors allows for the measurement of viscosity from 1-1000 centipoise, and the choice of rotor is important for ensuring precise measurements. Results on the viscosity of both inorganic and organic aerosol systems will be presented and the effect of relative humidity on aerosol viscosity will also be shown. The FLIM technique allows for the investigation of surface versus bulk characteristics of large supermicron particles. The variation of aerosol viscosity throughout the aerosol medium will be presented.

The FLIM technique shows great promise for aerosol research and potential future applications of the technique in this field will be highlighted. In particular, the technique will be extended to investigate the role of gas phase oxidant chemistry on aerosol viscosity, and the probing of glassy aerosol states.

This work was supported by the UK Natural Environment Research Council (NERC) studentship for C.F.

Koop, T. et al. (2011) Physical Chemistry Chemical Physics. 13(43) 19238.
Kuimova, M.K. et al. (2008) J. Amer. Chem. Soc. 130, 6672.
Kuimova, M.K. et al. (2009) Nature Chemistry, 1, 69.
Pfrang, C. Shiraiwa, M. Pöschl, U. (2011) Atmospheric Chemistry and Physics. 11, 7343.
Virtanen, A. et al. (2010) Nature, 467, 824.

Phase state and humidity-induced phase transition studies of SOA particles from biogenic and anthropogenic precursors

E. Saukko[1],A.T. Lambe, [2,3], P. Massoli, [3], T. Koop,[4], J.P. Wright[2], D.R. Croasdale[2], D.A. Pedernera[4,a], T.B. Onasch[2,3], A. Laaksonen[5,6],P. Davidovits[2], D.R. Worsnop[3,7] and A. Virtanen[1,b]

[1]Department of Physics, Tampere University of Technology, Tampere, Finland

[2]Chemistry Department, Boston College, Chestnut Hill, MA, USA

[3]Aerodyne Research Inc., Billerica, MA, USA

[4]Faculty of Chemistry, Bielefeld University, Bielefeld, Germany

[5]Finnish Meteorological Institute, Helsinki, Finland

[6]Department of Applied Physics, University of Eastern Finland, Kuopio, Finland

[7]Division of Atmospheric Sciences, Department of Physics, University of Helsinki, Helsinki, Finland

[a]Now at: Faculty of Mathematics, Astronomy and Physics, National University of Córdoba,Córdoba, Argentina

[b]Now at: [6]

Keywords: SOA, phase state, impactor, bounce, PAM.

Presenting author email: erkka.saukko@tut.fi

There is mounting evidence showing that tropospheric secondary organic aerosol (SOA) may exist in a phase state other than liquid, namely semi-solid or solid amorphous (Virtanen et al., 2010; Cappa and Wilson, 2011; Vaden et al. 2011). The solid or semi-solid, high viscosity material may have significantly higher lifetime in an oxidizing atmosphere than low viscosity liquid due to mass transfer limitations in the particle bulk (Shiraiwa, 2011).

In this work we report a systematic study of the phase state of SOA particles produced by photo-oxidation of several volatile organic compound (VOC) precursors in a potential aerosol mass (PAM) flow tube reactor. The phase state of the particles was studied by their bounce behaviour upon impaction on a polished steel plate in a low pressure impactor (Saukko et al., 2012). The SOA oxidation level (O/C) was determined by an Aerodyne high resolution time-of-flight aerosol mass spectrometer (HR-ToF-AMS)

The phase state for several types of SOA from different surrogate anthropogenic and biogenic precursors, produced at a wide range of oxidation conditions, were studied at a range of relative humidities. We report the solid or semi-solid phase state of SOA produced from cyclic and terpene precursors used in the study up to at least 50 % relative humidity. Furthermore, adding sulfur dioxide into the reaction chamber yielded liquefied particles, while particles formed from oxidation of pure organic precursor were solid or semi-solid. For a long-chain alkane precursor a liquid-like SOA at low oxidation level was produced, but upon increasing the oxidation level, the formed particles became more solid, which is shown in Fig. 1.

While the bounce behaviour of the particles had no single explaining factor for all experiments, the precursor molar mass was seen to correlate with more solid phase at higher humidities in cases with cyclic or terpene precursor.

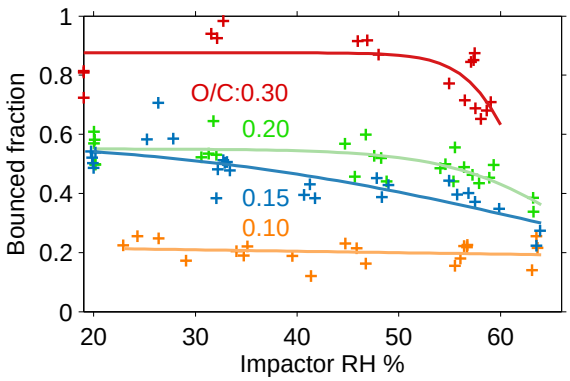

Figure 1: An increasing O/C level increases the fraction of bounced *n*-heptadecane-derived SOA particles at all humidities, while increasing humidity decreases the bounced fraction.

This work was supported by the Nessling Foundation, Office of Science (BER), Department of Energy (Atmospheric Science Program) grant No. DE-SC0006980 and the Atmospheric Chemistry Program of the National Science Foundation grants No. ATM-0525355 and ATM-0854916 and the EU integrated project 505390-GOCE-CT-2004.

Cappa, C. D. and Wilson, K. R. (2011) Atmos. Chem. Phys., 11, 1895–1911, doi:10.5194/acp-11-1895-2011.

Saukko, E., Kuuluvainen, H., and Virtanen, A. (2012) Atmos. Meas. Tech., 5, 259–265, doi:10.5194/amt-5-259-2012.

Shiraiwa, M., Ammann, M., Koop, T., and Pöschl, U. (2011) PNAS, 108, 11003–11008, 5 doi:10.1073/pnas.1103045108.

Vaden, T. D., Imre, D., Beránek, J., Shrivastava, M., and Zelenyuk, A. (2011) PNAS, 108, 2190–2195, doi:10.1073/pnas.1013391108.

Virtanen, A., Joutsensaari, J., Koop, T., Kannosto, J., Yli-Pirilä, P., Leskinen, J., Mäkelä, J., Holopainen, J., Pöschl, U., Kulmala, M., Worsnop, D. R., and Laaksonen, A. (2011) Nature, 467, 824–827, 2010.

Overview of ClearfLo Detling Site: Study of Aerosol Sources and Processing at a Rural Site Southeast of London

L. R. Williams[1], S. Herndon[1], J. Jayne[1], A. Freedman[1], B. Brooks[1], J. Franklin[1], P. Massoli[1], E. Fortner[1], P. Chhabra[1], M. Zahniser[1], H. Stark[1], T. Onasch[1], D. R. Worsnop[1], F. Lopez-Hilfiker[2], C. Mohr[2], J. Thornton[2], N. L. Ng[3], L. Xu[3], M. Kollman[3], W. B. Knighton[4], M. Dubey[5], A. Aiken[5], K. Gorkowski[5], T. Martin[6] and R. Coulter[6]

[1]Aerodyne Research, Inc., Billerica, MA 01821, USA
[2]Department of Chemistry, University of Washington, Seattle, WA 98195, USA
[3]School of Earth and Atmospheric Sciences, Georgia Institute of Technology, Atlanta, GA, 30332, USA
[4]Department of Chemistry and Biochemistry, Montana State University, Bozeman, MT 59717, USA
[5]Earth and Environmental Sciences Division, Los Alamos National Laboratory, Los Alamos, NM, 87545, USA
[6]Environmental Science Division, Argonne National Laboratory, Argonne, IL 60439, USA
Keywords: aerosol chemistry, atmospheric black carbon, field measurements
Presenting author email: Worsnop@aerodyne.com

Clean Air for London (ClearfLo) is a large, multidisciplinary study of the London urban atmosphere aimed at understanding the relationships between surface meteorology, gas-phase composition and particulate matter at a city street site, a city background site (away from local traffic sources) and at rural locations that sample the outflow from the London urban area. During the winter intensive (January to February, 2012) we deployed a suite of instruments at a rural site southeast of London in Detling, UK. We present an overview of the chemical, physical and optical properties of the aerosol, focusing specifically on black carbon containing particles, as well as correlations with gas-phase tracers and aerosol precursors.

Data were collected through several co-located inlets mounted on a 9 m tower. Real-time particle instruments included an Aerodyne high-resolution time-of-flight mass spectrometer (HR-ToF-AMS), an Aerodyne soot particle mass spectrometer (SP-AMS), a multi-angle absorption photometer (MAAP), photo-acoustic soot spectrometers (PASS), a scanning mobility particle sizer (SMPS), cavity enhanced phase-shift particle extinction monitors (CAPS PMex), and a single particle soot photometer (SP2). Particle properties were measured with and without a thermal denuder in order to understand the effect of coatings on optical properties. Bulk particle chemistry was measured with filter samplers, a rotating drum impactor and a semi-continuous elemental and organic carbon analyzer.

Gas phase measurements included air mass tracers (CO, CO_2, O_3, NO_x) and volatile organic compounds using a proton-transfer reaction spectrometer (PTR-MS) and gas-chromatograph/flame ionization detector (GC/FID). The micro-orifice volatilization impactor chemical ionization time-of-flight mass spectrometer (MOVI-CI-TOFMS), a recently developed chemical ionization instrument that measures organic acids in both the gas-phase and the particle-phase, was also deployed.

Over the course of the campaign, sampled air masses were of local (A249 motorway 200 m south of the site), regional (London to the northwest, industrial areas north of the site, or Maidstone city southwest of the site) or more distant (continental European) origin depending on the direction of the prevailing winds. Figure 1 shows wind and CO data for an example of continental outflow (top panel) and regional London outflow (bottom panel). Results will be presented for each of these regimes. For the air masses identified as containing London outflow, the results are correlated with measurements at the ClearfLo winter intensive site in downtown London (North Kensington).

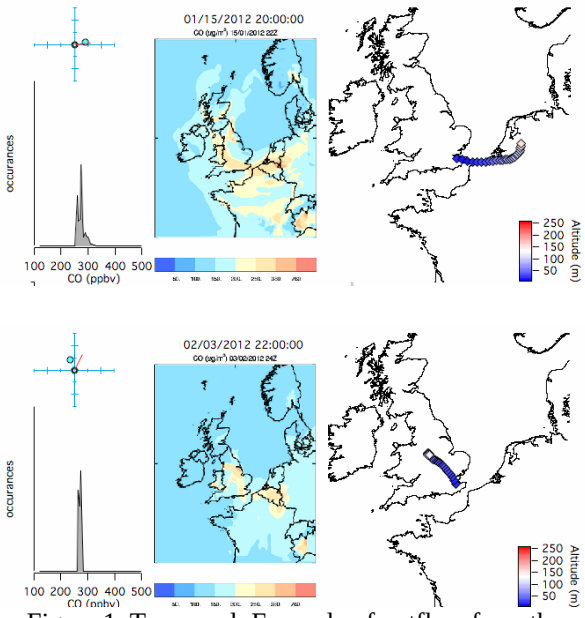

Figure 1. Top panel: Example of outflow from the continent. Bottom panel: Example of outflow from London. Both panels: Top left:wind direction and speed, bottom left: CO distribution over preceeding 4 hours (ppb), center University of Reading AQUM model CO average concentration (μg/m^3), right: Hysplit backtrajectory.

Acknowledgements: This project was funded by the US Department of Energy Atmospheric System Research Program and the UK Natural Environment Research Council.

Aircraft measurements of gases and particles during CAREBeijing-2008 in surrounded Beijing areas

W.J. Zhang[1*], Z.P Bai[1], T. Zhu[2], W. Yang[1], B.H. Yin[1]

[1]State Key Laboratory of Environmental Criteria and Risk Assessment, Chinese Research Academy of Environmental Sciences, Beijing 100012, China
[2] State Key Joint Laboratory for Environmental Simulation & Pollution Control, College of Environmental Sciences, Peking University, Beijing 100871, China
Keywords: Aircraft measurement, Gaseous pollutants, Particles, Back trajectory
Corresponding author email: zhangwj@craes.org.cn

At present, the air pollution around Beijing area has become a complex problem with a combination of different types of sources: coal smoke, traffic emission, dust re-suspension, and so on. Additionally, the transport of particulates seems to be a large-scale regional pollution. It is of great value to conduct aircraft measurements of pollutants at different altitudes (Wang et al., 2008).

Measurements of gaseous pollutants, including ozone (O_3), sulfur dioxide (SO_2), nitrogen oxides (NO_X = NO + NO_2), carbon monoxide (CO), particle number concentrations (5.6-560 nm and 0.47-20 μm), and meteorological parameters (T, RH, P) were conducted during the Program of Campaigns of Air Quality Research in Beijing and Surrounding Region (CAREBeijing) from August 27 through October 13, 2008. The data of total 18 flights (70 h flight time) from the ground to 2100 m were obtained by a Yun-12 aircraft in the southern surrounded areas of Beijing (38ºN-40ºN, 114ºE-118ºE). This measurement was to characterize the regional variation of air pollution during and after the Olympics of 2008, the impacts of different transport direction and possible influencing factors.

Results suggested that four different groups of transport sources influenced the pollution level of pollutants with the consideration of the backward trajectory analysis, including: (1) the pollutant transport of the southern direction with higher pollutants level. The higher SO_2 concentration especially at 2100 m may be a good tracer for the sources from southern transport. The higher NOx concentration may be more from the southern or southeastern transport of ground pollutants; (2) the cleaner long-range transport of the northern or northwestern direction with lower pollutants level. The flights showed lowest concentration of gases pollutants, at all three different heights, which may indicate the contribution of deserted areas; (3) the transport from the eastern direction with characteristics of sea sources, i.e. middle level of gases pollutants and higher particle concentration. This may be due to the characteristics of the sea sources, lack of gases pollutants but more sea salt particles; (4) the transport of mixing directions, i.e. lower altitudes from the pollutant transport direction or local pollution but higher altitudes from the clean transport direction. Additionally, the relatively long-lived CO was shown to be a possible transport tracer of long-range transport of northwestern direction especially on the higher altitudes. Three factors influenced the size distribution of particles, i.e. air mass transport direction, ground source emissions and meteorological influences were also discussed.

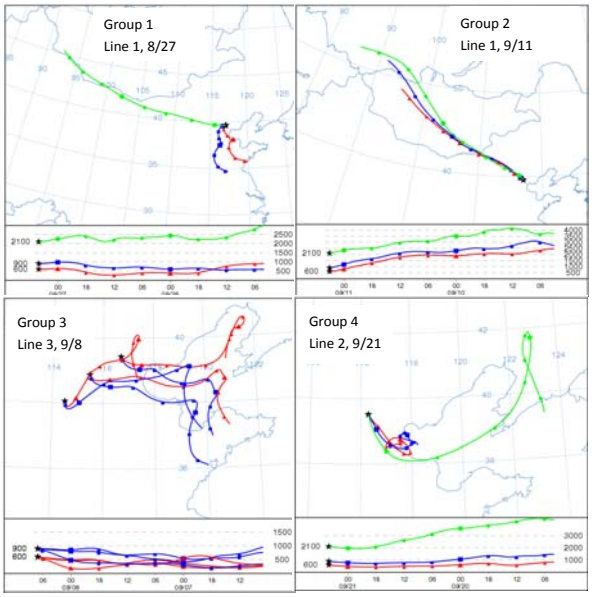

Figure 1. A 48 h back trajectories for the different group flights

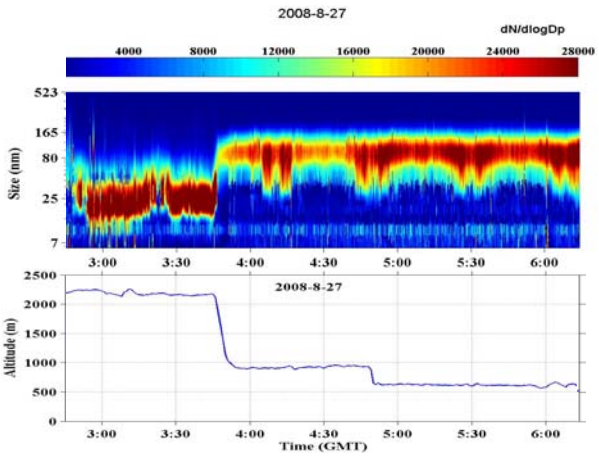

Figure 2. Variation of size distributions for 5.6-560 nm range with altitudes at different heights on Aug. 27 flight.

This work was supported by the CAREBeijing-2008 project, and the special fund of State Key Joint Laboratory of Environment Simulation and Pollution Control 11K02ESPCP.

Wang, W., Ma, J., Hatakeyama, S., Liu, X., Chen, Y., Takami, A., Ren, L., Geng, C. (2008) *Atmos Environ*, **42**, 5715– 5720.

Single particle characterization using a high resolution time-of-flight aerosol mass spectrometer: Atmospheric observation in Nagoya, Japan

T. Mihara and M. Mochida

Department of Earth and Environmental Sciences, Graduate School of Environmental Studies, Nagoya University, Furo-cho, Chikusa-ku, Nagoya 464-8601, Japan
Keywords: urban aerosol, single particle analysis, mixing state, organic aerosol, aerosol mass spectrometry
Presenting author email: mihara.toshiyuki@d.mbox.nagoya-u.ac.jp

Introduction

Physical and chemical properties of single particles (e.g., refractive index and hygroscopicity) are important for various atmospheric processes, such as scattering and absorption of solar radiation and cloud droplet formation. Chemical composition controls the properties; however, knowledge on single particle composition is still very limited. In this study, we investigated the composition of single particles in the urban atmosphere using a high resolution time-of-flight aerosol mass spectrometer (HR-ToF-AMS). The mass spectra of the particles were analyzed to explore the association of chemical components in single particles, and the temporal alternation of the aerosol mixing state.

Experiment

Measurements of atmospheric aerosols were performed in the urban area of Nagoya, Japan, from 31 October to 5 November, 2010. The aerosols were introduced to the HR-ToF-AMS and a scanning mobility particle sizer (SMPS) to measure the single particle composition and the size distribution, respectively. Prior to the measurement using the HR-ToF-AMS, the atmospheric aerosols were passed through a PM1 cyclone, three diffusion-dryer-type scrubbers (filled with activated carbon, silica gel, and molecular sieves), an aerosol neutralizer, and an aerosol humidifier (85% RH). The HR-ToF-AMS was operated in the mass spectrum (MS) mode, the particle time-of-flight (PToF) mode, and the brute-force single-particle (BFSP) mode alternatively. The unit mass spectra of size-resolved single particles were measured using the BFSP mode. In the analysis of the mass spectra collected using the BFSP mode, the baseline spectrum were subtracted to exclude the contribution from background gaseous species and to obtain the spectra originated from particles. Single particle detection events were extracted from the data using the threshold that is defined as the sum of the average and nine times the standard deviation of the baseline spectra. We regard that the particle was detected when the maximum of the sum of particle-related signals (i.e, those at mass numbers greater than or equal to *m*/*z* 30, but excluding *m*/*z* 32 and *m*/*z* 40) was above the threshold. The BFSP data were analyzed using the fragment table in the AMS analysis software (Squirrel, http://cires.colorado.edu/jimenez-group /ToFAMSResources/ToFSoftware/) to calculate the mass concentrations of sulfate, nitrate, and organics. These concentrations were compared with the concentrations measured in the MS and PToF modes, which were obtained using the AMS analysis software (Squirrel, Pika, Apes, PET).

Results and discussion

Particles were detected for 7,926 cycles in the 1,031,695 recorded cycles, whose diameter was in the range from 1 to 5,624 nm. The median diameter was 406 nm, and particle counts at <40 nm, which may not be real, was only 0.5 %. The pattern of the time series of the single particle counts were similar to that of the particle number concentrations measured using the SMPS. The mean concentrations of organics, sulfate, and nitrate in single particles were, respectively, 0.23, 0.05, and 0.05 μg m^{-3}. These values were one fifth of the mass concentrations measured in the MS mode. The delta analysis (Mihara and Mochida, 2011) was applied for the single particle mass spectra to assess the degree of oxidation of organics. The relationship of the proportion of organic mass with Δ values of 3, 4, and 5 in the total organic mass to the proportion of organic mass in the detected total mass (organics, sulfate, nitrate, ammonium, and chloride) was similar to that to the proportion of m/z 44 in the total organic mass (f44) (Aiken *et al.*, 2008). The results indicate that less oxygenated organics were more abundant in the particles with large fractions of organics. Oppositely, more oxygenated organics were abundant in the particles with large fractions of nitrate and sulfate. Alteration of the mixing state of aerosol was evident from the time series of the relationship of the proportion of organic mass with Δ values of 3, 4, and 5 in the total organic mass to the proportion of organic mass in the detected total mass; the internally-mixed condition changed to the externally-mixed condition from the evening of 4th to the noon of 5th of November. Although this analysis need processing of a large amount of data, this method makes it possible to analyze the chemical composition of single particles down to the size range (≥100 nm) that are not easy to analyze with the help of a laser scattering technique.

Acknowledgement This study was supported in part by a Grant-in-Aid for Young Scientists (S) (20671001).

References

Aiken, A. C. *et al.* (2008) *Environ. Sci. Technol.* **42**, 4478–8358.

Mihara, M. and Mochida, M. (2011) *Environ. Sci. Technol.* **45**, 9168–9174.

Long term measurements of chemical composition of ambient ions

Heikki Junninen[1], Mikael Ehn[2], Siegfried Schobesberger[1], Gustaf Lönn[1], Tuukka Petäjä[1], Douglas R Worsnop[1] and Markku Kulmala[1]

[1]Department of Physics, University of Helsinki, Finland, [2]Airmodus Oy, Helsinki, Finland,
[2] Institute for Energy and Climate Research (IEK-8), Forschungszentrum Jülich, 52425 Jülich, Germany
Keywords: Ambient ions, APiTOF, mass spectrometry
Presenting author email: Heikki.Junninen@helsinki.fi

Atmospheric aerosol formation consists of a complicated set of processes that include the production of nanometer-sized clusters from gaseous precursor vapours and their subsequent growth. Charge is known to change clustering energies and also the ions themselves might play a role in new aerosol formation. Since the very first steps of aerosol formation are still unclear also the role of ions is unresolved for certain. Long term parallel measurements with ion spectrometer and particle size distributions show that the fraction of ions participating in the particle formation is varying depending on ambient conditions and the chemical environment. These measurement techniques, however have had a low mobility resolving power and an ion cluster composition could not been determined.

Here we present recent achievements on developing instrumentation to detect the composition of ambient cluster ions in the masses up to 2000Th. The instrument is an Atmospheric Pressure Interface Time-of-Flight Mass Spectrometer (APi-TOF, Junninen et al 2010) with mass accuracy <20ppm and resolving power 3000Th/Th. The instrument can be operated on remote location unattended or remotely controlled. This makes possible long term measurements and time series analysis. Majority of the peaks can be associated with a confidence to elemental composition and further to molecular composition of atmospheric ions. The data analysis has been performed using a new tool for analysing large datasets of time-of-flight mass spectrometry data, tofTools.

The APi-TOF was sampling continuously in field station (SMEAR II, Hyytiälä, Finland) for 7 months from May to November 2010 covering seasons late spring, summer and autumn.

Recently, alpha-pinene oxidation experiments in plant chamber (Ehn et al. 2012) have shown remarkable similarities with spectrum measured in ambient boreal atmosphere. Among other negative clusters the time behaviour and seasonal variability these novel extremely oxidised organic C10 compounds will be presented and their time series will be correlated against other precursors of aerosol formation. General features of time seasonal behaviour can be seen in figure 1, where an average difference spectrum between summer and fall is presented. During light hours in summer time the spectrum is dominated by malonic acid its cluster ions while dark hours by extremely oxidized organic compounds. This will be the first time such a long term measurement of newly identified compounds will be presented.

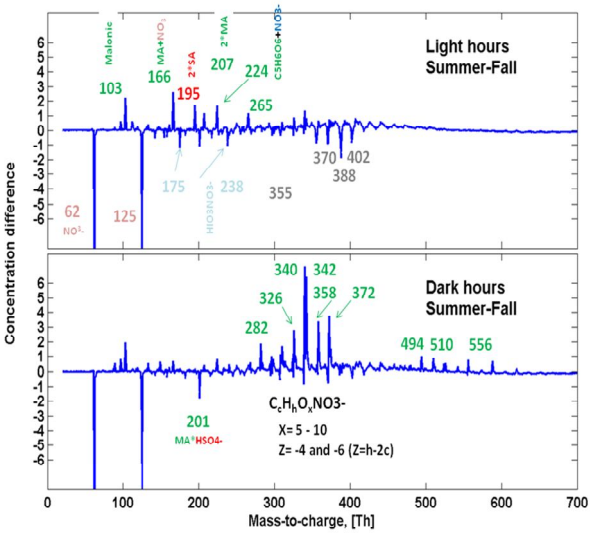

Figure1. Difference spectrum of summer and fall separated to light and dark hours. Positive peaks are dominant in summer while negative ones during fall.

This work was supported by Finnish Centre of Excellence (FCoE), Cryosphere-Atmosphere Interactions in a Changing Arctic Climate (CRAICC), and European Research Council (ERC).

Ehn, M. et al., *Atmos. Chem. Phys. Discuss.*, 12, 4589-4625, 2012.

Junninen, H. et al., *Atmos. Meas. Tech.*, 3, 1039–1053, 2010.

Using a new unified model to revisit the relationship between aerosol size and composition

D. Topping[1,2], A. Buchholz[2] and M. McFiggans[2]
[1]National Centre for Atmospheric Science, University of Manchester, Manchester, UK
[2]Centre for Atmospheric Science, University of Manchester, Manchester, UK
Keywords: Aerosol modeling, Organic aerosols, Aerosol Cloud Interaction, CCN.
Presenting author email: david.topping@manchester.ac.uk

Introduction

Aerosol particles, spanning orders of magnitude in size, are a complex mixture of many chemical compounds from both anthropogenic and biogenic sources. Despite this complexity, the present belief is that the relative importance of composition is second order to size and that the two remain uncoupled. Unfortunately, the theoretical tools which the community use as basis for such views, developed in the early 1930s, is not applicable to particulate composition we find in the atmosphere. Basic absorptive equilibrium partitioning models largely neglect the influence of curvature, leading to errors in predicted composition and volatility for conditions in which size is likely to play an important role. This includes the growth of very small particles and cloud activation potential. Similarly, empirical evidence often suggests it is not possible to reconcile water uptake in sub- and super-saturated environments using current instrumentation. This asks the question whether our knowledge of hygroscopicity derived using such tools is truly representative of behaviour in the atmosphere. Key to these problems is that the organic fraction of aerosol particles is comprised of multiple semi-volatile fractions. To attempt to address these problems we have developed a diameter depedent iterative equilibrium model that can predict partitioning between the gaseous phase and multiple condensed phases. We then apply it to two specific cases.

Case 1: CCN activation

As the particle is subject to changing environmental conditions, such as increasing/descreasing RH, the compounds comprising this fraction will re-partitioning between the gas and condensed phase accordring to their volatility, thus changing the particle size and chemical characteristics (figure 1). Existing theoretical tools cannot account for this. In this study we present new modelling and experimental work, carried out under the NERC funded programme ACID-PRUF, designed to reconcile the true effect of partitioning of all semi-volatile material on CCN activation potential, thus cloud droplet number. We show that the neglected effect of semi-volatile condensation as an aerosol particle approaches cloud activation has larger effects on activation potential than any other composition dependent phenomena included in equilibrium models. This directly challenges the widely held belief that size and composition remain uncoupled.

Case 2: Composition of ultrafine particles

The same numerical framework used in the previous section can be applied to study the predicted composition of ultrafine particles. It is still unclear what type of organic compunds may contribute to the initial stages of growth. Whilst insists from a non-dynamical model might be slightly resitrcted, in this study we apply this new iterative single particle modelling approach to ultrafine particles, first presenting an analysis on the type of organic compounds expected to contribute to their initial growth. Using output from state-of-the-art gas phase degradation mechanisms, with compound numbers ranging from 10^3 – 10^6, we are able to include the effect of non-ideality for each compound and account for depletion from the gas phase. We will show that the sensitivity to the surface energy of the particle increases as the size decreases, influencing the volatility boundaries required for aerosol growth.

Future outlook:

The development of a unified model enables the prediction of complex phenomena that might otherwise be limited by the numerical framework or availability of empirical data. With this in mind, we will also briefly show that the inclusion of non-ideality allows prediction of liquid-liquid phase separation, with subsequent effects on the equilibrium composition.

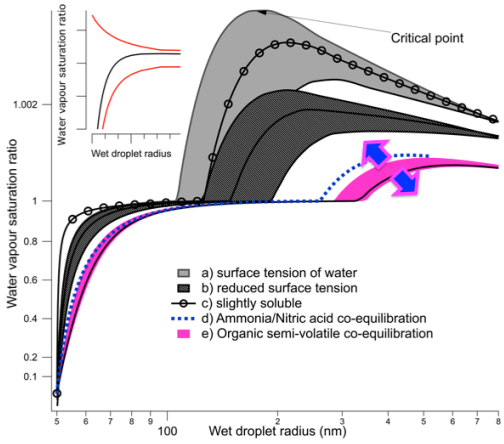

Figure 1. Traditional Kohler theory (grey areas) and the potential impact of organic co-condensation on CCN activation potential (cerise area). The up/down arrows highlight the effect of increasing or decreasing number concentrations respectively.

This work is supported by the National Centre for Atmospheric Science (NCAS) and the NERC funded programme ACID-PRUF(NE/I020121/1).

Wednesday, September 5, 2012

Session WG02S5O. Urban Aerosol Chemical and Physical Properties (II)

Comparative study of ultrafine aerosol within a city

I. Salma[1], T. Borsós[1], Z. Németh[1], P. Aalto[2] and M. Kulmala[2]

[1] Institute of Chemistry, Eötvös University, H-1525 Budapest, P.O. Box 32, Hungary
[2] Department of Physical Sciences, University of Helsinki, FIN-00014 Helsinki, P.O. Box 64, Finland
Keywords: DMPS, urban aerosol, number concentration, diurnal variation, atmospheric nucleation.
Presenting author email: salma@chem.elte.hu

Particle number size distributions were determined in the near-city background, city centre, street canyon and road traffic tunnel environments in Budapest. Measurements were performed by a flow-switching type differential mobility particle sizer (DMPS) in an electrical mobility diameter range of 6–1000 nm in 30 channels, with a time resolution of ca. 10 min.

Daily average particle number concentrations are shown in Table 1. Median daily concentrations varied by a factor of 33 from the background to the tunnel. The median and maximum number concentrations increased monotonically and substantially with the intensity of road traffic, which implies that the major source of particles is vehicular emission. The maximum measured concentration of 465×10^3 cm^{-3} was obtained in the tunnel. Mean contribution of ultrafine particles to the total particulate number and its standard deviation for the listed environments were (76±9)%, (79±6)%, (86±3)% and (85±2)%, respectively, which indicates that the combination of the primary emissions and atmospheric nucleation maintains more or less constant ultrafine contribution.

Mean diurnal variation of particles averaged by the time of day for the different environments exhibited similar structure. They contained three concentration peaks. The first peak occurred between 7:00 and 10:00 local time, and it was explained by vehicular emissions during morning rush hours. The third peak showed up in the evening between 19:00–22:00, and it was also related to traffic emissions but it was shifted from afternoon rush hours (that occurs between 16:30 and 18:00 in Budapest), mostly as a result of the daily cycling in meteorological parameters. The second peak appeared around midday for residential environments, and it was related to new particle formation and consecutive growth. The importance of atmospheric nucleation was clearly revealed by the diurnal variation of the mean ratio of ultrafine particles to the total particulate number, which exhibited a huge midday peak for the nucleation days, and no peak for the days without nucleation.

Table 1. Minimum (N_{min}), median (N_{med}) and maximum (N_{max}) daily number concentrations of aerosol particles in various environments in Budapest. The unit is 10^3 cm^{-3}.

Environment	N_{min}	N_{med}	N_{max}
Near-city background	1.25	4.3	10.1
City centre	2.7	11.8	20
Street canyon	4.9	23	41
Road tunnel	3.7	143	392

New particle formation occurred on 27% of all days in the city centre on a yearly scale. Its frequency showed an apparent seasonal variation. There were significant differences between the environments as far as nucleation frequency is concerned. It was the largest for the near-city background, and it was the smallest for the street canyon. No nucleation event was observed at all in the tunnel. Particle growth was usually finished within 1 day. Growth processes that were developing for two days were identified in the background. One of them is shown in Fig. 1. Special types of banana curves were also identified.

This work was supported by the Hungarian Scientific Research Fund under grant K84091.

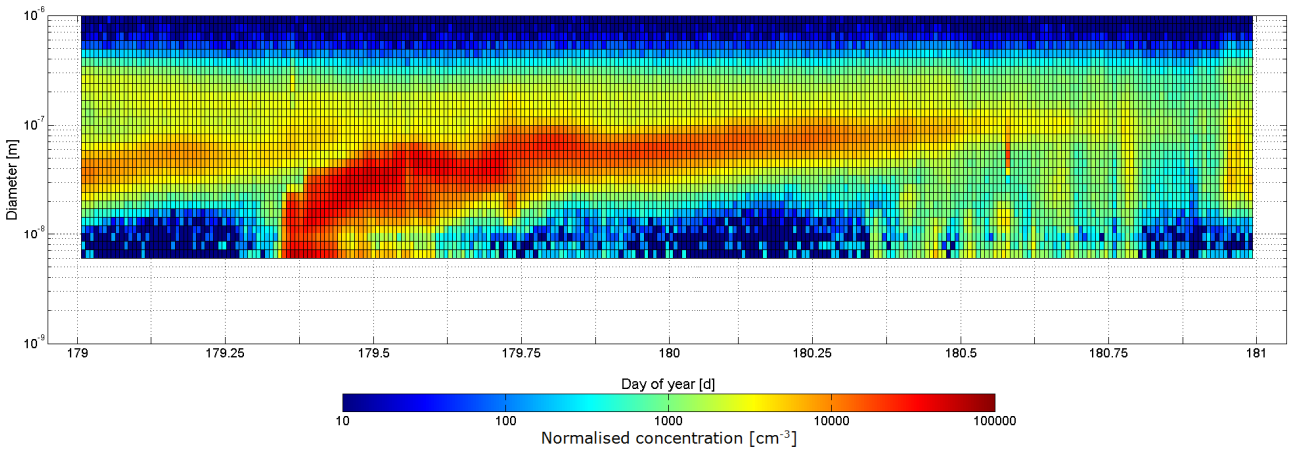

Figure 1. New particle formation event and consecutive growth developing for two days in the near-city background of Budapest on 28–29 June 2011 (Tuesday–Wednesday).

Summer ammonia measurements in a densely populated Mediterranean city

M. Pandolfi [1], F. Amato [1,2], C. Reche [1], A. Alastuey [1], R. P. Otjes [3], M.J. Blom [3] and X. Querol [1]

[1] Institute of Environmental Assessment and Water Research (IDAEA-CSIC), Barcelona, Spain
[2] TNO, Built Environment and Geosciences, Dept. of Air Quality and Climate, Utrecht, The Netherlands
[3] Energy Research Centre of the Netherlands, Department of Environ. Assessment, Petten, The Netherlands
Keywords: gas-phase ammonia, sources, PM
Presenting author email: marco.pandolfi@idaea.csic.es

Atmospheric ammonia (NH_3) is among the most abundant nitrogen compounds in the atmosphere and it plays an important role in: a) neutralisation of atmospheric acids to form ammonium salts, as ammonium sulfate ($(NH_4)_2SO_4$) and ammonium bisulfate ($(NH_4)HSO_4$) from sulfuric acid, ammonium nitrate (NH_4NO_3) from nitric acid and ammonium chloride (NH_4Cl) from hydrochloric acid, and b) eutrophication and acidification of the ecosystem by nitrogen (N) deposition (Flechard *et al.*, 2011). Overall, agriculture is estimated to contribute for 94% to the total NH_3 emission in Europe with livestock being the largest category in its emission inventory (EEA Report, 2011). Other sources of NH_3 include animal excreta, biomass burning, industries, coal burning, human breath, sweat and smoking, pets, sewage systems, wastes and vehicle emissions (Sutton *et al.*, 2000). Globally these sources form a minor part of the emissions but they might be relevant locally playing the greater role in ammonia emissions. At urban level for example there is a growing concern related with the emissions of ammonia after the introduction of gasoline-powered vehicles equipped with three-way catalytic converters and diesel-powered vehicles adopting selective catalytic reduction (SCR) system.

Measurements of ambient concentrations of gas-phase ammonia were performed in Barcelona (NE Spain) in summer between May and September 2011. Two measurement sites were selected: one in an urban background traffic-influenced area (UB) and the other in the historical city centre (CC). Levels of ammonia were higher at CC (5.6 ± 2.1 μg/m^3 or 7.5 ± 2.8 ppbv) compared with UB (2.2 ± 1.0 μg/m^3 or 2.9 ± 1.3 ppbv). This difference is attributed to the contribution from non-traffic sources such as waste containers and open markets more dense in the densely populated historical city centre. Under high temperatures in summer these sources had the potential to increase the ambient levels of ammonia well above the urban-background-traffic-influenced UB measurement station. The levels of NH_3 measured in Barcelona, especially high in the old city, may contribute to the high mean annual concentrations of secondary sulfate and nitrate measured in Barcelona compared with other cities in Spain affected by high traffic intensity. In Madrid (around 3 millions inhabitants) for example considerably lower concentrations of NH_3 have been observed compared with Barcelona. These high NH_3 concentrations in Barcelona may explain the increase of around 4 μg/m^3 in the mean annual concentrations of fine PM ($PM_{2.5}$) measured in Barcelona compared with Madrid. Finally, the concentrations of ammonia measured in Barcelona may also be the reason for the nucleation episodes involving NH_4HSO_4 formation which have been observed in Barcelona and which caused high levels of ultrafine particles (Reche *et al.*, 2011).

Ancillary measurements, including PM_{10}, $PM_{2.5}$, PM_1 levels (Particulate Matter with aerodynamic diameter smaller than 10 μm, 2.5 μm, and 1 μm), gases and black carbon concentrations and meteorological data, were performed during the measurement campaign. The analysis of specific periods (3 special cases) during the campaign revealed that road traffic was a significant source of NH_3. However, its effect was more evident at UB compared with CC where it was masked given the high levels of NH_3 measured in the old city. The relationship between SO_4^{2-} daily concentrations and gas-fraction ammonia ($NH_3/(NH_3+NH_4^+)$) revealed that the gas-to-phase partitioning (volatilization or ammonium salts formation) also played an important role in the evolution of NH_3 concentration in summer in Barcelona.

Acknowledgments
This work is supported by the MICINN (Spanish Ministry of Science and Innovation) and FEDER funds under the project CARIATI (CGL2008-06294/CLI), by Acción Complementaria GRACCIE CSD2007-00067, by the European Union (6th framework CIRCE IP, 036961). The authors thank the Department of Environment of the Autonomous Government of Catalonia for providing the concentrations of gaseous pollutants and the Faculty of Physics from Barcelona University for providing meteorological data.

References

EEA Technical report: Air quality in Europe, No 12/2011, doi:10.2800/83213, 2011.

Flechard, C. R., Nemitz, E., Smith, R. I., Fowler, D., Vermeulen, A. T., et al.: Dry deposition of reactive nitrogen to European ecosystems: a comparison of inferential models across the NitroEurope network, Atmos. Chem. Phys., 11, 2703–2728, 2011.

Reche, C., Querol, X., Alastuey, A., Viana, M., Pey, J., Moreno, T., et al.: New considerations for PM, Black Carbon and particle number concentration for air quality monitoring across different European cities, Atmos. Chem. Phys., 11, 6207–6227, 2011.

Sutton, M.A., Dragosits, U., Tang, Y.S., Fowler, D.: Ammonia emissions from non-agricultural sources in the UK, Atmos. Environ., 34, 855-869, 2000.

Seasonal variations of black carbon and number size distribution in Paris (France)

J. Sciare[1],T. Petäjä[2], J. Hakala[2], K. Lehtipalo[2], E. Herrmann[2], R. Sarda-Estève[1], J.B. Nicolas[1], N. Bonnaire[1] and P.P. Aalto[2]
[1]Laboratoire des Sciences du Climat et de l'Environnement (LSCE), CNRS-CEA, Gif/Yvette, 91191, France
[2]Deparment of Physics, University of Helsinki, Helsinki, 00560, Finland

Keywords: Black Carbon, number size distribution, fossil fuel, wood burning
Presenting author email: jean.sciare@lsce.ipsl.fr

Motivations. Road traffic and domestic wood burning emissions are two major contributors of particulate pollution in our cities. Because they are strong emitters of ultra-fine (soot containing) particles and are composed of highly toxic elements, these two incomplete combustion sources have important adverse health impacts, including increased morbidity and mortality from cardiovascular and respiratory conditions and lung cancer. A better characterization of soot containing aerosol sources (and their impact on aerosol number size distribution) in our major cities may provide useful information for policy makers, in the context of tackling air pollution issues affecting human health with additional benefits for climate change.

Experimental. As part of the EU-FP7 MEGAPOLI and the French ANR-MEGATOX & PRIMEQUAL-FRANCIPOL projects, seasonal variations of black carbon (BC) and number size distribution (NSD) were investigated at a background urban site of Paris (Laboratoire d'Hygiène de la Ville de Paris, LHVP, Paris, XIIIth district). Black carbon measurements in fine aerosols (PM2.5) were performed continuously for 2.5 years (July 2009 – December 2011) and achieved using a seven wavelength aethalometer (Magee Scientific, USA). Absorption measurements were corrected from the Weingartner et al. (2003) algorithm and source apportionment of BC between fossil fuel and biomass burning combustion source was obtained using the Aethalometer model developed by Sandradewi et al. (2008). The aerosol size distribution was measured in the same location with a flow switching Differential Mobility Particle Sizer (DMPS) over a period of one year (Aug. 2009 – Aug. 2010). In the flow switching DMPS, one Differential Mobility Analyzer (DMA) is operated with different sheath flows for a wider size range (6-800 nm). Also the total aerosol number concentration was measured with a Condensation Particle Counter (TSI CPC 3772) deployed in the DMPS by bypassing the DMA.

Results and discussion. Temporal variations of Black Carbon from wood burning (BC_{wb}) and fossil fuel (BC_{ff}) are reported in Figure 1 and clearly show distinct patterns. BC_{ff} is mainly dominated by traffic emissions and, for that reason, do exhibit a poor seasonal pattern. On the other hand, seasonal variations of BCwb are much more pronounced () and can be explained by domestic wood burning emissions which can be detected here for a period covering 7 consecutive months (October-April).
The sub-micron aerosol number size distribution had both diel and seasonal patterns, mainly governed by local emissions, boundary layer meteorology and long-range transport. The total number concentrations were typically higher during winter-time due to increased emissions and decreased vertical mixing.
Estimates of the PM contribution of traffic and domestic wood burning sources will be provided in the presentation as well as their impact on aerosol number size distribution will be discussed from previous observations performed in other European cities. Import of Black Carbon over the region of Paris will be addressed using similar (Aethalometer) measurements performed in parallel over a 1-year period at a rural site located at approximately 70km North-East of Paris center.

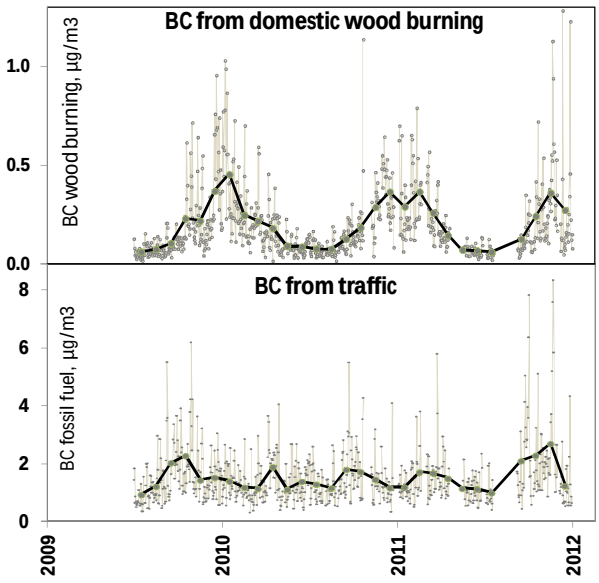

Figure 1. Daily and monthly mean concentrations of black carbon from domestic wood burning and fossil fuel (traffic) in the center of Paris.

Sandradewi, J., et al., Using aerosol light absorption measurements for the quantitative determination of wood burning and traffic emission contributions to particulate matter, Environ. Sci. Technol., 42, 3316–3323, 2008
Weingartner, E., et al., Absorption of light by soot particles: Determination of the absorption coefficient by means of aethalometers, J. Aerosol Sci., 34, 1445–1463, 2003

Effects of the Low Emission Zone on Black Carbon and Ultrafine Particles in Leipzig

A. Wiedensohler[1], W. Birmili[1], F. Rasch[1], K. Weinhold[1], M. Merkel[1], A. Sonntag[1], G. Löschau[2], A. Hausmann[2]

[1]Leibniz Institute for Tropospheric Research, Leipzig, Germany
[2]Saxon State Office for Environment, Agriculture and Geology, Dresden, Germany
Keywords: Low emission zone, black carbon, ultrafine particles

Presenting author email: alfred.wiedensohler@tropos.de

In Europe, the daily average values of ambient PM_{10} mass concentrations may not exceed the threshold of 50 µg/m³ more than 35 times per year (council directive 2008/50/EC) at governmental air quality sites. Many cities, however, find it hard to comply with this limit value. In Germany, low emission zones were established in many cities as part of a wider bundle of regulatory actions. The "green" low emission zone in Leipzig limits access to the city mainly to EURO4 equivalent of Diesel passenger cars as well as light and heavy duty vehicles. The main goal is to limit the direct tail pipe emissions, especially near traffic hot spots.

In Leipzig, a scientific cooperation between the Leibniz Institute for Tropospheric Research (IfT) and the Saxon State Office for Environment, Agriculture and Geology (LfULG) has analyzed possible beneficial impacts of the low emission zone. The Leipzig low emission zone, which covers most of the area of the city, was established on March 1, 2011. Black carbon and particle number size distributions have been determined continuously since June 2010 at 5 measurement sites (three IfT, two LfULG) in addition to the standard PM_{10} and $PM_{2.5}$ mass concentration measurements. The five measuring stations comprise two street sites (Leipzig-Mitte and Leipzig-Eisenbahnstrasse), two urban background sites (Leipzig-West and Leipzig-IfT) as well as a regional background site (Melpitz).

All stations are equipped with mobility particle size spectrometers such as a Twin Differential Mobility Particle Sizer (TDMPS) or a Scanning Mobility Particle Sizer (SMPS) to determine the particle number size distribution in the sub-µm size range. In Melpitz and Leipzig-Mitte, additional Aerodynamic Particle Sizer (APS) measure the number size distribution of coarse particle. At all stations, a Multi-Angel Absorption Photometer (MAAP) is used to determine the light absorption coefficient at 637 nm, which is converted into a black carbon mass concentration by using a mass absorption coefficient of 6.6 m²/g.

Figure 1 depicts the evolution of black carbon mass concentration in Leipzig between July 2010 and February 2012. The upper Figure illustrates the black carbon mass concentration at the street site Leipzig-Mitte and an urban background site, which exhibit significant short-term and seasonal variations. The lower graph visualizes the street site increment at Leipzig-Mitte, which was calculated as the difference between street site and background black carbon concentration.

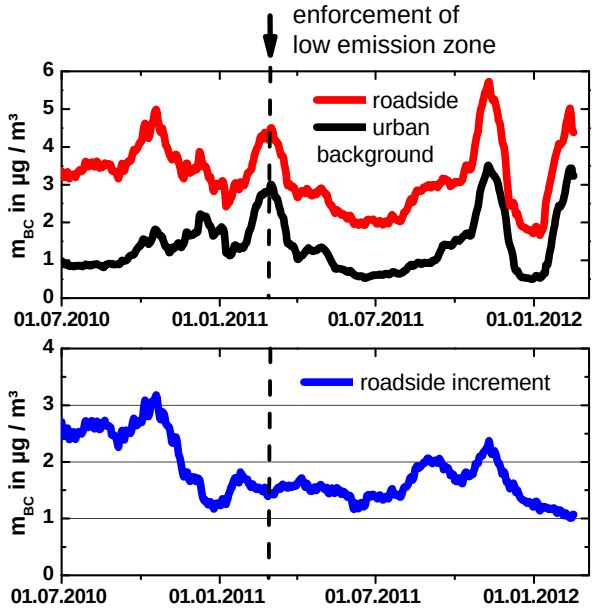

Figure 1: Upper graph: Black carbon mass concentrations at. two sites in Leipzig between July 2010 and February 2012. Red: street site Leipzig-Mitte; black: urban background site. Lower graph: roadside increment (i.e. background subtracted) at the roadside site Leipzig-Mitte.

The essential observation is that the street site increment shows a significant downward trend of 2010. The high levels of summer 2010 (24 h average), which exceeded 2µg/m^3 frequently, were hardly reached after this date. The reduction of the street site increment is approximately 25% in the black carbon mass concentration. However, this reduction corresponds to an black carbon mass concentration of 0.5-1.0 µg/m^3 only, which is modest compared to the overall PM_{10} level.This first analysis reveals beneficial effects of the low emission zone in Leipzig. It needs to be mentioned that black carbon accounts only for few percent of the PM_{10} mass concentration, but it is associated with adverse health effects. Black carbon caries especially heavy metal and polycyclic-aromatic hydrocarbons. Therefore, the benefits of the low emission zone might go significantly beyond the mere benefit of the associated reduction of the PM_{10} mass concentration. Furthermore, we will present the change in ultrafine number concentration at the street site due to the low emission zone.

Wintertime urban background measurements of PM_1, particle lung-deposited surface area, black carbon and particle number concentrations

U. Quass[1], H. Kaminski[1], T. A .J. Kuhlbusch[1] B. Bergmans[2], D. Muck[2], F. Lenartz[2]

[1]Air Quality & Sustainable Nanotechnology Unit, IUTA e.V., 47229 Duisburg, Germany
[2]Air Quality, Institut Scientifique de Service Public (ISSeP), Liège, B-4000 Belgium
Presenting author email: tky@iuta.

Particulate matter (PM) is known to cause adverse health effects when inhaled. Currently, air quality standards are in force for PM_{10} and $PM_{2.5}$. However, epidemiological and toxicological findings suggest that the driving characteristics for health effects are more strongly related to the sub-micron particles (Pope and Dockery 2006). This particle fraction can be characterised by different metrics. Besides the mass concentration of PM_1, which is dominated by particles larger than 300 µm, the lung-deposited surface area (LDSA, mainly 20-400 nm) and the particle number (dominated by ultrafine particles (UFP) with diameters below 100 nm) might be used. Further, the black carbon (BC) content is currently discussed as a particularly health relevant metric (Jansen et al. 2011) related to traffic and domestic wood burning which are important urban air pollution sources.

In a joined measurement campaign IUTA and ISSeP investigated the relationships between these metrics. Measured metrics and instruments deployed were: Number size distribution (SMPS two systems, ca. 10-800 nm, and Grimm spectrometer, 0.265-31µm), LDSA,(NSAM, 20-1000nm),, BC (2-wavelength aethalometer, PM_{10} inlet), PM_1 (TEOM-FDMS), meteo.

The measurements took place in Mülheim, Ruhr area, Germany, close to the LANUV air quality network site STYR. This urban background site is characterised by influences from a motorway located ca. 250 m to the North-East, the second important wind direction besides the predominant south-westerly winds

The campaign was carried out between Feb. 6th and March 2nd). At the beginning of this period cold Siberian air masses dominated the weather in entire Germany. After 5 days the wind changed to usually predominant south-westerly direction, and temperature rose to values above freezing and, surprisingly, PM_{10} and BC concentrations increased significantly (fig. 1).

From SMPS measurement the concentrations for the number of UFP (dp<100 nm) and >UFP (dp 100-800 nm) were calculated. The light absorption coefficient obtained from the aethalometer was converted to BC concentrations (µg/m³) with a sigma of 16.6 (880 nm) and 39.5 (370 nm). Delta-C values were calculated from BC data corrected as described in Wang *et al.* 2011.

Table 1: Pearson correlation coefficients between metrics (as available at time of abstract submission)

	PM_1	UFP	>UFP	LDSA	BC1
PM_1	1	-0.087	0.819	0.753	0.716
UFP		1	0.191	0.466	0.274
>UFP			1	0.935	0.721
LDSA				1	0.835
BC1					1

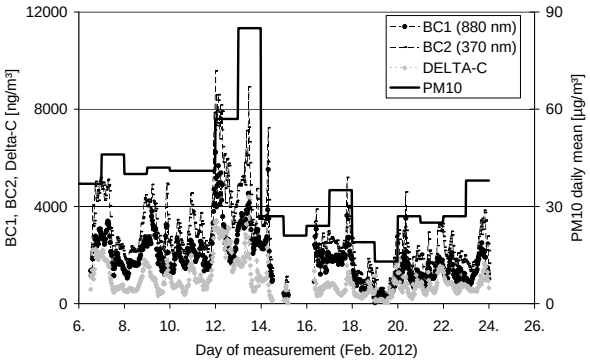

Figure 1: Time series of PM_{10} and BC concentrations

Delta-C data from aethalometer measurements (fig.1) indicate a significant influence of wood combustion which supports recent findings from levoglucosan analysis (Pfeffer *et al.* 2012). From correlation analysis (table 1) the five metrics reveal to provide rather complementary than redundant information.

Further evaluation of the full dataset (size distribution, LDSA, PM_1, BC, PM_{10}, NOx, meteo) for an indicative source apportionment following the approaches of Wang et al. 2011 as well as instrument intercomparisons will be presented.

This work was partly executed within the InterReg IV A project PM Lab. IUTA acknowledges financial support by the North Rhine Westphalia State Agency for Nature, Environment and Consumer Protection (LANUV)

Janssen N.A., Hoek G., Simic-Lawson M., Fischer P., van Bree L., ten Brink H., et al. (2011). Black Carbon as an Additional Indicator of the Adverse Health Effects of Airborne Particles Compared with PM_{10} and $PM_{2.5}$. Environ Health Perspect 119:1691-1699.

Pope C.A. and Dockery D.W. (2006). Health Effects of Fine Particulate Air Pollution: Lines that Connect J. Air & Waste Manage. Assoc. 56:709–742

Wang Y., Hopke P.K., Rattigan O.V., Xia X., Chalupa D.C., Utell M.J. (2011). Characterization of Residential Wood Combustion Particles Using the Two-Wavelength Aethalometer. Environ. Sci. technol. 45:7387-7393

Pfeffer U., Breuer L., Gladtke D. (2012): Contribution of wood burning to the exceedance of PM_{10} limit values in residential areas of the Rhine-Ruhr conurbation (Germany) Abstract submitted to EAC 2012

Soot externally mixed with Asian dust particles in the submicron range in the marine atmosphere

K.I. Lieke[1], D. Zhang[2], K. Kandler[3], S. Weinbruch[3], and M. Bilde[1]

[1]Copenhagen Center for Atmospheric Research, University of Copenhagen, 2100 Copenhagen, Denmark
[2]Environmental Science, Prefectural University of Kumamoto, Kumamoto 862-8502, Japan
[3]Environmental Mineralogy, Darmstadt University of Technology, 64287 Darmstadt, Germany
Keywords: soot, Asian dust, mixing state.
Presenting author email: kirstenlieke@gmx.de

Wide-spreading natural dust and anthropogenic soot in the atmosphere from the Asian continent are two important aerosols due to their influences on climate change, air quality, and ecosystem development. However, the available information does not provide clear knowledge on their mutual status in the outflow from the continent although they have been extensively studied. Here we show, with case data obtained in south-western Japan, that there were substantial amounts of soot particles in dust plumes arriving at Amakusa. In contrast to dust particles appearing in the size range of 1 to 30 µm geometric diameter, soot particles appeared in the submicron range of 0.5 µm and smaller. The observed soot particles were frequently isolated from dust particles and appeared in different morphologies as well as mixing state with secondary aerosol, most likely sulphate. These results indicate that anthropogenic soot externally mixed with dust particles in dust plume in the downstream offshore areas of the Asian continent and they could function as a place for sulphate formation in the submicron range.

Sampling and analysis

Samples of atmospheric particles were collected at Araoteke, a hill on the west coast of Amakusa peninsula, Japan (32.3550N and 129.9833E, 347 m a.s.l.) between 16 March and 18 March 2010. Weather reports issued by the Japanese Meteorological Agency indicated that a strong lower pressure system with fronts passed the desert and Gobi areas in north-western China, became loaded with dust on about 13 March and moved eastward. The low pressure system passed eastern China and the Korean peninsula on 14 and 15 March, and its centre arrived at the observation site in the afternoon on 15 March. On 16 and 17 March, the observation area was covered by a high pressure system following the low pressure system, Asian dust was reported at south-western Japan. Continuous records of an optical particle counter at the site revealed that the dust lasted until the afternoon of 18 March when a weak low pressure system arrived at the site. Therefore, the samples collected in the observation period were from the same dust event.

Samples were collected with a set of miniature cascade impactors on substrates suitable for electron microscopy. 3 Imapactor stages were used in the devices, covering a wide range in size: Particles from 40 nm up to tens of µm average diameter were collected. Single particle analysis was performed with an FEI ESEM Quanta 200 FEG and a FEI TEM CM200 at Darmstadt University of Technology. The instruments were equipped with energy-dispersive X-ray detectors for chemical analysis of elements with an atomic number larger than 5.

Results

During the spring dust episode, soot is found on all four samples of the dust event (listed in table 1, 11-3 is of a non-dust period). Soot is dominating the small particle size range. The size of primary soot spheres is 40-50 nm in average, showing typical graphitic layers under high resolution magnification in the transmission electron microscope. Lattice distances between 3.9 and 8 Å were measured in different soot particles. Combustion particles exist in different mixing states: pure different sized soot agglomerates in form of chains and balls; soot attached to secondary aerosol; soot encapsulated in secondary aerosol and internally mixed tar balls and fly ashes. The secondary aerosol was likely $(NH_4)_2SO_4$ and/or H_2SO_4.

Conclusions

Our results indicate that soot is transported with the dust from China. The large branched forms might arise from biomass burning, although the collapsed and internally mixed forms are occurring more frequently and thus proof that other sources as industrial plants and ships are contributing as well. A verification of sources and source apportionment is subject to further studies.

All over it is shown, that soot contributes significantly to the aerosol particles in the sub 500 nm size range in Asian dust plumes arriving at the Japanese coast in spring.

Acknowledgements

This studied was funded through a scholarship to Kirsten Inga Lieke by the Haiwa Nakajima Foundation.

Table 1. relative number abundance of particles with diameters smaller than 0.5µm.

date	*soot mixed*	*soot pure*	*secondary*	*other*	*total*
11-3	2.1 %	<1 %	6.6 %	90.4 %	825
16-3	13.9 %	45.8 %	14.6 %	32.6 %	144
17-3	11.2 %	22.9 %	14.7 %	51.2 %	170
17-3	3.2 %	45.6 %	5.8 %	45.6 %	329
18-3	8.1 %	39.3 %	4.7 %	47.9 %	211

Sources and processes affecting coarse aerosols at street canyon and urban locations in London, UK

David C Green and Gary W Fuller

MRC HPA Centre for Environment and Health, King's College London, London, SE1 9NH, UK
Keywords: Coarse aerosol, traffic emissions, Aerosol Particle Sizer.
Presenting author email: david.c.green@kcl.ac.uk

Introduction

Aerosols in the range 2.5 – 10 µm in aerodynamic diameter have important implications for health (WHO, 2003). They are also an important component of the wider PM_{10} fraction and are consequently subject to regulation (EU, 2008) and policies to control their emission (GLA, 2010). Many of the sources and processes which contribute to the production of these particles are independent of those governing the smaller size fractions and are therefore worthy of independent investigation.

Methods

Measurements of coarse aerosol (0.5 - 20µm) where made using the TSI 3321 Aerosol Particle Sizer (APS) at an urban background site and a street canyon site in London between July 2010 and October 2011. Aerosols were sampled at ambient temperature and humidity through a ¾" stainless steel tube protected from rain ingress by a TSP inlet. The instruments were collocated at the background site for a period of 10 days to ensure they were comparable. Regular sample flow and HEPA filter checks were undertaken and the instruments were calibrated regularly using PLS by the manufacturer.

An assessment was made of the 2.5 – 10 µm mass from the difference between PM_{10} and $PM_{2.5}$ mass measurements using the FDMS. Chemical composition, traffic and meteorological measurements were also available to determine the sources and processes affecting the concentration.

Measurements from the APS were converted to volumetric equivalent diameter using the method provided by Peters (2006). This was used to isolate the 2.5 – 10 µm mass fraction and to calculate the effective density when compared to the mass measurement.

Results and discussion

The difference between the urban background and street canyon locations (the traffic increment) was calculated for hours when both measurements were available. The mass concentration was calculated based on the mean effective density (1.8 gcm^{-3}) when the volume concentration was compared to the mass concentration measured using the FDMS. This is slightly higher than previous studies at the Marylebone Road site (1.5 gcm^{-3}) which examined the merged SMPS and APS datasets during a campaign (Beddows, Dall'osto et al., 2010) and a little lower than the densities of around 2 gcm^{-3} found during studies of coarse aerosol in the US (Peters, 2006).

Figure 1 shows the particle number and mass concentration spectra from each site and the traffic increment. The particle number concentration increment is dominated by the single sub 1 µm mode while the mass concentration increment is dominated by the >2.5 µm particles. This mass increment appears to be multi-modal, indicating that a number of different sources and processes influence this metric. By comparing the diurnal variation in the calculated APS 2.5 – 10 µm mass to the FDMS mass measurements, the density was shown to vary with time of day; this is also consistent with a multi-source hypothesis.

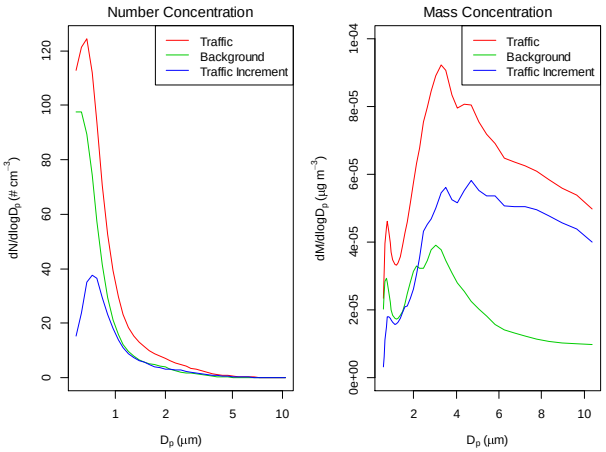

Figure 1: Particle number and mass concentration spectra

References

Beddows, D. C. S., M. Dall'osto and R. M. Harrison (2010). An Enhanced Procedure for the Merging of Atmospheric Particle Size Distribution Data Measured Using Electrical Mobility and Time-of-Flight Analysers. Aerosol Science and Technology 44(11): 930-938.

EU (2008). Directive of the European Parliament and of the council on ambient air quality and cleaner air for Europe. 2008/50/EC E. Union.

GLA (2010). Clearing the air. The Mayor's Air Quality Strategy. (ISBN 978 1 84781 411 1).

Peters, T. M. (2006). Use of teh Aerodynamic Particle Sizer to Measure Ambient $PM_{10-2.5}$: The Coarse Fraction of PM_{10}. Journal of Air and Waste Management Association 56: 411-416.

WHO (2003). Health Aspects of Air Pollution with Particulate Matter, Ozone and Nitrogen Dioxide. Geneva, World Health Organisation.

Highly time and size-resolved trace elemental composition of aerosols during CalNex-LA 2010

S. Visser[1], M. Furger[1], U. Flechsig[2], K. Appel[3], A. S. H. Prevot[1], U. Baltensperger[1]

[1] Paul Scherrer Institut, Villigen PSI, Switzerland
[2] Swiss Light Source, Paul Scherrer Institut, Villigen PSI, Switzerland
[3] Hamburger Synchrotronstrahlungslabor at Deutsches Elektronen-Synchrotron DESY, Hamburg, Germany
Keywords: trace elements, XRF, PM and source apportionment, aerosol emissions
Presenting author email: suzanne.visser@psi.ch

Size-resolved measurements of trace elemental composition provide a highly specific technique for the identification of primary aerosol sources. The utility of such measurements is enhanced by sampling with high time resolution and coordination with other aerosol composition measurements. Here we present highly time and size-resolved measurements of trace elements as part of the CalNex-LA field campaign. CalNex-LA 2010 focuses on complex interactions between climate change, atmospheric conditions, and pollution sources (local and global) on air quality in California and the eastern Pacific coastal region. The high time resolution enables identification of sources highly variable in time like shipping via vanadium, and traffic via iron.

Sampling was performed at a ground-based urban site (California Institute of Technology, Caltech) in Pasadena, CA, USA. Particulate matter (PM) was collected from 15 May to 16 June 2010 with a 3-stage Rotating Drum Impactor (RDI). The RDI stages enable particle size segregation in the ranges 10-2.5 µm, 2.5-1.0 µm and 1.0-0.1 µm (Richard et al., 2010). A high sampling time resolution of 2-h was applied, instead of more common 24-h sampling times. Simultaneous measurements of e.g. wind speed and direction, and organic aerosols help separating local from regional sources with fresh and aged air masses, respectively.

The trace elemental composition of the collected aerosols was determined with Synchrotron Radiation induced X-Ray Fluorescence Spectrometry (SR-XRF) at SLS (Paul Scherrer Institute, CH) and at HASYLAB (Deutsches Elektronen-Synchrotron, DE). With the high 2-h time resolution, SR-XRF allows quantification of ambient elemental concentrations with a detection limit on the order of a few pg. Calibration is performed using a standard containing known concentrations of the elements of interest. The SR-XRF analysis provides a quantitative time series for elements with atomic number 13 (aluminium) to 82 (lead). Fig. 1 shows the time series of the 3 stages for iron (Fe). The main source of Fe in the coarse fraction is typically mineral dust, while traffic emissions are important for the smallest sizes (Bukowiecki et al., 2005; Richard et al., 2011). The diurnal variations with elevated concentrations during the day also indicate anthropogenic influences. The higher and more variable values for the coarse fraction in June are probably caused by dry, sunny conditions resulting in increased dust resuspension by traffic.

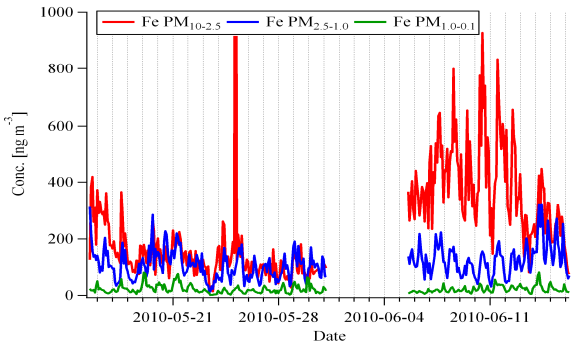

Fig. 1. Time series of size-segregated 2-h Fe conc. measured by RDI-SR-XRF during CalNex-LA 2010.

Fig. 2 shows the relative elemental contribution to the 3 stages averaged over the entire campaign. A high Cl fraction in $PM_{10-2.5}$ and $PM_{2.5-1.0}$ can indicate sea spray, as identified previously in Los Angeles with Na and Mg by Pakbin et al. (2011). The extreme S fraction, a known marker for secondary sulphate in $PM_{1.0-0.1}$, is in line with Richard et al. (2011). This fraction points at secondary and aged aerosol transported from LA to the sampling site in Pasadena. Further source identification during this campaign will be done with Positive Matrix Factorization.

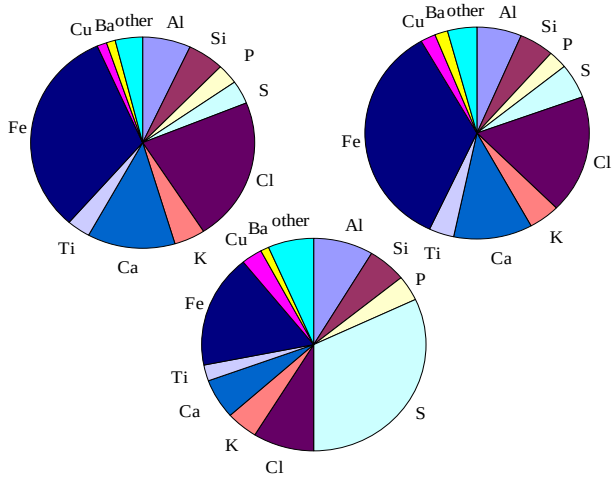

Fig. 2. Relative contribution of elements to $PM_{10-2.5}$ (left), $PM_{2.5-1.0}$ (right) and $PM_{1.0-0.1}$ (centre) identified by RDI-SR-XRF during CalNex-LA 2010.

Acknowledgments: This work was supported by CALTECH (J. Seinfeld), CARB, NOAA (J. de Gouw), the University of California, Los Angeles (J. Stutz) and the NSF.

Bukowiecki, N. et al. (2005) *Environ. Sci. Technol.* **39**, 5754-5762.
Pakbin, P. et al. (2011) *Aerosol. Sci. Tech.* ***45***, 949-963.
Richard, A. et al. (2010) *Atmos. Meas. Tech.* **3**, 1473-1485.
Richard, A. et al. (2011) *Atmos. Chem. Phys.* ***11***, 8945-8963.

Wednesday, September 5, 2012

Session WG07S3O. Gas phase synthesis of nanoparticles

Nanostructured catalytic layers for fuel cell electrodes prepared by electrospray

S. Martin, B. Martinez-Vazquez, P.L. Garcia-Ybarra and J.L. Castillo

Dept. Fisica Matematica y de Fluidos, Facultad de Ciencias UNED, Madrid, Spain
Keywords: Electrospray, Deposit morphology, Nanoparticles, Fuel cell
Presenting author email: smartin@dfmf.uned.es

The electrohydrodinamic atomization or electrospray has demonstrated to be a suitable technique for micro- and nano-thin-film deposition (Martin *et al*., 2005; Jaworek and Sobczyk, 2008). In our laboratory, the electrospraying of liquid suspensions containing catalytic nanoparticles is being successfully used in the production of porous catalytic layers for proton exchange membrane fuel cell (PEMFC) electrodes (Martin *et al*., 2010a, 2010b). One of the factors limiting the wide use of PEMFCs is the cost of the catalyst (platinum) in the electrodes. The goal of this study is to determine the electrospraying working conditions for obtaining electrodes with a low catalyst loading without compromising the fuel cell performance.

The electrospray deposition method enables the generation of nanostructured catalytic layers whose building blocks are clusters (of a few catalyst particles each) with a characteristic size of approximately 100 nm disposed in a dendritic arrangement (see Fig. 1).

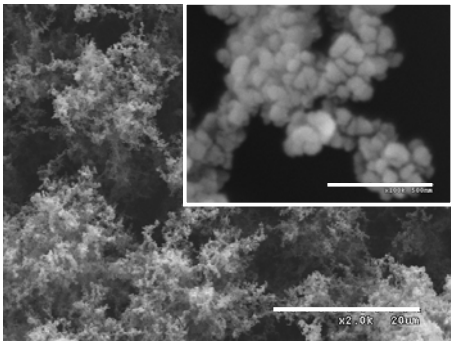

Figure 1. Dendritic structure of a catalyst layer with 0.01 $mg_{Pt}cm^{-2}$ Pt loading. The micron bar is 20 μm long for the main image and 500 nm for the inset.

This arrangement produces catalytic deposits with the appropriated morphology for PEMFC electrode preparation. On the one hand, the small size of the catalyst clusters leads to a high dispersion of the catalyst. On the other hand, the dendritic arrangement of the catalyst clusters results in a highly porous deposit with an enhanced permeability and increased electrochemical active surface area (Castillo *et al*., 2012).

The electrospray technique allows the preparation of efficient PEMFC electrodes with ultra-low platinum loadings (0.01 $mg_{Pt}cm^{-2}$). The conditions for achieving uniformly thin layers with the electrospray working in a stable cone-jet mode will be discussed. Figure 2 shows the fuel cell performance for several electrodes prepared under the same electrospraying parameters. The catalyst utilization (power per gram of platinum) delivered by these electrodes lies in the interval 30-35 kW g_{Pt}^{-1} what, to the best of our knowledge, represents the maximum platinum utilization reported up to now for any catalyst deposition method. Indeed, these results overcome in more than 50% the highest utilization achieved by sputtering (Cavarroc *et al*., 2009) and it is 3 times the Pt-utilization in our previous work (Martin *et al*., 2010b).

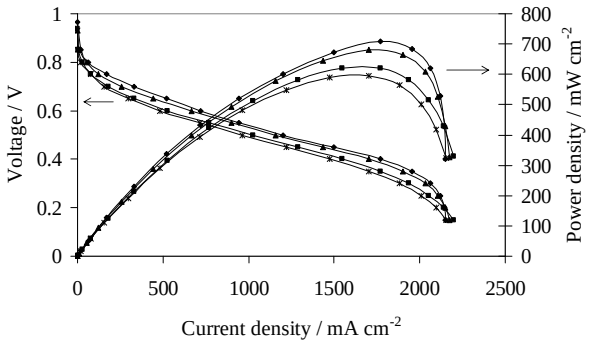

Figure 2. Fuel cell current-voltage and power density curves for electrodes with a Pt loading of 0.01 $mg_{Pt}cm^{-2}$.

The latter results were achieved using a fuel cell with small (5 cm^2) square electrodes. The scaling up to get 50 cm^2 square electrodes (delivering the same power density) will be discussed. In this way, the electrospray deposition method may be used to cover the entire range of required electrode sizes: from automotive or stationary applications down to portable units.

Work supported by Ministerio de Ciencia e Innovacion (Spain) (grants ENE2011-26868 and CSD2010-00011), and by Comunidad de Madrid (grant S2009ENE-1597).

Castillo, J.L., Martin. S., Rodriguez-Perez, D., Perea, A. and Garcia-Ybarra, P.L. (2012). *KONA Powder and Particle Journal*, **30** (2012), in press.

Cavarroc, M., Ennadjaoui, A., Mougenot, M., Brault, P., Escalier, R., Tessier, Y., Duran, J., Roualdès, S., Sauvage, T. and Coutanceau, C. (2009). *Electrochem. Comm.*, **11**, 859-861.

Jaworek, A. and Sobczyk, A.T. (2008). *Journal of Electrostatics*, **66**, 197-219.

Martín, S., Galán, D., Rodríguez-Pérez, D., Loscertales, I.G., Castillo, J.L., Barrero, A., García-Ybarra, P.L. (2005), in *Proceedings of the EAC*, Ghent, p. 637.

Martin, S., Garcia-Ybarra, P.L., and Castillo, J.L. (2010a). *J. Power Sources*, **195**, 2443-2449.

Martin, S., Garcia-Ybarra, P.L., and Castillo, J.L. (2010b). *J. Hydrogen Energy*, **35**, 10446-10451.

Aerosol synthesis of ZnO tetrapods for flexible and transparent UV sensors

Albert G. Nasibulin[1], Simas Rackauskas[1], Kimmo Mustonen[1], Terhi Järvinen[1], Marco Mattila[2], Olga Klimova[3], Hua Jiang[1], Oleg Tolochko[3], Harri Lipsanen[2], Esko I. Kauppinen[1]

[1] Department of Applied Physics, Aalto University, FI-00076, Espoo, Finland
[2] Department of Micro and Nanosciences, Micronova, Aalto University, Tietotie 3, 02015 Espoo, Finland
[3] State Polytechnical University, Polytechnicheskaya 29, 195251, Saint-Petersburg, Russia
Keywords: nanostructure, synthesis, tetrapod, ZnO, UV sensor.

Zinc oxide (ZnO) is a direct wide band gap (3.37 eV) semiconductor material with a large exciton binding energy (60 meV). It has gained significant attention because of the unique optical, piezoelectric and magnetic properties, as well as capability of band gap tuning (Rackauskas *et al.*, 2009). Non-catalytically grown ZnO nanostructures can be observed in various morphologies such as nanowires, nanobelts, nanobridges and nanonails, nanoshells, tetrapods. The latter is one of the most gorgeous structures with many promising applications in solar cells, lasers, field emitters, UV and gas sensors.

Zinc oxide tetrapods (ZnO-Ts) were discovered in smoke from zinc-smelting plants and first studied in chemical vapor deposition systems. ZnO-Ts were produced in the lab scale through hydrothermal process, vapor synthesis from ZnO and C mixture, or directly from Zn powder, when tetrapods are collected on reactor walls or filtered at the outlet. Direct synthesis of ZnO-Ts from the metal vapor has obvious advantages of low temperature process and high yield, still the control of uniform concentration is rather difficult.

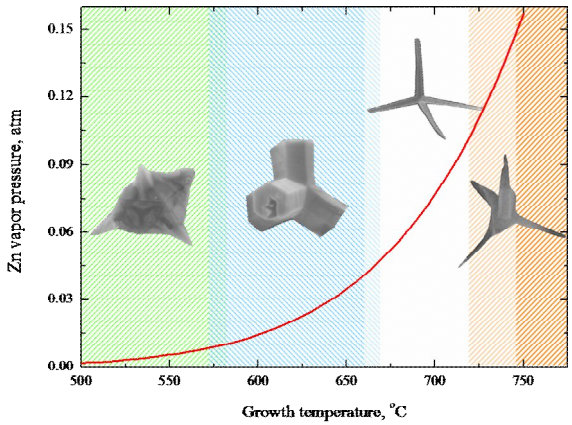

Figure 1. ZnO-T morphology at different temperatures and vapor pressures. Tetrapods shown are not in the scale.

In this work, we designed and constructed a vertical flow reactor for the controlled synthesis and collection of ZnO-Ts. In order to find favorable synthesis conditions, we varied the growth temperature and Zn vapor pressure. The overall trend of ZnO-T morphology change is summarized in Fig. 1. From our experimental data one can see that highly anisotropic structures were obtained above 650 °C (Rackauskas *et al.*, 2012). In order to modify the band gap and transparency of ZnO-Ts, we introduced magnesium vapor during the tetrapod growth.

Applicability of the produced ZnO-T structures was examined by fabricating transparent and flexible UV sensors. Flexible transparent UV sensor (Fig. 2) was made by drying droplet of ZnO-T solution in ethanol between two transparent single-wall carbon nanotube (SWCNT) film contacts, on a polyethylene terephthalate (PET) substrate. SWCNT electrode fabrication is described elsewhere, shortly,a one step process was used, filtered SWCNTs without any post processing were transferred from a filter by pressing it onto PET substrate. To obtain high optical transparency, sample synthesized at y_{Mg} = 2.3% and SWCNT electrodes with 95% transparency were used. UV sensing experiments were made under UV intensity of 30 μW/cm^2 at the wavelength of 365 nm. Inset in Fig. 2 shows a UV sensor response to the illumination. Initial current 0.032 pA increased to 1.45 pA under the UV illumination, which is 45 fold change. Response time to 90% of current change was 0.9 s.

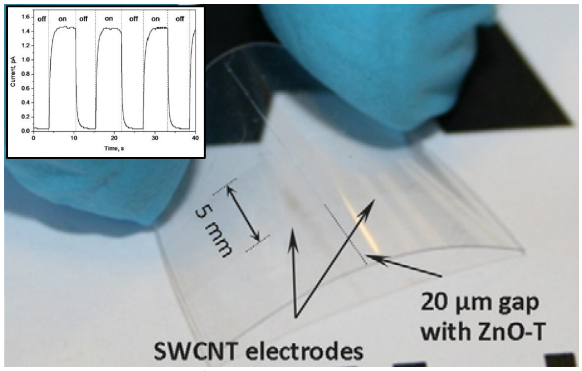

Figure 2. A photo of ZnO-T UV sensor. Inset shows the sensor response to excitation at 365 nm.

This work was supported by the Academy of Finland project No. 128445.

Rackauskas, S., Mustonen, K., Järvinen, T., Mattila, M., Klimova, O., Jiang, H., Tolochko, O., Lipsanen, H., Kauppinen, E.I., & Nasibulin, A.G. (2012). Nanotechnol., 23, 095502.

Rackauskas, S., Nasibulin, A.G., Jiang, H., Tian, Y., Statkute, G., Shandakov, S.D., Lipsanen, H., & Kauppinen, E.I. (2009). Appl. Phys. Lett., 95, 183114.

Synthesis of germanium-silicon hybrid particles in an aerosol reactor

C. Mehringer[1], R. Körmer[1], B. Butz[2], E. Spiecker[2] and W. Peukert[1]

[1]Institute of Particle Technology, Friedrich-Alexander-University Erlangen-Nuremberg, Cauerstr. 4, 91058 Erlangen, Germany
[2]Center for Nanoanalysis and Electron Microscopy (CENEM), Friedrich-Alexander-University Erlangen-Nuremberg, Cauerstr. 6, 91058 Erlangen, Germany
Keywords: nanoparticles, material synthesis, silicon, germanium.
Presenting author email: c.mehringer@lfg.uni-erlangen.de

Nanocrystalline silicon (Si) and germanium (Ge) are promising materials for the application in printable electronics (Holman et al, 2010). Nanoparticles (NPs) of these materials can be dispersed in organic liquids and deposited as thin functional films. As a prerequisite for the functionality of the film, good contacts between individual particles are necessary. A thin germanium layer around a silicon core might be a suitable composite material, because germanium has a much lower melting point, i.e. sintering is enhanced in comparison to Si, and Ge protects Si from oxidation.

A reactor system with two consecutive hot-wall reactors is used in the experiments. The first reactor stage is used for synthesis of Si NPs with defined properties from monosilane (Körmer et al, 2010). After the first reactor the aerosol is quenched by additional argon. Prior to the second reactor stage, monogermane is fed into the system. In the second reactor stage Ge is deposited on the Si NPs at temperatures between 500°C and 700°C. At the reactor exit the aerosol is quenched by nitrogen. The particles are collected with a membrane filter or sampled via a low pressure impactor by deposition on TEM grids or silicon wafers.

The structure of the nanoparticles is investigated by STEM analysis. Figure 1 shows a z-contrast image of representative particles synthesized at certain process parameters with a monogermane partial pressure of 0.08 mbar (Inset shows higher magnification). Under these reaction conditions Si particles with a faceted Ge patch are formed. This can be explained by energetically favoured sites for the initial island growth. Due to the slight misfit between the crystal lattices the Ge grows preferentially on itself and only partially around the Si core.

Figure 2 shows a HRTEM image of particles formed at reaction conditions with 0.83 mbar monogermane partial pressure, where the Ge patches cover an increased fraction of the Si particles´ surface. It is obvious, that the Si core, as well as the Ge patch is crystalline. Further, it can be seen that the Ge patch is no longer faceted. This fact is a hint to the growth mechanism of the patch. Starting from a wetting layer an initial Ge seed forms at the Si surface, which grows to a faceted patch. Further growth leads to relaxation and an altered form of the patch.

The progress on the synthesis of the germanium-silicon hybrid particles will be demonstrated, regarding the influence of the process parameters on their morphology and growth.

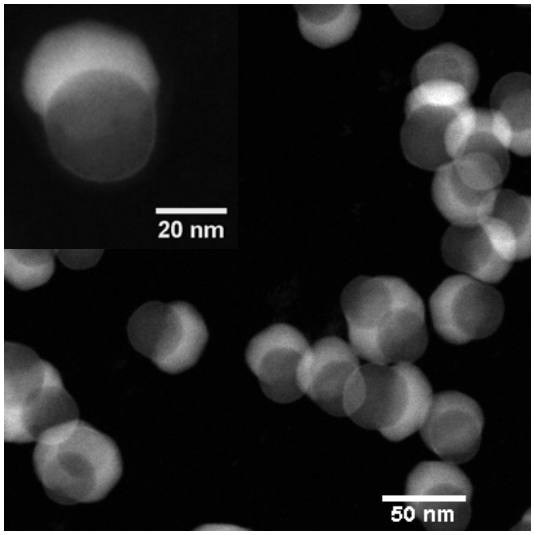

Figure 1. STEM image of Ge-Si hybrid particles (dark: Si, bright: Ge).

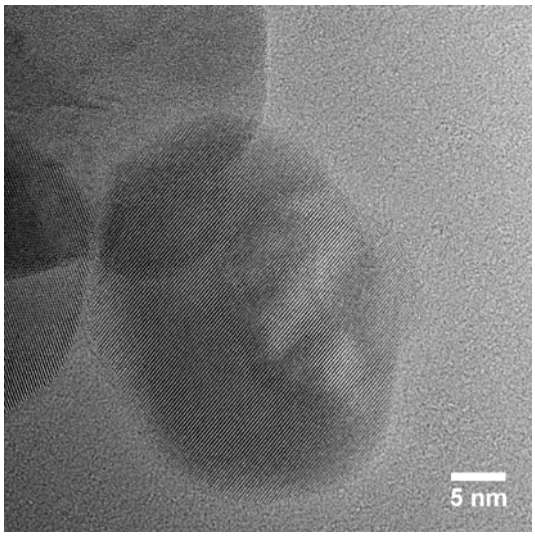

Figure 2. HRTEM image of Ge-Si hybrid particles

This work was supported by the German Research Council (DFG) and the Cluster of Excellence “Engineering of Advanced Materials” (EAM).

Holman, Z. C., Liu, C.-Y. & Kortshagen, U. R. (2010) *Nano Lett.* **10**, 2661-2666.
Körmer, R., Jank, M.P.M., Ryssel, H., Schmid, H.-J. & Peukert, W. (2010) *J. Aerosol Sci.* **41**, 998-1007.

Thermostability of flame synthesized core-shell TiO_2/SiO_2 nanoparticles and its photocatalytic activity

Qi, Fei[1], Moiseev, Anna[2], Deubener, Joachim[2], Weber, Alfred P.[1]

[1]Institute of Particle Technology, TU Clausthal, Leibnizstrasse 19, 38678, Clausthal-Zellerfeld, Germany
[2]Institute of Non-metallic Materials, TU Clausthal, Zehntnerstrasse 2a, 38678, Clausthal-Zellerfeld, Germany

Keywords: thermostability of anatase, core-shell nanoparticles, photocatalytic activity.

Nanosized TiO_2 is a well-established material used for development of environmental photocatalytic technologies and self-cleaning coatings as well as catalyst support. The anatase content and anatase particle size are crucial factors for its catalytic performance. For the application of nanosized TiO_2 at elevated temperatures (over 400 °C) the classical sintering problem of anatase particles must be avoided.

In the present study binary TiO_2/SiO_2 nanoparticles were synthesized by oxidizing $TiCl_4$ and $SiCl_4$ at about 900 °C in $CH_4/O_2/N_2$-premixed flame reactor described in detail in [1]. Tetrachlorosilane precursor was fed directly into the flame at different flow rates condensing as a SiO_2-layer on the surface of TiO_2 crystallites (ca. 18 nm) to build so-called core-shell particle morphology. The thermostability of anatase phase in synthesized products was studied in the temperature interval from 900 to 1200 °C. The photocatalytic activity of calcined samples was tested by degradation of dichloroacetic acid (DCA).

Fig. 1 shows the stability of anatase phase at different calcination temperatures dependent on Si/Ti-ratio in TiO_2/SiO_2 materials. For a certain minimum SiO_2-content the resulting fraction of anatase reaches a maximum for each calcination temperature. With increasing calcination temperature the necessary silica content increases, while the resulting fraction of anatase is reduced.

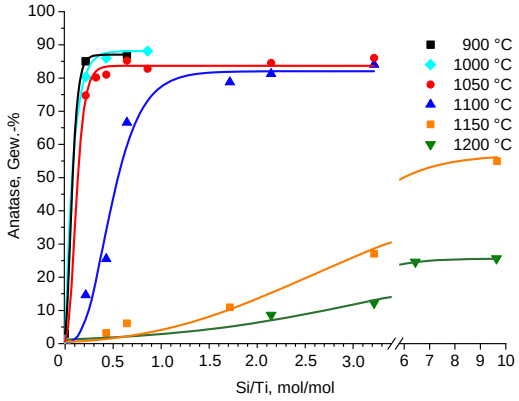

Fig. 1 Stability of anatase phase in core-shell particles versus Si/Ti-ratio at 900 - 1200 °C

Fig. 2 shows the oxidation rate of DCA, mgTOC/(l·min), versus Si/Ti-ratio. It was found that particles calcined at 1100 °C remained still notably photocatalytically active. Moreover, the samples calcined at 900 °C with Si/Ti-ratio up to 0.2 mol/mol exhibited the highest activity.

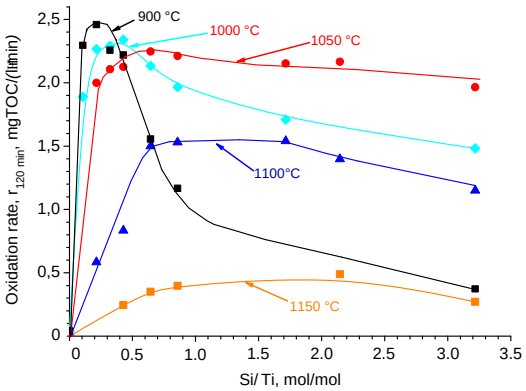

Fig. 2: Photocatalytic oxidation rate of DCA with calcined powders

Fig. 3 presents the binary TiO_2/SiO_2 powders after calcination procedure. The silica layer remained intact up to about 1050 °C. In the temperature range between 1050 and 1100 °C dramatic changes occurred in the material's morphology: cracks in the SiO_2-shell as well as coarse TiO_2 crystallites become now well observable by TEM. Calcination at 1150 and especially at 1200 °C nearly completely destroyed the protective effect of SiO_2-shell so that the TiO_2 particles sinter uninhibitedly rapidly to a µm-size.

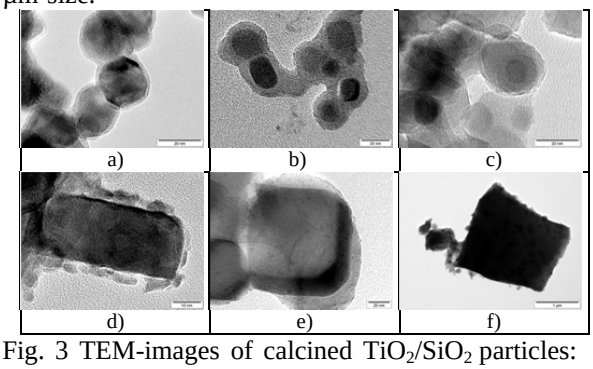

Fig. 3 TEM-images of calcined TiO_2/SiO_2 particles: a) - f) 900, 1000, 1050, 1100, 1150 and 1200 °C

This work is supported by the Deutsche Forschungs Gemeinschaft (DFG) under grant DFG-We 2331/12-2 and DFG-De 598/16-2.

[1] Qi, F., Moiseev, A., Weber, A.P., Deubener, J., J. Nanoparticle Res. (2011) 13: 1325-1334

Synthesis of aluminium nanoparticles with the aid of a customized atmospheric plasma spraying system

E. Daskalos[1], H. Mandilas[1], G. Karagiannakis [1] and A. G. Konstandopoulos[1,2]

[1]Aerosol &Particle Technology Laboratory, CPERI/CERTH, P.O. Box 60361, 57001, Thessaloniki, Greece
[2] Dept. of Chemical Engineering, Aristotle University, P.O. Box 1517, 54006, Thessaloniki, Greece
Keywords: atmospheric plasma spraying, aluminum nanoparticles, metallic nanoparticles
Presenting author email: emdaskal@cperi.certh.gr

The present study investigates the proof-of-concept feasibility to synthesize aluminium (Al) nanoparticles (NPs) from micron-sized Al powder with the use of a customized DC arc type Atmospheric Plasma Spraying (APS) technique. This technique facilitates synthesis of NPs via rapid sublimation of the precursor micrometric metallic particles (size ranges employed were 20-45 and 45-150 μm) and their subsequent re-nucleation. The process took place inside a sealed mantle/reactor system, which was designed and manufactured in-house. The reactor system equipped all necessary instruments for pressure, temperature and oxygen content measurements and provided the necessary inert environment (argon) to avoid any oxidation of the metal during plasma spraying. An additional argon flow, injected downstream of the plasma, promoted rapid quenching of the gasified metal. The particles formed were collected on a quartz filter. Typical production rate achieved was at 2gr·min^{-1}.

Post-characterisation of synthesised particles was performed via X-Ray Diffraction (XRD), Specific Surface Area measurement (BET), Transmission Electron Microscopy (TEM) coupled with Energy Dispersive Spectroscopy (EDS) and ThermoGravimetric Analysis (TGA) under air. It was found that the synthesised powders comprised metallic Al monocrystalline NPs of almost spherical shape. The NPs possessed a 2-5 nm oxide coating layer. By regulating the conditions inside the mantle, a variety of different size distributions was obtained.

Table 1. Overview of main properties of Al NPs synthesised

Exper. No	Average Primary Particle Size (nm)	Crystallite size (nm)	BET (m^2/gr)
1	31	23	51.33
2	47	49	27.20
3	68	67	20.60
4	82	57	18.07

Comparisons with respect to size distribution results of prepared samples provided strong indication that the effect of increasing precursor feed rate from 1 g·min^{-1} to 2 g·min^{-1} was more profound than that of decreasing precursor particle size from 45-150 μm to 20-45 μm. A more solid picture, however, emerged from a similar comparison for the synthesis runs performed with and without argon-accelerated quenching. It was evident that faster quenching led to smaller primary particles and narrower particle size distributions.

The size distribution and surface area features of Al NPs synthesised via the current system were found to be similar to those of Al NPs produced through similar plasma type systems. Dolbec *et al* (2008) produced Al NPs ranging from 25 to 100 nm (mainly dependent on quench rate) in size, using an inductively coupled plasma system under mild vacuum conditions. The mean size of Al NPs produced via H_2 plasma-metal reaction was reported at 46 nm by Liu *et. al.* (2003), while their BET surface area was measured at 48 m^2/g. Laser ablation of Al in liquid resulted in NPs production with a mean size of 30 nm (Kumar *et al*, 2010).

The amount of synthesised NPs deposited directly on the filter accounted to around 20% of the total quantity produced per experiment. The remaining quantity was deposited on the inner walls of the reactor/mantle (primarily) and near the APS gun (secondarily). Powder not deposited on, or near, the filter suffered from undesirable moderate-to-severe sintering phenomena as it failed to pass through the rapid quenching area of the reactor. The latter ascertainment implied the necessity for improvement of the current design in order to ensure that virtually all of the synthesised powder undergoes rapid quenching.

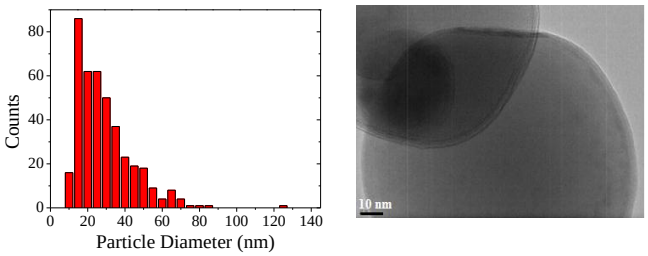

Figure 1. Representative size distribution of primary particles and HR-TEM image of Al NPs synthesised

This work was partially funded through the 7th Framework Programme (FP7), COMETNANO Project (Contract No: 229063). The authors would also like to acknowledge the valuable help of Dr. M. Vardavoulias and Dr. S. Kamnis from PYROGENESIS S.A.

Dolbec R. *et al* (2008) Nanotech **1**, ISBN: 978-1-4200-8503-7, 672-675

Liu T. *et al* (2003), *J. of Phys.: Cond. Mat.* **15** (17), 2507-2513

Kumar B. and Thareja R.K (2010). *J. Appl. Phys.* **108** 064906-1

Synthesis of Magnesium Hydride by Spark Discharge in Argon/Hydrogen Mixtures

T.V. Pfeiffer[1], A. Anastasopol[2], S.W.H. Eijt[2], and A. Schmidt-Ott[1]

[1]Nanostructured Materials, Department of Chemical Engineering, Faculty of Applied Sciences, Delft University of Technology, 2628 BL 136, Delft, the Netherlands
[2] Fundamental Aspects of Materials and Energy, Department of Radiation, Radionuclides & Reactors, Faculty of Applied Sciences, Delft University of Technology, 2629 JB 15, Delft, the Netherlands
Keywords: spark discharge, hydrogen storage, nanoparticles; generation, metal hydrides.
Presenting author email: t.v.pfeiffer@tudelt.nl

Hydrogen storage in metal/metal hydride systems is relevant as a safer alternative to high-pressure cryo-compressed storage. Magnesium based metal hydrides have the advantage of being relatively cheap, and having been studied extensively. An efficient process for the large scale production of metal hydrides is still lacking.

Previously we reported on spark discharge of magnesium in a mixture of 5% hydrogen / 95% argon. Nanoparticles of MgH_2 were formed, which showed low temperature hydrogen desorption. Apart from the typical β-MgH_2 phase, a significant amorphous fraction was found. This study aims to elucidate the formation of magnesium hydrides in hydrogen/argon mixtures, both in context of hydrogen storage properties and scale-up.

Hydrided magnesium nanoparticles were formed *in situ* by spark discharge using two electrodes of metallic magnesium 1.5 mm apart, and 1.0 SLM of 0-100% H_2 in Ar as carrier gas (figure 1). Production rates were determined from the mass collected on PVDF membrane filters over 5-17 hours. The structure of the as produced powders was investigated using XRD and TEM. Hydrogen storage properties were evaluated using Thermal Desorption Spectroscopy and a Sieverts apparatus.

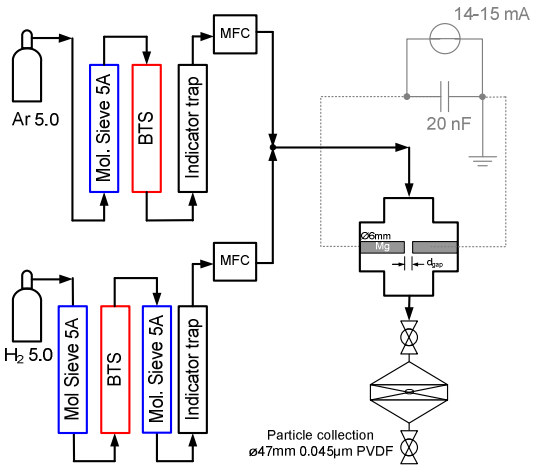

Figure 1. Spark discharge setup.

Increasing the hydrogen concentration in the carrier gas increases the breakdown voltage, and with it the power input into the spark. Power input levels off at 28 W for concentrations of 50% H_2 and up. Energy efficiency improves with increasing H_2 concentration: more mass is produced at the same plasma power input. When 100% H_2 is used, the nature of the plasma changes and the discharge becomes silent. The yield drops down to 5 ng/J, due to the absence of heavy Ar^+ ions in the ablation process. While the use of hydrogen is mostly limited to the production of hydrides, using less reactive gases that are heavy or have a large breakdown voltage, such as Ar, Xe or SF_6, in order to improve ablation efficiency could be more generally applicable.

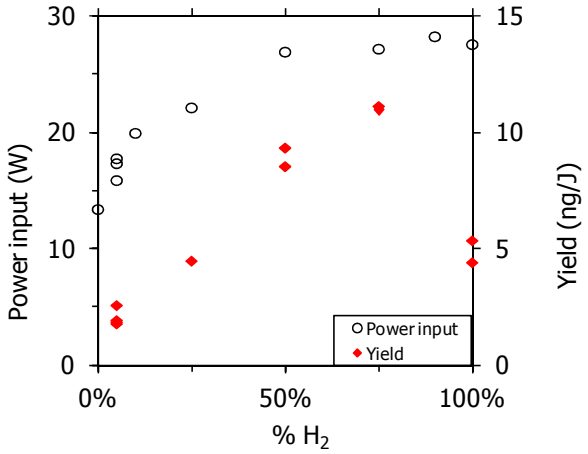

Figure 2. Power input and energy yield for various hydrogen concentrations.

For all samples, XRD shows the presence of nano-crystalline Mg, MgO and β-MgH_2. All samples produced with H_2/Ar mixtures have large amorphous fractions, but samples produced in 100% H_2 contain highly crystalline MgH_2 domains >100 nm. TEM confirms that the particles are surrounded by ~1-2 nm MgO shells. Sievert's analysis yields a decrease in desorption enthalpy to ~ 60 kJ/mol H_2 and increased equilibrium pressures at low temperatures, indicative of the nanostructure in the material.

The gas composition in spark discharge can be tuned to affect crystallinity and particle size of MgH_2. Power input and energy efficiency can also be affected, which is beneficial for larger scale production.

We acknowledge financial support by Agentschap NL, grant EOSLT07052.

Pfeiffer, T. V., Anastasopol, A., Vons, V.A., Legerstee, W.J., Eijt, S.W.H., Mulder, F.M., and Schmidt-Ott, A. (2010) *European Aerosol Conference 2011*, Manchester, 877.

WO_3-based thin films produced by Electrostatic Spray Deposition

J. Gaury[1, 2], E. M. Kelder[2], G. Biskos[1, 2, 3]

[1] LPCA, Université du littoral cote d'Opale, 59140 Dunkerque, France
[2] Faculty of Applied Sciences, Delft University of Technology, Delft, 2628-BL, The Netherlands
[3]Department of Environment, University of the Aegean, Mytilene 81100, Greece

Keywords: Aerosol spray pyrolysis, Nanoparticles, oxides, Particle deposition..
Presenting author email: j.f.m.m.gaury@tudelft.nl

Electrostatic Spray Deposition (ESD) is a method that combines Electrohydrodynamic atomization (in short electrospraying) and electrostatic deposition to form nano- or micro-structured materials. In this all-in-one-step technique that takes place in a controlled atmosphere, a precursor solution is pumped through a nozzle on which a high voltage is applied. As a result, the liquid jet breaks-up into micron-sized droplets under the influence of electrical forces and are deposited onto a substrate by the electrical field. By heating the substrate, one can enhance evaporation of the solvent and oxidation of the particles resulted from the solution during their flight from the nozzle to the substrate (cf. Figure 1).

By varying the operating conditions of the systems one can produce thin films having a wide variety of morphologies with building-block particles that range in size from the micrometer to the nanometer scale (Hartman and al, 2000). Despite the fact that temperature is the main parameter in the aerosol drying process and consequently in the morphology design of the film, a lot of other parameters should be taken into account such as the spraying parameters (voltage, flow rate, the nozzle to substrate distance) and the precursor properties (conductivity, surface tension, density, pH, etc).

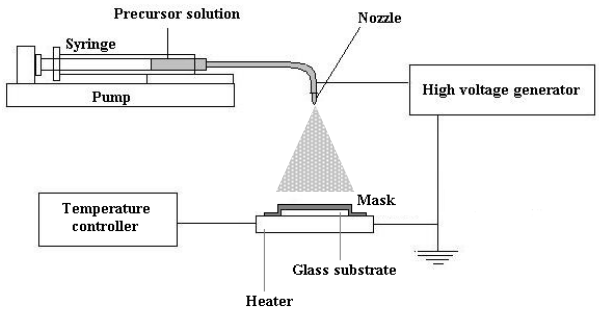

Figure 1. Schematic diagram of the Electrostatic Spray Deposition set up.

The ESD process has found valuable applications in the production of Metal Oxide Semiconductors (MOS), as well as thin films for Solid Oxide Fuel Cells (SOFC), Li-ion battery materials, or gas sensors. In this paper we demonstrate the fabrication of WO_3 films doped with niobium or tantalum using ESD. The modification of the spraying parameters offers the possibility to tune the morphology of our thin films in order to meet the requirements of building sensitive NO_x gas sensors. Doped and undoped samples have been produced and characterized by different techniques (e.g. SEM, TEM, EDX, XPS). Imaging analysis showed that we obtain homogeneous thin films, with highly porous morphologies and high surface to volume ratio, thereby offering a very efficient surface coverage that thereby enhances the gas sensing response.

The resulted Nb- and Ta-doped WO_3 thin films have dense, grain-like, flower-like or tree-like morphologies when the substrate temperature is increased from 250 to 400 °c. Reticulated structures have also been observed by using solvents with different boiling points. Based on the existing literature about the ESD theory (Hartman and al, 2000), droplet sizes have been estimated in the micrometer range and compared to the imaging spectroscopy performed on the films, showing particle sizes of about 150 nm. To explain this difference and the formation of the tree-like morphology, we developed a qualitative model (cf. Figure 2) in which the as-generated droplets undergo additional break-ups into smaller droplets by reaching the Rayleigh limit due to solvent evaporation (Tang and Gomez, 1994).

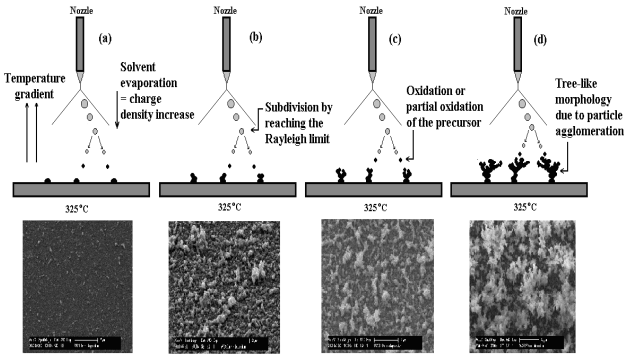

Figure 2. Deposition model and corresponding SEM pictures of WO_3 particles prepared at 325 °C, with a precursor flow rate of 0.2ml/h deposited for (a) 1; (b) 5; (c) 10 and (d) 20 minutes.

Acknowledgements
This work is supported by the European Commission, granted for the INTERREG IV project.

References

Hartman, Brunner, Camelot, Marijnissen and Scarlett, (2000) *Journal of Aerosol science* 31.

Tang and Gomez, (1994), *Journal of Aerosol Science*, 25, 1237-1249.

CCore-shell nanomagnets

Forsman, Johanna[1], Auvinen Ari[1], Tapper, Unto[1], Koskela, Pirjo[1], van Dijken Sebastiaan[2], Jokiniemi Jorma[1,3]

[1]Fine Particles, VTT Technical Research Centre of Finland, P.O. Box 1000, FI-02044 VTT, Finland
[2]NanoSpin, Department of Applied Physics, Aalto University School of Science, P.O. Box 15100, FI-00076 Aalto, Finland
[3]Department of Environmental Science, University of Eastern Finland, P.O. Box 1627, FI-70211 Kuopio, Finland
Keywords: core-shell nanoparticles, CVD, nanoparticle applications
Presenting johanna.forsman@vtt.fi

Nanomagnets with controlled size distribution are produced by continuous hydrogen reduction technique and coated in-situ by carbon or copper. Cobalt chloride is the precursor for the magnetic cobalt core of the particles. Copper chloride and ethene are applied as precursors for copper and carbon shells, respectively. The synthesis technique is presented in detail in previous articles (Forsman et al. 2008; Koskela et al. 2011). The copper layer can be oxidised ex-situ without oxidising the cobalt core. The magnetic cobalt cores are well protected against oxidation occurring over time or in elevated temperatures. The coating affects the optical and the electrical properties of the magnets and can be functionalised (Eiroma et al. 2011). The produced core-shell particles were characterised extensively with XRD, XRF, TEM, SAED, BET, TGA and squid magnetometer.

The number average diameter of the carbon coated cobalt core-shell particles (Co+C particles) varied between 17 and 78 nm (figure 1). The standard deviation of the particle size distribution increased with average particle diameter from 7 nm to 37 nm, while the specific surface area decreased from 27 to 7 m^2/g. The mass concentration ranged from 8 to 13 g/m^3 in these experiments. The number average diameter clearly correlated with the concentration of ethene in the reaction flow.

According to XRD and XRF data, the Co+C particles are very pure and well crystallized. The carbon mass fraction in the particles is 3-9 wt-% depending on ethene concentration. TGA analysis showed that oxidation of the Co+C particles started at 200°C. This indicates that the Co particles are uniformly coated with carbon.

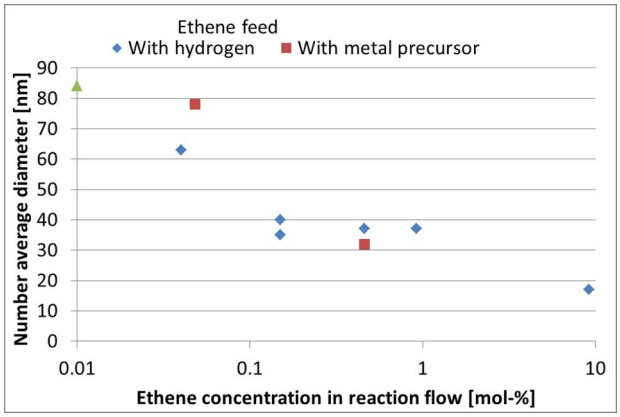

Figure 1. Number average diameter of particles as a function of ethene concentration in the reaction flow.

The mass fraction of copper in the copper coated cobalt particles (Co+Cu particles) was 31-92 wt-% according to XRF. XRD data showed that directly after production, both Co and Cu were in metallic form. After controlled oxidation of Cu, cobalt still remained metallic. The number average diameter of the Co+Cu particles ranged from 54 nm to 84 nm.

The saturation magnetization of the Co+C particles was close to that of bulk Co ($M_{s,\ bulk}$ = 159 emu/g) with the exception of the smallest (D_{ave} = 17 nm) particles. In that case, a large saturation magnetization of 239 emu/g was measured. This might indicate that the Co cores induce a magnetic moment in the C shell. Reports on induced ferromagnetism in C have attracted significant interest in recent years and this phenomenon still is a topic of intense scientific debate (Coey et al. 2002; Kusakabe and Maruyama 2003; H.-Ch. Mertins et al. 2004). In our experiments, we only observe an enhanced saturation magnetization for the smallest Co particles. In all studied Co+C samples hysteresis was low.

The saturation magnetization of Co+Cu particles was similar to bulk Co when normalized to Co weight. In comparison to Co+C particles, significant hysteresis was observed.

Coey, J. M. D., M. Venkatesan, C. B. Fitzgerald, A. P. Douvalis, and I. S. Sanders. (2002).*Nature* **420** (6912),156-159.

Eiroma, K.et. al. 2011. "Development of Conductive Carbon Coated Copper Nanoparticle Inkjet Fluid." Minneapolis, MN, The Society of Imaging and Technology, 2.-6.10.2011.

Forsman, J., U. Tapper, A. Auvinen, and J. Jokiniemi. (2008).*J. Nanopart. Res.* **10** (5),745.

Mertins, H.-Ch., S. Valencia, W. Gudat, P. M. Oppeneer, O. Zaharko, and H. Grimmer. (2004). *Europhys..Lett.* **66** (5),743-748.

Koskela, P. et. al. (2011). *Adv. Powder Technol.* **22** (5),649-656.

Kusakabe, K.and Masanori, M. (2003). *Phys. Rev. B* **67** (9),092406.

The authors acknowledge VTT Technical Research Centre of Finland and Tekes – The Finnish Funding Agency for Technology and Innovation (Magia project) for funding

Wednesday, September 5, 2012

Session WG09S1O. Aerosol Modelling: Atmospheric Applications

Secondary organic aerosol formation during summer 2010 over Central Europe

B. Langmann[1], K. Sellegri[2] and E. Freney[2]

[1] Institute of Geophysics, University of Hamburg, KlimaCampus, Hamburg, Germany
[2] Laboratoire de Meteorologie Physique, CNRS, Universite Blaise Pascal, Aubiere, France
Keywords: three-dimensional modeling, secondary organic carbon aerosol formation
Presenting author email: baerbel.langmann@zmaw.de

Introduction

Until recently, atmospheric models systematically underestimated measured OC aerosol mass concentrations in the atmosphere by a factor of up to 10 and more. Jimenez et al. (2009) proposed the concept of aging of organic vapors, thereby producing less volatile and higher oxygenated organic vapors with atmospheric mass concentrations comparable to sulfate. Based on these ideas, Yu (2011) developed a promising modeling strategy where the aging of organic vapors is considered and in addition to the traditional two compound thermodynamical gas-particle partitioning a third low volatile organic vapor is formed which kinetically undergoes condensation on pre-existing particles.

Model description

Here we use the regional three-dimensional atmosphere-chemistry-aerosol model REMOTE (Langmann et al., 2008) with the aerosol dynamics and thermodynamics module M7 (Vignati et al., 2004). The standard M7 has been extended by Anntila et al. (2010) by a thermodynamical two compound SOC aerosol formation mechanism. This one was further extended based on Yu (2011). We consider three classes of organic vapors where the low-volatile one is formed by aging form the more volatile ones. The low-volatile organic vapor is assumed to condense kinetically on pre-existing particles, while for the medium- and semi-volatile organic vapors the thermodynamical approach of Anntila et al. (2010) is used.

Model results

REMOTE model results over Central Europe are compared with measurements from a campaign at Puy-de-Dome, France during June 2010. Sulfate and chlorine aerosol mass concentrations are very well captured in the model simulation results - finally also organic carbon aerosol mass concentration. For illustrating the sensitivity of OC model results on SOC parameterizations, Fig. 1 shows results for the original two compound thermodynamical approach for isoprene only by Anntila et al. (2010) (grey line) and model results with additional VOC precursor gases (yellow line). Taking into account the SOC gases as additional trace species in the model, which undergo transport and removal (green line) leads to a considerable, however still insufficient increase in comparison with the measurements. The red line shows results from the simulation where aging of the most volatile SOC gas to the semi volatile SOC gas has been considered, finally generating OC aerosol mass concentrations in the range of the measurements. Taken into account the aging of the semi volatile SOC gas to the low volatile SOC gas (black line) does not modify OC aerosol mass concentrations much in comparison to the first aging step.

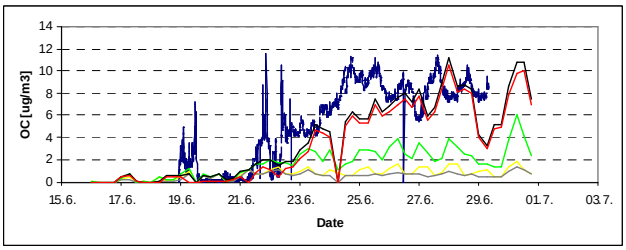

Fig. 1: AMS-measured (dark blue line) and modeled near surface OC mass concentration during June 2010 at Puy-de-Dome, France. Grey line: according to Anntila et al. (2010); yellow line: more VOC precursor gases; green line: SOC gas transport and removal; red line: 1. aging SOC gas; black line: 2. aging SOC gas - see text for more explanation

It should be noted however, that considerable differences in the aerosol size distribution are determined between the model simulations taking into account the first and second step of SOC gas aging. Due to kinetic condensation of the low volatile SOC gas, nucleation mode particles (up to 5 nm) grow into the aitken mode particle range (5 nm – 50 nm) which further grow into accumulation mode particle range (bigger than 50 nm).

This work was supported by the German and French Science Foundations DFG and CNRS within the joint project ATMOCHEM: Secondary organic aerosol production in the lower free troposphere over Western Europe.

Anttila, T. Langmann, B., Varghese, S. et al. (2010) Advances in Meteorology, doi:10.1155/2010/48203.
Jimenez, J.L., Canagaratna, M.R., Donahue, N.M. et al. (2009) *Science* **326**, 1525–1529.
Langmann, B., Varghese, S., Marmer, E. et al. (2008) *Atmos. Chem. Phys.* **8**, 1591–1607.
Vignati, E., Wilson, J., Stier, P. (2004) *J. Geophys. Res.* **109**, doi:10.1029/2003JD004485.
Yu, F. (2011) *Atmos. Chem. Phys.* **11**, 1083–1099.

Regional modelling of the tropospheric multiphase system using COSMO-MUSCAT: 2D-sensitivity-studies

R. Schrödner[1], A. Tilgner[1] and R. Wolke[1]

[1]Institute for Tropospheric Research, Leipzig, 04318, Germany
Keywords: Aerosol cloud interaction, Multiphase chemistry, Modelling (regional), Cloud microphysics.
Presenting author email: roland.schroedner@tropos.de

Clouds play a major role in the atmosphere due to their influence on the Earth's radiative budget, on the hydrologic cycle and on the tropospheric chemical composition (e.g. Ramanathan et al., 2001). Cloud lifetime is driven by the dynamics of the atmosphere at the synoptic scale and, in close interaction, by microphysical processes (e.g. nucleation of cloud droplets and ice crystals, condensation and evaporation, collision/coalescence processes, freezing, sedimentation of hydrometeor) on the small scale.

These processes depend on the chemical composition of particles and cloud droplets. In addition, microphysical processes redistribute chemicals among the various reservoirs: gaseous, particulate, liquid and ice phases. Clouds favor the development of "multiphase chemistry" since they are an ideal reaction medium for this: (1) clouds support very efficient photochemical processes inside droplets; (2) certain homogeneous chemical reactions within clouds can be usually faster than the equivalent reactions in the gas phase, and reactions such as those involving ionic species, can be important; (3) finally, interactions between the aqueous and solid phase can contribute additionally to chemical processes in clouds (for example dissolution of soluble particulate species). The evaluation of multiphase chemistry versus overall tropospheric chemistry and its role in the Earth's radiative budget is challenging since microphysical and chemical processes occurring at different time scales within clouds are still poorly known.

The model system COSMO-MUSCAT consists of MUSCAT (Wolke et al., 2004a) and the forecast model of the German Weather Service (DWD) COSMO (Schättler et al., 2008). Both models are coupled online. MUSCAT was extended to consider cloud-chemical processes (chemical aqueous phase reactions and phase transfer processes) on the regional scale replacing the former aqueous phase parameterization.

Based on the increasing kinetic and mechanistic knowledge on chemical aqueous phase reactions in the last two decades, advanced aqueous phase chemical mechanisms such as the Chemical Aqueous Phase Radical Mechanism (CAPRAM) are continuously developed (Tilgner and Herrmann, 2010). CAPRAM is an almost explicit mechanism which describes relevant chemical aqueous-phase conversions of both inorganic and organic compounds. A reduced version of the mechanism, applicable for 3D chemistry transport models was created (Deguillaume et al., 2009).

With the advanced model system, 2D-sensitivity-studies (air streaming over a mountain) have been conducted for an urban and a remote case. The comparison of two different mechanisms (simple inorganic (INORG) and detailed organic mechanism CAPRAM) have revealed agreements but also interesting differences for important chemical subsystems e.g. in the modeled multiphase HO_x budget and pH whereas the simple mechanism leads to always less acidic cloud droplets than CAPRAM. Invesigation of reaction fluxes show that this is due to additional organic acidification in CAPRAM. The difference in pH leads consequently to different regimes for e.g. the S(IV)-oxidation.

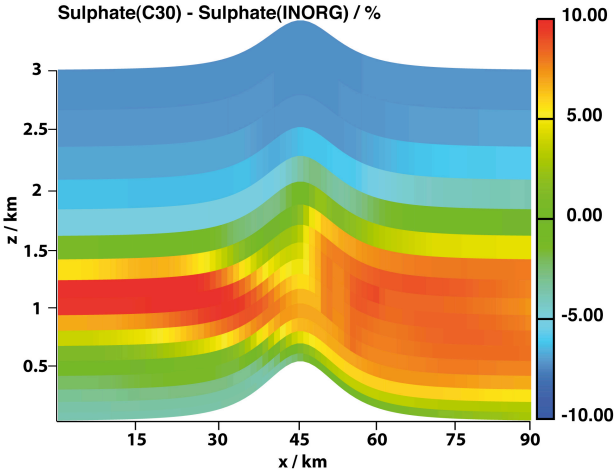

Figure 1. Height profile in x-direction of the simulated mass of S(VI) simulated with CAPRAM compared to the run with INORG. The cloud is located left of the mountain (red and yellow area). Species stream in from the left-hand side.

This work was supported by the Deutsche Bundesstiftung Umwelt (DBU).

Deguillaume, L., et al. (2010), *Journal of Atmospheric Chemistry*, *64*(1), 1-35.

Ramanathan, V., Crutzen, P. J., Kiehl, J. T. and Rosenfeld, D. (2001) *Science*. 294, 2119 - 2124

Schättler, U., Doms, G. and Schraff, C. (2008): *A Description of the Nonhydrostatic Regional COSMO-Model Part VII: User's Guide.*

Tilgner, A. and Herrmann, H. (2010) *Atmospheric Environment*, *44*(40), 5415-5422

Wolke, R., Knoth, O., Hellmuth, O., Schröder, W. and Renner, E. (2004a) *Parallel computing: Software technology, algorithms, architectures and applications*, 363-370

Simulating the impact of controlled sea salt emissions on cloud optical properties in the Southeast Pacific

K. Lundgren, T. Schad, M. Bangert, B. Vogel, A. Ferrone, and H. Vogel

Institute for Meteorology and Climate Research, Karlsruhe Institute of Technology (KIT), Karlsruhe, Germany
Keywords: climate engineering, Southeast Pacific, cloud formation, regional modelling.
Presenting author email: kristina.lundgren@kit.edu

Currently it is discussed in which way climate change can be delayed by using different methods known under the term climate engineering. One of the suggested methods involves the controlled emissions of sea salt particles with the purpose to increase the albedo of marine clouds. Previous investigations have suggested that the Southeast Pacific is the most favourable region for climate engineering with sea salt (e.g., Korhonen *et al.* 2010). The Southeast Pacific is known to be characterised by a persistent layer of stratocumuli clouds with high coverage near the coast of Chile and Peru. The reason for its existence is a result of a highly complex chain of interactions between several processes. Due to the complexity of the system and the fact that several of the processes happen at small un-resolved scales, that need to be parameterised, atmospheric models encounter difficulties in capturing this cloud layer in a realistic way.

In this study, we investigate the impact of controlled sea salt emissions for the Southeast Pacific with the regional scale online-coupled model system COSMO-ART (Vogel *et al.* 2009). Natural sea salt emissions are calculated as function of the wind speed and sea surface temperature. For the investigation of sea salt climate engineering, we add controlled sea salt emissions to the natural sea salt emissions following Korhonen *et al*. (2010). We use detailed two-moment cloud microphysics including six hydrometeor classes (Seifert and Beheng, 2006) that are coupled to the aerosol particles by a comprehensive parameterisation for aerosol activation (Barahona *et al*., 2010). The activation parameterization accounts for the competition of different aerosol particles for water vapour during their activation and considers the effect of giant CCN such as sea salt.

The first step is to reproduce the cloud cover in the region realistically with the model. Numerical simulations are performed for a time period in October-November 2008, in which the VOCAL-REX campaign took place (e.g., Bretherton *et al.* 2010). The simulated effective cloud droplet radius is compared to the effective radius that was retrieved from satellite observations during the VOCAL-Rex campaign (Fig. 1). Apart from a region along 20°S, where a too low temperature inversion suppressed the cloud droplet formation, the simulated effective radius compares well with the observed effective radius of water. Values in the order of 13-17 µm dominate in the satellite retrieved effective radius, and the corresponding values in the simulation are approx. 11-19 µm. The artificial sea salt emissions lead to strong increases in number density in the order of 200%, below the temperature inversion. . The effect on the effective cloud droplet radius these imposed sea salt emissions will be presented at the conference.

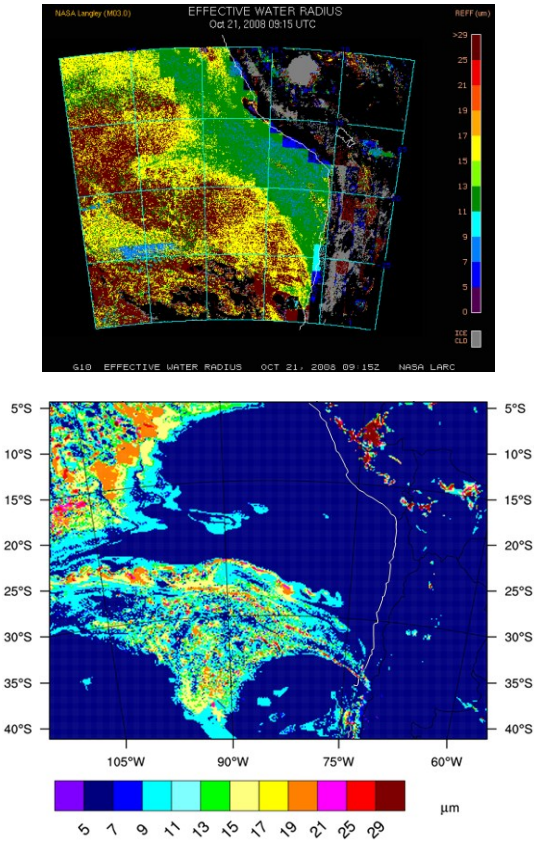

Figure 1. Observed and simulated effective radius at 21 October, 2008. Measurements are achieved from the VOCAL-Rex Field Catalog (www.catalog.eol.ucar.edu).

Bretherton, C. S. , Wood, R., George, R. C., Leon, D., Allen, G., and Zheng, X. (2010). *Atmos. Chem. Phys.,10*, 10639-10654.

Barahona, D., West, R.E.L., Stier, P. Romakkaniemi, S., Kokkola, H. and Nenes, A. (2010). *Atmos. Chem. Phys., 10,* 2467-2473.

Korhonen, H., Carslaw, K.S. and Romakkaniemi, S. (2010). *Atmos. Chem. Phys., 10,* 4133-4143.

Seifert, A. and Beheng, K.D. (2001). *Atmos. Res.*, 59-60, 265–281.

Vogel, B., Vogel, H., Bäumer, D., Bangert, M., Lundgren, K., Rinke, R., and Stanelle, T. (2009). *Atmos. Chem. Phys., 9,* 8661-8680.

Atmospheric boundary layer height estimation by different methods: Application to lidar measurements

D. Toledo[1], C. Córdoba-Jabonero[1], E. Cuevas[2] and M. Gil[1]

[1]Instituto Nacional de Técnica Aeroespacial (INTA), Atmospheric Research and Instrumentation Branch, Torrejón de Ardoz, Madrid, Spain
[2]Agencia Estatal de Meteorología (AEMET), Atmospheric Research Centre of Izaña (CIAI), Sta. Cruz de Tenerife, Spain
Keywords: Boundary layer, Lidar measurements, Mathematical methods, Saharan dust.
Presenting author email: toledocd@inta.es

The Atmospheric Boundary Layer (ABL) is the lowest part of the troposphere which is directly influenced by the Earth surface. Factors like the season, the orography, the time of the day and the weather act over the ABL.

The determination of the ABL height is decisive for pollution dynamic studies and weather forecasting modelling. Radiosoundings, typically used for this purpose, are launched in a 1-2/day basis, at best. Then they cannot provide a suitable evolution of the ABL along the day.

Higher concentrations of aerosols are usually present in the ABL respect to those are in the Free Troposphere (FT). This fact is used to estimate the ABL height by means of lidar measurements. Indeed, a sharp difference in backscatter signal is found by 'crossing' from BL to FT altitude. In addition, since lidar systems can be in full-time operation, they appear to be the most appropriate instrumentation for a continuous ABL top detection.

There are different methods to calculate the ABL top height from lidar signals. They are based on two approaches: 1) the vertical distribution of the aerosol concentration, as used by the Derivative Methods (DM) (Flamant, 1997), i.e. the Gradient Method (GM) and Logarithm Method (LGM), and the Wavelet Covariance Transform (WCT) (Brooks, 2003); and the statistic analysis as used by the Centroid/Variance Method (VM) (Hooper and Elorata, 1986). A new procedure combining both these approaches is also used in this work: the Cluster Analysis (CA). The goal of this work is the comparison of the results obtained from the application of each one of those methods to lidar measurements. Differences found are analysed in order to establish the most reliable method for ABL top height determination.

Daily measurements are performed by a Micro Pulse Lidar (MPL) system in routine operation at the subtropical station of AEMET/Sta. Cruz de Tenerife Observatory (SCO, 28ºN 16ºW, 52 m a.s.l.). Raw signal profiles are acquired with 1-min integrating time and vertical resolution of 75 m. Then, these 1-min profiles are averaged over 10 minutes, obtaining thus 6 profiles/hour (144 profiles/day). This study is focused on two scenarios: dusty and non-dusty cases. An example of the ABL top height calculated by the GM, VM, WCT CA methods is shown in Figure 1 for a dusty case (9 November 2005). The same by the LGM and IPM methods is shown in Figure 2.

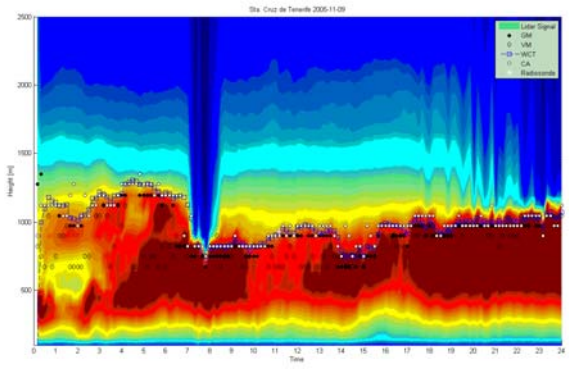

Figure 1. Daily range-corrected lidar signal on 09 November 2005, where the temporal evolution of the ABL top height calculated by GM, VM, WCT and CA methods (see legend) is shown. Radiosounding ABL estimation (11:00 UTC) is also included (white star) for reference.

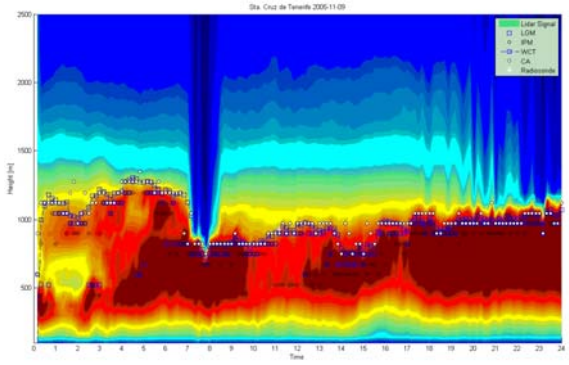

Figure 2. The same as Figure 1, but ABL top height is calculated by LGM, IPM, WCT and CA methods (see legend).

Results show that ABL heights determined by CA, WCT and LGM methods present the lowest differences respect to the radiosounding reference. VM provides a higher dispersion at the beginning and the end of the day. IPM shows, in general, lower height values than those obtained by all other methods.

This work is supported by the Spanish Ministry for Research and Innovation (MICINN) under grant CGL2011-24891 (project AMISOC).

Brooks, I. (2003) *J. Atmos. Ocean. Tech.* **20**, 1092-1105.
Flamant *et al.* (1997) *Bound.-Lay. Meteorol.* **83**, 247-284.
Hooper and Eloranta (1986) *J. Clim. Appl. Meteorol.* **25**, 990-1001.

The impact of the NAO on aerosol concentration levels in Europe

P. Jiménez-Guerrero[1], S. Jerez[2], J.P. Montávez[1] and R.M. Trigo[2]
[1]Department of Physics, University of Murcia, 30100 Murcia, Spain
[2]IDL, Universidade de Lisboa, Portugal
Keywords: aerosols, modeling, regional climate, NAO.
Presenting author email: pedro.jimenezguerrero@um.es

It is now widely accepted that the North Atlantic Oscillation (NAO) corresponds to the main mode of large-scale atmospheric circulation variability affecting the climate of the Atlantic and European sector. Positive phases of NAO promote the westerly winds in northern Europe and the northerly winds in the south-western Mediterranean basin. On the contrary, negative phases of NAO enhance (weaken) the zonal circulation and associated low-pressure systems in southern (northern) Europe.

Aerosols dispersion, deposition, transport and generation are intimately related to the predominant atmospheric conditions. Hence, the aforementioned NAO-impacts on climatic variables should display considerable signatures in terms of aerosols concentration levels. However, it is difficult to a priori establish them since (1) the aerosols response to the atmospheric conditions is highly non-linear, and (2) the NAO-impact on the various atmospheric variables could induce impacts of opposite signal, ones enhancing while others diminishing the concentration of aerosols. Therefore, the main objective of the present study is to characterize and quantify the NAO-impact on the aerosols concentration levels over Europe related to the well-known responses of its climate, identifying the prevailing underlying atmospheric processes.

The assessment is built on a 25-km resolution simulation performed with the CHIMERE chemistry transport model spanning from 1970 to 1999 and covering the whole European continent. The meteorological inputs were taken from a hindcasted climate simulation performed with the mesoscale model MM5 driven by the ERA40 reanalysis. The study is based on monthly values of aerosols total levels and their chemical composition. The monthly values of the NAO index are obtained from the Climate Prediction Center from the National Oceanic and Atmospheric Administration (NOAA). The analysis is mainly based on both, the correlation patterns depicting the temporal correlations between the evolution of the chemical variables and the NAO index, and the composites of the differences in the various aerosols concentration levels between positive and negative phases of NAO (>0.5 and <-0.5).

Results

The results show clearer changing signals during wintertime. A strong dipole north-south is depicted by the simulations. Months characterized with negative NAO values are associated with enhanced precipitation and positive temperature anomalies in southern Europe while northern European sectors present climatic anomalies of opposite signal. These patterns of anomalies reverse during months dominated by positive values of the NAO.

Therefore, a noticeable negative impact on ground-level aerosol concentrations (especially over southern Europe-Mediterranean area) is associated to the negative NAO phase, as clearly observed for the total levels of aerosols and most of their chemical components, such as sulphate, other secondary aerosols -not shown- and organic matter (Fig. 1). This is consequence, among others, of the higher precipitation associated to the negative values of NAO over the Mediterranean. However, this general behaviour for most aerosol species is not observed for those aerosols whose emissions depend on the wind module. The enhanced zonal circulation during negative phases of NAO promote the levels of sea salt aerosols, whose emission rate is a function of the surface wind speed raised to the power 3.41.

These results prove the structural role played by the NAO mode and would likely rebound on enhancing the short-term predictability of aerosols concentration levels over the entire European continent. Furthermore, the long-term future projections of air pollution could be reinterpreted and deeper understood taking into account these insights and possible trends in the NAO series.

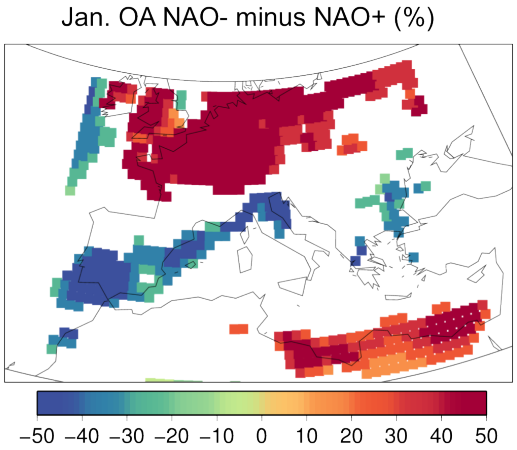

Figure 1: Difference (%) in the organic aerosols levels between January climatologies depicting NAO- minus NAO+.

This work was funded by project CORWES CGL2010-22158-C02-02 and the Ramón y Cajal Programme.

CCN formation from biogenic VOCs studied with the global climate model ECHAM5-HAM

R. Makkonen[1], A. Asmi[1], V.-M. Kerminen[1,2], M. Boy[1], A. Arneth[3], A. Guenther[4] and M. Kulmala[1]
[1]Department of Physics, University of Helsinki, Helsinki, FI-00014, Finland
[2]Finnish Meteorological Institute, Helsinki, FI-00101, Finland
[3]Institute of Meteorology and Climate Research, Karlsruhe Institute for Technology, Garmisch-Partenkirchen, 82467, Germany
[4]Atmospheric Chemistry Division, National Center for Atmospheric Research, Boulder, Colorado, 80301, USA
Keywords: BVOC, CCN, climate.
Presenting author email: risto.makkonen@helsinki.fi

The biosphere emits large quantities of biogenic volatile organic compounds (BVOCs), both in terms of number of species and emitted mass. For the quantification of the indirect effect of secondary organic aerosol (SOA) it is essential to know the size-dependent partitioning of the semi- and low-volatile organic compounds. By using thermodynamic equilibrium partitioning, the organic compounds condense according to available organic mass in the aerosol phase, which can not support the observational evidence of nanoparticle growth by organics. Also, the increase in condensation sink can hinder new particle formation. While organic compounds are globally important for providing particle growth, recent observations have shown that organic compounds can also affect the atmospheric nucleation rates directly (Metzger *et al*, 2010; Paasonen *et al*, 2011). Finally, the magnitude of the indirect effect is largely determined by the spatial distribution of the cloud condensation nuclei (CCN) concentration increase and cloud cover.

We study SOA formation from BVOCs with the global aerosol-climate model ECHAM5.5-HAM2. Biogenic monoterpene emissions are distributed evenly to the boundary layer, and the oxidation products are assumed to condense to the particle phase during one timestep. The partitioning is done by using the condensation sink of the aerosol population. We study aerosol formation mechanisms including sulphuric acid only, and sulphuric acid together with organics (Paasonen *et al*, 2011). In all nucleation schemes, organics can participate in particle growth already from 2 nm size. Three SOA precursor cases are applied: no BVOCs, and emissions of either MEGAN2 or LPJ-GUESS models. The global monoterpene emission of MEGAN2 (∼80 Tg/yr) exceeds that of LPJ-GUESS (∼30 Tg/yr), but most of the emission difference is located in the tropics. Regionally, the two models vary in terms of emission rates and intra-annual variation.

Turning on BVOC emissions and SOA formation increases CCN(0.2%) in the tropics and in Northern high latitudes above 40°N. The increase is over 20% in large areas in South America and the boreal forest regions. The global increase in the CCN(0.2%) concentration due to biogenic VOCs is about 1.5% with MEGAN2 emissions and 0.5% with LPJ-GUESS emissions. At the same time, there is an increase in the condensation sink, which leads to overall decrease in the simulated nucleation rates. While the global average total particle concentration is slightly decreased, there is some increase over boreal forests where the condensation sink is still low even with BVOC emissions turned on.

The application of the two BVOC emission models allows us to study the sensitivity of the particle concentrations to the underlying assumptions of biogenic properties. The differences in simulated CCN concentrations reflect the differences in the BVOC emission: emissions of LPJ-GUESS lead to generally more CCN between 0°N and 50°N, while MEGAN2 emissions produce more CCN in the tropics and northern high latitudes. Globally, MEGAN2 emissions lead to an increase of 0.5% in CCN(0.2%) concentration compared to LPJ-GUESS emissions. In all simulations, the decrease in nucleation rates together with an increase in particle growth rates lead to mixed results regarding total particle concentrations.

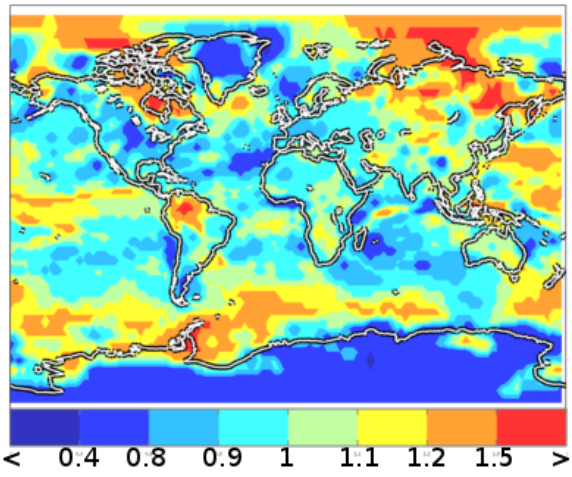

Figure 1: Ratio of CCN(0.2%) with MEGAN2 BVOC emissions to CCN(0.2%) without BVOC emissions.

This work was supported by the Academy of Finland Centre of Excellence program (project no. 1118615)).

Metzger, A. et al. (2010) Proc. Nat. Acad. Sci. 107, 6646-6651.

Paasonen, P. et al. (2010) Atmos. Chem. Phys. 10, 11223-11242.

Solar radiation management with high speed civil aircrafts and sulfur-enhanced fuel

A. Laakso[1], H. Kokkola[1], A-I. Partanen[1], A. Laaksonen[1], K.E.J. Lehtinen[1,3] and H. Korhonen[1]
[1]Finnish Meteorological Institute, Kuopio Unit, P.O. Box 1627, FI-70211, Kuopio, Finland
[2]Finnish Meteorological Institute, Climate Change, P.O. Box 503, FI-00101 Helsinki, Finland
[3]Department of Applied Physics, University of Eastern Finland, Kuopio Campus, P.O. Box 1627, FI-70211, Kuopio, Finland
Keywords: geoengineering, stratospheric aerosols, sulfate aerosols, modelling
Presenting author email: anton.laakso@fmi.fi

Geoengineering methods aim to increase the reflectivity of the Earth or remove greenhouse gases from the atmosphere as means to slow down global warming. One of the promising methods that have been suggested is injection of sulphate aerosols to the stratosphere. In the atmosphere, sulphate aerosols reflect solar radiation back to the space and thus cool the climate. Because of the stability of the stratosphere the lifetime of the sulphate aerosol is 1-2 years, when in the troposphere it is only a few days. Thus much smaller sulphur emissions would be required to obtain a similar cooling with stratospheric aerosol than with tropospheric sulfate aerosol.

Numerous methods have been proposed for delivering sulfate aerosol precursors. One of the methods that has been proposed but has not been sufficiently studied is using high-speed civil transport (HSCT) aircrafts and sulphur-enhanced fuel to emit aerosol precursors in a jet exhaust stream (Rasch, 2008). If aircraft fuel contained 1 weight per cent of sulfur, it would eventually generate roughly 4 Tg of sulphate aerosols. This method can be assumed to have relatively low cost since stratospheric sulfate production would be a by-product of civil air transport.

This study is performed with the global aerosol – climate model MAECHAM5.5-HAM2, a middle atmosphere version of ECHAM5.5-HAM2 (Stier et al. 2005). MAECHAM5 is integrated with a spectral truncation of 63 (T63) and 47 vertical levels up to 0.01 hPa and IPCC AR5 historic emission of air traffic has been used. For the geoengineering purpose, some of the flights are assumed to fly in the stratosphere.

Five-year long simulations have been made for six different cases: a control run for current flights and current fuel sulphur concentration and stratospheric flights with current sulphur concentration, with five times the current sulphur concentration (which is the current legal limit for aircraft fuel sulphur concentration), with 50 times the current sulphur concentration and with five times the sulphur concentration, but 5% of emissions are assumed to be converted as SO_4 (50 nm) immediately in the plume. To estimate the effect of future flight paths, we have used Representation Concentration Pathways (RCP) from IPCC Report 5 and in this case used five times the current sulphur concentration.

Results show that if stratospheric flights and current fuel content is used, the effect to the radiative forcing is insignificant. Also 5 x sulphur content has small effect to the aerosol radiative forcing, -0.11 W/m^2 by using current flight paths and -0.35 W/m^2 by using estimated air traffic for year 2050. If we enhance fuel sulfur concentration to 50 times the current concentration, the global aerosol radiative forcing at the surface is -0.9 W/m^2, but because commercial aircrafts fly mostly in the northern hemisphere, the effect of sulphate aerosols is much stronger in the northern hemisphere (-1.20 W/m^2) than in the southern hemisphere (-0.61 W/m^2). Thus if HSTC aircrafts were used for geoengineering, the aircraft fuel concentration would need to be enhanced much over the current legal limit for fuel sulphur concentration and some other delivering method would need to be used in the southern hemisphere to get similar effects for both hemispheres. If 5% of fuel sulfur emissions of the aircraft are assumed to be emitted as primary SO_4 particles, the effect to the aerosol radiative forcing is almost equal to the case where all sulphur is emitted only as SO_2.

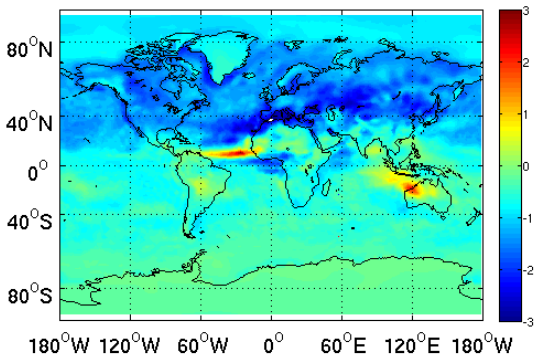

Figure 1: Radiative forcing when 50 x SO2 concentration is used

Acknowledgements. This work is supported by the Academy of Finland's Research Programme on Climate Change (FICCA).

Rasch, P. et al (2008), Phil. Trans. R. Soc. **366**, 1882 4007-4037

Stier, P et al (2005). Atmos. Chem. Phys., **5**, 1125-1156.

Modelling of particle number size distribution over Europe with chemistry transport model LOTOS-EUROS

Astrid Manders[1], Antoon Visschedijk[1], Hugo Denier van der Gon[1], Bas Henzing[1], Martijn Schaap[1].

[1]TNO, Department of Climate, Air and Sustainability, P.O.Box 80015, 3508 TA Utrecht, the Netherlands

Keywords: Particle size distribution, Aerosol modelling
Presenting author email: astrid.manders@tno.nl

There is a growing awareness of the significance of aerosol particles with diameters smaller than about 1 micron for human health as well as for their climatic impact. Particle number distributions are therefore gaining attention, both in measurements and modelling.

To study the particle number distribution over Europe with the regional chemistry transport model (CTM) LOTOS-EUROS, the model was extended with the aerosol dynamics module M7 which accounts for aerosol ageing effects (condensation, coagulation, hygroscopic growth) in 7 lognormal modes (Vignati et al.2004).

Model simulations with LOTOS-EUROS were performed using two different (anthropogenic) emission databases:

- MACC 2005 emissions. The first contains traditional PM2.5 and PM10 mass emissions (Kuenen et al., 2011). To be able to use these emissions, mass had to be redistributed over the species and size ranges used in M7.
- PN emissions. This database is the recently developed size-resolved particle number emission database for Europe. This database covers particles with dry diameters between 5 and 250 nm, distributed over 12 size bins (Denier van der Gon et al., 2010)

Modelling results are compared to EUSAAR SMPS/DMPS data for several European sites (Asmi et al. 2011).

Fall/winter concentrations, which are dominated by anthropogenic emissions, are modeled more realistically than spring/summer concentrations for which biogenic emissions and nucleation play a more important role. The PN inventory leads to a better correspondence with observations than the MACC inventory, showing the added value of the PN emission inventory.

In summer modeled Aitken mode concentrations tend to be underestimated as compared to measurements, in particular for the PN inventory. This may be due to a poor representation of SOA formation and an incomplete representation of SIA, combined with an underestimation of nucleation in the model.

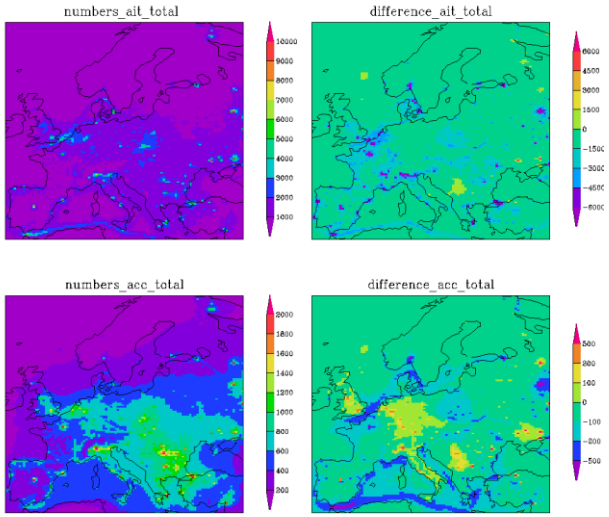

Fig. 1 Annual mean concentrations for Aitken and accumulation mode when using the PN emissions(left) and the difference with an-nual mean concentrations using the MACC emissions (PN-MACC)

Presentation

At the conference, it will be shown how the two emission databases are used in LOTOS-EUROS. The differences in the emission databases that are relevant for aerosol modeling are discussed.

Asmi, A. et al. (2011), ACP, Atmos. Chem. Phys., 11, 5505-5538, doi:10.5194/acp-11-5505-2011.

Denier van der Gon, H., Visschedijk, A., Johansson, C., Ntziachristos, L., and Harrison, R. (2010) Proceedings of the 2010 International Aerosol Conference, Helsinki, august/September 2010

Kuenen J., Denier van der Gon H.A.C., Visschedijk A., Van der Brugh H., Gijlswijk R., (2011). MACC European Emission Inventory for the Years 2003-2007, TNO-report TNO-060-UT-2011e00588 Utrecht.

Vignati, E., J. Wilson, and Stier P. (2004) *J. Geophys. Res.*, **109**, 8601-8616.

Thursday, September 6, 2012

Plenary 4

Secondary organic aerosol formation through aqueous chemistry: atmospheric evidence, chemistry, partitioning and prediction

B. J. Turpin[1]

[1]Department of Environmental Sciences, Rutgers University, New Brunswick, New Jersey, 08901, USA
Presenting author email: turpin@envsci.rutgers.edu

Organic aerosol, much of which is formed in the atmosphere (secondary), is a major component of fine particulate matter. The generally poor understanding of the formation of secondary organic aerosol (SOA) is a source of uncertainty in predictions of atmospheric aerosol concentrations and properties that affect climate, visibility and health. It is well accepted that SOA forms when semivolatile products of gas-phase photochemical reactions partition into preexisting particulate organic matter (SOA_{om}). SOA_{om} has been studied extensively through smog chamber experiments conducted at low relative humidity (RH). While clearly important, gas-phase chemistry and partitioning fails to explain several key atmospheric observations, including high O/C ratios, vertical profiles, correlations with sulfate and aerosol water, droplet mode size distributions, oxalate formation and formation of high molecular weight compounds (HMWC). Additionally and importantly, this chemistry does not consider the atmospheric abundance of liquid water in clouds, fogs and aerosols. For example, model predictions suggest that water is 2-3 times more abundant than all other aerosol species including organic matter, globally (Liao and Seinfeld, 2005).

In this presentation I present evidence that multiphase SOA formation involving gas followed by aqueous reactions in clouds, fogs and wet aerosols (SOA_{aq}) helps to explain these observations. I discuss chemistry leading to SOA_{aq} formation and how this chemistry is different in clouds/fogs versus in aerosols. I present information about the gas-particle partitioning of aqueous SOA products, and briefly review progress toward modeling $SOA_{aq.}$ Finally, I identify some important unresolved questions.

Gas phase oxidation of organic emissions frequently leads to the formation of smaller, more oxidized, water soluble compounds. After partitioning into water, these compounds can react further, e.g., with hydroxyl radical. The low volatility products of the aqueous reactions then remain in the particle phase, even after water evaporation, forming SOA_{aq} (Blando and Turpin, 2000).

We conducted aqueous photooxidation experiments by generating OH radicals (~10^{-12} M) in: filtered rainwater, aqueous solutions containing water-soluble gases scrubbed from ambient air, and single-compound solutions (30-3000 μM). Samples were analyzed by electrospray ionization mass spectroscopy (ESI-MS), ion chromatography (IC), IC-ESI-MS, Fourier transform ion cyclotron resonance mass spectroscopy (FT-ICR MS), and for total organic carbon. We have also taken solution from these reactions to generate and evaporate droplets using a Vibrating Orifice Aerosol Generator (VOAG). By comparing results with standards of known volatility, we determined the vapor pressure of the resulting aerosol.

Our experiments conducted with cloudwater surrogates suggest that SOA_{aq} precursors are predominantly aldehydes, organic peroxides and/or alcohols; products are predominantly organic acids. Our experiments and those conducted by others suggest that SOA_{aq} precursors include glyoxal, methylglyoxal, glycolaldehyde, acetic acid, and acetone. At cloud relevant concentrations, oxalate, glycolate and pyruvate are prominent products and the presence of sulfate and nitrate have little impact on the chemistry. OH radical chemistry in the much more concentrated solutions found in wet aerosols leads to the formation of high molecular weight compounds through organic radical-radical reactions (Lim et al., 2010; Tan et al., 2012). Non-radical chemistry can also play an important role in wet aerosols. We measured an effective liquid vapor pressure of ~10^{-7} atm for glycolaldehyde SOA (pH ~ 4) in droplet evaporation experiments. It should be noted that the volatility of SOA_{aq} will depend on whether organic acid products are present as acids or salts.

Several groups are now adding SOA_{aq} to chemical transport models. The approaches that are being taken and the insights these provide will be discussed, as will several yet unresolved questions that still hamper efforts at accurate SOA_{aq} prediction.

I gratefully acknowledge the contributions of Ho Jin Lim, Yong Lim, Ann Marie Carlton, Katye Altieri, Yi Tan, Diana Ortiz, Jeffrey Kirkland, and Anjuli Ramos. This work was supported by the US National Science Foundation (1052611), Environmental Protection Agency (83375101) and National Oceanic and Atmospheric Association (NA07OAR4310279).

Blando, J.D. and Turpin, B.J. (2000) *Atmos. Environ.* **34**, 1623–1632.

Liao, H. and Seinfeld, J. H. (2005) *J. Geophys. Res.*, **110**, D18208, doi:10.1029/2005JD005907.

Lim, Y. B., Tan, Y., Perri, M. J., Seitzinger, S. P., and Turpin, B. J. (2010) *Atmos. Chem. Phys.*, **10**, 10521–10539.

Tan, Y., Lim, Y. B., Altieri, K. E., Seitzinger, S., and Turpin, B. J. (2012) *Atmos. Phys. Chem.*, **12**, 801-813.

Thursday, September 6, 2012

Session WG01S5O. Physical and chemical properties + Transport (II)

Long Term Trends in Arctic Aerosol Composition at Kevo, Finland

P.K. Hopke[1], J.R. Laing[1], L. Hussain[2,3], V.A. Dutkiewicz[2], J. Paatero[4], and Y. Viisinen[4]

1Department of Environmental Health Sciences, School of Public Health, SUNY, Albany, NY. 12201, USA
2Wadsworth Center, NYS Department of Health, Albany, NY 12201-0509
3Center for Air Resources Engineering and Science, Clarkson University, Potsdam, NY 13699
4Finnish Meteorological Institute, Helsinki, Finland

Keywords: black carbon, Arctic, time series, Kevo
Presenting author email:hopkepk@clarkson.edu

Introduction

Carbon, primarily a byproduct of incomplete combustion of fossil fuel and biomass burning constitute only a few % of the total PM mass, but disproportionately affect the global climate by absorbing the incoming sunlight and directly warm the atmosphere. BC coated with sulfate is even more effective than externally mixed BC and SO4 particles. Recent studies have indicated that substantial radiative forcing in the Arctic is due to the indirect impact of BC on the albedo of snow and ice surfaces. We are determining the concentrations of BC, EC, MSA, SO_4, and selected trace elements in weekly samples collected at Kevo, Finland from 1964-2010 to assess the impact of aerosols on (1) radiative forcing, (2) source regions that have contributed to the burden of BC/EC and SO4 in the Arctic region, and (3) how the regional emissions impacting Arctic have changed with time.

Methods

Samples were collected over 7 day periods beginning in October 1964 through the present in Kevo [Yli-Yuomi et al., 2003a,b], Finland in an automated system to measure airborne radioactivity. The filters from 1964-1978 have been analyzed for trace metals by neutron activation (INAA) and inductively coupled plasma mass spectrometry (ICP-MS), major ions and methane sulfonate (MSA) by ion chromatography, black carbon, and elemental carbon [Yli-Tuomi 2003a,b]. Filters after 1978 have been analyzed for total and soluble trace elements by inductively coupled plasma mass spectrometry (ICP-MS), and major ions and methane sulfonate (MSA) by ion chromatography. Black carbon, and elemental carbon were analyzed using the approach developed by Li et al. [2002]. The light absorption of each new filter was measured with a Magee OT21 transmissometer. EC was measured using a Sunset Analyzer and the NIOSH protocol [Birch and Cary, 1996].

Results and Conclusions

Figure 1 shows the annual average BC values for 1965 to 2000. The concentrations of BC aerosols during 1965 were 430 ng m^{-3}. From 1966 thru 1987 it varied from ~250 to 430 ng m^{-3}. Beginning in 1989, concentrations showed a systematic decrease to about 150 ng m^{-3}. From 1989 to 2002, the concentrations have remained between 150 and 230 ng m^{-3}. The data from 2003 to 2010 is not yet available. These data show that there was a substantial decrease in BC concentrations around the time of the collapse of the Soviet Union and the change in political systems in eastern Europe.

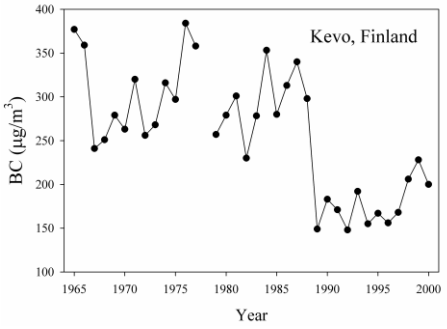

Figure 1. Time series of annual average concentrations of BC at Kevo, Finland

. The solubility of certain elements can provide information about the origin of the aerosol and formation processes. Trend analysis will be performed on individual species. The complete data set will be analyzed by Positive Matrix Factorization (PMF). The receptor modeling results will be connected with back trajectory data in a Potential Source Contribution Function (PSCF) analysis to determine possible source areas. Future work includes complete chemical analysis of the weekly filters through 2010 for trace elements and soluble trace elements by ICP-MS, major ions and methane sulfonate (MSA) by ion chromatography, and black carbon by light-absorption and thermo-optical techniques. This complete dataset will be able to provide insight into the long term trend of Arctic aerosol chemical species and the possible implications of global climate change in the Arctic.

Li, J., et al., 2002, Atmospheric Environ. 36, 4699–4704.
Yli-Tuomi, T., et al., 2003a. Atmospheric Environ. 37, 2355-2364.
Yli-Tuomi, T., et al., 2003b, .Atmospheric Environ. 37: 4381-4392.

Summer Campaign on Aerosol Optics, Microphysics, Chemistry and Mineralogy in Portugal - Overview

F. Wagner[1], K. Kandler[2], N. Schiavon[1,4], L. Tobias[1,4], S. Pereira[1], J. Preißler[1], A. Candeias[3,4] and J. Mirão[1,4]

[1]Centro de Geofísica, Universidade de Évora, Évora, 7000-671, Portugal
[2]Institut für Angewandte Geowissenschaften, Technische Universität Darmstadt, 64287, Germany
[3]Centro de Química, Universidade de Évora, Évora, 7000-671, Portugal
[4]HERCULES – Herança Cultural, Estudos e Salvaguarda, Universidade de Évora, Portugal

Keywords: field campaign, aerosol physical properties, aerosol chemical properties.
Presenting author email: frankwagner@uevora.pt

Introduction

Atmospheric aerosol particles play an important role in climate and air quality. Except for the Aerosol Characterization Experiment 2, optical, microphysical and chemical aerosol properties were not measured simultaneously and hence aerosol characterization is incomplete in Portugal. Thus in summer 2011 an intensive field campaign was performed at Évora, Portugal.

Data and Instrumentation

The Evora Geophysics Center is operating several instruments quasi continuously since several years in order to determine aerosol particle optical and microphysical properties. A nephelometer provides the particle scattering coefficient at three wavelengths; a MAAP provides the particle absorption coefficient at one wavelength. A TEOM is used to measure the particle mass concentration. A sun photometer included into the AERONET network is measuring the aerosol optical depth and a multi-wavelength Raman lidar was operated twice a day providing the vertical profile of atmospheric aerosols.

Particles were collected on TEM grids by a cascade impactor with nominal particle diameter cut-offs at 1.8, 0.7 and 0.45, and 0.1 µm, approximately, and subsequently analysed by VP-SEM+EDS to obtain morphological and chemical compositional data Furthermore, aerosol particles were collected on 3 different types of filters (quartz fiber, PTFE, glass fiber) over 24 hours. The filter change was done about noon. Each filter was weighted with an analytical balance before and after the sampling period, providing the particle mass concentration over 24 hours. The glass fibre filters were analysed by X-ray diffraction to provide the main minerals of the sample.

Results

The main summer campaign was conducted between 9 and 28 August. In comparison to previous years, the 2011 August was cooler, and clouds were more frequent than in average. On about half of the days, typical "background" conditions could be observed: an aerosol with a comparatively constant composition, consisting of sea sea-salt, ammonium sulfates, aluminosilicates, and calcite and with a low anthropogenic fingerprint. Two outbreaks of desert dust could be observed as well. Figure 1 shows mean hourly aerosol types identified from nephelometer and corresponding to the filter sampling period.

Figure 2 shows particle mass concentrations determined from the 3 different filter types and from the TEOM. Additionally, the aerosol optical depth determined by the sun photometer is shown. A general good correlation between all measurements is obvious. During desert dust outbreaks, the particle concentration increased by about a factor of 5 in mass concentration and in optical depths as well.

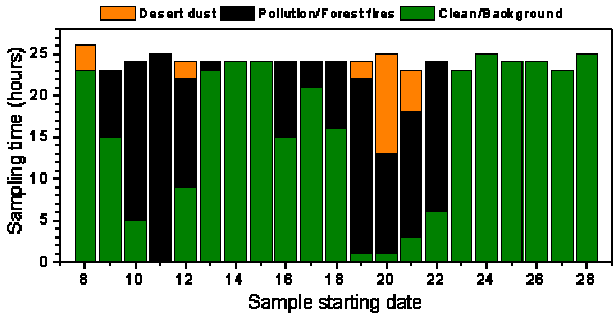

Figure 1. Aerosol types for the sampling period of the filter measurements in August.

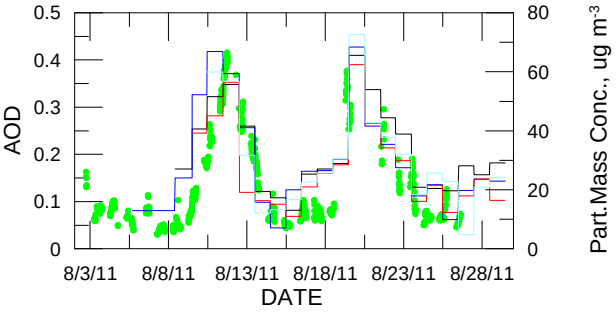

Figure 2. Particle mass concentration (black – TEOM; blue – glassfibre; cyan – PTFE; red – quartz) and aerosol optical depth (green dots) during the summer campaign

This work was supported by the Fundação para a Ciencia e a Technologia.

Climatology of aerosol optical properties in Amazonia

P. Artaxo[1], L.V. Rizzo[2], E. Swietlicki[4], A. Arana[1,5], E. T. Sena[1], A. Wiedensohler[3]

[1]Institute of Physics, University of Sao Paulo, Rua do Matao, Travessa R, 187, CEP 05508-090, Brazil.
[2] Department of Exact and Earth Sciences, Federal University of Sao Paulo, Diadema, 09972-270, Brazil
[3] Leibniz Institute for Tropospheric Research, Leipzig, 04318, Germany
[4] Department of Physics, Lund University, Lund, Sweden.
[5] INPA – Instituto Nacional de Pesquisas da Amazônia, LBA/CLIAMB, Manaus, Brazil.

Keywords: aerosol optical properties, biogenic aerosol, biomass burning, absorption and scattering coefficient.
Presenting author email: artaxo@if.usp.br

Aerosol physical and chemical properties were measured in two sites in Amazonia since January 2008. The clean site is at Central Amazonia and is located in a pristine Amazonian forest site. A second sampling site is located in Porto Velho, Rondonia, an area strongly affected by biomass burning emissions. Long term measurements, from February 2008 are being carried out in these two sites, as part of the EUCAARI (European Integrated Project on Aerosol Cloud Climate and Air Quality interactions) and AEROCLIMA (Direct and indirect effects of aerosols on climate in Amazonia and Pantanal) projects. The dataset obtained encompass the first long term aerosol measurements ever performed in Amazonia, elucidating the differences between the biogenic aerosol population naturally released by the forest metabolism and the anthropogenic aerosols.

In the pristine central Amazonia, measurements were taken at the Cuieiras forest site, tower TT34, with coordinates 2°35'40"S and 60°12'33"W, above the canopy (45m), under dry conditions (RH<40%). A MAAP 5012 absorption photometer in series with a nephelometer (TSI 3563) was used to measure aerosol absorption and scattering, respectively. Scattering coefficients were corrected for truncation errors. Observations were adjusted to 1000 mbar and 0°C. Aerosol size distributions were measure using a Lund DMPS system, as well as a TSI SMPS system. Aerosol composition, and several trace gases that helps to characterize aerosol sources were also measured.

In Rondonia, a sampling station was installed close to the city of Porto Velho, in the "Parque Natural de Porto Velho" at coordinates (8,69° S; 63,87° O). This region have with important land use change and biomass burning emissions. A MAAP 5012 absorption photometer and an Ecotech Aurora 3000 nephelometer are used to measure aerosol absorption and scattering. A TSI SMPS measure the aerosol size distribution continuously. Diffusion dryers are used to keep the relative humidity below 40%.

In the pristine Amazonian atmosphere, aerosol scattering coefficients ranged between 1 and 200 Mm^{-1} at 450 nm, while absorption ranged between 1 and 20 Mm^{-1} at 637 nm. A strong seasonal behavior was observed, with greater aerosol loadings during the dry season (Jul-Nov) as compared to the wet season (Dec-Jun). Although the forest site is locally well preserved, it receives the influence of regional biomass burning emissions during the dry season.

During the wet season in Manaus, aerosol scattering (450 nm) and absorption (637 nm) coefficients averaged, respectively, 14 ± 22 and 0.9 ± 0.8 Mm^{-1}. Both optical coefficients were greatly increased during the dry season, averaging 58 ± 58 Mm^{-1} and 4.1 ± 3.8 Mm^{-1}, correspondingly. Angstrom exponents for scattering were lower during the wet season (1.6 ± 0.4) in comparison to the dry season (1.9 ± 0.2), which is consistent with the shift from biomass burning aerosols, predominant in the fine mode, to biogenic and dust aerosols, predominant in the coarse mode. Single scattering albedo, calculated at 637 nm, did not show a significant seasonal variation, averaging 0.86 ± 0.06 and 0.86 ± 0.04, respectively for wet and dry season, even with that large variation in aerosol sources and magnitude of scattering and absorption coefficients.

In Porto Velho, even in the wet season it was possible to observe a strong impact from anthropogenic sources. Biomass burning emissions in the dry season. $PM_{2.5}$ aerosol concentrations of about 300 ug/m² were measured in August and September for most of the years. AOT values at 550 nm above 3 are frequently observed in Porto Velho with AERONET CIMEL sunphotometers. Black Carbon were measured at 20 ug/m³ in the dry season, showing strong aerosol absorption. Very high aerosol light scattering coefficients above 300 Mm^{-1} were measured.

Remote sensing techniques using a combination of MODIS and CERES sensors were used to measured large scale aerosol radiative forcing. The effect of land use change was calculated and is a significant factor for the aerosol radiative forcing due to change in surface albedo.

This work presents a general description of the aerosol optical properties in Amazonia, both during the Amazonian wet season, when the aerosol population is dominated by particles of biogenic origin, and during the dry season, when there is a strong influence of biomass burning emissions. It is important to describe accurately the optical behavior of these particles in order to assess the impact of anthropogenic changes on the regional climate.

This work was supported by FAPESP Thematic Project AEROCLIMA (08/58100-2) and the European Integrated project on Aerosol Cloud Climate and Air Quality Interactions, EUCAARI (036833).

Influence of water uptake on the aerosol light scattering at the regional continental site Melpitz, Germany

P. Zieger[1], R. Fierz-Schmidhauser[1], L. Poulain[2], W. Birmili[2], T. Müller[2], M. Nan[2,3], A. Wiedensohler[2], E. Weingartner[1], and U. Baltensperger[1]

[1]Laboratory of Atmospheric Chemistry, Paul Scherrer Institut, 5232 Villigen, Switzerland
[2]Leibniz-Institut für Troposphärenforschung e.V., Permoserstraße 15, 04318 Leipzig, Germany
[3]Department of Atmospheric and Oceanic Sciences, School of Physics, Peking University, Beijing, China

Keywords: light scattering, hygroscopic growth, field measurements, AMS
Presenting author email: paul.zieger@psi.ch

Atmospheric aerosol particles change in size due to water uptake which is determined by their chemical composition and the ambient relative humidity (RH). As a result also their optical properties - especially the aerosol light scattering - strongly depend on RH. Therefore, long-term measurements of aerosol physical and optical properties are generally recommended at dry conditions in order to keep measurements comparable (e.g. RH < 30 - 40% as recommended by (WMO 2003)). However, for the comparison of such ground-based measurements with other optical aerosol measurements, or for the use in climate models, accurate knowledge of the RH effect is very important.

The key parameter to describe the influence of RH on the aerosol light scattering is the scattering enhancement factor $f(\lambda,RH)$, which is defined as the scattering coefficient $\sigma_{sca}(\lambda,RH)$ at a certain RH divided by the dry scattering coefficient $\sigma_{sca}(\lambda,RH=dry)$:

$$f(\lambda, RH) = \frac{\sigma_{sca}(\lambda, RH)}{\sigma_{sca}(\lambda, RH = dry)},$$

where λ denotes the wavelength. The scattering enhancement can be directly measured e.g. with a humidified nephelometer.

Here, we will present results of a one-month field campaign at the regional continental site Melpitz, Germany performed in February/March 2009. A newly developed humidified nephelometer (WetNeph, Fierz-Schmidhauser et al. 2010) was operated together with a dry nephelometer, an Aerosol Mass Spectrometer (AMS), a Multi-Angle Absorption Photometer (MAAP), a Hygroscopic Tandem Differential Mobility Analyzer (H-TDMA) and other continuous aerosol instruments.

The scattering enhancement at Melpitz was found to be highly variable, e.g. $f(\lambda$=550nm,RH=85%) varied between 1.4 and 3.5 and depended on the air mass origin. The chemical composition was the main factor to determine f(RH), as can be seen in Fig. 1, where $f(\lambda$=550nm,RH=85%) is shown versus the inorganic mass fraction (inorganic mass fraction = (NO_3+SO_4) / $(NO_3+SO_4+Org+BC)$; with BC: black carbon) retrieved from AMS and MAAP measurements. The inorganic mass fraction and the scattering enhancement are clearly positively correlated. The aerosol size distribution played a minor role on f(RH) for that specific time period. A closure study showed that a good estimate on the aerosol chemical composition or on the aerosol hygroscopicity is of importance if f(RH) needs to be predicted from other auxiliary measurements.

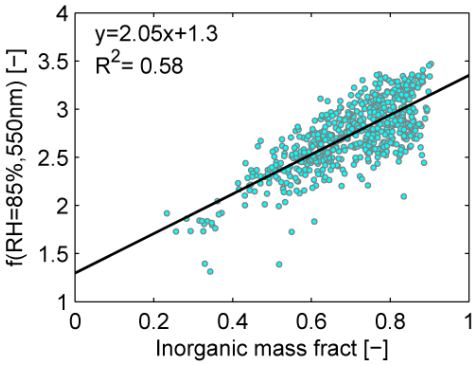

Figure 1: Scattering enhancement f(RH) (at 85% RH and λ=550nm) versus the inorganic mass fraction at Melpitz, Germany. The solid black line represents a weighted linear least squares regression.

This work was supported by the EC projects GEOmon (Global Earth Observation and Monitoring) and EUSAAR (European Supersites for Atmospheric Aerosol Research), as well as by the ESA project aerosol_cci.

Fierz-Schmidhauser, R., *et al.* (2010), *Atmos. Chem. Phys*. **10**(5): 2319-2333.

WMO (2003), *WMO/GAW Aerosol Measurement Procedures Guidelines and Recommendations,* GAW Report No. 153, World Meteorological Organization, Geneva.

Black carbon hygroscopic properties influenced by coating content and chemical compositions

Dantong Liu[1], James Allan[1], Brian Bandy[2], Hugh Coe[1], Zoe Fleming[3], Michael Flynn[1], Gordon McFiggans[1], James Whitehead[1] and Dominique Young[1]

[1]Centre for Atmospheric Science, University of Manchester, Manchester, UK, M13 9PL
[2]University of East Anglia, Norwich Research Park, Norwich, UK, NR4 7TJ
[3]Department of Chemistry, University of Leicester, Leicester, UK, LE1 7RH
Key Words: Black carbon, Hygroscopicity, Coating
Presenting author email: Dantong.liu@manchester.ac.uk

Black carbon aerosols (BC), as a strong absorber of solar radiation, significantly constrain the radiative forcing of climate system and contribute to climate change by heating the lower atmosphere (Ramanathan and Carmichael 2008). The time scale of BC removal from the atmosphere is a crucial factor for most climate and process model input. The removal rate determines both vertical and horizontal distributions of BC, as well as its dispersion on local and regional scale. The main mechanism of BC removal is wet deposition through nucleation scavenging so becoming incorporated into cloud droplets or directly scavenged via impaction onto cloud and rain droplets. Given its initial hydrophobic properties, for nucleation scavenging to take place BC needs to acquire a more hydrophilic composition. The time scale for BC hydrophobic/hydrophilic conversion is a crucial factor to determine how efficiently BC can be removed by wet deposition. Conversion to a more hydrophilic state occurs by a variety of processes such as: condensation of hygroscopic materials from the gas phase onto BC particles; repartitioning of soluble material from other aerosol; and coagulation of BC with hygroscopic aerosol. A simplified term BC coating is invoked by most models to quantitatively determine the amount of non-BC materials that have been associated with BC particles.

The single particle soot photometer (SP2) has been used extensively in recent studies to quantitatively determine BC coating state at various locations and under different atmospheric conditions. However, the link between the BC coatings and the hygroscopic properties of BC in the atmosphere has not been explored. To explicitly answer the question of how coatings influence the hygroscopic properties of BC is crucial to further investigate how efficiently BC will act as cloud condensation nuclei and hence be removed by wet deposition.

This study was conducted at the NCAS-operated Weybourne Atmospheric Observatory (06/11-07/11). Depending on the metrological conditions, this receives the air masses from various source regions, including central England, continental Europe and the North Sea. The HTDMA-SP2 (hygroscopicity tandem differential mobility analyser) system (McMeeking et al., 2011) was used to measure the hygroscopic properties of BC and associated coating state in real time. The HTDMA selects aerosol of a specific dry size then measures the size distribution after exposing the particles to a specified elevated relative humidity, hereby deriving hygroscopic growth factors (gf). The SP2 was measuring downstream of HTDMA so sampled particles of known growth factor, thus allowing the determination of BC particle loadings, size and coating state as a function of gf. In addition, the new Soot Particle AMS (SP-AMS) measured the chemical composition of the coatings on the BC, which is also linked to BC hygroscopic properties. This study provides information on BC hydrophilic properties by direct measurement and relates the coating chemical composition of the coating to these properties.

About 15-60% of BC particles are measured to be hydrophilic during the experiment. Increased BC coating thickness was observed to increase the water uptake ability of BC, however, the actual hydrophilic fraction of BC also depended on the chemical composition of coatings. The gf of BC was observed to be enhanced when significantly coated with nitrate however less so if with the coating that was dominated by organic matter. Given that nitrate is the major constituent of secondary aerosol in polluted air masses over European, the presence of nitrate coating on BC will considerably reduce the lifetime of BC and its radiative forcing effect.

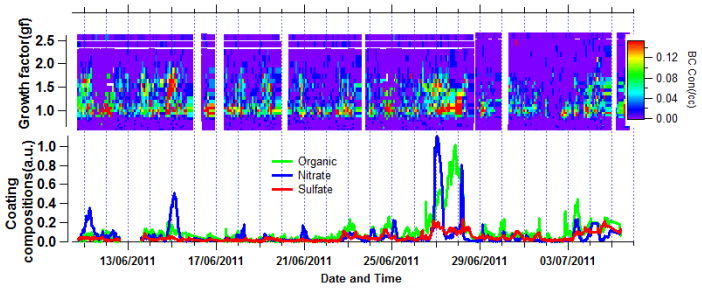

Figure 1. BC hygroscopic properties associated with coating content and compositions.

This work is funded by Multiscale Chemical Composition of Carbonaceous particles and Coatings (MC4) Grant No. NE/H008136/1

Ramanathan, V. and Carmichael, G.: Global and regional climate changes due to black carbon, Nat. Geosci., 1, 221-2-27,2008.

McMeeking, G. R., Good, N., Petters et al.: Influences on the fraction of hydrophobic and hydrophilic black carbon in the atmosphere, Atmos. Chem. Phys., 11, 5099-5112,acp-11-5099-2011, 2011.

Hygroscopicities, ethanol affinities and composition of nanoparticles in CLOUD

H. Keskinen[1], G. Tsagkogeorgas[2], J. Duplissy[3], F. Bianchi[4], J. Joutsensaari[1],P. Miettinen[1], J. Slowik[4], M. K. Kajos[3], S. Schobesberger[3], S. Schallhart[3], T.Ruuskanen[3], H. Wex[2], F. Stratmann[2], D. Worsnop[3], M. Kulmala[3], A. Virtanen[1] , and A. Laaksonen[1,5] (and CLOUD collaboration)

[1]Dept. of Applied Physics, University of Eastern Finland, 70211 Kuopio, Finland.
[2]Dept. of Physics, Leibniz Institute for Trophospheric Research, Leipzig 04318, Germany
[3] Division of Atmospheric Science, Dept. of Physics, University of Helsinki, Helsinki 00560, Finland
[4] Paul Scherrer Institute, Laboratory of Atmospheric Chemistry, Paul Scherrer Institut, Villigen, 5232, Switzerland
[5]Finnish Meteorological Institute, 00560 Helsinki, Finland.
Presenting author email:helmi.keskinen@uef.fi
Keywords: CLOUD, nanoparticles, hygroscopicity, composition

The aim of this study is to predict the size-selected composition of the nucleated nanoparticles and their ability to act as a cloud condensation nuclei. Particles were produced in CLOUD (Cosmic Leaving Outdoor Droplets) experiment, whose aim is to study possible link between galactic cosmic rays and cloud formation.

In the CLOUD experiment the atmospheric conditions were simulated in a chamber in which aerosols were formed. One can find detailed description of the CLOUD experiment elsewhere (Kirkby et al., 2011). To study the chemical composition of the formed particles and the particle-water vapour interactions we used data from hygroscopic and organic ethanol tandem differential analyzers (H- and OETDMA) (Joutsensaari et al., 2001), cloud condensation nuclei counter (CCN-c) (Droplet Measurement Technologies, Roberts and Nenes, 2005) and Aerodyne high resolution time-of-flight aerosol mass spectrometer (HR-ToF-AMS) (DeCarlo et al., (2006)). The smallest measured size was 15 nm for H- and OETDMA, 30 nm for CCN-c 30 nm and 50 nm for HR-ToF-AMS. For results interpretation also the gas phase chemistry studied by Proton Transfer Reaction Time-of-Flight Mass Spectrometer (PTR-TOF) and the ions composition (up to 2 nm) measured by Atmospheric Pressure Interface Time-of-Flight Mass Spectrometer (APi-TOF, Junninen et al., 2010) was used. Figure 1 illustrates the experimental system to analyze the nucleated nanoparticle properties during their growth.

From HTDMA and CCN-c measurements, we derived the hygroscopicity parameters (κ_{hgf} and κ_{ccn}, respectively) based on theory by Petters and Kreidenweis (2007). Same theory was also modified for calculating ethanol affinities (κ_{egf}):

$$\kappa_{egf} = (EGF^3 - 1) \cdot \left[\frac{1}{S} \cdot exp\left(\frac{4\sigma_e M_e}{RT\rho_e D_0 EGF}\right) - 1\right]$$

where EGF is measured ethanol growth factor, S is the saturation ratio, σ_e is the ethanol surface tension, M_e is the molecular weight of the ethanol, R is the gas constant, T is the temperature, ρ_e is the density of the ethanol and D_0 is the selected dry particles size in DMA. From HR-ToF-AMS we can derive the oxidation level of the particles and connect that to their hygroscopic properties (Massoli et al. (2010), Raatikainen et al. (2010)).

The analysis presented here will give valuable insight in the composition of the size-selected (from 15 nm) nucleated particles during their growth and further in their ability to act as cloud condensation nuclei in the atmosphere.

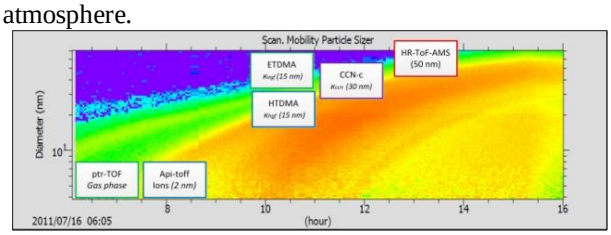

Figure 1. The experimental system to analyze the nucleated nanoparticles properties during their growth.

We would like to thank CERN for supporting CLOUD with important technical and financial resources, and for providing a particle beam from the CERN Proton Synchrotron. This research has received funding from the EC Seventh Framework Programme (Marie Curie Initial Training Network "CLOUD-ITN" grant no. 215072, and ERC-Advanced "ATMNUCLE" grant no. 227463), the German Federal Ministry of Education and Research (project no. 01LK0902A), the Swiss National Science Foundation (project nos. 206621_125025 and 206620_130527), the Academy of Finland Center of Excellence program (project no. 1118615), Academy of Finland (project 138951), the Austrian Science Fund (FWF; project no. P19546 and L593), the Portuguese Foundation for Science and Technology (project no. CERN/FP/116387/2010), and the Russian Foundation for Basic Research (grant N08-02-91006-CERN).

DeCarlo, P. F. et al. (2006), *Analytical Chemistry*, 78, 8281-8289.
Joutsensaari J., *et al*, (2001), *ACP*, 1, 51-60.
Junninen *et al.* (2010), *Atmos. Meas. Tech*. 3, 1038-1053.
Kirkby, J., *et al.*, (2011) *Nature*, 476, 429-U77.
Massoli *et al.*, (2010) *GRL*, 37, L24801.
Petters M.D., and Kreidenweis S.M. (2007), *ACP*, 7, 1961-1971.
Raatikainen *et al.*, (2010) *ACP*, 10, 2063-2077.
Roberts, G. C. and Nenes (2005), Aerosol Sci. Tech., 39, 206–2

Hygroscopicity and cloud forming properties of Arctic aerosol during one year

S. Silvergren[1], U. Wideqvist[2] , J. Ström[2], and B. Svenningsson[1]

[1]Division of Nuclear Physics, Lund University, Lund, 22100, Sweden
[2]Department of Applied Environmental Science, Stockholm University, Stockholm, 10691, Sweden
Keywords: Arctic, CCN, hygroscopicity, aerosol chemistry.
Presenting author email: sanna.silvergren@nuclear.lu.se

The Arctic aerosol has a strong seasonal variation in terms of number concentration. During the Arctic haze from February to May, aerosol numbers increase significantly. When the sunlight returns and the precipitation start, a period of cleaner air begins which lasts until fall. Long-term aerosol measurements of hygroscopicity and cloud forming properties are scarce in the Arctic region. Previous campaign studies suggest that local production of organic rich aerosol particles occur during the summer (Leck *et al*, 2002) and model calculations have indicated that these could be important for cloud droplet formation (Lohmann and Leck, 2005). A relationship between the number of CCN and aerosol sulphate content have been shown by Bigg and Leck (2001). In addition, ice nuclei concentrations influence the CCN concentration (Lance *et al*, 2011).

We are now presenting the chemical composition, hygroscopicity, CCN activity of aerosols collected at the Zeppelin station during one year.

From September -07 to August -08 twelve filters were collected with a high-volume sampler (PM10 cut-off) at the Zeppelin station, located at 474 m above sea level on Svalbard's west coast, a site that has been assessed as virtually free from local, anthropogenic particle emissions. The chemical composition was assessed from additional small filters with OC/EC analysis and ion chromatography (IC). The results are shown in figure 1. The water-soluble fraction was extracted and analyzed with respect to the ability to interact with sub- and supersaturated water vapor. For this we used a Hygroscopic Tandem Differential Mobility Analyser (H-TDMA) coupled with one or two Cloud Condensation Nuclei Counters (CCNC).

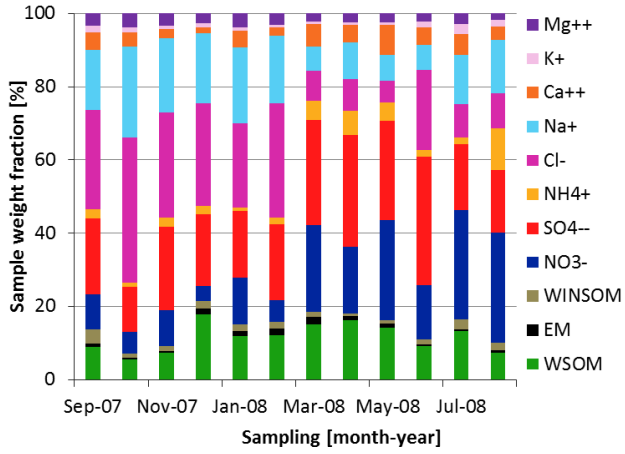

Figure 1. Chemical composition of Arctic aerosol.

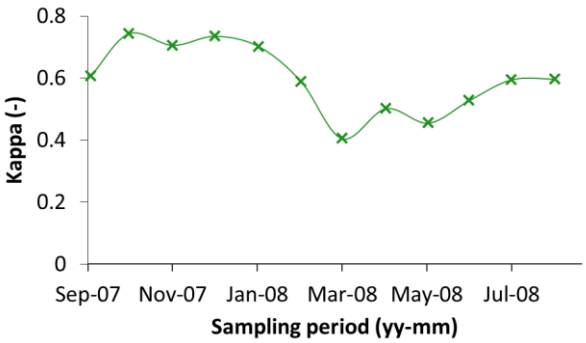

Figure 2. Annual CCN properties (preliminary results).

The kappa values derived from averaged CCNC measurements in figure 2 show that the cloud forming properties vary during the year. The fall aerosol particles are clearly more efficient CCN than the spring aerosol. Both are periods dominated by accumulation mode particles in number concentrations. The summer months have size distribution shifted to Aitken mode and these particles are slightly more favourable as CCN than spring aerosol of same size.

To investigate whether the statement that sulphate and/or organics are important for the CCN population is consistent with our results we plotted the relative amount of aerosol constituents against the kappa values. Sulphate, nitrate and ammonium had a weak negative correlation while sodium and chloride rich aerosol resulted in better CCN properties. It is not surprising that sodium chloride is efficient as CCN and is important to note that it is found mainly in coarse particles. However, in contradiction to previous findings no correlation between organic content and CCN efficiency was seen and more unexpectedly magnesium showed a slight positive correlation to the kappa value.

In addition to these results, the kappa values derived from growth factors at 90% relative humidity and a closure between chemical composition and hygroscopicity and CCNC will be presented.

Acknowledgement: W. Aas for providing IC analysis. This work was supported by Vetenskapsrådet, Formas and MERGE.

Bigg, E. K., and Leck, C. (2001) *J. Geophys. Res.*, **106**, 32,155-32,166.

Lance, S., Shupe, M. D., Feingold, G., *et al* (2011) *Atmos. Chem. Phys.*,**11**, 8003–8015.

Leck, C., Norman, M., and Bigg, E. K. (2002) *J. Geophys. Res.*, **107**, D12 4135.

Lohmann, U., and Leck, C. (2005) *Tellus*, **57B**, 261–268.

Particles measured in a low speed ship engine: cloud condensation nuclei and mixing state on the nano scale

K. I. Lieke[1], T. Rosenørn[1,2], A. C. Butcher[1], S. M. King[1], T. G. Frederiksen[2], K. Fuglsang[2], J. B. Pedersen[3], D. Larsson[3] and M. Bilde[1]

[1]Copenhagen Center for Atmospheric Research, Department of Chemistry, University of Copenhagen, 2100 Copenhagen, Denmark.
[2]Force Technology, Park Allé 345, 2605 Brøndby, Denmark.
[3]MAN Diesel & Turbo, Teglholmsgade 41, 2450 Copenhagen, Denmark

Keywords: ship emissions, CCN, mixing state, phase

Presenting author email: kirstenlieke@gmx.de

Transport by ship plays an important role in global logistics. Current international policy initiatives by the International Maritime Organization (IMO) are taken to reduce emissions from ship propulsion systems (NO and SO, primarily). However, particulate emissions (e.g. soot) from ships are yet not regulated by legislations. To date, there is still a lack of knowledge regarding the global and local effects of the particulate matter emitted from ships at sea. Particles may influence the climate through their direct effects (scattering and absorption of long and shortwave radiation) and indirectly through formation of clouds.

Many studies have been carried out estimating the mass and particle number from ship emissions (e.g. Petzold et al. 2008), many of them in test rig studies (e.g. Kasper et al. 2007). It is shown that particulate emissions vary with engine load and chemical composition of fuels. Only a few studies have been carried out to characterize the chemical composition and cloud-nucleating ability of the particulate matter (e.g. Corbett et al. 1997). In most cases, the cloud-nucleating ability of emission particles is estimated from number size distribution.

We applied measurements to characterize particulate emissions from a MAN B&W Low Speed engine on test bed. A unique data set was obtained through the use of a scanning mobility particle sizing system (SMPS), combined with a cloud condensation nucleus (CCN) counter and a thermodenuder - all behind a dilution system. In addition, impactor samples were taken on nickel grids with carbon foil for use in an electron microscope (EM) to characterize the mineral phase and mixing state of the particles. The engine was operated at a series of different load conditions and an exhaust gas recirculation (EGR) system was applied. Measurements were carried out before and after the EGR system respectively.

The measurements show significant changes in number size distribution and CCN activity with varying conditions. Results of transmission electron microscopy revealed salt condensates of nanometer size attached to soot particles. High resolution structural analysis of single particles shows that three different phases (graphitic soot, crystalline salt and amorphous condensed organic matter) may be present in the same particle volume. A closure between CCN activation curves, EM samples, and SMPS size distribution will be presented and used to identify climate active parts in single particles.

ACKNOWLEDGEMENTS

We thank the Danish Agency for Science, Technology and Innovation for support through the NaKIM project (www.nakim.dk).

REFERENCES

Corbett, J. J. and Fischbeck, P. (1997): Emissions from Ships, Science 278, 823–824.

Kasper, A., Aufdenblatten, S., Forss, A., Mohr, M. and Burtscher, H. (2007): Particulate Emissions from a Low-Speed Marine Diesel Engine, Aerosol Science and Technology 41, 24–32.

Petzold, A., Hasselbach, J., Lauer, P., Baumann, R., Franke, K., Gurk, C., Schlager, H. and Weingartner, E. (2008): Experimental studies on particle emissions from cruising ship, their characteristic properties, transformation and atmospheric lifetime in the marine boundary layer, Atmospheric Chemistry and Physics 8, 2387–2403.

Thursday, September 6, 2012

Session WG04S1O. Combustion and industrial aerosols

Results and experience of long-term study of reduction of fine particle emissions from wood combustion boiler by a compact electrostatic precipitator

A. Bologa, H.-R. Paur and K. Woletz

Institute for Technical Chemistry, Karlsruhe Institute of Technology
Hermann-von-Helmholtz-Platz 1, Eggenstein-Leopoldshafen, 76344, Germany
Keywords: biomass combustion, fine particles, emission control, electrostatic precipitator.
Presenting author email: andrei.bologa@kit.edu

In the Europe the combustion of wood is widely used for domestic heating. The power generation is mostly done by means of combustion of wood-logs, chips or pellets in small scale combustion appliances, e.g. stove and boilers.

Wood combustion it is responsible for emissions of fine particles which are associated with various diseases. Usually particles are composed of ash, elemental carbon and organic matter and particle chemical composition, particle size distribution, number and mass concentration vary greatly depending on the design of the boiler, fuel quality, mixing of air and fuel, combustion temperature, etc.

Last time various filter systems were developed for reduction of fine particle emissions from small scale biomass combustion. These devices include cyclones, wet scrubbers, condensers, bag filters, cartridge filters, electrostatic precipitators (ESPs'), etc. The electrostatic precipitators are the most attractive devices as they ensure high mass collection efficiency and are operated at low power consumption and low pressure drop in comparison with other gas cleaning equipment. The design of the ESPs' range from conventional to space charge ESPs', from dry to wet units, from precipitators integrated into the combustion appliances up to the ESPs' installed downstream the combustion units, inside of the gas duct and/or chimney and at the exit of the chimney.

By biomass combustion in the boilers with integrated hear exchangers, the electrostatic precipitators are operated at gas temperatures of 100-200°C and for wood-log stoves up to 300-400°C.

The purpose of the current work is to present the results of the study of reduction of fine particle emissions from a 100 kW wood-combustion boiler by use of the CAROLA electrostatic precipitators.

The CAROLA electrostatic precipitators are developed in the Karlsruhe Institute of Technology in the Institute of Technical Chemistry. In the ESPs' the gas cleaning technology is based on the particle charging in a corona ionizer and charged particles precipitation in the grounded, external electric field free collector. The DC negative corona discharge is used for particle charging in the precipitators (Bologa *et al*, 2010).

For effective reduction of fine particle emissions from the exhaust gas, the compact CAROLA-precipitators are designed for boilers with capacity of 10 kW, 25 kW and 50 kW. For the long-term tests, several electrostatic precipitators were manufactured and installed in parallel downstream the 100 kW wood-chips combustion boiler. The purpose was to study the long-term operation stability of the ESPs', power consumption and the mass and fractional collection efficiency of the precipitators.

The particle mass concentration in the gas flow upstream and downstream of the ESPs' was measured by gravimetric method according to the German norm VDI 2066. For the measurements of particle number concentrations in the gas flow, the Scanning Mobility Particle Sizer (SMPS, Fa. Grimm) was applied.

The stability of the operation of the precipitator was ensured by the protection of the high voltage insulator with a screen electrode from the direct particle loaded gas flow. The ESPs' were operated without any additional air input for the high voltage insulators protection from loading with fine particles (Bologa *et al*, 2011).

The CAROLA-precipitators were operated with relatively small electrode gaps in the ionizer at maximum operation voltage of 20 kV and corona current of 1,5 mA. Thus the designed precipitators were characterized by the low power consumption.

The designed CAROLA-electrostatic precipitators are the space-charge ESPs' in which particles are precipitated on the surface of the grounded brush electrodes installed in the collector stage of the unit (Bologa *et al*, 2012). A single brush electrode is currently used in the ESP modules up to 25 kW boiler and double brush electrodes are used in the ESPs' for the boilers with capacity of 50 kW. In the designed modules, the automatic cleaning of the collector stage is realised by the periodical rotation of the brush electrode(s).

Among the control of fine particle emissions, in the current work it is planned to discuss the results of the measurements of the gaseous emissions from the wood combustion boiler and the possibilities for their reduction.

Bologa A., Paur H.-R., Ulbricht T., Woletz K., (2010), *Chemical Engineering Transactions*, **22**, 119-124, DOI: 10.3303/CET1022019.

Bologa A., Paur H.-R., Woletz K. (2011), *International Journal on Plasma Environmental Science & Technology*, **5 (2)**, 168-173.

Bologa A., Paur H.-R., Seifert H., Woletz K., Ulbricht T. (2012), *Management of Environmental Quality: An International Journal*, **23 (**1), 36-55.

Effects of Zn on the physicochemical and toxicological properties of PM_1 in pellet combustion

T. Kaivosoja[1], O. Uski[1,2], H. Lamberg[1], J. Leskinen[1], A. Virén[1], T. Torvela[1], J. Tissari[1], O. Sippula[1], S. Paukkunen[3], M.-R. Hirvonen[1,2], J. Jokiniemi[1,4]

[1]Univ. of Eastern Finland, Department of Environmental Science, P.O. Box 1627, FI-70211 Kuopio, Finland
[2]National Institute for Health and Welfare, Department of Env. Health, P.O. Box 95, FI-70701 Kuopio, Finland
[3]North Karelia University of Applied Sciences, Centre for Natural Resources, Sirkkalantie 12 A, FI-80100 Joensuu, Finland.
[4]VTT Technical Research Centre of Finland, P.O. Box 1000, FI-02044 VTT, Espoo, Finland
Keywords: Zinc, Chemical composition, Combustion particles, Health effects of aerosols.
Presenting author email: Terhi.Kaivosoja@uef.fi

Significant amounts of transition metals such as Zn can be enriched in fine particle fraction in biomass combustion. A hypothesis exists that these metals may have an important role in the toxicity of particulate matter (PM) (Fernandez et al. 2001). However, the influence of the metals on toxicity of PM is not clear. In this study the fuel chemical composition was altered in order to enrich Zn fraction in PM. The aim of this study was to find out Zn behavior in biomass combustion and its role on toxicity of PM_1 (particle aerodynamic diameter <1 µm).

The fuel pellet was doped with Zn so that the concentrations were estimated to be 200, 500 and 2500 mg Zn/kg fuel. Also the reference pellet, which Zn concentration was not altered, was used. In addition, one experiment where the combustion conditions were intentionally degraded was made with 200 mg Zn/kg pellet. The combustion appliance was a pellet boiler (25 kW). Gaseous emissions were measured with FTIR (Gasmet technologies) from the stack. PM_1 samples for toxicological and chemical analyses were collected with Dekati Gravimetric Impactor (Dekati) and PM_1 samples for OC/EC analyses with filter holders (Gelman Sciences 2220) from diluted flue gas. Particle emissions were also measured with on-line measurement instruments: ELPI (Dekati), SMPS (TSI) and TEOM (Thermo Scientific).

The analyzed fuel Zn concentrations are presented in Table 1. With increasing fuel Zn content the size of the fine particles was found to grow and the particle number concentration to decrease. PM_1 emissions were found to increase as the fuel Zn content increased. CO and NO_x were found to decrease as the Zn concentration in the fuel increased.

Table 1. CO, NO_x and PM_1 emissions and GMD results with different Zn concentrations in the fuel

mg/MJ	11 mg/kg (reference)	170 mg/kg poor	170 mg/kg	480 mg/kg	2300 mg/kg
CO	74	340	48	52	41
NO_x	43	30	26	30	19
PM_1	12	42	20	24	57
Zn in PM_1	0.11	2.6	3.2	8.3	48
K in PM_1	2.2	2.6	2.6	2.0	1.7
GMD (nm)	62	129	87	89	145

The studied samples from Zn doped pellet and reference pellet combustion induced a dose-dependent decrease in cell viability (MTT assay). All samples had statistically significant decrease with all doses compared to the control (Fig. 1). Even the reference sample clearly caused cytotoxic effects. However, with the samples where Zn was added the toxicity was more severe.

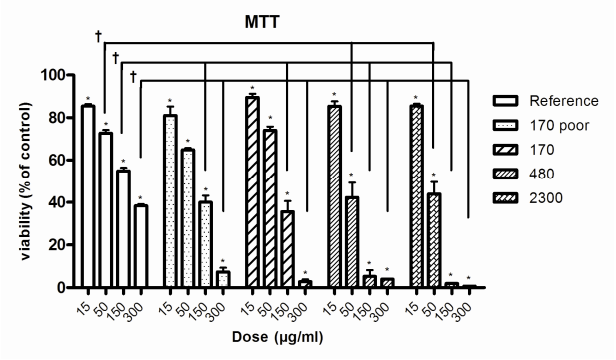

Fig. 1. Viability of RAW264.7 macrophages after exposure to four doses (15, 50, 150 and 300 mg ml^{-1}) of cell medium suspended particles emitted from a pellet boiler (the mean SEM). Asterisks (*) indicate a statistically significant difference from control cells as presented 100 % ($p < 0.05$, Dunnett's test), and crosses (†) denote statistically significant difference between the corresponding doses of the particles from the reference pellet and Zn doped pellet combustion ($p < 0.05$, Tukey's test). n=6 in total.

No major differences between the smallest doses were detected when the Zn doped samples were compared to the reference sample. However, with the 50 µg/ml dose the samples 480 and 2300 had statistically significant difference compared to the reference sample. With the 150 and 300 µg/ml dose all Zn doped samples had statistically different effect to cell viability when compared to the reference sample.

Results indicate that Zn can be one factor of the PM_1 induced health effects in biomass combustion. However, detected cytotoxic effects cannot be entirely explained by the PM_1 Zn content.

Fernandez, A., Davis, S.B., Wendt, J.O.L., Cennit, R., Young, R.S., Witten, M.L. (2001) *Nature*, **409**, 998.

Comparison of particle concentrations measured direct from hot flue gas and diluted sample gas from wood combustion

J. Tissari[1], H. Lamberg[1], O. Sippula[1], J. Jokiniemi[1,2]

[1]Department of Environmental Science, Univ. of Eastern Finland, P.O. Box 1627, FI-70211 Kuopio, Finland
[2]VTT Technical Research Centre of Finland, P.O. Box 1000, FI-02044 VTT, Espoo, Finland
Keywords: Aerosol sampling, Dilution, Wood combustion, Fine particles
Presenting author email: jarkko.tissari@uef.fi

Residential wood combustion (RWC) for heat production has been found to be a major source of e.g. fine particle mass emissions, but also polyaromatic hydrocarbons and several gaseous pollutants throughout Europe. The Air Quality Directive (2008/50/EC) sets stringent requirements on maximum levels of particle matter in the ambient air and thus, also stringent emission limits for RWC appliances have been recently set in different countries. However, there are significant problems in executing of emission reduction actions, because in RWC the obtained emission factor and chemical composition of the particle mass is strongly dependent on the measurement technique used. The most important question is, whether the sampler collects organic material or not. In many standard measurements, the particulate mass emission is measured directly from hot flue gas which gives too low emission factor because organic vapours partially penetrate the filter in a gaseous form. Because different measurement methods are used within Europe and national emission limit values are strongly connected to the measurement method, comparison of different methods and finding of relevant methods to determine particle matter emissions from RWC appliances is needed.

In this study, two different measurement methods were compared in two types of masonry heaters. In the conventional masonry heaters (CMH) there was no air staging (led to high organic emissions) while in the modern masonry heaters (MMH) the air supply was divided to primary air and secondary air (low organic emissions).

The PM (dust) samples were collected directly from the hot flue gas according to the EN 13284-1 standard. The fiberglass filters were heated before and after the sampling at temperature of 160 °C, stabilized for 4 h in desiccator and were weighed using a balance of 1 mg sensitivity. For fine particle measurements, a partial sample flow from the stack was led to the two step dilution system (Tissari et al., 2007) with porous tube diluter (PRD) and ejector diluter (ED). The PM_1 samples were collected on filters from diluted gas using a pre-impactor and the filter holders. The PM_1 samples for gravimetric and elemental analyses (IC, ICP-MS) were collected on Teflon membrane filters and for organic (OC) and elemental carbon (EC) analysis on quartz fiber filters. Also particle number emissions, number size distributions and mass size distributions were measured. The gaseous compounds were measured continuously with an analyzing rack for CO, CO_2, NO_x and O_2 and the organic gaseous substances (OGC) with a flame ionization detector.

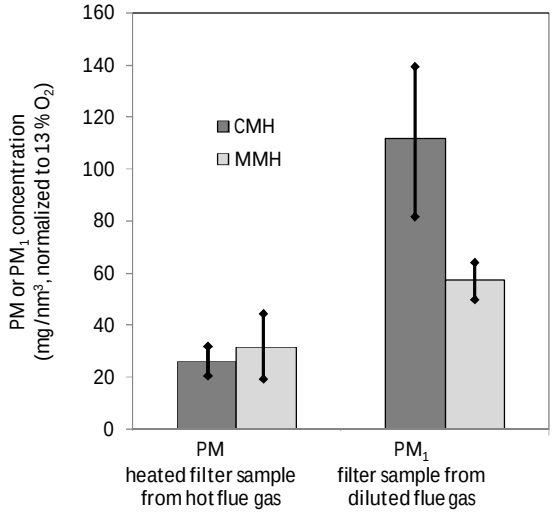

Fig.1. Comparison of PM and PM_1 measured from hot and diluted flue gas.

Table 1. OC, EC and fine ash concentrations in CMH (n=2) and MMH (n=5) appliances (mg/m^3, norm. to 13 % O_2 ± standard deviation) measured from diluted gas.

	OC	EC	Fine ash
CMH	60±20	50±30	3±2
MMH	20±7	33±8	3.4±1.1

PM_1 concentration (diluted and weighed sample) was 1.1 to 4.4 –fold as compared to total PM concentration collected from hot flue gas (Fig. 1) and it was not connected to the combustion quality (Table 1). The PM had also relatively large variation which can be due to several reasons. First, there were losses in the PM sampling, because rinsing of the sampling probe was not performed and the filters were heated after the sampling. Second, random existing of coarse particles in the flue gas is depending more on appliance structure and flow rates in the firebox than combustion conditions. Thus, the results indicate that particle emission measured from diluted flue gas is better connected to combustion efficiency i.e. highest PM_1 emissions with highest CO, OGC, EC and OC levels.

Tissari, J., Hytönen, K., Lyyränen, J. & Jokiniemi, J. (2007). *Atmospheric Environment*, 41, 8330–8344.

Continuous flow reactor for a defined measurement of the SOA formation potential of wood burning emissions

A. Keller, H. Burtscher
Institute for Aerosol and Sensor Technology, University of Applied Sciences Northwestern-Switzerland,
5210 Windisch, Switzerland
Keywords: SOA (Second. Organic Aerosols), Wood Combustion, Emissions, Measurement (characterization).
Presenting author email: alejandro.keller@fhnw.ch

Wood burning emissions, specially emissions from small combustion installation (SCI), contribute largely to the environmental particulate matter pollution. Current legislation considers only the control of primary particulate matter emissions and carbon monoxide. However, wood burning also produces organic gaseous carbon (OGC), that undergoes photooxidation and aging in the atmosphere and forms particles referred to as secondary organic aerosol (SOA, Grieshop et al., 2009; Heringa et al., 2011). Ambient measurements also show the importance of the organic fraction, which can reach values over 80% and become by far the single largest contributor to ambient anthropogenic particulate matter pollution (Szidat et al., 2007). For these reasons, it is desirable to monitor and limit the emissions of OGC and, ideally, base this control on its SOA production potential. There is however no standard tool for that.

We present a compact photo-oxidation continuous flow reactor as a conditioning system for real time monitoring of the SOA production potential of SCI. The SOA produced in our reactor can be measured using standard aerosol monitoring devices. We have tested our method using the gas phase emissions from different residential wood burning installations. The SOA production of our reactor expressed as an emission factor, in terms of SOA mass per emitted CO_2, closely matches the values found in the literature for smog chamber experiments. A short residence time of the order seconds allows us to give a time resolved picture of the emissions (see, e.g., figure 1).

The question of dimensioning the system in terms of requirements for light intensity, residence time and dilution is not trivial. If the system is not well dimensioned, a low OGC concentrations could result in a reduced SOA production rate whereas high OGC concentrations may not be completely transformed inside the reactor. Both cases will result in an underestimation of the SOA production potential.

We will present experiments using different wood burning devices, settings for dilution and residence time, and various UV wavelengths. Our results suggest that it is not enough to measure OGC or CO to establish the potential SOA formation. However, a photo-oxidation continuous flow reactor could be incorporated in type approval testing and emission control measurements as a way of including SOA in the legislation for emission control of SCI.

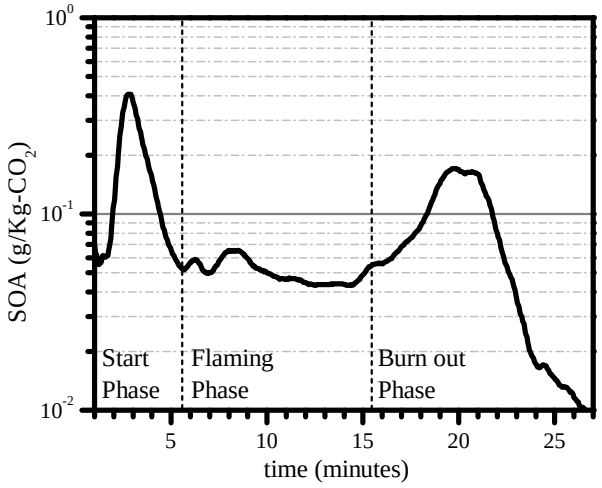

Figure 1: Time resolved SOA emission factor for a cold start from a log-wood stove as measured after a 3 second exposure to UVC followed by 3 seconds exposure to UVA.

This research was supported by the Swiss Federal Office for Energy (SFOE), the Swiss Federal Office for the Environment (FOEN) and the IMBALANCE project of the Competence Center Environment and Sustainability (CCES) from the ETH Zurich.

Grieshop, A., Logue, J., Donahue, N., and Robinson, A. (2009). *Atmos. Chem. Phys.*, 9:1263–1277.

Heringa, M., DeCarlo, P., Chirico, R., Tritscher, T., Dommen, J., Weingartner, E., Richter, R., Wehrle, G., Prévôt, A., and Baltensperger, U. (2011). *Atmos. Chem. Phys.*, 11:5945–5957.

Szidat, S., Prévôt, A., Sandradewi, J., Alfarra, M., Synal, H.-A., Wacker, L., and Baltensperger, U. (2007). *Geophys. Res. Lett.*, 34:L05820.

A two component optical absorption model for interpretation of different combustion conditions

Tanja Dobovičnik[1,2], Heidi Bauer[2], Hans Puxbaum[2], Andreas Petzold[3], Amir Ibrahim[3], Regina Hitzenberger[4], Griša Močnik[1]

[1]Aerosol d.o.o., Kamniska ulica 41, SI-1000 Ljubljana
[2]Vienna University of Technology, Getreidemarkt 9, A-1060 Vienna
[3]Institut für Physik der Atmosphäre, DLR, 82234 Oberpfaffenhofen, Germany
[4]Vienna University, Boltzmanngasse 5, A-1090 Vienna

Presenting author email: tanja.dobovicnik@aerosol.si

Brown carbon (BrC) originating from biomass combustion is very relevant in terms of health and climate. Light absorbing carbonaceous aerosols in general and black carbon (BC) in particular are all products of incomplete combustion. Optical methods are used for their detection and increased absorption in the short wavelength region (relative to black aerosols) is interpreted as presence of BrC.

We used an aerosol generator (CAST propane flame burner) as a source of aerosols, together with on-line measurements (Aethalometer Model AE31; TSI nephelometer 3563) and off-line measurements, performed on quartz fiber filters. The CAST burner was used as a model for combustion of carbonaceous fuels with varying ratio between the carbon in fuel and oxygen, available for combustion (C/O ratio). The study used a two component model to identify BrC and BC contributions to absorption, the Aethalometer model. The different wavelength dependence of the BC or BrC absorption coefficient (b_abs,i), proportional to $\lambda^{-\alpha(i)}$ (where λ is the wavelength and $\alpha(i)$ is the absorption Angstrom exponent of $i=BC, BrC$) was used to discriminate between BrC and BC (Sandradewi et al., 2008):

$$b_{abs}(\lambda) = b_{abs,\,BrC}(\lambda) + b_{abs,\,BC}(\lambda) \qquad \lambda = 470\ nm,\ 880\ nm \quad (1,2)$$

$$\frac{b\_abs,BrC(470)}{b\_abs,BrC\ (880)} = \left(\frac{470}{880}\right)^{-\alpha(BrC)} \quad (3)$$

$$\frac{b\_abs,BC(470)}{b\_abs,BC\ (880)} = \left(\frac{470}{880}\right)^{-\alpha(BC)} \quad (4)$$

We assumed the Angstrom exponent of pure BC α_{BC}=1, while α_{BrC} = 4.56 was determined from the experiment data, assuming that in the experiment with C/O=0.6, only BrC was generated (see Figs. 1 and 2). Values for $b_{abs,BrC}(470)$, $b_{abs,BrC}(880)$, $b_{abs,BC}(470)$, and $b_{abs,BC}(880)$ were computed with equations 1-4, using experimental data.

High α-values, up to six, were observed in the conditions with C/O ratio 0.60, in measurements with C/O ratio 0.21 we observe α value with values between 1.2 and 1.8. Contributions of BC and BrC for different values of C/O ratio were determined, two extreme examples C/O=0.21 and 0.6 are shown on Fig. 2. We see that for combustion conditions with high C/O, absorption from BrC dominates and can even surpass the BC absorption at low C/O conditions.

Biomass combustion in simple stoves, open fireplaces and forest fires also takes place at unfavorable C/O values. In our model we show that the absorption of BrC in such combustion processes needs to be taken into account when modeling climate effects of biomass combustion.

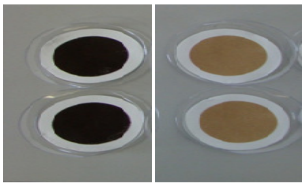

Fig. 1: Filters after sampling the exhaust air of C/O ratio 0.21 (left) and C/O ratio 0.60 (right).

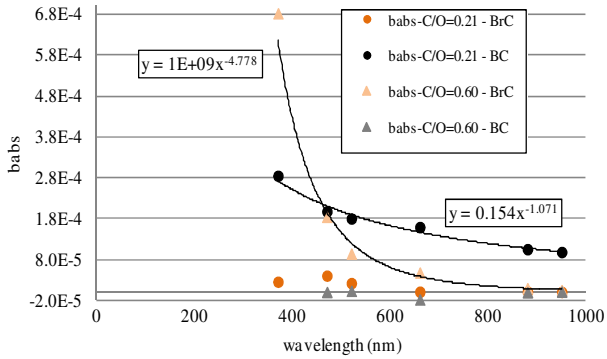

Fig. 2: Scatter plot of $b_{abs,BrC}$ and $b_{abs,BC}$ (1/m) at C/O ratio = 0.21, and of $b_{abs,BrC}$ and $b_{abs,BC}$ at C/O ratio = 0.6.

References

Sandradewi, J et al..: Using aerosol light absorption measurements for the quantitative determination of wood burning and traffic emission contributions to particulate matter, Environ. Sci.Technol., 42, 3316-3323, 2008.

Acknowledgements

Operation in part financed by the European Union, European Social Fund (P-MR-09/1). Part of this work was supported by the European Aviation Safety Agency under Contract EASA.2009.OP.18

Heavy metals contained in the Particulate Matter emitted from Foundries.

J.J. Rodríguez-Maroto[1], J.L. Dorronsoro-Arenal[1], D. Sanz-Rivera[1], E. Rojas-García[1], M. Fernández-Díaz[2], P. Galán-Valera[2] and E. Conde Vilda[2].

[1] Departamento de Medioambiente, CIEMAT, Avda. Complutense 40, 28040, Madrid, Spain
[2] Departamento de Tecnología, CIEMAT, Avda. Complutense 40, 28040, Madrid, Spain
Keywords: foundry, smelter, emissions, heavy metals, PM10, PM2.5, PM1
Presenting author email: jesus.maroto@ciemat.es

A big number of studies have showed the risk for the health and the environment of the fine and ultrafine particles issued from industrial sources. But this effect is not only due to the size of particles but also to their chemical composition by to the presence of specific toxic elements, as heavy metals. The metals are emitted both in elemental and compound (organic and inorganic) forms from many industrial process, that include among others the foundries.

These metallurgical processes represent one of source of the particles, and information regarding these emissions, including particle size distribution and metal partitioning between different particle sizes are likely important parameters to take into account in order to establish strategies to control the emissions.

In this study, the emissions of four sectors of Spanish metallurgy were investigated, zinc, copper, aluminium and steel and as part of it is included the distribution of metals by particle size in the emissions from fusion process. A total of 31 individual measurement results were obtained.

Table 1. Installations analyzed in this study.

Metallurgy		Nº of Installations
Primary º	Aluminium	3
	Copper	1
	Zinc	1
Secondary	Aluminium	13
	Copper	4
	Steel	7

Sampling and measurement was carried out in accordance with US EPA 201A and VDI 2066/5 procedures using three types of cascade impactors: Mark III and DEKATI 30LPM or KS207 Kalman System GMBH. The samples of collection substrates were chemically analyzed according to method EPA IO-3.1 as previous step to the determination by ICP-OES and/or ICP-MS and FAAS

Mass of particle and heavy metals, which apply a minimum threshold for releases to the atmosphere according to European Pollutant Release and Transfer Register (E- PRTR) were determined. Four ranges of particle aerodynamic diameter were analyzed, dp (in microns): dp>10, 10>dp>2.5; 2.5>dp>1; dp<1 and consequently PM10, PM2.5 and PM 1 could be studied.

The relationship between the mass of particles of a certain size (PM1, PM2.5, PM10) to the mass Total Particulate Matter (TPM), as well as the relationship between the mass of each metal found in a range of size and its total mass, are compared.

As an example, the results corresponding to PM1 size range are showed below. *(Specific values are avoided due to confidentiality agreements)*.

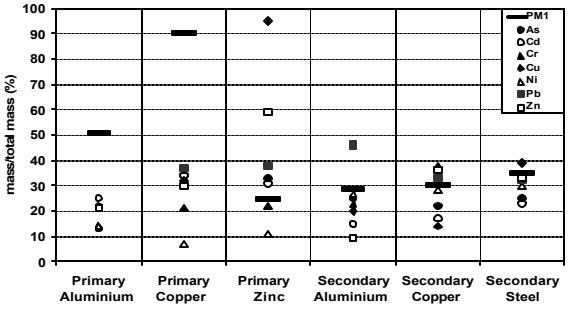

Figure 1. Ratio PM1/TPM and mass ratio of metal in PM1 to metal in TPM, versus foundry type.

In this size interval, the relation PM1/TPM varies in a wide range and you can see an enrichment or impoverishment of metals in this particle size depending on type of foundry. So in most of smelters, metals do not enrich PM1 particles, except for the primary zinc and secondary cooper foundries.

Knowledge of the distribution of heavy metals by size would allow perform a selective separation of particles containing metals of particular interest, either for its high toxicity or for being catalyst in the formation of other pollutants. This implies progress in the design of advanced systems for the control of emissions, based on the one hand in the multifunctionality of the equipments and on the other one the adaptation of emissions to separation and filtration conditions.

This work was supported by the Ministry of the Environment and Rural and Marine Environs. Special thanks to each one of the staffs of facilities.

European Commission. (2001). *IPPC. BREFT on BAT in the Non Ferrous Metals Industries*
European Commission. (2005). *IPPC. BREFT on BAT in the Smitheries and Foundries Industry.*
European Commission. (2006). *Guidance Document for the implementation of the European PRTR.*
Neil R Passant et al. (2002). *UK Particulate and Heavy Metal Emissions from Industrial Processes*. AEAT-6270 Issue 2
Ehrlich C. et al. (2007). *Atmospheric Environment 41* (2007) 6236–6254.

Coagulation of Combustion-Formed Nanoparticles in Medium Temperature Regime

M. Sirignano, and A. D'Anna
Department of Chemical Engineering, University of Naples, Naples, Italy
Keywords: nanoparticles, coagulation.
Presenting author email: marianosirignano@yahoo.it

Coagulation of combustion formed nanoparticles is a key issue in combustion and aerosol science (Smoluchowski, 1916, Bockhorn *et al*, 2007). It is widely known that this process controls the size distribution of the particles emitted from combustion sources and their evolution in the atmosphere.

Many insights have been gained on particle coagulation from in-situ optical measurements and on-line differential mobility analysis of the particles formed in combustion at high temperatures. Experiments have shown that nanoparticles with sizes lower than 10nm have a very low coagulation rate at flame temperatures with respect to that estimated by the gas-kinetic theory, allowing them to long live in the exhaust of combustion systems and be emitted and diluted in the atmosphere before coagulation occurs.

Experimental data have driven modelling attempts to determine the coagulation efficiency mostly based on the long-range interactions between colliding particles, their size and composition (Hamaker, 1937, D'Alessio *et al.,* 2005).

The temperature regimes of combustion plumes, i.e. conditions in which particle coagulate before being diluted and emitted in the atmosphere, are significantly different from flame temperatures as well as ambient temperature and particle coagulation in such conditions has never been measured. The aim of this study is to experimentally study the process of particle coagulation in temperature conditions (intermediate) typical of the plume of combustion devices. To this end a tubular reactor with a residence time of 1.65s, which can be operated at different temperatures up to 650K, is used. Particles, generated by premixed ethylene/air flames with equivalence ratios across the soot threshold limit, are fed to the tubular reactor allowing them to coagulate. The wide range of equivalence ratios used allows us to produce particles with very different size distributions, concentrations and chemical and morphological characteristics.

The evolution of the size distribution functions of the particles for effect of the change of the reactor temperature is measured by a differential mobility analyser with high sensitivity in the 2-100nm size range.

Particles exhibit different coagulation efficiency for the different operating temperatures. At room temperature, 2nm particles coagulate forming particles as large as 10-20nm, whereas at higher temperatures, particles size distribution does not change with respect to that measured at the entrance of the reactor. This turns in very ineffective coagulation. Larger particles (sizes larger than 10nm, do not exhibit high sensitivity to temperature, maintaining very effective coagulation efficiencies in the entire temperature range investigated.

Numerical simulations have been performed and a size dependent coagulation efficiency retrieved. The results confirm the also at low and intermediate temperature regimes, the use of a size dependent coagulation efficiency expression is mandatory to match the evolution of the particles during coagulation.

Additional information has been obtained on homogeneous and heterogeneous condensation of large polycyclic aromatic hydrocarbons by adding them in the tubular reactor in order to simulate exhausts conditions more similar to real systems. These latter results open the sight on a formation pathway that can be fundamental in certain flame conditions and in the post combustion zone of real combustion systems.

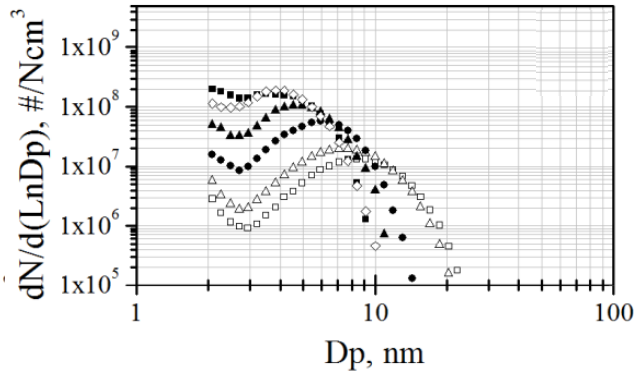

Figure: Evolution of the size distribution of particles generated in flames for fixed residence time (t=1.65s) and different temperatures in the reactor: inlet conditions (300K, t=0s (■), and 300K(□), 400K(△), 500K(●), 600K(▲), 650K(◇), t=1.65s.

H. Bockhorn, A. D'Anna, A.F. Sarofim, H. Wang, (Eds.), Combustion Generated Fine Carbonaceous Particles ,Karlsruhe University Press, Karlsruhe 2009

A. D'Alessio, A.C. Barone, R. Cau, A. D'Anna, P. Minutolo, Proc. Combust. Inst. 30 (2005) 2595–2603.

H.C. Hamaker, Physica 4 (1937) 1058

M.V. Smoluchowski, Phys. Z. 17 (1916) 557–585

Nucleation and growth of welding fumes on the vicinity of the welder: Implications on health effects assessment and protection strategy

Marroquin ML[1], C. Gutierrez-Canas[1], Egizabal[2], Aragon G. [1], Mugica I. [1], Casas N. [1], Flor B. [1] and Larrion M. [1]

[1]Department of Chemical and Environmental Engineering, University of Basque Country, Bilbao, 48011, Spain
[2]TECNALIA, Donosti, Postcode, Spain
Keywords: Welding fumes, nanostructure, nucleation, health effects.
Presenting author email: cristina.gutierrezcanas@ehu.es

Exposure to welding fume has been associated with both pulmonary and systemic health endpoints (Antonini, 2003). This has strong implications on booth design and protective equipment/materials. Regulations in industrialized countries specify a limit for total welding fume, e.g. 5 mg/m3 (TWA). Not very often, limits are identified for particular metals. The carcinogenic activity of welding fumes has usually been related exclusively to chemical features, in particular to the amounts of Ni and Cr in the bulk sample (McNelly *et al*, 2004). However, this approach does not take into account other important features, such as the structural distributions of metals or the surface characteristics (Moroni *et al*, 2009).

For both spatial and temporal variability are significant, a consensus about sampling strategies is crucial, probably depending on the intended results. (Lee *et al* 2007) report size distributions at different locations (Horizontal welding), concluding on differences of up to 3 orders of magnitude in the size range of 100-200 nm.

Earlier works study the temporal and spatial variability within experimental booths (Zimmer *et al*, 2001) and physicochemical characterization of fumes (Moroni *et al*, 2009). As stated in (Zimmer *et al*, 2001) "The arc welding aerosol is similar to a combustion aerosol and will be significantly altered with respect to where it is sampled". Therefore, the main aims of this work are: a more deeper understanding of the influence of welding process on aerosol characteristics and the study of the evolution of undisturbed.

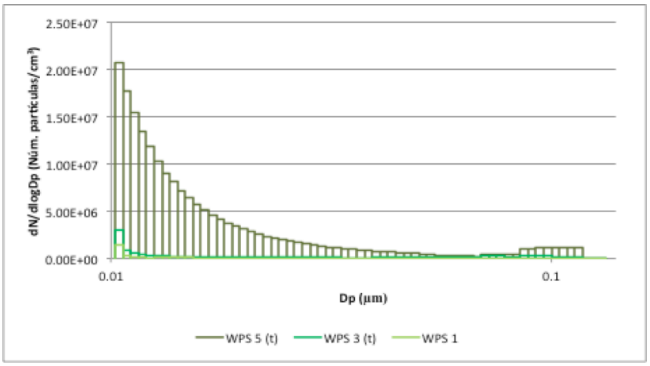

Figure 1. Mobility diameter distribution (as measured by scanning –WPS, MSP Corp) of the undisturbed plume, measured at 1,3 and 5 meters far from the welder.

Sampling and analytical methods have been described elsewhere (Gutierrez-Canas *et al*, 2011). To evaluate the gas to particle conversion rates, three SMPS systems (Figure 1) operate at fixed positions (1, 3 and 5 m far from the welder). Here are presented results for stainless steel welding (SS x5 Cr Ni 18 10) and two different welding processes: MIG (Metal Inert Gas) and SMAW (Shield Metal Arc Welding). Cascade impactors were used to collect size-seggregate samples. A MOUDI (MSP Corp) was used to collect the samples for toxi- and cito- analysis, whereas a HFI (MSP Corp) was used to collect samples for further elemental (ICP/MS) and mineralogical (XRD) analysis. TEM grids were located directly on a NAS (TSI Inc.) at different positions.

Welding procedure has been established as a critical factor for aerosol physics and chemistry. Figure 2 shows an example: whereas SMAW aerosol consists of spinel-like oxides formed during cooling and agglomerates of magnetite-like particles, MIG aerosol is structured by multiphase aggregates of globular to plate-like crystals characterized by variable amounts of different metals and slag-forming elements.

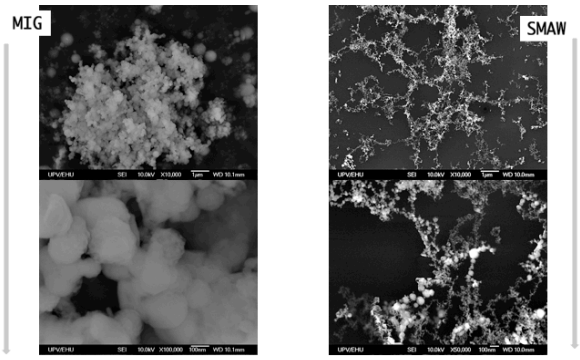

Figure 2. SEM images of stainless steel fume. (Left) Using a flux (Right) Using a inert gas shielding.

Chemical (speciation of toxics) and toxicological data will be discussed as size-seggregated ones.

This work was supported by the Basque Governments (Eusko Jaurlaritza) under grant NANOSOL 2009-2012.

Antonini JM (2003) Health effects of welding. Crit Rev Toxicol 2003, 33:61-103.
Gutierrez-Canas C. *et al.*, The effect of dilution and cooling on the chemistry and structure of samples from stainless steel and Al welding fumes, EAC 2011, Manchester
Lee M.-H., *et al.* (2007) J. Nanoparticle Research **9**:127-136
McNeilly JD *et al* (2004) *Toxicol Appl Pharmacol.*, **196:**95-107.
Moroni B. and Viti C. (2009) Aerosol Science **40**, 938-949
Zimmer A.T. and Biswas P., J. Aerosol Science 32(2001), 993-1008

Thursday, September 6, 2012

WG05S2O. Carbonaceous aerosol and wood burning contribution to PMx

Levels of carbonaceous aerosols in remote, rural, urban and industrial sites of Spain

Querol X.[1], Alastuey A.[1], Viana M.[1], Moreno T.[1], Reche C.[1], Minguillón M.C.[1], Ripoll A.[1], Pandolfi M.[1], Amato F.[1], Pérez N.[1], Pey J.[1], Cusack M.[1], Vázquez R.[1], de la Rosa J.[2], Sánchez de la Campa A.[2], Rodriguez S.[3], Pío C.[4], Alados-Arboledas L.[5], Titos G.[5], Atíñano B.[6], Salvador P.[6], García Dos Santos S.[7], Fernández Patier R.[7]

[1.] Institute of Environmental Assessment and Water Research, IDAEA, CSIC, Barcelona, Spain. [2.] University of Huelva, Spain. [3.] Izaña Observatory, AEMET, Santa Cruz de Tenerife, Spain. [4.] Aveiro University, Portugal. [5.] University of Granada, Spain. [6.] CIEMAT, Madrid, Spain. [7] Instituto de Salud Carlos III, Madrid, Spain.

The objectives of this study is interpreting the time and spatial variability of ambient air levels of particulate non mineral carbon (nmC), organic and elemental carbon (OC and EC) and BC in rural/remote, industrial, urban and traffic environments across Spain. To this end data obtained with similar methods in 72 monitoring sites across Spain in the period 1999-2011 is compiled and interpreted. Major focus on: a) Mean concentration ranges for nmC, OC, EC, BC reached in the above environments; b) Inter-annual and seasonal trends; c) OC/EC ratios; d) BC/EC ratios; e) possible origins of OC and EC. We obtained data on nmC from 72 monitoring stations across the Iberian Peninsula (IP), the Balearic and Canary Archipelagoes and the Spanish Northern African territories. For OC and EC we obtained data from 32 sites. The determinations were carried out in PM10, PM2.5 and PM1 samples. Below are summarized the sites from which we obtained Cnm, **OC/EC and BC** levels (**the two latter in bold and bold underlined letters,** respectively):

- 2 remote sites at NE Iberian Peninsula (**Monstec**) and the canary Islands (**Izaña**)
- 9 rural/regional background sites in the IP, including **Montseny, Monagrega**, Bemantes, El Perdón in the northern part of the IP Cortijo Endrinales, **San Jorge** in the central IP and Matalascañas, Valverde and Campillo in SW IP.
- 8 industrial-rural or industrial-suburban sites including **Ponferrada**, Plaza Castillo-Almeria and Poblado-Córdoba (power generation) and Torrelavega (chemical industry) in N IP, **Monzón** (metal and agro-industry) in NE IP, **Arenosillo** (metallurgy, petrochemical plants and fertilizers) and Punta Umbria (metallurgy and fertilizers) in SW IP and **Santa Cruz** (shipping and petrochemical emissions) in the Canary Islands.
- 19 industrial sites including Tarragona, Puertollano (both with large chemical and petrochemical estates), **Huelva**, **La Linea**, Puente Mayorga, Los Barrios and Aguadulce (with petrochemical and metallurgical estates), **L'Alcora, Onda,** Vila-real**, Borriana** and Almazora (influenced by ceramic and glass manufacture emissions form a large industrial estate), **Bailén** (manufacture of breaks), Llodio, **Bajo Cadagua** and **Zabalgarbi** (metallurgy), **Avilés** (coke production), Torredonjimena and **Montcada** (cement production).
- 7 suburban sites in the IP and the Balearic islands, including Palma, Chapineria, Burgos, Badajoz, Santa Ana-Cartagena, El Vacar-Córdoba, Nerva-Huelva. These are stations located in the outskirts of cities or villages.
- 18 urban background sites including, **Granada, Melilla,** Las Palmas de Gran Canarias, **Albacete**, **Santander**, Alcobendas, **Madrid**, **Barcelona, Sabadell**, Girona, Moguer, Cadiz, Córdoba, Sevilla, Jaén, 2 sites in **Bilbao** and **Zaragoza.**
- 9 road traffic sites in **Sabadell**, Girona, Barcelona, **Madrid**, Granada, Almería, **Barreda-Torrelavega**, **Bilbao** and Cartagena.

In all cases with the exception of the urban background from Madrid measurements were carried out by filter sampling of PMx with high or low volume samplers followed by sample treatment and laboratory analyses.

The presentation summarizes major finding on the interpretation of the time and spatial variability of levels of nmC, EC and OC.

Acknowledgements
This work was funded by the Spanish Ministry of Science and Innovation (VAMOS CGL2010-19464/CLI; DAURE CGL2007-30502-E/CLI, GRACCIE-CSD2007-00067), the Ministry of the Economy Competitivity, the Generalitat de Catalunya, Gobierno de Canarias and Junta de Andalucía.

Long term monitoring of black carbon at eight measurement sites in Switzerland

H. Herich[1], C. Hueglin[1], A. Fischer[1] and B. Buchmann[1]

[1]Empa, Swiss Federal Laboratories for Materials Science and Technology, Duebendorf, Switzerland

Keywords: Black Carbon, Aerosol Light Absorption, Source Apportionment

Presenting author email: hanna.herich@empa.ch

Beside their effects on radiative forcing, soot aerosols have been found to cause health effects as they are carcinogenic. Diesel engines and incomplete biomass burning are the major emission sources of soot particles. Especially during winter, the wood burning (WB) emissions from residential heating have been found to contribute significantly to the soot concentrations (Herich et al. 2011; Piazzalunga et al. 2011).

In this study we present continuous long-term measurements of black carbon (BC) at eight measurement stations in Switzerland from 2007 - 2011. All measurements were performed as part of the Swiss national air pollution monitor network (NABEL) and were either conducted by multi-angle absorption photometers (MAAP) or seven wavelength aethalometers. In addition, twenty-four hour high volume filter samples were collected at all stations in parallel and on a regular basis. The filters were analyzed for elemental carbon (EC) by thermo-optical analysis (TOT with EUSAAR 2 temperature protocol) and for light absorption (at 370 nm and 880 nm) by a SootScan Transmissometer (OT21, Magee Scientific Corporation).

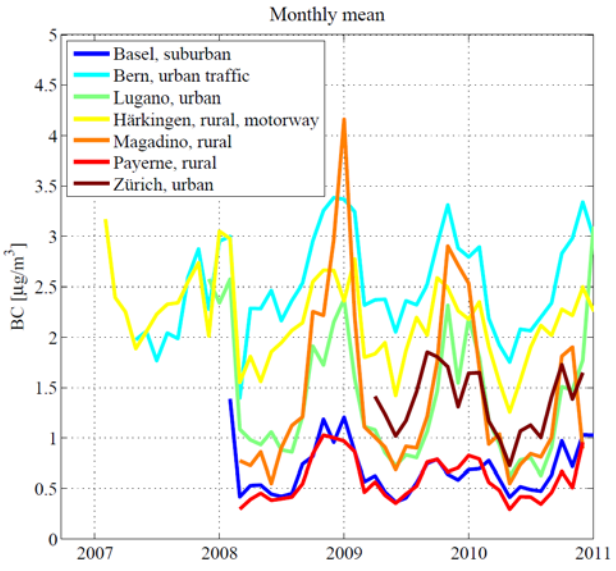

Figure 1. Monthly mean concentrations of BC at different measurement sites in Switzerland.

The site specific aerosol light absorption cross sections were calculated from the relationship between the measured optical absorption coefficient and EC as determined by TOT/EUSAAR 2. Consequently, the presented BC concentrations are consistent with EC. In addition, the aethalometer model (e.g. Sandradewi et al. 2008, Herich et al. 2011) is used for determination of the contribution of fossil fuel and WB emissions to total BC. Mean BC concentrations were highly dependent on the type of location, highest soot loadings were found at urban and traffic related sites, see Figure 1. The annual average concentration levels of BC ranged from 0.6 µg/m^3 (rural station) to 2.6 µg/m^3 (urban kerbside). At all stations the soot concentrations indicated a strong seasonal dependence with highest concentrations in winter compared to the other seasons. The contribution of WB emissions to total BC is negligible during summer but can contribute to more than 30% in winter at rural stations.

This study represents part of the research project IMBALANCE funded by the Competence Center Environment and Sustainability of the ETH Domain (CCES). Support from the Swiss Federal Office for the Environment (FOEN) is gratefully acknowledged.

Herich, H., C. Hueglin, and B. Buchmann (2011), A 2.5 year's source apportionment study of black carbon from wood burning and fossil fuel combustion at urban and rural sites in Switzerland, *Atmos. Meas. Tech.*, 4, 1409-1420.

Piazzalunga, A., C. Belis, V. Bernardoni, O. Cazzuli, P. Fermo, G. Valli, R. Vecchi (2011), Estimates of wood burning contribution to PM by the macro-tracer method using tailored emission factors, *Atmos. Environ.*, 45, 6642-6649.

Sandradewi, J., A.S.H. Prevot, S. Szidat, N. Perron, R. M. Alfarra, V. Lanz, E. Weingartner and U. Baltensperger (2008), Using aerosol light absorption measurements for the quantitative determination of wood burning and traffic emission contributions to particulate matter, *Environ. Sci. Technol.*, 42.

Cartography and long term trends (1998-2011) of polycyclic aromatic hydrocarbons (PAHs) in France

A. Albinet[1], M. Beauchamp[1], G. Harel[1], L. Malherbe[1] and E. Leoz[1]

[1] French National Institute for Industrial Environment and Risks (INERIS), Verneuil en Halatte, 60550, France
Keywords: PAH, Measurements, Ambient air pollution, Aerosol chemistry, Air quality.
Presenting author email: alexandre.albinet@ineris.fr

Polycyclic aromatic hydrocarbons (PAHs) are ubiquitous environmental contaminants widely studied due to their known toxicity. In the atmosphere, they are released in both, gaseous and particulate phases, as by-products from the incomplete combustion of organic matter and fossil fuel. In Europe, these compounds are regulated and their ambient air monitoring is required since 2004 by the introduction of the European directive 2004/107/CE (European Official Journal, 2005) with an application delay for the end of February 2007. A target value for benzo[a]pyrene in PM_{10} (B[a]P – as a marker for the suite of PAH compounds) has been set to 1 ng/m^3 on annual average for every single monitoring station.

As to date, no national cartography has ever been reported for any country and the study of long temporal trends of PAHs is poorly documented in the literature (e.g. Becker *et al.*, 2006; Meijer *et al.*, 2008; Menichini *et al.*, 1999; Schauer *et al.*, 2003). Additionally, to our knowledge, only one recent study reported results about the long term evolution of the contribution of B[a]P to the ambient air PAH mixture (Menichini *et al.*, 1999) while B[a]P was chosen as marker for the suite of PAH compounds.

The objective of this study was first, to realize a French cartography of atmospheric PAHs and to study their spatial and temporal variations concentration and profile (B[a]P/Σ_7PAHs and Σ_7PAHs/PM_{10}) at a national scale. Second, temporal trends were investigated on selected monitoring sites (monitoring periods > 5 years) in relation to emission time trends, location and seasonal effect.

In France, the monitoring of PAHs started in 1998 and a quasi-total coverage of the French national territory is now effective with about 90 sites instrumented for the monitoring of PAHs performed according to the European reference method of measurement EN15549. Concentration data were provided by each local air quality network (AASQA) and then computer processed by INERIS in order to build national cartographies and statistical analyses.

Overall, results obtained showed that, at a national scale, B[a]P annual mean concentration levels are lower than the target value of 1 ng/m^3 (Figure 1). Only industrial sites and some monitoring sites (mainly urban typology) located in specific regions, characterised by their important industrial activity, their relief and/or their geographical location (Nord-Pas-de-Calais (North), Lorraine (North-East) and Rhône-Alpes (East)), showed higher annual mean concentrations. High concentrations levels of PAH observed on suburban sites highlighted the importance of the monitoring of this site typology. The contribution of B[a]P to the mixture of the 7 regulated PAHs (European Official Journal, 2005) seemed stable in annual mean but highly variable between warm and cold seasons in relation to the photochemical activity and PAH source number (e.g. residential heating as additional source of PAHs in winter season) as for PAH concentration levels.

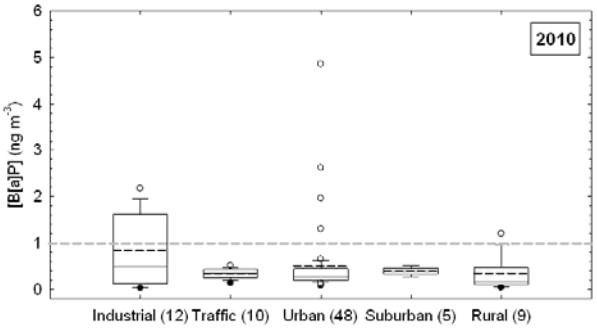

Figure 1. Box plot of B[a]P concentration levels according to the sampling site typology for 2010 in France (number of sites).

A statistical time-series model was used in order to decompose and analyse long term trends of PAHs (equation 1) (Becker *et al.*, 2006).

$$Y_t = T_t + S_t + e_t \qquad \text{(equation 1)}$$

where Y_t is the observed time series, T_t is a longer term trend, S_t is a seasonal component (period of 1 year) and e_t is an irregular or "noise" component. A statistical analysis (seasonal Mann Kendall) was then applied in order to evaluate the existence of a significant trend.

Results obtained showed a statistically significant decrease in PAH concentration levels (- 1 ng m^{-3} in 10 years) for all the selected sites. Moreover, results showed that the choice of B[a]P as representative of PAH chronicle contamination is questionable. Differences of temporal evolution of the contribution of B[a]P to the mixture of PAHs was clearly observed between monitoring sites of different regions. In Ile de France (Paris), the ratio B[a]P/Σ_7PAH increased significantly while the trends were largely decreasing (-50 % in 10 years) in Rhônes-Alpes region (Lyon/Grenoble).

Finally, all the results obtained highlighted the influence of local and regional influencing parameters such as the climatology, the nature of PAH sources and the topography.

This work was supported by the French Ministry of Environment (MEDDTL) and by the French central laboratory of air quality monitoring (LCSQA).

Becker, S.,C. J. Halsall,W. Tych,H. Hung,S. Attewell,P. Blanchard,H. Li,P. Fellin,G. Stern,B. Billeck and S. Friesen. (2006). *Environ. Sci. Technol.*, **40**, 3217-3222.

European Official Journal. (2005). *Official Journal*, **L23**, 3-16.

Meijer, S. N.,A. J. Sweetman,C. J. Halsall and K. C. Jones. (2008). *Environ. Sci. Technol.*, **42**, 3213-3218.

Menichini, E.,F. Monfredini and F. Merli. (1999). *Atmos. Environ.*, **33**, 3739-3750.

Schauer, C.,R. Niessner and U. Poschl. (2003). *Environ. Sci. Technol.*, **37**, 2861-2868.

On the contribution from wood burning to the PM10 aerosol in Flanders, Belgium

W. Maenhaut[1,2], R. Vermeylen[2], M. Claeys[2], J. Vercauteren[3], C. Matheeussen[3] and E. Roekens[3]

[1]Department of Analytical Chemistry, Ghent University, Gent, BE-9000, Belgium
[2]Department of Pharmaceutical Sciences, University of Antwerp, Antwerpen, BE-2610, Belgium
[3]Flemish Environment Agency (VMM), Antwerpen, BE-2000, Belgium
Keywords: PM10, OC, EC, levoglucosan, wood burning.
Presenting author email: willy.maenhaut@ugent.be

From February 2010 to February 2011 PM10 aerosol samples were simultaneously taken every 4th day at 7 monitoring sites in Flanders, Belgium. Two of the sites (i.e., Borgerhout and Gent) were urban background sites; one (i.e., Mechelen) a suburban background site, and the other four (i.e., Hamme, Lier, Retie, and Houtem) rural background sites, whereby Hamme and Lier were expected to be particularly impacted by biomass burning. The samplings were done for 24 h and 47-mm diameter Pallflex® Tissuquartz™ 2500 QAT-UP filters were used. After sampling the PM10 mass concentration was determined by weighing; organic and elemental carbon (OC and EC) were measured by thermal-optical transmission analysis using the NIOSH protocol (Birch and Cary, 1996) and the wood burning tracers levoglucosan, mannosan, and galactosan were determined by means of gas chromatography / mass spectrometry (Pashynska *et al.*, 2002).

The ratios of levoglucosan to mannosan (L/M) and of levoglucosan to the sum of mannosan and galactosan (L/M+G) have been proposed to assess the origin of the wood burning tracers (Fine *et al.*, 2004; Schmidl *et al.*, 2008; Fabbri *et al.*, 2009). The L/(M+G) ratio enables one to discriminate between biomass burning and lignite burning; L/(M+G) values for various source tests for biomass burning range from 0.4 to 18, whereas high ratios of about 50 are indicative of lignite burning (Fabbri *et al.*, 2009). The L/M ratio can be used to assess the relative importance of hardwood and softwood burning. Fine particles emitted from fireplace combustion of woods grown in the midwestern and western United States have L/M ratios in the 13-24 and 3.9-6.7 ranges, for hardwoods and softwoods, respectively (Fine *et al.*, 2004). Schmidl *et al.* (2008) found for fine particle emissions from wood stove combustion of common woods growing in mid-European Alpine regions L/M ratios of around 14-15 for hardwoods, while softwoods gave low ratios, 3.6-3.9. The annual average L/M ratios for our 7 sampling sites ranged from 6.2 to 7.1 and there was little variation with season; for winter and summer campaigns at Gent in 1998 and 2000-2001 (Zdráhal *et al.*, 2002; Pashynska *et al.*, 2002) the campaign average L/M ratios were in the range 4.1-7.2. This suggests that softwood burning was clearly more important than hardwood burning in Flanders in 2010-2011 and that this was also the case at Gent in 1998 and 2000-2001. Incidentally, the annual average L/(M+G) ratios at our 7 sites were in the range 4.5-4.9, while the winter and summer campaign average L/(M+G) ratios for Gent in 1998 and 2000-2001 were 3.4-5.6; these ratios are all within the range of 0.4-18 given above for various source tests for biomass burning.

From our L/M ratios we derived the relative contributions of softwood and hardwood burning, thereby using the same approach as used by Schmidl *et al.* (2008). It was found that softwood burning accounted, on average, for about 70%, and there was little variation in this percentage with site or with season. The levoglucosan data were used to assess the contribution of wood burning to the OC and to the PM10 mass, again following the approach of Schmidl *et al.* (2008). These contributions varied substantially with season (with largest percentages in winter, followed by fall) and there were also substantial differences between the sites, with largest percentages for the rural site of Hamme, where there are apparently large local sources of wood burning. The seasonal medians of the contribution from wood burning to the OC in Hamme were 19%, 5%, 48%, and 62% for spring, summer, fall, and winter, respectively. The percentages of the contribution from wood burning to the OC for 4 of the 7 sites (i.e., Gent, Borgerhout, Lier, and Retie) were very highly correlated with each other (all $r>0.9$), indicating that the impact from wood burning at these 4 sites was a regional phenomenon.

The yearly median percentage of the contribution from wood burning to the PM10 mass ranged from 2.1 to 4.3% for 6 of the 7 sites, but was as large as 8.3% at Hamme. These percentages are somewhat larger than the yearly median percentages of the contribution from EC to the PM10 mass; the latter ranged from 1.6 to 3.3% for 6 of the 7 sites, and was 4.8% at Borgerhout.

Birch, M.E. and Cary, R.C. (1996) *Aerosol Sci. Technol.* **25**, 221-241.

Fabbri, D., Torri, C., Simoneit, B.R.T., Marynowski, L., Rushdi, A.I. and Fabiańska, M.J. (2009) *Atmos. Environ.* **43**, 2286-2295.

Fine, P.M., Cass, G.R. and Simoneit, B.R.T. (2004) *Environ. Eng. Sci.* **21**, 387-409.

Pashynska, V., Vermeylen, R., Vas, G., Maenhaut, W. and Claeys, M. (2002) *J. Mass Spectrom.* **37**, 1249-1257.

Schmidl, C., Marr, I.L., Caseiro, A., Kotianová, P., Berner, A., Bauer, H., Kasper-Giebl, A. and Puxbaum, H. (2008) *Atmos. Environ.* **42**, 126-141.

Zdráhal, Z., Oliveira, J., Vermeylen, R., Claeys, M. and Maenhaut, W. (2002) *Environ. Sci. Technol.* **36**, 747-753.

Contribution of wood burning to the exceedance of PM_{10} limit values in residential areas of the Rhine-Ruhr conurbation (Germany)

U. Pfeffer, L. Breuer and D. Gladtke

North Rhine-Westphalia State Agency for Nature, Environment and Consumer Protection
Wallneyer Str. 6, 45133 Essen, Germany
Presenting author email: ulrich.pfeffer@lanuv.nrw.de
Keywords: PM_{10}, wood combustion, levoglucosan, emission reduction, air quality

European limit values for PM_{10} are still exceeded at many monitoring stations across Europe. 2011 was a year with long lasting episodes with unfavourable meteorological conditions in Germany. These episodes with high pressure, low wind speed and low inversion layers led to outstanding PM concentrations especially during winter/spring and in November 2011.

In order to reduce the PM burden in cities and agglomerations it is essential to have sound knowledge about relevant sources of particles and their contribution to PM levels in the breathing zone.

During the last years wood burning in private homes (open fire places, wood and pellet stoves) became more and more popular. This may be reasonable in respect to climate change (CO_2-neutral), but problematic for air pollution control.

Biomass smoke can be a very important constituent of organic particles in the mid and west European background (e. g. Puxbaum et al., 2007).

Recently, it was demonstrated that also in the large city of Milan wood burning may contribute 6.0 - 16.5 % to the PM_{10} concentration (Piazzalunga et al., 2011).

In densely populated areas of the Rhine-Ruhr conurbation (Germany) extensive measurements of PM_{10} were performed using high volume samplers with quartz filters and low volume samplers with glass fibre filters. In these dust samples concentrations of levoglucosan as a tracer for wood burning were determined. By comparing day (without) and night concentrations (with wood burning) at various sites an empirical factor relating levoglucosan to PM mass originating from biomass burning was evaluated and used for determining PM_{10} shares caused by wood burning. First results show that during unfavourable weather conditions (inversion episodes) like in November 2011 up to 25 % of the measured PM_{10} concentration may be caused by biomass burning in residential areas in the Rhine-Ruhr agglomeration. Even if the contribution of wood burning to annual averages is small (approximately only 1.5 to 2.5 µg/m³), the influence on the number of daily averages exceeding 50 µg/m³ can be very significant, because high wood burning activities logically coincide with low ambient temperatures where PM levels are already elevated due to bad dispersion conditions.

Figure 1 shows PM_{10} concentrations (number of days in exceedance of 50 µg/m³) and its share caused by biomass combustion measured at various sites in North Rhine-Westphalia (NRW) in November 2011 (stations mostly in densely populated cities).

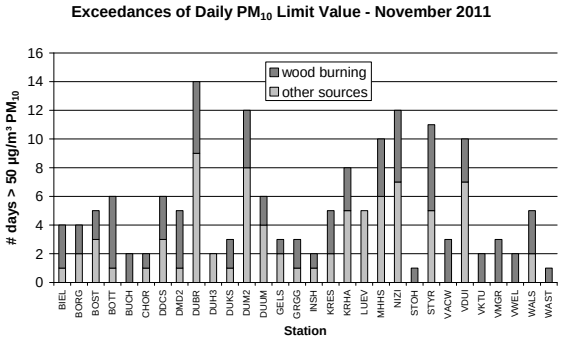

Figure 1. Contribution of wood burning to PM_{10} concentrations in NRW

It can be clearly seen that the number of days with PM_{10} values above 50 µg/m³ could be significantly reduced without wood burning.

Consequently, any measures lowering PM emissions from wood burning in domestic heating installations have a significant potential for the reduction of days exceeding the limit value of 50 µg/m³. In a first step old installations should be replaced or refitted by stoves with modern filter techniques which are already on the market.

Puxbaum, H., A. Caseiro, A. Sánchez-Ochoa, A. Kasper-Giebl, M. Claeys, A. Gelencsér, M. Legrand, S. Preunkert, C. Pio (2007), *Levoglucosan levels at background sites in Europe for assessing the impact of biomass combustion on the European aerosol background*, J. Geophys. Res., 112, D23S05, doi:10.1029/2006JD008114

Piazzalunga, A., C. Belis, V. Bernardoni, O. Cazzuli, P. Fermo, G. Valli, R. Vecchi, *Estimates of wood burning contribution to PM by the macro-tracer method using tailored emission factors*, Atmospheric Environment 45 (2011), 6642 - 6649

A UK-wide assessment of black carbon and PM from wood burning

Gary W. Fuller[1], David C Green[1] and David Butterfield[2]

[1] MRC HPA Centre for Environment and Health, King's College London, London, SE1 9NH, UK
[2] National Physical Laboratory, Teddington, Middx, TW11 0LW, UK
Keywords: PM source apportionment, black carbon, biomass burning, aethalometer.
Presenting author email: gary.fuller@kcl.ac.uk

Introduction

Member states of the European Union are committed to obtain 20% of their energy requirements from renewable sources, including biomass, by 2020 as part of a raft of proposals to reduce CO_2 emissions. In response the UK has announced financial incentives for homes and businesses to switch from fossil fuel to renewables in a strategy to 'de-carbonise' the generation of heat in the UK. Concern has been raised over the possible urban air pollution impacts arising from widespread installation and use of biomass heating. There is a risk that an increase in biomass burning may undermine the achievement of PM_{10} EU Limit Values and the EU exposure reduction target for $PM_{2.5}$. Although PM from biomass burning is a recognised problem in Scandinavian and Alpine countries, according to the UK Digest of Energy Statistics, wood heating in the UK is thought to be too small to quantify. It was therefore felt prudent to confirm this by establishing a baseline for the PM concentration from biomass across the UK.

Methods

Aethalometer measurements (370 & 880 nm, Magee Scientific) were analysed for 2009 and 2010 from background locations in 18 urban areas. Spot loading corrections (Virkkula et al, 2007) were undertaken and black carbon (BC) concentrations were apportioned between fossil fuel and wood burning assuming an Ångstrom absorption coefficient of 2.0 for wood burning and 1.0 for road traffic emissions on the basis of measurements next to a busy central London Road. PM concentrations from wood burning were estimated using coefficients derived by Sandrawei et al, 2008 and Favez et al, 2010 adjusted for the specific wavelengths used.

Results and discussion

Estimates of wood smoke PM were compared to campaign measurements (2 x 6 weeks) of levoglucosan (a wood smoke tracer) in London and gave correlation coefficients (r^2) of 0.76 and 0.77 confirming the ability of the aethalometer to detect PM from this source.

Mean BC concentrations were between 1.6 and 2.0 µg m^{-3} in urban areas in England, Scotland and Wales. Here BC was dominated by fossil fuel sources with wood burning comprising between 6 and 25%. A lower BC concentration of 0.5 µg m^{-3} was found in rural southern England, with 35% from wood burning.

Diurnal analysis of PM form wood burning (Figure 1) shows peak concentrations in each evening indicative of domestic heating. Weekend concentrations exceed weekdays by ratios of up to 1.3 indicating considerable discretionary or decorative wood burning. A lag between rural and urban concentrations shows PM from wood burning diffusing from cities into the surrounding countryside. Overall wintertime wood burning accounted for 5 to 10% of total PM_{10} in mainland urban areas and around 5% in rural southern England.

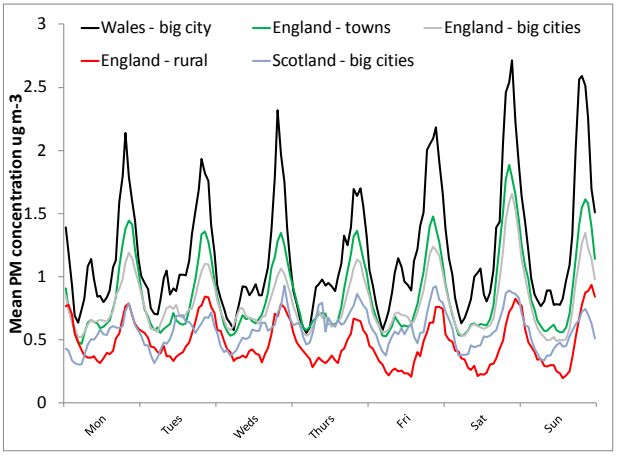

Figure 1 Mean PM from wood burning averaged by hour of day and day of week in England, Scotland and Wales.

Small towns in Northern Ireland are not on the UK natural gas grid. Here fuel use surveys and PAH concentrations suggest that coal burning is prevalent. Coal smoke has an Ångstrom absorption coefficient of around 1.4 (Yang et al, 2009) which would interfere with the aethalometer assessment of PM from wood burning and separate quantification of coal and wood burning is not possible. However, the mean evening Ångstrom coefficient of 1.7 during wintertime suggests a combination of coal and wood burning may be taking place in these areas.

References and acknowledgement

Favez et al . 2010. Atmos. Chem. Phys., 10, 5295–5314; Sandrawei et al 2008. Environ. Sci. Technol. 2008, 42, 3316–3323; Yang et al, 2009. Atmos. Chem. Phys., 9, 2035–2050.

The UK aethlometer network is funded by the Department for Environment Food and Rural Affairs.

Insight into the primary and secondary organic fraction of the organic aerosols in and around Barcelona

B.L. van Drooge, M. Alier, R. Tauler, J.O. Grimalt

Institute of Environmental Diagnostics and Water Research (IDÆA-CSIC), Jordi Girona 18, 08034 Barcelona, Catalonia, Spain
Keywords: Dicarboxylic acids, PAH, Hopanes, Levoglucosan
E-mail contact: barend.vandrooge@idaea.csic.es

Monitoring and chemical analysis of atmospheric fine particulate matter (PM1) is important due to its health impact and influence on climate change (Forster et al. 2007, Pérez et al. 2009). The air quality in the urban area of Barcelona is dominated by traffic related emissions. Moreover, the area is characterized by high levels of particulate matter and reactive chemical species due to emissions, the weak synoptic conditions and high solar radiation (Millán et al. 1997, Pérez et al. 2010). Ambient air filter samples were collected during intensive sampling campaigns during 2009 and 2010 (DAURE and SAPUSS) on urban background site (UB), road sites (RS) and a rural background at 780 m (RB). The samples were analyzed for organic tracer compounds, e.g. polycyclic aromatic hydrocarbons, hopanes, levoglucosan and nicotine, as well as secondary organic aerosols tracer compounds, e.g. dicarboxylic acids, for source characterization and identification of the organic patterns of primary and secondary aerosols. The obtained are compared with "on-line" data, such as those generated with Aerosol-Mass-Spectrometer. The results are discussed in terms of their relation to emission sources and influence of meteorological conditions in order to get an insight on the source contributions to the complex organic aerosol [5].

PM1 filter samples were collected with 12 or 24 hour resolution in background and road site in Barcelona (41º22"N; 2º11"E) and in a rural site in the Monseny natural park, using a Hivol-sampler. Polycyclic aromatic hydrocarbons, hopanes, levoglucosan, nicotine, and dicarboxylic acids were analyzed using GC-MS with TMS derivation of the polar compounds beforehand. Complementary data on meteorological conditions, and air-mass trajectories for the sampled days were recorded. Moreover, statistical tools, such as PCA (Principal Component Analysis) and MCR-ALS (Multivariate Curve Resolution - Alternating Least Squares), were used to analyze the variance in the database.

In the urban area, PCA analysis showed strong correlations between organic compounds separating them in three component groups: those related to primary emissions and those related to secondary aerosols and biomass burning. MCR-ALS analysis also resolved three components (Figure 1). The first component was related to regional air mass circulation and consequently accumulation of secondary aerosols, as well as an influence of regional biomass burning. The second component was related to anthropogenic activities (traffic and tobacco smoke) that was more intense in RS. A third component could be related to food cooking activities, or SOA formation other than described in the first component. The organic tracer compounds, representing the three identified components correlated very well with the organic aerosol analyses of the HR-AMS. From these analyses it was estimated that in UB about 50% of OA is secondary, and probably mainly biogenic, while this was about 40% in RS. Primary sources, mainly traffic, contributed to about 30% to the OA in UB and about 50% in RS.

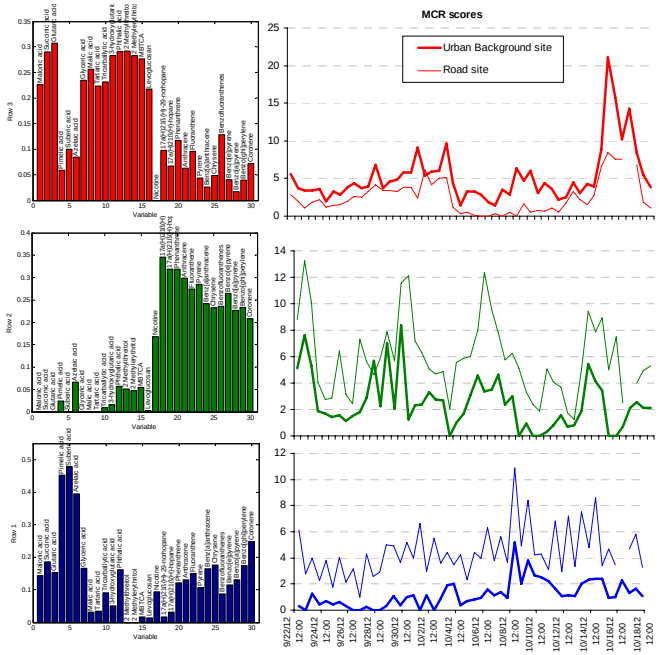

Figure 1. Organic tracer compounds per component (left) and the scores during the sampling days in UB and RS (right).

This work was supported by the scientic research projects GRACCIE (CSD2007-00067), AER-TRANS (CTQ2009-14777-C02-01), SAPUSS (FP7-PEOPLE-2009-IEF), DAURE (CGL2007-30502-E/CLI)

Forster et al. 2007, ISBN: 978 0521 88009-1.
Pérez et al., 2009. Environ. Sci. Technol. 43, 4707-4714.
Millán et al., 1997. J. Geophys. Res. 102, 8811-8823.
Pérez et al., 2010. Aerosol. Sci. Technol. 44, 487-499.
Alier et al., 2011. in preparation.

Thursday, September 6, 2012

Session WG09S2O. Aerosol Modelling: Emission inventories, transport and transformation

A 40-year retrospective high-resolution European radon flux inventory including climatological variability

I. López-Coto[1], J.L. Mas[2] and J.P. Bolivar[1]

[1]Dept. of Applied Physics, University of Huelva, Huelva, 21071, Spain
[2]Dept. of Applied Physics I, University of Seville, Seville, 41012, Spain
Keywords: Emissions, Fluxes, Modelling, Trace gases.
Presenting author email: israel.lopez@dfa.uhu.es

The natural radioactive noble gas radon, ^{222}Rn, is mainly terrestrial in origin and is dispersed in the air by atmospheric transport and mixing. Radon is a noble gas (no deposition, washout or chemical reactions), and the only loss mechanism is radioactive decay so the residence time of radon in the atmosphere is well-known.

The radioactive decay of radon and its progeny can lead to ionization of air molecules and consequently influence aerosol size distribution . Besides, simulating radon transport is currently one of the best tools for evaluating transport schemes in regional-to-global climate /atmospheric models. Yet the usefulness of this tool is limited by the quality of the radon emission rate in soil-to-atmosphere inventories.

In this work, a 40-year retrospective high-resolution European radon flux inventory has been calculated. Average values of the radon exhalation rate, probability distributions and seasonal fluctuations have been obtained. To achieve this, a numerical model of radon transport in finite, heterogeneous and porous media has been developed that has enabled us to calculate the exhalation rate of European soils by using geological, geochemical and climatological parameters with a horizontal resolution of 0.5 ' (~ 1 km).

Model and input databases

The theoretical model is based on the fundamental equation of radon transport in porous media, taking into account the dependency of the transport coefficient on temperature and humidity. It also includes a simple model that evaluates the effect of snow cover.

The Europe-wide scope of the model proposed requires knowledge of the different physical, chemical and thermodynamic parameters of soils with good spatial resolution. Thus, the activity concentration of ^{226}Ra was determined from total uranium concentration which was obtained from the FOREGS geochemical database. The geophysical properties were derived from the Harmonized World Soil Database (HWSD) of the FAO. Data on the temperature, soil moisture and thickness of snow cover have been obtained from the ECMWF's global ERA-40 re-analysis.

Results

In general, the results show wide variations depending on location and season of the year, with a spatial standard deviation close to the annual average value (30 Bq m^{-2} h^{-1}) In turn, the seasonal deviation is about 25% of the annual average value. Systematically lower latitudes exhibit the largest deviations, with greater amplitude in seasonal fluctuations.

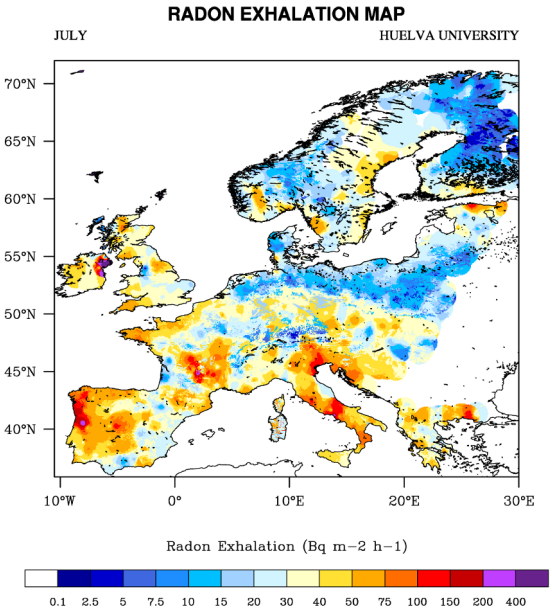

Figure 1. Radon exhalation rate of European soils for July of the composite year (40 years).

Conclusions

A numerical model of radon transport in finite, heterogeneous and porous media has been developed to calculate the exhalation rate of European soils by using geological, geochemical and climatological parameters with a horizontal resolution of 0.5 ' (~ 1 km).

A climatology of radon exhalation has been produced and the average values obtained, along with the probability distributions, seasonal anomalies and a European high resolution radon exhalation monthly average. The results were compared with experimental measurements of radon flux in the literature, and showed good general agreement.

The calculated inventory can be easily integrated into atmospheric transport models and also serve as a high-resolution baseline for policy decisions regarding the determination of areas of high risk of exposure to radon.

Modelling Contribution of Biogenic VOCs to New Particle Formation in the Jülich Plant Atmosphere Chamber

L. Liao[1], M. Boy[1], D. Mogensen[1,2], T. F. Mentel[4], E. Kleist[3], A. K.-Scharr[4], R. Tillman[4], H. Vuollekoski[1], M. Kulmala[1] and M. D. Maso[1,4]

[1] Division of Atmospheric Sciences, Department of Physics, University of Helsinki, Helsinki, 00014, Finland
[2] Helsinki University Centre for Environment, University of Helsinki, Helsinki, 00014, Finland
[3] Phytosphere (IBG-2), Forschungszentrum Jülich, Jülich, 52425, Germany
[4] Troposphere (IEK-8), Forschungszentrum Jülich, Jülich, 52425, Germany
Keywords: BVOCs, H_2SO_4, new particle formation.
Presenting author email: li.liao@helsinki.fi

Biogenic VOCs are substantially emitted from vegetation to atmosphere, and their emissions have been estimated to be of the order of 1150 Tg per year globally (Guenther et al., 1995). Isoprenoids and terpenoids, including e.g. isoprene (C5H8), monoterpenes (C10H16), and sesquiterpenes (C15H24) are the most abundant BVOCs, accounting for over 50% of BVOC emissions (Guenther et al., 1995). The oxidation of terpenes by OH, O_3, and NO_3 in air generating less volatile compounds may lead to the formation and growth of secondary organic aerosol, and thus presents a link to the vegetation, aerosol, and climate interaction system (Kulmala et al, 2004). Studies including field observations, laboratory experiments and modelling have improved our understanding on the connection between BVOCs and new particle formation mechanism in some extent (see e.g. Tunved et al., 2006; Mentel et al., 2009). Nevertheless, the exact formation process still remains uncertain, especially from the perspective of BVOC contributions.

The purpose of this work is using the MALTE aerosol dynamics and air chemistry box model to investigate aerosol formation from reactions of direct tree emitted VOCs in the presence of ozone, UV light and artificial solar light in an atmospheric simulation chamber. The measured chamber data, including both gas and aerosol phase measurements are used to evaluate the model. This model employs up to date air chemical reactions, especially the VOC chemistry, which may potentially allow us to estimate the contribution of BVOCs to secondary aerosol formation, and further to quantify the influence of terpenes to the formation rate of new particles.

Experiments were conducted in the plant chamber facility at Forschungszentrum Jülich, Germany (Jülich Plant Aerosol Atmosphere Chamber, JPAC). The facility consists of three Borosilicate glass chambers (164 L, 1150 L, and 1450 L) with Teflon floors. Either one of the two smaller chambers were served as plant chamber followed by the large chamber as reaction chamber (1450 L). The detail regarding to the chamber facility has been written elsewhere (Mentel et al., 2009). During the experiments, gas phase sulphuric acid was measured by CIMS. VOC mixing ratios were measured by two GC-MS systems and PTR-MS. An Airmodus Particle size magnifier coupled with a TSI CPC and a PH-CPC were used to count the total particle number concentrations with a detection limit close to the expected size of formation of fresh nanoCN. A SMPS measured the particle size distribution. Several other parameters including ozone, CO_2, NO, Temperature, RH, and flow rates were also measured.

MALTE is a modular model to predict new aerosol formation in the lower troposphere, developed by Boy, et al. (2006). In this study, we use modules that include aerosol dynamics, air chemistry, and organic chemistry of VOCs as a MALTE box model for the chamber simulation. Considering that each individual terpene compound may react quite differently, the generalized parameterizations of terpene chemistry in models are less used, and most biogenic VOCs will be accounted for individually when modelling the atmospheric new aerosol formation. We first evaluate the modelled results with measurements, and further we investigate the influence of different order of magnitude of terpene mixing ratios, especially isoprene and monoterpenes to the most important parameter of new particles formation, i.e. the formation rate (J_1). Also, the influence of varying organic source rates on the sulphuric acid concentration available for particle formation is discussed.

The Authors wish to thank the Maj and Tor Nessling foundation for financial support (grant No 2009362), as well as the Academy of Finland (Project No. 128731).

A. Guenther et al., (1995). *J. Geophys. Res.*, 100(D5), 8873–8892.
M. Boy et al., (2006). *Atmos. Chem. Phys.*, 6, 4499–4517.
M. Kulmala et al., (2004). *Atmos. Chem. Phys.*, 4, 557–562.
P. Tunved et al., (2006). *Science*, 14, 261–263.
Th. F. Mentel et al., (2009). *Atmos. Chem. Phys.*, 9, 4387–4406.

Development of emission inventories of recreational boats

Victoria Agranovski

Air Quality Sciences, Department of Environment and Resource Management, Brisbane, 4001, Australia
Keywords: Air pollution modelling, emission inventory, off-road transport, recreational watercrafts
Presenting author email: victoria.agranovski@derm.qld.gov.au

Accurate modeling of air quality can improve understanding of human exposure to ambient pollutants. Characterization of marine traffic emissions is particularly important for modelling air quality and atmospheric processes associated with air pollution in coastal regions. Investigation of individual pollutant sources and source apportionment is especially imperative for developing, monitoring and reviewing environmental policies, regulations and plans to make sure they meet specific requirements. This study was focused on the emissions from recreational vessel traffic as part of developing emission inventory for off-road mobile sources in the State of Queensland, Australia.

Recreational vessels emission inventories were developed for the two regions, Gladstone and the South East Queensland. The inventories were developed from bottom-up surveys of registered boat owners coupled with the local activity data gathered from the State's database on registered marine vessels, for 2006-2011 years. The advantage of using these two complimentary approaches is improved accuracy and reliability of the input data for modelling off-road emissions from this source category. In addition, this approach has enabled development of simplified technique for estimating emission projection based on average per vessel emission rates. This is especially beneficial for estimating air quality in the areas for which the input activity data is limited.

In 2011, there were more than 7,400 and 141,300 recreational vessels registered in Gladstone and SEQ (corresponds to 3 and 53% of State figure), respectively. The five-year trend analysis of relevant activity data revealed that recreational fleet in Queensland consists of vessels with a range of engine size (Fig.1) and fuel type.

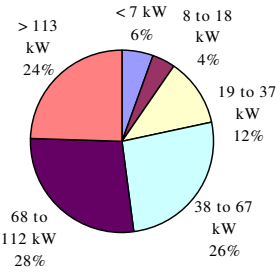

Figure 1. Distribution of vessels by engine power.

The fleet includes trailerable, small vessels (typically less than 8 m) that are launched at ocean or river boat ramps as well as larger, moored vessels, typically above 8 m which are not easily towed. The former includes sailing boats and larger cabin cruisers with auxiliary engines. The vast majority of vessels are however smaller than 8m (95%) and use outboard petrol engines (~88%). Emissions were estimated by applying appropriate emission factors listed in the Australian guidelines for developing emission inventories for recreational boats (Environment, 1999) to fuel usage. Fuel usage in the study regions were estimated from domestic surveys. To enable accurate estimates to be developed the vessels were categorised primarily on their engine/fuel type (Table 1).

Table 1. Annual emissions from recreational boats

Base year	2006	2009	2010	2011
Vessels, #	119,196	136,368	139,926	141,378
Pollutant	Emissions, tonnes/yr			
CO	5727.2	7600.7	8157.6	9963.1
NO_x	136.1	155.7	159.8	161.4
PM_{10}	184.3	210.9	216.4	218.6
$PM_{2.5}$	169.6	194.0	199.1	201.1
SO_2	17.0	19.4	20.0	20.2
VOC	2872.1	3285.9	3371.6	3406.6
1,3 Butadiene	5.8	6.6	6.8	6.9
Benzene	41.1	47.1	48.3	48.8
Formaldehyde	3.9	4.5	4.6	4.6
Xylene	234.6	268.4	275.4	278.3
PAH	8.0	9.2	9.4	9.5
Toluene	191.8	219.5	225.2	227.5

Average per vessel annual emission rates for selected pollutants by fuel/engine type are presented in Table 2.

Table 2. Average per vessel annual emission rates.

Pollutant	Emission rate (kg/vessel/year)		
	Petrol Outboard	Petrol Inboard	Diesel
CO	7.77E+01	5.47E+01	7.02E-01
PM_{10}	2.01E+00	6.80E-01	1.38E-01
$PM_{2.5}$	1.85E+00	6.23E-01	1.35E-01
SO_2	8.72E-02	6.31E-02	5.64E-01
NO_x	9.12E-01	1.26E+00	2.27E+00
VOC	3.15E+01	1.14E+01	2.22E-01
1,3 Butadiene	4.44E-02	9.99E-02	3.73E-04
Benzene	3.93E-01	3.95E-01	3.29E-03
Formaldehyde	2.77E-02	5.66E-02	2.68E-02
Xylene	2.56E+00	1.04E+00	3.80E-03
PAH	7.14E-02	9.50E-02	1.79E-03
Toluene	2.00E+00	1.17E+00	4.79E-03

Environment Australia (1999) *Emission Estimation Technique Manual for Aggregated Emissions from Commercial Ships/Boats and Recreational Boats.*

The Role of Compensating Errors in Reaction-Transport Models of Atmospheric Aerosol

P.A. Makar [1], R. Nissen[2], A. Teakles[2], J. Zhang[1], Q. Zheng[1], M.D. Moran[1], H.Yau[2]

[1]Air Quality Research Division, Environment Canada, Toronto, Ontario, M3H 5T4, Canada
[2]Air Quality Sicence Unit, Environment Canada, Vancouver, British Columbia, V6C 3S5, Canada
Keywords: Modelling (regional), Numerical Simulation, Urban Aerosols, Emissions.
Presenting author email: paul.makar@ec.gc.ca

Three dimensional aerosol models have the goal of simulating atmospheric aerosol formation and removal processes, but the accuracy with which they accomplish this aim will depend on the manner in which the processes are parameterized. Simplifications are often made to the science, and a seemingly arbitrary choice of methodologies can have a significant effect on model accuracy. The choices made to simulate one part of the equations describing aerosol creation and removal may have a profound effect on other parts of the system. This creates the potential for compensating errors in the results of the overall simulation.

In this study, A Unified Regional Air-quality Modelling System, AURAMS, v1.4.2, and the Community Multiscale Air-Quality Model, CMAQ, v4.6, were compared for a domain covering coastal north-western North America. The models were harmonized, with the same emissions inventory, horizontal grid, horizontal resolution (12km), and meteorological input information, for three one-month periods. The focus of the work described here will be the summer 2005 simulation, similar results having been noted for winter 2005 and summer 2004.

The models' performance differed greatly, in contrast with earlier comparisons, and the models were subsequently compared at the process parameterization level. The choice of process simplification and/or parameterization was found to have a profound effect on model results. In the case of AURAMS, revising the operator splitting methodology was shown to reduce positive biases in sea-salt aerosol predictions by a factor of three. For CMAQ, the use of a relatively high minimum cut-off in vertical diffusivity was largely responsible for improved night-time PM performance, but at the expense of reduced accuracy for ozone.

Once these parameterizations were improved and/or the simplifications were removed, it became clear that these choices were compensating for errors associated with the emissions and/or mixing of anthropogenic primary particulate matter. Model emissions were created from US EPA and Environment Canada data using the Sparse Matrix Operating Kernel Emissions (SMOKE) emissions processing system. The inputs for this system include information to allow the spatial and temporal allocation of annual political jurisdiction-based emissions into hourly gridded values, as well as into model-specific chemical species.

Time series showing the diurnal variation in primary PM emissions were reconstructed from SMOKE's library of temporal profiles and the emissions inventory. Some of the main sources of primary PM were found to be emitted at times inconsistent with the emitting activity, and Canadian spatial allocation fields were sometimes mis-assigned or contained errors. Corrections for these problems, updates to the Canadian emissions of ocean-going vessels, and parallel updates to the mobile emissions for the Canadian side of the grid, were incorporated into a second round of emissions generation and model simulations.

A marked improvement in some (though not all) of the $PM_{2.5}$ statistics for the models was noted, as were significant local improvements, though errors in primary PM speciation were still seen in urban regions.

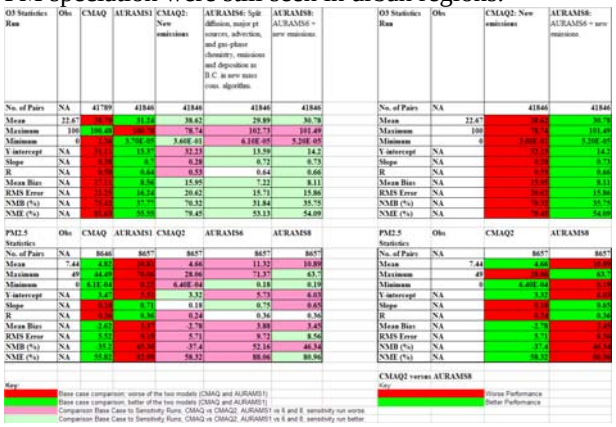

Table 1: Comparative statistics between CMAQ and AURAMS, for O_3 and $PM_{2.5}$, for five different model simulations.

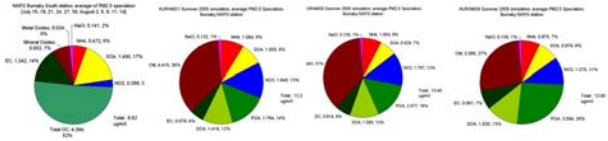

Figure 1: Comparison of particle speciation for Burnaby South Station (left: Observations, right: three AURAMS simulations).

A second examination of the primary PM emissions for downtown Vancouver was launched. A few key sources were found to contribute most of the urban primary PM, with temporal and spatial allocations that were once again inconsistent with expectations for those emitting activities. The effects of improving additional set of allocation factors will be discussed.

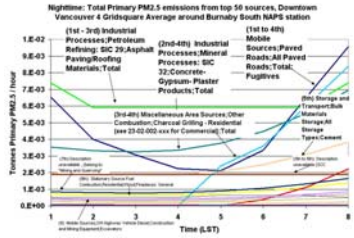

Figure 2: Time series showing major contributors to early morning primary $PM_{2.5}$ emissions in downtown Vancouver, using the first revision of the emissions database.

Application of Process Analysis in the CAMx model for evaluating physical and chemical processes affecting PM in Switzerland

G. Ciarelli, S. Aksoyoglu, J. Keller, D.C. Oderbolz, A.S.H. Prévôt

Laboratory of Atmospheric Chemistry (LAC), Paul Scherrer Institute, Villigen, CH-5232, Switzerland
Keywords: Modelling (regional), Aerosol modelling, Meteorology, Source apportionment.
Presenting author email: giancarlo.ciarelli@psi.ch

In this study, results from the Process Analysis (PA) tool provided with the Comprehensive Air Quality Model with extensions (CAMx) are presented for Switzerland. Process Analysis allows for in-depth analysis of photochemical model performance by revealing the contributions from individual physical and chemical processes operating within the model. This kind of investigation can be useful to improve model performance as well as to develop for control strategies. The process rates are integrated across each model output time interval (hourly). This information provides a complete description of temporal changes in species concentration due to different processes as well as their magnitude.

The air quality model system consists of the meteorological model Weather Research and Forecasting (WRF) version 3.2.1 and the Eulerian photochemical model CAMx version 5.30 (ENVIRON, 2010). A modular script called CAMxRunner was used to perform the simulations (Oderbolz et al., 2012). The model domain had a horizontal resolution of 0.25° x 0.125° and 14σ layer (lowest layer depth: 20m) covering Europe. Details about some of the model inputs are given in Aksoyoglu et al. (2011). We studied two periods in January and June 2006, in order to define the seasonal variation of the physical and chemical processes affecting the PM2.5 concentrations.

We investigated the contribution of the major physical (e.g. boundary advection tracking the inbound or outbound transport of the species) and chemical processes (e.g. production through gas-phase and aqueous chemistry) as well as direct emissions and removal, to the concentrations of particulate nitrate, sulfate, ammonium, primary and secondary organic aerosol in space and time. The focus was on the most populated area around Zurich in the Swiss Plateau.

Variations of processes rate in the vertical layers were also investigated. In particular, the diffusion term was used as a "tracer" in order to identify the layer height to use for the analysis (i.e. from the surface layer to the approximate height of the mixed layer).

Results are used to identify the main processes affecting the PM concentrations in the studied area. They also give us the information about whether particles are locally produced and/or transported from other regions. As an example, changes in sulfate concentration due to various processes are shown in Figure 1 for the first four days in June 2006. In this case advection from west and north directions are dominating over the local production for sulfate during the studied period in that region.

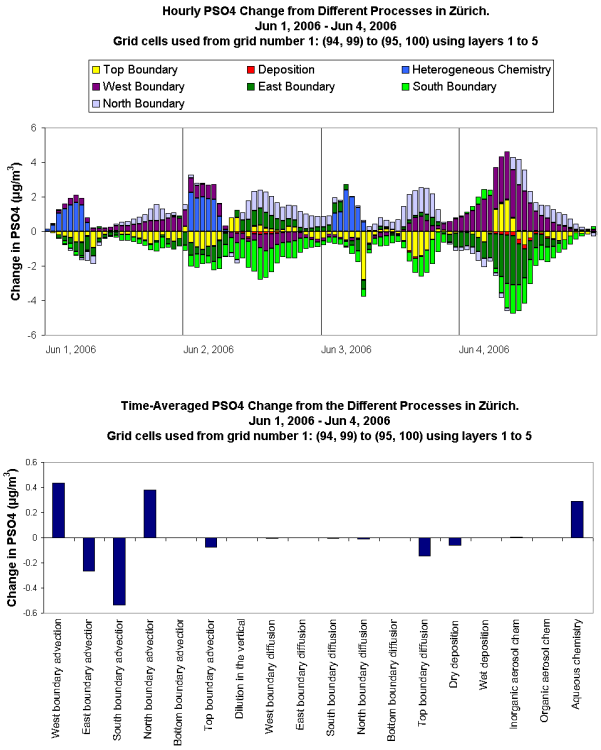

Figure 1. Example of hourly (top panel) and time-averaged (lower panel) change in sulfate due to different processes in Zürich (1-4 June 2006)

This work was supported by the Swiss Federal Office of Environment (FOEN).

Aksoyoglu, S., Keller, J., Barmpadimos, I., Oderbolz, D., Lanz, V. A., Prévôt, A. S. H., and Baltensperger, U. (2011) *Aerosol modelling in Europe with a focus on Switzerland during summer and winter episode*, Atmospheric Chemistry and Physics, 11 (14), 7355-7373.

ENVIRON (2010) U*ser's Guide, Comprehensive Air Quality Model with Extensions (CAMx). Version 5.30*, ENVIRON International Corporation, Novato.

Oderbolz, D. C., Barmpadimos, I., and Aksoyoglu, S. (2012) *CAMxRunner - a modular framework for efficient chemical transport modelling*, International Journal of Environment and Pollutions, in press

Modeling aerosol chemical properties: impact on cloud and precipitation formation

C. Barbet, L. Deguillaume and N. Chaumerliac
LaMP/CNRS, Clermont University, Blaise Pascal University, 24 Av. des Landais, 63177, Aubière, France

As observed at the Puy-de-Dôme monitoring site, which is located at an altitude of 1450m in the center of France, when the number concentration of aerosols is around 450 #.cm^{-3} it is estimated that the air mass is maritime whereas when the number concentration is nearly 2500 #.cm^{-3} it is a continental air mass. Then, if the atmosphere is poor in aerosol particles, the vapor condensation on aerosols leads to the formation of clouds droplets which reach easily the critical size to precipitate. So, it is necessary to study aerosols distributions native to different air masses in order to understand clouds droplets distributions. Detailed investigations of the properties of atmospheric aerosol particles were performed in autumn (September 2008), winter (March 2009) and summer (June 2010) using a Time-of-Flight Aerosol Mass Spectrometer (Freney et al., 2011).

These three cases, well documented for various seasons and for contrasted pollution levels native from various air masses are simulated with WRF-chem, using RADM2 (Stockwell et al., 1990) chemical mechanism associated with MADE/SORGAM aerosols (Ackermann et al., 1998). The proportion of various chemical components (ammonium, nitrate, sulfate, sodium, chloride, organic matter…) in aerosol chemical composition are quantified and compared to the observations. Sensitivity studies are conducted to assess the relative importance of anthropogenic vs biogenic emissions in SOA formation and their impact on cloud and precipitation formation.

Effect of precursor emissions on $PM_{2.5}$ concentrations over Europe

E. Tagaris, R.E.P. Sotiropoulou, N. Gounaris and S. Andronopoulos

Environmental Research Laboratory, NCSR Demokritos, Aghia Paraskevi Attikis, 15310 Athens, Greece
Keywords: particulate matter, emissions, modeling, Europe
Presenting author email: tagaris@ipta.demokritos.gr

Atmospheric pollution is a focus of attention because of its important role in many areas including human health (e.g., Seinfeld and Pandis, 2006; Peng et al., 2005). For this reason simulating air and particle concentrations as accurate as possible is fundamental in air quality planning and strategies for attainment of air quality standards. Although simulated meteorology could be compared with observation data spread throughout the domain suggesting the related uncertainties it is very difficult to accurately characterize emissions. Emission inventories are subject to significant uncertainties given that they are based on data sets of limited spatiotemporal coverage and always contain assumptions on interpolation and extrapolation of a limited set of sample data. The objective of this study is to modify appropriately precursor emissions improving air and particle concentrations predictions over Europe.

Meteorological fields are derived using the Penn State/NCAR Mesoscale Model (MM5) (Grell et al., 1994).

Emissions are processed by the Sparse Matrix Operator Kernel Emissions (SMOKE v2.6) Modeling System (http://www.smoke-model.org). The TNO gridded anthropogenic emissions inventory for the year 2006 over Europe in a 0.1 × 0.1 degrees resolution (ftp://neptunus.tno.nl) is used. The Biogenic Emission Inventory System, version 3 (BEIS3) is used for processing biogenic source emissions (http://www.epa.gov/asmdnerl/biogen.html) using the USGS gridded land use data in 1 Km resolution (http://edc2.usgs.gov/glcc/glcc.php).

The Community Multiscale Air Quality (CMAQ v 4.7) Modeling System with the Carbon Bond mechanism (CB05) (http://www.camx.com/publ/pdfs/CB05_Final_Report_120805.pdf) is used for the regional air quality modeling (177 × 217 grid cells of 35 km × 35 km, with 14 vertical layers) (Byun et al., 2006).

Emission scaling factors are applied for each country on NO_X, SO_2 and $PM_{2.5}$ emissions due to the significant number of monitoring data throughout the domain for these pollutants based on the country average ratio between observed and predicted concentrations.

Model performance is evaluated using the air quality information system maintained by the European Environment Agency (http://www.eea.europa.eu); a systematic bias for both air (i.e., NO_2, SO_2) and particle (i.e., $PM_{2.5}$) pollutants has been found. Application of scaling factors improves $PM_{2.5}$ and air pollutant model performance although the model still underpredicts $PM_{2.5}$ concentrations; this is related to the uncertain representation of secondary organic aerosol formation (Chen et al., 2005; Kroll et al., 2006).

Elevated $PM_{2.5}$ concentrations up to 40 ug/m^3 during winter are simulated over Europe (Figure 1). NO_3 is dominant during winter in Western Europe and in a few Eastern countries due to the high NO_2 concentrations. OC from biomass burning is a significant contributor in $PM_{2.5}$ components in Eastern Europe. During summer NO_3 is dominant only in regions with elevated NH_3 emissions such as the Netherlands and Northern Italy. For the rest of the domain SO_4 and OC are significant $PM_{2.5}$ components with SO_4 being dominant in the South and OC in the East.

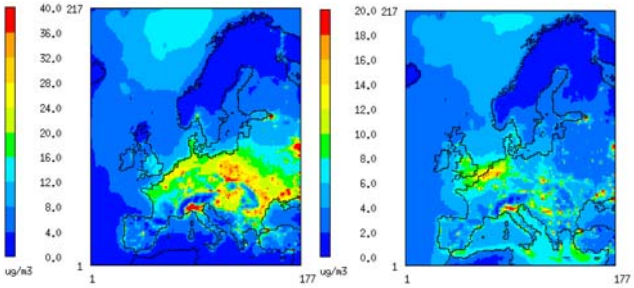

January, 2006 July, 2006

Figure 1: Daily average ground $PM_{2.5}$ concentrations

This work was supported by the FP7-REGPOT-2008-1grant No 229773 and the National Strategic Reference Framework (NSRF) 2007-2013 grand No 09SYN-31-667. We gratefully acknowledge the first Air Quality Model Evaluation International Initiative (AQMEII) activity. The following agencies have prepared the databases used in the study: TNO (European emissions processing), Laboratoire des Sciences du Climat et de l'Environment, IPSL, CEA/CNRS/UVSQ (gridded meteorology for Europe).

Byun, D. W., and K. L. Schere (2006), *Appl. Mech. Rev.*, **59**, 51–77.

Chen, J. et al., (2005), Atmos. Environ., **39**, 7731–7744.

Grell, G., et al. (1994), *Tech. Note NCAR/TN-398+STR*, Natl.Cent. for Atmos. Res., Boulder, Colo.

Kroll, J. H. et al., (2006), , *Environ. Sci. Technol.*, **40**, 1869–1877

Peng, R. D. et al., (2005), *Am. J. Epidemiol.*, **161**, 585–594.

Seinfeld, J., and S.N. Pandis (2006), *Atmospheric Chemistry and Physics*; John Wiley: Hoboken, NJ.

Thursday, September 6, 2012

Session WG10S1O. Aerosol Nucleation, Condensation and Coagulation

3D study of fractal combustion aerosols using Electron Tomography

D. Lottin[1], D. Ferry[2], D. Delhaye[1], F.-X. Ouf[3] and J. Yon[4]

[1]ONERA – The French Aerospace Lab, F-92322 Châtillon, France
[2]CINaM-CNRS UMR 7325, Aix-Marseille University, Campus de Luminy, 13009 Marseille, France
[3]IRSN-LPMA, BP 68, 91192 Gif-sur-Yvette, France
[4]CORIA-CNRS UMR 6614, University and INSA of Rouen, 76801 St-Etienne de Rouvray Cedex, France

Keywords: Soot nanoparticles, Fractals, 3D characterization, Electron Tomography.
Presenting author email: delphine.lottin@onera.fr

Atmospheric aerosol particles meet a growing interest in today's environmental concerns because of their potential impacts on the global radiative budget and human health. In this context, combustion aerosols are extensively studied as they originate from industrial and transport activities for a large part. They usually are in the form of more or less compact aggregates made of primary particles. The evaluation of their effects on the environment requires the knowledge of their microphysical properties.

One way to determine these properties is based on a Transmission Electron Microscopy (TEM) analysis. 2D characteristics of the aggregates' projection (Fig. 1 left) are measured on the micrographs and extrapolated to 3D using 2D-3D transposition relationships (Baron and Willeke, 2001). These mathematical relationships were established from studies of numerically generated aggregates of pre-defined fractal dimension and composed of monodisperse primary particles. They are nowadays widely used (Neer and Köylü, 2006). However, very few works have focused on the validity of these relationships when applied to real soot aggregates. Indeed, it is difficult to establish 2D and 3D characteristics of soot aggregates using a single experimental approach.

We investigate aircraft soot aggregates sampled at the exit of a turbofan engine by combining TEM and Electron Tomography (ET) analyses. Micrographs are processed using the "ImageJ" software (http://imagej.nih.gov/ij/). Statistical values for the population of aggregates are issued: primary particles mean diameter, aggregates mean gyration diameter.

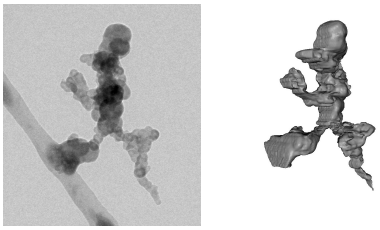

Figure 1. TEM micrograph of an aircraft soot aggregate (left) and the 3D visualization of its tomogram (right).

The 3D tomogram of this aggregate is built by ET using the plug-in "TomoJ" (Messaoudi *et al.*, 2007). We developed a plug-in *SootExpert* able to determine the 3D characteristics of an aggregate on its tomogram (volume, gyration diameter and fractal dimension). In a first step, we validate our plug-in on a numerically generated aggregate (Fig. 2), its volume and gyration diameter are known. The values determined by *SootExpert* are very close to the characteristics of this aggregate (Table 1), assessing the reliability of our plug-in.

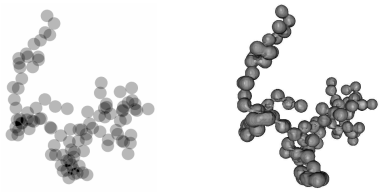

Figure 2. Projection of a numerical aggregate (left) and the 3D visualization of its tomogram (right).

	Known 3D characteristics	*SootExpert* 3D characteristics
Gyration diameter (nm)	310	298
Volume (nm^3)	$1\,456\times10^3$	$1\,616\times10^3$

Table 1. Comparison between the known and the determined 3D characteristics of a numerical aggregate.

In a second step, the ET analysis is applied to aircraft soot aggregates (Fig. 1 right). Van Poppel *et al.* (2005) and Adachi *et al.* (2007) have used ET to characterize atmospheric aerosols, with no special interest to the links between 2D and 3D characterizations. We study, for a single aggregate, the correlation between the 3D characteristics determined on its tomogram and the statistics resulting from the TEM analysis of the series of its projections. We can thus indicate the validity of the transposition relationships for aircraft soot aggregates. Then we compare this aggregate's 3D characteristics determined by *SootExpert* with the statistical values determined on the population, to investigate if a single aggregate is representative of its population.

Adachi, K., Chung, S.H., Friedrich, H., Buseck, P.R. (2007) *J. Geophys. Res.* **112**, D14202.

Baron, P.A. and Willeke, K. (2001) *Aerosol measurement. Principle, techniques, and applications* 2nd Edition, John Wiley & sons, Inc.

Messaoudi, C., Boudier, T., Sorzano, C.O.S., Marco, S. (2007) *BMC Bioinformatics* **8**, 288-297.

Neer, A. and Köylü, Ü.Ö. (2006) *Combust. Flame* **146**, 142-154.

Van Poppel, L.H., Friedrich, H., Spinsby, J., Chung, S.H., Seinfeld, J.H., Buseck, P.R. (2005) *Geophys. Res. Lett.* **32**, L24811.

Novel Features of (Re-)Crystallization and Particle Population Dynamics In Compressed Gas-Expanded Liquid

D. E. Rosner

Department of Chemical and Environmental Engineering, Yale University, New Haven CT, 06520-8286, USA
Keywords: Aerosol fundamentals, Multiphase processes, Coagulation, Supersaturation.
Presenting author email: daniel.rosner@yale.edu

With the ultimate objective of developing rational yet tractable continuous process models, attention is called here to novel features of a class of environments in which compressed gas (e.g., CO_2(g)) is employed as an "anti-solvent" to cause particle precipitation from conventional organic solvents. Under the acronyms: PCA (*precipitation with compressed antisolvent*), SASP (*supercritical anti solvent precipitation*), or GASP (*gas anti solvent precipitation*), this approach is currently being explored for continuously producing valuable ultrafine powders; e.g., to increase the bio-availability of sparingly soluble pharmaceutically active ingredient. We demonstrate the need for systematic modifications in the rate-laws governing organic crystal nucleation (N), growth (G) and coagulation (C) in these remarkable environments (neither liquid-like nor ideal gas-like). Consideration of such "transcritical" conditions not only provides the motivation for instructive new fundamental research, but uncovers opportunities for attractive process improvements.

In this overview of our recent research, we focus on some predicted consequences of:

1. "Intermediate" molecular volume fraction (neither liquid-like nor ideal gas!)
2. "Compressibility"---i.e. rapid "dilation" (see Rosner and Arias-Zugasti, 2011a) of solute-containing liquid solvent droplets
3. Temperature "Contrast"---i.e. exploiting large local temperature gradients to modify rates of particle coagulation (see Rosner and Arias-Zugasti, 2011b) and/or capture (Rosner and Arias-Zugasti, 2007)

We have also developed quadrature-based moment methods to include such N/G/C phenomena in suitably generalized yet tractable population-balance methods (see Rosner et al. 2003) compatible with state-of-the-art CFD simulation techniques.

Many of the techniques we have developed and recently applied to predict the performance of high-pressure continuous spray combustors (see, e.g., Rosner et al. 2011, Rosner and Arias-Zugasti, 2011c, Labowsky et al. 2011), or the evolution of restructuring nano-particles in counterflow diffusion flames (Rosner and Pyykonen 2002, Rosner 2005), are in fact relevant to these equally challenging (albeit milder temperature!) PCA-environments. Indeed, we must ultimately account for the interaction of at least two populations (Rosner 2009); i.e., the solute-charged solvent spray population with the precipitated population of submicron organic crystals---including its continuous efficient capture.

Labowsky, M., Rosner, D. E. and Arias-Zugasti, M. (2011) Int J Heat Mass Transfer **54** 2683-2695.
Rosner, D. E. and Pyykonen, J. J. (2002) AIChE J **48**(3) 476-491.
Rosner, D. E., McGraw, R. and Tandon, P. (2003) I&EC-Res **42** 2699-2711.
Rosner, D. E. (2005) I&EC-Res **44**, 6045-6055.
Rosner, D. E. and Arias-Zugasti, M. (2007) AIChE J **53**(7) 1879-1890.
Rosner, D. E., Arias-Zugasti, M. and Labowsky, M. B. (2008) Chemical Engineering Science **63** 3909-3920.
Rosner, D. E. (2009) I&EC-Res **48**(14) 6453-6464.
Rosner, D. E. and Arias-Zugasti, M. (2011a) AIChE J **57**(2) 307-318.
Rosner, D. E. and Arias-Zugasti, M. (2011b) I&EC-Res **50** 8932-8940.
Rosner, D. E. and Arias-Zugasti, M. (2011c) AIChE J **57**(12) 3534-3554.

New insight into organic driven particle formation and growth during the CLOUD experiment

F. Riccobono[1], E. Weingartner[1], U. Baltensperger[1] and the CLOUD collaboration

[1]Laboratory of Atmospheric Chemistry, Paul Scherrer Institut, CH-5232 Villigen PSI, Switzerland
Keywords: ion-induced nucleation, organics, growth, CLOUD
Presenting author email: francesco.riccobono@psi.ch

Formation of atmospheric aerosol has been observed in a wide range of atmospheric conditions in many different locations and altitudes all over the globe (Kulmala *et al.*, 2004). Nucleation and subsequent condensational growth alters the atmospheric aerosol size distribution and ultimately affects the climate. Despite extensive research, fundamental questions remain about the role played by organic compounds on the nucleation and growth mechanisms. The latest CLOUD experiment at CERN aimed to investigate how organic compounds and their interplay with cosmic radiation affect the formation and growth of new particles.

Several experiments have been performed in the CLOUD aerosol chamber at CERN in the presence of pinanediol, a first oxidation product of α-pinene. The CERN Proton Synchrotron provided an adjustable and precisely measurable beam of artificial cosmic rays, spanning the atmospheric ionization range from the upper troposphere to ground level (Kirkby *et al.*, 2011).

Integrated measurements by several instruments, such as an Atmospheric Pressure interface Mass Spectrometer (APi-TOF), Condensation Particle Counters (CPC) with different counting efficiency curves, a Scanning Mobility Particle Sizer (SMPS) together with a newly tailored diffusion technique (LDT, Laminar Diffusion Tube), provided a comprehensive picture of the processes governing the evolution of the particle size distribution inside the CLOUD chamber.

The effects of pinanediol on nucleation rates and growth rates are presented as nucleation and growth rate enhancement factors with respect to ternary nucleation of sulfuric acid, water and ammonia. Nucleation and growth rates enhancement factors as function of organic compounds and ion concentration will be discussed.

Special focus will be given to the size dependency of the growth rate enhancement factors obtained with the LDT. This instrument uses the 1.2 meter long sampling line of the CLOUD chamber as a diffusion tube, in which the particles are lost to the walls by diffusion as a function of the sample flowrate and of the particle diameter. Downstream of the LDT the particle concentration is determined with a Condensation Particle Counter.

The observed growth rates determine which fraction of the freshly nucleated particles can grow to CCN sizes and which fraction is lost by coagulation with larger pre-existing aerosol particles. Figure 1 depicts the steep increase of particle's lifetime as the diameter of the nucleated particle grows. The combination of low saturation vapor pressures of sulfuric acid and oxidized organic compounds increases the survival probability of nucleated particles. The role of sulfuric acid and organic compounds in speeding up the growth rates (i.e. increasing the survival probability) will be presented as a function of particle size.

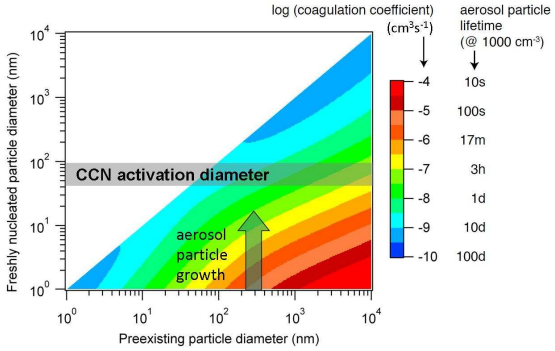

Figure 1. Grow or die: depending on the pre-existing surface area (number and size of pre-existing particles) the lifetime of freshly nucleated particles varies by 6 orders of magnitude (from red to blue). Rapid growth increases the probability of a nucleated particle to avoid coagulation and form a new CCN.

Acknowledgments: We would like to thank CERN for supporting CLOUD with important technical and financial resources, and for providing a particle beam from the CERN Proton Synchrotron. This research has received funding from the EC Seventh Framework Programme (Marie Curie Initial Training Network "CLOUD-ITN" grant no. 215072, and ERC-Advanced "ATMNUCLE" grant no. 227463), the German Federal Ministry of Education and Research (project no. 01LK0902A), the Swiss National Science Foundation (project nos. 206621_125025 and 206620_130527), the Academy of Finland Center of Excellence program (project no. 1118615), the Austrian Science Fund (FWF; project no. P19546 and L593), the Portuguese Foundation for Science and Technology (project no. CERN/FP/116387/ 2010), and the Russian Foundation for Basic Research (grant N08-02-91006-CERN).

Kulmala, M. et al. (2004). *J. Aerosol Sci.*, **35**, 143-176.
Kirkby, J. et al. (2011). *Nature.*, **476**,429-433.

Saturation Fluctuations and Rain Initiation

Charles Clement

15 Witan Way, Wantage, Oxon OX12 9EU, U.K.

Keywords: rain, condensation, turbulence, fluctuations

The initiation of raindrops in clouds is a longstanding problem which is still not well understood theoretically. It was recognised early that the usual coagulation processes between the numerous, but small (about 3 μm), cloud droplets are too slow to produce raindrops large enough to fall under gravity, and also to give the wide size distributions of droplets observed in clouds. In this paper we discuss how the more rapid condensation process can contribute to raindrop formation, including the recent suggestion (Wilkinson 2011) that the Ostwald ripening process plays a significant role.

Processes affecting the growth of activated droplets and subsequent redistribution of mass between them were summarised by Clement (2008), and include changes arising from interaction with radiation as well as the Ostwald ripening process which involves mass transfer from small droplets to large ones because of the greater equilibrium vapour pressure outside a curved surface. The difference in equilibrium saturation, S, of water for a droplet radius, R, from that for a plane surface is given by $R_\gamma(T) / R$, where $R_\gamma(T)$ is 1.2 nm at 0^0 C and 1.0 nm at 20^0 C. Thus the process is driven by changes of S of the order of 10^{-3} for 1 μm droplets, and 10^{-4} at 10 μm, and the theory describing it requires a uniform saturation surrounding a collection of droplets which is slowly reducing between these values as the mean droplet size increases between the two values of R.

Saturation fluctuations in the atmosphere were examined by Kulmala *et al* (1997) in connection with droplet growth, and the observations from aircraft discussed were found to lead to fluctuation values for S of 1-4 10^{-2}. Droplet growth and evaporation from such fluctuations will dominate over those from Ostwald ripening, and we now discuss whether they can lead to raindrop formation.

To simulate the effect of fluctuations on growth, Kulmala *et al* (1997) calculated growth of a droplet population containing a constant 0.01 ppb of nitric acid and included the Kelvin effect so that the initial droplets of size R_0 needed to be activated. The saturation was represented by a stochastic model changing with time with a Gaussian probability density of mean S_{av} and standard deviation σ_S. An exponential correlation function was used for changes with time:

$$< (S(t) - S_{av})(S(t + t') - S_{av})> = \sigma_S^2 \exp(-t'/\tau_c) \quad (1)$$

where τ_c is a correlation time.

Results were obtained for varying values of S_{av}, σ_S and τ_c which showed that wide size distributions could be produced, often with a separate unactivated peak, even for $S_{av} < 1$. We reproduce here some results obtained for the mean radius as a function of time for S_{av} =1 and correlation time τ_c = 100s except for 2.5 s when it was taken to be τ_c = 10 s. They clearly show that, with parameters not untypical of some atmospheric situations, droplet sizes of over 20 – 30 μm can be reached in timescales of 10-30 mins. At these sizes, the droplets start to fall with significant velocities (Stokes velocity of 0.15 ms^{-1} at 30 μm) with the ability to collide and coalesce with smaller droplets. Much more data on realistic fluctuations on different types of cloud are needed to apply this theory more widely.

The origin of saturation fluctuations, especially those in clouds, is still a difficult problem. The full equation for S (Clement 2008) has many components which have not yet been fully accounted for in calculations. Atmospheric calculations involving turbulence, such as those of Sidin *et al* (2009) concentrate on those arising from vertical motions. The possibility of other sources from diffusive processes and the interaction with radiation will be discussed.

Clement, C. F.(2008) Mass Transfer to Aerosols in *Environmental chemistry of Aerosols* ed. I. Colbeck, Blackwell Publishing, Oxford p.49-89.

Kulmala, M., Rannik, Ü., Zapadinsky, E. L. and Clement, C. F. (1997) *J. Aerosol Science*, 28, 1395-1409.

Sidin, R. S. R., IJzermans, R. H. A. and Reeks, M. W. (2009) *Physics of Fluids*, 21, 106603.

Wilkinson, M. (2011) Private communication..

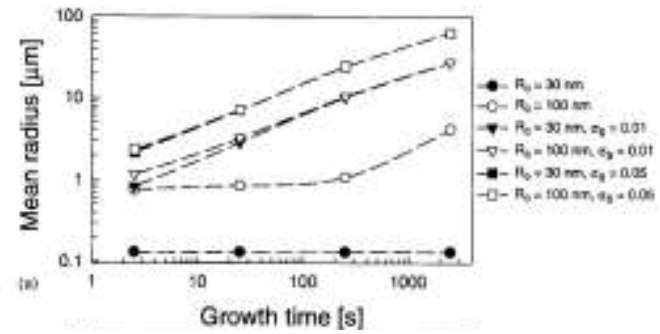

Fig. 1. Mean radius as a function of growth time for S_{av}=1. The different curves show the effect of changing σ_S, 0.01 for triangles and 0.05 for squares, as well as the initial radius, R_0.

Thermophoretic coating with molybdenum oxide nanoparticles

Lucija Boskovic[1] and Igor E. Agranovski[1]

[1]Griffith School of Engineering, Griffith University, Brisbane, 4111 QLD, Australia
Keywords: aerosol coating, thermophoresis, nanoparticles, oxides
Presenting author email: l.boskovic@griffith.edu.au

Dipping and spinning are the most extensively investigated sol-gel coating methods, however they suffer from the general requirements of axially or radially symmetric substrates, and the difficulty in achieving thick layers with a single coating Brinker and Scherer (1990). For these reasons, other coating methods such as electrophoresis, thermophoresis, sedimentation, and spraying have been investigated. The only viable deposition mechanisms for submicron particles are electrophoresis and thermophoresis. The electrophoretic coating is limited to conductive substrates that can serve as an electrode Dixen and Fissan (1999), on the other hand for thermophoresis no such limitation applies.

Many applications of hot wire and plate to plate thermophoretic precipitators (TP) were made in order to increase uniformity of the particle deposition. Messerer et al (2003) designed a plate to plate thermal precipitator with a flow channel length of 45cm to investigate the deposition of agglomerate soot aerosol particles under flow and temperature conditions relevant for heavy-duty diesel engine exhaust gas system. They have noticed the color change over the entry length at the inlet which indicates less soot deposition, and no visible treaces of particle deposition on the heated upper plate. Later, Gonzalez et al (2005) constructed a new TP for collection of nanometer-sized aerosol particles. Size of this precipitator was much smaller compared to Messerer et al (2003) design, with the length of 9.3 mm and precipitation area of 55.6 mm2. The deposition along the TP was shown to be homogenous on a millimeter scale for both NaCl and Fe particles collected on thin foil substrates and microscope grids, respectively at the aerosol flow rate of 50 sccm.

This paper investigates thermophoretic coating with molybdenum oxide nanoparticles, generated by a glowing wire generator, on different surfaces and at different flow rates.

Figures 1 (a), (b) and (c) show molybdenum oxide particles deposited on cold plate of the TP and on sixteen TEM grids distributed along the plate at three different flow rates 0.3, 1 and 1.5 l/min, respectively.

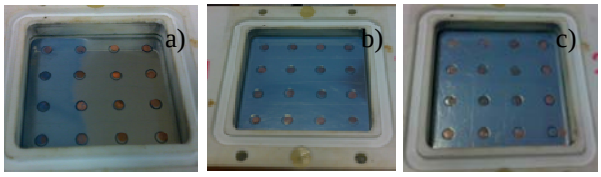

Figure 1. Molybdenum oxide nanoparticles deposited on the TP at flow rates a) 0.3 l/min, b)1 l/min and b) 1.5 l/min.

Figure 2 shows quantitative evidence of the particles collected by TP at three different flow rates (0.3, 1 and 1.5) l/min. The results are based on difference in mass of the TEM grids before and after particles deposition.

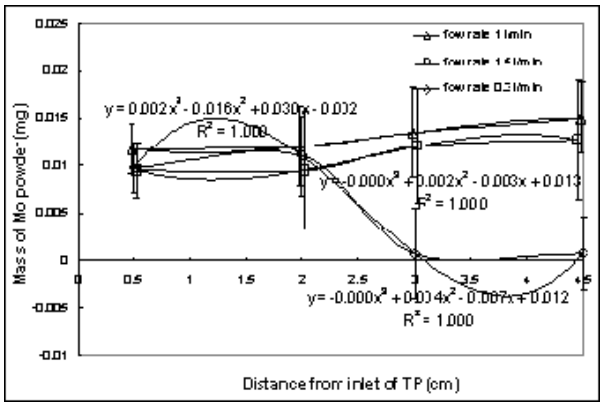

Figure 2. Quantitative evidence of the particles collected by TP at three different flow rates (0.3, 1 and 1.5) l/min

From the Figures it is clear that at 0.3 l/min flow rates vast majority of the particles settle closer to the entry of the precipitator with almost no particles collected close to the exit of the precipitator. With increase of the flow rate to 1 and 1.5 l/min results are showing that almost uniform collection of the particles is achieved along the whole area of the precipitator with slight increase in efficiency closer to the exit of the precipitator. The experimental curves were fitted with third order polynomial trendlines.

The uniformity of molybdenum oxide film generated on a glass slide at 1.5 l/min was investigated by Environmental SEM. The micrographs of the film confirmed that homogeneous densely packed network of molybdenum oxide particles is present along the precipitation area. Based on the results the thermophoretic precipitator described by Boskovic and Agranovski (2012) can be efficiently used for uniform coating with nanoparticles directly on various surfaces.

Boskovic, L. and Agranovski, I.E (2012) *CLEAN-Soil, Air, Water* (in press).
Brinker, C.J. and G.W. Scherer (1990) *Sol-Gel Science*, London Academic Press.
Dixkens, J. and Fissan, H. 1999. *Aerosol Sci. Tech*. **30**, 438-453.
Gonzalez, D. et al (2005) *Aerosol Sci. Technol*. **39**, 1064-1071.
Messerer, A. et al (2003) *J. Aerosol Sci.* **34**, 1009-1021.

Studies on thermal diffusion and Dufour effect in condensation of a trace gas and a near-pure vapor: water droplets on Earth and CO_2 ice crystals on Mars

C. Listowski[1], A. Määttänen[2], I. Riipinen[3], F. Montmessin[2], F. Lefèvre[1]

[1]LATMOS, UPMC, Paris, France
[2]LATMOS, UVSQ, Guyancourt, France
[3]University of Stockholm, Sweden
Keywords: condensation, cloud microphysics, clouds, ice clouds, planetology
Presenting author email: constantino.listowski@latmos.ipsl.fr

The growth or evaporation of droplets or crystals in a gas mixture is controlled by the balance of mass and heat transfer. The nature of the condensing vapor and above all its relative abundance in the atmosphere plays a major role in the mass transfer processes. We investigate the influence of molecular diffusion, thermal diffusion or Soret effect (mass transfer), and Dufour effect (heat transfer), with previous work done by Kulmala and Vesala (1991) as a starting point (hereafter KV91) and extending it to the case of high relative abundances of the condensing vapor.

Mars has a 95% CO_2 abundance in its atmosphere within which CO_2 ice clouds form. Those were first unambiguously observed by Montmessin *et al.* (2007). They present an unusual insight into cloud formation in the solar system because their formation involves the condensation of the major atmospheric component. Low atmospheric densities implies that the commonly-used continuum equations for mass transfer need to be modified by a correction factor (e.g. Fuchs and Sutugin, 1971) that accounts for the free molecular regime effects.

Soret effect and Dufour effect do not appear very important in cloud formation on Earth but might play a role on Mars in the formation of CO2 ice clouds. They are analogous terms in the sense that the former describes a mass flux rising from a temperature gradient and the latter a heat flux rising from a concentration gradient. The Dufour effect appears in the energy balance of the droplet or crystal:

$$D_{\mathrm{Duf}} I_{\mathrm{c}} - 4\pi r^2 K \frac{dT}{dr} = L_{\mathrm{sub}} I_{\mathrm{c}}$$

where I_c is the mass flow rate. From left to right appear the Dufour term (D_{duf}), the heat diffusion from Fourier's law, and the latent heat released by condensation (L_{sub}). Thus D_{duf} has to be compared to L_{sub}. Moreover we present the effect of thermal diffusion on the mass flow rate I_c as follows : $I_c = I_c^0/(1+Z_{th})$, where Ic^0 is the mass flow rate and Z_{th} a thermal diffusion-related term derived by assuming the simplest temperature profile above the droplet or crystal. Thus Z_{th} quantifies the effect of thermal diffusion on the mass flow rate. Importantly, in non-diluted conditions molecular diffusion has to account for the Stefan flow in Fick's law. Ic^0 accounts for it. Besides, in contrary to what KV91 did for water on Earth we could not simply used the classical mass flow rate of a condensing trace gas as 0^{th} order approximation to establish the thermal diffusion term. We had to rederive the equations and see how far the Stefan flow influences that coefficient. The result is that Z_{th} increases by 30% for the highest vapor concentration gradients between the crystal surface and the atmospheric background. Orders of magnitude of Z_{th} and D_{duf}/L_{sub} for typical Earth and Mars conditions are shown in Table 1.

Table 1. Z_{th} and L_{sub}/D_{duf} for tropospheric clouds and polar mesospheric clouds (PMC) on Earth, and CO_2 ice clouds on Mars

Planet - Cloud type	Z_{th}	$\frac{D_{\mathrm{Duf}}}{L_{\mathrm{sub}}}$
Earth - Tropo/H_2O_{liq}	10^{-2}	10^{-2}
Earth - PMC/H_2O_{ice}	10^{-5}	10^{-2}
Mars - Meso/$CO_{2,ice}$	≥ 10	$\leq 10^{-3}$

KV91 have studied the formation of a water droplet in Earth tropospheric conditions. Our results (Table 1) are valid in regards to KV91 conclusions in those specific conditions: Dufour effect dominates over thermal diffusion in tropospheric conditions. Indeed, using the values of Table 1 we observe that the energy balance puts the Dufour effect (through D_{duf}/L_{sub}) as a first-order correction term and the Soret effect (through D_{duf}/L_{sub} x Z_{th}) as a second-order correction term:

$$\frac{D_{\mathrm{Duf}}}{L_{\mathrm{sub}}} \frac{I_{\mathrm{c}}^0}{1+Z_{\mathrm{th}}} \simeq I_c^0 \left(\frac{D_{\mathrm{Duf}}}{L_{\mathrm{sub}}} - \frac{D_{\mathrm{Duf}}}{L_{\mathrm{sub}}} Z_{\mathrm{th}}\right)$$

We thus confirm in a different way the result of KV91.

A striking result is that thermal diffusion appears non negligible for CO_2 ice clouds on Mars ($Z_{th} \geq 10$) mainly because of high abundances of CO_2, while it is negligible for PMCs on Earth which form somewhat in similar atmospheric conditions but with very low abundances of water (< 250 ppm). These processes will be tested in a microphysical model presented in a companion abstract by Listowski et al.

Fuchs, N. A., and Sutugin, A. G., (1971) *Highly dispersed aerosols*, in Topics in *Current Aerosol Research*, **2**, 1-60, Pergamon, New York

Kulmala, M. and Vesala, T. (1991) *J. Aerosol Sci.,* **22**, 3, 337-346

Montmessin, F. et al. (2007) JGR, 112, E11S90, *Icarus,* **183**, 403–410

Design of well-mixed aerosol chambers for stable aerosol generation

J.T.N. Knijnenburg, M.L. Eggersdorfer and S.E. Pratsinis

Department of Mechanical and Process Engineering, ETH Zurich, Zurich, CH-8092, Switzerland

Keywords: aerosol dynamics, Brownian coagulation, population balance, CSTR.
Presenting author email: jesper.knijnenburg@ptl.mavt.ethz.ch

Agglomeration or coagulation is a common phenomenon in well-mixed particulate processes like gas-phase aerosol reactors (Pratsinis *et al*, 1986) and liquid-fed crystallizers. In aerosol reactors, agglomeration or coagulation is the dominant mechanism for particle growth at high particle concentrations, especially during materials manufacture (e.g. titania, silica, etc). Well-mixed conditions in these particulate processes either by stirring or by intense fluid turbulence resemble those of continuous stirred tank reactors (CSTR) of classic reactor engineering.

The shape of the steady state size distribution in CSTR-like processes has been widely studied for a range of in- and outflow terms and coagulation kernels (e.g. Camacho, 2001). For Brownian coagulation in batch systems, the shape of the distribution becomes invariant after a given time, and one can speak of the so-called self-preservation. Independent of the initial distribution, the size distribution will always approach the same shape, as indicated by its constant geometric standard deviation (Landgrebe and Pratsinis, 1989). To our knowledge it has not been studied whether continuous, CSTR-like systems are also self-preserving at steady state.

Recently Fritzsche *et al* (2010) presented a CSTR-like aerosol generator to produce submicron aerosols. In their experiments, well-stirred conditions were fulfilled and Brownian coagulation in the transition regime was the dominant mechanism for particle growth. The steady state particle size distribution is independent of process parameters when scaled accordingly, and the size distribution follows a power law for intermediate particle sizes, in agreement with theory (Fritzsche *et al*, 2010; White, 1982). Long residence times were used to ensure that the produced aerosol size is coagulation-controlled.

Here, we present a numerical model for Brownian coagulation in a continuously fed well-stirred chamber. The goal is to provide a systematic understanding of how the size distribution in a CSTR can be controlled by process parameters. A population balance model is used to describe the temporal evolution of the particle size distribution:

$$\frac{\partial n(v)}{\partial t} = R(v) n_0(v) + \frac{1}{2}\int_0^v \beta(v-u,u)\, n(v-u,t)\, n(u,t)\, du - n(v,t)\int_0^\infty \beta(v,u)\, n(u,t)\, du - \frac{n(v)}{\tau_{res}} - \beta_{wall}(v)\, n(v)$$

Here $R(v)$ is the particle inflow rate per unit or chamber volume, τ_{res} is the residence time in the chamber, and $\beta_{wall}(v)$ is the wall loss coefficient (Crump and Seinfeld, 1981). The size distributions are characterized by various performance indices, derived from their moments. The model is applied to predict the coagulation-controlled size distribution from Fritzsche *et al* (2010). Validation was done by coagulation in the continuum regime (Figure 1).

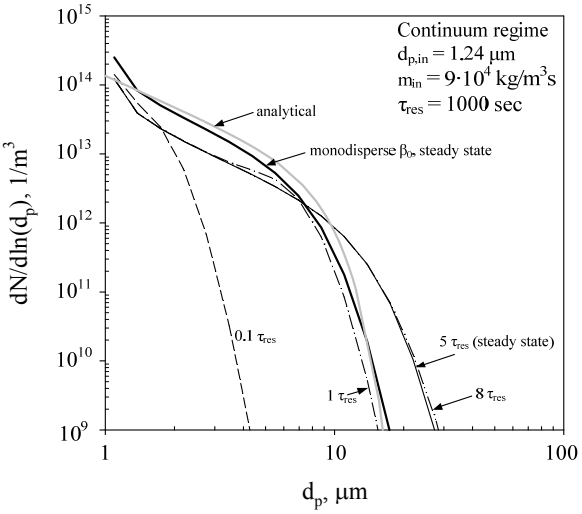

Figure 1. Evolution of particle size distribution over time by Brownian coagulation in the continuum regime. The monodisperse kernel β_0 gives good agreement with the analytical solution (Fritzsche *et al*, 2010; White, 1982).

The size distribution in CSTR-like processes does not evolve to an asymptotic self-preserving size distribution at steady state. The width of the size distribution is strongly dependent on the reactor residence time and the feed rate. Wall losses may have a strong influence on the size distribution but only for the large tail of the distribution for long residence times.

This work was supported by ETH Research Grant ETH-06 10-1.

Camacho, J. (2001) *Phys. Rev E.* **63**, 046112.
Crump, J.G. and Seinfeld, J.H. (1981) *J. Aerosol Sci.* **12**, 405-415.
Fritzsche, J., Pohlmann, G. and Koch, W. (2010) Abstract of the International Aerosol Conference 2010, Helsinki, Finland.
Landgrebe, J.D. and Pratsinis, S.E. (1989) *Ind. Eng. Chem. Res.* **28**, 1474-1481.
Pratsinis, S.E., Kodas, T.T., Dudukovic, M.P. and Friedlander, S.K. (1986) *Ind. Eng. Chem. Proc. Des. Dev.* **25**, 634-642.
White, W.H. (1982) *J. Coll. Interface Sci.* **90**, 204-208.

Nucleation and droplet growth measured by a pulse-expansion wave tube

M.A.L.J Fransen[1], J. Hrubý[2] and D.M.J. Smeulders[1]

[1]Department of Mechanical Engineering, Eindhoven University of Technology, Eindhoven, 5600 MB, The Netherlands
[2]Institute of Thermomechanics AS CR. v.i.i., Dolejškova 5, Prague, CZ-182 00, Czech Republic
Keywords: atmospheric aerosols, homogeneous nucleation, measurements, nucleation rate.
Presenting author email: m.a.l.j.fransen@tue.nl

Abstract

The determination of cloud formation, water nucleation properties, supersaturation, and droplet growth is of paramount importance for meteorology and global climate models. Homogeneous nucleation and droplet growth rates measured in mixtures of synthetic air and water vapour are reported.

Experimental setup

The nucleation experiments are performed by means of the so-called pulse-expansion wave tube (see Figure 1). This is a special shock tube design in which the nucleation pulse is created at the end wall (left) of the high pressure section (HPS). It is separated by a diaphragm (D) from the low pressure section (LPS). The latter contains a local widening (W) of the cross-sectional area.

An expansion wave and a shock wave are formed after rapid opening of the diaphragm. The expansion wave creates a strong isentropic expansion in the measurement section at the end wall (left) of the tube. The second, weak expansion wave, which is created by the interaction of the shock wave with the beginning of the local widening (W), arrives at the measurement section somewhat later. The nucleation pulse is terminated by the arrival of a weak compression wave caused by the interaction of the shock wave with the end of the local widening (W). The nucleation and growth stages of the water droplet are consequently separated in time in this nucleation pulse method.

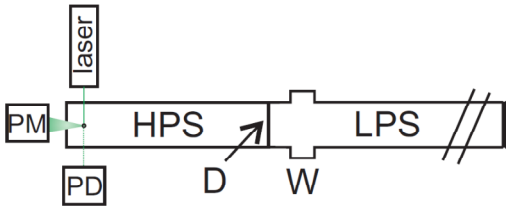

Figure 1. The pulse-expansion wave tube setup.

Droplet size and droplet number density can accurately be determined by a light extinction method (PD) and 90° Mie light scattering (PM).

The driving force for nucleation and condensation is the supersaturation, which therefore necessitates an accurate synthetic air/water vapour mixture preparation procedure. The latter is performed by means of a sophisticated mixture preparation device, in which gases are continuously premixed before injection in the high pressure section (Peeters *et al*, 2001). In this way, the synthetic air is the carrier gas charged with water vapour that will condense due to the sudden pressure decrease. The influence of the carrier gas on the condensation process and on the composition of the critical clusters is the subject of current research.

Critical cluster composition & classical nucleation theory corrections

Careful measurement of the dependence of the nucleation rate on supersaturation and total pressure allows us to determine the critical cluster composition in terms of air molecules and water molecules based on the nucleation theory for multi-component mixtures (Oxtoby and Kashchiev, 1994). The relatively high content of gas molecules in critical clusters is explained as adsorption of gas molecules on the surface of clusters.

At elevated pressures, appropriate corrections to the classical nucleation theory have to be applied. At high pressure, the solubility of vapor molecules in the gas phase in equilibrium with liquid is increased. This fact is quantified by the so-called enhancement factor, and leads to a decrease in the supersaturation for a given vapor molar fraction.

Another effect is the reduction of surface tension due to the adsorbed air gases. The effects of the gas on supersaturation and surface tension partially cancel. We analyze the gas effects by comparing the present results with the low-pressure nucleation data by Wölk and Strey (2001) with argon and Holten *et al.* (2005) with helium as carrier gas.

It is found that the carrier gas largely influences the composition of the critical clusters which is not predicted by the classical nucleation theory.

List of references

Peeters, P., Hrubý, J. and Van Dongen, M. (2001) *J. Phys. Chem. B* **105**, 11763-11771.

Oxtoby, D.W., and Kashchiev, D. (1994) *J. Chem. Phys.* **100,** 7665-7671.

Wölk, J., Strey, R. (2001) *J. Phys. Chem. B* **105,** 11683-11701.

Holten, V., Labetski, D.G., van Dongen, M.E.H. (2005) *J. Chem. Phys.* **123,** 104505.

Thursday, September 6, 2012

Session WG01S6O. Climate effects of aerosols

Model results of cirrus cloud modifications in a climate engineering framework.

H. Muri[1], J.E. Kristjánsson[1], T. Storelvmo[2], D. L. Mitchell[3] and M.A. Pfeffer[1]
[1]Department of Geosciences, University of Oslo, Oslo, Norway
[2]Department of Geology and Geophysics, Yale University, New Haven, Connecticut, US
[3]Desert Research Institute, Reno, Nevada, US
Keywords: cirrus, heterogenous freezing, climate engineering.
Presenting author email: helene.muri@geo.uio.no

Cirrus clouds are an important element of the climate system and they can have a large impact on the Earth's radiation budget. Recent observations of mid-latitude cirrus clouds forming at temperatures below -40°C suggest that they are primarily formed by homogeneous freezing (Mitchell et al., 2011). These clouds hence tend to mainly consist of numerous small ice crystals. However, if efficient ice nuclei are present, heterogeneous freezing will be favoured, due to the suppression of the required supersaturation with respect to ice (Kärcher and Lohmann, 2003).

Mitchell and Finnegan (2009) proposed a climate engineering technique exploiting this competition between homogeneous and heterogeneous freezing, in order to cool the global climate. The term climate engineering, or geoengineering, can be defined as intentionally interfering with the climate system in order to temporarily offset or reduce the increase in surface temperatures by global warming.

The idea is to inject ice nuclei into cirrus forming regions, then a small number of ice crystals would form heterogeneously and grow rapidly by vapour diffusion. The large ice crystals would gain large fall speeds. Sanderson et al. (2008) found that the ice fall speed from cirrus clouds strongly affect climate sensitivity. The cirrus cloud coverage, life cycle, optical depth and upper tropospheric water vapour amounts are dependent on the ice fall speed. Seeding the cirrus with an effective ice nuclei could outcompete any pre-existing natural ice nuclei for the water vapour. Larger ice crystals could form, leading to a fall out of the cloud and hence cloud removal. This facilitates for more outgoing longwave radiation (OLR) being able to escape the climate system. Targeting the highest and coldest cirrus would be the most effective at increasing the OLR.

As the upper tropospheric water vapour is exported to the lower troposphere, the water vapour greenhouse effect is reduced. The combination of water vapour and cirrus cloud reduction should combine to give a cooling to counteract the surface warming due to high CO_2 concentrations.

The suggested seeding material is bismuth tri-iodide (BiI_3) (Mitchell and Finnegan, 2009). It is non-toxic, relatively cheap and can be produced in aerosol form by combustion of BiI_3 alcohol solution. It has an atmospheric residence time of 1-2 weeks.

The idea of climate engineering of cirrus clouds is a new one and until now not tested in GCMs. We present results of model experiments investigating the potential of the proposed climate engineering method using the CAM5 global climate model and WRF-CHEM cloud resolving model. This is done in the framework of the Barahona and Nenes (2009) ice nucleation scheme. The cirrus cloud parametrisation takes both homogeneous and heterogeneous freezing into account, including their interaction, when calculating ice crystal number and size distribution.

Compared to other suggested climate engineering methods, the one explored here has the advantage of addressing the longwave radiation directly, which is the part of the spectrum that is being perturbed by anthropogenic greenhouse gases. This avoids some of the caveats of other proposed climate engineering methods, e.g. stratospheric sulphur injections or seeding of marine stratus clouds. I.e. solar radiation management techniques where the reflected solar radiation to space is increased. It should however be noted, that none of these methods tackle the ocean acidification issue.

Barahona, D. and Nenes, A. (2009) Atmos. Chem. Phys. **9**, 269-381.

Kärcher, B. and Lohmann, U. (2003) J. Geophys. Res. **108**, 4402.

Mitchell, D. L. and Finnegan, W. (2009) Environ. Res. Lett. **4**, 1-8.

Mitchell, D. L., Mishra, S. and Lawson, R.P. (2011) Planet Earth 2011 - Global Warming Challenges and Opportunities for Policy and Practice, 257-288.

Sanderson, B. M., Piani, C., Ingram, W. J., Stone, D. A. and Allen, M. R. (2008) Clim. Dyn. **30**, 175-190.

The influence of aerosols on the European heat-wave of 2003: a study with the regional model system COSMO-ART

A. Ferrone[1], H. Vogel[1], and C. Kottmeier[1], B. Vogel[1]

[1]Institute for Meteorology and Climate Research, Karlsruhe Institute of Technology, Eggenstein-Leopoldshafen, Baden-Würtemberg, 76344, Germany

Keywords: Aerosol modelling, Climate effect, Chemistry transport model, 3D, modelling (regional).

Presenting author email: andrew.ferrone@kit.edu

The year 2003 was marked by a strong heat-wave in June, July, and August (JJA). During this period a synoptic blocking situation and unusual clear skies caused a drying-out of the soil. The combinations of these factors induced unusually high surface temperatures, up and above 40°C in Mid-Europe (Black et al. 2004). These high temperatures favoured the chemical formation of ozone as well as the biogenic emission of its precursors. This together with an extremely high photolytic activity, due to the very clear skies, led to high levels of ozone concentrations. At the same time, the high temperatures led to large numbers of wild-fires and strong emissions of biogenic aerosol precursor gases that contributed to unusual high concentration of aerosols in Europe, favoured by the blocking situation of air-masses. All these aspects qualify this situation as a particular test for air-quality models (Vautard et al., 2005).

We perform detailed calculations with the comprehensive model system COSMO-ART (Vogel et al., 2009). COSMO-ART is online coupled, which makes it possible to investigate feedbacks between particles and the state of the atmosphere in a homogeneous framework. The natural emissions of primary particles are parameterized as function of the ambient conditions. Primary soot and organic particle emissions are considered and secondary aerosols are formed from gaseous precursors that are treated by complex photochemistry in the model.

In this study the model system is applied for a continuous integration of 2 months from 15th June to 20th August 2003 over the COSMO-EU domain (see figure 1) at a resolution of approx. 14km with 40 vertical layers, and driven at the borders by ERA-Interim (Dee et al., 2011). Two simulations have been performed. In the first one no interaction of aerosols and the state of the atmosphere is considered, whereas in the second the simulated aerosols can interact with the state of the atmosphere via scattering and absorption of long and short-wave radiation, depending on the nature of the aerosols. The direct interactions of aerosols and clouds are not considered in the present study.

As an example of feedbacks that can be represented, we analyse the impact of a prognostic calculation of aerosols on the 2m temperature here. In figure 1 some systematic effects can be discerned. The 2 months average temperatures around the Mediterranean were reduced by approx. 1 K associated to high loads of aerosols and in particular Saharan mineral dust from North Africa in these regions.

In the Eastern part of the domain some regions show an increase of the 2m temperature. This effect could be related to the absorbing effect of black carbon on the long wave radiation and/or a systematic change in cloud cover over the regions.

The statistical significance of the observed changes is however in general not very high and longer runs are needed to confirm if the observed signals are systematic or particularly related to the considered time period.

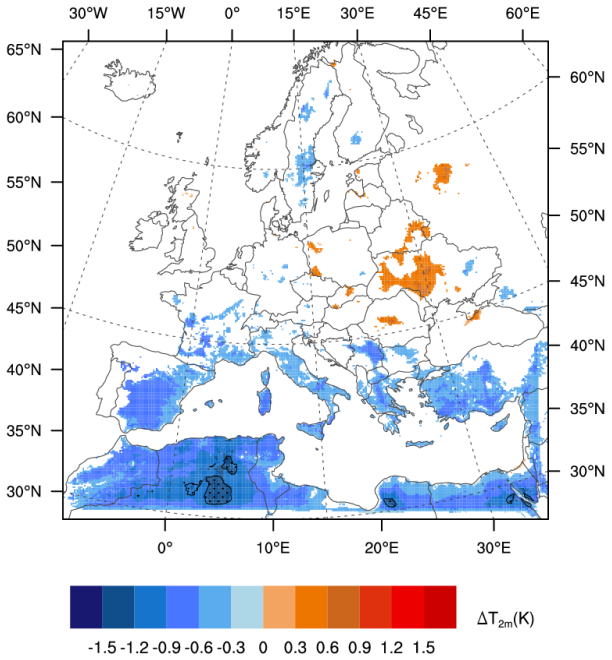

Figure 1. Absolute changes in average 2m-Temperature for the period from 15 June to 20 August 2003, from a run with COSMO-ART relative to a run with COSMO. White areas are where a t-test is not significant at the 66% level and stippled areas are where it is significant at least on the 90% level.

Black, E., Blackburn, M., Harrison, G., Hoskins, B., & Methven, J. (2004). *Weather*, 59(8), 217-223.

Dee, D. P., with 35 co-authors, (2011). *Quart. J. R. Meteorol. Soc.*, 137, 553-597.

Vautard, R., Honore, C., Beekmann, M., & Rouil, L. (2005). *Atmospheric Environment*, 39(16), 2957-2967.

Vogel, B., Vogel, H., Bäumer, D., Bangert, M., Lundgren, K., Rinke, R., and Stanelle, T. (2009). *Atmos. Chem. Phys.*, 9, 8661-8680.

Are indirect forcing estimates sensitive to cloud formation parameterizations, emission scenarios and meteorological fields?

R.E.P. Sotiropoulou[1], E. Tagaris[1],N. Meskhidze[2], J. Kouatchou[3], L. Oreopoulos[3], J.M. Rodriguez[3] and A. Nenes[4]

1 Environmental Research Lab, INT-RP, N.C.S.R. Demokritos, Aghia Paraskevi, Greece
2 School of Marine Earth and Atmospheric Sciences, North Carolina State University, Raleigh, NC, USA
3 NASA Goddard Space Flight Center, Greenbelt, Maryland, USA
4 Schools of Earth and Atmospheric Sciences and Chemical and Biomolecular Engineering, Georgia Institute of Technology, Atlanta, GA, USA
Keywords: Aerosol-cloud interaction, CCN, radiative forcing, clouds, modeling.
Presenting author email: rsot@ipta.demokritos.gr

Aerosol indirect effect (AIE) is one of the greatest sources of uncertainty in the assessment of anthropogenic climate change. Much of this uncertainty arises from the relationship used to link aerosol with cloud droplet number concentration (CDNC). In addition, variability in the predicted meteorology and emission inventories used contribute to the differences in predicted AIE between GCM studies. Here the sensitivity of the first AIE to cloud droplet parameterizations, emission inventories and meteorological fields used is assessed.

The sensitivities are computed with the 3D NASA Global Modeling Initiative (GMI) chemical-transport model. GMI allows easy interchange of different model components while maintaining all others identical allowing a direct intercomparison of results obtained between alternate representations of aerosol, chemistry and transport processes. CDNC is computed using both empirical correlations (i.e., Boucher and Lohmann - BL (1995), Menon et al., - LB (2002)), and physically-based parameterizations (i.e., Abdul-Razzak and Ghan - AG (2000), and Fountoukis and Nenes - FN (2005)). Emissions from the University of Michigan (UoM) and the IPCC CMIP5 (CMIP) are used. Sensitivities are examined under two meteorological fields (i.e., NASA GEOS4 finite volume GCM (FVGCM) and NASA GEOS1-STRAT (GEOS)). Computed CDNC is used to calculate the effective radius (Re). The CLIRAD-SW solar radiative transfer model is used online to calculate the cloud optical depth (COD) and the shortwave fluxes from the surface to the top of the atmosphere (TOA). COD is calculated as a function of the effective radius. Evaluation of modeling results (i.e., Re, COD) is performed against satellite products from Moderate Resolution Imaging Spectroradiometer (MODIS) platform.

Depending on the meteorological field, the emission inventory and the droplet scheme used the annual mean CDNC ranges between 57 and 218 cm^{-3} (Figure 1) with larger differences seen over heavily polluted regions (e.g., Europe, China, NE USA), regions affected by long range transport of pollution (e.g., Atlantic Ocean) and regions affected by biomass burning (e.g., S. Africa, S. America). The droplet scheme used seems to be the most important parameter affecting CDNC followed by meteorology; the sensitivity of CDNC to emission inventories is small. The results for the shortwave cloud radiative forcing and the first AIE are quite similar across the modeling experiments reflecting the main differences seen in CDNC between simulations that use current and preindustrial emissions.

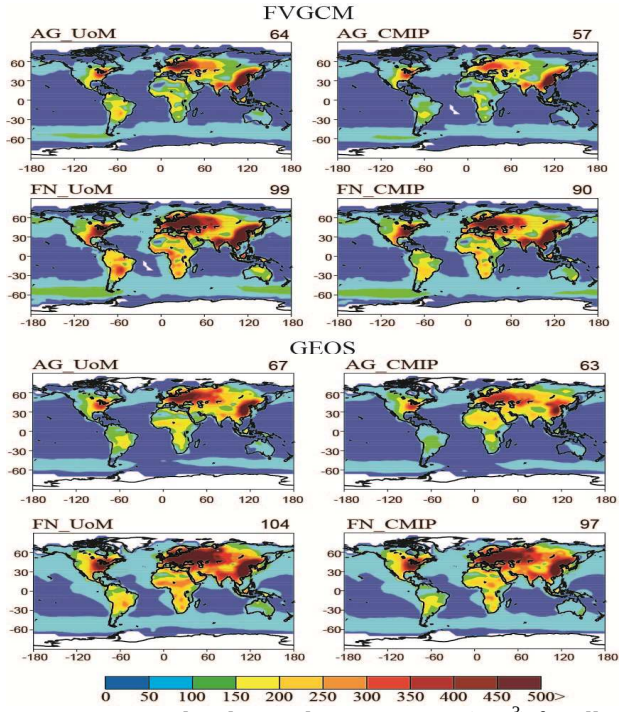

Figure 1. Simulated annual mean CDNC (cm^{-3}) for all emission inventories and meteorological fields used and the schemes of AG and FN. Global averages are shown in the upper right hand corner of each panel

This work was supported by NASA (New Investigator Award, EOS-IDS), an NSF CAREER Award, a Blanchard-Milliken Young Faculty Fellowship, DOE-ARM, FP7-REGPOT-2008-1grant No 229773 and the National Strategic Reference Framework (NSRF) 2007-2013 grand No 09SYN-31-667.

Abdul-Razzak, H. and Ghan, S. (2002), *J. Geophys. Res.*, **107**.

Boucher, O. and Lohmann, U. (1995). *Tellus B*, **47**, 281–300.

Fountoukis, C. and Nenes, A. (2005), *J. Geophys. Res.*, **110**(D11212), doi:10.1029/2004JD005 591.

Menon et al. (2002), *J. Atmos. Sci.*, **59**, 692-713

Airborne measurements of elevated aerosol layers over Central Europe

B. Weinzierl[1,2], F. Dahlkötter[1], D. Sauer[2,1], K. Heimerl[1], A. Minikin[1], A. Petzold[1], C. Voigt[1,3], H. Flentje[4], F. Schnell[2], V. Freudenthaler[2], M. Wiegner[2], and A. Ansmann[5]

[1]Deutsches Zentrum für Luft- und Raumfahrt (DLR), Institut für Physik der Atmosphäre, Oberpfaffenhofen
[2] Ludwig-Maximilians-Universität München (LMU), Meteorologisches Institut, München, Germany
[3] Johannes Gutenberg-Universität Mainz (JGU), Institut für Physik der Atmosphäre, Mainz, Germany
[4] Deutscher Wetterdienst (DWD), Albin-Schwaiger-Weg 10, D-82383 Hohenpeissenberg, Germany
[5] Leibniz-Institut für Troposphärenforschung (IfT), Leipzig, Germany

Keywords: airborne aerosol measurements, lidar, absorption, black carbon, coating thickness, radiative transfer
Presenting author email: bernadett.weinzierl@dlr.de

Satellite images impressively demonstrate that aerosol layers originating from biomass burning, anthropogenic pollution or from deserts regions are regularly transported over long distances, even reaching other continents. Although the aerosol optical depth of individual layers can significantly contribute to the aerosol optical depth of the total atmospheric column [Weinzierl *et al.*, 2011], the global importance and the impact of these aerosol layers on atmosphere and climate is not yet known well enough.

Within the framework of the Contrail and Cirrus Experiment (CONCERT 2011), the DLR Falcon research aircraft conducted 11 research flights with a comprehensive aerosol in situ and trace gas instrumentation over Central Europe in September 2011. The aerosol in situ payload included a multi-channel CPC, several optical particle counters of type Grimm SKY-OPC 1.129, UHSAS-A, and FSSP-300. In addition, a multi-wavelength Particle Soot Absorption Photometer (PSAP) and a Single Particle Soot Photometer (SP2) was deployed, and the non-volatile particle size distribution was measured.

The main aim of CONCERT 2011 was a better understanding of contrails and natural cirrus clouds in the UTLS region, but in 9 of the 11 flights, also elevated aerosol layers were detected (see Fig. 1). 75% of the aerosol layers showed enhanced black carbon (BC) mass concentrations. Backward trajectory calculations indicate that the observed aerosol layers originated from boreal forest fires in Northern America, but also from anthropogenic pollution sources. In most of the cases the aerosol layers were found at altitudes between 2 and 5 km, but in two cases extended forest fire layers were present between 9 and 13 km altitude (Fig. 1, left panel). BC mass concentrations (size range: 70 nm - ~440 nm) in the elevated aerosol layers reached up to 0.3 µg m^{-3}. For comparison, BC mass concentrations ranged between 0.05 and 0.8 µg m^{-3} in the polluted boundary layer over Munich. From our SP2 data, we calculated the coating thickness of the BC particles in the elevated aerosol layers and found particles with a coating thickness of up to several hundred nanometers, whereas the BC particles in the boundary layers had only minor coatings. Such coatings can enhance the absorption of solar radiation [Schwarz *et al.*, 2008; Shiraiwa *et al.*, 2010], and therefore amplify the climate impact of those aerosol layers.

In our presentation, we will contrast the properties of the individual aerosol layers and show the impact of the aerosol source region and transport time on the observed microphysical and optical aerosol properties. We combine airborne in situ and ground-based lidar data to get information on the vertical and horizontal extent of the aerosol layers which is necessary to quantify the radiative effects of the individual aerosol layers. Expected heating rates and their impact on atmospheric stability will be discussed.

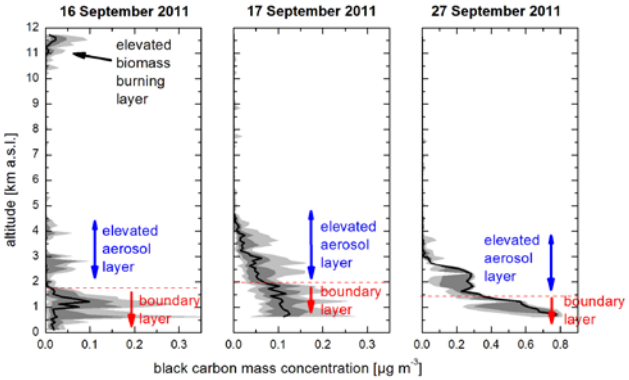

Fig. 1: Average vertical profiles of black carbon mass concentration for the research flights on 16, 17 and 27 September 2011. The black line denotes the median, and the light and dark grey shaded areas show the 10- and 90-, and 25- and 75-percentile values, respectively.

This work was funded by the Helmholtz Association (HGF) under grant number VH-NG-606 (Helmholtz Young Investigators Group AerCARE). The field experiment was organized and in part funded by the HGF grant VH-NG-309 (Helmholtz Young Investigators Group AEROTROP) and by the DLR project CATS.

Schwarz, J. P., et al. (2008), Coatings and their enhancement of black carbon light absorption in the tropical atmosphere, *J. Geophys. Res.*, *113*(3).

Shiraiwa, M., Y. Kondo, T. Iwamoto, and K. Kita (2010), Amplification of Light Absorption of Black Carbon by Organic Coating, *Aerosol Sci. Technol.*, *44*(1), 46-54.

Weinzierl, B., et al. (2011), Microphysical and optical properties of dust and tropical biomass burning aerosol layers in the Cape Verde region – An overview of the airborne in-situ and lidar measurements during SAMUM-2, *Tellus*, *63B*(4), 589-618.

The importance of wood burning as a source of absorbing aerosols in the European Arctic

K.E. Yttri[a], C. Lund Myhre[a], A. Stohl[a], C. Dye[a], D. Hirdman[a], J. Ström[b]

[a]Norwegian Institute for Air Research, P.O. Box 100, N-2027 Kjeller, Norway
[b]Stockholm University, SE-106 91 Stockholm, Sweden

Keywords: Arctic, black carbon, sources, wood burning
Presenting author email: clm@nilu.no

Improved understanding of processes and sources of absorbing aerosols (here called black carbon, BC) in the Arctic is crucial in order to predict future climate development and implement effective mitigation steps. Due to the high surface albedo of snow and ice, even weakly absorbing aerosol layers can heat the Earth/atmosphere system in the Arctic. Furthermore, absorbing aerosols deposited on the surface can affect the snow and ice albedo and increase the amount of solar radiation absorbed, enforcing melting of snow and sea ice. It can be argued that the largest uncertainties when studying the aerosols impact on the Arctic climate are attributed to the highly absorbing BC, which is generated by incomplete combustion of fossil fuel and biomass.

Recent studies have argued that agricultural and boreal wild fires with their high emissions and proximity to the Arctic could be the most important source of Arctic BC in years of high wild fire activity (Stohl, 2006; Warneke et al., 2009). Additionally, countries bordering the Arctic are known to use substantial amounts of wood for residential heating; e.g. residential wood burning accounts for 70 % of the Norwegian $PM_{2.5}$ emissions of which elemental carbon (EC) constitutes 20 – 25 % (Yttri et al, 2009). BC emissions from these countries might be more important with respect to contributing to the Arctic BC concentration, compared to emission sources situated further south (Hirdman et al., 2009).

The current study presents the first one-year time series (13th of March 2008 to the 13th of March 2009) of the wood burning tracer levoglucosan in the Arctic, measured at the Zeppelin observatory (78º54' N, 11º53' E 478 m asl). 24 hours mean concentrations of levoglucosan were obtained from ambient aerosol filter samples subjected to High-Performance Liquid Chromatography coupled with Time-of-Flight Mass Spectrometry. The levoglucosan measurements have been used to study the influence of residential wood burning emissions and boreal forest fire emissions as a source of BC in the European Arctic. Supplementary measurements of EC (Thermal-Optical Analysis), light absorbing particles (Particle Soot/Absorption Photometer) and CO are used to interpret the results.

The results show that the mean concentration of levoglucosan observed at the Zeppelin observatory in winter is typically 2 - 3 orders of magnitude less than that reported for European urban areas in winter and 1 – 2 orders of magnitude less than that of the European rural background environment. Elevated concentrations in winter (mean ± SD; 1019 ± 1769 pg m^{-3}) compared to summer (mean ± SD; 108 ± 180 pg m^{-3}) were observed, resembling the seasonal variation seen for e.g. sulphate and BC caused by the Arctic haze phenomenon.

Calculations are made with the Lagrangian particle dispersion model FLEXPART to assess dominating source regions for levoglucosan. The European areas bordering the European Arctic were found to have a large influence on the observed levoglucosan concentrations at Zeppelin in winter, likely being a combination of the widespread use of wood burning for residential heating in Northern Europe and its proximity to the Arctic, governing atmospheric transport.

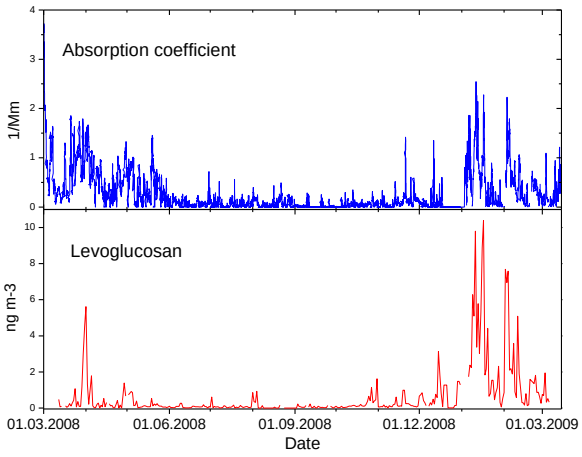

Figure 1: One year observations of levoglucosan and absorption coefficient at the Zeppelin Observatory

This work was supported by the Norwegian Research Council through the project POLARCAT (Polar Study using Aircraft, Remote Sensing, Surface Measurements and Models, of Climate, Chemistry, Aerosols, and Transport) which was an IPY (International Polar Year) project.

Hirdman D., et al. *Atmos. Chem. Phys*., 10, 669-693, 2010
Stohl, A., *J. Geophys. Res*. 111, D11306
Warneke C., et al., *Geophys., Res., Lett*, 37, L01801, 2010
Yttri, K.E., et al, *Atmos. Chem. Phys.*, 9, 2007-2020, 2009.

Horizontal Meter Scale Variability of Elemental Carbon in Surface Snow

J. Svensson[1,3], J. Ström[2], M. Hansson[2] and H. Lihavainen[1]

[1]Finnish Meteorological Institute, Helsinki, PO.Box 503, FI-00101 Finland
[2]Department of Applied Environmental Science, Stockholm University, Stockholm, SE-106 91, Sweden
[3]Department of Physical Geography and Quaternary Geology, Stockholm University, Stockholm, SE-106 91 Sweden
Keywords: Black Carbon, Arctic, Surface Snow, OCEC.
Presenting author email: jonas.svensson@fmi.fi

Investigations of Black Carbon (BC) have increased in recent years, as it has been proposed to significantly alter the climate, especially in the Arctic (e.g. Quinn et al. 2011). BC particles absorb solar heating (Flanner et al., 2007) and, if deposited in snow or ice it will lower the albedo and affect the radiative balance (Clarke and Noone, 1985). BC deposited on snow also contributes to earlier snowmelt (Flanner et al., 2007), which has the greatest effect in the spring when the highest amount of solar radiation is directed at the snowpack.

A comprehensive study of BC concentrations in snow in the Arctic was recently conducted by Doherty et al. (2010) and a variation from the different sampling sites was observed. The small scale (meter scale) variation, however, was not examined exhaustively and is in principle unstudied. The main objective of this study is to investigate the horizontal variation of BC on a high resolution scale (i.e. meter scale) in surface snow. The variation was further studied by comparing two sites with different character (clean vs. polluted). Due to the analysis method used, the thermal/optical method, elemental carbon (EC) is presented as a proxy of BC in this study.

Investigations were carried out in the vicinity of Stockholm, Sweden (representing the polluted site) and in Pallas, Arctic Finland (clean site). Individual surface snow (roughly the upper 5 cm) samples were collected in different grid-nets, with the most common grid-net consisting of a 20m by 20m square with samples taken every 5m within the square (see figure 1). Snow samples were melted and filtered through micro-quartz filters which were analyzed in a Thermal/Optical Carbon Aerosol Analyzer (OCEC) (Birch and Cary, 1996) for their apparent EC concentration.

A variability of EC in the sampled grid-nets was observed at both of the sites; however, the site with less pollution affecting it presented greater variation in comparison to the polluted site (figure 1 and 2). The higher variation at the Pallas site is probably explained by a higher degree of snow drift. Microphysics and snow metamorphism are also plausible factors which affect the variation of EC concentrations in the surface snow.

The results presented here on a meter scale will be compared with samples taken on a kilometer scale in Pallas. Additionally, a comparison between the Single Particle Soot Photometer (SP2) analysis method and the OCEC method for measuring BC in snow will be done.

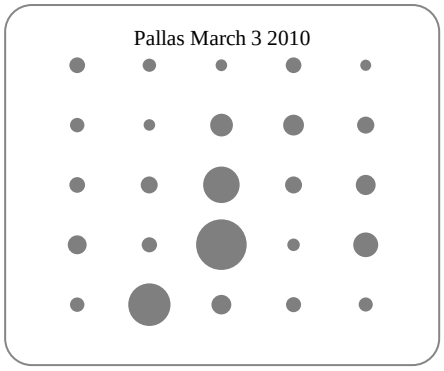

Figure 1. Grid-net from Pallas with a spatial scale of 5m between circles. The size of the filled circles reflects the corresponding sample's concentration size. The circle sizes are not proportional in size to the circles from Stockholm, as they are significantly higher.

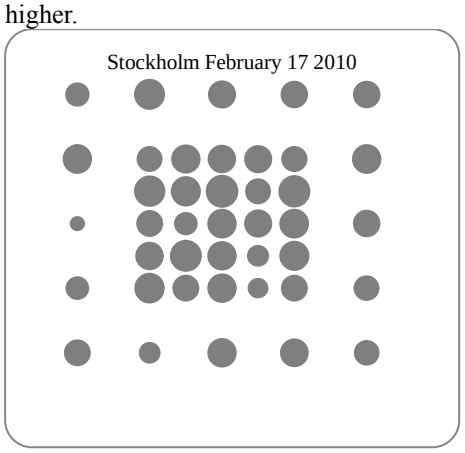

Figure 2. Grid-net from Stockholm with a spatial scale of 5m for the circles in the outmost square and 2.5m in the innermost part.

Birch, M. E. and Cary, R. A. (1996) *Aero. Sci. and Tech.* **25:3**,221-241.

Clarke, A. D. and Noone, K. J. (1985), *Atmos. Environ*., **19**, 2045–2053.

Doherty, S. J, Warren, S. G., Grenfell, T. C., Brandt, R. E. and Clarke, A. D. (2010). *Atmos. Chem. Phys.*, **10**, 11647–11680.

Flanner, M. G., C. S. Zender, J. T. Randerson, and P. J. Rasch (2007)., *J. Geophys. Res*., **112**, D11202, doi:10.1029/2006JD008003.

Quinn, P.K., Stohl, A., Arneth, A., Berntsen T., Burkhart, J.F., J. Christensen, J., Flanner, M., Kupiainen, K., Lihavainen, H., Shepherd, M., Shevchenko, V., Skov, H., and Vestreng, V. (2011), *AMAP*, 72pp.

Thursday, September 6, 2012

Session WG04S2O. Engines related emissions

Exhaust emissions and particle hygroscopicity with a diesel engine run with HVO fuel-oxygenate blend

M. Happonen[1], J. Heikkilä[1], P. Aakko-Saksa[2], T. Murtonen[2], K. Lehto[3], A. Rostedt[1], T. Sarjovaara[3], M. Larmi[3], J. Keskinen[1], A. Virtanen[1]

[1]Department of Physics, Tampere University of Technology, Tampere, 33540, Finland
[2]VTT Technical Research Centre of Finland, Espoo, 02044, Finland
[3]Aalto University, Department of Energy Technology, Espoo, 00076, Finland
Keywords: Diesel soot particles, Hygroscopic growth, fuel, oxygenate.
Presenting author email: juha.heikkila@tut.fi

The need to reduce greenhouse gas emissions as well as regulated emissions drives the need to study alternatives for fossil fuels.

Hydrogenated vegetable oil (HVO) is the newest commercially available bio-based diesel fuel. It is composed of paraffinic hydrocarbons and includes essentially no aromatics or sulphur. HVO fuel is reported to lower regulated emissions (Aatola *et al.*, 2008). Compounds containing oxygen (i.e. oxygenates) can be blended to the fuel to further reduce the particle emissions. Oxygen content in biodiesel (i.e. FAME) has been reported to increase the oxygen content in the emitted soot as well as alter the oxidation behaviour of the emitted soot (Song *et al*., 2006). Increased oxygen content in particles could also have an effect on particle hygroscopicity.

In this study (Happonen *et al.*, 2012), we investigated how the addition of oxygenate (Di-n-pentyl ether, DNPE) to HVO fuel alters particulate emissions and particle hygroscopicity. Oxygen content in the DNPE-HVO blend was 2 wt-%. The effect on NO_x-emissions was also studied.

The measurements were performed on an engine dynamometer with single-cylinder test engine modified from a commercial six-cylinder off-road common rail diesel engine.

Particle size distributions were measured using a Scanning Mobility Particle Sizer (SMPS) and the total number concentration with a Condensation Particle Counter (CPC). Particulate mass (PM) was measured according to the ISO 8178-1:2006 standard. Particle hygroscopicity was studied using a hygroscopic tandem differential mobility analyzer (HTDMA). We also performed organic/elemental carbon (OC/EC) analysis on collected particle filter samples.

Particulate matter (PM) emission was reduced 26-32% with all measured loads while particle number reduced 10-17%. With 75% and 100% loads NO_x-emission was slightly higher with oxygenate blended fuel, unlike with 50% load where NO_x – emission was 2-3% lower.

Growth factors are all within error limits (one standard deviation), as shown in figure 2. However, the growth factors measured with HVO were measured at approximately 2%RH higher humidity than HVO-DNPE growth factors and still the growth factors with HVO-DNPE are slightly higher than with pure HVO. The differences would be clearer if measured at the same RH. Thus, fuel seems to slightly affect the hygroscopic properties of emitted particles.

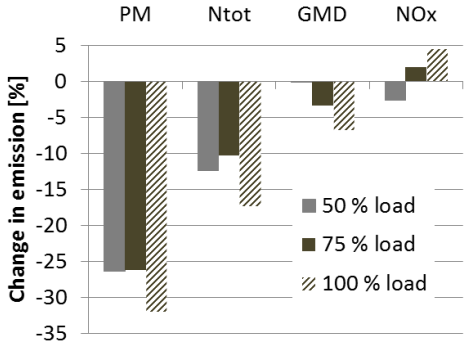

Figure 1. Relative changes in emissions caused by oxygenate blending with HVO fuel.

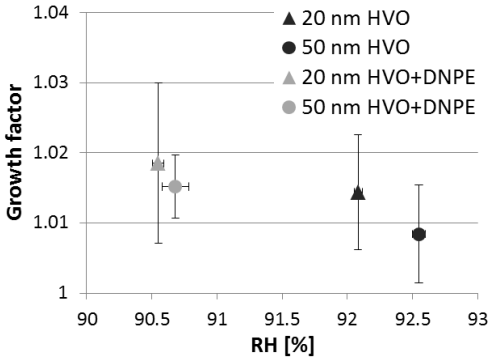

Figure 2. Growth factors of chosen particle sizes with and without oxygenate blending.

This study was funded by Tekes (Finnish Funding Agency for Technology and Innovation).

Aatola, H., Larmi, M., Sarjovaara, T., & Mikkonen, S. (2008). *Hydrotreated vegetable oil (HVO) as a renewable diesel fuel: trade-off between NOx, particulate emission, and fuel consumption of a heavy duty engine.* SAE Technical Paper Series, 2008-01-2500.

Happonen, M., Heikkilä, J., Murtonen, T., Lehto, K., Sarjovaara, T., Larmi, M., Keskinen, J., & Virtanen, A. (2012). *Diesel exhaust emissions and particle hygroscopicity with HVO fuel-oxygenate blend.* To be submitted in March 2012.

Song, J., Alam, M., Boehman, A. L., & Kim, U. (2006). *Examination of the oxidation behavior of biodiesel soot*. Combustion and Flame, 146,589–604.

Particulate matter emissions from a winter operation of a modern on-road diesel engine powered by heated rapeseed oil

M. Vojtisek-Lom, M. Pechout, M. Mazač

Department of Vehicles and Engines, Technical University of Liberec, Liberec, Czech Republic
Keywords: combustion, diesel engine, rapeseed oil, vegetable oil, biofuels
Presenting author email: michal.vojtisek@tul.cz

Introduction

Diesel engines powered by liquid fuels move the world, but also release, directly in the streets, nanoparticles hazardous to human health. New fuels and engine technologies must therefore be evaluated carefully for their effect on particle emissions.

Neat vegetable oils, typically used for the production of biodiesel, are often used as motor fuels, despite their use falling short of being widespread due to adverse effects on engines. One of such adverse effects is the inferior combustion of vegetable oils at low engine speeds and loads resulting in increased emissions of particulate matter (PM), while PM generally decrease at moderate and higher rpm and loads (Czerwinski 2008, Vojtisek-Lom 2009). The increase in PM emissions was attributed primarily to higher viscosity of rapeseed oil compared to diesel fuel, causing worse atomization of the fuel, and worsened evaporation in the combustion chamber, leading to a less complete combustion; the decrease in PM to the differences in chemical structure of rapeseed oil, notably the absence of aromatics and about 10% by weight oxygen content.

To decrease PM emissions, majority of currently produced diesel engines use a Common-Rail (CR) injection system. In a CR system, multiple injections are performed, with the timing and quantities of fuel injected controlled and optimized for petroleum diesel fuel. While this approach greatly reduces PM emissions when operating on diesel fuel, a question arises as to its performance with vegetable oils for which it is not optimized. Higher PM were reported by Dorn (2007).

Experimental

In this study, a 4.5-liter, 130 kW, four cylinder, turbocharged Cummins ISBe4 medium truck/bus engine with a Bosch CR injection system was tested on an engine dynamometer during steady-state operation. The engine was operated without any exhaust gas aftertreatment system on diesel fuel, neat biodiesel (FAME) and heated RO. The exhaust was routed in an improvised full-flow dilution tunnel, part of which was located outside of the laboratory. PM mass emissions were measured by the gravimetric method. Particle size distributions in the range of 5-500 nm were measured by EEPS spectrometer (model 3090, TSI, St. Paul, MN, USA). The testing was performed during the winter at outside temperatures 265-270 K and engine intake air temperatures 285-290 K.

The dilution apparatus and its operating temperature were favorable for nucleation and condensation of particles. No efforts were taken to evaporate volatile matter from the particles by a thermodenuder or by diluting with heated air. Therefore, this experimental setup was considered to represent reasonable worst-case scenario of an engine operated during the winter.

Results and discussion

The particle number emissions for FAME were typically similar to tens of percent lower compared to diesel fuel in all size ranges. For RO, particle concentrations were between diesel and FAME above 20-30 nm, but markedly higher at lower diameters with a strong nanoparticle peak (see figure below for an example). These small particles are believed to be organic carbon which would be in gaseous form at higher temperatures. Total particle number emissions for RO were compared to diesel lower at full load but higher at all other regimes. The effect on total PM mass over ESC and WHSC cycles was not uniform and relatively small. With the exception of the nanoparticle peak which is subject to future discussions, no major adverse effects on PM emissions were observed during operation of a modern CR diesel engine on heated RO.

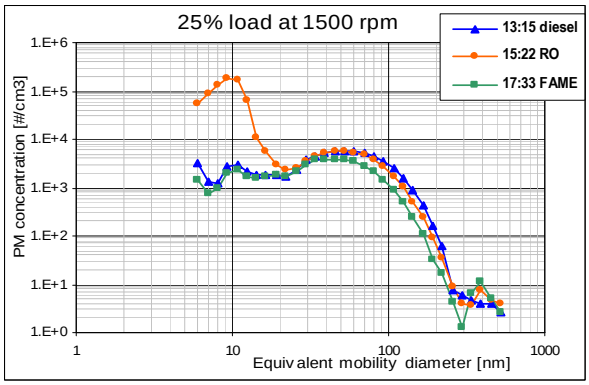

Funding: Czech Science Foundation grant 101/08/1717, Czech Ministry of Education project 1M0568, EU LIFE+ project MEDETOX, LIFE10 ENV/CZ/651.

References

Czerwinski, J.; Zimmerli Y.; Kasper, M.; Meyer, M. (2008). SAE Technical Paper 2008-01-1382 (Society of Automotive Engineers, www.sae.org).

DieselNet – www.dieselnet.com

Dorn, B.; Wehmann, C.; Winterhalter, R.; Zahoransky, R. (2007) SAE Technical Paper 2007-24-0127.

Vojtisek–Lom, M., Pechout, M., Blazek, J., Moc, L., Hlavenka,T. (2009). SAE Technical Paper 2009-01-1913.

Role of exhaust after-treatment devices in diesel exhaust nanoparticle formation processes

T. Rönkkö[1], J. Heikkilä[1], T. Lähde[1], L. Pirjola[2], F. Arnold[3], H. Schlager[4], D. Rothe[5] and J. Keskinen[1]

[1]Aerosol Physics Laboratory, Department of Physics, Tampere University of Technology, P.O. Box 599, FIN-33720, Tampere, Finland.
[2]Department of Technology, Metropolia University of Applied Sciences, P.O. Box 4000, FIN-00180, Helsinki, Finland.
[3]Atmospheric Physics Division, Max Planck Institute for Nuclear Physics (MPIK), P.O. Box 103980, D-69029 Heidelberg, Germany.
[4]Deutsches Zentrum für Luft- und Raumfahrt (DLR), Oberpfaffenhofen, Germany.
[5]MAN Truck & Bus AG, EMRE - Engine Research Exhaust Aftertreatment, Vogelweiherstr. 33, D-90441 Nürnberg, Germany.

Keywords: diesel exhaust, nucleation mode, sulphuric acid.
Presenting author email: topi.ronkko@tut.fi

The sulphuric acid, formed from fuel and lubricant oil sulphur compounds, is suspected to be one of the most important compounds in diesel exhaust nucleation mode particle formation. However, in several studies the nucleation mode particle formation conditions and physical characteristics of the particles do not indicate sulphuric acid driven process. In these cases the nucleation mode is repeatedly shown to include nonvolatile compounds (e.g. Rönkkö et al. 2007) and carry an electric charge. In general, it seems that exhaust after-treatment methods can have critical role in particle formation. Thus, in this study the focus was in the effects of exhaust after-treatment on diesel exhaust gaseous sulphuric acid and on nucleation mode particle formation and characteristics.

Measurements were performed at an engine dynamometer with a Euro IV heavy duty diesel engine without exhaust after-treatment and with three different oxidative exhaust after-treatment solutions: with diesel oxidation catalyst (DOC), with the combination of DOC and particle oxidation catalyst (DOC+POC) and with the combination of DOC and diesel particle filter (DOC+DPF). Thus the tested exhaust after-treatment devices represented typical technologies in modern vehicles and, on the other hand, formed interesting entity from the viewpoint of particle formation.

All exhaust after-treatment devices were tested using fuel and lubricant oil with sulphur contents 6 and 1600 ppm, respectively. In addition, particular tests were performed also using fuel with 36 ppm sulphur. Measurements were conducted at four steady state driving modes (ESC 10-13). Exhaust sampling and dilution for particle measurements was conducted using porous tube diluter, ageing chamber and secondary dilution. Particle size distribution and number concentration measurements were made using Nano-SMPS, SMPS, CPC and ELPI, and a thermodenuder was used to study particle volatility characteristics. Gaseous sulphuric acid (GSA) concentration was measured by using a CIMS instrument.

Results indicate that the formation and characteristics of nucleation mode particles are strongly depended on exhaust after-treatment. Without exhaust after-treatment or with the DOC, the particle formation seems to be based on non-volatile core particle formation at high temperatures and on particle growth by volatile compounds during the exhaust dilution and cooling process. With the DOC also the sulphuric acid driven particle formation seems to be possible. With a DOC+POC the nucleation mode was not observed (Figure 1) with low sulphur fuel. Instead, when the DOC+DPF was used, the nucleation mode occurred at high load and particles were volatile which, together with increased GSA concentrations, indicate sulphur driven particle formation.

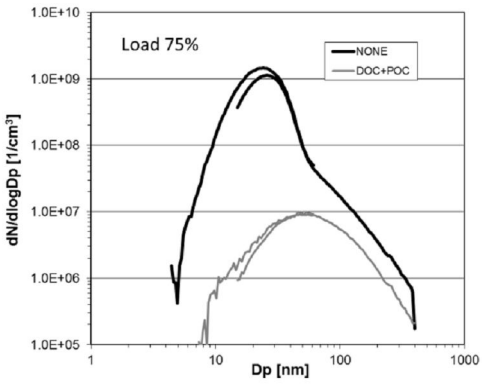

Figure 1. Particle size distributions of a heavy duty diesel engine without exhaust after-treatment (NONE) and with DOC+POC (Heikkilä et al. 2009).

This work was supported by The Finnish Funding Agency for Technology and Innovation (TEKES), Neste Oil Oyj and Ecocat Oy.

Heikkilä, J. et al. (2009). *J. Air & Waste Manage. Assoc.* 59:1148–1154

Rönkkö, T. et al. (2007). *Environ. Sci. Technol.* 41:6384-6389.

The influence of oxygenated organic aerosols (OOA) and its volatile organic content on the oxidative potential of diesel particulate mater

S. Stevanovic[1, 3], B. Miljevic[1], N.C. Surawski[1, 2], P.Vaattovaara[4], R. J. Brown[2], Z.D. Ristovski[1]

[1]International Laboratory for Air Quality and Health, Queensland University of Technology, 4001, Brisbane, Australia
[2]School of Engineering Systems, Queensland University of Technology, 4001, Brisbane, Australia
[3]ARC centre of Excellence for Free Radical Chemistry and Biotechnology, Queensland University of Technology, 4001, Brisbane, Australia
[4]Department of Physics, University of Eastern Finland,70211 Kuopio, Finland
Keywords: biofuels, reactive oxygen species, profluorescent nitroxide.
Presenting author email: s.stevanovic@qut.edu.au

Airborne particulate matter pollution is of concern for a number of reasons and has been widely recognised as an important risk factor to human health. A number of toxicological and epidemiological studies reported negative health effects on both respiratory and cardiovascular system. Despite the availability of a huge body of research, the underlying toxicological mechanisms by which particles induce adverse health effects are not yet entirely understood. The production of reactive oxygen species (ROS) has been shown to induce oxidative stress, which is proposed as a mechanism for many of the adverse health outcomes associated with exposure to particulate matter (PM). Therefore, it is crucial to introduce a technique that will allow rapid and routine screenings of the oxidative potential of PM.

In our previous studies we applied a new profluorescent nitroxide molecular probe (bis(phenylethynyl) anthracene-nitroxide; BPEAnit) [1], developed in an entirely novel, rapid and non-cell based assay, for assessing the oxidative potential of particles derived from various combustion processes (e.g. wood smoke and various diesel engines and fuels) [2,3].

One of the most important outcomes of our research thus far was that the oxidative potential per PM mass significantly varies for different combustion sources as well as different combustion conditions and feedstock used. However, possibly the most important finding from our studies was that there was a strong correlation between the organic fraction of particles and the oxidative potential measured by the PFN assay, which clearly highlights the importance of organic species in particle-induced toxicity [2,4] and reinforces the further investigations to explore this correlation.

To gain an insight into this relationship, additional measurements were conducted on an ethanol fumigated modern common rail diesel engine. In addition to running the engine with various levels of ethanol substitution several biofuels were used. Tests were designed to present emission differences due to changes in fuel and load settings.

A more detailed analysis of the organic content was performed to support the ROS measurements. This involved volatility measurement using a Volatility-Tandem Differential Mobility Analyser (V-TDMA) and particle composition using an Aerodyne Aerosol Mass Spectrometer (cToF-AMS). For detection of organic fraction we also used the ultrafine organic tandem differential mobility analyzer UFO-TDMA.

Volatility measurements indicating the overall organic coating on particles correlated with measured oxidative potential, but not as strong as in previous measurements. This indicated that ROS content is a function of organic particle composition but does not always exhibit a simple linear trend with volatility data. To investigate this relationship in more detail the data from the AMS were used. The fraction at the m/z of 44 (f44) was used as a tracer for the oxygenated organic aerosol (OOA) and 57 (f57) as the tracer for hydrocarbon like organic aerosol (HOA). The highest correlation was observed between the ROS concentration and the OOA.

Therefore the oxidative potential of the PM, measured through the ROS concentration, although proportional to the total volatile organic volume percentage shows a much higher correlation with the oxygenated organic fraction. This highlights the importance of the surface chemistry of particles for assessing the health impacts. It also sheds a light onto new aspects of particulate emissions that should be taken into account when establishing relevant metrics for health implications of various emissions.

1. Fairfull-Smith, K. E. and S. E. Bottle (2008). *Eur J Org Chem* 32: 5391-5400.
2. Miljevic, B., M. F. Heringa, et al. (2010). *Environ. Sci. Technol.* 44(17), 6601-6607.
3. Surawski, N. C., B. Miljevic, et al. (2010). *Environ. Sci. Technol.* 44(1), 229-235.
4. Surawski, N. C., B. Miljevic et al., (2011) *Environ. Sci. Technol.* 45 (24), 10337-10343

Size-resolved particle emission factors for individual ships

Å.M. Jonsson[1], J. Westerlund[2] and M. Hallquist[2]

[1]IVL Swedish Environmental Research Institute Ltd, Box 5302, 400 15, Gothenburg, Sweden
[2]Atmospheric science, Department of Chemistry and Molecular Biology, University of Gothenburg, 412 96, Gothenburg, Sweden
Keywords: ship emissions, emission factor, coastal area, number size distribution
Presenting author email: asa.jonsson@ivl.se

More than 80 % of world trade is transported by ships and shipping is projected to increase further in the future (Buhaug et al., 2009). Emissions from shipping are today poorly regulated in legislation. Shipping has therefore become a more and more important source for urban air quality in coastal and harbour cities. Shipping also contributes globally to climate effects. E.g. globally the contribution of particles from shipping is almost as large as from road traffic, 1.7 compared to 2.1 Tgy^{-1} (Eyring et al., 2005). For emission inventories both laboratory and field measurements are needed to complement each other. Measurements for large fleets on individual ship basis for nanoparticles are today very scarce.

A method previously used for road side measurements where particle emissions were related to CO_2 as a trace of combustion e.g. (Hak et al., 2009) was in this study used for ship emissions. A sample was extracted from passing exhaust plumes on an island next to a large fairway and characterized with an EEPS (Engine Exhaust Particle Sizer, model 3090, TSI Inc.), a CPC (Condensation Particle Counter, 3775, TSI Inc.) and a non-dispersive infrared gas analyser (LI-840, LI-COR Inc.) for CO_2. A thermodenuder was used in front of the EEPS to measure the volatile to non-volatile ratio of selected plumes. Emission factors (EFs) was calculated with the following formula:

$$EF_{part} = \frac{\Delta part}{\Delta gas} \times EF_{gas}$$

where $\Delta part$ and Δgas are changes in particle number/mass and CO_2 during ship passages and EF_{gas} is the EF for CO_2.

In these measurements particle emissions from individual ships have been characterized, both regarding number, mass and size distribution (Part 1) but also for volatility (Part 2) (Jonsson et al., 2011). The measurements were conducted in the entrance to the port of Gothenburg which is an environmental control area (ECA) where the maximum fuel sulphur content was limited to 1 % by weight. In total 734 EFs (Fig. 1) were derived. 92 ship passages were also selected to determine the thermal characteristics of the particles emitted (Part 2). Compared to diesel buses without particle filter the EFs in this study were a factor of 10 higher for number and a factor of 2 higher for mass (Jonsson et al., manuscript in preparation, 2012).

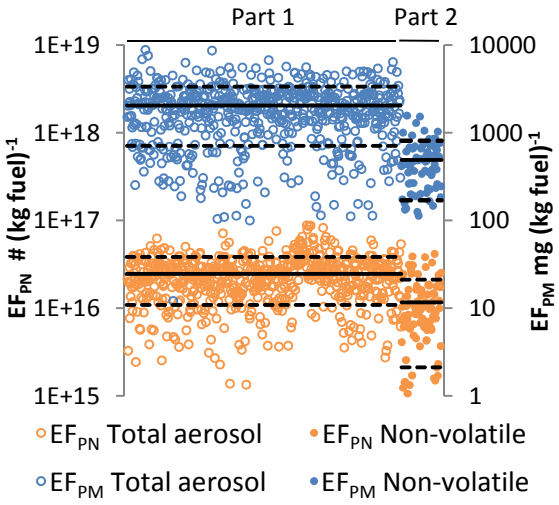

Figure 1. EF for 734 ship passages for number (EF_{PN}) and mass (EF_{PM}). The total aerosol was measured in Part 1 and the non-volatile fraction in Part 2. Solid lines represent averages and dashed lines represent 1 standard deviation.

Using a stationary measurement platform for ship emissions proved to be very successful both regarding reproducibility, cost and number of ships studied. Analysis of factors affecting the particle emissions e.g. ship speed and plume age are also considered (Westerlund et al., manuscript in preparation, 2012).

This work was financed by ÅForsk (Ångpanne-föreningen's Foundation for Research and Development), The Foundation for the Swedish Environmental Research Institute, SIVL and the Graduate School Environment and Health.

Buhaug, Ø., et al. (2009) *Second IMO GHG study 2009,* Int. Marit. Organ., London

Eyring, V., Köhler, H. W., van Aardenne, J., Lauer, A. (2005) *J. Geophys. Res,* **110**, doi:10.1029/2004JD005619

Hak, C. S., Hallquist, M., Ljungström, E., Svane, M., Pettersson, J. B. C. (2009) *J. Atmos. Environ,* **43**, 2481-2488.

Jonsson, Å, M., Westerlund, J., Hallquist, M. (2011) *Geophys Res. Lett,* **38**, L13809

Towards an identification of aircraft soot among urban background: focus on nanoparticles emitted by CFM56 turbofan engines

D. Lottin[1], D. Ferry[2], J.-M. Gay[2] and D. Delhaye[1]

[1]ONERA – The French Aerospace Lab, F-92322 Châtillon Cedex, France
[2]CINaM-CNRS UMR 7325, Aix-Marseille University, Campus de Luminy – case 913, 13009 Marseille, France

Keywords: Combustion aerosols, Size distribution, Morphology, Transmission Electron Microscopy.
Presenting author email: delphine.lottin@onera.fr

Today's scientific concerns incite to study both qualitatively and quantitatively the impact of combustion aerosols on the atmosphere because of the current questions of climate change and atmospheric pollution. For example, the combustion processes in aircraft turbofan engines produce particulate matter mainly composed of soot aggregates. These quasi-fractal, carbonaceous and submicron particles potentially act in the modification of the atmospheric radiative budget and in the degradation of the air quality in the airports vicinity (Lee *et al.*, 2009). This study focuses on the definition of size and morphological characteristics able to identify aircraft soot aggregates among urban aerosols.

Aircraft soot aggregates emitted by three different CFM56 turbofan engines (CFM International) are collected by impaction on Transmission Electron Microscopy (TEM) grids. The sampling is performed during engine cycles representative of combustion settings in airport areas. We analyze the TEM micrographs to determine the characteristic sizes of the aggregates, namely the primary particles diameters (d_p) and the aggregates gyration diameters (d_g) according to the usual methods of characterization (Baron and Willeke, 2001 and references therein). The geometric mean values calculated on the three populations of aircraft aggregates are compared to the characteristic sizes of diesel soot aggregates (Lapuerta *et al.*, 2012) and presented in Table 1. It appears that these aircraft soot aggregates are statistically smaller than diesel ones.

Characteristic sizes	$\langle d_p \rangle$	$\langle d_g \rangle$
Diesel	25 nm	110 nm
CFM56-5C	10 nm	70 nm
CFM56-5B	9 nm	40 nm
CFM56-7B	5 nm	60 nm

Table 1. Geometric mean primary particle diameter and gyration diameter for soot aggregates emitted by CFM56 and diesel engines (Lapuerta *et al.*, 2012)

The observation of TEM micrographs reveals that aircraft soot aggregates are generally more compact and less ramified than diesel ones (Figure 1). The determination of the statistical mass fractal dimension (Brasil *et al.*, 1999) does not highlight such morphological differences, since the values for CFM56 aggregates are very similar to values found in the literature for diesel aggregates (Lapuerta *et al.*, 2010 and references therein). Therefore, we use a complementary approach to describe the morphological characteristics of soot aggregates, based on a 2D analysis of the TEM micrographs. Firstly, we focus on the perimetric fractal dimension calculated on the aggregates as individuals using a covering-box method (Cleary *et al.*, 1990). Secondly, we describe the shape of the aggregates by using three shape descriptors, namely the roundness, the aspect ratio and the form factor (Chakrabarty *et al.*, 2006, Hentschel and Page, 2003). This approach seems efficient to distinguish soot aggregates according to their combustion source, i.e. diesel and aircraft ones.

However, further investigations will be undertaken to confirm the tendencies observed on size and morphology for soot aggregates emitted by technologically different aircraft engines. This could be used to complete the knowledge on the particulate matter emitted in the airport vicinity. To a further extent, this analysis has to be done for aggregates emitted by other urban, e.g. industrial or residential, combustion sources.

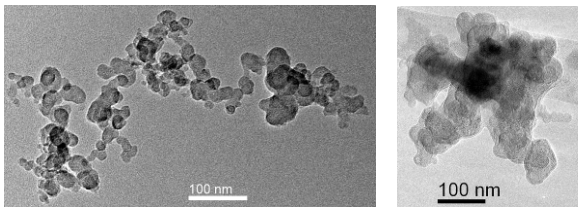

Figure 1. TEM pictures of diesel (left) and aircraft (right) soot aggregates.

Baron, P.A., and Willeke, K. (2001) *Aerosol measurement. Principle, techniques, and applications* 2nd Edition, John Wiley & sons.

Brasil, A.M., Farias, T.L., Carvalho, M.G. (1999) *J. Aerosol Sci.* **30**, 1379-1389.

Chakrabarty, R.K., Moosmüller, H., Garro, M.A., Patrick Arnott, W., Walker, J., Susott, R.A., Babbitt, R.E., Wold, C.E., Lincoln, E.N., Hao, W.M. (2006) *J. Geophys. Res.* **111**, D07204.

Cleary, T., Samson, R., Gentry, J.W. (1990) *Aerosol Sci. Tech.* **12**, 518-525.

Hentschel, M.L., and Page, N.W. (2003) *Part. Part. Syst. Charact.* **20**, 25-38.

Lapuerta, M., Martos, F.J., Martin-Gonzalez, G. (2010) *J. Colloid. Interf. Sci.* **346**, 23-31.

Lapuerta, M., Oliva, F., Agudelo, J.R., Boehman, A.L. (2012) *Combust. Flame* **159**, 844-853.

Lee, D.S., Fahey, D.W., Forster, P.M., Newton, P.J., Wit, R.C.N., Lim, L.L., Owen, B., Sausen, R. (2009) *Atmos. Env.* **43**, 3520-3537.

Evolution of Jet Engine Exhaust Aerosol in an Aging Plume

D.E. Hagen, P. Lobo, J. Keehn, M. Trueblood, and P.D. Whitefield

Center of Excellence for Aerospace Particulate Emissions Reduction Research, Missouri University of Science & Technology, 65409, Rolla MO, USA
Keywords: Combustion aerosols, Aircraft plumes, Hygroscopicity, Volatility.
Presenting author email: hagen@mst.edu

During Project AAFEX-II (**A**lternative **A**viation **F**uel **E**missions e**X**periment), PM emissions measurements were conducted on a CFM56-2C1 gas turbine engine in March-April 2011 in Palmdale CA. The engine was mounted on a NASA DC-8 aircraft, which was parked on a pad, and emission samples were extracted at the engine exit plane (1m), in the near field (30m), and in the advected plume (145m). The engine was operated at several power levels, and burned several fuels: JP-8, a coal-based Fischer-Tropsch (FT) fuel, and a Tallow-based Hydroprocessed Esters and Fatty Acids (HEFA) fuel. In addition, a blend of JP8 and HEFA fuels and FT fuel doped with with a 1000 ppm sulfur compound, Tetrahydrothiophene (THT) were also studied. The objectives of the AAFEX-II campaign were to evaluate alternative fuel effects on engine performance and fuel-handling equipment, determine fuel effects on engine PM and gas phase emissions, study the role of sulfur on exhaust PM, investigate the impact of sample line chemistry and line losses on emission measurements, and to support the development of standardized exhaust sampling methodology.

The chemical composition of atmospheric aerosol is an important but difficult to measure aerosol characteristic. In the absence of direct quantitative chemical analytic methods, the measurement of an aerosol's hydration and volatility properties contributes significantly to our understanding of the chemical nature of the aerosol and how it will evolve in the atmosphere. During project AAFEX-II PM total number and size distribution measurements were made at the engine exit plane and at distances of 30 m and 145 m downstream in the exhaust plume. Additionally non-volatile PM number, size distribution, and hydration measurements were made at the 145 m position. Condensation particle counters and electrical mobility-based size spectrometers were used for number and size distribution measurements, a thermal denuder operating at 300 C was used for volatility characterization (Schmid et al 2002), and a tandem differential mobility analyzer with saturator was used for hydration measurement (Whitefield et al 1993).

Figure 1 shows an example of the 145 m PM soluble mass fraction (Smf) and volatile mass fraction (Vmf) as a function of particle diameter (x) when the engine is operating at 85% power and burning JP8 fuel. Both Smf and Vmf decrease with increasing particle size and have a correlation coefficient of 0.86.

Particles are found to be generated in the near field between 1 and 30 m. This particle generation decreases as power increases; it is small at high power except for the case of high sulfur fuel. Non-volatile

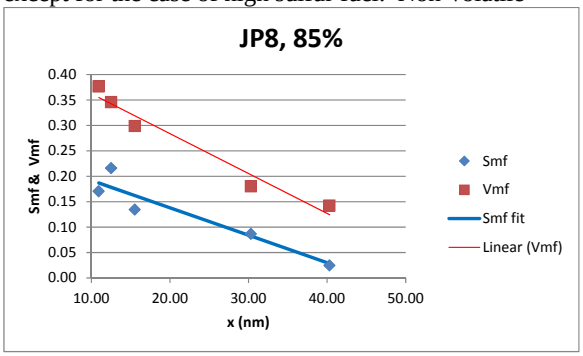

Fig. 1 Soluble mass fraction and volatile mass fraction vs. particle diameter

particles are generated between 1 and 145 m. This generation is observed to decrease with increasing engine power. JP8 and the HEFA-JP8 blends show the lowest proclivity for particle generation. At 145 m the volatile particle population is greater than the non-volatile by factors ranging from 10 to 300, with an average around 50. Particle mass is generated between 1 and 30 m; this generation decreases as power increases; it is small at high power except for the high sulfur fuel. PM non-volatile mass is generated between 1 and 145 m, perhaps due to scavenging. This effect decreases with increasing engine power, and it is small at high power for all fuel types. The volatile mass is greater than the non-volatile by factors ranging from 1 to 25, with an average around 7.

This work was sponsored by the Federal Aviation Administration under FAA Award No. 09-C-NE-MST Amendment No. 003. The opinions and conclusions expressed or implied in the presentation are those of the authors. They are not necessarily those of the program sponsor.

Schmid, O., B. Eimer, D.E. Hagen, and P.D. Whitefield (2002) Aerosol Sci. and Techn. **36**, 877-889.

Whitefield, P.D., M.B. Trueblood, and D.E. Hagen (1993) Particle Size & Techn. **11**, 25-36.

Thursday, September 6, 2012

Session WG05S3O. PMx source apportionment

Comparison of receptor models using synthetic organic aerosol mass spectra

H. Hagino[1], and T. Morikawa[1]

[1] Energy and Environmental Research Division, Japan Automobile Research Institute, Tsukuba, Ibaraki, 305-0822, Japan

Keywords: Aerosol mass spectrometry, Source Apportionment, PMF, CMB
Presenting author email: hhagino@jari.or.jp

The atmospheric aerosols, especially fine particles, are known to have adverse health effects on human populations. Understanding the composition of fine particles is necessary to identify their sources and to predict their effect on various atmospheric processes. Although organic aerosols are major components of the fine particles in urban atmospheres, the composition, formation mechanisms, and seasonal variation of concentrations of organic aerosols (OA) are not well understood. To study the organic aerosol source apportionment, several receptor models have been developed, such as the Chemical Mass Balance (CMB) and Positive Matrix Factorization (PMF) models. These receptor models have frequently been applied to $PM_{2.5}$ measurement for air quality management. However, few studies have applied receptor modelling to datasets of aerosol mass spectrometer (AMS). The AMS data has been used to chemically characterise the sources and evolution of OA at many worldwide (Zhang *et al*., 2007).

The CMB (CMB8J ; Hayakari and Hanaishi (2001)) and PMF (PMF2 ver4.2 ; Paatero (2000)) were demonstrated to synthetic datasets that suppose ambient organic aerosol mass spectra from two sources. Two different organic aerosol mass spectra scenarios using different sources were considered. The scenario assumed that the similar time variations occurred between diesel exhaust particles as primary organic aerosol (POA) and *m*-xylene-derived secondary organic aerosol (SOA) (Figure 1).

The time trend of PMF and CMB agree well with a good correlation. However, PMF separate out factors corresponding to POA and SOA, then two sources that made relatively uniform contributions to the synthetic dataset. In addition, PMF resolved factor profiles also have similar profile abundances. The CMB represented that the source apportionment with the POA and SOA profile has a better fit to the synthetic dataset.

Each receptor model has its strengths and weaknesses. These weaknesses include CMB might misspecify sources and have collinearity problem (Lowenthal, *et al*. 1992); for PMF, it should interpreted as sources and aerosol components. In addition, PMF might fail to separate out some factors (sources) (Brinkman *et al*., 2006).

The CMB is an ideal approache when the profiles of the emissions for all relevant sources are known and do not change with time. The more dataset from laboratory and field studies need to be analysed to evaluate the receptor models.

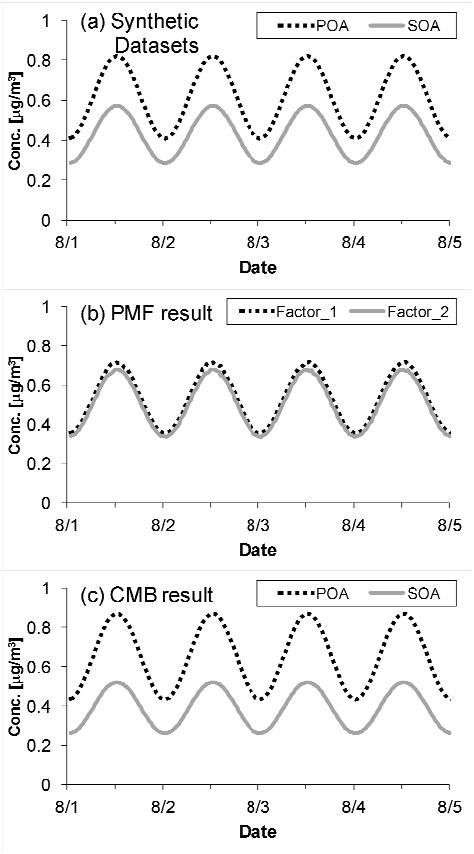

Figure 1. Time trends of synthetic dataset (a), PMF analytical result (b), and CMB analytical result (c).

This research was supported by the Environment Research and Technology Development Fund (C-1001) of the Ministry of the Environment, Japan.

Brinkman, G., Vance, G., Hannigan, M.P., and Milford, J.B. (2006) *Environ. Sci. Technol.* **40**, 1892–1901.

Hayakari, S. and Hanaishi, R.(2001) *J. Jpn. Soc. Atmos. Environ.*, **36**, 39–45.

Lowenthal, D.H., Chow, J.C., Watson, J.G., Neuroth, G.R., Robbins, R.B., Shafritz, B.P., Countess, R.J. (1992) *Atmos. Environ.* **26A**, 2341–2351.

Paatero, P. User's Guide for Positive Matrix Factorization Programs PMF2 and PMF3; University of Helsinki: Finland, 2000.

Zhang, Q. *et al*. (2007) *Geophys. Res. Lett.* **34**, L13801.

Tracer-based source-apportionment from the EUCAARI project and comparison with the EMEP model

D. Simpson[1,2], C. Alves[3], R. Bergström[4,5], S. Decesari[6], J. Genberg [7], S. Gilardoni [8], G. Kiss [9], E. Swietlicki [7] and E. Vignati [8]

[1]EMEP MSC-W, Norwegian Meteorological Institute, Oslo, Norway

[2]Dept. Earth & Space Sciences, Chalmers University of Technology, Gothenburg, SE41296, Sweden

[3] CESAM, Dept. of Environment, University of Aveiro, Aveiro, Portugal

[4] Dept. Chemistry, University of Gothenburg, Sweden

[5] Swedish Meteorological and Hydrological Institute, Norrkoping, Sweden

[6] ISAC-CNR, Istituto ISAC - C.N.R., 40129 Bologna, Italy

[7] Dept. Physics, Lund University, Lund, Sweden

[8] Joint Research Centre, Institute for Environment and Sustainability, TP 290 21027 Ispra (VA), Italy

[9] Air Chemistry Group of Hungarian Academy of Sciences at University of Pannonia, Veszprém, Hungary

Keywords: aerosol,source-apportionment,tracers,modelling

Presenting author email: david.simpson@met.no

Particulate carbonaceous matter (PCM) is found to constitute 10–40% of PM10 levels at rural and natural background sites in Europe Recent reviews have highlighted the complexity of the carbonaceous aerosol both in terms composition and formation mechanisms, but over the last few years a number of measurement results using tracer methods have become available which have started to shed light on the important sources of PCM in Europe (e.g. Gelencsér et al., 2007; Szidat et al., 2009).

Within the EUCAARI project, data on 14C, EC, OC and GC-MS analyses, and sometimes NMR and AMS, are available from a number of sites, including in Hungary, Finland, Germany, Italy (eg Gilardoni et al., 2011), and Sweden (Genberg et al., 2011). The link between tracers and their associated organic carbon amounts are of course very uncertain. Using method developed in Gelencsér et al. (2007) and Szidat et al. (2009) we define both a central best-estimate value for each factor and a plausible range of uncertainty. In order to tackle the multitude of possible combinations of these uncertain parameters, we have made use of an effective statistical approach known as Latinhypercube sampling (LHS). All valid combinations of parameters (i.e. excluding those producing negative contributions) are condensed in frequency distributions of possible solutions. This work focuses on the use of this method with EUCAARI and other observations to shed light on the sources of PCM in Europe. The LHS approach is used to calculate the relative contributions of the primary/secondary and anthropogenic/natural sources of the carbonaceous aerosol.

Finally, we will use model calculations using the EMEP MSC-W model (Simpson et al., 2012, Bergström et al., 2012), and variants of the so-called volatility basis set SOA schemes (eg Donahue et al., 2009) to illustrate how source-apportionment analysis can be used to discriminate between different SOA schemes, and to constrain model possibilities. An important finding of these studies is that large uncertainties exist in the emission inventories for residential wood-burning in Europe.

This work was supported by the the EU 6th Framwork programmes EUCAARI (Contract No. 34684), Swedish Research Programme for Clean Air (SCARP), and EMEP under UNECE

Bergström, R., et al. (2012) Modelling of organic aerosols over Europe (2002–2007) using a volatility basis set (VBS) framework with application of different assumptions regarding the formation of secondary organic aerosol, Atmos. Chem. Phys. Discuss, **12**, 5425–5485.

Donahue, N. M., Robinson, A. L., and Pandis, S. N. (2009) Atmospheric organic particulate matter: From smoke to secondary organic aerosol, Atmos. Environ., **43**, 94–106, 55.

Gelencsér, A. et al. (2007) Source apportionment of $PM_{2.5}$ organic aerosol over Europe: primary/secondary, natural/anthropogenic, fossil/biogenic origin, J. Geophys. Res., **112**, D23S04.

Genberg, J. et al. (2011) Source apportionment of carbonaceous aerosol in southern Sweden, Atmos. Chem. Phys., **11**, 11387–11400

Gilardoni, S. et al. (2011) Better constraints on sources of carbonaceous aerosols using a combined ^{14}C – macro tracer analysis in a European rural background site, Atmos. Chem. Phys., **11**, 5685–5700

Simpson, D. et al. (2012) The EMEP MSC-W chemical transport model – Part 1: Model description, Atmos. Chem. Phys. Discuss., **12**, 3781–3874

Szidat, S. et al. (2009) Fossil and non-fossil sources of organic carbon (OC) and elemental carbon (EC) in Göteborg, Sweden, Atmos. Chem. Phys., **9**, 1521–1535.

Intercomparison of source apportionment approaches within the EU-MED APICE project.

A. Detournay[1], D. Salameh[1], J.L. Jaffrezo[2], J. Cozic[2], J.Pey[3], N. Perez[3], X. Querol[3], P. Prati[4], M.C. Bove[4], E. Cuccia[4], D. Massabo[4], J. Bartzis[5], , D. Saraga[5], E. Tolis[5], K. Filiou[5], A. Latella[6], F. Liguori[6], S. Patti[6], A. Armengaud[7], D. Piga[7] and N. Marchand[1].

[1] Aix-Marseille Univ, CNRS, Laboratoire Chimie Environnement, 13331, Marseille, France
[2]Université Joseph Fourier-CNRS-LGGE, St-Martin d'Hères, France
[3] Institute of Environmental Assessment and Water Research –CSIC, Barcelona, Spain
[4] University of Genoa & INFN, Dept. of Physics, 16146 , Genoa, Italy
[5] University of West Macedonia, Dept of Mechanical Engineering, Env. Techn., Lab., 50100 Kozani, Greece
[6] ARPA Veneto - Regional Air Observatory , 30171 Mestre–Venice, Italy
7 AirPACA – Regional Air Observatory 13006, Marseille, France
Keywords: Source apportionment, PMF, CMB, organic markers, Marseille
Presenting author email: anais.detournay@univ-amu.fr

The EU-MED APICE project (Common Mediterranean strategy and local practical Actions for the mitigation of Port, Industries and Cities Emissions; www.apice-project.eu) aims to quantify the impact of harbour and harbour related activities to PM concentration observed in 5 Mediterranean harbours: Barcelona (Spain), Marseille (France), Genoa (Italy), Venice (Italy) and Thessaloniki (Greece). For that purpose, long term monitoring campaigns are currently underway in these 5 harbours by each of the local scientific partner of the project. In order to intercompare source apportionment approaches used by each partner and to harmonize the methodologies between areas under study, a 6 weeks intercomparison campaign has been conducted in Marseille during winter 2011.

Marseille is the most important harbour of the Mediterranean Sea. It handles twice the traffic compared to Genoa, and nearly three times the traffic of Barcelona or Valencia. A huge petrochemical area, among other industrial plants (steel mill, coke plant...), is also located close to Marseille, the second most populated city in France with more than 1 million inhabitants. Industrial and shipping emissions of PM are generally among the least well known sources in the field of atmospheric research and largely merit in depth studies in this context. Furthermore, this intercomparison campaign is also the ideal framework to test our ability to apportion such specific sources among many others in a densely populated area.

Comprehensive chemical characterization of PM2.5 and PM10 have been performed by each partner on the same 24h basis during this 6 week-long campaign, including measurements of major ions, OC/EC, metals/elements and organic markers (hopanes, levoglucosan, PAHs, n-alkanes, fatty acids, resin acids, methoxy phenol,..). Independent results from each partner are now intercompared. High temporal resolution measurements were also achieved with high-resolution time-of-flight aerosol mass spectrometers (HR-ToF-AMS), aethalometer, multi-angle absorption photometer (MAAP), scanning mobility particle sizer (SMPS) and proton transfer reaction mass spectrometer (PTR-MS) for VOC measurements. Positive Matrix Factorization (PMF) and Chemical Mass Balance (CMB) were used to apportion sources. Preliminary example of source apportionment is presented with figure 1.

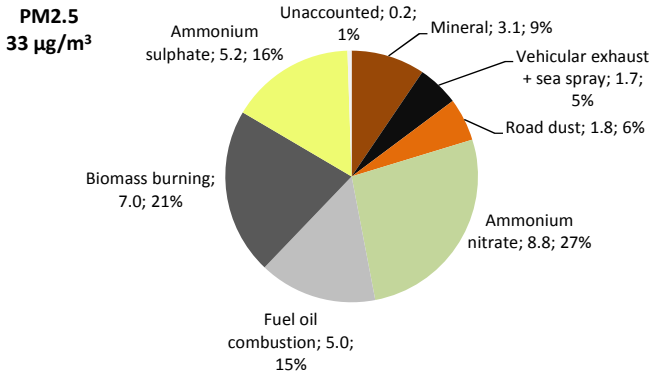

Figure 1. Example of source apportionment by PMF, using both organic markers and metals.

In this presentation, we will compare several source apportionment approaches:
- CMB with organics markers and elements/metals,
- PMF with elements/metals and major aerosol fractions (OC/EC, major ions),
- PMF with elements/metals, organic markers and major aerosol fractions (OC/EC, major ions) (figure 1),
- AMS/PMF.

Combination of CMB and PMF has also been performed (*i.e.* factors derived from PMF analysis have been injected as source profiles in CMB calculation). This combined approach is particularly interesting for sources such as mineral or road dust, for which no source profile exists (or presents too much variability between environments to be considered as scientifically sounded).

This work is supported by the MED programme under grant 2G-MED09-26.

European Intercomparison for Receptor Models: Preliminary Results

F. Karagulian[1], C.A. Belis[1], F. Amato[2,20], D.C.S. Beddows[3], V. Bernardoni[4], S. Carbone[5], D. Cesari[6], E. Cuccia[7], D. Contini[6], O. Favez[8], I. El Haddad[9], R.M. Harrison[3], T. Kammermeier[10], M.Karl[11], F. Lucarelli[12], S.Nava[12], J. K. Nøjgaard[13], M. Pandolfi[2], M.G. Perrone[14], J.E. Petit[8,15], A. Pietrodangelo[16], P. Prati[7], A.S.H. Prevot[9], U. Quass[10], X. Querol[2], D. Saraga[17], J. Sciare[15], A. Sfetsos[17], G. Valli[4], R. Vecchi[4], M. Vestenius[5], J.J. Schauer[18], J.R. Turner[19], P. Paatero[21], P.K. Hopke[22]

[1]European Commission, Joint Research Centre, Institute for Environment and Sustainability - Ispra, 21027, Italy [2]Institute of Environmental Assessment and Water Research (IDAEA), Barcelona, 08034, Spain [3]National Centre for Atmospheric Science, University of Birmingham, Birmingham, B15 2TT, UK [4]Department of Physics, Università degli Studi di Milano and INFN, Milan, 20133, Italy [5]Finnish Meteorological Institute, Helsinki, FI-00101, Finland [6]Istituto di Scienze dell'Atmosfera e del Clima, ISAC-CNR, Lecce, 73100, Italy [7]Department of Physics, Università degli Studi di Genova and INFN-Genova, Genoa, 16146, Italy [8]Institut National de l'Environnement Industriel et des Risques (INERIS), Verneuil-en-Halatte, 60550, France [9]Laboratory of Atmospheric Chemistry (LAC), Paul Scherrer Institut, Villigen, 5234, Switzerland [10]Air Quality and Sustainable nanotechnology (IUTA), D- Duisburg, 47229, Germany [11]Norwegian Institute for Air Research (NILU), Kjeller, NO-2027 Norway [12]Department of Physics, Università degli Studi di Firenze and INFN-Firenze, Sesto Fiorentino, 50019, Italy [13]Department for Environmental Science, Aarhus University, Roskilde, 4000, Denmark [14]Department of Environmental Science, Università di Milano Bicocca, Milan, 20126, Italy [15]Laboratoire des Sciences du Climat et de l'Environnement (LSCE), F-91191 Gif-sur-Yvette, France [16]Institute for Atmospheric Pollution, National Research Council, Rome, Monterotondo Staz., 00016, Italy [17]Environmental Research Laboratory (NCSR Demokritos, Athens, 15310, Greece [18]Dept of Civil and Environmental Engineering, University of Wisconsin, Madison, WI, USA [19]Energy, Environmental and Chemical Engineering Dept, Washington University in St. Louis, USA. [20]TNO, Built Environment and Geosciences, Dept Air Quality and Climate, 3508 Utrecht, The Netherlands [21]YP-Tekniikka Ky, FI-00970, Helsinki, Finland. [22]Center for Air Resources Engineering and Science, Clarkson University, Potsdam, NY 13699-5708, USA

Keywords: intercomparison, source apportionment, receptor models, PM
Presenting author email: claudio.belis@jrc.ec.europa.eu

Receptor models are commonly used to identify the sources of ambient particulate matter (PM) in Europe. However, the use of different tools and methodological approaches make it difficult to compare the results of different studies.

In order to promote harmonization in this field an intercomparison exercise involving 16 expert groups was organized and evaluated by the JRC within the framework of FAIRMODE.

The test DB consisted of 178 $PM_{2,5}$ speciated samples deriving from two real-world re-arranged DBs (Lee & Hopke, 2006 JGR; Jaeckels et al., 2007 EST). Concentrations and uncertainties of 46 inorganic and organic species were used to characterize the PM.

A total of 22 solutions obtained using the following models or model versions were reported for evaluation: EPA-PMF3 (8), PMF2 (6), EPA-CMB 8.2 (4), PCA (1), APCS (1), COPREM (1) and ME-2 (1).

Although data in the DB were partially pre-processed, participants had to scrutinize the DB in order to identify, solve and report typical imperfections of real world DBs (e.g. missing values, values below detection limits, outliers and unusual uncertainty patterns).

Participants reported the number and label of the identified sources, their contribution estimation (SCE) and uncertainty. In addition, the source/factor chemical profiles and the contribution of each source/factor in each sample were also requested.

The match between observed and modelled PM mass in every sample was assessed using regression analysis, centered RMSE and bias. More than 75% of the solutions reconstructed the PM mass satisfactorily.

The majority of participants reported between 7 and 11 source/factors. They were classified into 15 different source categories: biomass burning, gasoline, diesel, brakes, traffic, dust, sulphates, nitrates, Zn smelter, Cu metallurgy, Pb smelter, steel processing, industry & combustion, ship emissions, secondary.

The inclusion of every source/factor into a category was checked by comparing its chemical profile and time trend with all the other members of the same category and with reference source profiles, when available. The SCEs of the different solutions were compared with a reference value obtained by robust analysis (standard ISO 5725-5). The acceptability criterion was set to 50% relative standard uncertainty. For more details see Karagulian & Belis (2012, IJEP accepted for publication).

More than 90% of the 160 assessed source/factor contribution estimations met the acceptability criterion. Although no absolute reference values can be used in real-world DBs, a reasonable quantitative agreement in the SCEs is pointed out by these results. Indeed, the noise of experimental data, the variety of methodological approaches and the fact that the sampling site was completely unknown to participants (particularly crucial for those using CMB) shall be taken into account when interpreting the intercomparison outcome.

Identification of continental and marine aerosol sources in Paris using high resolution aerosol mass spectrometry

M. Crippa[1], DeCarlo Peter F.[1*], Slowik Jay G.[1], El Haddad Imad[1], Mohr Claudia[1], Heringa Maarten F.[1], Chirico Roberto[1**], Marchand Nicolas[2], Baltensperger Urs[1], Prévôt Andre. S. H.[1]

[1] Laboratory of Atmospheric Chemistry, Paul Scherrer Institut, PSI Villigen, 5232, Switzerland
[2]Aix Marseille Univ., Laboratoire Chimie Environnement (LCE), Equipe Instrumentation et Réactivité Atmosphérique (IRA), 3 Place Victor Hugo, 13 331 Marseille, France
*now at: Department of Civil, Architectural, and Environmental Engineering, Drexel University, Philadelphia, PA, USA, 19146
**now at Department of Atmospheric Sciences, University of Washington, Seattle WA 98195, USA
***now at: Italian National Agency for New Technologies, Energy and Sustainable Economic Development (ENEA), UTAPRAD-DIM, Via E. Fermi 45, 00044 Frascati, Italy
Keywords: AMS, source apportionment, urban environment, marine aerosols
Presenting author email: monica.crippa@psi.ch

An intensive one month long field measurement campaign was performed in the Parisian region during July 2009 within the MEGAPOLI project (Megacities: Emissions, urban, regional and Global Atmospheric POLlution and climate effects, and Integrated tools for assessment and mitigation). The "SIRTA" measurement site was located in an urban background environment, 20 km SW from Paris, and a suite of instruments was deployed to characterize the aerosol chemical composition and physical properties. This work is focused on the high resolution time-of-flight aerosol mass spectrometer (HR-ToF-AMS) data and on source apportionment techniques, such as positive matrix factorization (PMF), applied to discriminate aerosol sources. During the period of study, the site was often influenced by oceanic air masses, resulting in very low non-refractory PM_1 levels (on average 4.3 $\mu g/m^3$) accounting for 57.2% organic aerosol (OA), 28.7% sulfates, 6% nitrates, 7.6% ammonium and 0.5% chlorine. The high resolution PMF allowed the identification of both anthropogenic and biogenic organic aerosol (OA) sources. Table 1 reports the elemental ratios as well as OM:OC ratio of each PMF factor evaluated with the high resolution AMS data analysis.

Traffic (defined as hydrocarbon-like OA, "HOA") and cooking emissions (COA) were identified as the main primary anthropogenic sources, contributing for 12% and 14.7%, respectively. However, the major part of the organic aerosol was associated with secondary sources, comprising a low-volatility oxidized OA (LV-OOA, 25.2%) and a semi-volatile oxidized OA component (SV-OOA, 32.4%). Additionally, a component attributed to marine emissions (marine organic aerosol, MOA), due to its high correlation with methanesulfonic acid (R^2=0.84), was identified. This factor seemed to be dominated by SOA derived from marine precursors (high S:C and O:C ratios (Table 1)), and it contributed on average for 15.7% to the total OA, even in a continental megacity like Paris.

Marine emissions are also recognized as an important source of inorganic primary (e.g. NaCl) and secondary aerosol (e.g. SO_4) (O'Dowd and De Leeuw, 2007). Based on sodium concentrations, primary marine aerosol contributed on average to ~10% of the total $PM_{2.5}$ mass. In order to apportion the non sea salt SO_4 (nss-SO_4) sources, PMF was applied on the measured concentrations of organics and sulfates.

Over the whole campaign the influence of air masses coming from the Atlantic Ocean produced a significant amount of secondary marine nss-SO_4 (on average 48.9%), while the nss-SO_4 apportioned to the secondary formation from continental emissions over the continent made up 39.7% (Figure 1). A detailed discussion of the results including the diurnal variations and source mass spectra will be presented.

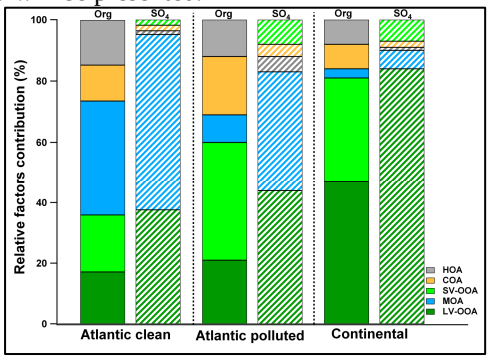

Figure 1. Organic (solid colors) and SO_4 (hatched colors) source apportionment for different air masses.

Table 1. Elemental ratios and OM:OC ratio of primary and secondary sources identified with HR-PMF.

Elemental ratios of the PMF factors					
	LV-OOA	**SV-OOA**	**HOA**	**COA**	**MOA**
OM:OC	2.12	1.66	1.38	1.32	1.94
O:C	0.73	0.39	0.16	0.13	0.57
H:C	1.33	1.52	1.84	1.74	1.57
S:C	0.0015	0.0009	0.0012	0.0005	0.013

This research in the context of the MEGAPOLI project is financially supported by the European Community's Framework Program FP/2007-2011 under grant agreement n°212520.

O'Dowd, C. D., and De Leeuw, G. Phil. Trans. R. Soc. A 365, 1753-1774, 2007.

PMF source apportionment of PM10 and PM2.5 daily and hourly aerosol data in Tuscany (Italy)

Lucarelli, Franco[1], Becagli, Silvia[2], Calzolai, Giulia[1], Chiari, Massimo[1], Giannoni, Martina[2], Martellini, Tania[2], Rugi, Francesco[2], Nava, Silvia[1], Traversi, Rita[2] & Udisti, Roberto[2]
[1]Department of Physics, University of Florence & INFN, Sesto Fiorentino, 50019, Florence, Italy
[2]Department of Chemistry, University of Florence, Sesto Fiorentino, 50019, Florence, Italy

Keywords: chemical composition, PM_{10}, $PM_{2.5}$, urban aerosols, 1 hour resolution.
Presenting author email: lucarelli@fi.infn.it

Two extensive field campaign for the PM10 and PM2.5 characterisation in Tuscany have been performed to investigate the aerosol composition and to identify its sources. Different sites representative of areas of different typology have been selected, six sites for PM10 and three sites for PM2.5, two in Florence (urban background and urban traffic) and one in Livorno (suburban-regional background). The two campaigns lasted 1 year (PM10: from September 2005 till September 2006; PM2.5: from March 2009 till March 2010). Aerosol samples were simultaneously collected, on a daily basis (00:01-23:59), by FAI-Hydra sequential samplers (EN 12341, 2.3 m^3/h), each of them equipped with two inlets (one equipped with Teflon filters and the other one with Quartz fibre filters). PM daily mass concentrations were obtained gravimetrically. Samples collected on Teflon filters were analysed by PIXE to measure the concentrations of all the elements with atomic number Z > 10, by IC to quantify the ion content and by ICP-AES (selected metals). Samples collected on Quartz filters were analysed by TOT to measure EC and OC concentrations, and by GC-MS to determine n-alkanes and PAHs concentrations. The comprehensive chemical characterisation allowed us to obtain the aerosol mass closure.

During shorter periods, the aerosol was collected also by means of a streaker sampler. PIXE analysis of these samples allowed the assessment of hourly resolution elemental time trends. It is worth noting that many aerosol sources can vary on a time scale of few hours or less. Therefore, the use of hourly concentration datasets can be of great help because the high resolved time patterns can improve the source identification and more accurate source profiles can be obtained.

Positive Matrix Factorisation (PMF) has been applied to the whole data set (daily and hourly samples separately). Input data were prepared using the procedure suggested by Polissar and PMF results for multiple values of FPEAK were systematically explored to find out the most reasonable solution.

From PM10 daily data two natural sources, marine and crustal aerosol, were identified, with an average contribution of 20-25% (but during a Saharan dust episode the contribution was more than 50%), a secondary sulphate source (20-30%), a traffic source (20-30%), a secondary nitrates/local combustion source (20-25%). In the most polluted site a biomass burning source was identified which is the responsible of the very high PM10 values during winter months.

For PM2.5 six main sources have been identified in all sampling sites: traffic, biomass burning, secondary sulphate, secondary nitrates, soil dust and marine aerosol (Figure 1). Two contributions to traffic emissions have been disentangled in Florence. In Livorno, an additional source, connected to ship emissions and harbour activities, has been detected. Traffic and secondary sulphate are the most important sources in Florence, but also biomass-burning gives an important contribution to PM2.5 mass. The contribution of the "natural" components (mineral dust and marine aerosols) to PM2.5 is on average moderate, but it reaches higher values during Saharan dust intrusions (in the most intense episode, the mineral dust component accounted for ~ 20% of the PM2.5 concentration).

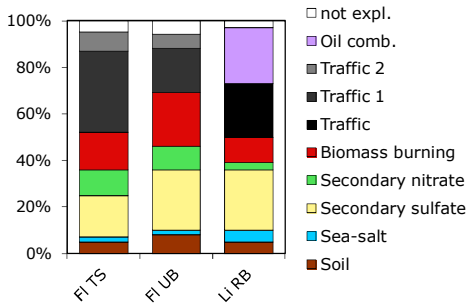

Figure 1: PM2.5 source apportionment.

High time resolution data were used to corroborate and validate these results. As an example the time trend of the BB source is reported for the winter samples (Figure 2). The BB source time pattern exhibits daily variations with peaks during evening-night period, typical of wood combustion for domestic heating; such a source is not present in the early autumn samples.

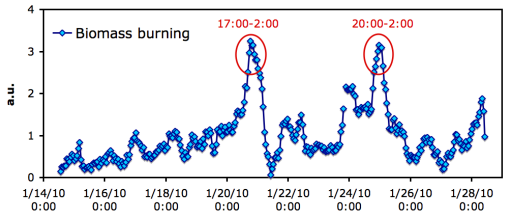

Figure 2: Hourly time trend of the BB source.

Source apportionment of indoor, outdoor and personal $PM_{2.5}$ exposure of pregnant women

M.C. Minguillón[1], M. Triguero-Mas[2,3,4], A. Schembari[2,3,4], A. de Nazelle[2,3,4], P. Dadvand[2,3,4], F. Figueras[5], J.A. Salvado[1], J.O. Grimalt[1], M. Nieuwenhuijsen[2,3,4], X. Querol[1]

[1]Institute of Environmental Assessment and Water Research (IDAEA), CSIC, 08034 Barcelona, Spain
[2]Centre for Research in Environmental Epidemiology (CREAL), 08003 Barcelona, Spain
[3]IMIM (Hospital del Mar Research Institute), 08003 Barcelona, Spain
[4]CIBER Epidemiología y Salud Pública (CIBERESP), Spain
[5]Department of Maternal-Fetal Medicine, ICGON, Hospital Clinic-IDIBAPS, University of Barcelona, 08028 Barcelona, Spain
Keywords: indoor/outdoor particles, personal sampling, source apportionment, PMF.
Presenting author email: mariacruz.minguillon@idaea.csic.es

Exposure to air pollution has been shown to adversely affect foetal development in pregnant women (e.g. Sapkota *et al*, 2010). The present study aims to investigate the PM composition and sources influencing personal exposure of pregnant women in Barcelona. To this end, indoor, outdoor and personal exposure measurements were carried out for a selection of 54 pregnant women between November 2008 and November 2009. $PM_{2.5}$ samples were collected during two consecutive days and then analysed for black smoke (BS), major and trace elements, and polycyclic aromatic hydrocarbons (PAHs) concentrations.

$PM_{2.5}$ concentrations were higher for personal samples than for indoor and outdoor environments. BS and sulphate concentrations showed strong indoor-outdoor-personal correlations, although some specific indoor and outdoor sulphate sources may exist. Average trace elements concentrations were quite similar indoor, outdoor and for personal exposure, but the correlations were moderate for most of them. PAHs concentrations indoor and outdoor were in general highly correlated. The ratios between different PAHs concentrations indicate that the influence from road traffic could be due to both gasoline and diesel vehicles.

A source apportionment analysis of the PM composition data by means of a Positive Matrix Factorization (PMF) resulted in the identification of six sources for the outdoor and indoor environments: secondary sulphate, fueloil+sea salt (characterized by V, Ni, Na and Mg), mineral, cigarette (characterized by K, Ce, Cd, benzo(k)fluoranthene and benzo(ghi)perylene), road traffic (characterized by BS and low weight PAHs), and industrial (characterized by Pb, Sn, Cu, Mn and Fe). Three of these sources were also identified in the personal dataset: sulphate, fueloil+sea salt, and cigarette, whereas the road traffic and industrial sources were merged in a single source, reflecting the influence of the urban background cocktail. For personal exposure two additional specific sources were found: cosmetics (characterized by abundance of Ca, Li, Ti and Sr and the absence of Al) and train/subway (characterized by Fe, Mn, Cu and Ba). Average contributions are shown in Figure 1, nevertheless, the contribution of the sources varied widely among women, especially for cigarette (from zero to up to 4 $\mu g/m^3$), train/subway (up to more than 6 $\mu g/m^3$) and cosmetics (up to more than 5 $\mu g/m^3$). The source contributions showed generally strong correlations indoor-outdoor although the infiltration efficiencies varied among homes. This study emphasizes the importance of relying on personal exposure in epidemiological studies assessing the impact of air pollution on human health.

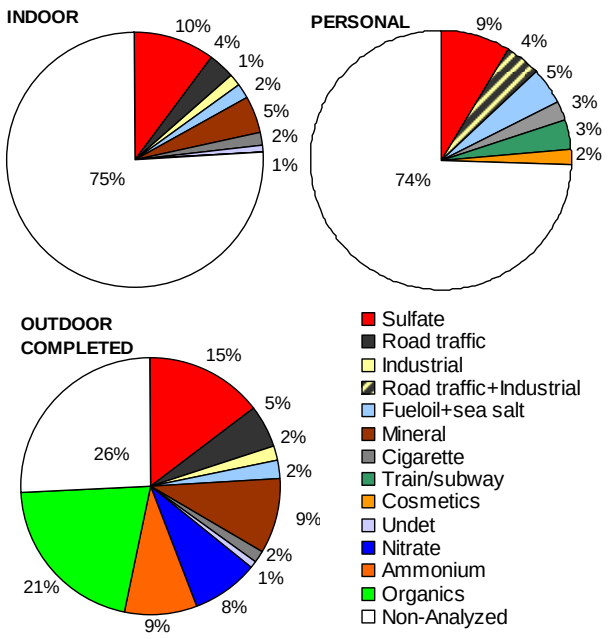

Figure 1. Average source contribution to $PM_{2.5}$ for indoor, personal and outdoor samples. Outdoor includes additional components measured in Barcelona.

The work was part of ARIBA, funded by a Fondo de Investigación Sanitaria (FIS) grant (PI081109) by the ISCIII. M.C. Minguillón was funded by JAE-Doc CSIC program, co-funded by the European Social Fund (ESF). A. Schembari was funded by an ISCIII grant (PFIS-FI10/00476). P. Dadvand was funded by the Spanish MICINN by a Juan de la Cierva grant (JCI-2011-09937).

Sapkota, A., Chelikowsky, A.P., Nachman, K.E., *et al* (2010). *Air Qual Atmos Health*, 1-13.

Thursday, September 6, 2012

Session WG09S3O. Aerosol Modelling: New particle formation and further topics

Determining the particle diameter growth rate from the fraction of charged particles

J. Leppä[1], S. Gagné[2], L. Laakso[1, 2, 3], K. E. J. Lehtinen[4], M. Kulmala[2] and V.-M. Kerminen[1, 2]

[1]Finnish Meteorological Institute, Climate Change, P.O. Box 503, 00101 Helsinki, Finland
[2]Department of Physics, University of Helsinki, P.O. Box 64, 00014 Helsinki, Finland
[3]School of Physical and Chemical Sciences, North-West University, Potchefstroom, South Africa
[4]Finnish Meteorological Institute, Kuopio Unit, and University of Eastern Finland, Department of Physics and Mathematics, P.O. Box 1627, 70211 Kuopio, Finland
Keywords: Atmospheric aerosols, Charged particles, Aerosol dynamics, Aerosol modelling.
Presenting author email: johannes.leppa@fmi.fi

New particle formation has been observed to take place in various conditions in the atmosphere. Atmospheric particles are known to affect the climate directly through reflecting the solar radiation and indirectly by affecting the properties of clouds. Both of these effects depend strongly on the size of the particle and thus knowledge of both the formation and the growth rate of the particles are needed to assess the climate effects caused by particles formed in the atmosphere.

Depending on the conditions, some of the atmospheric particles may be formed carrying an electric charge while others may be formed as electrically neutral. The fraction of charged particles in the nucleation mode changes as the particles grow to larger sizes due to various processes, including ion-aerosol attachment, self-coagulation and coagulation scavenging.

Iida *et al.* (2008) developed a method to estimate the particle diameter growth rate from the diameter dependence of the fraction of nucleation mode particles carrying a charge and the method was extended by Gagné *et al.* (2011) for situations in which it cannot be assumed that the concentrations of negative and positive small ions (diameter < ~2.0 nm) are equal.

In this study, we have conducted a simulation set with an aerosol dynamics model Ion-UHMA (Leppä *et al.* 2009), which includes neutral and charged particles as well as pools of negative and positive small ions. The simulated processes were, self-coagulation, coagulation scavenging and ion-aerosol attachment, while the condensational growth rate and the new particle formation rate were used as input in the model. The concentrations of negative and positive small ions were constant with values of 600 and 800 cm^{-3}, respectively.

We determined the particle growth rate, GR_{det}, from the simulated data using the method described by Gagné *et al.* (2011), which assumes that the ion-aerosol attachment dominates over the other processes affecting the charged fraction. We then compared GR_{det} to the real condensational growth rate, GR_{sim}, which was used as input in the model. The aim of this comparison was to assess how well we can estimate the growth rate from atmospheric measurements by using this method.

The correspondence between GR_{det} and GR_{sim} was good, if the changes in the charged fraction were dominated by ion-aerosol attachment (Figure 1), which was the assumption made in the method used to determine GR_{det}. Furthermore, the correspondence increased with increasing GR_{sim}.

If the difference in the negative and positive small ion concentrations was not taken into account when determining GR_{det}, the correspondence between GR_{det} and GR_{sim} was significantly worse than in the case in which the difference was taken into account. As a conclusion, the difference in the negative and positive small ion concentrations should be taken into account when determining the growth rate from the diameter dependence of the fraction of charged particles.

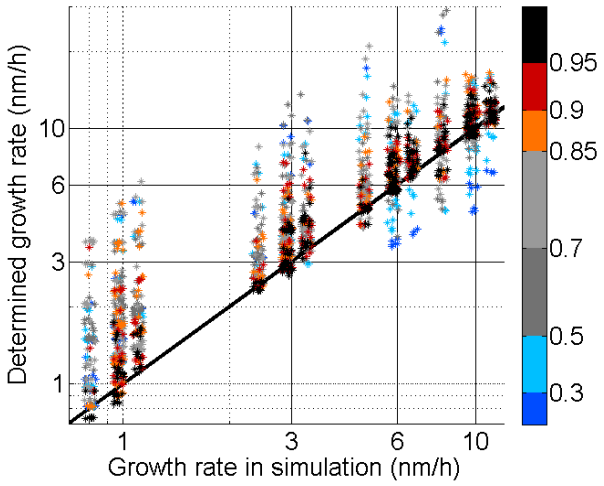

Figure 1. The particle diameter growth rates from the simulation set. Each star represents a single simulation. The colour indicates how big fraction of the change in the charged fraction is due to ion-aerosol attachment.

This work has been supported by European Commission 6th Framework program project EUCAARI, contract no. 036833-2 (EUCAARI), by Academy of Finland project ComQuaCC, project no. 135199, and the Academy of Finland Centre of Excellence program (project no. 211483, 211484 and 1118615).

Gagné, S., Leppä, J., Petäjä, T., McGrath, M. J., Vana, M., Kerminen, V.-M., Laakso, L. and Kulmala, M. (2011) *Atmos. Chem. Phys. Discuss.*, **11**, 15875-15920.

Iida, K., Stolzenburg, M. R., McMurry, P. H. and Smith, J. N. (2008) *J. Geophys. Res.*, **113**, D05207.

Leppä, J., Kerminen, V.-M., Laakso, L., Korhonen, H., Lehtinen, K. E. J., Gagné, S., Manninen, H. E., Nieminen, T. and Kulmala, M. (2009) *Boreal Env. Res.*, **14**, 559-575.

Nucleation rate parametrization in the CLOUD experiment over all tropospheric conditions

Almeida-Simões, João[1,2], Curtius, Joachim[1], Kirkby, Jasper[2], Carslaw, Ken[3], Dunne, Eimear[3], and the CLOUD collaboration

[1] Goethe-University of Frankfurt am Main, 60438 Frankfurt am Main, Germany
[2] Physics Department, CERN, CH1211, Geneva, Switzerland
[3] Institute for Climate and Atmospheric Science, University of Leeds, Leeds LS2 9JT, Leeds, United Kingdom

Keywords: CLOUD experiment, cosmic rays, atmospheric nucleation, nucleation rate, parametrisation.

The possible influence of cosmic rays on aerosols and clouds is of considerable interest (Carslaw, 2009). The CLOUD experiment at CERN aims to study under controlled conditions the effects of cosmic rays on nucleation, cloud droplets and ice particles.

The CLOUD experiment involves a 3m stainless steel aerosol chamber exposed to a pion beam from the CERN Proton Synchrotron. A suite of instruments continuously analyse the contents of the chamber via sampling probes. Each instrument has its own data acquisition system which delivers data in real-time to the CLOUD server. The CLOUD chamber is able to reproduce a wide range of well-controlled atmospheric conditions, including temperatures -90ºC to 100ºC, ion-pair concentrations 1-4000 cm^{-3} and relative humidities, RH, 0-100%. The nucleation and growth of new particles has been studied in the presence of various trace gases, including H_2SO_4 (10^6-10^9 cm^{-3}), NH_3 (35pptv to 1ppbv), amines and organics.

One of the primary goals of CLOUD is a quantitative evaluation of the dependency of the nucleation rate, J, on variables such as [H_2SO_4], [NH_3], [IONS], RH, T, etc. We have developed an accurate, automated method to determine the nucleation rate of critical clusters from the time evolution of the particle number concentration measured by each of the particle counters attached to the CLOUD chamber (CPC, DEG-CPC or PSM).

After the latest measurements in 2011 all atmospheric relevant conditions for ternary nucleation were covered by CLOUD. Using measurements from multiple instruments that analyse the CLOUD chamber, we have derived a J parametrisation based on physical equations that combines the measured J values with current theoretical understanding. The parametrisation is tuned using a nonlinear numerical Levenberg-Marquardt algorithm. The parametrisation successfully predicts all nucleation rates measured so far by CLOUD and is designed to be well-behaved when extrapolating outside the experimentally-explored region.

The CLOUD parametrisation is based on the most rigorous laboratory measurements of ion-induced and neutral atmospheric nucleation achieved so far including all ternary nucleation CLOUD results, and so constitutes an important new tool for evaluating the global contributions of nucleation in atmospheric models such as GLOMAP (Dunne, E.M., et al., this conference).

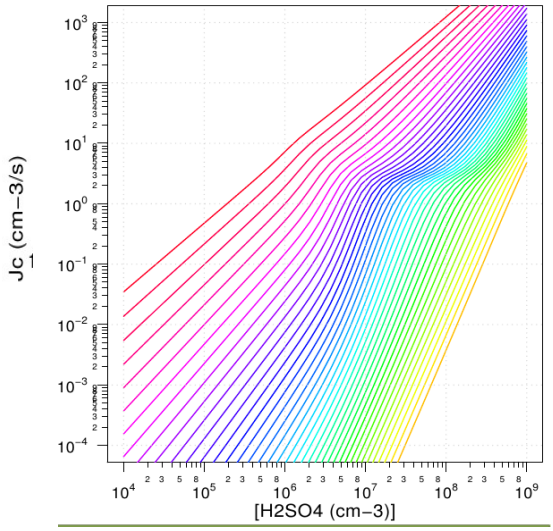

Figure 1. Nucleation rates predicted by the parameterisation over a wide range of temperatures (from -50C in purple up to 20C in red) in the presence of cosmic rays.

We would like to thank CERN for supporting CLOUD with important technical and financial resources, and for providing a particle beam from the CERN Proton Synchrotron. This research has received funding from the EC Seventh Framework Programme (Marie Curie Initial Training Network "CLOUD-ITN" grant no. 215072, and ERC-Advanced "ATMNUCLE" grant no. 227463), the German Federal Ministry of Education and Research (project no. 01LK0902A), the Swiss National Science Foundation (project nos. 206621_125025 and 206620_130527), the Academy of Finland Center of Excellence program (project no. 1118615), the Austrian Science Fund (FWF; project no. P19546 and L593), the Portuguese Foundation for Science and Technology (project no. CERN/FP/116387/2010), and the Russian Foundation for Basic Research (grant N08-02-91006-CERN)

Carslaw, K. (2009). Cosmic rays, clouds and climate. Nature, 460, 332-333.
Dunne, E.M., et al. (2011). The influence of ion-induced nucleation on atmospheric aerosols, this conference.

Modelling of ion-induced binary nucleation in the CERN CLOUD experiment

S. Ehrhart[1], L. Ickes[1], J. Kazil[2,3], K. D. Froyd[3], E. R. Lovejoy[3], J. Curtius[1] and the CLOUD collaboration
[1] Institute for Atmospheric and Environmental Sciences, Goethe University, Frankfurt am Main, Hessen, Germany
[2] CIRES, University of Colorado, Boulder, Colorado, USA
[3] NOAA Earth System Research Laboratory, Boulder, Colorado, USA
Keywords: nucleation modelling, ion induced nucleation, CLOUD experiment.
Presenting author email: ehrhart@iau.uni-frankfurt.de

Ion-induced aerosol nucleation could be an important mechanism to explain a substantial fraction of new particle production in the free troposphere (Lovejoy *et al*, 2004, Kirkby *et al*, 2011).

To improve the scientific knowledge about nucleation, ion-induced nucleation in particular, the CLOUD-project (Cosmics Leaving OUtdoor Droplets; Kirkby *et al*, 2011) was established at CERN (European Organization for Nuclear Research). The experimental setup consists of an aerosol chamber into which a beam of particles is sent from a Proton Synchrotron to investigate the effects of ions on the aerosol production under controlled laboratory conditions. The chamber itself provides a nearly perfectly clean environment. Concentrations of possible third nucleation agents are almost negligible or are controlled in order to study these. Furthermore the temperature of the chamber can be controlled down to 200 K.

We modelled the binary sulphuric acid/water nucleation processes in the CLOUD-chamber based on earlier work (Lovejoy *et al*, 2004; Kazil, J., and Lovejoy, E. R., 2007). The microphysical model is based on uptake and loss of single sulphuric acid molecules and spans a range from a single molecule to particles with a few nanometer size. The special conditions of a chamber experiment make certain adjustments to the model necessary for instance the main source of losses is the chamber wall. We compare measurements at low temperatures with the modelled evolution of particles. Measured cut-off functions for different particle counter are applied to the simulation for consistent conversion of calculated results to measurements.

The rate constants for charged nucleation are based on laboratory measurements, ab initio results and a smooth parameterisation to bulk phase properties as the particle size increases (Lovejoy *et al*, 2004). Neutral rate constants are currently based on the liquid drop model with corrections terms. These terms can be optimized with pure binary nucleation experiments. For the H_2SO_4 dimer and trimer measured thermodynanmic data are included in the neutral nucleation (Hanson, D. R, and Levoejoy, E. R., 2006). The detailed comparison of the measured and modeled temporal evolution of the particle concentrations for different particle sizes (Figure 1) gives a powerful tool for complete understanding and quantification of the dominant microphysical processes for a wide range of experimental conditions. The model can also be used to transfer the CLOUD results to conditions of the upper troposphere and stratosphere, i.e. lower pressures.

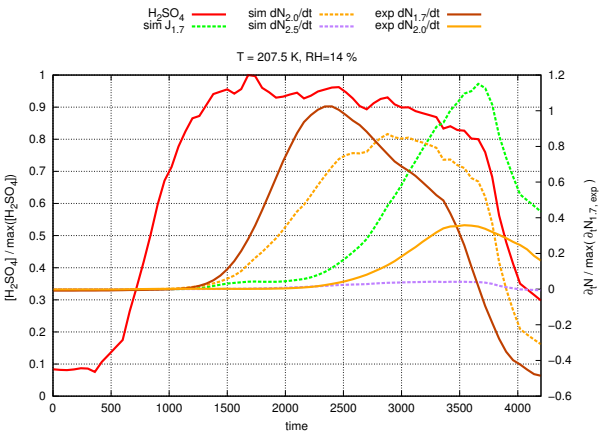

Figure 1: Example of model result without optimisation showing $\partial_t N$ vs time (right y-axis), normalised to the maximum of measured $\partial_t N$, for different particle counters. The normalised sulphuric acid is shown as function of time (left y-axis). Dashed lines are simulated results and solid lines are derived from measurements.

We would like to thank CERN for supporting CLOUD with important technical and financial resources, and for providing a particle beam from the CERN Proton Synchrotron. This research has received funding from the EC Seventh Framework Programme (Marie Curie Initial Training Network "CLOUD-ITN" grant no. 215072, and ERC-Advanced "ATMNUCLE" grant no. 227463), the German Federal Ministry of Education and Research (project no. 01LK0902A), the Swiss National Science Foundation (project nos. 206621_125025 and 206620_130527), the Academy of Finland Center of Excellence program (project no. 1118615), the Austrian Science Fund (FWF; project no. P19546 and L593), the Portuguese Foundation for Science and Technology (project no. CERN/FP/116387/2010), and the Russian Foundation for Basic Research (grant N08-02-91006-CERN).

Kirkby, J. et al (2011) Nature, **476**, 429-433.

Lovejoy, E. R., Curtius, J. and Froyd K. D. (2004) J. Geophys. Res. - Atmospheres, **109**, D08204.

Kazil, J., and Lovejoy, E. R. (2007) Atmos. Chem. Phys., **7**, 3447-3459.

Hanson, D. R. and Lovejoy, E. R. (2006) J. Phys. Chem. A, (110), 9525â9528.

Atmospheric new particle formation mystery unveiled?

I.K. Ortega[1], O. Kupiainen[1], T. Olenius[1], M. McGrath[3].T. Kurtén[2], P. Pasonen[1], M. Kulmala and H. Vehkamäki[1]

[1]Department of Physics, University of Helsinki, Finland
[2]Department of Chemistry, University of Helsinki, Finland
[3]Department of Biophysics, Kyoto University, Japan
Keywords: molecular clusters, quantum chemistry, sulfuric acid, amines, new particle formation.
Presenting author email: ismael.ortegacolomer@helsinki.fi

Atmospheric new particle is an important source of aerosol particles that can act as cloud condensation nuclei in the atmosphere. Despite the numerous efforts to determine the compounds involved in new particle formation, some of these remain unknown. Sulphuric acid certainly has a key role in atmospheric new particle formation, but, in realistic atmospheric conditions, cannot explain the observed new particle formation rates on its own. Recently, state-of-the-art experiments in CLOUD chamber at CERN (Kirby et al 2011), have showed how, although the presence of ammonia and ions can enhance new particle formation rates by a factor of 10000, the observed new particle formation rates are still far below those measured in the real atmosphere. This implies that other compound(s), yet unknown, is involved in atmospheric new particle formation.

In the recent years, many studies have suggested that amines may play a key role in atmospheric new particle formation. In the present work, we used the kinetic code ACDC (Atmospheric Cluster Dynamics Code) developed in our group (McGrath *et al*., 2011) to study the effect of ammonia and dimethylamine (DMA) on sulphuric acid new particle formation. We used the formation free energies calculated by quantum chemical methods (Ortega *et al*., 2011) as an input to obtain the evaporation rates needed in ACDC.

First we studied how the formation rate depends on sulphuric acid concentration, and how this varies with the presence of ammonia. To validate our results we have compared the model results with rates observed in the CLOUD experiment (Fig. 1). The modelled formation rates agree well with the experimental ones. Figure 2 shows how the presence of DMA, even at very low concentrations, leads to formation rates close to those observed in different field stations.

The main conclusions of this study are:

-ACDC model is able to reproduce experimental results, so it will be a useful tool to complement future experiments concerning especially the neutral clusters, which cannot be directly detected

-The presence of DMA together with sulphuric acid can explain observed atmospheric new particle formation rates

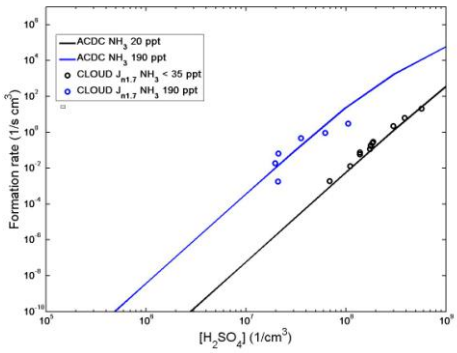

Figure 1. Formation rate versus sulfuric acid concentration at different ammonia concentrations, modelled and measured in CLOUD experiment (Kirby et al 2011)

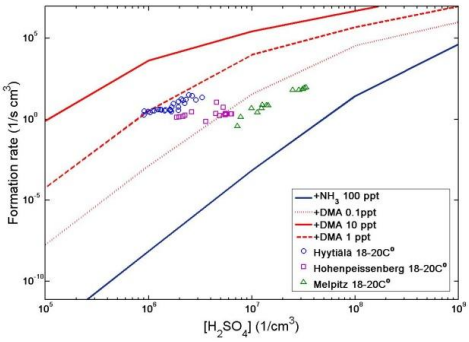

Figure 2. Formation rate versus sulfuric acid concentration at different ammonia and DMA concentrations, modelled and measured in different field stations.

This work was supported by FP7-MOCAPAF project No 257360 (ERC Starting Grant) and FP7-ATMNUCLE project No 227463 (ERC Advanced Grant). The authors thank the Scientific Computing Center (CSC) in Espoo, Finland, for the computing time and the CLOUD consortium for providing the experimental data.

Kirkby, J. *et al*. (2011) *Nature*, **476**, 429–433.

McGrath, M.J., Olenius, T., Ortega I.K., Loukonen V., Paasonen P., Kurtén T., Kulmala M., & Vehkamäki H. (2011) *Atmospheric Chemistry and Physics Discussions*, **11**, 25263-25295.

Ortega, I.K., Kupiainen, O., Kurtén, T., Olenius, T., Wilkman, O., McGrath, M.J., Loukonen, V. & Vehkamäki, H. (2012) *Atmospheric Chemistry and Physics*, **12**, 225-235.

Simulating the contribution of primary emissions and secondary formation to aerosol number concentrations in the European boundary layer

C. Fountoukis[1], I. Riipinen[2], D. Patoulias[3], H. D. van der Gon[4], P.E. Charalampidis[5], C. Pilinis[5], and S.N. Pandis[1,3]

[1]Institute of Chemical Engineering & High Temperature Chemical Processes, Foundation for Research & Technology-Hellas (FORTH), 26504, Patras, Greece
[2]Department of Applied Environmental Science & Bert Bolin Centre for Climate Research, Stockholm University, SE-11418, Stockholm, Sweden
[3]Department of Chemical Engineering, University of Patras, Patras, Greece
[4]TNO Built Environment and Geosciences, Netherlands
[5]Department of Environment, University of the Aegean, 81100, Mytilene, Greece
Keywords: PMCAMx-UF, Regional CTM, aerosol nucleation & growth, PEGASOS.
Presenting author email: cfountoukis@iceht.forth.gr

Aerosol formation by nucleation is important for climate because the newly formed particles can grow through condensation of vapors (e.g., sulfuric acid and ammonia, organics) from a few nanometers up to cloud condensation nuclei (CCN)-relevant particle sizes of ~100 nm or more influencing the formation and properties of clouds. Nucleation also enhances atmospheric levels of ultrafine particles which may be especially harmful to human health. Despite its importance, our understanding of the processes of formation and growth of atmospheric nanoparticles is currently limited.

In this work, a 3D CTM with detailed aerosol microphysics, PMCAMx-UF (Jung *et al.*, 2010), was applied to Europe to simulate the contribution of direct emissions and secondary formation to total particle number concentrations. A new size-resolved Pan-European anthropogenic Particle Number (PN) emission inventory was developed for the first time and the extracted aerosol number emissions were used as inputs for PMCAMx-UF. PMCAMx-UF uses the Dynamic Model for Aerosol Nucleation and the Two-Moment Aerosol Sectional algorithm (Adams and Seinfeld, 2002) to track both aerosol number and mass concentration using a sectional approach. We evaluate the model predictions for the European domain against field observations collected during a summer and a winter period.

For the summer simulation, the model reproduces more than 70% of the hourly concentrations of particles larger than 10 nm (N_{10}) within a factor of 2. Aerosol nucleation is predicted to increase the total particle number concentration by a factor of 20 or more in some high-SO_2 areas (Figure 1) and by a factor of 7 for particles larger than 10 nm. For N_{50}, nucleation is responsible for an increase of more than 100% in Southeast Europe. The effect of nucleation in the lower troposphere on particle number above 100 nm is, on average, small with the exception of the Mediterranean area where the model predicts that nucleation can increase the number concentration of CCN-sized particles by up to 20%. On average, approximately 50% of particles above 10 nm are predicted to come from aerosol nucleation. A systematic underprediction of N_{100} at almost all studied sites implies the need for improvement of either the size distribution of the emissions and/or the growth of the ultrafine particles to this size range.

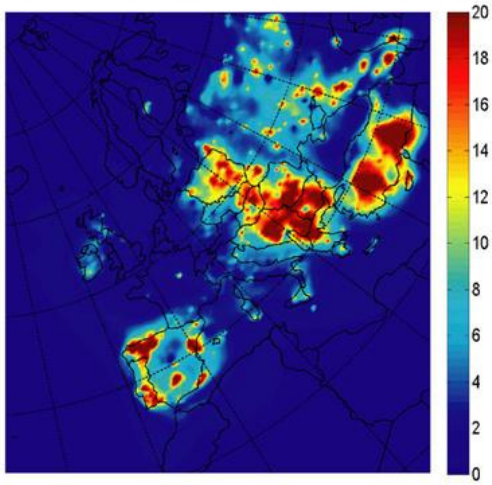

Figure 1. Ground level average fractional increase of PN concentration due to nucleation predicted for May 2008.

Results from 3 nucleation mechanisms that were tested suggest that i) the ternary mechanism performs better than the activation or the kinetic, and ii) future particle number emission inventory efforts should focus on improvements in the diurnal and geographical split of the particle numbers emitted. Reducing emissions of ammonia and sulfur dioxide impact differently certain parts of the size distribution. This could have important implications for emission control strategies that seek to mitigate future air pollution and climate change.

This work was funded by the European Community's 7th Framework Programme EU project PEGASOS.

Jung, J., Fountoukis, C., Adams, P.J., and Pandis, S.N. (2010) *J. Geophys. Res.*, 115, D3, doi:10. 1029/2009JD012313.

Adams, P.J., and Seinfeld, J.H. (2002) *J. Geophys. Res.*, 107(D19), 4370, doi: 10.1029/2001JD00 1010.

Modeling Reactive Aerosols in Oxidizing Atmospheres: Severe Accidents in Sodium Fast Reactors

M. García[1], L.E. Herranz[1]

[1]Unit of Nuclear Safety Research, CIEMAT, Madrid 28040, Spain
Keywords: In-containment SFR source term, Na-based aerosols.
Presenting author email: monica.gmartin@ciemat.es

Postulated Beyond Design Basis Accidents (BDBAs) in Sodium-cooled Fast Reactors (SFRs) might result in contaminated-coolant discharge at high temperature into the containment. As a consequence of the high chemical reactivity of sodium (Na) with air and steam, it would undergo Na-oxidation within the containment atmosphere. The exothermic nature of the chemical reactions taking place and the high level of turbulence in the reaction area, would determine to a good extent particle size and population. Hence, radioactive source term to the environment would depend on in-containment Na-aerosol behavior. Hence, it is of utmost importance for a full scope safety analysis of SFRs to have computation tools properly validated, particularly in the field of radionuclide transport in the containment.

Much of the analytical capability built-up until mid 80's for source term analysis of SFRs, was lost due to sharp reduction of resources spent worldwide. However, the major progress achieved in source term studies of Light Water Reactors (LWRs) and some existing similarities of LWR- and Na-based aerosols, highlights the interest of assessing the potential of LWR codes to deal with in-containment aerosol behavior in SFR scenarios. This is the goal of this work. Through a systematic application of the MELCOR code (Gauntt et al., 2005) to the ABCOVE-AB5 test, insights have been gained into drawbacks and capabilities of this computation tool. Hypotheses and approximations have been adopted so that differences in boundary conditions between LWR and SFR containments under BDBA can be properly accommodated.

The AB5 test of the ABCOVE experimental programme was conducted in the Containment System Test Facility (CSTF) vessel at the HEDL. A total of 223 kg of Na at high temperature (836.15 K) was sprayed over 872 s. The Na-air exothermic reactions yielded a source of aerosols into the atmosphere. This energetics is an intrinsic feature of Na-fire scenarios that requires some modeling hypotheses and approximations.

The energy released has been estimated by assuming that 90% of Na got oxidized to Na_2O_2 and 10% of Na reacted with steam and formed NaOH. These percentages were derived from the steam available in the containment atmosphere. This total energy is assumed to be distributed between the vessel atmosphere (50%) and the Na particles (50%). As MELCOR does not model aerosols-gas heat exchange, this 50% has been placed on an artificial surface introduced in the model. This surface is characterized by the same heat capacity as Na aerosols and its surface area (roughly 1 m^2) approximated by assuming all the Na-mass colapsed in a sphere ("fire ball"). The idea is that most Na particles are created in a relatively small region of the vessel; initially, the large amount of particles causes a heat transfer shielding effect that allows neglecting any exchange taking place within the particle cloud. In other words, most convection and radiative exchange would occur from particles at the most external layer of the cloud. This approach, called "fire ball" approximation, seems to provide a reasonable match of the thermal-hydraulic scenario (Fig. 1).

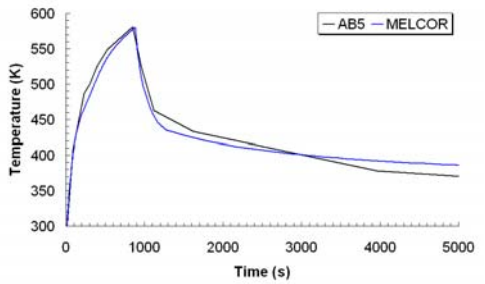

Fig.1. Gas temperature.

A systematic methodology has been developed to identify the most influencing aerosol parameters that can be chosen by the code user. Particles shape and turbulence seem to affect substantially aerosol evolution. In particular, dynamic (χ) and coagulation (γ) shape factors equal to 2.5 and turbulent energy dissipation rate (ε) equal to 10^{-3} $m^2 \cdot s^{-3}$, provided the closest agreement to data (Fig. 2). For comparison purposes, the default case (DC) is also shown ($\chi = \gamma = 1.0$; $\varepsilon = 10^{-3}$ $m^2 \cdot s^{-3}$).

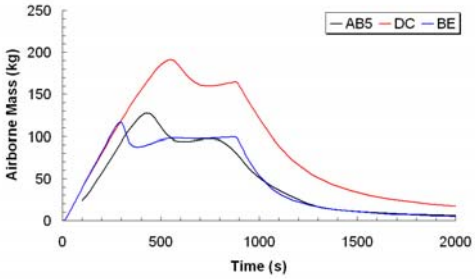

Fig. 2. Airborne mass as a function of time.

Non-spherical particles largely enhance the agglomeration process and compensate the slow-down effect of non-sphericity.

According to these results, sodium based particles produced during a spray fire might be non-spherical. Nonetheless, further experiments would be necessary.

Gauntt, R.O. et al. (2005). *MELCOR computer code manuals*. NUREG/CR-6119, SAND2005-5713.

The global distribution of aerosol model uncertainty

L.A. Lee[1], K.S. Carslaw[1], K.J. Pringle[1]

[1]School of Earth and Environment, University of Leeds, Leeds, LS2 9JT, UK
Keywords: aerosol modelling, model uncertainty, parametric uncertainty, statistical analysis.
Presenting author email: l.a.lee@leeds.ac.uk

Aerosols have been assessed in the last two IPCC assessments as the largest uncertainty in the radiative forcing of climate. An essential step towards reducing the uncertainty is to quantify the sources of uncertainty at the process level of global aerosol models. Here we use new techniques of statistical emulation to calculate the spatial pattern of parameter sensitivity in a complex global aerosol model. Gaussian process emulation enables a full variance based sensitivity analysis to be performed in every global grid box based on a relatively small number of model simulations.

We show global maps of simulated and emulated cloud condensation nuclei (CCN), including absolute and relative sensitivities to 8 parameters, the degree of interaction between the parameters, and probability density functions for CCN in selected grid boxes. The absolute variance is largest in polluted regions but the coefficient of variation (standard deviation divided by mean CCN) is greatest in remote regions. The maps show a high degree of spatial coherence in the causes of CCN uncertainty. In polluted regions and over the Southern Ocean the uncertainty is dominated by emissions but elsewhere the uncertainty is dominated by process parameters. The uncertainty in some regions is dominated by one or two parameters, while in other regions the overall uncertainty results from multiple parameters with up to 50% variance due to interaction effects. The variance analysis provides direct quantification of the reduction in variance that would result if a parameter could be specified precisely. When extended to all process parameters, the approach presented here will therefore provide a clear global picture of how improved knowledge of aerosol processes will translate into reduced model uncertainty.

We acknowledge funding from the Natural Environment Research Council AEROS project under grant NE/G006172/1.

Lee, L. A., Carslaw, K. S., Pringle, K. J., Mann, G. W., and Spracklen, D. V.: Emulation of a complex global aerosol model to quantify sensitivity to uncertain parameters, *Atmos. Chem. Phys.*, 11, 12253-12273

Thursday, September 6, 2012

Session WG10S2O. Aerosol Dynamics

Modeling of the behavior of droplets deposited on the smooth and rough fiber surfaces

J.M. Gac[1] and L. Gradoń[1]

[1]Faculty of Chemical and process Engineering, Warsaw University of Technology, Warsaw, 00-645, Poland
Keywords: Aerosol filtration, Droplets, Fibers, Modeling (microscale), Numerical simulation
Presenting author email: J.Gac@ichip.pw.edu.pl

The separation of the liquid droplets from the stable mist system is a crucial process in industrial technologies, natural gas cleaning, crank case ventilation systems and many other applications. The most efficient devices for such separations are fibrous filters (coalescers). A properly designed coalescer structure, defined through the space distribution of the local porosity and fiber diameter involves the phenomena of a droplet coalescing in the bulk, deposition of drops on the fiber, coalescing of the deposited droplet on the fibers and the drainage of the filter fibers.

In our presentation, a two-color lattice-Boltzmann method (LBM) is used for simulation of the behavior of droplets deposited on a fiber. This kind of well-known LBM scheme is an effective tool for simulating of two-phase flow, including surface tension effects. The interaction of the droplet with the gas flowing around a fiber having smooth and rough surfaces was analyzed.

As a results of our simulations, we derive the equilibrium of conformation of droplets. For a smooth fiber we obtain results consistent with analytical results presented in (Carrol, 1986). By contrast, the droplet on rough fiber takes often completely different conformations, what is explained by means of merging the theory of rough surfaces of Wenzel (1936) with the results of (Carrol, 1986).

Further, we investigate the axial and transversal motion of a droplet on a fiber. We have found that in case of smooth fibers the velocity of the asymmetric droplet is higher than the velocity of axisymmetric droplet, what is consistent with recent results of Gilet *et al* (2010). By contrast, the roughness of the fiber facilitates the motion of the droplet for the situation when the mean distance between the insets is big in comparison to the diameter of the droplet. The reason is that the droplet, moving through the inset, transits from the axisymmetric to the asymmetric conformation, for which the equilibrium velocity is higher. However, if the typical distance between the insets is smaller than the diameter of the droplet, its motion is rubbed. Both these situations are presented in Fig. 1.

The transverse motion of the droplet on rough fiber is slower than the motion of smooth one – so the roughness of the fiber impedes the detachment of the droplets. The difference of the times of detachment from rough and smooth fiber decreases with the value of contact angle, as it has been shown in Fig. 2.

The results of calculation show the distinguished patterns of the interaction depending on the structure of the fiber roughness and the fiber and droplet dimensions. The modeling data indicate a new approach for the designing of a novel generation of the efficient coalescers.

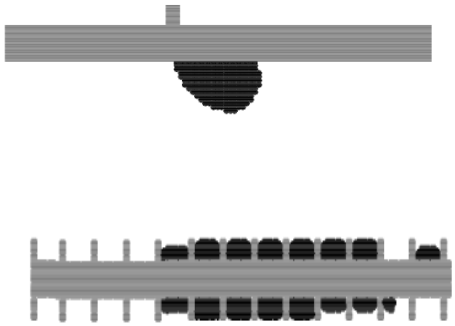

Figure 1. The shape of the droplet on rough fiber with low (a) and high (b) density of insets.

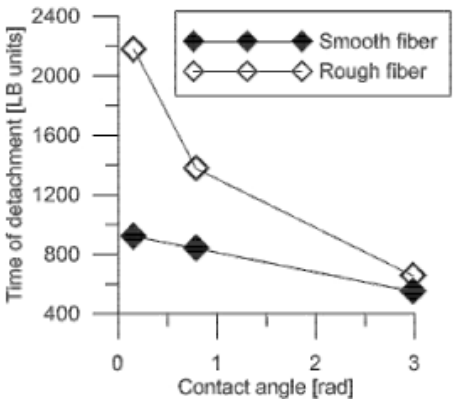

Figure 2. Dependence of time of detachment of the droplet on the contact angle for smooth and rough fiber at the same velocity of surrounding gas.

JMG thanks Foundation for Polish Science for financial support.

Carrol, B.J. (1986) *Langmuir* **2**, 248-250.
Wenzel, R.N. (1936) *Ind. Eng. Chem*. **28**, 988-994.
Gilet, T., Terwagne, D. and Vandewalle, N. (2010) *Eur. Phys. J. E* **31**, 253–262.

The mobility radius of small fractal aggregates in the slip-flow regime

A.D. Melas[1 2], A.G. Konstandopoulos[1 3] and Y. Drossinos[2]
[1]Department of Chemical Engineering, Aristotle University, Thessaloniki, 50006, Greece
[2]European Commission, Joint Research Centre, Ispra (VA), 21027, Italy
[3]Aerosol & Particle Technology Laboratory, CERTH/CPERI, P.O. Box 60361, 57001 Thessaloniki, Greece
Keywords: fractal aggregates, slip flow regime, mobility radius.
Presenting author email: Anastasios.Melas@jrc.ec.europa.eu

Aerosol particles may form complex structures that are fractal-like. Their fractal-like nature is described by the scaling law, $N = k_f(R_g/R_1)^{d_f}$, where N is the number of primary particles, k_f the fractal prefactor, d_f the fractal dimension, R_g the radius of gyration and R_1 the monomer radius.

Isella and Drossinos (2011) proposed a numerical method for the calculation of the mobility radius (R_m) of straight chains in the continuum regime which is applicable also to fractal aggregates. This method is based on experimental studies where it was shown that the total mass transfer times the aggregate mobility is approximately constant and independent of particle shape and chemical nature. The molecule-aggregate collision rate (K_N) is proportional to the mass transfer and consequently to the friction coefficient. By calculating the steady-state molecular diffusive flux over the aggregate surface we determine the collision rate. The appropriate boundary conditions in the continuum regime are fluid density $\rho = 0$ on the surface and $\rho = 1$ far away from it. Finally we calculate the mobility radius by

$$\eta_N = \frac{K_N}{NK_1} = \frac{R_m}{NR_1}, \qquad (1)$$

where η_N is the average monomer shielding factor.

In this study we expand this method to the slip-flow regime. The approach remains the same. The boundary condition that we use to solve the steady-state molecular diffusion equation is a Robin condition. On the aggregate surface the fluid density is $\rho(R_1) = \alpha(Kn)\frac{\mathrm{d}\rho}{\mathrm{d}r}\,|_{R_1}$ and far away from it, $\rho = 1$. Hence, from the analytical solution of the diffusion equation, we obtain

$$\frac{K_1(Kn=0)}{K_1(Kn)} = 1 + \frac{\alpha(Kn)}{R_1}, \qquad (2)$$

for a monomer where the constant $\alpha(Kn)$ is calculated from the Cunningham slip factor (Cn) to be $\alpha(Kn)/R_1 = Cn - 1$.

The diffusion simulations we carried out with the finite element software Comsol Multiphysics. In Table 1 we compare our results for a straight chain with 8, 15 monomers and different Knudsen numbers ($Kn = \lambda/R_1$, where λ is the gas mean free path) to Dahneke's (1982) calculations. The agreement is very good for $Kn = 0.1, 0.2$, getting worse for $Kn = 0.5$. This is expected as slip flow conditions should be appropriate for Kn around 0.1.

Straight chains		$Kn = 0.1$	$Kn = 0.2$	$Kn = 0.5$
8 monomers	Dahneke (1982)	0.414	0.436	0.499
	Collision rate	0.416 (0.48%)	0.447 (2.52%)	0.546 (9.42%)
15 monomers	Dahneke (1982)	0.344	0.365	0.427
	Collision rate	0.342 (0.58%)	0.372 (1.92%)	0.466 (9.13%)

Table 1: Comparison between collision rate calculations and Dahneke (1982). In parenthesis the relative difference is shown.

The R_m calculations will also be made for fractal aggregates and dynamic properties will be related to geometrical features (d_f, k_f, N). The fractals we will use are created with a tunable cluster-cluster aggregation method (CCA) proposed by Thouy and Jullien (1996). The monomers in the created fractals don't overlap, satisfy exactly the scaling law, and they have prescribed d_f, k_f, N. Figure 2 shows a typical fractal with 512 monomers, different monomer colours corresponding to the number of its nearest neighbors.

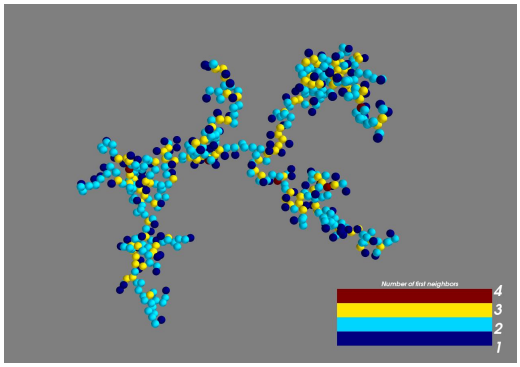

Figure 1: A 512-monomer fractal aggregate ($d_f = 1.8$, $k_f = 1.3$) created with a CCA algorithm.

This work was supported by the European Commission Doctoral Fellowship (ADM).

L. Isella, Y. Drossinos (2011), J. Colloid Interface Sci. **356**, 505.
B. Dahneke (1982), Aerosol Sci. Technol. **1**, 179.
R. Thouy, R. Jullien (1996), J. Phys. I France **6**, 1365.

Study of thermophoretic velocity of soot particles with a new device: the radial flow thermophoretic analyser

E. Brugière [1,2], F. Gensdarmes [1], F.-X. Ouf [1], J. Yon [2] and A. Coppalle [2]

[1] Aerosol Physics and Metrology Laboratory, IRSN, BP 68, 91192, Gif-sur-Yvette Cedex, France.
[2]UMR 6614 CORIA, Avenue de l'université, BP 8, 76801 Saint Etienne du Rouvray, France.
Keywords: thermophoresis, fractal aggregate, deposition.
Presenting author email: edouard.brugiere@irsn.fr

Thermophoresis is an important mechanism of micro-particle transport due to a temperature gradient in the surrounding medium. Extensive studies, both theoretical and experimental, have been carried out to understand the nature of this phenomenon which is well known for spherical particles contrary to non-spherical particles like soot particles. In fact, the soot particles are characterized by a complex morphology called "fractal" and, currently, the real impact of this morphology on deposition due to thermophoresis is not well known.

The existing theory of the thermophoresis for non-spherical particles is limited and there are few solutions to formulate thermophoresis velocity in the continuum and free molecular limits regime for several simple particle shapes. The reader is referred to a comprehensive review on thermophoresis of the two major categories, spherical and non-spherical particles, by Zheng (2002).

In order to determine particle morphology influence on the thermophoretic behavior, a new experimental device is presented. This new device is a radial flow thermophoretic analyser and it is based on the concept of the radial flow differential mobility analyser (DMA): the *Spectromètre de Mobilité Electrique Circulaire* (SMEC) developed by Pourprix (1989). This device consists of a parallel arrangement of two circular plates (hot and cold). A schematic diagram is given in figure 1; a sheath air flow (Qf) and an aerosol air flow (Qa) are passed between those two plates. For different flow rates and temperature gradients, this new device will enable to determine, with a high resolution, the mean thermophoresis velocity of monodisperse particles.

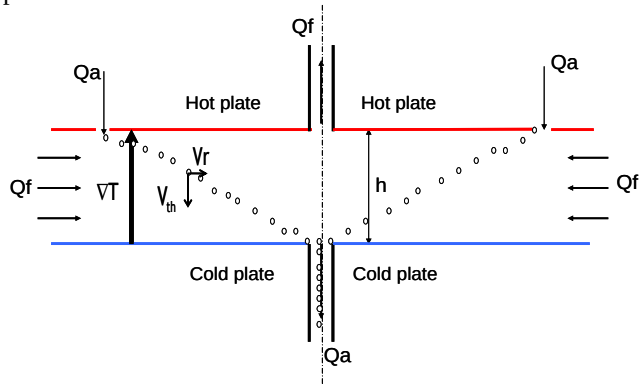

Figure 1: Schematic diagram of the radial flow thermophoretic analyser

We obtain experimental results for spherical PSL particles (polystyrene latex) in good agreement with the model proposed by Beresnev and Chernyak (1995).

A comparaison between mean thermophoretic velocity of spherical (PSL) and aggregate particles, produced by a diffusion flame propane/air generator (miniCAST), having same mobility diameters is realized. Our results show a significant difference between the thermophoretic velocity of aggregate and PSL particles. The measurements obtained with the radial flow thermophoretic analyser are reported in the figure 2. Contrary to the spherical particles, the thermophoretic velocity of aggregates increases with the diameter. For example, the thermophoretic velocity of an aggregate of 430 nm is 30 % higher than that of a PSL particle with the same mobility diameter.

The experimental results also show a dependance of the thermophoretic velocity of an aggregate with the number of primary particles and, for the first time, confirm the monte-carlo simulation of Mackowski (2006).

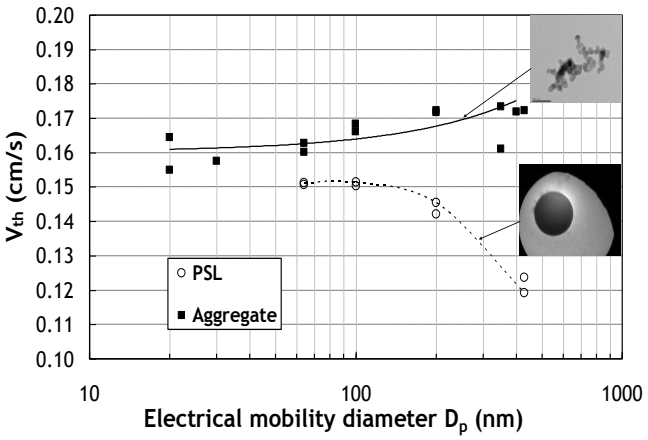

Figure 2: Relation between diameters and thermophoretic velocity for PSL and aggregate particles

Beresnev, S., and Chernyak, V. (1995). *Physics of Fluids* **7**: 1743-1756.

Mackowski, D.W. (2006). *J. Aerosol Sci*. **37**: 242-259.

Pourprix, M. (1989). French patent n° 89 08400.

Zheng, F. (2002). *Advances in Colloid and Interface Science* **97**: 255-278.

Forces on a porous particle in an oscillating flow

P. Vainshtein and M. Shapiro

Laboratory of Transport Processes in Porous Materials, Faculty of Mechanical Engineering, Technion – Israel Institute of Technology, Haifa 32000, Israel
Keywords: particle, permeability, oscillations, forces.
Presenting author email: mersm01@technion.ac.il

We considered dynamics of a single spherical porous particle oscillating in quiescent incompressible fluid when the instantaneous particle velocity is given by $U = U_\infty \exp(i\omega t)$. Here U_∞ is the velocity amplitude, ω is the angular frequency of harmonic oscillations, t is the time. The corresponding problem for impermeable solid particle was studied by Stokes (1851). The problem as formulated is relevant for dynamics in continuum regime of aerosol agglomerates (Shapiro et al., 2012).

We calculated theoretically the complex force reduction ratio, $\tilde{\Omega}$, between the drag force acting on an oscillating permeable sphere and the drag experienced by an impermeable oscillating particle. We solved the Stokes equations exterior to the particle and either by Darcy or Brinkman equations inside the particle. The velocity components and the pressure were required to be continuous at the particle boundary for both the Darcy and the Brinkman models. In the Brinkman model, boundary condition of the continuity of the tangential component of the stress vector, normal to the interface was also adopted. The equation of porous particle oscillations in the non-inertial frame of reference included the fictions body force $f = \rho_f \partial U / \partial t$ where ρ_f is the fluid velocity.

For the Darcy model we obtained $\tilde{\Omega}$ in the form

$$\tilde{\Omega} = \frac{2\beta^2}{2\beta^2 + 3 + 3[(1+i)Y + 2iY^2]} \qquad (1)$$

where $\beta = a/\sqrt{k}$, a is the particle radius, k is the permeability, $Y = \sqrt{a^2\omega/2\nu} = a/\delta$, ν is the dynamic viscosity, δ is the Stokes penetration depth. For the Brinkman model the real and imaginary parts of $\tilde{\Omega}$, namely Ω_r and Ω_i, were calculated numerically.

The force acting on the particle has the form

$$F = 6\pi\rho_f \nu a U C_{St} - \frac{4}{3}\pi\rho_f a^3 \frac{\partial U}{\partial t} C_{Ad} \qquad (2)$$

where the Stokes correction factor, C_{St}, and the added mass coefficient, C_{Ad} are

$$C_{St} = \Omega_r + (\Omega_r - \Omega_i)Y - \frac{2}{9}\Omega_i Y^2 \qquad (3)$$

$$C_{Ad} = \frac{1}{2}\Omega_r + \frac{9}{4Y}(\Omega_r + \Omega_i) + \frac{4}{9Y^2}\Omega_i \qquad (4)$$

The added mass coefficient in (4) describes the inviscid added mass (the first term on the r.h.s.) and also the unsteady effect of oscillations on the viscous resistance (Landau and Lifshitz, 1987). Figure 1 a, b shows the calculated dependences. For low permeability ($\beta >> 1$) C_{St} and C_{Ad} reproduce those for impermeable particles. In the limit of high-frequency oscillations of highly permeable particles, prevailing for inviscid flow, one has $C_{St} << 1$, $C_{Ad} << 1$. The inviscid added mass is always positive. However the effect of oscillations on viscous resistance gives rise to small negative values of C_{Ad} in the region approximately characterized by $\beta < Y$.

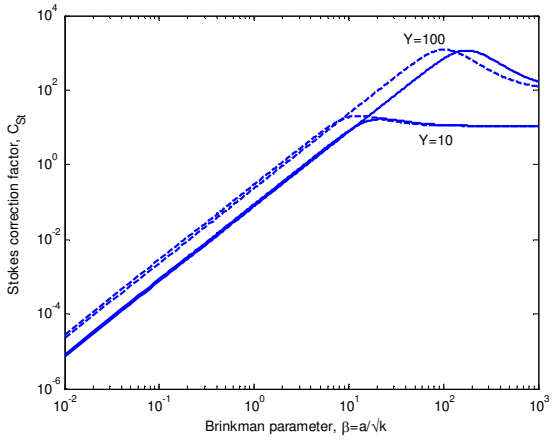

a)

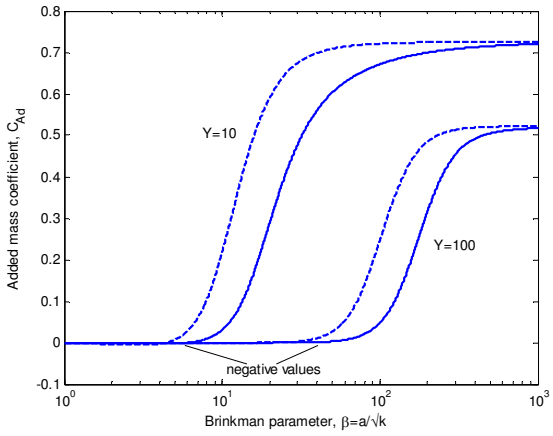

b)

Figure 1. Dashed and solid lines correspond to Darcy and Brinkman models, respectively.

Stokes, G.G. (1851) *Trans. Cambridge Philos. Soc.* **9**, 8-106,

Shapiro, M. et al., (2012) *Journal of Aerosol Sci* **44**, 24–45.

Landau, L.D. and Lifshitz, E. (1987) *Fluid Mechanics*, Pergamon, London.

Stick and rebound of single nanoparticles and nanoparticle agglomerates

S. Rennecke and A.P. Weber

Institute of Particle Technology, Clausthal University of Technology, Clausthal-Zellerfeld, 38678, Germany

Keywords: inertial impaction, bouncing, fragmentation.
Presenting author email: stephan.rennecke@mvt.tu-clausthal.de

When a particle impacts on a rigid surface it may stick to it, or, if the impact velocity is sufficiently high, may rebound from the surface being resuspended in the surrounding gas. Once a particle hits a surface its initial kinetic energy is reversibly transformed into elastic deformation and partly irreversibly lost i.e. in plastic deformation or heat, until all of it is consumed and the particle stops. Above a critical impact velocity, v_{cr}, the energy stored in elastic deformation is sufficient to overcome the energy of adhesion and the particle will be able to bounce. Thus, whether stick or rebound occurs is dependent on the mechanical properties of the particle and the acting adhesion force. These parameters also appoint the coefficient of restitution, e, the ratio of the final to the initial velocity, usually used to characterize particle impact events.

So far, there are no systematic measurements of both, e and $v_{cr,}$ for nanoparticles stated in the literature. This lack of knowledge arises most clearly in the discussion about a possible thermal rebound of nanoparticles. Wang and Kasper (1991) reported the possibility that nanoparticles may penetrate through personal protection filters when their size approaches the size of a cluster, as their mean thermal velocity due to Brownian motion may overcome v_{cr}. As the latter is unknown, the discussion did so far not lead to a closing result even after two decades. Thus, a new experimental technique is necessary that allows systematic investigations of the rebound of nanoparticles.

In this contribution a method for the investigation of particle bounce in a single stage low pressure impactor is presented. Size selected and singly charged spherical particles and dense spray dried agglomerates in the size range from 10 nm to 100 nm were impacted on a smooth surface at process conditions far above the critical Stokes number for deposition. The onset of particle rebound and the coefficient of restitution have been determined by using special structured collision substrates. The actual impact velocity of the nanoparticles has been determined numerically by calculating the particle trajectories with Lagrangian Particle tracking, similar to the methods recently published by Arffman et al. (2011). The setup allows defined collision experiments for impact velocities up to approximately 200 m/s.

Experimental results show that particles bounce with 100 % efficiency even at moderate impact velocities of some m/s, with v_{cr} increasing with decreasing particle size. An example dataset is shown in fig. 1 for dense silver particles. It can be clearly seen that with decreasing particle size the Stokes number necessary for particle bounce increases. The corresponding value for 10 nm particles is about 30 m/s.

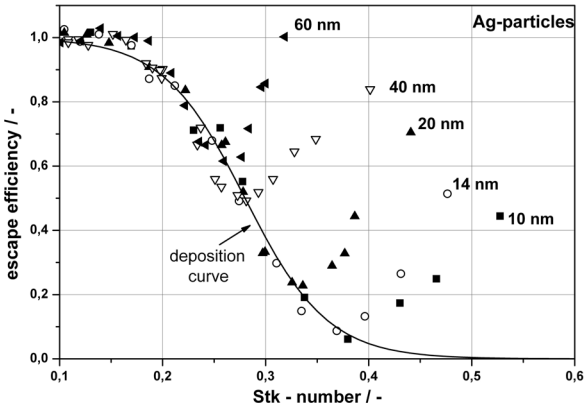

Figure 1. Escape efficiency as a function of Stk-number for silver particles of different size

Experiments were also performed with spherical dense silica particles and compared to spray dried silica agglomerates. The data shows that agglomerates bounce at much reduced v_{cr} values as their uneven surface (see fig. 2) acts as spacer, effectively reducing the contact area, and thus, adhesion force.

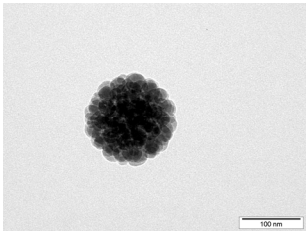

Figure 2. Dense, spray dried silica agglomerate

Further experimental results, including the coefficient of restitution and data on fragment bouncing, will be part of this contribution. The data will be used to identify an appropriate stick/bounce criterion for nanoparticles.

This work was supported by the Deutsche Forschungsgemeinschaft (DFG) under grant DFG-WE 2331/12-1.

Wang, H. C., & Kasper, G. (1991). Filtration efficiency of nm-size aerosol particles. J. Aerosol Sci., 22, 31–41.

Arffman, A., Marjamäki, M., & Keskinen, J. (2011), Simulation of low pressure impactor collection efficiency curves, J. Aerosol Sci., 42, 329-340

The Friction Factor and Collision Kernel for Aggregates in the Mass and Momentum Transition Regimes

Christopher J. Hogan Jr[1], Chonglin Zhang[2], Thaseem Thajudeen[1], Ranganathan Gopalakrishnan[1], Carlos Larriba[1], Tom Schwartzentruber[2]

[1]Department of Mechanical Engineering, University of Minnesota, Minneapolis, MN, 55455, USA
[2]Department of Aerospace Engineering and Mechanics, University of Minnesota, Minneapolis, MN, 55455,
USA Keywords: Aggregates, Direct Simulation Monte Carlo, Brownian Dynamics, Drag
Presenting author email: Hogan@me.umn.edu

The transport of aggregate aerosol particles is of considerable importance, given that particles fitting into this morphological class (ensembles of spherical primary particles connected in quasifractal configurations) are formed prevalently in combustion environments. Nonetheless, aggregates are difficult to examine: their non-spherical, complex geometries often preclude calculation of the drag force they experience as well as calculation of the rate of aggregate-aggregate collisions (aggregation). Further complicating analyses, for nanoparticle aggregates, both mass (aggregation) and momentum (drag) transfer processes occur within the transition regime, in which rates of mass and momentum transfer depend upon appropriately defined Knudsen numbers.

The purpose of the work shown in this presentation is two-fold. First, dimensional analysis is used to predict a functional form for the low Reynolds number, low Mach number drag on an arbitrarily shaped aerosol particle, such as an aggregate. The drag under these conditions is quantified in terms of the friction factor, for which dimensionless analysis provides a functional form similar to the adjusted sphere model of Dahneke (1973). This functional form for the friction factor is tested using direct simulation Monte Carlo (DSMC) of the flow field around test aggregate particles at selected Knudsen numbers, as shown in Figure 1. Good agreement is found between the predicted friction factor from dimensional analysis and the DMSC calculated friction factors in the transition regime.

Second, with the friction factor of an aggregate as input, an expression is developed to predict the collision rate (quantified by the collision kernel) of two arbitrarily shaped particles (such as aggregates) in the mass transfer transition regime, where the collision rate depends upon a suitably defined diffusive Knudsen number (in contrast to the traditional Knudsen number used in momentum transfer problems). For this purpose Brownian dynamics based mean first passage time calculations and dimensional analysis are employed, and it is found that a proper non-dimensionalization of the collision kernel (H), can be described solely as a function of the diffusive Knudsen number Kn_D (Figure 2), and that with suitable definitions of these parameters, the $H(Kn_D)$ relationship found applicable previously for sphere-sphere collisions applies to collisions between arbitrarily shaped particles as well.

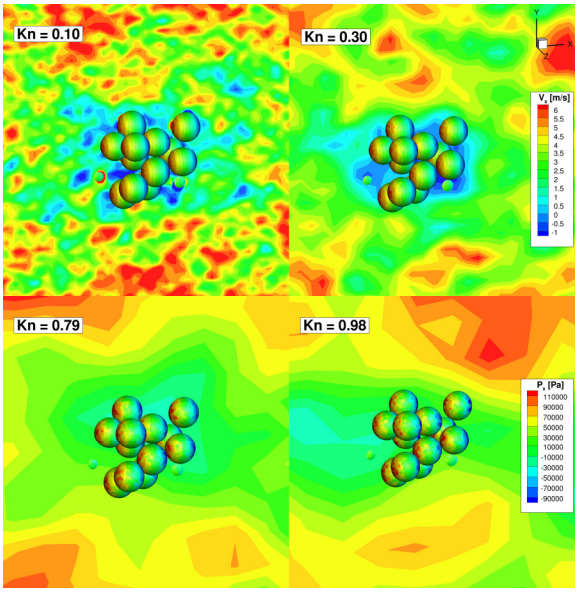

Figure 1. Contour plots of the x-direction component of the gas flow velocity around a 20-mer test aggregate at selected Kn. Also shown by contour plot are the x-direction stresses ($\mathbf{P_X}$) on the aggregate in a single DSMC time step.

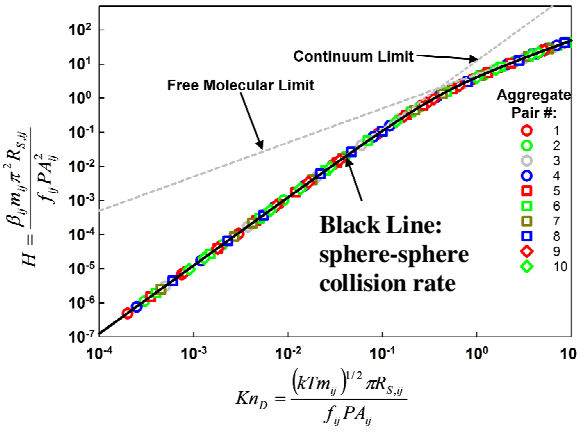

Figure 2. Summary of the $H(Kn_D)$ results obtained with mean first passage time simulations for the 10 test aggregate pairs.

Dahneke, B. E. (1973). Slip Correction Factors for Nonspherical Bodies- III The Form of the General Law. *Journal of Aerosol Science*, **4**, 163-170.

Separation of gas-borne nanoparticles in bubble columns

D. Koch, A.P. Weber
Institute of Particle Technology, Clausthal University of Technology, Clausthal-Zellerfeld, D-38678, Germany
Keywords: nanoscale carbon particles, surfactants, deposition, bubble column.
Presenting author email: koch@mvt.tu-clausthal.de

The transfer of nanoparticles from the gas phase into a liquid in bubble columns is employed for gas cleaning purposes (e.g. Pich and Schütz, 1991) and for the production of stable nanosuspensions (Verma *et al*, 2009). However, there are no systematic studies on the influence of particle size and structure, bubble size and surfactants on the particle separation efficiency. Therefore, the separation of gas-borne nanoparticles in bubble columns with heights of up to 1 m is studied. Nanoparticles used here are agglomerated carbon particles. In order to study the influence of surfactants on the separation efficiency, the results for pure water are compared with the ones obtained for polymeric stabilisers such as polyvinylpyrrolidone (PVP) K25 at various concentrations. The separation efficiency is determined from the measurements of the aerosol concentrations before and behind the bubble column. In addition, the concentrations in the solution is monitored on-line by an extinction technique.

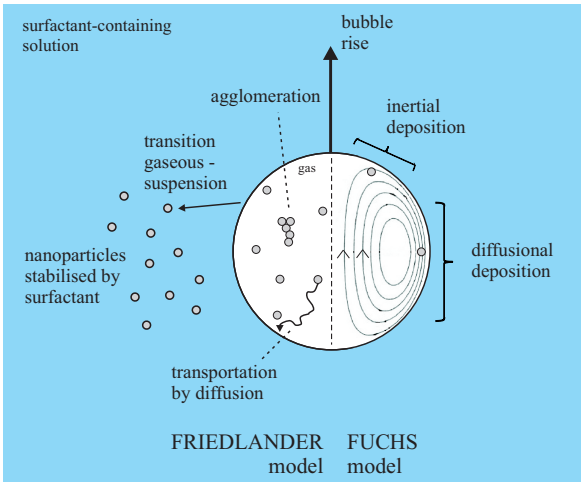

Figure 1: Processes inside the bubble with internal circulation

For pure water, the experimental results are compared to calculated values of the separation efficiency obtained with the Fuchs model (Fuchs, 1964) by using the experimental determined relative bubble rise velocity. The good agreement of theoretical and experimental results verifies the applicability of the Fuchs model to describe the separation efficiency of nanoparticles in pure water in the bubble columns, where mobile interfaces of the bubbles are assumed. In particular, it is shown that the particles exhibit a sticking probability of one at the gas-liquid interface. Supplementary, it was found that, for surfactants, the dissolved

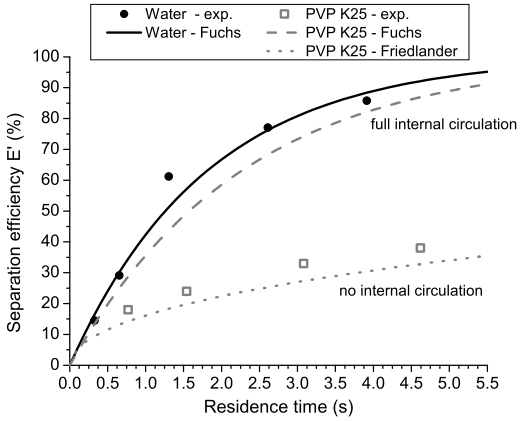

Figure 2: Influence of 0.4%(wt) PVP K25 on the separation efficiency

polymer in the solution reduces the internal circulation in the bubbles (shown in Fig. 1) due to reduced interface mobility and that, therefore, the Fuchs approach is no longer valid. For this case, the separation efficiencies are well described by the Friedlander model (Kronig and Brink, 1951; Friedlander, 2000) as shown in Fig. 2 for a 0.4%(wt) PVP K25 solution.

In this contribution, the Friedlander model, which takes only Brownian diffusion into account, will be discussed for surfactant solutions with changed interface properties by using surface active detergents.

This work was supported by the Deutsche Forschungsgemeinschaft (DFG) under grant DFG-We 2331/5-2.

S.K. Friedlander (2000) *Smoke, Dust, and Haze: Fundamentals of Aerosol Dynamics*, Oxford University Press Inc., New York.

N.A. Fuchs (1964) *The Mechanics of Aerosols*, Pergamon Press, Oxford.

R. Kronig and J. Brink (1951) *Applied Science Research A2, 142–154.*

Pich, J. and Schütz, W. (1991) *J. Aerosol Science, 22, 267-272.*

S. Verma, Y. Lan, R. Gokhale and D.J. Burgess (2009) *International Journal of Pharmaceutics 377 (1-2), 185–198.*

Biomass burning event in Spain: aerosol size distribution, aerosol optical properties and associated radiative forcing

E. Alonso-Blanco[1,2], V. Pont[3], A. Castro[1], A.I. Calvo[4], M. Mallet[3], R. Fraile [1]*

[1]Departamento de Física. Universidad León, León, 24071, España
[2]Centro de Investigaciones Energéticas, Tecnológicas y Ambientales (CIEMAT), Madrid, España
[3]Laboratoire d'Aérologie /OMP, UMR 5560, Université de Toulouse III, Toulouse, France
[4]Centre for Environmental and Marine Studies (CESAM), University of Aveiro, Portugal, 3810-193

*Corresponding author: Tel: 0034 987 29 15 43/ Fax: 0034 987 29 19 43
E-mail address: roberto.fraile@unileon.es (R. Fraile)
Keywords: Aerosol radiative forcing, Aerosol size distribution, Biomass burning.

The biomass burning particles have a direct effect on the global radiative balance, conditioning the energy balance by means of dispersion and absorption processes of the solar radiation reaching the Earth (Calvo *et al* 2010), so the study of these particles is crucial to identify energy variations in the atmosphere.

This study contains an analysis of the wildfires in the province of Leon on the 22nd and 23rd of August 2001 (400 ha were burnt) and their influence on the particulate matter concentration registered on the 23rd of August 2001 and on the size distributions. The optical characteristics of the aerosols and the associate radiative forcing were also analyzed.

The measurements were carried out in the district of Carrizo de la Ribera, in the center of the province of Leon, Spain, at 873 m asl, a rural farming area.

A PCASP-X laser spectrometer was installed in a field and 8 daily measurements during 15-minute intervals every 3 hours. The refraction index of the particles was estimated for each relative humidity. Then, raw size bins were corrected using a program based on Mie Theory from the estimated refraction indices.

The short-wave radiative forcing (SW) was analyzed using the Radiative Transference Model (RTM) GAME (Global Atmospheric Model) (Dubuisson *et al* 2004). The methodology used to compute the radiative impact is described in detail in Mallet *et al* (2008) and Roger *et al* (2006).

On the study day the measurements affected by the wildfires are the ones taken at 1300 UTC and at 1600 UTC, and the average increase in the number of aerosols is of around 500% when compared with the unaffected measurements. The increases corresponded mainly to particles smaller than 0.2 μm (fine mode).

The instantaneous surface forcing estimated by GAME (ΔFBOA) can reach up to -38.7 W/m^2 and -10.4 W/m^2. This significant decrease of solar energy at the surface might strongly modify the surface energy budget.

Moderate instantaneous forcing simulated at the top of the atmosphere (ΔFTOA) has been computed by GAME reaching up to -20.5 W/m^2 and -7.8 W/m^2. For most of our case studies, the aerosol forcing is negative (cooling effect) and much higher at the surface than at the top of the atmosphere due to absorption.

The estimation of the positive instantaneous radiative forcing (ΔFATM) given by GAME indicates the absorption of solar radiation in the atmosphere by the smoke aerosol considered. It ranges from + 2.7 to + 22.8 W/m^2. This positive atmospheric radiative forcing is reflected in an atmospheric heating by absorbing particles, which may affect both cloud cover and planetary albedo and atmospheric stability.

In Fig. 1 we can observe that the direct atmospheric radiative forcing reaches maximum values when fire events occur. Indeed, the aerosol number concentration is 8 times higher at 1300 UTC than during the morning for the fine mode. These high loads of aerosols in the fine mode clearly interact with visible radiation through absorption and scattering processes, which is reflected in a lower downward radiative flux reaching the surface (ΔFBOA highly negative).

The wildfires not only alter the atmospheric composition increasing the number of particles and modifying their size distributions, but they also alter the local radiative balance.

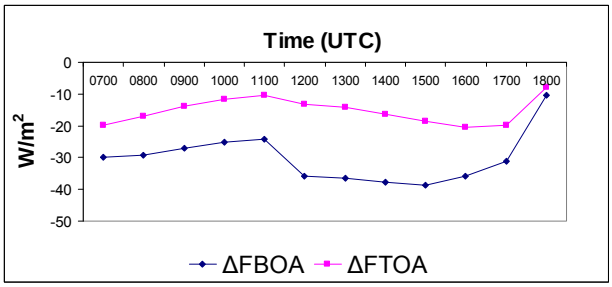

Figure 1. Daily variation of instantaneous aerosol radiative forcing at ΔFTOA and ΔFBOA

Calvo, A.I., Pont, V., Castro, A., Mallet, M., Palencia, C., Roger, J.C., Dubuisson, P. and Fraile, R. (2010) *J. Geophys. Res*. **115**, D08206.

Dubuisson, P., Dessailly, D., Vesperini, M. and Frouin, R. (2004) *J. Geophys. Res*. **109**, D19106.

Mallet, M., Pont, V., Liousse, C., Gomes. L., Pelon, J., Osborne, S., Haywood, J., Roger, J.C., Dubuisson, P., Marsical, A., Thouret, V. and Goloub, P. (2008) *J. Geophys. Res*. **113**. D00C01.

Roger, J. C., Mallet, M., Dubuisson, P., Cachier, H., Vermote, E., Dubovik, O. and Despiau, S. (2006) *J. Geophys. Res*. **111**, D13208.

Thursday, September 6, 2012

Poster Session C, Posters P001 - P292

Estimate of direct radiative forcing by aerosols over East Asia with the assimilated aerosol optical properties

C.H. Song[1], R.S. Park[1], C.E. Chung[1], J.H. Lee[2], and J. Kim[2]

[1]Advanced Environmental Monitoring Research Center (ADEMRC), School of Environmental Science and Engineering, Gwangju Institute of Science and Technology (GIST), 1 Oryong dong, Buk-gu, Gwangju 500-712, Republic of Korea

2 Institute of Earth, Astronomy, and Atmosphere, Brain Korea 21 Program, Department of Atmospheric Sciences, Yonsei University, Seoul, Republic of Korea

Keywords: data assimilation, direct radiative forcing, MACR
Presenting author email: chsong@gist.ac.kr

Direct radiative forcing (DRF) by aerosols over East Asia was investigated with the assimilated aerosol optical properties discussed in Park et al. (2011). For radiative transfer modeling, Monte-Carlo Aerosol Cloud Radiation (MACR) model, updated by Chung et al. (2010), was used, because it provides the more accurate radiative fluxes than those obtained with two-stream approximations (Baker et al., 2003). The input data for MACR simulation was described in Table 4.1. The angstrom exponents for AOD and SSA and the low-level, mid-level, high-level and convective cloud fractions and cloud optical depths were calculated, based on Chung et al. (2010).

Based on the seasonal variations of DRF by aerosols (Fig 1), the importance of dust was emphasized. At the top of atmosphere, the strong negative forcing was mainly affected by sulfate, and partly by nitrate, dust, and sea-salt. Especially, the dust effect was very strong in spring. At the atmosphere, the positive forcing was mainly affected by BC, and a little by organic matter,

Table 1. Description of input data used for MACR simulation.

Input data	Sources
AOD	combination of CMAQ-simulated and MODIS-retrieved AODs (Park et al., 2011)
SSA	CMAQ-simulated SSA (Park et al., 2011)
asymmetric factor	constant value (=0.69), which is based on AERONET data
angstrom exponents for AOD and SSA	using the parameterization in the literature (Chung et al., 2005)
cloud fractions	combination of ISCCP and terra MODIS data (Chung et al., 2010)
cloud optical thickness	combination of ISCCP and terra MODIS data (Chung et al., 2010)
albedo	ECMWF data
ozone	terra MODIS data
precipitable water	terra MODIS data
height	USGS data

***ISCCP: International Satellite Cloud Climatology Project**

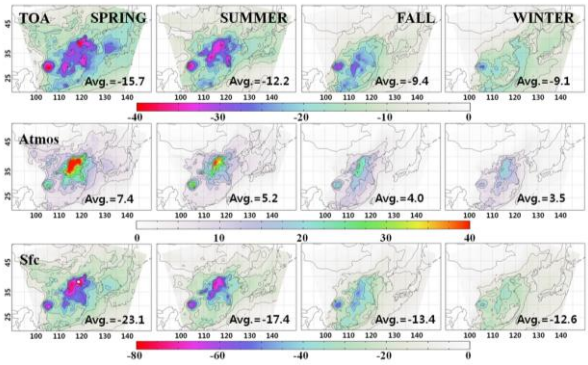

Figure 1. Seasonal variation of DRF (W m^{-2}) by aerosols at the surface, within atmosphere, and at the top of atmosphere with assimilated AOD.

but the DRF by organic matter is uncertain, because SSA for OC was controversial. The MACR-simulated DRF from assimilated AOD was evaluated with MODIS-retrieved DRF over ocean. The comparison was conducted only over ocean, but that over the Yellow sea and East China sea can be validation of MACR-simulated DRF, indirectly.

The DRF by aerosols, obtained from model simulation, have large uncertainty, caused by the uncertainty of aerosols and their properties. To reduce these uncertainties, the more accurate aerosol optical properties were applied for MACR model simulation, but there are still other uncertainties in several variables. SSA was already evaluated by Park et al. (2011), but can be improved through assimilating with AERONET SSA. The angstrom exponents and asymmetric factor could be developed, using Mie calculation. This study is only one of approaches to improve the modeled DRF by aerosols, and should be updated.

Barker, H. W., et al. (2003) *J. Clim.*, 16, 2676– 2699.
Chung et al. (2010) *Atmos. Chem. & Phys.*, **10**, 6007-6024.
Park et al. (2011) *Atmos. Chem. & Phys.*, **11**, 23801-23858.

9-year analysis of the aerosol radiative forcing over a Mediterranean urban coastal site

A.R. Esteve[1], V. Estellés[1,2], M.P. Utrillas[1] and J.A. Martínez-Lozano[1]

[1] Department of Earth Physics and Thermodynamics, University of Valencia, Burjassot, 46100, Spain.
[2] Department of Fundamental and Experimental Physics, University of La Laguna, La Laguna, 38207, Spain.
Keywords: atmospheric aerosols, aerosol radiative forcing, measurements.
Presenting author email: Anna.Esteve@uv.es

Atmospheric aerosols, both of natural and anthropogenic origin, directly affect the Earth's radiative balance through the scattering and absorption of the incident solar radiation (Charlson *et al.*, 1992; Kiehl and Briegleb, 1993). The determination of this effect, named direct aerosol radiative forcing, is still characterized by a great uncertainty, both at regional and global scale, due to the variability of the optical properties and the spatial-temporal distribution of the aerosols (IPCC, 2007).

In this study we present an analysis of the aerosol radiative forcing using measurements of global solar irradiance and aerosol properties, as well as simulated data, during the period from 2003 to 2011 in Burjassot, Spain, an urban coastal site on the western extreme of the Mediterranean, subject to the influence of particles brought from such distant regions as the Sahara, industrial continental Europe, and oceanic regions.

Measurements of global solar irradiance on a horizontal surface were made every 5 minutes with a Kipp and Zonen CM-6 pyranometer, which has a spectral range between 305 and 2800 nm. The solar irradiance without aerosols was simulated with the SBDART (Santa Barbara DISORT Atmospheric Radiative Transfer) multiple scattering model (Ricchiazzi *et al.*, 1998). The input parameters used by the SBDART were a mid-latitude model atmosphere, a fixed surface albedo of 0.15, the total ozone column from TOMS and OMI (ftp://toms.gsfc.nasa.gov), and the values obtained by a Cimel CE318 photometer of the water vapor amount. To obtain the solar irradiance with aerosols, the aerosol optical properties (aerosol optical depth, single scattering albedo, and asymmetry parameter) obtained by a Cimel CE318 photometer were also included as input parameters in the SBDART.

The aerosol radiative forcing, which is defined as the difference in net fluxes with and without aerosols, was calculated at 5 minutes intervals, and then integrated over 24 hours to obtain daily mean values for 200 complete days under cloud-free skies during the period from 2003 to 2011. The monthly mean aerosol radiative forcing (Figure 1) showed a clear variation during the year, ranging from -6 to -29 Wm^{-2} at the surface, and from -2 to -4 Wm^{-2} at the top of the atmosphere, with mean values for the whole period of -17 and -2 Wm^{-2}, respectively. The aerosol radiative forcing efficiency (Figure 2), which represents the change in net flux per unit of aerosol optical depth at 500 nm, was found to be -111 Wm^{-2} at the surface and -17 Wm^{-2} at the top of the atmosphere. These negative values, which correspond to cooling effects, show the important role of atmospheric aerosols in this urban site of the Mediterranean coast.

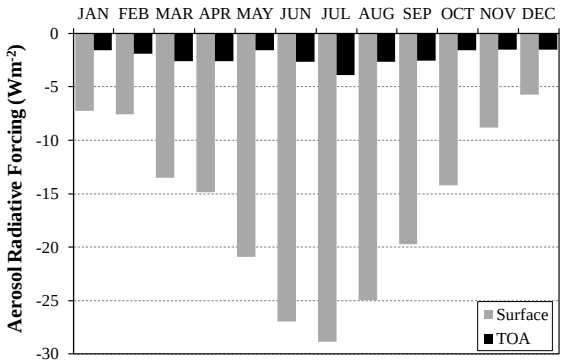

Figure 1. Monthly mean aerosol radiative forcing at the surface and at the top of the atmosphere.

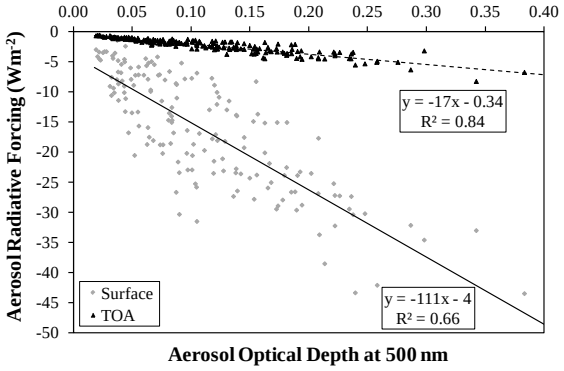

Figure 2. Aerosol radiative forcing as a function of the aerosol optical depth at 500 nm.

This work was funded by the Ministry of Economy and Competitiveness of Spain through projects CGL2009-07790 and CGL2011-24290, and the Valencian Autonomous Government through the project PROMETEO-2010-064. The collaboration of V. Estellés was possible thanks to the fellowship JCI-2009-04455.

Charlson, R. J., Schwartz, S. E., Hales, J, J. M., Cess, R. D., Coakley Jr., J. A., Hansen, J. E., and Hofmann, D. J. (1992), *Science*, **255**, 423-430.

Intergovernmental Panel on Climate Change (IPCC) (2007), *Climate Change 2007: The Physical Science Basis*. Cambridge University Press.

Kiehl, J. T., and Briegleb, B. P. (1993), *Science*, **260**, 311-314.

Ricchiazzi P., Yang, S., Gautier, C., and Sowle, D. (1998), *Bulletin of the American Meteorological Society*, **79**, 2101–2114.

6 years of continuous aerosol size distribution measurements from the foothills of Central Himalayas

A.-P. Hyvärinen[1], R.K. Hooda[1,3], M. Komppula[1,2], K. Neitola[1], E. Asmi[1], V.P. Sharma[3], T.S. Panwar[3,4], and H. Lihavainen[1]

[1]Finnish Meteorological Institute, Erik Palménin aukio 1, P.O. Box 503, FI-00101, Helsinki, Finland
[2]Finnish Meteorological Institute, Yliopistonranta 1F, P.O. Box 1627, FI-70211 Kuopio, Finland.
[3]The Energy and Resources Institute, Darbari Seth Block, IHC Complex, Lodhi Road, New Delhi 110 003, India
[4] WWF India, Lodhi Estate, New Delhi-110003, India

Keywords: aerosol size distribution, Himalayas

The Finnish Meteorological Institute together with The Energy and Resources Institute, TERI India have conducted continuous measurements of aerosol physical properties in Mukteshwar, India since September 2005. This is a background location in the foothills of Central Himalayas, and aerosol size distribution measurements with such a time span are unique from the area. Long-term trends in aerosol concentrations can be observed to emerge from the data set.

Mukteshwar is located about 350 km northeast of New Delhi. The site is at 2180 m above the sea level in a rural region at the Himalayan Mountains. The station is surrounded by an agricultural test field. No major local pollution sources are known to affect the site. The nearest towns, Nainital and Almora, are located 25 km to the west and north of the site, respectively. The size distribution measurements are made with a DMPS (Differential Mobility Particle Sizer) system. The instrument is set to measure the dry particle diameter in the size range 10–800 nm in about 5.5-min cycles (Komppula et al. 2009).

The total particle concentration for the 5-year measurement period shows high variability (Fig. 1). The maximum concentrations are observed in April, before the annual monsoon season (mid June-end of September). Not accounting year 2011, the maximum concentrations have shown an increase throughout the measurement period. This reflects the population growth, urbanization, and rapid industrial development occurring in India.

The highest concentrations which are observed during the warm summer are due to air lofted from the Indo-Gangetic plains below, when the boundary layer height is at its yearly maximum. This is also a time when nucleation mode particles are observed in Mukteshwar (Neitola et al. 2011). Typically the size distribution is unimodal, with a peak at ~ 100 nm (Fig. 2).

The seasonal concentration variation is similar for all the years: after the highest concentrations in spring, the monsoon season brings the concentrations down to the lowest values of the year with different wet deposition processes. These include impaction and diffusion scavenging by the falling rain drops and activation to mountain fogs and clouds. This also decreases the geometric mean diameter of the size distribution. Several studies suggest that the aerosol concentrations before the monsoon season may modulate the monsoon characteristics; this in turn would affect the aerosol concentrations during monsoon. In practice, such an observation is difficult to draw from *in situ* observations alone (Hyvärinen et al. 2011).

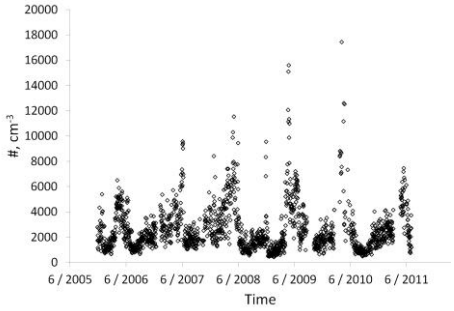

Figure 1. 1-day total particle concentrations from Mukteshwar.

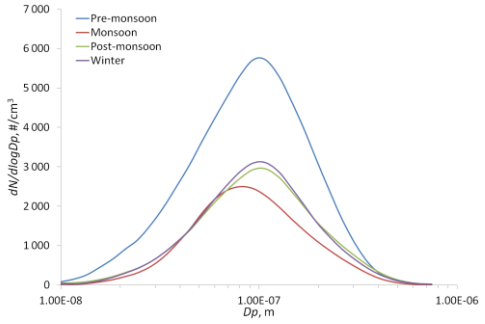

Figure 2. Seasonal average size distributions: Pre-monsoon 1.3-30.6.; Monsoon 1.7.-30.9.; Post-monsoon 1.10.-30.11.; Winter 1.12.-28.2

This work was supported by the Ministry of Foreign Affairs of Finland.

Komppula, M., et al. (2009), *Journal of Geophysical Research*, 114, D12202.

Neitola, K., et al. (2011), *Atmos. Chem. Phys.*, 11, 8447-8458, doi:10.5194/acp-11-8447-2011.

Hyvärinen, A.-P., et al. (2011), *Atmos. Chem. Phys.*, 11, 8283-8294, doi:10.5194/acp-11-8283-2011.

Description of the Soot on Snow experiment (SoS 2012) at Jokioinen, Finland

N. Kivekäs[1], D. Brus[1], A. Hyvärinen[1], O. Järvinen[2], J. Svensson[1], A. Aarva[3], O. Meinander[1], A. Heikkilä[1] and A. Virkkula[1,2]

[1]Research and Development, Finnish Meteorological Institute, Helsinki, PO.Box 503, 00101 Finland
[2]Department of Physics, Helsinki University, Helsinki, 00101, Finland
[3]Weather and safety, Finnish Meteorological Institute, Helsinki, PO.Box 503, 00101 Finland
Keywords: Soot particles, Absorption, Aerosol impacts, Climate effect.
Presenting author email: niku.kivekas@fmi.fi

Soot consists mainly of light absorbing carbon. When deposited on snow, it decreases the snow albedo, increases the absorption of radiation in snow and thereby enhances melting. This process has been studied for decades (e.g. Clarke and Noone, 1985) and it has been recognized to be one of the major sources of warming in the Arctic regions (Flanner et al., 2007). The link between soot, snow albedo, and climate change is still not known in enough detail for quantitative analysis (Hansen and Nazarenko, 2004). To provide more insight into these connections,the Finnish Meteorological Institute and Helsinki University have started the Soot on Snow (SoS 2012) measurement campaign for the whole melting season 2012 at Jokioinen, southern Finland. This project is a continuation of a similar experiment carried out at Nurmijärvi, southern Finland in spring 2011 (Virkkula et al., 2011).

On February 16th we produced three spots of different concentrations of soot on snow on an agricultural field. A fourth measurement spot was created as reference with no soot. The soot we used was produced in residential heating with wood and oil, and was collected by chimney cleaners in eastern and northern parts of Helsinki during winter 2012.

The soot was dispersed in air inside a closed barrel by blowing in ambient air. Then the air with the soot was led to a cyclone where larger particles were separated. The air with the smaller soot particles was led to a specially manufactured soot tent (an open-bottom cylinder 4 m in diameter, 1,3 m in height) via two inlets on the opposite sides of the tent. The sample inlet for the measurement devices was located approximately in the middle of the soot tent. Excess air was led out from the tent via a chimney on top of the tent.

Sample inlet was a six meters long approximately straight copper tube. Because the soot particle concentrations inside the tent were extremely high, the air sample was diluted with fraction: 1 part sample air, 25 parts filtered ambient air.

During the time when the tent was up, there were several instruments measuring the sampled air. Particle number concentration was measured with a Condensation Particle Counter (CPC) and particle size distribution with a Differential Mobility Particle Sizer (DMPS, 15-750 nm) and an Optical Particle Sizer (OPS 300 – 10 000 nm). The absorption of the airborne soot was measured with a three-wavelength Nephelometer and a three- wavelength Particle Soot Absorption Photometer (PSAP). The size distribution of the soot was measured with a Single Particle Soot Photometer (SP2, 70-500 nm).

After the soot was blown into the tent for a measured time and it was allowed to settle, the tent was carefully removed and snow samples were taken from the spot. These samples were melted and filtered. Filters were analysed with a Thermal/Optical Carbon Aerosol Analyzer (OC/EC) for their EC concentration. Each spot had also two poles for measuring the snow depth. Structure, grain size and temperature of the snow layer were also analysed.

Two broad band (300-42000 nm) albedo sensors were installed about 20 cm above the snow surface at each spot to measure the global net radiation. Each soot spot was also instrumented with a Scalar Irradiance Sensor (400-700 nm). These were installed on the ground in December before the snow pack was formed.

More snow samples will be taken and analysed during the spring. Also the evolution of the snow layer structure and temperature on the soot spots and on the reference spot will be monitored. The snow depth is measured daily, and the albedo and transmittance of the snow are measured continuously.

With this data our goal is to make a calibration curve for estimating how much soot is needed to cause observable differences in different parameters of the snow pack. We will also try to quantify of the effects of the soot on snow for modelling purposes. Other parameters of interest are the settling velocity of the soot, the aging of the soot in the snow and the transfer of radiation through the snow layers.

This work was supported by Tor and Maj Nessling foundation, Academy of Finland, and the international co-operation programs CRAICC and MACEB. We also thank Consti Talotekniikka for providing us the soot.

Clarke, A. D. and Noone, K. J. (1985), *Atmos. Environ.*, **19**, 2045–2053.

Flanner, M. G., C. S. Zender, J. T. Randerson, and P. J. Rasch (2007)., J. Geophys. Res., **112**, D11202, doi:10.1029/2006JD008003.

Hansen, J. and Nazarenko, L. (2004), *Proc. Nat. Acad. Sci.*,**101**, 423–428.

Virkkula, A., Järvinen, O., Lihavainen, H., Hyvärinen, A., Mäkelä, T., Kivekäs, N., Väänänen, R., Backman, J., Heikkilä, A., Aarva, A., Kyrö, E-M. and de Leeuw, G. (2011), *Proceedings of the CRAICC annual meeting*, 10-14.10.2011.

Influence of a kappa-Köhler theory based water uptake scheme on a global aerosol/climate model

D. O'Donnell[1]

[1]Climate Change Research, Finnish Meteorological Institute, 00101 Helsinki , Finland
Keywords: aerosol modelling, atmospheric aerosols, hygroscopic growth, climate effect.
Presenting author email: declan.odonnell@fmi.fi

The scattering of radiation by aerosol particles is a strong function of the aerosol size compared to the radiation wavelength. Furthermore, the number of particles in a given aerosol population that can act as cloud condensation nuclei (CCN) is also strongly size-dependent. Particle size is thus important for both the direct and indirect aerosol effects on climate. Hygroscopic growth can substantially alter both the size and optical properties of aerosol particles; moreover, observations in many regions show that condensed water makes up a significant proportion of the aerosol mass. It is thus deisrable that global climate/aerosol models are able to capture not only the regional and temporal distributions of particle mass and number, but also their hygroscopic growth with reasonable accuracy.

Kappa-Köhler theory is a comparatively recently developed method that allows the quantification of aerosol water uptake in terms of a single free parameter (κ) per compound in the aerosol phase (Petters and Kreidenweis, 2007). It obviates the need for detailed thermodynamic calculations and is for this reason highly attractive to global climate/aerosol modelling, where computation of aerosol physics is computationally very costly.

In this study, the global climate/aerosol model ECHAM5/HAM version 2 (Stier et al. 2005; Zhang et al. 2012) is used. The introduction of a based water uptake parameterization into this model is described. The impact of the new water uptake scheme is described in terms of observables by its influence on aerosol optical depth (AOD, a wide-area observable quantity), and in terms of aerosol direct effects on climate. Aerosol indirect effects are for future study.

Historically, ECHAM5/HAM (version 1) has been an outlier among the global models that have been compared within the AeroCom framework (Textor et al., 2006), with an annual mean global aerosol water burden of 75 Tg under year 2000 conditions, compared to the AeroCom median value of 35 Tg. With the introduction of the κ-Köhler based parameterization in its standard configuration, this figure falls to 51Tg for ECHAM5/HAM.

The global mean AOD falls from 0.16 to 0.13 with the introduction of the new scheme, with the largest reduction seen over the Southern Ocean. The modelled clear-sky aerosol forcing at the top of the atmosphere weakens from -4.2 Wm^{-2} to -3.6 Wm^{-2}.

The sensitivity of the model to the possible choices of the free parameter κ for each of the model hygroscopic compounds (sulphate, sea salt and organic carbon) is also studied and the results presented, again in terms of AOD and direct aerosol forcing,

Boxmodel studies

In order to better understand the model behaviour, the global modelling results are complemented by boxmodel studies in which dry aerosol size and composition, as well as ambient temperature and relative humidity, can be prescribed, and the resulting hygroscopic growth factors calculated.

It is found that, in the κ-Köhler based model, hygroscopic growth is:

i. insensitive to temperature
ii. moderately sensitive to κ
iii. highly sensitive to relative humidity (RH)

It is concluded that the κ-Köhler framework is well suited to global aerosol modelling. Indeed, it has already been adopted as the default water uptake scheme in ECHAM5/HAM2 (Zhang et al., 2012).

Petters, M. D. and Kreidenweis, S. M. (2007) *Atmos. Chem. Phys.* **7**, 1961-1971

Stier, P. et al. (2005) *Atmos. Chem. Phys.* **5,** 1125-1156

Textor, C. et al. (2006) *Atmos. Chem. Phys.* **6**, 1777-1813

Zhang, K.. et al. (2012) *Atmos. Chem. Phys. Discuss.*, submitted

Aerosol and cloud SW radiative forcing in the south of Portugal

V. Salgueiro[1], M.J. Costa[1,2], A.M. Silva[1], and D. Bortoli[1, 3]

[1]Évora Geophysics Centre (CGE), University of Évora, Évora, 7000, Portugal
[2]Department of Physics, University of Évora, Évora, 7000, Portugal
[3]Institute Atmospheric Sciences and Climate, ISAC-CNR, Bologna, 40129, Italy
Keywords: aerosols, clouds, radiative forcing
Presenting author email: vandasalgueiro@gmail.com

Clouds and to a certain extent aerosols, constitute the most important factors regulating the Earth's radiation budget because they absorb and scatter solar radiation and absorb and emit terrestrial radiation. Therefore, the characterization and understanding of their radiative effects are tremendously important.

Accordingly, the study of the variability of the solar radiation at the surface is highly dependent on clouds and aerosols and their optical properties, particularly the optical thickness is essential for any radiation parameterization, which are still major priorities for regional and global climate models (Kassianov et al., 2011; Santos et al., 2011).

In this work, results of the cloud and aerosol radiative forcings obtained from ground-based irradiance measurements in the shortwave (SW) spectral region are presented. These irradiance measurements are taken continuously in the Atmospheric Physics Observatory of the Evora Geophysics Center, with an Eppley Black & White Pyranometer that presents a spectral range comprehended between 285 and 2800 nm. Surface aerosol and cloud radiative forcings are defined as the instantaneous increase or decrease in net (downwelling minus upwelling) irradiances at the surface level, due to instantaneous changes of these atmospheric constituents. The clear sky irradiances are calculated with a radiative transfer model. Cloud and aerosol radiative SW radiative forcings are normalized dividing the absolute values by the net clear sky irradiances. This quantity is useful because it allows for eliminating the solar zenith angle dependence.

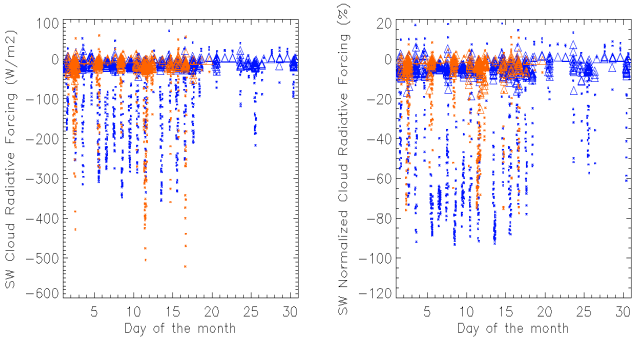

Figure 1. Absolute and normalized SW cloud radiative forcing at the surface, for January (blue dots) and July (red dots) 2008, in the region of Évora, south of Portugal. The triangles represent the latter quantities per unit cloud optical thickness.

Moreover the absolute and normalized SW cloud and aerosol radiative forcing values are also divided by the respective optical thickness, obtained from ground-based spectral measurements, to yield the cloud / aerosol radiative forcing efficiencies, and results are presented and analysed.

Figure 1 presents the absolute and normalized SW cloud radiative forcing values at the surface, for January (blue dots) and July (red dots) 2008, in the region of Évora, south of Portugal. To note that the strongest SW cloud radiative forcings are obtained in July, with values reaching -500 W/m^2, while the values obtained in January are around -350 W/m^2. When the normalized SW cloud radiative forcing is considered, the opposite situation is found, with the cloud radiative forcing in January reaching values around 95% and in July with values of about 75% (absolute values).

Figure 1 also shows both radiative forcing quantities per unit optical thickness, represented by the triangles. Results indicate that the summer and winter cloud radiative forcing efficiencies do not differ much, presenting a relatively constant behaviour.

The aerosol radiative forcing is also evaluated in terms of absolute and normalized values and results will be presented at the conference.

The work is financed through FEDER (Programa Operacional Factores de Competitividade – COMPETE) and National funding through FCT – Fundação para a Ciência e a Tecnologia in the framework of projects FCOMP-01-0124-FEDER-007122 (PTDC / CTE-ATM / 65307 / 2006), FCOMP-01-0124-FEDER-009303 (PTDC/CTE-ATM/102142/2008) and FCOMP-01-0124-FEDER-014024 (PTDC/AAC-CLI/114031/2009).

Kassianov, E., Barnard, J., Berg, L.K., Long, C.N., Flynn, C. (2011): Shortwave spectral radiative forcing of cumulus clouds from surface observations. Geophysical Research Letters, 38 (7), art. no. L07801.
doi: 10.1029/2010GL046282

Santos, D., M. J. Costa, A.M. Silva, R. Salgado, A. Domingues, and D. Bortoli, (2011): "Saharan desert dust radiative effects: a study based on atmospheric modelling". International Journal of Global Warming, 3, 88-102.

Investigating aerosol – radiation feedbacks in high-emission areas using WRF/Chem model

A.Balzarini[1], G.Pirovano[1], G.M. Riva[1]

[1]RSE S.p.A., via Rubattino 54, 20134 Milano, Italy
Keywords: WRF/Chem model, feedback, aerosol, climate
Presenting author email: alessandra.balzarini@rse-web.it

Aerosols are known to affect both weather and climate. The scattering of solar and terrestrial radiation by aerosol particles exerts a direct radiative forcing on climate system ("direct effect"; Foster et al., 2007). Additionally, aerosols, serving as cloud condensation nuclei, modified microphysical and optical properties of clouds and then precipitations ("indirect effect"; Forkel et al., 2011).

Also climate can influence air quality. The impact of climate on air quality may affect future air quality policy planning, especially in urban areas, through modifications of gas-phase chemistry, transport, diffusion, removal processes and natural emissions (Giorgi and Meleux, 2007).

Although the existence of these mechanisms has been documented in recent years, only few studies considered the interactions between aerosols and meteorology in air quality simulations over Europe (e.g. Forkel et al., 2011; Tuccella et al., 2012).

Traditional "off-line" chemical and transport models, in fact, do not allow the estimation of the coupled interactions between climate change and air quality and, hence, their effects on policies. Otherwise, in the fully coupled Weather Research and Forecasting/Chemistry model (WRF/Chem; Grell et al., 2005) the chemistry transformations are embedded into the meteorological model WRF (Skamarock et al., 2008), so that such interactions can be investigated with a full modular approach.

In order to evaluate the effect of direct and indirect effects of aerosols on meteorology and surface PM10 concentrations, numerical simulations of the WRF/Chem model (version 3.3.1; 2011) have been performed over the Italian Peninsula. Italy often suffers high PM concentrations, due to the interaction of both anthropogenic and natural emissions, enhanced by rather complex circulation conditions, making it a very interesting case study.

Particularly, this paper provides a quantitative evaluation of the interaction between aerosol and meteorological processes due to limited but strongly emitting areas, thus contributing to the investigation of possible regional climate impacts.

The fully coupled meteorology and chemistry model has been applied for both winter and summer episodes of the year 2005. WRF/Chem has been set up for the whole Italian domain with a grid resolution of 15 km, using emissions and configuration schemes adopted in previous studies and sensitivity test. The chosen gas phase chemistry and aerosol modules are coupled to some aqueous reactions and microphysics, as described in Peckham *et al.* (2011).

As a first step computed results have been evaluated against ground-based observations, providing PM10, PM2.5 mass concentrations together with their main components. Then, three WRF/Chem simulations have been compared in order to investigate aerosols-radiation feedbacks and their effect on clouds and precipitation. The first simulation does not account for any feedback mechanisms. The second simulation includes the direct aerosol effect and the third one accounts for the indirect effect of aerosols on clouds and precipitations.

For each simulation, the influence of the different model formulations is presented and discussed as well as the effects on meteorological processes and PM10 concentrations.

Moreover, whenever possible, the different impact of anthropogenic and natural aerosol loads is discussed.

References

Giorgi and Meleux (2007) *C. R. Geoscience* **339**, 721-733.

Forster, P., et al. (2007) *Contribution of Working Group I to the Fourth Assessment Report of the Intergovernmental Panel on Climate Change*, Cambridge University Press.

Forkel, R., Werhahn, J., Hansen, A. B., McKeen, S., Peckham, S., Grell, G., Suppan, P. (2011) *Atmos. Environ.*, article in press.

Grell, G. A., Peckham, S. E., Schmitz, R., McKeen, S. A., Frost, G., Skamarock, W. C. and Eder, B. (2005) *Atmos. Environ.* **39(37)**, 6957-6975.

Peckham, E. et al. (2011) *WRF/chem Version 3.3 User's Guide*

Tuccella, P., Curci, G., Visconti, G., Bessagnet, B., Menut, L., Park, R. J. (2012) *J. Geophys. Res.* **117**, D03303.

The Soot on Snow experiment 1 (SoS 2011): Soot from burning organics

A. Virkkula[1,2], O. Järvinen[2], H. Lihavainen[1], A. Hyvärinen[1], , J. Svensson[1], T. Mäkelä[1], N.Kivekäs[1], R. Väänänen[2], J. Backman[2], A. Heikkilä[1], A. Aarva[1], E.-M. Kyrö[2], and G. Leeuw[1,2]

[1] Finnish Meteorological Institute, P.O. Box 503, FI-00560 Helsinki, Finland
[2]University of Helsinki, Department of Physics, P.O Box 64, FI-00014 Univ. of Helsinki, Finland
Keywords: soot, snow, albedo, irradiance
Presenting author email: aki.virkkula@fmi.fi; aki.virkkula@helsinki.fi

Soot particles consist of light absorbing carbon, or black carbon (BC) and organics. If soot particles get deposited on snow they will absorb solar radiation, decrease the snowpack albedo and so heat the snow and accelerate its melting. This process has been studied for decades (e.g., Warren and Wiscombe, 1980; Clarke and Noone, 1985) and it is recognized as one of the most important climate forcers in the polar areas (e.g., Quinn et al., 2008). Hansen and Nazarenko (2004) concluded that there is a need for better quantification of the links of BC to snow albedo, melting ice, and climate change.

The Soot on Snow (SoS) project is aimed for studying and quantifying the effects of soot on snow, for example the effect on albedo, snow grain size, and melting. The plan is to make experiments during several consequent winters. The first one of the series was conducted in spring 2011, the second in spring 2012 (Kivekäs *et al.* 2012).

In the first campaign soot particles were produced and let them deposit on a snowpack on a farming field in southern Finland on Friday, 4 March 2011. Soot was produced by burning organics, such as rubber from used car tires in a wood-burning stove. The purpose was to get as high soot concentrations in air as possible, so that the effects become clear. The smoke was lead through a pipe, cooled by snow surrounding the pipe, and lead into a tent carage that was built on top of the snow. The other end of the tent carage was left open so that the smoke went out and a clear gradient was produced. An inlet was set at the open end of the carage tent and sample air was drawn to a measurement container approximately 5 meters apart. Aerosol number size distributions were measured with an SMPS, light scattering with a TSI 3λ nephelometer and absorption with a Radiance Research 3λ PSAP. Outside the tent aerosol number concentrations were measured at several locations to get an estimate of the dispersion.

After the soot production was over, the tent carage was removed carefully from the area. Snow samples were taken from the deposit area and a background reference area, to be analyzed for organic and elemental carbon. The albedo of the snowpack was measured both over the deposit and the reference area. Snowpack thickness was measured by inserting 18 measurement sticks in a grid around the deposit area and the reference area, and inspecting them regularly. On 1 April, just when the fastest melting started, two snow pits were dug, one in the deposit area and the other in the reference area. In both pits a physical characterization of snow stratigraphy was done, including thickness, density, hardness, grain size and shape. After that, temperature profiles were measured at a 5 cm intervals. In addition, the spectral irradiance at the depth of 20 cm was measured in the wavelength range 400 – 900 nm.

The experiment demonstrated very clearly the effects of soot on snow: the albedo decreased, the snow grain size, the whole stratigraphy and temperature profile in the snow pack changed compared with the reference site. All these lead to a faster melting of snow in the area where soot was deposited.

The problem in the experiment was the very large variation in aerosol concentrations. This, on the other hand, was due to the method of soot production: organics were burned in a simple wood-burning stove. The use of this kind of a stove results in batch-like burning: refilling is not continuous, the stove is filled in after the previous batch has burned. Therefore, in the following experiments soot will be produced by blowing cold soot particles without burning. This method was already used in the SoS 2012 campaign (Kivekäs *et al.*, 2012)

This work was supported by the EU Life+ project Mitigation of Arctic warming by controlling European black carbon emissions (MACEB) and Maj and Tor Nessling foundation. The work of Mr. Timo Vainio in constructing the measurement site and Mrs. Anita Virkkula in assisting in the snowbed thickness measurements are gratefully acknowledged.

Clarke, A. D. and Noone, K. J. (1985), *Atmos. Environ*., **19**, 2045–2053.

Hansen, J. and Nazarenko, L. (2004), *Proc. Nat. Acad. Sci*.,**101**, 423–428.

Quinn, P. K., Bates, T. S., Baum, E., Doubleday, N., Fiore, A. M., Flanner, M., Fridlind, A., Garrett, T. J., Koch, D., Menon, S., Shindell, D., Stohl, A., and Warren, S. G. (2008), *Atmos. Chem. Phys.*, **8**, 1723–1735, doi:10.5194/acp- 8-1723-2008

Warren, S., and W. Wiscombe (1980). *J. Atmos. Sci*., **37**, 2734– 2745.

Kivekäs, N., Brus, D., Hyvärinen, A., Järvinen, O., Svensson, J., Aarva, A., Meinander, O., Heikkilä, A. and Virkkula, A. (2012) Abstracts of the European Aerosol Conference 2012.

A4: Arctic Absorbing Aerosols and Albedo of Snow (2012-2015)

O. Meinander[1], A. Aarva[2], L. Backman[1], A. Heikkilä[1], P. Kolmonen[1], A. Kontu[3], E. Kyrö[3], H. Lihavainen[1], N. Kivekäs[1], J. Pulliainen[3], P. Räisänen[1], M. Sofiev[1], A. Virkkula[1] and G. de Leeuw[1,4]

[1]Research and Development, Finnish Meteorological Institute, Helsinki, PO.Box 503, 00101 Finland
[2]Weather and safety, Finnish Meteorological Institute, Helsinki, PO.Box 503, 00101 Finland
[3]Arctic Research Centre, Finnish Meteorological Institute, Tähteläntie 62, 99600 Sodankylä, Finland
[4]Department of Physics, University of Helsinki, P.O.Box 48, 00014 Helsinki, Finland
Keywords: Black Carbon, Albedo, Climate effect
Presenting author email: Outi.Meinander@fmi.fi

The effect of Black Carbon in snow layers is of importance to climate change and also for forecasting snow melt. Snow reflectivity, i.e. albedo, varies with wavelength, and therefore depends on a number of factors, such as the depth and age of the snow cover, snow grain size, solar zenith angle, cloud cover, and absorbing aerosols on snow. Currently, the effect of BC on snow albedo and melting is improperly understood. Our work on project A4 (Arctic Absorbing Aerosols and Albedo of Snow, 2012-2015) aims to reduce these uncertainties. On the basis of literature, the effect of BC on snow albedo is the larger, the shorter the wavelength. Therefore, as a special feature, we also consider snow albedo at ultraviolet (UV) wavelengths. Here an overview on the project is given, together with some preliminary results. The work forms a research ensemble for the life cycle of BC, effects on Arctic snow albedo, and using the elaborated information for modeling and satellite approaches.

The origin of airborne BC is studied by combining data from at least 5 measurement stations measuring BC and air mass transport history. We will use the Air Quality and Emergency modeling system SILAM to study the transport of soot from the sources in the Northern Hemisphere to the Arctic. The results will be verified against our experimental results on concentration of soot in snow. Multi-pollutant simulation outcome will also be compared with the remote-sensing AOD observations and in-situ PM measurements.

Our continuous albedo measurements are made at established measurement stations, north from 60 ^{o}N. In addition, short-term albedo experiments will be carried out. For the use of albedo data, ancillary data on snow properties, aerosols (BC) and various environmental parameters are essential. Albedo measurements will be analyzed in the context of atmospheric aerosols, BC in snow samples, snow grain size, and meteorological automatic weather station (AWS) data on the beginning of rain, snow depth, and cloud cover, etc.

We will also work to produce physically based improved albedo parameterizations that can be applied, for instance, in RT-models and in climate models with special emphasis on snow melt and BC; and to study the effect of BC on melting snow on the satellite measured top-of-atmosphere (TOA) reflectance; and to use the measured and modeled snow albedo to enable the retrieval of aerosol optical properties over snow covered areas during snow melt.

We will use continuous 1-min surface UV albedo data from the Sodankylä Arctic Research Centre (67^{o}22'N, 26^{o}39'E, 179 m asl); measurements started in 2007 by FMI as a part of the IPY activities. The site is also a WMO GAW station (www.wmo.int/gaw/). In addition, we will make use of long-term Sodankylä Arctic Centre mast albedo and weekly samples on BC in snow. In 2009, the maximum concentrations in snow were up to 38 ppb for BC, and 1734 ppb for organic carbon. On the other hand, on 23 April 2010, with new snow originating from an Eyjafjallajökull ash cloud, the snow sample contained 59 ppb elemental, and 4312 ppb organic carbon.

In 2012, the experiment Soot on Snow (SoS-2012), took place at the Jokioinen Observatory, a synoptic FMI weather station in the southern Finland. Three spots of different concentrations of soot on snow on an agricultural field were produced. A fourth measurement spot was a reference with no soot. The soot we used was produced in residential heating with wood and oil, and was collected by chimney cleaners. Two erythemally weighted UV-B sensors (280-310 nm) were installed about 20 cm above the snow surface to measure the UV albedo of the dirty snow continuously, until the end of snow melt. Also, albedo was measured periodically using a multichannel NILU-UV radiometer at UV and PAR channels.

The main objective of the A4 project is to quantify the interaction of Arctic snow albedo and absorbing aerosols, and to gain more in-depth understanding of the globally important aspects of BC and albedo feedback, as well as BC and snow melt in the Arctic.

This work is supported by the Academy of Finland.

Doherty, S. J., Warren, S. G., Grenfell, T. C., Clarke, A. D., and Brandt, R. E. (2010): Light-absorbing impurities in Arctic snow, *Atmos. Chem. Phys.*, **10**, 11647-11680, doi:10.5194/acp-10-11647-2010.

Experimental study of the surface shortwave aerosol forcing efficiency

J.L. Anastasio[1,2], I. Foyo-Moreno[1,2] , A. Valenzuela[1,2], M. Antón[1,2], F.J. Olmo and L. Alados-Arboledas[1,2]

[1] Andalusian Center for Environmental Research (CEAMA), Granada, 18006, Spain
[2]Department of Applied Physics, University of Granada, Granada, 18006, Spain
Keywords: Atmospheric aerosols, radiative forcing.
Presenting author email: jlal@correo.ugr.es

Ground-based measurements of aerosol optical depth (AOD) and surface shortwave irradiance carried out in South-Eastern Spain during 2006–2010 are used to evaluate the surface aerosol direct radiative forcing. The data were recorded at the radiometric station located on the rooftop of the Andalusian Center for Environmental Studies (CEAMA, 37.17°N, 3.61°W, 680 m a.s.l) in Granada, southeastern Spain. The station is operated by the Atmospheric Physics Group (GFAT) of Granada University.

The ground based station is equipped with a CM11 pyranometer (resolution better than ±5 W/m2) manufactured by Kipp & Zonen (Delft, Netherlands) for measuring the surface shortwave solar irradiance (310-3200 nm), recorded every minute by a data logger (CR10X model, manufactured by Campbell Scientific, Inc). This instrument was calibrated periodically with a reference CM11 pyranometer showing a great stability.

A CIMEL CE318 Sun photometer included in the NASA AERONET network (Holben et al., 1998) and located near the CM11 radiometer, provided AOD data at 340, 380, 440, 500, 670, 870 and 1020 nm. In this work, the AERONET AOD data of level 2 (cloud screened and quality assured), with accuracy of about ± 0.01 for λ>440 nm and ±0.02 for shorter wavelengths, were used. Furthermore the spectral dependency of the AOD has been considered through the Angström exponent evaluated in the range 440–870 nm. Cloud cover was characterized by the clearness index (kt) obtained from the ratio of the shortwave solar irradiance to the extraterrestrial shortwave solar irradiance on a horizontal surface. In addition, an All Sky Imager developed by the GFAT team was used to obtain the cloud cover in oktas (eighths of sky) (Cazorla et al., 2008).

The surface shortwave aerosol radiative forcing, ARF, is defined as the difference between the observed net shortwave irradiance (downward minus upward irradiances) at the Earth's surface and the aerosol-free surface shortwave net irradiance. The net irradiances in the presence and absence of atmospheric aerosols can be written in terms of the downward irradiance and the surface shortwave albedo.

Different methodologies can be used to estimate the surface shortwave aerosol forcing efficiency (AFE, aerosol forcing per unit of AOD). In this study we employed the direct method (e.g., Satheesh and Ramanathan, 2000) which is based on a linear fit of the net irradiance at the Earth's surface versus the AOD at a fixed solar zenith angle (SZA).

We evaluated the ARF and AFE for SZA ranging between 20º and 75º. Our results showed negative AFE values indicating that the atmospheric aerosols produce a cooling of the surface. In addition, AFE exhibited a clear dependence on SZA, increasing its absolute value from 20º to 60º, while a decreasing trend was observed for SZA larger than 60º. All these results are in agreement with previous studies developed in the study area using a different approach (Horvath et al., 2002; Lyamani et al.,2006).

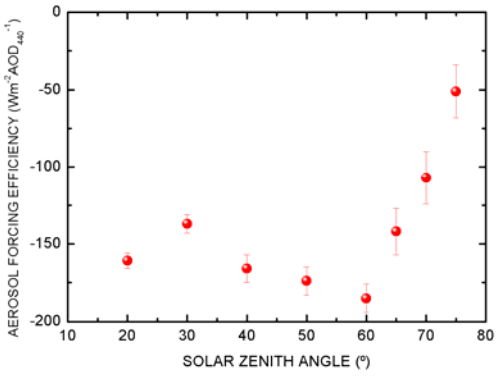

Figure 1: Aerosol forcing efficiency as a function of the SZA.

This work was supported by the Andalusia Regional Government through projects P08-RNM-3568 and P10-RNM-6299, by the Spanish Ministry of Science and Technology through projects CGL2010-18782, CSD2007-00067 and CGL2011-13580-E/CLI; and by EU through ACTRIS project (EU INFRA-2010-1.1.16-262254).

Cazorla, A. et al. (2008), Development of a sky imager for cloud cover assessment, J. Opt. Soc. Am. A., 25(1), 29–39.

Holben, B. N., et al. (1998), AERONET–A federated instrument network and data archive for aerosol characterization, Remote Sens. Environ., 66, 1–16.

Horvath, H. et al. (2002), Optical characteristics of the aerosol in Spain and Austria and its effect on radiative forcing, J. Geophys. Res., 107(D19), 4386.

Lyamani, H. et al. (2006), Atmospheric aerosols during the 2003 heat wave in southeastern Spain II: Microphysical columnar properties and radiative forcing, Atmos. Environ., 40, 6465–6476.

Satheesh, S.K. and V. Ramanathan(2000), Large differences in tropical aerosol forcing at the top of the atmosphere and Earth's surface, Nature, 405, 60– 63.

Aircraft Measurements of Aerosol, Cloud Droplet and CCN Distribution Characteristic over Northern China

Duan Ying[1], *Yin Yan*[2], *Duan Jing*[3]

[1]*Weather Modification Office of Hebei Province, 050021, China*
[2]*Nanjing University of Information Science & Technology, Atmospheric Physics, Nanjing, 210044, China*
[3]*Chinese Academy of Meteorological Sciences, Beijing, 100081, China*
Keywords: Aerosol size distribution, Number size distribution, Nucleation, Aerosol cloud interaction
Presenting author email: *hbwmo@heinfo.net*;duany2011@126.com

Hebei province is located in the north of China, Beijing and Tianjin is surrounded with it, the Bohai sea gulf is in the east of Hebei province. In this study, the data from the Piper Cheyenne twin urbo-prop aircraft was used to observe the clouds and precipitation, since 2005 year. The aerosol was measured by a PMI Aerosol Spectrum Probe (size range 0.1～3.0 micron). The cloud droplet was measured by a FSSP probe (size range set up as 2 ~ 47μm). The 2D – C (25 ~ 800μm) and 2D - P (150 ~ 9300μm) probes can provide two-dimensional particle image. In addition, the aircraft is also equipped with other devices to obtained corresponding data. CCN were measured by a DMT continuous flow streamwise thermal gradient CCN counter. The supersaturation is set at S=0.3% in observed period.

The concentration and size with spatial and temporal distribution of aerosol particles ,CCN and cloud droplet over Hebei area, northern China, are analyzed. The preliminary results show that the distribution of them are very different during the precipitation in stratiform. Synthetical research results show that the aerosols played an important role in formation of clouds and precipitation processes.

Figure 1 shows that the aerosols and cloud condensation nuclei (CCN) with spatial and temporal distribution in the aircraft detection time at May 27, 2010. The vertical left axis indicates the aerosol and cloud condensation nuclei concentration, the units is cm^{-3}. The vertical right axis indicates height of aircraft flight, its units is meter.

The results shown in the figure 1, light blue curve shows the altitude change with time, the red solid point is the temporal and spatial distribution of aerosol concentration, the black solid point is the spatial and temporal distribution of CCN concentration.

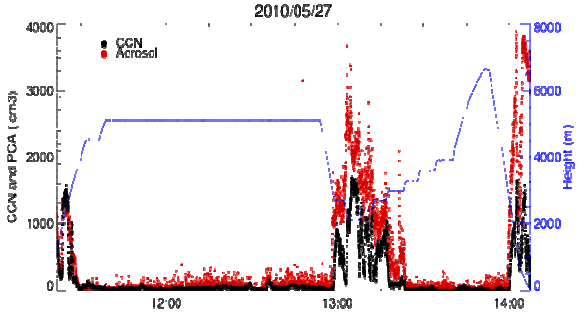

Fig. 1 the temporal and spatial distribution of aerosol and CCN concentration

In order to analyze aerosols, cloud condensation nuclei and cloud droplets in cloud base and cloud inside, the corresponding concentration and scale distribution between the spectra shown in figure 2. The results showed that the aerosol concentration and cloud condensation nuclei are very different, in two different conditions of inside and outside of cloud.

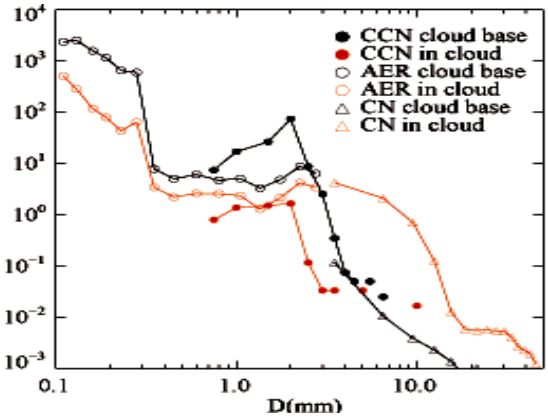

Figure 2. aerosol and CCN spectra comparison inside and outside of cloud

This research was Jointly funded by National Natural Science Foundation of China (Grant No. 40905058), the social commonweal research program (GYHY(QX)2007-6-36) funded by the Ministry of Science and Technology of the People's Republic of China.

Duan, J., and J. T. Mao（2009）, Influence of aerosol on regional precipitation in North China, Chinese Science Bulletin, 54(3), 474-483, doi: 10.1007/s11434-008-0447-6.

Duan ying et.al（2000）, an Analysis of the Evolution Characteristics and Physical Cause of Formation about Forty Years Natural Rainfall in Hebei Province .13th Internatoinal Conference on Clouds and Precipitation Proceeding-Volume 1,:395-397, Reno ,Nevada USA ,14-18.

Shi L. X., Y. Duan(2008), Observations of Cloud Condensation Nuclei in North China ,Acta Meteorologica Sinica, 22(1) , 97-106.

Yin yan et al, Airborne measurements of the spatial and spectral distributions of aerosol particles over Hebei area, northern China, PIAGENG 2009: Intelligent Information, Control, and Communication Technology for Agricultural

A note of caution concerning particle evaporation during measurements of their Cloud Condensation Nucleus potential

H. Wex[1], P. Herenz[1], J. Voigtländer[1] and F. Stratmann[1]

[1]Physics Department, Cloudgroup, Leibniz-Institute for Tropospheric Research, 04318 Leipzig, Germany
Keywords: CCN, volatile substances.
Presenting author email: wex@tropos.de

Particles consisting of either levoglucosan or of succinic acid were examined with respect to their ability to act as CCN (cloud condensation nucleus). Measurements of the activation were made with two different instruments, the Leipzig Aerosol Cloud Interaction Simulator (LACIS, Wex et al., 2006) and the Cloud Condensation Particle counter (CCNc) from DMT (Droplet Measurement Technologies, Roberts & Nenes, 2005). Both instruments were used to measure critical dry diameters (d_{crit}) for activation at different super-saturations. The calibration of both instruments (with respect to their supersaturation) was done by using ammonium sulphate particles.

In LACIS, super-saturations are produced via cooling of a humidified airstream, and the temperatures in LACIS are below 20°C at its inlet and go down to 2°C in the section where the particles are activated and where the activated droplets grow.

In the CCNc, super-saturation is produced by the effect that water vapour diffuses faster than heat, and the section responsible for the activation of the particles is heated from the inlet temperature (which usually is slightly above the temperature of the surrounding laboratory) up to almost 50°C, with the temperature-increase being linearly related to the super-saturation adjusted in the instrument.

Based on Köhler-theory, d_{crit} can be calculated when properties of the substances that make up the particle (as e.g. density and molecular weight) are known (e.g. Wex et al., 2007). As both, succinic acid and levoglucosan, are comparably well characterized substances, values for d_{crit} can be determined via Köhler-theory. Calculations were done for the super-saturations at which measurements had been performed. The resulting values were then compared to values obtained from the measurements, as shown in Figure 1.

In Figure 1 it can be seen that the measured activation of levoglucosan in LACIS and the CCNc are in agreement. This was also the case for the measured activation of succinic acid in LACIS. This can be taken as proof that in general the activation behaviour of the substances examined here can be modelled with Köhler-theory. However, for the activation of succinic acid derived from CCNc measurements, the measured d_{crit} was clearly larger than the calculated value for $d_{crit,measured} < 85$nm. For succinic acid, d_{crit} of 85nm corresponds to a super-saturation $> 0.32\%$, and to temperatures in the CCNc at the point of activation of the particles of roughly > 30°C.

The vapour pressure of succinic acid is about 3 orders of magnitude above that of levoglucosan. The results presented here can be used to deduce that a certain fraction of each succinic acid particle evaporates in the CCNc before it is activated to a cloud droplet, i.e. a larger particle than expected has to be fed into the instrument to account for loss of particle mass through evaporation. The evaporated fraction of the particles increased with increasing super-saturation and was up to 70% of the total particle mass at the highest super-saturations used in our measurements (1%).

Substances with vapour pressure as e.g. succinic acid can be present in the atmospheric aerosol, and therefore a note of caution has to be given here: It is possible that also some atmospheric aerosol particles may lose a certain fraction of their mass when their activation behaviour is measured with the CCNc we used for our study.

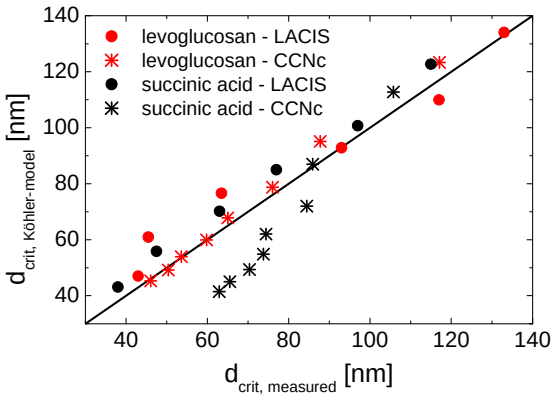

Figure 1. Comparison between calculated and measured critical diameters for the two examined substances and the two different instruments.

Roberts, G., and A. Nenes (2005), Aerosol *Sci. Technol.*, **39**, 206-221.

Wex, H., A. Kiselev, M. Ziese, and F. Stratmann (2006), *Atmos. Chem. Phys.*, **6**, 4519-4527.

Wex, H., T. Hennig, I. Salma, R. Ocskay, A. Kiselev, S. Henning, A. Massling, A. Wiedensohler, and F. Stratmann (2007), *Geophys. Res. Lett.*, **34**(L02818), doi:10.1029/2006GL028260.

Indirect aerosol effects estimated from Chemistry Transport model coupled to a Regional Climate model

M.A. Thomas[1], M. Kahnert[1,2], H. Kokkola[3], C. Andersson[1], R. Bergström[1,4], C. Bennet[1], L. Robertson[1], U. Hansson[5], C. Jones[5] and U. Willen[5]

[1]Swedish Meteorological and Hydrological Institute, Research Department, SE-601 76 Norrköping, Sweden
[2]Chalmers University of Technology, Department of Earth and Space Science, SE-412 96 Gothenburg, Sweden
[3]Finnish Meteorological Institute, Kuopio Unit, P.O Box 1627, FI-70211 Kuopio, Finland
[4]University of Gothenburg, Department of Chemistry and Molecular Biology, SE-41296, Gothenburg, Sweden
[5]Swedish Meteorological and Hydrological Institute, Rossby Center, SE-601 76 Norrköping, Sweden
Keywords: aerosol-cloud interaction, regional modelling
Presenting author email: Manu.Thomas@smhi.se

The scientific understanding of the climate effects of the different aerosol species as well as their representation in models and the physical and chemical transformation that the aerosols go through under different meteorological conditions is still low. Apart from the direct effects of aerosols on climate, the aerosols can also act as cloud condensation nuclei thereby altering the microphysical properties of clouds which is formulated as the indirect aerosol effect (IAE) (Lohmann and Feichter, (2005) and references therein). The uncertainty range of the IAE estimates is so high that in order to reduce this uncertainty one need to represent the aerosol dynamics and chemistry more accurately. In this study, we attempt to estimate the IAE from a full-fledged chemistry transport model that is coupled to a detailed aerosol dynamics model that also includes a cloud activation module.

The chemistry transport model, MATCH (Multiple-scale Atmospheric Transport and Chemistry) (Andersson et al., 2007) that accounts for transport, chemical transformation and deposition of chemical tracers in the atmosphere based on the EMEP emissions is used for this study. This model is coupled to an aerosol dynamics model, SALSA (Kokkola et al., 2008) that considers the physical processes such as nucleation of particles from gas phase, growth of particles by condensation and coagulation and thereby computes the size distribution, number concentration and chemical composition of the aerosol species in the different size classes. This information is coupled to a cloud activation model that computes the cloud droplet number concentrations (CDNC) based on the prognostic parameterization of Abdul-Razzak and Ghan (2002). By this scheme, the efficiency of an aerosol particle to be converted to cloud droplet depends on the size, number and chemical composition of the particle as well as the updraft velocity and maximum supersaturation of the air parcel. The CDNC thus obtained are offline coupled to the Rossby Center regional climate model, RCA4 (RCA4 is an improved version of RCA3 (Samuelsson et al., 2011)) that would give us information on the cloud microphysical properties such as cloud effective radius, cloud liquid water path as well as the radiative fluxes on the regional scale over Europe. The offline coupling is only one way for the present study. The merit of such a study is that more detailed description of emission, transport, particle growth, deposition processes of aerosols can be included and hence, such studies can give us a more accurate description of the climate impact of aerosols on a higher spatial resolution compared to global models. This can also help us assess the level of detail that will be needed in describing the effects on a regional climate. Also, the effects of future climate change on air pollution can be assessed in detail. Simulations are carried out for present day scenario with meteorology from RCA4. The seasonal distribution and vertical distribution of cloud microphysical properties resulting from this coupling will be presented. Also, comparisons with other studies and satellite observations will be discussed.

Abdul-Razzak, H. and Ghan, S. J.: A parameterization of aerosol activation 3. Sectional representation, *J. Geophys. Res.*, 107, doi:10.1029/2001JD000483, 2002.

Andersson, C., Langner, J. and Bergström, R.: Interannual variation and trends in air pollution over Europe due to climate variability during 1958-2001 simulated with a regional CTM coupled to the ERA-40 reanalysis, *Tellus* 59B, 77-98, 2007.

Kokkola, H., Korhonen, H., Lehtinen, K.E.J., Makkonen, R., Asmi, A., Järvenoja, S., Anttila, T., Partanen, A.-I., Kulmala, M., Järvinen, H., Laaksonen, A. and Kerminen, V.-M.: SALSA – a sectional aerosol module for large scale applications. *Atmos. Chem. Phys*, 8, 2469-2483, 2008.

Lohmann,U. And Feichter, J.: Global indirect aerosol effects: a review, *Atmos. Chem. Phys*, 5, 715-737, 2005.

Samuelsson, P., Colin, J., Willen, U., Ullerstig, A., Golvik, S., Hansson, U. Jansson, C., Kjellström, E., Nikulin, G. and Wyser, K.: The Rossby Center Regional Climate model RCA3: model description and performance, *Tellus A* – Special issue, 63, 4-23, 2011.

Mass spectrometric analysis of cloud residuals in tropical trade wind cumuli at Pico Este, Puerto Rico, during PRADACS 2011

J. Schneider[1], A. Roth[1], J. Schmale[1], S. Mertes[2], L. Schenk[2], O. L. Mayol-Bracero[3], C. J. Valle[3], F. Zurcher[3], and S. Borrmann[1,4]

[1]Particle Chemistry Department, Max Planck Institute for Chemistry, 55128 Mainz, Germany
[2]Leibniz Institute for Tropospheric Research, Leipzig, Germany
[3]Institute for Tropical Ecosystem Studies, University of Puerto Rico, San Juan, Puerto Rico
[4]Institute for Atmospheric Physics, Johannes Gutenberg University, 55128 Mainz, Germany
Keywords: Aerosol cloud interaction, Saharan dust, Single particle analysis, Mass spectrometry.
Presenting author email: johannes.schneider@mpic.de

During the dust season (April - October), Saharan dust is transported over long distances from Africa to the Caribbean, influencing the radiative properties and the cloud formation properties of the aerosol. The project PRADACS (Puerto Rico African Dust and Clouds Study) was established to study the role of Saharan dust in cloud formation over the Caribbean. Within PRADACS, we performed a one-month field campaign on the mountain station at Pico Este (1000 m asl), Puerto Rico (Figure 1).

The measurements were performed between August 16 and September 13, 2011. Cloud residuals, interstitial aerosol particles and out-of-cloud aerosol particles were sampled by a counterflow virtual impactor and by an interstitial inlet, respectively, and analyzed by two different types of aerosol mass spectrometers: One Aerodyne C-ToF-AMS and one single particle laser ablation instrument (ALABAMA). Additionally, we measured the number concentration, the black carbon mass concentration and the size distribution of the interstitial and out-of-cloud aerosol.

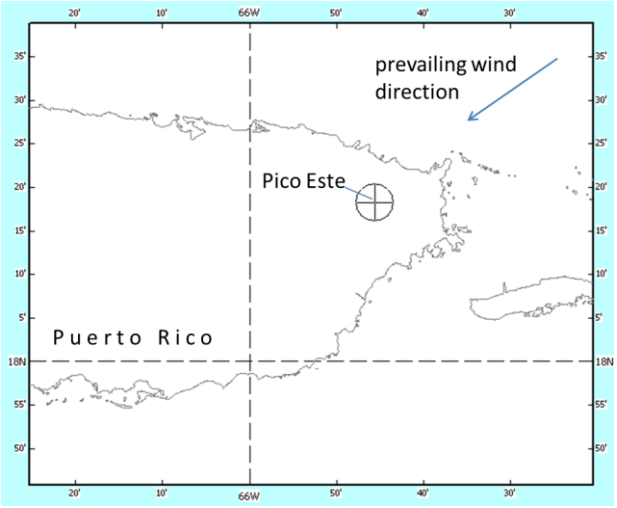

Figure 1. Map of the east coast of Puerto Rico showing the prevailing wind direction and the location of Pico Este.

Results show that the non-refractory fraction of the submicron cloud residual particles was mainly composed of sulfate. This finding is similar to the results of the RICO/PRACS (Rain In Cumulus over the Ocean experiment/Puerto Rico Aerosol and Clouds Study) that was performed at the same site in December 2004 (Allan et al., 2008; Gioda et al., 2009). In contrast to the 2004 study, the present study also included a single particle laser ablation instrument that detected the abundance of dust particles in the cloud residuals (Figure 2). These data allow for the determination of the importance of dust particles for cloud formation.

Additionally, the C-ToF-AMS was equipped with a light scattering probe that enables single particle analysis with the thermal desorption/electron impact ionization method (Freutel et al., 2011). These data will complement the single particle data obtained by the laser ablation method.

The black carbon content of the interstitial aerosol was generally low (below 100 ng m^{-3}), with a few exceptions that represented local pollution. Interstitial particle number concentrations ranged up to 4000 cm^{-3} in cloud-free periods while during intense cloud events the interstitial aerosol concentration was below 100 cm^{-3}.

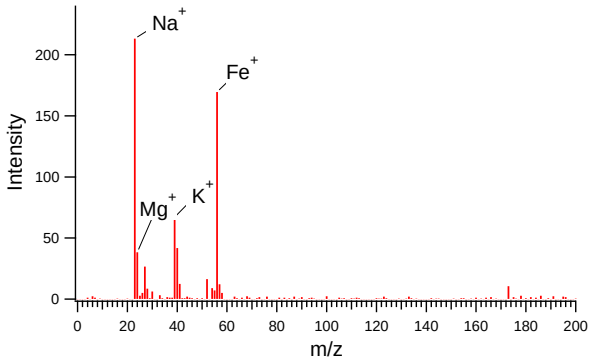

Figure 2. Example for a mass spectrum of a mineral dust particle detected by ALABAMA in the cloud residuals.

This work was supported by NSF ATM Grant #0936879 and by the Max Planck Society.

Allan, J. D., et al. (2008) *Atmos. Chem. Phys*. **8**, 1293–1309.
Freutel, F. et al. (2011) *European Aerosol Conference*, Manchester, UK.
Gioda, A., et al. (2009), *Water Air Soil Pollut.* **200**, 3–14.

New cloud chamber experiments on the crystallization and heterogeneous ice nucleation ability of sodium chloride dihydrate particles

R. Wagner, O. Möhler, H. Saathoff and M. Schnaiter

Institute for Meteorology and Climate Research, Karlsruhe Institute of Technology, Germany
Keywords: sea salt, crystallization, heterogeneous ice nucleation
Presenting author email: robert.wagner2@kit.edu

Recently, Wise *et al* (2012) have investigated the efflorescence of aqueous sodium chloride (NaCl) solution droplets as well as the heterogeneous ice nucleation ability of the crystallized particles in the temperature range between 221 and 238 K using optical microscopy coupled with Raman spectroscopy. The NaCl particles (size range 1 – 10 μm), used as a proxy for sea-salt aerosol, were deposited onto a hydrophobic quartz disc for analysis.

Raman spectroscopy allowed for differentiating between anhydrous sodium chloride crystals and the crystalline dihydrate form of NaCl ($NaCl \cdot 2H_2O$). According to the NaCl phase diagram, the dihydrate is the stable crystalline solid below the NaCl/ $NaCl \cdot 2H_2O$ peritectic at 273.3 K (Koop *et al*, 2000). In agreement with earlier results from Koop *et al* (2000), it was found that above 252 K only anhydrous NaCl effloresced. Between 252 and 236 K, the aqueous NaCl solution droplets effloresced into a mixture of anhydrous and dihydrate NaCl crystals whereas only $NaCl \cdot 2H_2O$ was observed below 236 K.

Concerning the heterogeneous ice nucleation ability of the crystallized particles in the deposition mode, Wise *et al* (2012) have detected that the dihydrate NaCl particles are highly efficient ice nuclei forming ice at about ice saturation (S_{ice} = 1.02 ± 0.04). Slightly higher threshold values were found for the anhydrous crystals (S_{ice} = 1.11 ± 0.07). The lower ice nucleation threshold of the dihydrate crystals could be related to a higher degree of surface roughness as revealed by the optical microscope images. In addition, the two molecules of hydration water could be particularly active sites for the further addition of water.

Using the new laboratory data as input in a trajectory model, the fraction of hydrated NaCl particles present in the troposphere at temperatures below 220 K was estimated to 40-80%. It was therefore concluded that deposition ice nucleation onto these crystals could be a new mechanism for ice formation in the troposphere.

In this contribution, we present novel results from crystallization and heterogeneous ice nucleation experiments with airborne NaCl particles which were performed in the large coolable cloud chamber AIDA at the Karlsruhe Institute of Technology. Our experiments cover the temperature range from 216 to 244 K using particles with median diameters between 0.1 and 0.9 μm. Ice formation was studied via controlled expansion cooling runs which mimic the adiabatic expansion cooling of rising air parcels in the atmosphere. We used in situ laser light scattering and depolarization measurements to detect the phase change between aqueous and crystalline NaCl particles and to infer the onset of ice nucleation. The chemical nature of the crystallized NaCl particles was probed by in situ infrared extinction spectroscopy. The spectrum of $NaCl \cdot 2H_2O$ particles bears a prominent signature in the mid-infrared regime due to the hydration waters which is absent for anhydrous NaCl crystals (Fig. 1).

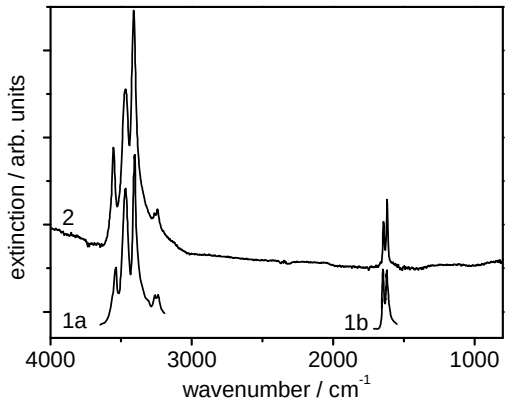

Figure 1. Infrared extinction spectrum of effloresced $NaCl \cdot 2H_2O$ particles at 226 K from this study (trace 2) in comparison with literature spectra of the dihydrate (traces 1a and 1b) from Schiffer and Hornig (1961).

In addition to determining the threshold saturation ratios for ice nucleation, the AIDA experiments allow for quantifying the ice nucleation ability in terms of the frozen fraction as well as the ice active surface site density of the seed aerosol particles. Our results corroborate the general findings from Wise *et al* (2012), namely the effect of temperature on the crystallization of either the anhydrous and/or the dihydrate form of NaCl and the good heterogeneous ice nucleation ability of $NaCl \cdot 2H_2O$ particles in the deposition mode. Closer inspection of the data, however, also reveals some variations: Firstly, the threshold where exclusively the dihydrate forms upon efflorescence is shifted in our experiments to a lower temperature, and, secondly, deposition mode ice nucleation onto the hydrated NaCl particles occurs at a somewhat higher threshold ice saturation ratio of about S_{ice} = 1.15 ± 0.05.

Koop, T.; Kapilashrami, A.; Molina, L. T.; Molina, M. J. (2000) *J. Geophys. Res. (Atmos.)* **105**, 26393-26402.

Schiffer, J. and Hornig, D. F. J. (1961) *Chem. Phys.* **35**, 1136-1137.

Wise, M. E.; Baustian, K. J.; Koop, T.; Freedman, M. A.; Jensen, E. J.; Tolbert, M. A. (2012) *Atmos. Chem. Phys.* **12**, 1121-1134.

Experimental and modelled characterization of diffuse spectral UV irradiance under cloudy conditions: impact of aerosol properties

D. Mateos[1], A. di Sarra[2], J. Bilbao[1], M. Cacciani[3], G. Casasanta[3], D. Meloni[2], G. Pace[2], and A. de Miguel[1]

[1]Atmosphere and Energy Lab, University of Valladolid, Valladolid, 47005, Spain
[2]UTMEA-TER, ENEA, Rome, 00123, Italy
[3]Physics Department, University of Rome Sapienza, Rome, 00185, Italy
Keywords: radiative properties, cloud microphysics, aerosol optics, cloudiness.
Presenting author email: dmateos@fa1.uva.es

Measurements of total and diffuse spectral UV irradiance, cloud optical thickness (COT), liquid water path (LWP), cloud effective radius (r_{eff}), cloud base and top heights, columnar ozone and spectral aerosol optical depth are used, together with radiative transfer simulations, to evaluate the spectral cloud transmittance or cloud modification factor (CMF) for the total and for the diffuse components under overcast conditions. The observations were carried out during a 2-month measurement campaign held in May and June 2010 at the ENEA-Trisaia Research Centre (40.16ºN, 16.64ºE, 40 m a.s.l.), in Southern Italy.

The total and diffuse UV irradiances were measured by an Ultraviolet Multifilter Rotating Shadowband Radiometer (UV-MFRSR) at seven narrowband channels. The HATPRO (Humidity And Temperature PROfiler) microwave radiometer allowed to derive the cloud LWP. With the spectral irradiance measurements by a visible MFRSR, COT and r_{eff} are derived, using the cloud LWP (Min and Harrison, 1996). Cloud top and base heights were measured by a LIDAR.

The spectral cloud transmittances (for the total and the diffuse components) of two cases with overcast conditions at the same solar zenith angle (SZA) are plotted in Figure 1. The two cases only differ in the cloud properties, i.e., the COT, LWP and r_{eff} values. Previous studies (e.g., Kylling *et al.*, 1997; Mateos *et al.*, 2011) showed that the total CMF decreases with wavelength above 315-320 nm and increases at shorter wavelengths (280-315 nm). These results for the total component were confirmed by the measurements of the campaign (see solid lines of figure 1). Conversely, the CMF of the UV diffuse irradiance component increases with wavelength throughout the spectral interval (the CMF depends also on SZA, not shown here), significantly different from the total CMF.

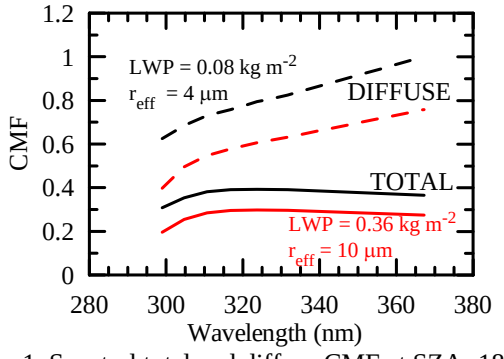

Figure 1. Spectral total and diffuse CMF at SZA=18º for overcast conditions with different LWP and r_{eff}.

A specific case was analyzed with the aim of understanding the aerosol impact on total and diffuse CMF comparing measurements and model simulations. The case study case presents an aerosol layer below the cloud during a desert dust event. The COT was 30, and the aerosol optical depth at 550 nm was 0.2. The radiative transfer model libRadtran was initialized with all the available measurements. The model reproduced both the experimental total and diffuse CMF within ±5% at all wavelengths. Varying the aerosol optical properties (single scatting albedo and asymmetry factor) did not significantly affect the total CMF, while did not allow the model to reproduce diffuse CMF within the same uncertainty range. Figure 2 shows the ratio of the spectral modelled and measured diffuse CMF as a function of the aerosol type.

This study highlights the need of an adequate characterization of the aerosol optical properties under cloudy conditions, if the effects on the diffuse component have to be analyzed.

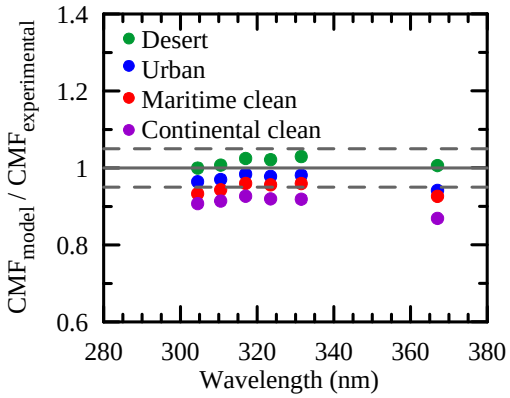

Figure 2. Ratio between modelled and experimental spectral diffuse CMF for different aerosol types.

This work was supported by the Spanish Government under the Projects CGL2010-12140E and CGL2011-25363 and the Italian Ministry for Environment through the MINNI Project.

Kylling, A., Albold, A., Seckmeyer, G. (1997) *Geophys. Res. Lett.* **24**, 397–400.

Mateos, D., di Sarra, A., Meloni, D., di Biagio, C., Sferlazzo, D.M. (2011) *J. Atmos. Sol.-Terr. Phy.* **73**, 1739–1746, doi:10.1016/j.jastp.2011.04.003.

Min, Q., Harrison, L.C. (1996) *Geophys. Res. Lett.* **23**, 1641-1644.

Overview of Puijo Cloud Experiments (PuCE 2010 & 2011)

Portin, Harri[1,2], Leskinen, Ari[1], Brus, David[3], Neitola, Kimmo[3], Hyvärinen, Antti-Pekka[3], Kortelainen, Aki[2], Hao, Liqing[2], Miettinen, Pasi[2], Jaatinen, Antti[2], Lihavainen, Heikki[3], Romakkaniemi, Sami[2], Laaksonen, Ari[2,3], Lehtinen, Kari E.J.[1,2] and Komppula, Mika[1]

[1]Finnish Meteorological Institute, Kuopio Unit, P.O.Box 1627, FI-70211, Kuopio, Finland
[2]University of Eastern Finland, Department of Applied Physics, P.O.Box 1627, FI-70211, Kuopio, Finland
[3]Finnish Meteorological Institute, Research and Development, P.O.Box 503, FI-00101 Helsinki, Finland
Keywords: aerosol-cloud interaction, atmospheric aerosols, cloud droplet activation, chemical composition.
Presenting author email: harri.portin@fmi.fi

It is known that both the size and chemical composition of aerosol particles affect cloud droplet activation (Dusek *et al.* 2006). Effect of particle size is already well known but the role of chemical composition is not yet completely understood. Some field studies have already been done (e.g. Drewnick *et al.* 2007) but more research is needed.

The Puijo measurement station has provided continuous data on aerosol-cloud interactions since summer 2006. The station is located on top of the Puijo observation tower (306 m a.s.l, 224 m above the surrounding lake level) near the town of Kuopio, Finland in a semi-urban environment (Portin *et al*, 2009). The top of the tower is covered by cloud about 15 % of the time, offering perfect conditions for studying aerosol-cloud interactions. With a special inlet setup (total and interstitial inlets) and a switching valve system we are able to separate the activated particles from the interstitial (non-activated) particles. The continuous twin-inlet measurements include aerosol size distribution (differential mobility particle sizer, DMPS), light scattering (nephelometer) and absorption (absorption photometer) (Leskinen *et al.* 2012). Activation properties of these parameters are retrieved continuously. In addition, cloud droplet size distribution is observed continuously with a cloud droplet probe (CDP) as well as weather parameters.

In autumns 2010 and 2011 intensive measurement campaigns were performed at the tower, during which the twin-inlet system was additionally equipped with aerosol mass spectrometer (AMS) and Single Particle Soot Photometer (SP-2). This way we were able to define the differences in chemical composition of the activated and non-activated particles. Other additional measurements included Hygroscopic Tandem Differential Mobility Analyzer (HTDMA) for particle hygroscopicity. Potential cloud condensation nuclei (CCN) in different supersaturations were measured with two CCN counters (CCNC). The other CCNC was operated with a Differential Mobility Analyzer (DMA) to obtain size selected CCN spectra. The full usage of this special data set will provide new information on the properties and differences of activating and non-activating aerosol particles.

In total, 38 cloud events took place during the campaigns, varying between 1-31 hours in duration. An example of the particle size distribution data from the twin-inlet system during a cloud event is shown in fig. 1. In this case, average out-of-cloud particle number concentration during the event was 820 cm^{-3}. Particles larger than 80 nm in diameter already form cloud droplets, and the diameter where 50 % of particles are activated (D_{50}), is 156 nm. For 400 nm particles, already 95 % are activated. Mean concentration difference between the sampling lines during this event was 230 cm^{-3}, representing the mean number concentration of activated particles. By comparing these activation data from different cloud events with AMS data, it is possible to get valuable information about the role of particle chemical composition in cloud droplet activation.

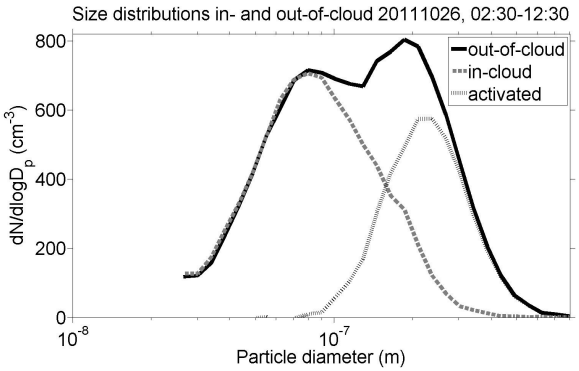

Figure 1. Example of cloud droplet activation during a cloud event. Mean size distributions during the event for out-of-cloud, in-cloud and activated particles are shown.

The authors acknowledge the financial support for instrumentation by the European Regional Development Fund (ERDF).

Drewnick, F., Schneider, J., Hings, S. S., Hock, N., Noone, K., Targino, A., Weimer, S. and Borrmann, S. (2007) *J. Atmos. Chem.*, **56**, 1-20.

Dusek, U., Frank, G. P., Hildebrandt, L., Curtius, J., Schneider, J., Walter, S., Chand, D., Drewnick, F., Hings, S., Jung, D., Borrmann, S. and Andreae M. O. (2006) *Science*, **312**, 1375-1378

Portin, H., Komppula, M., Leskinen, A., Miettinen, P., Romakkaniemi, S., Laaksonen, A. and Lehtinen, K.E.J. (2009) *Boreal Env. Res.*, **14**, 641-653.

Leskinen, A., Arola, A., Komppula, M., Portin, H., Tiitta, P., Miettinen, P., Romakkaniemi, S., Laaksonen, A. and Lehtinen, K.E.J. (2012) *Atmos. Chem. Phys. Discuss.*, **12**, 4719-4754.

Experimental study in situ conditions of below-cloud scavenging of aerosol particles

G. Depuydt[1], O. Masson[1], J.L. Brenguier[2], P. Boissery[3]

[1]IRSN/PRP-ENV/SESURE/LERCM, Cadarache, BP3, 13115 St Paul lez Durance, France
[2]CNRM/GMEI Météo-France - 42 Av Coriolis - 31057 Toulouse cedex 1, France
[3]Agence de l'Eau Rhône Méditerranée et Corse

Keywords: scavenging, wet removal, aerosol size distribution, in-situ measurements

Removal of atmospheric aerosols by the below-cloud scavenging is a wet deposition process particularly fast and efficient. This interaction between aerosols and raindrops is characterized by the washout coefficient Λ, which can be estimated from the temporal evolution of the size distribution of aerosols during rainfall events and macro-physical characteristics of this event (event duration, rain amount, rainfall intensity ...).

Up to now, few studies have defined below-cloud scavenging of particles from direct measurements of aerosol size distribution variations due to precipitation (Volken and Schumann, 1993; Laakso *et al.*, 2003). The large discrepancies noted between theory and field observations (Wang *et al.*., 2011) show the need to perform experimental in-situ studies of below-cloud scavenging in various environments.

For several months, two types of instruments were installed on sites in France having different features in terms of dust levels and climatic conditions, to have the largest scale of environmental conditions. A laser disdrometer PARSIVEL (for PARticule SIze and VELocity) measured hydrometeors size between 0.2 and 25mm and falling speed from 0.2 to 20m.s^{-1}. Particles were counted with an optical spectrometer with measuring range of 0.25 to 32µm or a wide range spectrometer (5nm to 32µm) depending on the site. Coupling of these two types of instruments allowed us to measure simultaneously, with high precision and short time interval, raindrops or snowflakes characteristics and aerosol size distributions during many various precipitations.

Washout coefficients (Λ) were calculated using the following formula :

$$\Lambda(D_p) = \frac{1}{\Delta t} \ln\left[\frac{c_0(D_p)}{c_1(D_p)}\right]$$

where Δt is the duration of precipitation, D_p the particle diameter, and c_0 and c_1 the concentration of particle respectively before and after precipitation.

Washout coefficients for each particle diameter have been calculated, and a typology of precipitation has been established according to their washout potential. Figure 1 is an illustration for one site of the mean washout coefficient vs. particle diameter accounting for data belonging from 20 to 80 different rain events. Dependence of washout coefficient with rainfall intensity has been estimated. Results were compared with previous experiments or theoretical models, and discussed.

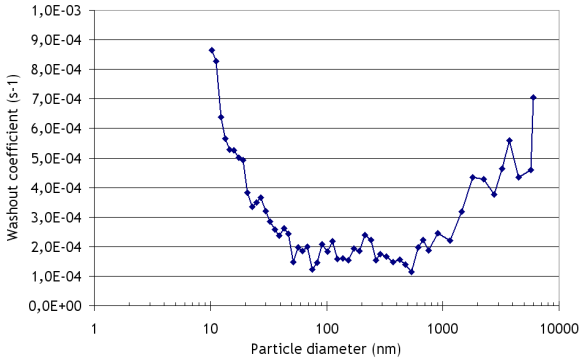

Figure 1. Washout coefficient vs. particle diameter (data of one site)

This work was cofunded by Meteo-France.and with the financial support of the Water Agency "Rhône Mediterrannée et Corse".

Association monitoring air quality ATMO-PACA and staff of the Laboratory of Glaciology and Geophysics of the Environment of Grenoble are also greatly thanked.

Laakso, L., Grönholm, T., Rannik, U., Kosmale, M., Fiedler, V., Vehkamäki, H., Kulmala, M. (2003) *Atmos. Environ.* **37**, 3605–3613.

Volken, M., Schumann, T. (1993) *Water Air Soil Poll.* **68**, 15–28.

Wang, X., Zhang, L., Moran, M.D. (2010) *Atmos. Chem. Phys.* **10**, 5685–5705.

Identifying cloud processed aerosol particles with light depolarization

D. Baumgardner[1], R. Newton[2], O.L. Mayol-Bracero[3], C.J. Valle-Diaz[3], F. Zurcher[3], S. Mertes[4]

[1]Centro de Ciencias de la Atmósfera, Universidad Nacional Autónoma de México, Mexico City, 04510, Mexico
[2]Droplet Measurement Technologies, Boulder, CO, 80301, USA
[3]Institute for Tropical Ecosystem Studies, University of Puerto Rico, Puerto Rico
[4]Leibniz-Institute for Tropospheric Research, Leipzig, Germany
Keywords: aerosol optics, aerosol/cloud interactions, dust, bioaerosols.
Presenting author email: Darrel.baumgardner@gmail.com

The interaction of aerosols and clouds is a complex process during which some aerosol particles form cloud droplets and crystals while others may be scavenged by diffusion or inertial collisions. The result of these interactions is often to transform the properties of the aerosol population such that after cloud processing the physical, optical and chemical characteristics are significantly different.

In an effort to better understand how cloud processing alters aerosol particle properties, an Aerosol Particle Spectrometer with Depolarization (APSD) was operated on Pico Este of Puerto Rico from August 19 to September 11, 2011 during the Puerto Rico African Dust and Cloud Study (PRADACS), attached to an inlet that selectively sampled interstitial aerosols or cloud droplet residuals derived from a Counterflow Virtual Impactor (CVI).

The APSD, developed by Droplet Measurement Technologies (DMT), measures the size distribution of aerosols between 0.5 and 20 µm and can distinguish the degree of asphericity or roughness of particles based upon the amount of depolarization caused by individual particles. An optical shape factor is derived by comparing backscattered light, from individual particles, measured with two detectors, one with and one without filters to detect the degree of depolarization.

As shown in Figures 1 and 2, the shape factor to optical diameter relationship is quite different depending on the source of the air mass and whether the particles are ambient (no cloud), droplet residual (CVI) or interstitial. Figure 1 shows the shape to size relationship for all periods when the air was coming from the islands upwind and southeast of Puerto Rico and Figure 2 are averages during a two day African dust event. The dashed lines show the shape to size relationships from reference particles measured in the laboratory.

From Fig. 1 we conclude that:

- Particles in SE flow look more like urban dust.
- Cloud residues have larger shape factors than cloud free particles.
- Particles > 5 µm during no cloud look like Azores (island) dust
-

From Fig. 2 we conclude that:

- Particles in SE flow + African dust look more like mixtures of urban and Azores dust.
- No interstitial particles > 5 µm (cloud removal?)
- Particles > 3 µm during no cloud look like pollen (biological?)

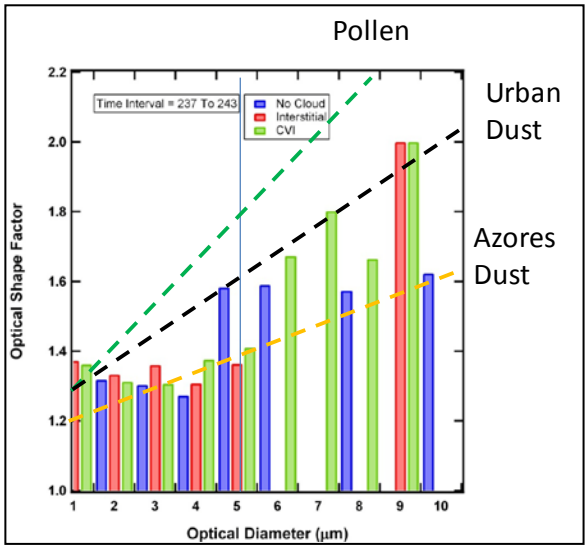

Figure 1. This graph shows how the average shape factor varies with optical diameter when air arrives at the mountain from the SE.

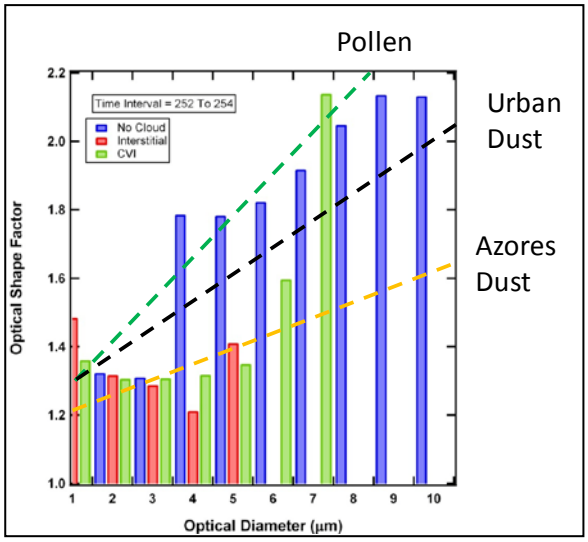

Figure 2. This graph shows how the average shape factor varies with optical diameter when air arrives at the mountain carrying African dust.

Inhibition of Heterogeneous Ice Nucleation of Mineral Dust Particles Exposed to Ozone

Z.A. Kanji[1], A. Welti[1], C. Chou[1, 2] and O. Stetzer[1]

[1]Institute for Atmosphere and Climate Science, ETH – Zurich, Zurich 8092, Switzerland
[2] Now at Science and Technology Research Institute, University of Hertfordshire, Hatfield AL10 9AB, UK
Keywords: Deposition, Immersion, Mineral Dust, Ice Nucleation.
Presenting author email: zamin.kanji@env.ethz.ch

Aerosols can cool or warm the atmosphere directly via interaction with incoming solar radiation (aerosol direct effect), or via their ability to act as cloud condensation or ice nuclei (IN) and thus play a role in cloud formation (indirect effect). The physical properties of aerosols such as size and solubility as well as chemical composition can influence their behavior and fate in the atmosphere. Ice nucleation is known to be especially sensitive to surface properties. Ice nucleation taking place via IN is termed as heterogeneous ice nucleation and can take place via deposition (ice forming on IN directly from the vapor phase), condensation/immersion (freezing via formation of the liquid phase on IN) or condensation (IN colliding with supercooled liquid drops).

Motivation for quantifying ice formation in the troposphere is many-fold. First, to understand the hydrological cycle since ice is the primary initiator of precipitation forming clouds. Second, the tropospheric budget of water vapour, an especially active greenhouse gas is strongly influenced by ice nucleation and growth. Third, ice surfaces in the atmosphere act as heterogeneous surfaces for chemical reactions of trace gases (e.g., SO_2, O_3, NO_x). Being able to quantify ice formation rates and ice surface concentrations allows an accurate calculation of trace gas budgets in the troposphere. This work addresses how mineral dust particles chemically aged from O_3 exposure influence deposition and immersion mode freezing under tropospherically relevant temperature (**T**) and relative humidity (**RH**) conditions.

Ice nucleation measurements were conducted using home-built chambers of the thermal gradient continuous flow diffusion principle capable of measuring immersion freezing (Lüönd *et al.*, 2010) (IMCA) and deposition freezing (Stetzer *et al.*, 2008) (PINC). In IMCA an ice optical depolarization detector was used to discriminate between frozen and liquid drops, whereas an optical particle counter was used to detect ice crystals in PINC. Poly-disperse samples of sub-micron diameter kaolinite and Arizona test dust were aerosolized in a stainless steel chamber and allowed to age for 15 – 90 minutes in known amounts of O_3 in the range 0.4 – 4 ppmv under dark conditions at ~298K. Destruction of O_3 was observed due to initial rapid decline of concentrations beyond background decay upon addition of dust particles to the aerosol tank. Deposition and immersion mode freezing experiments were conducted for both particles exposed to O_3 and unexposed particles.

Results for deposition mode freezing of kaolinite particles at RH_i = 130% are shown in Figure 1. It is observed that exposure to low levels of O_3 marginally enhance the ice active fractions as function of T. In contrast, when high O_3 concentrations are used for the ageing process, the ice active fractions are significantly repressed.

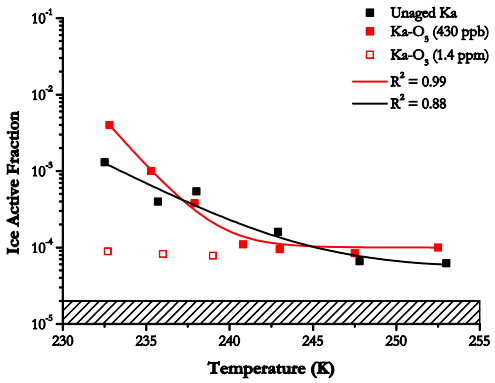

Figure 1. Ice active fraction as a function of T for kaolinite particles quoted at RH with respect to ice of 130%. The hashed region indicated the instrument background.

Ozone is known to react at surface sites of mineral dusts, including kaolinite (Karagulian and Rossi, 2005) to produce oxygenated surface species. It is possible that these surface species lower energies of ice germ formation for ice nucleation on the kaolinite surface. In contrast, when higher O_3 concentrations are used, the active surface species are chemically destroyed or physically occupied by adsorbed O_3, therefore making active sites for ice nucleation unavailable. Similar trends in ice nucleation behavior were observed for immersion freezing.

The results imply that mineral particles exposed to low ozone concentrations for longer periods of time in the atmosphere could have a significantly different ice nucleation behavior depending on the particle history compared to untreated particles typically used in laboratory measurements. These are the first results to show an inhibition of freezing in the immersion mode due to chemical ageing of aerosol particles.

Karagulian, F. and M. J. Rossi (2005), *Phys. Chem. Chem. Phys.*, 7(17): 3150-3162, DOI: 10.1039/b506750m.

Lüönd, F., O. Stetzer, A. Welti and U. Lohmann (2010), *J. Geophys. Res.-Atmos.*, 115(D14201)DOI: 10.1029/2009jd012959.

Stetzer, O., B. Baschek, F. Lüönd and U. Lohmann (2008), *Aerosol Sci. Technol.*, 42(1): 64-74, DOI: 10.1080/02786820701787944.

Aerosol activation behaviour in liquid-phase clouds at the Jungfraujoch: A comparison of in-situ measurements and box modelling data

E. Hammer[1], N. Bukowiecki[1], M. Gysel[1], C. R. Hoyle[1], Z. Jurányi[1], M. Leuenberger[2,3], U. Baltensperger[1] and E. Weingartner[1]

[1]Laboratory of Atmospheric Chemistry, Paul Scherrer Institut, Villigen, 5232, Switzerland
[2]Climate and Environmental Physics, Physics Institute, University of Bern, Bern, Switzerland
[3]Oeschger Centre for Climate Change Research, University of Bern,Bern, Switzerland.
Keywords: Aerosol cloud interaction, cloud condensation nuclei, CLACE, Activation.
Presenting author email: emanuel.hammer@psi.ch

Aerosols cause a radiative forcing directly through absorption and scattering of solar and infrared radiation in the atmosphere but also indirectly by modifying the properties of clouds. However, climate models still suffer from large uncertainties as a result of insufficient understanding of aerosol-cloud interactions.

An important parameter is the critical supersaturation, SS_{crit}, at which a particle forms a cloud droplet. SS_{crit} is described by the Köhler theory and depends on the particle's dry size and chemical composition. At ambient conditions, the prevailing supersaturation determines the activation diameter of the particles (i.e. the cut-off dry diameter above which all particles are able to act as cloud condensation nuclei, CCN, at a given supersaturation). We define the highest supersaturation that a particle experiences in an ambient cloud, leading to the formation of the cloud droplet, as the effective peak supersaturation (SS_{peak}). Since a higher updraft velocity results in a faster cooling of the surrounding air, this parameter is also dependent on the updraft velocity. To date no measurement device is available that is able to measure SS_{peak} within a cloud. Thus, the cloud peak supersaturation has to be retrieved indirectly from other measurements (e.g. Fors et al., 2011).

In summer 2010 and 2011, the Cloud and Aerosol Characterization Experiments (CLACE) were conducted at the high alpine research station Jungfraujoch (JFJ; 3580 m asl, Switzerland). Two different inlet systems were used to collect the total and interstitial aerosol separately. The in-cloud activation diameter was determined by comparing total and interstitial particle number size distributions. SS_{peak} was then inferred by comparing the in-cloud activation diameter with the supersaturation dependence of the activation diameter measured in parallel for the total aerosol using a CCN counter (CCNC) measuring at the JFJ (Jurányi et al., 2011).

The above approach yielded SS_{peak} values between 0.13% and 0.99% (10th and 90th percentile). While air masses coming from the north showed a wide range of values, SS_{peak} values for air masses coming from the south were more constant at around 0.2% (see Figure 1). This can most likely be explained by the different topography between south and north of the JFJ resulting in different cloud updraft velocities and thus higher cooling rates and higher SS_{peak} values.

The simulated influence of particle number concentration and size distribution on the SS_{peak} as a function of updraft velocity is currently being investigated in detail with a cloud box model. First results from a sensitivity study of the model show that SS_{peak} in convective clouds is strongly dependent on the accumulation particle number concentration. Hence, the difference in the SS_{peak} with air masses coming from south and north can to some extent also be explained by the difference in particle number concentration, additionally to the difference in topography.

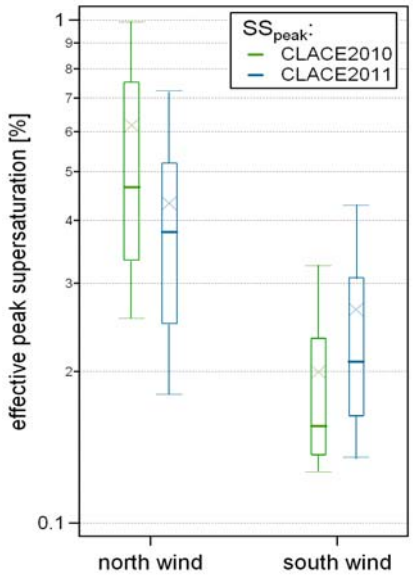

Figure 1. Effective peak supersaturation values distinguished by north and south wind conditions for CLACE2010 and 2011.

Currently, the model results (origin of cloud activation) are being validated with water isotope measurements from a Picarro H_2O isotope instrument provided by the Climate and Environmental Division of the Physics institute from the University of Bern.

This work was supported by MeteoSwiss in the framework of the Global Atmosphere Watch program. We thank the International Foundation High Altitude Research Stations JFJ and Gornergrat for the opportunity to perform experiments on the Jungfraujoch.

Fors, E.O., Swietlicki, E., Svenningsson, B., Kristensson, A., Frank, G. P., Sporre, M. (2011). *Atmos. Chem. Phys.* **11**, pp. 8343-8361.

Jurányi, Z., Gysel, M., Weingartner, E., Bukowiecki, N., Kammermann, L. and Baltensperger, U (2011). *J. Geophys. Res*. **116,** D10204

Cloud condensation nuclei (CCN) properties of mixed organic-sulphate particles

Å.K. Watne[1], R. K. Pathak[1], A. Eriksson[2], C. Wittbom[2], Th. F. Mentel[3], J. Pagels[4], B. Sveningsson[2], E. Swietlicki[2] and M. Hallquist[1]

[1]Department of Chemistry and Molecular Biology, University of Gothenburg, Gothenburg, SE-412 96, Sweden
[2]Department of Nuclear Physics, Lund University, Lund, SE-221 00, Sweden
[3]Institut für Energie- und Klimaforschung: Troposphäre (IEK-8),Forschungszentrum Jülich, D-52428 Jülich, Germany
[4]Ergonomics and Aerosol Technology, Lund University, Lund, SE-221 00, Sweden
Keywords: SOA, Aerosol Coating, AMS, CCN
Presenting author email: agot.watne@chem.gu.se

Mixed organic-inorganic particles will have different cloud condensation nuclei (CCN) properties compared with pure particles. In order to predict and represent the effect these mixed particles will have on cloud formation and climate, an accurate description of how changed organic mass loading of will affect the CCN properties is needed. The CCN properties and composition of mixed organic-sulphate particles were investigated in the Göteborg-Flow Reactor for Oxidation Studies at low Temperatures (G-FROST). The G-FROST facility has already shown to be valuable in studying properties and formation of pure SOA (e.g Jonsson et al., 2006; Jonsson et al., 2008). G-FROST is a laminar flow reactor where secondary organic aerosol (SOA) is produced under well-controlled conditions.

Mixed organic-sulphate particles were produced by condensation of secondary organic material (SOM) from dark ozonolysis of a SOA precursor on polydisperse inorganic seed particles. The CCN property of mixed organic-sulfate particles was measured as the supersaturation at which 50 % of the particles were activated as cloud droplets (SS_{50}) by a cloud condensation nuclei counter (CCNC, Droplet Measurement Technology DMT-100). The composition of the particles was measured by an aerosol mass spectrometer (AMS, Aerodyne Research Inc High-Resolution Time of Flight Aerosol Mass Spectrometer). The AMS and CCNC sampled monodisperse particles, size-selected by a Differential Mobility Analyser (DMA, TSI 3071), from the flow reactor. In each experiment, SS_{50} and composition was determined for 50, 75, 100 and 125 nm particles. In total six experimental conditions were carried out, see Table 1.

Table 1: List of experiments with corresponding conditions. Flow reactor kept constant at 298 K and at 30% RH.

	SOA precursor	Inorganic Seed	Ozone (ppb)
I	α-pinene	$(NH_4)_2(SO_4)$	500
II	Limonene	$(NH_4)_2(SO_4)$	500
III	Limonene	$(NH_4)(SO_4)$	4000
IV	Limonene	$(NH_4)_2(SO_4)$*	500
V	Limonene**	$(NH_4)_2(SO_4)$	500
VI	Limonene	NH_4HSO_4	500

*Seed particles were dried up-streams the flow reactor.
**2-butanol was used as OH scavenger.

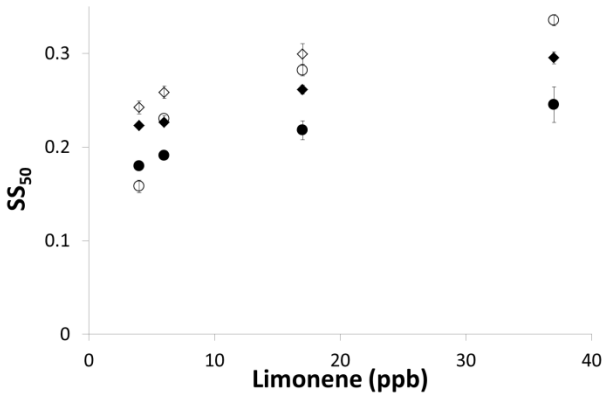

Figure 1: The SS_{50} for 100 nm particles in experiment II (open circle), III (open diamond), IV (closed circle) and VI (closed diamond) for 4, 6, 17 and 37 ppb of limonene.

Figure 1 shows the SS_{50} for 100 nm mixed organic-sulfate particles for four concentrations of limonene in four experiments. As can be seen, particles coated at higher limonene concentration were harder to activate compared to lower limonene concentrations. Furthermore, the 100 nm particles coated at high ozone concentration was harder to activate compared with lower ozone concentration. Interestingly, at high ozone concentration no activation of the 100 nm particles was seen for the highest limonene concentration.

These results demonstrated that the G-FROST facility, with its possibility to control and vary the conditions in the flow tube, combined with AMS and CCNC is a valuable tool in investigating the CCN properties of mixed organic-sulphate particles.

This project was supported by the Swedish Research Council (80475101), Formas (214-2010-1756) and the Swedish EPA research programme CLEO. The research presented is a contribution to the Swedish strategic research area ModElling the Regional and Global Earth system, MERGE.

Jonsson, Å. M., Hallquist, M., and Ljungström, E. (2006) *Environ. Sci. Technol.*, **40**, 188-194.
Jonsson, Å. M., Hallquist, M., and Ljungström, E. (2008) *ACP.*, **8**, 6541-6549.

Mixed-phase clouds observations at Pallas subarctic background site

D. Brus[1,2], K. Neitola[1], J. Svensson[1] and H. Lihavainen[1]

[1]Finnish Meteorological Institute, Erik Palménin aukio 1, P.O. Box 503, FI-00101, Helsinki, Finland
[2]Laboratory of Aerosol Chemistry and Physics, Institute of Chemical Process Fundamentals, Academy of Sciences of the Czech Republic, Rozvojová 135 Prague, 165 02, Czech Republic
Keywords: mixed-phase clouds, arctic, CAPS
Presenting author email: david.brus@fmi.fi

The Arctic region is slowly heading towards a new climatic state with substantially less permanent ice cover. The Arctic environment is very specific and full of not very well understood feedbacks, thus very hard to be predictable with current global models. Central role in these feedback processes are supposed to play Arctic clouds (Vavrus, 2004).

The winter cloud experiment has been conducted in first week of February 2012 at Finnish Meteorological Institute's Pallas-Sodankylä Global Atmosphere Watch (GAW) station located in northern Finland. The measuring site - Sammaltunturi station (67°58′N, 24°07′E) - resides on a top of the second southernmost fjeld, a round topped treeless hill, in a 50-km-long north and south chain of fjelds at an elevation of 565 m above sea level. Sammaltunturi station is due to topography of the surrounding terrain a great place for ground-based observations of orographic clouds. Thus providing an opportunity to investigate not only the cloud droplet activation of aerosol particles but also directly the cloud particle phase (Komppula *et al.*, 2005).

The Cloud, Aerosol and Precipitation Spectrometer (CAPS, DMT, CO, USA) which includes three instruments: the Cloud Imaging Probe (CIP), the Cloud and Aerosol Spectrometer (CAS) with depolarization, and the Hotwire Liquid Water Content Sensor (Hotwire LWC), were used in this campaign together with Cloud Condensation Nuclei counter (CCN-100, DMT, CO, USA) and Hygroscopic Tandem Differential Mobility Analyser (HTDMA). The CAPS probe was equipped with tailored inhalator to make it suitable for ground-based measurements. The average airspeed in the system was approximately 22 ms^{-1}. The shattering (Schwarzenboeck *et al.*, 2009) and thus overestimation of the concentrations of ice crystals obtained with the CIP probe is not expected to be observed.

Through the one week of intensive campaign five arctic cloud or freezing fog events lasting several hours were observed. The maximum and minimum temperature during the campaign was between -14 and -27°C. The maximum droplet concentrations were observed up to 100 cm^{-3} and 400 cm^{-3} for CIP-Greyscal probe and CAS-DPOL probe, respectively. Liquid water content was observed up to 1.5 g m^{-3}.

Figure 1 shows overlap of number concentration distributions obtained with CAS-DPOL and CIP-Greyscale probes in a range 0.5 μm – 1 mm. Images taken by CIP probe show both small spherical super-cooled drops together with larger irregular particles, figure 2.

The next step of the analysis will include all available experimental data on cloud particles together with physical and chemical properties, and activated fraction of aerosol particles (CCN and HTDMA).

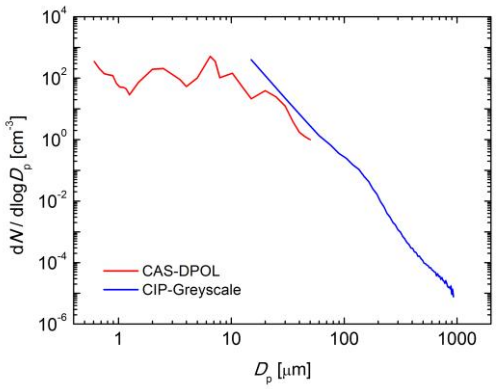

Figure 1. Example of raw size distributions obtained with CAS-DPOL and CIP-Greyscale probes during the campaign at Sammaltunturi, between 01:50-02:30, February 1st 2012.

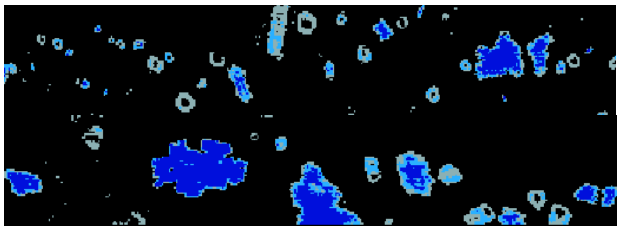

Figure 2. Example of image taken with CIP-Greyscale probe, particle sizes found on the picture are between 25-850 μm.

Authors would like to acknowledge financial support provided by Academy of Finland Centre of Excellence program (project no. 1118615)

Vavrus, S. (2004), *J. Climate*, **17**, 603-615

Komppula, M., H. Lihavainen, V.-M. Kerminen, M. Kulmala, and Y. Viisanen (2005), *J. Geophys. Res.*, **110**, D06204

Schwarzenboeck, A Shcherbakov, V., Lefevre, R., Gayet, J.-F., Pointin, Y., and Duroure, (2009), *Atmos. Res.* **92,** 220-228

First measurements of marine stratocumulus microphysical parameters at a subtropical Atlantic station (Friolera Peak Lab, FPL, 28.6ºN, 16.2ºW).

J.P. Díaz[1], F.J. Expósito[1], J.C. Pérez[1] and A. González[1]

[1]Group of Observation of the Earth and Atmosphere, University of La Laguna, S/C de Tenerife, 38200, Spain
Keywords: cloud microphysics, cloud condensation nuclei, aerosol, droplets.
Presenting author email: jpdiaz@ull.es

One of the most important uncertainties affecting the climate models are the processes related with cloud-aerosols interactions. The aerosols act as cloud condensation and ice nuclei, so they can modify the clouds in many ways. Thus it is essential to account with an accurate database of microphysics cloud and aerosols properties. The Canary Islands are located in one of the most important marine stratocumulus regions in the world. The orography of some of these islands allows us to locate a suitable station to establish long-term programs to measure the main mechanisms in cloud-aerosol interactions. With these aims, a new ground-based station has been installed in the North-East part of the Tenerife Island, Friolera Peak Lab. (28°33'1.16"N, 16°12'1.79"W, 720 masl). The main objectives for measurements programs taking place in this station are:

1.- Development of a measurements program with high-standard QA/QC requirements to obtain long-term time series.

2.- Study of the interrelations of the cloud properties with main aerosols types arriving to this region: marine, desert and anthropogenic aerosol from Europe.

3.- Estimation of the role of the marine stratocumulus in the energy budget

4.- Validation of satellite products with the data of microphysical properties made in this station.

In a first step two instruments have been installed: a FM100/DMT and an UFP 3031/TSI. The FM100 is a robust cloud-particle spectrometer, and allows for computation and real-time display of particle concentration, median volume diameter, equivalent diameter, and liquid water content. The UFP 3031 provides continuous size distribution and number concentration of particles between 20 and 850 nm, with six channels of size resolution: 20-30 nm, 30-50 nm, 50-70 nm, 70-100, 100-200 nm and 200-850 nm. It is an instrument specially designed for long-term monitoring with minimum maintenance.

The first results obtained are presented showing that this station is situated in a very clean environment, with values for the number of ultrafine particles lower than 1000 particles/cm^3 adding the six channels. An exception for this rule is clear when Saharan dust outbreaks reach the island. Thus it was recorded peak values that exceed the 20000 part/cm^3 during the last dust invasion in the second week of this year. Moreover, in cloudy conditions and a trade winds regime we observed for a minimal concentration of 300 droplets per cm^{-3}, an effective diameter of these droplets about 10 μm. The continuous monitoring of these parameters in a long term schedule will permit to analize any impact of climate change on processes related with the interaction cloud-aerosols.

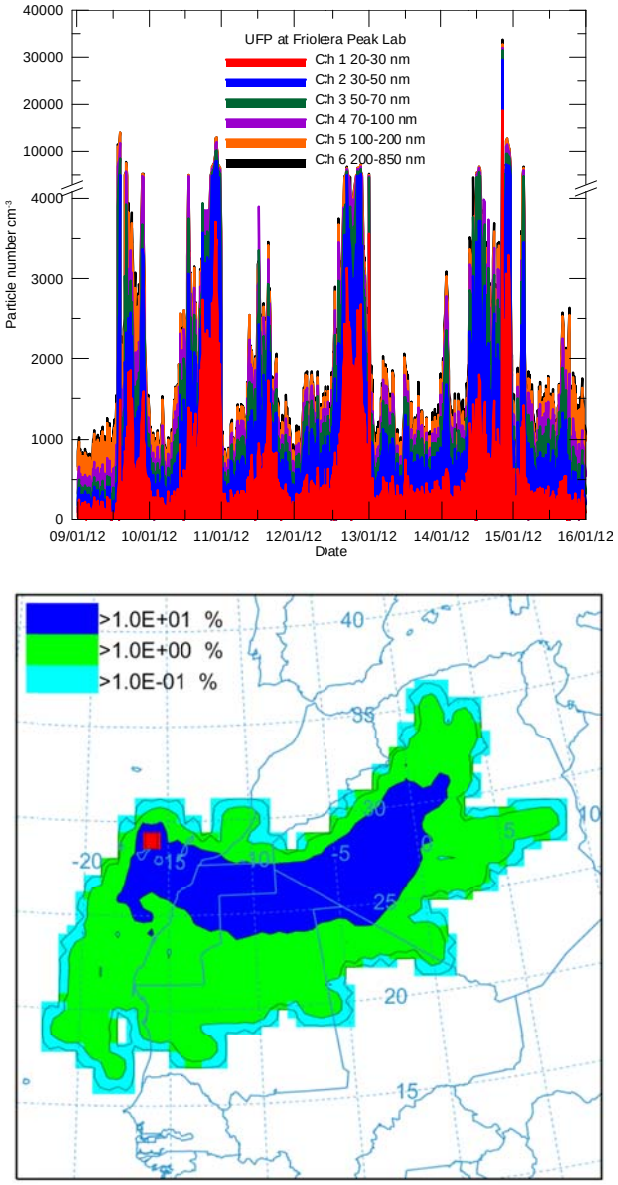

Figure 1. Particle concentration (upper) and frequency of backtrajectories (lower) during a Saharan dust invasion on January 09-16, 2012 recorded at Friolera Peak Lab.

We acknowledge to the MEC (Ministry of Education and Science, Spain) for the next supports: projects CGL2007-66477-C02-02/CLI, CGL2008-04740/CLI, CGL2010-21366-C04-01 and infrastructure project UNLL08-3E-007.

Combustion Particles as Ice Nuclei in an Urban Environment: Evidence From Single-Particle Mass Spectrometry

J.C. Corbin[1,2], P. J. G. Rehbein[2], G. J. Evans[2] and J.P.D. Abbatt[1]

[1]Department of Chemistry, University of Toronto, 80 St George St, ON, Canada
[2]Southern Ontario Centre for Atmospheric Aerosol Research, University of Toronto, 200 College St, Canada

The subset of atmospheric particles that trigger heterogeneous ice nucleation in the atmosphere can strongly influence the ice-crystal concentrations of cirrus and mixed-phase clouds. These particles, termed ice nuclei (IN), may catalyze ice formation under conditions ranging from a few degrees of supercooling down to about 237 K, below which a rapid increase in the rate of homogeneous ice nucleation renders heterogeneous nucleation less significant (Pruppacher and Klett, 1996). IN number concentrations affect cloud crystal size, number and shape, thereby influencing cloud precipitation and lifetime. However, the significance of IN to Earth's climate remains uncertain.

IN may trigger freezing from the vapour phase (deposition freezing), after immersion within liquid water (immersion freezing), or upon the collision of an IN with the surface of a liquid droplet (contact freezing). Aerosols that may contain IN include mineral dust, soot, biological material, and effloresced salts. Anthropogenic activity may affect the concentration of some of these IN via either direct emission, or the emission of precursors which may deposit upon pre-existing IN. However, most recent field studies have focused on relatively pristine environments, and the relative importance of anthropogenic IN is uncertain.

Direct measurements of the chemical composition of IN are a valuable tool for identifying potential IN sources. In this study, such measurements were made by activating IN to form ice crystals, using a counterflow virtual impactor to separate the ice crystals from background aerosol, and subsequently characterizing the evaporated crystals using a single-particle mass spectrometer (SPMS) (Cziczo et al., 2003). This CVI-SPMS technique provides valuable information on both the internal composition of IN and their external mixing state.

In this work, the CVI-SPMS technique was employed in the urban centre of Toronto, Canada, during winter 2011. The University of Toronto Continuous-Flow Diffusion Chamber (CFDC, Kanji and Abbatt, 2009) was used to activate IN before their introduction into a pumped counterflow virtual impactor (PCVI), followed by their chemical characterization using a TSI Aerosol Time-Of-Flight Mass Spectrometer (ATOFMS).

The CFDC was operated at 239 ± 1 K, 134 ± 2% RH_i (96 ± 2% relative humidity with respect to water, RH_w), under which conditions the chamber remains just below the experimentally-determined homogeneous freezing and droplet activation limits. Thus a maximal number of IN are activated under "deposition mode" conditions, although some degree of water was likely adsorbed to particle surfaces.

The number concentrations of particles measured by the CVI-SPMS at high RH_i (134%) and low RH_i (<105%) were compared to account for leakage by the PCVI. Single-particle mass spectra from the CVI-SPMS were sorted into 7 categories: dust, EC (elemental carbon), BB (biomass burning), metal-rich organic carbon (M/OC), potassium-rich OC (K/OC), OC potentially mixed with EC (OC/EC), and "unclassified." The resulting ratios, shown in Figure 1, were greater than unity for EC, BB, and dust particles. However, only the increase in EC was statistically significant (1 σ level) due to a low number of detected particles.

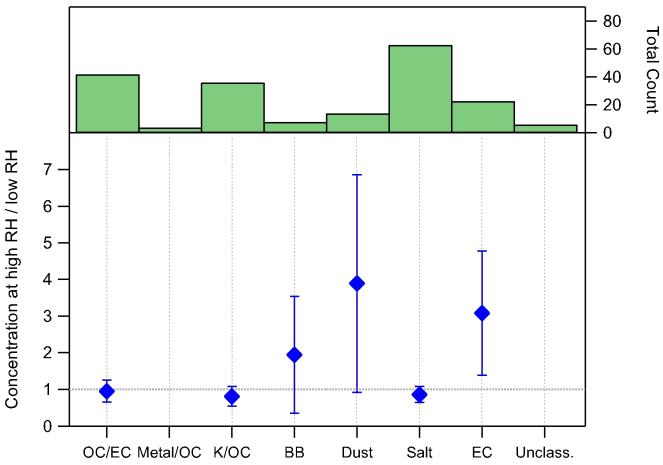

Figure 1. ***Upper panel:*** **Total numbers of particles measured by the CVI-SPMS at both high and low RH_i.** ***Lower panel:*** **Ratio of particle concentrations at 138% versus < 105% RH_i over ~35 measurement hours. No enhancement for metal/OC or unclassified particles is shown due to insufficient data. Error bars show one standard deviation.**

Finally, to complement the direct PCVI observations and enhance the number of spectra available, a second study was performed where particle composition and IN concentrations (C_{IN}) were measured in parallel. Backward elimination regression of C_{IN} against the same categories as above identified dust, BB and EC particles as the best C_{IN} predictors. Consistency between these two methods provides increased confidence in their individual results and encourages additional study of these potential IN.

Cziczo, D.J. *et al.* 2003. Aerosol Science and Technology 37, 460-470.
Kanji, Z.A., Abbatt, J.P.D., 2009. Aerosol Science and Technology 43, 730 - 738.
Pruppacher, H.R., Klett, J., D., 1996. Microphysics of Clouds and Precipitation. Springer.

A Case Study of Cloud Events by High Resolution Aerosol Mass Spectrometer in a Semi-urban Aerosol-cloud Interaction Observation Station

L.Q. Hao[1], A. Kortelainen[1], A. Jaatinen[1], P. Miettinen[1], S. Romakkaniemi[1], H. Portin[1,2], M. Komppula[2], A. Leskinen[2], A. Virtanen[1], J.N. Smith[1,2,4], D.R. Worsnop[1,3,5] and A. Laaksonen[1,3]

[1]Department of Applied Physics, University of Eastern Finland, Kuopio, P.O. Box 1627, Finland
[2]Finnish Meteorological Institute, Kuopio Unit, Kuopio, P.O. Box 1627, Finland
[3]Finnish Meteorological Institute, Helsinki Unit, Helsinki, P.O. Box 503, Finland
[4]National Centre for Atmospheric Research, Boulder, CO, P.O. Box 3000, USA
[5]Department of Physics, University of Helsinki, Helsinki, P.O. Box 64, Finland
Presenting author email: hao.liqing@uef.fi

Atmospheric aerosol can act as cloud condensation nuclei (CCN) to affect the amount of cloud on the earth and thus global climate. Such aerosol-cloud interactions comprise the largest uncertainties in our understanding of human-caused climate change. The composition of aerosol plays an important role determining its CCN activity. Thus direct and long-term observations of effects of chemical composition of aerosol on aerosol-cloud interactions are especially welcomed.

One campaign for the observation of cloud events was carried out in a aerosol-cloud interaction observation station in Kuopio, Finland in 2010 (Leskinen et al., 2009). We have succeeded to measure one intensive cloud event in this campaign. An Aerodyne high resolution aerosol time-of-flight mass spectrometer (TOF-AMS) was used to measure the chemical composition of cloud particles. During the cloud event, AMS sampled through two sampling lines: One is PM1.0 line. Samples from this line provides the chemical information of inactivated particles (cloud interstitial particles); The other is PMtot line, which collected all particles, presenting the information of cloud interstitial plus residual particles. We also applied positive matrix factorization (PMF) analysis to track the aerosol origin (Ulbrich et al., 2009).

Figure 1 displays the observation of cloud event along with meteorological conditions. There are several features shown in this figure: (1) wind direction and speed are roughly constant during cloud event, which can be roughly assumed the aerosol source to be constant, so does the chemical composition. Upon this assumption the information of cloud residual can be derived from the difference of PMtot to PM1.0 lines; (2)ratio of measured ammonia to predicted (orange curve) follows the trends of black curves and (3) the ratio of NO/NO_2 ions ($R_{NO/NO2}$, blue curve) shows an opposite trends to the orange curve.

Variations of $R_{NO/NO2}$ are able to indicate the nitrate origin. $R_{NO/NO2}$ for NH_4NO_3 is around 2.5 and much higher for organic nitrate. In this study, $R_{NO/NO2}$ from PMtot line is 4.7 and 3.7 for PM1.0 line during cloud event. Deconvolution of organic matrix plus NO/NO_2 ions extracts out ammonia nitrate factor and other four organic factors. The derived organic nitrate accounts for 27.7% of total nitrate for the cloud interstitial plus residual particles, 47.7% for cloud interstitial particles and 21.1% for cloud residual particles.

Contents of organic nitrate can further be estimated from AMS measurements. Assuming the possible contributions to nitrate included only organic nitrate and NH_4NO_3 in this campaign, we have:

$$NO_{org}+NO_{inorg}= NO_{tot} \quad (1)$$
$$NO_{2,org}+NO_{2,inorg}= NO_{2,tot} \quad (2)$$
$$NO_{org}/NO_{2,org}=10 \quad (3)$$
$$No_{inorg}/NO_{2,inorg}= 2.8 \quad (4)$$

where NO_{tot} and $NO_{2,tot}$ are from AMS measurement. From (1)-(4), we can estimate organic and inorganic nitrate fraction:

$$\text{Organic nitrate}=NO_{org}+NO_{2,org} \quad (5)$$
$$\text{Inorganic nitrate}=NO_{inorg}+NO_{2,inorg} \quad (6)$$

Based on this method, the estimated organic fraction to total nitrate is 48.1% for cloud interstitial particles and 22.6% for cloud residual, which are very close to the PMF deconvolution results.

Ratio of measured NH4 to predicted shows much lower values in PM1.0 lines, where the predicted $NH_4=18*(2*SO_4/96+NO_3/62+Chl/35.5)$. Much lower values in PM1.0 line indicated the higher fraction of NH_4HSO_4 in the cloud interstitial particle than in cloud residual particles.

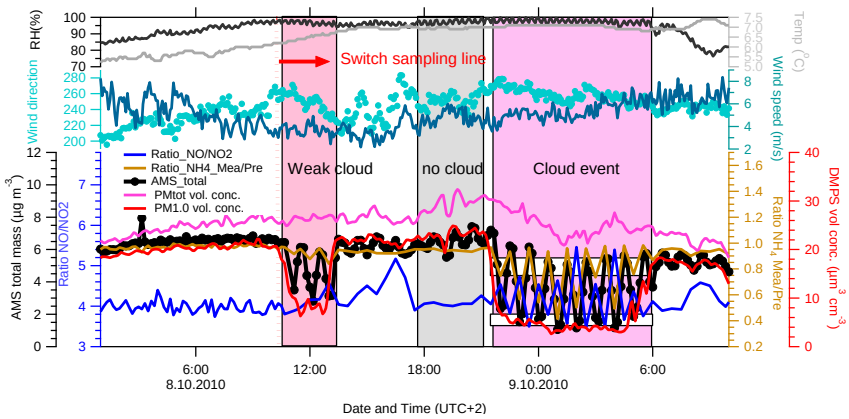

Figure 1 Observation of cloud event and meteorological conditions.

This work was supported by Academy of Finland Centre of Excellence program and Emil Aaltonen Foundation.

Leskinen, A., et al. (2009) *Boreal Environ. Res.*, **14**, 576-590.
Ulbrich, I.M., et al., *(2009) Atmos. Chem. Phys.*, *2891-2918*

A new ice selective inlet for the characterization of the atmospheric ice phase

P. Kupiszewski[1], P. Vochezer[2], M. Schnaiter[2], E. Weingartner[1]

[1]Laboratory of Atmospheric Chemistry, Paul Scherrer Institut, CH-5232 Villigen PSI, Switzerland
[2]Institute for Meteorology and Climate Research, Karlsruhe Institute of Technology (KIT), D-76021 Karlsruhe, Germany

Keywords: ice nucleation, mixed-phase clouds, CLACE 2013
Presenting author: ernest.weingartner@psi.ch

Uncertainties in climate projections are largely due to an insufficient understanding of aerosol-cloud interactions. One particularly poorly understood process is formation of mixed-phase clouds, where ice nuclei (IN), an aerosol sub-population, facilitate heterogeneous ice nucleation. IN influence the ice mass fraction, strongly affecting cloud radiative properties and lifetime. Meanwhile, the physico-chemical characteristics of IN in ambient mixed-phase clouds and the anthropogenic contribution to IN are not well known. Field studies of IN are hampered by difficulties with sampling the chemically complex ice residuals and separating them from liquid droplets.

A new Ice Selective Inlet (ISI) (Figure 1) is currently being developed. It is based on the design of an existing inlet (Mertes *et al.*, 2007) with the vital difference that the liquid droplets are separated from ice crystals in their airborne state via evaporation and thus minimizing artifacts like ice crystal breakup. Interstitial particles are removed by a pumped counterflow virtual impactor, ensuring only ice crystals remain in the sample air stream. The small crystals are evaporated and their residuals (considered representative of original IN) are transferred into the lab for physico-chemical analysis with state of the art instrumentation (e.g. AMS, SP2, SMPS).

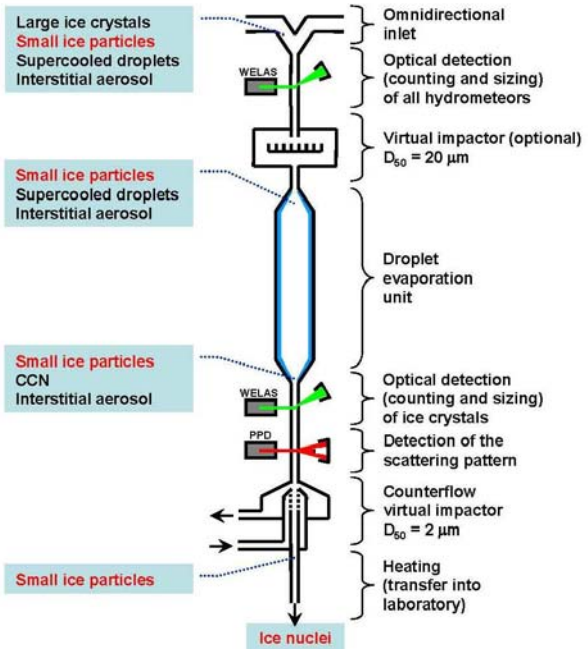

Figure 1. A schematic of the Ice Selective Inlet (ISI)

The new design includes an evaporation unit with ice-covered inner walls causing droplet evaporation using the Wegener-Bergeron-Findeisen process. The design is based on calculations of droplet evaporation rates (Figure 2), to allow for sufficient residence time of droplets to evaporate from a diameter of 20 µm (upper size limit of particles set by the virtual impactor) to 2 µm (particles smaller than 2 µm are removed by the counterflow virtual impactor).

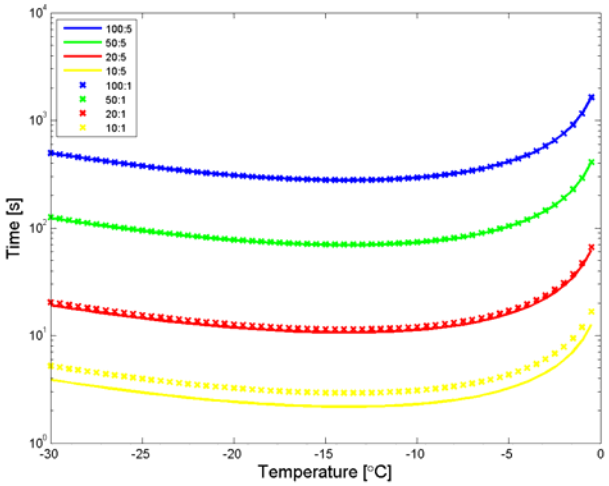

Figure 2. Evaporation times of cloud droplets in the evaporation unit for different droplet start and end diameters (in µm) as a function of temperature.

Optical particle counters are employed before and after the evaporation unit to retrieve information on droplet and ice crystal number size distributions. The ice particle microphysical properties, such as size, habit and surface roughness are inferred based on the scattering pattern measured with the novel Particle Phase Discriminator (PPD2). The PPD2 is also very important for the unambiguous detection of droplets that have survived the evaporation unit.

The inlet will first be tested in supercooled clouds generated at the AIDA cloud chamber at KIT. Subsequently, a field campaign (CLACE 2013) will be conducted at the high alpine Jungfraujoch site (3580 m.a.s.l) in order to characterize IN in ambient clouds.

This work is funded by the Swiss National Science Foundation and the German Research Foundation.

Mertes, S. *et al.* (2007) *Aerosol Sci. Technol.* **41**(9), 848-864.

Cloud resolving model simulations of geoengineering of marine stratocumulus cloud by sea salt injections

Z. Maalick[1], H. Korhonen[2] , H. Kokkola[2] , A. Laaksonen[1,3] and S. Romakkaniemi[1]

[1]Department of Applied Physics, University of Eastern Finland, Kuopio, 70211, Finland
[2]Finnish Matereological Institute, Kuopio unit, Kuopio, 70211, Finland
[3]Finnish Meteorological Institute, P.O.Box 503, 00101, Helsinki, Finland
Keywords: marine clouds, sea spray, aerosols.
Presenting author email: zubairm@uef.fi

Increase in the brightness of marine clouds through sea spray particles is considered as one of the quickest way to slow down global warming. The modification of marine clouds has received some attention as a relatively inexpensive method of achieving rapid cooling of climate.Hoverer, in most of the previous climate model studies a very high cloud droplet concentration is imposed on the clouds over the world's oceans and concluded that this geoengineering method can counteract warming from up to quadrupled CO_2 concentrations (Latham *et al* 2008).
Recent calculations using global models with size-resolved aerosol representations indicate that previously proposed sea spray producing vessel designs and emission fluxes are unlikely to lead to uniform cloud fields with such high drop concentrations, which may have important implications on the size of the spray vessel fleet required to achieve desired cooling (Korhonen *et al* 2010, Partanen *et al* 2011). Furthermore, in the recent study by Wang *et al* (2011) it was shown that this kind of geoengineering is efficient only in the cases where drizzle formation is suppressed by the increased number of cloud droplets.

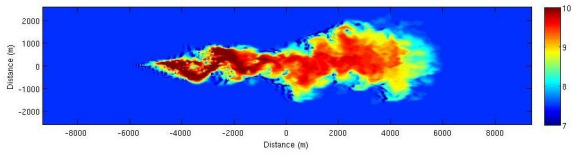

Figure 1. An example of the dispersion of particles emitted from the point source. The colour is logarithm of aerosol particle number concentration.

In this study we will use cloud resolving model UCLALES (Stevens and Seifert 2007) with the aerosol module SALSA (Kokkola *et al* 2007) to study aerosol cloud interactions in a cloud resolving scale. With SALSA we are able to represent aerosol size distribution found in marine environment and the number of cloud droplet formed is parameterized as a function of updraft velocity in the cloud base and aerosol size distribution present in the air parcel forming the cloud. With the model we are able to study aerosol cloud interactions in realistic conditions. We will use typical profiles for potential temperature and moisture content as well as surface fluxes to produce boundary layer dynamics with UCLALES.

In the simulations we will assumes that the moving vessel emits sea spray particles with a wind dependent flux similar to Wang *et al.* (2011) study. The results will show the changes in cloud drop number concentration with different wind speeds, emission rates and the size of the emitted particles. We will further study how well aerosol is dispersed in the boundary layer before they are removed through sedimentation. This will provide us information about how realistic is the proposed scheme and the number of vessels that should be employed to achieve the wanted change in cloud properties.

This study has been supported by the Academy of Finland (Project number 140907) and by the strategic funding of the University of Eastern Finland.

Latham, J., P. Rasch, C. Chen, L. Kettles, A. Gadian, A. Gettelman, H. Morrison, K. Bower and T. Choularton (2008) *Global temperature stabilization via controlled albedo enhancement of low-level maritime clouds, Phil. Trans. R. Soc*. A 366,3969-3987

Wang, H., P. J. Rasch, and G. Feingold (2011) *Manipulating marine stratocumulus cloud amount and albedo: a process-modelling study of aerosol-cloud-precipitation interactions in response to injection of cloud condensation nuclei, Atmos. Chem. Phys.*, 11, 885-916

Korhonen, H., K.S. Carslow. And S. Romakkaniemi (2010) *Enhancement of marine cloud albedo via controlled sea spray injections: a global model study of the influence of emission rates, microphysics and transport, Atmos. Chem. Phys.,* 10, 4133-4143

Partanen, A.-I., H. Kokkola, S. Romakkaniemi, V. Kerminen, K. Lehtinen, T. Bergman, A. Arola and H. Korhonen (2012) *Direct and indirect effects of sea spray geoengineering and the role of injected particle size. J. Geophysical research* 117, 0148-0227.

Kokkola, H., H. Korhonen, K. Lehtinen, M. Kulmula, A. Partanen and A. Laaksonen (2008) *SALSA- a sectional aerosol module for large scale application*. *Atmos. Chem. Phys.*, 8, 2469-2483

Stevens B. and A. Seifert (2008) *Understanding macrophysical outcomes of microphysical choices in simulations of shallow cumulus convection*, J. *Met. Soc. Japan* , 86A , 143_162

Size distribution and chemical composition of ice nuclei at a rural site in Germany

M. Ebert, T. Hermann, H. Bingemer, H. Klein, J. Curtius, and S. Weinbruch

[1]Environmental Mineralogy, Institute of Applied Geosciences, Technical University Darmstadt, 64287 Darmstadt, Germany
[2] Institute for Atmospheric and Environmental Sciences, Goethe - University, Altenhöferallee 1, D-60438 Frankfurt/M., Germany
Keywords: ice nuclei, electron microscopy, individual particle analysis
Presenting author email: mebert@geo.tu-darmstadt.de

By the static vacuum diffusion chamber FRIDGE. atmospheric ice nuclei (IN) concentrations are determined at Kleiner Feldberg (826 m asl, Rhein-Main Area, Germany) on a daily basis since more than 3 years (Bingemer et al., 2012).

The monthly mean number concentrations of IN vary by about one order of magnitude, with high values in early summer and low values in winter. This could have a significant effect on primary ice formation in mixed phased clouds and the development of precipitation over large areas of Central Europe.

Based on these measurements the aerosol optical thickness of mineral dust (AOD_{Dust}) turned out to be an especially important proxy for the IN-concentrations.

In order to proof the origin of the IN at Kleiner Feldberg the chemical composition, morphology and size of particles that had been identified as ice nuclei by FRIDGE were determined by environmental scanning electron microscopy (ESEM) combined with energy-dispersive X-ray microanalysis (EDX). In total more than 1000 individual IN were analyzed in 23 selected FRIDGE samples. The unambiguous identification of the analyzed particles as IN was enabled by a high precision laser engraved coordinate system on the substrates, which allowed to locate the positions of the ice crystals and the nucleating particles on the substrate both in FRIDGE and ESEM.

Nine groups of IN were distinguished: alumosilicates, quartz, Ca- and Mg-carbonates, Ca-sulfates, metal/metal oxides, biological particles, soot, other C-rich particles, and sulfates/nitrates/ chlorides. All other particles were summarized in a tenth “mixtures/other” group. This classification reflects the major composition of a particle. Minor compounds, which are present as coating, agglomerate or heterogeneous inclusion within individual particles were not considered for classification.

In total 30% of all identified IN belongs to the sulfates/nitrates/chlorides group. Because of methodical considerations this group was removed from the graphs in Figure 1 and 2

The size resolved particle group number abundance of the IN is shown in Figure 1, the total size distribution in Figure 2. Most abundant particle groups acting as IN are the soil groups alumosilicates, quartz and carbonates (orange bars) with in total 53%, followed by biological particles (plant fibers, pollen) with 27%, soot (8%) and metal/metal oxides (4%). While higher amounts of soot (average geometric diameter $d_{\varnothing}$ = 0.7 µm) were only found in the smallest size bin (<2 µm), biological particle dominate within the largest size bins (> 16 µm). Because of the large particle diameters of the biological IN ($d_{\varnothing}$ = 15.3 µm), these particles are very likely originating from local sources, while a major part of the alumosilicates ($d_{\varnothing}$ = 3,3 µm) also originates from long range transport (desert dust).

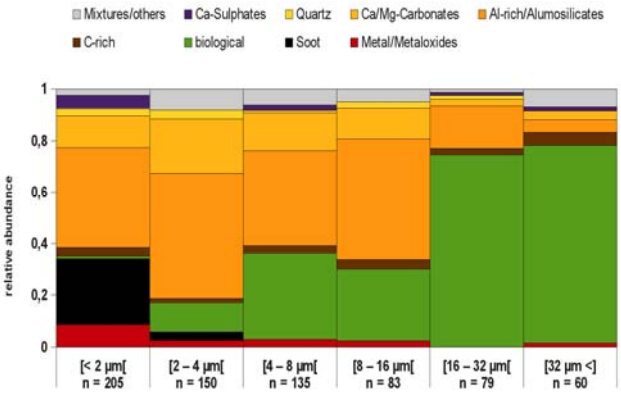

Figure 1. Relative particle group number abundance of IN at Kleiner Feldberg for six size classes.

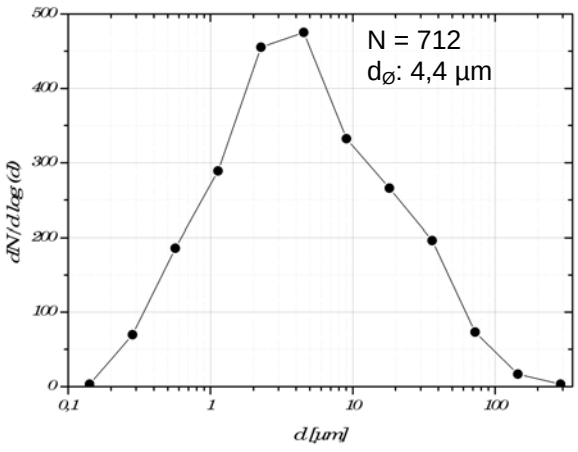

Figure 2: Size distribution of IN at Kleiner Feldberg (N = number of analyzed IN; d = average geometric diameter).

The regime dependency of the susceptibility of convective mixed-phase clouds and precipitation

Di Chang[1], Hang Su[1], Philipp Reutter[2], Jörg Trentmann[3], Meinrat O. Andreae[1], and Ulrich Pöschl[1]

[1]Max Planck Institute for Chemistry, Biogeochemistry Dept., Mainz, Germany

[2] Institute for Atmospheric Physics (IPA), Johannes Gutenberg University Mainz, Mainz, Germany

[3]Satellite Application Facility on Climate Monitoring, German Weather Service (DWD), Offenbach, Germany

Keywords: biomass burning, ice nuclei, clouds, precipitation and aerosol particles

Presenting author email: d.chang@mpic.de

Clouds have great influence on the vertical redistribution of energy and moisture, and consequently have impacts on weather and climate change from regional to global scales. Biomass burning is an important factor that could affect deep convection in clouds, and within this work, we used the ATHAM (Active Tracer High Resolution Atmospheric Model) model to study the properties of pyro-convective clouds and precipitation in 2- and 3-dimensional simulations. The two-moment microphysical scheme of Seifert (2002), including the hydrometeor categories cloud water, rain water, cloud ice, snow, graupel and hail, was utilized to investigate the interaction between atmospheric aerosols and cloud microphysics. The Chisholm fire that occurred in Alberta, Canada, in May 2001 was used as a base case. By assuming typical aerosol concentration conditions, we calculated the cloud droplet number concentrations under different fire intensity conditions and evaluated the effects of aerosol concentration and fire intensity on the formation of precipitation. The simulation results showed different control regimes for cloud and precipitation formation, including an aerosol-limited regime, a fire intensity-limited regime and a transitional regime, which are consistent with the results from a recent parcel model study (Reutter *et al* 2009).

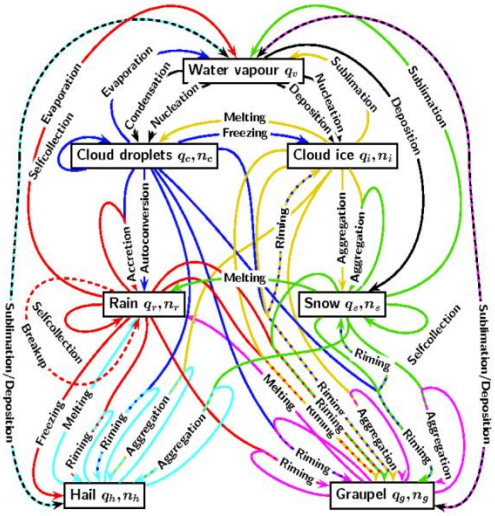

Figure 1. Simplified schematic diagram of the microphysical interactions in the two-moment Seifert scheme with respect to the particle classes cloud- and rain droplets, cloud ice, snow, graupel and hail.

Seifert, A. (2002) *Parameterisierung wolkenmikrophysikalischer Prozesse und Simulation konvektiver Mischwolken*, Ph.D. thesis, University of Karlsruhe.

Reutter, P., Su, H., Trentmann, J., Simmel, M., Rose, D., Gunthe, S. S., Wernli, H., Andreae, M. O., and Pöschl, U. (2009) *Atmos. Chem. Phys.* **9**, 7067-7080.

Measuring tropical maritime cumulus cloud particle residual composition and ice nuclei concentration during the ICE-T field campaign

A. Cazorla[1], K.J. Suski[1], G.R McMeeking[3], P.J. DeMott[3], S.G. Lasher-Trapp[4], C.H. Twohy[5] and K.A. Prather[1,2]

[1]Department of Chemistry and Biochemistry, University of California, San Diego. La Jolla, California, USA
[2]Scripps Institution of Oceanography, University of California, San Diego. La Jolla, California, USA
[3]Department of Atmospheric Science, Colorado State University, Fort Collins, Colorado, USA
[4]Department of Earth & Atmospheric Sciences, Purdue University, West Lafayette, Indiana, USA
[5]College of Earth, Oceanic and Atmospheric Sciences, Oregon State University, Corvallis, Oregon, USA
Keywords: aerosol cloud interaction, Saharan dust, biogenic particles, ice nuclei.
Presenting author email: cazorla@ucsd.edu

Ice nucleation is one of the most basic processes that leads to precipitation. Ice initiation and secondary ice multiplication in clouds are poorly understood processes that result in large uncertainties in the ability to model precipitation production and to predict climate change. Therefore, progress in modeling precipitation accurately requires a better understanding of ice formation processes.

In 2007, during the Ice in Clouds Experiment-Layer Clouds (ICE-L), measurements were focused on heterogeneous nucleation in clouds where secondary processes are not thought to occur. More recently, for the Ice in Clouds Experiment – Tropical (ICE-T), we turned our attention to tropical convective clouds, where both primary and secondary ice formation processes might play significant roles.

Tropical maritime cumulus clouds represent an important component of the global water cycle, but the relative roles of primary and secondary ice production in these clouds are poorly understood. Heterogeneous ice nuclei (IN) are responsible for ice initiation in towering tropical cumulus clouds, so information regarding their abundance, distribution, source compositions and dependence on cloud temperature is crucial to understanding the ice production processes.

We present recent measurements of cloud particle residual chemical composition and ice nuclei (IN) concentrations measured from an airborne platform (NSF/NCAR C-130) during the ICE-T field campaign, which took place in July 2011 over the Caribbean Sea.

Chemical composition of cloud particle residuals were measured with an Aircraft version of an Aerosol Time-of-Flight Mass Spectrometer (ATOFMS) (Pratt *et al* 2009a) sampling from a Counterflow Virtual Impactor (CVI) inlet. IN measurement techniques included airborne ambient (from an isokinetic inlet) and cloud particle residual (from the CVI inlet) measurements using a continuous flow diffusion chamber (CFDC) (Rogers *et al* 2001) and off-line analysis of samples collected from the aircraft. The presence of ice was confirmed with the cloud imaging probes installed on the wings of the C130, the Cloud Particle Imager (3V CPI) and the Two Dimensional Optical Array Probes 2D-P and 2D-C.

A total of 13 flights were performed during ICE-T and some of them had a strong Saharan dust influence. In particular, during the Research Flight 6, on 15 July 2011, dust particles were detected in ice crystal residuals with the ATOFMS and also resulted in higher IN concentrations compared to clean maritime conditions. Other flights showed the presence of biogenic particles detected in cloud ice crystals, suggesting that these also could be a source of ice nucleation, as identified also during ICE-L (Pratt *et al* 2009b).

Pratt, K.A., et al. (2009a). Observation of playa salts as nuclei in orographic wave clouds. *Analytical chemistry*, **81**, 1792–1800.

Pratt, K.A., et al. (2009b). In situ detection of biological particles in cloud ice-crystals. *Nature Geoscience*, **2**(6), 398-401.

Rogers, D.C., et al. (2001). A continuous flow diffusion chamber for airborne measurements of ice nuclei. *J. Atmos. Oceanic Technol.*, **18**, 725-741.

Hygroscopic and CCN properties of submicron atmospheric aerosol in a boreal forest environment during the summer of 2010

J. Hong[1], M. Paramonov[1] and T. Petäjä[1]

[1]Division of Atmospheric Science, Department of Physics, University of Helsinki, Gustaf Hällströmin katu 2, 00014, Helsinki, Finland

Keywords: hygroscopicity, CCN activity, κ, growth factor.

INTRODUCTION

Hygroscopic properties of atmospheric aerosol particles describe the interaction between the particles with ambient water molecules at both sub and super-saturated conditions in the atmosphere. Although the size of the particle is dominant factor (Dusek et al. 2006) determining whether a particle is a potential cloud condensation nuclei (CCN), the hygroscopicity plays a role at the size close to the limit of activation. Furthermore, hygroscopicity can give essential infor-mation on particle compositions (Swietlicki et al. 2008).

METHODS

This study was performed as a part of Hyytiälä United Measurement of Photochemistry and Particles – Comprehensive Organic Particle and Environmental Chemistry (HUMPPA-COPEC-2010) intensive field campaign (Williams et al. 2011).

Hygroscopicity properties measurements were per-formed using a Hygroscopicity Volatility Tandem Differential Mobility Analyzer (HVTDMA, Hakala et al. 2010), while the CCN properties were measured with a commercial continuous-flow Cloud Con-densation Nucleus Counter (CCNC, Roberts and Nenes, 2005).

PRELIMINARY RESULTS

In this study, preliminary results were obtained from CCNc measurements. For all data sets of super-saturation and activation diameters, derived from the CCN activation spectra, the effective hygroscopicity parameters κ were calculated from "*κ*-Köhler theory" equation (Petters and Kreidenweis, 2007). The effective hygroscopicity parameters (κ), were plotted against time during July of 2010, see Fig. 1. Larger particles activates earlier, thus have a larger kappa values, which means larger particles are more hygroscopic than smaller particles.

Critical diameters were plotted against supersaturation of this study from both CCN results and HTDMA data, with comparison of the ones from Sihto et al., 2010. The figure shows within the uncertainties, the results of this study agree well with Sihto et al., 2010, see Fig. 2.

Hygroscopic properties do not only depend on particle size, but also chemical composition. It is necessary to compare with the results from aerosol mass spectrometer to characterize the influence of chemical compositions.

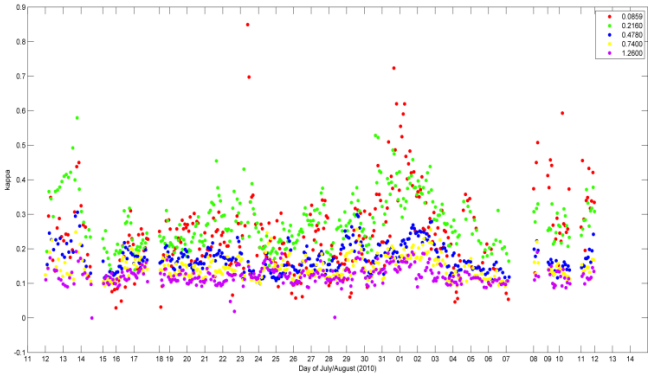

Figure 1. Hygroscopicity parameters obtained from CCN for different supersaturation as a function of time during July of 2010 for boreal environment aerosols.

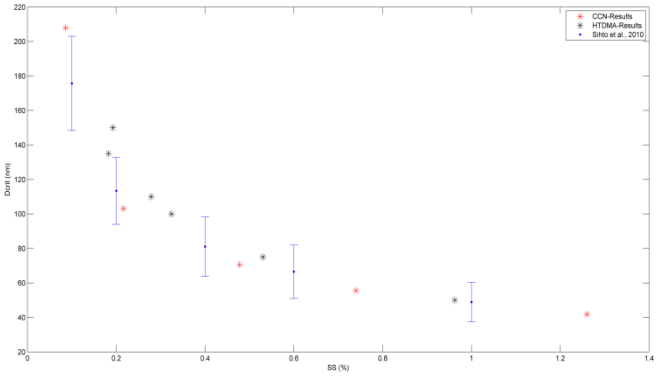

Figure2: Critical diameter as a function of critical supersaturation from this study and Sihto et al (2010).

ACKNOWLEDGEMENTS

This work was supported by Maj and Tor Nessling Foundation (project 2010143), and Academy of Finland via project 139656.

Reference

Desuk et al (2011). Size Matters More Than Chemistry for Cloud-Nucleating Ability of Aerosol Particles. *Sciences* 312(5778), 1375

Swietlicki et al (2008). Hygroscopic properties of submicrometer atmospheric aerosol particles measured with H-TDMA instruments in various environments-a review. *Tellus* 60B, 432-469.

Williams et al (2011). The summertime Boreal forest field measurement intensive (HUMPPA-COPEC-2010): an overview of meteorological and chemical influences. *Atmos. Chem. Phys. Discuss* 11, 15921-15973.

Roberts G. C.and Nenes A (2005). A Continuous-Flow Streamwise Thermal-Gradient CCN Chamber for Atmospheric Meausrements. *Aerosol Science and Technology* 39, 206-221.

Petters, M. D. and Kreidenweis, S. M (2007). A single parameter representation of hygroscopic growth and cloud condensation nucleus activity. *Atmos. Chem. Phys* 7, 1961-1971.

Ultra-fine aerosol particles above Amazon rainforest

M. Matisans[1], L. Rizzo[2], R. Krejci[1], P. Artaxo[2], P. Tunved[1], I. Riipinen[1], T. Hamburger[1], E. Swietlicki[3]

[1]Department of Applied Environmental science, Stockholm University, Stockholm, 10691, Sweden
[2]Departamento de Ciências Exatas e da Terra, Universidade Federal de São Paulo, São Paulo, 09972-270, Brazil
[3]Div. of Nuclear Physics, Dept. of Physics, Lund University, S-221 00 Lund, Sweden

Keywords: ultra-fine aerosol, Amazon, nucleation.
Presenting author email: modris.matisans@itm.su.se

Amazon rainforest undergo rapid changes due to increasing anthropogenic influence. Natural aerosol concentrations and pristine conditions are more perturbed by biomass burning associated with human driven deforestation. This study shows analysis of ultrafine aerosol number concentration over the rainforest canopy.

Events of new particle formation in tropics and over the rainforest followed by consecutive growth towards Aitken mode size range are sparse compared to mid-latitudes (Kulmala et al., 2004). More often short episodes of elevated ultrafine aerosol particles concentrations in a range of 20 – 40 nm are observed over the tropical rainforest, but their origin and process behind these episodes of new particle formation is unclear.

In this study scanning mobility particle sizer (SMPS) aerosol size distribution measurements in the range of 10 to 500 nm at the location of TT34 tower, 40 km NNW from the city of Manaus, Brazil were used. Measurements represent time period from April 2009 to February 2010. Ultra-fine particle range in this study is defined as smaller than 70 nm, including nucleation mode and Aitken mode. Meteorology, as wind speed/direction, temperature, relative humidity and solar irradiation, were measured nearby TT34 site.

Methods and results

The aerosol size distributions were analyzed using cluster analysis and 8 different clusters of characteristic size distributions were identified. One of the clusters includes data likely influenced by local pollution from diesel generator and were removed from dataset.

Obtained clusters were analyzed with respect to local meteorological data and mainly with respect to preferred source regions. Majority of measurements (~ 60 %) falls into clusters where aerosol size distribution is clearly dominated by accumulation mode aerosol, typical feature for Amazon during both, wet and dry seasons (Artaxo et al., 2002). Only modal size and magnitude of the accumulation mode is different with significantly higher concentrations during dry season when biomass burning take place. *Fig.1* shows median aerosol size distributions for various clusters. Accumulation mode dominated clusters were combined into one as they show very similar properties. Episodes with elevated concentrations of the ultrafine aerosol particles represent approximately 5 % of measurements. They are distinct by presence of aerosol mode with maxima around 20 – 30 nm and "closed" shape of size distribution indicating that new particle formation happened recently, but it is not still ongoing. Analysis of wind direction and other meteorological parameters does not show any preference to specific conditions. However, when seasonality is taken into account, ultrafine aerosol episodes occur dominantly during wet season when biomass burning is suppressed. The mechanism behind source and processes responsible for the ultrafine aerosol particle episodes are still under investigation. Hypothesis linking new particle formation in and in vicinity of shallow convective clouds is being at the moment in focus of ongoing analysis.

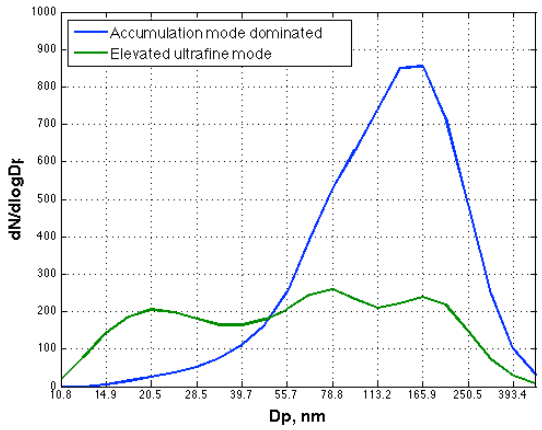

Fig 1. Median aerosol size distributions for clusters dominated by accumulation mode (blue) and for cluster with elevated ultrafine aerosol concentrations (green).

The data were collected with support from the AMAZE and EUCAARI project funded by National Science Foundation, Brazil LBA Millennium Institute, the Max Planck Society and European Union. Data analysis was supported also by Swedish Research Council.

Artaxo, P., Martins, J. V., Yamasoe, M. A., Procópio, A. S., Pauliquevis, T. M., Andreae, M. O., Guyaon, P., Gatti, L. V., and Leal, A. M. C. (2002):, *J. Geophys. Res.*, **107**.

Kulmala, M., Vehkamaki, H., Petajda, T., Dal Maso, M., Lauri, A., Kerminen, V. M., Birmili, W., and McMurry, P. H. (2004), *J Aerosol Sci*, **35**, 143-176,.

Impacts of Emission Controls and Perturbations on an Intense Convective Precipitation Event during the 2008 Beijing Olympic Games

Y. F. Cheng[1,2], C. Wei[1], P. Marrupu[1], P. Saide[1], S. Kulkarni[1], M. Lin[3], Q. Zhang[4], D. G. Streets[5], H. Su[2], A. Wiedensohler[6], G. R. Carmichael[1]

[1] Center for Global and Regional Environment Research, The University of Iowa, Iowa City, USA
[2] Max Planck Institute for Chemistry, Mainz, Germany
[3] Center for Sustainability and the Global Environment, University of Wisconsin-Madison, Madison, USA
[4] College of Environmental Engineer, Tsing Hua University, Beijing, China
[5] Argonne National Laboratory, Argonne, USA
[6] Leibniz-Institute for Tropospheric Research, Leipzig, Germany

Keywords: aerosol cloud interaction, emissions, megacity, Modelling (regional)

Presenting author email: yafang.cheng@mpic.de

A fully-coupled meteorology-chemistry-aerosol model (WRF-Chem) is used to assess the impacts of emission controls and perturbations on a summer intense convective precipitation event from August 9-11 during the 2008 Olympic Games. A four-nested domain configuration, from 81 km covering the whole China down to 3 km covering Beijing/surroundings, are used. Different emission scenarios are studied, including: (1) emissions targeting the 2008 Olympic period (OLY08); (2) INTEX-B emissions targeting the year 2006 (INTEXB06); (3) a zero-out of BC primary emissions in both anthropogenic (OLY08) and fire emissions (no-BC); and (4) a zero-out of anthropogenic emissions (no-AnthropE). MEGAN biogenic, MODIS fire and WRF-Chem embedded sea salt emissions are employed. INTEXB06 emissions are in general higher than OLY08 due to the long/short-term emission controls, especially for SO_2 and PM.

The WRF-Chem model (OLY08) is able to accurately predict both aerosol mass and number concentrations in the urban area of Beijing. The shapes of particle number size distributions are similar between observations and simulations. Column simulated aerosol optical depth (AOD) is also in a good agreement with MODIS AOD.

The emission scenario simulations suggest that even small perturbations in the concentration and/or compositions of aerosols can lead to either enhancement or suppression of this summer intensive precipitation event.

Compared with a pure WRF run (with no chemistry and feedbacks), WRF-Chem OLY08 simulations, including the coupled feedbacks, improve the predictions of precipitation and compare well with the satellite retrieval, while the WRF simulations predict a shift of ~ 1 to 2 degree in areal precipitation distribution and produces no convective rain in the Beijing area.

The pure WRF run produces the highest accumulated rainfall in the Beijing area. The next highest is produced by the no-AnthropE case, with over 50 mm more than predicted by the OLY08 scenario. Compared with OLY08, the INTEXB06 case produces slightly lower average rainfall accumulation, with nearly no change in convective precipitation but with suppression of non-convective precipitation by ~5 to 10 mm. The reduction of BC emissions makes nearly no change in non-convective precipitation, but suppresses convective precipitation by ~10 to 15 mm.

Without anthropogenic emissions, the predicted precipitation is strengthened in both precipitation area and intensity. Perturbation on emissions leads to a reorganization of precipitation. With OLY08 there are high precipitation patterns that sit at the center of Beijing and to the south. However, with INTEXB06, the precipitation center moves to the northwest mountain area, and with no-BC emissions, the high precipitation center shifts towards northeast of Beijing and with very low precipitation in the downtown area. The convective cloud-system in OLY08 case is more organized than that from INTEXB06 case, with maximum accumulated convective and non-convective precipitations, respectively over 50 and 20 mm more than the INTEXB06 case. With no-BC emission, the cloud-system is even more organized with double the differences in the extreme rainfall accumulation to the INTEXB06 case than the OLY08 case.

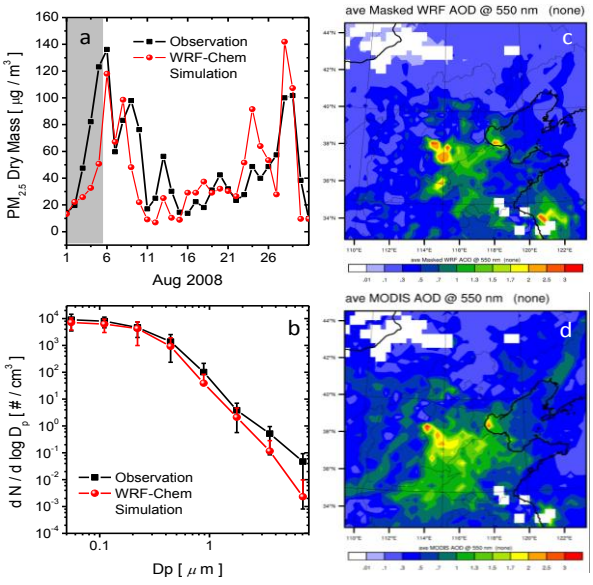

Figure 1. (a) PM2.5 at ground station on the campus of Tsinghua University, (b) particle number size distribution at ground station on the campus of Peking University site, (c) MOIDS AOD and (d) WRF-Chem simulated AOD.

Grell et al. (2005), Fully coupled "online" chemistry within the WRF model, *Atmospheric Environment*, 39, 6957-6975.

Relationships between aerosols, cloud condensation nuclei and cloud droplets on a background subarctic site

T. Anttila[1], D. Brus[1], A.-H. Hyvärinen[1], A. Jaatinen[2], N. Kivekäs[1], S. Romakkaniemi[2], H. Lihavainen[1]

[1] Finnish Meteorological Institute, Research and Development, Climate and Global Change, P.O. BOX 503, FI-00101 Helsinki
2 University of Eastern Finland, Kuopio Unit, Department of Physics, Finland

Keywords: aerosol-cloud interactions, cloud condensation nuclei, cloud microphysics
Presenting author email: tatu.anttila@fmi.fi

Incomplete understanding of the interactions between aerosols, clouds and climate form a large source of uncertainty in climate change predictions. The predictions are done with large scale models which rely on parameterizations of microphysical processes. One of the aims for the Pallas Cloud Characterization Experiment 3 (PaCE–3) was to provide more data on the microphysical processes related to the cloud formation. Such data is valuable in developing parameterizations that can be used in the global climate models.

The campaign took place during Autumn 2009 in a measurement located in a northern Finland. Here we present an analysis for measurement data for selected cloud periods. Measurements cover the particle size distribution, size resolved activated fraction of particles (performed within a dual DMPS set-up), particle hygroscopicity as well as their cloud condensation nuclei (CCN) activity at several different supersaturations ranging from 0.2 to 1.0%.

The average total particle concentrations, CN_{tot}, varied from 385 to 1518 cm^{-3} between the events. Table 1 shows further that particles with dry diameters above 100 nm, CN(>100 nm), made only a small contribution to the total number concentrations: the ratio between CN_{tot} and CN(>100 nm) varied in the range 0.07 to 0.25, implying that Aitken mode sized particles dominated the total particle concentrations. The average number of cloud droplets inferred from the dual-DMPS setup, CDNC, varied between 49 and 99 cm^{-3}. Such numbers are somewhat smaller than the average numbers obtained from an analysis of a longer data set from the site (Komppula et al., 2005) and are also smaller than observed in the previous campaign, PaCE-2, which took place in the same time of the year as the current campaign (Anttila et al., 2009).

The average value of the diameter at which 50% of the particles are activated into cloud droplets, D_{50}, varied in the range 80 to 102 nm between the cases. These numbers are somewhat lower than observed in the previous campaign (Anttila et al., 2009) but compare well to those reported by Komppula et al. (2005). Comparing the corresponding values of CN(>100 nm), CDNC and D_{50}, it can be concluded that Aitken mode particles made only a small contribution to the number of activated cloud droplets.

Table 1. Observed features of the analyzed cloud events. For each event, an average value of the quantity is shown followed by the value range during the event in parenthesis. Here CN_{tot} is the total particle number concentration, CN(>100 nm) is the concentration of particles with dry sizes above 100 nm, CDNC is the inferred number of cloud droplets and D_{50} is the diameter corresponding to the 50% activation efficiency.

Case	A	B	C	D	E
Time	9.9. 08:00-13:45	22.9. 06:45-8:15	22.-23.9. 22:30-08:30	25.-26.9. 23:30-04:15	4.10. 01:30 - 12:15
CN_{tot} (cm^{-3})	531	1518	449	385	499
CN(>100 nm) (cm^{-3})	127	131	100	29	119
CDNC (cm^{-3})	93	97	89	49	99
D_{50} (nm)	101	98	92	80	102
CDNC/ CN_{tot}	0.17	0.06	0.22	0.13	0.23

Here we have reported the key observed features of the cloud cases. In the future work, we will analyze the data further using the modelling tool presented in Anttila et al. (2009). Also, results from CCN closure study will be presented.

Anttila, T., P. Vaattovaara, M. Komppula, A.-P. Hyvärinen, H. Lihavainen, V.-M. Kerminen, and A. Laaksonen (2009). *Atmos. Chem. Phys*. **9**, 4841–4854

Komppula, M., Lihavainen, H., Kerminen, V-M., Kulmala, M., and Viisanen, Y. (2005) *J. Geophys. Res*. **110**, D06204, doi:10.1029/2004JD005200, 2005.

Fate of volatile and non-volatile elements from biomass burned in stoves and boilers

Torben Seidel & Hans Ruppert

Dept. of Sedimentology and Environmental Geology, Geoscience Center, Goettingen University, Goldschmidtstrasse 3, D-37077 Goettingen, Germany
Keywords: biomass burning, emission, concentration, fluxes, heavy metals
Presenting author email: tseidel1@gwdg.de

Biomass burning as an alternative energy supplier may play an essential future role due to the greenhouse effect, the shortage of fossil energy sources and the striving autonomy from fossil fuels. The growing contribution of biomass burning may have adverse effects such as higher emissions of harmful inorganic and organic substances in contrast to fossil fuels such as oil and gas.

Especially for in-house facilities burning biomass reliable measurements of concentrations and fluxes of heavy metals in the flue gas are lacking. For a reliable reconstruction of element fluxes and for input/output balances, the originating ashes such as grate ash, heat exchanger ash and fly ash are collected.

In the ideal case the amount of an element contained in the fuel should be identical with the combined element amounts in the different ash fractions. Especially the recovery rates of the environmentally and health relevant elements such as Cd, Zn, Sn, Tl, and Pb from burnt wood or straw in automatically fuelled furnaces are fairly low (Figure 1) suggesting that they either leave the chimney as molecules or ultrafine particles or that they "disappear" in the refractory lining material. The volatile property of these elements can be affirmed by a crucial lower presence in others than fly ashes. Other elements such as Co, Mo, Cr and Ni likewise show recovery rates lower than 100% attributed to a contamination of the fuel, but this may be caused by an abrasion of the cutting mill during preparation. On the other side elements like Ca, Ti, Mn, Ba, Fe, REE and Zr have recovery rates higher than 100% what may indicate a contamination by the refractory lining materials of the furnaces.

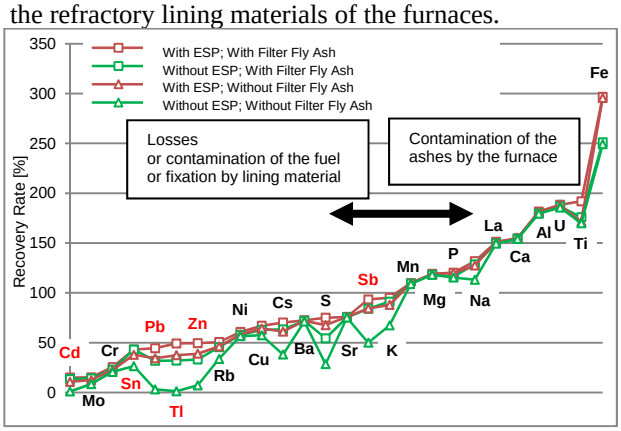

Figure 1. Recovery rate (%) of elements by burning wood-chips in a 30 kW boiler (combined element amounts in grate ash, internal heat exchanger ash and ESP ash (△) and fly ash (☐) divided by the element amounts contained in the wood chips).

Electrostatic precipitators (ESP) in the exhaust gas stream diminish the dust load e.g. from 55mg/Nm^3 to 18mg/Nm^3 at 13% O_2 respectively for a 30kW boiler fuelled by spruce wood-chips. Therefore the amount of risky elements can be diminished by the ESP if the elements are bound on particles but not if they are in an ESP non-retainable state. Figure 1 shows the recovery rates of elements in a 30kW boiler with downstream ESP. The boiler is fuelled by spruce wood-chips. The application of an ESP decreases the dust load and lowers the emission of associated elements such us Cd, Zn, Pb, and Tl. Nevertheless, main fractions of the most volatile elements are not retained what suggests either a very fine particulate or gaseous state of the elements which is not retained by ESP or by a baghouse filters.

The second explanation for the low recovery rate could be fixation by refractory lining materials such as chamotte. First analysis used lining materials show highly variable element concentrations and partly extreme enrichments especially of Cd in contrast to unused material form the same furnace or the continental crust (Table 1). The enrichment of some elements may be facilitated by the large open porosity (>20%) of these materials and may explain in part small recovery rates. But very high extraction efficiencies would be necessary to remove appreciable amounts of these elements from the flue gas. For example: 80% of Cd released during wood burning should be stored in the lining.

Table 1: Element concentration (µg/g) of used and unused refractory lining materials.

	Cd	Cr	Sn	Pb	Tl	Zn	Ni	Sb
1	0.12	156	0.26	3.29	0.38	99.5	143	0.02
2	20	54.5	20.7	89.2	1.29	47.0	59.7	2.92
3	109	155	1.51	157	0.41	186	134	1.47
4	0.06	56	8.22	27.2	0.23	12.1	52.1	0.33
5	0.09	92	2.1	17	0.9	67	47	0.4

1 From Wood-chip boiler, 30 kW; material used
2 From Stove, 8 kW; material used
3 From Pellet boiler, 25 kW; material used
4 From Wood-chips boiler, 30kW; material unused
5 Reference material, Upper Continental Crust

To assess the environmental impact of a furnace, flux calculations for elements are much more relevant than listing of simple concentration data. In addition, only element fluxes enable the comparison of emissions from different furnaces and fuels under different burning conditions, etc. But the fate of elements with low recovery rates has to be ascertained (losses by gaseous or fine particulate emission versus retention in refractory lining material versus contamination of the fuel).

Rudnick & Gao (2003): Composition of the Continental Crust. Treatise on Geochemistry, Volume 3. Editor: Roberta L. Rudnick. Executive Editors: Heinrich D. Holland and Karl K. Turekian. pp. 659. ISBN 0-08-043751-6. Elsevier, 2003., p.1-64.

Control of trace pollutants in fuidised bed biomass-residues co-combustion fly-ash.

D. Sanz[1], J. J. Rodríguez[1] , J. L. Dorronsoro[1] , E. Rojas[1] , R. Ramos[1], R. Escalada[1], M. E. Borjabad [1], M. A. Martínez[1], M. P. Sanz [1], A. De La Torre, P. Galán[1] , A. Bahillo[1] , C. Gutierrez-Cañas[2] , G. Aragón[2] and S. Astarloa[3]
[1]CIEMAT, Avda Complutense 40, Madrid, 28040, Spain
[2]Dpto. de Ingeniería Química y del Medio Ambiente, Universidad del País Vasco, Bilbao, Spain
[3]AIRg, Bilbao, Spain
Keywords: Aerosol characterization, Biomass burning, Combustion aerosols, Heavy metals, PCDD/Fs, Filtration
Presenting author email: david.sanz@ciemat.es

Introduction.

Combustion processes, such as waste incineration, are currently a relevant source of trace contaminants such as heavy metals or aromatic hydrocarbons, preferably contained in the particulate matter (PM) accompanying emissions. Heavy metals and other, such as copper or iron, can participate as catalysts in the formation process of dioxins and furans (PCDD/F) (Stanmore, 2004), along the way of flue gas through emissions control devices.

The behaviour of metals in general and heavy metals in particular, depends on several factors. These factors include their concentration and the chemical form in which they are incorporated, the type of matrix, the temperature and time of treatment, the composition and the speed of the gas flow, the presence of chlorine or other species, such as sulphur compounds, carbon monoxide or aluminium silicates.

The volatility of the elements depends not only on their boiling point, but also on the possibility of formation of more or less volatile compounds. In addition, mineral matter that forms the bulk of the fluidised bed may exhibit some ability to absorb some of the metals.

Table 1. Mass concentration reduction for selected metals in solid phase

Test	Fuel	% reduction Pb	% reduction Cu
A190Dx	A	84.73	93.94
B190-09	B	97.16	97.58
C190Dx	C	79.17	93.63

Experimental and results

A series of tests were done in a semi-industrial scale facility (Sanz, 2009). An hybrid filter comprising electrostatic precipitation (ESP) and baghouse (BH) modules was connected to a fluidised bed combustor. Tested fuels were olive tree pruning biomass (C), olive biomass/compost (A) and olive biomass/municipal waste RDF (B).

Fly-ash samples and fly-ash collected in hoppers of the hybrid filter was chemically analysed. The hybrid filter removes 99% of PM, thus reducing metals concentration (table 1).

Fly-ash collected in BH module, the fine fraction, is enriched in chloride, sulfates, K, Na, Pb, Cd and Hg compared to ESP module (table 2). Lower operating temperature in the filter resulted in higher content in volatile elements, such as mercury (figure 1) and cadmium, in the fly-ash collected in the filter.

Table 2. Average concentration in fly-ash collected in hybrid filter hoppers.

	Fuel A		Fuel B	
	ESP	BH	ESP	BH
Pb (ppm)	83	294	673	1350
Cu (ppm)	420	635	2667	4600
Cd (ppm)	1.82	6.76	10.00	23.00
K (%)	4.53	19.15	1.80	5.90
Fe (%)	0.80	0.44	2.63	1.50

Higher concentrations of PCDD/Fs were found downstream the filter in all the tests. This is probably related to high metals concentration in fly-ash. Formation of precursors in the ESP could also contribute to the effect (Kolluri, 1994).

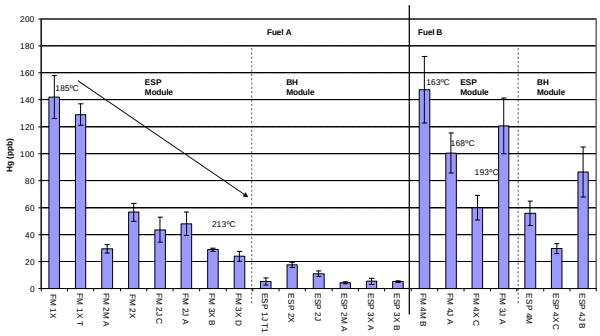

Figure 1. Mercury content in fly-ash collected in ESP and BH modules of the hybrid filter.

This work was supported by Ministerio de Medio Ambiente y Medio Rural y Marino of Spain under grant 220/PC08.

References

Kolluri, R. (1994) *Hazardous Waste & Hazardous Materials* 11 (1), 145-156

Sanz, D. (2009) *3rd International Congress on Energy and Environment Engineering and Management.* Portalegre, Portugal

Stanmore, B.R. (2004) *Combustion and Flame* 136, 398–427

Aerosol mass spectrometer measurements on wood combustion experiments

A. Kortelainen[1], J. Joutsensaari[1], A. Jaatinen[1], P. Miettinen[1], L. Hao[1], D. R. Worsnop[1,3,4] J. Jokiniemi[2] and A. Laaksonen[1,3]
[1]Department of Applied Physics, University of Eastern Finland, Kuopio, 70211, Finland
[2]Department of Environmental Science, University of Eastern Finland, Kuopio, 70211, Finland
[3]Finnish Meteorological Institute, Climate Change, Helsinki, 00101, Finland
[4]Aerodyne Research Inc., Billerica, MA, 01821, USA
Keywords: aerosol mass spectrometer, organics, combustion, PMF.
Presenting author email: aki-matti.kortelainen@uef.fi

Residential wood combustion is producing heat and high amounts of gaseous and particulate aerosol into atmosphere. The usual products, ash, carbon and alkali metals (Tissari, 2009), cause known climate and health effects, and therefore the evolution of combustion reactions need to be understood thoroughly. In many recent studies, the chemical composition of particulate emissions from residential wood combustion has been analyzed using filter samples. However, these methods don't share temporal information on aerosol chemical composition. This study aims to fill the gap in knowledge of real-time tracking of aerosol particles chemical composition in different combustion situations.

The experiments were performed by burning wood chips and controlling the air conditions in a grate fired burner (40 kW), and measuring the emission products with dilution ratio ranging approximately from 600 to 1000 depending on the emission yield. The experiments were distributed into efficient, medium and poor combustion conditions according to the emission rates of CO (low, elevated and high, respectively). Real-time size-dependent chemical composition of aerosol particles was measured by Aerodyne HR-TOF-AMS (High Resolution Time-Of-Flight Aerosol Mass Spectrometer) using 600°C vapourizer temperature.

Aerosol mass spectrometer found nitrate, chloride, sulphate, polycyclic aromatic hydrocarbons (PAH) and organics, which were divided into smaller subgroups by positive matrix factorization (PMF) (Ulbrich, 2009). Organics were split into formerly reported factors HOA (Hydrocarbon-like Organic Aerosol) and OOA (Oxygenated Organic Aerosol) and new factors named "Aromatics" and "Benzene". The proportion of each chemical compounds are presented in table 1.

Table 1. Relative abundance of the chemical compounds for combustion experiments.

Compound	Med. Combustion (%)	Poor combustion (%)
HOA	43	8
OOA	15	6
Aromatics	0	24
Benzene	12	26
PAH	0	31
SO_4	23	0
Chl	7	5

HOA had highest peaks C_2H_3O, C_4H_7, C_4H_9 and showed notable hydrocarbon series (i. e. $C_nH_{2n\pm1}$) with O/C ratio 0.1. OOA had high peaks of CO and CO2 and O/C ratio 0.75. Benzene had remarkably high contribution of C_6H_5 and $C_5H_3NO_4$ and O/C ratio 0.19. C_6H_5 was thought to be originating from the particles produced from the split of aromatic hydrocarbons contained aromatic ring retaining products. Aromatics had high contribution in hydrocarbon series of $C_{n+5}H_{n+1}$,n = 1,..,4 and O/C ratio 0.23. Aromatics had good correlation with PAH compounds in poor combustion as shown in figure 1.

Particles were not detectable in AMS at efficient combustion conditions due to their small size and low mass concentration. In medium combustion conditions main constituents were HOA, SO_4, OOA, Benzene and Chl whereas in poor combustion there were also PAH and Aromatics present simultaneously with constantly occuring CO/NO_X plumes. In the case of Poor combustion, no SO_4 was detected, but small amounts of nitrate (mainly NO fragment) were found. No ammonium was detected, hence we conclude that NO was originated mainly from organics.

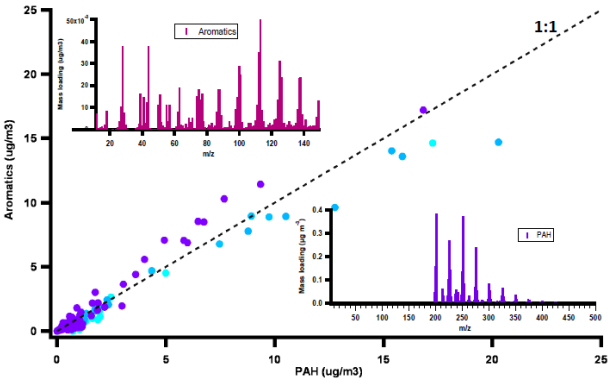

Figure 1. Aromatics vs. PAH, 1:1 line and mass spectra of the compounds.

The financial support by the Academy of Finland Centre of Excellence program (project no 1118615) and ERA-NET Bioenergy BioHealth project is gratefully acknowledged.

Tissari, J. Atmospheric Environment, 42, 7862-7873, 2009.
Ulbrich, I.M. Atmospheric Chemistry and Physics , 9(9), 2891-2918, 2009.

Effect of improved combustion technology on emissions in hybrid masonry heater from combustion of pellets and wood logs

A. Virén[1], H. Lamberg[1], T. Kaivosoja[1], O. Sippula[1], J. Tissari[1], J. Jokiniemi[1,2]

[1] University of Eastern Finland, Department of environmental science, Fine Particle and Aerosol Technology Laboratory, P.O. Box 1627, FI-70211 Kuopio, Finland
[2]VTT Technical Research Centre of Finland, P.O. Box 1000, 02044 VTT, Finland
Keywords: Wood combustion, combustion aerosols, emissions, abatement strategies, PM
Presenting author email: annika.viren@uef.fi

Batch-wise fired appliances that use pellets as fuel may provide an option to significantly decrease emissions from small-scale combustion of wood. In these appliances a single batch of pellets is burned for heating the appliance. In this study a hybrid masonry heater was used where the grate used for combustion of wood logs could be replaced with a specially designed pellet burner.

Previously, measurements were made with a hybrid masonry heater, where air staging was used only in pellet combustion, and in wood log combustion air was lead only from below the grate. After that, some improvements were made. Additional wall material was applied to the combustion chamber. This material was used to reflect part of the thermal radiation, and keep the combustion chamber temperature higher. Secondary air inlets were placed to the back wall of the combustion chamber to be used in (advanced) wood log combustion. In pellet combustion the tertiary air inlets were more efficiently directed towards the flame in order to achieve better mixing.

Three different measurements were made with the improved heater. In conventional wood log combustion there was no air staging, but good operational practices were followed (i.a. amount of fuel, ignition from top). In advanced wood log combustion the secondary air was used. In addition the primary air was reduced so that the combustion was operated mainly with secondary air. The pellet combustion was operated similarly as before. The measurements were compared to those made before the improvements (wood log and pellet).

Comprehensive measurement equipment was used. Gaseous compounds CO, CO_2 and O_2 were measured straight from the stack with FTIR, and OGC with FID. The sample gas was diluted with porous tube diluter and ejector diluter for the collection of PM_1 and particle mass size distribution (DLPI) samples. PM_1 samples were collected separately from ignition, steady firing and burn out phases and the mass size distribution sample from the total combustion in the pellet combustions. In wood log combustions the samples were collected from 1 to 2 batches. The organic (OC) and elemental carbon (EC) contents were analyzed from PM_1. Time-weighted average values $PM_{1,ave}$, were calculated for total combustion from the samples of different combustion phases. The flue gas was further diluted with another ejector diluter for online measurement of particle number size distribution (ELPI and FMPS), total particle number (CPC) and mass (TEOM) concentrations. In addition, the combustion air flow rates were measured from air supply ducts separately for primary air and combined for secondary and tertiary air.

In pellet combustion the PM_1 emission in ignition phase was previously rather high. With the improvements the emission in ignition was 3.6-fold lower. In the whole combustion cycle the PM_1 emissions was 3-fold lower. CO emission was nearly 2-fold lower than before the improvements, but OGC emission had increased by ~40%, being still below 14 mg/MJ. The PM_1 emission was found to be as low as 2.3 mg/MJ during the steady firing of the combustion.

The improvements in wood log combustion without air staging lead to a decrease in CO emission (nearly 4-fold lower) and in OGC emission (6-fold lower) compared to the combustion before the improvements. However, the PM_1 emission during the whole combustion cycle was nearly the same. It was noticed that in the previous measurements the PM_1 emission in the 1st batch was lower than in the 2nd batch, whereas in the current measurements the PM_1 emission decreased towards the subsequent batches.

With the air staging in wood log combustion CO and OGC emissions were 3-fold and 2-fold lower, respectively, compared to measurements before the improvements. However, the PM_1 emission in the whole combustion cycle was actually about 30% larger. The gasification rate of the fuel was most likely too high for the combustion air flow capacity. The combustions improved towards the end of the cycle but the emissions were still larger than without the air staging.

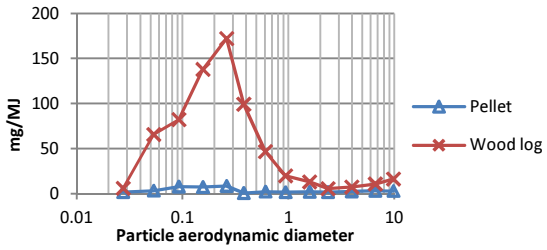

Figure 1. Mass size distributions in current study. Wood log combustion without air staging.

The authors thank Warma-Uunit Ltd. This work was supported by the Finnish Funding Agency for Technology and Innovation (TEKES) and University of Eastern Finland (strategic funding, SUBI).

Effective density of particles emitted from different biomass combustion conditions

J. Leskinen[1], A. Virén[1], H. Lamberg[1], T. Kaivosoja[1], T. Kettunen[1], I. Nuutinen[1], T. Torvela[1], O. Sippula[1], J. Tissari[1], J. Jokiniemi[1,2]

[1]Univ. of Eastern Finland, Department of Environmental Science, P.O. Box 1627, FI-70211 Kuopio, Finland.
[2]VTT Technical Research Centre of Finland, P.O. Box 1000, FI-02044 VTT, Espoo, Finland
Keywords: biomass burning, particle characterization, density measurement
Presenting author email: jani.leskinen@uef.fi

The properties of emitted particles from biomass combustion strongly depend on combustion conditions. When describing particle behaviour in human lungs (deposition), density is a key feature. Density is also a link between mobility size and aerodynamic size, and it is therefore important parameter for aerosol instruments.

In this study a novel fully logic operated and adjustable biomass combustion reactor (40 kW) was utilised to create different combustion conditions. These conditions were called efficient, erratic and poor combustion. They were achieved by adjusting fuel feeding and primary and secondary air flows. Fuel used was wood chips. The efficient case (~10 mg/MJ of CO) corresponds to optimal biomass combustion and the poor case (~2100 mg/MJ of CO) approaches conventional batch combustion. Whereas, the erratic case (~260 mg/MJ of CO) represents continuous biomass combustion with unideal burner settings.

The aerosol was diluted with porous tube diluter and two ejector diluters in series. Aerosol for collection samples was taken after the first ejector (DR ~ 25-50) and online instruments took sample after the second ejector (DR ~ 600-1000).

The effective density of (single) particles was measured using DMA (TSI), APM (Kanomax) and CPC (TSI) in series. According to demanded DMA (mobility size) and APM (single particle mass) operational parameters, only particles with certain effective density will penetrate them to CPC and will be counted. In order to cover the wanted range of particle densities and sizes, the parameters of the DMA (voltage) and APM (voltage and rotational speed) are varied [McMurry 2002].

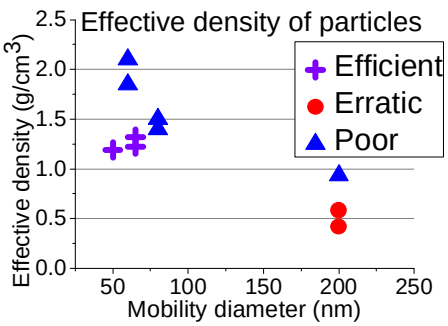

Figure 1. Preliminary results of the effective density of particles from different biomass combustion conditions.

Particle emissions from each combustion case were also characterised using ELPI (Dekati), SMPS (TSI) and TEOM (Thermo Scientific). In addition, OC, EC and ash contents of particle matter were analysed. Moreover gaseous emissions were measured using FTIR (Gasmet) and separate gas analysers (ABB).

Table 1. Typical averaged emission parameters.

Parameter	Efficient	Erratic	Poor
Mass Emission (mg/MJ)	10	180	300
GMD (ELPI, nm)	60	100	110
OGC (mg/MJ)	4	7	100
OC (mg/MJ)	0.2	41	49
EC (mg/MJ)	0.05	48	116
Ash (mg/MJ)	4	5	4

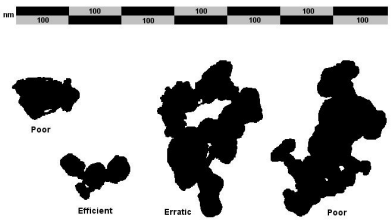

Figure 2. TEM-images (binary projection) of typical particles in each combustion cases from analysed size classes.

The effective density varied depending on the combustion conditions (Fig. 1). Generally speaking, density decreases as particle size increases. The small particles in the efficient case were mostly ash ($\rho_{bulk} \approx 2.7$ g/cm^3) which were quite loosely attached material (Fig 2). In the poor case the small particles (~ 60nm) seemed to be mainly elementary carbon (84 % of PM_1, $\rho_{bulk} \approx 2$ g/cm^3) and organic material and were more spherical in shape. Therefore these particles in the efficient case were less dense than in the poor case. With larger particles (~ 200 nm), poor conditions produced more organic matter than the erratic conditions. The organic matter is assumed to condense on the surface of the particles, which decreases the porosity of the particle and increases the effective density.

This study has been funded by Finish Institute for Technology and Innovation (TEKES, Eranet-Bio-energy programme), University of Eastern Finland (strategic funding, SUBI).

McMurry, P.H., X. Wang, K. Park, K. Ehara (2002). Aerosol Sci. Technol 36:227-238.

Zinc enrichment in ultrafine particles formed in biomass combustion

T. Torvela[1], T. Kaivosoja[1], O. Sippula[1], A. Virén[1], J. Leskinen[1], T. Kettunen[1], I. Nuutinen[1], H. Lamberg[1], J. Tissari[1], J. Jokiniemi[1,2]

[1]Department of Environmental Science, Univ. of Eastern Finland, P.O. Box 1627, FI-70211 Kuopio, Finland
[2]VTT Technical Research Centre of Finland, P.O. Box 1000, FI-02044 VTT, Espoo, Finland
Keywords: Biomass burning, Electron microscopy, Zinc, Combustion particles
Presenting author email: Tiina.Torvela@uef.fi

The link-up between chemical contents and morphology of particles formed in biomass combustion is an important issue yet still unclear. Description of single particle morphology types has been mostly qualitative, and the results can not usually be generalized. A semi-quantitative method using Energy Dispersive Spectroscopy (EDS) analysis with Transmission Electron Microscopy (TEM) analysis was evaluated. The applicability of the method in resolving chemical features of a certain morphology treated as group was of interest. The results suggest zinc enrichment in ultrafine particles of ash type morphology.

TEM-EDS analysis was carried out to interconnect chemical composition with typical soot and ash morphologies found in fine particles formed in biomass combustion. The combustion conditions were varied between efficient, erratic and poor, resulting in variation in organic carbon, elemental carbon and inorganic contents of PM_1. Chemical composition was determined with EDS both for 80-100 nm ultrafine size class (UFC) and for particles of non-classified sample (NCS). The UFC classification size was selected from the site where the number size distributions of the three setups overlapped. Analysis results were compared with ICP-MS analyses of PM_1 and SEM-EDS analyses on impactor samples having aerodynamic cut diameters in range of 30 nm to 10 µm.

TEM-EDS spectra were acquired in STEM mode using a spherical disk point selection tool. Constant emission current, magnification and signal collection times were used. Approximately 60-120 element spectra were acquired. Average of 8-10 background spectra were subtracted from the single particle spectra before the elemental mole fractions were quantified. The weighted averages of mole fractions were calculated for most abundant elements, K, S, O, C, Cl and Zn, using a parameter including disk area and acquisition parameters as weight. From previous studies it was known that large carbon content was indicative for soot morphology recognizable by eye from TEM samples. Therefore the results were recalculated using observed carbon mole fraction to make subclasses with soot and ash type morphologies, seen in TEM micrographs.

Table 1 shows average mole fractions of common elements showing differences both between the three combustion cases and between UFC and NCS.

From the results it can be concluded that there is a chemical link between morphological features seen in single particle TEM. The analyzed samples had high variation in carbon mole fraction. Subclasses of particle morphologies could therefore be described using carbon intensity as tool.

In addition it was concluded from the results that zinc was enriched in ultrafine particles, supporting previous studies. Moreover, efficient combustion of biomass seems to enrich zinc more than erratic and poor combustion as the particles of the same size class are compared. As shown in Fig. 1 this was observed in UFC particles. The feature was not observed in NCS, as well as was not in the bulk ICP-MS analysis. Instead the TEM analyses support the current findings.

As for conclusions more knowledge on particle characteristics was gained using this method on the side of bulk analyses. As for all quantitative analysis the more particles are analyzed the better would be the precision. However some qualitative selection has to be made to distinguish separate morphologies. With this condition the method can be utilized for describing variation in morphological features in biomass combustion origin fine particles.

Table 1. Average mole fractions of common elements before division to subclasses.

mol-%	Eff NCS	Err NCS	Poor NCS	Eff UFC	Err UFC	Poor UFC
Zn	4	8	0.4	34	10	2
K	26	23	2	38	71	5
O	36	30	5	30	15	7
S	5	2	0.2	5	4	0.3
C	19	32	84	11	1	85
gmd*	33	110	220	100	80	100

* electrical mobility geometric mean diameter, nm

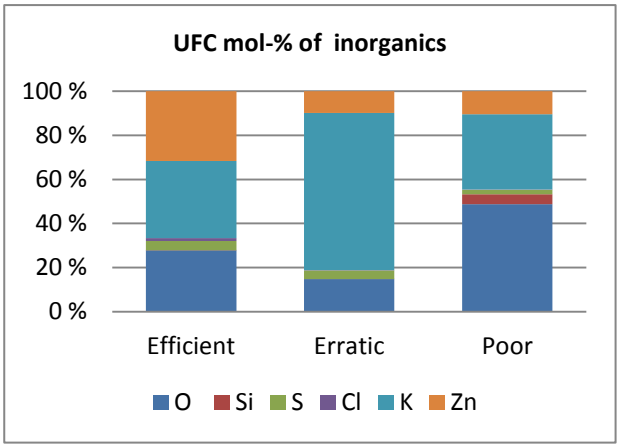

Figure 1. Comparison of inorganic element abundance in narrow ultra fine particle size class, between three combustion cases.

Particle formation during combustion of solid recovered fuels in a grate system

W. Baumann, H. Mätzing, H.-J. Gehrmann, M. Hauser, P. Nowak, H.-R. Paur and H. Seifert

Institute of Technical Chemistry (ITC), Karlsruhe Institute of Technology (KIT)
Hermann-von-Helmholtz-Platz 1, 76344 Eggenstein-Leopoldshafen, Germany
Keywords: Combustion aerosol, fine particle measurement, characterization of combustion aerosol, comparison of particle measurement methods
Presenting author email: w.baumann@kit.edu

Use of biomass materials and bio-waste in existing power and combined heat and power plants is widely recognized as an important means to meet internationally agreed green-house gas emissions reduction targets. According to CEN/TC 343 the input waste for SRF-production can be product specific waste, municipal solid waste, industrial waste, commercial waste, construction and demolition waste, sewage sludge etc. SRF can be used for electricity production and combined heat and power usage. Different technologies such as circulating and bubbling fluidised beds or continuous grate firings meeting best available techniques standards are used to demonstrate the highly efficient co-utilisation of low quality biomass together with SRF.

Present R&D activities at KIT are focused on studying combustion behaviour in continuous grate systems. In May 2011, a number of tests in the 500 kW pilot scale grate system, TAMARA, were performed to evaluate slagging, corrosion risk, forming of particles, emissions and assessment of ash utilization. Three fuels were fired: wood chips and two SRF's with high amounts of biomass (wood).

In this study, we report about our investigations on particle concentration, size distribution and chemical characterization of aerosol as a function of different solid fuel mixture. Particle samples were taken between the boiler and the bag filter. The particle concentrations were measured gravimetrically according to VDI 2066 with 50 mm plain filter. In addition to the gravimetric measurements, the size distribution was measured with a cascade impactor (Anderson Mark III impactor with 7 stages). The Anderson impactor was operated under isokinetic sampling conditions with a flow rate of 15 lpm. Under this operation conditions the size range of the impactor is from 0.4 to 20 µm.

From earlier investigation at TAMARA incineration plant, it is known that the unit has a good burnout and therefore the fly ash size distribution would be in the submicron range. The size distribution of the fly ash behind the boiler was measured with a scanning mobility analyser and an optical particle counter. Both of these online analyzers need a sample dilution if the particle concentration in the flue gas is too high.

Figure 1 shows the gravimetrically measured particle mass concentration in flue gas for different fuels. Wood chips, as reference material, has a mass concentration less than 100 mg/m³ and the solid recovered fuels having concentration 260 and 350 mg/m³, respectively.

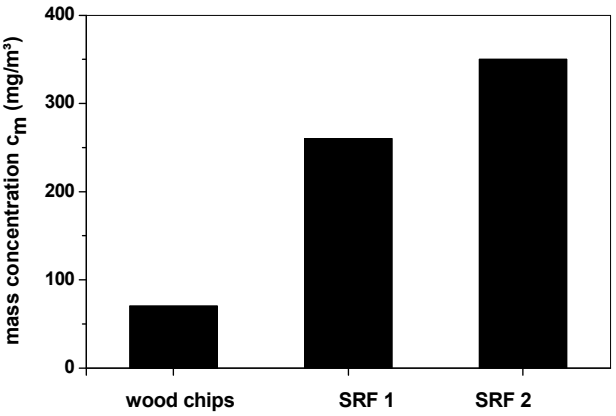

Figure 1. Particle mass concentration for different fuels

Figure 2 shows the size distribution of the fly ash from wood chips and the solid recovered fuels. The left part of the distributions is measured with the SMPS and the right part with the Anderson impactor. The impactor measures the mass distribution and the mobility analyser measures the number distribution. For data representation, the SMPS data were converted into the mass distribution (dm/dlog d_P). The size distribution of the fly ash for wood chips and solid recovered fuels showed nearly the same mean diameter in the range of 200 nm and therefore the burnout of all fuels was well.

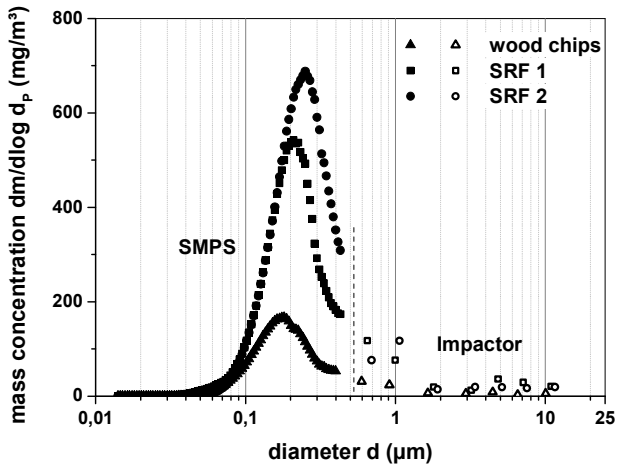

Figure 2. Particle size distribution of the fly ash

Particulate emissions from the co-combustion of forest biomass waste and sewage sludge in a bubbling fluidised bed

A.I. Calvo[1], L.A.C. Tarelho[1], E.R. Teixeira[1], T. Nunes[1], C. Alves[1], M. Duarte[1], E. Coz[2], A. Castro[3], B. Artiñano[2], R. Fraile[3]

[1]Centre for Environmental and Marine Studies (CESAM), Department of Environment and Planning, University of Aveiro, Aveiro, 3810-193, Portugal
[2]Centre for Energy, Environment and Technology Research (CIEMAT), Madrid, Spain
[3]Department of Physics, IMARENAB University of León, 24071 León, Spain
Keywords: aerosols, biomass waste, co-combustion, fluidised bed, sewage sludge
Presenting author email: anacalvo@ua.pt

Nowadays, the development of technologies/strategies able to produce energy in an efficient and environmental friendly way constitutes an important challenge and an unquestionable necessity. The use of biomass is taken an increasing interest regarding industrial heat and power production. Valorisation of industrial wastes constitutes a sustainable alternative in terms of safely manage industry wastes. In this way, co-combustion, i.e. the simultaneous combustion of two or more fuels in the same plant for energy production, constitutes a promising choice. Among the different alternatives available for co-combustion, fluidised bed combustion is one of the most advantageous methods due to its flexibility and parameter control (Leckner et al., 2004).

Some industries, such as the pulp and paper industries, can valorise both, the sewage sludge produced and the forest biomass waste generated during the activity. Co-combustion of these two waste products in fluidised bed offers a feasible alternative to manage these residues and, at the same time, generate income through energy recovery. However, special attention must be paid to operating and environmental problems associated with this process. Thus, focusing on air quality, particles and gases emissions acquire an important relevance when sewage sludge is used as an additional fuel (Leckner et al., 2004; Shao et al., 2008).

In this study, particulate emissions from the co-combustion of forest biomass residues with sewage sludge from a pulp and paper mill industry were studied. The combustion experiments were conducted in a pilot-scale bubbling fluidised bed combustor (BFBC) (Tarelho et al., 2011). The bed was operated with silica sand. Forest biomass residues resulting from eucalyptus felling for the cellulose industry were air dried, chopped and sieved in order to obtain particles in the size range of 1-5 mm. Sewage sludge was air dried and also sieving for the same particle range size. The final fuel was constituted by 40% of sewage sludge and 60% of forest biomass residues The combustion flue gas from the BFBC passes through a cyclone separator in order to minimise particle emissions to the atmosphere.

Particle sampling was carried out at the exhaust duct, before and after the cyclone separator with the reactor operating at steady state conditions. Fine particles ($PM_{2.5}$) were collected onto quartz filters using a low volume sampler. Carbonate fraction was determined by sample acidification with phosphoric acid. Organic and elemental carbon were determined by a thermal-optical transmission technique after removing carbonate fraction by exposing the filters to HCl vapour and then removing the HCl excess from the sample with NaOH. Ion chromatography was used for determining water-soluble inorganic ions.

Furthermore, before the cyclone, particles were analysed by using a laser spectrometer in order to determine aerosol size distributions between 0.1 and 10 µm. Morphology and elemental composition of individual aerosol particles onto polycarbonate filters (0.2 µm pore size) were investigated by Field Emission Scanning Electron Microscopy (FE-SEM).

An important fraction of particulate matter emitted is constituted by carbonates. This fact was confirmed by FE-SEM that showed that filters were loaded of crystallised submicrometric mineral particles. The analyses revealed a dominance of calcium products, mainly carbonates and oxides containing less than 5 wt % Mg, and sodium/potassium chlorides, calcium sulphates, and silicates in a lesser extent. The presence of needle-fibre elongated crystals was remarkable since non biogenic micro-rods are rare and it might have direct implications on lung disease.

The role of a cyclone on decreasing particle emissions to the atmosphere was evaluated.

An appropriate understanding of the emissions from biomass waste and sewage sludge combustion in fluidised beds is needed in order to establish proper control of combustion conditions and minimise the operational problems and environmental impacts.

This work was supported by Portuguese Science Foundation (FCT) through the projects PTDC/AAC-AMB/098112/2008 and PTDC/AMB/65706/2006 (BIOEMI). The electron microscopy was conducted at CNME-UCM through the AEROCLIMA project (Fundación Ramón Areces). Ana I. Calvo acknowledges the posdoc grant SFRH/BPD/64810/2009 from FCT.

Leckner, B., Amand, L.E., Lücke K., Werther J. (2004). *Fuel* **83**, 477-486.

Shao J., Yan R., Chen H., Yang H., Lee D.H., Liang D.T. (2008). *Energy Fuels* **22**, 2278–2283.

Tarelho, L.A.C., Neves, D.S.F., Matos, M.A.A. (2011). *Biomass Bioenergy* **35**, 1511-1523.

Ignition and combustion of coal dusts with different fuel mass concentrations

S.G. Orlovskaya, V.V. Kalinchak and O.N. Zuy
Department of Physics, Odessa National I.I. Mechnikov's University, Odessa, 65082, Ukraine
Keywords: heat and mass transfer, combustion particles, concentration, temperature.
Presenting author email: svetor@rambler.ru

Coal clean combustion remains a challenge. It is well known that reactions in pores affect significantly the combustion characteristics of coal particles, but this effect is not enough investigated in case of coal dusts.

The coal dusts ignition, burning and extinction processes are studied numerically with special attention to the reactions in pores. The effect of coal particles mass concentration on dust ignition characteristics is analyzed in details with account of porosity because the natural coals are usually porous (Pomerantsev, 1973).

The fuel mass concentration in dust depends on the particles countable concentration and mean particle diameter according to the next expression:

$$C_m = \frac{1}{6}\pi d^3 \rho C_N .$$

So the mass concentration (C_m) could be changed by varying the particles diameter (d) or particles concentration (C_N). The rate of heat transfer between the particle and surrounding medium as well as chemical heat release density depend strongly on the particle diameter (Kalinchak, 2005). In case of high concentration of small particles the total surface increases dramatically.

The simulation results of dust ignition delay time (t_{ind}) versus fuel mass concentration are presented in Figure. The curve 1 corresponds to specified value of the countable concentration C_N: the mass concentration increase is caused by the particle diameter growth. The curves 2 and 3 describe the ignition delay time dependence on the mass concentration $t_{ind}(C_m)$ for fixed particles diameters and increasing the particles concentrations.

It is shown that in the first case the dependence $t_{ind}(C_m)$ has a local minimum due to minimization of heat losses at some value of the particles diameter. Besides it is demonstrated that ignition delay times of coarse dusts are five times greater than those of fine dusts at the same values of fuel mass densities (when $C_m \geq 0.1$ kg/m^3).

The particles initial diameters range which corresponds to full fuel burnout is defined. It is shown that due to reactions in pores this range could be increased twofold.

In case of porous coal particles dusts the full burnout occurs in the range of air to fuel ratio is $3.5 < \eta < 1$, while for solid carbon particles dusts the corresponding range is $2 < \eta < 1.3$.

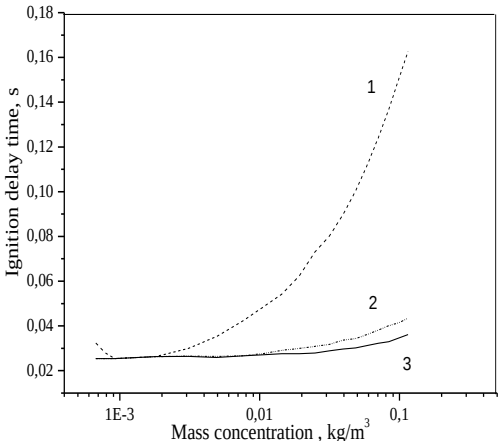

Figure 1. The ignition delay time of porous coal dusts versus mass fuel concentration at gas T_g =1300 K. 1 – C_N =1.9·10^{7}m^{-3}, 2 - d_b =50mcm, 3- d_b =40 mcm.

It is found that reactions in pores lead to significant decrease of ignition delay time and the critical diameter of particle ignition (when $d \leq d_{cr}$ the particle can't ignite).

It is determined that ignition delay time (t_{ind}) of porous particles is notably less then that of solid particles (Table 1), at the same time critical diameter of particles extinction (d_E) is twofold less.

Table 1. Combustion characteristics of porous (a) and solid (b) particles, d_b =100 mcm, T_g =1300 K, C_m =0.044 kg/m^3.

Characteristics	t_{ind}, msec	d_E, mcm	T_{bur}, K	t_{bur}, msec
a)	54	6	2282	244
b)	250	13	2265	264

The burning temperature (T_{bur}) and burning time (t_{bur}) are determined mainly by oxygen concentration at the particle surface, so depend slightly on particle porosity.

Pomerantsev V.V. (1973) *Basics of practical combustion theory, Energy. Leningrad.*
Kalinchak V.V., Zuy O.N., Orlovskaya S.G. (2005) *Teplofiz. Vys.Temp.[High Temp]*, **43** (5), 780 – 788.

Reduction of particulate matters emitted from a diesel-generator fuelled by waste-edible-oil biodiesel with acetone and isopropyl alcohol addition

J.H. Tsai[1], S.J. Chen[1,*], K.L. Huang[1], C.C. Lin[1] and W.Y. Lin[2]

[1]Department of Environmental Science and Engineering, National Pingtung University of Science and Technology, Pingtung County, Nei Pu, 91201, Taiwan
[2]Institute of Environmental Engineering and Management, National Taipei University of Technology, Taipei City, 10608, Taiwan

Keywords: waste-edible-oil biodiesel, acetone, isopropyl alcohol, diesel-generator.
Presenting author email: chensj@mail.npust.edu.tw

Because of the concerns of high international oil price and crude oil reserve depletion, increasing interest has been paid to the research and development of alternative energies. Biodiesels have received increasing attention as alternative fuels for diesel engines and generators. Many studies have shown that the use of biodiesel as an alternative fuel in diesel engines may improve combustion efficiency and reduce the emissions of carbon monoxide (CO), hydrocarbons (HC), particulate matter (PM), and polycyclic aromatic hydrocarbons (PAHs) (Subramanian *et al.*, 2004; Lin *et al.*, 2006; Tsai et al., 2011).

Acetone and isopropyl alcohol, two major industrial waste solvents (Lin and Wang, 2004), are widely used as cleaning and washing agents in electric and precision machineries. For a new generation semiconductor plant, over one thousand tons of isopropyl alcohol and acetone per year are consumed and then treated as waste after use. Recycling waste-edible-oil, isopropyl alcohol, and acetone as an alternative diesel fuel would reduce such environmental burden.

In this study, new blended fuels were prepared by adding 1–3 vol% of dehydrated acetone (A) and 1, 2, 3, 5, and 10 vol% of waste-edible-oil biodiesel (W) into a regular diesel (86–97 vol%) and using 1 vol% of isopropyl alcohol (P) as stabilizers. An auto-detector flow sampling system equipped with quartz fiber filters (with diameters of 47 mm) was installed downstream of the diesel-engine generator exhaust to determine suspended particles.

The preliminary results showed that using the tested biodieselhols (blends of isopropyl alcohols, acetones, and esterificated waste-edible-oils) fuels could reduce the PM emission concentration (6.97–30.6% reduction, average = 19.5%), compared to D100 (Figure 1). In particular, using 3 vol% acetone as a biodieselhol fuel in the diesel-generator had the highest reduction of PM emission (by an average of 27.5%), regardless of the ratio of waste-edible-oil-based biodiesel to premium diesel fuel. This phenomenon is similar to those reported by several researches that adding oxygenated additives into diesel fuels, such as ethanol or acetone, increased fuel oxygen content resulting in the improvement of fuel combustion reaction, and thus reduced PM emissions (Lin *et al.*, 2010; Lin *et al.*, 2012).

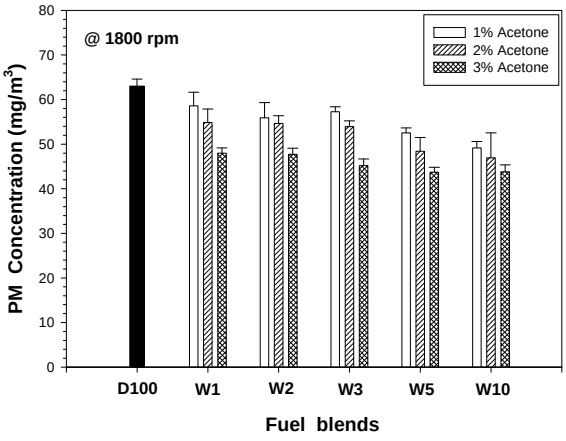

Figure 1. Concentrations of PM emitted from the diesel-engine generator fuelled by waste-edible-oil biodiesel with acetone and isopropyl alcohol addition.

Lin, S.H. and Wang, C.S. (2004) *J. Hazard. Mater.* **106**, 161–168.
Lin, S.L, Lee, W.J., Lee, C.F. and Chen, S.J. (2010) *Energy Fuels* **24**, 4522–4533.
Lin, S.L, Lee, W.J., Lee, C.F. and Wu, Y.P. (2012) *Fuel* **93**, 364–372.
Lin, Y.C., Lee, W.J., Wu, T.S. and Wang, C.T. (2006) *Fuel*, 85, 2516–2523.
Subramanian, M., Malhortra, R.K., and Kanal, P.C. (2004) *SAE Technical Paper*, No. 2004-28-0088.
Tsai, J.H., Chen, S.J., Huang, K.L., Lin, Y.C., Lee, W.J., Lin, C.C. and Lin, W.Y. (2010) *J. Hazard. Mater.* **179**, 237–243.

Study of paraffin droplets evaporation and burning

S.G. Orlovskaya, M.S. Shkoropado, F.F. Karimova

Department of Physics, Odessa National I.I. Mechnikov's University, Odessa, 65082, Ukraine
Keywords: n-alkanes, droplets, vapour, diffusion.
Presenting author email: svetor@rambler.ru

Investigations of droplets combustion are of great concern due to promising prospects of hybrid paraffin (n-alkanes) based propellants. The ground testing at Stanford University demonstrated that such fuel exhibits high regression rate and provides sufficiently high specific impulse Santos *et al* (2006). In addition paraffin based propellants are eco-friendly and safe in exploitation. High efficiency of paraffin-based propellants is explained by peculiarities of heat and mass transfer in combustion chamber. The charge surface melts under heat flux from reaction zone. High speed oxidizer flow pulverized melted paraffin and entrains the droplets, which ignite and burn quickly. So to model combustion process we have to know burning characteristics of single droplet.

To study kinetics of droplet evaporation and burning we use video microscopy and digital image analysis techniques. A paraffin droplet (n-Docosane or n-Octadecane) is suspended on tungsten filament loop. The droplet evaporation and burning are recorded on personal computer via two cameras: diameter decrease is recorded through microscope (x16) and the flame height is registered by another camera.

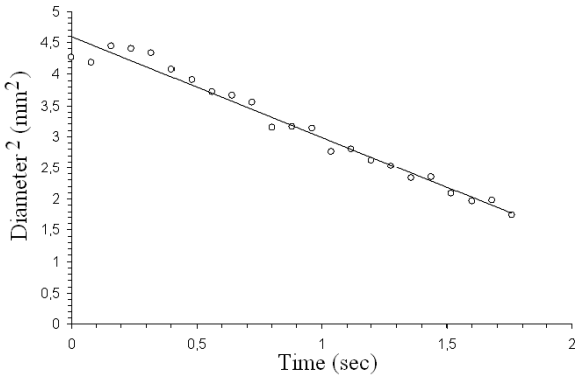

Figure 1. The history of n-Docosane droplet diameter squared.

At Figure 1 the square of the burning droplet diameter versus time (t_{bur}) is presented. The curve is close to linear one, so the d^2 law is true and the burning rate is limited by diffusion. The burning rate constant (K_{bur}) is calculated as tangent of the line inclination angle $d^2 = f(t)$ (Table 1).

Evaporation of n-Docosane and n-Octadecane droplets was studied in air at different temperatures.

Table 1. Burning characteristics of n-Docosane droplet.

Initial diameter (mm)	t_{bur}, s	K_{bur}, mm^2/s
1.87	1.36	0.013
1.99	1.52	0.016
2.04	1.84	0.016

The Sreznevsky law being applied, so the evaporation constants (K_{ev}) are defined as mentioned above. In Fig.2 the calculated values of K_{ev} versus air temperature (T) are presented.

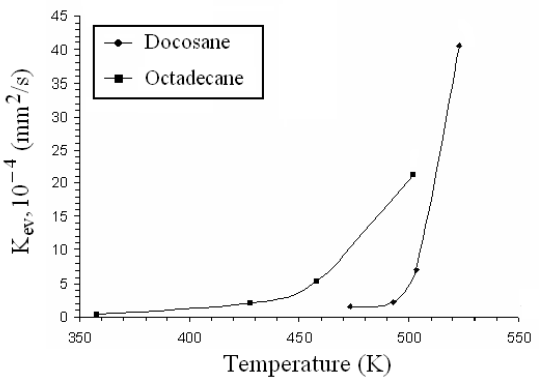

Figure 2. The temperature dependencies of the evaporation constants.

One can see that n-Octadecane evaporation coefficient increases significantly when the air temperature exceeds 450 K and in case of n-Docosane it rises abruptly above 500 K. These curves corresponds to Arrhenius dependence so we can estimate the evaporation heat by plotting $\ln(K_{ev})$ versus T^{-1}. In so way we obtain for n-Docosane value 91.7 kJ/mole, which is close to data of Chickos *et al* (1997) for the temperatures above 400 K.

The diffusion coefficient (D_c) of n-Docosane vapor in air at elevated temperature is estimated with account of natural convection (Table 2).

Table 2. Diffusion coefficients of n-Docosane vapor in air.

T, K	K_{ev}, 10^{-4} mm^2/s	D_c, 10^{-3} mm^2/s
493	2.23	1.4
523	40.56	8.1

Santos L.M.C., and roth. (2006) *Therm. Eng.* **53,** 8-12.
Chickos J.S. and Wilson J.A. (1997) *J. Chem. Eng. Data* **42**, 190-197.

Testing performance of fume hood in chemical laboratory

T. Jankowski
Department of Chemical, Aerosol and Biological Hazards, Central Institute for Labour Protection – National Research Institute, 00-701 Warsaw, Poland
Keywords: trace gases, fume hood, dust removal, ventilation system, ANSI/ASHRAE 110 test

The performance of a laboratory fume hood in providing protection for the worker at the face of the hood is strongly influenced by the aerodynamic design of the hood. It is important to study the effectiveness of the fume hood as specified in the ASHRAE 110-1995.

The CIOP-PIB studies are carried out flow visualization test, face velocity test and tracer gas containment test of the laboratory fume hoods. Smoke tubes and balls (Dräger, Germany) are used to map out the flow pattern which then enables us to improve on the flow dynamics generated by our fume hoods. Face velocity test was carried on using Testo 435-4 Transducer for measuring air velocity at the front of fume hood. The face velocity uniformity test evaluates the uniformity of the inflow velocity at various points across the sash opening while the final part, the SF_6 containment test, evaluates the containment efficiency. In tracer gas containment test, a manikin with clothing is used to simulate the actual human in front of the hood. A SF_6 particle detector - MIRAN SapphIRe 100E, capable of reading as low as 0.001ppm, is used in the detection of leaked SF_6 during the containment test. Detector probe is located at breathing zone of manikin to capture leakage of SF_6, simulating in actual operation the possibility of escaping fumes from the work chamber.

Figures 1, 2, 3 and 4 presents results of fume hood test in chemical laboratory.

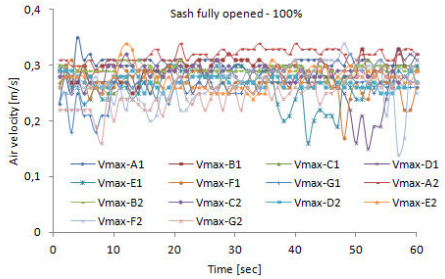

Figure 1. Air velocity distributions at sash full opening.

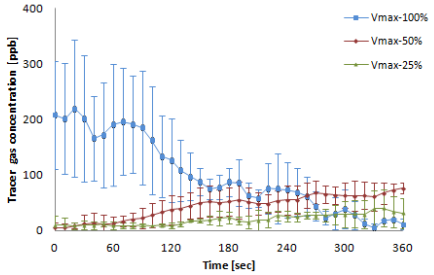

Figure 2. Distribution of SF_6 at tracer gas leak test.

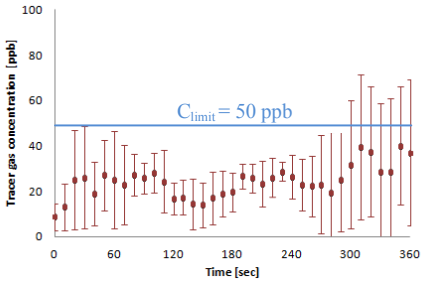

Figure 3. SF_6 distribution at face hood surface scan test.

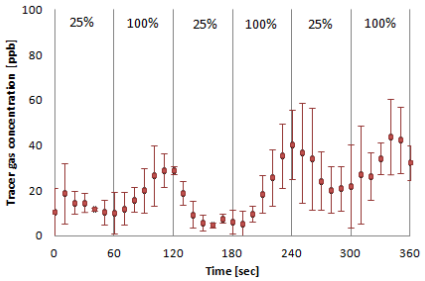

Figure 4. SF_6 distribution at sash movement effect test.

Figure 1 shows the variability of air velocity across the face of the fume hood in the range from 0.14 to 0.35 m/s. The study showed the value of air velocity dependence of the sash position, respectively: 0.28 m/s for 100%, 0.47 m/s for 50% and 0.69 m/s for 25% of the design hood opening.

According to the results shown in figure 2 only while the sash fully opened, SF_6 concentration exceed 50 ppb in the initial phase of the test (from 0 to 180 sec). As shown in figure 3 at any point during the face hood surface scan test, the SF_6 concentration does not exceed 50 ppb. In figure 4 can observe that SF_6 concentration decreased while the sash position was 25% and increased while the sash fully opened. Any surge in SF_6 levels outside the fume hood were not greater than 1000 ppb.

This paper has been prepared on the basis of the results of task 04.A.09 carried out within the National Programme “Improvement of safety and working conditions” partly supported in 2011-2013 within the scope of state services by the Ministry of Labour and Social Policy. The CIOP-PIB is the Programme's main co-ordinator.

Tseng L, Huang RF, Chen C, Chang C. (2007) *Ind. Health*, **45**, 199–208.
Standard No. ANSI/ASHRAE 110-1995.

Anthropogenic influence in bulk deposition fluxes in an urban-industrial area in the southwest of Spain

S. Castillo[1], J. de la Rosa[1], Y. González-Castanedo[1], A. Sánchez de la Campa[1], R. Fernández[1] and X. Querol[2]

[1]Unidad Asociada CSIC-Universidad de Huelva Contaminación Atmosférica, Universidad de Huelva, Spain
[2]Instituto de Diagnóstico Ambiental y estudios del Agua (IDAEA), CSIC, Barcelona, Spain
Keywords: deposition, insoluble particles, carbonaceous particles, trace elements, industrial aerosols
Presenting author email: sonia.castillo@dgeo.uhu.es

Areas close to industrial states are subject to an important influence of industrial emissions not only originating from the funnel emissions derived from the industrial processes, but also from other activities such as manipulation and transport of raw materials. The particulate matter originating from these anthropogenic activities may contribute notably in the levels and geochemistry of the deposition fluxes in these areas, and have influence on human health and in urban furniture. In 2006 was published the 151/2006 Spanish Decree to control the levels and methodology in air pollution in areas nearby to pollution zones (industrial and urban areas). This decree includes the control of the sedimentable particulate levels which establish limits of 300 mg/m^2.day.

Since 2006 a long time series of deposition sampling was performed in the city of Huelva. The sampling site (La Rábida) was located in the surrounding of the Ría de Huelva close to two important industrial states and near the harbour of the city. In 2008 were incorporated two more sampling sites, one with an urban influence in Huelva (Campus, 8km from La Rábida) and other one in Matalascañas close to the Doñana National Park with a rural influence (CIECEM, 45 km from La Rábida). The object of this sampling network was to evaluate the impact of the industrial activity in the deposition fluxes. In this work, we study and compare the deposition fluxes, both in the soluble and insoluble fractions for the bulk deposition sampled in three sites with an industrial influence in descending order.

The annual levels of bulk deposition show a decrease in the deposition levels as we move away from the industrial source. In La Rábida the deposition levels registered a mean of 21.4 g/m^2/yr, in Campus 18.6 g/m^2/yr, while in the rural area (CIECEM) registered only 10.7 g/m^2/yr (Table 1). The deposition levels registered in the urban and rural areas were normal in comparison with other sites with similar characteristic in Spain (Castillo, 2006).

Table 1. Annual deposition levels (g/m^2).

	La Rábida	Campus	CIECEM
	Industrial	Urban	Rural
Jun08-May09	25.8	22.4	9.5
Jun09-May10	18.8	15.8	8.7
Jun10-May11	19.8	17.6	14.0
mean	21.4	18.6	10.7

All the three locations present the same seasonal trend with the highest deposition levels during the summer period and lower in winter (Figure 1). In the summer, the high rate of soil resuspension due to the low precipitation levels registered during this period in the South of Europe and the most frequent African dust episodes above the Mediterranean basin caused this increase in the deposition levels in this period. Although this is the general trend, in La Rábida it was observed peaks along the year out of the general trend. These peaks show the local influence of the industrial and harbour emissions in this area.

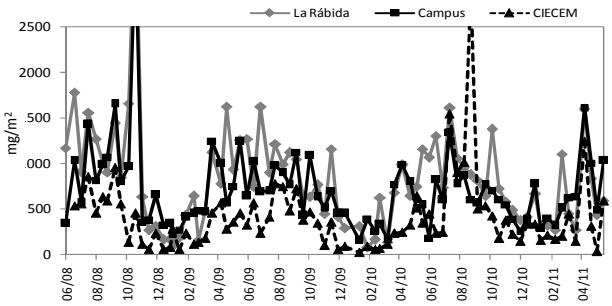

Figure 1. Seasonal trend of deposition levels (mg/m^2).

The high industrial influence was observed in the chemistry of the insoluble fraction. It´s observed that the carbonaceous species were the most elevated contributors to the total mass. This contribution was up to 15% of the total annual mass in La Rabida and less in Campus and CIECEM (11%). The levels of trace elements were notable also in La Rábida. Species such as Cu were the major contributors of trace elements (more than 50% in most cases) and minority Zn and Pb.

The meteorological analysis of the wind direction show a high correlation between the major amount of carbonaceous and trace species with three predominant wind directions, SW, NNE and minor NW, which favoured the transport of the anthropogenic emissions from the industrial states to the sampling stations.

The authors would like to express their gratitude to the Huelva Port Authority and the Environment Department of the Andalusia Government for their valuable collaboration.

Castillo S. (2006). Impacto de las masas de aire africano sobre los niveles y composición del material particulado atmosférico en Canarias y el NE de la península Ibérica. Tesis doctoral, Universitat Politècnica de Catalunya, 382pp.

Number size distribution of welding fumes

M. Manigrasso[1], C. Fanizza[1], P. Carrai[2], and P. Avino[1]
[1]INAIL ex- ISPESL, via Urbana 167, I-00184 Rome, Italy
[2]ASL2 Lucca, Dipartimento di Prevenzione, piazza Aldo Moro, I-55012, Lucca, Italy
Keywords: Combustion particles, Welding fumes, Nanoparticles, Number size distribution, FMPS.
Presenting author email: m.manigrasso@inail.it

Combustion derived nanoparticles are constantly inhaled in outdoor urban polluted atmosphere (Manigrasso and Avino, 2012) as well as in some workplace. Notably, exposure to welding fumes occurs in some occupational settings. The toxicity of welding fumes depends on both their chemical compositions and ability to penetrate and deposit deeply in the lungs. Fume chemical composition is determined by the composition of the base and of the filler metal. Its penetration and deposition in the regions of the respiratory system is mainly determined by their size. Therefore, the knowledge of the size distribution of welding fumes is a crucial information towards the estimate of the doses of toxic compounds delivered into the respiratory tract.

To this purpose particle number size distribution was continuously measured during Metal Inert Gas (MIG) welding of a mild carbon steel. Aerosol number size distributions were measured by means of a Fast Mobility Particle Sizer (model 3091, FMPS, TSI, Shoreview, MN, USA). FMPS counts and classifies particles, according to their electrical mobility, in 32 size-channels, in the range from 5.6 to 523 nm, with 1s time resolution.

Personal samples of the inhalable mass fraction of airborne particles were collected during welding with IOM personal sampler at flow rate of 2.0 L min^{-1}. Metal analysis was performed with an Inductively Couple Plasma Optical Emission Spectroscopy (ICP/OES). Metals detected in the breathing zone of the worker are reported in Table 1. It is worth noting the presence of Mn at concentration close to the ACGIH Threshold Limit Value-Time Weighted Average (TLV-TWA) of 200 µg m^{-3} (AIDII, 2011). The main target of the toxic effect of Mn and its compounds is the nervous system (Sińczuk-Walczak et al., 2001).

Figure 1 reports the temporal evolution of submicrometric particles (6-523 nm), nucleation mode particles (6-16 nm) and number Geometric Mean Diameter (GMD) before, during and after the welding operations performed without local exhaust ventilation. Before welding, nucleation mode particles represent about 7% of submicrometric particles and GMD is about 60 nm. After about 40 s from the welding start, the percent contribution of nucleation mode particles increases to 60% whereas GMD drops to about 18 nm. Total and nucleation mode particle concentrations increases from 2.1×10^4 to 2.0×10^6 and from 1.6×10^3 to 1.0×10^6, respectively. The contour plot in Figure 1 (in box) describes the temporal variation of the particle number size distribution across the peaks. It evidences the strong and fast-evolving contribution of nucleation mode particles: peak values are maintained for less than 10 s. The implication of such contribution on human health is linked to their high deposition efficiency in the alveolar interstitial region of the human respiratory system, where gas exchange occurs (ICRP, 1994).

Table 1. Heavy metal breathing zone concentrations (µg·m^{-3}) during MIG welding of a mild carbon steel.

Fe soluble	Cu	Mn	Cr total	Ni insoluble
18.8	18.1	148.4	3.7	2.0

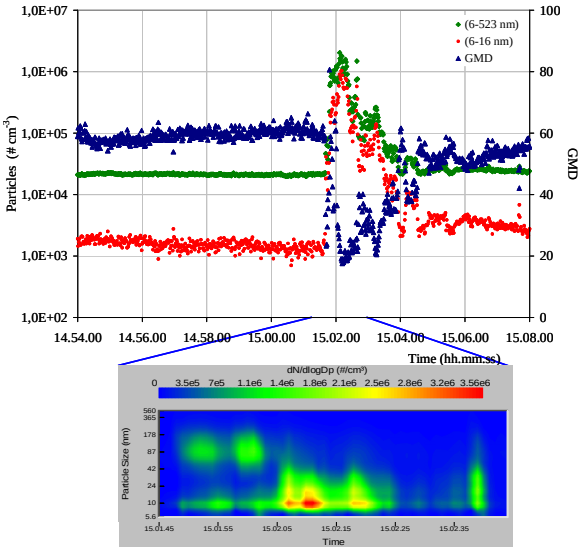

Figure 1. Temporal trend of submicrometric particles, nucleation mode particles, GMD and particle number size distribution during MIG welding of a mild carbon steel.

This work was supported by INAIL ex ISPESL under the grant ISPESL/DIPIA/P6 “Identificazione, analisi e valutazione delle conseguenze delle attività antropiche” L4 and L6.

AIDII (2011). *It J Occ Environ Hyg* **1** (Suppl). ISBN: 978-1-607260-28-8.

ICRP Publication 66 (1994). *Human Respiratory Tract Model for Radiological Protection*, International Commission on Radiological Protection.

Manigrasso, M., Avino, P. (2012) *Atmos Environ* in press. doi: 10.1016/j.atmosenv.2012.01.039.

Sińczuk-Walczak, H., Jakubowski M., Matczak W. (2001) *Int J Occup Environ Health* **14**, 329-337.

Clogging of industrial High Efficiency Particulate Air (HEPA) filters in case of fire: extension of an empirical model to realistic fire conditions.

F.-X. Ouf[1], V.-M. Mocho[1], S. Pontreau[1] and Z. Wang[1]

[1]Institut de Radioprotection et de Sureté Nucléaire (IRSN), BP 68, 91192 Gif-Sur-Yvette Cedex, France.
Keywords: clogging, HEPA pleated filter, fire, soot particles.
Presenting author email: francois-xavier.ouf@irsn.fr

AREVA NC and IRSN are conducting research on the impact of a fire on the behaviour of containment devices for radioactive materials such as High Efficiency Particulate Air (HEPA) pleated filters. The aim of the present work is to produce experimental results of clogging of industrial HEPA filters in case of fire involving realistic materials used in nuclear facilities, from medium to large scale.

For this purpose, an experimental test rig has been developed (Mocho and Ouf, 2011). This facility is composed of a 1 m^3 furnace where several types of fuel (liquids and solids) are burnt. It is surmounted by an exhaust duct where the ventilation flow rate is imposed with the help of an extraction device and two calibrated orifice plates, associated to two separate exhaust ducts and HEPA filter-housings, corresponding to a range of air flow from 50 to 500 m^3/h (filtration velocity from 0.23 to 2.1 cm/s). The clogging of HEPA filter is monitored by measuring the pressure drop of filters and the filtered air temperature at a given filtration velocity. Upstream of HEPA filters, combustion aerosols are characterized in terms of size distribution, mass concentration, composition and particle morphology respectively using a DMS500 (Cambustion Ltd), glass (mass concentration) and quartz fiber (organic to total carbon ratio OC/TC) filter samplings and transmission electron microscope (TEM) analysis of particles deposited on TEM grids.

First results deal with physico-chemical properties of particles produced by thermal degradation of several types of fuels. In most cases these particles are submicronic fractal aggregates with primary particle diameters ranging from 31 to 53 nm. A significant contribution of organic carbon components has been also reported and could be observed on TEM micrographs as a coating around fractal aggregates. A summary of the properties determined for all these sources is proposed in the table 1; figure 1 presents typical TEM micrographs of particles emitted by each fuel.

Table 1. Properties of aerosol emitted by thermal degradation of studied fuels.

Fuel	Morphology	D_m (nm)	D_{pp} (nm)	OC/TC (%)	Composition
TBP/TPH	Coated Fractal Compact	230 – 240	31 - 34	5 – 13	C / O / P
LEXAN	Coated Fractal	220 – 260	51 - 53	12 – 16	C / O
OIL	Coated Fractal	250 – 340	41 – 45	10 – 12	C / O
Electrical Cable	Coated Fractal Compact	300	48	11	C / O / Cl
KIOWAGLASS	Coated Fractal Fractal	237 – 274	35 – 39	5 – 8	C / O / Pb
Trash can	Compact	180 - 320	32 - 34	4 – 10	C / O / Sb / Zn / Al

Typical clogging behaviours of HEPA filters are presented on figure 2 for a filtration velocity of 2.1 cm/s.

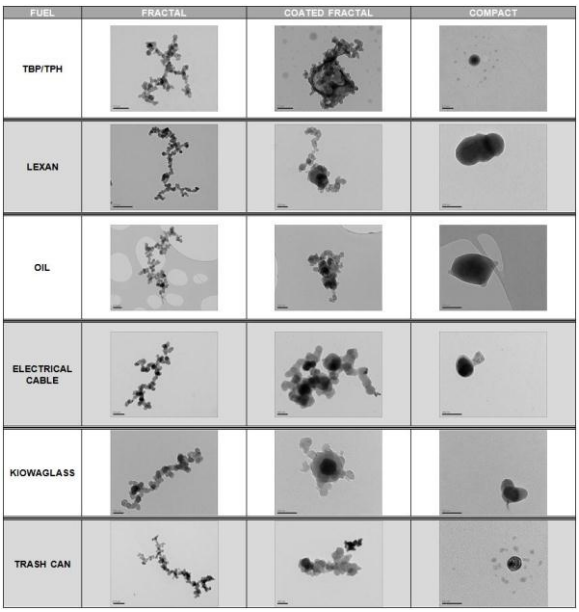

Figure 1. Typical TEM micrographs of particles emitted by thermal degradation of studied fuels.

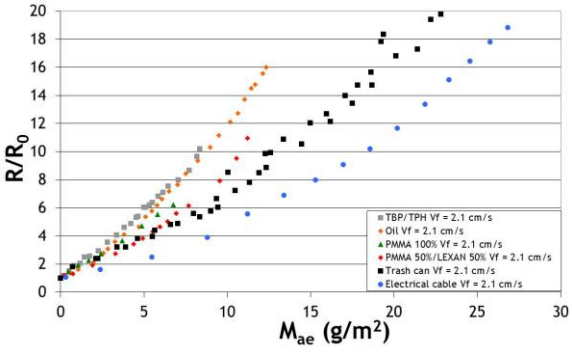

Figure 2. Evolution of non-dimensional airflow resistance (R/R_0) as a function of deposited mass of aerosol per filter surface area M_{ae}.

Results have confirmed the reliability of the empirical clogging model (Mocho and Ouf, 2011) for a large range of fuels, filtration velocities and fire conditions.

Finally, experiments have been performed on a large scale facility, for real scale scenarios (electrical cabinet, constant and variable filtration velocity). Once more, a fairly good agreement has been observed between experiments and the empirical model.

This work was supported by AREVA NC.

Mocho, V.-M. and Ouf, F.-X. (2011). *Nucl. Eng. Design.* 241, 1785-1794.

Elemental and morphological characterization of combustion by-products released from coal-fired thermal power plants in India

Rakesh Kumar[1] and Sudesh Yadav[2]
[1]Department of Environmental Sciences, University of Jammu, Jammu-18006, J&K, India
[2]School of Environmental Sciences, Jawaharlal Nehru University, New Delhi-110067, India
Keywords: coal combustion products, morphology, mineralogy, relative enrichment factor, elemental chemistry

Presenting Author: rakeshkumaratri@gmail.com

Utilization of coal for electricity generation produces large volumes of coal ash i.e. flyash and bottom ash as combustion waste along with flue gases. Particulate emissions from coal-fired thermal power plants have tendencies to accumulate higher amounts of toxic elements owing to their greater surface area (Vassilev and Vassileva, 1996; Xu et al, 2003). These potentially toxic elements are released into our immediate environments through resuspension triggered by winds and leached into surface and ground waters.

In this work feed coal (FC), bottom ash (BA) and flyash (FA) samples were collected from two thermal power plants in Northern India. FA samples were collected from different electrostatic precipitators (ESPs) field arranged in the series. These samples were then characterized for their morphological aspects and geochemistry (mineralogy, major and trace elements including rare earth elements-REE).

SEM micrographs revealed that the size of ash particles frequently decreased downstream towards the last end field of the electrostatic precipitators. Finer ash fractions are found to have homogeneous size range along with ideal spherical morphologies. However, coarser fraction FAs had irregular morphologies. Plerospheres which are the ash particles filled with microspheres (Goodarazi, 2006) are noticeable in FA samples. Plerospheres are suggested to exercise a morphological control on the emission of finer ash particles. Pleurospheres were present in large numbers in the ash collected from the ash ponds. Thus, under the extreme conditions of slurry transportation plerospheres remains relatively stable.

X-ray diffractograms of ash samples indicate the predominance of amorphous alumino-silicate glasses Quartz, mullite, sillmanite and magnetite and hematite are the dominant crystalline mineral phases in BA and FA. Among the FA samples the emergence of a strong mullite peaks is observed towards the finer fractions of FAs. However, a decrease in quartz peaks was also observed. The variations in the peak height indicates an increase in mullite content toward finer ash fraction whereas quartz proportion decreased. Emergence of hematite peak is also observed towards finer ash fractions.

Relative enrichment factors (Meij and Winkel, 2007) of FC, BA and FAs revealed that most of the trace elements present in the coal showed differential partitioning among different sized ash fraction.

$$REF = \frac{\text{Elemental concentration in ash}}{\text{Elemental concentration in fuel}} \times \frac{\text{\%age ash content in fuel}}{100}$$

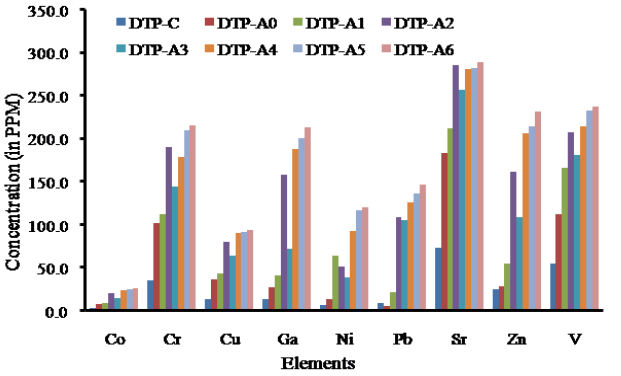

Figure 1. Showing enrichment of trace elements in the finer fraction of the flyash particle. (DTP-C is feed coal; DTP-A0 is bottom ash; DTP-A1 to DTP-A6 are flyash fraction (coarser to finer) collected from a series of electrostatic fields in power plant).

REF values indicates that Ba, Co, Cu and Mn remain relatively non-volatile during the combustion process and show uniform distribution on flyash fractions. Concentration of Ga, Pb, Tl, Ni, Zn and V were higher in FA than BA and increased with decreasing FA particle size. Finer particle at he latter ESP field accumulate greater amount of volatile trace metals due to their surface areas and being at high temperatures. However, REEs tends to remain non-volatile during the combustion process and observed no significant towards finer fractions.

Meij, R., and Winkel, H., (2007) *Atmospheric Environment* ***41***, 9262–9272.

Goodarzi, F. (2005) *Fuel* ***85***, 273-280

Vassilev, S. V., and Vassileva, C. G. (1996). *Fuel Processing Technology*, ***47***, 261-280.

Xu M., Yan R., Zheng C. C., Qiao Y., Han J. and Sheng C. (2003) *Fuel Processing Technology*, **85**, 215– 237.

Characterisation of particle number, nitrogen oxides and ozone concentrations in an urban background area located near a municipal waste incinerator

A.Donateo[1], D.Contini[1], F.Belosi[2], F. Prodi[2], F.M. Grasso[1]

[1]Institute of Atmospheric Science and Climate (ISAC-CNR), 73100, Lecce, Italy
[2] Institute of Atmospheric Science and Climate (ISAC-CNR), 40129, Bologna, Italy

Keywords: Industrial aerosol, NOx, Ozone, Particle concentration

In industrialized areas, the major contribution to the fine and ultrafine particles comes from anthropogenic activities, namely from emissions of industrial combustion processes and traffic-related emissions. In the waste treatment, incineration represents a favourable technique for reducing the volume of waste streams and recovering its energy content for the generation of electricity and district heating (Buonanno G. et al., 2009). The incineration sector has undergone rapid technological development over the last 10–15 years, due to specific legislation applied to industry that has obliged several European countries to reduce toxic emissions from municipal waste incinerators. However, the levels of environmental pollution linked with these activities and facilities are associated with a range of adverse health effects in humans. The principal contaminants include particles, nitrogen dioxide, sulphur dioxide, metals and heavy metals, (PAHs) and PCDD/Fs. Measurements have been taken in an urban background site nearby a municipal waste incinerator (Frullo) in the Emilia Romagna region (Italy) using a mobile laboratory.

Measurements were made between 6 June and 22 July 2008 (summer campaign) and from 20 January to 10 March 2009 (winter campaign). Particle number concentration has been measured using a CPC (Grimm model 5.403), coupled, for eddy correlation configuration, with a sonic anemometer (Gill, R3) at the top of a meteorological mast (10m) and a Rotronic (MP100A) thermo hygrometer. Mobile laboratory was also equipped with a nitrogen oxides detector (Teledyne T-API 200E) and an ozone detector (Teledyne T-API 400E). PM1 and PM2.5 measurements were also available at the site.

Measurements show a seasonal pattern with concentrations during winter larger than summer concentrations. A clear daily and weekly pattern was observed with weekdays concentrations larger than weekends concentrations, instead ozone concentration showed similar average values. Traffic-related emissions are the main causes of the observed concentration patterns.

All data were studied considering three principal wind direction sectors: wind direction directly from incinerator chimney at NW (292°-338°), from waste incinerator plant from W to N and from the city of Bologna at SW (200°-245°). In Fig.1 number particles concentration was reported as a function of wind direction. Different wind direction sectors were distinguished with three colours: cyan from the plant, yellow from the city of Bologna and green from chimney. A contribution from the plant is observed but the largest is coming from the urban area.

There is a limited correlation between NOx and particle hourly concentrations, especially in the summer campaigns due to the presence of particle number concentration peaks in the middle of the day. These were likely due to nucleation and/or growth of particles and their statistics will be discussed and compared with similar phenomena observed in urban background site in the area, where nucleation events frequency observed was high during spring and summer, in particular in July month (Hamed et al., 2007).

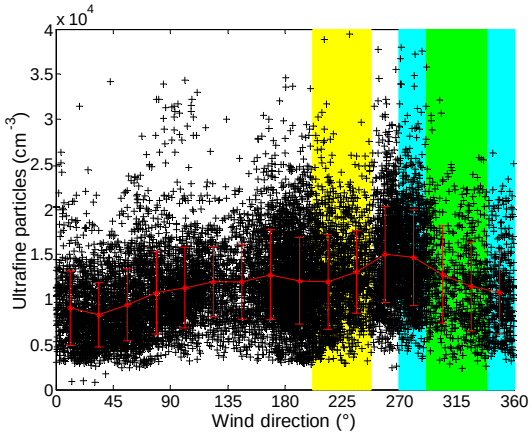

Figure 1. Number particle concentration against wind direction. In red the averages in bins of size direction (error bar represent a standard deviation).

The financial contribution of the project MONITER (Monitoraggio degli Inceneritori nel Territorio dell'Emilia Romagna) is acknowledged.
The authors wish to thank Mr. G. Trivellone (ISAC-CNR) for the technical help in preparing and implementing the campaign.

Buonanno G. et al., 2009. Waste Management, 29, 749-755.
Hamed et al., 2007.Atmospheric Chemistry and Physics, 7, 355-376.

Analysis of Soot deposit for post fire investigation: comparison between full scale experiment and theoretical approach

A. Bellivier[1], M. Vigreux[1], F.X. Ouf[2] and H. Bazin[1]

[1]Department of Physical Measure and Fire Sciences , Laboratoire Central de la Préfecture de Police
39bis rue de Dantzig, 75015 Paris, France
[2]Institut de Radioprotection et de Sûreté Nucléaire (IRSN), BP 68, 91192 Gif sur Yvette Cedex, France
Keywords: aerosol, soot, thermophoresis, particle deposition, fire.
Presenting author email: axel.bellivier@interieur.gouv.fr

One of the "Laboratoire Central de la Préfecture de Police" missions is to investigate on the causes of a fire that occurred in Paris and its suburb. A part of the soot produced during the fire is deposed on walls. In this context, the phenomenon of soot deposit is studied in order to evaluate the information that could be used for fire investigators.

Several phenomena of deposit could occur: sedimentation, Brownian diffusion, impaction under the effect of the centrifugal force, electrophoresis, deposit by turbulent diffusion and deposit by thermophoresis. The thermophoresis corresponds to the migration from the zones of high temperature towards zones of lower temperature. At the scale of a building fire, it is the main phenomenon of deposition because smokes temperatures are much higher than those of the walls.

Before analyzing the soot deposit during post fire investigation, laboratory tests are needed. An experiment in real scale, as a first approach, was conducted to study the phenomenon of thermophoresis. The experimental device BANCO (Ouf & al., 2008) was used to compare measurements to a theoretical model of thermophoresis (Talbot & al., 1980).

Experimental set up

The soot is produced by an acetylene burner. The deposition targets are placed in a holding area of hot smoke (approx. 85°C). There are three different targets corresponding to three different temperatures conditions: a "cold" (nearly 10 ° C imposed by a heat exchanger), an "ambient temperature" and a "hot" one (nearly 185 ° C imposed by a heat plate). Targets are exposed in the furnace to the smoke during 30 minutes. Deposit mass are measured by the weighing of the targets prior and after the soot deposition.

Theoretical description of thermophoresis

The thermophoresis velocity is given by (Talbot & al., 1980):

$$v_{th} = \frac{-H\,\mu_f\,Cu}{2\,\rho_f}\,\frac{dT}{dy}$$

where H is characterising the particles' internal thermal gradient, μ_f the fluid viscosity, Cu the Cunningham factor, ρ_f the fluid density and $\frac{dT}{dy}$ the thermal gradient.

Then the mass per unit area of soot deposition could be obtained by:

$$D = \rho_s\, v_{th}\, dt$$

where ρ_s is the soot concentration in smoke and dt the duration of the exposition.

Results

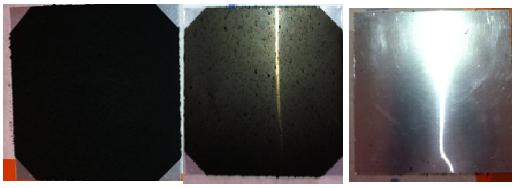

Figure 1. Visualisation of thermophoresis phenomenon on "cold" target (heavy deposition), "ambient temperature" target (medium deposition) and "hot" target (no deposition).

Qualitative observations of the thermophoresis deposition are shown in Figure 1.

Table 1 shows a comparison between experimental measurements and theoritical deposition based on the previously described approach.

Table 1. Comparison between experiment and theory.

Target	Measured soot deposition (g)	Theoretical soot deposition (g)
"Cold"	$1.6\cdot10^{-2}$	$1.9\cdot10^{-6}$
"Ambient"	$1.2\cdot10^{-2}$	$1.2\cdot10^{-6}$
"Hot"	< DL	Closed to 0

Conclusion

The experimental results are consistent: the deposition is more important on the coldest target. There is however a strong difference between measurements and predictions due to the assumptions made (spherical particles, steady state, etc.) to use the model. Nevertheless those firt results are encouraging for the investigation purpose. The next steps are to take into account the fractal morphology of soot particles and to compare these experimental results to a CFD simulation modeling of fire (customised FDS code).

F.X. Ouf & al. (2008), CST, 180: 674-698
L. Talbot & al.(1980), J. Fluid Mech., 101: 737-758
http://fire.nist.gov/fds/

Electrical Properties of Carbonaceous Particles Collected from Laminar Premixed Flames

G. De Falco[1], M. Commodo[2], V. Pagliarulo[3], G.P. Pepe[3]
P. Minutolo[2], A. D'Anna[1]

[1] Dipartimento di Ingegneria Chimica, Università Federico II, Napoli, ITALY
[2] Istituto di Ricerche sulla Combustione, C.N.R., Napoli, ITALY
***CNR-SPIN Napoli, Dipartimento Scienze Fisiche, Facoltà di Ingegneria, Napoli, Italy
Keywords: flame, carbonaceous particles, electrical properties.
Presenting author email: commodo@irc.cnr.it

Carbon particulate matter derived from combustion consists of a variety of organic compounds, which often present features similar to polymers and molecules used as photoactive layers in the most common organic solar cells (Zhu *et al*. 2009). This consideration has recently provided the inspiration to check out the possible applications of these products in the optoelectronic application such as the photovoltaic technology.

At the current state of knowledge the flame-formed carbon particulate matter mainly contain two different classes of materials: soot and nanoparticle of organic carbon (NOC) (D'Anna 2009). These two classes of particles present substantial differences on their sizes, optical properties and chemical features.

In this study, combustion-formed carbonaceous materials were collected from various fuel-rich laminar premixed flames of ethylene and air, in order to characterize both the optical and the electrical properties.

UV-visible absorption spectroscopy analysis has been used to measure the optical band-gaps of the materials by reporting the optical spectra in the Tauc plot (Tauc *et al*. 1966). The I-V characteristics, i.e. current vs. voltage plots, have been measured in order to estimate the electrical conductivity. Three different sampling procedures have been developed. A quartz substrate was rapidly inserted in flame, to collect by thermophoresis the carbon particulate matter, containing two main different classes of materials: soot and nanoparticles of organic carbon (NOC). The first class showed a band-gap ranging between 0.1 eV and 0.8 eV and a fair electrical conductivity, while the second class was characterized by a larger optical band-gap ranging between 1.9 eV and 3 eV and a low electrical conductivity.

The optical band-gap was investigated under a varying of flame conditions (C/O ratio and height above the burner) and residence time of the substrate in the flame.

A second particles collecting approach was realized by using a tube probe, positioned inside the flame, with a 0.8 mm orifice, followed by a particles impactor. This method was used to collect selected classis of particles.

A third method was a chemical procedure based on Soluble organic fraction (SOF) which was chemically extracted from the sampled particulate. In this later case the electrical characterization of the collected material showed an unusual presence of a hysteresis in the I quadrant of the I-V characteristic of SOF.

Finally by using the theoretical model proposed by Bruschi and Nannini 1991, the phenomenon of electrical conduction through a soot particles layer was simulated via tunnelling and percolative effect, which include both microscopic and macroscopic phenomena relative the charge transfer.

Zhu H., Wei J., Wang K. Wu D. (2009), Application of carbon materials in photovoltaic solar cells, *Sol. Energy Mater. Sol. Cells* 93: 1461-1470.

D'Anna A. (2009), Combustion-formed nanoparticles, *Proc. Comb. Inst.* 32: 593-613.

Tauc J., Grigorovici R. Vancu A. (1966), Optical properties and electronic structure of amorphous germanium, *Phys. Stat. Sol.* 15: 627-637.

Bruschi P., Nannini A., (1991), Current vs voltage characteristics of ion-beam-grown polymer-metal granular thin films, *Thin solid films* 201: 29-38.

Towards a discrimination between particle emission from wood/biomass combustion and road traffic by Raman microspectroscopy

N.P. Ivleva[1], C. W. Müller[2], I. Kögel-Knabner[2] and R. Niessner[1]

[1]Chair for Analytical Chemistry, Institute of Hydrochemistry, Technische Universität München, Munich, 81377, Germany
[2]Chair for Soil Science, Technische Universität München, Freising, 85354, Germany
Keywords: wood combustion, diesel soot, particle emission, Raman microspectroscopy (RM)
Presenting author email: natalia.ivleva@ch.tum.de

Aerosol particulate matter (PM) generated by combustion sources have a significant influence on atmospheric chemistry, Earth's climate and human health. Therefore, the detailed physicochemical characterization of combustion PM is crucial for understanding their impact on the environment. Moreover, the identification and quantification of anthropogenic and natural emission sources which govern global and regional aerosol abundances are essential for development of efficient emission reduction strategies. Besides engine exhaust particles, PM emitted by biomass burning (or, more specifically, wood combustion) is a seasonally important PM source in central Europe. It was shown that traffic and wood burning emission sources can be identified in ambient air by means of aerosol mass spectrometry (AMS), which allows for determination of organic and inorganic aerosol (Lanz *et al*, 2010). However elemental carbon (EC) cannot be detected by AMS. On the other hand, EC and inorganic species in combustion aerosols can be characterized by Raman microspectroscopy (RM). This non-destructive technique provides fingerprint spectra with the spatial resolution of an optical microscope and allows the identification and semi-quantitative analysis of soot, humic-like substances, nitrates, sulfates, and carbonates in size resolved samples of air particulate matter (Ivleva *et al*, 2007).

In order to demonstrate the feasibility of RM for discrimination between particle emission from wood/biomass combustion and road traffic, we firstly analyzed different reference compounds. Wheat (*Triticum aestivum*) straw as well as Norway spruce (*Picea abies*) branches, needles, roots and wood were dried, milled and heated at 450°C in ambient air for 2.5, 5 or 10 min. The Monarch 44 and Euro IV soot were used as examples for industrial soot (carbon black) and traffic particulate emission, respectively.

The RM analysis (λ_0 = 514 nm) of heated biomass samples revealed changes in their spectral features with the heating time, viz., the increase in the intensity of D (defect) peak around 1350 cm^{-1} compared to G (graphite) peak around 1600 cm^{-1}. This observation, which is in agreement with the Raman study on wood and bark of Japanese cedar pyrolyzed at increased temperature (Yamauchi, Kurimoto, 2003), indicates the ordering of amorphous carbon and increase of sixfold ring clusters area. Unlike all spruce samples, no differences were found in the spectra of wheat straw heated for 2.5, 5 or 10 min, indicating that pyrolysis was completed in less than 2.5 min of heating. Spectra of all analyzed biomass samples pyrolyzed for 10 min are very similar, with the exception of spruce wood sample, where slightly lower width of G and D peaks was found. The later suggests a slightly higher structural order of graphite-like carbon.

The comparison of spectra from pyrolyzed biomass, carbon black and diesel soot indicates significant differences in the width und relative intensity of D peak, which can be used for discrimination between combustion particles of different origin (Fig. 1).

The next step in our study will be the analysis of biomass burning aerosols of different origin, to extend our data base. Moreover, we plan to analyze the aerosol samples from various combustion sources, to prove the potential of RM for the discrimination between particle emission from wood/biomass combustion and road traffic.

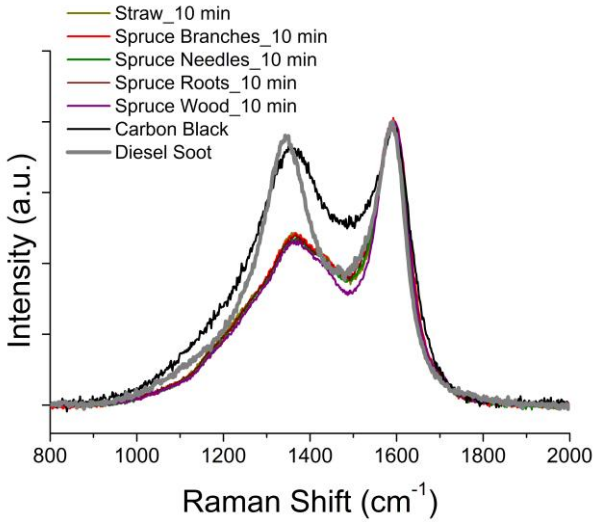

Figure 1. Spectra of wheat straw powder, and Norway spruce branches, needles, roots, wood powder heated at 450°C in air for 10 min., as well as carbon black (Monarch 44) and diesel soot (Euro IV).

Ivleva, N. P., McKeon, U., Niessner, R. and Pöschl, U. (2007) *Aerosol Sci. Technol.* **41**, 655-671.

Lanz, V. A., Prevot, A. S. H., Alfarra, M. R., Weimer, S., Mohr, C., DeCarlo, P. F., Gianini, M. F. D., Hueglin, C., Schneider, J., Favez, O., D'Anna, B., George, C. and Baltensperger, U. (2010) *Atmos. Chem. Phys.* **10**, 10453-10471.

Yamauchi, S. and Kurimoto, Y. (2003) *J. Wood Sci.* **49**, 235-240.

Field scale evaluation of ultrafine particles emissions from stationary combustion and industrial sources

S.Cernuschi[1], G. Lonati[1], M. Giugliano[1], S. Ozgen[1], G. Ripamonti[1]

[1]Department of Hydraulics, Environmental, Infrastructure and Surveying Engineering, Politecnico di Milano, Milan, 20133, Italy

Keywords: emissions, ultrafine particles, nanoparticles, combustion sources, emission factors

Presenting author email: stefano.cernuschi@polimi.it

Despite all recent attentions addressed to their presence in ambient air, ultrafine and nanoparticle emissions are still poorly characterized, particularly within stationary combustion and industrial activity sectors. Source effects related to process configurations and operating conditions, together with all technical issues associated with sampling and measurement procedures, result in limited and rather comparable informations, with a general lack of base data required for evaluating any intervention policy that should be eventually adopted for preserving air quality.

The paper reports on a broad research programme addressed to stack field testing at real scale operating conditions on several stationary combustion and industrial processes, conducted for evaluating total number concentrations and size distributions in a size range extended towards the evaluation of ultrafine and nanoparticles. The investigations interested municipal and industrial waste-to-energy (WTE) plants, a biomass power plant, residential scale boilers fed with different fuels (i.e., wood pellets, light oil, natural gas), a closed fired place burning wood logs and a thermal oxidizer treating emissions from thermal desorption for soil remediation. Field measurements were dedicated to the determination of primary particle concentrations at stack gas conditions and to the investigation of the contribution of any material of condensable origin, arising from cooling and dilution effects immediately following flue gas release into the atmosphere. For this purpose, measurements were performed using a specifically designed sampling line, equipped with a dilution system and a particle counting device.

Average concentration range detected as a whole is included between four orders of magnitude (10^{-3} cm^{-3} – 10^{-7} cm^{-3}; under all sampling conditions, ultrafine fractions largely prevail in number size distributions, with average diameters almost constantly located in the nanoparticle size range. Source and fuel type for residential heating units result in variations in concentration levels, with different effects arising from dilution sampling. For waste incineration, concentrations and emission factors are included in the lower range of all measured sources: some process and design configuration effects are observed, with stack concentrations influenced by the presence of wet scrubbing units and the baghouse operating temperature of dry removal processes.

This work, jointly conducted by Politecnico di Milano and LEAP consortium (Laboratory of Energy and Environment of Piacenza), was partially supported with a research fund from Italian Federation of Environmental Utilities (FederAmbiente).

Characterization of aerosols produced by a commercial combustion aerosol generator MiniCAST™ 5201: EC/TC, size distribution, morphology and optical properties.

F.-X. Ouf[1], E. Brugière[1,2], D. Ferry[3], S. Pontreau[1] and J. Yon[2]

[1]Institut de Radioprotection et de Sureté Nucléaire (IRSN), BP 68, 91192, Gif-sur-Yvette Cedex, France.
[2]UMR 6614 CORIA, Avenue de l'université, BP 8, 76801 Saint Etienne du Rouvray, France.
[3]CINaM-CNRS UMR 7325, Aix-Marseille University, Campus de luminy case 913, F-13009 Marseille, France.
Keywords: carbonaceous particles, TEM, fractal analysis, extinction coefficients.
Presenting author email: francois-xavier.ouf@irsn.fr

Since the last decades, the question of the global impact of combustion generated aerosols is of raising concern. Many researches have been conducted on the toxicological and global warming influences of particles emitted by wood combustion and aircraft engines or fire. Due to their complex composition and morphology, their reactivity and physical behaviour are not understood. Subsequently, the need of reference materials is growing over the years and recent developments allow to produce in a stable and repeatable way carbon particles assumed to be representative of combustion aerosol. Recently, Jing Ltd (*www.sootgenerator.com*) has proposed a combustion aerosol standard, called MiniCast, based on a propane diffusion burner, to be a candidate as a reference source of combustion generated particles. Since its beginning, this new device has been involved in many researches but few of those have proposed an overview of the physico-chemical properties of the particles produced by the MiniCast™ 5201.

The aim of this technical paper is to characterize the size distribution, morphology, elemental composition (EDX), microstructure (HRTEM), EC/TC (ratio of elemental carbon to total carbon) and optical properties of some selected set-points of the MiniCast™ burner. The corresponding set-points have been considered in order to produce a large range of EC to TC ratio ranging from 4 to 95 % of elemental carbon and are summarized in table 1.

Table 1. Experimental conditions of the MiniCAST™.

Propane (mL/min)	Nitrogen (mL/min)	Oxidation air (L/min)	Dilution air (L/min)
50	**0**	1.2	20
50	**50**	1.2	20
50	**100**	1.2	20
50	**150**	1.2	20
50	**200**	1.2	20
60	0	**0.8**	20
60	0	**1.0**	20
60	0	**1.1**	20
60	0	**1.2**	20
60	0	**1.5**	20

At the outlet of the MiniCAST™, a PALAS VKL10 ejector-type dilution device has been used to sample and dilute particles. The size distribution has been measured by a Scanning Mobility Particle Sizer (TSI SMPS 3936) and the morphology has been characterized by analysis of Transmission Electronic Microscopy micrographs of particles deposited on TEM grids (Ouf et al., 2010). In addition, the elemental to organic carbon ratio has been determined with the help of a thermo-optical method (Sunset Lab Inc.) using the "Improve" protocol, and the specific extinction coefficient has been retrieved with a turbidimetry optical bench described in Yon et al. (2011).

Figure 1 presents the evolution of elemental to total carbon ratio as a function of electrical mobility diameter.

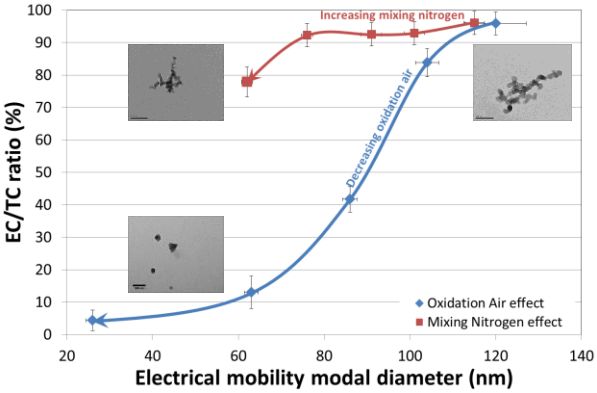

Figure 1. Evolution of EC/TC ratio as a function of electrical mobility diameter.

Considering an increase of mixing nitrogen flow rate, the EC/TC ratio does not change significantly while the mobility diameter significantly decreases. In this case, the evolution of size of particle is mainly due to coagulation inside the flame which does not modify the particles composition. On the other hand, as the oxidation air flow rate decreases, both the EC/TC and mobility diameter strongly decrease. In the most extreme case, the MiniCAST™ produces compact particles with a modal diameter of 25 nm and composed of nearly 4 % of EC. For this second case, a strong oxidation of combustion particles inside the flame could be suspected by incompletely burned gases. Despite the evolution of size, the change of EC/TC ratio as a function of oxidation air has been also reported to be linked with an evolution of morphology and optical extinction coefficient of these particles. Further analyses of TEM, HRTEM and EDX data are in progress and will bring more information on the nature and properties of such particles.

Ouf, F.-X., Yon, J., Ausset, P., Coppalle, A., Maillé, M. (2010). *Aerosol Sci. Technol.*, 44, 1005-1017.

Yon, J., Lemaire, R., Therssen, E., Desgroux, P., Coppalle, A. and Ren, K.F. (2011) *App. Phys. B.* 104, 253-271.

Selective catalytic NH_3 using rare-earth oxides of gasified biomasses fuels. Part 1. Materials structural characterization

Chang-Mao Hung[1], Shui-Jen Chen[2], Wei-Bang Lin[3] and Wen-Liang Lai[4]

[1]Department of Vehicle Engineering, Yung-Ta Institute of Technology and Commerce, 316 Chung-Shan Road, Linlo, Pingtung 909, Taiwan, Republic of China.
[2]Department of Environmental Science and Engineering, National Pingtung University of Science and Technology, 1 Shuefu Road, Neipu, Pingtung 912, Taiwan, Republic of China.
[3]Department of Mechanical Engineering, Chinese Military Academy, Fenshan, Kaohsiung County 830, Taiwan, Republic of China.
[4]Department of and Occupational Safety and Hygiene, Tajen University, 20 Wei-Shin Road, Yanpu Shiang, Pingtung 907, Taiwan, Republic of China.
Keywords: selective catalytic oxidation, ammonia, binary rare-earth oxides.
Presenting author email: hungcm1031@gmail.com

Nowadays, catalytic oxidation has been established to increase the effectiveness of AOP (Advanced Oxidation Processes) technology using dedicated catalysts, which potentially shorten the reaction times of oxidation, and allow it to proceed under milder operating conditions. The selective catalytic oxidation (SCO) of NH_3 in a stream to molecular nitrogen and water is one method for solving problems of NH_3 pollution. This work considers the oxidation of NH_3 from gasified biomasses fuels by selective catalytic oxidation (SCO) over binary rare-earth oxides (Cu-La nanomaterials) at temperatures between 150 and 400℃. To further understand the properties of the binary CuO/La_2O_3 composite catalyst, Figure 1 compares the FTIR spectra at various Cu-La molar ratios, and also confirms the presence of the CuO-like phase and the La_2O_3 phase on the surface of the CuO/La_2O_3 composite catalyst. Figure 1 reveals that the peaks associated with the CuO-like phase on the framework are associated with a peak at around 1384 cm^{-1}. Figure 1 also shows that the La^{3+} cations and the La_2CuO_4 phase adsorbed onto copper oxide clusters are at 1524 cm^{-1} and 520 cm^{-1} of the catalyst, respectively. Therefore, we suggest here that the catalytic activity of the binary $CuO\text{-}La_2O_3$ composite oxide catalyst system in oxidizing ammonia may be explained by the reversible redox behavior of $CuO\text{-}La_2O_3$ couples in promoting the functional mechanism. Figure 2 presents the X-ray diffraction (XRD) patterns at various Cu-La molar ratios, verifying the presence of CuO and La_2O_3 phases of the Cu-La composite metal catalyst. The dominant CuO diffraction peaks appeared near 2θ=35.4926 and 38.7593° for a CuO/La_2O_3 composite metal catalyst. La_2O_3 in a copper catalyst may be assumed promote the formation of the active phase of CuO under the conditions of ammonia oxidation, because La_2O_3 is well known that can be increased further thermal stability and oxygen storage capacity. Thus, the X-ray powder diffraction method confirmed the formation of copper (II) and lanthanum (III) oxide active sites on the binary CuO/La_2O_3 composite catalyst.

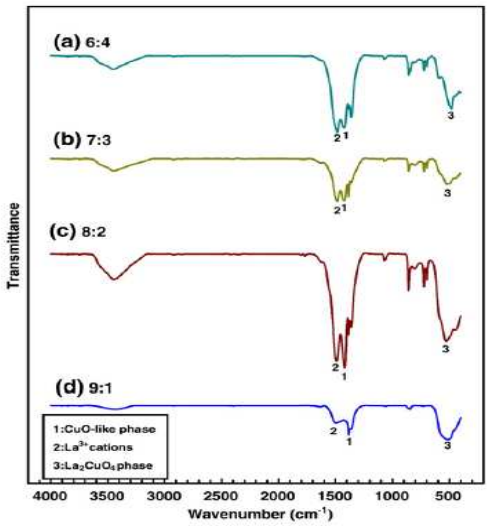

Figure 1. FTIR pattern of various metal content on the CuO/La_2O_3 catalyst for the conversion of NH_3. Test conditions: 1000 ppm NH_3 in He, O_2 = 4%, RH = 12%, GHSV = 92000 ml/h-g.

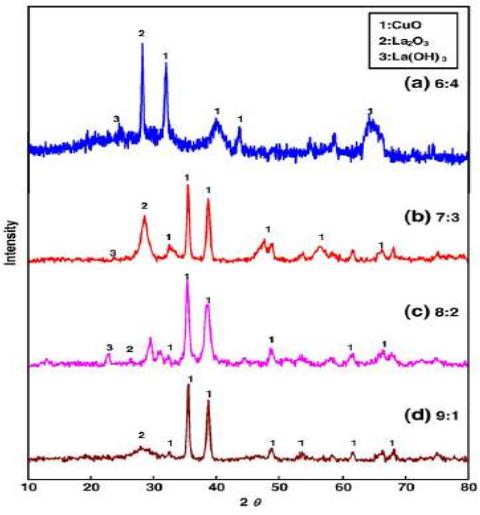

Figure 2. XRD pattern of various metal content on the CuO/La_2O_3 catalyst for the conversion of NH_3. Test conditions: 1000 ppm NH_3 in He, O_2 = 4%, RH = 12%, GHSV=92000 ml/h-g.

Selective catalytic NH_3 using rare-earth oxides of gasified biomasses fuels. Part 2. Catalytic activity and mechanism study

Chang-Mao Hung[1], Shui-Jen Chen[2], Wei-Bang Lin[3] and Wen-Liang Lai[4]

[1]Department of Vehicle Engineering, Yung-Ta Institute of Technology and Commerce, 316 Chung-Shan Road, Linlo, Pingtung 909, Taiwan, Republic of China.
[2]Department of Environmental Science and Engineering, National Pingtung University of Science and Technology, 1 Shuefu Road, Neipu, Pingtung 912, Taiwan, Republic of China.
[3]Department of Mechanical Engineering, Chinese Military Academy, Fenshan, Kaohsiung 830, Taiwan, Republic of China.
[4]Department of and Occupational Safety and Hygiene, Tajen University, 20 Wei-Shin Road, Yanpu Shiang, Pingtung 907, Taiwan, Republic of China.
Keywords: selective catalytic oxidation, ammonia, binary CuO/La_2O_3 composite catalyst.
Presenting author email: hungcm1031@gmail.com

NH_3 is a toxic inorganic gas with a pungent odor under ambient conditions, and is potentially harmful to public health reported in the literature. The selective catalytic oxidation (SCO) of NH_3 in a stream to molecular nitrogen and water is one method for solving problems of NH_3 pollution. This work considers the oxidation of NH_3 from gasified biomasses fuels by selective catalytic oxidation (SCO) over binary rare-earth oxides (Cu-La nanomaterials) at temperatures between 150 and 400℃. Figure 1 plots the measured catalytic activities over the binary CuO/La_2O_3 samples of interest as a function of temperature. NH_3 is converted even at 150℃, and more NH_3 was converted over the Cu-La (8:2) composite catalyst as the temperature increased, approaching 93% at 400℃. The extent of NH_3 conversion increased with temperature and approached 90%, 80% and 79% at 400℃ over Cu/La (9:1), Cu/La (7:3) and Cu/La (6:4) catalysts, respectively. Notably, more lanthanum corresponded to higher NH_3 conversion only at low temperatures. Conclusively, this work shows that the SCO process has the potential to treat highly concentrated streams of NH_3, helping industrial plants to meet discharge regulations. The overall selectivity of N_2 production varied from 12 to 53% and that of NO production varied from 0 to 45% over the range of 3-93% NH_3 conversion at NH_3 concentrations of 1000 ppm (Fig. 2). Nitrogen gas thought to be formed primarily by the dissociation of NO produced by oxidation of adsorbed NH_3. Therefore, according to the experimental results, we hypothesis that NH_3 and oxygen may be adsorbed onto specific sites on the binary CuO/La_2O_3 (8:2) composite catalyst, promoting the rapid conversion of NH_3 to nitrogen and water. Nitrogen was the dominant gaseous, and a small amount of NO was detected in the resultant stream.

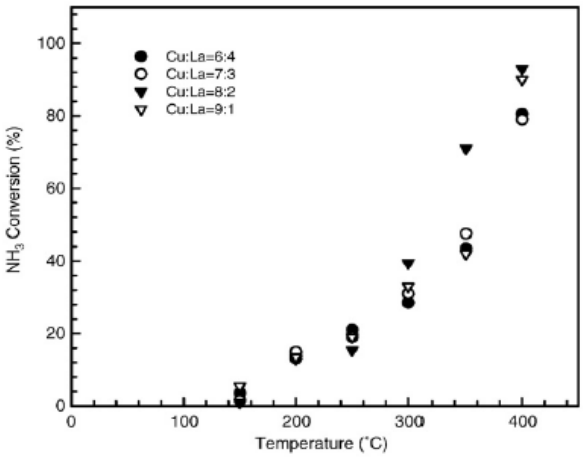

Figure 1. Dependence of the NH_3 content on the conversion, as function of temperature of the CuO/La_2O_3 catalyst. Test conditions: 1000 ppm NH_3 in He, O_2 = 4%, RH = 12%, GHSV = 92000 ml/h-g.

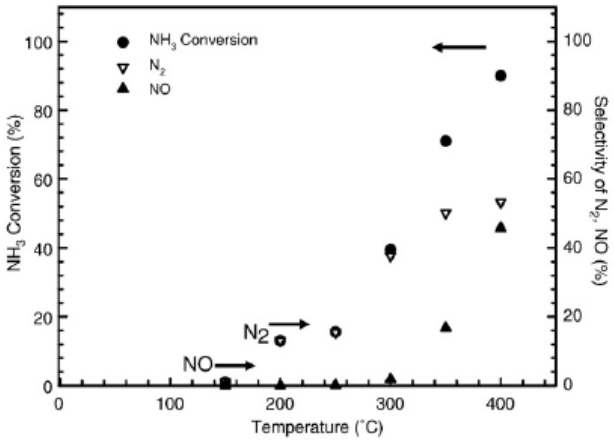

Figure 2. Relationship among NH_3 conversion, N_2 yield, and NO yield at various temperatures over the CuO/La_2O_3 (8:2) catalyst. Test conditions: 1000 ppm NH_3 in He, O_2 = 4%, RH = 12%, Temperature = 150-400℃, GHSV = 92000 ml/h-g.

Selective catalytic NH_3 using rare-earth oxides of gasified biomasses fuels. Part 3. Reaction kinetic behavior study

Chang-Mao Hung[1], Shui-Jen Chen[2], Wei-Bang Lin[3] and Wen-Liang Lai[4]

[1]Department of Vehicle Engineering, Yung-Ta Institute of Technology and Commerce, 316 Chung-Shan Road, Linlo, Pingtung 909, Taiwan, Republic of China.
[2]Department of Environmental Science and Engineering, National Pingtung University of Science and Technology, 1 Shuefu Road, Neipu, Pingtung 912, Taiwan, Republic of China.
[3]Department of Mechanical Engineering, Chinese Military Academy, Fenshan, Kaohsiung 830, Taiwan, Republic of China.
[4]Department of and Occupational Safety and Hygiene, Tajen University, 20 Wei-Shin Road, Yanpu Shiang, Pingtung 907, Taiwan, Republic of China.
Keywords: ammonia, binary CuO/La_2O_3 composite catalyst, kinetic model.
Presenting author email: hungcm1031@gmail.com

Ammonia (NH_3) is widely found in industrial processes and it is a valuable chemical product for using with a variety of purposes and its can be eliminated in several ways, including ammonium nitrate production industry, livestock feedlots, urea manufacture plants, nitrogen fertilizer application industry, biomass combustion or petroleum refineries, and refrigeration industry, which are either toxic inorganic gaseous and its pungent malodorous component under ambient conditions or have the potential harmful effects on the public. Moreover, the kinetic behavior of NH_3 oxidation with catalysis can be accounted by using the rate expression of the kinetic model. Kinetic parameters are also developed on the basis of the differential reactor data in this study. The adsorptive and catalytic behavior of a catalyst is strongly influenced by the capacity and texture of its exterior surface. Figure 1 summarizes the properties of test catalysts determined by BET (Brunauer-Emmett-Teller method) analysis, including specific surface area. The specific surface area was 72 m^2/g with molar ratios of 8:2. For the molar ratios of 6:4 on a CuO/La_2O_3 composite metal catalysts, the surface areas slightly decreased (4 m^2/g). This test showed that the catalysts were associated with a larger lattice surface of copper or lanthanum, and that higher loadings caused metal sintering, perhaps reducing catalytic activity. The change in the sizes of particles of the catalyst was determined using the laser light-scattering method, as depicted in Fig. 2. The mean particle size converged to approximately 12.3, 13.6, 9.3, and 8.7 μm, for fresh CuO/La_2O_3 composite catalysts with the four molar ratios, 8:2, 9:1, 7:3 and 6:4. However, the diameters of the catalyst decreased as the copper content declined, indicating that co-precipitation aggregates the low metal molar ratio. Moreover, a kinetic rate expression was developed to describe the data over the range of conditions investigated. Furthermore, correlation equations in the form of Arrhenius's law are derived from experimental data to predict the destruction efficiencies of ammonia from the temperatures and residence period in a catalytic process. A Langmuir-Hinshelwood model incorporating a first-order reaction appears to adequately represent the NH_3 oxidation, which shows fairly good agreements with experimental data. This kinetic model is appropriate for oxygen presence and high concentrations of NH_3.

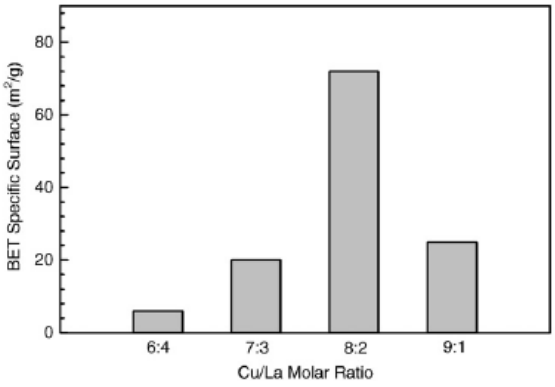

Figure 1. Effect of specific surface area on the CuO/La_2O_3 catalyst for the conversion of NH_3. Test conditions: 1000 ppm NH_3 in He, O_2 = 4%, RH = 12%, GHSV = 92000 ml/h-g.

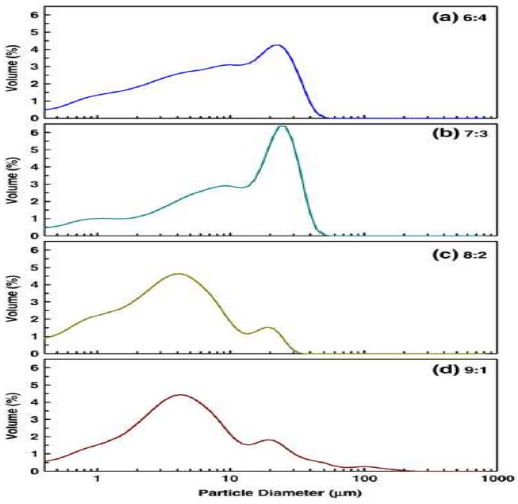

Figure 2. Changes in particle sizes distribution with various calcinations temperature on the CuO/La_2O_3 catalysts. Test conditions: 1000 ppm NH_3 in He, O_2 = 4%, RH = 12%, GHSV = 92000 ml/h-g.

Results and experience of long-term study of reduction of fine particle emissions from wood combustion boiler by a compact electrostatic precipitator

A. Bologa, H.-R. Paur and K. Woletz

Institute for Technical Chemistry, Karlsruhe Institute of Technology
Hermann-von-Helmholtz-Platz 1, Eggenstein-Leopoldshafen, 76344, Germany
Keywords: biomass combustion, fine particles, emission control, electrostatic precipitator.
Presenting author email: andrei.bologa@kit.edu

In the Europe the combustion of wood is widely used for domestic heating. The power generation is mostly done by means of combustion of wood-logs, chips or pellets in small scale combustion appliances, e.g. stove and boilers.

Wood combustion it is responsible for emissions of fine particles which are associated with various diseases. Usually particles are composed of ash, elemental carbon and organic matter and particle chemical composition, particle size distribution, number and mass concentration vary greatly depending on the design of the boiler, fuel quality, mixing of air and fuel, combustion temperature, etc.

Last time various filter systems were developed for reduction of fine particle emissions from small scale biomass combustion. These devices include cyclones, wet scrubbers, condensers, bag filters, cartridge filters, electrostatic precipitators (ESPs'), etc. The electrostatic precipitators are the most attractive devices as they ensure high mass collection efficiency and are operated at low power consumption and low pressure drop in comparison with other gas cleaning equipment. The design of the ESPs' range from conventional to space charge ESPs', from dry to wet units, from precipitators integrated into the combustion appliances up to the ESPs' installed downstream the combustion units, inside of the gas duct and/or chimney and at the exit of the chimney.

By biomass combustion in the boilers with integrated hear exchangers, the electrostatic precipitators are operated at gas temperatures of 100-200°C and for wood-log stoves up to 300-400°C.

The purpose of the current work is to present the results of the study of reduction of fine particle emissions from a 100 kW wood-combustion boiler by use of the CAROLA electrostatic precipitators.

The CAROLA electrostatic precipitators are developed in the Karlsruhe Institute of Technology in the Institute of Technical Chemistry. In the ESPs' the gas cleaning technology is based on the particle charging in a corona ionizer and charged particles precipitation in the grounded, external electric field free collector. The DC negative corona discharge is used for particle charging in the precipitators (Bologa *et al*, 2010).

For effective reduction of fine particle emissions from the exhaust gas, the compact CAROLA-precipitators are designed for boilers with capacity of 10 kW, 25 kW and 50 kW. For the long-term tests, several electrostatic precipitators were manufactured and installed in parallel downstream the 100 kW wood-chips combustion boiler. The purpose was to study the long-term operation stability of the ESPs', power consumption and the mass and fractional collection efficiency of the precipitators.

The particle mass concentration in the gas flow upstream and downstream of the ESPs' was measured by gravimetric method according to the German norm VDI 2066. For the measurements of particle number concentrations in the gas flow, the Scanning Mobility Particle Sizer (SMPS, Fa. Grimm) was applied.

The stability of the operation of the precipitator was ensured by the protection of the high voltage insulator with a screen electrode from the direct particle loaded gas flow. The ESPs' were operated without any additional air input for the high voltage insulators protection from loading with fine particles (Bologa *et al*, 2011).

The CAROLA-precipitators were operated with relatively small electrode gaps in the ionizer at maximum operation voltage of 20 kV and corona current of 1,5 mA. Thus the designed precipitators were characterized by the low power consumption.

The designed CAROLA-electrostatic precipitators are the space-charge ESPs' in which particles are precipitated on the surface of the grounded brush electrodes installed in the collector stage of the unit (Bologa *et al*, 2012). A single brush electrode is currently used in the ESP modules up to 25 kW boiler and double brush electrodes are used in the ESPs' for the boilers with capacity of 50 kW. In the designed modules, the automatic cleaning of the collector stage is realised by the periodical rotation of the brush electrode(s).

Among the control of fine particle emissions, in the current work it is planned to discuss the results of the measurements of the gaseous emissions from the wood combustion boiler and the possibilities for their reduction.

Bologa A., Paur H.-R., Ulbricht T., Woletz K., (2010), *Chemical Engineering Transactions*, **22**, 119-124, DOI: 10.3303/CET1022019.

Bologa A., Paur H.-R., Woletz K. (2011), *International Journal on Plasma Environmental Science & Technology*, **5 (2)**, 168-173.

Bologa A., Paur H.-R., Seifert H., Woletz K., Ulbricht T. (2012), *Management of Environmental Quality: An International Journal*, **23 (**1), 36-55.

Comparison of Methods for On-Line Measurement of Diesel Particulate Matter

Z. Liu, J. Swanson, D.B. Kittelson and D.Y.H. Pui

Department of Mechanical Engineering, University of Minnesota, Minneapolis, MN, 55455, USA
Keywords: Diesel emissions, Aggregates, Mass concentration, Soot size distribution.
Presenting author email: jswanson@me.umn.edu

Gravimetric analysis is the regulatory method for diesel particulate mass measurement. Due to inherent problems such as adsorption/volatilization artifacts, it faces obstacles in measuring ultra low level emissions from modern diesel engines. Alternative methods of suspended particle mass measurement have been developed that showed significant improvements in time resolution, sensitivity, and accuracy. Three size-resolved methods were considered here. Two methods rely on inverting number size distributions obtained using a scanning mobility particle sizer (SMPS). Inversion techniques were based on effective density measurements (Park *et al*., 2003) and the Lall-Friedlander (2006) aggregate model. The third method employed the Universal Nanoparticle Analyzer (UNPA) (Wang *et al*., 2010) to measure the aggregate size distribution, from which mass is calculated.

We compared the results with gravimetric analysis (Figure 1) and found correlations ranging from high (R^2 >0.99) to modest (R^2 =0.61), depending on the method. The ratio of alterative method to filter mass concentration was calculated to be 0.99 ± 0.04, 0.47 ± 0.03 and 0.45 ± 0.19 for the effective density method, the Lall-Friedlander inversion, and the UNPA, respectively over a wide range of engine operating conditions. A catalytic stripper (CS) was used to evaluate the impact of semi-volatile particles and hydrocarbons on mass measurement. Results obtained by comparing "CS and "no CS" results suggested there were no sampling artifacts due to adsorption of gaseous hydrocarbons on the filter.

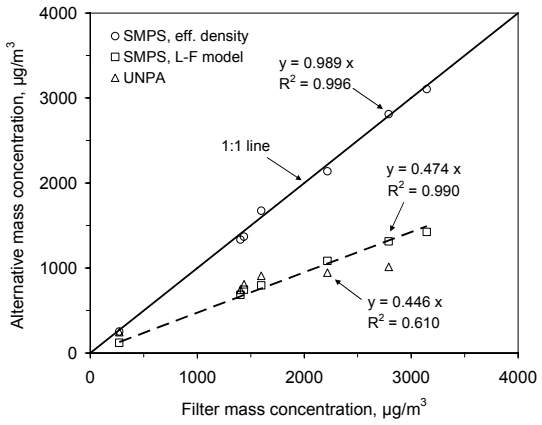

Figure 1. DPM mass concentrations by alternative methods in comparison to gravimetric analysis.

We also compared the diesel aerosol mass distributions obtained by the on-line methods. Figure 2 shows agreement to 15% - 20% in terms of mass mode measured by the different methods. As with the total mass concentration, the lower differential concentrations in reference to the effective density measurements are thought to arise from the fact that the diesel soot structure does not satisfy the loose aggregate assumption in the Lall-Friedlander model. Calculations based on particle counting uncertainty indicated that these on-line methods have a measurement sensitivity that is several orders of magnitude higher than that of the gravimetric analysis.

This study further demonstrated the robustness and value of the effective density measurement. Other results suggest that mass concentrations calculated using available aggregate models are limited in accuracy. Further work is needed to better understand the extent to which diesel particles can be modelled as loose aggregates. This will require better characterization of the charging and drag properties of particles found in diesel exhaust.

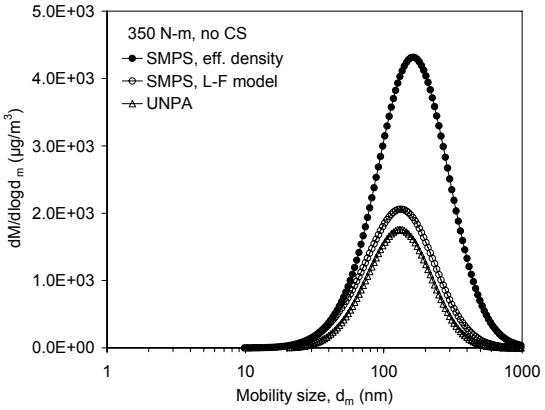

Figure 2. Comparison of DPM mass distributions measured by different on-line methods.

This work was supported by the Center for Filtration Research at University of Minnesota. Experiments were carried out in facilities of Center for Diesel Research at the same institution.

Park, K., Cao, F., Kittelson, D.B. and McMurry, P.H. (2003) *Environ. Sci. Technol.* **37**, 577-583.

Lall, A.A. and Friedlander, S.K. (2006) *J. Aerosol Sci.* **37**, 260-271.

Wang, J., Shin, W.G., Mertler, M., Sachweh, B., Fissan, H. and Pui, D.Y.H. (2010) *Aerosol Sci. & Technol.* **44**, 97-108.

Laboratory investigation of PAH transformation during NO_2-based DPF regeneration

J. C. Wolf and R. Niessner

Chair for Analytical Chemistry, Technical University of Munich, Marchioninistr. 17, 81377, Munich, Germany

Keywords: PAH, oxygenated PAH, NO_2, Diesel exhaust, Filter.
Presenting author email: jan.wolf@mytum.de

In the meantime Diesel Particle filters (DPF) are an inherent part of our present automotives. These filters drastically reduce the emitted mass of soot particles. Because soot is a known carcinogen, this technology seems to be very beneficial to human health. But the carcinogenic potential of soot is mainly attributed to the adsorbed pollutants on the soot surface. Especially polycyclic aromatic hydrocarbons (PAH) are considered responsible for the mutagenic potential. To prevent DPF plugging and engine damage in consequence, these filters have to be regenerated. In many cases this is achieved by increasing the amount of NO_2 in the exhaust stream to alleviate the soot oxidation. During this regeneration the PAH are affected as well and will most likely follow one of two possible reaction pathways. During reaction with NO_2 they can be either oxidized or nitrated. Both reactions would lead to more toxic PAH derivates as oxygenated PAH (OPAH) or nitrated PAH (NPAH).

Our research tries to identify whether PAH nitration or oxidation is the most predominant transformation reaction during DPF regeneration. Therefore a laboratory simulation system for diesel exhaust gas mimic was constructed. In this setup spark-discharge soot, which is PAH-free, is coated with a submonolayer of benzo[a]pyrene (B[a]P) and directed to a miniaturized DPF (PM-Kat®-like) structure, where it gets trapped. The regeneration of the filter structure can be controlled by temperature as well as the amount of NO_2 or oxygen passing through. Even different regeneration cycles can be simulated with this system, with the advantage, that only one PAH (here B[a]P) and its reaction products are monitored.

To ensure artifact free sampling a highly efficient NO_2 denuding system was placed in line after the DPF structure prior to sampling. Right after the NO_2 denuding system the gaseous reaction products were sampled by use of a XAD4 coated annular denuder. The particle phase was collected downstream on a quartz fiber filter. The NO_2 denuding system is limited to a sampling gas temperature of <200°C. So we investigate the temperature range of 25°C up to 200°C.

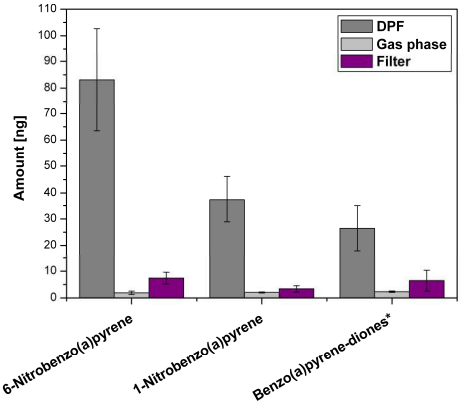

Figure 1.: Nitro- and oxy-B[a]P formation in the PM-Kat® like simulation system at 100°C and 50 ppm NO_2.(*sum of 1,6-, 3,6- and 6,12-B[a]P-dione)

Analysis was carried out by means of HPLC coupled to a high resolution mass spectrometer (*Thermo Fisher Exactive Orbitrap*). Ionization was performed by atmospheric pressure chemical ionization (APCI). This method is very sensitive for NPAH as well as for OPAH (LOD in the range of 0.05 – 0.50 Pg/µl; 10 µl injection Volume). Additionally the high resolution full mass scan (100-800 m/z) enables screening and identification of unknown reaction products.

Our experiments show that B[a]P is transformed into 1-,3- and 6-nitro-B[a]P as well as into B[a]P-diones. This transformation takes place exclusively in the DPF structure and is dependent on the NO_2 concentration passing the DPF. Our results find nitration is the preferred reaction mechanism at temperatures up to 100°C (see. figure 1). Nevertheless, our findings indicate oxidation might become the more important pathway with further temperature increase.

In summary, our results prove the transformation of B[a]P to nitrated and oxygenated derivates inside a DPF, continuously regenerated with NO_2.

Carrara M., Wolf J.-C., Niessner R. (2010), *Atmospheric Environment*, **44**, 3878-3885.

Wolf J.-C., Niessner R. (2012), *Analytical and Bioanalytical Chemistry* (submitted)

Comparison of genotoxicity of exhaust from a diesel, biodiesel and rapeseed oil powered engine – pilot study

J. Topinka[1], A. Milcova[1], J. Schmuczerova[1], M. Mazac[2], M. Pechout[2], M. Vojtisek-Lom[2]

[1]Department of Genetic Ecotoxicology, Institute of Experimental Medicine AS CR, Prague, 142 20, Czech Republic
[2] Department of Vehicles and Engines, Technical University of Liberec, Liberec, 461 17, Czech Republic
Keywords: diesel exhaust, biofuels, particulate matter, genotoxicity.
Presenting author email: jtopinka@biomed.cas.cz

Introduction

Last decades are characterized by massive use of alternative fuels, including biofuels. Since the reports on the toxic effects of exhaust from engines powered by biofuels are often contradictory, it might be of great interest to compare genotoxicity of standard diesel particulate emissions with that of the most frequently used biofuels. For this purpose we performed the pilot study with the aim to identify possible genotoxicity induced by organic extracts from the samples of exhaust of engines running on diesel fuel, biodiesel (neat methylester of rapeseed oil) and neat heated, fuel-grade rapeseed oil. The engines were tested in a laboratory using engine dynamometers.

Methods and Results

In one set of tests, a Zetor tractor engine with an inline mechanical injection pump and no exhaust gas aftertreatment device was tested using the NRSC cycle (also the ISO-8178 test with C-1 weighing, normally used for certification of non-road engines) and the ISO-8178 test with C-2 weighings, representing low-load operation. A sample of undiluted exhaust was drawn through a cartridge with a fluorocarbon-coated filter and two polyurethane foam plugs, with 2.0-3.5 m^3 of exhaust sampled. As a marker of the genotoxic potential, DNA adduct levels induced by extractable organic matter (EOMs) in an acellular assay of calf thymus DNA coupled with ^{32}P-postlabeling in the presence and absence of microsomal S9 fraction (contains enzymes for metabolic activation of genotoxic compounds such as PAHs) were employed. Simultaneously, chemical analysis of 16 priority PAHs in EOMs, including 7 carcinogenic PAHs (US EPA) was performed. The results suggest that on ISO-8178 non-road engine test cycle, C-2 schedule, representing low engine loads, the organic extract from standard diesel particulate emissions induces highest DNA adduct levels (53 adducts/10^5 nucleotides/ kWh), while rapeseed oil and methyl esters of rapeseed oil induce 5.8 and 2.4 adducts/10^5 nucleotides/ kWh, respectively. These results correlate with the content of carcinogenic PAHs (c-PAHs) and B[a]P in the corresponding EOMs.

In a second set of tests, the exhaust was routed to the laboratory main exhaust duct, which has served as an improvised full-flow dilution tunnel, with dilution ratio of approximately 1:100 at idle to 1:15 at full load. From this duct, diluted exhaust was sampled with high-volume samplers (Digitel) on the Teflon coated filters (Pallflex) normally used for ambient air quality measurements, at rates 500-1000 litres per minute, with a target accumulation on the order of 10 mg of particulate mass. Two engines were tested. One was a Cummins ISBe4 engine with a Common Rail fuel injection system and no exhaust gas aftertreatment device, tested using the World Harmonized Stationary Cycle (WHSC) and modified Engine Stationary Cycle (ESC). The ESC cycle was modified by altering the length of each of the 13 modes and including transitions between modes to facilitate continuous sampling. The other engine was the Zetor engine described above, which was tested using the NRSC cycle. Filters were extracted by dichlormethane and genotoxicity of extracts was analyzed by ^{32}P-postlabelling of DNA adducts by test described in the previous paragraph. Major results are described in Table 1.

Table1. Genotoxicity of the organic extracts from particulate emissions of selected fuels

Engine fuel injection	Fuel /cycle	PM mg/kWh	7c-PAH µg/kWh*	DNA add. /10^8 n./kWh**	
				+S9	-S9
Cummins ISBe4 Common Rail	D[1]/WHSC	6.9	0.59	271	119
	R[2]/WHSC	7.2	0.77	198	16
	D[1]/ESC	14.1	2.05	648	175
	R[2]/ESC	23.8	1.76	473	182
	B[3]/ESC	20.2	1.63	542	182
Zetor 1505	D[1]/NRSC	185	18.33	3678	1038
	R[2]/NRSC	202	11.39	2950	1096

*7 carcinogenic PAHs: benzo(a)anthracene, chrysene, benzo(b) fluoran-thene, benzo(k)fluoranthene, benzo(a)pyrene, indeno(1,2,3-cd)pyrene, dibenzo(a,h)anthracene; **DNA adducts/10^8 nucleotides/kWh; [1]D-diesel; [2]R-rapeseed oil; [3]B-biodiesel B-100

Conclusions

1. The emissions of classic diesel contain more of total PAHs, but much less B[a]P and other carcinogenic PAHs.
2. Genotoxicity of particulate emissions of selected biofuels is comparable with a classic diesel.
3. Metabolic activation (+S9) resulted in several fold higher genotoxicity suggesting major contribution of PAHs to the DNA adduct levels. However, directly acting genotoxicants (-S9) are also significant.
4. Genotoxicity is highly dependent on the test cycle (ESC vs. WHSC).
5. Genotoxicity of the emissions is dose dependent.

These results should be taken as preliminary and more detailed study is going on to verify these preliminary findings.

Acknowledgements: Supported by the LIFE+ project MEDETOX (LIFE10ENV/CZ/651) and by the Czech Science Foundation grants #101/08/1717 (rapeseed oil combustion) and P503/11/0142 (toxicology).

Experimental Investigations of Sensitivity of Lichens to Diesel Exhaust under Lab Conditions

U. Langmann[1], P. Madl[2], W. Hofmann[2], G. Brunauer[1], R. Türk[1]

[1]Department of Organismic Biology, University of Salzburg, A-5020 Salzburg, Hellbrunnerstr. 34, Austria
[2] Department of Materials Science & Physics, University of Salzburg, A-5020 Salzburg, Hellbrunnerstr. 34, Austria
Keywords:, Diesel exhaust, air pollution, laboratory experiments
Presenting author email: ulrike.langmann@stud.sbg.ac.at

The lichen vegetation reacts very sensitively to increased nitrogen-concentrations as well as to traffic exhaust and other pollutants in the air. Therefore, lichens are reliable indicators for air pollution. Recent environmental studies have shown that the loss of acidophytic lichen species and the increase of nitrophytic lichens can be explained by the increasing input of atmospheric generated nitrogen-compounds related to nanoparticles (Heinzelmann, 2007; Madl et al., 2010). This observed decreasing diversity of lichens due to increasing air pollution is followed and accompanied by a decrease in diversity of higher plants and animals and is therefore regarded as an optimal biomonitor for air pollution.

By the investigations presented here the effects of Diesel exhaust on the symbionts of six lichen species with different pollutant sensitivities are analysed. In a sealed stainless steel-chamber the pollution with Diesel exhaust was simulated for three weeks, which corresponds to the rhythmic rush hours cycles of a local highway. The closed chamber guarantees, that influences other than Diesel exhausts are excluded. Diesel Aerosols were fed into the chamber using a Tedlar-bag. Appropriate humidity levels were provided using an impiger powered with Hepa-filtered air. As a light source a HQ-400W lamp was used. A water-cooled system kept the tank temperature at physiologically optimal levels. Nanoparticles were quantified with an SMPS-system and the photosynthetic activity of lichens was measured with both a chlorophyll-fluorescence - Imaging-PAM as well as Mini-PAM devices. Vitality of lichens was determined by CO_2 gas exchange measurements.

The investigations provide explicit data, which show the negative effect on the photosynthesis of the lichens‘ photobionts. The measurements of treated lichens with Mini-PAM reveal that the electron-transport-rate ETR does not differ significantly from lichens, which are not exposed to Diesel exhaust.

The distinct quenching-rates qP and qN of fluorescence trends are evidence of the negative impact of Diesel pollutants (see Fig. 1 and Fig. 2). Therefore, we conclude: Diesel exhaust does not interfere directly with the photosystem II but affects the proton-gradient at the membrane between photosystem II and ATP-Synthase. Hence, ATP- and NADPH-yields along with the associated carbohydrate-synthesis of the Calvin-cycle of the photobiont are impaired. In effect the photobiont dies. The mycobiont is starved as it is dependent on the carbohydrate-synthesis of the photobiont.

Another remarkable result of this preliminary study is that the lichens are showing signs of regeneration when they are not exposed to Diesel-exhaust over week-ends as they regain nearly the same PAM-values as at the beginning of the investigations.

During these experiments we could also assess the optimal light, moisture and temperature conditions for the following long-term studies in order to eliminate light- and heat-stress.

To our knowledge this is the first study testing the impact of Diesel exhausts on lichens under laboratory conditions eliminating other interfering factors like in other environmental studies.

Heinzelmann E. (2007) *Highway exhaust aerosols and their effects on Alpine Lichen populations*, Diploma-Thesis, University of Salzburg, FB-Organismic Biology, Austria.

Madl P., Heinzelmann E., Hofmann W., Türk. R. (2010) *Motorway exhaust aerosols and their effects on epiphytic lichen populations*, Gefahrstoffe Reinhaltung der Luft, Springer-VDI-Verlag, Düsseldorf. **4**:147-153

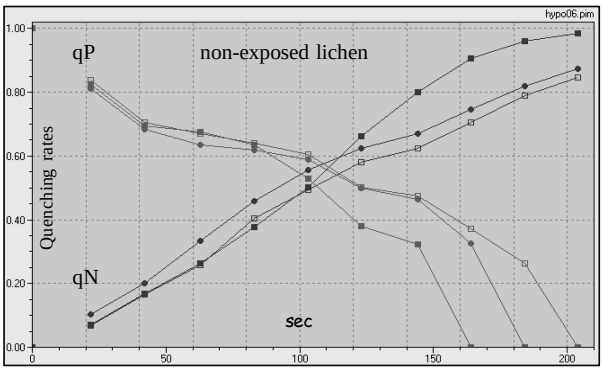

Figure 1: qP-Curves (down) and qN-Curves (up) at 3 measuring points of one non-exposed lichen (*Hypogymnia physodes*)

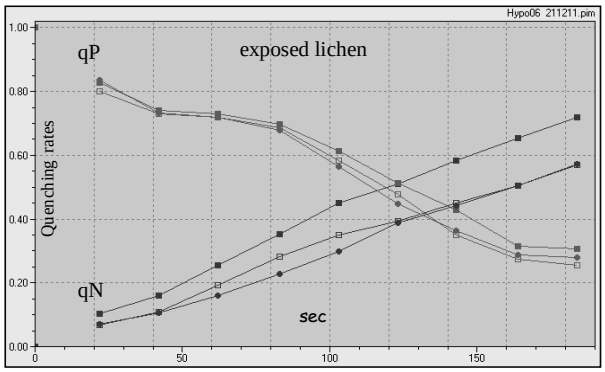

Figure 2: qP-Curves (down) and qN-Curves (up) at 3 measuring points of one exposed lichen (*Hypogymnia physodes*)

Nanoparticle emissions from ships calling the port of Gothenburg

J. Westerlund[1], M. Hallquist[1] and Å.M. Jonsson[2]

[1]Atmospheric Science, Department of Chemistry and Molecular Biology, University of Gothenburg, 412 96, Gothenburg, Sweden
[2]IVL Swedish Environmental Research Institute Ltd, Box 5302, 400 15, Gothenburg, Sweden
Keywords: shipping emissions, emission factor, coastal area, number size distribution
Presenting author email: jonathan.westerlund@chem.gu.se

Shipping is an important contributor to global emissions of air pollutants affecting both climate and health. Emissions from shipping are poorly regulated in legislation and 70 % of ship emissions occur within 400 km off land (Corbett et al., 1999). Ultrafine particles (UFP) are recognized to be one of the key elements in urban air pollution and particle number is believed to be a better measure for health effects than currently regulated mass standards (Kumar et al., 2010). In this study both number, mass and size of volatile and non-volatile particles are addressed.

Stationary ship plume measurements were conducted according to previous studies on shipping and road side measurements (Hak et al., 2009; Jonsson et al., 2011). The site was located in the entrance to the port of Gothenburg, the largest port of Scandinavia, which is an emission control area (ECA) with a newly introduced regulation limiting the fuel sulphur content to 1 % by weight. Particles were characterized using CO_2 as a tracer for fuel combustion and EFs (Emission Factors) were calculated using Eq.1:

$$\mathrm{EF_{part}} = \frac{\Delta \mathrm{part}}{\Delta \mathrm{gas}} \times \mathrm{EF_{gas}} \qquad (1)$$

where $\Delta part$ and Δgas are changes in particle number /mass and CO_2 during ship passages and EF_{gas} is the EF for CO_2.

The measurements were performed for real world dilution and for plume age time scales relevant to a harbour city (30-500 s), allowing plumes to travel several kilometres inland. Ship particle number EFs on individual basis are currently scarce and number emission factors cause the biggest uncertainty in dispersion modelling (Holmes and Morawska 2006).

In a previous study 734 EFs for particle number and mass were determined (Jonsson et al., 2011) and they have now been further extensively analysed. 613 ship passages were coupled to identifiable ships using AIS-data (Automatic Identification System) and were found to originate from 154 different ships. They were divided into 3 ship classes, as presented in Table 1. Significant differences were found between the ship classes both regarding particle number, mass, size and volatility. Engine load was found to be an important factor and was indirectly studied by comparing ship speed and acceleration differences between the ship passages. Age also seemed to have an effect on the EFs with a few older ships emitting more particles. An SCR-equipped passenger ship was analysed specifically. This ship had a remarkably high non-volatile number EF when leaving the harbour (2.3 times higher than the other departing ships).

In a typical harbour a number of supporting ships are in addition to the main cargo and passenger ship also active. It was demonstrated that for example tug and pilot ships had distinctly different particle emission characteristics. The differences between the individual ships and classes are important features and are discussed in relation to other studies and the air quality in harbour cities.

Table 1. Three ship classes with EFs for number and mass together with the log-normal distribution fit parameters CMD (count median diameter) and GSD (geometric standard deviation).

		Total particles (Non-volatile particles)			
Ship class	Speed ($m\ s^{-1}$)	EF_{PN} # $(kg\ fuel)^{-1}$ $\times 10^{16}$	EF_{PM} mg $(kg\ fuel)^{-1}$ $\times 10^{16}$	CMD (nm)	GSD
Cargo	8.49± 0.29	2.86±0.21 (1.39 ± 0.33)	2590±196 (521±110)	38.8 (13.3)	1.56 (1.57)
Non-cargo	10.4± 0.29	2.37±0.20 (1.33 ± 0.43)	2230±687 (432±92.2)	40.3 (13.7)	1.54/ 1.54
Tug/ Pilot	15.2± 1.68	1.67±0.27 (0.52±0.22)	1190±868 (404±251)	29.7[a], 10.3[a] (10.3)	1.73[a], 1.20[a] (1.35)

[a]Tugs and pilots had for the total particles a bimodal size distribution

This work was financed by ÅForsk (Ångpanne-föreningen's Foundation for Research and Development), The Foundation for the Swedish Environmental Research Institute, SIVL and the Graduate School Environment and Health.

Corbett, J, J., Fischbeck, P, S., Pandis, S, N. (1999) *J. Geophys. Res*, **104**, 3457-3470

Hak, C. S., Hallquist, M., Ljungström, E., Svane, M., Pettersson, J. B. C. (2009) *J. Atmos. Environ*, **43**, 2481-2488.

Holmes, N, S and Morawska, L. (2006) *J. Atmos. Environ*, **40**, 5902-592

Jonsson, Å, M., Westerlund, J., Hallquist, M. (2011) *Geophys Res. Lett*, **38**, L13809

Kumar, P., Robins, A., Vardoulakis, S., Britter, Rex. (2010) *J. Atmos. Environ*, **44**, 5035-5052

Detailed chemical characterization of PM and COV, and source apportionment near a French highway

L. Polo[1, 3], C. Piot[1, 2], A. Charron[3], J. Cozic[1], B. Temime-Roussel[4], N. Marchand[4], J.L. Besombes[2] and J.L. Jaffrezo[1]

[1]Université Grenoble 1-CNRS-LGGE, St-Martin d'Hères, France
[2]Université de Savoie-LCME, Le Bourget du Lac, France
[3]IFSTTAR, Bron, France
[4]Aix Marseille Univ., LCE, Marseille, France
Keywords: Traffic emissions, re-suspension, road dust, organic speciation, France.
Contact email: polo@lgge.obs.ujf-grenoble.fr

The relation between exposure to ambient fine particulate matter (PM) and human mortality is now well established, particularly in the roadway proximity. Further, Hoffman et al (2009) showed the link between long-term residential exposure to high level of PM and coronary atherosclerosis. Improving air quality for reducing morbidity and premature death has become an urgent need. In spite of the evolution of vehicle motorization, the PM_{10} level has not been decreasing proportionnally in urban environments during the last decade (Harrison, 2008). The characterization and quantification of traffic emissions are still poorly known for the French motor vehicle fleet. These emissions involved exhaust and non-exhaust emissions (i.e. road-traffic like re-suspension of road dusts, from brake, tyre and road-surface-wear, from the corrosion of vehicle components…). The PM_{10} emissions related to traffic can represent up to 60% non-exhaust emission (Bukowiecki, 2010). A detailed chemical characterization of exhaust and non-exhaust traffic related emissions is still needed.

In order to characterize the chemical composition of traffic sources, detailed measurements were performed in the vicinity a suburban highway characterized by regular traffic congestions in Grenoble-Echirolles (France). Measurements were simultaneously conducted at an urban background site (Grenoble-Les Frênes), 2.5km away. This two weeks campaign took place in September 2011 within the MOCOPO and PM-Drive programs. PM_{10} and Volatile Organic Compounds (VOCs) were sampled on a 4h basis at the two different locations. In addition, high time resolved measurements (HR-ToF-AMS, PTR-ToF-MS, MAAP, SMPS…) were performed at Grenoble-Echirolles. At the same time, the traffic on the highway was recorded with a high temporal resolution (loops and systems allowing vehicles identification).

HR-Tof-AMS has been used to measure the concentration and chemical composition of the non-refractory submicron aerosol. Figure 1 presents the temporal evolution of two well-known fragments derived from AMS measurements: mz 57 (mostly $C_4H_9^+$) and m/z 44 (mostly CO_2^+), considered as markers of HOA associated with fuel derivatives emissions and OOA associated with secondary organic aerosol respectively. The mz 57 fragment follows clear daily cycles highly correlated with traffic and BC (MAAP). The evolution of mz 44 is completely different, and is well related with that of ions from secondary origins like sulfate, nitrate, and ammonium. A strong link also exists with the weather pattern during this two-week campaign. These first results allow already a distinction between the traffic emissions and others sources, which is a good foundation for this study.

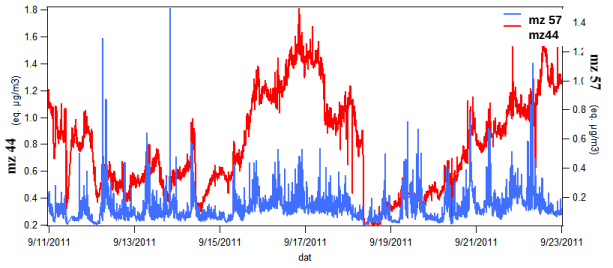

Figure 1: Temporal evolution of the fraction m/z 57 and m/z 44 at Echirolles (France)

Off-line sampling allows the detailed chemical characterization of aerosols notably the organic speciation with the aim of research of source tracers and determination of chemical fingerprints of large chemical families (hydrocarbons, PAH, saccharides…). About eighty compounds have been quantified. Further, a large array of trace metals was also measured on these filters. From these results, both the Chemical Mass Balance (CMB) and Positive Matrix Factorization (PMF) models will be used in order to apportion the contribution of influential sources including non-exhaust traffic emissions. These results will be presented and compared with on-line data and with traffic.

L. Polo and C. Piot thank the Rhône-Alpes Region for their PhD grants. Campaigns in France were supported by the French Ministry in charge of Transport (MOCOPO program) and by the French Environmental agency ADEME (PM-DRIVE program).

Hoffmann, B., Moebus, S., Dragano, N., Stang, A., Möhlenkamp S., Schmermund, A., Memmesheimer, M., Bröcker-Preuss, M., Mann, K., Erbel, R., Jöckel, KH. (2009) *Env.Health Pers. 117:8*

Harrison, RM., Stedman, J., Derwent, D., (2008) *Atmosph. Environ. 42:603-6*

Bukowiecki N., Lienenmann, P., Hill, M., Furger, M., Richard, A., Amato, F., Prévot ASH., Baltensperger, U., Buchmann, B., Gehrig, R. (2010) *Atmosph.Environ 44:2330-2340*

Time-resolved NO_2 analysis in the presence of soot

J. C. Wolf, K. Thaler, R. Niessner, and C. Haisch

Chair for Analytical Chemistry, Technische Universität München, Marchioninistr. 17, 81377, Munich, Germany

Keywords: NO_2, soot, transient analysis, Diesel exhaust, sampling artefact.
Presenting author email: Christoph.Haisch@ch.tum.de

Nitrogen dioxide plays a major role in Diesel exhaust aftertreatment technology as well as in atmospheric transformations. NO_2 is routinely monitored, either by FT/IR spectrometers or by chemiluminescence detectors. Both are commonly used in automotive exhaust measurements at test bench experiments, where a time resolution in the range of a second is required. Since soot particles cause contamination and artefacts in both measurement techniques, the soot particles are filtered in front of the measurement devices. Several authors did report about the heterogeneous reaction of NO_2 and soot. However, there are hardly any systematic investigations devoted to the consequence of these interactions on the precision of NO_2 measurement, and particularly to transient analyses. Over an instrument service period, the pre-filter of these instruments can acquire significant loads of soot, which can influence the NO_2 measurements to varying amounts. Even more severe, we observed this effect not only on filters, but also in the tubings and gas handling system, transferring the gas from the emission source to the analysis instrument.

Our investigations focus on the artefacts induced by soot-loaded filters and contaminated tubings on the total NO_2 concentration, and particularly to the influence on the temporal dynamics of the instrumentation. A propane burner (in-house made) and a spark discharge generator (Palas, GFG1000) were employed to systematically load tubings and filters with soot. In this investigation, PVC, Tygon®, Teflon®, stainless steel tubings, and quartz fiber filters were investigated. After weighting, the soot loaded tubings and filters were exposed for 3 minutes to high concentrations of NO_2 (~100 ppm). The transmitted NO_2 concentrations were measured using a newly developed photoacoustic sensor, which allows for the simultaneous detection of soot and NO_2 sensor with a response time below 1 s. Filter experiments were performed at different reaction temperatures between 20°C to 75 °C, while the tubing experiments were carried out at 20°C only.

Our first results show a significant influence of the soot load in tubings and filters on the rise time of the NO_2 and, depending on the experimental conditions, also on the absolute concentrations (see Fig. 1). These effects are more pronounced for spark discharge soot than for flame soot, which can be attributed to the higher reactivity of the former. This observation suggests the reaction mechanism proposed by Tabor et al., where NO_2 is adsorbed to the reactive sites in a first reaction. In a second step, the adsorbed molecules oxidize this active site and are released as NO, which results in a passivation of the soot surface. As it can be seen in Fig. 1, a second exposure period of the same filter to NO_2 was less affected by artefacts, which again favours the passivation of the surface during the first NO_2 exposure.

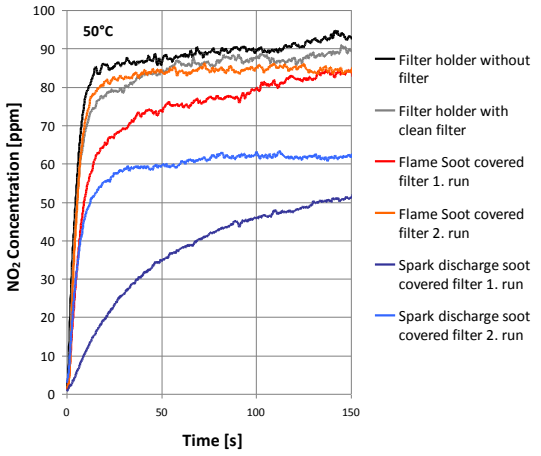

Figure 1.: NO_2 concentration (at 50 °C) downstream a filter holder: (black) without filter; (grey) with a clean quartz fiber filter; (red/orange) with a propane soot loaded filter; (dark blue/blue) with a spark discharge soot loaded filter.

Similar effects were observed for soot loaded tubings, where the tubing material influences the effects quantitatively. In contrast to the filter analyses, full transmission is reached for any material after a certain time (seconds to minutes).

In summary, our results suggest a significant risk of artefacts during NO_2 measurement in the presence of soot aerosol. This effect might be minimized by increasing the sampling gas flow and using PVC or Tygon® tubings.

Tighe C. J., Twigg M. V., Hayhurst A. N., Dennis J. S (2011) *Industrial & Engineering Chemical Research*, **50**, 10480-10492.

Schmid, J.; Grob, B.; Niessner, R.; Ivleva, N. P., (2011) *Anal. Chem.*, **83**, 1173-1179.

Particle size and number distribution of particles emitted by a modern diesel engine using mineral diesel and Biodiesel from Soybean

C. C. Barrios S, A. Domínguez-Sáez, C. Martín Jiménez
Environmental Department, CIEMAT, Avda. Complutense, 22. 28040, Madrid, Spain

Keywords: Biofuels, nanoparticles, particle size distribution and vehicles emissions.
Presenting author email: carmen.barrios@ciemat.es

For several decades, studies have shown the biodiesel of vegetal origin as a good substitute for mineral diesel in its application as a fuel for diesel engines because of its energy efficiency and emissions with less environmental impact (Chung *et al.*, 2008). However, the knowledge of the direct relationship between human health problems and the emission of nanoparticles from internal combustion engine has generated the necessity to know the physical characteristics of these particles when they come from the biodiesel blends combustion in different proportions and their differences with the particles from mineral diesel combustion (Avinash *et al.*, 2011). So far, studies on exhaust emissions from diesel engines have shown that particulate emissions from these engines are one of their biggest problems (Tzamkiozis *et al.*, 2012). The aim of this study is to make a comparative study of the distribution in size and number of particles emitted by a modern diesel engine (EURO 4, TDI) working with mineral diesel versus a blend of mineral diesel-biodiesel of vegetal origin (soybean) in a proportion of 30% by volume (B30). The choice of this blend proportion is because this is the maximum proportion of biodiesel which does not affect significantly the operating conditions of the inlet system elements of the motor and the ignition delay (Buyukkaya., 2010).

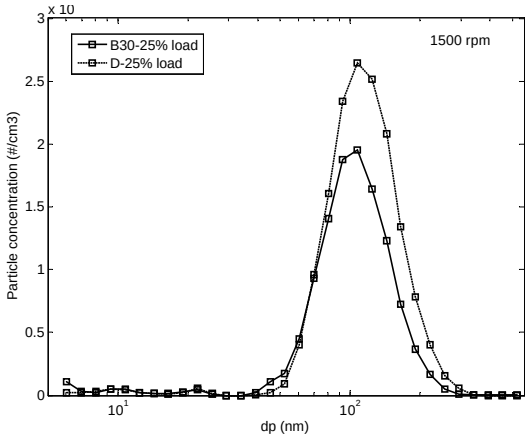

Figure 1- Particle size and number distribution at 25% rated engine load for 1500 rpm using mineral Diesel and Biodiesel (B30).

For load operating conditions tested (25%) at 1500 rpm, it have been observed a decrease in number of total particles of about 25% and an increase in particle sizes below 50 nm emitted by the motor operating with B30, in comparison to mineral diesel. Figure 1 shows the particle size and number distribution emitted during operation at 25% load with mineral Diesel and Biodiesel (B30) and it is important the differences in emission sizes lower than 50 nm from the B30 at same speed and engine load. In Figure 2 the same behaviour observed at 2500 rpm with 25% load, and a displacement of maximum of the curve toward smaller sizes.

The experience of this work has been very helpful, bringing us closer to understanding the physical characteristics of particles emitted by a diesel engine operating with Biodiesel from Soybean and the difference from the particle emitted by the same engine operating with mineral diesel. All experiments that provide results in an increase of the nanoparticles are an important source of information to evaluate the impact (over human health) of widespread use of biofuels in vehicle fleet, especially in urban areas.

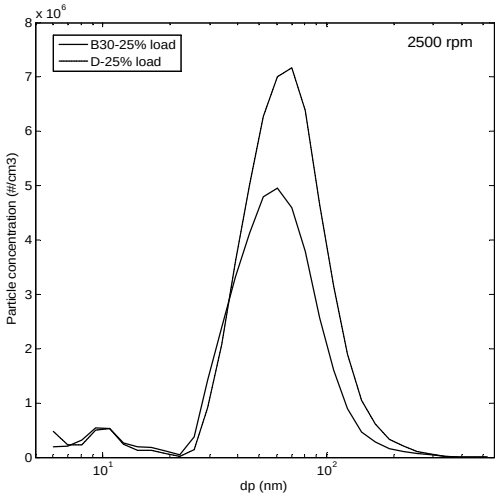

Figure 2- Particle size and number distribution at 25% rated engine load for 2500 rpm using mineral Diesel and Biodiesel (B30).

Chung, A. Lall, A.A. Paulson, S.E. (2008). Atmospheric environment. 42 2129-2140.
Avinash, K. Tarum, G. Abhishek, K. (2011). Renewable and Sustainable Energy Reviews. 15 3278–3300.
Tzamkiozis, T. Ntziachristos, L. Mamakos, A. Fontaras, G. and Samaras Z. (2012). Aerosol Science and technology. 45:5, 587-595.15.
Buyukkaya, E. (2010). Fuel, 89 3099-3105.

Measuring black carbon emission factors of cars in real driving conditions

I. Ježek[1], G. Močnik[1]

[1]Aerosol d.o.o., Ljubljana, SI-1000, Slovenia
Keywords: emission factors, cars, diesel emissions.
Presenting author email: irena.jezek@aerosol.si

Describing the influence of traffic on air pollution is complex. The amount of emitted pollutants depends on the vehicle engine, its maintenance, quality and consumption of fuel, filtering or processing of fuel, fluency of traffic, driving regime, topography, and weather conditions. For evaluation of the amount of pollutants emitted, several different tests can be used. Efficiency of combustion is given as an emission factor expressed as either mass of pollutant per fuel consumed or per driven kilometer. Tests for individual vehicles are usually performed in laboratories with dynamometers. With these tests we can get information about influence of used fuel, fuel additives, accelerations, engine type, temperature, dilution etc. These tests are expensive, time consuming and describe emissions of only few vehicles which are supposed to represent the fleet average. As shown in before, Kirchstteter et. al. (1999) and Wang et al. (2011), few individual vehicles (super emitters) can contribute significantly to the fleet emissions, much more than the average vehicle in the fleet.

In previously mentioned studies there have been two different approaches to measuring emissions of individual heavy duty vehicles. The first, performed by Kirchstetter et. al. (1999), measured transient increases of different pollutant concentrations emitted by individual vehicles passing a stationary measuring site. The second, performed by Wang et al. (2011), measured plumes of individual vehicles by chasing them on the road with a mobile station. Because the number of diesel cars is significant in Europe and therefore information on super emitters in the car fleet important, we wanted to test how these two methods work on cars, where the different pollutant emissions are much lower.

We have tested both methods on 4 different diesel cars. The first method was performed with the car passing the measuring site at two different speeds and while accelerating. We have measured concentrations of black carbon (prototype Aethalometer AE33), particle number concentration (FMPS, ELPI+) and CO_2 (Vaisala Carbocap343) on a safety training track field, where there were no other vehicles present at that time.

We have found that measured emission factors can be very versatile for one vehicle. One of the cars tested was a Euro 5 diesel. It emitted so little emissions that most plumes have not been detected by the stationary method. In Table 1 we report emission factors for three Euro 3 diesel cars while driving at two different speeds and while accelerating.

Table 1 Black carbon emission factors (average, std deviation) for three Euro 3 cars measured on two stationary sampling spots with different road slopes. Site 1 was on flat road, site 2 was on a slope.

Black carbon emission factors [g/kg]		Site 1			Site 2		
		car1	car2	car3	car1	car2	car3
50 km/h	average	0.08	0.03	/	0.03	0.09	0.41
	std	0.02	0.02	/	0.01	0.03	0.14
90 km/h	average	0.06	0.10	0.11	0.03	0.06	0.15
	std	0.02	0.03	0.01	0.02	0.03	0.10
acceleration	average	0.22	0.20	0.32	0.18	0.16	0.51
	std	0.15	0.07	0.21	0.12	0.15	0.23

First results show that black carbon emission factors for these three vehicles vary within each group and that measuring on slope did not increase the emission factor. We will show similar variation for particle numbers.

Table 2 Chasing emission factors for black carbon.

BC emission factor [g/kg]	car 1	car 2	car 3
EF	0.16	0.14	0.33
std	0.03	0.04	0.10

Chasing experiment showed slightly different results with higher EF values (Table 2). These are interpreted as being due to varying speed and acceleration during driving on the test circuit. We will show the importance of setting the right parameters for data processing, such as setting the baseline and errors that can be produced during data evaluation.

Operation is in part financed by the European Union, European Social Fund. We would also like to thank AMZS d.d., PE Center varne vožnje, for letting us use their safety training track to conduct our experiments.

Kirchstetter, T.W., Harley, A., Kreisberg, N.M., Stolzenburg, M.R., Hering, S.V., (1999) *On-road measurement of fine particle and nitrogen oxide emissions from light- and heavy-duty motor vehicles.* Atmosphric Environment 33, 2955–2968.

Wang, X., Westerdahl, D., Wo, Y., Pan, X., Zhang, K. M., (2011) *On-road emission factor distributions of individual diesel vehicles in and around Beijing, China*; Atmospheric Environment 45, 503-51.

2D study of the size and morphological properties of soot emitted by an aircraft advanced combustion chamber

D. Delhaye[1], D. Lottin[1], D. Ferry[2], J.-M. Gay[2] and X. Vancassel[1]

[1]ONERA – The French Aerospace Lab, F-92322 Châtillon, France
[2]CINaM-CNRS UMR 7325, Aix-Marseille University, Campus de Luminy, 13009 Marseille, France

Keywords: Soot nanoparticles, Fractals, Aircraft, Transmission Electron Microscopy.
Presenting author email: david.delhaye@onera.fr

Nowadays, particulate emissions of aircraft engines are a main concern for regulatory agencies because of their influence on the air quality decrease and also on the modification of the atmosphere composition. These particulate emissions are mainly constituted by soot aggregates, which are made of primary nanoparticles. Characterizing their size and their quasi-fractal morphology is required to monitor them through on-line measurement techniques or to evaluate their impact as a pollutant.

Since years, the European Aviation Safety Agency (EASA) funds scientific projects aiming to define a new certification requirement of aircraft engine exhausts, through several "SAMPLE" projects (Petzold et al., 2008, Marsh et al., 2009, Crayford et al., 2010). Part of these projects is devoted to characterize the size and morphology of soot aggregates emitted by a combustion chamber that is coupled to a hot end simulator (Wilson *et al.*, 2004). Eight different engine settings have been investigated, representing a range of running conditions that covers different Carbon/Oxygen ratios, namely the low smoke/low organic (LS/LO), low smoke/high organic (LS/HO) and high smoke/low organic (HS/LO) combustion conditions.

For each condition, soot aggregates have been sampled by impaction on Transmission Electron Microscopy (TEM) grids. We have determined the distributions of the primary particles size and the aggregates gyration diameter from TEM pictures (figure 1). Our results show that whatever the combustion conditions the geometric mean diameter of the primary particles is smaller than 10 nm and the geometric mean gyration diameter of the aggregates is below 100 nm. Moreover, the morphology of soot aggregates has also been investigated for each combustion condition in order to study a potential correlation between the aggregates morphology and the engine combustion settings.

Firstly, the aggregates mass fractal dimension has been determined using classical 2D-3D transposition relationships (Baron and Willeke, 2001) but no significant impact of the combustion settings on the mass fractal dimension has been revealed. Secondly, we used three shape factors, namely the roundness, the aspect ratio and the form factor (Chakrabarty *et al.*, 2006, Hentschel and Page, 2003) to characterize the morphology of soot aggregates according to the engine combustion settings. It appears that there is an impact especially on the ramification of the aggregates. Lower the Carbon/Oxygen ratio is, more ramified the aggregates are.

As a conclusion this work investigates relationship between engine setting and soot morphology. This new approach to characterize the real shape of combustion chamber soot is a more sensible methodology than the only quasi-fractal one. To a further extend it may be a complementary tool to distinguish combustion sources

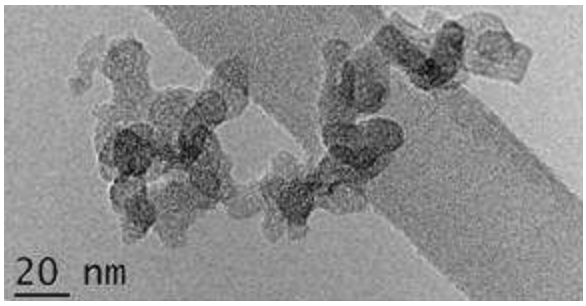

Figure 1. Soot aggregate collected behind a combustion chamber coupled with a hot end simulator

Baron, P.A., and Willeke, K. (2001) *Aerosol measurement. Principle, techniques, and applications* 2nd Edition, John Wiley & sons.

Chakrabarty, R.K., Moosmüller, H., Garro, M.A., Patrick Arnott, W., Walker, J., Susott, R.A., Babbitt, R.E., Wold, C.E., Lincoln, E.N., Hao, W.M. (2006) *J. Geophys. Res.* **111**, D07204.

Crayford, A., Johnson, M., Marsh, R., Sevcenco, Y., Walters, D., Williams, P., Christie, S., Chung, W., Petzold, A., Ibrahim, Delhaye, D., Quincey, P., Bowen, P., Coe, H., Raper, D., Wilson, C. (2010) EASA report. http://easa.europa.eu/safety-and-research/research-projects/environment.php.

Hentschel, M.L., and Page, N.W. (2003) *Part. Part. Syst. Charact.* **20**, 25-38.

Marsh, R., Crayford, A., Petzold, A., Johnson, M., Williams, P., Ibrahim, A., Kay, P., Morris, S., Delhaye, D., Lottin, D., Vancassel, X., Raper, D., Christie, S., Bennet, M., Miller, M., Sevcenco, Y., Rojo, C., Bowen, P. (2009) EASA report. http://easa.europa.eu/safety-and-research/research-projects/environment.php.

Petzold, A., Marsh, R. Johnson, M., Delhaye, D., Crayford, A., Morris, S., Kay, P., Bowen, P., Ibrahim, A., Bauer, H. (2008) EASA report. http://easa.europa.eu/safety-and-research/research-projects/environment.php.

Wilson, C.W., Petzold, A., Nyeki, S., Schumann, U., Zellner, R. (2004) *Aero. Sci. Tech.* **8**, 131-143.

Exhaust emissions and particle hygroscopicity with a diesel engine run with HVO fuel-oxygenate blend

M. Happonen[1], J. Heikkilä[1], P. Aakko-Saksa[2], T. Murtonen[2], K. Lehto[3], A. Rostedt[1], T. Sarjovaara[3], M. Larmi[3], J. Keskinen[1], A. Virtanen[1]

[1]Department of Physics, Tampere University of Technology, Tampere, 33540, Finland
[2]VTT Technical Research Centre of Finland, Espoo, 02044, Finland
[3]Aalto University, Department of Energy Technology, Espoo, 00076, Finland
Keywords: Diesel soot particles, Hygroscopic growth, fuel, oxygenate.
Presenting author email: juha.heikkila@tut.fi

The need to reduce greenhouse gas emissions as well as regulated emissions drives the need to study alternatives for fossil fuels.

Hydrogenated vegetable oil (HVO) is the newest commercially available bio-based diesel fuel. It is composed of paraffinic hydrocarbons and includes essentially no aromatics or sulphur. HVO fuel is reported to lower regulated emissions (Aatola *et al.*, 2008). Compounds containing oxygen (i.e. oxygenates) can be blended to the fuel to further reduce the particle emissions. Oxygen content in biodiesel (i.e. FAME) has been reported to increase the oxygen content in the emitted soot as well as alter the oxidation behaviour of the emitted soot (Song *et al*., 2006). Increased oxygen content in particles could also have an effect on particle hygroscopicity.

In this study (Happonen *et al*., 2012), we investigated how the addition of oxygenate (Di-n-pentyl ether, DNPE) to HVO fuel alters particulate emissions and particle hygroscopicity. Oxygen content in the DNPE-HVO blend was 2 wt-%. The effect on NO_x-emissions was also studied.

The measurements were performed on an engine dynamometer with single-cylinder test engine modified from a commercial six-cylinder off-road common rail diesel engine.

Particle size distributions were measured using a Scanning Mobility Particle Sizer (SMPS) and the total number concentration with a Condensation Particle Counter (CPC). Particulate mass (PM) was measured according to the ISO 8178-1:2006 standard. Particle hygroscopicity was studied using a hygroscopic tandem differential mobility analyzer (HTDMA). We also performed organic/elemental carbon (OC/EC) analysis on collected particle filter samples.

Particulate matter (PM) emission was reduced 26-32% with all measured loads while particle number reduced 10-17%. With 75% and 100% loads NO_x-emission was slightly higher with oxygenate blended fuel, unlike with 50% load where NO_x – emission was 2-3% lower.

Growth factors are all within error limits (one standard deviation), as shown in figure 2. However, the growth factors measured with HVO were measured at approximately 2%RH higher humidity than HVO-DNPE growth factors and still the growth factors with HVO-DNPE are slightly higher than with pure HVO. The differences would be clearer if measured at the same RH. Thus, fuel seems to slightly affect the hygroscopic properties of emitted particles.

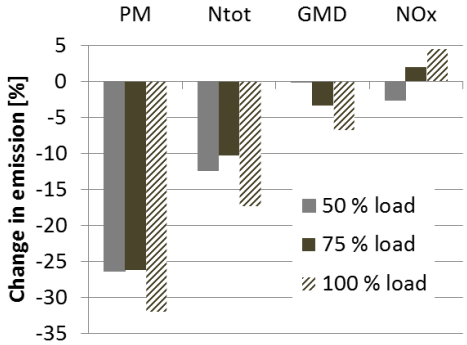

Figure 1. Relative changes in emissions caused by oxygenate blending with HVO fuel.

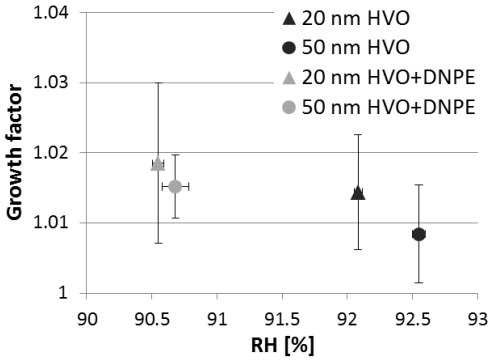

Figure 2. Growth factors of chosen particle sizes with and without oxygenate blending.

This study was funded by Tekes (Finnish Funding Agency for Technology and Innovation).

Aatola, H., Larmi, M., Sarjovaara, T., & Mikkonen, S. (2008). *Hydrotreated vegetable oil (HVO) as a renewable diesel fuel: trade-off between NOx, particulate emission, and fuel consumption of a heavy duty engine.* SAE Technical Paper Series, 2008-01-2500.

Happonen, M., Heikkilä, J., Murtonen, T., Lehto, K., Sarjovaara, T., Larmi, M., Keskinen, J., & Virtanen, A. (2012). *Diesel exhaust emissions and particle hygroscopicity with HVO fuel-oxygenate blend.* To be submitted in March 2012.

Song, J., Alam, M., Boehman, A. L., & Kim, U. (2006). *Examination of the oxidation behavior of biodiesel soot*. Combustion and Flame, 146,589–604.

Effective Density and Fractal–like Dimension of Diesel Soot Aggregates as a Function of Mobility Diameter

P. Baltzopoulou[1], E. Papaioannou[1,2] , M. Kostoglou[3], A.G. Konstandopoulos[1,2]

[1]Aerosol & Particle Technology Laboratory, CPERI/CERTH, P.O. Box 60361, 57001, Thessaloniki, Greece
[2] Dept. of Chemical Engineering, Aristotle University, P.O. Box 1517, 54006, Thessaloniki, Greece
[3] Div. of Chemical Technology, Dept. of Chemistry, Aristotle University, Thessaloniki, 54124, Greece
Keywords: soot aggregates, effective density, fractal-like dimension, oxidative fragmentation.
Presenting author email: pbaltzop@cperi.certh.gr

In the current study a simultaneous measurement of electrical-mobility-based (measured by SMPS, Scanning Mobility Particle Sizer, TSI) and aerodynamic-diameter-based (measured by ELPI, Electrical Low Pressure Impactor, Dekati) distributions is employed in order to study the morphology of soot aggregates produced by diesel engines at different operational conditions. This general approach has been used in the past to calculate an average fractal dimension for the entire aggregate size distribution (Virtanen *et al*, 2004).

A set of integral equations is constructed relating the output of each stage of ELPI to a weighted integral of the mobility diameter distribution. In the case of describing the entire aggregate population with just one fractal dimension the mathematical problem is a typical minimization problem with one unknown, that can be readily solved. In the present work it is assumed that the fractal dimension is in general a function of the aggregate size (i.e. mobility diameter). The reason behind this assumption is the existence of the oxidative fragmentation mechanism (Echavarria *et al*, 2011). The oxidative fragmentation of soot particles limits further aggregate growth while the resulting soot fragments may re-collide with the soot aggregates, leading to the establishment of a steady state at which point coagulation balances oxidative fragmentation and therefore the emergence of a size distribution with a "constant shape". The simultaneous action of these two processes, in general may lead to a distribution of soot aggregate morphologies (hence fractal dimensions), since both cluster-cluster and monomer-cluster aggregation events will be occurring within the same population.

The resulting mathematical problem that must be solved can take the form of a non-linear Fredholm integral equation of first kind which is well known to be ill-posed. Especially in the present case with the limited amount of experimental information (stemming from the few discrete ELPI stages) and considering that no knowledge exists for the shape of the unknown fractal dimension vs mobility diameter distribution an inversion approach seems hopeless. Instead, a reasonable approximation of the kernel functions with Dirac delta functions allows deconvolution of the data leading to the stabilization of the inverse problem and allowing the estimation of a different fractal dimension for each aggregate particle and corresponding mobility diameter.

The above approach leads to an effective density distribution from 2.5 to 0.3 g/cm^3 (Figure 1). Effective density values for the smaller soot aggregates (smaller than 100 nm) are very close to the density of carbon, slightly augmented, most likely due to existing inclusions from metal oxides.

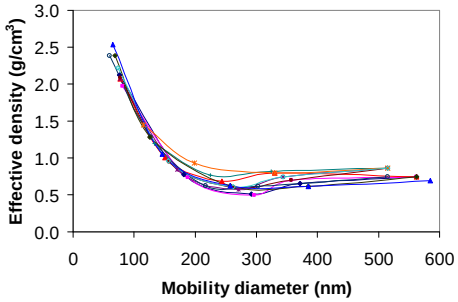

Figure 1. Effective density of soot aggregates for different operational conditions

Based on the work of Naumann (2003) we apply the following relation to calculate the fractal dimension, D_f from the effective density, ρ_{eff} and the mobility diameter, d_{me} :

$$\frac{\rho_{eff}}{\rho_o} = \frac{1}{f \cdot h_{KR}^{\,Df}} \left[\frac{d_{me}}{d_o} \right]^{Df-3} \qquad (1)$$

where, h_{KR} is the Kirkwood – Riseman ratio accounting for shielding effects and hydrodynamic interactions itself a function of D_f, f is the volume filling factor, d_o is the primary particle of the soot aggregates, while their density is, ρ_o, taken to be that of carbon. The results for D_f range between 3 and 1.75 and for the large soot aggregates tend to reach a value of 2.4 (Figure 2).

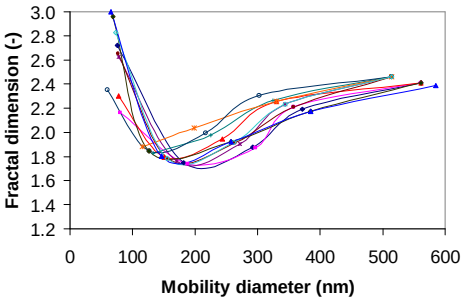

Figure 2. Fractal dimension of soot aggregates for different operational conditions

Virtanen A., Ristimaki J. and Keskinen J. (2004) *Aerosol Science and Technology*, **38**, 437–446.

K.-H.Naumann (2003) *Aerosol Science*, **34,** 1371–1397.

C.A.Echavarria, I.C.Jaramillo, A.F.Sarofim, J.S.Lighty (2011) *Proc. of the Combustion Institute*, **33,** 659–666.

PM10 is responsible for a greater IL-6 secretion after "in vitro" incubation with synoviocytes from patients with Rheumatoid Arthritis than in those with osteoarthrosis

V. Guercio[1], F. Cetta[1], F. Laghi Pasini[1], , E. Selvi[1], E. Balistreri[1]I. Santi[2], M. Monti [2], L. Cantarini[1], E. Bolzacchini [3] and M. Galeazzi[1]

[1] Dept. of Surgery and Thoracic Surgery, University of Siena, Siena, 53100, Italy
[2]Geriatric Institute "Pio Albergo Trivulzio" (PAT), Milan, 20146, Italy
[3]Dept. of Environmental Sciences, University of Milan, Milan, 20126, Italy
keyword: Rheumatoid Arthritis, osteoarthrosis, human fibroblast-like synoviocytes, IL-6
Presenting author email: guerciovalentina@libero.it

Autoimmunity and, in particular increased IL-6 secretion, play a crucial role in the occurrence of Rheumatoid Arthritis (RA). Genetic factors are thought to be responsible for about 50% of RA risk, suggesting that environmental factors could contribute to the development of RA in the genetically predisposed. In particular, pollution from traffic in adulthood has been considered as a newly identified environment factor for RA.

Aim of the study: to assess the "in vitro" effects of variable concentration of various types of PM when incubated with human Fibroblast-like synoviocytes (FSC), to evaluate the occurrence of proinflammatory effects.

Methods: daily levels of PM10 and PM2.5 and PM1 (diameter < 10 μm, 2.5 μm, 1 μm, respectively) were measured by PM detection units, both outside and inside 2 schools for children and 2 nursing homes for retired people, either in summer and in winter time in Milan, Italy. Both OPC detectors and low volume gravimetric detectors were used. Samples from Teflon filters were used after sonication in sterile phosphate buffer saline (PBS). Aliquots of these samples at various concentration of PM10 (10 μg/ml, 50 μg/ml, 70 μg/ml) were incubated at 37°C for 24, 48, 72 hours with human type B synoviocytes obtained from 5 patients with RA, and 5 with osteoarthrosis (OA) during hip replacement surgery.

Results: -Engulfment of particulate material within synoviocytes was observed even at lower concentrations and after 24 h incubation; -the penetration of PM into the cell was associated with an increased cytokine production. In particular, there was a considerable increase of IL6 concentration, namely after incubation with winter PM, up to 9-folds the basal values, already after 24 h (867,36 vs 100) in FSC obtained from RA patients ($p<0,001$), whereas summer PM determined a significant increase of IL6 (637,39) only after incubation for 72 h . This effect was likely due to the greater content of PAH rich OC in winter PM. In addition, after incubation for 24 h of the same type and the same concentration (10 μg/cm2) of PM10, collected during Summer and Winter, with alveolar type cells (A549 cell line), i.e. cells from front-line respiratory district (**Fig 1b**), the previous increase of IL6 observed in subjects with RA (**Fig 1a**) was not found (**Fig1**).

Conclusion: The inflammatory response elicited by PM is greater in RA-FLS, than in OA-FLS and other inflammatory or autoimmune diseases. Even if affected tissues are distant from the initial site of exposure, they are likely to be part of the health side-effects produced or facilitated by environment pollutants.

In particular, being RA a disease in which genetic predisposition plays a basic pathogenetic role, it could also be an interesting " new model" to evaluate host-particle interaction, and to try to weight the relative role of intrinsic toxicity of xenobiotics, including composition, structure, surface reactivity vs that of individual susceptibility, in the occurrence of clinical outcomes in humans. In particular, PM-related health effects seem to be not only determined by intrinsic toxicity of pollutants, mediated by oxidative stress, but are likely due to more complex responses, namely those typical of autoinflammatory and/or autoimmune diseases, which occur only or mainly in susceptible individuals.

In particular, if autoimmunity is crucial for RA occurrence and RA is part of the "pollution related syndrome", even low local concentration of PM could be sufficient to trigger pathological events in predisposed subjects.

a b

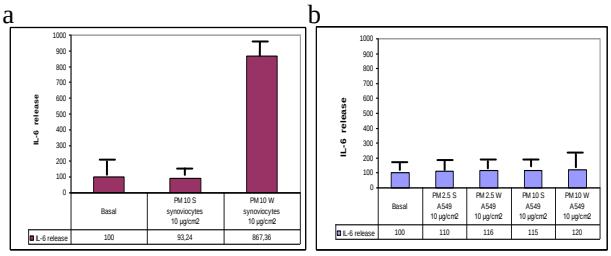

Figure 1a-b Comparison between IL-6 secretion in human synoviocytes from subjects with RA (a) and in alveolar type II cells (A549 cell line) (b).

This work was supported by the PROLIFE-Project, Milan, Italy.

Damage to newborns, in terms of risks for diseases occurring even decades after exposure to PM, as a crucial item in the global effects of air pollution to a given population

B. Lorenzi[1], F. Cetta[1], V. Guercio[1], P. Paladini [1], F. Granato[1], R. Zangari[1], M. Monti[2] , M. Giovannini[3], E. D'Auria[3], M. Mandelli[3] and M. Sala[3]

[1]Dept. of Surgery and Thoracic Surgery, University of Siena, Siena, 53100, Italy
[2]Geriatric Institute "Pio Albergo Trivulzio" (PAT), Milan, 20146, Italy
[3]Dept. of Pediatrics, University of Milan, Milan, 20122, Italy
Keywords: Particle concentration, health effects of aerosols, susceptibility window, newborn damage.
Presenting author email: lorenzi7@unisi.it

Aim of the study: Between 2007 and 2010, a comprehensive approach to health effects of air pollution was performed in Milan, Italy (Prolife Project): 1) measurement of PM concentration; 2) comparison between daily concentration of PM and other pollutants and hospital admission; 3) longitudinal studies in frail subpopulations, such as children attending primary school and elderly people living in nursing homes; 4) "*in vitro"* and "*in vivo"* experiments concerning host particle interactions.

The lack of adequate metrics of exposure, effect and susceptibility in epidemiological studies evaluating PM concentration and health effects is one of the main responsible for the conflicting results of these studies (Clark, 2010). In particular, the question of damage to human health by environmental pollutants has never been addressed exhaustively.

The current paradigm of environmental pollution included acute damage, usually measured as hospital admission for various diagnosis during "pollution peaks" - and chronic damage, i.e. the risk of developing cancer and/or chronic diseases as long -term effects. A dose and effect linearity, due to the intrinsic toxicity of pollutants has been presumed, but never proved, whereas the role of individual susceptibility in the occurrence of the final outcome has never been properly considered.

Results: The following results were obtained: 1) In a prospective study involving 118 children (63 males and 55 females) attending primary school, close to a park far from vehicular traffic, in 3 consecutive days very high peaks of indoor PM were detected for about one hour (8:15-9:15 in the morning), up to 1000 μg/m^3 indoor for PM10. There was no evident clinical outcome (increase of asthmatic bronchitis, upper or lower respiratory diseases) or different prevalence of spirometric or FeNO values in any of the 118 children who were evaluated during those days. 2) Functional alterations of human cells incubated in vitro with different types of PM10 and PM2,5 (10, 50, 75 μg/ml) and concentration greatly depended on individual susceptibility and on the pre-existing disease of the host. In particular, semiquantitative functional analysis showed that individual susceptibility of the host was responsible for more than 50% of the final outcome as compared with intrinsic toxicity of pollutants. 3) Comparison of the rate of asthmatic children in 2009 with historical series of 3 decades before, showed an evident increase of susceptible children, likely due to the effects of early life exposure to air pollution, during the critical "susceptibility window" involving the first months of life of newborns (Clark, 2010).

Conclusion: The question concerning the determinants of final outcomes and the measure of each component responsible for damage, - involving both toxic and harmful processes, but also repair mechanisms,- requires a multidisciplinary approach, involving clinicians and pathologists. In particular, the relative power of the damage due to intrinsic toxicity of pollutants, which can be without clinical evidence even at PM concentration of 1000 μg/m^3 - and that of individual susceptibility deserves further evaluation.

In the overall analysis of exposed population, the damage to newborns by pollutants usually escapes current evaluation of PM concentration and health effects, which is able to capture only damage expressed as "hospital admission, morbidity and mortality" measured within a 2- day lag.

A proper estimation of this damage, i.e. of the increased proportion of newborns - children of non susceptible parents - who will become susceptible to "pollution disease", because of exposure to pollutants in early life, is mandatory. Even if it will be measured some decades later, as a burden of diseases related to PM pollution, this damage actually is a major component of the total damage from environmental pollution, at a given time, which could also be transmitted to future generations.

This work was supported by the PROLIFE Project, City of Milan, Italy

Clark, N.A. et al. (2010) *Environ. Health Perspect.* **118**, 284-290.

A plea for greater caution before extending "in vitro" assessment of PM to risk assessment in humans

J. Martellucci[1], F Cetta[1] ,V. Guercio[1], D. Stergiou[1], B. Lorenzi [1], M. Monti[2] and E. Bolzacchini[3]

[1]Dept. of Surgery and Thoracic Surgery, University of Siena, Siena, 53100, Italy
[2]Geriatric Institute "Pio Albergo Trivulzio" (PAT), Milan, 20146, Italy
[3]Dept. of Environmental Sciences, University of Milan-Bicocca, Milan, 20126, Italy
Keywords: risk assessment, PM, intrinsic toxicity, individual susceptibility
Presenting author email: jamjac64@hotmail.com

Aim of the study to detect new tools, which could be useful for a better risk assessment in humans of effects of air pollutants, on the basis of *"in vitro"* studies of host-particle interactions.

Methods and results: the A549 (human alveolar epithelial cell) and the BEAS-2B (human bronchial epithelial cell-line), together with sperm cells and synoviocytes from humans with rheumatoid arthritis (RA) and osteoarthrosis (OA), were treated after 24-48h with both summer and winter PM_{10} and $PM_{2.5}$ sampled in Milan, Italy. Therefore, both human beings and cell-lines were exposed to the same pollutants. In addition, a cross comparison was performed between clinical and *in vitro* effects.

A549 cell viability wasn't significantly reduced after summer and winter PM exposure, and summer PM had no significant effects on BEAS-2B viability. Winter PM treatment induced a decrease in cell viability, at the dose of 25 and 50 mcg/cm^2. Moreover, winter PM_{10} induced a 5-fold increase in IL-8 release in treated cells, and summer PM_{10} induced a 20-fold increase in IL-8 expression. BEAS-2B resulted more responsive to PM treatment than A549. Short- term clinical effects in Milan were not related to PM daily concentration.

Discussion: "*In vitro*" studies confirmed potential toxicity of PM, but these studies cannot be used for clear-cut inferences to humans. In fact, in terms of health or biological effects, one cannot compare the effects of inhalation by breathing of diluted particles in a concentration equivalent to the one that can be introduced with a single breath in 1 sec with the effects of incubation, with a cell line of alveolar cells of particles deposited on filters, which contain aggregated and concentrated particles, that correspond to 60sec x 60min x 24h, i.e. 8640 folds the portion inhaled by a single breath. In particular, in humans each quantity can be partly cleared, and partly can rich the alveolar area. In addition, the final response includes not only the cellular and molecular response, but also includes the response of the "entire organism". Two main differences can be found between *"in vitro"* and in humans studies: 1)the human being gives not only biological, but also chemical and mechanical responses, which are able to clear completely inhaled particles; 2)the model used in analyzing host-particle interactions postulates a dose and effect linearity, whereas observed outcomes in humans show a "no threshold" behaviour. Therefore, in humans the prevalent causative mechanism cannot be the intrinsic toxicity of the pollutants with a linear progression (the greater the dose, the greater the health effect), but a different one. "*In vitro*" models, even if not immediately extensible to humans, may represent a surrogate for the experimental animal, in order to evaluate quantitatively parameters such as: inflammogenicity, mutagenicity, cell cycle alterations. The use of different cell lines and human samples, with different responses, has shown the great importance, not only of the intrinsic toxicity of the toxic agent, but also of the different type of targeted cell in triggering a different response. These differences- related to host response and individual susceptibility- can be one of the possible explanation for the "no threshold phenomenon" and for the inadequacy of the "pure" toxic model, characterized by dose and effect linearity, to capture the complexity of host-particle interactions. An adequate model of risk evaluation- applicable to human health- isn't available, mainly because of the persistent lack of knowledge, concerning pathogenetic and pathophysiological mechanisms, which are responsible for clinical outcomes in humans. In an ideal model, 2 different components should be distinguished: the particle-related component and the host-related one. However, at the moment we don't know yet the relative weight of each component.

Cetta, F. et al (2007) *Eur. Respir. J.* **30**, 805-806
Cetta, F. et al (2009) *GIMT* **63**, 381-384
Cetta, F. et al (2009) *Environ. Health Perspect.* **117**, A190.

Source-specific mutagenicity and carcinogenicity of $PM_{2.5}$-bound polycyclic aromatic hydrocarbons in a large city of North-eastern Italy

M. Masiol[1], S. Squizzato[1], A. Hofer[1], F. Benetello[1], G. Rampazzo[1], B. Pavoni[1]

[1]Dip. Scienze Ambientali, Informatica e Statistica, Università Ca' Foscari Venezia, Venice, 30123, Italy
Keywords: PM2.5, PAH(s), Source Apportionment, Health aspects of aerosols
Presenting author email: masiol@unive.it

Epidemiological studies directly correlated the exposure to airborne particulate matter with some adverse health effects (Pope et al., 2009), which are further enhanced by some chemical, physical and biological properties of the particles. Airborne particles can be composed of, or absorb on their surface, some substances having carcinogenic and/or mutagenic effects on humans. Among these compounds, Polycyclic Aromatic Hydrocarbons (PAHs) have been largely studied because of their known or suspected carcinogenic properties and their wide distribution in the urban atmospheres.

Up today, several approaches have been developed to assess the potential risk of exposure to complex mixtures of PAHs using equivalency factors based on Benzo(*a*)pyrene (BaP), which is recognized as class 1 carcinogen by IARC. Toxic Equivalency Factors (TEF) and Mutagenic Equivalency Factors (MEF) have been used in combination with measured concentrations of PAHs mixtures to compute the Carcinogenic (TEQ) and mutagenic equivalents (MEQ).

Unfortunately, most of conventional risk assessment studies are limited to estimating the carcinogenic potential of PAHs mixtures without providing information about the role of specific sources. This fact represents a great limitation, because equivalency factors can vary by some orders of magnitude amongst congeners and different emission sources potentially emit specific congeners.

In this study, 11 particle-phase PAHs, listed as carcinogenic and mutagenic agents by the IARC, were quantified in three sites of Venice-Mestre, Northern Italy. This large city was recently recognized as an ideal place to study the effects of the atmospheric circulation and long–range transports in the Po Valley. It is located between the eastern border of a wide continental plain and the Adriatic Sea and presents emissive scenarios common to other large European cities: high density residential areas, heavy traffic roads and motorways, coal and gas thermoelectric power plants, many industrial installations (Rampazzo et al., 2008; Masiol et al., 2010; Squizzato et al., 2012). These sites have been selected because of their different emissive scenarios and relative location with respect to the major winds. Analyses were carried out by Gas Chromatography-Mass Spectroscopy after solvent extraction of collected filters.

Some diagnostic ratios were calculated and a factor analysis was performed to detect the most probable emission sources. Three main sources were identified: traffic, domestic heating and heavy oils. A multi linear regression analysis was performed on the sum of analyzed congeners showing that domestic heating is the main source of PAHs in winter, whereas traffic mainly accounts for the carcinogenic and mutagenic risk during the whole year. In the same way, the source-specific mutagenicity and carcinogenicity have been computed (Figure 1).

In a second step, a chemometric approach using wind data was applied to group days with similar atmospheric circulation patterns. The study of the wind roses and their associated changes in PAH profiles, total carcinogenicity and mutagenicity discriminated the sources of particle-phase PAHs and their role in determining a serious hazard for human health.

Results, interpreted on the basis of seasonal variations and atmospheric conditions, have shown that even though domestic heating is the main source of total PAHs in winter, a background pollution including traffic mainly accounts for the carcinogenic and mutagenic risk during the whole year.

The proposed procedure has quantitatively pointed out the prevailing sources of organic air pollutants and particularly the very hazardous ones for human health.

It can be easily applied to other anthropized environments as a useful tool to design local and regional air pollution control strategies, including the use of better prevention technologies and traffic restrictions.

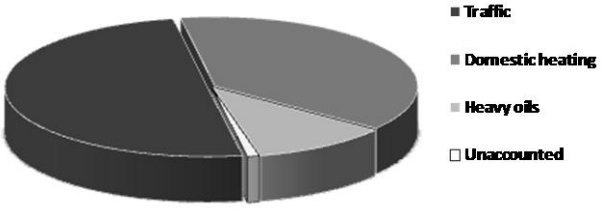

Figure 1. Results for a site.

Masiol, M., Rampazzo, G., Ceccato, D., Squizzato, S., Pavoni, B. (2010) *Chemosphere* **80,** 771–778.

Rampazzo., G., Masiol, M., Visin, F., Rampado, E., Pavoni, B. (2008a) *Chemosphere* **71**, 2068–2075.

Pope, C.A.III, Ezzati, M., Dockery, D.W. (2009). *N. Engl. J. Med.* **360**, 376-386

Squizzato, S., Masiol., M., Innocente, E., Pecorari, E., Rampazzo, G. and Pavoni, B. (2012). *J. Aerosol Sci.* **46**, 64-76

Quantitative and qualitative relationship between AOD obtained by AERONET and $PM_{2.5}$ from in situ measurements in Brazilian Amazonia over several years

M. Paixão[1], D. Mourao[2], A. Correia[1], S. Hacon[2], P. Artaxo[1]

[1]Institute of Physics, University of Sao Paulo, Sao Paulo, Brazil
[2]Escola de Saúde Pública da Fundação Oswaldo Cruz, Rio de Janeiro, Brazil
Keywords: Particulate Matter, $PM_{2.5}$, TEOM, AOD.
Presenting author email: melina@if.usp.br

Exposure to elevated levels of inhalable particulate matter has been associated to serious health threat such as cardiopulmonary and lung cancer mortality (Pope et al, 2002). The relationship between particulate matter measured on the surface and column averaged aerosol optical depth provided by remote sensing such as satellite sensors and ground-based measurements has been studied by several authors over the last years.

The Brazilian Amazonia, specifically the so-called Arc of Deforestation region, is heavily impacted by biomass burning aerosol particles with aerosol optical depth (AOD) reaching values as high as 5.0. Epidemiologic and health studies about the impact of inhalable particulate matter suffer from lack of surface measurements, especially in remote areas. Remote sensing data can improve monitoring air quality; in this sense the AERONET program provides reliable long-term measurements of AOD in key Amazonian sites.

In the present study it's explored the relationship between aerosol optical depth and *in situ* $PM_{2.5}$ concentrations measurements obtained by several campaigns from 1995 to 2006.

We noticed a change in the load of $PM_{2.5}$ in Alta Floresta about the year 2000, when PM concentrations dropped by half, but surprisingly the aerosol optical properties didn't follow the same trend. The hypothesis is that the site itself changed due to land use, and as the city grew the biomass burning spots went far from the measurement location. However, the columnar AOD measured by AERONET has an estimated area of representativity of more than 150 x 150 km according to (Hoelzemann et al., 2009), and might not be susceptible to such regional scale changes.

We found a significant correlation between AERONET AOD and $PM_{2.5}$ varying from 0.77 in Santarém, a pristine site, to 0.86 in biomass burning affected sites. Figure 1 shows the linear regression in Alta Floresta. It's proposed a linear relationship of $PM_{2.5}$ = (40±2)*AOD500 + (5±2) in µg/m³, evaluated from 2001-2006 for biomass burning sites. The method was validated using MODIS aerosol optical depth to estimate PM2.5 with the proposed regression, and compared with TEOM measurements in Ji Paraná, 2002, and Alta Floresta, 2006 (see Figure 2), with good agreement.

Although the Brazilian National Council for Environment doesn't contemplate a standard for $PM_{2.5}$, it's clear that the high loads in Brazil might affect the population and further policy discussions are needed.

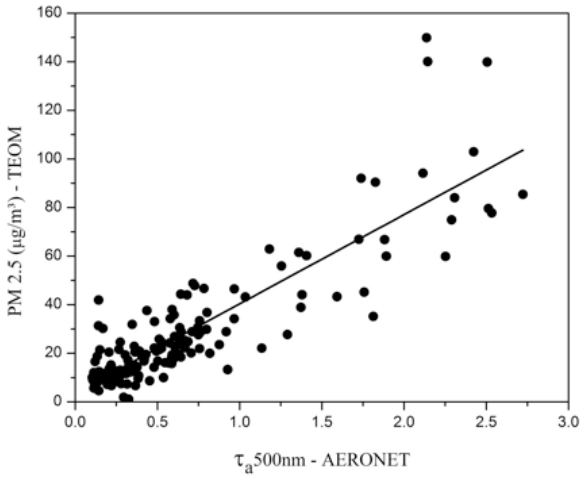

Figure 1. Correlation between $PM_{2.5}$ obtained by TEOM and AOD 500nm by AERONET in the site of Alta Floresta from September to December of 2006.

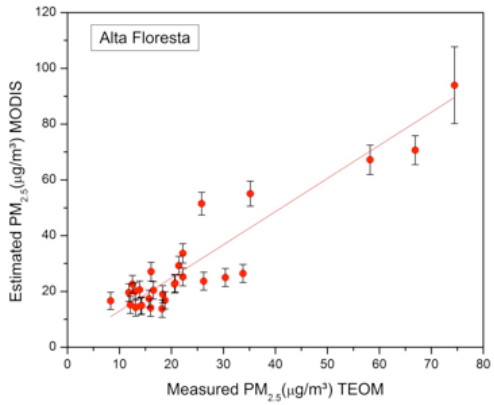

Figure 2. Comparison between estimated $PM_{2.5}$ to MODIS AOD and measured by TEOM in Alta Floresta for September to November of 2006.

The Brazilian National Council for Research, CNPq, supported this work.

Pope III, C. A. (2002) *JAMA: The Journal of the American Medical Association*, **287(9)**, 1132-1141.

Hoelzemann, J., Longo, K., Fonseca, R., do Rosário, N., Elbern, H., Freitas, S. and Pires, C. (2009) *J. Geophys. Res*. **114**, D13301.

Statistics of PM10 concentrations in Mazovia, central Poland (2007 – 2011)

A. Pietruczuk, J. Jarosławski and I. Pawlak

Institute of Geophysics Polish Academy of Sciences, Warsaw, Poland
Keywords: PM10, size distribution, statistical analysis.
Presenting author email: alek@igf.edu.pl

Results of PM10 concentrations measurements performed at four stations in central Poland (2007-2011) were analyzed in terms of levels, distributions of occurring concentrations, the number of exceedances of the limit values and the potential sources of aerosols.
Analyzed PM10 levels were similar at suburban and rural stations, except the station located in downtown of the cities or next to the busy street. The largest PM10 concentration was observed at Warsaw Kerb station, they were about 30% higher than in other stations.
Increase of PM10 concentration from year to year is observed during reported period. The number of days with exceeded daily limit value of PM10 is also rising. The number of exceedances is the highest at Warsaw Kerb station and decreases with the decrease of population density and road traffic in the vicinity of the measurement point.

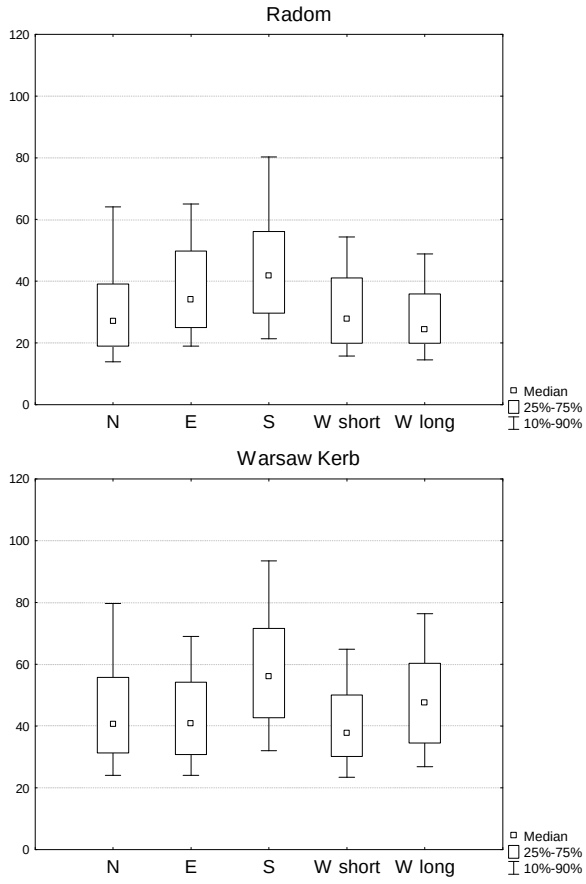

Figure 1. PM10 concentrations urban stations for different airmass origin.

Seasonal variability analysis of PM10 revealed additional maximum beyond the usual autumn-winter one. This maximum occurred in April at all stations corresponds to seasonal fires activity in Eastern Europe. Similar spring maximum is also seen at annual pattern of aerosol optical thickness (Jaroslawski and Pietruczuk, 2010). Elevated concentrations during cold part of the year could be associated to coal combustion, the main source of heat in Poland.
Cluster analysis of back-trajectories calculated by HYSPLIT model revealed that PM10 concentrations in the Mazovia region strongly depends on the origin of airmass. The highest values are registered for the air of the regional and Southern origin, while the lowest for the air-masses originating from the North and North-West direction. Air-mass advected from South direction could be polluted by industry in southern Poland (e.g. Silesia region) and industry in Czech Republic (e.g. Ostrava. PM10 concentrations related to air-mass advection from Western and Easter Europe are similar at all stations. This is rather surprising because one can expect that continental airmass from mostly rural areas of Belarus and Ukraine are cleaner than the airmass which could be polluted by European urban and industrial regions. However, regions east of Poland are the source of seasonal fires taking place mainly during spring (Barnaba et al., 2011).

This work was supported by the Polish Ministry of Science under grant 0281/B/P01/2009/36.

Barnaba F., F. Angelini, G. Curci, and G. P. Gobbi (2011), *An important fingerprint of wildfires on the European aerosol load*, Atmos. Chem. Phys., 11, 10487-10501,

Jarosławski J., Pietruczuk A. (2010), *On the Origin of Seasonal Variation of Aerosol Optical Thickness in UV Range over Belsk, Poland*, Acta Geophysica 58, 1134-1146, DOI: 10.2478/s11600-010-0019-4

Anions, Cations, Total Carbon and Water Soluble Organic Carbon in PM2.5 and PM1 samples monitored near a waste incinerator plant in the Po Valley (Bologna).

M. Rossi[1], L. Pasti[2], L. Tositti[3], S. Zappoli[4], E. Brattich[3], S. Parmeggiani[3], M. Stracquadanio[4]

[1]Regional Agency for Prevention and Environment ARPA - Emilia-Romagna, Rimini, 47923, Italy
[2]Department of Chemistry, University of Ferrara, Ferrara, 44121, Italy
[3]Department of Chemistry, University of Bologna, Bologna, 40126, Italy
[4]Department of Physical and Inorganic Chemistry, University of Bologna, Bologna, 40136, Italy
Keywords: PM2.5, PM1, Ions, Carbon, Water Soluble Organic Compounds, Air Quality, Monitoring, Modelling (microscale), Waste Incineration Impact.
Presenting author email: marossi@arpa.emr.it

It is well known that the problem of waste disposal is critical in advanced societies, characterized by increasing consumption of goods, and one of the technologies used to manage this problem is waste incineration. In Italy there is a high perception of health risk related to the presence of incinerating plants. For this reason, local communities are very interested in their air quality and in the possible presence of health-risk pollutants, related to the activity of these plants. The aim of this study is to characterize the inorganic ions and carbonaceous compositions in PM1 and PM2.5 samples collected in the surroundings of an incinerator.

To reach this goal two extensive monitoring campaigns were performed: the first one was held in summer 2008 and the second one in winter 2009. The plant under study is located in a suburban-farming area, less than 10 km away from northeast of Bologna (Italy), in the southeast of Po Valley, which is a well known atmospheric polluted critical area.

Seven out of eight monitoring stations were installed in a domain of 8x9 km^2 around the plant. The eighth station was placed far away, inside the urban area of Bologna, in a site used for urban background measurements by Arpa Environmental Agency.

A preliminary study with ADMS-Urban (Cerc, Cambridge, UK) dispersion model was performed in order to select coordinates of four monitoring stations, using PM10 emissions as a pollutant tracer (Bonafè and Rossi, 2011). Two stations representative of maxima deposition of plant emissions and two stations, used as "control" were chosen. The other stations were placed as to represent different air conditions in the domain: high traffic, rural and suburban area Inorganic ions (NH_4^+, K^+, Cl^-, NO_2^-, NO_3^-, SO_4^{2-} and Oxalate), total carbon (TC) and the associated water soluble organic fraction (WSOC) were determined in bi-daily aerosol samples. Extensive statistical analyses were performed, using both univariate and multivariate methods. In addiction some seasonal comparison were made.

Results

Principal Component Analysis was applied to the concentration data of the studied compounds. The data were normalized to the mass of PM. The compositions of PM2.5 were found significantly different from those of PM1 with respect inorganic ions in both the summer and the winter campaign.
The compositions of PM2.5 and PM1 were found to be different in both seasons.

PM2.5 samples collected in the first maximum were more rich in TC when compared to its control.

Seasonal variation were also observed in the composition of the inorganic fraction as reported in Figures 1 and 2, confirming results published by other authors. Nitrate and sulphate were found to be correlated to the ammonium in winter and summer respectively.

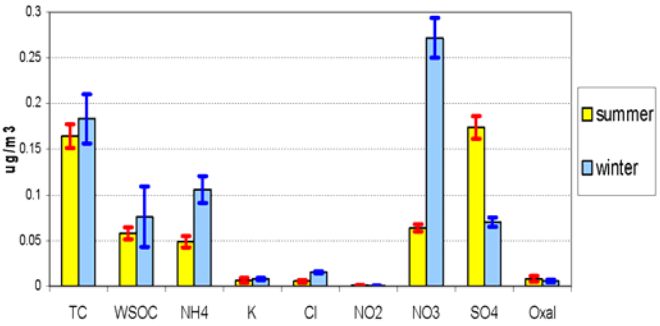

Figure 1. PM-normalized average concentrations of analytes, with standard deviations.

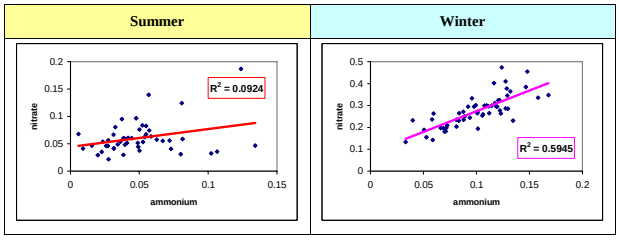

Figure 2. Correlation of nitrate and ammonium concentration in PM2.5 measured at the maximum of deposition of the incinerator

This work was part of the «Moniter Project». http://www.moniter.it

Bonafè, G., Rossi, M. (2011) *Proc of the.14th Int. Conf. on Harmonization within Atmospheric Dispersion Modelling for Regulatory Purposes*.

Water-soluble fraction Metals in PM2.5 and PM1 samples collected near a waste incinerator plant in the Po Valley (Bologna).

M. Rossi[1], L. Pasti[2], M. Remelli[2], A. Pagnoni[2] and E. Sarti[2]

[1]Regional Agency for Prevention and Environment ARPA - Emilia-Romagna, Rimini, 47923, Italy
[2]Department of Chemistry, University of Ferrara, Ferrara, 44121, Italy
Keywords: PM2.5, PM1, Metal, Air Quality, Monitoring, Waste Incineration Impact.
Presenting author email: marossi@arpa.emr.it

It is well known that the problem of waste disposal is critical in advanced societies, characterized by increasing consumption of goods, and one of the technologies used to manage this problem is waste incineration. In Italy there is a high perception of health risk related to the presence of incinerating plants. For this reason, local communities are very interested in their air quality and in the possible presence of health-risk pollutants, related to the activity of these plants. The aim of this study is to characterize the metal fraction in PM1 and PM2.5 samples collected in the surroundings of an incinerator. The samples were previously extracted in pure water to focus on the metals more biologically available.

To reach this goal two extensive monitoring campaigns were performed: the first one was held in summer 2008 and the second one in winter 2009. The plant under study is located in a suburban-farming area, less than 10 km away from northeast of Bologna (Italy), in the southeast of Po Valley, which is a well known atmospheric polluted critical area.

Seven out of eight monitoring stations were installed in a domain of 8x9 km^2 around the plant. The eighth station (MGA) was placed far away, inside the urban area of Bologna, in a site used for urban background measurements by Arpa Environmental Agency.

A preliminary study with ADMS-Urban (Cerc, Cambridge, UK) dispersion model was performed to select monitoring station coordinates, using PM10 emissions as pollutant tracer. A first station (MXW) representative of maximum falling out of plant emissions was placed in the east side, not too far from the incinerator, along the wind main-direction axis. A second station (CTW), used as a "control" of the first one, was chosen in a position representing both the minimum falling out of plant emission and whole extra-incinerator immission, according to the PM10 simulation (Bonafè and Rossi, 2011). A second maximum (MXS) was placed on the west side of the plant on the same wind axis, and a second control (CTS) was chosen. The other stations were placed as to represent different air conditions in the domain: high traffic (MXD), rural (MND) and suburban area (CAS).

Thirteen different metals were analyzed through atomic absorption spectroscopy GF-AAS with Zeeman background correction. Extensive statistical analyses were performed, using both univariate and multivariate methods. Furthermore some seasonal comparison were made.

Results

The ambient measurements showed that the metal compositions of PM2.5 and PM1 were not significatively different in the summer season. This was not true for the winter season, in which PM1 metal composition was found different from that of PM2.5 fraction and also variable among the monitoring stations. In both seasons aluminum, iron and zinc were the prevailing and most widespread elements. Summer PM2.5 or PM1 metals in both maxima were not different from their controls. The same behaviour was found in the winter season for PM2.5 particulate fraction only. On the contrary the PM1-metal composition was found different between the first maximum and its control samples.

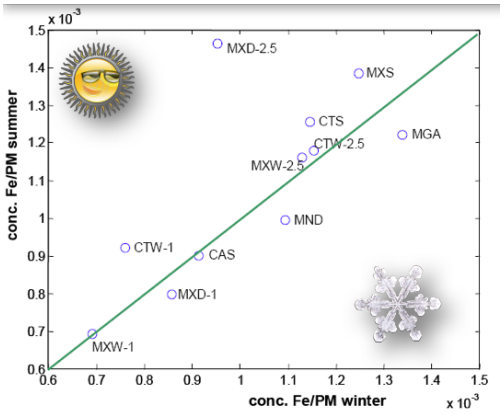

Figure 1. Average iron concentrations for both seasons and every monitoring station. The green line has slope one and intercept zero.

The typically crustal metals were widespread through the different stations samples in both seasons, while the other metals were found more seasonal influenced.

This work was part of the «Moniter Project». http://www.moniter.it

Bonafè, G., Rossi, M. (2011) *Proc of the.14th Int. Conf. on Harmonization within Atmospheric Dispersion Modelling for Regulatory Purposes*.

Polycyclic Aromatic Hydrocarbons and Nitro-Derivatives PAHs in PM2.5 and PM1 samples collected near a waste incinerator plant in the Po Valley (Bologna).

M. Rossi[1], L. Pasti[2], I. Scaroni[3] and P. Casali[3]

[1]Regional Agency for Prevention and Environment ARPA - Emilia-Romagna, Rimini, 47923, Italy
[2]Department of Chemistry, University of Ferrara, Ferrara, 44121, Italy
[3]Regional Agency for Prevention and Environment ARPA - Emilia-Romagna, Ravenna, 48121, Italy
Keywords: PM2.5, PM1, PAH(s), Air Quality, Monitoring, Modelling (microscale), Waste Incineration Impact.
Presenting author email: marossi@arpa.emr.it

It is well known that the problem of waste disposal is critical in advanced societies, characterized by increasing consumption of goods, and one of the technologies used to manage this problem is waste incineration. In Italy there is a high perception of health risk related to the presence of incinerating plants. For this reason, local communities are very interested in their air quality and in the possible presence of health-risk pollutants, related to the activity of these plants. The aim of this study is to characterize polycyclic aromatic hydrocarbons and some of their nitro-derivatives in PM1 and PM2.5 samples collected in the surroundings of an incinerator. Furthermore the plant accountability was also investigated.

To reach this goal two extensive monitoring campaigns were performed: the first one was held in summer 2008 and the second one in winter 2009. The plant under study is located in a suburban-farming area, less than 10 km away from northeast of Bologna (Italy), in the southeast of Po Valley, which is a well known atmospheric polluted critical area.

Seven out of eight monitoring stations were installed in a domain of 8x9 km^2 around the plant. The eighth station (MGA) was placed far away, inside the urban area of Bologna, in a site used for urban background measurements by Arpa Environmental Agency.

A preliminary study with ADMS-Urban (Cerc, Cambridge, UK) dispersion model was performed to select monitoring station coordinates, using PM10 emissions as pollutant tracer. A first station (MXW) representative of maximum deposition of plant emissions was placed in the east side, not too far from the incinerator, along the wind main-direction axis. A second station (CTW), used as a "control" of the first one, was chosen in a position representing both the minimum falling out of plant emission and whole extra-incinerator immission, according to the PM10 simulation (Bonafè and Rossi, 2011). A second maximum (MXS) was placed on the west side of the plant on the same wind axis, and a second control (CTS) was chosen. The other stations were placed to represent different air conditions in the domain:

- MXD as high traffic; it is also the highest polluted site in the preliminary simulation;
- MND as rural; it is also the lowest polluted site in the preliminary simulation;
- CAS as suburban area.

Twenty-three different PAHs and eleven nitro-derivatives PAHs (N-PAHs) were analyzed through GC-MS in PM1 and PM2.5. Extensive statistical analyses were performed, using both univariate and multivariate methods. Furthermore, markers and diagnostic ratios methods were used to complete the data interpretation.

ADMS-Urban dispersion model was eventually used to assess the plant accountability towards the ambient PAHs amounts, using direct emission measurements performed simultaneously at the smokestack.

The ambient measurements showed that there were different compositions between PM1 and PM2.5 PAHs, expecially during the winter season. Summer PM2.5-PAHs in the first max were not different from its control, but this cannot be retained true for N-PAHs, since they were more concentrated in the max station. In winter PM2.5-PAHs, on the contrary, were more concentrated in the control particulate.

The evaluation carried out by ADMS-Urban appears to ascribe to the incinerator a very small account, nearly about 2 ‰.

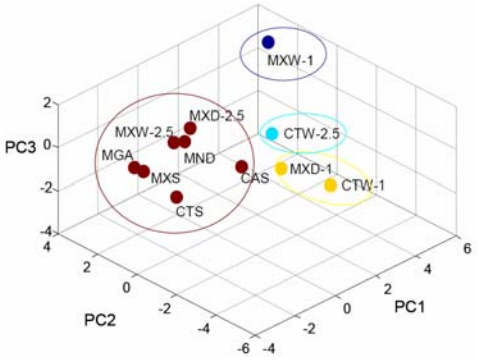

Figure 1. *K-means* clustering in the PC space able to describe more than 80% of the winter data variance.

Other complementary considerations lead us to think that the most of PAHs found in PM2.5 and PM1 aerosol are to be related to other sources, i.e. mainly to urban traffic.

This work was part of the «Moniter Project». http://www.moniter.it

Bonafè, G., Rossi, M. (2011) *Proc of the.14th Int. Conf. on Harmonization within Atmospheric Dispersion Modelling for Regulatory Purposes*.

PM2.5 and PM1 aerosol monitoring near a waste incineration plant located next to Bologna, in the Po Valley: the MONITER Project Campaign

M. Rossi[1], G. Bonafè[2], F. Scotto[2], A. Trentini[2], L. Pasti[3]

[1]Regional Agency for Prevention and Environment ARPA - Emilia-Romagna, Rimini, 47923, Italy
[2]Regional Agency for Prevention and Environment ARPA - Emilia-Romagna, Bologna, 40138, Italy
[3]Department of Chemistry, University of Ferrara, Ferrara, 44121, Italy
Keywords: PM2.5, PM1, Air Quality, Monitoring, Modelling (microscale), Waste Incineration Impact.
Presenting author email: marossi@arpa.emr.it

It is well known that the problem of waste disposal is critical in advanced societies, characterized by increasing consumption of goods, and one of the technologies used to manage this problem is waste incineration. In Italy, there is a high perception of health risk related to the presence of incineration plants. Nowadays, in Emilia-Romagna there are eight incinerators and a new one is under construction, so investigating the possible presence of pollution related to these plants activities is crucial.

The Emilia-Romagna Region promoted an applied researching project called MONITER (http://www.moniter.it). One of the aims of the project was acquiring new knowledge about the air quality in the proximity of an incinerator (also seeking pollutants not covered by current regulations), in order to understand if these plants should be considered a risk for the local communities' health.

To reach this goal two extensive monitoring campaigns were performed near a plant having these main features: 600 tons/day of incinerating capacity, two 80-meters-high stacks and BAT purification devices. The first monitoring campaign was carried out in summer 2008 and the second one in winter 2009. The plant under study is located in a suburban-farming area, less than 10 km away from northeast of Bologna (Italy), in the southeast of the Po Valley, which is unfortunately a well known atmospheric polluted critical area.

Seven out of eight monitoring stations were installed in a domain of 8x9 km^2 around the plant. The eighth station (GMA) was placed far away, inside the urban area of Bologna, in a site used for urban background measurements by Arpa Environmental Agency.

A preliminary study with ADMS-Urban (Cerc, Cambridge, UK) dispersion model was performed to select monitoring station coordinates, using PM10 emissions as pollutant tracer. A first station (MXW) representative of maximum deposition of plant emissions was placed in the east side, not too far from the incinerator, along the wind main-direction axis. A second station (CTW), used as a "control" of the first one, was chosen in a position representing both the minimum deposition of plant emission and whole extra-incinerator immission, according to the PM10 simulation (Bonafè, G. and Rossi, M., 2011). A second maximum (MXS) was placed on the west side of the plant on the same wind axis, and a second control (CTS) was chosen. The other stations were placed to represent different air conditions in the domain:
- MXD as high traffic; it is also the highest polluted site in the preliminary simulation;
- MND as rural; it is also the lowest polluted site in the preliminary simulation;
- CAS as suburban area.

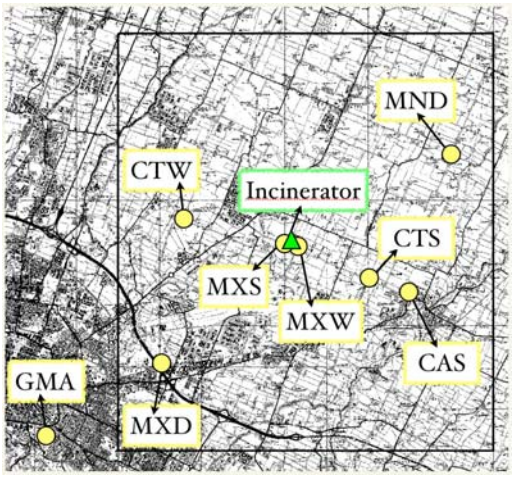

Figure 1. Location of the MONITER Project Campaigns. In the southwest corner is possible to see a part of the city of Bologna (I).

The MONITER Campaigns took into account various species of pollutants, for a total of more than 130 different chemical species sought into particulate. The data obtained were processed by extensive statistical analysis and the overall evaluation of results are the subject of this presentation.

A more detailed view of specific pollutants found in the particulate were presented in other specific communications of this same Conference.

This work was supported by Regione Emilia-Romagna and was conducted as part of the «Moniter Project». http://www.moniter.it

Peltier R. E., Lippmann M. (2011) *Spatial and seasonal distribution of aerosol chemical components in New York City: (1) Incineration, coal combustion, and biomass burning* J. Expos. Sci. Envir. Epid. **21**, 473-483

Bonafè, G., Rossi, M. (2011) *Proc of the.14th Int. Conf. on Harmonization within Atmospheric Dispersion Modelling for Regulatory Purposes.*

Concentrations of PM_x, NO_2 and NH_3 in the metropolitan area of Barcelona: APICE long monitoring campaign

J. Pey[1], N. Pérez[1], A. Alastuey[1], X. Querol[1], J. Cortés[2]

[1]Institute of Environmental Assessment and Water Research (IDAEA-CSIC), Barcelona, E-08034, Spain
[2]Autoritat Portuaria de Barcelona
Keywords: air quality, gaseous precursors, emission sources
Presenting author email: jorge.pey@idaea.csic.es

Concentrations of particulate matter (PM_{10} and $PM_{2.5}$) and NO_x are exceeding regularly the European standards in the Barcelona metropolitan area. As it's well known, NO_x concentrations recorded in urban areas are mostly anthropogenic in origin. Also PM_x levels are highly dependent of anthropogenic sources although natural contributions may be dominant in specific cases. The Barcelona region has a number of peculiarities that makes tricky the study of atmospheric pollutants, mainly concerning particulate matter. Thus, factors such as topography of the region, inputs of mineral dust particles from North Africa, local-regional meteorology, numerous anthropogenic emission sources, have to be taken into account. Previous studies revealed that around 1/4 of the PM_{10} concentration is mineral matter, mainly anthropogenic; 1/3 secondary inorganic aerosols; and the rest carbonaceous material and unaccounted mass (Pérez *et al.* 2008). A recent study revealed that formation of secondary inorganic aerosols in the Barcelona region occurs mainly inside the city (Pey *et al.* 2010). Accordingly, abatement plans for particulate matter need to consider both primary emissions but also gaseous precursors of secondary aerosols (such as NO_x, SO_x and NH_3) in order to be effective (Harrison *et al.* 2008).

In Barcelona, one of the major sources of atmospheric pollutants is road traffic, although other sources such as industry, power generation, construction-demolition, and harbour activities are relevant. Owing to the location of the harbour with respect to the city area and the wind regime (with high frequency of sea breezes), harbour pollution is affecting the city nearly half of the time.

The APICE (Common Mediterranean strategy and local practical Actions for the mitigation of Port, Industries and Cities Emissions) project pretends to reduce harbour emissions to the atmosphere by adopting mitigation strategies, that will be taken at two different scales: local (specific abatement measures for the harbour of Barcelona) and trans-national (common strategies to be applied in the five cities involved in the project). To fulfil the objectives of the project, a long monitoring campaign (one year study, 2011) was intended, mostly in the harbour area but also covering (for a number of atmospheric pollutants) the whole metropolis.

In this work we show the results of PM_{10}-$PM_{2.5}$, NO_2 and NH_3 concentrations obtained during the campaign. A first evaluation of the results indicates that the highest levels of PM_{10} are recorded in the harbour area (40-50 µg m^{-3}), whereas those of $PM_{2.5}$ are more elevated in the city centre, at traffic hotspots (22-25 µg m^{-3}). Out of the harbour area, PM_{10} levels are relatively homogeneous (25-33 µg m^{-3}), slightly higher at traffic sites. Regarding NO_2 concentrations, only shown for the harbour area, these are clearly parallel to traffic influence. Thus, the highest levels are observed in specific areas in the harbour. As far as we are away from road traffic lines, NO_2 levels decrease drastically. A different pattern is observed for NH_3, clearly higher in two specific sectors inside the harbour: where dusty materials are handled, and close to the water waste treatment plant..

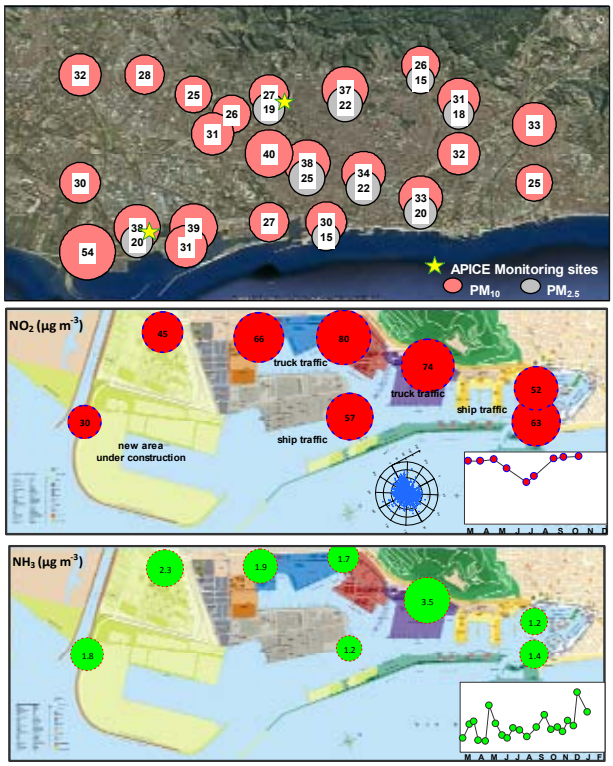

Figure 1. PM_{10}, $PM_{2.5}$, NO_2 and NH_3 (µgm^{-3}) spatial concentrations during APICE project.

This work has been supported by the MED programme (FEDER, CE) 2889 2G-MED09-026, in collaboration with *Autoritat Portuaria de Barcelona* and *Departament de Territori i Sostenibilitat (*Autonomous Government of Catalonia).

Harrison, R.M. Stedman, J. Derwent, D. (2008). *Atm. Env.* **42,** 603-606.

Pérez, N. Pey, J. Querol, X. Alastuey, A. López, J.M. Viana, M. (2008). *Atm. Env.* **42,** 1677-1691.

Pey, J. Querol, X. Alastuey, A. (2010). *Atm. Env.* **44,** 1587-1596.

Searching the relationship between PM_{10} and MODIS aerosol optical depth at Granada (Spain): urban location and background EMEP station

A.I. Calvo[1], J.L. Guerrero-Rascado[2,3], L. Alados-Arboledas[2,3], F.J. Olmo[2,3]

[1]Centre for Environmental and Marine Studies (CESAM), Department of Environment and Planning, University of Aveiro, Aveiro, 3810-193, Portugal
[2]Departament of Applied Physics. University of Granada. 18071, Granada, Spain.
[3]Group for Atmospheric Physics. CEAMA. Avd. del Mediterráneo s/n. 18006 Granada, Spain
Keywords: aerosol optical depth, MODIS, PM
Presenting author email: anacalvo@ua.pt

It has been widely recognized the important role of the atmospheric aerosol on different aspect such as climate, ecosystems, biogeochemical cycles or human health. In-situ measurements of atmospheric particles, carried out near the ground, constitute the most direct way to obtain information about the particulate matter (PM). However, surface monitors miss important information as often aerosol plumes are injected over higher atmosphere layer. At this point, it is important to pay attention to satellite observations, which can play an important role on supplementing the surface monitors (Guo et al., 2009).

In the last years, satellite remote sensing has been identified as a potential valuable tool for estimating ground-level PM concentration. Among the main advantages offered by satellite sensors, the extensive spatial resolution along with the cost effectiveness are highlighted. Several authors have studied the relationship between aerosol optical depth (AOD) retrieved from satellite data and the mass fraction PM_{10} or $PM_{2.5}$ at ground level. The AOD is retrieved as a measure of light extinction by columnar aerosol loading of the atmosphere during the satellite overpass.

Furthermore, the variation in this relationship across space and time has been investigated (e.g. Gupta et al., 2006; Tian and Cheng, 2010). However, it is not an easy task as different factors such as meteorological conditions, mixing layer height or site location, influence this relationship (Pelletier et al., 2007, Boyouk et al., 2010). As a consequence, different results have been reported by several authors at different study areas (Boyouk et al, 2010 and references therein).

Sensors such as MODIS (Moderate Resolution Imaging Spectroradiometer) are able to well retrieved AOD, an aerosol optical property that is also measured from ground-based sunphotometers in the frame of AERONET (Aerosol Robotic Network) network. Several authors have used MODIS data, as it has the unique ability to retrieve AOD with greater accuracy.

Ground-level particulate matter concentration (PM_{10}) at Granada (Spain), were analyzed: at a remote regional background EMEP station (EMEP: Cooperative Programme for the Monitoring and Assessment of Long Range Transport of Air Pollutants in Europe) installed in Víznar (37º 14' N, 03º 28' W and 1260 m a.s.l.) and at the urban place (four different locations included in the Air Quality Monitoring and Control Network of Andalusia). Víznar lies 12.5 km from Granada and is a rural area in a natural basin surrounded by mountains with the highest mountain range located to the southeast. Granada (37.16º N 3.58º W, and 680 m a.s.l.) is a city with 300 000 inhabitants, that increases up to 600 000 if the whole metropolitan area is considered.

For this study, the daily data set of AODs at 550 nm was obtained by MODIS Terra and Aqua (collection 5.1). Data used in this work are daily Level 2 data at the spatial resolution of 10x10 km (at nadir), including information from Terra (MOD04_L2) and Aqua (MYD04_L2) platforms. Only cloud-free pixels were considered.

In this study, several years of data were analysed aiming to compare the relationship between satellite retrieved AOD and surface-measured PM_{10}. The importance of mixing layer height will be highlighted.

Improving knowledge on this PM-AOD relationship constitutes an important challenge. The use of satellite AOD retrievals data for PM estimation will enable to obtain reliable PM information at global scale. Therefore, it is important to continue studying in depth this relationship as it constitutes a very useful tool for mapping PM distribution over large spatial domains and, hence, for monitoring air particulate pollution (Péré et al., 2009).

This work was supported by the Spanish Ministry of Science and Technology through projects CGL2010-18782 and CSD2007-00067; by the Andalusian Regional Government through projects P10-RNM-6299 and P08-RNM-3568; and by the EU ACTRIS project (EU INFRA- 2010-1.1.16-262254).

Beyouk, N., Léon, J.-F., Delbarre, Podvin, T., Deroo, C. (2010). *Atmos. Environ*. **44**, 271-277.
Guo et al., (2009). *Atmos. Environ.* **43** 5876–5886.
Gupta, P., Christopher, S., Wang, J., Gehrig, R., Lee, Y., Kumar, N. (2006). *Atmos. Environ.* **40**, 5880–5892.
Pelletier, B., Santer, R., Vidot, J. (2007). *J. Geophys. Res*. **112**. doi:10.1029/2005JD006737.
Péré, J.-C., Pont, V., Mallet, M., Bessagnet, B. (2009). *Atmos. Res*., **91**, 1-8.
Tian, J. and Chen, D. (2010). *Remote Sens. Environ*. **114**, 221-229.

Origin of $PM_{2.5}$ and Secondary Inorganic Aerosol (SIA) and relationship with gaseous pollutants in the Venice area

S. Squizzato, M. Masiol, E. Innocente, E. Pecorari, G. Rampazzo, B. Pavoni[1]

[1] Dipartimento di Scienze Ambientali, Informatica e Statistica, Università Ca' Foscari Venezia, Venice, 30123, Italy

Keywords:PM2.5, Secondary Inorganic Aerosol, local contribution, gaseous pollutants.

Presenting author email: stefania.squizzato@unive.it

Fine particles (AD ≤ 2.5 μm) mainly derive from industrial and residential combustion processes, motor-vehicle emissions and conversion of gaseous compounds to particulate phase. The particle mass deriving from gas-to-particle conversion is defined as secondary aerosol (SIA – secondary inorganic aerosol, SOA-secondary organic aerosol).

In the Venice area, $PM_{2.5}$ and NO_x emission are mainly related to road transport and combustion processes (combustion in energy and transformation industries and non industrial combustion plants) whereas SO_2 emission mostly derive from combustion in energy and transformation industries (ISPRA, 2012).

In this work, PM and major inorganic ions (NH_4^+, NO_3^-, SO_4^{2-}) are studied in relation to environmental conditions and gaseous precursors (SO_2 and NO_x) to highlight SIA formation patterns and origin.

One-year PM sampling campaign has been carried out from January 2009 to January 2010 in three sites, representing different emission scenarios and environmental conditions: (i) SRC, semi-rural-background costal site; (ii) UBG, urban background site; (iii) IND, industrial site. PM was collected simultaneously on 47 mm quartz fiber filters (Whatman QMA) using low volume automatic samplers equipped with $PM_{2.5}$ cut-off inlets and set according to EN 14907 standard.

Four sampling periods were selected to represent the four seasons and ultrasonic method was used to extract all filters for determination of major inorganic ions (NH_4^+, NO_3^-, SO_4^{2-}) by ion chromatography as proposed by Squizzato *et al.* (2012).

The concentrations of gaseous pollutants (SO_2, NO_x, NO, NO_2) in UBG and IND site were provided by local Environmental Protection Agency (ARPAV). Meteorological conditions (temperature, relative humidity, wind speed and direction) were recorded by Ente della Zona Industriale di Porto Marghera and ARPAV-Centro Meteorologico di Teolo.

The relationship between SIA and gaseous pollutant have been evaluated using SOR (Sulfur Oxidation Ratio) and NOR (Nitrogen Oxidation Ratio). SOR and NOR have been used to express the degree of atmospheric conversion of SO_2 to SO_4^{2-} and of NO_2 to NO_3^-. Then, wind speed and direction and back-trajectories have been combined with chemical data to point out the influence of local and external sources of PM and SIA and the Lenshow approach (Lenshow *et al.*, 2001) was used to estimate local contribution as described by Squizzato *et al.* (2012).

The $PM_{2.5}$ annual mean was 33 μg m^{-3} for the two mainland sites (UBG and IND) and 26 μg m^{-3} for SRC. $PM_{2.5}$ concentrations were inversely correlated with air temperature, with higher levels during the cold period. On a yearly basis, SIA accounts for 9.5 μg m^{-3} (27% of $PM_{2.5}$ mass) in UBG, 9.6 μg m^{-3} (28%) in IND and 9.5 μg m^{-3} (36%) in SRC.

Strong correlations were observed between NO_3^-, NO_2, NOR, NH_4^+, temperature and relative humidity (Table 1). This suggests a local origin for ammonium nitrate related to an increase in NO_x levels and particular environmental conditions (low temperature and high relative humidity). Heavy pollution events occur in days characterized by low atmospheric dispersion and air masses coming from Po' Valley. During these events the local contribution on PM and SIA increases. Nevertheless, considering the mass percentage, no significant variations were observed for all periods and samples. In conclusion, heavy SIA events are mainly due to a regional contribution and are enhanced by scarce atmospheric dispersion that traps pollutants.

Table 1. Correlation matrix between NO_3^-, NO_2, NOR, NH_4^+ temperature and relative humidity.

UBG	NO_3^-	NO_2	NOR	NH_4^+	T (°C)	R.H
NO_3^-	1.00					
NO_2	0.59	1.00				
NOR	0.96	0.48	1.00			
NH_4^+	0.89	0.59	0.87	1.00		
T (°C)	-0.44	-0.35	-0.51	-0.33	1.00	
R.H	0.35	0.04	0.43	0.33	-0.25	1.00

This work was supported by Ente della Zona Industriale di Porto Marghera. The authors are also grateful to Environmental Protection Agency of Veneto Region (ARPAV) for the valuable support and logistics.

ISPRA (Italian Institute for Environmental Protection and Research) (2012). Disaggregated emission inventory 2005.

Lenschow, P., Abraham, H.-J., Kutzner, K., Lutz, M., Preuß, J.-D. and Reichenbächer, W. (2001). *Atmos. Environ.* **35**, S23-S33.

Squizzato, S., Masiol., M., Innocente, E., Pecorari, E., Rampazzo, G. and Pavoni, B. (2012). *J. Aerosol Sci.* **46**, 64-76

Analysis of the episodes of high PM10 concentrations from January to April and October to November 2011 in Central and Western Europe with focus on North-Rhine Westphalia

S. Wurzler, H. Hebbinghaus, P. Bruckmann, A. Baltruschat, U. Romberg, J. Friesel, U. Pfeffer, W. Straub, J. Geiger

North Rhine Westphalia State Agency for Nature, Environment and Consumer Protection (LANUV), P.O. Box 101052, D-45610 Recklinghausen, Germany

Keywords: PM10, air quality.

Presenting author email: sabine.wurzler@lanuv.nrw.de

The year 2011 was an exceptional year, with a long period of cold weather in January and persistent sunny and dry weather conditions in October and November.

The year 2011 was also special with regard to the PM10 concentrations in Germany and NRW. Most of the exceedance days occurred in the time span from end of January to April and during an episode mainly in November. Especially in November very high particle concentrations occurred. These particle episodes led to a multitude of exceedance days. An exceedance day is a day with a daily average PM10 concentration of more than 50 µg/m³. The European air quality directive 2008/50/EC specifies a limit value of 35 allowed PM10 exceedance days. This situation reminded in the northern Ruhr area of the smog episodes in the eighties in NRW, leading to an increased mortality and as political consequence to traffic bans and restrictions for industrial facilities. Fortunately, the PM10 concentrations in 2011 did not reach this level.

In North-Rhine Westphalia (NRW) for example, we observed in 2011 limit value exceedances at more than 20 measurement sites (Fig. 1). For comparison: in 2008, 2009, and 2010 we had PM10 limit value exceedances on average at 5 measurement sites in NRW. Another novelty was that we had to report limit value exceedances for several urban background sites. The highest daily averages were found in NRW in the northern part of the Ruhr area with values up to 140 µg/m³.

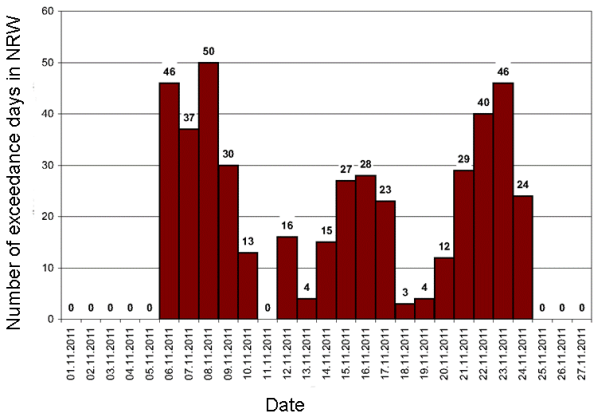

Figure 1: Number of exceedance days found at measurement stations in NRW during November 2011.

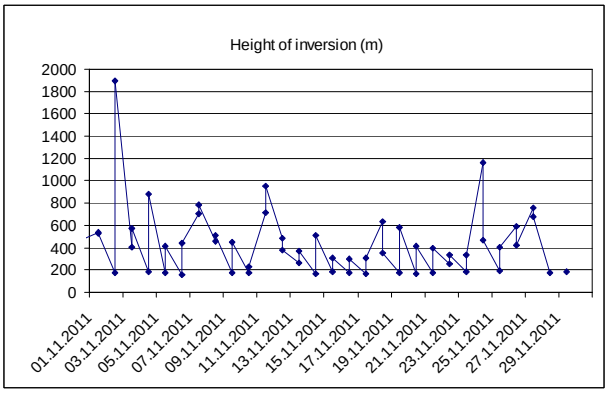

Figure 2: Height of inversion at Essen, NRW, Germany, during November 2011

Other parts of Germany showed high concentrations as well. In November, a first analysis showed exceedances on 18 days at rural background measurement sites in Germany (UBA, 2012). Over the whole year 2011, 11 rural background sites showed limit value exceedances (compared to 6 on average over the years 2005 to 2010), 19 urban background sites (13 over 2005 to 2010), and 33 traffic related sites (29 over 2005 to 2010).

EURAD simulations showed, at least for the November episode, that the high PM10 concentrations affected not only Germany but also large parts of Central Europe. The high PM10 concentrations covered Central Europe like a belt from west to east, sparing only the Scandinavian and Mediterranean countries.

Scope of the paper is to give an overview of the exceedance situation including the meteorological conditions. Additionally the origin of the particle burden will be investigated with focus on the questions whether the high particle loads were mainly home made or caused by long range transport. Figure 2 shows the height of inversion during November 2011 at the radiosounding station of the German Weather Service at Essen. It is clearly visible that during the whole month low heights of inversion persisted. This is certainly one of the causes leading to the high PM10 concentrations. Further investigations are currently under way.

UBA (2012) *Luftqualität 2011 – vorläufige Auswertung*.

Health relevant organic compounds on particulate matter ($PM_{2.5}$) at two urban sites in Munich: Critical data evaluation

J. Lintelmann, K. Fischer, R. Zimmermann

Cooperation Group "Comprehensive Molecular Analytics"
Helmholtz Zentrum Muenchen,
Ingolstädter Landstr.1, D-85764 Neuherberg

Keywords: PAH-derivatives, HPLC, LC-MS/MS, particulate matter, source apportionment

Recent studies underline the importance of the organic fraction of particulate matter for human health (Urch et al., 2004, Mauderly et al., 2008). Beside physical properties the chemical constitution of the particles determines their potency to cause severe health impairments.

During two consecutive years particulate matter ($PM_{2.5}$) was collected at two urban sites: In the Munich city center (2006) and at the Munich city border (2005) to aim for the characterization of representative, health relevant organic substances on $PM_{2.5}$ on the one hand, and for comparing concentrations, their time courses as well as information on respective sources on the other hand. Regularly sampling (every 3rd day for 24 hours) with a high volume sampler was performed. Particle-laden quartz-fibre filters were extracted and used for the determination of polycyclic aromatic hydrocarbons (PAH), nitro-PAH, and PAH-diones The HPLC-based methods applied were developed, validated and established in our laboratory (Lintelmann et al., 2006).

Data evaluation was performed applying different data analysis tools (e.g. multiple linear regression, principal component analysis (PCA) positive matrix factorization (PMF, Environmental Protection Agency, USA)). Additional information like temperature, wind speed, radiation, ozone-, CO- and PM-concentration was of course incorporated as far as available. Data analysis is a dynamic process meaning that not a *right* or *true* model/structure is found, but rather a reasonable, useful interpretation Stahel (2008). Some outlooks of this interpretation are:

Temperature and wind speed in contrast to radiation and ozone significantly influence concentrations of the organic compounds considered. As expected analyte concentrations are season dependent with higher and extreme values in autumn and winter.

PMF for the Munich city center samples leads to reasonable results concerning interpretation and regression diagnostics assessing four factors. One factor is assigned to diesel emissions due to a high load of 1-nitropyrene, which is regarded as a diesel marker, and coronene, 3- and 4-ring PAH as well (factor 1). A second factor is referred to residential heating emissions with high contributions in the cold seasons, dominated by PAH loadings (factor 2). A further factor probably is a mixture from combustion/heating emissions which have partly undergone atmospheric transformation processes. It is characterized by high loading of PAH-diones (factor 3). The last factor is ascribed to traffic (gasoline) emissions influenced by atmospheric transformation and transport processes (factor 4). It is dominated by nitro-PAH and low PAH-contributions.

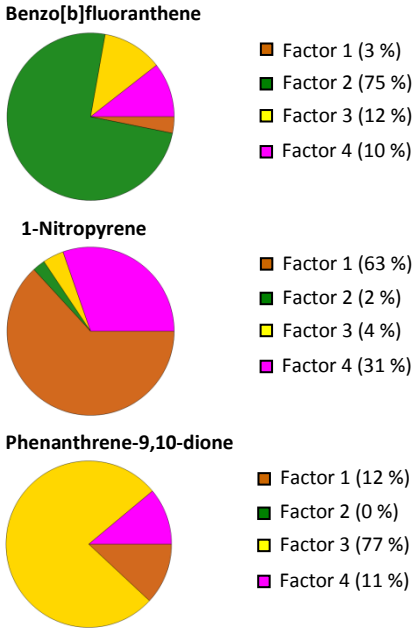

Figure 1: PMF-Factor pie charts for selected, representative health relevant organic compounds in $PM_{2.5}$, Munich, Germany.

Urch, B., Brook, J.R., Wasserstein, D., Brook, R.D., Rajagopalan, S., Corey, P, Silverman, F. (2004) *Inhal. Toxicol.* **16**, 345-352.

Mauderly, J.L., Chow J.C. (2008) *Inhal. Toxicol.* **20**, 257-288.

Lintelmann, J., Fischer, K., Matuschek, G. (2006) *J. Chromatogr.* A. **1133**, 241-247

Stahel, W. (2008). *Statistische Datenanalyse.* Vieweg + Teubner, Wiesbaden.

VARIATIONS OF PM-10 AND ITS RELATIONSHIP WITH BE-7 MEASUREMENTS USING A HIGH-VOLUME AIR SAMPLER AT MÁLAGA

C. Dueñas*[1], M.C. Fernández*[1], E. Gordo[1], S. Cañete[1] and M. Pérez[2]

[1]Department of Applied Physics I, Faculty of Science, University of Málaga, 29071 Málaga ,Spain
[2]Department of Radiology and Health Physics, Ophthalmology and OTL, Faculty of Medicine, University of Málaga, 29071 Málaga, Spain.
Keywords: Berylium-7, Atmospheric Aerosols, Gamma Spectrometry, Particulate Matter (PM10).

Presenting author email: mafeji@uma.es

Levels of particulate matter fraction PM10 were monitored between 2009 and 20011 in Málaga (Spain).

The station "Carranque" (4º 28' 4" W; 36º 43' 40"N), belongs to the Atmospheric Pollution Monitoring network managed by the Environmental Health Service of the Andalusian Government. PM10 concentrations were measured at "Carranque" station by the beta attenuation method. The ^{7}Be concentrations in air was weekly continuously monitored which a high-volume air sampler (ASS-500C). This sampler uses polypropylene square filters (44 x 44 cm^2) and collection efficiency 93-99%, at a flow rate of 90000 l/min. Measurements by gamma-spectrometry were performed to determine the ^{7}Be activities of the samples using an intrinsic REGe detector.

Long-term measurements of cosmogenic radionuclides such as ^{7}Be provide an important data in studying global atmospheric processes and comparing environmental impact of radioactivity from man-made sources to natural ones. The period of measurements was performed from 2009 to 2011. The variation of the data with time was studied by time series analyses and seasonal patterns were identified.

Table 1 provides arithmetic mean (AM) and related statistical information such as geometric mean (GM), standard deviation (SD), variation coefficient (CVDF), maximum (MAX) and minimum (MIN) value.

	AM	GM	SD	CV(%)	MAX	MIN
^{7}Be (mBq/m^3)	5.1	4.8	1.7	34.7	10.2	2.1
PM_{10} (µg/m^3)	40.3	37.8	14.3	35.5	86.3	17.4

Table 1. Statistical parameters of the different measurements.

Plots of the frequency distribution of ^{7}Be activities and PM10 show the histogram highly skewed (flat on the right) and a symmetric distribution. The concentration data of ^{7}Be and PM_{10} with meteorological variables were correlated to understand the week variation of these radionuclides in air. This study has shown that ^{7}Be and PM_{10} are associated with different source in Malaga, they may reach high concentration simultaneously. The reason for this is the concurrent occurrence of subsidence processes over North Africa (resulting in the downward transport of ^{7}Be from the mid-troposphere) and the suspension of mineral dust over desert region with a subsequent transport to Malaga. In other hand, in order to simplify the analysis, the events have been grouped into: (a) Low ^{7}Be and high PM_{10}; (b) high ^{7}Be and high PM_{10} (c) High ^{7}Be and low PM_{10}.

Several events of high ^{7}Be concentrations are mainly caused by downward transport of ^{7}Be from the mid-troposphere at mid-latitudes. The meteorological situation was characterised by an Atlantic anticyclone system with a low-pressure area over central European North Atlantic. Also found high ^{7}Be concentrations associated with low aerosol mass concentrations. These values were attributed to downward transport from mid-to-upper troposphere over the North Atlantic.

The meteorological situation was characterised by a south Europe anticyclone located in the South Atlantic Ocean that favoured the development of a blocking system with a low-pressure area over north Europe. Under these conditions, a slanting stratospheric air mass can penetrate into the troposphere (Hernandez et al., 2008)

Figure 1 shows the back-trajectories and map of atmospheric dust loads during a typical example of this type of events.

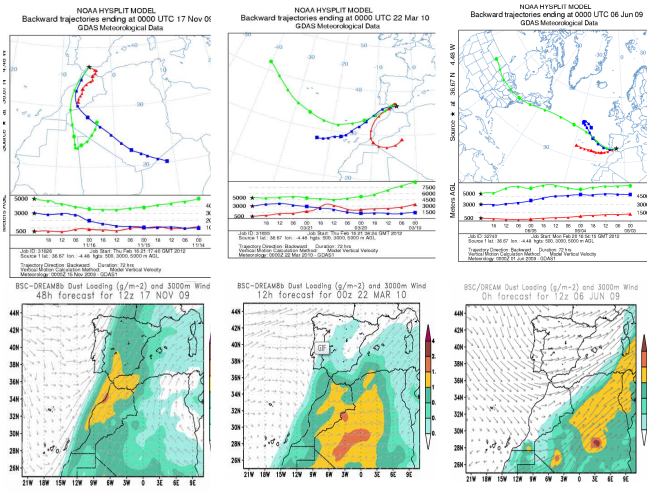

Figure 1. Map of atmospheric dust loads and back-trajectories

Hernandez F., Rodrıguez S., Karlssona L., Alonso-Perez S., Lopez-Pereza M., Hernandez-Armas J. and Cuevas E., (2008) *Origin of observed high 7Be and mineral dust concentrations in ambient air on the Island of Tenerife.* Atmospheric Environment 42, 4247–4256

EDXRF analysis of elemental composition of $PM_{2.5}$ particles sampled in Taif, Saudi Arabia

A. A. Shaltout[1,2], D. R. Almallway[1], Z. F. Shehadeh[1], J. Boman[3]

[1]Physics Department, Faculty of Science, Taif University, 21974 Taif, P.O. Box 888, Saudi Arabia
[2]Spectroscopy Department, Physics Division, National Research Center, El Behooth Str., 12622 Dokki, Cairo, Egypt
[3]Department of chemistry and molecular biology, Atmospheric Science, University of Gothenburg, SE-412 96 Göteborg, Sweden
Keywords: XRF, urban pollution, $PM_{2.5}$
Presenting author email: johan.boman@chem.gu.se

The present work is the first part of an initiative to evaluate the trace element composition of atmospheric aerosol particles smaller than 2.5 μm in aerodynamic diameter ($PM_{2.5}$) in two different areas of Taif city, Saudi Arabia. The selected industrial measurement site was situated at the largest industrial area in Taif whereas the residential measurement site was situated at the most crowded street in central Taif, namely on Television Street. $PM_{2.5}$ samples were collected during June and August 2011 on polycarbonate filters in a cyclonic sampler. The duration of the collection was 24 hours.

The knowledge of the chemical composition of air particulate matter is very important because it has an essential relation to health problems (Renwick et al., 2001). In addition, it gives important information on their origin and may also reveal whether they were emitted as primary or secondary particles. The smaller the particle, the more harm it may cause, as it penetrates deep into the lungs (Schwartz and Neas, 2000). Generally, there are two aspects to the importance of knowing the elemental content of atmospheric particles. First there are heavy elements such as Cd, Pb, As, and Sb, that are in themselves toxic to human health. It is of interest to follow the ecocycles of these metals as environmental hazards, once they are released into the atmosphere and biosphere. The second aspect is that single elements or ratios between elements can be used as a fingerprint of a special source emitting other hazardous species that are less stable and more difficult to measure.

An Energy Dispersive X-ray Fluorescence (EDXRF) spectrometer with Mo secondary target has been chosen for direct analysis of the filters with sampled aerosol particles. EDXRF was selected because of the relative simplicity of the analysis, no sample preparation is needed and the availability of the technique in many routine laboratories. The use of Mo secondary target is advantageous since it decrease the continuum radiation coming from the x-ray tube and creates a semi monochromatic excitation source for the elemental analysis. Quantitative X-Ray Analysis Software (QXAS/AXIL) has been used for the quantitative analysis of the sampled atmospheric particles. A certified reference material (SRM2783, Air Particulate on filter media, NIST, USA) has been used in order to validate the obtained results.

The analysis resulted in determination of thirteen elements; Br, Ca, Cl, Cu, K, Mn, Ni, Fe, Pb, S, Sr, Ti and Zn. One example of a XRF spectrum is shown in figure 1. The measured concentrations of the potentially hazardous trace elements As, Cu, Sb, Cr, Mn, Ni and Pb were below the limits defined by international guidelines and national standards of ambient air quality.

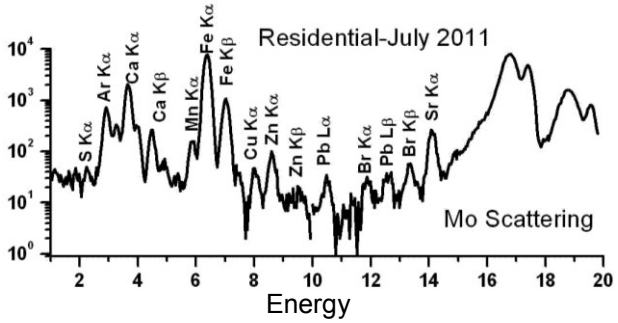

Figure 1. Example of the XRF spectrum of an aerosol particle sample collected in Taif.

This initial study is followed by long-term research required to validate the quantification of trace elements collected in this study. More samples are acquired at the two sites mentioned above and a newly added site dominated by traffic. In addition, the collected samples will be further studied using an Electron Spin Resonance (ESR) technique to investigate the existence of paramagnetic centers. These centers, if they exist in the samples, can be of great importance regarding the availability of radicals in the samples.

For this work we acknowledge the financial support by the Swedish Research Link program.

Renwick L.C., Donaldson K., Clouter A. (2001) *Toxicol Appl Pharmacol* 172 119–127..
Schwartz J., Neas L. (2000) *Epidemiology* 11(1) 6-10.

Time-resolved Measurements of Atmospheric Particulate Matter

M. Amodio, E. Andriani, P. R. Dambruoso, G. de Gennaro, A. Di Gilio

Department of Chemistry, University of Bari, Bari, Puglia, via Orabona, 4, 70126, Italy
Aerosol characterization, ionic fraction, PM2,5, AIM 9000D
alessia.digilio@uniba.it

Airborne particulate matter (PM) is a complex mixture of particles which show differences in size, physical and chemical properties and thus in the toxicological and carcinogenic effects they cause (Sager et al, 2009). The understanding of PM transport, mixing and transformation processes, and the identification of main factors influencing PM concentrations are relevant for developing appropriate control strategies for air quality. The determination of inorganic fraction in PM is very important to define the effective contribution of each source to fine PM. This fraction and in particular the ions, which constitute about 40-50% of total mass of PM2.5 and PM10, can be used as markers of different sources. Therefore, European Regulation suggest to characterize PM (ionic composition, organic carbon OC and elemental carbon EC) to obtain more detailed information concerning the different contributions to PM concentration (Annex IV of the air quality directive, EC, 2008).

The emitted pollutants undergo dilution with ambient air, and various types of transformations in atmosphere and during the transport process. The particle number concentrations, the information about the vertical diffusive properties of the low layers of the atmosphere, the meteorological data and the information obtained by aerosol models such as HYSPLIT and DREAM, and the characterization of ionic fraction of PM could be a useful tool to identify and characterize the different sources affecting PM concentrations (Amodio et al., in press).

In this work, the results obtained by applying an integrated approach in PM monitoring are shown. A system, located close to Chemistry Department of University of Bari was assembled with following instruments: SWAM Monitors, OPC monitor, PBL Monitor and Ambient Ion Monitor (AIM 9000D - URG Company). AIM instrument provides time-resolved direct measurements of anion and cation both in particulate (NO_3^-, SO_4^{2-}, Cl^-, NH_4^+, Na^+, K^+, Mg^{2+}, Ca^{2+}, found in PM2.5) and gases phases (such as HCl, HNO_3, HNO_2, SO_2 and NH_3).

Time-resolved data provided by system and collected from the 29th September to the 1st November 2011, allowed to identify and characterize time-limited events. In sampling period, the PM_{10} concentrations exceeded the limit value established by the EU Directive (50 ug/m^3) in nineteen days. The results showed an increase in concentration of secondary pollutants when low dispersive atmospheric conditions and high $PM_{2.5}/PM_{10}$ ratio were determined. In these days the hourly nitrate concentrations and the natural radiation counts showed the same trend. On the contrary, when high dispersive atmospheric conditions and lower $PM_{2.5}/PM_{10}$ ratio were registered, the long-range transport events, such as natural or anthropogenic outbreak, occurred. As example sulphate and ammonium concentration and the natural radiation counts in the period from the 29th September to the 12th October are reported in Fig.1. From the 10th and the 12th October, the natural radiation counts and $PM_{2.5}/PM_{10}$ ratio decreased respect to other days; this period was characterized by gust event and wind blew from North-East. High hourly sulphate and lower ammonium concentrations were observed. In these three days, the information provided by aerosol models and 5-days backward trajectories at event hour, identify the outbreak from North-East Europe in the Southern regions of Italy. The hourly concentration of sodium and chloride (not shown), calcium and sulphate in this period showed the same behaviour (Fig.2). These results suggested a synergic contribution to PM concentrations of crustal contribution, due to the pollutants resuspension caused by gust wind, and a marine aerosol.

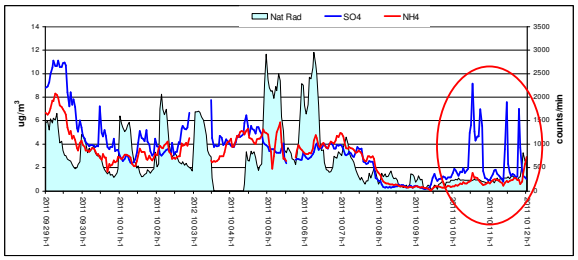

Fig. 1: natural radiative counts, ammonium and sulphate concentrations (ng/m^3)

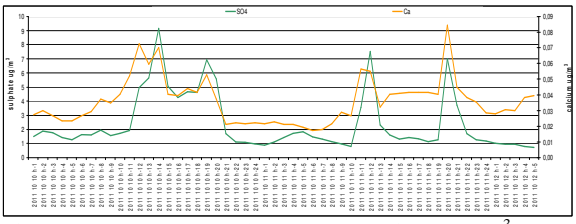

Fig. 2: sulphate and calcium concentrations (ng/m^3)

This work was supported by the Strategic Project PS_122 founded by Apulia Region.

Sager, T.M and Castranova, V. (2009) *Particle and Fibre Toxicology* 2009, **6**, 1-12.

Amodio M. et al, (2012) Env. Sci. Pol. Res. In press

The changes in chemical composition of fine PM between 1994 and 2010 at rural background site Košetice, Czech Republic

J. Schwarz[1], V. Havránek[2], R.Krejčí[3], P. Tunved[3], E. Swietlicki[4], and. V. Ždímal[1]

[1]Department of Aerosol and Laser Studies, Institute of Chemical Processes AS CR, Prague, 16502, Czech Rep.
[2]Department of Chemical Physics, Institute of Nuclear Physics AS CR, Řež, 25068, Czech Rep.
[3]Department of Applied Environmental Science, Stockholm University, S 106 91, Stockholm, Sweden
[4]Div. of Nuclear Physics, Dept. of Physics, Lund University, S-221 00 Lund, Sweden
Keywords: PM2.5, chemical composition, time trend, elemental composition
Presenting author email: schwarz@icpf.cas.cz

Elemental and ionic compositions of $PM_{2.5}$ were measured daily at rural backround site Košetice that is located about 80 km SE from Prague, Czech Republic. The Košetice site is a part of EMEP, ACTRIS, and GAW networks. The measurement was carried out from October 2009 till October 2010. The samples were taken using a sequential sampler Leckel equipped with $PM_{2.5}$ inlet at 2.3m3/h. TEFLO filters (Pall, 47mm in diameter, 3µm porosity) were used. The samples were analysed using ion chromatography for water soluble ions and by PIXE, PESA and RBS methods to determine content of up to 40 elements.

The results were compared with data measured daily at the same site for 14 months from Dec 1993 to January 1995 R. Krejčí who sampled the aerosol $PM_{2.5}$ fine fraction on polycarbonate Nuclepore filters and analysed samples using PIXE.

Meteorological data, and trace gases concentration are available for both campaigns. The air mass back trajectories were calculated for both campaigns. The results are compared both from view of individual elements and sources determined using PMF analysis of the data.

Ratios 1994/2010 of yearly median elemental concentrations are shown in Fig. 1.

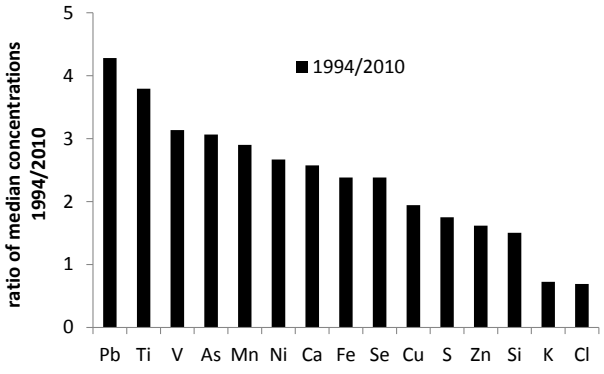

Figure 1. Ratios of median concentrations of individual elements in 1994 and 2010 data.

It is clear that most of elemental concentrations decreased during the time and some of them substantially. Lead and titanium decreased about 4 times, vanadium, arsenic, manganese, and nickel decreased about 3 times. Sulphur was found to be the most abundant element of the analysed ones. It decreased only 1.7 times despite much larger decrease of the SO_2 emissions. Potassium median concentrations were even higher in 2010 than in 1994.

An example of seasonal variation of several elements in both years is depicted in Fig. 2.

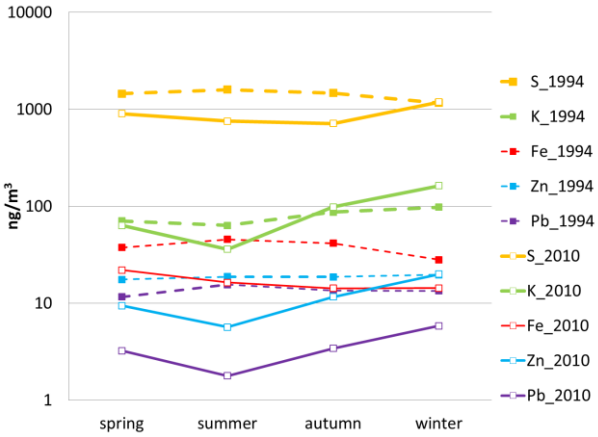

Figure 2. Seasonal median elemental concentration in aerosol fine fractions in 1994 and 2010 at the rural background site Košetice

Although seasonal trends may be influenced by year to year meteorological variations, it seems that residential heating plays an increasing role in total aerosol burden. The most pronounced differences can be seen in lead seasonal trend. In 1994, lead from the traffic exhibited a maximum in summer, while in 2010 it shows a clear minimum in the same season. Winter maxima are seen now for all depicted elements except iron, where the dust resuspension plays a major role Higher concentration of potassium found in the aerosol fine fraction in winter 2010 is probably related to an increasing use of biomass burning for residential heating due to supportive measures and lower price in comparison with the other fuels.

This work was supported by the Czech Science Foundation under the grants No. 205/09/2055 and 209/11/1342. The authors would like to thank Mr. Jan Čech from the Košetice station for operating the sequential sampler in the recent campaign and Dr. Milan Váňa from the same site for supporting data delivery.

Temporal and spatial variability of the total particle number concentration in the Venice area

Andrea Pigozzo[1], Alessio De Bortoli[2], Salvatore Patti[2], and Laura Manodori[3]

[1]Associazione CIVEN, Venezia, ,I-30175, Italy
[2]ARPAV, Venezia, I-30174, Italy
[3]Veneto Nanotech, Rovigo, I-45100, Italy

Keywords: CPC, number concentration, ultrafine particles.
Presenting author email: pigozzo@civen.org

Ultrafine airborne particles have been recognised to be toxic for the human health (Oberdörster, 2001) and they are becoming a primary concern in the air quality management and regulation. In a such framework, the present study aims to evaluate the temporal and spatial variation of ultrafine particles concentration at 5 sampling sites in the Venice mainland, where different human activities and sources of pollution could be identified

To collect a robust data-set, an intensive measurement campaign has been carried out over one year by means of a condensation particle counter (CPC Grimm, mod. 5.403; range of the detectable particles: 4 nm – 3 μm); samplings have been performed for 15 consecutive days at every site, with a temporal resolution of 1 minute. The sampling stations have been identified as rural, industrial, urban background, urban and traffic sites.

The analysis of the preliminary results allows to observe the presence of a clear seasonal trend at every site, with the highest concentrations detected in winter and the lowest ones in summer, as reported in Figure 1. Moreover, the obtained data-set has confirmed the expected spatial distribution of the particles concentration, in agreement with the surrounding anthropic sources and the results previously reported by Morawska *et al.* (2009). In detail, the rural site shows the minimum median concentration (total particle number concentration: $8x10^3$) whilst the traffic oriented site exhibits the maximum median concentration (total particle number concentration: 4.5×10^4).

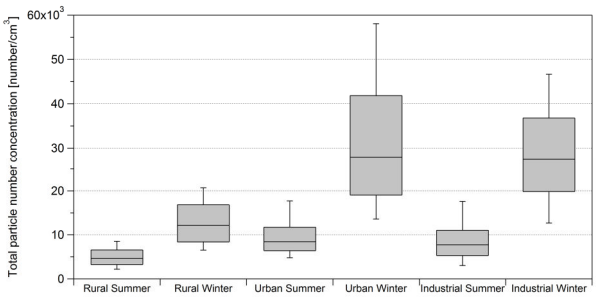

Figure 1. Box plot (minimum, 25th percentile, median, 75th percentile, maximum) of the particle number concentrations at the rural, urban and industrial sites in summer and winter

As depicted in Figure 2, a circadian variability of the particle concentration has been detected at the traffic site, with two maximum peaks in correspondence of the traffic rush hours in the morning and the late afternoon. These peaks may be related to the major input of fresh pollutants emitted by motor engines, which increase the formation of secondary aerosol that is the main responsible for the ultrafine fraction and the increasing of the total number concentration (Wang *et al*., 2010). The same trend has been observed at the urban site too, but it was completely lacking at the rural station.

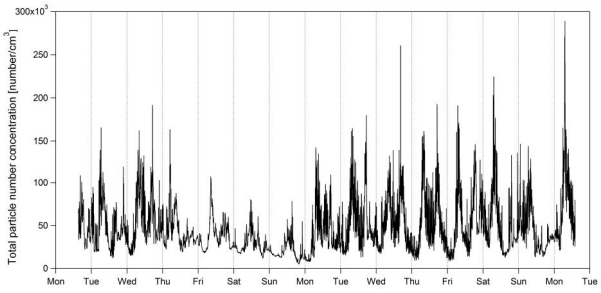

Figure 2. Smoothed trend of total particle number concentration at the traffic site.

This work has been supported by the Regione del Veneto under the project RESMIA.

Oberdörster, G. (2001) *Int. Arch. Occup. Environ. Health* **74,**1-8.

Morawska L, Ling X., and Jayaratne R. (2009) *European Aerosol Conference*, Karlsruhe, Abstract T043A04

Wang F., Costabile F., Li H., Fang D., Allegrini I. (2010) *Atmospehric Environment* **98**, 69-77.

Takeoff – but what was left behind? In an African perspective

M. J. Gatari[1], J. Boman[2], V. Kivaya[1], D. Maina[1] and A. Wagner[3]

[1]Institute of Nuclear Science and Technology, University of Nairobi, 00100 Nairobi, Kenya
[2]Department of Chemistry and molecular biology, Atmospheric Science, University of Gothenburg, SE-412 96 Gothenburg, Sweden
[3]Department of Applied Physics, Condensed Matter Physics, Chalmers University of Technology, SE-412 96 Gothenburg, Sweden
Keywords: Aerosol characterization, XRF, Nairobi
Presenting author email: johan.boman@chem.gu.se

This study was undertaken based on a growing global concern on the effect of airports on local air (Woody et al., 2011). It is the first to report trace element concentrations of aerosol particles at an international airport in Africa. Studies like this are important since a degraded air quality in a world of increasing urbanization and industrialization constitutes a direct threat to human health (Lighty et al., 2000).

Measurements were made at the Jomo Kenyatta International Airport, Nairobi, between May 6th 2011 and May 17th 2011. Outdoor aerosol particles were collected using an Andersen TM dichotomous impactor, whereas personal samplers were used for indoor particle collection. The Andersen impactor collect particulate matter of size segregated coarse and fine fractions on Teflon filters. Coarse and fine particle fractions are defined as particles between 2.5 and 10 µm aerodynamic diameter and particles smaller than 2.5 µm, respectively. Indoors only fine particles, also known as $PM_{2.5}$, were collected. Collection was carried out for 12 hours twice a day (day and night) outdoors and eight hours indoors. The shorter period indoors was chosen to mimic the normal working hours of the staff at the airport.

Mass concentration levels of particulate matter (coarse and fine) and Black Carbon (BC) were determined gravimetrically and by use of a Black Carbon photometer, respectively. Trace elements were determined using the secondary target based Energy Dispersive X-Ray Fluorescence (EDXRF) spectrometer at the Institute of Nuclear Science and Technology, University of Nairobi, Nairobi, Kenya. Quantification was done by the QXAS/AXIL software package.

The outdoor mass concentration range of PM_{10} and $PM_{2.5}$ at Jomo-Kenyatta International Airport were 18 – 67 µg m^{-3} and 4 – 28 µg m^{-3}, respectively. This is in most cases lower than the drafted Kenyan annual limits of 50 µg m^{-3} and 35 µg m^{-3}, respectively. Similarly the concentrations were higher than the World Health Organization (WHO) 24-hour guideline value of 50 µg m^{-3} and 25 µg m^{-3}, respectively, on a few occasions only. Median Pb mass concentration was 65 ng m^{-3} in the PM_{10} fraction. This is significantly lower than the WHO recommended limit of 500 ng m^{-3} in PM_{10}. The concentrations of PM, BC and detected elements indicate that the air at the airport is not more polluted than at other public places in Nairobi, and many other busy places in Africa and elsewhere.

It is anticipated that this study will provide baseline data that could help evolve a health related air pollution abatement program and provide evidence based advice to policy making.

The work is supported by International Science Programmes (ISP), Uppsala, Sweden.

Lighty J. S., Veranth J. M. and Sarofim A. F. (2000) Journal of the Air & Waste Management Association, 50, 1565-1618.

Woody M., Baek B.H., Adelman Z., Omary M., Lam Y. F., West J. J. and Arunachalam S. (2011) Atmospheric environment, 45, 3424-3433

Air Quality Monitoring Strategies for Urban Areas – A Data Base on New Monitoring Technologies, New Metrics and Proxies

T.A.J. Kuhlbusch[1], M. Viana[2], A. Borowiak[3], E.P. Weijers[4], K. Torseth[5], X, Querol[2], P. Quincey[6], R. Gehrig[7], C. Hüglin[7], K. Katsouyanni[8] and U. Quass[1]

[1] IUTA e. V., Air Quality & Sustainable Nanotechnology Unit, D-47229 Duisburg, Germany
[2] CSIC, Barcelona, Spain; [3] IES, JRC Ispra, Italy; [4] ECN, Petten, Netherlands; [5] NILU, Kjeller, Norway; [6] NPL, London, UK; [7] EMPA, Zürich, Switzerland; [8] University of Athens, Greece

Keywords: AirMonTech, Urban Air Quality, Online Monitoring Technology, Measurement Strategies
Presenting author email: tky@iuta.de

Urban air quality monitoring networks are requested to provide accurate and relevant data on air pollution levels which serve as basis to assess limit value compliance and the need of mitigation actions. Scientific and technological progress as well as new epidemiological and toxicological research results trigger a continuous demand to re-adjust the monitoring strategies and instrumentation.
On this background one major task of the EU FP7 project AirMonTech is to collect and evaluate information on recently developed and future monitoring technologies for regulated and potential future pollutants and proxy metrics. Metrics and available measurement technologies being reviewed are listed in Table 1.

Particulate Matter	**Gaseous pollutants**
Total number concentration	NO
Number size distribution	NO_2
Surface concentration	NO_x
Shape, morphology	SO_2
Mass concentration	O_3
Elemental composition	NH_3
Molecular composition	VOCs
Sulphate	HCl
Nitrate	HNO_3
Ammonium	HNO_2
Elemental carbon	
Organic carbon	
Light absorbing aerosols	
Reactive oxygen species	
Macrophage mobility decrease	
Polycyclic aromatic hydrocarbons	
Primary biological aerosol particles	

The information is obtained from scientific literature, manufacturer's files and researchers in the field of measurement technology development. It subsequently is processed in a standardised way to make it accessible via the AirMonTech database. The content of the database is based on hands-on experience and will be publicly available. It will facilitate the decision which metric to measure and which technique to use for a given situation and will also build on information coming from all stakeholders.

Although this process has not yet been accomplished, some general trends in monitoring instrumentation and regarding new metrics and proxies are already apparent. On the one hand, multi-component monitoring instruments increasingly gain attraction, on the other hand the development of miniaturised and mobile instruments offer new monitoring approaches which might be more suitable for exposure assessment than current approaches. The difficulties to translate the well-established health effects of particulate matter into toxicological mechanisms further motivates the development of monitoring technologies for specific physico-chemical particle proxies which are thought to better reflect the health relevant fraction of the ambient aerosol than its total mass. While some of these more advanced multi-component are already marketed and used in air pollution research, others still have to be further developed to make them usable within AQ monitoring networks.

This work was supported by the EU-FP7 Project AirMonTech.

Magnetic properties of PM10x collected at rural site during heating and non-heating seasons

E. Petrovsky[1], B. Kotlik[2], A. Kapicka[1], R. Zboril[3] and M. Roxer[1]

[1]Institute of Geophysics ASCR, Bocni II/1401, Prague 4, 14131, Czech Republic
[2]National Institute of Public Health, Srobarova 48, Prague 10, 10042, Czech Republic
[3]Center for Nanomaterial Sciences, Palacky University, Slechtitelu 11, Olomouc, 78371, Czech Republic
Keywords: PM10, magnetite, concentration, pollution, industrial source
Presenting author email: b.kotlik@szu.cz

Magnetic properties of environmental samples can serve as fast and relatively cheap proxy method to investigate occurrence of iron oxides. These methods are very sensitive in detecting strongly magnetic compounds such as magnetite and maghemite and can reveal concentration and assess grain-size distribution of these minerals (e.g., Sagnotti et al., 2009). This information can be significant in estimating e.g. the source of pollutants, monitoring pollution load, or investigating seasonal and climatic effects.

We studied magnetic properties of PM1, PM2.5 and PM10, collected over 32-48 hours in a small settlement in south Bohemia during heating and non-heating season. The site is remote, of rural character, with negligible traffic and industrial contributions to air pollution. Thus, the suggested seasonal effect should be dominantly due to local (domestic) heating, burning wood or coal.

Table 1. PMx concentration, magnetic moment and estimated concentration of magnetite in samples from non-heating and heating periods.

		Heating	Non-Heating
TSP	[μg/m³]	**40.6**	13.0
	Magnetic moment	6.26e-05	**7.09e-05**
	Magnetic conc.	1.48e-02	**6.20e-02**
PM10	[μg/m³]	**38.4**	9.4
	Magnetic moment	4.08e-05	4.36e-05
	Magnetic conc.	1.20e-02	**5.26e-02**
PM2.5	[μg/m³]	**36.8**	7.5
	Magnetic moment	**2.22e-05**	1.81e-05
	Magnetic conc.	0.74e-02	**2.95e-02**
PM1	[μg/m³]	**26.9**	6.5
	Magnetic moment	1.00e-05	**1.92e-05**
	Magnetic conc.	0.46e-02	**3.71e-02**

In our contribution we show typical differences in PMx properties in the two periods. Concentration is much higher in the winter (heating) period (Table 1). In both summer and winter samples, Fe-oxides of typical spherical shape with diameters below 5 μm were observed (Fig. 1). Fe-oxieds are observed mainly in PM10 fraction. Magnetic parameters sensitive to grain-size distribution of Fe-oxides are different for summer and winter PM10 samples, with clear shift towards finer particles in summer (Fig. 2). This may reflect different source of PM, with dominant natural particles from agriculture and land-use activities in summer, compared to those produced by domestic heating in winter.

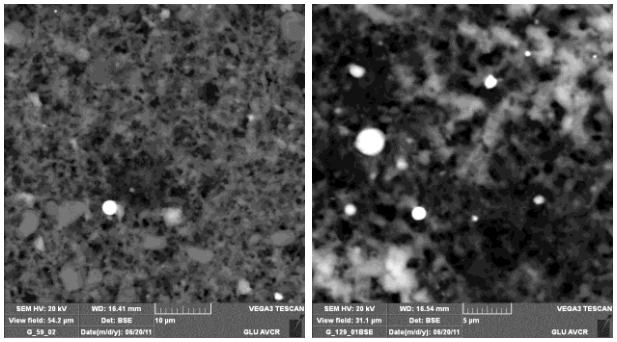

Figure 1. SEM of PM10 of sample from non-heating (left) and heating (right) period.

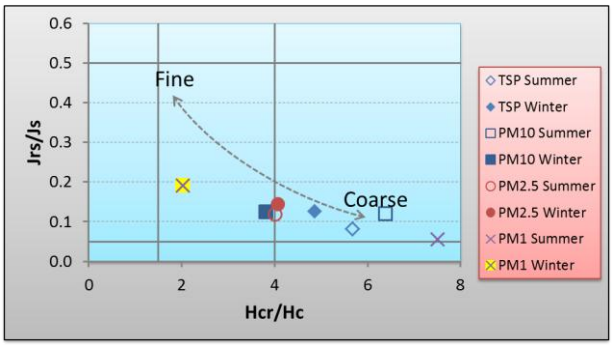

Figure 2. Diagram of magnetic parameters sensitive to grain-size distribution of magnetite/maghemite. Coarse is related to multi-domain magnetite (few μm and more), while Fine corresponds to single-domain magnetite (<0.5 μm).

Our results suggest that magnetic minerals reflect well specific seasonal properties of air pollutants in sites where domestic heating is the dominant source of pollution.

This work was supported by the Czech Science Foundation under grant P210/10/0554.

Sagnotti, L., Taddeucci, J., Winkler, A. and Cavallo, A., (2009) *Geochem. Geophys. Geosyst.* **10**, Q08Z06, DOI: 10.1029/2009GC002563 (2009)

Comparison of different operational parameters for thermal-optical EC/OC measurements of filter samples from Flanders, Belgium

W. Maenhaut[1,2], M. Claeys[2], J. Vercauteren[3] and E. Roekens[3]

[1]Department of Analytical Chemistry, Ghent University, Gent, BE-9000, Belgium
[2]Department of Pharmaceutical Sciences, University of Antwerp, Antwerpen, BE-2610, Belgium
[3]Flemish Environment Agency (VMM), Antwerpen, BE-2000, Belgium
Keywords: PM10, OC, EC, thermal-optical analysis, temperature protocol.
Presenting author email: willy.maenhaut@ugent.be

Within the framework of two research projects from the Flemish Environment Agency (VMM), PM10 samples, which were collected on 47-mm diameter Pallflex Tissuquartz filters, are analysed for organic, elemental, and total carbon (OC, EC, and TC). In the first project (P1), the samples were collected at 7 sites in parallel every fourth day from February 2010 to February 2011, whereas in the second project (P2) the samples are collected at 12 sites in parallel every fourth day from July 2011 through June 2012. All samples from P1 and all those taken in the course of 2011 within P2 were analysed by thermal-optical analysis with the NIOSH temperature protocol (Birch and Cary, 1996) and simultaneous measurement of transmission (TOT) and reflectance (TOR). A subset of 70 samples from P1 was also analysed with the EUSAAR2 protocol (Cavalli *et al.*, 2010) using TOT and TOR.

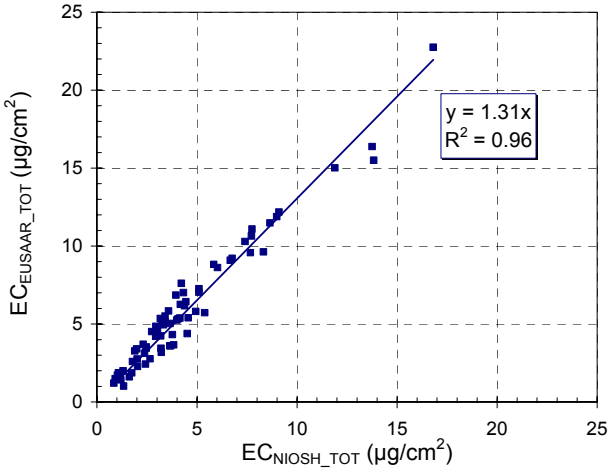

Figure 1. Comparison of EUSAAR2 and NIOSH TOT EC for the subset of 70 samples from project 1.

The scatterplot of EUSAAR2 TC versus NIOSH TC for the subset of 70 samples from P1 (not shown) indicated that there was very good agreement between the TC data from the two temperature protocols; the regression line, when forced through the origin, had a slope of 1.016 with R^2 = 0.995. Figure 1 shows the scatterplot of EUSAAR2 TOT EC versus NIOSH TOT EC for the same subset of samples; the slope is now 1.31 and thus substantially larger than 1. The scatterplot of EUSAAR2 TOR EC versus NIOSH TOR EC (not shown) had a slope of 1.09 with R^2 = 0.95. The average EUSAAR2/NIOSH ratios and associated standard deviations for EC in TOT and TOR for the 70 sample (70s) subset of P1 are given in the top part of Table 1. The two average ratios are somewhat larger than the slopes of the corresponding scatter plots, but that for TOT is again larger than that for TOR.

Table 1. Averages and associated standard deviations for two types of ratios for EC and different sample sets.

EUSAAR2/NIOSH ratio for EC	mean ± s.d.
P1_70s_TOT	1.36 ± 0.24
P1_70s_TOR	1.20 ± 0.18
TOR/TOT ratio for EC	**mean ± s.d.**
P1_70s_EUSAAR2	1.51 ± 0.32
P1_70s_NIOSH	1.73 ± 0.48
P1_all_NIOSH	1.77 ± 0.66
P2_all_NIOSH	1.30 ± 0.45

The average TOR/TOT ratios and associated standard deviations for EC, as obtained for the 70 sample subset of P1 with the EUSAAR2 and NIOSH protocols and for the samples of P1 and P2 (separately) with the NIOSH protocol, are given in the bottom part of Table 1. It appears that the average ratios with NIOSH in P1 for the subset of 70 samples and for all (644) samples are quite similar, which suggests that the subset was representative for the entire sample set of P1. The TOR/TOT ratio for EC obtained with EUSAAR2 is clearly lower than that obtained with NIOSH. It is further noteworthy that the difference between the TOR and TOT EC tends to be larger than the difference between the EUSAAR2 and NIOSH EC. One can also conclude from the standard deviations that the variability in the TOR/TOT ratio is larger than the variability in the EUSAAR2/NIOSH ratio. Finally, it appeared that the various ratios did not seem to depend much upon the filter loading, sampling site, or time of the year.

Birch, M.E. and Cary, R.C. (1996) *Aerosol Sci. Technol.* **25**, 221-241.

Cavalli, F., Viana, M., Yttri, K.E., Genberg, J. and Putaud, J.-P. (2010) *Atmos. Meas. Tech.* **3**, 79-89.

Road traffic impact on size-segregated atmospheric aerosols loading at Madrid

F. Mirante[1], C. Alves[1], C. Pio[1], [2]M. Fernandez, M.A. Revuelta[2] and B. Artiñano[2]

[1]CESAM, Department of Environment and Planning, Aveiro University, 3810-193 Aveiro, Portugal
[2]Centro de Investigaciones Energéticas, Medioambientales y Tecnológicas (CIEMAT), 28040 Madrid, Spain

Keywords: urban aerosol, size distribution, OC/EC, ions, metals
Presenting author email: casimiro@ua.pt

Road traffic and favourable climatic conditions for photochemical formation and dust re-suspension are the causes of atmospheric aerosol levels often above legislation limits. It is important to take strategies for urban particulate pollution control based on information concerning the sources of the aerosol. With these objectives, two campaigns were performed at two contrasting sites, in the city of Madrid.

Size-segregated (<0.5µm, 0.5-1µm, 1-2.5 µm, 2.5-10 µm) particulate matter was collected with hi-vol samplers simultaneously at two sites (roadside and urban-background) during two one-month long campaigns (summer 2009 and winter 2010). After collection, the organic and elemental carbon fractions were determined by a thermo-optical method, water-soluble ionic species were measured by ion chromatography, organic compounds by gas chromatography-mass spectrometry, while metals were analysed by inductively coupled plasma mass spectrometry.

Roadside enrichements (*REs*) were defined as the fractional difference between the concentrations at the roadside and urban background site:

$$RE_i(\%) = \frac{x_i^R - x_i^{UB}}{x_i^R} \cdot 100$$

where: *i* is a given chemical component (variable),
x is the concentration of the component *i*,
R and *UB* are the sampling sites for which the concentrations of component i are compared.

Differences in PM mass and composition between a kerbside station and an urban background station can be attributed to the adjacent traffic (Oliveira et al., 2010; Snyder et al., 2010).

In summer, the highest enrichments were in fine fraction, whereas in winter were in coarse fraction (Fig. 1). The *REs* were ≥ 80% for Mn, Ni, Cu, Zn, Cd, Sb, Sn, and Rb. In winter, these tracers of traffic emissions were lower, except for Zn. The mineral elements resulting from road dust re-suspension, such as Sr and La had a *RE* of 100 and 97%, respectively, in summer. Very low values were obtained in winter. The *EFs* for Ca^{2+} and Sm were 40-47% in summertime, while values of 70 and 27% were obtained in the cold season. A considerable difference was registered between EC and OC in summer; this difference was not so significant in winter. EC is only emitted as primary particles and it was enriched by 75, 71 and 68% in PM_1, $PM_{1\text{-}2.5}$ and $PM_{2.5\text{-}10}$, respectively in summer and 68, 55 and 72% in winter. OC could be primary and secondary. Their *Res* were 41% in all fractions in summer and 68, 76 and 65% in PM_1, $PM_{1\text{-}2.5}$ and $PM_{2.5\text{-}10}$, respectively, in winter. For $PM_{1\text{-}2.5}$ only five enrichements higher than 50% were obtained (Mn (59%), Zn (64%), Sb (75%), Sn (66%) and Ti (98%)) in summer, but in winter these elements were also higher than 50%. Lower enrichments were obtained in the coarse fraction than in the fine fraction for the tracers of traffic emissions and mineral matter in summer; the opposite happens in winter.

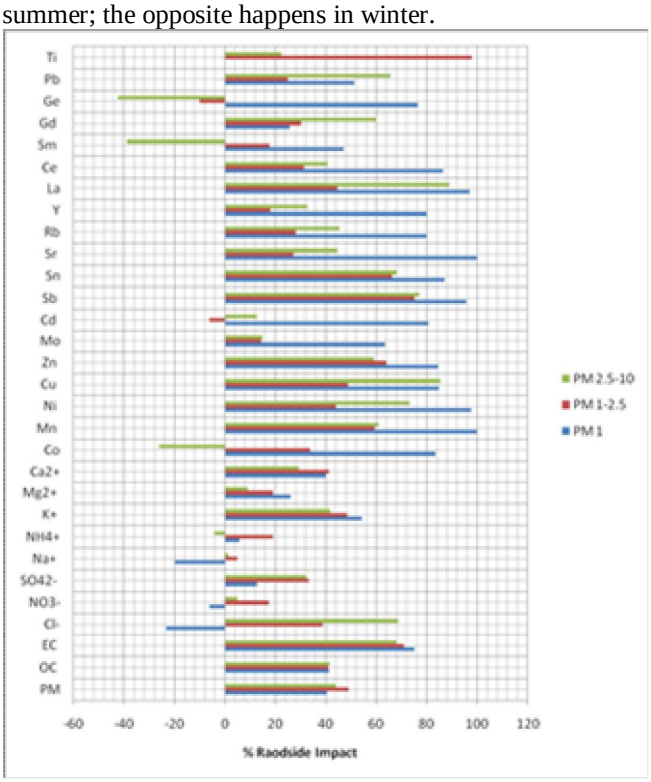

Figure 1.Roadside enrichments in summer.

This work was partially supported by the *Acción Integrada* PT2009-0151 funded by the Spanish Ministry of Science and Innovation or Action nº E-130/10 funded by CRUP. F. Mirante thanks the Portuguese Science Foundation for financial support of the training period at CIEMAT, as well for the PhD grant SFRH/BD/45473/2008.

Oliveira, C., Pio, C., Caseiro, A., Santos, P., Nunes, T., Mao, H., Luahana, L., and Sokhi, R. (2010) Atmos. Environ. **44**(26), 3147–3158.

Snyder, D. C., Rutter, A. P., Worley, C., Olson, M., Plourde, A., Bader, R. C., Dallmann, T., and Schauer, J. J. (2010) Atmos. Environ. **44**(13), 1597–1608.

Preliminary research on the ammonium content of particulate matter from indoor air of pig housing systems

T. Ulens[1], N. Van Ransbeeck[1], H. Van Langenhove[2] and P. Demeyer[1]

[1]Technology and Food Science Unit, Institute for Agricultural and Fisheries Research, Merelbeke, East Flanders, 9820, Belgium

[2]Department of Sustainable Organic Chemistry and Technology, Ghent University, Ghent, East Flanders, 9000, Belgium

Keywords: Aerosol characterization, Aerosol emissions, Aerosol generation, Aerosol sampling.

Presenting author email: tim.ulens@ilvo.vlaanderen.be

In a recent report, published by the Flemish Environment Agency (VMM) and the Flemish Institute for Technological Research (VITO), a method was formulated to map the different source contributions to PM10 and PM2.5 in Flanders. The conclusion in this report was that, apart from cross border contributions, the agricultural sector provides the largest contribution with regard to PM10 (54%) and PM2.5 (49%) (Deutsch *et al.*, 2010). These contributions were calculated by combining the emissions of primary particulate matter with the secondary particulate matter formation originating from ammonia emissions by agricultural activities.

In this approach however, it was not taken into account that secondary particulate matter (in this case ammonium salts) can possibly be formed indoor in the animal housing systems. Recent reports by the VMM indicate that ammonium, nitrate and sulphate contribute respectively about 7 %, 22 % and 12 % to the total atmospheric PM10 concentration and about 12 %, 21 % and 18 % to the total atmospheric PM2.5 concentration in Flanders (VMM, 2010;Vercauteren *et al.*, 2011;VMM, 2009). If ammonium salts are indeed formed indoor, the contribution of these salts is probably being counted twice: once as primary emissions from animal housing systems and again as secondary particulate matter, originating from ammonia emissions.

During the period of March to June 2012 experiments will be conducted to investigate this hypothesis. First, samples of PM10 and PM2.5 will be collected inside an experimental pig housing system at ILVO. These samples will be quantified gravimetrically and analysed on their ammonium content via colorimetric tests. Based on these results, a more extended sampling campaign will be carried out at three farms to verify the initial findings in real practice. The results and conclusions of these experiments will be presented at the conference.

If these experiments result in a clear indication that primary particulate matter from animal housing systems contain significant amounts of ammonium salts, a more in depth research approach will be set up to further investigate this phenomenon. This would also urge to review the contribution of agricultural activities to the PM10 and PM2.5 situation in Flanders.

This work was supported by the Boerenbond, a professional association for Flemish farmers.

Deutsch, F., Vankerkom, J., Veldeman, N., Peelaerts, W., Fierens, F., Vanpoucke, C., Trimpeneers, E., Vancraeynest, L., and Bossuyt, M. (2010) Verklarende factoren voor evoluties in luchtkwaliteit, studie uitgevoerd in opdracht van de Vlaamse Milieumaatschappij, MIRA, MIRA/2010/07, VITO. 2010.

Vercauteren J, Matheeussen C, Wauters E, Roekens E, van Grieken R, Krata A, Makarovska Y, Maenhaut W, Chi XG, Geypens B. (2011). *Atmospheric Environment* **45**, 108-116.

VMM. (2009) Chemkar PM10: Chemische karakterisatie van fijn stof in Vlaanderen, 2006-2007.

VMM. (2010) Chemkar PM10 'hotspots': Chemische karakterisatie van fijn stof in Vlaanderen, 2008-2009.

Seasonal variations of ions and metals in urban PM1 aerosol

P. Mikuška[1], K. Křůmal[1], M. Vojtěšek[1], N. Kubátková[1,2] and Z. Večeřa[1]

[1] Institute of Analytical Chemistry of the ASCR, v.v.i., Veveří 97, 602 00 Brno, Czech Republic
[2] Faculty of Chemistry, Brno University of Technology, Purkyňova 464/118, 612 00 Brno, Czech Republic
Keywords: atmospheric aerosols, metals, ions, PM1.
Presenting author email: mikuska@iach.cz

Epidemiological studies (Schwartz *et al.*, 1996; Pope, 2000; Brunekreef and Holgate, 2002) have suggested a statistical association between health effects and ambient fine particle concentrations, especially the submicron fraction (PM1) that can penetrate deep into the alveolar region of the lungs. Chemical composition of PM2.5 and PM10 is subject of many studies, however, relatively little attention has so far been paid to PM1 aerosols. Determination of their composition is essential to understand their properties and reactivity and hence their environmental and health effects (Singh *et al.,* 2010).

Daily samples of PM1 aerosol particles were collected in Brno and Šlapanice during a week in winter and summer of 2009 and 2010. Aerosols sampled using a high-volume sampler (DHA-80, Digitel, 30 m^3/h) on cellulose-nitrate filters (150 mm, Sartorius) were analysed for metals (Al, K, Ca, Fe, Mn, Zn, Cu, Pd, Cd, Ba, As, Pb, V, Ni, Sb) by ICP method. Aerosols sampled in parallel using a low-volume sampler (1 m^3/h) on Teflon filters (47 mm, Zefluor) were analysed for ions (nitrate, sulfate, nitrite, fluoride, chloride, oxalate, Na^+, K^+, NH_4^+, Ca^{2+}, Mg^{2+}) by IC. Application of annular diffusion denuder placed between cyclone inlet (1 µm, URG) and Teflon filter eliminates interference of gaseous pollutants like SO_2, HNO_3, NH_3 and others (Mikuška et al, 2012).

Brno represents a big city with 370 000 inhabitants while Šlapanice is a small town with 6 000 inhabitants.

Metals and especially ions form in winter season significant part of mass of PM1 aerosols, metals 4.5-4.9% (Šlapanice - Brno) and ions 37.1-40.7% (Šlapanice - Brno) while in summer their contribution to PM1 was much smaller, metals 1.4-1.8% (Šlapanice - Brno) and ions 24.6-18.7% (Šlapanice - Brno).

The concentrations of metals were, in general, in winter higher than in summer. In winter period, the concentrations of metals in Šlapanice were higher than those in Brno whereas summer concentrations of metals at both localities were comparable. The highest mean winter concentrations were found for lead and potassium originating from combustion of wood and coal (Figure 1) while in summer high concentrations were found for lead, potassium, calcium, aluminium and zinc.

Sulfate, nitrate and ammonium prevail among ions in winter while in summer the contribution of nitrate and ammonium decreases.

Local traffic in summer and coal and wood combustion during household heating in winter were identified as the main emission sources of PM1 aerosols in both towns. Secondary aerosol components formed a significant part of aerosols during the whole year.

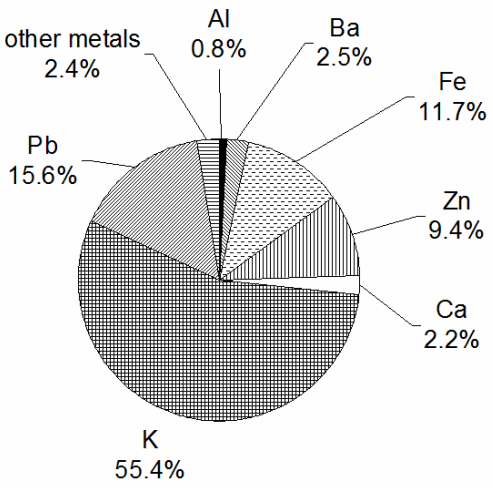

Figure 1. Relative mean contribution of analysed metals to the total metal content of PM1 aerosols in Brno during winter 2010.

This work was supported by Institute of Analytical Chemistry of ASCR under an Institutional research plan No. AV0Z40310501, by Grant Agency of the CR under grant No. P503/11/2315 and by Ministry of the Environment of the Czech Republic under grant No. SP/1a3/148/08.

Brunekreef, B. and Holgate, S.T. (2002) *Lancet* **360**, 1233-1242.

Mikuška, P., Večeřa, Z., Bartošíková, A. and Maenhaut, W. (2012) *Anal. Chim. Acta* **714**, 68-75.

Pope III, C.A. (2000) *Aerosol Sci. Technol.* **32**, 4–14.

Schwartz, J., Dockery, D.W. and Neas, L.M. (1996) *J. Air Waste Manage. Assoc.* **46**, 927–939.

Singh, R., Sharma, B.S. and Chalka, S.N. (2010) *Environ. Monit. Assess.* **168**, 195–203.

Comparison of online measurements with an Aethalometer and an HR-ToF-AMS and offline chemical analysis data for the characterization of $PM_{2.5}$ aerosols

V. Crenn[1,2], V. Riffault[1,2], I. Fronval[1,2] and D. Petitprez[1,3]

[1]Université Lille Nord de France, F-59000, Lille, France
[2]Département Chimie et Environnement, Ecole des Mines de Douai, F-59508, Douai, France
[3]Laboratoire de Physicochimie des Processus de Combustion et de l'Atmosphère (PC2A), UMR CNRS 8522, F-59655, Villeneuve d'Ascq, France
Keywords: Submicron particles, Urban aerosols, Coastal aerosols, Industrial aerosols.
Corresponding author email: veronique.riffault@mines-douai.fr /
Presenting author email: denis.petitprez@univ-lille1.fr

Atmospheric fine ($PM_{2.5}$) particulate matter are classically sampled by filter collection or impaction but these offline methods are often subject to sampling artifacts (volatilization and reactivity), partly due to the long sampling times. These methods are also labor intensive and time consuming due to sample treatment (collection, extraction) and analysis. Online techniques such as Time-of-Flight Aerosol Mass Spectrometry (Canagaratna *et al.*, 2007) with a few minutes temporal resolution have been developed to overcome these limitations.

In this work, we have coupled real-time measurements and offline analysis from filter sampling. The chemical composition of fine particulate matter sampled at an urban background site (Douai) and an industrialized coastal site (Grande-Synthe near Dunkirk) located in Northern France (summer and winter field campaigns for each site) was investigated in order to compare both measurement methods.

$PM_{2.5}$ were simultaneously collected on 12 quartz fiber filters during 24h using a low-volume sampler. Each filter was then extracted by pressurized fluid extraction before being concentrated and analyzed by specific methods according to the target compounds: Polycyclic Aromatic Hydrocarbons (PAH), mono- and dicarboxylic acids (Mirivel *et al.*, 2009; 2011). Elemental Carbon (EC) and Organic Carbon (OC) concentrations were also measured by the Thermo-Optical Transmittance method with a Sunset Lab EC/OC analyzer following the NIOSH protocol.

In addition, a High Resolution Time-of-Flight Aerosol Mass Spectrometer (HR-ToF-AMS) has been deployed to measure size-resolved average chemical composition of the non-refractory submicron ($NR\text{-}PM_1$) aerosols. Black Carbon (BC) concentrations were also monitored by an Aethalometer every 10 minutes.

Good agreements between online measurements and offline chemical analysis data have been shown for the whole campaign results, highlighting the relevance of coupling both methods. BC concentrations measured in $PM_{2.5}$ were well correlated with EC measurements at both sampling sites (Figure 1).

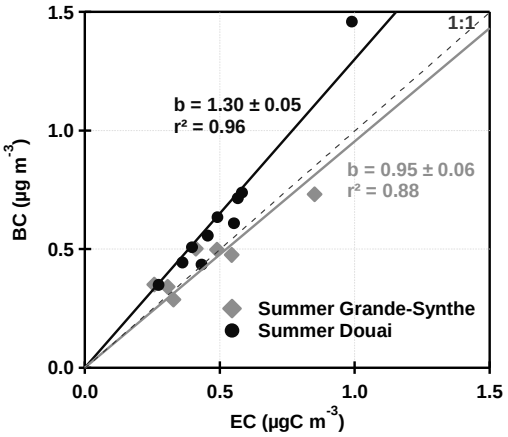

Figure 1. Comparison of BC and EC summer concentrations measured in $PM_{2.5}$ in Douai and in Grande-Synthe.

Another interesting comparison was made between 10 particulate PAH (2 C_{16}, 2 C_{18}, 3 C_{20} and 3 C_{22}) concentrations determined from filter analyses and the PAH concentrations measured by the AMS for the corresponding masses (m/z = 202, 228, 252, 276 and 278). Very similar time series were observed corresponding to a good linearity between measurements. Good correlations between OM/OC ratios have also been obtained in agreement with literature data. The results will be presented and discussed in details.

Our laboratory participates in the Research Institute of Industrial Environment (IRENI) which is financed by the Communauté Urbaine de Dunkerque, the Nord-Pas de Calais Regional Council, the French Ministry of Education and Research, the CNRS and European funds (FEDER).

Canagaratna, M.R., Jayne, J.T., Jimenez, J.L., Allan, J.D., Alfarra, M.R., Zhang, Q., Onasch, T.B., Drewnick, F., Coe, H., Middlebrook, A., Delia, A., Williams, L.R., Trimborn, A.M., Northway, M.J., DeCarlo, P.F., Kolb, C.E., Davidovits, P. and Worsnop, D.R. (2007) *Mass Spec. Rev.* **26**, 185-222.

Mirivel G., Riffault, V. and Galloo, J.C. (2009) *J. Chrom. A.* **1216**, 6481-6489.

Mirivel, G., Riffault, V. and Galloo, J.C. (2011) *Anal. Methods.* **3**, 1172-1179.

Spatial and seasonal distribution of dicarboxylic acids and sugars in the surroundings of a municipal waste incinerator near Bologna, Italy

M.C. Pietrogrande[1], D. Bacco[1], M. Rossi[2]

[1]Department of Chemistry, University of Ferrara, Ferrara, 44121, Italy
[2]Regional Agency or Prevention and Environment ARPA - Emilia-Romagna, Rimini, 47923, Italy
Keywords: water soluble organic compounds, GC-MS, air quality; waste incineration impact.
Presenting author email: marossi@arpa.emr.it

The aim of this study is to characterize the composition and seasonal variations of water-soluble organic compounds present in the atmospheric aerosol in the surroundings of a municipal waste incinerator (MWI) near to Bologna, a great urban centre in Northern Italy. This study is a part of an intensive environmental and epidemiological monitoring program (MONITER project) that has been designed and developed by the Environmental Protection Agency of Emilia Romagna Region (ARPAER), in order to evaluate the impact of the MPWI emissions on the ambient air and to estimate the exposure levels to toxic or carcinogenic compounds for a population living in the neighbourhood of this incinerator (www.moniter.it). Samples were collected during intensive summer 2008 and winter 2009 campaigns in 8 monitoring sites selected in order to compare points where the incinerator has the highest impact with those where the incinerator impact is negligible.

The analyzed compounds included 18 dicarboxylic acids and 7 sugars, as important chemical tracers that may give relevant information on the relative strengths of primary emission sources and secondary photochemical processes affecting air quality (Pietrogrande *et al*, 2010).

In both the seasons the most abundant compound is levoglucosan, as the major by-product from biomass burning.

The abundances of the main dicarboxylic acids -- C3-C9 n-alkanoic and pthalic acids --exhibit a seasonal pattern with higher winter concentrations (mean total concentrations are were 60±18 ngm^{-3} and 23±9 ngm^{-3}, in winter and summer, respectively).

The distribution profiles and the diagnostic ratios of these markers allowed to identify primary emission sources (power plants, vehicular circulation, biomass burning) associated with secondary constituents from both biogenic (e.g. pinonic acid) and anthropogenic precursors (e.g. phthalic and benzoic acids) (Pietrogrande *et al*, 2011). The distinct seasonal patterns of abundances (Figure 1) suggests that the contribution of primary sources is significantly enhanced in winter in comparison with summer, when secondary atmospheric processes are dominant

This result is consistent with the winter atmospheric conditions in Po valley, caracterized by lower mixing heights, possible formation of the inversion layers, and less chance of wet deposition that confine vertical distribution of pollutants to the first hundred meters of the atmosphere contributing to the accumulation of air pollutants. Consequently, the secondary production of diacids is promoted by higher abundance of the organic precursors.

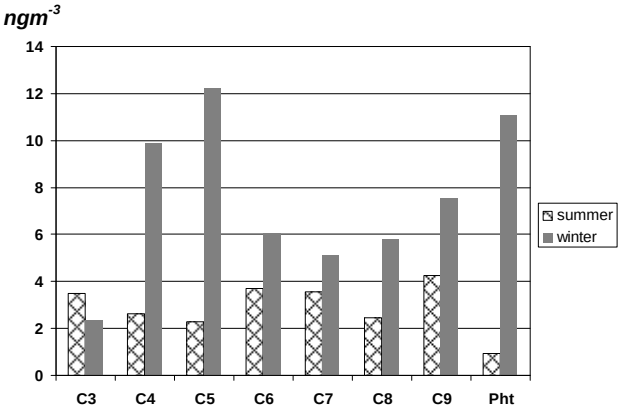

Figure 1. Seasonal pattern of the abundances of dicarboxylic acids (mean values computed on 8 sampling sites).

The spatial variations of the concentration of the target compounds show a homogenous PM composition in the sites around the municipal incinerator, reflecting the regional nature of primary sources and atmospheric processes, not significantly impacted by emissions from the MWI.

This work was financially supported by the Moniter project of the Environment Agency of Emilia Romagna region (ARPAER).

Pietrogrande, MC, Bacco D, Mercuriali M (2010) *Anal. Bioanl. Chem.* **396,** 877–885.
Pietrogrande, MC, Bacco D (2011) *Anal. Bioanal. Chem.* **689**, 257–264.

GC-MS method for the simultaneous analysis of water-soluble organic compounds in PM: response surface methodology for optimizing solvent extraction.

M.C. Pietrogrande, D. Bacco, S. Chiereghin

Department of Chemistry, University of Ferrara, Ferrara, 44121, Italy
Keywords: water soluble organic compounds, chemical analysis, GC-MS, air quality.
Presenting author email: mpc@unife.it

In recent years the increasing interest in water-soluble organic compounds (WSOCs) in the atmosphere is fuelled by their potential role in affecting the global climate, since they alter the hygroscopic properties of atmospheric particle, affecting their ability to act as cloud condensation nuclei and can also contribute to higher atmospheric absorption of solar radiation and atmospheric heating. In addition, some WSOCs – such as dicarboxylic acids and saccharides – are potentially useful molecular tracers, since they can have several different sources including primary emissions from biomass burning and fossil fuel combustion, as well as photochemical oxidation of organic precursors of both biogenic (e.g. pinonic acid) and anthropogenic precursors (e.g. phthalic and benzoic acids) (Pietrogrande *et al*, 2010).

GC–MS is the most widely applied technique for the characterization of organic aerosols since it yields excellent separation efficiency, sensitivity and high number of species analyzed. Due to their high polarity, hydrophilicity and low volatility, carboxylic acids and saccharides have to be converted into volatilizable and stable derivatives — i.e., trimethylsilyl derivatives using BSTFA(N,O-bis(trimethylsilyl)-trifluoroacetamide) as silylation reagent (Pietrogrande *et al*, 2011).

Indeed, multi-residue analytical methodologies, that achieve simultaneous analysis of several compounds, are useful for reducing the complexity and time required for sample preparation and analysis in order to provide a large amount of reliable data. With this aim, the proper selection of the extraction operating conditions is a critical step, since they are essential to achieve the highest yield for several target analytes with a wide range of water solubility and volatility.

This paper describes the optimization of the extraction operating conditions to develop a GC-MS procedure for the simultaneous analysis of carboxylic acids and saccharides in atmospheric aerosols, providing the low detection limits and the high reproducibility required by environmental monitoring.

The factors considered were the solvent type (characterized by polarity *p'* parameter) and extraction volume (10-20 ml). The response surface methodology (RSM) including central composite design (CCD) was applied to fully investigate the experimental domain of the operative parameters using a limited number of experiments (Basaglia *et al*, 2011). The response surface computed by the RSM model shows the simultaneous dependence of the extraction yield on the combination of the two variables, solvent polarity and volume (Figure 1).

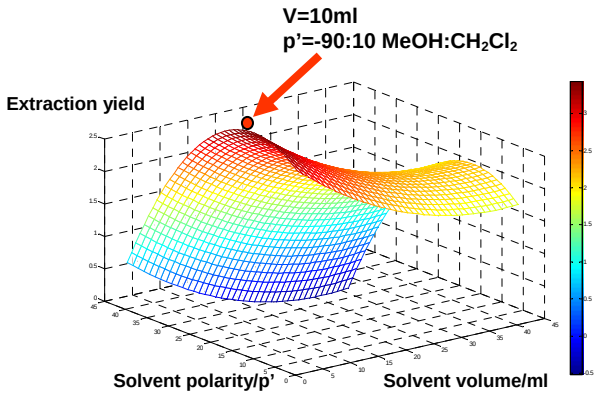

Figure 1. 3D surface plot showing the interacting effects of solvent polarity and extraction volume on extraction yield

The plot clearly shows that the optimum extraction solvent is a mixture of metane:dichlorometane (90:10) using a volume of 10 ml.

The optimized procedure provides low detection limits ($\leq$2 ngm^{-3}) and good reproducibility (RSD%$\leq$13%) that makes it suitable for environmental monitoring.

The developed protocol was extended to 22 target analytes that are relevant chemical markers, i.e., 15 carboxylic acids and 7 sugars.

In addition, the suitability of the optimized procedure was verified by application to PM filters collected under different conditions, i.e., different seasons (summer vs. winter), different sampling sites (urban vs. rural), different particle size dimensions ($PM_{2.5}$ vs. PM_1).

This work was partially supported by the Supersito project of the Environment Agency of Emilia Romagna region (ARPAER).

Pietrogrande, MC, Bacco, D, Mercuriali, M (2010) *Anal. Bioanl. Chem.* **396,** 877–885.

Pietrogrande, MC, Bacco, D (2011) *Anal. Bioanal. Chem.* **689**, 257–264.

Basaglia, G, Pasti, L, Pietrogrande, MC (2011) *Anal. Bioanl. Chem.* **399**, 2257–2265.

Total and water-soluble fraction trace element analysis of PM2.5 samples from the city of Patras, Greece

M. Manousakas[1], H. Papaefthymiou[1], K. Eleftheriadis[2]

[1]Department of Chemistry, University of Patras, Patras, Achaia, 26500, Greece
[2] E.R.L., Institute of Nuclear Technology and Radiation Protection, N.C.S.R, "Demokritos", Ag. Paraskevi, Attiki, 15310, Greece
Keywords: chemical analysis, chemical composition
Presenting author email: mmanousakas@yahoo.com

Airborne particulates are generated through a variety of processes and mechanisms and are emitted from numerous sources (both natural and anthropogenic). Toxicological studies have implicated metal content (particularly the water-soluble fraction) as a possible harmful component of particulate matter (2). Thus, elemental analysis of airborne particulates (both quantitative and qualitative) is of great importance.

In the current study PM2.5 samples were collected from the city of Patras, Western Greece, in order to investigate the city's air quality. Patras represents a common urban coastal environment (about 200,000 citizens) with no large industrial activities in the vicinity of the city. It is known from previous studies (1) that the city has high PM2.5 levels that in many cases exceed the safety limits. However results concerning PM elemental analysis on the water soluble fraction have not been reported yet.

PM2.5 sampling was performed in the city centre, from August 2010 to August 2011 using PTFE filters. A low volume sampler (PARTISOL-FRM MODEL 2000) was installed in the roof of a public building and was operated at 16.7 L/min for 24h in all cases. The sampler was approximately 25 meters above the ground level, thus having no immediate interaction with ground sources (traffic). Twenty samples were selected to be analyzed by ICP-MS. One half of each filter sample was digested and analyzed for total trace metal levels and the other half was leached for obtaining the water soluble metal fraction.

Microwave digestion of PM followed by chemical analysis by ICP-MS is one of the most accurate methods for the determination of trace elements (total) in particulate samples. For the digestion a mixture of HNO_3/HF was used. The water soluble fraction was extracted with ultra pure water using ultrasonication, and the extraction time was 30 min.

The efficiency of the digestion procedure was tested using the certified reference material, NIST SRM 1648a. The recoveries of the elements (with the exception of Al and Cr) ranged from 87 to125%.

Fifteen elements were analyzed in the PM2.5 samples (Al, As, Cd, Co, Cr, Cu, Fe, Mn, Ni, Pb, Rb, Sr, Ti, V, Zn). Al, Zn, and Fe displayed the highest concentrations, whereas Rb, As, Co the lowest ones. Tables 1 show the mean concentration and the solubility for each element.

The water soluble fraction of the analysed elements ranged between 5 to 42 %.

Table 1. Mean concentration, Standard Deviation and Solubility of the trace elements in the PM 2.5 samples.

Elements	**Mean Concentration (ng/m^3)**	**Standard Deviation**	**Solubility (%)**
Al	5532.3	5820.2	5
As	1.9	3.3	7
Cd	52.3	52.8	10
Co	0.7	0.9	11
Cr	5.8	3.0	9
Cu	10.5	20.3	42
Fe	163.3	190.6	7
Mn	6.9	8.9	37
Ni	11.7	14.3	29
Pb	15.4	31.9	16
Rb	2.7	4.8	7
Sr	9.6	13.1	13
Ti	99.3	90.6	6
V	4.3	2.7	24
Zn	402.9	603.5	35

Among the elements analyzed, the most water soluble and consequently bioavailable were the elements Cu, and Zn at a level of about 40%. Ti, Al and Fe were almost insoluble in the water (5-7 %). Cu and Zn are expected to originate from anthropogenic sources, are easily dissolved in water, while Ti, Al and Fe as refractory elements are not easily dissolved even in strong acids.

This work was supported by K. Karatheodoris Program Grant D.165 from the Research Committee of the University of Patras.

Bibliography

1. M. Psichoudaki, K. Eleftheriadis, M. Soupioni, H. Papaefthymiou, (2007), "Mass and chemical characterization of PM2,5 in ambient air of Patras, Greece. Proc. of the 5th International Conference on Instrumental Methods of Analysis-Modern Trends and Applications, 30 September - 4 October 2007, Rio-Patras, Greece, Book of Abstracts: p.245.
2. S.C., Delvin, R.B., Huang, Y.C.T. (2005). Seasonal variations in Air pollution particle-induced inflammatory mediator release and oxidative stress. Environ. Health Persp. 113, 1032-1038.

Recent changes in PM10 levels and associated ions in an industrial environment in Spain

E. Yubero[1], N. Galindo[1], J.F. Nicolás[1], D. Martínez[1], M. Santacatalina[3], and A. Carratalá[2]

[1]Department of Physics, Miguel Hernández University, Avda. Universidad, 03202, Elche, Spain
[2]Department of Chemical Engineering, University of Alicante, P.O. Box 99, 03080, Alicante, Spain
[3]University of Alicante's General Foundation, 03690, Alicante, Spain
Keywords: PM10, ions, industrial aerosols, Mediterranean.
Presenting author email: eyubero@umh.es

The present study was performed on the campus of the University of Alicante, located next to the town of San Vicente del Raspeig (55,000 inhabitants), approximately 6 km from the Spanish Mediterranean coast. A grey cement production plant that uses a dry manufacturing process is located 1.5 km southwest of the campus. Twenty-four hour PM10 samples were collected approximately every four days from January to December 2010 using a high volume Digitel DL77 sampler. The device was located 15 m above ground level, on the roof of the Faculty of Sciences. Ion chromatography analyses were carried out in order to obtain the concentrations of the main anions (Cl^-, NO_3^-, SO_4^{2-} and $C_2O_4^{2-}$) and cations (Na^+, NH_4^+, K^+, Mg^{2+} and Ca^{2+}).

Annual mean and daily maximum values were compared with those obtained at the same site between September 2005 and August 2006 (table 1), when another cement manufacturing facility, situated ~ 1 km northwest of the sampling site, was still operating (Yubero *et al*, 2010). This plant, which used the semi-wet process for white cement production, closed in May 2008.

Table 1. Concentrations for PM10 and associated ions ($\mu g/m^3$) measured in the University of Alicante.

	2010		2005/06	
	Mean	Max	Mean	Max
PM	21.6	59.7	40.5	120
Cl^-	0.58	3.48	0.91	3.81
NO_3^-	2.27	9.05	2.70	8.77
SO_4^{2-}	2.33	9.28	4.24	16.06
$C_2O_4^{2-}$	0.22	0.55	–	–
Na^+	0.66	2.96	0.78	2.91
NH_4^+	0.48	3.15	0.59	4.75
K^+	0.20	0.96	0.33	0.97
Mg^{2+}	0.11	0.34	0.13	0.37
Ca^{2+}	1.27	3.59	3.13	7.71

Mean and maximum PM10 concentrations in 2010 were considerably lower than the values previously measured. Such decline however cannot only be explained by annual changes in meteorological conditions. A factor that could play a part in the observed reduction is the closure of the white cement manufacturing plant. This facility represented an important contribution to local SO_2 emissions, which in the atmosphere is rapidly oxidised into particulate sulphate. Additionally, global emissions of gaseous precursors (NO_x, SO_x and NH_3) of particulate nitrate, sulphate and ammonium in Europe have experienced a decrease since the beginning of the economic crisis. Sulphur oxides emissions showed the highest reduction, which is consistent with the observed trend in sulphate concentrations. As can be calculated from the data presented in table 1, sulphate average levels in 2010 were 50% lower than in the period 2005-2006, while the decrease in nitrate and ammonium levels was only 16 and 19%, respectively.

Atmospheric levels of Ca^{2+} were also greatly reduced in 2010. In the study area, soluble calcium is mainly emitted by wind and traffic-induced dust resuspension (favoured by the scarce precipitation), Saharan intrusions, fugitive dust emissions from the nearby quarries that supply the cement plants with the necessary raw materials, and channelled emissions from cement kilns (Yubero *et al*, 2010). A fall in the demand for cement could have accounted for the decrease in Ca^{2+} emissions produced by the extraction, transport and storage of raw materials as well as from the cement manufacturing process. Another possible cause could be the increase in the number of rainy days in 2010 (63 against 38 in 2005-2006), although the annual accumulated precipitation was very similar (377 and 375 L/m^2, respectively).

Sodium and magnesium concentrations were similar for both study periods and the observed variations are most probably due to annual changes in sea-salt emissions. Finally, PM10 chloride can have both natural and anthropogenic origins. Coarse Cl^- (> 2.5 µm) mainly comes from the sea (Yubero *et al*, 2010), while fine Cl^- is primarily emitted from road traffic and combustion processes at the cement plants (*Galindo et al*, 2011). The higher reduction of Cl^- levels compared with those of Na^+ and Mg^{2+} can be attributed to a decrease in fine chloride emissions from anthropogenic sources.

This work was supported by CGL2009-08036 (PASSE) project.

Galindo, N., Yubero, E., Nicolás, J.F., Crespo, J., Pastor, C., Carratalá A. and Santacatalina, M. (2011). Atmos. Environ. **45**, 2043-2049.

Yubero, E., Carratalá, A., Crespo, J., Nicolás, J., Santacalina, M., Nava, S., Lucarelli, F. and Chiari, M. (2010) *Environ. Sci. Pollut. Res.* **18**, 64-74.

Particle source characterisation of a cement plant with automated scanning electron microscopy

M.F. Meier[1,2], T. Zünd[2] and B. Grobety[2]

[1]Department of Geosciences and FRIMAT, University of Fribourg, 1700 Fribourg, Switzerland
[2]Particle Vision GmbH, 6025 Neudorf, Switzerland
Keywords: CCSEM, cement particles, EDS, source characterisation.
Presenting author email: mario.meier@unifr.ch

Several mechanic processes, such as milling, lead to dust formation during cement production. Therefore cement plants can be important local sources for PM. The aim of this study was to obtain chemical/mineralogical fingerprints of two different potential dust sources.

For that reason two samples were taken in a cement plant with an active sampling device, depositing particles on polycarbonate filters. The first sample was obtained in the raw mix milling hall (RMH), the second one in the hall of clinker milling (CMH). The filters were analyzed by computer controlled scanning electron microscopy (CCSEM) coupled with energy dispersive spectroscopy (EDS). This setting allows to obtain data from several hundreds of particles in a few hours.

The filter from RMH was dominated by Calcite ($CaCO_3$) and clays. But also Pyrite, aluminium-hydroxides, iron-oxides, calcium-silicates, alkali-sulphates and silica fume particles could be detected in that sample. On the filter from CMH, most of particles were rich in calcium containing phases, such as calcium-silicates, -carbonates, -sulphates and - aluminates. Additional alkali-sulphates and silica fume particles could be found. All other phases observed on the first filter were almost absent.

Most of the analysed particles can be explained by processes of the cement production. Calcite and clays are the main raw material. Aluminium-hydroxides, iron-oxides and Pyrite are additive raw materials. During heating and sintering (clinker production), the raw mix materials undergo phase changes and clinker (calcium-silicates and -aluminates) gets formed. This process also produces alkali-sulphates. Calcite, calcium-sulphate and silica fume finally are cement additives, added before the clinker milling step.

The results show that the two sources can be distinguished clearly and give two different fingerprints which are shown graphically in Figures 1 and 2. Whereas the filter, containing mainly raw mix particles, shows a pattern which would be quite similar to the one of other sources (e.g. limestone quarry), the fingerprint of clinker milling is very characteristic and can be used for the local air quality assessments in the neighbourhood of cement plants. Because CCSEM analyses the chemical compositions of every single particle, this method is a very suitable to obtain chemical/mineralogical fingerprints of particle sources.

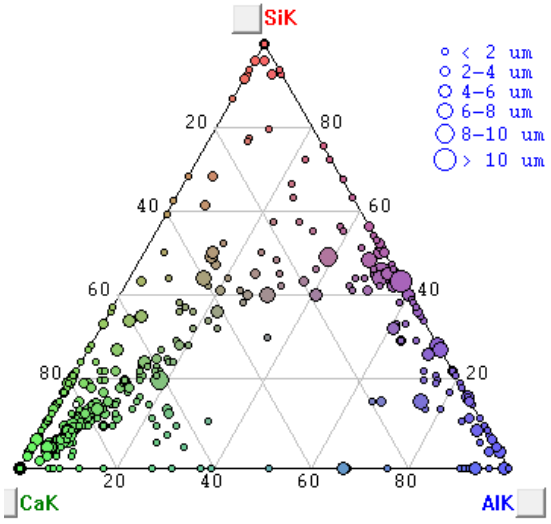

Figure 1. Ternary diagram (Si, Ca and Al). Every dot correspond to the chemical composition of particle analysed on the sample of the **raw mix milling hall**

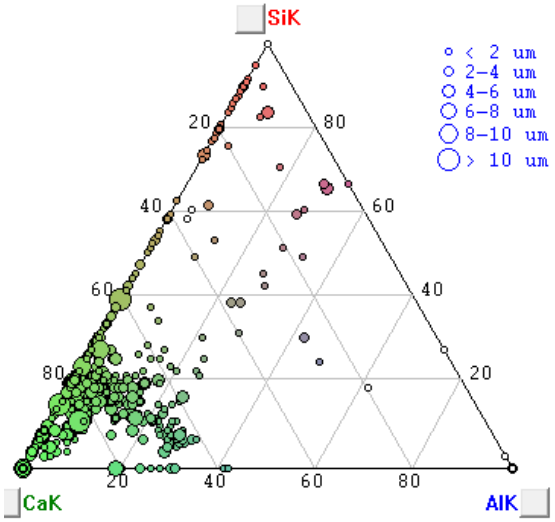

Figure 2. Ternary diagram (Si, Ca and Al). Every dot correspond to the chemical composition of particle analysed on the sample of the **clinker milling hall**

This work was supported by the Holcim (Schweiz) AG.

Indoor Air Quality in Gymnasiums

C.A. Ramos[1], S. M. Almeida[1], S. Cabo Verde[1], S. Viegas[2], C. Viegas[2]

[1]Technological and Nuclear Institute, URSN, E.N. 10, 2686-953 Sacavém, Portugal
[2] Lisbon College of Health Technology, Av. D. João II 4.69.01, 1990-096 Lisboa, Portugal
Keywords: indoor air quality; exposure; ventilation system; gymnasiums
Presenting author email: carla.ramos@itn.pt

Physical activity has become a social need among people, and is clearly proved that exercise is a way to prevent all-cause and cardiovascular-related death, diabetes mellitus and obesity (Warburton, Nicol, & Bredin, 2006; Zisser, Gong, Kelley, Seidman, & Riddell, 2011; Ruivo & Alcântara, 2012). However, athletes and the common individual can be at risk when they are practicing exercise in polluted environments due the fact that 1) the ventilation rates increase and the quantity of pollutants inhaled increase proportionally; 2) most of the air is inhaled through mouth, bypassing the normal nasal mechanisms for filtration of large particles and 3) the increased airflow velocity carries pollutants deeper in to the respiratory tract (Carlisle & Sharp, 2001). Physical activity can take place in two defined settings: outdoor (cycle lanes, sport campus, tennis court) or indoor (most of all in fitness centers). In Portugal, 12% of the people practice sport in fitness centers, little above the EU mean, with 11% (Eurobarometer 72.3, 2010). In fitness centers, physical activity is frequently performed in spaces with poor Indoor Air Quality (IAQ) due to the fact that large amount of people is concentrate in small spaces that often have deficient ventilation. The objective of this work was to assess the IAQ in three types of gymnasiums: health clubs, neighborhood gymnasiums and scholar gymnasiums. In each gymnasium all occupied spaces of the building were grouped by zones with expected similar IAQ. The groups were made according to the ventilation system in each zone, the type of activity, thermal loads and emission sources. In each zone at least one measurement was made.

Measurements of Particles with diameter lower than 10 µm (PM_{10}), CO_2, CO, H_2CO, VOCs and O_3 concentrations were performed in the selected indoor environments using automatic portable equipments. Measurements were performed during 24h in order to recognize daily patterns and identify pollutant sources. PM_{10} were sampled with a low volume sampler during the occupied period. Particles mass concentration was determined by gravimetry with a Mettler Toledo microbalance (UMT5). Filters were weighed before and after sampling in a humidity and temperature controlled room. Elemental analysis of PM_{10} sampled in the filters was performed by using Neutron Activation Analysis. Airborne microorganisms (fungi and bacteria) were collected by impaction method using a Microbial Air Monitoring Equipment. Microorganisms were also collected in surfaces (gymnasiums equipment) by swab. After sampling, processing and culturing (solid media) of the samples, quantitative (colony forming units counting) and qualitative (microscopy) results were obtained, with characterization and identification of microorganisms.

The high levels of CO_2 and microorganisms measured in the selected gymnasiums indicated that the ventilation systems were inadequate and highly contributed to the establishment of poor IAQ.

The author is gratefully acknowledge to Fundação para a Ciência e Tecnologia (FCT) for the PhD Grant - SFRH/BD/79277/2011.

Carlisle, A., & Sharp, N. (2001). *Br J Sports Med* , **35**, 214-222.

Eurobarometer 72.3. (2010). *Sport and Physical Activity*. European Comission.

Ruivo, J., & Alcântara, P. (2012). *Portuguese Jorunal of Cardiology* .

Warburton, D., Nicol, C., & Bredin, S. (2006). *CMAJ* , **174**, 801-809.

Zisser, H., Gong, P., Kelley, C., Seidman, J., & Riddell, M. (2011). *Int J Clin Pract Suppl* , **170**, 71-75.

Observations of elevated aerosol particle number and mass concentration events in Vilnius city

S. Kecorius, K. Plauškaitė, S. Byčenkienė and V. Ulevicius

Department of Environmental Research, SRI Centre for Physical Sciences and Technology, Savanoriu 231, 02300 Vilnius, Lithuania

Keywords: Number concentration, SMPS, Black carbon, Alpha Ångström coefficient.

Presenting author email: simolas2008@gmail.com

Aerosol particles have negative effects on human health regarding respiratory and cardiovascular diseases. Anthropogenic sources, such as industry and traffic, play an important role for overall atmospheric pollution throughout the year. Additionally, these constant emissions were superimposed by seasonal sources, especially to the wood combustion in winter and road dust in spring. Thus aerosol number, mass, size distribution and optical properties measurements are of great importance (Kennedy, 2007).

The aerosol particle number concentration, size distribution and optical properties were measured in Vilnius urban background site (54°38'36", 25°10'58") from 2011-09-01 to 2012-02-01 using a condensation particle counter (UF-02, sampling flow: 1 l/min, working liquid: butanol, cut-size: 4.5 nm), scanning mobility particle sizer (SMPS, sheath air flow: 5 l/min, sample flow: 1 l/min, size range: 8.693 – 839.6 nm) and a Magee Scientific company Aethalometer™, model AE31 Spectrum, (370, 450, 520, 590, 660, 880 and 950 nm). Simultaneously, aerosol particle mass (PM_{10}) and various gases (NO_X, CO, SO_2) concentrations were measured in The Environmental Protection Agency monitoring station (54°40'23", 25°14'56.81").

The absorption coefficient b_{abs} for airborne particles is defined with the Lambert-Beer's law (Eq. 1):

$$I = I_0 e^{(-b_{abs}x)}, \quad (1)$$

where I_0 is the intensity of light passing through a pristine portion of the filter and I – the intensity passing through a medium with thickness x. The wavelength-dependent optical absorption coefficient of the light can be described by: $b_{abs} \propto \lambda^{-\alpha}$, where α is the Ångström coefficient – an aerosol specific optical parameter (Sandradewi, 2008, Collaud Coen, 2010).

Unusually high pollution event was observed during the January 17 – 19, 2012. Aerosol particle size distribution with one high concentration mode was registered at the end of the January 17 (Fig. 1A, box a). This plume in all particle size ranges was related to specific meteorological and pollutant emission conditions. On the same day the highest aerosol number, black carbon and PM_{10} concentrations measured between 16:00 - 23:00 h were $13 \cdot 10^4$ 1/cm^3, 33 µg/m^3, 84.1 µg/m^3 respectively (Fig. 1B). Three distinct, well separated modes of aerosol particle size distribution were registered on the January 19, which represented different aerosol emission sources. Accumulation mode region with geometrical mean diameter d_g = 102 nm (Fig. 1A, box b) proclaims heating caused aerosols, while at the same time modes with geometrical mean diameters d_g = 8.36 nm and d_g = 80 nm (Fig. 1A, box c) represents traffic impact on high aerosol particle concentration.

The comparison of the diurnal cycle of the SO_2 and $\alpha_{660\text{-}950}$ showed that trends of the SO_2 and $\alpha_{660\text{-}950}$ were very similar, while cycles of the NO_X and CO were different. Analysis of the CO and NO_X ratio revealed, that the Ångström coefficient (Fig. 1A) values between 1 and 1.4 relate to the traffic impact, while values higher than 1.5 - to the wood combustion, which is explained by the domestic heating.

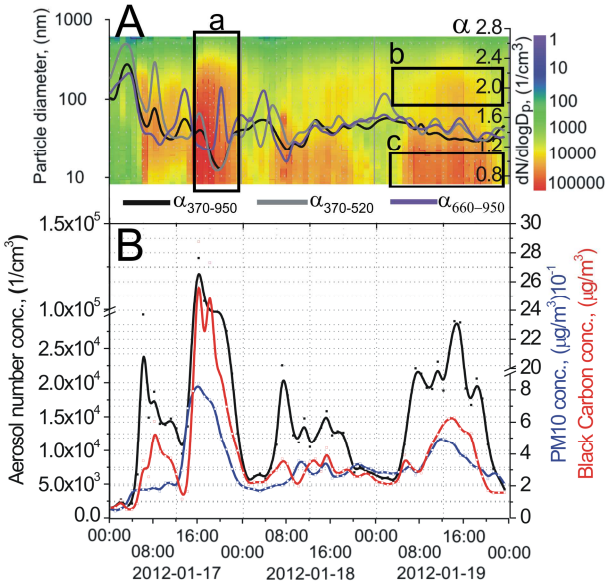

Figure 1. A - Ångström coefficient and particle size distribution, B - Aerosol number, mass (PM_{10}) and black carbon concentrations, January 17 – 19, 2012.

This work was partially supported by the FP7 TRANSPHORM project.

Kennedy, I. M. (2007). *Proc. of the Combustion Institute* 31, 2757-2770.

Sandradewi. J., Prevot, A.S.H., Weingartner, E., Schmidhauser, R., Gysel, M., Baltensperger, U. (2008). *Atmospheric Environment* 42, 101-112.

Collaud Coen, M., Weingartner E., Apituley A., Ceburnis D., Fierz-Schmidhauser R., Flentje H., Henzing J. S., Jennings S. G., Moerman M., Petzold A., Schmid O., Baltensperger U. (2010). *Atmos. Meas. Tech.*, 3, 457 - 474.

Mobile platform measurements of PM mass and number concentrations and black carbon in the Greater Athens Area

E. Diapouli[1], S. Vratolis[1], V. Vasilatou[1], M. Gini[1], A. Tsakis[2], L. Chasapidis[2], F. Akritidis[2], A. Konstantopoulos[2], G. Mocnik[3], S. Pothos[4] and K. Eleftheriadis[1]

[1] Institute of Nuclear Technology and Radiation Protection, Environmental Radioactivity Laboratory, National Centre for Scientific Research "Demokritos", 15310 Ag. Paraskevi, Attiki, Greece
[2] Chemical Process Engineering Research Institute, Laboratory of Aerosol and Particle Technology, Centre for Research & Technology Hellas,57001 Thermi, Thessaloniki, Greece
[3] Aerosol d.o.o, Ljubljana, Slovenia
[4] TSI GMBH, Aachen, Germany
Keywords: urban pollution, PM10/PM2.5, Number size distribution, Black carbon.
Presenting author email: ldiapouli@ipta.demokritos.gr

While air quality in Europe has improved substantially over the past decades, pollution from particulate matter (PM) remains a major environmental problem, especially in big urban agglomerations. The scope of this works was to examine the spatial variability of major aerosol parameters such as PM mass, particle number and black carbon concentrations across the Greater Athens Area (GAA), through the use of a mobile measurements platform (Mobilab). The city of Athens has been known to face air pollution problems over the last decades, with frequent exceedances of the daily PM_{10} air quality standard in certain stations (Aleksandropoulou et al., 2012). The main objectives of this survey were to examine the spatial distribution of PM (especially of their traffic-related components), to evaluate the effectiveness of the National Monitoring Network (NMN) in characterizing the Athens city population exposure and to identify potential local sources or "hot-spot"areas.

Measurements were conducted during 12–23/9/2011. The parameters measured were: particle size distribution (SMPS, OPC), PM mass concentration (photometer) and black carbon (portable aethalometer). All instruments were sampling from a thin walled tube inlet 6 mm in diameter situated on the top of the vehicle, extended well in front of the vehicle body, isoaxial to the incoming flow during movement in order to minimize losses and contamination. In addition, a GPS system was constantly monitoring Mobilab's exact position over time. During the day the vehicle was moving around the GAA, while at nights fixed measurements were performed at selected locations. During these night-time measurements, 12-hr gravimetric samples were also collected by a MOUDI impactor.

Table 1. Variation of aerosol parameters across the GAA

	Day-time	Night-time
PM_{10} ($\mu g\ m^{-3}$)	16 - 83	22 - 57
$PM_{2.5}$ ($\mu g\ m^{-3}$)	13 - 67	8 - 42
Total number conc. ($10^4\ cm^{-3}$)	1.8 – 12.0	0.6 – 3.2
BC ($\mu g\ m^{-3}$)	1.4 – 7.0	0.5 – 3.5

All measured parameters exhibited significant variability across the city (Table 1). Very high levels were measured in heavy-traffic areas during the day, especially for number concentration and BC. The obtained PM_{10} concentrations were compared to the levels measured by the NMN stations, selecting for each area the closest available station. Mean values were calculated both for the Mobilab campaign measurement period as well as for the last three years reported by the NMN (2008-2010). Day-time data were grouped in large regions covering areas in the North (N), Northeast (NE), Northwest (NW), East (E), West (W), South (S) and the city centre (Figure 1). The results indicate that in general the NMN stations provide a representative picture of population exposure in the wider area covered by them. Very high short-term exposures were measured on-road, especially for the traffic-related parameters, number concentration and black carbon (Figure 2).

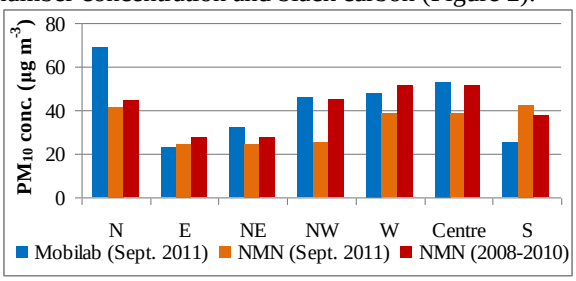

Figure 1. Comparison of mean day-time PM_{10} conc. measured by Mobilab with levels reported by NMN

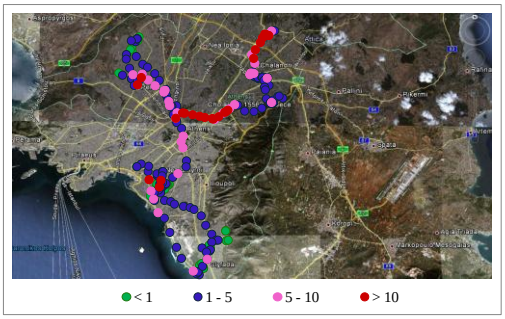

Figure 2. Variation of 2-min averages of black carbon ($\mu g/m^3$) during a 9-hr drive (23-9-2011, 8:00 – 17:00).

This work was supported by the European Commission LIFE+ Environment Policy and Governance programme.

Aleksandropoulou, V., et al. (2012) *J. Environ. Monitor.* **14**, 266-278.

PM concentration and chemical speciation measurements at two sites in Athens, Greece

S. Vratolis[1], E. Diapouli[1], V. Vasilatou[1], M. Gini[1], Th. Maggos[2], D. Saraga[2], Th. Ntoka[2] and K. Eleftheriadis[1]

Institute of Nuclear Technology and Radiation Protection,
National Centre of Scientific Research "Demokritos", 15310 Ag. Paraskevi, Attiki, Greece
[1] Environmental Radioactivity Laboratory
[2] Environmental Research Laboratory
Keywords: PM10/PM2.5, chemical composition, urban areas.
Presenting author email: vratolis@ipta.demokritos.gr

Particulate matter (PM) ambient concentration levels are still a major environmental problem in several urban areas in the E.U., while new evidence of its long term impacts on human health continues to emerge. As the E.C. is moving towards the implementation of the thematic strategy on Air Pollution, information on PM_{10} and $PM_{2.5}$ concentration levels, as well as their main constituents, will be very useful in developing new regulations and evaluating current measures. In this framework, Life+ project ACEPT-AIR is aiming, among others, in constructing an updated database on PM concentrations and chemical speciation for three big urban cities in Greece (Athens, Thessaloniki and Volos). The obtained data will be further utilized for source apportionment.

This work presents the results from the Athens measurement campaigns, conducted during warm and cold period of 2011 – 2012 (around 50 days per season). PM_{10} and $PM_{2.5}$ were measured gravimetrically on a 24-hr base, at two sites: (1) N.C.S.R. "Demokritos" urban background station (GAW-DEM, 2007) and (2) Nea Smyrni station of the National Monitoring Network (Figure 1). Two types of filters were used for each size fraction (Teflon / Quartz) in order to allow for detailed chemical speciation. Elemental (EC) and organic (OC) carbon will be determined through thermal-optical analysis. Atomic Absorption Spectrometry and X-Ray Fluorescence will be used for the determination of major and trace elements and Ion Chromatography for ionic species. Analysis of filters is still in progress.

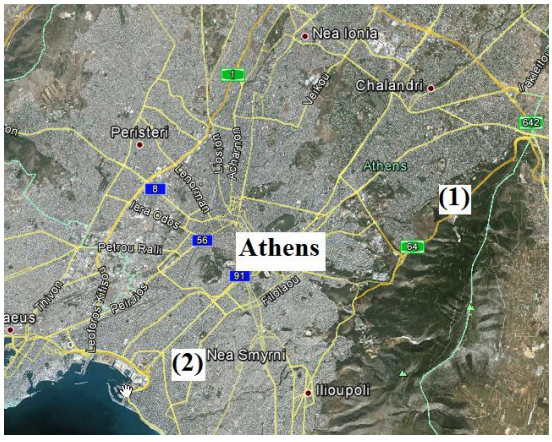

Figure 1. Map of Athens Greater Area and measurement sites: (1) Demokritos and (2) Nea Smyrni stations.

Basic statistical data on the measured PM_{10} and $PM_{2.5}$ concentrations at the two sites are presented in Tables 1 and 2, respectively. Similar PM levels were measured at the two sites during warm season. PM concentrations were low, indicating a background character for both sites. This was further supported by the initial results on chemical composition. Elemental and organic concentrations at both sites were relatively low with an average EC/OC ratio of 0.2.

Table 1. Basic statistics for PM_{10} concentrations measured at Demokritos (DEM) and N. Smyrni (NSM) stations (μg m^{-3}).

	Warm season		Cold season	
	DEM	NSM	DEM	NSM
Mean	24.4	23.7	16.5	41.1
St. Deviation	7.5	7.4	5.1	24.5
Minimum	6.2	11.4	5.3	17.0
Maximum	49.5	39.0	31.9	133.2

Table 2. Basic statistics for $PM_{2.5}$ concentrations measured at Demokritos (DEM) and N. Smyrni (NSM) stations (μg m^{-3}).

	Warm season		Cold season	
	DEM	NSM	DEM	NSM
Mean	12.4	16.2	10.8	22.8
St. Deviation	4.1	5.9	3.6	14.9
Minimum	4.9	6.0	4.4	7.5
Maximum	25.9	30.1	17.2	73.5

Demokritos station exhibited even lower concentration levels during cold season, which may be also attributed to the meteorological conditions (heavy rainfall during many of the measurement days). At N. Smyrni, on the contrary, the situation was very different during cold season. The measured levels were very high, with exceedances of both the 24-hr limit value for PM_{10} and the annual target value for $PM_{2.5}$. The higher residential density of the area, in comparison to N.C.S.R. "Demokritos" campus and the surrounding neighbourhood, in conjunction with the intensive use of fireplaces during this period may account for this great increase of both PM_{10} and $PM_{2.5}$ concentrations.

This work was supported by the European Commission LIFE+ Environment Policy and Governance programme.

GAW-DEM (2007) http://gaw.empa.ch/gawsis/reports.asp?StationID= 20 76202728.

Determination of refinery emission pollutants impact on an urban atmosphere

M.A. Barrero, M. Goikoetxea and L. Cantón

Department of Applied Chemistry, University of the Basque Country, 20018, Donostia-San Sebastián, Spain
Keywords: PM10, trace metals, volatile organic compounds, oil refinery
Presenting author email: miguelangel.barrero@ehu.es

The urban aerosol composition is directly related to the specific anthropogenic activities in the area. Though the road traffic is considered to be the main source of pollutants in urban areas, industrial emissions which can be of a very different nature, can also contribute with a wide range of contaminants. One special case of industrial facilities is oil refineries, which are known sources of gaseous pollutants such as sulphur dioxide or volatile organic compounds (VOCs) and particulate matter.

In this work, we evaluated the influence of refinery emissions in an urban area by analysing the variations of PM_{10} and VOCs concentrations and physicochemical and meteorological parameters.

The sampling sites were selected in two residential areas located in the immediate surroundings of an oil refinery, in the Basque Country coast. Site 1 was located less than 200 m to the Northwest from the refinery, and Site 2 was situated about 400 m to the Southwest.

PM_{10} and VOCs samples were collected during 24 h periods twice a week during one year, parallel at each site. PM_{10} samples, on quartz fibre filters, were analysed for metal composition by ICP-MS and for polycyclic aromatic hydrocarbon (PAH) by GC-FID and GC-MS. VOCs samples, on activated charcoal tubes, were analysed by GC-FID and GC-MS.

An automatic station of the Basque Government's Air Quality Monitoring Network measured the concentrations of some major pollutants (CO, NO_x, O_3, $PM_{2.5}$, SO_2) and meteorological variables (temperature, relative humidity, atmospheric pressure, solar radiation and wind speed and direction).

Some differences were found regarding the behaviour of particulate matter and the volatile organic compounds in the gas phase. While both sites showed similar composition and levels of PM components, VOCs exhibited large differences between sites. In Site 1 (the site located most of the time downwind the refinery), some samples exhibiting high levels of light hydrocarbons were collected. This was confirmed by a correlation analysis, that showed that particulate matter and VOCs in Site 2 (usually upwind the refinery) were significantly correlated while in the downwind site they did not correlate (Figure 1).

The concentrations of all the pollutants were evaluated with the wind direction. In general, both sites showed the highest levels of anthropogenic PM_{10} components with easterly winds, while VOCs were detected in higher concentrations with easterly winds in Site 1 and with northerly winds in Site 2.

These findings indicate that particulate matter pollution can be considered to be more general, disperse, while VOCs can be related with more punctual, local emissions.

In addition, a factor analysis was performed to help in the elucidation of the sources of air pollutants affecting the area of study.

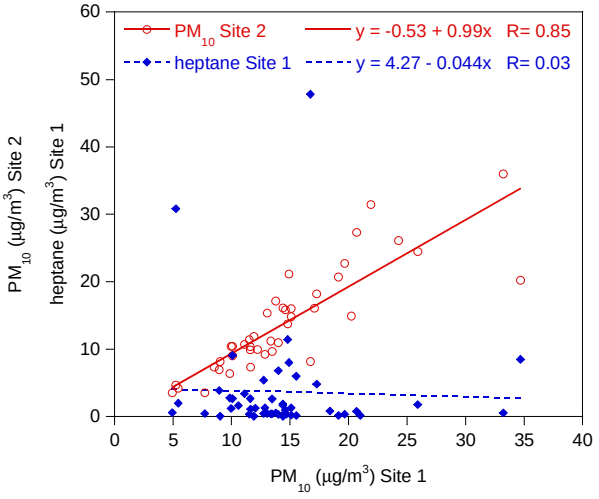

Figure 1. Dispersion plot of PM_{10} (Site 2) and heptane concentration (Site 1) with PM_{10} (Site 1).

Determination of water content in atmospheric particulate matter

C. Farao[1], C. Perrino[2], S. Canepari[1], E. Marconi[1], M.L. Astolfi

[1]Department of Chemistry, Sapienza University of Rome, Rome, 00185, ITALY
[2] C.N.R. Institute of Atmospheric Pollution Research, Monterotondo St., Rome, 00015, ITALY
Keywords: particulate matter, determination of water, chemical composition
Presenting author email: carmela_farao@libero.it

It is well known that water is able to interact with organic and inorganic hygroscopic compounds of atmospheric particulate matter (PM). This interaction has been widely studied and its influence on several chemical and physical characteristic of PM has been well documented (Hu et al., 2011). Several studies has evidenced the role of water in determining the position of ammonium salts vapor-solid equilibria that are responsible for one of the most relevant sampling artifact in PM collection (Vecchi et al., 2009), but the mechanism of this dependence is still largely unknown.
The quantitative determination of water in PM has been attempted in a few studies. Most of them are performed by a differential evaluation of the PM mass before and after exposing the sample to controlled relative humidity conditions (Kitamori et al., 2009). These studies demonstrate that the amount of retained water depends on the dimension and chemical composition of particles, but no information are given about the type and strength of water-particle interactions.
In a recent study concerning the application of thermogravimetric analysis (TGA) to PM samples (Perrino et al, 2012), we evidenced that the release of water occurs at different temperatures, depending on the strength of the interaction between water and PM. However, due to the presence of other volatile species evolving in the same temperature ranges, the TGA does not allow a reliable quantitative determination of water.

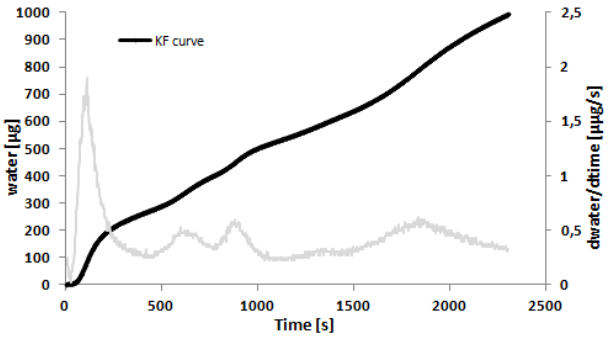

Figure 1. Karl-Fisher curve of NIST1648

In this work we report the optimization and validation of a new simple method for the quantitative determination of water in PM and its first application to a series of real PM_{10} samples. The analysis are performed by a coulometric Karl-Fisher system equipped with a controlled heating device. Different water contributes are separated by the application of a proper thermal ramp. The optimal heating condition, consisting in three heating steps (50°-120°C, 120°-180°C, 180°-250°C) allows to distinguish four different types of water in reference materials NIST1648 and NIST1649a (urban particulate matter; figure 1). The analytical performance of the method have been verified by using two standard materials, HYDRANAL Water Standard KF-Oven 220 ° C-230 ° C and Water Standard Oven 1%, containing 5.55 % and 1% by weight of water respectively. The recovery with both standards is greater than 95% and detection limits are of ca. 20 µg. A sufficiently good repeatability (ca. 10-15%) is obtained both on reference materials and real PM_{10} samples.
The application of the method to real PM_{10} samples has evidenced that the amount of water is subjected to very relevant variation, as a function of the PM chemical composition. Mass percentages of ca. 3-4 % have been obtained in most of the samples, but values up to about 15% have been reached when the chemical composition of PM was dominated by secondary inorganic ions and organic matter. Very different thermal profiles have been also evidenced. To try an identification of the type of the released water, the method has also been applied to some hygroscopic compounds (pure SiO_2, Al_2O_3, NaCl, Na_2CO_3, ammonium salts and carbohydrates) that are likely present in PM.

D. Hu, J. Chen, X. Ye, L. Li, X. Yang (2011). *Atmos. Environ.*, 45, 2349-2355.
Y. Kitamori, M. Mochida, K. Kawamura, (2009) *Atmos. Environ.*, 43, 3416-3423.
C. Perrino, E. Marconi, L. Tofful, C. Farao, S. Materazzi, S. Canepari (2012), *Atmos. Environ.*, In press, DOI: 10.1016/j.atmosenv.2012.02.078.
R. Vecchi, G. Valli, P. Fermo, A. D'Alessandro, A. Piazzalunga, V. Bernardoni (2009), *Atmos. Environ.*, 43, 1713-1720.

Long-range transport influence on PM2.5 measurements performed in Southern Italy

S. Trippetta[1], R. Caggiano[1], S. Fiore[1], A. Lettino[1], M. Macchiato[2] and S. Sabia[1]

[1] Istituto di Metodologie per l'Analisi Ambientale - Consiglio Nazionale delle Ricerche (IMAA - CNR), Tito Scalo (PZ), 85050, Italy
[2]Dipartimento di Scienze Fisiche (DSF), CNISM, Università Federico II, Napoli, 80126, Italy
Keywords: PM2.5, long-range transport, chemical composition, SEM.
Presenting author email: trippetta@imaa.cnr.it

Atmospheric aerosols are a complex mixture of suspended solid and liquid particles with different physical and chemical properties (e.g., size distribution, optical properties and chemical composition). They can originate both from anthropogenic sources – such as industrial activities, road traffic and residential heating – and natural sources – such as local soil, deserts, sea spray and volcanic eruptions.

The most relevant contribution to the atmospheric aerosol load in a given location is generally related to emissions from local anthropogenic and/or natural sources, although long-range transport contribution has been found to be often significant and needs considerations especially in Euro-Mediterranean regions (Nicolás et al., 2008).

Since the only PM concentration measurements are not enough to identify the PM origin, it would be of primary importance to characterize it from a chemical and mineralogical point of view and combine this information with model forecasts and remote sensing observations that allow the identification of the occurrence of long-range transport events over a study area (Caggiano et al., 2012).

In this context, PM2.5 daily samples were collected at the Institute of Methodologies for Environmental Analysis of the National Research Council of Italy (IMAA-CNR) located in Southern Italy (Tito Scalo - Potenza) from April to July 2010.

During this period, the PM2.5 daily concentrations ranged between 0.2 μg m^{-3} and 18 μg m^{-3}, with a mean value of 6 μg m^{-3}. Figure 1 shows the PM2.5 temporal pattern.

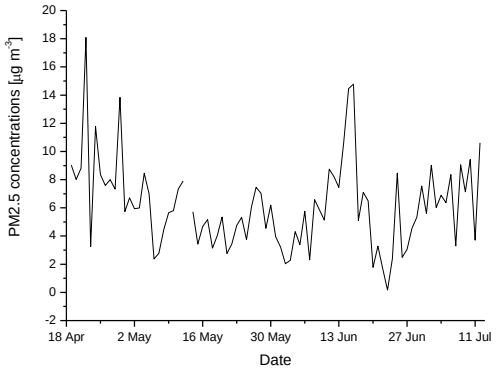

Figure 1. Temporal pattern of the PM2.5 concentrations measured at the CNR-IMAA site from April to July 2010.

The combined use of model outcomes and satellite observations allowed the identification of the occurrence of long-range transport events of different type over the area under study. In particular, two predominant long range transport events were identified: volcanic ash coming from the eruption of Eyjafjallajökull volcano located in Southern Iceland (63° 38' N, 19° 36' W, 1666 m a.s.l.) and dust particles coming from Sahara desert.

In order to evaluate the influence of these events on the PM2.5 measurements, PM2.5 chemical composition (Al, Be, Ca, Cd, Co, Cr, Cu, Fe, K, Li, Mg, Mn, Na, Ni, P, Pb, Ti and Zn) and mineralogical and morphological features of the PM2.5 single particles were analysed.

Results pointed out the falling to the ground both of volcanic ash and dust particles and their contribution to the increase in the PM2.5 concentrations.

Caggiano, R., Fiore, S., Lettino, A., Macchiato, M., Sabia, S., Trippetta, S. (2011) *Atmos. Res.* **102(1-2)**, 157-166.

Nicolás, J., Chiari, M., Crespo, J., Garcia Orellana, I., Lucarelli, F., Nava, S., Pastor, C., Yubero, E. (2008) *Atmos. Environ.* **42**, 8872–8882.

Particulate air pollution exposure during commuting in three European cities

P. Taimisto[1], A. Pennanen[1], E. Vouitsis[2], Z. Samaras[2], M.P. Keuken[4] and T. Lanki[1]

[1]Department of Environmental Health, National Institute for Health and Welfare (THL), Kuopio, FI-70210, Finland
[2] Laboratory of Applied Thermodynamics, Aristotle University, Thessaloniki GR-54124, Greece
[3]TNO, Netherlands Organization for Applied Scientific Research, Utrecht, NL-3508 TA, Netherlands
Keywords: Exposure, Measurements, Traffic emissions, PM10/PM2.5.
Presenting author email: pekka.taimisto@thl.fi

In the Transphorm study exposure to $PM_{2.5}$ (particles up to 2.5 micrometers in diameter), PM_{10} (particles up to 10 micrometers in diameter), PNC (particle number concentration) and BC (black carbon) during commuting was measured. Measurements were performed in three European cities: Helsinki, Thessaloniki and Rotterdam during spring 2011. Measured modes of commuting included a bike, a bus and a car (Ford Focus Wagon with 1.6 litres gasoline engine, model 2008-2010) driven with both open and closed windows.

Measurements were performed with TSI DustTrak DRX 8533 ($PM_{2.5}$ and PM_{10}), TSI P-Trak 8525 (PNC) and Magee Scientific microAeth AE51 (BC).

In Rotterdam, Thessaloniki and Helsinki 2, 3 and 6 study routes were chosen, respectively. The number of study routes per city depended on city's geometry and the actual commuting routes of the citizens. The local municipal authorities assisted in choosing of the routes.

Measurement campaigns lasted for 6 days. One measurement day included 4 one-way drives with a bike, a bus, a car with open windows and a car with closed windows; all drives within one day were performed on the same study route. The average exposures by commuting mode in three study cities are presented in table 1.

Table 1. The average concentrations of photometric $PM_{2.5}$ ($\mu g/m^3$), photometric PM_{10} ($\mu g/m^3$), PNC ($1/cm^3$) and BC ($\mu g/m^3$) by commuting mode in the three cities.

Mode of commuting	Particle fraction	City		
		Helsinki	Thessaloniki	Rotterdam
Bicycle	$PM_{2.5}$	24.4	37.7	27.0
	PM_{10}	35.4	45.3	30.6
	PNC	13000	42600	20300
	BC	3.2	6.9	3.1
Bus	$PM_{2.5}$	29.2	84.9	20.6
	PM_{10}	42.1	131.5	22.5
	PNC	15000	49200	17900
	BC	4.5	8.5	4.2
Car, closed windows	$PM_{2.5}$	14.3	28.2	23.7
	PM_{10}	14.8	33.8	25.2
	PNC	11400	24900	26000
	BC	3.0	4.7	6.3
Car, open windows	$PM_{2.5}$	33.2	62.6	30.7
	PM_{10}	41.4	79.0	34.3
	PNC	36900	60900	34000
	BC	7.3	10.9	6.4

Conclusions

The lowest particle concentrations were encountered in a car with closed windows and the highest in a car with open windows. The cars used in the study were of the latest model and presumably with recently installed filters for incoming air, which explains the highly protective effect of the car body. Opening the car window greatly reduces car body's capacity to protect persons inside from air impurities.

The differences in exposures between cyclists and persons taking a bus were rather small, showing that the body of a bus does not provide much protection against particulate air pollution (obviously because the doors are frequently open). Interestingly, in Thessaloniki $PM_{2.5}$ and PM_{10} concentrations inside a bus were extremely high, most likely because of resuspension of road dust accumulated inside the bus. Exposures of cyclist tended to be somewhat smaller than concentrations inside a car with open windows, obviously because the cyclists do not cycle all of the time in the middle of the vehicular traffic flow (i.e. next to emissions).

The differences in the levels of exposure were in the expected direction: the highest levels in Thessaloniki, the lowest in Helsinki, while Rotterdam was in-between the two. However, commuters' exposures to PM_{10} were higher in Helsinki than Rotterdam, obviously due to road dust accumulated during the winter because of sanding of icy roads and use of studded tyres. Further, exposure to black carbon were higher in Helsinki than in Rotterdam, perhaps depending on the proportion of diesel cars in the car fleet, or on the age of the car fleet, which is higher in Helsinki.

Two years of measurements at a regional background site in the Balearics: first results

J. Pey[1], C. Bujosa[2], S. Caballero[3], X. Querol[1], A. Alastuey[1], M Sicard[4,5], B. Artíñano[6]

[1]Institute of Environmental Assessment and Water Research (IDAEA-CSIC); [2]ENDESA; [3] Atmospheric Pollution Laboratory, Miguel Hernández University; [4]RSLab, Polytechnic University of Catalonia (UPC); [5]IEEC, UPC; [6]CIEMAT

Keywords: Western Mediterranean, ChArMEx, chemical composition

Presenting author email: jorge.pey@idaea.csic.es

In the context of the ChArMEx (The Chemistry-Aerosol Mediterranean Experiment, https://charmex.lsce.ipsl.fr) initiative, a number of atmospheric parameters are being measured at a regional background site (Can Llompart; CLP) in the Majorca Island (Balearic Islands, Spain). In January 2010, in addition to routine measurements of PM_{10}, NO, NO_2, SO_2 and O_3 levels (since January 2000), additional instruments were installed, including: 1) a sequential high-volume sampler for PM_{10} collection on quartz micro-fibre filters; 2) an optical particle counter to determine real time concentrations of PM_{10}, $PM_{2.5}$ and PM_1; 3) an automatic collector of dry and wet deposition of atmospheric particles. Currently, hourly levels of NO, NO_2, SO_2, O_3, PM_{10}, $PM_{2.5}$, PM_1, air temperature, wind direction and velocity, atmospheric pressure and precipitation are measured. Furthermore, 24-hour PM_{10} samples are collected every four days in order to perform a complete chemical characterization (Pey *et al.* 2009) and a subsequent source apportionment analysis. Furthermore, two intensive sampling campaigns were performed in 2011, one in early spring and the other in mid-summer. For these campaigns, sampling of PM was done everyday and additional instruments were deployed: 1) a sequential high-volume sampler for PM_1 collection on quartz micro-fibre filters; 2) an ultra-fine particle counter for number concentration between 5-1000nm; 3) a multi-angle absorption photometer monitor for continuous reading of black carbon concentrations.

Mean PM_{10}, $PM_{2.5}$ and PM_1 levels for the whole period (2010-2011) were 17, 11, and 8 µg/m^3. Seasonal trend of PM levels differs from winter to summer, with higher background levels in summer due to stagnant conditions over the Western Mediterranean. Intense peaks of coarse PM are observed along the year owing to African dust inputs. High PM levels, mainly fine particles, are observed occasionally under winds transported throughout Europe. PM_{10} composition (2010) is made up of organics (23% organic matter and 1% elemental carbon), mineral matter (17%), sulphate (14%), sea spray (10%) and nitrate (7%) and unaccounted mass (28%), mostly thought as water (Figure 1). Intensive sampling campaigns (Figure 2) were useful to assess on black carbon (BC) and number concentration (N) levels and time-variation. Thus, mean levels of BC were 560 ng/m^3 and number concentration was around 7100 cm^{-3} (spring campaign). Both parameters followed similar trends to those observed for PM_1 but BC also displayed fresh anthropogenic inputs from road traffic, and N peaked occasionally at midday because of new-formation of particles from photochemical reactions (Figure 3).

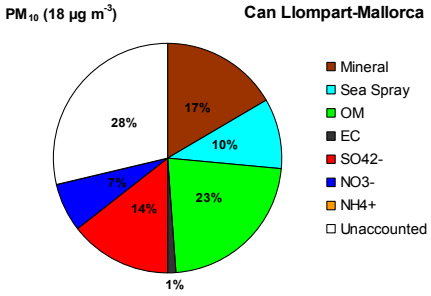

Figure 1. Mean PM_{10} composition in 2010 at CLP.

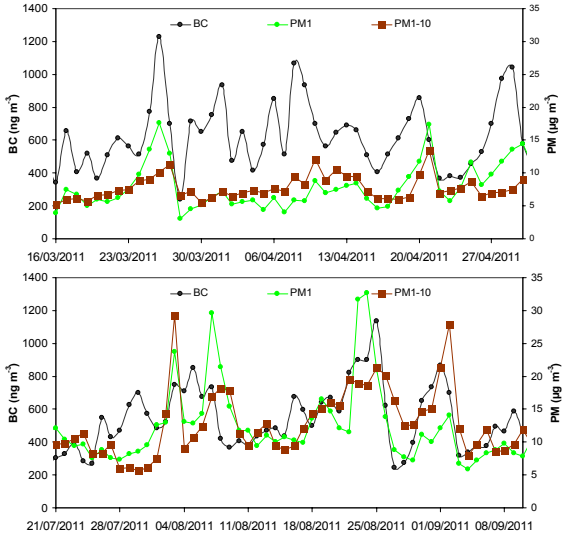

Figure 2. Daily PM_1, PM_{1-10} and BC levels during intensive campaigns.

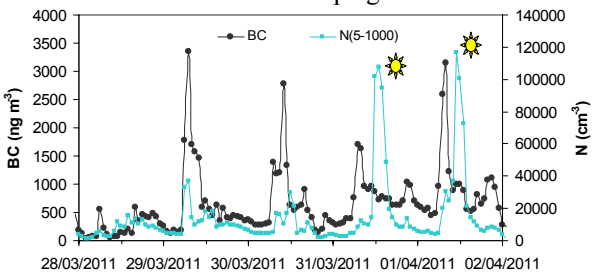

Figure 3. Hourly BC and N levels during intensive spring campaign: intense nucleation events.

This work is supported by the Spanish Ministry of Science and Innovation and FEDER funds (CGL2011-13580-E/CLI). ENDESA, through AMBILINE, is taking care of instruments and yielding gaseous and meteo data.

Pey, J. Querol, X. Alastuey, A. (2009). *Atm. Res.* **94,** 285-299.

Effect of flooring, cleaning and foot traffic on indoor air particulates

N. Mansouri[1], I. Colbeck[2]

[1]Science and Research Branch, Islamic Azad University, Tehran, Iran, 1998657151, Iran
[2]Department of Biological Sciences, University of Essex, Colchester, CO7 6LW, UK
Keywords: Floor cover, PM measurement, fine particle, PM_{10}, $PM_{2.5}$, PM_1
Presenting author email: colbi@essex.ac.uk

Indoor particulate matter is one of the major risk factors for chronic respiratory diseases (WHO, 2007). Scientific studies have shown that ordinary indoor activities such as walking over carpeted or hard floor areas can result in increased particulate concentrations in the indoor environment (Cheng et al., 2010). This current investigation was designed to assess the effect of foot traffic (FT) and type of floor covering (FC) on particle mass concentration (PMC) within various buildings in the University of Essex. Three types of hallways with different floor cover were included in the assessment: paint, carpet and concrete. PM_{10}, $PM_{2.5}$ and PM_1 concentrations were measured in 60-minute periods; with 1 minute intervals for each set of measurements, at 4 foot traffic modes : <2, 2-4, 5-8 and 9-12 persons per minute (p/m). This plan was repeated for three different points inside each hallway. FT in the hallways was measured by direct observation. Measurements were also undertaken in ambient air outside the building.

The measurements were carried out between 09.00 -17.00 at respiratory height. A GRIMM aerosol spectrometer, model 1.101 (Grimm Aerosol Technik GmbH, Ainring, Germany) was used for measurements. It had a sensitivity of 0.1 µg m^{-3} with a reproducibility of ±2%. All floors had been cleaned earlier in the day prior to sampling.

Table 1 shows the average concentrations and foot traffic for the various locations. Within the indoor environment carpeting resulted in the highest PM_{10} concentrations in comparison with other floor coverings for all foot traffic categories. Concrete floor coverings generally had lower PM_{10} concentrations than carpet and higher levels than painted floors. The one exception to this was for FT of 2-4 people per minute when the PM_{10} concentration for painted floors was higher.

The outdoor concentration was similar to that indoors at all locations with very low foot traffic. It is evident that both floor cover and foot traffic had effective role on resuspension of particles from floors. There was a statistically significant correlation between PM_{10} and foot traffic for all floor coverings ($p < 0.001$).

Earlier work has shown that an incremental foot traffic intensity of one person per minute over a carpeted hallway can increase the PM concentration by 1.0 µg m^{-3} and 0.8 µg m^{-3} for 1 to 5 µm and 5 to 7.5 µm particles, respectively (Cheng et al., 2010). The results in the current study indicate a near linear relationship between foot traffic and increasing PM_{10} with an increment of approximately 3.0 µg m^{-3} per person. For fine particulate the relationship was semi exponential (Fig 1). This means that human activity such as walking has more effect on the resuspension of coarse particles than fine ones. A number of factors can influence resuspension such as walking pace, walking style, dust loading, dust type, relative humidity and the effective indoor mixing volume.

Table 1. The average and standard deviation of outdoor and indoor air particulate concentrations (µg m^{-3}) for 3 different floor coverings

Flooring	PM size	Foot traffic (persons/minute)			
		<2	2-4	5-8	9-12
Fabric paint	PM_{10}	5.3 (0.96)	13.6 (1.61)	16.3 (1.89)	20.4 (3.51)
	$PM_{2.5}$	1.9 (0.35)	2.2 (0.26)	2.7 (0.43)	3.7 (0.29)
	PM_1	0.9 (0.10)	1.1 (0.15)	1.4 (0.34)	2.1 (0.13)
Carpet	PM_{10}	9.8 (1.24)	17.8 (3.34)	26.8 (4.66)	36.3 (6.00)
	$PM_{2.5}$	2.9 (0.15)	3.1 (0.35)	4.2 (0.28)	5.7 (0.57)
	PM_1	1.8 (0.13)	2.0 (0.25)	2.2 (0.19)	2.8 (0.47)
Concrete	PM_{10}	7.6 (1.00)	11.4 (1.64)	21.8 (2.58)	31.4 (3.74)
	$PM_{2.5}$	1.6 (0.16)	2.1 (0.18)	2.9 (0.43)	3.9 (0.37)
	PM_1	0.8 (0.12)	1.3 (0.22)	2.2 (0.19)	2.4 (0.28)
Outdoor	PM_{10}	4.6 (0.56)	Not measured		
	$PM_{2.5}$	0.74 (0.18)			
	PM_1	0.46 (0.15)			

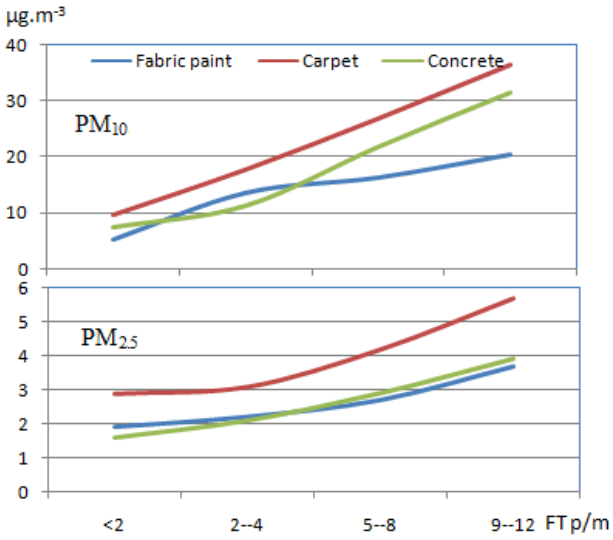

Fig1: Effect of FT on PM_{10} and $PM_{2.5}$ in 3 type3 of FC

Cheng K.C., Geobes M.D. and Hildemann L.M. (2010), Atmos. Environ., 44, pp 2062-2066.

WHO (2007), http://www.who.int/gard/publications/GARD%20Book%202007.pdf.

Evolution of PM_{10}, $PM_{2.5}$ and PM_1 in a semi-arid industrial environment

M. Santacatalina[1,2] and A. Carratalá[2]

[1]General Foundation, University of Alicante, 03690, Alicante, Spain
[2]Department of Chemical Engineering, University of Alicante, P. O. Box 99, 03080, Alicante, Spain

Keywords: Ambient PM, PM_{10}, $PM_{2.5}$, PM_1.
Presenting author email: milagros.santacatalina@ua.es

This work presents the evolution of ambient PM, PM_{10}, $PM_{2.5}$ and PM_1, in a semi-arid industrial environment, comparing two annual periods of study, May 2007 - April 2008 (before the economic crisis) and May 2010 - April 2011 (during the economic crisis). Levels of PM in the second period have decreased in concordance with the reduction of industrial activity due to the economic crisis. The three fractions present similar trends in the first period of study, with higher levels in winter months with the influence of several PM sources. In the second period, the seasonal variation is less noticeable due to the low levels in all months.

The study zone is a semi-arid industrial environment located in the southeast of Spain, with the mineral components of particulate matter as the main PM_{10} (Santacatalina *et al*, 2010) and $PM_{2.5}$ (Galindo *et al*, 2011) source. These characteristics have an effect on PM levels. Saharan dust events are common in the area due to the proximity of the African continent and they also have a lot of influence on PM levels. Three fractions of PM (PM_{10}, $PM_{2.5}$ and PM_1) were measured with a continue particle size analyzer (model Grimm 1.108). Data from two periods of study were compared, May 2007 - April 2008 and May 2010 - April 2011. The first one corresponds to a period previous to the height of the economic crisis, and the second one corresponds to a period during the economic crisis, with a significant decrease of the industrial activity in the area. The sampling point was located on the roof of the building of Research Technical Services of the University of Alicante, in the new Scientific Park of Alicante.

In the first period of study, levels of PM_{10} were high, with peaks of monthly average higher than 40 $\mu g/m^3$ (annual limit). In the case of $PM_{2.5}$, levels did not exceed the annual limit of 25 $\mu g/m^3$, and PM_1 levels were below 20 $\mu g/m^3$ (Figure 1). The annual averages were 34, 16 and 10 $\mu g/m^3$, respectively. In the second period, levels of PM decrease in the three fractions about 50% (Figure 1). The annual average were 17, 7 and 5 $\mu g/m^3$, respectively. Ratio values have not changed from the first period to the second period 0.5-0.4 $PM_{2.5}/PM_{10}$, 0.3-0.3 PM_1/PM_{10} and 0.6-0.7 $PM_1/PM_{2.5}$, and they have the same trend along the study periods. Data show the PM_{10} fraction as a critical pollutant in the area despite the low levels in the second period. PM levels in the second period can be considered as a baseline data that should not increase when the zone gets the industrial activity back.

Concerning the seasonality of the three fractions, the highest levels have occurred in winter months. This is more obvious in the first period of study, probably due to the influence of several PM sources as industrial activity, traffic, dust resuspension... and this is less marked in the second period, due to the decrease of levels in general.

African intrusions and meteorological factors were also studied and do not show a clear pattern explaining the decrease in the second period.

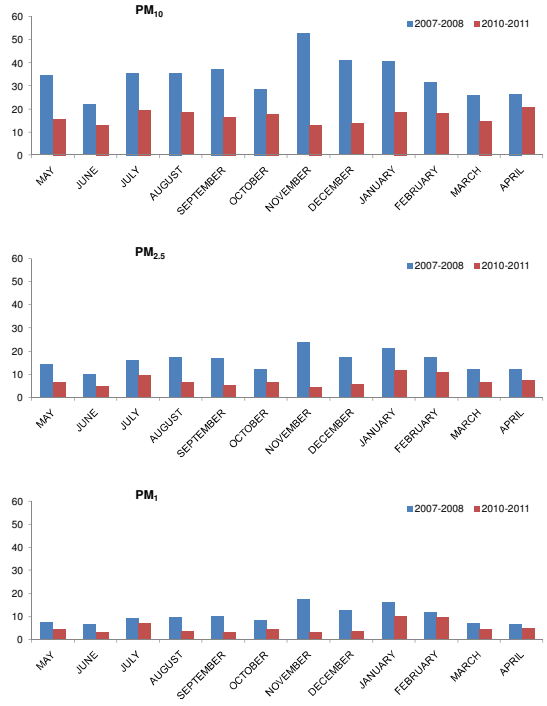

Figure 1. PM_{10}, $PM_{2.5}$ and PM_1 concentrations ($\mu g/m^3$) in both study periods.

This work was supported by the University of Alicante, the *Subprograma Torres Quevedo* (PTQ-10-03470) and the CGL2009-08036 (PASSE) project.

Santacatalina, M., Reche, C., Minguillón, M. C., Escrig, A., Sanfelix, V., Carratalá, A., Nicolás, J. F., Yubero, E., Crespo, J., Alastuey, A., Monfort, E., Miró, J. V. and Querol, X. (2010) *Sci. Total Environ.* 408 (21): 4999-5009.

Galindo, N., Yubero, E., Nicolás, J. F., Crespo, J., Pastor, C., Carratalá, A. and Santacatalina, M. (2011) *Atmos. Environ.* 45 (12): 2043-2049.

Emission measurement of PM size distribution from road wear

M. Maasikmets[1, 2], E. Teinemaa[1], T. Arumäe[1]

[1]Estonian Environmental Research Centre (EERC), Marja 4d, 10617Tallinn, Estonia; [2]Estonian University of Life Science (EULC), Institute of Agricultural and Environmental Sciences, Kreutzwaldi 5, 51014 Tartu, Estonia
Keywords: ELPI, road dust, resuspension, SEM.
Presenting author email: marek.maasikmets@klab.ee

In most developed countries, exhaust emissions from vehicles are controlled by legislation and therefore are expected to decrease drastically in forthcoming years. Non-exhaust emissions are more difficult to address and even zero emission vehicles will contribute to non-exhaust emissions. Non-exhaust emissions include particles from brake wear, tyre wear, road surface abrasion and resuspension in the wake of passing traffic. (Thorpe & Harrison, 2008). Suspended road dust will remain a problem because of an increasing number of vehicles in urban and rural areas. Only few real-world measurements of road dust resuspension have been performed to date. There is still a knowledge gap regarding the dominant mechanisms leading to road dust emissions, although resuspension of surface particle loading obviously plays an important role. (Pirjola et al. 2010). In practice, quantification of road dust emissions is complicated because of the many different factors that might need to be controlled —vehicle type and speed, tire type, pavement type and conditions, the use of road salt and sand (Hussein et al. 2008).

In current study the mobile measurement system was used to quantify the relative importance of road PM emission and suspension of accumulated dust versus direct pavement wear, tire type (studded and summer), pavement type, and vehicle speed. Measurements were performed during March-October on selected roads with different pavements and traffic conditions in Estonia. Particle number concentration and size distribution from 40 nm to 10 µm with 1-sec time resolution were measured by ELPI (Electrical low pressure impactor, Dekati Ltd.), behind the left rear tire with the sampling rate of 29.25 l/min. The minimum detection level at 1 stage for the mass concentration is 0.01 µg/m^3 and for the number concentration 142 1/cm^3. The upper concentration limit at 13 stage for the mass concentration is 8269 mg/m^3 and for the number concentration 2.7E+04 1/cm^3. PM samples on impactor plates were also analysed by SEM (scanning electron microscopy, Zeiss EVO MA15 with Inca EDS) technique for chemical composition and morphology.

Results

The initial data does not show very clear relationship between the vehicle speed and total PM emitted. With certain fractions there is quite strong correlation between emission and vehicle speed. Humidity of the road surface had strong implication on the PM emissions. Pavement composition has significant impact to the road wear and therefore PM emission.

The SEM chemical composition analysis of the PM fractions shows that the PM8.17 fraction contains mainly Si (36.79 %) and Ca (8.90 %), the PM2.5 fraction contains mainly Si (38.75%), Fe (19.20%), Cr (11.29%), K (3.34%) and Ca (2.36%) and in PM0.04 fraction mainly Si (32.30%), Ca (13.14%), Mg (6.65%) and Fe (5.47%) was detected.

Better characterization of road composition on selected sections before each measurement is needed. Measurement techniques and setup of the measurements is necessary to modify further to identify and subtract background levels including concentration spikes generated by passing cars and contribution of the exhaust emissions of own vehicle.

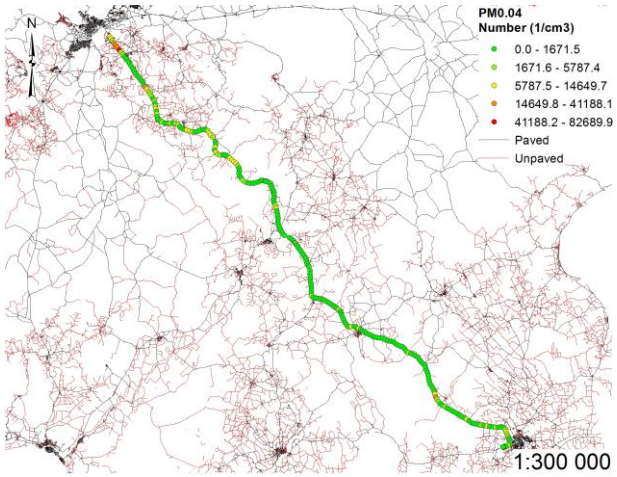

Figure 1. PM0.04 concentration (1/cm^3) along the Tallinn-Tartu road (186 km) during spring campaign in 2011.

Hussein, T., Johansson, C., Karlsson, H., Hansson, H.C. 2008. Factors affecting non-tailpipe aerosol particle emissions from paved roads: On-road measurements in Stockholm, Sweden. Atmospheric Environment. 688–702.

Pirjola, L., Johansson, C., Kupiainen, K., Stojiljkovic, A., Karlsson, H., Hussein, T. 2010. Road Dust Emissions from Paved Roads Measured Using Different Mobile Systems. Journal of the Air & Waste Management Association. 1422-1433.

Thorpe, A., Harrison, R.M. 2008. Sources and properties of non-exhaust particulate matter from road traffic: A review. Science of the total Environment. 270-282

PM_{10} sampling inlets comparison: EPA vs EU

P. Panteliadis, H.J.P.Helmink, P.C.Koopman, M.Hoonhout, D.de Jonge and J.H.Visser

Department of Air quality, Public Health Service Amsterdam, 1018WT, The Netherlands
Keywords: PM10, ambient air sampling inlet, low volume sampler, continuous particulate monitor
Presenting author email: ppanteliadis@ggd.amsterdam.nl

Uncommon deviations were observed between the continuous particulate monitor BAM (Met One instruments Inc, Oregon, USA) and the reference PM10 KFG/LVS sampler (Comde-Derenda GmbH, Stanhsdorf, Germany) during measurements at monitoring station Reijndersweg; located near the coastline of North Holland, at the west side fence of a 750 hectare steel production plant. The equivalence criteria between the continuous and the European reference, EN 12341 (1999) compliant method were met for 2010 despite the unexpected deviations. However, a greater, mainly slope, correction, had to be applied in the results of Reijndersweg monitoring station in comparison to other locations of the monitoring network of the Province of North Holland and Amsterdam.

A thorough investigation of monitors and samplers, including equipment exchange at the Reijndersweg monitoring station was initiated in response to the previously mentioned findings. Yet, the deviations between the two methods were not resolved.

In October and November 2011 two field comparisons of parallel measurements were performed at Reijndersweg with the use of the following sampling equipment:

First campaign (8-10-2011 / 26-10-2011):
- BAM with EPA PM10 inlet **(1)**
- TEOM 50°C EPA PM10 inlet **(2)**
- Derenda LVS with EU PM10 inlet 2,3 m^3/h **(3)**
- Derenda LVS with EPA PM10 inlet at 1 m^3/h **(4)**

Second campaign (28-10-2011 / 26-11-2011):
- BAM with EU Digitel 10/01/00 inlet **(5)**
- TEOM 50°C with EPA PM10 inlet **(2)**
- LVS with EU PM10 inlet 2,3 m^3/h **(3)**
- LVS with EPA PM10 inlet at 1 m^3/h **(4)**

During the first campaign, a Derenda LVS was connected to an EPA (BAM BX802) sampling inlet with the use of a special adapter. The actual flow of the LVS was lowered to 1 m^3/h **(4)** and showed a great match with the BAM-EPA inlet combination **(1)**. Secondly, the equivalence between TEOM **(2)** and LVS-BAM **(4),** after slope and intercept correction, was just below 25%, which is the limit value for the equivalence test. Finally, all reference measurements according to EN12341 **(3)** showed significantly lower results when compared to the LVS-EPA **(4)**.

Throughout the second campaign a Digitel (10/01/00) PM10 sampling inlet (1 m^3/h) was mounted on the BAM with use of a special designed adapter **(5)**, which showed good similarity with the reference method **(3).** The LVS-EPA **(4)** combination seemed to overestimate all daily-averaged PM10 concentrations. Indicative results of the second campaign are shown in Figure 1.

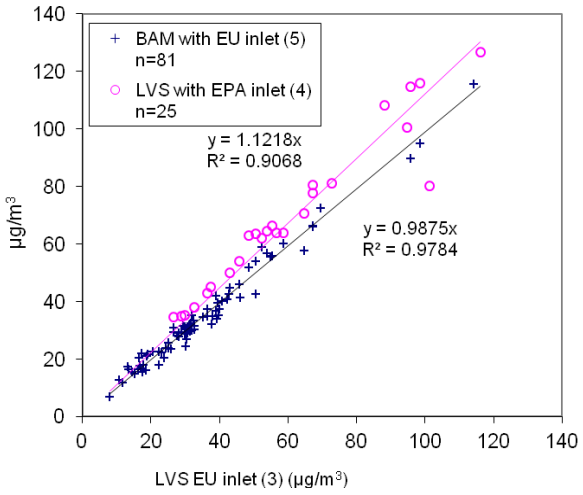

Figure 1. Comparison of Derenda LVS with EU inlet **(3)** vs BAM with EU inlet **(5)** and Derenda LVS with EPA inlet **(4)**.

Based on the limited dataset of the two campaigns, it can be concluded that significant deviations of PM10 measurements may occur due to specification differences between EPA and EU sampling inlets, in contradiction with TUEV report 2402 2605 – 2 (2000). The design of the Digitel PM10 inlet, besides the dimensional adaptation to the 1 m^3/h flow, is similar to the LVS Derenda, in accordance with EN12341 (1999). The BAM-Digitel combination can result to a significant improvement of both random and systematic deviation from the reference method, as described in EN 12341 (1999).

Extended research in additional locations, including PM2.5 sampling inlets has started in January and will conclude in April.

1. **TUEV Report 2402 2605 – 2 (2000).** *Comparability test according to DIN EN 12341 of a PM10 – Immission monitor Type described: SPM immission monitor FH 62 I-R using the PM10–sampling inlets-PM10 ESM and --- -DPM 10100*

2. **EN 12341 (1999)**. *Determination of the PM10 fraction of suspended particulate matter*. CEN/TC 264, 94/67/EG.

Source apportionment and sector analysis of organic aerosol in southern Sweden

J. Genberg[1], M. Sporre[1] and E. Swietlicki[1]

[1]Department of Physics, Lund University, Lund, Sweden
Keywords: Organic aerosols, Trajectory, Source apportionment.
Presenting author email: johan.genberg@nuclear.lu.se

The sources of organic aerosols have been extensively studied for several years since the data is valuable when verifying atmospheric models. In a newly published article a one-year source apportionment of organic aerosol from Vavihill in southern Sweden was presented (Genberg et al. 2011). The results showed significant differences in source contribution depending on the season of the sample. However, also within the seasons the sources varied. The low temporal resolution of the filter sampling did not permit a further analysis of the individual samples depending on air mass trajectories.

In this study a similar methodology has been used but filters where collected for 72 hours instead of one week. Four periods of constant air mass origin for the individual samples were found and used in this study.

The OC/EC results and temperature for the first interval is shown in figure 1a. The first period had air masses from the north and the daily mean temperature fluctuating between -10 and +5 °C. During the second period the air originated from the eastern sector and the daily mean temperature was stable at -2 °C for most of the period. The mean concentration from the four aerosol samples from the northern sector are 1.1 and 0.18 µg/m^3 for OC and EC. For the six east-samples the corresponding values are 2.59 and 0.33 µg/m^3.

The second interval is from the autumn months of October and November and the temperature is between -0 and +10 °C. During the first period the mean OC and EC concentrations are 6.2 and 0.61 µg/m^3. When the air mass origin shifts to the southern sector the OC and EC concentrations are 1.75 and 0.33 µg/m^3.

For these four investigated period both OC and EC are raised when the origin of the air mass changes from north or south to east. The results are consistent with what has been shown in Kristensson et al. (2008) where it was stated that air reaching Vavihill from the east contained more particles whereas the air is generally clean when originating from the north.

The results will be complemented with radiocarbon analyses and chemical tracers like anhydrosugars and several organic acids. This will enable a source apportionment with regard to the origin of the air masses.

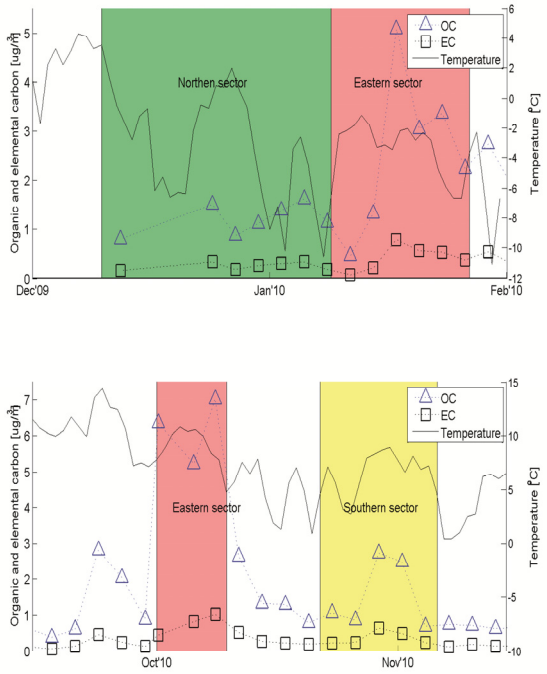

Figure 1. OC and EC results for the two studied intervals, both containing two periods with different wind directions. 1a shows results from December'09 to February'10. 1b shows results from mid-September'10 to mid-November'10

Genberg, J. Hyder, M. Stenström, K. Bergström, R. Simpson, D. Fors, E. Jönsson, J. Å. and Swietlicki, E. (2011), *Atmos. Chem. Phys.*, **11**, 11387-11400.

Kristensson, A. Dal Maso, M. Swietlicki, E. Hussein, T. Zhou, J. Kerminen, V. M. and Kulmala, M. *Tellus B*, **60**, 330-344

PM2.5 PCA-APCS Source Apportionment of a site monitored near a waste incinerator plant located in Bologna Area

M. Rossi[1], L. Pasti[2]

[1]Arpa Emilia-Romagna, Rimini, 47923, Italy
[2]Department of Chemistry, University of Ferrara, Ferrara, 44123, Italy
Keywords: Source apportionment, air quality, incinerator
Presenting author email: marossi@arpa.emr.it

Receptor modelling is one of the application of multivariate analysis dealing with the identification and quantitative apportionment of air pollutants to their potential sources (Hopke et al., 2006).

Various statistical multivariate models including principal component analysis-absolute principal component scores (PCA-APCS) have been proposed to identify and to ascertain the contribution of different sources to monitored ambient concentrations. Many studies have been reported on the apportionment of the PM, but most of them are focused only on the inorganic species of PM10, and there are only few works dealing with the apportionment of PM2.5 monitored near incinerator plants (Hopke et al., 2006). In this work the amount and distribution of both inorganic and organic components of PM2.5 were investigated and PCA-APCS method applied for source apportionment. The daily PM2.5 samples were collected in a monitoring station placed in the maximum impact area of the incinerator fallout previously determined by ADMS-Urban, a gaussian modified dispersion model.

Two extensive monitoring campaigns were performed: the first one was held in summer 2008 and the second one in winter 2009. The plant under study is located in a suburban-farming area, less than 10 km away from northeast of Bologna (Italy), in the southeast of Po Valley, which is a well known atmospheric polluted critical area.

PCA is generally employed to analyze the structure of multivariate datasets. PCA selects a smaller number of independent factors - starting from a large number of probably correlated variables - that can be used to explain the main sources of variance in the data. The factors are linear combinations of original variables.

APCS estimates the sources by employing the scores for each chemical species and for each day.

Results

Different sets of variables were selected. In the following the results referring to one of these sets are reported :

- Metals: Ni , Mn, Cd, Al, Fe, Sb, As;
- Inorganic ions: NH4+, K+ , Cl-, NO2-, NO3-, SO42-;
- Total Carbon (TC) e water solubile organic carbon (WSOC);
- Alcane: C29;
- PAHs: benzo[g,h,i]perylene, pyrene, fluoranthene

PCA-APCS method was applied and a 4 factors model was obtained. The predicted model seems to fit well the experimental data as can be seen in Figure 1. The adjusted square regression coefficient was 0.909. The 95% intervals of confidence of fitting parameters include their theoretical values of 1 for the slope and 0 for the intercept. The SSE is 1669 and RMSE is 4.848.

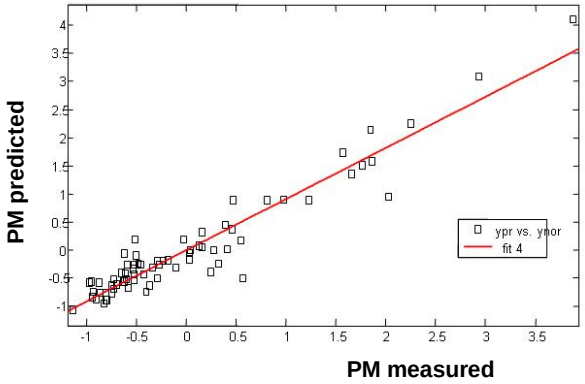

Figure 1. PM2.5 predicted by 4-factors PCA_APCS model vs. PM2.5 measured.

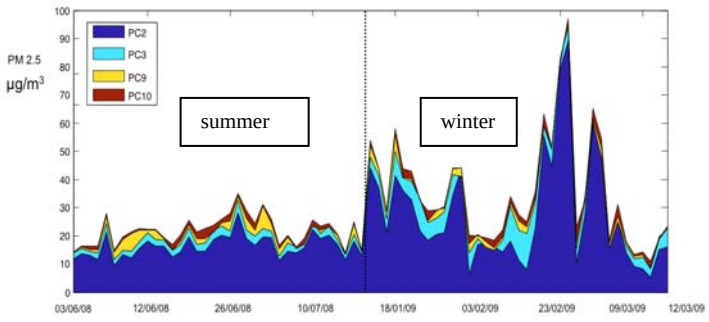

Figure 2. Temporal factors contribution to PM2.5 model.

The four factors shown in Fig.2 were associated with:
-Regional and secondary aerosol
-Vehicular emissions
-Biomass and/or secondary oxidized organic spiecies

This work was supported by Regione Emilia-Romagna and was conducted as part of the «Moniter Project». http://www.moniter.it

Hopke, P.K., Ito, K., Mar, T., Christensen, W.F., Eatough, D.J., Henry, R.C., Kim, E., Laden, F., Lall, R., Larson, T.V., Liu, H., Neas, L., Pinto, J., Stolzel, M., Suh, H., Paatero, P., Thurston, G.D., J. Expo. Sci. Env. Epid, 16, 275–286. 2006. *Intercomparison of source apportionment results*

Source apportionment of PM_1 aerosols sampled with an HR-ToF-AMS at an urban background site and an industrialized coastal site using PMF

V. Crenn[1,2], V. Riffault[1,2], S. Sauvage[1,2] and D. Petitprez[1,3]

[1]Université Lille Nord de France, F-59000, Lille, France
[2]Département Chimie et Environnement, Ecole des Mines de Douai, F-59508, Douai, France
[3]Laboratoire de Physicochimie des Processus de Combustion et de l'Atmosphère (PC2A), UMR CNRS 8522, F-59655, Villeneuve d'Ascq, France
Keywords: Submicron particles, Urban aerosols, Coastal aerosols, Industrial aerosols.
Corresponding author email: veronique.riffault@mines-douai.fr
Presenting author email: denis.petitprez@univ-lille1.fr

Fine particles have a major impact on human health due to their ability to penetrate deeper into the lungs, as well as on the Earth's climate through both direct and indirect climate forcing (Penner et al., 2006). French emission inventories indicate that in Northern France industrial activities could be responsible for as much as 40% of the $PM_{2.5}$ concentrations, while urban sources like traffic and residential heating correspond to 16 and 24%, respectively, of the total 17,522 tons emitted annually on average (CITEPA 2005).

Field campaigns have been conducted at two sites located in Douai and Grande-Synthe, Northern France and during two seasons to measure real-time mass concentrations, diurnal trends and size-resolved average chemical composition of the non-refractory submicron aerosols (NR-PM_1) by a High Resolution Time-of-Flight Aerosol Mass Spectrometer (HR-ToF-AMS). Offline chemical analyses were also performed, and result comparison is presented in a companion abstract.

Figure 1 shows the time series of the chemical species measured by HR-ToF-AMS and their contribution to the total mass of NR-PM_1 in Douai in winter. Nitrates and organics were on average the dominant species (accounting each for ~ 1/3 of the total mass), followed by ammonium (17%), sulfates (13%) and chlorides (2%). A similar work has been realized for each site, highlighting significant concentration differences between sampling sites and periods.

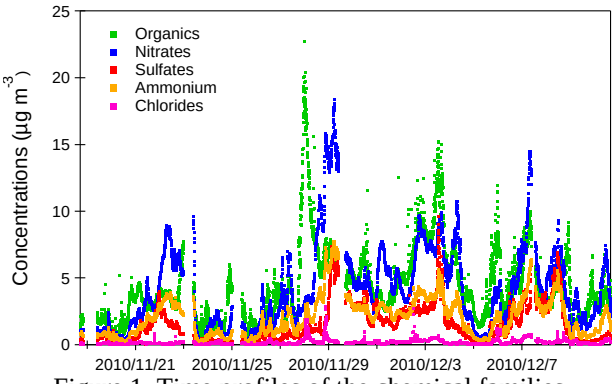

Figure 1. Time profiles of the chemical families measured by HR-ToF-AMS and their contribution to the total mass of NR-PM_1 in Douai in winter.

The HR-ToF-AMS has become a powerful tool for aerosol source apportionment (Baltensperger and Prévôt, 2008). Positive Matrix Factorization (PMF, version 3, Paatero and Tapper (1994)) can be applied to AMS data (Ulbrich *et al.* (2009)) to identify profiles related to emission sources or aerosol types, such as Hydrocarbon-like Organic Aerosol (HOA), Oxygenated Organic Aerosol (OOA), Biomass Burning Organic aerosol (BBOA) (Lanz *et al.*, 2007), or Cooking Organic Aerosol (COA) (Allan *et al.*, 2010). This approach has been applied to our HR-AMS data for all campaigns. Results will be presented and discussed in details.

Our laboratory participates in the Research Institute of Industrial Environment (IRENI) which is financed by the Communauté Urbaine de Dunkerque, the Nord-Pas de Calais Regional Council, the French Ministry of Education and Research, the CNRS and European funds (FEDER).

Allan, J.D., Williams, P.I., Morgan, W.T., Martin, C.L., Flynn, M.J., Lee, J., Nemitz, E., Phillips, G.J., Gallagher, M.W. and Coe, H. (2010) *Atmos. Chem. Phys.* **10,** 647-668.

Baltensperger, U and Prévôt, A.S.H. (2008). *Anal. and Bioanal. Chem.* **390,** 277-280.

CITEPA (2005) Emissions dans l'Air en France. Régions de la Métropole.

Lanz, V.A., Alfarra, M.R., Baltensperger, U., Buchmann, B., Hueglin, C. and Prévôt, A.S.H. (2007) *Atmos. Chem. Phys.* **7,** 1503-1522

Paatero, P. and Tapper, U. (1994) *Environmetrics* **5,** 111-126.

Penner, J.E., Quaas, J., Storelvmo, T., Takemura, T., Boucher, O., Guo, H., Kirkevâg, A., Kristjansson, J.E. and Seland, O. (2006) *Atmos. Chem. Phys.* **6,** 3391-3405.

Ulbrich, I.M., Canagaratna, M.R., Zhang, Q., Worsnop, D.R. and Jimenez, J.L. (2009) *Atmos. Chem. Phys.* **9,** 2891–2918.

The effect of local heating on indoor and outdoor air quality in a rural settlement

M. Braniš[1] and J. Kozáková[1]

[1] Charles University in Prague, Faculty of Science, Institute for Environmental Studies, Albertov 6, 128 43 Prague 2, Czech Republic

Keywords: air quality, indoor air quality, PM_{10}, $PM_{2.5}$, local heating, rural settlement

Presenting author email: brains@natur.cuni.cz

There is an increasing evidence that use of solid fuels for local heating significantly affects air quality of rural settlements. Particulate matter concentrations increase namely during winter inversions and/or in deep valleys *(Hellén et al., 2008, Caserini et al., 2009)*. It has also been documented that under natural ventilation conditions indoor air quality is influenced by infiltration of the outdoor air. *Koutrakis et al., 1991)* and that indoor air is significantly affected by indoor activities, including heating (He et al., 2004). The aim of the study was to characterize outdoor and indoor air quality in a small settlement in the Czech Republic and ascertain to what extent the indoor air is affected by infiltration from outside and by human activity (including heating) taking place indoors.

Concentrations of size-resolved PM were monitored by a small Personal Cascade Impactor Sampler (PCIS) during two winter and one summer seasons in a small village situated in West Bohemia. Continuous concentrations of $PM_{2.5}$ were measured in parallel by a photometer DustTrak. Basic meteorological parameters (temperature, relative humidity, wind velocity, wind direction, precipitation and sun radiation) were monitored as well. Presence of persons and their activities in the house were recorded in a diary.

The average PM_{10} concentrations in the village were higher than average PM_{10} concentration in the nearby town. The summer average PM_{10} concentrations in the village were lower than those in the town (15.5µg.m^{-3} vs 17. µg.m^{-3}) while the winter PM_{10} concentrations in the village were significantly higher (31.1µg.m^{-3} vs 24.3µg.m^{-3}). The average indoor concentrations (PM_{10} and $PM_{2.5}$) were lower in the summer (9.6µg.m^{-3} vs 8.3µg.m^{-3}) than in the winter season (24.0µg.m^{-3} vs 20.7µg.m^{-3}).

The presence of people indoors resulted in indoor $PM_{2.5}$ concentrations higher than outdoors (I/O ratio 1.41). In the absence of people the $PM_{2.5}$ concentrations as well as the I/O ratio (0.55) dropped down. Fig. 1 shows size resolved mass concentrations of aerosol in different microenvironments and situations. Presence of people caused increase in concentrations of quasi-ultrafine particles (< 0.25µm) presumably due to heating and coarse particles (10-2.5µm) due to resuspension. Regarding ambient PM levels the highest PM_{10} and $PM_{2.5}$ concentrations were recorded during low temperature and low wind velocity periods.

The PM_{10} concentrations in the village highly correlated with those from the nearest town during the winter season (0.92). The correlation dropped to 0.67 during the summer (Fig. 2). Analysis of wind direction showed that the town emissions affected the village levels only exceptionally. We conclude that the major source of pollution in the village is not the transport from the nearest town but local heating of houses burning wood and coal in stoves.

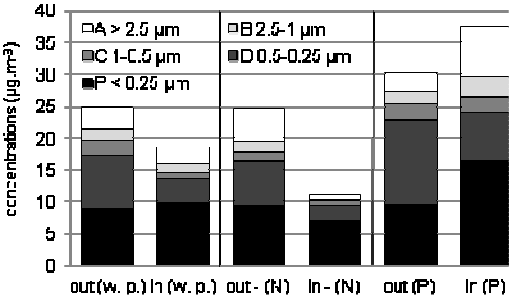

Figure 1. Size resolved mass concentrations of aerosol in different microenvironments (out-outdoor; in-indoor; w.p. - whole period; N - without people; P - with people.

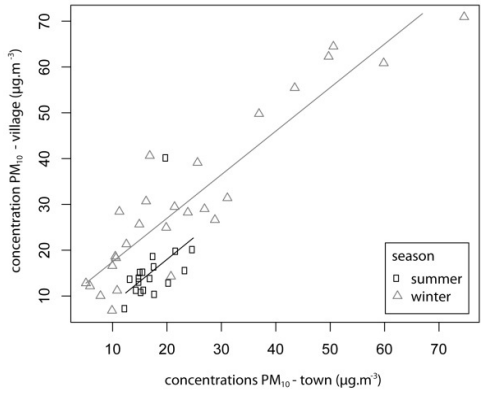

Figure 2. The association between PM_{10} concentrations in the village and the town in summer and in winter.

This work was supported by Ministry of Education, Youth and Sports of the Czech Republic under program NPV II, project No. 2B08077 INAIR.

Koutrakis, P., Brauer, M., Briggs, S.L.K. Leaderer, B.P. (1991) *Environ. Health Perspect.* **95**: 23-28.

Caserini S., Livio S., Giugliano M., Grosso M., Rigamonti, L. (2010) *Biomass and Bioenergy* **34**:474-482.

He, C.R., Morawska, L.D., Hitchins, J., Gilbert, D. (2004) *Atmos. Environ*. **21**: 3405-3415

Hellén, H., Hakola, H., Haaparanta, S., Pietarila, H., Kauhaniemi, M. (2008) *Sci. Tot. Environ*. 393:283-290.

Origin of low-molecular-weight mono and dicarboxylic acids in urban, industrial and suburban environments

G.A. Blanco[1], M.I. Turnes-Carou[2], P. López-Mahía[1,2], S Muniategui-Lorenzo[2] and D. Prada-Rodríguez[1,2]

[1]Instituto Universitario de Medio Ambiente (IUMA), Universidade da Coruña, Oleiros, A Coruña, 15179, Spain
[2]Department of Analytical Chemistry, Universidade da Coruña, A Coruña, 15008, Spain
Keywords: Organic acids, Source identification, Principal component analysis, Urban areas, Industrial aerosols.
Presenting author email: purmahia@udc.es

Water soluble ionic compounds represent always a significant part of the atmospheric particulate matter mass. The major compounds in this fraction are inorganic anions (chloride, nitrate and sulphate), inorganic cations (ammonium, potassium, calcium, magnesium and sodium) and a complex and poorly characterized mixture of organic compounds, among which mono and dicarboxylic acids are the most commonly identified species (Yang 2008). The main sources and formation pathways for inorganic compounds are well known. In contrast, the origin of dicarboxylic acids and variables affecting their levels remain unclear in many respects (Ho, 2011).

In this work we present the data obtained from the analysis of inorganic (Cl^-, NO^{3-}, SO_4^{2-}, NH_4^+, Na^+, Ca^{2+} ,Mg^{2+} and K^+) and organic (oxalic, malonic, succinic, malic, acetic and formic acids) in two PM fractions (PM2.5 and PM10) and three different environments (urban, suburban and industrial) for 45 days, comprising a total of 270 samples. The three sampling points were located in the surroundings of the city of A Coruña (Spain). The data obtained was employed to identify the origins of mono and dicarboxylic acids in the three environments. For this purpose, principal component analysis with Varimax rotation was employed based on the association of acids with components related to inorganic compounds sources. Although eleven mono and dicarboxylic acid were identified, only those detected in more than a 50 % of the samples were considered for origin estimation.

In every case, oxalic was the acid with higher concentration followed by malonic and succinic.

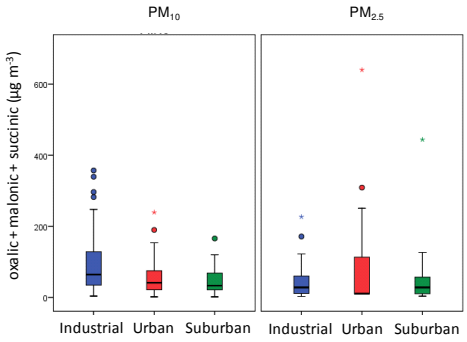

Figure 1. Distribution of major dicarboxylic acids in the three locations and two PM fractions.

As shown in figure 1, higher levels of organic acids were observed for industrial and urban environments, however, the distribution between fractions was different suggesting different formation mechanisms.

In all the locations the three main principal components were related to the three main sources of PM in this area: marine, crustal and secondary. In the suburban location a component related to biomass burning was also identified. The relation of dicarboxylic acids with these sources was employed to identify their sources.

In the industrial location, the dicarboxylic acids appear linked to secondary inorganic compounds (ammonium, nitrate and non-sea-salt sulphate) independently of the season and fraction considered, indicating a secondary origin.

In the urban location a clear distinction can be observed between cold and warm season. During winter, dicarboxylic acids show an origin independent of secondary generated compounds and the main origin can be related to direct emissions from traffic. During the warm season the contribution of photochemical generation increases and dicarboxylic acids appear related to inorganic secondary compounds.

In the suburban location dicarboxylic acids show an origin which can be interpreted as a combination of secondary formation and biomass burning.

Monocarboxylic acids present always an origin independent of the dicarboxylic and inorganic ions and are related to multiple anthropogenic and natural origins. The inclusion into the PCA of other compounds levels, which were available for the same samples (metals and organic compounds), was performed in order to clarify the origin of carboxylic acids.

This work was supported by *Dirección Xeral de Investigación, Desenvolvemento e Innovación,* (Ref. 10MSD164019PR).

Yang, L. and Lu, L. (2008) *Environ. Sci. Technol.***42 (24)** 9268-75

Ho, K. F. Ho, S. S. H. Lee, S. C. *et al.* (2011) *Atmos. Chem. Phys.* **11(5)** 2197-2208.

Modelling of particulate matter concentration at regional and local scale

P. Brotto[1], F. Cassola[1], A. Mazzino[1], T. Giannaros[2], K. Markakis[2], A. Poupkou[2], D. Melas[2] and P. Prati[1]

[1]Department of Physics & INFN, University of Genoa, Italy
[2]Aristotle University of Thessaloniki, Greece

Keywords: Shipping emissions, Chemical transport model, PM, source apportionment
Presenting author email: cassola@fisica.unige.it

Liguria is a very complex-topography region located in Northwestern Italy and consists of a narrow strip of land bordered by the Ligurian Sea, the Alps and the Apennines mountains, reaching elevations above 2000 m. Most of the population resides along the coast, where the main economic activities are concentrated as well. Environmental concerns are primarily associated with road and maritime transport, whereas industrial emissions are lower, apart from some local hot spots, typically corresponding to coal-fired power plants.

The Laboratory of Environmental Physics at the Department of Physics (DIFI) of the University of Genoa is currently involved in Transnational Action Plans projects (MED-APICE and Alcotra-AERA) aiming at the evaluation of air quality in the Liguria Region and in the urban area of Genoa, by means of numerical simulations as well as dedicated field measurement campaigns. In particular, the APICE (Common Mediterranean strategy and local practical Actions for the mitigation of Port, Industries and Cities Emissions) project is focused on the evaluation of the environmental impact of harbour activities on urban air quality and the definition of long-lasting measures and shared strategies to reduce air pollution in port cities.

In this framework, an integrated air quality forecasting system has been implemented at DIFI. Meteorological fields are obtained by the mesoscale model WRF-ARW (Skamarock et al., 2008), whereas air quality simulations are performed using the photochemical dispersion model CAMx (ENVIRON, 2010). By means of subsequent nesting procedures, meteorological and pollutant concentration fields are obtained up to resolutions of order of 1 km.

Initial and boundary conditions needed to drive WRF simulations are provided by the global model GFS, operational at NCEP (National Center for Environmental Prediction). Large-scale anthropogenic emissions data have been obtained by the Aristotle University of THessaloniki (AUTH) processing the 2005 European dataset by The Netherlands Organization (TNO) (Visschedijk et al., 2007) with the MOSESS (MOdel for the Spatial and tEmporal diStribution of emissionS) code (Markakis et al. 2011) while high-resolution (1 km) gridded emission data have been obtained from the Liguria Region inventory. Biogenic and natural emissions have been computed from WRF outputs using the AUTH NEMO (Natural Emission MOdel) model (Poupkou et al. 2010).

The analysis of available anemometric measurements from different stations suggests that favourable conditions for the pollutant transport from the harbour area towards the city are mostly encountered during the warm season, due to the onset of diurnal sea breezes, whereas during Autumn and Winter months intense northerly (offshore) winds are prevailing, thus contributing to improve air quality in the urban area. For this reason for the purposes of the APICE project we decided to choose a simulation period running from May to September 2011. In the same period, a dedicated PM monitoring campaign has been carried out in three different sites in town, providing a large amount of data to be used for source apportionment studies by means of receptor models and comparison with outputs from CAMx simulations.

In particular, PM source apportionment has been performed using the CAMx PSAT tool to investigate the impact of harbour activities, industry, residential heating and road transport. A major outcome of this analysis is the identification of the most relevant risk activities and the design of scenarios connected with possible mitigation measures and control strategies that could be adopted for a sustainable development and the improvement of urban air quality.

This work was supported by the Programme MED under the APICE grant and the Programme Alcotra under the AERA grant.

ENVIRON (2010) *User's Guide, Comprehensive Air Quality Model with Extensions (CAMx). Version 5.30*, ENVIRON International Corporation, Novato, CA.

Markakis, K., Katragkou, E., Poupkou, A., Liora, N., Giannaros, T. and Melas, D. (2011) *Environmental Policy* (submitted).

Poupkou, A., Giannaros, T., Markakis, K., Kioutsioukis, I., Curci, G., Melas, D. and Zerefos, C. (2010) *Environ. Modell. Softw.* **25**, 1845-1856.

Skamarock, W.C., Klemp, J.B., Dudhia, J., Gill, D.O., Barker, D.M., Huang, X.Z., Wang, W. and Powers, J.G. (2008) *A Description of the Advanced Research WRF Version 3*, Mesoscale and Microscale Meteorology Division, NCAR, Boulder, Colorado.

Visschedijk, A.J.H., Zandveld, P.Y.J. and Denier van der Gon, H. (2007) *High Resolution Gridded European Emission Database for the EU Integrate Project GEMS*, TNO-report 2007-A-R0233/B.

Comparison of receptor models using synthetic organic aerosol mass spectra

H. Hagino[1], and T. Morikawa[1]

[1] Energy and Environmental Research Division, Japan Automobile Research Institute, Tsukuba, Ibaraki, 305-0822, Japan

Keywords: Aerosol mass spectrometry, Source Apportionment, PMF, CMB
Presenting author email: hhagino@jari.or.jp

The atmospheric aerosols, especially fine particles, are known to have adverse health effects on human populations. Understanding the composition of fine particles is necessary to identify their sources and to predict their effect on various atmospheric processes. Although organic aerosols are major components of the fine particles in urban atmospheres, the composition, formation mechanisms, and seasonal variation of concentrations of organic aerosols (OA) are not well understood. To study the organic aerosol source apportionment, several receptor models have been developed, such as the Chemical Mass Balance (CMB) and Positive Matrix Factorization (PMF) models. These receptor models have frequently been applied to $PM_{2.5}$ measurement for air quality management. However, few studies have applied receptor modelling to datasets of aerosol mass spectrometer (AMS). The AMS data has been used to chemically characterise the sources and evolution of OA at many worldwide (Zhang *et al*., 2007).

The CMB (CMB8J ; Hayakari and Hanaishi (2001)) and PMF (PMF2 ver4.2 ; Paatero (2000)) were demonstrated to synthetic datasets that suppose ambient organic aerosol mass spectra from two sources. Two different organic aerosol mass spectra scenarios using different sources were considered. The scenario assumed that the similar time variations occurred between diesel exhaust particles as primary organic aerosol (POA) and *m*-xylene-derived secondary organic aerosol (SOA) (Figure 1).

The time trend of PMF and CMB agree well with a good correlation. However, PMF separate out factors corresponding to POA and SOA, then two sources that made relatively uniform contributions to the synthetic dataset. In addition, PMF resolved factor profiles also have similar profile abundances. The CMB represented that the source apportionment with the POA and SOA profile has a better fit to the synthetic dataset.

Each receptor model has its strengths and weaknesses. These weaknesses include CMB might misspecify sources and have collinearity problem (Lowenthal, *et al*. 1992); for PMF, it should interpreted as sources and aerosol components. In addition, PMF might fail to separate out some factors (sources) (Brinkman *et al*., 2006).

The CMB is an ideal approache when the profiles of the emissions for all relevant sources are known and do not change with time. The more dataset from laboratory and field studies need to be analysed to evaluate the receptor models.

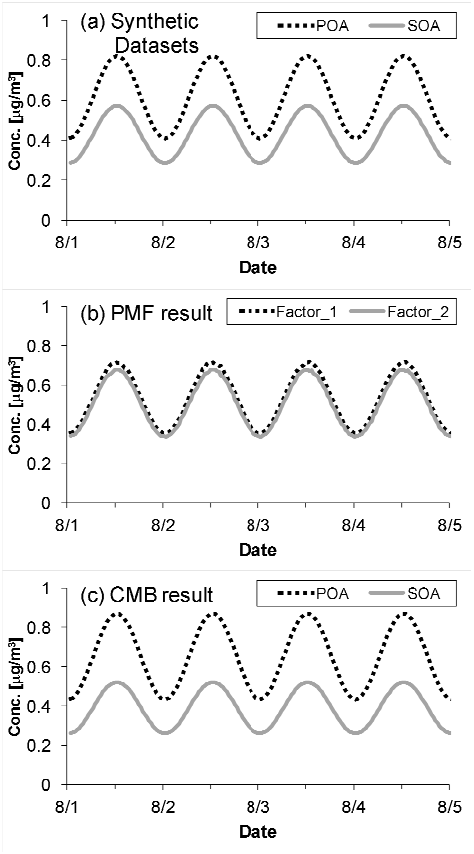

Figure 1. Time trends of synthetic dataset (a), PMF analytical result (b), and CMB analytical result (c).

This research was supported by the Environment Research and Technology Development Fund (C-1001) of the Ministry of the Environment, Japan.

Brinkman, G., Vance, G., Hannigan, M.P., and Milford, J.B. (2006) *Environ. Sci. Technol.* **40**, 1892–1901.

Hayakari, S. and Hanaishi, R.(2001) *J. Jpn. Soc. Atmos. Environ.*, **36**, 39–45.

Lowenthal, D.H., Chow, J.C., Watson, J.G., Neuroth, G.R., Robbins, R.B., Shafritz, B.P., Countess, R.J. (1992) *Atmos. Environ.* **26A**, 2341–2351.

Paatero, P. User's Guide for Positive Matrix Factorization Programs PMF2 and PMF3; University of Helsinki: Finland, 2000.

Zhang, Q. *et al*. (2007) *Geophys. Res. Lett.* **34**, L13801.

Indoor $PM_{2.5}$ Source Apportionment from Primary School in Rural Area, Portugal

N. Canha[1], S.M. Almeida[1], M.C. Freitas[1], H.T.. Wolterbeek[2], J. Cardoso[3,4], C.A. Pio[4], A. Caseiro[4]

[1]Instituto Tecnológico e Nuclear (ITN), URSN, E.N. 10, 2686-953 Sacavém, Portugal.
[2]Department of Radiation, Radionuclides and Reactors, Faculty of Applied Sciences, Delft University of Technology, Mekelweg 15, 2629 JB Delft, The Netherlands
[3]University of Cape Verde, Campus do Palmarejo, cp 279, Praia, Cape Verde
[4]Centre for Environmental and Marine Studies, University of Aveiro, 3810-193 Aveiro, Portugal
Keywords: source apportionment, indoor environment, $PM_{2.5}$, primary schools.
Presenting author email: nunocanha@itn.pt

Indoor air studies, with main focus on particulate matter, are a relevant subject nowadays, especially in environments like primary schools, where the occupants are characterized as very sensible to pollutants due to their specific physical characteristics. Due to its high penetrability and toxicity, the concern about $PM_{2.5}$ has increased and its characterization in environments like these is essential to understand the exposure level of the children.

Fig. 1 shows the primary school location (which village is characterized as a rural area).

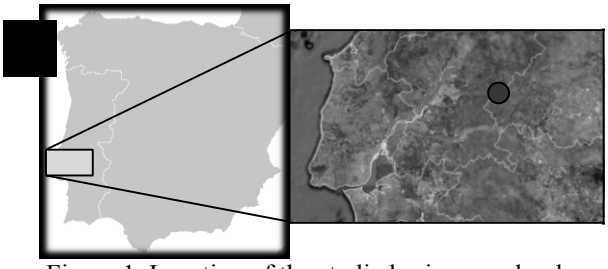

Figure 1. Location of the studied primary school.

A Partisol sequential sampler was placed inside of a classroom, where a slow combustion stove was in use for house heating (by means of wood burning), to collect $PM_{2.5}$. The sampling period was from 8 to 19 of March 2010. The sampler used Teflon^{TM} filters with a diameter of 47 mm to collect particles for the period of classes (09h-17h30) and the overnight period (17h30-09h), at an air-intake rate of 16.7 L min-1. For chemical identification, one half of the filter was analyzed by Instrumental Neutron Activation Analysis - INAA (As, Au, Br, Ce, Co, Cr, Fe, K, La, Na, Rb, Sb, Sc, Sm and Zn) and the other half was analyzed by ion chromatography for the determination of water soluble ions (Cl^-, NO_3^-, SO_4^{2-}, Na^+, NH_4^+, K^+, Mg^{2+} and Ca^{2+}).

Source apportionment was determined by Principal Component Factor Analysis (PCA) (Almeida et al., 2006) using STATISTICA software, for both types of periods.

Values of $PM_{2.5}$ concentrations above 200 $\mu g.m^{-3}$ were registered for 2 consecutive days, during classes. Mean values of $PM_{2.5}$ concentrations were 100 and 41 $\mu g.m^{-3}$ for classes and overnight periods, respectively. Table 1 shows the concentrations of the elements and soluble ions that were used for the source apportionment.

Table 1. Concentrations of the chemical elements and soluble ions determined in the $PM_{2.5}$. P. - Parameter.

P.	Concentration $ng.m^{-3}$			P.	Concentration $ng.m^{-3}$		
	Mean	Min	Max		Mean	Min	Max
As	0,92	0,15	3,75	Sc	0,27	0,01	0,98
Au	0,13	0,01	0,52	Sm	0,20	0,01	0,58
Br	4,7	2,3	7,1	Zn	20	6	42
Ce	3,8	0,7	10,4	Cl^-	253	8	658
Co	0,47	0,07	1,19	NO_3^-	1131	481	1829
Cr	10,4	0,7	40,6	SO_4^{2-}	1491	308	3461
Fe	882	124	2551	Na^+	315	15	753
K	1707	113	4986	NH_4^+	468	88	947
La	1,06	0,02	2,75	K^+	460	88	1492
Rb	8,7	2,5	18,0	Mg^{2+}	70	9	124
Sb	0,38	0,10	0,66	Ca^{2+}	600	174	1369

During classes' period, 4 factors were assessed and explained 93% of the variance. The overnight period displayed also 4 factors which explained 98% of the variance. Soil, secondary and marine aerosols, wood burn (through its fingerprint, K^+ (Canha et al., 2012)) and industry/traffic were identified as sources. The found sources differed in the 2 studied periods. The following up of this study is to determinate the sources contribution to $PM_{2.5}$ concentrations, by means of MLRA, to understand them, compare both types of sampling periods and propose mitigation measures.

This work was supported by the Fundação para a Ciência e a Tecnologia (FCT; Portugal) under research contract PTDC/SAU-ESA/65597/2006. N. Canha thanks FCT for his PhD grant (SFRH/BD/72272/2010).

Almeida, S.M., Pio, C.A., Freitas, M.C., Reis, M.A., Trancoso, M.A. (2006) *Sci. Total Environ.* 368: 663-674

Canha, N., Freitas, M.C., Almeida-Silva, M., Almeida, S.M., Dung, H.M., Dionísio, I., Cardoso, J., Pio, C.A., Caseiro, A., Verburg, T.G., Wolterbee, H.T. (2012) *J. Radioanal. Nucl. Chem.* 291(1): 83-88.

Almeida, S.M., Canha, N., Silva, A., Freitas, M.C., Pegas, P., Alves, C., Evtyugina, M., Pio, C.A. (2011) *Atmos. Environ.* 45: 7594-7599.

Characteristics of heavy metals in $PM_{2.5}$ at Fukuoka, Japan, based on daily analysis of year-round samples

N. Kaneyasu[1], A. Takami[2], K. Sato[2], S. Ymamamoto[3], Y-P. Kim[4], and I-S. Kim[4]

[1] National Institute of Advanced Industrial Science and Technology, Tsukuba 305-8569, Japan
[2] National Institute of Environmental Studies, Tsukuba 305-8506, Japan
[3] Fukuoka Institute of Health and Environmental Sciences, Dazaifu, Fukuoka 818-0135, Japan
[4] Department of Applied Chemistry, Ewha Womans University, Seoul 120-750, Korea
Keywords: $PM_{2.5}$, Heavy metals, Long-range transport, Source apportionment.
Presenting author email: kane.n@aist.go.jp

The emission rates of particulate matters and their precursory gases originating in East Asia are expected to increase in the first half of this century, and there is much concern about their influence on Japan, which is located on the leeward side of the westerlies. From this viewpoint, we measured the mass concentrations and chemical compositions of $PM_{2.5}$ in the upwind areas of Japan, including urban areas such as Fukuoka City (population 1,400,000; representative metropolis in western Japan), and isolated islands such as Fukue Island (population 40,000; located 190 km west of Fukuoka). The present study analyzes the behavior and seasonal characteristics of the metallic components in $PM_{2.5}$, which are important in view of their health effects and their use as tracers of emission sources.

At Fukuoka, year-round $PM_{2.5}$ filter samples are collected daily on quartz-fiber filters using a high-volume air sampler equipped with a $PM_{2.5}$ separation impactor. Metallic components are determined by ICP-AES after dissolution into HF-HNO_3-H_2O_2 mixed solution. $PM_{2.5}$ mass concentrations are monitored by TEOM 1400a. Figure 1 shows a comparison of the monthly averaged $PM_{2.5}$ concentrations in Fukuoka City, Nagasaki City (population: 300,000; located 100 km southwest of Fukuoka), and Fukue Island. The similarity in the concentrations and temporal variations of $PM_{2.5}$ suggests that even in a city as large as Fukuoka, the $PM_{2.5}$ mass concentration throughout the year is dominated by regional air pollution rather than domestic urban air pollution.

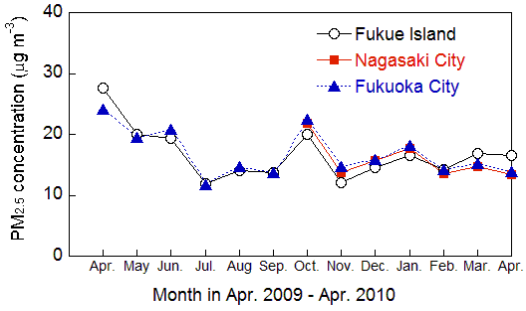

Figure 1 Time series of monthly average $PM_{2.5}$ concentrations in Fukue Island, Fukuoka City, and Nagasaki City.

Figure 2 shows the daily concentrations of metallic components in $PM_{2.5}$ at Fukuoka (Dazaifu district). Most metallic components show synchronous fluctuations, except V, Fe, and Al. The drastic increases in Fe and Al concentrations are apparently caused by the occurrence of Asian Dust (Kosa) events. The intervals of fluctuations for other metallic components, i.e., Pb, Zn, Mn, and Cd, is about 3 to 5 days, and the drastic increase in these concentrations corresponds to the passage of cold fronts. The relatively long-term (3 to 4 days) increase in concentrations, especially for Zn in spring, is accompanied by the passage of migrating anticyclones. This suggests that the increase in the Pb, Mn, and Cd concentrations is mainly caused by the long-range transported pollutants from the Asian continent and the increase in Zn concentration can be attributed to both domestic and long-range transported pollutants. The results of source apportionment analysis for the metallic components will be discussed in the presentation.

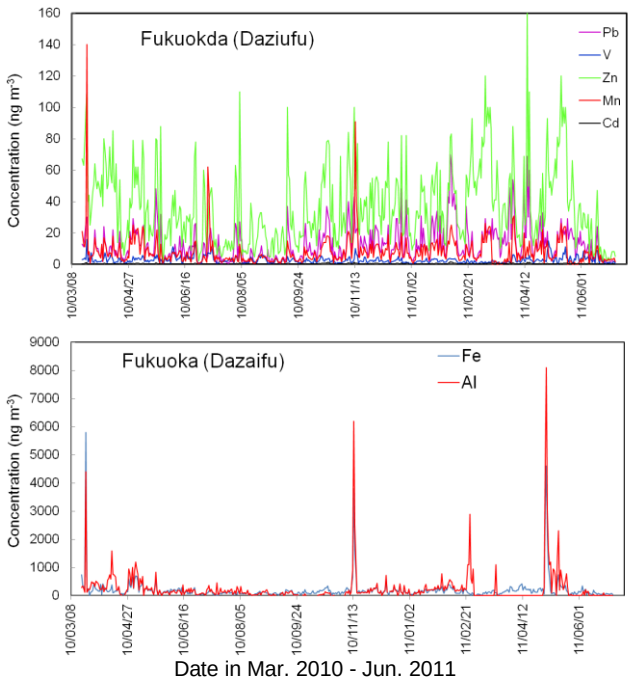

Figure 2 Daily concentrations of metallic components in $PM_{2.5}$ at Dazaifu district of Fukuoka. (Top) Concentrations of Pb, V, Zn, Mn, and Cd. (Bottom) Concentrations of Fe and Al.

This work was supported by a Grant-in-Aid for Scientific Research on Innovative Areas funded by the Ministry of Education, Culture, Sports, Science and Technology (MEXT), Japan.

An application of positive matrix factorization and cluster analysis to discriminate the sources of PM_{10} in a coastal site near Venice (Italy)

M. Masiol[1], S. Squizzato[1], D. Ceccato[2], G. Rampazzo[1], B. Pavoni[1]

[1]Dip. Scienze Ambientali, Informatica e Statistica, Università Ca' Foscari Venezia, Venice, 30123, Italy
[2]Dip. Fisica "Galileo Galilei", Università di Padova
Keywords: PM10, Source Apportionment, Statistical Analysis, Back trajectories.
Presenting author email: masiol@unive.it

This study combines a set of chemometric procedures for discriminating the role of weather conditions, local processes and remote contributions in determining the levels and chemical composition of airborne particulate matter. PM_{10} data were collected in a semi-rural coastal site near Venice (Italy), located on the eastern border of the Po Valley. This area is affected by worrying concentrations of several atmospheric pollutants causing a constant hazard for living inhabitants. This situation is favoured by a high level of urbanization, industries and some peculiar orographic features limiting air circulation (Rampazzo et al., 2008a;b; Squizzato et al., 2012). In particular, PM_{10}, known to be correlated to several adverse health effects, reaches levels frequently exceeding the limit and target values fixed by the European Directives.

A one year-long sampling campaign included the determination of PM_{10} mass concentration, the elemental and water soluble inorganic ions compositions using the gravimetric method, the Particle Induced X–ray Emission (PIXE) technique and ion chromatography, respectively. Finally, the concentrations of PM_{10}, 12 elements (Al, Si, K, Ca, Ti, V, Cr, Mn, Fe, Ni, Cu, Zn) and 6 ions (Cl^-, NO_3^-,SO_4^{2-}, Na^+, NH_4^+, Mg^{2+}) were determined and the relative analytical uncertainties quantified .

Seven sources were identified and apportioned using the Positive Matrix Factorization (PMF) model: sea spray, mixed combustions, pollution, aged sea salt, mineral dust, secondary sulphate and secondary nitrate. The factor profiles are reported in Figure 1.

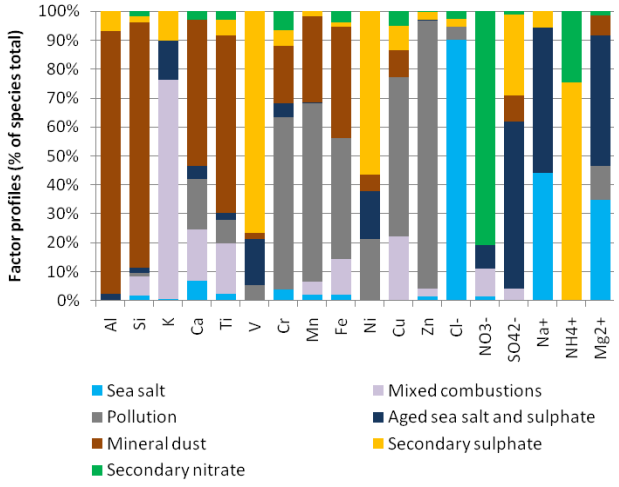

Figure 1. Factor profiles from PMF.

The relationships between PM_{10} mass, modelled source contributions and some weather parameters including solar radiation, temperature, relative humidity and precipitation were investigated. The importance of air temperature and relative humidity on secondary components, the direct relationship between sea spray and wind speed and the inverse correlation between pollution and wind speed were highlighted.

Using the approach proposed in Masiol et al. (2010), days with similar source profiles were grouped. Identified clusters were interpreted on the basis of their chemical composition, wind direction data and back-trajectories to extract further detailed information on potential source locations and possible links between meteorological conditions and PM_{10} chemical composition.

The differences in PM_{10} levels and source profiles between groups shows that the production of sea salt is strongly influenced by local winds. Differently, typical primary pollutants (i.e. combustion and pollution) increased during low wind regimes.

External contributions were investigated by using the air mass backward trajectories and by considering a forecast model analysis (ICoD-DREAM aerosol and dust maps). The increase of combustion and traffic-related pollutants was observed when air masses originated from Central and north-western Europe and the rise of secondary sulphate when air masses passed over the Po Valley. Conversely, anthropogenic contributions dropped when the origin was the Mediterranean area and Northern Europe.

The use of this approach gives detailed information on potential source locations and results may be used as a suitable instrument to design local and national air pollution control strategies.

This work was carried out using the AN2000 PIXE facility of the Legnaro laboratories of INFN, Padua (Italy).

Masiol, M., Rampazzo, G., Ceccato, D., Squizzato, S., Pavoni, B. (2010) *Chemosphere* **80**, 771-778.

Rampazzo, G., Masiol, M., Visin, F., Pavoni, B. (2008a) *Water Air Soil Pollut.* **195**, 161-176.

Rampazzo, G., Masiol, M., Visin, F., Rampado, E., Pavoni, B. (2008b). *Chemosphere* **71**, 2068-2075.

Squizzato, S., Masiol, M., Innocente, E., Pecorari, E., Rampazzo, G., Pavoni, B. (2012) *J. Aerosol Sci.* **46**, 64-76.

Source Apportionment of PM2.5 at Burnaby South and Abbotsford, British Columbia, using Positive Matrix Factorization

R. So[1], R. Vingarzan[1], S. Meyn[1], E. Dabek-Zlotorzynska[2], D. Mathieu[2], L. Ding[2], T. Dann[2], V. Celo[2], D. Wang[2]

[1]Air Quality Science Unit, Meteorological Service of Canada, Environment Canada, Vancouver, BC, Canada
[2]Analysis and Air Quality Division, Science and Technology Branch, Environment Canada, Ottawa, ON, Canada
Keywords: aerosol characterization, aerosol chemistry, receptor model, PMF
Presenting author email: Roxanne.Vingarzan@ec.gc.ca

INTRODUCTION

The Lower Fraser Valley of British Columbia is a complex airshed impacted by both urban sources from the metropolis of Vancouver and agricultural sources from adjacent agricultural areas. Although PM levels rarely exceed air quality guidelines or objectives, levels are of concern due to impacts on human health and visibility. In this study, a source apportionment analysis was performed on PM2.5 speciation data, collected at two monitoring sites. Positive Matrix Factorization (PMF) receptor modelling was employed to identify local sources and to inform airshed management efforts.

METHODOLOGY

Air quality monitoring data was collected from two stations, Burnaby South and Abbotsford, in the Lower Fraser Valley Airshed. Burnaby South is located in a suburban area bordering the eastern boundary of Vancouver, and Abbotsford is located in an agricultural-based area located 75 km east-southeast of downtown Vancouver. Both stations are part of the National Air Pollution Surveillance (NAPS) network and are run by Metro Vancouver and Environment Canada. Speciated 24-hour ambient aerosol samples were collected following a one-in-three day sampling schedule from December 2003 to December 2008.

PMF analysis was conducted using the EPA PMF3.0 software developed by the US Environmental Protection Agency. This graphical user interface employs the second version of the Multilinear Engine algorithm (Paatero, 1999) to determine the PMF solution.

Correlation analysis was applied to the PMF-resolved source contributions versus various gaseous pollutants (CO, NO, NO2, SO2, O3), individual VOCs and meteorological parameters (wind speed, relative humidity, temperature) to provide further insight into the identification of sources. Conditional Probability Function (CPF) analysis (Ashbaugh et al., 1985) was applied to resolved source contributions to estimate the likely direction of the individual sources from receptor sites.

RESULTS AND DISCUSSION

Eight and seven factor solutions were identified for Burnaby South and Abbotsford, respectively. The relative contributions of resolved factors relative to the total PM2.5 concentrations are illustrated in Table 1.

Factor	Burnaby South (%)	Abbotsford (%)
Secondary Nitrate	20	24
Secondary Sulphate	20	13
Vehicle Emission	20	21
Crustal Elements	12	16
Oil Combustion	6	9
Sea Salt	9	10
Burning	9	7
Diesel	4	-

Table 1. Contribution of resolved factors relative to total PM2.5 concentrations at Burnaby South and Abbotsford.

Overall, both sites exhibited similar source profiles and contributions. Strong seasonality was observed for burning, secondary sulphate, secondary nitrate, and oil combustion factors at both sites. Two vehicle related factors, vehicle emissions and diesel, were identified at Burnaby South, although the diesel factor only accounted for a small fraction of the total PM2.5. At the more rural location of Abbotsford, higher secondary nitrate was observed, as there was more NH_3 available to react with NOx from vehicles. Secondary sulphate was higher at Burnaby South due to the closer proximity to SO2 sources (marine and refineries).

Correlation analysis of PMF-resolved source contributions and individual VOCs helped confirm the validity of some of the sources. For example, the diesel factor was positively correlated with several diesel-related VOCs such as toluene, xylene, nonane, styrene, and decane. Significant contributions from crustal elements were identified at both sites. Conditional probability function (CPF) results identified the general direction of local sources from receptors. These included industrial, residential, agricultural, vehicle and marine vessel emissions. Other sources, such as emissions from oil refineries and marine biogenic influences were also identified. Results from studies such as this can help provide policy makers and air quality managers the information needed to develop effective air quality management plans.

REFERENCE

Ashbaugh, L.L., Malm, W.C, and Sadeh, W.Z. (1985) *Atmospheric Environment* 19: 1263-1270.

Paatero, P. (1999) *Journal of Computational and Graphical Statistics* 8 (4): 854–888.

Application of Positive Matrix Factorization to particle size distribution data from a suburban site in South East Queensland, Australia

Mark Hallas, Adrian J. Friend, Godwin A. Ayoko*

International Laboratory for Air Quality and Health, School of Chemistry, Physics and Mechanically Engineering, Queensland University of Technology, Brisbane, QLD 4001, Australia

Keywords: PMF, Source apportionment, PM.

Presenting author email: g.ayoko@qut.edu.au

The adverse effects of the size of airborne particles on human health have been well established. Therefore to facilitate the formulation of mitigating measures information that aid the understanding of the source, transport and accumulation of particles is critically required. Although extensive studies have been performed on the spatiotemporal variation of particle number concentration as a functions size distribution in indoor and outdoor in South East Queensland, there is a dearth of information on the sources of particles as a function of particle size distribution in this region (Friend et al, 2012).

The objective of the current study was to apply Positive Matrix Factorization to particle number size distribution data collected at a suburban site located at latitude -27.5441º and longitude 152.9987º on Sherwood road in Rocklea Queensland. The site was close to the Brisbane Produce Markets and Oxley Creek, and its air quality was influenced by local sources such as commercial and private vehicles, farming fields, and waterways, including the Brisbane River and Pacific Ocean to the east. Ipswich Motorway is about 2 kilometres to the east of the site, and railway lines and residential areas are also located nearby. This site was used for some of our previous air quality studies (Friend et al, 2011a and 2011b).

Particle number concentration was recorded at the site every 15 minutes from 1 September to 13 October 2009. The data obtained were pre-treated before Positive Matrix Factorisation (PMF) and other statistical analyses. This process involved the removal of obvious outliers and the grouping of the particle size data into six groups: 20-30nm, 30-50 nm, 50-70 nm, 70-100 nm, 100-200 nm and >200 nm. Subsequent analysis of the data by Positive Matrix Factorization revealed instructive details about the possible sources of the particles. Thus, four sources were identified and these are tentatively assigned as : unknown source, Traffic I, Traffic II and nucleation. These sources contributed 5.4%, 24.6%, 34.5% and 35.5% respectively to the particles at the site. The variations of the weekend/weekday, hourly and PM/AM contributions of each source were also examined, with the representative result shown in Figure 1 below. To facilitate the identification of the possible sources of the particles, meteorological information has been incorporated into the results obtained from PMF analysis.

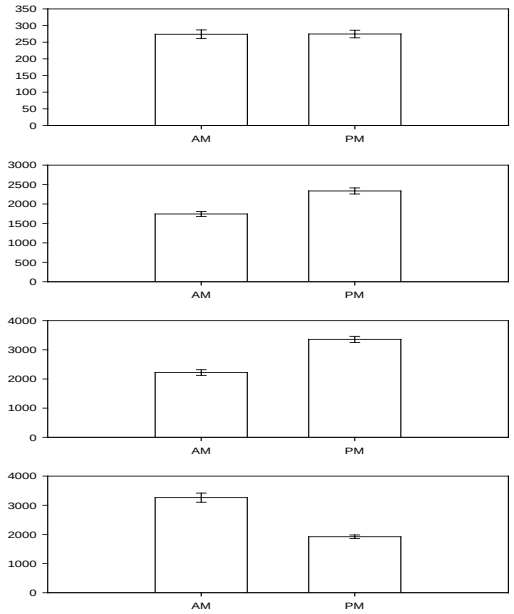

Fig 1: PM/AM source contribution for the four factors.

It was hoped that the comprehensive information provided by the overall results about the receptor site, would aid the development of appropriate measures for controlling and reducing the potential effects of air pollution in the area.

Acknowledgement

We thank the former Queensland Environmental Protection agency for the data used for this work.

Friend, A.J., Ayoko, G.A. , Jayaratne, E.R., Jamriska, M., Hopke, P.K., Morawska, L., (2012) Source apportionment of ultrafine and fine particle concentrations in Brisbane,Australia, Environmental Science and Pollution Research, DO!,10.1007/s11356-012-0803-6, Published online 19 February 2012.

Friend, A.J., Ayoko, G.A.,Elbagir, S.G.,(2011a) Source apportionment of fine particles at a suburban site in Queensland, Australia, Environmental Chemistry, 8, 163-173.

Friend A., Ayoko G. A., Stelcer, E., Cohen D., (2011b) Source Apportionment of PM2.5 at two receptor sites in Brisbane, Australia, Environmental Chemistry, 8, 569-580.

Impact of the Traffic on the Air Particulate Matter from the Urban Area of Setúbal, Portugal

S.M. Almeida[1], Alexandra V. Silva[1], A.I. Pedro[2], A. Ferreira[2]

[1]Instituto Tecnológico e Nuclear (ITN), URSN, E.N. 10, 2686-953 Sacavém, Portugal
[2]Escola Superior de Tecnologia da Saúde de Lisboa (ESTeSL), Av. D. João II, Lote 4.69.01, 1900-096 Lisboa, Portugal

Keywords: $PM_{10}/PM_{2.5}$, Urban Areas, Traffic, Source Apportionment

Presenting author email: smarta@itn.pt

At urban areas in the South Europe, PM_{10} and $PM_{2.5}$ levels frequently exceed the legislated limits as a consequence of road traffic and favourable climatic conditions for photochemical formation and dust suspension.

The main objective of this study was to characterize the Air Particulate Matter (APM), in Setúbal (Portugal) and to evaluate the impact of traffic emissions in the concentration and composition of respirable particles.

In order to evaluate the influence of the traffic emissions on atmospheric particles, sampling was performed simultaneously at two locations: one directly impacted by fresh car emissions (traffic station) and the other considered as urban background (background station) (Fig.1).

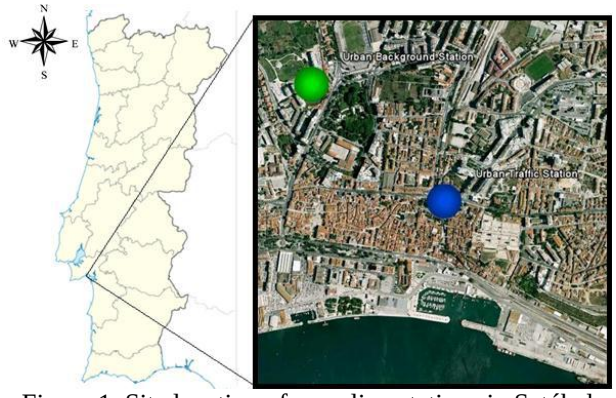

Figure 1. Site location of sampling stations in Setúbal (background and traffic station).

At each site, a Gent Sampler was used to collect $PM_{2.5}$ and $PM_{2.5-10}$. Sampling was made during two 12 hour periods, one during the day and the other during the night. The exposed filters were analysed by k_0 based Instrumental Neutron Activation Analysis (k_0-INAA) for elemental characterization. Hourly PM_{10} concentrations were also measured with beta attenuation monitors.

In order to apportion the contribution of traffic for the concentration and composition of the particles, complementary statistical methods were used: 1) Principal Component Analysis (PCA) and Multilinear Regression Analysis (MLRA) were applied; 2) comparisons between sampling stations (traffic and background) were made and 3) comparisons between different time periods (day/night and weekday/ weekend) were performed.

Figure 2 shows the average hourly PM_{10} concentrations in traffic and background stations. The ratio traffic/background (r=1.27) indicated that as expected the traffic station had higher PM_{10} concentrations than the background station.

Results show that there was an increase of PM_{10} concentration at around 9h00 to 12h00, reaching 27µg.m^{-3}, on traffic station. After that there was a decrease of the concentrations followed by a second peak with a maximum value at 22h00 that reached the value 40 µg.m^{-3} on the traffic station. This increase can be explained by the formation of a strong atmospheric stability and a low mixing layer height during this time period.

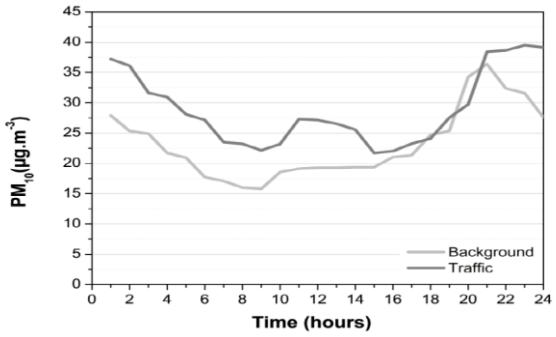

Figure 2: Hourly average PM_{10} concentrations in traffic and background stations (values in µg.m^{-3}).

Chemical analysis showed that the elements associated with traffic (Zn, Sb and As) and dust re-suspension (Fe, Sc, La and Sm) presented higher concentrations in the traffic station, during the day and in the weekdays.

PCA/MLRA results showed that the comparison between source contribution a) for roadside and urban background stations, b) for day and night periods and c) for weekday and weekend, constitutes a suitable approach to assess the contribution of the traffic to the air suspended particles.

This work was supported by the Fundação para a Ciência e Tecnologia (FCT) for the funding of the project PTDC/AAC-AMB/098825/2008 – PMfugitive - Mitigating the Environmental and Health Impacts of Particles from Fugitive Emissions.

Contribution of Residential Wood Combustion to Ambient $PM_{2.5}$ in a Suburb in Eastern Finland

T. Yli-Tuomi[1], T. Siponen[1], R.P. Taimisto[1], M. Aurela[2], K. Teinilä[2], A. Frey[2], R. Hillamo[2], J. Pekkanen[1,3], R.O. Salonen [3], T. Lanki[3]

[1]Department of Environmental Health, National Institute for Health and Welfare (THL), FI-70701, Kuopio, Finland
[2]Finnish Meteorological Institute, Air Quality Research, FI-00101, Helsinki, Finland
[3]Institute of Public Health and Clinical Nutrition, University of Eastern Finland, FI-70211, Kuopio, Finland
Keywords: biomass burning, wood smoke, $PM_{2.5}$, source apportionment.
Presenting author email: Tarja.Yli-Tuomi@thl.fi

In order to assess the exposure to and health effects of current residential wood combustion, outdoor $PM_{2.5}$ samples were collected in Kuopio, Finland, at a residential area favouring residential wood combustion during heating season (Nov 2008 - May 2009). At the same time, a cohort of 37 elderly residents was followed for home outdoor, home indoor, and personal exposure concentrations as well as health endpoints. The aim of this work was to determine the temporal variation of wood combustion related $PM_{2.5}$ at the central outdoor monitoring site.

Two EPA-WINS impactors (EPA Well Impactor Ninety-Six, BGI Inc, Waltham, MA, USA) were used to collect daily $PM_{2.5}$ samples on Teflon and quartz fibre filters. Teflon filters were used to analyse concentrations of inorganic ions, while levoglucosan, EC and OC were analysed from the quartz fibre filters.

A number of chemical species have been used as particle phase biomass burning emission tracers. A commonly used organic tracer is levoglucosan, a sugar anhydride produced during the combustion of cellulose (Simoneit, 1998). Jordan *et al* (2006) have shown that levoglucosan is stable during atmospheric transport and present at expected levels. Furthermore, levoglucosan emissions from woodstoves are relatively constant (Jordan and Seen, 2005).

Oxalate can originate from primary emissions of biomass burning (Yamasoe *et al*, 2000) and/or be formed as a secondary product by the oxidation of gaseous organic compounds (Kawamura and Ikushima, 1993). In Kuopio, the ratio of oxalate to levoglucosan increased in spring with increasing solar radiation, and thus, oxalate could not be used as a tracer of biomass burning.

Smoke from biomass burning is known to be high in potassium, but K^+ is present also in particles from other sources. Thus, K^+ is not an ideal tracer for wood combustion, but was included in the dataset for source apportionment.

EPA PMF 3.0.2.2 was applied to analyse $PM_{2.5}$ sources. Five factors were resolved and interpreted as long/regional range transported aerosol (LRT), salt, soil, traffic emissions and wood combustion. The factor associated with wood combustion was characterized by high concentrations of levoglucosan, K^+, EC and OC. This factor explained 96 % of levoglucosan and 64 % of K^+ concentrations, on average. Interestingly, over 20 % of the K^+ concentration was associated with the LRT factor.

The average ambient $PM_{2.5}$ concentration was 6 µg/m³ of which wood combustion related particles, $PM_{2.5wood,}$ composed 23 %. Concentration of $PM_{2.5wood}$ varied from 0 to 5 µg/m³ during the heating season (Fig.1). Correlation between outdoor temperature and $PM_{2.5wood}$ was only moderate (r= -0.36), possibly because wood smoke was emitted also from sauna stoves.

A remarkable portion of ambient $PM_{2.5}$ was associated to residential wood combustion. Although the concentrations were low, the results can be used in epidemiological time series study to assess the health effects.

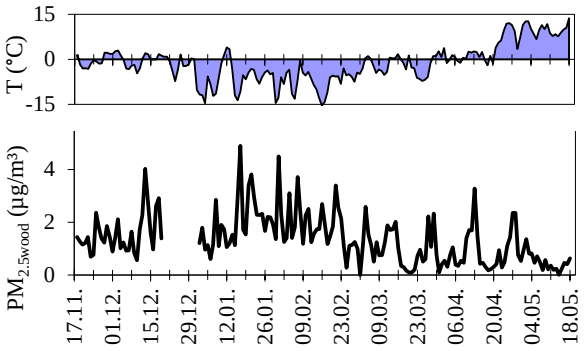

Figure 1. Temporal variation of outdoor temperature and wood combustion related $PM_{2.5}$ in a residential area in Kuopio.

This work was supported by Academy of Finland Contract No: 10155 and intramural funding from THL.

Jordan, T.B. and Seen, A.J. (2005) *Atmospheric Environment*, 39, 3601-3610.

Jordan, T.B., Seen, A.J. and Jacobsen, G.E. (2006) *Atmospheric Environment*, 40, 5316-5321.

Kawamura, K. and Ikushima, K. (1993) *Environmental Science&Technology*, **27**, 2227-2235.

Simoneit, B.R.T. (1999) *Environmental Science and Pollution Research*, ***6****, 159-169.*

Yamasoe, M.A., Artaxo, P., Miguel, A.H., Allen, A.G. (2000) *Atmospheric Environment*, **34**, 1641–1653

Aerosol chemical characterization and source quantification in a semi-urban area of Indo-Gangetic plains

Hooda, Rakesh K[1, 2], A.-P. Hyvärinen[1], S. Gilardoni [3, a], V.P. Sharma[2],
E. Vignati[3], T.S. Panwar[2, b], Viisanen, Y.[1] and H. Lihavainen[1]

[1] Finnish Meteorological Institute, P.O.Box 503, FIN-00101 Helsinki, Finland
[2] The Energy and Resources Institute, IHC, Lodi Road, New Delhi -110003, India
[3] European Commission, Joint Research Centre, 21027 Ispra, Italy
[a] ISAC-CNR, via Gobetti 101, 40129 Bologna, [b] WWF India, Lodhi Estate, New Delhi-110003, India
Keywords: aerosol characterization, Indo-Gangetic plains

The Finnish Meteorological Institute (FMI), The Energy and Resources Institute (TERI) and Joint Research Centre (JRC) conducted aerosol mass measurements in Gual Pahari, Gurgaon, India from April 2008 to March 2009. The work belongs to the frame of the EUCAARI (European Integrated project on Aerosol Cloud Climate and Air Quality interactions) project (Kulmala et al. 2009). Chemical speciation of particulate matter of such a long-term dataset and identification & quantification of sources at a location near to "hot spot- Delhi" is of utmost importance.

Coarse ($PM_{2.5-10}$) and fine ($PM_{2.5}$) aerosols were sampled using a Dichotomous Partisol Plus 2025-D sequential air sampler, (Rupprecht & Patashnick Co., Inc. USA). Here, we present the results analysed for the fine fraction. The 24-hours weekly sampling was carried out, and filters were analyzed for water soluble ions (Cl^-, NO_3^-, SO_4^{2-}, Na^+, NH_4^+, Ca^{2+}, K^+, Mg^{2+}), OC and EC. The measurements in Gual Pahari ($28^0 43'$ North, $77^0 15'$ East, 243 m above sea level), were conducted in an open area surrounded mainly by light vegetation. The surroundings represent a semi-urban environment, Delhi is located north of the station about 25 km.

The temporal pattern of overall aerosol concentrations shows distinct variability (Hyvärinen et al. 2010). The highest concentrations were observed during the winter months (Dec to Feb) due to the low and stable boundary layer. Concentrations decreased in March-June due to increasing temperatures and a higher boundary layer. The lowest concentrations were observed during the rainy months (June to August/Sept) due to wet deposition. Similar seasonal trend was observed for OC, EC and WSIS (water soluble inorganic species) (Fig.1&2). The WSIS constituted 30% of annual average $PM_{2.5}$ with SO_4^{2-}, NH_4^+ and NO_3^- being the dominant ions followed by K^+. It is noteworthy that variability of SO_4^{2-}, NH_4^+ and NO_3^- exhibits similar pattern (Fig. 2) suggesting their dominant occurrence as $(NH_4)_2SO_4$ and NH_4NO_3 salts, the scattering aerosols in nature.

During the post-monsoon and winter periods there were high concentrations of source markers such as K^+, OC, EC, SO_4^{2-}, NH_4^+ and NO_3^-. Peaks for K^+ and OC may be due to higher biomass burning. NO_3^- is high in winters which could be due to emissions from biomass burning, vehicles and important role of meteorology. These relate to greater emissions of both primary and secondary PM precursors during winter due to the higher cooking, heating load and photo-chemistry. The higher OC to EC during winter ratio supports higher secondary organic aerosol (SOA) formation in this season.

Primarily, biomass burning and vehicular exhausts are the major sources that seem to dominate the aerosol $PM_{2.5}$ composition over this region. Further work is aimed at quantifying the sources as to use chemical tracers and Positive Matrix Factorization (PMF).

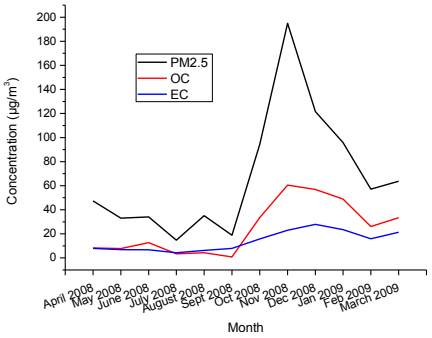

Figure 1. OC and EC in $PM_{2.5}$.

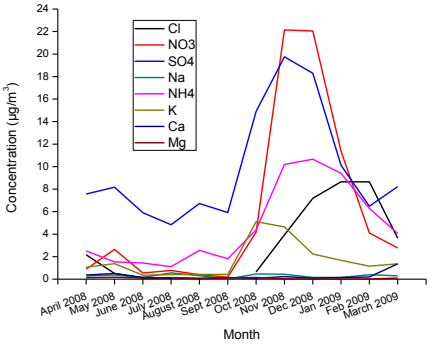

Figure 2. Soluble ions in $PM_{2.5}$

This work was made as part of the project EUCAARI, which is funded by the European Commission.

Kulmala, M., et al. (2009), *Atmos. Chem. Phys.*, 9, 2825–2841, doi:10.5194/acp-9-2825-2009.
Hyvärinen, A.-P., et al. (2010), *Atmos. Chem. Phys.*, 10, 7241–7252, doi:10.5194/acp-10-7241-2010.

Determination of the elemental composition and the source profiles of particulate matters in Bolu

E. Özlü[1] and S. Yenisoy-Karakaş[1]

[1]Department of Chemistry, Abant Izzet Baysal University, Bolu, 14280,Turkey

Keywords: receptor modeling, metals, ions, total carbon
Presenting author email: bayindir_e@ibu.edu.tr

The variation of the sources of PM (natural or anthropogenic) causes the changes in particle diameter. The size of the particles is significant to determine the sources of pollutants, investigate health effects, and understand the effects on climate and residence and removal mechanisms of pollutants. Aerosols also affect the balance of global radiation by scattering or absorbing light. Absorbing radiation by fine particles causes heating whereas, scattering light by coarse particles causes cooling (Rastogi, 2009).

Distribution of elemental concentration of particles, relationship between each parameter and meteorological aspects and quantitative analysis results of all components can be determined by statistical evaluation.

Daily aerosol samples were collected during two campaigns (summer and winter) in Abant Izzet Baysal Universty campus in Bolu. Fifteen metals (Al, Cd, V, Mg, Ca, Fe, Pb, K, Cr, Mn, Ni, Cu, Zn, Co, As), ions (Cl^-, NO_3^-, SO_4^{2-}, Na^+, NH_4^+, K^+, Mg^{2+}, Ca^{2+}) and total carbon were determined in both $PM_{2.5-10}$ and $PM_{2.5}$ size fractions.

Among the all parameters, contribution of SO_4^{2-} to $PM_{2.5}$ (28.3%) was the highest and the average concentration was 2.7 μg m^{-3}. In $PM_{2.5-10}$ the maximum concentration percent ratio belongs to Al (17.4 %) with 1.62 μg m^{-3} and Ca (37.5 %) with 3.3 μg m^{-3}. Total carbon showed no significant difference in both $PM_{2.5}$ and $PM_{2.5-10}$ samples. According to the ion balance calculations in $PM_{2.5}$ the anion/cation ratio is 1.03 and in $PM_{2.5-10}$ this ratio is calculated as 0.82. In fine particles all anions and cations were determined however, in coarse particles 18% of the anions could not be explained. The reason is the disability of the determination of CO_3^{2-} and HCO_3^- which are important among anions. In order to determine the sources of the parameters $PM_{2.5}/PM_{2.5-10}$ ratio in summer period was calculated. This ratio was greater than 1 for SO_4^{2-}, NH_4^+, Cl^- and Pb. In winter the ratio for As, K, SO_4^{2-}, NH_4^+, NO_3^- and Pb was greater than 1. In winter period this indicated that As, K and NO_3^- were mostly originated from the anthropogenic sources and they show seasonal variation due change of transboundary movement of pollutants with respect to meteorological parameters and change in human activities.

In this study for the determination of the source profiles of each pollutants, basic receptor modeling methods like enrichment factor analysis and factor analysis are used and for the determination of source regions of pollutants wind sector analysis was applied.

In enrichment factor analysis, Mn, Al, V and Co are found as crustal origin in both size of particles. Magnesium, K, Ca, Cu and Cr are moderately enriched and Ni, Pb, Zn, As and Cd are highly enriched (anthropogenic origin (Yenisoy-Karakaş, 2008)) again in both size.

Wind sector analysis summarize that in fine particles ($PM_{2.5}$) As, Pb, Cd, Cu and Cr were emitted from residential areas. Manganese, Pb, As, Ni, Cr and total carbon are due to traffic emission. In coarse particles ($PM_{2.5-10}$) all crustal elements come from agricultural zone in Nort-East, East-South-East and South-South-East directions. Arsenic and NO_3^- were emitted from coal and local traffic, respectively.

In factor analysis the 69% of whole data in $PM_{2.5}$ and 72% of the whole data in $PM_{2.5-10}$ can be explained with 5 factors. In $PM_{2.5}$ Al, Fe and NH_4^+ are in first factor (impure soil) which explains the 23.6% of variance. The second factor (traffic, anthropogenic) explains the 15.1% of the total variance. Nitrate, Pb, SO_4^{2-} and TC have high factor scores. In the third factor (coal, traffic) Ni, Cr and Mn have high factor scores and this factor explains the 12.8% of the variance. Arsenic, NH_4^+ and SO_4^{2-} are included in the fourth factor (secondary aerosols) which explains the 10.4% of the variance. The last factor (iron-steel works) explains only 8.7% of the total variance. In this factor Mn, Zn and SO_4^{2-} have high factor scores.

In $PM_{2.5-10}$ Factor 1 (soil) explains the 25.9% of the total variance and where Ca, $PM_{2.5-10}$, Fe, K, Mg, TC have high factor scores. The second factor (impure soil) explains the 15.3% of the variance. Aluminum and Fe have high scores whereas K, Mg and Mn have low factor scores. Nickel and Mn are included in Factor 3 (iron-steel works) which explains the 11.4% of the total variance. Manganese and Ni are the tracers of the iron-steel works. The fourth factor (coal) includes only Cr with factor score 0.86 and it explains 10.4% of the total variance. The last factor (traffic) explains only the 8.7% of the total variance. High factor score of lead (0.80) implies the source of factor is traffic emission.

This study was funded by TUBITAK-(The Scientific and Technological Research Council of Turkey) scientific research project with the grant number 108Y089.

Rastogi, N. and Sarin, M. M. (2009) *Atmospheric Environment.* **43**, 3481-3488

Yenisoy-Karakaş, S. and Tuncel, S. G. (2008) *Environmental Engineering Science.* **25**, 1263-1271

Characterization of $PM_{2.5}$ in a residential area of Beijing, China

R.R. Shen[1], K. Schäfer[1], P. Suppan[1], N. Schleicher[2,3], U. Kramar[3], S. Norra[2,3], J. Schnelle-Kreis[4], L.Y. Shao[5], J. Wang[5], J. Y. Wang[5], K. Cen[6], Y.S. Wang[7], S. Schrader[1,2]

[1]Institute of Meteorology and Climate Research (IMK-IFU), Karlsruhe Institute of Technology (KIT), 82467 Garmisch-Partenkirchen, Germany; [2]Institute of Geography and Geoecology (IGG), Karlsruhe Institute of Technology (KIT), 76128 Karlsruhe, Germany; [3]Institute of Mineralogy and Geochemistry (IMG), Karlsruhe Institute of Technology (KIT), 76128 Karlsruhe, Germany; [4]Joint Mass Spectrometry Centre, Comprehensive Molecular Analytics, Helmholtz Zentrum München, 85764 Neuherberg, Germany; [5]Department of Resources and Earth Sciences, China University of Mining and Technology (CUMTB), 100083 Beijing, P. R. China; [6]School of earth sciences and resources, China University of Geosciences (CUGB), 100083, Beijing, P.R. China [7]Institute of Atmospheric Physics, Chinese Academy of Sciences (CAS), 100029, Beijing, P. R. China

Keywords: Ambient PM, meteorological parameters, Aerosol characterization, Asian dust

Presenting author email: rongrong.shen@kit.edu

Beijing suffers from air pollution since the 1980s and ambient PM becomes a major problem now (Garland et al., 2009). A lot of emission reduction measures were performed to improve the air quality during the Olympic Summer Games in 2008, which has cut down coarse particles largely (Schleicher et al. 2011). The $PM_{2.5}$, which is more harmful than PM_{10}, is still a problem and related investigation becomes more important.

To discuss typical aerosol characteristics during different seasons together with meteorological influences, two sequential high volume samplers (Digitel DHA-80, Hegnau, Switzerland) were used to collect automatically $PM_{2.5}$ samples at the campus of the CUGB which is located in the North West of Beijing from June 2010 to June 2011. Meteorological parameters including wind speed and direction, temperature, relative humidity and atmospheric pressure were obtained from the site ZBAA whose data are available at an internet page of the University of Wyoming (http://weather.uwyo.edu/upperair/sounding.html).

During the research period, the annual average $PM_{2.5}$ concentration determined by gravimetry was 27 $\mu g\ m^{-3}$ which is lower than the results documented by Shi et al (2003) for 2001. They found an annual average $PM_{2.5}$ mass concentration of 106 $\mu g\ m^{-3}$, which is approximately seven times higher than the annual average of the National Ambient Air Quality Standard of the United States (NAAQS) for $PM_{2.5}$ (15 $\mu g\ m^{-3}$). Our $PM_{2.5}$ concentration ranged from 3 to 107 $\mu g\ m^{-3}$. The lowest $PM_{2.5}$ mass concentration was in January 2011 and the highest in April 2011. However, these values are obviously lower than those monitored before 2008 Olympic Games.

The comparisons of $PM_{2.5}$ mass concentrations with meteorological parameters, provide some correlations with wind speed and relative humidity. It is also influenced by wind direction and precipitation and it is influencing visibility.

Minor and trace elements are measured by PEDXRF (Polarized Energy Dispersive X-ray Fluorescence). Factor analysis is used to identify the sources of $PM_{2.5}$ in Beijing. From this can be concluded that the aerosols are originated from geogenic sources (found from Fe, Ti and Ba), which is like to be resuspended road dust and dust storm, and also from anthropogenic sources (found from Zn, As and Pb), such as vehicle exhaust, chemical industry, coal combustion and fertilizer application.

In order to identify the source of the dust storm which happened on 30/04/2011 in the Beijing area, the HYSPLIT model (Hybrid Single Particle Lagrangian Integrated Trajectory) was applied. It was originated from the Gobi desert.

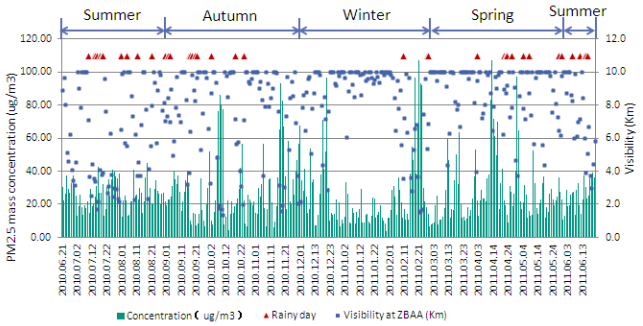

Figure 1. $PM_{2.5}$ mass concentration, visibility and precipitation

This work is supported by the China Scholarship Council (CSC), NSFC grant (41175109) and the KIT Center for Climate and Environment.

Garland, R.M., Schmid, O., Nowak, A., Achtert, P., Wiedensohler, A., Gunthe, S.S., Takegawa, N., Kita, K., Kondo, Y., Hu, M., Shao, M., Zeng, L.M., Zhu, T., Andreae, M.O. and Pöschl, U. (2009) *Journal of Geophysical Research*, 114(D00G04), 1–12.

Schleicher, N., Norra, S., Dietze, V., Yu, Y., Fricker, M., Kaminski, U., Chen, Y. and Cen, K. (2011) *Science of the Total Environment*, 412-413, 185-193.

Shi, Z.B., Shao, L.Y., Jones, T.P., Whittaker, A.G., Lu, S.L., Bérubé, K.A., He, T.E. and Richards, R.J. (2003) *Atmospheric Environment*, 37, 4097–4108.

Anthropic and natural sources of PM10 in central Mediterranean Sea by bulk and size-segregated samples

S. Becagli[1], R. Traversi[1], M. Marconi[1], C. Ghedini[1], S. Nava[2], M. Chiari[2], F. Lucarelli[2], G. Calzolai[2], A. di Sarra[3], G. Pace[3], D. Meloni[3], C. Bommarito[4], D. M. Sferlazzo[4] , R. Udisti[1]

[1]Dept. of Chemistry, University of Florence, Sesto Fiorentino, Florence, I-50019, Italy
[2]Department of Physics, University of Florence and INFN Sez. Firenze, Sesto F.no, Florence, I-50019, Italy
[3]UTMEA-TER, ENEA, I-00123, S. Maria di Galeria, Roma – Italy
[4]UTMEA-TER, ENEA, I-92010, Lampedusa, Agrigento, Italy

Keywords: PM10, chemical composition, aerosol source, Central Mediterranean Sea.
Presenting author email: silvia.becagli@unifi.it

Due to the relevant role of aerosol in affecting climate, studies of variability in aerosol chemical composition at marine sites coupled with optical properties are requested in order to understand the complex aerosol-climate interactions, and reduce the uncertainty in the determination of the aerosol radiative forcing. In particular the Mediterranean region has been identified as one of the "Hot-Spots" in future climate change projections (Giorgi and Lionello, 2008).

In order to understand the contribution of natural and anthropic sources and the aerosol optical properties in the Central Mediterranean Sea, continuous observations of greenhouse gases concentration, aerosol properties, total ozone, ultraviolet irradiance, and other climatic parameters are routinely carried out at Lampedusa (35° N, 12.6° E). Since June 2004, a continuous campaign of PM10 sampling has been performed. A spot campaign with 8-stage impactor was also carried out in spring 2008. Each filter was analyzed for main and trace ions, and selected metals (HNO_3, pH = 1.5). Half of PM10 filters were analysed by PIXE for total elemental content.

Since 2010, PM10 was sampled on quartz filter, thus allowing EC and OC determination by thermo-optical methods as well.

In figure 1 the mean composition of PM10 is shown.

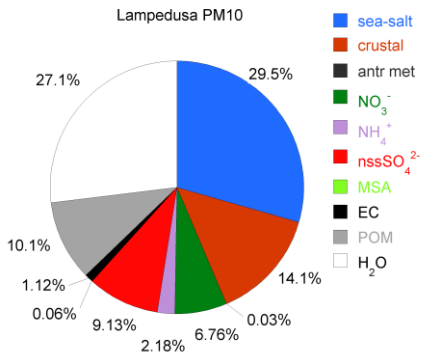

Figure 1. Pie plot of PM10 mean composition over 2004-2010 sampling periods at Lampedusa Island. Mean values of EC and POM are refer to a shorter time period than other measurements.

Crustal content was evaluated by Al, Si, Ca, non-sea-salt Na, K and Fe oxides, revealing that during strong Saharan dust events PM10 is often higher than 50μg m^{-3} and dust contribution is about 50%. The crustal aerosol amount and contribution to PM10 shows a very small seasonal dependence; conversely, the aerosol optical depth displays an evident annual cycle, with a strong summer maximum (monthly average aerosol optical depth at 500 nm up to 0.28 in June-August). When cases influenced by dust are excluded, also the aerosol optical depth displays a very small seasonal change, suggesting that the limited variations of the marine boundary layer produce a limited variability of the surface and lower tropospheric dust contribution.

The Positive Matrix Factorization (PMF) model has been applied to the chemical data in order to obtain the source apportionment of the PM10 at Lampedusa. The main sources impacting the site are: Saharan dust, primary marine, secondary anthropic and natural from biogenic emission.

Among the anthropic sources reaching the remote site of Lampedusa, heavy oil combustion emissions are identified using V and Ni as specific marker of this source. Back trajectory analysis shows that the selected events are affected by sea going ship and not by local pollution (i.e. Lampedusa harbour) or long range transport from refineries or power plants, confirming their provenience from the ship tracks crossing the Strait of Sicily (Becagli et al , 2011).

The campaign with 8-stage impactor shows that Al and Fe in Saharan dust events are distributed in the coarse fraction. Conversely, in events characterized by high contribution of aerosol from heavy oil combustion the same elements other than the specific marker of this source (V, Ni) are distributed in the sub-micrometric aerosol fraction.

Giorgi, F., Lionello, P., (2008) *Global and Planetary Science*, **63**, 90-104.

Becagli S., Sferlazzo D. M., G. Pace, A. di Sarra, C. Bommarito, G. Calzolai, Ghedini C., Lucarelli F., Meloni D., Monteleone F., Severi M., Traversi R., and Udisti R. (2011) *Atmos. Chem. Phys. Discuss.*, 11, 29915–29947. Doi:10.5194/acpd-11-29915-2011

The contribution of Rome-Ciampino airport to the surrounding air quality

A. Di Menno di Bucchianico[1], G. Cattani[1], A. Gaeta[1], A. Caricchia[1], F. Troiano[2], R. Sozzi[2], A. Bolignano[2], F. Sacco[2], S. Damizia[2], S. Barberini[2], R. Caleprico[2], T. Fabozzi[2], C. Ancona[3], L. Ancona[3], G. Cesaroni[3], F. Forastiere[3], G.P. Gobbi[4], F. Costabile[4], F. Angelini[4], F. Barnaba[4], M. Inglessis[5], F. Tancredi[5], L. Palumbo[5], L. Fontana[6], A. Bergamaschi[6], I. Iavicoli[6]

[1] ISPRA Italian National Institute for Environmental Protection and Research, V.Brancati 48, 00144, Rome, Italy
[2]ARPA Lazio Environmental Protection Agency, Via Giuseppe Saredo 52, 00173, Rome, Italy
[3]ASLRME Local Health Authority, Department of Epidemiology, Via di Santa Costanza 53, Rome, Italy
[4]ISAC CNR Institute of Atmospheric Sciences and Climate, Via Fosso del Cavaliere, 100, 00133, Rome, Italy
[5]ISS Italian National Health Institute, Viale Regina Elena 299, 00161, Rome, Italy
[6]UCSC Università Cattolica del Sacro Cuore, Largo Francesco Vito 1, 00168, Rome, Italy
Keywords: aircraft, airports, source apportionment, number concentration, urban pollution.
Presenting author email: alessandro.dimenno@isprambiente.it

Rome-Ciampino airport is a military and civilian airport located 14 km south of the centre of Rome (Italy).
This one runway airport, the second of the city, became in recent years a hub for low-cost carriers that in the last decade have increased in flight frequency, making it now the tenth busiest airport by passenger traffic in Italy.
The purpose of this study was to investigate the impact of aviation traffic emissions on the air quality of the area: a conurbation just outside the circular motorway Greater Ring Road (GRA) around Rome, impacted by a number of different anthropogenic sources and where residential homes, commercial activities and schools border the Terminal.
The effect of Ciampino aircraft noise exposure on the residents was recently investigated (S.E.R.A. project), but no information about the airport apportion to air quality and its health effects in a such polluted area was available yet.
To this scope, two air monitoring campaigns were carried out during the 2011 (summer) and the 2012 (winter) in the area surrounding the airport.
Two mobile stations were placed 400 m south of the end of the runway, under the take-off route followed in prevailing wind conditions. In this sampling site the parameters listed below were continuously measured:

- Particulate Matter mass concentration (PM_{10}, $PM_{2.5}$);
- Particle Number Concentration > 10 nm (PNC);
- Particle Size Distribution, 0.3-10 µm (PSD);
- Carbon Monoxide (CO);
- Nitrogen Oxides (NO, NO_2, NO_X);
- Sulfur Dioxide (SO_2);
- Ozone (O_3);
- Aromatic and Carbonyl Volatile Organic Compounds (VOCs)
- Light-scattering Coefficient of atmospheric aerosols;
- Light-absorption Coefficient;
- Aerosol Vertical Profile and Planetary Boundary Layer (PBL) height.

Additionally, in the same period, two 15 days campaigns in 46 sites with diffusive samplers (Nitrogen Dioxide, NO_2, Aromatic and Carbonyl compounds) were realized to implement a Land Use Regression model (LUR) in a 8x8 km domain, that helped to highlight the differences in spatial distribution of measured pollutants, in relation with the main pollution sources existent in the area.
Preliminary results showed that combining radar flight tracks and continuous sampling data, the direct contribution of take-off operations to the air quality of nearby areas was revealed (see Figure 1: Particle Number Concentration, 0.01 µm - 3 µm, temporal profile with one minute resolution).

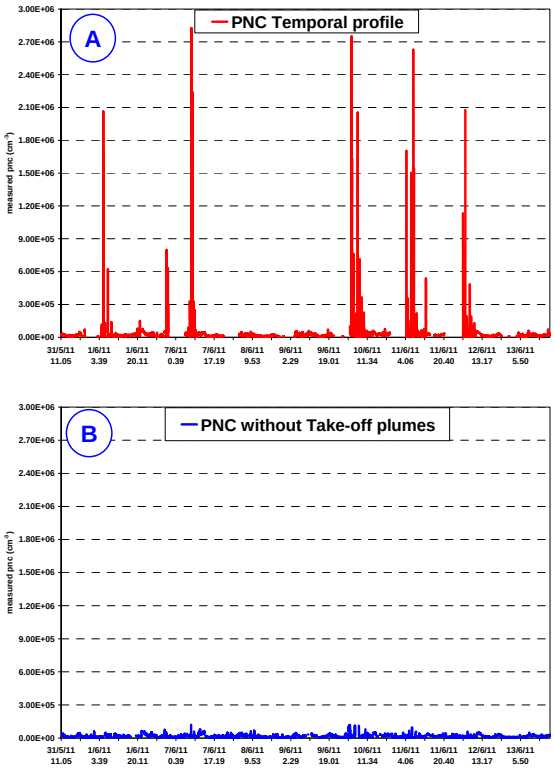

Figure 1. Summer campaign: comparison between with/without take-off plumes (A and B) PNC temporal profile measured by the Condensation Particle Counter placed 400 m south of the end of the runway.

This relation between PNC and the airport activities was an aspect otherwise invisible using standard averaging periods (hour or day), since confused or hidden in the complex mix of urban activity emissions.

PM2.5 source apportionment in Milan by UNMIX receptor model

G. Lonati[1], C. Colombi[2] and S. Cernuschi[1]

[1] DIIAR – Politecnico di Milano, P. za L. da Vinci, 32, 20133, Milano, Italy
[2] ARPA Lombardia – Dipartimento di Milano – Via Juvara, 22 - 20129 Milano, Italy
Keywords: recptor modeling, source apportionment, PM2.5, urban areas
Presenting author email: giovanni.lonati@polimi.it

Milan is a well-known "hot spot" for particulate matter pollution in Europe, facing severe problems for compliance with PM10 and PM2.5 air quality limits. Source apportionment studies mainly focused on PM10 through Chemical Mass Balance and Positive Matrix Factorization receptor modelling whereas only few works considered PM2.5 and none by means of the UNMIX model (Henry, 2002; 2003)

In this work the UNMIX receptor model has been applied for the PM2.5 source apportionment of to a rather extended set of daily samples (about 120) collected at an urban background site in Milan. The samples, representative of the different seasonal PM2.5 levels, have been speciated for the chemical composition in terms of carbon components (elemental and organic carbon), major inorganic ions (Cl^-, NO_3^-, SO_4^{2-}, NH_4^+) and 13 trace elements (Lonati et al., 2008).

The model has a good ability in reconstructing the measured PM2.5 mass (Figure 1) based on 8 chemical species: EC, OC, NO_3^-, SO_4^{2-}, NH_4^+, Cu, Pb, Zn. Correlation between measured and modelled concentration data is in excess than 0.81 for all the chemical species and up to 0.99 for the ionic species.

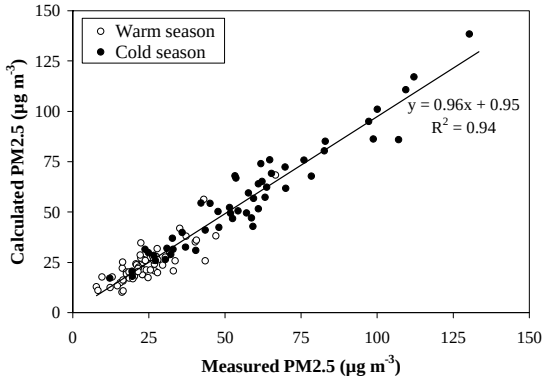

Figure 1. Scatter plot of the measured and calculated PM2.5 mass concentrations.

The model apportions the PM2.5 mass among four sources, identified as traffic emissions, combustion processes, secondary nitrate and secondary sulphate, based on the corresponding source profiles; only a small fraction of the mass (~2%) is not apportioned to any source. On annual basis the average contributions to the PM2.5 mass vary in a rather narrow range (Figure 2), with very similar values for traffic, combustion, and secondary nitrate source (~11 µg m^{-3}) and a smaller contribution from secondary sulphate (~7 µg m^{-3}). Overall, the secondary inorganic sources account for almost half of the total PM2.5 mass, in agreement with the results obtained by Marcazzan et al. (2003) through Principal Components Factor Analysis technique applied to a different dataset. Conversely, the model does not recognize a source related to soil resuspension.

The estimated source contributions are characterized by a remarkable seasonal and daily variability. During the cold season (Oct-Mar), combustion processes and secondary nitrate each account for about 33% of the PM2.5 mass, with the traffic source responsible for 22% and the secondary sulphate source for 10% only. In the warm season (Apr-Sep) both traffic and secondary sulphate account for about 30% of the PM2.5 mass whereas secondary nitrate and combustion processes for 16% only. The huge increase in the winter contribution of these latter sources, both in absolute and relative terms, is consistent with the additional emission of domestic heating and with the meteorological conditions fostering the ammonium nitrate atmospheric presence in the urban atmosphere.

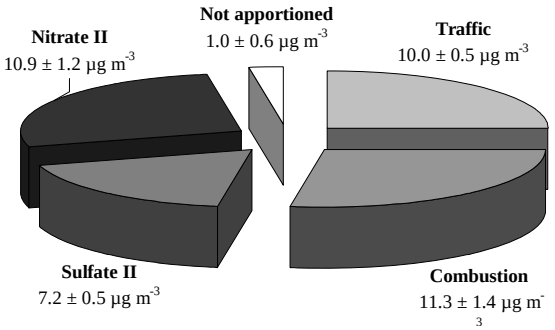

Figure 2. PM2.5 source apportionment in Milan (annual mean ± mean standard deviation).

Henry, R.C. (2002) *Chemometrics and intelligent laboratory systems* **60**, 43-48.

Henry, R.C. (2003) *Chemometrics and intelligent laboratory systems* **65**, 179-189.

Lonati G., Giugliano M., and Ozgen, S. (2008). *Environment International* **34**, 665-670.

Marcazzan, G.M., Ceriani, M., Valli, G. and Vecchi, R. (2003) *The Science of the Total Environment* **317**, 137–147

Source apportionment of ambient PM_{10-1} and PM_1 in Granada

G. Titos[1,2], H. Lyamani[2], A.Alastuey[3], M. Pandolfi[3], J.A. Bravo-Aranda[1,2] and L. Alados-Arboledas[1,2]

[1]Centro Andaluz de Medio Ambiente, Universidad de Granada, Junta de Andalucía, Granada, 18006, Spain.
[2]Department of Applied Physic, University of Granada, Granada, 18071, Spain.
[3]IDÆA, Department of Geosciences, CSIC, Barcelona, Spain
Keywords: source apportionment, PM1, PM10.
Presenting author email: gtitos@ugr.es

PM_{10} is one of the most used parameters to assess the air quality in Europe. The identification of its sources is one of the main goals of environmental research and plays an important role in PM abatement strategies. In this study, a Principal Component Analysis (PCA) has been applied to chemical composition in the coarse (PM_{10-1}) and fine (PM_1) fractions in order to determine the main sources contributing to these size fractions. In this sense, a multilinear regression analysis (MRLA) has been then conducted to determine the contribution of each source to each fraction. In addition, we have studied the influence of dust intrusions from North Africa in PM_{10} speciation levels. These cases have been selected according to calima database (www.calima.ws).

The measurements were performed in Granada (37.16º N, 3.58º W, 680 m a.s.l.) from 2006 to 2010 using two high-volume samplers (flow rate 30 m^3 h^{-1}) for sampling PM_{10} (CAV-A/MSb) and PM_1 (Digitel DHA-80). Quartz fibre filters (150 mm) were used to collect particulate matter and were conditioned and treated pre- and post-sampling. Sampling usually starts at 7:00 GMT and ends 24h later. More information about the measurement station and the sampling procedure can be found in Lyamani et al. (2010) and Titos et al. (2012). Once the levels of bulk particulates were obtained by weighting the filters using gravimetric techniques, we apply to the filters different laboratory treatments for determining the levels of major and trace components following the procedure of Querol et al. (2009). With this procedure we obtained the concentration of major species (Total Carbon, SiO_2, CO_3^{2-}, Al, Ca, Na, Mg, K, Fe, SO_4^{2-}, NO_3^-, Cl^- and NH_4^+) and trace elements (Li, P, Ti, V, Cr, Mn, Co, Ni, Cu, Zn, As, Se, Rb, Sr, Mo, Cd, Sn, Sb, Ba, La, Ce, Hf, Pb, Bi, Th, U, among others). Quantitative errors have been estimated to be less than 10% for most of the components, and around 15% for K and P.

A varimax rotated PCA was applied to selected variables using the STATISTICA 8 software. PM_{10-1} and PM_1 were analysed separately. For the coarse fraction, the first component (PC1) is clearly identified with mineral dust. It exhibits high factor loadings (>0.70) for SiO_2, Al_2O_3, Ca, K, Mg, Fe, Li, P, Ti, Cr, Mn, Ga, As, Se, Rb, Sr, Cs and Ba, and explains 58% of the variance. This mineral matter is associated with dust re-suspension from roads, construction/demolition activities and dust intrusions from North Africa. PC2 explains 10% of variance and is characterized by high factor loadings for carbon, Sn and Sb (these latter elements are mainly associated to tyre and brake abrasion). The third component explains 5% of the variance and presents high factor loadings for Cl and Na, thus, being associated with marine aerosols.

For PM_1, the first component is also related with mineral particles although the factor loadings and the explained variance are lower than for PM_{10-1}. PC2 presents high factor loadings for carbon, Pb, NO_3^- and Sb being associated with traffic emissions (17% explained variance). PC3 is highly loaded with Ni, Co and V and it is related to fuel-oil combustion. PC5 presents high factor loadings for Se, SO_4^{2-} and As. The contribution of each source to PM_1 is shown in Figure 1.

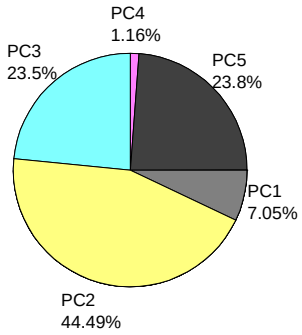

Figure 1. Source contribution to PM_1.

Considering the dust events, levels of PM_{10} increase significantly, which is especially marked for the mineral fraction (Σ SiO_2, CO_3^{2-}, Al, Ca, Mg, K, Fe). Surprisingly, other species such as non marine SO_4^{2-} or NO_3^- also increase during African dust outbreaks.

Aknowledgments: This work was supported by the Andalusia Regional Government through projects P08-RNM-3568 and P10-RNM-6299, by the Spanish Ministry of Science and Technology through projects CGL2010-18782, CSD2007-00067 and CGL2011-13580-E/CLI; and by EU through ACTRIS project (EU INFRA-2010-1.1.16-262254).

Lyamani, H., F. J. Olmo, and L. Alados-Arboledas (2010), Atmos. Chem. Phys., 10, 239–254.

Querol, X., A. Alastuey, J. Pey, M. Cusack, N. Pérez, N. Mihalopoulos, C. Theodosi, E. Gerasopoulos, N. Kubilay, and M. Kocak (2009), Atmos. Chem. Phys., 9, 4575–4591.

Titos, G., I. Foyo-Moreno, H. Lyamani, X. Querol, A. Alastuey, and L. Alados-Arboledas (2012), J. Geophys. Res., 117, D04206.

The effect of local wood combustion on fine particles in suburban small house areas in Helsinki Metropolitan Area, Finland

A. Kousa[1], J. Niemi[1], A. Svens[1], K. Teinilä[2], R. Hillamo[2] and T. Koskentalo[1]

[1]Helsinki Region Environmental Services Authority, P.O. Box 100, FI-00066 HSY, Helsinki, Finland
[2]Air Quality Research, Finnish Meteorological Institute, P.O. Box 503, FI-00101 Helsinki, Finland
Keywords: black carbon, biomass burning, urban pollution, PM.
Presenting author email: anu.kousa@hsy.fi

Residential wood burning has a remarkable effect on fine particles concentrations during cold season even on urban areas where heating of buildings is mainly based on centralized district heating system. Large amounts of PM are still emitted e.g. in heat storing fireplaces and sauna stoves in suburban small house areas. In the recent study it was estimated that during the average cold season the contribution of wood combustion emissions to fine particles ranged from 18 % to 29 % at the urban sites and from 31 % to 66 % at the suburban areas in Helsinki Metropolitan area, Finland (Saarnio et al 2012). In addition it was estimated that occasionally the local wood combustion emissions caused an addition of even 10-15 µg/m^3 to the daily mean concentration of $PM_{2.5}$ while the average addition to the daily concentrations of $PM_{2.5}$ was about 1-3 µg/m^3.

Wood combustion in suburban small house areas

The measured concentrations of benzo(a)pyrene have been at the same level in an urban background site at least since year 2007 (Table 1). It seems that local traffic does not have an effect on the concentrations of benzo(a)pyrene because the concentration levels are equal with the urban background and street canyon sites. The highest benzo(a)pyrene concentrations are measured in the suburban small house areas where local wood burning exists. It seems that there is quite large spatial variation between different suburban small house areas. The EU's target value for benzo(a)pyrene (1 ng/m^3) is exceeded in some suburban small house areas clearly when in some other areas the concentrations are well below the target value .

Table 1. The concentrations of benzo(a)pyrene in an urban background, different street canyons and suburban small house areas .

	Concentration of Benzo(a)pyrene (ng/m^3)		
Year	Urban background	Street canyons	Small house areas
2007	0.3	0.3	
2008	0.2		1.1
2009	0.3		0.5
2010	0.3	0.3	0.5
2011	0.3		1.2

Black carbon (BC) concentrations in year 2009 were measured in the suburban small house area (the annual BC concentration was 0.8 µg/m^3) and in year 2010 in one of the most polluted street canyon (the annual BC concentration 2,6 µg/m^3) in the Helsinki Metropolitan Area. The strong effect of local sources can be clearly seen in variation of BC concentrations between day of week and time of day (Figure 2). In the busy street canyon the concentrations were the highest during morning rush hours in weekdays while in the suburban small house areas the BC concentrations were highest on Saturday evenings. Also on Wednesday evenings the BC concentrations were elevated in the small house areas. This can be explained by the fact that Wednesday and Saturday are the days when sauna stoves are traditionally heated in Finland.

The annual $PM_{2.5}$ concentration was 8.1 µg/m^3 so it can be estimated that 11 % of total $PM_{2.5}$ concentration was caused by BC in the suburban small house area.

Correlations between the concentrations of levoglucosan and benzo(a)pyrene in an urban background site and suburban small house areas are also studied.

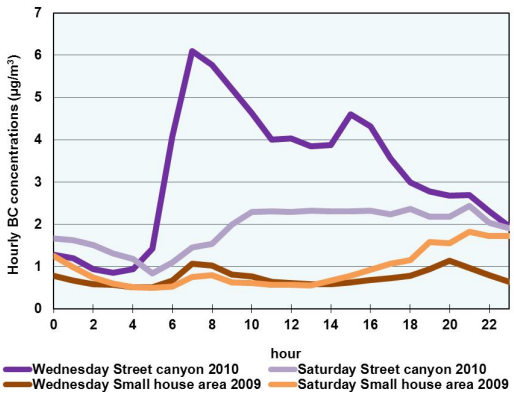

Figure 2. Daily variation of BC concentration in the street canyon and suburban small house area.

This study was partly funded by MMEA Programme (Measurement, Monitoring and Environmental Assessment). MMEA is supported by Tekes (the Finnish Funding Agency for Technology and Innovation) and coordinated by the Finnish energy and environment cluster - CLEEN Ltd.

Saarnio, K., Niemi, J., Saarikoski, S., Aurela, M., Timonen, H., Teinilä, K., Myllynen, M., Frey, A., Lamberg, H., Jokiniemi, J. and Hillamo, R. (2012) *Boreal Environment Research*, **17**, in press.

Overview of the impact of wood burning emissions on carbonaceous aerosols and PM in the Alpine region

H. Herich[1], M.F.D. Gianini[1], Ch. Piot[2,3], J. Cozic[2], J.L. Jaffrezo[2] , J.L. Besombes[3], A.S.H. Prevot[4], and Ch. Hueglin[1]

[1]Empa, Swiss Federal Laboratories for Materials Science and Technology, Duebendorf, Switzerland
[2]UJF-Grenoble 1 / CNRS, LGGE UMR 5183, Grenoble, F-38041, France
[3]Université de Savoie-LCME, Le Bourget du Lac, France
[4] Paul Scherrer Institut, Laboratory for Atmospheric Chemistry, Villigen, Switzerland

Keywords: Wood combustion, source apportionment, macro-tracer method
Presenting author email: christoph.hueglin@empa.ch

Wood burning for domestic heating is an important source of carbonaceous aerosols and ambient particulate matter (PM). The importance of wood burning as a source of particulate air pollutants has been shown in many studies carried out in different countries. At locations in the Alpine region during the cold season, wood burning can be the dominating source of carbonaceous aerosols and PM (Szidat *et al.*, 2007; Gilardoni *et al.*, 2011; Piot, 2011).

During the past years, implemented measures for the reduction of PM emissions have been focused in many European countries on road traffic emissions. Conversely, much less attention has been paid to emissions from domestic wood burning. As shown recently by Gianini *et al.* (2012), average road traffic contributions to PM10 have in Switzerland declined during the past ten years, whereas the contributions from wood burning remained unchanged. As a consequence, the contribution of wood burning to PM10 is today comparable to (or even higher than) the contributions from road traffic on annual average at many locations in Switzerland. Same results are observed in France by Piot (2011).

This presentation provides an overview of the impact of wood burning emissions on carbonaceous aerosols and PM in the Alpine region. The overview is based on results of recently published studies using different methods, such as multivariate statistical models (Positive Matrix Factorization, PMF), Chemical Mass Balance (CMB), ^{14}C-method and evaluation of the wavelength dependence of the optical aerosol absorption (Aethalometer model). In addition, available data of specific wood combustion tracers such as levoglucosan are used together with published source emission ratios and PMF-derived emission ratios in macro-tracer analyses to estimate contributions of wood burning emissions to carbonaceous aerosols and PM.

As an example, Fig. 1 shows average wood burning contributions to PM10 as derived by PMF versus average concentrations of levoglucosan at sites in Switzerland and the Lombardy region (Northern Italy; data from Piazzalunga et al., 2011). The content of levoglucosan in PM10 from wood burning is constant for the Swiss sites that are located north of the Alps (Bern, Zurich, Payerne; levo/$PM10_{WB}$ = 0.045) and clearly lower than at the Swiss site south of the Alps (Magadino; levo/$PM10_{WB}$ = 0.069) and the average of the sites in Northern Italy (Piazzalunga et al., 2011; levo/$PM10_{WB}$ = 0.059). These and other PMF-derived emission ratios are used for estimation of wood burning impacts on particulate air pollutants and for comparison with results obtained by other source apportionment approaches.

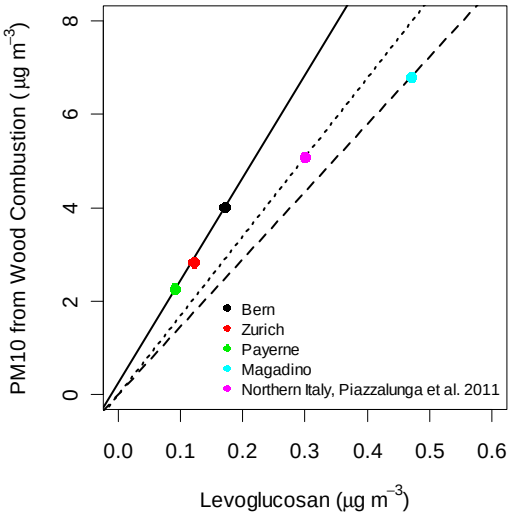

Figure 1. PMF-derived average contribution of PM10 from wood combustion versus average concentration of levoglucosan at sites in Switzerland and Northern Italy.

Gianini, M.F.D., Gehrig, R., Fischer, A., Ulrich, A., Wichser, A., Piot, Ch., Besombes, J.L. and Hueglin, Ch. (2012) *Atmos. Environ.*, accepted.

Gilardoni, S., Vignati, E., Cavalli, F., Putaud, J.P., Larsen, B.R., Stenström, K., Genberg, J., Henne, S. and Dentener, F. (2011) *Atmos. Chem. Phys.*, **11**, 5685-5700.

Piazzalunga, A., Belis, C., Bernardoni, V., Cazzuli, O., Fermo, P., Vialli, G. and Vecchi, R. (2011). *Atmos. Environ.*, **45**, 6642-6649.

Piot, C. (2011). Thesis of the University of Grenoble, 294 pp.

Szidat, S., Prevot, A.S.H., Sandradewi, J., Alfarra, M.R., Synal, H.A., Wacker, L. and Baltensperger, U. (2007) *Geophys. Res. Lett.*, **34**, L05820.

Indoor-outdoor relationships of airborne particles and nitrogen dioxide inside Parisian buses

R. Molle[1,2], E. Géhin[2], S. Mazoué[1] and A. Ionescu[2]

[1]RATP, Paris Public Transport, Paris, 75012, France
[2]Université Paris-Est Créteil, CERTES, 61 avenue du Général de Gaulle, 94010,Créteil

Keywords: Ambient air pollution, PM2.5, Cars, Diesel exhaust
Presenting author email: romain.molle@ratp.fr

Studies measuring air pollutants in the living areas determine the city-dwellers' exposure to urban air pollution. In 2008, measures were made in Paris on the passengers' exposure to traffic air pollution inside the main modes of transport during rush hour periods by Delaunay et al. (2010). The results have revealed that passengers travelling on bus line 91 are more exposed to fine particles and nitrogen dioxide compared to those using the bus line 56 in Paris.

New works were scheduled to confirm these preliminary results and to identify the sources and parameters determining the concentrations of pollutants measured inside the buses.

The regulated pollutants in the outdoor air were firstly selected, moreover pollutants from AIRPARIF data (the monitoring network of Paris and its suburbs) and 2008 measuring campaign were also selected for comparison. For all of the above reasons, NO_2 concentration, PM2.5 mass concentration and particle number concentration between 0.3 and 20 µm were measured in this study. Portable devices were used to measure simultaneously pollutants at the front, middle and rear positions inside buses in order to determine the spatial distribution and the most exposed position to these pollutants. This study evaluated passengers' exposure to traffic air pollution inside the buses of the line 91 in Paris during 10 working days in May, 2010 in the presence of passengers. Twenty buses were studied on 32 routes of 40 minutes each from 8 a.m. to 9 a.m. and from 4 p.m. to 5 p.m., time periods corresponding to the peak traffic and travellers.

Results

According to the results, the NO_2 and PM2.5 exposure is greater inside the instrumented buses in comparison to the outside air.

In 2010, the nitrogen dioxide concentration average obtained inside the instrumented buses is 203±21µg.m^{-3} therefore lower compared to air monitoring stations means range from 58±3 to 128±4 µg.m^{-3}. The conclusions are the same for in-cabin PM2.5 mass concentrations with 82±4 µg.m^{-3} against 46±7 µg.m^{-3} for air monitoring station. Moreover, the particle number concentration (0.3-20 µm) inside buses is variable and depends on the sampling date.

This experiment reveals the negligible role of the sampling position in the bus to PM2.5 mass concentration and for the particle number concentration (0.3-20 µm) thereby the levels are considered equal between the three sampling positions. However, in-cabin NO_2 concentrations increase when the sampling positions move from the front to the back of the bus.

The campaign confirmed the NO_2 levels found in 2008 therefore the NO_2 concentrations are repeatable and vary little if the factors (line, rolling stock, ventilation conditions, outdoor level) do not vary. The campaign confirmed also the PM2.5 levels despite fluctuations of PM2.5 concentrations measured by air monitoring station.

A correlation (Pearson, Spearman) is calculated with 2010 results to identify correlations between the in-cabin air and the outside air. These calculations have been made by comparing the average in-cabin concentration to air monitoring station concentration mean for each trip on identical time periods.

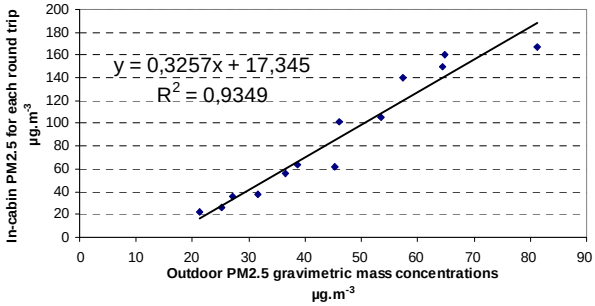

Figure 1. Linear regression between in-cabin PM2.5 and outdoor PM2.5.

The correlation coefficients between in-cabin and outdoor PM2.5 concentrations are highly correlated (greater than 0.9), despite the variability of PM2.5 mass concentrations inside the cabin.

However, it is still difficult to conclude. Indeed, the air monitoring stations are not present in the route of the studied bus line, the comparison between outside monitoring station data and in-cabin data are distorted.

Therefore the next campaign scheduled for autumn 2010 has included a laboratory vehicle in order to sample the air near the instrumented buses.

Delaunay,C., Mazoué, S., Morawski, F., Goupil, G., Ravelomanantsoa, H., Person, A. (2010). *City-dwellers exposure to atmospheric pollutants when commuting in Paris urban area*. Primequal/Predit (RATP, LCPP, LHVP).

Fungal Bio-Aerosols Quantification - Comparison between q-PCR and Ergosterol Analysis

Naama Lang-Yona[1], Karen Dannemiller[2], Naomichi Yamamoto[2], Noa Burshtein[1], Jordan Peccia[2], Oded Yarden[3], Yinon Rudich[1]

[1]Department of Environmental Sciences, Weizmann Institute of Science, Rehovot, 76100, Israel.
[2]Department of Chemical and Environmental Engineering, Yale University, 9 Hillhouse Avenue, New Haven, CT, 06520-8286, USA.
[3]Department of Plant Pathology and Microbiology, The Faculty of Agriculture, Food and Environment, The Hebrew University of Jerusalem, Rehovot 76100, Israel.

Keywords: Health aspects of aerosols, fungal spores, particulate matter, allergens, biomarkers, ergosterol.

Presenting author email: naama.lang-yona@weizmann.ac.il

Airborne fungal spores are an important fraction of atmospheric particulate matter and are major causative agents of allergenic and infectious diseases. Predicting the variability and species of allergy-causing fungal spores requires detailed and reliable methods for identification and quantification. There are diverse methods for fungi detection in the atmosphere and in the indoor environments; yet, it is important to optimize suitable methods for their characterization in atmospheric samples.

In this study we sampled and characterized total and specific airborne fungal spores from PM10 samples collected in Rehovot, Israel over an entire year.

The total fungal spore concentrations vary throughout the year although the species variability was nearly the same (Figure 1).

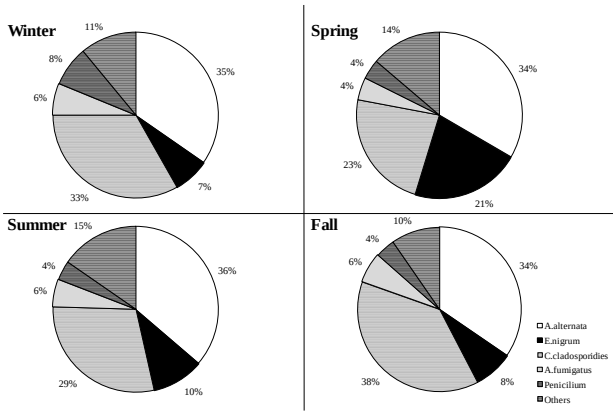

Figure 1: Seasonal distribution of selected allergy-inducing fungal species.

Seasonal equivalent spore concentrations analyzed by real-time quantitative-PCR-based methods were fall > winter > spring > summer. Reported concentrations based on ergosterol analysis for the same samples were fall > spring > winter > summer (Table 1, Burshtein, 2011).

Table 1: Seasonal correlation coefficients between Ergosterol and spore concentrations.*

Season	Ergosterol ng m^{-3}	Spore m^{-3}	Correlation coefficient, r	P-value
Winter	0.42±0.38	2044.6±2772.5	0.03±0.40	0.95
Spring	0.76±0.74	1380.6±2090.5	0.61±0.63	0.10
Summer	0.28±0.23	356.6±265.7	0.06±0.24	0.84
Fall	0.94±0.71	2896.9±2240.1	-0.15±0.72	0.55
Whole year	0.61±0.61	1873.8±2195.0	0.18±0.61	0.21

*Ergosterol and spore values are presented by the season mean value.

Correlation between the two analytical methods was found only for the spring season (Figure 2). These poor associations may be due to the per-spore ergosterol variations that arise from both varying production rates, as well as molecular degradation of ergosterol.

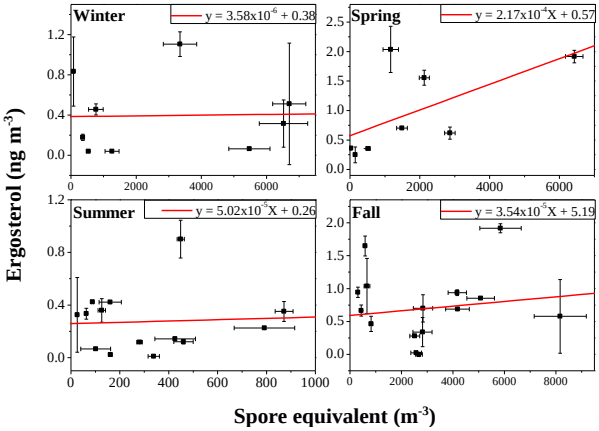

Figure 2: Seasonal correlation between equivalent total fungal spore concentrations analyzed from q-PCR measurements, and ergosterol mass concentrations (Burshtein 2011). The error bars represent the standard deviation of ergosterol (vertical) and fungi spore sampling replicates (horizontal).

While conversion of genome copies to spore concentration is not yet straightforward, the potential for improving this conversion and the ability of q-PCR to identify groups of fungi or specific species makes this method preferable for environmental spore quantification.

Identifying tools for establishing the relation between the presence of species and the actual ability to induce allergies is still needed in order to predict the effect on human health.

This research was supported by a research grant from the Dr. Angel Faivovich foundation for Ecological Studies. N. Lang-Yona was supported by a grant from the Environmental Health Fund, K. Dannemiller was supported by a U.S. National Science Foundation fellowship, and N. Yamamoto is supported by the Japan Society for the Promotion of Science. Y.R. acknowledges support by the Helen and Martin Kimmel Award for Innovative Investigation.

Burshtein, N., Lang-Yona, N., Rudich, Y. 2011
Ergosterol, arabitol and mannitol as tracers for biogenic aerosols in the eastern Mediterranean. Atmospheric Chemistry and Physics 11(2):829.

Comprehensive evaluation of dust cleaning in a subway indoor

W. R. Kim, H. W. Park, Y. M. Jo†

Department of Environmental Engineering, Kyung Hee University, Yongin, Gyeonggi-do, 446-701, Korea
Keywords: Indoor aerosol, Filtration, PM_x, IAQ, Subway
Presenting author email: woojoa@hanmail.net

Air quality of underground railway is of a critical interest in Seoul, Korea. The local government has paid a great attention to the IAQ(Indoor Air Quality) of metro-subway. In order to reduce the fine dust concentration of public indoor spaces, an integrated managing system including intelligent control network, on-line detects and double filters lay-out has been installed in a test field station. The effects of automatic operation of two stage filters: pre-filter and electret filter, were examined with a real-time analysis focusing on PM10 and PM2.5 at several points of the platform and tickets. The present study attempted to estimate the time-lag of conveyed air from the MVAC (Mechanical Ventilation Air Chamber) to the passengers' standing rooms.

Main purpose of this work is to provide the reasonable data for the integrated control program, which can give an order to operate the filtration system; individually or simultaneously. In order to meet an appropriate operation, an accurate estimation of the dust distribution inside is essential beforehand. Two particle monitors: Grimm-portable aerosol spectrometer 1.109(Germany) and HCT-PM sensor(Korea), were used to measure the quantitative analysis.

Table 1. Dust concentration of the flows at duct outlets from MVAC

[$\mu g/m^3$]

	Outdoor	Platform	Tickets	Filtration efficiency
PM10	56.3	10.9	12.4	78.3%
PM2.5	35.4	8.2	9.9	75.3%

Table 1 shows a typical tendency of dust levels just right after cleaning and conveying through long ducts. Filtration efficiency of the two stage filters including pre-filter and an electret filter screen was quite fair about 80% for fine dust aerosols. Nevertheless the supplied clean air from the MVAC would be combined with the ambient air insides of ticket waiting room and platforms. As can be seen in Fig. 1, therefore, the detected level of dust in ticket room and platform was quite high. Fig. 1 indicates the time delay of cleaning; for example of a certain day, the second electret filter in the MVAC initiated working at 9:00, but the cleaning effect on the internal spaces appeared at least one hour later. It implies that the artificial intelligence control system should consider the time delay as long as the predicted.

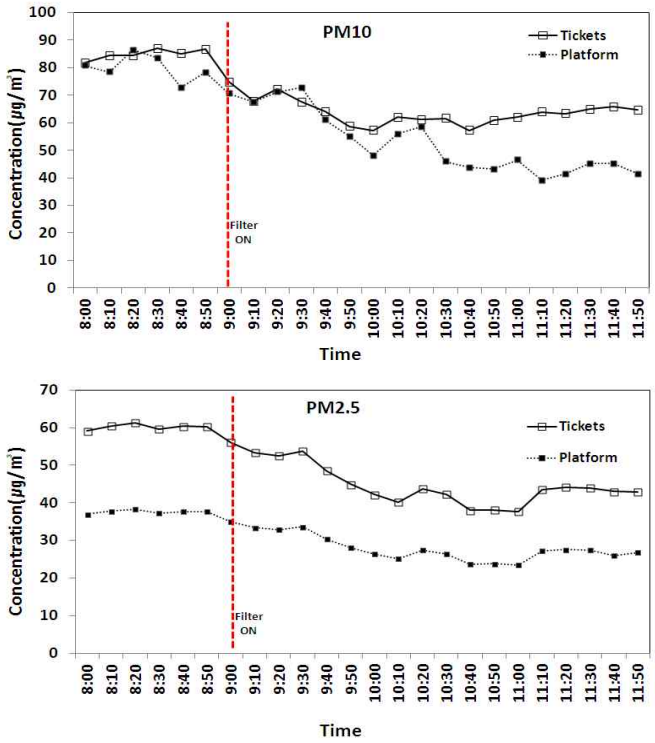

Figure 1. Dust concentration change with time at test indoor spaces.

Dust filtration of MVAC was more effective on platform than tickets because while the space of tickets was widely open to the external air, the standing corridors of platform in the second basement would be relatively isolated from the outdoor. In addition, the screen doors prevents inflowing the dust from the tunnel. In accordance, the platform composed of the limited air volume must be more effectively controlled by the central ventilation.

This research was supported by Seoul R&BD Program (CS 070160 : Development of artificial intelligence air quality control and management system for subway stations and tunnels)

Jang. J. H. K. Li and Y. M. Jo(2009) *Characterization of subway MVAC system in Seoul*, Korea Society for Indoor Environment, **6**(4), 237~250

Oh, J. T, (2011) *A Study on Artificial Intelligence Air Quality Control and Management System for Subway Stations and Tunnels,*164-184.

Results from the second Netherlands Research Program on Particulate Matter (BOP II)

E. van der Swaluw[1], M. Keuken[2], E. Weijers[3], M. Schaap[2], G. Kos[3], J. Matthijsen[4], H. Denier van der Gon[2] and R. Hoogerbrugge[1]

[1]National Institute for Public Health and the Environment (RIVM), PO Box 1, 3720 BA Bilthoven, The Netherlands
[2]Netherlands Organisation for Applied Scientific Research, TNO, PO Box 80015, 3508 TA Utrecht, The Netherlands
[3]Energy research Centre of the Netherlands (ECN), P.O. Box 1, 1755 ZG Petten, The Netherlands
[4]Netherlands Environmental Assessment Agency (PBL), PO Box 303, 3720 AH Bilthoven, The Netherlands
Keywords: PM10/PM2.5, monitoring, modelling, source apportionment
Presenting author email: Eric.van.der.Swaluw@rivm.nl

Introduction

A *review* is given of the results from the *second* Netherlands Research Program on Particulate Matter (BOP II). The BOP programs in the Netherlands are aimed at performing *policy-oriented* research on particulate matter, funded by the ministry of Infrastructure and the Environment. The BOP II framework was a co-operation between the institutes RIVM, ECN and TNO. The focus of BOP II addressed three main issues:

1. The concentrations of secondary inorganic aerosols (SIA) have been underestimated in the past in the Netherlands. BOP II provides an answer on 'how to continue' with analysis of models and measurements of SIAs.
2. PM_{10} and $PM_{2,5}$ are limited indicators to monitor the population based impact on health from the combustion aerosol. BOP II performed research in EC/OC on the local (city) scale and the more regional scale around Rotterdam. This to provide more insights in the contribution from sources within and outside of cities to the EC/OC concentrations in cities.
3. The first BOP program provided insights into the contribution of several sources to PM. However from the measurements performed in BOP it is difficult to determine whether the sources are originating from within or outside of the Netherlands. In BOP II this aspect will be investigated in more detail by means of model calculations which take into account source apportionment/labeling techniques.

Secondary inorganic aerosols

From the first BOP program it was concluded that the concentrations of SIAs had been underestimated by 50% in the Netherlands. In BOP II the mismatch between the old low-volume sampler (LVS) and the reference low volume sampler (Leckel) are further investigated: it was found that measurements as performed by the Leckel are more representative for ambient SIA concentrations than the ones measured with the old LVS method. Furthermore, fudge factors are derived in order to achieve comparability between the old LVS and recent Leckel annual values. Furthermore, depletion effects on the filters of the Leckel instrument were investigated: it was found that nitrate and chloride mass loss occurs on days with high temperature and low relative humidity.

Additionally, in BOP II new simulations were performed with the LOTOS-EUROS model which included new improved modules: height distribution of the emissions; cloud chemistry; implementation of compensation point approach for ammonia; improved dry deposition module for particles; implementation of new thermodynamic equilibrium module and including the formation of coarse nitrate mode. The underestimation of SIAs in the Netherlands in PM_{10} was reduced from 50% to 20% with the new simulations.

EC/OC

A measurement campaign was performed in Rotterdam from November 2010-November 2011. The campaign was focused on measurements of PM_{10}, $PM_{2.5}$ and EC/OC at urban background and kerbside locations. From this campaign it was shown that PM_{10} and $PM_{2.5}$ only partly reflect exposure to traffic-related PM. Contrary, EC showed elevation up to 100%, both near urban and motorway traffic.

Source apportionment

In BOP II source apportionment was implemented into the 3D chemistry-transport model LOTOS-EUROS (LE) model. With this new module in the LE model, one can now distinguish between national and foreign source contributions to the PM_{10} and $PM_{2.5}$ levels in the Netherlands. This information in both spatial and temporal variability of the source contribution to PM levels is a valuable tool for policy discussions.

BOP II reports can be downloaded from:
http://www.rivm.nl/Onderwerpen/Onderwerpen/F/Fijn_stof/BOP_II_het_vervolg_op_het_Nederlands_onderzoeksprogramma_fijn_stof

Single molecule water catalysis of atmospheric OH oxidation reactions

Theo Kurtén[1], Ditte Linde Thomsen[2], Solvejg Jørgensen[2], Signe Baggesen[2], Cecilie Aalling[2], Henrik Kjærgaard[2]

[1]Laboratory of Physical Chemistry, University of Helsinki, P.O. BOX 55, FI-00014 Finland
[2]Department of Chemistry, University of Copenhagen, Universitetsparken 5, DK-2100 København Ø, Denmark
Keywords: aerosol chemistry, precursors, molecular clusters, amines
Presenting author email: theo.kurten@helsinki.fi

Atmospheric chemical reactions have traditionally been divided into gas-phase and condensed-phase reactions. Elementary gas-phase reactions are typically assumed to involve at most two reactant molecules, with possible third bodies only playing the role of inert collision partners. Recent computational and experimental evidence has begun to nuance this picture, as the clustering (complexation) of reactants with just one or two condensable trace gas molecules such as water or formic acid has been shown to catalyse several key reactions. From an aerosol perspective, the most important example is the SO_3+ H_2O => H_2SO_4 reaction, which is speeded up many orders of magnitude due to catalysis by one or more water molecules (Kolb et al, 1994).

Atmospheric new-particle formation from gas-to-liquid nucleation is believed to involve sulfuric acid, water, nitrogen-containing base molecules such as ammonia or amines, and oxygenated organic compounds such as diacids. Water catalysis is already known to be important for sulfuric acid formation, and may possibly play a role also in key oxidation reactions involving nitrogen- and carbon-containing aerosol precursors.

We have investigated the effect of a water molecule on hydrogen abstraction by OH radicals from the central carbon atoms of a series of substituted, saturated organic compounds of the type $HCY_{1...2}X$. The series includes both amines (X = NH_2), alcohols (X = OH) and aldehydes (X = O): all relevant functional groups for aerosol formation and growth processes.

For molecules containing polar functional groups such as those mentioned above, the transition states for the hydrogen abstraction reactions by OH typically resemble those shown on the left-hand side of Figure 1. Water molecules are able to stabilize the transition states (lower the activation energy of the reaction) by forming hydrogen bonds with both the OH hydrogen atom and the polar group, as shown on the right-hand side of Figure 1. Our calculations indicate that the magnitude of the stabilization is at most a few kcal/mol, implying an increase in the reaction rate by around one order of magnitude at room temperature.

Since simultaneous three-body collisions in the atmosphere are extremely improbable, a necessary precondition for water catalysis is that water is already complexed with either the molecule being oxidized, or with OH. Unfortunately, neither OH nor any of the studied organic compounds of type $CY_{1...2}XH$ (including for example methylamine) form strong enough complexes with water to be significantly hydrated at temperatures and humidities encoutered in the troposphere. For example at 298 K and 50% RH, computed equilibrium constants indicate that at less than 0.03% of any of the reactants will be complexed to water.

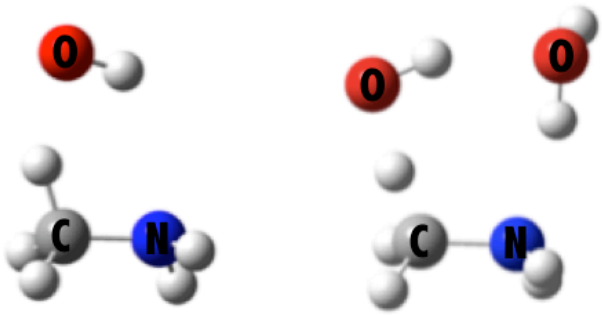

Figure 1. Transition states for the oxidation of methylamine by OH in the absence (left) and presence (right) of a water molecule.

Thus, despite the existence of a moderately strong *intrinsic* water catalysis effect (increase of the reaction rate when one of the reactants is complexed with water), the *net* catalytic effect of water on OH oxidation reactions in the atmosphere is likely to be quite small – certainly smaller than the typical error margins of reaction rate coefficients. The catalytic effects observed in the laboratory for OH oxidation reactions of, for example, acetaldehyde (Vöhringer-Martinez et al, 2007) were measured at very low temperatures and high absolute water concentrations – conditions unlikely to occur in the atmosphere. We therefore conclude that atmospheric chemistry models (for example, chemistry-transport models used in many types of aerosol modelling) do not need to include the effect of water catalysis on OH hydrogen abstractions from saturated organic compounds.

Calculations were performed at the B3LYP/aug-cc-pVTZ//CCSD(T)-F12/VDZ-F12 level using Gaussian 09 (Frisch et al, 2009) and Molpro 2010.1. (Werner et al, 2010). We thank the CSC IT Centre for Science in Espoo, Finland for computer time.

Frisch, M. J. *et al.* (2009) Gaussian 09, Gaussian, Inc., Wallingford CT, U.S.A.

Kolb, C. E. *et al.* (1994) *J. Am. Chem. Soc.* **116**, 10314–10315.

Vöhringer-Martinez, E. *et al.* (2007) *Science* **315**, 497-501.

Werner, H.-J. *et al.* (2010) MOLPRO, version 2010.1, http://www.molpro.net

Intercomparison of dust prediction models in the framework of the WMO SDS-WAS programme

E. Terradellas[1], S. Basart[2], M. Schulz[3], J. M. Baldasano[2], J.-J.Morcrette[4], G. Pejanovic[5], L. Menut[6], A. Benedetti[4], O. Jorba[2], S. Nickovic[7] and F. Benincasa[2]

[1]Agencia Estatal de Meteorología, carrer de l'Arquitecte Sert 1, 08005 Barcelona, Spain
[2]Earth Sciences Department, Barcelona Supercomputing Center, Jordi Girona 29, 08034 Barcelona, Spain
[3]Norwegian Meteorological Institute, Henrik Mohns Plass 1, 0313 Oslo, Norway
[4]ECMWF, Shinfield Park, RG2 9AX Reading, United Kingdom
[5]SEEVCCC-RHMSS, Kneza Višeslava 66, 11000 Belgrade, Serbia
[6]Laboratoire de Meteorologie Dynamique IPSL, Ecole Polytechnique, 91128 Palaiseau Cedex, France
[7]World Meteorological Organization, 7 bis Avenue de la Paix, 1200 Geneva, Switzerland
Keywords: dust, aerosol modelling, AOD
Presenting author email: eterradellasj@aemet.es

Sand and Dust Storm Warning Advisory and Assessment System (SDS-WAS) is a program of the World Meteorological Organization (WMO) with the mission to enhance the ability of countries to deliver timely and quality sand and dust storm forecasts, observations, information and knowledge to end users. The Regional Center for Northern Africa, Middle East and Europe, hosted by the Spanish State Meteorological Agency (AEMET) and the Barcelona Supercomputing Center (BSC-CNS), supports a network of research and operational partners implementing the objectives of the SDS-WAS program in the region.

A system to routinely exchange forecast model products has been established as the basis for a model intercomparison that includes common near real-time evaluation, verification, and generation of multimodel products. Six modelling systems: BSC-DREAM8b (Pérez et al., 2006), MACC-ECMWF (Morcrette et al, 200)), LMDzT-INCA (Schulz et al, 2009), DREAM8-MACC (Nickovic et al., 2001), CHIMERE (Menut et al., 2009) and NMMB/BSC-Dust (Pérez et al., 2011) provide daily dust forecast products (surface concentration and dust optical depth at 550 nm) for a reference area extending from 25ºW to 60ºE and from 0º to 65ºN with a 3-hourly basis until a lead time of 72 hours.

The forecasts of dust optical depth are compared with the total AOD provided by the AERONET network for 36 selected dust-prone stations. Version 2-Level 1.5 of AERONET products are used, that is, data that have been automatically cloud screened, but without the final calibrations applied. Since AERONET sun photometers do not yield AOD at 550 nm, it is calculated from AOD at 440, 675 and 870 nm and the Ångström exponent (AE) 440-870 using the Ångström law.

Bias error (BE) and root mean square error (rmse) are computed on a monthly basis. Because there might be other aerosol types not simulated by some of the participating models, negative BE could be expected. In order to minimize this source of error, it is intended to restrict the comparison to situations in which mineral dust is the dominant aerosol type. A threshold discrimination is made by discarding observations with AE higher than 0.6.

Multimodel products are generated from the values of the different prediction models. In order to produce them, the model outputs are bilinearly interpolated to a common grid mesh of 0.5 x 0.5 degrees. The median multimodel product could provide in principle a more reliable forecast than individual models. Its performance is assessed by comparing the respective verification scores. The range of variation of the models at every grid point is also displayed in order to evaluate the dispersion of the models and to allow identification of areas where there is a better match between the predictions of the different models.

Menut, L., Chiapello, I., and Moulin, C. (2009), *Previsibility of mineral dust concentrations: The CHIMERE-DUST forecast during the first AMMA experiment dry season*, J. Geophys. Res. - Atmospheres, 114, D07202

Morcrette, J.-J., Boucher, O. et al. (2009), *Aerosol analysis and forecast in the ECMWF Integrated Forecast System. Part I: Forward modelling*, J. Geophys. Res., 114, D06206 .

Nickovic, S., Kallos, G., Papadopoulos, A., and Kakaliagou, O. (2001), *A model for prediction of desert dust cycle in the atmosphere*, J. Geophys. Res., 106, 18113 - 18129.

Perez, C., Nickovic, S., Baldasano, J. M., Sicard, M., Rocadenbosch, F., and Cachorro, V. E. (2006), *A long Saharan dust event over the western Mediterranean: Lidar, Sun photometer observations, and regional dust modeling*, J. Geophys. Res., 111, D15214

Pérez, C., Haustein, K., et al. (2011), *Atmospheric dust modeling from meso to global scales with the online NMMB/BSC-Dust model–Part 1: Model description, annual simulations and evaluation.* Atmos. Chem. Phys., 11, 13001–13027

Schulz M., Cozic, A., and Szopa, S. (2009), *LMDzT-INCA dust forecast model developments and associated validation efforts*, IOP Conf. Ser.: Earth Environ. Sci. 7 012014

Secondary organic aerosol formation during summer 2010 over Central Europe

B. Langmann[1], K. Sellegri[2] and E. Freney[2]

[1] Institute of Geophysics, University of Hamburg, KlimaCampus, Hamburg, Germany
[2] Laboratoire de Meteorologie Physique, CNRS, Universite Blaise Pascal, Aubiere, France
Keywords: three-dimensional modeling, secondary organic carbon aerosol formation
Presenting author email: baerbel.langmann@zmaw.de

Introduction

Until recently, atmospheric models systematically underestimated measured OC aerosol mass concentrations in the atmosphere by a factor of up to 10 and more. Jimenez et al. (2009) proposed the concept of aging of organic vapors, thereby producing less volatile and higher oxygenated organic vapors with atmospheric mass concentrations comparable to sulfate. Based on these ideas, Yu (2011) developed a promising modeling strategy where the aging of organic vapors is considered and in addition to the traditional two compound thermodynamical gas-particle partitioning a third low volatile organic vapor is formed which kinetically undergoes condensation on pre-existing particles.

Model description

Here we use the regional three-dimensional atmosphere-chemistry-aerosol model REMOTE (Langmann et al., 2008) with the aerosol dynamics and thermodynamics module M7 (Vignati et al., 2004). The standard M7 has been extended by Anntila et al. (2010) by a thermodynamical two compound SOC aerosol formation mechanism. This one was further extended based on Yu (2011). We consider three classes of organic vapors where the low-volatile one is formed by aging form the more volatile ones. The low-volatile organic vapor is assumed to condense kinetically on pre-existing particles, while for the medium- and semi-volatile organic vapors the thermodynamical approach of Anntila et al. (2010) is used.

Model results

REMOTE model results over Central Europe are compared with measurements from a campaign at Puy-de-Dome, France during June 2010. Sulfate and chlorine aerosol mass concentrations are very well captured in the model simulation results - finally also organic carbon aerosol mass concentration. For illustrating the sensitivity of OC model results on SOC parameterizations, Fig. 1 shows results for the original two compound thermodynamical approach for isoprene only by Anntila et al. (2010) (grey line) and model results with additional VOC precursor gases (yellow line). Taking into account the SOC gases as additional trace species in the model, which undergo transport and removal (green line) leads to a considerable, however still insufficient increase in comparison with the measurements. The red line shows results from the simulation where aging of the most volatile SOC gas to the semi volatile SOC gas has been considered, finally generating OC aerosol mass concentrations in the range of the measurements. Taken into account the aging of the semi volatile SOC gas to the low volatile SOC gas (black line) does not modify OC aerosol mass concentrations much in comparison to the first aging step.

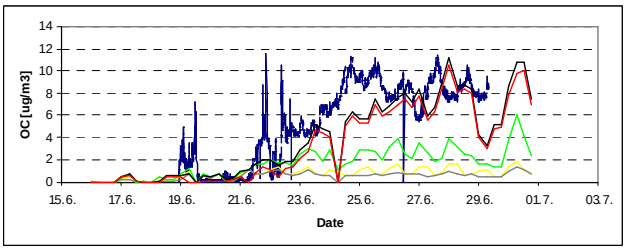

Fig. 1: AMS-measured (dark blue line) and modeled near surface OC mass concentration during June 2010 at Puy-de-Dome, France. Grey line: according to Anntila et al. (2010); yellow line: more VOC precursor gases; green line: SOC gas transport and removal; red line: 1. aging SOC gas; black line: 2. aging SOC gas - see text for more explanation

It should be noted however, that considerable differences in the aerosol size distribution are determined between the model simulations taking into account the first and second step of SOC gas aging. Due to kinetic condensation of the low volatile SOC gas, nucleation mode particles (up to 5 nm) grow into the aitken mode particle range (5 nm – 50 nm) which further grow into accumulation mode particle range (bigger than 50 nm).

This work was supported by the German and French Science Foundations DFG and CNRS within the joint project ATMOCHEM: Secondary organic aerosol production in the lower free troposphere over Western Europe.

Anttila, T. Langmann, B., Varghese, S. et al. (2010) Advances in Meteorology, doi:10.1155/2010/48203.
Jimenez, J.L., Canagaratna, M.R., Donahue, N.M. et al. (2009) *Science* **326**, 1525–1529.
Langmann, B., Varghese, S., Marmer, E. et al. (2008) *Atmos. Chem. Phys.* **8**, 1591–1607.
Vignati, E., Wilson, J., Stier, P. (2004) *J. Geophys. Res.* **109**, doi:10.1029/2003JD004485.
Yu, F. (2011) *Atmos. Chem. Phys.* **11**, 1083–1099.

Simulation and evaluation of ozone and its precursor gases over Indian region using the high resolution CHIMERE chemical transport model

Chinmay Jena, Sachin D. Ghude, G. Beig and D.M. Chate

This study presents annual simulations of ozone and its precursors made for the first time using CHIMERE regional chemistry transport model over the Indian domain. The model simulations are made using EDGAR emissions (v4.1) on 50 km by 50 km grid resolution for the year 2005. The model simulated ozone and its precursors are evaluated against ground-bashed and space-borne observations. The comparison of model results with seasonal variation of surface ozone observations from eleven sites and diurnal variation of ozone, CO and NO_X observations from two sites are presented. In addition, surface ozone measurements aboard 'Sagar Kanya' over the Bay of Bengal during 2009 are compared with the model simulations. The spatial and temporal variabilities of ozone, CO and NO_X are simulated very well by the model. The model in general compare well with the OMI observations during pre-monsoon and monsoon season, but underestimates tropospheric column NO_2 retrievals during post-monsoon and winter season. Model results indicate regional differences in surface ozone seasonality over Indian region. This study shows that CHIMERE model captures many important features of the observations and lends confidence to the use of model for understanding spatio-temporal variability of ozone over India. However, improvement of India emission inventories is also essential for accurately quantifying ozone production in this region.

Climate change impacts on atmospheric gas and particulate mercury levels and deposition rates

A. G. Megaritis[1,2], B. N. Murphy[3], and S. N. Pandis[1,2,3]

[1]Department of Chemical Engineering, University of Patras, Patras, 26500, Greece
[2]Institute of Chemical Engineering and High Temperature Chemical Processes, Foundation for Research and Technology Hellas (FORTH), Patras, 26504, Greece
[3]Department of Chemical Engineering, Carnegie Mellon University, Pittsburgh, PA 15213, USA
Keywords: CTM, Climate change, Mercury, Deposition
Presenting author email: athmegaritis@chemeng.upatras.gr

Despite its low concentration in the atmosphere, there is an increasing interest on atmospheric mercury (Hg) due to its ability to accumulate in the food chain in the form of methylmercury, a neurotoxin to living organisms and human beings (Satoh, 2000). In addition, atmospheric mercury is a global pollutant subject to long-range transport due to the long atmospheric lifetime of gaseous elemental mercury (0.5–2 years).

Recent studies have addressed the sensitivity of ozone and PM concentrations to climate change (Tagaris *et al*, 2007) pointing out that climate change could have an appreciable effect on future air quality. In this study, for the first time, we applied the global-regional climate-air pollution modeling system (GRE-CAPS) (Dawson *et al*, 2009) over the eastern United States to study the impact of climate change on concentration and deposition of atmospheric mercury in three distinct forms: gaseous elemental mercury (Hg^0), gaseous oxidized mercury (Hg^{2+}) and primary particulate mercury Hg(p).

The GRE-CAPS modeling system includes three models, spanning the global to the regional scale: the GISS II' GCM global CTM with online chemistry (Racherla and Adams, 2006), the MM5 regional meteorological model (Grell *et al*, 1994), and the PMCAMx regional CTM (Karydis *et al*, 2007) which was modified in order to simulate also mercury. A set of ten present-day Januaries and Julys was simulated using GRE-CAPS and the present-day model predictions (2000s) were compared to model predictions for a set of ten future Januaries and Julys. The future climate period studied was 2050s according to the Intergovernmental Panel on Climate Change A2 scenario.

Figure 1 shows the predicted changes in average July Hg^{2+} concentrations due to climate change. In most areas of the model domain, Hg^{2+} is predicted to increase in the future (3% on average), mainly due to increased temperature which favours the oxidation of Hg^0 and the subsequent formation of Hg^{2+}. The predicted increase was found to be highest in the Southeast (up to 25 pg m^{-3} or 35% in Florida). Similar results were predicted during January (5% increase on average) while Hg(p) was found to have a similar response to climate change as Hg^{2+}. On the contrary Hg^0 was not significantly changed, with a small decrease predicted in both periods.

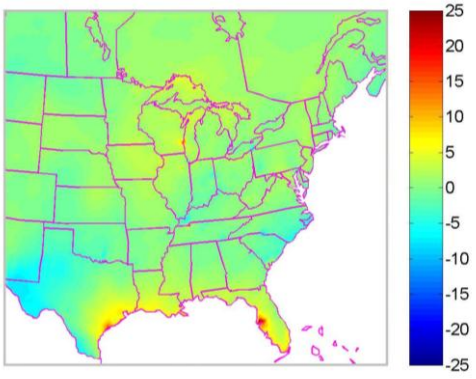

Figure 1. Changes (future-present) in average July Hg^{2+} concentrations (pg m^{-3})

Climate change has also a significant effect on mercury deposition. In both periods the response of mercury deposition to climate change varies spatially with an average increase of 3% during July and 5% during January to be predicted for the entire model domain. The predicted mercury deposition response is mainly explained from the changes in rainfall which largely affects mercury wet deposition.

This work was funded by the European Commission 7th Framework Programme project MEGAPOLI.

Dawson, J. P., Racherla, P. N., Lynn, B. H., Adams, P. J., and Pandis, S. N. (2009) *Impacts of climate change on regional and urban air quality in the eastern United States: Role of meteorology*, J. Geophys. Res., 114, D05308.

Grell, G. A., Dudhia, J., and Stauffer, D., (1994) *A description of the fifthgeneration Penn State/NCAR Mesoscale Model (MM5)*, NCAR Tech. Note, TN-398 + STR, Natl. Cent. for Atmos. Res., Boulder, Colo.

Karydis, V. A., Tsimpidi A. P., and Pandis S. N. (2007) *Evaluation of a three-dimensional chemical transport model (PMCAMx) in the eastern United States for all four seasons*, J. Geophys. Res., 112, D14211.

Satoh, H. (2000) *Occupational and Environmental Toxicology of Mercury and Its Compounds*, Industrial Health-Kawasaki, 38(2), 153– 164.

Tagaris, E., Manomaiphiboon, K., Liao, K. J., Leung, L. R., Woo, J. H., He, S., Amar, P., and Russell, A. G. (2007) *Impacts of global climate change and emissions on regional ozone and fine particulate matter concentrations over the United States*, J. Geophys. Res., 112, D14312.

Air Quality in Paris - A modeling study

A. G. Megaritis[1,2], K. Skyllakou[1,2], C. Fountoukis[2], and S. N. Pandis[1,2,3]

[1]Department of Chemical Engineering, University of Patras, Patras, 26500, Greece
[2]Institute of Chemical Engineering and High Temperature Chemical Processes, Foundation for Research and Technology Hellas (FORTH), Patras, 26504, Greece
[3]Department of Chemical Engineering, Carnegie Mellon University, Pittsburgh, PA 15213, USA
Keywords: PMCAMx-2008, Air Quality, Emissions Sources, $PM_{2.5}$
Presenting authors email: athmegaritis@chemeng.upatras.gr; ksakousti@chemeng.upatras.gr

Large urban population centers, also known as Megacities (Gurjar and Lelieveld 2005) are substantial sources of anthropogenic pollutants having adverse effects on human health, visibility and ecosystems (Seinfeld and Pandis 2006). In order to improve air quality in a Megacity like Paris we need to understand what fraction of the pollution comes from local and regional sources and to determine the response of the system to emission controls. Three-dimensional chemical transport models (CTMs) are well suited to help address these source receptor questions since they model all the necessary processes that impact air pollution concentrations and transport in the domain.

In this study we applied PMCAMx-2008 (Fountoukis *et al* 2011) a detailed 3-D chemical transport model (CTM) to simulate the chemical composition and mass of the major PM components during a summer and a winter period. The PMCAMx-2008 model includes state-of-the-art organic and inorganic aerosol modules which make it well suited for the purpose of this study. We focused our analysis on the Paris metropolitan area evaluating the performance of the model against Aerosol Mass Spectrometer ground measurements taken from different sites (LHVP, SIRTA and GOLF) in the Paris greater area. In addition, the contribution of air pollution originating from local and regional sources was examined through sensitivity analysis.

The model performance against the AMS measurements is encouraging especially during summertime. For example, for the suburban site in SIRTA the model reproduces both the observed diurnal variation in PM_1 organic aerosol (OA) and the measured average levels (predicted average 1.9 μg m^{-3} compared to a measured average of 1.85 μg m^{-3}) (Figure 1). The model performance for OA was similar in other sites. In general, OA is predicted to be the dominant species in both periods, accounting for 25% of total PM_1.

In order to examine the contribution of local and regional emissions sources to Paris air quality we performed a sensitivity analysis applying different emissions scenarios (e.g. an "annihilation" scenario zeroing all anthropogenic emissions in Paris). The results showed that local emissions sources accounted for approximately 20% of total PM_1 within Paris during summertime while during winter their contribution on PM_1 levels is higher (more than 30%). The impact of local sources is even higher for BC levels (more than 45% in both periods). At the same time, Paris emissions do not influence only the local air quality, but their impacts extend to the surrounding regions up to an average distance of 200 km.

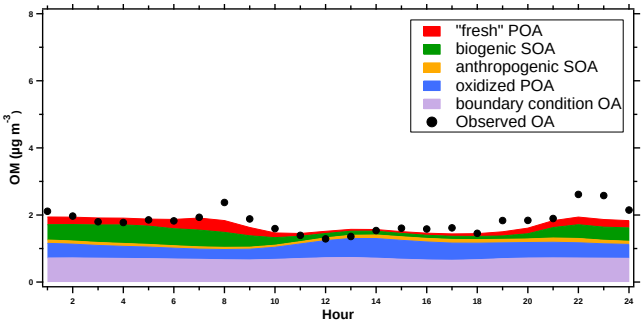

Figure 1. Summertime average diurnal profile of PM_1 organic aerosol and its component (in μg m^{-3}) in SIRTA.

In our study for the simulation of the contribution of different emissions source areas to Paris region we also utilized the Particulate Matter Source Apportionment Technology (PSAT) in PMCAMx-2008 to quantify the contributions from local emissions and short range, mid range and long range pollutant transport to Paris PM concentrations. The results of these simulations will be presented.

This work was funded by the European Commission 7th Framework Programme project MEGAPOLI.

Fountoukis, C., Racherla, P. N., Denier van der Gon, H. A. C., Polymeneas, P., Charalampidis, P. E., Pilinis, C., Wiedensohler, A., Dall'Osto, M., O'Dowd, C., and Pandis, S. N. (2011*) Evaluation of a three-dimensional chemical transport model (PMCAMx) in the European domain during the EUCAARI May 2008 campaign*, Atmos. Chem. Phys., 11, 10331-10347.

Gurjar, B. R., and Lelieveld, J. (2005) *New directions: megacities and global change*, Atmos Environ, 39, 391-393.

Seinfeld, J. H., and Pandis, S. N. (2006) *Atmospheric chemistry and physics: From air pollution to climate change*, 2nd ed.; John Wiley and Sons, Hoboken, NJ.

Development of a microphysical model for the H_2SO_4 – H_2O clouds on Venus

A. Määttänen[1], S. Bekki[2], F. Montmessin[1], S. Lebonnois[3]

[1]Laboratoire Atmosphères, Milieux, Observations Spatiales, Université Versailles St Quentin, CNRS, IPSL, Guyancourt, France.
[2]Laboratoire Atmosphères, Milieux, Observations Spatiales, Université Pierre et Marie Curie, CNRS, IPSL, Paris, France.
[3]Laboratoire de météorologie dynamique, Université Pierre et Marie Curie, Paris, France.
Keywords: cloud modeling, planetology, sulfuric acid.
Presenting author email: anni.maattanen@latmos.ipsl.fr

Clouds on Venus are formed of sulfuric acid aerosols. The clouds are optically very thick in the visible, inhibiting visual observation of the surface. The clouds are organized in three quite distinct layers with differing properties in terms of particle size distributions and possibly composition. Some early observations hint to the existence of other species in the clouds, but recent missions have not been able to verify their composition. The lowest cloud layers are very dynamic and the reason for the bi- and trimodal size distributions could be partly explained by mixing and distinct altitudes of nucleation. However, the possibility of mixed phase clouds and different chemical compositions of the droplets have not yet been evaluated.

Both the clouds of Venus and aerosols found in the Earth's stratosphere are composed of sulfuric acid droplets. On the Earth, the sulfur in the stratosphere originates from OCS, a long-lived sulfur species emitted at the surface and transported by the general circulation, and from volcanic eruptions that can inject material above the tropopause. It is thought that the water – sulfuric acid droplets form by binary homogeneous nucleation on both planets. However, the existence of condensation nuclei on Venus has not been ruled out.

We use a model developed for the sulfuric acid aerosols and polar stratospheric clouds (PSCs) in the terrestrial stratosphere (Jumelet et al., 2009; Larsen et al., 2000). The model describes several key microphysical processes, including nucleation via a parameterization for two-component nucleation (Vehkamäki et al., 2002) of water and sulfuric acid. This parameterization is in principle quite applicable for the Venusian atmosphere, but we discovered that the lower limit of relative humidity is still too high considering the extremely dry Venusian atmosphere. We are extending the parameterization of (Vehkamäki et al., 2002) to lower relative humidity (see another abstract by Määttänen et al., this conference). In addition to formation of droplets via nucleation, the model includes their subsequent growth by condensation, evaporation of droplets, coagulation, and sedimentation. The model describes explicitly the size distribution with 50 size bins. It can handle several particle modes described with a log-normal size distribution. In the future, we will explore simplifications of the fully size-resolved model in order to develop a moment model for coupling with a global atmospheric model (Lebonnois et al., 2010). We are planning to include the effects of (in)soluble condensation nuclei in the model at a later stage.

First tests of the model are carried out with a standard temperature profile from the Venus International Reference Atmosphere (VIRA, Kliore et al. 1986) and a compilation of water vapor and sulfuric acid concentration profiles, as in McGouldrick et al. (2007). Further sensitivity tests with profiles from the LMD Venus GCM (Lebonnois et al., 2010) are performed. Preliminary results will be evaluated against a range of cloud observations from Venus Express. The infrared channel of SPICAV instrument can scan the highest cloud levels and give profiles and microphysical properties, and for observations of the deeper cloud levels we will use the VIRTIS instrument.

We have developed an aerosol dynamics model for the Venusian clouds by adapting a model of terrestrial stratospheric aerosols and PSCs to the Venusian case. We will present the first results and some improvements included in the model during the development phase. The development is still ongoing, but we aim, after a full phase of testing, at developing a simplified version of the model for implementation into the LMD Venus GCM.

Jumelet J., S. Bekki, P. Seifert, N. Montoux, J.-P. Vernier and J.-P., Pelon J, J. Geophys. Res., 114, D00H03, 2009.

Kliore, A., Moroz, V., Keating, G., 1986. Pergamon, Oxford.

Larsen, N., Mikkelsen, I. B., Knudsen, B. M., Schreiner, J.,Voigt, C., Mauersberger, K., Rosen, J. M., Kjome,T., J. Geophys. Res.,105(D1), pp.1491, 2000.

Lebonnois, S., Hourdin, F., Eymet, V., Crespin, A., Fournier, R. and Forget, F., J. Geophys. Res.,115(E14), E06006, 2010.

McGouldrick, K. and Toon, O. B., Icarus 191, pp.1, 2007.

Vehkamäki, H., Kulmala, M., Napari, I., Lehtinen, K. E. J., Timmreck, C., Noppel, M., and Laaksonen, A.: J. Geophys. Res., 107(D22), pp. 4622, 2002.

Evaluation of the Marco Polo Venice and the Antonio Canova Treviso airports impact: two hot spots areas

E. Pecorari[1], G. Valotto[1], G. Rampazzo[1], S. Sollecito[2], D. Bassano[2], F. Bertoldo[3]and E. Rampado[3]

[1]Department of Environmental Science Informatics and Statistics, University Ca' Foscari, Dorsoduro 2137, I-30123 Venezia, Italy
[2]SAVE S.p.A., Marco Polo Venice airport viale G. Galilei 30/1, I-30173 Tessera-Venezia, Italy
[3]Ente Zona Industriale di Porto Marghera, via dell'Elettricità 39, I-30175 Porto Marghera-Venezia, Italy
Keywords: airport impact, aircraft emissions, Aircraft plumes
Presenting author email: eliana.pecorari@unive.it

Aircraft pollutant emissions have been of concern since the beginning of commercial aviation. The continuing growth in air traffic and the increasing public awareness have made environmental considerations one of the most critical aspects of commercial aviation (Kurniawan, 2011). This effect of airports close to urban areas is of growing concern and current emission regulations have focused on local air quality in the vicinity of airports (ICAO, 1993; ICAO, 2007a; ICAO, 2007b).

Ca' Foscari University in collaboration with SAVE S.p.A., Are Tre S.p.A. and Ente Zona Industriale (EZI) started in 2009 a research project in order to understand the role of the airports in two particular areas: Venice and Treviso. The two areas represent two important hot spots in the study of air pollution impact: i)the Venice Marco Polo airport, for the presence of the lagoon, a very delicate ecosystem and; ii) the Treviso airport for its closeness to urban sites. The project involved both measurements and modelling studies to characterize principal pollutants dispersion (SO_2, PM_{10}, O_3, NO, NO_X NO_2, CO, methane and non-methane hydrocarbons). A characterization of both Venice and Treviso aircraft emissions were made adopting the EMEP/CORINAIR methodology (EMEP, 2009). A 3D Lagrangian particle dispersion model, SPRAY, (Tinarelli et al., 1994) was applied to assess the impact of aircrafts in both the study sites. Predicted data were correlated to measurements and to the other emission sources of the areas. Results presents a low impact of both the airports respect to the close urban and natural areas.

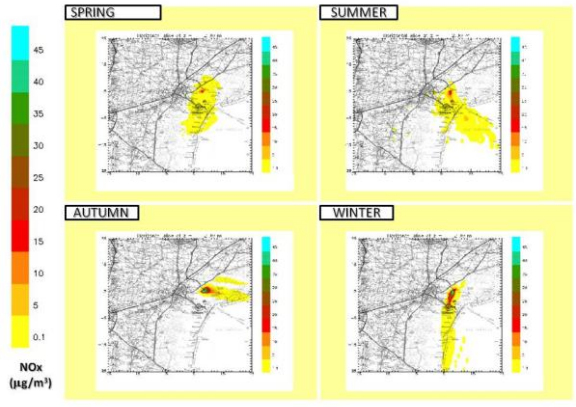

Figure 1. An example of aircraft dispersion in Venice Marco Polo airport during winter.

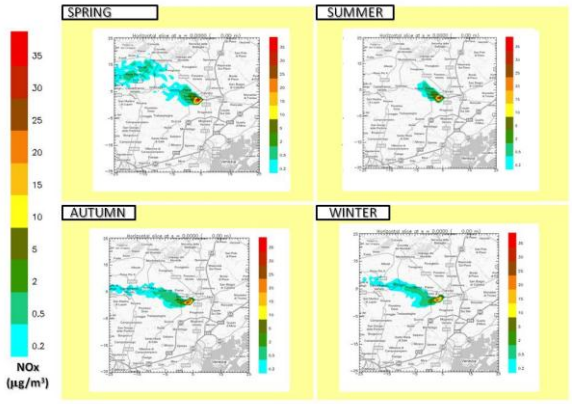

Figure 2. An example of aaircraft dispersion in Treviso airport during winter.

References

EMEP, 2009. "EMEP/CORINAIR Emission Inventory Guidebook—2009 UPDATE, Technical Report, Shipping Activities—Sub sector 0804, European Environment Agency http://www.eea.europa.eu/publications/emep-eea-emission-inventory-guidebook-2009.

ICAO. International Standards and Recommended Practices, Environmental Protection Annex 16. Volume II Aircraft Engine Emissions. second ed. 1993.

ICAO. Airport Local Air Quality Guidance Manual; 2007a.

ICAO. Environmental Report; 2007b.

Kurniawan Jermanto S. and Khardi S., (2011). Comparison of methodologies estimating emissions of aircraft pollutants, environmental impact assessment around airports. Environmental Impact Assessment Review, 31, 240 – 252.

Tinarelli G., Anfossi D., Brusasca G., Ferrero E., Giostra U., Morselli M.G., Moussafir J., Tampieri F., Trombetti F. (1994). Lagrangian particle simulation of tracer dispersion in the Lee of a schematic two-dimensional hill. Journal of Applied Meteorology, 33, pp. 744–756.

Nucleation studies with regional aerosol-climate model REMO-HAM

J.-P. Pietikäinen[1], S. Mikkonen[2] and A. Laaksonen[1]
[1]Finnish Meteorological Institute, P.O. Box 503, 00101 Helsinki, Finland
[2]Department of Applied Physics, University of Eastern Finland, P.O. Box 1627, 70211 Kuopio, Finland
Keywords: nucleation, climate models, statistical proxy.
Presenting author email: Joni-Pekka.Pietikainen@fmi.fi

Nucleation of aerosol particles is an important part of the climate system. It occurs around the world and has a potential to influence regional cloud condensation nuclei (CCN) concentrations (e.g. Kulmala *et al* (2004), Laaksonen *et al* (2005)). Different types of mechanisms for nucleation have been proposed in the past few years. It is still unkown which of the different mechanisms is the dominant one, or whether nucleation can be only explained with a combination of different mechanisms. In any case, sulfuric acid (H_2SO_4) is concidered to be the most important species contributing to nucleation. Moreover, many studies have also indicated the importance of organic compounds to nucleation and particle growth.

In this work, we have concentrated on the boundary layer activation nucleation. In this mechanism, the nucleation rate J_{nuc} is taken to be a function of gas phase sulfuric acid concentration $[H_2SO_4]$:

$$J_{\mathrm{nuc}} = A \times [H_2SO_4], \qquad (1)$$

where A is the activation coefficient. We have used this mechanism in a regional aerosol-climate model REMO-HAM (Pietikäinen *et al* (2012)). In REMO-HAM, the H_2SO_4 concentration mainly depends on the availability of sulfur dioxide (SO_2) and dimethyl sulfide (DMS), and the oxidative species OH (daytime chemistry, for SO_2 and DMS) and NO_3 (night-time chemistry, only for DMS) (Stier *et al* (2005)). For H_2SO_4 concentrations, SO_2 oxidation by OH during daytime is the most important process. The normal approach for determining the concentrations of the oxidative species in the model is to use monthly mean fields derived from the chemical transport model MOZART. In addition an artifical cosine based diurnal cycle has been applied for OH. This improves the treatment of OH inside the model, but does not link its concentrations directly to radiation (OH is known to be formed by photochemistry in the atmosphere). Therefore, reduction of radiation intensity below clouds does not affect the OH concentrations.

In order to improve the calculation of H_2SO_4 concentrations in REMO-HAM, we have implemented a statistics-based proxy for the OH concentrations. The proxy is a non-linear function of solar radiation intensity and is based on OH measurement data from Europe. In this way, the 3-D OH oxidation fields become radiation dependent, and are thus affected by the cloudiness inside the model. The improved representation of OH leads to more realistic H_2SO_4 concentrations. This is important, because in our previous studies we have shown that the model has too much sulfuric acid in the gas phase (Pietikäinen *et al* (2012)).

We have done series of detailed simulations for Europe with 50×50 km^2 horizontal resolution. The simulations included the the new OH proxy approach. In addition, we have tested a range of values for the activation nucleation coefficient. Fig. 1 shows the sulfuric acid concentrations from Hyytiälä and San Pietro Capofiume for both model versions. Measured daily maximum values at Hyytiälä are about $[2]\times10^7$ molec/cm^3 (data for the years 2003 and 2007), and about $[5]\times10^7$ molec/cm^3 at San Pietro Capofiume(data for the year 2009) (Mikkonen *et al* (2011)). As we can see from the Fig. 1, the new model version gives much more realistic results than the old one.

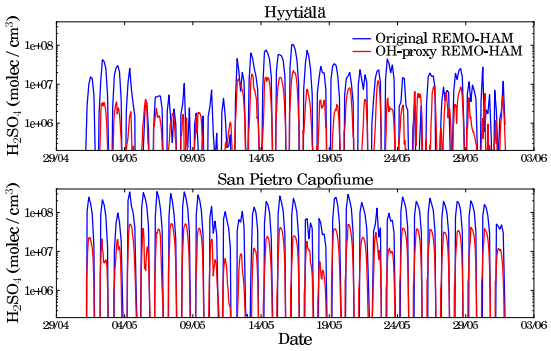

Figure 1: Original and OH-proxy REMO-HAM sulfuric acid conconcentrations from Hyytiälä and San Pietro Capofiume for May 2005.

If we consider $J_{\mathrm{nuc}} = 1.0$ cm^{-3} s^{-1} as a limit for nucleation event, we get slight overestimation for the number of event days. This naturally depends on the activation coefficient A. With $A = 4\times10^{-7}$ s^{-1}, we get for May 2005 at Hyytiälä 18 nucleation days (observations: 12), and at San Pietro Capifueme 28 days (observations: 22).

Kulmala, M. *et al* (2004), J. Aer. Sci., **35**, 143-176.
Laaksonen, A. *et al* (2005), Geophys. Res. Let., **32**, L06812.
Mikkonen, S. *et al* (2011), Atmos. Chem. Phys., **11**, 11319-11334.
Pietikäinen, J.-P. *et al* (2012), Geosci. Model Dev., submitted.
Stier, P. *et al* (2005), Atmos. Chem. Phys., **5**, 1125-1156.

Research Needs Identified In a First-Generation Regional Air Quality Model for Polycyclic Aromatic Hydrocarbons

E. Galarneau[1], P.A. Makar [1], Q. Zheng[1], J. Zhang[1], and M.D. Moran[1]

[1]Air Quality Research Division, Environment Canada, Toronto, Ontario, M3H 5T4, Canada
Keywords: air quality model, chemical transport model, polycyclic aromatic hydrocarbons, PAHs
Presenting author email: elisabeth.galarneau@ec.gc.ca

AURAMS is a regional air quality model developed by Environment Canada to examine issues relating to ground-level ozone, size-resolved particulate matter, and acid deposition. The model has now been extended to simulate the atmospheric fate of polycyclic aromatic hydrocarbons (PAHs). Seven PAH species that span a range of volatilities and reactivities were selected for the first formal AURAMS-PAH simulation in order to examine interspecies differences in model performance.

The model was run for a full-year period (2002) using two alternate particle/gas partitioning schemes: Junge-Pankow adsorptive partitioning and Dachs-Eisenreich dual sorption partitioning. Model outputs were compared to ~5,000 PAH measurements from ~50 sites in southern Canada and the continental USA. Model performance was assessed for simulation accuracy of total (gas plus particle) PAH concentration, particle/gas partitioning, and particle size distribution. As a result of this first assessment, a list of research needs has been developed and is described below.

The first group of research needs relates to the PAH emissions that are used as model inputs (Galarneau et al., 2007). Model performance in predicting PAH concentrations was found to vary systematically by month of year (see Figure 1) and by day of week. This implies that the factors used to disaggregate annual emissions require adjustment. Extreme underestimation of anthracene concentrations near a large industrial facility in Canada led to the discovery that this commonly-reported species was excluded from mandatory reporting through the National Pollutant Release Inventory of facility emissions data in Canada. PAH particle sizes calculated with Dachs-Eisenreich partitioning were erroneously bimodal because of errors in a default emitted elemental carbon size distribution which have since been corrected.

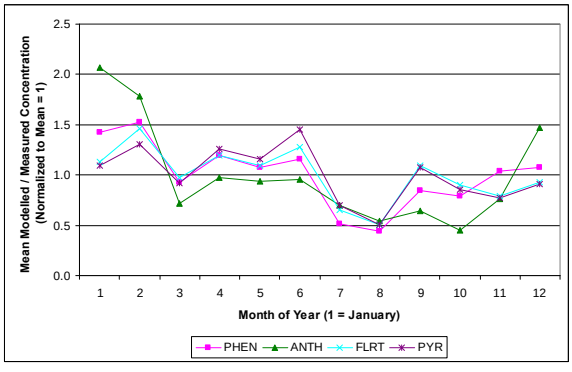

Figure 1: Concentration Simulation Variation by Month of Year for Four PAHs

The second group of research needs relates to physicochemical process representations in the model. The addition of PAH species to AURAMS required modifications to many existing model routines that handle reactivity, aqueous-phase chemistry, and deposition. Furthermore, a novel routine was added to calculate particle/gas partitioning according to the two aforementioned parametrisations thought to be relevant to PAHs. For the modified model to simulate PAH fate with reasonable accuracy, not only must the relevant processes be included but their associated physicochemical parameters must be also be correct.

Reactive particulate compounds such as benzo[a]pyrene (BaP) tended to be overestimated in the simulations; this may be due to the absence of particle-phase degradation in the model. However, no relationship was found between the degree of BaP overestimation and ozone concentration. Particle/gas partitioning was greatly biased toward the gas phase for volatile species but performance improved with decreasing volatility (increasing molecular weight). This behaviour was seen for both partitioning expressions and suggests that the physicochemical properties used in those expressions need adjustment. The simulated size distributions of all PAHs were identical because quantitative expressions to describe the inter-species differences observed in numerous field studies have not yet been developed and incorporated in the model.

The third and final group of research needs relates to shortcomings in the base AURAMS model that are not related to PAHs. For example, the total PM mass simulated by the model tends toward underestimation. As a result, the available pool of particle surface or mass available for partitioning of PAHs is not accurately represented. Improvements to PM accuracy in the model are expected to lead to improvements in the simulation of partitioning and particle size distribution of PAHs.

Observed inaccuracies in model simulations may be due to a combination of causes. For example, BaP overestimation may have contributions from both overestimated emissions and unrepresented reactions. Further analysis of these factors, including sensitivity of model results to their adjustment, will be conducted in order to prioritize research needs for the development to the second-generation version of AURAMS-PAH.

Galarneau, E., Makar, P.A., Sassi, M., and Diamond, M.L. (2007) *Environ. Sci. Technol.* **41**, 4205-4213.

Modelling dust aerosol impacts on heating rate profiles over the Iberian Peninsula and Atlantic Ocean

D.Santos[1], M. J. Costa[1,2], R. Salgado[1,2] and A. M. Silva[1,2]

[1]Évora Geophysics Centre, University of Evora, R. Romão Ramalho, 59, 7000 Évora. Portugal
[2]Department of Physics, University of Evora, R. Romão Ramalho, 59, 7000 Évora. Portugal.
Keywords: Atmospheric Aerosol Modelling, Desert Dust radiative effects, Radiation
Presenting author email: dinas@uevora.pt

It is well known that the Sahara desert acts as the strongest source of mineral dust aerosol in the world.

Several studies have been dealing with estimation of direct effects associated with major aerosol types, especially mineral dust, and related changes of the radiative budget at the surface, top of atmosphere (TOA) and within the aerosol layer.

The effect of dust particles is very complex because of their capacity to interact both in the shortwave and longwave spectral ranges.

Over a given region, the desert dust radiative effects, occurring at different atmospheric levels (surface, TOA and within the aerosol layer), all contribute to a climatic response. Thus it is very important to understand how these effects can alter the earth energy budget at regional and/or global scales.

The Iberian Peninsula and surrounding Atlantic Ocean are affected by considerable mineral dust loadings able to significantly modify the regional radiative budget (Santos *et al* 2011).

The present study investigates the mineral dust potential impact in terms of heating rate profiles.

This work has been carried out by using the MesoNH meso-scale forecasting model (Lafore *et al* 1998) fully coupled with a dust production and transport model (Grini *et al* 2006), a radiation scheme and an explicit land surface model. The MesoNH model has then the ability of investigate how the aerosols have a direct radiative forcing upon the surface-atmosphere system.

Initialization and lateral boundary conditions of the domain used (10×10 km resolution) were taken from the ECMWF analysis. A case study for intense dust events occurring during May 2006, September 2007 and April 2011 is analysed.

Figure 1 present the simulated atmospheric heating rate at TOA level for 27 May 2006 (1200UTC).

From this Figure it is possible to observe the atmospheric heating rate changes due to the presence of desert dust in the atmosphere. An increase of the atmospheric heating rate is observed when the mineral dust layer is present in the atmosphere (probably due to the absorption of the incoming radiation).

For the other days under analysis the same situation occurs, being the warming more pronounced within the mineral dust layer.

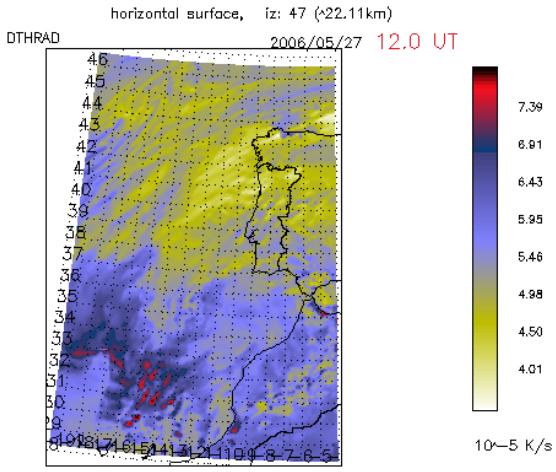

Figure 1. Simulated atmospheric heating rate for 27 May 2006 (1200UTC) at TOA level.

The work was supported through FEDER (Programa Operacional Factores de Competitividade – COMPETE) and National funding through FCT (Fundação para a Ciência e a Tecnologia) in the framework of projects FCOMP-01-0124-FEDER-007122 (PTDC / CTE-ATM / 65307 / 2006) and FCOMP-01-0124-FEDER-009303 (PTDC/CTE-ATM/102142/2008).

Lafore, J.-P., J. Stein, N. Asencio, P. Bougeault, V. Ducrocq, J. Duron, C. Fischer, P. Héreil, P. Mascart, V. Masson, J.-P. Pinty, J.-L. Redelsperger, E. Richard, and J. Vilà-Guerau de Arellano (1998) *The Meso-NH Atmospheric Simulation System. Part I: adiabatic formulation and control simulations, Scientific objectives and experimental design*, Ann. Geophys., 16, 90-109. http://www.ann-geophys.net/16/90/1998/.

Grini, A., Tulet, P., and Gomes, L. (2006) *Dusty weather forecasts using the MesoNH mesoscale atmospheric model*, J. Geophys. Res., 111, D19205, doi:10.1029/2005JD007007.

Santos, D., M. J. Costa, A. M. Silva, R. Salgado, A. Domingues, and D. Bortoli (2011) *Saharan desert dust radiative effects: a study based on atmospheric modelling*,Int. J. Global Warming, 3, 88-102.

Modelling $PM_{2.5}$ chemical composition with CAMx in southwest Spain

C. Milford[1,2], N. Castell[3], C. Marrero[2], A. Sánchez de la Campa[1], R. Fernández-Camacho[1], S. Rodríguez[2,1], J. D. de la Rosa[1] and A. F. Stein[4]

[1]University of Huelva, Joint Research Unit to CSIC, Campus El Carmen, Huelva, Spain
[2]Izaña Atmospheric Research Centre, AEMET Joint Research Unit to CSIC, Spain
[3]NILU-Norwegian Institute for Air Research, PO Box 100, NO-2027 Kjeller, Norway
[4]Earth Resources and Technology on assignment to Air Resources Laboratory, NOAA, Maryland, USA
Keywords: aerosol modelling, $PM_{2.5}$, chemical composition.
Presenting author email: cmilford@aemet.es

Background $PM_{2.5}$ concentrations (rural) are rather high in the southwest region of Spain (Andalusia). The region has high anthropogenic emissions including substantial industrial emissions (e.g. power plants, petrochemical refineries, fertiliser industry), on-road traffic, shipping traffic passing through the Gibraltar strait, agricultural emissions and also biogenic emissions. It also experiences a high frequency of African dust intrusions and its low rainfall, dry soils and high photochemical activity plus the availability of aerosol precursors all contribute to the enhanced concentration of atmospheric aerosols.

As a result of these factors the AER-REG project was initiated to study the formation and transport of atmospheric aerosol in western Andalusia. It involved intensive measurement campaigns at two rural sites and one urban site in 2008 and 2009. Chemically speciated $PM_{2.5}$ measurements of all major aerosol components (sulphate, nitrate, ammonium, total carbon, black carbon, sea-salt, dust) plus trace elements were made during daytime and nighttime with high volume samplers (30 m^3 h^{-1}) using quartz micro-fibre filters. In addition highly time resolved (15 minute mean) measurements of Black Carbon (BC) were made at one of the rural sites and the urban site using a Multi-Angle Absorption Photometer, see Fernández-Camacho *et al* (2010) for more details. Gaseous measurements of O_3, SO_2, NO and NO_2 were also conducted.

In parallel to the chemically speciated measurements the three-dimensional eulerian photochemical model CAMx v4.51 (Environ) was implemented to investigate the complex dynamics of aerosol formation and transport in this region and their spatial and temporal resolution. CAMx was run with three nested domains with 18 km, 6 km and 2 km resolution. The outer domain covers the Iberian Peninsula while the inner domain covers the southwest region of Spain (western Andalusia). The non-hydrostatic mesoscale meteorological model (MM5) v3.7 was used to drive the photochemical model.

Emissions in the inner domain are based on Castell *et al* (2010) and include industrial point and area sources; on-road and shipping traffic; NH_3 emissions from fertiliser application to agricultural land and biogenic sources of non-methane volatile organic compounds (NMVOC). Emissions in the outer domains are from EMEP plus biogenic NMVOC emissions.

The combination of the high quality chemically speciated measurement dataset and the modelling system is now being utilised to explore the seasonal differences in both primary and secondary chemically speciated aerosol. The model performs well for ammonium in both summer and winter periods (although tending to underestimate the magnitude of concentrations) while for sulphate the performance is better during the summer period. The highly resolved measurements of $PM_{2.5}$ BC and CAMx simulated $PM_{2.5}$ primary elemental carbon (PEC) at the urban site in Huelva in winter and summer (Fig. 1) show that the model captures the diurnal and seasonal variability of this primary aerosol. Peak concentrations are observed during a winter anticyclonic episode in the first half of the March campaign and these are well captured by the modelling system (Fig. 1a), although the model underestimates concentrations in the latter half of the campaign. During the summer campaign, concentrations are generally much lower reflecting enhanced dispersive conditions (Fig 1b).

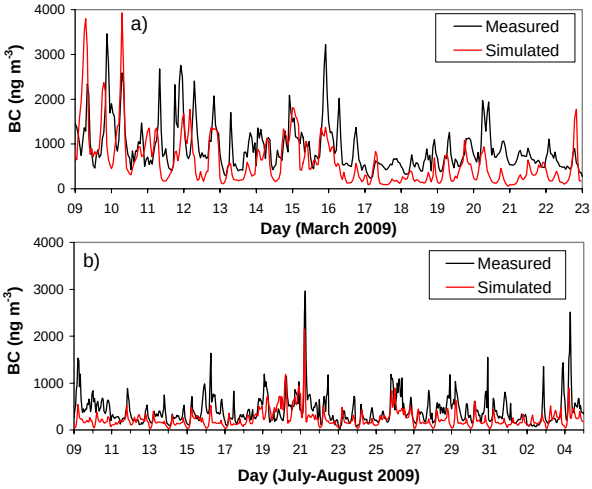

Figure 1. Measured BC ($PM_{2.5}$) and simulated $PM_{2.5}$ PEC concentrations at University Campus, Huelva.

The authors gratefully acknowledge funding from the Department of Innovation, Science and Enterprise (Andalusia Government) through the projects AER-REG (P07-RNM-03125) and SIMAND (P07-RNM-02729).

Castell, N., Mantilla, E., Salvador, R., Stein, A.F. and Millán M. (2010) *J. Environ. Manage.* **91**, 662-676.
Fernández-Camacho, R., Rodríguez, S., *et al.* (2010) *Atmos. Chem. Phys.* **10**, 9615–9630.

Simulation of mineral dust particle contribution to urban aerosol loading in Greater Beijing with the model system COSMO-ART

S. Schrader[1,3], B. Vogel[2], H. Vogel[2], K. Schäfer[3], R. R. Shen[3], P. Suppan[3], S. Norra[1]

[1]Institute of Geography and Geoecology, Karlsruhe Institute of Technology (KIT), 76128 Karlsruhe, Germany
[2]Institute of Meteorology and Climate Research – Troposphere Research (IMK-TRO), Karlsruhe Institute of Technology (KIT), 76128 Karlsruhe, Germany
[3]Institute of Meteorology and Climate Research – Atmospheric Environmental Research (IMK-IFU), Karlsruhe Institute of Technology (KIT), 82467 Garmisch-Partenkirchen, Germany
Keywords: Modelling (regional), Asian dust, air pollution, megacity
Presenting author email: stefanie.schrader@kit.edu

Sand- and dust storms frequently occur in spring in Northern China causing very high geogenic particle mass concentrations in the atmosphere (Wu *et al.*, 2009). Dust particles can be transported over long distances towards the highly urbanized areas of Eastern China. These geogenic particles influence the state of the atmosphere and provide effective surfaces for heterogeneous chemical reactions (Huang *et al.*, 2010). In megacities like Beijing, the combined anthropogenic and geogenic aerosol loadings can lead to severe reduction of air quality and harm the human health (Chen *et al.*, 2011). Still, a lack of information exists about the impact of these geogenic particles on the urban atmosphere and aerosol pollution.

To investigate the contribution of geogenic particles on the urban particle loading in Beijing and their impact on the state of the atmosphere the comprehensive online coupled model system COSMO-ART (Vogel *et al.*, 2009) has been set up for Northern China. COSMO-ART consists of the meteorological weather forecast model COSMO of the German Weather Service (DWD) and ART for the treatment of aerosols and reactive trace gases. The model domain covers whole Northern China which allows the investigation of the influence of mineral dust from all Chinese desert areas to the particle loading in Beijing. COSMO-ART is applied for the spring season 2011 with a 28x28 km² horizontal resolution.

Model results are compared to $PM_{2.5}$ data measured by KIT. Daily measurements were conducted with two high volume samplers at one station in Beijing since June 2011. Meteorological data for model and measurement comparison is taken from the Beijing WMO official meteorological station.

COSMO-ART is applied for the Asian dust storm event that hit Beijing at April 30th in 2011 lasting for about 1 day. The Beijing meteorological station reported blowing sand conditions and wind speeds up to 20 m/s from north-western directions. There is also a rapid drop of relative humidity from 90 to 10% with arrival of the dust storm air masses. Observed $PM_{2.5}$ concentrations showed a sudden peak up to 100µg/m³. The simulated mass concentrations are reproducing the timing of this peak quite well. This confirms that the high particle concentrations observed in Beijing during this episode are of geogenic origin. In a next step we will also include in addition to the natural ones the anthropogenic emissions to quantify the contributions of each source category to PM_{10} in Beijing.

The horizontal distribution of simulated mass concentrations of mineral dust particles for April 30th 03h UTC is shown in figure 1. It can be seen that near surface wind is coming from north-western directions indicating that Gobi desert in Western Inner Mongolia is the main source of the geogenic particles transported to Greater Beijing. The fast decrease of relative humidity down to 10% is also supporting the assumption of the arrival of dry air masses from these desert areas.

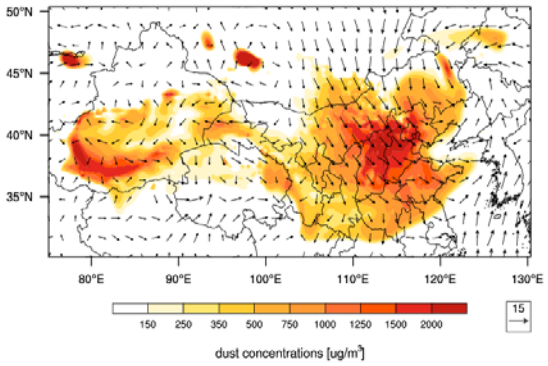

Figure 1. Simulated dust particle mass concentrations for April 30th 2011, 03h UTC and near surface wind conditions

This work is partly funded by the Graduate School for Climate and Environment (GRACE) of KIT and the KIT Centre for Climate and Environment.

Chen, R., Li, Y., Ma, Y., Pan, G., Zeng, G., Xu, X., Chen, B. and Kan, H. (2011) *Sc. Tot. Environ.*, 409, 23, 4934-4938.

Huang, K., Zhuang, G., Lin, Y., Li, J., Sun, Y., Zhang, W. and Fu, J. S. (2010) *J. Geophys. Res.*, 115, D00K16.

Vogel, B., Vogel, H., Bäumer, D., Bangert, M., Lundgren, K., Rinke, R. and Stanelle, T. (2009) *Atmos. Chem. Phys.*, 9, 8661-8680.

Wu, Z. J., Cheng, Y. F., Hu, M., Wehner, B., Sugimoto, N. and Wiedensohler, A. (2009) *Atmos. Chem. Phys.*, 9, 6915-6932.

Effects of modal representation of aerosol distribution on aerosol activation and optical properties

Korhola, T.[1], Kokkola, H.[2], Korhonen, H.[2], Partanen, A.-I.[2], Laaksonen, A.[1,3], Romakkaniemi, S.[1]

[1] Department of Applied Physics, University of Eastern Finland, Finland
[2] Finnish Meteorological Institute Kuopio Unit, Kuopio, Finland
[3] Finnish Meteorological Institute, Climate change, Helsinki, Finland
Keywords: modelling, modal representation, size distribution, activation, extinction coefficient
Presenting author email: tapani.korhola@uef.fi

In atmospheric modelling there are several applications where an aerosol microphysics module is coupled with a general circulation model. Many of these modules use a modal representation for aerosol distribution. For example, four modes can be used to cover the aerosol size range from nucleation to coarse mode. In 3D-transport model applications modes are often restricted to certain particle size ranges. If the larger edge of the mode grows over its set size limit, particles are moved, reallocated to the next mode (Binkowski and Roselle 2003).

When used in large scale models, modal modules reallocate the distribution to account for the changes in mode radius from microphysical processes and air mass mixing over a simulation step. The distributions before and after reallocation routine should describe the same physical situation (Figure 1). Nevertheless, in case of a rapid growth of one or several modes these two distributions can differ greatly. When the difference is in Aitken, accumulation and coarse mode size range, it affects the number of activated particles during cloud droplet formation when calculated from these modal representations. If the distributions before and after reallocation differ in accumulation and coarse mode size range, also the total extinction coefficient of aerosol particles can be clearly affected by the difference.

In this study we explore how the reallocation affects climate relevant model parameters such as cloud droplet number concentration (CDNC) and extinction coefficient. First, a base distribution is defined so that none of the modes exceed their size limit and there is no need for reallocation. Then the average radius and/or number concentration of a single mode is increased in small increments, creating a large set of distributions. When the mode grows enough, some of the particles will be reallocated to the next mode. Then the number of cloud droplets and the extinction coefficient are calculated before and after the reallocation routine. The number of cloud droplets is calculated by using a parametrization by Abdul-Razzak et al (2000) and the extinction coefficient by using libRadtran library.

From the CDNC and extinction coefficient we calculated the relative difference between the before and after reallocation cases. In our simulations we found out that the relative difference in CDNC and extinction coefficient can be from few to tens of percents.

Figures 1 and 2 are the results from a simulation where the accumulation mode properties were varied (average radius from 150 to 210 nm and number concentration from 10 to 1000 1/cm^3). Figure 1 shows the most "extreme" case where the overgrowth of the right most mode (accumulation mode) is the largest in the simulation, corresponding to the rightmost edge of Figure 2. In Figure 1, the number concentration of accumulation mode is 500 1/cm^3 before the reallocation. In Figure 2 the axes show the values of the diameter and number concentration of an accumulation mode through the simulation, and the colour describes the relative difference of the extinction coefficient. From Figure 2 we can see how strongly the difference between distributions affects the extinction coefficient.

An artificial data set was used in this simulation. The next step is to see if similar results can be obtained from the development of the real atmospheric aerosol distributions, for example in the case of a realistic nucleation event followed by growth of the aerosol particles.

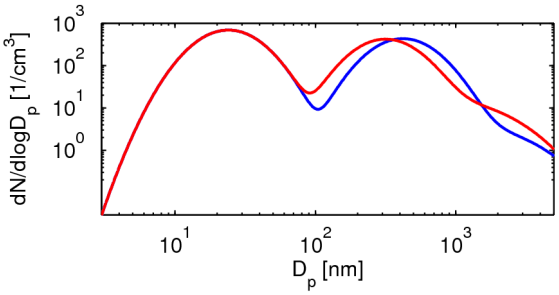

Figure 1. Distributions before (blue) and after (red) reallocation routine.

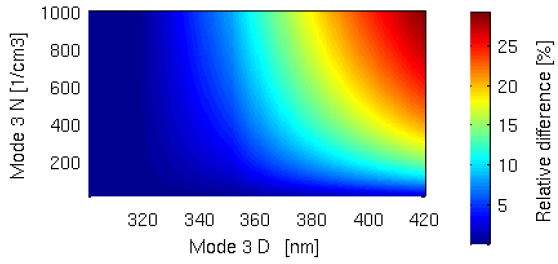

Figure 2. The relative difference of the extinction coefficient calculated before and after reallocation.

Binkowski, F., Roselle S., *Models-3 Community Multiscale Air Quality (CMAQ) model aerosol component 1. Model description.* J. Geophys. Res., 108, 4183, 18 PP, 2003

Abdul-Razzak, H., Ghan, S. T., *A Parameterization of Aerosol Activation. Part 2: Multiple Aerosol Types.* J. Geophys. Res. D. (Atmospheres) 105:6,837-6,844, 2000

Aerosol observations and predictions in the southeastern Europe during the extreme summer 2007

E. Athanasopoulou[1], E. Gerasopoulos[1], H. Vogel[2], S. Kazadzis[1], E. Liakakou[1], M. Gratsea[1], and B. Vogel[2]

[1] Institute for Environmental Research and Sustainable Development, National Observatory of Athens, Greece
[2]Institute for Meteorology and Climate Research, Karlsruhe Institute of Technology (KIT), Germany
Keywords: PM10, optical depth, Mediterranean, Chemistry transport model, 3D.
Presenting author email: eathana@gmail.com

Summer 2007 was exceptionally hot for many parts of the southeastern Europe, the Balkans and particularly Greece. Comparisons with regional model projections showed that this summer can serve as a strong indicator of what eastern Mediterranean summers could resemble in future (Founda and Giannakopoulos, 2009). Since atmospheric chemistry is strongly dependent on temperature conditions, this episode has been selected for an air quality assessment over Greece, both by means of observations and regional modelling.

Observations utilised here include: PM_{10} measurements from the municipality networks of Athens and Thessaloniki, obtained and retrieved within the FP7 CITYZEN project. Aerosol optical depth (AOD at 550nm) measurements over Athens have been acquired using a Multi-Filter Rotating Shadowband Radiometer (Gerasopoulos et al., 2011). Finally, satellite derived AOD was obtained from the MODIS sensor onboard the Terra platform **(**Kaufman et al., 1998**).**

The numerical tool used is COSMO-ART (Vogel et al., 2009), which is established and applied for the first time in Greece. COSMO-ART is a regional chemistry transport model (ART stands for Aerosols and Reactive Trace gases) online-coupled to the COSMO weather prediction model (Baldauf et al. 2011). Simulations are performed between August 15 and September 15 with a horizontal resolution of 2.8 km and a vertical extend up to 20 km. The initial and boundary meteorological data are retrieved from a coarser COSMO simulation performed by the German Weather Service. The anthropogenic emission database used is the TNO/MACC (Kuenen et al. 2011), while biogenic and sea-salt emissions are calculated online.

A preliminary comparison between observations and measurements showed that PM_{10} predictions were significantly lower than observations. This was partly attributed to the unrealistically high $PM_{2.5}/PM_{10}$ values (higher than 90% for all sites), compared to the ratio measured during August (51%). This fraction was applied to predictions and the new results are presented in Table 1. Model performance has been improved approximately around 30% and is found optimal according to the metrics proposed by Boylan and Russell (2006) (MFB $\leq \pm$ 30%). Nevertheless, PM_{10} values are still underestimated. AOD is also investigated and found in a good correlation, especially concerning its spatial distribution and maximum values (Figure 1).

Current results are used for the optimization of COSMO-ART applications over Greece. In specific, local dust emissions will be incorporated. Then, the inorganic chemistry module will be modified so that sea-salt and dust particles are chemically active. Results will be presented during the conference.

Table 1. Comparison of daily average PM_{10} ($\mu g/m^3$) and AOD values between COSMO-ART predictions and measurements over Greece (17-24/08/2007).

Area/quantity	Measured	Predicted	MFB[1] (%)
Athens (7sites)/PM_{10}	41±14	22±12	-16
Thesaloniki (5 sites)/PM_{10}	53±16	34±14	-12
Athens (1 site)/AOD	0.21±0.11	0.13±0.04	-

[1]Mean fractional bias: normalize the bias by the average of the prediction and observation.

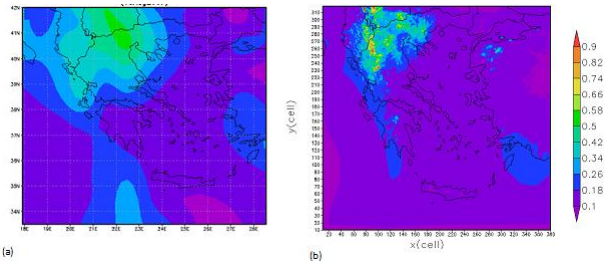

Figure 1. AOD (550nm) as measured by MODIS (a) and estimated by COSMO-ART (b) on 18/08/2007.

Part of this work, related to observations has received funding from the project CITYZEN (FP7/2007-2013, under Grant Agreement no. 212095)

Baldauf M, Seifert A, Forstner J, Majewski D, Raschendorfer M, Reinhardt T (2011*) Mon Wea Rev*. doi:10.1175/MWR-D-10-05013.1 (e-view).

Boylan JW and Russell AG (2006) *Atmos Environ* **40** (26), 4946-4959.

Founda D. and Giannakopoulos C. (2009) *Global and Planetary Change* **67**, 227-236.

Gerasopoulos E., Amiridis, V., Kazadzis, S., et al. (2011), Atmos. *Chem. Phys.*, **11**, 2145–2159.

Kaufman, Y.J., Herring, D.D., Ranson, K.J., and Collatz, G.J. (1998) *IEEE T. Geosci. Remote*, **36(4)**, 1045–1055.

Kuenen J, Denier van der Gon H, Visschedijk A, van der Brugh H (2011). *TNO-report-060-UT-00588*.

Vogel, B., Vogel, H., Baumer, D., Bangert, M., Lundgren, K., Rinke, R. And Stanelle T. (2009) *Atmos. Chem. Phys*. **9**, 8661–8680.

Application of a SOA parameterization for α-pinene and limonene photooxidation to different conditions

Manuel Santiago[1], Marta G. Vivanco[1] and Ariel F. Stein[2]

[1] *Atmospheric Pollution Divison. CIEMAT (Research Center for Energy, Environment and Technology). 28040 Madrid. SPAIN*

[2] *ERT on assignment of NOAA's Air Resources Laboratory, Silver Spring MD*

Presenting author email: manuel.santiago@ciemat.es

Secondary organic aerosol (SOA) is an atmospheric pollutant that has received increasing attention during the last decade. Because of its inclusion in environmental directives, 3-D air quality models are evolving to include SOA formation pathways in their code. However, due to the computational efforts needed by the models to perform mesoscale simulations, SOA treatment is still simple, being so a source of considerable uncertainty in air quality model predictions.

The two product model, first presented by Odum et al. (1996), represents an easy to implement parameterization used in several models. In the two product model, the oxidation of a certain volatile organic compound (VOC) drives to the formation of two semivolatile compounds ($SVOL_i$), that later partition to the particle phase to form individual SOA species (SOA_i). The formation and partition of the semivolatile compounds is governed by an stoichiometric coefficient (α_i) and a partitioning constant (Kp_i) respectively:

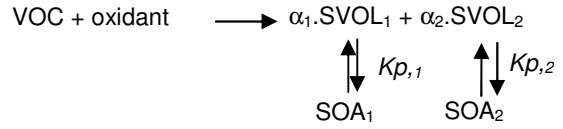

While this approach has the advantage of its straight-forward implementation in the model, it also represents a "black-box" conception of the overall process, as the parameters α_i and Kp_i are generally obtained empirically based on smog chamber experiments where the SOA formation potential of VOCs under certain experimental contitions are studied. Because of this, the application of a certain set α_i and Kp_i parameters to conditions different from which they were obtained may be difficult.

In this work, we present a evaluation of a two product model set of parameters obtained for the photooxidation of a 50:50 α-pinene:limonene mixture in a set of experiments performed in the EUPHORE smog chamber (EUropean PHOto-REactor, CEAM, Valencia) by the authors in a previous study (Santiago et al., 2011).

First, the parameterization is evaluated against some experiments performed by Li et al. (2007) for a similar α-pinene:limonene mixture in a different chamber (Figure 1). Based on the good simulation of the SOA growth curve obtained in an adapted version of CMAQv4.7 where the EUPHORE parameters were implemented, we have calculated the individual parameters for each of the components of the mixture and tested their ability to simulate the SOA yields (Y) obtained by other authors in different photooxidation experiments.

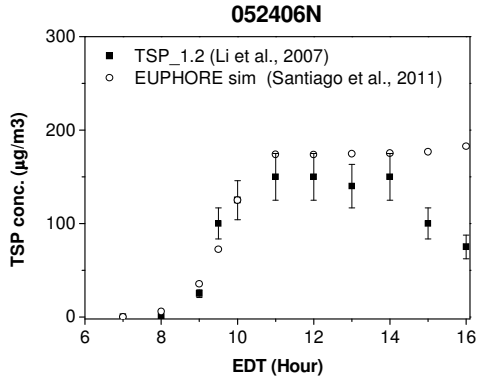

Figure 1. Simulation of the experiment 052406N by Li et al. (2007) using the EUPHORE parameters in an adapted version of CMAQv4.7

The results of this evaluation show that, while the parameters obtained in the EUPHORE chamber experiments generally represent a reasonable approximation of the experimental data from different studies, two product model parameters may present limitations when there is a change in experimental conditions such as the NOx level or the OH initiator.

This study has been financed by the Spanish Science and Innovation Ministry (CGL2008 02260/CLI) and the Spanish Ministry of Environment. We gratefully acknowledge all the EUPHORE team members.

Li Q., Hu D., Leungsakul S. and Kamens R. M.,2007. Large outdoor chamber experiments and computer simulations: (I) Secondary organic aerosol formation from the oxidation of a mixture of d-limonene and a-pinene. Atmospheric Environment 41 9341–9352.

Odum J. R., Hoffmann T., Bowman F., Collins D., Flagan R. C. and Seinfeld J. H.,1996. Gas/Particle Partitioning and Secondary Organic Aerosol Yields. Environmental Science and Technology 30 2580-2585.

Santiago M., Vivanco M. G. and Stein A. F.,2011. Modeling SOA formation from the photooxidation of α-pinene and limonene with CMAQ4.7: Evaluation of different parameterizations against smog chamber data., *Submitted to Atmospheric Environment on December 23th 2011*.

PM modelling: old challenges and new possibilities

S. Tsyro[1], D. Simpson[1,2], H. Fagerli[1], W. Aas[3] and M. Schulz[1]

[1]Research and Development Department, Norwegian Meteorological Institute, Blindern, 0313, Oslo, Norway
[2]Chalmers University of Technology, Gothenburg, Sweden
[3]Norwegian Institute for Air Research, P.O. Box 100, N-2027, Kjeller, Norway
Keywords: regional modelling, PM10/PM2.5, aerosol chemical composition, AOD
Presenting author email: svetlana.tsyro@met.no

Model assessment of air pollution with Particulate Matter (PM) in Europe has started over a decade ago. Ever since, a sound model reproduction of PM_{10} and $PM_{2.5}$ fields and the temporal variation of concentrations has remained a challenging task.

Clearly, accurate PM calculations are essential for reliable assessment of the compliance with regulatory target values. Still, most of regional models tend to under-predict observed PM due to the underestimation of one or several PM components, or due to incomplete PM mass closure. Not less important is the model's ability of correct representation of PM chemical composition, which is necessary for trustworthy calculations of PM source allocation and the impact of emission reductions. Due to scarce observations, modelled PM chemical composition facilitates health effect studies of different PM components. Furthermore, in order to estimate the effects of climate change on PM levels, the models should be capable of reproducing meteorological dependencies of formation and depletion rates of different PM components.

The lack of appropriate observational data was for many years a serious obstacle to the improvement of models' results with respect to PM. However in the recent years, more measurements of PM_{10} and $PM_{2.5}$ mass closure and simultaneous measurements of several PM components have become available for models evaluation. In addition to surface in-situ measurements, aerosol observations from remote measurement systems have been more and more widely used for comparison with models, allowing model testing in the areas not covered with monitoring stations. Great possibilities for evaluating transport processes have been provided by LIDAR measurements of aerosol vertical profiles.

The EMEP model (Simpson et al., 2012) has recently undergone a substantial refinement aimed at improving the accuracy of PM_{10} and $PM_{2.5}$ calculations. Comparing model results with EMEP intensive measurements of PM mass closure in June 2006 and January 2007 (Aas, Tsyro et al., 2012) we have identified the most problematic PM components. Making extensive use of the size-segregated PM chemical composition data, as well as hourly measurements of Secondary Inorganic Aerosols (SIA) and gas-aerosol partitioning (Nemitz at el., 2012), the importance of different parameters and processes has been investigated and will be presented. Among the most important are the effect of cloud water acidity on sulphate production and gas-aerosol equilibrium calculation of ammonium nitrate and formation of coarse nitrate on sea salt and dust particles. The focus has been on completing the mass closure in modelled PM, which now includes SIA, EC, primary and secondary OC, sea salt, mineral dust and particle water (Fig. 1). The main features of geographical and seasonal variations of PM chemical composition and the ability of the model to reproduce those is discussed. We will also summarise the recent findings with respect to the effects of meteorological input and model resolution of PM results.

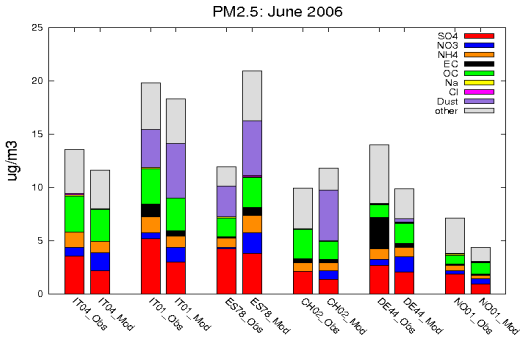

Figure 1. Measured and modelled chemical composition of $PM_{2.5}$. June 2006.

The performance improvement of the EMEP model for PM_{10} and $PM_{2.5}$ will be shown through comparison with EMEP and Airbase observations. Aerosol Optical Depth (AOD) data from satellites and AERONET sun-photometers within AEROCOM system (http://aerocom.met.no/) allows further model evaluation for extended areas (also on a global scale). Finally, first evaluation results will be presented of modelled aerosol vertical profiles, comparing 3D extinction coefficients from the EMEP model and the CALIOP LIDAR on board the CALIPSO satellite.

This work was supported by the EMEP Programme and the Norwegian Space Agency.

Aas, W., Tsyro, S. et al. (2012). *Atmos. Chem. Phys. Discuss,* 12, 3731-3780.

Nemitz, E. et al (2012). European submicron aerosol chemical composition derived from a campaign-based Aerosol Mass Spectrometer network, in preparation.

Schulz, M., Chin, M., Kinne S. (2009). *IGAC Newsletter*, No 41, May 2009.

Simpson, D. et al. (2012). *Atmos. Chem. Phys. Discuss*, 12, 3781-3874.

Modelling the microphysics of Martian CO_2 ice clouds

C. Listowski[1], A. Määttänen[2], F. Montmessin[2], F. Lefèvre[1]

[1]LATMOS, UPMC, Paris, France
[2]LATMOS, UVSQ, Guyancourt, France
Keywords: modelling, condensation, cloud microphysics, ice clouds, planetology
Presenting author email: constantino.listowski@latmos.ipsl.fr

The first unambiguous spectroscopic observation of CO2 ice clouds on Mars came from Montmessin *et al.* (2007), but observations have been reported for a decade now (Clancy *et al.* 2003). The CO2 ice clouds are a rare phenomenon in the Solar System, since 95% of the martian atmosphere consist of CO2 gas, and thus on Mars we are dealing with the condensation of the main component of the atmosphere. The condensation is moreover occuring in a rarefied atmosphere (large Knudsen numbers) that can have dramatic consequences on the crystal growth through the limiting effect of the heat transfer.

CO2 ice cloud modeling has turned out to be challenging : recent efforts (e.g. Colaprete *et al.* 2008) fail in explaining typical small sizes (80 nm-130 nm) observed in equatorial mesospheric ice clouds (Montmessin *et al.* 2006). Recent modelling studies suggest that the effect of the thermal tide in cooling the mesosphere is a prerequisite for the cloud formation (Gonzalez-Galindo *et al.* 2011), but other perturbations are required to attain the CO2 condensation temperatures. A recent study has shown a strong correlation between mesospheric ice cloud observations and the filtering of gravity waves through the atmosphere (Spiga *et al.* 2012). Those waves could create cold pockets in wich $T \leq T_{cond}$, and thus provoke a supersaturated environment in which the clouds can form. However, the nature of the key microphysical processes in the formation of CO2 ice clouds remains unclear, especially in the mesosphere.

We have adapted a microphysical model previously developed for water ice clouds formation on Mars (Montmessin *et al.* 2004) for modeling these CO2 ice clouds. The gas mixture considered here is CO2/N2, N2 being the second most abundant gas in the atmosphere. A hybrid radius grid is used and prevents numerical diffusion during crystal growth. We adopt classical nucleation theory assuming that nucleation is only heterogeneous, as it most probably is on Mars (Määttänen *et al.* 2005). The condensation and the sedimentation both use an implicit scheme for computing derivatives, which guarantees numerical stability whatever the chosen time step. To account for the free molecular regime a Fuchs and Sutugin (1971) correction is applied to the the heat conductivity of the mixture $K_{th,CO2+N2}$, and to the binary diffusion coefficient $D_{CO2/N2}$. Another approach would consist in using equations valid in both continuum and kinetic regimes as Wood (1999) did. It is however still not clear if one approach is better than the other one (see Colaprete *et al.* 2003) and we first aim at fully investigating the first option.

The model is used in a 1D mode with atmospheric pressure and temperature profiles taken from the European Mars Climate Database v.4.3 (Millour et al. 2008) that do not present any excursion below T_{cond} We simulate the presence of cold pockets, formed by gravity waves, by imposing a gaussian disturbance at the altitude where we wish to form a cloud (see Figure 1). We follow the evolution of the cloud during one or several daily cycles. We investigate the influence of different parameters and processes (see below) on the formation of the cloud, its evolution, and its microphysical parameters

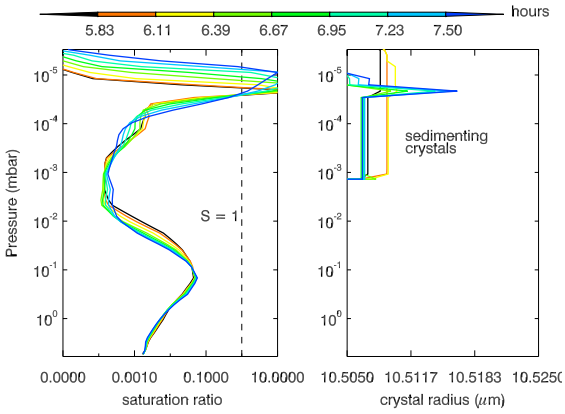

Figure 1. An ice cloud forming at an altitude >80km, in a cold pocket onto 10nm radius dust particles.

A companion abstract by Listowski et al. explains aspects of continuum equations that need to be considered when the major component of the atmosphere condenses (namely the Stefan flow, the thermal diffusion term and the Dufour effect). These processes could be part of the explanation for the small observed radii.

Clancy et al. (2003), *JGR*, **108** (E9), 5098
Colaprete et al. (2003), *JGR*, **108** (E4), 5025
Colaprete, A., et al., (2008) *PSS*, **56**, 150C
Fuchs, N. A., and Sutugin, A. G., (1971) *Highly dispersed aerosols*, in Topics in *Current Aerosol Research*, **2**, 1-60, Pergamon, New York
Gonzalez-Galindo, F., (2011), Icarus, **216**, 10–22
Määttänen, A., et al., (2005) *JGR*, **110**, E02002.
Millour, E., et al., (2008) *LPI Contributions,* **1447**, 9029–+., 2008
Montmessin, F. et al. (2007) *JGR,* **112**, E11S90,
Montmessin, F., et al., (2006) *Icarus*, **183**, 403–410
Montmessin, F., et al., (2004) *JGR,* **109**, E10004
Spiga, A., (2012), *GRL,* **39**, L02201
Wood, S. E., (1999), *Ph.D. thesis*, UCLA

Aerosol generation in atmosphere – data development and modelling

V.A. Zagaynov[1], D.V.Vodyanik[1], S.F. Timashev[1], A.A. Lushnikov[1], Yu.G. Biryukov[1], I.E. Agranovski[1,2], V.V. Maksimenko[1]

[1]Karpov Institute of Physical Chemistry, 105064 Moscow, Russia
[2]School of Engineering, Griffith University, Brisbane, 4111 QLD, Australia
Keywords: atmospheric aerosols, flicker noise spectroscopy, modelling
Presenting author email: zagaynov@cc.nifhi.ac.ru

Atmospheric aerosols significantly contribute towards physical and chemical properties of the ambient air. In fact atmospheric aerosol is a conclusive phase of atmospheric pollution, and the particle size distribution is a key problem of transport and kinetics of disperse media. Monitoring of atmospheric aerosols is related to (1) measurements of the particle size distribution and concentrations at various locations, and (2) analysis of data bases and modeling of the particle behavior. A very important part of analysis of substantially sized data arrays is selection of the procedure for rearrangement of the information in a way, convenient for following mathematical modeling. We propose a procedure based on employment of flicker noise spectroscopy (*Timashev et al, 2008*) enabling to convert the data base into an order very convenient for integration. This method uses autocorrelations $\sigma_i(\tau)$ and correlations $q_{ij}(\tau,\theta)$ between different parameters (particle size, concentration and so on) leading to the following mathematical expression:

$$\sigma_i(\tau) = (< (V_i(t) - V_i(t+\tau))^2 >)^{\frac{1}{2}} \qquad (1)$$

$$q_{ij}(\tau;\vartheta) = < \frac{(V_i(t) - V(t+\tau))(V_j(t+\vartheta_{ij}) - V(t+\vartheta_{ij}+\tau))}{\sqrt{2}\sigma_i \sqrt{2}\sigma_j} >$$

where τ – is time delay for autocorrelation, ϑ - time delay for correlation between two measured values, $V_i(t)$ – time dependant monitoring values.

The suggested approach allows refining important aerosol parameters from raw data sets, i.e. the information on particle growth rate or evaporation, particle generation and so on.

Then, the next step of mathematical modeling could be logically made. It is required for evaluation of time related evolution of dispersed phase and validation of the results against measured data. The modeling procedure could be based on the equation of aerosol kinetics written in the form:

$$\frac{\partial c_g}{\partial t} = I(g) + \frac{1}{2}\int_0^g K(g-n,n) c_{g-n} c_n dn + c_g \int_0^G K(g,n) c_n dn \qquad (2)$$

where c_g time dependant concentration of particles containing g monomers, $I(g)$ - source of particles, $K(g,n)$ – collision frequency between aerosol particle of various sizes with g and n monomers. This equation could be solved and the results obtained for a range of particle sizes. The procedure allows covering particle size range from 1 nm up to 10 micrometer by a number of specially selected size fractions. Direct integrations of equation (2) enables to get a set of N differential equations, which describes the particle evolution over time periods. To validate this approach and ensure that it is feasible to achieve accurate results, the equation (2) could be solved for the cases when K(g,n)=1, and K(g,n)=g+n. For this regime of particle collisions, the equation could be solved analytically and provide accurate solutions, which could be compared against the experimental data acquired for real collision regimes and different generation scenarios presented by the term I(g).

The results obtained by this procedure will be presented at the conference.

Timashev, S. F., Zagaynov, V. A., Lushnikov, A. A., Biryukov, Yu.G., Agranovskii, I.E., Lamukhin, E. M. (2008) Flicker Noise Spectroscopy in an Analysis of the Dynamics of Atmospheric Aerosol *Russian Journal of Physical Chemistry A*, **82,** No. 10, pp.1756-1768,

.

Evaluation of the hydrophobic SOA species estimated by the CHIMERE model considering experiments in a chamber

Marta G. Vivanco[1] and Manuel Santiago[1]

[1] *Atmospheric Pollution Divison. CIEMAT (Research Center for Energy, Environment and Technology). 28040 Madrid. SPAIN*

Keywords: secondary organic aerosols, modelling

Presenting author email: m.garcia@ciemat.es

Simulating secondary organic aerosol (SOA) formation presents a great number of uncertainties. Representative groups of aerosol species of the main oxidation products can be defined in different ways. For example, approaches based on two oxidation products (*Odum et al.*, 1996) are extensively used to determine the amount of aerosol formed from the oxidation of a specific volatile organic compound (VOC). Other approaches are based on the hydrophobic or hydrophilic characteristics of the aerosol species. In all of these approaches, mass stochiometric coefficients, vaporization enthalpies (Hv) and vapor pressures (Pv) for the aerosol species must be defined in order to estimate SOA concentration. In this paper we present an evaluation of the CHIMERE model performance when simulating some experiments in an outdoor chamber. These experiments were designed to study the oxidation of four VOCs assossiated to anthropogenic emissions: toluene (TOL), trimethylbenzene (TMB), o-xylene (OXYL) and octane (OCT). The experiments were carried out in the EUPHORE facility located in CEAM (Valencia, Spain) in 2008, 2009, 2010 and 2011 (*Vivanco et al.*, 2011). Experimental conditions are summarized in Table 1.

The CHIMERE model was applied to simulate 17 experiments. The model was first modified to reproduce EUPHORE conditions. In the model, SOA formation is governed by the production of a group of semivolatile compounds from the oxidation of biogenic and anthropogenic volatile organic compounds, that partition to the particle phase to form individual SOA species. According to the set of reactions included in the model AnBmP is the main SOA species formed from the oxidation of the precursors introduced into the chamber. This specie includes the hydrophobic aersosol compounds with a medium vapour pressure coming from the oxidation of anthropogenic VOCs. Pv and Hv values for this specie in 2011 CHIMERE version (2x10-3 Pa and 156kJ/mol respectively), do not produce organic aerosols. A lower Pv is required. Pv and Hv values proposed by Kim et al. (2011) for this specie (4x10-4 Pa and 88 kJ/mol, respectively) drove to an increase of aerosol formation Even lower Pv values taken from Jordan (2000) (4.8x10-5) drove to better results. This reference was used as according to SOA CHIMERE scheme, AnBmP is the only product coming from octane oxidation and thus thermodynamic properties of octane oxidation products could be assigned to AnBmP specie. Moreover, Hv value in the 2011 CHIMERE version (156 kJ/mol) leads to an unrealistic temporal behaviour. Other enthalpies, such as that in CMAQ (around 40 kJ/mol) improved model results. Nevertheless, an overall overestimation is found in most of the experiments (Figure 1).

Table 1. Initial concentration of the chemcial species introduced into the chamber for each experiment

ANTHROPOGENIC EXPERIMENTS									
	TMB	TOL	OXYL	OCT	HONO	NO	NO_2	SO_2	RH
6/16/08	49	76	9	40	29				0
20080617	99	151	17	80	98				20
20080618	197	302	34	159	98				20
20080619	49	76	9	40	98				20
20080620	99	151	17	80	155				20
20080623	99	151	17	80	51				20
20080624	99	151	17	80	98				0
20080626	99	151	17	80	98			990	20
20080701	99	151	17	80	98			23	20
20090610**	131	87	22	87	122	59			17-4
20090622**	19	116	29	10	119	57			14-17
20090623**	101	81	22	75		34	69		17-18
20091006*	129	86	24	73	90	31			37-28
20091007**	122	82	19	71	79	118	57		46-52
20091008*	121	84	23	72	292	261	80		0.5-1
20091030*	118	82	19	64	281	128	17		17-22
20091103*	239	200	47	154	198	169	24		19-16
20091116*	116	84	21	72	57	182	128	514	47-62
20100608*	204	106	23	87	89	126	36	582	16-25
20110616**	102	49	23	48	85	55			63-71

Figure 1. SOA concentration for the experiment on 27102009

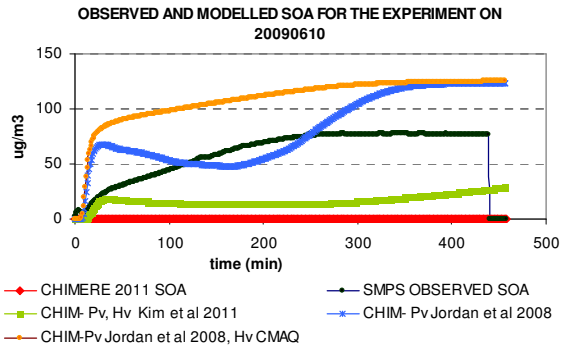

Acknowledgments

This study has been financed by the Spanish Ministry of Science and Innovation (CGL2008-02260/CLI) and by the Spanish Ministry of Environment.

References

Odum, J. R., T. Hoffmann, F. Bowman, D. Collins, R. C. Flagan, and J. H. Seinfeld,1996, Gas/Particle Partitioning and Secondary Organic Aerosol Yields, Envir. Sci. and Techn. 30, 2580-2585.

Jordan, C. E., Ziemann, P. J., Griffin, R. J., Lim, Y. B., R.Atkinson and Arey, J., 2008. Modeling SOA formation from OH reactions with C8-c17 n-alkanes. Atm. Env. 42, 8015-8026

Y. Kim, K. Sartelet, and C. Seigneur (2011). Formation of Secondary aerosols over Europe: comparison of two gas-phase chemical mechanisms. Atmos. Chem. Phys., 11, 583–598.

Vivanco, M. G., M. Santiago, A. Martínez-Tarifa, E. Borrás, M. Ródenas, C. García-Diego, and M. Sánchez,2011, SOA formation in a photoreactor from a mixture of organic gases and HONO for different experimental conditions, Atm. Env. 45, 708-715.

Influence of Schmidt Number on dispersion modelling using CFD tools: Assessment of urban breathability for urban design and management

M. Tomé[1], C.A. Alves[2], R.Santos[3]

1Escola Superior de Tecnologia e Gestão; Instituto Politécnico de Viana do Castelo ; Avenida do Atlântico; 4900-348 Viana do Castelo; Portugal
2Centre for Environmental and Marine Studies, Department of Environment and Planning, University of Aveiro, Aveiro, 3810-193, Portugal
3LSRE - Laboratory of Separation and Reaction Engineering; Chemical Engineering Department; Faculdade de Engenharia da Universidade do Porto; Rua do Dr. Roberto Frias; 4200-465 Porto; Portugal
Keywords: Dispersion, aerosol, PM_{10}, urban
Presenting author email: celia.alves@ua.pt

We present and discuss a novel approach for modelling the dispersion of aerosols emitted by mobile sources in an urban environment using k-ε model with varying the Schmidt number in order to model the dispersion intensity of PM_{10} in the urban canyons. The study area, Lisbon downtown, is frequently surpassing the air quality limits, mainly in the main avenue of Lisbon: "Avenida da Liberdade". The main factors influencing this bad air quality are the high emissions and low dispersion due to atmospheric stability, urban structure (buildings and trees) and wind speed and direction. The integral modelling approach includes the emission estimation using fine traffic data, modelling the flow field through the urban canopy and the dispersion of the pollutants and the concentration of PM_{10} at pedestrian height. Dispersion is computed by both eulerian and lagrangian approaches. In the eulerian dispersion, one evaluates the influence of the Schmidt number upon the concentration field modelled. These results are compared with those obtained by the lagrangian approach and with the measurements available through the local air quality network. Results are in agreement with those published in the literature (Hagler et al., 2011; Tominaga & Stathopoulos, 2007). The influence of the Schmidt number is an important parameterization for any eulerian model and is being somehow addressed as a fine tuning for fitting the experimental measurements (Buccolieri, Sandberg, & Di Sabatino, 2010; Hang, Li, Buccolieri, Sandberg, & Di Sabatino, 2012).

Most modelling applications in the literature parameterize Schmidt number as a single value in the range 0.2-1.3 (Tominaga & Stathopoulos, 2007). However, there are studies that concluded that a Schmidt value of 0.04 can produce better results in specific conditions, namely when the wind direction is perpendicular to the street canyon axis (Di Sabatino, Buccolieri, Pulvirenti, & Britter, 2008).

We review the main physics behind Schmidt number and its importance for eulerian modelling based on the significant study of (Konrad, 2000) who studied the vertical profile of Schmidt number and thus reveals that the use of a single/uniform value for modelling domain is physically false. In our study we used a vertical Shmidt number vertical profile based on Konrad results, fitted as:

$$Sc = \begin{cases} 0.3 & if \quad \frac{z}{\delta} < 0.05 \\ -10.2\left(\frac{z}{\delta}\right)^4 + 25.161\left(\frac{z}{\delta}\right)^3 - 22.667\left(\frac{z}{\delta}\right)^2 + 8.1597\left(\frac{z}{\delta}\right) - 0.043 & if \\ 0.05 \le \left(\frac{z}{\delta}\right) \le 1 & \\ 0.4 & if \quad \frac{z}{\delta} > 1 \end{cases}$$

Buccolieri, R., Sandberg, M., & Di Sabatino, S. (2010). City breathability and its link to pollutant concentration distribution within urban-like geometries. *Atmospheric Environment, 44*(15), 1894-1903.

Di Sabatino, S., Buccolieri, R., Pulvirenti, B., & Britter, R. E. (2008). Flow and pollutant dispersion in street canyons using FLUENT and ADMS-Urban. *Environmental Modeling & Assessment, 13*(3), 369-381.

Hagler, G. S. W., Tang, W., Freeman, M. J., Heist, D. K., Perry, S. G., & Vette, A. F. (2011). Model evaluation of roadside barrier impact on near-road air pollution. *Atmospheric Environment, 45*(15), 2522-2530.

Hang, J., Li, Y., Buccolieri, R., Sandberg, M., & Di Sabatino, S. (2012). On the contribution of mean flow and turbulence to city breathability: The case of long streets with tall buildings. *Science of the Total Environment, 416*(0), 362-373.

Konrad, K. (2000). The height dependence of the turbulent Schmidt number within the boundary layer. *Atmospheric Environment, 34*(7), 1147-1151.

Tominaga, Y., & Stathopoulos, T. (2007). Turbulent Schmidt numbers for CFD analysis with various types of flowfield. *Atmospheric Environment, 41*(37), 8091-8099.

The influence of ion-induced nucleation on atmospheric aerosols based on data from the CERN CLOUD experiment

E.M. Dunne[1], K.S. Carslaw[1], J. Almeida[2,], and the CLOUD collaboration[3]

[1]School of Earth and Environment, University of Leeds, Leeds, LS2 9JT, UK
[2]CERN, Geneva, Switzerland
[3]Refer to author list of Kirkby *et al.,* (2011)
Keywords: aerosol modelling, ion-induced nucleation.
Presenting author email: E.Dunne@leeds.ac.uk

A range of observations support a connection between cosmic ray intensity and the Earth's climate, on time-scales from days (Pudovkin and Veretenenko, 1995) to centuries (Eichler *et al*, 2010) to millennia (Bond *et al*, 2001). Away from the surface, ion concentrations are controlled by cosmic-ray induced ionization. One likely candidate for the mechanism connecting cosmic rays and the climate is the ion-induced nucleation of aerosol.

Because ions stabilise sub-critical nuclei, ion-induced nucleation is likely to act as a nucleation pathway in remote regions with low concentrations of precursor vapours. When determining the impact of this phenomenon on the climate, a global aerosol microphysics model is a vital tool due to its inclusion of the various processes which affect particle growth and deposition.

The CERN CLOUD experiment is designed to accurately measure both ion-induced and neutral nucleation rates in unprecedented detail, as described in (Kirkby *et al.*, 2011) and its online Methods and Supplementary Materials. The experiment has found that the presence of both ions and ammonia enhance nucleation rates beyond the binary neutral, but that inorganic precursor vapours are not sufficient to reproduce atmospheric observations of new particle formation events.

Using the GLOMAP aerosol microphysics model, we quantify the contribution of ion-induced nucleation to global aerosol based on new results from the CLOUD experiment at CERN. We will present the results of the implementation within a global model of the first parametrisation of ion-induced nucleation based on experimental observations rather than theoretical predictions. This parametrisation is the result of work in the ternary H_2SO_4-NH_3-H_2O system by the CLOUD collaboration at CERN. Low-temperature measurements have been used to extend the region of validity of the parametrisation below 250 K.

The simulations have been compared with other simulations which used binary homogeneous nucleation and an activation-based boundary-layer nucleation mechanism. Changes in aerosol concentrations over a solar cycle have also been evaluated.

We would like to thank CERN for supporting CLOUD with important technical and financial resources, and for providing a particle beam from the CERN Proton Synchrotron. This research has received funding from the EC Seventh Framework Programme (Marie Curie Initial Training Network "CLOUD-ITN" grant no. 215072, and ERC-Advanced "ATMNUCLE" grant no. 227463), the German Federal Ministry of Education and Research (project no. 01LK0902A), the Swiss National Science Foundation (project nos. 206621_125025 and 206620_130527), the Academy of Finland Center of Excellence program (project no. 1118615), the Austrian Science Fund (FWF; project no. P19546 and L593), the Portuguese Foundation for Science and Technology (project no. CERN/FP/116387/2010), and the Russian Foundation for Basic Research (grant N08-02-91006-CERN).

Bond, G.C., B. Kromer *et al.* (2001) *Persistent solar influence on North Atlantic climate during the Holocene*. Science 294:2130–2136

Eichler, A., S. Olivier *et al.* (2009) *Temperature response in the Altai region lags solar forcing*. Geophysical Research Letters 36:L01808

Kirkby, J. *et al.* (2011) *Role of sulphuric acid, ammonia and galactic cosmic rays in atmospheric aerosol nucleation.* Nature 476:429-433

Pudovkin, M.I., Veretenenko, S.V. (1995) *Cloudiness decreases associated with Forbush decreases of galactic cosmic rays.* Journal of Atmospheric and Terrestrial Physics 11:1349-1355

Numerical study of the effect of dilution process on the measurement of particle number emissions

Yan Wang[1], Bo Yang[2], Eric M. Lipsky[3], Allen L. Robinson[4], Topi Ronkko[5], Jorma Keskinen[5], K. Max Zhang[1]

[1]Sibley School of Mechanical and Aerospace Engineering, Cornell University, Ithaca, NY, USA
[2]College of Automotive Engineering, Jilin University, Changchun, China
[3]Engineering, Pennsylvania State Greater Allegheny, McKeesport, PA, USA
[4]Department of Mechanical Engineering, Carnegie Mellon University, Pittsburgh, PA, US
[5]Aerosol Physics Laboratory, Tampere University of Technology, Tampere, Finland
Keywords: aerosol sampling, turbulent mixing, numerical simulation, CFD, design.
Presenting author email: yw365@cornell.edu

The development of emission inventories relies on the laboratory emission testing. Numerous experimental results have indicated that particle emission measurements are sensitive to how dilution is conducted. The objective of our study is to investigate the effect of dilution process in fabricated dilution systems on particle emission measurement. An environmental turbulent reacting flow model, the Comprehensive Turbulent Aerosol Dynamics and Gas Chemistry (*CTAG*), developed by Energy and Environment Research Laboratory (*EERL*) in Cornell University, is employed to simulate the coupling of aerosol dynamics and turbulent mixing processes inside different types of diluters.

We first investigate the aerosol dynamics during the dilution process inside two dilution tunnels, one is a variation of the T-mixing Caltech lab dilution tunnel (noted as lab tunnel), and the other is a portable *CMU* field dilution tunnel (noted as field tunnel) with a type of coaxial mixing. The highly turbulent dilution process inside the dilution tunnels is simulated using the Large Eddy Simulation (*LES*) model, which is coupled with aerosol dynamical processes. Simulation result of particle size distribution *(PSD)* shows a reasonable agreement with the experimental data for the dilution of diesel exhaust (Lipsky and Robinson, 2005), illustrated in Figure 1. Our results indicate that nucleation has a strong relationship with the mixing rate, which is determined by the configuration of the dilution tunnel (especially the mixing type of the exhaust and dilution gas), dilution ratio *(DR)* and the turbulence level of the incoming dilution gas. The T-mixing lab tunnel tends to favor the formation of the ultrafine particles due to the faster mixing rate, shown in Figure 2. The process of aerosol dynamics inside the dilution tunnel is also affected by the property of dilution gas (e.g., temperature, relative humidity) and exhaust (e.g., the level of sulfuric acid), of which the sensitivity analysis have been conducted.

Furthermore, the turbulent flow field and aerosol dynamics inside several widely used sampling diluters (e.g., the ejector diluter and the porous diluter used in "Particulates" research program of EU (Ronkko *et al*, 2006)) are studied to characterize the different dilution processes, shown in Figure 3. The numerical study inside diluters can help understanding the dilution process and its effect on aerosol dynamics, and can provide useful information for the development of a harmonized sampling methodology.

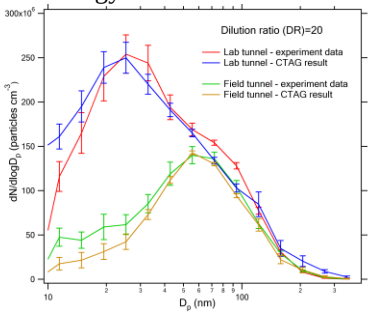

Figure 1. Simulated vs measured *PSDs* within two tunnels under dilution ratio (*DR*)=20.

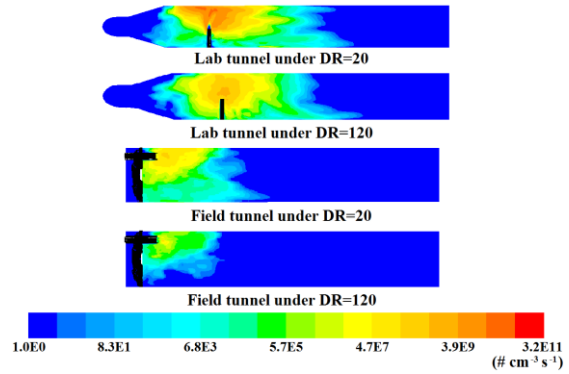

Figure 2. Nucleation rate of ultrafine particles within two tunnels (Injection area) under *DR*=20 and *DR*=120.

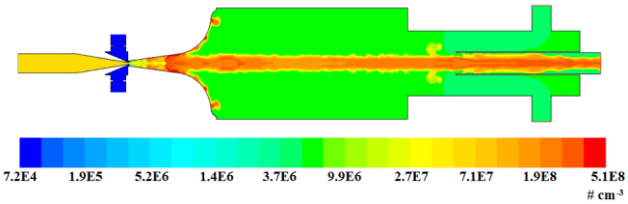

Figure 3. Distribution of particle number concentration within the ejector diluter under Mach number=2.4.

Lipsky, E. M. and Robinson, A. L. (2005) *Aerosol Science & Technology 39(6): 542-553.*
Ronkko, T., Virtanen, A., Vaaraslahti, K., Keskinen, J., Pirjola, L., and Lappi, M. (2006) *Atmospheric Environment 40: 2893-2901.*

This work was supported by the US Environmental Protection Agency (USEPA).

Water bus emission factor model in Venice area

E. Pecorari[1], G. Rampazzo[1], A. Ferrari[2], G. Cuzzolin[2]

[1]Department of Environmental Science Informatics and Statistics, University Ca' Foscari, Dorsoduro 2137, I-30123 Venezia, Italy
[2]ACTV S.p.A. Isola Nova del Tronchetto 32, 30135 Venezia
Keywords: emission factor, source apportionment. shipping emissions
Presenting author email: eliana.pecorari@unive.it

Human activities in urban areas strongly affect air quality. In order to characterize the main sources, emission inventories are requested by legislation. The water cities, in particular, need an appropriate regulation that take into account boats and ships for inland waters. The general concern for the impact of air pollutant emissions on the environment has led to the introduction of numerous regulations targeting land based emission sources. In contrast, marine emissions to the air from ships have largely been exempt from this development. Over the past decades, however, the air emissions from shipping have been the subject of increasing attention. Research and development efforts have focused on characterizing the problem at hand (Lloyd's Register Engineering Services, 1995; Cooper et al., 1996; EMEP, 2009) and offering suitable abatement solutions (Swedish Maritime Administration, 1994; Cooper and Andreasso, 1999). In the wake of these advances, regulatory work on a global scale is being dealt with by the International Maritime Organisation (IMO, 2002). Despite this some specific scenarios could not be considered because of their peculiarity. Venice, as a *water town* in its historical part, is a very distinctive case where transport is supplied by marine systems. In the historical center the canals serves as roads and beyond the road/rail land entrances at the northern edge of the town, transportation within it remains entirely on water or on foot. Venice is the largest urban car-free area of Europe. The main transportation means are motorized public and private boats. In order to better investigate on the impact of these vehicles on the Venice area, an emission factor model was implemented: *Water Bus Emission factor Model (WATERBUS)*. The WATERBUS model was developed using a bottom-up approach and tested on the public ACTV boats that furnished the data. The preliminary results were obtained and compared with local measurements.

Figure 1. Water bus transport plan (ACTV).

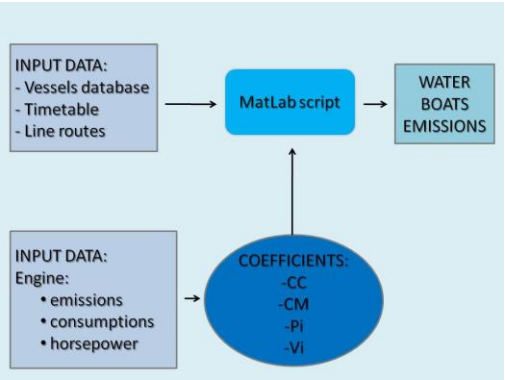

Figure 2. Flow chart of the waterbus model.

Acknowledgments
The authors would like to thank ACTV S.p.A. for aid in collecting data.

References

Cooper D.A., Peterson K., Simpson D., 1996. Hydrocarbon, PAH and PCB emissions from ferries: a case study in the Skagerak-Kattegatt-OGresund region. Atmospheric Environment, 30(14), 2463-2473.

Cooper D.A., Andreasson K., 1999. Predictive NOx emission monitoring on board a passenger ferry. Atmospheric Environment, 33, 4637-4650.

EMEP, 2009. "EMEP/CORINAIR Emission Inventory Guidebook—2009 UPDATE, Technical Report, Shipping Activities—Sub sector 0804, European Environment Agency http://www.eea.europa.eu/publications/emep-eea-emission-inventory-guidebook-2009.

IMO, International Maritime Organisation, 2002. MARPOL 73/78, Consolidated edition, 2002.

Lloyd's Register Engineering Services, 1995. Marine Exhaust Emissions Research Programme. London, England.

Swedish Maritime Administration, 1994. Air pollution and control measures for the marine sector (in Swedish). Report 45-9371263, SjoKfartsverket, NorrkoKping, Sweden.

Verification of the NOx emission inventories over South Korea

Na Kyung Kim[1], Yong Pyo Kim[1], Yu Morino[2], Junichi Kurokawa[3], and Toshimasa Ohara[2]

[1] Department of Environmental Science and Engineering, Ewha Womans University, Seoul, 120-750, Korea
[2] National Institute for Environmental Studies, Tsukuba, Ibaraki, 305-8506, Japan
[3]Atmospheric Research Department, Asia Center for Air Pollution Research, Niigata, 950-2144, Japan
Keywords: Aerosol emissions, REAS, CAPSS, top down NOx estimation.
Presenting author email: yong@ewha.ac.kr

In this study, the emission inventories of NOx, which is a major air pollutant of South Korea were compared and analyzed.

The two bottom-up emission inventories, Regional Emission inventory for ASia (REAS) (Ohara et al., 2007) and Clean Air Policy Support System (CAPSS) (NIER, 2009), which are the latest emission inventories about the air pollutant emissions about South Korea were compared to find out the trend of NOx emission from the past to the present. Also, these two emission inventories compared to the top down NOx estimation by inverse modeling to estimate the accurate amount of NOx emitted from South Korea.

The total NOx emission trends, sectoral and regional comparisons were carried out. In total NOx emissions, REAS was bigger than CAPSS about 3.0E+05 ton per year.

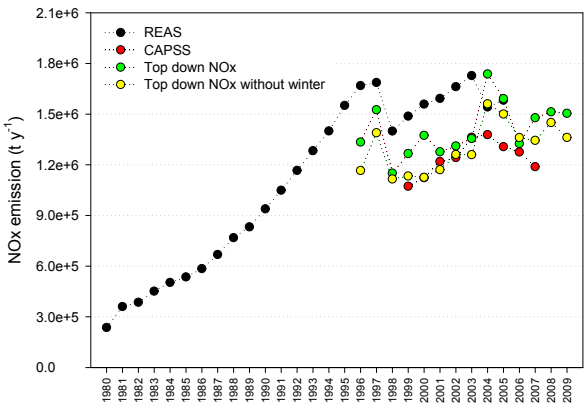

Figure 1. Trends and absolute values of NOx emissions of REAS, CAPSS, and top down NOx.

This difference was mainly caused by the difference in Transport sector, especially emissions from diesel buses (REAS was bigger than CAPSS about 2.5E+05 ton per year) and diesel cars (REAS was bigger than CAPSS about 5E+05 ton per year).

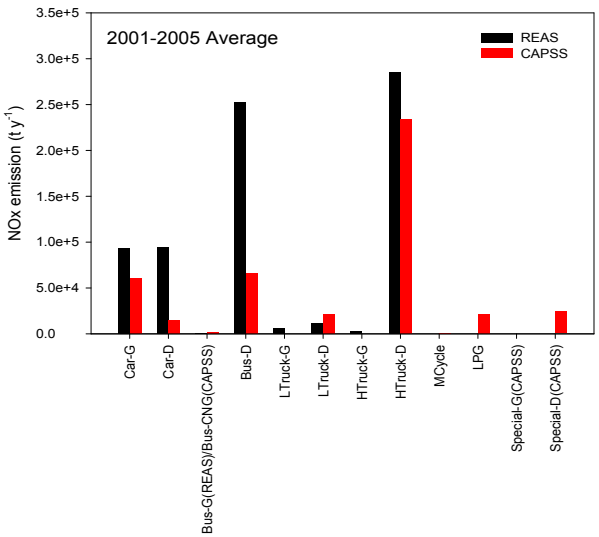

Figure 2. NOx emissions according to the types of vehicles.

The NOx emission of REAS was bigger than that of CAPSS in Seoul and Busan. On the other hand, the NOx emission of REAS was smaller than that of CAPSS in North and South area in Korea. These differences could be explained by the difference in Vehicle Kilometers Travelled (VKT) and emission factors (EF) used in REAS and CAPSS. REAS used longer VKT in Busan, Seoul, and Incheon than CAPSS. Also, REAS used bigger EF than CAPSS for diesel buses and diesel cars (5.01 times bigger for Diesel Buses, and 3.85 times bigger for diesel cars).

For the problems in the estimation of absolute amount of NOx emission, spatial distributions in bottom up inventories, inverse modeling could be a powerful method that solves the problems.

This work was supported by the Global Internship program by National Research Foundation of Korea (NRF) and the NRF grant funded by the Korea government (MEST) (2011-0016297).

National Institute of Environmental Research (2009) Incheon, Korea.

Ohara, T., Akimoto, H., Kurokawa, J., Horii, N., Yamaji, K., Yan, X., Hayasaka, T. (2007), *Atmospheric Chemistry and Physics*, **7**, 4419–4444.

Modelling the chemically speciated $PM_{2.5}$ over the French Northern region using the WRF-Chem system coupled to EMEP and regional emission inventories.

Maxence Mendez [1], Vincent Crenn[2], Valérie Fèvre-Nollet[1] , Patrick Lebègue[1], Denis Petitprez[1], Véronique Riffault[2], Nicolas Visez[1], Rafael Borge[3]

[1] Laboratoire de Physico-Chimie des Processus de Combustion et de l'atmosphère, PC2A, UMR 8522 CNRS/Lille 1, Université Lille1, Villeneuve d'Ascq, F-59655, France
[2] Département Chimie et Environnement, Ecole des Mines de Douai, Douai, F-59508, France
[3] Department of Chemical and Environmental Engineering, Technical University of Madrid (UPM), c/ Jose Gutierrez Abascal 2, 28006 Madrid, Spain
Keywords: aerosol speciation, air quality modeling, emission inventory generation
maxence.mendez@ed.univ-lille1.fr

INTRODUCTION

The lack of information about aerosol chemical and physical properties in modelling systems is a critical step to enhance the emission reduction policies and the knowledge about aerosol impacts over radiative forcing and health.

Since heterogeneous reactivity experiments are conducted in our laboratory, we would like to add measured parameters and mechanisms in the air quality models. Such simulations can be useful to determine how the heterogeneous processes are important in the chemical balance of the main tropospheric oxidants or the evolution of chemical composition of aerosols. To achieve this goal, WRF-Chem has been chosen as the most suitable model because of the KPP module (Kinetic Pre-Processor) which permits to simulate the reactivity of new chemical families.

METHODOLOGY

The first step is to create software to generate emissions. At the same time, in order to improve the accuracy of air quality monitoring, we have adapted the USEPA chemical speciation profiles to a CORINAIR based emission inventory. A data processing system, EMEP2WRF, has been developed to generate chemical information which is compatible with the WRF-Chem specificities from any emission inventory based on CORINAIR architecture and methodology.

Using the RADM2 mechanism, we converted "emission species" into "model species" using the SAPRC methodology. An aerosol chemical speciation profile processing completes EMEP2WRF. Coming from the adaptation of US EPA $PM_{2.5}$ profiles (Borge et al. 2007), those data separate the unspeciated $PM_{2.5}$ emission into five chemical families: sulfate, nitrate, elemental carbon, organic aerosol and unspeciated particulate matter.

RESULTS

EMEP2WRF 1.0 has been created mixing SMOKE and CORINAIR methodologies. The EMEP2WRF 1.0 code has been developed using the Python programming language and PostgreSQL database system in order to evaluate their respective performances. Algorithms defining the EMEP, regional inventory and WRF-Chem projections maps and grids have been coded to adapt the program to any European domain and resolution. Since $PM_{2.5}$ speciation modelling has never been evaluated in Europe, we will statistically compare the simulated values with the measured ones in order to validate the chemical speciation of anthropogenic particles on a regional scale. A HR-ToF-AMS has been deployed over 2 measurements areas (Dunkerque and Douai), the first one is an urban station and the second one is an industrially influenced urban station. The measurements have been done during winter and summer seasons on both sites over about 20-day periods. From those measurements, we obtain hourly profiles of the mass of each chemical class for the ultrafine particles. Both measurements and simulations have the same information levels, this makes it possible to evaluate the new emission speciation methodology and chemical mechanism part developed in this work. EMEP2WRF 1.0 will be operational and available on poqair.univ-lille1.fr.

REFERENCES

Borge R., Lumbreras J., Rodríguez E., 2008. Development of a high-resolution emission inventory for Spain using the SMOKE modelling system: A case study for the years 2000 and 2010, Environmental Modelling & Software, 23, 1026-1044.

New method for estimating cigarette smoke emissions

Victoria Agranovski

Air Quality Sciences, Department of Environment and Resource Management, Brisbane, 4001, Australia
Keywords: Air pollution modelling, emissions, inventory, cigarette smoke
Presenting author email: victoria.agranovski@derm.qld.gov.au

Environmental Tobacco Smoke (ETS) emissions are the complex mixture of gases and fine particles, with thousands of individual toxic air contaminants (Daisey et al, 1998) emitted by the burning of tobacco products (cigarettes, cigars, and pipes) and from smoke exhaled by the smokers.

The composition of ETS emissions vary depending on the tobacco content, additives present and the type of paper and filter material used. Among other tobacco products, cigarettes are the principal source of ETS emissions in Australia (ABS, 2000). The environmental and health impacts of ETS emissions from cigarettes are therefore of concern to regulatory agencies.

There has been an increasing interest in developing emission inventories as a tool for air quality management. Accurate inventory development is however a difficult, time-consuming task due to diversity and large number of individual emission sources. Development of simplified techniques for estimating emissions using readily available activity data will facilitate the process and thus is highly desirable. The simplified techniques can be based on the typical, average emission rates derived from the analysis of relevant data specific to a particular geographical area. Such data can subsequently be used as the default input parameters for developing national emission inventories.

The purpose of this research was developing per smoker emission rates (PSER) for ETS emissions as a cost-effective mean for modeling emissions over large geographic areas containing numerous pollution sources.

The PSER, were estimated from the annual levels of pollutants emitted during smoking cigarettes divided by the number of cigarette smokers in a particular base year. The total annual ETS emissions were estimated using smoking prevalence data from the Australian national tobacco consumption surveys, coupled with cigarette sales figures gathered from the manufacturers.

For the purposes of this study, the emission rates were derived from the emissions factors (µg/cigarette) specific to Australian conditions. Specifically, they were based on the latest data available for cigarette brand variants manufactured and sold in Australia.

A selection of the default per smoker emission rates derived from this research is presented in Table 1. These figures are the mean values of relevant data over period 2000-2007 years.

The default PSER values were developed under assumption that the Australian adult smokers (older than 15 years) consume on average approximately 5150 cigarettes annually, based on the data from the Australian national surveys conducted over the last decade.

Table 1. Per smoker emission rates (PSER) for selected pollutants from cigarette smoke.

Compound	PSER (κg/smoker/yr)	
	Mean	SD
1,3 Butadiene	2.06E+00	8.67E-02
Acetaldehyde	9.60E+00	4.04E-01
Acetone	5.96E+00	2.51E-01
Acrolein	1.96E+00	8.24E-02
Acrylonitrile	5.57E-01	2.35E-02
Benzene	1.70E+00	7.16E-02
Benzo[A]Pyrene	6.24E-04	2.63E-05
Cadmium	2.17E-03	9.12E-05
Carbon Monoxide	3.28E+02	1.38E+01
Catechol	6.37E-01	2.68E-02
Chromium	1.05E-03	4.44E-05
Ethylbenzene	7.24E-01	3.05E-02
Formaldehyde	2.63E+00	1.11E-01
Hydrogen Cyanide	7.00E-01	2.95E-02
Methyl Ethyl Ketone	1.03E+00	4.32E-02
Oxides of Nitrogen	1.16E+01	4.90E-01
$PM_{2.5}$	7.60E+01	3.20E+00
Phenol	1.61E+00	6.79E-02
Styrene	5.92E-01	2.49E-02
Toluene	3.39E+00	1.43E-01
Total VOC	2.44E+01	1.03E+00
Xylenes	2.62E+00	1.11E-01

Daisey, J.M., K.R.R. Mahanama and A.T. Hodgson. (1998) *J. Exposure Analysis and Environmental Epidemiology*, 8, 313-334.

ABS (2000) Australian Social Trends, Australian Bureau of Statistics 2000, Cat. No. 4102, Canberra.

Effect of the Lagrangian integral time scale estimation on particle deposition

G. Lecrivain[1], T. Barth[1] and U. Hampel[1]

[1]Institute of Fluid Dynamics, Helmholtz-Zentrum Dresden-Rossendorf, Dresden, 01328, Germany
Keywords: nuclear aerosols, deposition velocity, numerical simulation, CFD.
Presenting author email: g.lecrivain@hzdr.de

In a high temperature pebble-bed reactor, carbonaceous dust is conveyed by the cooling carrier phase and eventually deposits in the primary circuit of the reactor (Moorman, 2008). In hypothetical severe accident, a dose of radioactive graphite dust may escape the system boundaries. The accurate prediction of transport and deposition of graphite particles is therefore a key primary safety issue.

The numerical dispersion and deposition of aerosol particles in a turbulent flow involving Reynolds-averaged Navier-Stokes simulations frequently make use of the Lagrangian integral time scale T_L. It is the correlation of successive velocities along a particle path throughout the duration of particle travel. Each component T_{Li} of the time scale T_L is defined as:

$$T_{Li} = \int_0^{t_\infty} \frac{\overline{u_i(t) \cdot u_i(t+\tau)}}{u_i(t) \cdot u_i(t)} d\tau$$

where the subscript $i = 1,2,3$ denotes the streamwise, the wall normal and the spanwise component respectively, t_∞ is a long period of time and u_i is the instantaneous fluid velocity seen by the particle. T_L as seen by the moving particle is difficult to obtain, especially in the turbulent boundary layer. Multiple estimations of T_L were derived in homogeneous turbulence, and yet very scarce literature data are available on accurate estimations of T_L in the inhomogeneous and anisotropic turbulent viscous sublayer. Bocksell and Loth (2006) performed a Direct Numerical Simulation (DNS) in which thousands of fluid tracer particles were released within the boundary layer. At the wall most sample values of the wall normal component T_{L2}^+ were found to lie in the interval [2-5]. T_L^+ denotes here the non-dimensional counterpart of T_L. Luo et al (2010) reported the average value at the wall $T_{L2}^+ = 4$, thus supporting the results numerically determined by his predecessors. T_{L2}^+ values at the wall of up to 10 were also estimated in some other literature sources.

The effect of T_{L2} estimation in the near wall region on the numerical prediction of particle deposition is here investigated. The stochastic continuous random walk model is used. It correlates the velocity fluctuation u_i' from the previous time-step through a Markov chain, with the inclusion of a zero mean, unit variance distributed random number $N(0,1)$. The following first order approximation of the normalised Langevin equation which accounts for inhomogeneous turbulence is implemented in the OpenFOAM code:

$$u_i'(t+\Delta t) = u_i'(t) \cdot (1 - \frac{\Delta t}{T_{Li}}) + u_i^{rms} \cdot \sqrt{2\frac{\Delta t}{T_{Li}}} \cdot N(0,1)$$

where Δt is the simulation time step and u_i^{rms} the root mean square local fluctuation velocity taken from DNS data in the near wall region. The mean velocity field and its corresponding turbulence field are derived from a numerical simulation carried out with a Reynolds stress turbulence model. The turbulent flow is simulated in a vertical square duct flow (gravity in the flow direction) at Reynolds Number $Re = 42000$. The diameter of the particles is varied from 0.01 μm to 50 μm to cover the particle size range experimentally observed in a high temperature reactor. T_{L2} is varied as follows:

$y^+ < 5$	T_{L2}^+ =3, 4, 6 and 10
$5 < y^+ < 100$	T_{L2}^+ fitted value to DNS data
$y^+ > 100$	$T_{L2} = C \cdot \frac{k}{\varepsilon}$

The effect T_{L2} has on the particle deposition velocity can be seen in Figure 1. Findings form this study show that $T_{L2}^+ = 3$ at the wall results in an accurate match with particle deposition velocities previously determined. The "V-shape" variation of the deposition velocity is accurately reproduced. The deposition velocity seems very sensitive to T_{L2}^+ near the wall. A slight overestimation will produce large errors.

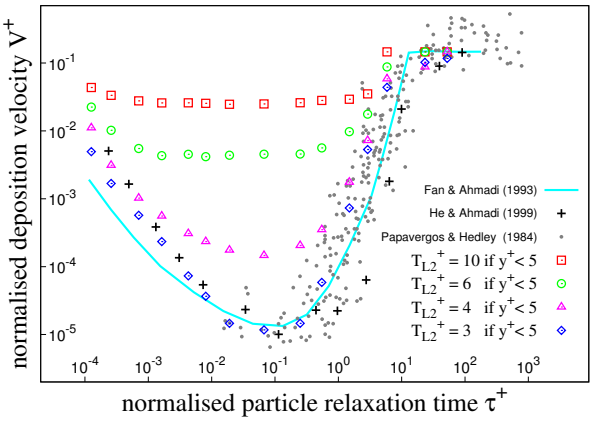

Figure 1: Effect of T_{L2}^+ on aerosol particle deposition.

This work was supported by the European Commission under the grant 249337 of the THINS project.

Bocksell, T.L. and Loth, E. (2006) *Int. J. of Multiphase Flow* **32**, 1234-1253.

Luo, J.P., Lu, Z.M. and Liu, Y.L. (2010) *Applied Mathematics and Mechanics* **14**, 71-75.

Moormann, R. (2008) *Science and Technology of Nuclear Installations*, 1-14.

Sulphuric Acid Aerosols in Industrial Processes – Simulation, Estimation of Coagulation and CPC measurement

L. Brachert[1], S. Sinanis[1] and K. Schaber[1]

[1]Institute for Technical Thermodynamics and Refrigeration, Karlsruhe Institute of Technology, Karlsruhe, 76131, Germany

Keywords: Absorption, Coagulation, CPC, Homogeneous nucleation, Industrial aerosols

Presenting author email: leonie.brachert@kit.edu

The formation of sulphuric acid aerosols is a phenomenon which emerges frequently in industrial processes such as absorption, mixing and cooling. An important domain is for example the absorption-based flue gas cleaning in power plants using fossil fuels. It is crucial to be able to predict the number concentrations and droplet diameters which will emerge in industrial applications in order to improve and facilitate the design of precipitation systems.

The simulation tool AerCoDe has been developed at the Institute of Technical Thermodynamics and Refrigeration to predict aerosol formation initiated by heterogeneous (Wix, 2008) as well as homogeneous nucleation (Wix *et al*, 2010). In sulphuric acid – water systems homogeneous nucleation has to be considered. The reason for this is the occurrence of high supersaturations as a result of the extreme phase equilibrium of this binary system. The simulation yields small aerosols (<200 nm) and high number concentrations up to 10^{10} 1/cm³ (Wix *et al*, 2010). The number concentration is slightly lower when the parameterisation of Vehkamäki et al (2003) is used to take the formation of hydrate clusters into account (Figure 1).

For heterogeneous nucleation the simulation tool has been validated by experiments with the systems H_2O-HBr and H_2O-HCl in the past (Wix, 2008). The validation of the homogeneous nucleation model is currently conducted at the semi-industrial flue gas cleaning facility at the institute. Therefore the number concentration of the aerosol is measured by means of a condensation particle counter (CPC) in combination with a dilution cascade. The measurements show high number concentrations of $>10^8$ 1/cm³ within the entire concentration range of H_2SO_4 in the flue gas (Figure 1). The measured concentration is slightly decreasing at smaller inlet concentrations of H_2SO_4.

Two competing depletion mechanisms of supersaturation affect the resulting number concentration: nucleation and growth. At low inlet concentrations, the binary system H_2SO_4-H_2O reveals a steep descent of the saturation pressure with increasing concentrations of H_2SO_4 (and subsequently high supersaturations). Hence, at low inlet concentrations the driving force for nucleation is high, whereas there is not much substance in the gas phase which would enforce growth. As a consequence, the resulting number concentration is high even for low inlet concentrations of H_2SO_4 combined with small diameters of the aerosol. The higher the inlet concentration, the higher the driving force for growth. However, the number concentration does not increase significantly as the supersaturation does not augment in the same manner. The simulation reveals even decreasing number concentration at higher inlet concentrations.

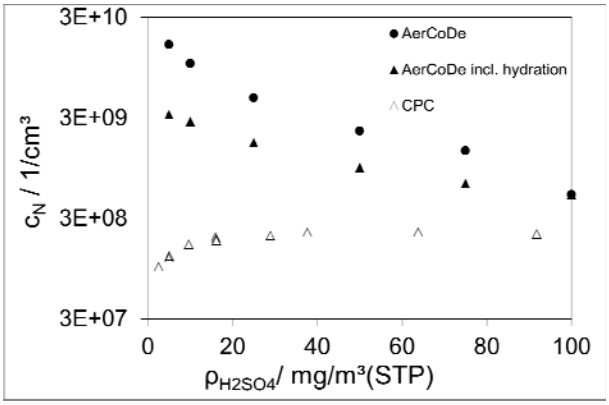

Figure 1. Total number concentration in the absorption column outlet as a function of the H_2SO_4 inlet concentration from AerCoDe and CPC measurement

For the homogeneous nucleation no coagulation model is implemented in AerCoDe so far because it is computationally expensive as a polydisperse model has to be used. It can be seen in Figure 1 that high number concentrations are obtained and coagulation has to be considered in order to compare simulation and experiments. This is essential at low inlet concentrations in particular because the prevalent small diameters increase the effect of coagulation. As a consequence, several approaches for coagulation (monodisperse as well as polydisperse) are investigated and will be presented at the conference.

The aim of the investigation is to provide information about the sulphuric acid aerosol formed during flue gas cleaning and thus provide a base for the improvement of absorption processes in industrial applications.

Vehkamäki, H.; Kulmala, M.; Lehtinen, K.E.J., (2003) *Environmental Science and Technology* **37**, 3392-3398

Wix, A., Brachert, L., Sinanis, S. and Schaber, K. (2010) *Journal of Aerosol Science* **41**, 1066-1079

Wix, A. (2008) *Fortschritt-Berichte VDI*, Reihe 3, Nr. **894** VDI-Verlag

Microscopic observation of aerosol particle deposition in turbulent channel flows

T. Barth, G. Lécrivain, J. Preuß and A. Lehmann

Institut für Fluiddynamik, Helmholtz-Zentrum Dresden-Rossendorf,
Bautzner Landstraße 400, 01328 Dresden, Germany

Keywords: Turbulent flow, particle deposition, microscopic observation, isokinetic sampling, spectrometry
Presenting author email: t.barth@hzdr.de

The transport behaviour of carbonaceous dust in the primary circuit of a High Temperature Reactor (HTR) plays an important role in the safety assessment during a Design Basis Accident (DBA). Carbonaceous dust is formed mainly due to friction between graphite fuel elements (Kissane, 2009). In a pebble bed reactor the dust forms due to abrasion of graphite material between the pebbles. During reactor operation it is a safety issue to precisely predict the dust deposition and the corresponding resuspension rate of particles released into the containment during a DBA.

Deposition of aerosol particles has been investigated e.g. by Sippola & Nazaroff (2004). These experiments have been performed in steel ducts at Reynolds numbers and with particle relaxation times observed in a HTR. Their results follow the "v-shaped" curve of the non-dimensional deposition velocity against particle relaxation time and show a dependency on flow speed, particle size and orientation of the duct.

More recently, an Euler-Lagrange CFD simulation of particle deposition in a turbulent square duct flow has been performed by Lecrivain (2012). It was found that the friction velocity significantly influences the particle deposition velocities.

Deposition experiments of liquid and solid particles in a fully developed horizontal turbulent square duct flow are performed to further study the deposition behaviour of aerosol particles. The oil liquid particles (DEHS) are generated by a condensational aerosol generator (TOPAS, SLG 270). The aerodynamic particle size distribution and the particle number concentration of the suspended particles are determined by isokinetic sampling using an Aerodynamic Particle Sizer Spectrometer (TSI. APS 3321). The particle size distributions are fairly monodisperse for particles with $d_{aero} = [1.5, 2.5, 3.5, 4.5]\ \mu m$. The solid aerosol particles are microspheres (AkzoNobel, Expancel DU, $d_{50} = 6.5\ \mu m$) and are injected into the flow field by means of a solid aerosol generator (TOPAS, SAG 410). The particle mass flow rate and the particle concentration are precisely adjusted by the feed rate of the SAG. The particle size distribution of the airborne particles is measured by means of Scanning Electron Microscopy (SEM). The size distributions gained by the APS and the SEM analysis are used to calibrate the size distributions obtained by an optical microscope.

A commercial light microscope equipped with a CMOS camera is mounted underneath the test section of the channel. It is focused on the inside surface of the channel floor which consists of a glass plate coated with indium tin oxide to remove electrostatic charges. This allows a time-resolved *in situ* observation of the particle deposition processes. A standard LED light source illuminates the microscope's *6 x 4 mm²* field of view and the CMOS camera records the scatter light of the wall deposited particles. The measurement uncertainty for particles larger than *2 µm* is assumed to be *24%*.

Figure 1 illustrates the time averaged deposition velocities for varying friction velocities. The CFD results of Lecrivain (2012) and Sipolla & Nazaroff (2004) are also plotted for comparison purposes. In the particle relaxation time range $\tau^+ = 0.001..10$ the deposition velocity increases with decreasing friction velocity. which is also observed elsewhere. It is assumed that the effect of gravitational settling leads to an increase of deposition velocity for decreasing flow speed. The results of this study also capture this tendency. Nevertheless, the scatter in the data has to be further investigated.

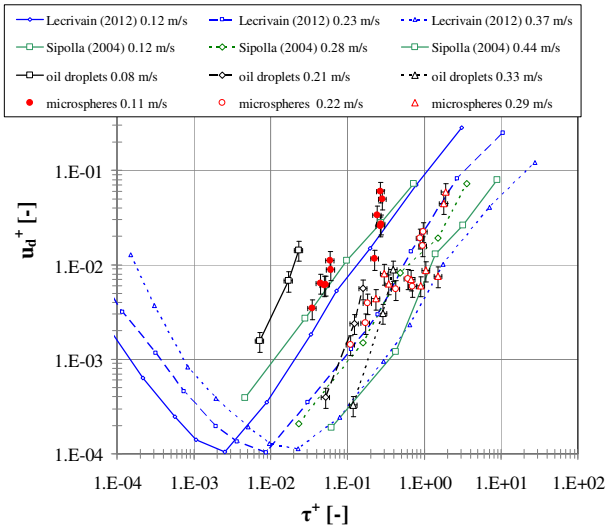

Figure 1. deposition velocity against relaxation time with respect to different friction velocities

This work is supported by the the EC (Project THINS, grant agreement no. 249337).

Kissane, M. A. (2009). *Nucl. Eng. Des.* **239**, 3076 - 3091.

Lecrivain G., Barth T. & Hampel U. (2012), *European Aerosol Conference*, Granada, Spain.

Sippola, M. R. & Nazaroff, W. W. (2004), *Aerosol Sci & Techn*, **38**, 914 – 925.

Experimental and Numerical Investigation of Hygroscopic Aerosols Transport, Kinetics and Deposition in an Enclosure

M.A. Zatevakhin[1], A.A. Ignatiev[1],
Y.N.Vashlyaev[2], A.A. Zaitsev[2], A.A. Lukyanov[2], A.S.Mikheev[2], D.V.Sumin[2], O.V.Supotnitskaya[2]

[1] JSC SPAEP, 9/2a, 2nd Sovetskaya street, 191036, Saint Petersburg, Russia
[2] SSC RF-IPPE named after A.I.Leypunsky, 1 Bondarenko Sq., 249033, Obninsk, Russia

Keywords: aerosol dynamics, CFD, deposition, diffusiophoresis, hygroscopicity

Hygroscopic aerosols behaviour in an enclosure at certain thermohydraulic conditions was studied. Processes of aerosol transport, kinetics and deposition were modelled simultaneously under conditions of air-steam atmosphere. The soluble NaCl (sodium chloride) aerosol particles with size on the order of 1–2 μm were used. Experiments were conducted at the VKM test facility located in the SSC RF-IPPE territory (Obninsk). The scheme of the VKM is showed in figure 1. The volume of the vessel is 9 m^3.

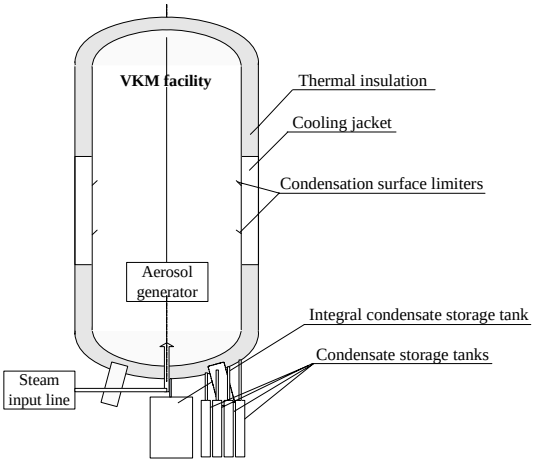

Figure 1. Scheme of the VKM test facility.

The experiments were carried out at 350 kPa pressure and 410 K temperature. Water steam was supplied into vessel containing some amount of air and condensed on vessel walls. Following parameters were measured during experiments:
- pressure;
- temperatures of gas and walls;
- volume of condensate at special wall collectors and vessel bottom;
- concentration of dissolved sodium chloride.

Hydrodynamic code integrated with aerosol block was used for numerical simulation. The code was based on Reynolds averaged hydrodynamic equations solution. To simulate the transport of low-inertia particles in turbulent flow Eulerian diffusion-inertia model (Zaichik et al. 2010) was employed. Boundary conditions at walls were set with taking into account gravitational settling, Brownian diffusion, thermophoresis and deposition by Stefan flow (diffusiophoresis).

Kinetic block was based on numerical solution of condensation/coagulation kinetic equations. Sodium chloride solubility and its influence on vapor pressure at particle surface were taking into account.

Simulation results showed that Stefan flow totally determines deposition onto lateral walls. Equilibrium between incoming and condensing water vapor was achieved at relative humidity of the order of 99.3%. Appreciable growth of water droplets on soluble NaCl nuclei occurs at this humidity level. These droplets deposit onto bottom of the vessel due to gravity sedimentation. This process provides good agreement between simulation results and experimental data. Meanwhile, results obtained without taking into account solubility differs considerably from described above and experimental data. It can be clearly seen in figure 2.

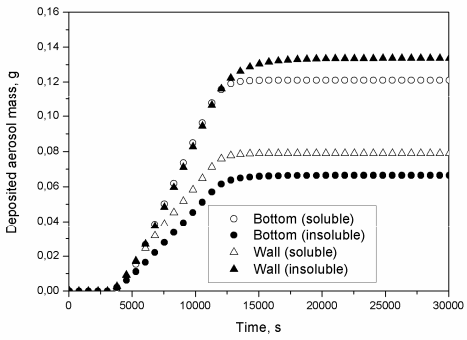

Figure 2. Deposited aerosol masses.

Zaichik L.I., Drobyshevsky N.I., Filippov A.S., Mukin R.V., Strizhov V.F. (2010) *Int. J. Heat and Mass Transfer*. 53. 154–162.

Mathematical study of inhalable fraction in low velocity conditions

A.K. Gilfanov, I.T. Mukhametzanov, S.K. Zaripov

Kazan Federal University, Kazan, Russia, 420008

Keywords: inhalable fraction, sampler, calm air, CFD
Presenting author email: artur.gilfanov@ksu.ru

The CFD model and parametrical investigations of the particle inhalable fraction for the human manikin in low velocity air including a calm air case are presented. Obtained dependences of the inhalable fraction on the particle size are compared with experimental data and the aspiration efficiency of a spherical sampler.

The particle inhalability for a realistic human head was studied numerically for low air velocity by Antony&Flynn (2006). Presently, there is little information regarding the human inhalability under calm air condition (Dai et al., 2006). In the present work a realistic digital model of human head and an idealized spherical sampler facing the wind are used to calculate the inhalable fraction of coarse dust particles up to very low velocity values including the calm air case.

In the first model the velocity field of the air flow is found by numerical solution of the Navier-Stokes equations of viscous flow of incompressible fluid using the FLUENT code. To describe the gas flow for the spherical sampler the potential flow model developed by Galeev&Zaripov (2003) is used. The particle motion equations are integrated in the velocity field, which is found numerically or analytically.

In the undisturbed air flow far from the human head and sampler particles move with the velocity $\bar{U}_1 = \bar{U}_0 + \bar{V}_s$, where $\bar{U}_0$ is the air velocity, $\bar{V}_s = \tau \bar{g}$ is the settling velocity, $\tau = \rho_p d^2 / 18\mu$ is the relaxation time, ρ_p and d are the particle density and diameter, μ is the air viscosity. Breathing is simulated by an stationary air suction through the elliptical mouth orifice. On the base of calculating particle trajectories the tube of limiting trajectories is calculated, which divides the sampled particles from the unsampled ones. The cross section area S_p of the tube of limiting trajectories far from the manikin allows to calculate the aspiration efficiency (inhalable fraction) by the formula

$$A = \frac{U_1 S_p}{Q} = \frac{S_p \sqrt{U_0^2 + V_s^2}}{S_m U_a},$$

where $Q = S_m U_a$ is air flow rate through mouth with area S_m, $\bar{U}_0$ is the aspiration velocity.

Some trajectories of particles in the vicinity of the human head at two values of wind velocity are shown in fig.1. The shape and size of the area S_p depends on the ratio of the wind and sampling velocities and the particle diameter. In the calm air case the human head screens a part of particles that could be aspirated. The aspiration efficiency as a particle diameter function is shown in fig.2. The obtained values of aspiration efficiency for moving air agree well with experimental data of Kennedy&Hinds (2002) and the theoretical curve of Anthony&Flynn (2006). Comparison with the criterion for inhalable particulate mass (IPM) aerosol samplers is given. The aspiration efficiency of the spherical sampler in moving air also agrees well with mentioned curves. Thus the model of an idealized spherical sampler can be used to estimate the inhalable fraction in low velocity environment.

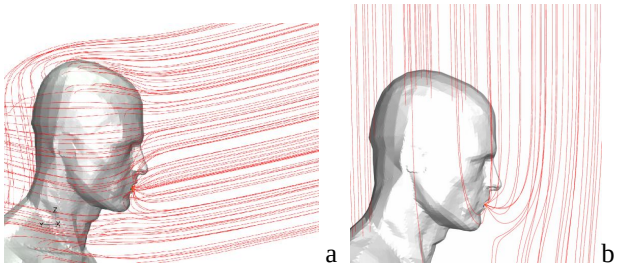

Figure 1. The trajectories of particles at d=37μm for two wind velocities: a-U_0=0.2 m/s, b - U_0=0

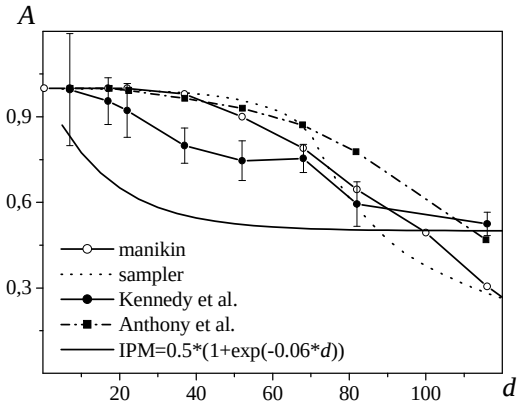

Figure 2. A as a function of the particle diameter d

Anthony, T. R., Flynn, M. R. (2006) J. of Aerosol Sci., P. 750-765.

Dai, Y-T, Juang, Y-J, Wu, Y., Breysse, P.N., Hsu, D-J. (2006) J. of Aerosol Sci., 967-973.

Galeev, R.S., Zaripov, S.K. (2003) J. of Aerosol Sci., 1135-1150.

Kennedy, N.J., Hinds, W.C. (2002) J. of Aerosol Sci., 237-255.

Transnational assessment of emerging health relevant air quality parameters (Joaquin)

S. Adriaenssens[1], F.Fierens[1], E.Trimpeneers[1], D.Celis[2], E. Van der Swaluw[3], R. Hoogerbrugge[3] and K.V. Wyche[4]

[1]Belgian Interregional Environment Agency (IRCEL), Brussels, B-1000, Belgium
[2]Flemish Environment Agency (VMM), Antwerp, B-2000, Belgium
[3]National Institute for Public Health and the Environment (RIVM), 3721, Netherlands
[4]University of Leicester, LE1 7RH, UK
Keywords: Modelling (regional), Abatement strategies, Ultrafine particles
Presenting author email: adriaenssens@irceline.be

Background of the Joaquin project

Air pollution and health effects has been the subject of extensive research for many years (Brunekreef and Holgate, 2002). Although air quality has improved considerably in Europe in recent decades (EEA, 2011), airborne fine particles still have a significant impact on our health and life expentancy (Amman *et al*., 2005).

Recent research shows that other pollutants, such as the smaller ultra fine particles (UFP) and "Elemental Carbon (EC)" are more likely to be linked to health problems, than the current parameters of NO_2 (nitrogen dioxide) and PM_{10} (PM with a diameter less than 10μm) (Sioutas *et al*., 2005, Janssen *et al.*, 2011). At present there is no clear understanding of the presence of these particles, especially at local and regional level. Furthermore, the links between air quality research and policy are missing (Morawska *et al*., 2008). Air pollution, especially of the current parameters, is by its nature a truly transnational problem, e.g. emissions of air pollutants in one region can have a detrimental effect on the air quality of other regions and vice versa. A jointly identified and implemented transnational approach is therefore an essential requirement for a successful reduction of air pollution.

The aim of the Joaquin project is to support health-oriented air quality policies in the Northwest European Region (NWE). To achieve this, the project is broken up in three work packages. The first work package consists of capacity building, in which innovative knowledge will be gained by e.g. setting up a novel monitoring infrastructure for UFP and EC. In the second work package, measures are assessed to identify, pilot and evaluate the most efficient and cost-effective measures to reduce exposure. In the third work package, communication is set-up between the involved policy levels, stakeholder groups and the general public.

Transnational assessment

Within the second work package, is a transnational assessment of health relevant parameters will be conducted. Currently there is no insight in the relative importance of health relevant pollutants across the NWE region and no maps of UFP and EC emissions and concentrations exist.

The first part of this action is the comparison of four currently used regional models with regard to EC (and UFP) concentrations, i.e. Lotos-Euros, BelEuros, Chimere and Aurora (EEA Model Documentation System). The results of this exercise will be validated with the measurements carried out in work package one of the project.

Secondly, the Lotos-Euros and BelEuros model will be used to assess the contribution of emissions from surrounding regions to the air quality in one region. To this aim, the NWE region will be divided in 10-15 regions. In the BELEuros model de contribution of one region to the other regions will be assessed based on emission reductions of the concerned region. In the Lotos-Euros model, emission data of each region are labelled and their distribution over the regions is tracked.

In the third part, local models are extended for UFP modelling. For this purpose, the high resolution bigaussian IFDM model and the TREDM model (EEA Model Documentation System) will be used.

The last part of this action involves the assessment of different measures on yearly average PM_{10}, $PM_{2.5}$, NO_x EC and UFP concentrations for 2020. The impact of several measures with regard to traffic (permanent speed reduction, greening of the car park), energy use (e.g. shift from oil fuel to natural gas or biomass) and agriculture (ammonia emission reductions) on air quality will be assessed.

This work was supported by the European Union through the Interreg IV-B NWE program.

Brunekreef, B., Holgate, S.T. (2002) *Lancet,* **360**, 1233-1242.

Amman M., Bertok, I., Cofala, J., Gyarfas, F., Heyes, C., Klimont, Z., *et al.*, (2005) *Baseline Scenarios for the Clean Air for Europe (CAFE) Programme* , IIASA, Austria

EEA (2011) *Air quality in Europe 2011*, European Environment Agency, Denmark.

EEA, Model Documentation System (2012), http:// acm.eionet.europa.eu/databases/MDS/index_html

Janssen N., Hoek, G., Simic-Lawson, M., Fisher, P., van Bree, L., *et al.*, (2011) *Environ Health Perspect*., **119**,1691-1699.

Morawska, L., Ristovski, Z., Jayaratne, E.R., Keogh, D.U., Ling, X. (2008) *Atmos. Environ*., **42**, 8113-8138.

Sioutas, C., Delfino, R.J., Singh, M. (2005) *Environ. Health Persp.* **113**, 947-955.

Development of a workflow for integration of fresh slaughterhouse porcine lungs into an active lung simulation

K. Stiglbrunner[1], M. Forjan[1], Z. Bureš[2,3] and A. Drauschke[1]

[1]Institute for Biomedical Engineering, University of Applied Sciences Technikum Wien, Vienna, Austria
[2]Department of Electrotechnics and Informatics, College of Polytechnics, Jihlava, Czech Republic
[3]Institute of Experimental Medicine, Academy of Sciences of the Czech Republic, Prague, Czech Republic
Keywords: Lung Deposition, Lung/Particle Interaction, Workplace Safety, Porcine Lung.
Presenting author email: katharina.stiglbrunner@technikum-wien.at

Working place safety is an important topic of recent discussions. Different institutions, like companies or R&D laboratories, are interested in enhanced research, containing environmental factors at the workplace, leading to knowledge of local particle distributions in the human lung. (Ruzer and Harley, 2005) Using measurements of the actual particle number entering the respiratory system, the possible effects or hazards of the inhaled aerosols can thereby be evaluated. The amount of particles is of interest as well as the local distribution on a cellular basis. Making this observation as realistic as possible, an anatomically realistic model, such as an isolated porcine lung, should be used, as well as an integrated circulatory system. The main advantage of the fresh slaughterhouse porcine lung in combination with the developed lung simulator (the i-Lung) is the possibility to use the setup as an alternative to animal testing, which will be necessary due to legal provisions. (European Commission, 1976)

The lung simulator has been developed and measurements have verified the functionality of both, physiological and pathological breathing patterns. (Forjan *et al*, 2011)

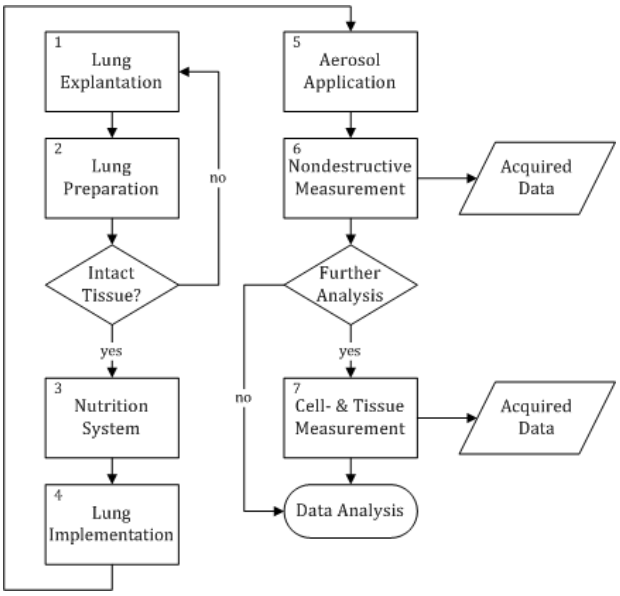

Figure 1. Workflow diagram of the measurement setup.

The workflow starts with the explantation of a porcine lung, (1) in Figure 1, during a common slaughtering process. In addition, prepared porcine lungs or other lung equivalents are used in aerosol measurements. The next step is the preparation and usage of the fresh porcine lung (2). If the tissue of the lung and the pharyngeal area is intact for the integration into the lung simulator, the nutrition system of the circulatory system has to be connected (3). Afterwards the porcine lung is implemented into the i-Lung (4). In combination with the either actively breathing or passively ventilated lung simulator, the aerosols are applied to the completed setup (5). The acquired data from the non-destructive aerosol concentration measurements of the porcine lung (6) is the basis for further analysis on a cellular level (7). The entire system is therefore designed to allow work place aerosol inhalation measurements with an anatomically correct model and to provide information about local particle distribution within the lung tissue.

The active lung simulator i-Lung is used as core element for this workflow. With either lung equivalent, aerosol concentration measurements have been performed and showed a significant degree of separation of inhaled particles using a porcine lung. (Forjan et al, 2012) In addition cooperation has been established for elaborating adequate slaughterhouse process integrated explantation techniques for porcine lungs. Furthermore the use of porcine lung tissue provides an anatomically and physiologically realistic model, comparable to a human lung. (Stiglbrunner, 2011) The next steps in this workflow development include the decision for a proper tissue preparation and nutrition solution. A further goal is the integration of a nutrition circulatory module for tissue life prolongation into the i-Lung system. In a last step the cell- & tissue measurement techniques for the workflow have to be defined and integrated.

European Commission. (1976) *Council Directive (76/768/EEC).*
Forjan, M., Stiglbrunner, K., Bureš, Z. and Drauschke, A. (2011) *Proceedings of Biomech-2011,* ACTA Press.
Forjan, M., Stiglbrunner, K., Bureš, Z. and Drauschke, A. (2012) *Proceedings of WC8,* ALTEX **29**.
Ruzer, LS., Harley, NH. (2005) *Aerosols Handbook: Measurement, Dosimetry and Health Effects*, CRC Press.
Stiglbrunner, K. (2011) *Aerosol Measurement Technologies for Respiratory Research Purposes*, UAS Technikum Wien.

Ion-induced vs. base-induced sulfuric acid nucleation

O. Kupiainen[1], T. Olenius[1], I.K. Ortega[1], T. Kurtén[2], and H. Vehkamäki[1]
[1]Department of Physics, University of Helsinki, Gustaf Hällströmin katu 2 A, P.O. Box 64, FI-00014 Finland
[2]Department of Chemistry, University of Helsinki, A.I. Virtasen aukio 1, P.O. Box 55, FI-00014 Finland
Keywords: Sulfuric acid, Molecular clusters, Modeling, Ion-induced nucleation.
Presenting author email: oona.kupiainen@helsinki.fi

A large fraction of atmospheric aerosols are formed in the atmosphere by gas-to-particle nucleation, but their birth-mechanism remains unclear. Sulfuric acid is believed to have a major role, but the observed new-particle formation rates cannot be explained by homogeneous nucleation of sulfuric acid and water alone. Instead, some additional compound is needed to stabilize the small sulfuric acid clusters and enable them to grow into particles.

Since acids and bases bind strongly together, bases are likely to enhance sulfuric acid cluster formation. We have studied the role of ammonia, which is a weak base and abundant in the atmosphere, and dimethylamine (DMA), which is a stronger base but has a lower concentration.

Nucleation can also be enhanced by ions through several mechanisms. Firstly, ions attract polar and polarizable molecules and clusters, which leads to higher collision rates compared to neutral cluster formation. Secondly, ionic clusters are more strongly bound, leading to lower evaporation rates. Finally, the recombination of oppositely charged clusters may enable the formation of neutral clusters even in conditions where purely neutral nucleation would be negligible.

We have computed formation Gibbs free energies of neutral and negatively and positively charged sulfuric acid – ammonia – DMA clusters up to four acids and four bases using a multi-step quantum chemistry method (Ortega *et al*, 2012). These energies were used to calculate evaporation rates of the clusters, assuming classical collision rates and barrierless reactions. Cluster formation was then studied using the Atmospheric Cluster Dynamics Code, ACDC (McGrath *et al*, 2011).

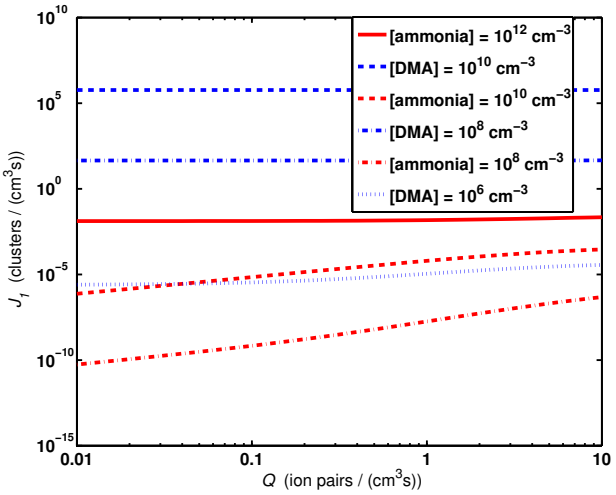

Figure 1: Formation rate of 1 nm clusters as a function of ion pair formation rate at a sulfuric acid concentration of 10^6 cm^{-3} and different ammonia and dimethylamine concentrations.

We have found that the charged clusters are overall more stable than neutrals, although the optimal acid-base ratio varies depending on the charge. In all charging states, DMA stabilizes the clusters more effectively than ammonia. On the other hand, ammonia concentrations in the atmosphere are typically a few orders of magnitude higher than amine concentrations, resulting in more frequent collisions with sulfuric acid molecules and clusters.

We have simulated the formation and growth of clusters at various concentrations of sulfuric acid, ammonia and DMA, and different ion formation rates. We have also compared our cluster formation rates with results from chamber experiments and field measurements, and studied the effect of charge in different conditions.

Figure 1 shows the effect of ions on our simulated cluster formation rate at a sulfuric acid concentration of 10^6 cm^{-3} and different ammonia and dimethylamine concentrations. It can be seen that DMA enhances cluster formation much more strongly than ammonia. For both bases, ion-induced nucleation may play a major role when the base concentration is low, but neutral cluster formation dominates at higher base concentrations.

Our results indicate that the first steps of atmospheric new-particle formation could be explained by the formation of sulfuric acid – amine clusters, whereas ammonia and charge may play a larger role in the absence of amines.

This work was supported by FP7-ATMNUCLE project No 227463 (ERC Advanced Grant), FP7-MOCAPAF project No 257360 (ERC Starting grant) and Academy of Finland LASTU project No 135054. The authors thank CSC - IT Center for Science in Espoo, Finland, for computing time.

McGrath, M. J., Olenius, T., Ortega, I. K., Loukonen, V., Paasonen, P., Kurtén, T., Kulmala, M., and Vehkamäki, H. (2011) Atmos. Chem. Phys. Discuss. **11**, 25263-25295.

Ortega, I. K., Kupiainen, O., Kurtén, T., Olenius, T., Wilkman, O., McGrath, M. J., Loukonen, V., and Vehkamäki, H. (2012) Atmos. Chem. Phys. **12**, 225-235.

Parameterization for two-component H_2SO_4 – H_2O nucleation applicable for very low relative humidities and correct at the one-component limit

A. Määttänen[1], J. Julin[2,3], I. K. Ortega[2] and H. Vehkamäki[2]

[1]Laboratoire Atmosphères, Milieux, Observations Spatiales, Université Versailles St Quentin, CNRS, F-78280 Guyancourt, France
[2]Department of Physics, Division of Atmospheric Sciences, PO Box 64, FI-00014 University of Helsinki, Finland
[3]Department of Applied Environmental Science (ITM), Stockholm University, SE-10691 Stockholm, Sweden
Keywords: nucleation, sulfuric acid.
Presenting author email: anni.maattanen@latmos.ipsl.fr

We have extended the Vehkamäki et al. (2002) two-component nucleation parameterization for sulfuric acid and water in stratospheric conditions to very low relative humidities where nucleation of pure sulfuric acid becomes possible. Our motivation for this work was an application to the extremely dry atmosphere of Venus, where relative humidities can fall below the lowest limit of the Vehkamäki et al. (2002) parameterization, RH=0,01%.

According to observations, sulfuric acid aerosols are the main component forming the clouds on Venus. The clouds are optically thick in the visible wavelengths masking the surface of the planet from visual observation. The clouds are organized in three quite distinct layers with differing droplet size distributions and probably differing composition. Hints from early observations on possible existence of other species than sulfuric acid in the clouds have not yet been confirmed by recent missions.

It is thought that the water – sulfuric acid droplets form by binary homogeneous nucleation in both the Earth's stratosphere and the atmosphere of Venus. In this study we focus on homogeneous nucleation only. However, the existence of condensation nuclei on Venus cannot be ruled out in lack of observational evidence.

We have used the thermodynamically consistent version of the Classical Nucleation Theory (Noppel et al., 2002). The 2002 model was improved by deriving analytical formulae for the second derivatives of the formation free energy, since the numerical derivatives were unstable at the limit of one-component system.

Instead of the cluster distribution based on the dihydrate used in the 2002 model, we have used the self-consistent distribution of Wilemski and Wyslouzil (1995, hereafter WW95), which reduces to the one-component distribution at the one-component limit. We have studied analytically the one-component limit of the kinetic part of the two-component model, which differs from a one-component kinetic model, and verified that the numerical models behave as predicted by the analytical studies. In developing the parameterization, for continuity and consistency, the two-component model is used also at the one-component limit at the extremely low relative humidities that enable pure sulfuric acid nucleation. The data were calculated for the temperature range of 150-400 K, relative humidities ranging from 1e-6 to 100%, and sulfuric acid concentrations of 1e4 to 1e17 m^{-3}.

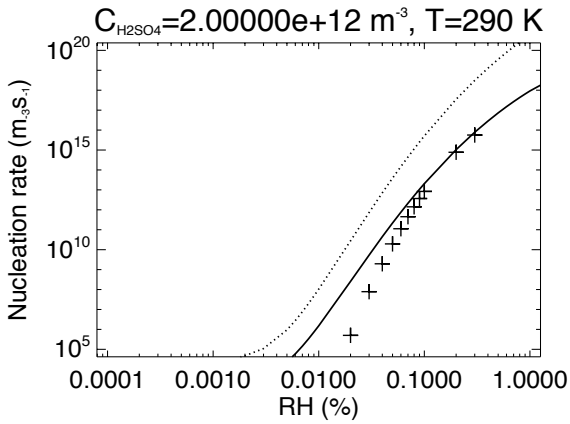

Figure 1. Example of the difference in nucleation rate between the old parameterization (+), old data (solid line, Noppel et al. 2002 hydrate distribution), and new data (dotted line, WW95 hydrate distribution). Validity range of the old parameterization goes down to RH=0.01%

Figure 1 presents a comparison of the old parameterization and the data calculated using the hydrate distributions of the 2002 model and WW95. The large difference between the solid line (Noppel distribution) and the dotted line (WW95 distribution) comes from the difference in cluster distributions. This example also illustrates that the old parameterization and the old data may differ by an order of magnitude or more in certain conditions.

The parameterization has been developed mainly for the needs of a Venus cloud model (see another abstract by Määttänen et al. in this conference), but it can naturally be applied to other, for example stratospheric, conditions as well.

M. Noppel, H. Vehkamäki, and M. Kulmala (2002). J. Chem. Phys., 116, pp. 218.

H. Vehkamäki, M. Kulmala, I. Napari, K. E. J. Lehtinen, C. Timmreck, M. Noppel, and A. Laaksonen (2002) J. Geophys. Res., 107(D22), pp. 4622.

G. Wilemski and B. E. Wyslouzil (1995) J. Chem. Phys. 103, pp.1127.

First modelling study on new particle formation and growth in Southern African savannah environment

R. Gierens[1], L. Laakso[1,2,3], V. Vakkari[1], D. Mogensen[1], and M. Boy[1]

[1]Department of Physics, Division of Atmospheric Sciences, University of Helsinki, Helsinki, 00014, Finland
[2]Finnish Meteorological Institute, Research and Development, P.O. BOX 503, FI-00101, Finland
[3]School of Physical and Chemical Sciences, North-West University, Potchefstroom, South Africa
Keywords: aerosol modelling, particle formation and growth, boundary layer, South African savannah.
Presenting author email: rosa.gierens@helsinki.fi

Africa is one of the least studied continents in respect to atmospheric aerosols. In this study measurements from a relatively clean savannah environment in South Africa were used to model new particle formation and growth. There are already some combined long-term measurements of trace gas concentrations together with aerosol and meteorological variables available (Laakso *et al.*, 2008), but to our knowledge this is the first time detailed simulations, that include all the main processes relevant to particle formation, were done.

MALTE (Model to predict new Aerosol formation in the Lower TroposphereE) is a one-dimensional model, which includes modules for boundary layer meteorology, emissions from the canopy as well as aerosol dynamical and chemical processes (Boy *et al.*, 2006, Lauros *et al.*, 2011). The aerosol dynamic processes are simulated with UHMA (University of Helsinki Multicomponent aerosol model) using two different nucleation approaches, the kinetic nucleation and organic induced nucleation. Previous studies indicate that this model is able to predict new particle formation events at the surface (Boy *et al.*, 2006 and Lauros *et al.*, 2011) and in the boundary layer with good agreement compared with measurements.

The measurements utilized in this study were done at a relatively clean background savannah site in central southern Africa (Laakso *et al.*, 2008). The location is characterized with relatively low pollutant concentrations with occasional polluted air masses from the industrial areas 100-300 km to the east. New particle formation at the site has been found to take place during most of the sunny days, 69 % of the days showing clear nucleation with additional 14 % of the days with non-growing nucleation mode (Vakkari *et al.*, 2011). The measurements include meteorological variables (temperature, relative humidity, wind speed and direction, precipitation, and radiation), trace gas concentrations (SO_2, NO_x, CO, and O_3), aerosol number size distribution, and concentrations of volatile organic compounds.

The observational data was used for input and comparisons with the simulations. We selected a couple of days of continuous data and varying conditions of clean and polluted background air. Figure 1 shows the measured and modelled particle size distributions for one day (the 10th of October 2007), during which a relatively polluted air mass was advected on the site. The model was able to reproduce the nucleation event and the growth of the particles, but the particles grow to the detected size, which is shown in the figure with a white line, later than observed. For this day the kinetic nucleation approach also underestimated the number concentrations.

The frequent new particle formation events and particle growth for the simulated days was evaluated in detail. We were able to simulate the aerosol number concentrations of newly formed particles with a reasonable good agreement with the measurements. This work will present new model results to give a better understanding on the new particle formation process in South Africa and discuss the reasons for high frequency of nucleation episodes observed.

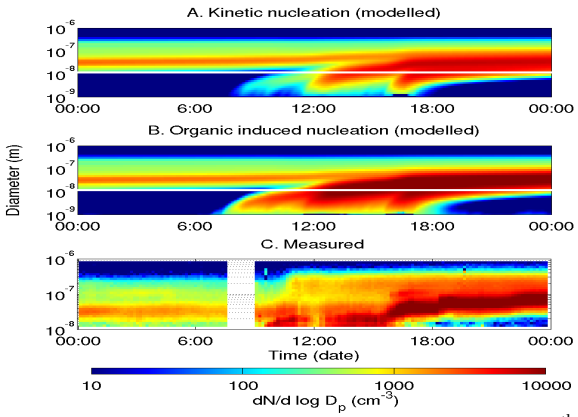

Figure 1. Particle number size distribution on the 10th of Oct assuming a) kinetic nucleation and b) organic induced nucleation in the simulation, and c) from the measurements. The white line in a and b show the detection limit of the instrument at 10nm.

Boy, M., Hellmuth, O., Korhonen, H., Nilsson, E. D., ReVelle, D., Turnipseed, A., Arnold, F. , and Kulmala M. (2006) Atmos. Chem. Phys. **6**, 4499-4517.

Laakso, L.,Laakso, H., Aalto, P. P. , Keronen, P., Petäjä, T., Nieminen, T., Pohja, T., Siivola, E., Kulmala, M., Kgabi, N., Molefe, M., Mabaso, D., Phalatse, D., Pienaar, K., and Kerminen,V.-M. (2008) Atmos. Chem. Phys., **8**, 4823–4839.

Lauros, J., Sogachev, A., Smolander, S., Vuollekoski, H., Sihto, S.-L., Laakso, L., Mammarella, I., Rannik, Ü., and Boy, M. (2011) Atmos. Chem. Phys. **11**, 5591-5601.

Vakkari, V., Laakso, H., Kulmala, M., Laaksonen, A., Mabaso, D., Molefe, M., Kgabi, N. and Laakso, L. (2010) Atmos. Chem. Phys. **11**, 3333-3346.

Comparing simulated and experimental molecular cluster distributions

T. Olenius[1], I.K. Ortega[1], O. Kupiainen[1], T. Kurtén[2], S. Schobesberger[1] and H. Vehkamäki[1]

[1]Department of Physics, University of Helsinki, Gustaf Hällströmin katu 2 A, P.O. Box 64, FI-00014 Finland
[2]Department of Chemistry, University of Helsinki, A.I. Virtasen aukio 1, P.O. Box 55, FI-00014 Finland
Keywords: molecular clusters, sulfuric acid, modelling, nucleation.
Presenting author email: tinja.olenius@helsinki.fi

The first step in the formation of secondary atmospheric aerosols involves nucleation of gas phase molecules into small molecular clusters. Today high-resolution mass spectroscopy enables the detection and unambiguous chemical characterization of electrically charged clusters from molecular scale upward, but experimental observation of electrically neutral clusters smaller than 1 nm in diameter still remains impossible. This results in a need for theoretical methods able to link the observed concentrations of charged clusters with the concentrations of neutral clusters.

We have used the kinetic code ACDC (Atmospheric Cluster Dynamics Code) (McGrath *et al*., 2011) to simulate a set of small molecular clusters containing sulfuric acid and ammonia molecules. As an input for the code we have used formation free energies of the clusters calculated with quantum chemical methods (Ortega *et al*., 2012). The code solves the birth-death equations of the clusters by using evaporation rates derived from the formation free energies. In this way we have examined the steady-state cluster distributions in different conditions, and compared the results to the concentrations measured in CLOUD experiments at CERN (Kirkby *et al*., 2011). We have included in the simulation both neutral clusters and negatively and positively charged cluster ions that contain up to four sulfuric acid and four ammonia molecules. The set of clusters was chosen based on the relative stability of the clusters, and therefore the unstable charged clusters were left out.

We have studied how the ratio between the concentrations of charged pure sulfuric acid clusters of different sizes varies with sulfuric acid and ammonia concentrations. Figure 1 shows the ratio of tetramer and trimer concentrations as a function of sulfuric acid concentration. According to the simulations the effect of ammonia becomes more important as the temperature decreases. At 278.65 K lines with different ammonia concentration are clearly separated, whereas at 292.15 K they fall on top of each other. The modelled ratios are qualitatively consistent with experimental observations.

We have shown that ACDC is capable of qualitatively reproducing the results measured in CLOUD. ACDC can also be used to simulate the distribution of neutral clusters that cannot be experimentally observed, leading to a better understanding of atmospheric cluster formation and nucleation mechanisms.

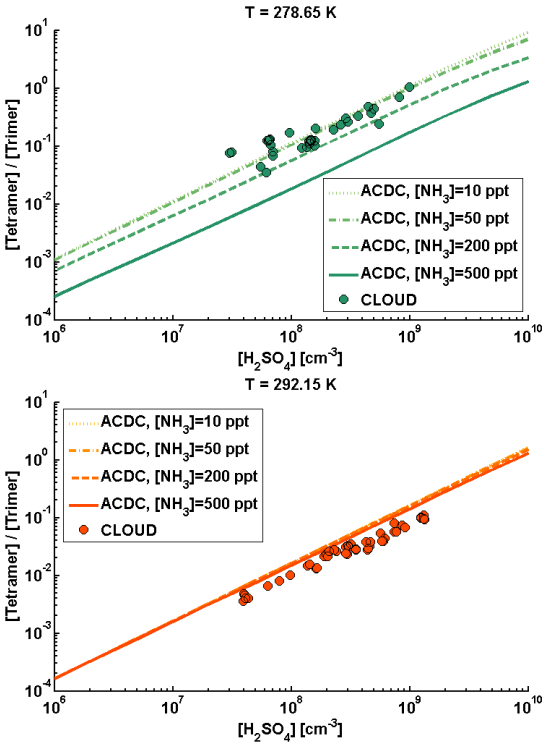

Figure 1. The simulated and experimental ratios between sulfuric acid tetramer and trimer concentrations versus sulfuric acid concentration for different temperatures and ammonia concentrations. The ammonia concentration in the experimental data points is uncertain and is estimated to vary between 0-500 ppt.

This work was supported by FP7-MOCAPAF project No 257360 (ERC Starting Grant) and FP7-ATMNUCLE project No 227463 (ERC Advanced Grant). The authors thank CSC- IT Center for Science in Espoo, Finland for the computing time and the CLOUD consortium for providing the experimental data.

Kirkby, J. *et al*. (2011) *Nature*, **476**, 429–433.

McGrath, M.J., Olenius, T., Ortega I.K., Loukonen V., Paasonen P., Kurtén T., Kulmala M., & Vehkamäki H. (2011) *Atmospheric Chemistry and Physics Discussions*, **11**, 25263-25295.

Ortega, I.K., Kupiainen, O., Kurtén, T., Olenius, T., Wilkman, O., McGrath, M.J., Loukonen, V. & Vehkamäki, H. (2012) *Atmospheric Chemistry and Physics*, **12**, 225-235.

Simulation of Aerosol Nucleation Bursts: A Case Study

J. Salm, A. Luts, U. Hõrrak, M. Vana and H. Tammet

Institute of Physics, University of Tartu, Tartu, 50090, Estonia
Keywords: tropospheric aerosols, nucleation bursts, nanoparticles, simulation.
Presenting author email: jaan.salm@ut.ee

Tammet and Kulmala (2005, 2007) have developed a numerical tool for the simulation of atmospheric aerosol nucleation bursts. The tool takes into account a number of various processes and relationships, which probably affect the generation and growth of aerosol particles in the atmosphere. This report presents a development of the preliminary attempt by Salm (2007) to simulate a measured nucleation burst.

Complex measurements were performed at SMEAR II Station, Hyytiälä, Southern Finland (61 51'N, 24 17'E, 170 m above sea level), from March 20 to April 20, 2000, at the annual maximum of the new particle burst occurrence (Salm, 2007). The main novel apparatus was a set of two identical DMPS with different pre-charging conditions. One of these DMPS operated at the very customary mode: the aerosol particles were charged in a bipolar charger. Another DMPS was identical, but without the charger; thus it measured only naturally charged aerosol particles. In both DMPS, negatively charged particles were analyzed.

The same nucleation burst of April 8, 2000, as previously (Salm, 2007), was chosen for an advanced study. In the previous study, the output graphs of the simulator calculations were visually compared with the measurement graphs. In the present study, one of the authors compiled a special shell, which links the initial data of a simulation and the simulation results with MS Excel tables, and enables automation of the calculations.

From measurements, we have the concentrations of negative nanoparticles in the size interval of 2.8–8.6 nm, the concentrations of neutral nanoparticles in the same size interval, and the concentrations of negative cluster ions recorded as average values for successive 30 min intervals. The particular nucleation burst began about 09:00 of LST and dropped about 14:30 LST. The time series of these three concentrations serve as targets for simulation (see Figure 1).

The simulation tool has 61 physical input parameters. Several parameters are kept as in the previous study, e.g., the electric mobility of cluster ions, the recombination coefficient of cluster ions etc. The meteorological and the background aerosol parameters are taken from the measurements. 44 parameters were varied in the process of calculations by means of the abovementioned shell using random number function. Thus every trial of calculations had an independent set of input parameters. The accuracy of every individual trial was rated through the sum of the squares of deviations between simulated values and measured values of the concentrations. The realization of about 1000 trials gives us a high probability that a satisfactorily simulated nucleation burst has been found (see Figure 1).

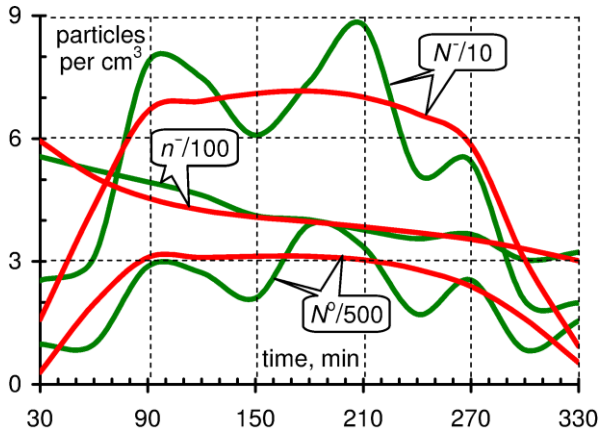

Figure 1. Simulation results for the fraction concentrations of charged and neutral aerosol particles and of cluster ions. n^- is the concentration of negative cluster ions, N^- and N^o are the concentrations of negative, and neutral particles in the diameter interval of 2.8–8.6 nm. Green lines represent the measured values and red lines the simulations.

The majority of obtained parameter values are comparable with the results of (Salm, 2007). However, several values turned out to be different, e.g.

- initial ionization rate 3.0 $cm^{-3}s^{-1}$
- halftime ionization rate 2.6 $cm^{-3}s^{-1}$
- final ionization rate 4.9 $cm^{-3}s^{-1}$
- max nucleation rate for + particles 0.06 $cm^{-3}s^{-1}$
- max nucleation rate for – particles 0.07 $cm^{-3}s^{-1}$
- max nucleation rate for neutral particles
  0.8 in free air and 1.1 $cm^{-3}s^{-1}$ in forest
- the time of steady nucleation activity 240 min
- the birth size of particles 1.0 nm.

A special calculation showed that the birth size of particles is a sensitive parameter, i.e. its increase or decrease rapidly worsens the accuracy of simulation.

Two condensing substances were considered. The initial, halftime and final growth rate of particles was 2.2–3.7 nm/h for both the substances.

This work was supported by the Estonian Science Foundation through grants 8342 and 8779, and the Estonian Research Council Project SF0180043s08.

Salm, J. (2007) *Nucleation and Atmospheric Aerosols, C. D. O'Dowd and P. E. Wagner (eds.)*, Springer, 245-249.

Tammet, H. and Kulmala, M. (2005) *J. Aerosol Sci*. **36**, 173-196.

Tammet, H. and Kulmala, M. (2007) *Boreal Env. Res.* **12**, 421-430.

Efficient second-order time-integration for simulation of single-species aerosol dynamics

C. Winkelmann[1,*], M. Nordlund[1], A. Kuczaj[1], S. Stolz[2] and B.J. Geurts[2,3]

[1]Philip Morris International R&D, Philip Morris Products SA, 2000 Neuchâtel, Switzerland
[2]Department of Applied Mathematics, University of Twente, 7500 AE Enschede, The Netherlands
[3]Department of Applied Physics, Eindhoven University of Technology, 5600 MB Eindhoven, The Netherlands
Keywords: CFD, aerosol formation, aerosol dynamics, time integration.
[*]Presenting author email: christoph.winkelmann@pmi.com

The dynamics of a single-species aerosol composed of water droplets in air is described in terms of nucleation, evaporation and condensation processes. Fast nucleation bursts that initiate formation of aerosol droplets co-exist with comparably slow condensation, which is responsible for the subsequent growth of the droplets. In order to accurately represent the dynamical consequences of the fast nucleation process, while retaining numerical efficiency, a new time-integration method for the nucleation, evaporation and condensation terms is proposed.

The new time-integration method is second-order accurate in time also in the general case of solution-dependent transport coefficients. The computational costs per time step were found to be increased by less than 50% compared to the reference Euler forward method. For a spatially homogeneous model system, a speed-up with a factor of up to several hundred was observed in selected cases.

The second order method is also applied in spatially varying situations involving convection-diffusion transport of the aerosol forming vapor inside a pipe geometry. We employ first order upwinding for the spatial discretization to capture sharp spatial variations, e.g., in the aerosol number density. Comparison with the Euler forward method allows identifying physical and numerical parameters for which the benefits of the new method, in terms of both accuracy and efficiency, are significant.

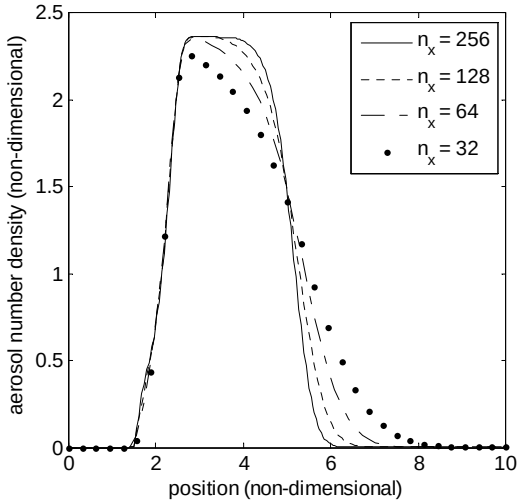

Figure 1: Convergence of aerosol number density with refinement of spatial discretization (n_x). Shown is the solution at the characteristic dimensionless time *t=5* at which a nucleation burst clearly developed.

We concentrate on the development of a front of rapid nucleation. In Figure 1, we observe the aerosol number density at a characteristic time for several spatial resolutions. A clear convergence is observed towards a sharp profile. The convergence with respect to a reduction of time step is illustrated in Figure 2. In the case shown, the Euler forward method is about a factor of 10 less accurate at equal time step. Conversely, at given desired accuracy level, the computational cost is reduced by a factor of up to 10 by the proposed scheme, even though only first order convergence is achieved in view of the selected spatial discretization.

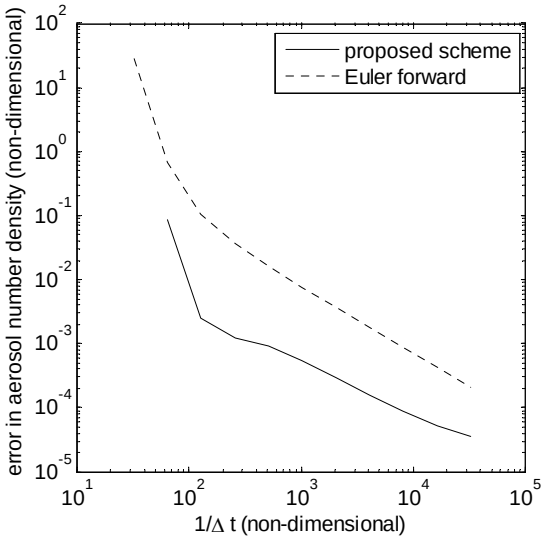

Figure 2: Convergence of aerosol number density with refinement of time discretization.

A complete overview and analysis of the new method for a range of physically realistic parameters will be presented at the conference. Extension to multi-dimensional nucleation fronts is subject of current research.

C. Winkelmann, M. Nordlund, A. Kuczaj, S. Stolz and B.J. Geurts (2012) *Second-order time-integration of single-species aerosol dynamics.* In preparation

To the theory of drop shattering in high-speed flows

A. G. Girin

Odessa National Maritime University, Odessa, 65029, Ukraine
Keywords: dispersion, aerosol generation, aerosol modelling, generation of combustion aerosol.
Presenting author email: club21@ukr.net

The mechanism in force of tearing-off of daughter droplets is a base of the theory of parent drop shattering in gas flows. It was shown earlier that hydrodynamic instability of "gradient instability" type describes adequately the known features of the process for weak-viscosity liquids. It is grounded on the concept of quasi-continuous high-frequency periodic dispersion of daughter droplets from unstable part $\varphi_{cr}<\varphi<\pi/2$ of parent drop surface due to action of gradient instability in conjugated boundary layers with due regard to changing of velocity profile across the boundary layers. In speedy flows, when the criterion of gradient instability $\mathrm{GI}\equiv \mathrm{We_d}\,\mathrm{Re_d^{-0.5}} \gg \mathrm{GI_{cr}} \approx 0.3$, values of polar angle of critical point are small: $\varphi_{cr} \ll \pi$, so, most part of drop surface generates a mist of droplets. This mechanism differs from that of Kelvine – Helmholtz type and it is caused by a large enough velocity gradient inside liquid boundary layer.

The foundations of drop breakup theory for speedy flows were laid in (Girin, 2011, a, b, c), where the application of approximative analytical approach, based on gradient instability mechanism, allowed to derive the governing differential equations of shattering process: of drop mass efflux (ablation law) and of torn-off droplets quantity together with the characteristic scales for their sizes and quantity. These equations demand simultaneous solution of drop motion equation in order to determine relative velocity, and of equation for transient critical conditions of instability – to determine $\varphi_{cr}(\tau)$. Their integration provides all the necessary relations of the theory of shattering process.

For speedy flows and spherical shape of drop we have obtained by integration the law of drop ablation $M(\tau)=\left(1-A\left(\tau-\alpha^{1/2}X_{\mathrm{d}}(\tau)\right)/3\right)^3$, that indicates the direct influence of drop motion law $X_{\mathrm{d}}(\tau)$. Then at approximation of experimental data for drop velocity versus time in the form $W=1-\exp(-H\tau)$, or $\alpha^{1/2}X_{\mathrm{d}}(\tau)=\tau-(1-\exp(-H\tau))/H$, we have integrated the equation of drop mass efflux and have obtained the drop mass history: $M=\left(1-h(1-\exp(-H\tau))\right)^3$ (here $h=A/3H$ is the ratio of initial mass efflux rate $A=0.46\left(1+(\alpha\mu)^{1/3}\right)^{-1}\left(\mu^2/\alpha\right)^{1/6}$ to the rate $H=2\alpha^{1/2}$ of relaxational decreasing of relative velocity of shattering drop and gas flow, $\alpha=\rho_{\mathrm{g}}/\rho_l$ and $\mu=\mu_{\mathrm{g}}/\mu_l$ are density and viscosity ratios of gas and liquid).

The distribution function $f_{\mathrm{n}}(r,\tau)$ was then obtained by integrating the equation of torn droplets quantity and the distributions $\Delta n(\tilde{r})=f_{\mathrm{n}}(r)\Delta r$ for various h, Re_∞ were calculated. Formula for $f_{\mathrm{n}}(r,\tau)$ allows to calculate intermediate distribution of droplets torn-off to arbitrary time moment. The analysis showed, that values of h slightly higher than $h=1$ are inherent to flows behind shock and detonation waves, the values $h>4$ correspond to ablation of liquid meteoroids and the case $h<1$ – to incomplete shattering of viscous drops. When $h>1$, the entire drop is dispersed to the moment $\tau_{\mathrm{b}}=H^{-1}\ln\left(h/(h-1)\right)$. When $h<1$ dispersing terminates before the drop is completely shattered, because of quick reducing of main reason of dispersing – relative velocity.

In view of lack of empirical data about laws of drop motion for various gas-droplets systems the main relations of shattering drop kinetics were obtained again, but on reliable ground of theoretical laws. They were found analytically as solutions of a system of non-linear differential equations of drop motion, drop mass efflux and quantity of torn droplets in a speedy uniform gas stream at neglecting by drop deformation influence. The two approaches of determination of drop motion law, which are based on empirical and theoretical methods, have lead eventually to similar distribution functions, but theoretical approach has the advantage being independent from lack of empirical data, so obtained formula is applicable to any gas – droplets system.

Obtained theoretically main regularities of shattering process: distribution function of torn daughter droplets by sizes, law of motion of shattering in gas stream parent drop and law of parent drop mass ablation give the opportunity to build mathematical model for further processes of rapid acceleration and evaporation of the mist of stripped daughter droplets in a wake of shattering parent drop.

Girin A.G. (2011a) *Journ. of Engin. Phys. and Thermophys.* **84**, 262–269.
Girin A.G. (2011b) *Journ. of Engin. Phys. and Thermophys.* **84**, 872–880.
Girin A.G. (2011c). *Journ. of Engin. phys. and Thermophys.* **84**, 1009–1015.

Particulate Fugitive Emissions in Harbours: characterization and emission factors estimation

A.V.Silva[1,2], S.M.Almeida[1], A.I. Miranda[2], F. Martín[3]

[1] URSN, Instituto Tecnológico e Nuclear, E.N. 10, 2686-953 Sacavém, Portugal.
[2]CESAM, Universidade de Aveiro, 3810-193 Aveiro, Portugal
CIEMAT, Atmospheric Pollution Unit.. Avda. Complutense, 22. 28040 Madrid, Spain

Keywords: fugitive emissions, emission factors, harbour, particles
Presenting author email: alexandra.silva@itn.pt

Fugitive emissions pose problems both for general air quality as well as for the operational management of facilities. Harbours activities such as loading, unloading and transport of dusty materials, are important sources of particles fugitive emissions. Therefore, harmful health effects of atmospheric particles in harbours may be originated by the handling of huge amounts of pulverulent raw material (including hazardous chemicals) that are managed in harbours (Gupta *et al*, 2002; Lucialli *et al*, 2007 and Gómez-Ollés *et al*, 2007).

The aim of this study was: 1) to characterize particulate matter emitted during unloading operations of fertilizer, phosphorite from Syria, phosphorite from Morocco, and sugar; 2) to compile an inventory of the main characteristics of $PM_{2.5}$ and $PM_{2.5-10}$, and; 3) to determine the emissions factors associated with these activities.

Results showed that manipulation of materials during harbour operations produced high emissions of particles, especially from the coarse fraction ($PM_{2.5-10}$). Figure 1 shows that the highest average concentrations were registered for phosphorite provided from Syria followed by phosphorite provided from Morocco. The lowest concentrations were measured during the handling of fertilizer and sugar.

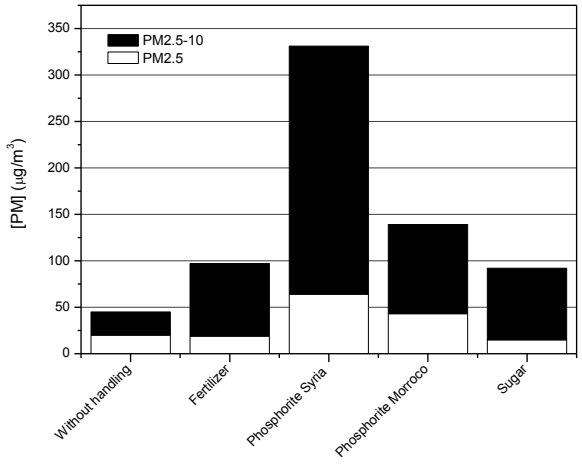

Figure 1. PM average concentrations measured in the harbour during the bulk materials handling (values in $\mu g.m^{-3}$).

PM10 concentrations discriminated by wind direction confirmed that the location of the sampling stations in relation to the wind direction is essential to evaluate the impact of fugitive emissions.

Emission estimations are usually based on emission factors provided by classical handbooks, U. S. Environmental Protection Agency reports labeled as AP-42 available at the EPA web page (http://www.epa.gov/ttn/chief/ap42/index.html) for different bulk handling and batch drop operations. Unfortunately, there are not specific harbour operation emission factors which take into account the unique conditions that exist in these coastal places.

This study processed experimental data to estimate the emission rate variation during the experiments, and the emission factors from each handling operations. This was done by applying a reverse dispersion modeling technique applying a high resolution Lagrangian puff model. This approach uses particulate matter concentration measured values and the atmospheric conditions to estimate emission rates, assuming that the contribution of a source to the concentration at a receptor is the product of the source emission rate and an atmospheric dispersion factor (Henry *et al* (1984). Crossing results with the quantities of handled material, for each period of time, provided specific emission factors.

Finally the comprehensive analysis of measured values and modeling results allowed to better characterize fugitive emissions in harbours and to develop specific emission factors from the handling operations, considering different types of raw material.

This work was supported by the Fundação para a Ciência e Tecnologia (FCT) for the funding of the project PTDC/AAC-AMB/098825/2008 – PMfugitive - Mitigating the Environmental and Health Impacts of Particles from Fugitive Emissions.

Gupta, A.K., Patil, R.S., and Gupta, S.K. (2002). *Emissions of gaseous and particulate pollutants in a port and harbour region in India*, Environmental Monitoring and Assessment, vol**. 80**, pp. 187–205.

Gómez-Ollés, S., Cruz, M.J., Bogdanovic J., M. Wouters, G. Doekes, I. Sander, F. Morell, and M.J.

Rodrigo, (2007). *Assessment of soy aeroallergen levels in different work environments*, Clinical and Experimental Allergy, vol. **37**, 1863–1872.

Henry, R. C., Lewis, C.W., Hopke, P.K. and Williamson, H.J., (1984). *Review of receptor model fundamentals*. Atmospheric Environment 28, 1507-1515.

Lucialli, P., Ugolini, P.and Pollini, E. (2007*). Harbour of Ravenna: the contribution of harbour traffic, Atmospheric Environment*, vol. **41**, 6421–6431.

Simulation of aerosol growth in chamber conditions

M. Vesterinen[1], H. Kokkola[1], H. Korhonen[1], H. Keskinen[2] and K.E.J. Lehtinen[1]

[1]Finnish Meteorological Institute, Kuopio Unit, Kuopio, 70211, Finland
[2]University of Eastern Finland, Kuopio, 70211, Finland
Keywords: condensation, absorption, chamber modelling.
Presenting author email: milko.vesterinen@fmi.fi

Detailed understanding of the partitioning of biogenic hydrocarbons to the aerosol phase is important when trying to quantify their aerosol forming potential. Several different processes can be associated with secondary organic aerosol (SOA) and information is required about the forming mechanisms of low- and semi-volatile organics. For example, semi-volatile compounds can either be locked in the condensed phase or be present in both the gas and particle phase. Modeling-based studies suffer from the lack of quantitative information of different partitioning processes and therefore, aerosol (smog) chamber data is needed to offer an optimal platform for both model verification and development.

The dynamical model applied in this study is SALSA (Kokkola *et al*, 2008) which includes subroutines for aerosol condensational growth, coagulation and nucleation, as well as for aerosol size distribution and its time-dependent behaviour. SALSA model running time was 8 hours and nucleation was handled by inserting measured data for the first two bins in the model. Next, the particle number concentration time evolution predicted by SALSA was compared to the chamber measurement data and first model run results can be seen in Figure 1.

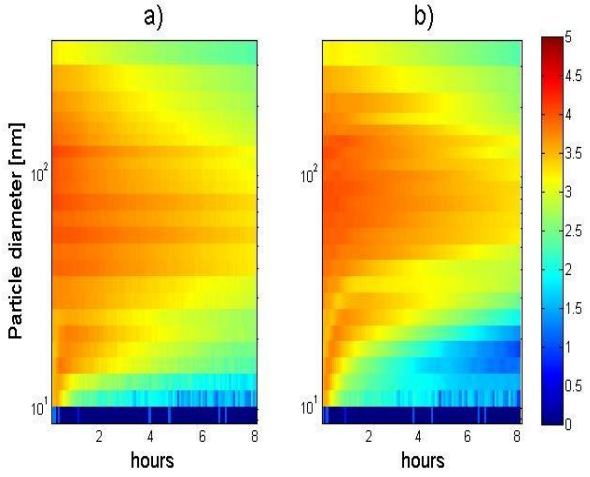

Figure 1. Left: the measured particle number concentration (cm^{-3}) as a function of time (h) and diameter (nm). Right: simulated particle number concentration. The particle number concentration is presented in a logarithmic scale with a maximum of 10^5 cm^{-3}.

For the condensing species, a basic two – product model was applied (for example, see Bowman *et al* (1999). In addition, wall loss of the gases was included in the calculations. The simple precursor gas – phase chemistry was based on the reaction between ozone and alpha-pinene that was similar to the measurement. Aerosol wall deposition rate was determined by fitting a first-order wall loss curve for each size class (by using data 4.5 hours after the outset of the measurement) and by combining the fit results to obtain a wall loss function for polydisperse aerosol population (see Figure 2). Measurement was performed in a Teflon coated chamber with a volume of 5.8 m^3; details of the chamber can be found in Hao *et al* (2009).

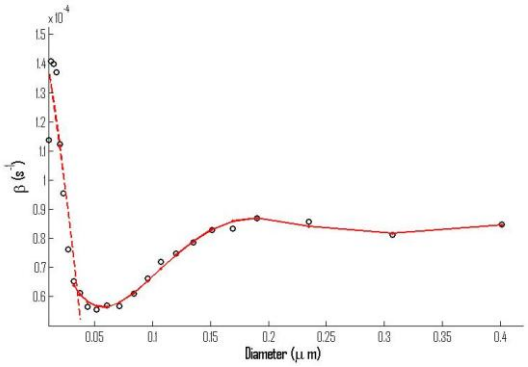

Figure 2. Particle wall deposition rate (s^{-1}) as a function of the particle diameter (μm). Two separate fits were performed (for small and for larger particles) and the results were combined to obtain a polydisperse wall loss function.

This work is supported by the Maj and Tor Nessling Foundation under grant 2012358.

Bowman, F., Odum, J.R., Seinfeld, J.H. and Pandis, S.N. (1997). *Atmos. Environ.* **31**, 3921-3931.

Hao, L., Yli-Pirilä, P., Tiitta, P., Romakkaniemi, S, Vaattovaara, P., Kajos, M., Rinne, J., Heijari, J., Kortelainen, A., Miettinen, P., Kroll, J., Holopainen, J., Smith, J., Joutsensaari, J., Kulmala, M., Worsnop, D. and Laaksonen, A. (2009). *Atmos. Chem. Phys.* **9**, 8121-8137.

Kokkola, H., Korhonen, H., Lehtinen, K., Makkonen, R., Asmi, A., Järvenoja, S., Anttila, T., Partanen, A.-I., Kulmala, M., Järvinen, H., Laaksonen, A. and Kerminen, V.-M. (2008). *Atmos. Chem. Phys*. **8**, 2469-2483.

Oxidation of SO_2 by $O_2^-(H_2O)_n$ molecular clusters – a density functional theory study

N.T. Tsona[1], N. Bork[1,2] and H. Vehkamäki[1]

[1]Department of Physics, University of Helsinki, Helsinki, 00014, Finland
[2]Department of Chemistry, University of Copenhagen, Copenhagen, 2100, Denmark
Keywords: Ion-induced nucleation, aerosol catalysis, charged particles, molecular clusters.
Presenting author email: narcisse.tsonatchinda@helsinki.fi

One of the most active areas of atmospheric chemistry is related to understanding cloud formation. The first step in this mechanism is known as nucleation, and despite much research dedicated exclusively to this process, it is still not properly understood.

Although clouds are mainly composed of water, it is well known that at least one other particle or chemical is needed to initiate the nucleation. In numerous studies sulphuric acid has been identified as the primary candidate for this (Kulmala *et al.* (2004)).

The most important mechanism of H_2SO_4 formation is the well known UV induced oxidation of SO_2. It follows a neutral pathway.

$$OH + SO_2 + M \rightarrow HSO_3 + M \quad (R1)$$
$$HSO_3 + O_2 \rightarrow SO_3 + HO_2 \quad (R2)$$
$$SO_3 + H_2O \rightarrow H_2SO_4 \quad (R3)$$

Currently, the properties of atmospheric ions are receiving increased attention from both theoretical, field based, and chamber studies. It has thus firmly been established that ions increase nucleation rates and hence aid cloud formation. However, the underlying mechanism is currently unknown. Several possible mechanisms may be responsible but since ionic chemistry also opens a mechanism for formation of sulphuric acid this might explain the observations.

It is well known that the majority of atmospheric ions originate from cosmic ray impacts, producing free electrons and a variety of cations. A free electron may easily attach to O_2 with an energy gain of ca. 40 kJ/mol. The resulting ion has been found to form stable clusters with at least 5 water molecules (Bork *et al.* (2011)).

Few chemical properties of $O_2^-(H_2O)_n$ clusters have been investigated but experiments have shown that

$$O_2^-(H_2O)_n + SO_2 \rightarrow SO_4^-(H_2O)_n \quad (R4)$$

for n = 1 and 2. Further, it has been shown that the reaction is fast at ambient temperatures (Möhler *et al* (1992)). Also in recent field measurements SO_4^- has been observed (Ehn *et al* (2010)). SO_4^- is hence known to be stable and it seems plausible that SO_4^- may react further to H_2SO_4 or a related species and thereby contribute to nucleation and cloud formation. This confirms the need to understand the origin of SO_4^-.

However, neither the structures, the reaction mechanism, nor the possible catalytic effects of water molecules are properly understood.

The main goal of this research is to provide a plausible mechanism and reaction rates for the formation of SO_4^-. We have used density functional theory calculations and basis sets successfully used in previous studies.

Since it is known that the reactants are containing at least 5 water molecules, we have included that amount in our studies. We model the entire reaction from the initial collision and clustering, over intermediate structures (see Figure 1) to products.

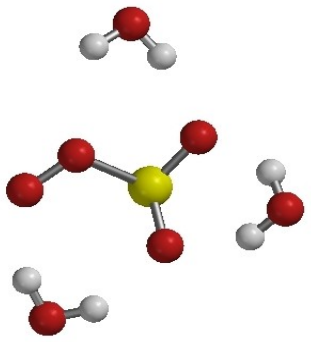

Figure 1. Stable configuration of the $SO_2O_2^-(H_2O)_3$ cluster. Sulphur (yellow), oxygen (red) and hydrogen (white). The cluster is stabilized by hydrogen bonds.

The following results will be reported and analysed:

- the structures of hydrated clusters
- the thermodynamics of the reactions
- the cluster populations at varying conditions
- the dynamics of the reactions
- the kinetics of the reactions
- comparison to experimental results and field studies
- the atmospheric relevance of the reaction

This work is supported by the CSC IT Centre for Science in Espoo, Finland.

Bork, N., Kurten, T., Enghoff, M.B., Pedersen, J.O.P., Mikkelsen, K.V. and Svensmark, H. (2011) *Atmos. Chem. Phys.,* **11,** *7133–7142.*

Ehn, M., Junninen, H., Petäjä, T., Kurten, T., Kerminen, V.-M., Schobesberger, S., Manninen, H. E., Ortega, I. K., Vehkamäki, H., Kulmala, M. and Worsnop, D. R. (2010) *Atmos. Chem. Phys.,* **10**, *8513–8530.*

Kulmala, M., Vehkamäki, H., Petäjä, T., Dal Maso, M., Lauri, A., Kerminen, V.-M., Birmili, W. and McMurry, P.H. (2004) *J. Aerosol Sci.,* **35**, *143-176.*

Möhler, O. Reiner, T. and Arnold, F. (1992) *J. Chem. Phys.,* **97(11),** *8233-8239.*

Determining the proton affinity of atmospheric molecular ions

K. Ruusuvuori[1], T. Kurtén[2], I. K. Ortega[1] and H. Vehkamäki[1]

[1]Division of Atmospheric Sciences, Department of Physics,
University of Helsinki, P.O. BOX 64, FI-00014, Finland
[2]Laboratory of Physical Chemistry, Department of Chemistry,
University of Helsinki, P.O. BOX 55, FI-00014, Finland
Keywords: Atmospheric aerosols, aerosol thermodynamics, modelling.
Presenting author email: kai.ruusuvuori@helsinki.fi

Understanding the birth and interaction mechanisms of atmospheric aerosols is essential if we are to understand e.g. climate change and the health effects of aerosols.

Our aim is to study the absolute values of proton affinities using quantum chemical methods. These methods will be applied to several molecular ion species that have been observed by Ehn *et al.* (2010). Proton affinity is a measure of gas-phase basicity and is an important thermodynamic quantity. However, absolute gas-phase proton affinities are hard to measure, which makes theoretical methods a valuable tool in determining these absolute values.

We have begun our study by a series of benchmark calculations, where several different computational methods have been used to calculate the proton affinities of ammonia (NH_3) and pyridine (C_5H_5N). The obtained values have been compared to results listed in the National Institute of Standards and Technology (NIST) database. For the case of ammonia and pyridine, the NIST values for the proton affinity are from a review article by Hunter and Lias (1998) and are theoretical values calculated at the G2 level of theory.

Quantum chemical calculations of proton affinity have been performed using Gaussian 09 and Turbomole 6.3 quantum chemistry programs at the following levels of theory: G2MP2, G2, G3, G4, CBS-QB3, CBS-APNO, W1BD and B3LYP/6-31++G(2df,2pd)//RI-MP2-F12/cc-pVDZ-F12. Due to computational limitations, the W1BD method has only been used for ammonia. The resulting proton affinities are listed in Table1.

Table 1. Proton affinities in kcal/mol for the reactions $NH_3 + H^+ \rightarrow NH_4^+$ and $C_5H_5N + H^+ \rightarrow C_5H_6N^+$ calculated from standard enthalpies (1 atm, 298.15K).

Method	PA(NH_3) [kcal/mol]	PA(C_5H_5N) [kcal/mol]
G2MP2	204.008	222.238
G2	204.040	222.232
G3	204.619	222.407
G4	204.363	222.505
CBS-QB3	204.186	221.600
CBS-APNO	204.420	222.366
W1BD	204.062	-
A*	202.540	219.605
NIST(G2)	204.015	222.275

*B3LYP/6-31++G(2df,2pd)//RI-MP2-F12/cc-pVDZ-F12

The results of the benchmark calculations show that only results obtained with the B3LYP/6-31++G(2df,2pd)//RI-MP2-F12/cc-pVDZ-F12 method differ from the NIST values by more than 1 kcal/mol. Out of all the listed methods, the W1BD method should, at least in principle, provide the most accurate results. The W1BD is also the most demanding computationally and computational resources will not permit its use in the remaining part of our study. All the CBS-methods proved to be quite similar to each other in performance as did the different G-methods. In addition, comparison between the CBS- and G-methods shows that similar accuracy is obtained. Since the CBS-QB3 method should be significantly faster than the G-methods and is also available for second row atoms in Gaussian 09, whereas the CBS-APNO is available only for first row atoms, it would make a good choice for the remaining proton affinity calculations. However, the benchmark calculations of CBS-4M are still underway and since the Gaussian 09 manual recommends it for new studies over the CBS-QB3, our final choice of method is still at the moment undetermined.

Once the CBS-4M results are obtained and the choice of theoretical method made, we will proceed to calculate the proton affinities of positively charged ions observed by Ehn *et al*. (2010).

We thank the CSC – IT Center for Science Ltd. for computer time and technical assistance. The financial support by the Academy of Finland Centre of Excellence program (Project No. 1118615) and ERC StG 257360-MOCAPAF is gratefully acknowledged.

Ehn, M., Junninen, H., Petäjä, T., Kurtèn, T., Kerminen, V.-M., Schobesberger, S., Manninen, H.E., Ortega, I.K., Vehkamäki, H., Kulmala, M., and Worsnop, D.R. (2010) *Atmos. Chem. Phys.* **10**, 8513-8530.

Hunter, E.P.L., and Lias, S.G., *J. Phys. Chem. Ref. Data* **27**, 413-656.

Frisch, M.J. *et al.* (2009). Gaussian 09, Revision C.01, Gaussian, Inc., Wallingford CT.

TURBOMOLE V6.3 (2010), a development of University of Karslruhe and Forschungszentrum Karslruhe GmbH, 1989-2007, TURBOMOLE GmbH, since 2007

Particle generation in electric arc: experiment and modelling

V.A. Zagaynov[1], E.V. Zhukova[1], A.A. Lushnikov[1], Yu.G. Biryukov[1], I.E. Agranovsky[1,2], V.V. Maksimenko[1]

[1]Karpov Institute of Physical Chemistry, Vorontsovo Pole, 10, 105064 Moscow, Russia
[2]School of Engineering, Griffith University, Brisbane, 4111 QLD, Australia

Keywords: electric field, particle generation, modelling
Presenting author email: zagaynov@cc.nifhi.ac.ru

Particle generation in atmospheric and laboratory conditions is very important part of aerosol dynamics. The matter of fact, very often the particles of different sizes are generated in electric arc and electric discharges. There are great experimental data on the particle generation in these conditions; at the same time till now the corrected theory on this subject is absent. During electric discharge there are several physical processes, which can lead to particle generation and to extract most important is hard problem. The flow of free electrons and ions collide with metal surface, they knock out electrons, selected atoms, and molecular clusters. The temperature in this local space exceeds several thousand degrees, and when this vapor finds themselves in cold air, it begins to create aerosol particles of different sizes. At the same time metal molecular clusters and particles, which were kicked out from metal surface. At high temperatures they become liquid and take spherical form. This picture was found under electron microscope after sampling particles from arc discharge.

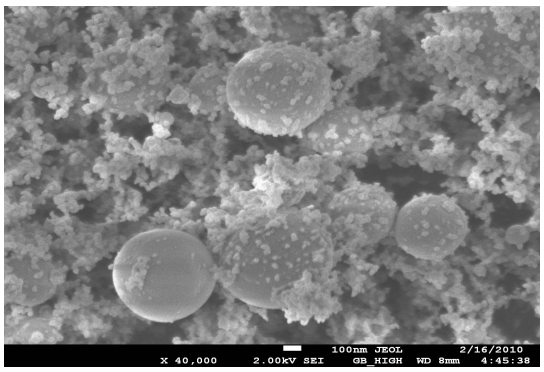

Figure 1. Photo image, obtained under electron microscope of silver particles, created in arc discharge.

It may be seen from this picture, that two mode particle size distributions was formed. There are large particles, which size is in the range between 300 and 700 nm, and small particles which size in the range between 10 and 30 nm. It may explain by two processes which responsible for particle generation. First of all large particle were kicked out from metal surface as molecular or atomic clusters, at large temperatures they become liquid and take spherical form, as may be seen from the picture. They have not enough time to be evaporated and after cooling save their spherical form. Secondly, there are many small particles, which were formed by volume condensation of metal vapors.

To control particle generation diffusion aerosol spectrometer and SMPS were used. They showed the same results. To get more information on particle generation in these conditions the computer modeling was involved. To this end the kinetic equation of particle coagulation was written:

$$\frac{\partial c_g}{\partial t} = I(g) + \frac{1}{2}\int_0^g K(g-n,n)c_{g-n}c_n dn + c_g \int_0^G K(g,n)c_n dn$$

here c_g –concentration of the particles, which composed of g monomers, $I(g)$ – source power of particles, consisted of g monomers, $K(g,n)$ – collision frequency between particles consisted of g and n monomers. To adjust it to computer calculations the axis of particle sizes was divided into fractions by logarithmic scale (Zagaynov and Lushnikov, 1988). It allowed to cover particle size range between 1 nm and 10 micrometers. To approach modelling results to reality the random factor was used (Lushnikov and Zagaynov, 1989).

The results allowed to clear up processes of particle generation.

Zagaynov, V.A., Lushnikov, A.A (1988). Modelling of coagulating processes in the atmosphere. - *Lecture Notes Physics*, Pergamon Press, pp.93-96,

Lushnikov, A.A., Zagaynov, V.A. (1989) Random factors in aerosol kinetics. - *J.Aerosol Sci.*, v.20, n.8, pp.987-990,

Impact of horizontal grid resolution on predicting fine PM with a regional 3-D Chemical Transport Model

C. Fountoukis[1], A.G. Megaritis[1,2], D.S. Koraj[2], H.A.C. Denier van der Gon[3], P.E. Charalampidis[4], C. Pilinis[4], and S.N. Pandis[1,2,5]

[1]Institute of Chemical Engineering & High Temperature Chemical Processes, Foundation for Research & Technology-Hellas (FORTH), 26504, Patras, Greece
[2] Department of Chemical Engineering, University of Patras, Patras, Greece
[3]TNO Built Environment and Geosciences, Netherlands
[4]Department of Environment, University of the Aegean, 81100, Mytilene, Greece
[5]Department of Chemical Engineering, Carnegie Mellon University, Pittsburgh, PA 15213, USA
Keywords: PMCAMx, Regional air quality, high resolution emissions, AMS data, MEGAPOLI.
Presenting author email: cfountoukis@iceht.forth.gr

Three dimensional Eulerian Chemical Transport Models (CTMs) are often used for the design and assessment of air pollution mitigation policies. Grid resolution is a critical factor for these models since a large model grid size cannot capture inhomogeneities in emission rates, meteorology and land cover while a very small grid size makes the simulation inefficient due to the large computational cost. The lack of adequate resolution limits also the ability of the model to accurately simulate individual processes and their interactions.

In this work, we use the regional CTM PMCAMx (Fountoukis et al., 2011) in a two-way nesting configuration to study the impact of different grid resolutions on fine particulate matter predictions at two domains, the North Eastern United States and Western Europe during a summer and winter period. In the US domain we use model grids of 36 and 12 km and PM measurements taken by the IMPROVE and STN monitoring networks, while for the European domain high time resolution AMS measurements were used to evaluate the performance of the model at 36 km and 4 km grids. For the US nested subdomain the model interpolates the input emission data from the coarse grid while for the European nested grid high resolution (~ 1 × 1 km) emissions are used.

During the July 2001 period use of both grid resolutions results in very similar predictions for $PM_{2.5}$ sulfate and organics over the Eastern US. The higher resolution slightly improves predictions of OA for the mostly rural (IMPROVE) sites, while for the mostly urban (STN) sites the model underpredicts both major $PM_{2.5}$ components with either the 36- or the 12-km grid spacing with roughly the same magnitude. During the January 2002 period there is a clearer improvement in the model predictions in both monitoring networks mainly for fine organic aerosol and elemental carbon.

In an effort to stress more the differences between the two model grid configurations we combined high resolution emissions (1 × 1 km) with AMS measurement data and applied an even higher model grid resolution (4-km) over a Megacity in Europe. For particulate sulfate, the model predicts negligible differences in the two simulations at all sites (both urban and suburban) even on an hour-by-hour basis during both the July 2009 and the January 2010 period. Similarly to the Eastern US domain, the differences between the two grid simulation results in the Paris area are, on average, small for all species during the summer period. During the winter period there are some significant differences in model predictions of mainly primary organics (Fig. 1) and black carbon. The major differences are seen for the maximum (morning peak) values in the two most polluted sites (LHVP and GOLF). The 4-km grid simulation captures the average diurnal concentration of fine organic aerosol better than the coarse grid.

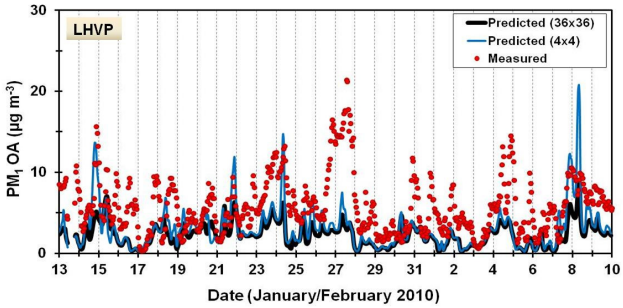

Figure 1. Timeseries comparison of predicted vs. observed PM_1 OA concentration in Paris center (LHVP station) during winter 2010.

Overall, the improvement in model predictions with the fine grid is modest during the summer and somewhat more significant during wintertime at both domains. The use of very high resolution emissions in the Megacity of Paris does not reveal a significant improvement in the predictions of the fine grid simulation. These results suggest that the major reasons for the discrepancies between the model predictions and observations in both seasons and at both domains are not due to the grid size used, but to other problems (e.g. emissions, process description, and meteorology).

This work was funded by the European Community's 7th Framework Programme EU project PEGASOS.

Fountoukis, C., et al. (2008) Evaluation of a three-dimensional chemical transport model (PMCAMx) in the European domain during the EUCAARI May 2008 campaign, *Atmos. Chem. Phys.*, 11, 10331–10347.

Development of an observation-based box model to investigate secondary inorganic particle behaviours in the urban atmosphere

J. Xue[1], Z.B. Yuan[2], J.Z. Yu[1], A.K.H. Lau[1] and T. Yao[1]

[1]Division of Environment, Hong Kong University of Science and Technology, Clear Water Bay, Hong Kong

[2]Atmospheric Research Centre, HKUST Fok Ying Tung Graduate School, Nansha IT Park, Guangzhou, China

Presenting author email: zibing@ust.hk

In this study, a mechanistically complete and time-dependent model, Observation-BAsed Model for Ambient Particulates (OBAMAP), is developed for resolving chemistry processes, thermodynamic equilibriums and size distribution of secondary inorganic aerosols (SIA) in an urban atmosphere. OBAMAP uses in-situ atmospheric and meteorological observations to determine the sensitivity of sulfate and nitrate concentrations to changes in their precursors (i.e., volatile organic compounds, nitrogen oxides and sulfur dioxide). OBAMAP is relatively easy and inexpensive to operate and makes use of data that are increasingly available in China and other developing countries, thereby offering a cost-effective tool for the analysis of SIA-precursor relationships in an urban atmosphere.

To demonstrate the applicability of OBAMAP, we first compare the simulation results of hydroxyl radicals with ambient observations. The OBAMAP is then applied on a wintertime pollution episode in Hong Kong to gain insight into relevant physical and chemical processes of SIA formations and to shed light on ways of effective control strategy formulation in Hong Kong. The results suggest local processes contrite more significantly on ambient NO_3^- and SO_4^{2-} levels during the episode period than the normal period. The major pathway responsible for the production of NO_3^- is the reaction of OH and NO_2 in the gas phase, while the aqueous phase oxidation of $S_{(IV)}$ by NO_2 shows the most significant contributions on SO_4^{2-} production. Local processes contribute 78.4% enhancement of NO_3^- and 14.0% enhancement of SO_4^{2-} in the episode hours (hours with Air Pollution Index>100). Formation of $PM_{2.5}$ NO_3^- is somewhat more sensitive to the reduction of NO_x and anthropogenic volatile organic compounds (AVOC) concentration. For each percent reduction in NO_x and AVOC, a 0.53 and 0.66% reduction in mass of NO_3^- formation would result in, respectively. Reduction of SO_4^{2-} formation is most sensitive to reduction of SO_2 and it would become more effective when more SO_2 has been reduced.

This work was supported by the Research Grant Council of Hong Kong (615406) and Joint Fundings of the National Science Foundation of China – Guangdong Province (U1033001). We thank Dr. Peter Louie of the Hong Kong Environmental Protection Department for providing the VOC speciation data at Tung Chung and Prof. Dui Wu of the Institute of Tropical Marine Meteorology, Chinese Meteorology Administration for providing the gas and particle data at Panyu.

Simulation of Droplet Nucleation and Growth in a Laminar Counterflow via the Quadrature Method of Moments

A.O. Alshaarawi, K. Zhou and F. Bisetti
Clean Combustion Research Center, King Abdullah University of Science and Technology,
Thuwal, 23955-6900, Kingdom of Saudi Arabia
Keywords: Aerosol Transport, Quadrature Method of Moments, Brownian Diffusion, CFD.
Presenting author email: amjad.shaarawi@kaust.edu.sa

The solution of the General Dynamic Equation (GDE) is an essential step for simulating multiphase flows. Applications include the study of soot formation, spray combustion and air pollution.

In the current study, the dynamics of the nucleation and growth of di-butyl-phthalate (DBP) droplets are simulated in a counterflow configuration. A cold stream of nitrogen mixes with a hot one saturated with DBP vapor. Near the stagnation plane, temperature drops and nano-size droplets of DBP nucleate and grow due to heterogeneous nucleation. As the number density of particles increases, coagulation affects the population balance.

The flow field is simulated with a stream-function formulation due to Kee et al. (1989). The GDE of the particle size distribution (PSD) is integrated to obtain transport equations for moments. The Quadrature Method of Moments (QMOM) (McGraw (1997)) is used for closure. Moments are transported using a second-order upwind scheme in space and an adaptive variable-order scheme in time. Homogeneous nucleation is described by classical Becker-Döring theory and heterogeneous nucleation is modelled using the generalization of Mason's formula due to Loyalka and Park (1988).

Realizability of the transported moments was treated carefully to ensure the existence of a corresponding PSD. For this purpose, Stieltjes conditions were monitored and shown to guarantee a physical solution.

Droplets start nucleating at the cold side (right side in Figure 1) of the stagnation plane. These droplets are then convected towards the stagnation plane where they diffuse to the hot side. As particles are convected, they grow in size due to heterogeneous nucleation and the volume-averaged diameter increases.

Mass diffusion of particles modifies the spatial distribution of each moment differently, making diffusion more significant for the moments of low order, such as the number density. Nucleating droplets have a diameter equal to the critical diameter (2.3 nm). Such small particles have a high diffusion coefficient corresponding to a Schmidt number $\sim \mathcal{O}(10)$.

On the other hand, large particles with a diameter of size $\sim \mathcal{O}(1\,\mu\mathrm{m})$ have a very low diffusion coefficient corresponding to a Schmidt number $\sim \mathcal{O}(10^6)$. For higher moments such as the volume fraction, the strong dependence of the mass diffusion coefficient on the particle size results in two flow regions: a hyperbolic convective-reactive zone away from the stagnation plane and a diffusive-convective-reactive zone near the stagnation plane, where velocity vanishes and diffusion dominates.

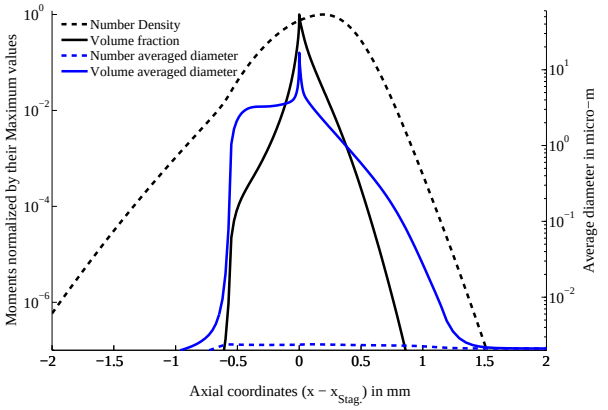

Figure 1: Distribution of different normalized Moments (in black), distribution of the number/volume averaged diameters (in blue). The flow has a nominal strain rate of 20 s^{-1} with boundaries at $T_c = 0\,^{\circ}\mathrm{C}$ and $T_h = 160\,^{\circ}\mathrm{C}$. DBP concentration at the hot inlet is 2600 ppm.

References

Kee, R., Miller, J., Evans, G., and Dixon-Lewis, G. (1989). A computational model of the structure and extinction of strained, opposed flow, premixed methane-air flames. In *Symposium (International) on Combustion*, volume 22, pages 1479–1494. Elsevier.

Loyalka, S. and Park, J. (1988). Aerosol growth by condensation: a generalization of mason's formula. *Journal of colloid and interface science*, 125(2):712–716.

McGraw, R. (1997). Description of aerosol dynamics by the quadrature method of moments. *Aerosol Science and Technology*, 27(2):255–265.

Vertical wind as the dominating factor for spatial-temporal distribution of stratospheric aerosol

V.I. Gryazin* and S.A. Beresnev

Aerosol Physics Laboratory, Ural Federal University, Ekaterinburg, 620083, Russia
Keywords: aerosol modelling, stratospheric aerosols, aerosol dynamics, vertical wind
Presenting author email*: Gryazin.Victor@mail.ru

This report continues and summarizes analysis and estimations of transport opportunities of the vertical wind in stratosphere. The developed method is based on the inclusion of the averaged fields of vertical wind retrieved from the assimilation global circulation model UKMO (http://badc.nerc.ac.uk) in the standard statistical atmospheric models. We are limited in analysis only to the monthly-averaged or annual-averaged profiles of a vertical wind (synoptic and global temporal scales for stratosphere). For the description of mechanical characteristics of motion of particles with different sizes and densities under action of gravity and vertical wind the gas-kinetic expression for resistance force, being by generalization of Millikan empirical formula, and well-worked in various problems of aerosol mechanics is used (Gryazin and Beresnev, 2011).

In this study the standard climatological analysis of vertical wind field in stratosphere over a period of a total solar cycle is presented, and surprising capabilities of the averaged vertical wind to the aerosol transport in comparison with other mechanisms (gravitational sedimentation and turbulent diffusion of particles) are demonstrated. High-altitude, temporal, and latitude dependences of zonal-mean averaged vertical wind velocity for the period of 1992-2006 from the UKMO atmospheric general circulation model are analysed. It is shown that monthly averaged amplitudes of the vertical wind are approximately ±5 mm/s, while annual averaged ones are ±1 mm/s (Beresnev et al, 2008). We have carried out the comparison of the received results with the NCEP-NCAR reanalysis data, and have found out their qualitative agreement.

The upward wind can provide the vertical lifting against gravity for sufficiently large (up to 3-5 μm) aerosol particles with a density up to 1.0-1.5 g/cm^3 at stratospheric and mesospheric altitudes. The vertical wind is a substantial factor for particles motion up to altitudes of 30-40 km, and can change essentially the sedimentation velocities and the residence times of stratospheric aerosols. The structure of the averaged fields of vertical wind supposes the opportunity of formation of dynamically stable aerosol layers in the middle stratosphere (Beresnev et al, 2009).

For the problem about action of a permanent source of monodisperse particles near the stratopause, it is shown that action of the averaged vertical wind along with the gravitational sedimentation and turbulent diffusion changes the standard vertical profiles of the relative concentration of particles cardinally. Estimations for the levitation heights for particles of different densities and sizes in the stratosphere under action of gravity and vertical wind are presented also (Gryazin and Beresnev, 2010).

Transport capabilities of the vertical wind will be especially noticeable for fractal-like particles (for example, soot particles and volcanic aerosol). It is possible that the proposed approach would allow clarifying mechanisms of accumulation of soot particles from the air transport and the ground-based biomass burning at altitudes of the lower and middle stratosphere.

The method of comparison of vertical motion characteristics for spherical and fractal-like aerosol particles in stationary atmosphere and in atmosphere under action of the averaged vertical wind is introduced. It is shown, that subsidence velocities of compact spherical and fractal-like particles can differ essentially in this case.

Thus, the advanced aerosol transport models should include with necessity the vertical wind factor for the correct analysis of post-volcanic or background stratospheric aerosol at rather long time scales. On one hand, the used database of high-altitude profiles of the averaged vertical wind contains extensive information on its latitudinal and seasonal variability for the period of 1993-2006 and useful not only for a convenient mathematical approximation, but also a rather simple parameterization of the vertical wind profiles for the following analysis. On the other hand, the question regarding the reliability and representativeness of this parameterization remains open because of the high variability of the circulation processes in the stratosphere, including the data for the vertical wind as well. We believe that this problem can be solved partly by comparing the results for several different databases, for example, the UKMO model used in this paper and the NCEP/NCAR reanalysis data.

We are grateful to the BADC which provided us with access to the UKMO Stratospheric Assimilated Data. This work was supported by the Ministry of Education and Science of the Russian Federation (research project implemented by leading scientist at Russian institution of higher education, No.11.G34.31.0064).

Beresnev, S.A., Gryazin, V.I. and Gribanov, K.G. (2008) *Atmos. Oceanic Opt.* **21(6)**, 448-454.

Beresnev, S.A., Gryazin, V.I. and Gribanov, K.G. (2009) *Rus. Meteor. Hydrol.* **34 (11)**, 724-731.

Gryazin, V.I. and Beresnev, S.A. (2010) *Atmos. Oceanic Opt.* **23(3)**, 174-180.

Gryazin, V.I. and Beresnev, S.A. (2011) *Meteor. Atm. Phys.* **110(3-4)**, 151-162.

Presents to the nearest neighbours: contribution of transboundary transport to the PM10 and PM2.5 concentrations in Central Europe with focus on NRW

H. Hebbinghaus[1], S. Wurzler[1], M. Memmesheimer[2], G. Piekorz[2], E. Friese[2], H. J. Jakobs[2], C. Kessler[2], A. Ebel[2]

[1] North Rhine Westphalia State Agency for Nature, Environment and Consumer Protection (LANUV), P.O. Box 101052, D-45610 Recklinghausen, Germany
[2] Rhenish Institute for Environmental Research (RIU), EURAD-Project, University of Cologne, Aachener Strasse 201-209, D-50931 Cologne, Germany

Keywords: Aerosol modelling, PM10/PM2.5, air quality, air pollution modelling.
Presenting author email: sabine.wurzler@lanuv.nrw.de

Despite a series of measures to improve air quality there still remains a rather high PM background concentration over highly industrialized and densely populated Central Europe. High particle concentrations pose a threat for health. Even though compliance to the EC air quality limit value for the annual average PM10 concentration (40 µg/m³) does no longer pose a major problem, the allowed number of exceedance days (35 days with daily average PM10 concentrations > 50 µg/m³), which is linked to the annual average PM10 concentration, still presents a challenge.

Source apportionments in North-Rhine Westphalia (NRW) for measurement sites with limit value exceedance show that about 75 % of the PM10 burden stems from background concentration. The background concentration is dominated by transboundary transport, especially in the western part of NRW (Fig. 1), owing to the main wind direction (west). Therefore, local measures alone are not sufficient to comply with the limit values, especially in years with adverse meteorological conditions like 2011. But how high is the contribution of the neighbouring countries to the background concentration – on their own and in comparison to the effect of a reduction of emissions until 2015?

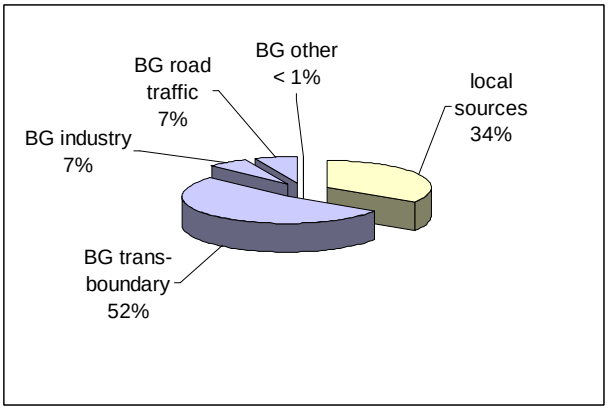

Figure 1: Source apportionment for PM10 at a curb site, Düsseldorf, Corneliusstraße, with focus on the background concentration (BG).

Scope of this paper is to estimate the contribution of Germany to the PM10 and PM2.5 loads of its neighbours downwind and the contribution that Germany, with focus on NRW, receives from its nearest neighbours upwind. For this reason simulations have been performed with the European Air Pollution Dispersion Model (EURAD, Memmesheimer et al., 2004). The EURAD model simulates the concentration due to emissions, transport, and chemical transformation. The meteorological data is computed with the dynamic model MM5. The atmospheric, transport model CTM2 solves the 3-D advection and diffusion equation together with the transformation of constituents through gas phase and heterogenous chemistry. Within CTM2 the Modal Aerosol Dynamics Model (MADE) is used to account for secondary aerosol generation (Schell et al., 2001). The EURAD model has been applied in a one-way nesting mode with two grids, spanning Europe in a horizontal resolution of 125 x 125 km² and a nested domain covering the area of Germany with 25 x 25 km². This allows the consideration of long-distance transport across Europe while retaining sufficient resolution in NRW to analyse regional changes.

Simulations were performed for the year 2009 with baseline emissions, without emissions from the Netherlands, and without emissions from Belgium and for the year 2006 without emissions from Germany. Additionally, a simulation with an emission forecast for the year 2015 was done.

For annual averages, the contributions from Germany, Belgium, and the Netherlands are of similar magnitude, though the effect from Belgium is more pronounced in the south western part of NRW, while the effect from the Netherlands is stronger in the north western part of NRW. Assuming a scenario without emissions from Belgium or the Netherlands leads to a reduction of annual average PM10 background concentration of about 5 to 10 µg/m³. The reduction in PM2.5 background concentration is smaller with up to 5 µg/m³. The contribution of Germany to the PM load in Poland and Czech Republic is of the same order.

The European wide reduction in emissions until 2015 leads to a reduction of about 5 µg/m³ PM10 and about the same for PM2.5 for all of Europe Thus, successful abatement of air pollutants is a European issue.

Some further analyses of special episodes and on further details are currently under way.

Memmesheimer, M., Friese, E., Ebel, A., Jakobs, H. J., Feldmann, H., Kessler, C., Piekorz, G. (2004), IJEP, **22**, 108 – 132.

Schell, B., Ackermann, I.J., Hass, H., Binkowski, F.S., and Ebel, A. (2001) *J. Geophys. Res.*, 106, 28275-28293.

Validation of ECHAM5-SALSA aerosol climate model against EARLINET lidar network

H. Niskanen[1,2], E.,Giannakaki[2,3], H. Korhonen[2], K. E. J. Lehtinen[1,2], T. Mielonen[2], A. Lindfors[2], M. Komppula[2], L. Alados-Alboledas[4], U. Wandinger[5], D. Balis[3], G. Pappalardo[6] and H. Kokkola[2]

[1]Department of Applied Physics, University of Eastern Finland, Kuopio, FI-70211, Finland

[2]Finnish Meteorological Institute, Kuopio Unit, Kuopio, FI-70211, Finland

[3]Laboratory of Atmospheric Physics, Aristotle University of Thessaloniki, Thessaloniki, GR-54124, Greece

[4]Applied Physics Department Sciences Faculty, University of Granada, Granada, ES-18071, Spain

[5]Leibniz Institute for Tropospheric Research, Leipzig, DE-04318, Germany

[6]National Research Council - Institute of Methodologies for Environmental Analysis, Potenza, IT-85050, Italy

Keywords: aerosol modelling, extinction, lidar, optical properties.

Presenting author email: heidi.niskanen@fmi.fi

Aerosols and the uncertainty related to their climatic impact have gained increasing interest in recent years because of the on-going climate change. In order to study the effect of the aerosols on various processes of the atmosphere and on climate, modelling and different kind of observations are used. However, due to the complexity of the aerosol-climate coupling, such as the impact of aerosols on clouds and their feedback on climate, the results from the different models may show a great deviation. Thus, the comparison of different modelled aerosol properties with observational data is a useful method to improve the models and the understanding related to atmospheric processes affecting the aerosol fields.

In this work, the aerosol extinction vertical profiles achieved from the global circulation model ECHAM5-SALSA (Roeckner *et al* 2003, Kokkola *et al* 2008) are compared with the observations provided by European Aerosol Research Lidar Network (EARLINET) (Bösenberg *et al* 2003) at various stations. EARLINET is the first coordinated aerosol lidar network, established in 2000, with the main goal to provide a comprehensive, quantitative, and statistically significant database for the aerosol distribution on a continental scale. The locations of the measurement sites are shown in Fig.1. One of the main objectives of this network is to provide the necessary database for validating and improving numerical models describing the evolution of aerosol properties and their influence on climate and environmental conditions.

For the comparison in this study four EARLINET stations were selected on the basis of different predefined regions including central Europe (Leipzig), western Mediterranean (Granada), Central Mediterranean (Potenza) and East Mediterranean (Thessaloniki). The purpose of the comparison is to address two issues. First point is to study whether the model estimates the altitude of the aerosols correctly and if so, to investigate if their size distribution and composition are depicted properly in order to reproduce the observed extinction profiles. In the first stage, we study the seasonal variation and geographical distribution of aerosol over Europe. In addition, to study how the model performs in describing the different aerosol types the extinction profiles from the model are compared with the observations at different sites and regions.

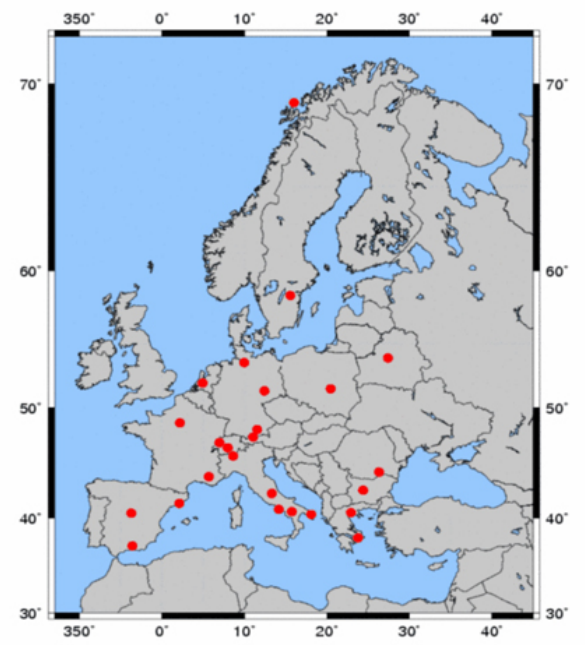

Figure 1: The locations of EARLINET measurement sites.

The results of the comparison in this study can be used to improve the representation of the emissions and removal processes in the ECHAM5-SALSA model.

The authors acknowledge EARLINET for providing aerosol lidar profiles available from the EARLINET database accessible at http://access.earlinet.org/.

Bösenberg, J. et al. (2003) Report 348, Max Planck Institute for Meteorology, Hamburg, Germany.

Kokkola, H. et al. (2008) Atmos. Chem. Phys. **8**, 2469-2483.

Roeckner, E. et al. (2003) Report 349, Max Planck Institute for Meteorology, Hamburg, Germany.

Numerical simulations of mixing conditions and aerosol dynamics in the Cern CLOUD chamber

J. Voigtländer[1], J. Duplissy[2], L. Rondo[3], A. Kürten[3], F. Stratmann[1], and the CLOUD collaboration

[1]Leibniz Institute for Tropospheric Research, Leipzig, Germany
[2]CERN, PH Department, Geneva, Switzerland
[3]Institute for Atmospheric and Environmental Science, Goethe-University, Frankfurt/Main, Germany
Keywords: CLOUD, cloud chamber, modelling, mixing state, sulphuric acid, particle formation
Presenting author email: jensv@tropos.de

The Cosmics Leaving OUtdoor Droplets (CLOUD) project was established to investigate the effect of galactic cosmic rays on aerosols and clouds by studying the nucleation of sulphuric acid (H_2SO_4) particles and its dependence on ionizing radiation and additional other substances such as ammonia [Kirkby et al., 2011]. Experiments are carried out at a cylindrical electro polished stainless steel tank with a volume of 26.1 m^3, which is located at CERN (Switzerland). For the experiments it is necessary to attain spatial homogeneity regarding the prevailing thermodynamic conditions, gas concentrations and particle properties. To investigate the mixing state of the CLOUD chamber, numerical simulations were performed using a coupled computational fluid dynamics (CFD) – particle dynamics model, the so-called CLOUD-FPM [Voigtländer et al, 2011]. The model is the combination of the commercially available CFD code FLUENT (ANSYS Inc., Canonsburg, PA, USA) and the Fine Particle Model (FPM, Particle Dynamics GmbH, Leipzig, Germany). CLOUD-FPM is capable of handling the coupled fluid and particle dynamical processes taking place inside the CLOUD chamber as all relevant properties like velocity, temperature, pressure, turbulence parameters, wall losses of the condensable gas phase species and particle nucleation/growth are treated explicitly.

The flow field in the CLOUD chamber was investigated by adjusting the model to measured 1-D velocity profiles. With the adjusted model, the calculated temporal evolution of the H_2SO_4 concentration was found to be in good agreement with the experimental data. Time resolved calculations were also carried out to estimate time scales for mixing the tank's contents and to simulate nucleation and growth of H_2SO_4 particles. The simulations showed that two fans are necessary to mix the tank properly [Voigtländer et al., 2011].

Here, we present simulation results of the current set up of the CLOUD chamber in addition to prevailing measurements of the flow field, H_2SO_4 concentration and particle nucleation. These simulations are the consequent continuation of the previous investigations with the CLOUD-FPM model [Voigtländer et al., 2011]. Aim of the calculations is to evaluate the mixing conditions, controlled by fan speed and fan configuration, and their dependence on the ongoing modifications at the chamber. Calculated volume-to-surface exchange times were compared to internal mixing times. Thereby, internal mixing was simulated using a small regional source of a tracer species. The simulations show that the volume-to-surface exchange and therewith the wall loss of several trace gases increases with increasing fan speed. On the other hand the simulations indicate that at low fan speeds the exchange between lower and upper half of the tank decreases due to the low efficiency of the fan hoods and the resulting divergent flow field at low flow velocities. It can be concluded that sufficiently high fan speeds have to be used to ensure internally well mixed conditions in the CLOUD chamber.

Acknowledgement: We would like to thank CERN for supporting CLOUD with important technical and financial resources, and for providing a particle beam from the CERN Proton Synchrotron. This research has received funding from the EC Seventh Framework Programme (Marie Curie Initial Training Network "CLOUD-ITN" grant no. 215072, and ERC-Advanced "ATMNUCLE" grant no. 227463), the German Federal Ministry of Education and Research (project no. 01LK0902A), the Swiss National Science Foundation (project nos. 206621_125025 and 206620_130527), the Academy of Finland Center of Excellence program (project no. 1118615), the Austrian Science Fund (FWF; project no. P19546 and L593), the Portuguese Foundation for Science and Technology (project no. CERN/ FP/116387/2010), and the Russian Foundation for Basic Research (grant N08-02-91006-CERN).

Kirkby, J., et al. (2011), Nature, 476, 429–433.
Voigtländer, J., et al. (2011), Atmos. Chem. Phys. Discuss., 11, 20013-20049.

Experimental Studies on Tin Oxide Dry Aerosol Deposition in Piping assembly under Flow and High Thermal Gradient conditions: Comparison with SOPHAEROS code

Rajni Modi[1], Arshad Khan[1], Sunil Ganju[2], Manish Joshi[1], Pallavi Khandare[1], B. K. Sapra[1] and Y. S. Mayya[1]

[1]Radiological Physics and Advisory Division, [2]Reactor Safety Division,
Bhabha Atomic Research Centre, Mumbai 400085, India
Keywords: Reactor accident, piping assembly, aerosol, deposition, SOPHAEROS.
Presenting author email: rajnimodi@gmail.com, rajnim@barc.gov.in

During a severe nuclear reactor accident involving core melt down condition, the deposition of fission product (FP) aerosols in the primary heat transport (PHT) system will lead to a reduction in the source term to the containment and subsequently to the environment.

This study aims to experimentally quantify the deposition in the PHT and to explore the capability of SOPHARERROS (a module of the Accident Source Term Evaluation Code (ASTEC) dealing with transport and retention of FP aerosols in the PHT of a reactor system) to reproduce the experimental results. In line with this, a small scale piping assembly has been fabricated and installed at Nuclear Aerosol Test Facility (NATF) at Bhabha Atomic Research Centre, India. This assembly, having a total length of 3m, consists of nine pipe sections, of which six are straight cylindrical sections and three are 90° bend sections. To simulate the reactor accident conditions, tin oxide aerosols have been generated using a plasma torch aerosol generator based on the evaporation-condensation technique (Sapra et al. 2008). The generated aerosols were transported to the assembly via a double walled water cooled plenum chamber using Argon carrier gas.

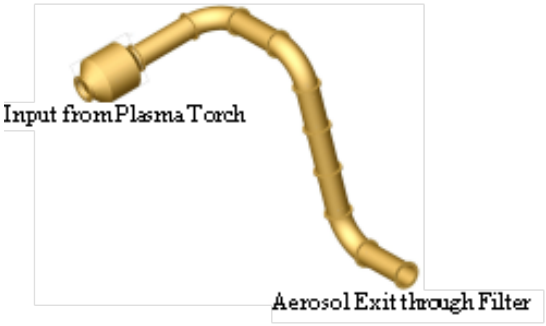

Figure1: Piping assembly

Experiments have been performed at two carrier flow rates of 135.5 lpm (laminar regime) and 237.5 lpm (Transition regime). The results showed that 47.36% and 40.75% deposition of tin oxide aerosols occurs in the whole system in experiment I and II respectively. However, a deposition of 17.40% and 15.50% was found in the piping system alone excluding the plenum chamber. SOPHAEROS results were within 7.96% and 17.51 % in case of experiment I and II respectively. The code predicted depositions of 76.48% and 23.16% due to thermophoresis and settling respectively in experiment I; while the respective depositions in experiment II were 88.19% and 11.38%. The increase in the thermophoretic deposition is attributed to increased thermal gradient in the latter experiment. Bend impaction and laminar diffusion did not play a significant role.

The XRD of deposited tin oxide particles confirms the formation of both SnO_2 and SnO.

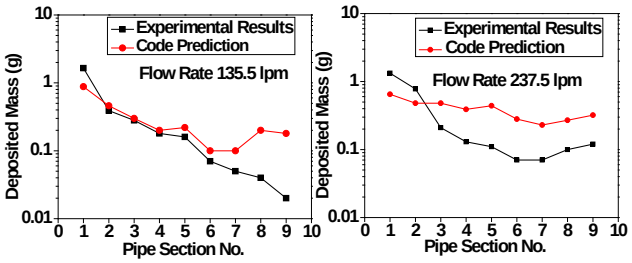

Figure 2. Comparison of experimental and code predicted results

Also, as analyzed by TEM pictures, primary particles showed a mode at around 15nm present in all pipe sections. Although some bigger particles in the size range of 50 to 100nm are also seen, it is difficult to say that the distribution is bimodal at this point.

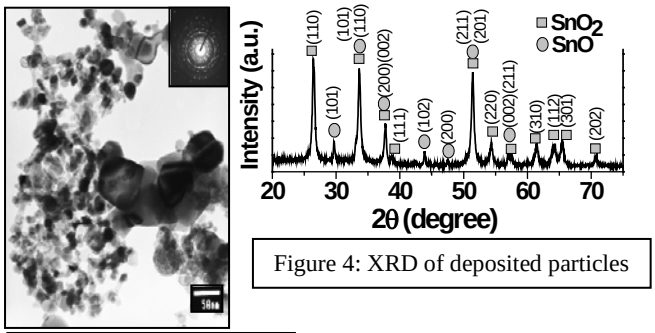

Figure 4: XRD of deposited particles

Figure 3: TEM of deposited particles

Sapra, B.K., Mayya, Y.S., Khan, A., Sunny, F., Ganju, S., Kushwaha, H.S., (2008) *Nuclear Technology*, 163, 228-244.

Evaluation of black carbon estimations by the regional aerosol-climate model REMO-HAM

A.I. Hienola, J.-P. Pietikäinen, A.-P. Hyvärinen, H. Lihavainen and A. Laaksonen
Finnish Meteorological Institute, Helsinki, FI-00101, Finland
Keywords: black carbon, regional modelling.
Presenting author email: anca.hienola@fmi.fi

Black carbon (BC), a product of incomplete combustion of fossil fuels and biofuels, is thought to contribute to global warming since pre-industrial times. When emitted into the atmosphere, BC directly warms the air by absorbing the incoming solar radiation and subsequently emitting thermal-infrared radiation into the surrounding space. Due to the complex mechanisms through which BC affects the radiation balance, estimating the impact of black carbon on climate change remains largely uncertain.

In this study, we evaluate black carbon model prediction from the regional aerosol-climate model REMO-HAM by comparing modeled data with available measurements from five remote sites in Finland (Hyytiälä, Pallas, Puijo, Virolähti and Ujö) for the year 2005 (Hyvärinen *et al.* (2011)), with focus on Hyytiälä station as a case study. The model-measurement comparison includes black carbon surface concentrations, the seasonal trends and black carbon concentrations in relation to some meteorological factors. We also used nonparametrical statistical tools for quantifying the agreement between the model and the observations.

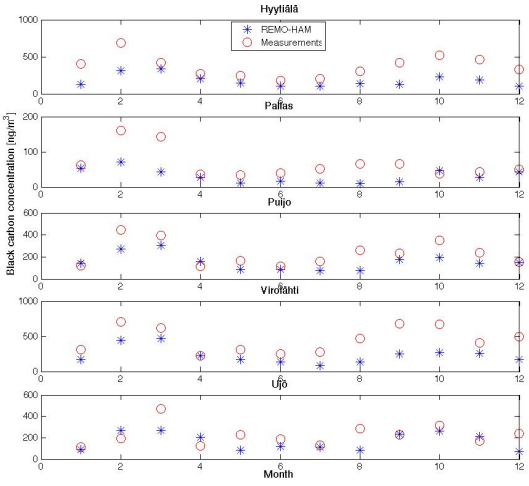

Figure 1: Monthly means of experimental (circles) and modeled (stars) black carbon concentrations in 5 Finnish stations for 2005.

The tool used in this study is the aerosol-climate model REMO-HAM, an improved version of the regional climate model REMO (Jacob(2001)), in which Pietikäinen *et al.* (2012) has recently implemented the aerosol module HAM-M7.

The monthly means of modeled and measured black carbon surface concentration for the 5 station are shown in Figure 1. A seasonal variation is detected for all stations, with a maxima in late winter/early spring and a second maxima in the autumn, potentially due in part to lower mixing height levels during this time of the year. The model reproduces to a certain extent the cycle. However, REMO-HAM agrees better with the measured values during the non-maxima period, while for the maxima periods the model underestimate is more evident.

The (dis)agreement between the model and the observation in can be accurately described by the overlap coefficient (OVL) of the probability distribution curves and the Mann-Whitney test (the Z-coefficient). The disadvantage of OVL is that its magnitude does not show where the common area is. As such, nonparametric density functions

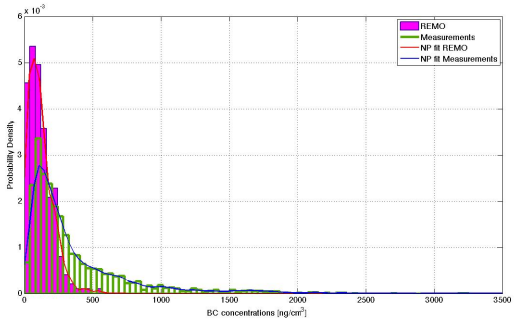

Figure 2: Histograms and nPDFs for black carbon concentrations - Hyytiälä 2005.

(nPDF) for the measured and computed 3-hourly resolution black carbon concentrations were used for Hyytiälä (Figure 2). The model fails in providing concentrations higher than 500 ng/m^3. This underestimation might be caused either by an excessive loss of black carbon in the model or by missing emissions during these periods of time. These hypothesis are discussed.

This work was supported by the Finnish Meteorological Institute and by Helsinki University Center for Environment HENVI .

D. Jacob(2001), Meteorol. Amtos. Phys. 77, 61.
J.-P. Pietikäinen *et al.*(2012), Geosci. Model Dev.- submitted
A.-P. Hyvärinen *et al.*(2011), Atm. Environ. 45, 4042 .

Effects of vapor properties on modelled particle growth in the model UHMA

A. Rusanen[1] and M. Boy[1]
[1]Department of Physics, University of Helsinki, Helsinki, Finland
Keywords: Organic aerosols, Particle growth, Aerosol modelling, Aerosol dynamics.
Presenting author email: anton.rusanen@helsinki.fi

The effect of changing the physical properties of a condensing vapor in a model run was tested and the effects on particle growth and composition were observed. The model used for this task was the University of Helsinki Multicomponent Aerosol model, abbreviated UHMA, which was first introduced in Korhonen *et al* (2004).The results were also compared with theory. The properties investigated were vapor density, surface tension and molar mass. In addition, effects of changes in ambient temperature and pressure, were tested.

Since the amount of possibly important organic compounds in the atmosphere is too large to simulate in most cases, we are currently using representative vapors. These sum up the contributions of several compounds into a single species. This results in the problem of determining appropriate physical properties for these representative vapors so that they can still accurately represent growth and particle composition.

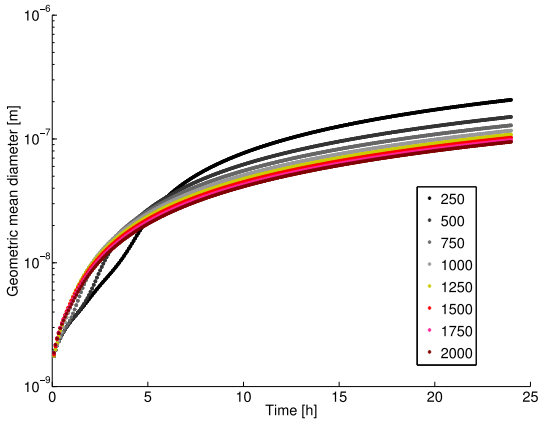

Figure 1: The geometric mean diameter of simulated particles with several different densities for one vapor. Vapor density is in units kg/m^3.

The simulation runs for these tests were done for identical conditions, only changing one parameter at a time. The runs had a single, initially monodisperse, peak that was allowed to grow for a day. Aerosol dynamics considered were coagulation and condensation. Three vapors were included, sulfuric acid with two generic organic compounds. Since only particle growth was investigated, constant vapor supersaturations for all vapors were chosen.

As an example of the results there are plots of geometric mean diameter and vapor volume fraction of a organic vapor for simulations with different vapor densities. The

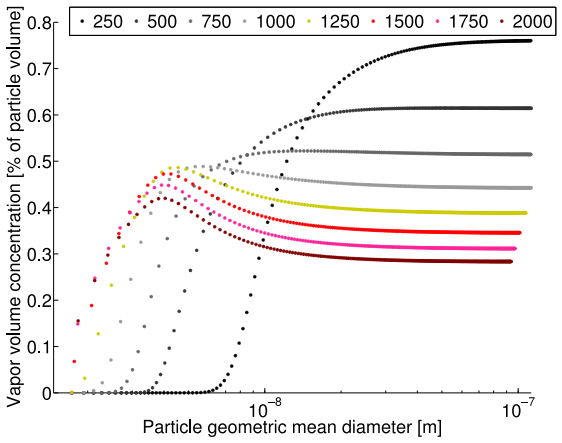

Figure 2: The volume fraction of the same simulated particles consisting of a specific vapor with several different densities for the vapor. Vapor density is in units kg/m^3.

simulation was of a initially monodisperse peak of pure sulfuric acid particles growing in constant vapor supersaturation. Initially growth is suppressed with decreasing density, but once the vapor starts condensing smaller densities result in more growth. In the volume fraction plot one can clearly see the kelvin effect in the delayed onset of vapor condensation.

While the study is limited to one model, the results are possibly useful in determining factors relevant to combining different organics into representative groups and determining which physical properties are important in a growing multicomponent aerosol system.

H. Korhonen, K. E. J. Lehtinen, and M. Kulmala (2004) Multicomponent aerosol dynamics model UHMA: model development and validation, Atmos. Chem. Phys., 4, 757–771, 2004

Scanning Mobility Particle Sizer: Fast data Inversion and uncertainty analysis

L. Coquelin[1,2,3], N. Fischer[1], T. Mace[1], C. Motzkus[1], F. Gensdarmes[2], G. Fleury[3], L. Lebrusquet[3]

[1]Department of Mathematics and Statistics, National Laboratory of Metrology and Testing, Trappes, FRANCE
[2]Aerosol Physics and Metrology Laboratory, Institute for radiation protection and nuclear safety, Saclay, FRANCE
[3]E3S, SUPELEC Science of Systems, EA4454, Gif-sur-Yvette, FRANCE

Keywords: SMPS, uncertainty, data inversion, sensitivity analysis.
Presenting author email: loic.coquelin@lne.fr

Introduction

SMPS (Scanning Mobility Particle Sizer) is the most widely used device to characterize particle sizes below 0.1 µm and it takes part in a large range of applications such as toxicology testing, indoor air quality measurement, etc.

Yet, a dimensional uncertainty on the size distribution isn't provided to SMPS users when the instrument operates under scanning mode. Since it has been proved that ultra-fine particles can pass through human barriers (lung, blood-brain barrier, etc.), assessing uncertainties on the estimated size distribution has become of primary interest. Present study aims at simulating SMPS measurements and at proposing a fast and accurate inversion technique to estimate the particle size distribution, as well as providing a sensitivity analysis to determine the influent parameters of the system. A 95% confidence region on the output size distribution is finally obtained by performing Monte-Carlo simulations.

Model and Inversion

Aerosol measurement using a SMPS is based on particle electrical mobility, that is defined as the ratio of the particles drift velocity to the magnitude of the electric field; particle electrical mobility is then linked to its mobility diameter d_p and electrical charge p. Once selected by DMA (Differential Mobility Analyser), particles are gathered into canals, enlarged and detected by a CPC (Condensation Particle Counter). Wang and Flagan (1990) developed the theory of particle classification when the instrument operates under scanning mode, and precision on the voltage ramp is given by Collins *et al.* (2004).

Raw data extracted from the SMPS represent a concentration over a certain class of mobility diameters. If we denote r_i as the concentration over the class i, n the size distribution, p the number of charges carried by a particle, $d_{1,i}$ and $d_{2,i}$ respectively the left and right extremity of the class i, t_i the counting time for the class i, $t_{0,i}$ being the time at which the count begins in the class i, f describes particle electrical mobility selected according to scanning time and k_i the kernel function (product of the charge distribution, the detection efficiency of the CPC, the DMA transfer function), then:

$$r_i = \frac{1}{t_{0,i}} \cdot \iint_{[d_{1,i},d_{2,i}]\times[t_i,t_i+t_{0,i}]} k_i\left(f(t), p, d_p\right) \cdot n(d_p) \cdot dd_p \times dt \ .$$

Starting from the deterministic model, next step is to focus on the variability of the measurements. Indeed, a model of noise based on experimental results that takes into account the CPC counting modes (single particle counting, live-time counting and photometric mode) is created.

Knowing the concentrations for each class, data inversion consists in retrieving the size distribution. It is a minimization problem with the constraint of positivity of the solution. Regularization technique of Tikhonov and Arsenin (1977) that penalizes non-smooth solutions is performed. In our case, the inversion has been proved to be fast and stable to perturbations in the input space and can then be used for the sensitivity analysis.

Primary Results

Since the number of parameters involved in the model is high, sensitivity analysis would require too much computing time, that's why analysis based on the decomposition of the variance is carried out by using indices defined by Sobol (1993). Then, according to experts in aerosol physics, the range of variation for each influent parameter of the system is chosen and a 95 % confidence interval is computed using Monte-Carlo simulations as shown in figure 1 for a typical atmospheric aerosol size distribution (Whitby, 1978).

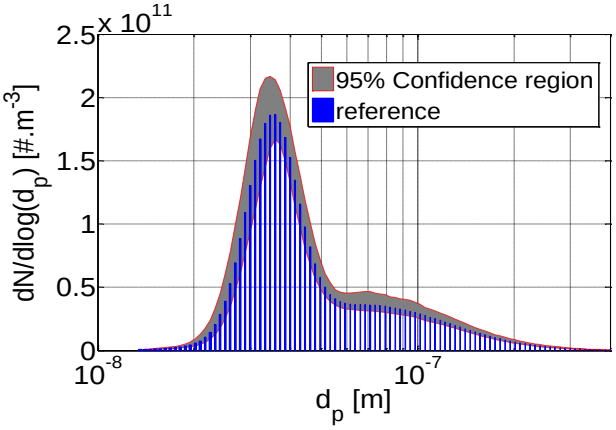

Figure 1. 95% confidence region when simulating SMPS measurement of an atmospheric aerosol

Collins, D. R., Cocker, D. R., Flagan, R. C., and Seinfeld, J. H. (2004) *Aerosol Science and Technology*, **38**, 833-850.

Wang, S. C. and Flagan, R. C. (1990) *Aerosol Science and Technology*, **13**, 230-240.

Sobol, I. M. (1993) *Mathematical Modelling and Computational Experiments*, **1**, 407–414.

Tikhonov, A. N. and Arsenin, V. A. (1977) Solution of Ill-posed Problems. Winston & Sons, Washington.

Whitby, K. T. (1978) *Atmospheric Environment*, **12**, 135-159.

Novel informatics software for automated individual aerosol component property predictions and complex ensemble predictions – an online community facility

D. Topping[1,3], M. Bane[2], M. Barley[3], D. Lowe[3], R. Pinning[2] and M. McFiggans[3]
[1]National Centre for Atmospheric Science, University of Manchester, Manchester, UK
[2]IT Services, University of Manchester, Manchester, UK
[3]Centre for Atmospheric Science, University of Manchester, Manchester, UK
Keywords: Aerosol modeling, Organic aerosols, Informatics.
Presenting author email: david.topping@manchester.ac.uk

Introduction:
Atmospheric aerosols are known to be an important yet highly uncertain component of the earth's climate and air quality (Solomon et al 2007). Owing to the complexity and diversity of atmospheric aerosol components, quantification of the properties that determine their highly uncertain climatic and human health impacts requires the development of novel technological applications. Inorganic material is restricted to a few well-understood compounds. However, organic material can comprise many thousands, as yet largely unidentified, compounds with a vast range of properties.

We must be able to predict however many thousands of components can exist in particulate matter. Predicting the evolution of aerosol requires calculating the distribution of all components between the gas and aerosol phase. This requires knowledge of all component vapour pressures and other thermodynamic properties. The many thousands of individual aerosol components ensure that explicit manual calculation of these properties is laborious and time- consuming. The emergence of explicit automatic mechanism generation techniques (Aumont, 2005; Jenkin, 2003) including up to many millions of individual gas phase products as aerosol precursors renders the process impossible and automation is necessary.

It can require significant resource to develop methods for automating these processes, but also to develop efficient numerical frameworks that drive the complex calculations. In this presentation we showcase development and application of a new online facility that combines benchmark aerosol models with open source informatics software to provide a new community service.

The model system:
The facility is written in python, a high-level language is widely used as a scripting language for web applications. It supports both fixed-point and floating-point numeric calculations, string manipulation and facilities for structures and multi-dimensional arrays. It is distributed under a permissive free software license and is available for all major operating systems, which will enable our software to be highly portable. Also, a PYTHON interface has been developed for the chemical informatics software of our choice (Open Babel) as described by O'Boyle et al (2008).
The SMILES chemical informatics syntax is used to automate extraction of molecular substructure information from individual compound identifiers (figure 1). Commonly employed in commercial and public software, it can be imported by most molecular editors and has a wide base of software support and extensive theoretical backing (www.daylight.com).

We will demonstrate the need for developing libraries that capture all functionality of compounds expected in the atmosphere, a problem that occurs in other available online services used by the community.

Example applications:
Important uncertainties are in those parameters which dictate the aerosol water content and gas / aerosol partitioning. To this end we will demonstrate the use of this facility to calculate fundamental properties, such as pure component vapour pressures, for an unlimited set of compounds. Absorptive partitioning simulations carried out on the facility will demonstrate the ability to predict secondary organic aerosol loading and composition using output from complex gas phase degradation mechanisms. Specifically we will use output from the Master Chemical Mechanism (MCM Jenkin (2003)) to simulate the detailed composition of aerosol in multiple scenarios.

Future outlook:
The facility is also designed to act as a springboard for collaborative purposes, the inclusion of specific visualization techniques enabling the modeling and measurement community to directly compare outputs from models and instruments. In addition we will present progress on using GPGPUs (General purpose graphical processing units) to obtain large increases in computational performance on the complex models hosted on the website. This is an exciting area of research and is already being explored for chemical models that are often heavily reduced to reduce numerical complexity.

This work is supported by the National Centre for Atmospheric Science (NCAS), NERC grant NE/H002588/1 and NERC grant NE/J013471/1.

Aumont, B., Szopa, S., and Madronich, S. Atmos. Chem. Phys., 5, 2497-2517, (2005).
Jenkin, M. E., Saunders, S. M., Wagner, V., and Pilling, M. J.: Atmospheric Chemistry and Physics, 3, 181-193, (2003).
O'Boyle,N.M. Morley, C., and Hutchison, G. R.: Chem. Cent. J., 2, 1–7. (2008).
Solomon, S., Qin, D., Manning, M., Chen, Z., Marquis, M., Averyt, K. B., Tignor, M., and Miller, H. L., IPCC: Climate change 2007

Contributions of Traffic Emissions to the Ambient Aerosol in an Industrial Area

Sílvia M. Garcia1[1], Gonçalo Domingues [1], Clara Santos[1], Carla Gomes [1,2] Alexandra V. Silva[2], S. Marta Almeida [2]

[1] Núcleo de Ambiente, Instituto de Soldadura e Qualidade, Taguspark, 2740-120 Porto Salvo, Portugal
[2] Instituto Tecnológico e Nuclear, URSN, E.N. 10, 2686-953 Sacavém, Portugal
Keywords: air quality, road traffic, PM10, NOx, CO, HC, air dispersion models, emissions factors.
Presenting author email: smgarcia@isq.pt

The scale and seriousness of impacts of air pollution on health that have been detected by scientific investigations over the past decade is the subject of media reports and policy debate throughout Europe.

Particle size is one of the indicators can be used to describe airborne particulate matter (APM), since it is associated with the origin of the particles, their transport in the atmosphere and their ability to be inhaled into respiratory system. PM10 (particles with a diameter <10 µm) and PM2.5 (those with a diameter <2.5 µm) are nowadays commonly used to describe emissions and ambient concentrations of APM. An APM impact on mortality (life expectancy) seems to be attributable to PM2.5 while PM10 may have more visible impacts on respiratory morbidity.

Comprehensive evaluation of this evidence is needed in order to formulate effective APM pollution reduction strategies and national and international policies for reducing health risks due to pollution. For this reason, the European Directive 2008/50/EC, on ambient air quality and cleaner air for Europe, reinforces the need and obligation of Member-States to monitor the average exposure level of their populations to the particulate matter and to adopt measures to reduce these levels. Nevertheless, concerning the local authorities, managing local APM concentrations can be a rather frustrating affair, due to the existence of a quite number of different sources.

Therefore, in order to plan appropriate actions, it is necessary to have a deeper knowledge of the mains sources and their relative contributions to the formation of the ambient aerosol. This assessment, by providing concrete indications of the most important emission sources, helps decision and policy-makers to define appropriate mitigation actions and thus assuring a more effectiveness management of air quality.

The present study was accomplished in a port industrial area, which holds huge panoply of different fugitive and stationary sources such as industrial stacks, emissions from sea-going and berthed ships, harbour stock piles and road traffic (Figure 1).

This work focused it attention on road traffic emissions and aims to quantify the relative contribution of it to the solid fraction of the atmospheric aerosol in this industrial area.

Road traffic is one of the APM major anthropogenic emission sources, especially for finer particles. In fact, compliance with air quality standards requires control of this source emission. Fine exhaust particles are already subject to regulation but vehicle fleets increase whilst the non-exhaust emissions are totally uncontrolled and not well known. This kind of emissions comprise not only the only tailpipe vehicle exhaust emissions but also non-exhaust emissions derived mostly from the vehicle-induced ressuspension of dust deposited on the road.

Therefore, in this assessment special attention was given to the contribution of vehicles exhausted versus dust ressuspension.

For this propose the air dispersion model, using the computational tool TAPM - The Air Pollution Model, was performed according to Figure 2.

Results showed that the highest contribution of traffic resulted from dust ressuspension and not from vehicles exhausted. The heavy vehicles were the classes that that most contributed to the APM concentration.

Figure 1 - Studied area and target road

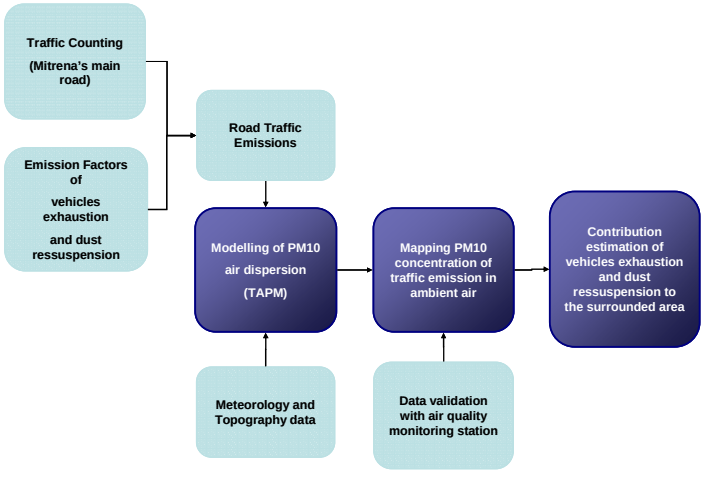

Figure 2 - Diagram of the global applied methodology

Evaluating the impact of flooring types on exposure to fine ($PM_{2.5}$) and coarse ($PM_{2.5-10}$) particles within the residential micro-environment

Lisa Bramwell[1], Jing Qian[1], Sumona Mondal[3], Andrea R. Ferro[1]

[1]Department of Civil and Environmental Engineering, Clarkson University, Potsdam, NY, 13699, USA
[3]Department of Mathematics and Computer Science, Clarkson University, Potsdam, NY, 13699, USA

Keywords: Resuspension, indoor air quality, modeling, fine particles
Presenting author email: bramweld@clarkson.edu

People spend almost 70% of their time within a residence (Klepeis et al., 2001). During this time, typical resuspension activities within the home have been estimated to contribute 30 % of exposures to PM_{10} (Yakovleva et al., 1999). Chamber studies have also shown that for moderate walking intensities, for a wide cross section of participants, flooring type can impact the rate at which particles are re-entrained into the air column (Qian & Ferro, 2008). For this study, human activity patterns were randomly selected from the USEPA's National Human Activity Pattern Survey (NHAPS) to evaluate the impact flooring types may have on overall exposures to fine and coarse particles. The NHAPS 24-hr diaries were used to develop particle exposure schedules using NIST's multizone ventilation and mass transport model CONTAM. CONTAM was then used to assess the influence of flooring types on the daily (24-hr) average contribution of resuspended settled house dust to both $PM_{2.5}$ and $PM_{2.5-10}$ exposure concentrations (Figure 1).

The exposure assessment comparison was made for a range of floor loading and resuspension rate estimates found in the literature. For the purposes of this study, total floor loading represents the total mass of settled dust on floorings collected by studies cited in the literature. Owing to the wide variety of collection methods used the particle size collected in these studies, ranged from 5 µm to less than 500 µm (Adgate et al., 1995, Fortune et al., 2000).

From this study, reducing floor loading with a regular cleaning schedule would aid in reducing the impact of flooring type on exposures to fine ($PM_{2.5}$) and coarse ($PM_{2.5-10}$) particles. For a total floor loading of 0.1 g/m2 and resuspension rate of 10-3/hr for carpets and 10-4/hr for hard floors, the flooring type did not significantly affect the exposure to PM2.5. However, flooring type significantly affected exposure to course particles. Further when the resuspension rate was increased by one order of magnitude, that is of the order of 10^{-2}/hr for carpets and 10^{-3}/hr for hard floors, flooring type became significant for both flooring particle size ranges.

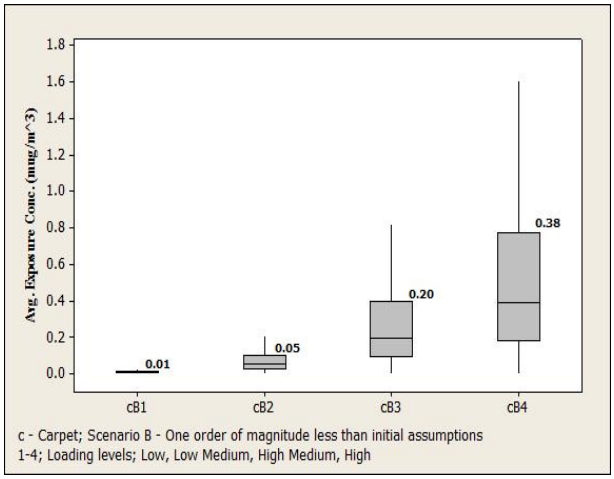

Figure 1 Contribution of resuspended $PM_{2.5}$ to average daily exposure concentration (Carpet)

This work is supported by the U.S. Department of Housing and Urban Development Healthy Homes Technical Studies Grant Number NYLHH0168-08. Any opinions, findings, and conclusions or recommendations expressed in this material are those of the authors and do not necessarily reflect the views of the agency.

Adgate, J., Weisel, C., Wang, Y., Rhoads, G., & Lioy, P. (1995). Lead in house dust: Relationships between exposure metrics. *Environmental Research, 70*(2), 134-147.

Fortune, C. R., Blanchard, F. T., Ellenson, W. D., & Lewis, R. G. (2000). Analysis of aged in-home carpeting to determine the distribution of pesticide residues between dust, carpet, and pad compartments. *Contract, 68*, D5-0049.

Klepeis, N. E., Nelson, W. C., Ott, W. R., Robinson, J. P., Tsang, A. M., Switzer, P., et al. (2001). The national human activity pattern survey (NHAPS): A resource for assessing exposure to environmental pollutants. *Journal of Exposure Analysis and Environmental Epidemiology, 11*(3), 231-252.

Qian, J., & Ferro, A. R. (2008). Resuspension of dust particles in a chamber and associated environmental factors. *Aerosol Science and Technology, 42*(7), 566-578.

Yakovleva, E., Hopke, P. K., & Wallace, L. (1999). Receptor modeling assessment of particle total exposure assessment methodology data. *Environmental Science & Technology, 33*(20), 3645-3652.

Dynamics of Spray Flames in Oscillating Flow with Droplet Grouping

D. Katoshevski[1] and J. B. Greenberg[2]

[1]Environmental Engineering Unit, Ben-Gurion University of the Negev, Beer-Sheva, 84105, Israel
[2]Faculty of Aerospace Engineering, Technion – Israel Institute of Technology, Haifa 32000, Israel

Keywords: Spray, Droplets, Combustion
Presenting author email: davidk@bgu.ac.il

The co-flow laminar spray diffusion flame in an oscillating flow field is investigated. A velocity lag is permitted between the droplets and their host surroundings and droplet grouping resulting from the host flow oscillations is accounted for (Katoshevski, 2006; Greenberg and Katoshveski, 2011; Katoshevski et al., 2008&2010). The spray is modeled using the sectional approach (Greenberg, 1989) and a perturbation analysis using a small sectional Stokes number is utilized for solving the liquid phase governing equations. The effect of droplet grouping is described through a specially constructed model for the vaporization Damkohler number. The large chemical Damkohler number assumption is adopted and a formal analytical solution is developed for Schwab-Zeldovitch parameters through which the dynamics of the spray flame front shapes and thermal fields are deduced. Computed results based on the solutions demonstrate how the phenomenon of droplet grouping can lead to the existence of multiple flame sheets as a result of the dynamic change in the *type* of the main homogeneous flame from under- to over-ventilated as the flow field oscillates. Concomitant fluctuating thermal fields are also shown to be present **indicating a potential impact on undesirable pollutants production.**

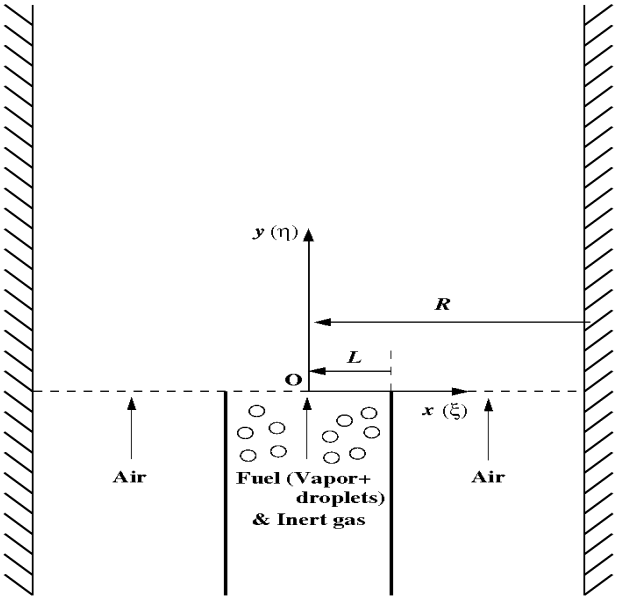

Figure 1. Schematic configuration.

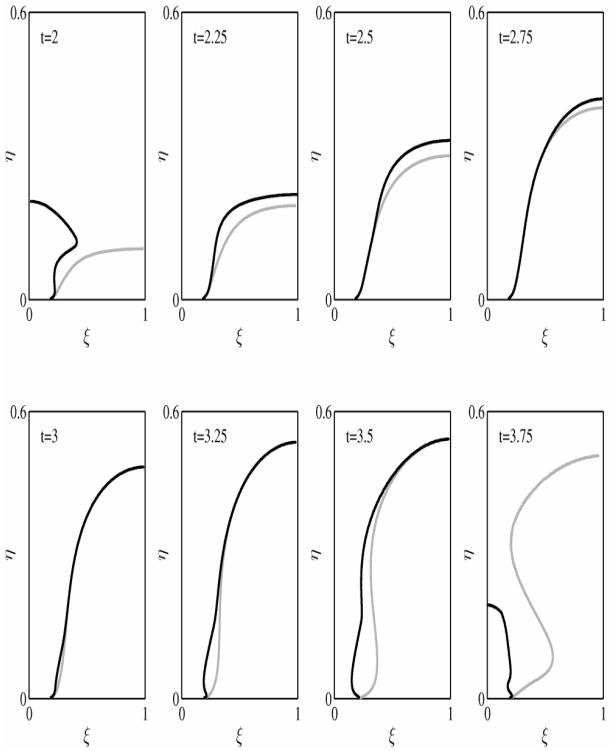

Figure 2. Stages in the evolution of a spray flame. The zone is at $x>0$ of Fig.1. Notation: black lines are flame fronts when ***droplet grouping*** is modeled, gray lines are flame fronts when droplet grouping is not accounted for.

The remarkable influence that grouping can have on the flame dynamics is illustrated in Fig. 2 where a typical cycle of a homogeneous spray flame is drawn, with and without droplet grouping.

JBG gratefully acknowledges the support of the Lady Davis Chair in Aerospace Engineering and the Technion Fund for the Promotion of Research. JBG and DK acknowledge the support of the ISF Grant no. 621/11.

Greenberg, J. (1989) Combust. Flame **77** , 229-240.
Greenberg J. B. and D. Katoshevski, (2011) *Proc. Comb. Inst.*, **33**, 2055-2062.
Katoshevski, D. (2006) *Aerosol & Air Quality Res.* **6**, 54-66.
Katoshevski, D., Crua, C., Sazhin, S. and Heikal, M. R. (2008) *Int. J. Heat & Fluid Flow*, **29,** 415-426.
Katoshevski, D., Ruzal, M., Shakked, T. and Sher, E. (2010) *Fuel **89***, 2411-2416.

Nonlinear oscillations and deposition of aerosol in tubes

D.A. Gubaidullin, R.G. Zaripov, A.L. Tukmakov and L.A. Tkachenko

Institute of Mechanics and Engineering, Kazan Science Center, Russian Academy of Sciences, Kazan, 2/31, Lobachevsky str., 420111, Russia

Keywords: aerosol, coagulation, deposition, particles, oscillations.

Presenting author email: damirgubaidullin@gmail.com

In the present work, longitudinal oscillations of an aerosol of different initial number concentration and dynamics of particles is considered in tubes of different length with various geometry on the end near to resonant frequencies.

Experimental investigations oscillations of an aerosol were carried out for different length of tubes in a shock-wave and no shock-wave modes near to subharmonic and natural resonances. Di-ethyl-hexyl-sebacate $C_{26}H_{50}O_4$ was used as the working fluid to generate aerosol. The majority of droplets have the geometric diameter 0.863 μm. Number concentration of drops for all experiments monotonously decreases with time and with growth of the excitation frequency. In the case of a closed tube, this process is defined by the coagulation of aerosol and deposition of droplets on the tube walls. In an open tube, the discharge of aerosol to the environment is observed in addition to the coagulation of aerosol and deposition of droplets on the tube walls. The dependence of the time of coagulation of aerosol on the excitation frequency likewise exhibits a nonmonotonic pattern with a maximum and a minimum when passing the resonance. It is established, that presence of a flange slows down process of a coagulation of an aerosol. Reduction of internal diameter of a flange results in increase in the time of coagulation. In so doing, the time of coagulation of aerosol in the case of an open tube is reduced by a factor of two and more compared to the time of coagulation in a closed tube. Nonlinear dependence of the time of coagulation of droplets is established at nonlinear oscillations of an aerosol in a tube from initial number concentration of an aerosol. It has been found that a decrease in the tube length and increase oscillation intensity results in a decrease in the time of coagulation of aerosol. It is shown, that with increase of intensity of the oscillations, the caused increase of amplitude, time of coagulation and deposition of an aerosol decreases. Time of a coagulation and deposition of drops of an aerosol in no shock-wave mode in 2-4 times is lower, than at a natural deposition. Ordered space-time structures of different densities have been revealed in the visible region in the vicinity of the middle of a closed tube.

The numerical modeling of a drift of the solid spherical particles were in a suspension in a nonlinear wave field of the closed tube and open flat channel at excitation of oscillations of a gas column on three first fundamental frequencies is executed. These researches have been carried out about use of model of a single particle and with application of model of interpenetrating continuums. It is obtained, that easy particles drift under an operation of acoustical current, and heavy are displaced under an action of wave pressure. In result easy and heavy particles concentrate in different areas of the resonator: easy are displaced to antinodes of a standing wave of velocity, heavy – to nodes. Depending on a steepness of a wave front of compression, the same particles can behave as easy at small nonlinearity, or as heavy at steep enough fast-head wave front. Drift of heavy particles in the open channel proceeds in two stages. The first quickly proceeding stage is connected to the mechanism of drift due to asymmetry of a wave, and the second with drift under action of developed acoustic stream. Influence of radius of particles on distribution of temperature and average density of a disperse phase along an axis of the channel is revealed.

Dynamics of a single particle with various physical and geometrical parameters is experimentally investigated at the longitudinal oscillations gas in tubes. Along an axis of a tube the particle moves from the closed (open) end to the piston, near to a wall – to the return side, making longitudinal oscillations with increase in the oscillations swing that is caused by acoustic streaming. In a radial direction, the oscillating particle moves from an axis to a wall of the tube up to a boundary point. Outside of a tube, the particle moves from the open end to an exterior wave field practically without oscillations with nonlinear increase of coordinate from time. It is revealed, that the increase in lengths of a tube and excitation frequency of gas in up to - resonant modes gives in growth of an oscillations swing of a particle and increase of its average velocity. Nonmonotonic character for dependence of oscillations swing and average velocity of a spherical particle from excitation frequency of gas is detected. At approach to a resonance oscillations swing and average velocity are incremented, attain the maximum value on a resonance frequency and decrease behind a resonance. Effect of a weight and diameter of a particle on its oscillations swing and average velocity is investigated. Shift of a curve maximum for dependence of a particle average velocity from oscillation frequency aside magnifications of frequency is shown at increase of a weight or diameter of a particle.

This work was supported by the Russian Fund of Foundation Investigation under grant 10-01-00098 and within the framework of the Federal target program "Scientific and scientific and pedagogical shots of innovative Russia for 2009-2013" (state contract №14.740.11.0351).

Dispersion and dissipation of weak waves in aerosols

Gubaidullin Damir, Nikiforov Anatoly, Teregulova Eugenia and Fedorov Yury

Institute of Mechanics and Engineering, Kazan Science Center, Russian Academy of Sciences,
Kazan, 2/31, Lobachevsky str., 420111, Russia
Keywords: aerosol, waves, damping, heat and mass transfer.
Presenting author email: damirgubaidullin@gmail.com

Propagation of acoustic waves in two-fractional mixtures of gas with vapor, with polydispersed particles and drops and in *n*-fractional mixtures of gas with particles is investigated. The mathematical model is presented, the dispersion relation is received, asymptotic at high and low frequencies is deduced, and dispersion curves are calculated. Influence of polydispersity of drops and particles or *n*-fractionality on dispersion and dissipation of small perturbations is analysed.

In Figures 1 the effect of polydispersity of water drops and ash particles on the form of dependences of decrement of attenuation on length of wave from dimensionless frequency of oscillations $\Omega_{5,3}$ is illustrated. ($\Omega_{5,3} = \omega\tau_{va5,3}$, where ω – frequency of oscillations, $\tau_{va5,3}$ – characteristic relaxation time of velocity of disperse phase, $a_{5,3}$ – average radius). Variables with an index *a* correspond water drops of radius *a*, with an index *b* – to particles of ash of radius *b*.

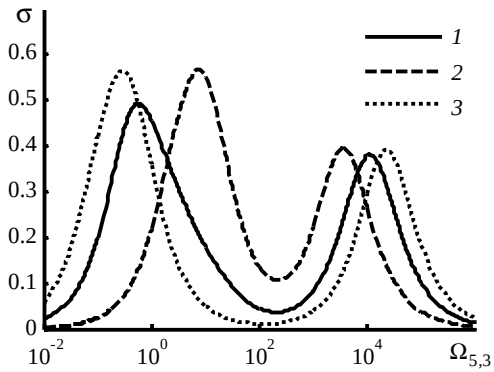

Figure 1. Dependences of decrement of attenuation on dimensionless frequency of oscillations: *1* – $a \in [10^{-5}, 10^{-4}]$, $b \in [10^{-7}, 10^{-6}]$, *2* – $a_0 = 2 \cdot 10^{-5}$, $b_0 = 10^{-6}$, *3* – $a_0 = 10^{-4}$, $b_0 = 4 \cdot 10^{-7}$

At calculations it was assumed: relative mass content of water drops $m_a = 0.3$, ash particles $m_b = 0.3$, pressure of bearing phase $p_1 = 10^5$ Pa ($T_0 = 271$ K). Distribution functions of drops and particles on sizes are accordingly equal $N(a) = a^{-3}$ and $N(b) = 1/\sqrt{2\pi}s \exp(-b_1^2/(2s))$, $s = (b_{\max} - b_{\min})/10$, $b_1 = b - (b_{\max} + b_{\min})/2$. Units of measure are given in SI system.

In Figure 2, The calculations are performed for a mixture of air with particles of ice, aluminum and carbon black particles with different mass concentration *m* of the ice, aluminum and soot. The radius of particles of aluminum was made $r_a = 10^{-5}$[m], by a ice – $r_l = 10^{-6}$[m] and by a soot –$r_s = 8 \cdot 10^{-5}$[m].

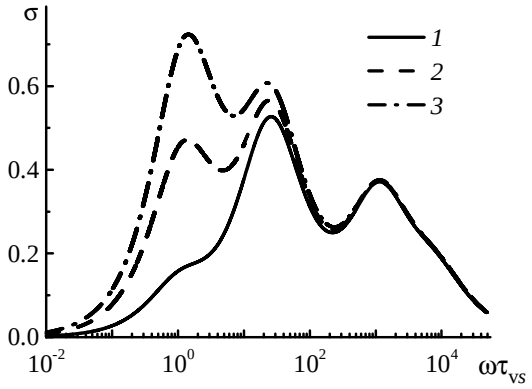

Figure 2. Dependences of decrement of attenuation on dimensionless frequency of oscillations: *1* – $m = 0.3$, *2* – $m = 0.5$,*3* – $m = 0.7$

Accounting for the three-fractional composition and difference in thermophysical properties of fractions gives rise to three peaks for the dependence of the decrement of attenuation at a wavelength at the characteristic values of the dimensionless frequency $\omega\tau_{vl}$, $\omega\tau_{va}$, $\omega\tau_{vs} = 1$. The increase in the mass concentration of one or several fractions (line *2* and *3* in Fig.2) of the dispersed phase significantly affects the dispersion and dissipation of weak waves in aerosols.

This work was supported by the Russian Fund of Foundation Investigation under grant 10-01-00098 and within the framework of the Federal target program "Scientific and scientific and pedagogical shots of innovative Russia for 2009-2013" (state contract №14.740.11.0351).

Gravito-potophoresis of aerosols: the insufficiency of “accommodation” forces action

M.S. Vasiljeva* and S.A. Beresnev

Aerosol Physics Laboratory, Ural Federal University, Ekaterinburg, 620083, Russia
Keywords: fundamental aerosol physics, stratospheric aerosols, photophoresis, accommodation coefficient
Presenting author email*: mary_ru@mail.ru

The description of gravito-photophoresis is based on the semi-empirical theory developed during some years by the Austrian scientist Rohatschek (1984). A simplified model of the physical mechanism of initiation of the gravito-photophoretic forces amounts to the following. A spherical particle with large heat conductivity is placed in the field of directed radiation, its mean volumetric temperature at the cost of absorption differs from the temperature of ambient gas but is homogeneous (in this case the force of radiometric photophoresis is negligible). The frontal to radiation and rear hemispheres of the particle are characterized by asymmetry of surface properties expressed, in particular, in the difference of energy accommodation coefficients on the particle surface.

To calculate the arising force the results of solution of the problem about the force acting in rarefied gas on a heated thin plate with different accommodation properties of surfaces (the plate radiometer) are used. This problem was analyzed earlier by Knudsen (1930), and formal transfer of this result to the problem of a spherical radiometer leads to a simple expression for the gravito-photophoretic force (Rohatschek, 1984). The obtained result predicts a very high efficiency of gravito-photophoretic forces in the vertical transport of stratospheric and mesospheric aerosol particles against gravity, with which none of the known force mechanisms can compete (including radiometric photophoresis). This theory, in particular, was proposed later for explaining the observed phenomenon of accumulation of soot particles from air transport engines at altitudes of the middle stratosphere (Pueschel *et al*, 2000). Recently this kind of vertical motion of particles at the high altitudes was discussed again as means of aerosol albedo modification for mitigation of global warming (Keith, 2010).

The goals of this report are, first, the independent development of the consecutive and rigorous gas-kinetic theory of the phenomenon for the free-molecular regime with detailed consideration of gas-surface interaction features and, second, an attempt of the measurement of predicted forces using an experimental technique with model macroparticles for quantitative comparison with the theoretical predictions.

Gas-kinetic theory of “accommodation” force. Consider a spherical particle of radius R_p suspended in infinite gas volume in the field of unidirectional electromagnetic radiation of intensity I and wavelength λ. The particle heat conductivity is λ_p, the complex refractive index is $m = n + ik$. The particle has a model asymmetry of surface properties: frontal and rear to the radiation direction hemispheres are characterized by constant but various values of the phenomenological accommodation coefficients of energy and momentum of gas molecules. The volume thermo-physical and optical characteristics for both hemispheres are the same. Thus, the physical model of this Janus particle fully corresponds to the model proposed by Rohatschek (1984). The obtained expression for gravito-phoretic force has the form (Beresnev *et al*, 2012):

$$F_{acc} = \frac{\pi}{8} R_P^2 \frac{1}{\bar{v}_g} I Q_{abs} \Delta A_n \text{, where}$$

$$\Delta A_n = \alpha_n(2) / [1 - \frac{9\pi}{32}(1 - \alpha_n(2))] - \alpha_n(1) / [1 - \frac{9\pi}{32}(1 - \alpha_n(1))] \cdot$$

This result can be reduced to the form obtained by Rohatschek (1984) at the same assumptions (free-molecular regime and the neglected radiation cooling of a particle). However, instead of the difference between energy accommodation coefficients $\Delta\alpha_E$, the complex ΔA_n occurs which is responsible for accommodation of the normal momentum of gas molecules on different particle hemispheres. The estimations with the use of known values of show that in the stratosphere the “accommodation” forces can be comparable with the radiometric photophoretic forces, but do not exceed the gravity force. These conclusions both qualitatively and quantitatively differ from the conclusions of the semi-empirical theory of gravito-photophoresis of Rohatschek (1984).

The experimental verification of “accommodation” forces. The measurements conducted in the model experiment with macroparticles have confirmed the existence of “accommodation” forces affecting a particle with artificial asymmetry of surface characteristics together with the forces of radiometric photophoresis. The experimental values for the system “steel particle–helium” are in good agreement with theoretical predictions, and the ratio of the “accommodation” force to the photophoretic force does not exceed 3%.

Thus, the action of "accommodation" forces, in our opinion, is not capable to provide effective vertical transport of aerosol particles against gravity at stratospheric altitudes.

This work was supported by the Ministry of Education and Science of the Russian Federation (research project implemented by leading scientist at Russian institution of higher education, agreement No.11.G34.31.0064).

Rohatschek, H. (1984) *J. Atmos. Chem.* **1(4)**, 377–89.
Beresnev, S.A., Vasiljeva, M.S. and Suetin, D.V. (2012) *Vacuum* (to be published).

The Polydispersity of Primary Particles in Aggregates undergoing Sintering

M.L. Eggersdorfer and S.E. Pratsinis

Department of Mechanical and Process Engineering, ETH Zurich, CH-8092 Zürich, Switzerland

Keywords: Aggregates, Particle size distribution, Particle surface area, Sintering.
Presenting author email: meggers@ptl.mavt.ethz.ch

Nanoparticles often exhibit unique properties which are confined to a certain size range, like quantum dots or plasmonic nanoparticles. A narrow distribution of primary particles is desired for these applications. Aerosol processes allow a rapid and scalable production of nanoparticles over a wide range of sizes. In such processes, particles grow, however, typically by coagulation that places a lower limit to the width of the size distribution, the so called self-preserving size distribution with a geometric standard deviation of σ_g = 1.45. If primary particles with different high temperature residence time histories (e.g. different streamlines) are mixed, agglomerates with quite polydisperse primary particle size distributions are obtained. This polydispersity can be overcome by sintering of primary particles in their agglomerates. Furthermore accounting for primary particle polydispersity is important as the characteristic sintering time depends strongly on primary particle size (Sander et al., 2009).

Heine and Pratsinis (2007) investigated the polydispersity of primary particles in agglomerates during coagulation and sintering by a two-dimensional sectional model. The detailed agglomerate and primary particle size distribution of TiO_2 formation was simulated. The narrowest primary particle size distribution was obtained when aggregates (particles with sinter necks) were produced. This effect could be observed for ZnO nanocrystallites which showed a blueshift of the absorption spectrum with decreasing crystallite size (1.5 – 12 nm, Mädler et al., 2002). Their average primary particle size by nitrogen adsorption measurements was larger than their X-ray diffraction crystal size, indicating multicrystalline aggregates. A narrow crystal size distribution is required to exhibit this so-called quantum-size effect.

Here, aggregate sintering by viscous flow (polymers, SiO_2, Eggersdorfer et al., 2011), lattice and grain boundary diffusion of crystalline materials (Ni, Ag, ZnO_2, TiO_2, Eggersdorfer et al., 2012) is simulated to track the primary particle growth. The change in particle distance, dx/dt, and particle radius, dr_p/dt, are calculated by energy and mass balances (Eggersdorfer et al., 2011). The restructuring during sintering from fractal-like agglomerates to aggregates and eventually compact particles (e.g. spheres) is simulated. The effect of initial primary particle size distribution and sintering mechanisms on the primary particle polydispersity and surface area mean diameter are investigated. The initial primary particle size distributions are log-normal with σ_g = 1, 1.45 and 2. Each sintering mechanism exhibits a different primary particle size distribution evolution but almost identical growth in surface area mean diameter. Grain boundary diffusion has the strongest impact among all densifying sintering mechanisms and results rapidly in the narrowest primary particle size distributions (Fig. 1). Nevertheless, the relations between surface area mean primary particle and mobility diameter as well as the power law scaling between projected area and number of primary particles are independent of sintering mechanism. So these relations can be readily used for the characterization of agglomerates and aggregates regardless of material and sinter mechanism.

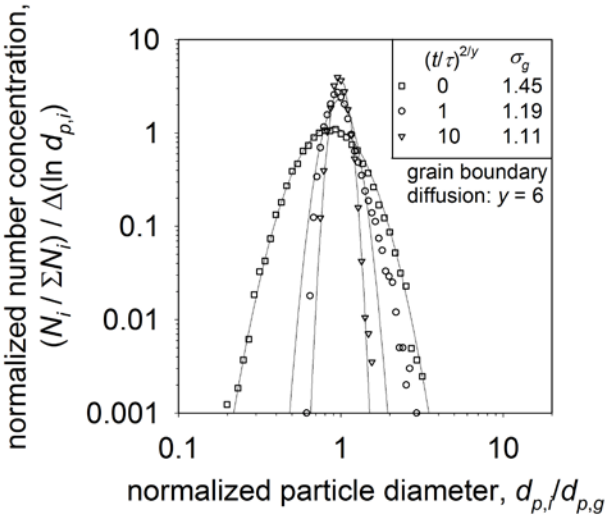

Figure 1. Evolution of the primary particle size distribution of agglomerates during sintering by grain boundary diffusion as a function of scaled time.

Financial support by ETH Research Grant (ETHIIRA) ETH-11 09-1 and the European Research Council is gratefully acknowledged.

Heine, M.E. and Pratsinis, S.E. (2007) *J. Aerosol Sci.* **38**, 17-38.

Eggersdorfer, M.L., Kadau, D., Herrmann, H.J. and Pratsinis, S.E. (2011) *Langmuir* **27**, 6358-6367.

Eggersdorfer, M.L., Kadau, D., Herrmann, H.J. and Pratsinis, S.E. (2012) *J. Aerosol Sci.* **46**, 7-19.

Mädler, L., Stark, W.J. and Pratsinis S.E. (2002) *J. App. Phys.* **92**, 6537-6540.

Sander, M., West, R.H., Celnik, S. and Kraft, M. (2009) *Aerosol Sci. Technol.* **43,** 978-989.

Temperature and particle vertical profiles: suitability of the ML concept under weak cyclonic conditions

J. Giménez[1], J.F. Nicolás[1], C.Pastor[1], R.Castañer[1], E. Yubero[1], M.J. Cuesta-Bolao[1], J. Crespo[1] and S. Caballero[1]

[1]Department of Applied Physics, Miguel Hernández University, Elche, 03202, Spain
Keywords: Particle number concentration; Mixing Height; Weak cyclonic conditions
Presenting author email: j.gimenez@umh.es

Several studies have shown good correspondence between the Mixed Layer Depth (MLD) or Mixing Height (MH) calculated from aerosol profiles and the MH estimated from meteorological parameters (Giménez *et al* (2010); Ferrero *et al* (2011)). The MH is only determined under anticyclonic scenarios because in low pressure regions the upward motions carry boundary layer air away from the ground to large altitudes throughout the troposphere. In this work, we show that under weak cyclonic conditions aerosol profiles and MH estimated from meteorological parameters fit like we were under anticyclonic situation.

The vertical profiles of particle number concentrations and meteorological parameters were obtained using a motorized paraglider. The instrument used to obtain the particle number concentration was a GRIMM 1.109 aerosol spectrometer. This instrument determines particle number concentrations in 31 particle size channels from 0.25 to 32 µm. A Delta Ohm ultrasonic anemometer, model HD 2003, was used to record the temperature, relative humidity and pressure. No wind data was available. Altitude data was supplied from GPS and from meteorological parameters with good agreement between them.

Two flights were performed under weak cyclonic conditions on 22 September 2009 in flat terrain in southeast Spain (38°11´19.7´´N; 0°49´47.3´´W; 60 m a.s.l.), approximately 20 km from the Mediterranean coast. All heights refer to meters above ground level (a.g.l.). In the first flight, the paraglider took off at 07:45 UTC. In the second flight, the paraglider took off at 10:45 UTC. We use the following nomenclature: F1A (flight 1-ascent), F1D (flight 1-descent), F2A (flight 2-ascent) and 2D (flight 2-descent) to refer to the four vertical profiles, two per each flight. The horizontal displacement from the launch site in both cases was almost negligible. We calculated the hypothetical heights of the Stable Boundary Layer (SBL) and the Convective Boundary Layer (CBL) as if the flights had taken place under anticyclonic conditions. To determine the hypothetical SBL heights in flight 1, we focused on the heights where the temperature gradient vanishes ($\partial T/\partial z=0$; inversion top), (Stull, 1988). To determine the hypothetical CBL heights in flight 2, the parcel method (Seibert *et al.* (2000)) was used.

Fig. 1 shows the particle concentration, temperature and relative humidity (RH) vertical profiles in the two flights during the ascents and descents.

In F1A, the hypothetical SBL height was about 300 m. This height decreases until ~100 m when the inversion is disappearing (F1D), and we can appreciate

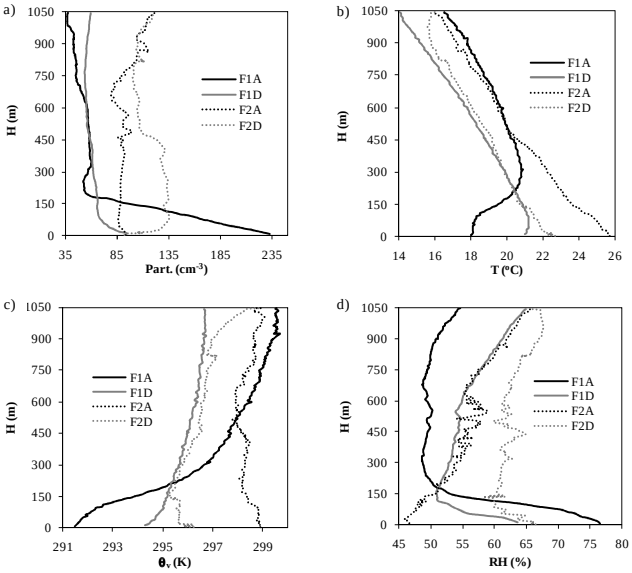

Figure 1. Profiles of: a) total particle concentration, b) temperature, c) virtual potential temperature, d) RH

that these inversion heights roughly coincide with the changes in particles vertical profiles slopes (Fig. 1a and 1b).

Between F1D and F2A around two hours passed and in that time weak convective movements developed. The CBL heights were ~950 m (F2A) and ~400 m (F2D) (Fig. 1c). This could be because of stratiform clouds formed and the entry of a cold air mass with higher RH (Fig. 1b and 1d). In F2D, particle profile decrease at ~400 m (CBL height). In F2A, the coincidence is not clear. However, it seems as if the atmospheric thermal effect prevails over the convergence dynamic effect.

Ferrero L, Riccio A, Perrone MG, Sangiorgi G, Ferrini BS, Bolzacchini E (2011) *Mixing height determination by tethered balloon-based particle soundings and modeling simulations.* Atmos Res **102**, 145-156.

Giménez J, Pastor C, Castañer R, Nicolás JF, Crespo J, Carratalá A (2010) *Influence of Saharan dust outbreaks and Atmospheric stability upon vertical profiles of size-segregated aerosols and water vapor*. Atmos Environ **44**, 338-346.

Seibert, P, Beyrich F, Gryning SE, Joffre S, Rasmussen A, Tercier P (2000) *Review and intercomparison of operational methods for the determination of the mixing height*. Atmos Environ **34**, 1001-1027.

Stull RB (1988) *An introduction to Boundary Layer Meteorology*. Kluwer Academic Publisher, Dordrecht

Two-phase polydisperse spray in a wake of shattering drop

A. G. Girin

Odessa National Maritime University, 65029, Odessa, Ukraine
Keywords: dispersion, aerosol generation, aerosol modelling, evaporation.
Presenting author email: club21@ukr.net

A mathematical model of evaporation aerodynamics of a mist in the wake of a shattering drop in uniform gas stream is elaborated. It is grounded on the distribution function $f_{\text{n.p.}}(r,t)$ for stripped daughter droplets by sizes, which was obtained earlier on the base of concept of quasi-continuous stripping of daughter droplets from unstable part of parent drop surface due to action of high-frequency periodic gradient instability. Stripped droplets are considered as a polydisperse multi-velocity continuum and a system of three partial differential equations of two-phase spray dynamics is composed, which consists of equations of torn droplets motion, of evaporation and of transient density of their number distribution. The dependencies of droplets drag coefficient on velocities and sizes as well as intensification of evaporation due to their streamlining are taken into account. The system allows to describe quantitatively the evaporation and acceleration of each stripped droplet and thereby – the process of formation of liquid-phase jet and vapor cloud in a wake.

Spatial structure of two-phase wake spray has transient complicated character since every droplet has its own values of velocity, radius, evaporation rate and distances between droplets vary due to non-uniform field of accelerations. To take into account all the peculiarities of evaporation ballistics we have introduced into consideration the transient distribution function of daughter droplets by sizes $f_{\text{n.d.}}(r,x,t)$ as it exactly reflects the entire evolution of stripped droplets in time t, in space x, as well as in sizes r. The parent drop is considered as located in spray origin $x=0$ source of daughter droplets with a given source distribution function $f_{\text{n.p.}}(r,t)$. The daughter droplets are moving in a direction of spray axis OX with velocity $w_{\text{d}}(r,x,t)$. As well, each daughter droplet is regarded as a moving point source of vapor, and they altogether form the distribution of a vapor mass $m_{\text{v}}(x,t)$ in a wake.

At one-dimensional spatial approximation of a wake flowfield the mathematical problem is formulated and solved in a closed form in dynamic 3D space. A detailed calculation of the ballistics of evaporating spray, generated in the wake of a kerosene drop fragmented by air stream, is performed and the formation of liquid-phase jet and vapor cloud in a wake is described. Calculations showed, that times of living of finest and largest droplets are the characteristics of liquid jet formation in spray. Soon after moment of entire evaporation of droplets of minimum in spray radius, that were stripped at the beginning, the evaporation mass rate and current value of liquid-phase mass in spray exceed their maximum values because of droplets vanishing begins. After moment of vanishing of droplets of maximum radius the vanishing of droplets of new radii doesn't occur, and this is the necessary condition for stabilization of length of liquid-phase jet.

The proposed model allows to calculate spray mean diameters, so, the evolution of the dispersive characteristics of the liquid-phase jet of spray is studied. Parameters of two kinds were considered: the first are defined at any cross section of jet and characterize its spatial structure at fixed moment, while the second are calculated at any moment for the whole set of droplets and describe temporal changing of jet dispersity in total. At the beginning the bunch of first set of curves is narrow, that testifies to weak polydispersity of jet, but after droplets vanishing starts, the polydispersity increases. The stabilization proceeds gradually along jet from astern part to the tip. The dependencies of the second set of curves confirm the conclusions. In final state the jet polydispersity is much greater than that, produced by source. In the case considered the stabilization of jet is discovered and the range of a jet is found. The internal structure of the spray is investigated as related to the dynamic process of spray formation.

The process of vapor cloud formation in spray was studied. At the beginning the intensification of evaporation due to rapid growth of liquid surface is so large, that vapor wave appears which has sharp front similar to blast wave. After losing contact with liquid phase this wave has convectional drift, keeping its form invariable. Gradual weakening of droplets source capacity generates rarefied wave in vapor mass distribution, so, far from the source the distribution tends to "triangle" form. Analysis of the processes of jet and vapor cloud formations is done and their structures are described thus.

By rough estimations, in the case of a fuel drop, combustible mixture in wake of a shattering drop is substantially overreached in average, as vapor density several times exceeds the stoichiometric value. Vapor oversaturation leads to cooling of the mixture. Equation of heat balance for process of vapor – air mixing yields the temperature dropping in about 300°K which means that delay of ignition may jump several orders high.

The proposed model can serve as a core of the entire model of formation, ignition and combustion of homogeneous inflammable mixture in a wake, and thereby – of heterogeneous detonation wave, but also of some kinds of engine furnaces.

Ab initio molecular dynamics study of sulfuric acid clusters with ammonia/dimethylamine

V. Loukonen[1], I-F. W. Kuo[2], M. J. McGrath[2] and H. Vehkamäki[1]
[1]Department of Physics, University of Helsinki, Helsinki, FI-00014 University of Helsinki, Finland
[2]Department of Biophysics, Kyoto University, Kyoto 606-8502, Japan
[3]Lawrence Livermore National Laboratory, Livemore, CA 94550, USA
Keywords: atmospheric clusters, *ab initio* molecular dynamics
Presenting author email: ville.loukonen@helsinki.fi

Previously

Arguably, during the recent years various *ab initio* calculations have increased our understanding on the first steps of atmospheric new-particle formation.

Most of these studies concentrate on finding the minimum energy structures for small molecular clusters and often the characterizing quantity is the formation free energy. Lately, the formation energies have also been converted into evaporation rates (Ortega et al., 2012) and these in turn have been used in kinetic models to obtain insight on how the cluster concentrations evolve (McGrath et al., 2012).

On the other, in the atmosphere all the molecules are under constant thermal motion. However, in the static minimum energy calculations the effect of non-zero temperature is most often taken into account as a correction term to the electronic energies. Furthermore, this correction term is typically obtained by approximating the clusters as rigid rotors and harmonic oscillators. The static calculations are inherently unable to capture the real dynamics of the system.

This study

In the current study, we have used *ab initio* molecular dynamics simulations to probe the actual dynamics of sulfuric acid - ammonia and sulfuric acid - dimethylamine clusters.

In *ab initio* molecular dynamics the forces acting on atomic nuclei - and thus driving the dynamics of the system - are calculated from the electronic structure of the cluster in question. The advantage of the method is its ability to keep track of both the kinetic and potential energy, thus providing a full picture of the energetics and dynamics at the chosen level of computational sophistication. The downside is large computational cost.

We used a timestep of 0.5 fs and simulated the clusters in NVT ensemble ($T = 300$ K) for 45 ps. The chosen clusters

$$(\text{sulfuric acid})_n \bullet (\text{ammonia})_{n-1}$$

$$(\text{sulfuric acid})_n \bullet (\text{dimethylamine})_n,$$

where $n = 2,3,4$ were found the be very stable in a recent minimum energy structure study (Ortega et al., 2012), and as such are good initial structures for the current study probing the dynamics and stability.

The simulations show that the stability of the clusters in non-zero temperature is largely dependent on the hydrogen bonding patterns, similarly to the static minimum energy calculations. In most of the studied clusters the equilibrium was reached between 0-10 ps. However, even after the equilibrium was reached there was notable bond rearrangement in both the ammonia and dimethylamine containing clusters: the number of hydrogen bonds stayed the same but the individual atoms forming the bonds changed (cf. Figure 1).

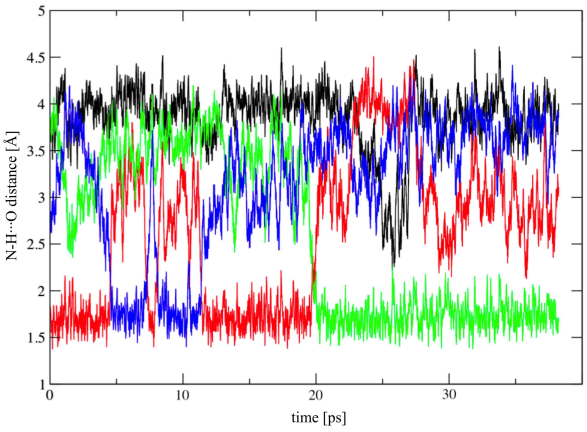

Figure 1: One particular H-bond as a function of time in $(\text{sulfuric acid})_2 \bullet (\text{dimethylamine})_2$ cluster. Different colors correspond to different O atoms in H_2SO_4 participating in the bond.

Regardless of the bond rearrangement the clusters remained bound together during the simulation period. It is likely that similar bond forming and breaking will take place also during the initial formation of atmospheric molecular clusters.

This work has been supported by the Maj and Tor Nessling Foundation.

McGrath, M. J., Olenius, T., Ortega, I. K., Loukonen, V., Paasonen, P., Kurtén, T., Kulmala, M. and Vehkamäki, H. (2012) Atmos. Chem. Phys., *in press*.

Ortega, I. K., Kupiainen, O., Kurtén, T., Olenius, T., Wilkman, O., McGrath, M. J., Loukonen, V., and Vehkamäki, H. (2012) Atmos. Chem. Phys., **12**, 225-235.

A turbulent model for the study of dust mobilisation in closed enclosures

J.R. García-Cascales[1], F.J. Sánchez-Velasco[2], R. Otón-Martínez[1] and F. Vera-García[1]
A. Bentaib[3], N. Maynet[3]

[1]Department of Thermal and Fluids Engineering, Universidad Politécnica de Cartagena, 30202 Murcia, Spain
[2]Centro Universitario de la Defensa, Academia General del Aire, 30720 Santiago de la Ribera, Murcia, Spain
[3]Institute de Radioprotection et Sureté Nucléaire, 92262 Fontenay-aux-Roses Cedex, France
Keywords: aerosol dynamics, dispersion, dust, gas particle distribution.
Presenting author email: jr.garcia@upct.es

This paper focuses on dust mobilisation problems. It describes a finite volume approach to approximate solutions of a *k-ε* turbulent model which is applied to the analysis of transient two-phase flows with gas and particles. This development has been carried out in the context of the fusion reactor ITER and its application is restricted to high dilute mixtures of gas and particles which are the type of mixtures expected to have inside the tokamak. This development has been implemented inside the DUST code (García-Cascales, 2010). The model includes the effect of particle-wall interaction, interfacial friction, interfacial heat transfer, and lift forces. The closure laws used in the model are realistic enough for the problems studied. Gas phase is modelled as a perfect gas and the solid phase is considered incompressible. Despite its specific application, the model can be extrapolated to study other dust mobilisation and/or explosion problems in industry.

In fusion devices such as the ITER, the interaction of plasma with the surfaces that comprise the vacuum vessel of a fusion reactor may produce certain amount of dust which may adhere or deposit on to such surfaces. This is expected to be formed by a polydisperse mixture of particles of carbon, beryllium, stainless steel, and tungsten. The geometric median diameter of the particles will be of about 2 μm and a standard deviation ranging 2-5. Estimates for ITER point out that the expected amount of dust may range from several kg to hundreds kg depending on the case (Winter, 2000). Associated to its existence, a great amount of problematic scenarios have been reported:

Dust causes tritium uptake and its deposition may make difficult the facility maintenance. Its mobilisation, due to a loss of vacuum accident, may lead to the exit of radioactive, reactive or toxic chemicals which can contaminate the surroundings and be a potential risk for the public. In a loss of coolant event, dust can contribute to hydrogen generation (e.g. Be or C in the presence of water or steam), which in presence of air may deflagrate or detonate.

Dust might also ignite if the necessary conditions were met. Its permanent deposition may reduce heat transfer and therefore the cooling capacity of the refrigeration system. In general, it may be the cause of plasma disruptions, impede start-up or breakdown, and globally contribute to the malfunction of the system.

The understanding of dust sources, the characterization of its effects, and the performance of experiments which simulate fusion plasma conditions will help to improve the development of reliable tools for the analysis of such problems (Sharpe et al., 2002). At the same time, this will avoid problems in operation and prevent accidents. Their validation with suitable benchmark tests will contribute to reduce the uncertainties in safety analysis and safety limits.

During the last years, several works have appeared in the existing literature. Great effort has been done in order to develop and validate numerical codes for the analysis of the kind of scenarios that may be encountered inside the vacuum vessel of a fusion reactor. Examples of them are Takase (2001) or Porfiri (2006) who experimental and numerically studied the mobilisation of particles in closed reservoirs.

Considering our previous work (García-Cascales et al., 2008) and the physical laws added to the code (García-Cascales et al. 2010), in this paper, the k-ε model and the system of equations adopted in DUST are presented. Some details about the finite volume model implemented are given and numerical results are provided. Finally, some conclusions are drawn.

García-Cascales J.R., Mulas-Pérez J., Paillère H. (2008), Extension of some numerical schemes to the analysis of gas and particle mixtures *International Journal for Numerical Methods in Fluids*, **56**, 845-875.

Garcia-Cascales J.R., Vera-García F., Zueco-Jordán J., Bentaib A., Meynet N., Vendel J., Perrault D. (2010) Development of a IRSN code for dust mobilization problems in ITER, *Fusion Engineering and Design*, **85**, 2274-2281.

Porfiri, M.T. and Forgione, N. and Paci, S. and Rufolini, A. (2006) Dust mobilization experiments in the context of the fusion plants, *Fusion Engineering and Design*, **81**, 1353-1358.

Sharpe, J.P. Petti, D.A. Bartels, H.W. (2002) A review of dust in fusion devices: implications for safety and operational performance, *Fusion Engineering and Design*, **63-64**, 153-163.

Takase, K. (2001), Three-dimensional numerical simulations of dust mobilization and air ingress characteristics in a fusion reactor during a LOVA event, *Fusion Engineering and Design*, **54**, 605-615.

Winter, J. (2000) Dust: a new challenge in nuclear fusion research, *Physics of Plasmas*, **7**, 3862-3866.

Microgravity experiments on particle motion in the region of negative thermophoresis

A.A. Vedernikov[1], S.A. Beresnev[2] and A.V. Markovich[1]

[1]Université Libre de Bruxelles, Brussels, B-1050, Belgium
[2]Ural Federal University, Ekaterinburg, 620083, Russia
Keywords: aerosol dynamics, thermophoresis, microgravity, accommodation coefficient
Presenting author email: sergey.beresnev@usu.ru

Thermophoresis (motion of particles due to temperature gradient in a gas) is a subject of many-year experimental and theoretical investigations of great significance for fundamental and applied aerosol physics.

Substantial improvement of accuracy and sensitivity due to diminishing convective effects is possible to get in microgravity conditions performing experiments in drop towers, in parabolic airplane flights, or onboard the orbital space station. Microgravity conditions are the most advantageous, if not the only suitable for decisive experiments in tackling the problem of "negative thermophoresis", i.e. predicted for high-conductivity aerosol particles at small Knudsen numbers motion in the direction of temperature gradient and not against as for the traditional thermophoresis.

According to theoretical analysis the thermophoretic force and velocity are very sensitive to the variation of energy accommodation coefficient α_E. The value of α_E governs the magnitude of the heat flux normal to the surface, which, in its turn, controls the competition of oppositely directed thermal creep and thermal stress gas flow near the particle surface so that the thermophoretic velocity can be positive even for high-conductivity particles at very small Kn numbers. Experimental analysis of negative thermophoresis thus splits into two tasks: 1) testing which theories are adequate – those taking into account the thermal stress slip or without it and 2) which model most accurately takes into account peculiarities of these phenomena.

Experiments were performed at Bremen Drop Tower (Germany) with 4.7 s duration of high quality microgravity (better than 10^{-5}g). We used two types of particles *a*) high heat conductivity ($\Lambda = \lambda_p/\lambda_g$ =20500) polydisperse copper spherical particles with mean diameter of 74 μm and *b*) low conductivity ($\Lambda = 1.8$) hollow glass spheres with about the same particle size distribution. Particles were injected separately into the cubic cell filled with nitrogen at normal pressure with four windows for stereoscopic observation in back illumination. The gradient was created by a heated wire in the cell center. Velocities were analyzed for the particles, for which three-dimensional trajectories were identified. Radial components of particle velocities were related to the thermophoretic motion. Previous results (Vedernikov *et al* (2008) and Beresnev *et al* (2008)) are here completed with the analysis of motion of low conductivity particles and detailed three-dimensional simulation of residual convective motion.

Typical velocities of low conductivity particles were around 0.3-0.5 mm/s depending on their distance from the wire and showed excellent agreement with the theory of Brock (1962). Velocities of copper particles appeared to be 30-50 times lower under the same conditions. Reduced thermophoretic velocities of copper particles are presented on Fig. 1 after refinement on residual convective motion.

These results meet predictions of gas-kinetic theories that take into account the thermal stress slip flow. As for the second task mentioned at the beginning, the experiments were still not sensitive enough to define the sign of the motion and relate it to a particular set of accommodation coefficients. Using the same experimental approach in future in a wider range of Kn number, different ratio of heat conductivities and different accommodation coefficients should allow solving most current problems of the theory of negative thermophoresis.

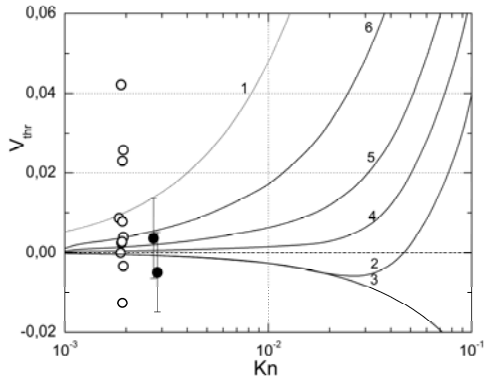

Figure 1. The dimensionless thermophoretic velocity V_{thr} for copper particles. Microgravity experiments: black circles stand for particles close to the wire where negative thermophrsis is dominant; open circles stand for particles far from the wire where dominates residual convection. Theory: 1 – Brock (1962) with $C_{ts} = 1.17$, $C_t = 2.18$, $C_m = 1.14$; 2-6 – Beresnev et al (1995): 2 – calculations and 3 – asymptotic solution at $\alpha_\tau = \alpha_E = 1.0$; 4 – calculations at $\alpha_\tau = 1.0$; $\alpha_E = 0.95$; 5 – at $\alpha_\tau = 1.0$; $\alpha_E = 0.90$; 6 – at $\alpha_\tau = 1.0$; $\alpha_E = 0.80$.

ESA PRODEX Program, Belgian Federal Science Policy Office and Bremen Drop Tower Operation and Service Company ZARM FABmbH (Germany) are greatly acknowledged for their support.

Vedernikov, A., Beresnev S. and Markovich A. (2008) *J. Jap. Soc. Micrograv. Appl.* **25**, 267-272.
Beresnev S.A., Vedernikov, A.A. and Markovich, A.V. (2008) *Atmos. Oceanic Opt*. **21(7)**, 508-513.

High order operator splitting adaptive time marching Monte Carlo for aerosol dynamics

Kun Zhou and Fabrizio Bisetti
Clean Combustion Research Center, King Abdullah University of Science and Technology (KAUST),
Thuwal, 23955, Saudi Arabia
Keywords: Monte Carlo simulations, aerosol dynamics, particle size distribution.
Presenting author email: kun.zhou@kaust.edu.sa

Aerosol dynamics are usually described by the population balance equation (or general dynamics equation). Direct discretization and moment methods are two popular ways to solve the population balance equation. In principle, Monte Carlo (MC) methods are more flexible than both direct discretization and moment methods in that they can readily accommodate complex physical models for aerosol dynamics, e.g., a bi-variate volume-surface description of aerosol particle morphology. In this work we develop and validate a new Monte Carlo method that distinguishes itself from available methods for accuracy, adaptivity, and ease of use. The algorithm combines a stochastic modeling of coagulation and a deterministic description of nucleation and particle growth processes adopting a high-order operator splitting technique.

Figure 1 shows the flowchart. The dynamic equations for nucleation and surface growth are integrated via an adaptive Runge-Kutta method within every time step δt. Within δt, coagulation is modeled by the stochastic scheme of Gillespie (1975). Gillespie's scheme is parallized with MPI and the parall version of the algorithm exhibits nearly linear (optimal) speedup with increasing CPUs at fixed number of Monte Carlo particles N. First order and second order (Strang) operator splitting techniques are compared. It is found that the second order symmetric Strang splitting produces signficantly more accurate results at the same cost of the first order splitting. The operator splitting error is controlled by the adaptive time step δt, which is set according to two criteria based on number density and volume fraction rate of change.

Stochastic noise in the ensemble quantities is one of the key issues in Monte Carlo methods. The stochasticity comes from three steps in the current MC method (filled blocks in the flowchart in Fig. 1). Re-sampling is necessary to increase or decrease the total number of simulation particles N, according to a underlying probability distribution function. The number of particles N cannot be too large due to the algorithmic complexity. Here we present a mathematical proof that re-sampling will not introduce any statistic bias. The other stochastic steps are the draw of the event time increment from its probability density function and the random selection of the two coagulating particles.

As expected, it is found that the variance tied to coagulation modeling is inversely proportional to N. Conversely, the computational cost is proportional to N^2. Hence, increasing N to reduce the variance is not a good strategy. Detailed numerical simulations on various test cases show that repeated Monte Carlo simulations are independent of each other and can be used to reduce the sample variance. The total cost of repeating the simulation m times is CmN^2, where C is a constant. The expression for the cost suggests to chose N as small as possible while increasing m to reduce the variance.

The numerical efficiency and error of the MC method are studied in four cases: (i) constant kernel coagulation, (ii) free molecular regime coagulation, (iii) constant nucleation and constant kernel coagulation, and (iv) constant nucleation and free molecular regime coagulation. For cases (i) and (iii) analytical solutions are available. It is found that for N equal to several hundred to thousand particles, and m equal to several hundred iterations, the MC method provides very good results for lower order moments of the particle size distribution function. This sort of simulation needs only a few hours on a typical multi-core engineering workstation. Conversely, if one is interested in predicting high order moments (i.e., the tail of the particle particle size distribution function), a rather large N is needed.

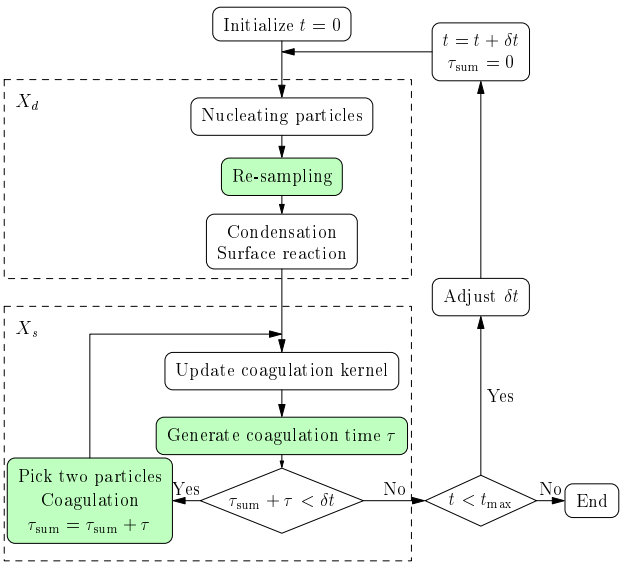

Figure 1: Flowchart of the MC method. Filled blocks denote stochastic steps. X_d and X_s denote different operators in the operator splitting method, which can be grouped in various ways to achieve numerical efficiency and accuracy.

Gillespie, D. T. (1975) J. Atmos. Sci. **32**, 1977–1989.

Modeling of the behavior of droplets deposited on the smooth and rough fiber surfaces

J.M. Gac[1] and L. Gradoń[1]

[1]Faculty of Chemical and process Engineering, Warsaw University of Technology, Warsaw, 00-645, Poland
Keywords: Aerosol filtration, Droplets, Fibers, Modeling (microscale), Numerical simulation
Presenting author email: J.Gac@ichip.pw.edu.pl

The separation of the liquid droplets from the stable mist system is a crucial process in industrial technologies, natural gas cleaning, crank case ventilation systems and many other applications. The most efficient devices for such separations are fibrous filters (coalescers). A properly designed coalescer structure, defined through the space distribution of the local porosity and fiber diameter involves the phenomena of a droplet coalescing in the bulk, deposition of drops on the fiber, coalescing of the deposited droplet on the fibers and the drainage of the filter fibers.

In our presentation, a two-color lattice-Boltzmann method (LBM) is used for simulation of the behavior of droplets deposited on a fiber. This kind of well-known LBM scheme is an effective tool for simulating of two-phase flow, including surface tension effects. The interaction of the droplet with the gas flowing around a fiber having smooth and rough surfaces was analyzed.

As a results of our simulations, we derive the equilibrium of conformation of droplets. For a smooth fiber we obtain results consistent with analytical results presented in (Carrol, 1986). By contrast, the droplet on rough fiber takes often completely different conformations, what is explained by means of merging the theory of rough surfaces of Wenzel (1936) with the results of (Carrol, 1986).

Further, we investigate the axial and transversal motion of a droplet on a fiber. We have found that in case of smooth fibers the velocity of the asymmetric droplet is higher than the velocity of axisymmetric droplet, what is consistent with recent results of Gilet *et al* (2010). By contrast, the roughness of the fiber facilitates the motion of the droplet for the situation when the mean distance between the insets is big in comparison to the diameter of the droplet. The reason is that the droplet, moving through the inset, transits from the axisymmetric to the asymmetric conformation, for which the equilibrium velocity is higher. However, if the typical distance between the insets is smaller than the diameter of the droplet, its motion is rubbed. Both these situations are presented in Fig. 1.

The transverse motion of the droplet on rough fiber is slower than the motion of smooth one – so the roughness of the fiber impedes the detachment of the droplets. The difference of the times of detachment from rough and smooth fiber decreases with the value of contact angle, as it has been shown in Fig. 2.

The results of calculation show the distinguished patterns of the interaction depending on the structure of the fiber roughness and the fiber and droplet dimensions. The modeling data indicate a new approach for the designing of a novel generation of the efficient coalescers.

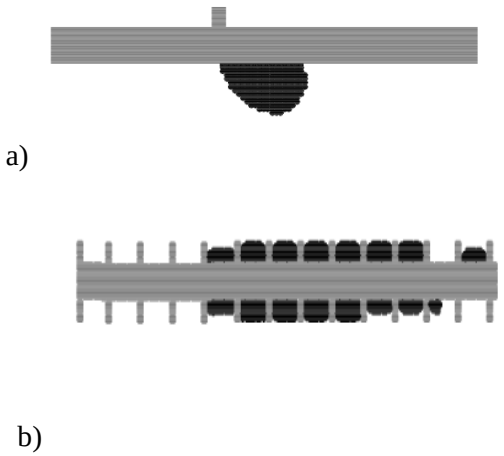

Figure 1. The shape of the droplet on rough fiber with low (a) and high (b) density of insets.

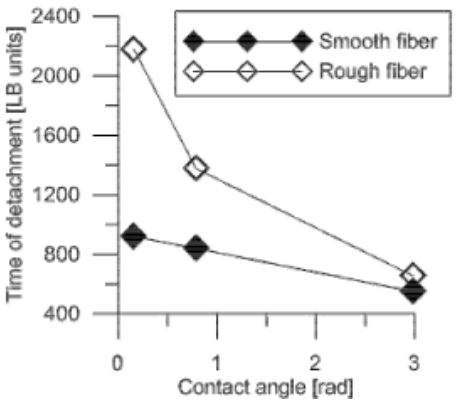

Figure 2. Dependence of time of detachment of the droplet on the contact angle for smooth and rough fiber at the same velocity of surrounding gas.

JMG thanks Foundation for Polish Science for financial support.

Carrol, B.J. (1986) *Langmuir* **2**, 248-250.
Wenzel, R.N. (1936) *Ind. Eng. Chem*. **28**, 988-994.
Gilet, T., Terwagne, D. and Vandewalle, N. (2010) *Eur. Phys. J. E* **31**, 253–262.

Parameters affecting deposition on fibrous filters

Sarah J. Dunnett[1], Charles F. Clement[2]

[1]Department of Aeronautical and Automotive Engineering, Loughborough University, Loughborough, Leics. LE11 3TU, U.K.
[2]15 Witan Way, Wantage, Oxon, OX12 9EU, U.K.

Keywords: fibrous filter, filtration, numerical simulation, particle deposition

INTRODUCTION

The separation of particles from a flow by the use of fibrous filters is common practise. Such filters generally consist of numerous fibres, of varying sizes, which are positioned more or less normal to the flow. The flow passes through the regions between the fibres and particles are removed by attaching to the fibre surface. The mechanisms by which the particles are removed depend on various particle and flow properties, such as flow velocity, particle size, etc. As the deposit accumulates inside the filter the flow through it, and hence the efficiency with which further particles is collected, is altered. Hence an understanding of the areas in which deposit collects on the fibres and its effect upon the flow field is crucial in predicting the performances of filters. This is dependent on numerous parameters making this is a complex problem. In this work the numerical model that we have developed in previous papers, Dunnett and Clement (2009), is used to investigate this dependence.

NUMERICAL MODEL AND PARAMETERS

The numerical model we have developed previously investigates the performance of fibrous filters in the early stages of particle loading for particles for which diffusion and interception with the fibre are the main mechanisms of deposit. In the model the Boundary Element Method is used to determine the flow field around a single fibre containing deposit. The neighbouring fibres are taken into account in the model by the application of the boundary conditions. The deposit collected on the fibre is assumed to form a smooth porous layer and the flow through the porous layer is assumed to be modelled by Darcy's law. In this work we consider the effects upon filter performance of the various parameters in the problem.

In the literature there are various expressions available for the filter efficiency if deposition is dominated by one mechanism, Brown (1993). Results obtained by our model have found that the parameter **s** defines whether diffusion or interception are the dominant mechanism. This parameter is a function of particle and fibre size, fluid velocity, filter packing fraction and diffusivity, D. It is given by $s = \frac{d_p k_h}{d_f Pe^{1/3}}$. Where d_p and d_f are the particle and fibre diameter respectively and k_h is a hydrodynamic factor given by $k_h^3 = -2\ln\alpha - 3 + 4\alpha - \alpha^2$, α is the filter packing fraction. Pe is the Peclet number $Pe = d_f U_0 / D$ where U_0 is the freestream velocity. It has been found that diffusion dominates for $s<1$ and interception for $s=O(1)$. The numerical model has also shown that the value of s is important in determining whether or not porosity in the deposit subsequently increases the deposition rate.

Another important parameter identified by the model is the dimensionless permeability of the porous deposit, k'. This parameter is dependent upon the deposit porosity and the particle size. There are various expressions available in the literature for k' and these have been investigated and the effects they have upon the predicted flow field will be reported on. An example of the different expressions is shown in Figure 1 where k' is shown as a function of porosity, φ using 3 different expressions from the literature.

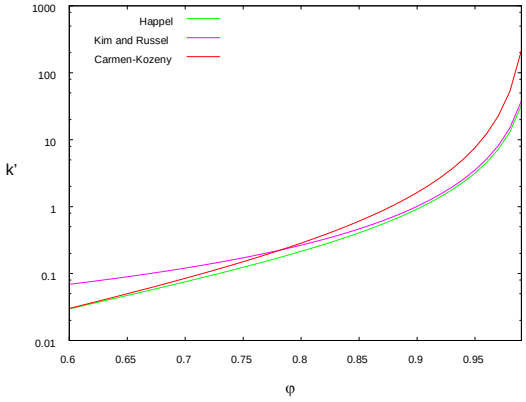

Figure 1. k' as a function of φ

As with all numerical models assumptions have been made, and the range of validity of the model as a result of these will be discussed.

REFERENCES

Brown, R.C. (1993) Air filtration. An integrated approach to the theory and application of fibrous filters, Pergamon Press, Oxford.

Dunnett, S.J. and Clement, C.F. (2009) Eng. Anal. Boundary Elem. 33, 601-610.

Application of filter utility factor in the filtration of dust and liquid aerosol

T. Jankowski
Department of Chemical, Aerosol and Biological Hazards, Central Institute for Labour Protection – National Research Institute, 00-701 Warsaw, Poland
Keywords: oil mist, aerosol, dust, filtration efficiency, fibrous filters

The melt-blown nonwovens are important part of fibrous filters used in local exhaust ventilation. The filtration efficiency and pressure drop are fundamental parameters which determine operation of fibrous filter.

According to a classic filtration theory (Brown, 1993), the quality factor (QF) was introduced for evaluation of relationships between filtration efficiency (E_{total}) and pressure drop (Δp) through filtration systems in the steady state process.

$$QF = \frac{-\ln(1 - E_{total})}{\Delta p} \quad (1)$$

In the transient state of air filtration process Podgórski (2003) proposed to use the filter utility factor (FUF) takes into account the actual investment and operating costs the use of filtration system.

$$FUF = \left(\frac{C_0 \cdot \eta_p}{\Delta p_0 \cdot u_{pe}} \right) \left[\frac{\int_0^{t_f} E_{total}(t)dt}{t_c + \int_0^{t_f} \frac{\Delta p(t)}{\Delta p_0} dt} \right] \quad (2)$$

This article presents results of tests of influence of changes of the pressure drop and filtration efficiency on the QF and FUF of systems used to filtration of oil mists and dust. Tests were conducted using the melt-blown nonwovens made from polypropylene fibers.

Table 1. Structural characteristic of filter systems.

Filter No.	Filter thickness	Fiber diameter	Porosity	Main pore size
	[mm]	[μm]	[%]	[μm]
PP2	2.55	2.86	97.08	11.26
PP6	1.93	6.71	95.32	42.13
PP12	1.75	12.38	94.59	75.56

Calculations of QF and FUF values were carried out for experimental conditions and the conditions of use filtration system during metal machining. Summary of variables parameters used in the calculation of QF and FUF of systems PP2, PP6, PP12 shown in Table 2.

Table 2. Calculation parameters of FUF.

Ratio $C_{0,exp}/C_{0,real}$	Unit price of electricity	Mechanical effic. of fan	Price of unit mass of filter	Testing time
[-]	[PLN/kWh]	[%]	[PLN/m^2]	[min]
10^3	0.2555	100	29; 35; 50	120

Investigations are performed synthetic dust (ASHRAE 52.1) and liquid aerosol (DEHS) test using a setup composed of aerosol generator AGF 2.0 iP, powder disperser RGB-1000, TSI DMA 3080L, CPC 3022A and CPC 3775.

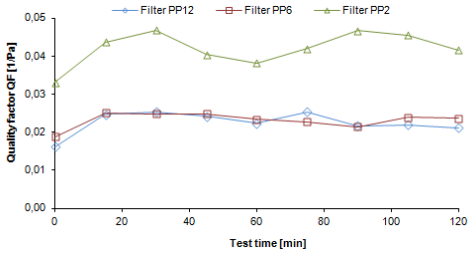

Figure 1. QF of tested filter in testing time.

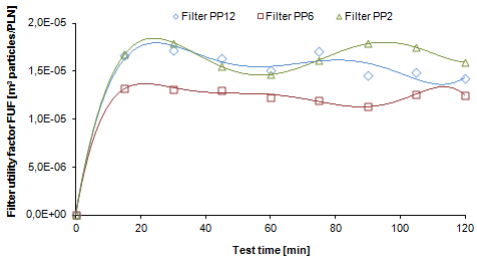

Figure 2. FUF of tested filter in testing time.

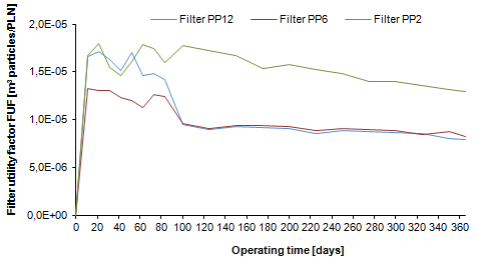

Figure 3. FUF of tested filter in operating time.

It was found that for the initial stage filtration the highest QF value for system PP2 (0.028 1/Pa) was observed. In systems PP6 and PP12 was observed similar values of QF in the range of 0.017 ÷ 0.019 1/Pa (Fig. 1). The highest FUF value for tested systems were similar and ranged from $1.3 \cdot 10^{-5}$ do $1.8 \cdot 10^{-6}$ m^3 particles/PLN (Fig. 2). The optimal time of use PP6 and PP12 was 85 days (Fig. 3), while in the case of PP2 almost twice and it was 150 days (Fig. 3).

This paper has been prepared on the basis of the results of research task I.B.11 carried out within the National Programme partly supported in 2011-2013 within the scope of research and development by the Ministry of Science and Higher Education. CIOP-PIB has been the Programme main coordinator.

Brown R.C. (1993). Air filtration. Pergamon.
Podgórski A., Bałazy A. (2003) *Journal of Aerosol Science, vol. II, 1197-1198.*

Simultaneous removal characteristics of particulate and nitrogen oxides by the SCR catalyst packed high temperature pleated filter bags

Y.O. Park[1], N.Hasolli[1]

[1]Clean Fuel Research Center , Korea Institute of Energy Research, Deajeon, Deaduk Science Town, 305-343, Korea

Keywords: high temperature pleated filter bag, SCR catalyst, particulate, nitrogen oxide, NOx and particulate removal system

Presenting author email: yopark@kier.re.kr

Removal of hamful nitrogen oxides(NO, NO_2 and N_2O) from the exhaust presents a great challenge to the ctalysis community. A variety of investigations have been undertaken to reduce nitrogen oxide emissions, with selective catalytic reduction(SCR) being the mos widly used worldwide. A number of tudies on catalysts for SCR processes have been carried out. The catalysts used most frequently to reduce nirogen oxides emissions from stationary sources(incinerastors, coal-fired power plants and sinter plants) are V_2O_5/TiO_2(anatase) catalysts mixed with WO_3 or MoO_3. The V_2O_5 catalysts exert high effiecncy between 250 and 350oC. To meet this temperature ranges, SCR equipment can be installed before pariculate removal facility and desulurization equipment. In this case, however, SO_2 and particulate may cause catalyst deactivation and poisioning . Furthermore, after the particulate removal facility and desulfurization equipment whose temperature range is about 250^{o}C, the effluent gas must be reheated. The reheating creates an extra opreational cost. To reduce operational costs, SCR equipment can be installed between the particulate removal facility and desulfurization equipment. However, in such a layout, effluent gas also contains SO_2 and As which may cause catalyst deactivation. Accordingly, extensive effort have been made to develop low-temperature SCR catalysts capable of activation under 250^{o}C.

The catalyst packed high temperature filter bags are special multifunctional reactors capable of carrying out two operations at the same time: particulate removal and catalytic abatement of noxious gases such as VOCs, dioxin and furan, nitrogen oxides. This might entail a potential reduction in space requirements as well as energy and investment cost, as pointed out in a recent review.

A pulse jet baghouse , placed downstream of the desulfurization equipment, is a widely used industrial separator for particulate removal to prevent the contamination of catalyst in the SCR equipment. A filter bag installed in the pulse jet baghouse must be operates at high temperature up to 250 ^{o}C. A high temperature pleat filter bags have been developed for high temperature flue gas filtration from coal-fired boilers, waste incinerators and sinter plants. These filter elements are constructed from a patent-pending high density unsupported needle felt media that is stiffened by a state of the art thermal bonding process. These elements are a direct replacement for standard filter bags and cages. Their shorter length keeps the filter element out of the inlet gas stream, reducing abrasion problems and providing for a large drop-out area.

In this study, the SCR catalyst packed high temperature pleated filter bag containing V_2O_5/TiO_2 installed in the Nox and pariculate removal system (DDN-System) was exaimed in the pilot-scale unt and also in a demonstration plant to determne its feasibility in a real system.

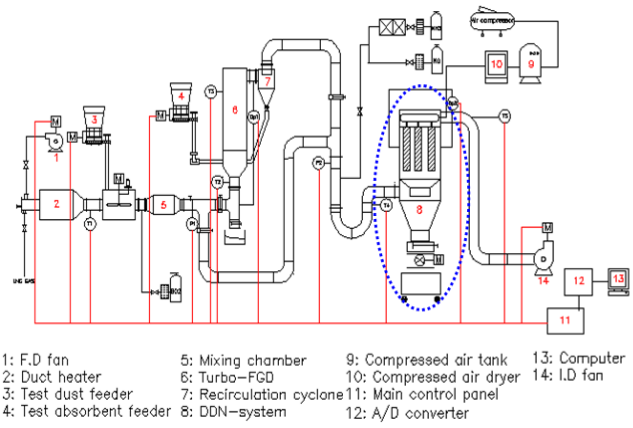

Figure 1. A schematic flow diagram of the particulate and NOx removal system.

The hot flue gas generated from the duct heater was introduced into the new developed desulfurization equipment (Turbo-FGD), particulate, reacted sorbent and nitrogen oxides flow in the particulate and NOx removal system (DDN-System) as shown in Figure 1. The DDN-System had 12 the SCR catalyst packed high temperature pleated filter bags arranged in 4 rows. The system was equipped to conduct cleaning based on pressure set points. The pulse jet cleaning parameters were as follows-cleaning pressure of 3.5 kg/cm^2, pulse time of 0.15 seconds, and time between pulses of 6 seconds.

This work was supported by the Korea Environment for the Eco-Innovation Technology Development project under grant 402-222-004.

Y.O. Park and H.J. Park (2011) *Proc. SETAC 21st Annual Meeting on Ecosystem Protection in a Sustainable Worrd.*

S.R. Ness, G.E. Dunham, G.F. Weber and D.K. Ludlow (1995) *Environ. Prog. 14(1). PP69.*

Dust Cake Cleaning Characteristics of PPS Pleated Bags with Double Venturi and Standard Venturi

Y.O. Park[1], N. Hasolli[1,2]

[1] Clean Fuel Research Center, Korea Institute of Energy Research, Daejeon, 305-343, Korea
[2]Graduate School of Green Energy Technology, Chungnam University, Daejeon, 305-764, Korea
Keywords: Surface filter media, Bag cleaning efficiency, Dust cake, Filter clogging.
Presenting author email: yopark@kier.re.kr

Introduction

Recently pleated filter bags are used for cleaning of dust laden gas in various industrial applications. Pleated filter bags made of cleanable filter media have been used in combination with the pulse jet cleaning unit. Surface filter media are designed to hold the particles on their outer surface so that efficient removal of dust cake and dislodging of particles form the filter media means the regeneration of the filter after pulsing by pressurized air. Since the operation mode does not change during the pulsing the air flows back through the pleated filter soon as the pulsing impact is reduced and the filtration process can start again. At this stage if the dust is not dislodged properly the dust will reintrain and mix with the incoming air flow. In complex flue gas treatment facilities, filter bags are loaded with particles generated through the combustion process and other solid matter reactants for removal of gaseous pollutants. Therefore it is very important to optimize the bag cleaning unit by finding proper setting for pulsing unit as well as the venturi. In order to investigate the effect of the venturi design on the pleated filter bag cleaning efficiency we have prepared two types of venturi.

Experimental method and material

Experimental conditions are set constant for all three tests as displayed in the Table 1. Terminal pressure drop was chosen 100 mmH_2O and the pulsing pressure was set for the initial stage as $3kg_f/m^2$. Solenoid valve was opened during pulsing for 150 ms. These tests were run on the clean-on-demand mode where the pulse was triggered after the total pressure drop reaches the value of terminal pressure drop.

Table 1. Experimental conditions.

Conditions	Value
Reaction temp.	180°C
Filtration area	35.2 m^2
Filtration velocity	0.5, 0.6, 0.7 m/min
Gas flow rate	17.6, 21.1, 25 m^3/min
Dust inlet conc.	5 g/m^3

Tests were performed in our integral test unit which contains 8 pleated bags of 2 meter in length together with the air pulsing unit and clean air plenum.

Results and Discussion

Filtration velocity was varied from 0.5, 0.6 and 0.7 m/min. At the higher filtration velocity the pulsing interval is very short and the residual pressure drop increases very fast due to the re-entrainment of the dust. The standard venturi used in traditional baghouse has shown almost no advantage noticed compared to the arrangement without venturi. On the other hand the arrangement with double venturi shows better results in bag cleaning performance as shown in Figure 1.

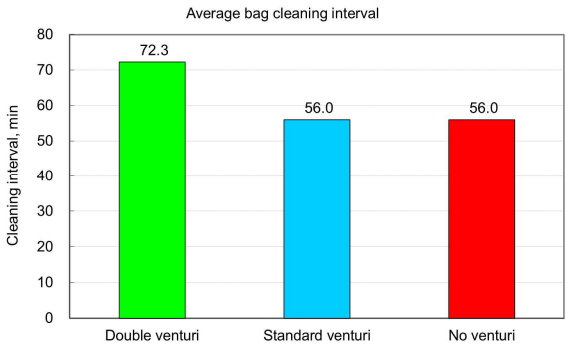

Figure 1. Comparison of bag cleaning efficiency.

The unique design of the double venturi is responsible for the secondary air flow after induction of primary high pressurized air flowing directly through the center of the pleated filter bag opening. This enables the higher pressure impact inside the filter bag down to the bag bottom thus resulting in better cleaning efficiency. As result the pulsing interval was longer and the residual pressure drop lower than the remaining two arrangements with standard and without venturi.

This work was supported by the Korean Environment for the Eco-Innovation Technology Development Project

Donovan, R.P., (1985) *Fabric Filtration for Combustion Sources, Fundamentals and Basic Technology*, Marcel Dekker.

Brauer, H., Varma, Y.B.G., (1981) *Air Pollution Control Engineering*, Springer Verlag.

Lo, L.M., Chen, D.R., Pui, D.Y.H., (2010) *Powder Technology* 197, 141-149,.

Filtration of airborne carbon nanotubes with nanofiber filters

Y.K. Bahk[1, 2] and J. Wang[1, 2]

[1]Institute of Environmental Engineering, ETH Zurich, Zurich, ZH, CH-8093, Switzerland
[2]EMPA, Analytical Chemistry, Dubendorf, ZH, CH-8600, Switzerland
Keywords: airborne CNT, filtration, nanofiber filter.
Presenting author email: ykbahk@ifu.baug.ethz.ch

Carbon nanotubes (CNTs) have been used as a structural material for a decade in many applications such as sports equipment, semiconductor devices, etc. The amount of CNT production is increasing every year, at the same time, toxicity of CNTs has raised increasing concerns. For this reason, filtration of airborne CNTs is an important issue for inhalation protection of workers (Kim *et al*, 2010, Wang *et al*, 2011). Nanofiber filter media may possess a larger specific surface area and higher permeability for air flow than conventional filter media (George, 2007, Wang *et al*, 2008). In this study, several nanofiber filters, with different solidities, were tested against airborne CNTs.

Fig. 1 shows a schematic of CNT filtration experiments with nanofiber filters. Airborne CNTs were generated by an atomizer or electrospray. In order to classify the generated airborne CNTs, a differential mobility analyser (DMA) was used. The mobility size distribution was obtained by using the scanning mobility particle sizer (SMPS). Classified airborne CNTs by the DMA were carried by the air flow with controlled flow rate to challenge the filters. A neutralizer (Kr-85) was used to avoid electro static precipitation. Concentration of CNTs was measured by condensation particle counters (CPC) at upstream and downstream of the filters. The tested filters were composed of a nanofiber layer and micrometer fiber substrate. Different numbers of layers were tested and the CNT penetrations compared. Polystyrene latex particles (PSL) were used to provide the penetration of spherical particles as a comparison with CNT penetration.

Experimental results of different types of CNTs, including multi-walled CNTs (MWCNTs) with diameters of 8-10 nm, 15-20 nm and 20-30 nm, are reported in the study. These CNTs were aerosolized from suspensions with either an atomizer or electrospray. For example, MWCNTs Baytubes, BMS, Germany with diameters about 15-20 nm, which were functionalized by the nitric acid refluxing method, were dispersed in DI water.

Fig. 2 shows CNTs captured by nanofiber filters. The results show significantly higher collection efficiency for CNTs than spherical particles when nanofiber filters with higher solidities were used. Due to the geometrical characteristics of CNTs, which possess extremely high aspect ratios, CNTs were easily captured by interception in the tested mobility size range. The experimental results are also compared with model calculation, which includes mechanical mechanisms for particle capture by diffusion, interception and inertial impaction.

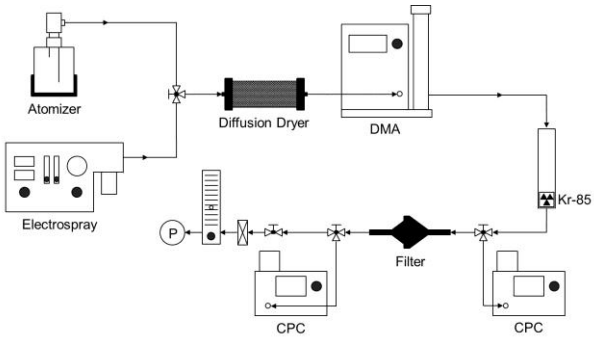

Figure 1. Experimental system for CNT filtration tests.

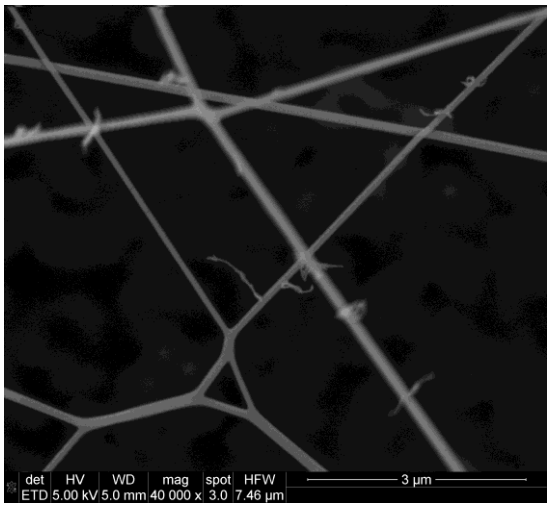

Figure 2. SEM image of captured CNTs by a nanofiber filter.

George, J. (2007) *20th Annual Conf. of American filtration & separations society.*

Kim, S.C., Chen, D.R., Qi, C., Gelein, R.M., Finkelstein, J.N., Elder, A., Bentley, K., Oberdorster, G. and Pui D.Y.H. (2010) *Nanotoxicology*, **4(1)**, 42-51.

Wang, J., Kim, S.C. and Pui, D.Y.H. (2008) *J. Aerosol Sci.* **29**, 323 – 334.

Wang, J., Kim, S.C. and Pui, D.Y.H. (2011) *Aerosol Sci. & Tech.* **45**, 443 – 452.

Cellulose nanofibrils filters for environmental applications

L. Alexandrescu[1], K. Syverud[1], F.Belosi[2], G.Santachiara[2], F. Prodi[2], A. Donateo[3]

[1]PFI Paper and Fibre Research Institute, Trondheim, 7491-Norway
[2]Institute of Atmospheric Science and Climate (ISAC-CNR), Bologna, 40129 - Italy
[3]Institute of Atmospheric Science and Climate (ISAC-CNR), 73100, Lecce - Italy
Keywords: Nanofibre, filtration efficiency, nanoparticles.
Presenting author email: f.belosi@isac.cnr.it

Worldwide, filters for air purification are predominantly produced of synthetic and non-biodegradable materials. This includes filters in air conditioning systems for homes, offices, vehicle cabins and clean rooms in addition to air intakes for engines and in respirators worn by humans.

Environmental concerns have increased the general interest in renewable materials, such as cellulose; and microfibrillated cellulose (MFC) has remarkable properties both derived from composition (high strength and the ability to adhere to each other and make strong inter-fibril bonds) and from the fibers small size (high surface area). Indeed, this class of nanomaterials have spanned out the volume of application every year by creating new products in new domains.

The development of microfibrillated cellulose filters are very promising to enhance aerosol filtration at the nanosize aerosol particles (below 100 nm) and could help in the prevention of nanoparticles connected pathologies (nanopathologies).

In this work, a range of various air filters have been prepared from microfibrillated cellulosic material using freeze-drying technique, with the aim to create alternative air filters which are completely biodegradable.

In freeze drying, the material is frozen below its triple point with subsequent sublimation. The solvent is thus transferred directly from solid to gaseous state by reducing the surrounding pressure to avoid the liquid-gas transition.

During the freezing process, the nanocellulose fibrils are separated from the growing ice crystals and are confined to the interstitial regions between them.

.

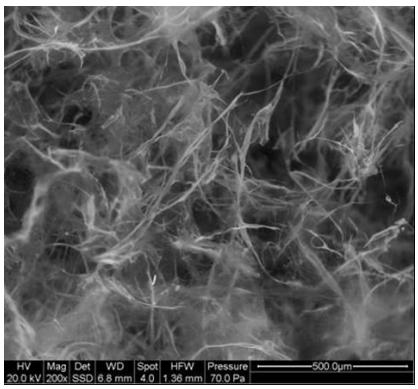

Figure1. Filter structure, 20gm^{-2}, 0.1% dry content of the initial MFC suspension

When the ice crystals in a frozen cellulose-water suspension are removed by sublimation, gas-filled pores are left behind. The pore structure of the freeze-dried filter is therefore a direct reflection of the original distribution of ice crystals. The ice crystal size in the frozen MFC suspension is highly dependent on how the water in the suspension is frozen.

All synthesized filters had tensile strengths above the required for air filters used in commercial and residential filtration systems. Filtration tests have been carried out on freeze-dried filter samples made of 0.1 - 0.2 % dry content of the initial MFC suspension having 5 – 30 gm^{-2} gramages (Figure 1).

The challenge particles for the filter transmission efficiency were NaCl obtained through a Collison nebulization (0.6 bar pressure) of a water solution. The filter face velocity was set at 5.5 cms^{-1}. Particle number concentration upstream and downstream the filter was measured by means of an SMPS+C system (CPC model 5.4 with DMA model 5.5, Grimm GmbH). Pressure drop across the filter was measured using an electronic manometer (Testo mod. 511 AG, Germany). The filter Figure of Merit (FOM), given by the ratio between the logarithim of the particle penetration and the pressure drop, was measured.

Results show a better capture efficiency of these filters, respect to the previously studied impregnated ones, although the filtration efficiency is modest for 100-500 nm particle size domain.

The most penetrating particle size (MPPS) varies for the same type of nanofibrils type used for films fabrication and lies between 100-300 nm.

This work was supported by PFI project 196119/V30 – Nanofilter: Nanofibril filter for environmental nanoparticles, financed through the Research Council of Norway.

Eichhorn S. J., Dufresne A., Aranguren M., Marcovich N. E., Capadona J. R., Rowan S. J., Weder C., Thielemans W., Roman M., Renneckar S., Gindl W., Veigel S., Keckes J., Yano H., Abe K., Nogi M., Nakagaito A. N., Mangalam A., Simonsen J., Benight A. S., Bismarck A., Berglund L. A., Peijs T., (2010) *J Mater Sci*.,45,1–33

Eninger R.M., Honda T., Adhikari A., Heinonen-Tanski H., Reponen T., Grinshpun S. A. (2008) A*nn. Occup. Hyg*., 52, 385-396.

Syverud, K. and Stenius P. (2009). *Cellulose* 16, 75-85.

Aerosol retention in the secondary side of a tube bundle: Insights into a key scenario for nuclear safety

R.D. Tardáguila*, C. Lopez, L.E. Herranz, M. García

Unit of Nuclear Safety Research, CIEMAT, Madrid, 28040, Spain
Keywords: aerosol surface interaction, deposition efficiency, measurements, nuclear aerosols, particle nature
rosario.delgado@ciemat.es

The Pressurized nuclear water reactors rely on shell-and-tube heat exchangers to generate the steam that expands in the turbine stage of a Rankine cycle. Under the highly unlikely conditions of a reactor core melt accident, a tube rupture in the heat exchanger could result in a release of radioactive particles to the environment. This scenario, generally called severe accident Steam Generator Tube Rupture (SGTR), is of an outstanding importance in nuclear safety. Previous investigations (Auvinen et al, 2005), showed that the most challenging condition from the safety point of view would be the absence of water in the secondary side of the steam generator. However, even under these unfavorable conditions, the secondary side of the steam generator is capable of retaining a fraction of particles carried by the gas (Herranz et al., 2006).

In order to explore the SGTR scenario and build up a sound database on aerosol retention during this accidental sequence, ambitious research programs (EU-SGTR, Auvinen et al, 2005; ARTIST, Guntay et al, 2004; and the current ARTIST2) have been developed. As a contribution to the ARTIST2 project, an experimental campaign (CAAT2, CIEMAT Aerosol ARTIST Tests # 2) aimed at measuring the aerosol retention in the break stage of a dry steam generator has been performed. In particular, the influence of particle nature (agglomerates formed from primary TiO_2 nano-particles; and spherical, single- or few-particle aggregates of SiO_2, Figure 1), the breach size (fish-mouth break: 1D, 0.5D and 0.25D sizes) and the gas mass flow rate has been investigated. Comparison of present results with previous experimental CAAT series performed under guillotine configuration (Sánchez-Velasco et al, 2010) have allowed to explore the effect of the breach shape on the aerosol retention too.

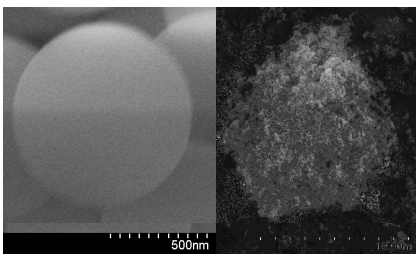

Figure 1. SEM images of SiO2 (left) and TiO2 (right).

The CAAT2 campaign has been conducted at the PECA-SGTR facility of the Laboratory of Analysis of Safety Systems (LASS). A mock-up of 11x11 tubes with the broken tube placed in the 3th row from the bundle edge mid-plane position was set-up in the PECA. The experimental rig consisted of a gas supply system, the Fluid Bed Generator where aerosols are produced, and a measuring system (i.e. sampling and instrumentation). The instrumentation used (i.e. APS®, ELPI®, cascade impactors, membrane filters) characterized the aerosol size distribution and concentration upstream the broken tube and at the bundle exit. The aerosol deposits on tubes surfaces were also collected and weighted to characterize the deposition pattern on the tube bundle.

Particles entering through the breach deposit to some extent, no matter the particle type. However the amount of material collected on tubes surface is highly dependent on its physical nature. The SiO_2 average collection efficiency (η) resulted to be more than one order of magnitude higher than the TiO_2 ones. In case of SiO_2 the net η values have been shown to be consistent with the η distribution as a function of size (Figure 2). Other system variables investigated like breach size and/or shape are of less relevance for net η. Nevertheless, in-bundle deposition patterns have been found to be largely dependant on the breach shape: guillotine breaches result in deposition patterns that only depend on jet penetration, whereas fish-mouth breach profiles do also on orientation.

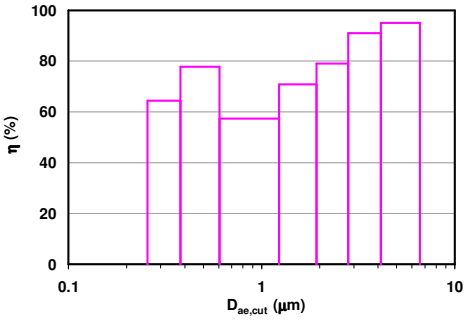

Figure 2. SiO_2 collection efficiency distribution.

This work was supported by the Spanish Nuclear Safety Council (CSN). The authors are indebted to PSI and other ARTIST2 partners for their technical support.

Auvinen, A, et.al., (2005). *Nuc. Eng. Des.*, 235, 457-472.
Güntay, S., Suckow, D., Dehbi, A., Kapulla, R., (2004). *Nuc.Eng. Des.*, 231, 109-120.
Herranz, L.E. Velasco, F.J., del Prá, C., (2006). *Nuc.Tech*, 154, 85-94.
Sánchez-Velasco., Del Prá, Herranz, (2010). *Aerosol Science and Technology,* 44, 349-361

Deposition efficiency of charged aerosol particles in cylinder array

T.S. Zaripov, A.G. Egorov

Kazan Federal University, 420008, Kazan, Russia

KEYWORDS: aerosol filtration, collection efficiency, charged particles, CFD
Presenting author email: zaript@gmail.com

The transport and deposition of aerosol particles in the porous medium have many experimental and industrial applications. The diffusion, impaction and gravity actions are not enough to provide the deposition of aerosol particles in the intermediate range of sizes ~0.1-1 μm. In this case the particle charging is used to increase the deposition by the electrostatic force action (Alonso&Alguacil, 2007, Yu&Chandra, 1977).

The aerosol flow with charged particles in a periodic bar of height *H* of an array of circular cylinders of radius R_f .at initial velocity U_0 is studied. The motion of two-phase flow with charged particles is described by the system of non-dimensional equations

$$\nabla \cdot \bar{u} = 0 \quad (1)$$

$$\mathrm{Re}(\bar{u} \cdot \nabla)\bar{u} = -\nabla p + \Delta \bar{u} \quad (2)$$

$$\bar{u} \cdot \nabla c - \mathrm{Pe}^{-1} \Delta c + \beta \nabla \cdot \left(c \nabla \varphi\right) = 0 \quad (3)$$

$$\Delta \varphi = -c \quad (4)$$

$\bar{u} = \frac{\bar{U}}{U_0}$, $p = \frac{PL_0}{\mu U_0}$, $\varphi = \frac{F\varepsilon_0}{qC_0 L_0^{\,2}}$, $c = \frac{C}{C_0}$, $\mathrm{Re} = \frac{\rho U_0 L_0}{\mu}$, $\mathrm{Pe} = \frac{L_0 U_0}{D}$, $\beta = \frac{q^2 b C_0 L_0}{U_0 \varepsilon_0}$, where $\bar{U}$ is the gas velocity, P is the pressure, C is the particle concentration, F is the potential of electric field, L_0, U_0, C_0 are scales of length, velocity and concentration, D is the diffusion coefficient, q is the particle charge quantity, ε_0 is the permittivity of the air. To express the inertia of gas flow the Reynolds number Re is used. Nondimensional parameters Peclet number Pe and β characterize the influence of diffusion and electrostatic force on the particle deposition. The boundary conditions for the hydrodynamics problem (1), (2) include unity values of gas velocity at the bar inlet, the symmetry conditions on top and bottom lines of the bar, zero value of pressure on the right boundary. As a boundary conditions for problem (3), (4) zero values of concentration and potential on the cylinders surfaces are taken. The relative input concentration of particles is equal unity. Zero periodic conditions are takes for electric potential along the flow.

The Navier-Stokes equations (1), (2) are solved independently, then joint solution of equations (3), (4) gives the distributions of concentration and electric potential on the found velocity field. The distributions of particle concentration and electric potential and particle deposition efficiency are studied numerically at the various values of particle size, initial particle concentration, quantity of particle charges, array porosity and flow Reynolds number.

Dependencies of capture efficiency of single cylinder on Peclet number are shown in fig. 1. The formula for capture efficiency due to diffusion η_D within the boundary layer flow model was obtained by Stechkina (1966)

$$\eta_D = 2.9 Ku^{-1/3} Pe^{-2/3} + 0.624 Pe^{-1}$$

where $Ku = -0.5\ln\alpha - 0.75 + \alpha - 0.25\alpha^2$, α is the solidity. The dependence $\eta_D(\mathrm{Pe})$ is shown in fig.1 (dotted line). Calculations for neutral particles give very close curves $\eta(\mathrm{Pe})$. In the case of charged particles the deposition efficiency tends to constant values that are determined by the parameter β. It is possible to provide high deposition of submicron particles by increase the charge quantity q of particles.

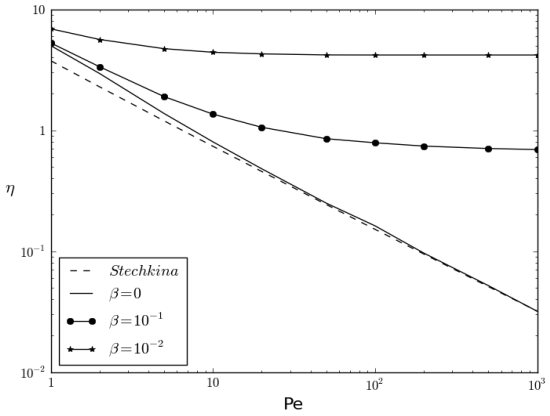

Figure 1. The dependence of capture efficiency on Peclet number Pe .

Alonso, M., Alguacil, F.J. (2007) J. *Aerosol Sci*. 38: 481-493.

Stechkina, I.B. (1966) *Dokl. Acad. Nauk SSSR*, 167:.1327-1330.

www.ansys.com

Yu, C.P., Chandra, K. (1977) J. *Aerosol Sci*.. .9: 175-180.

Inertial deposition of aerosol particles on a porous cylinder

O.V. Grigorieva[1], S.K. Zaripov[2]
[1]Kazan State Power University, 420066, Kazan, Russia
[2]Kazan Federal University, 420008, Kazan, Russia

Keywords: inertial deposition, collection efficiency, porous cylinder, CFD
Presenting author email: rara_avis86@mail.ru

In the process of air filtration suspended particles deposited on filter elements form a porous layer that acts on the flow around a single fiber and the process of particle settling. In addition, porous fibers can be used as single filter elements. It was shown (Kirsh, 2007) that the use of porous cylinders as an element of aerosol filters significantly increases the efficiency of diffusion capture of small particles. The presence of an additional gas flow through a porous body also affects the inertial capture. In this paper the problem of aerosol flow through a porous cylinder is solved.

A two-dimensional flow of an incompressible gas flow with suspended particles around the porous cylinder radius r_c is considered. In the assumption that particle concentration is small the influence of the dispersed phase is neglected. The air motion around the cylinder and in porous area is described by the equations (Bhattacharyya et.al., 2006):

$$\nabla \bar{u} = 0 \qquad (1)$$

$$\varepsilon^{-2} \rho \bar{u} \nabla \bar{u} = -\nabla p + \frac{\mu}{\varepsilon} \Delta \bar{u} - b \frac{\mu}{k} \bar{u} \qquad (2)$$

where $\bar{u}$ is the gas velocity, μ and ρ are the coefficient of dynamic viscosity and the air density, p is the pressure, ε is the porosity, k is the permeability of the porous medium. The parameter b equals to zero outside the cylinder and to one inside the cylinder. The gas velocity $\bar{u}$ averaged over the volume of pore space is associated with flow rate $\bar{u}_f$ by the relation $\bar{u} = \varepsilon \bar{u}_f$.

In the region outside the cylinder ($\varepsilon = 1, b = 0$) equations (1), (2) become the Navier – Stokes equations for an incompressible gas. Inside the porous body they are extended Darcy– Brinkman equation. The equations of the carrier medium (1), (2) are solved by finite volume method using CFD FLUENT software. The equations of motion of suspended particles are numerically integrated in the obtained velocity field. The particulate flow is characterized by the dimensionless parameters: the Reynolds number $\mathrm{Re} = \rho U_\infty 2r_c / \mu$ (U_∞ – velocity of the undisturbed flow), the Darcy number $\mathrm{Da} = k / r_c^2$, the Stokes number $\mathrm{Stk} = U_\infty / r_c \tau$ (τ – the relaxation time of a particle).

To calculate the deposition efficiency E the particle trajectories are traced outside the porous cylinder. The coefficient E can be expressed as a product of the efficiency E_e of the particles that reach the surface of cylinder and the efficiency E_i of their deposition within the porous body: $E = E_e E_i$. To find E_e it is suggested that all the particles reached the surface of the porous cylinder should be settled. In the absence of gas flow through the cylinder the inertial deposition efficiency drops to zero at a finite number of Stokes. For a porous cylinder at sufficiently small values Stk the quantity E_e remains finite. Under the assumption that the cylinder is consisted by packed fibers of equal radius r_f the coefficient E_i of particle deposition inside the porous body is expressed through the integral ($\tilde{y} = y / r_f$ – dimensionless ordinate):

$$E_i = \int_0^1 \left[1 - \exp\left(-\frac{\sqrt{1-\tilde{y}^2}(1-\varepsilon)\mathrm{Stk}}{0.0058} \right) \right] d\tilde{y} \qquad (3)$$

The approximate formula for the depth of penetration of dispersed particles in the porous structure obtained in [1] is taken into account in (3). Fig. 1 shows the dependence of the efficiency E on the Stokes number. With the increase ε the efficiency of deposition of particles inside the cylinder drops. It is seen that the additional advantage in the total deposition efficiency decreases for large values of porosity due to the lower efficiency of deposition of particles inside the cylinder.

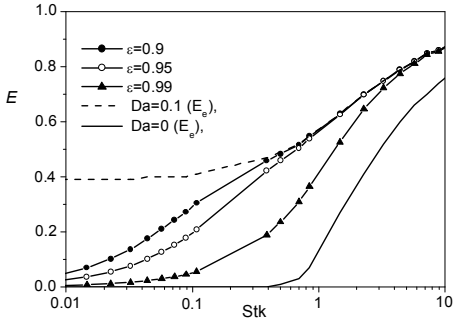

Fig. 1. The deposition efficiency as a function of Stk number.

REFERENCES

Araujo A.D., Andrade J.S., Herrmann H.J. (2006) *Physical Review Letters,* **97**, 1-4.

Bhattacharyya S., Dhinakaran S., Khalili A. (2006) *Chemical Engineering Science,* **61**, 4451–4461.

Kirsh V.A. (2007) Separation and Purification Technology, **58**, 288–294.

Soot Nanoparticle Aggregate Filtration in Layer-Coated Diesel Particulate Filters

N. D. Vlachos[1], A.G. Konstandopoulos[1,2]

[1]Aerosol & Particle Technology Laboratory, CPERI/CERTH, P.O. Box 60361, 57001, Thessaloniki, Greece
[2] Dept. of Chemical Engineering, Aristotle University, P.O. Box 1517, 54006, Thessaloniki, Greece
Keywords: filter wall microstructure, digital reconstruction, gradient porosity.
Presenting author email: ndv@cperi.certh.gr

An ideal filter wall microstructure should provide high filtration efficiency at the expense of low pressure drop, targets that cannot be independently pursued due to the porosity – filtration efficiency trade-off. To overcome this, filtration media with so-called gradient (or asymmetric) structures have been introduced into industrial (liquid) filtration since 1962 (Loeb *et al*, 1962) and a first attempts to introduce to the Diesel filtration field were made by Yoshida *et al* (1989) and more recently in a publicly-funded project ("CERFIL", 1998). Multifunctional layers, having also catalytic action, have also been developed for modern DPFs, e.g. Ogyu *et al* (2008) and Lorentzou *et al* (2008). Similar layers, only with filtration action, have been suggested for commercial application by Mizuno *et al* (2008). In the present work we outline the first principles (ab initio) simulation of such gradient filter wall microstuctures, focusing on the prediction of nanoparticle filtration behaviour.

In support of the above task, we have developed a set of process-mimetic reconstruction techniques to numerically generate realistic 3-D representations of DPF porous wall microstructures (Vlachos *et al* 2006). Using such digital materials and microflow simulation the flow field in the pore spaces of the filter wall can be obtained (Konstandopoulos *et al* 2007). Such calculations have shown that, inside typical DPF materials, there can be more than an order of magnitude variation of the filtration (approach) velocity. This feature is not accounted for in traditional mean-field type filtration theory which therefore cannot be used in developing new material structures but only for describing existing ones, provided that a proper calibration of the phenomenological parameters of the model is performed.

The framework employed here relies also on the use of realistic representations of the soot aggregates, generated by a dedicated computational engine that matches morphology and mobility of the digital soot to distributions derived from Diesel exhaust by methods similar to e.g. Virtanen *et al* 2004. Size-specific filtration efficiency can thus be calculated for the clean filter wall as well as during transient soot deposition in the filter wall, the latter being carried out by iterating between soot aggregate deposition and flow field updates.

To illustrate the application of this framework we examine the influence of a thin coating layer on DPF filtration and pressure drop. We consider a realization of a grain-sintered porous wall with a wall-thickness of 180 μm, representing a SiC DPF wall with a porosity of 42% and an average pore size of 11 μm (as determined by mercury porosimetry). Such a wall structure is typical of a down-sized DPF which, due to the higher filtration velocities expected, features a thinner wall for reduced pressure drop. The needed filtration efficiency is recovered by coating the upstream side of the wall with a nanoparticle-based layer of 20 μm thickness and 62% porosity, results for which are shown in Figure 1 below.

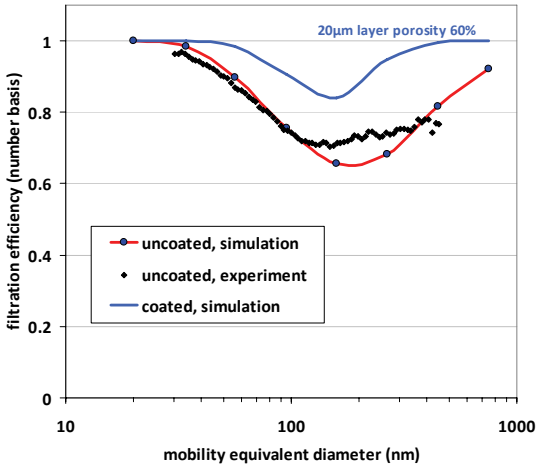

Figure 1. Filtration efficiency of a grain-sintered DPF wall with and without a nanoparticle-based layer.

Loeb S. and Sourirajan S. (1962) Adv. in Chem. Series, 38, 117.

Yoshida K., Makino S., Sumiya S., Muramatsu G., Helferich R. (1989) SAE Technical Paper 892046, doi:10.4271/892046.

CERFIL Project (1998) http://cordis.europa.eu/projects/45748_en.html

Ogyu K., Oya T., Ohno K., Konstandopoulos A.G. (2008) SAE Technical Paper No 2008-01-0621, doi:10.4271/2008-01-0621.

Lorentzou S., Pagkoura C., Konstandopoulos A.G., Boettcher J. (2008) SAE Technical Paper No 2008-01-0483, *SAE SP2154, Diesel Exhaust Emission Control*.

Mizuno Y., Miyairi Y., Katsube F., Ohara E., Takahashi A., Makino M., Mizutani T., Yuki K., Kurachi H. (2008) SAE Technical Paper No 2008-01-0618, , doi:10.4271/2008-01-0618.

Vlachos N., Konstandopoulos A.G. (2006) SAE Technical Paper No 2006-01-0260, *SAE Trans., J. Fuels & Lubricants*, 115, 79-89.

Konstandopoulos A.G., Vlachos N., Patrianakos G., (2007) SAE Technical Paper No 2007-01-1131, *Diesel Exhaust Emission Control Modeling SAE SP2140*.

Virtanen A., Ristimaki J. and Keskinen J. (2004) *Aerosol Science and Technology*, 38:437–446.

Experimental study on small cyclones for combustion engine gas cleaning

B. Sagot and J. Giardi

[1]Thermo-Fluids Laboratory, ESTACA, 92300, Levallois-Perret, France
Keywords: cyclone separator, collection efficiency, pressure drop.
Presenting author email: benoit.sagot@estaca.fr

Cyclone separators are widely used in industry for separating dispersed particles from their carrying gas. Theses devices are frequently used in large-scale industrial processes, for both separation and drying applications. However, small cyclones have also found various applications, such as personal cyclone samplers which are used in environment control. Small cyclones are also widely used in combustion engines, for the separation of oil mist from blow-by gases. Theses so-called “blow-by gases” result from leakage between the combustion chamber and the crankcase, especially when piston rings wear occurs. An important function of crankcase venting systems is the separation of the oil mist resulting from the circulation of these blow-by gases through the crankcase, which contains lubricating oil.

The size of the sampling cyclone is of great importance for its collection efficiency: a reduction of this size produces an increase of the collected oil flow, but also results in an increase of the pressure drop.

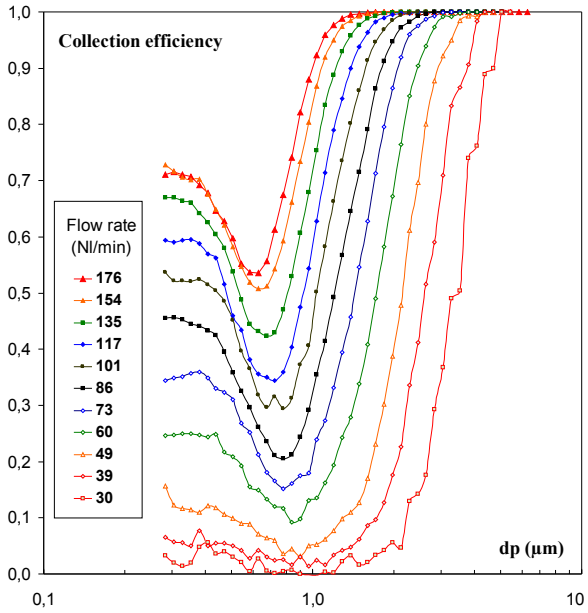

Figure 1. Collection efficiency measurements for a cyclone with 35 mm diameter.

Few data are currently available for small cyclones operating with high flow rates. We present in this study a new set of experimental data on the particle collection efficiency and pressure drop, for three different cyclones which are systematically studied, for combustion engine operating conditions (80°C), and with droplet size in the range 0.3 to 10 µm. For this purpose, we developed a temperature controlled flow bench, with an aerosol generator (PALAS), measurements of the aerosol particle concentrations upstream and downstream of the cyclone (WELAS). As illustrated in figure 1, the collection efficiency curves demonstrate that different mechanisms generate deposition (inertia for large particles, turbulent and Brownian diffusion for small particles).

Every cyclone geometry is normalized, all internal dimensions within the cyclone being proportional to its diameter, which has been varied from 25 to 45 mm.

The measurement results are compared with available models, as reported by Cortés and Gil. (2007), Avci and Karagoz (2003), and Zhu and Lee (1999), for the evaluation of both cumulative collection efficiency and pressure drop.

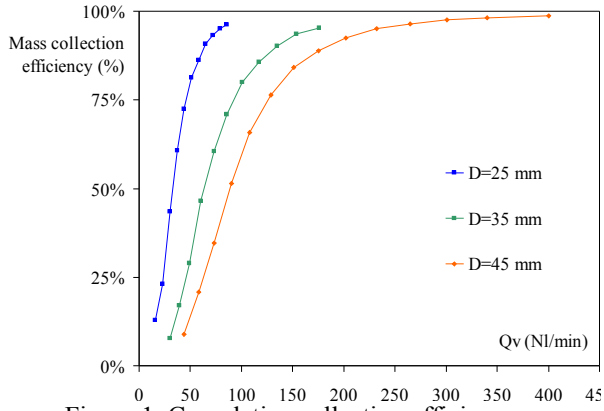

Figure 1. Cumulative collection efficiency.

The aim of this study is to provide a consistent comparison between a new set of measurements and available models, to identify the most relevant models for the design and optimization of cyclone separators applied to liquid droplet aerosol filtration.

Avci, A., Karagoz I. (2003) Effect of flow and geometrical parameters on the collection efficiency in cyclone separators. J. Aerosol Sci., 34, 937–255

Zhu, Y., Lee, K. W. (1999) Experimental study on small cyclones at high flowrates, J. Aerosol Sci., 30, 1303-1315.

Cortés, C., Gil, A. (2007) Modeling the gas and particle flow inside cyclone separators, Progress in Energy and Combustion Science, 33, 409-452.

The calculating method of resuspension based on the combination deterministic and statistical approaches

D.V.Tsaplin and V.N. Piskunov

Russian Federal Nuclear Center – VNIIEF; Sarov, Nizhniy Novgorod region, 607190, Russia
Keywords: aerosol dynamics, resuspension, aerosol-surface interaction, particle size, modelling
Email: tsaplindv@mail.ru, v-n-piskunov@yandex.ru

Resuspension, this is the process of detaching the particles from the underlying surface to the near-surface layer of the atmosphere under the wind flow. It plays the important role in transporting the contaminations.

It is possible to allocate the statistical and deterministic approaches to the description of resuspension. The statistical approach determines the resuspension rate of particles from the surface under the wind flow, taking into account the fluctuations of aerodynamic forces, the turbulent bursts and the spread of adhesive force (e. g., the rock'n roll model (Reeks and Hall, 2001; Zhang, Reeks and Kissane, 2010)). The deterministic approach allows estimating the threshold velocity of a stream to begin with the resuspension of the particles of the set size. In many models (Ziskind et al., 1997; Ibrahim et al., 2003) this threshold velocity is determined by the balance of the moments acting on a particle to start its rolling on a surface as the particle resuspension often begins after their rolling. Thus it is necessary to consider, that rolling and immovable particles are in different conditions for resuspension as the force of adhesion acting on the rolling particles, is much less.

In the given report there is the calculating method of the resuspension uniting the deterministic and statistical approaches to description of resuspension of immovable and rolling particles on a surface. This method uses rock'n roll model based on the statistical approach for representation of resuspension of immobile particles, which size is less than threshold diameter D_{th}.

Quantity of the threshold diameter D_{th} is evaluated from the balance of adhesive M_A and drag M_D moments, operating on the particles:

$$D_{th} = 0.489\left(\frac{\left(F_A(D)\right)^3 \gamma}{\rho_f^3 E u_*^6}\right)^{1/7}, \qquad (1)$$

where γ is the surface energy and E is the composite Young's modulus of the particle-surface contact, ρ_f is the fluid density, u_* is the friction velocity. Dependence of the adhesion force on the particle's diameter is set by the adhesion model taking into account of a surface roughness.

The resuspension rate of small particles ($D<D_{th}$) is calculated, using expression for the resuspension rate constant p under the action of the fluctuating aerodynamic force, obtained in model rock'n roll (Reeks and Hall, 2001). Resuspension of rolling large particles of diameter $D>D_{th}$, which doesn't undergo any significant adhesion, occurs immediately if aerodynamic lift force F_L acting on them exceeds their weight:

$$F_L > m_P g = \pi \rho_P D^3 g/6, \qquad (2)$$

where m_P is the particle mass, ρ_P is the density of the particle's material and g is the gravitational acceleration. Too large and as a consequence too heavy particles, for which the inequality (2) is not suitable, still rolling on a surface, not taking part in resuspension. The full fraction of the particles, which has been resuspended in time t from surface unit under the wind flow, is evaluated by sum of a fraction of the rolling particles, for which the inequality (2) is satisfied, and a fraction of immovable particles, which resuspension is defined by the rock'n roll model.

On basis of the described algorithm of the resuspension calculation the program for estimation short-term resuspension was written by using the application package MATLAB. Figure 1 illustrates that the calculations carried out by this program are better close to the experimental data, then the predictions of the usual rock'n roll model.

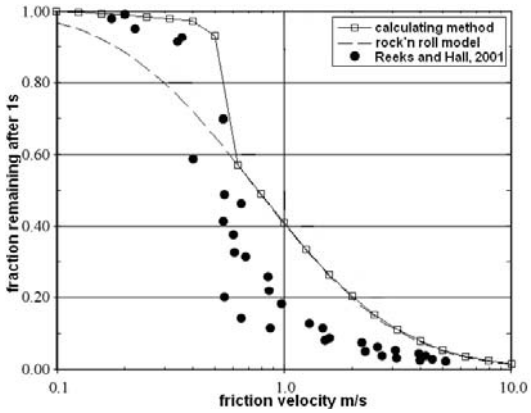

Figure 1. Comparison of the calculated and measured fractions of alumina particles of nominal size 20 μm, which have remained on a surface at various friction velocity.

The suggested method can be used for the account redistribution of contaminations on a surface after their deposition.

Reeks, M. and Hall, D. (2001) *J. Aerosl Sci.*, **32**, 1–31.

Zhang, F., Reeks, M. and Kissane, M. (2010) *Report 11F5 at the IAC 2010*, Helsinki.

Ziskind G., Fichman M. and Gutfinger C. (1997). *J. Aerosol Sci.* Vol. 28, No. 4, pp. 623-634.

Ibrahim, A., Dunn, P. and Brach, R. (2003) *J. Aerosol Sci.* **34**, 765–782.

Analysis of asymptotic behavior of disperse systems with particle coagulation and breakage

V.N.Piskunov

Russian Federal Nuclear Center – VNIIEF; Sarov, Nizhni Novgorod region, 607190, Russia

Keywords: particle formation, coagulation, fragmentation, asymptotic behavior, self-similar spectra

Presenting author email: piskunov@vniief.ru

In general terms, the following three regimes can be implemented in coagulation and breakage systems at large times $t \to \infty$:

- Eventually, the loss of small particles due to their merging is compensated for large particle fragmentation into small ones; steady spectra are shaped in the system.

- The breakage process is too slow as compared to coagulation; particle spectrum evolves into the range of large sizes, similar to free coagulation.

- Breakage results in spectrum cumulation in the initial range of sizes; either quasi-stationary singular or non-steady (including self-similar) spectra are shaped.

Analysis show that the following self-preserving types can be formed.

1. Spectra governed by self-preserving hypothesis (Friedlander, 1960):

$$c(g,t) = \frac{N^2(t)}{\rho}\Psi(x),\ x = \frac{gN(t)}{\rho},$$

$$\int_0^\infty \Psi(x)dx = \int_0^\infty x\Psi(x)dx = 1\ , \qquad (1)$$

where $N(t)$ and ρ – are number and mass concentrations. In this case the asymptotic behavior of $L_\alpha(t)$ spectrum moments at $t \to \infty$ is as follows:

$$L_\alpha(t) = \int_0^\infty g^\alpha c(g,t)dg \approx B_\alpha \rho^\alpha N^{1-\alpha}(t)\ ;\ B_\alpha = \int_0^\infty x^\alpha \Psi dx \quad (2)$$

2. Self-similar singular spectra (Lushnikov and Piskunov, 1976), for which function $\Psi(x)$ is not integrable in zero: $\Psi(x)\,|_{x\to 0} \approx \varphi(x)/x^\gamma$; $\varphi(0) \neq 0$: $1<\gamma<2$.

3. Self-similar collapsing spectra.

The breakage can provide a different type of self-similarity corresponding to spectrum accumulation (collapse) in zero ($g \to 0$). Equation (1) does not vary for integrable $\Psi(x)$. Formally, the behavior of moments (2) $L_\alpha(t) \sim N(t)^{1-\alpha}$ remains the same, but in this case moments with $\alpha < 1$ increase, and with $\alpha > 1$ decrease, opposite to a general coagulation pattern.

4. Slowly decreasing self-similar collapsing spectra.

Divergence of moments $L_\alpha(t)$ is valid for self-similar collapsing distributions, but physically it should be generated by too slow decrease of $\Psi(x)$ at $x >> 1$: $\Psi(x)\,|_{x\to\infty} \approx A/x^\Gamma$, $\Gamma > 2$.

Moments asymptotic behavior $L_\alpha(t)$ can be defined by increase exponent $F(\alpha)$:

$$F(\alpha) = \lim_{t\to\infty} \frac{d\left[\ln L_\alpha(t)\right]}{d\left[\ln N(t)\right]};\ L_\alpha(t) \sim N(t)^{F(\alpha)} \qquad (3)$$

The possibility of self-similarity regime formation in particle coagulation and breakage system can be predicted according to the diagram of Figure 1 using moments asymptotic behavior $L_\alpha(t)$ for $t \to \infty$ derived either analytically, or with numerical computations.

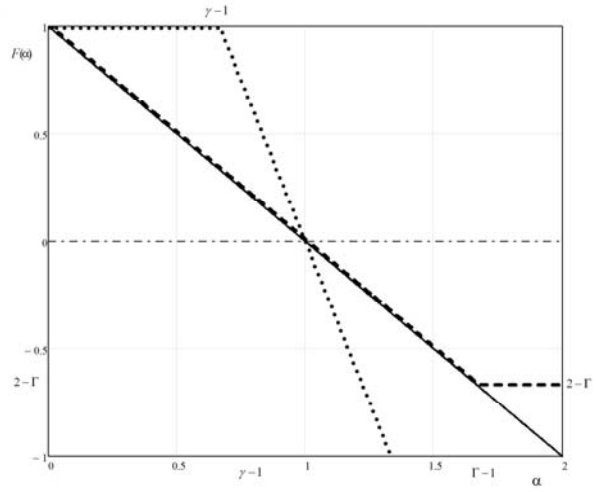

Figure 1 – Increase exponent behavior $F(\alpha)$ for different types of self-similarity: ——— dependence (2) for ordinary and collapsing self-preserving spectra (1), - - - for singular spectra; — — for slowly decreasing collapsing spectra; — · — steady-state regime

For homogeneous coagulation kernels $K(g,n)$ and breakage rates $f(g,n)$:

$$K(ag,an)=a^\lambda K(g,n)\ ,\qquad f(ag,an)=a^\mu f(g,n) \quad (4)$$

(λ and μ - are homogeneity corresponding parameters) the following condition has been obtained required for self-similar regimes existence in coagulation and breakage systems:

$$2 - \lambda + \mu = 0\ , \qquad (5)$$

Condition (5) means range boundary $2-\lambda+\mu > 0$, where steady-state regimes are implemented according to (Vigil and Ziff, 1989).

References

Friedlander S.K. (1960) *J. Meteorol.* **17**, 479-483.

Lushnikov A.A. and Piskunov V.N. (1976) *Doklady Akad. Nauk SSSR*. **231**, 1166-1169.

Vigil R.D. and Ziff R.M. (1989) *Journal of Colloid and Interface Science.* **133**, 257–264.

Analytical tests for simultaneous coagulation and condensation of composite particles

V.N.Piskunov

Russian Federal Nuclear Center – VNIIEF; Sarov, Nizhni Novgorod region, 607190, Russia

Keywords: aerosol formation, coagulation, condensation, composite particles, analytical solutions, numerical program verification

Presenting author email: piskunov@vniief.ru

A short description is considered to be efficient for kinetics numerical simulation of composite particles when one of the components (impurity) is taken integrally – by zero $n(g,t)$ and first $m(g,t)$ moments of entire spectrum (Simons, 1981; Piskunov, Golubev, Goncharov and Ismailova, 1997):

$$n(g,t)=\int_0^\infty C(g,\alpha,t)d\alpha\,;\quad m(g,t)=\int_0^\infty \alpha C(g,\alpha,t)d\alpha \quad (1)$$

where $C(g,\alpha,t)$ - is particle concentration with total mass g and impurity mass α at time t, and $\overline{\alpha}(g,t) = m(g,t)/n(g,t)$ – is impurity average mass in a particle. For simultaneous processes of coagulation and condensation, the complete kinetic equation is given by (Piskunov, 1999):

$$\partial_t C(g,\alpha,t)+\partial_g\left[V(g,\alpha,t)C(g,\alpha,t)\right]+$$

$$+\,\partial_\alpha\left[U(g,\alpha,t)C(g,\alpha,t)\right]\;=S(C;g,\alpha,t)\;, \quad (2)$$

where S – is Smoluchowski operator, $d_t g = V(g,\alpha,t)$ – is total condensation rate, and $d_t\alpha = U(g,\alpha,t)$ is impurity condensation rate. Taking

$$V(g,\alpha,t)\cong V(g,\overline{\alpha},t)\equiv v(g,t)\;;\;\; U(g,\alpha,t)\cong U(g,\overline{\alpha},t)\equiv u(g,t)$$

and integrating (2) between 0 and g over α (with weights 1 and α), we get the following system of equations:

$$\partial_t n(g,t)+\partial_g\left[v(g)n(g)\right]\;=$$

$$=\frac{1}{2}\int_0^g K(g-s,s)n(g-s)n(s)ds - n(g)\int_0^\infty K(g,s)n(s)ds \quad (3)$$

$$\partial_t m(g,t)+\partial_g\left[v(g)m(g)\right]-u(g)n(g)=$$

$$=\int_0^g K(g-s,s)n(g-s)m(s)ds - m(g)\int_0^\infty K(g,s)n(s)ds \quad (4)$$

In case when the impurity is condensed, and the ballast substance (core) is relocated due to coagulation, it must be assumed that $u(g,t) = v(g,t)$, simplifying solution (3) – (4). In this case, for impurity particles we have:

$$\partial_t c(g,t)+\partial_g\left[v(g)c(g)\right]=$$

$$=\frac{1}{2}\int_0^g K(g-s,s)c(g-s)c(s)ds \;- c(g)\int_0^\infty K(g,s)n(s)ds \quad (5)$$

Equations (3), (5) agree with kinetic equations for water-ice phase transitions obtained in (Piskunov, 2000; Piskunov, Petrov, 2002), but they have more general meaning. Equation (4) is additional and describes impurity relocation between the particles.

The following statement is true.

Theorem 1. Let $u(g,t) = v(g,t) = \beta g$ and $n(g,t)$ be solution of (3). Let the initial conditions be arbitrary, but $m(g,0) = gF_0/A_0\, n(g,0)$. Then (4) is given by:

$$m(g,t)=\varphi(t)gn(g,t)\;;\;\; \varphi(t)=e^{-\beta t}\left(D+\beta\int_0^t e^{\beta s}ds\right), \quad (6)$$

where D – is arbitrary constant.

The proof consists in forward substitution of function $m(g,t)=\varphi(t)gn(g,t)$ in (4) accounting for (3). g quadratic terms are canceled, and linear terms are reduced to equation $\frac{d\varphi}{dt}+\beta\varphi-\beta=0$ with solution

$$\varphi(t)=e^{-\beta t}\left(D+\beta\int_0^t e^{\beta s}ds\right)$$

Conclusion

Solution (5) for free impurity is a separate task, but, for example, for kernels $K_c(g,n)=2$, $K_+(g,n)=g+n$ and $K_*(g,n)=2gn$ it is solved in (Piskunov, 2000; Piskunov, Petrov, 2002). Thus, we can talk about the complete solution of chain of equations (3)-(5) for composite particles. Certainly, what is meant here is short (integral) moment description of impurity particles distribution functions and for a particular type of condensation rates. It is reasonable to use the analytical solutions obtained for numerical program verification.

References

Piskunov V.N., Golubev A.I., Goncharov E.A. and Ismailova N.A. (1997) *J. Aerosol Sci.* **28**, 1215–1231.

Piskunov, V.N. (1999). Kinetic of precipitations formation with phase transition. *J. Aerosol Sci.* **30**, S233-S234.

Piskunov, V. N. (2000) *J. Aerosol Sci.* **31**, S576–S577.

Piskunov, V. N., Petrov A. M. (2002) *J. Aerosol Sci.* **33**. 647–657.

Simons S. (1981) *Annals of Nuclear Energy.* **8**, 287–294.

Collapsing self-similarity in systems with coagulation and fragmentation of particles

V.N.Piskunov, I.V.Piskunova

Russian Federal Nuclear Center – VNIIEF; Sarov, Nizhni Novgorod region, 607190, Russia

Keywords: particle formation, coagulation, fragmentation, self-similarity, collapsing spectra

Presenting author email: piskunov@vniief.ru

The possible types of self-similarity in particle breakage and coagulation systems have been analyzed in report (Piskunov, 2012). For homogeneous coagulation kernels *K(g,n)* and breakage rates *f(g,n)*:

$$K(ag,an)=a^{\lambda} K(g,n) \quad , \qquad f(ag,an)=a^{\mu} f(g,n) \qquad (1)$$

the following condition required for self-similar regimes should be fulfilled:

$$2 - \lambda+\mu = 0 \quad , \qquad (2)$$

The possibility of collapsing regime formation when spectrum is accumulated (collapsed) in zero ($g \to 0$), is mentioned the report.

The analysis shows the additional constraints for self-similar collapsing spectra:

$$2 - \lambda + \mu = 0 \; ; \quad \lambda > 1 \; ; \quad \mu > -1 \qquad (3)$$

We take coagulation kernel *K(g,n)* = *gn* and breakage rate *f(g,n)=a.* In this case, the required conditions (3) are fulfilled. Equation for number concentration $N(t)$ is:

$$\frac{dN}{dt} = \frac{\rho}{2}(a-\rho) \; ; \quad N(t) = N_0 + \frac{\rho}{2}(a-\rho)\cdot t \; , \qquad (4)$$

i.e. $N(t)$ increases at $a > \rho$ and decreases at $\rho > a$. Let us analyze the first case $a > \rho$, when breakage is dominant. Since $N(t)$ increases in time, spectrum collapse in zero ($g \to 0$) is possible.

Let us represent the self-similar solution in the form of:

$$c(g,t) = \frac{N^2(t)}{\rho}\Psi(x) \qquad , \qquad x = \frac{gN(t)}{\rho},$$

$$\int_0^{\infty} \Psi(x)dx = \int_0^{\infty} x\Psi(x)dx = 1$$

Insertion in breakage coagulation kinetic equation gives:

$$(Q-1)\left(2\Psi + x\frac{d\Psi}{dx}\right) = \int_0^x \Psi(x-y)\Psi(y)(x-y)ydy - \qquad (5)$$

$$-(2+Q)x\Psi + 2Q\int_x^{\infty} \Psi(y)dy \; , \quad Q = a/\rho > 1$$

Function $\Psi(x)$ has finite value in zero $\Psi(0) = a/(a-\rho)$. If there is no coagulation, i.e. *K(g,n)* = 0, *h(g)=a,* then (5) is given by $\Psi(x) = \exp(-x)$, corresponding to collapsing self-similarity only for breakage (Fillipov, 1961).

In the general case, moments behavior at large times resulting from (5), is as follows:

$$L_{\alpha}(t) = \int_0^{\infty} g^{\alpha} c(g,t)dg \approx B_{\alpha}\rho\left(\frac{a-\rho}{2}\right)^{1-\alpha} t^{1-\alpha} \; ;$$

$$B_{\alpha} = \int_0^{\infty} x^{\alpha}\Psi(x)dx \qquad (6)$$

Integrals B_{α} are taken convergent. Hence, moments with α < 1 should increase, and moments with α > 1 should decrease (which is opposite to a general pattern for free coagulation).

GA-computations (Piskunov and Golubev, 2002) were used to verify that for α = {0, 1/3, 1/2, 2/3, 1, 2} asymptotic moments behavior also agrees with (6), proving the existence of self-similar regime (5), (6). Solution (5) can be found either with Laplace transformation or numerically.

At $\rho > a$ critical phenomena similar to free kernel coagulation, are valid (Lushnikov, 1978). Critical phenomena with mass disbalance occur at time $t_c = 1/L_2(0)$. Criterion of this occurrence is the second moment $L_2(t)$ becoming infinite. GA-computations formerly successfully applied in (Piskunov, Golubev, Barrett et al., 2002) to detect critical phenomena in free coagulation, have been used to determine the behavior of $L_2(t)$ at arbitrary a. Computations t_c were carried out at $\rho = 1$ and $L_2(0)$=1. The results are given Table 1. As it must be according to physical content, the moment of critical phenomena is pulled by breakage.

Table 1 – Computational results t_c for different $a < \rho$ at ρ=1, $L_2(0)$=2

a	0	0.2	0.5	0.6	0.8	0.9	0.95
t_c	1	1.340	2.106	2.416	3.266	3.904	4.338

References

Piskunov, V.N. (2012) Analysis of asymptotic behavior of disperse systems with particle coagulation and coagulation. *EAC 2012 Report*.

Fillipov, A.F. (1961) *Probability theory and its applications*. **6**, 299-318.

Lushnikov, A. A. (1978) *Journal of Colloid and Interface Science.* **65**, 276–285.

Piskunov V. N. and Golubev A. I. (2002) *J. Aerosol Sci.* **33**, 51–63.

Piskunov, V. N., Golubev, A. I., Barrett, J.C. and Ismailova, N.A. (2002) *J. Aerosol Sci.* **33**, 65–75.

Thermophoretically Modified Brownian Coagulation

M. Arias-Zugasti[1] and D. E. Rosner[2]
[1]Departmento de Física Matemática y de Fluidos, UNED, Madrid, 28040, Spain
[2]Department of Chemical and Environmental Engineering, Yale University, New Haven, CT, 06520, USA

Keywords: Coagulation, Fundamental aerosol physics, Aerosol modeling.
Presenting author email: *maz@dfmf.uned.es*

For particle populations in a highly non-isothermal carrier gas, size-dependent particle thermophoresis provides an often-neglected coagulation mechanism (Rosner and Arias-Zugasti 2011a), which can either induce the coagulation of non-Brownian particles, or systematically alter the coagulation frequency for Brownian particles. In the present work we focus on this second scenario, in which an aerosol of Brownian particles evolves under the simultaneous influence of both coagulation mechanisms: the well-known Brownian coagulation first studied by Smoluchowski, and thermophoresis-induced coagulation (Arias-Zugasti and Rosner 2011b, Rosner and Arias-Zugasti 2011c). In the present case all particles in the population are assumed to have the same thermal conductivity and, except for their rapid coalescence upon contact, behave like solid spheres.

We first derive a combined coagulation frequency based on a thermophoresis-modified continuum-limit coagulation frequency of Smoluchowski. The Brownian + thermophoresis combined coagulation frequency is modeled in a way similar to the Brownian + sedimentation coagulation frequency (Simons et al. 1986), but with the gravitational sedimentation velocity replaced by the size-dependent near-continuum thermophoretic velocity.

We show that the relative intensity of each coagulation process is characterized by a dimensionless Peclet number, defined by the ratio of the characteristic coagulation frequencies. Introducing the combined coagulation frequency as a kernel into a Smoluchowski-type population-balance integro-PDE, we perform a systematic parametric study of the time evolution of a coagulation-aged, initially log-normal population, as a function of the Peclet number (Pe) and the particle/gas Fourier thermal conductivity ratio, kp/kg. We also investigate the errors associated with the frequently made “additive kernel” approximation.

Our results show that in the long-time limit a quasi-self-preserving population (QSPP) is reached. Regarding the dependence of this QSPP on Pe and kp/kg, we find that when the reference Peclet number is much smaller than, say 0.1, we recover the previously well-studied Brownian self-preserving populations. However, for intermediate Pe-values characteristic distortions set in, corresponding to increased spread and skewness, and slightly smaller departures from log-normality. Ultimately (for Pe-values larger than about 10) our QSPP become indistinguishable from our previously reported TP-dominated results (Rosner and Arias-Zugasti 2011a). It has been observed that the dependence on kp/kg reduces to a slight modification of the characteristic time- and size- scales (for kp/kg > 10), and, hence, our results for the self-similar normalized PDF reached in the long-time limit are almost independent of kp/kg over the entire range of Peclet numbers.

This recent work was supported, in part, by Comunidad de Madrid (S2009/ENE-1597), Ministerio de Ciencia e Innovación (CSD2010-00011, ENE2011-26868), and NSF(USA)-CBET (Grant 1037733). Extensions currently in progress deal with composition-dependent thermal conductivity, thermocapillary effects for mists, and dense carrier vapour effects.

Rosner, D. E. and Arias-Zugasti, M. (2011a) Phys. Rev. Lett. **106**(1), 015502.
Arias-Zugasti, M. and Rosner, D. E. (2011b) *Phys. Rev. E* **84**(2), 021401.
Rosner, D. E. and Arias-Zugasti, M. (2011c) *Ind. & Eng. Chem. Res.* **50**, 8932-8940.
Simons, S. Williams, M. M. R., and Cassell J. S. (1986) *J Aerosol Sci.* (**17**), 789.

Calculation of the mobility radius of fractals in the continuum regime from their geometry

A.D. Melas[1 2], A.G. Konstandopoulos[1 3], L. Isella[4] and Y. Drossinos[2]
[1]Department of Chemical Engineering, Aristotle University, Thessaloniki, 50006, Greece
[2]European Commission, Joint Research Centre, Ispra (VA), 21027, Italy
[3]Aerosol & Particle Technology Laboratory, CERTH/CPERI, P.O. Box 60361, 57001 Thessaloniki, Greece
[4]European Commission, DG Energy, L-2530, Luxemburg
Keywords: fractal aggregates, continuum regime, mobility radius.
Presenting author email: Anastasios.Melas@jrc.ec.europa.eu

We calculated the mobility radius of fractal aggregates in the continuum regime as suggested by Isella and Drossinos (2011) who related it to the molecule-aggregate collision rate. We created the fractal aggregates with the cluster-cluster aggregation method proposed by Thouy and Jullien (1996).

The fractals used in our simulations have different fractal dimension (d_f), fractal prefactor (k_f) and they consist of 8 up to 64 monomers. In each case the scaling law is exactly satisfied. In Fig. 1 the mobility radius (R_m) is plotted as a function of the radius of gyration (R_g). Both of them are scaled with R_1 (as all length scales are).

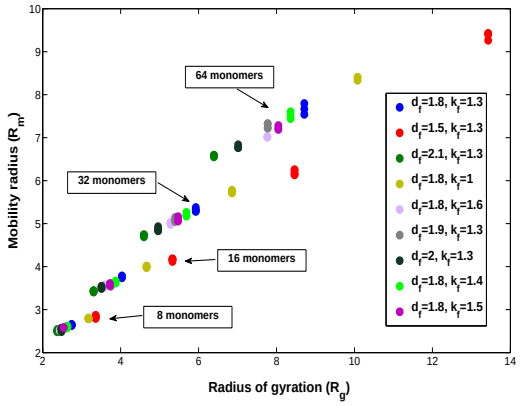

Figure 1: The mobility radius as a function of the radius of gyration for fractals with different N, d_f, k_f.

For a number of monomers N a linear relationship between R_m and R_g is observed. By fitting we obtain:

$$R_m = 0.512\left[1-\frac{1}{\ln(2N)}\right]R_g + 0.72N^{0.413}. \qquad (1)$$

We used a Levenberg-Marquardt algorithm to perform the fit, and we found it to be stable. As expected Eq. 1 reproduces the $R_m - R_g$ relationship shown in Fig. 1. We used the same equation to calculate $\beta = \frac{R_m}{R_g}$ for a large number of monomers ($N = 1000$). The fractal aggregates we chose have the same fractal dimension and prefactor as DLCA ($d_f = 1.85, k_f = 1.17$) and RLCA ($d_f = 2.05, k_f = 0.94$) clusters. We find $\beta = 0.769$ for DLCA and $\beta = 0.86$ for RLCA clusters, in good agreement with the literature values 0.765 and 0.831, correspondingly (Lattuada et al., 2003).

Two very important conclusions can be exctracted from Eq. 1: (1) R_m can be estimated for a single fractal; (2) both d_f, k_f are very important as far as they influence the radius of gyration according to the scaling law,

$$R_g/R_1 = N^{1/d_f}k_f^{-1/d_f}. \qquad (2)$$

The dependence on N may be eliminated by scaling R_m and R_g with a characteristic length which we call outer radius (R_o). This radius is the largest distance in a fractal between its center of mass and the center of mass of a monomer. In Fig. 2 we replot the data of Fig. 1 scaled with R_o.

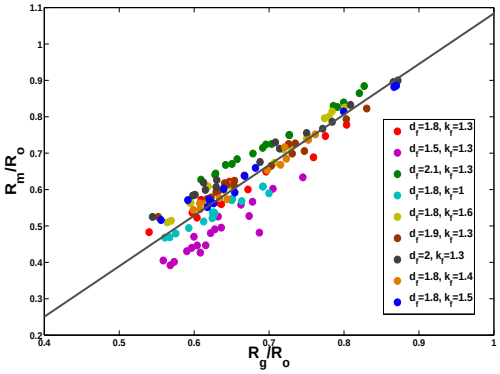

Figure 2: Fractal mobility radii as a function of radii of gyration scaled by their outer radius.

By fitting all the data we get

$$\frac{R_m}{R_o} = 1.389\frac{R_g}{R_o} - 0.305. \qquad (3)$$

Equation 3 relates three different radii of a fractal, two based on geometrical properties and one on dynamical; it reproduces our calculations to a good accuracy.

This work was supported by the European Commission Doctoral Fellowship (ADM).

L. Isella, Y. Drossinos (2011), J. Colloid Interface Sci. **356**, 505.
R. Thouy, R. Jullien (1996), J. Phys. I France **6**, 1365.
M. Lattuada, H. Wu and M. Morbidelli (2003), J. Colloid Interface Sci. **268**, 96.

Virtual generation of realistic soot particles: Impact to their morphological and optical properties.

A.Bescond[1], J.Yon[1], C. Rozé[1], F. X. Ouf[2]

[1] UMR 6614 CORIA, Avenue de l'université, 76801 Saint-Etienne du Rouvray, France.
[2]Institut de Radioprotection et de Sureté Nucléaire (IRSN), 91192 Gif-sur-Yvette Cedex, France
Keywords: Nanoparticle aggregates, generation, Numerical simulation, light scattering, cirrus clouds
Presenting author email: alexandre.bescond@coria.fr

Since the emergence of the fractal concept (Jullien and Botet, 1987), the taking into account of soot particles non sphericity gave rise to multiple studies. The experimental interpretation of light scattering by fractal aggregates by Static Light Scattering (SLS), light extinction or their visualization by Transmission Electron Microscopy (TEM) implied the development of adapted theory for light-particle interaction (Dobbins and Megaridis, 1991) or establishment of $3D \rightarrow 2D$ projections laws (Brasil, et al., 1999; Köylü, et al., 1995). These studies enabled theoretical calculations of angular scattering cross sections related to the particle fractal dimension d_f, amount of absorbed light, albedo or methods for analyzing TEM images for the determination of particle size (gyration radius R_g) and morphology. Up to now, all the studies meaning with aggregate particles usually employ these results.

For these studies, virtual aggregates are usually generated by using DLCA (Diffusion Limited Cluster Aggregation) or RCA (Reacted Limited Cluster Aggregation) (Meakin, 1999). The resulting aggregates are most of the time made of primary spheres monodisperse in size and characterized by one point contact between two spheres. Moreover, for the optical calculations, uniform optical index have been considered. Though, visualization of real soot particles put in evidence a more complex morphology (figure 1-a).

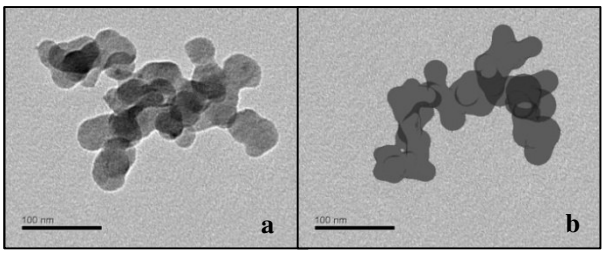

Figure 1, Aggregate of Ethylene flame ($\overline{D_p} = 34.19nm$); a) Real TEM pictures; b) Virtual TEM pictures for $Cov = 0{,}2$; $\zeta = 2$ obtained with PovRay

Indeed, primary spheres present an amount of overlapping and a coating that may increase the surface of contact between two spheres. The impact of spheres overlapping on fractal prefactor has been evaluated by Brasil, et al., (2001) who introduced the overlapping parameter $\boldsymbol{Cov}$. Eggersdorfer, et al. (2011) simulated the thermal sintering effect which creates aggregates with softered outlines but they did not evaluated the impact of this smoothed shape on interpretation of SLS, extinction or TEM measurements.

The aim of this work is firstly to present a method for generating more realistic aggregates by using a 3D level set function (figure 1-b). Additionally to the overlapping coefficient $\boldsymbol{Cov}$, we introduced a coating parameter $\boldsymbol{\zeta}$. The second objective of the present work is to evaluate the impact of this realistic morphology on the optical and morphological properties of soot aggregates.
It will be seen if the parameters of the fractal law, which links the aggregates size R_g and the number of primary spheres $N_p = k_f \left(\frac{R_g}{R_p}\right)^{d_f}$, are affected by the adjunction of overlapping and coating. So, the analysis of TEM images based on the maximum projected length L and the projected area A_a have to be checked. We will observe the impact of $\boldsymbol{Cov}$ and $\boldsymbol{\zeta}$ parameters on the classical relationships between 2D and 3D parameters, i.e. κ, k_a and α, $\left(L = \kappa R_g\,, N_p = k_a \left(\frac{A_a}{A_p}\right)^{\alpha}\right)$ where A_p is the projected area of a primary particles. The evaluation of angular or total light scattering and extinction cross sections for realistic aggregates is based on the Discrete Dipole Approximation Code DDSCAT7.1 (Draine and Flatau, 2010) It will be seen if fractal dimension measurement by SLS is affected by $\boldsymbol{Cov}$ and ζ parameters. Additionally, the impact on light scattered depolarization and albedo will be also presented.

Finally, one of the advantages of the level set method for generating realistic aggregates resides in its ability to control a space dependent optical property. Indeed, we will evaluate the albedo of soot aggregates covered by a thin layer of ice (Hong, et al., 2008) for the practical study of aeronautics emissions.

This work was supported by the French DGAC in the framework of the Mermose project.

Brasil, A., Farias, T. and Carvalho, M. (1999) *Journal of Aerosol Science*, **30**, 1379.
Brasil, A.M., Farias, T.L., Carvalho, M.G. and Koylu, U.O. (2001) *Journal of Aerosol Science*, **32**, 489-508.
Dobbins, R.A. and Megaridis, C.M. (1991) *Applied Optics*, **30**, 4747-4754.
Draine, B.T. and Flatau, P.J. (2010).
Eggersdorfer, M.L., Kadau, D., Herrmann, H.J. and Pratsinis, S.E. (2011) *Langmuir*.
Hong, G., *et al.* (2008) *Journal of Quantitative Spectroscopy and Radiative Transfer*, **109**, 2635-2647.
Jullien, R. and Botet, R. (1987) *Aggregation and fractal aggregates*. Word Scientific.
Köylü, Ü.Ö., Faeth, G.M., Farias, T.L. and Carvalho, M.G. (1995) *Combustion and Flame*, **100**, 621-633.
Meakin, P. (1999) *J. Sol-Gel Sci. Technol.*, **15**, 97-117.

3D study of fractal combustion aerosols using Electron Tomography

D. Lottin[1], D. Ferry[2], D. Delhaye[1], F.-X. Ouf[3] and J. Yon[4]

[1]ONERA – The French Aerospace Lab, F-92322 Châtillon, France
[2]CINaM-CNRS UMR 7325, Aix-Marseille University, Campus de Luminy, 13009 Marseille, France
[3]IRSN-LPMA, BP 68, 91192 Gif-sur-Yvette, France
[4]CORIA-CNRS UMR 6614, University and INSA of Rouen, 76801 St-Etienne de Rouvray Cedex, France

Keywords: Soot nanoparticles, Fractals, 3D characterization, Electron Tomography.
Presenting author email: delphine.lottin@onera.fr

Atmospheric aerosol particles meet a growing interest in today's environmental concerns because of their potential impacts on the global radiative budget and human health. In this context, combustion aerosols are extensively studied as they originate from industrial and transport activities for a large part. They usually are in the form of more or less compact aggregates made of primary particles. The evaluation of their effects on the environment requires the knowledge of their microphysical properties.

One way to determine these properties is based on a Transmission Electron Microscopy (TEM) analysis. 2D characteristics of the aggregates' projection (Fig. 1 left) are measured on the micrographs and extrapolated to 3D using 2D-3D transposition relationships (Baron and Willeke, 2001). These mathematical relationships were established from studies of numerically generated aggregates of pre-defined fractal dimension and composed of monodisperse primary particles. They are nowadays widely used (Neer and Köylü, 2006). However, very few works have focused on the validity of these relationships when applied to real soot aggregates. Indeed, it is difficult to establish 2D and 3D characteristics of soot aggregates using a single experimental approach.

We investigate aircraft soot aggregates sampled at the exit of a turbofan engine by combining TEM and Electron Tomography (ET) analyses. Micrographs are processed using the "ImageJ" software (http://imagej.nih.gov/ij/). Statistical values for the population of aggregates are issued: primary particles mean diameter, aggregates mean gyration diameter.

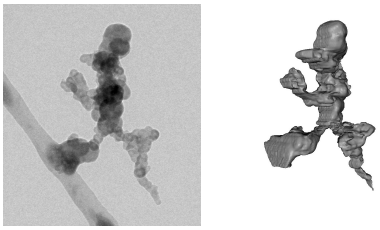

Figure 1. TEM micrograph of an aircraft soot aggregate (left) and the 3D visualization of its tomogram (right).

The 3D tomogram of this aggregate is built by ET using the plug-in "TomoJ" (Messaoudi *et al.*, 2007). We developed a plug-in *SootExpert* able to determine the 3D characteristics of an aggregate on its tomogram (volume, gyration diameter and fractal dimension). In a first step, we validate our plug-in on a numerically generated aggregate (Fig. 2), its volume and gyration diameter are known. The values determined by *SootExpert* are very close to the characteristics of this aggregate (Table 1), assessing the reliability of our plug-in.

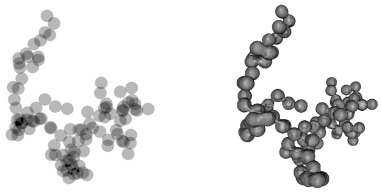

Figure 2. Projection of a numerical aggregate (left) and the 3D visualization of its tomogram (right).

	Known 3D characteristics	*SootExpert* 3D characteristics
Gyration diameter (nm)	310	298
Volume (nm^3)	$1\,456\times10^3$	$1\,616\times10^3$

Table 1. Comparison between the known and the determined 3D characteristics of a numerical aggregate.

In a second step, the ET analysis is applied to aircraft soot aggregates (Fig. 1 right). Van Poppel *et al.* (2005) and Adachi *et al.* (2007) have used ET to characterize atmospheric aerosols, with no special interest to the links between 2D and 3D characterizations. We study, for a single aggregate, the correlation between the 3D characteristics determined on its tomogram and the statistics resulting from the TEM analysis of the series of its projections. We can thus indicate the validity of the transposition relationships for aircraft soot aggregates. Then we compare this aggregate's 3D characteristics determined by *SootExpert* with the statistical values determined on the population, to investigate if a single aggregate is representative of its population.

Adachi, K., Chung, S.H., Friedrich, H., Buseck, P.R. (2007) *J. Geophys. Res.* **112**, D14202.

Baron, P.A. and Willeke, K. (2001) *Aerosol measurement. Principle, techniques, and applications* 2nd Edition, John Wiley & sons, Inc.

Messaoudi, C., Boudier, T., Sorzano, C.O.S., Marco, S. (2007) *BMC Bioinformatics* **8**, 288-297.

Neer, A. and Köylü, Ü.Ö. (2006) *Combust. Flame* **146**, 142-154.

Van Poppel, L.H., Friedrich, H., Spinsby, J., Chung, S.H., Seinfeld, J.H., Buseck, P.R. (2005) *Geophys. Res. Lett.* **32**, L24811.

Impaction dynamics of TiO_2 agglomerates with different properties

M. Ihalainen[1,2], T. Lind[1], T. Torvela[2], K.E.J. Lehtinen[3,4] and J. Jokiniemi[2,5]

[1]PSI Paul Scherrer Institut, The Laboratory for Thermal-Hydraulics, CH-5232 Villigen PSI, Switzerland
[2]Fine Particle and Aerosol Technology Laboratory, Department of Environmental Science, University of Eastern Finland, P.O. Box 1627, FI-70211 Kuopio, Finland
[3]Department of Physics, University of Eastern Finland, P.O. Box 1627, 70211 Kuopio, Finland
[4]Finnish Meteorological Institute, Kuopio Unit, P.O. Box 1627, 70210 Kuopio, Finland
[5]VTT Technical Research Centre of Finland, Fine Particles, P.O. Box 1602, 02044 VTT, Espoo, Finland
Keywords: inertial impaction, deagglomeration, bouncing.
Presenting author email: jorma.jokiniemi@uef.fi

During certain severe nuclear reactor accidents, e.g., a Steam Generator Tube Rupture, radioactive agglomerates may impact onto surfaces in near sonic conditions (Guntay et al. 2004). Due to this impaction, the physical properties of these agglomerates may change which may affect their transport in the power plant and possible release into the surrounding environment. The determining factors to solve the outcome in these situations are the interactions within the agglomerate, and the interactions between the surface and the agglomerate. Whether the agglomerates adhere onto the surface, bounce and/or break-up under certain conditions remains a question to be answered. For this purpose agglomerate impaction behavior was studied.

A combination of a single stage Micro Uniform Deposit Impactor (MOUDI) and a low pressure sampling chamber was used to carry out the impaction studies. TiO_2 agglomerates were impacted onto an impaction plate located in the MOUDI and the sampling chamber was used to collect the aerosol at low pressure after the impactor. The particles which deposited to the impaction plate were studied using a Transmission Electron Microscopy (TEM). The TEM-grid for this purpose was located on the impaction plate. The bounced particles were collected from the sampling chamber at ambient pressure for analysis with the TEM and a Scanning Mobility Particle Sizer (SMPS). The measurement system is described in details in Ihalainen et al. (2010).

The following parameters of the TiO_2 agglomerates were varied to find out how they affect the impaction behavior: the primary particle size, agglomerate size and degree of sintering. The TiO_2 agglomerates were generated through chemical vapor synthesis (CVS) in a hot wall reactor while controlling the primary particle size with the temperature of the reactor. A Differential Mobility Analyzer (DMA) was used for the size classification of the generated particles. The degree of sintering of TiO_2 agglomerates was altered by placing another hot wall reactor downstream the DMA.

Both the primary particle size and the degree of sintering affected the break-up and bounce of the TiO_2 agglomerates (Figure 1.). For instance, the geometric mean diameter (GMD) of the bounced particles increased as the primary particle size was decreased from about 27 nm to 16 nm, meaning that on average fewer bonds per agglomerate broke up during the impaction. The GMD of the bounced particles also increased as the degree of sintering of the agglomerates was increased, indicating that fewer bonds per agglomerate broke up. Decreasing the primary particle size and increasing the degree of sintering lowered the number concentration of the bounced particles. Further data analysis will be carried out to estimate the mass based bounced particle fraction of the impacted particles.

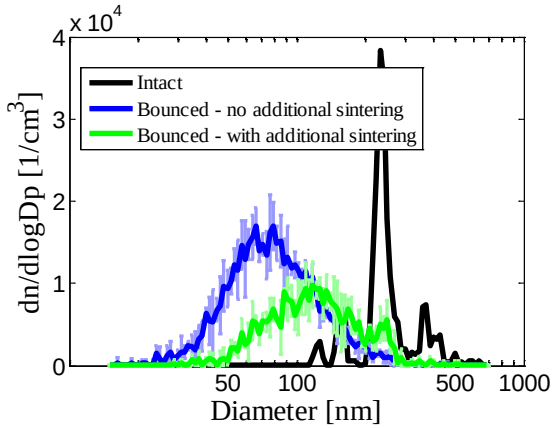

Figure 1. The number size distributions of the intact and bounced particles measured with the SMPS. The impaction results of agglomerates with and without additional sintering are shown.

This work was carried out in support of the international ARTIST II program. The authors express their gratitude to those members of the Laboratory for Thermal-Hydraulics at PSI and of the Fine Particle and Aerosol Technology Laboratory at the University of Eastern Finland that participated in the experimental work and construction of the facility.

Güntay, S.,Suckow, D., Dehbi, A. and Kapulla, R., (2004) *Nuclear Engineering and Design*, **231**, 109-120.

Ihalainen, M., Lind, T., Güntay, S., and Jokiniemi, J., (2010) Abstract. *International Aerosol Conference* 2010.

Study of fluorescent imaging quantitative evaluation in protective equipment validation

S. Yang[1], C.H. Luo [2], M.Y. Syu[2], C.Y. Wen[4], K.H. Lin[3], S.H. Chiu[3] and C.P. Chang[5]

[1] Department of Environmental and Occupational Health, Toko University, Chiyai, Taiwan
[2] Department of Safety, Health and Environmental Engineering, Hungkuang University, Taichung, Taiwan
[3] Department of Materials Science and Engineering, National Taiwan University of Science and Technology, Taipei, Taiwan
[4] Department of Forensic Science, National Central Police University, Taoyuan, Taiwan
[5]Division of Occupational Hygiene, Institute of Occupational Safety and Health, New Taipei City, Taiwan
Keywords: aerosol exposure; image processing; protective clothing; pumping effect.
Presenting author email: shinhaoyang@ntu.edu.tw

Clothing surface safety has been a consideration in many studies. When motions are performed, the air exchange increases and results in a functional loss of clothing insulation. This phenomenon is called the pumping effect (Havenith and Nilsson, 2004), or clothing ventilation. In addition, this phenomenon occurs at the collar, cuff, waistline, and hemline body- clothing boundaries. Several studies have simulated or estimated the pumping effect on thermal insulation loss of work wear and cold-weather clothing in wind conditions (Aoyagi et al., 1994; Havenith et al., 1990). However, there has been little research into the pumping effect on leakage of airborne pollutants. The purpose of this study is to determine if particulate leakage into protective clothing worn by volunteer simulated workers would happen after a series of designed exercises. Finally, a leakage ratio was introduced to assess the pumping effect on protective clothing in various conditions, such as exposure time and body parts.

For simulating the intensity and range of activities in hospitals and factories, simplified and disciplined exercises were taught to volunteers wearing protective clothing before exposure-and-leakage tests. The designed exercises included squatting, standing, raising elbows, turning left and right, holding arms across the chest, and stooping. All action sets were performed and finished successively in one minute, and repeated for the next minute if necessary. Therefore, the ten-repetitions of designed exercises lasted ten minutes. Volunteers wearing protective clothing performed designed exercises in a stabilized chamber, described below, for two- and ten-repetitions. Protective clothing was a one-piece coverall of high-density polyethylene fibers, registered as Tyvek® of DuPont.

For controlling the physical conditions, a closed chamber 360 cm (length) × 213 cm (width) × 180 cm (height), was fanned with a wind velocity of 1.3 m/s to simulate an indoor environment. The temperature was set at 21(±3) ℃ by an air conditioner, and relative humidity was controlled at 50 ± 3 % by a dehumidifier. The aerosol solution was prepared by a mixture of SiO_2 powders, an ethanol solution of 20% (v/v), and the Hoechst 33258 fluorescent dye ($C_{25}H_{24}N_6O$•3HCl, Aldrich Inc.). A nebulizer consists of air-extractor and flow-presser was used to disperse the aerosol solution to produce challenged aerosols with fluorescence. The fluorescent aerosols with a count median diameter of 0.15 μm were dispersed into the chamber through a nozzle (model 8012/1010L, Natural Fog® , Taiwan) with a caliber of 0.80 mm. The concentration detected by a portable aerosol spectrometer (model 1.109, Grimm Aerosol Technik GmbH & Co., Germany) was 10^5－10^6 particles/cm^3.

After a series of designed exercises, volunteers left the chamber, removed protective clothing, and stood in a darkroom. If boundary leakage of protective clothing happened, the selected boundary parts deposited by challenged aerosols presented fluorescent in a UV scanner of 365 nm. Fluorescent pictures were taken with a digital camera (Nikon D3000) equipped with a manual and automatic focusing lense (Nikon AF NIKKOR 50mm 1.8D, Japan). Its charge-couple device's (CCD) picture quality is 3872 × 2592 pixels. A digital comparison of the photograph of the chart and the chart confirmed the constancy of CCD quality. Finally, fluorescent areas were segmented and analyzed for their fluorescent gray levels (or brightness) by an image processor developed using an entropy-based algorithm

The results imply the exposure time was a major factor for evaluating leakage of protective clothing. An increase of leak ratio occurred on the neck, chest, and wrists with increased exposure time. The neck, comparatively, presents the most multiplicative increase of leak ratio at the end of exposure. The highest contamination possibility of aerosols transmitted from the neck to nose and mouth happens during the removal of personal protective clothing.

This work was supported by the Institute of Occupational Safety and Health and National Science Council, Taiwan under Contract NSC 96 -2221-E-241-011-MY3.

Havenith, G. and Nilsson, H.O. (2004). *European Journal of Applied Physiology*. 92, 636-640.

Havenith, G., Heus, R. and Lotens, W.A. (1990). *Ergonomics*. 33, 89-1005.

Aoyagi, Y., McLellan, T.M. and Shephard, R.J. (1994). *European Journal of Applied Physiology and Occupational Physiology*. 68, 234-245.

Vibrational Spectroscopy of the Atmospherically Relevant Ions $A^-(H_2SO_4)_m(HNO_3)_n(H_2O)_o$ with $A^- = HSO_4^-, NO_3^-$

N. Heine[1], T.I. Yacovitch[2], C. Hock[2], D.M. Neumark[2,3], C. Brieger[1], T. Wende[1], G. Meijer[1] and K.R. Asmis[1]

[1]Department of Molecular Physics, Fritz-Haber-Institut, Berlin, Berlin, 14195, Germany
[2]Department of Chemistry, University of California, Berkeley, Berkeley, CA 94720, USA
[3]Chemical Science Division, Lawrence Berkeley National Laboratory, CA 94720, USA
Keywords: acid solvation, vibrational spectroscopy, stratosphere, cluster ions.
Presenting author email: heine@fhi-berlin.mpg.de

Ions influence various chemical and physical processes in the atmosphere, such as the electrical conductivity and the formation of polar stratospheric clouds (PSC).They also play a critical role in aerosol formation through ion nucleation. Among the most abundant anions in the troposphere and stratosphere are nitrate (NO_3^-) and bisulfate (HSO_4^-), in particular, clusters of these ions with nitric acid, sulfuric acid and water (Heitmann and Arnold, 1983). While below ~30 km, nitrate- core cluster are dominant, bisulfate-core clusters are more abundant above this height (Viggiano, A.A., Arnold, 1981). The negative ion $NO_3^-(HNO_3)_2$, for example, accounts for over 90% of all negative ions at heights around 27-30 km. In order to understand the chemical and physical properties of these anionic clusters, as well as to test the structural predictions from previous computational studies (Galvéz *et al*, 2006), experimental information on the cluster structure is required.

Here, we present first results on the vibrational action spectroscopy of the atmospherically relevant clusters $A^-(H_2SO_4)_m(HNO_3)_n(H_2O)_o$ with $A^- = HSO_4^-$, NO_3^-. In particular, we focused on the series $NO_3^-(HNO_3)_{1-3}(H_2O)_{1-2}$, as well as small mixed acid clusters. Infrared multiple photon dissociation (IR-MPD) spectra, measured using the tunable and intense radiation from the infrared free electron laser FELIX (Oepts *et al*, 1995), are reported in the fingerprint region (550 – 1800 cm^{-1}), directly probing the NO/SO-stretching and -bending modes. The assignment of the spectra is aided by comparison with calculated B3LYP/TZVPP structures and harmonic frequencies, as well as with higher-level calculations.

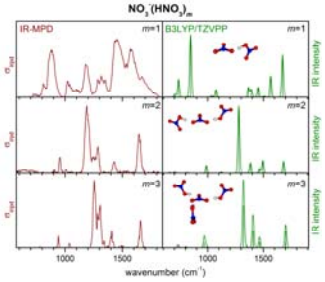

Figure 1. Experimental (left) and simulated (right) vibrational spectra of $NO_3^-(HNO_3)_m$ with m = 1 - 3.

The IRMPD spectra of $NO_3^-(HNO_3)_{1-3}$ are shown in Figure 1. Reasonable agreement is observed for the predicted lowest energy structures. DFT predicts that the nitrate–nitric acid clusters prefer non-planar structures at 0 K, but these become effectively planar at higher temperatures due to vibrational averaging. The biggest discrepancy between the experimental IRMPD and simulated harmonic spectra is observed for m=1. This is due to the presence of strong low-barrier hydrogen bond in hydrogen dinitrate ($^-O_2NO\cdots H\cdots ONO_2^-$), which is not well described within the harmonic approximation. With increasing cluster size, the hydrogen bond strength decreases, evidenced by an increase in the O-O distance of the O-H···O moiety from 2.43 Å (m=1) to 2.62 Å (m=3).

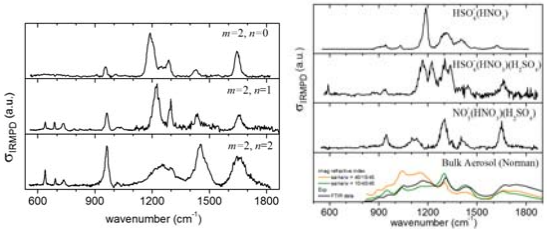

Figure 2. IRMPD spectra of $NO_3^-(HNO_3)_m(H_2O)_n$ (left) and of mixed NO_3^-/HSO_4^--acid clusters (right).

The IRMPD spectra of microhydrated $NO_3^-(HNO_3)_m(H_2O)_n$ clusters are shown for m=2 and n=0-2 in the left part of Figure 2. The vibrational features observed for n=0 remain discernible throughout all three spectra, indicating that binding of water to nitrate is weaker compared to nitric acid and consequently the addition of water does not perturb the $NO_3^-(HNO_3)_2$ core structure substantially.

IRMPD spectra of mixed sulfuric acid/nitric acid anion clusters are shown and compared with FTIR-spectra of bulky aerosols containing H_2SO_4, HNO_3 and H_2O taken by Norman *et al* (2002) on the right of figure 2. Two interesting observations can be made. First, a core switching behaviour is observed. Depending on the number and nature of the neutral ligands, evidence for either a nitrate or a bisulfate anion is found. Second, the best agreement between bulk and cluster can be found within the small systems, containing HSO_4^-.

Heitmann, H., Arnold, F. (1983) *Nature* **306**, 747-751.
Viggiano, A.A., Arnold, F. (1981) *Planetary and Space Science* **29**, 895-906.
Gálvez, O., Gómez, P.C., Pacios, L.F. (2006) *J. Phys. Chem. A* **110**, 3750-3758.
Norman M.L., Miller, R.E., Worsnop, D.R. (2002) *J. Phys. Chem. A* **106**, 6075 – 6083.
Oepts, D., van der Meer, A.F.G., van Amersfoort, P.W. (1995) *Infrared Phys. Technol.* **36**, 297–308.

Microhydration of Conjugate Base Anions Probed by Gas Phase Vibrational Spectroscopy

K.R. Asmis[1], N. Heine[1], T. Wende[1], L. Jiang[1], G. Meijer[1], T.I. Yacovitch[2], D.M. Neumark[2,3]

[1]Abteilung Molekülphysik, Fritz-Haber-Institut der MPG, 14195 Berlin, Germany
[2]Department of Chemistry, University of California, Berkeley, Berkeley, CA 94720, USA
[3]Chemical Science Division, Lawrence Berkeley National Laboratory, CA 94720, USA
Keywords: cluster ions, acid solvation, vibrational spectroscopy, density functional theory.
Presenting author email: asmis@fhi-berlin.mpg.de

Conjugate base anions are ubiquitous species in aqueous phase chemistry. However, how these anions are hydrated at the molecular level is far from completely understood. A molecular-level understanding of ion hydration is also important in understanding the surface speciation and reactivity of aerosols, which play a key role in atmospheric and oceanic chemical cycles.

We use infrared multiple photon dissociation (IRMPD) spectroscopy over the spectral range of 550-4000 cm^{-1} as a structural probe of size-selected clusters in which the polyatomic anions HCO_3^-, NO_3^-, HSO_4^-, SO_4^{2-}, $H_2PO_4^-$ and $(CH_2)_n(COO^-)_2$ are hydrated by a known number of water molecules *n*. (Asmis and Neumark, 2012) The experiments follow how the H-bonded solvent network around these anions evolves, one water molecule at a time. Structural assignments are made by comparing the experimental IR spectra to those obtained from electronic structure calculations. Our results show how changes in anion structure, symmetry, charge state and acidity have a profound effect on the structure of the solvent network and, vice versa, how hydration can markedly affect the structure of the anion core in a microhydrated cluster.

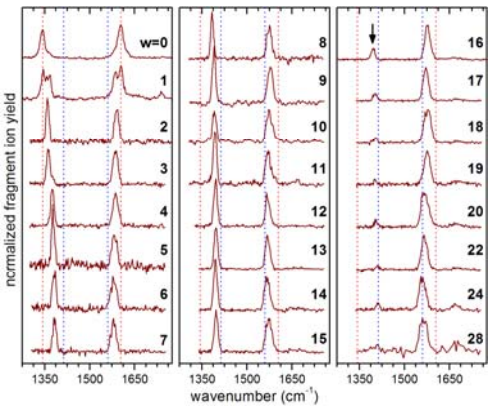

Figure 1: IRMPD spectra of $(CH_2)_6(COO^-)_2(H_2O)_n$.

Some key results include the following. The first few water molecules bind to the anion terminal oxo groups in a bridging fashion. Each oxo group can form up to three hydrogen bonds. When there are more than three hydrating water molecules, the formation of a particularly stable four-membered water ring is observed for NO_3^- and HCO_3^-. In the case of HCO_3^-, additional water molecules then add to this water ring rather than directly to the anion, indicating a preference for surface hydration. In contrast, doubly charged sulfate dianions are internally hydrated and characterized by the closing of the first hydration shell at $n = 12$. The situation is different for dicarboxylate dianions, which adapt to the hydration network by changing from a linear to a folded structure (see Fig. 1) at $n > 15$. (Wende *et al.* 2011)

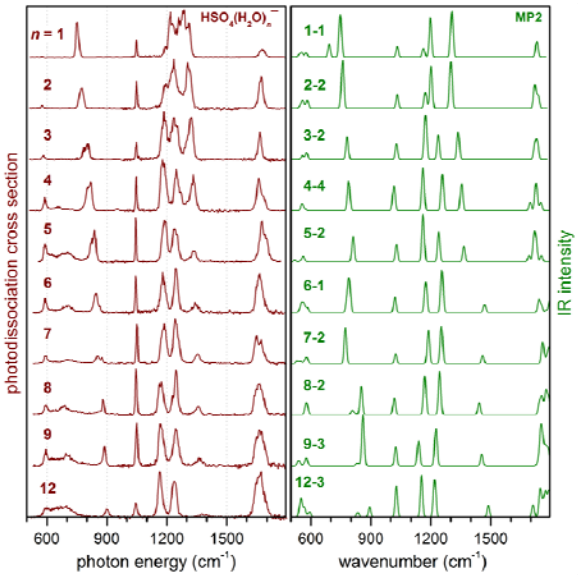

Figure 2. IRMPD (left) and simulated IR absorption spectra (right) for $HSO_4^-(H_2O)_{1\text{-}9,12}$.

For $HSO_4^-(H_2O)_n$ the comparison with electronic structure calculations (see Fig. 2) suggests that the acidic proton of HSO_4^- is involved in the formation of a hydrogen bond from $n \geq 1$. (Yacovitch *et al.* 2011) The blue shifting of the SOH bending mode accompanied by a dramatic decrease in its IR intensity suggests increased incorporation of the bisulfate hydrogen atom into the H-bonding network, the first step toward acid dissociation.

Asmis, K.R., Neumark, D.M. (2012) *Accts. Chem. Res.* **45**, 43–52.

Yacovitch, T.I., Wende, T., Jiang, T., Heine, N., Meijer, G. Neumark, D.M., Asmis, K.R. (2011) *J. Chem. Phys. Lett.* **2,** 2135-2140.

Wende, T., Wanko, M., Jiang, L., Meijer, G., Asmis, K.R., Rubio, A. (2011) *Angew. Chem. Int. Ed.* **50**, 3807-3810.

Heat effects at self-similar regime of droplet diffusion growth and the vapor-gas outflow

A.E. Kuchma and A.K. Shchekin

Department of Statistical Physics, St Petersburg State University, St Petersburg, 198504, Russian Federation
Keywords: droplet growth, nonstationary diffusion and heat conduction, nonisothermal condensation.
Presenting author email: akshch@list.ru

It is a well known fact that release of the latent heat at condensation on aerosol particles plays a key role in dynamics of the Earth atmosphere (Colbeck (2008)). The aim of this report is to consider how the condensation heat affects the character of vapor-passive gas flow produced around a droplet at diffusion regime of the droplet growth. A novelty in our approach is finding new self-similar solutions for the vapor density and temperature profiles at the nonstationary nonisothermal droplet growth and showing their importance for existence of a vapor-gas inflow at small distances from a droplet and an outflow at larger distances.

We will consider the problem of nonstationary diffusion growth of the droplet with allowance for the motion of droplet surface, nonstationary Stefan's flux of the vapor-passive gas medium, thermal diffusion and thermal conduction in the vapor-gas mixture as a result of releasing of the latent heat at vapor condensation onto droplet. In the coordinate system with an origin in the droplet center, the equation of vapor diffusion to the growing droplet at fixed total pressure of the vapor-gas medium can be written (Landau and Lifshitz (1987), Frank-Kamenetskii (1969)) as

$$\frac{\partial n_1}{\partial t}+\frac{\partial j_1}{\partial r}+\frac{2}{r}j_1=0 \qquad (1)$$

where vapor flux density j_1 is determined in the form

$$j_1=-D\left[\partial n_1/\partial r+n_1\left(1+\frac{\rho^2}{m_1m_2n_1n}k_T\right)\partial\ln T/\partial r\right]+n_1\mathrm{v}, \qquad (2)$$

n_i and m_i are the volume density and the mass of molecules of gaseous component i ($i=1$ and $i=2$ refer to vapour and passive gas, respectively), t is the time, r is the radial coordinate, $\rho=n_1m_1+n_2m_2$ and $n=n_1+n_2$ are the total mass and volume densities of the vapor-gas medium, $T=T(r,t)$ is the local temperature, $\mathrm{v}=\mathrm{v}(r,t)$ is the radial velocity of hydrodynamic flow of the vapor-gas medium caused by vapor condensation, $D=D(n_1,T)$ and $k_T=k_T(n_1,T)$ are the vapor diffusion and thermal diffusion coefficients in the vapor-gas medium.

Let us denote the radius of the growing droplet at time moment t as $R(t)$. In order to find the radial velocity $\mathrm{v}(r,t)$, we consider a mobile sphere of a certain radius $R_1(t)>R(t)$ surrounding the droplet. If the rate $\dot R_1(t)$ of variation of $R_1(t)$ with time coincides with the radial velocity $\mathrm{v}(r,t)$, one can write

$$4\pi n_l R^3(t)/3+4\pi\int_{R(t)}^{R_1(t)}r^2n(T(r,t))dr=const \qquad (3)$$

where n_l is the volume density in the liquid droplet. By differentiating Eq.(3) with respect to time, assuming $T(r\to\infty,t)=T_0$, $T(R,t)=T_d$, and $n(T)T=n(T_0)T_0$, we obtain the following relationship

$$\mathrm{v}(r,t)=\dot R\frac{R^2}{r^2}\frac{T(r,t)}{T_d}\left[1-\frac{T_dn_l}{T_0n(T_0)}+\frac{T_d}{R^2\dot R}\int_{R(t)}^{r}dr_1r_1^2\frac{1}{T^2(r_1,t)}\frac{\partial T(r_1,t)}{\partial t}\right]. \qquad (4)$$

In the case of isothermal condensation at $T(r,t)=T_d=T_0$, Eq.(4) gives $\mathrm{v}(r,t)=-\dot R(t)\left(R^2(t)/r^2\right)[n_l/n(T_0)-1]$ (Kuchma and Shchekin (2012)). This result corresponds to the inflow of the vapor-gas medium at any distance from the droplet. The presence of the positive third term in the brackets on the right-hand side of Eq.(4) gives the possibility of an outflow of the vapour-gas medium at some distances from the droplet. It may be of importance for explaining the cloud floating in the Earth atmosphere. Note that this term disappears at stationary regime of diffusion.

It can be shown that equation of heat conduction in the form

$$\frac{\partial T(r,t)}{\partial t}=\kappa\Delta T(r,t) \qquad (5)$$

(where κ is the coefficient of the thermal conductivity of the vapor-gas medum) provides a sufficient accuracy for finding the profiles of vapor density $n_1(r,t)$ and flow velocity $\mathrm{v}(r,t)$ around a droplet at nonisothermal condensation. For self-similar solutions of Eqs.(1) and (5) (similar to that in Grinin et al (2011) and Kuchma and Shchekin (2012)), approximate expression for $\mathrm{v}(r,t)$ has a form

$$\mathrm{v}(r,t)=\dot R\frac{R^2}{r^2}\left[1-\frac{n_l}{n(T_0)}+\frac{T_d-T_0}{T_0}\frac{\kappa}{R\dot R}\left(1-\exp\left(-\frac{R\dot R}{2\kappa}\left(\frac{r^2}{R^2}-1\right)\right)\right)\right]. \qquad (6)$$

This work was supported by the Russian Foundation for Basic Research (pr. 10.03.00903) and the Program of Development of St. Petersburg State University (pr. 0.37.138.2011).

Colbeck I. (Ed.) (2008), *Environmental Chemistry of Aerosols*, Blackwell.

Frank-Kamenetskii, D.A. (1969) *Diffusion and Heat Transfer in Chemical Kinetics*. Plenum Press.

Grinin, A.P., Gor, G.Yu., Kuni, F.M. (2011) *Atmos. Res.* **101**, 503-509.

Kuchma A.E., Shchekin A.K. (2012) *Colloid Journal*, **74**, 215–222.

Landau, L.D., Lifshitz, E.M. (1987). *Fluid Mechanics*. Butterworth-Heinemann.

High temperature oxidation of tungsten particles with account of Stefan flow

S.G. Orlovskaya, M.S. Shkoropado and F.F. Karimova

Department of Physics, Odessa National I.I. Mechnikov's University, Odessa, 65082, Ukraine
Keywords: metal, combustion particle, modelling, temperature.
Presenting author email: svetor@rambler.ru

Wide applications of tungsten and molybdenum alloys at high temperatures require detailed data on these metals heat and mass transfer in oxidized media. Effect of Stefan flow arising as a result of chemical reactions and phase transitions on the particle surface isn't clarified till now. At elevated temperatures the oxide scale forms on the metal surface which melts at the temperature further rise. Evaporating oxides forms the flow outwards the particle (so called Stefan flow) which affects its ignition and burning characteristics (Kalinchak, 2001; Orlovskaya, 2009).

It is known that oxide scale properties affect significantly the metal oxidation kinetics. The tungsten particle high temperature oxidation is modeled mathematically to obtain the oxide scale thickness history. The maximum on this dependence is found which is explained by concurrence of oxide formation and evaporation processes. When the scale thickness passes through this maximum its value decreases fast, as a result the oxidation rate increases and the particle temperature quickly rises up the metal melting point.

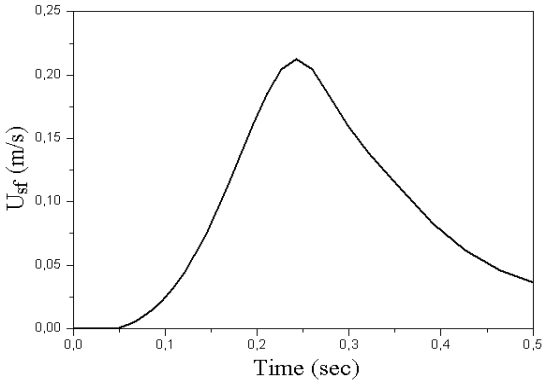

Figure 1. Stefan flow velocity versus time at the tungsten particle surface.

In case of small particles (d<200 μm) the Stefan flow direction changes during the oxidation process. At relatively low temperatures it is directed towards the particle due to solid oxide formation. At higher temperatures the Stefan flow is directed outwards the particle as a result of intense oxide evaporation. So the Stefan flow effect is ambiguous and depends on gaseous oxidizer temperature. For example, for the tungsten particle with diameter 200 μm at the gas temperature T_g = 1500 K and oxygen mass fraction ($n_{O_2\infty}$) 0.5, the oxide scale formation prevails the oxide evaporation so the Stefan flow is directed towards the particle (Fig.1).

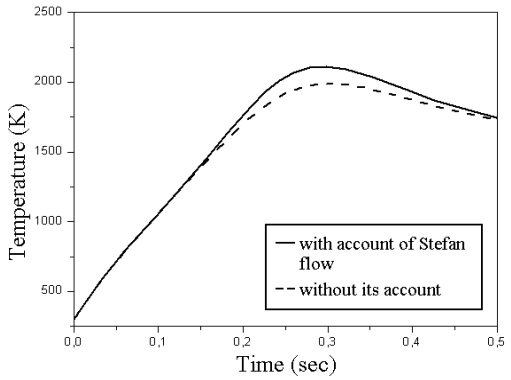

Figure 2. Tungsten particle temperature histories. d =200 μm, $n_{O_2\infty}$ =0.5, T_g =1500 K.

Stefan flow account leads to calculated temperature increase and oxide scale thickness growth. It is found that estimated value of the particle ignition delay increases and its burning time decreases.

It is established that Stefan flow effect on the particle burning characteristics is more pronounced at high gas temperatures and increased oxygen content (Table). Stefan flow account leads to significant burning time decrease in case of small particles.

Table. Ignition delay (t_d) and burning time (t_b) of the tungsten particle at T_g = 1800 K, $n_{O_2\infty}$ = 0.5.

(n/a – no Stefan flow account; w/a – with its account)

Stefan Flow	d, μm	200	300	500
n/a	t_d, ms	117	205	398
w/a		123	234	466
n/a	t_b, ms	167	311	760
w/a		91	231	642

V.V. Kalinchak, S.G. Orlovskaya, and Yu.V. Prudnikova. (2001) Combustion Explosion and Shock Waves. **37** (4), 402-405.

S.G. Orlovskaya, F.F. Karimova, and M.S. Shkoropado (2009). *Proc. 1st Int. Conf. on Chemical and Radiation Physics.*

Heat and mass transfer and thermal decomposition of firm aerosols when laser radiation action

L.I. Ryabchuk and S.K.Protas

Department of Physics, Odessa National I.I. Mechnikov's University, Odessa, 65082, Ukraine
Keywords: heat and mass transfer, firm aerosols decomposition, ferosol-surface reactions, laser radiation action.
Presenting author email: svetor@rambler.ru

Process of firm aerosols burning and the chemical characteristic of burning has been studied on an example of a laser irradiation of the organic fuel rich with oxygen (peat).The theoretical model of laser irradiation of fuel with high humidity is submitted. Process of heat and mass transfer, thermal decomposition and burning of solid organic fuel at its laser irradiation is described by the presented model.

The model includes chemical reactions: oxidation of carbon to CO and CO_2, oxidation of CO_2 to CO, oxidation of carbon by hydrogen from steams of water and combustion of hydrogen. Heterogeneous reactions of oxidation of carbon take place on a surface of the sample and change its thermal balance. It was supposed that at heating of a fuel tablet, even before ignition, there was a thermal decomposition of fuel. Decomposition is accompanied by emission of coal-volatile matter and their emission is described by equation Arrenius. Ignition of flying substances of coal in an boundary layer warms up a gas phase Rise in temperature of a gas phase heats up a surface of the sample by convection and a radiating heat transfer and stimulates chemical reactions and decomposition. The model take into account: diffusive thermal conductivity, which determine endo- and exothermal chemical reaction; flow of coal-volatile matter from sample's surface; convection and molecular heat transfer between gas phase of the boundary layer and gas: radiation heat transfer.

The samples which thickness at considered parameters of process corresponds to a semi-infinite body, were studied. $H \succ\succ (at_i)^{1/2}$, τ - duration of an impulse a - thermal conductivity of peat.

The system of the equations for a considered problem contents:

The heat conductivity equation which defines distribution of temperature of a surface and in volume of the sample $mc\dfrac{dT}{dt} = P(t)A(x_1,...x_n) + \sum_i P_{ex}^i - P_{loss}(T)$,

where *m, c* – weight and a system thermal capacity; *P (t)* – capacity of radiation falling on the sample; A_λ – absorb ability of of a target at laser radiation wavelength; $x_i = x_i(t)$ – concentration of reacting substances; P^i_{ex} – capacity of power allocation of chemical sources – the reactions which are passing in the condensed phase; P_{loss} *(T)* – capacity of heat losses.

1) Partial absorption of laser radiation, thermal streams for the account thermolysis and the chemical reactions which are taking place on a surface, and also convective and radiating losses considers a boundary condition on an irradiated surface;
2) To define boundary layer temperature next factors were taken into account: inflows of heat from combustion coal-volatile matter and at the expense of diffusive heat conductivity coal-volatile matter and components of chemical reactions from an irradiated surface; convection-molecular heat transfer from surface of sample to gas of a boundary layer and also from boundary layer to environment, radiating heat transfer.

Intensity and the form of an impulse of a laser irradiation was various during researches. The irradiation of the sample with three various time dependences of impulses has been studied..

Two triangular form of an impulse $I(t) = \begin{cases} I_{\max}\cdot A_\lambda \cdot t/(\tau / t_{\max}) \\ I_{\max}\cdot A_\lambda \cdot t/(\tau /(\tau - t_{\max})) \end{cases}$, were I_{max} - the maximum value of laser radiation intensity, A_λ - absorb ability of a target at laser radiation wavelength, t_{max} - time when the impulse reaches the maximum value (t_{max} =1 - fast increase of intensity to I_{max} and its slow reduction to zero; t_{max} =3 - slow increase of intensity to I_{max} and its fast reduction to zero). The irradiation of the sample has been studied by the laser impulse which time form looks like curve Gaussa $I(t) = I_{\max}\left(\dfrac{\ln 2}{t}\right)^{1/2}\left\{-\left[\dfrac{r(\ln 2)^{1/2}(t - t_{\max})}{t_p}\right]\right\}$, were t_p - achievement time capacities I_{max} /2, t_{max} - time of achievement of the maximum capacity.

The thermal picture of warming up has been studied: main parameters of ignition and behavior of system after the termination of action of an impulse. Distributions of concentration and oxygen in a boundary film has been received. Influence of the processes occurring in a gas phase on propagation of burning, has been studied. The received data on minimal-necessary energy for ignition and propagation of burning of fuel as functions of intensity and forms of impulses represents as the diagrams.

Flow and Heat Transfer in a Particle Laden Differentially Heated Cavity

J. Kalilainen[1,2], P. Rantanen[1], T. Lind[2], A. Auvinen[1], A. Dehbi[2], S. Güntay[2] and J. Jokiniemi[1,3]

[1] VTT Technical Research Centre of Finland, P.O.box 1000, BI7, FI02044 VTT Espoo, Finland
[2]Paul Scherrer Institut, CH-5232 Villigen PSI, Switzerland
[3]Univ. of Eastern Finland, Department of Environmental Science, P.O. Box 1627, FI-70211 Kuopio, Finland
Keywords: particle image velocimetry, deposition, fission product, severe accident.
Presenting author email: jarmo.kalilainen@vtt.fi

In severe nuclear accidents the containment has the vital role of preventing the release of radioactive particles to the outside environment. A turbulent natural convective flow is induced in the containment by a temperature difference between the walls and hot gas. The turbulence can significantly influence the fraction of particles deposited to the walls and the floor of the containment.

DIfferentially heated cavity with **A**erosol in turbulent **NA**tural convection (**DIANA**) facility was constructed in order to experimentally investigate the effects of turbulent natural convection on aerosol deposition inside the cavity. The results from the experimental work will also be used in validation of the DNS (Puragliesi, 2010) and LES simulation results obtained at the Paul Scherrer Institut (PSI). DIANA facility contains two heated / cooled walls made of aluminium. The top, front and back walls have adiabatic boundary conditions and are made of glass in order to allow optical access to the cavity. Particle Image Velocimetry (PIV) is applied in measuring the flow fields and particle concentrations inside the cavity.

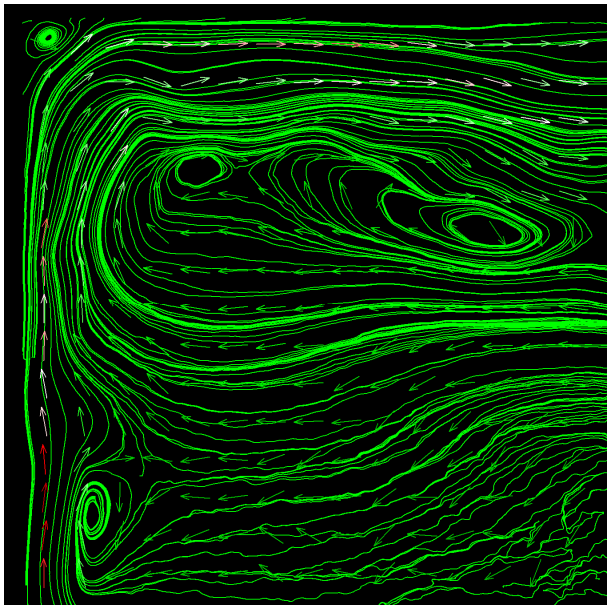

Fig. 1 *Instantaneous streamlines and part of the velocity vectors in the top corner of the differentially heated cavity on the hot side, measured with PIV. Vortexes moving slowly up and right.*

After the construction of the DIANA facility, three preliminary measurements were done to investigate the feasibility of the PIV measurements in this system. Particles were illuminated with a double pulse laser sheet. Laser beam was conducted from the laser to sheet optics with a guiding arm. Parallel laser sheet was formed with an adjustable telescope and a convex lens. The laser sheet was directed into the cavity from the top through a double layer window. Sheet thickness was about 1 mm. Duration of a laser pulse was about 5 ns and energy of one pulse was 10 to 250 mJ at wavelength of 532 nm.

Three measurement planes are situated at 330 mm, 210 mm and 70 mm from the front adiabatic wall. For each measurement, the imaged plane was divided into 16 200 x 200 mm sections. A double frame CCD camera with 2048 x 2048 pixel sensor was used for imaging. Interframe delay for PIV measurements was 10 ms to 100 ms. 500 images were taken from each imaging plane. Oil aerosol was used as tracer particles in PIV measurements. The cavity atmosphere consisted of air and the hot and cold wall temperatures were set to approximately 57 °C and 19 °C, respectively. This sets the Rayleigh number of the flow to an approximate value of 10^9, which was also used in the DNS simulation work (Puragliesi, 2010).

The preliminary flow measurements showed that there are slowly moving vortexes between the high velocity side flow and slowly moving centre. In the corners, there are obviously small stable vortexes. Fig. 1 shows the instantaneous streamlines and velocity vectors at the top corner near the heated wall. Also, other larger vortexes could be seen in the average flow fields, calculated from the PIV data.

After the flow field measurements have been completed, the particle depletion on the cavity walls is investigated. This is done using PIV to measure the change in particle concentration due to particle deposition and settling on the cavity walls and floor. Also, Condensation Particle Counter (CPC) and Tapered Element Oscillating Microbalance (TEOM) are used to help determine the change of particle concentration in time. Latex and/or hollow glass beads with 2 or 3 different particle diameters, varying from 1 to 20 µm are applied in the concentration measurements.

Puragliesi, R. (2010) *Numerical Investigation of Particle-Laden Thermally Driven Turbulent Flows in Enclosure*, Ph.D. thesis. no:4600, École Polytechnique Fédérale de Lausanne. Lausanne.

Modelling of spray drying of multicomponent aerosols

J.M. Gac[1] and L. Gradoń[1]

[1]Faculty of Chemical and Process Engineering, Warsaw University of Technology, Warsaw, 00-645 Poland
Keywords: heat and mass transfer, medicinal aerosols, numerical simulation, particle formation.
Presenting author email: J.Gac@ichip.pw.edu.pl

The spray drying process is widely used in various aerosol techniques in aerosol technologies, as e.g. manufacturing of drug particles for inhalation. The main advantage of spray drying is possibility of obtaining of regular-shaped spherical particles with nearly uniform dimensions (contrary to e.g. crystallization followed by milling). Another advantage may be special segregation of components in particles formed. This segregation may improve the storage characteristics and facilitate the controlling of drug delivery.

Typically, the spray drying process consists on two stages. During the first one the droplet of solution gets a sensible heat from the surrounded gas and the evaporation occurs resulting in diameter shrinking. Following that, the mean concentration of all the components grows up. When the concentration of one of components exceeds its critical value (typically, it takes place near the droplet surface first), the solid porous crust forms and the second stage of drying starts. During this stage the evaporating water diffuses through the porous crust and the farther growing of the concentration of components takes place, resulting in increasing of crust thickness. The segregation of components may take place as a result of difference in their diffusivity (Wang and Langrish, 2009).

The aim of our work is to build numerical model of spray drying such multicomponent droplets. Because of moving boundaries (decreasing of droplet diameter in a first stage and increasing of crust thickness in the second one) the direct numerical solution of heat and mass transport in droplet seems to be quite difficult (Mezhericher *et al*, 2008). To solve this problem we adopt the shell model, first present by Parentia *et al* (2011). In this model the droplet is considered as a set of concentric shells between which the heat and mass is moving. The thickness of each shell decreases as a result of water evaporation. Contrary to the original work (Parentia *et al*, 2011), in our model we take into account the crystallization of components and solid crust formation.

As a result of our investigations, we describe the kinetics of spray drying of mulitcomponent droplet (see Fig. 1 for example). We have also examined the influence of drying agent temperature, initial droplet diameter and concentration of all the components, its diffusivity, solubility etc. on properties of particle formed: its diameter and composition. We have found that in most cases two regions of particle can be distinguished – the outer shell, where the composition strongly changes and the inner one where the concentration of each component is nearly constant, as it is seen in Fig. 2. The thickness of the inner shell depends mainly on the solubility ratio of all the components and has been also estimated in our investigations.

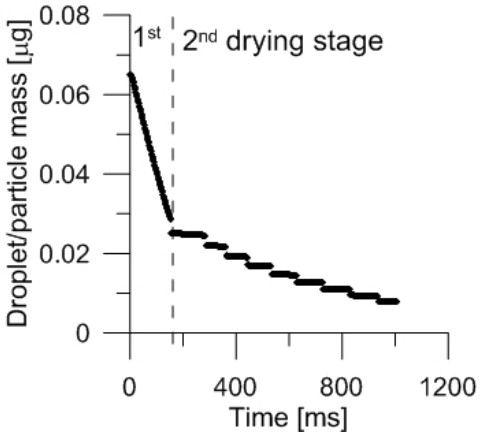

Figure 1. Droplet/wet particle mass as a function of time of drying.

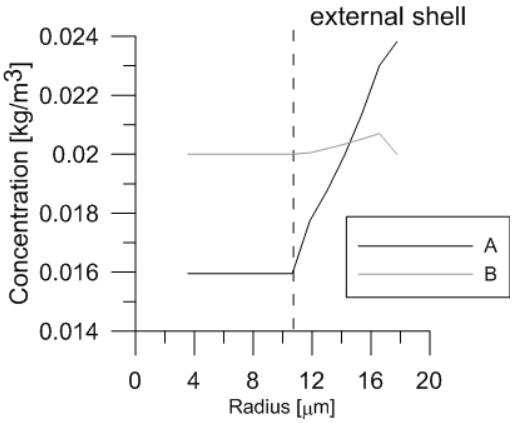

Figure 2. The composition of spray drying formed particle contained two components, *A* and *B*.

Mezhericher M., Levy A. and Borde I. (2008) *Chem. Eng. Process.* **47**, 1404-1411.

Parentia D., Morawska L., Johnson G.L.,. Ristovski Z.D., Hargreaves M., Mengersen K., Corbett S., Chao C. Y. H., Li Y. and Katoshevski D. (2011) *J. Aero. Sci.* **42**, 1-10.

Wang S. and Langrish T.A.G. (2009) *Adv. Powder Technol.* **20**, 220-226.

The effect of droplet size on the evaporation and mass accommodation processes of water: a molecular dynamics study

Jan Julin and Ilona Riipinen

Department of Applied Environmental Science (ITM), Stockholm University, SE-10691 Stockholm, Sweden
Keywords: mass accommodation, fundamental aerosol physics, molecular dynamics, water.
Presenting author email: jan.julin@itm.su.se

The majority of atmospheric particle number consists of particles in the ultrafine sub-100 nm size-range, thus understanding their growth processes has a central role in understanding the climate effects of aerosols. The condensational growth of ultrafine particles is quite sensitive to their ability to uptake various gaseous species, an ability which is quantified by the mass accommodation coefficient. Unfortunately, there still exists some controversy on the value of the mass accommodation coefficient even for the case of water-on-water, for which values ranging from 0.1 to 1 have been reported (see e.g. review by Kolb *et al.* and references therein).

On a molecular level the mass accommodation coefficient α is commonly defined as the fraction of incoming molecules that are absorbed to the surface. As such, the coefficient can be readily studied by using molecular dynamics (MD) simulations, where the trajectories of individual molecules can be followed as a function of time. Several such studies have reported a mass accommodation coefficient $\alpha \approx 1$ (e.g. Morita *et al.*, 2004, Neshyba *et al.*, 2009, Takahama and Russell, 2011), for various temperatures, water potential models, and even different bulk phases. However, to our knowledge all MD mass accommodation studies consider a planar interface. This practice can be considered quite reasonable if one is interested in relatively large particles, but nonetheless for smallest droplets size-dependent factors may affect the process.

We are performing MD simulations to study the effect of droplet size on the mass accommodation and the evaporation processes, and we have also simulated the familiar mass accommodation on a planar surface to facilitate a consistent comparison with the droplet simulations. This set of simulations allows us to examine how well the simulated evaporative flux agrees with the theoretical predictions, which are derived using bulk thermodynamic considerations. Furthermore, the size-dependence, or lack of one, of the various processes and properties help in the assessment of the validity of assumptions used in different kinetic mass-transport models. The simulations are performed with the GROMACS software (Hess *et al.*, 2008), using the TIP4P-Ew water model. After an initial equilibration of the target droplet, or the target liquid slab, incident molecules are generated at set time intervals with velocities pointing towards the target surface. The incoming water molecules are generated at a set distance but random locations around the droplet, with different initial orientations, and the velocities are drawn from the Maxwell-Boltzmann distribution corresponding to the desired temperature. A total of 1000 impact events are simulated per target surface, with a fresh simulation started after a set of ten incident molecules to ensure that the target droplet remains roughly at a constant size.

First results show that at T=273.15 K the accommodation coefficient on clusters consisting of as few as 1000 molecules (a radius of only about 2 nm) is ≈1, which is same as for a planar surface. In addition to the absorption and scattering of the incoming molecules, evaporation events are observed during the simulations. Conceivably some of them could be induced by the accommodation of an incident molecule, and the actual accommodation coefficient could therefore be lower. However, the trajectories suggest that from an already low number of evaporation events only few occur both spatially and temporally close to the location of an impact, thus reaffirming that α will be close to unity.

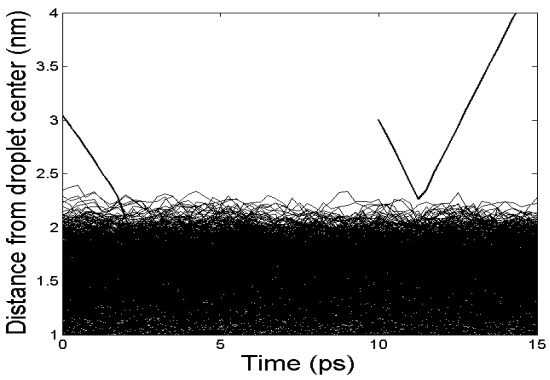

Figure 1. Example trajectories: absorption and recoil events.

This work was supported by the European Research Council ATMOGAIN (No. 278277). Computational resources were provided by PDC Center for high performance computing.

Hess, B., Kutzner, C., van der Spoel, D., Lindahl, E. (2008). *J. Chem. Theory Comp.* **4**, 435-477.

Kolb C. E. *et al.* (2010). *Atm. Chem. Phys.* **10**, 10561-10605.

Morita, A., Sugiyama, M., Kameda, H., Koda, S. And Hanson D. R. (2004). *J. Phys. Chem. B* **108**, 9111-9120.

Neshyba, S., Nugent, E., Roeselova, M., and Jungwirth, P. (2009). *J. Chem. Phys. C* **113**, 4597-4604.

Takahama S. and Russell, L. M. (2011). *J. Geophys. Res.* **116**, D02203.

Design of a simulation facility for workplace relevant aerosols of semi-volatile organic hydrocarbons: Set-up and first results

G.C. Dragan[1,2], E. Karg[1], H. Nordsieck[3], J. Schnelle-Kreis[1] and R. Zimmermann[1,2]

[1]Joint Mass Spectrometry Centre, Cooperation Group Comprehensive Molecular Analytics, Helmholtz Zentrum München, Ingolstädter Landstr. 1, 85764 Neuherberg, Germany
[2]Joint Mass Spectrometry Centre, Chair of Analytical Chemistry, University of Rostock, Dr.-Lorenz-Weg 1, 18059 Rostock, Germany
[3]bifa Environmental Institute, Am Mittleren Moos 46, 86167, Augsburg, Germany
Keywords: mineral oil mist, SVOC aerosol, mixed phase measurement, sampling strategy.
Presenting author email: constantin.dragan@helmholtz-muenchen.de

The measurement and risk assessment of semi-volatile organic hydrocarbons in workplace air is complicated by their readiness to condense and form particles, evaporate from filters and adsorb onto surfaces.

Mineral oil fractions, frequently used as a coolant, lubricant or cutting fluid during the machining of metal components in many industrial processes are known to form oil mist. The used mineral oil fractions mainly contain a mixture of straight-chain, aliphatic hydrocarbons from $C_{12}H_{26}$ to $C_{23}H_{48}$ (Raynor, 1999). In the case of oil mist, the particulate phase is considered to be of greater toxicological concern than the vapour, even though the vapour is often present in much higher concentration (Simpson, 2008). Due to mist separation between vapour and particle phase, artefacts are likely to occur in workplace aerosol samplers (filter blow-on, blow-off, evaporation, condensation, particle penetration) and may lead to errors in risk assessment as a consequence.

Due to the different toxicological effects of particle and vapour there is an increasing need to accurately differentiate between particle bound mass and gas-phase concentration in workplace sampling and monitoring. Because traditional filter-denuder sampling may induce sampling artefacts we are now investigating a new online method that can accurately distinguish between the vapour and particle mass.

Our second aim is to study the dynamic processes related to oil mist formation, ageing and sampling. For this purpose our study focuses on a simulation facility for SVOC test aerosols and on the development of a theoretical evaporation model.

For the theoretical part we have developed a particle evaporation model that predicts the evaporation rate of a single component aerosol and for the experimental part we have designed an aerosol simulation facility inside two temperature controlled chambers.

The chambers are operated at constant temperatures ranging from 10 to 40 °C. The setup allows the simulation of the three phases in an aerosol life cycle: generation, transport/ ageing and deposition/ analysis. The experimental system consists of:

- a Sinclair-La Mer type aerosol generator (Topas SLG 270) to produce particles from the test substances by vapour deposition on condensation nuclei.
- a mixing head designed to obtain an homogenous aerosol - dilution gas mixing.
- a flow-tube reactor to study the dynamic processes during and directly after the aerosol production.
- a white light particle sizer (Palas WELAS 3000) and a FID hydrocarbon gas analyser (JUM 109A) coupled with a heated transfer line for quantification of particle- and gas phase concentration.
- a 300 l Tedlar ageing bag that allows 10 to 60 minutes of residence time to simulate aerosol ageing.

The particle diameter and lifetime are the most important factors in relationship to the inhalation risk. Our model shows that a 1µm aerosol particle can have a lifetime between a few fractions of a second and several hours depending on the droplet components, partial pressure and temperature. The particle lifetime can also influence the amount of inhaled aerosol as larger particle lifetimes lead to an enhanced transport distance and exposed area.

Our experimental data is in good agreement with the model prediction for 1-component systems. Multicomponent-mixture experiments are in preparation.

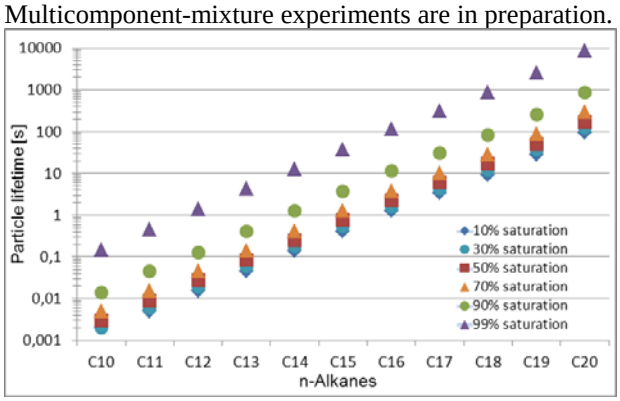

Figure 1. Estimated lifetime for 1µm droplet of n-alkanes ($C_{10}H_{22}$ - $C_{20}H_{42}$) depending on the gas phase saturation at 25°C and 1 atm.

This work is supported by the German Statutory Accident Insurance (DGUV) under Research Contract FP 299. The health effects of organic compounds in aerosols are currently further investigated in the framework of the Helmholtz Virtual Institute of Complex Molecular Systems in Environmental Health, HICE (www.hice-vi.eu).

Raynor, P.C., & Leith, D. (1999). *Ann. Occup. Hyg.*, 43(3), 181-192.

Simpson, A.T., & Wright, M.D. (2008). *Ann. Occup. Hyg.*, 52(4), 249-257.

Measurement of neutral sulphuric acid dimer concentration during CLOUD

A. Kürten, L. Rondo, S. Ehrhart, J. Curtius and the CLOUD collaboration

Institute for Atmospheric and Environmental Sciences, University of Frankfurt, Frankfurt, 60438, Germany
Keywords: CIMS, CLOUD, nucleation, sulphuric acid, cluster
Presenting author email: kuerten@iau.uni-frankfurt.de

The nucleation of aerosol particles is an important process affecting atmospheric chemistry, visibility, weather and climate as well as human health.

Observations show that under atmospherically relevant conditions the particle nucleation rate is strongly dependent on the concentration of sulphuric acid. However, recent studies have shown that the binary system of sulphuric acid and water cannot explain atmospheric nucleation (Kirkby *et al* (2011)). Therefore, the influence of ternary substances is increasingly discussed. Likely candidates for enhancing the nucleation are basic molecules, and it has indeed been shown that the addition of ammonia at very low concentrations in the pptv-range can increase the nucleation rate by several orders of magnitude compared to the pure binary case (Kirkby *et al* (2011)). In addition to ammonia, modelling studies and experiments suggest that other ternary substances like amines and oxidized organic compounds can enhance the nucleation tremendously as well – potentially even stronger than ammonia (Kurten *et al* (2008), Metzger *et al* (2010), Zollner *et al* (2012)).

During the CLOUD (Cosmics Leaving OUtdoor Droplets) experiments conducted at CERN the effect of ammonia, dimethylamine and organic oxidation products on the particle nucleation rates has been studied systematically. During these experiments a certain concentration of sulphuric acid is established within a very clean stainless steel chamber. Adding different concentrations of ternary substances allows quantifying the enhancement of these substances on the nucleation rates. In addition to adding gas-phase substances, the effect of ions on the nucleation can be investigated as well by means of an ionizing particle beam provided by the CERN proton synchrotron.

The concentration of sulphuric acid during CLOUD is measured through chemical ionization mass spectrometry (CIMS). This method allows the accurate and precise measurement of sulphuric acid at concentrations above ~$5x10^5$ molecule/cm^3. In addition to measuring the monomer concentration, the CIMS instrument can be used to determine the sulphuric acid dimer concentration. This measurement is important because it allows identifying at which stage of the nucleation process the stabilizing effect of a base molecule becomes effective. In a recent study evidence has been found that the stabilizing effect is already affecting the dimer formation for the neutral nucleation pathway (Petäjä *et al* (2011)). This speculation was supported by the unexpectedly high dimer concentrations measured during nucleation studies conducted in a laminar flow tube as well as through modelling studies. However, the study by Petäjä *et al* (2011) was lacking the direct measurement of ammonia or amines and could therefore only link the enhanced sulphuric acid dimer concentrations to the presence of an unknown contaminant with unknown concentrations.

Here, we present results related to the measurement of neutral sulphuric acid dimers during the CLOUD experiment. The measured dimer concentrations will be discussed for the cases of binary sulphuric acid and water nucleation as well as ternary nucleation experiments involving ammonia and dimethylamine, respectively. The dimer formation rates will be presented with respect to the observed nucleation rates derived from various condensation particle counters. In contrast to most other studies, the concentration of ternary substances like ammonia and dimethylamine in the pptv-range has been measured with state-of-the-art instruments during CLOUD. Therefore, sulphuric acid dimer formation will also be discussed regarding different concentrations of these ternary substances.

We would like to thank CERN for supporting CLOUD with important technical and financial resources, and for providing a particle beam from the CERN Proton Synchrotron. This research has received funding from the EC Seventh Framework Programme (Marie Curie Initial Training Network "CLOUD-ITN" grant no. 215072, and ERC-Advanced "ATMNUCLE" grant no. 227463), the German Federal Ministry of Education and Research (project no. 01LK0902A), the Swiss National Science Foundation (project nos. 206621_125025 and 206620_130527), the Academy of Finland Center of Excellence program (project no. 1118615), the Austrian Science Fund (FWF; project no. P19546 and L593), the Portuguese Foundation for Science and Technology (project no. CERN/FP/116387/2010), and the Russian Foundation for Basic Research (grant N08-02-91006-CERN).

Kirkby, J., Curtius, J., Almeida, J., *et al* (2011) *Nature* **476**, 429 – U77.

Kurten, T., Loukonen, V., Vehkamäki, H. and Kulmala, M. (2008) *Atmos. Chem. Phys.* **8**, 4095 – 4103.

Metzger, A., Verheggen, B., Dommen, J., *et al* (2010) *PNAS* **107**, 15, 6646 – 6651.

Petäjä, T., Sipilä, M., Paasonen, P., *et al* (2011), *Phys. Rev. Lett.* **106**, 22, 228302.

Zollner, J.H., Glasoe, W.A., Panta, B., *et al* (2012) *Atmos. Chem. Phys. Discuss.* **12**, 1117 – 1150.

Nucleation and condensation on presence of aerosols in boundary-layer flows

L.L. Bonilla[1] and M.D. Camejo[1]

[1]Gregorio Millán Institute, University Carlos III, Leganés, Madrid, 28911, Spain
Keywords: Boundary layer, Condensation, Nucleation, Deposition.
Presenting author email: mdcamejo@ing.uc3m.es

Condensation of vapours is a very well phenomenon that occurs in a wide variety of scenarios ranging from nature to industry and, of course, at different spatial scales. Air flowing in the open atmosphere at the seafront carries water vapour molecules in a suspension of saline aerosols [1]. In combustion chambers, hot air carries a mixture of soot and vaporized substances produced by the combustion of fuels [2,3]. In both cases, flow contents are very aggressive.

The relatively colder walls of tall buildings or combustion chambers allow the formation of neighbouring condensation layers where active processes of nucleation and condensation take place and result in the subsequent deposition of condensate.

Wall temperature (considered to be constant) and density and size of suspended particles are the main controlling parameters for the problem while physical properties of substances and air are, in general, temperature-dependent. Depending on droplet size, condensation may occur according to a free molecular regime or by diffusion, so this aspect needs also to be considered.

We propose a thermophysical model to describe homogeneous and heterogeneous condensation in simple laminar boundary-layer flows near cold walls assuming that the supersaturated vapours are diluted [4]. Then the air velocity and temperature fields are independent of the condensation process. We determine the position of the condensation layers and obtain the profiles of vapour density, density and size of droplets, and the deposition rates on the walls. Droplet nucleation is modelled by the Zeldovich stationary flux of supercritical clusters. The droplet distribution resulting from nucleation is approximately monodisperse although we have also considered the polydisperse case.

We have solved numerically the thermophysical model and interpreted the results by using singular perturbation techniques. These approaches lead to a reduction of the problem and basically work by uncoupling the droplet density balance equation from the rest, estimating it, solve the remaining equations and iterate to improve the approximation.

The figure shows total deposition rates (vapour and condensate) as obtained by solving numerically the whole model (plot indicated as n) and by an asymptotic approach (plot indicated as a). The results are good for a very wide range of wall temperatures.

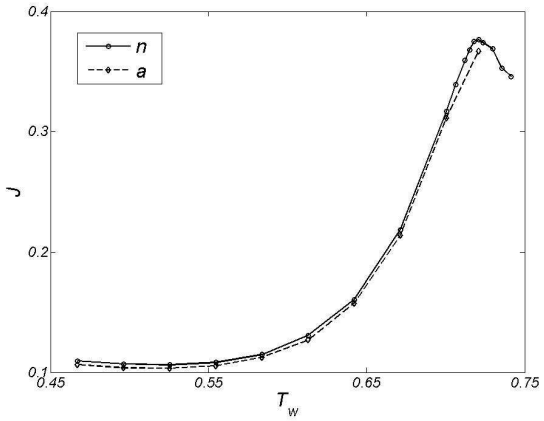

Figure 1. Total deposition rates on the wall (J) vs. wall temperature (Tw)

This work has been supported by the Spanish Ministry of Economy and Competitiveness grant FIS2011-28838-C02-01 and by the Autonomous Region of Madrid grant P2009/ENE-1597 (HYSYCOMB).

[1] Friedlander, S.K. (2000) *Smoke, dust, and haze. Fundamentals of aerosol dynamics*, 2nd ed. Oxford U. P., New York.
[2] Castillo, J.L. and Rosner, D.E. (1989) *Chem. Eng. Sci.* **44**, 925-937.
[3] Neu, J.C., Bonilla, L.L. Carpio, A. (2009) *J. Fluid Mechanics* **626**, 183-210.
[4] Camejo, M.D. and Bonilla, L.L. (2011) **(submitted)**.

Particle nucleation in urban subtropical atmosphere

F. Salimi, L. Morawska, Z. Ristovski and M. Mazaheri

ILAQH, IHBI, QUT, Brisbane, QLD, 4001, Australia
Keywords: Nucleation, Particle growth, Condensation sink, Urban areas.
Presenting author email: f.salimi@qut.edu.au

New particle formation (NPF) and growth have been observed in different environments all around the world and NPF affects the environment by forming cloud condensation nuclei (CCN). Detailed characterisation of NPF events in a subtropical urban environment is the main aim of this study. Particle size distribution (PSD) of atmospheric aerosol particles in range 9-414 nm were measured using a Scanning Mobility Particle Sizer (SMPS), within the framework of the "Ultrafine Particles from Traffic Emissions and Children's Health" (UPTECH) study, which seeks to determine the relationship between exposure to traffic related ultrafine particles and children's health (http://www.ilaqh.qut.edu.au/Misc/UPTECH%20Home.htm). The UPTECH study includes measurements of air quality, meteorological and traffic parameters in 25 randomly selected state primary school within the Brisbane metropolitan area, in Queensland, Australia. Measurements at 17 schools have been completed so far.

SO_2, NO_x, CO, PM_{10} and $PM_{2.5}$ concentration, as well as solar radiation (SR), humidity, wind speed/direction and other air quality parameters were measured in each school. Data which were not measured or missed due to instrument faults were obtained from the nearest Department of Environment and Resource Management (DERM) or Bureau of Meteorology (BOM) site.

Several nucleation events were identified based on the method presented by dal Maso et al (2005) and the condensation sinks (CS) for all PSDs during these events were calculated. H_2SO_4 concentration was substituted with a proxy as follows (Salma et al. 2010):

$$[H_2SO_4] \propto \frac{[SO_2] \times Rad}{CS}$$

PSD, CS, SR, and SO_2 concentration during an NPF event at one of the schools (S09) is illustrated in Figure **1**. The temporal trend of PSD is illustrated by an image plot which shows a significant increase in particle concentration in the nucleation mode (<25nm) during the late morning, followed by an increase in particle size for several hours. The dashed line illustrates the geometric mean diameter (GMD) of particles in the nucleation mode, which shows an increase at the beginning of the event and then the particles exceed the nucleation size range. SR, SO_2 and O_3 concentration increased during event, however CS was at its minimum value throughout.

This study is part of an ongoing project and further measurements and analysis are currently in progress, including measurements for the last eight sites. The development of an automatic NPF identification procedure in the Igor Pro environment and a detailed analysis of the main parameters affecting new particle formation events are also still in progress.

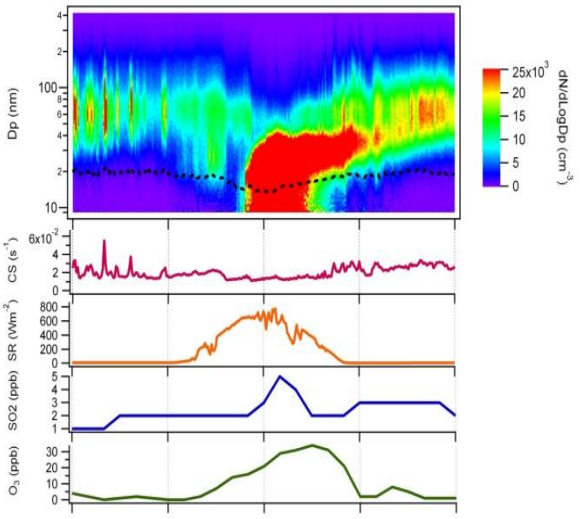

Figure 1. PSD, CS, SR, SO2, and CO concentration at S05 during an NPF event.

This work was supported by the ARC, DTMR and DET through Linkage Grant LP0990134. We would also like to thank all members of the UPTECH project, including R. Fletcher, A. Monk, G. Marks, P. Robinson, K. Mengersen, G. Ayoko, C. He, R. Jayaratne, G. Johnson, S. Low Choy, W. Ezz, G. Williams, L. Crilley, M. Falk, M. Mokhtar, N. Mishra, R. Laiman, C. Duchaine, H. Salonen, X. Ling, J. Davies, L. Toms, F. Fuoco, A. Cortes, B. Toelle, A. Quinones, P. Kidd and R. Appleby

Dal Maso, M., M. Kulmala, I. Riipinen, R. Wagner, T. Hussein, P. P. Aalto & K. E. J. Lehtinen (2005) Formation and growth of fresh atmospheric aerosols: eight years of aerosol size distribution data from SMEAR II, Hyytiälä, Finland. *Boreal Environment Research*, 10**,** 323-336.

Salma, I., T. Borsós, T. Weidinger, P. Aalto, T. Hussein, M. D. Maso & M. Kulmala (2010) Production, growth and properties of ultrafine atmospheric aerosol particles in an urban environment. *Atmospheric Chemistry and Physics Discussions*, 10**,** 13689-13721.

Growth of sulfuric acid nano-particles at dry and wet conditions

L. Škrabalová[1, 2], D. Brus[3], V. Ždímal[1] and H. Lihavainen[3]

[1]Laboratory of Aerosol Chemistry and Physics, Institute of Chemical Process Fundamentals, Academy of Sciences of the Czech Republic, Rozvojová 135 Prague, 165 02, Czech Republic
[2]Department of Physical Chemistry, Faculty of Science, Charles University in Prague, Hlavova 8 Prague, 128 43, Czech Republic
[3]Finnish Meteorological Institute, Erik Palménin aukio 1, P.O. Box 503, FI-00101, Helsinki, Finland
Keywords: sulfuric acid, nano-particles, particle growth.
Presenting author email: skrabalova@icpf.cas.cz

This work presents measurements of sulfuric acid nano-particles produced by homogenous nucleation. Since sulfuric acid has a key role in atmospheric new particle formation (Sipilä et al, 2011), it has been intensively studied for a long time, however the exact mechanism of atmospheric nucleation and subsequent growth (Biskos et al., 2009) has not been fully understood yet.

The experiments presented here were conducted in a laminar flow tube which was kept at a constant temperature. A steady stream of particle free air saturated with high purity sulfuric acid (97% w.t.) was mixed with a mixing stream of particle free air saturated with water vapor and then the stream flowed through the tube. Temperature and humidity of the gaseous mixture were measured using probes (PT100 and Vaisala HMI38).

The measurements were performed at relative humidities ~1% and ~30% and at 4 residence times 30, 45, 60 and 90 seconds. The nucleation temperatures investigated were 10, 20 and 30°C. Temperature of the acid saturator was changed in seven small increments during the experiment resulting in gradually increasing concentration of sulfuric acid in the gaseous mixture. At the outlet of the flow tube there were measured number concentrations of produced particles using Ultrafine Condensation Particle Counter (UCPC TSI 3776) and particle size distributions using Differential Mobility Particle Sizer (DMPS with a short HAUKE type DMA and UCPC TSI 3025A). In Figure 1 is presented the observed variation in particle size distribution and particle number concentration with time obtained from inversion process of raw DMPS data from a single experiment. The increasing particle concentration and particle diameter correspond with increasing sulfuric acid concentration due to gradually growing temperature of acid saturator.

Figure 2 illustrates the dependency of particle median diameter on temperature of acid saturator at different residence times. As the concentration of sulfuric acid increases, the particle size generally increases at all residence times.

This work was supported by the Grant agency of the Academy of Sciences of the Czech republic (Grant no. IAA200760905).

Sipilä, M., Berndt, T., Petäjä, T., Brus, D., Vanhanen, J., Stratman, F., Patokoski, J., Mauldin III, R. L., Hyvärinen, A.-P., Lihavainen, H. and Kulmala, M. (2010) *Science* **327**, 1243-1246.

G. Biskos, P. R. Buseck, S. T. Martin (2009) *J. Aerosol Sci.* **40**, 4, 338-347.

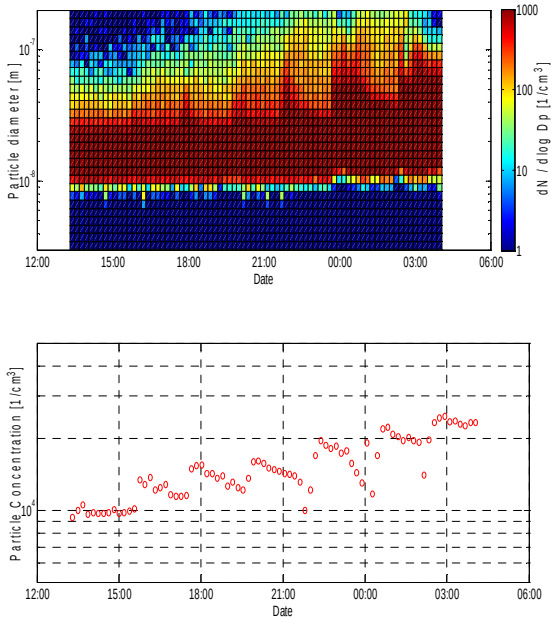

Figure 1. Variation in particle size distribution and number concentration during a single measurement at RH = 34%

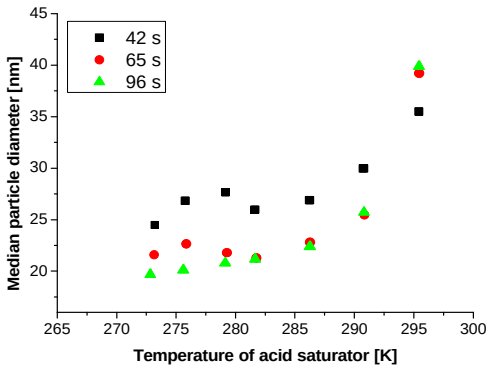

Figure 2. Dependency of median particle diameter on temperature of acid saturator at residence times 42, 65 and 96s at RH = 30%

Using A09 Particle Size Magnifier for resolving formation and growth rates below 2 nm

K. Lehtipalo[1,2], A. Franchin[1], T. Nieminen[1], S. Schobesberger[1], J. Kangasluoma[1], J. Mikkilä[2], J. Vanhanen[2], T. Petäjä[1], and M. Kulmala[1]

[1]Department of Physics, University of Helsinki, 00560 Helsinki, FINLAND
[2]Airmodus Oy, 00560 Helsinki, FINLAND

Keywords: nucleation, condensation particle counters, nano-particles, growth rates
Presenting author email: katrianne.lehtipalo@helsinki.fi

A reason why the molecular level processes leading to new particle formation are not yet completely understood has been the inability to detect neutral particles below 3 nm. Typically, the formation rate is calculated for larger particles, and then scaled back to the size of the nucleating clusters using assumptions of growth rate, particle losses *etc.* New kinds of condensation particle counters, like the A09 Particle Size Magnifier, allow deriving parameters describing the new particle formation process, *e.g.* the formation and growth rates, directly from measurements also in the size range well below 2 nm, *i.e.* exactly at the size of the critical clusters.

The Airmodus A09 Particle Size Magnifier (PSM) can be used to resolve the size distribution of particles below 2 nm. The PSM is a mixing-type condensation particle counter using diethylene glycol to activate particles. An external CPC is then used for growing and counting the activated particles. The nominal cut-off size of the Particle Size is about 1.5 nm (Vanhanen *et al.* 2011). However, the cut-off size of the instrument can be varied between about 1 – 2.5 nm by changing the mixing ratio of saturator and aerosol flow and thus changing the supersaturation created. Exact laboratory calibrations are needed for establishing the relation between the size and the mixing ratio.

The A09 PSM was tested and calibrated in University of Helsinki laboratory facilities using negatively charged ammonium sulphate clusters, which were produced in a tube furnace and size-selected with high-resolution Herrmann DMA. The exact composition of the produced clusters and the cleanliness of the sample were verified with an APi-TOF mass spectrometer (Junninen *et al.,* 2010). The detection efficiency was measured also for mobility standards, NaCl and silver ions. Since the activation probability of small particles and clusters in a CPC can depend on their charge and composition, the calibration strictly holds only for the measured compounds.

The formation rates and growth rates below 2 nm have been determined from the size distribution measured with the PSM, for example for nucleation experiments in the CLOUD-chamber (Duplissy *et al.,* 2010; Kirkby *et al.,* 2011) and for field measurements at the Hyytiälä SMEAR II measurement station (Kontkanen *et al.,* 2012). The growth rates (GR) were calculated from the difference between the appearance times of the newly formed particle population with different cut-off sizes of the PSM. The growth rates below 2 nm were also compared to the appearance times of differently sized charged clusters measured with the APi-TOF, and to the growth rates of 1.6-3 nm ions from ion spectrometers. However, the PSM gives additional information on the behaviour of the smallest neutral particles at the beginning of the new particle formation. This is crucial since nucleation in the boundary layer is most probably dominated by neutral mechanisms (*e.g.* Manninen *et al.*, 2010). The initial growth rates determine what fraction of the newly formed particles eventually reach sizes, where they can act as CCN and influence the climate.

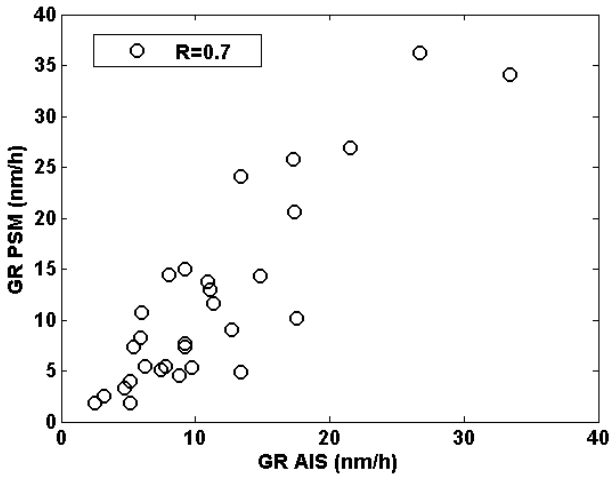

Figure 1. Comparison of the growth rate of the total particle population below 3 nm measured with the PSM and the growth rate of positive 1.6-3 nm ions measured with the AIS ions spectrometer.

Duplissy, J. *et al.* (2010) *Atmos. Chem. Phys.,* **10**, 1635-1647.
Junninen, H. *et al.* (2010) *Atmos. Meas. Tech.*, **3**, 1039-1053.
Kirkby, J. *et al.* (2011) *Nature* **476**, 492-433.
Kontkanen, J. *et al.* (2012). This abstract collection.
Manninen, H.E. *et al.* (2010). *Atmos. Chem. Phys.*, **10**, 7907-7927.
Vanhanen, J. *et al.* (2011) *Aerosol Sci.Tech.* **4**, 533-542.

Two amine campaigns; H_2SO_4 detection with different methods

K. Neitola[1], D Brus[1], U. Makkonen[1] and H. Lihavainen[1]

[1]Finnish Meteorological Institute, Erik Palménin aukio 1, P.O. Box 503, FI-00101, Helsinki, Finland
Keywords: nucleation, sulphuric acid, amine, flow tube.
Presenting author email: kimmo.neitola@fmi.fi

Atmospheric new particle formation is an important source of aerosol particles. Sulphuric acid is known to play key role in nucleation but third species is expected to participate in the first steps of nucleation. Laboratory studies have been recently focusing on the effect of amines and ammonia on the nucleation (e.g. Berndt et al., 2010).

Two similar campaigns have been conducted in the Finnish Meteorological Institute using flow tube technique to investigate the effect of four different base molecules (ammonia, monomethyl-, dimethyl- and trimethyl amine) on sulphuric acid-water gas to liquid-nucleation. Flow tube is a vertically positioned two meter long thermally controlled stainless steel cylinder. Sulphuric acid was produced from pure liquid sulphuric acid in a thermally controlled saturator.

In the first experiment, sulphuric acid concentration was detected with Chemical Ionization Mass Spectrometer (CIMS, Petäjä et al., 2009) or with Atmospheric pressure interface Time of Flight mass spectrometer (Api-TOF, Junninen et al., 2010) used with similar Chemical Ionization inlet as the CIMS. In the second experiment Sulphuric acid concentration was determined with the instrument for Measuring AeRosols and Gases (MARGA, ten Brink et al., 2007) from SO_4^{2-} concentration separately from gas and aerosol phase. Major difference in these methods is that with MARGA total sulphate concentration was determined and with CIMS/Api-TOF only the H_2SO_4-monomer concentration was measured. MARGA is able to detect five different acidic gases and eight major inorganic species from aerosol phase, so it can be used also to detect amines.

Particle concentration was measured with Ultra Fine Condensation Particle Counter (UFCPC, TSI model 3776) and custom made Differential Mobility Particle Sizes (DMPS) was used for measuring the number size distribution from 3 to ~260nm.

Measured nucleation rates covered several order of magnitudes, from 0.1 to ~500 #/cm^{3}s with sulphuric acid concentrations ranging from 10^5 to 10^7 mol./cm^3 (CIMS/Api-TOF) or 10^8 to 10^{10} mol./cm^3 (MARGA) depending which instruments were used for sulphuric acid detection. Mean particle size was always below 30nm, usually between 10-20nm.

Figure 1 presents particle number concentrations as a function of H_2SO_4 monomer measured by CIMS (lower x-axis) and as a function of total SO_4^{2-} measured by MARGA (upper x-axis) for sulphuric acid-water nucleation only. In both measurements the temperature of the saturator is only changed variable. It is clear that depending on the measuring instruments, similar nucleation rates are produced with sulphuric acid concentration that differs by orders of magnitude.

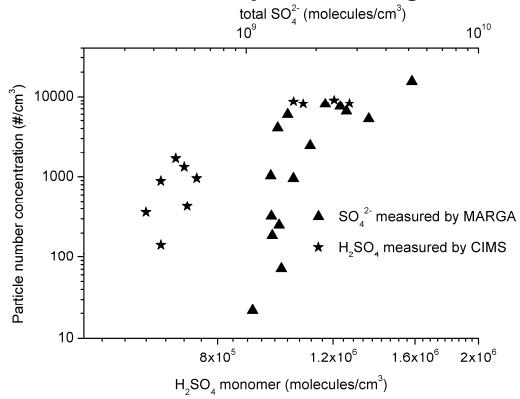

Figure 1. Particle number concentrations as a function of SO_4^{2-}/H_2so_4 monomer concentrations.

Amine enhancement of nucleation was detected when trimethyl amine was added in campaign one but the results of the base molecules in campaign two has not been analyzed yet. Figure 2 shows the enhanced particle count as a function of added trimethyl amine with constant sulphuric acid concentration with standard deviation as an error bar in campaign one. Next step is to compare the effect of the amines and ammonia to the nucleation rates and the size distribution of the particles.

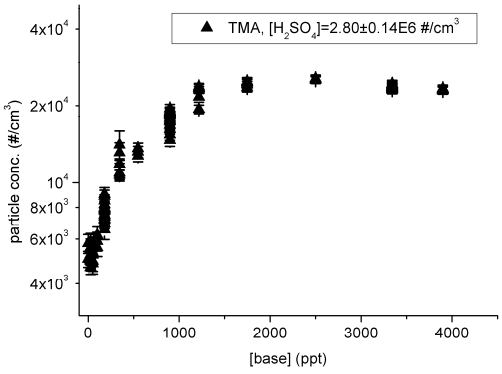

Figure 2. Particle concentration as a function of added trimethyl amine with constant sulphuric acid concentration in campaign one.

This work was supported by the Maj&Torr Nessling foundation.

Berndt et al., (2010), *Atmos. Chem. Phys.*, **10**, 7101-7116.

Petäjä et al., (2009), *Atmos. Chem. Phys.*, **9**, 7435-7448.

ten Brink et al., (2007), *Atmos. Env.*, **41**, 13, 2768-2779.

Investigation of proton behaviour in water-sulphuric acid clusters using Path Integral Molecular Dynamics

J.L. Stinson[1], I.J. Ford[1], S.M. Kathmann[2] and A. Michaelides[3]

[1]Department of Physics and Astronomy, University College London, Gower Street, London, WC1E 6BT, U.K.
[2]Chemical and Material Sciences Division, Pacific Northwest National Laboratory, Richland, WA 99352, U.S.A.
[3]London Centre for Nanotechnology, University College London, 17-19 Gordon Street, London, WC1H 0AH, U.K.
Keywords: Charge exchange, Nucleation, Sulphuric acid.
Presenting author email: j.stinson@ucl.ac.uk

Sulphuric acid/water (SAW) aerosols are thought to play a major role in the climate. The low vapour pressure of sulphuric acid means it readily condenses, particularly in association with water and other species. These aerosols are thought to have a direct and indirect effect on the climate: the first is due to their light scattering properties and the second is where they act as cloud condensation nuclei. For these reasons sulphuric acid aerosols have been of particular interest in research concerning geoengineering schemes, but a better understanding of their formation is still needed.

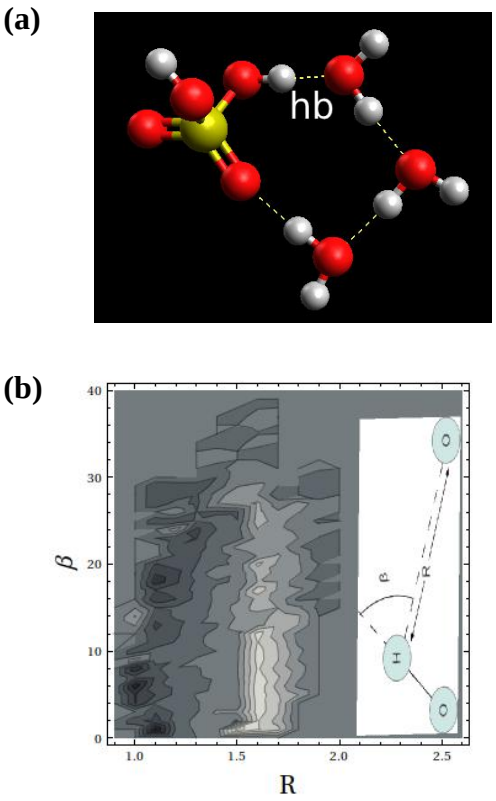

Figure 1: We study the hydrogen bond indicated in (a). The bond is identified in figure 2. The potential of mean force (PMF) indicates the work required to remove a particle from a given position to infinity. The difference between the PMF for standard DFT MD and PIMD (with 32 beads) is shown in (b). R and β are defined in the inset and contours are of width kT. The darker regions indicate where the PIMD PMF is deeper, and the lighter regions indicate where the standard DFT PMF is deeper. The background grey indicates zero change. The comparison shows that the PIMD simulation produces a shorter bond on average.

Classical nucleation theory does not reproduce nucleation rates well for SAW clusters and alternative theories have been suggested (Napari et al 2010) to improve upon it. Amongst these, Molecular Dynamics (MD) stands out as a method for the simulation of clusters and can be used to predict nucleation rates.

The work presented here concerns the creation of an MD-based method that improves upon schemes such as that of Ding et al. (2004) by explicitly treating proton transfer events. The charged species $[HSO_4]^-$ and $[SO_4]^{2-}$ have recently been shown to affect the nucleation rate significantly (Kirkby et al, 2011).

Configurations of sulphuric acid trihydrated (SATH) and tetrahydrate were studied using density functional theory (DFT) MD and path integral MD (PIMD), with the CASTEP code, to investigate the importance of quantum nuclear dynamics in small hydrated sulphuric acid clusters. This builds on work by several groups using both MD and geometry optimisations at the DFT level. The extra cost incurred using PIMD may be justifiable as suggested by Sugawara et al. (2011).

The results indicate that quantum effects change the dynamics of certain hydrogen bonds in the system. Figure 1(b) compares the potentials of mean force, with and without a quantum treatment of the nuclei, for hydrogen bond hb in Figure 1(a). The mean bond length shortens from 1.47Å to 1.36Å. However it does not seem to affect the gross stability of a configuration, such as the degree of hydration required for proton transfer. The importance of quantum nuclear dynamics to cluster nucleation at 300K therefore appears to be limited.

Additionally the DFT MD level of theory reveals effects not seen if the focus is on geometry optimisation alone. Another SATH configuration is expected to adopt a stable ionised state at $T = 0$ K according to such studies. However our DFT MD simulations at 300 K show this structure to exhibit a complex bimodal behaviour of proton hopping between ionised and neutral states. Current effort is being devoted to the parameterisation of an empirical valence bond potential to represent these effects.

This work was funded by UCL and PNNL.

Ding C.-G.. et al., Chem. Phys. **287**, 7-19, 2004.
Napari I. et al, J. Chem. Phys. **133**, 154503, 2010.
Kirkby J. et al., Nature **476**, 429–433, 2011.
Sugawara S. et al. J. Phys. Chem. A, **115**, 11486−11494, 2011.

Absorbing aerosols at high relative humidity: closure between hygroscopic growth and optical properties

J. Michel Flores,[1,2,a] R. Z. Bar-Or,[3] N. Bluvshtein,[3] A. Abo-Riziq,[3] A. Kostinski,[4] S. Borrmann,[1,2] I. Koren,[3] and Y. Rudich[3]

[1] Max Planck Institute for Chemistry, Particle Chemistry Department, Mainz, 55128,Germany
[2] University of Mainz, Institute for Atmospheric Physics, Mainz, 55128,Germany
[3] Weizmann Institute of Science, Environmental Science Department, Rehovot 76100, Israel
[4] Department of Physics, Michigan Technological University, Houghton, Michigan, 49931,USA
[a] Now at Weizmann Institute of Science, Environmental Science Department, Rehovot, Israel.

Keywords: Optical properties, hygroscopic growth, refractive index, volume weighted mixing rule, twilight zone

Presenting author email: flores@weizmann.ac.il

One of the major uncertainties in the understanding of Earth's climate system is the interaction between solar radiation and aerosols in the atmosphere. This interaction is dependent on the physical and chemical properties of the aerosols and the wavelength of the incident light. Aerosols exposed to high humidity areas will change their chemical, physical, and optical properties. To model hydrated aerosols, atmospheric chemistry models use the volume weighted mixing rule to predict the complex refractive index (RI) of aerosols when they interact with high relative humidity areas, and, in general, assume homogeneous mixing. The validity of these assumptions is explored. Furthermore, the laboratory results were used as a basis to model the change in the total extinction, the single scattering albedo (ω), and the asymmetry parameter (g) in the twilight zone of clouds at 355 nm and 532 nm.

The extinction coefficient and growth factor of humidified aerosols, at 80% and 90% RH, and at 532 nm and 355 nm wavelengths was measured for size-selected aerosols with different degrees of absorption; from purely scattering to highly absorbing particles. The ratio of the humidified extinction coefficients to the dry (fRH$_{ext}$(%RH,Dry)) is explored and compared to theoretical calculations based on Mie theory. Using the measured hygroscopic growth factors and assuming homogeneous mixing the expected RIs using the volume weighted mixing rule are compared to the RIs derived from the extinction measurements. The differences between assuming a core-shell structure or a homogeneous mixing of the substances is also examined.

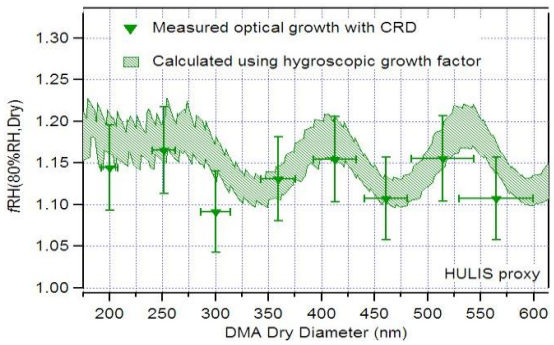

Figure 1. Size dependence of fRH$_{ext}$(80%RH,Dry) for IHSS Pahokee peat at 532 nm. The shaded areas represent the theoretical size dependence calculated from the measured growth factors from the SMPS.

We found either a moderate linear slope or no dependence of fRH(%RH,Dry) with size for absorbing substances in contrast to the decreasing exponential behavior with size for purely scattering substances, but no discernible difference could be made between the two wavelengths used. Less than 5% differences were found between the real parts of the RIs derived and those calculated using the volume weighted mixing rule, and the imaginary parts (k) had up to a 20% difference.

The total extinction as a function of distance from the nearest cloud was found to be independent of k of the dry RI of the absorbing aerosols modeled. The single scattering albedo, as expected, decreased with larger values of k, whereas the asymmetry parameter increased suggesting a reduction in the reflectivity of the twilight zone with more absorbing aerosols and a reduction of cloud edge 3D radiative effects.

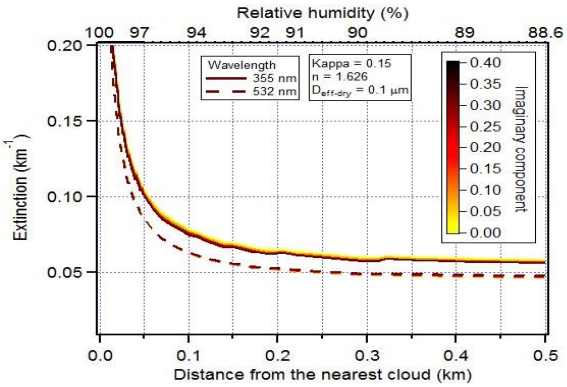

Figure 2. Extinction as a function of distance from the nearest cloud. The hygroscopicity parameter (κ) was set at 0.15, the real part of the RI (n) at 1.626, and the dry effective diameter ($D_{eff\text{-}dry}$) at 0.1 µm. A typical relative humidity field for the marine boundary layer was used. Two wavelengths: 355 nm (solid lines) and 532 nm (dashed lines), are shown. The imaginary component (color scale) was varied from 0 to 0.4.

Funding was provided by the Israel Science Foundation (Grant #196/08) 20 and by FP7-ENV-2010-265148-PEGASOS. This research was also funded by the Max Planck Institute internal funding. MF is supported by a research grant from the Jinich Postdoctoral Fellowship.

Flores, J. M., Bar-Or, R. Z., Bluvshtein, N., Abo-Riziq, A., Kostinski, A., Borrmann, S., Koren, I., and Rudich, Y. (2012) *Atmos. Chem. Phys. Discuss.*, **12**, 1019-1052.

Detecting correlations between the morphological parameters of multi-fractal samples of fractal-like aggregates

M. Woźniak[1,2], F.R.A. Onofri[1], S. Barbosa[3], J. Yon[4], C. Caumont[4], J. Mroczka[2]

[1]CNRS, IUSTI-UMR6595, 13453 Cedex13, Marseille, France
[2]Chair of Electronic and Photonic Metrology, Wroclaw University of Technology, Wroclaw 50-317, Poland
[3]IUSTI-UMR 6595, Aix-Marseille University, 13453 Cedex13, Marseille, France
[4]CORIA-UMR 6614, INSA de Rouen, 76801, Saint Etienne du Rouvray, France
Keywords: Fractals, Nanoparticle aggregates, Morphology, Soot agglomerates, TEM
Presenting author email: mariusz.wozniak@pwr.wroc.pl

Various aerosol systems lead to the formation of self-organized fractal-like aggregates of nano-sized primary particles, whose formation mechanisms and morphological properties are not yet fully understood. Over the last few decades a huge effort has been devoted for developing a Transmission Electron Microscopy (TEM) based method for estimating the size distribution and average fractal dimension of collected samples (Koylu et al. 1992, Yon et al. 2011). This widely used method, referred here as the Minimum Bounding Rectangle method (MBR) is based on the multi-scale analysis of an entire aggregate sample. So that, in principle, this method is not suitable for aggregate samples that do not have homogeneous fractal dimension.

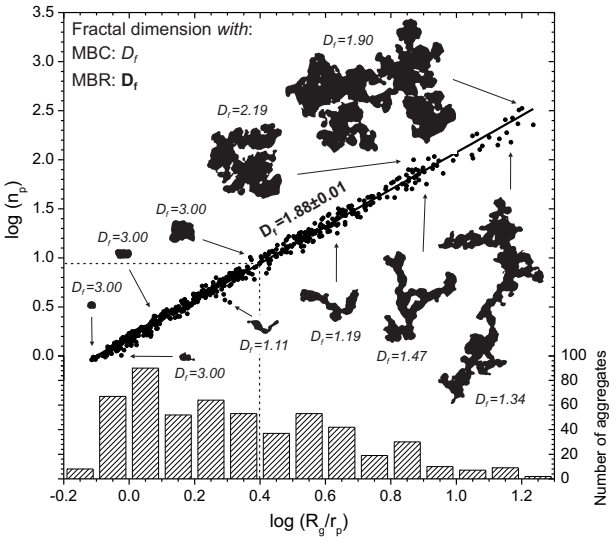

Figure 1. TEM-based analyses of experimental sample of diesel soot. The fractal dimension (D_f) is obtained with the conventional MBR method (average value in bold) and the MBC method (value for each aggregate in italics). R_g,r_p,n_p stand respectively for the radius of gyration, the radius and number of monomers within aggregates

The work we would like to present at the EAC-2012 conference will be focused on solutions to overcome the latter limit (Wozniak et al. 2012). It is will be shown in particular that the average fractal dimension estimated with MBR is severely biased by the smallest aggregates that do not exhibit self-similarity properties. On the other hand, we will detail the principle of a Modified Box-Counting (MBC) method that provides a less noisy estimation for the evolution of the fractal dimension with the size of aggregates, giving at the same time a criterion to reject the aggregates within sufficient self-similarity properties. Tests and validations results will be based on experimental soot aggregates as well as synthetic TEM images produced with a tunable Diffusion Limited Aggregation code (Wozniak et al. 2012).

As an illustration, Fig. 1 shows TEM-based analyses for 543 soot aggregates produced by a diesel flame (Yon et al., 2011). Several results, which will be detailed in the final paper, are presented in this Figure: (i) the number distribution of the normalized radius of gyration of all soot aggregates; (ii) the fractal dimension of the whole sample estimated with MBR method and (ii) typical binarized TEM images of soot aggregates with their fractal dimension estimated by MBC. From a quick view of the binarized TEM images, one may intuit that the smallest aggregates have a significantly greater fractal dimension than the largest ones. If such a correlation exists (i.e. the experimental sample is multi-fractal but not necessarily the aggregate themselves (Vicsek et al., 1990; Kravchenko et al., 2009)), one of the main hypothesizes of the multi-scale analysis is not satisfied. More profoundly, the detection of such a correlation could have major implications for our understanding of nanoparticles aggregation and growing mechanisms. For instance, going back to the results related to Fig. 1, the MBC method clearly show that the fractal dimension of this soot sample is much lower (1.66±0.02) than that the one derived with the MBR analysis (1.88±0.02). This fractal dimensions is, for some extend, in agreement with recent investigations (Chakrabarty et al., 2009).

Chakrabarty, R.K., Moosmuller, H., Arnott, W.P., Garro, M.A., Tian, G., Slowik, J.G., Cross, E.S., Han,J. H., Davidovits, P., Onasch, T.B., and Worsnop, D.R. (2009), *Phys. Rev. Lett.*, **102** (23), 235504.

Koylu, U. O. and Faeth, G. M. (1992), *Combust. Flame* **89**:140-156.

Kravchenko, A.N., Martin, M.A., Smucker, A.J.M., and Rivers, M.L. (2009), *Vadose Zone J.*, **8** (1), 220–226.

Vicsek, T., Familly, F., and Meakin,P. (1990), *Europhys. Lett.*, **12**(3), 217–222.

Wozniak, M., Onofri, F. R. A., Barbosa, S., Yon, J. and Mroczka, J. (2012), *Journal of Aerosol Science* **47**: 12-26.

Yon, J., Lemaire, R., Therssen, E., Desgroux, P., Coppalle, A., and Ren, K.F. (2011), *Applied Physics B*, **100**(2), 253–271.

Electrostatic and diffusion loss of charged nanoparticles in cylindrical tube connections with electric potential difference

D.K. Song[1], W.S. Hong[1] and W.H. Shin[1]

[1]Department of Eco-Machinery Systems, Korea Institute of Machinery and Materials, Daejeon, 305-343, KOREA

Keywords: Charged particles, Electrical mobility, Numerical simulation, Particle losses, Penetration.

Presenting author email: dksong@kimm.re.kr

For the real-time measurement of a detailed size distribution, a differential mobility analyzer (DMA) is widely used to measure size distributions of ultrafine particles.

When measuring the size distribution of atmospheric particles using a DMA, the electrical mobility distribution of particles is obtained, rather than the size distribution. Hence, the so-called reduction or inversion process must be used to derive the size distribution of atmospheric particles from the measured electrical mobility distribution. However, the electrical mobility distribution measured by DMA-CPC or DMA-FCE system is different from the size distribution of the airborne particles, due to the following: diffusional broadening during transport by Brownian diffusion, transport loss caused by inertial impaction, gravitational settling and interception in tube connections, and limitations in the efficiency of instruments for counting the number of particles.

Diffusional losses in particle sampling systems that contain bends and elbows, the detection efficiency of a condensation particle counter and the diffusional transfer function of DMA has been studied by numerous researchers. However, there is no report of any analysis of the phenomenon that electrostatic loss results in a decrease of the penetration of charged particles when they pass through a connection of cylindrical tubes whose electrical voltage differs.

We here present a theoretical and numerical analysis of the effect of the electrode setup geometry on the penetration efficiency of charged particles in transport through a cylindrical tube connection that has an electrical difference. The trajectory of charged particles was analyzed and penetration efficiencies for various cases are presented.

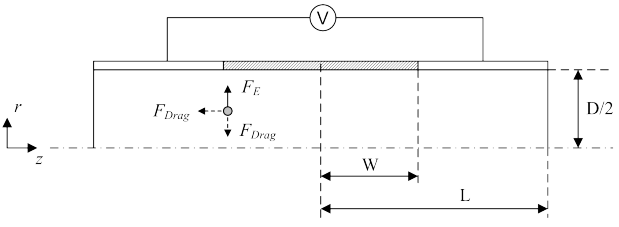

Figure 1 Schematics of cylindrical tube connection with electrical voltage difference.

A cylindrical tube connection that has a voltage difference and is separated electrically by an insulator was modelled (Figure 1), and electrostatic and diffusion loss of charged nanoparticles passing through the connector tube was numerically investigated. To assess the effect of the electrode geometry, various lengths of electric insulator W, tube diameter D, total connection length L and aerosol flow rate Q_a were used when investigating electrostatic loss.

Particle loss was calculated by analyzing particle trajectories and comparison of electrostatic loss for various electrode geometry setups, and Eulerian approach was also performed for solving convective-diffusion equation. We calculated the penetration efficiency for various particle diameters and applied voltages. The range of particle size and applied voltage used in the calculation were 2 – 500 nm and 0.01 – 5 kV, respectively. The ratio W/L of the insulator length to the total length was also changed from 0.1 – 0.4. In the numerical calculations, all particles were assumed to be spherical and singly charged with positive polarity.

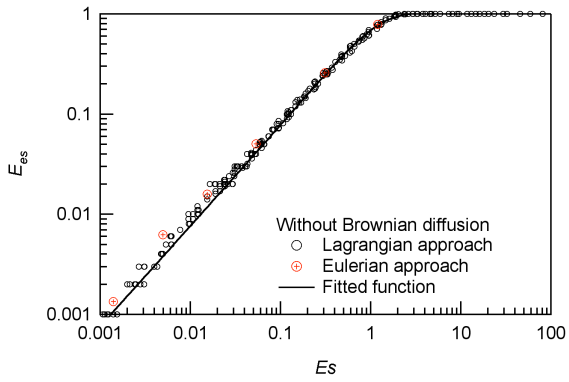

Figure 2 Electrostatic loss of charged particles presented as a function of a non-dimensional parameter, Es.

It suggests that the electrostatic loss can be described as a function of a new non-dimensional parameter,

$$Es = \frac{Z_p V}{U_{avg} W} = \frac{Z_p V}{Q_a W} \frac{\pi D_{tube}^2}{4}.$$

An explicit form for electrostatic loss is provided as a function of Es and given as

$$E_{es} = \frac{1}{1 + \left\{-0.0948 + 1.4137 e^{-0.947 Es}\right\} / Es}.$$

This work was supported by the Ministry of Knowledge Economy of KOREA.

Charge control of particles in air using centrifugal force acting under applied electric field

S. Matsusaka and K. Satoh

Department of Chemical Engineering, Kyoto University, Nishikyo-ku, Kyoto 615-8510, Japan
Keywords: tribocharging, particle charge control, centrifugal contact, electric field.
Presenting author email: matsu@cheme.kyoto-u.ac.jp

When particles are handled in air, their surfaces become triboelectrically charged by coming in contact with walls or solid bodies made of different materials. As a result, charged particles may adhere to walls. If the particles are excessively charged, an electrostatic discharge can occur. Electrostatic forces can be used to control the motion of charged particles, and many such applications have been developed, e.g., electrostatic precipitation and particle separation. To prevent unexpected particle behavior and to improve the process performance, it is necessary to control the charge on the particles. In the present study, we propose a new charge control system for gas-solid pipe flow, which uses centrifugal force produced in an applied electric field, and evaluate the performance of the proposed system both theoretically and experimentally.

The contact charging of particles based on electron transfer depends on the contact potential difference V, which again depends on several factors, e.g.,

$$V = V_c - V_e - V_b + V_{ex} \quad (1)$$

where V_c is the potential difference caused by the surface work functions; V_e, image charge effect; V_b, space charge effect; and V_{ex}, applied electric field effect. To obtain the charge q as a function of the number of collisions n, we use a continuous quantity as follows:

$$\frac{dq}{dn} = k_c CV \quad (2)$$

where k_c is the charging efficiency and C is the capacitance between contact surfaces. Solving Eq. (2) with initial conditions $n = 0$ and $q = q_0$, we obtain the following exponential equation:

$$q = q_0 \exp\left(-\frac{n}{n_0}\right) + q_\infty \left\{1 - \exp\left(-\frac{n}{n_0}\right)\right\} \quad (3)$$

where q_∞ is the equilibrium charge. When the particle concentration is sufficiently low, $V_b = 0$, and q_∞ is expressed as

$$q_\infty = k_1 E_{ex} + k_2 V_c \quad (4)$$

where k_1 and k_1 are constants. Therefore, the equilibrium charge can be controlled by the applied electric field.

Figure 1 shows a schematic of the charge control system. Particles dispersed in air were charged using an inverted truncated cone-shaped device with inner and outer electrodes. Particles introduced into the device in a tangential direction from the top flow spirally downward and exit from the bottom. The particles came in contact with the side wall because of the centrifugal force acting in an electric field and became charged. The diameter of the particles was 80 μm, and their surface was coated with different resins to induce a positive or negative charge. The performance of the charge control system was evaluated by estimating the specific charge of the particles. Experimental results showed that the particle charging efficiency of a single system was approximately 90% and that of a combination of two charge control systems was 98%–99%.

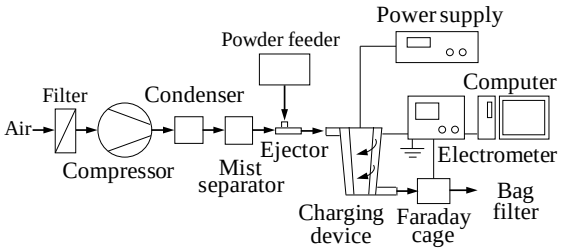

Figure 1. Charge control system.

Figure 2 shows that the specific charge varies with the applied electric field and type of resin. This figure also indicates an interesting feature: the relationship between specific charge and applied electric field can be classified into two categories, linear (Eq. (4)) and nonlinear.

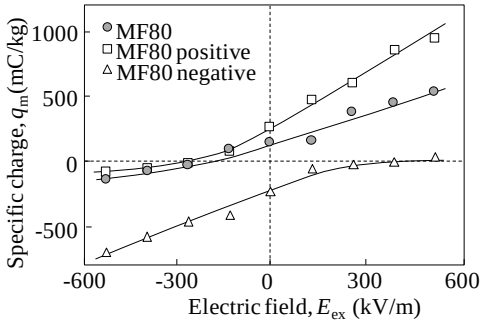

Figure 2. Effect of applied electric field on specific charge of particles.

This work was supported by a Grant-in-Aid for Scientific Research (B) (No. 23360341) from the Japan Society for the Promotion of Science and Grant no. S0901039 from MEXT, Japan.

Matsusaka, S. and Masuda, H. (2003) *Adv. Powder Technol.*, **14**, 143-166.

Matsusaka, S., Maruyama, H., Matsuyama, T. and Ghadiri, M. (2010) *Chem. Eng. Sci.*, **65**, 5781-5807.

Matsusaka, S. (2011) *KONA Powder and Particle*, **29**, 27-38.

Data inversion and calibration of a particle number concentration monitor

L. Hillemann[1], A. Zschoppe[2]
[1]Institute of Process Engineering and Environmental Technology, TU Dresden, 01062 Dresden, Germany
[2]Topas GmbH, Oskar-Röder-Str. 12, 01237 Dresden, Germany
Presenting author email: lars.hillemann@tu-dresden.de

The concentration of particle matter in ambient air is quantified in air quality monitoring networks. The classical mass-based methods are more and more completed by number-based methods. This enables to quantify the concentration of submicron particles, which especially show adverse health effects (Peters *et al*, 1997). In the European project UFIPOLNET a particle number concentration monitor has been developed, which combines an unipolar corona-jet charger, a DMA and an aerosol electrometer to measure the particle number concentration in six size classes from 20 to 800 nm.

Data inversion

The raw data measured by the number concentration monitor is the rate of particle-bound charge measured as electrical current versus the classifier voltage $I(U)$. Objective of the data inversion is to derive from these raw data the distribution of the number concentration versus the particle size $c_n(d)$. The analysis of the inverse problem delivers the connection between $I(U)$ and $c_n(d)$ by the charge distribution $f(d,n_e)$, the transfer function of the DMA $\Omega(Z(d,n_e),U)$ and the inlet flow Q if losses can be neglected.

$$I(U) = \int \mathrm{e} Q \sum_{n_e} f(d,n_e) n_e \Omega(Z(d,n_e),U) c_n(d) \mathrm{d}d \quad (1)$$

Due to the stepwise variation of the classifier voltage and the indication of the concentration in discrete size channels the inversion problem can be written in matrix notation.

$$\mathbf{I} = \mathbf{K}(\mathbf{U},\mathbf{d})\mathbf{C}_n \quad (2)$$

The kernel data can be calculated from the charge distribution by

$$K(U,d) = \mathrm{e} Q \sum_{n_e} f(d,n_e) n_e \Omega(Z(d,n_e),U) \quad (3)$$

or derived experimentally in calibration measurements.

The data inversion algorithm bases on the Tichonov regularization and minimizes the third differences of the concentration vector. The regularization parameter is fixed and was chosen empirically.

Calibration

Objective of the calibration of the number concentration monitor is to determine the values of the kernel matrix $\mathbf{K}(\mathbf{U},\mathbf{d})$. This is done in a parallel measurement of the monitor and a reference method, typically a SMPS or DMPS. The raw data of the monitor and the concentration data of the reference system are stored in the columns of the matrices **IM** and **CM** respectively. From these matrices the kernel matrix is derived by minimization

$$||\mathbf{K} \cdot \mathbf{CM} - \mathbf{IM}||_2 \Rightarrow Min \quad (4)$$

This minimization can be decomposed, which enables the calculation of the rows of the matrix separately. Fig. 1 shows a kernel matrix derived by this method.

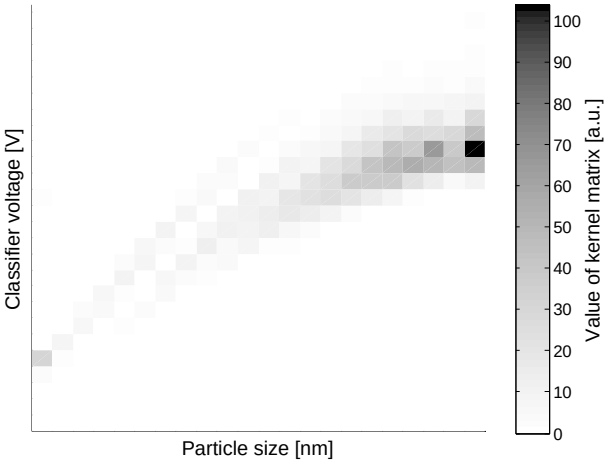

Figure 1: Kernel matrix of the particle number concentration monitor.

A. Peters et al. (1997), *Am. J. Respir. Crit. Care Med.*, **155**, 1376-1383.

Structured chain-like aggregates by coagulation of charged particles

L. Knobel[1] and H.-J. Schmid[1]

[1]Chair of Particle Technology, University of Paderborn, Paderborn, 33098, Germany
Keywords: structured aggregates, unipolar charging, coagulation, charged particles
Presenting author email: lena.knobel@upb.de

Intention is to build a chain-like aggregate with alternating sequence of different materials.

Application could be a lamellar structured polymer with new properties. The structure is to be reached by adding the chain, structured nanoparticle aggregates during polymerization.

The structure of the aggregate will be realized by mixing a positively charged aerosol flow with a negatively charged aerosol flow which consists of another material. To realize the chain shape, the coagulation process needs to be faster than the neutralization by recombination in the contact point. Therefore the materials need to be dielectric. To slow down the charge mobility on the surface as well as in the bulk phase, temperature and humidity conditions have to be adjusted.

Chain-like structures were realised by e.g. Kasper *et al.* (1980) based on magnetic dipoles. DallaValle *et al.* (1954) showed formation of chain aggregates of ammonium chloride particles depending on the charge of the particles. Gutsch (1995) investigated the coagulation of sodium chloride particles forced by multi-stage bipolar charging by simulation and experimentally. Concurrent results showed the decreasing of the form factor (to the point of long-chain aggregates) by increasing the charges of the particles. The simulation results showed even the alternating structure of the oppositely charged particles.

To realize the structure with two different materials, two aerosol flows will be charged unipolar in each case in another polarity by corona charger. An advantage of the unipolar charger is the higher number of charges on the particles.

After forming doublets the impact of the opposite charged particles on the coagulation time will decrease (Figure 1). In order to keep the characteristic coagulation time short particle concentration and temperature have to be adjusted.

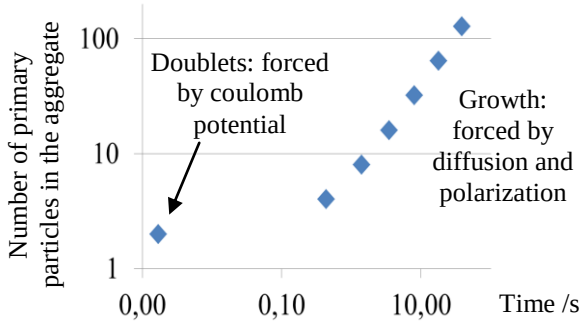

Figure 1: Coagulation time of charged 100 nm particles with an initial particle concentration of 10^{14}/m³

The particle materials, which are first investigated, are silicon dioxide and aluminium oxide. Both are synthesized in a hot wall reactor. The liquid precursors will be evaporated and fed to the process flow. Preliminary for the following coagulation we need at first spherical primary particles. The particle concentration is limited by the synthesis of those particles, because the characteristic coagulation time needs to be much longer then the characteristic sintering time. Figure 2 shows the maximum concentrations and production rate based on the facility design and the calculation of the sintering time by Kirchhof (2008).

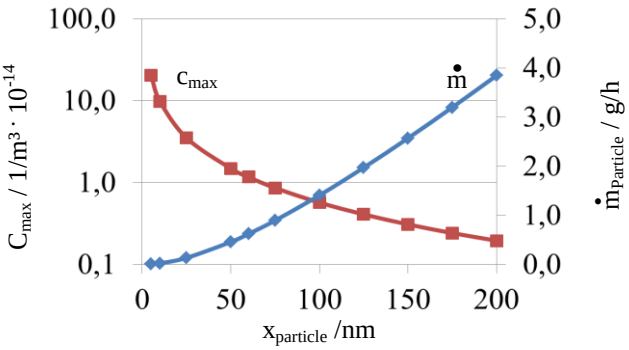

Figure 2: Max. particle concentration and production rate for SiO_2 dependent on the primary spherical particle size, residence time: 900 ms, T= 1700 °C

Downstream of the high-temperature kilns the streams will be charged unipolar separately from each other. The next step is the mixing for the coagulation process.

The analysis of the complex structure in dependency of particle charge, particle size and residence time can only be done by simultaneous application of different measurement technics like mobility analysis, measurement of chargeability (Wang *et al.*, 2011), low-pressure impaction and image analysis.

The charging process will be monitored by a Faraday Cup Electrometer in combination with a Condensation Particle Counter.

DallaValle, J.M., ClydeOrr, J., Hinkle, B.L. (1954) *Br. J. Appl. Phys.*, 5, 198-206

Gutsch, A. (1995) *Universität Karlsruhe*, PhD Thesis

Kasper, G., Shon, S.N., Shaw, D.T. (1980) *AIHA Journal*, 41, 4, 288-296

Kirchhof, M.J., Förster, H., Schmid, H.-J., Peukert, W. (2011) *J. Aerosol Science*, 45, 26-39

Wang, J., Shin, W.G., Mertler, M., Sachweh, B., Fissan, H., Pui, D.Y.H. (2011) *Aerosol Science and Technology*, 44:2, 97-108

Influence on the bipolar stationary charge distribution

L. Knobel[1], A. Jain[2] and H.-J. Schmid[1]

[1]Chair of Particle Technology, University of Paderborn, Paderborn, 33098, Germany
[2]Department of Chemical Engineering, Indian Institute of Technology, Bombay, India
Keywords: bipolar charging, charge distribution, SMPS, charger downstream
Presenting author email: lena.knobel@upb.de

The prediction of the aerosol charge distribution in a bipolar ion environment is an essential part of the mobility analysis. The Fuchs theory (1963) is a widely-used method to calculate the distribution. The temperature, mass of gas molecules, ion mobility and ion mass are necessary independent input parameter. The species of the ions is again influenced by trace gases, humidity, aging time and ionisation energy. The last point is not physically understood jet, but experimental results suggest a difference in the charge distribution (e.g. Lee *et al*., 2004)

The Wiedensohler approximation (1988), derived from the Fuchs model, is a widely-used method in mobility analysis. However, it relies on fixed input parameters.

The first part is a sensitivity analysis on the Fuchs calculation to determine the range of the resulting charge distribution depending on the input parameters and to determine the dominating parameters. It is shown that, in the free molecular regime the charge process is driven by the mobility and in the near-continuum regime it is driven by the mass.

Lots of different values for the ion mobility are known by measurements from the literature. Based on these values for the mobility and the adapted values for the mass by the Kilpatrick relation (1971), we calculated the possible results for the fraction of singly charged particles. The results pointed out, that the mobility difference between negative and positive ions in the near-continuum regime is more important than the absolute values of the mobility. Figure 1 shows four cases for varied mobility differences. The dashed line in the middle shows the result for equal mobility of positive and negative Ions. The three other values for the mobility difference are chosen by reasonable values of the literature. The green line presents the values chosen by Wiedensohler (1988) for his approximation.

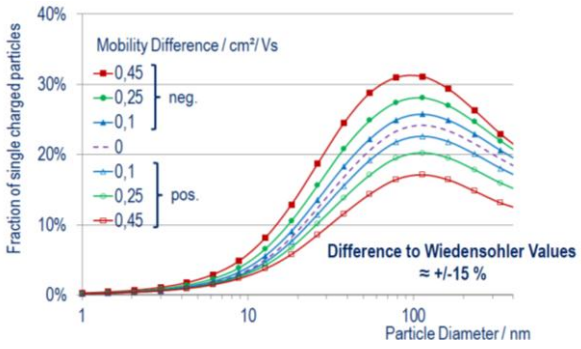

Figure 1: Effect of the mobility difference

The range of the variation is significant and should be taken into account when analysing results from measurements with a SMPS system.

The second part was about the development of the charge distribution downstream of the charger. Hoppel *et al.* (1990) calculated the modification of the ion concentration downstream of the charger and emphasize the non-equilibrium character of the charge distribution, because of not dispensable pluming.

We expanded this calculation. To describe first the ion concentration a coupled population balance for ions and particles were solved along a tube. The following effects were taken into account for the ions: Recombination, charging of particles, electrostatic dispersion, convection and diffusion. In the model the particle flux is driven by dispersion and convection. Particles with the charge of -2 to +2 were examined. The boundary conditions for the model case were selected based on the conditions in a conventional SMPS system.

An interesting aspect is the decay of ion concentration dependent on the initial ion and particle concentration. Based on this result the modified charge probability was calculated. Figure 2 shows, that for the application of the SMPS this effect is negligible.

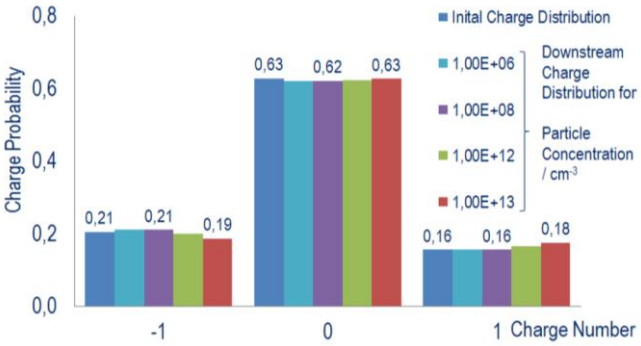

Figure 2: modification of the charge distribution downstream of the charger

Fuchs, N.A. (1963) *Pure and Applied Geophysics*, 56, 1, 185-193

Hoppel, W.A., Frick, G.M. (1990) *Aerosol Science and Technology*, 12, 3, 471-496

Kilpatrick, W.D. (1971) *Proc. Annu. Conf. Mass. Spectrosc.*, 19th, 320-325

Lee, H.M., Kim, C.S., Shimada, M., Okuyama, K. (2004). *J. Aerosol Science*, 36, 813-129

Wiedensohler, A. (1988) *J. Aerosol Science*, 19, 387-389

Break-up of charged ionic salt solution droplets at super-Rayleigh limits

Asit Ray and Kuo-Yen Li

Department of Chemical Engineering, University of Kentucky, Lexington, KY 40506, USA
Keywords: droplet charge limit, evaporation, solute precipitation
Presenting author email: akray@engr.uky.edu

Evaporation of neutral solvent from a charged solution droplet causes reduction in the droplet size, and as a result the charge density at the droplet surface increases. Ultimately, the charge density level attains a critical limit where the droplet becomes unstable resulting in the formation of smaller progeny droplets from the break-up of the parent droplet. The break-up process lowers the charge level below the instability limit, but continual evaporation causes the droplet to break-up intermittently. The charge density level at which droplet break-ups occurs is known as the Rayleigh limit, which has been confirmed by numerous experiments. We have examined the charge stability limits of single evaporating microdroplets of ionic salt solutions. Single charged droplets were suspended in an electrodynamic balance, and a resonance-based light scattering technique was used to determine the size and the size change of a droplet at a charge instability induced break-up. The dc voltages required to gravitationally balance the droplet prior to and following the break-up were used to calculate the charge level and the charge loss at the break-up. We have examined diethylene glycol (DEG) and triethylene glycol (TEG) droplets containing lithium chloride as well as calcium chloride at varying concentrations.

Our previous studies [Li et al. (2005) and Hunter and Ray (2009)] on single component droplets and droplet doped with ionic compounds, such as ionophores or ionic liquids, show that droplet break-ups occur at the Rayleigh limit, and the concentration of ions in a droplet has no effect on the charge limit. The results also show that the fractional charge loss increases, while the mass loss decreases as the ion concentration in a droplet increases. Through an analysis we have shown that the presence of nonuniform ion distributions in a droplet enhances the electrical conductivity at the droplet surface, and established that the charge-to-mass ratio of progeny droplets is proportional to the conductivity at the surface of the parent droplet. The results of the present study on DEG and TEG droplets containing ionic salts show that droplet break-ups occur at significantly higher charge levels than the Rayleigh limit, and droplets can remain stable at charge levels greater than three times the Rayleigh limit. The charge limit at a break-up depends on the salt concentration in a droplet and increases as the concentration increases. During evaporation the salt concentration in a droplet increases due to the reduction in the size, and when the droplet undergoes multiple break-ups we observed that the charge limit of the succeeding break-up always exceeds that of the prior break-up due the concentrating effect of the salt. As long as the salt concentration in a droplet remains below the saturation point, the observed charge limit increases linearly with the salt concentration and approaches the Rayleigh limit at low concentration levels. Between the salts, lithium chloride has more pronounced effect on the charge limit than calcium chloride. Even though the observed charge limit increases with increasing salt content when the salt concentration in a droplet exceeds the saturation value, the dependence of the charge stability limit on the concentration changes considerably due to the precipitation of solute at the droplet surface. In addition, we also observed that the fractional mass loss at a droplet break-up is below the detection limit (i.e., about 0.03%) of our measurement technique. The fractional charge loss at a droplet break-up increases with increasing charge stability limit, and each break-up results in the reduction of the droplet charge to a level lower than the Rayleigh limit. We developed a model to explain the observed behaviour.

This work was supported by the National Science Foundation (grant # ATM-0634789), and National Institute for Occupational Safety and Health (grant # 1R01OH009802-01).

K.-Y. Li, Tu H. and Ray, A. K. (2005) *Langmuir*, **21**, 3786-3794.

Hunter, H. C. and Ray, A. K. (2009) *Phys. Chem. Chem. Phys.* **11**, 6156 - 6165.

Performance of ^{85}Kr, Soft X-ray and AC Corona Charging Sources for Particles <20 nm

J.J. Swanson[1], A.M. Boies[1], A. Collins[2]

[1]Department of Engineering, University of Cambridge, Cambridge, UK, CB2 1PZ
[2]MSP Corporation, Shoreview, Minnesota, 55126, USA
Keywords: electrical mobility, electrometer, electrostatic precipitator
Presenting author email: js2011@cam.ac.uk

Aggregates consisting of clusters of primary particles are ubiquitous in ambient and industrial aerosols. Soot emitted by Diesel engines or biomass burning is a primary source of aggregates in the atmosphere. Similarly, spherical particles are generated in the laboratory for calibration or synthesis. In many cases, measurement of these particles depends on the knowledge of the distribution of charges they have acquired, either naturally or from a "neutralizer." Variations in neutralization techniques may lead to different charging characteristics and other parameters such as particle size, shape, composition, concentration, and ambient air properties impact the charging process.

The objective of this work is to evaluate the performance of different neutralization techniques. In a typical neutralizer, particles pass through a cloud of ions and acquire a steady state distribution of charges that is nearly symmetrical [1]. Many techniques are available to generate these ions but this work focuses on radioactive sources (^{85}Kr, NRD, Inc), x-rays (3087 Soft X-ray Charger, TSI, Inc [2]), and corona discharge (1090 Electrical Ionizer, MSP Corp). These methods differ in the way they ionize surrounding N_2 and O_2 molecules. The de-facto standard, ^{85}Kr, emits highly energetic beta particles. Similarly, the X-ray Charger generates energy x-rays that peak in energy at ~6 keV. The Electrical Ionizer uses corona discharge operated with AC voltage to generate positive and negative ions. For all cases, ions are generated in equal proportions to achieve a near symmetric charge distribution.

To better quantify the impact of neutralization technique for particles <20 nm, our measurements have focused on the following phenomena.

- Particle charged and neutral fractions
- Particle generation due to photochemistry & radiolytic effects and electrode erosion
- Direct charging of individual particles

Measurement of the particle charged fraction provides an indication as to whether the aerosol is charged according to the assumed equilibrium charge distribution. The charged fraction (f_C), which is a function of particle size (D_p), is the summation of the singly, doubly, etc negatively and positively charged particles, where *n* is an integer index representing the number of charges:

$$f_{C,D_p} \equiv \sum_{n=-\infty}^{-1} f_{n,D_p} + \sum_{n=1}^{\infty} f_{n,D_p}$$

Likewise, the neutral fraction, f_{0,D_p}, is $1 - f_{C,D_p}$. It can be measured by taking the ratio of neutral particle concentration of the given size D_p (N_{0,D_p}) and the total particle concentration of size D_p (N_{T,D_p}):

$$f_{0,D_p} = \frac{N_{0,D_p}}{N_{T,D_p}}$$

A schematic of the apparatus used to measure f_{0,D_p} is shown in Figure 1. A DMA is used to classify a mono-mobility aerosol. The classified particles traverse a bipolar charger to reach an equilibrium charge state. An electrostatic precipitator (ESP) is used to remove all the charged particles by applying a high voltage and a condensation particle counter (CPC) downstream is used to measure neutral concentration ($N_{0,D}$). The total concentration is measured by turning off the ESP.

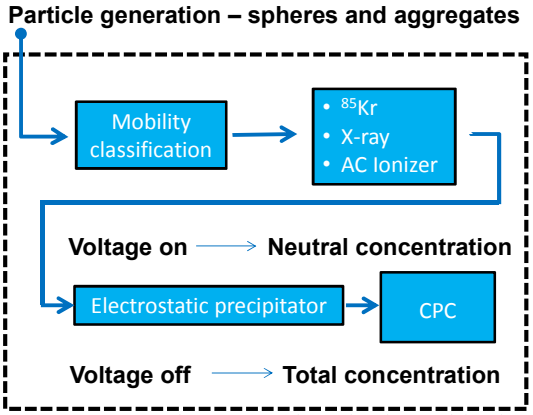

Figure 1. Apparatus used to measure charged and neutral fractions

Additional experiments were performed to investigate the formation of particles during neutralization due to the ionization of molecules into reactive species followed by nucleation and condensation (formation of radiolytic particles), as well as the direct charging for particles, rather than molecules. These effects depend on ambient air and trace gas chemistry. Overall, results obtained from these measurements provide further insight into the nature of particle charging for very small particles.

[1] Fuchs, N. A. (1963). On the stationary charge distribution on aerosol particles in a bipolar ionic atmosphere. *Pure and Applied Geophysics*, 56, 185-93.

[2] Lee, H.M, Kim, C.S., Shimada, M., Okuyama, K. (2004). Bipolar diffusion charging for aerosol nanoparticle measurement using a soft X-ray charger. *Journal of Aerosol Science*, 36, 813-829.

Characterization of charging effects on different particles and discharge electrodes

Wen-Yinn Lin[1], Yuan-Yi Chang[1], Jin-Yuan Syu[1], Shao-Hao Lu[1], Chih-Chieh Chen[2]

1Institute of Environmental Engineering and Management, National Taipei University of Technology, Taipei, TAIWAN
2 Institute of Occupational Medicine and Industrial Hygiene, College of Public Health, National Taiwan University, Taipei, TAIWAN

Keywords: Electrostatic precipitator, Electrical resistivity coefficient

Presenting author email: wylin@ntut.edu.tw

Abstract

The performance of ESP and generation of the corona discharge is influenced by many parameters. Particle charge is influenced by electrical resistivity that influences the particle collection efficiency. However, not many studies were about measuring the effect of electrical resistivity of particles. Various types of electrostatic precipitator were set up in this study. The objectives of this research included studying the characteristic of two different electrical resistivity of particles (polydispere NaCl and monodisperse PMMA) and discussing corona onset voltage, particle charge, collection efficiency, ozone concentration and filter quality of different types of ESP. The experimental results indicated that the lowest value of particle penetration was obtained for the Point-Plate ESP. The penetration of PMMA of 1.7μm was 0.19%, 9.4% and 64.66% for Point-Plate, Plate-Wire and Flate-Plate, respectively. The particle charge was measured under the same ESP and it was found that the particle charge of PMMA was lower than NaCl because the higher electrical resistivity of particles was difficult to be charged. However, the corona current of Point-Plate ESP was higher than other types of ESP that resulted in generating higher ozone concentration.

Experimental

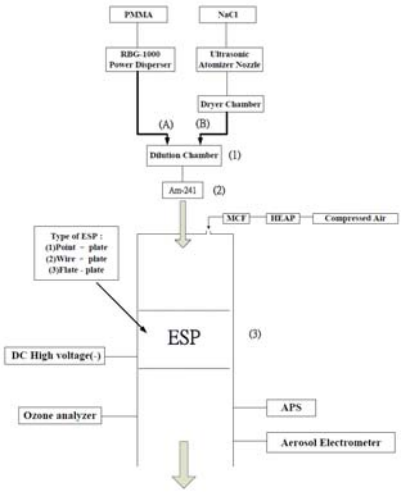

Figure 1. experimental set-up.

The experimental set-up, shown in figure 1, experimental apparatus included three major systems, i.e. The aerosol generator, the discharge electrode and collector system, and the aerosol measurement system, etc.

Results and Conclusions

The results show that the input current increased as the input voltage increases. Besides, the point-plate had largest input current than wire-plate and flat-plate of discharge electrode of ESP based on the same input voltages (figure 2).

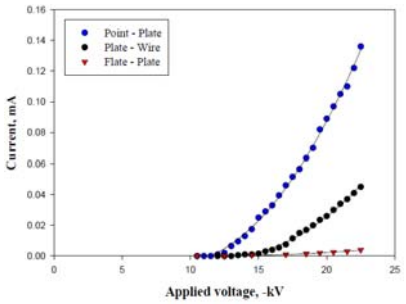

Figure 2. Input voltage vs. current of different discharge electrodes.

And it suggested that the particle charge and removal efficiency (Figure 3) of PMMA were lower than NaCl because the higher electrical resistivity of particles was difficult to be charged (Navarrete et al.,1997).

However, the corona current of Point-Plate ESP was higher than other types of ESP that resulted in generating higher ozone concentration (Viner et al., 1992; Jaworek et al. 2007).

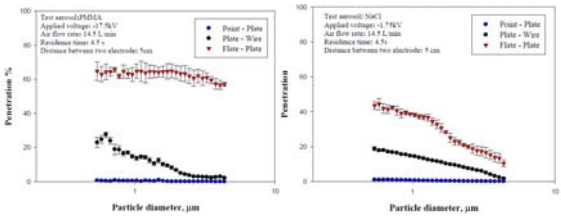

Figure 3. PMMA(left) and NaCl(right) particle penetrations vs. size distributions of different discharge electrodes.

Viner, A. S., Lawless, P. A., Ensor, D. S. and Sparks, L. E. (1992) *Industry Applications*, IEEE Transactions on 28:504-512.

Navarrete B., Canadas L., Cortes V., Salvador L., and Galindo J. (1997) *Journal of Electrostatics*, 39: 65-81.

Jaworek, A., Krupa, A. and Czech, T. (2007) *Journal of Electrostatics*, 65:133-155.

Selective electrostatic deposition of airborne engineered nanoparticles on a patterned substrate of silicon cantilever sensor

H. S. Wasisto[1*], S. Merzsch[1] , A. Waag[1], E. Uhde[2], I. Kirsch[2] and E. Peiner[1]

[1]Institute of Semiconductor Technology, TU Braunschweig, Braunschweig, D-38106, Germany
[2]Department of Material Analysis and Indoor Chemistry, Fraunhofer WKI, Braunschweig, D-38108, Germany
Keywords: particle deposition, airborne particles, personal sampling, deposition efficiency
*E-mail: h.wasisto@tu-braunschweig.de

Recently, there is increasing demand for air quality monitoring equipments to assess the release of airborne nanoparticles (NPs) to the environment due to the wide-spread use of nanotechnology. From the previous research, MEMS-based cantilever resonators are proven to highly contribute to the development of low-cost and compact sensors for monitoring ~20 nm airborne carbon NPs mass with a mass sensitivity of 8.33 Hz/ng (Wasisto *et al*, 2012). However, the NPs are still trapped on the whole cantilever surface, including its supporting frame which can definitely reduce the sampling efficiency because of their deposition location. Meanwhile, the most sensitive location of cantilever sensor for detecting the micro/nano-sized particles is its free-end (Dohn *et al*, 2005). The use of electrostatic forces is found to be the most effective method to position airborne charged particles (Tsai *et al*, 2007). Therefore, motivated by the need of high-sensitive mass detection of NPs adhered to the microcantilever on a selective area, a method of electrostatic-directed deposition of NPs by using a *p*-*n* junction patterned Si substrate is investigated and analyzed in this work.

Results

The cantilevers are successfully fabricated using a Si bulk micromachining process. The selective patterned area (*p*-type Si) for NPs collection is located close to the cantilever free-end and is formed by boron diffusion. A self-built miniaturized NP sampler is integrated with the patterned Si cantilever during 15-min TiO_2 aerosol sampling in the chamber having concentration of ~3500 NP/cm^3 (V = 1 m^3, T = 23 °C, rH = 30 %, P = 1 atm) (Fig 1). The aerosol consists of positively and negatively charged NPs. Upon reverse bias, an additional electric field is established in the charge depletion zone. From SEM images, a high number concentration of positively charged TiO_2 NPs with diameter of 6 to 523 nm is clearly deposited uniformly on the *p*-type Si region, indicating that positively charged particles were being repelled by *n*-type Si region and attracted to the *p*-type Si region (Fig. 2). A positive voltage of the NP sampler tube has also created additional electrostatic forces which push the positively charged NPs down to the substrate and keep the negatively charged NPs away from the substrate. In regard to the NP sampler flow rate of 0.68 l/min, the NP collection efficiency of 0.457 % is obtained. Further tests with the other types of aerosol will be addressed.

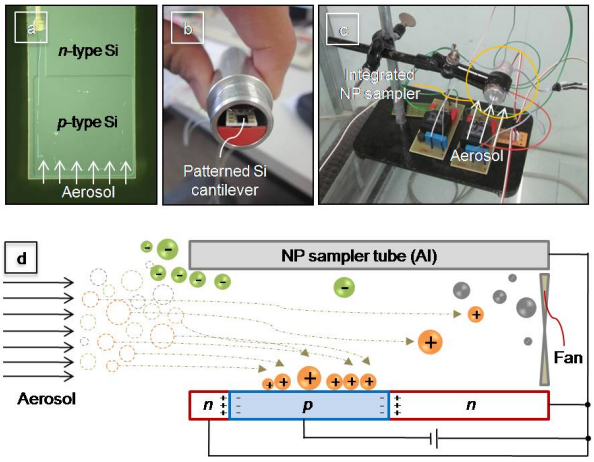

Figure 1. (a) The patterned Si cantilever integrated with (b) NP sampler in (c) TiO_2 aerosol sampling. (d) The mechanism of electrostatic-directed NP deposition.

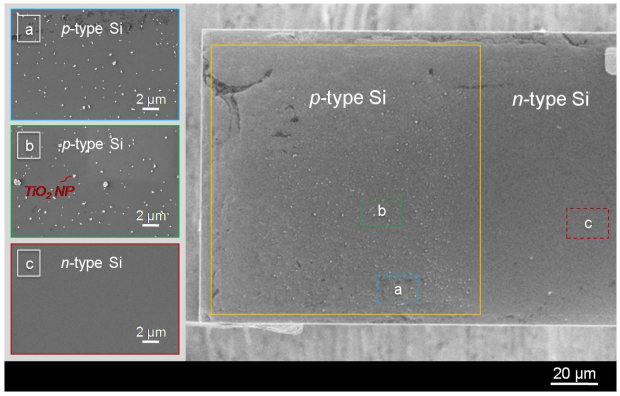

Figure 2. The polluted cantilever showing (a, b) the arrangement of trapped NPs on *p*-type Si and (c) the clean area on *n*-type Si.

This work is supported by the German Federal Ministry of Education and Research (BMBF) within the cluster “NanoCare” under no. 03X0098A.

Wasisto, H. S., Merzsch, S., Waag, A., Kirsch, I., Uhde, E., Salthammer, T., Peiner, E. (2012) *Microsyst. Technol*. DOI: 10.1007/s00542-011-1405-9.

Dohn, S., Sandberg, R., Svendsen, W. and Boisen A. (2005) *Applied Physics Letters* 86, 233501.

Tsai, D-H., Hawa, T., Kan, H-C., Phaneuf, R. J. and Zachariah, M. R. (2007) *Nanotechnology 18*, 365201 (10pp). DOI: 10.1088/0957-4484/18/36/365201.

Post-corona diffusion charging versus radial ion profile in axisymmetric arrangement

Jidenko Nicolas[1], Alonso Manuel[2] and Borra Jean-Pascal[1]

[1]Equipe Décharges Electriques et Aérosols du Laboratoire de Physique des Gaz et des Plasmas (UMR 8578 CNRS – Université Paris-Sud Orsay, F-91405) SUPELEC, Plateau de Moulon, F-91192, Gif-sur-Yvette, France
[2]National Center for Metallurgical Research (CSIC), Gregorio del Amo, 8. 28040, Madrid, Spain.

Keywords: aerosol charging, diffusion charging, charge distribution, corona discharge

This work addresses the comparison of measured and calculated charge distributions in a post-discharge unipolar charger. The main objective is to evaluate the range of charging conditions (Ni.τ products, as time integrated ion densities Ni on particle trajectories) induced by radial and axial decreasing ion densities.

The negative corona discharge occurs around a needle of 100 µm radius in air at atmospheric pressure (Trichel 1938). Ions are extracted from the discharge gap using a 1-2 lpm gas flow rate through a hole in the anode plane. The charger operates with ion and aerosol flow velocities ratio between 0.1 and 2 that controls the ion radial profile. The charging zone has been designed to limit ion and aerosol losses.

A model developed for aerosol and ion mixing (Alonso et al. 2009) is used for the evaluations of Ni profile, mean Ni.τ product and charge distributions in realistic conditions using Fuchs' theory (Fuchs 1963) in the transition regime (30-300 nm). The zone of mixing is axisymmetric. Radial and axial profiles of ion density are stationary. The model calculates these profiles taking into account diffusion, space charge effects (for ion and particle) as well as the evolution of the charge level of particles.

Ni.τ products and the decrease of ion density along the charging zone have been characterized by current measurements at different locations. The related mean Ni.τ product is $6 \cdot 10^{12}$ s.m^{-3}. This value fits with calculation within 10 %.

The average particle charge and aerosol charge distributions are measured and compared to calculations. In that respect, aerosols of controlled size (related to DMA voltage) and concentration (controlled by the furnace temperature and maturation time after furnace) are injected in post-discharge.

Aerosol losses through the charger are determined with the CPC. Maximal aerosol losses are reached for smallest particles tested and remains below 10 % for a charge fraction of 40 % at 10 nm.

The neutral fraction is defined using the CPC after an electrostatic precipitator to collect charged aerosols. Aerosol charge distributions are obtained from mobility spectra measured with a Radial Differential Mobility Analyser (RDMA).

Previous estimation for flat radial ion density profile with decreasing axial density has proven that the radial profile has to be taken into account. Indeed, the measured charge distribution is broader than the calculated one with less than 8 % difference in population of each charge level, when neglecting the radial ion density profile.

Then, taking into account the calculated radial ion profiles, figure 1 shows the evolution of the calculated charge distribution for particles of 30 nm along the charging zone that will be compared with measured charge distributions.

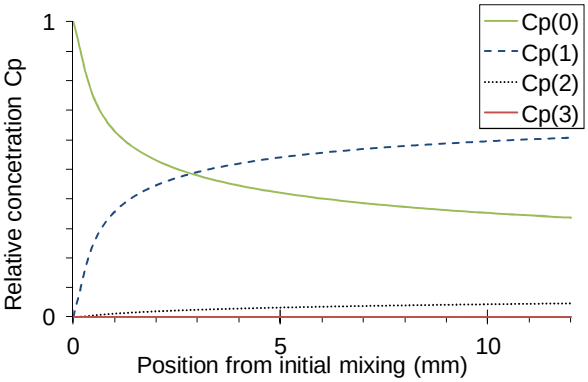

Figure 1. Evolution of the charge distribution for particles of 30 nm along the charging zone.

Measured charge distributions will be compared with the calculated ones at different location in the charging zone, for different radial ion density profiles induced by flow different velocity ratio at constant initial ion density and reversely.

References

Trichel GW (1938) *Phys. Rev*. **54**, 1078-84
Alonso M and Alguacil FJ 2003 *J. A. S.* **34** 1647-64
Fuchs N (1963) *Geofis. Pura Appl*. **56**, 185-92
Alonso M et al. (2009). *J.A.S.*, **40-8**, pp 693-706

Sub-second diffusion charging

N. Jidenko*(1), D. Maro(2), F. Gensdarmes(2), D. Boulaud(2) and J.-P. Borra(1)

[1]Laboratoire de Physique des Gaz et des Plasmas (CNRS – Univ. Paris XI F-91405) SUPELEC, F-91192 Gif-sur-Yvette cedex, France
[2]Institut de Radioprotection et de Sûreté Nucléaire, BP 68, 91192, Gif-sur-Yvette cedex

Keywords: aerosol charging, diffusion charging, charge distribution, corona discharge
nicolas.jidenko@u-psud.fr

Numerous aerosol processes are based on the charging of aerosol by ions (filtration, size measurement, electrostatic agglomeration …) (Intra 2011). The present work focuses on diffusion charging in short time (below 50 ms). The final aim is to measure the time evolution of the aerosol size distribution with a frequency of 10 Hz. The short charging time is thus required to preserve the temporal information. The ions are produced by an electrical discharge in air at atmospheric pressure and the aerosols are charged in post-discharge to prevent from the destabilization of the discharge due to the collection of aerosol on the electrode when the aerosol is injected in the discharge (Borra 2006).

Two scientific aspects are presented. The first one is the optimization of the ions extraction from the corona discharge and the evaluation of the charging conditions (Ni.τ product which is the critical parameter for diffusion charging). The second one concerns the charge-diameter relation including the influence of aerosol concentration on this relation.

The discharge occurs around a needle of 50 µm radius. The discharge current (-30 µA) is typical of the negative corona regime (Trichel 1938, Goldman et al. 1978). Ions are extracted from the discharge gap through a hole in the anode by convexion. Only a small fraction (about 1 %) of the discharge current is extracted from the discharge. To increase the ion flux, three processes have been studied: the distribution of the ion in the discharge gap, the electro-collection in the extractor by self repulsion and re-collection below the anode.

The charger has been designed to control the charging time below 50 ms. The originality of the charger lies on the strong heterogeneity of the ion density that decreases by 4 orders of magnitude in 50 ms. Indeed, the loss of ions to the walls by electrostatic repulsion requires high initial ion densities to achieve aerosol charging in the short charging time.

The product Ni.τ is defined by integration of the density of ions along the trajectory of the particles obtained by measuring the ion current in post-discharge. The product Ni.τ depends on the ion extraction on the one hand and hydrodynamic conditions of ion-aerosol mixture on the other hand, affecting the ion density profile in post-discharge and the path particles. The estimation of the mean Ni.τ is $2{\cdot}10^6$ s.cm^{-3}.

Under these conditions, the average charge levels are measured on calibrated aerosol size (10 nm - 1 micron) and concentration (10^3-$3{\cdot}10^5$ cm^{-3}). In our charging conditions, the ion density is very heterogeneous; we have highlighted the lack of ions per particle for aerosol concentration higher than 10^9 m^{-3} (cf. figure 1).

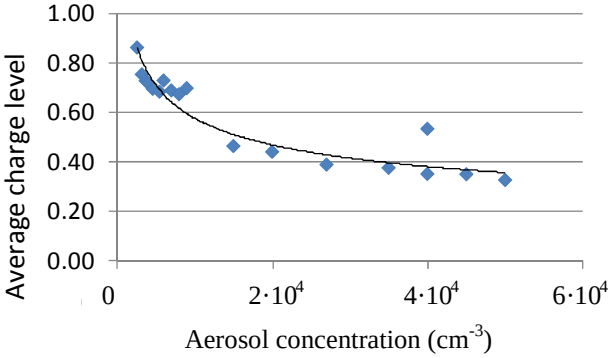

Figure 1. Number of charge per 100 nm particle for a given Ni.τ product of $2{\cdot}10^6$ s.cm^{-3}

The average charge level per particle decreases with the concentration of aerosol, despite constant initial ion density and charging time. Indeed, the charging laws are only valid when in very a large excess of ions per particle (Fuchs 1963). In this experiment, this is only true at the entrance, but this is no longer the case at the end of the charging zone. The numbers of ion per particle evolve from 10^5-$2{\cdot}10^4$ with the aerosol concentration at the entrance but fall down to 10 to 2 at the end of the charging zone. Hence, this effect of aerosol concentration on charge level can be attributed to different real Ni.τ that can be related to a faster decrease of ion density due to collection on the particle for higher aerosol concentration. The estimation of the real Ni.τ product using Fuchs' theory gives Ni.τ between of $3{\cdot}10^5$ and $8{\cdot}10^5$ s.cm^{-3}.

These values are in the same order of magnitude but smaller than the one estimated by ion current measurements without aerosol ($2{\cdot}10^6$ s.cm^{-3}) and account for the maximal aerosol concentration for any post-discharge aerosol charger.

References

Intra P and Tippayawong N 2011 *Aerosol and Air Quality Research* **11** 187-209
Borra J-P 2006 *J. of Physics D: Appl. Phys* **39** R19-R54
Fuchs N A 1963 *Pure and Appl. Geophysics* **56** 185-93
Goldman M and Goldman A 1978 *Gaseous Electronics 1, Electrical discharges* ed M N Hirsh and H J Ascam (New York: Academics Press) pp 119-66
Trichel G W 1938 *Physical Review* **54** 1078

Atmospheric small-ion mobility downwind and upwind of AC high-voltage power lines

M.D. Wright[1,2], A.J. Buckley[1], J.C. Matthews[1,2] and D.L. Henshaw[1,2]

[1]H H Wills Laboratory, School of Physics, University of Bristol, Bristol BS8 1TL, UK
[2]Atmospheric Chemistry Research Group, School of Chemistry, University of Bristol, Bristol BS8 1TS, UK
Keywords: Ions, ion mobility, corona discharge, particle charging.
Presenting author email: matthew.wright@bristol.ac.uk

Diffusion charging of atmospheric aerosols is chiefly governed by the mobility and concentration of small-ions. Near to corona-emitting high voltage power lines (HVPLs), a higher ion mobility may lead to enhanced aerosol charging and possibly a higher particle deposition efficiency in the lung (Fews *et al*, 1999). Several previous studies report elevated small-ion concentrations near to AC HVPLs (e.g. Jayaratne *et al*, 2008). Ion mobility measurements have been made near DC lines (Suda and Sunaga, 1990) and from corona sources in the laboratory (Alonso *et al*, 2008). We present measurements of ion mobility upwind and downwind of AC HVPLs in the Bristol, UK area.

Positive and negative ion mean mobilities at 8 HVPL sites were calculated from mobility spectra obtained using Gerdien-type Aspiration Condenser Ion Mobility Spectrometers (ACIMS, Fews *et al*, 2005). Where possible, two ACIMS were used to measure at upwind (UW) and downwind (DW) sites simultaneously. Laboratory intercomparison of the mobility response of each ACIMS (Figure 1) showed reasonable agreement, and was used to correct data obtained in the field. 28 individual measurements were made on 17 days. Wind speed and direction were measured and used to estimate transit times from HVPL to measurement location.

Figure 2 shows DW against UW mobility for positive and negative ions, with mean values given in Table 1. Of 28 (negative) and 27 (positive) individual measurements, only 5 (negative) and 4 (positive) did not show an increased mobility DW compared to UW. Ion mobility for both polarities was higher DW than UW of high-voltage power lines by ~15%, implying that aerosol charging may occur faster, and reach higher peak levels, than if typical background mobilities are assumed. The ratio of negative/positive mobility was 1.32 UW and 1.27 DW. The mobilities reported here are higher than in some previous studies, possibly due to lower than expected airflow through the ACIMS. However, the relative response of the two devices (Figure 1) suggests that the DW/UW ratio was not affected.

Ion mobility is related (in a non-trivial manner) to ion mass and composition. Higher mobilities are often taken to imply that ions are newly-produced. However, most previous studies report that 'ageing' of ions is expected to terminate within a few seconds. In these measurements, transit times from the line to site ranged from 22−290 s, implying that the ageing process may take longer than previously thought, a finding also reported by Luts *et al* (2011), and/or that the components of the cluster are smaller at creation and remain so despite chemical ageing. However, measurements here on 8 days at more than one DW site show no significant difference between mean DW/UW mobility ratios at different transit times from the line. Thus, the present data suggests, but does not provide solid evidence for, further growth at ages > 20 s.

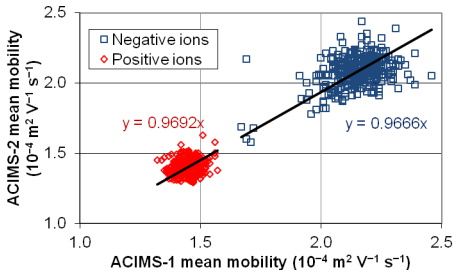

Figure 1. Results of laboratory intercomparison between two ACIMS for positive and negative ions.

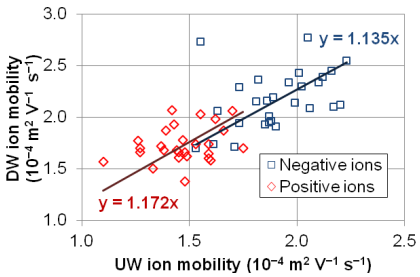

Figure 2. Scatterplot showing individual data for DW against UW mobility. DW=UW shown as dashed line.

Table 1. Mean mobilities DW/UW for each polarity

	Mobility (10^{-4} m^2 V^{-1} s^{-1})		Ratio
	UW	DW	(DW/UW)
Positive	1.47	1.73	1.18
Negative	1.90	2.17	1.14

This work was supported by Children with Cancer UK, Registered Charity No. 298405.

Alonso, M., Santos, J.P., Hontañón, E. and Ramiro, E., (2009). *Aerosol Air Qual. Res.* **9**, 453-457.

Fews, A.P., Wilding, R.J., Keitch, P.A., Holden, N.K. and Henshaw, D.L. (1999). *Int. J. Radiat. Biol.* **75**, 1523-1531.

Fews, A.P., Holden, N.K., Keitch, P.A. and Henshaw, D.L. (2005). *Atmos. Res.* 76, 29-48.

Luts, A., Parts, T.-E., Hõrrak, U., Junninen, H. and Kulmala, M. (2011). *J. Aerosol Sci.* **42**, 820-838.

Jayaratne, E.R., J-Fatokun, F.O. and Morawska, L. (2008). *Atmos. Environ.* **42**, 1846-1856.

Suda, T. and Sunaga, Y. (1990). *IEEE Trans. Power Delivery* **5**, 247-253.

Charging and collection of fine mists from a wet scrubber using activated oxidation catalysts

Bangwoo Han, Hak-Joon Kim and Yong-Jin Kim

Environmental and Energy Systems Research Division, Korea Institute of Machinery and Materials, Daejoen, 305-343, Korea
Keywords: Carbon fiber, Dielectric film, Electrostatic precipitator, Recovery
Presenting author email: bhan@kimm.re.kr

Wet scrubbers spraying fine water droplets into gas streams have been widely used to remove toxic or odorous gases in many industrial places such as food waste disposal facilities or semiconductor manufacturing factories. Fine white mists generated via the rapid condensation of humid air at the outlet of the wet scrubber can be one of main sources of civil appeals from the residents near the places. Therefore it needs to remove fine visible white mists generated at the chimney of the facilities or the factories. Recently, to improve the performance of the wet scrubbers, spraying water has been activated via electric oxidation catalysts (Chung et al., 2009). The electric activated scrubbing water contains acid solvents such as H_2SO_4 and a small amount of metal catalysts. The mists generated from the scrubbers which use these activated solutions need to be collected to minimize the toxic mist emission and restore valuable catalyst metals from the mists. In this study, a two stage non-metallic electrostatic precipitator (ESP) using a carbon fiber charger and a dielectric film collector has been investigated to charge and collect fine mists from the scrubber with the activated liquids containing a valuable metal catalyst. Carbon fiber charger was composed of 16 carbon fiber ionizers (Han et al., 2008) and dielectric film collector was made of parallel aluminum plates coated by polypropylene films (Kim et al., 2010). Scrubber was packed by a lot of 1 inch balls with a height of 1,200 mm and 40% H_2SO_4 aqueous solution with 0.1 M Co as a scrubbing liquid was sprayed. At the downstream of the scrubber the non-metallic ESP was located to remove fine mist particles generated from the scrubber. Mist size distributions were measured by a scanning mobility particle sizer (Model 3936, TSI) and an aerosol spectrometer (Model 1.109, Grimm) at the downstream of the ESP. High voltages of 4-8 kV were supplied to both the charger and collector of the ESP. Particle size and concentration were increased by about 4-10 times due to the sprayed mist droplets after turning scrubber on. Figure 1 shows the average charge number per particle obtained by the carbon fiber charger when the scrubber was operated on and off. The average charge number per particle was linearly increased with the applied voltage to the charger. After operating scrubber on, charge number per particles was increased by about 4 times compared to indoor particles without scrubbing water. It indicates that mist particles have larger sizes compared to indoor particles and can obtain a larger number of charges at the same particle charging condition. These charged mist particles can be easily collected at the dielectric film collector of our ESP system. Particle loss at the charger and collection efficiency at the collector of the ESP were measured for the various applied voltages at the charger and collector at the gas face velocity of 0.25 m/s. Particle loss was in the range of 5-20% at the applied voltage to the charger of 4-6 kV. Collection efficiency of the charger was increased from 92% to 95% by increasing applied voltage to the charger from 4 kV to 6 kV with an applied voltage to the collector of 4 kV. At the applied voltage to the charger of 4 kV, increase of applied voltage to the collector from 4 kV to 8 kV could improve the collection efficiency from 92% to 98%. At the applied voltage to the charger of 6 kV, it could improve the efficiency from 95% to 98.5%. Therefore, applied voltage of 4 kV at the charger seems to be much proper at the point of view of particle loss in the charger. In our further studies, pH variation at the second scrubber located after the ESP and the fraction of Co catalyst at the collector will be investigated to evaluate our system whether our system can properly remove harmful acid mists and collect valuable metal catalysts from the mists.

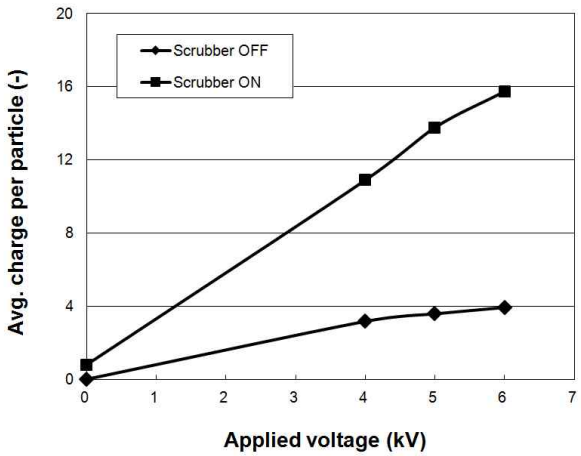

Figure 1. Comparison of average charge number per particle between the indoor particles with scrubber off and the mist particles with scrubber on.

This work was supported by Korean Ministry of Environment as “The Eco- Innovation project”.

Chung, S.J., Pillai, C. and Moon, I.S. (2009) Separation and Purification Technol., 65, 156-163

Han, B., Kim, H.-J., Kim Y.-J. and Sioutas C. (2008) *Aerosol Sci. Technol.,* **42**, 793-800

Kim, H.-J., Han, B., Kim, Y.-J. and Yoa (2009) *J. Aerosol Sci.*, **40**, 285-294

Removal performance of an electrostatic precipitator with edge to plate geometry for particulates in combustion gases for marines

H.J. Kim, B. Han, G.B. Cho and Y.J. Kim

Department of Eco-Machinery System, Korea Institute of Machinery and Materials (KIMM), Daejeon, 171 Jangdong, Yuseong-gu, 305-343, Korea
Keywords: Marine, electrostatic precipitator, particulates, removal.
Presenting author email: diayolk@kimm.re.kr

Even though NO_x and SO_x have been already regulated by international maritime organization (IMO), PMs which are known to be a source of respiratory diseases have not been regulated. However, Due to strong regulation trend on PMs from other machineries such as on and off road combustion machineries such as vehicles, construction machineries, the PMs from marines will be regulated by IMO in the near future.

Generally, to remove particles from combustion engines for on and off load transportation and machinery, DPFs (Diesel Particulate matter Filter) are being widely used. However, the filters have a technical problem to be applied for high volumetric engines such as marines because of significant pressure drop.

In this study, for removal of particles from combustion used in marines, we applied an ESP (electrostatic precipitator) which was generally used for removal of particulates in high volumetric flow rates such as coal firing combustion, and manufacturing industries. Shown in Figure 1, the ESP was one field and two channel geometry with hammer type rappers. The ESP was evaluated with a 12 L diesel engine and a Bunker C boiler with an exhaust gas flow rate of 3000 m^3/hr, based on particle numbers. The concentration was measure by a SMPS (CPC 3076, Classifier 3081, TSI, US), combined with dilutors, and a high voltage power supply of Max. 80 kV/20 mA for negative polarity was used in this study.

Figure 2 shows the particle collection efficiency of the ESP against specific corona power for different combustion conditions. The collection efficiency showed a correlation with a specific corona power which was determined with applied voltage, current, temperature, and flow rate. Specially, with the specific corona power more than 10 W/m^3/min, the ESP achieved high collection efficiency over 80 %, based on number, regardless of types of combustion and temperature. This correlation could be used for a design of the ESP for larger scale of marine diesel engines and boilers. Figure 3 shows the long term PM collection performance of the ESP for different operation conditions such as exhaust flow rate, temperature, and rapping. The collection efficiency was calculated with the total number concentrations measured by a CPC (Model 3076, TSI, US), and it was approximately 95% with the specific corona power of 30 W/m^3/min. This performance was maintained even at high temperature, particle load and flow rate. In particular, during the continuous rapping of 5 min period over one hour, the collection performance was also maintained.

Figure 1. Experimental set-up for this study.

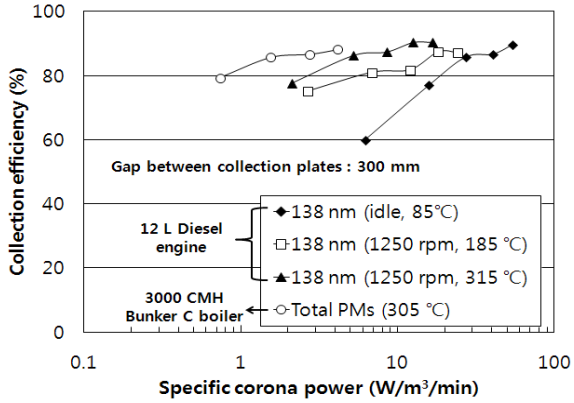

Figure 2. The variation in collection efficiency of the ESP plotted against specific corona power for different combustion conditions.

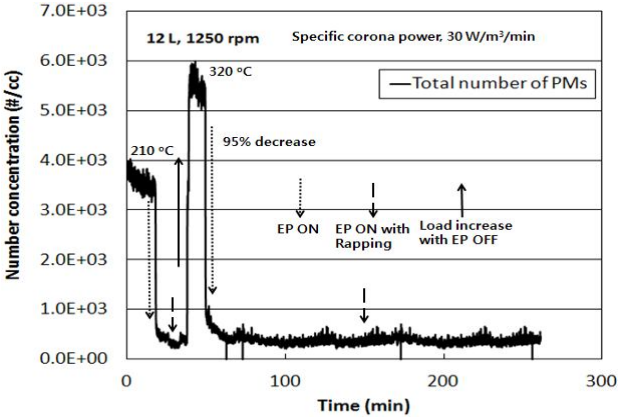

Figure 3. Long term PM collection performance of the ESP.

This work was supported by a Basic Research Fund (SC0820) of the KIMM.

Enhancement of the filtration performance of metallic foam filter for diesel particulates by electrostatic charging and collection

H.J. Kim, B. Han, G.B. Cho and Y.J. Kim

Department of Eco-Machinery System, Korea Institute of Machinery and Materials (KIMM), Daejeon, 171 Jangdong, Yuseong-gu, 305-343, Korea
Keywords: metallic foam filter, electrostatic, charging, collection, diesel particulates.
Presenting author email: diayolk@kimm.re.kr

In order to decrease both diesel particulate matter (PM) mass and number in exhaust gas from diesel engines, the filtration system with the ceramic DPF (Diesel Particulate Filter) is being on commercialization for light and heavy duty diesel vehicles. Even if the wall flow type ceramic filters, which are coated with metal catalysts, have shown over 90 % filtration performance for the diesel PMs, the DPFs still have problems such as insufficient reliability, excessively high pressure drop at low exhaust temperature, and mechanical crack and failure. To decrease pressure drop and avoid the numerous problems related to DPF, metallic filters as an alternative were developed in Germany and South Korea. However, the filtration systems have shown lower efficiency than DPF especially for removal performance, based on PM number.

To increase particle removal performance of the metallic foam filter for a newly reinforced regulation, based on number of the PMs from diesel engines, a novel metallic foam filtration system assisted by electrostatic charging and collection has been developed. The system was evaluated by comparison with a standalone metallic foam filter and a commercialized DPF filter, using 3000 cc diesel engine with engine dynamo at steady-state engine operation conditions with constant rpms and loads, shown in Figure 1.

The cylindrical diesel PM filtration system in this study was consisted of a novel high voltage electrode which is used for charging particles and imposing electrostatic field to the metallic filter at the same time, and metallic foam filter. Figure 2 shows the curves of corona voltage against current at different temperatures. The curves for the system were moved to the left, and the corona current was higher for the same applied voltage, when the temperature increased. In particular, the sparkover was observed at lower applied voltages at higher temperature. However, the high electrical potential was maintained at the voltage and current up to 16 kV and 1.5 mA even at 300 ^{o}C, due to a special air slit insulation. Figure 3 shows the comparison of the particle collection and pressure drop performance of the filtration system in this study and DFP filter for particles ranged at a peak size of the PMs from the diesel engine, 50 nm. Even though the collection efficiency with only foam filter was 50 % which was much lower than that with the DPF, the pressure drop was significantly lower by a maximum of only 20 % of the DPF. In particular, with the filtration system combined with electrostatic precipitation device, the collection efficiency exceeded over 95% using 10 W/m^3/min, similar to that of DPF.

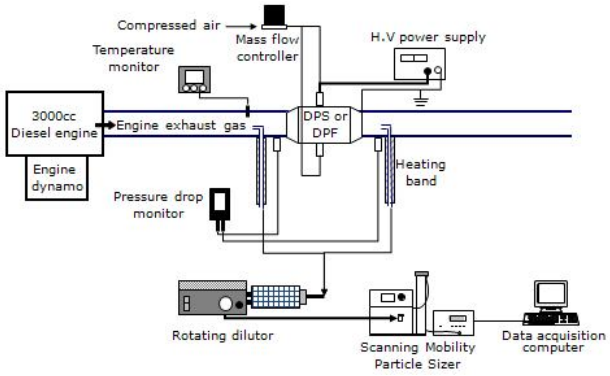

Figure 1. Experimental set-up for this study.

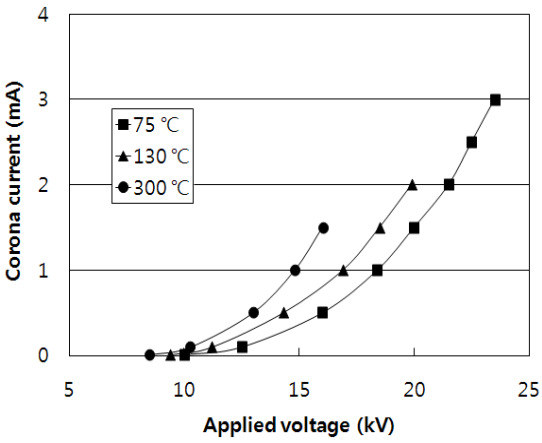

Figure 2. The changes in voltage to current curves plotted for different temperature of the diesel exhaust

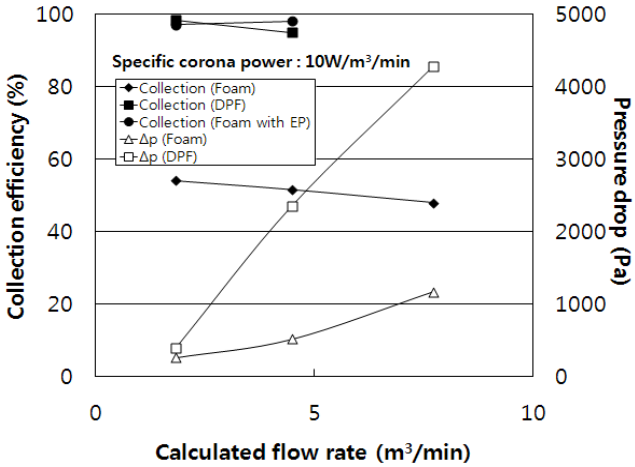

Figure 3. Comparison of performances between standalone foam filter and ceramic DPF.

This work was supported by a Basic Research Fund (SC0820) of the KIMM.

Numerical simulations of electrosprays including induced gas flow

A.K. Arumugham[1], J. Grifoll[1] and J. Rosell-Llompart[1,2]

[1]Department of Chemical Engineering, Universitat Rovira i Virgili, Tarragona, Catalonia, E-43007, Spain
[2]Catalan Institution for Research and Advanced Studies (ICREA), Barcelona, Catalonia, E-08010, Spain
Keywords: electrospray, electric wind, numerical simulation, drag force.
Presenting author email: joan.rosell@urv.cat

When aerosol particles move collectively with a net velocity relative to the surrounding gas exert a drag force on the gas which can cause the gas to flow. In electrosprays, this gas motion is induced by the highly charged microdrops moving under the action of electrostatic forces, and can be significant. Because of the difficult experimental accessibility to gas velocity, there are only a handful of reports on this important question, however. In the systems studied by Gomez and Tang (1994) and by Hartman et al. (1999) the surrounding gas velocity was determined to be about 1/3 of the mean droplet axial velocity.

Numerical simulations of electrosprays thus far have neglected the gas flow (Grifoll and Rosell-Llompart, 2012, and works cited therein). In this contribution, we report on our recent efforts to simultaneously compute the droplet and gas motions in steady state. Correct computation of this effect is of paramount importance for the correct numerical simulation of electrosprays, and of multiplexed electrospray systems, and is a requirement in the modelling of droplet evaporation and vapor concentration in electrosprays.

Because the transport equations for each phase (gas and droplets) are coupled, steady state solutions are sought by an iteration procedure using two separate codes. Our droplet dynamics code is based on a 3D Lagrangian model that simplifies the far droplet-droplet electrostatic interactions without any significant loss in accuracy. This coarse-graining scheme, called Lumped Space Charge (LSC) approximation has been proposed recently (Grifoll and Rosell-Llompart, 2012). Our gas flow code seeks steady state solutions to the 2D cylindrical equations for flow vorticity and stream function, modified to include source terms associated to the spray drag. The spray drag force function (force/volume) is a smoothed approximation of the spray drag which is defined piecewise within each of the grid cells used by the flow code. We have assumed that all of the space within the spray is available to the gas, which is approximately valid so long as the volume fraction of the droplet phase is much smaller than unity.

The integration procedure proceeds iteratively as follows. Initially, quiescent gas (zero gas velocity) is assumed and the droplets trajectories are integrated using the LSC code until steady state is reached and about 0.1 seconds of real time data is available. Next, the droplet's velocity and position data are pooled-averaged to compute the corresponding drag force density field, and a steady state gas flow solution caused by this force field is determined. The vorticity and stream function values are then used to define the corresponding gas velocity field. This initial gas velocity solution is then fed to the particle dynamics code, and a new spray configuration is obtained to produce a second estimate for the drag function, from which a second steady gas flow is computed using the gas flow code. The procedure is repeated iteratively until a convergence criterion based on a small predefined difference between the solutions obtained in two consecutive iterations is satisfied.

This methodology is applied to recalculate our previously simulated sprays based on the experimental scenarios of Park et al (2004) comprising droplets of lognormally distributed diameters with count mean of 8.84 μm, and of Tang and Gomez (1994) for a bimodal spray with primary droplets count mean diameter of 32.5 μm. Our methodology can also be useful to simulate systems in which an external co-axial gas flow around the needle is present.

This work was supported by Grant CTQ2008-05758/PPQ from the Spanish Ministry of Science and Innovation, and Grant 2009-SGR-1529 from the Government of Catalonia, Spain.

Grifoll, J. and Rosell-llompart, J. (2012) *J. Aerosol Sci.* **47**, 78-93.

Hartman, R.P.A., Borra, J.-P., Brunner, D.J., Marijnissen, J.C.M., & Scarlett, B. (1999) *J. Electr.*, **47**, 143–170.

Park, H., Kim, K., & Kim, S. (2004) *J. Aerosol Sci.*, **35**, 1295–1312.

Tang, K. and Gomez, A. (1994) *Phys. Fluids*, **6**, 2317-2332.

Hybrid QMOM-Orthogonal-Collocation Method: Application to Aerosol Dynamics under Coagulation

M. Arias-Zugasti

Departmento de Física Matemática y de Fluidos, UNED, Madrid, 28040, Spain
Keywords: Coagulation, Aerosol evolution, Aerosol fundamentals.
Presenting author email: maz@dfmf.uned.es

Spectral methods, as Orthogonal Collocation, are an extremely accurate and stable numerical tool for solving partial differential equations. However, this kind of numerical methods is restricted to cases where the dependent variables are very smooth functions. In many cases this condition limits the applicability of spectral methods in aerosol science (in particular in aerosol dynamics under coagulation). In the present work it is shown that a possible way of solving that difficulty is by using time-dependent mappings, based on the dynamics of the region of interest, defined as the region in state variables space where the distribution function is mainly located. This strategy relies on information on the dynamics of that region, which can be defined in terms of the moments of the aerosol's distribution function. Hence, the Quadrature Method of Moments (QMOM) (see McGraw 1997) seems the ideal tool to calculate the dynamics of the region of interest, since the information that this method provides is all that is needed to track the position and size of the region of interest and, on the other hand, QMOM is extremely efficient and its applicability range is extremely broad.

In the case of aerosol dynamics under coagulation, a difficulty that arises when time-dependent mappings are used to solve the General Dynamic Equation (GDE) is that, in general, the coagulation kernel in terms of the mapped variable depends explicitly on time. This difficulty appears as a consequence of the time-dependent mapping, even if the coagulation kernel in terms of the physical variable (e.g. particle size) does not depend on time. Thus, in order to solve the GDE in terms of the mapped variable one needs to re-calculate the integrals that define the coagulation term at every time step. In principle this is too expensive (time-consuming) task, which makes this strategy un-practical. However, this difficulty can be avoided solving the GDE using orthogonal collocation and computing the coagulation term by means of the Fast Algorithm (Arias-Zugasti 2006, 2012). As shown in Arias-Zugasti (2006, 2012), the use of the Fast Algorithm factors the dependence of the coagulation term on the spectral basis used on one hand, and on the coagulation kernel on the other hand. This solves the former numerical difficulty, since by means of the Fast Algorithm the orthogonal collocation expansion of the coagulation term can be computed as the product of the coagulation kernel evaluated at the collocation abscissae, times a set of N integrals that only depend on the spectral basis used (N is the number of functions used in the spectral basis), but not on the coagulation kernel. Since the spectral basis does not depend on time, these integrals can be pre-calculated, thus enabling the efficient evaluation of the coagulation term, even in cases of time-dependent kernels. The present method enables the numerical integration of the GDE from an arbitrary initial condition until the self-preserving size distribution function is reached.

This hybrid QMOM-orthogonal collocation strategy, enabled by the Fast Algorithm, is totally general. I.e., it is not restricted to: (*a*) any particular form of the coagulation kernel, (*b*) the spectral basis used, or (*c*) the conservation law that relates the state variables of the emerging particle to those of the colliding particles. This method has been successfully used in recent studies on the dynamics of Brownian coagulation in expanding gases (Rosner and Arias-Zugasti 2011), the coagulation induced by thermophoresis in the case of non-Brownian particles (Rosner and Arias-Zugasti 2011a) and the thermophoresis-modified coagulation of Brownian particles (Arias-Zugasti and Rosner 2011b, Rosner and Arias-Zugasti 2011c). It is also shown that this method can be extended to the case of multivariate distributions, regardless of the number of state variables and their conservation properties under coagulation. On the other hand, it is shown that the Fast Algorithm leads to the correct evolution equations of the moments of the distribution, which explains its accuracy and stability.

This work was supported by Comunidad de Madrid (S2009/ENE-1597), Ministerio de Ciencia e Innovación (CSD2010-00011) and (ENE2011-26868).

McGraw, R (1997) *Aerosol Sci. and Technol.* **27**(2), 255-265

Arias-Zugasti, M (2006) *J. of Aerosol Sci.* **37**(10), 1356-1369.

Arias-Zugasti, M (2012) *J. of Aerosol Sci.* submited.

Rosner, D. E. and Arias-Zugasti (2011), M. *AIChE J.* **57**(2), 307-318.

Rosner, D. E. and Arias-Zugasti, M. (2011a) *Phys. Rev. Lett.* **106**(1), 015502.

Arias-Zugasti, M. and Rosner, D. E. (2011b) *Phys. Rev. E* **84**(2), 021401.

Rosner, D. E. and Arias-Zugasti, M. (2011c) *Ind. & Eng. Chem. Res.* **50**, 8932-8940.

Friday, September 7, 2012

Plenary 5

Photophoresis – the forgotten force

Helmuth Horvath

University of Vienna, Faculty of Physics, Aerosol.and Environmental Physics
Boltzmanngasse 5, 1090 Vienna, Austria
Presenting author email: Helmuth.Horvath@univie.ac.at

Particles illuminated by a beam of light having sufficient flux density can move in various directions under the influence of the light. Since light is the cause for the motion, the expression photophoresis has become common. Preining (1966) gives a concise description of the important factors influencing photophoretic motion: *"This motion can depend on the illumination, colour, structure and shape of the light beam, on pressure and composition of the gas, on the particles size, shape and material, and on additional fields such as electric, magnetic, and so on"*

The momentum transferred by photons hitting a particle and absorbed or deflected obviously exerts a force on a particle. Except for extremely intense radiation this direct photophoresis (radiation pressure) is of minor importance in aerosol science and can be neglected. The indirect photophoretic force, as treated below, is much stronger, but needs the presence of gas molecules which are always available in an aerosol.

On a microscopic scale, the gas molecules impact on the surface of an aerosol particle and are reflected. The reflection can be specular, diffuse, or with accommodation. For a particle moving through a gas, the molecules impacting at the front side are reflected with a higher velocity compared to the back side. This asymmetry in velocities leads to a momentum transferred to the particle and causes the friction force acting on the particles when moving through a gas.

Reflection of gas molecules at the particle's surface with accommodation is of special importance for photophoresis. A particle which absorbs (visible of IR) radiation is heated to a higher temperature T_p than the temperature T_g of the surrounding gas. A gas molecule hitting the particle's surface can acquire some of the thermal energy of the hot particle and be emitted with a velocity corresponding to a higher temperature, T, compared to the surrounding gas. The probability of taking up additional thermal energy is characterized by the accommodation coefficient $\alpha = (T - T_g)/T_p\text{-}T_g)$. With $\alpha = 0$ for no and $\alpha = 1$ for full accommodation. The value of α depends on both the material forming the particles as well as the surface structure.

If the accommodation coefficient of the surface of the particles is $\alpha > 0$ and the particle is heated by light, a photophoretic force can act on the particle. Two different possibilities have to be distinguished:

(a) Constant accommodation coefficient but variation in surface temperature. This e.g. occurs for an illuminated light absorbing particle. The surface of the particles is warmer than the backside; molecules at the side facing the radiation source leave the surface faster, resulting in a force away from the light source (positive photophoresis). For a slightly absorbing particle the maximum absorption may be at the backside, resulting in a motion towards the light source (negative photophoresis). The direction of the photophoretic force is determined by the direction of the radiation and is almost independent on the orientation of the particle.

(b) Variable accommodation coefficient on the surface but constant temperature. At the location of higher accommodation coefficient the molecules are reflected with a higher velocity resulting in a thrust on the particle similar to the jet of an airplane. The direction of the force on the particle is determined by the orientation of the particle and independent on the direction of the illumination (body fixed force). Upon change of the orientation of the particle the direction of the force changes likewise. Since all particles perform Brownian rotation, the net force is zero. If an orientating torque acts on the particle, the photophoretic force will predominantly be in one direction, thus the average photophoretic force will be nonzero. The orientation can be due to inhomogeneous distribution of the mass on the particle in the gravitational field, or magnetic or electric dipoles in the corresponding field.

(c) Obviously a combination of (a) and (b) is possible.

The photophoretic force depends on many factors: Flux density of radiation, particle size and optical properties, mean free path of the gas molecules, gas pressure, thermal conductivity of gas and particle, temperature of gas and particle, asymmetry of the particle, strength of external fields. Generally the photophoretic force reaches a maximum value for particle sizes comparable to the mean free path of the gas molecules. Despite these many influencing factors, a theory of photophoresis could be developed (Rohatschek 1955, 1995).

Positive photophoresis can be used as a tool for on line separation of absorbing and non absorbing particles. Particles are illuminated by an intense laser (808 nm), obtain a velocity into the direction of the light and perpendicular to the flow velocity due to the photophoretic force and can be collected in a secondary

flow (Haisch *et al*. 2008). Also photophoretic particle trapping and levitation is possible.

In the stratosphere and mesosphere the air molecule's mean free path is between 1 and 100µm due to the lower pressure thus photophoresis can occur for all particles found there. Since an irregular particle or one with a magnetic moment has a preferred orientation in the gravitational or magnetic field, gravito- of magneto-photophoresis are important. This has been proven experimentally (Jovanovic 2005). The existence of layers of particles in the stratosphere and mesosphere can be explained by photophoresis, as well as the transport of soot particles in the atmosphere (Cheremisin *et al*., 2005, 2011, Pueschel *et al*. 2000).

Photophoresis is an important force involved in planet formation. In a gas rich, optically thin circumstellar disk the motion of particles ranging from 1 µm to 10 cm will be dominated by photophoresis, moving the particles opposite to gravity to a distance from the star, where the gas density reaches a value at which photophoresis equals all other forces at work. Thus the formation of ring like structures of dust distribution around a star can naturally be explained (Krauss and Wurm, 2005) and the formation of protoplanets is significantly influenced by photophoresis (Wurm and Krauss, 2006).

For fighting global warming by geo-engineering, particles should be positioned in the stratosphere or mesosphere, which reflect sunlight and remain suspended as long as possible. The photophoretic force can be very helpful, since a long residence time can be achieved this way. A particle optimized for this purpose can be a 10 µm disk with a layer of Al_2O_2 at the top, Al in the middle and $BaTiO_3$ at the bottom with a micro-magnet attached to it (Keith 2010).

For completeness it is mentioned, that the term photophoresis is also used for motion of hydrocolloids illuminated by a laser beam. In that case actually it is the radiation force, which makes the particle migrate (Helmbrecht *et al*. 2007).

Cheremisin A.A, Vassilyev Yu.V., and Horvath H. (2005), Gravito-photophoresis and aerosol stratification in the atmosphere, *Journal of Aerosol Science*, **36**, 1277-1299.

Cheremisin, A. A., I. S. Shnipov, H. Horvath, and H. Rohatschek (2011), The global picture of aerosol layers formation in the stratosphere and in the mesosphere under the influence of gravito-photophoretic and magneto-photophoretic forces, *J. Geophys. Res.*, 116, D19204, doi:10.1029/2011JD015958.

Haisch, C., Kykal, C., Niessner, R. (2008), Photophoretic velocimetry for the characterization of Aerosols, *Analytical Chemistry* **80**, 1546-1551.

Helmbrecht C., Niessner R., Haisch C. (2007), Photophoretic velocimetry for colloid characterization and separation in a cross-flow setup, *Anal. Chem*. **79**, 7097 – 7103.

Jovanovic, O. (2005), Gravitophotophorese stark absorbierender Partikel für den stratosphärischen Druckbereich (Gravitophotophoresis of strong absorbing particles for stratospheric range of preassures), PhD. Dissertation, University of Vienna, 129 pp.

Keith D.W. (2010), Photophoretic levitation of engineered aerosols for geoengineering. *PNAS* **107**, 16428-16431 doi:/10.1073/pnas.1009519107.

Krauss O., and Wurm G. (1995), Photophoresis and the pile up of dust in young circumstellar disks, *The Astrophysicsl Journal* **630**: 1088 – 1092.

Preining O. (1966), Photophoresis. Chapter V of *Aerosol Science*, C.N. Davies, Ed. Academic Press, London and New York pp 111-135.

Pueschel R.F., S Verma, H. Rohatschek, G.V. Ferry, N. Boiadjeva, S.D. Howard, A.W. Strawa (2000), Vertical transport of anthropogenic soot aerosol into the middle atmosphere, *J. Geophysical Research*, **105**, 3727 – 3736.

Rohatschek H. (1955) Theorie der Photophorese – Ergebnisse und Probleme. *Staub* **39**, 45 – 64.

Rohatschek H. (1995), Semi empirical model of photophoretic forces for the entire range of pressures, *J. Aerosol Science* **26**, 717 – 734.

Wurm G. and Krauss O. (2006), Concentration and sorting of chondrules and CAIs in the late solar nebula, *Icarus* **180**(2) 487 - 495.

Friday, September 7, 2012

Session SS03S1O. Source apportionment

PMF vs CMB for source apportionment of PM: advantages, limitations, complementarity of the two models explored by applications at different types of environments

C. Piot[1,2], M.F.D. Gianini[3], J. Cozic[2], L. Polo[2,4], J.-L. Besombes[1], J.-L. Jaffrezo[2] and C. Hueglin[3]

[1]Université de Savoie-LCME, Le Bourget du Lac, France
[2]Université Joseph Fourier-CNRS-LGGE, St-Martin d'Hères, France
[3]EMPA, Materials Science and Technology, Duebendorf, Switzerland
[4]LTE, IFSTTAR, Bron, France
Keywords: source apportionment, Chemical Mass Balance, Positive Matrix Factorization.
Presenting author email: christine.piot@lgge.obs.ujf-grenoble.fr

Compliance with the tougher regulations of ambient particulate matter (PM) in the European Union will require detailed and quantitative information about the sources of PM. Such information can be provided by source apportionment studies based on determination of the chemical composition of PM and application of receptor models (RM). These RM can be applied to on-line measurements or off-line PM sampling. Off-line PM sampling is developing largely because of the ease of implementation, especially by air quality networks throughout Europe. From the off-line chemical characterization of PM, different RM have been proposed in the literature (see review of Viana *et al.*, 2008), including the Molecular Marker - Chemical Mass Balance (MM-CMB) and multivariate statistical models, e.g. Positive Matrix Factorization (PMF).

MM-CMB is commonly based on the organic speciation of PM while PMF is typically applied to major components, metals and traces elements. Given differences between the two models (mass balance or statistical analysis) and the chemical speciation used, identified sources and estimated contributions may be different and intercomparisons of these two models are necessary. Just a few of these intercomparisons have been published so far (Ke *et al.*, 2008 ; Shrivastava *et al.*, 2007). In this work, the two models were applied on the same set of PM10 samples collected in various types of environments and seasons, representing various sources and chemical composition of PM: urban background, urban kerbside, rural and alpine valley sites in France and in Switzerland.

Results obtained in the urban background site of Zurich (Switzerland) and in the rural site of Payerne (Switzerland) for the estimation of PM10 show a reasonable agreement between the two models (Fig. 1) particularly in winter and confirm the estimated contributions. Differences are observed in summer for vehicular emissions due probably to an underestimation of this source by CMB (organic tracers of this source are lower than limits of detection in this season). Estimations of secondary inorganic (sulphates and nitrates) and organic aerosols (SOA) are almost equivalent despite the method of estimation: in MM-CMB they are indirectly estimated while in PMF they represent some individual factors (containing inorganics and SOA in same factors).

The presentation will also cover comparisons of the estimation of OC and EC in various types of environments. From these comparisons, MM-CMB seems to be more adapted to primary organic sources and source apportionment of OC. PMF allows estimation of a greater number of inorganic sources but by reconstructing the total mass of PM it can overestimate the fraction of each source. All this will be discussed in the presentation focusing on the complementarity of the two models.

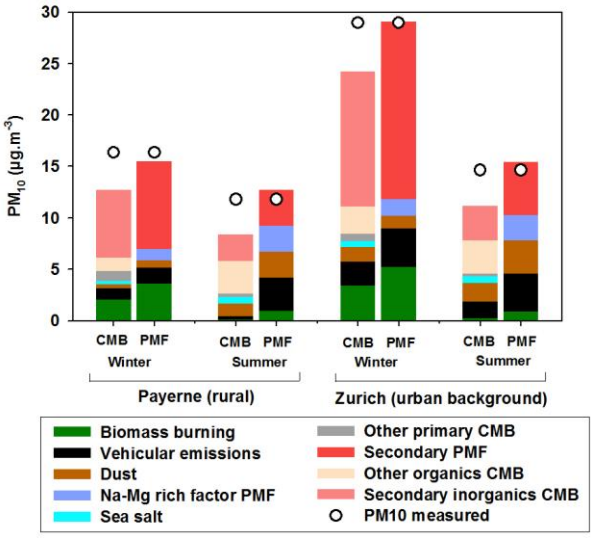

Figure 1. Contributions to PM10 estimated by PMF and MM-CMB in Zurich and Payerne.

C. Piot and L. Polo thank the Région Rhône-Alpes for their PhD grant. The activities at the Swiss sites were supported by the CCES- IMBALANCE and by the Swiss FOEN. Campaigns in France were supported by the MOCOPO program funded by the French Ministry in charge of Transport or studies of AASQA, and several activities were funded by ADEME.

Ke, L., Liu, W., Wang, Y., Russell, A.G., Edgerton, E.S. and Zheng, M. (2008) *Sci. Total Environ.* **394**, 290-302.

Shrivastava, M.K., Subramanian, R., Rogge, W.F. and Robinson, A.L. (2007) *Atmos. Environ.* **41**, 9353-9369.

Viana, M., Pandolfi, M., Minguillon, M.C., Querol, X., Alastuey, A., Monfort, E. and Celades, I. (2008) *Atmos. Environ.* **42**, 3820-3832.

Towards a European Common Protocol for Receptor Modelling

C.A. Belis[1], F. Karagulian[1], B. R. Larsen[2], F. Amato[3,4], O. Favez[5], I. El Haddad[6], R.M. Harrison[7], A. Prevot[6], U. Quass[8], R. Vecchi[9], M. Viana[3], P. Paatero[10], P.K. Hopke[11]

[1]European Commission, Institute for Environment and Sustainability - Joint Research Centre, Ispra, 21027, Italy
[2]European Commission, Institute for Health and Consumer Protection - Joint Research Centre, Ispra 21027, Italy
[3]Institute of Environmental Assessment and Water Research (IDAEA), Barcelona, 08034, Spain
[4]TNO Buil Environment and Geosciences, Dept. Air Quality and Climate, TA 3508,Utrecht, The Netherlands
[5]Institut National de l'Environnement Industriel et des Risques (INERIS), Verneuil-en-Halatte, 60550, France
[6]Laboratory of Atmospheric Chemistry (LAC), Paul Scherrer Institut, Villigen, 5234, Switzerland
[7]National Centre for Atmospheric Science, University of Birmingham, Birmingham, B15 2TT, UK
[8]Air Quality and Sustainable nanotechnology (IUTA), D- Duisburg, 47229, Germany
[9]Department of Physics, Università degli Studi di Milano and INFN, Milan, 20133, Italy
[10]YP-Tekniikka Ky, FI-00970, Helsinki, Finland
[11]Center for Air Resources Engineering and Science, Clarkson University, Potsdam, NY 13699-5708, USA

Keywords: source apportionment, receptor models, model harmonization, guidelines
Presenting author email: claudio.belis@jrc.ec.europa.eu

The identification of sources is one of the prerequisites for the implementation of the Air Quality Directive (AQD). It provides scientific support to the development and periodic revision of air quality plans and short term action plans and to the quantification of categories with special status like long range transport, natural sources and winter road salting and sanding.

The suitability of receptor models (RM) for the apportionment of pollutant sources in the implementation of the AQD is testified by the amount of published studies in 2005 and 2010 in correspondence with the entry into force of new provisions for PM10 and PM2,5, respectively.

In recent years, Member States were requested to provide official estimations of source contribution to the Commission like the quantification of natural sources in 2006 and PM_{10} time extension reports in 2009 (Fragkou et al., 2011). These experiences have shown that although this kind of methodology is used by about 60% of the European experts involved in source apportionment there is a considerable variability in the methodological approaches and adopted tools. Furthermore, there are critical steps that require strict quality assurance standards and skilled practitioners (e.g. identification of the appropriate number of sources).

In order to foster harmonization in this field, the JRC has promoted a number of interconnected initiatives linked to FAIRMODE. One of those was to set up a group of experts with skills in different areas to assess RM methodologies and propose common criteria and procedures for source apportionment studies. The information collected was summarized in a document which is intended to serve as a basis for a common Receptor Model Technical Protocol (RMTP).

The RMTP is addressed to different kinds of users: Policy makers and managers interested in the output of RMs for development of mitigation measures, air quality experts and scientists unfamiliar with these techniques, and RM practitioners involved in the model execution and interpretation of results.

In order to address such heterogeneous readership the document was designed to be accessible at different levels. The RMTP is organized in three sections:

- an introduction to present the methodology to the unskilled reader, illustrating its capabilities and recommending when and how to use it.
- a core section concerning the most common RM methodologies for source apportionment with in-depth analysis boxes for more experienced readers. The section is structured in 13 chapters following, as a check list, the logical steps to accomplish a source apportionment study. The first chapters deal with preliminary activities like the evaluation of the study area, collection of existing information and experimental design. In the following chapters data collection and data treatment are discussed. The section includes also chapters regarding specific aspects of widely used methodologies like CMB, Factor Analysis, and PMF. The evaluation of test performance and reporting are discussed in the last part of this section.
- the third section of the document was conceived to give an insight on the capabilities and the possible future trends in RM methodology. It consists of four chapters dealing with advanced, innovative techniques for which ready- to-use tools are already available or under development: trajectory analysis combined with RM, constrained and expanded models, AMS data processing, and the aethalometer model.

The document includes a number of annexes to provide additional and practical information on specific topics, and examples.

References

Fragkou et al., 2011
http://www.harmo.org/Conferences/Proceedings/_Kos/publishedSections/H14-290.pdf

Application of PMF to the Source Apportionment of Polycyclic Aromatic Hydrocarbons

Roy M. Harrison[1,2], Eunhwa Jang[1] and Mohamed S. Alam[1]

[1]Division of Environmental Health & Risk Management, School of Geography, Earth & Environmental Sciences, University of Birmingham, Edgbaston, Birmingham, B15 2TT, United Kingdom
[2]Centre of Excellence in Environmental Studies, King Abdulaziz University, PO Box 80203, Jeddah (21589) Saudi Arabia
Keywords: Positive Matrix Factorisation, polycyclic aromatic hydrocarbons, source apportionment.
Presenting author email: r.m.harrison@bham.ac.uk

The fact that polycyclic aromatic hydrocarbons comprise a large number of individual compounds emitted in different proportions by their various sources offers many opportunities for application of source apportionment methods. Historically, source apportionment of PAH has generally been based upon the use of diagnostic ratios but recent reports, e.g. Galarneau (2008), have cast doubt on this approach. Problems include the frequently large number of contributory sources and the very significant chemical reactivity of some PAH. Nonetheless, application of Principal Component Analysis has yielded valuable insights into the major sources of PAH in urban air (Harrison et al., 1996; Mari et al., 2010).

Positive Matrix Factorisation (PMF) is generally recognised to be a more powerful technique than PCA as it uses weighting and is constrained not to produce negative factors. For this reason, PMF has been applied to several large databases of PAH concentrations measured in the United Kingdom and has yielded valuable outcomes which challenge the conclusion of Katsoyiannis et al. (2011) that "atmospheric sources of PAH in the UK are probably not dominated by any single clear and strong source type, so the mixture of PAHs in air is quickly 'blended' away from the influence of the few major point sources which exist and further weathered in the environment by atmospheric reactions and selective loss processes.".

An example of the results shown in Figure 1 is a factor enriched in benzo(b)naph(2,1-d)thiophene whose abundance declined rapidly after 2004 coincident with the reduction in the sulphur content of motor fuels. This factor is associated with diesel vehicle emissions whose profile has changed as a result of the changing fuel composition.

Other identified sources include wood combustion, gasoline vehicles and steel industry emissions, and further refinements to the methods may yield additional insights.

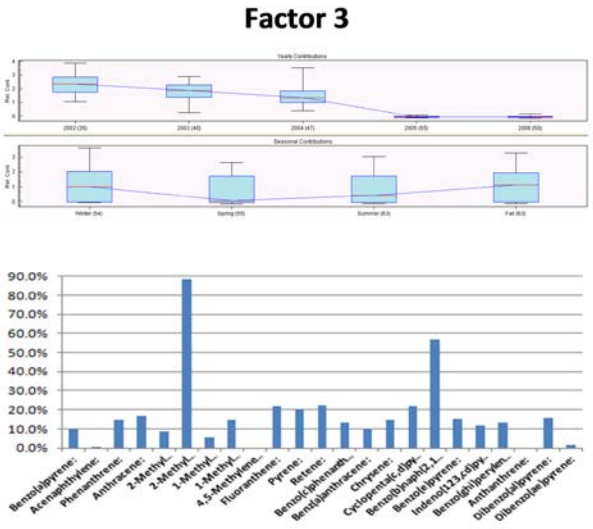

Figure 1. Factor profile and temporal variation in a factor related to diesel emissions.

The authors acknowledge support from the U.K. Natural Environment Research Council and a Chevening Scholarship (to Eunhwa Jang).

Galarneau, E. (2008) *Atmos. Environ.* **42**, 8139-8149.
Harrison, R.M., Smith, D.J.T. and Luhana L. (1996) *Environ. Sci. Technol.* **30**, 825-832.
Katsoyiannis, A., Sweetman, A.J. and Jones, K.C. (2011) *Environ. Sci. Technol.* **45**, 8897-8906.
Mari, M., Harrison, R.M., Schuhmacher, M., Domingo, J.L. and Pongpiachan S. (2010) *Sci. Tot. Environ.* **408**, 2387-2393.

Comparing source apportionment results by a chemistry transport model against PMF analyses for north western Europe

M. Schaap[1], C. Hendriks[1], R. Kranenburg[1], T.A.J. Kuhlbusch[2], U. Quass[2] and J. Vercauteren[3]

[1] TNO, Department of Climate, Air and Sustainability, P.O.Box 80015, 3508 TA Utrecht, the Netherlands
[2]IUTA e. V., Air Quality & Sustainable Nanotechnology Unit, D-47229 Duisburg, Germany
[3]VVM, Kronenburgstraat 45, 2000 Antwerp, Belgium
Keywords: PM and source apportionment, Modelling (regional), PMF.
Presenting author email: martijn.schaap@tno.nl

To develop effective mitigation strategies to reduce concentrations of particulate matter its origin needs to be established. To identify and apportion observed PM concentrations to source categories, a statistical receptor model (Positive Matrix Factorization (PMF)) is often applied to comprehensive experimental data sets. Although this technique provides general categories, it cannot cope with non-linear components. A complementary detailed source attribution study with a chemistry transport model (CTM) is therefore recommended to gain further insight in the origin of PM.

For the CTM LOTOS-EUROS a new module was developed that tracks the origin of primary as well as secondary aerosol components in each modeled process. The source apportionment module was validated with dedicated simulations. It enables to quantify the source contributions of a set of sources at a computational effort of 20% compared to performing a "source off/on" scenario based assessment. Moreover, the module is mass conserving and provides the source attribution under one chemical regime, which is not the case for a source apportionment based on scenario simulations.

The new module was used to establish the source attribution of PM10 and PM2.5 in the Netherlands at a SNAP 1 level, distinguishing between national and foreign sources, for the period 2007-2009. Based on modelled PM, 70-80% of PM_{10} and 80-95% of $PM_{2.5}$ in the Netherlands is estimated to be man-made. About 1/3 of anthropogenic PM_{10} is of Dutch origin and 2/3 originates in foreign countries. For $PM_{2.5}$, a Dutch share of 30% was found. These figures change with location, with highest domestic contributions in the densely populated western part of the country. During peak episodes, natural sources are less important than under normal conditions, whereas especially emissions from road transport and agriculture become more important.

To evaluate the quality of the source apportionment the model results were compared to mass concentration measurements throughout Europe. To gain further insight in the quality of the source apportionment a study was set up to compare the model results to those obtained by PMF. Experimental data sets on PM_{10} and $PM_{2.5}$ from the Netherlands, Belgium and Germany were collected and a combined PMF analysis was performed for 23 sites. The analysis resulted in a 7 factor solution. Three of these factors were identified as industrial process emissions, fossil fuel combustion in general and heavy oil combustion. The latter is indicated by V/Ni tracers (Fig. 1). To compare the model results to the PMF a new LOTOS-EUROS simulation was performed that discriminates between major fuel types. Emissions from industrial process emissions as well as agriculture are classified as unknown. The model results enable a large number of analyses, such as assessing the source contributions as function of modelled PM10 mass concentration (Fig. 2) and its components.

Comparison of the model and PMF results are on-going and will be presented. Besides using the PMF factors special attention is given to tracer concentrations for different sources. First results indicate that modelled international shipping contributions are too high. Anthropogenic sodium contributions are low on average, but both the model and the PMF analysis indicate higher non-marine sodium contributions in the Ruhr area and during days with high PM10 concentrations.

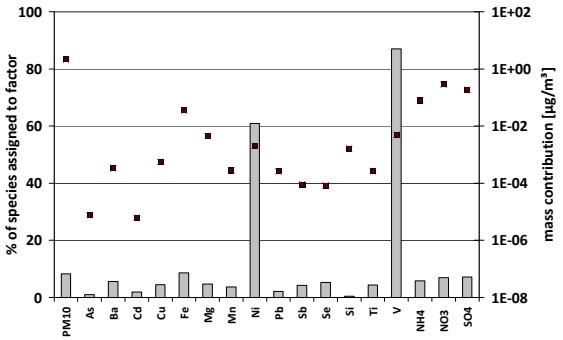

Figure 1. PMF factor profile for "oil combustion/ship emissions". Bars denote to % of species assigned to factor, dots indicate species mass contribution.

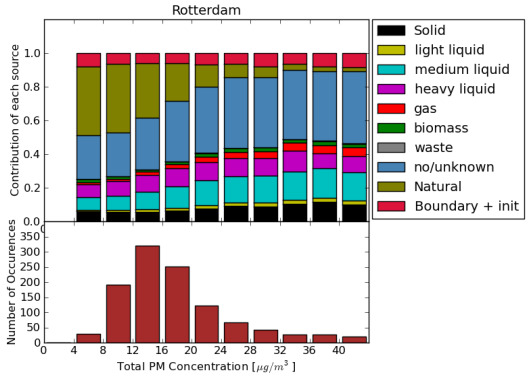

Figure 2. Modelled contribution of 10 labelled sources as function of modelled PM10 concentration at Rotterdam.

This work was supported by the FP7 project ENERGEO.

Multilinear engine 2 applied to long-term on-line data of non-refractory submicron aerosol in the city of Zurich

F. Canonaco[a], J. Slowik[a], U. Baltensperger[a], A.S.H. Prévôt[a]

[a]Laboratory of Atmospheric Chemistry, Paul Scherrer Institut, 5232 Villigen PSI, Switzerland
Keywords: AMS, PMF, ME2, ACSM
Presenting author email: francesco.canonaco@psi.ch

The role of aerosols in the atmosphere is of pivotal importance, because they affect climate (Forster *et al.*, 2007), human health (Peng *et al.*, 2005), ecosystems, e.g., acidification (Matson *et al.*, 2002), and visibility (Watson, 2002). These effects are controlled by particle concentration, composition, and size, which are in turn governed by sources and formation processes. Thus, the identification and quantification of formation mechanisms and sources is of high priority. However, this task is complicated due to the complexity of particle composition.

Long-term monitoring of aerosol composition provides a powerful tool for the analysis of the effects described above. This approach enables elucidation of the seasonal variability of different aerosol constituents, which is not possible with shorter-term campaigns. Long-term measurement records also allow for evaluation of emissions control strategies. Furthermore, long-range, mesoscale, and local air quality models can be improved through comparison with long-term datasets. Finally, the existence of long-term sampling records at a given site provides a framework for the interpretation of datasets from short-term intensive measurement campaigns.

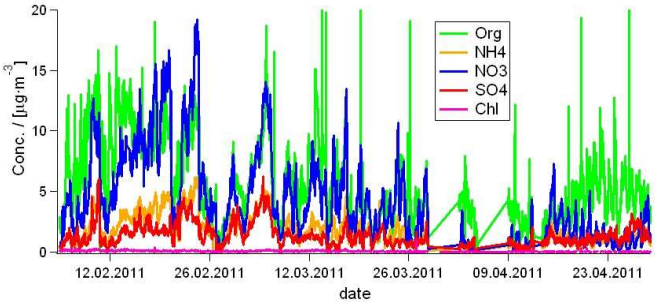

Figure 1. Preliminary time series of the ACSM including SO_4, NO_3, NH_4, Cl and organics. For the sake of simplicity the figure comprises only the winter data.

We present measurements of submicron aerosol composition from an aerosol chemical speciation monitor (ACSM, Aerodyne Research, Inc.) deployed in downtown Zurich. The ACSM yields quantitative mass spectra of the non-refractory aerosol component with an averaging period of 15 minutes. These are the first full year measurements in Europe using this technique. As shown in Fig. 1, the ACSM is capable of resolving inorganic species such as NH_4, SO_4, NO_3, Cl, and the organic fraction. The data can be further deconvolved in order to identify and apportion the inorganic and organic fraction to important sources and processes.

There are several possible techniques for the deconvolution of a data set. In particular positive matrix factorization (PMF) is extensively used for this purpose. However, the multilinear engine 2 (ME2) comprises more advantages compared to PMF. The user has the possibility to run ME2 in the normal PMF algorithm allowing the engine to model the factor solutions or imply constraints on single parts of the factors or to the factors themselves (Paatero, 1999). The use of constraints is justified in many cases, e.g., if the source contributions are known in advance or if an unconstrained model does not lead to plausible ambient results at all.

Therefore, the aim of this work is to exploit the multiple advantages of ME2 on a large dataset, in particular on the obtained data from downtown Zurich during the full year 2011. For this purpose we implemented a user-friendly interface in the software IGOR wavematrics which might be shared in the next future with other environmental science groups.

During the winter period, PMF did not succeed in resolving the factors probably caused by the high correlation of various components due to the prevailing meteorology, similar to Lanz et al. (2008). ME2 was therefore effectively applied on the full winter period, i.e., between January and April using different constraining techniques.

We will discuss identification and source apportionment of AMS and ME2 data at an urban site over the full year of 2011. Aerosol composition and source apportionment will be used to investigate the seasonal variability of specific emission sources and processes in the city of Zurich.

This work was supported by the Swiss Federal Office for the Environment (FOEN).

Forster, P. et al. (2007) *Changes in Atmospheric Constituents and in Radiative Forcing, in: Climate Change 2007*, Cambridge University Press, Cambridge, United Kingdom and New York, NY, USA.

Lanz, V.A. et al. (2008) *Environ. Sci. Technol.* **42**, 214-220.

Matson, P. et al. (2002) *Ambio* **31**, 113-119.

Peng, R. et al. (2005) *Am. J. Epidem.* **161**, 585-594.

Paatero, P. (1999) *J. Comp. Graph. Stat.* **8**, 854-888.

Watson, J.G. (2002) *J. Waste Air Manage.* **52**, 628-713.

Aging fingerprints on the carbon functional groups in 2-stroke scooter exhaust particles with STXM/NEXAFS

E. Coz[1], S. Platt[2], I. El Haddad[2], J. G. Slowik[2], A. S. H. Prévôt[2], S. Steimer[3,4], G. Grzinic[3,5], M. Lampimäki[3], B. Artíñano[1] and M. Ammann[3]

[1]Department of Environment. CIEMAT, Madrid, 28040, Spain
[2]Laboratory of Atmospheric Chemistry, PSI, Villigen-PSI, 5232, Switzerland
[3]Laboratory of Radiochemistry and Environmental Chemistry, PSI, Villigen-PSI, 5232, Switzerland
[4] Department of Environmental Systems Science, ETHZ, Zurich, Switzerland
[5] Department of Chemistry and Biochemistry, University of Bern, Bern, 3012 Bern, Switzerland
Keywords: Scooter emissions, STXM/NEXAFS, morphology, photochemical processes
Presenting author email: esther.coz@ciemat.es

The physical state and the microstructure of individual particles with a typical, complex chemical composition is an important issue in assessing the significance of aerosols. It has been shown that oxidative degradation of reactive organic compounds may be controlled by the morphology of the particles they are contained in. Despite of its scientific relevance, the number of studies relating aerosol morphology and microstructure from an individual perspective with atmospheric physicochemical processes is still scarce. The light scattering and absorption properties of internally mixed and possibly mixed phase aerosol particles strongly depend on their phase state and their microstructure (Zhang *et al.*, 2008).

Recent results suggest that the emissions of organic compounds from scooters are much higher than from other vehicles (Chirico, 2008). In addition, secondary organic aerosol (SOA) from 2-stroke scooters can be distinguished by aerosol mass spectrometry from that of diesel vehicles, wood burning or alpha-pinene oxidations products (Heringa *et al.,* 2011). These findings prompt the scientific motivation to study in detail the microstructural changes associated to the photooxidation processes of scooter emissions. Thus, the present study seeks the identification of distinctive changes to the carbon functional groups in individual particles from 2-stroke scooter experiments at the PSI mobile smog chamber at different degrees of aging.

The aging experiments were performed in the new mobile smogchamber of the PSI Laboratory of Atmospheric Chemistry under UV-light. Samples collected at different stages during an experiment were analyzed offline using scanning transmission X-ray microscopy (STXM) and near edge X-ray absorption fine structure spectroscopy (NEXAFS), which allow the retrieval of spatially resolved information about carbon functional group composition and the O/C ratio (Vernooij *et al*., 2009). Particle samples were collected by inertial impaction on silicon nitride membrane windows on Si wafers. The wafers were mounted into the standard sample holder fitting into the STXM at the PolLux beamline at SLS. Images and NEXAFS spectra were taken at the carbon and oxygen K-edges in the energy ranges 280 – 320 eV and 520 – 560 eV, respectively.

The carbon K-edge spectra for the 2-stroke scooter exhaust particles before and after photooxidation exhibited clear changes. The main distinguishing features are found at the peak energies of the C 1 s→π* transitions of aromatic (285.2 eV), phenolic or ketone carbon (286.7 eV), the carboxylic carbon (288.3 eV), and the aliphatic and/or aromatic carbon (292 eV). The aromatic fraction was predominant in the structure of the recently formed particles. As the particles were processed, there was a pronounced decrease in the aromatic fraction and a corresponding gradual increase in the phenolic and carboxylic groups. Particles within 1-2 hours of photooxidation showed significant particle to particle variation, representing a variety of stages between the unprocessed and heavily processed spectra. However, the changes in the particle internal structure were homogeneously developed and no coatings were found. Similar spectral changes, but to a much lesser extent, were observed in a previous study with wood burning and diesel vehicle exhaust (Zelenay *et al*., 2011).

J. Raabe and B. Watts kindly supported the STXM measurements at PolLux at SLS. M. Lampimäki and G. Grzinic are supported by the Swiss National Science Foundation. S. Steimer is supported the EU FP7 project PEGASOS. Jay Slowik and Imad El Haddad are supported by Swiss NSF. The mobile smogchamber project is funded by the Swiss Federal Office of the Environment and the Federal Road Office. E.Coz is supported by the Spanish National Research Plan (CGL2011-27020) and Fundación Ramón Areces (AEROCLIMA Project).

Chirico, R., PhD Thesis, ETH No. 19237, 2010.
Heringa, M.F., DeCarlo, P.F et al. (2011) Atmos. Chem. Phys. **11**, 5945–5957.
Vernooij, M. G. C., Mohr, M., et al. (2009) Environ. Sci.Technol. **43**, 5339.
Zhang, R., Khalizov, et al. (2008) PNAS **105**, 10291-10296.
Zelenay, V. Mooser, R.,. et al. (2011). Atmos. Chem. Phys. **11**, 11777–11791.

Considering the different thermal behaviour of wood-burning and diesel emissions for ^{14}C-based source apportionment of elemental carbon

S. Szidat[1,2], Y.L. Zhang[1,2,3], G. Ciobanu[3], P. Zotter[3], N. Perron[3,4], M.C. Minguillón[3,5], L. Wacker[6], U. Baltensperger[3], and A.S.H. Prévôt[3]

[1]Department of Chemistry and Biochemistry, University of Bern, 3012 Bern, Switzerland
[2]Oeschger Centre for Climate Change Research, University of Bern, 3012 Bern, Switzerland
[3]Paul Scherrer Institut, 5232 Villigen-PSI, Switzerland
[4]Now at: Division of Nuclear Physics, Lund University, 22100 Lund, Sweden
[5]Institute of Environmental Assessment and Water Research (IDAEA), CSIC, 08034 Barcelona, Spain
[6]Laboratory of Ion Beam Physics, ETH Hönggerberg, 8093 Zurich, Switzerland
Keywords: Source apportionment, ^{14}C, carbonaceous particles, elemental carbon, wood combustion
Presenting author email: szidat@iac.unibe.ch

Radiocarbon (^{14}C) analysis is a powerful tool to help apportion the sources of carbonaceous aerosols (Szidat *et al*, 2006), due to its ability to differentiate between contemporary and fossil emissions. Since elemental carbon (EC) and organic carbon (OC) may have different origins, source apportionment of both fractions separately (as opposed to only total carbon, TC) provides additional valuable information. However, this strategy requires complete chemical separation of OC and EC, which cannot be achieved for ambient samples due to the indeterminate transition between both fractions (Minguillón *et al*, 2011).

We present an optimized procedure for the isolation of OC and EC for ^{14}C analysis conducted with a commercial thermo-optical OC/EC analyser. In particular, we show how different conditions of temperatures and carrier gases influence the separation of OC and EC and the ^{14}C results of the removed carbon fractions. An optimized thermo-optical protocol (Swiss_4S) with four steps was developed to isolate only the carbon fractions of interest (i.e. OC and EC) with minimized biases from charring and premature EC oxidation. For the isolation of EC for ^{14}C analysis, the thermal treatment is applied to water-extracted filters, as this substantially reduces charring by removal of water-soluble organic and inorganic compounds. For monitoring positive and negative biases of EC, the laser transmission signal of the OC/EC analyser is used.

The Swiss_4S protocol involves these consecutive four steps:

1. Combustion in pure O_2 at lower temperature for separation of OC for untreated filters and water-insoluble OC (WINSOC) for water-extracted filters without any premature EC evolution
2. Combustion in O_2 at intermediate temperatures
3. Further heating in helium; steps 2 and 3 yield mixtures of refractory WINSOC and non-refractory EC aiming at complete OC removal before step 4
4. Complete oxidation of the remaining refractory EC in O_2

In addition, water-soluble OC (WSOC) is determined by subtraction of the water-soluble fraction of TC from complete TC.

Optimum temperatures and durations were investigated for all steps in order to confine the reaction for OC within steps 1-3 and for EC within steps 2-4. This was possible with maximum EC recoveries for step 4 of 70-85%. Although the ^{14}C analysis of CO_2 from step 4 already gives a good indication of EC sources, it cannot provide the full information of all emissions. As wood-burning EC tends to be less refractory than diesel EC, ^{14}C analysis of step 4 alone may underestimate the wood-burning contribution. Additional ^{14}C analyses of step 1 (WINSOC) and steps 2+3 (mixture of refractory WINSOC and non-refractory EC) eliminate this bias and allow a full source apportionment of EC.

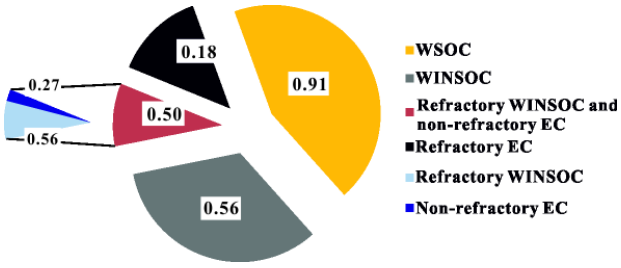

Figure 1. Composition of different carbon fractions of the carbonaceous aerosol (pies) and their ^{14}C signature (numbers) based on the Swiss_4S separation protocol for a typical winter sample.

Figure 1 presents an example of this approach. Whereas the refractory EC from step 4 reveals a more fossil ^{14}C signature (fraction of modern, f_M, ranging from 0 for fossil to ~1.1 for non-fossil emissions; Szidat *et al*, 2006), the less-refractory fraction of EC shows a substantially larger contribution from wood burning. For this sample, the f_M value for the total EC is determined to be 0.23 from isotope-mass balancing. Consequently, the analysis of step 4 alone would underestimate the wood-burning contribution by ~20% so that the more comprehensive approach presented here is required for correct ^{14}C source apportionment.

Minguillón, M.C. *et al* (2011) *Atmos. Chem. Phys.* **11**, 12067-12084.
Szidat, S. *et al* (2006) *J. Geophys. Res.* **111**, D07206.

Safe PMF: Minimizing the Impact of Erroneous Data in Source Apportionment

P. Paatero[1] and P.K. Hopke[2]
[1]Department of Physics, University of Helsinki, Finland
[2] Institute for a Sustainable Environment, Clarkson University, Potsdam, NY, USA 13699
Keywords: Positive Matrix Factorization, gross errors, data errors
Presenting author email: hopkepk@clarkson.edu

Gross data errors may seriously distort the results of source apportionments based on speciated particulate measurements. The worst effects are due to data where a very small value (zero or practically zero) and a very low uncertainty estimate are mistakenly reported for one or several measurements.

Visual screening of such errors by the user is not practical. Both the time and the training for such work are missing. Also, the so-called *Robust Mode* in program PMF often fails, especially with points where an unrealistically small uncertainty was specified.

High-leverage values

The mathematical concept of *Leverage* (L) indicates how powerful any data value is in commanding the fitted value to be close to itself. If L=100%, then the fitted value cannot deviate from the measurement. In contrast, L=0% means that the measured value has no effect at all on the fitted value.

Figure 1 illustrates a least squares fit of a straight line to five points, two of them having high leverage.

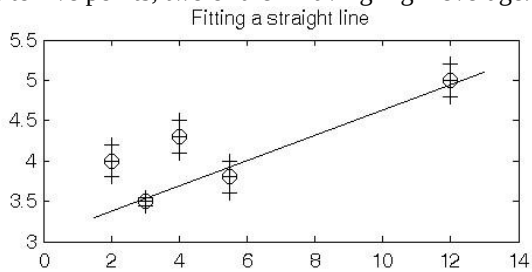

Figure 1. Least-squares fit to a line illustrating points with high leverage.

The second point has very small uncertainty (short error bar). Its power overrides that of its neighbors. The last point has a "long lever" for forcing the fitted line. Both points have almost L=100%. In practice, points 2 and 5 control the position of this least squares line.

A high-leverage value has excessive influence on the outcome of any factor analysis (FA). Omitting or accepting one such point may significantly change the results. The whole idea of source apportionment is to determine the normal or repetitive patterns of particulate matter (PM) concentrations. High-leverage points contradict this idea. Thus, it is advantageous to source apportionments to eliminate high-leverage values from the data matrix.

The following is a simplification of an algorithm that has been successfully used against high-L points. First, run PMF in the customary way. Then compute L values for all data points in the matrix. Identify all matrix elements whose L values exceed a chosen limit, e.g. L>25%. Downweight all these high-L elements by a large coefficient, e.g. by 100. Finally, rerun PMF.

Edge outliers

Figure 2 illustrates real data from PM measurements. One point is on the wrong side of the invisible "fence" or *Edge*. This *Edge Outlier* point may be caused by a gross error in SO_4 (too large value) or in NH_4 (too small value). Alternatively, it might also be caused by a transient or local source of acidic SO_4

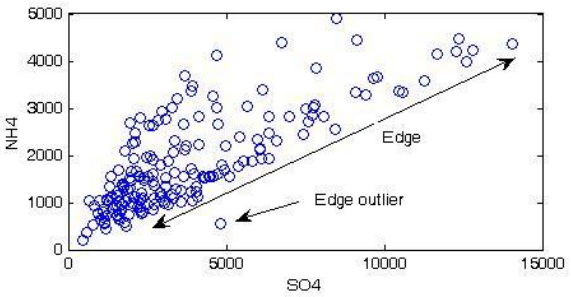

Figure 2. Plot of ammonium and sulphate ion concentrations illustrating an edge outlier.

Clean edges, without outliers, are valuable for determining a realistic rotation of the computed factors. Edge outliers often force the PMF model to a wrong, unrealistic rotation, preventing identification and evaluation of sources. Thus, one wishes to eliminate edge outliers, even if their causes remain unknown.

In this work, an algorithm is developed for automatic detection and downweighting of edge outliers.

Avoiding false rejection of good values

On rare occasions, good matrix elements may have high leverage. This effect may occur when some values have been measured by an enhanced technique so that uncertainties of such values are exceptionally low. The investigators must be aware of such special conditions. They have the option to declare some data "untouchable" by the high-leverage algorithm.

Unusual natural conditions may create a "good" edge outlier. This would happen if a source is always active, except during a rare interruption. For the traffic source, such an interruption might be caused by heavy snowfall, so that all roads are blocked by the snow. Good data corresponding to such special conditions should be declared untouchable by the edge outlier algorithm.

Practical results

In this talk, examples will be shown for real data where the two types of errors have been identified and eliminated.

Detailed chemical characterization of PM and COV, and source apportionment near a French highway

L. Polo[1, 3], C. Piot[1, 2], A. Charron[3], J. Cozic[1], B. Temime-Roussel[4], N. Marchand[4], J.L. Besombes[2] and J.L. Jaffrezo[1]

[1]Université Grenoble 1-CNRS-LGGE, St-Martin d'Hères, France
[2]Université de Savoie-LCME, Le Bourget du Lac, France
[3]IFSTTAR, Bron, France
[4]Aix Marseille Univ., LCE, Marseille, France
Keywords: Traffic emissions, re-suspension, road dust, organic speciation, France.
Contact email: polo@lgge.obs.ujf-grenoble.fr

The relation between exposure to ambient fine particulate matter (PM) and human mortality is now well established, particularly in the roadway proximity. Further, Hoffman et al (2009) showed the link between long-term residential exposure to high level of PM and coronary atherosclerosis. Improving air quality for reducing morbidity and premature death has become an urgent need. In spite of the evolution of vehicle motorization, the PM_{10} level has not been decreasing proportionnally in urban environments during the last decade (Harrison, 2008). The characterization and quantification of traffic emissions are still poorly known for the French motor vehicle fleet. These emissions involved exhaust and non-exhaust emissions (i.e. road-traffic like re-suspension of road dusts, from brake, tyre and road-surface-wear, from the corrosion of vehicle components…). The PM_{10} emissions related to traffic can represent up to 60% non-exhaust emission (Bukowiecki, 2010). A detailed chemical characterization of exhaust and non-exhaust traffic related emissions is still needed.

In order to characterize the chemical composition of traffic sources, detailed measurements were performed in the vicinity a suburban highway characterized by regular traffic congestions in Grenoble-Echirolles (France). Measurements were simultaneously conducted at an urban background site (Grenoble-Les Frênes), 2.5km away. This two weeks campaign took place in September 2011 within the MOCOPO and PM-Drive programs. PM_{10} and Volatile Organic Compounds (VOCs) were sampled on a 4h basis at the two different locations. In addition, high time resolved measurements (HR-ToF-AMS, PTR-ToF-MS, MAAP, SMPS…) were performed at Grenoble-Echirolles. At the same time, the traffic on the highway was recorded with a high temporal resolution (loops and systems allowing vehicles identification).

HR-Tof-AMS has been used to measure the concentration and chemical composition of the non-refractory submicron aerosol. Figure 1 presents the temporal evolution of two well-known fragments derived from AMS measurements: mz 57 (mostly $C_4H_9^+$) and m/z 44 (mostly CO_2^+), considered as markers of HOA associated with fuel derivatives emissions and OOA associated with secondary organic aerosol respectively. The mz 57 fragment follows clear daily cycles highly correlated with traffic and BC (MAAP). The evolution of mz 44 is completely different, and is well related with that of ions from secondary origins like sulfate, nitrate, and ammonium. A strong link also exists with the weather pattern during this two-week campaign. These first results allow already a distinction between the traffic emissions and others sources, which is a good foundation for this study.

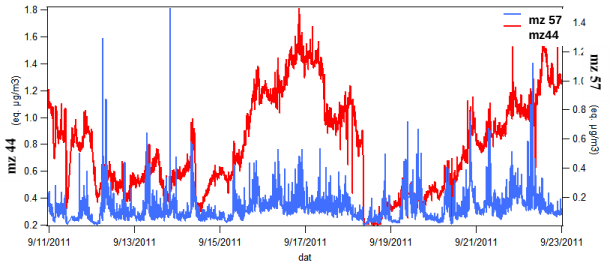

Figure 1: Temporal evolution of the fraction m/z 57 and m/z 44 at Echirolles (France)

Off-line sampling allows the detailed chemical characterization of aerosols notably the organic speciation with the aim of research of source tracers and determination of chemical fingerprints of large chemical families (hydrocarbons, PAH, saccharides…). About eighty compounds have been quantified. Further, a large array of trace metals was also measured on these filters. From these results, both the Chemical Mass Balance (CMB) and Positive Matrix Factorization (PMF) models will be used in order to apportion the contribution of influential sources including non-exhaust traffic emissions. These results will be presented and compared with on-line data and with traffic.

L. Polo and C. Piot thank the Rhône-Alpes Region for their PhD grants. Campaigns in France were supported by the French Ministry in charge of Transport (MOCOPO program) and by the French Environmental agency ADEME (PM-DRIVE program).

Hoffmann, B., Moebus, S., Dragano, N., Stang, A., Möhlenkamp S., Schmermund, A., Memmesheimer, M., Bröcker-Preuss, M., Mann, K., Erbel, R., Jöckel, KH. (2009) *Env.Health Pers. 117:8*

Harrison, RM., Stedman, J., Derwent, D., (2008) *Atmosph. Environ. 42:603-6*

Bukowiecki N., Lienenmann, P., Hill, M., Furger, M., Richard, A., Amato, F., Prévot ASH., Baltensperger, U., Buchmann, B., Gehrig, R. (2010) *Atmosph.Environ 44:2330-2340*

Friday, September 7, 2012

Session SS04S1O. Chemical characterization of combustion aerosols

Soot aerosol – hard nuts to crack for an analyst

R. Niessner

[1]Institute of Hydrochemistry, Chair of Analytical Chemistry, Technical University of Munich, Marchioninistrasse 17, D-81377 München, Germany
Keywords: soot, chemistry, electrical conductivity, health effect, morphology, reactivity
Presenting author email: reinhard.niessner@ch.tum.de

Soot is emitted from many sources all around the world. There is common consensus about the harmfulness of ambient or occupational soot exposure. Ca. 30 % mass of aerosol sampled in urban areas is consisting of soot. The role of soot aerosol on radiation budget, thus influencing climate forcing, is heavily discussed among climate scientists.

But what is "soot"? Are there special properties with soot particles, which are unique, and can be used for proper identification, characterisation, and quantification? So far, there does not even exist a reference material for soot, not to mention a procedure to generate such soot aerosol in a representative way for mimicking where it comes from: incomplete combustion.

Obviously, one has to consider the situation where soot is an actor. In the presentation different features of soot are discussed:

- *cardiovascular health effect*: results of experiments with a still beating heart perfused by blood serum enriched with flame-derived soot, in comparison to other nano-engineered materials, are shown.
- *carbon particle morphology*: high resolution TEM measurements show the individual types of soot, ranging from completely mixed to well ordered nano-crystallinity, depending on history of formation.
- *electrical conductivity* of soot is the latest soot sensor priciple. Conductivity is dependent on nano-crystallinity and twinned metal oxides attached.
- *photoelectron emission* under X-ray stimulation. ESCA spectra reveal distinct differences among different soot types because of surface chemistry.
- *photon absorption* can be probed threefold: the subsequent heating up of individual carbon particles can lead to photon emission (*laser-induced incandescence*), may causes subsequent optoacoustic effects (*photoacoustic soot sensor*), or undergo photophoretic movement (*thermo-photophoretic velocimetry*).
- *chemical reactivity*: is very important for current and future diesel exhaust aftertreatment. *Thermally programmed oxidation (TPO)* reveals a huge span among various types of soot – from completely inert graphite up to highly reactive spark discharge soot. Again, the degree of nano-crystallinity governs the scene: best probed by *Multi-wavelength Raman microspectroscopy.*

Organic Emissions from Modern Small Scale Wood Combustion Appliances – Chemical Characterization and Toxic Potential of Fine Particulate Matter

J. Orasche[1, 2, 3], J. Schnelle-Kreis[2], G. Abbaszade[2], H. Hartmann[4],H. Ruppert[1], R. Zimmermann[2, 3]

[1]Department of Sedimentology & Environmental Geology, Georg-August University, Göttingen, Germany
[2]Joint Mass Spectrometry Centre, Comprehensive Molecular Analytics, Helmholtz Zentrum München, Germany
[3]Joint Mass Spectrometry Centre, Chair of Analytical Chemistry, University of Rostock, Rostock, Germany
[4]Technology and Support Centre (TFZ), Straubing, Germany

Keywords: ambient aerosols, health aspects of aerosols, PAH, wood combustion
Presenting author email: juergen.orasche@helmholtz-muenchen.de

In this century the use of renewable energies is enforced by many European countries. In Germany an effort was started to replace even nuclear power plants. The new energy mix must involve next to solar power, wind power and geothermal power also energy crops and wood for generation of heat, electrical power and gaseous and liquid fuels. But the combustion of wood for residential heating or in biomass power plants is accompanied by considerable emissions of particulate matter (PM) with particle sizes in the fine (< 2.5 µm) and ultrafine fraction (< 100 nm). So it is now discussed which part of energy supply can be solved by wood combustion. How much additional PM will be generated and how dangerous are the effects of generated PM to human health? Moreover the release of high amounts of different organic species is responsible for a lot of not well known chemical processes in the atmosphere. In order to further investigate the impact of wood combustion on atmospheric processes and human health and to apportion the contribution of wood combustion to ambient PM concentrations a comprehensive characterization of source emissions is essential.

Therefore an investigation was done to study the emissions of state of the art small scale wood combustion furnaces under different firing conditions. Additionally emissions from straw combustion were studied. A detailed characterization of organic species of PM of all combustion systems was done by filter sampling and analysis by in-situ derivatization thermal desorption gas chromatography time-of-flight mass spectrometry (IDTD-GC-TOFMS) (Orasche, 2011).

An approach was done to estimate toxicity of the emitted PM by the content of polycyclic aromatic hydrocarbons (PAH). It is based on the proposal of the German Research Foundation (DFG) that the health risk is proportional summarised by different PAH with different health risk potentials (Greim, 2008). Although this tool has been developed to estimate work place exposure this approach can be transferred for assessing health effects associated with PAH in wood combustion PM. This allows a rough but fast comparison of different furnaces by determination of toxic equivalents (TEQ) and emission of PM.

Best results were obtained by combustion of wood pellets in a modern pellet boiler (PM = 4 - 9 mg MJ^{-1}, TEQ = 0.01 - 0.03 µg MJ^{-1}). On the opposite of the emission scale the toxic potential of common log wood stoves were found to be about 1000-fold higher (PM up to 119 mg MJ^{-1} and TEQ up to 27 µg MJ^{-1} during the inflaming phase – Fig. 1)!

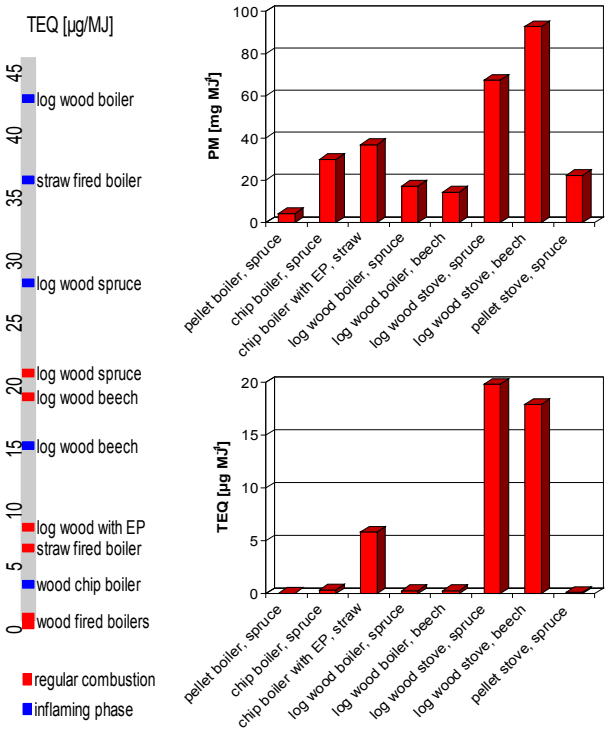

Figure 1. Right: Comparison of emissions from different types of wood combustion during regular combustion (EP = electrostatic precipitator). Left: toxicity scale of the wood combustion systems by the toxicity of released PM distinguishing inflaming phase (blue) and regular combustion (red).

This work was supported by the Federal Ministry of Science and Culture, Lower Saxony, Germany.
The health effects of organic compounds in aerosols are currently investigated in the framework of the Virtual Helmholtz Institute HICE (www.hice-vi.eu).

Greim, H.: *Gesundheitsschädliche Arbeitsstoffe - Toxikologisch-arbeitsmedizinische Begründungen von MAK-Werten und Einstufungen*, Wiley, 2008.

Orasche, J., Schnelle-Kreis, J., Abbaszade, G., and Zimmermann, R.: *Technical Note: In-situ derivatization thermal desorption GC-TOFMS for direct analysis of particle-bound non-polar and polar organic species*, ACP, 11, 8977-8993, 2011.

On-line Characterization of Aerosols from Transient Biomass Combustion

E. Z. Nordin[1], A. C. Eriksson[2], R. Nyström[3], E. Pettersson[3,4], J. Rissler[1], E. Swietlicki[2], M. Bohgard[1], C. Boman[3] and J. Pagels[1]

[1]Ergonomics and Aerosol Technology, Lund University, P.O. Box 118, SE-22100, Lund, Sweden
[2]Nuclear Physics, Lund University, P.O. Box 118, SE-22100, Lund, Sweden
[3]Energy Technology and Thermal Process Chemistry, Umeå University, SE-901 87, Umeå, Sweden
[4]Energy Engineering, Luleå University of Technology, SE-971 86 Luleå, Sweden

Keywords: APM, AMS, morphology, biomass combustion
Presenting author email: Erik.Nordin@design.lth.se

Combustion of biomass fuels for residential heating is considered to be a climate friendly option and is increasing globally. However, this implies potentially increased emissions of aerosol particles. $PM_{2.5}$, which is to a large extent comprised by combustion generated particle matter, co-varies with cardio vascular diseases (Kocbach Bølling *et al.*, 2009). The composition of biomass combustion aerosol can be divided into three main components, soot, alkali salts/ash and organic aerosol and is determined by combustion conditions like oxygen supply and temperature as well as the fuel. Soot and organic aerosol are a result of poor combustion conditions and are considered to be more harmful to human health than ash particles produced under optimal combustion conditions (Kocbach Bølling *et al.*, 2009). A combustion cycle for example in a wood stove can emit episodes of poor combustion even when the overall combustion is relatively complete. The start-up phase is very sensitive to flash-over which results in air-starved conditions with emissions of soot and polycyclic hydrocarbons. The aim of this paper is to study the change in aerosol properties due to different combustion conditions and phases using on-line aerosol measurement techniques.

A total of five combustion cases were studied using three residential wood combustion appliances; *i*) a conventional wood stove operated with high burn rate *ii*) a conventional wood stove operated with nominal burn rate, *iii*) a modern pellet burner operated under optimal conditions *iv*) a novel pellet reactor operating on optimal conditions *v*) a novel pellet reactor operating under air starved conditions. Mean flue gas and particle characteristics from the combustion cases are shown in table 1.

Table 1: Particle characteristics and gas concentrations.

Case	O_2 (%)	CO (mg/MJ)	Total conc. (#*10^7/cm^3)	Org (mg/MJ)
i	9.3±5,4	3020	2.7±1.1	9.4
ii	11.8±2,4	2590	1.6±0.8	8.6
iii	8.2±1.0	110±38	8.4±0.4	0.32
iv	11.1±1.2	120±67	6.1±0.2	0.45
v	5.3±2.0	700±1390	3.0±0.8	6.5

The aerosol from the combustion appliances was diluted 1000-3000 times to concentrations relevant for ambient air before sampling. A high resolution aerosol mass spectrometer (HR-TOF-AMS, Aerodyne research Inc.) was used for size resolved composition of compounds vaporised at 600°C. A scanning mobility particle sizer (SMPS) was used for mobility size distributions (10-600 nm) and an aerosol particle mass analyser operated downstream a differential mobility analyser and an optional thermodenuder (DMA-TD-APM) was used to determine the mass mobility relationship and assess the size dependent organic mass fraction. Particles for TEM analysis were collected using an electrostatic precipitator. For highly transient conditions like the start-up phase the time-resolution of the APM is not sufficient. By utilizing a relationship in (DeCarlo *et al.*, 2004) that the effective density is the ratio between the vacuum aerodynamic diameter (AMS) and mobility diameter (SMPS), the effective density can be derived by from SMPS and AMS size distributions. Combining this method with APM measurements will give novel and detailed information about the aerosol composition in all phases of the combustion cycle.

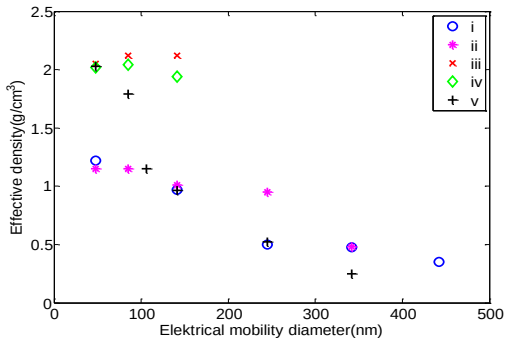

Figure 1: The effective density

The effective density from DMA-APM measurements (figure 1) gives an indication of the particle shape and composition. Salt aerosols have a relatively high effective density, which does not change with increasing mobility diameter, due to their spherical shape. Soot particles on the other hand have a lower effective density which is decreasing with increased size, due to their agglomerated shape.

This work was supported by the Swedish Energy Agency, the ERA-NET project Biohealth, FORMAS and METALUND.

DeCarlo P. *et al.*, (2004) Aerosol Sci. Technol. 38: 1185–1205
Kocbach Bølling A. *et al.*, (2009) Particle & Fibre Toxicology, 6:29

Impact of iron content on structure and thermo-chemical characteristics of multicomponent soot aerosol

H. Bladt[1], J. Schmid[1], E. Kireeva[2], O. B. Popovicheva[2], N. P. Ivleva[1] and R. Niessner[1]

[1]Chair for Analytical Chemistry, Technische Universität München, Munich, 81377, Germany
[2]Skobeltsyn Institute of Nuclear Physics, Moscow State University, Moscow, 119991, Russia
Keywords: combustion aerosol, metal, contamination, SEM/EDX, Raman microscopy, soot reactivity.
Presenting author email: bladt@tum.de

Soot aerosol which is a major pollutant in the atmosphere of urban areas often contains not only carbonaceous matter, but also inorganic material. As specifically iron contaminations can be derived from various sources, e.g. impurities in heavy fuel oil or lubricating oil used for shipping, engine wear or fuel-borne catalysts, they can be frequently found to a high content in ambient aerosols (Moldanová et al., 2009). Thus, our research focuses on iron species and their impact on the chemical and physical properties of soot.

We studied in-depth the change of composition, structure and oxidation reactivity of laboratory-produced soot of various iron content. For this purpose, iron-containing soot aerosol was generated in a propane/air diffusion flame. By adjusting the doping amount of iron pentacarbonyl to the flame, soot types without Fe addition and with various iron content were produced. Additionally, diesel flame soot without and with ferrocene addition was combusted to give further soot types without and with iron contamination. Scanning Electron Microscopy and Energy-dispersive X-ray Spectroscopy (SEM/EDX) were combined with cluster analysis (CA) to characterize the individual particles by separating them into definable groups of similar chemical composition representing the particle types in dependence of the iron content in soot. Raman Microspectroscopy (RM) and Infrared Spectroscopy (IR) were applied for the structural investigation of the carbonaceous soot structure as well as the characterization of hydrocarbons and iron species. For the analysis of the soot oxidation reactivity, Temperature-Programmed Oxidation (TPO) and Desorption (TPD) were applied and the temperature of maximum CO and CO_2 emission T_{max} throughout the TPO experiment was used as criterion for soot reactivity (Schmid et al., 2011).

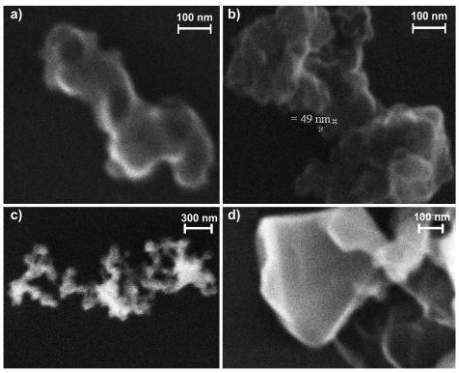

Figure 1. SEM images of different particle types: "typical soot" (a), "elemental carbon" (b), "oxidized soot" (c) and "soot with iron oxide" (d).

Individual soot particles are classified by combined SEM/EDX and CA into four different groups according to their elemental composition in dependence of iron content: "typical soot", "elemental carbon", "oxidized soot" and "soot with iron oxide" (Fig. 1).

Moreover, it could be demonstrated, that iron is most dominantly present in the form of amorphous Fe (III) oxide that crystallizes upon the thermal treatment of soot to form hematite α-Fe_2O_3. Iron contaminations do not change the soot microstructure significantly, but doping of the flame with iron pentacarbonyl impacts the hydrocarbon composition.

Soot oxidation reactivity strongly depends on the content of the catalyst iron, as T_{max} follows an exponential decay with increasing iron content in soot (Fig. 2). Thus, especially at low iron contents, soot reactivity increases significantly with increasing iron content. For iron contents above ~30 % (m/m), soot reactivity cannot be enhanced by further increase in iron content.

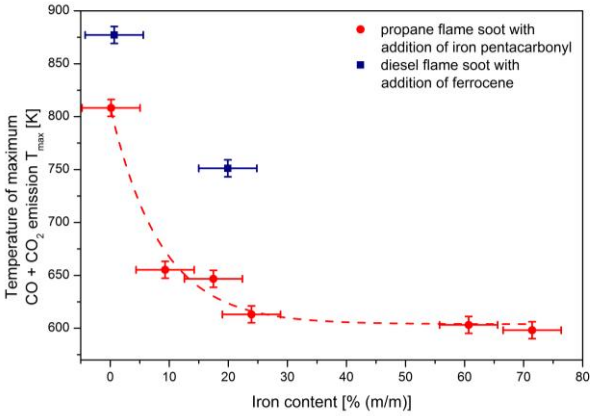

Figure 2. Relation of T_{max} and iron content in soot.

Our results of the thermo-chemical characterization of laboratory-produced internally mixed iron-containing soot raise severe questions on the applicability of commonly used thermo-optical techniques for the quantification of organic carbon (OC) and elemental carbon (EC) in ambient aerosol samples contaminated with inorganic compounds.

Financial support by the DFG, the RFBR and the DAAD is gratefully acknowledged.

Bladt, H. et al. (2012) *Aerosol Sci. Technol.* (submitted).
Moldanová, J. et al. (2009) *Atmos. Environ*. **43**, 2632-2641.
Schmid, J. et al. (2011) *Anal. Chem.* **83**, 1173-1179.

Black Carbon Sources Characterized using the Soot-Particle Aerosol Mass Spectrometer (SP-AMS)

J.C. Corbin[1], A. A. Mensah[1], M. Gysel[2], M. Laborde[2], A. Keller[3], J. Kim[4], A. Petzold[4], and B. Sierau[1]

[1]Institute for Atmosphere and Climate Science, ETH Zürich, Universitätstrasse 16, 8092 Zürich, Switzerland.
[2]Laboratory of Atmospheric Chemistry, Paul Scherrer Institut, 5232 Villigen, Switzerland.
[3]Institute of Aerosol and Sensor Technology, FHNW, Klosterzelgstrasse 2, 5210 Windisch, Switzerland.
[4]Institut für Physik der Atmosphäre, DLR, 82234 Oberpfaffenhofen, Germany.
Keywords: BC, EC, soot, AMS, SP-AMS.
Presenting author email: joel.corbin@env.ethz.ch

Aerosol particles play important direct and indirect roles in climate. Particles composed of black carbon (BC) are key absorbers of radiation in the atmosphere, thereby affecting planetary warming, circulation patterns and cloud formation (Ramanathan and Carmichael, 2008). By acting as condensation or ice nuclei, BC particles may enhance cloud formation. Conversely, they may inhibit cloud formation or precipitation by radiative heating within-cloud.

The climate effects of BC depend on its degree of oxidation and on the presence of heterogeneous coatings. These in turn vary between different BC sources. For example, emissions from sulphur-rich coal combustion may lead to sulphate-coated BC, affecting the radiative and cloud effects mentioned above. To determine the importance of such effects, field measurements need to describe BC according to its source and mixing state.

In order to characterize the composition and coating of BC aerosols, the Aerodyne Soot Particle Aerosol Mass Spectrometer (SP-AMS, Onasch et al. 2012) has been developed based on the original AMS (Jayne et al., 2000). This new instrument complements other BC-measurement techniques by providing information on the chemical composition of BC particles and their coatings in real time. In the SP-AMS, BC particles are vapourized by a continuous-beam laser operated at 1064 nm. The resulting vapour is then ionized by electron impact at 70 eV; ions are then mass-analysed within a high-resolution time-of-flight chamber. In this study, the SP-AMS was also operated with a 600°C tungsten vapourizer positioned directly behind the laser. With the laser switched on or off, the SP-AMS detected either both refractory and non-refractory species (laser on), or non-refractory species only (laser off).

The SP-AMS was employed in the laboratory to characterize five different BC types along with a suite of mass- and optically-based instrumentation. The BC sources were: propane-flame soot ("CAST", Jing Ltd.), graphite-spark-generated soot ("GFG", PALAS GmbH), a commercial carbon black ("Regal Black", REGAL 400R pigment black, Cabot Corp.) and fullerene soot (Sigma-Aldrich Corp.). The CAST propane burner was operated under two different regimes, fuel-lean ("black" soot) and fuel-rich ("brown" soot).

The mass spectral signatures of these five BC types were analysed and compared with the goal of identifying mass spectral characteristics unique to each sample. As an example, the ratio of signals at mass-to-charge ratios (*m/z*) +12 to *m/z* +36 are shown in Figure 1 below for three BC types: GFG, CAST black (fuel-lean) and CAST brown (fuel-rich) soot. For these three types, the slopes of a linear-regression fit were 0.85, 0.57 and 0.95, respectively. When the SP laser was switched off so that particles saw only the 600°C vapourizer, the signals at *m/z* +12 and *m/z* +36 fell to zero for all three samples. The results therefore demonstrate a distinct chemical structure of BC for these three soot types.

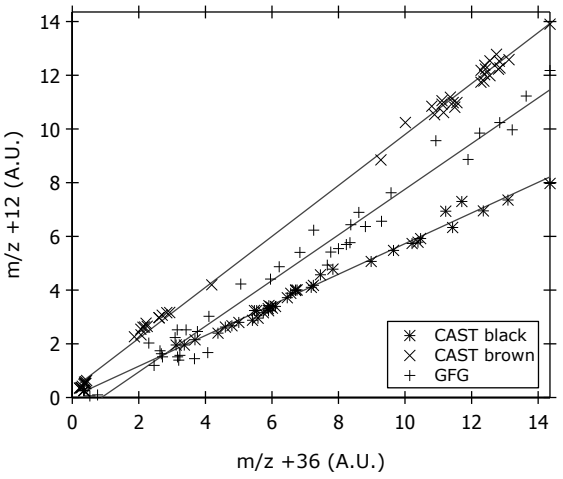

Figure 1. SP-AMS signal at *m/z* 12 and *m/z* 36 for graphitic soot (GFG), and two types of propane flame soot: CAST black and CAST brown. Error bars omitted for clarity.

In this presentation, similarities and differences between the mass spectra of five BC types will be detailed, supported by independent measurements of soot mass and optical properties (SP2, APM, MAAP, nephelometer, PSAP). The results provide a reference against which ambient measurements of BC may be compared.

Onasch, T. B., A. Trimborn, E. C. Fortner, J. T. Jayne, G. L. Kok, L. R. Williams, P. Davidovits, and D. R. Worsnop (2012), *Aerosol Science and Technology*, in press.

Ramanathan, V., and G. Carmichael (2008), *Nature Geosci*, *1*(4), 221-227.

Jayne, J. T., D. C. Leard, X. Zhang, P. Davidovits, K. A. Smith, C. E. Kolb, and D. R. Worsnop (2000), *Aerosol Science and Technology*, *33*(1-2), 49-70.

Chemical and physical characterization of combustion aerosol

J. Jokiniemi[1,2]

[1]Fine Particle and Aerosol Technology Laboratory, Department of Environmental Science, University of Eastern Finland, FI-70211 Kuopio, Finland
[2]VTT, Technical Research Centre of Finland, Fine Particles, FI-02044 VTT, Espoo, Finland
Keywords: biomass combustion, fine particles, characterisation, chemistry, measurement.
Presenting author email: jorma.jokiniemi@uef.fi

Fine particle emissions from combustion sources have gained attention recently due to their climate effects and adverse effects on human health. Here the effects of fuel quality, boiler type and control devices on particle emissions from energy production by combustion and some other industrial sources (Lind et al., 2007) are reviewed. Several fossil and biomass based fuels are used for energy conversion processes. Here we consider coal, peat, heavy fuel oil, biomass and waste derived fuels and their effects on fine particle formation in boilers. Boiler types considered are pulverized combustion, bubbling fluidized boilers, circulating fluidized boilers, grate fired boilers, gasification-combustion boilers, small scale combustion (Ruusunen et al., 2011; Hytönen et al., 2009; Kaivosoja et al., 2012) appliances and oil burners. The emission control devices have the most important effect on particle matter (PM) emissions. Several PM removal devices are used like multicyclones, scrubbers, electrostatic precipitators, fabric filters with and without sulphur removal. Measurements have been performed for boilers with fuel power from few kW up to several hundred MWs. Extensive chemical and physical characterisation methods are used to understand the role of different species on emissions. Understanding all these factors helps us to design the energy production units to meet the emission regulations and to assess the environmental fate of different alternatives in energy production.

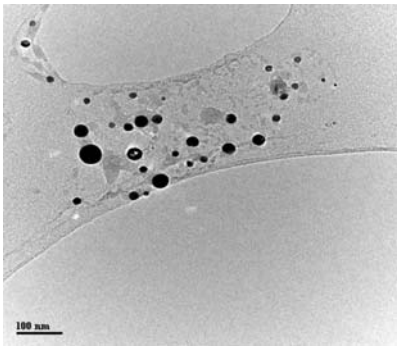

Figure 1. TEM image of waste combustion particles.

Lind, T., J. Hokkinen, J. K. Jokiniemi (2007) Fuel Processing Technology, 88(737-746).

Ruusunen, J., M. Tapanainen, O. Sippula, P. I. Jalava, H. Lamberg, K. Nuutinen, J. Tissari, M. Ihalainen, K. Kuuspalo, J. Mäki-Paakkanen, P. Hakulinen, A. Pennanen, K. Teinilä, U. Makkonen, R. O. Salonen, R. Hillamo, M.-R. Hirvonen and J. Jokiniemi (2011). Analytical and Bioanalytical Chemistry September 401(10) 3183-3195.

Hytönen, K., Yli–Pirilä, P., Tissari, J., Gröhn, A., Riipinen, I., Lehtinen, K.E.J. and Jokiniemi (2009) Aerosol Sci. and Technol. 43:442-454.

Kaivosoja, T., A. Viren, J. Tissari, J. Ruuskanen, J. Tarhanen, O. Sippula, and J. Jokiniemi (2012). Accepted in Chemosphere February 2012.

Friday, September 7, 2012

Session SS05S1O. Field observations and modeling of special events

Physico-chemical properties of airborne radiocesium released from the Fukushima nuclear accident

N. Kaneyasu[1], H. Ohashi[2], F. Suzuki[2], and T. Okuda[3]

[1]National Institute of Advanced Industrial Science and Technology, Tsukuba, 305-8569, Japan
[2]Department of Chemical Physics, Tokyo University of Marine Science, Tokyo, 108-8477, Japan
[3]Department of Applied Chemistry, Keio University, Yokohama, 223-8522, Japan
Keywords: Radioactive aerosol, Sulfate, Soluble fraction, Wet removal.
Presenting author email: kane.n@aist.go.jp

The accident of Fukushima Dai-ichi nuclear power plant, triggered by the great Tohoku earthquake and Tsunami that hit eastern Japan on March 11, 2011, released a large amount of radioactive materials into the environment. Although the radioactive particles have been collected by use of High-Volume air sampler in numerous sites, the activity size of radionuclides and their mixing state with other aerosol components have not yet been reported since the occurrence of the accident. We thus have started the sampling of size segregated aerosol at Tsukuba City, Japan, located 170 km south of the plant since 28 April, 2011.

A low-pressure cascade impactor (12-stages plus backup filter, Tokyo Dylec LP-20) was operated on the fourth-floor balcony of a building in Tsukuba. As impaction substrates, aluminium foil sheets were used for the first and third samples (LPI-AIST-1 and 3), and quartz fiber filters (Pallflex 2500 QAT-UP) were used for the second and fourth sample (LPI-AIST-2 and 4). As the backup filter, a quartz fibre filter was placed after the 12th stage. The radioactivity of ^{134}Cs and ^{137}Cs in aerosols collected at each stage were determined by gamma-ray with a high sensitivity Germanic detector. After the gamma-ray spectrometry analysis, the ionic species in the aerosols were extracted from one-fourth of the substrates into ultra-pure water and were determined by ion chromatography

The activity size distributions of ^{134}Cs and ^{137}Cs in aerosols measured from the first sample (LPI-AIST-1) reside mostly in the accumulation mode size range and showed the double peak structure. These activity size distributions almost overlapped with the mass size distribution of non-sea-salt sulfate aerosol. From the results, we can regard that sulfate is the main transport medium of these radionuclides, and re-suspended soil particles that attached radionuclides were not the major airborne radioactive substances by the end of May, 2011 (Kaneyasu *et al*., 2012).

Temporal changes in the Activity Median Aerodynamic Diameter (AMAD) of ^{137}Ce and the Mass Median Aerodynamic Diameter (MMAD) of non-seasalt (nss.)SO_4^{2-} are listed in Table 1. From the three sample sets analyzed so far, we can recognize two aspects on the size of radiocesium: (a) AMADs of ^{137}Ce are monotonously increasing with time, and (b) AMAD of ^{137}Ce are almost the same as MMAD of nss.SO_4^{2-} in the first two samples. In other words, the activity size distribution of the first two samples follows the mass size distribution of nss.SO_4^{2-}, while this character diminishes in the latest (LPI-AIST-4) aerosol sample. These suggest that the radiocesium included in sulfate aerosol had become a minor contributor to the airborne radionuclides by that time, and the re-suspended soil dust that attached the radiocesium has started to replace the position. This is probably caused by two factors: the direct emission of radiocesium from the damaged plant had almost halted, and the transport of radioactive materials from the plant was depressed by weather conditions.

During the Chernobyl nuclear accident in 1986, Bondietii *et al.* (1988) conducted a successive extraction experiment of radionuclides from aerosols collected on glass-fiber filters (aerodynamic diameter < 0.41 μm) in Tennessee, USA, with water, 0.01M HCl, and 0.1 M HCl. Their results indicated that water-extractable fraction of $^{134, 137}$Cs were less than 25%, and those of non-extractable fraction to 0.1 M HCl were above 30%.

We then conducted the successive extraction experiment of radiocesium from the aerosol deposits on the aluminum sheet substrate (8th stage of LPI-AIST-1, 0.5–0.7 μm in aerodynamic diameter) with water and 0.1M HCl. In contrast to the relatively insoluble property of Chernobyl radionuclides, those in aerosols collected at Tsukuba are exceedingly water-soluble (~100%). This may reflect the difference in the nature of the Chernobyl and Fukushima accidents, of which the former exposed the damaged reactor core directly to the ambient air whereas the latter did not. The possible formation mechanism of sulfate-radiocesium internal mixing particles will further be discussed in the presentation.

Table 1. Comparison of ^{137}Cs AMAD and nss.SO_4^{2-} MMAD of aerosols collected in Tsukuba, Japan, after the Fukushima accident.

Sample ID	Sampling period	^{137}Cs AMAD (μm)	nss.SO_4^{2-} MMAD (μm)
LPI-AIST-1	Apr.28– May 12	0.54	0.53
LPI-AIST-2	May12– May 26	0.63	0.63
LPI-AIST-3	May 26–Jun.9	under meas.	under meas.
LPI-AIST-4	Jun.9 – Jul.19	0.89	0.66

Bondietti, E. A., Brantley, J. N., and Rangarajan, C. (1988) *J. Environ. Radioactivity* **6**, 99-120.

Kaneyasu, N., Ohashi, H., Suzuki, F., and Okuda, T. (2012) submitted to *Environ. Sci. Tech*.

Environmental Impact of Fukushima Fallout in Southeast Spain

F. Piñero-García, J. Drożdżak and M.A. Ferro-García

Radiochemistry and Environmental Radiology Laboratory (LABRADIQ), Department of Inorganic Chemistry, University of Granada, Granada, 18071, Spain
Keywords: Nuclear Reactor, Accident, Radioactive Aerosols, Back Trajectories.
Presenting author email: franciscopigar@ugr.es

The aim of this research is to study the impact of the Fukushima fallout in Southeast Spain. Based on backward and forward trajectory, the movement of the radioactive cloud toward Southeast Spain was reconstructed. Furthermore, the transfer of fission products to different matrixes was studied.

On March 11th, 2011, an earthquake of magnitude 9.0 occurred in the Pacific Ocean near the east coast of Japan (epicenter 38.32ºN-142.37ºE), followed by a tsunami. As consequence, the backup diesel generators of Fukushima Dai-ichi nuclear plant were dangerously affected. The lack of electrical power subsequently caused extensive damage to the reactor cooling system. Subsequent explosions inside the reactors projected fission product (^{131}I, ^{132}I, ^{132}Te, ^{134}Cs, ^{137}Cs) into the atmosphere. Fifteen days after, traces of the Fukushima nuclear accident, was detected at Southeast Spain.

Samples of aerosols, rainwater and food, were taken in Granada, Spain, from March 11th to April 19th. Air samples were collected weekly by an air pump with two filters. Aerosols were collected in AAWP04700 cellulose filter, 4.7 10^{-2} m diameter and 0.8 μm size pore. The ^{131}I was collected in a CP-100 Radioiodine Sampler with activated charcoal traps for gaseous iodine. Dry and wet deposition was collected weekly using a slightly tilted stainless steel tray, 1m^2, connected to a 50L vessel. After the rainfall, samples of food, vegetables and cheese, were taken to check the transfer of the fission products from the atmosphere to the human food chain.

Some of experimental values found were; the highest concentration of ^{131}I in air (gas 2.63±0.12 mBq/m^3 and aerosols 0.82±0.08 mBq/m^3) was detected between March 23 and 30 and in rainwater samples (1.10±0.16 mBq/L) between March 30 and April 6. In addition, the maximum concentrations in air of ^{134}Cs (0.10±0.03 mBq/m3) and ^{137}Cs (0.09±0.02 mBq/m3) were measured between March 30 and April 6. ^{131}I remains mainly in gaseous form during transport due to activity levels for the gaseous fraction (2.6-0.4 mBq/m^3) were always higher than particulate fraction (0.82-0.14 mBq/m^3). After rainfall on April 3rd, 131I concentrations fell by 33.5% as a result of the scavenging of the atmosphere. The ratio ^{131}I/^{137}Cs, was similar in different countries, suggesting a quick movement of the radioactive cloud around the world (Manolopoulou, 2011). In addition, the high level of the ratio confirms that the fallout was rich in ^{131}I.

After the nuclear accident the air masses transported the radioactive cloud from Fukushima toward the Pacific Ocean and northern Japan in the direction of the Arctic Ocean, Canada and northern USA. Subsequently, polar maritime air masses, which had been originated as continental air masses over North America, moved the radioactive plume toward the Atlantic Ocean on the way to southeast Spain (Figure 1), (Piñero-García et al 2012). However, the rainfall and the change in the air mass origin (polar and arctic air masses passing over the British Isles and Western Europe, and Mediterranean and European Continental air masses), from April 16 to April 19, decreased the activity of radioactive fission product to background levels.

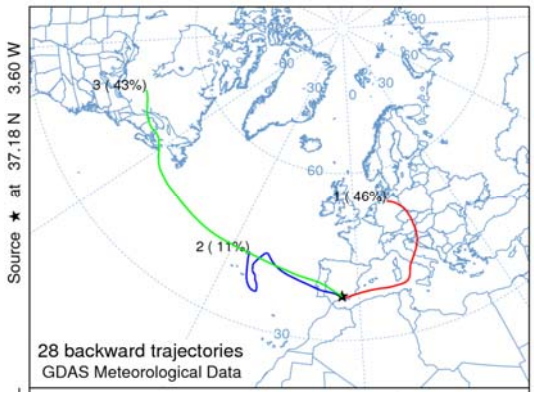

Figure 1. This is a representative air mass origin during Fukushima fallout exposure over Granada, Spain.

The concentrations of fission product detected in southeast Spain due to Fukushima fallout are so low that there is no impact on human health or the environment. Furthermore the Annual Limits on Intake (ALI), calculated for ingestion of food was 130±30 nSv/y, 0.013% of the annual effective dose limit for members of the public, 1mSv/y. Therefore the ingestion of vegetable and cheese, in Southeast Spain after the nuclear accident does not represent any risk to human health.

In summary, this research shows the importance of the climatic events in the evolution of the Fukushima fallout, and the importance of environmental radiology laboratories for nuclear safety in the world.

The Spanish Nuclear Safety Council (CSN) supported this work.

Piñero-García, F., Ferro-García, M.A., (2012) *Traces of fission product in southeast Spain after the Fukushima nuclear accident J. Environ. Radioact. Doi:10.1016/j.jenvrad.2012.01.011Proc.*

Manolopoulou et al (2011) *J. Environ. Radioact.* ***102****, 796-797.*

Atmospheric dispersion and ground deposition induced by the Fukushima Nuclear Power Plant accident at local scale: simulation and sensitivity study

I. Korsakissok[1], A. Mathieu[1] and D. Didier[1]

[1]Institute of Radiation Protection and Nuclear Safety, Fontenay-aux-roses, 92262 Cedex France
Keywords: Fukushima, Accident, Dispersion, Meteorology, Numerical Simulation, Deposition, Scavenging
Presenting author email: irene.korsakissok@irsn.fr

On March 11th 2011, an earthquake of magnitude 9.0 occurred off northeastern Japan, causing a tsunami and damaging the Fukushima Daiichi Nuclear Power Plant (FNPP1). As a result, radioactive products were released in the atmosphere. During the emergency phase, the Institute of Radiation Protection and Nuclear Safety (IRSN) was asked to provide its expertise on the plume dispersion and radiological consequences, in support of the French Government. Since then, the institute has been working on improving its assessment of the environmental contamination (Mathieu *et al*, 2012).

Understanding the formation process of highly contaminated areas cannot be achieved through measurements only. Indeed, many devices (radiation and meteorological monitoring stations) had been damaged by the earthquake and tsunami and were unavailable. Thus, improving atmospheric dispersion simulations remains a key issue. This paper presents the evolution of atmospheric and ground activity simulated at local scale (within 80 km of FNPP1), sensitivity studies and comparisons with environmental monitoring data.

IRSN's Gaussian puff model pX is used for the simulations. Dry deposition is modelled through apparent deposition velocities (cf. Table 1), and the scavenging coefficient is given by $\Lambda s = \Lambda_0 \times p_0$, with $\Lambda_0 = 5 \times 10^{-5}$ h/mm/s and p_0 the rain intensity in mm/h.

Table 1. Deposition velocities used in the simulation

	Particles	Organic iodine	Gaseous iodine
v_d (m/s)	2×10^{-3}	1×10^{-4}	7×10^{-3}

The source term was evaluated using available information on the reactors status (pressure, water level) and events chronology (ventings and explosions). 73 isotopes were included. Additional information was inferred from air dose rate measurements at local and Japan scales, to help determine each release's time and duration and the quantity of each radioisotope. However, the source term remains a key uncertainty.

The meteorological data used are ECMWF forecasts at 0.1° resolution, with a 3-hour time step. At this resolution, the model fails to reproduce the complex orography, leading to uncertainties in the wind fields. Thus, wind observations at FNPP1 are used during crucial time periods. Since wet deposition is a key process in the contamination, rain radar data at a 10-minutes time period are used to model the precipitations.

The reference simulation was carried out using the aforementioned deposition and scavenging values. The release height was split between 50 m above the ground (70% of the emission) and 150 m (30 % of the release). The results compare well with gamma air dose rates measured in Fukushima prefecture (cf. Figure 1).

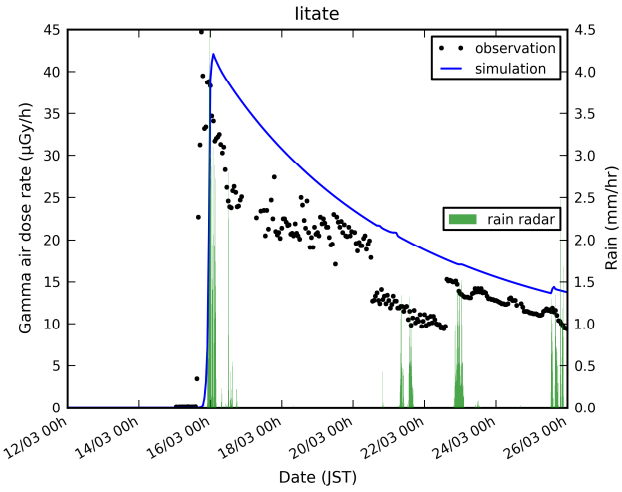

Figure 1. Comparisons between gamma air dose rate measured (dots) and simulated (line) at Iitate (about 40 km north-west of FNPP1).

Additional simulations are used to evaluate the results sensitivity to some parameters, such as the release height, the isotopic composition (e.g., proportion of noble gas in the release), the deposition and scavenging constants, and the dispersion parameterizations. A particular focus is made on the wet deposition process, which is probably responsible for the formation of the north-western high dose rate zone. Gamma air dose rate data are used to evaluate a simulation ability to forecast (1) the plume arrival time, (2) the peak intensity and (3) the deposition rate. Ground deposition measurements are used as a complement to this analysis.

Acknowledgements: the meteorological forecasts used in this work have been provided by Météo-France. The source term evaluation was done in collaboration with D. Corbin and J. Denis (IRSN).

Mathieu, A. *et al.* (2012). *Modeling of atmospheric dispersion and ground deposition induced by the Fukushima Daiichi nuclear power plant accident*, Submitted to Elements (special Fukushima issue).

Observations in Germany, France, and Great Britain during eruptions of the Eyjafjallajökull volcano in 2010

S. Wurzler[1], P. Bruckmann[1], J. Friesel[1], J. Geiger[1], H. Hebbinghaus[1], W. Straub[1], D. Gladtke[1], U. Pfeffer[1], T. Kuhlbusch[2], R. Lumpp[3], S. Heupel Santos[4,1], M. Memmesheimer[5], H. Jakobs[5], E. Friese[5], L. Nieradzik[5], H. Elbern[5], D. Klugmann[7], S. Gilge[6], O. Favez[8], A. Colette[8], L. Chiappini[8]

[1] LANUV NRW, Wallneyer Str. 6, 45133 Essen, Germany
[2] IUTA e.V., Bliersheimer Strasse 60, 47229 Duisburg, Germany
[3] LUBW, Postfach 10 01 63, 76231 Karlsruhe, Germany
[4]Institute for Landscape Ecology, University of Münster, Robert Koch Str. 28, 48149 Münster, Germany
[5] RIU-EURAD, IGMK, University of Cologne, Aachener Straße 209, 50931 Köln, Germany
[6] German Meteorological Service, Hohenpeissenberg Met. Observatory, Albin-Schwaiger-Weg10, 82383 Hohenpeissenberg, Germany
[7] Met Office, Observations R&D, FitzRoy Road, Exeter, Devon EX1 3PB, UK
[8] Laboratoire Central de Surveillance de la Qualité de l'Air, INERIS, Parc Technologique Alata, BP2, 60550 Verneuil-en-Halatte, France
Keywords: volcanic particles, measurements, modelling
Presenting author email: sabine.wurzler@lanuv.nrw.de

In spring 2010 the Icelandic volcano Eyjafjallajökull erupted high loads of pyroclastic material into the atmosphere. The eruption cloud reached heights between 4 and 7 km. The volcanic ash advisory centre London, the responsible institution for making forecasts of ash coming to Europe, decided the complete shut down of the air traffic over wide parts of Europe for a sequence of days.

From April 13th to 20th there was a stable high pressure system over the Atlantic Ocean. Thus, a rather constant air flow from north-west to south-east prevailed over Europe in the upper and middle troposphere. Due to that the volcanic ash was transported from Iceland over the UK to Central Europe. Furthermore, the weather conditions were sunny, dry, and stable, preventing the ash from being mixed throughout the atmosphere or from being washed out by precipitation. These weather conditions led not only to long range ash transport but also to high PM10 concentrations in the boundary layer from other sources. Thus the question arises whether the volcanic ash contributed to the high PM10 levels near ground or if the reason for the high PM10 concentrations measured by the ground based stations has to be found elsewhere.

The aim of this paper is to give a review of some of the findings of the ground based measurements, model calculations, and remote sensing in Central Europe during the volcanic event two years ago, with focus on Germany, France, and Great Britain.

A large variety of modelling results on the dispersion of the Eyjafjallajökull plume over Europe can be found in the recent literature. They all showed that the ash plume reached the air space over Central Europe and these findings compare rather nicely to satellite pictures, Lidar measurements, and measurements from aircrafts. In the present paper as an example EURAD and Chimere model simulations will be presented.

With regard to lidar and satellite measurements, we will concentrate on the findings by the German Weather Service, the Met Office and of the volcanic ash advisory centre in Great Britain.

As an example for the ground based measurements, we will show the findings of Germany and France. To figure out whether and to what extend the elevated PM10 concentrations are influenced by the transported volcanic ash the PM10 samples were analysed for heavy metals, chloride, nitrate, sulphate, and ammonium. The composition was compared with the one of the erupted material as measured by Óskarsson (2010). An additional indicator for volcanic material is the occurrence of elevated SO_2 concentrations and of unusual particle shapes that can be detected by scanning electron microscope analyses.

The results of the ground based observations in Germany and France are quite similar. There was volcanic ash that reached the surface, especially at the Black Forest as well as in the Alsace region (Colette et al., 2011, LUBW, 2010), where part of the sampled particles have the same chemical composition than the erupted material. Thus about 25 $\mu g/m^3$ of the PM10 can be ascribed to volcanic ash there, in good agreement with long-range transport modelling studies. Nevertheless in other places, for example in North Rhine-Westphalia (LANUV), the volcanic ash fraction contributed merely about 5 $\mu g/m^3$ to the PM10 burden in the latter regions.

This shows that a combination of all existing methods and a close collaboration should be used to predict the impact of future events.

Óskarsson (2010): Chemical Composition. http://www.earthice.hi.is/page/IES-EY-CEMCOM (27.02.2012)

A. Colette, O. Favez, F. Méleux et al. (2011): Assessing in near real time the impact of the April 2010 Eyjafjallajökull ash plume on air quality, Atmos. Environ., 45, 1217-1221.

LUBW (2010): Ausbruch des Eyjafjallajökull im April 2010. Auswirkungen auf die Feinstaubkonzentrationen in Baden-Württemberg. Karlsruhe

VOLCANIC ASHES, DESERT DUST AND FLYING ASHES FROM FOREST FIRES: All RADIOACTIVE CLOUDS !

O. Masson[1], J.C. Sabroux[2], D. Piga[1], R. Gurriaran[3], J. Loyen[3]
[1]Nuclear Safety and Radioprotection Institute (IRSN), bât 153, BP3, Saint Paul lez Durance, 13115, France
[2] IRSN, Bât. 389, BP68, Gif sur Yvette, 91192, France
[3] IRSN, 31 rue de l'écluse, BP35, Le Vésinet, 78116, France

Keywords: radioactive aerosol, volcanic particles, desert dust, wood smoke.
Presenting author email: olivier.masson@irsn.fr

Desert dust events, volcanic eruptions and soot emissions from forest fires are natural events that emit large amount of particles into the atmosphere. Depending on their magnitude, such event can yield sometimes air travel disruption at a local or continental scale. Beside the large amount of emitted material, airborne particles bear also in common some traces of radionuclides, either of natural or anthropogenic origin (table1).

During the first three days of the Eyjafjallajökull eruption in April 2010, roughly 200 million tonnes of basaltic tephra (Gudmundsson, 2010) having a uranium concentration close to 2 ppm (Schleicher, 2012) were emitted into the atmosphere. This corresponds to *ca.* 400 tonnes of uranium and 1300 tonnes of thorium (assuming a 3.3 Th/U ratio). Most of those particles were deposited close to the volcano on soil having the same specific activity level. Moreover, a large plume spread over northern Europe. In France, IRSN conducted measurements of ^{210}Po, known as a specific tracer of volcanic plumes (Nho et *al.* 1997). Results were in the range of the north hemisphere background level (~ 50 µBq/m^3), excluding a specific volcanic contribution at ground level. This was also consistent with Lidar detections showing that the plume remained mainly at around 1 km a.g.l. over France before being so diluted that the signal became too weak to be measured.

Desert sandstorms are responsible for the transport of hundreds million tonnes of particles a year. Most atmospheric nuclear bomb tests where performed in the northern hemisphere and yielded to a latitudinal dependent deposition with maximum rate between 30 et 50° of North latitude. Wind eroded clay and silt particles have trapped small traces of former deposited anthropogenic long-lived radionuclides. Traces of caesium and plutonium can thus be transported over long distances. This is the case when winds are blowing from Sahara to France. The specific contribution of the French nuclear tests performed in the early 1960's in Sahara cannot currently be distinguished from the global radioactive fallout as the ^{238}Pu/$^{239+240}$Pu, ^{241}Pu/$^{239+240}$Pu and ^{240}Pu/^{239}Pu ratios remain close to ratios characteristic of the global fallout (Masson *et al.* (2010). Additionally, weighted activity levels in Saharan soils (except very close to ground zero test site) are similar to what can be observed in France. Similar observations were noticed in Japan regarding sandstorm originating from East Asian arid areas (Hirose, 2007).

Fires in boreal forests may also act as a diluted and widespread source that can redistribute up to 10% of formerly deposited radionuclides still present in the forest litters, or that have migrated into biomass. In summer 2004, fires occurred in territories contaminated by the Chernobyl fallout in Belarus, Ukraine and western part of Russia. Airborne ^{137}Cs, normally at trace levels, was slightly enhanced during eastern wind conditions over France (Piga, 2010). Apart from forest fires, usual biomass burning for heating purposes or agricultural practices can slightly affect its current background level at local and regional scales. This is especially the case during winter as shown by Bourcier *et al.* (2010) using simultaneous ^{137}Cs and Levoglucosan determinations.

Table 1: Comparison of some radionuclide amounts (Bq) emitted to the atmosphere by natural events

	^{137}Cs	^{238}U
Sahara desert export (*per* year)	10^{12} Bq	10^{12} Bq
Eyjafjöll 2010 eruption (first 3 days)	not concerned	5.10^{12} Bq
Europe and Russia forest fires export (*per* year)	10^{13} Bq	n.d.

Despite the amounts of released or re-emitted radionuclides, airborne levels remains after dispersion at trace levels (~ 1-50 µBq/m^3) and of no concern for public health.

Masson, O., Piga, D., Gurriaran, R. and D'Amico, D. (2010). *Atmos. Env.*, **44**: 2478-2486.

Hirose, K., Igarashi, Y. and Aoyama, M. (2007). *J. Radioanal. Nucl. Chem.*, **273**(1): 115–118.

Piga, D. (2010). Rémanence au niveau du compartiment atmosphérique du ^{137}Cs. PhD thesis (in French).

Bourcier, L., Sellegri, K., Masson, O., Zangrando, R., Barbante, C., Gambaro, A., Pichon, J.-M., Boulon, J. and Laj, P. (2010). *Atmos. Environ.*, **44**: 2280-2286.

Gudmundsson, M.T., Pedersen, R., Vogfjörd, K., Thorbjarnardóttir, B., Jakobsdóttir, S. and Roberts, M.J. (2010). *EOS*, **91**(21): 190-191.

Schleicher, N., Kramar, U., Dietze, V., Kaminski, U. and Norra, S. (2012). *Atmos. Environ.*, **48**: 113-121.

Nho E.Y., Le Cloarec M-F, Ardouin B., Ramonet M. ^{210}Po, an atmospheric tracer of long-range transport of volcanic plumes. Tellus B: Chemical and Physical Meteorol.. Vol. 49, 4, 09/97, 429-438.

Eyjafjallajokull volcanic dust characteristics from LIDAR data and in-situ aerosol size distributions

Massimo Del Guasta[1], Paolo Cristofanelli[2], Angela Marinoni[2], Paolo Bonasoni[2]
[1]Institute of Applied Physics (IFAC) CNR, Via Madonna del Piano 10, 50019 Sesto Fiorentino (Italy)
[2]Institute of Atmospheric Science and Climate (ISAC) CNR,Via Gobetti 101, 40129 Bologna,(Italy)

Keywords: volcanic dust, LIDAR, light scattering, depolarization
Presenting author email: m.delguasta@ifac.cnr.it

In this experiment the LIDAR backscatter and depolarization of Eyjafjallajokull volcanic dust measured continuously at 532 nm at IFAC CNR (60 m asl, Sesto Fiorentino, Italy) are compared with calculated quantities derived from aerosol observational activity in high mountain site during the period 18-22 May 2010.

The simulations rely on aerosol size distributions that are continuously measured by means of DMA and Optical counters at the O. Vittori Mt. Cimone station, Italy (MTC, 2165 m asl), which is located 50 km away from the IFAC LIDAR site. Different dust compositions and aspect ratios were considered in the simulation..

A closure experiment was then attempted by comparing the calculated and measured LIDAR quantities at the altitude of MTC. The goal is to improve the derivation of the characteristics of volcanic dust with the synergic use of LIDAR and mountain-site aerosol data.

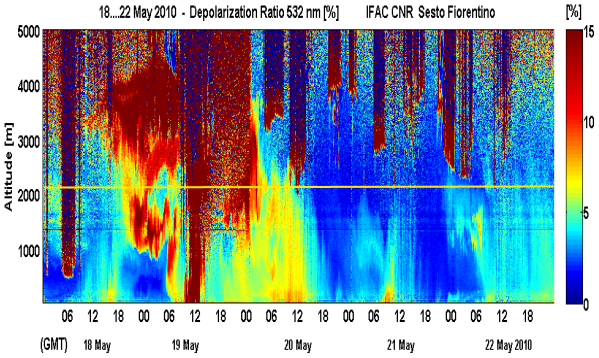

Figure 1. The LIDAR depolarization of the volcanic plume of 18-22 May 2010 at Sesto Fiorentino (Italy). The altitude of the MTC station is line-marked

Optical simulations

The scattering properties of volcanic dust were simulated at 532 nm by assuming axisymmetric spheroids with the refractive index of Obsidian, Basaltic glass, Basalt and Andesite (Pollack et al.,1973). The scattering simulations were performed by means of the "Null Field method with discrete sources" approach to T-matrix developed by Doicu *et al*. (2006).

The final results of simulations were LIDAR quantities, such as depolarization, calculated for randomly-oriented particles of different sizes (0.01-20 um), composition and aspect ratios (1.2<AR<2). LIDAR depolarization is a powerful indicator of the presence of non-spherical particles: simulations showed that large volcanic spheroids can depolarize less than small ones, and that 15-17% depolarization is expected from large volcanic spheroids, regardless of their shape and composition (Fig.2).

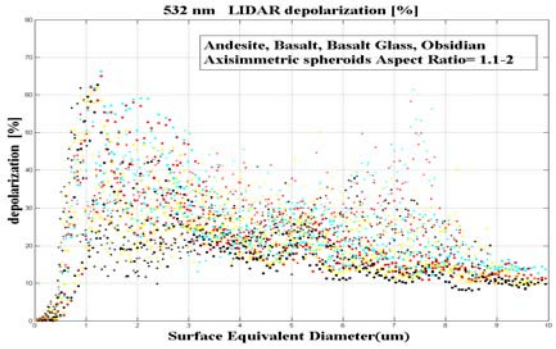

Figure 2: LIDAR Depolarization as obtained from simulations with different dust composition

Comparison with in-situ aerosol information

IFAC LIDAR data and MTC in-situ aerosol size distributions (0.01-20μm) were both analysed for the Eyjafjallajokull cloud of 18-22 May, 2010. LIDAR quantities were calculated from MTC size distributions by splitting them into three lognormal modes. The LIDAR backscatter and depolarization were calculated by using the Mie theory for the two small modes, and the T-matrix results for the third, dust mode. All the different, simulated ash compositions and aspect ratios were considered. The calculated LIDAR quantities were compared with the measured ones for the altitude of MTC (2165 m) (Fig.1).

A closure experiment was thus carried out in order to show, as suggested e.g. by Hervo *et al*.,(2012) the benefits of the synergic use of LIDAR data and aerosol data from high mountain sites in deepening our knowledge about volcanic dust.

Doicu A., Wriedt T., Eremin Y. A.,(2006) *Light Scattering by Systems of Particles Null-Field Method with Discrete Sources Theory and Programs*. Springer Verlag

Hervo M., B. Quennehen, N. I. Kristiansen, J. Boulon, A. Stohl, P. Freville, J.-M. Pichon, D. Picard,P. Labazuy, M. Gouhier, J.-C. Roger, A. Colomb (2012) Physical and optical properties of 2010 Eyjafjallajokull volcanic eruption aerosol: ground-based, Lidar and airborne measurements in France. Atmos. Chem. Phys., 12, 1721–1736

Pollack J.B., O.B.Toon, B.N.Khare (1973) Icarus **19**, 372-389

Eyjafjallajökull volcanic ash number concentration retrieval at Lyon (France) with a UV-polarization Lidar

G. David[1], B. Thomas[1], A. Miffre[1] and P. Rairoux[1]

[1]Laboratoire de Spectrométrie Ionique et Moléculaire, CNRS UMR 5579, Université Lyon 1, Villeurbanne, 69622, France

Keywords: remote sensing, volcanic particles, number concentration

Presenting author email: amiffre@lasim.univ-lyon1.fr

The volcanic ash particles released from the Eyjafjallajökull 14th April 2010 eruption caused a six days airspace closure over Western Europe. After long-range transport, volcanic ash aerosols were aged and highly dispersed with irregularly shaped volcanic ash particles, mixed with sulfate particles (Schumann et al., 2011). We have traced these non-spherical volcanic ash particles with a sensitive and accurate UV-polarization Lidar at Lyon (France), at the border of the airspace closure, after advection over more than 2,600 km. We then applied this field measurement to develop a new methodology (Miffre et al., 2012b) to remotely evaluate the volcanic ash particles number concentration in the troposphere, with high sensitivity and accuracy. It only requires a single Lidar laser wavelength and it is ash particles specific, which is new (Miffre et al., 2012b).

The spatial and temporal dispersion of the volcanic ash cloud at Lyon is displayed in figure 1 from April 17th to 20th 2010, between 0.5 to 7 km, by representing the particles parallel backscattering coefficient $\beta_{p,//}$. Between 3 and 7 km, an unusually high backscattering coefficient is observable in a thin filament, tilting into the low troposphere, in nice agreement with FLEXPART ash numerical dispersion model and 7-days air mass back-trajectories (Miffre et al., 2012a), showing evidence of volcanic ash presence above the Lidar station.

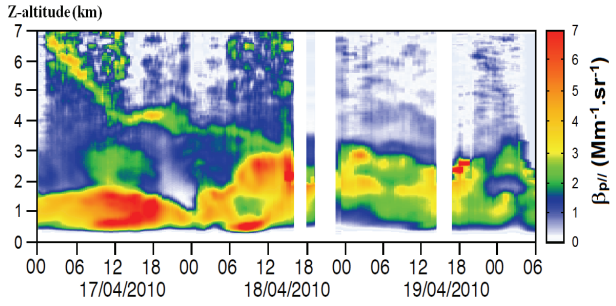

Figure 1. UV-Lidar time-altitude map of the particles parallel backscattering coefficient $\beta_{p,//}$ at Lyon (France).

Since the perpendicular Lidar channel is, by construction, only sensitive to non-spherical particles backscattering, it is in this study volcanic ash particles specific. As volcanic ash particles are detected on both Lidar polarization channels, the volcanic ash particles backscattering coefficient β_{ash} can be determined as follows (with obvious notation for $\beta_{p,\perp}$):

$$\beta_{ash} = \beta_{ash,\perp} + \beta_{ash,//} = \beta_{p,\perp} (1 + 1/\delta_{ash}) \quad (1)$$

The volcanic ash depolarization ratio $\delta_{ash} = 40.5 \pm 2$ % has been determined from laboratory scattering matrix measurements on volcanic ashes, mechanically sieved to remove the largest particles, as after long-range transport (Muñoz et al., 2004). Then, at altitude z, the volcanic ash number concentration N_{ash} has been retrieved from the β_{ash}-definition ($N_{ash} = \beta_{ash} / \langle (d\sigma/d\Omega)_{ash} \rangle$), by computing the size-averaged ash backscattering cross-section $\langle (d\sigma/d\Omega)_{ash} \rangle$, using Muñoz's ash particles size distribution and refractive index, assuming surface equivalent spheres, while including sedimentation processes (Schumann et al., 2011). $\langle (d\sigma/d\Omega)_{ash} \rangle$ is hence known with 15 %-uncertainty. Figure 2 displays vertical profiles of $\beta_{p,//}$, $\beta_{p,\perp}$ and N_{ash}. The sensitivity and accuracy of our Lidar enable to distinguish different volcanic ash layers. Moreover, the retrieved N_{ash}-values well compare with in-situ optical particle counter measurements (Schumann et al., 2011).

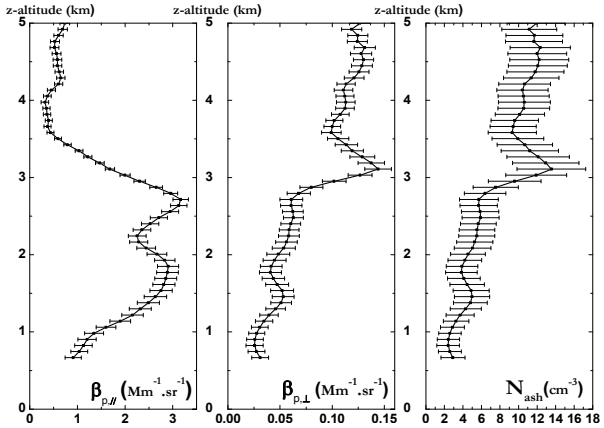

Figure 2. Vertical profile of $\beta_{p,//}$, $\beta_{p,\perp}$ and N_{ash} on April 19th at 0 h UTC at Lyon (France).

The presentation will detail our field observation of the Icelandic volcanic ash cloud at Lyon, in nice agreement with FLEXPART ash numerical dispersion model (Miffre et al., 2012a, Eyjafjallajökull Special Issue). Then, we will point out the robustness of our N_{ash}-retrieval methodology (Miffre et al., 2012b), which is new and easily applicable to other volcanic ash events as only one Lidar wavelength is required.

We thank A. Stohl's group for providing FLEXPART ash numerical dispersion model, CNRS and Région Rhône-Alpes for financial funding.

Muñoz O. et al., (2004), *J. Geo. Res.* **109**, D16201.
Miffre A. et al., (2012a), Eyjafjallajökull Special Issue, *Atm. Env.*, **48**, 76-84.
Miffre A. et al., (2012b), *J. Atm. Ocean. Tech.*, accepted.
Schumann U. et al., (2011), *Atm. Chem. Phys.*, **11**, 2245-2279.

Friday, September 7, 2012

Session WG01S7O. Aerosol Cloud Interaction

Inhibition of Heterogeneous Ice Nucleation of Mineral Dust Particles Exposed to Ozone

Z.A. Kanji[1], A. Welti[1], C. Chou[1, 2] and O. Stetzer[1]

[1]Institute for Atmosphere and Climate Science, ETH – Zurich, Zurich 8092, Switzerland
[2] Now at Science and Technology Research Institute, University of Hertfordshire, Hatfield AL10 9AB, UK
Keywords: Deposition, Immersion, Mineral Dust, Ice Nucleation.
Presenting author email: zamin.kanji@env.ethz.ch

Aerosols can cool or warm the atmosphere directly via interaction with incoming solar radiation (aerosol direct effect), or via their ability to act as cloud condensation or ice nuclei (IN) and thus play a role in cloud formation (indirect effect). The physical properties of aerosols such as size and solubility as well as chemical composition can influence their behavior and fate in the atmosphere. Ice nucleation is known to be especially sensitive to surface properties. Ice nucleation taking place via IN is termed as heterogeneous ice nucleation and can take place via deposition (ice forming on IN directly from the vapor phase), condensation/immersion (freezing via formation of the liquid phase on IN) or condensation (IN colliding with supercooled liquid drops).

Motivation for quantifying ice formation in the troposphere is many-fold. First, to understand the hydrological cycle since ice is the primary initiator of precipitation forming clouds. Second, the tropospheric budget of water vapour, an especially active greenhouse gas is strongly influenced by ice nucleation and growth. Third, ice surfaces in the atmosphere act as heterogeneous surfaces for chemical reactions of trace gases (e.g., SO_2, O_3, NO_x). Being able to quantify ice formation rates and ice surface concentrations allows an accurate calculation of trace gas budgets in the troposphere. This work addresses how mineral dust particles chemically aged from O_3 exposure influence deposition and immersion mode freezing under tropospherically relevant temperature (**T**) and relative humidity (**RH**) conditions.

Ice nucleation measurements were conducted using home-built chambers of the thermal gradient continuous flow diffusion principle capable of measuring immersion freezing (Lüönd *et al.*, 2010) (IMCA) and deposition freezing (Stetzer *et al.*, 2008) (PINC). In IMCA an ice optical depolarization detector was used to discriminate between frozen and liquid drops, whereas an optical particle counter was used to detect ice crystals in PINC. Poly-disperse samples of sub-micron diameter kaolinite and Arizona test dust were aerosolized in a stainless steel chamber and allowed to age for 15 – 90 minutes in known amounts of O_3 in the range 0.4 – 4 ppmv under dark conditions at ~298K. Destruction of O_3 was observed due to initial rapid decline of concentrations beyond background decay upon addition of dust particles to the aerosol tank. Deposition and immersion mode freezing experiments were conducted for both particles exposed to O_3 and unexposed particles.

Results for deposition mode freezing of kaolinite particles at RH_i = 130% are shown in Figure 1. It is observed that exposure to low levels of O_3 marginally enhance the ice active fractions as function of T. In contrast, when high O_3 concentrations are used for the ageing process, the ice active fractions are significantly repressed.

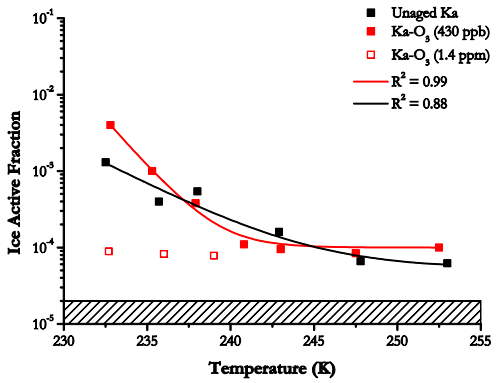

Figure 1. Ice active fraction as a function of T for kaolinite particles quoted at RH with respect to ice of 130%. The hashed region indicated the instrument background.

Ozone is known to react at surface sites of mineral dusts, including kaolinite (Karagulian and Rossi, 2005) to produce oxygenated surface species. It is possible that these surface species lower energies of ice germ formation for ice nucleation on the kaolinite surface. In contrast, when higher O_3 concentrations are used, the active surface species are chemically destroyed or physically occupied by adsorbed O_3, therefore making active sites for ice nucleation unavailable. Similar trends in ice nucleation behavior were observed for immersion freezing.

The results imply that mineral particles exposed to low ozone concentrations for longer periods of time in the atmosphere could have a significantly different ice nucleation behavior depending on the particle history compared to untreated particles typically used in laboratory measurements. These are the first results to show an inhibition of freezing in the immersion mode due to chemical ageing of aerosol particles.

Karagulian, F. and M. J. Rossi (2005), *Phys. Chem. Chem. Phys.*, 7(17): 3150-3162, DOI: 10.1039/b506750m.

Lüönd, F., O. Stetzer, A. Welti and U. Lohmann (2010), *J. Geophys. Res.-Atmos.*, 115(D14201)DOI: 10.1029/2009jd012959.

Stetzer, O., B. Baschek, F. Lüönd and U. Lohmann (2008), *Aerosol Sci. Technol.*, 42(1): 64-74, DOI: 10.1080/02786820701787944.

Combustion Aerosol over Marine Stratus: Long Range Transport, Subsidence and Aerosol-Cloud Interactions over the SE Pacific

Antony D Clarke[1], Jan Kazil[2, 3], Graham Feingold[3], Steffen Freitag[1], C. McNaughton[1], Jefferson Snider[4], Teresa Lynn Campos[5], Vera Breckhovskikh[1],
[1]School of Ocean & Earth Sci & Tech, Univ. of Hawaii, Dept Oceanography, Honolulu, HI, 96822, USA.
[2]CIRES, Boulder, CO, USA. [3] NOAA, Boulder, CO, USA. [4]University of Wyoming, Laramie, WY, USA.
[5] NCAR, Boulder, CO, USA.
Keywords: combustion aerosols, long-range transport, cloudiness, CCN
Presenting author email: tclarke@soest..hawaii.edu

The world's largest stratus deck over the South East Pacific (SEP) was a study target for the VOCALS (http://www.eol.ucar.edu/projects/vocals/) experiment in October 2008. Aerosol-cloud interactions were one major goal of several ship and aircraft studies including results from 14 flights of the NCAR C-130 aircraft reported here. Each flight covered about a 1000 km range with multiple profiles and legs below, in and above the Sc deck.

Strong aerosol sources along the coast of Chile were expected and found to influence cloud condensation nuclei (CCN) in coastal clouds. However; "rivers" of elevated CO, black carbon (BC) associated with combustion aerosol effective as CCN at <0.3%S were also common in subsiding free troposphere (FT) air overlying the extensive Sc deck for over 1000km offshore (Shank et al., 2012). This subsidence brought in aerosol from sources over the western Pacific as well as South America. Observed entrainment of this aerosol appeared linked to cloud related turbulence. When present, entrained combustion aerosol increased the CCN in the marine boundary layer (MBL) (Fig.1) leading to decreased effective radius compared to clouds in "clean" MBL air advected from the South Pacific.

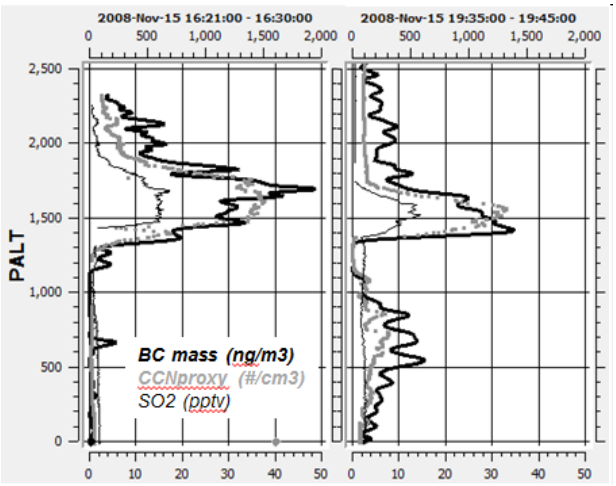

Figure 1. An example from flight 14 on Nov. 15 for descent (left) and ascent (right) ~3hrs later in same location near isolated cloud in an MBL air mass advected with the wind. Combustion plume aloft with elevated BC, SO2 and CCNproxy at 0.2%S (Here non-volatile CN heated to 350C are shown as proxy for CCN at 0.2%S) initially lies above inversion near 1,300m with a clean MBL below. Three hours later (right) plume is lower and about 1/3 is mixed into MBL. This suggests a localized entrainment near this cloud of about 1.4 cm/s and 2-3 times regional expected entrainment values.

Previous modeling results using LES (Wang and Feingold, 2009) show that drizzle in the clean marine boundary layer depletes aerosol and leads to a transition from closed cell convection to the formation pockets of open cells (POC), with much reduced cloud cover. These clean conditions are similar to MBL conditions in Fig. 1 (left) before entrainment of pollution. New, preliminary simulations, with a pollution layer located in the FT above the cloud deck, using measured aerosol size distributions, suggest that entrainment of the pollution aerosol can maintain MBL CCN concentrations and prevent the transition to POC conditions (Figure 2).

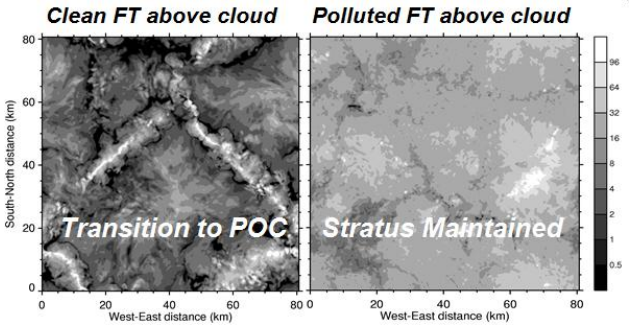

Figure 2. Modeled LES cloud optical depth after 21hr simulation of cloud evolution in clean SC topped MBL resulting in transition to POC (left). Similar model for case with pollution layer located above cloud (Fig. 1, right) showing no evidence of transition to POC.

We hypothesize that such entrainment of pollution and the resulting elevated CCN concentrations in the MBL can help buffer clouds over the SEP against depletion of CCN by drizzle. This may suppress the transition of closed cell to open cell convection, leading to increased lifetimes of Sc clouds that entrain such aerosol. If confirmed by additional ongoing investigations this would be important because increased cloud cover, caused by suppressed POC formation, would have significant regional radiative effects. These are expected to add to but greatly exceed those caused by an albedo increase from associated increases in CCN.

Kazil, J., et al., ACP, 11, 7491–7514, 2011.
Shank et al., ACP, 12, 557-576, 2012.
Wang, H., and Feingold, G., J. Atmos. Sci., 66, 3237- 3256, 2009

Aerosol cloud interactions of trade wind cumuli
A single cloud contact analysis

F. Ditas[1], B. Wehner[1], H. Siebert[1], R.A. Shaw[2], H. Wex[1], T. Schmeißner[1], G. Roberts[3,4], A. Wiedensohler[1]

[1]Leibniz Institute for Tropospheric Research (IfT), 03418 Leipzig, Germany
[2]Department of Physics, Michigan Technological University, Houghton, Michigan, USA
[3]Centre National de Recherche Scientifique - Météo France, Toulouse, France
[4]Scripps Institution of Oceanography, Center for Atmospheric Sciences, La Jolla, United States
Keywords: aerosol cloud interactions, activation properties, critical supersaturation, trade wind cumuli
Presenting author email: ditas@tropos.de

Aerosol and cloud microphysical properties of trade wind cumuli were observed during the CARRIBA (Clouds, Aerosol, Radiation, and tuRbulence in the trade wInd regime over BArbados) experiment in November 2010 and April 2011. Measurements were performed by the helicopter-borne measurement platform ACTOS (Airborne Cloud Turbulence Observation System, Siebert et al. 2006) with high temporal and spatial resolution. For detailed information about the aerosol instrumentation the reader is referred to Wehner et al. 2011.

A single cloud contact analysis is carried out, providing statistical information about e.g., activation diameter and critical supersaturation (S_{crit}) of each observed cloud. The analysis is based on two different methods: a) deriving the activation diameter by comparison of aerosol number size distributions (NSDs) inside and outside the cloud, b) calculating the fraction of activated particles by comparison of interstitial aerosol and cloud free aerosol number concentration. Simultaneous measurements of cloud microphysical properties allow aerosol – cloud condensation nucleus – cloud droplet number concentration closure studies to evaluate both methods.

Figure 1 demonstrates method a), it shows NSDs inside and outside of a trade wind cumuli observed on Nov. 15th 2010. NSDs under cloud free conditions show a typical bimodal structure, whereas for the NSDs of the interstitial aerosol inside the cloud the accumulation mode is vanished due to cloud droplet activation. The black line indicates the fraction of activated particles (η), the shaded area corresponds to the number of activated particles of $N_{act} = 100$ cm^{-3}. From $\eta = 0.5$ we derive an activation diameter of $d_{p50} = 80$ nm which is close to the Hoppel-minimum of the number size distribution. For particles in this size range a critical supersaturation of $S_{crit} = 0.3\%$ is required to activate to cloud droplets (for ammonium sulfate, 70% soluble fraction).

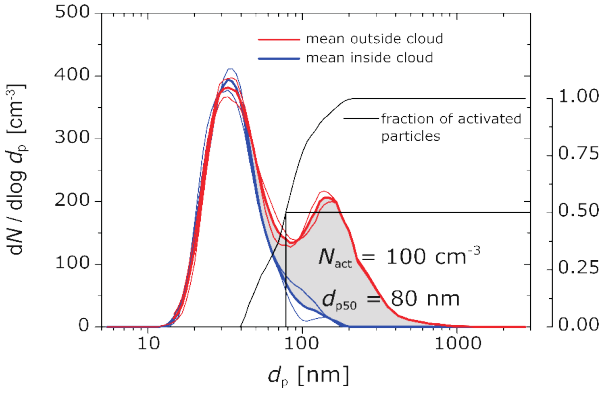

Fig. 1. Aerosol number size distributions inside (blue) and outside (red) clouds. Black line indicates the fraction of activated particles.

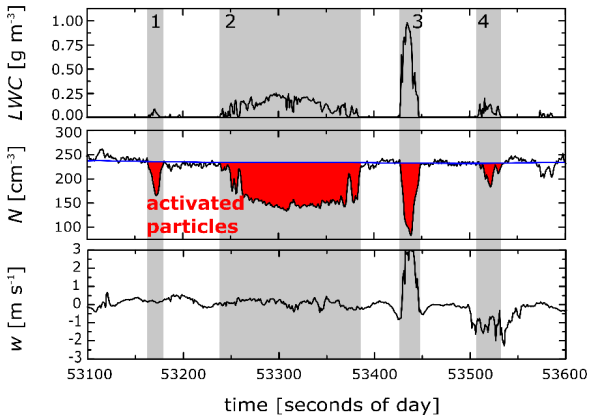

Fig. 2. Time series of liquid water content (*LWC*), interstitial aerosol particle concentration (*N*) and vertical wind velocity during a typical flight leg at cloud level. Grey shaded areas mark 4 cloud contacts, fraction of activated particles is indicated in red.

Figure 2 shows a time series at cloud level and illustrates partly method b). The red area refers to the fraction of activated particles which is related to the activation diameter with the help of integrating the aerosol number - size - distribution. Furthermore, the critical supersaturation is calculated by using Köhler theory. First results of single measurement flights under clean, marine conditions show for actively growing cumuli lowest activation diameter of $d_p = 40$ nm, corresponding to a critical supersaturation of $S_{crit} = 0.7\%$ (for similar chemical properties as used above).

Finally, this analysis is applied to measurement flights of both campaigns in November 2010 and April 2011 covering different meteorological conditions and aerosol types.

We thank the CIMH (Caribbean Institute for Meteorology and Hydrology), Horizon Helicopters, enviscope GmbH, and Barbados Concorde Experience. This project was funded by DFG-grant SI 1534/3-1 and the IfT.

Siebert, H., H. Franke, K. Lehmann, R. Maser, E. W. Saw, D. Schell, R. A. Shaw, and M. Wendisch (2006). *Probing Fine-Scale Dynamics and Microphysics of Clouds with Helicopter-Borne Measurements, Bull. Amer. Met. Soc.*, 87, 1727 – 1738

Wehner, B., H. Siebert, A. Ansmann, F. Ditas, P. Seifert, F. Stratmann, A. Wiedensohler, A. Apituley, R. A. Shaw, H. E. Manninen, and M. Kulmala (2010). *Observations of turbulence-induced new particle formation in the residual layer, Atmos. Chem. Phys.*, 10, 4319-4330, doi:10.5194/acp-10-4319-2010, 2010.

Aerosol optical properties before, during, and after cloud events at Puijo

A. Leskinen[1], A. Arola[1], H. Portin[1,2], S. Romakkaniemi[2], A.-P. Hyvärinen[3], A. Laaksonen[3], K.E.J. Lehtinen[1,2] and M. Komppula[1]

[1]Finnish Meteorological Institute, Kuopio Unit, P.O.Box 1627, FI-70211, Kuopio, Finland
[2]University of Eastern Finland, Department of Applied Physics, P.O.Box 1627, FI-70211, Kuopio, Finland
[3]Finnish Meteorological Institute, Research and Development, P.O.Box 503, FI-00101 Helsinki, Finland
Keywords: aerosol cloud interaction, atmospheric aerosols, optical properties, scavenging.
Presenting author email: Ari.Leskinen@fmi.fi

The direct effect of aerosols to radiative forcing arises from light extinction by aerosol particles, i.e. light scattering from and absorption to the aerosols, and it still has a great uncertainty. Evaluation of its magnitude is complicated, because the optical properties depend on the wavelength of the incident light and the angular distribution of the scattered light, which, in turn, depends, e.g., on the size, concentration, and chemical composition of the aerosol particles.

The Puijo measurement station on the top of an observation tower (306 m a.s.l. and 224 m above the surrounding lake level) near the town of Kuopio in Finland has provided continuous data on aerosol-cloud interactions since 2006. Since then the station has been covered by clouds 15 % of the time and is occasionally influenced by e.g. sulphurous compounds and black carbon emitted from local sources. The former are good scatterers of light and the latter absorbs light efficiently.

With a special inlet setup (total and interstitial inlets) and a switching valve system we are able to separate the activated particles from the interstitial (non-activated) particles. This enables us to define the activation properties for aerosol size distribution between 3–800 nm, measured with two differential mobility particle sizers, light scattering at the wavelengths of 450, 550, and 700 nm, measured with a nephelometer (TSI Model 3563) and light absorption at the wavelength of 670 nm, measured with a Multi-Angle Absorption Photometer (Thermo Model 5012).

The level of cloud scavenging depends not only on the aerosol size but also its chemical composition and atmospheric age. We have found that during a cloud event the scattering and absorption values for non-activated particles compared to those for the activated particles are sometimes smaller and sometimes not (Leskinen *et al.* 2012). The decrease is stronger for scattering than for absorption. This may be due to the fact that the absorptive material, e.g. fresh soot, is generally hydrophobic and therefore inhibits activation.

The stronger decrease in scattering results in a decrease in the single scattering albedo (SSA), which is the ratio of scattering to extinction (scattering + absorption). The SSA determines whether an aerosol layer causes net heating or cooling. For example, during two cloud events the SSA dropped from its initial value of 0.80–0.85 to as low as 0.4–0.5, on an average (Figure 1). A similar, but not as intensive, decrease in the SSA was observed by Berkowitz *et al.* (2011) in a foggy situation.

The scavenging is less efficient when the wind blows from the direction of local pollutant sources (the first cloud event in Figure 1) than when it blows from a cleaner sector with no local sources (the second cloud event in Figure 1). A similar observation was done by Sellegri *et al.* (2003) who concluded that the scavenging efficiency in clouds is enhanced by aging of organic species and subsequent mixing.

After the second cloud event the incoming air was clean and the scattering and absorption coefficients decreased to the same levels as during the second cloud. The low SSA values can be explained by the uncertainties in the low scattering and absorption coefficients and by the sensitivity of the SSA to the scattering coefficient value, especially in dry conditions.

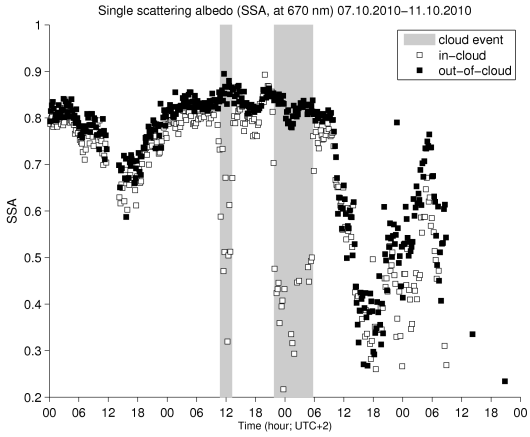

Figure 1. Single scattering albedo (SSA) before, during and after two cloud events at Puijo in October 2010.

The authors thank the support for instrumentation by the European Regional Development Fund (ERDF).

Berkowitz, C.M., Berg, L.K., Yu, X.-Y., Alexander, M.L., Laskin, A., Zaveri, R.A., Jobson, B.T., Andrews, E. and Ogren, J.A. (2011) *Atmos. Environ.* **45**, 2559-2568.

Leskinen, A., Arola, A., Komppula, M., Portin, H., Tiitta, P., Miettinen, P., Romakkaniemi, S., Laaksonen A. and Lehtinen, K.E.J. (2012) *Atmos. Chem. Phys. Discuss.* **12**, 4719-4754.

Sellegri, K., Laj, P., Dupuy, R., Legrand, M., Preunkert, S. and Putaud, J.-P. (2003) *J. Geophys. Res.* **108**, D11, 4334.

Mixing state resolved hygroscopicity closure between sub- and supersaturation in Paris

Zs. Jurányi[1, 2], M. Gysel[1], T. Tritscher[1, 3], E. Weingartner[1], M. Laborde[1] and U. Baltensperger[1]

[1]Laboratory of Atmospheric Chemistry, Paul Scherrer Institut, CH-5232 Villigen PSI, Switzerland
[2]now at: IAST, University of Applied Sciences Northwestern Switzerland, Windisch, 5210, Switzerland
[3]now at: TSI GmbH, Particle Instruments, Aachen, 52068, Germany

Keywords: cloud condensation nuclei, mixing state, hygroscopicity, megacity
Presenting author email: zsofia.juranyi@fhnw.ch

Ambient aerosols are usually complex mixtures of particles with different physical and chemical properties and consequently distinct hygroscopic behaviour. The hygroscopicity of a particle determines its water uptake at subsaturated relative humidity (RH) and influences its ability to form a cloud droplet at supersaturated RH. These processes influence the Earth's climate and the atmospheric lifetime of the particles as well.

HTDMA measurements are widely used and accepted to determine the size-resolved hygroscopicity mixing state of aerosols. Several studies on ambient aerosol were performed where, next to the overall hygroscopicity, the mixing state of the particles was investigated as well. The same hygroscopicity mixing state can be also derived from cloud condensation nuclei (CCN) counter measurements (Su et al. 2010), however it is barely done, and to our knowledge no hygroscopicity closure study was performed that does not only compare the agreement between the average hygroscopicity but also its proper distribution.

The CCN number size distributions covering 10 different supersaturations (0.1-1.0%) and total particle (CN) number size distributions from 10 to 440 nm were measured for a 10-day period during the MEGAPOLI campaign in winter 2010 in Paris. This was achieved by adding a CCN counter (CCNC) in parallel to the condensation particle counter of an SMPS (Scanning Mobility Particle Sizer) system. In addition, the mobility diameter growth factor probability density functions (GF-PDF) below saturation (at 90% RH) at 6 different dry diameters (35-265 nm) were determined from Hygroscopicity Tandem Differential Mobility Analyser (HTDMA) measurements.

Distributions of the commonly used κ parameter (Petters and Kreidenweis, 2007) were derived from both HTDMA and CCNC measurements. The CCNC derived mean particle hygroscopicity was as low as κ=0.14 averaged over all dry particle sizes and decreased with increasing supersaturation (SS) (corresponding to a decreasing dry activation diameter) from 0.09 to 0.24 at SS=1.0-0.1%. During the measurement period the aerosol was often highly externally mixed, HTDMA measurements revealed often bi- or tri-modal GF distributions, and the time dependent average GF values show significant variability as well. As an example, for the 110-nm particles ~80% of the performed scans had more than 1 GF mode and the mean GF varied between 1.1 and 1.48 within the 10 days of measurement.

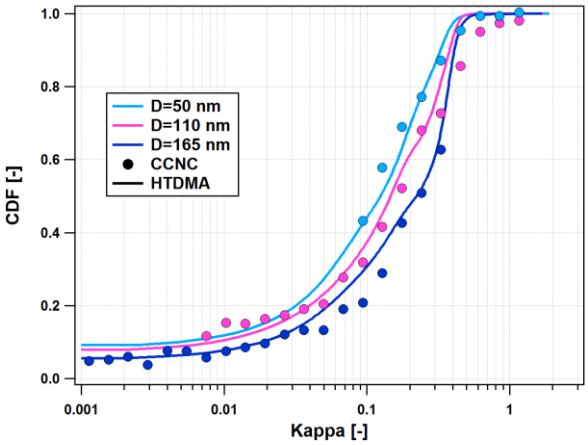

Figure 1. κ hygroscopicity parameter cumulative distribution functions (CDF) at different dry diameters as derived from hygroscopicity measurements.

Figure 1 shows the hygroscopicity (κ) cumulative distribution functions for 3 selected dry sizes (diameter D = 50, 110 and 165 nm) determined for sub- and supersaturation. It can be seen that not only the average hygroscopicity (median κ) but also its distributions agree very well between sub- and supersaturation. Based on these results, we can state that the hygroscopicity mixing state can also be successfully derived from CCN number size distribution measurements and that the assumptions used in the closure such as κ parameterisation, use of the surface tension of pure water were valid.

The success of the closure for this fast-changing, highly externally mixed, complex aerosol also suggests that significant differences between sub- and supersaturation reported in some previous hygroscopicity closure studies, might originate from measurement uncertainties and/or from insufficient time- and size-resolution.

This work was supported by MeteoSwiss in the framework of the Global Atmosphere Watch program, the Swiss National Science Foundation and the European Commission FP7 project MEGAPOLI.

Petters, M. D. and Kreidenweis, S. M. (2007) *Atmos. Chem. Phys.*, **7**, 1961-1971.

Su, H., Rose, D., Cheng, Y. F., Gunthe, S. S., Massling, A., Stock, M., Wiedensohler, A., Andreae, M. O., and Pöschl, U. (2010) *Atmos. Chem. Phys.*, **10**, 7489-7503.

Immersion freezing of biological particles

S. Hartmann[1], T. Š. Temkiv[2,3], B. G. Pummer[4], S. Augustin[1], T. Clauss[1], D. Niedermeier[1], H. Wex[1], J. Voigtländer[1], U. G. Karlson[2], H. Grothe[4] and F. Stratmann[1]

[1]Department of Physics, Leibniz Institute for Tropospheric Research, Leipzig, 04318, Germany
[2]Department of Environmental Science, Aarhus University, Roskilde, 4000, Denmark
[3] Department of Bioscience, Aarhus University, Aarhus, 8000, Denmark
[4]Institute of Materials Chemistry, Vienna University of Technology, Vienna, 1060, Austria
Keywords: ice nuclei, biogenic particles, mixed phase clouds.
Presenting author email: hartmann@tropos.de

Atmospheric observations indicate that heterogeneous ice nucleation in mixed-phase clouds can already occur at a temperature higher than - 20 °C (Seifert *et al.*, 2010). In contrast, laboratory studies showed that, e.g., mineral dust and soot particles, which are two of the major components of ice crystal residues (e.g., Pratt *et al.*, 2009), function as ice nuclei (IN) at lower temperatures. One possible explanation for the observed temperature differences might be the presence of biological particles (one out of three particles have biological origin, Pratt *et al.*, 2009) acting as IN already at temperatures above - 20 °C. Biological particles such as bacteria and pollen possess membrane proteins and non-proteinaceous macro-molecules, respectively, acting as template for ice cluster formation reducing the energy barrier required for ice nucleation. Nevertheless, the dominating freezing mechanism, the properties inducing ice nucleation, and the relative importance of biological particles in the atmosphere are still unclear.

In our study, the immersion freezing behaviour of different size-segregated biological particles is investigated at the laminar flow tube LACIS (Leipzig Aerosol Cloud Interaction Simulator, Hartmann et al., 2011). SNOMAX®, outer membrane vesicles (OMV) and surface material of pollen was used for the analysis. SNOMAX® is considered as convenient surrogate for bacterial IN and contains ice nucleation active proteins. Bacterial strains, here extracted and cultured from rain samples (Temkiv *et al.*, 2011), have the ability to produce outer membrane vesicles, which might also contain ice nucleation active proteins. Surface material washed off from pollen grains (e.g. birch) includes macro-molecules which induce ice nucleation (Pummer *et al.*, 2011).

Figure 1 shows the ice fraction f_{ice} (number of frozen droplets per sum of frozen and unfrozen droplets) as function of temperature for all biological particles investigated. For 800 nm SNOMAX® the freezing curve is very steep in a temperature range from -5 °C to -10 °C and levels off to constant values of about 0.4, i.e., 40 % of SNOMAX® particles are ice active. The ice fractions observed for the OMV containing particles where close to the detection limit (in the order of 1 % and lower). This indicates that only a small fraction of the OMV particles nucleate ice. However, considering the small size of the OMV particles (ranging between 50 nm and 160 nm as shown in Temkiv *et al.*, 2011) it might be possible that compared to SNOMAX®, the significantly reduced IN ability is mainly due to size effects. The IN contained in the washing water of birch pollen grains nucleated ice below -18 °C with f_{ice} curve having a slightly shallower slope than observed for SNOMAX®. About 80 % of the 800 nm particles might include at least one ice nucleation macro-molecule.

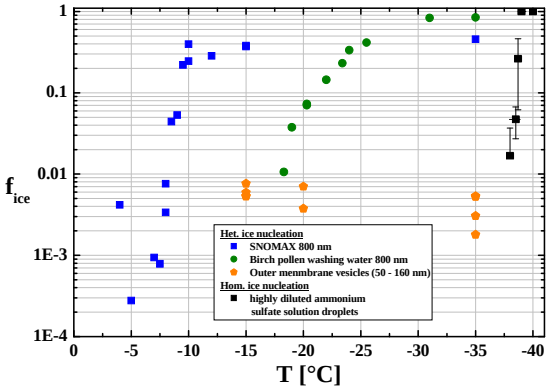

Figure 1. Ice fraction f_{ice} as function of temperature for 800 nm SNOMAX® and birch pollen washing water as well as different sized outer membrane vesicles as well as highly diluted ammonium sulphate solution droplets.

In conclusion, investigating the ice nucleation behavior of quasi monodisperse biological IN, SNOMAX® was found to be the most ice nucleation active substance, followed by the residues of birch pollen washing water. Outer membrane vesicles featured the lowest ice nucleation potential.

This work is part of the DFG research unit INUIT, under contract WE 4722/1-1.

Hartmann, S. et al. (2011) *Atmos. Chem. Phys.*, **11**, 1753-1767.
Pratt, K. et al. (2009) *Nat. Geosci.*, **2,** 397-400.
Pummer, B. G. et al. (2011) *Atmos. Chem. Phys. Discuss.*, 11, 27219-27241.
Seifert, P. et al. (2010) *J. Geophys. Res.-Atmos.*, **115**, 13.
Temkiv, T. Š. et al. (2011) Bacteria in Clouds. *PhD dissertation,* Graduate School of Science and Technolopgy, Aarhus University, Denmark.

Ice formation via deposition mode nucleation on hydrophobic and hydrophilic surfaces

J.B.C. Pettersson[1], X. Kong[1], E.S. Thomson[1], and N. Markovic´[2]

[1]Department of Chemistry and Molecular Biology, Atmospheric Science, University of Gothenburg, SE-412 96 Gothenburg, Sweden
[2]Department of Chemical and Biological Engineering, Physical Chemistry, Chalmers University of Technology, SE-412 96 Gothenburg, Sweden
Keywords: ice nucleation, cirrus, deposition freezing, soot
Presenting author email: janp@chem.gu.se

Deposition of water on aerosol particles contributes to ice cloud formation in the atmosphere with implications for the water cycle and climate on Earth. Heterogeneous ice nucleation is influenced by physico-chemical properties of substrate particles, but the mechanisms remain incompletely understood.

Here we investigate heterogeneous ice nucleation via deposition mode freezing on graphite and alcohol-covered graphite surfaces. The overall aim is to identify and characterize governing mechanisms in ice formation by deposition freezing, which can be used to guide the further development of a molecular-level description of the process. The investigated surfaces have pronounced hydrophobic and hydrophilic properties. They are simplified compared to systems found in the atmosphere, but display some characteristics that mimic properties of soot, soot coated with organics, and secondary organic aerosol particles. We describe the results from studies of pure water, and water-methanol and water-butanol mixtures at temperatures up to 213 K using elastic helium scattering and light reflection techniques. Surface science experiments at these relatively high temperatures are made possible by the use of a recently developed Environmental Molecular Beam (EMB) method that allows for experiments at pressures up to $\approx 10^{-2}$ mbar (Kong *et al.* 2011; Thomson *et al.* 2011).

We observe that nucleation of ice on a bare graphite crystal becomes increasingly inefficient as the surface temperature decreases below 200 K. The hydrophobic graphite also prevents efficient wetting in this temperature range, resulting in rough ice surfaces (e.g., Figure 1).

Adsorption of a monolayer of methanol on the graphite surface changes it from hydrophobic to highly hydrophilic. The methanol molecules provide sites for efficient hydrogen-bonding of water molecules, which stabilizes water on the surface compared to the bare graphite. Ice nucleation on the hydrophilic surface takes place at lower supersaturations than on the hydrophobic surface, and the adsorbate thus influences the absolute nucleation rate at a given temperature. Pre-adsorption of methanol also results in the growth of smooth crystalline ice (Figure 1) in sharp contrast to the rough ice surfaces grown on bare graphite (Kong *et al.* 2012).

Adsorption of a butanol monolayer results in an ice nucleation efficiency intermediate between the other systems. Butanol forms a highly stable solid layer on graphite. Water does not appear to wet the butanol layer efficiently and the water stability on the surface is lower

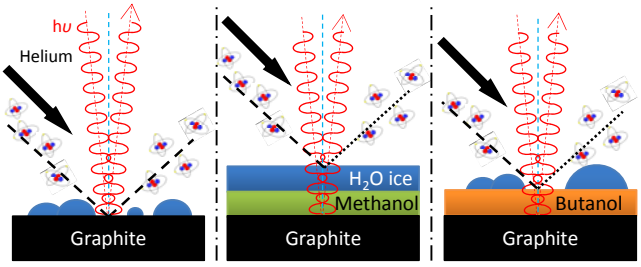

Figure 1. Schematic illustration of ice growth on bare and alcohol-covered graphite surfaces. Elastic helium scattering and light scattering were used to probe ice formation on the substrate.

than on the methanol layer. We conclude that the hydrophilicity of the different investigated surfaces influences the absolute nucleation rate. However, the supersaturation required for nucleation increases rapidly with decreasing temperature, and the overall trend with temperature is similar for all systems.

The combination of the present investigations of carbon-based hydrophobic and hydrophilic systems with existing literature provides us with a sufficient data set to allow us to generalize the behaviour of the deposition freezing process at low temperatures. Although the substrate plays a role, the overall trends with temperature are similar for different surfaces and therefore the explanation for the observed inefficient nucleation at low temperatures must be related to the inherent properties of water. The importance of the results for cloud formation processes in the Earth and Martian atmospheres are discussed.

This work was supported by the Swedish Research Council and by the Nordic Top-level Research Initiative through the program CRAICC (Cryosphere-atmosphere interactions in a changing Arctic climate).

Kong, X., Andersson, P. U., Markovic´, N. and Pettersson, J. B. C. (2011) *Physics and Chemistry of Ice 2010*, Eds. Furukawa, Y., Sazaki, G., Uchida, T. and Watanabe, N., Hokkaido University Press, 79-88.

Thomson, E., Kong, X., Andersson, P. U., Markovic´, N. and Pettersson, J. B. C. (2011) *J. Phys. Chem. Lett.* **2**, 2174–2178.

Kong, X., Thomson, E., Andersson, P. U. and Pettersson, J. B. C. (2012) *J. Phys. Chem. C,* submitted.

Cloud particle detection at the AIDA chamber & over the UK and Northern Canada

M. Krämer[1], J. Meyer[1], A. Afchine[1] M. Schnaiter[2] O. Möhler[2] S. Benz[2] A. Abdelmonem[2]
M. Gallagher[3], J. Dorsey[3], P. Brown[4], A. Wooley[5], C. Schmitt[6], R. Newton[7] and D. Baumgardner[7,8]

[1] Research Center Jülich, Institute for Energy and Climate Research (IEK-7), Wilhelm-Johnen-Str. 1, 52425 Jülich, Germany
[2] Karlsruhe Institute of Technolgy, IMK-AAF, Karlsruhe, Germany
[3] University of Manchester, Manchester, UK, [4] Met Office, Exeter, UK
[5] FAAM, Cranfield University, Cranfield, UK
[6] NCAR, Boulder, CO, USA,[7] Droplet Measurement Technologies, Boulder, USA
[8] Universidad Nacional Autonoma de Mexico, Mexico City, Mexico

Keywords: Instrument intercomparison, cloud drops and ice crystals, mixed phase clouds.
Presenting author email: m.kraemer@fz-juelich.de

To understand the formation and evolution of clouds in the atmosphere, airborne in-situ measurements of liquid and ice cloud particle sizes and concentrations are essential. Recently, the particle measurement techniques are under revision to rule out possible scientific misinterpretations due to particle artifacts, i.e. ice crystals shattered or drops splashed at the instruments edges.
Here, we present NIXE-CAPS single droplet and ice crystal measurements in the temperature range between -40 C and 0°C observed at the AIDA cloud chamber, in mixed-phase clouds over the UK during the COALESC field campaign in 2011 and over Northern Canada during the VERDI campaign in 2012. NIXE- CAPS (Novel Ice EXpEriment - Cloud and Aerosol Particle Spectrometer, manufactured by DMT) is a cloud particle spectromete which measures the cloud particle size and phase in the size range 0.6 - 945μm. The AIDA chamber is especially suitable for testing the cloud instrumentation performance without influences induced by aircraft. Comparison of NIXE-CAPS to a number of other instruments such as SMPS, APS, WELAS, SID3, PHIPS and VIPS shows an overall good agreement.

In both the chamber and the natural clouds ice crystals in the size range of 1 to several 100μm are detected. We found that the shape of the ice size distributions mirrors the drop spectra. They are unimodal in nonraining clouds with one cloud drop mode and bimodal in clouds where precipitation sized drops have developed.
The mean total ice crystal number concentration observed in the natural clouds during COALESC agrees well with the number of ice nuclei reported by DeMott et al. (2010), PNAS. On average, the mass of cloud water that is converted to ice increases with decreasing temperature. Slightly below 0°C the clouds were liquid, the highest ice mass fraction is found to be 80%. Complete glaciation is not detected in the stratocumulus mixed phase clouds over the UK.

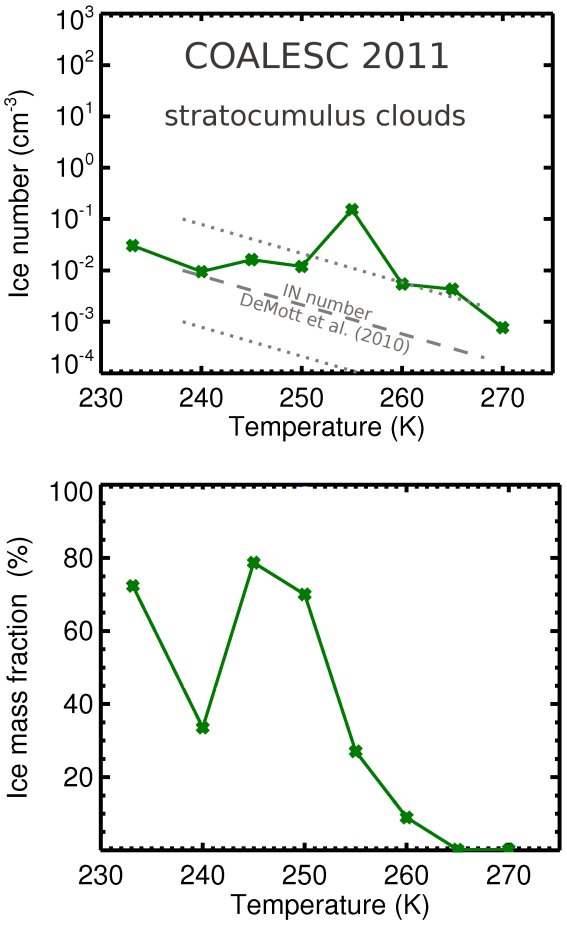

Figure 1: Mean total ice crystal number and ice mass fraction in stratocumulus mixed phase clouds during COALESC 2011 (UK).

DeMott et al. (2010) PNAS, 107:1121711222, doi:10.1073/pnas.0910818107.

Friday, September 7, 2012

Session WG11S1O. Electrical effects

Indirect Photoelectric Diffusion Charging of Aerosols

B. Grob[1] and R. Niessner[1]
[1]Chair for Analytical Chemistry, Technical University of Munich, Munich, Bavaria, 81377, Germany
Keywords: particle charging, particle counting
Presenting author email: benedikt.grob@mytum.de

Black carbon has a big impact on the public health as well as to the climate. Therefore the upcoming exhaust emission standards Euro 5b and 6 for diesel engines include a strict limit of 6.0×10^{11} particles/km of non-volatile particles. To measure the particle emission of engines, complicated measurement set-ups are necessary, which can handle high particle concentrations, prevent coagulation, separate non-volatile and volatile particles and count efficiently particles in the low nanometer-range. The idea of the car manufacturers currently is to use condensation nucleus counters (CNC), which causes many problems due to measurement reproducibility and to their susceptibility to chemical particle composition (Giechaskiel, 2009 and 2011). An alternative is the counting of unipolar charged particles by a aerosol electrometer. However, a unipolar charging method is necessary, which can charge particles in a range of 10 to 100 nm efficiently.

In this study we are using a modified set-up published by Bucholski and Niessner (1991). It consists of an elliptically grooved, electrically grounded alumina block (Figure 1). A UV lamp is fixed in one focus of the ellipse to concentrate the light to the second focus. The aerosol flux is pumped through a quartz tube placed in the second focus. In the medial axis of the tube a metal rod is installed. On the rod a voltage can be applied. The idea is to emit electrons on the metal surface, due to the photoeffect. The photoelectrons can charge directly by diffusion the aerosol particles or form negative ions by attachment processes, which itself collide with the aerosol particles. It was shown that the set-up is working for NaCl particles, with a gold or nickel rod at a wavelength of 185 nm (Bucholski & Niessner, 1991).

The challenge for charging black carbon particles is to find a material for the rod which has a lower work-function then the particle. It has to be avoided to perform the photoelectric charging directly on the particle surface. Additionally the ozone formation has to be prevented, which will take place in a combustion aerosol by radiation with 185 nm photons. Therefore we changed the set-up to a UV lamp of 254 nm and a magnesium rod.

With this method it seems to be possible to charge the particles with a efficiency of over 90% (Figure 2). To prove the system we study several questions like influence of particle size, surface morphology, particle concentration and effect of multiple charging. We think with our approach of the indirect photoelectric diffusion charging we can overcome the disadvantages of the directly photoelectric aerosol charging and we provide an alternative to the particle counting by a CNC.

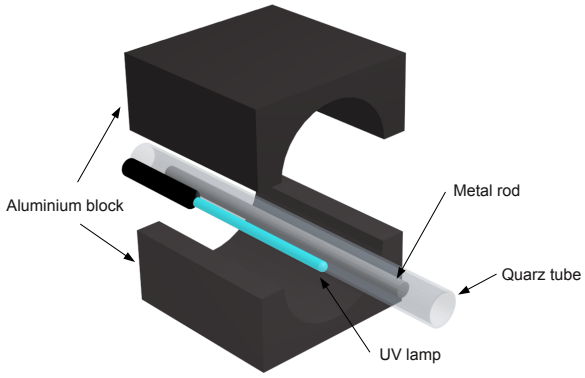

Figure 1: Set-up for the production of low energy photoelectrons

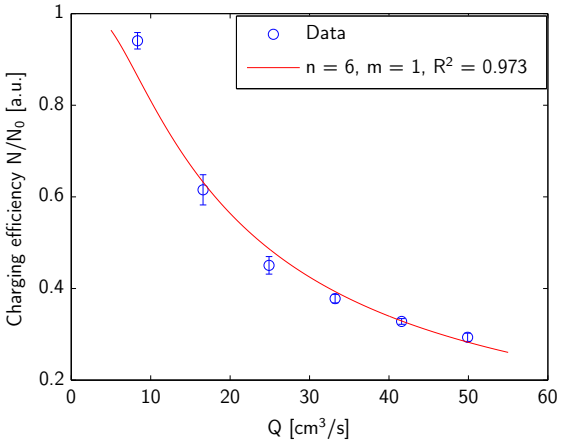

Figure 2: Charging efficiency versus aerosol flux Q of 40 nm spark discharge soot particles with an applied potential on the rod of -4.5 kV and a irradiation wavelength of 254nm

Bucholski, A., Niessner, R. (1991) *Journal of Aerosol Science* **22**, 111-115.
Giechaskiel, B., Wang, X., Horn, H.G., Spielvogel, J., Gerhart, C., Southgate, J., Jing, L., Kasper, M., Drossinos, Y., Krasenbrink, A. (2009) *Aerosol Science and Technology* **43**, 1146-1173
Giechaskiel, B., Wang, X., Gilliland, D., Drossinos, Y. (2011) *Journal of Aerosol Science*, **42**, 20-37.

High resolution mobility and mass spectra of corona-generated ions

H.E. Manninen[1], A. Franchin[1], E. Järvinen[1], J. Kangasluoma[1], S. Schobesberger[1], T. Petäjä[1] and M. Kulmala[1]

[1]Department of Physics, University of Helsinki, Helsinki, FI-00014 University of Helsinki, Finland
Keywords: corona discharge, ions, DMA, aerosol mass spectrometry.
Presenting author email: hanna.manninen@helsinki.fi

We present mobility distribution measurements of both positive and negative ions produced by corona discharge under different conditions. Here, the measured mobilities of the corona-generated ions are converted to Millikan-Fuchs equivalent mobility-diameters (Mäkelä et al., 1996). The chemical composition of the ions was measured in parallel with the mobility measurements. The aim was to characterise both the mobility and chemical composition of the ions generated by a corona-needle charger from the Neutral cluster and Air Ion Spectrometer (NAIS, Manninen et al. 2009) with state-of-art instrumentation.

The corona-generated ions were characterized with a high resolution Herrmann Differential Mobility Analyzer (H-DMA), which has nearly monomobile transfer functions (sample to sheath flow ratio ~1:100). The negative corona ions were < 1.6 nm (0.8 $cm^2 V^{-1} s^{-1}$ in mobility) in all the tested gas mixtures (nitrogen, air with variable mixing ratios of water vapour), whereas the positive ions were < 1.7 nm (0.7 $cm^2 V^{-1} s^{-1}$). An Atmospheric Pressure Interface Time-Of-Flight mass spectrometer (APi-TOF, Ehn et al. 2011) was used to measure the mass/charge ratios of corona-generated ions, from which we can find quite accurately (<20 ppm) their exact masses which correspond to certain elemental compositions.

Our results indicate that in the corona discharging process the mobility and the concentration of ions depend both on the corona voltage and on the physical and chemical properties of the carrier gas mixture. The role of the water vapour is pronounced. The chemical composition of corona-generated ions has been observed to depend on the trace gas composition and time for reactions, as one could expect. The results of this study help in understanding the large scattering of ion mobility values given in earlier publications.

The mobility distribution of the positive and negative corona-generated ions, shown in Fig. 1, illustrates the effects of carrier gas and impurities in the sample lines on the size distribution observed during laboratory experiments. Asmi et al. (2009) and Manninen et al. (2011) both used the corona discharger of the NAIS to generate these ions. Basically, the only difference between the experiments is the design of the sample lines and the exact composition of the carrier gas, as the charger current stayed constant in both experiments. In Fig. 1, the black dots represent corona-generated ions carried by filtered compressed air and the gray stars represent ions carried by room air. The room air contains e.g. more water vapour compared to the compressed air.

This result found an agreement with earlier publications and indicated that the mobility and concentration of charger ions generated in the corona charging process depend strongly on the properties and composition of the carrier gas. Therefore, in field conditions the corona-generated ion mobility and composition changes with time when the corona discharger is used to charge the aerosol sample.

Therefore, the corona-generated ions complicate NAIS particle detection in the measurement range which overlaps the mobility range of charger ions. The positive and negative corona-generated ions were smaller than 1.8 and 1.6 nm, respectively, which results in the lower detection limit of approximately 2 nm for the NAIS particle measurements. Thus, particles below a diameter of ~2 nm cannot be reliably distinguished from the corona-generated ions. An efficient filtering of these ions, but not the charged particles, at different operating conditions is essential for achieving the lowest possible size limit for the electrical detection of charged particles.

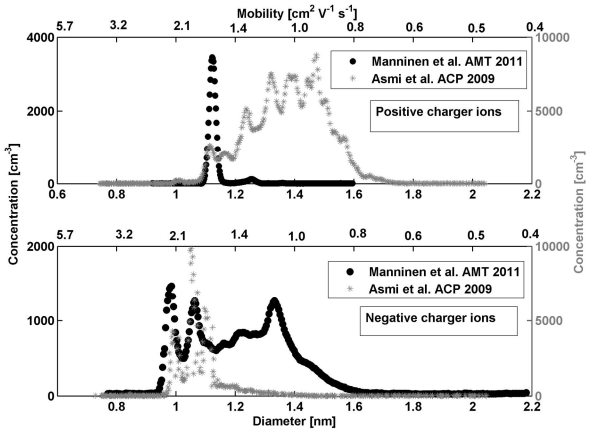

Figure 1. The size distribution of positive and negative corona charger ions measured with a high resolution H-DMA by Asmi et al. (2009) and Manninen et al. (2011).

The financial support by the Academy of Finland Centre of Excellence program (Project No. 1118615) is gratefully acknowledged.

Asmi, E. et al. (2009) *Atmos. Chem. Phys*., 9, 141-154.
Ehn, M. et al. (2011) *Aerosol Sci. Technol.* 45: 522-532.
Manninen, H.E. et al. (2009) *Boreal Env. Res.* 14, 591-605.
Manninen, H. E. et al. (2011) *Atmos. Meas. Tech.*, 4, 2767-2776.

Study of the corona discharge in the syngas at various gas temperatures and pressure

A. Bologa, H.-R. Paur, H. Seifert and K. Woletz

Institute for Technical Chemistry, Karlsruhe Institute of Technology
Hermann-von-Helmholtz-Platz 1, Eggenstein-Leopoldshafen, 76344, Germany
Keywords: corona discharge, gas composition, temperature, pressure
Presenting author email: andrei.bologa@kit.edu

The use of corona discharge opens broad possibilities for developments in many fields such high temperature / high pressure electrostatic precipitators (HT/HP ESPs'), electrohydrodynamic pumps, heat exchangers, decomposition of toxic gases, etc. (Chang *et al*, 1995, Bologa *et al*, 2011,a).

The corona discharge occurs when a high voltage is applied between two electrodes with substantially different radii of curvature. The charge generation and transport in the gaseous media is one of the key-points of corona discharge which characteristics strongly depend on gas composition, velocity, temperature, humidity and pressure; electrode system geometry; form, value and polarity of applied voltage and electrogasodynamic phenomena in electrode system, etc. (Bologa et al. 2011,b) By gas cleaning in electrostatic precipitators, the corona discharge characteristics depend on particle mass and number concentration in the exhaust gas, particle physical properties, aerosol space charge, loading of the electrode system with precipitated aerosol, etc. The objective of the current work is the study of the corona discharge at various temperatures and pressures in the syngas (a gas mixture which contains varying amounts of H_2 and CO). The 1st purpose is to define the conditions of stable corona discharge which ensure effective charging of particles and their precipitation. The 2nd purpose is to observe the phenomena in the HT/HP syngas in the corona discharge ionizer. The aim is the development of the new type of high temperature / high pressure electrostatic precipitator.

The experimental studies are carried out with a high temperature / high pressure ionizer (Bologa *et.al*, 2011,a,b). The ionizer is installed inside of a high pressure vessel (gas pressure up to 2,0 MPa and temperature up to 500°C). The electrode gap between the high voltage and grounded electrodes is 10 mm. The tests were carried out with two different gas mixtures. The first one contained 25,7 Vol.% H_2; 38,0 Vol.% CO; 18,3 Vol.%CO_2; 0,2 % of CH_4 and rest (17,8 Vol.%) was N_2. The second one contained 40 Vol.% of H_2 and 60 Vol.% of CO.

The current-voltage characteristics of the negative corona discharge in the 1st gas mixture for various temperatures and pressures are presented in the Figure 1 and 2. The corona current by the negative polarity of applied voltage was higher than for positive polarity of applied voltage. At room temperature conditions the increase of gas pressure strongly suppresses the corona discharge (Fig.1). By increase of gas temperature, the conditions of stable corona discharge are extended to higher gas pressures (Fig.2).

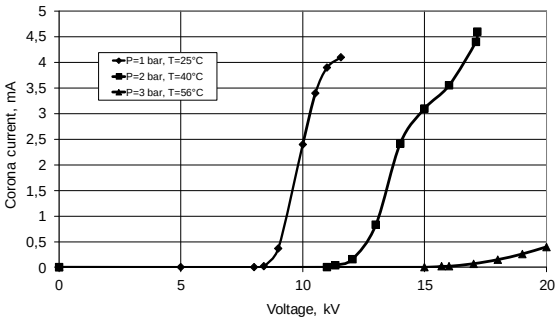

Figure 1 Corona discharge at room conditions.

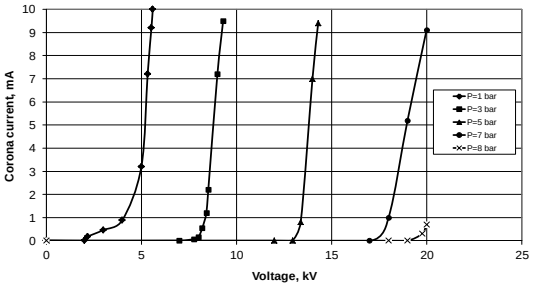

Figure 2 Corona discharge at 500°C.

By the experimental studies the following phenomena were observed. By high temperatures, the application of corona discharge:
(i) can change the composition of the 1st gas mixture. It was observed the increase of CO_2 and corresponding decrease of CO concentrations;
(ii) can provoke the generation of nanoparticles in the ionizer stage from the 1st gas mixture which are precipitated inside of the ionizer under the influence of the electric field forces;
(iii) by special design of the electrodes, in the 2nd gas mixture a large quantity of aerosol can be generated during relative short period of time. By aerosol generation, the decrease of gas pressure inside of the HT/HP vessel was observed.

Chang J.S., Kelly A.J., and Crowley J.M. (1995), *Handbook of electrostatics processes*, Marcel Dekker, New York.

Bologa A., Paur H.-R., Seifert H. and Woletz K. (2011), *International Journal on Plasma Environmental Science & Technology*, **5(2),** 110-116.

Bologa A, Paur H.-R., Seifert H. and Woletz K. (2011), *Proc. of European Aerosol Conference, Manchester.*

Stability of the cone-jet mode in electrohydrodynamic spraying

J.L. Castillo, S. Martin, A. Perea and P.L. Garcia-Ybarra

Dept. Fisica Matematica y de Fluidos, Facultad de Ciencias UNED, Madrid, Spain
Keywords: Electrospray, Particle deposition, Deposit morphology, Material synthesis
Presenting author email: jcastillo@ccia.uned.es

Granular materials with a given microstructure may be efficiently prepared via an aerosol route starting with the electrohydrodynamic atomization of a liquid suspension. The liquid is pumped through a needle under the presence of strong voltage differences between the needle and the surroundings. Then, the electrosprayed charged droplets evaporate along their pathway leaving a dry residue that deposits on a collecting plate (Martin et al., 2010a, 2010b). For attaining a highly porous material at the deposit, the collecting plate must be kept relatively far from the electrospray ejecting needle as the solvent must have enough time to evaporate during the flight of the droplets. On the other hand, the efficiency in the capture of the dry particles substantially improves when a negative voltage is applied to the collector plate, leading to an electric field that forces the charged particles to deposit preferentially over the plate. Under these conditions, the intensity of the *electric field at the needle exit* controls the operating mode of the electrospray whereas the strength and homogeneity of the *electric field at the plate* surface determines the deposition features of the charged particles and thus, the morphological properties (bulk porosity, compactness and surface roughness) of the formed deposit (Rodriguez-Perez et al, 2005, 2007).

The electrospray should work in a stable mode to be used as a steady generator of almost monodisperse droplets. A steady cone-jet mode (consisting of a Taylor cone formed at the needle exit and a very thin jet emerging from the cone tip) is only achieved in a range of flow rates and voltage differences.

In the classical electrospray configuration (Cloupeau and Prunet-Foch, 1989) a high positive voltage (V_n) is imposed at the needle and the liquid is ejected at a given flow rate, Q, toward a collecting plate connected to ground. Then, Q and V_n remains as the control parameters and the cone-jet mode is stable in a stability island on the (Q, V_n) space. The borders of the island depend on the liquid properties (electrical conductivity, viscosity and surface tension) and in minor extend on geometrical aspects.

However, other configurations may lead to significant changes in the stability island. Indeed, an opposite polarity at the plate is required when the main objective of the electrospraying process is to collect the charged particles emitted at the needle. This configuration introduces a new degree of freedom in the experimental set-up; that is, the voltage applied to the plate (V_p), with some additional parameters that affect the electric field at the needle exit: the needle-plate distance and the plate dimensions.

The present work (Castillo et al, 2012, Martin et al, 2012) extends previous studies by performing an experimental investigation on the stable cone-jet domain when a voltage is also applied to the plate. For completeness, positive as well as negative polarities of the plate voltage are investigated, showing the changes induced in the range of liquid flow rates compatible with a stable cone-jet mode configuration.

Thus, the stability island corresponding to the electrohydrodynamic spraying of different liquids [a pure liquid (ethanol), a liquid mixture (isopropanol+Nafion®) and liquid suspensions (Pt on carbon nanoparticles in ethanol)] has been experimentally determined. A broader range of liquid flow rates compatible with a stable cone-jet mode is observed. Thus, the two-dimensional cone-jet domain in the classical needle voltage-flow rate diagram (for a grounded plate) is recovered as embedded in the three-dimensional parameter space (Q, $V_n - V_p$, V_p). When the voltage polarity applied to the plate is opposite to the needle polarity, the maximum flow rate compatible with the cone-jet regime is much larger than for an electrically grounded plate. This amplification factor increases with the liquid electrical conductivity. Also, when liquid suspensions (based on Pt/C nanoparticles in ethanol) are electrosprayed, the maximum flow rate is more than twice the value for a grounded plate.

This configuration allows a suitable control of the whole process (electrospray + deposit formation + deposit morphology) and opens the door for preparing new materials as those required for fuel cell electrodes.

Work supported by Ministerio de Ciencia e Innovacion (Spain) [grant ENE2011-26868 and Consolider-Ingenio 2010 (CSD2010-00011)], and also by Comunidad de Madrid (project HYSYCOMB, S2009ENE-1597).

Castillo, J.L., Martin. S., Rodriguez-Perez, D., Perea, A. and Garcia-Ybarra, P.L. (2012). *KONA Powder and Particle Journal*, **30** (2012), in press.

Cloupeau, M., and Prunet-Foch, B. (1989). *Journal of Electrostatics*, **22**, 135-159.

Martin, S., Garcia-Ybarra, P.L., and Castillo, J.L. (2010a). *J. Power Sources*, **195**, 2443-2449.

Martin, S., Garcia-Ybarra, P.L., and Castillo, J.L. (2010b). *Int. J. Hydrogen Energy*, **35**, 10446-10451.

Martin, S., Perea, A., Garcia-Ybarra, P.L. and Castillo, J.L. (2012) *J. Aerosol Science*, **46**, 53-65.

Rodriguez-Perez, D., Castillo, J.L., and Antoranz, J.C. (2005). *Phys. Rev. E*, **72**, 021403.

Rodriguez-Perez, D., Castillo, J.L., and Antoranz, J.C. (2007). *Phys. Rev. E*, **76**, 011407.

Electrospray deposition of nanoparticles onto airborn microparticles

C.U. Yurteri[1], N. Ellis[2], J.R. van Ommen[1]

[1] Delft University of Technology, Faculty of Applied Science, Julianalaan 136, 2628 BL Delft, The Netherlands
[2] University of British Columbia, Chemical and Biological Engineering, 2360 East Mall, Vancouver, BC V6T 1Z3, Canada

Keywords: coating, nano_particles, electrospray.
e-mail: c.u.yurteri@tudelft.nl

Coated particles are common in industrial and pharmaceutical applications. Coating surfaces of micron-sized particles (host particles or carriers) with nanoparticles (guest particles) can set up chemical or biological contact points allowing diagnosis and treatment of respiratory diseases, adding functionalities, such as changing the hydrophobic or hydrophilic behaviour, anti-reflex performance or the catalytic activity. In case of inhalation, nanoparticles can also be more efficiently transported using micro vehicles [1-3].

Coating can be realized via either dry or wet coating techniques. However, dispersing dry nano-sized particles in the former case, and use of liquid solvents and dispersants requiring evaporative removal during dispersion steps in the latter case are among major challenges. A solution for dispersing and directly depositing nanoparticles in one step can be realized by Electrohydrodynamic atomization (EHDA), also called electrospraying, a process where a liquid jet breaks up under the influence of electrical forces. EHDA comes with unique advantages: a narrow droplet size distribution; and self dispersing of droplets due to unipolar charged droplets. Electrospraying suspensions of nanoparticles results in a charged spray of nanoparticles, overcoming the challenges of dispersing and depositing nanoparticles on a substrate.

The charged nature of nanoparticles via EHDA can be utilized to coat host particles charged with opposite polarity by means of tribocharging, field, diffusion, or inductive charging to enhance the efficiency of deposition. Furthermore, mechanical, or electrostatic interactions can also be utilized to combine particles. In the latter case, a bipolar coagulation due to the mutual electrostatic attraction force between the negative and positive charges will take place. Thus, guest particles deposit on the surface of host particles while airborne. Figure 1 is a typical result from such interaction. Once coated, the van der Waals forces keep nanoparticles from detaching from host particles. The coating level is controlled by the interaction time, the concentration of the suspension, and the charge of host particles in the spray.

Several possibilities to accomplish mutual interaction of oppositely charged particles in order to deposit electrosprayed or electrospray formed nanoparticles on micron-sized particles have been studied by our group. By controlling the electrostatic charge of host particles relative to the charge of nanoparticles, the coating quality can be optimized.

We will present results from various process lay-outs and demonstrate a novel approach for continuous production of nanostructured particles. The approach is based on various processes: fluidization, tribocharging, elutriation, and electrohydrodynamic atomization.

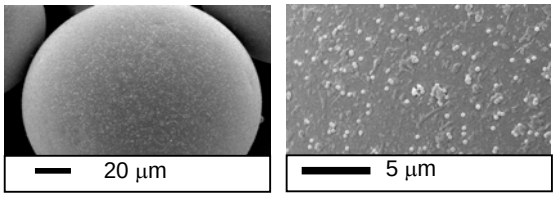

Figure 1. 125 um glass bead coated with 260 nm Zeta diameter PS spheres (D10 = 150 nm, D50 = 220 nm, D90 = 345 nm as measured with Malvern ZetaSizer)..

Funding from the Natural Sciences and Engineering Research Council of Canada (NSERC) is graciously acknowledged.

References:

1. F. Schulz, S. Franzka, G. Schmid, Nanostructured surfaces by deposition of metal nanoparticles by means of spray techniques, Adv. Funct. Mater. 12(8) (2002) 532-536.
2. N. Ellis, C.U. Yurteri, Ruud van Ommen, J. Continuous process to deposit nanoparticles onto microparticles, Chemical Engineering Journal 181– 182 (2012) 798– 805
3. M.A.T. Cardoso, M. Talebi, P.A.M.H. Soares, C.U. Yurteri, J.R. van Ommen, Functionalization of lactose as a biological carrier for bovine serum albumin by electrospraying. Int J Pharmaceut (2011), 414 (1-2) (2011) 1-5.

Determination of the Transition Regime Collision Rate in the Presence of Potential Interactions from Mean First Passage Time Calculations

Christopher J. Hogan Jr.[1], Ranganathan Gopalakrishnan[1], Hui Ouyang[1]

[1]Department of Mechanical Engineering, University of Minnesota, Minneapolis, MN, 55455, USA
Keywords: Coagulation, Diffusion Charging, Transition Regime, Brownian Dynamics
Presenting author email: Hogan@me.umn.edu

The behaviour of aerosol nanoparticles is strongly influenced by collisions between particles (leading to adherence; coagulation), as well as particles with ions (leading to charge transfer; diffusion charging). Complex about these processes is that 1). collision processes for nanoparticles in atmospheric pressure environments occur in neither in the mass transfer continuum nor mass transfer free molecular regimes (they occur in the transition regime), and 2). particle-particle and particle-ion interactions also influence collision rates. Traditionally, the flux matching approach of Fuchs (1963) has been used to predict collision rates in the mass transfer transition regime, and in comparison to experimental results this approach has been shown to be quite successful in the absence of potential interactions. Recent work (Gatti & Kortshagen, 2008), however, reveals that in the presence of strong attractive potential interactions between colliding entities, application of the flux matching approach to collision rate calculation may be problematic. Specifically, in the standard application of flux matching, a limiting sphere concept is employed, whose radius defines the boundary between continuum and free molecular motion. Problematic in the use of this concept is that on the limiting sphere radius, the velocity distribution of particles is not known in the presence of strong potential interactions, and, in the case of strong attractive interactions, completely free molecular motion does not describe well particle motion inside the limiting sphere (Gopalakrishnan & Hogan, 2012).

We describe an alternative approach for the examination of collision rates in the transition regime in the presence of potential interactions between colliding entities: mean first passage time calculations. In this method, the relative motion between colliding entities in the gas phase is monitored by a Langevin equation. From determination of the average time necessary for entities to collide under specified conditions (the mean first passage time), the collision rate is inferred. In conjunction with mean first passage time calculations, it is shown that regardless of the functional form for the potential between colliding entities, the collision rate coefficient, β_{ij}, can be non-dimensionalized as:

$$H = \frac{\beta_{ij} m_{ij} \eta_C}{f_{ij} (a_i + a_j)^3 \eta_{FM}^2} \qquad (1)$$

where m_{ij} is the reduced mass of the colliding entities, f_{ij} is their reduced friction factor, a_i and a_j are the radii of the colliding entities, and η_C and η_{FM} are the potential dependent enhancement factors for the collision process in the continuum and free molecular regimes, respectively. The dimensionless collision rate coefficient, H, is found to depend on the diffusive Knudsen number, $\mathrm{Kn_D}$:

$$\mathrm{Kn_D} = \frac{(kTm_{ij})^{1/2} \eta_C}{f_{ij} (a_i + a_j) \eta_{FM}} \qquad (2)$$

where kT is the thermal energy. As shown in figure 1 for the image potential, provided the potential energy/thermal energy ratio is sufficiently low, mean first passage time calculations reveal a near universal relationship to describe collisions, $\mathrm{H(Kn_D)}$ is found:

$$H = \frac{4\pi \mathrm{Kn_D^2} + C_1 \mathrm{Kn_D^3} + (8\pi)^{1/2} C_2 \mathrm{Kn_D^4}}{1 + C_3 \mathrm{Kn_D} + C_4 \mathrm{Kn_D^2} + C_2 \mathrm{Kn_D^3}} \qquad (3)$$

where C_1 =25.836, C_2 = 11.211, C_3 = 3.502, and C_4 = 7.211.

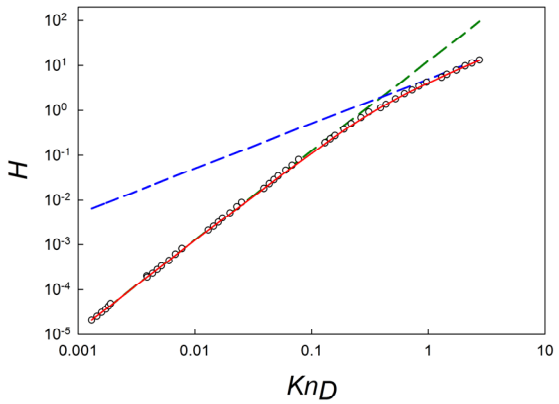

Figure 1. $\mathrm{H}(Kn_D)$ in the continuum limit (green), free molecular limit (blue), from equation (3) (red), and from mean first passage time calculations considering the image potential (open circles).

Fuchs, N. A. (1963). On the Stationary Charge Distribution on Aerosol Particles in a Bipolar Ionic Atmosphere. *Geofis. Pura Appl.*, **51**, 185-193.

Gatti, M. & Kortshagen, U. (2008). Analytical model of particle charging in plasmas over a wide range of collisionality. *Physical Review E*, **78**(4), 046402.

Gopalakrishnan, R. & Hogan, C. J. (2012). Coulomb Influenced Collision in Aerosols and Dusty Plasmas. *Physical Review E*, **In Press**.

Charge Distribution of Primary Nanoparticles Generated by Spark Discharge

K.Barmpounis[1], T.V. Pfeiffer[1],G. Biskos[1], A. Schmidt-Ott[1]

[1]Department of Chemical Technology, Delft University of Technology, Delft, 2628-BL, The Netherlands
Keywords: Spark discharge, Charge Distribution, Particle Coagulation
Presenting author email: K.Barmpounis@tudelft.nl

Spark discharge generators are widely used for a controllable and stable production of high-purity aerosol nanoparticles down to sizes in the range of 1 nm (Schwyn et al. 1988). The mechanism of particle formation is caused by an evaporation/condensation type process based on a capacitive spark discharge between two target electrodes. During spark discharge, material is evaporated from the electrodes, and is immediately quenched in a flow of inert carrier gas. Through coalescence, these clusters grow into bigger primary particles, which are carried away from the discharge zone by the carrier gas.

While little is known about the mechanism of the charging process within the spark discharge, it appears to lead to a much higher charging probability than the Boltzmann-type equilibrium distribution (Tabrizi 2008). Knowledge of the charge distribution would be of great importance, since combining spark generators with mobility classifiers represents a versatile method of producing well-defined nanoparticles. Spark discharge nanoparticle generators usually produce a particle concentration that leads to rapid coagulation, changing the charge distribution.

We report a measurement, which allows derivation of an estimate of the primary particle charge distribution for the size range around 2 nm using Pt as electrode material. In order to calculate the portion of charged primary particles, the total number concentration of particles needs to be measured, and this is the greatest challenge. Due to their small size it is not possible to apply condensation nucleus counters, and charging methods are hardly efficient enough to allow the use of an Aerosol Electrometer (AEM) for the fraction that is initially neutral.

To overcome this limitation, we allowed our primary particles to coagulate in a controlled manner and measured their growth by means of electrical mobility analysis. Particle growth due to coagulation is a function of the particles total number concentration, and the coagulation coefficient, which, in turn, depends on particle size and charge. Coagulation theory (Huang 1990) can then be used to derive the total number concentration of primary particles, if the other parameters are known. With such an approach, due to the dependence of the coagulation coefficient on the charged state of the particles (Maisels 2002), the charged state of primary particles can be outlined.

Measurements of the size distribution of the charged fraction of the generated particles were performed using a High-Flow DMA coupled with an aerosol electrometer (AEM). Primary particles of both polarities were classified in terms of their electrical mobility while preserving their initial charge distribution. In a second run, an agglomeration chamber was placed between the spark generator and the DMA, allowing particles to grow for a very short residence time (ca. 0.6 sec). Shift of mean particle size after agglomeration is the parameter used in the agglomeration model in order to calculate the total concentration of the primary particles.

Results

There is strong evidence for the multiply charged nature of Pt primary particles eroding from the spark discharge. They appear having significantly larger electrical mobility, than the “neutralized” size distribution (fig.1). Calculations showed that higher charged state (mostly 3 charges) defines particle charged state. The portion of triply charged particles was calculated to 0.70% of the total number concentration of primary particles.

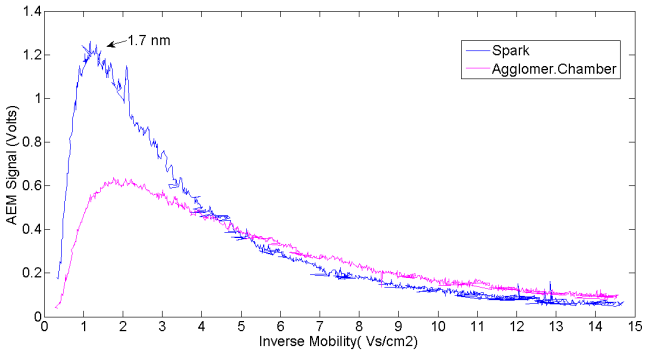

Figure 1. Mobility distribution of Pt negatively charged primary particles as measured in three different setups.

Schwyn, S., Garwin, E. & Schmidt-Ott, A. (1988), *J. Aerosol Sci.*, 19(5), 639-642.

Tabrizi N.S., Ullmann M., Vons V. A., Lafont U., Schmidt-Ott, A (2008). *J. Nanopart. Res.*, 11(2), 315-332.

Huang, D. D., and Seinfeld, J. H., J. Colloid Interface Sci. 139, 213 (1990)

Maisels A., Einar Kruis F. And Fissan H., Journal of Colloid and Interface Science 255, 332–340 (2002)